

# TRANSACTIONS

*American Society for Metals*

VOL. XLIII

1951

## TECHNICAL PROGRAM AND REPORTS OF OFFICERS AMERICAN SOCIETY FOR METALS—32nd ANNUAL CONVENTION, CHICAGO, OCTOBER 21 to 27, 1950

FOR purposes of record and for the benefit of members who were not in attendance at the Thirty-second Annual Convention of the Society, held in Chicago, October 21 to 27, 1950, the Programs of the Technical Papers and Educational Lectures together with the Reports of Officers for 1950 are herewith published in full.

### TECHNICAL PAPERS PROGRAM

#### Seminar on Atom Movements

Saturday, October 21

*Normandie Lounge, Stevens Hotel, 9:30 A.M.*

Chairman: J. H. Hollomon, General Electric Co.

*Formal Basis of Diffusion Theory*, by L. Darken, U. S. Steel Co. Research Laboratories.

*Chemical Techniques and Analysis of Diffusion Data*, by Cyril Wells, Carnegie Institute of Technology.

*Tracer and Other Techniques of Diffusion Measurements*, by R. Hoffman, General Electric Co., Research Laboratory.

*Normandie Lounge, Stevens Hotel, 2:00 P.M.*

Chairman: Frederick Seitz, University of Illinois

*Mechanisms of Diffusion*, by H. Huntington, Rensselaer Polytechnic Institute.

*Diffusion in Alloys and the Kirkendall Effect*, by J. Bardeen and C. Herring, Bell Telephone Laboratories.

*Volume Diffusion—An Empirical Survey*, by C. E. Birchenall, Carnegie Institute of Technology.

Sunday, October 22

*Ballroom, Palmer House, 9:30 A.M.*

Chairman: Clarence Zener, University of Chicago

*Grain Boundary and Surface Diffusion*, by D. Turnbull, General Electric Co., Research Laboratories.

*Diffusion and High-Temperature Oxidation of Metals*, by C. Wagner, Massachusetts Institute of Technology.

*Gas-Metal Diffusion and Internal Oxidation*, by F. N. Rhines, Carnegie Institute of Technology.



Ballroom, Palmer House, 2:00 P.M.

Chairman: J. K. Stanley, Westinghouse Electric Corp.

*Diffusion in Sintering*, by P. Duwez, California Institute of Technology.

*The Migration of Grain Boundaries*, by J. Burke, General Electric Co., Knolls Atomic Power Laboratory.

*Summary*, by R. F. Mehl, Carnegie Institute of Technology.

General Discussion

### Monday, October 23

#### Surface Phenomena Session

Ballroom, Palmer House, 9:30 A.M.

Co-Chairmen: V. H. Patterson, Climax Molybdenum Co.

W. A. Pennington, Carrier Corp.

*The Carbonitriding Process of Case Hardening Steel*, by G. W. P. Rengstorff, Battelle Memorial Institute, M. B. Bever and C. F. Floe, Massachusetts Institute of Technology.

*Constitution of Carbonitrided Cases*, by G. W. P. Rengstorff, Battelle Memorial Institute, M. B. Bever and C. F. Floe, Massachusetts Institute of Technology.

*Effect of Bath Composition on Aluminum Coatings on Steel*, by D. O. Gittings, D. H. Rowland and J. O. Mack, Carnegie-Illinois Steel Corp.

*Formation of Oxides on Some Stainless Steels at High Temperatures*, by H. M. McCullough, Sylvania Electric Products Inc., and M. G. Fontana and F. H. Beck, Ohio State University.

*The Oxidation of Pure Iron*, by J. K. Stanley and Miss J. vonHoene, Westinghouse Research Laboratories, and R. T. Huntoon, Carnegie Institute of Technology.

#### Physical Metallurgy Session

Ballroom, Palmer House, 2:00 P.M.

Co-Chairmen: A. J. Herzig, Climax Molybdenum Co.

E. S. Rowland, Timken Roller Bearing Co.

*Recovery and Cold Working of 52S Commercial Aluminum Alloy*, by Gerard H. Boss, Metallurgy Division, Oak Ridge National Laboratory.

*A Metallurgical Investigation of Silver Chloride*, by R. D. Moeller, F. W. Schonfeld, C. R. Tipton, Jr., and J. T. Waber, Los Alamos Scientific Laboratory.

*Molybdenum Plating by Reduction of the Pentachloride Vapor*, by W. J. Childs, J. E. Cline, W. M. Kisner and John Wulff, Massachusetts Institute of Technology.

*Structure of Permanent Magnet Alloys*, by A. H. Geisler, General Electric Co.

### Tuesday, October 24

#### High Temperature Metallurgy Session

Ballroom, Palmer House, 9:30 A.M.

Co-Chairmen: J. K. Stanley, Westinghouse Electric Corp.

L. P. Tarasov, Norton Co.

*Transformations in Ferritic Chromium Steels Between 1100 and 1500 °F (595 and 815 °C)*, by F. J. Shortsleeve and M. E. Nicholson, Standard Oil Co.

*Hardening of High-Chromium Steels by Sigma Phase Formation*, by John J. Gilman, Crucible Steel Co. of America.

*Nickel-Aluminum-Molybdenum Alloys for Service at Elevated Temperatures*, by H. V. Kinsey, Department of Mines and Technical Surveys, Ottawa, and M. T. Stewart, National Research Council of Canada.

*Sigma Phase Formation in a Wrought Heat Resisting Steel*, by A. E. Bindari, Illinois Institute of Technology; P. K. Koh, Allegheny Ludlum Steel Corp., and Otto Zmeskal, Illinois Institute of Technology.

*Long-Time Elevated-Temperature Test of Chromium-Molybdenum Steels*, by A. B. Wilder and J. O. Light, National Tube Co.

#### High Temperature Metallurgy Session

Ballroom, Palmer House, 2:00 P.M.

Co-Chairmen: N. J. Grant, Massachusetts Institute of Technology  
J. J. Kanter, Crane Co.

*Formation of Austenite in High-Chromium Stainless Steels*, by C. B. Post and W. S. Eberly, Carpenter Steel Co.

*Influence of Austenitizing Time and Temperature on Austenite Grain Size of Steel*, by O. O. Miller, Research Laboratory, U. S. Steel Co.

*Carbide Precipitation in AISI Type 304 Stainless Steel—an Electron Microscope Study*, by E. M. Mahla and N. A. Nielsen, E. I. du Pont de Nemours & Co.

*Some Aspects of Graphitization in Steel*, by G. V. Smith, J. A. MacMillan and E. J. Dulis, Research Laboratory, U. S. Steel Co.

#### Wednesday, October 25

##### ASM Annual Meeting

Ballroom, Palmer House, 9:30 A.M.

*Edward deMille Campbell Memorial Lecture*, by Earle C. Smith, Chief Metallurgist, Republic Steel Corporation, entitled *Iron Smelting Problems*.

E. R. Johnson, Republic Steel Corp., Chairman

##### Heat Treatment Session

Ballroom, Palmer House, 2:00 P.M.

Co-Chairmen: J. B. Austin, United States Steel Co.  
G. A. Roberts, Vanadium-Alloys Steel Co.

*A Hardenability Test for Deep Hardening Steels*, by W. Wilson, Jr., Armour Research Foundation.

*An Examination of the Quenching Constant, H*, by D. J. Carney and A. J. Janulionis, Carnegie-Illinois Steel Corp.

*The Tempering of Chromium Steels*, by R. W. Balluffi, Sylvania Electric Products Inc.; Morris Cohen and B. L. Averbach, Mass. Inst. of Tech.

*Austenite Transformation*, by Axel Hultgren, Professor of Metallography, K. Tekniska Hogskolan, Stockholm, Sweden; being an abbreviated presentation of the following two papers: *The Isothermal Transformation of Austenite in Low-Alloy Steels*, by Axel Hultgren and others, and *Partition of Alloying Elements in Transformed Low-Alloy Steels*, by Kehsin Kuo and Axel Hultgren.

#### Thursday, October 26

##### Fracture Session

Ballroom, Palmer House, 9:30 A.M.

Co-Chairmen: L. A. Carapella, Westinghouse Electric Corp.  
Finn Jonassen, National Research Council

*Grain and Grain Boundary Compositions: Mechanism of Temper Brittleness*, by J. W. Spretnak and Rudolph Speiser, Ohio State University.

*Effect of Strain Rate on Toughness of Temper Brittle Steel*, by D. C. Buffum and L. D. Jaffe, Watertown Arsenal.

*The Influence of Chromium on the Mechanical Properties of Plain Chromium Steels*, by W. O. Binder and Howard R. Spendelow, Jr., Union Carbide and Carbon Research Laboratories, Inc.

*Rheotropic Embrittlement of Steel*, by E. J. Ripling and W. M. Baldwin, Jr., Case Institute of Technology.

*Embrittlement of Stainless Steel by Steam in Heat Treating Atmospheres*, by C. A. Zapffe and R. L. Phebus, Research Metallurgists.

#### **Constitution of Alloys Session**

*Room 14, Palmer House—9:30 A.M.*

Co-Chairmen: M. G. Fontana, Ohio State University  
M. Hansen, Armour Research Foundation

*The Ternary System Chromium-Molybdenum-Iron*, by J. W. Putman, Massachusetts Institute of Technology; R. D. Potter, University of California; and N. J. Grant, Massachusetts Institute of Technology.

*The Ternary System Indium-Cadmium-Zinc*, by S. C. Carapella, Jr., and E. A. Peretti, University of Notre Dame.

*The Determination of Solidus Temperatures in Magnesium Alloys by Dilatometric Measurements*, by Heinrich Adenstedt, Wright-Patterson Air Force Base, and Jay R. Burns, Dow Chemical Co.

*Constitution and Mechanical Properties of Zirconium-Iron Alloys*, by E. T. Hayes, A. H. Roberson and W. L. O'Brien, Bureau of Mines, Albany, Ore.

#### **Fracture Session**

*Ballroom, Palmer House, 2:00 P.M.*

Co-Chairmen: M. Gensamer, Columbia University  
B. J. Lazan, Syracuse University

*Fracturing of Silicon Ferrite Crystals*, by C. F. Tipper, Cambridge University, England, and A. M. Sullivan, Naval Research Laboratory, Washington, D. C.

*A Study of Cleavage Surfaces in Ferrite*, by E. P. Klier, University of Maryland.

*Fractographic Registrations of Fatigue*, by C. A. Zapffe and C. O. Worden, Research Metallurgists.

*Effect of Alloying Elements on Notch Toughness of Pearlitic Steels*, by J. A. Rinebolt and W. J. Harris, Jr., Naval Research Laboratory.

#### **Friday, October 27**

#### **Plasticity Session**

*Ballroom, Palmer House—9:30 A.M.*

Co-Chairmen: W. M. Baldwin, Case Institute of Technology  
W. T. Lankford, Carnegie-Illinois Steel Corp.

*The Stress-Strain Energy Relationship for Metals*, by D. J. McAdam, Jr., Consulting Metallurgist.

*Tension-Compression Biaxial Plastic Stress-Strain Relations for Aluminum Alloys 24S-T and 2S-O*, by J. H. Faupel, E. I. du Pont de Nemours & Co., and Joseph Marin, Pennsylvania State College.

*Hot Forming of Aluminum and Magnesium Alloys*, by T. E. Piper, Northrop Aircraft, Inc.

*Strain Hardening of Mild Steel in the Torsion Test as a Function of Temperature*, by Hugo Larson, Massachusetts Institute of Technology, and E. P. Klier, University of Maryland.

#### **Physical Metallurgy Session**

*Room 14, Palmer House—9:30 A.M.*

Co-Chairmen: E. I. Larsen, P. R. Mallory & Co., Inc.  
W. E. Mahin, Armour Research Foundation

*The Powder Metallurgy of Beryllium*, by H. H. Hausner and Norman P. Pinto, Sylvania Electric Products Inc.

*The Dimensional Behavior of Invar*, by B. S. Lement, University of Notre Dame; B. L. Averbach and Morris Cohen, Massachusetts Institute of Technology.

*Preparation and Properties of Titanium-Chromium Binary Alloys*, by D. J. McPherson, Armour Research Foundation, and M. G. Fontana, Ohio State University.

*Statistical Analysis of the Effect of Alloying Elements on Mechanical Properties of Seamless Steel Tubes*, by W. T. Rogers, National Tube Co.

*Grindability of Tool Steels*, by L. P. Tarasov, Norton Co.

### ASM EDUCATIONAL LECTURES

#### High-Temperature Properties of Metals

**Monday, October 23**

Ballroom, Palmer House

Chairman: I. R. Kramer, Office of Naval Research

*Creep*, by Earl R. Parker, University of California.

*Stress-Rupture Testing*, by N. J. Grant, Massachusetts Institute of Technology.

*Fatigue Testing*, by H. J. Grover and Howard C. Cross, Battelle Memorial Institute.

*Oxidation*, by Carl Wagner, Massachusetts Institute of Technology.

*Service Experience*, by John J. B. Rutherford, Babcock and Wilcox Tube Co.

#### Interpretation of Tests and Correlation With Service

**Tuesday, October 24**

Ballroom, Palmer House

Chairman: K. L. Fethers, Youngstown Sheet & Tube Co.

*Correlation of Laboratory Tests and Service Performance*, by M. F. Garwood, H. H. Zurburg, and M. A. Erickson, Chrysler Corp.

*Limitations of Mechanical Testing*, by M. Gensamer, Columbia University.

*Wear Tests and Service Performance*, by J. T. Burwell, Massachusetts Institute of Technology.

*Corrosion Tests and Service Performance*, by Frank LaQue, International Nickel Co.

#### Metallurgy of Titanium

**Wednesday, October 25**

Ballroom, Palmer House

Chairman: B. W. Gonser, Battelle Memorial Institute

*Historical Development, Extractive Metallurgy, General Properties of the Metal of Commercial Grades*, by W. J. Kroll, Bureau of Mines.

*Melting, Casting, Working, Fabrication, and Testing*, by W. L. Finlay, Remington Arms Co.

*Alloys of Titanium*, by Robert Jaffee, Battelle Memorial Institute.

### ASM SALES CLINIC

**Sunday, October 22**

Ballroom, Palmer House—8:00 P.M.

Presiding: Arthur E. Focke, President ASM

*The Three Bogeymen*, by C. T. Burg, general sales manager, Iron Fireman Mfg. Co.

*Making a Profit on Your Investment in an Industrial Show*; Panel Discussion and Open Forum.

Philip Salisbury, editor, *Sales Management*

Herbert L. Stephen, field editor, *Printers' Ink*

Harold E. Green, Midwest editor, *Printers' Ink*

S. R. Bernstein, editor, *Advertising Age*

R. S. Aitchison, editor, *Industrial Marketing*



**ASM HIGH PRODUCTION MEETINGS***Saddle & Sirloin Club, International Amphitheatre***Monday, October 23—2:00 P.M.****Fabrication of Nonferrous Metals**

Chairman: Harvey A. Anderson, Engineer, Raw Materials, Western Electric Co.  
*Casting*, by H. C. Snyder, Plant Superintendent, Stewart Die Casting Div.,  
Stewart-Warner Corp.

*Forming*, by Kent R. Van Horn, Associate Director of Research, Aluminum  
Co. of America.

*Machining*, by J. S. Gillespie, Products Sales Manager, Carboloy Co., Inc.

**Tuesday, October 24—2:00 P.M.****Forming of Metals (Hot and Cold)**

Chairman: J. W. Armour, Manager, Mfg. Research, International Harvester Co.

*Forging*, by E. O. Dixon, Chief Metallurgical Engineer, Ladish Co.

*Stamping and Drawing*, by C. R. Cory, Fisher Body Div., General Motors Corp.

*Powder Metal Molding*, by L. G. Klinker, Chief Engineer, Metals Refining Co.  
Div. of Glidden Co.

**Wednesday, October 25—2:00 P.M.****Cutting**

Chairman: A. H. d'Arcambal, Vice-President and Consulting Metallurgist,  
Pratt & Whitney Div., Niles-Bement-Pond Co.

*High Cost of Obsolescent Machine Tools*, by Tell Berna, General Manager,  
Machine Tool Builders' Association.

*Cutting Tools for High Production*, by S. K. Rudorf, Superintendent of Tools  
and Maintenance, General Machinery Plants, Allis-Chalmers Mfg. Co.

*Metals Selection From the Viewpoint of Machinability*, by Walter C. Troy,  
Assistant Chairman, Metals Research Dept., Armour Research Foundation.

**Thursday, October 26—2:00 P.M.**

Chairman: Lewis C. Walgash, General Production Manager, Continental Can Co.

*Production Management*, by Emil F. Gibian, Chief Industrial Engineer,  
Thompson Products, Inc.

**ASM BUSINESS FORUM****Thursday, October 26***Red Lacquer Room, Palmer House—9:30 A.M.*

Chairman: Earl L. Shaner, Editor, *Steel*

Speakers represented producers of both ferrous and nonferrous metals, and  
also the consuming industries—namely, the automotive industry, electrical equip-  
ment manufacturers and the railroads.

*Representing ferrous metal producers:*

Edward L. Ryerson, Chairman, Inland Steel Company.

*Representing nonferrous metal producers:*

C. Donald Dallas, Chairman, Revere Copper & Brass, Inc.

*Representing the Railroads:*

Wayne A. Johnston, President, Illinois Central Railroad.

*Representing Electrical Equipment Manufacturers:*

William V. O'Brien, Commercial Vice-President, General Electric Co.

*Representing the Automotive Industry:*

Charles E. Wilson, President, General Motors Corp.

## ANNUAL MEETING OF AMERICAN SOCIETY FOR METALS

*Chicago, Wednesday, October 25, 1950*

The meeting was called to order by President A. E. Focke, who announced that the first order of business was the President's report. He then asked Vice-President W. E. Jominy to occupy the chair while he read his report. This is published in full beginning on this page of TRANSACTIONS.

VICE-PRESIDENT JOMINY: You have heard the report of the President. There being no objections, the report will stand approved as read. I now return the chair to the President.

PRESIDENT FOCKE: The next order of business will be the annual report of the treasurer, R. L. Wilson.

Treasurer Wilson presented his report which appears in full beginning on page 11.

PRESIDENT FOCKE: You have heard the report of the Treasurer. There being no objections, it will stand as read. The next order of business is the report of the Secretary.

Secretary Eisenman presented his report which appears in full beginning on page 15.

PRESIDENT FOCKE: You have heard the report of the Secretary. There being no objections, it will stand as read. The next order of business is the election of officers. (See page 22.)

---

## ANNUAL ADDRESS OF THE PRESIDENT

ARTHUR E. FOCKE, *President*

*Thirty-second Annual Meeting, Chicago, October 25, 1950*

IN some societies, the President makes his principal address upon installation. At that time, he can talk glibly of his aims and his hopes. With our practice, your President must either recount items with which you are already familiar or tell about his disappointments. This reports contains a bit of both.

It is my pleasant duty to report to you that under the watchful, vigorous and ingenious care of our Executive Secretary, Bill Eisenman, our Society continues to move forward successfully. You will hear the details of these successes in the reports of your Secretary and of your Treasurer.

For his part, in spite of the coal strike, the railroad strike, the

strike of the airline pilots and the flu, your President traveled 30,000 miles during the past year to visit 44 chapters, 4 regional meetings, 4 meetings of the Board of Trustees, 6 meetings of standing or special committees and to represent our Society at three other special events.

Also, in spite of using the long distance whenever it seemed even remotely reasonable, referring everything possible to the Cleveland office and, when writing to Bill, including at least six subjects in each letter, your President sent out over 600 letters from his own office.

It has been fun. It has been stimulating, but it has taken a lot of time. Without the sympathetic cooperation of Mr. Guy A. Wainwright, President, and Mr. George G. Mize, Chief Engineer, of the Diamond Chain Company, Incorporated, it would not have been possible for your President to have done this.

We know that our local chapters are the backbone of our Society. Have you ever stopped to realize how much our individual members and their companies contribute when making our local chapter meetings possible and effective by presenting their technical talks? If we ignore the time spent in preparation and assume that each speaker spends 4 days on each talk—one traveling to the meeting, one there, one returning home and one getting over it—with our 79 chapters each holding about 7 technical meetings each year, you can begin to see that at the rate of over 2000 man-days it is truly a very sizable contribution.

In his meeting with the chapter chairmen this morning, your President emphasized the importance of making these chapter visits as valuable as possible for the speaker and his company.

In addition to carrying Bill's stereopticon slides and becoming proficient enough to substitute for him in a few cases, your President in his talks to the chapters this year experimented with an unorthodox type of presentation. It included audience participation, repetition, and association. It was not original. The oral repetition part, at least, was an old teaching device when John Adams went to school to Mr. Cleverly. Since it was an experiment, an effort was made to measure the results by arranging for each member of the audience to indicate his preference and his job classification. There is some question that the results are truly representative. Some people insist that many present did not feel free to express themselves. One man did, however, for he wrote on his slip, "Art, it stinks!" So, for what it may be worth:

- a. Of those attending the 37 chapter meetings on which this



technique was tried, 82% stated that they preferred the unorthodox presentation.

- b. The highest vote in favor of the presentation at any chapter was 98% and the lowest was 66%.
- c. There was evidence that this type of talk was more acceptable to the smaller chapters (fewer than 150 members) than to the larger (over 500 members). For example, of the nine chapters in which the favorable vote for the special method was greater than 90%, 4 were small, 3 were medium, and 2 were large. While of those nine that showed less than 78% in favor, there were no small chapters, 3 medium and 6 large. More directly, the average of the ten large chapters included in the survey was 80%, while that of the ten small chapters was 89% in favor of the different method.
- d. It was interesting that, while your President expected that his unconventional presentation would be accepted better by the practical man than by the technical, two of the highest scores were made in chapters that one would consider well above the average in technical competency. Also, while those primarily concerned with technical problems did have the lowest average favorable score (78%) and sales the highest (85%), the difference is much less than might be expected.

It is certainly not your President's intention to suggest that his unconventional presentation be generally adopted. He is not sure he liked it himself. But these results should tend to encourage every chapter speaker to consider whether or not there are new or different techniques that would help to make his talk more useful to our members.

From the summary of the job classification on these votes, while the make-up of the attendance at these chapters varied widely, the average showed that 49% had technical activities as their primary interest, 32% were concerned with problems of production supervision, and 14% were in sales.

It seems important to note that these average figures for chapter attendance correspond closely to the Audit Bureau of Circulations reports for METAL PROGRESS. Referred to the same basis, these show about 45% technical, 42% production supervision, and 11% sales. This would appear to confirm our general feeling that our chapter and national activities are well coordinated.

One new chapter was added during the past year. It was your President's pleasant duty to present the charter to the Northern Ontario Chapter at Sault Ste. Marie on April 27, 1950. In addition,



student groups were organized with the New York Chapter at the Brooklyn Polytechnic Institute and with the West Michigan Chapter at Michigan State College.

On the national basis, your Board of Trustees held four meetings—on October 21, 1949, and May 17, August 24 and October 24, 1950. At these meetings, in addition to concerning themselves closely with the problems of finances, the members of the Board have given serious attention to several important phases of ASM activities. These have all been concerned with considering methods whereby the ASM may be more useful to its members and how our Society can help to raise still further the status of the metallurgical profession. At this time, special mention should be made of the faithful services of the retiring members of the Board of Trustees—Harry Croft and Fred Robbins. Both of these men have unusually important responsibilities in their own industries, but each of them gave freely of his precious time to travel long distances to maintain a perfect record of attendance at Board meetings.

By now, perhaps, you are saying, "What about the disappointments you promised to mention?" Well, for one, it would have been nice to have visited all 79 chapters. Your President regrets exceedingly that it was not possible for him to accept all the invitations that were extended.

Also, early this year, it was suggested that our Society, through the facilities and with the assistance of the Economic Cooperation Administration, expand this National Metal Congress into a World Metallurgical Congress, at which several hundred top scientists in the metals field from all over the world would participate. Bill Eisenman prepared a fine outline of the possibilities of this Congress. This was accepted with enthusiasm by the ECA, and your President, your Secretary and several other members of your national office spent many hours working with their representatives in an effort to make this event possible for this year. But we finally had to admit that the time was just too short to do the job properly and it was necessary to postpone this event until next year.

It is customary for your President to record in his report the outstanding events of the previous Congress. In Cleveland, in 1949, the President's Medal was awarded to Francis B. Foley. The Howe Award made to B. L. Averbach, Morris Cohen, and S. D. Fletcher. The 1949 Campbell Lecture was presented by Edgar H. Dix, Jr., of the Aluminum Company of America, and the Sauveur Achievement Award was granted to Marcus A. Grossmann, director of research, Carnegie-Illinois Steel Corporation. The Gold Medal was presented

to Edgar C. Bain, vice-president in charge of research and technology, Carnegie-Illinois Steel Corporation, and the ASM Medal for the Advancement of Research was given to Fred H. Haggerson, president of the Union Carbide and Carbon Corporation.

In conclusion, I wish to extend, on behalf of the Board of Trustees, our appreciation for the splendid support and cooperation of the participating societies—the American Institute of Mining and Metallurgical Engineers, American Welding Society, and the Society for Non-Destructive Testing. They have prepared attractive programs and contributed greatly to the success of this Congress.

Finally, your President wishes to express his thanks to all the members of the national office, the Board of Trustees, the chairmen and members of national committees and those of the local chapters, and to all of you who have contributed so much of your time and effort to the success of our Society.

### TREASURER'S REPORT

RALPH L. WILSON, *Treasurer*

It is a pleasure to report that your Society has completed another prosperous year. A condensed balance sheet presenting the financial position of the Society at August 31, 1950, which is the end of the fiscal year, is given below:

ASSETS	August 31, 1950
Cash .....	\$ 301,718.27
Securities .....	1,450,667.31
Cash surrender value of life insurance .....	72,968.96
Accounts receivable .....	47,160.09
Inventories .....	130,294.60
Other Assets .....	11,447.73
Real Estate .....	57,611.01
Office furniture, fixtures and equipment .....	59,825.09
Deferred charges .....	54,892.95
	<u>\$2,186,586.01</u>
LIABILITIES, RESERVES, AND SURPLUS	
Accounts payable .....	\$ 29,180.86
Reserves .....	202,139.50
Deferred income .....	191,264.75
Surplus .....	1,764,000.90
	<u>\$2,186,586.01</u>

Total assets have shown an increase of \$121,885.80. Cash has gained \$30,447.98 and holdings of securities have been increased \$67,963.66. During the year there were a number of changes in the investment portfolio. Several bonds were called for redemption. All the industrial bonds and a few common stocks were sold, while

government bonds and different common stocks were acquired. The net effect of these transactions was to increase moderately the proportion of common stocks in the portfolio, with the expectation of improving the yield on the Society's investments. In planning and executing investment programs of this nature, the Society follows the recommendations of the Cleveland Trust Co. as Agent, with whom the Finance Committee and the Board of Trustees have regular meetings to review the status of the ASM portfolio.

The distribution of securities in the portfolio by classes is now as follows:

SECURITIES	Carrying Amount August 31, 1950	Per Cent
U. S. Government Bonds .....	\$ 955,907	65.9
Canadian Government Bonds ...	10,000	0.7
Public Utility Bonds .....	39,070	2.7
Railroad Bonds .....	12,267	0.8
Total Bonds .....	<u>\$1,017,244</u>	<u>70.1</u>
Common Stocks .....	\$ 364,352	25.1
Preferred Stocks .....	18,694	1.3
Total Stocks .....	<u>\$ 383,046</u>	<u>26.4</u>
Land Trust Certificates .....	43,524	3.0
Accrued Interest .....	6,853	0.5
Total Securities .....	<u>\$1,450,667</u>	<u>100.0</u>

The market value of these investments on August 31, 1950, was approximately \$1,570,031.02, with the stocks accounting for about 33% of the total. Dividends and interest earned came to \$56,852.52 or 3.92% based on the carrying value as compared to a corresponding figure of 3.65% for last year.

Total income and expense for the year ending August 31, 1950, were:

Income .....	\$934,918.93
Expense .....	<u>793,488.60</u>
Net Income .....	<u>\$141,430.33</u>

The income dollar of the Society may be divided as follows to indicate the sources of income and the items of expense:

Where it came from	Where it went
METAL PROGRESS .....	35¢
Metal Exposition .....	23
Membership Dues .....	21
Book Publishing .....	8
Interest and Dividends ....	7
METALS HANDBOOK .....	3
METALS REVIEW .....	1
Miscellaneous .....	2
	<u>100</u>
	METAL PROGRESS .....
	Metal Exposition .....
	Dues Returned to Chapters ..
	Books and Misc. Mdse. ....
	Membership Expense .....
	TRANSACTIONS .....
	METALS REVIEW .....
	METALS HANDBOOK .....
	General Administration ...
	Added to Surplus .....
	<u>100</u>

## AUDITED BALANCE SHEET

## AMERICAN SOCIETY FOR METALS

August 31, 1950

ASSETS		
CASH (includes \$9,186.93 of Canadian dollars) ..		\$ 301,718.27
SECURITIES (approximate market or redemption prices aggregate \$1,570,031.02)		
Bonds, stocks, and land trust certificates—		
at cost .....	\$1,443,814.25	
Accrued interest .....	6,853.06	1,450,667.31
CASH SURRENDER VALUE OF LIFE INSURANCE		72,968.96
ACCOUNTS RECEIVABLE		
Advertising accounts .....	\$22,016.48	
National Metal Exposition—Chicago—		
October, 1950 .....	15,401.75	
Miscellaneous .....	11,741.86	\$ 49,160.09
Less allowance for doubtful accounts .....	2,000.00	47,160.09
INVENTORIES—at cost or lower		
Bound and unbound publications, books, paper stock, etc. ....	\$ 136,294.60	
Less allowance for obsolescence .....	6,000.00	130,294.60
OTHER ASSETS		
Officers, employees, and sundry accounts and deposits .....		11,447.73
REAL ESTATE (at cost less allowances for depreciation) .....		57,611.01
OFFICE FURNITURE, FIXTURES, AND EQUIPMENT (at cost less allowances for depreciation) .....		59,825.09
DEFERRED CHARGES		
Prepaid exposition expenses:		
National Metal Exposition—Chicago—		
October, 1950 .....	\$40,142.68	
Western Metal Show—Oakland—		
March, 1951 .....	1,118.30	\$ 41,260.98
Prepaid publication and sundry expenses .....	11,246.82	
Prepaid insurance .....	2,385.15	54,892.95
		<u>\$2,186,586.01</u>
LIABILITIES, RESERVES, AND SURPLUS		
ACCOUNTS PAYABLE		
For purchases, expenses, etc. ....	\$ 24,183.98	
For apportionment of dues to local chapters .....	2,448.98	
Taxes withheld from employees .....	1,657.90	
Rental deposits—Western Metal Show .....	890.00	\$ 29,180.86
RESERVES		
For METALS HANDBOOK .....	\$ 67,139.50	
For conventions .....	60,000.00	
For dues paid in advance .....	50,000.00	
Campbell Memorial lecture fund .....	15,000.00	
H. M. Howe medal fund .....	5,000.00	
Sauveur achievement award .....	5,000.00	202,139.50
DEFERRED INCOME		
National Metal Exposition—Chicago—October, 1950 .....		191,264.75
SURPLUS		
Balance at September 1, 1949 .....	\$1,622,570.57	
Add net income for the year .....	141,430.33	1,764,000.90
		<u>\$2,186,586.01</u>



# **AUDITED INCOME AND EXPENSE STATEMENT** **AMERICAN SOCIETY FOR METALS**

Year ended August 31, 1950

INCOME	
METAL PROGRESS—monthly publication .....	\$355,889.76
National Metal Exposition .....	239,765.70
Memberships .....	127,941.41
Dividends and interest earned .....	56,852.52
Book sales .....	53,229.50
ASM METALS HANDBOOK sales .....	32,788.00
METALS REVIEW—monthly publication .....	31,454.82
TRANSACTIONS sales .....	9,097.30
General reprints .....	7,728.17
Net gain on sales of securities .....	6,880.94
Sundry sales, etc. ....	5,785.66
Discount earned .....	5,222.42
Increment in cash value and dividends on life insurance .....	1,824.77
Sale of purchased books .....	457.96
<b>TOTAL INCOME .....</b>	<b>\$934,918.93</b>
EXPENSES	
METAL PROGRESS—monthly publication .....	\$326,620.50
National Metal Exposition—Cleveland—October, 1949 .....	148,832.17
Books published .....	48,930.39
METALS REVIEW—monthly publication .....	48,130.79
TRANSACTIONS .....	39,390.41
Memberships .....	38,081.23
General expenses .....	37,433.54
Secretary's office .....	27,979.04
ASM METALS HANDBOOK .....	24,824.79
Accounting department .....	15,809.55
Headquarters .....	15,518.02
Trustees .....	5,605.25
President's office .....	4,550.60
National Committees .....	4,380.40
Miscellaneous merchandise, etc. ....	3,170.61
Technical books .....	1,083.78
Library .....	808.23
Medals and awards .....	792.00
Booth equipment—storage .....	615.02
Lectures .....	520.00
Research and educational contribution .....	250.00
Medal funds .....	162.28
<b>TOTAL EXPENSES .....</b>	<b>\$793,488.60</b>
<b>NET INCOME .....</b>	<b>\$141,430.33</b>

Board of Trustees,  
American Society for Metals,  
Cleveland, Ohio.

We have examined the balance sheet of American Society for Metals as of August 31, 1950, and the related statements of income and expense and surplus for the year then ended. Our examination was made in accordance with generally accepted auditing standards, and accordingly included such tests of the accounting records and such other auditing procedures as we considered necessary in the circumstances.

In our opinion, the accompanying balance sheet and statement of income and expense present fairly the financial position of American Society for Metals at August 31, 1950, and the results of its operations for the year then ended, in conformity with generally accepted accounting principles applied on a basis consistent with that of the preceding year.

ERNST & ERNST  
Certified Public Accountants

Cleveland, Ohio  
September 22, 1950

Dues paid by members were the largest source of net income to the Society. Gross income from dues amounted to \$216,156.14, of which \$88,733.35 was returned to the chapters. However, it has long been known that the members of ASM receive from the Society services that exceed the cost of the membership. In the fiscal year just ended the Society spent about \$44 per member.

The Metal Expositions continue to make substantial contributions to net income. METAL PROGRESS showed a smaller excess of income over expense this year than last. Publishing and sales of books, including METALS HANDBOOK and ASM REVIEW OF METAL LITERATURE, provided a net income of \$26,732. Interest and dividends are growing in amount and are becoming an increasingly important part of the income of the Society. TRANSACTIONS and METALS REVIEW, which are not self-sustaining, were distributed at a net cost to the Society of \$30,293 and \$25,804, respectively.

The METALS HANDBOOK reserve, being accumulated to take care of the publication of the next revision, received an addition of \$18,895, bringing the total to \$67,139.50.

Since the local chapters must have money to promote the aims of the Society effectively, it is reassuring to know that the combined assets of the chapters are about \$205,000, an increase of nearly \$5000 in the year.

In concluding this report your Treasurer wishes to acknowledge the generous assistance he has received throughout the year from Secretary Eisenman, Assistant Treasurer A. A. Hess, Messrs. W. W. Horner and A. W. Marten of the Cleveland Trust Co., members of the Finance Committee, and the Board of Trustees.

## ANNUAL REPORT OF THE SECRETARY

W. H. EISENMAN, *Secretary*

The American Society for Metals on October 1, 1950, had a total membership of 20,016. Of this number 16,802 or 83.9% were the member classification; 1706 or 8.5% were sustaining members; while 1464 or 7.3% were junior members. There were 42 honorary and founder members.

### TRANSACTIONS

Since the last National Metal Congress, Vol. 42 and Vol. 42A of the TRANSACTIONS were published and distributed to the membership in April 1950. Vol. 42 totals 1356 pages and constitutes 51 articles with their discussions. It contains all of the papers presented

at the October 1949 Convention held in Cleveland, together with papers presented at the Western Metal Congress held in Los Angeles in April 1949, and interim papers received during the year. The president, secretary and treasurer's report for 1949 and other current items of record were included in Vol. 42, together with a report of the Convention.

Vol. 42A contains the 14 papers (319 pages) presented at the seminar on "Thermodynamics in Physical Metallurgy" held on Saturday and Sunday, October 15 and 16, 1949, during the National Metal Congress and Exposition, Cleveland. This seminar was sponsored by the American Society for Metals, the subject being selected by a committee appointed by the Board of Trustees. The personnel of the committee was: M. Gensamer, Chairman; R. M. Brick, Lloyd Jackson, J. H. Hollomon, Morris Cohen, and C. Zener. The preparation and coordination of the series of subjects and solicitation of speakers was carried on by Dr. C. Zener.

#### PUBLICATIONS COMMITTEE

Seventeen persons constitute the membership of the Publications Committee for 1950, under the chairmanship of A. R. Troiano, Professor of Metallurgy, Case Institute of Technology, Cleveland. The members of the Committee and their Chapter affiliation are: W. M. Baldwin, Jr., Cleveland; J. A. Bennett, Washington; Edgar Brooker, Los Angeles; C. D. Donoho, Birmingham; C. T. Evans, Jr., Northwest Pa.; M. G. Fontana, Columbus; A. J. Herzig, Detroit; E. I. Larsen, Indianapolis; W. E. Mahin, Chicago; W. A. Pennington, Syracuse; G. C. Riegel, Peoria; G. A. Roberts, Pittsburgh; H. Solakian, New Haven; L. P. Tarasov, Worcester; C. A. Zapffe, Baltimore; and Ray T. Bayless, Secretary, Cleveland.

During the year the Committee has reviewed 76 papers. Of this number 45 were approved for presentation at this Convention and publication in *TRANSACTIONS*, and of this number 42 were made available to the membership in preprint form; 5 papers were approved for *TRANSACTIONS* as interim papers; 4 were recommended for publication in *METAL PROGRESS*; 22 were not approved for printing in ASM publications. Three papers are now in the process of review.

The Publications Committee held one formal meeting on June 14 and 15, 1950, at which time all of the members of the committee except one were present. The final arrangements of the technical program for this Convention were made, including the selection of two chairmen for each of the sessions.



## METAL PROGRESS

Data on total editorial pages since the 1946 peak are as follows:

Fiscal Year	Editorial Pages
1946 .....	832
1947 .....	722
1948 .....	628
1949 .....	621
1950 .....	622

The editorial resources of METAL PROGRESS were improved by the appointment of Adolph Bregman and Harold J. Roast, experts respectively in the fields of cleaning and finishing, and of nonferrous foundry work. Notable articles from their pens have been printed during the year. Much attention has also been given to modern methods of heat treatment, alloys for ultra-high temperature service, and the once-rare metals now available in commercial quantities—all subjects where great progress is currently being made. The thanks of the Society are due to over a hundred of its members who have contributed to the editorial success of their magazine, METAL PROGRESS.

During the year the Society has donated considerable of Ernest E. Thum's time to the U. S. Atomic Energy Commission as chairman of the "Working Committee on Technological Information for Industry". The task undertaken by this committee is to examine in detail the formidable mass of documents in the files of the various A.E.C. centers now classed as secret and to recommend which, if any, can be declassified and made public with profit to American industry without endangering the security of the United States.

## METALS REVIEW

METALS REVIEW continues to serve as the monthly news digest magazine of the Society, reporting local chapter meetings, activities of members, and news from headquarters. Of the total of 632 pages published during the 12 months from October 1949 through September 1950, 194 pages or 31% were devoted to material of this nature.

Reporters and publicity chairmen for the local chapters were responsible for securing most of this information. Altogether, 307 reports of chapter meetings were contributed and printed.

The bulk of the remaining pages was devoted to the ASM Review of Metal Literature, which covered 362 printed pages, or 57% of the total. In February 1950 a new classification system was adopted for the Review of Metal Literature, developed after two years of work by a joint committee of the American Society for Metals and the Special Libraries Association. The new classification



has resulted in a distinct improvement in the method of classifying and indexing the literature references by subject matter.

An offshoot of this project was the publication of the ASM-SLA Metallurgical Literature Classification, and also the development of a standardized punched card system for literature indexing and filing, which is available to ASM members and to librarians at manufacturer's cost.

#### METALS HANDBOOK

METALS HANDBOOK continues to make a name for itself with all new members, and is doing yeoman service in the hands of 27,162 individuals.

The METALS HANDBOOK Committee is inactive during the lull following the publication of the last edition and will remain so for two years, when plans will begin to mature for the new edition.

#### EDUCATIONAL COMMITTEE

The Educational Committee for the year 1950 was composed of the following personnel: J. F. Kahles, Chairman; R. H. Aborn, M. J. Day, K. L. Fethers, N. J. Grant, H. Y. Hunsicker, I. R. Kramer, C. L. Lewis, Ray McBrien, and Ray T. Bayless, Secretary.

This Committee held one formal meeting on January 17, 1950, at which time the three educational lecture courses for the 1950 Convention were selected and planned. These lectures are:

1. "High Temperature Properties of Metals", by 6 authors:

E. R. Parker, University of California  
N. J. Grant, Massachusetts Institute of Technology  
H. J. Grover, Battelle Memorial Institute  
H. C. Cross, Battelle Memorial Institute  
C. Wagner, Massachusetts Institute of Technology  
J. J. B. Rutherford, Babcock and Wilcox Tube Co.

2. "Interpretation of Tests and Correlation with Service", by 6 authors:

M. F. Garwood, Chrysler Corp.  
H. H. Zurburg, Chrysler Corp.  
M. A. Erickson, Chrysler Corp.  
J. T. Burwell, Massachusetts Institute of Technology  
F. LaQue, International Nickel Co.  
M. Gensamer, Carnegie-Illinois Steel Corp.

3. "Metallurgy of Titanium", by 3 authors:

W. J. Kroll, Bureau of Mines  
W. L. Finlay, Remington Arms Co.  
Robert Jaffee, Battelle Memorial Institute

In addition, plans were laid for the making of a third motion

picture film entitled "The Heat Treatment of Steel". The tentative scenario was prepared by Prof. J. O. Lord and carefully reviewed by members of the Committee and others. At the present time about one-half of the photography has been completed and it is hoped that the entire film will be available by January 1, 1951. This will be a color, sound, 16-mm motion picture film with an approximate running time of 30 minutes.

### BOOKS

During the past year, a total of 18,125 books published by the Society were sold to members and others. This figure includes 1681 copies of the 1948 METALS HANDBOOK.

During this period eight titles were added to the publication list. These are:

Transactions of the ASM, Vol. 42  
ASM Review of Metal Literature, Vol. 6  
ASM-SLA Metallurgical Literature Classification and Work Sheets  
Casting of Brass & Bronze—By D. R. Hull  
Machining—Theory and Practice—By 15 authors  
Thermodynamics in Physical Metallurgy—Seminar by 14 authors  
Mechanical Wear—By 22 authors  
Crystallography of the Elements—By W. B. F. Mackay and H. S. Jerabek  
(a series of pamphlets for the student, researcher or engineer on  
Metallurgical Data—No. 1)

The following titles are now in preparation:

The Story of Metals—Techbook by John W. W. Sullivan  
The Nature of Metals—Techbook by B. A. Rogers  
Atmosphere Heat Treatment of Steel—By Floyd E. Harris  
High Temperature Properties of Metals—By 6 authors  
Interpretation of Tests and Correlation With Service—By 6 authors  
Metallurgy of Titanium—By 3 authors

### ADVISORY COMMITTEE ON METALLURGICAL EDUCATION

The Advisory Committee on Metallurgical Education, under the chairmanship of Dr. John W. W. Sullivan, worked on a number of projects during the past year. Among them were:

1. Teaching award.
2. Securing information through local chapters re vocational schools.
3. Formation of counselors for high school students by chapters.
4. A progress report on laboratory manual on process metallurgy.
5. A continuation of the analysis of replies to the occupational questionnaire sent out last year.
6. Consideration of an ASM visiting lectureship.

Some of them have already been placed in effect and others are being given serious consideration by the Board.

## PREPRINTS

Of the 45 papers being presented at this Convention, 42 were prepared in preprint form and distributed to those members of the Society who requested them. The total number of pages for the 1950 preprints is 846. A total of 45,000 preprint copies was distributed free to the membership.

## SEMINAR ON ATOM MOVEMENTS

The Seminar on Atom Movements this year was an outstanding success. It was divided into four important and interesting sessions with the meeting room filled to capacity. This interest is a great compliment to the committee and the seminar speakers and assures a continuance of this important annual event.

The Committee on Arrangements consisted of the following personnel: Clarence Zener, Chicago, Chairman; J. B. Austin, New York; R. M. Brick, Philadelphia; M. Cohen, Boston; M. Gensamer, Pittsburgh; J. H. Hollomon, Eastern New York, Coordinator of the Seminar; L. R. Jackson, Columbus; L. K. Jetter, Oak Ridge; and Don McCutcheon, Detroit.

## METAL CONGRESS

The 32nd National Metal Congress enters on its third day. Those of you who are in attendance are well able to judge the fine success this activity will be.

There have been two added features this year.

1. The sales clinic held Sunday evening
2. The business forum to be held tomorrow (Thursday) morning at 10:00 o'clock in the Red Lacquer Room at the Palmer House, when the following men will discuss the business outlook in their respective fields:

W. A. Johnston, President, Illinois Central Railroad Co., speaking for the railroads;  
Edward L. Ryerson, Chairman of the Board, Inland Steel Co., representing the ferrous metal producers;  
C. Donald Dallas, Chairman of the Board, Revere Copper and Brass, Incorporated, representing the nonferrous metal producers;  
William V. O'Brien, Commercial Vice-President, General Electric Co., representing the electrical equipment manufacturers; and  
Charles E. Wilson, President, General Motors Corporation, representing the automotive industry.

This program has been prepared at the direction of the Board of Trustees by Mr. Earl L. Shaner, Editor in Chief of *Steel* and Chairman of the Board of the Penton Publishing Company. We are confident this will be an outstanding program.

### HIGH PRODUCTION SESSIONS

High Production meetings from management's viewpoint are being held on Monday, Tuesday, Wednesday, and Thursday afternoons at the Saddle & Sirloin Club at the International Amphitheatre. These sessions are being devoted to increasing output.

The subjects being discussed are: "Fabrication of Nonferrous Metals", "Forming of Metals (Hot and Cold)", "Cutting", "Production Management".

### THE EXPOSITION

The Chicago Exposition has lived up to all expectations. It is having a magnificent attendance and proving to be a great success.

Following the usual practice, approximately 400 exhibitors reserved space, and it is estimated the attendance will be approximately 50,000, with a registration of 35,000.

### WESTERN METAL CONGRESS AND EXPOSITION

The Western Metal Congress and Exposition will be held in Oakland, March 19-23, 1951.

Floor plans have already been distributed and we have received many reservations.

The west coast show is held every two years alternating between Los Angeles and the San Francisco Bay territory.

### 1951 EXPOSITION

Since last July the National Headquarters has worked diligently on the 33rd National Metal Congress and Exposition which will be held in Detroit the week of October 15, 1951.

The Exposition will be located in the buildings at the State Fair Grounds. Since the National Metal Congress and Exposition have not been in Detroit for 13 years, due to our inability to secure adequate exposition facilities, we contemplate that this exposition will be the largest ever held by the Society.

The Detroit Exposition will be of outstanding size and significance, and the 33rd Metal Congress with its magnificent array of highly technical papers, combined with the World Metallurgical Congress, will place Detroit as the national center of the world during the week of October 15th.

### WORLD METALLURGICAL CONGRESS

As your President mentioned in his report, plans were initiated to hold in this country a World Metallurgical Congress simulta-



neously with this convention and exposition. However, the amount of time involved, as far as communications were concerned, brought the acceptance too late in order to complete satisfactory plans for this event.

Therefore, it was wisely decided by the Board that the World Metallurgical Congress should be postponed until the Metal Congress in Detroit next year.

In November, this year, invitations will go to all the free countries of the world inviting them to send groups of at least 20 members on the top scientific level to discuss world metallurgical practices according to the 10 divisions of the Congress.

The ASM has had a wonderful year, as you have been able to judge from the reports of the President, the Treasurer, and the Secretary.

Speaking for the National Office staff I can assure you it has been a pleasure to serve you, and in the same breath may I add that our continued endeavor will be to perfect the present services for the members and to strive constantly to increase the services.

### ELECTION OF OFFICERS

PRESIDENT FOCKE: We will now proceed with the election of officers. Complying with the constitution, I appointed in March 1950 the following nominating committee, selected from the list of candidates suggested by the eligible chapters prior to March 1, 1950:

Harold L. Geiger, Chairman—Chicago Chapter	
Neil Waterbury, St. Louis Chapter	Mars G. Fontana, Columbus Chapter
Columbus Floyd, Akron Chapter	Joseph Gray Jackson, Philadelphia Chapter
E. C. Wright, Birmingham Chapter	
Morris Cohen, Boston Chapter	George A. Nelson, Golden Gate Chapter
Henry Hauseman, Jr., Cedar Rapids Chapter	

The Committee met in Cincinnati on May 22, 1950, and made the following nominations for the following offices:

#### FOR PRESIDENT

Walter E. Jominy, Staff Engineer, Chrysler Corp.,  
Detroit—1 year.

#### FOR VICE-PRESIDENT

John Chipman, Prof. of Metallurgy, Massachusetts Institute of Technology,  
Cambridge—1 year.

#### FOR TRUSTEES

J. B. Austin, Director of Research, U. S. Steel Co., Research Labs.,  
Kearny—2 years.  
James T. MacKenzie, Technical Director, American Cast Iron Pipe Co.,  
Birmingham—2 years.

The committee to nominate the Secretary, which consists of the

six immediate past presidents, nominated William H. Eisenman for 2 years. A report of these nominations duly appeared in the *METALS REVIEW*, June 1950.

I have been informed by the Secretary that no additional nominations were received prior to July 15, 1950, for any of the vacancies appearing on the Board of Trustees. Consequently, the nominations were closed. I now call upon the Secretary to carry out the provisions of the constitution in respect to the election of officers.

SECRETARY EISENMAN: Conforming with the provisions and requirements of the constitution of the American Society for Metals, I hereby cast the unanimous vote of the members for the election of the aforementioned candidates who were nominated May 22, 1950.

PRESIDENT FOCKE: I hereby declare the nominees as duly elected to their respective offices.

President Focke then introduced the newly-elected officers, and President-Elect Jominy gave a few words of acceptance.

PRESIDENT FOCKE: Has anyone present anything to bring before this meeting for the good of the Society? If not, a motion to adjourn is in order.

President Focke then introduced Mr. E. R. Johnson of Republic Steel Corp., chairman of the Campbell Memorial Lecture meeting, who in turn introduced the lecturer, Dr. Earle C. Smith, Chief Metallurgist, Republic Steel Corp., who then presented his lecture entitled "Iron Ore Smelting Problems". This is published in full beginning on page 651 of this volume of *TRANSACTIONS*.

---

### ASM ANNUAL DINNER

On Thursday evening, October 26, members and guests assembled in the Ballroom of the Palmer House for the Annual Dinner of the Society. The attendance was well over 500.

Those persons seated at the speakers' table were: W. E. Mahin, Armour Research Foundation, Chicago—Chairman, Chicago Chapter, ASM; T. G. Digges, National Bureau of Standards, Washington—Trustee, ASM; Elmer Gammeter, Globe Steel Tubes Co., Milwaukee—Trustee, ASM; H. P. Croft, Kennecott Copper Corp., New York—Trustee, ASM; L. W. Ball, United States Naval Ordnance Laboratory, Washington—President, Society for Non-Destructive Testing; E. L. Shaner, Penton Publishing Co., Cleveland; C. E. Sims, Battelle Memorial Institute, Columbus—Recipient of the Albert Sauveur Achievement Award; Clyde E. Williams, Battelle Memorial Institute, Columbus; E. C. Smith, Republic Steel Corp.,

Cleveland—1950 Campbell Memorial Lecturer; Morris Cohen, Massachusetts Institute of Technology, Cambridge; Axel Hultgren, Royal Institute of Technology, Stockholm, Sweden—Recipient of Honorary Membership in ASM; H. K. Work, New York University, New York—Past-President, ASM; Zay Jeffries, General Electric Co., Pittsfield, Mass. (Retired)—Honorary Member and Past-President, ASM, and Dean of American Metallurgists; A. E. Focke, Diamond Chain Co., Inc., Indianapolis—President, ASM; C. E. Wilson, General Motors Corp., Detroit—Recipient of the ASM Medal for the Advancement of Research; W. E. Jominy, Chrysler Corp., Detroit—Vice-President and President-Elect, ASM; A. E. White, University of Michigan, Ann Arbor—Founder Member and Past-President, ASM; R. L. Wilson, Timken Roller Bearing Co., Canton—Treasurer, ASM; G. T. Hook, *Iron Age*, New York; John Chipman, Massachusetts Institute of Technology, Cambridge—Vice-President-Elect, ASM; W. O. Binder, Union Carbide and Carbon Research Labs., Niagara Falls, N. Y.—Recipient, with C. M. Brown and Russell Franks, of 1950 Henry Marion Howe Award; W. V. O'Brien, General Electric Co., Schenectady; O. B. J. Fraser, International Nickel Co., New York—President, American Welding Society; J. B. Austin, U. S. Steel Corp., Kearny, N. J.—Trustee-Elect, ASM; James T. MacKenzie, American Cast Iron Pipe Co., Birmingham, Ala.—Trustee-Elect, ASM; W. H. Eisenman, Secretary, American Society for Metals, Cleveland.

#### *Presentation of President's Medal*

The annual presentation of the President's Medal was made by A. E. Focke to H. K. Work, the twenty-ninth president, who served the Society so ably in 1949.

#### *Presentation of Howe Medal*

In honor of Dr. Henry Marion Howe, the distinguished scientist, often called the dean of American metallurgists, the Board of Trustees in 1922 established the first of its medals. The rules governing the award of this medal make the provision that it be awarded to the author or authors of the paper judged of highest merit, presented before the ASM and published during any one year in the TRANSACTIONS of the Society.

The 1950 award was made to the authors of the paper entitled "Resistance to Sensitization of Austenitic Chromium-Nickel Steels of 0.03% Max. Carbon Content" which was published in Vol. 41 of TRANSACTIONS, 1949, page 1301. The authors who were honored



are W. O. Binder, C. M. Brown and Russell Franks. Each of these authors was presented with a certificate, a gold medal and a bronze replica.

#### *Edward deMille Campbell Memorial Lecture*

In 1926 the Society established the Edward deMille Campbell Memorial Lecture and each year since that time has invited a distinguished scientist to present this lecture. The 1950 lecturer was Dr. Earle C. Smith, Chief Metallurgist, Republic Steel Corp., and to commemorate this lecture a scroll certifying to that event was presented to Dr. Smith.

#### *Albert Sauveur Achievement Award*

In 1934 the Board of Trustees established an award consisting of a metal plaque and certificate in honor of Dr. Albert Sauveur, distinguished metallurgist and for many years an honorary member of the ASM. The purpose of this award is to recognize a metallurgical achievement which has stood the test of time and stimulated others along similar lines to the extent that a marked basic advance has been made in the metal arts and sciences. The 1950 candidate was Clarence E. Sims, Assistant Director, Battelle Memorial Institute, who was presented by Clyde E. Williams, following the reading of the citation of Mr. Sims' accomplishments. President Focke then conferred the award. The presentation and citation is as follows:

"The Albert Sauveur Achievement Award has been established to recognize pioneering metallurgical achievements which have stimulated work along similar lines to such an extent that a basic advance has been made in our knowledge. This year the award is to Clarence E. Sims, who for nearly two decades has studied the origin and effects of inclusions in cast steels.

"His first contribution in a long series was published in 1932. Written with G. A. Lillieqvist as co-author, it aroused so much interest that the discussions far exceeded the original paper in length. It later received the Robert W. Hunt Award. This paper pointed out for the first time that the normal non-metallic inclusions in solid steel do not exist as mechanical entities while the steel is molten but are formed by precipitation during solidification and cooling. Such inclusions, therefore, cannot be removed by levitation from the liquid steel bath. This thesis has stood the test of time and is now generally accepted both nationally and internationally.

"The continuing phase of Sims' work dealt with the nature



of the sulphide inclusions as related to deoxidation practice. Three types were distinguished; one of them is quite harmful to the toughness and ductility of the product. These harmful inclusions were not only recognized, but their origin demonstrated, and means for avoiding them clearly pointed out. This study has had a profound influence on the steel casting industry. As a result, it is possible to deoxidize steel castings with aluminum, eliminate pinhole porosity and, at the same time, avoid the formation of harmful sulphide inclusions.

"These and other researches in later years have not only extended the original thesis but have also stimulated many other workers in a long line of allied investigations of the greatest importance to the foundry industry.

"Mr. President, it gives me much pleasure, therefore, to present to you Clarence E. Sims, as a worthy candidate to receive the Albert Sauveur Achievement Award for 1950."

#### *Conferring of the ASM Medal for the Advancement of Research*

The 1950 ASM Medal for the Advancement of Research was awarded to Charles E. Wilson, President of General Motors Corporation, in recognition of his consistent sponsorship, foresight, and influence in financing and prosecuting metallurgical research, which have helped substantially to advance the arts and sciences relating to metals.

In presenting Mr. Wilson, A. L. Boegehold read the citation engrossed on the scroll which accompanies the medal. President Focke then conferred the award. The citation is:

"Metallurgical Research has for many years been an integral part of a general research program maintained by General Motors Corporation. Mr. Charles E. Wilson, President of General Motors, has made available the necessary funds and has given his personal encouragement to this work ever since becoming an official of the corporation. His education and early training as an engineer engender a keen interest and intelligent appreciation of the problems connected with research.

"Some of the metallurgical accomplishments that have been made possible by this encouragement are:

"Hardenability test for determining this characteristic of steels; wear-resistant machinable cast iron; a more wear-resistant zinc-base casting alloy for forming sheet steel; process for aluminum coating steel; development of diffusion treatments of aluminum-coated steel for obtaining greatest degree

of high temperature resistance; three-layer steel-back, copper-nickel cushion, corrosion-resistant lead-base surface layer bearings for increased service requirements of modern engines; grid-type heavy-duty bearings; application of pearlitic malleable iron to combat material components; aluminum-base bearing alloy; powdered iron oil pump gears and process for making iron powder; permanent mold centrifugally cast bimetal brake drums; tin-plated groove piston rings.

"The entire Nation has benefited both during time of peace and during time of war, for which the Society wishes to tender its recognition in the form of the Medal for the Advancement of Research."

### *Honorary Membership*

Dr. Morris Cohen was called upon to introduce Professor Axel Hultgren for the award of honorary membership in the Society. He said:

"Mr. President, Ladies and Gentlemen: Each year the members and friends of the American Society for Metals look forward to the Annual Banquet when the honors and medals of the Society are awarded. There is, however, one distinguished honor in the Treasure-house of the Society that is not awarded each year; in fact, it has not been awarded within the past decade. I refer, of course, to the post of Honorary Membership.

"The Constitution of the American Society for Metals states specifically that the total number of living Honorary Members is not at any time to exceed twenty-five. Actually, we have only four Honorary Members at present, and only fifteen men have been so appointed throughout the entire history of our Society. The first Honorary Member was Henry Marion Howe, whose name we commemorate each year in the award of the Howe Medal. We have just witnessed this ceremony. The last Honorary Member to be appointed was Dr. Zay Jeffries who is to be our principal speaker this evening.

"Because metallurgical science and technology recognize no national boundaries, it is entirely fitting that our Society should pay tribute to metallurgical greatness wherever it is found. We find such greatness in Professor Hultgren of Sweden, whom I am about to present to you.

"Professor Hultgren's influence in metallurgical circles extends the world over through his students, his discoveries, his

writings and his incisive discussion of the writings of others. His contributions range from the practical development of salt baths for high speed steel treatment to important theories on the nature of steel microconstituents, from studies on the solidification of massive ingots to the electrolytic extraction of minute carbides from steel. His research covers the fields of heat treatment, equilibrium diagrams, phase transformations, steel quality, nonmetallic inclusions, mechanical properties and many others too numerous to mention here.

"But, above all, we desire to honor Professor Hultgren as one of the world's most esteemed metallographers whose microscope has opened new vistas in metallurgy. For he has been among the foremost in probing the microstructure and macrostructure of metals to reveal the intricate physical and chemical changes that occur therein. One would find it difficult indeed to designate any other subject that has proved so vital to the interests of the American Society for Metals. Accordingly, in April 1950 the name of Professor Hultgren was duly placed in nomination before the Board of Trustees of the American Society for Metals, and by unanimous vote the Board elected him to Honorary Membership. It is our firm conviction that Professor Hultgren not only merits the distinguished recognition that goes with this high post, but that this appointment will prove a source of lasting honor to the Society itself.

"Mr. President, it is with immense personal pleasure and pride that I now present to you the Professor of Metallurgy of the Royal Institute of Technology in Stockholm, Axel Gustav Emanuel Hultgren."

President Focke then presented Professor Hultgren with the scroll of Honorary Membership in the American Society for Metals.

#### *Address of the Evening*

Dr. Zay Jeffries, Retired Vice-President of General Electric Co., Past President of the American Society for Metals, and Leonard Case Professor at Case Institute of Technology, presented the main address of the evening entitled "Security", printed in full herewith.

Fortunately the American Society for Metals faces no foreseeable crises. The younger members, however, should not gain the impression that the present healthy status was achieved without hard work and clear thinking. I recall that many earlier activities of the Society centered right here in Chicago. In the main, they were very



serious affairs but they were not without their amusing incidents. I attended a board meeting here back in the 1920's when the predecessor society (The American Society for Steel Treating) was struggling to establish its place in the sun. Our genial secretary, the same Bill Eisenman who sits at this table now but not quite so heavy and with no gray hair at all, was excused from the meeting for a half hour to meet with a group of Chicago business men to try to sell them some space in the forthcoming exhibit. When he returned to our meeting one of the members said: "Bill, did you sell them any space?" "No, I didn't," Bill replied, "but I bought ten shares of the best damned preferred stock you ever heard of." After the gloom had lifted a bit, another member asked Bill if he would mind taking off his coat. "Why should I take off my coat?" Bill inquired. "Well," said the member, "your shirt looks all right from the front, but I just wanted to see whether it still had a back in it."

If those board members had guessed that by 1950 there would be more than two million dollars in the Society's treasury and that much of this success could be attributed to Bill's management and financial genius, I am sure they would have had no worries about the condition of his shirt.

It would be pleasant to report that our country faces no foreseeable crises, but you know that this is not so. By many earlier standards, we should be very happy about current conditions. Business is good, employment is high, companies and individuals are seemingly prosperous and we are not engaged in any great hot war. Yet there is great fear and unrest. Many people are mindful that our great unemployment problem of the 1930's was only solved by the big defense program and active war; that we are saddled with an enormous debt; that more than five years after the cessation of the active fighting in World War II, there is no peace; that we are and have been since 1945 engaged in a cold war for which our experience, our noble objectives, and our temperament have not prepared us; that the cold war has warmed up considerably in Korea and may even get hot; that we have had to finance other countries to help them combat communism; that the value of our dollar has greatly depreciated in the past ten years; that it may decrease more and that we face another large defense program, the duration and magnitude of which cannot be predicted.

Perhaps we might agree that the main fears are those pertaining to Russia and those relating to the home front. Both of these are aspects of security, one representing fear from without, and the other,



fear from within. I hope we can profitably explore both of these this evening.

Let us consider the Russian situation first. It is obvious that Russia's objective is to overtake us in strength. It can do so only by building itself up or weakening us. It is trying to do both at the same time. The building process is not fast enough to suit the dictators and there is no hope in this direction anyway; so a full-fledged campaign to tear us down is and for years has been under way. Why some people over here are willing to aid Russia in the process is evident enough. They hope to profit by our downfall. Others probably have good intentions, but do not realize that they are furthering an unworthy cause. But why any intelligent American citizen should think that a Communist police state is preferable to what we have is totally beyond my comprehension.

Notwithstanding Russia's potency for world disturbance, I believe it is fundamentally weak. It has no mechanism like ours for progress through the correction of the mistakes of millions of free people. It is busy copying the industrial advances of the West, but beyond a certain point we can't be copied. It doesn't have the strength which only free markets can provide. In short, Russia is not fundamentally strong because its people and institutions are not free.

A country can be free but not strong. We freed the Philippines, but they did not become strong enough to protect themselves from outside attack. Several European countries were freed after World War I, but they did not become strong. On the other hand, no country can become really strong without free individuals. It is not accidental that we in the United States of America have the most efficient industrial establishment, the highest standard of living and the greatest potential military might in the world. We admit the favorable influence of our size, the oceans and our natural resources. But without the strength deriving from our free individuals, free institutions, elective government and free enterprise, we could be weak and defenseless.

I do not have time to elaborate on the reasons for the dependency of strength on freedom. In essence, however, our strength can be measured by our economic health and this is reflected in our standard of living. Economic health requires free markets in order to insure that the goods produced and services rendered will be exactly what we people want. Free individuals making billions upon billions of free choices in a free market not only make possible a sound economy but also national strength. This is what has made

America strong. A country can be free and yet not be strong, but it can't be strong without freedom.

Maybe you think that Russia is not free but it is strong. Is a country strong that won't allow its citizens to travel in other countries, for fear they will become dissatisfied with their own miserable lot at home? Is a country strong that won't allow free elections? Is it not probable that Hitler would have conquered Russia had it not been for the help of Britain and America?

If so, was not Nazi Germany a country that was strong without freedom? I visited Germany several times before Hitler came to power and again in 1935 after the blood purge. I saw that dictators can do things which the heads of democratic countries cannot. They can decide the working hours and Hitler did decree a 60-hour work week. They can provide full employment by having the otherwise unemployed make military equipment. They can avoid the losses caused by work stoppages, slowdowns and strikes by putting the recalcitrant into concentration camps. I saw too what wrecks the loss of liberty can make of strong men and institutions. When I had recovered from the first shock, I saw in a new, clear light the blessings we enjoy because of the wisdom and sacrifices of our forefathers. I felt sure that the all-powerful Nazi ruling clique could not muster the wisdom necessary to make Germany fundamentally strong. Hitler's regime fell.

I am not unmindful of the Russian menace. It is real. It is surely the most important factor in world security and must be dealt with the same as many other anti-social movements have been dealt with throughout history. Fortunately, Russia's objective to gain domination of the world is now generally recognized and its low and ruthless methods have been exposed for all with a desire to know the truth to see.

With the fighting war successfully concluded five years ago, we still have no peace. Why? Because Russia doesn't want peace. With the rest of the world willing to implement a workable plan to make atomic energy a boon to a world at peace, Russia holds out. Why? In part, because it cannot afford to have the world inspectors see how bad conditions are inside the country. Who has prevented the United Nations from making greater headway? Russia. Why? Because planned chaos fits Stalin's program better than order.

We must face up to the fact that Russia has considerable strength. Its size, manpower and resources alone would permit it to overrun small countries. Some strength is derived from unified policies determined by a small group for the whole population. Also,

there is temporary strength in extreme ruthlessness. A stick-up man with a loaded gun which he is willing to use can hold many unarmed citizens at bay. There is appearance of strength too if fast destructive action can be used to gain ends which otherwise would require tedious constructive procedures. Such practices, however, represent too flagrant a violation of the Golden Rule to have lasting strength.

What forces are there to deal with this menace? There are welcome bright spots in some parts of the world, including much of the Western Hemisphere. The desire to help is present in a considerable part of Europe but the outlook there, as you know, is not as favorable as we should like to see it. However, there is great strength in Europe if it can be mobilized. People who have carried the torch of freedom for more than two thousand years, who provided the foundations for our freedom and who have emerged from many severe crises with enhanced strength are not to be brushed aside with a sweep of a dictator's arm. We should be profoundly thankful that they are on our side.

Naturally, most of the peace-loving nations of the world look to America to take the lead. So far, Russia has elected to shun conventional methods. We earnestly hope that it will accept peaceful procedures for settling international differences, but the prospects seem slim. Therefore, we must be ready for any eventuality. Of one thing we can be sure. Russia will ever be watching for weaknesses in our armor.

The action of the United Nations this past summer in connection with the Korean affair should give us a much-needed lift in morale. The League of Nations failed because it had no "teeth". The United Nations in addition to having splendid objectives has shown great courage in facing the knotty world problems. It is not to be doubted that if Russia is determined to have a hot war, the United Nations will demonstrate that it has a full complement of sharp teeth.

In recent times so much has been said about security at home that I hesitate to spend more time on the subject. Many people have a passion for talking about it, coupled with a determination to do things which will add to our insecurity.

There are many aspects of security. Among other things, we want safety of person. We want safety of property. We want to be assured of a fair opportunity to earn a living. We do not want to be dependent on anybody in our old age. We want our children to be educated and, in general, to have the good things of life. We want protection from the untimely death of our breadwinners. We want to secure the opportunity to study and enjoy the wonders and



beauties of nature, to enhance cultural values and to give exercise to our many and various creative faculties. We want our nation to be secure against any kind of attack. There is nothing much new in these desires.

But of late the security urge has developed some new facets or at least some new reflections from the old. We have so-called "social security". We have unemployment compensation. Some kind of a "ham and eggs" scheme is up for consideration most of the time. We have parity prices for several farm products. Pension plans fill the air. Minimum wage rates are written into the law of the land. Government proposals to provide for the people are so numerous and embracive that they have given rise to the expression "from the cradle to the grave".

We should ask ourselves who is to be guaranteed security and by whom, for what duration and to what extent. We should try to find out whether the so-called security is phony or the real thing. We should even try to ascertain whether the right emphasis is put on security. The least we can do is to inform ourselves on this vital subject.

Often an individual or group strives for security at the expense of the security of others. Stalin, for example, is taking the steps which he thinks will mean security for him, for the Politburo and probably for the Russian government. Is he taking the steps designed to provide security for the Russian people? The Germans who managed the weird Dachau establishment were gaining security for themselves, at least temporarily, by making the lives of the prisoners insecure. A gangster gains security for himself by being loyal to the gang at the expense of the security of various good citizens. Some labor groups in this country want security for themselves at the expense of others, which means millions of stockholders and still more millions of customers. Many farmers want security for themselves clearly at the expense of the public.

I believe there are some kinds of security that we can't have, or wouldn't want even if we could have them—for example, security at the expense of others, security at the expense of our government, security without freedom and security with scarcity.

Even though we might be willing to accept security at the expense of others, we can't have it. If a group tries to gain security for itself within a country, at the expense of other groups, there is civil strife and if a country tries to gain security for itself at the expense of other countries, there is danger of war. So only by helping all deserving people can there be lasting security.



Although the doctrine that the government can provide security for the people has many advocates, it is unsound. The government derives its strength from the people, and patronizing practices by the government not only weaken it but soften and weaken the citizens also. Security at the expense of the government is a myth, the same as all other "something for nothing" schemes.

If we merely want to be assured of a living, how better can we achieve it than a life sentence in a high-walled penitentiary? We would have food, shelter and clothing, and possibly, with a modicum of political pull, we could get intra-mural work. Of course, we don't want security at the expense of our liberty. "Give me liberty or give me death!" is not a hollow or meaningless expression. When Kravchenko escaped from the Russian vise and wrote about it, he entitled his book "I Chose Freedom". When Einstein quit Germany, he told the world his reason. He wanted to live in a place where individuals were free. But cherished as freedom is for its own sake, it is not a luxury. It is a practical necessity for sustained strength.

Aside from our normal desire for abundance, there is another compelling reason for discarding the idea of security with scarcity. Even if we as individuals might be satisfied with such an economy, our national sovereignty would be insecure. Therefore, we want security with abundance, of course, *balanced* abundance. We don't need so many potatoes.

So we want security with freedom, with balanced abundance, and with all deserving people sharing in its blessings. America today represents the nearest approach to this ideal of any nation at any time. We should be most grateful for this magnificent heritage. Yet we know that there is room for much improvement. It is our privilege, our responsibility and our challenge to preserve the past gains and to advance to higher levels.

We have much strength but we must not be complacent about this. There is no danger of our becoming too strong. Also, we may not be as strong as we appear to be. A person can be infected with pneumonia germs and they can be multiplying at a dangerous rate before there is appearance of sickness. I have seen many metal test specimens subjected to rapid alternating stresses. At loads around half those required to produce quick rupture, the test pieces may stand up for months and then suddenly break. An hour before rupture they may appear sound. An individual or a nation appears prosperous while spending borrowed money, but the pains come during the paying-back period. Are there reasons for thinking that we are not as strong as we appear? I believe there are.

Some of our number are saying that our freedoms are being steadily eroded away. Rent control removes an area of enterprise activity from the free market. Price support of certain farm products is impairing another part of the free market. There is fear that the welfare program may deprive us of more of our freedom. Bonneville, TVA, Hoover Dam and Grand Coulee remove a part of the power business from the free market and perhaps impose on us an added tax burden. The government has also taken over some of the prerogatives of our financial institutions.

The great danger in these governmental activities lies in the impairment of our dynamic strength. As long as markets are free, there is competition, and as long as competition is healthy and active, there is hope, not only of maintaining but of enhancing our strength. We are strong enough to stand a little statism and survive but too much will surely destroy our free enterprise system and, hence, our strength. If we should go too far, there is no assurance that we can turn back. We know that some unfortunate countries have not found it possible to do so. And since no one knows exactly where the dividing line is, we shouldn't play with dangerous fire—we should keep the government encroachment to a minimum.

The purchasing power of the dollar has decreased alarmingly since the war. I know a man who bought German marks in 1919 for five cents each. He said that it was unthinkable to him that the mark could go any lower. A few years later it went, as you know, to zero. In 1914 about five French francs could be exchanged for one dollar. Now it requires 350 francs to buy a smaller dollar. What is dollar depreciation doing to our internal security? How about endowed institutions, pensioners, life insurance beneficiaries and those who have saved all of their lives that they might have enough to live on in their old age? Ridiculing the possibility of dangerous inflation here will not in itself keep us from having it.

Another cause for concern is the labor union movement. Beginning with the passing of the Wagner Act in 1935, this situation has steadily worsened. For over fifty years industrial employee relations had been improving. Owners, management and other employees were learning that each was dependent on the other and that all were dependent on the buying public. While the progress graph had its ups and downs, the long-range direction was upward. The standard of living was increasing. All were moving up together. This is not to say that all shared equally. People never have shared equally and they never will. But each group had ways of getting its fair share.

Then came the Wagner Act. Internal war was instigated by certain labor unions against companies. War terms came into use. War methods were used. The war spirit was whipped up. Class warfare was encouraged. The right to stop work was legalized while the right to work was all but forgotten. Unfortunately, some government people, instead of functioning as impartial umpires, helped the unions to gain unprecedented power.

Having acquired the power to close down plants, stop the wheels of industry and even shut off the supply of food and fuel from the citizens of this country, some union leaders are trying to control the government partly by direct action and partly by open threats to defeat congressional candidates who dare to vote against measures designed to give the unions still more power. Perhaps the coal debacle this past winter will arouse the good citizens to corrective action.

I am not complaining about labor unions as such. We had labor unions long before we had the Wagner Act. I am complaining about labor leaders who are undermining American institutions and American strength and who, among other things, are forcing wage increases at a faster rate than production can be increased by the orderly technological improvement processes. Kaiser Wilhelm couldn't wait for the orderly growth processes, so we had World War I. Hitler wanted short-cuts and we had World War II. Some labor leaders should heed the fable about the goose that laid the golden eggs. The proved sense of irresponsibility of these leaders demands that the power of the unions be drastically limited. If there are historians in the future free to express their real thinking, and I am optimistic enough to believe that there will be, it may be that they will rate the Wagner Act as the worst piece of legislation ever enacted by our Congress.

Our huge public debt and the heavy tax burden pose problems which will demand our attention for years or even decades. Some measures designed to give security, at least to some groups, will obviously weaken the country as a whole. While giving lip service to a sage like Thomas Jefferson, we are doing violence to many of his teachings. For example, he said, "I place enomomy among the first and most important virtues, and public debt as the greatest of dangers. . . . . We must make our choice between economy and liberty or profusion and servitude. If we can prevent the government from wasting the labors of the people under the pretense of caring for them, they will be happy."

Although there are many prophets of gloom and doom, I believe



we can look forward with hope. I don't say that the road will be smooth nor that we can make progress without conscious effort, clear thinking and courageous action. Nothing will happen overnight that will improve the present status materially. Building processes are slow while destructive processes can be fast and dramatic. There is no way to produce a 50-year-old human being with all of his knowledge and experience in less than 50 years, but he can be destroyed in an instant. One may spend years building a house, but it can be destroyed with a single match in an hour. A nation that has been building for decades or even centuries can be quickly destroyed.

But even though the destructive processes are faster, the constructive forces are stronger. There is ample evidence all around us that for hundreds of millions of years the constructive forces have gained the upper hand. Do you know of any good reason why these great constructive forces should not be made to work for us now?

It would seem that we ought to be able to stop or greatly retard the inflation trend. Who wants inflation anyway? The answer is that nobody here wants it. Then why have we such a dose of it? The main reasons are well understood—government fiscal policy and union power. Our economy at present seems to have taken on something of the nature of a ratchet—it moves readily in a single direction—toward inflation. We have reached the point where many candidates for office cannot be elected unless they support measures which, directly or indirectly, promote inflation. It is difficult to find anyone who is helped by our inflation unless it be Russia. The control of inflation essentially demands our willingness to do the right things. Are we so shortsighted that we will rush headlong into destructive inflation? It is hard to believe that the American people will be so foolish.

Nor are we as dependent on election outcomes as our emotions might lead some to believe. For example, the American Society for Metals had its birth when Wilson was president and since has functioned under five additional presidents, three Republican and two Democratic. Yet it has made steady progress year by year. Its status may have been better if some elections had turned out differently, but strong national and local officers and committeemen have always done the best they knew how under the existing conditions. In a broad sense, this is true of the lives of each of us. We try to progress all of the time—not merely when the party we favor is in power. Also, the same can be said about businesses, large and small,



professional men, our educational organizations from kindergarten to post-graduate, churches, farmers, ranchers, fishermen, lumbermen, hospitals and others. For the greater part, these represent private enterprise where efficiency is rewarded and excessive inefficiency meets economic punishment.

This process results in the survival of the efficient and the death or shrinkage of the inefficient and thus leads to a general strengthening of our people and their institutions. This is, in fact, the real, hard core of strength of our nation.

The people of this country are united on some other important objectives. We all want peace. Each of us is a customer for the goods and services incident to our economic life. If Russia insists on a hot war, horrible as it is to contemplate, we will unite in the struggle and will not quit until there is complete victory for the forces of decency on this earth.

We are not worthy of our priceless heritage as Americans if we accept any part of the philosophy of despair. Let the aggressors wage war for conquest and power if they can find nothing constructive to do. To enjoy national security, we must *be* stronger and *keep* stronger than any would-be aggressor. We *can* do this if we *will*. And we can enjoy security at home too if we shun the "something for nothing" schemes and vigorously wage FREEDOM, PEACE and PROSPERITY.

## A METALLURGICAL INVESTIGATION OF SILVER CHLORIDE

BY R. D. MOELLER, F. W. SCHONFELD, C. R. TIPTON, JR.,  
AND J. T. WABER

### *Abstract*

*Data and information concerning microstructures, deformation, and mechanical and physical properties are presented for the purpose of establishing an analogy between silver chloride and metals. Although differences do exist (e.g. electrical resistivity, ionic bonding), the similarities demonstrated seem sufficient to allow the use of silver chloride as a "transparent metal" in metallurgical investigations.*

*Silver chloride can be cast, rolled, forged, extruded and machined by common metallurgical techniques. Its deformation mechanism, thermal expansion, elastic constants, crystal structure and behavior during deformation and recrystallization are similar to those of many common metals. Rolling and drawing result in preferred orientations of the types exhibited by copper and aluminum. Stress-strain curves and the strain hardening exponent are similar to those obtained from nonferrous metals. Silver chloride alloys with other metallic chlorides and bromides forming phase diagrams exhibiting varying degrees of solid miscibility and eutectic and peritectic reactions. Solid solubilities appear to vary in accordance with a rule similar to Hume-Rothery's "size-factor" rule for metals. Photomicrographs and macrographs are presented showing silver chloride in the as-cast and the cold-worked conditions and in various stages of recrystallization. Micrographs taken with reflected light show structures indistinguishable from those of metals, while those taken with transmitted light exhibit several unusual features such as showing grain boundaries on both sides of thin sheet. Data obtained by use of a recording spectrophotometer show that silver chloride remains adequately transparent over periods in excess of one year.*

THE fact that metals are opaque to visible light has placed limitations on investigatory methods. Knowledge of metallurgical phenomena would be more readily attained if it were possible to observe and record the behavior of the interior of a

A paper presented before the Thirty-second Annual Convention of the Society, held in Chicago, October 21 to 27, 1950. The authors, R. D. Moeller, F. W. Schonfeld, C. R. Tipton, Jr., and J. T. Waber, are staff members, Los Alamos Scientific Laboratory, Los Alamos, N. M. Manuscript received April 3, 1950.

metallic specimen during a reaction or test. Lacking such an ability, an alternative is the development or discovery of a material possessing the desired properties.

If such a material could be found it would then be possible to carry on three-dimensional studies during melting, phase transitions, precipitations, and other solid-state phenomena. In an optically anisotropic substance it might be possible to determine grain orientation relationships resulting from metallurgical reactions. In addition, stress analyses could be made by photoelastic methods on a micro and macro scale during these studies and during deformation of polycrystalline structures.

Most of these desired investigations can be made by existing but rather cumbersome and time-consuming techniques. A transparent metal would contribute to the flexibility, selectivity, and ease in application of investigative methods.

The exceptional plasticity of silver chloride has long been known in scientific circles, and silver chloride has been utilized in production of lenses, valves, and other articles. In certain instances it has been called a transparent metal, but no attempt has heretofore been made to establish the analogy on a firm basis. It is the purpose of this paper to establish that a transparent material (namely AgCl) exists which is sufficiently metallic in behavior to allow its use in metallurgical research.

#### LITERATURE SURVEY

Tammann (1),<sup>1</sup> in 1932, pointed out that during the rolling of silver chloride the changes in hardness and density were similar to those occurring in metal. Cagliotti (2), in 1933, investigated the structure of cold-worked silver chloride and its subsequent recrystallization and observed a duplex fiber structure identical to that occurring in some face-centered cubic metals. His work on recrystallization indicated a recrystallization temperature above 160 °C and a strongly oriented texture. At the same time Levi and Tabet (3) published data concerning the fiber structure resulting from cold rolling and wire drawing of silver chloride. Rolling produces the (111) type texture up to 230 °C and the (100) type above this temperature. In 1934, Stepanov (4) investigated the plastic properties of single crystals and in the following year published stress-strain diagrams of the polycrystalline material. These diagrams closely resembled those obtained from nonferrous metals. Fugassi and McKinney (5), in 1942, reported that they were able to roll

<sup>1</sup>The figures appearing in parentheses pertain to the references appended to this paper.



thin sheets and extrude thin wall tubing. In 1943, Fetters and Dienes (6), during an investigation of silver chloride as a material for the study of ingot structure, noted their ability to cold reduce specimens more than 50% by rolling. Investigations by Cagliotti (7) in 1935 demonstrated that the presence of 0.01% cuprous chloride, calcium chloride or magnesium chloride and 0.4% rubidium chloride destroyed the workability of silver chloride; whereas 1.25% sodium chloride or 0.25% lithium chloride had no effect. In 1949, Tsobkallo (8) published detailed information concerning the preparation of sheet and bar specimens for photoelastic analysis.

Orowan (9), Nye (10), Prigorovskii (11), Stepanov (12), and West and Makas (13) have utilized silver chloride as a media for photoelastic stress analysis.

The physical constants of silver chloride have been established by many investigators. For the sake of brevity they will be included only as is necessary for correlating the results obtained by the authors.

#### MELTING AND CASTING

Powdered silver chloride of Baker's analytical reagent grade was used as melting stock. It contained 5 ppm of nitrate, 5 ppm of iron and less than 10 ppm of copper. Kremers (14) has pointed out that for high transparency to infra-red radiation, reagent grade material is unsatisfactory and the silver chloride must be carefully precipitated and dried.

Melting was done in an open pot-type electric resistance furnace. Various types of crucibles were used but the only wholly satisfactory crucible materials were porcelain and platinum. High-fired magnesia crucibles were found to be entirely unsatisfactory and fused silica crucibles were subject to slow attack by molten silver chloride. The charge was melted and brought to the desired temperature as rapidly as the furnace would allow and immediately cast. Molten silver chloride is very fluid and is readily cast at a temperature only slightly above the melting point. Rapid manipulation is advantageous in that it shortens the time that the silver chloride is in the molten state and subject to decomposition. A relatively low casting temperature allows a wider selection of mold materials by decreasing the possible reaction time in the mold. Mold materials used were, in order of preference, pyrex, fused silica, platinum, porcelain, and tantalum. Pyrex is a very versatile mold material for production of relatively simple shapes. The shapes readily available in fused silica are limited, and this fact, combined with



the higher cost, relegates fused silica to a secondary position as a mold material. Platinum and tantalum are expensive but provide rapid means of chilling a casting. The reactivity of tantalum with silver chloride is considerably greater than that of the other materials mentioned and can be used only under conditions where very rapid handling is feasible. The impossibility of working porcelain in the average laboratory makes this material largely unsatisfactory.

The specimens used were cast into cool molds except where a large grain size was required. Unless silver chloride is chill cast it will solidify with an extremely large grain size, and even when chill cast the grains are quite large. Most castings exhibited some degree of macroporosity, probably due to the granular nature of the melting stock. The solidification shrinkage of silver chloride is approximately 5% and is illustrated in Fig. 6.

The ingots after casting were slightly cloudy, possibly because of precipitation of colloidal silver formed by decomposition of the chloride in the liquid state. In an effort to eliminate this cloudiness, chlorination was attempted. Chlorine was bubbled through a melt by means of a fused silica tube inserted into the molten silver chloride. This method was quite satisfactory and resulted in the production of very clear ingots. These ingots were used in the studies concerning the effects of exposure to light on light transmissions. It was found that ingots of good clarity could be obtained without chlorination by shortening the melting and cooling cycle to a minimum; therefore, such material was used for the metallurgical operations.

The effect of light on the salts imposed a less serious problem than was expected and it was found that the usual metallurgical operations could be carried out under fluorescent lighting without serious discoloration, although tungsten incandescent light has been recommended for the production of the optical grade of silver chloride (14). Many statements are to be found in the literature (15) which indicate that the transmissibility of silver chloride decreases in the ultraviolet region. The absorption spectrum of silver chloride in the vapor state lies between 3100 and 3400 Å (16), but solidification causes broadening of the band as is characteristic of the spectra of metals (17).

The absorption spectrum in the visible range was determined with the aid of a General Electric Hardy-type recording spectrophotometer. A plate of silver chloride  $\frac{1}{8}$  inch thick was chill cast into pyrex by melting and casting in a darkened room. The spectro-

photometer trace obtained is shown in Fig. 1. The ordinate (density) in this figure is plotted as the logarithm of the reciprocal of transmittance. Similar curves, also in Fig. 1, were obtained from the same sample after 10 and 50 hours' exposure to fluorescent light, 20 foot-candles having been received by the sample. It will be noted that the exposure resulted in increased absorption in the

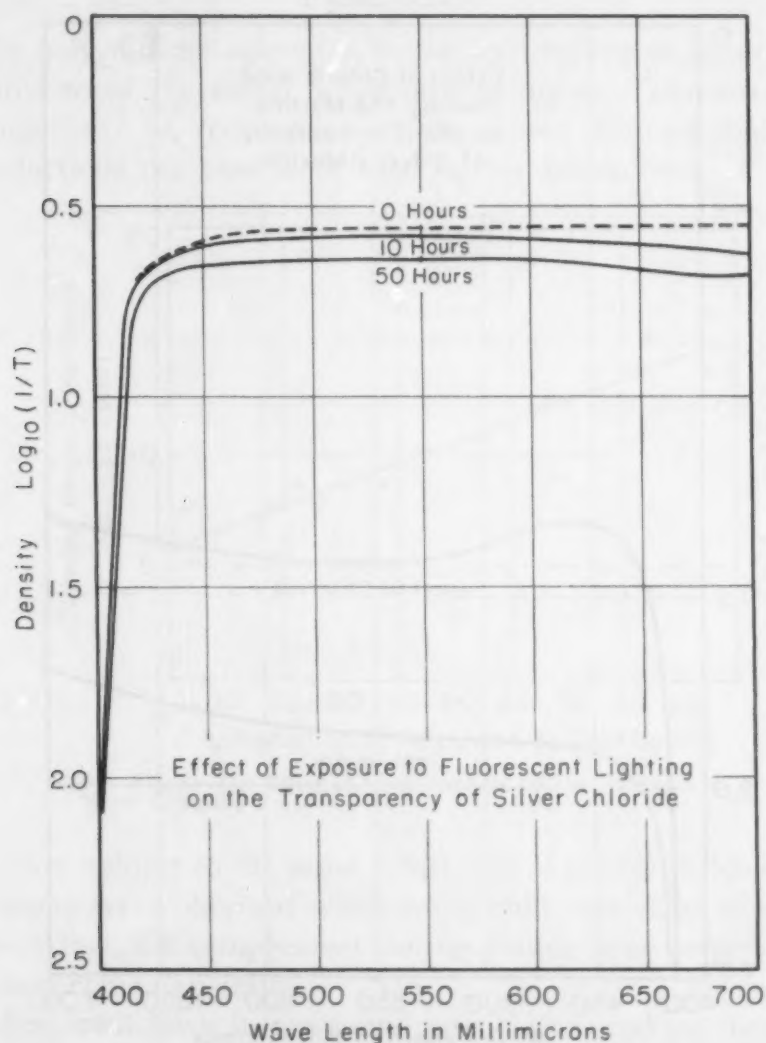


Fig. 1—The Effect of Exposure to Fluorescent Lighting on the Transparency of Silver Chloride.

red end of the spectrum. Although there was no further large change after 50 hours, there was a general increase in opacity and significantly stronger absorption in the red.

A reasonable explanation of this behavior is the formation of F-centers<sup>2</sup> which frequently have the peak of their characteristic

<sup>2</sup>Mott and Gurney explain in their book, "Electronic Processes in Ionic Crystals", that an F-center is an area of local anionic deficiency.

absorption curves near 6000 Å. The illumination by light thus created these F-centers both by formation of a cationic excess (i.e., by evolution of chlorine) and by electron trapping. On the basis of such reasoning, one would predict that the density of free silver atoms could be reduced by contact with chlorine and as a result the transparency would be increased. Pursuant to this prediction,

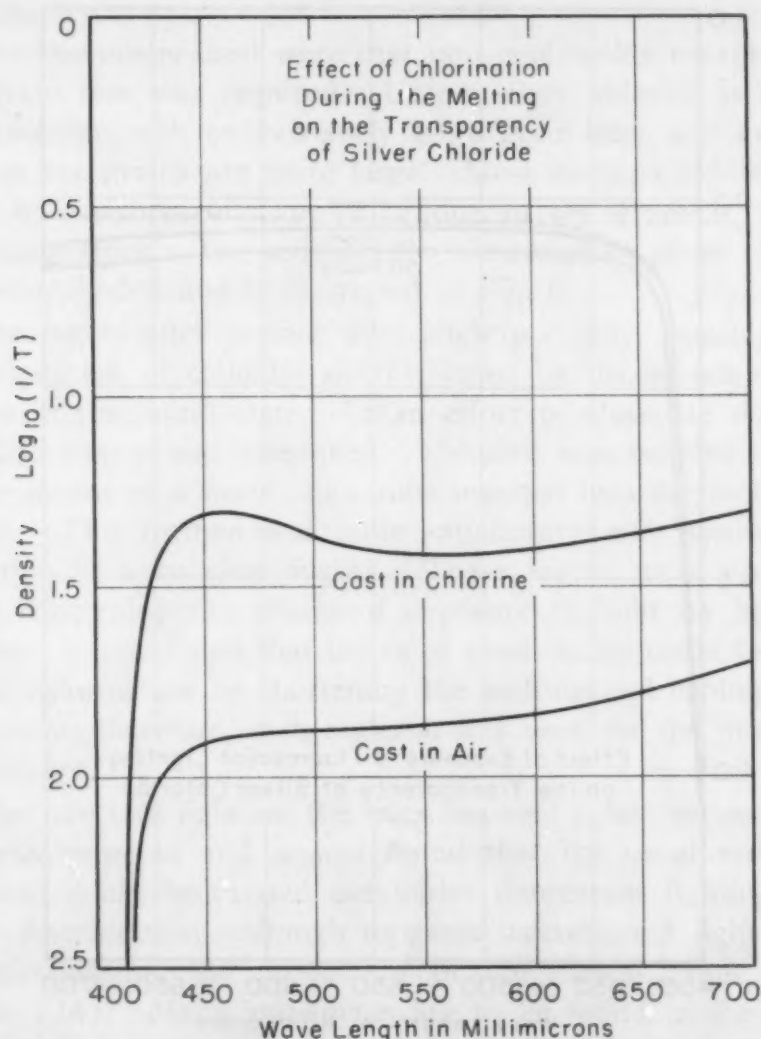


Fig. 2—The Effect of Chlorination, During Melting, on the Transparency of Silver Chloride.

similar samples were melted in air and under bubbling chlorine gas. Comparative spectrophotometric traces for the freshly cast specimens are presented in Fig. 2. Herein the logarithm of the reciprocal of the transmittance is plotted against the wavelength as in Fig. 1. (The differences in optical density values between Figs. 1 and 2 are due to different specimen thicknesses.) A five-fold increase in



transmission can be observed for the chlorine treated sample in the spectral region of 5000 Å. This experiment confirms the prediction and agrees with what is known about the theory of photographic processes. In spite of the difference in transmission, the air-melted material was found to be sufficiently transparent to allow its use in all investigations described herein.

#### FABRICATION

The only difficult operation in the cold rolling of silver chloride was found to be the initial breakdown of ingots. The coarse grain and "ingotism" of rectangular ingots caused fracture unless very light reductions per pass were used during breakdown. Cylindrical

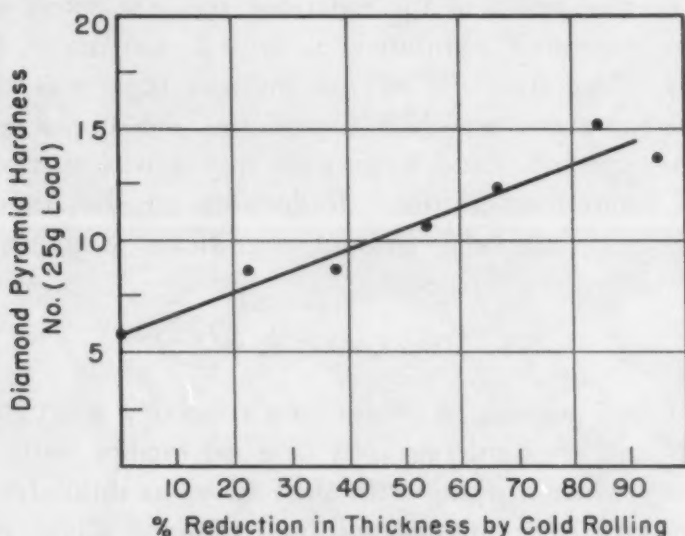


Fig. 3—The Effect of Cold Working on the Hardness of Silver Chloride.

ingots were subject to the same defect, but of course in lesser degree. Best results were obtained when using chill cast slabs of such conformation that the compression during rolling was perpendicular to the as-cast columnar grains.

After breakdown it was found possible to produce sheet of high quality with reductions per pass as high as 50%, although the usual procedure was to reduce 10 to 15% per pass. Strip of 0.0007 inch in thickness was successfully produced cold, with no intermediate anneals. This lower limit on thickness was not due to excessive work hardening of the specimens but rather to the mechanical deficiencies of the bullion rolls which were used. Hot rolling, at a temperature of about 200 °C, was found to produce more nearly perfect sheet in thicknesses greater than 1/4 inch and was utilized for such purpose.

The effects of cold rolling on the hardness of silver chloride are shown in Fig. 3. Hardness values were obtained on a Tukon hardness tester utilizing a Vickers-type indenter under a 25-gram load. As is seen from this graph, silver chloride seems to behave in a normal metallic manner. Cold-rolled silver chloride was found to have a considerably higher yield point than the annealed material and possessed a metallic ring when lightly struck.

A typical microstructure of a coarse-grained rolled sheet is shown in Fig. 4; the transmitted light delineates a number of elongated grains with nearly parallel grain boundaries.

A cast cylindrical ingot of silver chloride  $\frac{1}{2}$  inch in diameter and 4 inches in length was extruded to form 16 inches of  $\frac{1}{4}$ -inch rod. The surface finish of the extruded rod was excellent and the last portion extruded exhibited a typical extrusion pipe. An austenitic stainless steel die of the indirect type was used. The extrusion temperature was 175 °C and the pressure was 5000 psi.

As was expected, hand forging of ingots was successfully carried out at room temperature. Reductions of the order of 75% were successfully attained without significant amounts of edge cracking or other forging defects.

#### METALLOGRAPHY

It was found possible to obtain, in a relatively short time, photomacrographs and photomicrographs of good quality with less effort than necessary when working with such alloys as mild steel or brass.

The authors have microscopically examined silver chloride in the as-cast, as-extruded, and as-rolled conditions; after recrystallization and grain growth treatments; and after varying amounts of cold deformation.

Surface preparation of specimens for macrography and micrography followed well-established metallurgical routine. Specimens were cut with a hacksaw and rough grinding was carried out by filing. Fine grinding was done on metallurgical abrasive papers beginning with No. 1 grit and continuing through 3/0 grit, utilizing oil of lavender or kerosene as lubricant. Polishing operations, when necessary, were carried out in two steps on a rotating wheel covered with Gamal cloth, utilizing first Gamal alumina, and finally a suspension of magnesium oxide in water, with green oil soap added to provide lubrication. Suitable precautions were taken during polishing to avoid excessive surface flow.

It was found that no preparation beyond the use of the abrasive papers prior to etching was necessary for specimens to be utilized

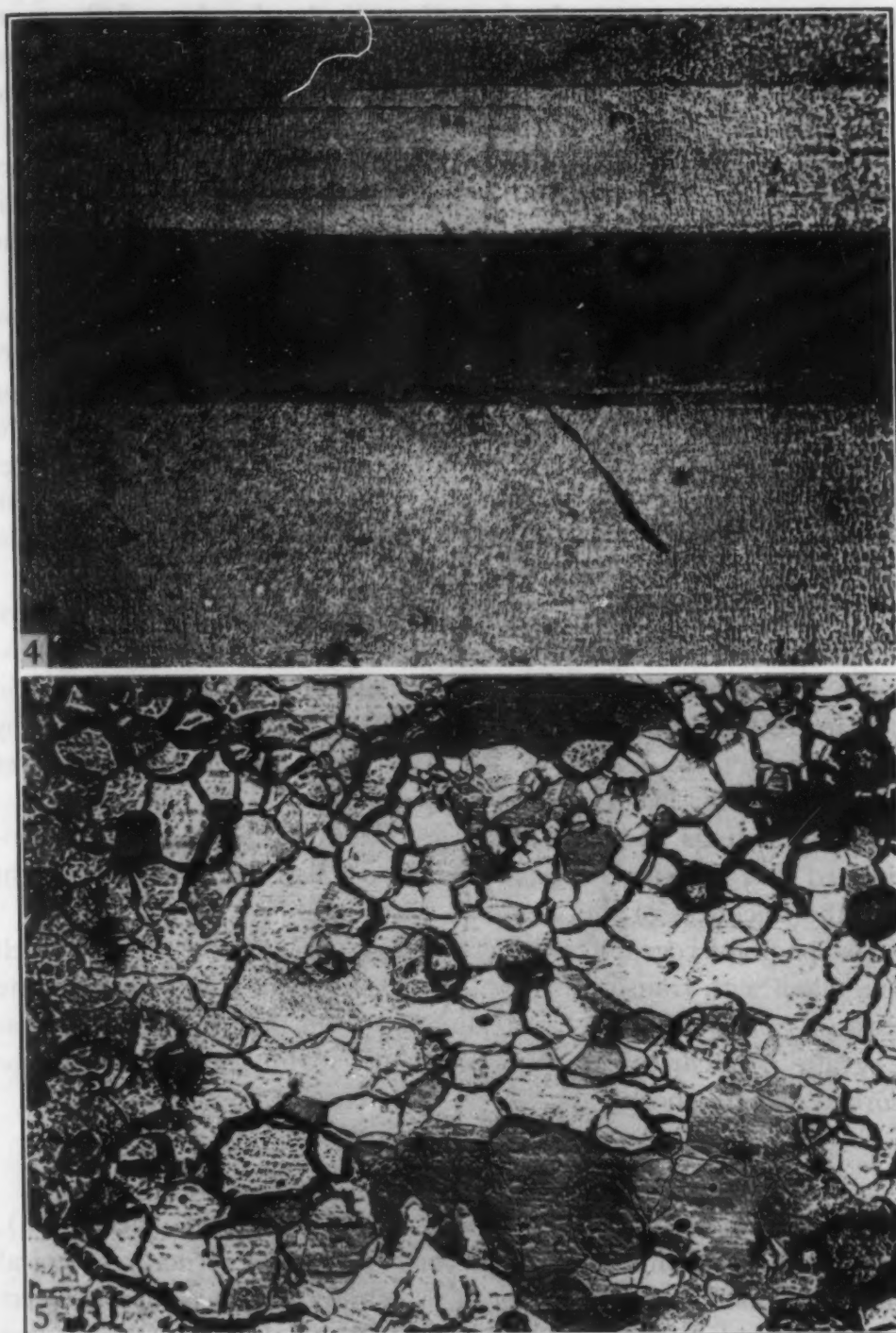


Fig. 4—A Typical Microstructure of Cold-Worked Silver Chloride, Photographed Using Transmitted Light. This photomicrograph illustrates the typically elongated grains. The rough appearing texture of the individual grains is apparently the result of localized internal stresses causing anisotropy.  $\times 100$ .

Fig. 5—Transmitted Light Photomicrograph of a 0.001-Inch Thick Specimen of Rolled Silver Chloride After Recrystallization (12 Minutes at  $340^{\circ}\text{C}$ ). This photomicrograph shows the intersection of the grain boundaries with both surfaces of the specimen, which has a thickness of less than the average grain size.  $\times 100$ .



in macrographic work. In fact, if meticulously clean 3/0 papers were used, it was found possible to dispense with the polishing operations in all cases except when preparing micrographic specimens larger than about 1 square inch in area. Those specimens which were prepared by rolling with well-polished rolls needed no surface preparation at all prior to etching, even after heat treatment. This fact made possible the examination of thin sheet by transmitted light without troublesome mounting and dismounting procedures.

Attempts were made to prepare several specimens by electropolishing, but the results were inconclusive. Best results were obtained in an aqueous solution of nitric acid (5%), utilizing alternating current at 6-volt potential, with a platinum electrode. Polishing times were of the order of 3 to 4 minutes. The surfaces were in all cases unevenly polished and reproducibility was not attained. Since excellent results were obtained by other methods, this line of attack was discontinued.

Among various reagents tested for use as etchants were hydrochloric acid, nitric acid, ammonia, and sodium thiosulphate. Best results were obtained by using 15 grams of Eastman Kodak acid fixer in 100 ml of distilled water. Etching was carried out by immersion for 2 to 4 minutes, followed by a rinse in running water and drying by air blast.

Examinations of microstructures were carried out under non-polarized and polarized reflected light and also by transmitted light when the thickness of the specimen permitted.

A photomicrograph of a recrystallized specimen 0.001 inch thick, taken with transmitted light, is presented in Fig. 5 to illustrate the results obtained with this technique. The figure illustrates that the grain boundaries on both sides of a thin specimen can be recorded on one photograph.

#### CASTING

In agreement with the findings of Fетters and Dienes (6), ingots of silver chloride were observed to possess structures typical of metallic castings. The material is subject to the common defect of ingotism. Fig. 6 is a photomicrograph of a sectioned ingot which had been cast into a pyrex glass centrifuge tube of  $\frac{1}{2}$  inch maximum diameter. Piping due to solidification shrinkage is illustrated in the same figure. Much finer and relatively equiaxed grains were obtained by chill casting.

Through utilization of polarized light, it was found that the microscopic stresses resulting from freezing could be observed in

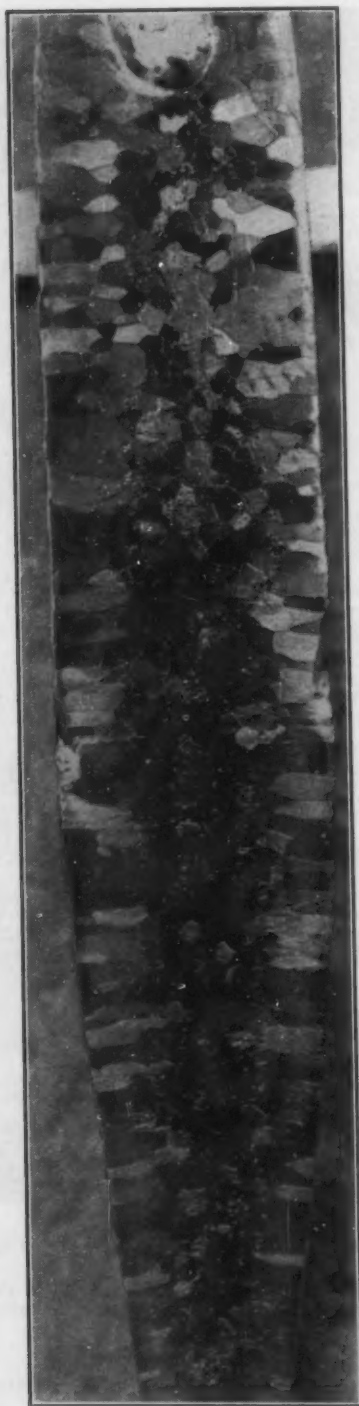


Fig. 6—Photomacrograph of a Cast Ingot Illustrating Ingotism and Solidification Shrinkage. Photographed using reflected light.  $\times 2$ .

individual grains. Unfortunately, the color fringes did not show enough contrast to permit successful photography. The same was found to be true when working with cold-rolled specimens, although

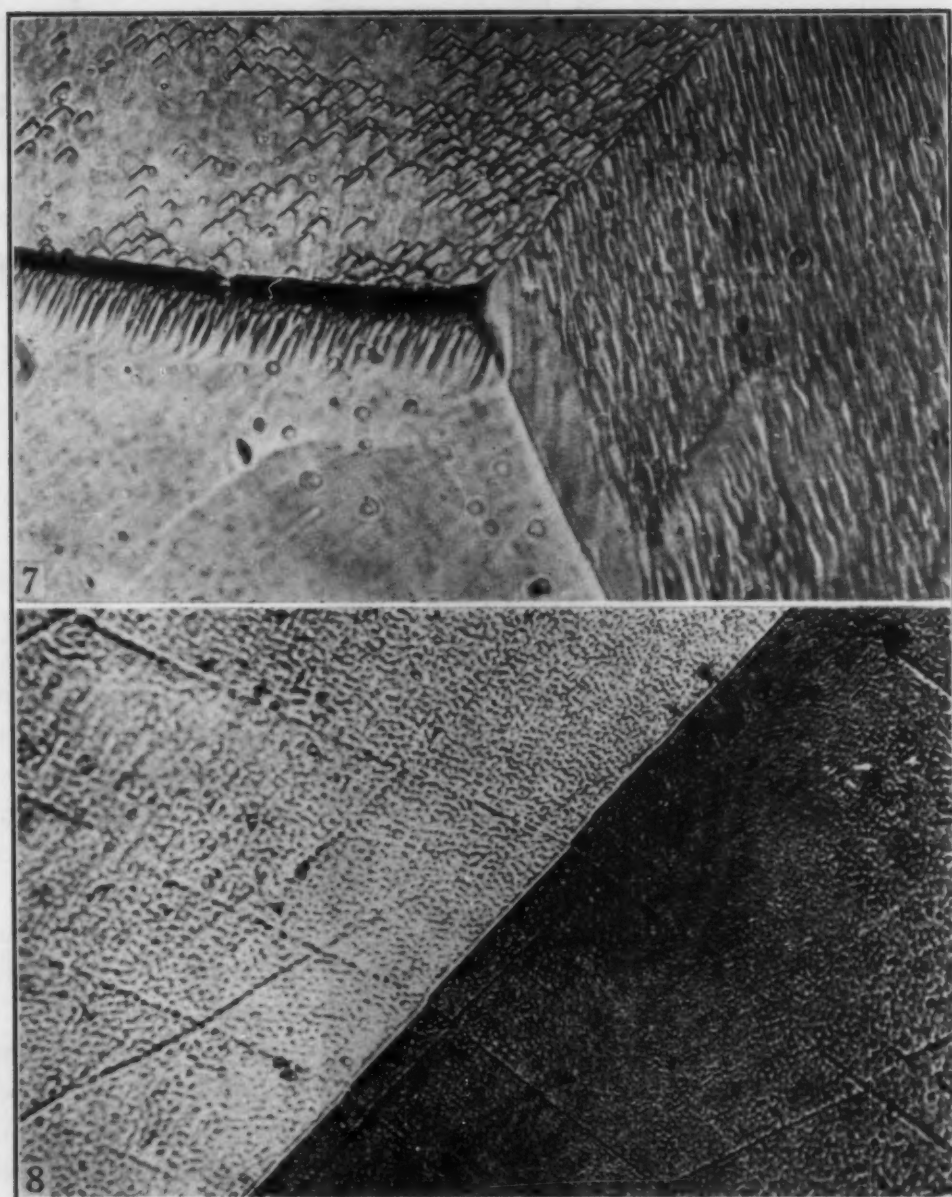


Fig. 7—Deep Etched Specimen of Silver Chloride Photographed Using Reflected Light.  $\times 1500$ .

Fig. 8—Slip Lines in Silver Chloride. The deformation of silver chloride appears to be mechanically the same as that for face-centered cubic metals and alloys. Reflected light.  $\times 1500$ .

the magnitude of stresses was, of course, considerably larger. In an annealed specimen the grain boundaries are, in general, visible under polarized light without an etch.

Fig. 5, a photomicrograph of an etched specimen with transmitted light, exhibits numerous broad grain boundaries. The phenomenon causing this seems to be similar to the Becke effect used by petrographers in the determination of differences in refractive indices and, in an isotropic material such as silver chloride, would



indicate the presence of stresses or impurities at the grain boundaries.<sup>3</sup> The magnitude of the effect varies considerably between various grains, which seems to indicate an orientation effect either on the stresses or on the amount of impurities.

Deep etching of as-cast specimens revealed etch pits as illustrated in Fig. 7. Many metals exhibit similar etch pits after prolonged etching. The variation of etch attack with crystallographic

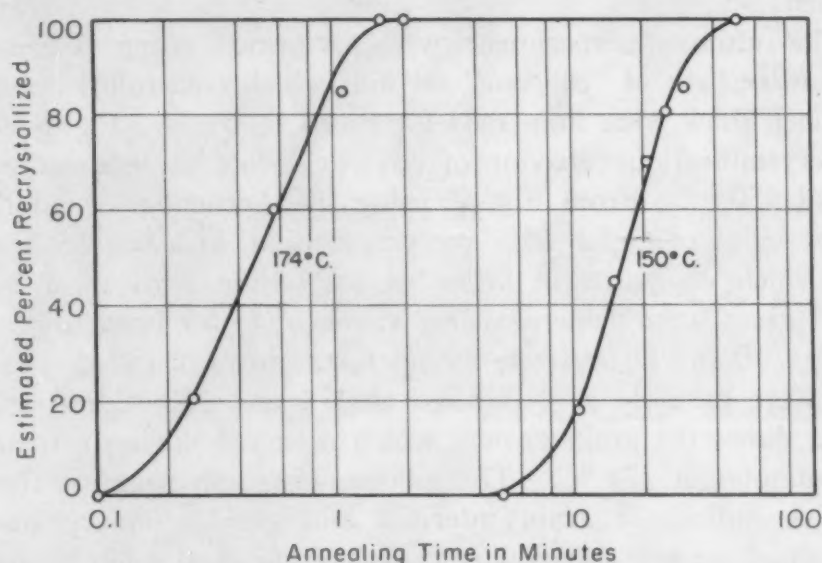


Fig. 9—The Recrystallization Behavior of Cold-Rolled Silver Chloride at Temperatures of 174 and 150°C.

orientation is obvious and, in addition, two of the three grains show a further variation of attack between the body of each grain and the material near the grain boundaries. It is noteworthy that the dihedral angles between the grains approximate 120 degrees, thus agreeing with the angle predicted by C. S. Smith (18) in the case of single-phase equilibrated metals.

*Cold-Worked Silver Chloride*—Fig. 8 is a photomicrograph of a specimen after plastic deformation of less than 1% in compression. The slip lines are similar to those formed in most face-centered cubic metals and are believed to result from movement of the (111) planes. The figure suggests that the deformation of AgCl is mechanically the same as the deformation of common metals and alloys of face-centered cubic structure. The photomicrograph of Fig. 4 serves to illustrate the typically elongated grains of a specimen which had been cold-rolled to 90% reduction in thickness.

#### RECRYSTALLIZATION

Recrystallization and grain growth were first investigated by

<sup>3</sup>The unhomogeneous stressing of a cubic isotropic material produces anisotropy and variations in the refractive index.

placing rolled specimens 0.020 inch thick in ovens at temperatures of 343, 276, 250, 200 and 150 °C for several hours. When recrystallization was observed in all the specimens and grain growth noted for those treated above 200 °C, the temperatures of the experiment were reduced to 100 and 75 °C. After 1 hour, signs of recrystallization were noted in the 100 °C specimen and after 16 hours at 75 °C recrystallization appeared to have begun in the second specimen.

The ultimate experiment was performed using a constant-temperature bath of "Silicone" oil into which cold-rolled specimens 0.020 inch thick were immersed for timed intervals. Fig. 9 depicts the recrystallization behavior of silver chloride at temperatures of 174 and 150 °C. From Fig. 9, using the Arrhenius equation, one gets the value of  $Q$  for 50% recrystallization, of about 55 kcal per mole, which compares in order of magnitude with most metals. Table I gives some data regarding values of  $Q$  for brass and nickel.

Figs. 10 and 11 illustrate the microstructures of rolled specimens which were partially recrystallized at 174 and 150 °C respectively. Fig. 12 shows the grain growth which occurred during a treatment of 16 minutes at 174 °C. This photomicrograph suggests that the refractive indices of grain interiors and grain-boundary material differ, since one sees "shadow patterns" of unetched grain boundaries within the interior of the specimen when those boundaries approach the normal to the surface.

Table I  
Values of " $Q$ " for Brass and Nickel (19)

Cartridge Brass		
Deformation		$Q$ (for Recrystallization)
20.9% cold rolling	.....	53.8 kcal
42.8% cold rolling	.....	41.5 kcal
60.4% cold rolling	.....	32.3 kcal
"A" Nickel		
Deformation		$Q$ (for Recrystallization)
20% cold rolling	.....	75.8 kcal
40% cold rolling	.....	73.3 kcal
60% cold rolling	.....	69.5 kcal

*Stress Relief Anneal*—When specimens which had been plastically deformed were mounted on a hot-stage microscope and heated to about 100 °C and examined with polarized transmitted light, successive changes in the interference fringes at the grain boundaries were observed, thus indicating stress relief before recrystallization. Unfortunately, suitable photographs could not be obtained.

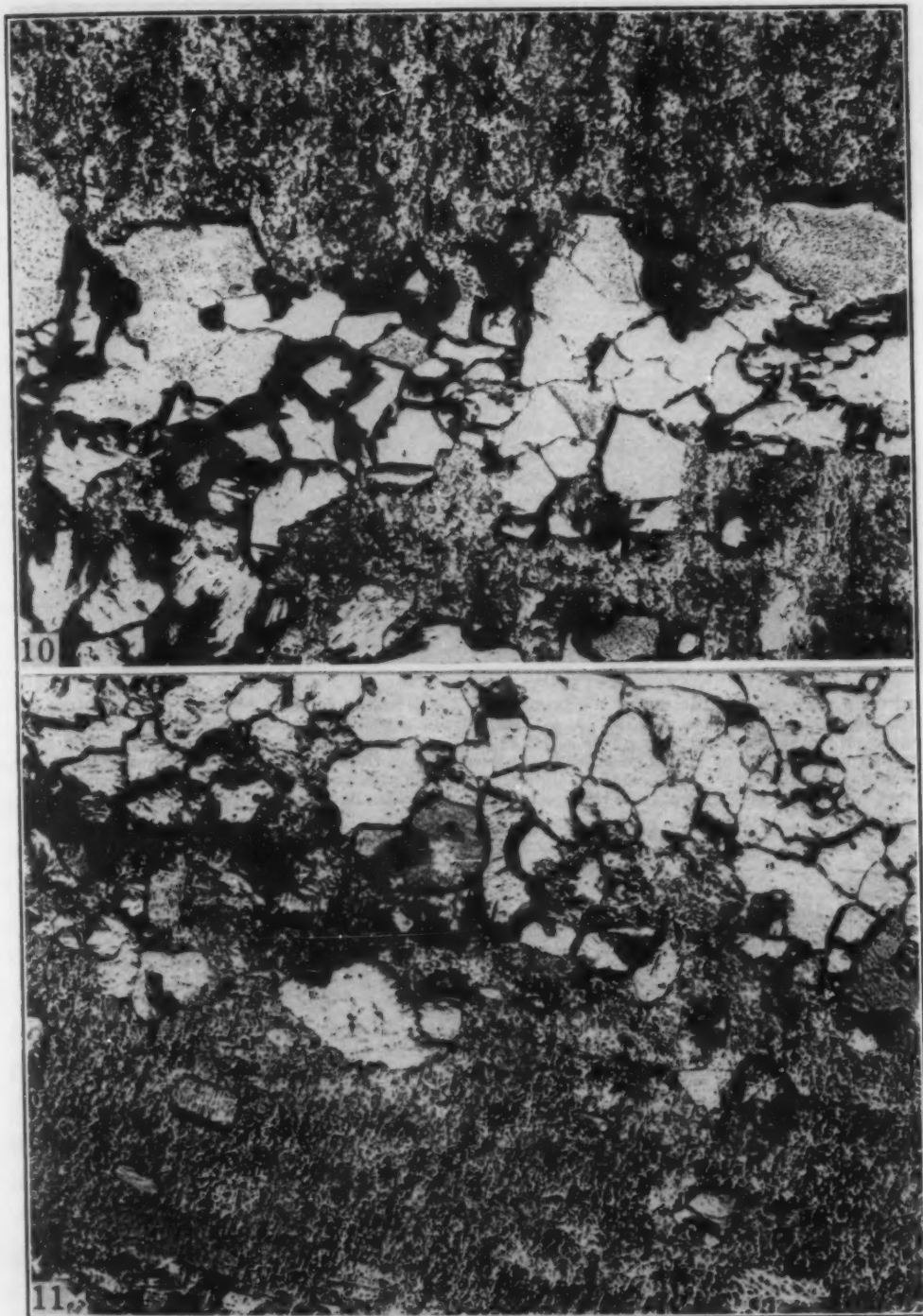


Fig. 10—Microstructure of Specimen of Cold-Rolled Silver Chloride Partially Recrystallized by Heating for 0.5 minute at 174°C. The unrecrystallized areas of the specimen are stressed grains in which the apparent roughness is the result of internal anisotropy. Transmitted light.  $\times 100$ .

Fig. 11—Microstructure of a Specimen of Cold-Rolled Silver Chloride Partially Recrystallized by Heating for 10 Minutes at 150°C. Structural features same as in Fig. 10. Transmitted light.  $\times 100$ .





Fig. 12—Microstructure of a Specimen of Cold-Rolled Silver Chloride Recrystallized by Heating for 16 Minutes at 174°C. Exhibits grain growth. This photomicrograph suggests that the refractive indices of grain interiors and grain-boundary material differ, since one sees "shadow patterns" of unetched grain boundaries within the interior of the specimen when those boundaries approach the normal to the surface. The abnormally wide grain boundaries result from an optical effect similar to the Becke effect. Transmitted light.  $\times 100$ .

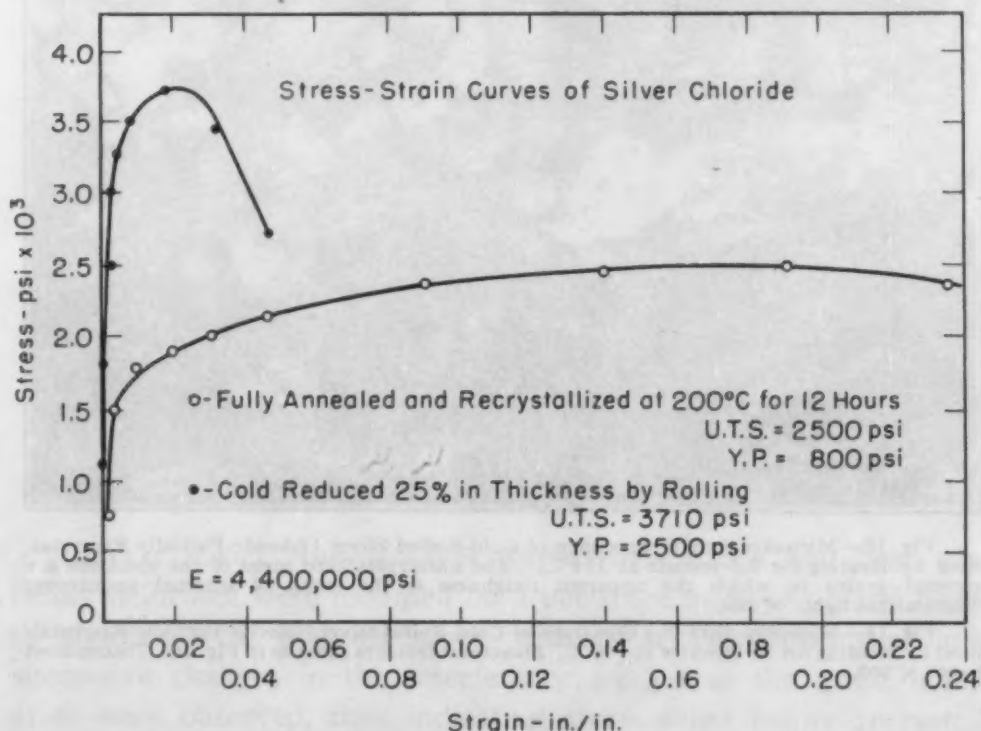


Fig. 13—Stress-Strain Curves for Fully Annealed and Recrystallized Silver Chloride and for Cold-Reduced Silver Chloride.

## MECHANICAL PROPERTIES AND ELASTIC CONSTANTS

The hardness of fully annealed silver chloride, measured on a Tukon hardness tester, utilizing a Vickers-type indenter and a 25-gram load, was found to be 6.5 (DPH No.). The work hardening of silver chloride is illustrated in Fig. 3. In several instances it was noted that large cold reductions caused the appearance of the phenomena of overwork. Appearance of overwork was incon-

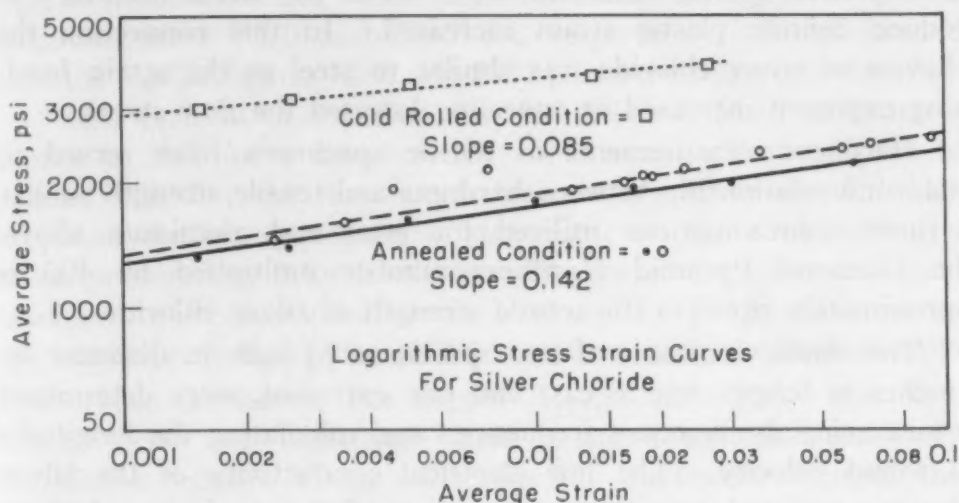


Fig. 14—Log-Log Plot of Stress-Strain Curves (Fig. 13) for Determination of Strain Hardening Exponent.

sistent but may be associated with exposure to light prior to or during cold deformation.

Typical stress-strain curves obtained by conventional methods, shown in Fig. 13, were obtained from full-annealed and work-hardened stock respectively. Test specimens used conformed to the ASTM specifications for sheet materials having a  $\frac{1}{8}$ -inch thickness and a 2-inch gage length. Stress-strain curves were obtained using a motor-driven Dillon tensile tester, and an Olsen averaging extensometer. The ultimate tensile strength of the material in the dead-soft condition was found to be 2500 psi, with a yield strength of 800 psi. Rolling at room temperature to 25% reduction in thickness raised the yield strength to 2500 psi, and the ultimate tensile strength to 3700 psi. The modulus of elasticity, as measured from the data used to construct both curves in Fig. 13, was found to be  $4.4 \times 10^6$  psi. Elongation of the cold-worked specimen was 4.6% and of the full-annealed specimen 24% (2-inch gage length). Specimens were cut from a sheet rolled from a single large ingot.

In addition to the conventional stress-strain curves, the log-

arithmic plot of Fig. 14 has been included for the purpose of determining the strain hardening exponent,  $n$ , in the relation developed by Ludwik (20), namely:  $\alpha = K\Delta^n$  where  $\alpha$  is the stress,  $\Delta$  the strain and  $K$  a material constant. The values of  $n$  increase from 0.085 for the cold-rolled material to 0.14 after annealing. These values are of the same order as those observed for carbon steel by Gensamer (21). Hollomon (22) noted that the strain hardening exponent of brass decreased as the yield strength increased and that this exponent decreased for carbon steels as the stress necessary to produce definite plastic strain increased. In this connection the behavior of silver chloride was similar to steel as the strain hardening exponent increased as annealing lowered the flow stress.

Hardness measurements of tensile specimens have served to establish a relationship between hardness and tensile strength similar to those approximations utilized for steel and aluminum alloys. The Diamond Pyramid Hardness number multiplied by 400 is approximately equal to the tensile strength of silver chloride.

The elastic constants of two specimens  $\frac{1}{4}$  inch in diameter by 4 inches in length, one as-cast and one extruded, were determined by measuring the resonant frequencies and calculating the longitudinal sound velocity. The low electrical conductivity of the silver chloride prevented satisfactory grounding of the specimen, which in turn caused a large direct pick-up of the applied electrical oscillations. This difficulty was overcome by completely filming the surfaces of the specimens with metallic silver by treatment with commercial photographic developer.<sup>4</sup> Excellent data were obtained by use of the "filmed" bars. In the case of the extruded bar the sixteenth harmonic of the fundamental frequency was sufficiently strong to be measured. The modulus is related to the velocity of sound in the medium and to the density of the medium (23). The velocity of sound in silver chloride was found to be  $2.305 \times 10^5$  centimeters per second. The calculation of the value of the modulus was made utilizing the measured density of the test specimens and was found to be  $2.835 \times 10^{11}$  dynes per square centimeter or  $4.112 \times 10^6$  psi.

Using the data on the velocity dispersion, it was possible to estimate Poisson's ratio as 0.41. The values of the modulus obtained from the tensile data and the above method agree rather well and are comparable to those of several common metals; e.g., lead— $2.6 \times 10^6$  psi, bismuth— $4.6 \times 10^6$  psi, tin— $6 \times 10^6$  psi and magnesium— $6.5 \times 10^6$  psi.

Stepanov (4) measured the elastic properties of cold-rolled and

<sup>4</sup>Eastman Kodak Developer—DK-19.



recrystallized silver chloride. He found that the ultimate strength of the annealed material was 1970 psi and that of the cold-rolled material 6050 psi. Young's modulus in these experiments was reported to be  $6.34 \times 10^6$  psi.

Levi and Tabet (3, 24), in the course of an investigation of the fiber structure produced by wire drawing of such compounds as the silver halides, measured the tensile strength of the chloride. By choice of temperature they could produce a (111) or a (100) type of orientation and found that the tensile strengths in the two directions were 7310 and 5340 psi, respectively. Silver bromide gave the similar figures 8980 and 5520 psi in the same two directions.

This relation of the data for the different fiber structures is similar to that for a face-centered cubic metal. Barrett (25) has pointed out that the directional dependence of the elastic moduli in polycrystalline aggregates is dependent on the preferred orientation produced by prior treatment. The maximum value of Young's modulus for face-centered metals is along the [111] direction and the minimum is along the [100] direction, with the former almost three times the latter. For copper  $E_{[111]} = 27.6 \times 10^6$  and  $E_{[100]} = 9.69 \times 10^6$  psi. Although there is not a complete and unique correlation between Young's modulus and the tensile strength, there is in general a linear relation between them. Hence the statements just made about moduli in different directions are almost equivalent to saying that the tensile strength of face-centered cubic metals is highest in the [111] direction and minimum in the [100].

The face-centered cubic metals usually have a double fiber texture on wire drawing (26). In this connection it should be pointed out that at low temperatures aluminum slips on the (111) plane in the [101] direction but at higher temperature the (100) plane becomes operative. Although rigorous correlation has not been attempted, on casual inspection the effect of temperature on the change of wire texture of silver chloride appears to be reasonably analogous to the effects on face-centered cubic metals.

The large variation in the elastic modulus of wires with annealing must arise from alteration of the texture, since the elastic constants are almost unaffected by cold work and recovery. For example, the annealing of hard drawn copper wire (27) causes a drop in Young's modulus from  $18.0 \times 10^6$  to  $13.4 \times 10^6$  psi. On the basis of Barrett's (28) calculation, the hard drawn wire is composed of 73% (111) texture and the remainder (100) texture; whereas after annealing, the fraction which has the (111) texture is only 43%. Hence the variation in tensile strength of the silver

chloride wire with the different textures appears to be in agreement with the behavior of face-centered cubic metals such as copper and aluminum.

#### MACHINABILITY

The machinability of silver chloride was investigated and found to be similar to that of aluminum. The cutting speed was limited only by the melting of the silver chloride; no lubrication was necessary. A heavy cut could be taken on a lathe if the tool had a top rake angle in the vicinity of 45 degrees. Because of the high plasticity of silver chloride, large curling chips were obtained. A finely machined surface could be obtained without difficulty. However, due to tool pressure and the low modulus of rigidity, the specimens showed a slight running bow or barrel-like distortion when finished on a lathe. A carefully machined piece of silver chloride 4 inches long and  $\frac{1}{4}$  inch in diameter was 0.0003 inch larger in diameter near the center of the rod than at the ends. These facts indicate that silver chloride is a satisfactory material to machine by conventional methods.

#### CRYSTAL STRUCTURE AND ALLOTROPY

The compounds silver chloride and bromide are isomorphous with sodium chloride and possess the lattice parameters 5.455 kX and 5.755 kX units respectively at room temperature. Silver iodide has two crystallographic modifications. The alpha or higher temperature form is cubic and isomorphous with zinc blende (ZnS), having a lattice constant 6.47 kX. The room temperature modifications are hexagonal and isomorphous with ZnO or Wurtzite. The lattice constants are 4.58 and 7.59 kX with  $c/a = 1.633$ .

The transition temperature of the iodide is 146.5 °C, although it can be lowered by the application of pressure as Tammann has shown (29).

Bridgman (30) has demonstrated that the silver halides undergo allotropic changes at high pressures. On the basis of compressibility measurements he has shown that the increasing order of stability of cubic structures is Wurtzite, sodium chloride and cesium chloride lattices. In agreement with this rule, the silver chloride and bromide transform under high pressures from the "face-centered" sodium chloride lattice to the cesium chloride type.

#### ALLOYING OF SILVER CHLORIDE

Some of the properties of metals which are best known are the

great changes in strength which arise from the addition of alloying elements to commercially available pure metals. The effects on strength, hardness, workability and recrystallization temperatures are so well known as to require no recitation here. If the analogy of silver chloride as a transparent metal is to be valid, it must undergo the same changes as metals do when alloyed.

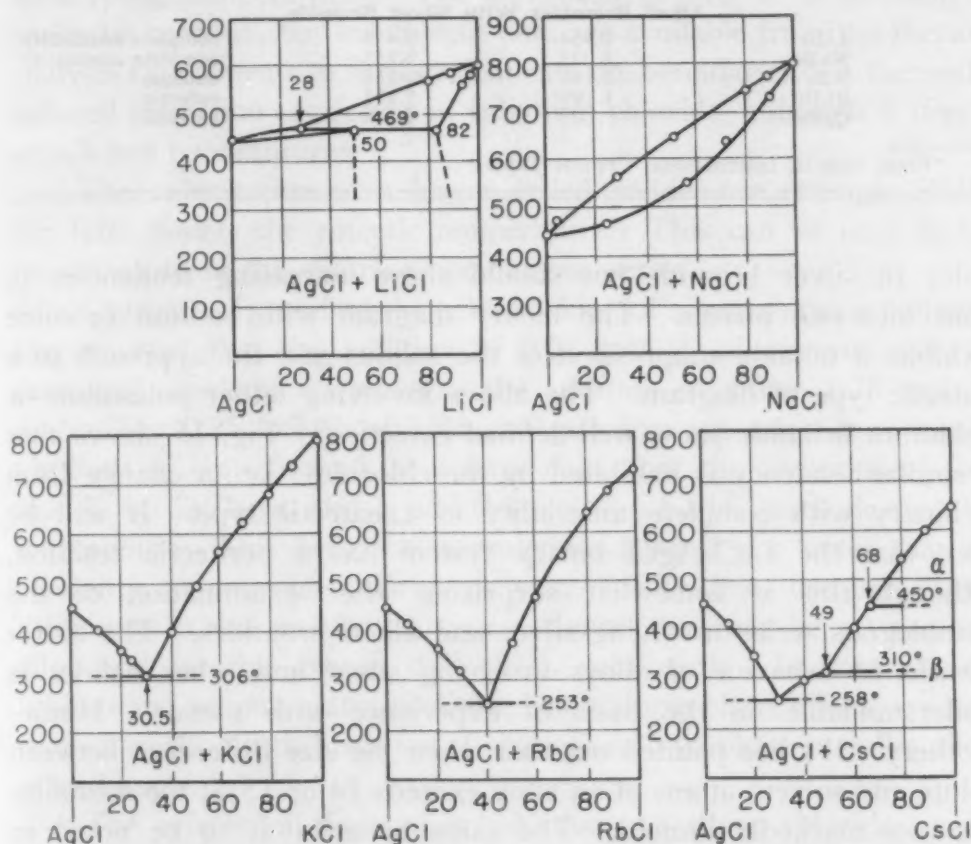


Fig. 15—The Phase Diagrams Involving Silver Chloride and the Chlorides of Lithium, Sodium, Rubidium and Cesium.

It seems reasonable to believe that one could form solid solutions of silver bromide in silver chloride of an extended range and that the addition of other halides would be interrupted by the precipitation of these halides from solution as the affinity and solubility were satisfied. In fact, there are sufficient data available in the literature to permit a much more extended discussion of the phenomenon of "alloying" than will be attempted here.

Most of the following data are compiled from the International Critical Tables. The homologous series of lithium bromide, sodium bromide and potassium bromide have increasing lattice parameters, although they are isomorphous with silver chloride and bromide. Therefore, on the basis of experience with metals, they should dis-



**Table II**  
**Alkali Chlorides With Silver Chloride\***

Solute	$a_0/a$	$r/r$	Phase Diagram
LiCl	0.927	0.476	peritectic
NaCl	1.015	0.755	complete miscibility
KCl	1.13	1.055	eutectic
RbCl	1.19	1.175	eutectic
CsCl	....	1.340	eutectic

Alkali Bromides With Silver Bromide			
LiBr	0.954	0.476	complete miscibility
NaBr	1.033	0.755	complete miscibility
KBr	1.143	1.055	eutectic
RbBr	1.195	1.175	eutectic
CsBr	.....	1.340	eutectic

\*From data in International Critical Tables.

solve in silver bromide but should show increasing tendencies to split into two phases. The binary diagram with sodium bromide exhibits a notable suppression of the solidus and the approach to a eutectic type of diagram. The alloys involving either potassium or rubidium bromide show well-defined eutectics.<sup>5</sup> Fig. 15 shows that a similar tendency is exhibited by the chlorides; i.e., a change from a binary with complete miscibility to a eutectic type. It will be seen that the LiCl-AgCl binary system has a peritectic reaction, although this is somewhat surprising after examination of the homologous series involving silver and alkali bromides. The aforementioned behavior of alloys involving silver and other halides is understandable on the basis of experience with metals. Hume-Rothery (31) has pointed out that when the size difference between solute and solvent atoms of an alloy exceeds 14 or 15%, the solubility becomes markedly limited. The same behavior is to be noted in homologous series of the halides. In Table II, the ratio of lattice constants of the solute halide and silver chloride is included with the type of phase diagram. The ratio of alkali ionic radii to that of the silver has been included to indicate that there is a small likelihood that the ionic radii are the proper criteria.

It does not appear reasonable that ions half as large as silver could be tolerated when ions only 5% larger produce a eutectic. In contrast to this anomalous behavior, the limit between complete miscibility and eutectic formation seems to occur at a  $\pm 5$  to 6% difference in lattice parameters. These data indicate the validity of a size-factor rule similar to Hume-Rothery's rule for metals based upon the lattice parameters. Electronegativity effects may be important in producing "intermetallic" phases, as is indicated by the

<sup>5</sup>The phase transition of the rubidium bromide is from the room temperature body-centered cubic or cesium chloride-type structure to sodium chloride structure.

fact that several compounds of the type AB and AB<sub>2</sub> may be found in the AgCl-AlCl<sub>3</sub> and AgBr-AlBr<sub>3</sub> systems. The "valence" rule is undoubtedly applicable in these phase systems but data concerning precise limits of solubility for a proper series are not available.

The binary diagram involving cesium chloride shows that the body-centered to face-centered cubic transition occurs at 450 °C with rising temperatures. The transition at 310 °C is probably a peritectic reaction, but insufficient data are available from the thermal analysis experiments to further delineate the boundaries. A thermally induced transition is present in rubidium chloride, although it occurs at subzero temperatures.

The substitution of a larger celled halide, for example RbBr, for KBr lowers the eutectic temperature. This can be seen in the bromide and in the chloride homologous series.

Cagliotti (2) studied the cold working of silver chloride "alloys". He reported that the addition of 0.01 mol % of cuprous chloride destroyed workability, whereas the addition of either 1.25 mol % of NaCl or 0.25 mol % of LiCl or AgCl does not affect it seriously. Cagliotti (7) also found, at a later date, that the additions of 0.01 mol % of CaCl<sub>2</sub> or MgCl<sub>2</sub> and 0.4 mol % of RbCl each destroy the workability. This behavior is understandable if one notes that the solubility of cuprous chloride is undoubtedly low, because of the difference in size and lattice type. Hence, this may be a two-phase alloy and for this reason difficult to cold work. In contrast, the lithium and sodium chloride alloys, being single-phase alloys, are easy to cold work. Such behavior of single- and two-phase metallic alloys is well known.

The effects of these alloy additions to silver chloride on the recrystallization temperature have also been evaluated by Cagliotti (2). He states that the addition of 0.25 mol % of LiCl lowers the recrystallization temperature to 160 °C and the addition of 0.5 mol % of NaCl lowers the temperature to 150 °C. This lowering of the temperature of recrystallization is in contrast to the behavior of metals. However, the available abstract of this Italian paper did not present the recrystallization temperature of the pure silver chloride, which on the basis of our data was found to be appreciably lower than 100 °C. On the basis of the rule of 0.4 of the absolute melting point, the recrystallization temperature should be about 20 °C. It is possible that Cagliotti was describing the minimum temperature for rapid grain growth, which the authors have found to lie in the vicinity of 200 °C.

## PHYSICAL PROPERTIES

The coefficient of linear thermal expansion of AgCl is similar to metals in exhibiting a marked increase upon approaching the melting temperature. The authors have confirmed this effect first noted by Strelkov and associated with the easily deformable ion of silver.

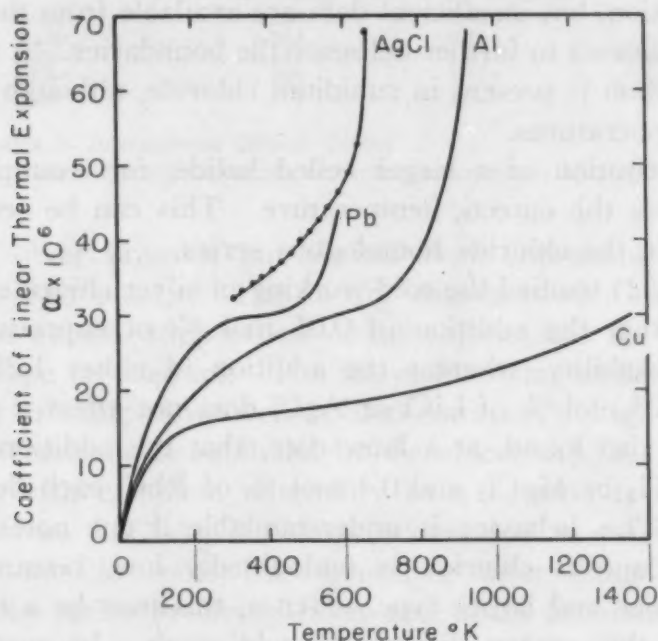


Fig. 16—The Variation of the Coefficient of Linear Thermal Expansion With Temperature for Silver Chloride, Aluminum, Copper and Lead. The data for the three metals are from the work of Richards.

Table III  
Heat Capacities of Some Silver Halides

Compound	Solid (34)	Liquid*
AgCl	$9.60 + 9.29 \times 10^{-3}T$	14.05
AgBr	$8.58 + 14.1 \times 10^{-3}T$	14.90
$\alpha$ -AgI	$8.58 + 14.1 \times 10^{-3}T$	.....
Cu	$5.44 + 14.62 \times 10^{-3}T$	7.50
Al	$4.80 + 3.22 \times 10^{-3}T$	7.00
Au	$5.61 + 1.44 \times 10^{-3}T$	7.00

\*In unit cal/°K/mole.

The coefficient of expansion is considerably higher than most metals at room temperature but at higher temperatures seems to be comparable to several common metals. In Fig. 16 the coefficient of expansion is compared with Pb, Cu and Al. The data for the three metals were derived from the original work of J. W. Richards (32).

The observed densities of silver chloride and bromide as



minerals are 5.56 and 6.473 gm/cm<sup>3</sup> at 23 °C. The variation in density with temperature and prior treatment is largely due to large population of lattice vacancies in the silver halides. Seitz (33) has developed expressions for the population of lattice vacancies in the silver halides. The population ratio is

$$r(\text{AgCl}) = 36 \exp \left( \frac{-6250}{T} \right)$$

$$r(\text{AgBr}) = 29 \exp \left( \frac{-5050}{T} \right)$$

wherein  $r$  is the ratio of vacant lattice sites to the number of normally occupied positions.

Silver chloride melts at 457.5 °C with a latent heat of fusion of 3155 calories per mole or an entropy change on melting of 4.335 entropy units. Silver chloride boils at 1431.3 °C with an enthalpy change of 42.43 kilocalories per mole and an entropy change of 24.90 units.

The heat capacities of these silver halides have been measured from room temperature up to the melting point and beyond. Reference to Table III shows that the heat capacities are large in comparison to metals but are less than the value of 12.4 to be expected on the basis of the Kopp-Neuman rule for diatomic solids. No other significant data are available except for the compressibility measurements.

Bridgman (30), working at pressures up to 50,000 kg/cm<sup>2</sup> (approximately fifty thousand atmospheres), has measured the compressibilities of chloride, bromide and iodide to be 0.0838, 0.0893 and 0.2525, respectively, at room temperature. The data agree in direction with the refractive indices of these compounds; i.e., the compressibility and the refractive index are both measures of the ease of deformation.

#### DISSIMILARITIES

This review of the properties of silver chloride shows them to be similar to those of metals in kind and in degree. The principal exception is that silver chloride is an ionic crystal and as a consequence has neither the electrical conductivity nor the metallic bonding with which one is familiar in the case of metals.

A further dissimilarity arises from the fact that silver chloride has a lattice in which many cation vacancies are thermodynamically stable because of the two valences of silver, namely one and two. Kirkwood (35) has suggested that the facility of forming and

moving dislocation is related to these lattice vacancies, and hence the abnormally high plasticity of silver halides is indirectly due to the bivalent state of silver in the lattice.

One of the obvious ways in which silver chloride and a metal differ is in the phenomenon of electrical conduction. Ions conduct the electricity to a large extent in ionic salts, whereas electrons conduct it in metals. A second dissimilarity is the fact that the conductance of salts increases with increasing temperatures according to the formula

$$\alpha = A \exp (-u/RT) + B \exp (-w/RT) \quad \text{Equation 1}$$

whereas the conductance of metals decreases with increasing temperatures according to the formula

$$\alpha = \alpha_0 - a T \quad \text{Equation 2}$$

In short, the former is an exponential increase and the latter a linear decrease.

Near room temperature, the conductivity of silver chloride is  $10^{-8}$  mhos/cm, and the first exponential term of Equation 1, which alone is important at room temperature, relates to the movement of lattice defects.

The effect of alloying on the electrical resistance of metals is to increase it as the alloy content is increased. In contrast, the effect of dissolving other halides in silver chloride is generally to decrease the resistance, particularly if the valence of the cation is greater than one (33, 36).

#### SUMMARY

An attempt has been made to bring together the existing scattered and sometimes conflicting data, and to produce supplementary information to provide a basis for the use of this transparent medium in general metallurgical investigations.

Silver chloride can be cast, worked, and formed by common metallurgical techniques. Its deformation mechanism, mechanical properties, elastic constants and such physical properties as compressibility, thermal expansion and crystal structure are similar to those of many common metals. Differences from metals exist, such as electrical resistivity, because of ionic bonding. However, it is hoped that the similarities demonstrated are sufficient to encourage the use of silver chloride as a transparent metal in metallurgical research.

#### ACKNOWLEDGMENTS

The authors wish to make acknowledgment to the University

of California, Los Alamos Scientific Laboratory, for the use of its facilities; for permission to publish this paper, and for the cooperation and assistance of many of its staff members.

Special acknowledgment is made to Messrs. H. A. Lacy, for his contributions on machinability; H. L. Laquer, for his determination of elastic constants by sonic methods; and G. W. Wensch, for his valuable assistance in several experimental determinations; to Mrs. Evelyn Meierkord for preparation of the references, and to Mrs. B. P. Wellborn for assistance in preparation of the manuscript.

### References

1. G. Tammann, "Change in Qualities of Nonmetallic Substances on Cold Working", *Naturwissenschaften*, Vol. 20, 1932, p. 958-960.
2. V. Cagliotti, "The Structure of Cold-Worked Silver Chloride and Its Recrystallization", *Atti della accademia nazionale dei Linzei*, II, Vol. 18, 1933, p. 570-574.
3. G. R. Levi and M. Tabet, "Fibrous Structure in Ionic Lattices", *Atti della accademia nazionale dei Linzei*, II, Vol. 18, 1933, p. 574-579.
4. A. V. Stepanov, "The Plastic Properties of AgCl and NaCl Crystals", *Physikalische Zeitschrift der Sowjetunion*, Vol. 8, 1935, p. 25-40.
5. P. Fugassi and D. S. McKinney, *Review of Scientific Instruments*, Vol. 13 (8), 1942, p. 335-337.
6. K. L. Fetters and M. Dienes, "AgCl as a Medium for Study of Ingot Structures", American Institute of Mining and Metallurgical Engineers, Tech. Pub. No. 1570, 1943.
7. V. Cagliotti, "The Hardness that Accompanies the Formation of Mixed Crystals in AgCl", *Chemical Abstracts*, Vol. 29, 1935, p. 7145.
8. S. O. Tsobkallo, "Production of Test Specimens from AgCl for the Study of Stresses by an Optical Method", *Zavodskaya Laboratoriya*, Vol. 15, March 1949, p. 338-345.
9. E. Orowan, "Classification and Nomenclature of Internal Stresses", *Journal*, Institute of Metals, Symposium on Internal Stresses in Metals and Alloys, Preprint No. 1077, 1947.
10. J. P. Nye, "Photoelastic Investigation of Internal Stresses in AgCl Caused by Plastic Deformation", *Nature*, Vol. 161, 1948, p. 367-368.
11. N. I. Prigorovskii, "Contemporary Development of an Optical Polarization Method for Determination of Stresses", *Zavodskaya Laboratoriya*, Vol. 15, March 1949, p. 305-321.
12. A. V. Stepanov, "New Optical Method for Study of Stresses by Polarized Light", *Zhurnal Tekhnicheskoi Fiziki*, Vol. 19, February 1949, p. 205-217.
13. C. D. West and A. S. Makas, "Technical Crystals with Abnormally Large Stress Birefringence", *Journal of Chemical Physics*, Vol. 16, 1948, p. 427.
14. H. C. Kremers, "Optical Silver Chloride", *Journal*, Optical Society of America, Vol. 37, 1947, p. 337-341.
15. C. Ellis and A. A. Wells, "Chemical Action of Ultraviolet Rays", Reinhold Publishing Company, New York, 1941, p. 378.
16. J. Franck and Kuhn, *Zeitschrift für Physik*, Vol. 44, 1927, p. 6071.
17. F. Seitz, "Modern Theory of Solids", McGraw-Hill Publishing Company, New York, 1940, p. 225.
18. C. S. Smith, "Grains, Phases and Interfaces; An interpretation of Microstructure", *Metals Technology*, TP 2387, Vol. 15, June 1948, p. 3-4.



19. G. W. Wensch, "Coalescence and Recrystallization of Cold-Rolled Nickel", Ph.D. Thesis, University of Illinois, Champaign, Ill., October 1949.
20. P. Ludwik, "Elements der Technologischen Mechanik", J. Springer, Berlin, 1909.
21. M. Gensamer, "Strength and Ductility", *TRANSACTIONS, American Society for Metals*, Vol. 36, 1946, p. 30-60.
22. J. H. Hollomon, "Tensile Deformation", *Transactions, American Institute of Mining and Metallurgical Engineers*, Vol. 162, 1945, p. 268-289.
23. H. L. Laquer, "The Elastic Constants of Uranium", *TRANSACTIONS, American Society for Metals*, Vol. 42, 1949, p. 771-784.
24. G. R. Levi and M. Tabet, "Fibrous Structure in Ionic Lattices", *Atti della accademia nazionale dei Lincei*, II, Vol. 19, 1934, p. 723-725.
25. C. S. Barrett, "Structure of Metals", McGraw-Hill Publishing Company, New York, 1943, p. 382.
26. E. Schmid and G. Wasserman, *Zeitschrift für Physik*, Vol. 42, 1927, p. 779.
27. A. J. Phillips and A. Smith, *Proceedings, American Society for Testing Materials*, Vol. 36, Part II, 1936, p. 263.
28. C. A. Barrett, loc. cit., p. 458.
29. G. Tammann, "The States of Aggregation", Van Nostrand, New York, 1925, p. 175.
30. P. W. Bridgman, "The Compression of 21 Halogen Compounds and 11 Other Simple Substances to 100,000 kg/sq. cm.", *Proceedings, American Academy of Arts and Sciences*, Vol. 76, 1945, p. 1-7.
31. Hume-Rothery, "The Structure of Metals and Alloys", Institute of Metals, London, 1944, p. 59.
32. J. W. Richards, "The Overall Linear Expansion of Three Faced Cubic Metals from 190 °C to Near Their Melting Points", *TRANSACTIONS, American Society for Metals*, Vol. 30, 1942, p. 326.
33. F. Seitz, "Nature of Lattice Defects in AgBr Crystals", *Physical Review*, Vol. 54, 1938, p. 1111-1112.
34. J. H. Perry, "Chemical Engineers Handbook", McGraw-Hill Publishing Company, New York.
35. Personal Communication, 1949.
36. C. Sandonnini, "The Conductivity of Mixtures of Solid Salts", *Atti della accademia nazionale dei Lincei*, Vol. 24, 1915, p. 842-849.

## DISCUSSION

**Written Discussion:** By J. F. Nye, Cavendish Laboratory, University of Cambridge, Cambridge, England.

I am sure that I am only one of many who are using, or are contemplating using, silver chloride as an aid to understanding the properties of metals and who will be grateful to the authors for bringing together and supplementing what is known of its rather surprising properties.

A recent series of experiments<sup>6, 7</sup> has shown that the glide direction in silver chloride is  $\langle 110 \rangle$ , the direction of closest packing of like ions. The glide plane is variable and, macroscopically, irrational but is often not far from  $\{111\}$ . The glide elements are thus formally similar to those of, say, aluminum at low temperatures, and, as the authors say, this is no doubt why the fiber structure after wire drawing is also similar.

<sup>6</sup>J. F. Nye, "Glide Bands in Silver Chloride", *Nature*, Vol. 162, 1948, p. 299.

<sup>7</sup>J. F. Nye, "Plastic Deformation of Silver Chloride". "I. Internal Stresses and the Glide Mechanism", *Proceedings, Royal Society*, Vol. 198, 1949, p. 190-204; "II. Photoelastic Study of the Internal Stresses in Glide Packets", *Proceedings, Royal Society*, Vol. 200, 1949, p. 47-66.

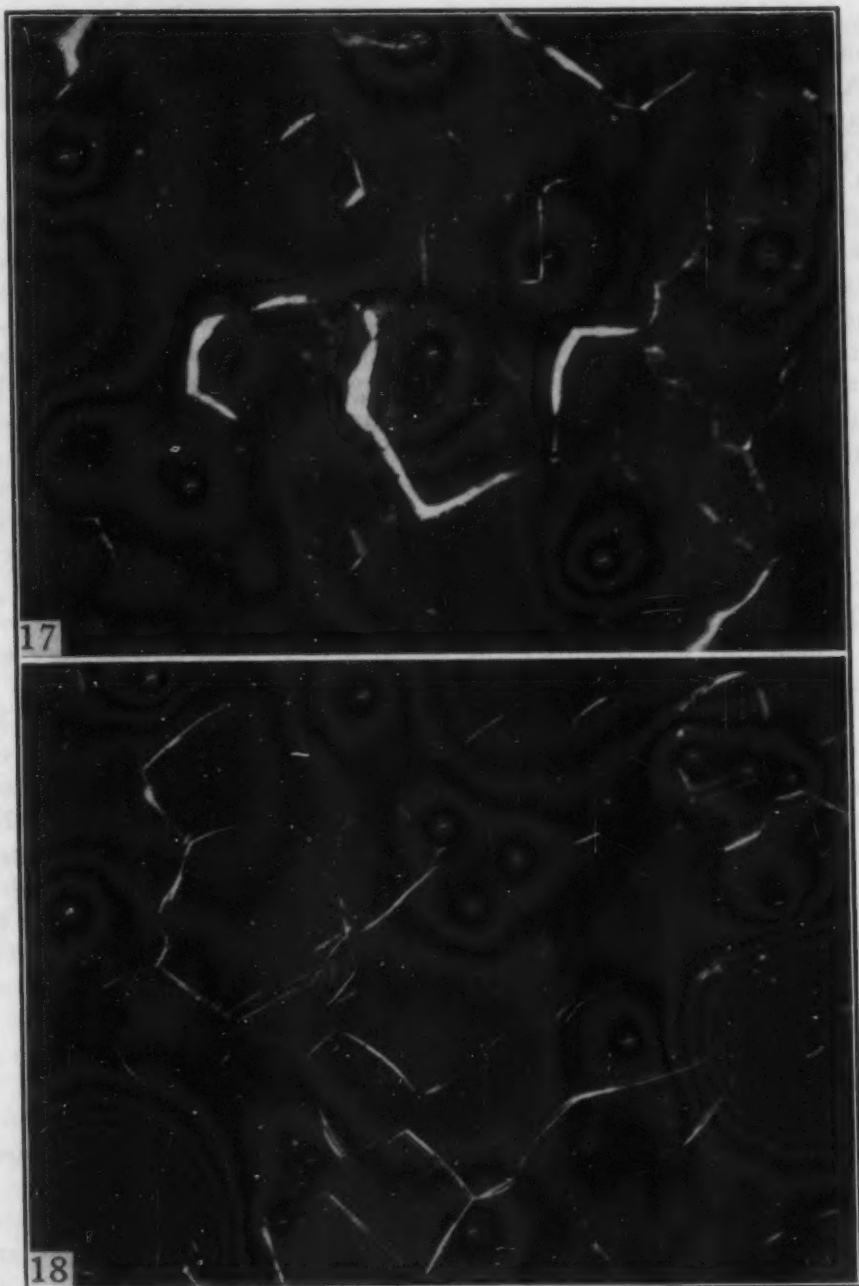


Fig. 17—Recrystallized Silver Chloride Sheet Bent Elastically Between Crossed Nicols. The sheet is one grain only in thickness. The grain boundary areas are birefringent.  $\times 22$ .

Fig. 18—Recrystallized Silver Chloride Sheet Between Crossed Nicols. The grain boundaries on both faces of the sheet are visible, probably owing to rotation of the plane of polarization.  $\times 22$ .

But the analogy with the face-centered cubic metals ceases here, for the mechanism of plastic glide seems to be more like that of the body-centered metals. The irrationality of the glide plane, the phenomenon of pencil glide, and the formation of wavy slip lines are reminiscent of the behavior of alpha iron and make it seem very likely that, as with

many body-centered metals, the critical shear stress for glide is nearly the same on a number of different planes.

A further similarity to the plastic deformation of metals is the appearance in silver chloride of deformation bands. These have been observed recently by Dr. Orowan and myself.

I think that the apparent change in refractive index at the grain boundaries noted by the authors on their twelfth page may possibly be connected with a phenomenon that appears whenever polycrystalline sheets of recrystallized silver chloride are elastically bent or twisted. If the bending is done between crossed nicols the grain boundaries (or, more precisely, any areas in the sheet where two grains overlap) light up in a spectacular way (Fig. 17). The effect is quite reversible; when the bending couples are removed the lightening vanishes. The explanation of this effect, which has also been reported by West and Makas (Ref. 13 in main paper), has been given in Ref. 10 of the main paper. The point of interest is that, although the birefringence is confined to the grain boundaries, a close examination shows that this does not at all indicate a concentration of stresses there.

One can also often observe a separate optical phenomenon at the grain boundaries which, unlike the one just described, is a surface effect. Between crossed nicols the grain boundaries on the two surfaces of a sheet show up as fine bright-colored lines (Fig. 18). It seems most likely that the reason for this is that the boundaries are really fine grooves produced by thermal etching. A similar effect is seen if a fine smooth scratch on a glass slide is viewed by transmission under a polarizing microscope. Between crossed nicols the scratch shows up, in general, as a bright line on a dark background. The reason is that, at the sloping walls of the scratch on the glass slide and of the grooves on the silver chloride sheet, rays of plane polarized light are striking a surface between two transparent media obliquely. In these circumstances, owing to the difference in the transmission coefficients for the components in and perpendicular to the plane of incidence, the plane of polarization is, in general, rotated, and thus a component passes through the analyzer. The plane is not rotated, however, if the direction of polarization in the incident rays happens to be either in or perpendicular to the plane of incidence.

In accordance with this explanation the scratch on the glass slide extinguishes when the vibration directions of the nicols are either parallel or perpendicular to it. The grain boundaries also frequently show "straight extinction", but this is not always so. I am not sure why there should be these exceptions. It may be because the grain boundaries are not the smooth curves that they appear to be under the microscope, but are really a series of steps. However, this is merely a speculation at present. Perhaps the authors may be able to throw some light on the problem.

#### Authors' Reply

The authors wish to thank Dr. Nye for his discussion, which was most instructive. As yet, we have had no opportunity to closely examine



the phenomena described, but are certainly in accord with the general argument.

It seems quite possible that the critical shear stress for glide may be nearly the same on a number of different planes, as suggested by Dr. Nye, but Fig. 8 (of the text) seems to indicate (at least in the case of a small deformation) that primary slip does occur on preferred planes. We have not as yet observed deformation bands.

We agree that "the apparent change in refractive index at the grain boundaries" does not necessarily indicate the concentration of stress or impurities but might alternatively be explained by "fine grooves produced by thermal etching".

In addition to the observations of Dr. Nye, we have noted other effects under polarized light. In some cases grain boundaries have appeared dark rather than brilliant, and individual grains have shown differences in their opacities.

In the case of etched specimens it is thought that the dark grain boundaries result from the scattering and refraction of light at the sloping walls at the grain boundaries.

The hypothesis of Dr. Nye regarding the roughness of grain boundaries is supported by Fig. 7, of the main text. This deeply etched specimen, although admittedly an extreme case, gives clear evidence that sufficient roughness exists to give scratch birefringence.

## STRUCTURE OF PERMANENT MAGNET ALLOYS

BY A. H. GEISLER

### *Abstract*

*A correlated summary of the constitution and structure of the various materials that are used commercially as permanent magnets has been made. The particular transformation that these materials undergo in the course of the heat treatment was identified as precipitation in Cunico, Cunife, Silmanal, Vectolite and all of the Alnicos and as order-disorder in Vicalloy. New data on the structure of these materials were obtained by metallography and X-ray diffraction analyses. It was shown that cobalt, copper and titanium additions to the basic Fe-Ni-Al alloys from which the Alnicos were derived did not alter the type of decomposition process but appeared in solid solution. Cobalt decreased the difference in lattice parameter of the decomposition products, whereas titanium increased this difference. All of the transformations involved the formation of fine plate-like particles of a new phase which at first had an anisotropically strained crystal lattice. Permanent magnetism was attributed to the fine, strained particles consistent with the modern physical theory. The particles in most of the materials were oriented with the lateral dimensions parallel to one of the three cube planes of the matrix crystal; however, Alnico 5, which was cooled in a magnetic field after the solution heat treatment, exhibited plate in only two of the three possible orientations.*

THE properties of the permanent magnet alloys depend upon a transformation in a solid solution. The older alloys were magnetically strong and hard because of the martensitic structure which was developed on quench hardening these carbon-containing steels; thus, they depended upon the eutectoid reaction for good properties. On the other hand, the newer alloys depend upon precipitation or ordering in a solid solution. The properties change during aging treatments concurrent with changes in structure promoted by the reaction. While a few investigations have been made on the structure of these latter materials, notably those by Bradley and co-workers (1-4),<sup>1</sup> a correlated survey of the structures of many of

<sup>1</sup>The figures appearing in parentheses pertain to the references appended to this paper.

A paper presented before the Thirty-second Annual Convention of the Society, held in Chicago, October 21 to 27, 1950. The author, A. H. Geisler, is research associate, General Electric Research Laboratory, The Knolls, Schenectady, N. Y. Manuscript received April 10, 1950.

the commercial materials has not yet been made. The nature of the reaction in alloys such as the Alnicos, Silmanal and Vicalloy has been inconsistently defined as precipitation or ordering. The structural influence of additions such as cobalt, copper and titanium as they appear in the Alnicos has not been determined previously. The nature of the reaction in Vectolite, the oxide magnet, has not yet been established. Finally, the recognition of features of structure which are common to all three transformations and which may be the origin of good magnetic properties awaits a comprehensive survey of the structures of these materials. The object of the present paper is to report new data directed at a better understanding of permanent magnets.

The results were obtained by X-ray diffraction and metallographic techniques. The compositions of the materials are summarized in Table I.

Table I  
Nominal Composition of Permanent Magnet Materials

Alloy	Per Cent					
	Fe	Ni	Al	Co	Cu	Others
349	78	14	8	..	..	..
Alnico 3	63	25	12	..	..	..
348	46	38	16	..	..	..
Alnico 4	55	28	12	5	..	..
Alnico 5	51	14	8	24	3	..
Alnico 12	33	18	6	35	..	8 Ti
Cunife	20	20	..	..	60	..
Cunico	..	21	..	29	50	..
Silmanal	..	..	4.4	..	..	86.8 Ag, 8.8 Mn
Vectolite	..	..	..	..	..	30 Fe <sub>2</sub> O <sub>3</sub> , 44 Fe <sub>3</sub> O <sub>4</sub> , 26 Co <sub>2</sub> O <sub>3</sub>
Vicalloy 1	38.5	..	..	52	..	9.5 V
Vicalloy 2	35	..	..	52	..	13 V

Crushed powders of the Alnicos and Vectolite and fine wires of the other alloys were used for X-ray diffraction specimens. Filtered cobalt radiation and a cylindrical camera of 10 centimeters diameter were used except where noted otherwise. The specimens were prepared from 1/2-inch square cast bars of the Alnicos, 1/4-inch thick pressed and sintered slabs of Vectolite, and 0.050-inch thick strip of the other alloys. Specimens of the metals were heat treated in a hydrogen atmosphere, while the heat treatments of Vectolite and some of the low temperature aging were conducted in air.

The structure was studied after various aging treatments which are listed in subsequent tables. It was generally necessary to greatly overage the specimens in order to make the precipitate particles large enough to be resolved by microscopic examination, although evidence of the reaction could be detected by X-ray analyses after the speci-



mens had been aged to provide optimum magnetic properties. The most convenient overaging treatment consisted merely of slowly cooling (25 to 50 °C per hour) the specimens from the solution heat treating temperature. That this treatment had resulted in inferior properties is apparent from the data in Table II.<sup>2</sup> This emphasizes the structural dependence of the properties of these materials.

Table II  
Properties of the Permanent Magnet Materials

Alloy	Optimum Properties				Overaged Properties (Slowly Cooled)			
	Coercive Force, $H_c$	Residual Induction, $B_r$	Energy Product, $BH_{max}$	Vickers Hardness	Coercive Force, $H_c$	Residual Induction, $B_r$	Energy Product, $BH_{max}$	Vickers Hardness
349	90	9,900	$0.34 \times 10^6$	508	22	9,100	$0.10 \times 10^6$	301
Alnico 3	450	6,700	1.38	530	55	2,600	0.05	346
348	750	3,700	0.86	511	37	280	0.003	233
Alnico 4	700	5,200	1.30	554	61	980	0.02	370
Alnico 5	575	12,000	5.00	579	89	3,700	0.09	432
Alnico 12	950	5,800	1.75	780				
Cunife	550	5,400	1.55	251	20	1,600	0.008	116
Cunico	710	3,400	0.85	265	120	2,000	0.09	...
Silmanal	6,000*	550	0.09	181				
Vectolite	900	1,600	0.50	...				
Vicalloy 1	290	8,800	1.10	...				
Vicalloy 2	450	10,500	3.30	...				

\* $H_{c1}$ —intrinsic coercive force.

The results for the various materials will be correlated with previous knowledge in the following sections according to material.

### THE ALNICOS

The Alnicos, developed independently by Mishima in Japan and Ruder (5) in this country, are basically iron-nickel-aluminum alloys modified in regard to properties by additions of other elements such as cobalt, copper and titanium. Since it will subsequently be shown that these additions do not alter the nature of the transformation, a review of the constitution of the ternary system will serve to illustrate the basic concepts inherent in this group of alloys. The

<sup>2</sup>The magnetic properties—coercive force, residual induction and maximum energy product—are the ones used to specify the magnetic quality of permanent magnets. They are all derived from the second quadrant of the hysteresis loop. This portion is called the demagnetization curve. The residual induction ( $B_r$ ), as the name implies, is the magnetic induction or flux density left in the specimen when the magnetizing field is removed. This may be regarded as the strength of a magnet, for it is akin to the magnetic field strength supplied by the magnet. Coercive force ( $H_c$ ) is the field strength required to reduce the induction to zero and thus demagnetize the magnet. It may be regarded as the resistance to demagnetization and thus magnetic hardness analogous to mechanical hardness which is the resistance to deformation.

The energy product ( $BaHa$ ) is the product of the coordinates of points on the demagnetization curve. It represents the available potential energy which the magnet can furnish for external use at the various flux densities on the curve. At some point on the demagnetization curve the energy product will attain a maximum ( $BH_{max}$ ) and at this flux density the magnet will give the maximum energy output. The maximum energy product is directly related to coercive force and residual induction, the intercepts of the demagnetization curve with the  $H$  and  $B$  axes, and to the shape of the demagnetization curve.

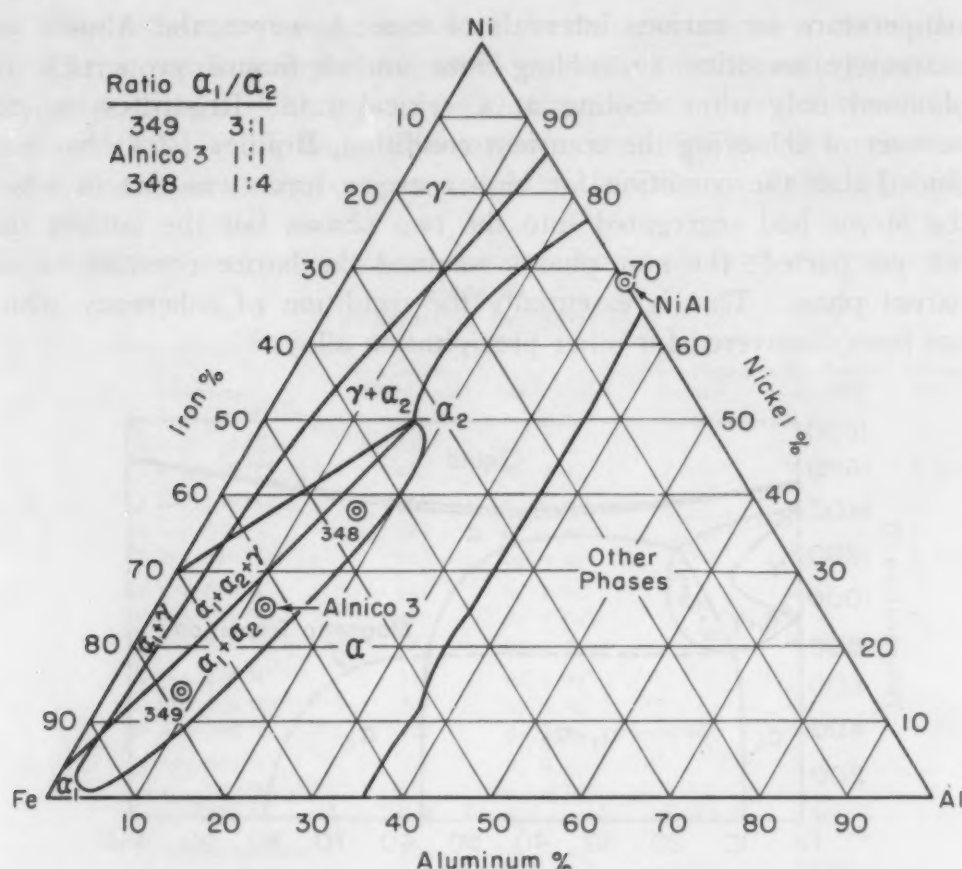


Fig. 1—Constitution of Slowly Cooled Fe-Ni-Al Alloys According to Bradley and Taylor (7).

phase diagram was first determined by Köster (6), but subsequent work by Bradley (7), Kuiti (8) and Dannöhl (9) has shown the earlier diagram to be incorrect.

The latter investigators independently agree that a miscibility gap exists at low temperatures in the broad ferrite field that extends from  $\alpha$ -iron across to the intermetallic compound NiAl, as shown by Fig. 1. Alloys with compositions in this gap are those which are of interest for their magnetic properties. These alloys are susceptible to heat treatment, for at high temperatures they consist of a single body-centered cubic phase which decomposes by precipitation at low temperatures into two body-centered cubic phases of differing lattice parameters, one rich in iron and one rich in NiAl, as shown by Fig. 2.

The phase diagram defines the initial and final states of equilibrium of these alloys. On the other hand, the important changes in properties occur in the course of the reaction. These could be followed in the conventional manner of rapidly cooling from high temperatures to retain supersaturated  $\alpha$  and then reheating to the aging

temperature for various intervals of time; however, the Alnicos are extremely sensitive to cooling rate and optimum properties are obtained only after cooling at a critical rate. Regardless of the manner of achieving the transient condition, Bradley (2-4) has concluded that the condition for high coercive force was one in which the atoms had segregated into the two phases but the lattices had not yet parted; the new phases retained the lattice constant of the parent phase. This is essentially the condition of coherency which has been discovered for other precipitation alloys.<sup>3</sup>

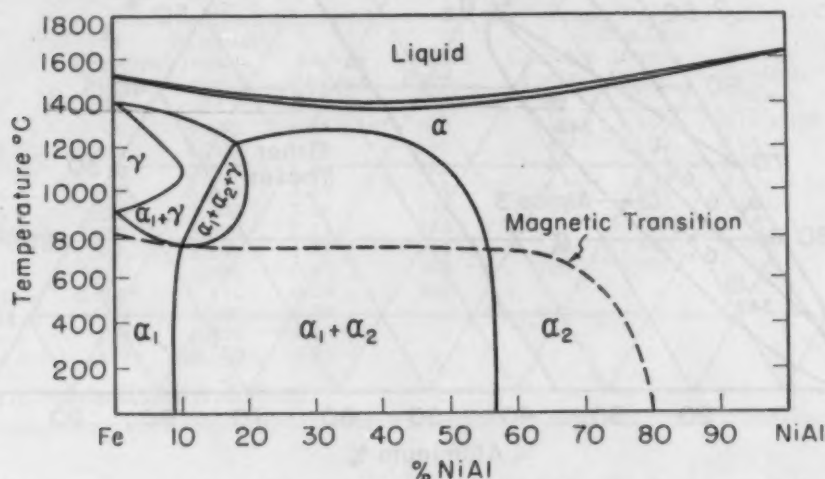


Fig. 2—Vertical Section of Fe-Ni-Al Phase Diagram According to Kuiti (8).

The results of X-ray studies on the three ternary alloys marked in Fig. 1 are listed in the upper portion of Table III. The prime designation (') is used to distinguish the coherent transition structures from equilibrium phases. The disregistry was calculated from the difference in parameter of the two phases. This is a measure of the strain involved at the coherent stage where the lattices match each other. The NiAl-rich phase,  $\alpha_2$ , has a regular atomic arrangement of nickel atoms on the corner sites and aluminum atoms on the center sites of the body-centered cell characteristic of the compound NiAl. This arrangement produces extra lines in the diffraction pattern which were observed for all of the specimens listed in the table. Since the intensity of these lines generally increased with aging temperature, the amount of the NiAl-rich phase and thus the extent of precipitation attained in a 16-hour aging interval increased in the expected manner with temperature over the range 600 to 800 °C (1110 to 1470 °F).

<sup>3</sup>See review in course of publication (10).



The difference in parameter of the two phases in some of the Alnicos is small and the expected splitting of the main lines is difficult to detect. This renders a distinction between the transition state and final equilibrium state even more difficult. The criterion which was used in arriving at some of the data in Table III was

Table III  
Structure of the Alnicos

	Treatment	Vickers Hardness	Structure	Parameters, Å		Disregistry*
				Fe-rich	Ni-Al-rich	
349	16 hrs. 600 °C	504	$a_1' + a_2'$			
	16 hrs. 700 °C	434	$a_1' + a_2'$			
	16 hrs. 800 °C	402	$a_1 + a_2$	2.879	2.874	0.17%
Alnico 3	16 hrs. 600 °C	508	$a_1' + a_2'$			
	16 hrs. 700 °C	454	$a_1' + a_2'$			
	16 hrs. 800 °C	422	$a_1 + a_2$	2.880	2.874	0.21%
348	16 hrs. 600 °C	511	$a_1' + a_2'$			
	16 hrs. 700 °C	449	$a_1' + a_2'$			
	16 hrs. 800 °C	375	$a_1 + a_2$			
Alnico 4	16 hrs. 600 °C	533	$a_1' + a_2'$			
	16 hrs. 700 °C	467	$a_1' + a_2'$			
	16 hrs. 800 °C	427	$a_1 + a_2$	2.877	2.873	0.14%
Alnico 5	16 hrs. 600 °C	...	$a_1' + a_2'$			
	16 hrs. 700 °C	...	$a_1' + a_2'$			
	16 hrs. 800 °C	484	$a_1 + a_2$	2.866	2.864	0.10%
Alnico 12	Normal treatment	780	$a_1' + a_2'$			
	16 hrs. 600 °C	...	$a_1' + a_2'$	{2.878	2.878	
	16 hrs. 700 °C	...	$a_1' + a_2'$	{2.908	2.838	
	16 hrs. 800 °C	557	$a_1 + a_2$	2.899	2.853	1.59%

\*Between equilibrium phases; that between matrix and precipitate approximately  $\frac{1}{2}$  to 1 times this.

based on diffuseness of the lines. When the equilibrium state was attained, the high-angle  $K\alpha$  radiation doublets were resolved, although the line for  $K\alpha_1$  of the one phase in Alnico 4 superimposed on that for  $K\alpha_2$  of the other phase. Measurements could be made by ordinary techniques when precautions were taken to assure maximum resolution in the patterns. However, diffuseness and lack of resolution at earlier stages were assumed to be evidence for the transition state in which the lattices are strained. The transition state will be more fully analyzed and compared with Bradley's conclusions subsequently when Alnico 12 is described.

Since the three compositions of ternary alloys lie approximately on a "tie line" in the  $a_1 + a_2$  field of Fig. 1, the compositions (and lattice parameters) of the respective phases are the same in all three alloys. On the other hand, the relative amounts of the two phases in equilibrium at low temperatures change with alloy compo-

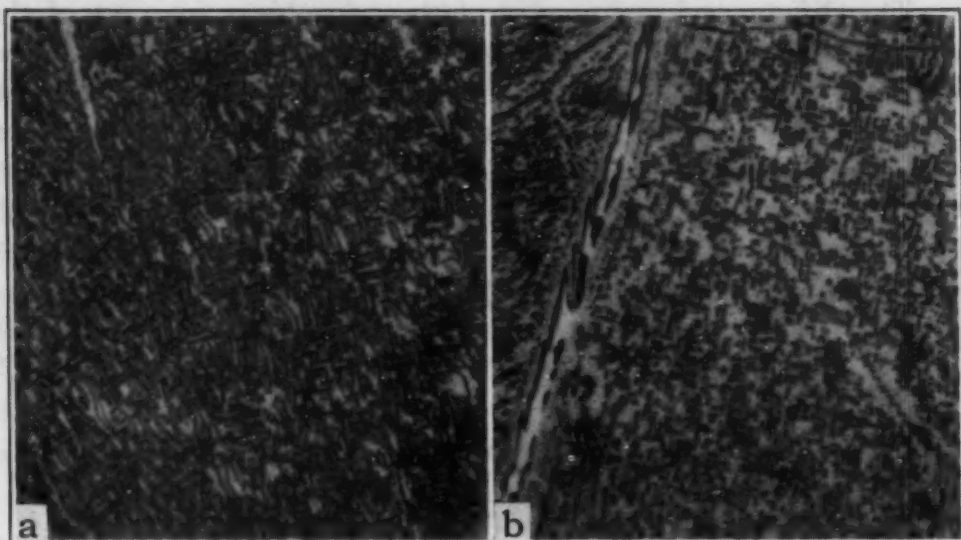


Fig. 3—Microstructure of Two Fe-Ni-Al Alloys Which Had Been Slowly Cooled From 1250 °C. Etchant,  $\text{CuCl}_2$  in  $\text{HCl}$ .  $\times 1000$ . a—Alloy 349 in which iron-rich precipitate is the major phase. b—Alloy 348 showing iron-rich precipitate in NiAl-rich matrix.

sition as shown by the data listed in Fig. 1. The relationship is also apparent from the microstructures which are illustrated by Fig. 3. Here plate-like particles of precipitate which are parallel to  $\{100\}$  planes of the parent matrix are visible. The iron-rich phase apparently is the precipitate, regardless of alloy composition. In Fig. 3a the darker etching, discontinuous phase appears to predominate while, according to Fig. 1, the iron-rich phase should exceed the other phase by three-fold. In Fig. 3b, the darker etching precipitate is the minor phase, which again agrees with the relative amount expected for the iron-rich phase. Apparently it is easier for the iron-rich phase to nucleate and grow to leave a depleted matrix which becomes the more complex NiAl-rich phase rather than vice versa.

The changes in properties which accompany the change in composition along a "tie line" of the  $\alpha_1 + \alpha_2$  field are noteworthy. For the first three alloys in Table II, the optimum coercive force increases with decreasing amount of the iron-rich phase, while the residual induction decreases in this same direction. The energy product which is dependent on these two properties goes through a maximum. The decreasing residual induction is not difficult to explain, for this property is related to the degree of ferromagnetism of the alloy as measured by its saturation induction. The induction decreases with decreasing quantity of the ferromagnetic element (iron) in the alloy. An explanation of the increasing coercive force is possible, based on increasing lattice strain, if one assumes that the

strains in the more ferromagnetic, iron-rich phase are more important than those in the other phase. The disregistry and thus potential strain between the parent matrix and the iron-rich phase increase as more nickel and aluminum are added and the lattice parameter of the parent matrix departs more and more from that of the iron-

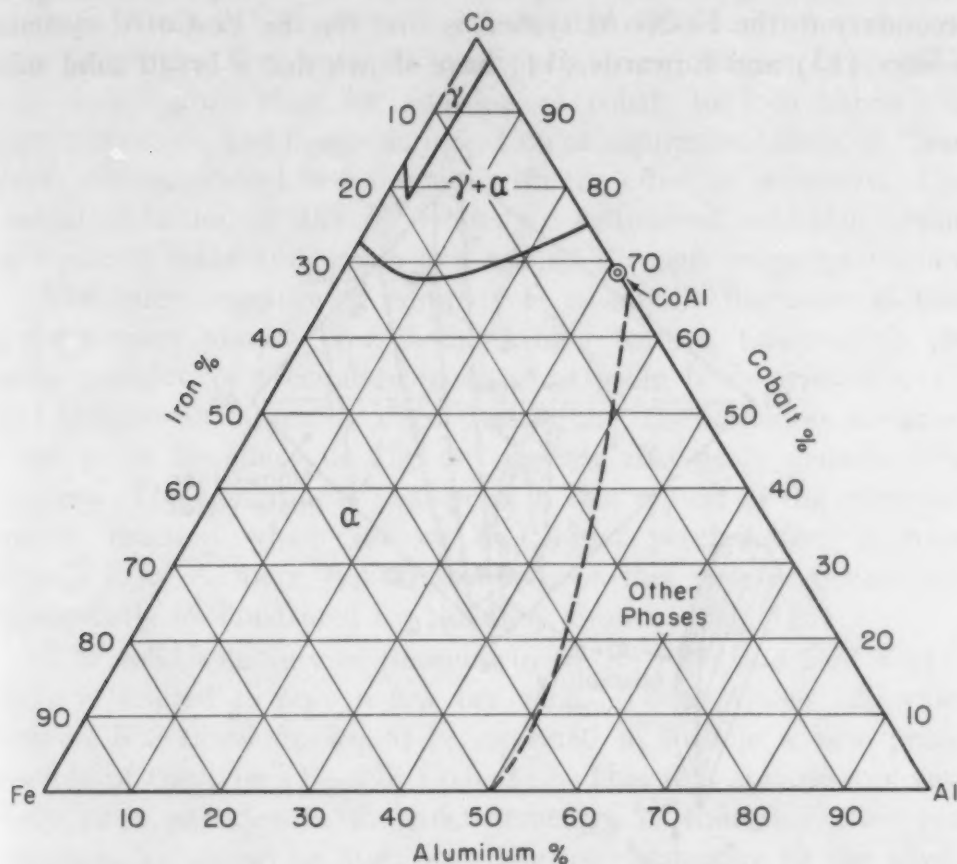


Fig. 4—Constitution of Fe-Co-Al Alloys Quenched From 800 °C According to Edwards (14).

rich phase.<sup>4</sup> A similar effect has been reported for structurally analogous nickel-gold alloys (11) and the relationship of structure to properties has been discussed in more detail elsewhere (12).

The addition of cobalt to the ternary compositions was of practical value, since it made the reaction more sluggish and decreased the critical cooling rate necessary to obtain optimum magnetic properties. This permitted the casting of larger magnets. The data for Alnico 4 in Table III show that cobalt does not change the nature of the precipitation process. Decomposition into an

<sup>4</sup>In this respect the figures listed in Table III are somewhat misleading for they represent total strain between final, equilibrium phases. The strains between parent matrix and iron-rich phase are about 0.5, 0.10 and 0.15%, respectively, for the three ternary alloys in the order listed in Tables II and III.



iron-rich and a NiAl-rich phase is likewise the basis for the hardening of cobalt-containing Fe-Ni-Al alloys. The explanation of the effect on reaction rate can be inferred from the constitution of Fe-Ni-Al-Co alloys. Although the quaternary phase diagram has not been experimentally established, it can be hypothesized from the contributing ternary diagrams. The most important diagram secondary to the Fe-Ni-Al system is that for the Fe-Co-Al systems. Köster (13) and Edwards (14) have shown that a broad solid solu-

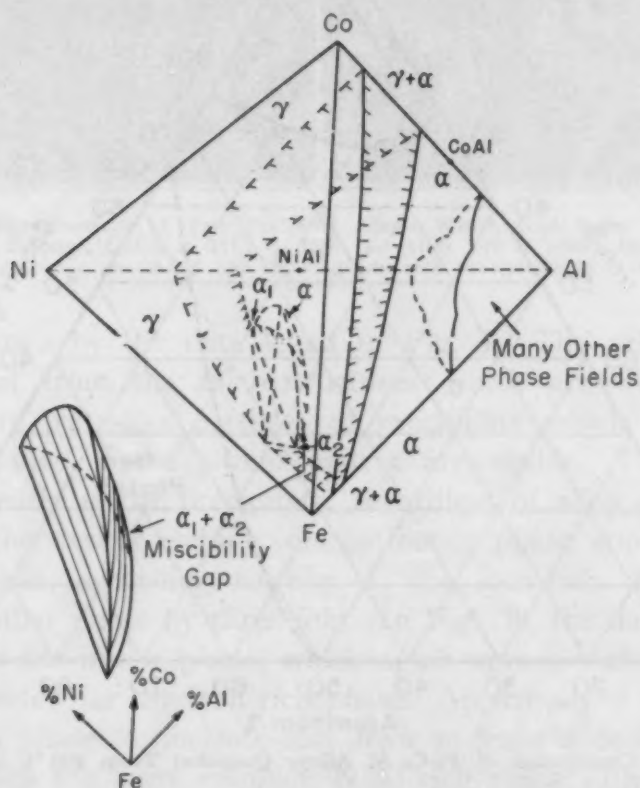


Fig. 5—Hypothetical Section of Fe-Ni-Co-Al Phase Diagram at 1000 °C.

tion field extends from  $\alpha$ -iron to the compound CoAl as in Fig. 4. It is significant that a miscibility gap in the  $\alpha$  field does not occur as in the Fe-Ni-Al system. In the Fe-Co-Ni system a continuous series of austenitic solid solutions exists above 910 °C (1670 °F), while in the Ni-Co-Al system the compounds NiAl and CoAl form a continuous series of solid solutions as shown by Schramm (15). Thus, one would expect an extensive field of body-centered cubic solid solutions extending from  $\alpha$ -iron to NiAl to CoAl, as illustrated by Fig. 5. This would be interrupted by the miscibility gap on the Fe-Ni-Al side, which would taper off as cobalt is added, since a gap

does not exist in the  $\alpha$  fields of the Fe-Co-Al or Ni-Co-Al systems.

In effect, cobalt increases the solubility of  $\alpha_1$  and  $\alpha_2$  in each other and lowers the temperature at which decomposition starts. With a lowered degree of supersaturation at the higher temperatures where diffusion is fast, the rate of reaction would be expected to be decreased in accordance with the observation. While this is the main structural function of cobalt, the additions influence two other properties that promote good permanent magnet properties. It is well known that the addition of cobalt to iron raises the magnetostriction and magnetic induction at saturation. Both of these effects are considered to cooperate with the effect of structure. The residual induction is directly related to saturation induction, while the coercive force and strain are related through magnetostriction.

The microstructure of Alnico 4 is essentially the same as that of the ternary alloys. One distinguishing feature, however, is the coarse network of precipitate particles at grain boundaries of over-aged samples as shown by Figs. 6a and 6b. The waviness imparted to the grain boundary in Fig. 6b suggests that grain growth is in progress. The structure is analogous to that typical of the recrystallization reaction which follows the initial precipitation in some alloys (10). A more typical example of this type structure will subsequently be illustrated for the alloy Cunico (Fig. 11d).

The solid solubility of titanium in Fe-Ni (16) and Fe-Co (17) alloys is limited to only a few per cent. Thus, Alnico 12, which contains 8% titanium, would be expected to include a new phase, possibly of the type  $(\text{Fe, Ni, Co})_3 \text{Ti}$ . This was apparent as relatively large particles in the microstructure of the alloy after heat treatment, as shown by Fig. 6c. The microstructure of the slowly cooled alloy exhibited more than one precipitate in Fig. 6d. In the background of the latter micrograph a Widmanstätten pattern is faintly visible. It is considered that this represents the precipitate which is hardening the alloy and not the relatively large particles of insoluble phase. This is confirmed by the results of X-ray diffraction analyses which reveal that the basic decomposition inherent in Fe-Ni-Al alloys also occurs in Alnico 12, as shown by the data in Table III. The essential reaction is likewise one in which decomposition proceeds into two body-centered cubic phases, one rich in iron and one rich in NiAl.

The principal virtue of Alnico 12 in regard to this study of structure is that part of the titanium addition goes into solid solution in the iron-rich phase and expands its unit cell to the extent that the diffraction lines of the two phases are clearly resolvable. The dis-

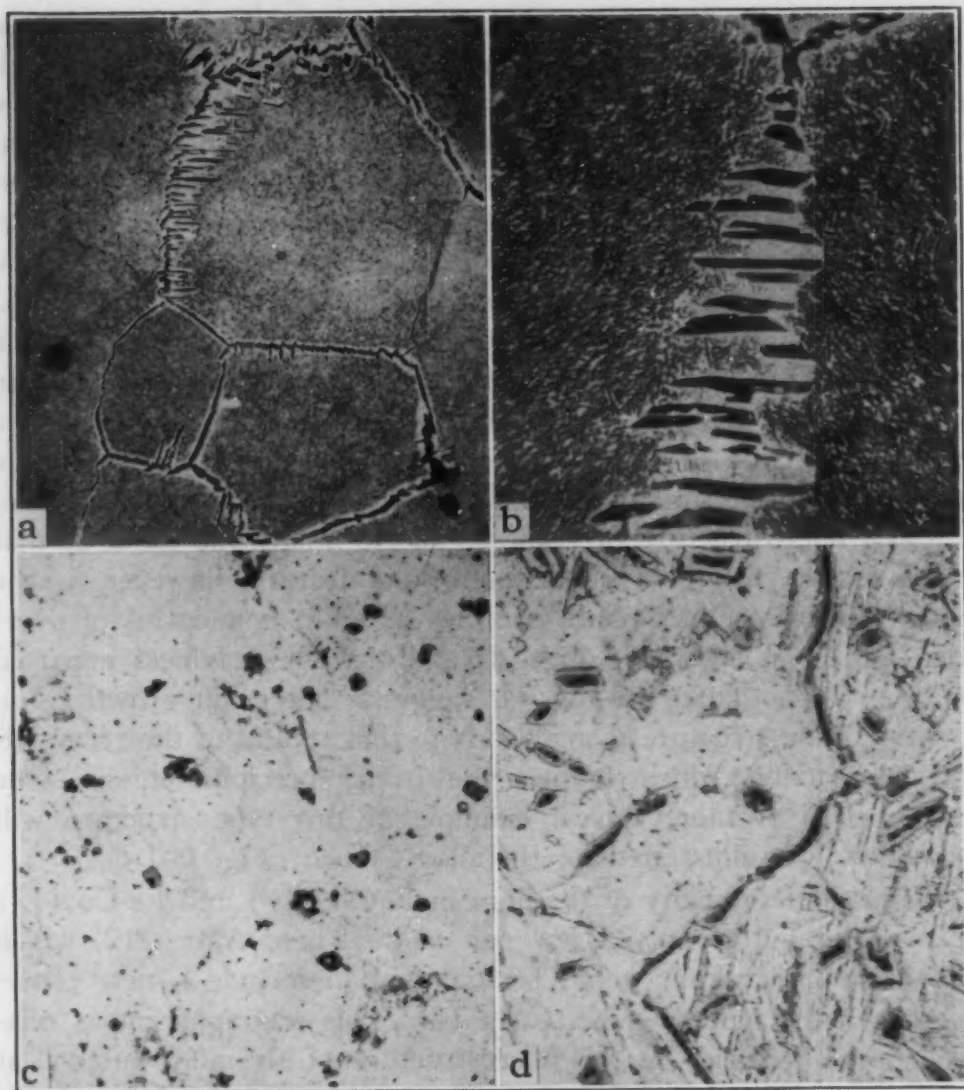


Fig. 6—Microstructure of Some of the Alnicos. Etchant,  $\text{CuCl}_2$  in  $\text{HCl}$ . a—Alnico 4 slowly cooled from  $1250^\circ\text{C}$ .  $\times 250$ . b—Same as a.  $\times 1000$ . c—Alnico 12 after normal heat treatment.  $\times 1000$ . d—Alnico 12 slowly cooled from  $1200^\circ\text{C}$ .  $\times 500$ .

registry is increased from 0.2% or less to 1.6% for the equilibrium state. This permits an analysis of the structure at the transition state. Although the lines in the pattern for the specimen aged to optimum properties are diffuse, only certain lines are doubled, whereas others such as the (200) are flanked by side lines.

Similar conditions have been observed for the alloys Cunife (2, 3) and Cunico (18) and it has been shown that the phases instead of being cubic are distorted into tetragonal cells. The sequence of crystallographic structures is illustrated by Fig. 7 for Alnico 12. At the transition state, the decomposition products retain lattice matching on the (001) plane. The iron-rich phase is elongated in one direction, whereas the NiAl-rich phase is contracted in this



same direction. Presumably the same condition obtains during the hardening of the other Alnicos, but detection is limited by the very small changes in lattice parameters. This suggests that instead of coherency in all directions, as Bradley concluded for ternary alloys, coherency is obtained only in the two directions in the (001) plane of the plate-like particles. The precipitate particles are nucleated at random throughout the parent matrix. The particles and their surrounding envelope of the conjugate phase (depleted

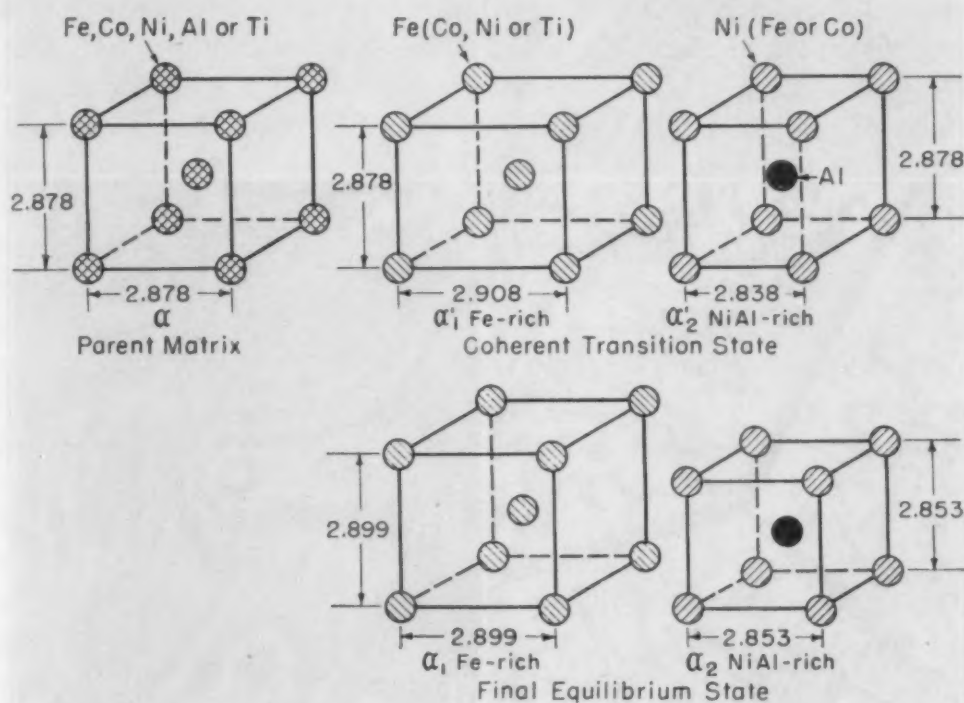


Fig. 7—Unit Cells of Structures That Participate in Precipitation in Alnico 12.

matrix) grow as plates parallel to one of the planes of the {100} family while retaining lattice matching in the planar expanse of the particle. Subsequently, the decomposition products assume their cubic lattices.

The addition of copper to the Alnicos plays an analogous role to that of cobalt; it retards the rate of precipitation. Structurally, it goes into solution in the  $\alpha$  phases, for at high temperatures the body-centered cubic compound  $\text{Cu}_3\text{Al}$  forms continuous solid solutions with  $\alpha\text{-Fe}$  (19) and  $\text{NiAl}$  (20-21). Bradley (7) has pointed out that these three phases appear to be linked together into a single solid solution field in the quaternary diagram. The condition is analogous to that in the  $\text{Fe-Ni-Co-Al}$  diagram, Fig. 5. The addition of copper

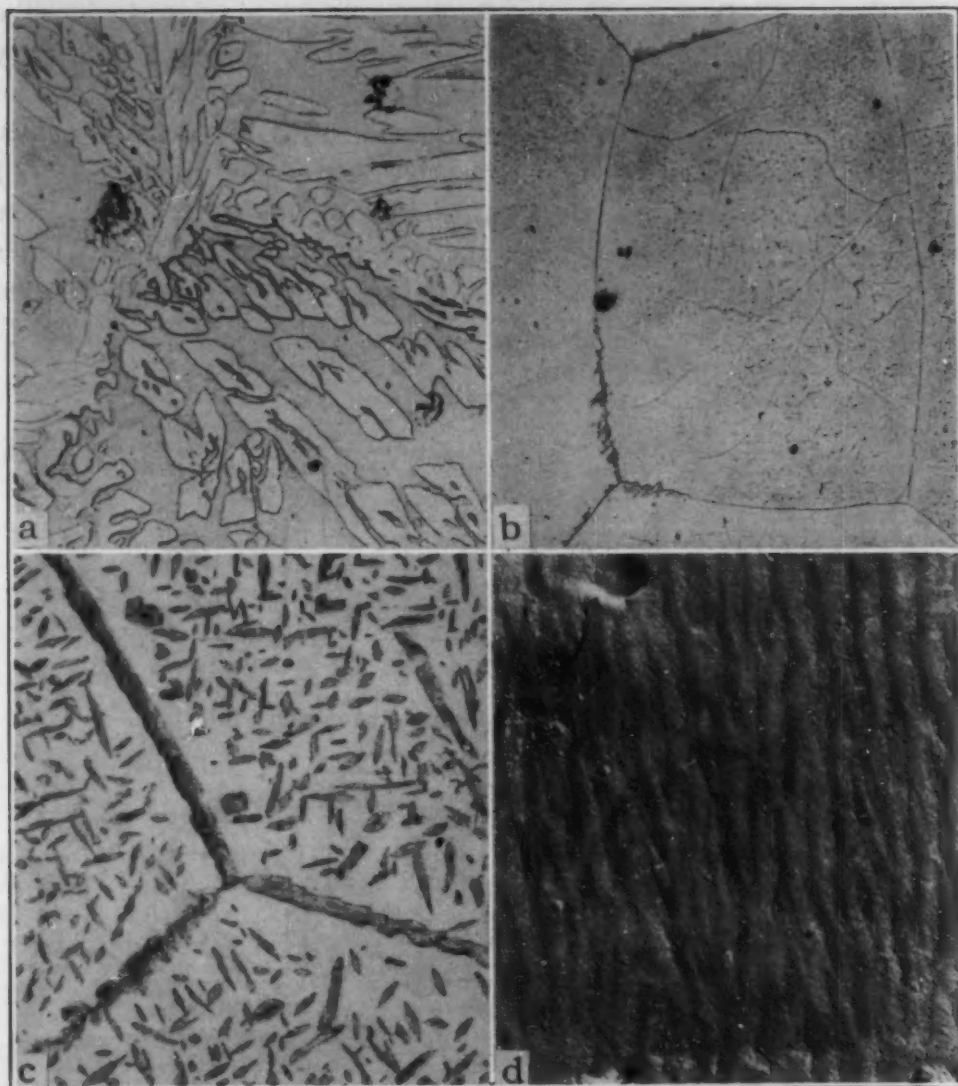


Fig. 8—Microstructure of Alnico 5. Etchant,  $\text{CuCl}_2$  in  $\text{HCl}$ . a—As cast.  $\times 100$ . b—Normal heat treatment.  $\times 250$ . c—Slowly cooled from  $1250^\circ\text{C}$ .  $\times 250$ . d—Electron micrograph of shadow-cast silica replica from single crystal that had received normal treatment followed by slow reheating to  $800^\circ\text{C}$ , held 16 hours.  $\times 8000$ .

could likewise increase the mutual solubility of  $\alpha_1$  and  $\alpha_2$  and lower the decomposition temperature to retard the reaction. In Alnico 5, copper and cobalt work together to achieve this end.

Microstructures of Alnico 5 are shown by Fig. 8. In the as-cast condition, Fig. 8a, the structure consisted of massive particles of a light phase in a matrix of darker phase which probably is the iron-rich phase. After the normal heat treatment, which consisted of a solution heat treatment, cooling at a controlled rate in a magnetic field and aging, the precipitate was too fine to resolve microscopically as shown by Fig. 8b. The "feathery precipitate" at grain boundaries which is occasionally observed is analogous to that in Alnico 4, Fig.

6a. The presence of much of the precipitate in this form detracts from the magnetic properties. After slow cooling, the precipitate was easily resolvable microscopically as in Fig. 8c. The darker phase was identified by etching tests and microhardness as the iron-rich precipitate which is embedded in a matrix of the NiAl-rich phase.

In Alnico 5, the disregistry between phases after overaging was found to be the least of all those for the alloys of this group, Table III. The low disregistry permits an explanation of the anisotropic properties that are obtained on cooling this alloy in a magnetic field after the solution heat treatment and prior to aging. The latter treatment produces properties that are much better in the direction of the applied field than in the transverse directions. Such a condition in regard to mechanical properties originates in a preferred orientation. Magnetic properties are likewise dependent on orientation and the dependence would be particularly prominent in the case of the small plate-like precipitates in a permanent magnet material. Since the orientations of the particles relative to the matrix grains are fixed on a discrete family of matrix planes by crystallographic considerations, the orientation of the particles relative to the outward form of the magnet can be controlled in general only by controlling the orientation of matrix grains in the aggregate. A preferred orientation of matrix grains is achieved in alloys such as Cunife and Vicalloy by cold working and in Alnico 5 DG by directional solidification in casting. Under normal conditions of precipitation the formation of plate-like particles is equally favorable on all planes that constitute the family; however, the author suggested some time ago that the anisotropy promoted by cooling Alnico 5 in a magnetic field originates in the preferential nucleation of particles on one or two of the three possible {100} planes (12). Good evidence for preferential nucleation in this alloy has been obtained more recently. Direct examination of Alnico 5 after the usual thermal treatments was not successful, but by very slowly heating a sample to temperatures at which the particles could grow to resolvable sizes, it was found possible to retain the distribution of precipitate characteristic of the normally aged condition. In Fig. 8d, the microstructure of a single crystal that had been cooled with the magnetic field along the [001] direction (vertical) and then reheated shows cross sections through plates on (100) and (010) planes only. The plane of polish was approximately parallel to the (110) plane and the absence of horizontal traces shows that no precipitate particles had been nucleated on the (001) plane which is normal to the direction of the field. The explanation of this phenomenon probably involves



amount of disregistry, as it determines the strain energy term in the equation for change in free energy of precipitation, modified anisotropically by a contribution of some form of magnetic energy. Apparently, equilibrium disregistry which specifies the strain at the coherent state is important, for only when the disregistry is small, as in Alnico 5, is the treatment effective. Alloys with higher disregistry, such as Alnico 12 and Cunico, are not improved by the magnetic treatment.

Three types of magnetic energy could be influencing the nucleation process in Alnico 5. First, the magnetic energy associated with shape would be high for particles oriented with their smallest dimension parallel to the field. For this reason the activation energy for plates on the (001) plane might be prohibitively high and precipitation would proceed by the normal process on (100) and (010) planes only. Such a condition would be expected to obtain for other alloys also, regardless of equilibrium disregistry, since the lattices are always coherent at the early stages of aging and precipitates are generally plate-like in shape. Second, magnetocrystalline anisotropy energy would be a minimum for plates in the orientation in which the field is along the easy direction of magnetization. The easy direction would be along the expanded C-axis of the tetragonal precipitate parallel to the thickness of the plates and on this basis plates on the (001) plane would be preferred, which is contrary to observations. Finally, magnetostriction of the matrix could produce preferred orientations in which the strains on the surface of coherency would be less than normal. Iron and iron-cobalt alloys expand spontaneously when they are subjected to a magnetic field along one of the  $\langle 100 \rangle$  directions. If the matrix were expanded by magnetostriction in the [001] direction prior to precipitation, then the iron-rich precipitate would have to be strained 10 to 15% less to make it fit onto planes of coherency that include this direction, i.e., (100) and (010). When disregistry is small, as in Alnico 5, the magnetostrictive energy term would be significant compared with strain energy and it would contribute to the energy change. Magnetostriction of the matrix thus lowers the activation energy for particles on (100) and (010) planes and raises it for particles on the (001) plane. The observed preferred orientation would be effected on this basis also. Regardless of the specific form of magnetic energy, it is apparent from Fig. 8d that magnetic energy contributes to the nucleation process and that the nuclei are established during cooling from the solution heat treatment with growth occurring only during subsequent aging. In order for the treatment to be

effective, obviously the Curie temperature of the alloy must be above the temperature at which nucleation is rapid.

### THE COPPER-BASE ALLOYS

The constitutions of the Cu-Ni-Fe (1, 22) and Cu-Ni-Co (23) systems have been completely determined. The alloys Cunife and Cunico are analogous in regard to constitution and structure; there-

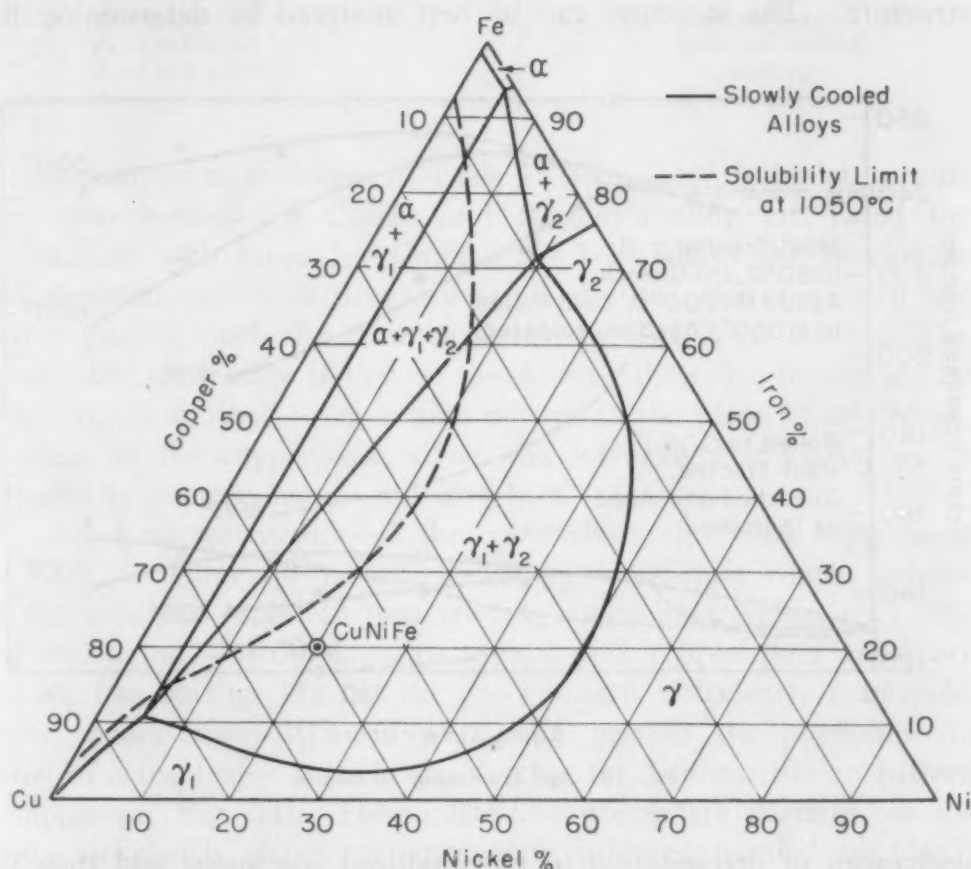


Fig. 9—Constitution of Cu-Ni-Fe Alloys According to Bradley, et al (1).

fore, they will be discussed simultaneously. The prerequisite precipitation process originates in a simple binary miscibility gap between copper and the ferromagnetic metal (Fe or Co) which is narrowed to complete solubility by the addition of the third metal (nickel), Fig. 9. The solubility between  $\gamma_1$  and  $\gamma_2$  contracts toward the Cu-Fe side of the diagram on raising the temperature, so that an alloy such as Cunife is a single-phase solid solution at high temperatures and decomposes by precipitation into two solid solutions at low temperatures (24). A vertical section of the phase diagram would be similar to Fig. 2. The reaction is analogous to that in the

Alnicos, with the minor difference that here face-centered cubic phases are involved.

The properties of the copper-base alloys have been rather extensively investigated (23-26); however, a comprehensive correlation with structure has been made for the commercial alloy Cunico only (18). A correlation for the alloy Cunife is more difficult to make, since the commercial treatment involves cold rolling after preaging which introduces its own complications in the interpretation of the structure. The structure can be best analyzed by determining the

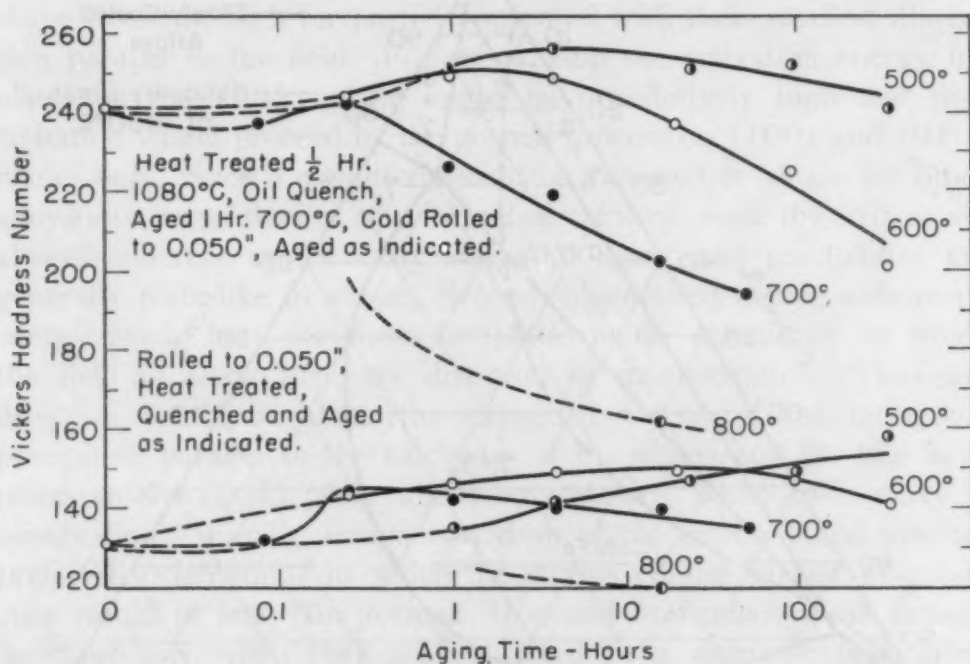


Fig. 10—Age Hardening of Cunife.

mechanism of precipitation in recrystallized specimens and then by considering the added effect of cold working. A comparison of the age hardening of recrystallized and cold-worked samples is given by Fig. 10.

The results of X-ray diffraction analyses are summarized in Table IV. A coherent transition state in the decomposition of  $\gamma$  to  $\gamma_1 + \gamma_2$  was identified for Cunife analogous to that which Bradley had discovered earlier for a different Cu-Ni-Fe alloy (2, 3).

Comparison with Fig. 10 will show that the presence of the transition structure ( $\gamma_1' + \gamma_2'$ ) is concurrent to hardening, while much softening had occurred when the decomposition was complete and only the normal phases were present (see Table II for magnetic properties). Patterns for cold-worked samples were too diffuse to



**Table IV**  
**Structure of Cunife**

Treatment	Structure
As-rolled	$\gamma_1 + \gamma_2$
Heat treated and quenched	$\gamma$
Above aged 1 hr. 625 °C	$\gamma + \gamma_1' + \gamma_2'$
Aged 16 hrs. 625 °C	$\gamma + \gamma_1' + \gamma_2'$
Aged 16 hrs. 800 °C	$\gamma_1 + \gamma_2$
Slowly cooled from 1050 °C	$\gamma_1 + \gamma_2$
Heat treated, aged 1 hr. 700 °C, cold-rolled 80%	$\gamma$ diffuse lines
Above aged 1 hr. 625 °C	Lines not resolved
Aged 16 hrs. 625 °C	Lines not resolved
Aged 16 hrs. 800 °C	$\gamma_1 + \gamma_2$

permit analysis as indicated in Table IV. In Table V lattice parameter measurements of Cunife and Bradley's alloy are listed for comparison with those for Cunico. In both alloys the precipitate and depleted matrix lattices are strained into coherency with the parent matrix much the same as shown by Fig. 7 for Alnico. The outstanding difference is that in the Alnicos the more ferromagnetic phase,  $\alpha_1$ , is strained by extension normal to the plane of coherency, whereas in the copper-base alloys the ferromagnetic phase,  $\gamma_2$ , is strained by compression in this direction.

Some microstructures of the copper-base alloys are reproduced in Fig. 11. After the normal treatment for Cunife which consists of the sequence—solution heat treating, quenching, aging, cold rolling and aging—distorted grains typical of a cold-worked metal are apparent as in Fig. 11a but the precipitate is not clearly resolvable. Slow cooling from 1050 °C (1920 °F) permits the precipitate to grow to a resolvable particle size so that the Widmanstätten pattern is apparent, Fig. 11b. Here plate-like precipitate particles of the iron–nickel-rich phase are apparently oriented parallel to {100} planes of the more abundant copper-rich matrix. A similar microstructure also had been identified for slowly cooled Cunico pre-

**Table V**  
**Lattice Parameters (Å) of Structures in Cunife and Cunico**

Alloy	Condition	Phases	$\gamma_1$ (Cu-rich)		$\gamma_2$		Disregistry
			a	c	a	c	
Cunife	As-quenched	$\gamma$	3.596	.....	.....	.....	.....
	Equilibrium state	$\gamma_1 + \gamma_2$	3.607	.....	3.590	.....	0.5%
52 Cu-36 Ni- 12 Fe (2, 3)	As-quenched	$\gamma$	3.583	.....	.....	.....	.....
	Transition state	$\gamma_1' + \gamma_2'$	3.583	3.617	3.583	3.550	.....
	Equilibrium state	$\gamma_1 + \gamma_2$	3.594	.....	3.572	.....	0.6%
Cunico	As-quenched	$\gamma$	3.564	.....	.....	.....	.....
	Transition state	$\gamma_1' + \gamma_2'$	3.562	3.647	3.565	3.487	.....
	Equilibrium state	$\gamma_1 + \gamma_2$	3.593	.....	3.539	.....	1.5%

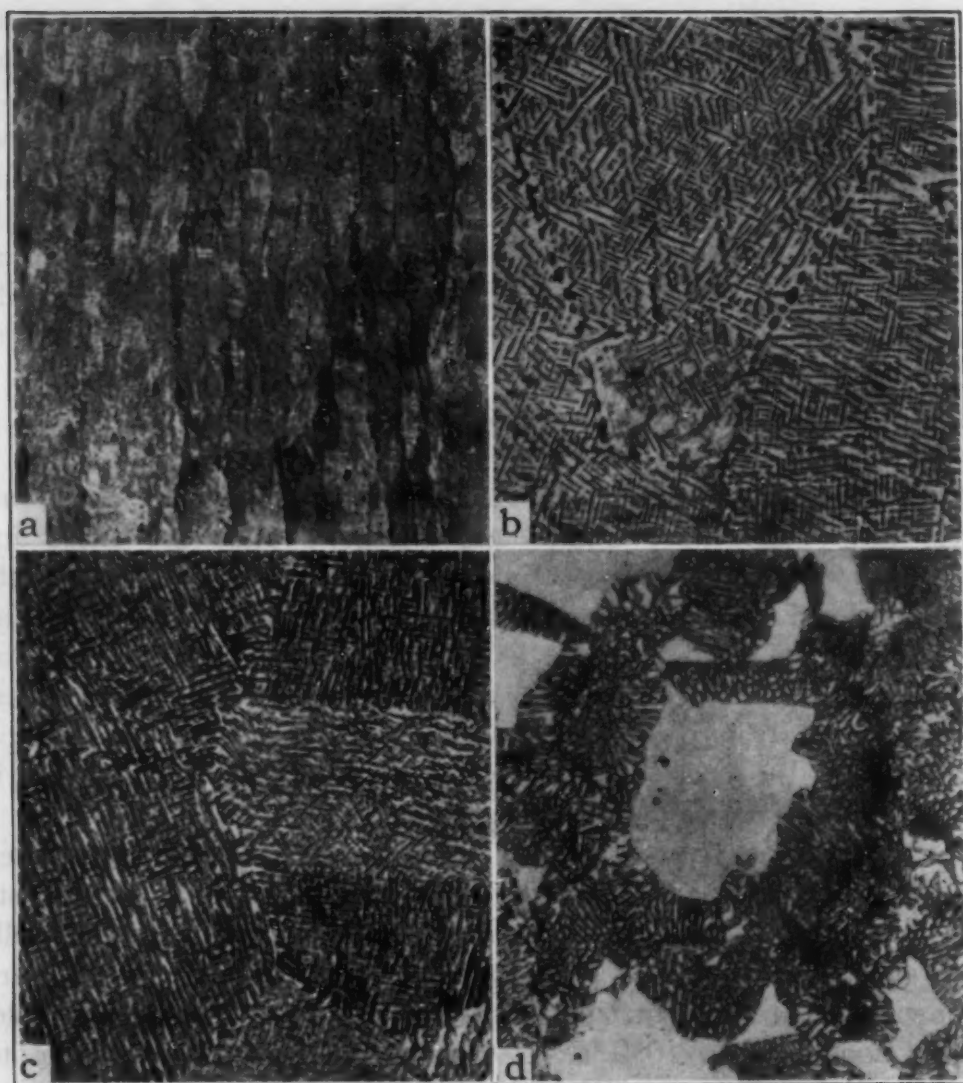


Fig. 11—Microstructure of the Copper-Base Alloys. Etchant,  $K_2Cr_2O_7$ . a—Cunife after normal heat treatment and cold rolling.  $\times 500$ . b—Cunife slowly cooled from  $1080^\circ C$ .  $\times 1000$ . c—Cunico slowly cooled from  $1100^\circ C$ .  $\times 1000$ . d—Cunico aged 49 hours at  $900^\circ C$ .  $\times 500$ .

viously, Fig. 11c. In both alloys the recrystallization reaction has also been observed. This was well advanced in Fig. 11d. Here a coarse aggregate of the two decomposition products has partially consumed the parent grain structure. This reaction starts at points on the original grain boundaries and proceeds by nodular growth analogous to recrystallization. The very fine, general precipitate within the parent grains apparently is redissolved during this process. It is a softening reaction, for the strains of precipitation are being relieved and the unstrained lattices of the equilibrium phases are being formed. Actually, the precipitate of immediate interest from the standpoint of the hardening of these alloys is the one that is uniformly distributed

throughout the parent grains and has the appearance shown by Figs. 11b and 11c when the particles are permitted to grow to a microscopically resolvable size. Here there are plate-like particles in one of three orientations parallel to  $\{100\}$  planes of the parent grains. The effect of cold working alloys such as Cunife after the solution heat treatment is probably two-fold. First, cold working produces a preferred orientation of the parent grains. Thus, the particles of the magnetic precipitate will bear a preferred orientation relative to the direction of working. This accounts for the anisotropic properties of the material. Second, cold working accelerates the precipitation

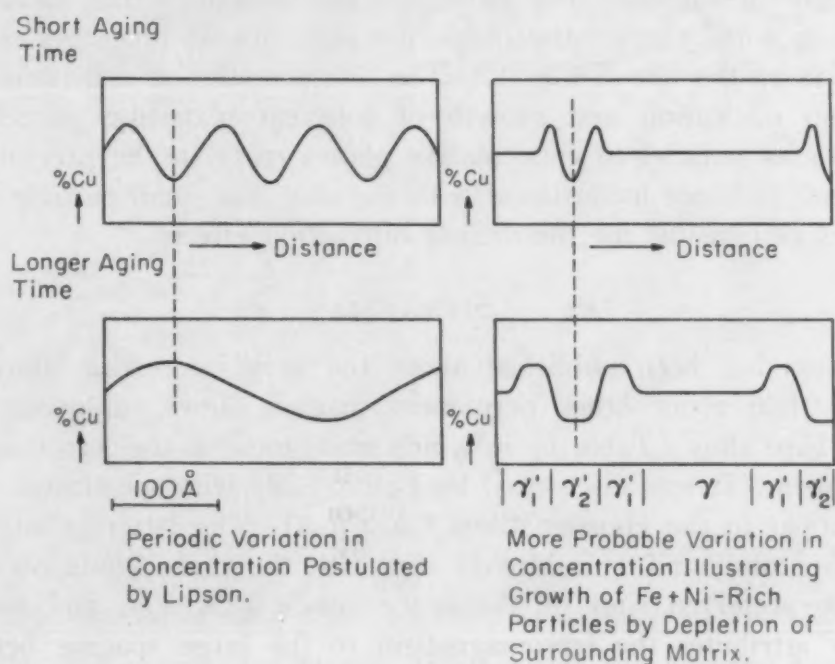


Fig. 12—Concentration Fluctuations in Aged CuNiFe.

reaction (see data in Fig. 10). This should permit obtaining a larger number of small particles by aging at temperatures lower than those which could be practically used without working.

The early stages of precipitation in alloys such as the Alnicos, Cunico and Cunife are associated with diffuse X-ray diffraction effects analogous to those which have been identified with other types of precipitation alloys. Although these generally have been attributed to a small dimension of the particles (platelets too thin to afford sharp diffraction in the thickness dimension), it is of interest here to consider the explanation proposed for Cu-Ni-Fe alloys. Daniel and Lipson (27) observed a phenomenon in the



aging sequence prior to the tetragonal structures of Bradley. This appeared as diffuse "side bands" on the pattern for the parent matrix. They found that the diffraction effects could be explained by assuming a periodic variation of lattice parameter in the direction of cube edges. This could originate in concentration differences in the solid solution at regular intervals while the coherence of the single-phase lattice remains. The period of modulation increased from 100 to 250Å, with aging time as illustrated in Fig. 12. While Daniel and Lipson assumed a pure sinusoidal variation of lattice parameter because of the ease of handling this in calculating predicted intensity distributions, it is more likely that the actual case is as illustrated at the right in Fig. 12. The latter has the advantage that subsequent peaks in copper concentration do not later appear at earlier depressions as on the left of Fig. 12. The interpretation is consistent with random nucleation and growth of coherent plate-like particles of the phases parallel to cube matrix planes early in the precipitation process. It is not inconsistent with the idea that small particle thickness is responsible for the diffuse diffraction effects.

#### SILMANAL

Less has been published about the very interesting alloy Silmanal than about other permanent magnet alloys. Silmanal is a silver-base alloy (Table I) in which manganese is the ferromagnetic component. It was discovered by Potter (28) who substituted silver for copper in the Heusler alloy, Cu-Mn-Al. The latter is an intermetallic compound ( $\text{Cu}_2\text{MnAl}$ ) in which the three kinds of atoms assume preferred sites on the space lattice (29, 30), and modern theory attributes the ferromagnetism to the large spacing between manganese atoms inherent in this structure. The regular arrangement of atoms has led to the supposition that an order-disorder (superlattice) reaction plays an important role in dictating the properties of these materials (31). High temperature X-ray work has shown, however, that the ordered arrangement in many of the Heusler compounds is retained up to the melting point, while the present work will show that Silmanal is a precipitation-hardening alloy rather than an ordering alloy. Potter was not able to detect any phase other than a random silver solid solution with  $a_0 = 4.06$  in X-ray patterns of Silmanal.

The nature of the reaction in Silmanal was readily identified by metallographic examinations. Some of the microstructures are shown by Fig. 13. After the normal treatment, which involves cold working after the solution heat treatment interspersed with aging treatments,

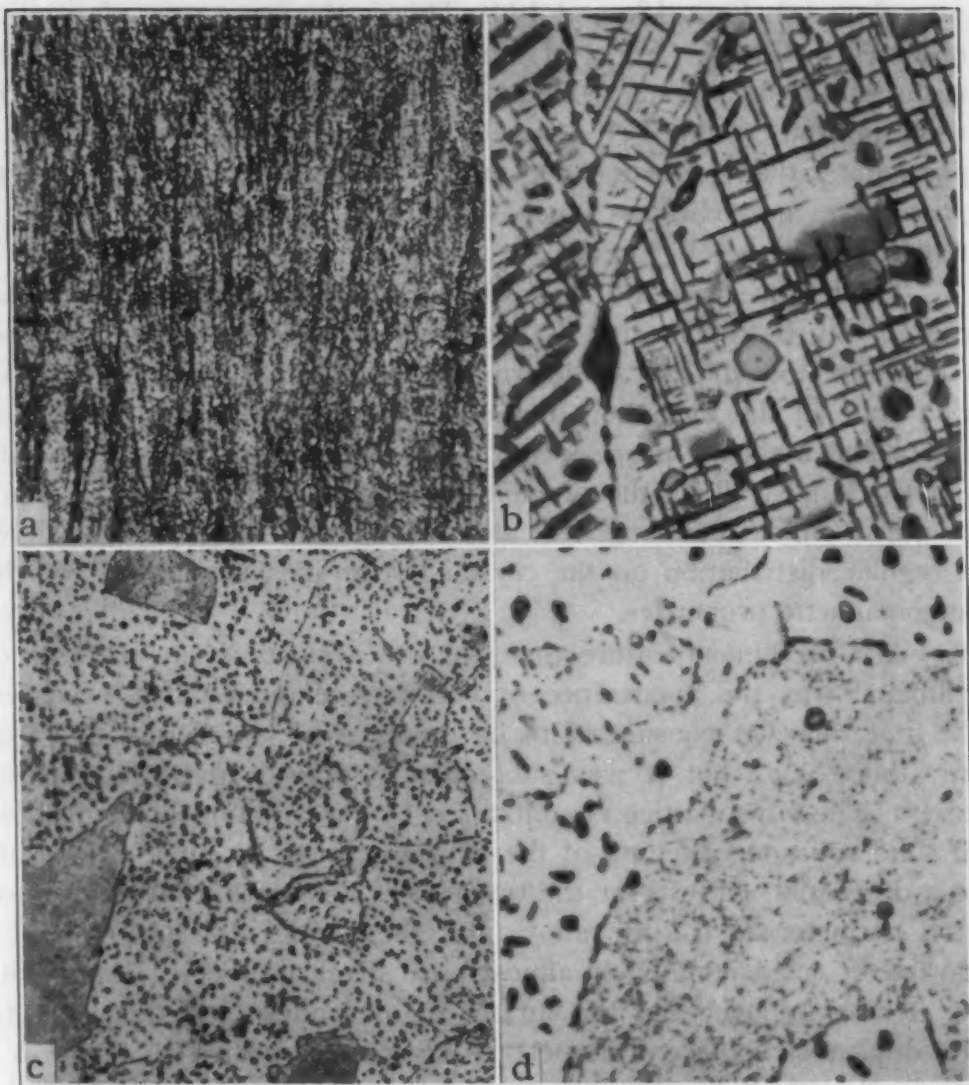


Fig. 13—Microstructure of Silmanal. Etchant,  $\text{CrO}_3\text{-H}_2\text{SO}_4$ . a—Normal heat treatment and cold rolling.  $\times 500$ . b—Slowly cooled from  $800^\circ\text{C}$ .  $\times 1500$ . c—Heat treated 1 hour at  $800^\circ\text{C}$ , water-quenched and aged 16 hours at  $500^\circ\text{C}$ .  $\times 250$ . d—Same as c.  $\times 1000$ .

the microstructure exhibited a fine dispersion of precipitate in a matrix of distorted grains as in Fig. 13a.

Heating to  $800^\circ\text{C}$  ( $1470^\circ\text{F}$ ) followed by slow cooling produced a typical precipitate structure at boundaries and within recrystallized grains, Fig. 13b. Again the precipitate is plate-like, oriented parallel to cube planes, as may be concluded from certain grains which are so oriented that two sets of traces of the plate-like precipitate are at right angles, while the third is almost parallel to the plane of polish. When a specimen was aged directly after the solution heat treatment and quench without cold working, the discontinuous reaction in which strains are relieved by recrystallization

was observed, Figs. 13c and 13d. This is the same type of reaction observed in Cunico (Fig. 11d) and other precipitation alloys, but the nature is rather unique. In most alloys the second phase in the recrystallized nodules is generally much coarser than the initial precipitate that is being consumed. In Silmanal the secondary precipitate apparently is finer than that in the matrix which is redissolved.

While the reaction responsible for the hardening of Silmanal can readily be determined as precipitation, the identity of the precipitate is more difficult to determine. Presumably a coherent transition state in the formation of the precipitate accounts for the good permanent magnetic properties. On the other hand, by analogy with the Cu-Mn-Al alloys the precipitate must be an intermetallic compound in which the manganese atoms are far enough apart and have a regular distribution on the crystal lattice sites to account for the ferromagnetic properties.

The prominent feature that was observed in X-ray patterns of Silmanal was the appearance of two face-centered cubic  $\delta$  phases. At first this was considered to be evidence for a reaction like that in Cunico, etc., but it was subsequently proved to be an etching effect. The silver lattice is contracted by the addition of manganese in solid solution. Etching of the wire specimens in nitric acid leads to a diffraction pattern for the two phases, one with a lattice parameter characteristic of the alloy, and the second (4.084Å) with a parameter corresponding to almost pure silver (4.086Å). Apparently, etching impoverishes the surface in manganese and this leads to the duplex structure. Parameter measurements listed in Table VI are for  $\delta$  in the base alloy, the terminal solid solution in silver. Subsequently, one or two faint lines for the second phase in aged Silmanal were detected in patterns for most of these samples. These lines seemed to be of two different types corresponding to different phases which are designated  $\gamma$  and  $\beta$  in the upper part of Table VI.

In order to identify these phases, the four alloys were made up of the compositions and hypothetical formulas listed at the bottom of Table VI. None of these was a single-phase alloy according to microstructure and X-ray pattern, for they all contained a variable quantity of the silver solid solution,  $\delta$ , in addition to other phases after most heat treatments. Some of these other phases were the same as those in Silmanal. Since manganese is soluble in silver to rather large amounts and these metals do not form intermetallic compounds, the Al-Ag system should be consulted in lieu of any prior data on the ternary Ag-Mn-Al phase diagram. Silver forms



Table VI  
Structure of Ag-Mn-Al Alloys

Alloy*	Treatment	Vickers Hardness	Parameter of f.c.c. Phase, $\delta$	Phases Present Other Than $\delta$
Silmanal	As-received	181	.....	None detected
Silmanal	48 hrs. 250 °C	196	.....	$\gamma$ (?)
Silmanal	168 hrs. 250 °C	181	4.075	None detected
Silmanal	1 hr. 300 °C	116	.....	$\gamma$ (?)
Silmanal	16 hrs. 300 °C	174	4.066	$\gamma$ (?)
Silmanal	48 hrs. 300 °C	171	.....	$\beta$
Silmanal	186 hrs. 300 °C	165	4.074	None detected
Silmanal	1 hr. 400 °C	161	4.071	$\beta$ (?)
Silmanal	16 hr. 400 °C	148	4.069	$\beta$ (?)
Silmanal	1 hr. 500 °C	141	4.071	None detected
Silmanal	16 hrs. 300 °C plus 2 hrs. 500 °C	...	.....	$\beta$ (?)
Silmanal	16 hrs. 400 °C plus 2 hrs. 500 °C	...	.....	$\gamma$ (?)
Silmanal	16 hrs. 500 °C	121	.....	$\beta$
Silmanal	6 hrs. 500 °C plus 1 hr. 600 °C	99.2	.....	$\beta$
Silmanal	1 hr. 800 °C, quenched	...	.....	None detected
Silmanal	16 hrs. 800 °C, quenched	...	.....	None detected
Silmanal	16 hrs. 800 °C, furnace cool	96	.....	$\gamma$ (?)
Silmanal	1 hr. 800 °C plus 16 hrs. 500 °C	...	.....	$\beta$
"Ag <sub>2</sub> MnAl"	As-cast	...	.....	$\beta$
"Ag <sub>2</sub> MnAl"	Ground—2 hrs. 500 °C	...	4.063	$\beta$
"Ag <sub>2</sub> MnAl"	44 hrs. 500 °C	...	.....	$\beta$
"Ag <sub>2</sub> MnAl"	16 hrs. 700 °C	...	.....	$\beta$
"Ag <sub>2</sub> MnAl"	16 hrs. 840 °C	...	.....	$\beta$
"Ag <sub>2</sub> MnAl"	4 hrs. 750 °C, W. Q.	...	.....	$\beta + \gamma$
"AgMnAl"	Ground—5 hrs. 500 °C	...	4.063	$\beta$
"AgMnAl"	18 hrs. 750 °C	...	.....	$\gamma$
"AgMn <sub>2</sub> Al"	Ground—4 hrs. 500 °C	...	4.075	$\beta$
"Ag <sub>3</sub> Al"	As-cast	...	.....	$\gamma (+\delta)$
"Ag <sub>3</sub> Al"	Ground—4 hrs. 500 °C	...	.....	$\beta'$ (tr. $\delta$ )
"Ag <sub>3</sub> Al"	72 hrs. 400 °C	...	.....	$\beta'$ (no $\delta$ )
"Ag <sub>3</sub> Al"	44 hrs. 500 °C	...	.....	$\beta' (+\delta)$
"Ag <sub>3</sub> Al"	2 hrs. 750 °C, W. Q.	...	.....	$\gamma (+\delta)$

\*The compositions of these alloys were as follows:

	Ag	Mn	Al
Silmanal	86.8	8.8	4.4
"Ag <sub>2</sub> MnAl"	72.5	18.4	9.1
"AgMnAl"	56.9	28.9	14.2
"AgMn <sub>2</sub> Al"	44.1	44.9	11.0
"Ag <sub>3</sub> Al"	93.0	....	7.0

three intermetallic compounds with aluminum, all stable in the composition range of 5 to 10% aluminum, which roughly corresponds to Ag<sub>3</sub>Al. These exist at different temperature ranges and transform into each other on cooling. The high temperature form,  $\beta$ , has a body-centered cubic lattice and is stable above 600 °C; the intermediate form,  $\gamma$ , is hexagonal close packed and is stable from 600 to 450 °C, while below 450 °C the  $\beta'$  form with a  $\beta$ -Mn-type structure is stable. The latter phase appeared only in the alloy "Ag<sub>3</sub>Al" after annealing at 400 to 500 °C (Table VI). On the other hand, the other two phases were detected in Ag-Mn-Al alloys. Although the high temperature body-centered cubic  $\beta$  phase could not be retained by quenching the Ag-Al alloy, it was present in most of the ternary alloys. Apparently, the addition of manganese lowers its temperature range of stability. Its structure is similar to Cu<sub>2</sub>MnAl and it has a lattice parameter of 6.075Å; however, it

probably does not have as much silver as the copper alloy has copper, for the alloy "Ag<sub>2</sub>MnAl" contained an excess silver as the  $\delta$  phase. The  $\beta$  probably is the ferromagnetic phase for, although there was some questionable evidence for the  $\gamma$  phase in Silmanal, this hexagonal phase does not have the required regular arrangement of atoms. The results on Silmanal, although not complete, show that this is a precipitation-type alloy and that the precipitate is not a  $\beta$ -Mn-type structure but probably a body-centered cubic structure like Cu<sub>2</sub>MnAl.

#### VECTOLITE

A study of Vectolite, the oxide magnet, affords an opportunity to apply to inorganic compounds some of the principles of precipitation from solid solution formulated in the study of metals. Although Vectolite is based upon the oldest known permanent magnet material—lodestone—the structural dependence of its properties has not previously been reported. It is known that many oxides form continuous series of solid solutions with Fe<sub>3</sub>O<sub>4</sub> (or FeO·Fe<sub>2</sub>O<sub>3</sub>). These mixed oxides which have been named "ferrites" have the cubic structure of the spinel type and have the general formula MO·Fe<sub>2</sub>O<sub>3</sub> in which M is another bivalent ion of about the same size as iron (Mg, Zn, Cu, Ni, Mn, Co). Some such combinations are found to have interesting soft magnetic properties (32). These are prepared by mixing the oxide powders, pressing to shape and sintering to insure complete solution of the solid components. On the other hand, a mixture of Fe<sub>3</sub>O<sub>4</sub> plus CoO·Fe<sub>2</sub>O<sub>3</sub> (cobalt ferrite) forms the basis of the hard magnetic material, Vectolite (33, 34). The oxides are intimately mixed, pressed, sintered at 1000 °C and aged by controlled cooling in a magnetic field. By analogy with the permanent magnet alloys, it would be expected that Vectolite would owe its permanent magnet properties to a transformation in the solid state in contrast with the magnetically soft ferrites which must be stable solid solutions.

The results of X-ray diffraction analyses listed in Table VII show that Vectolite is susceptible to a precipitation reaction. After the optimum heat treatment the structure consisted of two phases, a solid solution like cobalt ferrite (CoFe<sub>2</sub>O<sub>4</sub>) with the spinel-type structure, and  $\alpha$ -Fe<sub>2</sub>O<sub>3</sub> with a rhombohedral lattice. The latter could be dissolved by heating to temperatures above 1000 °C (1830 °F) and could be precipitated by aging at temperatures below 800 °C (1470 °F). It is suspected that Fe<sub>2</sub>O<sub>3</sub> when it first forms also has a spinel-type structure characteristic of the  $\gamma$ -Fe<sub>2</sub>O<sub>3</sub> modifi-

Table VII  
Structure of Vectolite

Treatment	Type of Phases	$a_0$ of Spinel Phase, Å
As-received (optimum heat treatment)	$\text{CoFe}_2\text{O}_4 + \alpha\text{-Fe}_2\text{O}_3$	8.375
Above aged 16 hrs. 800 °C	$\text{CoFe}_2\text{O}_4 + \alpha\text{-Fe}_2\text{O}_3$	8.394
Heat treated 1 hr. 1050 °C	$\text{CoFe}_2\text{O}_4$	8.381
Heat treated 1 hr. 1150 °C, furnace-cooled	$\text{CoFe}_2\text{O}_4$	8.383
Heat treated 3 hrs. 1150 °C, $\text{H}_2\text{O}$ quench	$\text{CoFe}_2\text{O}_4$	8.393
Heat treated—aged 10 hrs. 500 °C	$\text{CoFe}_2\text{O}_4$	.....
Heat treated—aged 10 hrs. 600 °C	$\text{CoFe}_2\text{O}_4 + \text{tr. } \alpha\text{-Fe}_2\text{O}_3$	8.362
Heat treated—aged 10 hrs. 700 °C	$\text{CoFe}_2\text{O}_4 + \alpha\text{-Fe}_2\text{O}_3$	8.377

cation, but either the lattice parameter ( $8.32\text{\AA}$ )<sup>5</sup> is too near that of  $\text{CoFe}_2\text{O}_4$  to be readily distinguishable in the X-ray pattern or more likely the transformation to  $\alpha\text{-Fe}_2\text{O}_3$  occurs rapidly and the amount of  $\gamma\text{-Fe}_2\text{O}_3$  at steady state is small. The discrepancy between the spinel-type structures is about 0.7%. Although it has not been possible to obtain all the data which would be desired, the reaction in Vectolite could well be analogous to that in the Alnicos, Cunico, and Cunife where the precipitate first forms in a strained coherent condition to cause magnetic hardening. In Vectolite, however, the cubic precipitate is not stable and the rhombohedral modification appears rapidly.

#### VICALLOY

The hardening of the cobalt-iron-base alloy has been attributed by Nesbitt (35) to the precipitation of an austenitic phase in a ferritic matrix. According to the work of Köster and Lang (36), the addition of vanadium depresses the  $\gamma$  to  $\alpha$  transformation in cobalt-iron to provide an open  $\gamma$  field analogous to the Fe-Mn and Fe-Ni binary alloy systems. After quenching and cold working, Vicalloy consists of only the ferritic phase, but on aging some of the austenitic phase appears. This precipitation may be the source of hardening, but the absence of pronounced hardening in the analogous systems, Fe-Ni and Fe-Mn, does not lend support to the concept. On the other hand, consider an alternate explanation. Ellis and Greiner (37) have shown that binary alloys near 50:50 atomic per cent Co-Fe are susceptible to an ordering reaction. A superlattice on the ferritic phase is formed in such a manner that iron atoms occupy the corner sites and cobalt atoms the center sites of the body-centered cubic lattice. The lattice parameter increases from  $2.854\text{\AA}$  to  $2.857\text{\AA}$ . It is well known that such a superlattice reaction in alloys like Co-Pt (38, 39) and Fe-Pt (40) leads to outstanding permanent magnet

<sup>5</sup>Handbook value for  $\gamma\text{-Fe}_2\text{O}_3$ . The analogous phase in Vectolite may contain some cobalt which would alter this parameter slightly.



Table VIII  
Structure of Vicalloy I

Treatment	Structure
As cold drawn	$\alpha$
Aged 500 hrs. 400 °C	$\alpha$
Aged 500 hrs. 500 °C	$\alpha + \gamma$
Aged $\frac{1}{4}$ hr. 600 °C	$\alpha + \text{tr. } \gamma$
Aged 1 hr. 600 °C	ord. $\alpha + \text{tr. } \gamma$
Aged 4 hrs. 600 °C	ord. $\alpha + \text{tr. } \gamma$
Aged 16 hrs. 600 °C	ord. $\alpha + \gamma$
Aged 100 hrs. 600 °C	ord. $\alpha + \gamma$
Aged 500 hrs. 600 °C	ord. $\alpha + \gamma$
Aged 500 hrs. 700 °C	ord. $\alpha + \gamma$
Aged 500 hrs. 800 °C	$\gamma + \text{some } \alpha$

properties. Possibly the ordering reaction inherent in Co-Fe alloys plays a part in the hardening of Vicalloy.

The results of X-ray diffraction analyses summarized in Table VIII show that ordering in the ferrite occurs during the aging of Vicalloy. Ordering was not as readily detectable in this alloy as was the appearance of  $\gamma$ , but the presence of superlattice lines in patterns made with cobalt radiation was unmistakable. The superlattice lines increased in intensity with aging, but the change in lattice parameter on ordering was too small to be detectable, particularly when cold-worked samples were used.

While an analysis of the transition state in the ordering process was not possible, it was found that the addition of vanadium increased the parameter of the ordered phase to 2.863Å for the 9.5% vanadium alloy. Ordering was also detected in alloys of lower vanadium contents in which  $\gamma$  did not form at aging temperatures below 800 °C (1470 °F). On the other hand, hardening occurs at low aging temperatures (400 °C) and low vanadium contents (2%) under conditions at which  $\gamma$  would not be expected to form, although higher vanadium contents are required for greatest hardening.<sup>6</sup> While the structure dependence of the properties of these alloys has not yet been completely established, it seems possible to treat the formation of  $\gamma$  as incidental in regard to the main hardening reaction. On the other hand, this is a nonmagnetic phase and its formation detracts from the magnetic induction. One result of cold working is the acceleration of the decomposition of retained  $\gamma$ , as Nesbitt pointed out (35). The preferred orientation also produces anisotropic properties with an increased residual induction and energy product in the direction of working analogous to the effect of cold working Cunife.

<sup>6</sup>The results on alloys of other vanadium contents will appear in a future publication of D. L. Martin.

## DISCUSSION

The structural aspects of the precipitation process in alloys have become fairly well established and, after the limitations of the various analytical techniques were duly recognized, valid correlations of structure with properties have been formulated.

On the other hand, only recently has the order-disorder reaction come under critical study with the objective of rationalizing the phenomena of this reaction (39). This process is also one of nucleation and growth in which particles of the ordered phase form and grow at the expense of the disordered phase. The particles may have plate-like shapes which are oriented parallel to some family of crystallographic planes in the matrix crystal. Anisotropic strains and coherency are involved in the formation of the new phase, while recrystallization of the strained ordered phase may supplement the initial ordering process. Although these phenomena which have their analogs in the precipitation reaction have been rationalized for only Co-Pt alloys, one can well consider them general for alloys of the order-disorder type. In this light the ordering reaction in Vicalloy can be regarded as precipitation of a body-centered cubic phase of somewhat different lattice parameter from the matrix analogous to precipitation in Alnico, while ordering in Co-Pt and Fe-Pt is analogous to precipitation in Cunico and Cunife, since face-centered phases are formed in a face-centered cubic matrix. The one principal difference is that the final equilibrium state of the precipitation process is a two-phase mixture, whereas that of the ordering process is generally a single phase.<sup>7</sup> The optimum magnetic properties, however, are obtained in both cases at some transient step in the process or after a certain degree of partial transformation.

Transformations in solid solutions apparently have certain features in common which should be examined in seeking an explanation of magnetic hardening. First, they all involve the formation of small particles of anisotropic shapes oriented in a discrete manner relative to the crystal lattice of the parent grains in which they form. Second, the crystal lattice of the small particles is homogeneously strained by virtue of coherency with the parent matrix. Both of these factors are consistent with modern theory of ferromagnetism which attributes high coercive force to small particle size (41). This is based on the theory that the formation of domain boundaries is energetically unfavorable in very small particles, and changes in

<sup>7</sup>This is true for the normal ordering temperatures and compositions, but the existence of a two-phase field separating order from disorder in the phase diagram has been established (39).

magnetization must proceed by the relatively difficult process of rotation of the total magnetic moment of the particle rather than by the easy process of domain boundary movement. When the particles are small, coercive force depends on shape, on differences in ease of magnetizing in different crystal directions (magnetocrystalline anisotropy), and on anisotropic straining. The theory was developed to explain the moderately high coercive force of powders of iron and some of its soft alloys when the particle size is in the colloidal range. It can also explain magnetic hardening in alloys where a fine precipitate forms. The basic problem is to decide which of the above three types of anisotropy is the most prominent. The plate-like shape of the precipitate particles and their discrete orientations enhanced further by magnetic aging or cold working favor good permanent magnet properties on the basis that shape anisotropy (without strain) is important. On the other hand, the state of coherency influences the other two types of anisotropy. Magnetocrystalline anisotropy of the strained coherent precipitate is different from that of the incoherent phase, for the crystal symmetry of the former is lower. The crystal lattice of the coherent precipitate is tetragonal rather than cubic and it has only one or two directions of easy magnetization rather than three.

The role of anisotropic strains is also associated with magnetocrystalline anisotropy, but through magnetostriction rather than directly through change in symmetry of the lattice. When a material is magnetized it will dilate in such a manner as to reduce its magnetocrystalline anisotropy energy. If this dilation were hindered by external stresses, a greater energy would be required to reverse the direction of magnetization and the material would be hardened magnetically. Studies of the effect of elastic strains produced by stressing in tension or compression on the magnetization of iron and nickel have shown that this is the case. The paramount difference is that the elastic strains of coherency are many times greater than those which can be imposed by external stressing.

The changes in magnetic properties during aging of materials such as Cunico when correlated with structure favor the strain theory (18). Although hardening occurs during the formation of small plate-like particles of a coherent precipitate, the subsequent pronounced softening is concurrent with relief of the strains through the appearance of the equilibrium phase rather than with any pronounced change in size and shape of the precipitate particles.

In general, however, a clear identification of the controlling factor is not yet possible and much remains to be learned about the



mechanism of magnetic hardening. Results on fine powders cannot yet be accepted by the critical observer as experimental evidence that the particle size of a pure phase alone is an important factor, for the powders generally contained a large percentage of impurities such as oxides, and interfacial strains between the oxide layer and metal particle might well be a contributing factor as their prototype in alloys. Certainly the oxidation product of Fe-Co alloy powders would make a good magnet, since it is the basis of the commercial material, Vectolite. Properties such as magnetostriction of bulk alloys cannot be considered as characteristic of the coherently strained precipitate particle. Likewise, calculations based on the assumption of isotropic properties of pure metals such as iron do not give a very good representation of the properties of a precipitate such as that in Alnico 12 which is unquestionably different from iron in both composition and structure.

The present study of the structures of the commercial permanent magnet materials shows that both fine particles and strains are involved in the reactions in solid solution to which the materials are susceptible. The nature of the strains and their dependency on alloy composition which controls the disregistry between phases are amenable to identification. It is hoped that this study will represent a step toward the goal of designed permanent magnet alloys on the basis of constitution and structure.

#### ACKNOWLEDGMENT

The author wishes to express his appreciation to Miss J. K. Hill for conducting the X-ray diffraction analyses; to the Metallography Group for preparing the micrographs; and to Dr. D. L. Martin for supplying the samples of Vicalloy.

#### References

1. A. J. Bradley, W. F. Cox and H. J. Goldschmidt, "An X-ray Study of the Iron-Copper-Nickel Equilibrium Diagrams at Various Temperatures", *Journal, Institute of Metals*, Vol. 67, 1941, p. 189-201.
2. A. J. Bradley, W. L. Bragg and C. Sykes, "Researches into the Structures of Alloys", *Journal, Iron and Steel Institute*, Vol. 141, 1940, p. 63-142.
3. A. J. Bradley, "X-ray Evidence of Intermediate Stages During Precipitation from Solid Solution", *Proceedings, Physical Society*, Vol. 52, 1940, p. 80-85.
4. A. J. Bradley, et al, "Magnetism", Institute of Physics Monograph, 1938.
5. W. E. Ruder, U. S. Patents 1,947,274 and 1,968,569, 1934.
6. W. Köster, "The System Fe-Ni-Al", *Archiv für das Eisenhüttenwesen*, Vol. 7, 1933, p. 257-262.
7. A. J. Bradley and A. Taylor, "An X-ray Study of the Iron-Nickel-Aluminum System", *Proceedings, Royal Society*, Vol. 166A, 1938, p. 353-375.

8. S. Kuiti, "On the Mechanism of a New Transformation and Some Associated New Reactions in the Iron-Nickel-Aluminum System", Report of the Aeronautical Research Institute, Tokyo Imperial University, Vol. 15, 1940, p. 601-720. See also *ibid.*, Vol. 14, 1939, p. 563-580; Vol. 16, 1941, p. 167-204, 271-298.
9. W. Dannöhl, "The Equilibrium Diagram of the Iron-Nickel-Aluminum System", *Archiv für das Eisenhüttenwesen*, Vol. 15, 1942, p. 321-330.
10. A. H. Geisler, "Precipitation from Solid Solutions of Metal", Cornell Conference National Research Council, 1948.
11. W. Köster and W. Dannöhl, "Precipitation Hardening of Gold-Nickel Alloys", *Zeitschrift für Metallkunde*, Vol. 28, 1936, p. 248-253.
12. A. H. Geisler, "Structure and Properties of the Permanent Magnet Alloys", *Electrical Engineering*, Vol. 69, 1950, p. 37-44.
13. W. Köster, "The System Fe-Co-Al", *Archiv für das Eisenhüttenwesen*, Vol. 7, 1933, p. 263-264.
14. O. S. Edwards, "An X-ray Study of the Al-Co-Fe System", *Journal, Institute of Metals*, Vol. 67, 1941, p. 67-77.
15. J. Schramm, "The Ternary System Ni-Co-Al", *Zeitschrift für Metallkunde*, Vol. 33, 1941, p. 403-412.
16. R. Vogel and H. J. Wallbaum, "The System Fe-Ni-Ni<sub>3</sub>Ti-Fe<sub>3</sub>Ti", *Archiv für das Eisenhüttenwesen*, Vol. 12, 1938, p. 299-304.
17. W. Köster and W. Geller, "The System Fe-Co-Ti", *Archiv für das Eisenhüttenwesen*, Vol. 8, 1935, p. 471-472.
18. A. H. Geisler and J. B. Newkirk, "Mechanisms of Precipitation in a Permanent Magnet Alloy", *Transactions, American Institute of Mining and Metallurgical Engineers*, Vol. 180, 1949, p. 101-120.
19. A. J. Bradley and H. I. Goldschmidt, "An X-ray Study of Slowly Cooled Fe-Cu-Al Alloys. I—Alloys Rich in Fe and Cu", *Journal, Institute of Metals*, Vol. 65, 1939, p. 389-418.
20. A. J. Bradley and H. Lipson, "An X-ray Investigation of Slowly Cooled Cu-Ni-Al Alloys", *Proceedings, Royal Society*, Vol. 167A, 1938, p. 421-438.
21. W. D. Alexander, "Cu-Rich Ni-Al-Cu Alloys. II—The Constitution of the Cu-Ni-Rich Alloys", *Journal, Institute of Metals*, Vol. 63, 1938, p. 163-183.
22. W. Köster and W. Dannöhl, "The System Cu-Ni-Fe", *Zeitschrift für Metallkunde*, Vol. 27, 1935, p. 220-226.
23. W. Dannöhl and H. Neumann, "Permanent Magnet Alloys of Cobalt, Copper and Nickel", *Zeitschrift für Metallkunde*, Vol. 30, 1938, p. 218-231.
24. K. E. Volk, W. Dannöhl and G. Masing, "The Precipitation Process in Cobalt-Copper-Nickel Alloys in the Solid State", *Zeitschrift für Metallkunde*, Vol. 30, 1938, p. 113-122.
25. H. Neumann, A. Büchner and H. Reinboth, "Mechanically Soft Permanent Magnet Alloys of Copper, Nickel and Iron", *Zeitschrift für Metallkunde*, Vol. 29, 1937, p. 173-185.
26. H. G. Müller, "A Permanent Magnet Alloy with Anisotropic Magnetic Properties", *Zeitschrift für Elektrochemie*, Vol. 45, 1939, p. 674-678.
27. V. Danial and H. Lipson, "An X-ray Study of the Dissociation of an Alloy of Copper, Iron and Nickel", *Proceedings, Royal Society*, Vol. 181A, 1943, p. 368-378; Vol. 182A, 1944, p. 378-387.
28. H. Potter, "Some Magnetic Alloys and Their Properties", *Philosophical Magazine*, Vol. 12, 1931, p. 255-264.
29. E. Persson, "Structure of Heusler Alloys", *Zeitschrift für Physik*, Vol. 57, 1929, p. 115-133.
30. A. J. Bradley and J. W. Rodgers, "The Crystal Structure of the Heusler Alloys", *Proceedings, Royal Society*, Vol. 144A, 1934, p. 340-359.

31. J. K. Stanley, "Metallurgy and Magnetism", published by the American Society for Metals, 1949, p. 67, 118.
32. J. L. Snoek, "New Developments in Ferromagnetic Materials", *Elsevir*, 1947.
33. Y. Kato and T. Takei, "Metal Oxide Magnet", *Journal, Society of Chemical Industry, Japan*, Vol. 36, 1933, p. 172-173.
34. R. J. Studders, "Permanent Magnets of Sintered Oxide", *Product Engineering*, February 1948, p. 120-122.
35. E. A. Nesbitt, "Vicalloy—A Workable Alloy for Permanent Magnets", *Transactions, American Institute of Mining and Metallurgical Engineers*, Vol. 166, 1946, p. 415-425.
36. W. Köster and K. Lang, "The Cobalt Corner of the System Iron-Cobalt-Vanadium", *Zeitschrift für Metallkunde*, Vol. 30, 1938, p. 350.
37. W. C. Ellis and E. S. Greiner, "Equilibrium Relations in the Solid State of the Iron-Cobalt System", *TRANSACTIONS, American Society for Metals*, Vol. 29, 1941, p. 415-432.
38. E. Gebhardt and W. Köster, "The Platinum-Cobalt System with Particular Consideration of the CoPt Phase", *Zeitschrift für Metallkunde*, Vol. 32, 1940, p. 253-261.
39. J. B. Newkirk, et al, "The Ordering Reaction in Cobalt-Platinum Alloys", *Transactions, American Institute of Mining and Metallurgical Engineers*, Vol. 188, 1950, p. 1249-1260.
40. H. Lipson, D. Schoenberg and G. V. Stupart, "The Relation Between Atomic Arrangement and Coercivity in an Alloy of Iron and Platinum", *Journal, Institute of Metals*, Vol. 67, 1941, p. 333-339.
41. C. Kittel, "Physical Theory of Ferromagnetic Domains", *Review of Modern Physics*, Vol. 21, 1949, p. 541-583.

### DISCUSSION

**Written Discussion:** By C. Kittel, visiting associate professor of physics, University of California, Berkeley, Calif.

The beautiful experimental results on the microstructure of Alnico 5 presented in this paper appear to be in agreement with the predictions of recent theoretical work.\* It may be remarked that the anisotropy of the demagnetizing energy may be expected to exceed considerably the anisotropy of the magnetostrictive energy, so that the former cause is the more likely explanation of the response of Alnico 5 to heat treatment in a magnetic field. The demagnetizing effect may amount to

$$(1/2) N (\Delta M_s)^2 \approx (2\pi) (500)^2 \approx 1.5 \times 10^6 \text{ e-rgs/cc}$$

whereas the magnetostrictive effect can only be of the order of

$$(1/2) c e^2 \approx 10^{12} (5 \times 10^{-5})^2 \approx 2.5 \times 10^3 \text{ ergs/cc}$$

Here  $N$  = demagnetizing factor;  $M_s$  = saturation magnetization;  $c$  = elastic modulus;  $e$  = strain.

**Written Discussion:** By J. E. Goldman and R. Smoluchowski, Carnegie Institute of Technology, Pittsburgh.

Dr. Geisler's work is a welcome addition to the literature of permanent magnet materials. Many voids still exist in our knowledge of the physics of these materials and the source of their high coercive properties. Only by work of this sort coupled with theoretical analysis of the fun-

\*C. Kittel, E. A. Nesbitt and W. Shockley, "Theory of Magnetic Properties and Nucleation in Alnico 5", *Physical Review*, Vol. 77, 1950, p. 839.



damental nature of coercive force can we hope to understand these mysteries.

Dr. Geisler has called attention to the various types of magnetic energy which could influence the nucleation process in Alnico 5. The writers have recently proposed a theory<sup>9</sup> for the Alnico 5 effect in which a preferred orientation of the precipitated particles is suggested as arising from the anisotropic elastic energy of the nuclei in a magnetic field due to magnetostriction. Analysis of the quaternary diagram discussed by Dr. Geisler indicates that the composition of the precipitated phase is approximately 30% cobalt with the balance iron. Measurements of the magnetostriction in single crystals of an alloy of this composition have been made<sup>10</sup> and indicate its value to be a minimum in the [100] direction. If one may extrapolate these results as measured at room temperature to the nucleation temperature, one is led to the conclusion that nuclei, whose [100] axes are reasonably close to the direction of the field present during cooling, have a lower elastic energy than others and hence will grow preferentially. Since the [100] direction is also the direction of easy magnetization in this alloy, the precipitated particles maintain this direction (of the cooling field) as the preferred direction of magnetization. The greatest influence would thus be upon the remanence in agreement with observation. One is able, with this mechanism, to explain other unusual characteristics of this alloy, such as the extreme sensitivity of the entire effect to small changes in composition.

We wish to make another point concerning the role of order in influencing such magnetic properties as the coercive force to which Dr. Geisler has alluded briefly. It has been the opinion of the writers<sup>11</sup> that in many magnetic alloy systems the state of order can exert a great deal of influence on such properties as coercive force through its effect not so much on the state of internal strain as by the role it plays in influencing crystal anisotropy and magnetostriction. In an iron-cobalt alloy in which, according to Geisler, the ordering reaction may be the critical factor in determining the properties of Vicalloy, we have found that the magnetostriction is increased by 50% on ordering.<sup>12</sup> Since, according to the presently accepted theories, magnetostriction and coercive force are closely related, this observation tends to support Geisler's proposal, although further examination of the system seems desirable.

#### Author's Reply

I wish to thank Dr. Kittel and Drs. Goldman and Smoluchowski for their contributions. Both discussions pertain to the preferential nucleation of certain orientations of the precipitate in Alnico 5 induced by an applied field; however, somewhat conflicting viewpoints on the cause of the phenomenon are presented. Agreement apparently exists only in

<sup>9</sup>J. E. Goldman and R. Smoluchowski, "Theory of Magnetic Anisotropy in Alnico 5", *Physical Review*, Vol. 80, Oct. 15, 1950, p. 302.

<sup>10</sup>J. E. Goldman, "Single Crystal Magnetostriction Constants of an Iron-Cobalt Alloy", *Physical Review*, Vol. 80, Oct. 15, 1950, p. 301.

<sup>11</sup>J. E. Goldman, "The Influence of Atomic Order on Magnetic Properties", *Journal of Applied Physics*, Vol. 20, 1949, p. 1131.

R. Smoluchowski, Proceedings of the Grenoble Conference on Magnetism, to be published, 1950.

<sup>12</sup>J. E. Goldman and R. Smoluchowski, "Magnetostriction and Order-Disorder", *Physical Review*, Vol. 75, 1949, p. 140.

attributing the anisotropic properties of commercial Alnico 5 to a preferred orientation of the plate-like precipitate particles as suggested earlier by the author (Ref. 12 of the paper).

The rough calculations by Dr. Kittel would seem to suggest that the anisotropy of the demagnetizing energy is more likely responsible for the preferred nucleation of certain orientations of the precipitate. As pointed out in the paper, however, this explanation does not appear to be sufficient, for the anisotropy of demagnetization energy which originates in the plate-like shape of the precipitate obtains for all precipitation alloys, but only certain ones are susceptible to the magneto-thermal treatment.

On the other hand, the explanation proposed by Drs. Goldman and Smoluchowski is similar to that of the author in that the anisotropic strain energy of the nuclei and magnetostriction are involved. According to their explanation, the direction of minimum elastic strain energy due to magnetostriction—the  $\langle 100 \rangle$  directions in the precipitate—develop preferentially parallel to the direction of the field during cooling. The relation of particle shape orientation to field direction is not clear, however, for there are  $\langle 100 \rangle$  directions both in the lateral directions as well as in the thickness direction of the plate-like precipitate particles.

It is apparent that the magnetic energy contribution to change in free energy for nucleation of precipitation is not sufficient to change the inherent nature of the process. The habit plane remains  $\{100\}$  and the  $\langle 100 \rangle$  directions in the precipitate remain parallel to  $\langle 100 \rangle$  directions of the matrix. Thus, one must look at terms in the expression for the usual change in free energy for nucleation of the precipitate which could be affected slightly by magnetic energy. One such term is the strain energy. This is already an anisotropic property; compressive strains are involved in the habit plane of the coherent iron-rich precipitate and a tensile strain occurs normal to the habit plane in the thickness direction of the plate-like particles. In the absence of all magnetic fields, the situation is the same for each of the three orientations of the plates. When a field is applied along a  $[100]$  direction, magnetostriction of positive sign (tensile strain) in the matrix would reduce the required compressive strains for precipitation of particles which contain the field direction in their planar expanse. In this way the magnetostriction energy would alter the strain energy for the differently oriented particles; it could lead to a lowered strain energy for two orientations and an increased strain energy for the third or suppressed orientation.

Goldman and Smoluchowski have done some nice work on the measurement of magnetostriction. Contrary to other workers who have attempted to discount the role of this property on the basis of measurements on polycrystalline samples of the heterogeneous alloy, they have undertaken the extra effort to make their measurements on single crystals and to specify compositions simulating the precipitate rather than the bulk alloy. This is the best that the precipitate can be synthesized for a study of its properties, but perhaps it is not good enough; the synthetic product has a cubic structure, while the precipitate has a tetragonal structure due to coherency strains. These homogeneous strains would also be expected to contribute to the properties of the precipitate.

While the properties of the ordered phase referred to in the con-

cluding paragraph of the remarks by Goldman and Smoluchowski must be considered in comparing various alloys, basically they alone are not the source of coercive force. The 50% increase in magnetostriction on ordering an iron-cobalt alloy does not produce a high coercive force, since the fully ordered alloy is a good, soft, magnetic material. The coercive force of the ordering cobalt-platinum alloys goes through a maximum in the course of ordering and approaches zero as ordering approaches completion. Thus, the coercive force becomes significant only at some intermediate stage of ordering when the ordered phase is present as a precipitate in a matrix of the disordered phase. This requirement of a heterogeneous structure with interfacial strains is the whole thesis which has been developed from a study of the structure of permanent magnet alloys. On the other hand, the relative degree of hardening between various permanent magnet alloys may well depend upon the properties of the precipitate, its disregistry with the matrix at equilibrium (strain), its magnetostriction, its shape, and its magneto-crystalline anisotropy. These are the properties which will have to be investigated in order to understand why the addition of vanadium to iron-cobalt makes hard magnetic materials from a soft base alloy.



## MOLYBDENUM PLATING BY REDUCTION OF THE PENTACHLORIDE VAPOR

BY W. J. CHILDS, J. E. CLINE, W. M. KISNER AND JOHN WULFF

### *Abstract*

*In this investigation the plating of molybdenum by the hydrogen reduction of molybdenum pentachloride vapor was studied. A coarse-grained structure of the molybdenum, deposited at pressures of 20 millimeters of mercury or lower and in the temperature range 800 to 1100 °C (1470 to 2010 °F), was found to have the best physical properties. The effect of interdiffusion between molybdenum and various basis metals on the adhesion of the plate was investigated. An excellent bond was formed when molybdenum was deposited on nickel at 950 °C (1740 °F).*

MOLYBDENUM possesses a wide variety of useful properties, both physical and chemical. Among the more useful properties are its high melting point, 2625 °C (4725 °F), its resistance to chemical corrosion and its high temperature strength. There are many possible objectives, therefore, that might be realized by coating other metals or alloys with an adherent nonporous layer of molybdenum of adequate thickness.

A coating of molybdenum on other metals or alloys may be useful in some applications where the surface of an object is raised to excessively high temperatures, causing failure due to progressive attack initiated at the heated surface although the interior remains at a lower temperature. In a similar manner a molybdenum coating would be expected to confer corrosion resistance in many types of gaseous or liquid media. Molybdenum-coated articles could well be used as an economical substitute for those made entirely of molybdenum, and in some cases the physical properties may be superior to those of pure molybdenum. Since the fabrication of molybdenum is rendered difficult by the metal working which is necessary to impart adequate ductility, a further advantage may well be realized in the molybdenum coating of a basis metal which can be more easily fabricated.

A paper presented before the Thirty-second Annual Convention of the Society, held in Chicago, October 21 to 27, 1950. Of the authors, W. J. Childs is associate professor of metallurgy, Lafayette College, Easton, Pa.; J. E. Cline is physical chemist, Division of Industrial Cooperation; W. M. Kisner is research assistant, Department of Metallurgy, and John Wulff is professor of metallurgy, Massachusetts Institute of Technology, Cambridge, Mass. Manuscript received April 19, 1950.

There have been many suggested methods of the electro-deposition of molybdenum in the literature (1),<sup>1</sup> but as yet there has been no definite support for these claims. Since no industrial applications of the methods of electroplating molybdenum have been made, it seems reasonable to assume that a practical method for electrodeposition of a molybdenum plate of adequate quality has not yet been developed. According to Lander and Germer (2), pure molybdenum has not been electroplated successfully.

Molybdenum coatings have been applied by sputtering (3), but the process is very complex and long periods of time are required to obtain only very thin deposits. According to Cartwright and Strong (4), evaporation is much easier and requires less time than sputtering, but the boiling point of molybdenum is too high for this process to be of practical importance.

Coatings of some metals have been obtained (5, 6) by the thermal decomposition or the hydrogen reduction of a volatile compound of the metal. For example, iron, nickel, tungsten, and molybdenum can be deposited from the corresponding carbonyls; titanium, zirconium and chromium from the iodides; and tantalum, molybdenum and columbium from the volatile chlorides. In such methods a volatile compound of the metal is passed over the piece to be coated, which is heated to a temperature high enough to decompose or reduce the volatile compound and to form a coating on the surface. The by-products of the reaction can be removed by a vacuum pump or by a stream of carrier gas. In many cases a coating can be applied in this way at a temperature well below the melting point of the metal or at a temperature at which the vapor pressure of the metal is negligible.

Lander and Germer (2) have investigated very thoroughly the deposition of molybdenum on steel by decomposition of the carbonyl. In this process it was found necessary to keep the plating temperature below 800 °C (1470 °F) and the pressure below 0.1 millimeter of mercury. Higher pressures and temperatures caused excessive gas-phase decomposition with the formation of colloidal particles, producing a powdery or a poorly-coherent coating. An X-ray diffraction study showed that these deposits contained the hexagonal carbide,  $\text{Mo}_2\text{C}$ , which is formed only in the gas phase. Any coating that contained even a small amount of this carbide was found to lack strength. Coatings from the carbonyl process as soft as 300 Vickers were obtained by plating at 600 °C (1110 °F) in wet hydrogen and as hard as 1560 Vickers by plating at 450 °C (840 °F)

<sup>1</sup>The figures appearing in parentheses pertain to the references appended to this paper.

in dry hydrogen. Plating of molybdenum from the carbonyl was found to be rather slow; the maximum rate obtained was 0.0022 inch per hour.

#### STUDY OF PLATING PROCEDURE

In this investigation the plating of molybdenum by the hydrogen reduction of molybdenum pentachloride vapor was studied. The apparatus was designed so that the following six plating variables could be controlled: temperature of the specimen, rate of flow of the vapor, pressure of the vapor, composition of the vapor, duration of the coating process and the composition of the basis material. In the apparatus constructed, the range of pressures was from  $10^{-5}$  millimeters of mercury to atmospheric, and the maximum temperature of the specimen was  $1100^{\circ}\text{C}$  ( $2010^{\circ}\text{F}$ ).

The molybdenum pentachloride used in this investigation was prepared by passing chlorine over powdered molybdenum metal at  $300^{\circ}\text{C}$  ( $570^{\circ}\text{F}$ ). The apparatus was constructed entirely of glass and so designed that the molybdenum pentachloride could be prepared, resublimed and transferred to the plating apparatus without coming in contact with the atmosphere. By this technique chlorine and oxychlorides of molybdenum were removed from the pentachloride, and reaction with moisture in the atmosphere was prevented.

The apparatus for plating molybdenum on small specimens is shown in Fig. 1. The sealed capsule containing the resublimed pentachloride was attached to the apparatus, and a magnetically-operated hammer, made of iron enclosed in glass, was placed in position to open the capillary seal when necessary. That part of the apparatus between the two stopcocks could then be evacuated and tested for leaks with a high-frequency discharge.

The pressure head of the incoming hydrogen was maintained at 13 millimeters of mercury by a pressure stabilizer consisting of a glass piston fitting loosely in a glass cylinder. A similar stabilizer constructed of metal has been previously described (7). The flow-meter, shown in Fig. 1, contained dibutyl phthalate as manometer liquid and calibrated in liters per hour at atmospheric pressure. The hydrogen was passed through copper gauze at  $500^{\circ}\text{C}$  ( $930^{\circ}\text{F}$ ) to remove any oxygen. The rate of flow of the hydrogen was controlled by stopcock 1. Water vapor or any other condensable impurities were removed from the hydrogen in trap 1, which was immersed in liquid nitrogen.

To introduce the molybdenum pentachloride into the vapor



stream the capillary seal was broken by the magnetically-operated hammer. The pentachloride was then sublimed into the hydrogen stream by raising the temperature of the heater to about 85 °C above that of the oil thermostat. In this way some of the pentachloride was removed from the vapor in the tubing immersed in the oil thermostat, and the vapor mixture then contained the equilibrium partial pressure of pentachloride. From the thermostat

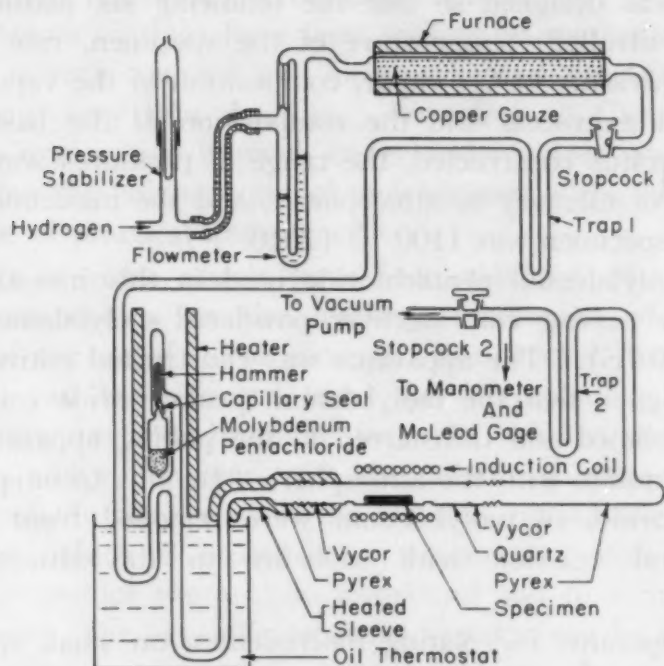


Fig. 1—Apparatus for Vapor Deposition Plating.

temperature the partial pressure of the pentachloride was then determined using the following equation derived from rough measurements in this laboratory:

$$\log P = -5210/T + 13.1$$

where  $P$  is the partial pressure of molybdenum pentachloride over the solid in millimeters of mercury, and  $T$  is the absolute temperature (°K).

Between the thermostat and the plating zone a heated sleeve was used to prevent precipitation of the pentachloride. The specimen to be plated was placed in a fused-quartz tube which was connected at both ends to Vycor glass. The Vycor tubes were connected to the Pyrex portion of the apparatus through Vycor-Pyrex seals.

The specimen was heated by a high-frequency induction coil operating from a spark generator. The temperature of the specimen was determined by an optical pyrometer in the range above 800 °C

(1470 °F). Below this, the temperature was controlled by the current in the induction coil, using a calibration chart. To avoid contamination of the vacuum pump, the products of the plating reaction were condensed out in trap 2.

It was soon found that the pressure of the vapor mixture had a very strong influence on the molybdenum plate. At atmospheric pressure, it was necessary to keep the partial pressure of the pentachloride below 1.5 millimeters to avoid excessive formation of powdery, nonadherent deposits. Under these conditions molybdenum coatings could be obtained at temperatures as low as 500 °C (930 °F), but only very slow rates of plating were achieved.

At pressures of 20 millimeters of mercury and lower, molybdenum plates were obtained from 800 to 1100 °C (1470 to 2010 °F), and no difficulty was experienced with powder formation. The partial pressure of hydrogen was generally about 10 times that of the pentachloride, leaving a large excess of hydrogen over that required for complete reduction to the metal. At a pressure of 5 millimeters a plating rate of 0.020 inch per hour was reached at 900 °C (1650 °F), and a rate of 0.005 inch per hour at 800 °C (1470 °F).

In order to learn more about the possible intermediate steps in the deposition of molybdenum, a series of experiments was performed in which vapor mixtures of hydrogen and molybdenum pentachloride at atmospheric pressure and at 20 millimeters were passed through a quartz tube at temperatures increased in 50-degree steps. At the lower pressure, the vapor entered the tube at 200 °C (390 °F), and no reaction was observed until the temperature had reached 350 °C (660 °F). In the temperature range 350 to 600 °C (660 to 1110 °F), a brown deposit of molybdenum tetrachloride was found in the cooler tube following the reaction zone, but no deposit was found in the heated zone itself. The vapor pressure of the tetrachloride, although lower than that of the pentachloride, is evidently high enough to prevent precipitation above 350 °C (660 °F). On increasing the temperature of the quartz tube to 650 °C (1200 °F) a metallic deposit of molybdenum was formed as a mirror.

At atmospheric pressure quite different results were obtained. At low gas flows a red deposit of molybdenum trichloride was deposited in the heated zone at temperatures above 350 °C (660 °F). As the rate of gas flow was increased the temperature of the initial deposit of trichloride increased up to 550 °C (1020 °F). At this temperature and above, metallic molybdenum was deposited.

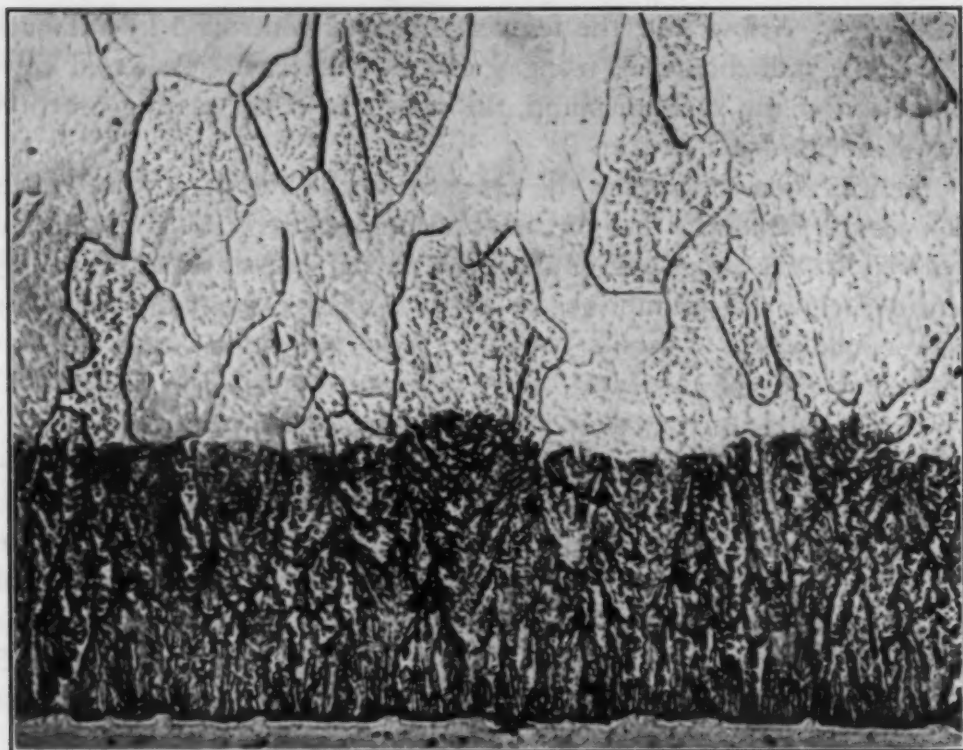


Fig. 2—Coarse-Grained (Upper Layer) and Fine-Grained (Lower Layer) Deposits of Molybdenum.  $\times 500$ .

It seems evident that the elimination of the tendency to deposit the trichloride at the lower pressures is closely related to the elimination of the powder formation. Possibly at the higher pressures the gas phase reaction to form particles of the trichloride leads to formation of nuclei of molybdenum metal on which fine powdery deposits can grow. For a more complete understanding of the mechanism of the plating reaction, a thorough study of the thermodynamics of the lower chlorides of molybdenum might be helpful.

#### STRUCTURE OF THE PLATE

Formation of a nonadherent black powder was often observed when the concentration of molybdenum pentachloride in the vapor or the total pressure of the vapor phase was too high. The atomic ratio of Cl:Mo was shown by chemical analysis to be only 0.089, and the X-ray diffraction pattern showed only lines corresponding to metallic molybdenum. These lines were quite broad, due probably to the fine particle size. After a 2-hour hydrogen anneal at  $900^{\circ}\text{C}$  ( $1650^{\circ}\text{F}$ ), the powder assumed a gray metallic appearance and gave an X-ray diffraction pattern with sharper lines, also agreeing with those of molybdenum. It is believed from these results



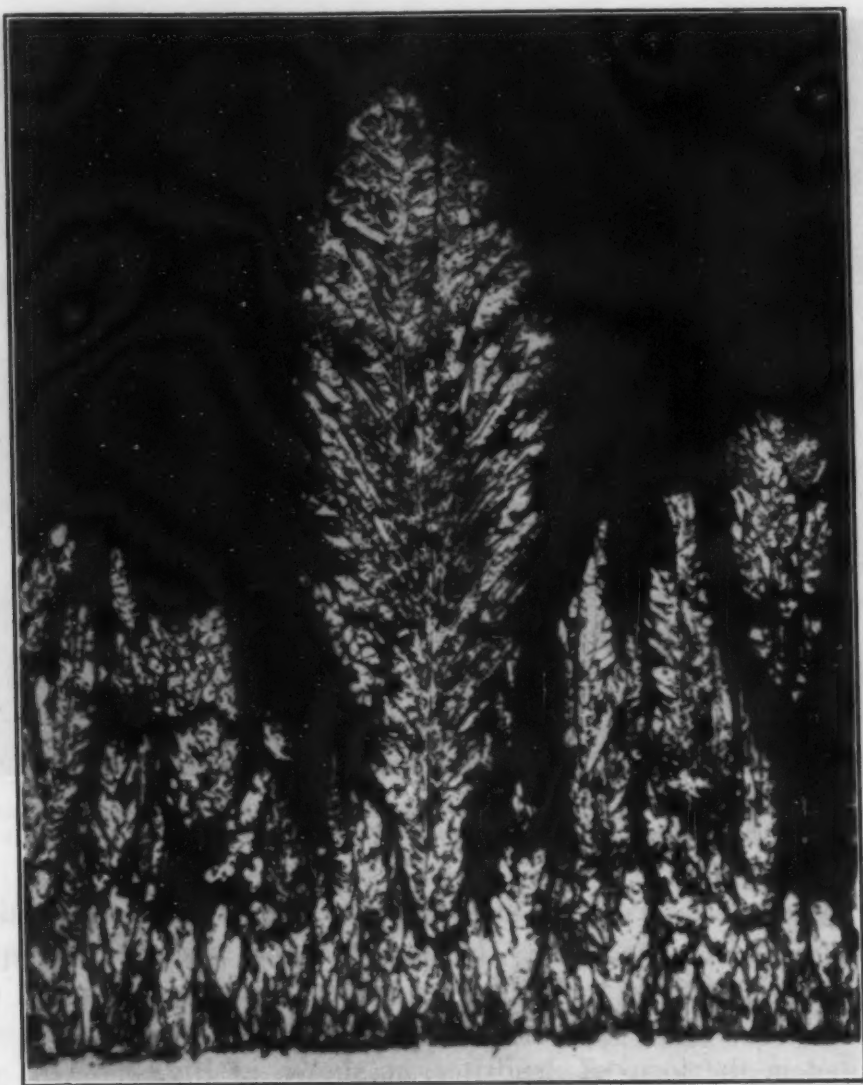


Fig. 3—Molybdenum Deposited in the Form of Dendrites.  $\times 500$ .

that the black powder is finely-divided molybdenum metal with small amounts of a lower chloride of molybdenum as an impurity.

Three distinct types of structure were found in molybdenum coatings deposited under different conditions. These structures are referred to in this work as: (a) fine-grained, (b) coarse-grained and (c) laminated. The fine-grained molybdenum was deposited at the lower temperatures, about  $600^{\circ}\text{C}$  ( $1110^{\circ}\text{F}$ ). The coarse-grained deposit was formed at temperatures of about  $850^{\circ}\text{C}$  ( $1560^{\circ}\text{F}$ ) and higher and at total pressures below 25 millimeters of mercury. Both types of plate can be compared in Fig. 2, showing a cross section of a coating which was deposited under two different sets of conditions so that the fine-grained deposit was overlaid by a coarse-grained one. It is seen that the fine-grained molybdenum is

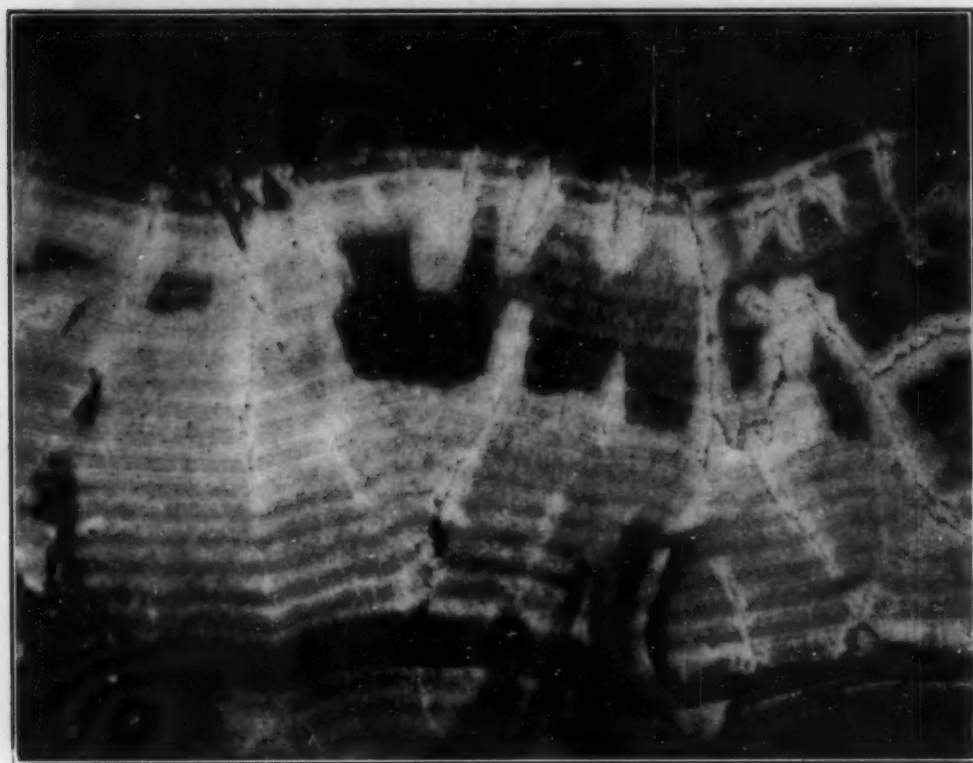


Fig. 4—Deposition of Molybdenum on Pyrex at 650 °C (1200 °F) Showing a Laminated Structure and More Complete Reduction Around the Cracks.  $\times 500$ .

more easily attacked by the etchant (potassium ferricyanide—potassium hydroxide). This indicates that the fine-grained deposit contains an impurity, quite likely a lower chloride, as in the case of the black powder deposits. Occasionally the molybdenum was deposited in the form of dendrites, as shown in Fig. 3. This may well represent a borderline condition between deposits of black powder and the fine-grained deposit.

When the plating conditions were intermediate between those that produced a fine-grained deposit and those that produced a coarse-grained deposit, it was found that a laminated structure was produced, as shown in Fig. 4. The darker, more easily etched areas are apparently not so completely reduced as the lighter areas. It is interesting to note that lighter areas surround the cracks in the deposit where hydrogen could more easily diffuse into the coating and the gaseous products of the reduction could more easily diffuse out. On annealing the laminated type of plate in hydrogen for 2 hours at 970 °C (1780 °F) a recrystallized, completely reduced molybdenum coating was obtained. However, since the reduced structure contained some voids at the grain boundaries, the mechanical properties were still unsatisfactory.

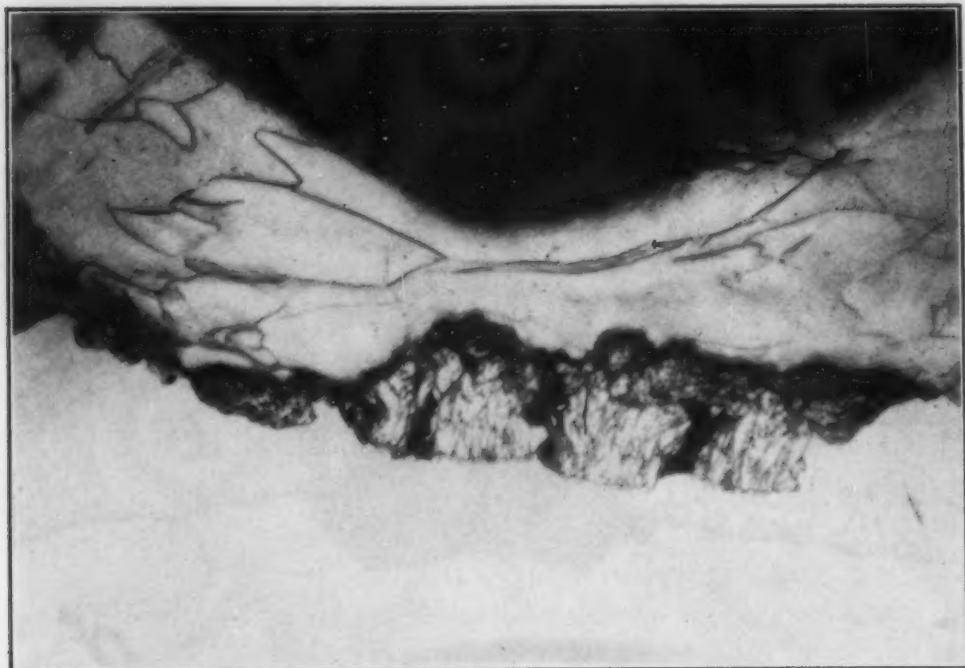


Fig. 5—Effect of Chisel Impression on Coarse-Grained and Fine-Grained Deposits of Molybdenum.  $\times 500$ . Upper light zone deformed, coarse-grained molybdenum; center zone fine-grained molybdenum; lower zone nickel.

Of the three types of structure, the coarse-grained deposits had the best properties. The superior ductility of the coarse-grained deposit was demonstrated by driving a chisel into the plate containing both coarse- and fine-grained coatings. As can be seen in Fig. 5, the originally columnar grains of the coarse-grained deposit were greatly distorted by this test. The fine-grained deposit, on the other hand, was broken up into a number of smaller sections, and there is no indication of plastic deformation. Similarly, in measurements of hardness, a series of cracks radiated out from the impression made in the fine-grained deposit. The hardness of the coarse-grained deposit of molybdenum was about 230 Knoop, while that of the fine-grained deposit varied between 220 and 340 Knoop, depending on the coherence of the plate.

Even in the coarse-grained deposit the strength was better in compression than in tension. For example, when a molybdenum-coated specimen was bent with the molybdenum on the outside of the bend, the tensile forces caused the plate to crack along the grain boundaries, as shown in Fig. 6. It was believed that the columnar structure decreased the strength of the plate in tension, and some attempts were made to improve the structure by cold working the plate followed by an anneal to cause recrystallization. Due to the brittleness of the plate, sufficient cold working was not obtained.



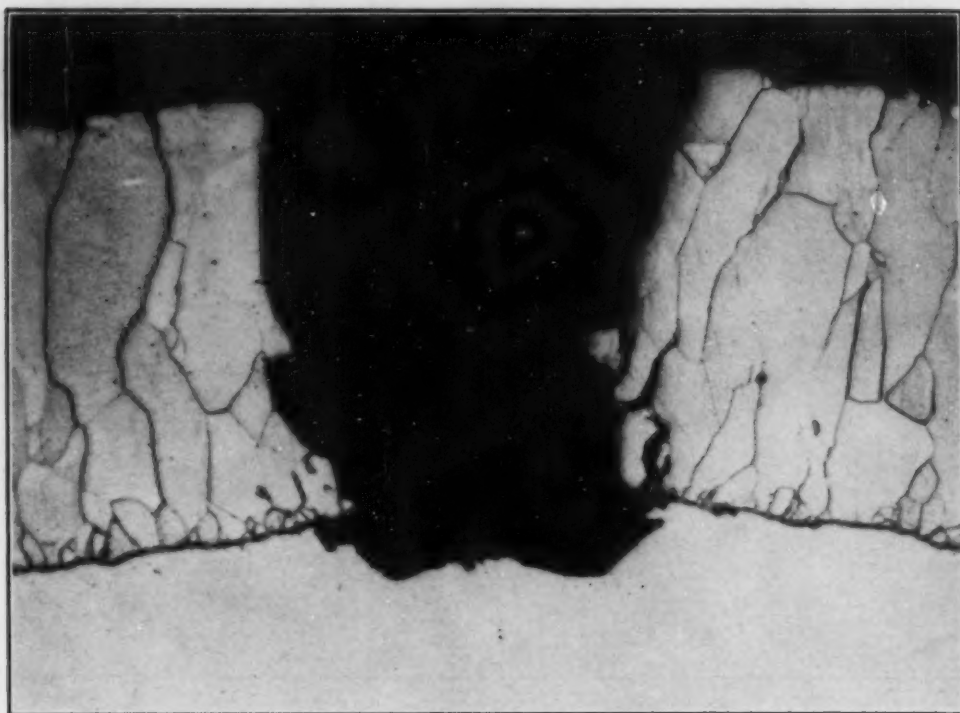


Fig. 6—Specimen of Molybdenum Deposited on Nickel at 900°C (1650°F) After Test in Bending Jig.  $\times 500$ .

Hot working the plate may offer a better opportunity for improvement of the structure.

The lattice parameter of the coarse-grained deposit, determined by X-ray diffraction, was found to be the same as that of pure molybdenum. The density of the plate, 10.2, also agreed with that of molybdenum.

#### ADHESION OF THE PLATE

In applications where the molybdenum-coated article must withstand mechanical or thermal stresses, the adhesion of the molybdenum to the basis metal is of utmost importance. As a qualitative test for adhesion, the plated specimen,  $\frac{1}{8}$  inch thick, was bent to an angle of 90 degrees with the coating on the outside. The tendency of the plate to spall off was then observed. Although cracking of the coating under the tensile stresses always took place, no spalling of the plate was observed in the most favorable cases. Since the bending test was believed adequate for determining the relative degree of adhesion of the molybdenum coating on the various basis metals, no attempt was made to reduce the results to a quantitative measure of the adhesion.

The cleanliness of the metal to be coated was not found to be a determining factor in securing adequate adhesion. The specimens

were cleaned with emery paper and given a preliminary treatment at the plating temperature with hydrogen to reduce surface oxides. Intimate contact of the molybdenum coating with the basis metal was indicated by the absence of voids or inclusions at the interface and by interdiffusion between the molybdenum and the basis metal. Although in some cases a rough finish of the basis metal gave slightly better adhesion of the plate than a smooth finish, it was found that the most important factors in securing good adhesion were the kind of basis metal and the amount of interdiffusion with the molybdenum deposit.

The main factors influencing the amount of diffusion which will occur are the diffusion coefficients at the temperature of the plating operation and the duration of the plating. The diffusion coefficients at a given temperature depend to a large extent on the solubility of the metals in one another. No diffusion can take place if the metals are completely insoluble. As diffusion progresses, any intermediate phases which are present in the phase diagram of the binary system will appear as distinct layers. If there is sufficient time for the diffusion to proceed, these intermediate layers will be thick enough to be identified metallographically in the interface (8).

Fig. 7 shows the structure of the diffusion zone between low carbon steel and a molybdenum coating which had been deposited at 900 °C (1650 °F) for 35 minutes. The phase diagram of the iron-molybdenum system at this temperature shows two terminal solid solutions and one intermetallic phase, epsilon corresponding to  $\text{Fe}_3\text{Mo}_2$  (9). The epsilon phase, approximately 0.0002 inch in thickness, is clearly visible in the photomicrograph in Fig. 7. The molybdenum-rich terminal solid solution, or eta phase, is more difficult to detect, since it etches similarly to pure molybdenum. The molybdenum has diffused into the iron about 0.003 inch to produce the iron-rich solid solution, the alpha phase.

It was found that the brittle intermetallic epsilon phase was the cause of poor adhesion in molybdenum deposited on iron or steel. Separation of the plate from the basis metal, due either to thermal stresses set up on cooling the material from plating temperature or to mechanical stresses, took place in the layer of intermetallic phase. Although, in the case of iron, poor adhesion was caused by too much diffusion and the formation of too thick a layer of intermetallic phase, in the case of copper, poor adhesion of the molybdenum coating resulted from lack of sufficient diffusion.

The bond between nickel and molybdenum was found to be much stronger. On metallographic examination of the interface,

evidence of the formation of at least one intermediate phase was found. The phase diagram (10) for the molybdenum-nickel system shows only one intermetallic phase existing above 890 °C (1635 °F), the delta phase corresponding to NiMo. Below this temperature two other intermediate phases with lower molybdenum content are

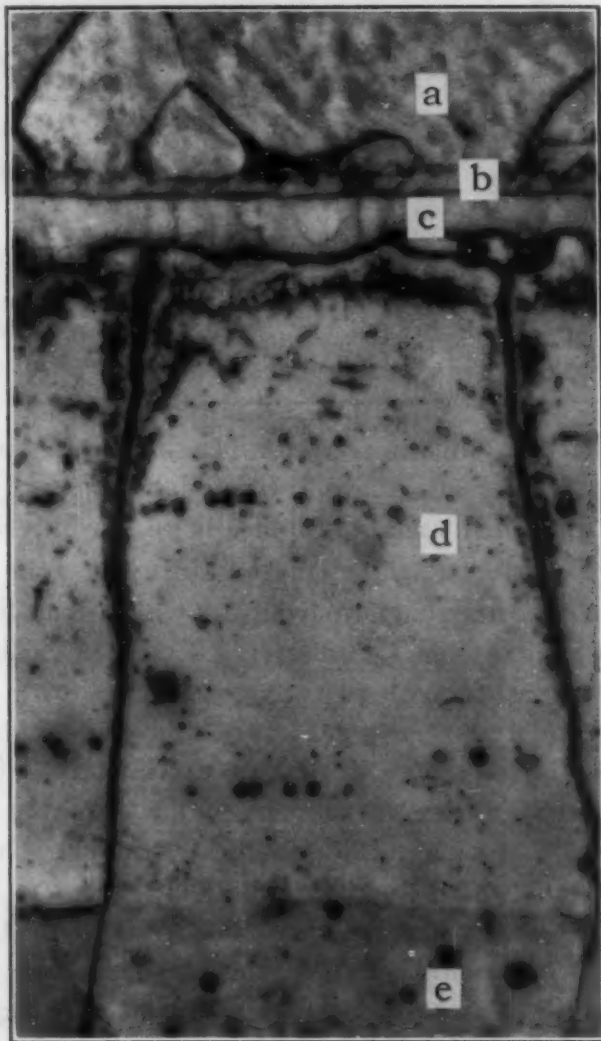


Fig. 7—Molybdenum on Low Carbon Steel, Plated at 900 °C (1650 °F) for 35 Minutes.  $\times 1000$ . (a) Molybdenum; (b) Eta phase; (c) Epsilon phase; (d) Alpha phase; (e) Steel.

present. In Fig. 8 a cross section of molybdenum deposited on nickel at 900 °C (1650 °F) is shown. The thickness of the intermetallic phase is about 0.00004 inch, or about  $1/5$  the thickness of the molybdenum-iron intermetallic phase. To test the bond, a specimen of nickel  $1/8$  inch thick and plated with 0.004 inch of molybdenum was bent 90 degrees with the coating on the outside.



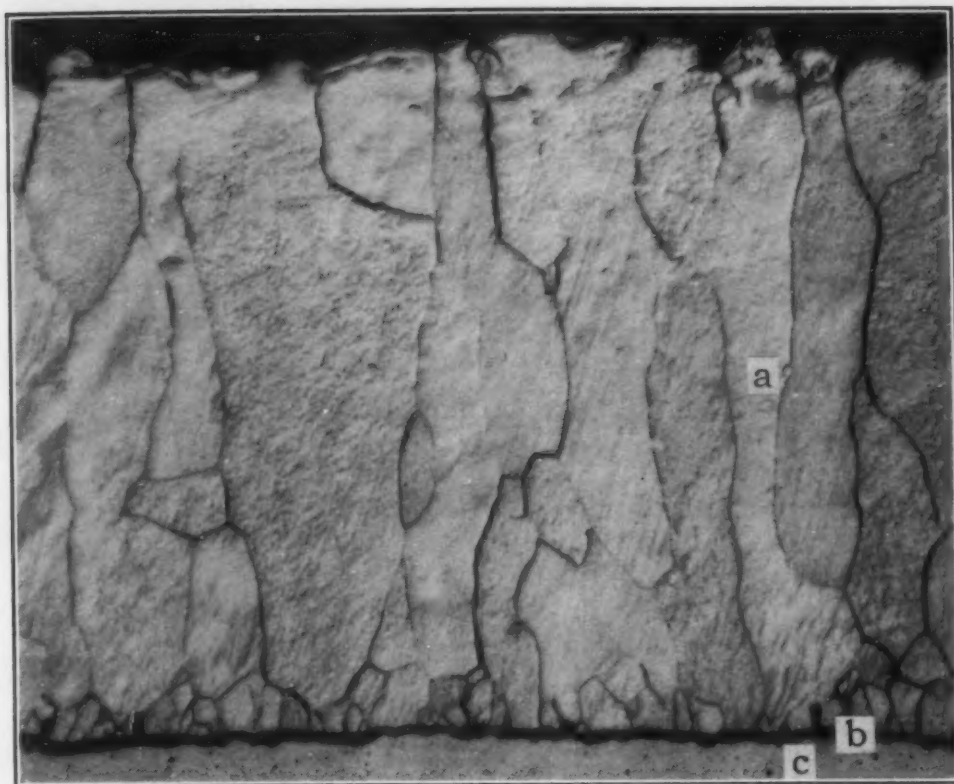


Fig. 8—Molybdenum Deposited on Nickel at 900°C (1650°F).  $\times 750$ . (a) Molybdenum; (b) Intermetallic layer; (c) Nickel.

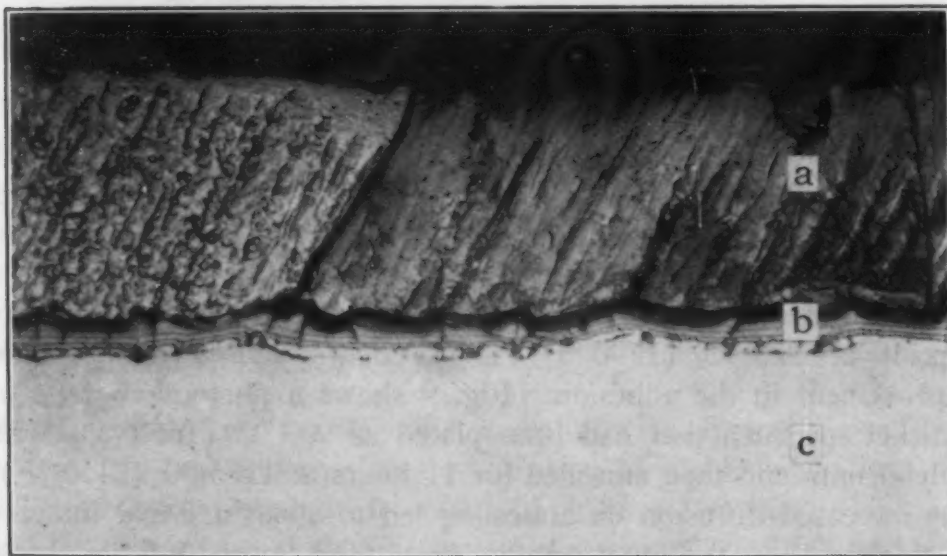


Fig. 9—Molybdenum on Nickel. Annealed at 1175°C (2145°F) for 11 Hours.  $\times 500$ . (a) Molybdenum; (b) Intermetallic layer; (c) Nickel.

The tensile stress caused the plate to crack, as shown in Fig. 6, but the molybdenum bond did not fail. In this test the bond appears to be stronger than either the molybdenum coating or the nickel basis metal.

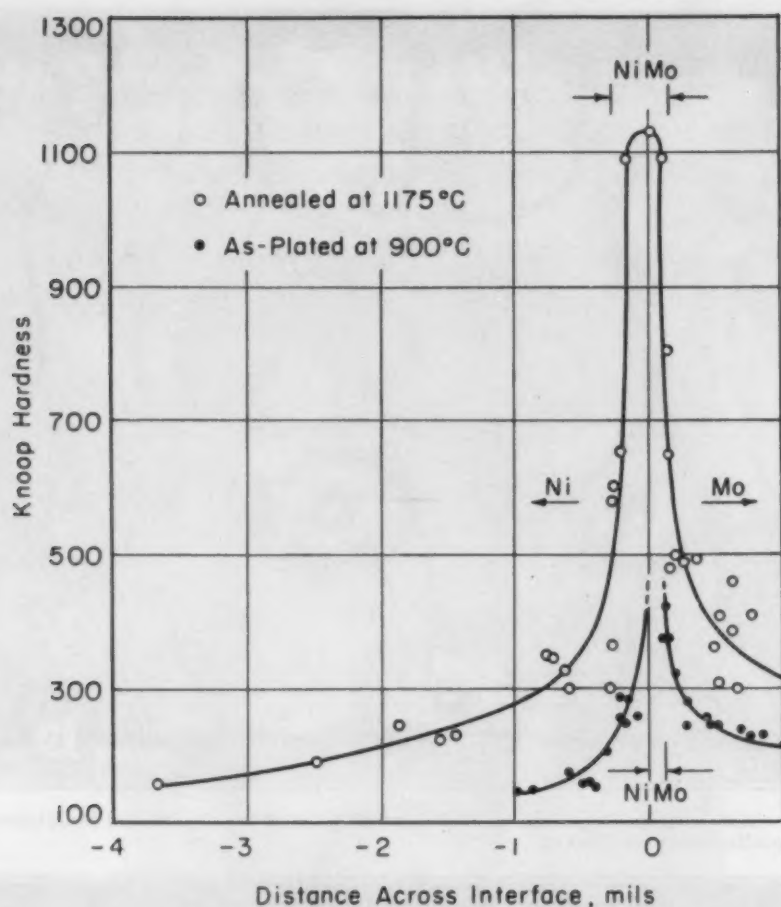


Fig. 10—Hardness Survey Across Interface of Molybdenum Deposited on Nickel.

The bond strength between molybdenum and nickel was found to be strongly influenced by the amount of diffusion taking place. When the plating temperature was  $750^{\circ}\text{C}$  ( $1380^{\circ}\text{F}$ ) the amount of diffusion and the strength of the bond were both lower than in a deposit formed at  $900^{\circ}\text{C}$  ( $1650^{\circ}\text{F}$ ). Annealing the low temperature deposit at  $975^{\circ}\text{C}$  ( $1790^{\circ}\text{F}$ ) for 2 hours caused a noticeable improvement in the adhesion. Fig. 9 shows a photomicrograph of a nickel specimen that had been plated at  $900^{\circ}\text{C}$  ( $1650^{\circ}\text{F}$ ) with molybdenum and then annealed for 11 hours at  $1175^{\circ}\text{C}$  ( $2150^{\circ}\text{F}$ ). The increased diffusion on annealing led to about a 5-fold increase in thickness of the intermetallic layer and much inferior bond strength. It is thus apparent that there is an optimum amount of diffusion to produce the maximum bond strength. It was found that the best bond strength between molybdenum and nickel was obtained at a plating temperature of about  $950^{\circ}\text{C}$  ( $1740^{\circ}\text{F}$ ).

To demonstrate the extent of the interdiffusion between the molybdenum coating and nickel, hardness surveys were made on

the specimen plated at 900 °C (1650 °F), before and after annealing for 11 hours at 1175 °C (2150 °F). The results are plotted in Fig. 10. In the unannealed specimen the intermetallic layer was thinner than the diamond indenter, and it was thus impossible to get accurate hardness readings of the intermetallic layer itself. However, the hardening of the molybdenum and of the nickel on

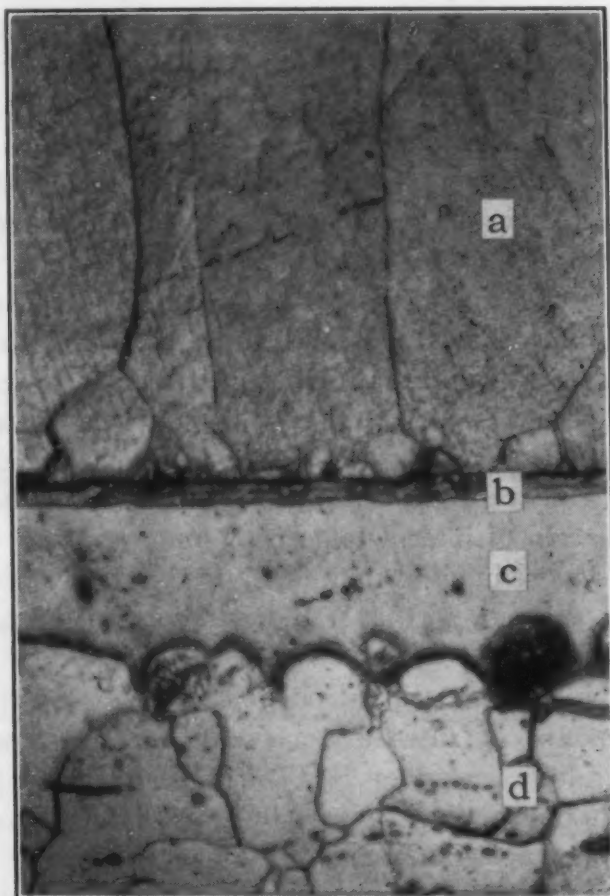


Fig. 11—Molybdenum on Nickel-Plated Low Carbon Steel.  $\times 1000$ . (a) Molybdenum; (b) Diffusion layers; (c) Nickel; (d) Low carbon steel.

either side of the intermetallic layer due to interdiffusion was evident. It can be seen that the diffusion of molybdenum into the nickel has progressed at least 0.0005 inch. This method is not suitable for precise determination of the extent of diffusion since, according to Grube and Schlecht (11), the hardening of nickel by molybdenum is not appreciable until the amount of molybdenum exceeds 20%, the limit of the solubility in the alpha phase.

The hardness survey of the annealed specimen was taken with a 50-gram load. The hardness of the intermetallic layer was shown to be about 1150 Knoop. The diffusion of molybdenum has caused



hardening of the nickel up to a distance of 0.004 inch from the interface. The extent of the diffusion of nickel into molybdenum could not be measured in this case, since the plate was only about 0.002 inch thick.

In order to secure adequate adhesion of molybdenum on steel, it was necessary to prevent the formation of too thick a layer of brittle intermetallic compound. It was found possible to accomplish this by first electrodepositing a layer of nickel on the steel before depositing the molybdenum from the pentachloride vapor. A cross section of this type of plate is shown in Fig. 11. In studying the interdiffusion, use was also made of the taper section technique (12), in which the apparent width of the diffusion layers was increased 25-fold by taking a section which intersects the surface at a very small angle. This technique was especially useful in the identification of the various intermetallic phases and solid solutions present in the interdiffusion region. Since there are no intermetallic phases formed in the interface between nickel and steel, the interdiffusion produced a solid solution with a gradual change in composition. This forms an excellent bond between the nickel and steel at the plating temperature used in depositing the molybdenum. The excessive formation of intermetallic compound between the steel and molybdenum was eliminated by the nickel layer, leading to an adhesion much superior to that found without the intermediate layer of nickel.

When molybdenum was deposited on copper, there was no appreciable amount of interdiffusion and the adhesion was poor. However, the addition of 5 or 10% of nickel to the copper gave an alloy on which the coating of molybdenum adhered as well as on pure nickel. The possibility exists that copper might be useful in reducing the formation of intermetallic phase between steel and molybdenum, and that an improvement in adhesion could result in this way.

#### CONCLUSIONS

(a) Molybdenum coatings were obtained by hydrogen reduction of molybdenum pentachloride vapor. It was found advisable to keep the total pressure at or below 20 millimeters of mercury and the temperature in the range 800 to 1100 °C (1470 to 2010 °F) for maximum plating rate and optimum structure of the plate.

(b) Of three distinct types of structure of the molybdenum plate—fine-grained, coarse-grained and laminated—it was found that the coarse-grained structure had the best physical properties.

(c) Adhesion of the molybdenum coating to nickel or to a copper-nickel alloy containing at least 5% nickel was found much better than to steel or to pure copper.

(d) The proper amount of interdiffusion was shown to be essential for securing optimum adhesion. In the case of molybdenum on nickel, a plating temperature of 950 °C (1740 °F) was recommended for producing the best adhesion.

(e) An intermediate electroplated layer of nickel was found to improve the adhesion of molybdenum on steel.

#### ACKNOWLEDGMENT

The authors wish to express their appreciation to the United States Army Ordnance Department for financial support of this investigation and for permission to publish these results.

#### References

1. H. J. Seim and M. L. Holt, "The Electrodeposition of Molybdenum Alloys", *Journal, Electrochemical Society*, Vol. 96, 1949, p. 205-213.
2. J. J. Lander and L. H. Germer, "Plating Molybdenum, Tungsten and Chromium by Thermal Decomposition of Their Carbonyls", *Metals Technology*, Vol. 14, No. 6, Technical Publication No. 2259, September 1947.
3. E. O. Hulburt, "The Preparation of Sputtered Metal Films", *Review of Scientific Instruments*, Vol. 5, 1934, p. 85-88.
4. C. H. Cartwright and J. Strong, "An Apparatus for the Evaporation of Various Materials in High Vacuums", *Review of Scientific Instruments*, Vol. 2, 1931, p. 189-193.
5. I. E. Campbell, C. F. Powell, D. H. Nowicki and B. W. Gonser, "The Vapor-Phase Deposition of Refractory Materials. I—General Conditions and Apparatus", *Journal, Electrochemical Society*, Vol. 96, 1949, p. 318-333.
6. C. F. Powell, I. E. Campbell and B. W. Gonser, "The Deposition of Tantalum and Columbium from Their Volatilized Halides", *Journal, Electrochemical Society*, Vol. 93, 1948, p. 258-265.
7. E. H. Brown, J. E. Cline, M. M. Felger and R. J. Howard, Jr., "Continuous Determination of  $\text{NH}_3$  Activity in Ammoniacal Solutions", *Industrial and Engineering Chemistry, Analytical Edition*, Vol. 17, 1945, p. 280-282.
8. F. N. Rhines, "Diffusion Coatings on Metals", *Surface Treatment of Metals*, published by American Society for Metals, 1941, p. 122.
9. W. P. Sykes, "Iron-Molybdenum", *ASM Metals Handbook*, 1948 Edition, p. 1210.
10. R. M. Parke, "Molybdenum-Nickel", *ASM Metals Handbook*, 1948 Edition, p. 1230.
11. G. Grube and H. Schlecht, "Electrical Conductivity and Phase Diagrams of Binary Alloys. XXIII—The System Nickel-Molybdenum", *Zeitschrift für Elektrochemie*, Vol. 44, 1938, p. 413-422.
12. H. R. Nelson, "Proceedings of the Special Summer Conferences on Friction and Surface Finish", Massachusetts Institute of Technology, Cambridge, June 1940, p. 217-237.

## RECOVERY AND COLD WORKING OF 52S COMMERCIAL ALUMINUM ALLOY

BY GERARD H. BOSS

### *Abstract*

*This paper reports the results of experiments on the recovery and recrystallization of commercial aluminum. In order to explain some of the results, it is postulated that there is an intrinsic difference between the modes of deformation during rolling and stretching. The essential features of the postulate are that deformation during rolling occurs mainly by fragmentation of the crystals so that continuity of the crystal is broken, and during stretching many of the planes are bent but not broken, resulting in no marked discontinuity of the planes.*

THIS paper is a report of an investigation of recovery in 52S aluminum alloy sheet which was studied through its effect on the mechanical properties of the metal. Incidental opportunities for the study of recrystallization were utilized.

The changes which take place in a metal when heated below its recrystallization temperature are the results of a process called recovery or partial annealing. Mehl sums up most of the present knowledge of recovery (1).<sup>1</sup> Generally, recovery decreases the electrical resistance and the speed of solution in an acid. In addition to the above, recovery frequently results in a sharpening of the lines of the X-ray diffraction pattern and an apparent increase in Young's modulus. This last is the result of a partial overcoming of the departure from Hooke's law, which is typical of cold-worked metal. In most metals recovery is manifested by a decrease in hardness and yield strength. Mehl (1) mentions that recovery cannot be separated from recrystallization in certain metals, among which are copper, silver, and gold, because the two processes occur simultaneously in these metals. Barrett (2) points out that the difference between the recovery and recrystallization temperatures of tungsten may be as much as 1000 °C (1830 °F).

Basically, recovery may be considered to be the relief of the

<sup>1</sup>The figures appearing in parentheses pertain to the references appended to this paper.

Taken from the author's thesis submitted in partial fulfillment for the degree of Master of Science in Engineering, University of Pennsylvania, January 1949.

A paper presented before the Thirty-second Annual Convention of the Society, held in Chicago, October 21 to 27, 1950. The author, Gerard H. Boss, is associated with the Metallurgy Division, National Laboratory, Oak Ridge, Tenn. Manuscript received April 20, 1950.



microstresses existing among the individual planes in cold-worked crystals. These stresses are a result of bending or other distortion of crystal planes which occurs during cold deformation. It is this bending of the crystal planes which causes a large portion of the line broadening that is typical of the diffraction patterns of cold-worked metals. Recovery may be considered principally as the localized straightening of these bent planes, resulting in a series of steps instead of curves.

### MATERIALS STUDIED

It was necessary that the metal chosen for this work have no marked solution or precipitation responses to heat treatment, i.e., no age hardening properties. It was also desirable that its strength and ductility be variable over a range of sufficient magnitude that the changes caused in them by the usual cold working and annealing processes would be sufficient for easy determination. As Alloy 52S has a desirable combination of strength and ductility, it was used in this investigation. This alloy is sold in the annealed, O, condition, and in various work-hardened states. The work-hardened metal is usually given an anneal between 300 and 350 °F for several hours to stabilize it against changes which would otherwise occur because of the metal's tendency to recover at room temperature. In this report, when  $\frac{1}{4}$ -H metal is spoken of, it will mean commercial metal, the more recent designation being H-32 which has been given the recovery anneal.

The metal used in this investigation came from several sources, so that there was an opportunity to check most of the results on metal from two or more different sources or lots. All samples were obtained in the usual commercial conditions, which means that the S-O metal had really been stretched or rolled to a reduction of 1 or 2% to straighten or stiffen it slightly. All the test specimens were 1 inch wide by 0.051 or 0.064 inch thick. The average composition of the materials tested was:

Magnesium	Chromium	Manganese	Fe + Si	Others
2.50%	0.25%	0.10%	0.45%	0.10%

### RECOVERY EXPERIMENTS

#### *Test Procedures*

The purpose of this section was to investigate recovery completely isolated from recrystallization. For these experiments the S-O specimens were stretched from 2 to 14% in increments of 2% and the  $\frac{1}{4}$ -H specimens were stretched 0 to 6%. They were heated at temperatures ranging from 212 to 1000 °F in 50-degree increments or to the recryst-

tallization temperature, if it was lower. The S-O pieces stretched 2 to 10% were heated 20 minutes in the temperature range 212 to 450 °F; but for the higher temperatures the heating periods were 20, 40 and 60 minutes, and 16 hours for some scattered temperatures. The heating period for all the  $\frac{1}{4}$ -H specimens and for the S-O metal stretched 12 and 14% was 30 minutes.

Hardness tests were made with the  $\frac{1}{16}$ -inch ball and 60-kg load, the Rockwell F scale. There was some penetration to the bottom side by the hardness indenter, anvil effect, on all specimens tested. While this affected the absolute hardness, it did not change the qualitative relationships among the various results.

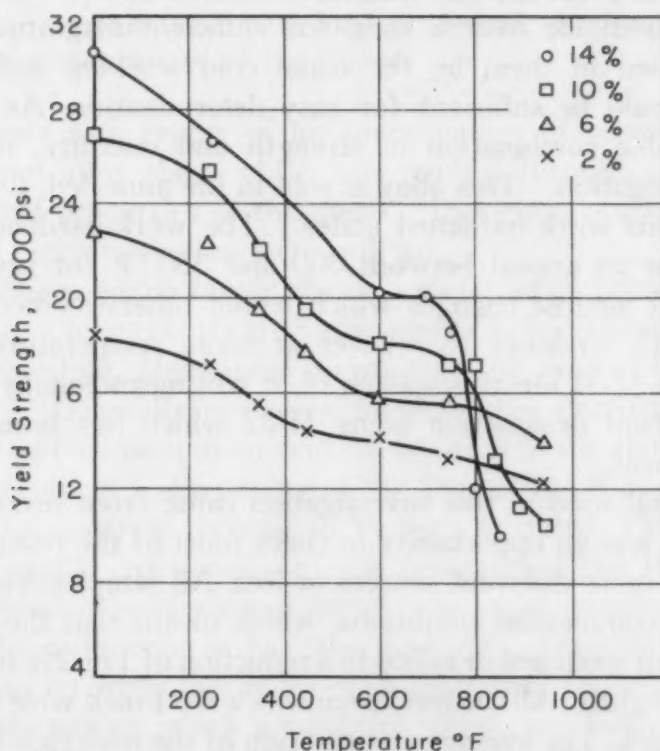


Fig. 1—Yield Strength of Stretched S-O Metal Plotted Against Temperature of Annealing. Each curve is for metal stretched the indicated amount.

All tensile tests were made on standard sheet specimens with the 2-inch gage length milled down to  $\frac{1}{2}$ -inch width. The specimens were pulled in a Baldwin-Southwark hydraulic tensile testing machine.

The hardness and tensile data of all the above specimens were plotted in Figs. 1 to 8 against the annealing temperature as abscissa. Each point on the curves represents the average of three tests not necessarily heated for the same time interval. Averaging the values for specimens annealed various periods was possible, since it was observed

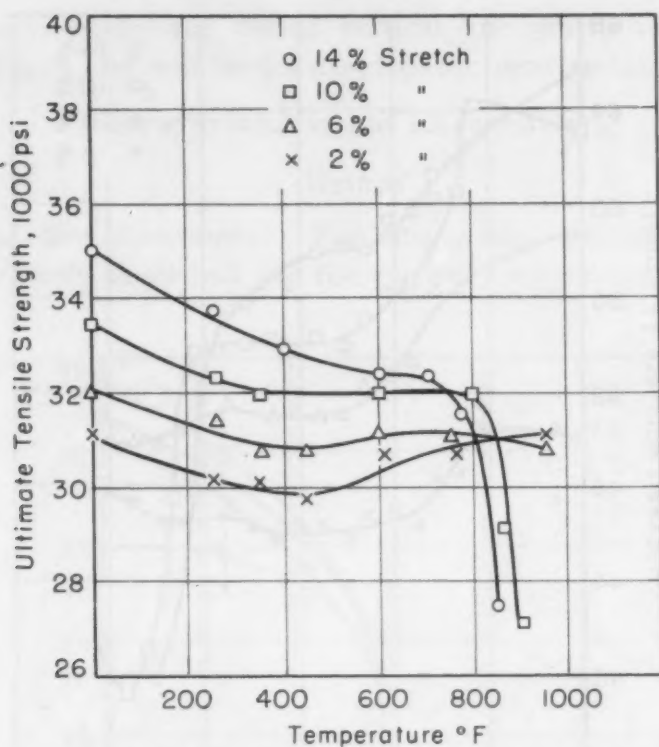


Fig. 2—Ultimate Strength of Stretched S-O Metal Plotted Against Temperature of Annealing. Each curve is for metal stretched the indicated amount.

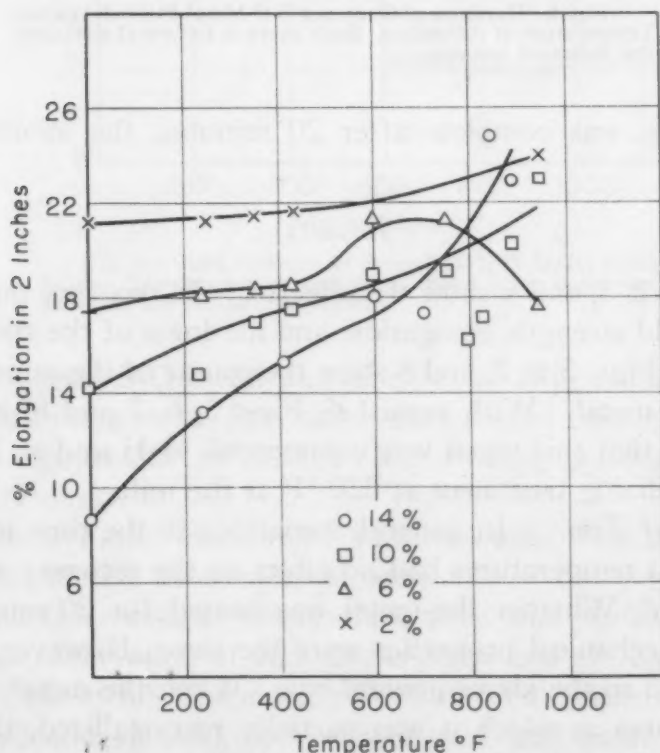


Fig. 3—Elongation of Stretched S-O Metal Plotted Against Temperature of Annealing. Each curve is for metal stretched the indicated amount.



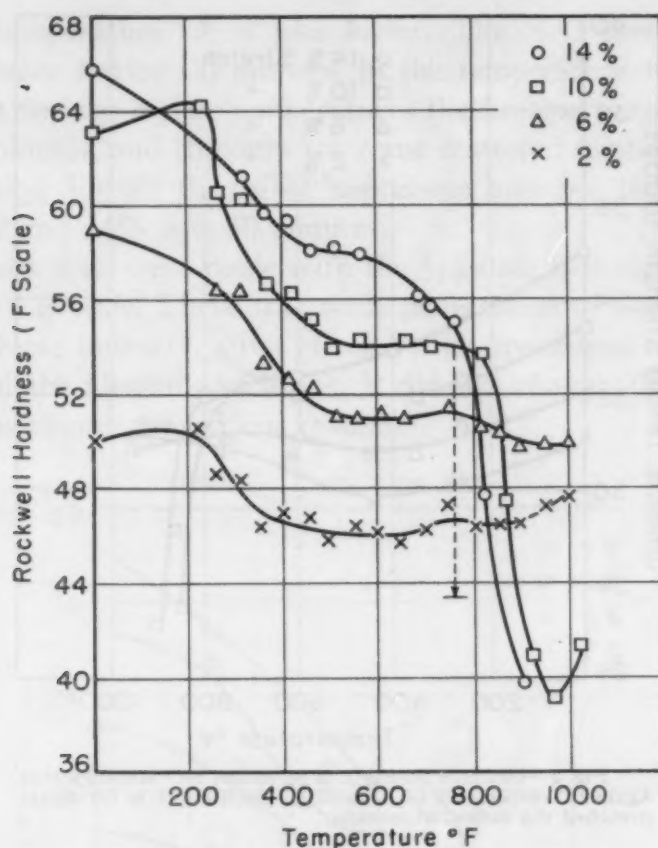


Fig. 4—Hardness of Stretched S-O Metal Plotted Against Temperature of Annealing. Each curve is for metal stretched the indicated amount.

that recovery was complete after 20 minutes, the shortest heating period used.

### Results

Figs. 1, 2, 3, and 4 show the effects of the recovery on the tensile strength, yield strength, elongation, and hardness of the stretched S-O metal, while Figs. 5, 6, 7, and 8 show the course of the same properties in the  $\frac{1}{4}$ -H metal. With regard to Figs. 5, 6, 7 and 8, it should be remembered that this metal was commercial  $\frac{1}{4}$ -H and so it had been given a stabilizing treatment at 320 °F at the mill.

*Effect of Time:* In general, variations in the time in excess of 20 minutes at temperatures had no effect on the recovery of the cold-worked metal. Whether the metal was heated for 20 minutes or 16 hours, the mechanical properties were the same. However, there was one exception to the above general rule. When the metal was heated to temperatures at which it was partially recrystallized, there was a continuous drop in hardness with time at the temperature which continued until the metal was almost as soft as after recrystallization.

This is indicated by the dotted vertical line drawn from the 10% curve in Fig. 4 and will be discussed in the next section.

### RECRYSTALLIZATION EXPERIMENTS

#### Method

*Preparation Specimens:* For this work, specimens similar to those previously described for the recovery experiments were used.

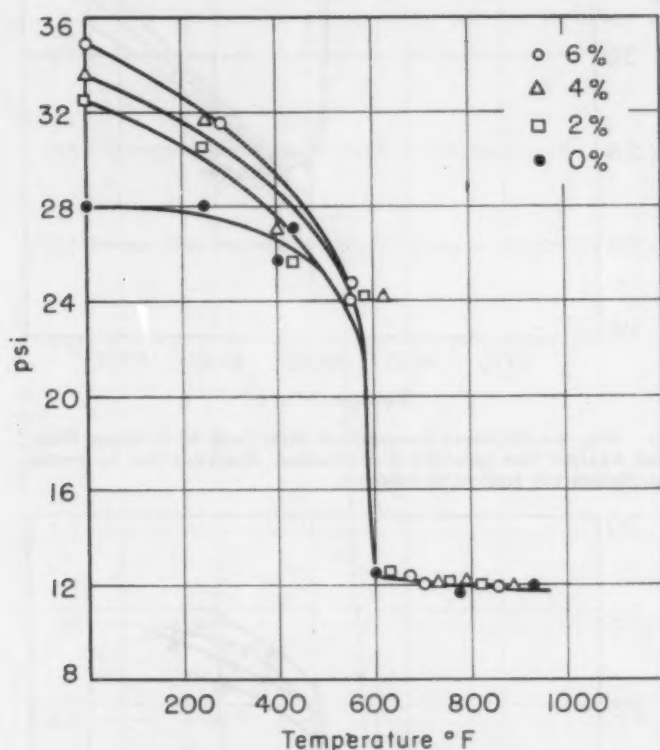


Fig. 5—Yield Strength of Stretched  $\frac{1}{4}$ -H Metal Plotted Against Temperature of Annealing. Each curve is for metal stretched the indicated amount.

In addition, some S-O metal was rolled to an 18% reduction in thickness in small increments. Specimens were heated throughout the temperature range of 550 to 1030 °F. The heating periods varied from  $\frac{1}{2}$  hour to 7 days.

*Hardness Test:* Rockwell F hardness tests were made on specimens representative of every treatment.

*Crystal Observation:* Recrystallization was studied by means of both optical observation of etched specimens and of X-ray diffraction patterns of the metal. The etching solution used consisted of one-third each of hydrofluoric acid, hydrochloric acid, and water. The surfaces with the usual commercial finishes were etched without preparation by polishing or grinding. The grain size was determined by counting the

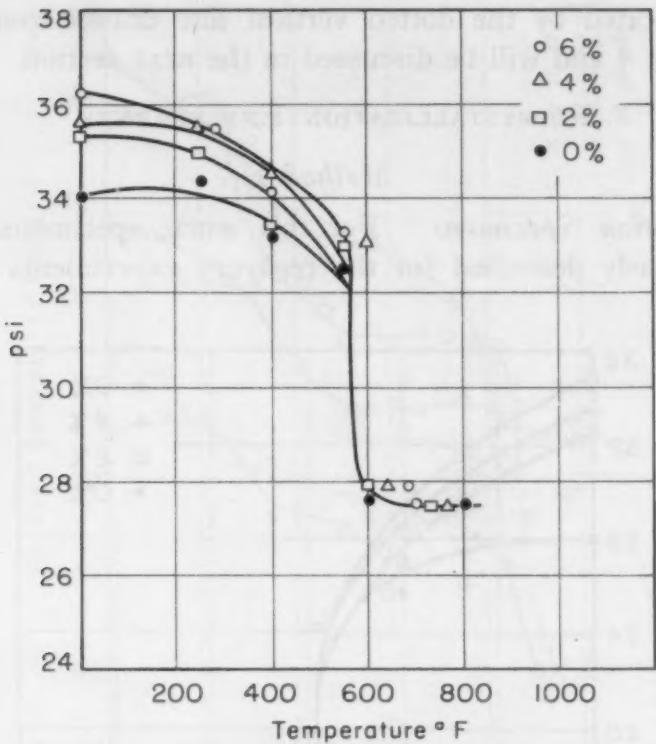


Fig. 6—Ultimate Strength of Stretched  $\frac{1}{4}$ -H Metal Plotted Against Temperature of Annealing. Each curve is for metal stretched the indicated amount.

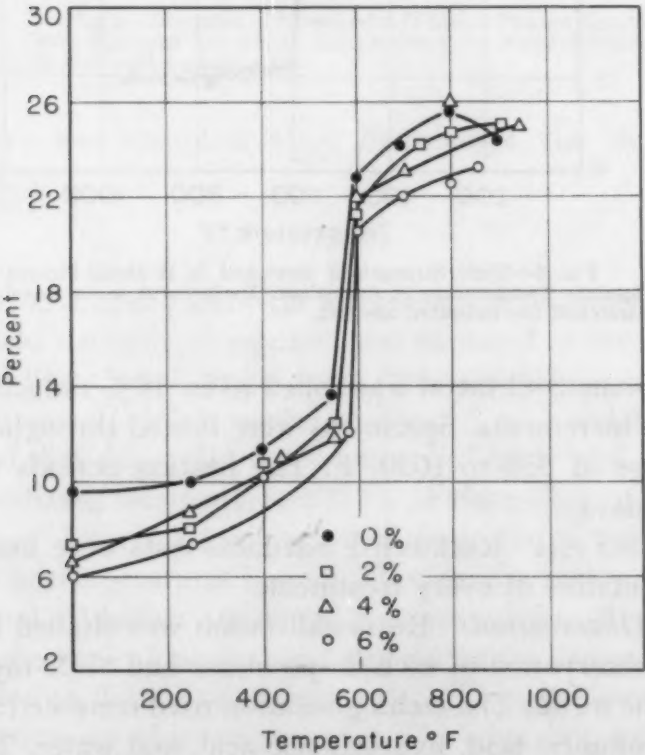


Fig. 7—Per Cent Elongation of Stretched  $\frac{1}{4}$ -H Metal Plotted Against Temperature of Annealing. Each curve is for metal stretched the indicated amount.



number which intercepted a line of measured length. Knowing this number and the length of the line, it was then possible to calculate the average diameter. For the smaller grains, at least 30 were included in the measurement, and since they were not resolvable by the unaided eye, a low-power microscope was used. For the larger grain sizes, the diameters of 10 to 15 grains were determined individually and then

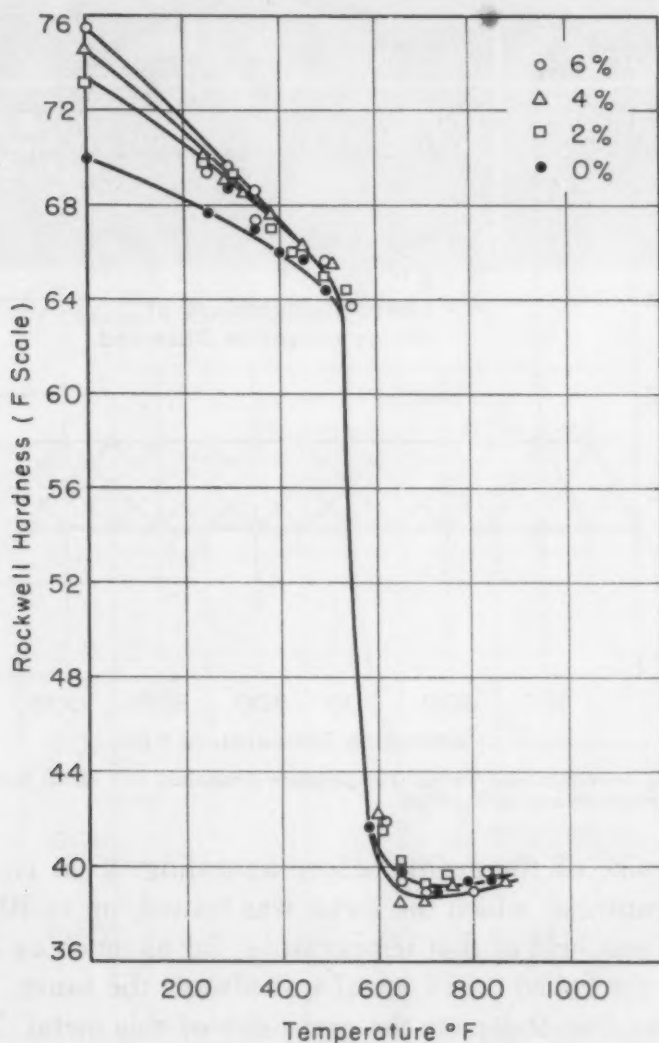


Fig. 8—Hardness of Stretched  $\frac{1}{4}$ -H Metal Plotted Against Temperature of Annealing. Each curve is for metal stretched the indicated amount.

the average was calculated. All grains except those next to the edges were equiaxed.

Since some of the specimens recrystallized without change in grain size, as determined by the method described above, X-ray diffraction patterns were made of all specimens whose hardness was below Rockwell F-45 and whose grain size was unchanged after heating. For this

purpose, simultaneous back reflection and transmission patterns were obtained by the Hull method.

### Results

**Rolled Metal:** The grain size of all fully annealed, i.e., recrystallized,  $\frac{1}{4}$ -H specimens was 0.0025 to 0.0017 inch in diameter. This

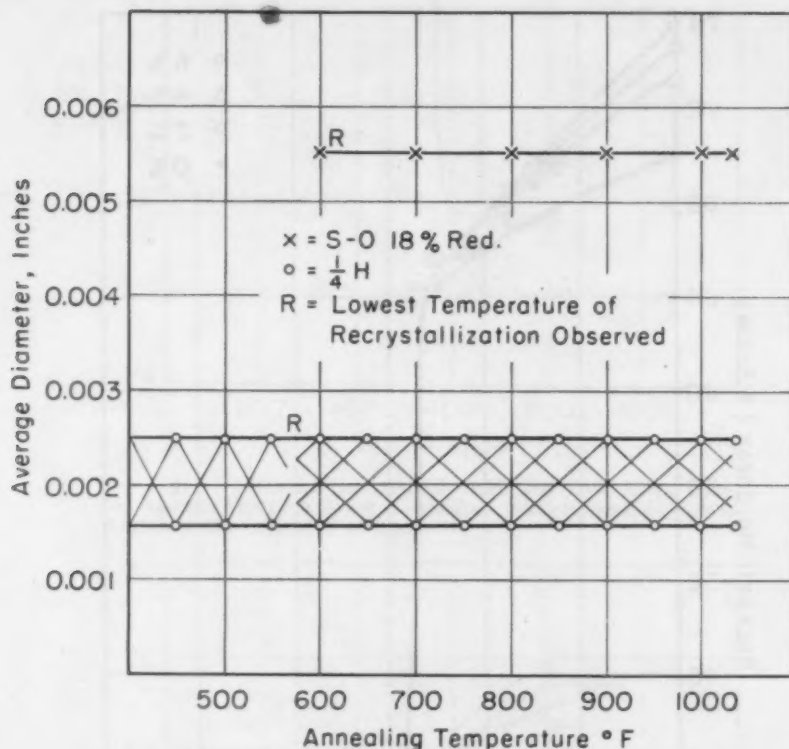


Fig. 9—Grain Size Versus Temperature Annealing S-O Metal Rolled 18% Reduction and  $\frac{1}{4}$ -H Metal.

was also the size of the grains before annealing. That is, regardless of the temperature at which the metal was heated, up to 1030 °F, and of the time it was held at that temperature, for as much as 7 days, the grain size of the rolled  $\frac{1}{4}$ -H metal was always the same. The cross-hatched area of Fig. 9 depicts the grain size of this metal. The curves are continued below the recrystallization temperature, as there was no change in grain size at that point. Since the recrystallization of the  $\frac{1}{4}$ -H metal was accomplished without any apparent change in grain size, it was necessary to examine the X-ray diffraction pattern instead of the etched surface to determine whether or not a piece had recrystallized and to what extent. Figs. 10b and 10c show the back reflection and transmission patterns of two pieces of  $\frac{1}{4}$ -H metal which had been heated to 570 °F for 24 and 48 hours respectively. The metal of Fig. 10b had a hardness of Rockwell F-44, while that of Fig. 10c had a

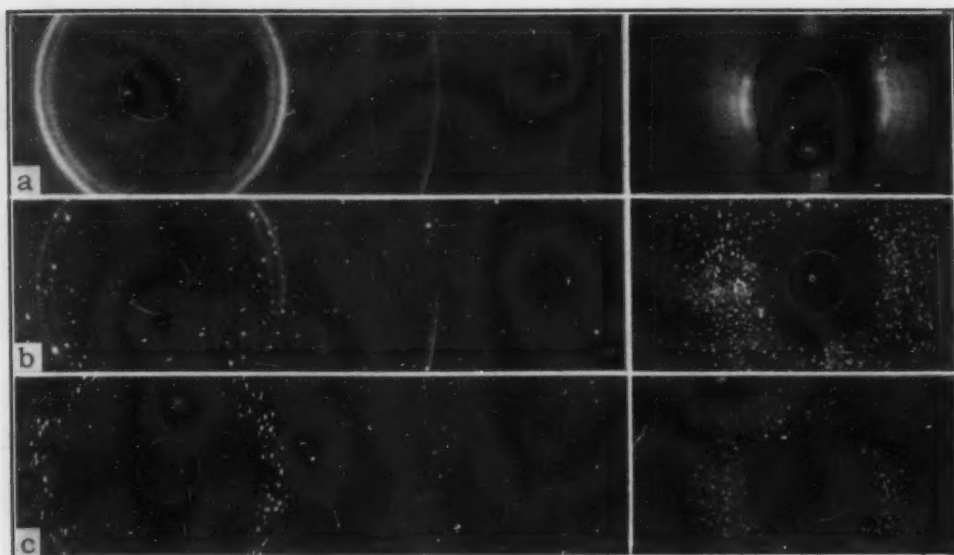


Fig. 10—X-Ray Diffraction Patterns of  $\frac{1}{4}$ -H Metal Treated as Described: a—As  $\frac{1}{4}$ -H rolled; b—570°F, 24 hours; c—570°F, 48 hours.

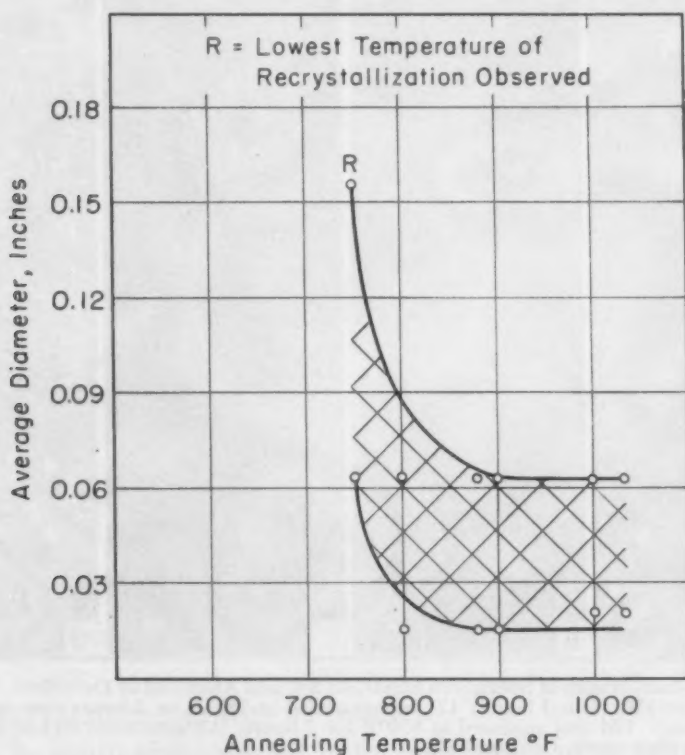


Fig. 11—Grain Size Versus Temperature Annealing S-O Metal Stretched 8%.

hardness of F-42. Fig. 10c shows the effect of complete recrystallization on the X-ray diffraction pattern, while Fig. 10b is the pattern of metal which has only partially recrystallized. Fig. 10a is the pattern of the as-received  $\frac{1}{4}$ -H metal, whose hardness was Rockwell F-72. The three patterns of Fig. 10 depict the progress of recrystallization in this metal.



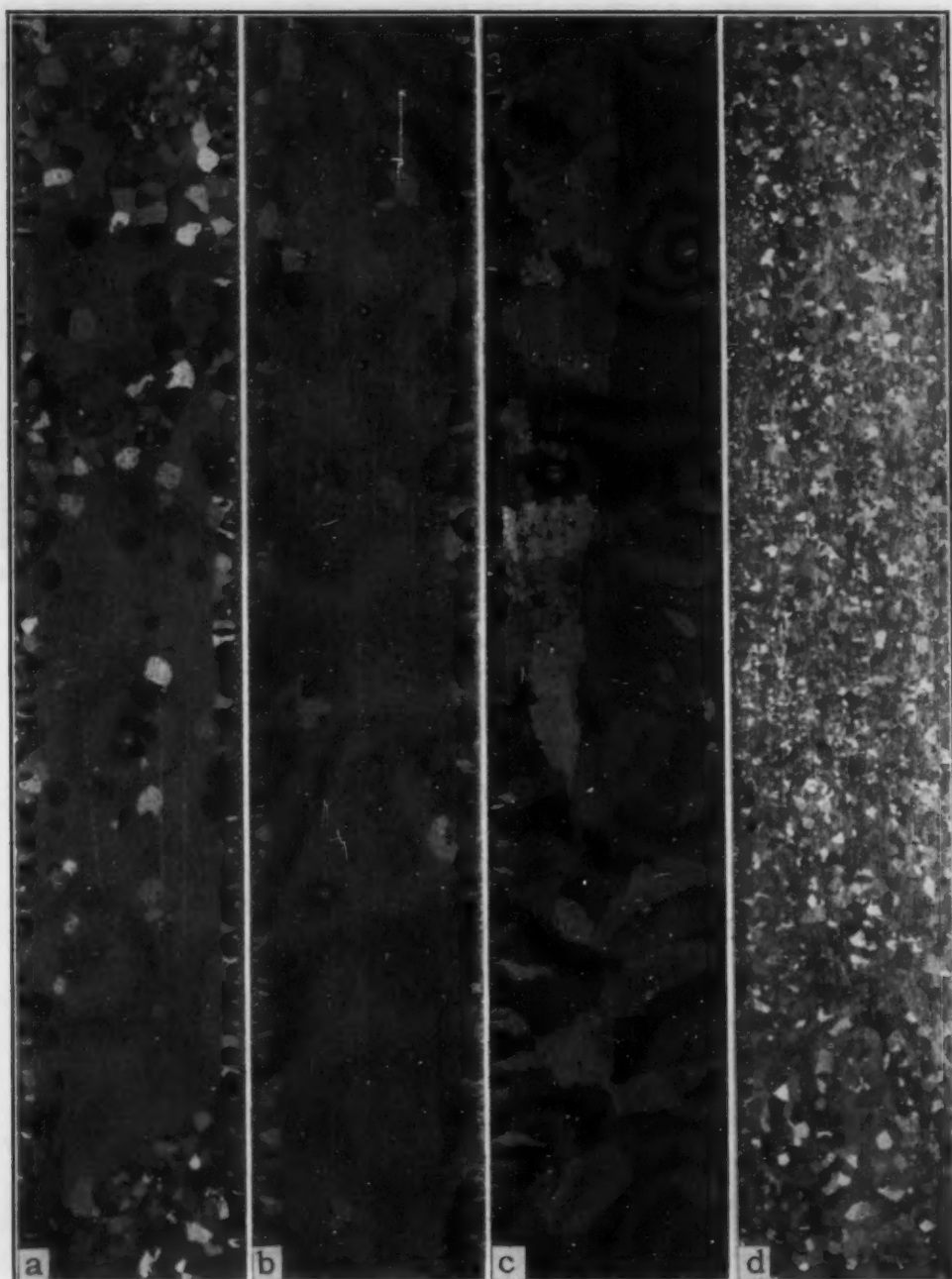


Fig. 12—Macrographs of Specimens Stretched 8% and Annealed as Described. 12a and 12b were annealed at 750 °F for 2 hours. 12c was annealed at 750 °F for 2 hours then reannealed at 850 °F for 3 hours. 12d was annealed at 850 °F for 2 hours. All specimens etched in a solution consisting of  $\frac{1}{8}$  each water, HF, and HCl.

The recrystallized grain size of the S-O metal rolled to 18% reduction in thickness was also not affected by the temperature of recrystallization. The original grain size of this metal was 0.0025 to 0.0014 inch in diameter, while its recrystallized size was 0.0055 inch in diameter, whether recrystallized at 600 or 1000 °F. Fig. 9 shows the relation between temperature of recrystallization and grain size of the

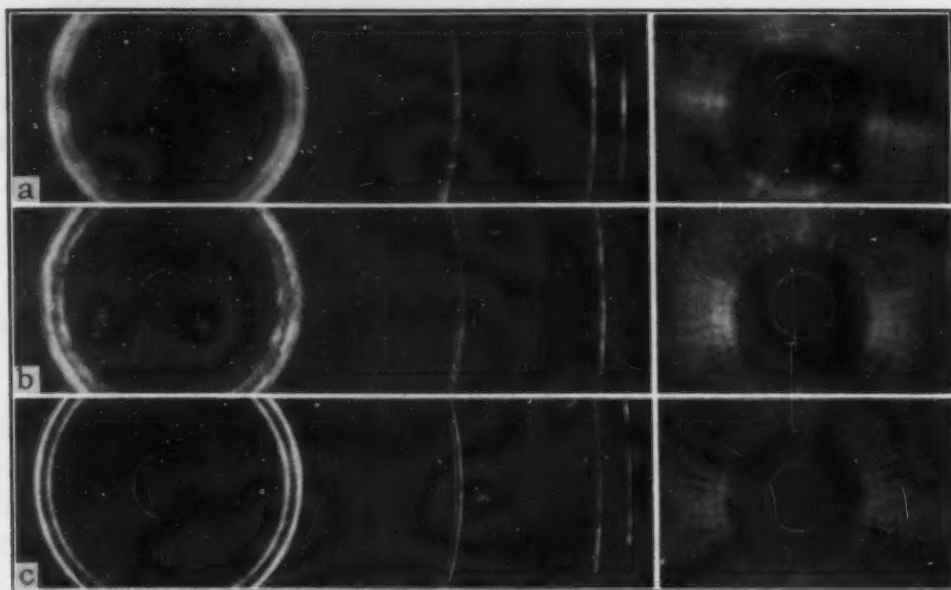


Fig. 13—X-Ray Diffraction Patterns of S-O Metal Stretched 8% and Treated as Described: a—As-stretched; b—4 hours at 750 °F—shows no recrystallization; c—4 hours at 750 °F—signs of recrystallization in transmission pattern.

rolled  $\frac{1}{4}$ -H metal and S-O specimens which were reduced 18% in thickness by rolling.

*Stretched Metal:* It was found that the recrystallized grain size increased as the temperature of annealing was decreased from 1030 °F to the lowest temperature of recrystallization. This same effect of decreasing temperature on grain size of stretched metal was noted on all specimens which recrystallized. Fig. 11 shows the variation of grain size with temperature of annealing of S-O metal stretched 8%. This phenomenon was previously observed by Eastwood (5). The pieces shown in Figs. 12a, 12b, and 12d were S-O metal stretched 8%. The pieces shown in Figs. 12a and 12b were annealed at 750 °F while the piece of Fig. 12d was annealed at 850 °F. The effect of temperature on grain size is apparent.

Another point noted was that at temperatures of partial recrystallization it was possible to have very large recrystallized and very small unrecrystallized grains in contact. This is shown in Figs. 12a and 12b. The grain size contrast in these pieces is interesting, especially so when one considers that it is maintained during long periods at the temperature at which it occurred. The unrecrystallized grains are 0.0014 to 0.0025 inch in diameter, which is much too small to be revealed without magnification, while the other grains are  $\frac{1}{8}$  to  $\frac{3}{16}$  inch in diameter. The hardness of the small grains varied, being as low as Rockwell F-44, while the large grains had a hardness of F-38. That this fine-grained metal with the low hardness was not recrystallized

was proved by its X-ray diffraction pattern. Fig. 13b shows the diffraction pattern of a piece of S-O metal stretched 8% and then annealed 4 hours at 750 °F. Like the sample shown in Fig. 12b, this metal had a duplex grain size. The X-rays were directed against a fine-grained portion of the piece. The hardness of the metal in the neighborhood of

A = As-Stretched	B = Heated to 650°F For 20 Hrs.	C = Heated to 750°F For 20 Hrs.
A	B	C
65 65	55.5	39 44
65	54 55	44
65 64	54	43 50
65	54 53	51
64 64	53.5	48 47
63	52 52	52
65 66	53	36 40
66	55 55	45
66 65	55	41 38
64	53.5 52	43

Fig. 14—Hardness Surveys of Pieces Stretched 8%.

impingement of the rays was Rockwell F-44. Fig. 13c shows the pattern from an area of a similar piece, with a hardness of Rockwell F-42, in which the back-reflection pattern shows almost complete recovery without recrystallization.

In Fig. 12 the crystals are much finer along the edges of the strips, since the shearing operation has added enough extra deformation to the edges to cause a noticeable reduction in the grain size. Time at temperature had very little effect on the grain size of the stretched pieces. Thus, pieces stretched 14% and heated for as much as 72 hours at various temperatures from 700 to 1000 °F showed the same grain size, regardless of the time at temperature.



Fig. 15—Diffraction Pattern of Specimen Whose Hardness Is Shown in Fig. 14B.

It was found that metal with a hardness of Rockwell F-42 or lower was always at least partially recrystallized, as revealed by its X-ray pattern; and if its hardness was Rockwell F-44 or higher, it was completely unrecrystallized. The results of hardness surveys of three pieces of S-O metal which had been stretched 8% are shown in Fig. 14. The hardness of the as-stretched piece lay between Rockwell F-63 and F-66, the variation of 3 points being slightly more than the known limits of the instrument. The hardness of the piece annealed at 650 °F for 20 hours varied between Rockwell F-52 and F-55.5. Fig. 15 shows the diffraction pattern of this metal. The piece heated to 750 °F for 20 hours had a low hardness of Rockwell F-36 and a high of Rockwell F-52, a variation of 16 points. Etching this piece revealed that it was partially recrystallized; and it was observed that the recrystallized metal included, or was adjacent to, all areas of Rockwell F-42 or lower. The unrecrystallized areas varied between Rockwell F-44 and F-52, a difference of 8 points.

*Double Anneal:* The unrecrystallized grains in the partially recrystallized metal present an example of advanced recovery. It was thought that a second anneal at a higher temperature would be interesting. Accordingly, some of the metal which was stretched 8% and heated to 750 °F, so that it contained the small unrecrystallized grains and large recrystallized grains, was reheated to either 850 or 950 °F. In both cases, the entire piece was recrystallized with very large grains; however, as in the other experiments, the lower temperature resulted in the large grains. The piece heated to 850 °F had an appearance similar to that of the large-grained piece in Fig. 12. On the other hand, a piece of 1/4-H which was given the double anneal had the same small grains found in all the 1/4-H metal after annealing. As numerous investigators have previously reported (1-4), the grain size after recrystallization increased as the amount of cold work decreased.

#### DISCUSSION

The observation, that the lower the temperature at which the



stretched S-O metal was recrystallized, the larger its grain size became, is explained as follows: At the lower temperatures, recrystallization occurs very slowly; hence there is time enough for recovery to destroy some of the potential recrystallization nuclei before they can become active. With the fewer potential nuclei thus available, the recrystallized grain size is quite large. Now, with rising temperature, the rate of recovery does not increase so fast as the rate of recrystallization; accordingly, at the higher temperature more of the potential nuclei are

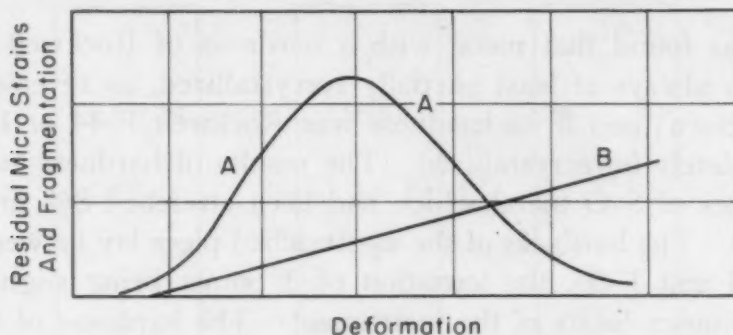


Fig. 16—Schematic Curves for Rolled Metal Showing Relation Between Total Deformation and Residual Stress, Curve A, and Fragmentation, Curve B.

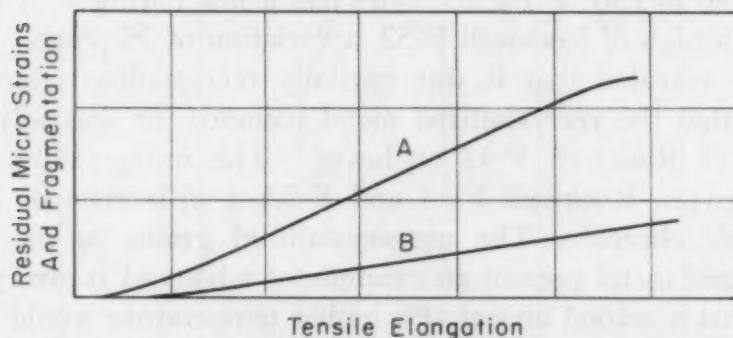


Fig. 17—Schematic Curves Showing Postulated Relation Between Total Tensile Elongation and Residual Stress, Curve A, and Fragmentation, Curve B.

utilized before they can be destroyed by recovery. As a result, the grain size is smaller at the higher temperatures.

The above explanation is based on the postulate, herewith offered, that most of the potential recrystallization nuclei in stretched metal are furnished by lattice distortion, which causes microstresses, and that fragmentation plays an unimportant role, regardless of how far the metal is stretched.

The destruction of potential recrystallization nuclei by recovery also explains the extremely large grains developed in the stretched piece given the recovery anneal. As described, this piece was partially recrystallized at 750 °F and then completely recrystallized at 850 °F.

The lower temperature destroyed a significant proportion of potential nuclei so that further heating at the higher temperature caused recrystallization which was nucleated by a small number of nuclei, hence the large grain size.

It is postulated here that the principles illustrated by Fig. 16 represent rolled metal and that the condition for stretched metal is shown in Fig. 17. The curves of Figs. 16 and 17 are postulated as an explanation of the data reported here. The belief that microstresses increase indefinitely with stretching is based on the following conclusions made during the course of this work:

- (A) The very marked changes observed in the mechanical properties of the stretched metal during recovery were due to the relief of microstresses. Also, the extent of these changes increased as the degree of deformation by stretching increased.
- (B) The destruction of potential recrystallization nuclei by recovery anneal of the stretched metal indicates that these nuclei must have had their source in the microstrains set up during the stretching operation.

The recrystallized grain size of the metal reduced 18 to 20% by rolling was not affected by the temperature, nor was it affected by any sort of double heat treatment. Recrystallization nuclei furnished by fragmentation would not be destroyed by recovery, hence the conclusion is reached that fragmentation is the predominating source of potential nuclei in this rolled metal. This puts the metal reduced 18 to 20% by rolling well beyond the peak of Curve A in Fig. 16 and accounts for the fine grains of the recrystallized  $\frac{1}{4}$ -H metal.

Based on the curves of Figs. 16 and 17, a theory has been postulated: During stretching there is little fragmentation and the different portions of a stretched crystal tend to maintain registry with each other. As a result, relatively intense microstrains are set up in the crystal. In rolling, on the other hand, many portions of the deformed crystal cannot maintain registry, and so we get fragmentation. There will be a relatively large number of stresses set up in the fragments but none of them will be very great. The total energy contained in all these numerous small stresses may be quite large; however, their intensity is so low that they do not exceed the yield strength of the metal during recovery annealing; hence, they are not removed by it. In the early stages of rolling there are probably stresses similar to those found in stretched metal. These may be removed by the later stages of rolling as described by Taylor (7).

In regard to the discussion which has been presented here, one other observation should be recorded. It was found that metal rolled

on the small laboratory power rolls in the laboratory of the University of Pennsylvania had the same recovery characteristics as the stretched metal. The results as described here were duplicated many times, but only when the rolled metal was commercially rolled. Industrial rolls are larger than laboratory-type rolls and are driven at much faster velocities; also, it may be important that the specimens rolled in the laboratory were only 1 inch wide, whereas industrially rolled sheets are 30 inches or over in width. Since the wide piece was under a greater lateral restraint than the narrower piece, its flow pattern may have been different.

References 9 and 10 describe some rolling and annealing experiments on their alloy resembling duralumin. These papers report a recovery effect on their rolled metal which was reduced cold 25 to 90%. Their metal behaved in the same manner as the metal rolled on the small power rolls at the University of Pennsylvania. It is possible that these authors also used small power rolls, but in any event their metal contained a much higher percentage of alloys. It may be that solute atoms can influence the type of deformation.

Reference 11 describes some cold rolling and annealing experiments on pure copper. In it, the authors put forward the idea that, during cold work, up to 50% of the reduction proceeds by slip within the grains; thereafter it occurs by block movement along "flow layer". Apparently the term "flow layer" is another name for deformation band. Wood in discussing the paper took issue with the authors. His idea was that deformation always occurs by breaking down of the grains into components having orientations very different from that of the parent grains. He also said that there was a limit to degree of fragmentation and that this varied with the metal. In Reference 12, Gough and Wood express some of these same ideas.

#### SUMMARY

A. As measured by the hardness test, it was possible to obtain about 90% recovery in 52S commercial alloy which had been stretched 8%. This advanced recovery always occurred in samples in which some portions had recrystallized.

B. The grain size of 52S alloy rolled to 18% or more reduction in thickness is independent of the temperature at which it is recrystallized. It is also independent of the time at the annealing temperature, at least up to one week.

C. The same degree of reduction by rolling or stretching does not produce the same grain size after recrystallization. It appears that

the same grain size is produced by that deformation by each process whose lowest temperature of recrystallization is the same. This deserves further checking.

D. Stretched metal, stretched up to 14%, always recrystallized with fairly large grains, and the lower the temperature at which the metal was recrystallized, the larger the grain size. That is, the nearer to the lowest temperature of recrystallization for the degree of cold working, the larger the recrystallized grains.

E. Within the heating periods used in this work, this alloy was not subject to grain growth.

#### ACKNOWLEDGMENTS

Dr. Brick, Professor of Metallurgy at the University of Pennsylvania, made many helpful criticisms, corrections and suggestions during the course of the work and the preparation of the report. His interest and assistance are gratefully recorded. The cooperation of management at the Reynolds Metals Company and at the Air Materials Laboratory of the Naval Air Center in Philadelphia is acknowledged.

#### References

1. R. F. Mehl, "Recrystallization", *ASM Metals Handbook*, 1939 Edition, p. 207-213.
2. Charles S. Barrett, "Structure of Metals", First Edition, p. 373-377. McGraw-Hill Book Co., New York, N. Y.
3. R. L. Kenyon and R. F. Mehl, "Effect of Cold Work on the Properties of Iron", *ASM Metals Handbook*, 1948 Edition, p. 436-438.
4. Sachs and Van Horn, "Practical Metallurgy", p. 140-141. Published by the American Society for Metals.
5. L. W. Eastwood, R. W. James and F. Bell, "Some Aspects of the Recrystallization of Cold Work Aluminum and Aluminum Alloys", *Transactions*, American Institute of Mining and Metallurgical Engineers, Vol. 133, 1939, p. 124.
6. Walter Boas, "Physics of Metals and Alloys", First Edition, p. 90-91. John Wiley & Sons, New York, N. Y.
7. A. Taylor, "X-ray Metallography", First Edition, 1945, p. 233-235. John Wiley & Sons, New York, N. Y.
8. W. A. Wood and S. L. Smith, "A Stress-Strain Curve for the Atomic Lattice of Aluminum", *Journal*, Institute of Metals, Vol. 67, Part 10, October 1941, p. 315-324.
9. M. Cook and T. L. Richards, "Observations on the Annealing Characteristics of an Aluminum-Copper-Magnesium Alloy", *Journal*, Institute of Metals, Vol. 74, 1948, p. 583.
10. R. Chadwick, T. L. Richards and K. G. Sumner, "The Effect of Rolling and Annealing Procedures on the Structures and Grain-Size of Aluminum-Copper-Magnesium Alloy Strip", *Journal*, Institute of Metals, Vol. 75, 1949, p. 627.
11. M. Cook and T. L. Richards, "The Structural Changes in Copper Effected by Cold Rolling and Annealing", *Journal*, Institute of Metals, Vol. 66, 1940, p. 1.



12. H. J. Gough and W. A. Wood, "A New Attack upon the Problem of Fatigue of Metals Using X-ray Methods of Precision", *Proceedings, Royal Society, Series A*, Vol. 154, 1936, p. 510.

## DISCUSSION

**Written Discussion:** By R. J. Raudebaugh, School of Chemical Engineering, Georgia Institute of Technology, Atlanta, Ga.

The observations reported by Mr. Boss concerning the temperature-insensitive recrystallized grain size of rolled 52S alloy as contrasted with the temperature-dependent recrystallized grain size of stretched material is extremely interesting. The theory he proposes in explanation of the experimental behavior is reasonable but very probably oversimplified. Further study and more data are required for a more thorough understanding of contributing factors.

Experimentation concerning the influence of variables associated with rolling such as temperature of the stock, amount of front and back tension on the stock, roll roughness, and those items cited by the author (roll diameter, roll speed, and width of stock being rolled) should be profitable.

Broadening the investigation to include high-purity aluminum and other wrought aluminum alloys should also be fruitful.

Fully recrystallized material of mixed grain size commonly tends to assume a uniformly coarse structure on prolonged heating above the minimum recrystallization temperature. In view of this fact, the persistence of small unrecrystallized grains in the presence of relatively large recrystallized grains, throughout a long time at the temperature where the latter were formed, is difficult to explain. Could this be due, in part, to chemical segregation?

In looking over the graphs in this paper, it appears to me that the author might have been justified in constructing his elongation versus temperature curve for material stretched 10% to exhibit a sharper increase in ductility at about 825 °F (Fig. 3). This would be in keeping with yield, tensile, and hardness data which indicate some recrystallization above 800 °F.

**Written Discussion:** By U. Dehlinger, professor, Max Planck Institut für Metallforschung, Stuttgart, Germany.

The difference between stretching and rolling found in this paper is very interesting. Another difference of this sort was found many times in the textures of rolled and of stretched metals. Here one sees that, in the case of rolling, the pressure of the rolls causes a much more complicated bending of the lattice than in stretching. Therefore a large part of the hardening by rolling is due to this bending, whereas in stretching most hardening is due to gliding. But the glide hardening may disappear by recovery without recrystallization at lower temperatures, whereas bending needs recrystallization at temperatures, increasing with decreasing deformation. Therefore the recrystallization nuclei in the rolled metal would not be destroyed by recovery.

**Author's Reply**

The author wishes to thank Drs. Dehlinger and Raudebaugh for their discussions of this paper. Dr. Raudebaugh has made some very good constructive suggestions which should prove fruitful. It is pleasing to have Dr. Dehlinger concur in that deformation during rolling and stretching takes place by two different mechanisms. If his terminology is correctly understood, it appears that his theory of the mechanisms of the two processes is substantially the same as that postulated by the author. This is gratifying.

# TRANSFORMATIONS IN FERRITIC CHROMIUM STEELS BETWEEN 1100 AND 1500 °F (595 AND 815 °C)

By F. J. SHORTSLEEVE AND M. E. NICHOLSON

## Abstract

*An X-ray diffraction study was made of the ferrite/ferrite plus sigma phase boundary on the iron side of the iron-chromium diagram and of the characteristics of sigma formation in iron-chromium alloys of simulated commercial purity. It was found that the small amounts of silicon and manganese, which are usually introduced into ferritic chromium steels during the process of steelmaking, shift the phase boundary from the high-purity position toward lower values of chromium and higher temperatures. Sigma was detected in a low (0.1%) carbon alloy containing 18% chromium after aging at 1100 °F (595 °C). Carbon, which combines with chromium and iron to form cubic chromium-iron carbide, shifts the boundary to higher chromium contents. The threshold time for sigma formation is influenced by temperature and chromium content in the manner normally expected for a transformation proceeding by thermal nucleation and growth. The rate of formation of sigma is greatly accelerated by the presence of carbides and by the other steelmaking elements. The solubility of carbon in sigma was found to be less than 0.016% at 1100 °F (595 °C).*

AS early as 1927 some investigators (1, 2)<sup>1</sup> suggested that a compound exists in the iron-chromium system at about 50 atomic per cent chromium. However, it was not until 1936 that the intermetallic compound, FeCr, now commonly referred to as sigma, was identified definitely (3, 4). Although several investigators (5, 6) had attempted to establish the location of the ferrite/ferrite plus sigma phase boundary on the iron side of the diagram,<sup>2</sup> it was not until 1943, when Cook and Jones (7) reinvestigated the system using high-purity alloys, that the limits of this 2-phase region were established with reasonable certainty. The diagram

<sup>1</sup>The figures appearing in parentheses pertain to the references appended to this paper.

<sup>2</sup>Since this investigation was restricted to the iron side of the iron-chromium diagram, in the discussion, the ferrite/ferrite plus sigma phase boundary on the iron side of the diagram will be called, simply, the ferrite/ferrite plus sigma boundary.

A paper presented before the Thirty-second Annual Convention of the Society, held in Chicago, October 21 to 27, 1950. Of the authors, F. J. Shortsleeve is research engineer, and M. E. Nicholson is assistant section head, in the Materials Division, Engineering Research Department, Standard Oil Company (Indiana), Chicago. Manuscript received April 15, 1950.

proposed by Cook and Jones, Fig. 1, showed, at 1110 °F (600 °C), that the single-phase sigma region extended from 42 to 48% chromium and that sigma existed in alloys containing as little as 24% chromium.

From a study of the work of Andersen and Jette (3) and of Burgess and Forgeng (8) there was good reason to suspect that this boundary might be considerably altered by the small amounts of silicon and manganese which are usually introduced into ferritic chromium alloys during the process of steelmaking. Since no

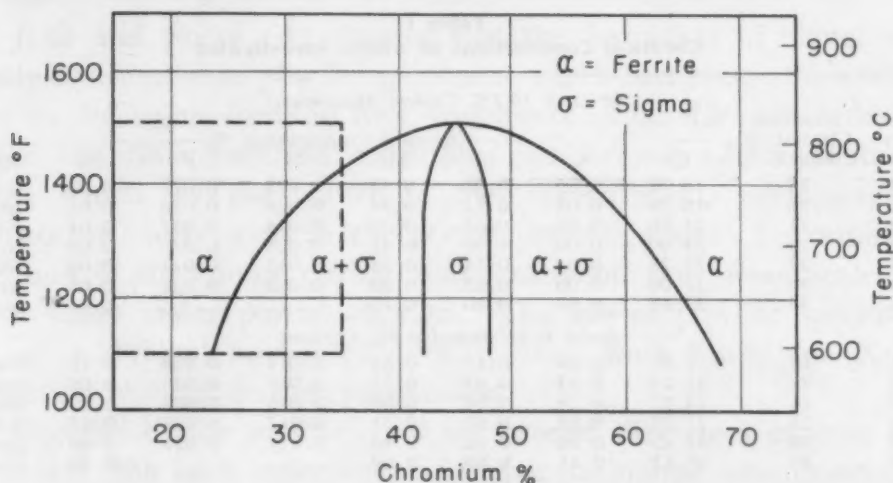


Fig. 1—Iron-Chromium Phase Diagram, After Cook and Jones (7). The dashed lines, on the left, outline the temperature and composition range covered in the present investigation.

reliable information was available showing the location of the ferrite/ferrite plus sigma boundary for commercial alloys,<sup>3</sup> the present investigation was undertaken.

The purpose of this study was to determine the location of the ferrite/ferrite plus sigma boundary for alloys of simulated commercial purity. Since we were concerned, therefore, only with the over-all effects of silicon and manganese, this work was not extended to a study of the individual effects of these elements on the phase boundary. The study was limited to alloys containing from 15 to 35% chromium and to temperatures from 1100 to 1500 °F (595 to 815 °C), i.e., the region enclosed by the dashed lines in Fig. 1. In addition to the determination of the phase boundary for simulated commercial alloys, the investigation included a study of the effects of carbon on the ferrite/ferrite plus sigma boundary, and the effect of temperature, of chromium, of carbon, and of the other steel-making elements on the rate of formation of sigma.

<sup>3</sup>Commercial alloys are considered as those containing up to about 0.3% carbon, about 0.5% each of manganese and silicon, and about 0.025% each of sulphur and phosphorus.



# TRANSFORMATIONS IN FERRITIC CHROMIUM STEELS BETWEEN 1100 AND 1500 °F (595 AND 815 °C)

By F. J. SHORTSLEEVE AND M. E. NICHOLSON

## Abstract

*An X-ray diffraction study was made of the ferrite/ferrite plus sigma phase boundary on the iron side of the iron-chromium diagram and of the characteristics of sigma formation in iron-chromium alloys of simulated commercial purity. It was found that the small amounts of silicon and manganese, which are usually introduced into ferritic chromium steels during the process of steelmaking, shift the phase boundary from the high-purity position toward lower values of chromium and higher temperatures. Sigma was detected in a low (0.1%) carbon alloy containing 18% chromium after aging at 1100 °F (595 °C). Carbon, which combines with chromium and iron to form cubic chromium-iron carbide, shifts the boundary to higher chromium contents. The threshold time for sigma formation is influenced by temperature and chromium content in the manner normally expected for a transformation proceeding by thermal nucleation and growth. The rate of formation of sigma is greatly accelerated by the presence of carbides and by the other steelmaking elements. The solubility of carbon in sigma was found to be less than 0.016% at 1100 °F (595 °C).*

AS early as 1927 some investigators (1, 2)<sup>1</sup> suggested that a compound exists in the iron-chromium system at about 50 atomic per cent chromium. However, it was not until 1936 that the intermetallic compound, FeCr, now commonly referred to as sigma, was identified definitely (3, 4). Although several investigators (5, 6) had attempted to establish the location of the ferrite/ferrite plus sigma phase boundary on the iron side of the diagram,<sup>2</sup> it was not until 1943, when Cook and Jones (7) reinvestigated the system using high-purity alloys, that the limits of this 2-phase region were established with reasonable certainty. The diagram

<sup>1</sup>The figures appearing in parentheses pertain to the references appended to this paper.

<sup>2</sup>Since this investigation was restricted to the iron side of the iron-chromium diagram, in the discussion, the ferrite/ferrite plus sigma phase boundary on the iron side of the diagram will be called, simply, the ferrite/ferrite plus sigma boundary.

A paper presented before the Thirty-second Annual Convention of the Society, held in Chicago, October 21 to 27, 1950. Of the authors, F. J. Shortsleeve is research engineer, and M. E. Nicholson is assistant section head, in the Materials Division, Engineering Research Department, Standard Oil Company (Indiana), Chicago. Manuscript received April 15, 1950.

proposed by Cook and Jones, Fig. 1, showed, at 1110 °F (600 °C), that the single-phase sigma region extended from 42 to 48% chromium and that sigma existed in alloys containing as little as 24% chromium.

From a study of the work of Andersen and Jette (3) and of Burgess and Forgeng (8) there was good reason to suspect that this boundary might be considerably altered by the small amounts of silicon and manganese which are usually introduced into ferritic chromium alloys during the process of steelmaking. Since no

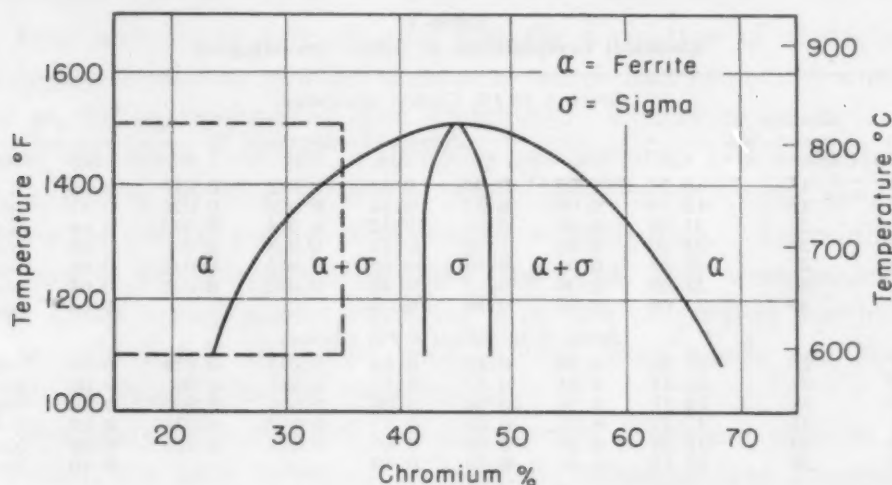


Fig. 1—Iron-Chromium Phase Diagram, After Cook and Jones (7). The dashed lines, on the left, outline the temperature and composition range covered in the present investigation.

reliable information was available showing the location of the ferrite/ferrite plus sigma boundary for commercial alloys,<sup>3</sup> the present investigation was undertaken.

The purpose of this study was to determine the location of the ferrite/ferrite plus sigma boundary for alloys of simulated commercial purity. Since we were concerned, therefore, only with the over-all effects of silicon and manganese, this work was not extended to a study of the individual effects of these elements on the phase boundary. The study was limited to alloys containing from 15 to 35% chromium and to temperatures from 1100 to 1500 °F (595 to 815 °C), i.e., the region enclosed by the dashed lines in Fig. 1. In addition to the determination of the phase boundary for simulated commercial alloys, the investigation included a study of the effects of carbon on the ferrite/ferrite plus sigma boundary, and the effect of temperature, of chromium, of carbon, and of the other steel-making elements on the rate of formation of sigma.

<sup>3</sup>Commercial alloys are considered as those containing up to about 0.3% carbon, about 0.5% each of manganese and silicon, and about 0.025% each of sulphur and phosphorus.

## MATERIALS

Two series of iron-chromium alloys of simulated commercial purity, denoted as A and B, were obtained from Crane Company; series A contained, nominally, 0.1% carbon, and series B, 0.3% carbon. In both series, the chromium content ranged from 15 to 35%, and silicon, manganese, nickel, molybdenum, phosphorus, and sulphur were present as steelmaking impurities. The chemical composition of each of these alloys is shown in Table I. The 35%

Table I  
Chemical Compositions of Alloys Investigated

Alloy No.	Nominal Chromium Content, %	Series A (0.1% Carbon Maximum)							
		Chemical Composition, %							
		Cr	C	Si	Mn	S	P	Ni	Mo
A-1	15	15.37	0.04	0.40	0.33	0.022	0.022	0.05	0.02
A-2	18	18.29	0.08	0.47	0.34	0.026	0.026	0.04	0.09
A-3	21	21.76	0.06	0.61	0.32	0.014	0.032	0.04	None
A-4	24	24.60	0.06	0.59	0.31	0.008	0.026	0.05	None
A-5	27	27.78	0.04	0.54	0.38	0.015	0.024	0.08	None
A-6	30	31.00	0.06	0.65	0.36	0.008	0.024	0.08	None
A-7	35	33.03	0.08	0.80	0.72	.....	.....	0.05	None
Series B (Nominal 0.3% Carbon)									
B-1	18	17.96	0.29	0.42	0.63	0.014	0.028	0.10	None
B-2	21	21.14	0.33	0.63	0.77	0.017	0.026	0.08	None
B-3	24	24.17	0.28	0.54	0.50	0.016	0.026	0.10	None
B-4	27	27.33	0.28	0.61	0.51	0.017	0.024	0.18	0.01
B-5	30	31.25	0.20	0.63	0.46	0.017	0.026	0.10	None
B-6	35	35.13	0.41	0.80	0.69	.....	.....	0.10	None
Series C (High Purity)									
		Cr	C	N					
C-1	35	34.75	0.01	0.002					
C-2	43	43.15	0.016	0.003					

chromium alloys were received in the cast condition, but all others were received in the hot-rolled condition.

Two high-purity iron-chromium alloys were obtained from Union Carbide & Carbon Research Laboratories. They contained, nominally, 35 and 43% chromium and are listed in Table I as alloys C-1 and C-2.

## EXPERIMENTAL PROCEDURE

*Carbide Precipitation*

Although the principal consideration of this investigation was the determination of the ferrite/ferrite plus sigma boundary, a preliminary study was made of the precipitation of cubic chromium-iron carbide to determine its relationship to the formation of sigma. In general, the techniques used for the carbide precipitation study were the same as those used for the determination of the ferrite/ferrite plus sigma boundary. Since the carbides frequently were

present in quantities so small that they could not be detected by the normal X-ray powder techniques, it sometimes was necessary to concentrate them by preferentially dissolving away the ferrite matrix in 1:1 HCl (specific gravity, 1.20). From these experiments it was found that, at sigma-forming temperatures, the precipitation of cubic chromium-iron carbide from ferrite was substantially complete before any sigma could be detected.

*Determination of the Ferrite/Ferrite Plus Sigma Boundary  
in the Presence of Carbides*

Jette and Foote (4) showed that the formation of sigma was greatly accelerated in powder specimens which had been cold-worked prior to the sigma-forming heat treatment. Therefore, in order to reduce the time required to attain equilibrium, 170-mesh metal filings, which, by the nature of their preparation, were severely cold-worked, were used in the present investigation. To minimize oxidation of the filings during heat treatment, they were sealed in Vycor tubes under partial vacuum. The use of powder specimens had an additional advantage because they were ready for X-ray diffraction without further preparation.

Because of the similarity of the atomic diameters of iron and chromium, the back reflection parametric technique was unsatisfac-

**Table II**  
**Heat Treatments Used to Establish Ferrite/Ferrite Plus Sigma Boundary**

Series A (0.1% Carbon Maximum)				
Alloy No.	Nominal Chromium Content, Weight %	Temperature		Time at Temperature, Hours
		°F	°C	
A-1	15	1100	593	1000
A-2	18	1100	593	310
A-4	24	1200	649	165
A-4	24	1225	663	120
A-4	24	1275	690	43
A-4	24	1300	704	65
A-6	30	1300	704	65
A-6	30	1375	746	64
A-6	30	1425	774	52
A-6	30	1475	801	46
A-7	35	1300	704	65
A-7	35	1375	746	64
A-7	35	1425	774	6
A-7	35	1450	788	9
A-7	35	1475	801	46
Series B (Nominally 0.3% Carbon)				
B-1	18	1100	593	935
B-2	21	1100	593	25
B-2	21	1200	649	500
B-3	24	1175	635	235
B-3	24	1225	663	163
B-3	24	1300	704	65
B-5	30	1300	704	65
B-5	30	1375	746	232
B-5	30	1425	774	152
B-5	30	1475	801	140
B-6	35	1450	788	70
B-6	35	1480	804	180
B-6	35	1500	816	150



tory for locating the ferrite/ferrite plus sigma boundary. Therefore, the disappearing phase method was selected. Since the extremely low rate of sigma formation near the phase boundary had led to errors in the work of other investigators, in the present study two specimens of the same alloy were aged at each temperature. Prior to the aging treatment, one of these was heat treated to develop sigma so that a specimen containing sigma and a sigma-free specimen were aged simultaneously. It was assumed that equilibrium had been attained when the X-ray diffraction patterns showed that both specimens contained the same phases. In this way the ferrite/ferrite plus sigma boundary in the presence of carbides was determined between 1100 and 1500 °F (595 and 815 °C) for the series A and series B alloys. Throughout these experiments the heat treating temperatures were controlled within plus or minus 5 °F of the desired temperature. The heat treatments used are listed in Table II. The X-ray diffraction patterns were made using a 143-mm diameter powder camera and unfiltered chromium radiation.

#### *Determination of the Rate of the Reaction:*

##### *Ferrite to Ferrite Plus Sigma, in the Presence of Carbides*

In order to study the influence of temperature on the rate of sigma formation in the presence of carbides, a series of powder specimens of alloys A-4 (24% chromium), A-6 (31% chromium) and A-7 (33% chromium) were aged isothermally at various temperatures between 1050 and 1450 °F (565 and 790 °C). X-ray powder patterns were made of these samples in order to determine the minimum aging time required to develop enough sigma to produce detectable X-ray diffraction lines. This time will be referred to as the threshold time.

The influence of chromium, of carbon, and of the other steel-making elements on threshold time was investigated by employing similar techniques.

## RESULTS

The ferrite/ferrite plus sigma boundary, in the presence of carbides, is shown in Fig. 2, for the series A low (0.1%) carbon steels, and in Fig. 3, for the series B high (0.3%) carbon steels. All points on the diagrams represent equilibrium conditions, as determined by the two-specimen technique, except the points at 1100 °F (595 °C) for the 15% chromium low carbon and the 18% chromium high carbon alloys. Because of the very low reaction rate at lower temperatures it was not practical to develop sigma in

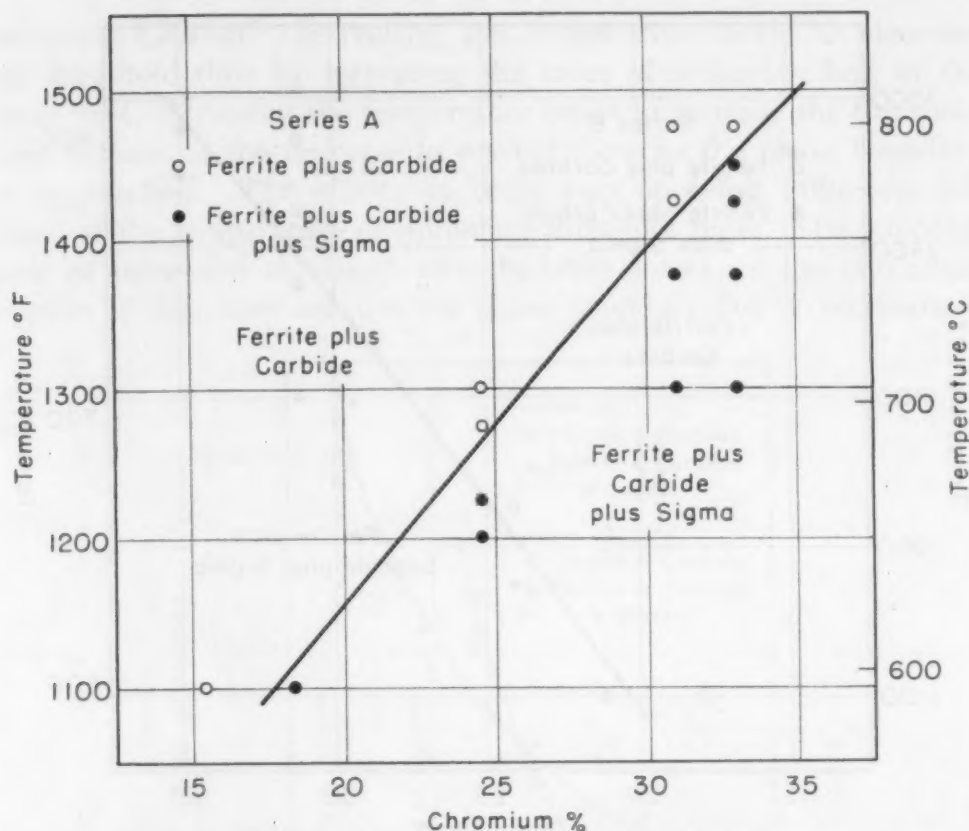


Fig. 2—Ferrite/Ferrite Plus Sigma Boundary, in the Presence of Carbides, for Iron-Chromium Steels Containing Less Than 0.1% Carbon.

either of these alloys before aging them at 1100 °F (595 °C). Therefore, these two points indicate only that sigma could not be developed in powder specimens of these alloys by holding them 1000 hours at 1100 °F (595 °C). The signature lines of sigma were detected readily in the low carbon 18% chromium alloy (A-2) and in the high carbon 21% chromium alloy (B-2) after aging at 1100 °F (595 °C). Since a certain minimum quantity of sigma had to be present before it could be detected by X-ray diffraction methods, the boundary of the ferrite plus sigma region, at 1100 °F (595 °C), was conservatively located at 17.5% chromium for the low carbon (series A) alloys and at 20.5% chromium for the high carbon (series B) alloys.

The times required to develop the equilibrium phases in these alloys varied substantially, depending upon alloy composition and temperature. In Fig. 4, the sigma threshold times for cold-worked powder specimens are plotted as a function of temperature for the 24, 31 and 33% chromium alloys of series A. These curves show the effect of two opposing influences and exhibit the characteristic shape expected for the usual thermal nucleation and growth type

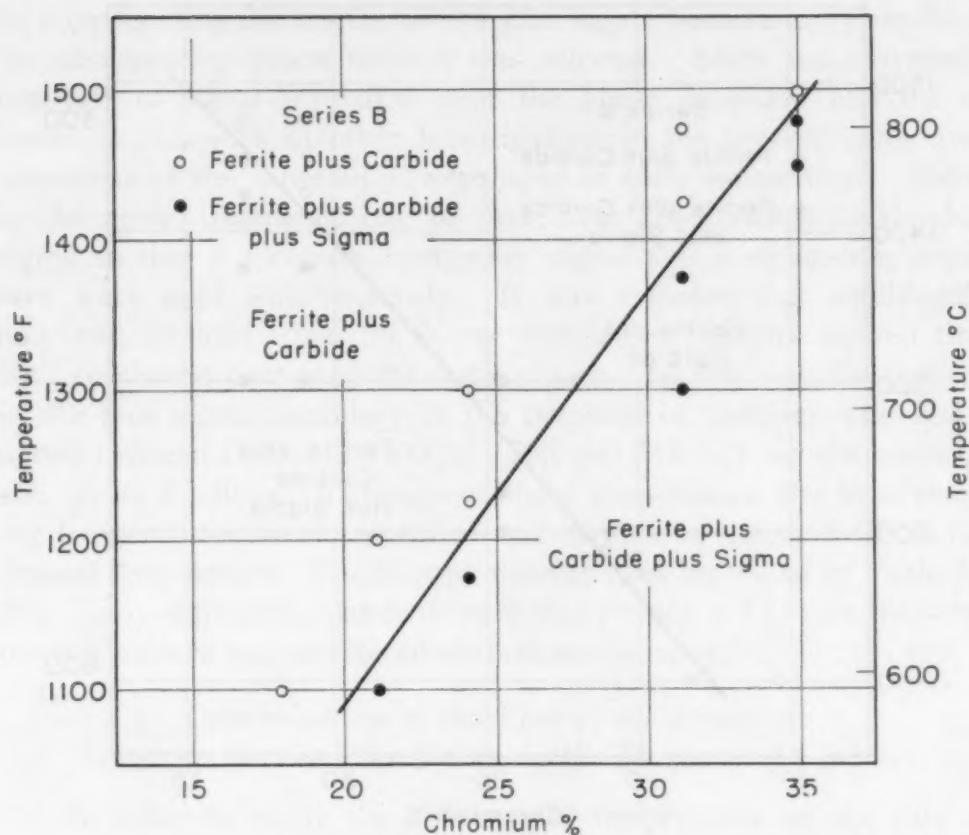


Fig. 3—Ferrite/Ferrite Plus Sigma Boundary, in the Presence of Carbides, for Iron-Chromium Steels Containing, Nominally, 0.3% Carbon.

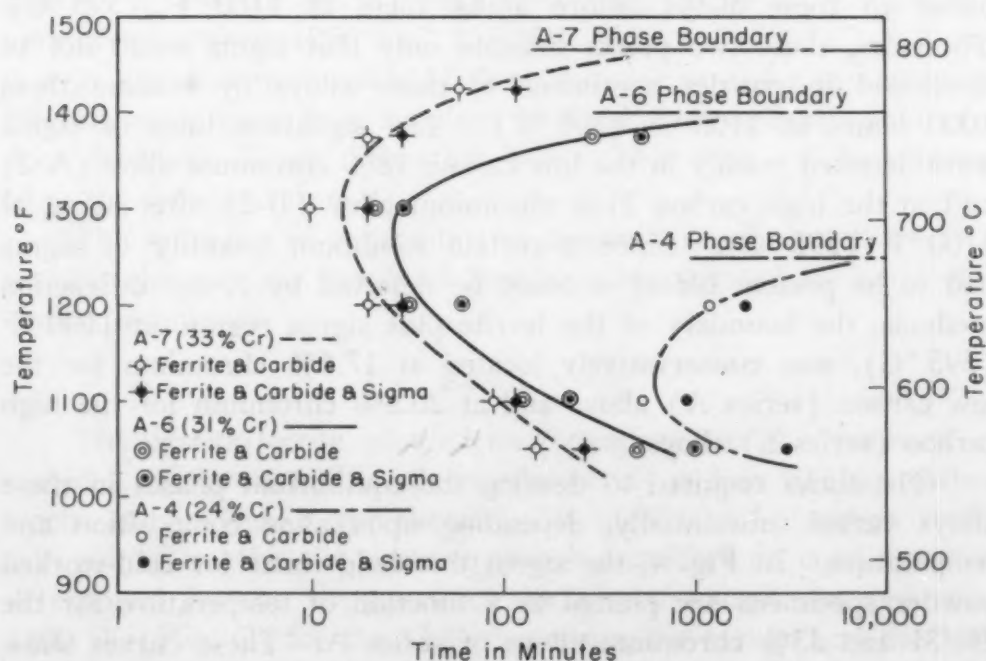


Fig. 4—Time-Temperature-Transformation Curves of the Ferrite to Ferrite Plus Sigma Transformation in the 24, 31 and 33% Chromium Alloys of Series A.

of transformation. Increasing the temperature tends to decrease the threshold time by increasing the rates of diffusion; but, at the same time, increasing the temperature tends to increase the threshold time because of the decrease in driving force as the phase boundary is approached. The effects of these two opposing influences are equal at the temperature of minimum threshold time. The temperature of minimum threshold time becomes lower as the chromium content is decreased because the phase boundary lies at successively

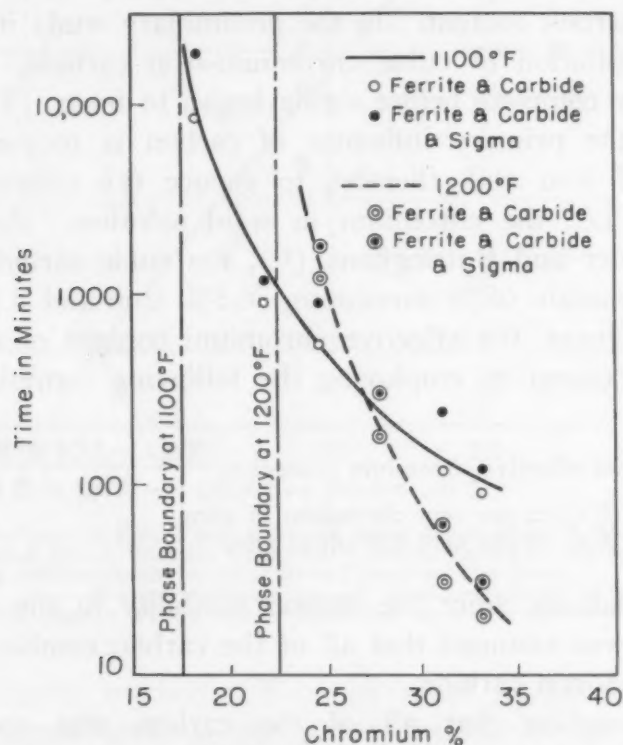


Fig. 5—The Effect of Chromium Content on the Threshold Times of Sigma Formation in the Alloys of Series A at 1100 and 1200°F (595 and 650°C).

lower temperatures as the chromium content decreases. It will be noted also that, as the temperature of minimum threshold time decreases, the threshold time itself increases.

The threshold times of sigma formation at 1100 and 1200 °F (595 and 650 °C) are plotted as a function of chromium content in Fig. 5. At either 1100 or 1200 °F (595 or 650 °C), decreasing the chromium content markedly increases the threshold times for sigma formation. Both of these curves appear to approach the phase boundary composition asymptotically.

In considering the significance of the data in Figs. 4 and 5 it must be remembered that cold-worked powder specimens were used for the determinations and that the rates of sigma formation



are more rapid than those which would be encountered in process equipment.

### DISCUSSION OF RESULTS

#### *Influence of Minor Elements on the Ferrite/Ferrite Plus Sigma Boundary in the Presence of Carbides*

The difference in phase boundary location for the series A and series B alloys (cf. Figs. 2 and 3) is principally the result of the difference in carbon content. In the preliminary study it was found that the precipitation of cubic chromium-iron carbide,  $(\text{Cr,Fe})_4\text{C}$ , was apparently complete before sigma began to form. Therefore, it appears that the primary influence of carbon is to combine with chromium and iron and, thereby, to reduce the effective amount of chromium, i.e., the chromium in solid solution. According to Tofaute, Küttner and Büttinghaus (9), the cubic carbide for these alloys should contain 68% chromium, 26.5% iron and 5.5% carbon. Using these figures, the effective chromium content of each of the alloys was calculated by employing the following formula:

$$\text{Per cent effective chromium content} = \frac{\% \text{ Cr} - 12.4 \times \% \text{ C}}{1 - 0.182 \times \% \text{ C}}$$

where % Cr = per cent chromium in alloy  
% C = per cent carbon in alloy

In these calculations, since the carbon solubility in the ferrite was very small, it was assumed that all of the carbon combined to form cubic chromium-iron carbide.

The assumption that all of the carbon was combined as chromium-iron carbide can be made only if there is no appreciable solubility of carbon in sigma. To determine the order of magnitude of the carbon solubility in sigma, alloy C-2 (43.15% chromium, 0.016% carbon) was aged at 1400 °F (760 °C) for 48 hours, and at 1100 °F (595 °C) for 6 hours, and then water-quenched. This treatment was sufficient to transform all of the ferrite to sigma. After concentration in 1:1 HCl (specific gravity, 1.20) the residue from this specimen was found, by X-ray diffraction methods, to contain cubic chromium-iron carbide. Since the original specimen contained only 0.016% carbon, the carbon solubility in sigma at 1100 °F (595 °C) must be less than this amount.

In Fig. 6, the data for the series A and B alloys have been replotted as a function of temperature and effective chromium content. When the data are replotted in this way, it is apparent that the two phase boundaries are identical within the limitation of

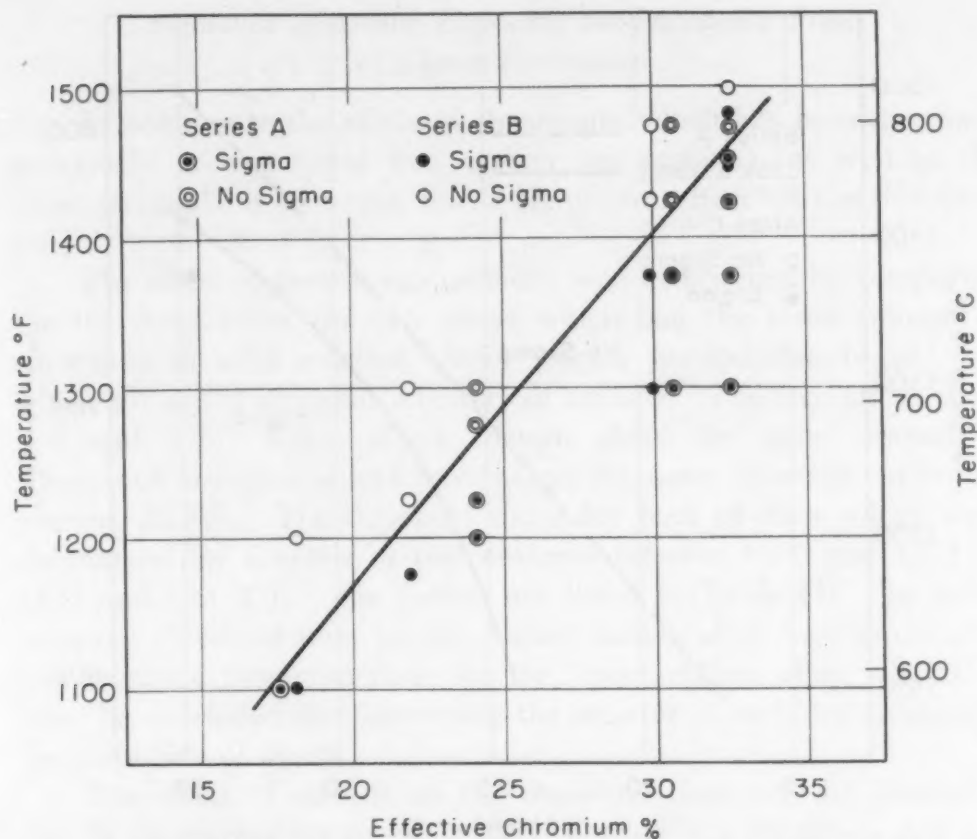


Fig. 6—Data of Figs. 2 and 3, for the Series A and Series B Alloys, Replotted as a Function of the Effective Chromium Content, Showing That the Two Phase Boundaries Are Practically Identical When Plotted on This Basis.

Note: Since effective chromium content is plotted instead of total chromium content, this diagram should not be considered as a true constitutional diagram.

the experimental method. Thus, it must be concluded that the major difference between the phase boundaries for the series A and series B alloys is the result of a reduction in the chromium content of the ferrite brought about by the formation of cubic carbide.

In order to show the difference between the location of the phase boundary for high-purity alloys and that for the simulated commercial alloys in series A, both boundaries have been redrawn in Fig. 7. In general, the phase boundary for alloys of simulated commercial purity extends to lower chromium contents and to higher temperatures than the boundary for high-purity alloys. This difference is not unexpected in the light of work by Andersen and Jette (3) and by Burgess and Forgeng (8). Nevertheless, it was observed with considerable interest that as little as about 0.5% silicon and 0.5% manganese appeared to shift the boundary as much as about 7% chromium at 1100 °F (595 °C).

In order to demonstrate that the boundary shift was real and not simply the result of a difference in the two experimental tech-

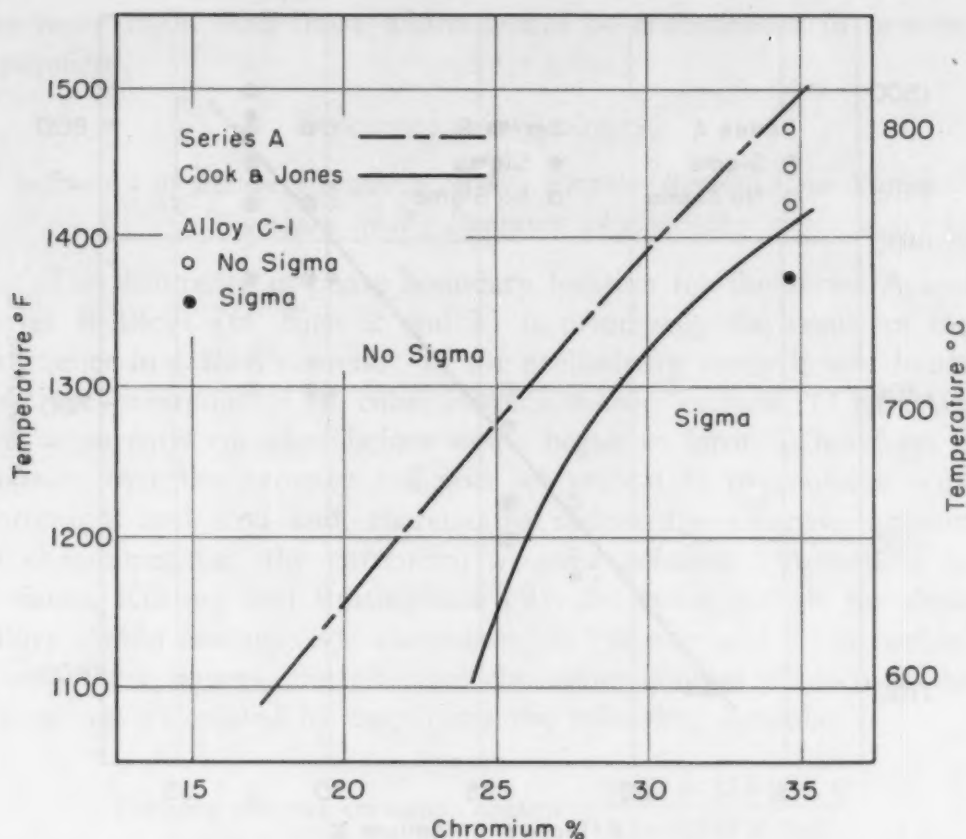


Fig. 7—A Comparison of the Phase Boundary for the Series A Alloys With the Boundary for High-Purity Alloys, After Cook and Jones (7). Also plotted are the equilibrium phase results for the high-purity alloy C-1.

niques, the high-purity phase boundary was checked with a 35% chromium alloy, C-1, using the 2-specimen technique. The results of this experiment, also included in Fig. 7, indicate that the Cook and Jones boundary represents equilibrium conditions at 35% chromium. On the other hand, it appears that the lower limit of the Cook and Jones ferrite plus sigma region at 1100 °F (595 °C), determined from the results with a 24% chromium alloy, may not represent equilibrium conditions. Based on our work, it would seem that, if the 24% chromium alloy which was aged only 720 hours at 1112 °F (600 °C) had been aged for about 2500 hours, sigma might have developed. Therefore, at a temperature of 1100 °F (595 °C) the boundary shift may not actually be as great as 7% chromium, but something less, perhaps 5%.

Although it cannot be stated with absolute certainty which of the four steelmaking elements present were most effective in shifting the phase boundary, it appears likely that only the influence of the silicon and manganese is important.

*Influence of Minor Elements on Threshold Time  
of Sigma Formation*

In addition to the effect of chromium, which has been discussed previously, it was found that carbon (as carbide), as well as the other steelmaking elements, had a significant effect on the threshold time.

The effect of carbon (as carbide) was determined by comparing the threshold times for two alloys which had the same amount of chromium in solid solution (before sigma precipitation began) but which contained different amounts of carbide. The two alloys were A-7 and B-6. These alloys contain about the same amount of silicon and manganese and have about the same effective chromium content, 32.5%. The threshold times for both of these alloys were determined for a series of temperatures between 1100 and 1375 °F (595 and 745 °C). The results are listed in Table III. In every case, the threshold time for the higher carbon alloy was appreciably less than the threshold time for the lower carbon alloy. Thus, it must be concluded that increasing the amount of carbides accelerates the formation of sigma.

The effect of carbide on the threshold time may be illustrated also by comparing the times at 1050 °F (565 °C) for alloys A-6 and B-5. Both of these alloys have substantially the same chromium, silicon and manganese contents, as shown in Table III, but B-5

**Table III**  
**Effects of Carbide on the Threshold Time of Sigma Formation**

Alloy No.	Chemical Composition, %				Effective Chromium Content	Threshold Time of Sigma Formation, in Minutes, at				
	Cr	C	Si	Mn		1050 °F (565 °C)	1100 °F (595 °C)	1200 °F (650 °C)	1300 °F (705 °C)	1375 °F (745 °C)
A-7	33.03	0.08	0.80	0.72	32.5	.....	90-120	20-30	20-30	20-30
B-6	35.13	0.41	0.80	0.69	32.5	.....	45-60	10-20	0-10	0-10
A-6	31.00	0.06	0.65	0.36	30.6	540-915	.....	.....	.....	.....
B-5	31.25	0.20	0.63	0.46	29.9	300-540	.....	.....	.....	.....

has a somewhat higher carbon content than A-6 and consequently a lower effective chromium content. Despite the decreased driving force which results from this decreased chromium content of the ferrite, the threshold time for alloy B-5 is less than that for A-6. This can be only the result of the accelerating effect of the greater amount of carbide in alloy B-5.

The effect of the other steelmaking elements on the threshold time can be shown by comparing the times at 1100 °F (595 °C) for alloys C-1 (high purity), A-7 and B-6. These data are listed



**Table IV**  
**Effect of Steelmaking Elements on the Threshold Time of Sigma Formation**

Alloy No.	Chemical Composition, %				Threshold Time of Sigma Formation, in Minutes, at 1100°F (595°C)
	Cr	C	Si	Mn	
C-1	34.75	0.01	....	....	1440-2160
A-7	33.03	0.08	0.80	0.72	90- 120
B-6	35.15	0.41	0.80	0.69	45- 60

in Table IV. Although the ferrite of the series A alloy contains less chromium than the ferrite of the high-purity alloy (before sigma precipitation begins), the threshold time of the high-purity alloy is many times greater than that for the simulated commercial alloy. This marked difference undoubtedly results from the presence of the steelmaking elements other than carbon. Although it has been established that an increase in the amount of carbide will accelerate the formation of sigma, a comparison of the three alloys in Table IV shows that an increase of 0.07% carbon, 0.72% manganese and 0.80% silicon (C-1 to A-7) produces a much greater acceleration than an increase of 0.33% carbon (A-7 to B-6).

#### CONCLUSIONS

As a result of this investigation, it may be concluded that, for ferritic chromium steels containing less than 35% chromium:

1. The small amounts of silicon and manganese, usually found in commercial alloys, displace the ferrite/ferrite plus sigma phase boundary to lower values of chromium than were found by Cook and Jones for high-purity alloys. As a result of this displacement, at 1100°F (595°C), sigma can be formed in 0.1% carbon iron-chromium alloys of simulated commercial purity containing as little as 18% chromium.
2. Carbon in excess of its solubility limit in ferrite depletes the ferrite of chromium by forming cubic chromium-iron carbide,  $(\text{Cr,Fe})_4\text{C}$ , thus causing a displacement of the ferrite/ferrite plus sigma boundary to higher values of total chromium.
3. The effective chromium content of the alloy, i.e., the chromium content of the ferrite, may be computed with reasonable accuracy from the formula:

$$\text{Per cent effective chromium content} = \frac{\% \text{ Cr} - 12.4 \times \% \text{ C}}{1 - 0.182 \times \% \text{ C}}$$

where % Cr = per cent chromium in alloy  
 % C = per cent carbon in alloy

4. The formation of cubic chromium-iron carbide occurs much more rapidly than the formation of sigma.
5. The time, at constant temperature, required to form sufficient sigma to be detected by X-ray powder diffraction methods increases

as the chromium content is decreased and appears to become asymptotic to the phase boundary composition.

6. The threshold time versus temperature curves for the ferrite to ferrite plus sigma reaction have the shape characteristic of transformations which proceed by thermal nucleation and growth.

7. The ferrite to ferrite plus sigma reaction is accelerated appreciably by increasing the amount of carbide particles present.

8. The ferrite to ferrite plus sigma reaction is accelerated greatly by the steelmaking elements, other than carbon, that are dissolved in the ferrite.

9. In a high-purity iron-chromium alloy containing 43% chromium, the solubility of carbon in sigma at 1100 °F (595 °C) is less than 0.016%.

#### ACKNOWLEDGMENTS

The authors are indebted to Standard Oil Company (Indiana) for permission to publish the results of this investigation which was part of a cooperative research program on stainless steels undertaken by Standard Oil Company (Indiana) and Crane Co.

The assistance of Messrs. J. P. Magos, N. A. Ziegler, W. L. Meinhart and J. R. Goldsmith, of Crane Co., and of Dr. P. K. Koh, now of Allegheny Ludlum Steel Corporation, in securing the alloys of simulated commercial purity, and of Dr. A. B. Kinzel, of Union Carbide & Carbon Research Laboratories, in securing the high-purity alloys, also is gratefully acknowledged. Without the encouragement and advice of Mr. G. W. Watts, Dr. C. H. Samans and the Crane Co. group, and the assistance of our colleagues in the Engineering Research Department, this work never would have been possible.

#### References

1. P. Chevenard, "Recherches experimentales sur les alliages der fer, de nickel, et de chrome", *Trav. Mém. Bur. Int. Poids et Mesures*, Vol. 17, 1927, p. 90.
2. E. C. Bain and W. E. Griffiths, "An Introduction to the Iron-Chromium-Nickel Alloys", *Transactions*, American Institute of Mining and Metallurgical Engineers, Vol. 75, 1927, p. 166-213.
3. A. G. H. Andersen and E. R. Jette, "X-ray Investigation of the Iron-Chromium-Silicon Phase Diagram", *TRANSACTIONS*, American Society for Metals, Vol. 24, 1936, p. 375-419.
4. E. R. Jette and F. Foote, "The Fe-Cr Alloy System", *Metals and Alloys*, Vol. 7, 1936, p. 207-210.
5. F. Wever and W. Jellinghaus, "Zur Kenntnis des Zweistoffsystems Eisen-Chrom", *Mitteilungen aus dem Kaiser-Wilhelm-Institut für Eisenforschung*, Vol. 13, 1931, p. 143-147.
6. E. C. Bain and R. H. Aborn, "Constitution of Iron-Chromium Alloys", *Metals Handbook*, American Society for Metals, Cleveland, 1939, p. 374-376.

7. A. J. Cook and F. W. Jones, "The Brittle Constituent of the Iron-Chromium System (Sigma Phase)", *Journal, Iron & Steel Institute*, Vol. 148, No. II, 1943, p. 217-223.
8. C. O. Burgess and W. D. Forgeng, "Constitution of Iron-Chromium-Manganese Alloys", *Transactions, American Institute of Mining and Metallurgical Engineers*, Vol. 131, 1938, p. 277-302.
9. W. T. Tofaute, C. Küttner and A. Büttinghaus, "Das System Eisen-Chrom-Chromkarbid  $\text{Cr}_7\text{C}_3$ -Zementit", *Archiv für das Eisenhüttenwesen*, Vol. 9, 1936, p. 606-616.

## DISCUSSION

**Written Discussion:** By Francis B. Foley, International Nickel Co., Research Laboratory, Bayonne, N. J.

One of the most interesting observations in this very valuable and carefully conducted investigation of sigma formation is that bearing on the effect of carbon on the transformation. The authors' work leads to the very logical statement: "It must be concluded that increasing the amount of carbides accelerates the formation of sigma."

It has been my observation, and I am sure that of others as well, that sigma is habitually associated with the carbides in commercial alloys in which they are both present. This habitual juxtaposition of these two phases in the microstructure has led me to suspect and to state in discussions that the sigma transformation may be nucleated by carbides. This thought was prompted by the necessity of attaining a local enrichment in chromium (and sometimes other elements normally present in carbide form) in order to form sigma, the higher chromium being present in the chromium carbide from which it might diffuse into the adjacent ferrite.

In the present work the authors show that the presence of carbides shortens the "threshold time" for sigma formation, at the same time increasing the percentage of chromium at which sigma begins to be formed. This latter effect is rightly attributed to a decrease in the amount of "effective" chromium remaining in the alloy after the chromium carbide has been formed. If, as I have suggested above, chromium then diffuses back from the carbide into the alloy in order to supply the amount necessary to form sigma, the presence of carbides would not have the effect of shifting the incidence of sigma to higher chromium contents as shown by these investigators. It would seem, then, that the effect of carbides in shortening the "threshold time" is not one of chemical nucleation through chromium enrichment of the neighboring metal but, more likely, a local straining of the lattice, incident to the formation of the carbide, a very effective means of starting the transformation. If the carbide formation could be followed by strain relieving prior to "sigmatizing", the nature of this effect of the presence of carbides might be clarified. In the case of the present work this might be accomplished by precipitating the carbides at a temperature above that of sigma formation, cooling rapidly, obtaining the 170-mesh cold-worked filings and reheating them to produce sigma.

**Written Discussion:** By Carl A. Zapffe, consulting metallurgist, Baltimore, Md.

This paper presents some information which metallurgists interested



in stainless steels will welcome. In preparing the recent book, "Stainless Steels",<sup>4</sup> the problem arose of submitting to the more or less practical reader a constitutional diagram for the sigma area which would be theoretically sound, and yet would be helpful to people experiencing problems with sigma. Cook and Jones had brought the iron-rich boundary down to 24% at 1110 °F (600 °C), but a number of persons handling the ferritic stainless steels had encountered difficulties readily attributed to sigma phase, except that the steels had only 20% chromium, and sometimes as low as 17% chromium. German investigators had at one time or another extended the sigma boundary down toward 17%, but their argument rested largely upon including "890 °F (475 °C) embrittlement" as an expression of sigma phase. There is not much reason as yet for accepting this to be true.

While the development of sigma phase in the studies of the present authors has been greatly expedited by utilizing cold-worked powders, nevertheless their placement of the sigma boundary has full validity from theoretical standpoints, and now provides a basis for understanding the occurrence, occasional as it may be, of sigma-phase problems in such Class II steels as Type 442 (21% Cr) and Type 430 (17% Cr). Some of these steels serve tens of thousands of hours within the embrittling range, and it is not surprising therefore that equilibrium is closely approached and that the farthest reaches of the sigma area are exploited.

**Written Discussion:** By J. J. Heger, research associate, Carnegie-Illinois Steel Corp., Pittsburgh.

We are indebted to Messrs. Shortsleeve and Nicholson for their excellent contribution to our knowledge of the existence of sigma phase in the ferritic chromium steels. Too often, investigators of these steels neglect the fact that reaction times required to produce sigma phase are extremely long. Fortunately, Messrs. Shortsleeve and Nicholson have recognized this fact and, as a result, their investigation is one of the few of the nature that can be accepted with confidence.

Investigations which are now being conducted in Carnegie-Illinois Steel Corp. on the ferritic chromium steels indicate that the boundary established by the authors between the ferrite and ferrite-sigma regions for the 0.10% carbon steels is substantially correct, at least over the temperature and composition ranges investigated. At lower temperatures, a slight disagreement occurs.

In our investigations, cold-worked samples of 12 and 14% chromium steels were heated for 5000 hours at 900 and 1050 °F (480 and 565 °C). Metallographic examination of these samples revealed that sigma had formed in the 14% chromium steel but not in the 12% chromium steel. At 1050 °F (565 °C), these results agree with those of the authors, at least within experimental error; however, at 900 °F (480 °C), the absence of sigma in the 12% chromium sample is not predicted by an extrapolation of the authors' boundary line. Undoubtedly, one explanation for this lack of agreement is that the exposure time of 5000 hours at 900 °F (480 °C) is not long enough for equilibrium, even in drastically cold-worked samples. Another explanation is that an extrapolation of the authors' boundary to lower temperatures is unjustified because probably

<sup>4</sup>Published by the American Society for Metals, 1949, 368 pages.



the boundary bends sharply downward at about 10 or 12% chromium. In any event, the heating of these cold-worked samples is being continued, and examinations will be made at the end of 10,000 and 20,000 hours' exposure.

**Written Discussion:** By Howard R. Spendelow, Jr., and W. O. Binder, research metallurgists, Union Carbide & Carbon Research Laboratories, Niagara Falls, N. Y.

The authors are to be commended for their work in establishing the ferrite/ferrite plus sigma phase boundary of the iron-chromium system, particularly at the lower levels of chromium, and in showing the dependency of this phase boundary on the normal steelmaking impurities. There is still another impurity, however, perhaps overlooked because of the fact that often no attempt is made to control it, and that impurity is nitrogen. In air-melted steels, this element varies with the chromium content, and would be expected to combine with chromium in much the same manner as does carbon, resulting in the precipitation of chromium nitrides, and the further depletion of chromium in solid solution. While the total influence of nitrogen on effective chromium in solid solution is probably less than that of carbon because of its lower content, its influence on the rate of sigma formation must not be overlooked.

In a paper presented before this Society,<sup>5</sup> we have studied the influence of small amounts of carbon and nitrogen on the toughness of chromium-iron alloys and have shown that at certain levels of chromium, carbon and nitrogen appear to be interchangeable in their effects, and in view of this, we wonder whether the influence of nitrogen on the ferrite/ferrite plus sigma phase boundary shift would not be additive to that of carbon.

The authors show the phase boundary for a high-purity 35% chromium alloy to be of the order of 1400 °F (760 °C), which raises another interesting point. The high temperature embrittlement of high-chromium alloys is generally believed to be due to the formation of sigma phase, and from this work it would appear that there should be some difference in the mechanical properties of specimens of this alloy heated to temperatures a little above and a little below 1400 °F (760 °C). We have studied the embrittlement characteristics of this steel over a wide range of temperatures, and found that the embrittlement range does not coincide with the observed ferrite/ferrite plus sigma boundary. Though the alloy possessed a notched Izod impact strength of some 80 foot-pounds when quenched from 1650 °F (900 °C), heating the alloy at temperatures from 750 to 1520 °F (400 to 825 °C) for 100 hours reduced this to the order of 5 foot-pounds.

Hence, one must conclude either that the X-ray method for establishing phase boundaries is not entirely accurate under these conditions, or that embrittlement by sigma phase in high-chromium alloys may be affected either by very small amounts of the compound, or by its precipitation in a particle size less than the critical necessary for detection by X-rays.

<sup>5</sup>W. O. Binder and H. R. Spendelow, Jr., "The Influence of Chromium on the Mechanical Properties of Plain Chromium Steels", see this volume, p. 759.

## Authors' Reply

The comments of the discussers are especially appreciated, since they come from such authorities on stainless steels as Messrs. Foley, Zapffe, Heger, and Binder and Spendelow.

Mr. Foley has suggested that carbides may reduce the threshold time for sigma formation by producing strain in the neighboring lattice during their formation, thereby making it easier for sigma to form in the vicinity of a carbide particle. We agree that the formation of carbide is accompanied by a severe lattice distortion which influences the rate of sigma formation. However, since a linear expansion of about 2% occurs, this distortion is probably both elastic and plastic when  $\text{Cr}_7\text{C}_3$  ( $\text{Cr}_{23}\text{C}_6$ ) precipitates from a chromium steel. Thus, even though a specimen was stress-relieved, a region of atomic disorder, which would accelerate the rate of sigma formation in these regions, still would remain around the carbide particle.

Experiments which show the effect of pretreatment on the rate of sigma formation indicate that the factors governing this reaction are more complex than have been outlined in the paper. This is evident from the data summarized in Table V, which shows the phases developed in a 30% chromium steel in 100 hours at 1100 °F (595 °C) after pretreating 24 hours

Table V  
Phases Present in 30% Chromium Steel After Aging 100 Hours at 1100 °F Following Various Pretreatments

Pretreating Temperature	Sigma Present
None	Strong
1400 °F	Moderately Strong
1600 °F	None
2000 °F	None
2200 °F	None

at the indicated temperatures. All of the specimens were cold-worked in a mortar and pestle between the pretreatment and the 1100 °F (595 °C) aging. After 24 hours at 1400 °F (760 °C) the sample undoubtedly was completely stress-relieved and the maximum amount of carbide had formed. Therefore, according to the stress-relief hypothesis, this specimen should have transformed much more slowly than the reference specimen which had no pretreatment. Actually, the rates of formation for these two specimens were not markedly different. At 1600 °F (870 °C) the specimen should have been completely stress-relieved but less carbide should have been formed than at 1400 °F (760 °C). Therefore, upon subsequent aging at 1100 °F (595 °C), additional carbide should precipitate. This additional carbide should have accelerated sigma formation so that the amount of sigma formed should have been intermediate between the 1400 °F (760 °C) specimen and the specimen which received no pretreatment. This was not observed. In fact, the 1600 °F (870 °C) pretreatment greatly reduced the rate of sigma formation. Similar behavior was observed in specimens pretreated at 2000 and 2200 °F (1095 and 1205 °C), temperatures at which the carbide was almost completely dissolved. According to the stress-relief hypothesis, these specimens should have

developed about the same amount of sigma as in the sample without pretreatment. Thus, it appears that the sigma transformation is influenced by:

1. Temperature and time of aging in the sigma-forming region.
2. Presence of carbides.
3. Presence of alloying elements in solid solution in ferrite.
4. Prior treatment.

It is possible to explain these results on the basis of the Hollomon-Turnbull nucleation theory. However, critical experiments to support this theory have not been performed.

There are certain unpublished indications that secondary transformations, which influence the rate of embrittlement at 885 °F (475 °C), may be occurring in the iron-chromium system outside the region of sigma formation. It may be these transformations which cause the embrittlement observed by Binder and Spendelow after aging above the sigma-forming temperatures.

Regarding Mr. Heger's comments on a straight-line extrapolation of our phase boundary to 12% chromium, we have no data to show whether this extrapolation is justified. However, additional data for the 15% chromium (low-carbon) alloy A-1 shows that the phase boundary at 15% lies between 1080 and 1100 °F (580 and 595 °C). Therefore, it would appear that alpha/alpha plus sigma phase boundary must change direction abruptly between 12 and 15% chromium, if sigma cannot be formed in a 12% chromium alloy of commercial purity. We shall look forward with a great deal of interest to seeing the results from Mr. Heger's 10,000-hour 12% chromium specimen.

## HARDENING OF HIGH-CHROMIUM STEELS BY SIGMA PHASE FORMATION

By JOHN J. GILMAN

### *Abstract*

*The hardening of four high-chromium austenitic-ferritic steels by sigma formation is discussed. The mechanism of the hardening phenomenon is indicated by a correlation between the logarithm of the average path in the austenite and the hardness. The effects of the following variables on the hardening phenomenon are discussed:*

- A. Composition*
- B. Temperature*
- C. Initial ferrite content*
- D. Cold working*
- E. Annealing*
- F. Rolling temperature*
- G. Casting method*
- H. Cast versus wrought material*
- I. Recrystallization*

*Data are presented which indicate the effect of the composition of commercial steels on the rate of sigma formation at a given temperature, the upper limit of the sigma formation range, and the temperature below which sigma forms at a negligible rate.*

THE steels of the group which will be called sigma-hardenable high-chromium steels have the important ability to harden at high temperatures (1200 to 1600 °F) and to retain their hardness for an indefinite period of time at the hardening temperature. Because of this ability, they are useful for applications involving high temperature erosion or wear. They are high-chromium steels (20 to 30%) containing medium carbon, and various amounts of manganese and nickel to render them partially austenitic, and silicon, molybdenum, and manganese to promote the formation of the sigma phase in them.

Most steels, which are hardened by the formation of martensite, or by age hardening, soften when heated at high temperatures because of tempering or overaging. In contrast, sigma-hardenable

A paper presented before the Thirty-second Annual Convention of the Society, held in Chicago, October 21 to 27, 1950. The author, John J. Gilman, is associated with the Research Laboratory, Crucible Steel Company of America, Harrison, N. J. Manuscript received April 15, 1950.



high-chromium steels are hardened to Rockwell C-38 to 43 by the formation of the sigma phase and show no indications of softening after as long as 1000 hours at 1400 °F (760 °C). The mechanism of this hardening phenomenon will be discussed in this paper.

The fact that these steels, which contain large amounts of the sigma phase (approximately 35%) in their service structures, have been extensively used as internal-combustion-engine exhaust valves is interesting because many metallurgists look upon the sigma phase as a constituent of high-chromium steels which is to be avoided whenever possible. The embrittlement that accompanies the appearance of the sigma phase in steels such as 25-20 stainless and 27 chromium-iron has caused this attitude. The sigma-hardenable high-chromium steels are not exempt from sigma-phase embrittlement but this disadvantage is counterbalanced by their excellent hot hardness. Thus, while their toughness is low compared to many steels, sigma-hardenable high-chromium steels have performed very well under the somewhat adverse conditions imposed upon engine exhaust valves. Of course, the composition of these steels must be properly balanced in order to avoid extreme embrittlement.

It is the purpose of this paper to discuss the formation of the sigma phase in sigma-hardenable high-chromium steels as it is affected by composition, heat treatment, and deformation. The structure and behavior of the sigma-hardenable steels is very complex but it is felt that they are representative of a large number of steels containing 20 to 30% of chromium and having duplex austenitic-ferritic structures.

The literature up to 1947 on the sigma phase has been extensively reviewed by Foley (1)<sup>1</sup> and some of the more recent literature by Oliver (2); therefore no review will be made here.

#### COMPOSITION AND GENERAL CONSTITUTION OF THE STEELS USED

Four steels were used in this investigation. The analyses of the steels were as follows:

Characteristic Elements	Code	C	Mn	Si	Ni	Cr	Mo
Cr-Ni-Mo	CN	0.42	0.81	0.72	4.65	23.31	2.6
Cr-Ni-Mo	CNO	0.37	0.87	0.50	6.37	24.52	4.41
Cr-Ni-Mn	CNM	0.26	4.68	0.74	3.76	25.36	0.14
Cr-Ni-Mn-Si	CNMS	0.34	5.08	1.49	3.29	23.97	0.12

At the left of the table the alloying elements which are felt to determine the character of the steel are listed. Next to these are the code letters by which reference will be made to the steels. These code

<sup>1</sup>The figures appearing in parentheses pertain to the references appended to this paper.

letters are suggestive of the characteristic alloying elements in each steel. Thus, the steel called CNM is the one characterized by chromium, nickel, and manganese, etc. The steels called CN and CNO are both characterized by chromium, nickel and molybdenum, but steel CNO contains considerably more molybdenum than steel CN which changes its behavior appreciably.

Steel CN is the commercial valve steel known as XCR which has been used in the manufacture of exhaust valves for many years. Steel CNO is also a commercial steel while CNM and CNMS are experimental steels.

The steels were received at the laboratory in the form of 1-inch round hot-rolled bars. Specimens were in the form of  $\frac{5}{8}$ -inch disks. The most data were collected for the CN analysis and it is therefore considered to be the norm in the discussion.

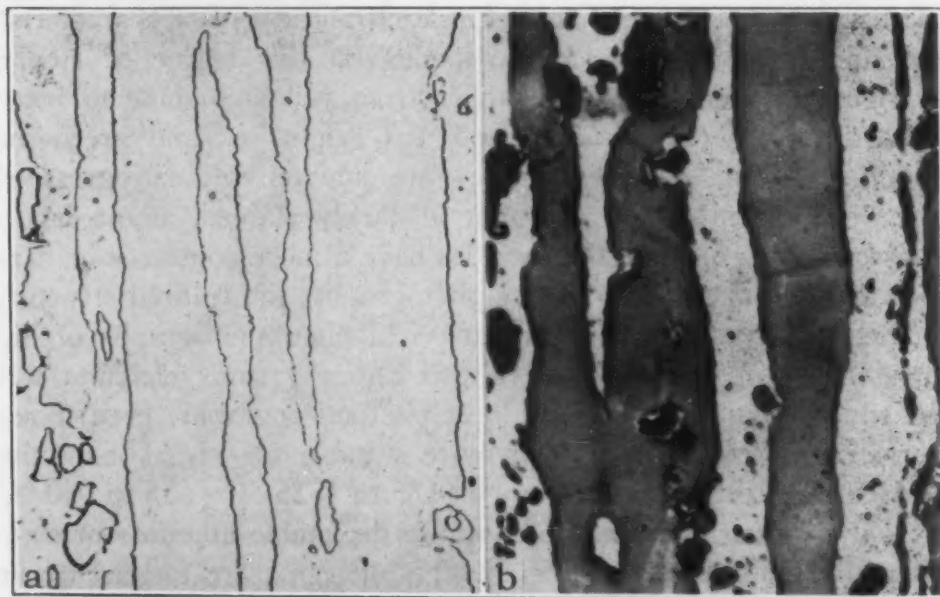


Fig. 1—CN, As-Rolled.  $\times 1000$ . (a) Oxalic acid etch; (b) Concentrated Murakami etch.

### *Constitution of CN*

Because of its high chromium-nickel ratio, steel CN normally has a duplex austenite-ferrite structure at high temperatures. This duplex structure is retained when the steel is air-cooled following rolling. Thus, the as-rolled room-temperature structure consists of austenite, delta ferrite, and complex carbides (predominantly the cubic chromium carbide,  $(\text{Cr}, \text{M}_x)_{23}\text{C}_6$ ). Figs. 1a and 1b show the microstructure of the as-rolled material. Fig. 1a shows the arrangement of austenite and ferrite in stringers or bands. Fig. 1b shows

the ferrite as differentiated from the austenite by the modified Murakami etch (30g. KOH - 30g.  $K_3Fe(CN)_6$  - 60cc.  $H_2O$ ), introduced by Burgess and Forgeng (11). The ferrite is stained brownish-red after fairly long immersion. The white bands across the ferrite stringers are caused by splitting of the stain film. Oxalic acid (10g. oxalic acid - 90cc.  $H_2O$ ) distinguishes between the ferrite and the austenite by roughening the ferrite slightly and not attacking the austenite as rapidly. On the other hand, Vilella's picral reagent (5cc. HCl - 1g. picric acid - 95cc.  $C_2H_5OH$ ) has the opposite effect; it attacks the austenite in preference to the ferrite.

Under certain conditions, sigma, ferrite, austenite, and carbides coexist in steel CN and the other hardenable high-chromium steels. The etchants which, in the author's opinion, distinguish among these four phases most readily are the modified Murakami reagent and alkaline sodium picrate (2g. picric acid, 25g. sodium hydroxide, 100cc. water). These etchants stain each phase with a characteristic color and texture. The color depends on the degree of etching. For sigma the color usually changes from yellow to blue to brown as the time of etching is increased, but bright red and green may sometimes be observed. Carbides are stained with progressively deeper shades of brown. Until it is darkly stained, sigma has an opalescent texture, while the carbides have a more contrasty or harsh appearance. For black-and-white photography, the colored structures developed by these etchants do not yield photomicrographs of high contrast. Therefore, throughout this paper various etchants were used which seemed to yield the best photomicrographs, even though other etchants might have been more suitable for visual inspection.

Heating steel CN in the range 1175 to 1725 °F (635 to 940 °C) causes the formation of microscopically detectable amounts of sigma in it within 16 hours. Larger amounts of sigma are formed toward the middle of the range. The sigma starts to form at the ferrite-austenite interfaces and as time at temperature is increased it grows until it fills the volumes formerly occupied by ferrite stringers. At this time it takes the shape of a loose, lacelike network. Fig. 2 shows the structure when the sigma phase has grown until it fills about half the volume formerly occupied by the stringers of ferrite. Fig. 3 shows the structure after the formerly ferritic volumes have been completely converted to sigma plus austenite. On the basis of hardness measurements which will be discussed later, and the microstructures, the sigma reaction substantially halts when the formerly ferritic volumes have been converted to sigma, but after some more time has elapsed, sigma begins to form in the sigma-free



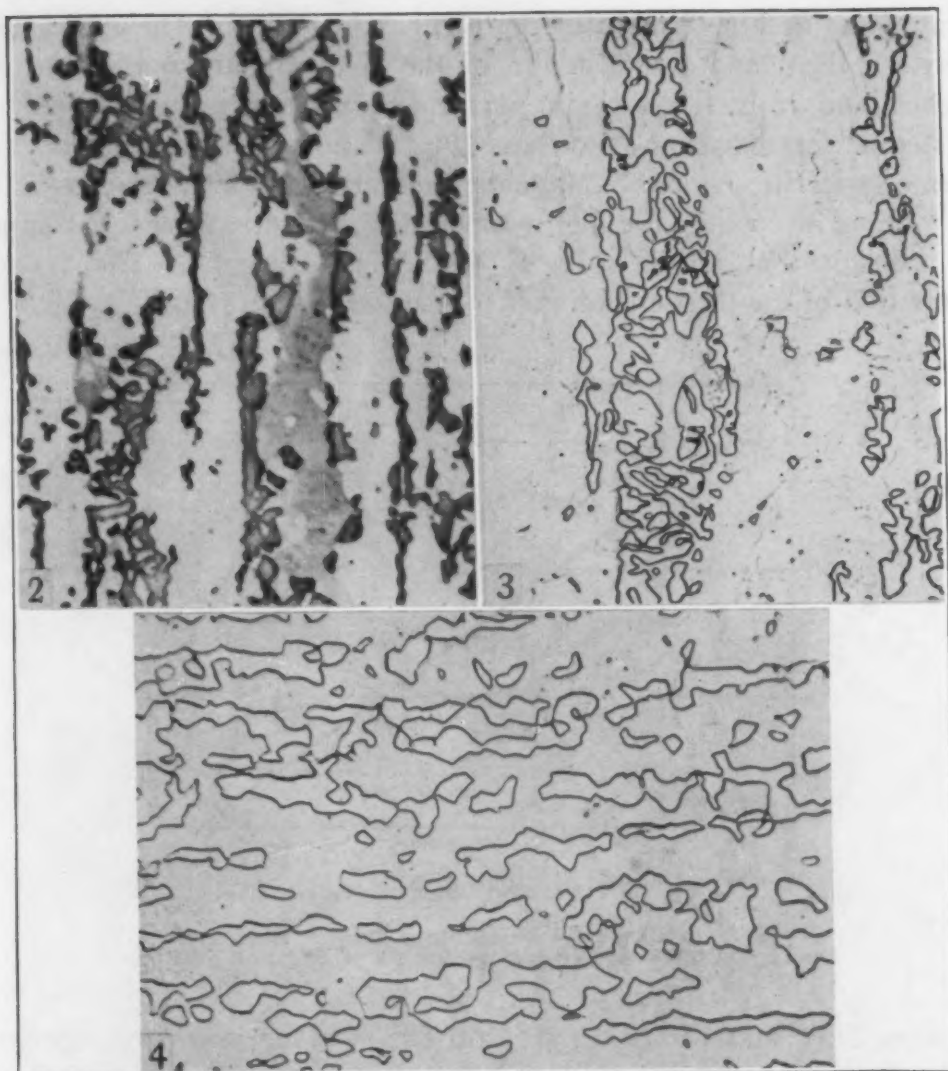


Fig. 2—CN, Heated 8 Hours at 1400°F.  $\times 1000$ . Concentrated Murakami etch. White—*austenite plus carbides*; Light gray—*ferrite*; Dark gray—*sigma*.

Fig. 3—CN, Heated 16 Hours at 1400°F.  $\times 1000$ . Oxalic acid etch. White particles—*sigma*; Background—*austenite plus carbides*.

Fig. 4—CN, Heated 1000 Hours at 1400°F. Oxalic acid etch.  $\times 1000$ .

volumes of the austenite. At the same time, the sigma which formed in the beginning slowly coalesces and the microstructure shown in Fig. 4 finally results. In Figs. 2, 3 and 4, the carbides do not appear: only the sigma is etched because the etchants attack it more rapidly than the carbides.

Apparently, the rate at which the ferrite transforms to austenite plus sigma is equal to the rate at which the sigma grows. This is indicated by Fig. 5 which shows that there is a direct correlation between the volumes which appear to be ferrite (see Fig. 2) and the amount of sigma present. However, it is not certain that the light



gray areas in Fig. 2 actually represent only ferrite. The interfaces between them and the austenite of the structure are not distinctly etched and it is felt that in part they may represent regions of austenite formed from and having a similar composition to the formerly ferritic regions. Magnetic measurements also indicate this.

On slow cooling, the high temperature ferrite in steel CN begins to transform at about 1675 °F (915 °C) to sigma. The transformation of the ferrite continues to about 1550 °F (845 °C). Thus

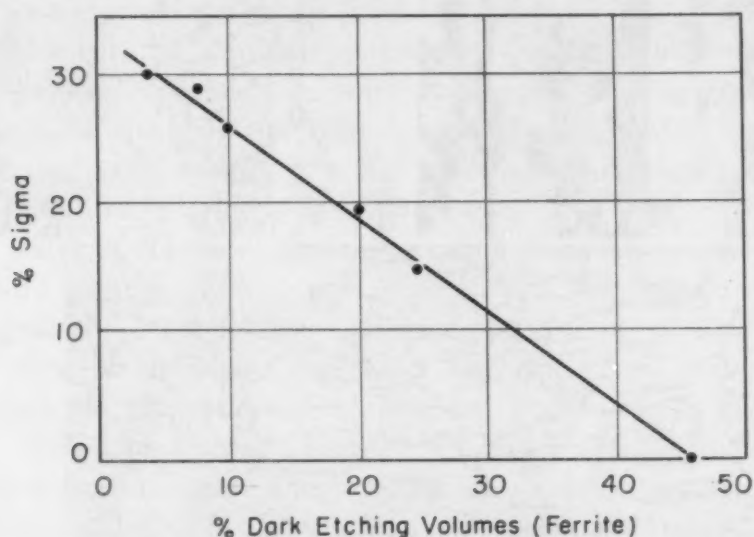


Fig. 5—Relationship Between Sigma Content and Apparent Ferrite Content in CN During the Growth of Sigma at 1400°F.

between 1675 and 1550 °F (915 and 845 °C) the structure consists of austenite, ferrite and sigma plus carbides (see Fig. 6). Below 1550 °F (845 °C), all the ferrite has transformed to sigma as well as some of the austenite, so that the structure consists of austenite and sigma plus carbide. The austenite of the structure that is stable below 1550 °F (845 °C) persists on slow cooling to about 80 °F (the exact temperature depends on the elevated temperature history) where part of it transforms isothermally to a ferritic transformation product. Cooling to lower temperatures results in further transformation of the austenite to the ferritic product. The reactions at low temperatures are considerably affected by the sigma reaction previous to cooling.

#### *Constitution of CNO*

The second steel, CNO, contains more molybdenum than steel CN. This increases the rate of sigma formation in the steel. CNO's

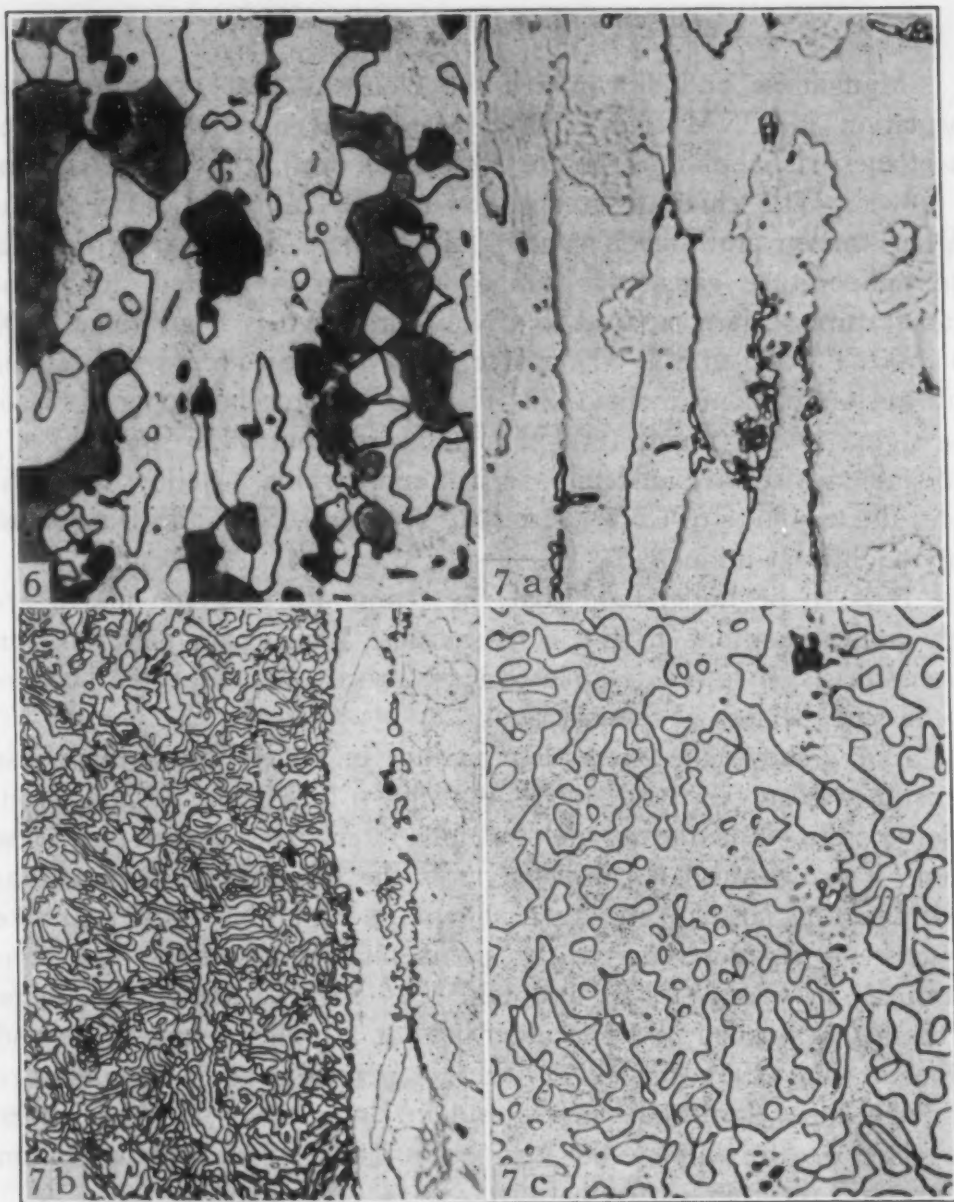


Fig. 6—CN, Heated 16 Hours at 1600°F. Etched in Vilella's picral reagent followed by Murakami's reagent.  $\times 1000$ . White—sigma; Black—carbides; Background—  
austenite; Gray—ferrite.

Fig. 7—CNM,  $\times 1000$ . (a) Heated 1 hour at 1300°F—oxalic acid etch; (b) Heated 16 hours at 1300°F—oxalic acid etch; (c) Heated 500 hours at 1400°F—concentrated Murakami etch.

higher nickel content balances the composition so that below about 1700 °F (925 °C) its matrix consists of austenite. Sigma forms in CNO at temperatures from 1100 to 1800 °F (595 to 980 °C) within 16 hours. The austenitic matrix of CNO is more stable than that of CN at low temperatures. Cooling it to the temperature of liquid nitrogen (minus 320 °F) causes no detectable transformation of the austenite.

*Constitution of CNM and CNMS*

Manganese and silicon are the elements that promote sigma formation in CNM and CNMS instead of molybdenum. Since manganese is a mild austenite former as well, the nickel content is lower. The chief difference between CNM and CNMS is the higher carbon and silicon content of CNMS. In these two steels, the temperature range for sigma formation is shifted down the temperature scale compared to CN. The range is from about 1100 to 1600 °F (595 to 870 °C). Also, delta ferrite coexists with sigma and austenite from about 1475 °F (800 °C) to the upper limit of the sigma range (about 1600 °F). Below about 1475 °F (800 °C) the stable phases are austenite, sigma, and carbide. At low temperatures the austenite of CNM is stable to minus 105 °F and transforms only slightly at minus 320 °F.

It is to be understood that the temperatures given above are only approximations to the constitutional limiting temperatures in these steels. It is not feasible to state precise temperatures because of the sluggishness of the reactions.

Fig. 7 shows an interesting manner in which the sigma phase sometimes grows in these steels. As shown in Fig. 7a it starts from a few points along the ferrite-austenite interfaces. From these few points it grows until it completely fills the formerly ferritic regions with the fine lacelike structure shown in Fig. 7b. This mazelike structure is characteristic of the sigma phase's growth at low temperatures in CNM, CNO and CNMS. Fig. 7c shows the shape of the sigma formed in a specimen held at a higher temperature and a longer time. The mazelike structure persists over a temperature range of a few hundred degrees and for long times, but the longer the time or the higher the temperature the more agglomeration occurs and the coarser the pattern.

An important characteristic of the manner in which sigma-phase formation takes place is the fact that a large amount of growth proceeds from relatively few nuclei leading to structures such as that in Fig. 7b.

#### MECHANISM OF HARDENING IN SIGMA-HARDENABLE HIGH-CHROMIUM STEELS

The general hardening characteristics of CN, CNO and CNM are shown in Fig. 8. At first glance, these curves appear to be typical age hardening curves. However, there are important differences and it will be shown shortly that this hardening is not an age

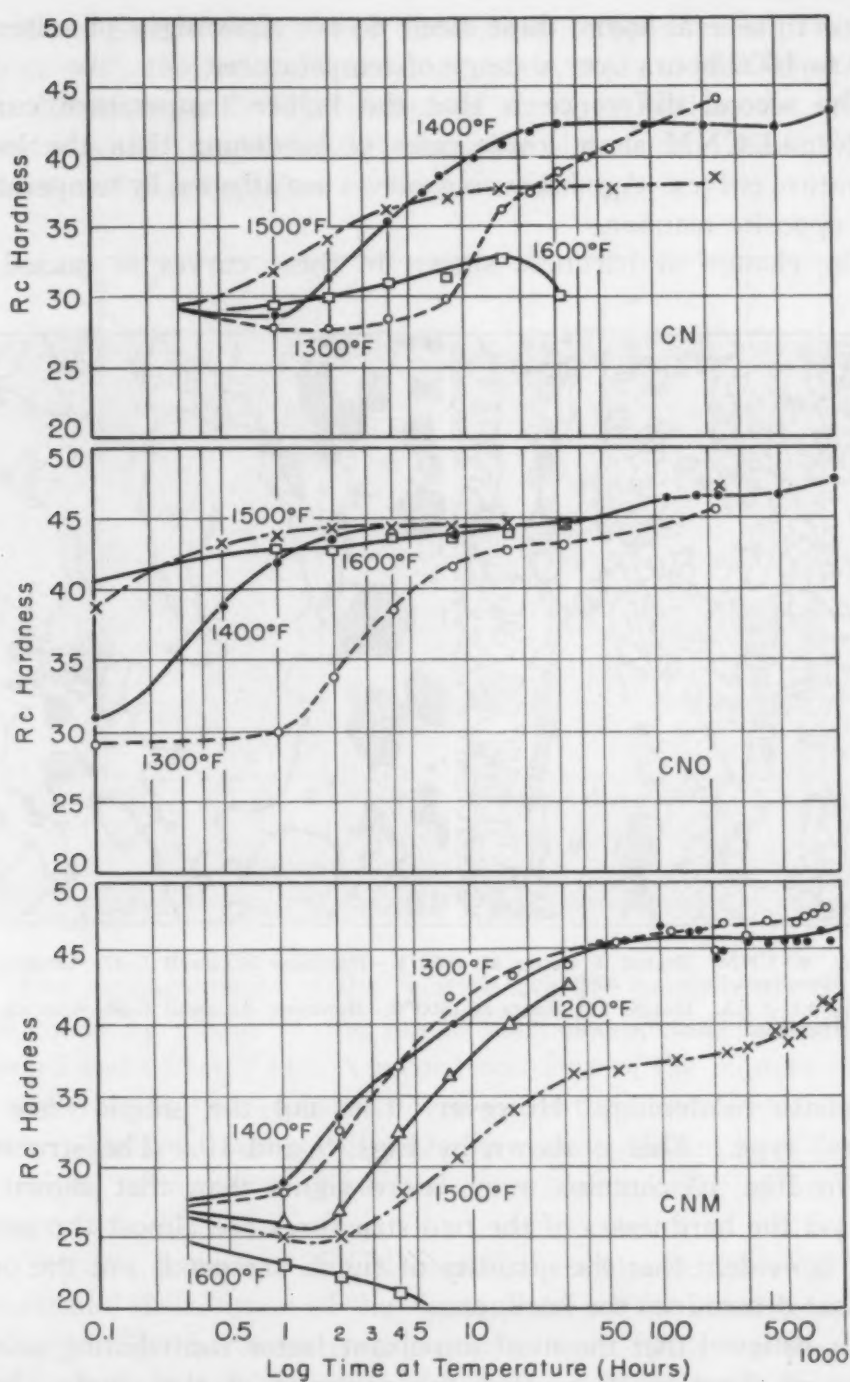


Fig. 8—Hardening Characteristics of CN, CNO, and CNM. All specimens originally in as-rolled condition.

hardening phenomenon, but that it is simply mixed-phase hardening. The curves for CNMS are very similar to those for CNM and therefore were not included.

The first difference between these curves and age hardening curves is the absence of overaging. Having once reached maximum



hardness in several hours, these steels do not show signs of softening in 200 to 1000 hours over a range of temperatures.

The second difference is that the higher temperature curves for CN and CNM show lower rates of hardening than the lower temperature curves. Age hardening curves are affected by temperature in the opposite manner.

The change of hardness shown in these curves is caused by

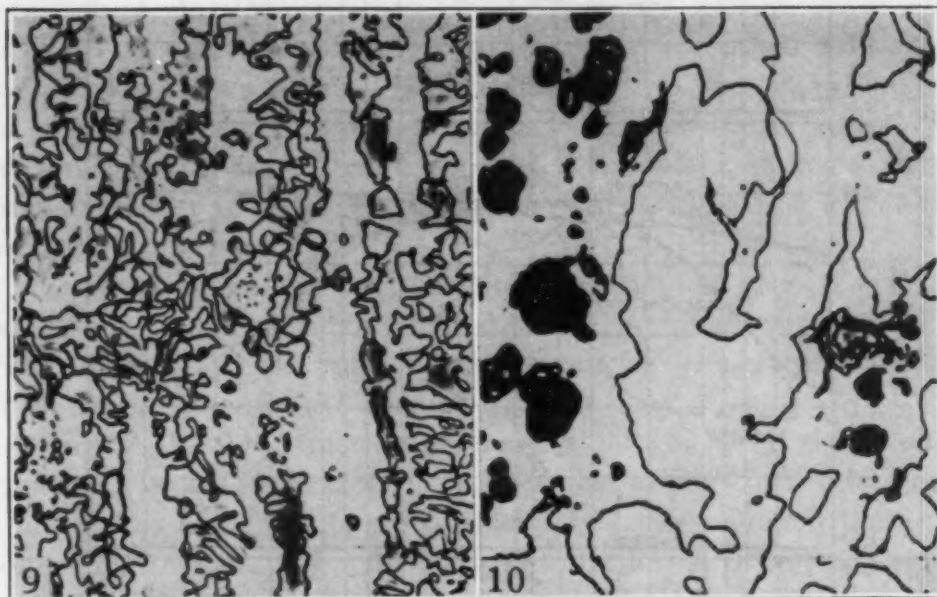


Fig. 9—CNM, Heated 4 Hours at 1400°F—Hardness Rockwell C-37—Concentrated Murakami Etch.  $\times 1000$ .

Fig. 10—CNM, Heated 234 Hours at 1500°F—Hardness Rockwell C-38—Concentrated Murakami Etch.  $\times 1000$ .

mixed-phase hardening. However, it is not the simple "law of mixtures" type. This is shown by Figs. 9 and 10. The structure shown in Fig. 10 contains much more sigma than that shown in Fig. 9, yet the hardnesses of the two structures are almost the same. Thus it is evident that the quantity of sigma present is not the only factor that determines the hardness.

It is believed that the most important factor contributing to the hardness of these steels is that the presence of the sigma phase blocks off the austenitic matrix into small volumes. That is, the sigma phase reduces the average path in the austenite. The test of this hypothesis is shown in Fig. 11. In this figure, the hardness is plotted as a function of the logarithm of the average path in the austenite. The correlation is good. The scatter shown is to be expected on account of the extremely fine and irregular distribution of the sigma in many of the specimens. The experimental points

cover a range of temperatures, times, and compositions. This correlation with the austenitic average path explains the dependence of the hardness on the distribution of sigma as well as the quantity present. A similar correlation is found in plain carbon steels between hardness and the logarithm of the mean ferrite path (10).

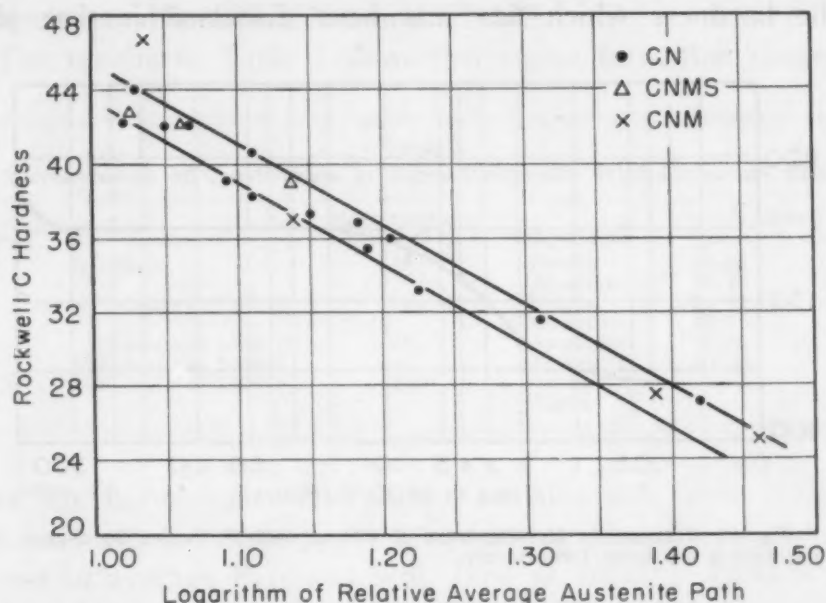


Fig. 11—Correlation Between Rockwell Hardness and Average Austenite Path in CN, CNM, and CNMS During Sigma Formation in These Steels.

The measurements of the relative average paths in the austenite were made by means of the lineal analysis apparatus described by Howard and Cohen (3). A record was kept of the number of times the austenite key was pushed for a given total number of austenite counts. The total number of austenite counts divided by the number of regions of austenite traversed gave the relative value for the average path.

The hot hardness of CN shows the same dependence on the amount and distribution of the sigma phase as the room temperature hardness. Hot-hardness measurements were made by the method described by Fetz (12). Fig. 12 shows the hot hardening of CN at 1400 °F. The structures formed in CN at 1300 and 1500 °F both have lower hot hardness (160 impact BHN) when tested at 1400 °F (760 °C) than the structure formed at 1400 °F (760 °C). This is the same trend as that indicated by the room temperature hardening characteristics of Fig. 8; therefore, the hot hardness correlates with the room temperature hardness, and hence with the average austenite path.

The dependence of the hardness on the average austenite path explains the shape of the curves in Fig. 8 completely. At the lower temperatures, the rate of hardening is relatively low because it is limited by the low rates of sigma formation. At the higher temperatures, the sigma is massive and hence large amounts of it are necessary to cause hardening.

The hardness which has just been discussed is that of the

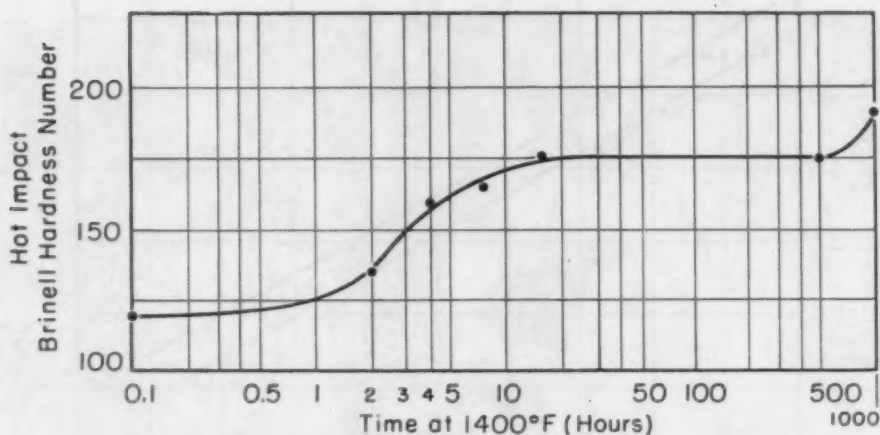


Fig. 12—Increase in Hot-Hardness of CN at 1400°F Caused by Sigma Formation at the Same Temperature.

structure as a whole—the macrohardness. It is believed that this is determined by the amount and distribution of the sigma only. That is, no age hardening mechanism is involved. However, the sigma forms preferentially in the former ferritic volumes of the steels and therefore is not randomly dispersed in the austenite. Fig. 3 shows this. Thus the possibility must be considered that the first sigma that forms causes age hardening of the ferrite which has a negligible effect on the macrohardness. In an attempt to detect age hardening in the ferrite, microhardness measurements were made.

The microhardness measurements were made with a Bergsman microhardness tester (13). A Vickers diamond and 25-gram load were used. The results are given in Table I. Both the range and average hardnesses are reported because, although many determinations were made, one never knows whether a hard constituent lies just below the point at which the penetrator enters the surface of the specimen. With the four phases present in these steels, this creates a large amount of uncertainty in the significance of average hardness values.

Only in CNM were the sigma particles large enough to allow hardness determinations to be made on the sigma phase itself. It would be interesting to know if composition affects the hardness



of sigma, but its extreme brittleness prevents one from determining the hardness with the necessary accuracy. The penetrator invariably causes some crushing of the sigma. Therefore, the hardness number that is obtained is a minimum value and not necessarily the true indentation hardness. For these reasons the hardness of the sigma in CNM (Rockwell C-64) is assumed to be approximately that of the sigma found in CN, CNO and CNMS.

The results in Table I show that sigma formation causes little

**Table I**  
**Microhardness of Constituents in Sigma-Hardenable High-Chromium Steels**

Material	Treatment	Macrohardness Rockwell C	Constituent	Rockwell C	
				Range	Average
CN	As-rolled	29	Ferrite	11-28	19
			Austenite	12-27	25
	2 hours at 1400 °F	32	Ferrite	14-21	16
			Austenite	19-26	25
	16 hours at 1400 °F	41	Austenite	25-35	31
	1000 hours at 1400 °F	43	Austenite	30-33	31
CNM	500 hours at 1400 °F	46	Austenite	.....	17
			Sigma	.....	64

if any age hardening. The matrix remains soft, even though the macrohardness increases appreciably during sigma formation. The increase in average hardness with time at 1400 °F (760 °C) from Rockwell C-25 to 31 of the austenite in CN is probably attributable to the low-temperature transformation of some of the austenite. Thus the austenite would be of constant hardness during the sigma reaction. This conclusion is based on the fact that the low-temperature transformation is known to affect the macrohardness by as much as five points Rockwell C and therefore it would affect the microhardness to a similar extent. The results show that the hardness of the ferritic volumes in which the sigma is concentrated is unaffected by the early stages of sigma formation. Of course, the ferritic volumes are not present during the later stages.

In addition to the evidence already presented, it was found that appreciable amounts of sigma were present in the microstructures before any increase in the hardness was observed. The results of measurements of the quantities of sigma present after various periods of heating at 1400 and 1500 °F (760 and 815 °C) are given in Fig. 13. The measurements were made by means of lineal analysis. The data show that the hardness did not begin to increase rapidly until about 15% of sigma had formed in the structure, but that to a first approximation the hardness is proportional to the sigma content.

It is concluded that the hardening which is observed to accompany the formation of the sigma phase in the steels of this group



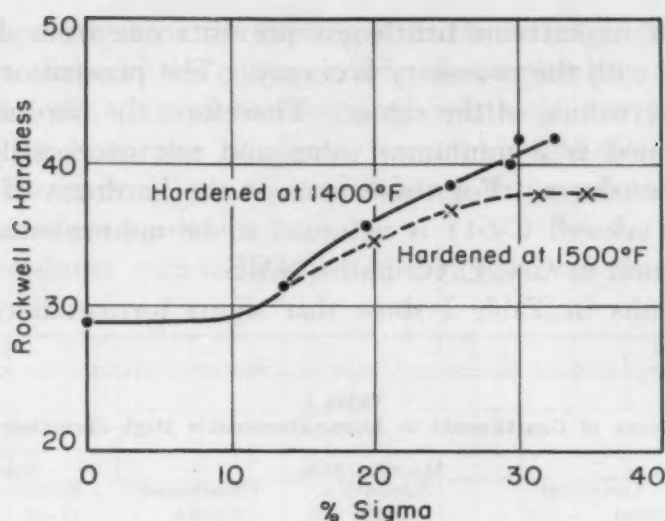


Fig. 13—Rockwell Hardness Versus Quantity of Sigma Present in CN for Two Temperatures of Sigma Formation.

is the result of mixed-phase hardening. It is dependent on the amount and distribution of the sigma phase present, inasmuch as this affects the average path in the austenite. No appreciable age hardening is caused by the formation of the sigma phase in these steels. This conclusion is intended to apply only to this type of steel. In other types it may be true that sigma formation is accompanied by age hardening.

#### EFFECT OF ALLOYING ELEMENTS ON SIGMA FORMATION IN SIGMA-HARDENABLE HIGH-CHROMIUM STEELS

There are several ways in which alloying elements can affect the rate of formation of the sigma phase. First, they may affect the matrix material. By affecting the free energy of the matrix or the diffusion of sigma-forming elements through the matrix they may affect the rate of formation of sigma. This may be the role of interstitially dissolved elements such as boron (7), nitrogen (4) and carbon (4, 7) which affect sigma formation in austenitic steels. Second, they may be dissolved in the sigma phase itself. This will affect the free energy of the sigma phase relative to the matrix. If the free energy of the sigma phase is lowered relative to the matrix, its rate of formation will increase. This may be the mechanism by which elements such as silicon and molybdenum affect the rate of sigma formation. Third, if the initial structure is duplex austenitic-ferritic, alloying elements may change the amount of ferrite in the structure. Usually, the greater the amount of ferrite in the initial structure, the greater is the rate of sigma formation.

Carbon and nitrogen may affect the rate of sigma formation in still another manner. They may combine with chromium or other strong sigma formers such as titanium and columbium (4) and thereby reduce the tendency toward sigma formation.

In the course of the development of the sigma hardening steels, a large number of alloy combinations were tested for their ability to harden when heated at 1400 °F (760 °C). Thus the effects of several elements on the rate of sigma formation were determined, since, to a first approximation, the amount of sigma present is

**Table II**  
**Effect of Alloy Elements on Rate of Hardening (Rate of Sigma Formation)**  
**of High-Chromium Austenitic-Ferritic Steels**

Alloy	Amount Added in Combination With Other Elements %	Effectiveness
Chromium	20.0 to 27.5	Most effective
Molybdenum	1.3 to 5.6	Very effective
Manganese	0.75 to 14.5	Effective
Silicon	0.25 to 4.1	Very effective
Nickel	0.5 to 12.0	Depends on balance
Carbon	0.15 to 0.5	Decreases
Nitrogen	0.04 to 0.28	Decreases slightly
Cobalt	1.3 to 5.0	Slightly effective

proportional to the hardness. Screening was on the basis of the amount of hardening that occurred in a steel when heated at 1400 °F (760 °C) for 16 hours. Therefore, the data are related to the rate of sigma formation and not to the final equilibrium amount that might form. The effects of the various alloying elements are reported in Table II. The elements are listed with the ones on which the most data were collected at the top. The effects of some of these elements have been reported before in other grades of steel (1, 4). The ranges of the additions that were made are reported in order to give some idea of the scope of the work because it was not feasible to report all the specific analyses.

It must be remembered that these alloying elements were added to duplex austenitic-ferritic steels and therefore their effect on sigma formation may have been either direct or indirect. That is, they may have promoted sigma formation either by entering into the reaction themselves, or they may have affected the amount of ferrite present and thereby affected the rate of sigma formation indirectly.

The effects of some elements other than those shown in Table II were investigated but the data were not extensive. However, it may be said tentatively that vanadium, tungsten, aluminum, and phosphorus seem to be effective in increasing the rate of sigma formation, while boron seems to decrease the rate slightly.

Composition also affects the temperature range of sigma formation. This is shown by Fig. 14 which shows that CNO hardens rapidly over a much wider temperature range than the other steels. This indicates that molybdenum has a quite powerful effect on the temperature range of sigma stability. The temperature at which

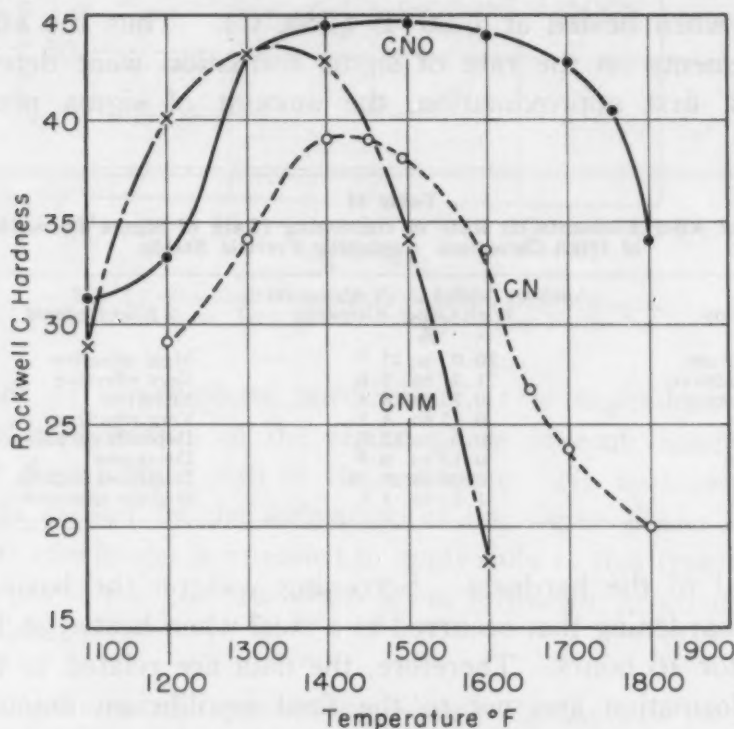


Fig. 14—Effect of Composition on the Temperature Range of Sigma Formation. Each steel heated for 16 hours at each temperature.

CNM and CNMS harden most rapidly is lower than that for CN. This indicates that manganese increases the tendency toward sigma formation at relatively low temperatures.

The effects of composition on the rate of formation of sigma are probably all related to the effects of the various elements on the equilibrium diagram, but since equilibrium structures are not being considered, it seems more apt to discuss the effects in terms of the rate of sigma formation at a given temperature, the upper limiting temperature of the sigma formation range, and the temperature below which sigma forms at a negligible rate.

#### EFFECT OF FERRITE ON THE RATE OF FORMATION OF SIGMA

When composition allows, the sigma phase forms in both austenite and ferrite. It is known, however, that if ferrite is initially present in the structure, sigma forms with a high degree of prefer-

ence in the ferritic volumes (5, 6). This phenomenon is certainly partly attributable to the fact that the ferrite-forming elements which are concentrated in the ferritic regions of the steel are all strong sigma-phase promoters. The degree of partition of the elements between the ferrite and the austenite is not known but it is evident from equilibrium diagrams that it is appreciable. Also, Kirby and Morley (9) showed by means of microradiographs that the ferritic

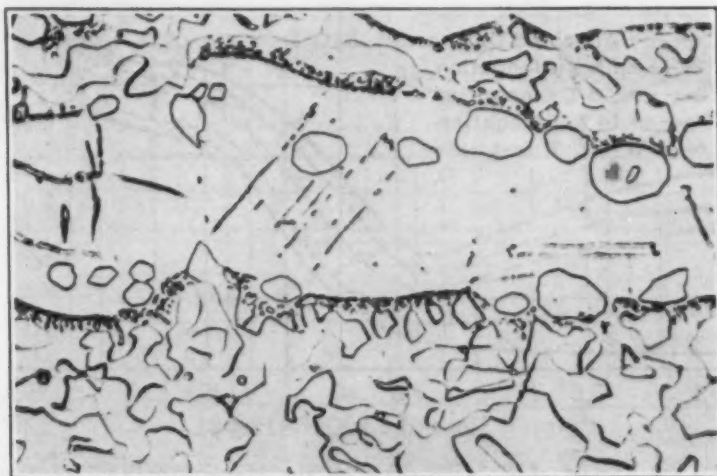


Fig. 15—CNMS. Heated for 3 Hours at 2100°F. Water Quench  
—Then Heated 500 Hours at 1400°F. Oxalic acid etch.  $\times 1000$ .

phase contains more chromium than the austenitic phase in a duplex-chromium steel.

An estimation of the partition of the elements between the ferrite and the austenite can be obtained by means of preferential electrolytic dissolution. Vilella's picral reagent (5cc. HCl, 1g. picric acid, 99cc.  $C_2H_5OH$ ) attacks the austenite of these steels more rapidly than the ferrite. Therefore it can be used to separate the two phases electrolytically. Analyses of ferrite residues obtained by this have shown that, indeed, the alloying elements are partitioned between the austenite and ferrite. The ferrite-formers concentrate in the ferrite and the austenite-formers in the austenite. Further work is necessary, however, to establish the degree of partition definitely.

Sigma does eventually form in the initially austenitic volumes of the sigma hardening steels. This is clearly shown by Fig. 15 where plates of sigma appear along certain planes of the initially austenitic regions. The rate of formation of sigma in the austenite is considerably less than that in the ferrite, as is evident from this picture. Thus, while sigma appeared in the ferritic regions in a



matter of minutes at 1400 °F (760 °C), hundreds of hours were required for the appearance of sigma in the austenitic regions.

In addition to the massive sigma in the initially ferritic regions and the plates of sigma in the initially austenitic regions, Fig. 15 also shows massive carbides that were not dissolved by the 2100 °F (1150 °C) treatment and precipitated carbides at the initial ferrite-austenite interfaces.

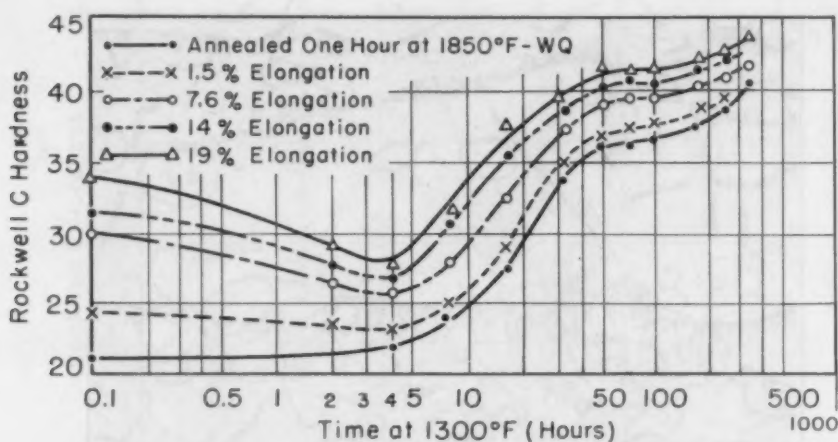


Fig. 16—Effect of Cold Working on the Hardening (Rate of Sigma Formation) of CN at 1300 °F.

The hardness curves of Fig. 8 also indicate the formation of sigma in the austenitic regions after sufficient time has elapsed. This is indicated by the secondary hardness increases in all three steels after several hundred hours had elapsed at temperatures in the sigma range.

The same sequence for the sigma formation process was observed by Rees, Burns and Cook (8) in pure iron-nickel-chromium alloys. What the maximum extent of the reaction within the austenitic volumes might eventually be is not known, but the rate of the reaction is still measurable after 1000 hours at 1400 °F (760 °C).

#### EFFECT OF COLD WORKING ON THE RATE OF FORMATION OF SIGMA

Tensile bars were cut from CN that had been annealed at 1850 °F (1010 °C) for 1 hour and water-quenched. These were then pulled in tension to various amounts of permanent elongation (1.5 to 19%). Specimens were cut from the centers of the gage length and held at 1300 and 1400 °F (705 and 760 °C). The hardening curves are shown for the specimens held at 1300 °F (705 °C) in Fig. 16.

The curves of Fig. 16 show that the rate of sigma formation

in CN is increased by any amount of tensile cold work up to the maximum that the steel will endure (about 20%). The curves for the specimens heated at 1400 °F (760 °C) are similar in shape.

Fig. 17 shows the relationship between the hardening of as-rolled, annealed, and annealed plus cold-worked CN. The time

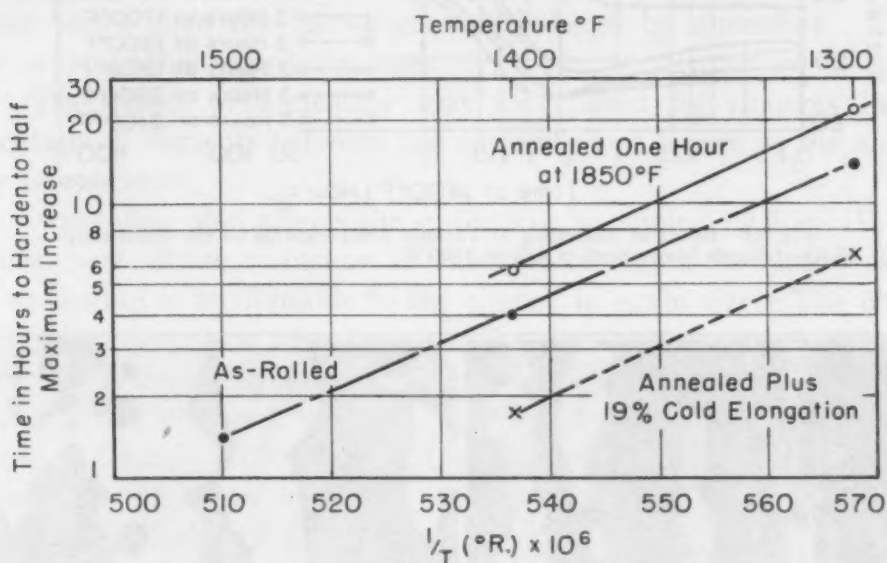


Fig. 17—Time-Temperature Dependence of the Sigma Reaction in CN for Various Initial Conditions.

required for specimens to increase in hardness by one-half of the maximum increase is plotted against the reciprocal of the absolute temperature. The relative behavior of the initial states and the temperature dependence of the reaction should be clear from this graph. The straight lines in this figure are meant only to indicate the data; they have no special significance. The great importance of the initial condition of the steel on the sigma reaction is evident, for example, for the data on 1400 °F (760 °C). The half-hardening time for the as-rolled initial condition was 4 hours; when the steel was cold-worked by a 19% elongation this time was reduced by a factor of two to about 1.8 hours; and when the steel was annealed at 1850 °F (1010 °C) for 1 hour the half-hardening time increased by 50% to about 6 hours. The temperature dependence of the reaction is also very pronounced. Thus decreasing the temperature used for hardening the as-rolled material from 1400 to 1300 °F (760 to 705 °C) changes the half-hardening time from 4 hours to about 15 hours. These effects are partly attributable to differences in amounts of sigma present in the various specimens and partly to differences in the distributions of sigma.

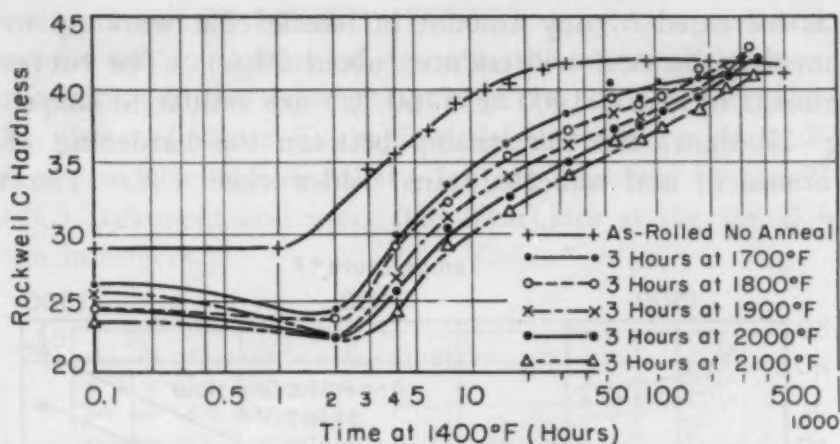


Fig. 18—Effect of Annealing at Various Temperatures on the Hardening (Rate of Sigma Formation) of CN at 1400°F.

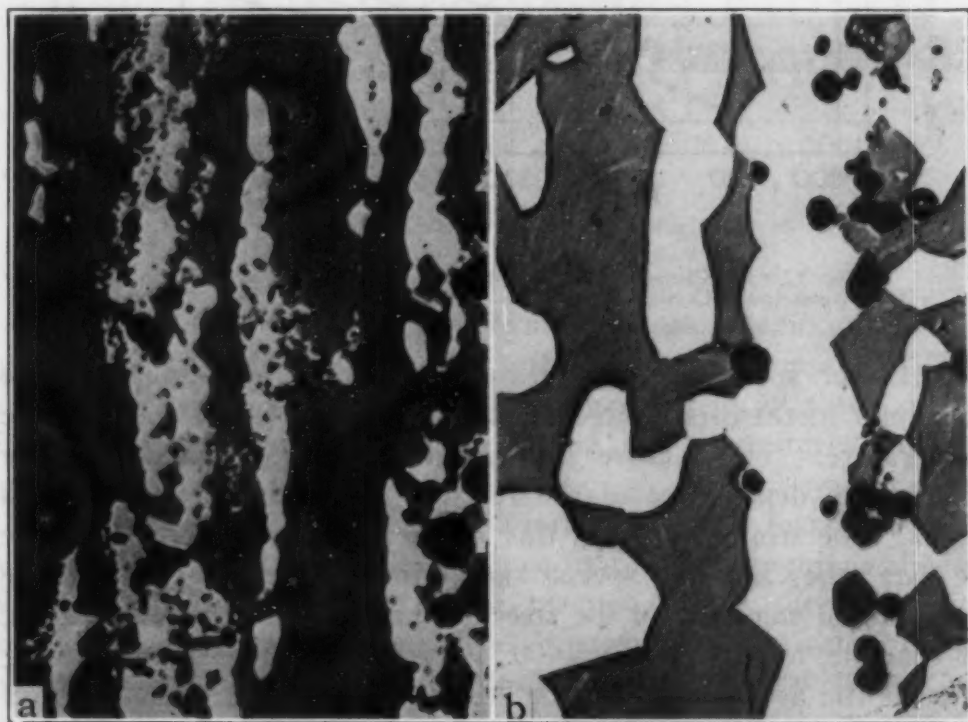


Fig. 19—CN, Concentrated Murakami Etch.  $\times 500$ . Black—carbides; Gray—ferrite; White—austenite. (a) 3 hours at 1800°F—WQ; (b) 3 hours at 2200°F—WQ.

#### EFFECT OF ANNEALING ON THE RATE OF SIGMA FORMATION

Specimens of CN were annealed at 100-degree intervals from 1700 to 2200 °F (925 to 1205 °C). The time of annealing was 3 hours. All specimens were water-quenched. The hardening characteristics of these specimens are shown in Fig. 18. The curves show that there is a direct relationship between annealing tempera-

ture and the rate of sigma formation. A similar set of hardening curves was obtained for specimens heated at 1300 °F (705 °C) subsequent to annealing.

There was not a direct relationship between the initial ferrite content (as measured by magnetic susceptibility) and the annealing temperature. Therefore, the effect of annealing was related to some other factor than the ferrite content induced by annealing. There are several other possible causes.

The effect of annealing may be caused by changes in the partition of elements between the austenite and ferrite at the annealing temperature.

Annealing also affects the grain size, as shown by Fig. 19. No doubt, part of the reduction in the rate of sigma formation caused by annealing is attributable to the change in grain size. The change in grain size does not seem to be the entire cause, however. Increasing the annealing temperature from 1800 to 2200 °F (980 to 1205 °C) changed the half-hardening time from about 9 to 56 hours, a change of 6 times. Corresponding to this large change in the rate of sigma formation, the grain size was changed only by a factor of about two (Fig. 19).

Other factors that might affect the rate of sigma formation are the degree of solution of carbides at the higher annealing temperatures and homogenization of any segregations that might exist. When a specimen of CN is heated to 1000–1700 °F (540–925 °C), any carbon that was dissolved at high annealing temperatures precipitates very rapidly at the ferrite-austenite interfaces. This would prevent sigma from nucleating at these favorable sites and may be one of the reasons for the slower rate of sigma formation following annealing. Segregations would have an effect similar to that of ferrite in promoting sigma formation. Thus homogenization should reduce the rate of sigma formation.

#### EFFECT OF MANUFACTURING VARIABLES ON RATE OF SIGMA FORMATION

As might be suspected from the data of the foregoing sections, the entire prior history of a steel determines the rate at which sigma will form in it. The casting conditions, whether the ingot is reduced by rolling or hammering, fabricating procedures such as extrusion, heat treatments, etc., all have an effect.

One example is the effect on the hardening of the temperature at which the final rolling of billets is begun. Fig. 20 shows the hardening characteristics of two 1-inch bars from different billets



of the same heat of CN. One billet was heated to 1925 °F (1050 °C) prior to rolling and the other to 2025 °F (1105 °C). Individual specimens were used for each period of time at temperature. The curves show that in the material rolled at the higher temperature sigma formed slightly less rapidly than in the material rolled at the lower temperature.

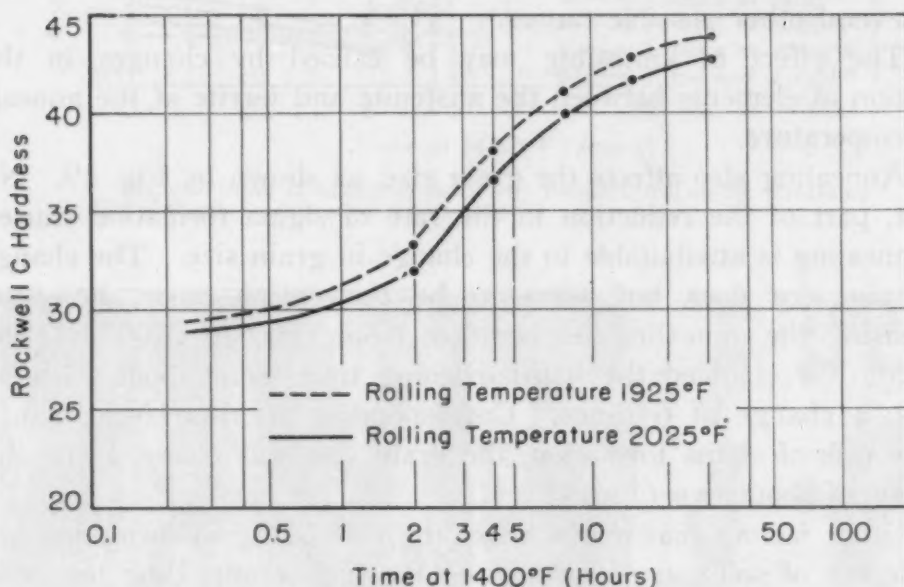


Fig. 20—Effect of Rolling Temperature on the Hardening (Rate of Sigma Formation) of CN at 1400°F.

A more striking example of the effect of prior structure on the rate of formation of the sigma phase is the difference in hardening characteristics of cast and annealed wrought material of the same composition. Complete recrystallization of the wrought material does not render its behavior similar to that of the cast material. The rate of sigma formation remains much more rapid in the recrystallized wrought material as compared to cast material of essentially the same composition and grain size. The reason for this difference in behavior is not known, but one is tempted to attribute it to differences in crystalline perfection.

The steel in which this phenomenon was investigated was CNO. It was available in three conditions: investment castings, graphite castings, and a hot-rolled bar. Thus the effects of two rates of solidification and of hot working could be compared. The analyses of the materials were sufficiently alike that the steels should have had very similar behaviors with respect to sigma formation if their histories had been identical. The analyses were as follows:

	C	Mn	Si	Ni	Cr	Mo
Investment castings	0.37	0.40	0.40	6.35	24.28	4.51
Graphite castings	0.38	0.70	0.71	6.47	24.30	4.45
Wrought bar	0.375	0.87	0.51	6.37	24.52	4.41

Specimens were heated at 1300 °F (705 °C) for various periods of time up to 80 hours. The hardnesses were measured and are plotted in Fig. 21. The difference in the rates of sigma formation

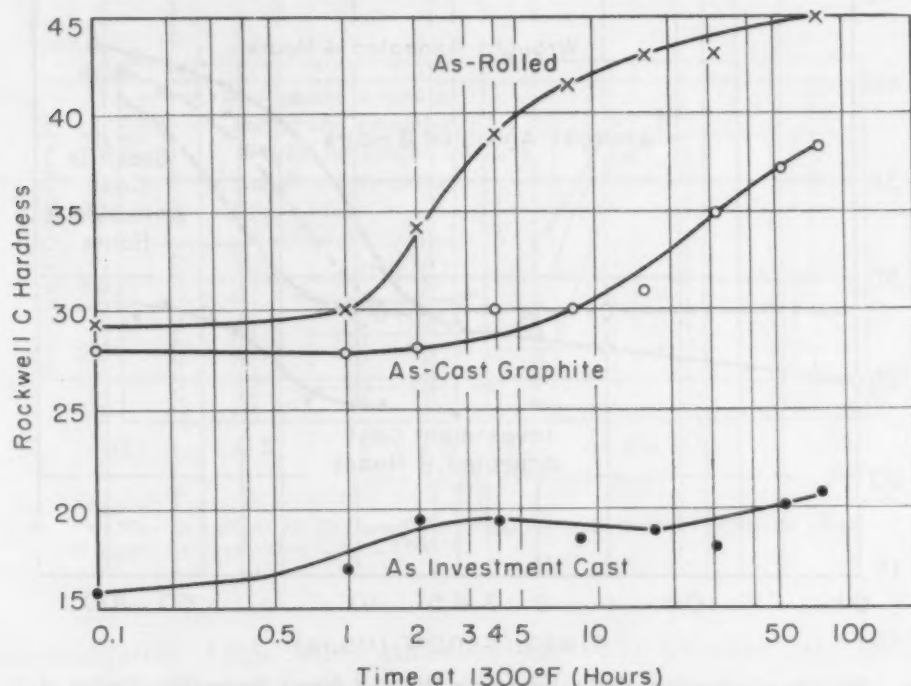


Fig. 21—Comparison of the Hardening (Rate of Sigma Formation) Curves of Cast and Wrought CNO.

in these materials is striking. Although the data are rather meager, it is indicated that the greater the rate of solidification, the greater the rate of sigma formation. Segregation does not account for the difference, because the material cast in graphite should be less segregated and therefore have a lower rate of sigma formation than the investment-cast material. There was some difference in grain size but not enough to account for the large difference in reaction rates.

In order to recrystallize the wrought material, homogenize the specimens, and equalize the grain sizes, specimens of each prior condition were heated for 8 hours at 2200 °F (1205 °C) and water-quenched. These specimens were then heated at 1300 °F (705 °C) and hardness measurements were made. The results are plotted in Fig. 22. The rate of sigma formation was decreased appreciably in the wrought material, remained about the same in the graphite-

cast material and increased slightly in the investment-cast material. The latter effect may have been due to the strains caused by quenching from 2200 °F (1205 °C), as indicated by the higher initial hardness of the cast and annealed as compared to the cast material. The grain sizes after annealing were essentially the same.

The hardening curves show that even after the effect of plastic

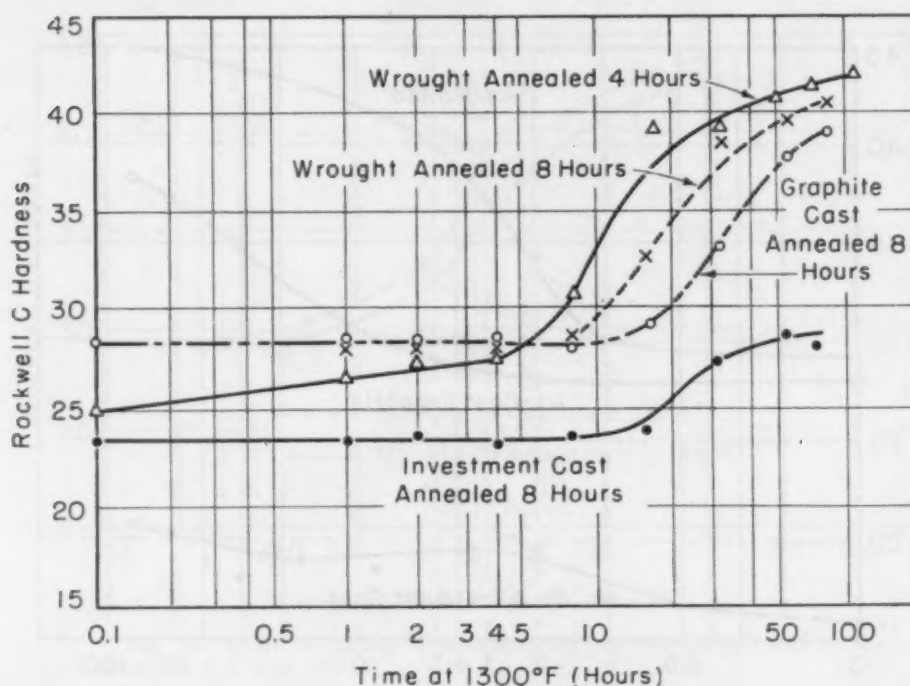


Fig. 22—Comparison of the Hardening (Rate of Sigma Formation) Curves of Cast and Wrought CNO After Annealing for 8 Hours at 2200 °F.

strain was removed by annealing, the wrought material hardened appreciably faster than the material cast in graphite and considerably faster than the material cast in investment material. The difference between the wrought and graphite-cast materials might be attributed to an incidental difference such as composition or grain size, but it is not believed that the very large difference between the investment-cast specimens and the wrought specimens can be explained away so easily. This difference in behavior seems to reflect a fundamental difference between the wrought and cast structure, the nature of which is not known.

The phenomenon just discussed has practical importance in that it indicates that cast heat-resistant alloys will be much less susceptible to sigma-phase embrittlement than wrought alloys. Also, the susceptibility of chromium steels such as 18-8 to intergranular sensitization by sigma-phase precipitation should be less in cast steels than in wrought steels.

### EFFECT OF REPEATED RECRYSTALLIZATIONS ON RATE OF FORMATION OF SIGMA

An attempt was made to determine whether the effect of cold working could be removed completely by annealing or whether it is cumulative. Tensile specimens were machined from rolled CN that had been annealed 1 hour at 1850 °F (1010 °C). These were then

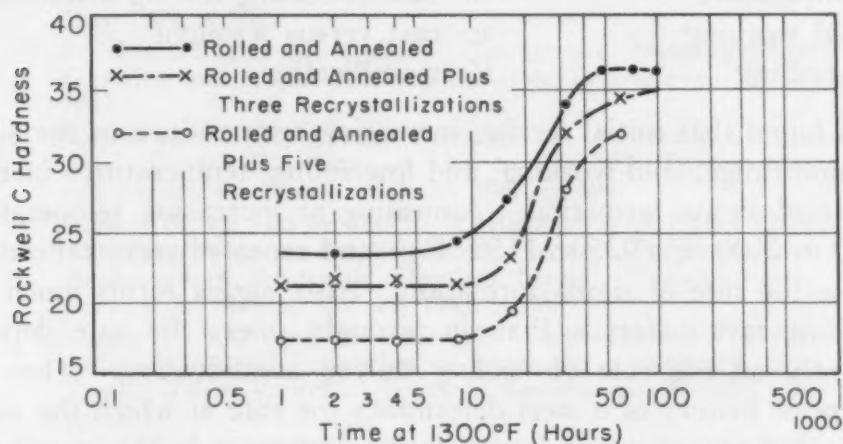


Fig. 23—Effect of Repeated Recrystallizations on the Hardening (Rate of Sigma Formation) of CN at 1300°F.

cold-elongated 15% and annealed for 15 minutes at 1850 °F (1010 °C). For one set, the cold elongation and annealing were repeated twice and for another they were repeated four times. The final annealing treatments were 1 hour at 1850 °F (1010 °C). For the set that was recrystallized five times, the last cold elongation was 10% instead of 15% because the tensile bars began to neck down. Specimens were then cut from the centers of the gage lengths and heated at 1300 and 1400 °F (705 and 760 °C).

The change of hardness with time at 1300 °F (705 °C) is shown in Fig. 23. The curves show that sigma formed much less rapidly in the specimens which were recrystallized five times than in the specimens which were only annealed after rolling. Similar curves were obtained for the specimens heated at 1400 °F (760 °C). Thus the effect of cold working does not appear to be cumulative; rather, the effect of annealing seems to be cumulative. The reason why sigma formed less rapidly in the repeatedly recrystallized specimens than in the rolled and annealed specimens is not known. However, the grain growth and homogenization that would result from recrystallization may account for the phenomenon.



## SUMMARY

The rate at which the sigma phase forms in several high-chromium austenitic-ferritic steels has been studied by means of hardness measurements and microscopy. The effects of the following variables on the rate of sigma formation are discussed:

- |                            |  |
|----------------------------|--|
| 1. Composition             | 6. Manufacturing variables               |
| 2. Initial ferrite content | a. rolling temperature                   |
| 3. Temperature             | b. rate of cooling during solidification |
| 4. Cold working            | c. cast versus wrought                   |
| 5. Annealing               | 7. Recrystallization                     |

It was found that initial ferrite, increasing temperature in the sigma formation range, cold working, and low rolling temperatures increase the rate of sigma formation. Annealing at increasing temperatures—1700 to 2100 °F (925 to 1150 °C)—and repeated recrystallizations decrease the rate of sigma formation. Also, sigma forms much less rapidly in cast materials than in wrought ones; the rate depends apparently on the rate of cooling during solidification. Thus the entire prior history of a steel determines the rate at which the sigma phase may form in it and is equally as important in this connection as the composition of the steel.

The steels which were investigated are considerably hardened by the sigma phase as it forms in them. The mechanism of this hardening phenomenon was discussed. It was found that the hardening mechanism could not be considered either as an age hardening effect or as simple mixed-phase hardening. However, a correlation was found between the hardness and the logarithm of the average free path in the austenite for steels containing various amounts and distributions of sigma. Thus the sigma-phase hardening in these particular steels is of the mixed-phase type but depends on both the amounts and distributions of the phases.

Composition was found to affect the behavior of these steels with respect to sigma formation in three ways; it affected the:

- a. rate of sigma formation at a given temperature
- b. upper limit of the sigma formation range
- c. temperature below which sigma forms at a negligible rate.

## ACKNOWLEDGMENTS

The author wishes to acknowledge the assistance of Dr. L. C. Chang, who obtained the data for Fig. 11. He is much indebted to Mr. P. Payson for the opportunity to perform this work and for his

valuable guidance. Mr. G. Stefanelli supervised the preparation and treatment of the specimens and Mr. F. Baureis prepared the illustrations. The facilities of the Crucible Steel Company of America were used throughout the work.

### References

1. F. B. Foley, "The Sigma Phase", *Bulletin*, Research Institute of Temple University, 1947, and *Metallurgia*, Vol. 34, 1946, p. 139.
2. D. A. Oliver, "The Sigma Phase in Stainless Steels", *METAL PROGRESS*, May 1949, p. 665.
3. R. T. Howard and M. Cohen, "Quantitative Metallography by Point Counting and Lineal Analysis", *Metals Technology*, TP 2215, August 1947.
4. P. Payson and C. H. Savage, "Changes in Austenitic Chromium-Nickel Steels During Exposures at 1100 to 1700 °F", *TRANSACTIONS*, American Society for Metals, Vol. 39, 1947, p. 404.
5. R. Franks, W. O. Binder and C. R. Bishop, "The Effect of Molybdenum and Columbium on the Structure, Physical Properties and Corrosion Resistance of Austenitic Stainless Steels", *TRANSACTIONS*, American Society for Metals, Vol. 29, 1941, p. 35.
6. J. Gilman, P. Koh and O. Zmeskal, "Delta Ferrite Formation and Its Influence on the Formation of Sigma in a Wrought Heat Resisting Steel", *TRANSACTIONS*, American Society for Metals, Vol. 41, 1949, p. 1371.
7. Unpublished data of Research Laboratory, Crucible Steel Company of America.
8. W. P. Rees, B. D. Burns and A. J. Cook, "Constitution of Iron-Nickel-Chromium Alloys at 650 to 800 °C", *Journal*, Iron and Steel Institute, Vol. 162, 1949, p. 325.
9. H. Kirby and J. Morley, "The Formation of the Sigma Phase in Duplex Chromium-Nickel-Molybdenum Corrosion-Resisting Steels", *Journal*, Iron and Steel Institute, Vol. 158, 1948, p. 289.
10. M. Gensamer, E. Pearsall, W. Pellini and J. Low, "The Tensile Properties of Pearlite, Bainite and Spheroidite", *TRANSACTIONS*, American Society for Metals, Vol. 30, 1942, p. 983.
11. C. Burgess and W. Forgeng, "Constitution of Fe-Cr-Mn Alloys", *Transactions*, American Institute of Mining and Metallurgical Engineers, Vol. 131, 1938, p. 277.
12. E. Fetz, "Dynamic Hardness Testing of Metals and Alloys at Elevated Temperatures", *TRANSACTIONS*, American Society for Metals, Vol. 30, 1942, p. 1419.
13. E. B. Bergsmann, "A Simple, Accurate Microhardness Testing Device", *METAL PROGRESS*, August 1948, p. 183.

### DISCUSSION

**Written Discussion:** By Otto Zmeskal, director, Department of Metallurgical Engineering, Illinois Institute of Technology, Chicago.

Mr. Gilman has presented a most excellent paper covering his comprehensive study of the factors affecting sigma-phase formation in certain valve steels. These steels are remarkably suited for hardness measurements as a means of following the formation of sigma phase since they attain such high levels of hardness.

Mr. Gilman has presented a good case to substantiate his conclusion regarding the mechanism of hardening.

Bindari, Koh and Zmeskal have also noted gray areas in a different steel, as shown in Fig. 2 of Gilman's paper, and agree with his analysis that they are austenite of the same composition as the ferrite from which they formed.

Mr. Gilman has shown that not all of the sigma forms from the ferrite; some sigma forms out of the austenite. The impoverishment of the matrix austenite in chromium as a result of the process must have a profound effect upon its stability. Would Mr. Gilman care to elaborate on this matter?

**Written Discussion:** By Harry K. Herschman, metallurgist, National Bureau of Standards, Washington, D. C.

With respect to the amount of sigma formed during heating, the author states, "Usually, the greater the amount of ferrite in the initial structure, the greater the rate of sigma formation", and indeed he supports this with experimental evidence. However, he makes no reference to this factor as a possible contributing cause for the greater hardening obtained in the steels annealed at 1700 °F (925 °C) than for those annealed at 2200 °F (1205 °C) and subsequently heated at 1400 °F (760 °C), as shown in the author's Fig. 18. An examination of the micrographs of Fig. 19 in the paper indicates that the amount of austenite present in the specimen quenched from 2200 °F (1205 °C) is considerably greater than that in the specimen quenched from 1800 °F (980 °C). If this assumption is correct and is characteristic of the steels heated at the higher temperatures, then it is suggested that the author's reasoning quoted above may be considered as possibly applicable in explaining the results shown in his Fig. 18.

#### Author's Reply

In reply to Mr. Herschman, I refer to my discussion of the annealing effect in the paper. It was stated that no correlation was found between the ferrite content of the solution-treated material and the rate of sigma formation in the steel. However, I shall give some of the data in order to make this point clear.

Table III  
Relative Magnetic Susceptibilities (Ferrite Contents) of Specimens of Steel CN  
After Annealing Treatments and Prior to Hardening

Annealing Temperature (°F) Time—3 Hours—WQ	Relative Magnetic Susceptibility
1700	575
1800	650
1900	675
2000	675
2100	400
2200	400

Table III shows that the ferrite content of steel CN increases with annealing temperature until about 1950 °F (1065 °C) is reached, and then decreases. On the other hand, the rate of sigma formation subsequent to the annealing treatment decreases monotonically with increasing anneal-

ing temperature (Fig. 18 of the paper). Thus there is a lack of correspondence between the two phenomena. This is not to say that the variable initial ferrite content has no effect on the rate of sigma formation; it very probably does have. I desire only to say that this is not the controlling factor.

Dr. Zmeskal's question is the answer to an author's prayer. In fact, considerable attention was paid to the effect of sigma-phase formation on the stability of the matrix austenite. The work was not included in the paper because it was felt that this would give the paper undue bulk. The results of this work I shall summarize briefly now.

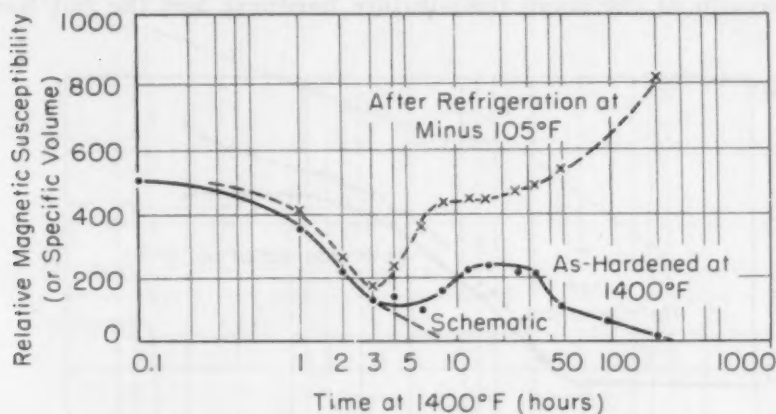


Fig. 24—Changes in the Magnetic Susceptibility of As-Rolled CN Caused by Holding at 1400 °F and Refrigeration.

In the solution-treated condition, the steels used for the investigation were quite stable with respect to transformation of the austenitic matrix when cooled down to about minus 105 °F. When they were heated in the sigma-formation temperature range they became less stable as sigma formation progressed. This effect depended on the composition. The austenite of steel CN was affected most, that of steel CNM was affected less, and the austenite of steel CNO was quite stable down to minus 320 °F after appreciable amounts of the sigma phase had formed. I shall discuss the effects of sigma formation on the austenite of steel CN in further detail.

The way in which the stability of the austenite in steel CN is affected by sigma formation is shown by Fig. 24. In this figure the relative magnetic susceptibilities (or specific volumes) of various specimens are plotted against the time that they were held at the sigma-phase formation temperature. These quantities are directly related to the ferrite content of the steel (by X-ray examination the transformation product of the austenite was confirmed as ferrite). The results for two sets of specimens are plotted. The continuous line is for specimens which were cooled in air from 1400 °F (760 °C) and then tested. The dotted line represents specimens which were air-cooled from 1400 °F (760 °C) and then cooled in a dry ice-acetone mixture to about minus 105 °F, where they were held for 1 hour. The difference in the vertical coordinates of the continuous and the dotted curves indicates transformation. Similar curves



were obtained for specimens heated at 1300 °F (705 °C). These curves were displaced about 10 hours to the right, however. For specimens heated at 1500 °F (815 °C), effects were observed but they were much smaller; and at 1200 °F (650 °C) the sigma phase formed so slowly that its effects on the austenitic stability were not investigated.

Fig. 25 presents the results of hardness measurements on the specimens of Fig. 24. It will be seen that the low temperature transformation of the austenite caused a measurable increase in the hardness of the material when large amounts of the transformation product were formed. The fact that the austenitic transformation had no appreciable effect on the room temperature hardness (of nonrefrigerated specimens) is shown by a comparison of the room temperature hardness and the hot hardness

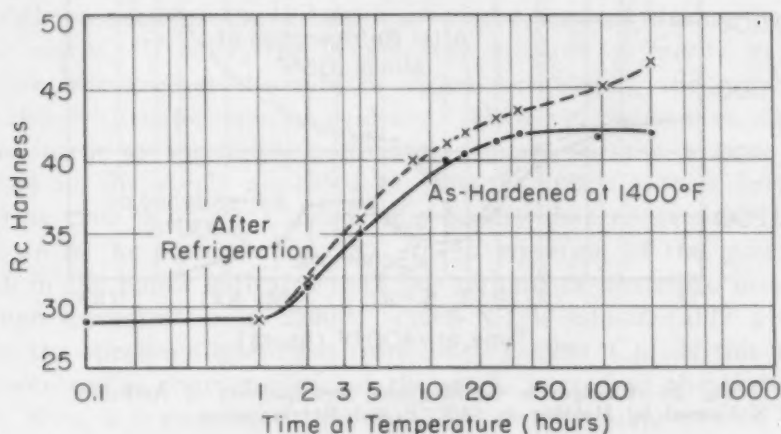


Fig. 25—Effect of Refrigerating for 1 Hour at  $-105^{\circ}\text{F}$  on the Hardness of As-Rolled CN After Holding at  $1400^{\circ}\text{F}$  for Various Amounts of Time.

curves. (See Fig. 12.) They have very similar shapes. This would not be the case if a large part of the room temperature hardness were attributable to the transformation product.

A characteristic of the austenitic matrix which changes during sigma-phase formation in steel CN is its lattice parameter. This was measured using chromium radiation and a symmetrical back-reflection focusing camera. The specimens were ground to the curvature of the camera and deeply etched. As shown in Fig. 26, the lattice parameter of the matrix austenite which was stable at room temperature decreased with increasing time at  $1400^{\circ}\text{F}$  ( $760^{\circ}\text{C}$ ) up to 200 hours. This decrease indicates a change in the alloy content of the matrix austenite and therefore partly explains the change in stability of the austenite. The lattice parameter of the austenite which transformed upon cooling to room temperature was not measured, of course. This localized austenite probably had a lattice parameter which was quite different from those shown in Fig. 26. Perhaps the scatter of points in the 5-to-20-hour region of the curve is related to this.

The somewhat unusual shapes of the curves in Fig. 24 require some interpretation. There are two peculiarities of these curves which invite explanation. One is the increase in the amount of magnetic phase at

room temperature with time at 1400 °F (760 °C) in the range from 5 to 16 hours, and the subsequent decrease from 20 to 200 hours. The second is the increase in the amount of magnetic transformation product for the refrigerated specimens in the range from 20 to 200 hours, while the amount of magnetic phase present at room temperature decreased in the same time range.

The increase in quantity of the magnetic phase present at room temperature is attributed to localized regions of the austenitic matrix which, because of sigma-phase formation, were impoverished in the elements which promote austenitic stability. If this had not occurred,

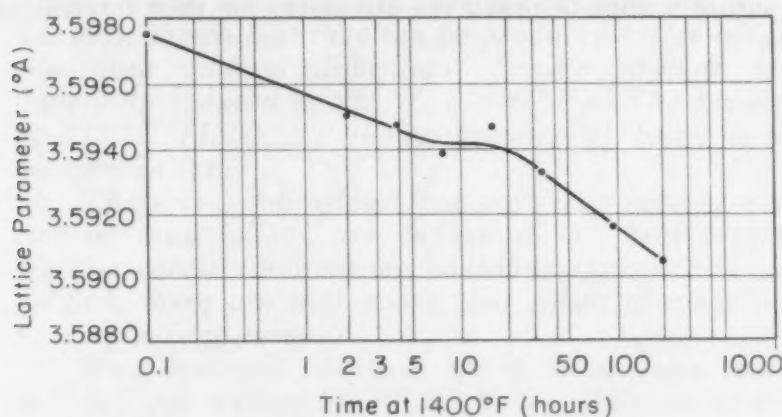


Fig. 26—Change in the Lattice Parameter of the Austenite in As-Rolled CN Caused by Holding at 1400 °F.

it is believed that the continuous curve would follow the schematic dashed line instead of its actual course. After large amounts of time at 1400 °F (760 °C), it is believed that the locally impoverished regions gained somewhat in alloying elements and thus became stable with respect to cooling to room temperature. However, now the whole matrix became lower in alloy content than it was initially. That is, there was a mild over-all impoverishment of the austenitic matrix as the time increased at 1400 °F (760 °C). Being less severe than the localized decreases in alloy content, this over-all depletion of the austenite did not render it unstable with respect to room temperature transformation but did cause it to transform when cooled to minus 105 °F. Thus, in the region beyond about 20 hours in Fig. 24, the amount of localized impoverishment of the austenite decreased from 20 to 200 hours and thereby caused the amount of magnetic phase present at room temperature to decrease in this range. On the other hand, the over-all alloy depletion of the austenitic matrix progressed in the 20-to-200-hour range and caused the amount of magnetic phase which was present after refrigeration to increase.

Another feature of the low temperature transformation of the austenite in steel CN is the fact that it occurs isothermally when the material is cooled below some critical temperature. This was concluded from dilatometric measurements. Also, this was shown by measurements of specific volume (Archimedes' method) and magnetic susceptibility made on specimens heated back to room temperature from minus 105 °F. For

example, if steel CN in the as-rolled condition was heated at 1400 °F (760 °C) for 16 hours and then cooled moderately rapidly (mild air blast) to minus 105 °F, its specific volume increased with time at minus 105 °F. The increase was exponential, being comparatively rapid at first and then approaching some constant value asymptotically. The half time for the reaction was about 1 hour, but measurable increases could be determined up to 16 hours at minus 105 °F.

In summary, the formation of the sigma phase in particular steels has a marked effect on the stability of the austenitic matrix with respect to low temperature transformation. Magnetic, density, dilatometric, hardness and X-ray measurements have shown this.

The author wishes to thank the discussers for their interest and kind comments.



## NICKEL-ALUMINUM-MOLYBDENUM ALLOYS FOR SERVICE AT ELEVATED TEMPERATURES

BY H. V. KINSEY AND M. T. STEWART

### *Abstract*

*The results presented in this paper indicate that alloys consisting of nickel, aluminum and molybdenum possess mechanical properties at 815 °C (1500 °F) that are at least the equivalent of the best cobalt-base casting alloys. These new alloys require no strategic materials. It has been shown that they can be produced under industrial conditions without difficulty. Tensile strength is not materially reduced at 815 °C (1500 °F). The tensile test at 815 °C (1500 °F) shows promise of being a useful acceptance test.*

*There are indications that the creep-rupture properties of these alloys are influenced by heat treatment. Neither cobalt nor tungsten additions appear to be useful. In fact, there are indications that cobalt above 5% may be decidedly injurious.*

*Two tentative chemical specifications, one based on a 35,000-psi rupture life of 150 hours minimum at 815 °C (1500 °F) and the other based on a 35,000-psi rupture life of 200 hours minimum at 815 °C (1500 °F), are developed.*

**I**N a search for a new and better alloy that might prove suitable for gas-turbine blades and other high temperature applications, the nickel-rich corner of the nickel-aluminum-molybdenum system was investigated.

Exploratory work previously reported (1)<sup>1</sup> indicated that these alloys showed promise. Furthermore, the fact that these alloys required no metals that might be classified as "strategic" made a more thorough investigation of their characteristics mandatory.

During the course of this preliminary work (1) it became apparent that the properties of the alloy could be related to two

<sup>1</sup>The figures appearing in parentheses pertain to the references appended to this paper.

Published by permission, Director General of Scientific Services, Department of Mines and Technical Surveys, Ottawa, and by permission of the National Research Council, Ottawa, Canada.

A paper presented before the Thirty-second Annual Convention of the Society, held in Chicago, October 21 to 27, 1950. Of the authors, H. V. Kinsey is metallurgical engineer, head of High Temperature Metals Section, Division of Physical Metallurgy, Mines Branch, Department of Mines and Technical Surveys, Ottawa, and M. T. Stewart is junior research officer, Associate Committee of High Temperature Metals, National Research Council of Canada, Ottawa, Canada. Manuscript received April 17, 1950.



variables of composition—namely, the ratio of nickel to aluminum, and the molybdenum content. Accordingly, for convenience, a system of naming an alloy in terms of these two variables was evolved. The following examples will serve to illustrate this system.

1. Alloy 116M203 has a nickel to aluminum ratio of 11.6:1 and a molybdenum content of 20.3%.

2. Alloy 86M241 has a nickel to aluminum ratio of 8.6:1 and a molybdenum content of 24.1%.

In the work presented here, in addition to a more intensive investigation of the nickel-aluminum-molybdenum system, two modifications of the basic alloys were also explored. These are:

- (a) the replacement of part of the nickel with cobalt,
- (b) the replacement of molybdenum with tungsten.

It therefore became necessary to expand the system of nomenclature described above to accommodate these more complex compositions.

A suffix is used to indicate the presence of cobalt, and the ratio number expresses the ratio of (nickel plus cobalt) to aluminum. Thus, Alloy 88M223-61K has a (nickel plus cobalt) to aluminum ratio of 8.8:1, a molybdenum content of 22.3%, and a cobalt content of 6.1%.

The means employed to indicate the presence of tungsten are illustrated in the following example:

Alloy 93M152W78 has a nickel to aluminum ratio of 9.3:1, a molybdenum content of 15.2%, and a tungsten content of 7.8%.

#### INFLUENCE OF COMPOSITION VARIABLES ON CREEP-RUPTURE PROPERTIES

Exploratory work (1) indicated that the ratio of nickel to aluminum, and the molybdenum content, were composition variables that influence properties both at room temperature and at elevated temperatures. Therefore, the first part of the current program was designed to study the properties of alloys within composition limits defined as follows:

Ratio of nickel to aluminum	12:1 to 8:1
Molybdenum content	12 to 28%

In order to evaluate the effect of replacing some of the nickel with cobalt, Alloy 100M250 was selected. Cobalt was substituted for nickel in 5% increments up to 25%.

Alloy 80M250 was modified by substituting tungsten for molybdenum in increments of 5% up to 25% tungsten.

*Production of Alloys and Test Bars*—Commercially pure nickel,

aluminum, and molybdenum were used to make these alloys. All melting was done by high-frequency induction in a magnesia-lined crucible. Five-pound melts were cast into sand ingot molds. A chemical analysis was made on each melt.

The alloy thus produced was used to make up melts from which test bars were cast. Minor corrections for chemical composition and melting losses were made to the test-bar melts by additions of nickel, aluminum, or molybdenum, according to requirements. These melts

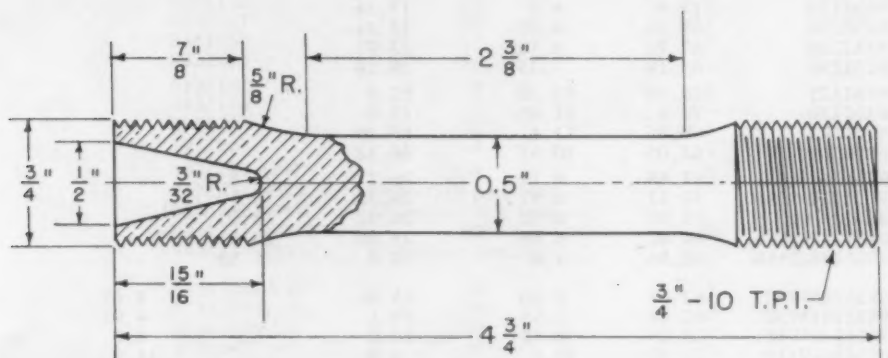


Fig. 1—P.M.R.L. Precision-Cast 0.5-Inch Diameter Creep Test Bar for High Temperature Alloys.

were protected with a flux consisting of silica, soda and fluorspar. Just prior to casting they were treated by plunging calcium metal into them. About 1 gram of calcium was used per 5-pound melt.

A platinum-rhodium immersion couple was used to measure the metal temperature. The casting temperature was 1600 to 1650 °C (2910 to 3000 °F).

The test bars were cast centrifugally in molds heated to 675 °C (1250 °F). These molds were produced by the lost-wax process.

A half-inch-diameter test bar (see Fig. 1) was used for the first part of this work.

*Composition and Creep-Rupture Properties of Alloys Produced*—The alloys produced for the first part of this program are listed in Table I. Iron and silicon were both kept below 0.15%. A maximum of 0.10% carbon was permitted.

A creep-rupture test at 815 °C (1500 °F) using a stress of 35,000 psi was used to evaluate these alloys. Where a test result appeared to be questionable, a second, and sometimes a third, test was made. The highest test result obtained for each alloy is reported. The results of these creep-rupture tests at 35,000 psi are summarized in Table II.

The alloys that showed merit on the basis of the results listed

Table I  
Chemical Analyses of Alloys Tested

Alloy	Chemical Analysis, %				Cobalt	Tungsten
	Nickel	Aluminum	Molybdenum			
135M156	78.46	5.77	15.63			
122M165	76.98	6.28	16.52			
127M185	75.4	5.94	18.53			
119M254	68.59	5.75	25.4			
104M132	79.04	7.6	13.2			
103M159	76.51	7.45	15.85			
96M203	72.07	7.47	20.30			
104M247	68.54	6.57	24.72			
107M297	64.09	6.0	29.7			
86M135	77.43	8.98	13.5			
85M173	73.8	8.7	17.34			
83M224	69.26	8.35	22.24			
83M240	67.72	8.18	23.97			
86M293	63.19	7.35	29.26			
61M125	74.99	12.38	12.5			
64M150	73.41	11.45	15.0			
59M193	69.45	11.1	19.26			
59M261	63.08	10.67	26.12			
99M267-48K	61.58	6.72	26.7	4.83		
97M254-101K	57.42	6.97	25.35	10.10		
108M270-150K	51.05	6.62	26.95	15.03		
102M231-209K	49.07	6.86	23.10	20.85		
98M248-255K	42.54	7.0	24.8	25.55		
67M240W47	62.97	9.26	23.96			4.67
85M191W50	67.93	7.95	19.1			4.97
78M140W88	68.39	8.75	14.0			8.8
65M48W119	72.97	10.2	4.8			11.9
80M110W186	62.27	7.8	11.0			18.6
56W162	71.4	12.6	.....			16.2

in Table II were subsequently tested in creep rupture at 815 °C (1500 °F) at stresses between 27,500 and 40,000 psi. The results of these tests are summarized in Table III.

Typical time versus per cent elongation curves of alloys having nickel to aluminum ratios of 11.9:1, 10.4:1, and 8.3:1 are shown in Figs. 2, 3 and 4, respectively.

### Discussion of Results

Since most of the data obtained in the work thus far presented are representative of single heats of each analysis and in many cases are based on only one test, no attempt has been made to place too rigorous an interpretation on this portion of the program. At this stage, general trends were of primary interest. An examination of the data presented in Tables I, II and III permits the following general observations to be made:

1. *Effect of Molybdenum*—In the ternary nickel-aluminum-molybdenum alloys, the optimum molybdenum range for best elevated temperature properties appears to be 20 to 25%.

2. *Effect of Nickel to Aluminum Ratio*—(a) As the ratio of nickel to aluminum decreases from 12:1 to 8:1, the creep-rupture strength of the alloy decreases and the ductility, as measured by

**Table II**  
**Summary of Creep-Rupture Results at 815 °C (1500 °F) and 35,000 Psi**

Alloy	Hours to Rupture	Total Elongation, %
135M156	0	0
122M165	21	1
127M185	8	0
119M254	464	0.5
104M132	13	0
103M159	53	0
96M203	115	0
104M247	306	3
107M297	244	2
86M135	36	0
85M173	89	1
83M221	217	7
83M240	157	5
86M293	66	2
61M125	1	2
64M150	2	3
59M193	1/4	1
59M261	1	2
99M267-48K	338	5
97M254-101K	Defective test bars	
108M270-101K	Defective test bars	
102M231-209K	50	0
98M248-255K	Defective test bars	
67M240-W47	89	2
85M191W50	128	3
78M140W88	122	1
65M48W119	20	2
80M110W186	127	1
56W162	0	1

**Table III**  
**Summary of 815 °C (1500 °F) Creep-Rupture Tests at Various Stresses**

Alloy	Stress, psi	Time, Hours				Rupture	Total Elong. After Fracture, %
		0.2% Creep Strain	0.5% Creep Strain	1.0% Creep Strain	2.0% Creep Strain		
119M254	30,000	400				750	1.0
	35,000		No extensometer			464	0.5
	40,000	40				307	0
96M203	30,000	80	408			508	2.0
	35,000		No extensometer			115	
104M247	30,000	20	105	332		402	
	35,000	18	74	210		306	3.0
	40,000	9	38	94		118	
107M297	32,500	30	135			350	
	35,000		No extensometer			244	2.0
83M224	32,500			118	288	310	7.0
	35,000			70	135	217	7.0
83M240	30,000		No extensometer			314	5.0
	35,000			55	103	157	5.0
99M267-48K	30,000		72	184	365	497	4.0
	35,000		40	110	245	338	5.0
	40,000		28	55		106	6.01
80M110W186	35,000	10	50			127	1

elongation after rupture in a creep-rupture test, increases.

(b) The usefulness of the alloy disappears when the ratio of nickel to aluminum becomes 6:1 or less. This deterioration of properties coincides with the appearance of a phase (Fig. 15) identified as NiAl.



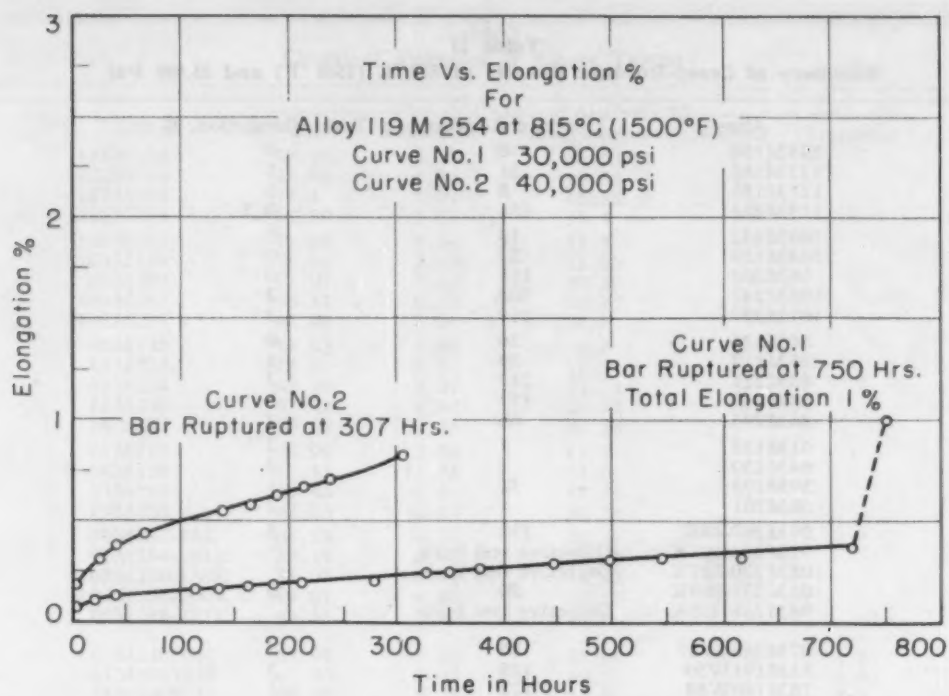


Fig. 2—Time Versus Per Cent Elongation for Alloy 119M254 at 815 °C (1500 °F).

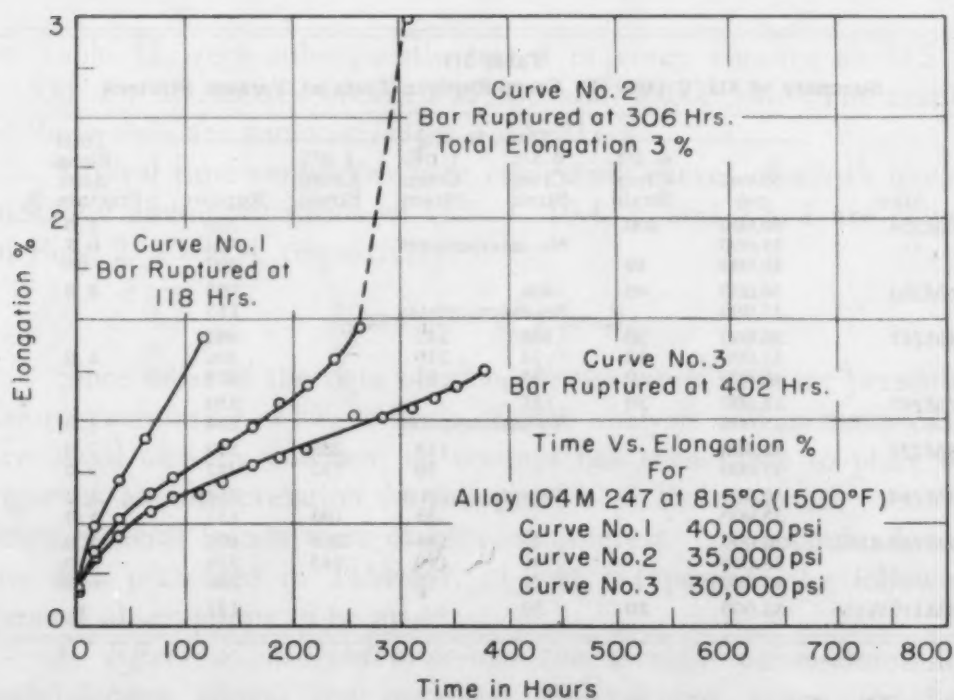


Fig. 3—Time Versus Per Cent Elongation for Alloy 104M247 at 815 °C (1500 °F).

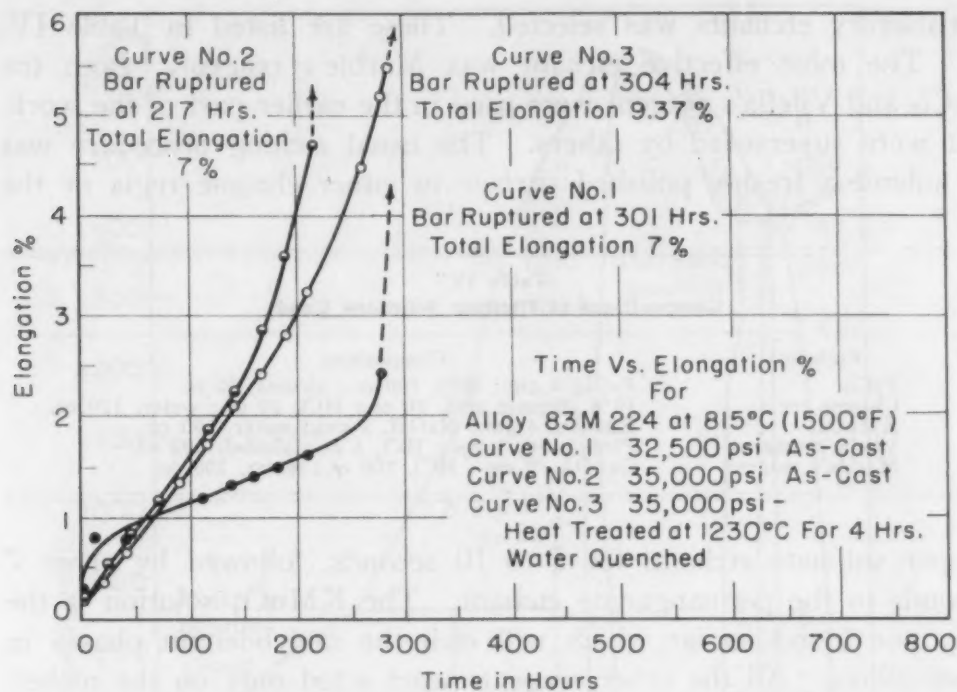


Fig. 4—Time Versus Per Cent Elongation for Alloy 83M224 at 815 °C (1500 °F).

3. *Effect of Cobalt*—Cobalt, up to 5%, has no apparent effect on the creep-rupture properties. However, over 10% cobalt makes the alloy difficult to cast and, by causing the occurrence of NiAl (Fig. 24) destroys the creep-rupture properties.

4. *Effect of Tungsten*—Replacing up to two-thirds of the molybdenum with tungsten apparently is neither beneficial nor harmful.

5. *Thousand-Hour Rupture Stress at 815 °C (1500 °F)*—From the data presented in Table IV, the thousand-hour rupture stress at 815 °C (1500 °F) is apparently about 25,000 psi.

#### INFLUENCE OF COMPOSITION VARIABLES ON METALLOGRAPHIC CHARACTERISTICS

This phase of the work was planned to observe how changes in composition would influence the microstructure. Preliminary work (1) had indicated that certain characteristic microstructures identified useful alloy compositions, while other characteristic microstructures identified useless alloy compositions.

#### Etching

The etching of these nickel-aluminum-base alloys presented some unusual problems. After considerable work, a group of

satisfactory etchants was selected. These are listed in Table IV.

The most effective etchant was Marble's reagent. Both the  $\text{FeCl}_3$  and Vilella's reagent were used in the earlier part of the work, but were superseded by others. The usual etching procedure was to submit a freshly polished surface to either chrome regia or the

Table IV  
Compositions of Etching Solutions Used

Etchant	Composition
$\text{FeCl}_3$	$\text{FeCl}_3$ , 4 gm.; $\text{HCl}$ , 100 cc.; alcohol, 50 cc.
Chrome regia	10% chromic acid, 10 cc.; $\text{HCl}$ , 20 cc.; water, 120 cc.
$\text{KMnO}_4$	$\text{KMnO}_4$ , 4 gm.; $\text{NaOH}$ , 2 gm.; water, 100 cc.
Vilella's reagent	Picric acid, 1 gm.; $\text{HCl}$ , 5 cc.; alcohol, 100 cc.
Marble's reagent	$\text{CuSO}_4$ , 20 gm.; $\text{HCl}$ , 100 cc.; water, 100 cc.

copper sulphate etchant, for 5 to 10 seconds, followed by about 7 seconds in the permanganate etchant. The  $\text{KMnO}_4$  solution is the only one found so far which will etch the molybdenum phases in these alloys. All the other reagents used acted only on the nickel-aluminum phases. This makes the two-stage etching procedure necessary.

Except where otherwise indicated in the caption, all specimens were polished mechanically, the final surface being obtained by the use of Linde "B" on a gamal cloth. Little difficulty was encountered in the polishing of these alloys. Flowed surfaces were never bothersome. Only a freshly polished surface could be etched, but after etching, the surfaces deteriorated only slightly during storage over a period of months.

#### Binary Nickel-Aluminum Alloys

The starting point for this project was provided by the work of Alexander and Vaughan (2) on the nickel-aluminum system. The constitution diagram developed by these investigators is reproduced in Figs. 5 and 6.

From this diagram, four alloy compositions were chosen such that each would lie in one of the four phase zones between 75 and

Table V  
Analyses of Binary Alloys

Alloy No.	% Ni	% Al	Ni: Al Ratio	Anticipated Phases
1	73.08	26.92	2.7:1	NiAl
2	83.19	16.81	4.9:1	NiAl + $\text{Ni}_3\text{Al}$
3	84.70	15.30	5.6:1	$\text{Ni}_3\text{Al}$
4	92.2	7.8	11.8:1	$\text{Ni}_3\text{Al}$ + Alpha

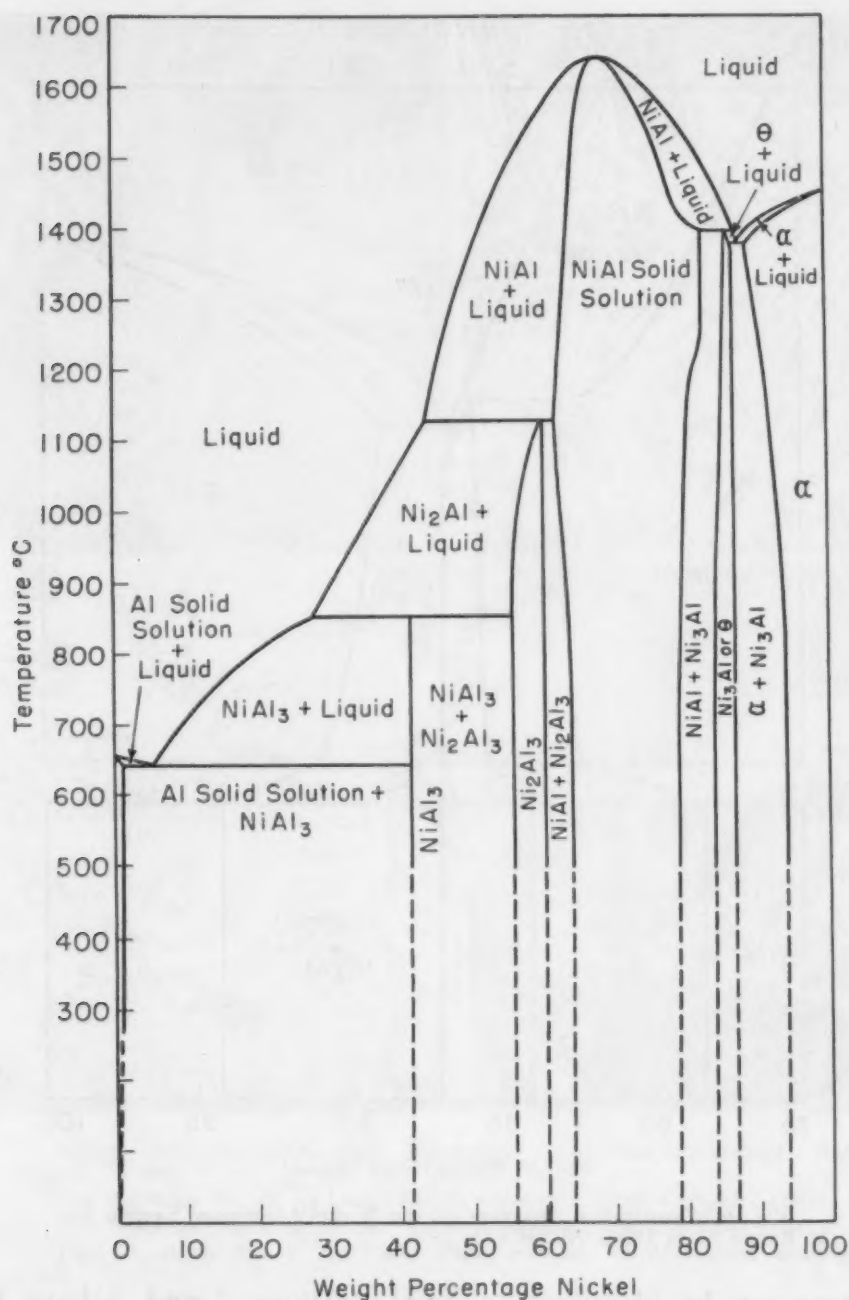


Fig. 5—Constitution Diagram of the Nickel-Aluminum System. Alexander and Vaughan (2).

95% nickel at room temperature. These alloys were cast into sand molds. Photomicrographs of their structures are reproduced in Figs. 7 to 10 inclusive. Table V gives the chemical analyses of these heats and the phases expected to be present in their microstructures.

Alloy No. 1, with a Ni:Al ratio of 2.7:1, shows only one phase, as was expected. By reference to the equilibrium diagram,



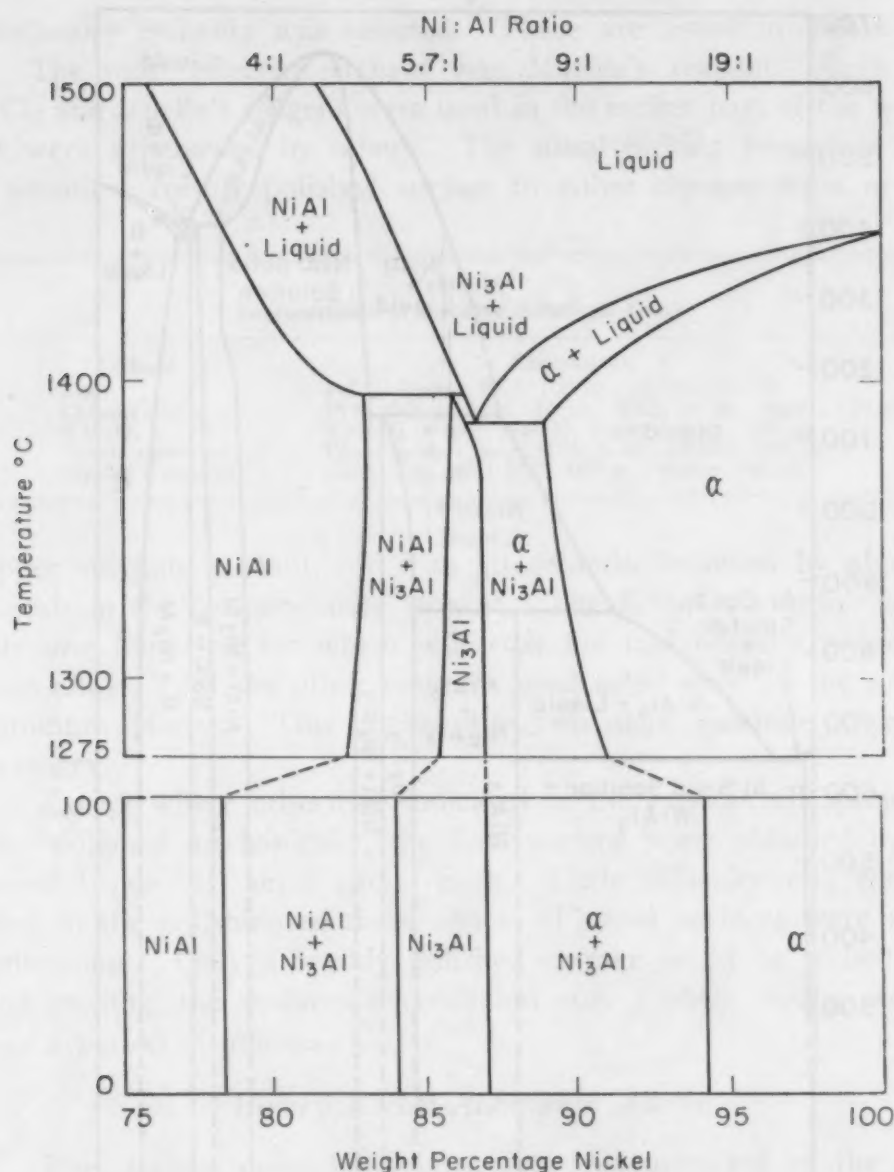


Fig. 6—Constitution Diagram of the Nickel-Aluminum System for the Range 75 to 100% Nickel (2).

this phase can be identified as NiAl. Alloys 2 and 3 have two phases. This also was to be expected in Alloy 2, the phases being NiAl and Ni<sub>3</sub>Al; but under equilibrium conditions only one phase should appear in Alloy 3. The NiAl, formed at the time of freezing, should dissolve in the Ni<sub>3</sub>Al on cooling past about 1200 °C (2190 °F). Actually, the rate of cooling has been too rapid to permit this solution to take place, and NiAl is retained in the as-cast alloy. The dark-etching phase present in Alloys 2 and 3 is identified as NiAl, since there is more of this phase present in the alloy containing the higher percentage of aluminum. The typical appearance

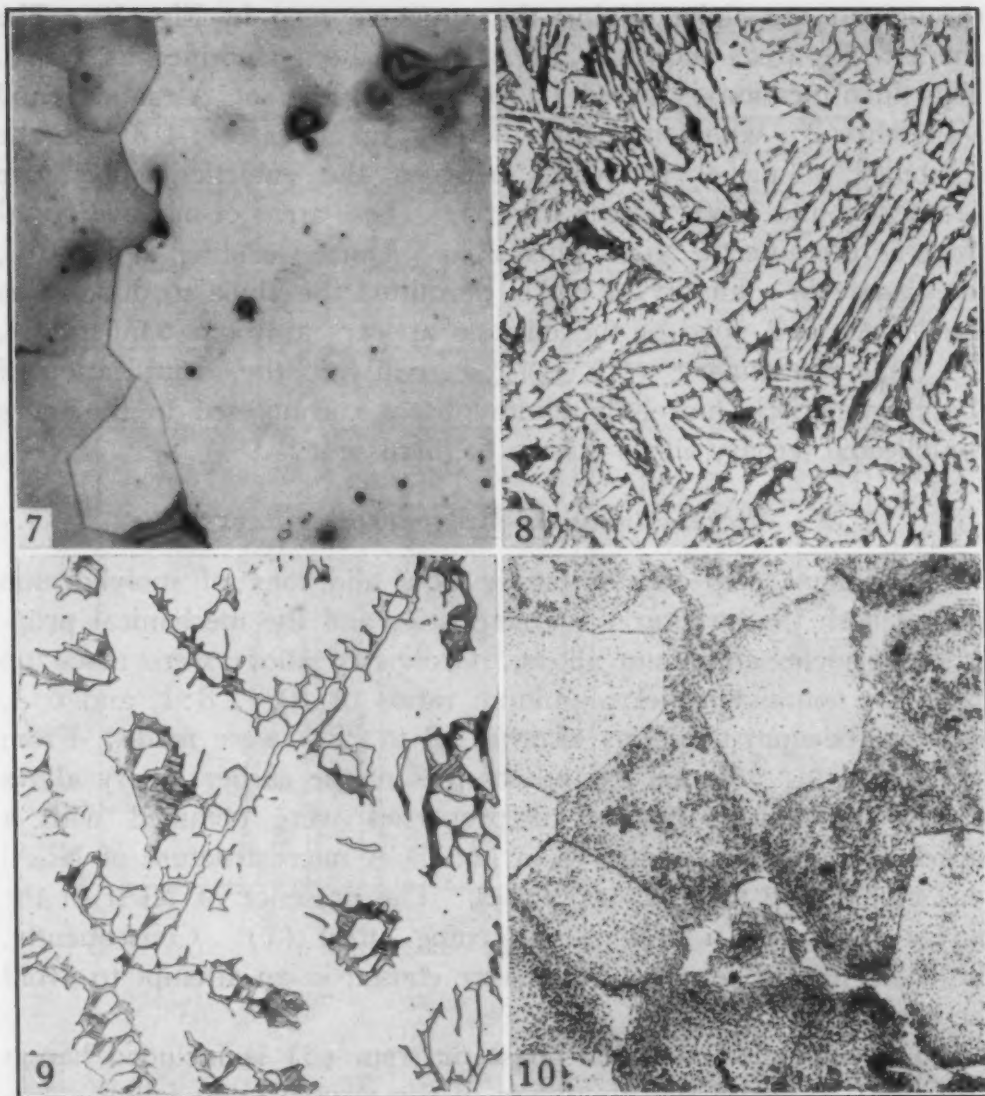


Fig. 7—Alloy No. 1, As Cast. Electrolytic polish, Vilella's etchant. NiAl solid solution.  $\times 200$ .

Fig. 8—Alloy No. 2, As Cast. Vilella's etchant. NiAl + Ni<sub>3</sub>Al (white).  $\times 200$ .

Fig. 9—Alloy No. 3, As Cast. Vilella's etchant. Ni<sub>3</sub>Al + NiAl (dark).  $\times 200$ .

Fig. 10—Alloy No. 4, As Cast. FeCl<sub>3</sub> etchant. Ni<sub>3</sub>Al + alpha solid solution.  $\times 200$ .

of NiAl, as seen in these binary alloys, aided a great deal in its subsequent identification in the ternary nickel-aluminum-molybdenum alloys.

Alloy 4 consists of two phases, identified as Ni<sub>3</sub>Al in a matrix of alpha solid solution. Alexander and Vaughan (2) pointed out that there is a decrease in the solubility of aluminum in nickel between 1385 and 1000 °C (2525 and 1830 °F). Immediately after freezing, the alloy consisted almost entirely of alpha solid solution. During cooling to room temperature, Ni<sub>3</sub>Al was precipitated

throughout the alpha, giving the structure seen in Fig. 10. The small white areas shown in Fig. 10 have been identified as  $\text{Ni}_3\text{Al}$ . This identification is based on the same work of Alexander and Vaughan (2), who found that there is an increase of 0.3% in the solubility of nickel in  $\text{Ni}_3\text{Al}$  between the eutectic temperature ( $1385^\circ\text{C}$ ) and  $1360^\circ\text{C}$  (see Fig. 6). These areas of massive  $\text{Ni}_3\text{Al}$  froze as the eutectic  $\text{Ni}_3\text{Al}$  plus alpha. During cooling to  $1360^\circ\text{C}$ , the change in solubility of nickel permitted the alpha to dissolve in the  $\text{Ni}_3\text{Al}$ , and none of the eutectic appears at room temperature.

This preliminary work assisted greatly in the identification of the characteristic nickel-aluminum phases encountered in the more complicated ternary alloys now to be discussed.

#### *Nickel-Aluminum-Molybdenum Alloys*

The next step was to study how additions of molybdenum altered both the structural characteristics and the mechanical properties of nickel-aluminum alloys. Groups of alloys were made up based on nominal nickel:aluminum ratios of 10:1, 8:1, and 6:1, and molybdenum additions of from 12 to 25% were made. From mechanical tests carried out on samples of the earlier binary alloys it was established that useful properties were obtained with a nickel:aluminum ratio of 6:1 to 12:1. A microstructure of  $\text{Ni}_3\text{Al}$  plus alpha gave the best properties. The presence of  $\text{NiAl}$  in the binary alloys had a decided weakening effect (1). Consequently, the bases for the ternary group were chosen in an attempt to avoid the occurrence of  $\text{NiAl}$ .

The molybdenum-nickel phase diagram (3) is included herein (Fig. 11) to aid in the discussion of the structures to follow.

*Nickel: Aluminum Ratio 10: 1*—As was expected, the first heats of 10:1 ratio alloys, which contained small quantities of molybdenum, showed microstructures similar to that of the binary nickel-aluminum alloy, No. 4. The matrix was fine  $\text{Ni}_3\text{Al}$  in alpha solid solution, and a few clear islands of  $\text{Ni}_3\text{Al}$ , evolved from the  $\text{Ni}_3\text{Al}$  plus alpha eutectic, were present. No change in this structure was noticeable until the molybdenum content reached 15%. At this point a new phase began to appear, the amount of which increased with increased molybdenum. Fig. 12 shows the first occurrence of this phase, which has appeared associated with the clear  $\text{Ni}_3\text{Al}$  areas. Fig. 13 shows this same phase in larger quantity, and displaying a eutectic appearance. No  $\text{Ni}_3\text{Al}$  is visible here, which fact is accounted for by the slightly higher nickel:aluminum ratio of this particular heat. Thus, in the 10:1 ratio group, the addition of





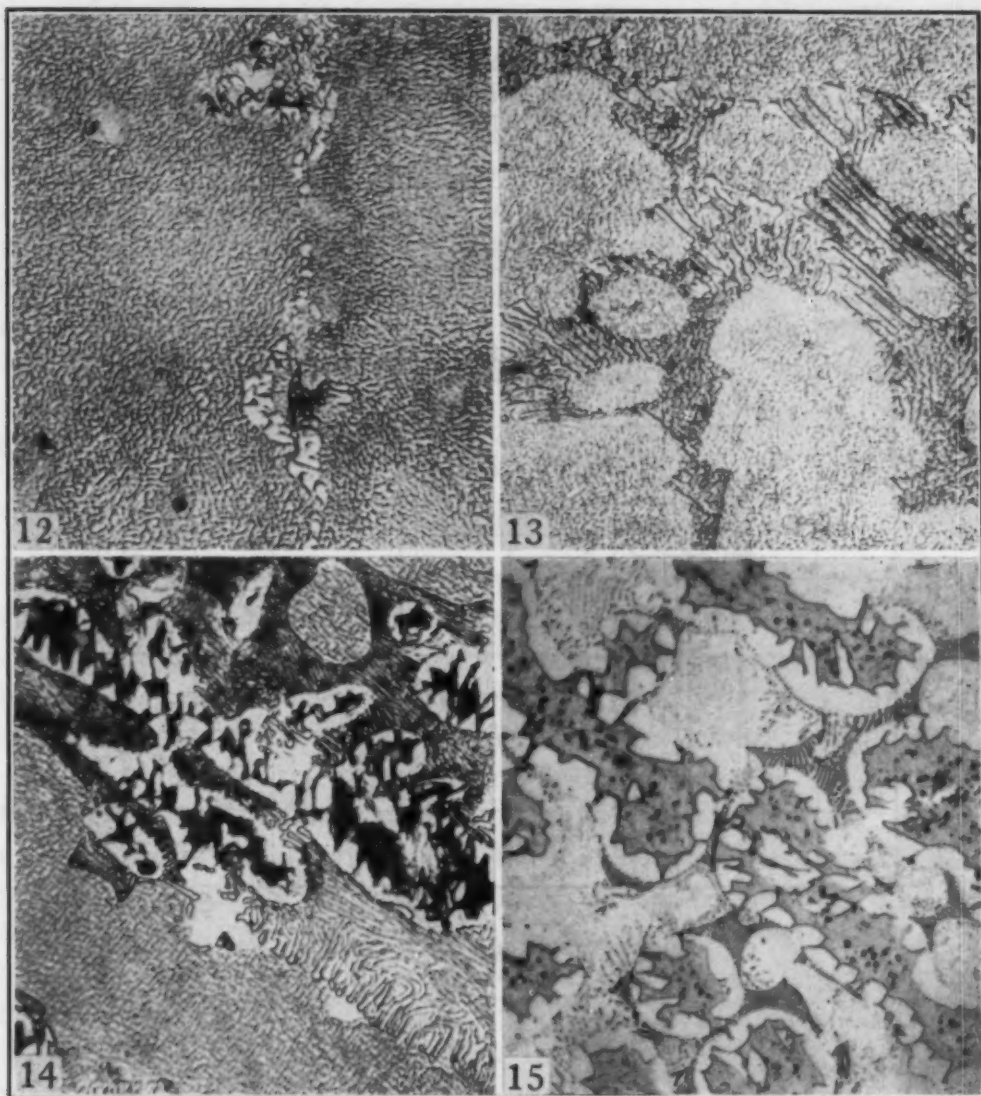


Fig. 12—Alloy 102M158, As Cast. Chrome regia etch. Alpha +  $\text{Ni}_3\text{Al}$  with traces of  $\text{NiMo}$  (black).  $\times 750$ .

Fig. 13—Alloy 104M252, As Cast. Chrome regia etch. Alpha +  $\text{Ni}_3\text{Al}$  with  $\text{NiMo}$  eutectic.  $\times 750$ .

Fig. 14—Alloy 84M236, As Cast. Chrome regia etch. Alpha +  $\text{Ni}_3\text{Al}$  in the background, with  $\text{NiMo}$  eutectic and  $\text{NiAl}$  (black) surrounded by white  $\text{Ni}_3\text{Al}$ .  $\times 750$ .

Fig. 15—Alloy 58M117, As Cast. Chrome regia and  $\text{KMnO}_4$  etch.  $\text{Ni}_3\text{Al}$  (white),  $\text{NiAl}$  (gray), and  $\text{NiMo}$  eutectic.

amounts of both  $\text{NiMo}$  and  $\text{NiAl}$  present. A structure typical of this condition is shown in Fig. 14, of Alloy 84M236. Here are seen the matrix of  $\text{Ni}_3\text{Al}$  in alpha, the blackened  $\text{NiAl}$ , clear white areas of  $\text{Ni}_3\text{Al}$ , and a good deal of  $\text{NiMo}$ . The  $\text{NiAl}$ ,  $\text{Ni}_3\text{Al}$ , and  $\text{NiMo}$  have been found to be generally associated, as indicated in this figure. Thus, in the 8:1 ratio group, the addition of molybdenum, from 10 to 25%, causes the appearance of  $\text{NiMo}$ , and above

15% molybdenum NiAl also occurs. Both of these phases increase in quantity with increased molybdenum content.

*Nickel: Aluminum Ratio 6:1*—In this group of heats based on a nominal nickel:aluminum ratio of 6:1, the presence of little more than 10% molybdenum is required to cause NiAl to appear, as well as NiMo. Fig. 15, of Alloy 58M117, is typical of the structures found in the low molybdenum range of this group. Fig. 16, of Alloy 61M222, shows the structure produced when more molybdenum is present. Here the matrix appears to be Ni<sub>3</sub>Al, with large quantities of both NiAl and NiMo appearing. The blackened phase is NiMo which was concentrated sufficiently in certain areas to be overly darkened by the etchant. So it is apparent that in the 6:1 ratio alloys, it is not feasible to introduce any appreciable quantity of molybdenum, because of the early appearance of NiAl. As has been previously stated, with respect to the binary nickel-aluminum alloys, the presence of NiAl is to be avoided, because this phase imparts very poor mechanical properties when it is present to any great degree (1).

As a result of these observations, it can be stated that the introduction of molybdenum into binary nickel-aluminum alloys in the high nickel range causes a shift to the right of the phase zones in the nickel-aluminum diagram. This shift is roughly proportional to the amount of molybdenum introduced.

All the alloys discussed above were cast into test bars which were tested at 815 °C (1500 °F). The results of these tests, which are presented in the earlier part of this paper, confirm the fact that the presence of NiAl is deleterious, and indicate that the best type of microstructure—that is, the structure associated with the best properties—is one consisting of a matrix of Ni<sub>3</sub>Al in alpha solid solution, with an almost continuous network of NiMo.

#### *Heat Treatment of Selected Alloys*

Some exploratory work has been done to learn how the microstructure of these alloys is altered by various heat treatment cycles.

*Elimination of NiAl*—The fact that the alloys examined were not under equilibrium conditions could explain the presence of NiAl in the 8:1 ratio group of alloys. To establish this fact, Alloy 81M265 was given homogenizing treatments at 1000 and 1150 °C (1830 and 2100 °F). It was found that after 22 hours at 1000 °C (1830 °F), all the NiAl had been removed from this alloy. A much shorter time at 1150 °C (2100 °F) gave the same result. In *neither* case was the remainder of the structure perceptibly altered. The

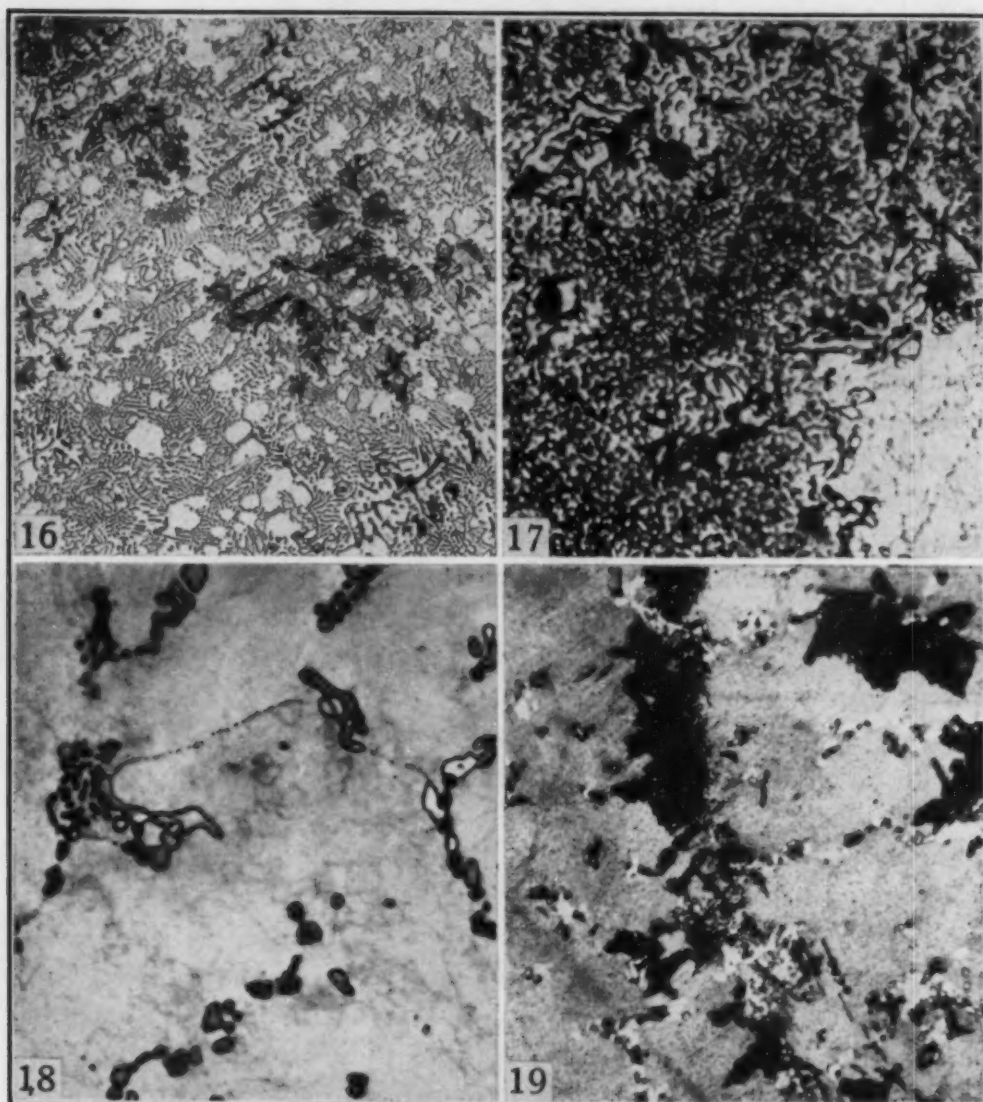


Fig. 16—Alloy 61M222, As Cast. Chrome regia and  $\text{KMnO}_4$  etch.  $\text{Ni}_3\text{Al}$  matrix (white) with  $\text{NiAl}$  and  $\text{NiMo}$ . Some of  $\text{NiMo}$  blackened.  $\times 200$ .

Fig. 17—Alloy 119M254, As Cast. Chrome regia and  $\text{KMnO}_4$  etch. Alpha +  $\text{Ni}_3\text{Al}$  matrix, with  $\text{Ni}_3\text{Al}$  (white) and  $\text{NiMo}$  (black).  $\times 1000$ .

Fig. 18—Alloy 119M254, Solution-Treated 5 Hours at  $1250^\circ\text{C}$ . Chrome regia and  $\text{KMnO}_4$  etch. Alpha matrix, with agglomerated  $\text{Ni}_3\text{Al}$  (gray) and  $\text{NiMo}$  (black).  $\times 200$ .

Fig. 19—Alloy 119M254, Solution-Treated 5 Hours at  $1250^\circ\text{C}$ , Aged 75 Hours at  $815^\circ\text{C}$ . Chrome regia and  $\text{KMnO}_4$  etch. Alpha matrix with fine  $\text{Ni}_3\text{Al}$  precipitate. Residual  $\text{Ni}_3\text{Al}$  (white) and gamma  $\text{NiMo}$  phase (black).  $\times 200$ .

prolonged exposure of Alloy 60M151 to a temperature of  $1150^\circ\text{C}$  ( $2100^\circ\text{F}$ ) did not remove any  $\text{NiAl}$ .

*Solution and Aging Treatment*—Another aspect of the heat treatment of these alloys was the possibility of improving the properties of those which had a matrix of  $\text{Ni}_3\text{Al}$  in alpha, by a suitable solution and aging treatment. To explore this theory, Alloy 119M254 was selected and solution treated at  $1250^\circ\text{C}$  ( $2280^\circ\text{F}$ )



for 5 hours, followed by a water quench. The as-cast structure (see Fig. 17) consisted of a matrix of  $\text{Ni}_3\text{Al}$  in alpha, with some areas of clear  $\text{Ni}_3\text{Al}$  around the grain boundaries. A small amount of  $\text{NiMo}$  was associated with this  $\text{Ni}_3\text{Al}$ . It is worthy of note that  $\text{Ni}_3\text{Al}$  and  $\text{NiMo}$  can form a ternary eutectic with alpha, in which the  $\text{Ni}_3\text{Al}$  and  $\text{NiMo}$  are almost indistinguishable. It is necessary to etch very carefully to permit a differentiation of these two phases in this condition.

Heating this alloy at  $1250^\circ\text{C}$  ( $2280^\circ\text{F}$ ) served to dissolve the  $\text{Ni}_3\text{Al}$  which had been present in the matrix and, in addition, caused the  $\text{Ni}_3\text{Al}$  and  $\text{NiMo}$  at the grain boundaries to agglomerate into larger, more spherical particles. This may be seen by reference to Fig. 18.

Following this solution treatment at  $1250^\circ\text{C}$  ( $2280^\circ\text{F}$ ) samples of this alloy were subsequently aged at  $815^\circ\text{C}$  ( $1500^\circ\text{F}$ ) for 25, 50, 75 and 100 hours. After 25 hours, a darkening of the field could be seen, presumably due to precipitation of  $\text{Ni}_3\text{Al}$ , although the particles could not be resolved at a magnification of 2000 diameters. It was not until the aging time had reached 75 hours that any further change appeared, but this change was quite striking. A new phase had appeared (see Fig. 19) in the form of small nests which could be resolved into clusters of very fine particles etched black by the  $\text{KMnO}_4$  reagent. Since the aging temperature was so close to the alpha plus gamma region of Ellinger's molybdenum-nickel diagram, it is thought that this is the gamma phase, which has been brought into existence by the prolonged heat treatment. Further aging caused these nests to grow and become less distinct, while the precipitated  $\text{Ni}_3\text{Al}$  became readily visible under the microscope at 750 diameters, as shown by Fig. 20.

A sample of this same alloy overaged at  $980^\circ\text{C}$  ( $1800^\circ\text{F}$ ) showed the microstructure seen in Fig. 21, consisting of a matrix of alpha, in which appears a large quantity of coarsened  $\text{Ni}_3\text{Al}$ .

In an effort to establish the equilibrium structure of this alloy, a sample was homogenized by holding for 8 hours at  $1260^\circ\text{C}$  ( $2300^\circ\text{F}$ ), furnace cooling to  $1070^\circ\text{C}$  ( $1960^\circ\text{F}$ ) and quenching after 60 hours at that temperature. Here the structure, as shown in Fig. 22, is entirely  $\text{Ni}_3\text{Al}$  plus alpha. It is possible that the material in this condition might be forgeable.

*Hardness of Heat Treated Samples*—During this brief solution and aging treatment investigation, Vickers hardness measurements were made of samples in each of the conditions discussed. These readings appear in Table VI.



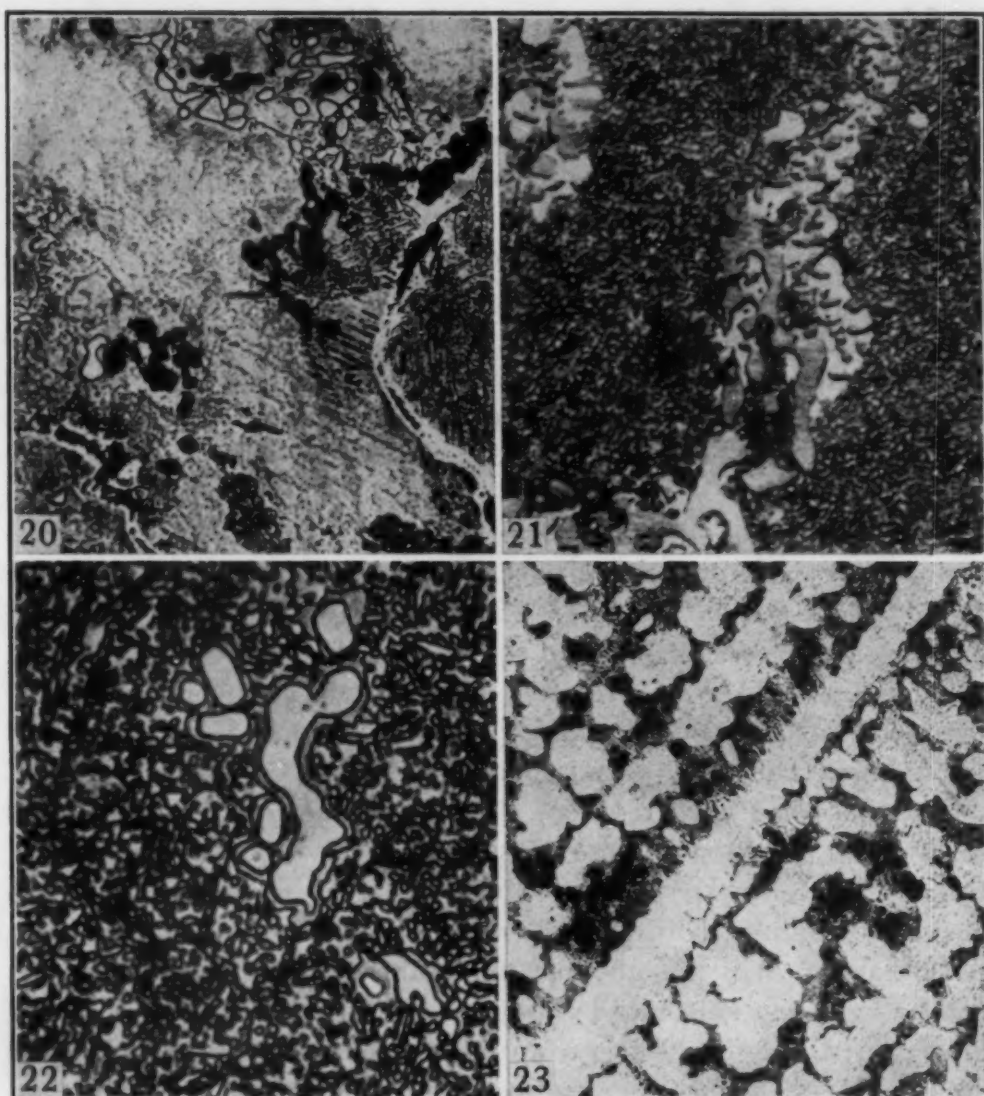


Fig. 20—Alloy 119M254, Solution-Treated 5 Hours at 1250 °C, Aged 100 Hours at 815 °C. Chrome regia and  $\text{KMnO}_4$  etch. Precipitate of  $\text{Ni}_3\text{Al}$  and gamma merged. White areas are  $\text{Ni}_3\text{Al}$ .  $\times 750$ .

Fig. 21—Alloy 119M254, Solution-Treated 5 Hours at 1250 °C, Aged 36 Hours at 980 °C. Chrome regia and  $\text{KMnO}_4$  etch. Alpha matrix with coarsened  $\text{Ni}_3\text{Al}$ . White areas are massive  $\text{Ni}_3\text{Al}$ .  $\times 1000$ .

Fig. 22—Alloy 119M254, Held at 1260 °C 8 Hours, Furnace-Cooled to 1070 °C, Held for 60 Hours, Water-Quenched. Chrome regia and  $\text{KMnO}_4$  etch, alpha matrix with  $\text{Ni}_3\text{Al}$ .  $\times 750$ .

Fig. 23—Alloy 92M247-90K. 59.22% nickel, 7.43% aluminum, 24.7% molybdenum, 8.98% cobalt. Black areas are  $\text{NiAl}$ . Network is  $\text{NiMo}$  eutectic.  $\times 200$ .

It is apparent from these readings that the hardness of the solution-treated material is not appreciably lowered by aging at 815 °C (1500 °F) for periods up to at least 100 hours. The effects of this treatment on mechanical properties other than hardness have yet to be determined.

Similar attempts to alter the microstructure of alloys which

Table VI  
Vickers Hardness of Heat Treated Samples

Condition	Hardness (30-Kg. Load)
As cast .....	518
Solution-treated, 1250 °C (2280 °F), 5 hr., W.Q. ....	557
Solution-treated, aged 25 hr. 815 °C (1500 °F) .....	596
Solution-treated, aged 50 hr. ....	578
Solution-treated, aged 75 hr. ....	596
Solution-treated, aged 100 hr. ....	594
Solution-treated, aged 36 hr. 980 °C (1800 °F) .....	480
Homogenized—8 hr. at 1260 °C (2300 °F), cooled to 1070 °C (1960 °F), held 60 hr., W.Q. ....	444

had a nominal nickel:aluminum ratio of 8:1 have so far been unsuccessful.

*Creep-Rupture Test of Solution-Treated Samples*—Since some of these alloys will respond structurally to a heat treatment of the solution and aging type, some idea as to how such a treatment would alter creep-rupture properties at 815 °C was sought. Two test bars of Alloy 88M215 were used for this experiment. One bar was tested in the “as-cast” condition. The other bar was given a solution treatment at 1250 °C (2280 °F) for 5 hours followed by a water quench, prior to testing. Both of these bars were tested in creep rupture at 815 °C (1500 °F), using a stress of 35,000 psi.

Fig. 24 shows the time versus elongation curves obtained from these tests. It is obvious that such a treatment can radically alter the creep-rupture properties of these alloys at 815 °C (1500 °F).

#### *Effect of Cobalt Additions*

At one stage of this work, it was felt that some benefit might be derived from the inclusion of cobalt in the nickel-aluminum-molybdenum alloys. Accordingly, a group of heats was made in which part of the nickel was replaced by an equal weight of cobalt. These were based on a nickel:aluminum ratio of 8:1. It was found that the addition of up to 5% cobalt had little effect on the microstructure, but more than this amount brought about a premature appearance of NiAl (Fig. 23) with a consequent lowering of properties. Therefore, it was not considered worthwhile to pursue this avenue of investigation.

#### BEHAVIOR OF A NICKEL-ALUMINUM-MOLYBDENUM ALLOY PRODUCED UNDER INDUSTRIAL CONDITIONS

In view of the promising properties exhibited by some of the alloys reported in the earlier part of this paper, it was decided to try to obtain some idea of how these alloys would behave when pro-

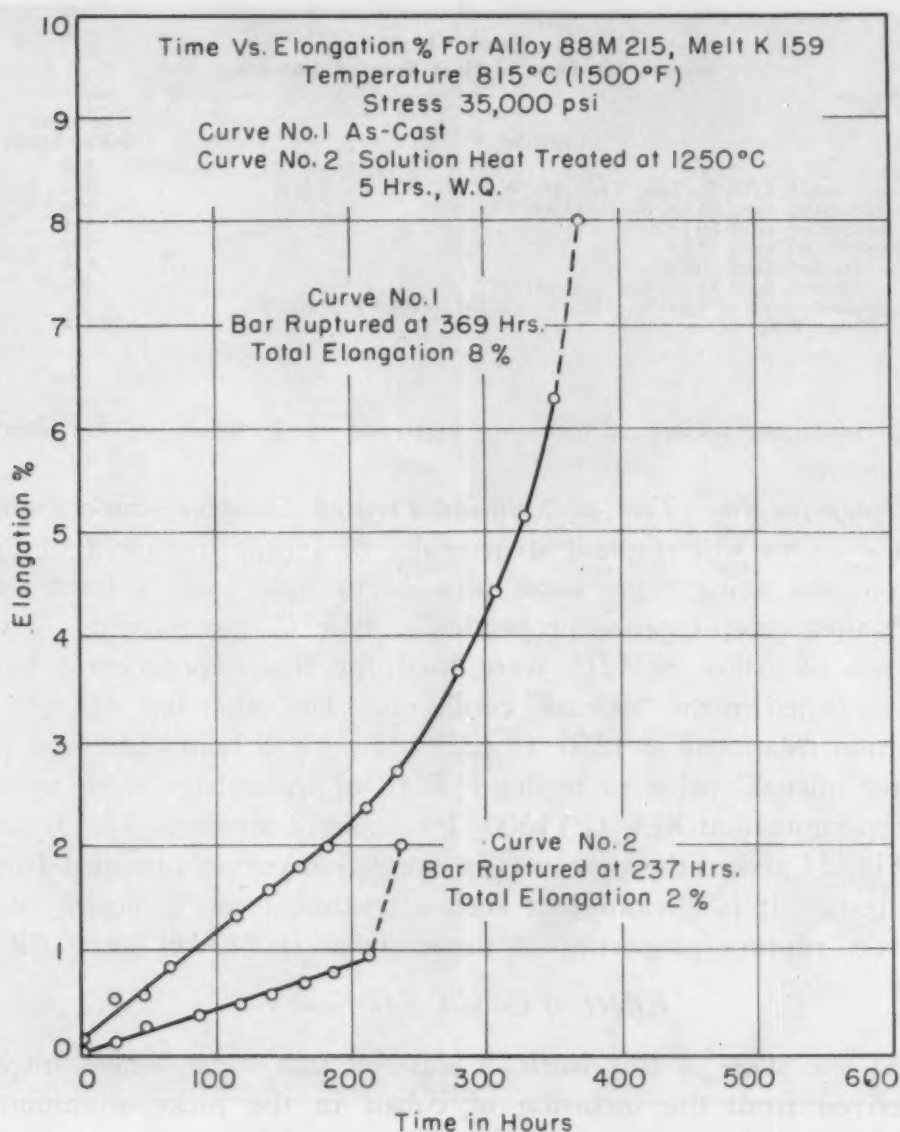


Fig. 24—Influence of Solution Treatment on Creep-Rupture Characteristics of Alloy 88M215.

duced under industrial conditions. In this matter we received full cooperation from C. R. Whittemore, Research Metallurgist of the Deloro Smelting and Refining Company, Deloro, Ontario; and from Winnett Boyd, Chief Design Engineer, and G. E. Anderson, Chief Metallurgist, of the Gas Turbine Engineering Division, A. V. Roe Canada Ltd., Toronto, Ontario.

From an examination of the data collected during the first part of the program, it was decided that Alloy 83M224 offered the best compromise between ductility and creep strength. Based on this alloy, the following tentative chemical specification was drawn up:

	Per Cent
Nickel .....	68-72
Molybdenum .....	21-24
Aluminum .....	7- 8.2
Carbon .....	0.10 max.
Silicon .....	0.25 max.
Iron .....	0.15 max.
Manganese .....	0.3 max.
Ratio of nickel to aluminum—	8.3:1 to 10.3:1
Preferred—	8.3:1 to 8.5:1

*Production of Alloy*—Five 100-pound melts of alloy were produced to the above chemical specifications by the Deloro Smelting and Refining Company. Commercially pure nickel, aluminum and molybdenum were used. The melting was done in a "Detroit"-type rocking arc furnace lined with magnesia. The alloy was cast into piglets of a size suitable for small melts for precision casting.

No unusual difficulties were encountered at this stage of the work. The usual problems of melting loss, melting procedure, etc., responded to orthodox treatment.

*Production of Test Bars*—This alloy was then turned over to A. V. Roe Canada Ltd. Here it was remelted in small quantities and cast into tensile test bars, fatigue bars, and nozzle guide vanes. The tensile bars used in this part of the work had a 2-inch gage length,  $\frac{1}{4}$  inch in diameter. Thirty-eight test-bar melts were cast. Four tensile test bars and two fatigue bars were made from each melt.

These melts were made in zircon-lined crucibles by high-frequency induction on a centrifugal casting machine of commercial design. A protective blanket of argon was used. The metal casting temperature was reported to be 1525 °C (2775 °F) as measured by an optical pyrometer. The mold temperature was reported to be 925 °C (1700 °F) for most of the melts. The alloy was used just as it came from Deloro. However, no attempt was made to keep each of the five original melts separate. A test-bar charge might contain metal from two or more of the alloy melts and also scrap castings or sprues from previous test-bar melts. Melts K59 to K148 inclusive were made up from 100% virgin alloy; melts K150 to K157 inclusive contained 50% virgin alloy, and melts K158, K159 and K160 were 100% returns (sprues and defective castings).

*Testing Procedure and Results*—All test bars were radiographed prior to acceptance.

The fatigue bars have been reserved for a high temperature fatigue testing program.

One tensile test bar was pulled at room temperature by A. V. Roe Canada Ltd. The remaining three bars were forwarded to the



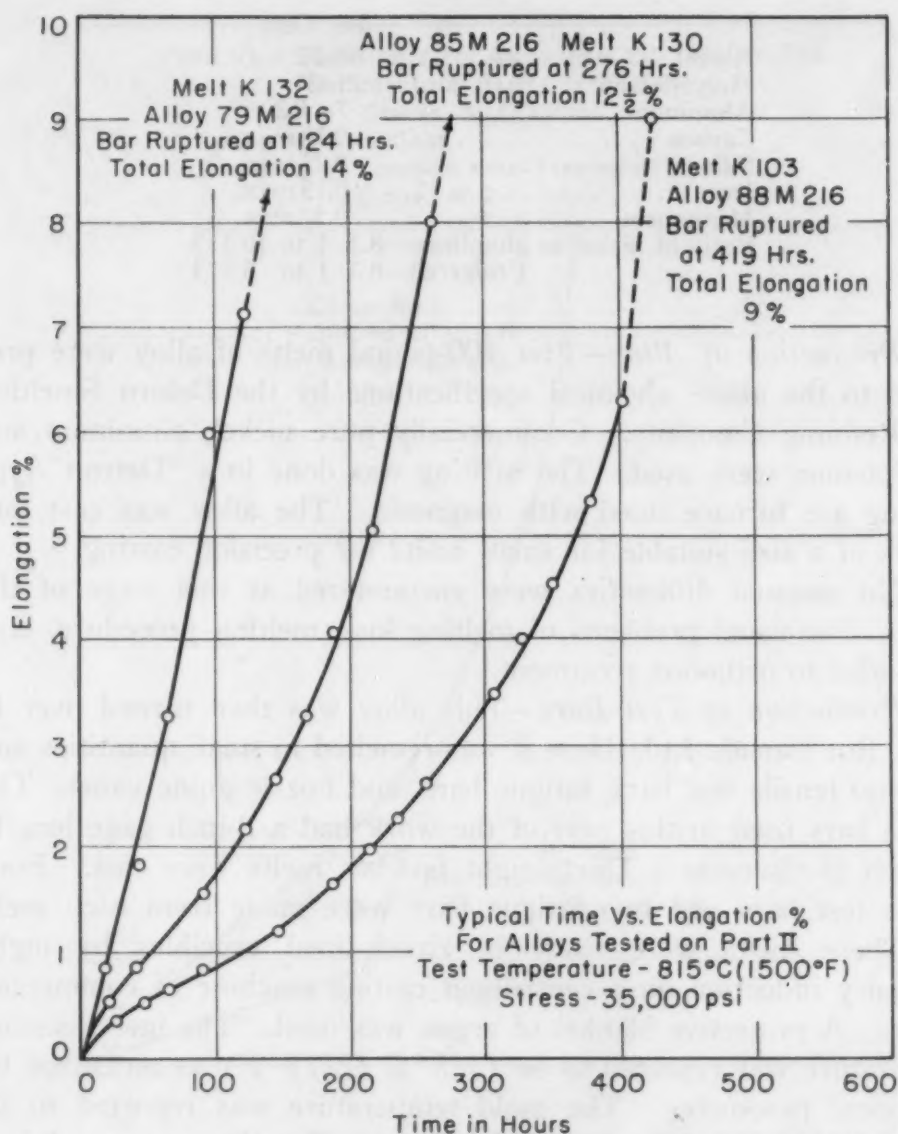


Fig. 25—Typical Time Versus Per Cent Elongation Curves at 815 °C (1500 °F) and 35,000 Psi, for Alloys Listed in Table VII.

Physical Metallurgy Research Laboratories where the following test were conducted:

1. Room Temperature Tensile Test.
2. Tensile Test at 815 °C (1500 °F).
3. Creep-rupture at 815 °C (1500 °F) using a stress of 35,000 psi.
4. Chemical Analyses.

Table VII lists the melts tested and their chemical analyses. Tensile test results at room temperature and 815 °C (1500 °F) are presented in Table VIII. Table IX summarizes the results of the creep rupture tests at 815 °C (1500 °F). Typical Time Versus Per Cent Elongation Curves are presented in Fig. 25.

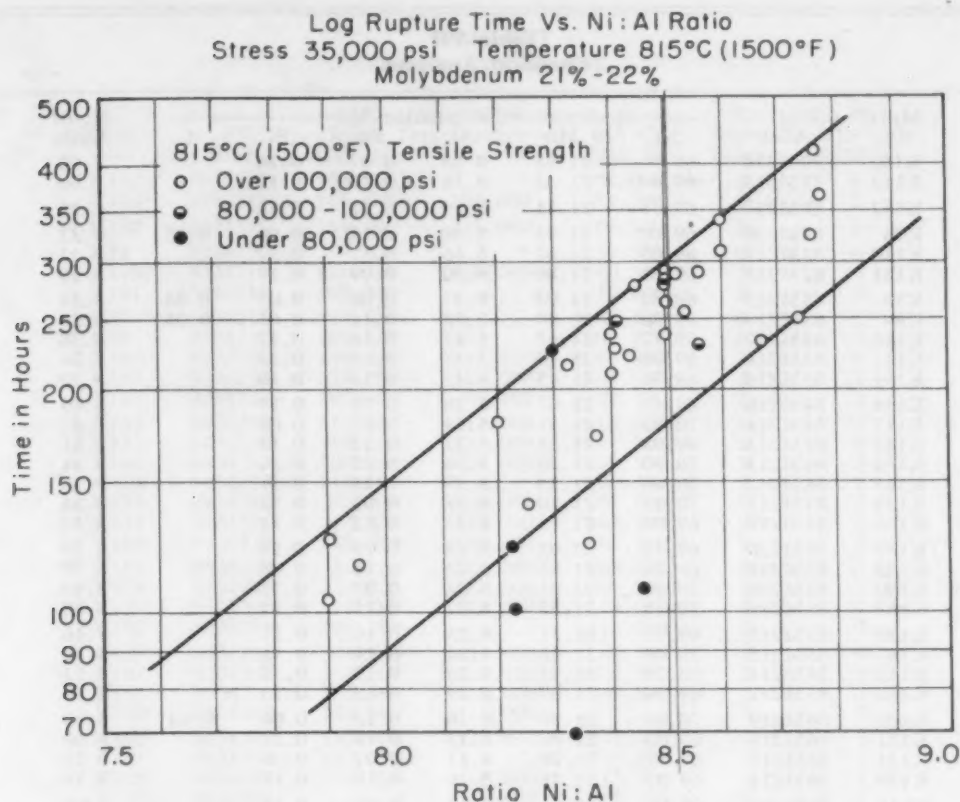


Fig. 26—Nickel-Aluminum Ratio Versus Log Rupture Time at 815 °C (1500 °F) and 35,000 Psi.

### Discussion of Results

At first glance, the elevated temperature properties of these alloys appeared to be rather erratic. The tensile strength at 815 °C (1500 °F) varied between 55,800 and 118,200 psi. The 35,000-psi rupture life at 815 °C (1500 °F) ranged from 31 to 419 hours.

However, a closer inspection of the data presented in Tables VIII and IX indicated that there might be some order to this variation. It is to accentuate this order that the alloys have been grouped according to their nickel:aluminum ratio in Tables VII, VIII, and IX.

*Nickel to Aluminum Ratio Versus 815 °C Creep-Rupture Life Versus 815 °C Tensile Strength*—In order better to illustrate the general trends observed, the logarithm of the rupture time has been plotted against the ratio of nickel to aluminum (see Fig. 26). On this chart an attempt has also been made to indicate the significance of the tensile test values at 815 °C (1500 °F) by identifying the points corresponding to melts having tensile strengths below 80,000 psi, at 815 °C (1500 °F).

Table VII  
Chemical Analyses

Melt No.	Alloy	Composition, %					C	Ni:Al Ratio
		Ni	Mo	Al	Fe	Si		
K132	79M216	69.95	21.58	8.86	0.07	0.10		7.90
K143	79M213	69.43	21.32	8.76	0.16	0.18		7.90
K152	80M217	69.75	21.71	8.76	0.11	0.16		7.95
K74	82M220	69.00	21.95	8.38	0.12	0.06	0.05	8.23
K140	82M219	69.65	21.67	8.46	0.17	0.12		8.23
K131	82M218	69.66	21.80	8.50	0.09	0.12		8.20
K59	83M219	69.82	21.93	8.37	0.06	0.05	0.05	8.33
K89	83M219	69.34	21.90	8.32	0.14	0.05	0.04	8.33
K146	83M217	69.77	21.68	8.42	0.16	0.12		8.30
K142	83M214	69.76	21.40	8.45	0.19	0.13		8.26
K151	83M214	69.81	21.45	8.42	0.13	0.16		8.30
K144	84M216	69.46	21.61	8.26	0.15	0.13		8.40
K137	84M214	70.03	21.41	8.34	0.07	0.08		8.41
K141	84M213	69.98	21.28	8.32	0.22	0.13		8.41
K154	84M213	70.50	21.30	8.36	0.15	0.16		8.44
K145	84M212	70.06	21.23	8.39	0.15	0.17		8.36
K134	84M211	70.15	21.10	8.38	0.07	0.15		8.38
K155	84M219	69.02	21.93	8.25	0.12	0.14		8.40
K158	85M220	69.72	22.02	8.25	0.16	0.16		8.50
K133	85M218	69.76	21.85	8.23	0.16	0.08		8.50
K130	85M216	70.40	21.61	8.34	0.07	0.12		8.45
K153	85M216	70.38	21.55	8.27	0.15	0.11		8.50
K139	85M215	69.75	21.51	8.25	0.16	0.11		8.46
K147	85M215	70.09	21.48	8.24	0.14	0.11		8.50
K148	85M214	70.29	21.45	8.25	0.17	0.15		8.53
K150	85M217	69.56	21.69	8.19	0.15	0.13		8.50
K102	86M219	70.07	21.90	8.16	0.12	0.06	0.03	8.60
K157	86M218	69.73	21.80	8.13	0.14	0.22		8.60
K135	86M217	69.97	21.70	8.17	0.07	0.10		8.56
K138	86M214	69.82	21.38	8.16	0.18	0.19		8.56
K136	87M217	70.04	21.64	8.08	0.07	0.15		8.68
K156	87M216	70.04	21.55	8.02	0.14	0.13		8.74
K160	87M213	70.50	21.30	8.05	0.19	0.14		9.76
K103	88M216	70.15	21.60	8.00	0.06	0.06	0.04	8.77
K159	88M215	70.29	21.50	8.02	0.15	0.11		8.78

Virtually all the points on this chart can be contained in a band. This band will include the creep-rupture results on all melts showing hot tensile strengths over 80,000 psi, with the exception of two melts. It excludes the creep-rupture results on all those melts showing hot tensile strengths below 80,000 psi, with the exception of one melt. Of these three vagrant results, one is so far out of line (rupture life 31 hours for melt K151) that a gross flaw in the rupture test bar is suspected.

Furthermore, this band has a clearly defined slope, indicating that, as the nickel:aluminum ratio increases from 7.9:1 to 8.8:1, the 35,000-psi rupture life at 815 °C (1500 °F) also increases.

This chart indicates also that:

1. The frequency of occurrence of subnormal melts based on tensile tests at 815 °C (1500 °F) is high when the nickel:aluminum ratio is below 8.4:1 and zero when it is above 8.5:1.
2. The tensile test at 815 °C (1500 °F) shows evidence of being a useful criterion of creep-rupture characteristics at 815 °C (1500 °F).

Table VIII  
Tensile Test Results

Melt No.	Alloy	Ultimate Tensile Strength, psi			Elongation, %	
		Room Temperature	815 °C	815 °C	Room Temp.	815 °C
		A.V. Roe	Mines Br.	(1500 °F)		(1500 °F)
K132	79M216	106,000	.....	101,000	2	2
K143	79M213	108,600	108,000	102,700	2	2
K152	80M217	104,300	111,000	103,500	2	2
K74	82M220	99,600	.....	57,200	0	0
K140	82M219	126,320	120,000	50,300	3	0
K131	82M218	109,500	.....	110,600	2	2
K59	83M219	116,500	.....	58,800	0	2
K89	83M219	107,600	.....	109,300	0	2
K146	83M217	116,600	117,000	63,900	2	0
K142	83M214	117,700	113,000	107,700	2	2
K151	83M214	107,300	93,400	108,700	2	2
K144	84M216	115,700	114,000	118,200	2	2
K137	84M214	118,300	123,000	81,000	2	0
K141	84M213	120,100	109,000	109,500	2	2
K154	84M213	111,200	.....	102,300	2	2
K145	84M212	102,400	110,000	105,800	2	2
K134	84M211	113,500	111,000	104,100	2	2
K155	84M219	123,300	110,000	107,500	2	2
K158	85M220	56,700	109,000	108,800	0	2
K133	85M218	120,900	115,000	91,200	2	2
K130	85M216	119,700	124,000	114,000	2	2
K153	85M216	107,300	.....	113,200	2	2
K139	85M215	77,716	122,000	62,700	3	0
K147	85M215	108,500	119,000	107,200	2	2
K148	85M214	111,300	118,000	103,800	2	2
K150	85M217	111,900	115,000	.....	2	2
K102	86M219	115,500	122,000	115,400	5	2
K157	86M218	112,500	.....	113,600	2	2
K135	86M217	124,300	116,000	113,000	2	2
K138	86M214	.....	117,000	89,300	2	2
K136	87M217	113,500	120,000	102,300	2	2
K156	87M216	120,500	70,000	108,300	2	2
K160	87M213	113,800	116,000	112,200	2	2
K103	88M216	119,700	.....	107,000	2	2
K159	88M215	124,400	.....	105,200	2	2

*Per Cent Elongation at 815 °C (1500 °F)*—These alloys displayed a rather unusual behavior with respect to elongation. It is considered normal when an alloy exhibits greater elongation when pulled in a hot tensile test than when it is pulled in a creep-rupture test at the same temperature. However, test bars of the nickel-aluminum-molybdenum alloys elongate only about 2% when pulled in a tensile test at 815 °C (1500 °F) but give an elongation figure of from 7 to 14% when pulled in a 35,000-psi creep-rupture test at 815 °C (1500 °F). In general, the higher elongation values are associated with the lower nickel:aluminum ratios.

*Subnormal Hot Tensile Properties*—The reason for the tensile strengths at 815 °C (1500 °F) of less than 80,000 psi is not definitely known. However, in the authors' opinion, porosity or other types of casting defects can be ruled out. Otherwise those melts that displayed subnormal tensile strengths at 815 °C (1500 °F) would also be expected to possess subnormal tensile strengths at room temperature. An examination of Table VIII will show that



**Table IX**  
**Creep-Rupture Results at 35,000 Psi and 815 °C (1500 °F)**

Melt No.	Alloy	2% Creep Stress	Hours to 4% Creep Stress	Rupture	Total Elongation, %	Reduction in Area, %
K132	79M216	45	74	124	14	13
K143	79M213	37	65	104	8	9.4
K152	80M217	46	82	116	10	10
K74	82M220	62	...	102	6	7
K140	82M219	60	108	125	5	10.5
K131	82M218	64	113	180	12	15
K59	83M219	61	...	69	3	2.4
K89	83M219	100	168	216	9	12.5
K146	83M217	94	158	224	9	10.8
K142	83M214	62	...	138	11	11.8
K151	83M214	...	...	31	2	2
K144	84M216	110	178	238	8	10.8
K137	84M214	114	182	249	9	12.7
K141	84M213	90	158	228	9	13
K154	84M213	83	140	224	11	13.3
K145	84M212	82	...	124	4	11.8
K134	84M211	73	108	172	12	10
K155	84M219	88	152	214	8	13
K158	85M220	123	200	273	10	11.5
K133	85M218	118	200	279	10	10
K130	85M216	110	198	276	12.5	14.4
K153	85M216	129	210	288	8	13.0
K139	85M215	80	...	110	5	2.4
K147	85M215	122	195	262	9	14
K148	85M214	119	180	257	8	8.6
K150	85M217	135	217	286	9	10.8
K102	86M219	160	242	312	8	8
K157	86M218	152	248	340	9	15
K135	86M217	110	171	289	9	13.5
K138	86M214	107	174	233	7	7
K136	87M217	130	184	235	9	13
K156	87M216	122	198	250	8	10
K160	87M213	168	265	328	8	13
K103	88M216	212	334	419	9	9.5
K159	88M215	190	295	369	8	12.5

this is not so. Therefore, it is reasonable to assume that some variation in structure or phase distribution caused by variations in casting conditions might be the cause. However, if there is such a structural variable, it is a fairly subtle one, since careful metallographic examination has not yet revealed it.

#### PROPOSED SPECIFICATIONS

The data presented in this paper could form the basis for a tentative specification for nickel-aluminum-molybdenum alloys.

Two such specifications are presented below. The first is based on a minimum 35,000-psi rupture life of 150 hours at 815 °C (1500 °F). The other is based on a minimum 35,000-psi rupture life of 200 hours at 815 °C (1500 °F).

#### SPECIFICATION NO. 1

*Tensile Properties at 815 °C (1500 °F):*

Ultimate tensile strength—80,000 psi min.

Per cent elongation—2 min.

*Creep-Rupture Properties at 815 °C (1500 °F):*

35,000-psi rupture life—150 hours min.

Total per cent elongation—7 min.

*Chemical Composition:*

	Per Cent
Nickel .....	69.3 -70.74
Aluminum .....	7.76- 8.36
Molybdenum .....	21.0 -22.0
Silicon .....	0.15 max.
Iron .....	0.15 max.
Carbon .....	0.10 max.
Ni: Al ratio .....	8.4: 1 to 9: 1

## SPECIFICATION NO. 2

*Tensile Properties at 815 °C (1500 °F):*

Ultimate tensile strength—90,000 psi min.

Per cent elongation—2 min.

*Creep-Rupture Properties at 815 °C (1500 °F):*

35,000-psi rupture life—200 hours min.

Total per cent elongation—7 min.

Nickel ..... 69.44-70.74 |*Chemical Composition:*

	Per Cent
Aluminum .....	7.76- 8.27
Molybdenum .....	21.0 -22.0
Silicon .....	0.15 max.
Iron .....	0.15 max.
Carbon .....	0.10 max.
Ni: Al ratio .....	8.5: 1 to 9: 1

## SUMMARY

On the basis of the work presented herein, it would appear that sufficient data are available on alloys of nickel, aluminum and molybdenum to justify the opinion that these alloys are practical and useful for elevated temperature applications. The properties available are quite promising, the materials used are not highly strategic, and there appear to be no complications in melting and casting.

## References

1. H. V. Kinsey and M. T. Stewart, "A Nickel-Aluminum-Molybdenum Creep-Resistant Alloy", *Canadian Journal of Research*, Vol. 27, No. 2, Section F, February 1949.
2. W. O. Alexander and N. B. Vaughan, "The Constitution of the Nickel-Aluminum System", *Journal, Institute of Metals*, Vol. 61, No. 2, 1937, p. 247-260.
3. F. H. Ellinger, "The Nickel-Molybdenum System", *TRANSACTIONS, American Society for Metals*, Vol. 30, No. 3, September 1942.

## DISCUSSION

**Written Discussion:** By N. J. Grant, professor of metallurgy, Massachusetts Institute of Technology, Cambridge, Mass.

I agree that the alloys in the subject paper are very interesting and may be developed into useful commercial alloys. I shudder, however, when I look at the extremely narrow chemical limits shown in the suggested specifications on the last two pages of the paper. In Specifi-

cation No. 1, the range for aluminum is 0.60% and for nickel and molybdenum 1.4 and 1% respectively. For Specification No. 2 they are 0.5% aluminum, 1.3% nickel, and 1.0% molybdenum. Our chemist professes that he cannot hope to attain better than  $\pm 0.15\%$  for aluminum just for the analysis alone. Yet a change of 0.30% aluminum changes the nickel: aluminum ratio from 8.75 to 8.44 in a sample calculation. This alone would result in a change in rupture life from 280 to 420 hours. Throw in, on top of this, melting variations, and what is the chance of foundries melting to such close specifications?

In re-examining Tables VIII and IX and Fig. 26, the following is noted:

(In Table VIII)

- (a) Heats K150 through K157 all contain 50% scrap melt but show 815 °C tensile values of 102,300 to 113,600 psi.
- (b) Heats K158 through K160 are all 100% scrap remelt but show 815 °C tensile value of 105,200 to 112,200 psi.
- (c) All the low 815 °C tensile values are among the virgin melts.

(In Table IX and Fig. 26)

- (a) All values for heats K150 through K157, except one, are in the upper half of the range shown in Fig. 26. (These are 50% scrap heats.)
- (b) Heats K158 through K160 are in the upper half of Fig. 26. (These are 100% scrap heats.)

Does this suggest that scrap is beneficial and desirable because of possible effects on melting and solidification? The points are not too numerous but such an effect is indicated. Certainly it indicates that if remelting practice is used, the effect is not a harmful one, provided that the very narrow specification limits can be met.

**Written Discussion:** By H. P. Evans, metallurgist, Boeing Airplane Co., Seattle, Wash.

The authors are to be congratulated for the thorough manner in which they have explored the nickel-aluminum-molybdenum system in their search for an alloy with optimum elevated temperature properties. The development of their finally chosen alloy is particularly timely, since it requires no highly strategic materials.

Most alloys now in use for such applications as gas turbine blades contain considerable amounts of highly critical materials, such as cobalt and columbium. It is rather shocking to realize that if jet engines and other wartime facilities were required in considerable quantities, the supply of cobalt and columbium and certain other strategic materials would be entirely inadequate. The composition of this nickel-aluminum-molybdenum alloy is, therefore, quite a fortunate one.

Alloy	Temperature		Short-Time Tensile, psi	Stress-Rupture psi	S. R. Life, Hours
	°F	°C			
Ni-Al-Mo Spec. No. 1	1500	815	80,000	35,000	150
Ni-Al-Mo Spec. No. 2	1500	815	90,000	35,000	200
Stillite Spec. No. 21	1500	815	59,000	22,000	100
Stillite Spec. No. 30	1500	815	64,000	27,200	100
Stillite Spec. No. 31	1500	815	59,600	28,700	100

The data above give the reader an opportunity of comparing the short-time tensile and stress-rupture values quoted for this alloy with those of representative cast alloys used for such applications as cast gas

turbine blades. Values reported for these alloys are average values reported by the manufacturer.

It is evident that the short-time tensile and stress-rupture values shown for the nickel-aluminum-molybdenum alloys are quite attractive. There are, however, a number of additional factors which influence the life of such a part as a gas turbine blade, i.e., castability, weldability if welded, creep strength, fatigue strength, modulus of elasticity, and oxidation resistance, to name a few.

Experience has shown that most failures of turbine wheels have been fatigue failures. Fatigue stresses may be accentuated if the frequency of the revolving wheel assembly at critical speeds coincides with the natural frequency of the assembly. Since the natural frequency is a function of the modulus of elasticity, it is advantageous that the modulus should remain as constant as possible so that the assembly may be designed to operate outside its natural frequency.

Certain alloys containing considerable amounts of molybdenum have shown unsatisfactory oxidation resistance; in fact, some such alloys have failed at elevated temperatures due to so-called catastrophic oxidation.

In view of the encouraging short-time tensile and stress-rupture values quoted for the Ni-Al-Mo alloy discussed in this paper, every effort should be made to facilitate the task of obtaining these additional properties. If these properties are satisfactory, a new and highly important alloy will have been added to our list of alloys for elevated temperature services.

**Written Discussion:** By G. E. Anderson, chief metallurgist, Gas Turbine Engine Division, A. V. Roe Canada Limited, Toronto.

The authors of this interesting paper are to be congratulated upon their contribution to the development of high temperature alloys. The properties reported for these alloys at 1500 °F are greatly in excess of those reported for commercial alloys at present employed in gas turbines, with the added virtue that no strategically scarce materials are required for their production.

The history of the gas turbine has shown a close correlation between advances in the development of high temperature alloys and increases in the thrust and efficiency of gas turbines. There is no reason to doubt that this trend will continue and that the future development of gas turbines will to a large extent be dependent upon the continued improvement of high temperature alloys. Hence the series of alloys reported upon in this paper seem to be well worth attention.

It might be of interest to mention our experience with the alloy nominally designated as 83M225 (i.e., 69.0 to 70.5% nickel, 8.0 to 8.9% aluminum, 21.1 to 21.9% molybdenum). We have found this alloy possesses excellent castability, even with pouring temperatures as low as 1450 °C (2640 °F), and using the "lost wax" process we have been able to cast quite complicated parts. Although some experimenting is always necessary to establish the proper "gating" technique, we have been able to produce castings free from porosity, dross inclusions or other casting defects.

It would be interesting to know if the authors can advance any explanation of the apparently anomalous results for the elongations obtained



in the creep-rupture and short-time tensile tests performed at 815 °C (1500 °F). In an earlier paper (Ref. 1), the authors described the metallography of certain specimens that had been creep-tested and it is possible that a further study along these lines might throw some light on the problem.

With reference to the authors' remarks regarding the correlation of subnormal tensile strengths at 815 °C (1500 °F) with Ni:Al ratios below 8.5:1, it seems doubtful if there are sufficient data to warrant any statistically significant conclusions being drawn. We would therefore urge the authors to study this matter further, for the occurrence of subnormal results naturally raises doubts in the minds of potential consumers unless some explanation is forthcoming, together with a reasonably certain criterion for acceptance or rejection of material.

**Written Discussion:** By G. S. Farnham, assistant manager, Canadian Development & Research, The International Nickel Company of Canada, Ltd., Toronto.

Messrs. Kinsey and Stewart are to be congratulated on their thorough work in a difficult field. This paper and other papers emanating from the Physical Metallurgy Research Laboratories of the Canadian Bureau of Mines point to the excellence of that organization and to the fact that Canadians have come of age in a physical metallurgy sense.

As the authors point out, the composition of this alloy is such that it can be produced from materials available in the North American continent. I would feel that their reference to these materials as being non-strategic might be out of order at the present time in view of the current scarcity of metals.

The portion of the paper dealing with the heat treatment of the alloy was of considerable interest and one would think that there is a good chance of materially improving its rupture values by some type of precipitation hardening treatment. In this regard, the possibilities of titanium and magnesium additions should not be overlooked.

The peculiar decrease in elongation exhibited by the alloys when they are tested at higher temperatures is definitely a curiosity. Would the authors care to comment further on this point?

**Written Discussion:** By J. D. Nisbet, Metallurgical Division, General Electric Co., The Knolls, Schenectady, N. Y.

The paper by Messrs. Kinsey and Stewart again emphasizes the fact that some of the strongest high temperature alloys tend to be very, very brittle. Mechanical engineers do not get enthusiastic about alloys which show elongation values of 0, 1, 2, 3, 7, and 5%. For this reason, the alloys developed might have very limited applications. The work reported indicates, as pointed out by the authors, that neither chromium, cobalt, nor niobium (very strategic metals) is essential in high temperature materials. This is an important conclusion and opens a new field of possibilities for alloy development.

To take advantage of the low strategic elements employed in the alloys described, would it be reasonable to expect that higher elongation could be obtained by a sacrifice in high temperature strength to a level still competitive with materials now used for applications up to 815 °C (1500 °F)?

The compositions explored have been plotted in a ternary chart in Fig. 27. The 815 °C (1500 °F) rupture strength reported was also charted in a similar way. From this plot, I cannot agree with the general observations 1, 2, and 3 claimed on pages 196, 197, and 198.

In several places in the paper it is claimed that the compound Ni-Al is deleterious. Do the authors think that this might be because of the

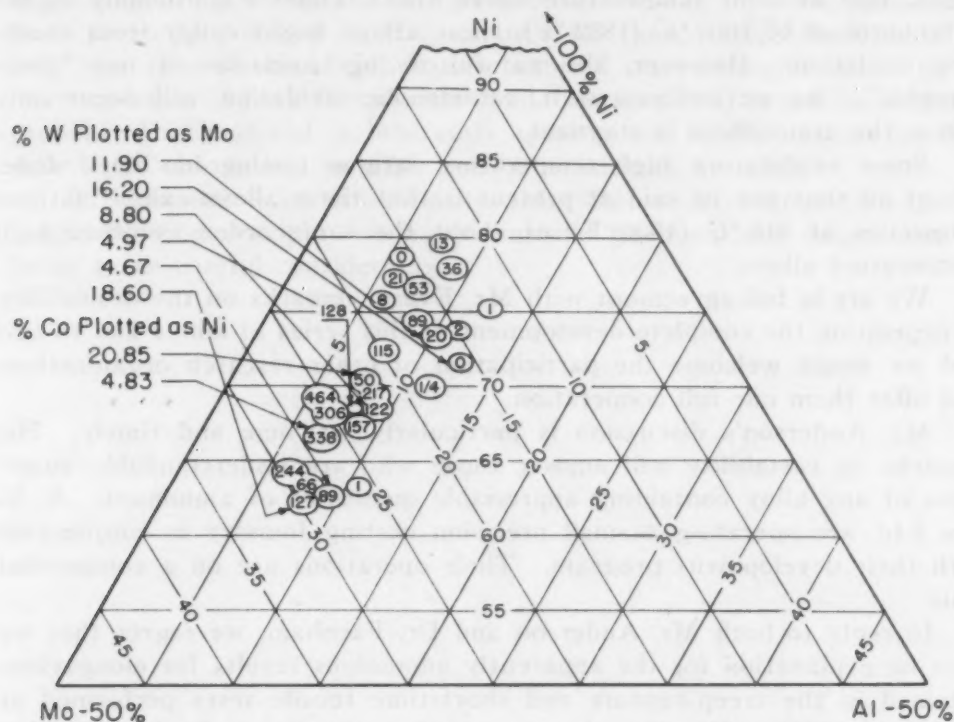


Fig. 27—Rupture Life in Hours for Molybdenum-Nickel-Aluminum Alloys at 1500 °F.

really extreme brittleness of this compound at room temperature, and at 815 °C (1500 °F), which could cause difficulties in testing to the extent that real values are not measured?

#### Authors' Reply

We sincerely thank those who partook in this discussion for the careful attention they gave our paper in preparing their remarks.

Professor Grant is quite correct in his remarks on aluminum analysis. As a matter of fact, we suspect that this inability to determine the aluminum content within closer limits than  $\pm 0.15\%$  is one of the major factors causing the scatter shown in Fig. 26. However, we cannot agree with the criticism of the narrow chemical limits. While these limits are admittedly narrow, we have a commercial precision casting foundry in Canada that is willing to work to these limits.

The information on remelting was included in the paper merely to demonstrate that the alloy can be remelted. Professor Grant's analysis of this data uncovers a probable and very interesting relationship that we were not aware of.

In reply to Mr. Evans' discussion, all that we can say at present is that we appreciate the need for more complete determination of other properties of these alloys before they can be pronounced commercially useful. We are reasonably certain that up to 815 °C (1500 °F) these alloys possess adequate oxidation resistance. However, there are some indications, resulting from work subsequent to the presentation of this paper, that at some temperature above 815 °C (1500 °F), probably in the neighborhood of 1000 °C (1832 °F), these alloys might suffer from excessive oxidation. However, the nature of this oxidation is not "catastrophic". As we understand it, catastrophic oxidation will occur only where the atmosphere is stagnant.

Some exploratory high temperature fatigue testing has been done. About all that can be said at present is that these alloys exhibit fatigue properties at 815 °C (1500 °F) of about the same order as other high temperature alloys.

We are in full agreement with Mr. Evans' remarks on the desirability of expediting the complete development of this series of alloys and to this end we would welcome the participation of other research organizations and offer them our full cooperation.

Mr. Anderson's discussion is particularly welcome and timely. His remarks on castability will answer those who are understandably suspicious of any alloy containing appreciable quantities of aluminum. A. V. Roe Ltd. are operating a small precision casting foundry in conjunction with their development program. Their operations are on a commercial scale.

In reply to both Mr. Anderson and Dr. Farnham, we regret that we have no explanation for the apparently anomalous results for elongations obtained in the creep-rupture and short-time tensile tests performed at 815 °C (1500 °F). We thought at one time that it might be an aging effect. To get an answer to this, a test bar was aged at 870 °C (1600 °F) for 100 hours, air-cooled, and then pulled in a tension test at 815 °C (1500 °F). The elongation measured on this test bar after fracture was still only 2%.

We admit that as yet there are not sufficient data to permit a statistically significant conclusion to be drawn concerning the relationship existing between the Ni:Al ratio and the tendency toward subnormal tensile properties at 815 °C (1500 °F). However, we do submit that there is rather conclusive experimental evidence to indicate that the tensile test at 1500 °F, together with the Ni:Al ratio, could probably become useful criteria of acceptance.

Mr. Nisbet brings up the question of brittleness. This appears to be a highly controversial point. The British are using Nimonic 80, which certainly does not exhibit any great amount of ductility at their service temperatures (about 700 °C). Two-hundred-hour rupture tests give total elongation figures in the order of 2 to 5% at this temperature. This is appreciably lower than the elongation values reported for alloy 85M220. Also there appears to be a considerable amount of activity directed toward the utilization of ceramics or cermels as blade materials. Such materials could by no stretch of the imagination be termed ductile. We submit that the utilization of the less ductile alloys or the brittle cermels

is a design problem and there are indications that this problem is not an impossible one to solve.

We have produced test bars consisting completely of NiAl. These bars would literally fall apart on handling, apparently from lack of cohesion between the grains. However, in the preparation of metallographic specimens, the polished surface metal flowed very readily during polishing, filling in all the scratches. Subsequent etching of what appeared to be a perfectly polished surface exposed all these scratches again. The only way that we could polish this material was electrolytically. So we have evidence of both "brittleness" and "softness". It is our opinion that probably this material is inherently quite weak so that pieces of NiAl distributed throughout an alloy can be considered as voids.

Dr. Farnham's contribution to this discussion is appreciated. His suggestions on precipitation hardening and titanium and magnesium are being given careful consideration.



## SIGMA-PHASE FORMATION IN A WROUGHT HEAT RESISTING STEEL

BY AHMED EL BINDARI, P. K. KOH AND OTTO ZMESKAL

### *Abstract*

*Previous investigators had concluded that steel of the type analysis 0.12% (max.) carbon, 18.5 to 19.5% chromium, 8.5 to 9.0% nickel, 0.5 to 1.5% tungsten, 0.25 to 0.50% molybdenum, 0.25 to 0.50% columbium, 0.15 to 0.40% titanium was immune to sigma-phase formation. It is shown in this investigation that sigma phase can form in a steel of this type. The rate of sigma-phase formation is extremely slow for the steel in the annealed condition but is greatly accelerated in the steel that has been strain hardened.*

*Sigma forms in the sites formerly occupied by ferrite stringers. It has been clearly identified by means of X-ray diffraction, using an etch-concentrating technique. Because of the variation in rates at which magnetism decreases, it is proposed that most of the ferrite rapidly transforms to austenite, and it is this austenite and the untransformed ferrite from which sigma slowly forms.*

THE work of Gilman et al. (1)<sup>1</sup> has shown that for a wrought heat-resistant steel of the composition given in Table I, Column A, sigma phase appears after holding the specimen 100 hours at 1400 to 1600 °F (760 to 870 °C). It was brought out by Evans (2) that no sigma could be found in a somewhat similar material whose analysis is given in Table I, Column B. The exact history of the bar stock was not revealed by Evans, but the steel was probably hot-rolled and stress-relieved at 1200 °F (650 °C). Delta ferrite present was estimated from the photomicrographs at about 30%. X-ray diffraction studies with the Geiger counter spectrometer, made on samples after various heat treatment procedures that had produced sigma phase in the steel studied by Gilman, gave no evidence of sigma. The only transformation appeared to be that of ferrite to austenite. The attempts to reveal sigma with Vilella's

<sup>1</sup>The figures appearing in parentheses pertain to the references appended to this paper.

A paper presented before the Thirty-second Annual Convention of the Society, held in Chicago, October 21 to 27, 1950. Of the authors, A. E. Bindari is a graduate student, Department of Metallurgical Engineering, Illinois Institute of Technology, Chicago; P. K. Koh is research engineer, Allegheny Ludlum Steel Corp., Brackenridge, Pa.; and Otto Zmeskal is director, Department of Metallurgical Engineering, Illinois Institute of Technology, Chicago. Manuscript received April 20, 1950.

reagent, Vilella's reagent followed by Murakami's, and 1:1 HCl followed by 10% alkaline ferricyanide were unsuccessful.

Although the analyses of the steels are quite similar, the carbon and molybdenum contents of the steel studied by Gilman are in a higher range. It was believed at first that the lower percentage of molybdenum in the steel reported by Evans may have slowed down tremendously the rate of formation of sigma (discussion of Ref. 1, authors' closure). It will be shown that strain hardening promotes the formation of sigma nuclei.

Table I  
Composition of Steels Studied

%	Steel Studied by Gilman et al. (1) A	Steel Reported by Evans (2) B	Steel of This Research C
C	0.27	0.084	0.10
Mn	1.20	0.44	0.46
Si	0.66	0.61	0.54
S	0.01	0.013	0.014
P	0.02	0.013	0.022
Cr	18.82	18.50	19.27
Ni	9.59	8.78	8.70
W	1.39	1.38	0.97
Mo	1.34	0.28	0.34
Cb	0.54	0.47	0.32
Ti	0.32	0.38	0.19

#### EXPERIMENTAL PROCEDURE

The analysis of the steel studied in this research is given in Table I, Column C. It was supplied through the courtesy of Mr. Frank Garratt. Since strain hardening has been demonstrated to be the most effective agent for the acceleration of sigma-phase formation, the steel was rolled to produce a high level of strain energy in the material and yet be in the province of hot-mill practice. The operations were as follows:

12 $\frac{1}{16}$ -inch ingot hammer-cogged to 4-inch square, heated to 2100 °F (1150 °C). Three reheatings used in cogging.

4-inch billet roll-cogged to 2 $\frac{1}{4}$ -inch square. Billet ground.

Billet rolled from 2 $\frac{1}{4}$ -inch square to  $\frac{3}{4}$ -inch round.

Starting temperature 2100 °F (1150 °C), finishing temperature 1500 °F (815 °C).

Held at last pass until 1500 °F (815 °C), then rolled in final pass.

Not annealed or stress-relieved.

The temperatures and times chosen for this investigation were: 1400, 1500, 1600 °F (760, 815, 870 °C) and 0.1, 1, 10, 50, 100, 200, 400, 800, 1000, 2000, 3500 hours.

In addition to the as-received condition, specimens were studied in the as-solution-treated condition (2300 °F) to obtain a comparison between the sigma nucleating effects of strain energy and of delta ferrite.

After aging, the specimens were cut longitudinally and prepared for microstructure examination. Each specimen was etched electrolytically in 10% oxalic acid. The steel resisted strongly the modified Murakami's etch (1) and no particular advantage was found in its

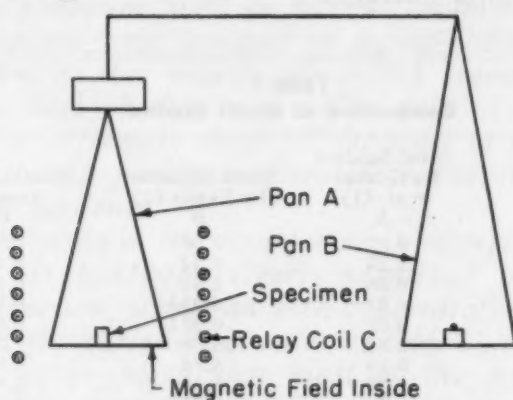


Fig. 1—Apparatus for Measuring Magnetic Intensity in Stainless Steels.

use. Short-time etching in the oxalic acid solution electrolytically outlined the sigma phase while long time darkened it.

Measurements of the magnetic intensity of the steel have been used to follow the formation of sigma (1, 3, 4) in austenite-ferrite steels. A very simple apparatus was used by the authors to detect the presence of ferrite in the steel (Fig. 1).

A small pan A, calibrated to be in equilibrium with the usual pan B of an analytical balance, is surrounded by a relay coil C. This small pan A is free to move inside the coil. Specimens were weighed without the coil surrounding the pan A, to be sure that any remanent magnetism in the coil would not lead to errors. The decreased weight required to restore the system to balance was divided by the original weight to determine the magnetization intensity of the specimens.

This method revealed itself to be simple and to be sufficiently sensitive. When the magnetism of a material was strong enough (ferritic steels) to project the pan A to one side of the relay coil, friction against the wall of the coil obviated the use of this method. With stainless steels of the 18-8 type, however, the magnetism is very small and this apparatus is satisfactory for the detection of the amounts of magnetic phase.

X-ray analysis throughout the present investigation was made using the grazing technique discussed previously (1). Also Troiano's (5) anodic  $\text{FeCl}_3$  etch on 00 emery paper finished small solid wedge samples, chromium K-radiation, and a General Electric 143.2 Debye camera were used. Microhardness determinations were made with a Tukon tester using a 25-gram weight.

## EXPERIMENTAL RESULTS

### *Microstructural Changes*

*Prior Condition Strain-Hardened*—The microstructure of the steel as-received is given in Fig. 2. The ferrite grains are in the form of stringers in the direction of rolling, and are delineated by very small particles, most probably carbides. The titanium-rich

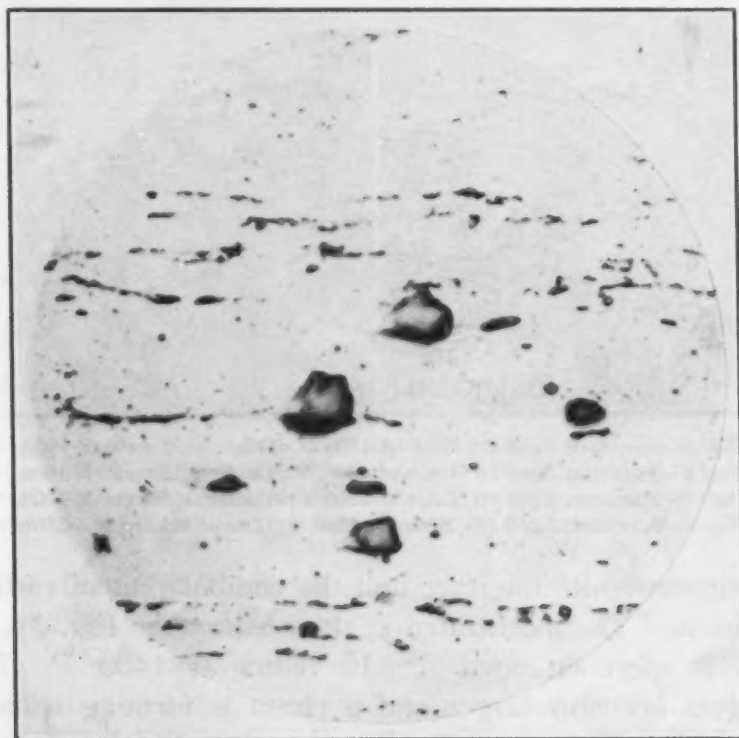


Fig. 2—Specimen in the As-Received Condition. Oxalic acid etch.  $\times 1000$ .

carbides, which can be recognized by their regular square form, are very refractory and persisted to a high temperature ( $2300^\circ\text{F}$ ). The columbium-rich carbides are distinguished by their large size and their irregular shape.

Carbide precipitation occurs on short-time aging, causing the ferrite stringers to appear more in relief. These carbides tend to concentrate at the ferrite grain boundaries, due to the retreating



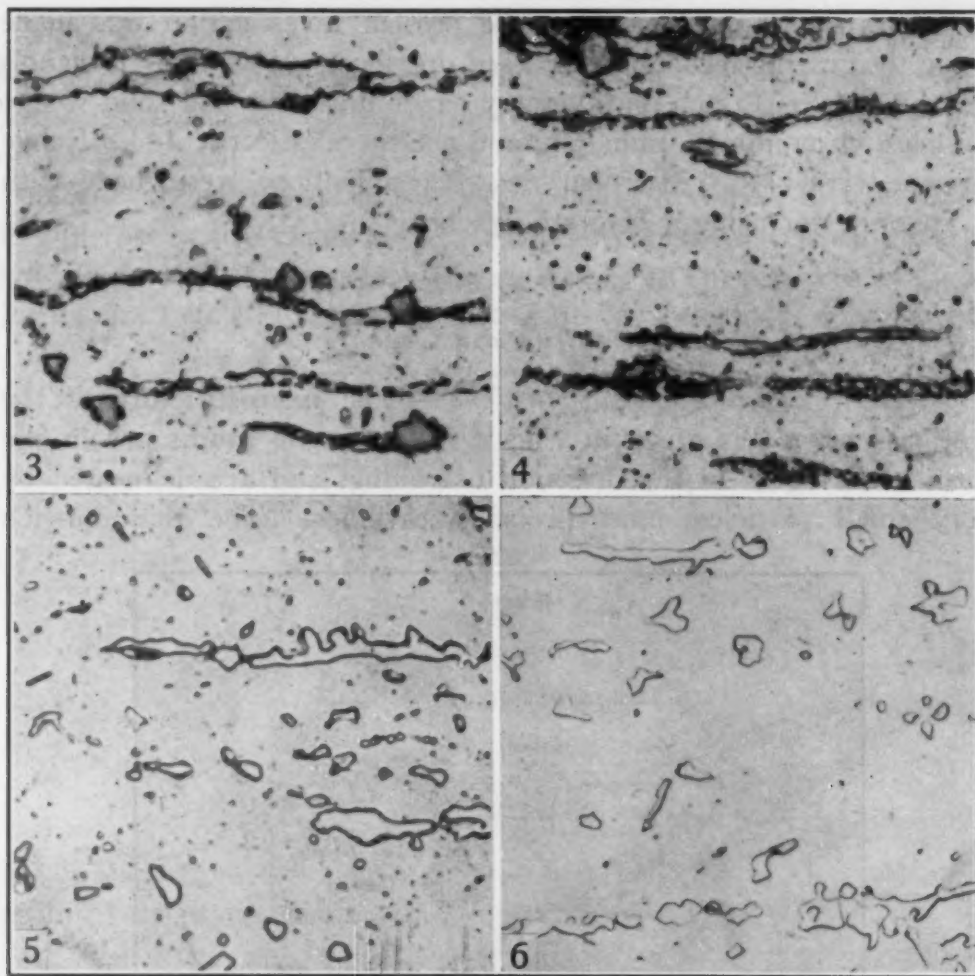


Fig. 3—Specimen Aged 0.1 Hour at 1500°F. Oxalic acid etch.  $\times 1000$ .

Fig. 4—Specimen Aged 10 Hours at 1400°F. Oxalic acid etch.  $\times 1000$ .

Fig. 5—Specimen Aged 50 Hours at 1500°F. Oxalic acid etch.  $\times 1000$ .

Fig. 6—Specimen Aged 100 Hours at 1600°F. Oxalic acid etch.  $\times 1000$ .

of the ferrite-austenite interface and the combination of carbon with Cr, W, Mo, and Ti concentrated at these sites (see Fig. 3). Fig. 4 represents a specimen aged for 10 hours at 1400°F (760°C). The stringers are now larger and a phase is forming within these stringers. After 50 hours (Fig. 5) the original stringers have disappeared completely and a new phase has definitely taken shape and grows with increasing time (Figs. 6 to 10). When the time of aging has reached 1000 hours the growth of that phase seems to have reached a maximum (Fig. 7), and at 2000 hours (Fig. 8) the irregular contour of the phase has been significantly reduced. In Figs. 9 and 10, representing specimens held 3500 hours at 1400°F and 3500 hours at 1600°F, respectively, clustering of the grains occurs, although the amount of the phase has not changed appreciably. The stable maximum amount of this new phase at

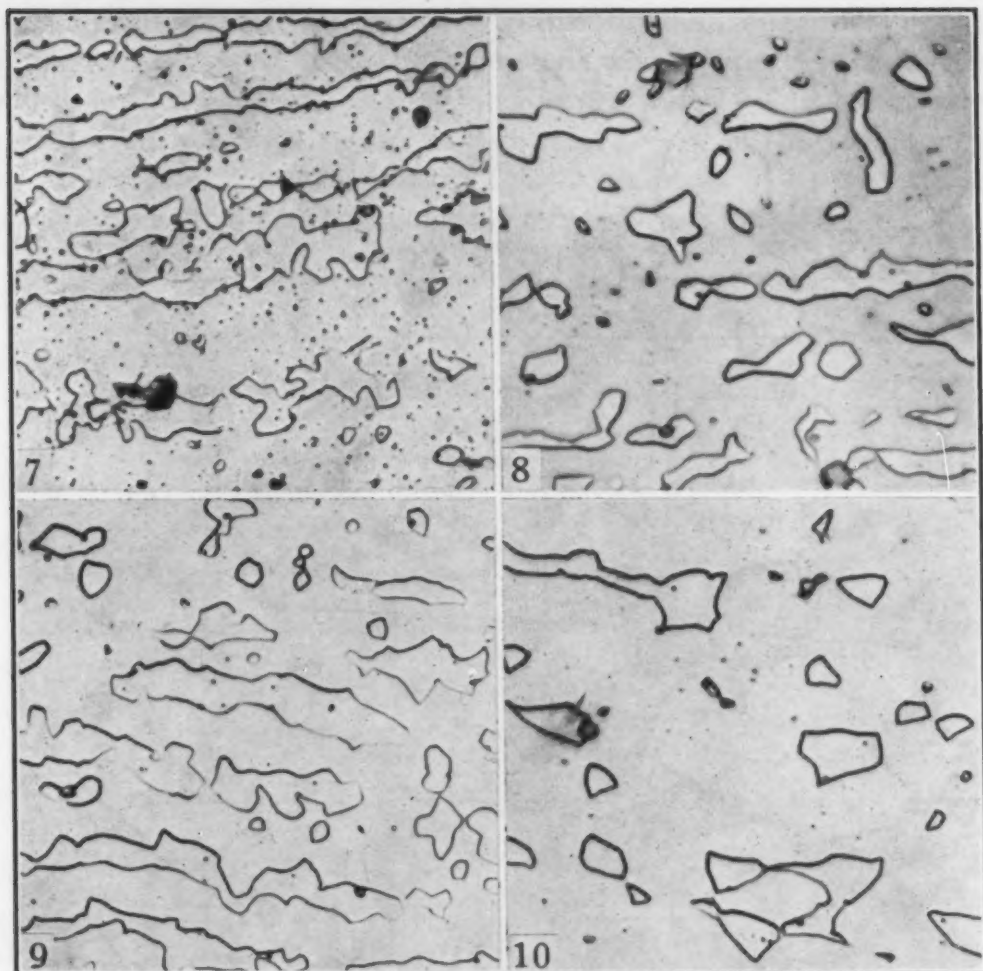


Fig. 7—Specimen Aged 1000 Hours at 1400°F. Oxalic acid etch.  $\times 1000$ .

Fig. 8—Specimen Aged 2000 Hours at 1500°F. Oxalic acid etch.  $\times 1000$ .

Fig. 9—Specimen Aged 3500 Hours at 1400°F. Oxalic acid etch.  $\times 1000$ .

Fig. 10—Specimen Aged 3500 Hours at 1600°F. Oxalic acid etch.  $\times 1000$ .

each aging temperature is, of course, different, being greatest at 1400 °F and lowest at 1600 °F.

*Prior Condition Solution-Treated*—The ferrite-austenite mixture obtained in the specimen water-quenched from 1 hour at 2300 °F (1260 °C) is shown in Fig. 11. The regularity of the grain boundaries of the ferrite is in sharp contrast to the irregular boundaries of the phase produced by aging of the strain-hardened material (Fig. 7). After 0.1 hour aging at 1500 °F (Fig. 12) the precipitation of the carbides in the ferrite grains is lamellar. After 1 hour at 1500 °F (815 °C) the pearlitic appearance of the specimen has disappeared to be replaced by a nodular one (Fig. 13). No carbides are present, except the highly refractory ones after 13.5 hours of aging (Fig. 14) and the amount of ferrite has decreased. Also, there is no evidence of the formation of a new phase.

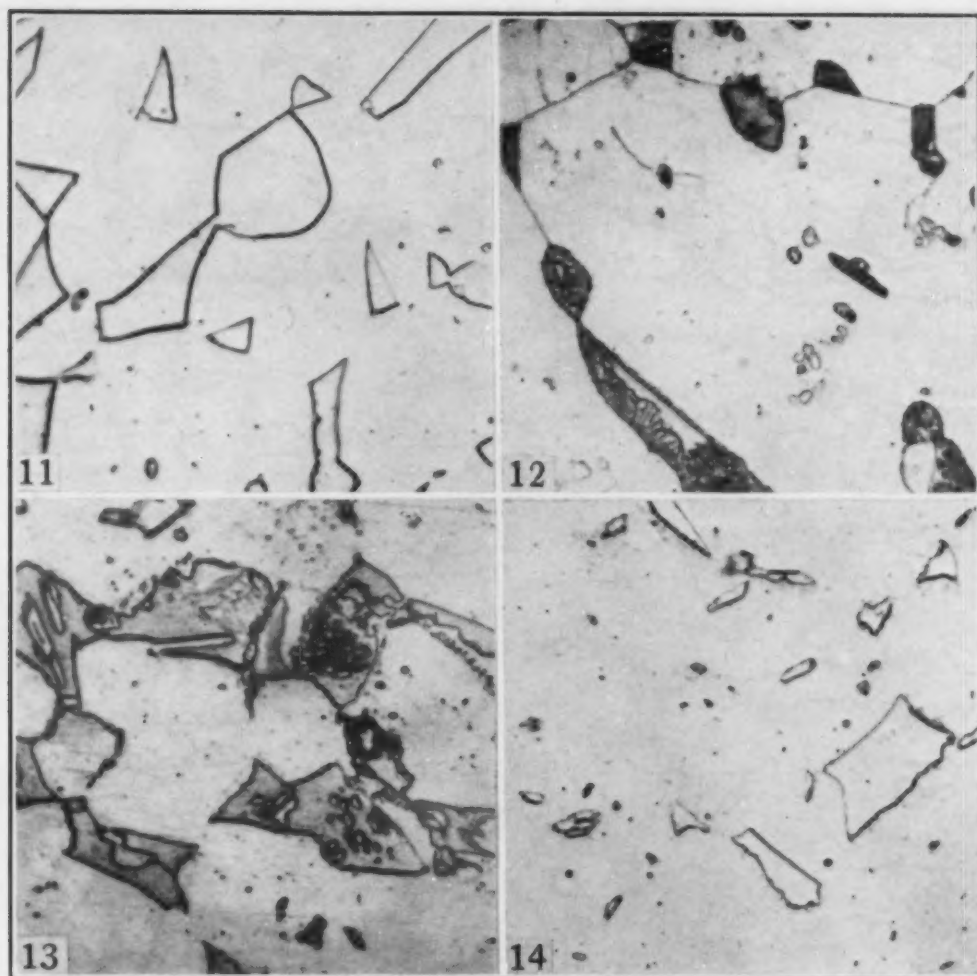


Fig. 11—Specimen Solution-Treated at 2300°F 1 Hour and Quenched. Oxalic acid etch.  $\times 1000$ .

Fig. 12—Specimen Quenched From 1 Hour at 2300°F. Aged 0.1 hour at 1500°F. Oxalic acid etch.  $\times 1000$ .

Fig. 13—Specimen Quenched From 1 Hour at 2300°F. Aged 1 hour at 1500°F. Oxalic acid etch.  $\times 1000$ .

Fig. 14—Specimen Quenched From 1 Hour at 2300°F. Aged 13.5 hours at 1500°F. Oxalic acid etch.  $\times 1000$ .

### *Magnetic Examination*

*Prior Condition Strain-Hardened*—The results of the magnetic measurements are given in Fig. 15. Some ferrite was still present after 1000 hours of aging at 1400 °F. At 1500 °F the ferrite completely disappeared after 50 hours of aging. At 1600 °F a trace persisted after 100 hours of aging.

It may be speculated that these curves consist of two parts. The first part, with the steeper slope, would represent the transformation of ferrite into austenite until a point is reached where the equilibrium ferrite-austenite of the duplex structure is attained. Aging within the relatively short-time period required for the

consummation of this stage of transformation does not result in sigma formation. From that point on, the ferrite, as well as the newly formed austenite, would transform to sigma. The slower rate of this transformation results in a decreased slope of the second part of the curve. The temperature of 1400 °F seems to be the one at which the rate of transformation of ferrite is maximum.

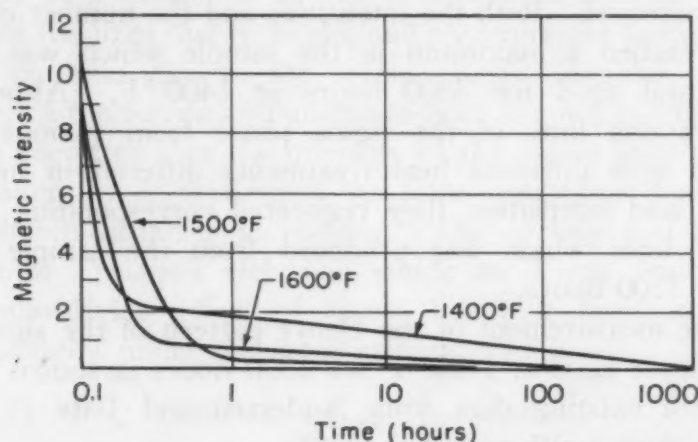


Fig. 15—Magnetic Intensity of Specimen in the As-Received Condition and Then Annealed at 1400, 1500 and 1600 °F.

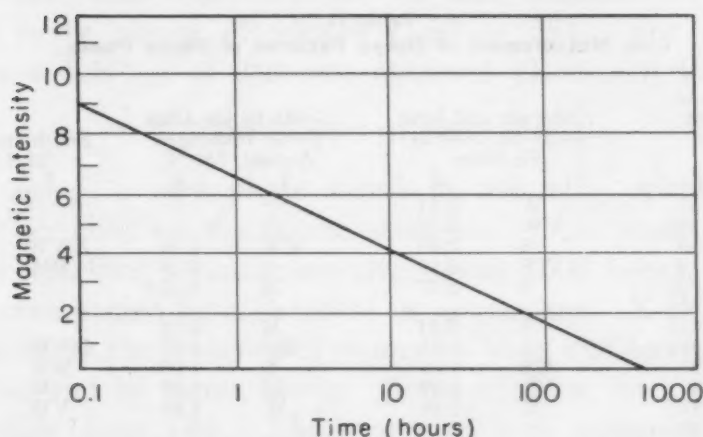


Fig. 16—Magnetic Intensity of Specimen Solution-Treated at 2300 °F for 1 Hour and Then Annealed at 1500 °F.

*Prior Condition Solution-Treated*—Magnetic measurements on the specimens quenched from 2300 °F and aged at 1500 °F are shown in Fig. 16. No change in the slope of the curve is apparent, indicating that no sigma formed within the maximum time of aging used for the solution-treated specimens (100 hours). This was confirmed by the photomicrographs (Figs. 11 and 12). The fact that the solution treatment has removed any trace of strain hardening produced during the rolling operation would remove an important factor in the hastening of the sigma formation.



*X-Ray Analysis*

Numerous Debye diffraction lines of unknown crystal structure were observed on all the samples examined; a few were observed even on the hot-rolled and as-received condition. With an increasing amount of sigma phase, which was observed under the microscope, the intensities of the lines and the number of the visible diffraction lines both increased. Both the intensities and the number of diffraction lines reached a maximum in the sample which was partially cold-rolled and aged for 3500 hours at 1400 °F. Although the Debye diffraction lines of the sigma phase from various samples of the alloy with different heat treatments differed in number of visible lines and intensities, they registered corresponding positions in a set of lines which was produced from the sample aged at 1400 °F for 3500 hours.

The line measurement of the Debye pattern of the sigma phase from the sample aged at 1400 °F for 3500 hours is shown in Table II along with existing data from Andersen and Jette (6), Goldschmidt (7), and Smith and Bowen (3).

Table II  
Line Measurement of Debye Patterns of Sigma Phase

Steel Studied in This Research 3500 Hours at 1400 °F		Andersen and Jette 44.76 Cr, 7.50 Si Fe Alloy		Goldschmidt Alloy Fe-Cr Prolonged Anneal, 750 °C		Smith and Bowen 18-8-3 Ti	
I	d	I	d	I	d	I	d
VVW	2.57	W	2.51				
VW	2.385	VW	2.37				
M	2.29	S	2.29	MW	2.26	VVW	2.284
VS	2.14	VS	2.13	S	2.14	VW	2.128
VS	2.080	S	2.07	M	2.075		
W	2.055						
S	2.030	S	2.03	M	2.01		
VS	1.985	VS	1.98	MS	1.97	MVW	1.977
VS	1.94	VS	1.93	S	1.925	MW	1.932
S	1.89	VS	1.89	M	1.88	W	1.888
M	1.85	M	1.84	W	1.84	VW	1.843
W	1.80						
M	1.77	W	1.765	VW	1.76		
VVW	1.67						
VVW	1.645						
VVW	1.615						
VVW	1.57						
VVW	1.54	VW	1.392			VW	1.395
VW	1.380	VW	1.375	W	1.375		
M	1.33	W	1.325	MW	1.33		
W	1.292						
W	1.282						
M	1.270						
S	1.259	VS	1.254	MS	1.259	Tr	1.262
VS	1.240	S	1.240	MS	1.241	M	1.244
M	1.232	M	1.23				
S	1.228	M	1.226	W	1.228	VW	1.232
M	1.222	SM	1.22				
S	1.208	SM	1.202	MW	1.208	MW	1.210
M	1.200	M	1.195			VVW	1.202
M	1.187	M	1.185	VW	1.188	VVW	1.191
M	1.178	S	1.171	M	1.172		
S	1.168	VS	1.165				

By comparison of the present data with that from the literature it is clear that the Debye diffraction pattern of the steel used, aged at 1400 °F for 3500 hours, contained lines reported as sigma phase plus some extra lines. The additional lines may be due to a mixture of additional phases, such as titanium carbide and columbium carbide, among others.

There is a likelihood of the existence of a small amount of ferrite, but the lines due to ferrite and austenite are frequently superimposed on lines due to the sigma phase. Besides, the relative intensities of the ferrite and austenite lines are not in order.

It is regretted that the intensity of the sigma lines on the same sample taken under apparently the same conditions depends on the uncontrollable variables in etching. The peeling and dropping of the scale in Troiano's etch (on which an X-ray beam is spotted to get intensifying effect of sigma lines) is hard to predict on various samples under the same etching conditions.

#### *Microhardness Examination*

On the specimen aged for 2000 hours at 1500 °F a KHN<sub>25</sub> (Knoop Hardness Number) of 453 was obtained for the phase assumed to be sigma (Rockwell C-50 to 55). For the matrix, austenite, a KHN<sub>25</sub> of 246 was obtained (Rockwell C-25 to 30).

#### DISCUSSION OF RESULTS

On aging, a new phase forms in this alloy within the sites formerly occupied by the ferrite stringers. This phase grows continuously, reaching a maximum after about 1000 hours. Its formation is accompanied by a decrease in magnetism. X-ray diffraction studies disclose the presence of numerous lines that have been shown to be produced by sigma phase. Some of those lines also coincide with carbide lines (8). The grains of both austenite and sigma phases coarsened with aging time.

#### SUMMARY AND CONCLUSIONS

This work is an attempt to reveal the presence of sigma and to study its rate of formation in a wrought heat-resistant steel previously reported as immune to sigma formation. The following conclusions can be drawn:

1. Sigma forms in the sites occupied by ferrite in the duplex austenite-ferrite structure.
2. The ferrite decreases in amount with aging time:
  - a. Its maximum rate of transformation is at 1400 °F.

- b. Precipitation of carbides from ferrite occurs within a short time.
  - c. These carbides are completely dissolved in the austenite with increasing aging time. (Exception is made for the highly refractory ones.)
3. There is some indication that during aging at 1400 to 1600 °F there occur:
- a. A high rate of transformation of some of the ferrite to austenite.
  - b. A low rate of transformation of the remaining ferrite and newly formed austenite to sigma.
4. Strain hardening is one of the most important factors in increasing the rate of formation of sigma in this steel.

#### References

1. J. J. Gilman, P. K. Koh and Otto Zmeskal, "Delta Ferrite Formation and Its Influence on the Formation of Sigma Phase in a Wrought Heat Resisting Steel", *TRANSACTIONS, American Society for Metals*, Vol. 41, 1949, p. 1371.
2. C. T. Evans, Jr., Discussion to aforementioned paper, *ibid.*, p. 1388.
3. L. Smith and K. W. J. Bowen, "The Occurrence and Some Effects of Sigma Phase in a Molybdenum-Bearing Chromium-Nickel Austenite Steel", *Journal, Iron and Steel Institute*, Vol. 158, 1948, p. 295.
4. Simpkinson and Lavigne, "Detection of Ferrite by Its Magnetism", *METAL PROGRESS*, Vol. 55, 1949, p. 164.
5. W. J. Barrett and A. R. Troiano, "X-Ray Identification of Sigma Phase in 25-20 Cr-Ni Stainless", *METAL PROGRESS*, Vol. 54, 1948, p. 366.
6. A. G. H. Andersen and E. R. Jette, "X-Ray Investigation of the Fe-Cr-Si Phase Diagram", *TRANSACTIONS, American Society for Metals*, Vol. 24, 1936, p. 375.
7. Goldschmidt, *Metallurgia*, Vol. 49, June 1949, p. 103.
8. B. M. Rosenbaum, "X-Ray Diffraction Investigation of Minor Phases of 20 High Temperature Alloys", Technical Note No. 1580, National Advisory Committee for Aeronautics, July 1948.

#### DISCUSSION

**Written Discussion:** By C. T. Evans, Jr., chief metallurgist, Elliott Company, Jeannette, Pa.

Sigma is getting to be almost as certain as death, taxes and the Democratic Party! It used to be considered a rarity, but it is now an exceptional heat resisting alloy in which someone has not uncovered sigma.

This is an excellent companion paper to the previous work of the same laboratory. The authors are to be particularly congratulated on their simple, but effective, magnetic balance.

The inference is clear that the reason the N.A.C.A. at Cleveland could not find sigma in samples of this same alloy, as reported in Ref. 2, was probably that these samples had not received the degree of strain

hardening achieved in the samples studied by the authors. This again emphasizes the influence of processing variables in the constitution and properties of heat resisting alloys.

**Written Discussion:** By John J. Gilman, Crucible Steel Company of America, Harrison, N. J.

The authors of this paper have convincingly demonstrated the susceptibility of the heat resisting steel, known as 19-9WMo, to sigma-phase formation. However, Bindari, Koh and Zmeskal report, on the sixth page of their paper, a result which seemed very unusual to me. This is the re-resolution of precipitated carbides at 1500 °F (815 °C) in a specimen which had been previously solution-treated at 2300 °F (1260 °C) for 1 hour (shown in Figs. 11, 12, 13, and 14 of their paper). In order to verify this result, I repeated the experiment using some 19-9WMo strip stock which was available at our laboratory, and some of the bar stock which had been used by the authors. The latter was kindly furnished to me by them. I will refer to these as Heats B and A, respectively. For comparison, the analyses are given below:

	C	Mn	Si	S	P	Cr	Ni	W	Mo	Cb	Ti
Heat A	0.10	0.46	0.54	0.014	0.022	19.27	8.70	0.97	0.34	0.32	0.19
Heat B	0.08	0.62	0.36	0.019	0.013	18.80	9.33	1.39	0.40	0.30	0.40

Specimens of both heats were solution-treated at 2300 °F (1260 °C) for 1 hour, water-quenched, and then heated for various amounts of time at 1500 °F (815 °C). Microsections were prepared and examined. The times used for the 1500 °F (815 °C) treatments were 0.1 and 16 hours for specimens of Heat A, and 0.1, 1, 13.5, and 100 hours for specimens of Heat B. Fig. 17 shows the microstructures of specimens heated at 1500 °F (815 °C) for 0.1, 16, and 100 hours, subsequent to the 2300 °F (1260 °C) solution treatment. Fig. 17a shows dark untransformed ferrite surrounded by a fringe of fine precipitated carbides. This is similar to the result of Bindari, Koh and Zmeskal. Fig. 17b shows the structure of the specimen which was heated for 16 hours at 1500 °F (815 °C). There are two points to be noted about this structure: first, many precipitated carbides are present in contradiction to the authors' statement that the carbides which originally precipitate are redissolved within 13.5 hours at 1500 °F (815 °C); second, the larger particles within the former ferrite areas, such as those which are etched darkly in Fig. 17b, are believed to be particles of the sigma phase. These particles are distinctly different from the other phases in the steel with respect to their etching characteristics and morphology. The particles are identified by referring to Fig. 17c. This figure shows the structure of the specimen which was heated at 1500 °F (815 °C) for 100 hours. The dark-etching particles in Fig. 17c will be shown definitely to be particles of the sigma phase. Since the larger particles in Fig. 17b have etching characteristics similar to the sigma particles of Fig. 17c, it is believed that some sigma phase was present in the specimen heated for 16 hours at 1500 °F (815 °C). Only a few scattered former ferrite patches contained the sigma-phase particles. These seemed to be in greater concentration toward the center of the bar. The total amount of sigma was less than 1% and hence it is not expected that X-ray methods would detect it. However, various etching reagents were used on the specimens shown in Fig. 17, and because of the distinct



etching behavior of the sigma phase and its characteristic morphology, the larger dark particles in the former ferrite areas are believed to be composed of this phase.

Fig. 18 serves to show the existence of the sigma phase in appreciable quantities in the specimen of Heat B which was heated at 1500 °F (815 °C) for 100 hours. Fig. 18a shows the structure of this specimen as it was developed by Vilella's reagent. The smooth white particles are

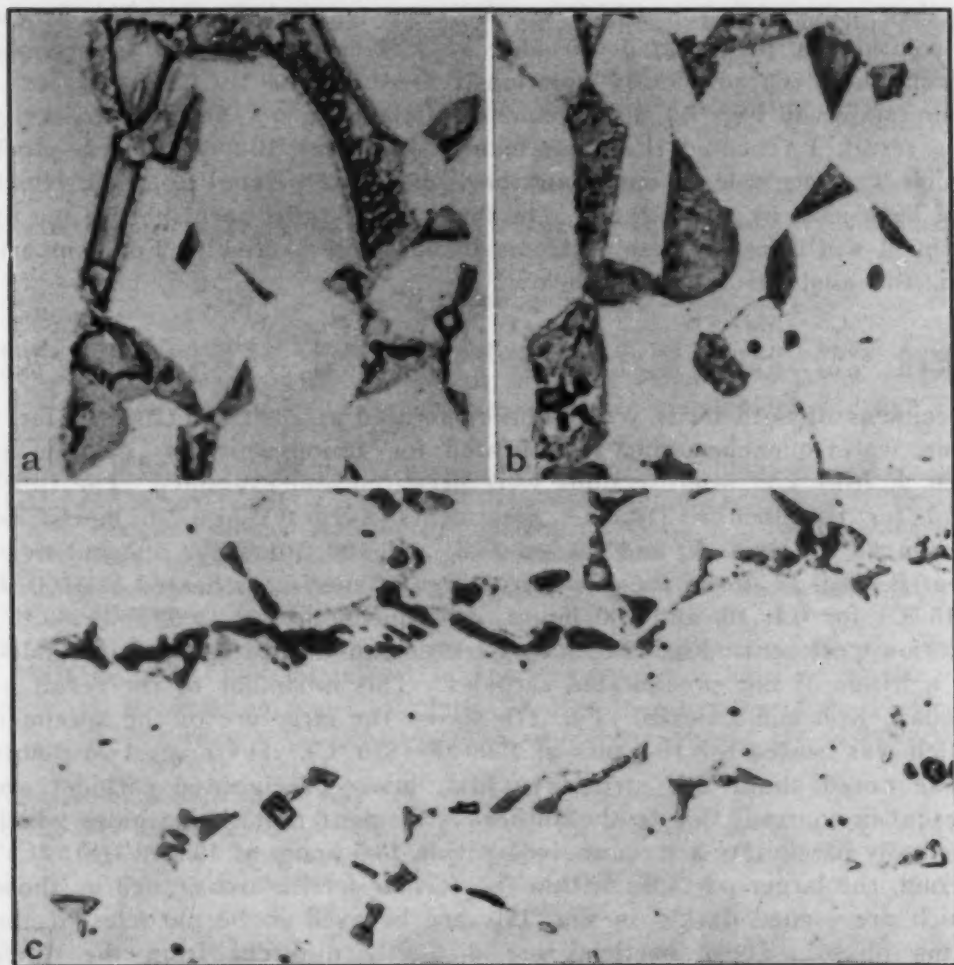


Fig. 17—19-9WMo—Specimens Etched Electrolytically in 10% Normal  $\text{NaOH}$ —1.5 Volts.  $\times 650$ . a—Solution-treated 1 hour at 2300 °F and water-quenched—reheated 0.1 hour at 1500 °F and air-cooled—Heat A. b—Same but heated 16 hours at 1500 °F—Heat A. c—Same but heated 100 hours at 1500 °F—Heat B.

believed to be sigma phase. The fine precipitated particles are carbides. The austenitic matrix is rough because of attack by the etchant. Fig. 18a shows the entire microstructure of the steel through the preferential attack of the austenitic matrix by Vilella's reagent. Chromic acid was used to develop the structure shown in Fig. 18b. This reagent is known to attack sigma-phase boundaries more rapidly than those of carbides. Therefore, this photograph provides evidence that the smooth white particles in Fig. 18a consist of the sigma phase. Further evidence is provided by Fig. 18c. This structure was developed by etching with

ammonium hydroxide. I have learned that this reagent attacks the carbides in stainless steels much more rapidly than it attacks the sigma phase. The microstructure shown in Fig. 18c does not show the white particles of Fig. 18a and therefore provides evidence that the white particles are not carbides and hence perhaps sigma.

Photographs were not made of the other specimens, but their struc-

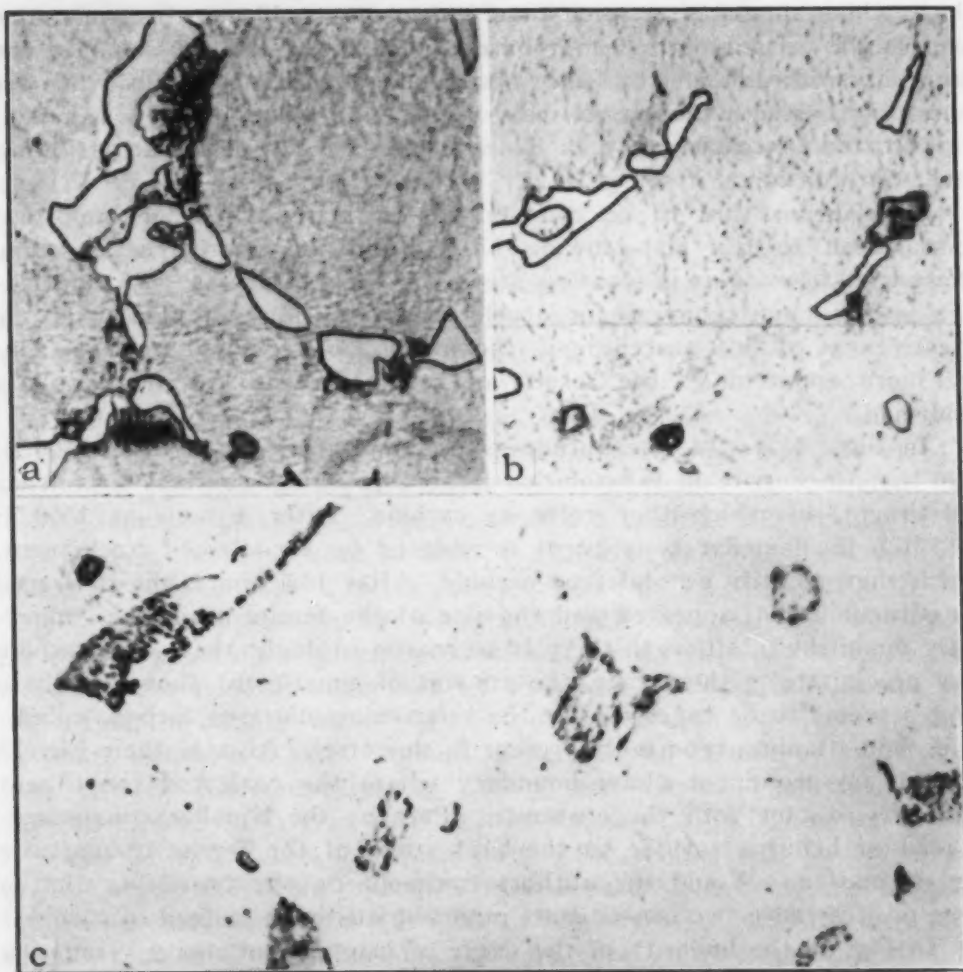


Fig. 18—19-9WMo—Heat B—Specimen Was Heated 1 Hour at 2300 °F and Water-Quenched. Then it was reheated at 1500 °F for 100 hours.  $\times 1500$ . a—Etched in Vilella's reagent. b—Etched electrolytically in 10% chromic acid—1.5 volts. c—Etched electrolytically in concentrated  $\text{NH}_4\text{OH}$ —1.5 volts.

tures as observed visually were just as would be expected on the basis of the structures described here. To summarize, the changes in solution-treated 19-9WMo which occur when it is heated at 1500 °F (815 °C) seem to be as follows: partial transformation of delta ferrite and precipitation of carbides within 0.1 hour, local appearance of sigma phase and some agglomeration of carbides within 16 hours, appearance of several per cent of the sigma phase and further agglomeration of carbides up to 100 hours. These results do not agree entirely with those of Bindari, Koh and Zmeskal. In particular, the phenomenon of re-solution of precipitated carbides was not observed.

I would also like to point out a peculiarity in the mode of sigma precipitation in this type of steel. I refer to the relatively rapid growth of the sigma phase in comparison to the few nuclei of this phase which form in a given amount of time. Thus, solution-treated specimens, if they are heated in the sigma-phase formation range, are characterized by multitudes of tiny particles of carbide which appear immediately but agglomerate or grow very slowly, and by a very few particles of the sigma phase which appear after some time, but grow steadily so that they soon surpass the carbides in size. Apparently, nuclei of the sigma phase can form only with difficulty but once formed they grow readily until they are in equilibrium with the matrix material.

**Written Discussion:** By H. S. Link and J. O. Mack, Carnegie-Illinois Steel Corporation, Pittsburgh.

The authors are to be commended for making another important contribution to the fast-growing bibliography on microstructures and phase transformations in stainless steels. The use of drastic cold deformation is a sound technique for accelerating diffusion reactions, and the effectiveness of this procedure in the forming of sigma phase is becoming more apparent as the results of several recent investigations are published.

In Figs. 11 to 14, the authors show that after 0.1 hour at 1500 °F (815 °C), the ferrite in the solution-treated specimen contains a lamellar constituent, to which they refer as carbide. After 1 hour at 1500 °F (815 °C), the lamellar constituent is replaced by a coalesced constituent, which they identify as coalesced carbide. After 13.5 hours, the coalesced constituent has disappeared and the size of the ferrite grains has apparently diminished. Although there is no reason to doubt that some carbide may precipitate in the ferrite, the amount of constituent shown in these figures seems to be excessive for the relative amounts of carbon, columbium, and titanium reportedly present in this steel. Also, in their Fig. 13 there is no prominent phase boundary where the coalesced constituent comes in contact with the austenite. Perhaps the lamellar constituent, instead of being a carbide, is the first stage of the ferrite-to-austenite transformation. Would the authors comment on the possibility that a large part of these two constituents might be austenite instead of carbide?

In Fig. 16 the linearity of the curve of magnetic intensity versus log time is unexpected for a ferrite-to-austenite reaction. Actually, magnetic intensity is a measure of per cent ferrite in the steel; the decrease in magnetic intensity with time at temperature should follow the laws of reaction rates, which are not linear but are S-shaped when plotted against log time. For example, Austin and Rickett<sup>2</sup> produced linear curves from comparable magnetic measurements by plotting the data on log-probability paper. It is unfortunate that individual data points are not plotted in Fig. 16; if the data truly show a linear relation, then some complex reaction must be operative rather than the simple decomposition of ferrite to austenite.

If the data used to plot the curves in Fig. 15 were obtained at the time intervals of 0.1, 1, 10, 100, and 1000 hours as reported in the Experi-

<sup>2</sup>J. B. Austin and R. L. Rickett, "Kinetics of the Decomposition of Austenite at Constant Temperature", *Transactions, American Institute of Mining and Metallurgical Engineers*, Vol. 135, 1939, p. 396, Fig. 7.



mental Procedure, we would like to ask the authors how they determined the paths of the curves in the time interval 0.1 to 1 hour. With data for only 0.1 and 1 hour, it is conceivable that the three curves could nearly coincide in this interval rather than cross one another.

In the absence of the data points in Fig. 15, the reader cannot observe the experimental error in the curves and particularly cannot determine if the indicated sequence of the 1500 °F (815 °C) and the 1600 °F (870 °C) curves for times of more than 1 hour is significant or if these curves are essentially coincident. Coincidence or even a reversal in sequence would be more understandable to us than the sequence shown. In this connection, we would like to ask the authors if each point used in plotting the curves in Fig. 15 was an average value, and if so, what was the range of values obtained?

#### Authors' Reply

We thank Mr. Evans for his comments on this paper. He has in the past contributed a great deal to the development of special processing of high temperature alloys. We are pleased to note his agreement with our findings.

Mr. Gilman and Messrs. Link and Mack brought out an interesting point in the mechanism of sigma formation based upon Figs. 11 to 14 in our paper. In light of the discussion, we re-examined by X-ray the following four samples: (a) Solution-treated 1 hour at 2300 °F (1260 °C); (b) Solution-treated 1 hour at 2300 °F (1260 °C) followed by a 6-minute reheat at 1500 °F (815 °C); (c) As in (b) except 1 hour at 1500 °F (815 °C); (d) As in (b) except 100 hours at 1500 °F (815 °C). To concentrate the minute amounts of precipitated carbides and sigma phase,  $\text{FeCl}_3$  electrolytic extraction, as suggested by Professor Troiano, was used. We found that the 2300 °F (1260 °C) solution-treated sample contained mostly austenite and also a small amount of ferrite—no carbide or sigma lines were visible. After reheating at 1500 °F (815 °C) for 6 minutes, besides austenite lines,  $\text{Cr}_{23}\text{C}_6$  type carbide lines appeared. On reheating at 1500 °F (815 °C) to 1 hour, no sigma lines were visible, only austenite and  $\text{Cr}_{23}\text{C}_6$  carbide lines were present. Intense sigma lines were visible in the sample reheated at 1500 °F (815 °C) to 100 hours. The  $\text{Cr}_{23}\text{C}_6$  lines were definitely weaker than the same carbide lines in the sample heated for 6 minutes at 1500 °F (815 °C). The above results showed that the visible sigma formation is preceded by a precipitation of alloyed carbides. As sigma phase increases in quantity upon prolonged aging, the amount of precipitated carbides decreases. Mr. Gilman's theorization on the stages of the formation of sigma is very interesting, and seems to agree in general with our observation. The exact percentage of ferrite-to-austenite transformation at 1500 °F (815 °C) is hard to measure microscopically or by X-ray. The nuclei of sigma, if they exist, are difficultly distinguished microscopically from carbides, and will be too weak for visible X-ray lines. We believe that probably the decrease in the intensity of  $\text{Cr}_{23}\text{C}_6$  carbide lines as reheating at 1500 °F (815 °C) goes on could be explained by a resolution of alloy carbides into the matrix to form sigma.

One point on the Troiano electrolytic etch for sigma concentration seems to be worth mentioning. If a sigma-containing specimen is etched



electrolytically according to Professor Troiano, a thin dark film forms gradually, but if this electrolytic etching is allowed to continue beyond 4 or 5 minutes, the dark film begins to float away. In order to catch the dark film on the specimen, it is impossible to wash the film sufficiently.  $\text{FeCl}_2 \cdot \text{H}_2\text{O}$  lines were observed in the film by X-ray. The dark film when X-rayed proved to contain not only sigma phase but also carbides and residual amount of matrices. One sample which was 2300 °F solution-treated and then reheated for 1 hour at 1500 °F was etched electrolytically according to the Troiano technique and its extraction residue was collected on a glass bottom filter and washed. The extraction residue showed strong  $\text{Cr}_7\text{C}_3$  lines, weak austenite lines and weak face-centered cubic carbide lines of 4.43 Å lattice parameter which could probably be CbC.

In regards to the magnetic data, the curves were plotted to fit the points obtained from a single set of specimens. The departure of these curves from those previously obtained for simple carbon steels arises from the complexity of the transformations. Some ferrite is transforming to austenite and some to sigma, each process having a different reaction rate.

## FORMATION OF AUSTENITE IN HIGH-CHROMIUM STAINLESS STEELS

By C. B. POST AND W. S. EBERLY

### *Abstract*

*High-chromium stainless steels of the AISI Type 446 are generally assumed to be 100% ferritic at high temperatures. Pure binary alloys of chromium and iron are completely ferritic at high temperatures, but commercial alloys can contain austenite at high temperatures because of the presence of such elements as carbon, manganese, silicon, nickel, and nitrogen.*

*The presence of these residual elements has a direct bearing on the phases present at elevated temperatures, say 1600 °F (870 °C) and above. A mixed structure of ferrite and austenite at elevated temperatures can be retained, if cooled fairly rapidly, and thereby change the expansion properties of the alloy. This change in expansion properties near room temperature can be harmful in special applications, such as glass-to-metal sealing.*

*The chromium equivalent has been determined for the elements carbon, manganese, silicon, nickel and nitrogen. Using these equivalents, it is possible to calculate the minimum chromium content necessary to obtain a 100% ferritic structure at elevated temperatures. The higher the temperature, the more chromium is needed to obtain a completely ferritic structure. The influence of chromium content and temperature on the resulting high temperature structure is shown by means of a diagram.*

FERRITIC stainless steels of the AISI Type 446 containing approximately 0.15% carbon, 0.50% manganese, 0.50% silicon, 24 to 30% chromium and the balance substantially iron are presently used in high temperature applications and in making glass-to-metal seals. These ferritic steels have good high temperature oxidation resistance and can be used in applications that do not require much strength at temperatures over 1500 °F (815 °C). Expansion characteristics of these steels from room temperature to about 1900 °F (1040 °C) are almost linear, and these properties make possible

---

A paper presented before the Thirty-second Annual Convention of the Society, held in Chicago, October 21 to 27, 1950. Of the authors, C. B. Post, metallurgist, and W. S. Eberly are associated with the Metallurgical Department, The Carpenter Steel Company, Reading, Pa. Manuscript received April 15, 1950.

glass-to-metal seals when the metal is used with a glass having similar expansion properties.

This type of high-chromium stainless steel matches the expansion of several sodium- and lead-bearing glasses. A desirable glass sealing property of these alloys is the formation of a green surface oxide during a wet hydrogen annealing treatment. This green oxide is tightly adhering to the metal surface and also soluble in the glass, and makes an excellent bond between the metal and the glass. A glass-to-metal seal is generally considered to be good when the bond between the metal-oxide and oxide-glass is stronger than the glass itself.

The binary alloys of iron and chromium are ferritic when more than 16% chromium is present (1).<sup>1</sup> However, commercial alloys are never binary in nature and are influenced more or less by carbon, manganese, silicon, nickel and nitrogen, even though the range of these elements might be classed as "residual". In the case of these high-chromium stainless steels, the carbon, manganese, silicon, nitrogen and nickel contents can cause the appearance or absence of austenite at high temperatures. This austenite will be retained on rapid cooling to room temperature or it can be substantially eliminated by transformation to the ferritic phase by holding at about 1700 °F (925 °C) after the alloy is subjected to high heat.

Carbon, manganese, nickel and nitrogen are classified as austenite-forming elements. Silicon and chromium are known as ferrite-forming elements. The carbon, manganese, nickel and silicon additions are a result of present-day steelmaking techniques, and it is only recently that nitrogen has been used in the range of 0.10 to 0.20%. Franks (2) summarized the known effects of nitrogen in high-chromium ferritic stainless steels. Nitrogen in the range of 0.10 to 0.20% refines the grain size and improves the strength, ductility, and toughness of the alloys with slight effect on the hardness.

Franks (2) observed that the presence of nitrogen in a 25% chromium ferritic stainless steel caused the appearance of an austenitic phase when the alloy was heated to approximately 2000 °F (1095 °C) and rapidly cooled. He attributed the retarding of grain growth at elevated temperatures to the presence of the austenite phase, but this cannot be true in general because of the grain refinement in completely ferritic steels. Nitrogen was introduced in high-chromium stainless steels containing 24% or more chromium to obtain fine-grained ductile and malleable wrought products.

In making glass-to-metal seals, the range of 26 to 28% chro-

<sup>1</sup>The figures appearing in parentheses pertain to the references appended to this paper.

mium was established for specification purposes to insure uniform expansion properties from heat to heat. Occasionally, excessive breakage of glass-to-metal seals was encountered, and it was found that a 26% chromium stainless steel with a low nitrogen content (say below 0.10%) produced satisfactory seals, whereas the same composition having about 0.15% nitrogen had to be rejected from production. These seals were defective due to breakage and difference in expansion between the metal and glass. In order to eliminate this condition, the chromium content was increased to the range of 27 to 30% when 0.10 to 0.20% nitrogen was present. In view of the importance of the presence or absence of small quantities of austenite in this type of analysis when treated at high temperatures and subsequently used in making glass-to-metal seals, the following data are designed to show the effect of analysis on the formation of austenite at high temperatures in commercial high-chromium stainless steels containing 16 to 30% chromium. This includes the investigation of such austenite-forming elements as carbon, manganese, nickel and nitrogen, and ferritic elements such as silicon and chromium. Observations were made on the behavior of the austenite at temperatures ranging from 1600 to 2350 °F (870 to 1290 °C), with particular emphasis on the properties necessary for glass-to-metal seals.

To study the effect of a particular element on the alpha-gamma field at high temperatures, a base analysis was selected as follows:

Carbon	Manganese	Silicon	Nickel	Chromium	Nitrogen
0.08%	0.60%	0.40%	0.15%	25 to 30%	0.15%

In studying an austenite-forming element, a chromium content of 30% was used in the base analysis to insure that the alloy would be in a ferritic condition with the other elements at their selected values. The amount of a single austenitic element was then increased until austenite formed at elevated temperatures, particularly in the range of 1800 to 2300 °F (980 to 1260 °C). For ferritic elements, a chromium content of 25% was used in the base analysis to insure the presence of austenite in the base alloy. Increasing amounts of a single ferritic element were added until all austenite was eliminated at elevated temperatures.

Table I shows the analyses studied in this investigation. These analyses were cast into 15-pound ingots, 3 inches square, which were hot-worked to about 1/2 inch square. This corresponds to 90% reduction and is sufficient to break up any form of dendritic structure. For the purpose of checking the results shown by the Type 446 analyses, several Type 430 analyses (Alloys 36 to 39, Table I) were studied in the same manner.



Table I  
Analyses Investigated

	C	Mn	Si	Cr	Ni	Mo	N <sub>2</sub>	Cr Available*
Alloy 1	0.096	0.61	0.50	28.85	0.17	.....	0.130	21.29
Alloy 2	0.090	0.57	0.36	26.04	0.19	0.02	0.147	20.54
Alloy 3	0.094	0.56	0.36	28.11	0.19	0.02	0.149	22.40
Alloy 4	0.090	0.59	0.38	30.01	0.15	0.02	0.145	24.70
Alloy 5	0.086	0.59	0.36	32.06	0.15	0.02	0.146	26.70
Alloy 6	0.096	0.66	0.45	25.61	0.15	0.02	0.16	19.90
Alloy 7	0.096	0.66	0.61	25.61	0.15	0.02	0.16	20.50
Alloy 8	0.096	0.66	0.74	25.61	0.18	0.02	0.16	21.10
Alloy 9	0.096	0.66	0.89	25.61	0.18	0.02	0.16	21.70
Alloy 10	0.093	0.66	1.30	25.61	0.18	0.02	0.15	23.60
Alloy 11	0.092	0.61	0.41	30.60	0.22	0.04	0.16	24.80
Alloy 12	0.132	0.61	0.41	30.60	0.22	0.04	0.16	23.90
Alloy 13	0.167	0.61	0.41	30.60	0.22	0.04	0.16	23.10
Alloy 14	0.199	0.61	0.41	30.60	0.22	0.04	0.17	22.40
Alloy 15	0.231	0.61	0.41	30.60	0.22	0.04	0.17	21.80
Alloy 16	0.11	0.50	0.25	23.66	0.19	.....	0.071	19.60
Alloy 17	0.116	0.46	0.25	25.05	0.19	.....	0.074	20.80
Alloy 18	0.116	0.51	0.29	25.71	0.15	.....	0.151	19.40
Alloy 19	0.114	0.50	0.64	25.66	0.15	.....	0.149	20.70
Alloy 20	0.116	0.58	0.28	23.92	0.07	.....	0.114	18.75
Alloy 21	0.114	0.54	0.26	23.87	0.45	.....	0.115	18.00
Alloy 22	0.114	1.02	0.24	23.75	0.43	.....	0.111	16.21
Alloy 23	0.29	0.97	0.24	23.59	0.44	.....	0.111	9.92
Alloy 24	0.090	0.57	0.36	22.40	0.19	0.02	0.12	17.70
Alloy 25	0.090	0.56	0.40	28.20	0.14	0.02	0.14	23.15
Alloy 26	0.093	0.63	0.45	29.52	0.45	0.02	0.15	23.80
Alloy 27	0.093	0.63	0.45	29.52	0.75	0.02	0.15	23.40
Alloy 28	0.092	0.63	0.45	29.52	0.98	0.02	0.15	23.00
Alloy 29	0.092	0.63	0.45	29.52	1.43	0.02	0.15	22.40
Alloy 30	0.091	0.63	0.45	29.52	1.61	0.02	0.15	22.10
Alloy 31	0.099	0.92	0.45	30.12	0.19	0.01	0.15	24.50
Alloy 32	0.098	1.22	0.45	30.12	0.19	0.01	0.15	24.40
Alloy 33	0.097	1.43	0.45	30.12	0.19	0.01	0.15	24.30
Alloy 34	0.097	1.96	0.45	30.12	0.19	0.01	0.15	24.00
Alloy 35	0.096	3.04	0.45	30.12	0.19	0.01	0.15	23.50
Alloy 36	0.060	0.43	0.39	16.93	0.44	0.02	0.041	15.05
Alloy 37	0.058	0.43	0.39	16.93	0.86	0.02	0.041	14.47
Alloy 38	0.066	0.45	0.34	16.72	0.06	0.02	0.046	14.90
Alloy 39	0.156	0.45	0.34	16.72	0.06	0.02	0.046	12.96

\*Available chromium as calculated by Equation 1.

Small microspecimens (approximately  $\frac{1}{2}$  inch square and  $\frac{1}{4}$  inch thick) of each heat were prepared for heat treatment. Heat treatment consisted of holding at a given temperature for at least 5 minutes and quenching in brine so as to retain the structures present at the temperature in question. Temperatures employed covered the range of 1900 to 2300 °F (1040 to 1260 °C). Tests were generally made at intervals of 50 °F.

After heat treatment, microspecimens were polished and etched in a ferric chloride reagent containing 20 grams of ferric chloride, 60 cc. of HCl and 240 cc. of water. Structures were examined at a magnification of  $\times 750$ . As a further check on the presence of austenite, most microspecimens were heat tinted at a temperature of 1200 °F (650 °C). At this temperature, the austenite has a tendency to oxidize more readily than the ferrite. Generally, the austenite has a tendency to form in the grain boundary and also at

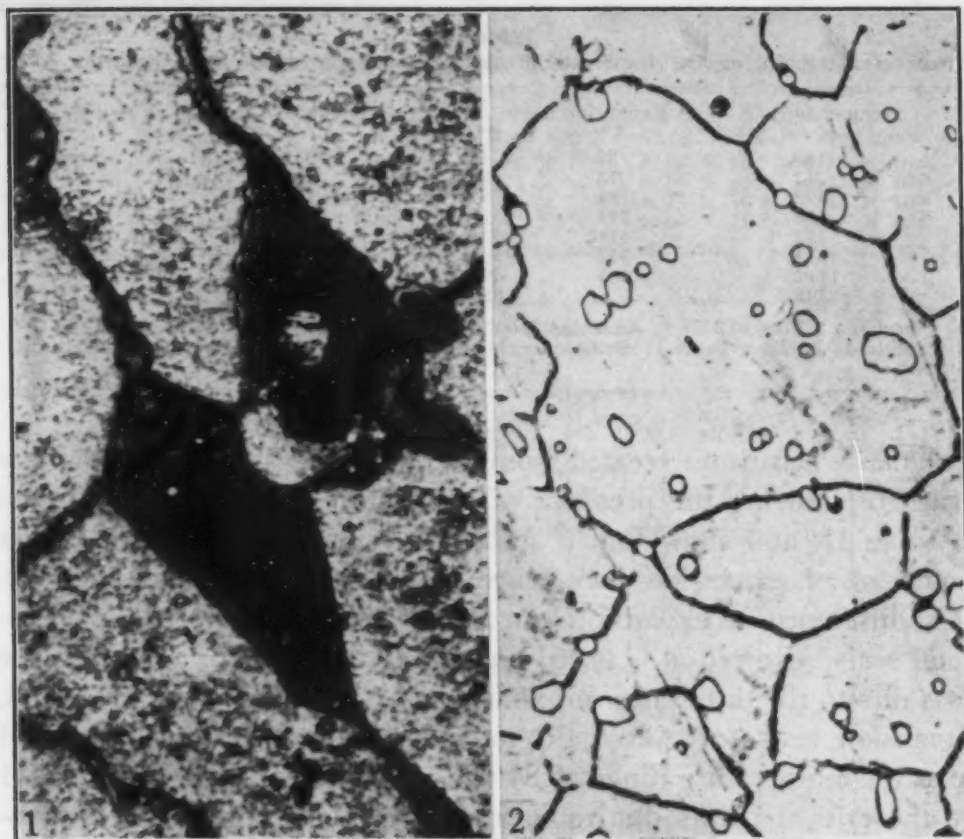


Fig. 1—Microstructure of a 26.04% Chromium-Iron Alloy Containing Ferrite (Light) and Austenite (Dark) Structures. Brine-quenched from 2150 °F.  $\times 1000$ .

Fig. 2—Ferritic Structure of a 30% Chromium-Iron Alloy. Brine-quenched from 2250 °F.  $\times 1000$ .

points caused by converging grains. Very rarely was austenite detected inside a grain.

An attempt was made to determine the percentage of austenite present to the nearest 5% to obtain the alpha-gamma field for that element over the temperature range investigated.<sup>2</sup> Fig. 1 is a photomicrograph of a chromium-iron alloy containing 26.04% chromium when heated to 2150 °F (1175 °C) and brine-quenched. The dark areas represent tinted austenite and show a large percentage present (Alloy 2, Table I). Fig. 2 is a microstructure of a chromium-iron containing 30% chromium when heat tinted after a quench from 2250 °F (1230 °C). No austenite is present and the structure is ferritic (Alloy 4, Table I).

Expansion tests (size  $\frac{1}{4}$  inch round by 4 inches long) were made on Alloy 2, Table I, when annealed and slowly cooled to insure a ferritic structure. An expansion test was also made on the same

<sup>2</sup>Percentage austenite in a given structure was determined by projecting an average of 5 fields on a screen having the area subdivided into 100 square parts. By counting the sections, two observers determined the amount of austenite present.

**Table II**  
**Effect of Austenite on the Expansion Properties of a Chromium-Iron Stainless Alloy**

Temperature, °F 68 to	Expansion in./in. $\times 10^{-5}$		Coefficient in./in./°F $\times 10^{-4}$	
	A*	B†	A	B
140	37	42	5.1	5.7
212	78	86	5.4	5.9
392	184	195	5.7	6.0
572	297	317	5.9	6.3
752	417	433	6.0	6.4
932	542	565	6.2	6.5
1112	663	696	6.3	6.7
1292	...	859	...	7.0

\*Specimen 2 Alloy, Table I: Annealed 2100°F and slow-cooled. Ferritic in structure.

†Specimen 2 Alloy, Table I: Brine quench from 2100°F. Ferrite plus 10% austenite in structure.

specimen when water treated from 2150 °F (1175 °C) and having a structure showing the presence of austenite. These data are found in Table II, and show that a structure with austenite has a higher coefficient of expansion than when the alloy is completely ferritic. This difference in expansion can be the cause of rejected glass-to-metal seals. Rejection is based on too high stresses or failure of the glass due to the difference in expansion between the glass and metal. Expansion tests for Alloys 36 to 39 are found in Table III and cover the temperature range of 84 to 1400 °F. Included in Table III are the critical points due to formation of austenite and the micro-structure of the respective alloys.

Based upon the micro-examination of the heats to study the effect of a particular element and estimating the percentage of austenite present, alpha-gamma field diagrams were sketched for the following elements:

Austenitizing elements:

Carbon—Fig. 3; Manganese—Fig. 4; Nickel—Fig. 5.

Ferrite elements:

Silicon—Fig. 6.

The diagrams for the austenitizing elements have the average base analysis of:

Carbon	Manganese	Silicon	Chromium	Nitrogen
0.09%	0.60%	0.40%	30.00%	0.12 to 0.15%

The diagram for the ferritic element silicon has the base analysis of:

Carbon	Manganese	Chromium	Nitrogen
0.09%	0.60%	25.50%	0.12 to 0.15%

In Figs. 3, 4, 5, and 6, the lines in the fields labeled 0, 5, 10%, etc., refer to the estimated percentages of austenite at the temperature and composition noted.

Table III  
Expansion Properties and Critical Points of Several Type 430 Analyses

Alloy No.	Available Chromium, %	Critical Point °F	77 to 800 °F	77 to 1200 °F	77 to 1400 °F
36	15.05	1650	$5.98 \times 10^{-6}$	$6.14 \times 10^{-6}$	$6.18 \times 10^{-6}$
37	14.28	1590	$5.75 \times 10^{-6}$	$6.14 \times 10^{-6}$	$6.25 \times 10^{-6}$
38	14.84	1650	$5.78 \times 10^{-6}$	$6.45 \times 10^{-6}$	$6.48 \times 10^{-6}$
39	12.96	1560	$5.47 \times 10^{-6}$	$6.04 \times 10^{-6}$	$6.15 \times 10^{-6}$

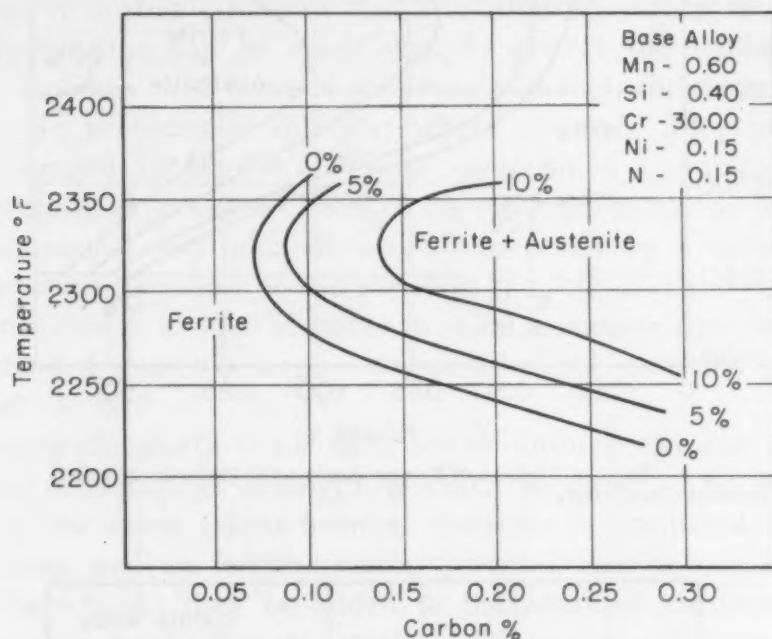


Fig. 3—Effect of Carbon and Temperature on the Structure of a 30% Chromium-Iron Alloy.

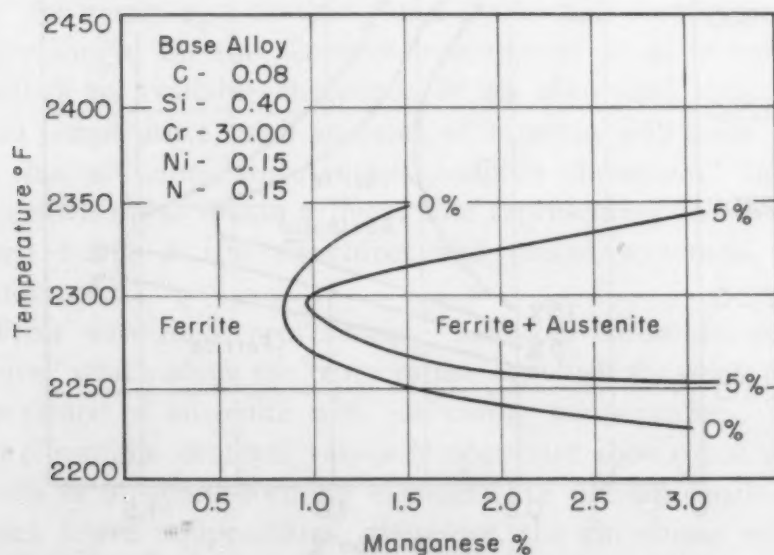


Fig. 4—Effect of Manganese and Temperature on the Structure of a 30% Chromium-Iron Alloy.



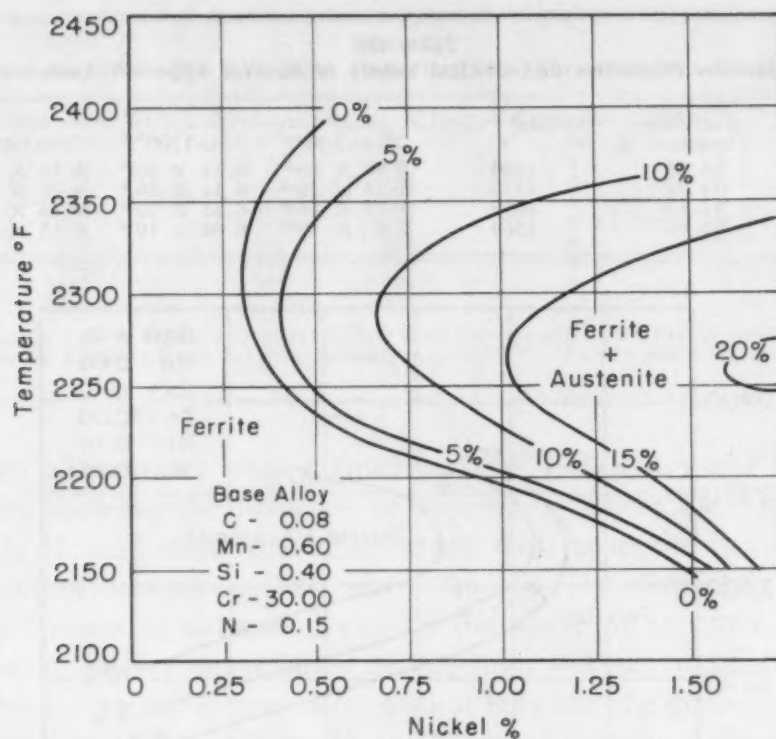


Fig. 5—Effect of Nickel and Temperature on the Structure of a 30% Chromium-Iron Alloy.

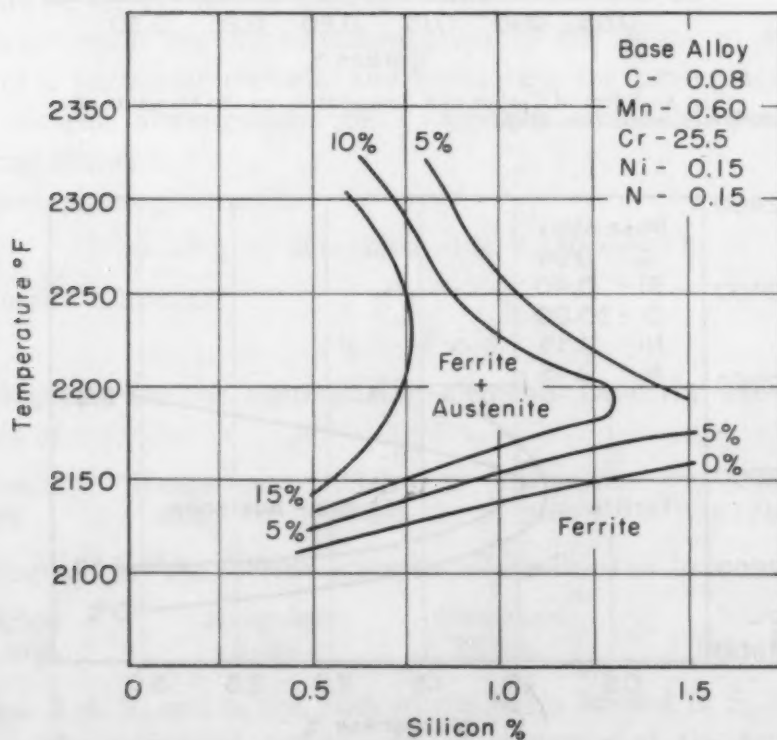


Fig. 6—Effect of Silicon and Temperature on the Structure of a 25.5% Chromium-Iron Alloy.

Figs. 3, 4, 5, and 6 can be used to show the maximum amount of austenitizing element permitted in the alloy to insure 100% ferrite in the matrix under the temperature investigated. Also the minimum amount of ferritic alloy (silicon in this case) necessary to insure 100% ferrite in a 25.50% chromium-iron alloy can be determined.

The treating temperatures at which these alloys first show the presence of austenite indicate that a relationship incorporating chemical composition can be established to predict the temperature at which austenite will form in this range of high-chromium stainless steels. In problems of this sort where a specific alloy property is being studied in terms of several composition variables, it is of advantage to express the effects of the elements by means of a linear-type equation. Any function can be represented by a linear equation over a small variation of the variables, in this case the composition elements, and it should be borne in mind that such equations cannot be extended over too large a variation of the elements nor extrapolated too far.

Since chromium is the basic ferrite-forming element, its ferrite-forming tendency, or strength, is taken as unity. The strength of each of the other ferrite-forming elements is compared to that of chromium, and its ferrite-forming potential can be expressed as a value which can then be added to the analyzed chromium figure. Austenite-forming elements replace chromium and therefore their relative value in proportion to chromium is subtracted from the analyzed chromium content. The final result is the "available chromium" for retaining a ferritic phase at elevated temperatures. Factors are sought for the elements investigated so as to calculate the percentage of available chromium in an alloy and thus determine at what temperature small amounts of austenite will form. In order to do this, a "temperature versus available chromium" diagram has to be drawn up to obtain a linear line representing the dividing line between 100% ferrite structures and mixed structures of ferrite and austenite.

Plots were made representing "analyzed chromium versus temperature" which show the temperature at which the alloy first shows the presence of austenite with increasing temperatures. A plot of actual chromium contents versus temperature shows that when large amounts of austenite-forming elements are present, austenite forms at much lower temperatures; therefore, the chromium value has to be changed, depending on the amount of austenitizing and ferrite-forming elements present.

The effect of each of the elements was studied individually to determine its strength factor to obtain the chromium equivalent. Trial-and-error methods had to be used to determine the factors. The numerical value of the factor was varied until a diagram of "available chromium versus temperature" showed a straight-line boundary between the ferritic-type structures and ferrite-austenite

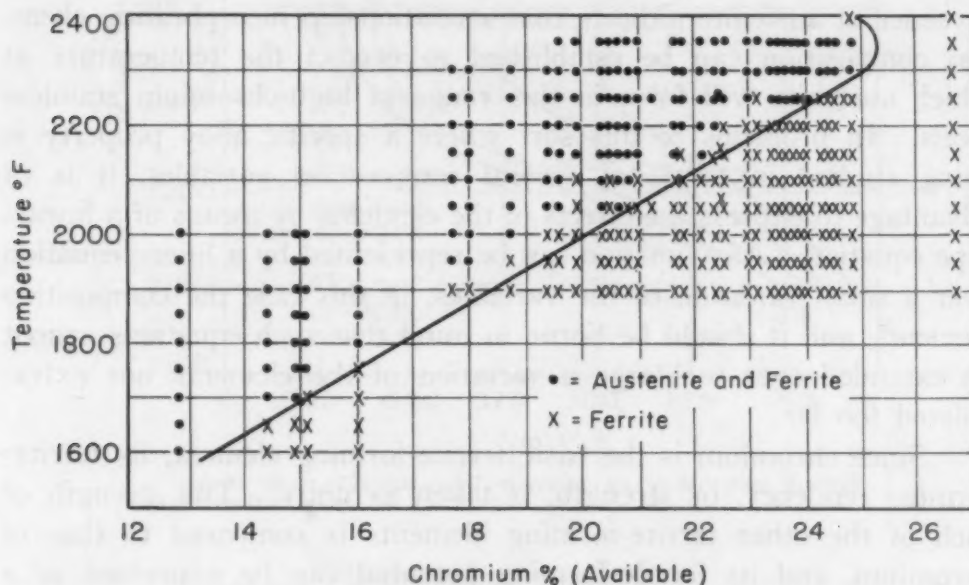


Fig. 7—Boundary Line of Ferrite - Ferrite and Austenite Structures as Determined by Analyses Investigated.

structures. The diagram had to represent a range of chromium contents and also a range of the element in question. Finally each complete analysis was evaluated on the basis of these factors and slight adjustments made to obtain a clear-cut boundary between ferrite and ferrite-austenite structures.

The final strength factors determined by this method are:

Chromium	Silicon	Manganese	Nickel	Carbon	Nitrogen
+1.0	+4.0	-0.5	-1.5	-22	-30

A positive factor means ferrite-forming tendencies, whereas a negative factor indicates austenite-forming tendencies. Value of the factor is an indication of its potency compared to chromium.

Using these factors, it is possible to set up a relationship to calculate the percentage available chromium by knowing the composition of the alloy. This relationship is as follows:

$$\% \text{ Cr (available)} = \% \text{ Cr} + 4\% \text{ Si} - 22\% \text{ C} - 0.5\% \text{ Mn} - 1.5\% \text{ Ni} - 30\% \text{ N}_2 \quad (\text{Equation 1})$$

**Table IV**  
**Comparison of Multiplying Factors**

Element	Newell (4) Fleischman	Post (5) Eberly	Thielemann (6) (Converted)	Campbell (7) Thomas	Schaeffler (3)	Post Eberly
Chromium	1	1	1	1	1	1
Molybdenum	2	1.5	4.2	1.5	1.8	...
Silicon	...	...	5.2	...	2.5	4
Nickel	1	1	1	...	1	1.5
Carbon	30	35	13.1	...	30	22
Manganese	0.5	0.5	0.67	...	0.5	0.5
Nitrogen	...	...	...	...	...	30
Type Alloy	18-8 type	14/25 Cr 7/21 Ni	Cr-Ni-Fe	20 Cr 2 Ni	Cr-Ni-Fe	16-30 Cr-Fe

Fig. 7 shows the available chromium calculated for each of the alloys in Table I using Equation 1. The separation of the alloys into ferrite and ferrite-austenite structures is possible on the basis of Equation 1 and is its main justification when used in conjunction with Fig. 7. Once again it is necessary to state that Equation 1 is based on trial-and-error methods and has been used to correlate the data shown in Table I. This equation can be used only for extrapolating purposes where the range of the element is relatively small. The estimated valid range of Equation 1 is:

Carbon	Manganese	Silicon	Nickel	Chromium	Nitrogen
0.09 to 0.29%	0.60 to 3%	0.25 to 1.50%	0.15 to 3%	16 to 30%	0.07 to 0.18%

Factors for the elements carbon, manganese, silicon, nickel, chromium and nitrogen as determined by the conditions discussed in this report are compared with factors for the same elements determined under different conditions. A comparison of these factors can be found in Table IV which includes factors determined under six different conditions and a wide range of chromium-nickel-iron and chromium-iron alloys. Generally speaking, it can be said that the values obtained in this investigation are in fair agreement with those discussed in other reports (3-7).

Tests were made to determine if the austenite would transform back to ferrite at elevated temperatures and, if so, the length of time for this transformation to take place. Samples of Alloy 2, Table I, were held at 2150 °F (1175 °C) for 5 minutes at heat to insure the presence of austenite. Specimens were then immediately transferred to another furnace held at 1700 °F (925 °C), and it was found that at least 3 minutes were necessary to permit the austenite to transform over to ferrite at that temperature. Percentages of ferrite remaining after being held various times at 1700 °F (925 °C) were as follows:



Time in Minutes	% Austenite in Ferrite
0	20
$\frac{1}{2}$	20
1	15
2	5
3	0

These data indicate that if austenite is present, at elevated temperatures, its presence can be removed by annealing at a lower temperature, say 1700 to 1400 °F (925 to 760 °C), for a given time. The alloys must be held longer at the lower temperatures for this treatment to be effective.

### SUMMARY

This study of high-chromium stainless steels, Type 430 and Type 446, within the analysis range of:

Carbon	Manganese	Silicon	Chromium	Nickel	Nitrogen
0.09 to 0.29	0.60 to 3	0.25 to 1.50	16 to 30	0.15 to 3	0.07 to 0.18

shows that austenite can be produced in these alloys in the temperature range of 1600 to 2350 °F (870 to 1290 °C). The occurrence of austenite depends both on temperature and composition, particularly such austenite-forming elements as carbon, manganese, nickel and nitrogen and such ferrite-forming elements as silicon and chromium.

The formula:

$$\% Cr_A = \% Cr + 4\% Si - 22\% C - \frac{1}{2}\% Mn - 1.5\% Ni - 30\% N_2$$

where  $\% Cr_A$  is the per cent of available chromium for producing ferrite, can be used to determine approximately at what temperature austenite will commence to form by reference to the following tabulation:

Temperature, °F	Minimum Available Chromium for No Austenite—%
1700	15.25
1800	16.70
1900	18.20
2000	20.00
2100	21.80
2200	23.00
2300	25.00

In the glass-to-metal sealing industry, the presence of austenite is detrimental to glass-to-metal seals made from these alloys, due to the change in expansion properties near room temperature after the glass has set. The change in expansion properties generally results in defective seals by breakage of the glass near the seal or such high stresses in the glass that the seals are brittle and fragile.

The presence of the austenite can be removed by annealing at lower temperatures than the sealing temperature, but in many applications this is impossible, due to the design of the glass-to-metal seal. Small metallic parts to be sealed to thin sections of glass generally have to be heated to a very high temperature to obtain a good seal, and are then permitted to cool to room temperature on their own account. If the composition is such that austenite is formed at the sealing temperature, the glass-to-metal seal would have to be held at a lower temperature to transform the austenite back to ferrite so that the alloy would have the expected match in expansion with the glass. Generally, this annealing is impracticable, due to the softening point of the glass and because automatic, high production, glass sealing machines usually do not have sufficient space for such annealing procedures. In the case of large objects, the annealing is possible, since the metal part itself has a high heat content and the part to be sealed can be held several minutes in an annealing chamber. An example of this is the large television tube which incorporates a metal conic section. For this particular application, the chromium content can be reduced, since the sealing between the glass and metal is done at a lower temperature, and at this temperature little if any austenite is produced. The annealing of these large objects immediately after the sealing operation also insures the transformation of austenite to ferrite before the glass becomes excessively brittle.

Small glass-to-metal seals such as fluorescent light tubes, radio tubes, and so forth, require a much higher temperature and therefore will require alloys having the higher chromium content, such as 28 to 30% chromium.

#### ACKNOWLEDGMENT

The generous cooperation of the staff of the Metallurgical and Chemical Laboratories of the Carpenter Steel Company in carrying out this investigation is gratefully acknowledged. The authors wish to thank J. H. Parker, Chairman of the Board, F. R. Palmer, President, and B. H. DeLong, Vice-President, of the Carpenter Steel Company, for permission to publish these results.

#### References

1. A. B. Kinzel and W. Crafts, "Alloys of Iron and Chromium", Engineering Foundation, McGraw-Hill Book Co., New York, 1937, p. 25.
2. Russell Franks, "Chromium Steels of High Nitrogen Content", TRANSACTIONS, American Society for Metals, Vol. 23, 1935, p. 968-994.
3. Anton L. Schaeffler, "Selection of Austenitic Electrodes for Welding Dissimilar Metals", *Welding Journal Research Supplement*, October 1947.

4. H. D. Newell and M. Fleischman, U. S. Patent No. 2,118,683.
5. C. B. Post and W. S. Eberly, "Stability of Austenite in Stainless Steels", *TRANSACTIONS, American Society for Metals*, Vol. 39, 1947, p. 868-890.
6. R. H. Thieleman, "Some Effects of Composition and Heat Treatment on the High-Temperature Rupture Properties of Ferrous Alloys", *Proceedings, American Society for Testing Materials*, Vol. 40, 1940, p. 798.
7. H. C. Campbell and R. D. Thomas, Jr., "The Effect of Alloying Elements on the Tensile Properties of 25-20 Weld Metal", *The Welding Journal*, Vol. 25 (11), *Research Supplement*, November 1946, p. 760-S to 768-S.

### DISCUSSION

**Written Discussion:** By A. E. Nehrenberg, supervisor, Research Laboratory, Crucible Steel Company of America, Harrison, N. J.

In their microstructural studies of high chromium stainless steels water-quenched from various temperatures, the authors have used a heat tinting procedure to distinguish between the austenite and ferrite. Their

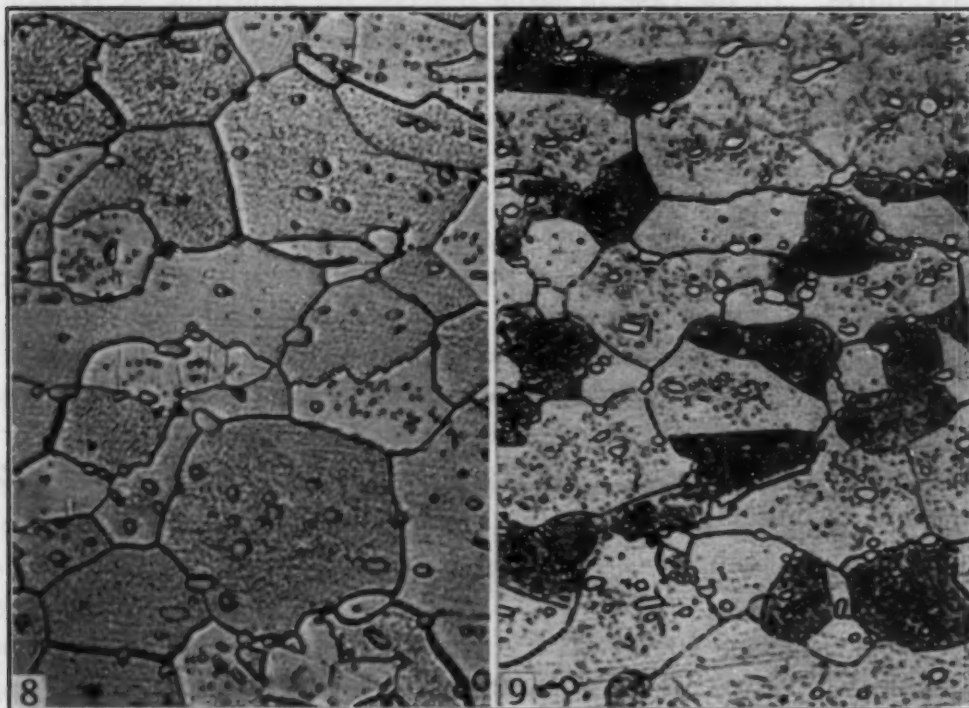


Fig. 8—Mixture of Austenite and Ferrite in Type 446 Stainless Heated 5 Minutes at 2000 °F (1095 °C) and Water-Quenched.  $\times 500$ .

Fig. 9—Mixture of Ferrite and a Dark-Etching Transformation Product of Austenite Produced by Reheating the Sample Shown in Fig. 8 at 1300 °F (705 °C) for  $\frac{1}{2}$  Hour.  $\times 500$ .

Fig. 1 indicates that this procedure provides good contrast between these phases.

In the laboratory with which the writer is associated, a different procedure has also been successfully used for the same purpose. Our method is based on the fact that the austenite which forms in Type 446 stainless has an  $M_s$  temperature below room temperature but transforms quite readily to a dark-etching high temperature transformation product if given an opportunity to do so. In our work, we quenched samples in water



from the temperature being investigated, and then reheated them at 1300 °F (705 °C) for ½ to 1 hour to permit the transformation to take place.

The microstructure of a sample of Type 446 stainless water-quenched from a temperature above that at which austenite forms in the steel in question is illustrated by Fig. 8. There is seen to be little contrast between the austenite and ferrite. Fig. 9 illustrates the effect of a ½-hour reheating at 1300 °F (705 °C). Dark-etching areas of the high temperature transformation product occupy regions which were initially austenite. If quantitative measurements are to be made, it is desirable to use a somewhat longer time than ½ hour, that is, 1 hour or so, to assure that all of the austenite present will have been transformed.

**Written Discussion:** By D. Niconoff, Metallurgical Laboratory, Republic Steel Corp., Canton, Ohio.

The correlation of the composition of high chromium ferritic steels with their propensity toward formation of austenite is highly interesting and timely in view of the rapidly increasing number of applications for this steel. Equally interesting is the reference to the effect of the coefficient of thermal expansion of these alloys upon their ability to form a satisfactory glass-to-metal seal.

The authors state that the expansion of high chromium steels matches the expansion of certain glasses, and give some representative coefficients for stainless Types 446 and 430 without, however, showing the corresponding coefficients for the glasses. It is the writer's impression that the latter values are usually below the coefficients for most of steels, particularly those consisting wholly or partially of austenite, and that the principal advantage of introducing high chromium steels for this application is due to the lowering of the expansion coefficient and making it change more uniformly with the temperature.

Comparison of the data reproduced in Table II for Alloy 2 containing 20.54% available chromium with the data for several heats of 430 type containing only 13 to 15% available chromium shows that the latter group possesses somewhat lower coefficients in spite of the fact that all the heats have measurable critical points and presumably contain some austenite. Can the authors offer an explanation for this apparent inconsistency?

In the writer's experience with similar steels of the modified 430 type he encountered occasionally some heats lying apparently on the boundary line of ferrite-ferrite and austenite structures shown in Fig. 7 which were found to possess a satisfactory coefficient of thermal expansion. On air cooling or water quenching from 2200 to 2100 °F (1205 to 1150 °C) their structure was ferritic with only a trace of austenite. But on interrupting the cooling for several minutes at lower temperatures prior to quenching it was found that the austenitic constituent gradually increased with decreasing temperature, reaching a concentration of about 5% at 1800 to 1700 °F (980 to 925 °C). It appeared as if under certain conditions the familiar gamma loop of the iron-chromium system became restricted and sagged downward to such an extent that it was intersected by the cooling curve at this temperature range. The austenite thus formed could be readily decomposed at temperatures below 1700 °F (925 °C) as stipulated by the authors.



The writer would like to know if similar phenomena were not encountered in this investigation. The data reproduced in Fig. 7 give no indication whether the austenite formed immediately above the curve in the low-available-chromium range was stable at temperatures above 2000 °F (1095 °C).

**Written Discussion:** By Arnold S. Rose, Engineering Department, Special Products Division, I-T-E Circuit Breaker Co., Philadelphia.

Messrs. Post and Eberly have capably presented a review of the effect of the various alloying elements on the formation of austenite in the 17 to 28% chromium-iron alloy used for glass sealing applications. However, their interpretation of the role of the austenite transformation in the glass sealing operation is not entirely in accord with that previously presented by this writer.<sup>3, 4</sup>

The authors correctly indicate by their data the increased coefficient of expansion which results when the structure of a 26% chromium-iron alloy is found to be partially austenitic as contrasted to a wholly ferritic structure. It is an error to assume, however, that the mere presence of austenite in the metal adjacent to the seal will cause glass failure. Since the increase in the expansion coefficient is directly proportional to the amount of austenite formed in the alloy, it is obvious that small amounts of austenite will have only a negligible effect on the expansion. In actual practice many thousands of metal cone kinescopes have been manufactured where the chromium-iron alloy has undergone the transformation to a partially austenitic structure. The limiting factor on the amount of austenite which may be tolerated is, of course, the resultant coefficient of expansion. The tubemaking industry has established a maximum value for this coefficient of  $6.4 \times 10^{-6}$  inch/inch/°F over the range 80 to 980 °F for the 28% chromium-iron alloy and this figure actually allows for the presence of a small amount of austenite in the steel.

The stability of the austenite which is formed during glass sealing is a most critical factor affecting the quality of the seal. In the Type 446 alloys, the austenite has been found to be stable to below room temperature so that the only detrimental effect upon the seal is the resultant increased mismatch between the expansivity of the glass and the metal. In Type 430 alloys, on the other hand, the austenite is not stable, and, during the cooling cycle following the sealing, a transformation to the alpha martensite phase occurs. This transformation is accompanied by a sudden expansion of the metal at a temperature below the setting point of the glass, which, contracting normally, is caused to crack away.

The data presented by the authors in Table III regarding the expansion properties and critical points of the Type 430 alloys give only an incomplete and somewhat misleading picture of the possibility of sealing glass to this analysis. The low expansion values cited are insignificant in view of the transformation which occurs after sealing. The 17% chromium alloys which have been stabilized to prevent any transformation through addition of suitable ferrite-promoting elements have become available only recently. Before the advent of these stabilized alloys it was

<sup>3</sup>A. S. Rose and J. C. Turnbull, "The Evaluation of Chromium-Iron Alloys for Metal Kinescope Cones", *RCA Review*, Vol. X, No. 4, December 1949.

<sup>4</sup>A. S. Rose, "Stainless Steel for Television", *METAL PROGRESS*, Vol. 57, June 1950, p. 761.

impossible to seal glass successfully to a 17% chromium-iron alloy. At present, however, the stabilized Type 430 alloys have completely supplanted the more expensive and difficult to fabricate Type 446 alloy for metal cone television tubes.

In the authors' summary the suggestion is put forth that holding at a temperature lower than the sealing temperature is a practical expedient to eliminate any austenite which may have formed. It should be pointed out that the technique of sealing glass to metal in the manufacture of the large metal cone kinescope is subject to the same critical factors that the authors acknowledge for small assemblies. In view of the increasing plasticity of the glass at temperatures over 950 °F (510 °C), it would be extremely difficult to maintain the shape of the glass face plate of the tube during the 3-minute period at 1700 °F (925 °C) which is required to permit the austenite to transform to ferrite.

#### **Authors' Reply**

A. E. Nehrenberg's suggestion for distinguishing the austenitic phase from the ferritic phase in Type 446 stainless bears comment. This procedure is somewhat more foolproof than the procedure as described in the paper. The heat-treating operation is generally done for a very short time so that little or none of the austenite converts into martensite.

Referring to D. Niconoff's question about the expansion properties as appearing in Tables II and III, we would like to point out that these expansion data represent tests conducted on two types of equipment. Data shown in Table II were obtained on a recording Sylvania dilatometer and can be considered accurate. The data appearing in Table III were obtained on a special homemade apparatus capable of determining expansion properties up to 2100 °F (1150 °C), and the information is not too reliable. Therefore, any discrepancy between Tables II and III should be taken very lightly. Data in Table III were intended primarily to show the presence of a critical point.

Mr. Niconoff is correct in stating that the expansion properties of stainless Type 430 are slightly higher than Type 446. In many applications, Type 430 would be suitable for glass-to-metal sealing, providing 100% ferritic phase would persist during the sealing operation.

Regarding the abnormality of the iron-chromium diagram, this phenomenon was not found, since tests were primarily designed to determine only the percentage of austenite present when quenched from the range of temperatures used during the investigation.

Referring to Arnold Rose's discussion, it is possible that some glass-to-metal sealing applications will permit a small amount of austenite. No doubt the making of metal cone kinescopes is in this category. Nevertheless, there are many other known applications where the presence of austenite is not tolerated for making glass-to-metal seals. Applications not tolerating the presence of austenite are those used in manufacturing electric light bulbs and radio tubes.

There also is an application using stainless Type 430 for a glass-to-metal sealing where the part is cooled very slowly to room temperature, thereby permitting the austenite phase to transform to ferrite.

# INFLUENCE OF AUSTENITIZING TIME AND TEMPERATURE ON AUSTENITE GRAIN SIZE OF STEEL

By O. O. MILLER

## *Abstract*

*This investigation furnishes data on influence of austenitizing time up to 5000 hours and of austenitizing temperature up to 2300 °F (1260 °C) on austenite grain size of representative carbon and low alloy steels differing in mode of deoxidation, alloy content and type of steel-making process used for their production. The results are discussed in relation to the general phenomena associated with grain growth in metals.*

A REVIEW of published work on austenite grain size of steel indicates that it is influenced by six factors: (a) austenitizing time, (b) austenitizing temperature, (c) presence of small inclusions, (d) heating rate, (e) prior microstructure and (f) special heat treatments. The present investigation furnishes new data on the first three factors, these being generally of more significance in heat treating than the others. Such information is needed because published data on influence of austenitizing time (1-4)<sup>1</sup> are meager, data on austenitizing temperature (2, 4-10) are, in general, limited to austenitizing periods of 2 hours, or less, and are not so quantitative as might be desired, especially at heat treating temperatures used prior to forging or hot rolling, and the data are incomplete on variables which control effectiveness of small, sometimes submicroscopic, inclusions (2, 5, 7-9, 11-17) such as alumina, aluminum nitride, zirconia, vanadium carbide, sulphides or tellurides.

The influence of heating rate (1, 4, 7, 10, 18-20) is, in general, small; it is on the order of one grain size number (ASTM scale) for very large differences in rate of heating of the types of steel in this investigation. The effect of prior microstructure (4, 15, 19, 21, 22) is small also, the difference in grain size being on the order of one number (ASTM scale) for wide variations in microstructure.

<sup>1</sup>The figures appearing in parentheses pertain to the references appended to this paper.

This paper was presented to the University of Pittsburgh in partial fulfillment of the requirements for the degree of Doctor of Philosophy. The investigation was carried out at the Research Laboratory, United States Steel Co., Kearny, N. J.

A paper presented before the Thirty-second Annual Convention of the Society, held in Chicago, October 21 to 27, 1950. The author, O. O. Miller, is associated with the Research Laboratory, United States Steel Co., Kearny, N. J. Manuscript received April 12, 1950.



The influence of special heat treatments (2, 4, 23) may be small or large in magnitude but none was used in this investigation; such treatments probably alter the size and distribution of the inclusions which retard grain growth.

#### STEELS INVESTIGATED AND EXPERIMENTAL PROCEDURE

Pertinent data on the steels investigated, which are of the "fully" deoxidized or "killed" type, are given in Table I. Bars of each steel were pretreated by austenitizing at 1650 or 1700 °F (900 or 925 °C) and cooling in air or in the furnace to minimize microstructural differences between specimens of the same steel. Specimens were cut from the pretreated bars so that the surface used for metallographic study would be parallel to the rolling direction and would represent either the entire range from center to surface of the ingot or the midportion.

The specimens were austenitized in sealed silica bulbs evacuated at room temperature to a pressure of not more than 0.004 atmosphere of air, except for a few which were austenitized in air when the combination of austenitizing time and temperature was known to be too mild to oxidize a significant portion of the deoxidizing elements, such as aluminum or zirconium, in the steel (9). Oxidation of these elements in the specimens that were sealed in silica was minimized by removing scale and rust completely from the specimens prior to sealing (9). To minimize significant transport of carbon from one specimen to another (24), only specimens with essentially identical carbon content were sealed in the same bulb. No precautions to prevent transport of other alloying elements were considered necessary.

The specimens were heated relatively rapidly by placing them in a furnace at austenitizing temperature. The austenitizing treatments covered a series of time intervals (0.1, 0.5, 2, 10, 50, 200, 1000 and 5000 hours) at a series of temperatures (1400, 1500, 1600, 1700, 1800, 1900, 2100 and 2300 °F). A *different* specimen was used for *each combination* of austenitizing time and temperature, the longer times being investigated only in the lower portion of the temperature range. At the end of the austenitizing period and after cooling to room temperature, all specimens were mounted in bakelite, ground to remove metal possibly not representative of the interior of the specimens, polished and etched to reveal the austenite grains. Steels 1, 2 and 13 were quenched in brine from the austenitizing temperature to form ferrite at the austenite grain boundaries and martensite elsewhere in these low carbon steels; etching was with



Table I  
Type and Chemical Composition of Steels Investigated

Steel	Type of Steel	Deoxidizer	C	Mn	Si	Ni	Cr	Mo	V	Al (%) <sup>*</sup>	Al <sub>2</sub> O <sub>3</sub>	Zr	ZrO <sub>2</sub>	N†
1	AISI C1008	Si	0.08	0.30	0.10	...	...	...	...	0.004	0.003	...	...	0.004
2	AISI C1006	Al	0.06	0.34	0.01	...	...	...	...	0.04	0.01	...	...	0.005
3	AISI C1020	Si	0.20	0.61	0.23	...	...	...	...	0.008	0.002	...	...	0.004
4	AISI C1020	Si+Al	0.20	0.53	0.24	...	...	...	...	0.032	0.008	...	...	0.003
5	0.15% C	C+Si+2.5 lb. Al/ton	0.15	0.47	0.23	...	...	...	...	0.032	0.009	...	...	0.015
6	AISI C1060	Si	0.60	0.89	0.13	...	...	...	...	0.006	0.001	...	...	0.004
7	AISI C1060	Si+0.5 lb. Al/ton	0.59	0.89	0.15	...	...	...	...	0.020	0.009	...	...	0.003
8	AISI C1060	Si+2.0 lb. Al/ton	0.59	0.89	0.15	...	...	...	...	0.10	0.010	...	...	0.004
9	0.88% C	Si	0.83	0.34	0.16	...	...	...	...	0.009	0.001	...	...	0.007
10	V	Si+Zr	0.83	0.33	0.32	...	...	...	0.24	0.012	0.001	0.03	0.01	0.003
11	Mo	Si	0.20	0.84	0.22	...	...	0.48	...	0.005	0.006	...	...	0.005
12	Mo	Si+Zr	0.20	0.73	0.23	...	...	...	...	0.004	0.004	0.04	0.03	0.004
13	Cr-Mo	Si+1.2 lb. Al/ton	0.10	0.34	0.12	...	2.26	0.56	...	0.027	0.008	...	...	0.015
14	Mn-Mo	Si+Zr	0.89	1.68	0.23	...	...	0.28	...	0.004	0.001	0.04	0.02	0.010
15	AISI 4815	Si+Al	0.16	0.52	0.27	3 36	...	0.19	...	0.016	0.006	...	...	0.011
16	NE 8339	Si+Al	0.37	1.46	0.23	0 19	0.13	0.26	...	0.030	0.007	...	...	0.007
17	AISI 8740	Si+Al	0.40	0.83	0.34	0 48	0.48	0.25	...	0.022	0.009	...	...	0.011

\*Check analyses of rolled material similar to that investigated.

Phosphorus and sulphur are less than 0.035%, except that phosphorus is 0.084% in Steel 5.

†Total nitrogen by fuming sulphuric acid method; nitrogen soluble in hydrochloric acid is not significantly different.

Note: Steel 5 is acid bessemer. Steels 13, 14, 15, 16 and 17 are basic electric. Others are basic open-hearth.

An umpire method, described by Lundell, Hoffman and Bright (30), was used for aluminum and alumina.

a 5% solution of ferric chloride (25). Steels 6, 7 and 8, C1060 type, were transformed isothermally at 1250 °F (675 °C) to form ferrite at the austenite grain boundaries and pearlite elsewhere (26); etchant was a solution of equal parts by volume of saturated Picral and 1% Nital. The other steels in Table I were quenched in brine to yield martensite, tempered for 15 minutes at 450 °F (230 °C) and etched in picric-hydrochloric acids (9, 26).

#### TREATMENT OF DATA

Grain size was measured by use of the ASTM standard scale for ferrous metals (27), though modified (6) by the use of —1 for 00, —2 for 000, etc. The percentage of each grain size present in a specimen was observed and recorded. The numerical grain size reported is a weighted average calculated from the percentage of each grain size (9). Such a weighted average is a satisfactory measure when grain sizes are fairly uniformly distributed about the average, as in specimens illustrated in Figs. 1a, 1b, and 1c; however, it does not indicate the two ranges of grain size present during the abrupt coarsening of a fine-grained steel such as is illustrated in Fig. 1d. It is necessary to emphasize that the weighted average has little, if any, more absolute accuracy than plus or minus 0.5 grain size number (ASTM scale); however, it is reported to 0.1 grain size number largely because differences (as opposed to absolute values) of approximately this order of magnitude can be detected between specimens in a series. In several instances the ASTM standard for nonferrous metals (28) is used, the data having been transposed from ferrous to nonferrous standard (29).

#### RESULTS AND DISCUSSION

The data indicate that austenite grain size increases with an increase in austenitizing time at any constant temperature in the austenitic region; this isothermal growth is illustrated by the photomicrographs in Fig. 1. For any constant austenitizing time, austenite grain size also increases with austenitizing temperature, except as noted below.

The influence of time and temperature on austenite grain size differs considerably between "coarse-grained"<sup>2</sup> and "fine-grained" steels. In a typical coarse-grained steel the grains gradually grow larger with an increase in austenitizing time or temperature, as

<sup>2</sup>Steels fall into two general patterns of austenite grain growth, known as "coarse grained" and "fine grained", usually set by the steelmaking practice. Both "coarse-grained" and "fine-grained" steels initially have relatively small austenite grains just above the  $A_3$  temperature. In Table I the "coarse-grained" steels are those deoxidized with silicon, or principally with silicon, whereas the "fine-grained" steels are those deoxidized finally with aluminum or zirconium, with or without prior deoxidation by silicon.

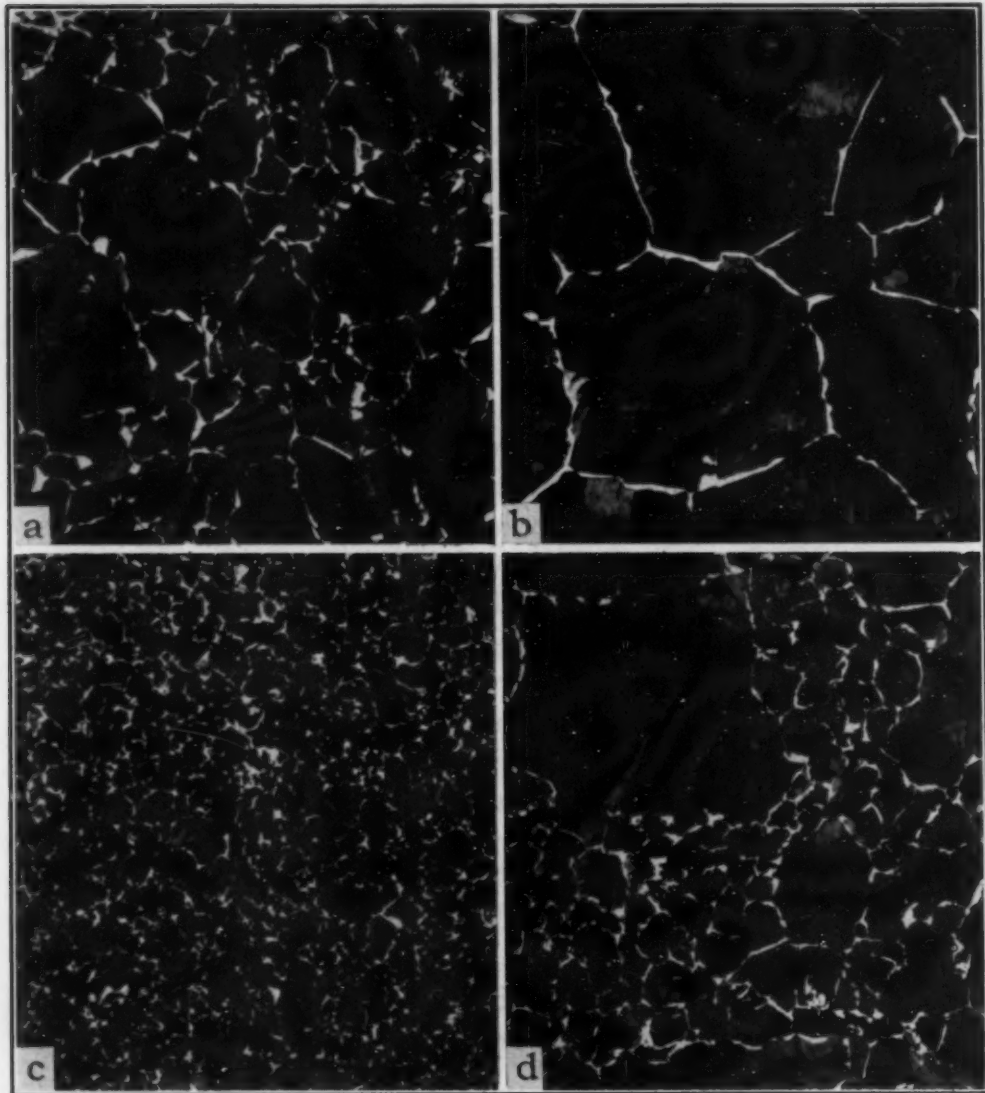


Fig. 1—Influence of Time at Austenitizing Temperature of 1500 °F on Austenite Grain Size. Fig. 1a and 1c, 0.5 hour; Fig. 1b and 1d, 5000 hours. a and b—Coarse-grained Steel 6. c and d—Fine-grained Steel 8. Picral-nital etch.  $\times 100$ .

illustrated in Fig. 2. In a typical fine-grained steel the pattern of austenite grain growth is more complex, with grain size increasing always with time but not always with temperature, as illustrated in Fig. 3. This complex pattern of growth may be described as follows: (a) at low austenitizing temperatures growth proceeds very slowly; (b) at somewhat higher temperatures, such as 1700 to 1800 °F (925 to 980 °C), a few grains grow very rapidly to a huge size, thus producing a mixture of small and very large grains, and after longer austenitizing only very large grains remain; (c) in the neighborhood of 1900 °F (1040 °C) more grains grow but this appears to be associated with a lessening of the average rate of growth;

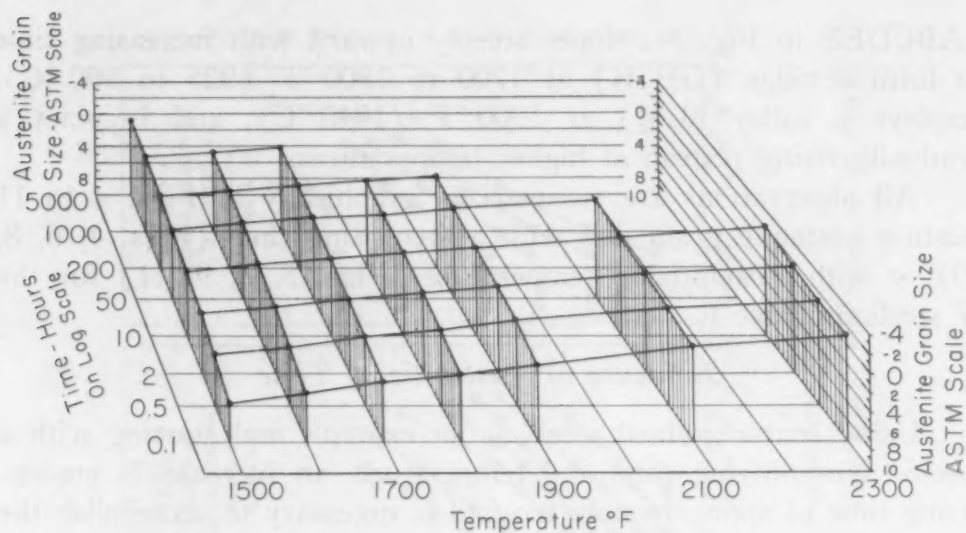


Fig. 2—Influence of Austenitizing Time and Temperature on Austenite Grain Size of a Coarse-Grained Steel Deoxidized With Silicon, Steel 6.

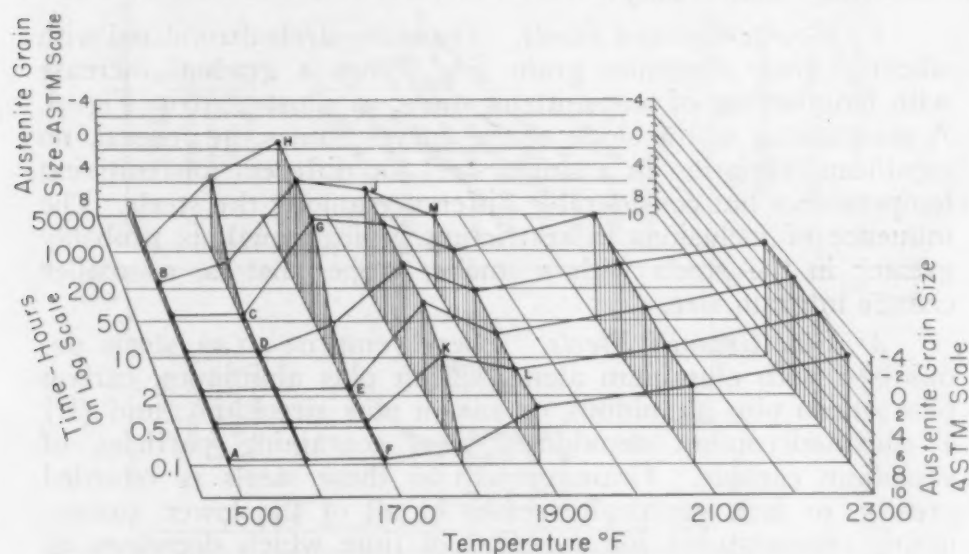


Fig. 3—Influence of Austenitizing Time and Temperature on Austenite Grain Size of a Fine-Grained Steel Deoxidized With Silicon Plus Aluminum, Steel 17.

consequently, both maximum and average size are actually smaller than at 1700 or 1800 °F (925 to 980 °C); and (d) at 2100 and 2300 °F (1150 and 1260 °C) the grains grow very rapidly so that both maximum and average size are larger than at any lower temperature for the same austenitizing period. Thus the surface or "roof" of the chart representing average grain size in Fig. 3 is low and nearly flat around 1500 to 1700 °F (815 to 925 °C)



(ABCDEF in Fig. 3), slopes steeply upward with increasing time to form a ridge (GHJK) at 1700 to 1800 °F (925 to 980 °C), displays a valley (LM) at 1900 °F (1040 °C), and becomes a gradually rising plateau at higher temperatures.

All observations are summarized graphically in Figs. 4 to 11 relating austenite grain size with austenitizing time (Figs. 4, 6, 8, 10) or with austenitizing temperature (Figs. 5, 7, 9, 11) for the 17 steels in Table I.

### *Influence of Austenitizing Time*

Using coarse-grained steels as an example and starting with a specific austenitizing time and temperature, an increase in austenitizing time of approximately ten-fold is necessary to accomplish the same grain growth as an increase in temperature of 100 °F.

The coarse- and fine-grained steels are strikingly different and are described individually:

1. *Coarse-Grained Steels.* These are steels deoxidized with silicon;<sup>3</sup> their austenite grain size shows a gradual increase with lengthening of austenitizing time, as illustrated in Fig. 4. A comparison of the slope of the curves shows, in general, no significant variation in a single steel for different austenitizing temperatures but considerable difference among the steels. The influence of inclusions in restricting grain growth is probably greater in the steels with a smaller slope, that is, a smaller change in grain size.

2. *Fine-Grained Steels.* These comprise: (a) steels deoxidized with aluminum alone, silicon plus aluminum, carbon plus silicon plus aluminum, or silicon plus zirconium; and (b) a silicon-zirconium deoxidized steel containing particles of vanadium carbide. Grain growth in these steels is retarded greatly, in fact, practically ceases at all of the lower austenitizing temperatures for a period of time which decreases as austenitizing temperature is increased, as shown in Figs. 6, 8 and 10.

These results indicate that austenite grains grow larger at any temperature at which austenite is the stable phase, though the rate of growth may be very slow just above the  $A_3$  temperature. The data also show that isothermal austenite grain growth continues at 1500 °F (815 °C) for as long as 5000 hours, the longest time investigated, which suggests that such growth may continue indefinitely.

### *Influence of Austenitizing Temperature*

The data in Figs. 4, 6, 8 and 10 have been replotted in Figs.

<sup>3</sup>These steels contain 0.004 to 0.009% metallic aluminum which is too little to produce a fine-grained steel.

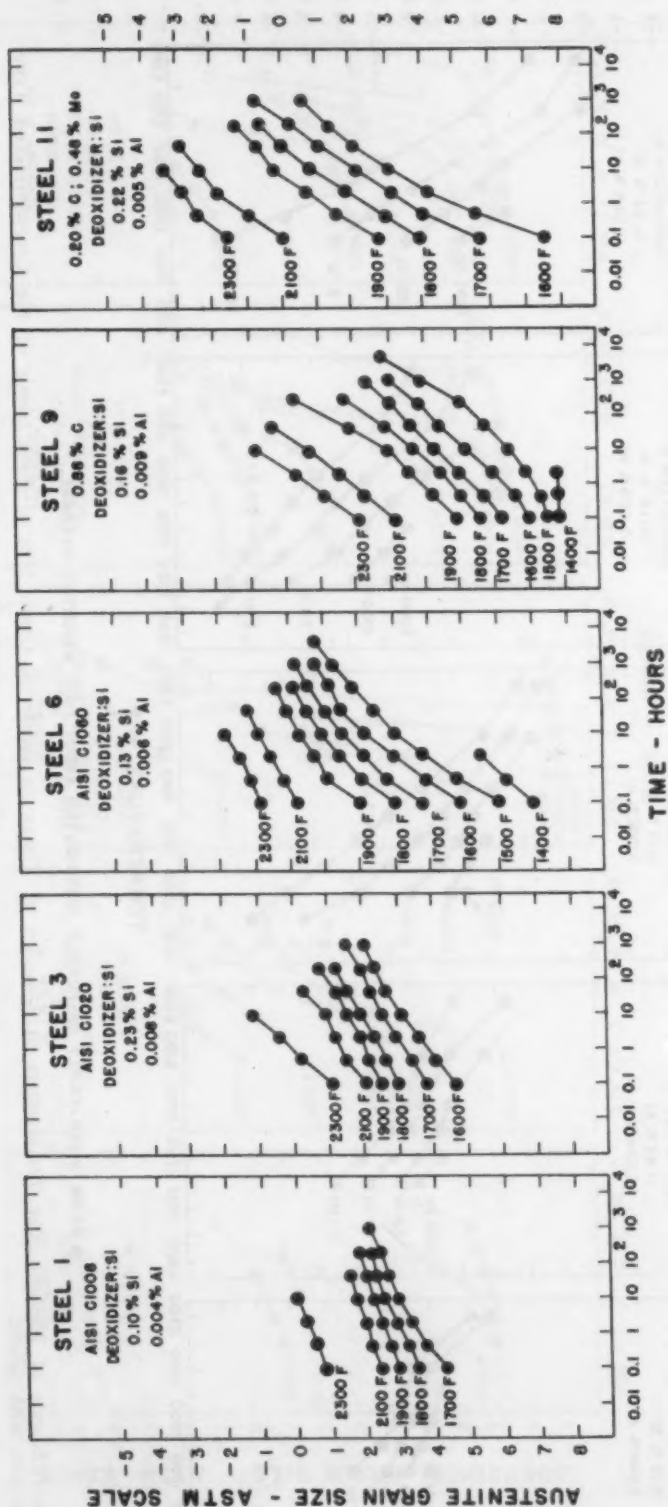
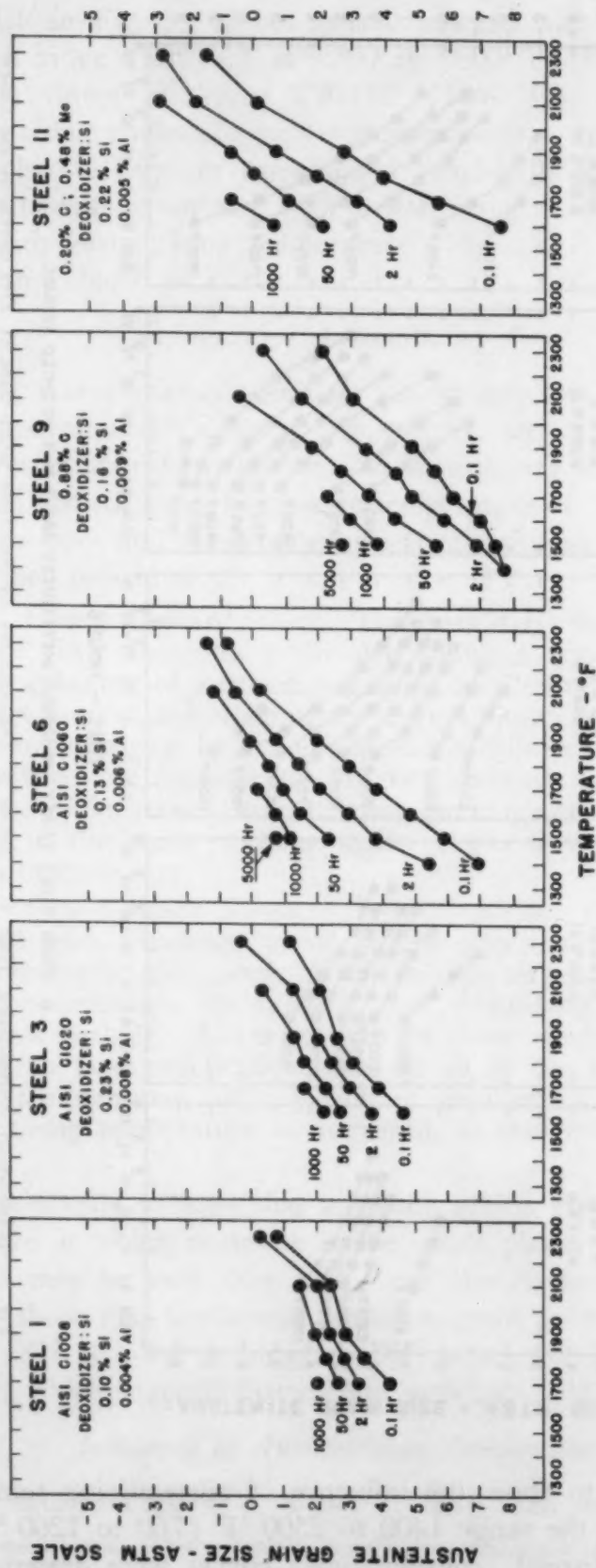


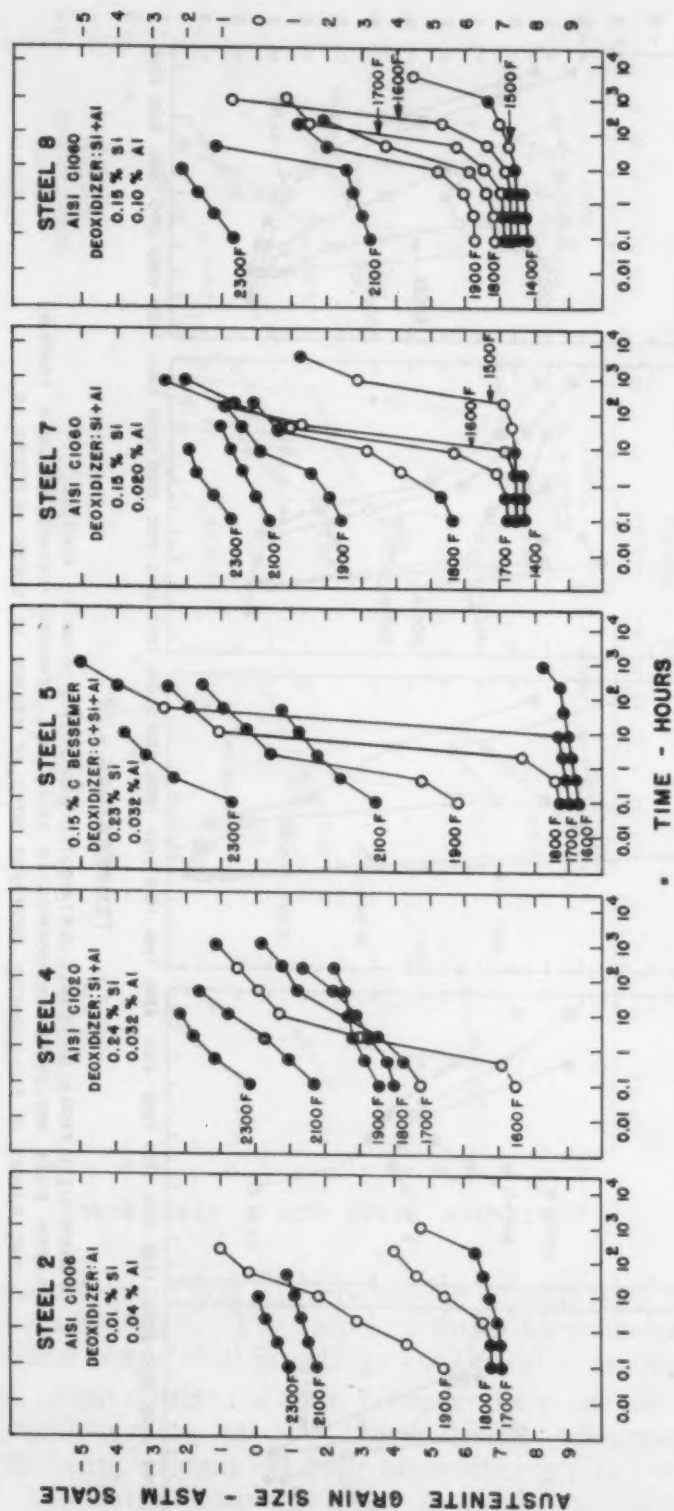
Fig. 4—Influence of Austenitizing Time at a Series of Temperatures on Austenite Grain Size of Five Steels of the Coarse-Grained Type. Deoxidation was with silicon.

5, 7, 9 and 11 to show the influence of austenitizing temperature on grain size in the range 1400 to 2300 °F (760 to 1260 °C); not all of these isochronal (constant-time) curves were drawn, because



● GRAIN SIZES FAIRLY UNIFORMLY DISTRIBUTED ABOUT THIS WEIGHTED AVERAGE.

Fig. 5—Influence of Austenitizing Temperature at a Series of Times on Austenite Grain Size of Five Steels of the Coarse-Grained Type. Deoxidation was with silicon.



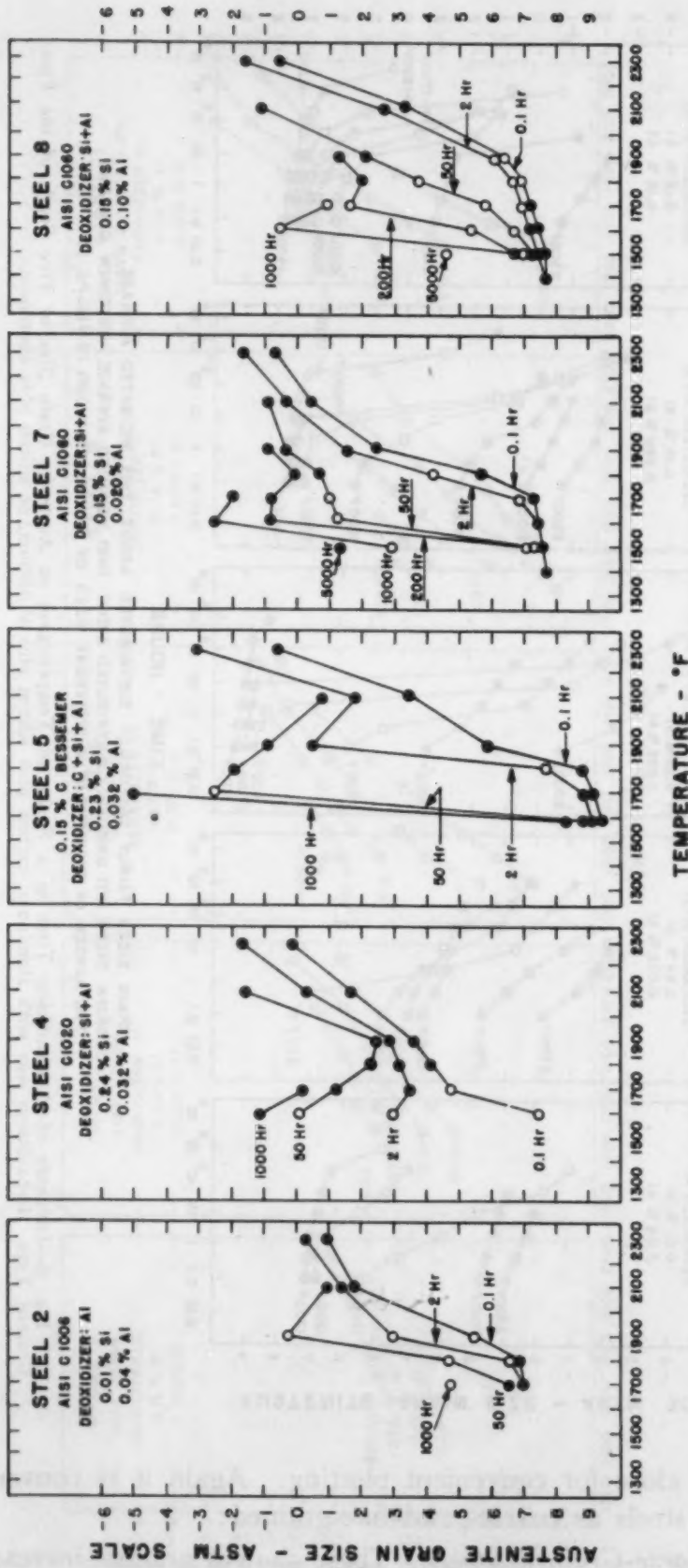
● GRAIN SIZES FAIRLY UNIFORMLY DISTRIBUTED ABOUT THIS WEIGHTED AVERAGE.  
○ GRAIN SIZES NOT UNIFORMLY DISTRIBUTED ABOUT THIS WEIGHTED AVERAGE; SPECIMEN CONTAINS TWO RANGES OF SIGNIFICANTLY DIFFERENT SIZES OF GRAINS, AS SHOWN IN FIGURE 1D.

Fig. 6—Influence of Austenitizing Time at a Series of Temperatures on Austenite Grain Size of Five Steels of the Fine-Grained Type. Deoxidation was with aluminum, carbon plus silicon plus aluminum, or silicon plus aluminum.

some are too close for convenient plotting. Again it is convenient to group the steels as coarse- and fine-grained:

1. *Coarse-Grained Steels.* These show a gradual increase





● GRAIN SIZES FAIRLY UNIFORMLY DISTRIBUTED ABOUT THIS WEIGHTED AVERAGE.  
○ GRAIN SIZES NOT UNIFORMLY DISTRIBUTED ABOUT THIS WEIGHTED AVERAGE; SPECIMEN CONTAINS TWO RANGES OF SIGNIFICANTLY DIFFERENT SIZES OF GRAINS, AS SHOWN IN FIGURE 1D.

Fig. 7—Influence of Austenitizing Temperature at a Series of Times on Austenite Grain Size of Five Steels of the Fine-Grained Type. Deoxidation was with aluminum, carbon plus silicon plus aluminum, or silicon plus aluminum.

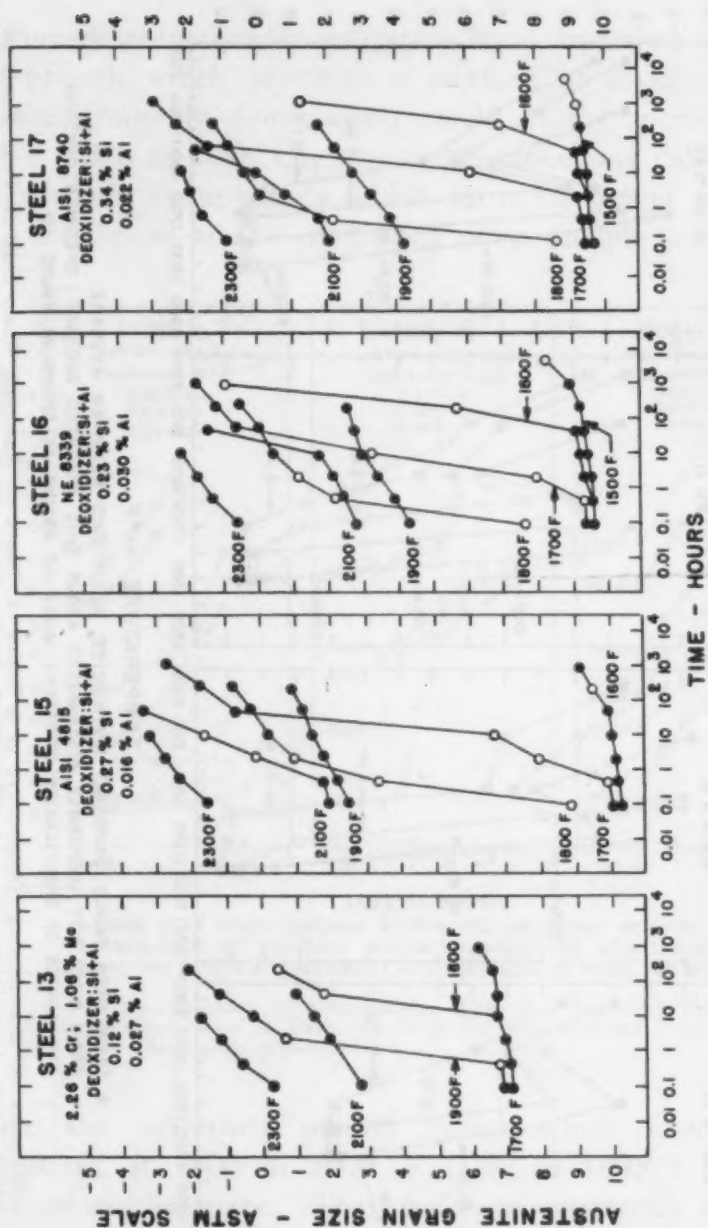
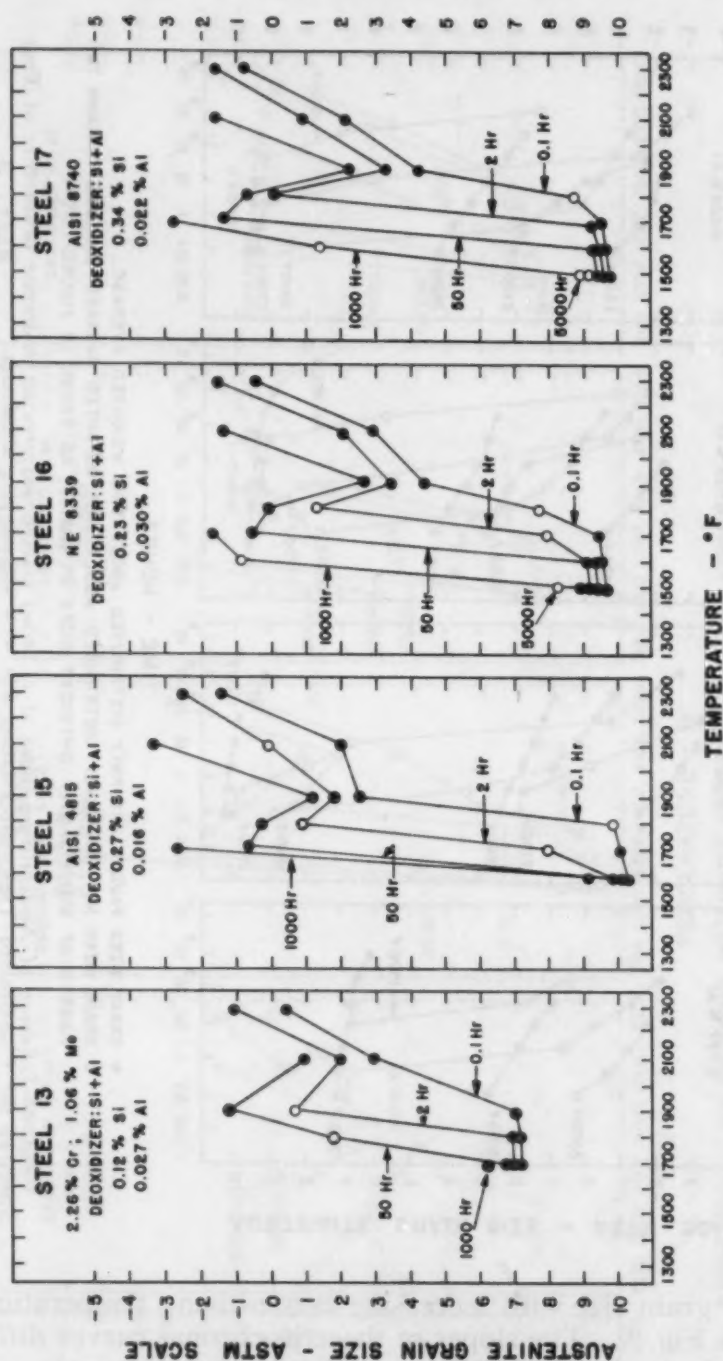


Fig. 8—Influence of Austenitizing Time at a Series of Temperatures on Austenite Grain Size of Four Steels of the Fine-Grained Type. Deoxidation was with silicon plus aluminum.

in austenite grain size with increasing austenitizing temperature, as shown in Fig. 5. The slopes of these isochronal curves differ little for a single steel but differ considerably among steels.

**2. Fine-Grained Steels.** These show in varying degree: (a) small grains at low austenitizing temperatures, some growth being evident on long austenitizing; (b) a mixture of small and large grains with a marked tendency for a few grains to absorb all of the others, especially after long austenitizing periods, thereby producing uniformly large grains and a peak in the coarsening curve in the vicinity of 1600, 1700 or 1800 °F (870, 925 or 980 °C), the exact temperature depending on deoxidation and pretreatment; (c) smaller grains



● GRAIN SIZES FAIRLY UNIFORMLY DISTRIBUTED ABOUT THIS WEIGHTED AVERAGE.  
 ○ GRAIN SIZES NOT UNIFORMLY DISTRIBUTED ABOUT THIS WEIGHTED AVERAGE; SPECIMEN CONTAINS TWO RANGES OF SIGNIFICANTLY DIFFERENT SIZES OF GRAINS, AS SHOWN IN FIGURE 10.

Fig. 9—Influence of Austenitizing Temperature at a Series of Times on Austenite Grain Size of Four Steels of the Fine-Grained Type. Deoxidation was with silicon plus aluminum.

in the neighborhood of 1800, 1900 or 2000 °F (980, 1040, 1095 °C), thus producing a recession in the coarsening curve; and (d) a return to larger grains at higher austenitizing temperatures. The difference in grain size between the 1600 to 1800 °F (870 to 980 °C) maximum and the 1800 to 2000 °F (980 to 1095 °C) minimum in the coarsening curve varies between steels and is pronounced for final deoxidation with aluminum, Figs. 7 and 9, whereas it is small, or was not detected, with zirconium, Fig. 11.

Though numerous investigators have discussed the exaggerated grain growth which produces a mixture of small and very large austenite grains in fine-grained steels in the vicinity of 1600 to 1800 °F (870 to 980 °C), apparently none has called attention to the uniformly large grains which form on longer austenitizing to give a maximum on the coarsening curve in this temperature range

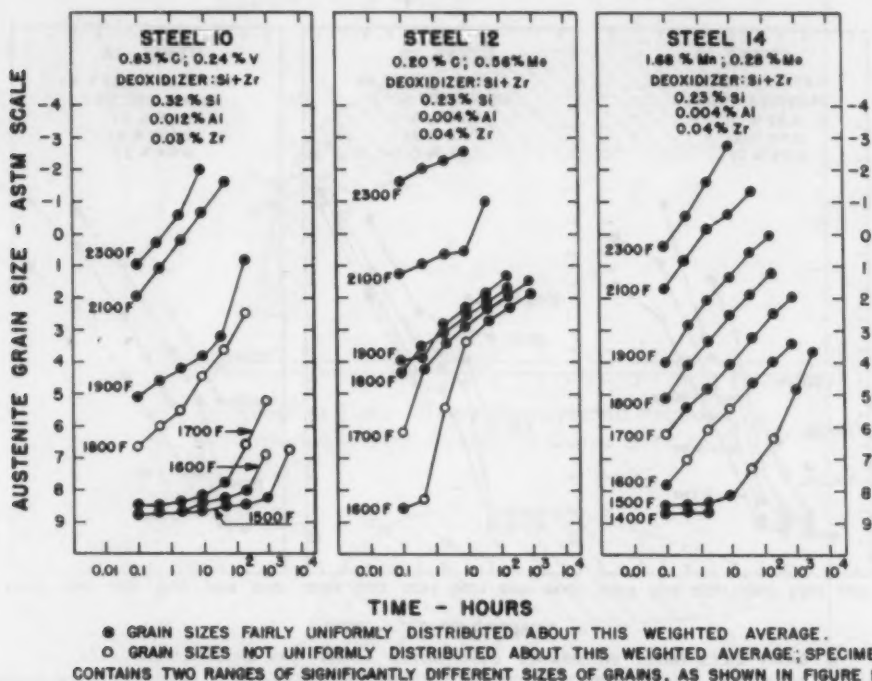


Fig. 10—Influence of Austenitizing Time at a Series of Temperatures on Austenite Grain Size of Three Steels of the Fine-Grained Type. Deoxidation was with silicon plus zirconium.

and to the uniformly smaller grains which form in specimens austenitized at 1800 to 2000 °F (980 to 1095 °C) to produce a minimum on the curve. The maximum apparently results from the growth of a few grains to relatively enormous size by absorption of the small ones; this behavior is probably associated with the beginning of breakdown in effectiveness of small inclusions or particles in retarding grain growth, and is an example of the phenomenon of germination (31). At a somewhat higher temperature more grains grow simultaneously to produce a smaller grain size and a minimum in the curve. At still higher austenitizing temperatures, very large grains are produced again, reflecting the normal influence of a higher temperature.

#### *Influence of Deoxidation Practice and Inclusions*

It is well known that the effectiveness of an aluminum addition



in retarding austenite grain growth is associated with the amount of acid-soluble aluminum in the finished steel; presumably the effectiveness of small inclusions of aluminum oxide or nitride in retarding grain growth is controlled by the amount of acid-soluble aluminum. Steels 7 and 8 in Figs. 6 and 7 show that the higher the aluminum, the greater the resistance to grain growth; however, there is

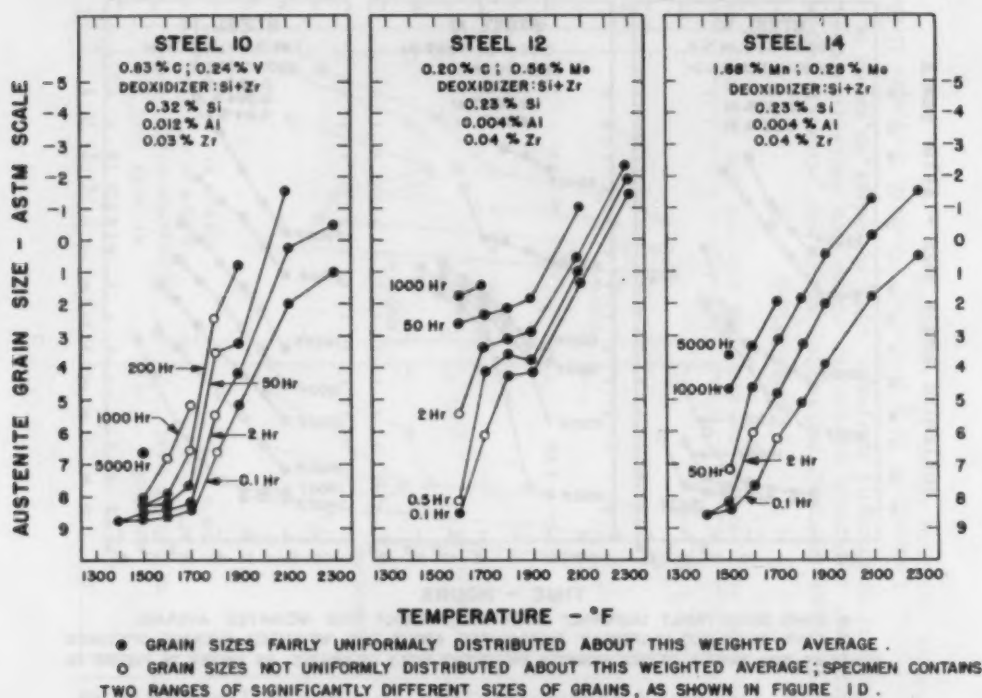


Fig. 11—Influence of Austenitizing Temperature at a Series of Times on Austenite Grain Size of Three Steels of the Fine-Grained Type. Deoxidation was with silicon plus zirconium.

probably an optimum amount of aluminum above which resistance to grain growth becomes less with increase in aluminum. This optimum amount is not accurately known and has been observed (13, 32, 33) to vary greatly among steels.

The data in Fig. 12 relate aluminum content to coarsening temperature for a 2-hour austenitizing period and to time required for coarsening at 1700 °F (925 °C). The latter relation is not so well known as the former. These results support the earlier observation that in the range of low aluminum content, the higher the aluminum, the greater the resistance to coarsening, and suggest that the optimum percentage of aluminum may be little, if any, greater than 0.04%. The curves in Fig. 12 are broken between 0.04 and 0.1% aluminum because of lack of data between these amounts and uncertainty as to whether there is a maximum in this

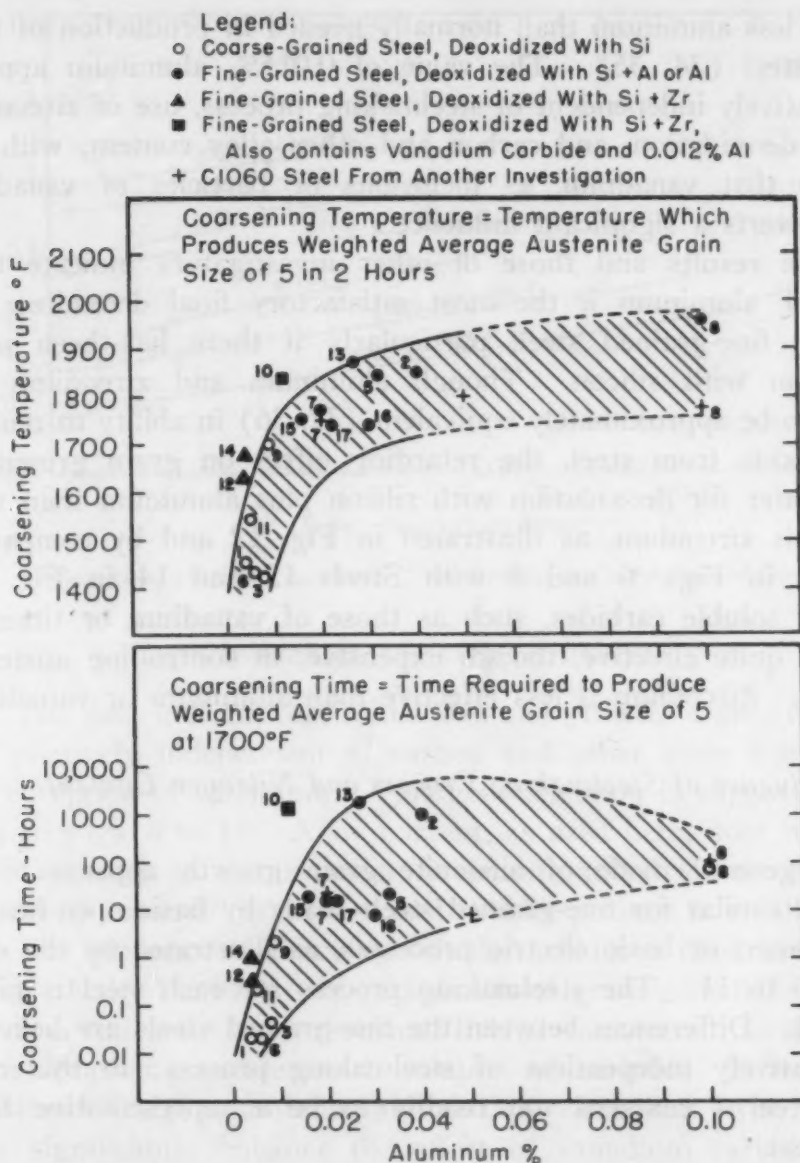


Fig. 12—Relation Between Austenite Grain Coarsening and Metallic Aluminum Remaining in Steel After Deoxidation. Note 1. Steels are indicated by numbers adjacent to plotted points. Note 2. Basic open-hearth steels: 1, 2, 3, 6, 7, 8, 9, 10, 11 and 12. Acid bessemer steel: 5. Basic electric steels: 13, 14, 15, 16 and 17. Note 3. Order of increasing carbon in carbon steels: 2, 1, 5, 3, 7, 8, 6, 9. Order of increasing alloy content in low-alloy steels: 10, 11, 12, 14, 16, 17, 13, 15. Note 4. Coarsening temperatures for Steels 1, 3, and 11 and coarsening times for Steels 1, 3, 6, and 13 were obtained by short extrapolations.

range. Further work is needed to determine the optimum percentage of aluminum for greatest resistance to austenite grain growth in various types of steel.

Of the steels represented in Fig. 12, those containing less than 0.015% aluminum are of the coarse-grained type, whereas those containing more are of the fine-grained type; however, this is

probably less aluminum than normally needed in production of fine-grained steel (34, 35). The value of 0.015% aluminum appears to be relatively independent of steelmaking process, use of zirconium for final deoxidation, and carbon and other alloy content, with the exception that vanadium, as inclusions or particles of vanadium carbide, exerts a significant influence.

These results and those of other investigators indicate that, in general, aluminum is the most satisfactory final deoxidizer for producing fine-grained steel, particularly if there has been prior deoxidation with silicon. Though aluminum and zirconium are believed to be approximately equivalent (32, 36) in ability to remove ferrous oxide from steel, the retarding effect on grain growth is much greater for deoxidation with silicon plus aluminum than with silicon plus zirconium, as illustrated in Fig. 12 and by comparing the steels in Figs. 6 and 8 with Steels 12 and 14 in Fig. 10. Difficultly soluble carbides, such as those of vanadium or titanium (33), are quite effective, though expensive, in controlling austenite grain size. Zirconium is less effective than aluminum or vanadium.

#### *Influence of Steelmaking Process and Nitrogen Content*

The general mode of austenite grain growth appears to be essentially similar for fine-grained steels made by basic open-hearth, acid bessemer, or basic electric processes, as illustrated by the data in Figs. 6 to 11. The steelmaking process for each steel is given in Table I. Differences between the fine-grained steels are believed to be relatively independent of steelmaking process; in this connection Steel 4 coarsens too readily to be a representative fine-grained heat.

The hypothesis has frequently been advanced that nitride, not oxide, is the effective agent in retarding austenite grain growth in steels whose final deoxidation was with such elements as aluminum or zirconium. The data give no indication that resistance to austenite grain growth increases with increase in nitrogen; however, resistance does increase with increase in the *product* of the percentages of aluminum and nitrogen, which suggests, but does not prove, that nitrogen may enhance the effect of aluminum or act in the form of small particles of aluminum nitride. Though further work is needed, it seems possible that aluminum nitride may retard grain growth and, on going into solution, permit abrupt coarsening. Such a mechanism was observed (37) in aluminum-manganese alloys when an intermetallic compound went into solid solution.

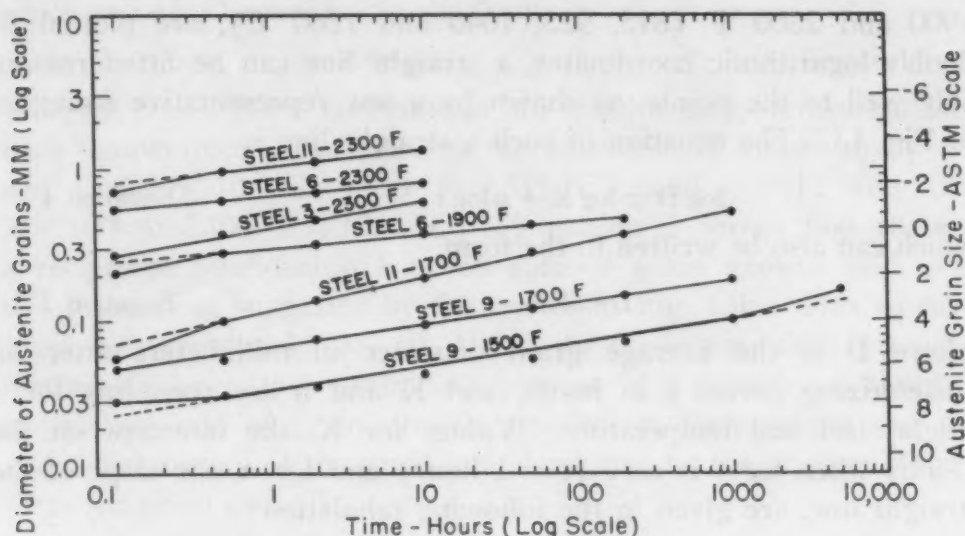


Fig. 13—Isothermal Austenite Grain Growth in Coarse-Grained Steels.

### *Influence of Alloying Elements*

The data indicate that initial size and growth of austenite grains are relatively independent of carbon and other alloy content, with the exception of vanadium. This generalization is supported by the data in Figs. 4 to 11. Alloy content, as used here, does not include elements, such as aluminum or zirconium, added for deoxidation or control of austenite grain size and usually present in small amounts.

The influence of difficultly soluble carbides is illustrated in Figs. 10 and 11 by the extensive retardation of grain growth in Steel 10, which contains 0.83% carbon and 0.24% vanadium. Disappearance of retardation coincides with solution of carbide. This steel also contains 0.012% aluminum and 0.03% zirconium, which together may significantly enhance the effect of vanadium carbide. Easily soluble carbides, if present, can also restrain grain growth. An example occurs in Steel 9, a coarse-grained carbon steel containing 0.88% carbon, which has a slightly retarded grain growth during short austenitizing periods at 1400 and 1500 °F (760 and 815 °C), Fig. 4, when easily soluble carbides are present. In Steel 9 carbide is a stable phase at 1400 °F (760 °C) but not at 1500 °F (815 °C) at which solution is complete in 2 hours though not in 30 minutes.

### FUNDAMENTAL ANALYSIS OF DATA

#### *Equations for Isothermal Austenite Grain Growth*

When austenitizing time and average grain diameter of the five coarse-grained steels at four austenitizing temperatures, 1500, 1700,



1900 and 2300 °F (815, 925, 1040 and 1260 °C), are plotted on double logarithmic coordinates, a straight line can be fitted reasonably well to the points, as shown by a few representative examples in Fig. 13. The equation of such a straight line is

$$\log D = \log K + n \log t \quad \text{Equation 1}$$

which can also be written in the form

$$D = Kt^n \quad \text{Equation 2}$$

where  $D$  is the average grain diameter in millimeters after an austenitizing period  $t$  in hours, and  $K$  and  $n$  are constants for a single steel and temperature. Values for  $K$ , the intercept on the  $D$ -axis when  $\log t$  is zero ( $t = 1$  hour) and for  $n$ , the slope of the straight line, are given in the following tabulation:

Austenitizing Temperature (°F)	Steel 1		Steel 3		Steel 6		Steel 9		Steel 11	
	K	n	K	n	K	n	K	n	K	n
1500	—	—	—	—	0.10	0.13	0.03	0.16	—	—
1700	0.12	0.08	0.14	0.08	0.19	0.10	0.07	0.15	0.12	0.22
1900	0.17	0.05	0.20	0.09	0.30	0.09	0.11	0.19	0.29	0.15
2300	0.36	0.06	0.40	0.17	0.66	0.09	0.33	0.23	1.00	0.11

This tabulation shows no evidence of a consistent relationship between  $n$  and austenitizing temperature. The dependence of rate of grain growth on austenite grain size present (discussed in next section), as well as on temperature, excludes the probability of finding such a relationship. These results on isothermal growth, and those reported for similar studies of aluminum (38) and brass (39), disprove the generally accepted belief that metals reach a stable grain size characteristic of the annealing or austenitizing temperature after only a few hours at temperature.

#### *Influence of Austenite Grain Size Present on Rate of Grain Growth*

When grain size is plotted directly against time, as in Fig. 14a, a coarse-grained steel gives a family of curves whose slope at any point is the rate of grain growth. This rate,  $R$ , may also be obtained from the relation

$$R = \frac{dD}{dt} = Knt^{n-1} \quad \text{Equation 3}$$

which results from differentiation of Equation 2, above. When  $R$  and average grain diameter,  $D$ , are plotted on double logarithmic coordinates, a straight line can be fitted reasonably well to the points for each austenitizing temperature. Such lines (not illustrated) have an equation of the type

$$\log R = \log C - p \log D \quad \text{Equation 4}$$

which can also be written in the form

$$RD^p = C$$

Equation 5

in which  $p$  and  $C$  are constants at any specific temperature but vary with temperature. For Steel 6 the approximate values are  $p = 6$  and  $C = 1 \times 10^{-8}$  at  $1500^\circ\text{F}$  ( $815^\circ\text{C}$ ), and  $p = 12$  and  $C = 3 \times 10^{-4}$  at  $2300^\circ\text{F}$  ( $1260^\circ\text{C}$ ). Equation 5 shows that there is a reciprocal relationship between rate of grain growth and grain size present, as suggested by the curves in Fig. 14b. This equation supports recent work (38, 40, 41) in the nonferrous field, providing further evidence that grain size present is a significant factor in controlling rate of grain growth at constant temperature and that interfacial energy of the grain boundary may be the primary driving force for grain growth.

#### *Influence of Austenitizing Temperature on Rate of Grain Growth and Activation Energy for Grain Growth*

The influence of temperature on rate of austenite grain growth is indicated in Fig. 14a for typical steels. In Steel 6, a coarse-grained type, the rate increases gradually with increase in austenitizing temperature. In Steel 17 the influence of austenitizing temperature is irregular, coinciding with the retardation of grain growth and its breakdown in this fine-grained steel, as illustrated also in Figs. 3, 8 and 9.

The dependence of rate of grain growth on temperature is illustrated further in Fig. 15, which shows the austenitizing time required to obtain an average austenite grain size of 2, on ASTM scale, for five coarse-grained steels in relation to the reciprocal of absolute temperature.<sup>4</sup> The points for each steel fall quite close to a straight line, those for Steel 3 showing more scatter than the others. These straight lines suggest some inner consistency in the data and form the basis for estimating that the activation energy (42) associated with isothermal austenite grain growth in these five coarse-grained steels varies from 90 to 113 kilocalories per gram atom. This range can be compared with a value of 61.8, recently reported (39) to be associated with isothermal grain growth in 70-30 brass. Too little is known about the mechanism of austenite grain growth to assess the significance of these values for activation energy.

#### *Austenite Grain Shape and Growth*

No evidence was found to support Whiteley's observations (4)

<sup>4</sup>The reciprocal of the time in Fig. 15 may be used as a convenient measure of relative rate of grain growth (42).

Legend for a:

- Grain Size Fairly Uniformly Distributed About This Weighted Average
- Grain Size Not Uniformly Distributed About This Weighted Average; Specimen Contains Two Ranges of Significantly Different Sizes of Grains, as Shown in Fig. 1 d

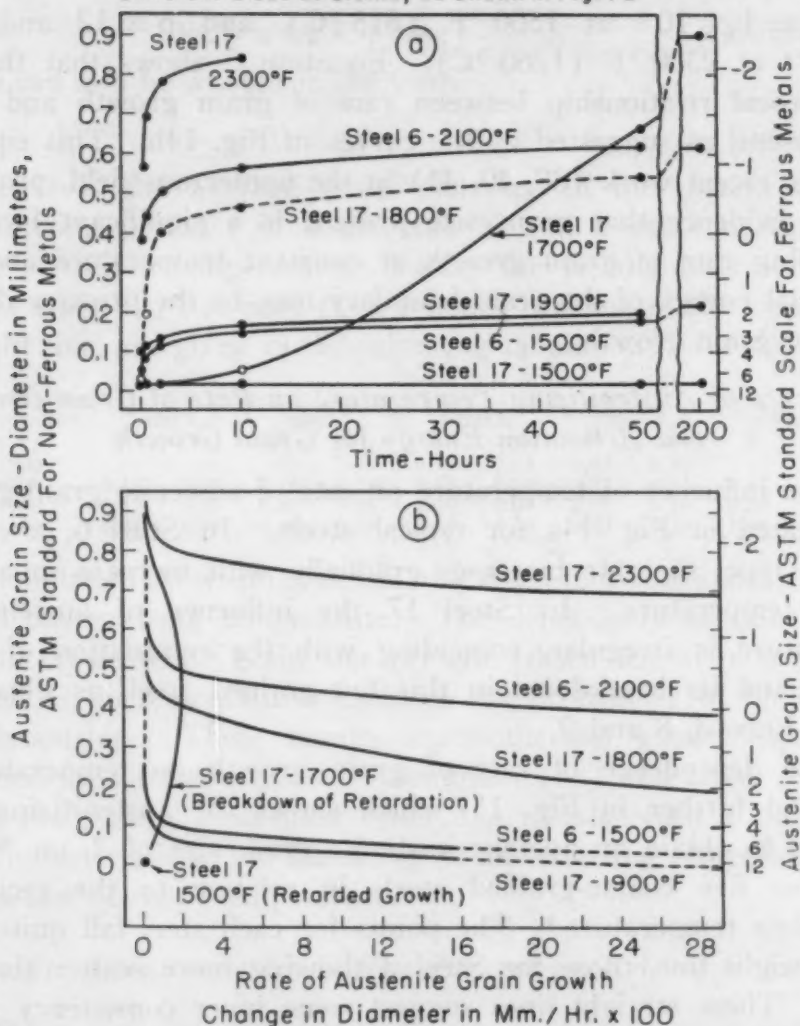


Fig. 14—Influence of Grain Size and Austenitizing Temperature on Rate of Grain Growth in Typical Steels. Steel 6: Coarse-grained type. Steel 17: Fine-grained type. a—Influence of austenitizing time on grain size; the slope at any point on one of these curves is the instantaneous rate of grain growth. b—Influence of grain size on average rate of grain growth; rate is slope of corresponding curve in a.

that grains reach a virtually stable size in isothermal growth, but his conclusion that grain growth is accompanied by a gradual straightening of grain boundaries to give a more uniform network is confirmed, as shown by Figs. 16a and 16b. Prior to the recent work of Beck, Kremer, Demer and Holzworth (38), it was generally accepted that a relatively short treatment yields a stable grain size determined by the temperature.

Several years ago Harker and Parker (43) proposed that grain shape, not grain size, determines the ability of grains to grow. The present investigation indicates that, as they predicted, grain shape approaches that of a geometric solid<sup>5</sup> with face-junction angles of 120 degrees; however, isothermal grain growth in austenite con-

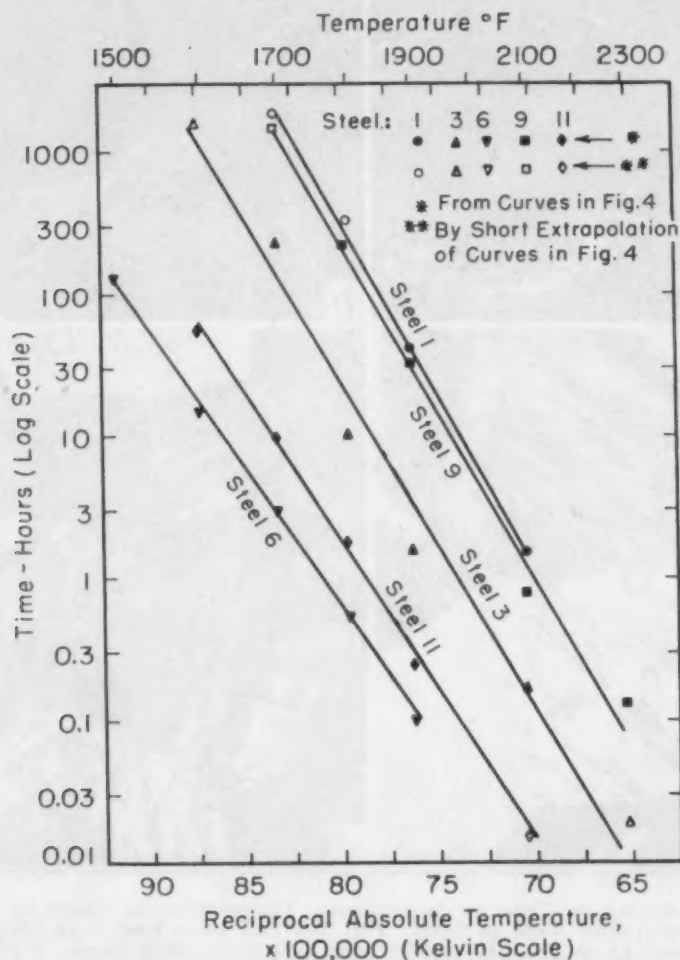


Fig. 15—Austenitizing Time Required to Obtain an Average Austenite Grain Size of 2 on ASTM Scale in Coarse-Grained Steels Versus Reciprocal Absolute Temperature.

tinues after substantial attainment of angles of this size, in disagreement with their hypothesis.

To check the influence of austenite grain shape on grain growth, austenite grain junction angles were measured on two specimens of Steel 11 by the prescribed procedure (43), and the cumulative distribution of these angles was compared with Harker and Parker's ideal curve, based on a solid composed of rhombic dodecahedron-

<sup>5</sup>Smith (40), in discussing surface tension in metals, states that the minimum-area tetrakaidecahedron of Lord Kelvin (44), rather than the rhombic dodecahedron (43), is the only stable shape of grain. He does not postulate, however, that grain growth stops when such a shape is reached.



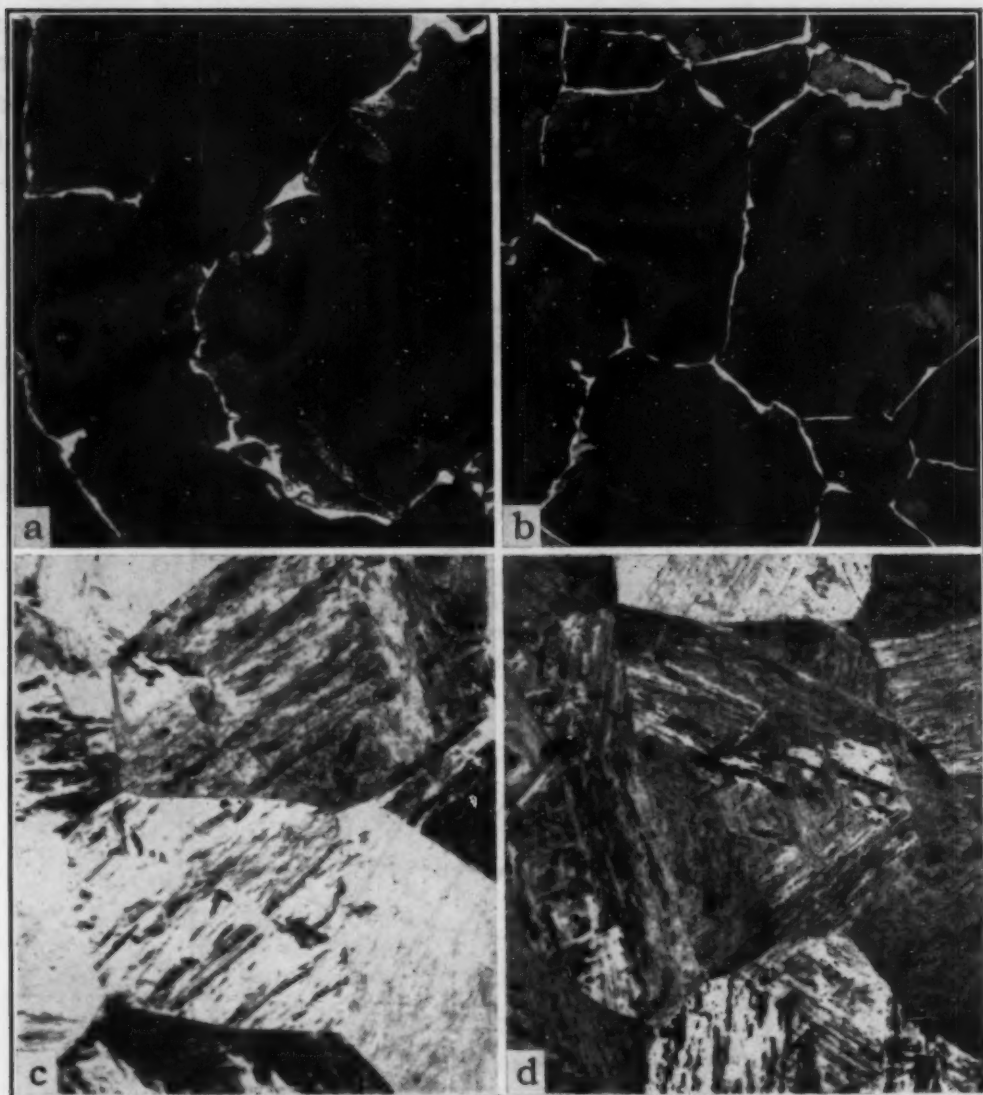


Fig. 16—Influence of Time at Austenitizing Temperature on Shape of Austenite Grains in Coarse-Grained Type of Steel. Fig. 16a and 16b—Steel 6 at 1500 °F; Fig. 16c and 16d—Steel 11 at 1900 °F. a—0.5 hour,  $\times 400$ ; b—5000 hours,  $\times 100$ ; c—0.1 hour,  $\times 350$ ; d—200 hours,  $\times 100$ .

shaped<sup>6</sup> grains, by plotting both on the same chart as shown in Fig. 17. The curves for Steel 11 are sufficiently similar to the ideal curve that, in accord with their examples (43), no further grain growth would be predicted for either specimen at 1900 °F (1040 °C); however, after 0.1 hour the average grain size was 2.8 and after 200 hours it was  $-0.7$  (ASTM scale), representing extensive isothermal growth.

Austenite grains in Steels 6 and 8 show a tendency, similar to

<sup>6</sup>Since each face-junction or dihedral angle in a tetrakaidecahedron and in a rhombic dodecahedron is 120 degrees, presumably a discussion on distribution of observed face-junction angles should apply reasonably well to a random section of a solid body comprised of either geometric unit.

that in Steel 11, to grow after face-junction angles of 120 degrees have been substantially attained; consequently, it appears that such measurements of face-junction angles are not a sufficient criterion of the ability of austenite grains to grow. Dunn and Lionetti (45) observed that the face-junction angles reach 120 degrees long before the grain boundaries straighten out to an equilibrium condition. A

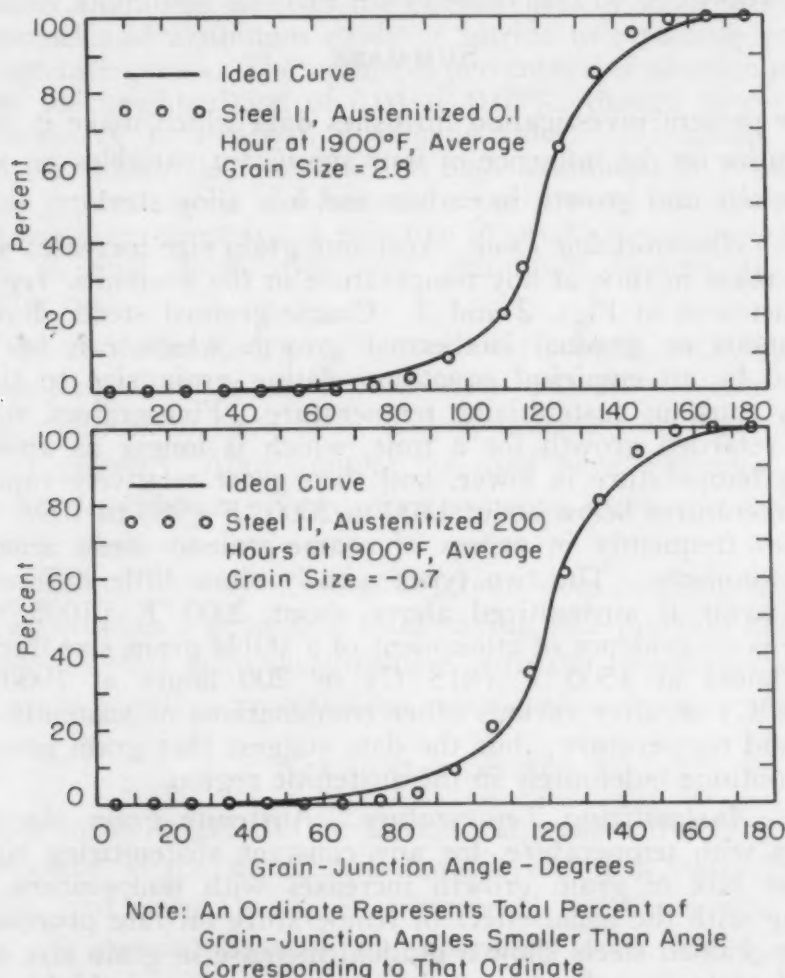


Fig. 17—Cumulative Distribution of Austenite Grain-Junction Angles for Steel 11 Compared With Ideal Curve Based on a Solid Composed of Rhombic Dodecahedron-Shaped Grains; Showing That Approach to Such an Ideal Shape Does Not Stop Growth.

true criterion of stability must include grain-boundary contour as well as face-junction angles (40, 43). Possibly unstable grain-boundary contours were a significant factor in the austenite grain growth discussed above; examples of boundary contours, before and after grain growth, in Fig. 16 show some change for Steel 6 but little, if any, for Steel 11.

The present work and recent work on nonferrous alloys (38, 39)

indicate rather conclusively that no stable grain size is reached. Burke (41) has suggested that changes occurring during grain growth may make the growth process self-perpetuating. It appears that during grain growth the stable shape is not quite reached, thus allowing growth to continue through operation of surface tension phenomena which, however, produce slower growth as the grains become larger.

### SUMMARY

The present investigation furnishes data which make it possible to generalize on the influence of four significant variables on austenite grain size and growth in carbon and low alloy steels:

1. *Austenitizing Time.* Austenite grain size increases with an increase in time at any temperature in the austenitic region, as illustrated in Figs. 2 and 3. Coarse-grained steels show a continuous or gradual isothermal growth which can be described by an empirical equation relating grain size to time, at any constant austenitizing temperature. Fine-grained steels show retarded growth for a time, which is longer as austenitizing temperature is lower, and then grow relatively rapidly at temperatures below about 1800 to 2000 °F (980 to 1095 °C) to sizes frequently in excess of coarse-grained steels austenitized similarly. The two types usually show little difference in behavior if austenitized above about 2000 °F (1095 °C). There is no evidence of attainment of a stable grain size during 5000 hours at 1500 °F (815 °C) or 200 hours at 1900 °F (1040 °C) or after various other combinations of austenitizing time and temperature; thus the data suggest that grain growth may continue indefinitely in the austenitic region.

2. *Austenitizing Temperature.* Austenite grain size increases with temperature, for any constant austenitizing time, because rate of grain growth increases with temperature, in keeping with the usual effect of temperature on rate processes. Coarse-grained steels show a gradual increase in grain size and rate of grain growth as austenitizing temperature is higher, as illustrated in Figs. 2 and 14. Fine-grained steels provide an exception to the above generalization by having a minimum in grain size and rate of grain growth in the neighborhood of 1800 to 2000 °F (980 to 1095 °C), as shown in Figs. 3 and 14.

3. *Austenite Grain Size Present.* The rate of austenite grain growth is determined by the austenite grain size present, as well as by temperature. The rate decreases markedly as the grains become larger; in fact, an empirical equation has been derived to show that for coarse-grained steels the rate is related reciprocally to grain size, probably through interfacial energy associated with grain boundaries. This general trend on rate of growth applies equally well to coarse- and

fine-grained steels, as indicated in Fig. 14, except for the irregular variation in rate associated with retardation of grain growth and breakdown of this retardation in fine-grained steels.

4. *Inclusions.* In final deoxidation with aluminum, preferably enhanced by prior deoxidation with silicon, a minimum excess of approximately 0.015% acid-soluble or "metallic" aluminum is necessary to produce a fine-grained steel; presumably aluminum controls the effectiveness of small inclusions or particles of aluminum oxide or nitride in retarding growth of austenite grains. The optimum percentage of aluminum may be in the neighborhood of 0.04 to 0.05%, though more work is necessary to establish a reliable value. Zirconium, as a final deoxidizer, is less effective than aluminum in producing a fine-grained steel. Inclusions or particles of vanadium carbide are approximately as effective in producing a fine-grained steel as final deoxidation with aluminum, though at much greater cost.

Type of steelmaking process and alloy content, including carbon but excluding alloy elements which form difficultly soluble carbides, generally appear to have little, if any, influence on austenite grain size and growth. Alloy content, as used here, excludes elements added for deoxidation or control of austenite grain size and usually present in small amount.

Isothermal growth of austenite grains does not stop when grain shape approaches a geometric solid having face-junction angles near 120 degrees; this is in disagreement with the hypothesis, advanced a few years ago, that growth stops when such a shape is approached.

#### ACKNOWLEDGMENT

The author is grateful for advice and constructive criticism from his associates at the Research Laboratory, United States Steel Corporation, and from Dr. G. R. Fitterer of the University of Pittsburgh. In certain phases of the laboratory work, Mr. E. T. Gioia gave valuable assistance.

#### References

1. H. Tobin and R. L. Kenyon, "Austenitic Grain Size of Eutectoid Steel", *TRANSACTIONS, American Society for Metals*, Vol. 26, 1938, p. 133.
2. K. Malishev, "Mechanism of Grain Growth in As-Cast and As-Forged Steel with Additions of Aluminum, Vanadium and Titanium", *Metalurg*, Vol. 14, 1939, p. 30.
3. J. R. Vilella, "The Grain Size of Steel", *Mechanical Engineering*, Vol. 62, 1940, p. 293.
4. J. H. Whiteley, "Austenite Grain Growth in Medium-Carbon Steels", *Journal, Iron and Steel Institute (London)*, Vol. 148, 1943, p. 513.
5. E. C. Bain, "Factors Affecting the Inherent Hardenability of Steel", *TRANSACTIONS, American Society for Steel Treating*, Vol. 20, 1932, p. 385.



6. E. S. Davenport and E. C. Bain, "General Relations Between Grain-Size and Hardenability and the Normality of Steels", *TRANSACTIONS, American Society for Metals*, Vol. 22, 1934, p. 879.
7. C. H. Herty, D. L. McBride and S. O. Hough, "Effect of Deoxidation on Grain Size and Grain Growth in Plain Carbon Steels", *Mining and Metallurgical Investigations, Carnegie Institute of Technology Mining and Metallurgical Advisory Boards, Cooperative Bulletin 65*, 1934.
8. S. Epstein, J. H. Head and T. S. Washburn, "Grain Size Control of Open-Hearth Carbon Steels", *TRANSACTIONS, American Society for Metals*, Vol. 22, 1934, p. 942.
9. O. O. Miller and M. J. Day, "Heat Etching as a General Method for Revealing the Austenite Grain Size of Steels", *TRANSACTIONS, American Society for Metals*, Vol. 30, 1942, p. 541.
10. T. G. Digges, "Influence of Austenite Grain Size on the Critical Cooling Rate of High-Purity Iron-Carbon Alloys", *TRANSACTIONS, American Society for Metals*, Vol. 29, 1941, p. 285.
11. H. W. McQuaid, "Importance of Aluminum Additions in Modern Commercial Steels", *TRANSACTIONS, American Society for Metals*, Vol. 23, 1935, p. 797.
12. E. Houdremont and H. Schrader, "On the Question of Grain Size of Steel; Its Estimation, Effect on Properties and Methods of Influencing It", *Stahl und Eisen*, Vol. 56, 1936, p. 1412.
13. E. Houdremont and H. Schrader, "Effect of Aluminum on Plain Carbon Steel", *Archiv für das Eisenhüttenwesen*, Vol. 12, 1939, p. 393.
14. G. Derge, A. R. Kommel and R. F. Mehl, "Some Factors Affecting Austenite Grain Size in High-Purity Steels", *TRANSACTIONS, American Society for Metals*, Vol. 26, 1938, p. 153.
15. M. Baeyertz, "Effects of Initial Microstructure on Austenite Grain Formation and Coarsening", *TRANSACTIONS, American Society for Metals*, Vol. 30, 1942, p. 458.
16. C. Benedicks, "Capillarity of Grain Boundaries of Metals. Effect upon Grain Growth and Its Importance for Steel", *Kolloid-Zeitschrift*, Vol. 91, 1940, p. 217.
17. M. J. R. Morris, "Steel Containing Tellurium", U. S. Patent 2,236,716, April 1, 1941; Reissue 22,021, Feb. 10, 1942.
18. S. J. Rosenberg and T. G. Digges, "Effect of Rate of Heating Through the Transformation Range on Austenite Grain Size", *TRANSACTIONS, American Society for Metals*, Vol. 29, 1941, p. 638.
19. T. G. Digges and S. J. Rosenberg, "Influence of Initial Structure and Rate of Heating on Austenite Grain Size of 0.5 Per Cent Carbon Steels and Iron-Carbon Alloy", *TRANSACTIONS, American Society for Metals*, Vol. 31, 1943, p. 777.
20. M. A. Grossmann, "Grain Size in Metals with Particular Reference to Growth in Austenite", *TRANSACTIONS, American Society for Metals*, Vol. 22, 1934, p. 861.
21. M. A. Grossmann, "On Grain Size and Grain Growth", *TRANSACTIONS, American Society for Steel Treating*, Vol. 21, 1933, p. 1079.
22. D. F. Pavlenko, "The Effect of Heterogeneity of Steel Ingots on the Grain of Austenite", *Teoriya i Praktika Metallurgii*, Vol. 12, No. 7, 1940, p. 38.
23. J. E. Dorn and O. E. Harder, "Relation of Pre-Treatment of Steels to Austenitic Grain Growth", *TRANSACTIONS, American Society for Metals*, Vol. 26, 1938, p. 106.
24. L. S. Darken, "Diffusion of Carbon in Austenite with a Discontinuity in Composition", *Transactions, American Institute of Mining and Metallurgical Engineers*, Vol. 180, 1949, p. 430.
25. O. O. Miller and M. J. Day, "Ferric Chloride Etchant for Austenite Grain Size in Low-Carbon Steel", *METAL PROGRESS*, Vol. 56, 1949, p. 692.

26. E. C. Bain and J. R. Vilella, "Austenite Grain Size in Steel", *ASM Metals Handbook*, 1948, p. 399.
27. "Austenite Grain Size in Steels", ASTM Standards, Part I-A, Ferrous Metals, 1946, p. 682.
28. "Preparation of Micrographs of Metals and Alloys", ASTM Standards, Part I-B, Non-Ferrous Metals, 1946, p. 803.
29. J. J. B. Rutherford, R. H. Aborn and E. C. Bain, "The Relation Between the Grain Areas on a Plain Section and the Grain Size of a Metal", *Metals and Alloys*, Vol. 8, 1937, p. 345.
30. G. E. F. Lundell, J. I. Hoffman and H. A. Bright, "Chemical Analysis of Iron and Steel", John Wiley & Sons, 1931, p. 348.
31. Z. Jeffries and R. S. Archer, "The Science of Metals", McGraw-Hill Book Co., 1924.
32. T. S. Washburn, "Deoxidation of Basic Open-Hearth Steel", *Transactions, American Institute of Mining and Metallurgical Engineers*, Vol. 162, 1945, p. 658.
33. J. W. Halley, "Grain Growth Inhibitors in Steel", *Transactions, American Institute of Mining and Metallurgical Engineers*, Vol. 167, 1946, p. 224.
34. "Basic Open-Hearth Steelmaking", American Institute of Mining and Metallurgical Engineers, 1944, p. 235.
35. H. W. McQuaid and John Chipman, "The Use of Aluminum for Deoxidation and Control of Grain Size in Steel", *ASM Metals Handbook*, 1948, p. 341.
36. John Chipman, "Application of Thermodynamics to the Deoxidation of Liquid Steel", *TRANSACTIONS, American Society for Metals*, Vol. 22, 1934, p. 385.
37. P. A. Beck, M. L. Holzworth and P. R. Sperry, "Effect of Dispersed Phase on Grain Growth in Al-Mn Alloys", *Transactions, American Institute of Mining and Metallurgical Engineers*, Vol. 180, 1949, p. 163.
38. P. A. Beck, J. C. Kremer, L. J. Demer and M. L. Holzworth, "Grain Growth in High-Purity Aluminum and in an Aluminum-Magnesium Alloy", American Institute of Mining and Metallurgical Engineers, Technical Publication 2280, *Metals Technology*, Vol. 14, No. 6, 1947.
39. P. A. Beck, J. Towers and W. D. Manly, "Grain Growth in 70-30 Brass", American Institute of Mining and Metallurgical Engineers, Technical Publication 2326, *Metals Technology*, Vol. 15, No. 2, 1948.
40. C. S. Smith, "Grains, Phases and Interfaces: An Interpretation of Microstructure", American Institute of Mining and Metallurgical Engineers, Technical Publication 2387, *Metals Technology*, Vol. 15, No. 4, 1948.
41. J. E. Burke, "Some Factors Affecting the Rate of Grain Growth in Metals", *Transactions, American Institute of Mining and Metallurgical Engineers*, Vol. 180, 1949, p. 73.
42. S. Glasstone, K. J. Laidler and H. Eyring, "The Theory of Rate Processes", McGraw-Hill Book Company, 1941.
43. D. Harker and E. R. Parker, "Grain Shape and Grain Growth", *TRANSACTIONS, American Society for Metals*, Vol. 34, 1945, p. 156.
44. William Thompson (Lord Kelvin), "On the Division of Space with Minimum Partitional Area", *Philosophical Magazine*, Vol. 24, 1887, p. 503.
45. C. G. Dunn and F. Lionetti, "The Effect of Orientation Difference on Grain Boundary Energies", *Journal of Metals*, Vol. 1, 1949, p. 125.

## DISCUSSION

**Written Discussion:** By Paul A. Beck, head, Department of Metallurgy, University of Notre Dame, Notre Dame, Ind.

I would like to congratulate the author on the large amount of excel-

lent data he obtained and on the soundness of his conclusions. For the first time now, extensive and systematic information is available on grain growth in steels. I was particularly interested in the isothermal data for long periods of annealing, such as 5000 hours. It is gratifying to note that all the information amassed by the author supports the view that grain growth in steel proceeds in a manner basically similar to that found in nonferrous metals.

**Written Discussion:** By Cyril Stanley Smith, director, Institute for the Study of Metals, University of Chicago, Chicago.

I would like to amplify somewhat the quotation from an earlier paper of mine that the author makes on page 281. I most certainly did mean, by my statement that "the minimum area tetrakaidecahedron of Lord Kelvin is the stable shape of grain", that an aggregate of grains of this shape could not and would not undergo any further change either in size or shape. However, it should be emphasized that this state can never be reached or even approached by growth of a random distribution of grains, and is itself unstable unless perfect. Any departure from the ideal array, either within the metal or at the surface of a metal, results in instability. Provided that one is concerned only with surface tension factors, a single grain face with the wrong number of sides to it will result in eventual migration and elimination of all boundaries. It should be understood that there is no direct connection between the attainment of the 120-degree angles called for by local surface tension equilibrium, and the stability of the grains. It is the curvature of the sides that is important, and this depends more on the number of contacts with neighboring grains than on any slight departure from 120 degrees that may occur in practice. A mass of soap froth wherein the uniformity of surface tension gives 120-degree angles exactly does not consist of rhombic dodecahedra nor even of tetrakaidecahedra. It consists of an array of bubbles with a widely varying number of faces (though the average tends closely to slightly less than 14) and each face may have any number of edges tending, however, to average very nearly  $5\frac{1}{7}$ . Because the pentagon comes closest to this topologically required average, the most frequently observed simple regular polyhedron is the pentagonal dodecahedron, but no single shape except the Kelvin body will by multiplication satisfy the criteria both for space-filling and for surface tension equilibrium. In reality, there is an assortment of grain shapes that, taken together, fulfill the topological requirements, but only at the cost of a diversity of shapes instead of a single shape. It is the curvatures that are inevitably reduced in such an assembly that are responsible for grain growth and, though curvatures decrease as grains are eliminated, they never become zero unless grain boundaries spread completely across the specimen. One can tell nothing about these factors by measuring the angles at grain corners. Neither, unfortunately, can one determine anything by measurements of curvature on a two-dimensional section. True mean curvature measured on the surfaces of three-dimensional grains is what is needed. The matter is of considerable mathematical complexity, beyond that of the average metallurgist, and for the moment one must be satisfied with analogy with the simple growing soap froth which demonstrates the geometrical principles so beautifully.

I would like to re-emphasize that grain growth need not stop when



120-degree angles are reached; the fact is that it would stop if 120-degree angles were not required. The setting up of surface tension equilibrium at nonequal angles as a result of the variations of surface energy with orientation between grains is actually one of the principal possible reasons for the cessation of grain growth when extremely large grains have been reached in pure materials. An additional method of stopping grain growth is by inclusions, for the grain boundary clings to the foreign particles in its desire for minimum area, for exactly the same reason that a bubble sticks to a particle of ore in flotation. A second phase will be more effective the more numerous its particles, and aluminum is probably effective in controlling grain size in steel because of the extremely fine size and hence large number of the oxide or nitride particles produced. A given distribution of inclusions will have a critical curvature above which it will not restrain grain boundary motion, and if for some local reason a grain becomes somewhat larger than its neighbors, which are inclusion blocked at the limiting size, the boundary between the large grains and the small ones will obviously be more strongly curved and hence will not be restrained. Abnormal grain growth therefore results. It is obtained only when normal grain growth is blocked for some reason or other.

#### Author's Reply

I wish to thank Dr. Beck for his highly complimentary remarks and Dr. Smith for his excellent amplification concerning the reference to one of his earlier papers. The data in my paper are in agreement with Dr. Smith's remarks that attainment of 120-degree face-junction angles does not constitute equilibrium and that grain growth continues after angles of this size are reached.



## CARBIDE PRECIPITATION IN TYPE 304 STAINLESS STEEL—AN ELECTRON MICROSCOPE STUDY

By E. M. MAHLA AND N. A. NIELSEN

### *Abstract*

*Electron microscope studies have been made of carbides isolated in an unchanged state from sensitized AISI Type 304 (18 Cr–8 Ni–0.08 C max.) stainless steel by means of a solution of bromine in methanol. The size, form, and distribution of the carbide precipitates, identified as  $\text{Cr}_{23}\text{C}_6$  by electron diffraction analysis, were studied with reference to the time and temperature of alloy heat treatment and the effect of 80% alloy cold reduction. It was found that the carbide precipitate undergoes an isothermal change in form in which the particles tend to assume more stable energy configurations with time at the sensitizing temperature. The sequence of transformation appears to be: precipitation of dendrites  $\rightarrow$  growth of dendrites  $\rightarrow$  fragmentation of dendrites  $\rightarrow$  change to more stable geometric forms.*

*No obvious correlation of carbide form alone was found with the standard nitric acid corrosion rates of the respective alloy specimens, but these and continuing studies are designed to shed more light on the actual mechanism of intergranular corrosion of stainless steel.*

THE corrosion resistance of the stainless steels is a matter of great importance in the chemical industry. These alloys are widely used in most chemical processes, but the serious limitations in their corrosion resistance induced by certain heat treatments are a continuing matter of concern and necessitate fundamental research on corrosion mechanisms and alloy development. Although intergranular corrosion and carbide precipitation have been the subject of many independent investigations, the exact role of carbides in the corrosion of stainless steel is still unknown. This has been due mainly to limitations in the methods of physically studying carbide precipitation and of observing the complex corrosion cell process localized at grain boundaries. In the present work, electron microscopy has been the principal tool in a detailed study of the influence

---

A paper presented before the Thirty-second Annual Convention of the Society, held in Chicago, October 21 to 27, 1950. The authors are members of the Engineering Research Laboratory, Engineering Department, E. I. du Pont de Nemours and Co., Inc., Wilmington, Del. Manuscript received April 15, 1950.

of alloy heat treatment and the effect of cold work on the size, shape, and distribution of carbide particles in AISI Type 304 (18 Cr-8 Ni-0.08 C max.) stainless steel. The authors also have included parallel observations on the nitric acid corrosion rates of the heat treated alloys. Most of the information developed on carbides is new and, in certain respects, entirely unexpected. These studies, besides adding to our knowledge of precipitation from the solid state, are considered a necessary step in attaining a more fundamental understanding of the mechanism of intergranular corrosion. The present publication must be considered in the nature of a progress report, for the work to date, although extensive, is still far from complete and many old questions, along with many new ones arising from this work, remain unanswered.

Although there are numerous references in the literature to investigations of isolated carbides, actual references to electron microscope studies of carbides are few and none on carbides in stainless steel are reported. Koch (1),<sup>1</sup> Koch and Wiester (2) and Crafts and Lamont (3, 4, 5) have in recent years published work on carbides electrolytically isolated from low alloy steels and included electron photomicrographs of the residue particles. Crafts and Lamont have made an extensive study of the carbide particles precipitated in vanadium-chromium-molybdenum steels after long-time tempering and have also investigated carbides in isothermally transformed chromium steels.

Although most information in the literature indicates that it is the carbides themselves which are seen when a sensitized stainless steel specimen is etched for light microscopic examination, our previous studies of polished and etched specimens have indicated that what are usually termed carbides are actually only holes indicating local cell corrosion at the grain boundary (6). Continued exposure of a sensitized 18-8 specimen to a corrosive medium results in the formation of continuous "trenches" along the grain boundaries. Ordinary metallographic procedures are entirely inadequate to study the phenomena present. Since the carbide particles themselves, in the isolated state, have too fine a detail to be resolved by light microscopy, the use of electron microscopy is mandatory. The results which have been obtained with it, along with the method of carbide isolation, later described, have led us to question many of the conclusions of previous metallographic studies. Investigators of carbides in stainless steel actually have not seen the true detail of the precipitates which they have described in numerous papers.

<sup>1</sup>The figures appearing in parentheses pertain to the references appended to this paper.

## EXPERIMENTAL PROCEDURE

The identification and chemical analyses of the different AISI Type 304 stainless steels used in this study are shown in the following table:

Table I  
Compositions of Stainless Steels Employed in Carbide Studies

Code No.	C	Cr	Ni	Mn	Si	S	P
AN9	0.05	18.51	9.76	0.37	0.49	0.014	0.014
DT2	0.06	18.30	10.66	0.98	0.45	0.008	0.014
BQ9	0.05	18.20	9.25	0.41	0.56	0.017	0.023
EN3	0.065	18.43	9.51	0.63	0.74	.....	.....
EX1	0.061	18.22	8.97	0.56	0.58	0.011	0.025
819A	0.07	18.65	8.92	0.52	0.30	0.018	0.020

*Alloy Heat Treatment*—In order to establish the maximum corrosion resistance in Type 304 stainless steel, it must be "annealed". Annealing in this alloy is defined as water quenching from about 1950 to 2000 °F (1065 to 1095 °C). This heat treatment results in an essentially homogeneous, supersaturated, solid solution of carbon in austenite. On reheating an annealed Type 304 stainless steel within the temperature range of 1100 to 1500 °F (595 to 815 °C), carbides are precipitated, principally in the grain boundaries. With the carbides thus precipitated, this alloy is sensitive to intergranular corrosion in certain media. Heat treating annealed stainless steels in this fashion has become known as sensitization.

Heat treatments given the annealed alloys listed in Table I covered the entire sensitization temperature range and particularly the following heat treatments:

1. Holding 1 hour at the sensitizing temperature, followed by water quenching, or in other cases by air cooling. With a constant time of sensitization, the effects of temperature on the carbide form were investigated.
2. With constant temperatures of 1200 and 1300 °F (650 and 705 °C), the effect of time of sensitization was investigated. The longest sensitization times investigated at the above temperatures were 2000 hours and 18 hours respectively.
3. The effect of time of sensitization on the carbide form was also investigated for specimens sensitized either by a direct quench to the sensitizing temperature from the higher annealing temperature, or by heating up into the sensitizing zone for very short lengths of time. These heat treatments have permitted an estimation of the severity of the sensitization effect as related to the direction from



which the temperature zone of sensitization was approached.

Although this paper deals only with the behavior of carbides in Type 304 stainless steel, enough evidence from studies of Type 316 (18-8-S-Mo) material has been accumulated to say that the carbide phenomena discussed for 18-8-S also hold for 18-8-S-Mo. Studies are also being made of the extra low carbon stainless alloys and in the stainless steels Types 321, 347, 430 and 446.

*Method of Carbide Isolation*—In the studies of carbides isolated as residues from alloy steels, reported in the literature, anodic solution of the material in a hydrochloric acid electrolyte or other acid solutions has been the technique generally utilized to obtain nonmetallic residues for study. This method was tried in the present work and found to give very inferior results in comparison with a chemical solution method developed in earlier film-stripping studies (7). The latter method employs a solution of bromine in anhydrous methanol (for example, 5 to 10 ml of  $\text{Br}_2$  per 100 ml of  $\text{CH}_3\text{OH}$ ), which rapidly dissolves all the metallic phases in the sensitized stainless steel, leaving behind a layer of carbides, together with other nonmetallic constituents which are unattacked by the bromine solution. (Since the presence of water is avoided, there is no decomposition of isolated carbides by acid hydrolysis.) The carbides can then be collected for experimental study. Carbide samples in the form of residue layers on the metal sample are washed several times by successive immersion in dishes of fresh methanol.

*Electron Microscopy and Electron Diffraction*—All samples of carbides for electron microscope examination and for electron diffraction were prepared as follows: Specimen-supporting bases consisted of  $\frac{1}{8}$ -inch diameter screens of stainless steel wire covered with a very thin film of Formvar resin which served as a carrier film for the fine carbide particles while being itself essentially transparent to the electron beam. The usual procedure in mounting carbides on a "Formvar screen" consisted first in dipping the metal sample with its layer of methanol-wet carbide residue into a small volume of distilled water. The differential surface tension forces of the methanol and water result in the carbide residue being dispersed throughout the water and also in spreading a layer of carbide particles on the surface of the water. This latter film of carbide particles is easily caught on a "Formvar screen" and excess water is drawn away by touching the screen to a piece of filter paper. The screen dries within a few seconds and is then ready for examination in the electron microscope. This procedure generally results in a good dispersion of carbide particles. For electron



diffraction samples, a somewhat heavier dispersion of material is preferable.

The oxide replicas of stainless steel surfaces included in this paper were made by a technique described in detail elsewhere (8).

*Carbides in Cold-Reduced Stainless Steel*—The material employed for the study of the effect of cold work on the form and distribution of carbides was again Type 304, 18-8-S stainless steel (coded herein as 819A). Annealed material, 0.125 inch thick, was cold-rolled by hand on a jeweler's roll to a thickness of 0.025 inch (80% cold reduction). Several heat treatments of this material were investigated with regard to corrosion rates and the form and distribution of the carbides formed.

### RESULTS AND DISCUSSION

The marked decrease in intergranular corrosion resistance of austenitic stainless steel specimens upon sensitization has generally been explained by the chromium depletion theory. Briefly, this theory attributes intergranular corrosion susceptibility to the formation of narrow paths of chromium-depleted austenite. Chromium carbide ( $\text{Cr}_{23}\text{C}_6$ ) precipitation at grain boundaries is held to be responsible for chromium depletion in the matrix and for the formation of the intergranular zones of poor corrosion resistance. Supposedly, the inability of the chromium-depleted areas to maintain passivity results in intergranular corrosion in many media in which the stainless steel would ordinarily be resistant.

The evidence for this theory is largely indirect. It is hoped that the continuation of this study will help to clarify the mechanism of intergranular corrosion.

*Effect of Temperature of Sensitization on the Carbide Precipitate*—Fig. 1 shows a series of electron photomicrographs illustrating the changes in form and size undergone by the carbide precipitate as the 18-8-S alloy is heated at increasingly higher temperatures for a constant period of 1 hour. (All of the alloy samples in this series were air-cooled from the temperature of sensitization. Water-quenched samples showed a similar sequence in precipitate form.) The corrosion rate of the alloys in the standard  $\text{HNO}_3$  test is also shown. In other figures the  $\text{HNO}_3$  corrosion rate has been included whenever it was available.

In interpreting Fig. 1 and all other electron photomicrographs of carbides presented in this paper, it must be emphasized that the carbides are samples isolated and collected from the stainless steel alloys. The photomicrographs give no idea of the total volume of

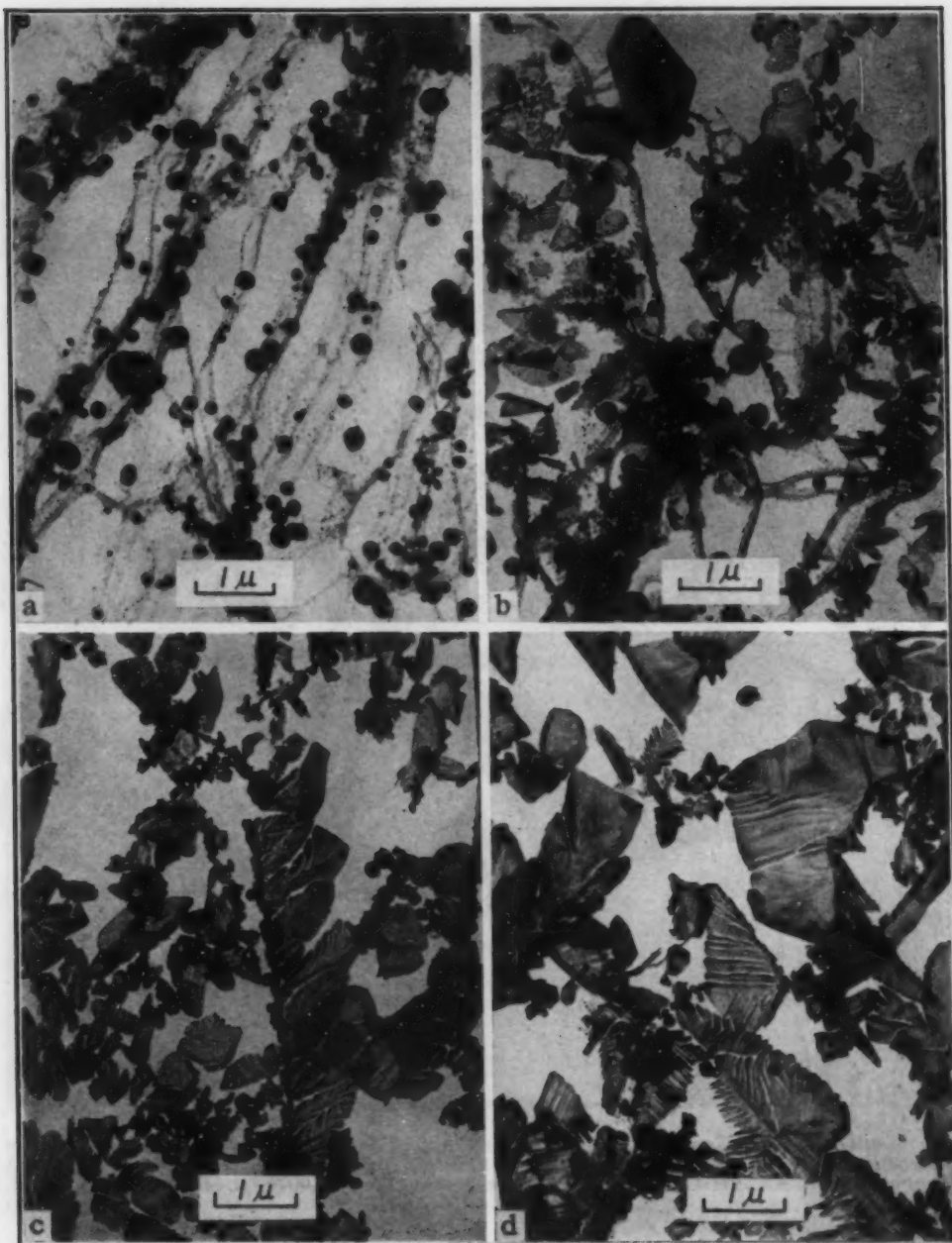


Fig. 1—Effect of Temperature on Carbide Form (Alloy AN9).  $\times 13,000$ . (Reduced  $\frac{1}{4}$  in reproduction.) Heat treatment: a—Annealed; b—1 hour at  $1100^{\circ}\text{F}$ , A.C. (air-cooled); c—1 hour at  $1150^{\circ}\text{F}$ , A.C.; d—1 hour at  $1200^{\circ}\text{F}$ , A.C.  $\text{HNO}_3$  corrosion rate, inch per month: a—0.0005; b—0.00539; c—0.011; d—0.0119.

carbide isolated. Each succeeding picture shows only new forms of carbide not found to exist in the residue isolated from the previous sample. It should be understood that many of the forms found in previous pictures may also coexist with the new forms.

*Residue From Annealed Material (Fig. 1a)*—The residue shown here is typical of the types of particle which appear in the residue layer from annealed 18-8-S stainless steel. Both small and large



Fig. 1—Effect of Temperature on Carbide Form (Alloy AN9).  $\times 13,000$ . (Reduced  $\frac{1}{8}$  in reproduction.) Heat treatment: e—1 hour at 1250°F, A.C.; f—1 hour at 1300°F, A.C.; g—1 hour at 1400°F, A.C.  $\text{HNO}_3$  corrosion rate, inch per month: e—0.00767; f—0.00663; g—0.00332.

globular constituents with a lacy, flocculent background material are obtained.

The composition and structure of this residue are unknown. Our work has included only electron and X-ray diffraction studies and the authors have not been able to interpret the complex pattern. It is not  $\text{Cr}_{23}\text{C}_6$ . The presence of the residue in the alloy apparently has no effect on the nitric acid corrosion rate. Undoubtedly the residue contains a mixture of oxides, silicates, and other non-metallic inclusions undissolved by the bromine-methanol solution. It is hoped that spectrographic and chemical analysis will develop more information on this. Although some of these globules go



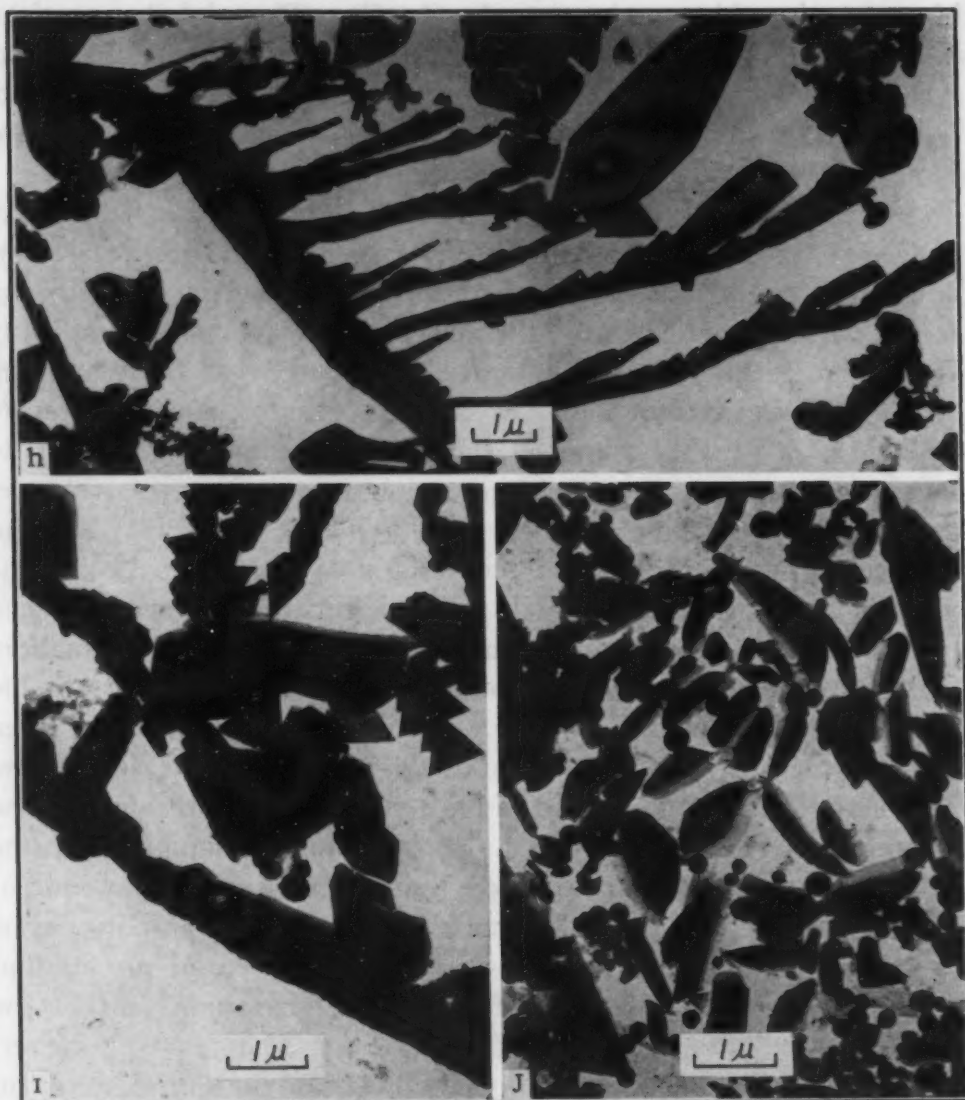


Fig. 1—Effect of Sensitization Temperature on Carbide Form (Alloy AN9).  $\times 13,000$ . (Reduced  $\frac{1}{4}$  in reproduction.) Heat treatment: h—1 hour at 1500°F, A.C.; i—1 hour at 1600°F, A.C.; j—1 hour at 1700°F, A.C.  $\text{HNO}_3$  corrosion rate, inch per month: h—0.00155; i—0.00121; j—0.00055.

through the entire series of heat treatments unchanged, others apparently disappear when the recognizable forms of carbides appear. In some instances these globules also seem to be transforming to what appear to be carbides. Further information on this point is being developed.

Fig. 1b representing 1 hour exposure at 1100°F (595°C) discloses a small amount of the globular residue and in addition a considerable quantity of small carbide flakes and dendrites. At a temperature 50°F higher (1150°F or 620°C), the carbides have grown somewhat larger and appear as dendrites and isolated flakes or "leaves" (Fig. 1c). Electron diffraction studies have shown



this type of residue to be entirely  $\text{Cr}_{23}\text{C}_6$ . The globular particles so evident in Fig. 1a have almost entirely disappeared. This may be a case only of "disappearance by dilution", since the volume of residue obtained from sensitized samples is much greater than the amount that can be isolated from annealed material.

At a temperature of 1200 °F (650 °C) the carbide flakes have changed only in size, becoming visibly larger (Fig. 1d). The same comment is true for higher temperatures, as shown in Figs. 1e and 1f; the carbide particles are still increasing in area and complexity of dendritic form. It will be noticed, however, that the maximum  $\text{HNO}_3$  corrosion rate of the alloy samples occurred at a temperature of 1200 °F (650 °C) (Fig. 1d). From this temperature on up to the annealing temperature, the corrosion rate is progressively declining and approaching the initial value (Fig. 1a). The form of the carbide precipitate is also accordingly approaching the residue forms isolated from the initial sample, but this is accomplished through an interesting and complex process of transformation. Fig. 1g shows an elongated carbide dendrite found in the residue of the 1400 °F (760 °C) sample. While large particles are often found, they are always coexistent with smaller carbide forms and some of the original globular residue. Although the residue on the microscope screen is regarded as a fair random sampling of the carbide forms, it should be stated that each electron photomicrograph represents only a small fraction of the original sampling. For this paper the photomicrographs have been chosen in an attempt to show the general direction of change in size and form of the carbide particles with alloy heat treatment. There are, however, several figures included which do not illustrate the entire range in residue forms. These will be mentioned as they are encountered.

At a temperature of 1500 °F (815 °C) the alloy corrosion rate has declined to 0.00155 in./mo. and a noticeable change takes place in the form of the carbide particles (shown in Fig. 1h). At this temperature and time the particles are noticeably thicker and coarser in structural detail. Perhaps at these higher temperatures surface tension forces predominate and the precipitate particles are more dense and start to assume angular outlines. This is more evident in Fig. 1i. In Fig. 1j surface tension forces are still higher and the particles appear to be spheroidizing. At this temperature (1700 °F or 925 °C) more of the original globular constituents are present and the alloy has regained its original corrosion resistance. In this state the material, on the basis of corrosion rate, would be regarded as fully annealed. Carbides, however, still are present in

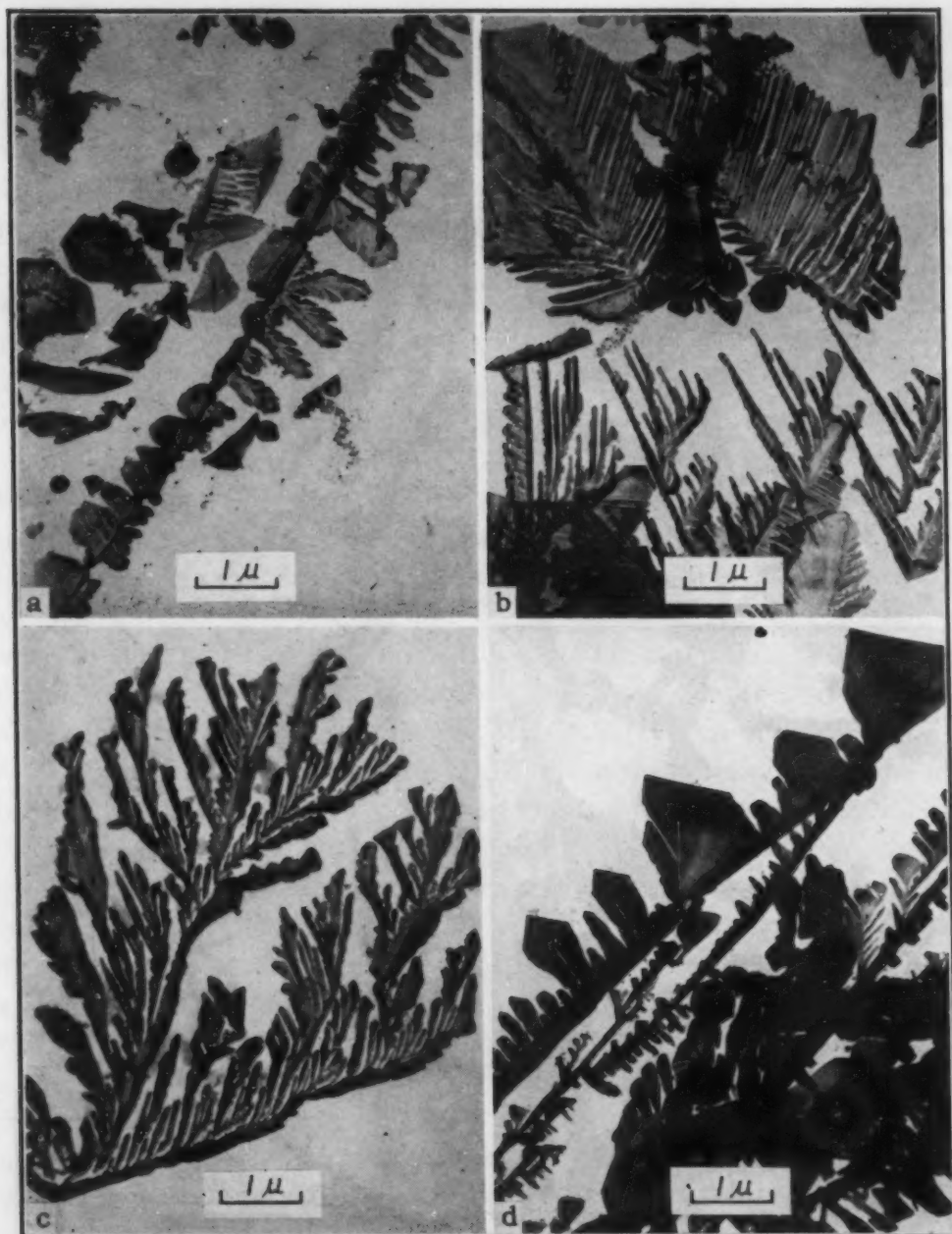


Fig. 2—Effect of Time of Sensitization on Carbide Form (Alloy DT2).  $\times 13,000$ . (Reduced  $\frac{1}{4}$  in reproduction.) Heat treatment: a—15 minutes at 1200°F, W.Q.; b—30 minutes at 1200°F, W.Q.; c—3 hours at 1200°F, W.Q.; d—10 hours at 1200°F, W.Q.

the alloy matrix (confirmed by an electron diffraction pattern of this residue) although they should theoretically be in solid solution, since 1700 °F (925 °C) is just within the single-phase  $\gamma$  region (for 0.06% carbon) according to the constitution diagram (9).<sup>2</sup>

Exposures of 1 hour at higher temperatures do not affect the  $\text{HNO}_3$  corrosion rate, and the type of residue encountered is iden-

<sup>2</sup>It is probable that the limit of carbon solubility in austenite should be displaced to higher temperatures.

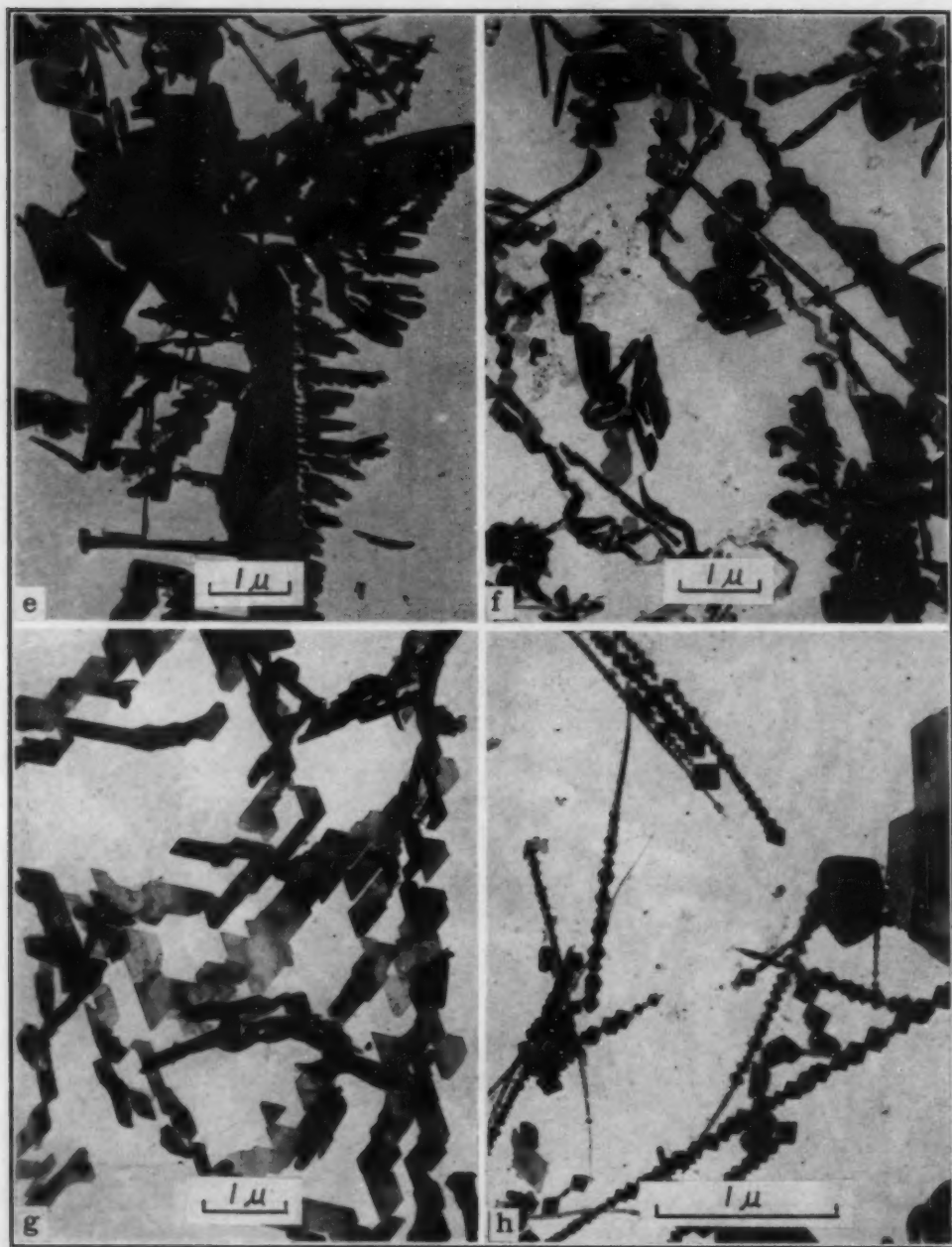


Fig. 2—Effect of Time of Sensitization on Carbide Form (Alloy DT2).  $\times 13,000$ . (Reduced  $\frac{1}{2}$  in reproduction.) Heat treatment: e—15 hours at  $1200^{\circ}\text{F}$ , W.Q.; f—50 hours at  $1200^{\circ}\text{F}$ , W.Q.; g—185 hours at  $1200^{\circ}\text{F}$ , W.Q.; h—2000 hours at  $1200^{\circ}\text{F}$ , W.Q. (Alloy AN9).  $\times 30,000$  (reduced  $\frac{1}{2}$  in reproduction).

tical with that shown in Fig. 1a.

*Effect of Time of Sensitization on Carbide Form*—Fig. 2 shows a series of photomicrographs of carbide residues obtained from 18-8-S (Alloy DT2), which was sensitized at  $1200^{\circ}\text{F}$  ( $650^{\circ}\text{C}$ ) for times varying from 15 minutes up to 185 hours. (These alloy samples are water-quenched from the sensitizing temperature.) Residue from Alloy AN9 heat treated for 2000 hours at  $1200^{\circ}\text{F}$



(650 °C) is also included in the series.

The progression illustrated in Figs. 2a, 2b, and 2c, representing specimens having sensitization times of 15, 30 and 180 minutes, respectively, shows how the dendritic carbides grow progressively with time. (The pictures unfortunately do not give any information about the quantity of carbide precipitated in the alloy, and again no accurate inference of the quantity can be drawn from the individual photomicrographs.) In the above progression the 15-, 30- and 180-minute specimens produced increasing volumes of residue. The period of 180 minutes might be regarded as stage 1 in the (1200 °F or 650 °C) process as it occurs isothermally. Under these conditions of time and temperature, the carbide dendrites reach a maximum size, whereupon the dendrite arms start to thicken and become less transparent to the electron beam. Fig. 2d (10-hour exposure) shows the dense dendrites whose branches are now assuming angular contours. Figs. 2e and 2f, representing 15 and 50 hours' sensitization times, respectively, further illustrate this process; the dendrites actually appear to fragment or recrystallize and assume a regular crystallographic habit. Fig. 2g represents one portion of carbide precipitate isolated from a sample sensitized for 185 hours, which is completely recrystallized into a cluster of ribbons characterized by 60 and 120-degree angles. The electron micrograph presents a striking example of a precipitate whose outward form is apparently controlled by the {111} lattice planes in the matrix. (The atoms on the {111} planes in the cubic lattice exhibit an hexagonal symmetry.) This geometric structure represents a form of intermediate stability of the precipitate. These form changes may be presumed also to represent an effort of the system to minimize lattice strain energy and interfacial area. It can be assumed that the cluster of ribbon carbides existed pseudomorphic with the metal in the same orientation (of ribbon to ribbon) as shown in the photograph, since the side of any one of the ribbons is generally parallel to only one of three directions. This geometric ribbon form of carbide is first formed after about 15 hours at 1200 °F. Structurally, the precipitate has the form of  $\text{Cr}_{23}\text{C}_6$ , as shown by electron diffraction.

In carbide residues from samples of 18-8-S stainless steel sensitized for thousands of hours at 1200 °F (650 °C), particles similar to those in Fig. 2h are always found. (Times beyond 4000 hours have not been investigated. In this case the residue is from Alloy AN9 sensitized for 2000 hours.) These are stringers made up of small cubes linked edge to edge. Except in length, the



dimensions of the cube-stringers are very small. In the photomicrograph, which has been printed at a higher magnification, the stringers taper off into invisibility, suggesting a terminal crystal of molecular dimensions. These figures and many other electron photomicrographs studied by the writers indicate that it is erroneous to speak of an agglomeration of carbides with time at temperature. Also the present use of "fine" and "coarse" carbides on the basis of photomicrographic observation can be misleading. The average carbide particle size does not increase as stated in the literature, but actually decreases. It is probable that the formation of clusters of small geometric carbide particles after long periods of time simulate in their etched appearance under light microscopy a large single particle. The inability of light microscopy to resolve carbide precipitates and the erroneous identification of etch attack and localized corrosion as "carbide precipitation" is responsible for many of the prevalent but questionable (on the basis of the present work) conclusions about the actual physical condition and form of the precipitate.

A similar study of the effect of time of sensitization on the carbide form was carried out at the higher temperature of 1300 °F (705 °C). In this case the series covered times only of 1, 5, and 18 hours, but within this period the sequence of the change in habit that appears to be: dendrites → fragmented products → geometrical carbides was observed again, as illustrated in Fig. 3a to Fig. 3d. Here Figs. 3c and 3d show oriented structures whose mode of growth has again been influenced by the orientation of the metal lattice in which the carbides precipitated. In Fig. 3c the recrystallized carbide consists of a cubic or rectangular network of small carbide cubes. Whether the gross cubic cross-hatch pattern of the system is related to a mosaic block structure in the alloy is conjectural. Its size is of the right order of magnitude ( $10^{-5}$  cm). Fig. 3d shows a precipitate consisting of small equilateral triangular crystals lined up apex-to-base in extended stringers. In this case the {111} planes in the metal crystal lattice have again presumably been the orienting influence, as postulated for the carbides in Fig. 2g. It should be noted that the residues from which these latter two photomicrographs were made still contained some dense dendrites and also dendritic fragments. All of the carbide had not yet changed to the geometric form.

Carbide precipitation has also been studied in specimens sensitized by an interrupted quench from an annealing temperature of 2000 °F (1095 °C) to the sensitizing temperature. It has been

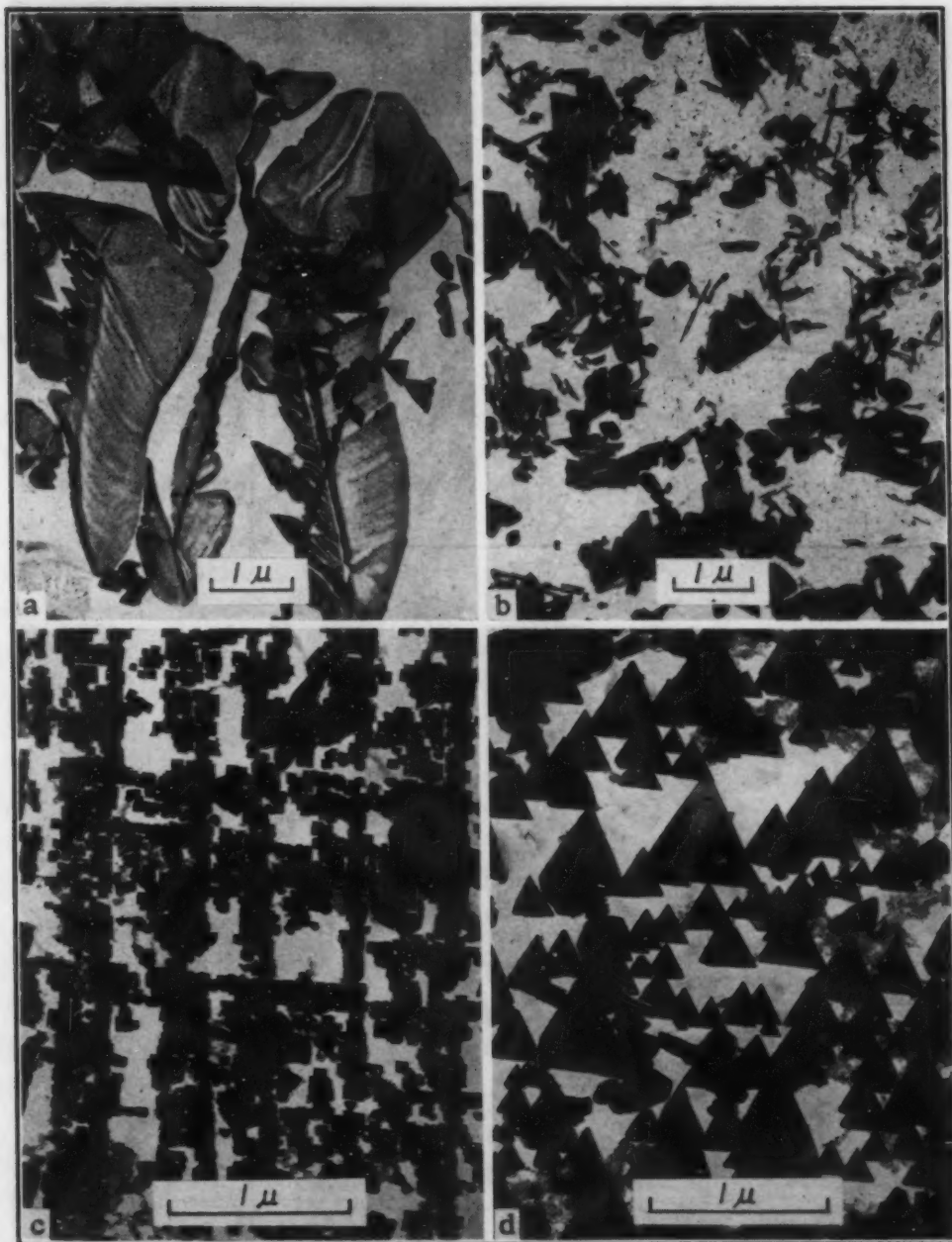


Fig 3—Effect of Time of Sensitization on Carbide Form (Alloy BQ9). Heat treatment: a—1 hour at 1300°F, W.Q.; b—5 hours at 1300°F, W.Q.; c—18 hours at 1300°F, W.Q.; d—18 hours at 1300°F, W.Q. a and b— $\times 13,000$ . (Reduced  $\frac{1}{2}$  in reproduction.) c and d— $\times 30,000$ . (Reduced  $\frac{1}{2}$  in reproduction.)

shown (Fig. 4) that entering the temperature zone of sensitization from a temperature above the range results in less severe sensitization than when the sensitization zone is entered from a temperature below it. The explanation for this may be found in a consideration of the rate of nucleation with temperature (10). Thus, on cooling through the sensitization range, the rate of carbide nucleation is at first relatively low. Presumably the stable nucleus size is large and

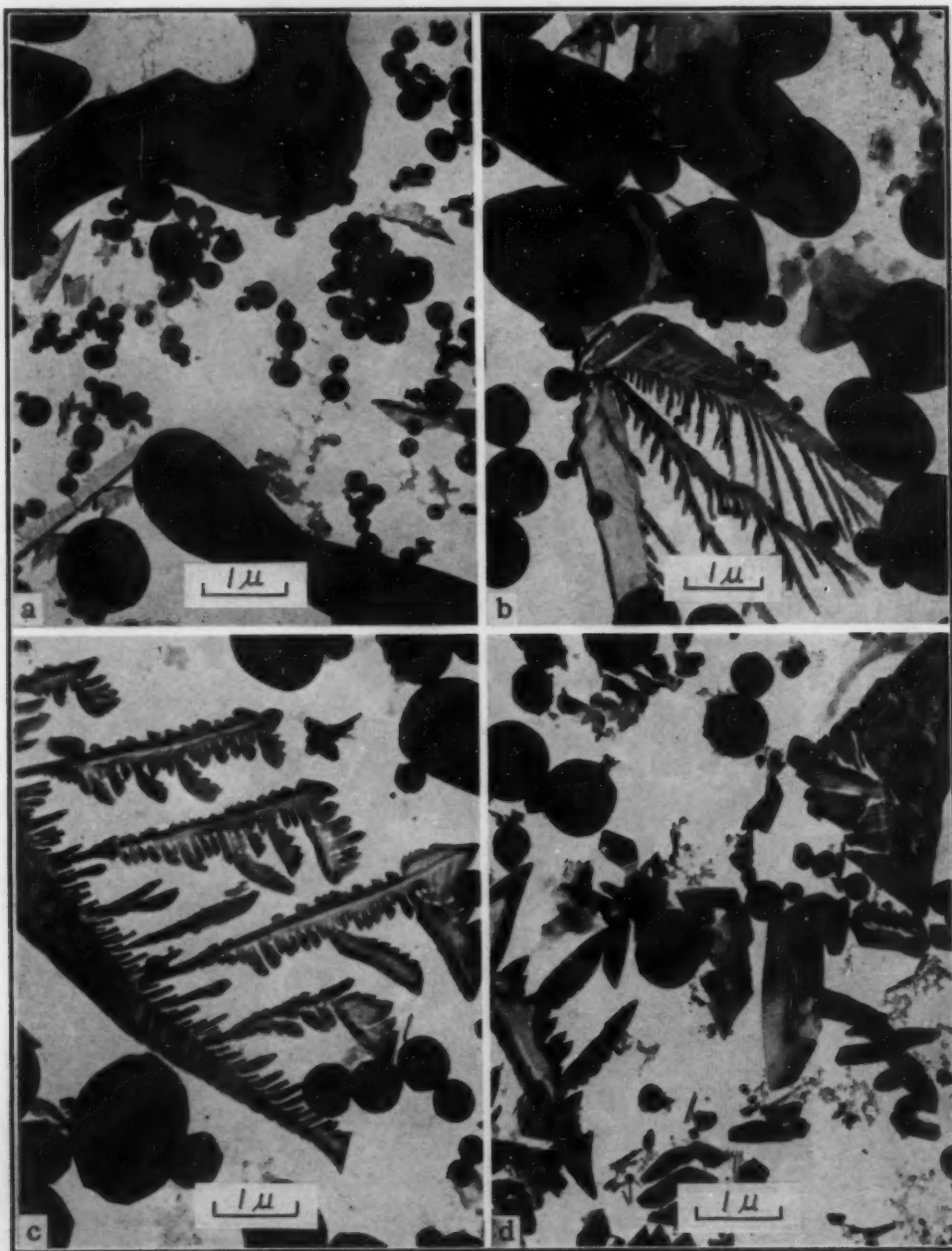


Fig. 4—Effect of Time of Sensitization on Carbide Form (Alloy EN3).  $\times 13,000$ . (Reduced  $\frac{1}{5}$  in reproduction.) All samples heated 5 minutes at  $2000^{\circ}\text{F}$  and quenched into fused salt for the temperatures and times indicated, then water-quenched. a—30 seconds at  $1400^{\circ}\text{F}$ ; b—5 minutes at  $1400^{\circ}\text{F}$ ; c—15 minutes at  $1400^{\circ}\text{F}$ ; d—45 minutes at  $1400^{\circ}\text{F}$ .  $\text{HNO}_3$  corrosion rate, inch per month: a—0.00076; b—0.00091; c—0.00283; d—0.0026.

therefore the number of nuclei so formed will be fewer than at lower temperatures where the nucleation rate is higher and critical nucleus size for stability is probably smaller. On this basis more carbide nuclei have a better likelihood of forming and growing upon heating an 18-8 alloy up through the temperature zone of sensitization than they would in the same specimen on cooling from an



elevated temperature and passing through the sensitization zone in the same length of time.

In Fig. 4, although carbides are present in the residues from the samples exposed for 30 seconds and 5 minutes at 1400 °F (760 °C), they are relatively few and have not produced much of an increase in the HNO<sub>3</sub> corrosion rate. However, after 15 minutes very large dendrites have formed and the HNO<sub>3</sub> corrosion rate is at its maximum. The entire sequence of carbide precipitates again follows the same order observed in Figs. 2 and 3. Thus fragmentation of the large dendrites appears to occur after 45 minutes' exposure as shown in Fig. 4d and the particles are becoming angular. In this case the isothermal transformation process is occurring more rapidly than in the previous two cases because of the higher temperature involved and the consequent greater atomic mobility. Higher temperatures should increase the rate of attainment of a more stable configuration by the chromium carbide precipitate.

For the samples from which the residues shown in Fig. 5 were obtained, the same kind of heat treatment was carried out except that the quench was interrupted at 1200 °F (650 °C) for varying lengths of time. At this temperature, even in times up to 30 minutes, the carbide dendrites did not grow appreciably and the HNO<sub>3</sub> rate has increased only 50% relative to the 2-minute sample (Fig. 5a) which showed only a very few carbide flakes. It is concluded that the interrupted-quench method of sensitization is less damaging to corrosion resistance than sensitization occurring on heating and that maximum sensitization by the former method takes place at higher temperatures.

The unanswered question of identity of the dense spheroids which appear in the residues, particularly of annealed material and the semisensitized samples of Figs. 4 and 5, must eventually be settled.

Very short times of sensitizing on heating up into the sensitization zone have been found to result in recognizable carbide precipitates (Fig. 6). Here 0.6 second in the range 1200 to 1210 °F (650 to 655 °C) resulted in the formation of a few small carbide flakes (Fig. 6a). Two and one-half seconds in the range 1200 to 1400 °F (650 to 760 °C) produced further precipitation (shown in Fig. 6b). In Fig. 6c most of the carbides shown [from a sample sensitized for 10 seconds in the range 1200 to 1450 °F (650 to 790 °C)] are still in small flake forms, while Fig. 6d indicates that a considerable amount of precipitation occurred during 12 seconds in the temper-



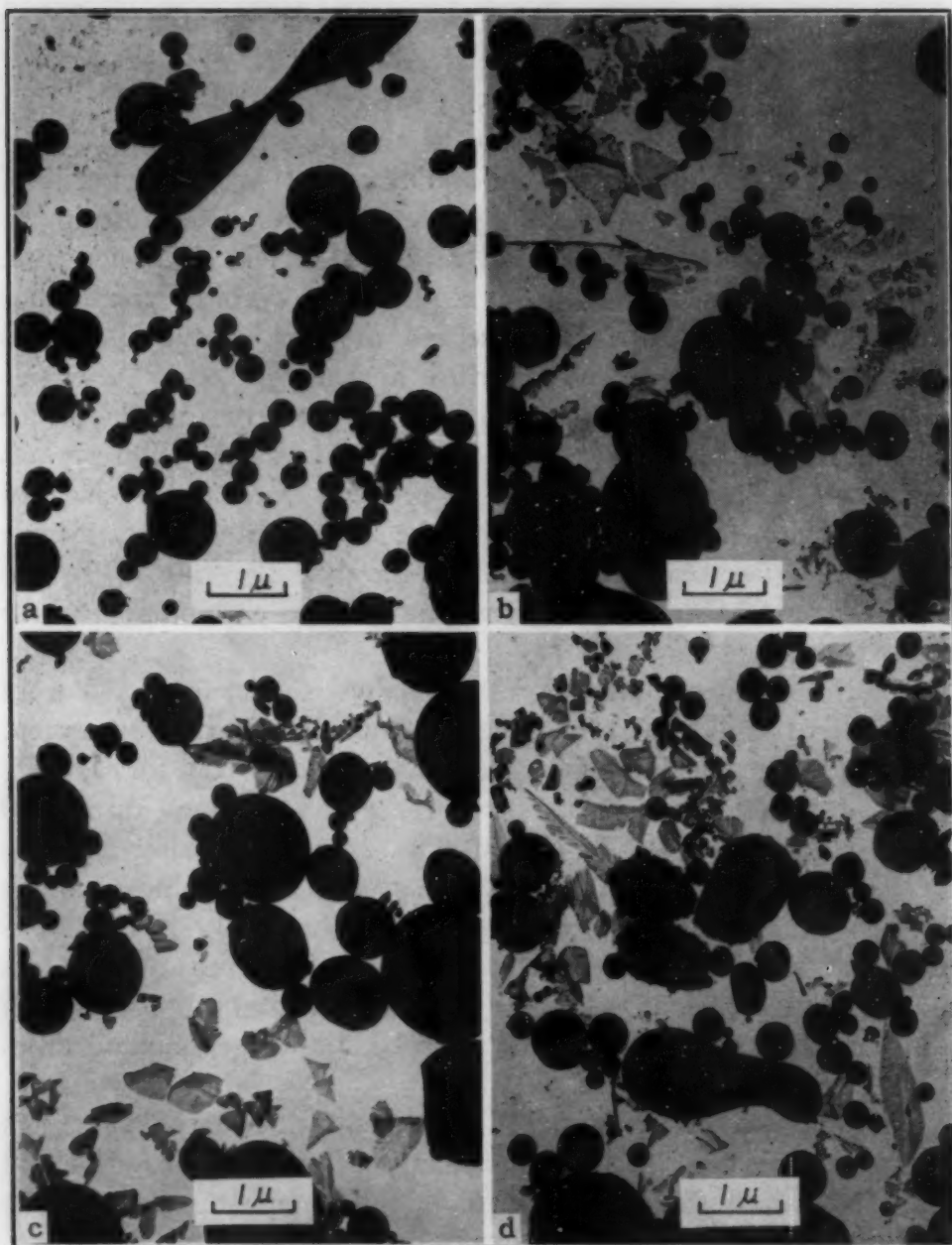


Fig. 5—Effect of Time of Sensitization on Carbide Form (Alloy EN3).  $\times 13,000$ . (Reduced  $\frac{1}{2}$  in reproduction.) All samples heated 5 minutes at 2000 °F and quenched into fused salt for the temperatures and times indicated, then water-quenched. a—2 minutes at 1200 °F; b—5 minutes at 1200 °F; c—15 minutes at 1200 °F; d—30 minutes at 1200 °F.  $\text{HNO}_3$  corrosion rate, inch per month: a—0.00077; b—0.00071; c—0.0011; d—0.00105.

ature range 1200 to 1350 °F (650 to 730 °C) and the carbides have recognizable dendritic forms. Other electron microscope studies have shown that these carbides can also be taken back into solid solution in the same length of time required to precipitate them, provided they are heated to the annealing temperature for only a few seconds. Only seconds at a temperature within the single-phase

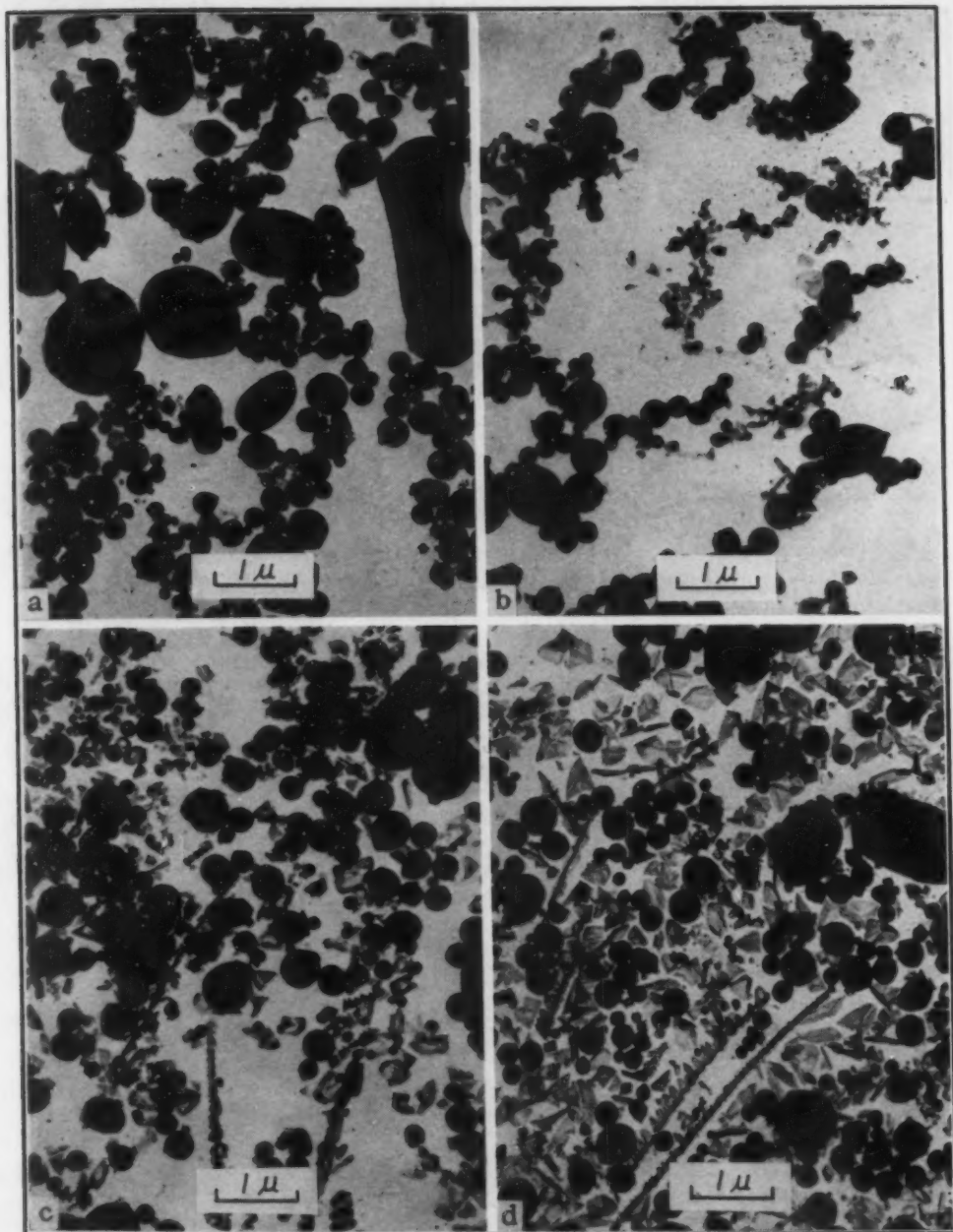


Fig. 6—Effect of Very Short Sensitization Times on Carbide Form (Alloy EX1).  $\times 13,000$ . (Reduced  $\frac{1}{3}$  in reproduction.) Heat treatment in range 1200 to 1600°F: a—0.6 second; b—2.5 seconds; c—10 seconds; d—12 seconds. Maximum temperatures attained: a—1210°F; b—1400°F; c—1450°F; d—1350°F.

$\gamma$  zone are necessary to redissolve completely the amount of carbide precipitation which occurs in times up to an hour at temperatures around 1250 °F (675 °C). The form of the carbide precipitate itself helps to explain the rapidity of sensitization and recovery. The carbide flakes and dendrites as shown in many of the preceding figures are essentially two-dimensional, being so thin that they are transparent to the electron beam and actually only a relatively few

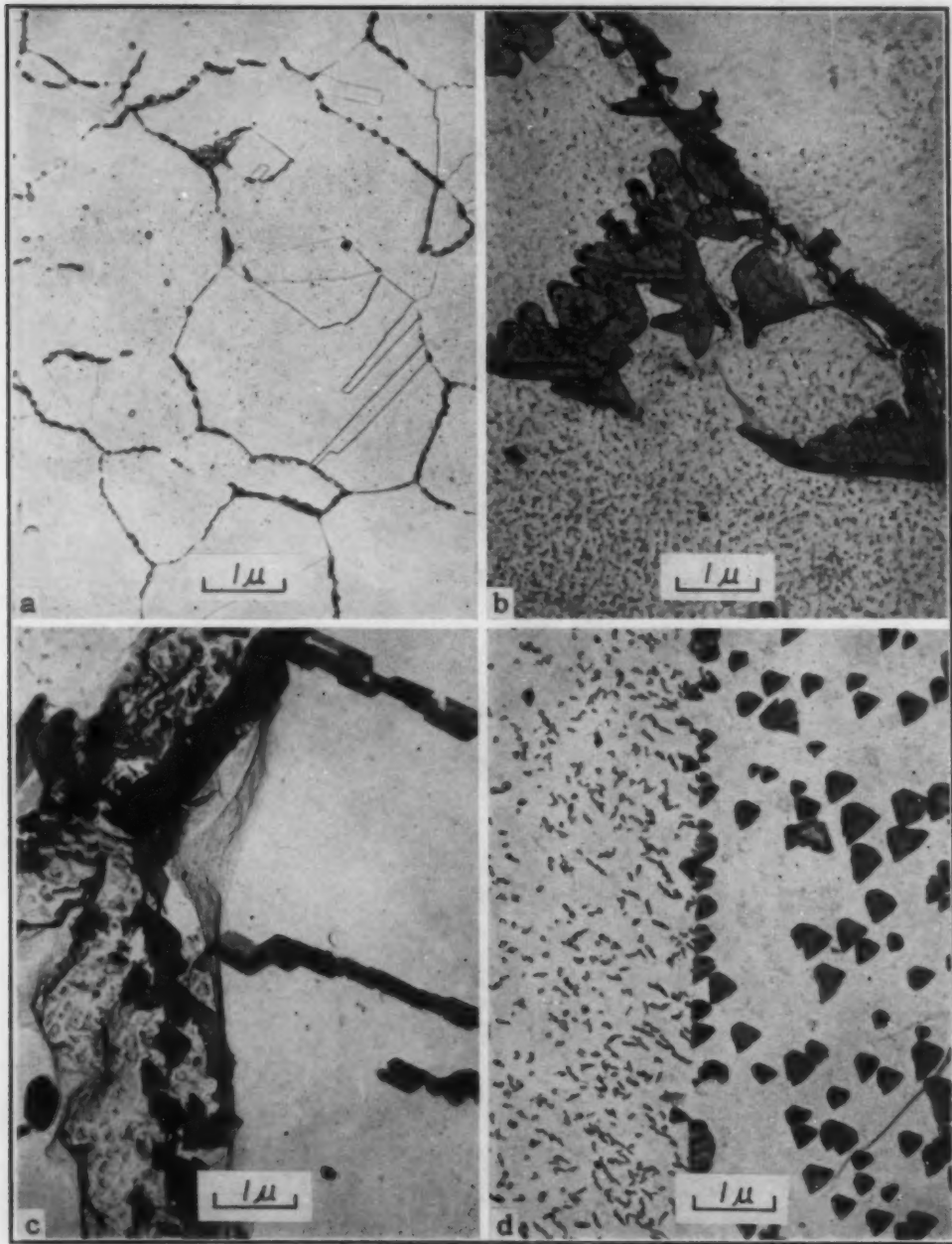


Fig. 7—Locus of Carbide Precipitation in Type 304 Stainless Steel. a—Photomicrograph of polished and etched (electrolytic oxalic acid) surface sensitized 1 hour at 1200°F. W.Q.  $\times 750$ . (Reduced  $\frac{1}{2}$  in reproduction.) b—Oxide replica of polished and etched ( $H_2SO_4$ -citric acid, electrolytic) surface after similar sensitization.  $\times 13,000$ . (Reduced  $\frac{1}{2}$  in reproduction.) c—Same but after sensitization for 185 hours.  $\times 13,000$ . (Reduced  $\frac{1}{2}$  in reproduction.) d—Carbides on passive film showing original loci of precipitation.  $\times 13,000$ . (Reduced  $\frac{1}{2}$  in reproduction.)

unit cells of chromium carbide thick.

*Locus of Carbide Precipitation in Type 304 Stainless Steel—*

In the past, studies of carbide precipitation in sensitized stainless steel have been based on metallographic observation of polished and etched alloy surfaces. The photomicrograph shown in Fig. 7a may



be regarded as typical of such a sample. Carbide precipitation is assumed to have occurred by reason of the sensitivity of the grain boundaries to selective, accelerated attack during etching. For this reason it has also been assumed that carbide precipitation takes place primarily at grain boundaries and not generally throughout the alloy matrix as, for example, is the case with age hardening alloys. Electron microscopy carried out with the aid of surface replicas has cast further light upon the precipitation mechanism, in particular the loci of precipitation. In Figs. 7b and 7c oxide replicas have successfully been adapted to studying carbides in situ in the alloy. Fig. 7b shows that during a 1-hour sensitization at 1200 °F (650 °C) (water quench) carbides were nucleated in the grain boundary and grew as dendrites into the metal. It is believed that Fig. 7b shows not the actual carbides but instead the etched-out impressions of the sites of carbide precipitation. The figure also shows that carbide precipitation at grain boundaries is not in the form of a complete continuous envelope as has been mentioned in the literature but is characterized rather by a discontinuous, irregular line of chromium carbide particles.

Fig. 7c is an oxide replica of the alloy sample from which the "ribbon-carbides" of Fig. 2g were isolated. Here actual carbides are shown in situ (clinging to the oxide film which replicated the polished and etched surface). In this figure the grain boundaries were etched very deeply and are seen to contain small, dense individual carbide particles.

Carbide precipitation is by no means confined to grain boundaries (and the ends of twin-bands) although these regions often appear to be selective loci for precipitation to occur. Fig. 7d shows an isolated film from a stainless steel sample which had been sensitized 1 hour at 1250 °F (675 °C), (water quench). This is an electron photomicrograph of an exceedingly thin oxide film formed by air exposure (room temperature) of a previously corroded metal surface. When the film was examined in the electron microscope, it was found to "contain" carbide particles of two varieties separated by what appears to be a grain or twin boundary existent in the underlying alloy and reproduced in the film. This figure may indicate that carbide precipitation does occur at locations other than at grain boundaries. The larger "flake" carbides in the right-hand grain have a definite orientation and it is evident that the boundary served as a selective limit for the precipitation of these larger particles. Work on Type 302 stainless steel has also shown that carbide precipitation may be more general than previously assumed.



*Cold-Worked Stainless Steel and Carbide Precipitation*—In the case of heavily cold-worked austenitic stainless steel it has become an accepted hypothesis that carbide precipitation due to sensitization heat treatments occurs generally throughout the alloy with no especial preference for grain boundaries. Multifold slip planes in

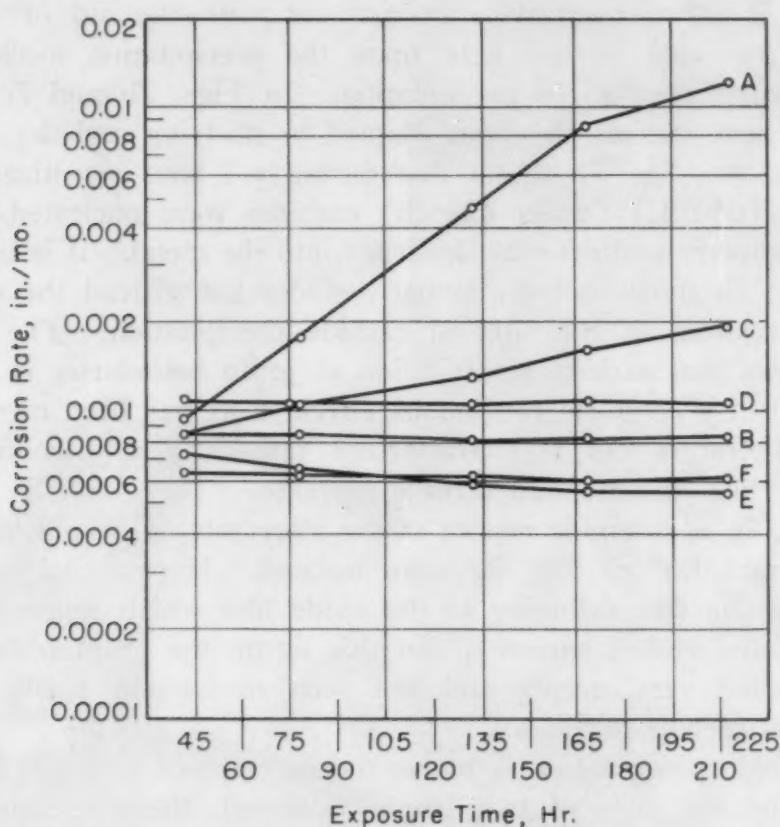


Fig. 8—Effect of Cold Reduction and Heat Treatment on  $\text{HNO}_3$  Corrosion Rates of 18-8-S Stainless Steel. A—Sensitized 1 hour at  $1250^\circ\text{F}$ , W.Q.; B—80% cold-reduced, sensitized; C—Sensitized, 80% cold-reduced; D—Sensitized, 80% cold-reduced, sensitized; E—Annealed; F—As cold-reduced 80%.

the cold-deformed alloy serve as nucleation loci to distribute the carbide relatively uniformly throughout the alloy matrix (11, 12). This hypothesis has been checked by electron microscope examination of the precipitated carbides and verified.

Data are summarized in Figs. 8 and 9, which correlate the effect of 80% cold reduction (both prior to sensitization and after sensitization) with the form of the carbide precipitate and the corrosion rate in 65%  $\text{HNO}_3$ .

Corrosion rate curve (A) in Fig. 8 is that of the unstrained, annealed and sensitized alloy which contains the large dendritic carbide flakes shown in the photomicrograph, Fig. 9a. Curve B

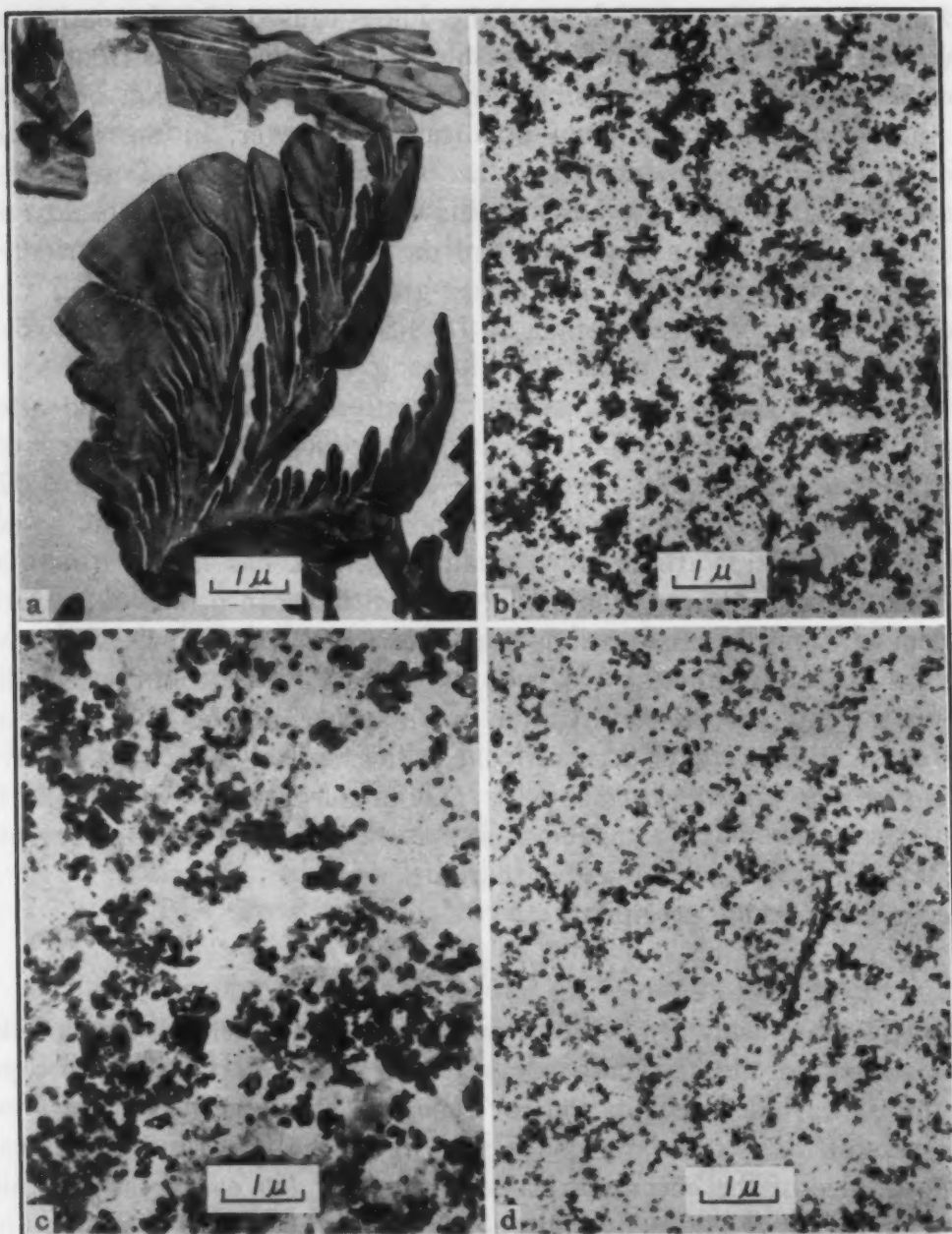


Fig. 9—Effect of Cold Reduction on the Form of Carbide in 18-8-S.  $\times 13,000$ . (Reduced  $\frac{1}{2}$  in reproduction.) a—Sensitized 1 hour, 1250°F, W.Q.; b—80% cold-reduced, sensitized; c—Sensitized, 80% cold-reduced; d—Sensitized, 80% cold-reduced, sensitized.

(Fig. 8) shows the beneficial effects of 80% cold reduction prior to sensitization on corrosion resistance. The corrosion rate of this sensitized material is low and not greatly above the corrosion rate curves of the annealed or the cold-reduced (both unsensitized) samples. Cold working sufficient to reduce the thickness of this sample 80% resulted in a uniform precipitation of very fine carbide particles throughout the alloy as illustrated in the photomicrograph,

Fig. 9b. Severe straining of the alloy caused the formation of countless slip planes, and the resulting fine uniform distribution of carbides is mainly responsible for the improved corrosion behavior. Another factor of unknown importance, however, in the improvement in corrosion resistance is the mechanical effect of grain distortion, which so "keys" the grains together that none are lost in the  $\text{HNO}_3$  corrosion test. None of the weight loss can be attributed to the "dropping out" of surface grains such as occurs in any undeformed, sensitized sample of 18-8-S given a standard corrosion test in  $\text{HNO}_3$ .

Curve C (Fig. 8) illustrates the effect of cold reduction after sensitization on corrosion rate. Cold reduction to the extent of 80% has considerably lowered the corrosion rate, and here again the mechanical disruption of grain boundaries and the breaking up of the dendritic carbides into small fragments has had a beneficial effect (see photomicrograph, Fig. 9c). Still more benefit is derived from a second sensitization heat treatment (Curve D, Fig. 8) which, paradoxically, has reduced the corrosion rate to an acceptable figure. The second sensitization treatment eliminates the magnetic  $\alpha$ -phase which is developed on cold rolling and also appears to have refined the carbide particle size (photomicrograph, Fig. 9d). If the latter has actually happened, it may be ascribed either to recrystallization of the fragmented carbide dendrites or possibly to a secondary carbide precipitation.

#### SUMMARY AND CONCLUSIONS

The application of the bromine-methanol method of carbide isolation and the use of oxide replicas in an electron microscope study of carbide precipitation in Type 304 stainless steel have been successful. The techniques have shown, for the first time, the actual appearance of the chromium carbide particles (in every case in this paper  $\text{Cr}_{23}\text{C}_6$ ) whose precipitation in grain boundaries results in sensitization of the alloy or an appreciable decrease in intergranular corrosion resistance. The effect of time and temperature on the crystalline form and habit of carbide particles has been clarified. Important conclusions are listed below:

1. The bromine-methanol technique of isolating carbides has been found superior to electrolytic methods which employ aqueous solutions, since the presence of water is avoided in the isolation procedure, thereby minimizing acid hydrolysis and decomposition of the metal carbides.

2. Electron microscopy of carbides formed by sensitization

times of the order of 1 hour has shown that these carbides have a dendritic form, typical of a high rate of diffusion-controlled particle growth. Carbides in the form of thin, effectively two-dimensional dendrites can easily account for observed rapid sensitization and recovery on very short-time heat treating cycles. The carbides, being only a few molecules in thickness, can be precipitated and redissolved in a matter of seconds or less.

3. When the conditions of time and temperature are such as to allow the carbide crystal to assume its characteristic state at the temperature and time in question, the unstable, dendritic carbide transforms to a carbide of geometrical habit determined by the metal lattice planes on which it is growing. This behavior appears to be new in the study of solid-solid transformations. The isothermal form change of chromium carbide appears to follow the progression: small carbide flakes and dendrites  $\rightarrow$  large dendrites  $\rightarrow$  dendritic fragmentation  $\rightarrow$  geometrical particles (of small average particle size but which may form stringers or oriented clusters). The habit changes occur more rapidly at high temperatures of sensitization.

4. Electron photomicrographs of carbides isolated from sensitized 18-8-S stainless steel after prior cold deformation (80% thickness reduction) have verified the hypothesis that carbides precipitate generally and in a finely divided form throughout the alloy matrix, thereby markedly diminishing the harmful effects of "heavy" carbide precipitation localized at grain boundaries.

5. The distribution and form of carbide precipitates in general have an important influence on the susceptibility of the alloy to intergranular attack. No definite correlation of carbide form alone with standard  $\text{HNO}_3$  corrosion rates of the heat treated alloys was established.

#### ACKNOWLEDGMENT

The authors wish to express their appreciation to M. H. Brown, W. B. De Long and P. H. Permar of the Engineering Research Laboratory and to R. F. Mehl of Carnegie Institute of Technology for their assistance in this work.

Acknowledgment is made to the Electron Microscope Laboratory of the Chemical Department who took the electron micrographs.

#### References

1. W. Koch, "Elektrolytische Isolierung der Karbide in legierten und unlegierten Stählen", *Stahl und Eisen*, No. 1, 1949, p. 1.
2. W. Koch and H. J. Wiester, "Neue Beiträge zur Kenntnis der Karbide in legierten Stählen", *Stahl und Eisen*, No. 3, 1949, p. 73.



3. W. Crafts and J. L. Lamont, "Secondary Hardening of Tempered Martensitic Alloy Steel", *Transactions, American Institute of Mining and Metallurgical Engineers*, Vol. 180, 1949, p. 471.
4. W. Crafts and J. L. Lamont, "Carbides in Long-Tempered Vanadium Steels", *Transactions, American Institute of Mining and Metallurgical Engineers*, Vol. 188, March 1950; *Journal of Metals*, p. 561.
5. W. Crafts and J. L. Lamont, "Carbides in Isothermally Transformed Chromium Steels", *Transactions, American Institute of Mining and Metallurgical Engineers*, Vol. 185, 1949, p. 957; *Journal of Metals*, December 1949; T.P. 2709.
6. E. M. Mahla and N. A. Nielsen, "Application of the Electron Microscope to Corrosion Studies", Pittsburgh International Conference on Surface Reactions, 1948, p. 60. Corrosion Publishing Company, Pittsburgh, Pa.
7. E. M. Mahla and N. A. Nielsen, "A Study of Films Isolated from Passive Stainless Steels", *Transactions, Electrochemical Society*, Vol. 93, No. 1, p. 1.
8. E. M. Mahla and N. A. Nielsen, "An Oxide Replica Technique for the Electron Microscope Examination of Stainless Steel and High Nickel Alloys", *Journal of Applied Physics*, Vol. 19, No. 4, 1948, p. 378.
9. A. B. Kinzel and R. Franks, "The Alloys of Iron and Chromium", Vol. II, 1st ed., 1940, p. 275, McGraw-Hill Book Company, Inc., New York.
10. R. F. Mehl and L. K. Jetter, "The Mechanism of Precipitation from Solid Solution. The Theory of Age Hardening", *Age Hardening of Metals*, 1940, p. 342, published by the American Society for Metals, Cleveland, Ohio.
11. E. C. Bain, R. H. Aborn and J. J. B. Rutherford, "The Nature and Precipitation of Intergranular Corrosion in Austenitic Stainless Steels", *TRANSACTIONS, American Society for Steel Treating*, Vol. 21, 1933, p. 481.
12. E. C. Rollason, "Some Effects of Cold Rolling on the Intergranular Corrosion of the 18-8 Stainless Steels", *Journal, Iron and Steel Institute*, Vol. 129, 1934, p. 311.

## DISCUSSION

**Written Discussion:** By A. M. White, Stamford Research Laboratories, American Cyanamid Co., Stamford, Conn.

The authors are to be congratulated on the excellent electron micrographs which they have presented in this paper. The time-consuming and painstaking nature of the work can be appreciated only by those who have worked with the electron microscope.

The derived concept of carbide precipitation in the form of essentially two-dimensional dendrites rather than as continuous envelopes or spheroidal particles randomly distributed at grain boundaries is novel. It is difficult to visualize how such ribbon-shaped carbides would be distributed around the three-dimensional austenitic grains. Confirmatory evidence in the form of electron micrographs of polished specimens might be of assistance in interpreting the results and a synthetic three-dimensional model might also be of value.

In October 1947, evidence that carbide precipitation tends to form continuous envelopes was obtained in our laboratory and is illustrated by two electron micrographs. Fig. 10 shows an electron micrograph of Type 304 stainless steel which was held at 1075 °F (580 °C) for 400 hours. The specimen was mechanically polished and then etched electrolytically with

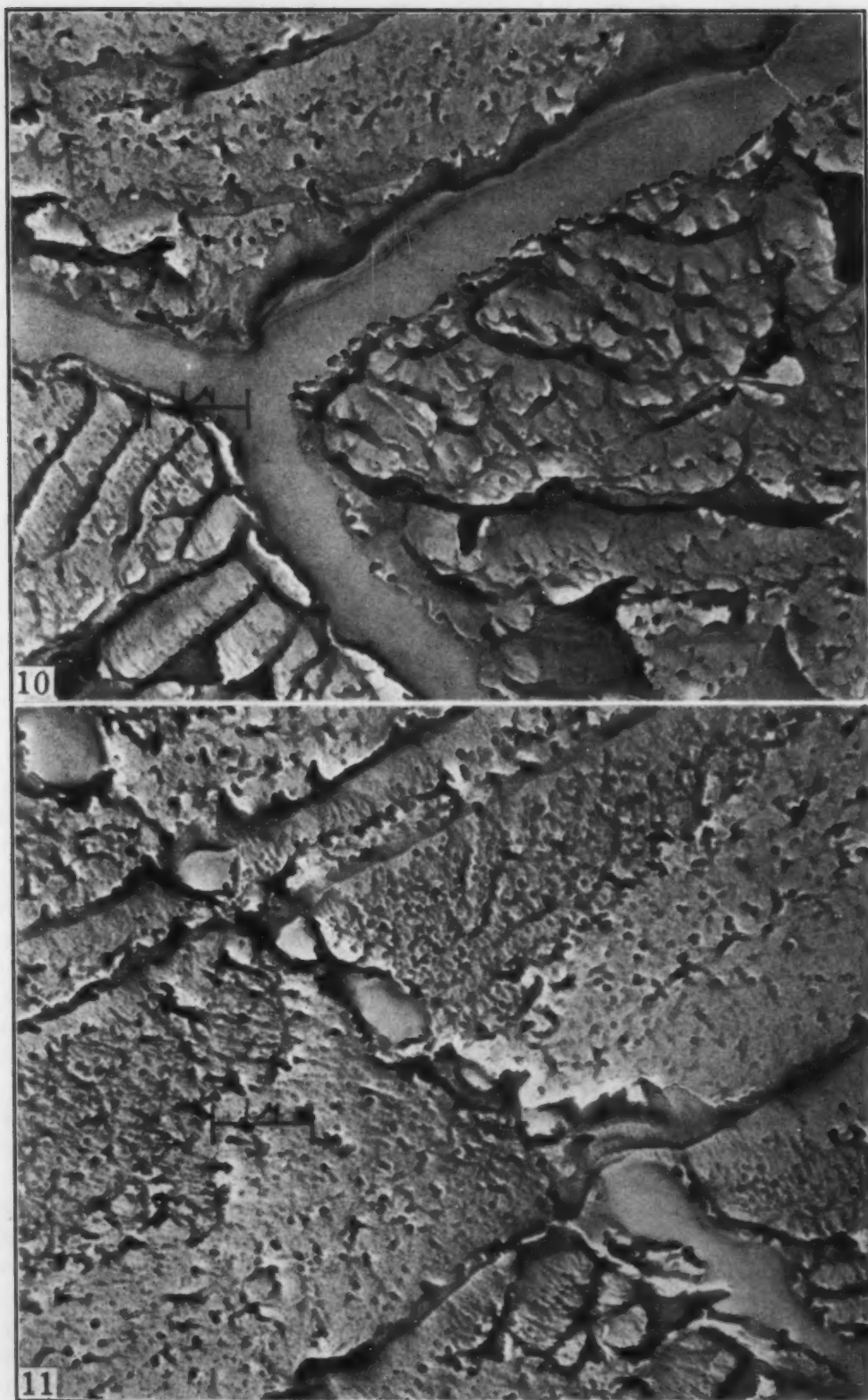


Fig. 10—Electron Microstructure of Type 304 Stainless Steel After Exposure at 1075 °F for 400 Hours. Specimen was mechanically polished, then etched electrolytically with chromic acid.  $\times 11,800$ .

Fig. 11—Adjacent Field of Specimen of Fig. 10.  $\times 11,800$ .

10% chromic acid. The polystyrene-silica replicating technique was used without shadowing. We believe that this micrograph represents the intersection of three grains and that the material at the grain boundaries is carbide. This continuous carbide, when considered on a three-dimensional basis, must be representative of complete envelopes around the grains. The structures in the grains are believed to be at least partly artifacts, probably resulting from polishing. Fig. 11 is an electron micrograph of an adjacent area of the same specimen. In this area the carbide is not continuous but there is some indication that a continuous envelope was being formed when the reaction was arrested.

Our study of this problem was by no means exhaustive and we made no attempt to confirm our observations with other types of data. It will be appreciated if the authors, using the background of their experience, will comment on our photomicrographs.

**Written Discussion:** By Carl A. Zapffe, research metallurgist, Baltimore, Md.

Before the technical features of this paper come up for discussion, it is necessary and highly appropriate to congratulate Drs. Mahla and Nielsen for presenting one of the finest set of electron micrographs of any yet appearing in metallurgy, and certainly the only set of its kind referring to the important problem of sensitization in austenitic stainless steels. It will be studies such as this, in combination with surface-tension thermodynamics as currently being presented by Drs. Spretnak and Speiser, that will promise an ultimate explanation for sensitization, which so far remains virtually unexplained.

While there is little reason to doubt that these patterns principally concern carbide formation, nevertheless it seems proper to have the authors define more clearly whether these forms are entirely carbides, or whether it is possible that other precipitations are included. Nitrogen has already figured in discussions of sensitization as being a possible partner with carbon, whereupon it becomes possible that nitrides are included in the micrographs. Also, stainless steels are known to contain an important quantity of oxygen, and the presence of a solubility boundary in the temperature range of sensitization is not unlikely. Microchemical methods have come in for much development in recent years, and it is an intriguing possibility that these residues studied by the present authors might submit to microchemical analysis, both for determining the presence of noncarbide forms, and for ascertaining the stoichiometry of the carbide.

**Written Discussion:** By W. D. Forgeng, Union Carbide and Carbon Research Laboratories, Inc., Niagara Falls, N. Y.

The authors have made a valuable contribution to the study of the mechanism of carbide precipitation in 18% chromium-8% nickel steels. Isolation methods and particularly the bromine-methanol procedure have been shown to yield interesting results.

We have had occasion to examine, by light and electron microscopy, residues which were isolated electrolytically by means of an aqueous hydrochloric acid solution from Type 304 steels that had been heated for one week at 1020, 1200, 1380, and 1560 °F (550, 650, 750, and 850 °C). At the two lower temperatures, the material most commonly observed in our residues was unlike any of the structures shown in the paper and was an



agglomerate of very narrow fibers arranged in a triangular pattern. Constituents identical with those shown in Fig. 3d of the paper were the chief types found in the samples heated at 1380 and 1560 °F (750 and 850 °C). The presence of austenite as well as chromium carbide was indicated by X-ray diffraction in the residues, and since the triangular structures bore a marked resemblance to etch-pit configurations, the possibility arose that they might be thin flakes of the original metal that were perforated by topochemical attack during electrolysis. Examining the residues by means of the optical microscope, however, we were able to correlate the appearance and size of the flakes with those of the carbides in the polished and etched specimens. Incidentally, some of the perfect equilateral triangles measured as much as 9 microns on a side and were too large to provide satisfactory subjects for electron microscopy. From these observations, we are inclined to agree with the authors that the triangular structures are in fact chromium carbide and we confirm their observation that the bromine-methanol procedure is more satisfactory for separating carbides from austenite than one in which electrolysis in aqueous hydrochloric acid is employed.

**Written Discussion:** By Samuel J. Rosenberg, metallurgist, National Bureau of Standards, Washington, D. C.

The authors of this unique paper make an interesting observation on the effect of direction of temperature change on the sensitization of stainless steel. They conclude that direct cooling from the annealing temperature to the sensitizing temperature results in less severe sensitization than results when the annealed steel is cooled to room temperature and then heated to the sensitizing temperature. Examination of their data indicates that this conclusion is justified.

It should be pointed out, however, that the effect of direction of temperature change on corrosion was obtained on two different steels. Apparently this particular subject was but a minor part of their study, but since it was included, it is difficult to understand why the variable of composition was not eliminated by the simple expedient of using the same steel.

When mention is made of sensitization of stainless steel, most metallurgists think of intergranular embrittlement. It is the writer's opinion that this particular property is better evaluated by the boiling copper sulphate-sulphuric acid test than by the boiling nitric acid test. In view of the fact that results obtained with these two boiling solutions frequently show considerable disagreement, the data submitted by the authors would be enhanced in value, and the effect of direction of temperature change, if any, more definitely established, if the authors would or could include such additional tests.

**Written Discussion:** By M. G. Fontana, professor and chairman, Department of Metallurgy, The Ohio State University, Columbus, Ohio.

The authors are to be congratulated for a fine piece of painstaking work. They present a new approach to the problem of carbide precipitation in austenitic stainless steels. Studies of this type should be of great value in obtaining a more complete understanding of the phenomenon of intergranular corrosion of these steels.

Of particular interest are the data showing recovery of corrosion



resistance of sensitized 18-8-S as a result of cold working after sensitization. Does this simply mean that the susceptible intergranular paths or network are broken up and become discontinuous or is it a hint that perhaps the commonly accepted chromium depletion theory may not be correct? The authors' comments would be appreciated.

**Written Discussion:** By Morton C. Smith, associate professor, Department of Metallurgy, Colorado School of Mines, Golden, Colo.

In tracing the initial appearance and subsequent changes in form of chromium carbide particles precipitated during sensitization of an 18-8 type stainless steel, Mahla and Nielsen have made a significant contribution to our knowledge of the behavior of this versatile group of alloys, and have beautifully demonstrated another important field of usefulness for the electron microscope in metallographic research. The evidence which they present leaves little doubt that, in the past, nearly all of us have been misled with regard to the shape and distribution of the carbides precipitated in stainless steel. The powerful etching solutions required to prepare an austenitic stainless steel for routine metallographic examination undoubtedly result in galvanic corrosion between carbide particles and the austenitic matrix so intense that only the resulting corrosion pits can normally be resolved optically, and these are grossly enlarged in comparison with the actual carbide areas adjacent to which they have originated.

The precise geometric form eventually approached by  $\text{Cr}_{23}\text{C}_6$  particles (and best illustrated by the authors' Fig. 2h) deserves comment, since it illustrates an effect which is perhaps not sufficiently emphasized by the authors, and which is certainly not well understood by most metallurgists. Any stable precipitate particle, when heated to a temperature at which diffusion occurs at an observable rate, approaches a condition of minimum surface energy which is typical both of the material of which the particle is composed and of the matrix in which it is contained. The total surface energy of any given particle is, of course, the product of its total surface area and of the surface energy per unit area exposed to its environment. There are, then, two principal means by which total surface energy of any given particle may be decreased: total surface area may be reduced, or energy per unit area of actual surface may be reduced.

$\text{Fe}_3\text{C}$ , the most familiar metallic precipitate of all, has a rather complex orthorhombic crystal structure, and consequently is one of the rather rare metallic materials which is almost isotropic in its properties, including its surface energy. The energy condition of an  $\text{Fe}_3\text{C}$  particle is, therefore, almost independent of the family of crystallographic planes which happens to be exposed at its surface, and upon prolonged heating  $\text{Fe}_3\text{C}$  particles attain the condition of minimum surface energy by forming spheres, thus minimizing surface area without regard to the types of planes ultimately exposed at the surface of each sphere. This behavior is typical of isotropic materials (e.g., of liquids). It is not typical of crystalline materials, but, unfortunately, is the behavior expected of them by most metallurgists simply because spheroidizing of  $\text{Fe}_3\text{C}$  in plain carbon steels is so familiar to them.

Like most other metallic phases,  $\text{Cr}_{23}\text{C}_6$  differs markedly from  $\text{Fe}_3\text{C}$  in having a relatively simple crystal structure of high symmetry (based,

in this case, upon a face-centered cubic lattice); it is quite strongly anisotropic in its surface energy as well as in its other properties. Within such simple, symmetrical crystal structures there are always one or a few families of crystallographic planes on which atomic packing is unusually dense; such planes, in general, have outstandingly low surface energy per unit area when they are exposed at a crystal face. The tendency of  $\text{Cr}_{23}\text{C}_6$  particles to reduce surface energy by reducing surface area is beautifully illustrated by the authors' sequences of pictures showing steps in the consolidation of feathery, almost two-dimensional dendrites into compact, three-dimensional bodies. This process is not, however, carried to the same conclusion finally attained by  $\text{Fe}_3\text{C}$ , since, at the surface of a sphere, every plane within the crystal (whether of high energy or of low energy) is somewhere exposed. Instead, in  $\text{Cr}_{23}\text{C}_6$ , the process terminates when compact idiomorphic crystals have been developed, on which only low-energy planes appear as crystal faces. In the case of this chromium carbide, the lowest-energy form is evidently a cube, on which only (100) type planes are exposed; in other metallic phases the equilibrium form is often an octahedron or a dodecahedron, etc. In strongly anisotropic materials, spheroids, if originally present, would actually revert to regular polyhedra such as these upon prolonged heating, a process which is exactly the reverse of spheroidizing. With the notable exception of  $\text{Fe}_3\text{C}$ , and of a few other complex and almost isotropic metallic phases, spontaneous formation of idiomorphic crystals is the behavior to be expected of any stable metallic precipitate upon prolonged heating.

Fragmentation of relatively large  $\text{Cr}_{23}\text{C}_6$  dendrites as one step toward formation of compact geometrical shapes, as is postulated by the authors, would apparently involve a temporary increase in surface area, and probably also in surface energy, since there is no evident means by which it could produce a compensating reduction in energy per unit area of surface exposed. Spontaneous fragmentation of dendrites, therefore, appears very unlikely. Both Figs. 1h and 2e suggest that an early step in the progressive consolidation of dendrites is a pronounced thickening of dendrite arms near their tips, where, initially, surface energy must be abnormally high because of very large surface area per unit of mass. The thickened tips appear to remain attached to the axis of each dendrite only by relatively thin branches. Is it possible that the observed fragmentation is not spontaneous, but instead is purely mechanical—a result of fracturing of these dendritic branches during handling incidental to dissolution of the specimen and embedding of carbides in the Formvar screen?

In the remarkable photograph of Fig. 7d, it appears that the "large" carbide particles in the right half of the field of view may actually be identical with the "small" ones in the left half, differing only in orientation. Essentially flat carbide plates (such as those of Fig. 3d), precipitated parallel, for example, to (111) type planes of the austenite matrix, might have this appearance on opposite sides of a twinning plane through the austenite, which the vertical dividing line of Fig. 7d might well represent.

Corrosion testing is mentioned only incidentally in connection with the subject matter of this paper, although the conclusions drawn from it are given some prominence. It seems, however, that corrosion resistance

was evaluated simply by measuring loss of weight during exposure of specimens to  $\text{HNO}_3$  solutions of standard concentration. Where intergranular attack predominates, this appears to be a very questionable criterion of relative corrosion resistance.

Mahla and Nielsen have developed a new and very promising technique for the study of precipitation reactions, and have completed some truly fundamental work on the behavior of 18-8 type stainless steels. Unfortunately, such work has been rare, and when undertaken it deserves both recognition and applause. I am very happy that this program of investigation is to be continued, and look forward to publication of its future results.

#### Authors' Reply

We wish to thank all of the discussers of our paper. We are grateful for the interest evidenced in this work.

Specifically, in reply to A. M. White's comments, we believe that the carbides do not constitute continuous envelopes around the grain boundaries but rather nucleate in the grain boundaries and grow into the body of the grains. Figs. 7b and 7c, which are electron micrographs of replicas of stainless steel surfaces, illustrate this phenomenon.

It is dangerous to attempt an interpretation of electron micrographs prepared by techniques with which we are unfamiliar. However, we would speculate that the replicas which Mr. White shows are representative of the chromic acid etched structure and not of stainless steel carbides. Fig. 12 shows a light micrograph at  $\times 500$  of an annealed Type 304 stainless sample which has been etched with 10% boiling chromic acid for 18 hours. It is evident that intergranular grooves have developed along grain boundaries, even when the material was annealed prior to exposure to the chromic acid. We believe that grooves similar to these are being reproduced in Mr. White's micrographs.

Dr. Zapffe's comments are highly complimentary. We too feel the need for further and active extension of information of the kind presented in the paper. For that reason this paper must be considered in the nature of a progress report, and we hope to present further information at a later date. We have not been able to identify forms other than carbide in the samples that we have isolated from 18-8 to date. However, we do believe that other precipitates may be included. Quantitative separation and analysis of these residues is being undertaken, and we should be able to answer Dr. Zapffe's questions more certainly at some future time. In the isolation of carbides from heat treated ferritic chromium steels which were not discussed in this paper, some evidence for  $\text{CrN}_2$  has been obtained.

We are appreciative of Mr. Forgeng's discussion and confirmation of our work. We are not surprised that Mr. Forgeng has found equilateral triangles of carbides measuring as much as 9 microns on a side. Fig. 1g shows a carbide whose over-all dimensions taken on two successive negatives in a panoramic fashion is in excess of 18 microns; approximately 16 microns are shown in Fig. 1g.

Dr. Rosenberg has raised a question about the effect of interrupted quenching on the degree of sensitization of stainless steels. The samples used in this work were available from a previous research and therefore



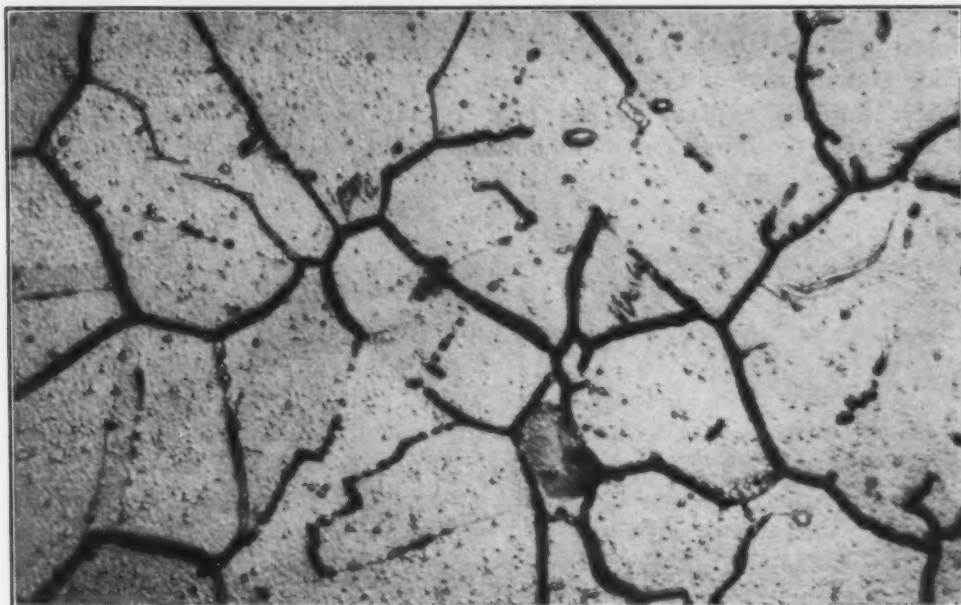


Fig. 12—Annealed 18-8-S Stainless Steel After 18 Hours in Boiling 10%  $\text{CrO}_3$ .  $\times 500$ .

the authors had no control over the compositions of steels used. However, these previous studies have shown that there is no question about the validity of the effect of direction of temperature change on the sensitization of stainless steels. It has been confirmed on several other different heats of 18-8.

Again in the cases where  $\text{HNO}_3$  acid test data are included, these samples were obtained from previous researches. As has been shown in the recent ASTM Symposium on Tests for Stainless Steels, there is good agreement between the nitric acid test and the boiling  $\text{H}_2\text{SO}_4$ - $\text{CuSO}_4$  test for Type 304 stainless steels.

We appreciate Dr. Fontana's discussion. In answer to his question on the reason for the recovery of the corrosion resistance of sensitized 18-8 as a result of severe cold working, we believe that his first suggestion is probably right. Whether or not there is an indication that the commonly accepted chromium depletion theory may not be correct is questionable, since the breaking up of the intergranular material could explain the result in either event. We do believe, however, that the chromium depletion theory is not necessary to explain the facts of intergranular corrosion as presented in this paper. Further work will be required to conclusively disprove the theory.

We are pleased with Mr. Smith's comments. That the fragmentation process is, as indicated in the paper, to be part of a continuous process in the change of carbide precipitates to more stable geometric forms, apparently bothers Mr. Smith as much as it does the authors. In this instance we are reporting the facts as we see them; however, we agree that Mr. Smith's explanation presents a possible mechanism for fragmentation. It may also be that the thin connections of branches to main dendrites may themselves be spontaneously broken on isolation. It is also possible, however, that sufficient lattice accommodation accompanies frag-



mentation to result in a reduction in energy per unit area of surface exposed and the process may thus be a valid part of the sequence of carbide transformations.

Mr. Smith's explanation of Fig. 7 may be right; however, there appears to be a difference in population density on opposite sides of the twin boundary.



Fig. 7. Micrograph showing a network of lines, likely representing grain boundaries or twin boundaries in a metal specimen.

The micrograph shows a network of lines, likely representing grain boundaries or twin boundaries in a metal specimen. The lines are irregular and intersect, forming a complex web-like pattern across the field of view. The lines are more densely packed in some areas than others, suggesting a difference in population density on opposite sides of the twin boundary. The overall appearance is that of a metal specimen that has undergone some form of transformation, possibly related to the carbide transformations mentioned in the text.

## LONG-TIME ELEVATED TEMPERATURE TEST OF CHROMIUM-MOLYBDENUM STEELS

BY A. B. WILDER AND J. O. LIGHT

### *Abstract*

*The stability of over one hundred different types of steel at 900, 1050 and 1200 °F (480, 565 and 650 °C) is being evaluated over a period of 10 years. Welded samples are included in the investigation. The results obtained in an examination of 35 of the molybdenum-bearing steels for evidence of structural changes, oxidation characteristics and impact properties after exposure for 10,000 and 34,000 hours are presented.*

*Typical carbon-molybdenum, molybdenum-vanadium, chromium-molybdenum and chromium-molybdenum-vanadium steels were investigated. Some of the material was obtained from commercial pipe. The steels containing less than 1% chromium were severely oxidized in air during 10,000 hours' exposure at 1200 °F (650 °C). No significant oxidation was observed in the 9 and 12% chromium steels after 10,000 hours' exposure at this temperature. The carbon-molybdenum steels with fine-grained deoxidation practice, the  $\frac{1}{4}\%$  Cr -  $\frac{1}{2}\%$  Mo steel and the Mo-V steels graphitized after 10,000 hours' exposure. The other steels exposed for 10,000 hours and in certain cases for 34,000 hours did not graphitize. This includes all the steels containing  $\frac{1}{2}$  to 12% chromium and the carbon-molybdenum steels melted to coarse-grained deoxidation practice.*

*Several post-heat treatments of weld specimens did not prevent graphitization during exposure at 1050 °F (565 °C) in steel which otherwise graphitized. The Charpy impact test results at ambient temperature of the 1 to 12% chromium-molybdenum steels were not adversely affected by exposure at the elevated temperatures. Impact properties of the carbon-molybdenum and  $\frac{1}{2}\%$  chromium-molybdenum steels were to some extent decreased by exposure with the exception of the quenched and tempered  $\frac{1}{2}\%$  chromium-molybdenum steel.*

---

A paper presented before the Thirty-second Annual Convention of the Society, held in Chicago, October 21 to 27, 1950. Of the authors, A. B. Wilder is chief metallurgist, National Tube Company, U. S. Steel Company Subsidiary, Pittsburgh, and J. O. Light is chief metallurgist, National Tube Company, Lorain Works, Lorain, Ohio. Manuscript received July 12, 1950.

GRAPHITIZATION, first observed in power plant piping systems in 1943, was reported by Emerson (1).<sup>1</sup> Seamless steel pipe with approximately 0.15% carbon and 0.50% molybdenum, melted to fine-grained deoxidation practice, graphitized in the weld heat-affected zone and parent metal. It was soon observed by Kerr, Eberle (2) and others that steel melted to coarse-grained deoxidation practice (3) was less susceptible to graphitization. Later the beneficial effects of chromium in the control of graphitization were recognized by various investigators.

The recognition of coarse-grained deoxidation practice and the use of chromium in the control of graphitization in seamless pipe for power plant service led to the production of this type of steel. As a result of the work at Battelle Memorial Institute by Hall and Hoyt (4) and other laboratories, it developed that steel containing 0.5 to 1.0% chromium and 0.5% molybdenum with 0.15% carbon would be desirable for steam power plant piping systems operating at temperatures in the neighborhood of 1000 °F (538 °C). Properties of experimental heats with approximately 0.15% carbon and 0.50% chromium were described by Fitzgerald, Wilder, Smith and White (5). One of the heats was melted to coarse-grained deoxidation practice, and the other to fine-grained deoxidation practice. Both heats of steel are in power plant piping services. The fine-grained heat was investigated to determine if this type of steel would graphitize in the presence of chromium, and no graphitization has been observed after nearly four years' exposure at 900 and 1050 °F (480 and 565 °C). Recently, Weisberg (6) described steel for 1050 °F (565 °C) steam temperatures containing 2 and 3% chromium with 1% molybdenum. The trend is apparently toward the use of higher chromium contents for increased operating temperatures without restrictions in deoxidation practice.

#### PURPOSE OF THE INVESTIGATION

Due to the importance of preventing graphitization in steam power plant piping systems, a wide variety of steels has been investigated in many laboratories during the past few years. Most of these steels have been included in the present investigation which describes exposure tests of weld samples at 900, 1050 and 1200 °F (480, 565 and 650 °C) for periods up to 34,000 hours. In addition to studies of the microstructure of weld bead specimens, oxidation characteristics, impact and hardness properties of unwelded material were evaluated. A considerable amount of data has already been

<sup>1</sup>The figures appearing in parentheses pertain to the references appended to this paper.

reported in previous papers (7, 8, 9) and, as the experimental work progresses, additional results will be presented.

### MATERIALS INVESTIGATED

Chemical composition, deoxidation practice with respect to the use of aluminum and the carburized austenitic grain size of the steels investigated are shown in Table I. Phosphorus and sulphur

Table I  
Chemical Composition, Deoxidation Practice and Grain Size

Code	Grade	Process	C	Mn	Si	Cr	Mo	Other	Deoxi- dation Lbs/N.T. Al	Austen- itic Grain Size
7B	C- $\frac{1}{2}$ Mo	OH	0.16	0.85	0.24	0.03	0.51	.....	0	1-3
7C	C- $\frac{1}{2}$ Mo	OH	0.22	0.51	0.17	0.05	0.50	.....	0.4	1-3
7D	C- $\frac{1}{2}$ Mo	OH	0.13	0.52	0.16	0.06	0.52	.....	1.6	6-8
8D	C-1 Mo	I	0.14	0.45	0.16	0.01	0.97	.....	2.0	(2-4) (6-8)
9D	$\frac{1}{4}$ Cr- $\frac{1}{2}$ Mo	I	0.12	0.41	0.11	0.21	0.57	.....	2.0	6-8
12B	$\frac{1}{2}$ Cr- $\frac{1}{2}$ Mo	E	0.13	0.51	0.22	0.48	0.58	.....	0	1-3
12D	$\frac{1}{2}$ Cr- $\frac{1}{2}$ Mo	I	0.14	0.47	0.17	0.48	0.51	.....	2.0	6-8
12DX	$\frac{1}{2}$ Cr- $\frac{1}{2}$ Mo	E	0.11	0.46	0.14	0.43	0.58	.....	1.3	5-7
12DY	$\frac{1}{2}$ Cr- $\frac{1}{2}$ Mo	E	0.11	0.46	0.14	0.43	0.58	.....	1.3	5-7
12DZ	$\frac{1}{2}$ Cr- $\frac{1}{2}$ Mo	E	0.11	0.46	0.14	0.43	0.58	.....	1.3	5-7
15C	1 Cr- $\frac{1}{2}$ Mo	E	0.12	0.45	0.74	1.13	0.50	.....	0.5	1-3
16D	2 Cr- $\frac{1}{2}$ Mo	E	0.11	0.50	0.34	2.18	0.51	.....	2.3	3-5
17D	5 Cr- $\frac{1}{2}$ Mo	E	0.13	0.42	0.22	4.69	0.47	.....	3.0	5-7
18D	5 Cr- $\frac{1}{2}$ Mo-Si-Ti	E	0.07	0.80	1.14	4.71	0.84	0.29 Ti	1.5	6-8
19D	5 Cr- $\frac{1}{2}$ Mo-Ti	E	0.05	0.40	0.32	5.19	0.51	0.55 Ti	1.5	5-7
20D	5 Cr- $\frac{1}{2}$ Mo-Cb	I	0.09	0.54	0.41	5.05	0.53	0.89 Cb	2.0	5-7
21D	9 Cr-1 Mo	E	0.09	0.44	0.66	8.94	0.89	.....	1.0	6-8
48	12 Cr- $\frac{1}{2}$ Mo	E	0.07	0.40	0.30	12.26	0.49	.....	0*	...
52D	3 Cr-1 Mo	E	0.11	0.45	0.39	3.21	0.97	.....	0.75	5-7
55	$1\frac{1}{2}$ Mo- $\frac{1}{4}$ V	I	0.16	0.35	0.41	0.03	1.43	0.16 V	0	7-8
56	$1\frac{1}{2}$ Mo- $\frac{1}{4}$ V	I	0.17	0.39	0.46	0.03	1.40	0.16 V	0.4	6-8
57	$1\frac{1}{2}$ Mo- $\frac{1}{4}$ V	I	0.17	0.38	0.45	0.03	1.48	0.17 V	1.3	7-8
70	1 Mo- $\frac{1}{4}$ V	E	0.20	0.58	0.27	0.09	0.99	0.22 V	0.5	7-8
70A	1 Mo- $\frac{1}{4}$ V	E	0.20	0.58	0.27	0.09	0.99	0.22 V	0.5	7-8
72	1 Cr- $\frac{1}{2}$ Mo	E	0.14	0.45	0.15	0.95	0.52	.....	0	1-3
73	$\frac{1}{2}$ Cr- $\frac{1}{2}$ Mo	E	0.14	0.47	0.21	0.48	0.50	.....	0.5	1-3
74	$\frac{1}{2}$ Cr- $\frac{1}{2}$ Mo	E	0.11	0.54	0.15	0.49	0.52	.....	0.13	1-3
75	1 Cr- $\frac{1}{2}$ Mo	E	0.11	0.51	0.28	0.94	0.56	.....	0	3-5
76	1 Cr- $\frac{1}{2}$ Mo	E	0.07	0.51	0.17	1.09	0.61	.....	0	1-3
77	1 Cr- $\frac{1}{2}$ Mo	E	0.13	0.53	0.30	0.91	0.51	.....	0.13	3-5
78	1 Cr- $\frac{1}{2}$ Mo	E	0.13	0.56	0.19	0.89	0.51	.....	0.13	3-5
79	C- $\frac{1}{2}$ Mo-Al	I	0.18	0.44	0.25	0.06	0.54	.....	4.0	6-8
80	$\frac{1}{2}$ Cr- $\frac{1}{2}$ Mo-Al	I	0.18	0.50	0.26	0.55	0.56	.....	4.0	6-8
81	$\frac{1}{2}$ Cr- $\frac{1}{2}$ Mo- $\frac{1}{4}$ V	E	0.13	0.36	0.24	0.56	1.03	0.23 V	0	7-8
81A	$\frac{1}{2}$ Cr- $\frac{1}{2}$ Mo- $\frac{1}{4}$ V	E	0.13	0.36	0.24	0.56	1.03	0.23 V	0	7-8

OH—Open-Hearth. E—Basic Electric. I—Induction. \*Calcium Silicon.

were below 0.035%. The steels in the form of 1 by 1-inch surface-ground bars with code identification 7B to 57, inclusive, were exposed 34,000 hours and steels 70 to 81A, inclusive, were exposed 10,000 hours at 900, 1050 and 1200 °F (480, 565 and 650 °C). Heat treatment of the material prior to exposure and type of electrode used for the bead welds are shown in Table II. Some of the steels as indicated in Table II were selected from heavy wall pipe samples and exposed in the original heat treated condition.



**Table II**  
**Heat Treatment and Welding Electrode**

Code	Material	Heat Treatment (°F)	Welding Electrode
7B*-7C-7D*-79	Forged	1650 Air Cool	E-7010
8D	Forged	1650 Air Cool	E-7010
9D*	Forged	1650 Air Cool	E-7010
12B-12DX	Pipe	1650 Air Cool	E-7010
73-74	Pipe	1200 Stress Relief	E-7010
12DY	Pipe	1650 Furnace Cool	E-7010
12DZ*	Pipe	1650 WQ; 1200 Draw	E-7010
12D*-80	Forged	1650 Air Cool	E-7010
72-75-76-77-78	Pipe	1200 Stress Relief	5 Cr - ½ Mo
15C*	Forged	1650 Air Cool; 1300 Draw	5 Cr - ½ Mo
16D	Forged	1650 Air Cool; 1300 Draw	5 Cr - ½ Mo
52D	Forged	1550 Anneal, Cool 50°/hr.	5 Cr - ½ Mo
17D	Forged	1500 Anneal, Cool 50°/hr.	5 Cr - ½ Mo
18D	Plate	1550 Anneal, Cool 50°/hr.	5 Cr - ½ Mo
19D-20D	Forged	1375 Anneal, Cool 50°/hr.	5 Cr - ½ Mo
21D	Forged	1550 Anneal, Cool 50°/hr.	25 Cr - 20 Ni
48	Forged	1450 Air Cool	25 Cr - 20 Ni
55-56-57	Forged	1650 Air Cool	E-7010
70	Pipe	As-Rolled	E-7010
70A	Pipe	1925 FC to 1750 AC; 1300 Draw	E-7010
81	Forged	1650 Air Cool	E-7010
81A	Forged	1925 FC to 1750 AC; 1300 Draw	E-7010

\*Additional weld beads were post-heated. See Table IV.

### TESTING PROCEDURE

*Exposure Furnaces and Graphitization Chart*—The electric furnaces employed for exposing the specimens and the graphitization rating chart used in this investigation have been described (7).

*Weld Bead Tests*—Two 6-inch weld beads with different heat inputs were deposited on opposite sides of each bar as previously described (7). Structural changes are reported only for the small weld beads which were deposited with a ⅛-inch diameter coated electrode using 100 amperes at 24 volts and an arc travel speed of 10 inches per minute. No preheat or post-heat was employed. The electrodes used are shown in Table II.

A transverse section of the weld bead samples was examined at 500 magnifications as follows: Zone 1, in the coarsened grain structure immediately beneath the weld metal; Zone 2, in the relatively fine grain structure beneath Zone 1; Zone 3, near the boundary of the heat-affected zone where grain size is similar to the parent metal; and Zone 4, in the unaffected metal.

*Impact, Oxidation and Hardness Tests*—Standard Charpy impact tests of the unwelded material before and after 10,000 hours' exposure were made in accordance with ASTM designation E-23-47T. Results reported are the average of duplicate specimens tested at ambient temperature.

Oxidation resistance in air was determined by descaling un-

Table III  
Graphite Rating of Welds

Code	Hours Exposure	900 °F	1050 °F			
		3*	1*	2*	3*	4*
7D	10,000	0	0	0	100B	3F
	34,000	200A	6B	100A	110B	3F
79	10,000	75A	2B	60A	125B	3F
8D	10,000	0	0	10A	75B	2D
	34,000	60A	12B	100A	100B	4D
9D	10,000	0	0	0	16A	0
	34,000	0	0	0	16A	0
55	10,000	0	0	0	75B	2B
	34,000	25A	0	0	60A	5B
56	10,000	0	0	0	75A	2A
	34,000	75A	0	0	50A	2A
57	10,000	0	0	0	60A	2A
	34,000	50A	0	0	25A	4A
70	10,000	Trace	0	0	8A	0

\*Designates Zone—See description of weld bead tests.  
No graphite observed in Zones 1, 2, 4 at 900 °F.

welded 1 by 1 by 20-inch bars after exposure on racks in the electric furnace for 10,000 hours. A sodium hydride bath was used for descaling. Results are reported as per cent loss in weight.

The Rockwell "B" hardness of unwelded bars was determined before and after 1000 and 10,000 hours' exposure. Hardness measurements were made of the unaffected parent metal of weld bead samples after 34,000 hours' exposure.

#### MICROSTRUCTURE OF WELD BEADS<sup>2</sup>

*Carbon-Molybdenum Steels*—Graphite ratings of the carbon-molybdenum steels are shown in Table III. Steel 7B with no aluminum and 7C with 0.4 pounds of aluminum for deoxidation had no graphite after 34,000 hours' exposure at 900 and 1050 °F (480 and 565 °C). Graphitization did occur, however, in steels 7D, 79 and 8D where 1.6 pounds of aluminum or more was used. In addition, it is significant to observe that in the steels deoxidized with 4 pounds of aluminum, graphite was observed in the heat-affected zone after 10,000 hours' exposure at 900 °F (480 °C). The steel containing 1% molybdenum was similar to the 0.5% molybdenum steels with respect to graphitization.

The only structural changes observed, other than graphitization, were spheroidization and decarburization. Oxidation of these steels after 10,000 hours at 1200 °F (650 °C), as shown in Table V, was so advanced that a discussion of the properties would be misleading. The type of graphitization observed is shown in Fig. 1. The weld heat-affected zone, Fig. 1b, and the parent metal, Fig. 1c,

<sup>2</sup>The microstructure of steels containing less than 1% chromium after 34,000 hours' exposure at 1200 °F (650 °C) are not included due to the severity of oxidation.

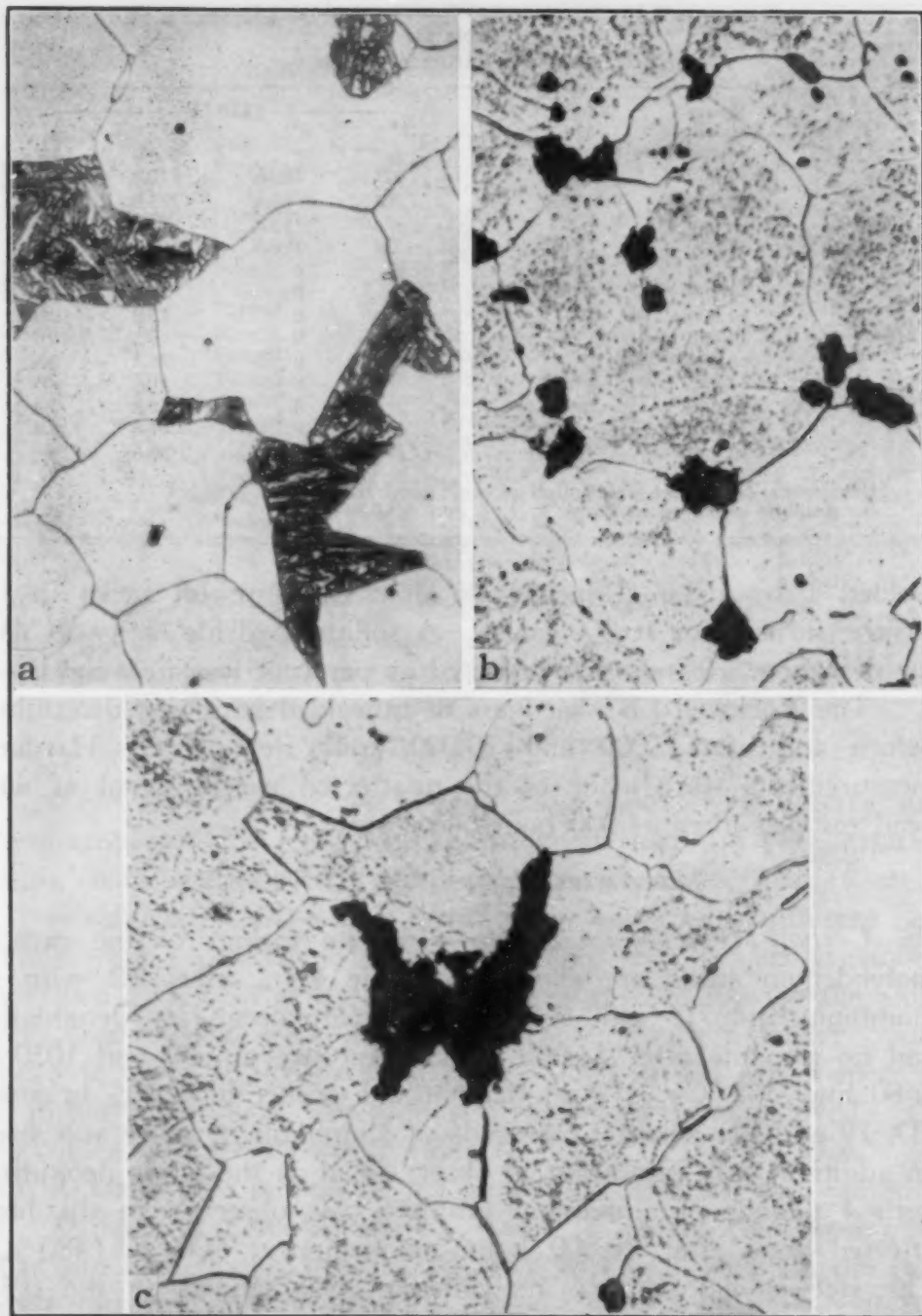


Fig. 1—Carbon-Molybdenum Steel 7D. ~ Picral etch.  $\times 1000$ . a—Unexposed parent metal. b—Heat-affected weld zone 3, 34,000 hours' exposure at 1050 °F. c—Parent metal, 34,000 hours' exposure at 1050 °F.

not only show evidence of graphitization, but after an exposure period of 34,000 hours at 1050 °F (565 °C) the steel had completely spheroidized.

In Figs. 1c, 2c and 2d, it was observed that two grain boundary patterns were present. In many areas the spheroidization of car-



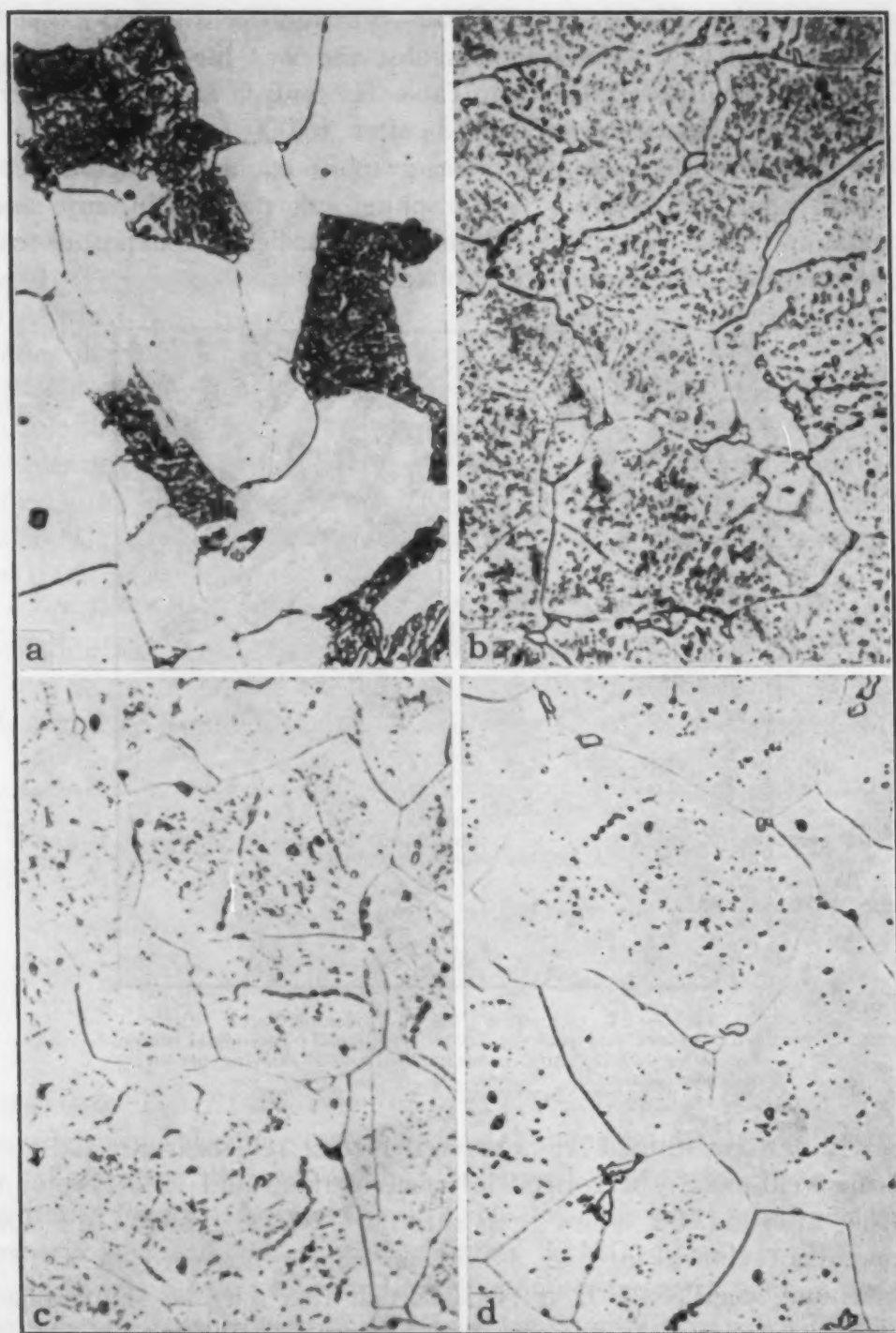


Fig. 2—Carbon-Molybdenum Steel Parent Metal 7D. Picral etch.  $\times 1000$ . a—1000 hours' exposure at 1050 °F. b—10,000 hours' exposure at 1050 °F. c—1000 hours' exposure at 1200 °F. d—10,000 hours' exposure at 1200 °F.

bides was associated with the secondary pattern of grain boundaries. This occurred at 1050 °F (565 °C) after 34,000 hours of exposure and at 1200 °F (650 °C) after 1000 hours of exposure.



*Chromium-Molybdenum Steels*—The only chromium-molybdenum steel in which graphite was observed was the  $\frac{1}{4}\%$  Cr -  $\frac{1}{2}\%$  Mo steel 9D. As indicated in Table III, only a small amount was present, and that only in Zone 3, after 10,000 hours' exposure at 1050 °F (565 °C). No additional graphite could be observed after 34,000 hours' exposure. No graphite was present in any steels containing 0.5% or more chromium, regardless of exposure conditions, prior heat treatment, or material.

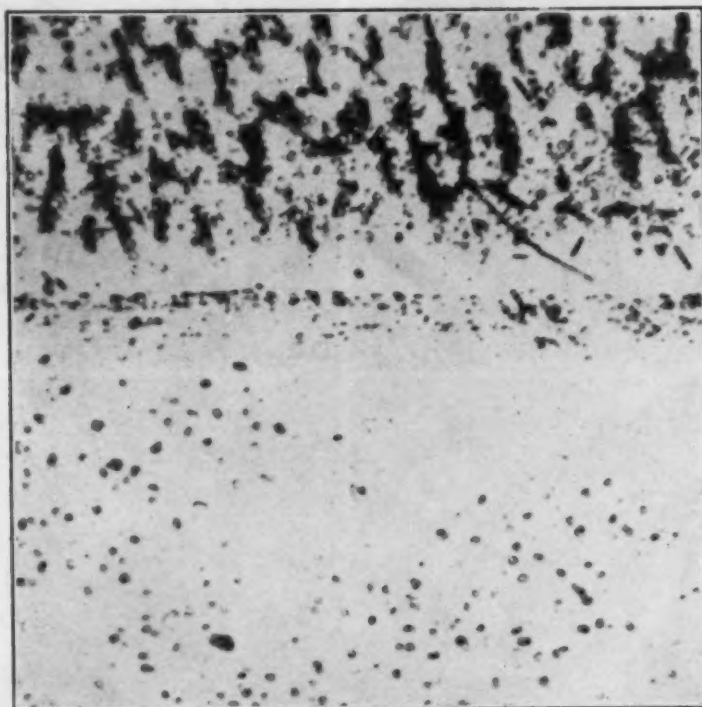


Fig. 3—9% Chromium - 1% Molybdenum Steel. Electrolytic chromic acid etch.  $\times 1000$ . Weld-metal-base-metal interface after 34,000 hours' exposure at 1200 °F showing presence of a new phase.

A new constituent was observed in the weld heat-affected zone at the weld-metal - base-metal interface of the 9 and 12% chromium steels after 34,000 hours' exposure at 1200 °F (650 °C). This constituent shown in Fig. 3 was previously observed in a 17% chromium steel (8). It is possible that this may be sigma phase in a restricted zone of analysis due to alloy diffusion from the 25-20 weld metal utilized for the bead welds.

*Molybdenum-Vanadium Steels*—Graphitization encountered in these steels is reported in Table III. The occurrence of graphite in Zone 3 after 34,000 hours at 900 °F (480 °C) is significant. At 1050 °F (565 °C) exposure, less graphite was observed in Zone 3 after 34,000 hours than after 10,000 hours. No explanation of this

phenomenon is offered, but it should be observed that all three of the 1½% Mo – ¼% V steels behaved similarly.

Steel 70 was obtained from as-rolled pipe containing 1% Mo – ¼% V. Since this steel was recently included, only the 10,000-hour exposure samples are available. Graphite in small quantities was observed in Zone 3 at the 1050 °F (565 °C) exposure, as shown in Table III. Its presence in this same zone at 900 °F (480 °C) is questionable, due to extreme fineness. This same steel 70A when heat treated prior to welding did not develop graphite under the same exposure conditions.

*Chromium-Molybdenum-Vanadium Steels*—No graphite was visible in steel 81 or 81A after 10,000 hours at any of the exposure temperatures. The addition of ½% chromium had a pronounced effect on spheroidization. Even after 10,000 hours at 1200 °F (650 °C), virtually all carbides were of the dot type, unresolvable at 1000 magnifications.

*Post-Heating*—Post-welding heat treatments were performed on additional bead-welded bars of steels 7B, 7D, 9D, 12D, 12DZ and 15C to determine the effects on graphitization as suggested by the work of Smith, Brambir and Benz (10). The weld beads were

Table IV  
Effect of Post-Welding Heat on Graphitization of Carbon – ½% Molybdenum Steel  
After 10,000 Hours at 1050 °F

Post-Heat	Zone			
	1	2	3	4
None	0	0	100B	3F
1300 °F	0	2B	2E	2E
1425 °F	10A	30A	30A	30A
1650 °F	1B	3C	5E	10D

heated to 1300, 1425 and 1650 °F (705, 775 and 900 °C) for 1 hour, air-cooled, and exposed for 10,000 hours at 1050 °F (565 °C). The effect of the post-welding treatments on steel 7D in which graphite formed is presented in Table IV. Graphitization was also observed in steel 9D but not in steels 7B, 12D, 12DZ and 15C.

In the ¼% chromium-molybdenum steel 9D only a small amount of graphite was visible in Zone 3 without post-heating, but after the 1300 and 1425 °F (705 and 775 °C) treatments no graphite was observed. With the 1650 °F (900 °C) treatment, however, a small quantity of graphite was present in Zone 3.

Post-welding treatments influenced behavior of the steels which graphitized without the special heat treatment, but it is apparent that treatments of this nature will not always prevent graphitization.

It should be observed that, in the 7D and 9D steels, normalizing after welding did not prevent graphitization. This is significant in that the structure resulting from the thermal welding gradient was recrystallized by the normalizing treatment.

#### OXIDATION CHARACTERISTICS

The degree of oxidation of the steels exposed to air for 10,000 hours at 900 to 1200 °F (480 to 650 °C) is shown in Table V.

Table V  
Oxidation After 10,000 Hours' Exposure

Code	Weight Loss—%		
	900 °F	1050 °F	1200 °F
7B	0.9	2.0	30.4
7C	0.9	2.2	27.0
7D	1.0	2.4	23.9
8D	1.0	1.8	28.6
9D	1.0	1.9	21.6
12B	0.8	1.6	24.0
12DX	0.7	1.8	....
12DY	1.0	1.8	22.9
12DZ	0.9	1.7	24.2
12D	0.9	1.8	21.8
15C	1.0	1.8	9.5
16D	1.0	1.6	11.1
52D	0.8	1.4	6.3
17D	1.0	1.6	12.6
18D	0.9	1.1	1.0
19D	0.7	0.8	2.6
20D	0.8	1.1	1.1
21D	0.7	0.7	0.7
48	0.6	0.6	0.5

It will be observed that considerable oxidation was encountered at 1200 °F (650 °C) in all steels containing less than 1% chromium, but that little oxidation was observed at 900 and 1050 °F (480 and 565 °C).

Considering the oxidation incurred at 1200 °F (650 °C), several distinct changes are observed as the chromium content increases. The addition of  $\frac{1}{4}$  to  $\frac{1}{2}$ % chromium apparently offers only limited benefits; however, 1% up to 5% chromium serves to reduce oxidation to less than half that observed in the lower chromium or chromium-free steels. The addition of silicon, titanium or columbium as alloying elements to the 5% chromium steels appears to be beneficial. No significant oxidation loss could be detected in either the 9% chromium–1% molybdenum or the 12% chromium– $\frac{1}{2}$ % molybdenum steels.

#### IMPACT PROPERTIES

Impact properties of the steels exposed for 10,000 hours at the various temperatures are presented in Table VI. The carbon-

molybdenum steels maintained their impact strength at 900 °F (480 °C) and at 1050 °F (565 °C) for 1000 hours; after 10,000 hours' exposure at 1050 °F (565 °C), however, there was a substantial reduction in impact value. After 10,000 hours at 1200 °F

Table VI  
Ambient Temperature Impact Properties

Code	Charpy Full Size Keyhole Notch Specimens—Ft-Lbs— Before Exposure	Exposed 10,000 Hours		
		900 °F	1050 °F	1200 °F
7B	39	31	13	61
7C	37	32	19	25
7D	62	66	39	78
8D	57	54	33	66
9D	67	69	24	79
12B	35	33	44	62
12DX	69	74	54	..
12DY	63	58	51	98
12DZ	67	70	76	94
12D	61	61	32	79
15C	69	70	55	53
16D	59	51	53	60
52D	67	52	..	41
17D	48	44	45	27
18D	50	38	..	33
19D	107	111	..	75
20D	60	..	46	56
21D	63	50	32	37
48	45	56	56	54

(650 °C) a completely ductile fracture was obtained due to decarburization and structural changes in the specimens.

The ¼% chromium – ½% molybdenum steel performed in a like manner. The ½% chromium – ½% molybdenum steels were similar to the carbon-molybdenum steels except that a smaller reduction in impact value after 10,000 hours at 1050 °F (565 °C) was observed. The quenched and drawn steel 12DZ did not exhibit the characteristic drop in impact properties and maintained completely ductile fractures for all the exposure conditions.

The chromium-molybdenum steels containing 1 to 5% chromium maintained their impact properties reasonably well. The 9% chromium – 1% molybdenum steel yielded somewhat erratic impact values after exposure. Direct correlation, however, was observed between the per cent granular fracture and the severity of the exposure condition. Impact strength of 12% chromium – ½% molybdenum steel was not decreased by exposure.

In a previous paper (9) the authors observed a characteristic pattern of changes in the impact properties of various AISI alloy steels after exposure at elevated temperatures. A similar pattern is shown in Fig. 4. With the exception of the high chromium (9 and 12%) and the quenched and drawn steel 12DZ, all of the



steels investigated conform to the pattern shown in Fig. 4. For values exceeding 260 on the abscissa scale, the increase in impact values was associated with decarburization and resulting changes in internal structure. The exposure factors varied between 0.8 and 1.2, depending upon the grade of steel.

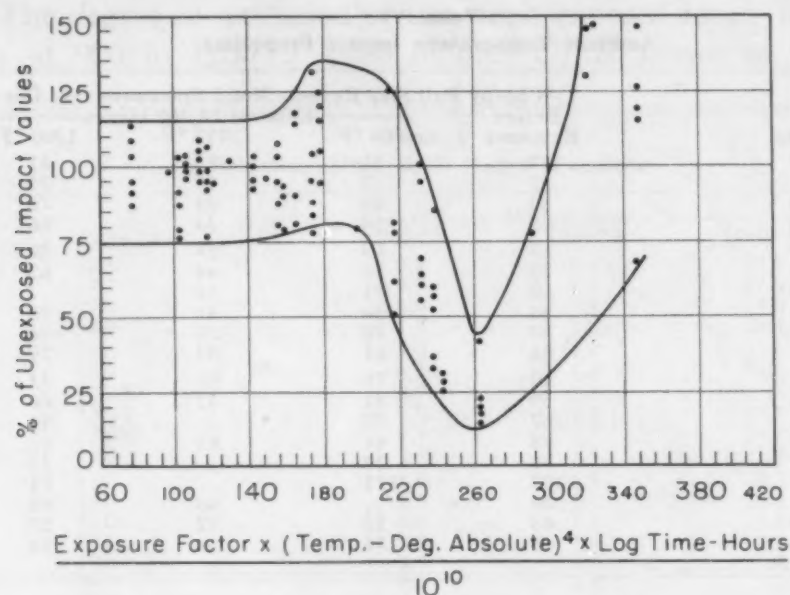


Fig. 4—Impact Properties.

#### HARDNESS PROPERTIES

A small decrease in hardness, depending on the severity of exposure, was observed in the carbon-molybdenum steels with the exception of the 7D and 8D steels exposed for 34,000 hours at 900 °F (480 °C). The  $\frac{1}{4}$  and  $\frac{1}{2}$ % chromium-molybdenum steels, with the exception of steel 12B, also showed a small decrease in hardness which may be associated with the degree of exposure. The 1 to 12% chromium-molybdenum steels did not appreciably change in hardness due to exposure, except in a few instances a slight decrease in hardness was observed. The changes in hardness observed were probably associated with size and distribution of carbides in the exposed material.

#### CONCLUSIONS

1. Coarse-grained deoxidation practice in the carbon-molybdenum steels prevented graphitization during 34,000 hours' exposure at 900 and 1050 °F (480 and 565 °C).
2. A minimum chromium content of 0.50% in the chromium-molybdenum steels melted to both coarse- and fine-grained de-

oxidation practice prevented graphitization during 34,000 hours' exposure at 900 and 1050 °F (480 and 565 °C). The 1 to 12% chromium-molybdenum steels were also exposed at 1200 °F (650 °C) and did not graphitize.

3. Several post-heat treatments of certain weld specimens did not prevent graphitization during exposure at 1050 °F (565 °C) in steels which otherwise graphitized.

4. Graphitization was not observed in the chromium-molybdenum-vanadium steels after 10,000 hours' exposure at 900 and 1050 °F (480 and 565 °C), but was observed in the molybdenum-vanadium steels.

5. The steels containing less than 1% chromium were severely oxidized during 10,000 hours' exposure at 1200 °F (650 °C). Addition of silicon, titanium or columbium to the 5% chromium - ½% molybdenum steel appears to be beneficial.

6. The Charpy impact test results at ambient temperature of the 1 to 12% chromium-molybdenum steels were not adversely affected by exposure at the elevated temperatures.

7. Impact properties of the carbon-molybdenum and ½% chromium-molybdenum steels were to some extent decreased by exposure. Quenched and tempered ½% chromium-molybdenum steel had increased impact properties after exposure.

8. Hardness of the steels investigated was, in general, not appreciably changed after exposure. The 1 to 12% chromium-molybdenum steels appeared to be more stable in this respect.

#### ACKNOWLEDGMENT

The authors wish to express their appreciation for the assistance received from the management and operating personnel of National Tube Company and United States Steel Company Research Laboratory. They are particularly indebted to Mr. D. B. Collyer of Lorain Works under whose direction the experimental work was conducted.

#### References

1. R. W. Emerson, "Carbide Instability of Carbon-Molybdenum Steel Piping", *Transactions, American Society of Mechanical Engineers*, Vol. 66, April 1944, p. 5.
2. H. J. Kerr and F. Eberle, "Graphitization of Low Carbon and Low Carbon-Molybdenum Steels", *Transactions, American Society of Mechanical Engineers*, Vol. 67, September 1945, p. 1.
3. American Society for Testing Materials, "Austenitic Grain Size in Steels", 1946 Standards Designation E19-46.

4. A. M. Hall and S. L. Hoyt, "Further Investigation on the Graphitization of Piping for the EEI and AEIC", *Transactions, American Society of Mechanical Engineers*, Vol. 70, November 1948, p. 847.
5. F. C. Fitzgerald, A. B. Wilder, G. V. Smith and A. E. White, "A Study of the Properties of 0.5 Per Cent Chromium-0.5 Per Cent Molybdenum Pipe Steel", *Transactions, American Society of Mechanical Engineers*, Vol. 70, November 1948, p. 867.
6. H. Weisberg, "Cyclic Heating Test of Main Steam Piping Joints Between Ferritic and Austenitic Steels", Sewaren Generating Station, *Transactions, American Society of Mechanical Engineers*, Vol. 71, August 1949, p. 643.
7. A. B. Wilder and J. D. Tyson, "Graphitization of Steel at Elevated Temperatures", *TRANSACTIONS, American Society for Metals*, Vol. 40, 1948, p. 233.
8. A. B. Wilder and J. O. Light, "Stability of Steels at Elevated Temperatures", *TRANSACTIONS, American Society for Metals*, Vol. 41, 1949, p. 141.
9. A. B. Wilder and J. O. Light, "Stability of AISI Alloy Steels at Elevated Temperatures", *TRANSACTIONS, American Society for Metals*, Vol. 42, 1950, p. 917.
10. G. V. Smith, S. H. Brambir and W. G. Benz, "Comparative Graphitization of Some Low Carbon Steels with and without Molybdenum and Chromium", *Transactions, American Society of Mechanical Engineers*, Vol. 68, 1946, p. 589.

## DISCUSSION

**Written Discussion:** By S. L. Hoyt and A. M. Ball, Battelle Memorial Institute, Columbus, Ohio.

The authors have presented another timely progress report of results coming out of the comprehensive long-range program of studying steels under exposure at temperatures up to 1200 °F (650 °C). The results reported in this paper on the structural changes occurring in carbon-molybdenum and chromium-molybdenum steels, when heated in air, offer important confirmation of results obtained by other investigators. Of considerable practical interest is the corroboration by the authors of the observation<sup>3</sup> that, while the addition of ¼% chromium to a high-aluminum deoxidized carbon-molybdenum steel did not prevent it from graphitizing, an addition of ½% chromium definitely did. This observation has been the basis for determining composition limits for chromium-molybdenum steels for use in steam lines operating in the higher temperature ranges.

The finding of graphite formation by the authors in their molybdenum-vanadium test steels also confirms previous findings.

With regard to the influence of post-weld heat treatment on graphite formation in a graphitization-susceptible steel, the data given in Table IV (if we interpret them correctly) support an observation previously reported.<sup>4</sup> The substance of this observation was that, while post-weld stress relieving or normalizing did not inhibit graphitization, it did tend to eliminate concentrations of graphite at the low temperature edge of

<sup>3</sup>S. L. Hoyt and A. M. Hall, Continuation of Joint EEI-AEIC Investigation on Graphitization, *Transactions, American Society of Mechanical Engineers*, Vol. 69, 1947.

<sup>4</sup>S. L. Hoyt, R. D. Williams and A. M. Hall, Summary Report on the Joint EEI-AEIC Investigation of Graphitization of Piping, *Transactions, American Society of Mechanical Engineers*, Vol. 68, 1946.



the weld heat-affected zone. The results given in Table IV appear to bear this out.

Finally, we noted in their discussion of impact properties that the authors referred to "per cent granular fracture". We would like to make the brief comment that our experience with notched-bar tests has led us to place more reliance upon the numerical value obtained from the test as a criterion of the metal's performance, rather than upon the appearance of the fracture. It frequently occurs that a metal takes considerable deformation before breaking with what appears to be a "granular" or brittle fracture.

The notched-bar behavior is interesting for the light it throws on possible deterioration at elevated service temperatures. The writers suggest that it would be of great interest if the authors would write up that phase of the investigation separately with a discussion of the pertinent factors. Since all of the steels contained molybdenum, the effect of that element does not show up, though some of the materials do appear to be more harmed than others, at least in the room temperature test.

**Written Discussion:** By F. Eberle, chief metallurgical engineer, Research & Development Department, The Babcock & Wilcox Company, Alliance, Ohio.

The paper, by Messrs. Wilder and Light, represents another valuable contribution by these authors to our knowledge of high temperature steels.

One statement in this paper is not quite clear to us. We refer to the second paragraph of page 328 which reads: "In Figs. 1c, 2c and 2d, it was observed that two grain boundary patterns were present. In many areas the spheroidization of carbides was associated with the secondary pattern of grain boundaries."

May we ask the authors to give us a definition of what they call "secondary pattern of grain boundaries"?

We note with satisfaction that the high-aluminum deoxidized  $\frac{1}{2}\%$  Cr- $\frac{1}{2}\%$  Mo steel 12D did not graphitize within 34,000 hours at temperatures up to 1200 °F (650 °C), which is another evidence of the effectiveness of the addition of chromium as an inhibitor of graphitization. However, since graphite formation has been observed by other investigators in  $\frac{1}{2}\%$  Cr- $\frac{1}{2}\%$  Mo castings deoxidized with similar amounts of aluminum, the absence of graphite in the authors' wrought specimen should not be taken as an indication that the generally observed aluminum restriction for the wrought  $\frac{1}{2}\%$  Cr- $\frac{1}{2}\%$  Mo steel may be dispensed with.

The graphitization results obtained by the authors with different types of post-weld treatments, summarized in Table IV of their paper, suggests that subcritical annealing at 1300 °F (705 °C) is more effective in minimizing graphitization than annealing at and air cooling from temperatures just above the  $A_1$  and  $A_2$  transformation points. This observation is interesting, since it is believed by some that a post-weld normalizing treatment represents the best safeguard against dangerous graphite formation in inherently susceptible steels.

The occurrence of graphite in molybdenum-vanadium steel 55 which had received no aluminum in the deoxidation practice definitely indicates that molybdenum is not very effective in preventing graphitization. One would not expect vanadium to be very helpful in this respect, since the



amount of vanadium present in this steel is insufficient to combine with all of the carbon.

#### Authors' Reply

The authors wish to express their appreciation for the discussions.

Messrs. S. L. Hoyt and A. W. Hall have stated that our results, based on 34,000 hours' exposure at elevated temperatures, confirm observations previously reported with respect to (a) inhibiting characteristics of chromium with reference to graphitization, (b) graphitization susceptibility of molybdenum-vanadium steels, and (c) graphitization susceptibility of steels with post-weld heat treatments. We plan to further confirm these results with exposure periods extending up to ten years.

Our notched-bar tests were performed at ambient temperature. The transition temperature of ductile to brittle failure after long periods of exposure at elevated temperatures would be more significant. Messrs. Hoyt and Hall suggest that the subject be treated separately. Dr. G. V. Smith of the United States Steel Company Research Laboratory has conducted an investigation of the transition temperature for ductile to brittle failure of various alloys after exposure at 900, 1050 and 1200 °F (480, 565 and 650 °C) for 10,000 hours. We hope Dr. Smith will publish these results, as they will add considerably to our knowledge of the impact properties of high temperature alloys.

Dr. Eberle has raised a question regarding the interpretation of "a secondary pattern of grain boundaries". Others have observed, under entirely different conditions, two sets of grain boundaries in certain types of material. In our investigation we observed the usual distinct type of grain boundaries after etching. In addition, we also observed another pattern (a secondary pattern) of grain boundaries which were lightly developed during etching. This secondary pattern of grain boundaries is difficult to depict, but clearly visible under direct observation with the microscope. In our studies it was observed that carbides tend to coalesce after long periods of exposure (34,000 hours) in the secondary pattern and, as a result, these grain boundaries become more distinct. The phenomenon was not observed after 10,000 hours' exposure and the significance of the observation is not clearly understood. It would appear that the secondary pattern of grain boundaries may be associated with prior austenitic or ferritic grain structures.

We are in agreement with Dr. Eberle that the lack of graphitization in the  $\frac{1}{2}\%$  Cr -  $\frac{1}{2}\%$  Mo steels deoxidized with large amounts of aluminum will require additional confirmation before it can be concluded that all wrought alloys of this type will not graphitize. However, the powerful influence of chromium in retarding graphitization is again demonstrated. Further, the advantages of thorough deoxidation with aluminum should also be recognized in that this practice provides a sounder and tougher steel.

In the post-weld treatments it was not our intention to indicate that subcritical annealing at 1300 °F (705 °C) would be more effective in minimizing graphitization. We wish to imply that the post-heat treatment of a weld to prevent graphitization may not achieve the desired objective.

In reply to Dr. J. K. Stanley's oral question raised during the presen-

tation of the paper, i.e. "Do the authors have creep data for steels exposed at the elevated temperatures?", we have tensile and creep-rupture data for some of the steels before and after 10,000 hours' exposure at 900 and 1050 °F (480 and 565 °C). These results were obtained by Messrs. D. T. Boughner and G. R. Lynch in the National Tube Company Research Laboratory. The tensile and creep-rupture test specimen is shown in Fig. 5.

Tensile properties summarized in Table VII were obtained at ambient temperature before and after exposure at the elevated temperature. No appreciable change in tensile properties, due to exposure for 10,000 hours at 900 and 1050 °F (480 and 565 °C), were observed except in steel 12DZ. In this particular steel the yield and ultimate strengths were lowered after exposure at 1050 °F (565 °C), due to the fact that this material was in the quenched and tempered condition.

Creep-rupture properties are summarized in Table VIII. The creep-rupture properties of steel 12B, with no aluminum used for deoxidation, were appreciably changed after 10,000 hours' exposure at 1050 °F (565 °C). This result is particularly significant, as the apparent creep strength of this material before exposure was very high and similar to steel 82 which was also melted to coarse-grained deoxidation practice. The creep strength of the low-aluminum steels before exposure should be interpreted

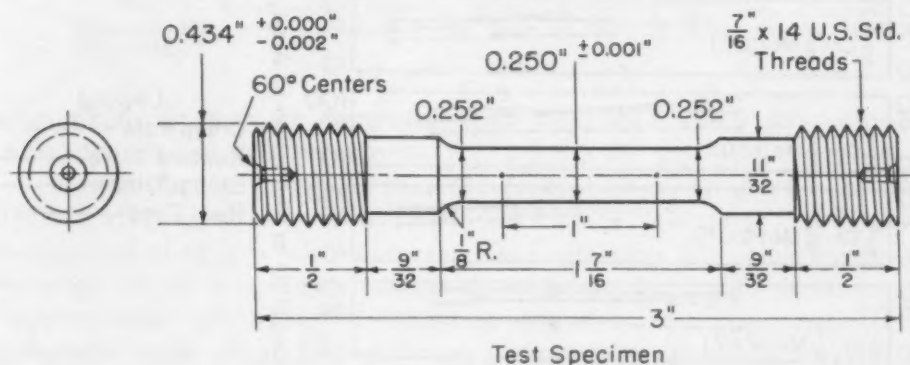


Fig. 5—Test Specimen.

**Table VII**  
**Tensile Properties of  $\frac{1}{2}\%$  Cr -  $\frac{1}{2}\%$  Mo Steels**  
**at 70 °F After 10,000 Hours' Exposure at 900 and 1050 °F**

Code	Yield (1000 psi)			Ultimate (1000 psi)			Elongation in 1 in. (%)			Reduction of Area (%)		
	A*	B*	C*	A*	B*	C*	A*	B*	C*	A*	B*	C*
12B	38	51	47	72	72	66	34	34	34	68	68	77
12D	39	49	42	70	70	64	36	36	38	72	73	75
12DX	40	45	41	63	64	62	40	40	37	78	78	81
12DY	38	37	38	59	59	60	38	39	38	72	73	77
12DZ	77	71	63	88	87	75	29	30	30	80	78	81
82	49	..	..	72	..	..	31	..	..	66	..	..
84†	57	..	..	80	..	..	32	..	..	80	..	..
52D†	37	39	35	72	72	71	37	40	38	78	76	72

\*A—Unexposed; B—Exposed at 900 °F for 10,000 Hours; C—Exposed at 1050 °F for 10,000 Hours. Yield, 0.5% elongation under load.

†2¼% Cr-1% Mo Grade.

‡3% Cr-1% Mo Grade.

Table VIII  
Creep-Rupture Properties of  $\frac{1}{2}\%$  Cr- $\frac{1}{2}\%$  Mo Steels  
at 900 and 1050 °F After 10,000 Hours' Exposure

Code	Stress (1000 psi) for Rupture in 1000 Hr.				Stress (1000 psi) for Rupture in 10,000 Hr.*			
	900 °F		1050 °F		900 °F		1050 °F	
	Exposed	Unexposed	Exposed	Unexposed	Exposed	Unexposed	Exposed	Unexposed
12B	59.5	64.0	14.5	28.0	53.5	59.0	11.2	20.0
12D	56.5	65.0	12.0	19.5	51.5	....	8.7	10.2
12DX	54.5	60.0	13.0	20.0	....	....	9.7	12.0
12DY	47.0	49.0	12.0	16.5	....	....	9.2	10.2
12DZ	51.0	65.0	15.0	18.5	47.0	62.0	11.3	9.0
82	....	58.0	....	29.0	....	....	....	21.0
84†	....	46.0	....	25.0	....	36.5	....	18.0
52D‡	32.5	34.5	14.0	15.0	27.5	29.0	10.5	11.3

\*Values obtained by extrapolation.

† $2\frac{1}{4}\%$  Cr-1% Mo Grade.

‡3% Cr-1% Mo Grade.

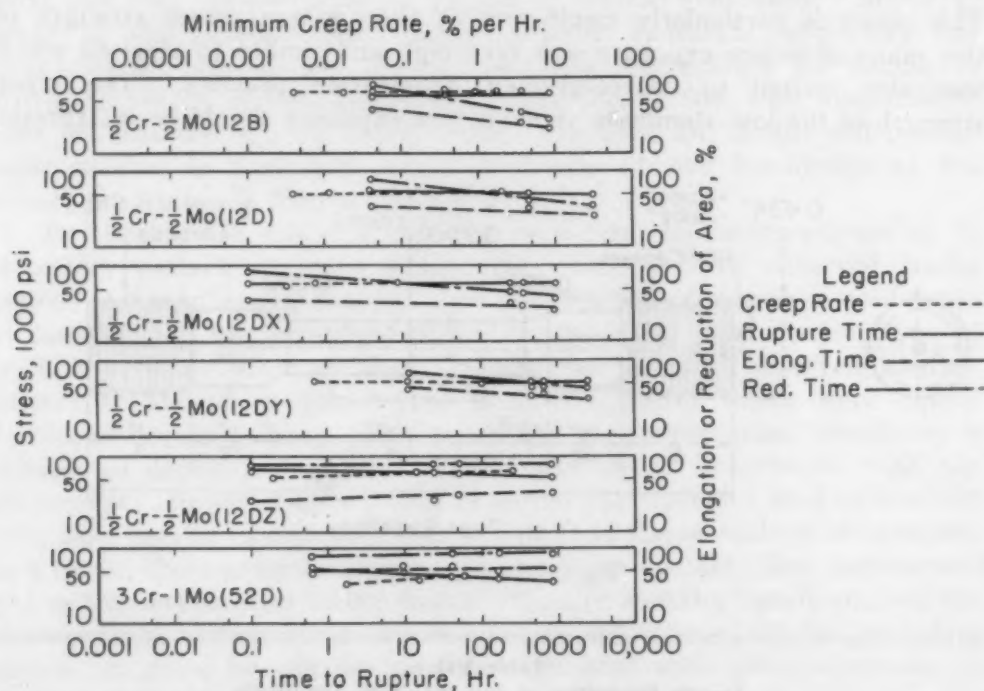


Fig. 6—Relationship Between Stress, Reduction of Area, Elongation, Rupture Time and Minimum Creep Rate at 900 °F After 10,000 Hours' Exposure.

with caution, as the creep strength after exposure is similar in this investigation to the other steels. The working stresses for the coarse-grained  $\frac{1}{2}\%$  Cr- $\frac{1}{2}\%$  Mo steels should, therefore, not be based in this particular case on the creep-rupture values obtained in the usual way.

The creep-rupture properties of steel 82, which is a coarse-grained  $\frac{1}{2}\%$  Cr- $\frac{1}{2}\%$  Mo steel, have not been completed after exposure and it will be interesting to see if the results obtained with this steel after exposure are similar to steel 12B. This also applies to steel 84 with  $2\frac{1}{4}\%$  Cr-1% Mo, and in this particular case the results, when available



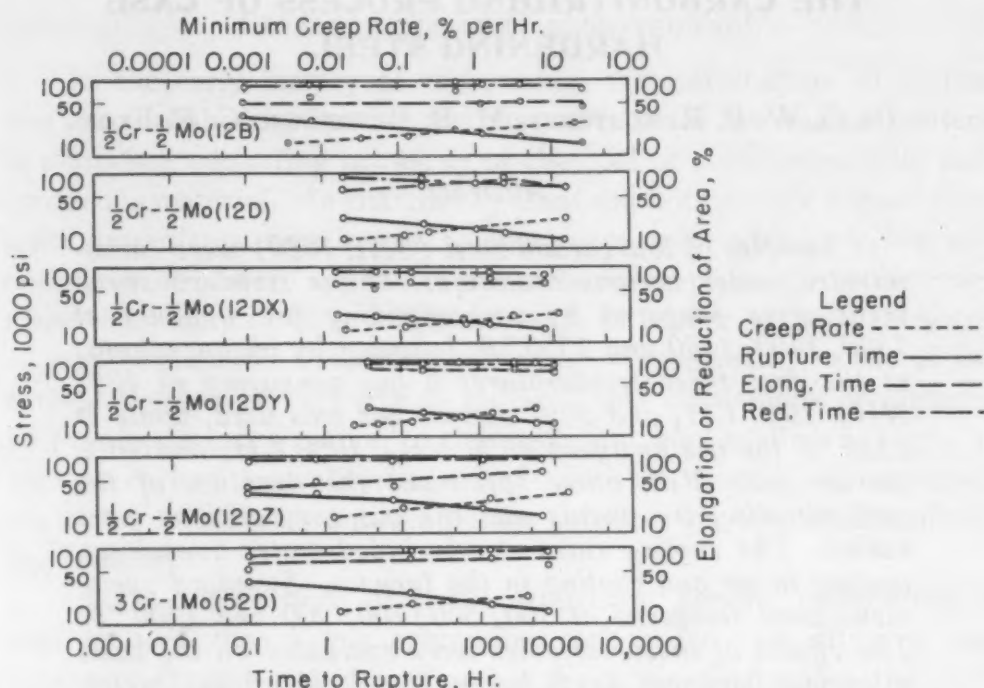


Fig. 7—Relationship Between Stress, Reduction of Area, Elongation, Rupture Time and Minimum Creep Rate at 1050 °F After 10,000 Hours' Exposure.

after exposure, may be compared with steel 52D which also contains 1% molybdenum but 3% chromium.

It will also be observed that the creep-rupture properties of 3% Cr-1% Mo steel were inferior to the 1/2% Cr-1/2% Mo steels. It is generally recognized that low chromium steels containing 1% molybdenum have superior creep properties compared with similar steels containing 1/2% molybdenum. However, deoxidation practice, structure and treatment influence creep properties and are apparently responsible for the results observed. This suggests that the working stresses assigned to steel containing 1% molybdenum should be reviewed, as the results in Table VIII do not support higher working stresses for this type of material. The stability of steel 52D with respect to creep-rupture properties obtained before and after exposure indicates that the material is quite stable under exposure conditions of 10,000 hours at 900 and 1050 °F (480 and 565 °C).

The relationship between stress, reduction of area, elongation, rupture time, and minimum creep rate at 900 and 1050 °F (480 and 565 °C) after 10,000 hours' exposure are shown in Figs. 6 and 7. The relationship between stress and minimum creep rate was fairly constant at 900 °F (480 °C), but at 1050 °F (565 °C) the minimum creep rate increased with stress. The relationship in the 1/2% Cr-1/2% Mo steels of rupture time to stress was reasonably constant at 900 °F (480 °C), but at 1050 °F (565 °C) the stress decreased with increasing time to rupture and a pronounced change in slope of the curve was observed.

There were some changes observed in the elongation and reduction of area after exposure but they will not be discussed at this time.



## THE CARBONITRIDING PROCESS OF CASE HARDENING STEEL

BY G. W. P. RENGSTORFF, M. B. BEVER AND C. F. FLOE

### *Abstract*

*Samples of low carbon steel (SAE 1020) were carbonitrided under various conditions. Four standard specimens were prepared by carbonitriding for 4 hours at 1300, 1400, 1500 and 1550 °F, followed by oil quenching; at the first three temperatures a gas consisting of 40% NH<sub>3</sub>, 10% CH<sub>4</sub> and 50% carrier gas was used, while at 1550 °F the gas analyzed 20% NH<sub>3</sub>, 10% CH<sub>4</sub> and 70% carrier gas. With other specimens the duration of the carbonitriding treatments and the gas compositions were varied. The cooling rates also included water quenching, cooling in air and cooling in the furnace. Standard specimens were tempered at 300, 500, 700, 900 and 1100 °F. The effects of these variables were evaluated on the basis of surface hardness, depth hardness, microhardness, metallographic features and case depth.*

THE carbonitriding process of case hardening steel consists of the simultaneous absorption of carbon and nitrogen from a suitable gas mixture at elevated temperature followed by cooling at a rate which produces the desired properties. This process was introduced less than twenty years ago, and its development has been rapid. It is now used extensively, especially in mass production industries, but small batch installations are also being made.

The development of carbonitriding came about through concentrated efforts devoted to operating techniques and practical applications, but understanding of the principles underlying the operations and particularly of the nature of the case produced has lagged. In the work reported here the major variables of the process were investigated. In particular, the effects of case hardening temperature and time, gas composition and tempering on the properties of cases produced were determined. Subsequent papers will report on the constitution of carbonitrided cases and on other aspects of the process.

---

This paper is based on a portion of a thesis submitted by G. W. P. Rengstorff in February 1950 to the Department of Metallurgy at the Massachusetts Institute of Technology in partial fulfillment of the requirements for the degree of Doctor of Science.

A paper presented before the Thirty-second Annual Convention of the Society, held in Chicago, October 21 to 27, 1950. Of the authors, G. W. P. Rengstorff is associated with Battelle Memorial Institute, Columbus, Ohio, and M. B. Bever and C. F. Floe are associated with the Department of Metallurgy, Massachusetts Institute of Technology, Cambridge, Mass. Manuscript received April 14, 1950.

DEVELOPMENT OF CARBONITRIDING<sup>1</sup>

In the early history of carburizing, the introduction of carbon was accomplished by heating ferrous materials of low carbon content in a mixture consisting primarily of charcoal or some other solid carbonaceous material. As charcoal by itself did not produce a good case, other ingredients, now known as energizers, were added. When scientific methods were applied to the carburizing process, it was recognized that many of these additions, such as leather or hair, consisted of organic material containing nitrogen. Consequently, some of the earliest theories of carburizing required that compounds of nitrogen be present to carry carbon to the steel, and implied that nitrogen as well as carbon was absorbed (2).<sup>2</sup> In this manner an erroneous theory of carburizing anticipated the principle on which carbonitriding is based.

As the mechanism of pack carburizing became understood, it was realized that a gas containing carbon but not nitrogen was necessary for the transfer of carbon from the charcoal to the steel. Attempts were then made to use a gas rather than a solid as a source of carbon, but gas carburizing was not an immediate success. Carbon monoxide, the most obvious gas to use, must be present in very high concentrations. Most of the other gaseous sources of carbon, such as the hydrocarbons, are so unstable at carburizing temperatures that operations become difficult because of soot formation.

Machlet successfully reduced sooting by diluting hydrocarbons with a neutral gas (3-9). One of the gases which he attempted to use as a diluent was ammonia. He soon found that ammonia introduces nitrogen into the steel. This discovery led to the original process of nitriding plain carbon steel (8, 9) which was not successful because of the brittle nature of the case.

Bramley and his co-workers in an investigation of the fundamentals of carburizing treated ingot iron in pure carbon monoxide and in mixtures of carbon monoxide with other gases. They also tried other carburizing gases such as pyridine and methyl cyanide (10) which produced exceptionally good cases. Nitrogen as well as carbon were found to be absorbed and their distribution in the case was studied. Another series of experiments showed that a mixture

<sup>1</sup>The process is also known by a variety of other names, such as gas cyaniding, Nitriding, nitrocementation and nitrocarburizing. The term "carbonitriding" is now accepted by the Joint Committee on Definitions of Terms Relating to Heat Treatment of the American Society for Metals, The American Foundrymen's Society, The American Society for Testing Materials, and the Society of Automotive Engineers (1). The authors prefer the term "nitrocarburizing", since the process is a modification of carburizing rather than of nitriding.

<sup>2</sup>The figures appearing in parentheses pertain to the references appended to this paper.

of carbon monoxide and ammonia (11) resulted in a harder case than either carbon monoxide alone or carbon monoxide plus hydrogen.

These discoveries of the effect of nitrogen and carbon absorbed simultaneously from a gas atmosphere were not developed commercially, probably in part because industrial techniques of gas carburizing had not been worked out. Another deterring factor was that carbon-nitrogen cases did not soften sufficiently for final machining, even with rather slow cooling from the case hardening temperature.

In the development of the nitriding process, it was found that a nitrided case formed on a decarburized surface tends to spall. Various investigators attempted to overcome this difficulty by passing the ammonia over hot charcoal, or by adding carburizing gases to the nitriding furnace (12-14). The resulting gas mixtures were expected to recarburize the surface of the material simultaneously with the nitriding action. This procedure was not successful, however, mainly because the nitriding temperature was too low for the introduction of carbon in appreciable amounts.

Other investigators (15) attempted to achieve the absorption of both carbon and nitrogen into steel by the use of various mixtures of ammonia and hydrocarbon gases. The cases obtained, although apparently satisfactory, did not seem to be radically different from those formed in ordinary carburizing. These investigators encountered severe operating difficulties. Soot was deposited from ammonia-propane mixtures, and ammonium carbonate formed in the exhaust lines when carbon dioxide was used as a diluent.

The first detailed publication reporting successful carbonitriding operations was a paper by Cowan and Bryce in 1938 (16). During the period 1935-1940 patents were issued to Machlet (17, 18, 19) and to Cowan (20, 21). The paper of Cowan and Bryce described some of the advantages and techniques of carbonitriding, and interest in the process arose in this country (22-24), Russia (25-28), and in England (29).

#### RELATION OF CARBONITRIDING TO CARBURIZING, NITRIDING AND CYANIDING

The term carbonitriding, as well as the term nitrocarburizing preferred by the authors, suggests relations with carburizing and nitriding. Some aspects of these two older processes and of another closely allied method of case hardening, cyaniding, are in fact pertinent to a discussion of carbonitriding.



In carburizing, the objective of case hardening is achieved by adding carbon to the surface layer of a steel so that by appropriate heat treatment the case can be hardened while the core remains in a softer condition. In pack carburizing and gas carburizing, the medium which supplies carbon to the steel is a carbon-bearing gas.

Traditionally, carbon monoxide has been considered to be the effective gas in pack carburizing, but methane formed in the carburizing box may also be important (30, 31). In gas carburizing, hydrocarbons or mixtures of hydrocarbons and inert gases are used. Carbon monoxide alone is not satisfactory, since a very small concentration of the reaction product, carbon dioxide, suppresses any further reaction of carbon monoxide with steel. The concentration of carbon dioxide cannot be kept sufficiently low unless excess carbon is present, as in pack carburizing.

Soot deposition is prevented in gas carburizing by dilution with a neutral gas known as a carrier gas. Such a gas is usually made by incompletely oxidizing a hydrocarbon in the presence of a suitable catalyst or by passing air through a thick bed of incandescent charcoal. The resulting gas mixture is composed of carbon monoxide, hydrogen, nitrogen and small amounts of methane. Carbon dioxide and water vapor must be kept low (31).

The minimum amount of hydrocarbons in the furnace atmosphere to maintain the necessary carbon potential for carburizing can be calculated from known equilibrium data (31). This concentration is only a few per cent of the total gas, but several times this equilibrium value is necessary to counteract localized depletion and to assure adequate rates for the process.

Water vapor is very harmful in carburizing, since it may cause soft spots and sometimes entirely prevents the formation of a case. Water vapor interferes with carburizing by its oxidizing and decarburizing action and it may also affect the rate of decomposition of hydrocarbons. Some experiments, however, have suggested that very small amounts of water vapor are not only harmless but are actually required to keep the hydrocarbons from decomposing without any reaction with the steel (32).

Temperatures of 1700 to 1750 °F (925 to 955 °C) are normally used for carburizing, because it is necessary to operate above the transformation range to obtain absorption and penetration of carbon in a reasonable time. At these high temperatures, considerable distortion may occur; distortion also results from stresses set up on quenching. Finishing operations are therefore required on many carburized parts in order to maintain dimensional tolerances.



Nitriding differs from carburizing in the operating conditions and in the hardening mechanism. The nitriding atmosphere consists only of ammonia which decomposes at the nitriding temperature; this decomposition would be almost complete at equilibrium (33). The rate of decomposition is therefore the important factor in maintaining the necessary ammonia concentration.

The temperature of nitriding (approximately 975 °F) is well below the transformation range of steel, and no change in the properties of the core results from the operation. Hardening of the case is caused by precipitation of alloy nitrides and for this reason special alloy steels containing nitride-forming elements must be used. The time of nitriding is very much longer than for carburizing, due primarily to low diffusion rates at the nitriding temperature. Finishing is usually necessary to remove the brittle layer of iron nitrides ("white layer") which forms on the surface.

In the search for improved energizers for pack carburizing, it was discovered that immersing steel into molten cyanides produced a hard case (2). This case was correctly attributed to the simultaneous absorption of carbon and nitrogen, and the process was called cyaniding. Cyanided cases harden by the same mechanism as carburized cases. The time of cyaniding is short, usually less than 2 hours, and the cases produced are shallow.

During the last two decades, much effort has been expended on obtaining a greater variety of cyanided cases (34, 35). As simple mixtures of sodium and potassium cyanide are not stable at high temperatures, other compounds have been added to allow higher operating temperatures. It has also been considered desirable to vary the proportion of nitrogen to carbon in the case. Nitrogen absorption is increased in several special processes. On the other hand, activated baths have been developed which promote carbon absorption while suppressing nitrogen absorption. Such baths are operated at temperatures above those of normal cyaniding and the resulting case resembles a carburized case.

#### CURRENT PRACTICE IN CARBONITRIDING

Carbonitriding can be carried out under a wide variety of operating conditions (16, 22, 36-39). A close control of the case properties, however, calls for control of temperature, time, gas composition, quenching rate and type of steel. Operating conditions are also determined by the size and type of furnace used, the carburizing gas available, and the nature of the parts treated (37, 40, 41).

Temperatures used for carbonitriding range from 1200 to 1600

°F (650 to 870 °C). With increasing temperature, the amount of nitrogen absorbed decreases and the process approaches carburizing more closely. At low temperatures, cases consisting largely of a high-nitrogen compound layer are formed (42). These cases do not have as desirable characteristics as cases formed at high temperatures and are used chiefly to avoid distortion. Most carbonitriding is done at 1500 to 1550 °F (815 to 845 °C). This is the lowest temperature at which the formation of a nitrogen-bearing compound layer can be suppressed.

The duration of carbonitriding varies from 15 minutes to 4 hours or more. The cases produced in such treatment times are similar in thickness to those formed in cyaniding at the same temperatures.

Natural gas, city gas, propane and butane are commonly used as sources of carbon. In order to reduce soot formation and to improve the uniformity of results, carrier gases are often employed (43-48). The proportions of ammonia to carburizing gas are varied in practice over a wide range. At low temperatures, ammonia-rich mixtures are preferred and are believed to lead to higher nitrogen contents, while at high temperatures the ammonia concentration in the gas is reduced (42). A common gas composition used in the low temperature range is 40% ammonia, 10% natural gas and 50% carrier gas (39). For temperatures above 1450 °F (790 °C) a gas composition of 10% ammonia, 10% natural gas and 80% carrier gas is typical.

In carburizing, 1 to 3% ammonia is sometimes added to the gas mixture. It is claimed that this addition results in more uniform cases, although the reason for the improvement is not definitely known. This procedure is not a carbonitriding process, however, because the amount of nitrogen absorbed is not likely to be large enough to impart the characteristic properties of a carbonitrided case.

The effects of water vapor in carbonitriding are controversial (49). It has been suggested that water vapor causes the same difficulties as it does in carburizing (16). There are, however, indications that the presence of water vapor in the inlet gas is not as harmful as originally suspected (49, 50).

The standard grades of carburizing steel, including plain carbon steel, are commonly used for carbonitriding (16, 36, 37, 51, 52). Steels are also sometimes carbonitrided in order to restore the carbon content of decarburized surfaces. Attempts have been made to carbonitride other ferrous materials such as tool steels (53, 54) or malleable iron.

Carbonitrided parts are quenched in oil, cooled in air, or cooled at even slower rates. The ideal cooling rate is one which will harden the case, result in the desired core structure, and keep distortion due to quenching within tolerable limits (42). Water quenching is employed only when full case hardness cannot be achieved with an oil quench. Parts carbonitrided at above 1450 °F (790 °C) are usually quenched in oil, since their hardness depends on the formation of martensite. Cases formed below 1450 °F (790 °C) may be quenched, but are often cooled at a slower rate. These cases may contain enough nitrogen for high hardenability, but some hardness is obtained even at cooling rates so slow that martensite is not formed (55, 56). This moderate hardness is due to compounds present at the surface of the case.

In a special cycle, carbonitriding is carried out at two temperatures (16). During the first period the steel is treated at above 1500 °F (815 °C). The characteristic case for this temperature is formed fairly rapidly. The temperature is then dropped to below 1400 °F (760 °C). If the second period is very short, the advantage gained is that of quenching from a lower temperature. If the second period is longer, substantial amounts of compounds may form, and properties characteristic of the lower temperature are approached. In another cyclic treatment which has much promise, the second period is carried out at a temperature below the transformation range for the core. In this way toughness of the core is assured.

#### CLAIMS MADE FOR CARBONITRIDING

A number of advantages have been claimed for carbonitriding. Some of these claims have been contradicted in the literature and many have not been substantiated by conclusive evidence. Without attempting to assess their merits, one may summarize these claims as follows:

(a) Since carbonitriding is done at lower temperatures than carburizing, distortion of the parts in the furnace is reduced (16, 27, 38, 57, 64). Fuel costs are lowered and furnace maintenance is simplified (22).

(b) Lower quenching rates are possible (22, 27, 37, 52, 55, 57), which results in softer cores. Distortion and cracks resulting from quenching are reduced (55, 56).

(c) Since nitrogen introduced in carbonitriding increases the hardenability of the case, plain carbon steels may be substituted for alloy steels.



(d) Cases produced by carbonitriding are more resistant to tempering than carburized cases (59, 63).

(e) Carbonitrided cases are more uniform than carburized cases, because carbon dioxide and water vapor in the atmosphere are less detrimental in the presence of ammonia. It has, however, also been stated that water vapor has just as bad effects in carbonitriding as in carburizing (16).

(f) The wear resistance is claimed to be better than for carburized cases (64). This has been attributed to the presence of large amounts of retained austenite (27) or of a phase other than austenite or martensite (42). Also, the coefficient of friction of carbonitrided cases is believed to be lower (58).

(g) Corrosion resistance is claimed to be improved by carbonitriding (37, 38, 58). This is attributed to compounds present at the surface.

(h) A greater depth of hardness penetration for a given treatment time and temperature than for other processes has been claimed for carbonitriding (64).

(i) The process has been claimed to result in greater surface hardness than carburizing (37, 52).

(j) Carbonitriding, like gas carburizing, is readily applicable to mass production methods (22, 37, 61-64). The conversion of gas carburizing furnaces to carbonitriding is simple. Parts carbonitrided at low temperatures and with high ammonia concentrations air harden and therefore simple conveyor-type furnaces without quenching facilities may be used. Special batch-type furnaces have been developed for short-time carbonitriding (40, 65).

(k) The process is claimed to have advantages over liquid cyaniding in quantity production (27, 37, 38, 60, 64). The working conditions are better and safer, the surface is cleaner, and the cost may be considerably less.

The research reported here has investigated the facts bearing on several of the major claims contained in the foregoing list. Some other claims remain unsettled, although in several instances tentative conclusions may be reached on the basis of general principles (66).

#### EXPERIMENTAL PROCEDURES

The experimental work reported in this paper was carried out on hot-rolled, low carbon steel (SAE 1020), which was obtained in the form of 1½-inch rounds and had the following heat analysis: carbon 0.23%, manganese 0.43%, phosphorus 0.014% and sulphur 0.035%. Sections about 6 inches in length were normalized by



heating at 1700 to 1750 °F (925 to 955 °C) for 1 hour followed by air cooling. Specimens to be used for chemical analysis were then turned to a diameter of about  $\frac{3}{4}$  inch. All other specimens were milled to a cross section of  $\frac{3}{4}$  inch square and were surface ground.

The gases used were anhydrous ammonia, methane, propane, nitrogen and compressed air. The methane was of technical grade containing not over 2% ethane and propane, about 2% nitrogen, and not over 0.1% oxygen; its dew point was approximately -23 °F. So-called "natural propane" analyzing 96% was used. The pre-purified nitrogen was guaranteed to contain less than 0.002% oxygen and 0.002% hydrogen, and to have a dew point below -67 °F. Compressed air in cylinders was prepared for a few of the runs by mixing 20.5% oxygen and 79.5% water-pumped nitrogen. For most of the work, air compressed by oil pumping was available.

Carrier gas was prepared by passing air and propane in the ratio of seven to one over a catalyst in a silica tube at 1800 to 1850 °F (980 to 1010 °C). The catalyst was made by soaking small cubes of refractory brick in a saturated nickel nitrate solution. The cubes were dried at 220 °F and then heated rapidly to 700 °F in a stream of air. In a typical analysis the carrier gas contained 31.0% hydrogen, 20.5% carbon monoxide, 0.6% methane, 0.07% carbon dioxide, and had a dew point of 10 °F. Analyses during several runs showed that the extreme range of the dew points of the carrier gas was from 5 to 32 °F.

The flow rates of ammonia and methane were measured by meters of a patented design. The flow rates of air and propane for making the carrier gas were determined by the pressure drop across a restricted orifice calibrated with a standard wet test gas meter. The rate of flow of the carrier gas was checked by inserting a meter similar to that used for measuring ammonia and methane. The ammonia content of the exhaust gases in most runs was found by an absorption and titration method.

Case hardening was carried out in an electric furnace equipped with automatic temperature control. This furnace is shown schematically in Fig. 1.

Before introducing a specimen, the hot furnace was flushed with nitrogen. After the specimen was placed in the furnace the temperature recovered in 5 to 10 minutes, but about 30 minutes elapsed before it became completely stabilized. The active gases were turned on immediately after introducing the specimen. At the end of a run, the system was flushed with nitrogen before the specimen was removed. The duration of the runs was measured from the time the

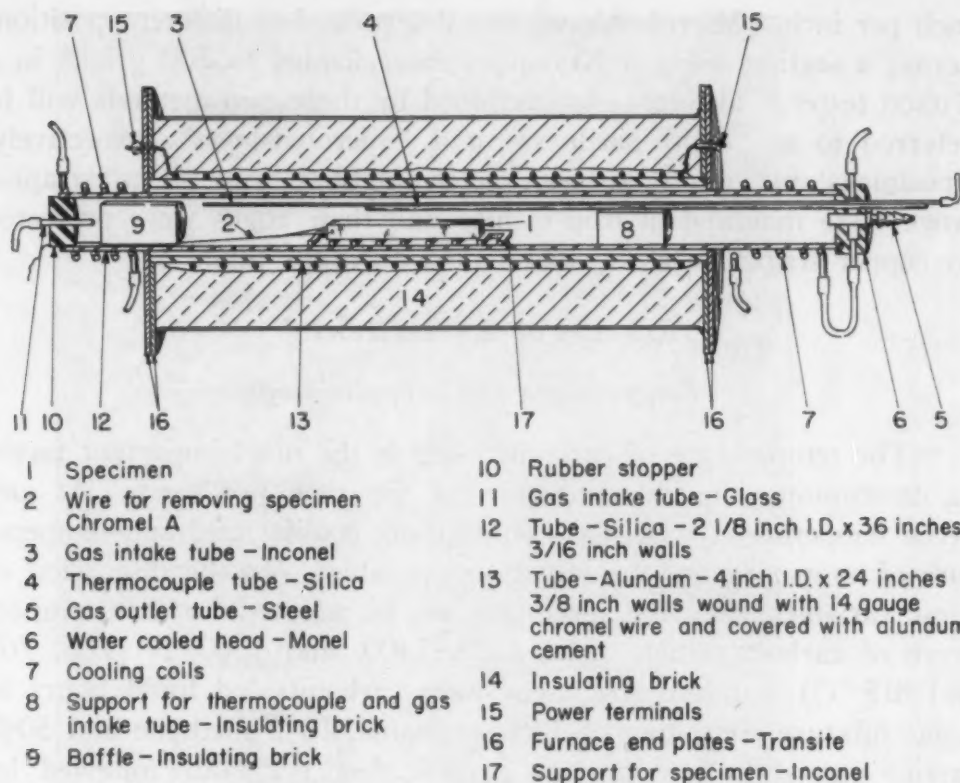


Fig. 1—Diagram of Carbonitriding Furnace.

specimen was placed in the furnace to the time the nitrogen was turned on for final flushing.

In order not to chill the specimen, the carrier gas was preheated by passing through the Inconel tube indicated in Fig. 1, but the ammonia and methane were introduced through a short tube without preheating. This arrangement provided mixing and preheating of the entire mixture before it came into contact with the specimen. Unless otherwise stated, the total flow of gas into the furnace was 5 cubic feet per hour and the time of a run was 4 hours. For quenching, the specimens were pulled from the furnace and were rapidly plunged into agitated oil at 110 °F. For air cooling, the specimens were suspended in still air. For furnace cooling the specimens were cooled to 1150 °F in the gas atmosphere; the active gases were then turned off and the specimens were cooled in prepurified nitrogen to room temperature. Tempering was carried out by heating in an air atmosphere followed by air cooling.

All grinding of specimens was done on a wet wheel with light cuts in order to reduce heating. Depth-hardness measurements were made by taking Rockwell N-15 readings at intervals of 1/10 or 1/20 of an inch along a case hardened surface ground to a taper of 0.015

inch per inch. Microhardness was determined at different positions across a section using a Knoop indenter loaded to 500 grams in a Tukon tester. The curves determined by these two methods will be referred to as "depth-hardness" and "microhardness" respectively. Specimens for microhardness determinations and metallographic work were mounted in iron clamps and their edges were protected by copper strips. Etching was done with dilute nital.

### RESULTS OF EXPERIMENTS<sup>3</sup>

#### *Temperature of Carbonitriding*

The temperature of carbonitriding is the most important factor in determining the characteristics of the case produced. At any given temperature, time, gas composition, cooling rate and temperature of tempering are the important variables. In the discussion of these variables, standard specimens will be adopted for each temperature of carbonitriding. The 1300, 1400, and 1500 °F (705, 760 and 815 °C) standard specimens were carbonitrided for 4 hours in a gas mixture consisting of 40% ammonia, 10% methane and 50% carrier gas at a flow rate of 5 cubic feet per hour followed by quenching in oil. The standard specimen for 1550 °F (845 °C) differs in that the gas composition was 20% ammonia, 10% methane and 70% carrier gas.

The microstructures of the standard specimens are shown in Figs. 2 and 3. Microhardness and depth-hardness curves for the standard specimens are shown in Figs. 4 and 5 respectively.

*The 1300 °F Standard Specimen*—The case formed at 1300 °F (705 °C) consists of two distinct layers, each approximately 0.004 inch thick as shown in Fig. 2a. Fig. 3a shows the entire outer layer and part of the inner layer. It can be seen in this figure that the outer layer is not composed of a single phase throughout its entire depth, but that a dark and a light etching constituent are present near the surface. The presence of two phases in this area is confirmed by X-ray diffraction results, which will be described in another paper (68). This multiphase region grades into a single-phase region which appears to have a columnar structure. The inner layer throughout its entire depth apparently consists of two phases, one of which predominates at the outer edge and the other at the inner edge.

The structure of the case of the 1300 °F standard specimen could be described in terms of three or even four separate layers

<sup>3</sup>The results given here are only a part of the total experimental data reported in Reference 67.



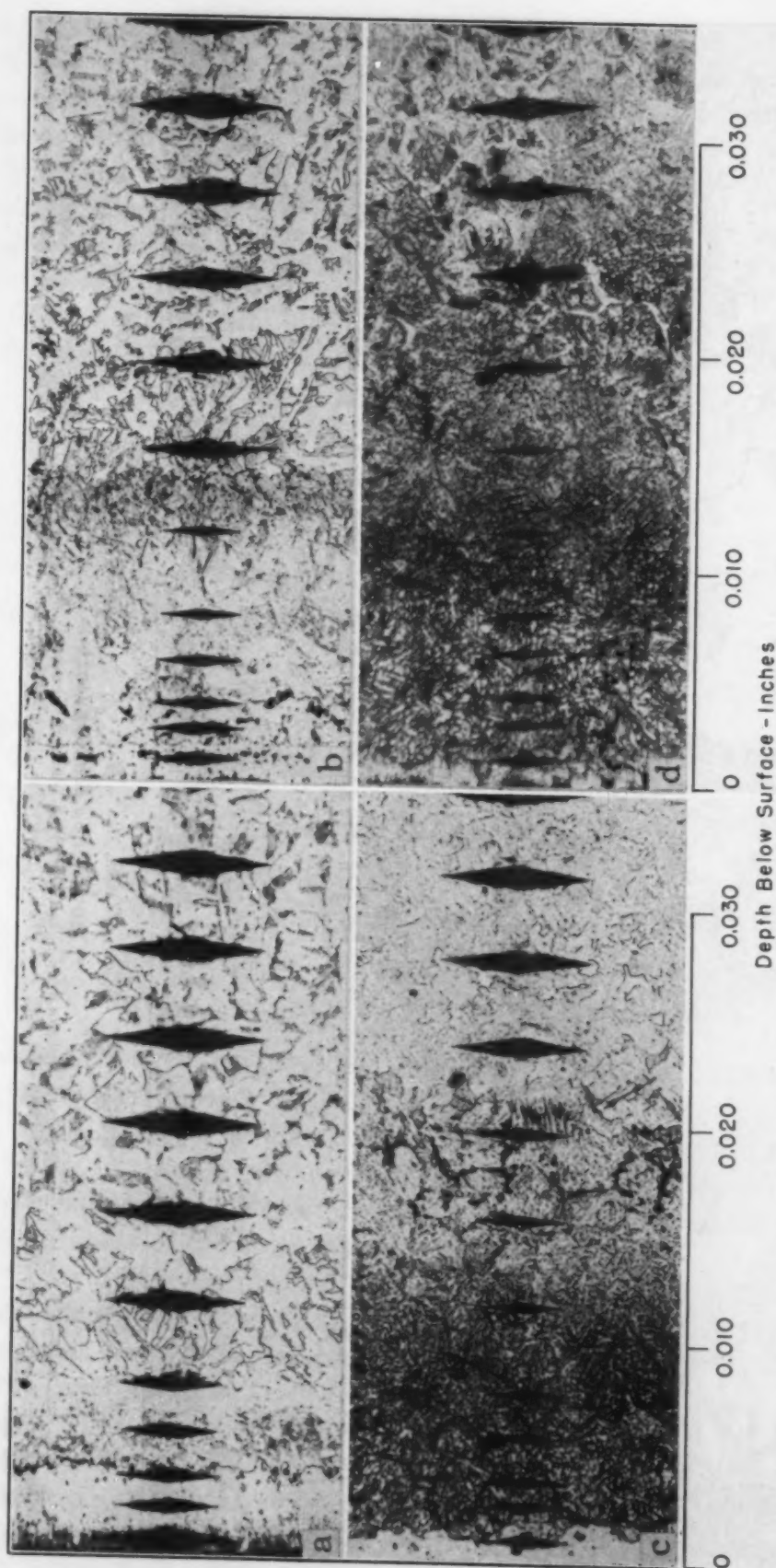


Fig. 2—Photomicrographs of Standard Specimens Carbonitrided 4 Hours at Various Temperatures and Oil-Quenched.  $\times 100$ . Carbonitriding temperatures: (a) 1300 °F, (b) 1400 °F, (c) 1500 °F, (d) 1550 °F. Gas compositions: (a), (b) and (c) 40%  $\text{NH}_3$ , 10%  $\text{CH}_4$ , 50% carrier gas, (d) 20%  $\text{NH}_3$ , 10%  $\text{CH}_4$ , 70% carrier gas. Photomicrographs are placed so that the edge representing the surface of the specimen is at the left.



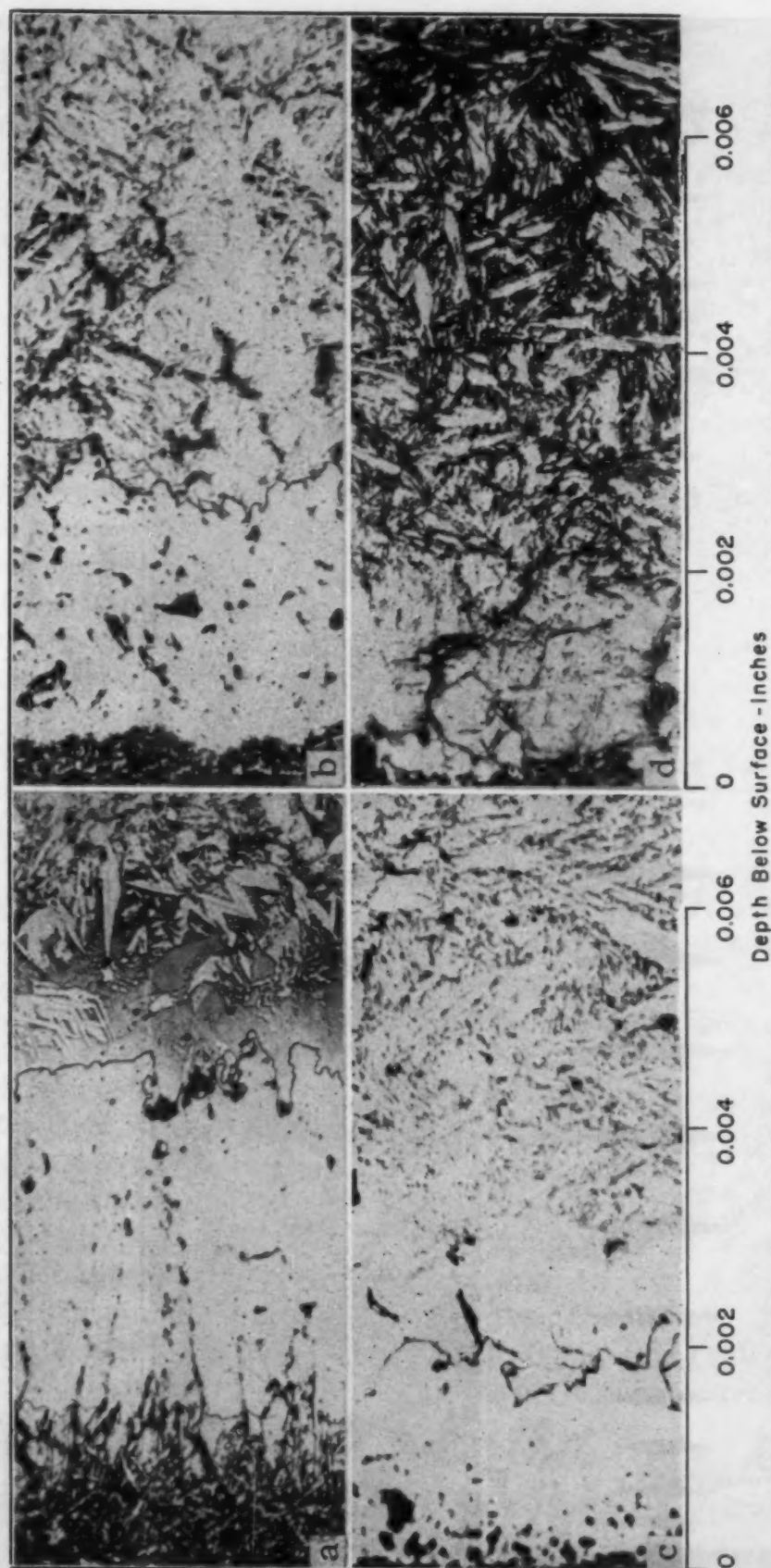


Fig. 3—Photomicrographs of Standard Specimens Carbonitrided at Various Temperatures—(a) 1300 °F, (b) 1400 °F, (c) 1500 °F, (d) 1550 °F.  $\times 500$ . For other carbonitriding conditions see Fig. 2. Photomicrographs are placed so that the edge representing the surface of the specimen is at the left.

and the cases of some other specimens, for example those shown in Figs. 7 and 10, could be similarly subdivided. Such subdivision, however, is subject to objections. The outer and inner layers as defined in the preceding paragraph have fairly discrete interfaces, while their constituent strata tend to grade into each other. The several constituents of the outer layer as defined here have the common characteristic that they consist of iron-carbon-nitrogen compounds, while the inner layer consists of iron-carbon-nitrogen austenite and its decomposition products (68). This latter distinc-

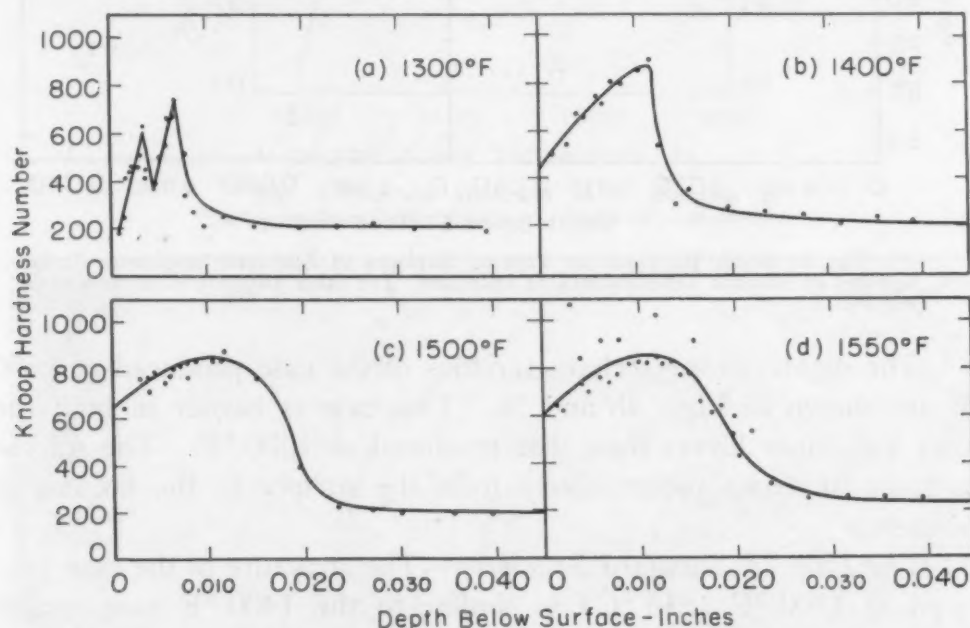


Fig. 4—Microhardness Across the Case of Standard Specimens Carbonitrided at Various Temperatures as Indicated. For other carbonitriding conditions see Fig. 2. Hardness expressed in Knoop numbers obtained with a load of 500 grams.

tion clearly separates the outer and inner layers of all cases discussed in this paper.

The case produced at 1300 °F is only moderately hard as shown in Figs. 4a and 5a. There is considerable scatter of the microhardness readings for different traverses, largely because of variation in the thickness of the outer layer.

*The 1400 °F Standard Specimen*—The standard specimen carbonitrided at 1400 °F (760 °C) also shows two distinct layers, but the outer layer is thinner than that produced at 1300 °F, while the inner layer is considerably thicker (Fig. 2b). At higher magnification (Fig. 3b) the surface of the outer layer again appears to be made up of a dark and a light etching constituent. The inner layer shows a structure resembling high carbon martensite-austenite mixtures.

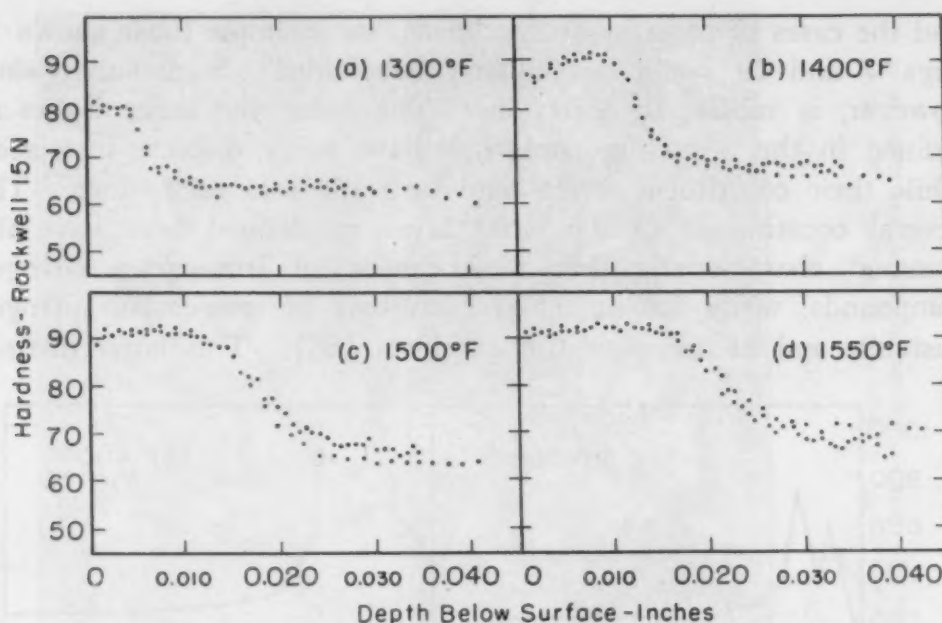


Fig. 5—Depth Hardness on Tapered Surfaces of Standard Specimens Carbonitrided at Various Temperatures as Indicated. For other carbonitriding conditions see Fig. 2.

The depth-hardness characteristics of the case produced at 1400 °F are shown in Figs. 4b and 5b. This case is harder in both the outer and inner layers than that produced at 1300 °F. The micro-hardness increases progressively from the surface to the bottom of the case.

*The 1500 °F Standard Specimen*—The structure of the case produced at 1500 °F (815 °C) is similar to the 1400 °F case except that the outer layer is slightly thinner, as shown in Figs. 2c and 3c. The depth-hardness curves, Figs. 4c and 5c, show that the outer layer is somewhat harder and that the inner layer is more uniform in hardness. The total case depth increases with increasing temperature.

*The 1550 °F Standard Specimen*—This temperature is the one most commonly used in industrial practice. The structure of the case produced is similar to the 1500 °F case except that the outer layer is exceedingly thin. The depth-hardness characteristics, Figs. 4d and 5d, are also similar except that a deeper case is produced at the higher temperature.

*Surface Hardness*—Fig. 6 shows the surface hardness of the standard specimens as a function of carbonitriding temperature. The progressive increase in surface hardness with temperature can be attributed to several factors. First, the inherent hardness of the compound layer increases with increasing temperature; secondly, the compound layer becomes thinner and therefore the contribution



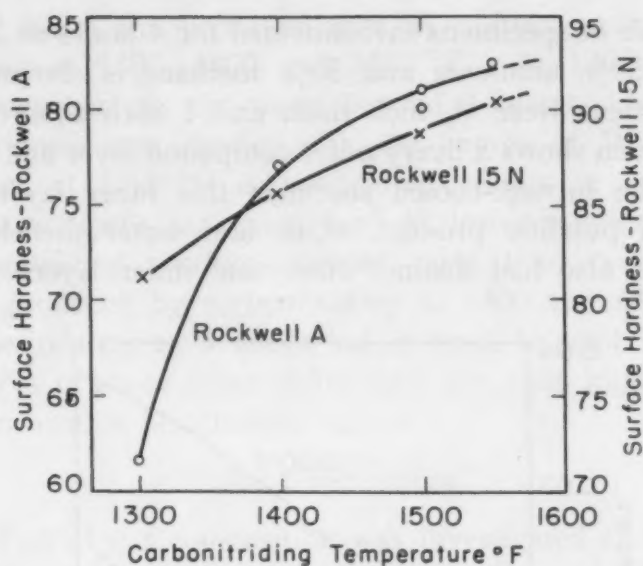


Fig. 6—Surface Hardness as a Function of Carbonitriding Temperature of Standard Specimens.

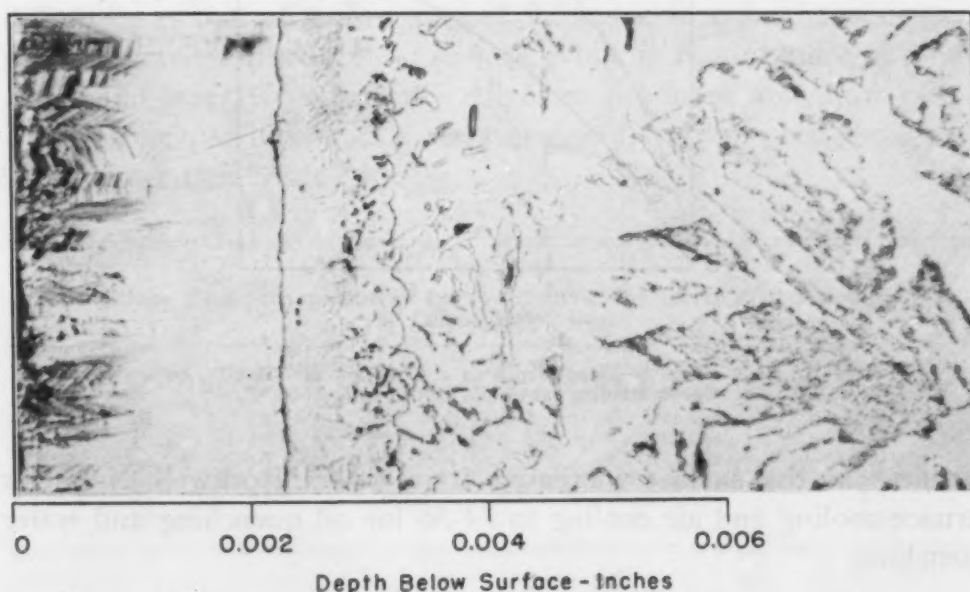


Fig. 7—Photomicrograph of Specimen Carbonitrided 4 Hours at 1204 °F, Air-Cooled.  $\times 500$ . Gas composition: 50%  $\text{NH}_3$ , 50%  $\text{CH}_4$ . Flow rate: 1.6 cubic feet per hour. Photomicrographs are placed so that the edge representing the surface of the specimen is at the left.

of the inner layer to the surface hardness becomes relatively more important, and thirdly, the inner layer itself is harder after carbonitriding at the higher temperatures.

*Carbonitriding at Other Temperatures*—Specimens were also carbonitrided at temperatures above 1550 °F (845 °C). Even with the use of gas mixtures containing 50% ammonia, the nitrogen contents were considerably less than those resulting from carbonitriding at lower temperatures.



A sample of specimens carbonitrided for 4 hours at 1204 °F in a mixture of 50% ammonia and 50% methane is shown in Fig. 7. These specimens were  $\frac{3}{16}$  inch thick and 1 inch square. The air-cooled specimen shows a heavy outer compound layer and a thin inner layer. In the furnace-cooled specimen this inner layer has transformed to a pearlitic product. Oil- and water-quenched samples in this series also had distinct outer and inner layers (67). The

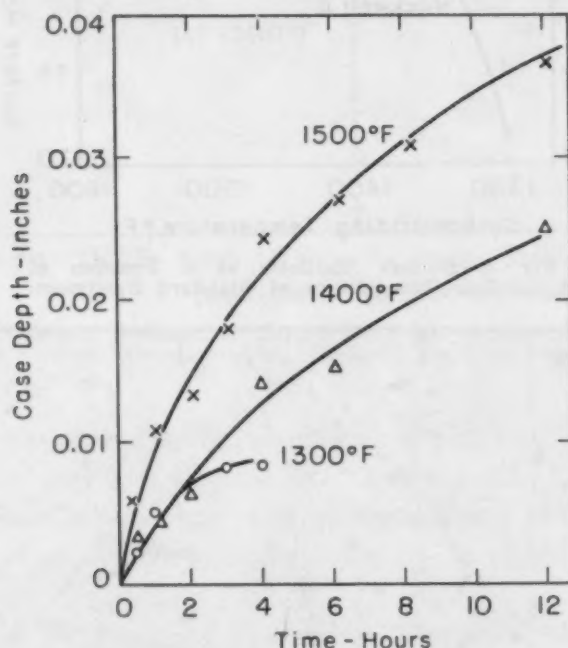


Fig. 8—Case Depth as a Function of Time of Carbonitriding at 1300, 1400, and 1500 °F.

hardness at the surface increased from 68-69 Rockwell N-15 for furnace cooling and air cooling to 74-76 for oil quenching and water quenching.

#### *Time of Carbonitriding*

At a given temperature, the time of carbonitriding determines the thickness of the case produced. While all definitions of case depth are arbitrary, case depth is here defined as the depth at which the maximum slope of the depth-hardness curve of a taper-ground specimen intersects the core hardness. The depth of case was also observed under the microscope.

The effect of carbonitriding time was investigated for periods ranging from  $\frac{1}{2}$  to 15 hours at temperatures of 1300, 1400 and 1500 °F, the other conditions being the same as for the standard specimens.

Fig. 8 shows the depth of case as a function of time after carbonitriding at 1300, 1400 and 1500 °F. At 1300 °F the case depth was very erratic for times beyond 4 hours. A comparison of the maximum case depths with the curves of Waterfall (34) suggests that at 1500 °F carbonitriding results in approximately the same case depths as cyaniding. At lower temperatures, however, carbonitriding produces deeper cases than cyaniding. The case depth produced by carbonitriding at 1300 and 1400 °F is the same for periods up to 3 hours but it must be kept in mind that the structures of these cases differ and also that high accuracy of measurement cannot be attained.

### Gas Composition

The effect of gas composition was investigated at 1500 °F with oil-quenched specimens treated under the conditions listed in Table I. The structures of all cases produced were similar. The principal difference is that at a flow rate of 2.5 cubic feet per hour no compound layer is formed on the surface, while in the presence of air the compound layer is very thin. All cases produced at a flow rate of 5 cubic feet per hour did show a compound layer, even though the ammonia content varied widely.

Table I  
Conditions Used in Experiments for Determining the Effect of Gas Composition on Carbonitrided Cases

Ammonia %	Methane %	Carrier Gas, %	Air %	Gas Preheated	Rate of Flow (cu. ft. per hr.)
20	10	70	0	Carrier gas	5.0
40	10	50	0	Carrier gas	5.0
20	0	80	0	Carrier gas	5.0
50	0	50	0	Carrier gas	5.0
85	15	0	0	None	2.5
27	46	0	27	Air	7.5

The presence of the compound layer does not affect the surface hardness which averaged about 91 Rockwell N-15 on most of these samples. The lack of a compound layer may alter the service performance and also may be associated with a lower nitrogen content of the case and thus with lower hardenability.

*Effects of Water Vapor*—The effect of water vapor in the gas mixture on the cases produced was investigated. Specimens were carbonitrided under the same conditions as the 1400 and 1500 °F standard specimens, except that the carrier gas had a dew point of -30 °F in one case and +82 °F in the other. The cases formed may also be compared with the regular runs in which the carrier gas

had a dew point between 5 and 32 °F.

The metallographic investigation of the specimens carbonitrided under standard conditions and of specimens carbonitrided with low and high water vapor contents in the inlet gas showed no difference in structures, despite the variation in water vapor content of the atmospheres used. The case depths were comparable, although increased water vapor may have caused a slight decrease in case depth. The hardness curves were also similar (67). It is concluded that within the wide concentration limits of these experiments water vapor in the inlet gas did not affect the case produced to any appreciable extent. It should be emphasized that the water vapor concentrations refer to the entering gas mixture. The water vapor content of the gas actually in contact with the specimens may have differed considerably from its content in the entering gas.

*Composition of Exhaust Gas*—Analyses showed that even when the specimen size, gas composition and flow rates of the inlet gases were the same, the ammonia content of the exhaust gas from the carbonitriding furnace was quite variable. With a flow rate of 5 cubic feet per hour and a gas mixture containing 40% ammonia, 10% methane and 50% carrier gas, the exhaust gas analyzed between 8 and 20% ammonia in runs at 1300 °F, between 5 and 12% in runs at 1400 °F and between 2 and 6% in runs at 1500 °F. With the same flow rate and a gas containing 20% ammonia, 10% methane and 70% carrier gas, the exhaust gas analyzed between 2 and 4% in runs at 1500 °F and between 1.2 and 2.0% in runs at 1550 °F. Lower flow rates gave lower ammonia contents in the exhaust. For example, the run with a flow rate of 2.5 cubic feet per hour using 85% ammonia and 15% methane at 1500 °F resulted in an exhaust analyzing only 0.8% ammonia.

*General Comments*—Gas composition is the most elusive of all the variables of carbonitriding, chiefly because the atmosphere introduced into the furnace changes in composition even before it reaches the surface of the work. This change results mainly from the thermal decomposition of ammonia, the rate of which is affected by temperature, gas flow, dilution and catalytic effects. The extent to which this decomposition takes place cannot be predicted. For this reason the optimum amount of ammonia in the inlet gas cannot be calculated but must be found by trial and error. It should not be concluded, however, that in industrial operation the choice of an atmosphere for adequate performance is particularly difficult. The results of this investigation confirm industrial experience that satisfactory cases can be produced with many different gas mixtures.



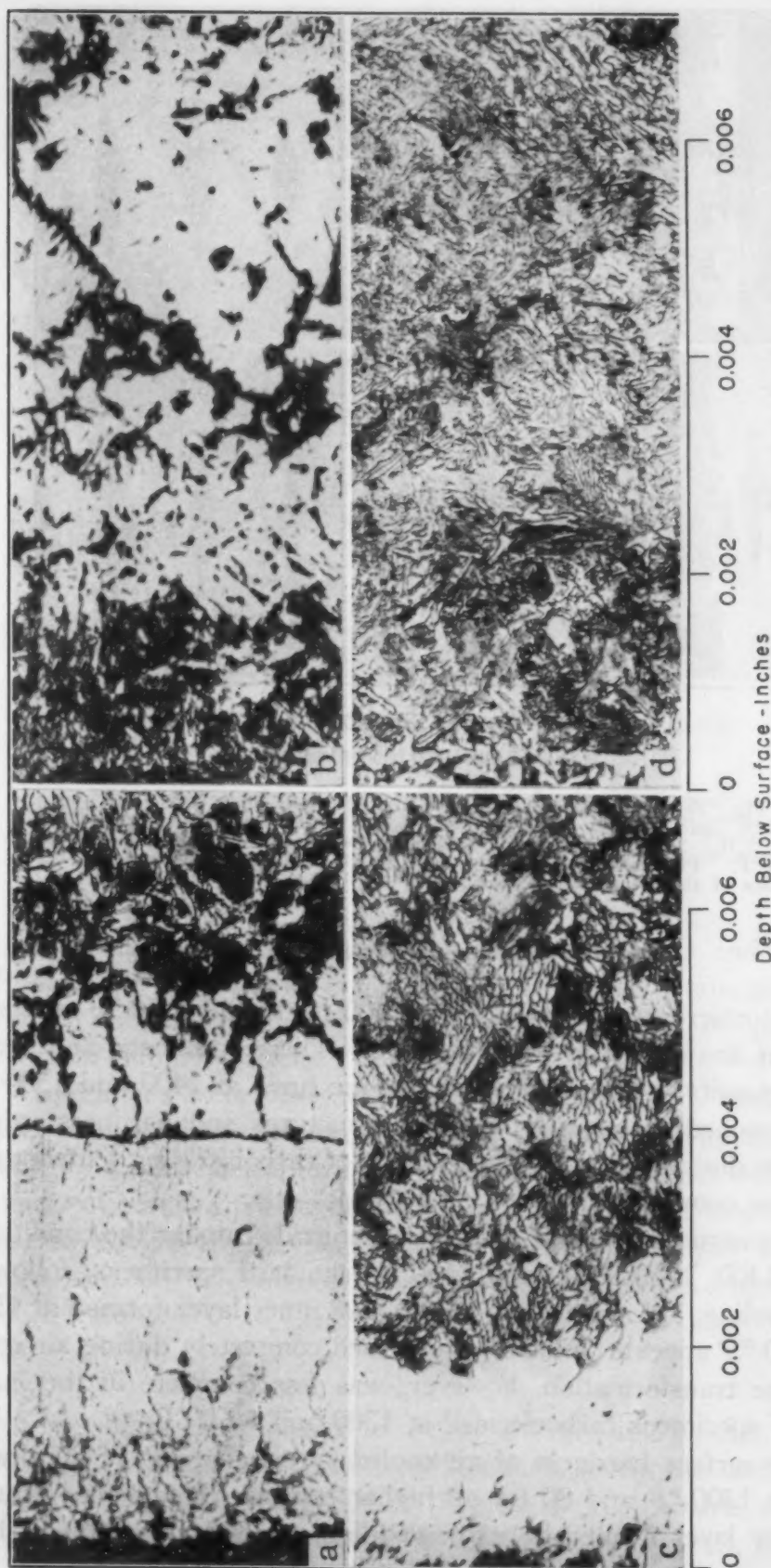


Fig. 9—Photomicrographs of Specimens Carbonitrided at Various Temperatures—(a) 1300 °F, (b) 1400 °F, (c) 1500 °F, (d) 1550 °F and Air-Cooled.  $\times 500$ . Gas compositions: (a), (b) and (c) 40%  $\text{NH}_3$ , 10%  $\text{CH}_4$ , 50% carrier gas, (d) 20%  $\text{NH}_3$ , 10%  $\text{CH}_4$ , 70% carrier gas. Photomicrographs are placed so that the edge representing the surface of the specimen is at the left.



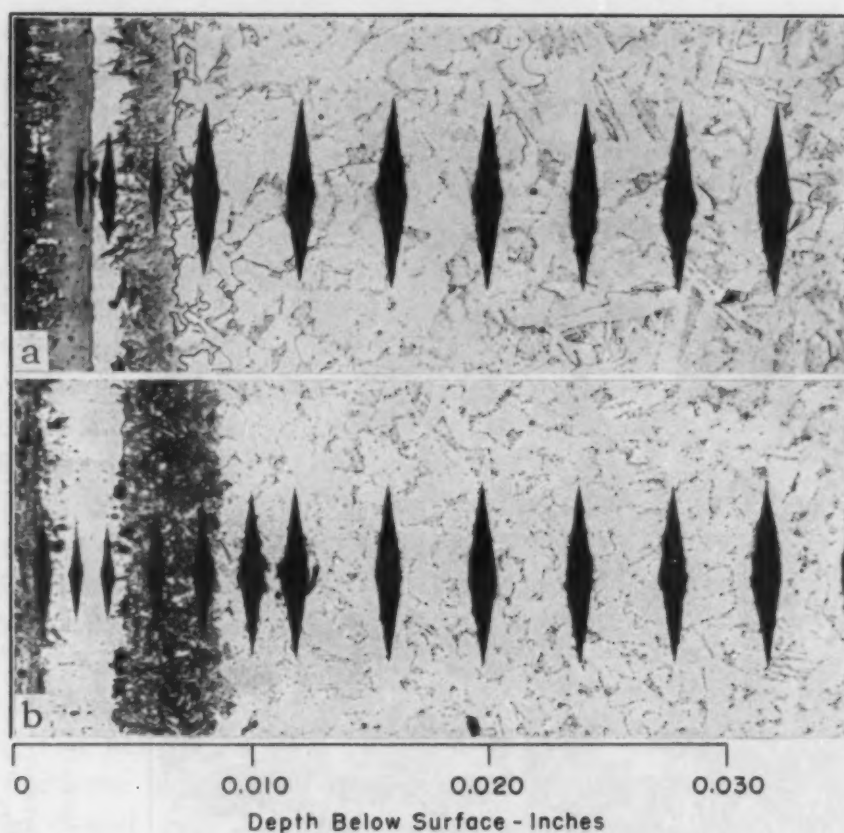


Fig. 10—Photomicrographs of Standard Specimens Carbonitrided at 1300 °F, Oil-Quenched and Tempered.  $\times 100$ . Gas composition: 40%  $\text{NH}_3$ , 10%  $\text{CH}_4$ , 50% carrier gas. Tempering temperatures: (a) 500 °F, (b) 1100 °F. Photomicrographs are placed so that the edge representing the surface of the specimen is at the left.

### *Cooling Rate*

Photomicrographs of the 1300, 1400, 1500 and 1550 °F standard specimens are shown in Figs. 2 and 3. These specimens and specimens carbonitrided with different gas mixtures at 1400 and 1500 °F were quenched in oil; the resulting structures and hardness values have been discussed under the headings of carbonitriding temperature and of gas composition.

Microstructures of specimens carbonitrided under the conditions for the 1300, 1400, 1500 and 1550 °F standard specimens, followed by air cooling, are shown in Fig. 9. The inner layer formed at 1500 and 1550 °F appears to have transformed completely during air cooling. The transformation, however, was less complete in the inner layers of specimens carbonitrided at 1300 and 1400 °F.

The surface hardness of air-cooled specimens was 75 Rockwell N-15 for 1300 °F and 80 for all higher carbonitriding temperatures. The outer layer formed by carbonitriding at 1300 and 1400 °F had

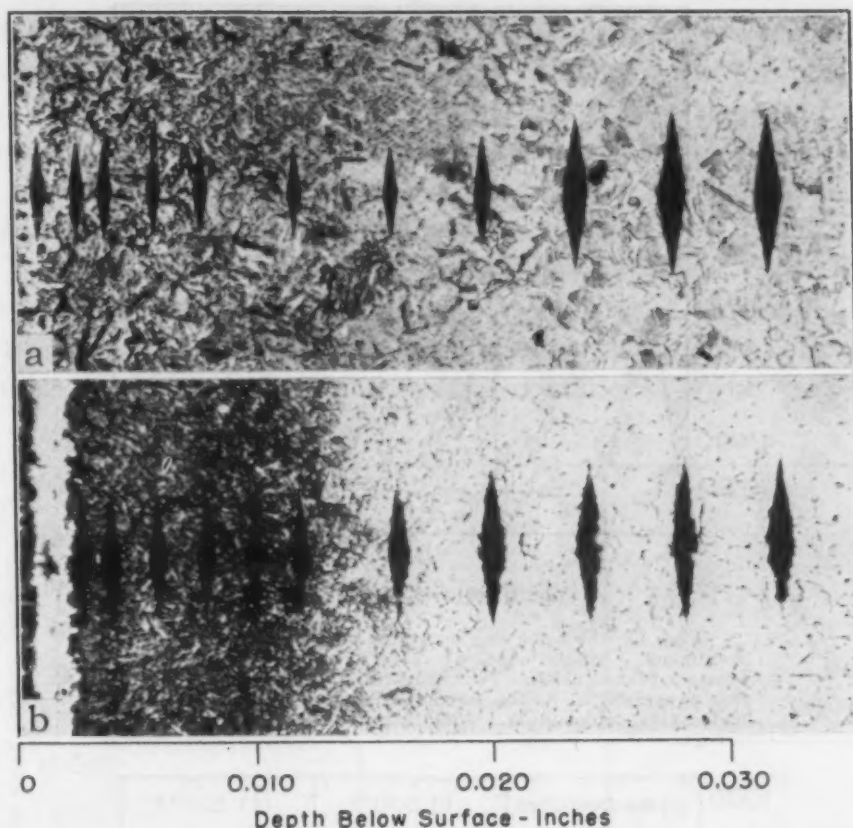


Fig. 11—Photomicrographs of Standard Specimens Carbonitrided at 1500 °F, Oil-Quenched and Tempered.  $\times 100$ . Gas composition: 40%  $\text{NH}_3$ , 10%  $\text{CH}_4$ , 50% carrier gas. Tempering temperatures: (a) 500 °F, (b) 1100 °F. Photomicrographs are placed so that the edge representing the surface of the specimen is at the left.

a greater microhardness than that formed at 1500 and 1550 °F. Although air cooling was not sufficiently rapid to obtain good hardening of the case in any of these specimens, it may be quite satisfactory in thinner sections.

Specimens were also carbonitrided at 1300, 1400 and 1500 °F under the conditions of carbonitriding the standard specimens followed by cooling in the furnace. All of the cases underwent a large amount of transformation in the inner layer, and the microhardness was lower than for the faster cooling rates. The outer layer produced at 1300 °F, however, has the same hardness regardless of cooling rate.

### *Tempering*

The effect of tempering in air for 2 hours at 300, 500, 700, 900 and 1100 °F was investigated on standard specimens carbonitrided at 1300, 1400, 1500 and 1550 °F. Typical microstructures are shown in Figs. 10 and 11 and microhardness curves in Figs. 12, 13 and 14.

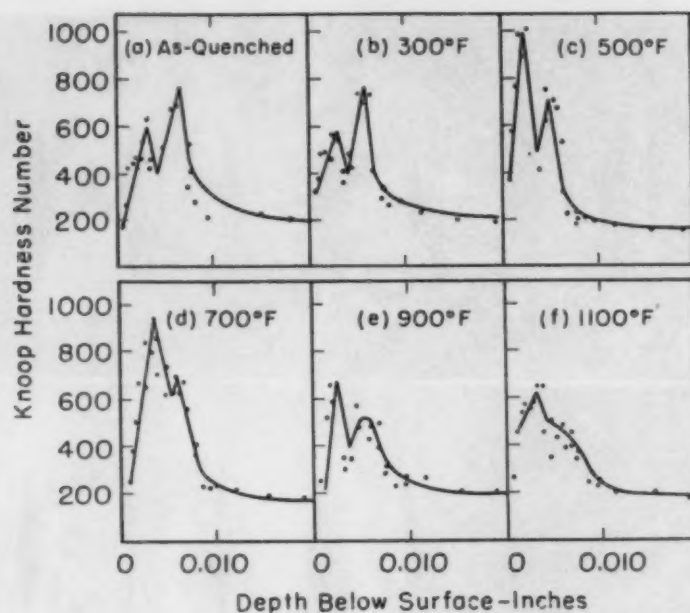


Fig. 12—Microhardness Across the Case of Standard Specimens Carbonitrided at 1300 °F, Oil-Quenched and Tempered at Various Temperatures as Indicated. Hardness expressed in Knoop numbers obtained with a 500-gram load. Gas composition: 40%  $\text{NH}_3$ , 10%  $\text{CH}_4$ , 50% carrier gas.

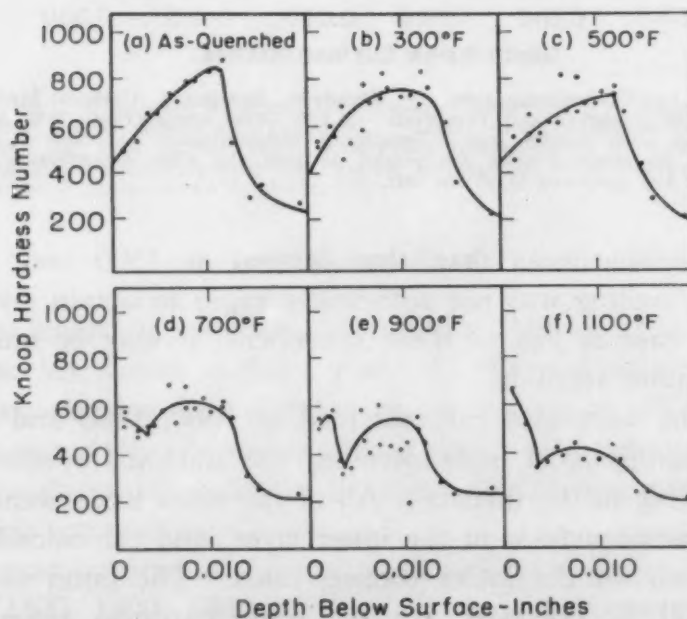


Fig. 13—Microhardness Across the Case of Standard Specimens Carbonitrided at 1400 °F, Oil-Quenched and Tempered at Various Temperatures as Indicated. Hardness expressed in Knoop numbers obtained with a 500-gram load. Gas composition: 40%  $\text{NH}_3$ , 10%  $\text{CH}_4$ , 50% carrier gas.

The microhardness of the outer or compound layer in the 1300 °F standard specimen increases on tempering, reaching a maximum at 500 °F; this increase varied considerably with time of tempering.

Similar increases were not observed in the outer layers of specimens carbonitrided at higher temperatures. The hardness of the inner layer of samples produced at all carbonitriding temperatures is maintained fairly well up to tempering temperatures of about 700 °F. The effects of tempering on the microstructure of the inner layer progressively increase as the temperature is raised.

To compare the resistance to tempering, specimens of SAE 1020 were also carburized at 1700 °F for 1¼ hours. This carburizing treatment resulted in approximately the same case thickness as carbonitriding at 1500 °F under standard conditions. The carburized

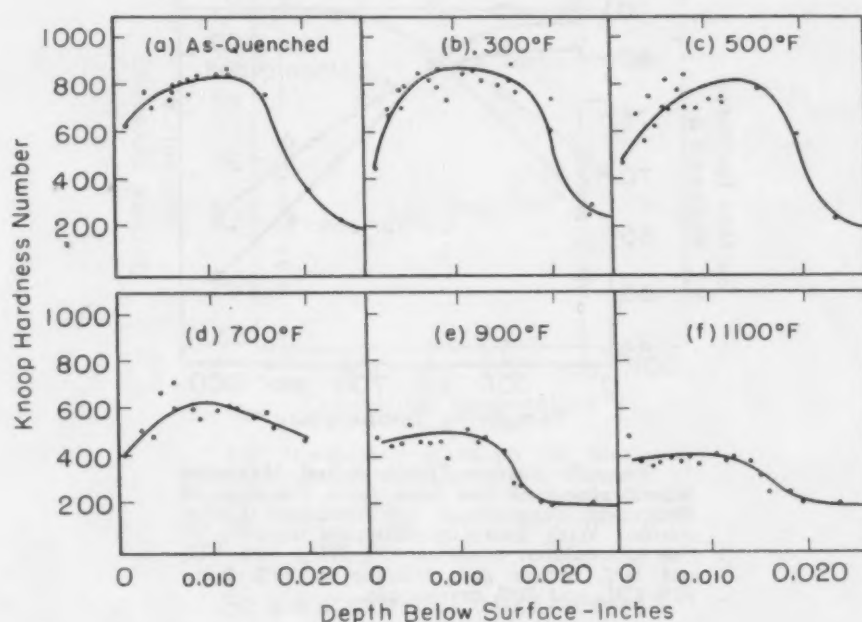


Fig. 14—Microhardness Across the Case of Standard Specimens Carbonitrided at 1500 °F, Oil-Quenched and Tempered at Various Temperatures as Indicated. Hardness expressed by Knoop numbers obtained with a 500-gram load. Gas composition: 40%  $\text{NH}_3$ , 10%  $\text{CH}_4$ , 50% carrier gas.

specimens were tempered under the same conditions as the carbonitrided specimens.

The changes in maximum microhardness and in surface hardness of the carbonitrided standard specimens were compared with the values for the carburized specimens as a function of tempering temperature. Such comparisons for specimens carbonitrided at 1500 and 1550 °F are shown in Figs. 15 and 16. These plots indicate that carbonitrided specimens retain their hardness somewhat better than do carburized specimens, especially at higher tempering temperature. For example, the 1500 °F standard specimen is harder than the carburized specimen after tempering at 700 °F or higher temper-



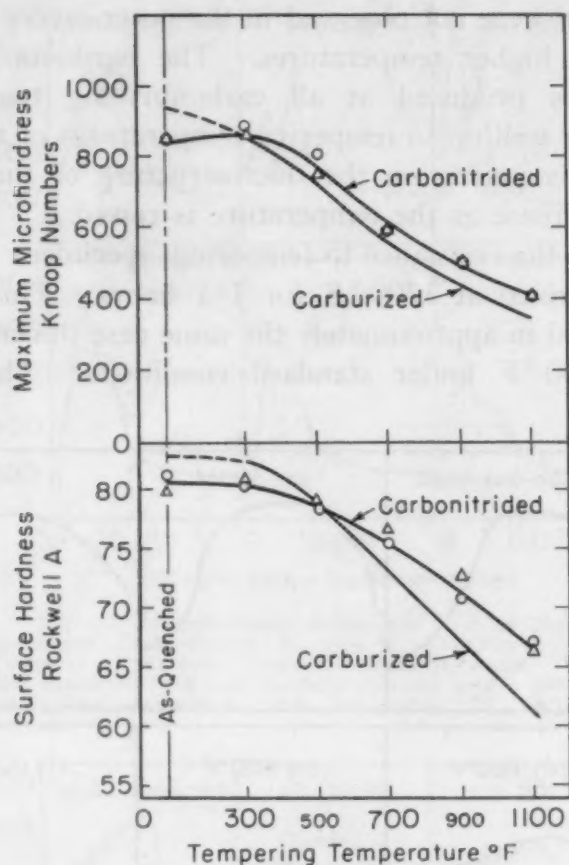


Fig. 15—Surface Hardness and Maximum Microhardness of the Case as a Function of Tempering Temperature for Specimens Carbonitrided With Two Gas Mixtures at 1500 °F. Gas composition: circle = 40%  $\text{NH}_3$ , 10%  $\text{CH}_4$  and 50% carrier gas; triangle = 20%  $\text{NH}_3$ , 10%  $\text{CH}_4$  and 70% carrier gas.

atures, although in the as-quenched condition its hardness is slightly lower. It should be emphasized, however, that carbonitrided cases fall far short of nitrided cases which withstand high tempering temperatures before softening.

#### Core Structures

At 1300 °F the core is below the transformation range and the only effect of the treatment is to spheroidize the pearlite. At 1400 °F the pearlitic regions changed to austenite during carbonitriding and some proeutectoid ferrite was dissolved. On oil quenching, these austenite areas were changed to very fine pearlite. At higher temperatures the structural changes were similar except that more proeutectoid ferrite was dissolved, which resulted in a greater proportion of very fine pearlite after quenching.

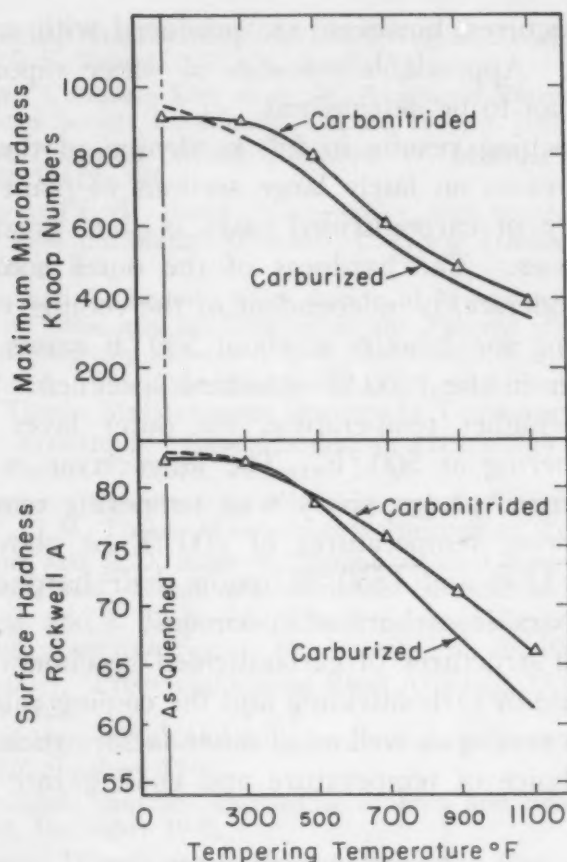


Fig. 16—Surface Hardness and Maximum Microhardness of the Case as a Function of Tempering Temperature for Specimens Carbonitrided at 1550 °F. Gas composition: 20%  $\text{NH}_3$ , 10%  $\text{CH}_4$  and 70% carrier gas.

### SUMMARY AND CONCLUSIONS

1. The temperature of carbonitriding is the most important single variable in determining the composition of the case and, together with the cooling rate, its constitution and properties. The case produced at 1300 °F (705 °C) has a thick compound layer at the surface and an inner layer which consists of a decomposition product of carbon-nitrogen austenite and retained austenite. At higher temperatures the thickness of the compound layer decreases. Cases produced at 1500 to 1550 °F (815 to 845 °C) have the highest hardness, the thinnest compound layer and the greatest case depth.

2. The time and temperature of carbonitriding determine the depth of the case produced. The case depth after carbonitriding at 1500 °F is approximately equal to that resulting from cyaniding for the same treatment time.

3. Gas composition is an elusive variable in carbonitriding, primarily because of unpredictable rates of dissociation of ammonia.

Similar case structures, however, are produced with widely varying gas composition. Appreciable amounts of water vapor in the inlet gas were found not to be detrimental.

4. Oil quenching results in full hardening of the inner layers of carbonitrided cases on fairly large sections of plain carbon steel. The hardenability of carbonitrided cases is thus greater than that of carburized cases. The hardness of the outer compound layer, although only moderate, is independent of the cooling rate.

5. Tempering for 2 hours at about 500 °F raises the hardness of the outer layer in the 1300 °F standard specimen. In specimens carbonitrided at higher temperature, the outer layer remains unaffected by tempering at 500 °F. The inner layer of all standard specimens is softened progressively with tempering temperature and time. At tempering temperatures of 700 °F or above, specimens carbonitrided at 1500 and 1550 °F retain their hardness somewhat better than comparable carburized specimens.

6. The core structures of carbonitrided specimens are affected by the temperature of carbonitriding and the cooling rate. Considerations of core properties as well as of other factors such as distortion enter into the choice of temperature and cooling rate in industrial carbonitriding.

#### ACKNOWLEDGMENTS

The investigation reported in this paper was made possible through a fellowship sponsored by the Ammonia Division of Armour and Company of Chicago. The authors also wish to acknowledge gratefully the counsel and encouragement received from Prof. V. O. Homerberg. Special thanks are due Mrs. Gloria F. Johnson, who carried out many of the tests. Finally, the authors wish to record their great indebtedness to metallurgists in industry for very generously given advice.

#### References

1. Joint AFA-ASM-ASTM-SAE Committee on Definitions of Terms Relating to Heat Treatment, "Definitions of Metallurgical Terms", *ASM Metals Handbook*, 1948, p. 1.
2. F. Giolitti, *Cementation of Iron and Steel*, McGraw-Hill Book Company, New York, 1915.
3. A. W. Machlet, "Improvements in Case Hardening Apparatus", U. S. Patent 884,180, April 1908.
4. A. W. Machlet, "Case Hardening Apparatus", U. S. Patent 1,013,190, January 1912.
5. A. W. Machlet, "Case Hardening Apparatus", U. S. Patent 1,013,191, January 1912.
6. A. W. Machlet, "Improvements in Annealing Processes", U. S. Patent 1,065,697, June 1913.

7. A. W. Machlet, "Improvements in Hardening or Treatment of Steel, Iron, etc.", U. S. Patent 1,092,925, April 1914.
8. Anonymous, "Complete List of A. W. Machlet's Patents", *TRANSACTIONS, American Society for Metals*, Vol. 28, 1940, p. 1009.
9. Anonymous, "Sauveur Medalist, Adolph W. Machlet", *METAL PROGRESS*, Vol. 40, 1941, p. 46.
10. A. Bramley and G. H. Beeby, "Cementation with the Nitrogenous Vapours of Pyridine and Methyl Cyanide", *Carnegie Scholarship Memoirs*, Vol. 15, 1926, p. 71.
11. A. Bramley and G. Turner, "The Action of Mixtures of CO and NH<sub>3</sub> on Iron and Steel and Its Bearing on the Process of Cementation", *Carnegie Scholarship Memoirs*, Vol. 17, 1928, p. 23.
12. J. P. Walsted, "The Case Hardening of Special Steels with Ammonia", Sc.D. Thesis, Massachusetts Institute of Technology, 1929.
13. P. A. E. Armstrong, "Case Hardening (Nitriding) Ferrous Articles", U. S. Patent 1,748,378, February 1930.
14. G. E. Claussen, "Simultaneous Nitriding and Carburizing of Special Alloy Steels", S.M. Thesis, Massachusetts Institute of Technology, 1931.
15. U. L. Chang and J. D. Rumsey, "Simultaneous Carburizing and Nitriding of Steel", S.M. Thesis, Massachusetts Institute of Technology, 1934.
16. R. J. Cowan and J. T. Bryce, "The Process of Dry Cyaniding", *TRANSACTIONS, American Society for Metals*, Vol. 26, 1938, p. 766.
17. A. W. Machlet, "Process of Casing Steel Articles", U. S. Patent 1,995,314, March 1935.
18. A. W. Machlet, "Case-Hardening of Ferrous Articles", U. S. Patent 2,188,226, January 1940.
19. A. W. Machlet, "Surface Hardening of Iron and Steel", German Patent 700,964, December 1940.
20. R. J. Cowan, "Composite Carbide and Nitride Case on Steel Articles", U. S. Patent 2,151,190, March 1939.
21. R. J. Cowan, "Case Hardening of Ferrous Articles", British Patent 518,726, March 1940.
22. Anonymous, "Dry Cyaniding", *Iron Age*, Vol. 141, No. 9, 1938, p. 58.
23. Anonymous, "Dry Cyaniding", *Steel*, Vol. 102, February 1938, p. 62.
24. Discussion by J. F. Wyzalek of E. F. Davis, "Production Carburizing", *TRANSACTIONS, American Society for Metals*, Vol. 26, 1938, p. 642.
25. V. I. Prosvirin, "Diffusion of Nitrogen and Carbon in Iron", *Metallurg*, Vol. 12, No. 8, 1937, p. 26; *Chemical Abstracts*, Vol. 32, 1938, p. 6997.
26. V. I. Prosvirin, "Gaseous Nitrocarburizing", *Metallurg*, Vol. 13, No. 11, 1938, p. 84; *Chemical Abstracts*, Vol. 34, 1940, p. 2759.
27. M. P. Braun, A. M. Vlasov and P. M. Goldina, "The Dry Cyaniding of Steel", *Metallurg*, Vol. 15, No. 7, 1940, p. 32; (Brutcher Translation 1820).
28. N. F. Vjasnikov and A. A. Jurgenson, "Dry Cyaniding (Nitrocementation)", *Metallurg*, No. 7, 1940.
29. D. W. Rudorff, "Recent Investigations of the Dry Cyaniding Process", *Metallurgia*, Vol. 23, 1941, p. 99.
30. I. Jenkins, "Gas Carburizing", *Journal, Iron and Steel Institute*, Vol. 154, 1946, p. 195.
31. I. Jenkins, *Controlled Atmospheres for the Heat Treatment of Metals*, Chapman and Hall, London, 1946.
32. C. R. McCloskey and J. H. Loux, "A Theory of the Mechanics of Carburization", *Steel Processing*, Vol. 32, 1946, p. 53.
33. F. Haber and R. Le Rossignol, "Über die technische Darstellung von Ammoniak aus den Elementen", *Zeitschrift für Elektrochemie*, Vol. 19, 1913, p. 53.



34. F. D. Waterfall, "Casehardening Steels in Cyanide-Containing Salt Baths", *Metallurgia*, Vol. 40, 1949, p. 29.
35. H. B. Northrup, "Cyaniding", *ASM Metals Handbook*, 1948 Edition, p. 694.
36. Anonymous, "Case Hardening A La Carte", *Iron Age*, Vol. 148, September 1941, p. 48.
37. J. F. Wyzalek and M. H. Folkner, "The Nicarb Process of Case Hardening", *Heat Treating and Forging*, Vol. 28, 1942, p. 39, 89.
38. E. R. Woodward and R. J. Quinn, "Ammonia for Processing Metals", *Metals and Alloys*, Vol. 22, 1945, p. 418.
39. W. H. Holcroft, "Carbo-Nitriding of S.A.E. Steel", *METAL PROGRESS*, Vol. 52, 1947, p. 380.
40. J. A. Dow, "A New Batch-Type Gas Cyaniding Furnace", *METAL PROGRESS*, Vol. 52, 1947, p. 984.
41. D. K. Bullens, "Steel and Its Heat Treatment", Vol. II, John Wiley and Sons, Inc., New York, 1948.
42. J. A. Dow, "Carbonitriding (Gas Cyaniding)", *ASM Metals Handbook*, 1948 Edition, p. 696.
43. J. F. Wyzalek, "Case Hardening", *Heat Treating and Forging*, Vol. 27, 1941, p. 297.
44. J. W. Donaldson, "Surface Hardening of Steel", *Metal Treatment*, Vol. 7, 1942, p. 131, 168.
45. Anonymous, "Dry Cyaniding in Surface Combustion Furnaces", Advertising Brochure, Surface Combustion Company, 1945.
46. Anonymous, "Carburizing Treatments", *Steel*, Vol. 119, No. 21, 1946, p. 101.
47. E. G. De Coriolis, "The Growing Use of Prepared Atmospheres", *Industrial Gas*, Vol. 25, No. 1, 1946, p. 10.
48. E. G. De Coriolis, "The Growing Use and Importance of Prepared Atmospheres", *Industrial Heating*, Vol. 14, 1947, p. 226.
49. S. Tour, "Facts and Fancies about Ammonia Carburizing", *METAL PROGRESS*, Vol. 55, 1949, p. 495.
50. S. Damon, "Dry Cyaniding, an Examination of Some Variables", Unpublished Report of Materials Engineering Department, Westinghouse Electric Corporation, 1948.
51. Anonymous, "Hardening Small Parts Aided by Unusual Furnace", *Steel*, Vol. 108, April 1941, p. 70.
52. R. Trautschold, "Surface Hardening", *Steel*, Vol. 111, No. 17, 1942, p. 64.
53. N. A. Yakhonin and V. T. Chirikov, "Nitrocarburization of Cutting Instruments", *Tyazheloc Mashinostronie*, Vol. 1, No. 5, 1941, p. 11; *Chemical Abstracts*, Vol. 39, 1945, p. 4827.
54. B. I. Kostetskii and G. D. Kuruklis, "Deep Nitrocementation of Cutting Tools", *Stanki i Instrument*, Vol. 17, No. 6, 1946, p. 16; *Chemical Abstracts*, Vol. 41, 1947, p. 361.
55. O. E. Cullen, "Gas Chemistry. Its Role in Metallurgy", *Steel*, Vol. 121, No. 1, 1947, p. 86.
56. O. E. Cullen, "Applications of the Science of Gas Chemistry to Heat Treating Processes", *Industrial Heating*, Vol. 14, 1947, p. 1450.
57. H. M. Parshall, "Gas Cyaniding", *Steel*, Vol. 119, No. 25, 1946, p. 86.
58. Anonymous, "Modern Gas Carburizing Processes and Equipment", Advertising Brochure, Surface Combustion Company, 1947.
59. Anonymous, "Mass Production Heat Treating", *Steel*, Vol. 120, No. 12, 1947, p. 88.
60. J. A. Dow, "Carbo-Nitriding", *Industrial Heating*, Vol. 11, 1944, p. 1426.
61. Anonymous, "Case Hardening of Buick Parts", *Industrial Heating*, Vol. 8, 1941, p. 364.

62. I. Stewart, "Dry Cyaniding or Nitro-Cementation", *Mechanical World*, Vol. 111, 1942, p. 413.
63. L. L. Clark and C. H. Leland, "Dry Cyaniding in the Production Heat Treat", *Heat Treating and Forging*, Vol. 29, 1943, p. 295.
64. E. C. Boyer and M. R. Larson, "Carbonitriding—A Casehardening Process", *Steel Processing*, Vol. 34, 1948, p. 264.
65. H. N. Ipsen, "Gas Cyaniding Small Parts", *Iron Age*, Vol. 161, No. 22, 1948, p. 84.
66. G. W. P. Rengstorff, M. B. Bever and C. F. Floe, "The Carbonitriding Process of Case Hardening Steel", *METAL PROGRESS*, Vol. 56, 1949, p. 651.
67. G. W. P. Rengstorff, "The Carbonitriding Process of Case Hardening Steel", Sc.D. Thesis, Massachusetts Institute of Technology, 1950.
68. G. W. P. Rengstorff, M. B. Bever and C. F. Floe, "Constitution of Carbonitrided Cases", published in this Volume of TRANSACTIONS, p. 378.

---

### DISCUSSION

**Written Discussion:** By C. O. Sundberg, process metallurgist, Diamond Chain Co., Inc., Indianapolis.

The authors are to be commended for this excellent presentation on a process of such current interest to industry. Fundamental data of the sort provided in this and the companion paper<sup>4</sup> fill a long-sought need for those of us who are concerned with such processes in our everyday endeavors.

Conclusion 3 wherein similar case structures are said to be produced with widely varying gas compositions is interesting. Can it be that this conclusion is based upon results for the longer time cycles (4 hours) and might not hold true for shorter cycles?

Taylor<sup>5</sup> indicates that absorption rates for carbon, and presumably nitrogen, vary during the carburizing period from an initial instantaneous rate approaching infinity to considerably reduced rates, depending upon the length of time involved. Should this be the case, the composition of exhaust gas could be expected to vary during the cycle when constant input flow rates are employed. Similarly, the input gas compositions might be more critical during the shorter carbonitriding cycles of  $\frac{1}{2}$  to 1 hour.

The question about the necessity for having the core in solution on carburized and cyanided work has been subject to general debate for some time. In most instances it is resolved by service testing and individual preference. The advent of the carbonitriding process in which the dissociation temperature for ammonia tends to preclude the possibility of having the core in solution (for plain carbon steels especially) has not clarified this problem. Logical reasoning would suggest that there should be an optimum distribution of stresses in the case and core which should answer this question. Such a fundamental study might very well be a good thesis subject.

---

<sup>4</sup>G. W. P. Rengstorff, M. B. Bever and C. F. Floe, "Constitution of Carbonitrided Cases", see this volume, p. 378.

<sup>5</sup>J. Taylor, "The Diffusion of Carbon and the Carburizing Process", *Journal, Iron and Steel Institute*, March 1950.

**Written Discussion:** By W. H. Holcroft, executive vice-president, Holcroft & Co., Detroit.

This paper shows the results of a tremendous amount of work, both in the laboratory and in searching of the literature. It is unfortunate that the laboratory work was done with such low flows of gas and with such high percentages of ammonia in the inlet gas, especially in the higher temperature runs. With dew points of the carrier gas varying from +5 to +32 °F with consequent variations in the CO<sub>2</sub> content and with the low partial pressures of CO and CO<sub>2</sub> caused by the thermal breakdown of the ammonia, we feel that results will of necessity be erratic. Our own laboratory tests confirm this.

The results shown in Fig. 6 (surface hardness as a function of carbonitriding temperature) and the statement in conclusion, "Similar case structures, however, are produced with widely varying gas composition. Appreciable amounts of water vapor in the inlet gas were found not to be detrimental", we believe were due to the choice of gas composition and flow rates.

These results and conclusions are not borne out in practice where it is by varying and controlling the composition of the gas atmosphere enveloping the work that we are able to produce many different types of case structures for a given temperature. These different types result in varying hardness and wear-resistant values.

Careful analyses which we have made in both continuous furnaces and in our laboratory indicate that the carbon gradient in the case is that which might be expected from the equilibrium values of the CO and CO<sub>2</sub>. Further work indicates that increasing ammonia flows result in more nitrogen being added to the case for any given temperature. For the reaction  $2\text{CO} \rightleftharpoons \text{CO}_2 + \text{C}$ , the equilibrium constant  $K$  is a function of the

$$\frac{(\text{partial press CO})^2}{\text{partial press CO}_2}$$

The ammonia added to generator gas in the inlets to carbonitriding furnaces breaks down in the furnace forming two volumes of nitrogen plus hydrogen for each volume of ammonia, thus decreasing the partial pressure of the CO and CO<sub>2</sub>. For the 1500 °F runs where the authors used an inlet gas comprising 40% NH<sub>3</sub>, 10% CH<sub>4</sub> and 50% carrier gas they would have approximately 7% CO in the furnace atmosphere. Percentages of CO<sub>2</sub> too small to measure would thus upset the carburizing potential of the gas.

That this does happen and that increasing ammonia flows cause increasing nitrogen addition is shown in Fig. 17. This is part of a series of laboratory tests using samples of 0.07% carbon shim stock. The samples were weighed before and after carbonitriding and the gain in weight recorded. After carbonitriding the samples were analyzed for carbon and the difference between weight gained by carbon and total weight gain was assumed to be nitrogen. For the tests shown in Fig. 17 the temperature was a constant at 1550 °F; time in furnace was 1 hour; carrier gas flow 32 cfh and natural gas addition 1 cfh. The ammonia flow was the only variable and was varied to give inlet ammonia percentages as shown. It will be noted that increasing ammonia flows increased the nitrogen



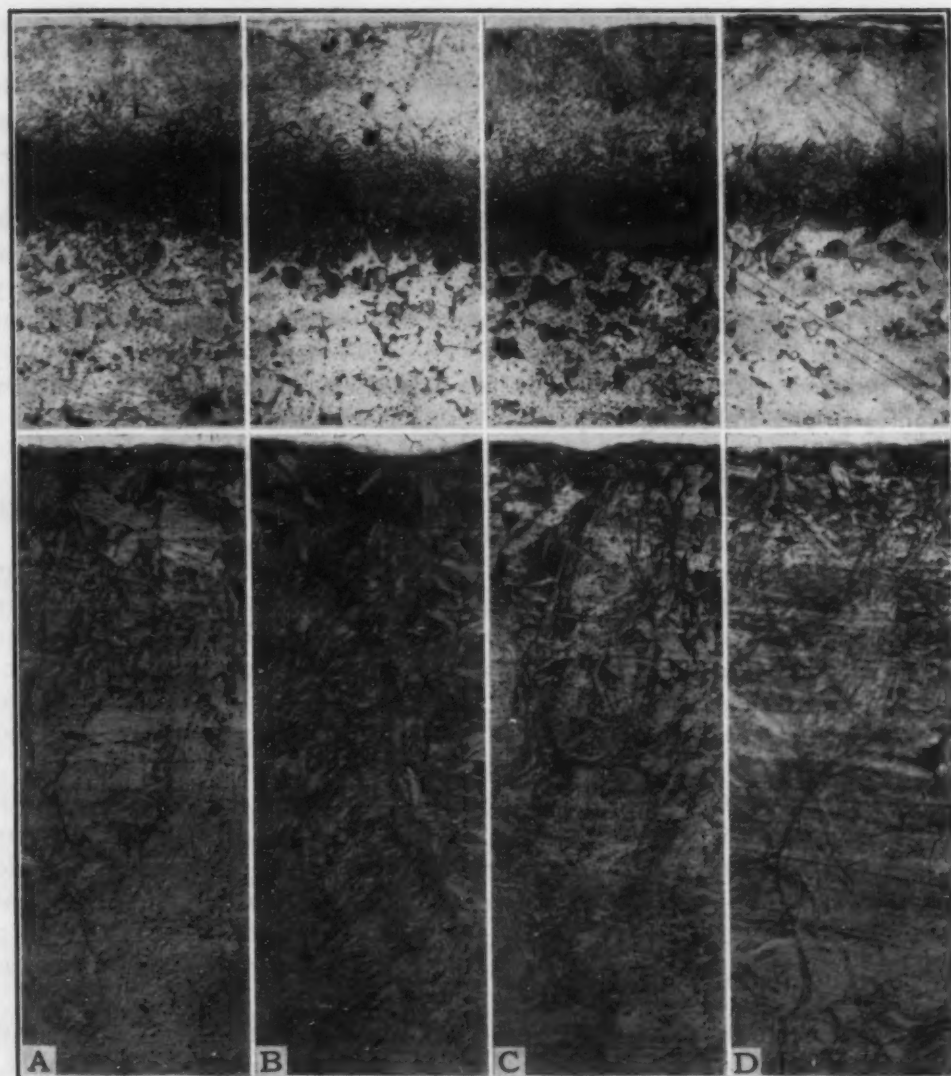


Fig. 17—Photomicrographs of Specimens, Oil-Quenched at 1550 °F. Generator gas (CFH)—32; Raw gas (CFH)—1. Upper  $\times 100$ ; Lower  $\times 500$ . (Reduced 20% in reproduction.)

	A	B	C	D
Per Cent $\text{NH}_3$ Inlet .....	3.00	9.00	23.00	33.00
Rockwell Hardness (RC) .....	62	60	56	52
Per Cent Carbon .....	0.22	0.22	0.21	0.18
Per Cent Nitrogen .....	0.10	0.16	0.22	0.29

addition and as the increasing ammonia appreciably decreased the partial pressure of CO and  $\text{CO}_2$  the carbon addition decreased. To check our reasoning relative to effect of partial pressure of CO- $\text{CO}_2$ , a further test was made using 33% ammonia and the same flows of carrier gas and natural gas but in which the percentage of CO in the carrier gas was increased. With the resultant higher partial pressure of carbon monoxide the carbon addition came back up to 0.22%.

**Written Discussion:** By Hans J. Heine, chief metallurgist, Rockwell Manufacturing Co., Pittsburgh.

The authors should be congratulated on presenting, for the first time, systematically collected data regarding the respective effects of time and



temperature on the structural characteristics and chemical composition of the "nitrocarburized" case.

From our own limited practical experience with this new method in production, we should like to emphasize what we have come to consider these major advantages of the process over other conventional case carburizing procedures:

1. Judging from the data here presented, the addition of nitrogen slows down the rate of transformation to a degree sufficient to obtain fully hardened cases with oil quenching. In intricate parts the tendency toward distortion is minimized because of the lower quenching rates realized.

It appears then that carbon-nitrogen austenite differs from ordinary austenite in the following respects:

- a. It is stable at lower temperatures than plain carbon austenite.
- b. It transforms more slowly on cooling.
- c. It has a strong tendency not to transform at all on cooling, which results in the retention of austenite in the case.

2. One of the most obnoxious causes of recurrent gear wear in one of our applications employing AISI A-4615 steel has been incomplete meshing of gears, which may lead to tooth breakage because of extreme loads. Nonuniform case depths have materially accelerated the occurrence of this undesirable condition. We have found carbonitriding to produce more uniform cases both with respect to thickness and freedom from soft spots, and tooth failures have materially decreased.

It was interesting to observe that the authors obtained relatively discrete interfaces between the outer and inner layers, although there was no such clear distinction between the constituents which tended to grade into each other. Some of the previously published work did not reveal such clearly defined interfaces. We are wondering if that is due to a special metallographic technique used by the authors or variations in carbonitriding practice.

That appreciable amounts of water vapor in the inlet gas were found to be not detrimental is reassuring and certainly of eminent significance, inasmuch as water vapor has always been considered to be very obnoxious in carburizing, causing soft spots. We are wondering, because of the controversy which these findings may undoubtedly unleash, if the authors are planning to clarify not only this point, but on a larger scale the effects of gas composition, particularly ammonia, as a whole, since this variable appears to have yielded the least clear-cut conclusions.

**Written Discussion:** By O. E. Cullen, chief metallurgist, Surface Combustion Corp., Toledo, Ohio.

The authors and their sponsor are to be commended for their choice of a subject which is of such immediate and future interest to a large portion of the membership of the American Society for Metals.

The information they have supplied should materially aid the increasingly large number of metallurgists and others who are using or considering the use of the carbonitriding process.

From a practical standpoint it might be well to elaborate a little on some of the points mentioned in the paper.

The authors confirmed their work to single-sized test specimens of SAE 1020 steel. In commercial applications a number of different SAE

and AISI steels are treated, with excellent results. Proper choice of the alloying elements manganese, nickel and chromium makes it possible to control and sometimes eliminate the outer layer described in this paper. As the authors point out, temperature plays an important part in this matter but experience has shown that the alloying constituents actively affect the surface and underlying structures and tend to promote a definite surface layer or eliminate it, depending upon the choice of alloying elements.

The authors touched briefly on the type of case produced by cooling at rates slower than can be obtained by liquid quenching. Their opinion that size of the work and consequently cooling rate definitely affect the structure and hardness is of practical importance and has been borne out in commercial use of the process. Even SAE 1010 steel in thin section can be cooled sufficiently fast in a cooling chamber or in air to produce case structures similar to those shown by the authors in Fig. 3a. It has been our experience that proper choice of metal cross section and alloying elements will permit complete or almost complete elimination of the surface constituents and the columnar structure beneath, so that the surface of the work apparently consists of the partially transformed austenite structure shown to the right in Fig. 3a.

For wearing quality the partially transformed austenite structure appears to be beneficial and is oftentimes sought when friction under light loads is an important consideration. When properly processed this surface is file hard.

It is the writer's opinion that the file hardness test is the most practical one for evaluating the cases produced in the temperature ranges of 1300 to 1400 °F (705 to 760 °C).

We believe the effects of water vapor are more important than the authors intimate in the paper. It has been our experience in commercial applications of the process that the dew point of the atmosphere surrounding the work should be below +40 °F and preferably not more than about +30 °F. Of course it is conceivably possible to introduce gases to the furnace with a considerably higher dew point if sufficient hydrocarbon gas and ammonia are present to react and lower the dew point in the furnace. However, this is not always easy to do and certainly does not make for efficient operation. In our opinion the dew point of the carrier gas should be held at or below +20 °F for most satisfactory treatment in the furnace.

The authors have made an excellent start toward the better understanding of the carbonitriding process and it is hoped that further work can be carried on to make the process of more value to the heat treating field.

#### Authors' Reply

The authors greatly appreciate the contributions made by the discussions and wish to express their thanks to Messrs. Sundberg, Holcroft, Heine and Cullen.

It is possible, although not very likely, that the structure of carbonitrided cases is more sensitive to variations in gas composition in shorter treatment cycles, as Mr. Sundberg suggests. Concerning the composition

of the exhaust gas, there is probably not sufficient variation to give any sure indication of the progress of the carbonitriding reaction in a single run. At the higher carbonitriding temperatures and with alloy steels it should be possible to produce hardened cores if this is desirable. The authors concur with Mr. Sundberg on the importance of the relation of core and case properties, which is indeed a promising subject for further work.

The main points raised by Mr. Holcroft pertain to the atmospheres used in this investigation and the conclusions concerning them. Whether a given flow rate is adequate depends largely on the size and shape of the furnace. The volume of the furnace chamber in this investigation was so small that the atmosphere turned over about 70 times per hour, which is considerably higher than industrial practice. The authors would agree, however, with an argument that a small furnace, especially one of tubular shape, requires large flow rates because of the large ratio of surface to volume which favors such atmosphere-wasting reactions as the decomposition of ammonia. In this investigation the catalytic action of the furnace surface was somewhat reduced by the use of a quartz rather than metal tube.

Mr. Holcroft also states that the ammonia concentrations in the inlet gas used in this investigation were unduly high. This objection would be justified by a comparison of inlet gas analyses used in current carbonitriding practice, although high ammonia concentrations are not without industrial precedent. These high concentrations in the inlet gas were chosen deliberately in an attempt to compensate for the fast decomposition of ammonia in a small tubular furnace. In other words, it was reasoned that a higher concentration of ammonia in the inlet gas than used industrially would lead to an approximately equal concentration near the workpiece. The analyses of the exhaust gas, especially in the runs at higher temperatures, tend to confirm this reasoning. High ammonia concentration would also, at least in some respects, compensate for low over-all flow rates.

It is unfortunate that the paper gives a range of dew points from 5 to 32 °F without adding that very probably in most runs the dew point was below about 12 °F. Moreover, the effects of the water vapor in the carrier gas were lessened by the fact that the other constituents of the atmosphere were consistently very dry.

The authors are quite ready to agree with Mr. Holcroft that the effects of gas composition on carbonitriding are not yet clear in all respects. In particular, work with lower concentrations of ammonia in the inlet gas is desirable and will be undertaken. There may well be a critical range in which the case properties vary markedly with ammonia concentrations. Special thanks are due to Mr. Holcroft for having stressed this point.

Mr. Holcroft's experimental results are of real interest but it is difficult to correlate them with the results of this paper because of the low methane content and the fact that the rate of total gas flow varied in his experiments. Differences in furnace characteristics and in absolute flow rate must also have existed between the two investigations.

The advantages of reduced distortion and greater uniformity of case



depth of carbonitrided cases mentioned by Mr. Heine are of great importance and it is very gratifying to have his confirmation of these points based on practical experience. The sharp interface between the outer and inner layers need not be considered as unusual; it does not require a special metallographic technique.

Mr. Cullen's remarks are greatly appreciated, especially in that they relate the results of this investigation to various practical problems. It is particularly interesting that retained austenite has been found beneficial for certain types of friction wear. The controversy concerning the role of retained austenite is undoubtedly owing to the large differences in conditions of wear and will only be settled on the basis of detailed practical observations. Research into the carbonitriding of alloy steels is currently in progress but with maximum temperatures of 1550 °F so far used a compound outer layer has been found in all of the three or four steels studied.



## CONSTITUTION OF CARBONITRIDED CASES

BY G. W. P. RENGSTORFF, M. B. BEVER AND C. F. FLOE

### *Abstract*

*Samples of low carbon steel (SAE 1020) were carbonitrided under various conditions; some carbonitrided samples were also tempered. The carbon and nitrogen concentrations in these samples as a function of position in the case were studied by chemical analysis. The structural constituents were investigated by X-ray diffraction. The amounts of retained austenite in various samples were determined by quantitative metallography using the lineal analysis method.*

IN the carbonitriding process of case hardening, steel absorbs carbon and nitrogen from a suitable gas mixture at elevated temperatures and is then cooled at a rate which produces the desired properties. The results of an investigation of the effects of process variables on carbonitrided cases are reported in a concurrent paper (1).<sup>1</sup> The purpose of the research reported here was to determine the compositions of carbonitrided cases by chemical analysis and to investigate their structures by X-ray diffraction and metallographic analysis.

### SURVEY OF LITERATURE

The literature contains little information directly concerned with the constitution of carbonitrided cases. Some data on the chemical composition of carbonitrided cases have been published (2, 3, 4); data are also available for cases produced by procedures much different from industrial carbonitriding practice (5a, 5b). X-ray investigations of the surface of carbonitrided cases showed that as a result of some treatments a hexagonal phase occurs, while after other treatments mixtures of hexagonal with body-centered cubic or face-centered cubic structures were found (6a, 6b). No detailed data or

<sup>1</sup>The figures appearing in parentheses pertain to the references appended to this paper.

This paper is based on a portion of a thesis submitted by G. W. P. Rengstorff in February 1950 to the Department of Metallurgy at the Massachusetts Institute of Technology in partial fulfillment of the requirements for the degree of Doctor of Science.

A paper presented before the Thirty-second Annual Convention of the Society, held in Chicago, October 21 to 27, 1950. Of the authors, G. W. P. Rengstorff is associated with Battelle Memorial Institute, Columbus, Ohio, and M. B. Bever and C. F. Floe are associated with the Department of Metallurgy, Massachusetts Institute of Technology, Cambridge, Mass. Manuscript received April 14, 1950.

description of the techniques used in these investigations have been published.

A complete understanding of the nature of carbonitrided cases presupposes a knowledge of the phases existing in the iron-carbon-nitrogen system and of the kinetics of phase changes in this system, but such knowledge is very meager. Only part of an isothermal section of the ternary phase diagram for iron, carbon and nitrogen has been published. The iron-carbon and iron-nitrogen binary diagrams must be used to furnish some clues for the ternary system. Information on the rates and mechanisms of phase changes is available only for the binary systems.

While the iron-carbon phase diagram is known in great detail, several points in the high carbon region are still unsettled, especially in the metastable iron-iron carbide system. Iron carbide ( $\text{Fe}_3\text{C}$ ) has an orthorhombic structure (7-9) in which the iron atoms are nearly close packed and carbon atoms fill the largest interstices. According to a convention which has been proposed (10) and which will be adhered to in this paper, any phase with the crystal structure of  $\text{Fe}_3\text{C}$  is referred to as cementite, even though some of the iron or carbon atoms are replaced by other elements. That such replacement of iron by other elements occurs has been shown (11). Substitution of nitrogen for some of the carbon in cementite is also very probable. There is some evidence of the existence of a range of solubility of carbon in cementite (10, 12-14), but this has been questioned for several reasons, in particular because no iron-carbon cementite has been observed with lattice dimensions appreciably different from those of  $\text{Fe}_3\text{C}$ . Some evidence that another compound in addition to cementite exists in the iron-carbon system was published prior to 1935 (15, 16). Recently, such a compound was identified (16) and was named iron percarbide. It has a small solubility range for carbon which includes the formula  $\text{Fe}_{20}\text{C}_9$ . Iron percarbide is less stable than cementite and decomposes to give cementite and carbon.

The iron-nitrogen phase diagram has been redetermined (17) and is shown in Fig. 1. Nitrogen dissolves in alpha ferrite but the associated change in lattice parameter is small. The gamma phase exists at high temperatures and corresponds to carbon austenite. With larger nitrogen concentrations the gamma prime phase occurs; it is close to the composition of  $\text{Fe}_4\text{N}$  and resembles the gamma phase in that the iron atoms have a face-centered cubic structure but nitrogen occupies only certain preferred interstitial positions in the gamma prime phase. Epsilon exists over a wide solubility

range and its lattice parameter changes appreciably with nitrogen content. Another high nitrogen phase, zeta, was first reported in 1929 (18) and has been confirmed (17, 19). This phase exists at 11.3% nitrogen and has an orthorhombic structure.

An investigation of the iron-carbon-nitrogen system has found

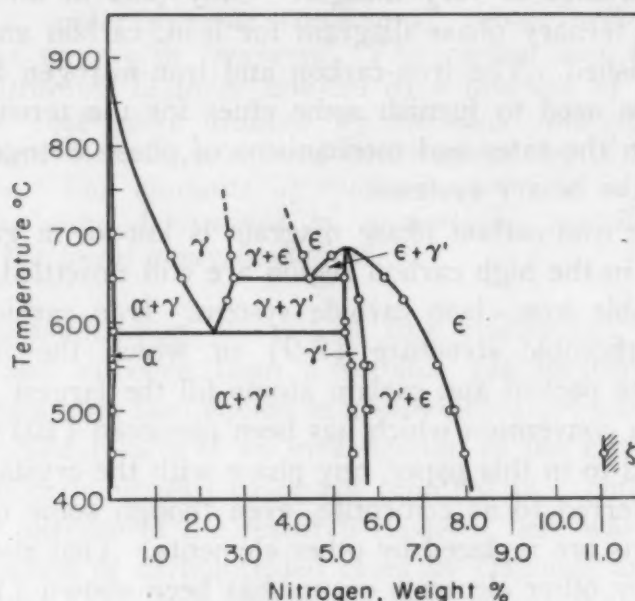


Fig. 1—The Iron-Nitrogen Phase Diagram (Ref. 17).

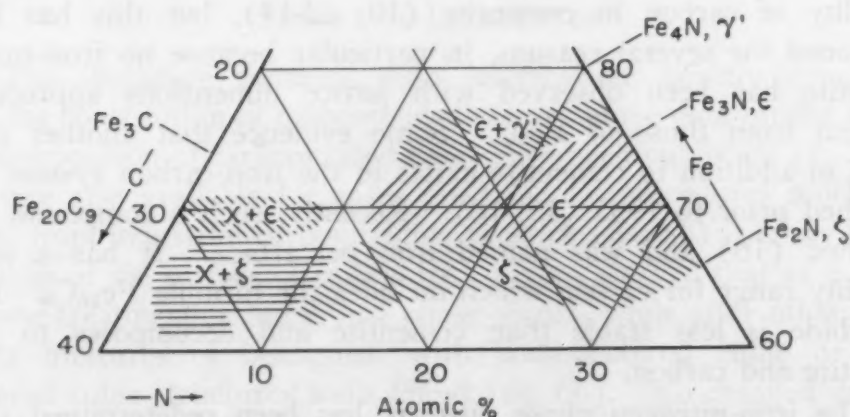


Fig. 2—Part of Isothermal Section of the Iron-Carbon-Nitrogen System at 450°C (After Ref. 20).

that carbon can replace some of the nitrogen in the lattice of gamma prime, epsilon, and zeta (20) and resulted in part of an isothermal section for 450 °C (840 °F) shown in Fig. 2. It is probable that ferrite in the iron-nitrogen system is continuous with carbon-bearing ferrite, and that gamma in the iron-nitrogen system (nitrogen austenite) is continuous with carbon-bearing austenite.



Martensite, a nonequilibrium constituent, can occur in either iron-carbon or iron-nitrogen alloys. The crystal structure of this constituent is body-centered tetragonal; the distortion in one direction is due to the presence of carbon or nitrogen atoms in preferred positions.

The kinetics of the decomposition of austenite and the factors favoring the retention of austenite need not be reviewed here. It should be mentioned only that, depending on the cooling rate, nitrogen austenite (gamma phase) decomposes into a nitrogen-bearing pearlitic or martensitic constituent. Recent work (21) has shown that the isothermal transformation of eutectoid iron-nitrogen alloys is slower than of iron-carbon alloys at all temperatures; nitrogen austenite is also more sluggish with respect to transformation to martensite.

#### GENERAL EXPERIMENTAL METHODS

Samples of low carbon steel (SAE 1020) were carbonitrided under various conditions. Four standard specimens were prepared by carbonitriding for 4 hours at 1300, 1400, 1500 and 1550 °F (705, 760, 815 and 845 °C), followed by oil quenching; at the first three temperatures a gas consisting of 40% NH<sub>3</sub>, 10% CH<sub>4</sub> and 50% carrier gas was used, while at 1550 °F (845 °C) the gas analyzed 20% NH<sub>3</sub>, 10% CH<sub>4</sub> and 70% carrier gas. With other specimens the duration of the carbonitriding treatments and the gas compositions were varied. The cooling rates also included water quenching, cooling in air and cooling in the furnace. Standard specimens were tempered at 300, 500, 700, 900 and 1100 °F (150, 260, 370, 480 and 595 °C). The effects of these variables were evaluated on the basis of surface hardness, depth hardness, microhardness, metallographic features and case depth. The details of this research may be found in a concurrent paper (1).

In the work reported here, the constitution of carbonitrided cases produced in the manner outlined above was studied by means of chemical analysis, X-ray diffraction analysis and metallographic investigation, consisting of quantitative metallography by lineal analysis.<sup>2</sup>

#### CHEMICAL ANALYSIS

##### *Procedures*

The standard specimens as well as other specimens were analyzed for carbon and nitrogen content as a function of position in

<sup>2</sup>Reference 22 reports the results of this investigation in considerably greater detail, including tables of numerical data.



the case. In this work, cylindrical specimens were used. These specimens were air-cooled because with slower cooling an appreciable amount of nitrogen would probably have been lost, while faster cooling rates would have resulted in a case that could not be machined.

Four sections were marked off along each carbonitrided specimen. A few thousandths of an inch were then removed from each section on a lathe and the chips were collected. Because of the rapid variations in composition near the surface, cuts of 0.0025 inch were attempted, although machining difficulties often interfered. The remainder of the case machined satisfactorily and the variations in composition were gradual. Therefore, cuts of 0.005 inch were made. Duplicate samples from two sections were analyzed for carbon by the classical combustion method and the other two samples were analyzed for nitrogen by a modified micro-Kjeldahl method. Samples taken from a specimen before it was case hardened showed that the steel originally contained 0.23% carbon and 0.0065% nitrogen.

The depths reported are somewhat uncertain because the high hardness of carbonitrided cases interfered with accurate machining. An additional reason was that case depth on a given specimen was not always uniform. This latter factor interfered especially with the accurate locating of the interface between the outer and inner layers. Also the growth of the specimen occurring in carbonitriding may have been uneven in some specimens. Most values, however, are probably correct within 0.0015 inch.

#### *Results of Chemical Analysis*

Carbon and nitrogen gradients in cases carbonitrided at various temperatures are shown in Figs. 3 to 7. The existence of an outer layer at the surface of carbonitrided specimens, which was found by metallographic observation (1) and confirmed by X-ray analysis, justifies a discontinuity in the curves at the depth of the interface between the compound layer and the inner layer of the case. The position of the interface was determined by averaging the metallographic observations made on several specimens or sections. The method of sampling was not sufficiently accurate, however, to determine adequately the carbon and nitrogen concentrations and gradients within the narrow compound layer and they are therefore shown only approximately as dotted lines.

*Nitrogen Gradients*—Considering the effect of temperature, the nitrogen content at the surface decreased continuously from about

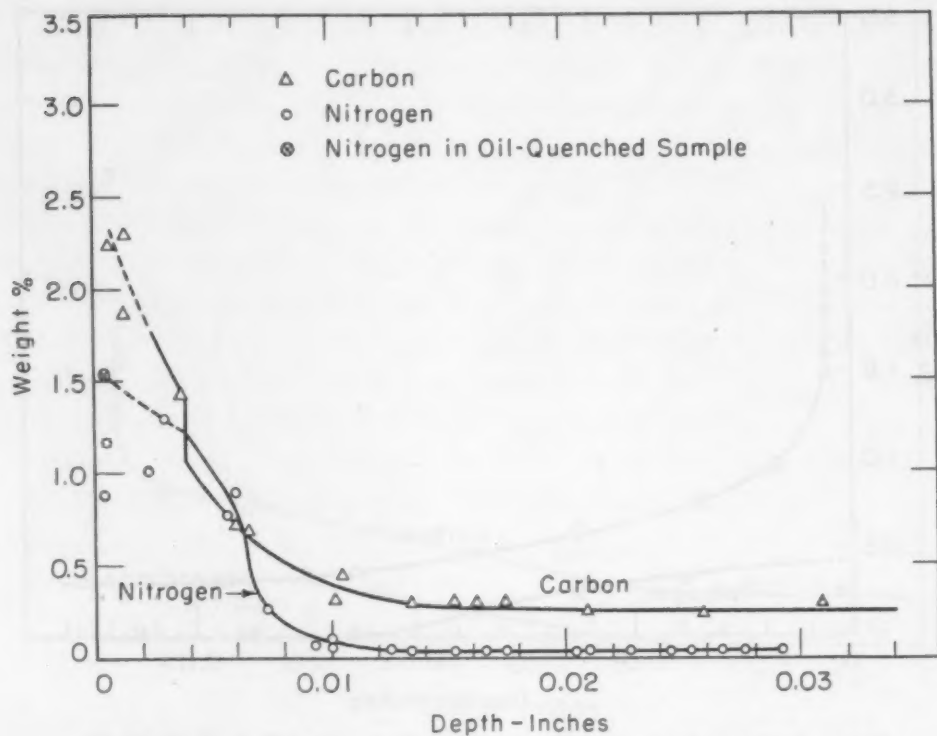


Fig. 3—Carbon and Nitrogen Concentrations in Specimen Carbonitrided 4 Hours at 1300°F Followed by Air Cooling. Gas composition: 40%  $\text{NH}_3$ , 10%  $\text{CH}_4$ , 50% carrier gas.

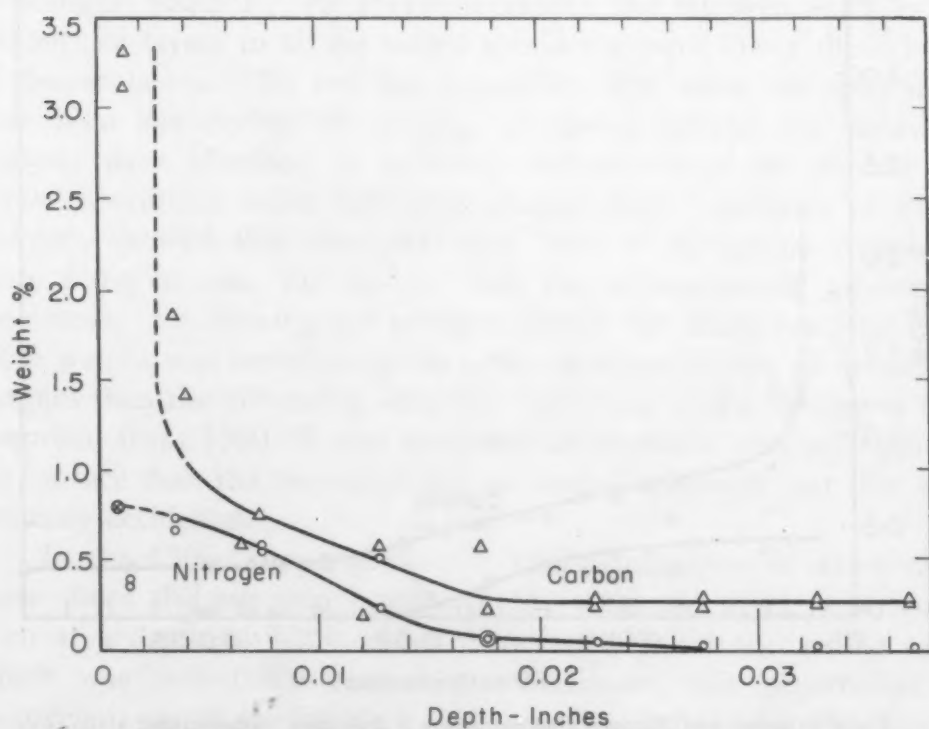


Fig. 4—Carbon and Nitrogen Concentrations in Specimen Carbonitrided 4 Hours at 1400°F Followed by Air Cooling. Gas composition: 40%  $\text{NH}_3$ , 10%  $\text{CH}_4$ , 50% carrier gas.

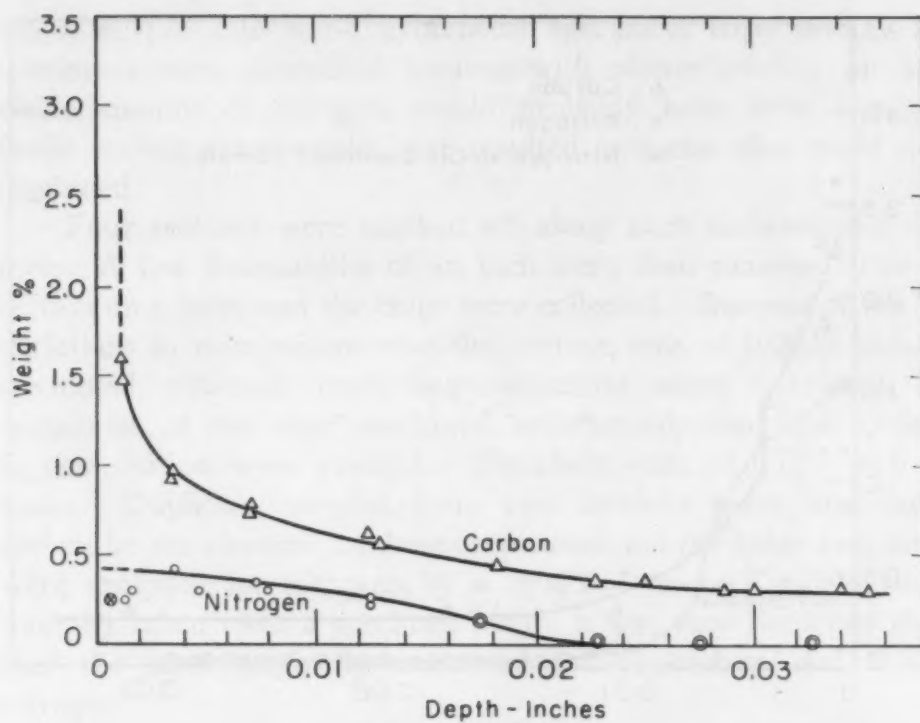


Fig. 5—Carbon and Nitrogen Concentrations in Specimen Carbonitrided 4 Hours at 1500°F Followed by Air Cooling. Gas composition: 40%  $\text{NH}_3$ , 10%  $\text{CH}_4$ , 50% carrier gas.

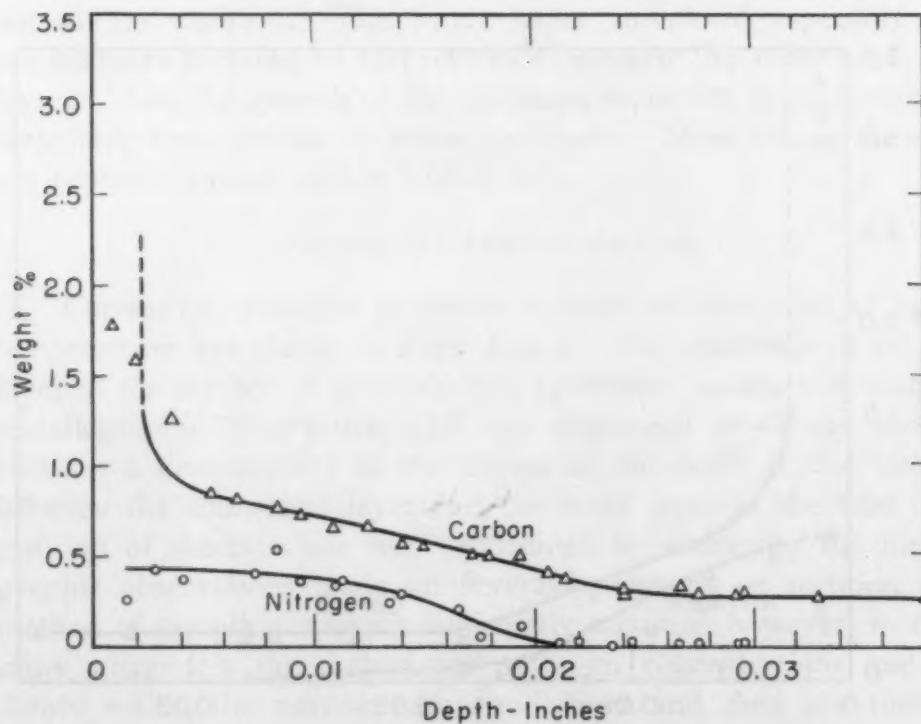


Fig. 6—Carbon and Nitrogen Concentrations in Specimen Carbonitrided 4 Hours at 1500°F Followed by Air Cooling. Gas composition: 20%  $\text{NH}_3$ , 10%  $\text{CH}_4$ , 70% carrier gas.

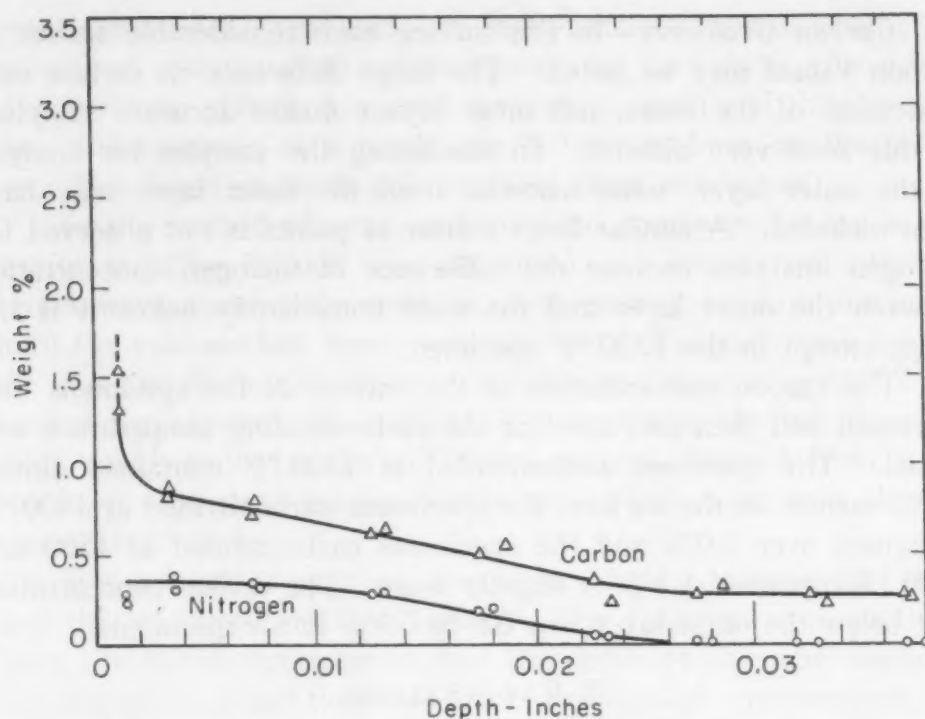


Fig. 7—Carbon and Nitrogen Concentrations in Specimen Carbonitrided 4 Hours at 1550°F Followed by Air Cooling. Gas composition: 20%  $\text{NH}_3$ , 10%  $\text{CH}_4$ , 70% carrier gas.

1.5% after carbonitriding at 1300 °F to less than 0.4% after carbonitriding at 1550 °F. At any temperature, the nitrogen analyses of the surface layers in all air-cooled specimens were lower than those of deeper layers. To test the possibility that some nitrogen may have been lost during air cooling, powdered samples for chemical analysis were obtained by scraping material from the surface of special specimens which had been oil-quenched. Analyses of these powders showed that the 1300 and 1400 °F specimens contained more nitrogen near the surface than the corresponding air-cooled specimens. In drawing the nitrogen curves for these temperatures, more weight was therefore given to the analyses of the oil-quenched samples than the air-cooled samples. Only one of the specimens oil-quenched from 1500 °F was analyzed; it contained less nitrogen at the surface than the corresponding air-cooled specimen, but this was probably accidental.

In the 1300 °F specimen, over 0.02% nitrogen, or more than three times the nitrogen content of the untreated steel, was found even at a depth of 0.030 inch. This is far below the visible case, which was only 0.008 inch deep. Moreover, this penetration of nitrogen is much deeper than in specimens carbonitrided at higher temperatures, probably because of the greater diffusion rate and smaller solubility of nitrogen in ferrite than in austenite.



*Carbon Gradients*—In the surface zone considerable scatter of carbon values may be noted. The large difference in carbon concentration of the outer and inner layers makes accurate sampling in this zone very difficult. In machining the samples for analysis of the outer layer, some material from the inner layer may have been included. A similar large scatter of points is not observed for nitrogen analyses because the difference of nitrogen concentration between the outer layer and the zone immediately below it is not large, except in the 1300 °F specimen.

The carbon concentration at the surface of the specimens first increased and then decreased as the carbonitriding temperature was raised. The specimen carbonitrided at 1300 °F contained almost 2.5% carbon on the surface, the specimens carbonitrided at 1400 °F contained over 3.0% and the specimens carbonitrided at 1500 and 1550 °F contained 1.5% or slightly more. The carbon concentration just below the outer layer was 0.8 to 0.9% in all specimens.

## X-RAY ANALYSIS

### *Procedures*

Specimens analyzed by X-ray diffraction included the 1300 1400 and 1500 °F (705, 760 and 815 °C) standard specimens quenched in oil and tempered at 300, 500, 700, 900 and 1100 °F. Furnace-cooled specimens and a specimen nitrided at 1300 °F and oil-quenched were also analyzed. Determinations were made on a specimen air-cooled after carbonitriding at 1400 °F, on a specimen oil-quenched after carbonitriding at 1204 °F and on a powder specimen carbonitrided at 1400 °F, as-quenched and after tempering at 700 °F.

For low-angle diffraction lines a Norelco recording spectrometer was used with chromium radiation;  $K_{\beta}$  radiation was absorbed by a vanadium carbide filter. Diffraction lines from planes of higher indices were obtained with cobalt radiation and a Phragmen No. 2 camera covering the range from  $\theta = 29$  degrees to  $\theta = 57$  degrees. The pattern showed predominantly the cobalt  $K_{\alpha}$  lines because the high iron content of the sample absorbed most of the  $K_{\beta}$  radiation. For the few samples available in powder form, a diffraction pattern was made with a Debye-Scherrer camera, using cobalt radiation or chromium radiation filtered with vanadium carbide.

*Preparation of Specimens*—Specimens had to be prepared in a manner which permitted accurate determination of the position in the case from which each diffraction pattern was obtained. If taper-

ground specimens prepared for depth-hardness measurements (1) were used and the area radiated was large enough to give a sufficiently strong pattern, too great a range in depth and thus in structure was covered; as a result, the diffraction lines on the pattern were broadened so much that many of them overlapped.

In the method adopted, carbonitrided specimens having a cross section of  $\frac{3}{4}$  by  $\frac{3}{4}$  inch were cut into 1-inch lengths and successive layers were removed by grinding and etching in 30% nitric acid until the cold-worked layer was dissolved. The difference between the final and the initial thickness, which was known to  $\pm 0.0002$  inch, located the exposed flat surface with respect to the initial surface. With cobalt radiation the diffraction pattern obtained from a steel specimen represents predominantly the surface layer to a depth of about 0.0005 inch.

For successive analyses, the same side was ground and etched and the thickness measured again. This thickness was subtracted from the initial thickness to find the depth of the new surface in the original case and therefore errors in thickness measurement were not cumulative.

*Recording Spectrometer*—The amplitudes and damping of the recording unit were adjusted so that the peaks of the lines would be as high as possible without producing too uneven a background. The maximum angle which the spectrometer was able to analyze was  $2\theta = 88$  degrees. All runs were started at this angle, and the specimens which showed a complicated pattern were carried to an angle of  $2\theta$  approximately equal to 30 degrees.

The location of the diffraction lines represented by peaks on the record was listed in terms of the angle  $2\theta$  and of the lattice spacing ("d" values). The angle  $2\theta$  was measured to the nearest tenth of a degree, and the "d" values were calculated to the nearest five-thousandth of an Angstrom.

The heights of lines above the background were measured in arbitrary units, and relative intensities were determined by reference to the strongest lines. Many of the patterns included one or two peaks which fell off the scale, but these lines occurred in simple crystal structures and could be separated from those resulting from more complicated structures.

The relative intensities were plotted as a bar graph against the "d" values where the lines were found. These graphs were compared with similar graphs made from intensities and "d" values of various known phases, and the unknown crystal structures were determined by matching. The data for the known structures were

taken from the detailed report (23) of an investigation by Jack, the results of which have been published (16, 19, 20).

Many of the patterns obtained had very broad lines indicating distortion of the phases or lack of uniformity in composition. In these cases it was found better to approximate the shape of the lines in the recorded pattern than to use simple bar graphs.

*Cameras*—The patterns made with a Phragmen No. 2 camera and cobalt  $K\alpha$  radiation included lines from planes of higher indices than could be obtained with the spectrometer. Even when care was taken that the flat surfaces of the solid specimens were located on the circumference of the camera at the same spot at which the X-ray beam intersected the circumference, the lines in the films were broadened. Some broadening was caused by distortion, but much of it was due to the fact that the incident X-ray beam had some width and that the specimen could not be placed on the circumference of the camera throughout the whole width of the beam.

The films made with the Phragmen camera were measured to the nearest tenth of a millimeter. A correction was made for film shrinkage and the  $\sin \theta$  value for the lines was obtained from calibration curves of the camera. These values of  $\sin \theta$  were converted to "d" values. The intensities of the lines were estimated roughly and plotted against the measured "d" values. The crystal structures were again found from the resulting bar graphs by comparison with data for known structures.

### *Results of X-Ray Analysis*

The constituents found in the standard specimens at various depths are summarized in Figs. 8, 9 and 10. The symbols used in

Table I

Explanation of Symbols Used in Figs. 8, 9 and 10

- $\vee$  Position of sample analyzed
- $\ominus$  One or more of the phases indicated for that zone were not found in the sample analyzed
- $\oplus$  Lines from phases not indicated for that position were found in the sample analyzed
- $\leftarrow \vee$  One or more of the phases indicated for the adjoining zone (lying in the direction of the arrow) found in the sample analyzed

M = Martensite

F = Ferrite or Tempered Martensite

$\gamma$  = Austenite

$\gamma'$  = Gamma Prime (Iron Carbonitride)

C = Cementite

XC = X-Cementite

$\epsilon$  = Epsilon (Iron Carbonitride)



these figures are explained in Table I. The constitution of the surfaces of the various specimens in these figures could not be determined, since the patterns obtained were too complex. A thin film consisting of several phases was present at the surface of the quenched specimens, probably because of a reaction of the specimen with the atmosphere or the quenching oil.

*Specimens Carbonitrided at 1300 °F*—As shown in Fig. 8, X-ray analysis indicates that the specimen quenched from 1300 °F con-

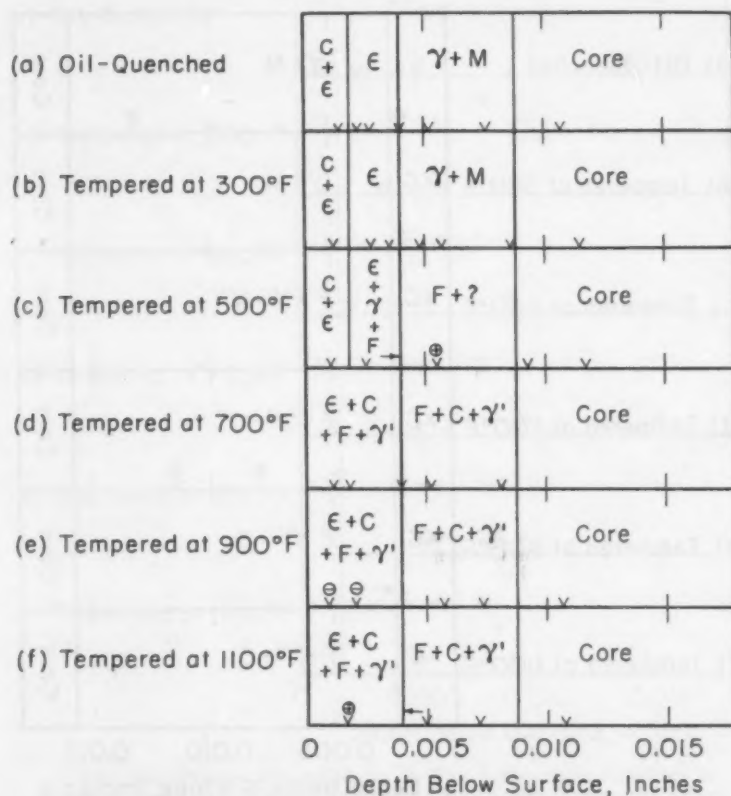


Fig. 8—Phases Identified by X-Ray Diffraction Analysis in Standard Specimens Carbonitrided at 1300 °F and Tempered. For explanation of symbols, see Table I.

tained an outer layer composed primarily of epsilon carbonitride and that at the outer edge of this layer some cementite was present. In the spectrometer record of the epsilon carbonitride phase formed under these conditions the (100) line was much stronger with reference to the (002) line than would have been expected from the values of Jack (23); also the (101) line was very much weaker. All the lines were shifted to higher angles, giving smaller "d" values.

In order to check whether the epsilon carbonitride phase was formed in a preferred orientation, a specimen was nitrided in ammonia at 1300 °F and then analyzed by X-ray diffraction. This



specimen showed differences in intensity and displacement of lines similar to those found in the specimen carbonitrided at 1300 °F. As further evidence that the phase found was epsilon carbonitride having a preferred orientation rather than some other phase, it was noted that both spectrometer and Phragmen patterns of those specimens which did not show cementite lines consisted only of lines which could be identified as resulting from a contracted epsilon carbonitride. Finally, patterns taken from near the surface showed

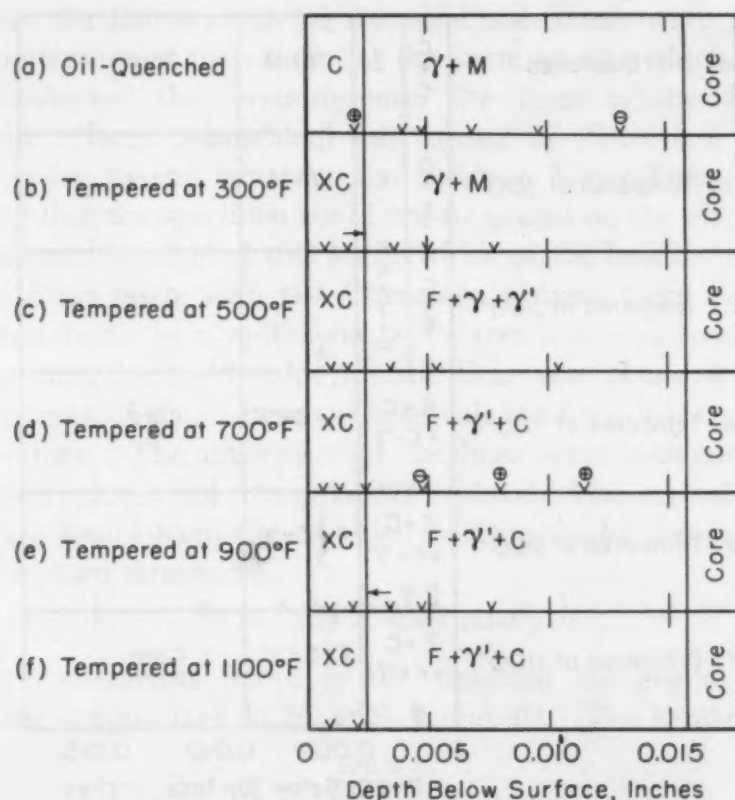


Fig. 9—Phases Identified by X-Ray Diffraction Analysis in Standard Specimens Carbonitrided at 1400 °F and Tempered. For explanation of symbols, see Table I.

intensities and "d" values more nearly in agreement with those given by Jack for epsilon carbonitride.

The X-ray results agree with the metallographic evidence. The epsilon carbonitride appears to be the white etching constituent in the outer layer of the as-quenched samples (see Fig. 3a, Ref. 1). The multiphase region observed in the microstructures near the surface is made up of mixtures of cementite and epsilon.

Beneath the compound layer of the 1300 °F standard specimens, diffraction patterns of body-centered cubic and face-centered cubic structures were found. The body-centered cubic phase had approxi-

mately the lattice parameter of alpha iron. While no tetragonality was detected, the lines were broad and may be attributed to martensite on the basis of the combined X-ray and metallographic evidence. The face-centered cubic structure had approximately the lattice parameter of gamma iron, but the recorded lines were also broad. The corresponding phase is identified as austenite. Austenite was found by X-ray diffraction even a little below the case depth deter-

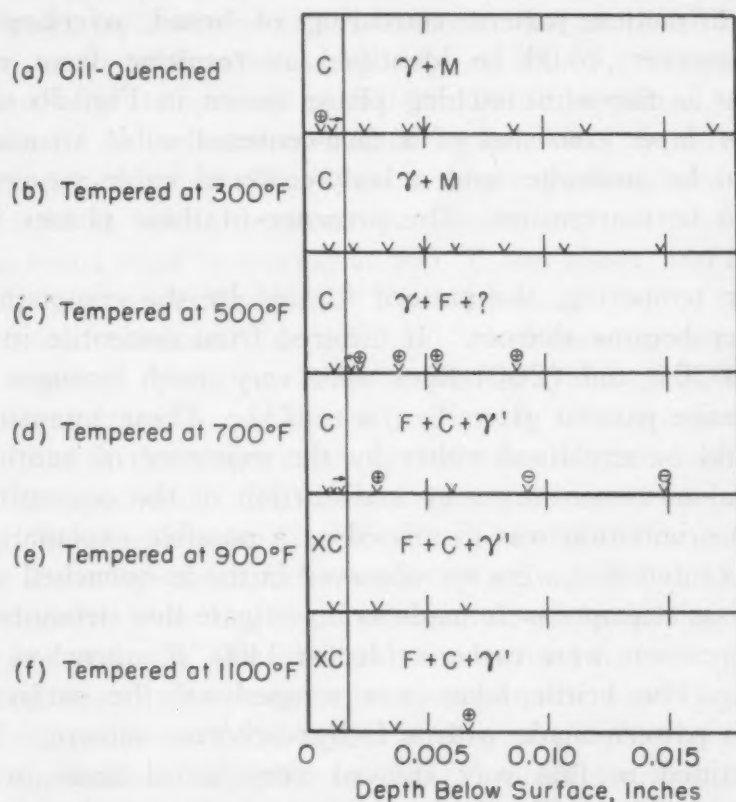


Fig. 10—Phases Identified by X-Ray Diffraction Analysis in Standard Specimens Carbonitrided at 1500°F and Tempered. For explanation of symbols, see Table I.

mined by simple metallographic observation. In agreement with this finding, photomicrographs (Fig. 2a, Ref. 1) show patches of austenite in ferrite for a few thousandths of an inch below the inner layer of the case.

The cementite present near the surface of the outer layer appeared to remain unchanged at all tempering temperatures investigated. Epsilon carbonitride showed no change after tempering at 300 °F, but at higher temperatures it partially decomposed to ferrite and the gamma prime phase. After tempering at 500 °F, some austenite was also found in the compound layer, but this probably originated in the underlying zone.

In the inner layers of specimens tempered at 300 °F only austenite and martensite were found. The structure formed after tempering at 500 °F was greatly distorted and there was considerable uncertainty as to what phases were actually present. On tempering at higher temperatures, cementite, gamma prime, and alpha were found in the inner layer.

*Specimen Carbonitrided at 1400 °F*—The compound found in the outer layer of the oil-quenched specimen carbonitrided at 1400 °F gave a diffraction pattern consisting of broad, overlapping lines which, however, could be identified as resulting from cementite. This layer is the white etching phase shown in Fig. 3b of Ref. 1. The inner layer consisted of a face-centered cubic structure, considered to be austenite, and a body-centered cubic structure, considered to be martensite. The presence of these phases is shown in Fig. 9.

After tempering, the pattern formed by the compound in the outer layer became sharper. It differed from cementite in that the (111), (020), and (200) lines were very much stronger than for the cementite pattern given by Jack (23). These intensity differences could be explained either by the existence of another phase in addition to cementite or by a distortion of the cementite lattice. Preferred orientation was dismissed as a possible explanation, since anomalous intensities were not observed in the as-quenched specimen.

Various attempts were made to investigate this structure further. Round specimens were carbonitrided at 1400 °F, quenched and also tempered. The brittle layer was scraped off the surface and a diffraction pattern made with a Debye-Scherrer camera. The patterns obtained in this way showed very broad lines in the as-quenched condition. The lines in both the as-quenched and tempered specimens were intermingled so much with lines from the oxide layer of the surface that no identification of the phases from the film was possible. Another sample was made by carbonitriding a pure iron powder at 1400 °F, quenching in oil and tempering part of the sample at 700 °F. Diffraction patterns obtained from these samples indicated a true cementite structure but did not contribute to the problem because it was found that this sample contained only very little nitrogen, probably because the large surface area of the powdered sample had caused rapid dissociation of the ammonia at these temperatures to inert nitrogen and hydrogen.

The structure designated as "x-cementite" in this paper consists of the phase or phases producing the X-ray diffraction pattern discussed above, which is similar to cementite but shows certain



anomalies in intensities. The methods used were not able to decide definitely whether the pattern attributed to x-cementite was produced by two phases or by a distorted cementite. While photomicrographs of the outer layer of the 1400 °F specimens (Fig. 3b, Ref. 1) suggest that a second phase may be present, in view of the entire evidence, it is more probable that x-cementite is really cementite with a distorted lattice. Such a distortion may be expected from the simultaneous presence of nitrogen and carbon.

The inner layer of specimens carbonitrided at 1400 °F showed no change in structure after tempering at 300 °F. Austenite was still present after tempering at 500 °F, but disappeared at higher temperatures. A body-centered cubic phase was found after all tempering temperatures. The lines were always broad, and no distinction could be made between martensite and ferrite. Gamma prime was found after tempering at 500 °F and above, and cementite was found after tempering at 700 °F and above.

*Specimens Carbonitrided at 1500 °F*—Phases present in the 1500 °F standard specimen, both as-quenched and after tempering at various temperatures, are shown in Fig. 10. The compound layer was very thin in these specimens and consisted of cementite in the as-quenched specimen. This cementite remained unchanged at tempering temperatures up to 700 °F. The diffraction patterns of the outer layer of the specimens tempered at 900 and 1100 °F differed slightly from the cementite found on tempering at lower temperatures and was identified as x-cementite.

Austenite and martensite were found in the inner layer of the as-quenched specimen. Although in photomicrographs the martensite was darkened after tempering at 300 °F, austenite and martensite were the only phases found by X-ray diffraction. After tempering at 500 °F, austenite and martensite or ferrite were present. The X-ray diffraction pattern indicated the presence of other phases but these were not identified. On tempering at 700 °F, ferrite, cementite and gamma prime were found and photomicrographs of this specimen showed that the inner layer had transformed. After tempering at 900 and 1100 °F, ferrite and gamma prime were found, but x-cementite was identified instead of cementite.

*Other Specimens*<sup>3</sup>—Furnace- and air-cooled specimens were also investigated by diffraction analysis. Although the details of distribution varied from the oil-quenched and tempered specimens discussed above, no new phases were found. Ferrite, cementite, x-cementite, gamma prime and epsilon were present in these speci-

<sup>3</sup>Detailed results are reported in Ref. 22.



mens at various depths. An X-ray diffraction pattern at a depth of 0.0051 inch was taken of the specimen which was air-cooled after carbonitriding at 1400 °F. The predominant structure was that of austenite which may therefore be identified with the large white patches in the photomicrographs of this specimen (shown in Fig. 9b of Ref. 1).

An X-ray diffraction pattern was also made of the compound layer of a specimen oil-quenched after carbonitriding at 1204 °F. The only phase found was epsilon carbonitride. Lines from this epsilon phase had approximately the same intensities as those given by Jack, and the lattice parameters of epsilon carbonitride formed under these conditions were almost equal to Jack's values (23). Apparently, there was no preferred orientation. The phase was almost saturated with interstitial atoms.

#### *Correlation of Chemical and X-Ray Analyses of the Outer Layer*

Consideration of the chemical analyses of the 1300, 1400 and 1500 °F specimens shows that the outer layer of these specimens did not contain enough nitrogen plus carbon to equal the formula  $\text{Fe}_3\text{X}$  (equivalent to  $\text{Fe}_3\text{C}$ ) in which X represents both interstitial atoms (carbon and nitrogen). On the other hand, X-ray analysis shows that the outer layer of the specimen carbonitrided at 1500 °F contained cementite. This apparent contradiction may be resolved by assuming that cementite can exist with a deficiency of interstitial atoms. Such deficiency is in agreement with the work of Schwartz (10, 13, 14) which shows that cementite can exist with less than the number of carbon atoms required by the formula  $\text{Fe}_3\text{C}$ .

The results discussed in this section strongly suggest that nitrogen can replace some of the carbon atoms in cementite. Aside from the nitrogen content found analytically in the outer layer, the inner layer of the 1500 °F specimen, for example, could not contain nitrogen unless this element is also soluble in the outer layer of cementite. While Jack found only a negligible solubility of nitrogen in cementite at much lower temperatures, this solubility may increase with temperature.

Epsilon carbonitride and mixtures of epsilon carbonitride and cementite were found in the 1300 °F specimen at combined concentrations of carbon plus nitrogen lower than the lower composition limits for nitrogen in the iron-nitrogen epsilon phase. Carbon therefore appears to shift the range of stability of the epsilon phase as well as to replace nitrogen in the crystal structure.

The iron-nitrogen diagram shows that epsilon can exist over a

wide range of nitrogen concentrations and Jack (20) proved that the ratios of carbon and nitrogen in epsilon carbonitride can vary greatly. The work reported here indicates that cementite also may have a range of composition. The fact that the composition of the compound layer formed in carbonitriding is variable should be important in determining the carbon and nitrogen concentrations of the inner layer, which affect its properties. If gas composition can be adjusted so that varying concentrations of carbon and nitrogen exist in the compound layer, the composition of the inner layer in contact with this can also be varied.

### LINEAL ANALYSIS

#### *Procedure*

Quantitative determinations of retained austenite as a function of location in the layer were made by lineal analysis. Specimens to be analyzed by lineal analysis were held for 1 minute in a salt bath at 600 °F to darken the martensite and make it distinguishable from retained austenite. The specimens were then polished and etched, and Knoop indentations were made at 3, 6, 9, 12 and 15 thousandths of an inch from the surface. These indentations were used as reference marks to determine the location of counts. Four sets of indentations, two on each of the sides of a specimen adjacent to the mount clamp, were made. The specimens were then placed under a microscope equipped with a stage as described by Howard and Cohen (24), and the counts were made while the specimen was moved parallel to a surface. Four series of counts were made, one at each set of reference indentations. The depths of counts of specimens carbonitrided at 1400 and 1500 °F were measured from the surface. The amount of retained austenite in specimens carbonitrided at 1300 °F was found to change rapidly with depth below the interface of the compound and inner layer. Since the thickness of the compound layer was not constant in these specimens, austenite counts are reported with reference to the interface of the layers rather than the surface of the specimens.

#### *Results of Lineal Analysis*

The amounts of retained austenite present in standard specimens are summarized in Fig. 11. The retained austenite content immediately below the outer layer was found to decrease with increasing carbonitriding temperature from over 90% in the specimen carbonitrided at 1300 °F to less than 30% in the specimen carbonitrided at 1500 °F. The amount of retained austenite at the inner edge

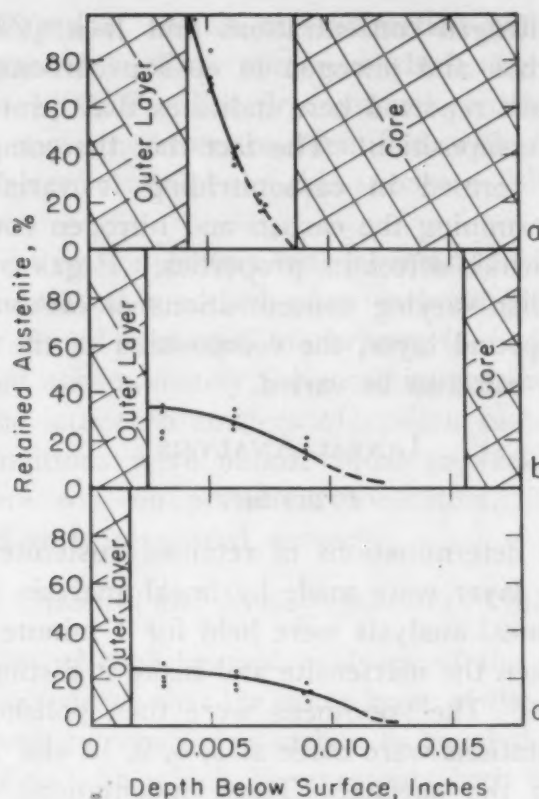


Fig. 11—Retained Austenite in the Inner Layer of Standard Specimens Carbonitrided for 4 Hours at (a) 1300°F, (b) 1400°F, (c) 1500°F, and Quenched in Oil. Gas composition 40%  $\text{NH}_3$ , 10%  $\text{CH}_4$ , 50% carrier gas.

of the case was so small in all specimens that it could not be measured.

For every temperature of carbonitriding, the content of retained austenite and the concentrations of nitrogen and carbon in the inner layer decrease with case depth. A corresponding decrease in hardness across the case was shown in Figs. 4 and 5 of Ref. 1. The increase in surface hardness with increasing carbonitriding temperature, discussed in Ref. 1, is in part caused by the decrease of retained austenite with temperature shown in Fig. 11.

#### SUMMARY AND CONCLUSIONS

The structure of carbonitrided cases is characterized by the presence of an outer and inner layer. With increasing carbonitriding temperature the thickness of the outer layer decreases, while that of the inner layer increases.

The outer layer formed in carbonitriding at 1300 °F consists of a mixture of cementite and epsilon carbonitride. At higher temperatures cementite only, containing nitrogen atoms substituting for



carbon, was found. The nitrogen content near the surface decreases from approximately 1.5% at 1300 °F to less than 0.4% at 1550 °F. The corresponding carbon contents are approximately 2.5% at 1300 °F, over 3.0% at 1400 °F and 1.5% or slightly more at 1500 and 1550 °F.

Beneath the compound layer a nitrogen-carbon austenite is formed at the carbonitriding temperature. This decomposes on quenching in oil to mixtures of martensite and retained austenite. The amount of retained austenite is a function of the amount of nitrogen present, thus decreasing with increasing temperature.

This investigation confirms that nitrogen reduces the lower transformation temperature of steels. It is also of interest that nitrogen penetrated far below the visible case in carbonitriding at 1300 °F; this penetration is greater than in specimens carbonitrided at higher temperatures, probably because of a larger diffusion rate and the smaller solubility of nitrogen in ferrite than in austenite.

#### ACKNOWLEDGMENTS

The investigation reported in this paper was made possible through a fellowship sponsored by the Ammonia Division of Armour and Company of Chicago. The authors also wish to acknowledge gratefully the advice and assistance received from various members of the Department of Metallurgy at the Massachusetts Institute of Technology. Special thanks are due to Mr. Allan Sloane of Watertown Arsenal, Watertown, Mass., who conducted the nitrogen analyses.

#### References

1. G. W. P. Rengstorff, M. B. Bever, and C. F. Floe, "The Carbonitriding Process of Case Hardening Steel", published in this Volume of *TRANSACTIONS*, p. 342.
2. R. J. Cowan and J. T. Bryce, "The Process of Dry Cyaniding", *TRANSACTIONS*, American Society for Metals, Vol. 26, 1938, p. 766.
3. R. Trautschold, "Surface Hardening", *Steel*, Vol. 111, 1942, p. 64.
4. W. H. Holcroft, "Carbo-Nitriding of S.A.E. Steel", *METAL PROGRESS*, Vol. 52, 1947, p. 380.
- 5a. A. Bramley and G. H. Beeby, "Cementation with the Nitrogenous Vapours of Pyridine and Methyl Cyanide", *Carnegie Scholarship Memoirs*, Vol. 15, 1926, p. 71.
- 5b. A. Bramley and G. Turner, "The Action of Mixtures of CO and NH<sub>3</sub> on Iron and Steel and Its Bearing on the Process of Cementation", *Carnegie Scholarship Memoirs*, Vol. 17, 1928, p. 23.
- 6a. V. I. Prosvirin, "Gaseous Nitrocarburizing", *Metallurg*, Vol. 13, No. 11, 1938, p. 84; *Chemical Abstracts*, Vol. 34, 1940, p. 2759.
- 6b. D. M. McCutcheon: Unpublished research. See Ref. 4 and J. A. Dow, "Carbonitriding (Gas Cyaniding)", *ASM Metals Handbook*, 1948, p. 696.



7. A. Westgren and G. Phragmen, "X-ray Studies on the Crystal Structure of Steel", *Journal, Iron and Steel Institute*, Vol. 105, 1922, p. 241.
8. S. B. Hendricks, "The Crystal Structure of Cementite", *Zeitschrift für Kristallographie*, Vol. 74, 1930, p. 534.
9. H. Lipson and N. J. Petch, "The Crystal Structure of Cementite,  $\text{Fe}_3\text{C}$ ", *Journal, Iron and Steel Institute*, Vol. 142, 1940, p. 95.
10. H. A. Schwartz, K. R. Van Horn and C. H. Junge, "Transformation in the Carbide Phase During Graphitization", *TRANSACTIONS, American Society for Steel Treating*, Vol. 21, 1933, p. 463.
11. A. Westgren, G. Phragmen and T. Negresco, "On the Structure of the Iron-Chromium-Carbon System", *Journal, Iron and Steel Institute*, Vol. 117, 1928, p. 383.
12. A. A. Bates, D. E. Lawson and H. A. Schwartz, "Metastable Equilibrium in Hypereutectoid Iron-Carbon Alloys", *TRANSACTIONS, American Society for Steel Treating*, Vol. 18, 1930, p. 659.
13. H. A. Schwartz, H. H. Johnson and C. H. Junge, "Graphitization of Pre-quenched White Cast Iron", *TRANSACTIONS, American Society for Steel Treating*, Vol. 17, 1930, p. 383.
14. H. A. Schwartz, "The Conversion of Solid Cementite into Iron and Graphite", *Journal, Iron and Steel Institute*, Vol. 138, 1938, p. 205.
15. G. Hägg, "Pulverphotogramme eines Neuen Eisen-Carbides", *Zeitschrift für Kristallographie*, Vol. 89, 1934, p. 92.
16. K. H. Jack, "Binary and Ternary Interstitial Alloys, III. The Iron-Carbon System: The Characterization of a New Iron Carbide", *Proceedings, Royal Society*, Vol. 195, 1948, p. 56.
17. V. G. Paranjpe, M. Cohen, M. B. Bever and C. F. Floe, "The Iron-Nitrogen System", *Transactions, American Institute of Mining and Metallurgical Engineers*, Vol. 188, 1950, p. 261.
18. G. Hägg, "X-ray Studies on the Binary Systems of Iron with Nitrogen, Phosphorus, Arsenic, Antimony and Bismuth", *Nova Acta Regiae Societatis Scientiarum Upsaliensis*, Vol. 7, 1929, p. 1.
19. K. H. Jack, "Binary and Ternary Interstitial Alloys, I. The Iron-Nitrogen System: the Structures of  $\text{Fe}_4\text{N}$  and  $\text{Fe}_2\text{N}$ ", *Proceedings, Royal Society*, Vol. 195, 1948, p. 34.
20. K. H. Jack, "Binary and Ternary Interstitial Alloys, II. The Iron-Carbon-Nitrogen System", *Proceedings, Royal Society*, Vol. 195, 1948, p. 41.
21. B. N. Bose and M. E. Hawkes, "Kinetics of the Eutectoid Transformation in Alloys of Iron and Nitrogen", *Transactions, American Institute of Mining and Metallurgical Engineers*, Vol. 188, 1950, p. 307.
22. G. W. P. Rengstorff, Sc.D. Thesis, Massachusetts Institute of Technology, 1950.
23. H. K. Jack, Unpublished Report, Study of Interstitial Alloys of the Iron-Carbon-Nitrogen System, Project MG/C/26, Metal Physics Committee, Metallurgy (General) Division, The British Iron and Steel Research Association, 1947.
24. R. T. Howard and M. Cohen, "Quantitative Metallography by Point-Counting and Lineal Analysis", *Transactions, American Institute of Mining and Metallurgical Engineers*, Vol. 172, 1947, p. 413.

## DISCUSSION

**Written Discussion:** By W. H. Holcroft, executive vice-president, Holcroft & Co., Detroit.

The work reported in this paper should prove of great interest and value to all who are interested in carbonitriding. The X-ray diffraction work is particularly interesting.

The carbon and nitrogen concentrations shown in Figs. 3 and 4 are very similar to what we would expect. The high surface carbons shown at 1400 °F (760 °C) are typical in this temperature range. The lack of difference in nitrogen content shown in Figs. 5 and 6 with varying ammonia flow is very unusual. Our experiments all show that increasing ammonia flows increase the nitrogen content in this temperature range.

As mentioned in the discussion of Ref. 1, attention should be called to the fact that the high flows of ammonia used for Figs. 5, 6 and 7 are far above the flows used in commercial work. Most commercial carbonitriding is done in the temperature range of 1450 to 1650 °F (790 to 900 °C), with ammonia additions approximating 5% of the total inlet gas flow.

**Written Discussion:** By Hans J. Heine, chief metallurgist, Rockwell Manufacturing Co., Pittsburgh.

The authors are to be congratulated for the contribution they have made to our knowledge of the case hardening process by carbonitriding and for the concise yet comprehensive manner in which the information was presented.

Without wishing to detract from the excellence and completeness of the paper, we are wondering if the slight discrepancies noted between Fig. 11c (retained austenite in the inner layer of standard specimens carbonitrided for 4 hours at 1500 °F and quenched in oil) and Fig. 3 in the paper previously published by the same authors<sup>4</sup> are due to additional research work since presentation of the earlier article. We feel that the replacement of retained austenite by martensite is probably the most significant feature of those case hardening processes which result in the formation of carbon-nitrogen austenite.

The presentation of the constituents found in standard specimens at various depths as summarized in Figs. 8, 9 and 10 is unusually lucid and interesting. We should like to know if the only instance of the presence of austenite, found after carbonitriding at 1300 °F (705 °C) and tempering at 500 °F (260 °C) in the compound layer, is significant and how the mechanism of its existence may be explained.

**Written Discussion:** By Don M. McCutcheon, supervisor, Applied Physics Unit, Manufacturing Research, Ford Motor Co., Dearborn, Mich.

The authors have presented information on the carbonitriding process which is of considerable interest to commercial users of this process. We have been using carbonitriding<sup>5</sup> for a number of years with good success, although adequate fundamental information on the process has never been available.

A large amount of experimental work has been carried out at the Ford Motor Co. on one phase of the carbonitriding process. Specifically, we have been treating low carbon body steel formed into cylinder liners with a carbonitriding atmosphere at approximately 1340 °F (725 °C). The atmosphere consists essentially of:

<sup>4</sup>G. W. P. Rengstorff, M. B. Bever and C. F. Floe, "The Carbonitriding Process of Case Hardening Steel", *METAL PROGRESS*, Vol. 56, 1949, p. 651.

<sup>5</sup>G. Vennerholm, N. D. Ford and F. C. Young, "Method of Heat Treating Steel", U. S. Patent No. 2,472,320 dated June 7, 1949. Application, Feb. 5, 1941.

*Carbonitriding Atmosphere*

- (a) 3200 cubic feet of ammonia gas per hour
  - (b) 1600 cubic feet of generator gas per hour
- Generator Gas Analysis
- |                                    |                       |
|------------------------------------|-----------------------|
| 2.5% CO <sub>2</sub>               | 5.2% H <sub>2</sub>   |
| 3.1% C <sub>2</sub> H <sub>4</sub> | 25.4% CH <sub>4</sub> |
| 0.5% O <sub>2</sub>                | 9.8% N <sub>2</sub>   |
| 6.7% CO                            |                       |
- (c) 20 cubic feet of propane per hour
  - (d) Regulated air cooling after treatment.

Considerable experimental work was carried out to determine the most favorable temperature cycle and gas composition for the service requirements of an automotive engine cylinder liner. Since the initiation of production operations on carbonitrided cylinder liners, our efforts have been devoted to studying the factors which affect the quality of the product and to investigate suitable quality control methods on production operations.

The authors have performed a valuable service in pointing out the complexity of the carbonitriding process under laboratory conditions and offering reasonable explanations for these factors. I would like to offer some supplementary information on the low temperature (1300 °F) carbonitriding process and point out that production operations introduce additional complications.

The effect of increasing the ammonia flow to the production furnace<sup>a</sup> is well illustrated by comparing Fig. 12 with Fig. 13. Fig. 12, with 1000 cubic feet of ammonia gas per hour, shows a rather thin acicular outer layer with no evidence of cementite as determined by X-ray diffraction. The secondary zone is predominantly austenite and the original micrograph shows the presence of coarse martensitic needles throughout this zone.

Increasing the ammonia gas to 1500 cubic feet per minute per hour more than doubles the thickness of the primary zone and seems to indicate that the acicular structure has a precipitate phase. The electron micrograph, in Fig. 14, shows that even very fine acicular primary layers have a precipitate phase in the striations. X-ray diffraction shows both the hexagonal phase ( $\epsilon$ -carbonitride with anomalous line shifts) and the face-centered iron nitride. We must conclude that the hexagonal nitride is primarily a precipitate phase in the outer zone and only occasionally appears as a continuous phase. Some evidence indicates that if a case structure is produced with a pronounced white outer layer of hexagonal nitride, a brittle condition exists and a tendency to spalling may occur in service. Unfortunately, the X-ray diffraction line intensities of the hexagonal close-packed and the face-centered cubic phases show little change between good carbonitride cases and brittle cases except in very unusual examples.

Excessively brittle carbonitrided cases have been observed and their cause is still open to question. The distinction between a moderately brittle case and the so-called ductile case is easy to demonstrate by a destructive test, but difficult to identify by laboratory test methods. Nitrogen analysis, X-ray diffraction studies, and micrographic examina-

<sup>a</sup>Furnace supplied by the Holcroft Company, Detroit, Mich.



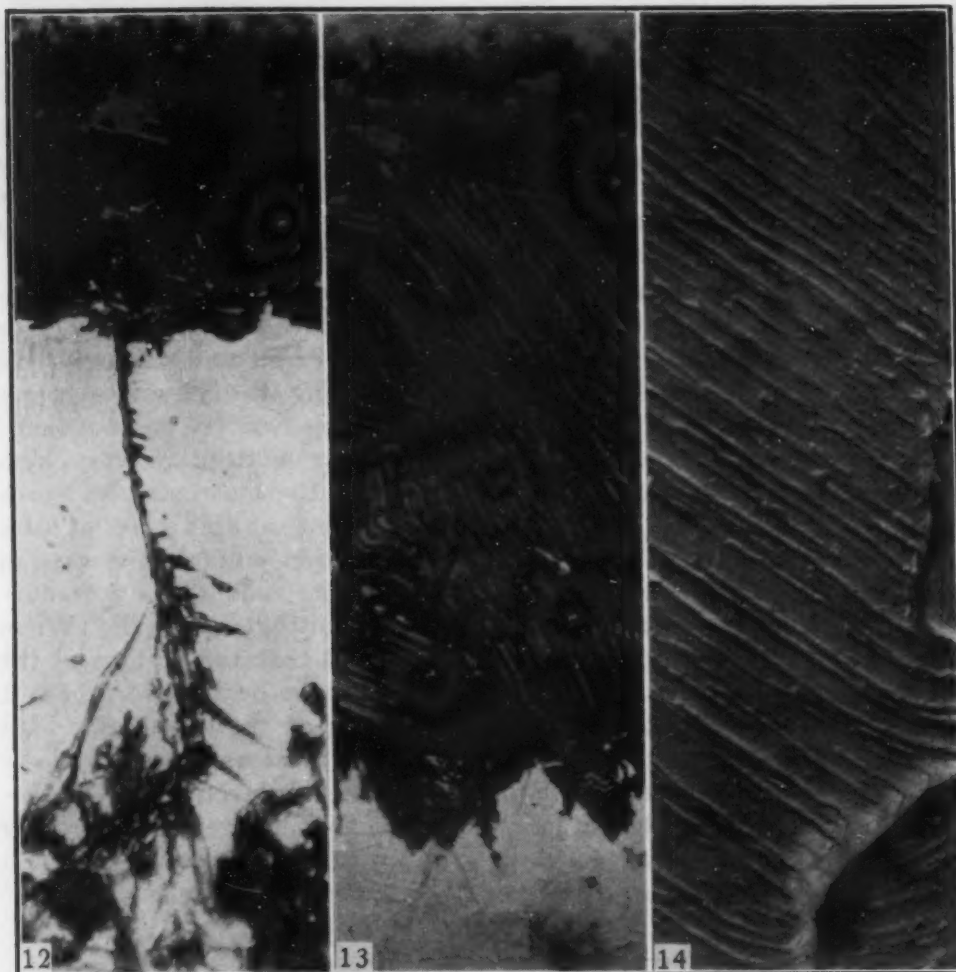


Fig. 12—Primary Layer of Carbonitride Case on Low Carbon Steel Using 1000 Cubic Feet of Ammonia Gas per Hour at 1350 °F. Etchant, Nital and sodium picrate.  $\times 2500$ .

Fig. 13—Primary Layer of Carbonitride Case on Low Carbon Steel Using 1500 Cubic Feet of Ammonia Gas per Hour at 1350 °F. Etchant, Nital and sodium picrate.  $\times 2500$ .

Fig. 14—Electron Micrograph of Acicular Structure in Primary Case of Carbonitrided Low Carbon Steel Using 3200 Cubic Feet of Ammonia Gas per Hour. Precipitate phase believed to be hexagonal iron nitride.  $\times 15,000$ .  
(Reduced  $33\frac{1}{3}\%$  in reproduction.)

tion all failed to show a clear-cut distinction between borderline good and bad cases. Microhardness<sup>7</sup> traverse data through the case are very useful in explaining abnormal carbonitride conditions, but also fail to distinguish clearly between acceptable and brittle cases. The development of internal stresses may play an important role here.

Most of the laboratory tests mentioned above readily detect carbonitrided cases which are too soft to show good wearing properties in service. The X-ray diffraction method is very sensitive in detecting case structure which will give below normal service life. If the X-ray collimated beam is brought in through one end of the cylinder liner and the reflected rays picked up on a photographic film placed over the other end, a nondestructive test method requiring only 5 minutes exposure is possi-

<sup>7</sup>Eberbach, Micro-brinell indenter.



ble. Experience has shown that X-ray diffraction from the surface layers should show a definite ratio of the hexagonal phase to the face-centered cubic nitride phase for acceptable carbonitrided cylinder liners.

For production control, the simplest and lowest-cost method appeared to be a hardness measurement. The procedure finally adopted requires the spot checking of cylinder liners at specified intervals for surface hardness using a microindenter<sup>7</sup> and microexamination for measurement of the case depth.

Experience has shown that many factors can contribute to the production troubles encountered in the low temperature carbonitriding. One particular type of defect occasionally experienced but, unfortunately, the most difficult to trace, is the effect of processing variables or furnace conditions which produce a poor diffusion of nitrogen in the case. Micro-traverse curves across such a case show a narrow band of very high hardness near the outer layers. In such a case, the macrostresses reach a very high value. We had an excellent example of this type of case where an attempt was made to remove a very thin layer of the case in the laboratory, using a fine diamond-tipped cutting tool. This procedure is common for preparing samples for carbon and nitrogen analysis. When the diamond tool started cutting, it was observed that the surface of the case appeared to shatter and break up into fine microcracks for about 1 inch ahead of the cutting tool. The true cause of the apparently high surface concentration of nitrogen in such brittle cases as described above has never been clearly settled. It is suspected, however, that the dissociation of ammonia in the furnace is unusual and in severe cases of this kind the only remedy has been to shut the furnace down and clean and readjust everything. Generally, the defect is cleared up by such drastic action.

I have only compliments and no criticism of the authors' very excellent presentation and have offered the above remarks only as a commentary on the production end of carbonitriding.

#### Authors' Reply

The authors wish to express their sincere appreciation of the contributions made by Messrs. Holcroft, Heine and McCutcheon. Concerning the points raised by Mr. Holcroft, it is likely that a change in nitrogen content would accompany a change in ammonia concentration, but this effect would probably be more noticeable below some critical ammonia content in the atmosphere. Specifically, in lowering the ammonia below 20% some gas composition would probably be reached below which the nitrogen content of the case would decrease more rapidly. It should also be emphasized that the nitrogen contents shown in Figs. 5 and 6 refer to the inner layer and that the outer layer, although it is of variable nitrogen content, may tend to hold the nitrogen content of the inner layer uniform. As explained more fully in the authors' closure of Ref. 1, the high flow rates of ammonia were used in an attempt to have the gas in contact with the specimen approximate commercial practice, as more rapid dissociation in a small tube furnace calls for higher ammonia content in the inlet gas. It also is the authors' impression that current prac-

tice, while commonly using less than 20% ammonia, often exceeds the 5% mentioned by Mr. Holcroft.

In reply to Mr. Heine, Fig. 11c of this paper and Fig. 3 of the paper previously published in METAL PROGRESS are based on the same experimental data but are plotted on different scales. The presence of austenite in the outer layer, carbonitrided at 1300 °F (705 °C) and tempered at 500 °F (260 °C) is probably not significant and as suggested in the paper may be due to the accidental inclusion of some of the underlying material.

The application of low temperature carbonitriding described by Mr. McCutcheon is indeed interesting. His searching analysis well illustrates the problems met with in the application of advanced experimental techniques to the control of production. The authors are especially grateful for the excellent photomicrographs contributed by Mr. McCutcheon.

## FORMATION OF OXIDES ON SOME STAINLESS STEELS AT HIGH TEMPERATURES

BY H. M. McCULLOUGH, M. G. FONTANA AND F. H. BECK

### *Abstract*

*A continuous weighing apparatus was used to study the course of oxide growth on stainless steels, Type 304 (18-8S), Type 430 (16% Cr), and Type 410 (12.5% Cr) in the temperature range 1500 to 1800 °F (815 to 980 °C). Dried oxygen, nitrogen and mixtures of these gases constituted the controlled furnace atmospheres.*

*Oxidation in the early stages followed the equation  $Y^n = Kt$  with  $n$  constant, and then the rate of oxidation increased abruptly because of rupture of the scale. The time for this change in rate to occur was dependent on the alloy composition, the partial pressure of oxygen in the atmosphere, and temperature. At 1800 °F (980 °C) in a 100% oxygen atmosphere, Types 304, 430 and 410 showed the rupture of the oxide to take place after 40 minutes, 20 minutes and 10 minutes, respectively. This time increased as the oxygen partial pressure or the temperature was decreased. A combination of visual observations, chemical analyses, and electron diffraction examinations indicated that an initial oxide of  $\text{FeO} \cdot \text{Cr}_2\text{O}_3$  spinel formed on the Type 304 or 430 materials. After the rupture occurred, a second oxide consisting primarily of  $\text{Fe}_2\text{O}_3$  started to grow at a more rapid rate.*

*Pre-oxidation treatments to form selected oxides showed that  $\text{FeO} \cdot \text{Cr}_2\text{O}_3$  scale is more protective than alpha  $\text{Fe}_2\text{O}_3$ .*

*The difference in oxidation behavior for Type 410 at 1700 and 1800 °F (925 and 980 °C) as compared to 1500 and 1600 °F (815 and 870 °C) (aside from temperature effects) may be related to the fact that at the lower temperatures the metal is alpha iron and at the higher temperatures mixed alpha plus gamma phases exist.*

**T**HE purpose of this investigation was to study oxidation mechanisms of stainless steels at high temperatures. Types 304, 430 and 410 stainless steels were exposed to oxidizing atmospheres in

A paper presented before the Thirty-second Annual Convention of the Society, held in Chicago, October 21 to 27, 1950. Of the authors, H. M. McCullough is associated with Sylvania Electric Products Inc., Long Island, N. Y.; M. G. Fontana is professor and chairman, Department of Metallurgy; and F. H. Beck is assistant research professor, Engineering Experiment Station, The Ohio State University, Columbus, Ohio. Manuscript received April 14, 1950.



which the partial pressure of oxygen was varied by using oxygen-nitrogen mixtures. The course of oxidation with time was followed by continuous weighing of the specimens. Chemical analyses and electron diffraction examinations were used to identify the oxides formed at various stages during the progress of oxidation. By controlling the temperature, time, and oxygen partial pressure it was possible to form selected oxides. The effect of phase transitions in Type 410 stainless steel on oxidation characteristics was studied.

Careful control in regard to surface preparation of specimens increased the degree of reproducibility; the preparation varied slightly with the material. A bromine-alcohol solution was used to strip the thin oxides from the base metal.

#### SURVEY OF LITERATURE

Evans (1)<sup>1</sup> shows the following integrated equations to express oxidation as a function of time:

$$\begin{aligned}y &= K_1 t + K_2 \\y &= K_3 \log (K_4 t + K_5) \\y^2 &= K_6 t + K_7\end{aligned}$$

When a metallic surface is exposed to an oxygen atmosphere, Evans (2) states that oxygen molecules attach themselves to the surface instantaneously by intermolecular forces and then combine with the metal by transferring or sharing electrons. Once the surface of the metal has been covered with a monolayer of oxide, growth perpendicular to the metal surface commences. According to the Pilling and Bedworth (3) rule 2, if the volume of unconstrained oxide for heavy metals is greater than the volume of metal required to form the oxide, the oxide is highly constrained. Stress relief is possible by cracking or plastic flowing of the oxide. At high temperatures a smooth oxidation curve was found by Pilling and Bedworth (3) for copper, whereas at lower temperatures a broken curve was obtained showing sudden increases in weight gain. At the higher temperatures the more plastic nature of the scale permitted stress relief without cracking.

The variation of oxidation rates with temperature can be expressed by the classical Arrhenius equation  $K = Ae^{-Q/RT}$ . The slope of the straight line obtained by plotting  $K$  versus the reciprocal of the absolute temperature relates the activation energy. Gulbransen (4) has applied the transition-state theory to oxidation processes and has developed equations whereby the entropy and energy of activation can readily be calculated. All these derivations are based

<sup>1</sup>The figures appearing in parentheses pertain to the references appended to this paper.



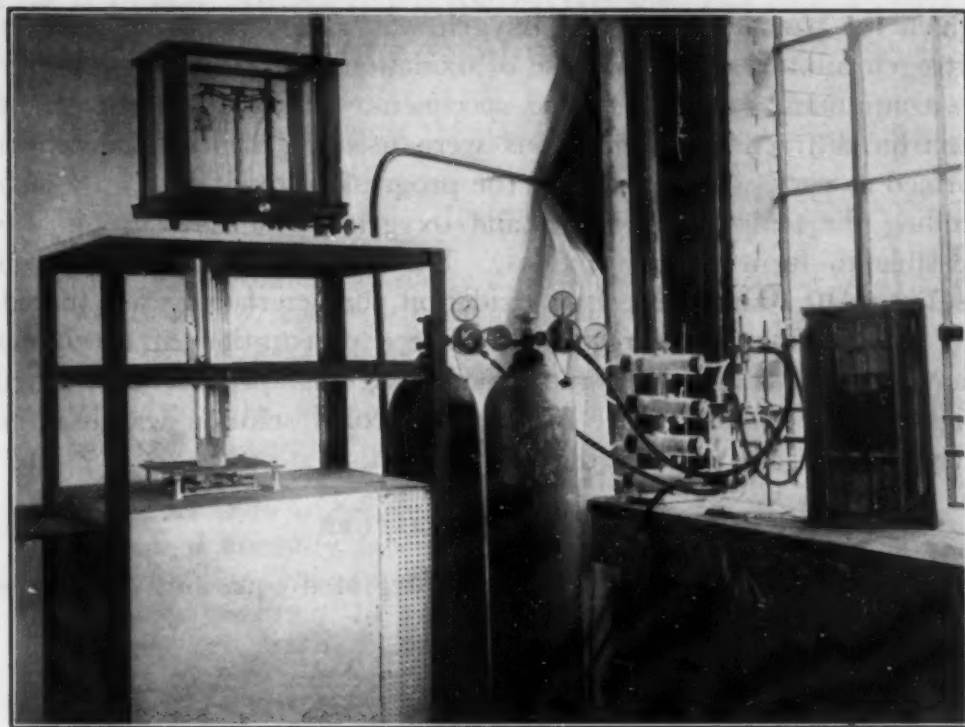


Fig. 1—General View of Controlled Atmosphere Furnace and Weighing Arrangement.

on the parabolic equation of the second order; however, this second-order equation is quite limited, since most metals follow this type of oxidation rate over a very limited time. A more general equation would be one of the  $n$ th order. It was pointed out by Lustman in the discussion of Gulbransen's paper (6), that very seldom does the equation become of the second order. Lustman proceeded to plot recalculated values of the exponent from Gulbransen's data and found that they varied considerably. Upon plotting these values of  $n$  versus temperature, a maximum or minimum point was observed. Lustman pointed out that the maximum or minimum points occurred at temperatures of phase transitions of the metal or alloy.

Vernon (5) found marked differences in the properties of oxides formed on iron above and below 390 °F (200 °C). Above 390 °F a parabolic relationship was found; whereas below 390 °F a curve approximating  $W^{2.5} = Kt$  was followed. By plotting weight gain versus the reciprocal of absolute temperature, a line of greater slope existed above the transition point.

Numerous references are available in the literature on oxidation of metals. Only a few are mentioned here in order to save space and because it is not the purpose of this paper to present a complete literature review.

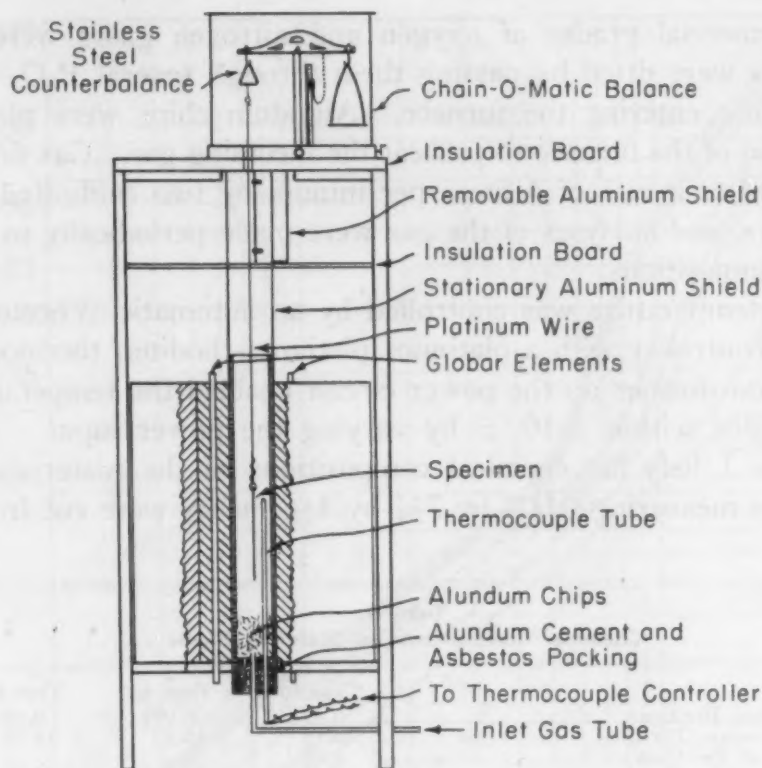


Fig. 2—Schematic Diagram of Furnace and Balance.

#### PROCEDURE AND EQUIPMENT

Figs. 1 and 2 are photograph and schematic diagram, respectively, of the continuous weighing apparatus used in this investigation. An alundum tube, 36 inches long by 2 inches I.D., is located vertically in a Globar-type controlled atmosphere furnace with a 16-inch heating zone. A Chain-O-Matic balance is positioned above the furnace so that the weight-pan hook is on the centerline of the furnace tube. The weight pan is replaced by a counterbalance and a 22-gage platinum wire for supporting the specimens. Protection of the balance from the heat of the furnace is accomplished by placing two widely spaced insulation boards between the balance and the furnace.

An aluminum shield is placed around the platinum wire to protect it from being deflected by air currents. The section of the shield between the insulation boards consists of two parts, with one removable. Each specimen was lowered into the furnace through this part; and, when in position, a transite cap with a hole just sufficiently large to accommodate the platinum wire was placed over the end of the furnace tube. The removable portion of the aluminum shield was then fastened into place.

Commercial grades of oxygen and nitrogen gases were used. The gases were dried by passing them through several  $P_2O_5$  drying tubes before entering the furnace. Alundum chips were placed in the bottom of the furnace to preheat the incoming gas. Gas flow was maintained at a rate of 4 liters per minute by two calibrated Linde flowmeters, and analyses of the gas were made periodically to insure proper compositions.

The temperature was controlled by an automatic Wheelco temperature controller with a platinum/platinum-rhodium thermocouple. An autotransformer on the power circuit enabled the temperature to be controlled within  $\pm 10^\circ F$  by varying the power input.

Table I lists the chemical compositions of the materials used. Specimens measuring 0.004 by  $7\frac{3}{4}$  by  $1\frac{1}{4}$  inches were cut from the

Table I  
Chemical Compositions of Stainless Steels

	Type 304	Type 430	Type 410
Carbon, Per Cent .....	0.072	0.071	0.083
Chromium, Per Cent .....	19.19	15.82	12.59
Nickel, Per Cent .....	8.66	...	...
Silicon, Per Cent .....	0.61	0.60	0.34

stock, polished on grit number 120 emery cloth, washed, dried, pickled, rewashed, dried with ethanol, weighed cold, and finally placed in the furnace.

Pickling solutions varied with the type of steel being used. Aqua regia or boiling 10% sulphuric acid was satisfactory for Type 304 stainless steel. Although aqua regia was more difficult to control, the corrosion product was easier to remove than that resulting from the boiling 10% sulphuric acid pickle. For Types 430 and 410 steels, a bright pickling solution (120 cc. 70%  $HNO_3$ , 20 cc. 48% HF, and 10 cc. 37% HCl per liter of solution) heated to  $175^\circ F$  was used. The pickling treatments were sufficiently long to remove the cold-worked surface resulting from mechanical abrasion (polishing).

Before starting a test, the furnace was brought to temperature and the tube flushed with the desired gas composition. A specimen, previously pickled and weighed, was then suspended in the furnace tube. The cap and shield were placed in position, and weight measurements were made at desired intervals. The first reading was taken 15 to 30 seconds after the specimen hit the hot zone. At the completion of the test, the specimen was pulled from the furnace and allowed to cool in air before being reweighed and stripped of its oxide.



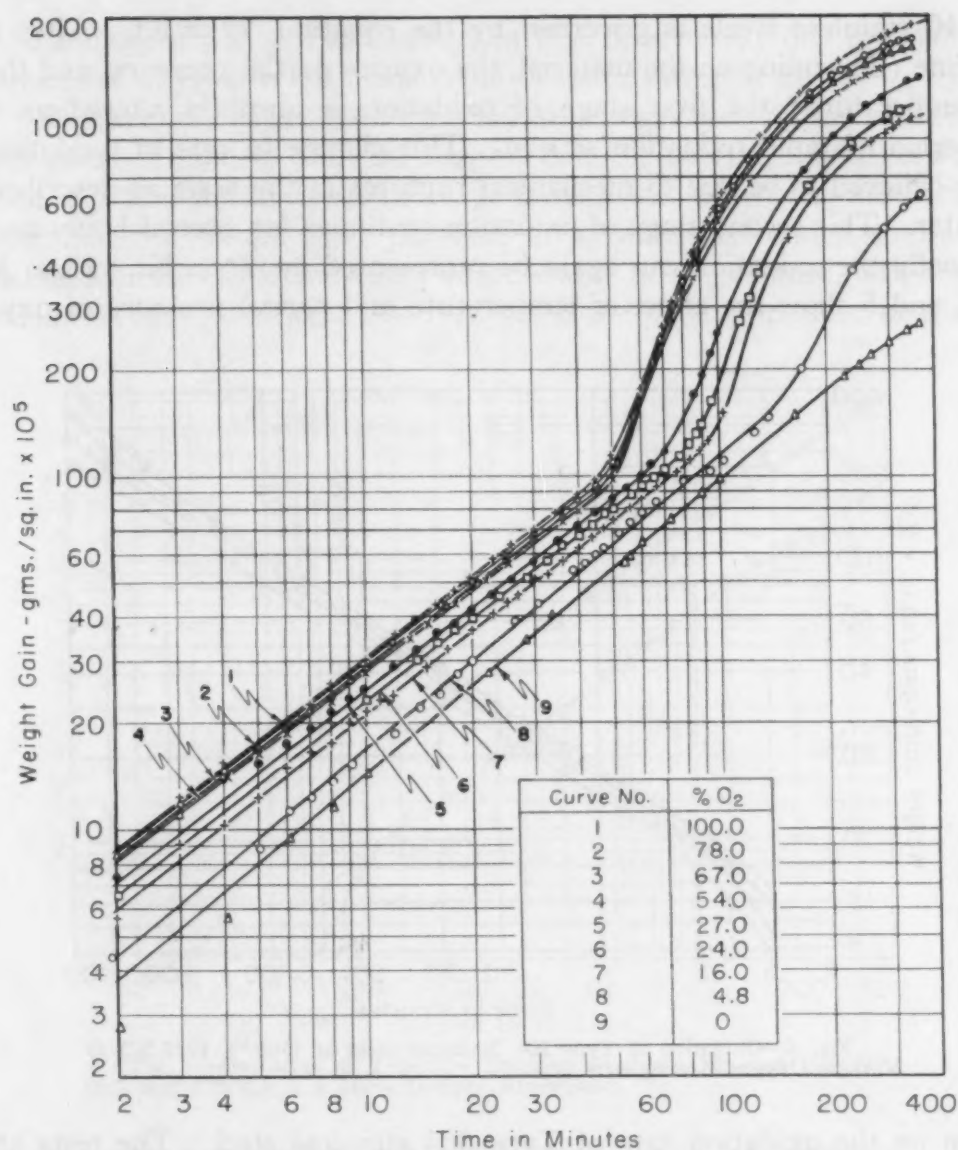


Fig. 3—Oxidation of Type 304 Stainless Steel at 1800 °F (980 °C).

Stripping of oxides from the metal was accomplished by scribing the oxide to expose the underlying metal and immersing the specimen in a 10% solution of bromine in absolute alcohol. The solution dissolves the metal and undercuts the oxide until it drops free. Then the solution containing the oxide is filtered through a 200-mesh stainless steel screen and the retained oxide washed several times with ethanol. Finally the oxide is sealed in a glass vial containing ethanol, where it is kept until ready for chemical analyses.

#### RESULTS AND DISCUSSION

*Effect of Time, Temperature and Oxygen Partial Pressure—*  
The first stage of oxidation on the specimens of Types 304, 430 and



410 stainless steels is governed by the equation  $Y^n = Kt$ . After a time (depending on the material, the oxygen partial pressure, and the temperature) the first stage of oxidation is abruptly altered as a period of rapid oxidation sets in. This change in rate of oxidation is believed to be due to mechanical ruptures in the scale as described later. This second stage of oxidation continues for several hours and finally the oxidation can again be represented by  $Y^n = Kt$ . Figs. 3, 4, and 5 show the effect of temperature and partial pressure of oxy-

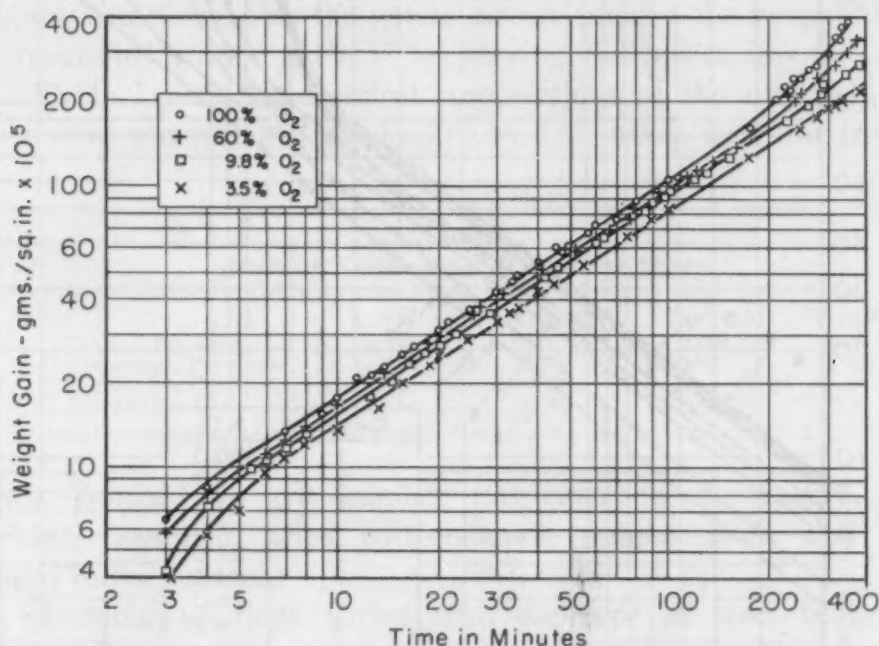


Fig. 4—Oxidation of Type 304 Stainless Steel at 1700 °F (925 °C) in Various Oxygen Atmospheres.

gen on the oxidation rate of Type 304 stainless steel. The tests at 1800 °F (980 °C), Fig. 3, illustrate the period of rapid oxidation and show the effect of oxygen partial pressure on the time for the break to occur. That is, at lower oxygen pressures, a longer time is required before the break occurs. Forty-four hours at 1800 °F (980 °C) did not reveal any subsequent breaks in the curves. At 1700 °F (925 °C), Fig. 4, 3 hours in a 100% oxygen atmosphere was required before rupture of the oxide occurred—the time for rupture to occur at 1800 °F (980 °C) was 45 minutes. Here again, as in the case of the 1800 °F tests, a decrease in the oxygen pressure affects a delay in the time for rupture to occur. At 1500 or 1600 °F (815 or 870 °C), Fig. 5, no rupture occurs (some tests were conducted for as long as 44 hours) at any oxygen pressure (curves illustrated are for a 100% oxygen atmosphere). The weight gain

in "0% oxygen", shown as Curve 9 in Fig. 3, is mostly due to small amounts of oxygen in the commercial cylinder nitrogen used.

*Rupture of Scales*—Since the failure of the oxide appears to be mechanical in nature, it would suggest that the rupture might result when a critical thickness of the oxide is reached. However, the data show that the weight gain per unit area, which is related to the thickness of the oxide, may vary considerably before rupture. Higher over-all weight gains were observed when the partial pressure of the

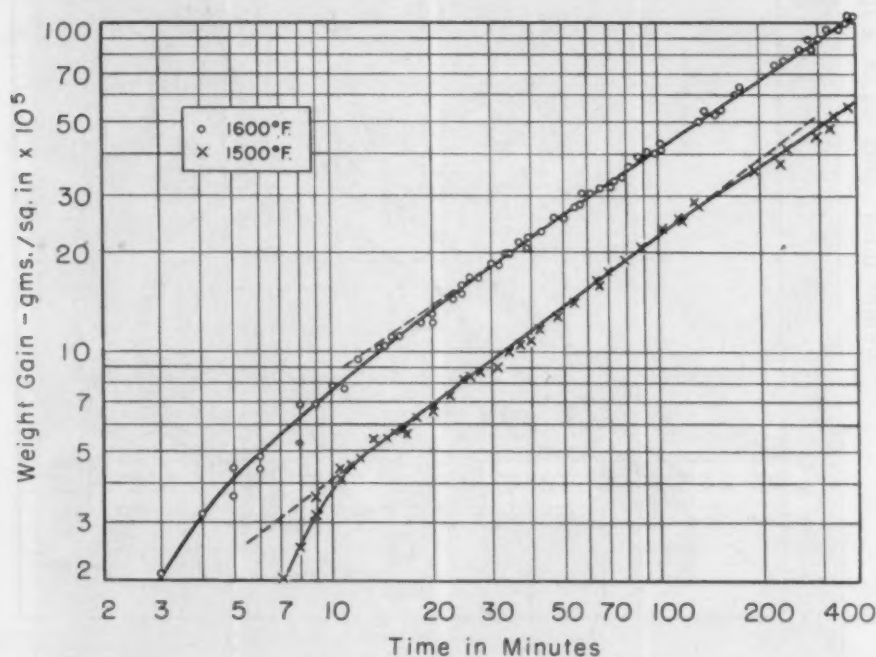


Fig. 5—Oxidation of Type 304 Stainless Steel at 1500 and 1600 °F (815 and 870 °C) in a 100% Oxygen Atmosphere.

oxygen was decreased or when the temperature was lowered. In other words, the oxides attained a greater thickness without rupture if the rate of formation was lowered by either a reduction in the temperature or the partial pressure of oxygen. Since the time for rupture is related to the rate of oxide formation, the rate must have a pronounced effect on the nature of the resulting oxide and, therefore, on the stresses within that oxide. This explanation would infer that the rapidly forming oxides would be more highly stressed and would rupture before reaching the thicknesses observed for slower forming oxides.

Once rupture has occurred, the oxygen can easily make its way through the scale, and rapid oxidation begins. Evidence that rapid oxidation occurred at the points of rupture was found when the metal surface was examined after the removal of the oxides. This evidence

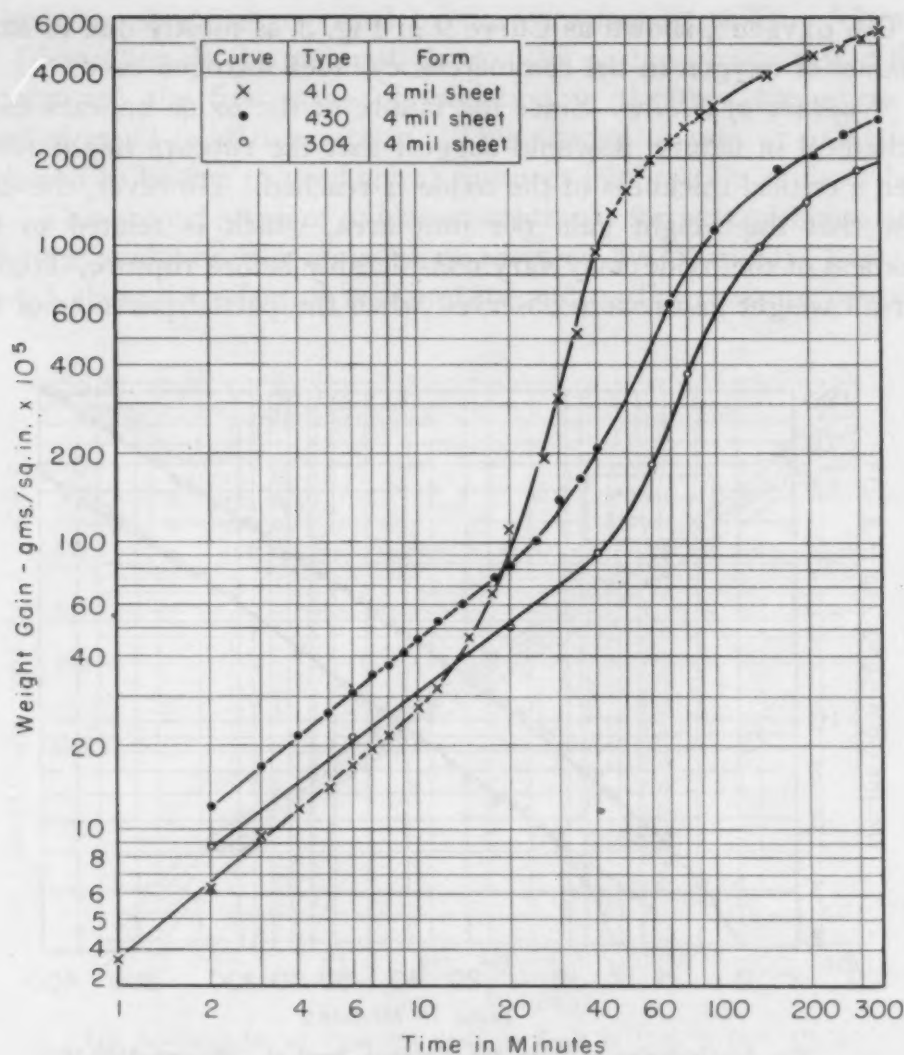


Fig. 6—Oxidation of Types 304, 430 and 410 Stainless Steels in 100% Oxygen at 1800 °F (980 °C).

was in the form of pitting in the metal surface at points where the second oxide layer was starting to form. The inability of this secondary oxide to seal the fissures or heal the scale is evident from the extended period of rapid oxidation. Oxidation slows down only after the new oxide has reached an appreciable thickness.

Fig. 6 shows that the rupture effect was not a peculiarity of the Type 304 material, since it was also apparent on the Type 410 and 430 steels. The effect of composition on the time for rupture to occur and on the oxide thickness prior to rupture is illustrated. An increase in chromium and nickel content decreases the rate of oxidation, extends the time before rupture and promotes thicker (higher weight gains) scales before rupture occurs. Note that the time for rupture decreases from 45 minutes for Type 304 to 10 minutes for

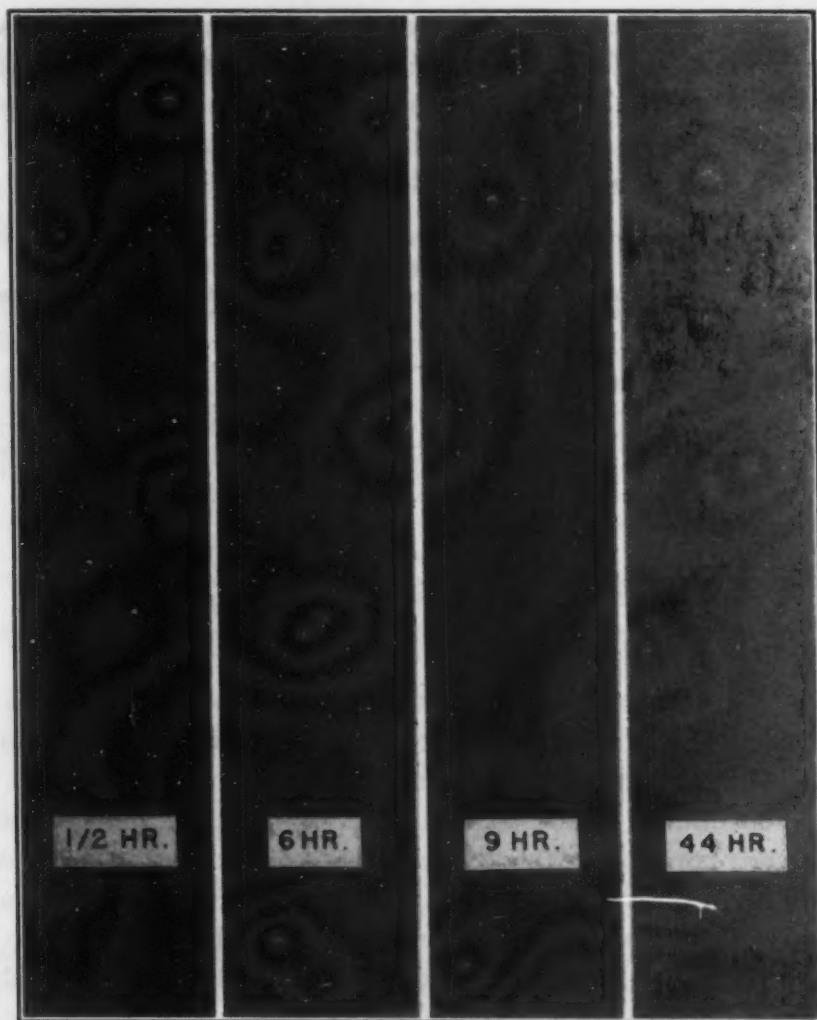


Fig. 7—Oxides Formed on Type 304 Stainless Steel in a 100% Oxygen Atmosphere at 1800 °F (980 °C).

the Type 410 material and that the oxide formed on Type 304 reaches a thickness three times that observed on the Type 410 material. The scale on Type 430 steel shows the break after 20 minutes and reaches a thickness approximately  $\frac{4}{5}$  that of the Type 304 material before rupture.

*Chemical Analyses and Electron Diffraction Studies of Oxides—*

In an attempt to better understand the mechanism of oxidation, chemical analyses and electron diffraction studies of the oxides formed on Types 304 and 430 stainless steels were made.

Fig. 7 is a photograph of four Type 304 stainless steel specimens which were exposed to 100%  $O_2$  at 1800 °F (980 °C) for varying lengths of time. Note that the secondary scale on the 6, 9, and 44-hour specimens is light gray in color, whereas the initial oxide ( $\frac{1}{2}$ -hour specimen) is black. The secondary oxide has not appeared



on the  $\frac{1}{2}$ -hour specimen, since the rupturing had not yet occurred, but the 6, 9, and 44-hour specimens show increasing amounts of the secondary oxide. The 44-hour specimen was completely covered with the gray oxide. During handling of the 44-hour specimen, some of the oxide flaked, exposing the dark substrate.

**Table II**  
Chemical Analyses of Oxides Formed on Type 304 Cold-Rolled Stainless Steel Sheet in a 100% Oxygen Atmosphere at 1800 °F, for Various Times

	Minutes					
	10	20	30	40	50	60
Iron, Per Cent .....	11.62	6.57	5.36	5.73	4.04	3.91
Chromium, Per Cent .....	54.64	59.32	60.38	61.38	56.21	54.19
Nickel, Per Cent .....	0.87	0.26	0.15	0.16	Nil	0.84
Silicon, Per Cent .....	1.00	0.55	0.47	0.46	4.67	5.17

	Hours				
	2	4	6	9	44
Iron, Per Cent .....	5.34	20.14	34.00	39.48	40.16
Chromium, Per Cent .....	49.81	43.58	28.48	24.22	24.58
Nickel, Per Cent .....	8.36	0.74	5.51	4.73	3.81
Silicon, Per Cent .....	3.70	0.56	2.40	0.39	0.47

Chemical analyses of oxides formed on Type 304 stainless steel in a 100% oxygen atmosphere at 1800 °F (980 °C) are listed in Table II. The analyses show that, with increasing time, the ratio of iron to chromium in the oxide decreases until the rupture occurs. Although the rupture of the oxide is not evident from the analyses until 60 minutes oxidation, weight gain data (Fig. 3) show that the break-through occurs within 45 minutes from the start of the test. After the rupture, the ratio of iron to chromium in the oxide increases rapidly. After approximately 9 hours this ratio becomes almost constant.

The trend of the nickel content is rather interesting. Nickel decreases in per cent concentration during the first 50 minutes of oxidation, then increases rapidly for the next hour, then decreases again. Since nickel diffuses at an extremely low rate into oxides, the increase of nickel in the oxide is attributed to the rapid oxidation

**Table III**  
Electron Diffraction Results of Oxide Formed at Various Times at 1800 °F and for 6 Hours at Various Temperatures on Type 304 Cold-Rolled Sheet in a 100% Oxygen Atmosphere

Treatment	Appearance of Oxide	Electron Diffraction Results
$\frac{1}{2}$ hr. at 1800 °F (980 °C)	Black	Fe <sub>3</sub> O <sub>4</sub> Spinel
6 hrs. at 1800 °F (980 °C)	Black and gray	$\alpha$ -Fe <sub>2</sub> O <sub>3</sub>
9 hrs. at 1800 °F (980 °C)	Gray	$\alpha$ -Fe <sub>2</sub> O <sub>3</sub>
44 hrs. at 1800 °F (980 °C)	Gray	$\alpha$ -Fe <sub>2</sub> O <sub>3</sub>
6 hrs. at 1700 °F (925 °C)	Black with few gray spots	Fe <sub>3</sub> O <sub>4</sub> Spinel
6 hrs. at 1600 °F (870 °C)	Black	Fe <sub>3</sub> O <sub>4</sub> Spinel
6 hrs. at 1500 °F (815 °C)	Black	Fe <sub>3</sub> O <sub>4</sub> Spinel

at the metal surface just after the oxide ruptures. Once the fissures are filled with the secondary oxide, the rate of nickel pickup in the oxide is again retarded.

Electron diffraction studies of these oxides, Table III, show the initially formed oxide to be an  $\text{Fe}_3\text{O}_4$ -type spinel and the oxide formed after the rupture to be  $\text{Fe}_2\text{O}_3$ . By coupling these results with the chemical analyses, the initially formed oxide is identified as an  $\text{FeO}\cdot\text{Cr}_2\text{O}_3$ -type spinel, and the secondary formation as primarily  $\text{Fe}_2\text{O}_3$ .

Electron diffraction studies have also shown the  $\text{Fe}_3\text{O}_4$ -type spinels to be the initial oxides formed on the Type 304 material at the lower temperatures (see Table III). This information and

Table IV  
Chemical Analyses of Oxide Formed on Type 430 Cold-Rolled Sheet in a 100%  $\text{O}_2$  Atmosphere at 1800 °F for Various Times

	Minutes					
	5	10	15	20	30	55
Iron, Per Cent .....	4.27	7.14	6.84	5.77	9.52	11.00
Chromium, Per Cent .....	19.85	54.19	53.21	56.42	52.68	48.12
Silicon, Per Cent .....	29.15	4.47	4.94	3.40	3.28	5.97
	Minutes					
	85	150	360			
Iron, Per Cent .....	18.61	32.89	55.92			
Chromium, Per Cent .....	49.31	32.19	29.29			
Silicon, Per Cent .....	0.89	2.27	2.11			

chemical analyses of the oxides again identify them as  $\text{FeO}\cdot\text{Cr}_2\text{O}_3$ -type spinels. It is this spinel-type oxide which provides greatest resistance toward oxidation.

Table IV lists the chemical analyses of the oxides formed on the Type 430 alloy. The trend of the change in iron to chromium ratio in the oxide is similar to that noted for the Type 304 alloy. An  $\text{FeO}\cdot\text{Cr}_2\text{O}_3$  spinel-type oxide is formed during the first stage of oxidation.

*Pretreatment of Type 304 to Form Preferential Oxides*—Since oxygen partial pressure and temperature had an effect on the type of oxide formed, experiments for producing and testing selected oxides were devised. This experiment involved 1-hour pre-oxidation treatments on specimens at various temperatures and oxygen pressures, with subsequent exposure at 1800 °F (980 °C) for 6 hours.

Fig. 8 shows the results of specimens pretreated for 1 hour in a 100% oxygen atmosphere at 1800, 1700, 1600 and 1500 °F (980, 925, 870 and 815 °C) with subsequent tests for 6 hours in a 100% oxygen atmosphere at 1800 °F. Only the 6-hour portions of the tests are illustrated. The 1700 °F pretreatment produced the most

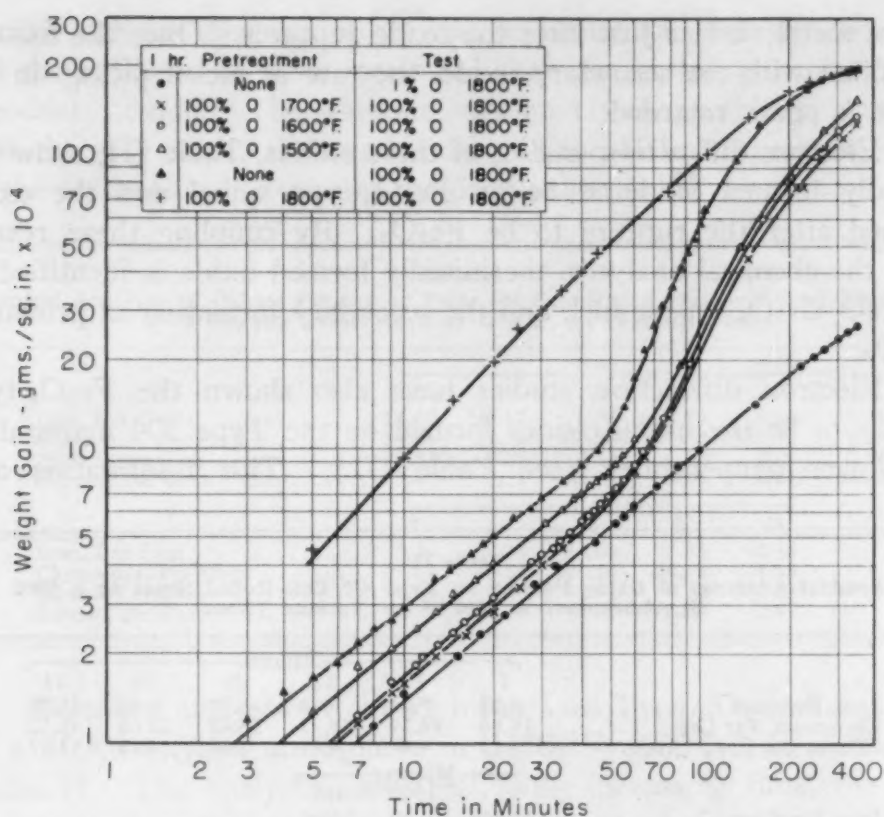


Fig. 8—Oxidation of Type 304 Stainless Steel With Various 1-Hour Pretreatments at Various Temperatures in a 100%  $O_2$  Atmosphere Followed by 6-Hour Tests in a 100% Oxygen Atmosphere at 1800 °F (980 °C).

protective oxide. The 1500 °F pretreatment produces a scale, which from the standpoint of chemical composition (high in chromium content) should show good resistance; however, the thickness of this preformed oxide was not sufficient to withstand the more severe attack at 1800 °F. The oxide formed during the 1800 °F pretreatment was nonprotective because it had already ruptured.

Pre-oxidation treatments at various oxygen concentrations at 1800 °F show that at low oxygen concentrations the spinel-type oxide was formed; whereas at the higher oxygen concentrations the nonprotective  $Fe_2O_3$ -type oxide was predominant.

Fig. 9 shows the results of tests in which the specimens were given 1-hour pretreatments in 5 and 95% oxygen atmospheres at 1800 °F (980 °C), with subsequent tests for 6 hours in a 20% oxygen atmosphere at 1800 °F. The specimen given the 95% oxygen pretreatment did not show much resistance to oxidation in the subsequent 20% oxygen test. Specimens pretreated in a 5% oxygen atmosphere at 1700 °F with subsequent tests for 6 hours in a 20% oxygen atmosphere at 1800 °F showed only slightly better performance. Again the thickness of the preformed oxide was not sufficient



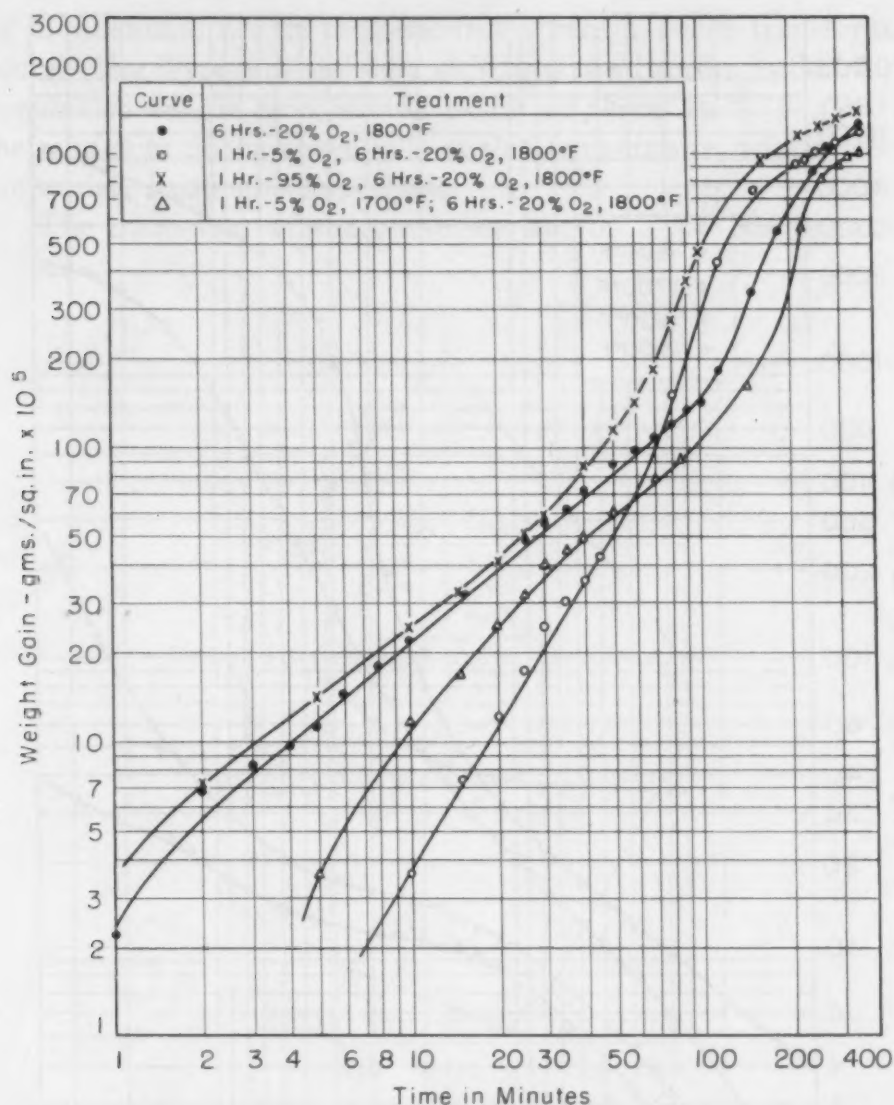


Fig. 9—Oxidation Tests on Type 304 Stainless Steel With Various Pretreatments.

to withstand the attack at the higher oxygen concentration.

*Effect of Metal Structure on Oxidation Characteristics*—Fig. 10 is a plot of weight gain against time for Type 410 stainless steel in a 100% oxygen atmosphere at several temperatures. The differences in oxidation behavior (note shapes of curves) at 1700 and 1800 °F as compared to 1500 and 1600 °F—aside from temperature effects alone—may be related to the fact that at the lower temperature the metal is of the alpha phase, and at the higher temperature mixed alpha plus gamma phases exist. Additional study of this item is underway. The effects of cold working and recrystallization are also being studied.

*Mathematical Representation of the Rate Law*—Equations for



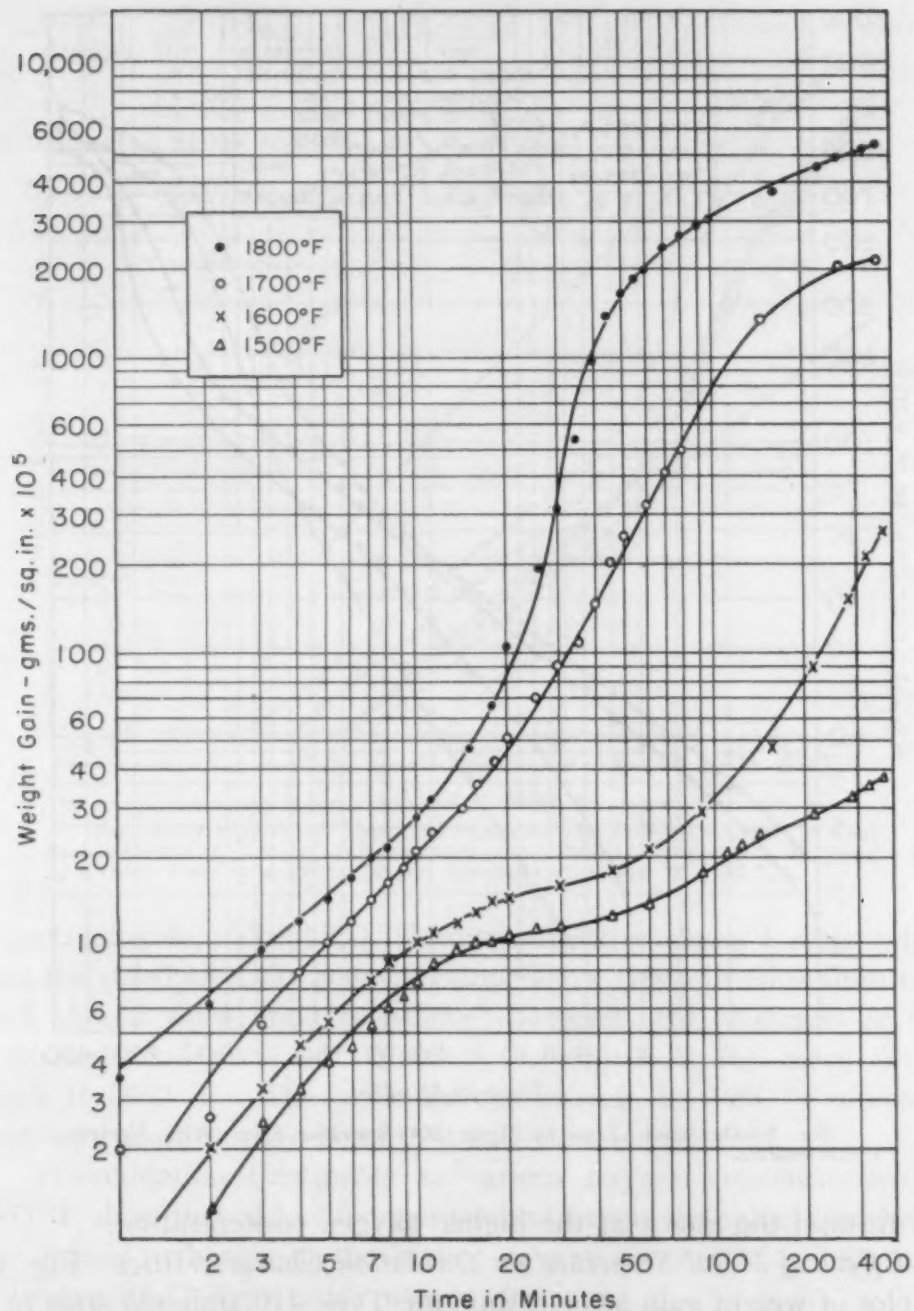


Fig. 10—Oxidation Tests on Type 410 Stainless Steel in a 100% Oxygen Atmosphere at Various Temperatures.

the straight-line portions of the curves on a log-log plot are of the order  $Y^n = kt$ , where  $Y$  is the weight gain,  $t$  the time, and  $k$  and  $n$  are constants. Fig. 11 shows a plot of the exponent  $n$  versus temperature for Types 304, 430 and 410 stainless steels. Note the maximum in the curve for Type 304 and the minimum for Type 410. This phenomenon was pointed out by Lustman in the discussion of Gulbransen's paper (6). The maximum or minimum points, accord-

ing to Lustman, are at temperatures where a phase transformation occurs. For Type 410 stainless steel, a phase transformation for this composition of the steel should occur at about 1670 °F (910 °C). The minimum of the curve falls at this temperature, which seems to substantiate Lustman's hypothesis.

The maximum of the curve shown for Type 304 is at about

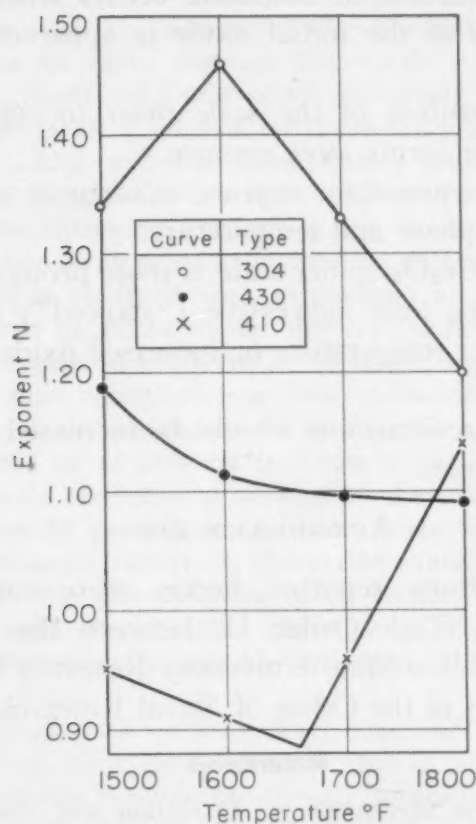


Fig. 11—Plot of the Exponent  $n$  Versus Temperature for the 4-mil Types 304, 430 and 410 Stainless Steel Oxidized in a 100% Oxygen Atmosphere.

1600 °F. Since the phase transformation of the ferrite resulting from cold working probably occurs at a much lower temperature, some other explanation must be found.

The value  $k$  can be related to the activation energy. Since there is some controversy as to whether the value  $k$  from equations other than of the second order can be used to calculate activation energies, an assumption is made that  $k$  can be used. This, at least, gives some values for comparison. The calculated values for the activation energies for Types 304 and 430 steels between 1600 and 1800 °F are 32,000 and 27,000 calories per gram mole, respectively. The activation energies for Type 410 stainless steel are 23,000 calories between

1700 and 1800 °F, and 38,000 calories between 1500 and 1600 °F. Here, again, the effect of different structures upon oxidation rates is illustrated.

#### SUMMARY AND CONCLUSIONS

1. Types 304, 430 and 410 stainless steels oxidize with respect to time according to the relation  $Y^n = Kt$  until the oxide ruptures.
2. A rapid increase in oxidation occurs when the oxide ruptures. Breakdown of the initial oxide is apparently mechanical in nature.
3. The composition of the scale prior to rupture is different from the oxide that forms after rupture.
4. The time required for rupture to occur is a function of alloy composition, atmosphere and temperature.
5. The  $\text{FeO} \cdot \text{Cr}_2\text{O}_3$  spinel scale is most protective. This spinel tends to form in the least aggressive ("starved") atmospheres, i.e., lower oxygen, lower temperature or increased oxidation resistance of the alloy involved.
6. Oxidation resistance in air can be increased by pretreatments to form selected oxides.

#### ACKNOWLEDGMENT

The investigations reported herein were carried out under Contract N6ori-17, Task Order II, between the Office of Naval Research and The Ohio State University Research Foundation. The interest and support of the Office of Naval Research are appreciated.

#### References

1. U. R. Evans, "The Mechanism of Oxidation and Tarnishing", *Transactions, Electrochemical Society*, Vol. 91, 1947, p. 547-572.
2. U. R. Evans, "The Mechanism of the Formation of Films on Metals", *Pittsburgh International Conference on Surface Reactions*, June 1948, p. 71-76.
3. N. B. Pilling and R. E. Bedworth, "Oxidation of Metals at High Temperatures", *Journal, Institute of Metals*, Vol. 29, 1923, p. 529-591.
4. E. A. Gulbransen, "The Kinetics of Oxide Film Formation on Metals and Alloys", *Transactions, Electrochemical Society*, Vol. 91, 1947, p. 573-604.
5. W. H. J. Vernon, "A Laboratory Study of the Atmospheric Corrosion of Metals", *Transactions, Faraday Society*, Vol. 31, 1935, p. 1668-1700.
6. E. A. Gulbransen, "The Transition State Theory of the Formation of Thin Films on Metals", *Transactions, Electrochemical Society*, Vol. 83, 1943, p. 301-317.

#### DISCUSSION

**Written Discussion:** By S. W. Poole, Metallurgical Laboratory, Republic Steel Corp., Central Alloy District, Canton, Ohio.

The authors have performed an interesting study incorporating a large amount of work on the oxidation of stainless Types 304, 430 and 410. The information presented on oxidizing pretreatments to form a protective spinel-type oxide layer should be of practical interest.

Examination of the data presented in Tables II and III raises some interesting questions concerning the nature of the oxide constituents formed on Type 304 stainless at 1800 °F (980 °C). From a chemical point of view, the analyses listed in this table for the oxides formed for periods of oxidation in a 100% oxygen atmosphere up to a 2-hour period are of interest with respect to the nature of the chromite-type spinel oxide layer. The ferrous chromite formula  $\text{FeO} \cdot \text{Cr}_2\text{O}_3$  contains, in stoichiometric proportions, 25.0% iron and 46.4% chromium. Analyses up to a 2-hour period of the scale produced on these tests indicates iron values not higher than 11.62% and chromium values ranging from 49.81 to 61.38%. The spinel compounds can have widely varying compositions so that in this case the chromium content of the chromite layer can exceed the stoichiometric requirement by solid solution of  $\text{Cr}^{+++}$  ions in the spinel lattice. This effect is observed with magnesium aluminate spinel where excess  $\text{Al}^{+++}$  ions can be taken up by the crystal lattice. The low iron content of the chromite spinel layer is no doubt supplemented by solid solution of  $\text{Mn}^{++}$  ions resulting from the oxidation of the manganese present in this analysis which should oxidize in a manner similar to chromium. It would be of interest to know if the high nickel contents reported for the scale produced at several of the oxidizing periods noted in Table II may not be present at the inner scale layer contiguous with the metal as microscopic nickel or nickel-rich metallic particles. Nickel as  $\text{Ni}^{++}$  ions could enter the chromite spinel lattice, but it is more probable that nickel exists as metallic particles at the inner scale layer. Metallographic examination, if possible with these thin scale layers, might settle this point.

Lattice parameter data on the spinel constituent of the scales produced for the various time periods might also be of value in developing more information on the mechanism of scale formation.

**Written Discussion:** By C. A. Siebert, University of Michigan, Ann Arbor, Mich.

The authors have shown that a very interesting phenomenon occurs in the oxidation of stainless steels. The heading of Table II, namely, "Chemical Analyses of Oxides Formed on Type 304 Stainless Steel Sheet in a 100% Oxygen Atmosphere at 1800 °F, for Various Lengths of Time", is somewhat misleading. The analyses represent the results obtained on the scale remaining after the bromine descaling treatment, and this scale may not necessarily be the entire scale which was formed in the oxidation test.

It is a well-known fact that scale formed on steels is composed of several layers, and that the thickness and composition of these layers are functions of the time, temperature, and atmosphere used in the oxidizing treatment. It is possible that some layer or layers are dissolved by the bromine solution, depending upon the degree of oxidation of the iron. Selective solution of some constituents within any one layer may also take place, depending upon the degree of oxidation of the constituents



in that layer. The results reported in Table II indicate that the above is true, as it is not reasonable to expect that diffusion occurs at such a rate to account for the analysis shown for the 10-minute scaling test.

One might postulate that the iron in the inner layer of the scale was present essentially as FeO in the initial stages of oxidation, and as  $\text{Fe}_3\text{O}_4$  after cracking of the scale occurred, which allowed the rich oxygen atmosphere to raise the layer to a higher degree of oxidation. If the bromine solution will dissolve FeO and not dissolve  $\text{Fe}_3\text{O}_4$ , it would account for the marked change in the iron-chromium ratio with length of time of scaling.

It would be appreciated if the authors would tell us if they have checked the dissolving power of the bromine solution on FeO,  $\text{Fe}_3\text{O}_4$ , NiO, and solid solutions of Ni and Si in FeO.

**Written Discussion:** By Carl A. Zapffe, research metallurgist, Baltimore, Md.

This paper constitutes an important contribution, and it contains suggestions within its results which can lead to some new thought in this type of work.

For many years there have accumulated increasing evidences for protoxide forms active in high temperature metallurgical reactions. The oxides of iron, also of manganese, have been well explored, and the monoxide forms FeO and MnO are well understood and readily enter calculations. However, the lower oxide forms of such companion metals as aluminum, silicon, chromium, and so forth, have received little attention. A review of available information a few years ago<sup>2</sup> brought out much that should be of interest to metallurgists for interpretation of metal-oxide systems; and a study of inclusions<sup>3</sup> later illustrated some specific activities of the two monoxides, CrO and SiO.

In brief, there remain to be explored a number of oxide systems involving such forms as CrO, SiO, AlO, BO, VO, and so forth. It is not yet customary to speak of these oxides in studies such as the present one; nevertheless, it is known that the caustic hydride pickling process for stainless steels reduces all of the surface oxides down to some remanent form largely comprising CrO. Since CrO is an intermediate form in the process of oxidizing Cr to the common  $\text{Cr}_2\text{O}_3$ , one's attention is drawn to the two-stage nature of the present work. The first stage would be likely to concern the formation of a lower oxide, or complex lower oxides. This would be the thin adherent scale first observed during oxidation, and remaining after such deoxidation processes as the one just mentioned. Its course would be expected to be prolonged in atmospheres of lower oxygen contents, as noted by the present authors. Also, a decrease in chromium analysis would be expected with increasing stages of oxidation, exactly as reported in Table II. The electron diffraction identification of an  $\text{Fe}_3\text{O}_4$ -type spinel should perhaps be watched more closely to find whether a protoxide form can be distinguished. Spinel, chromites, fayalites, and similar complex oxides based upon a protoxide constitution remain to be investigated.

<sup>2</sup>C. A. Zapffe, "Conversion of Certain Refractory Oxides to a Suboxide Form at High Temperatures", *Journal, American Ceramic Society*, Vol. 27, 1944, p. 293-298.

<sup>3</sup>C. A. Zapffe, "Dissociation Reactions Within Inclusions", *Journal, Iron and Steel Institute*, Vol. 154, No. 2, 1946, p. 155; *disc.*, p. 160.

Finally, there is an interesting point regarding the pickling procedure previous to oxidation which should be watched. A treatment with nitric acid, alone or mixed, causes little or no hydrogen absorption by the metal; but cleansing by the reducing acids will carry hydrogen into the metal, which will then later effuse during the oxidation treatment. This will have an effect upon the course of oxidation. Tests should be run sometime using material deliberately charged with hydrogen to find whether recognizable effects are produced during such treatments as those described by the present authors. Certain chemical effects of effusing hydrogen have been noticed at ordinary temperatures, and there is an indication that this phenomenon may be responsible for certain oxidation anomalies encountered during vitreous enameling.

**Written Discussion:** By W. J. Moore, The Catholic University of America, Washington, D. C.

This extremely interesting paper will repay careful study by anyone concerned with high temperature gaseous corrosion of metals and alloys, because it illustrates very well a principle that we often tend to forget—namely, that the kinetic laws followed in relatively complex systems may bear little resemblance to those in simple systems. Those of us who have been engaged in the study of the kinetics of the reactions between pure gases and elementary metals have found that in almost every case the results can be fitted very well by one of these basic laws:

$$\begin{array}{ll} \text{the linear} & dy/dt = k \\ \text{the parabolic} & dy/dt = k/y \\ \text{the exponential} & dy/dt = k_1 e^{-k_2 y} \end{array}$$

Here  $y$  is the thickness of the oxide film, and  $t$  is the time. The physical interpretation of these laws has been quite well established by the work of Wagner, Mott, Evans, and others. A linear law denotes a rate-controlling interface reaction; the parabolic law denotes diffusion control; an exponential law arises from a mechanism of gas attack through fissures of varying depth in a protective film.

One's first thought would be that the present results might be interpreted by a combination of interfacial reaction and diffusion control, leading to an equation, due originally I believe to Fischbeck,

$$\frac{dy}{dt} = \frac{k_1}{y} + k_2$$

I was unable, however, to satisfactorily fit such an expression to the data, and of course this failure is hardly surprising when one contemplates the results in Tables II, III, and IV, on the compositions of the oxides formed. No theoretical equation based on a constant value for the diffusion coefficient could be expected to apply. The parabolic rate constant, according to the Mott equation, is  $k = 2Df$ , where  $D$  is the cation diffusion coefficient and  $f$  is the fraction of lattice defects. In the present work,  $D$  is not a constant, but depends on the iron content in the surface film. It might be physically more reasonable to assume that the scale has a layered structure, with different diffusion coefficients for each layer.

We are as yet in no position to test this suggested interpretation for the observed oxidation kinetics, but I am inclined to believe that future

studies of cationic diffusion in spinels and other oxides may substantiate this picture.

#### Authors' Reply

The authors wish to thank Messrs. Poole, Siebert, Zapffe and Moore for their valuable comments and discussion.

As a result of Dr. Poole's discussion, we made a metallographic examination of oxides formed on Type 304 stainless steel and no metallic nickel particles were observed. The oxides in these specimens were still attached to the base metal. If metallic nickel were present, however, it would probably be dissolved by the bromine solution during the stripping operation and would not show up in the chemical analyses of the oxides. In addition, some selective attack occurs at the interface. The nickel reported in the paper probably exists primarily as NiO in solid solution with the remainder of the oxides. Dr. Poole's other remarks are also appreciated.

In reply to Dr. Siebert's remarks, we wish to point out that the chromium contents listed in Table II are within reason and are based on the following factors: (a) chemical analyses (as shown in Table II), (b) after 10 minutes of oxidation only one scale was observed and this oxide was identified by electron diffraction to be  $\text{FeO} \cdot \text{Cr}_2\text{O}_3$  spinel, (c) the color of the scale after 10 minutes of oxidation was greenish-brown, indicating a high chromium content, (d) the protective nature of the oxide during the early stages of oxidation (slow rate of oxidation) would indicate an oxide high in chromium.

It should also be pointed out that the oxide layer (as illustrated by the small increase in weight in the curves) is quite thin at the end of a 10-minute test and also that the diffusion of chromium is rapid at 1800 °F (980 °C). In addition to the rapid diffusion of chromium, it does not necessarily diffuse over a great distance.

Vernon, Wormwell and Nurse<sup>4</sup> show that on highly polished 18-8 stainless steel, oxide films containing as high as 90% chromium oxide are formed, the balance being ferric oxide. This is added as a matter of interest.

Some work was done to check the dissolving power of the bromine solution on  $\text{FeO}$ ,  $\text{Fe}_3\text{O}_4$ , and  $\text{Fe}_2\text{O}_3$ . The results show that there is selective attack at the metal- $\text{FeO}$  interface, the  $\text{FeO}-\text{Fe}_3\text{O}_4$  interface, and the  $\text{Fe}_3\text{O}_4-\text{Fe}_2\text{O}_3$  interface. Also, the  $\text{FeO}$  is attacked at a greater rate than the other oxides. In the case of the two oxides,  $\text{FeO} \cdot \text{Cr}_2\text{O}_3$  spinel and the  $\text{Fe}_2\text{O}_3$ , the  $\text{Fe}_2\text{O}_3$  layer is attacked more rapidly than the spinel. However, for the 10-minute oxidation test the  $\text{Fe}_2\text{O}_3$  layer is not present. The rapid increase in iron content during the later stages of oxidation (second layer present) indicates again that differential solution of the oxides is not great enough to appreciably change the trend of results indicated in Table II.

We have not made any studies to check the dissolving power of the bromine solution on NiO, and solid solutions of Ni and Si in  $\text{FeO}$ .

With regard to Dr. Zapffe's discussion, the possibility of a protoxide

<sup>4</sup>W. H. J. Vernon, F. Wormwell and T. J. Nurse, "A Study of the Surface Films on Chromium-Nickel (18-8) Stainless Steel", *Journal, Iron and Steel Institute*, Vol. CL, 1944, p. 81-91.



form of oxide should not be overlooked; however, for the work described in this paper the pattern for the scale matched that of the  $\text{Fe}_3\text{O}_4$ -type spinel. This, of course, does not mean that the protoxide form does not exist in the very early stages of oxidation. Unfortunately, electron diffraction is not very precise for this work.

Specimen preparation is one of the most important, or perhaps the most important, factor to be considered in these fundamental oxidation studies. Even with the great care used in handling specimens, one can often observe patterns on oxidized specimens indicating that the surface had been altered or contaminated prior to the test. Although we have no direct evidence to show that absorbed hydrogen (resulting from pickling treatment) causes any recognizable effects during the oxidation test, it is felt that hydrogen may enter the picture during the early stages of oxidation.

With reference to Professor Moore's remarks, additional knowledge concerning diffusion rates of cations in oxides would indeed be valuable in making a theoretical interpretation of complex systems such as the one encountered in the oxidation of stainless steels. Our attempts at developing an equation to fit the data presented were unsuccessful. More fundamental information should be developed to aid in the interpretation of oxidation mechanisms in complex alloys. Perhaps a good approach would be one of studying simple systems using various combinations of the elements in Type 304 stainless steel before trying to interpret the mechanism for the more complex alloys.



## THE OXIDATION OF PURE IRON

By J. K. STANLEY, MISS J. VON HOENE AND R. T. HUNTOON

### Abstract

*The oxidation of high-purity iron in air was studied from 500 to 900 °C. The oxidation was found to proceed by the common parabolic rate law,  $W^2 = Kt + C$ , where  $W$  is the weight gain,  $t$  is time and  $K$  and  $C$  are constants. The oxidation process as a function of temperature follows the usual exponential law. The rate constant,  $K$ , shows the temperature dependence*

$$K = 0.37 e^{-33,000/RT}$$

*where  $R$  is the gas constant and  $T$  the absolute temperature.*

*The nature of the oxide films was investigated with the Geiger counter X-ray spectrometer. Only one oxide,  $Fe_3O_4$ , was found at 500 °C, but three oxides,  $\alpha$ - $Fe_2O_3$ ,  $Fe_3O_4$  and  $FeO$ , were found at the higher temperatures.*

*Metallographic examination made possible the resolution of the various oxide strata.*

*It was found that  $FeO$  could be cooled to room temperature without decomposition to  $Fe$  and  $Fe_3O_4$ .*

WHILE many data have been obtained on the oxidation of commercial ingot iron and low carbon steels, there is little on the oxidation of high-purity iron. The available data on the oxidation of pure iron is not particularly complete with respect to the kinetics of the oxidation, the structure and composition of the oxide layers. The mechanism of the oxidation of even the element iron is not well understood, although several theories have been advanced. If our understanding of the oxidation is to increase, more basic information on the nature and structure of the oxide layer or layers is necessary. The present study is a report on the kinetics of oxidation and the structure and nature of the oxides formed.

### LITERATURE

The literature can be considered under the headings: kinetics of the reaction, structure and composition of the oxides, the metallography of the oxide-metal composite, and the mechanism of the reaction.

A paper presented before the Thirty-second Annual Convention of the Society, held in Chicago, October 21 to 27, 1950. Of the authors, J. K. Stanley and Miss J. von Hoene are associated with the Westinghouse Research Laboratories, East Pittsburgh, and R. T. Huntoon is a student, Carnegie Institute of Technology, Pittsburgh. Manuscript received April 15, 1950.

**Kinetics of the Reaction**—Many workers have studied the kinetics of oxide formation on iron (1-4).<sup>1</sup> Iron is known to oxidize by the parabolic rate law,  $W^2 = Kt + C$ , where  $W$  is the weight gain per unit area,  $t$  is the time, and  $K$  and  $C$  are constants. The constant  $K$  is called the parabolic rate constant; it is also sometimes referred to as the scaling constant. This law does not hold for very thin films formed below 200 °C (5).

**Structure and Composition**—Gulbransen and Hickman (6) were among the first to study the oxidation of high-purity iron. They used low-pressure oxidation (1 mm oxygen) in order to form thin films which could be examined by electron diffraction. These workers made electron diffraction measurements on the films at the temperatures at which they were formed, since Jackson and Quarrell (7) had demonstrated that oxides formed on iron at high temperatures underwent transformations when cooled to room temperature. Gulbransen and Hickman found that the oxide formed on iron depends on the temperature of oxidation and may also depend on the oxide thickness. The oxides found by electron diffraction, which are claimed by Hickman (8) to be identical with bulk oxides, are given in Table I. Structures found on iron by other investigators are given in Table II.

Table I  
Oxides Formed at Various Temperatures\*  
(by Hickman)

Temperature °C	°F	Oxide	Crystal Structure	Remarks
200	390	$\gamma\text{-Fe}_2\text{O}_3$	Cubic; $a = 8.4$	$\gamma\text{-Fe}_2\text{O}_3 \rightarrow \alpha\text{-Fe}_2\text{O}_3$ at about 225 °C
300	570	$\alpha\text{-Fe}_2\text{O}_3$	Rhombohedral	$\alpha\text{-Fe}_2\text{O}_3 \rightarrow \text{Fe}_3\text{O}_4$ at 225 to 450 °C
400	750	$\text{Fe}_3\text{O}_4$	Cubic; $a = 8.4$	$\text{Fe}_3\text{O}_4 \rightarrow \text{FeO}$ at 450 to 550 °C;
500	930	$\text{Fe}_3\text{O}_4$	Cubic; $a = 8.4$	reaction is reversible and appears
600	1110	FeO	Cubic; $a = 4.294$	to depend on film thickness; i.e.,
700	1290	FeO	Cubic; $a = 4.294$	the thicker the film the higher the transition.

\*A rare hexagonal oxide of iron ( $a = 4.64$ ;  $c = 6.50$ ) forms sometimes when the films are thin.

**Metallographic Study**—Bénard and Coquelle (14) reported the relative thickness of FeO,  $\text{Fe}_3\text{O}_4$  and  $\text{Fe}_2\text{O}_3$  found by micrographic inspection in iron scales formed after heating 5 hours at temperatures of 650 to 1050 °C (1200 to 1920 °F). Most of the scale consisted of FeO up to about 900 °C (1650 °F), at which temperature the amount of  $\text{Fe}_3\text{O}_4$  and  $\text{Fe}_2\text{O}_3$  started to increase rapidly.

Tesche (4) has also reported some metallographic work up to 700 °C (1290 °F), which appears in agreement with Bénard and

<sup>1</sup>The figures appearing in parentheses pertain to the references appended to this paper.

Table II  
Oxides Found on Iron by Other Investigators

Investigator	Temperature, °C	Sample	Oxides Observed	
Jackson & Quarrell (7)	400 to 1200	Iron	Fe <sub>3</sub> O <sub>4</sub>	Studied at room temp.
	350 to 400	Armco Iron	Fe <sub>3</sub> O <sub>4</sub>	
	400 to 515	Armco Iron	FeO and Fe <sub>3</sub> O <sub>4</sub>	Studied at indicated temperature
	515 to 900	Armco Iron	FeO	
Gulbransen, Phelps and Hickman (9)	900	Armco Iron	Fe <sub>3</sub> O <sub>4</sub>	
	400	Pure Iron	Fe <sub>3</sub> O <sub>4</sub>	
	500	Pure Iron	{ FeO (1 min.) Fe <sub>3</sub> O <sub>4</sub> (1 min.)	Studied at room temp.
Pfeil (10, 11)	600	Pure Iron	FeO	
	850	Iron	FeO	
	1050	Iron	Fe <sub>3</sub> O <sub>4</sub>	
Goldschmidt (12)	650 to 1000	Iron	Fe <sub>2</sub> O <sub>3</sub>	Studied at room temp.
			FeO	
			Fe <sub>3</sub> O <sub>4</sub>	
Bénard (13)	650 to 1050	Iron	Fe <sub>2</sub> O <sub>3</sub>	Studied at room temp.
			FeO	
			Fe <sub>3</sub> O <sub>4</sub>	

Coquelle. Tesche finds that below 625 °C (1155 °F) the oxide is single layered and consists of Fe<sub>3</sub>O<sub>4</sub>. Above 625 °C the oxide occurs in two layers, with the FeO adjacent to the metal and Fe<sub>3</sub>O<sub>4</sub> on the outside.

*Mechanism of the Reaction*—The mechanism of the oxidation of metals, and iron in particular, is not well understood. Theories, of course, have been advanced for the oxidation of iron (15, 19), but they are far from satisfactory because of the lack of information on the nature and structure of the phases, the variation of oxygen and iron contents at the various interfaces and through the phases, and the diffusion of both the oxygen and iron ions through the oxide lattices.

There is little doubt that our qualitative picture of the mechanism is correct. It appears that the iron ions diffuse from the iron base into the oxide layers, but countercurrent to this process is the diffusion of oxygen ions from the gas-oxide interface into the oxides to the metal. At the oxidizing temperature, several layers are maintained. Bénard (13) indicates that the formation of FeO allows a parabolic rate law, whereas the formation of the  $\alpha$ -Fe<sub>2</sub>O<sub>3</sub> and Fe<sub>3</sub>O<sub>4</sub> follows a linear rate law.

#### DATA

*Kinetics of Oxidation of Iron*—The iron used for the experiments is a product of the Westinghouse Electric Corporation known as Puron. It is a specially purified electrolytic iron. The metallic impurities occur only as traces; the greatest impurities are oxygen and carbon, being about 0.04 and 0.005%, respectively. The iron content is about 99.95%.

The iron was prepared from an induction-melted ingot which had been forged to  $1\frac{1}{2}$  by  $\frac{1}{2}$ -inch bars. These bars were hot-rolled at  $900^{\circ}\text{C}$  ( $1650^{\circ}\text{F}$ ) to 0.05 inch and were then cold-rolled to 0.025 inch. The samples were abraded with No. 1 metallographic paper. A small hole was punched in the edge for support from a quartz rod when in the furnace. The samples were then washed in

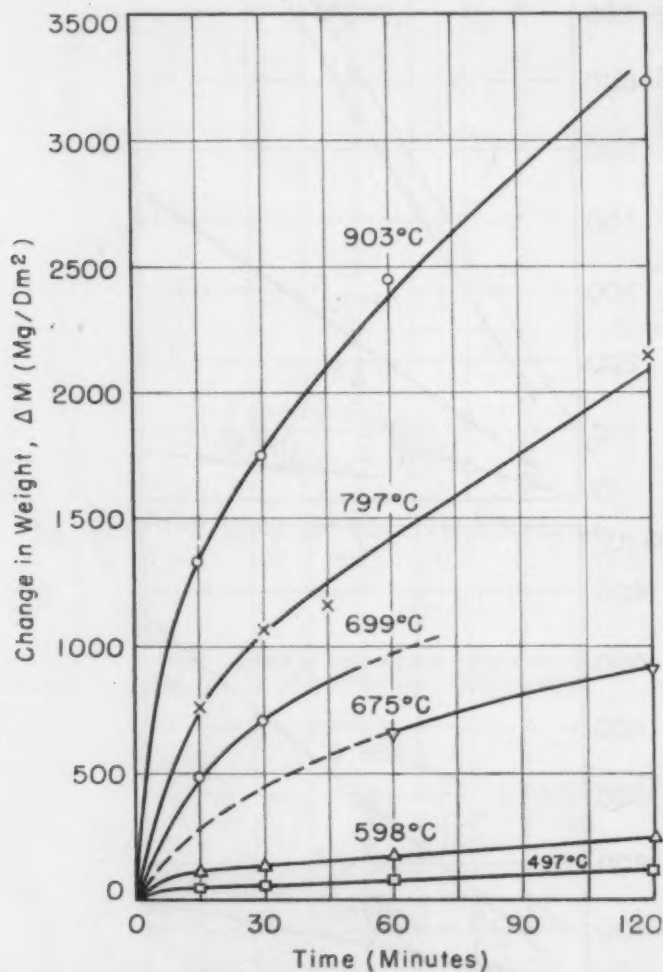


Fig. 1—Oxidation of Pure Iron (Puron) in Air.

acetone and were stored in a desiccator until weighed. The iron was then oxidized in an air muffle at 500, 600, 700, 800 and  $900^{\circ}\text{C}$  ( $930$ ,  $1110$ ,  $1290$ ,  $1470$  and  $1650^{\circ}\text{F}$ ) for 15, 30, 60 and 120 minutes. The relative humidity of the atmosphere during oxidation varied from 52 to 74%. At the end of the oxidation period the samples were withdrawn from the furnace and were cooled in a desiccator.

The results of the oxidation of iron at the various temperatures are given in Fig. 1 where the weight increase in milligrams per



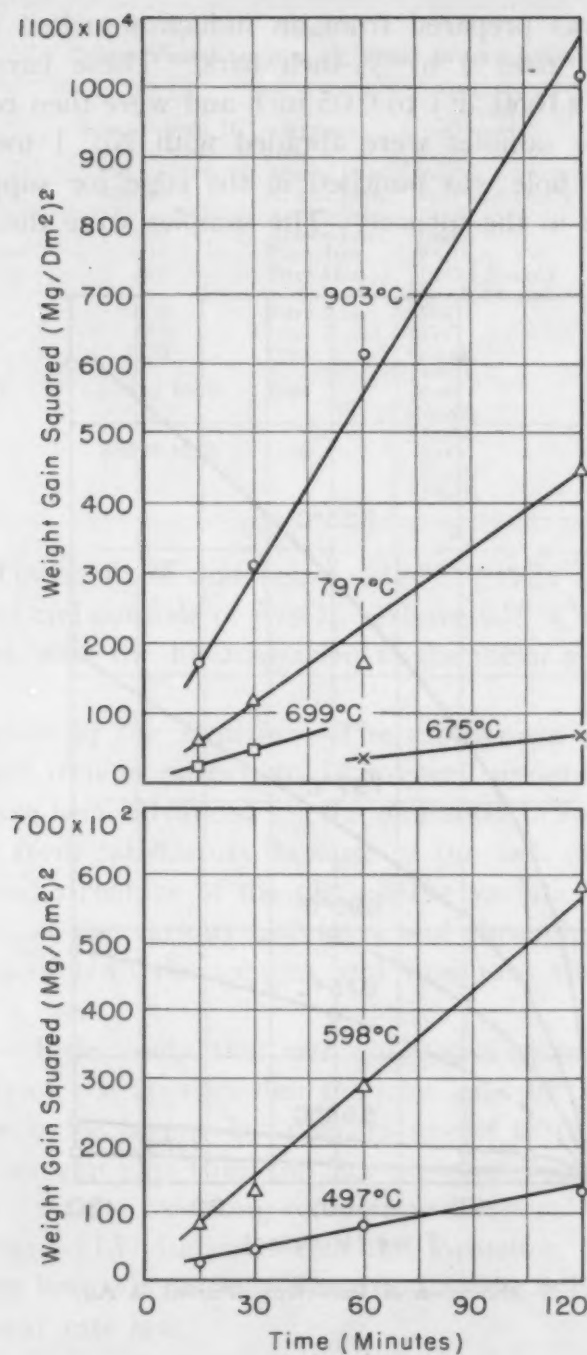


Fig. 2—Oxidation of Pure Iron (Puron) in Air.

square decimeter is plotted against time. To show that the curves obey the parabolic rate law, the data were replotted with the weight gain squared against time to show that straight lines result (Fig. 2).

A calculation of  $K$ , the parabolic rate constant, was made for the oxidation at each temperature; values are given on next page.

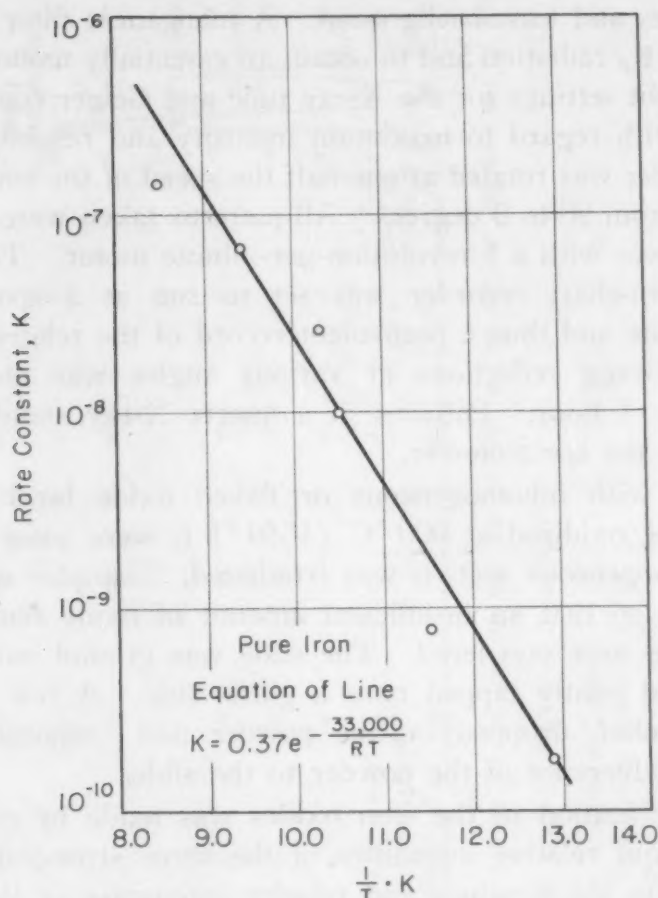


Fig. 3—Rate Constant Plotted Against the Reciprocal of the Absolute Temperature.

°C	K
497	$1.7 \times 10^{-10}$ (grams/cm <sup>2</sup> ) <sup>2</sup>
598	$7.9 \times 10^{-10}$ sec
675	$9.7 \times 10^{-9}$
699	$2.5 \times 10^{-8}$
797	$6.1 \times 10^{-8}$
903	$1.5 \times 10^{-7}$

The constant plotted against the reciprocal of the temperature gives a straight line whose slope is  $Q/R$  where  $Q$  is the activation energy (Fig. 3). The temperature dependence of the oxidation of pure iron can be given by the equation

$$K = 0.37 e^{-33,000/RT}$$

*X-Ray Study of the Oxide Films*—In the present study the chemical nature of the oxide films was determined using the Geiger counter X-ray spectrometer. Front reflection X-ray patterns were made. An iron target<sup>2</sup> was employed, since this radiation gave the

<sup>2</sup>The tube was operated at 36 KV and 6 ma. The voltage across the counter was maintained at 1350.

best intensities and least background. A manganese filter was used to absorb the  $K_{\beta}$  radiation and to obtain an essentially monochromatic beam. The slit settings for the X-ray tube and Geiger counter were determined with regard to maximum intensity and resolution. The specimen holder was rotated at one-half the speed of the counter tube which scans from 90 to 0 degrees. All patterns taken were run from 86 to 26 degrees with a 1 revolution-per-minute motor. The Brown electronic strip-chart recorder was set to run at a speed of  $\frac{1}{2}$  inch per minute and thus a permanent record of the relative intensities of the Bragg reflections at various angles was obtained in approximately 1 hour. Patterns of a quartz X-ray standard were used to check the spectrometer.

Samples with inhomogeneous or flaked oxide layers, as, for example, those oxidized at 900 °C (1650 °F), were placed so that the most homogeneous section was irradiated. Samples which had scaled heavily so that an insufficient amount of oxide remained on the metal base were powdered. The scale was ground with mortar and pestle and gently tapped onto a glass slide. A few drops of denatured alcohol, dropped on the powder and evaporated, were sufficient for adherence of the powder to the slide.

The identification of the iron oxides was made by correlating the d-values and relative intensities of the three strongest lines of the unknown to the d-values and relative intensities of the known compound as given in the Hanawalt tables. Records were kept of the angular value, d-value and absolute intensity of the lines on each pattern. A typical pattern is shown in Fig. 4. To speed up the analyses, a standard pattern of  $\text{Fe}_3\text{O}_4$  was superimposed on a pattern of  $\alpha\text{-Fe}_2\text{O}_3$  and each sample was read from this. A pattern of a synthetic mixture of 50%  $\text{Fe}_2\text{O}_3$  and 50%  $\text{Fe}_3\text{O}_4$  showed that these compounds have a damping effect upon each other by decreasing the intensities of lines and giving usually wide and overlapping reflections. Thus it was often difficult to decide whether  $\text{Fe}_3\text{O}_4$  was present or not, even though the absence of the strong lines would seem to indicate that it was not. The oxides on the various samples thus identified are given in Table III; they are also included in a summary of the data in Table IV.

According to Barrett (16), some substances will produce a pattern in a mixture if they represent only 1%, many will not show if less than 10%, and some will not show even for 50%. In numerous samples of the present work, weak lines of  $\text{Fe}_3\text{O}_4$  appeared strong, while strong lines were weakened or absent. In several instances, involving a possible superposition of two strong lines, a

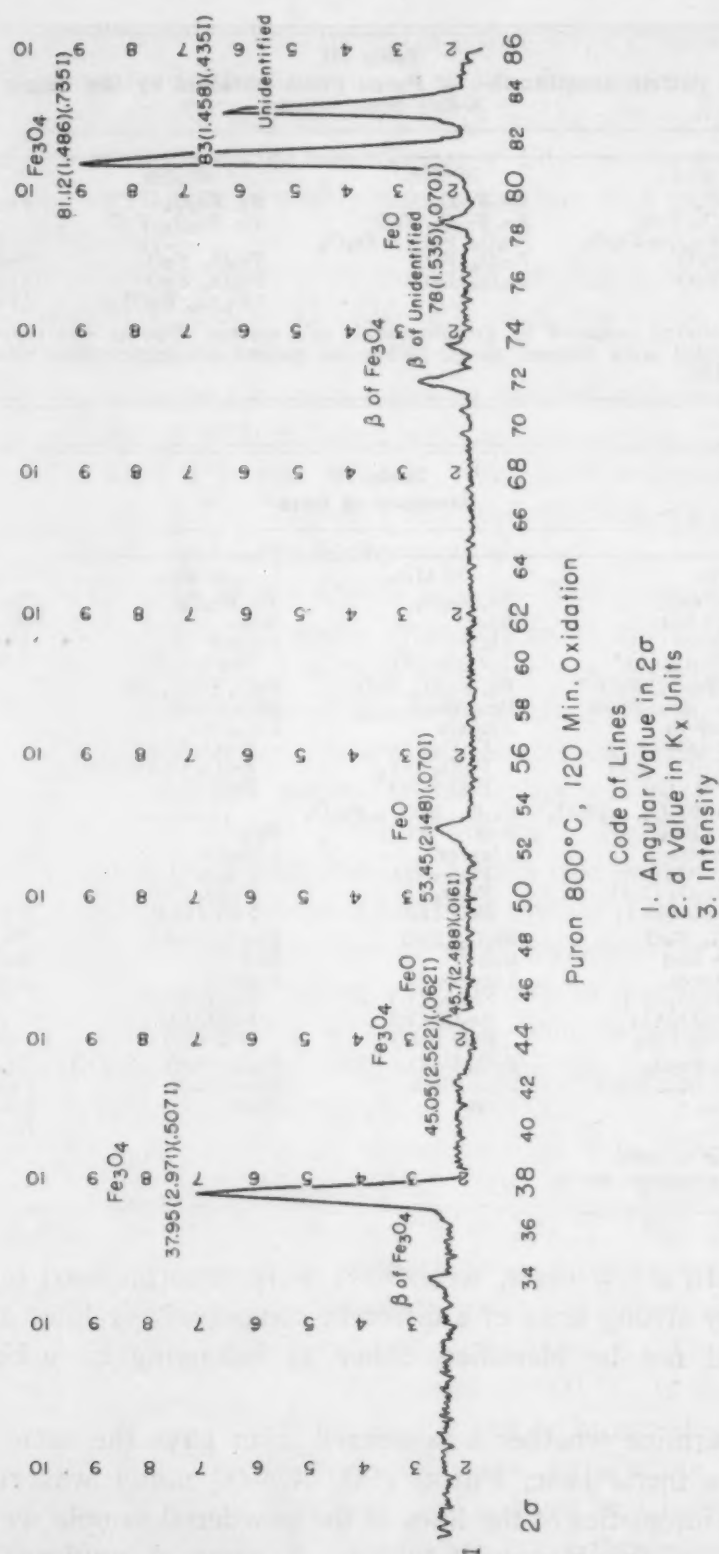


Fig. 4—Typical X-ray Diffraction Record Taken on a Geiger Counter Spectrometer.

clear-cut decision could not be made on the basis of intensity. If the line appeared thick, however, and especially if it showed strength, both compounds were considered present if additional weak lines



**Table III**  
Diffraction Pattern Identification of Puron Films Obtained by the Gelger Counter  
X-Ray Spectrometer

Temp. °C	°F	Period of Oxidation			
		15 Min.	30 Min.	60 Min.	120 Min.
500	930	Fe, Fe <sub>3</sub> O <sub>4</sub>	Fe, Fe <sub>3</sub> O <sub>4</sub>	Fe, Fe <sub>3</sub> O <sub>4</sub>	Fe, Fe <sub>3</sub> O <sub>4</sub>
600	1110	Fe, Fe <sub>3</sub> O <sub>4</sub> , FeO	Fe, Fe <sub>3</sub> O <sub>4</sub> , FeO	Fe, Fe <sub>3</sub> O <sub>4</sub> , FeO	.....
700	1290	Fe <sub>3</sub> O <sub>4</sub> , FeO, α-Fe <sub>2</sub> O <sub>3</sub>	Fe <sub>3</sub> O <sub>4</sub> , FeO, α-Fe <sub>2</sub> O <sub>3</sub>	.....	.....
800	1470	Fe <sub>3</sub> O <sub>4</sub> , FeO	Fe <sub>3</sub> O <sub>4</sub> , FeO	Fe <sub>3</sub> O <sub>4</sub> , FeO	Fe <sub>3</sub> O <sub>4</sub> , FeO
900	1650	Fe <sub>3</sub> O <sub>4</sub> , FeO	Fe <sub>3</sub> O <sub>4</sub> , FeO	Fe <sub>3</sub> O <sub>4</sub> , FeO [Fe <sub>3</sub> O <sub>4</sub> , FeO]	Fe <sub>3</sub> O <sub>4</sub> , FeO [Fe <sub>3</sub> O <sub>4</sub> , FeO, α-Fe <sub>2</sub> O <sub>3</sub> ]

[ ]—Powdered specimens prepared by grinding scale in a mortar. Powder was tapped onto a glass slide and a few drops of alcohol were dropped on it. When the alcohol evaporated there was sufficient adherence of the powder to the slide.

**Table IV**  
Summary of Data

Temp.	Oxidation Time			
	15 Min.	30 Min.	60 Min.	120 Min.
500 °C (930 °F)	X-ray: Fe, Fe <sub>3</sub> O <sub>4</sub> Appearance: Blue Metall.: 1 layer Fe <sub>3</sub> O <sub>4</sub> (6)*	Fe, Fe <sub>3</sub> O <sub>4</sub> Blue 1 layer Fe <sub>3</sub> O <sub>4</sub> (8)	Fe, Fe <sub>3</sub> O <sub>4</sub> Blue 1 layer Fe <sub>3</sub> O <sub>4</sub> (10)	Fe, Fe <sub>3</sub> O <sub>4</sub> Blue 1 layer Fe <sub>3</sub> O <sub>4</sub>
600 °C (1110 °F)	X-ray: Fe, Fe <sub>3</sub> O <sub>4</sub> , FeO Appearance: Blue-Black Metall.: 3 layers Fe <sub>2</sub> O <sub>3</sub> (0.5) Fe <sub>3</sub> O <sub>4</sub> (5.5) FeO (2)	Fe, Fe <sub>3</sub> O <sub>4</sub> , FeO Blue-Black 3 layers Fe <sub>2</sub> O <sub>3</sub> (1) Fe <sub>3</sub> O <sub>4</sub> (5) FeO (4.5)	FeO, Fe <sub>3</sub> O <sub>4</sub> , Fe Blue-Black 3 layers Fe <sub>2</sub> O <sub>3</sub> (1.5) Fe <sub>3</sub> O <sub>4</sub> (4.0) FeO (8.5)	.....
700 °C (1290 °F)	X-ray: FeO, Fe <sub>3</sub> O <sub>4</sub> , α-Fe <sub>2</sub> O <sub>3</sub> Appearance: Red Metall.: 3 layers Fe <sub>2</sub> O <sub>3</sub> (1) Fe <sub>3</sub> O <sub>4</sub> (2.5) FeO (30.5)	Fe <sub>3</sub> O <sub>4</sub> , FeO, α-Fe <sub>2</sub> O <sub>3</sub> Red 3 layers Fe <sub>2</sub> O <sub>3</sub> (1) Fe <sub>3</sub> O <sub>4</sub> (3) FeO (50)	..... Red 3 layers Fe <sub>2</sub> O <sub>3</sub> (1.0) Fe <sub>3</sub> O <sub>4</sub> (3.0) FeO (67.0)	.....
800 °C (1470 °F)	X-ray: Fe <sub>3</sub> O <sub>4</sub> , FeO Appearance: Red Metall.: 3 layers Fe <sub>2</sub> O <sub>3</sub> (1.) Fe <sub>3</sub> O <sub>4</sub> (3) FeO (58)	Fe <sub>3</sub> O <sub>4</sub> , FeO Red 3 layers Fe <sub>2</sub> O <sub>3</sub> (1.) Fe <sub>3</sub> O <sub>4</sub> (5.) FeO (77.)	Fe <sub>3</sub> O <sub>4</sub> , FeO Red 3 layers Fe <sub>2</sub> O <sub>3</sub> (2) Fe <sub>3</sub> O <sub>4</sub> (4) FeO (96)	Fe <sub>3</sub> O <sub>4</sub> , FeO Red 3 layers Fe <sub>2</sub> O <sub>3</sub> (2) Fe <sub>3</sub> O <sub>4</sub> (6) FeO (156)
900 °C (1650 °F)	X-ray: FeO, Fe <sub>3</sub> O <sub>4</sub> Appearance: Blue-Black Metall.: None	FeO, Fe <sub>3</sub> O <sub>4</sub> Blue-Black None	Fe <sub>3</sub> O <sub>4</sub> , FeO, [Fe <sub>3</sub> O <sub>4</sub> ]† Blue-Black None	Fe <sub>3</sub> O <sub>4</sub> , FeO [Fe <sub>3</sub> O <sub>4</sub> , FeO, α-Fe <sub>2</sub> O <sub>3</sub> ]† Blue-Black None

\*Thickness in mm. at × 1000.

†X-ray analysis on powdered scale.

appeared. In a few cases, weak lines were superimposed on reflections of very strong lines of a different compound; or lines appeared which could not be identified either as belonging to α-Fe<sub>2</sub>O<sub>3</sub> or Fe<sub>3</sub>O<sub>4</sub>.

To determine whether a powdered layer gave the same pattern as one on a metal base, Puron (900 °C—60 min.) was run both ways. The intensities of the lines of the powdered sample were similar to those of the Hanawalt tables. A common unidentified line (d-2.296), present in the unpowdered sample, was not present in the powdered sample, however. Furthermore, the relative intensities of the oxide lines on the metal indicated considerable departure from

the given intensities. This indicates either large crystals or the presence of preferred orientation. Another line having a  $d$ -value of approximately 1.458 was assigned to  $\alpha$ - $\text{Fe}_2\text{O}_3$ , although the strongest line of the compound did not appear. This would indicate a high degree of orientation, probably due to the fact that the iron had been initially cold-rolled.

The lattice parameter of iron was readily calculated from the samples oxidized at 500 °C (930 °F), since the oxide on these samples was thin and the iron lines were strong. The lattice parameter of iron was obtained from a mean of the reflections of the (110) and (200) from a pattern taken with an iron target. The parameter obtained on pure iron was 2.869 Å. This is in reasonable agreement with Farquhar (17), Taylor (18) and Barrett (16) who found 2.8662, 2.86624, and 2.86678, respectively.

*Metallography of the Oxide Layers*—The preparation of specimens for metallographic study departed from the normal mounting and polishing procedures in that special precautions were necessary to prevent the destruction of the oxide coatings during the mounting and polishing operations. Since the oxides on many of the sheets were soft and fragile, a method of mounting was required which did not require conventional pressure curing. For this, a catalyzed monomer Bio Plastic<sup>3</sup> was used. Mounts cast with this preparation need only be oven cured for 3 hours at 65 °C.

After mounting, the specimens were sectioned on a liquid-cooled cutoff wheel. Rough grinding on conventional metallographic paper followed. Final polishing was done by hand lapping with diamond paste on onionskin paper. After polishing, the samples were etched in 10% nital and were examined at  $\times 1000$ .

The oxide structures are shown in Figs. 5 to 8 for the oxidation of iron at 500, 600, 700 and 800 °C (930, 1110, 1290 and 1470 °F), respectively. The oxidation of iron at 500 °C (Fig. 5) shows only one layer but at the other temperatures three layers can be seen. Where the three layers occur, there exist differences in color, which help to differentiate the layers, Figs. 6, 7 and 8. Under the microscope the outside  $\text{Fe}_2\text{O}_3$  layer, formed at 600 °C, is bluish-black but, when formed at 700 and 800 °C, it is red or brownish-red and photographs, surprisingly enough in all cases, as a white layer. Under the microscope the intermediate  $\text{Fe}_3\text{O}_4$  layer is a light gray and the  $\text{FeO}$ , adjacent to the metal, is a darker gray; these layers also photograph in much the same way. The mottled appearance of the layers is probably caused by etching with 10% nital, and the large voids

<sup>3</sup>Bio Plastic is a plastic obtainable from the Ward Natural Science Establishment Inc., Rochester, N. Y.

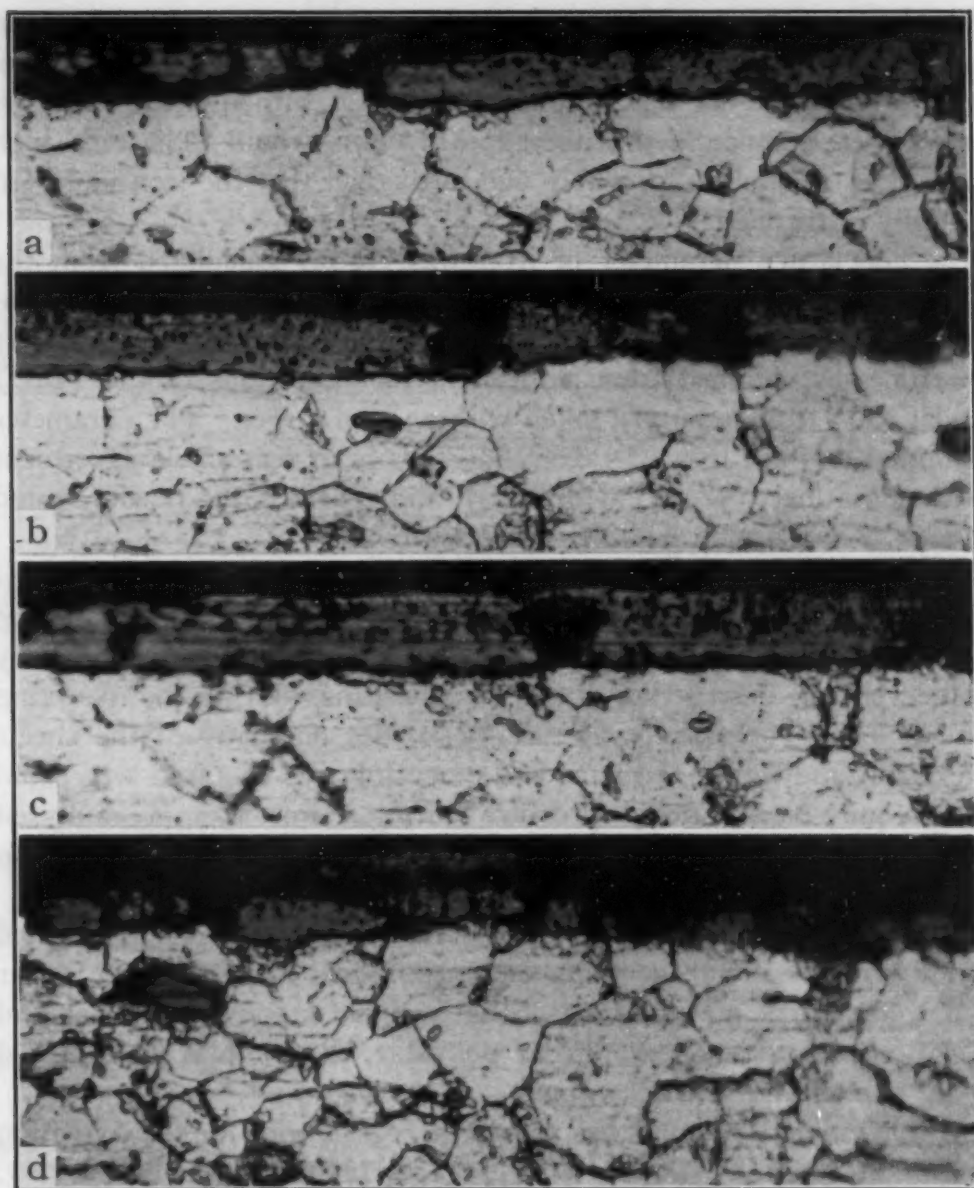


Fig. 5—Oxide Layers Formed on Pure Iron at 500 °C (930 °F).  $\times 1000$ . a—15 minutes; b—30 minutes; c—60 minutes; d—120 minutes.

are probably cavities or holes where the brittle oxide was torn out by the polishing operation.

The thickness of the total oxide and the thickness of the respective layers was measured on the ground glass of the microscope at several places on each specimen and the thickness values were averaged. This information is tabulated in Table IV and is referred to in the discussion.

#### DISCUSSION

*Oxidation at 500 °C*—There is little doubt that a single layer of



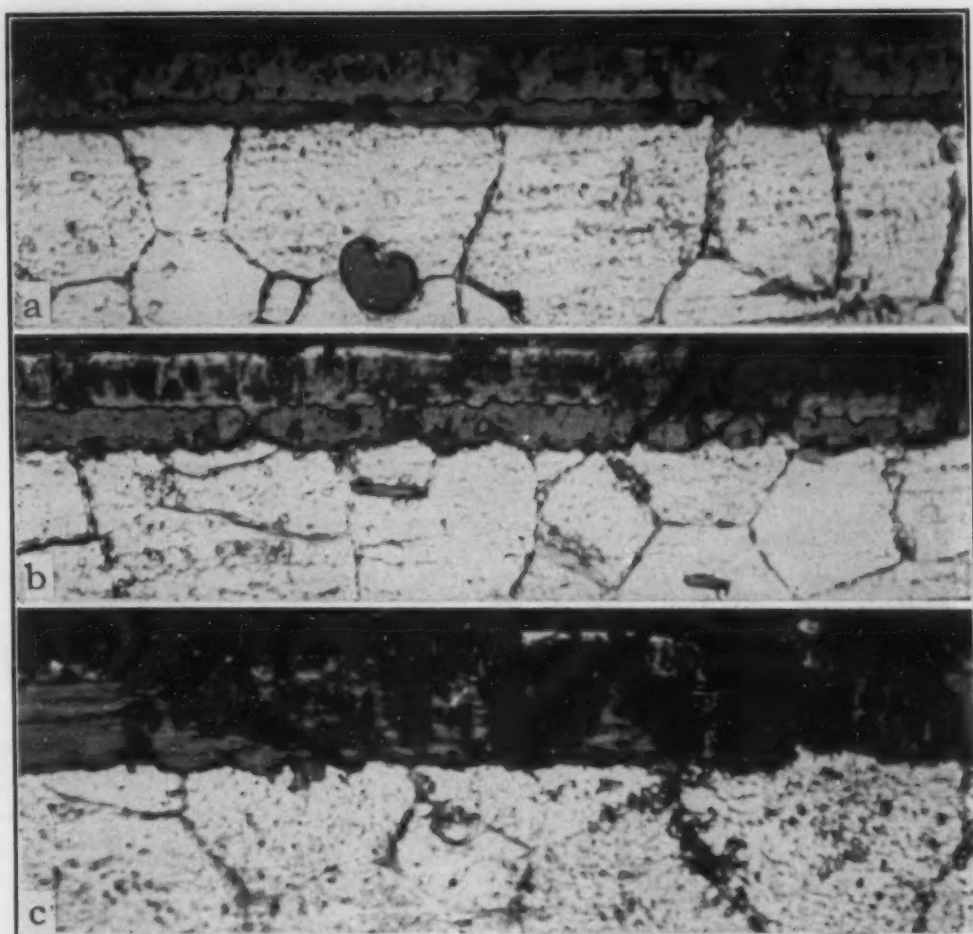


Fig. 6—Oxide Layers Formed on Pure Iron at 600 °C (1110 °F).  $\times 1000$ . a—15 minutes; b—30 minutes; c—60 minutes.

$\text{Fe}_3\text{O}_4$  forms on pure iron oxidized at 500 °C (930 °F). The X-ray study shows iron lines but this is due to the diffraction of the X-rays by the iron, since the thickness of the oxide is only of the order of 0.004 to 0.008 millimeters (0.00016 to 0.00032 inch). Metallographic examination (Fig. 5) shows only one oxide phase and the appearance of the strip in reflected light is bluish-black, generally indicative of  $\text{Fe}_3\text{O}_4$ .

*Oxidation at 600 °C*—Above 570 °C (1060 °F)  $\text{FeO}$  forms and one obtains layers of oxides forming on the iron. Our work shows that the three oxides,  $\alpha\text{-Fe}_2\text{O}_3$  (30.0% oxygen),  $\text{Fe}_3\text{O}_4$  (28.6%), and  $\text{FeO}$  (22.2%), form in that order on the iron, with the  $\text{FeO}$  being adjacent to the iron; these layers can be readily differentiated; see Fig. 6.

The X-ray examination shows only the two phases,  $\text{Fe}_3\text{O}_4$  and  $\text{FeO}$ , as well as iron. This is a result which might be expected because the  $\alpha\text{-Fe}_2\text{O}_3$  layer is too thin (about 1 millimeter at  $\times 1000$ )



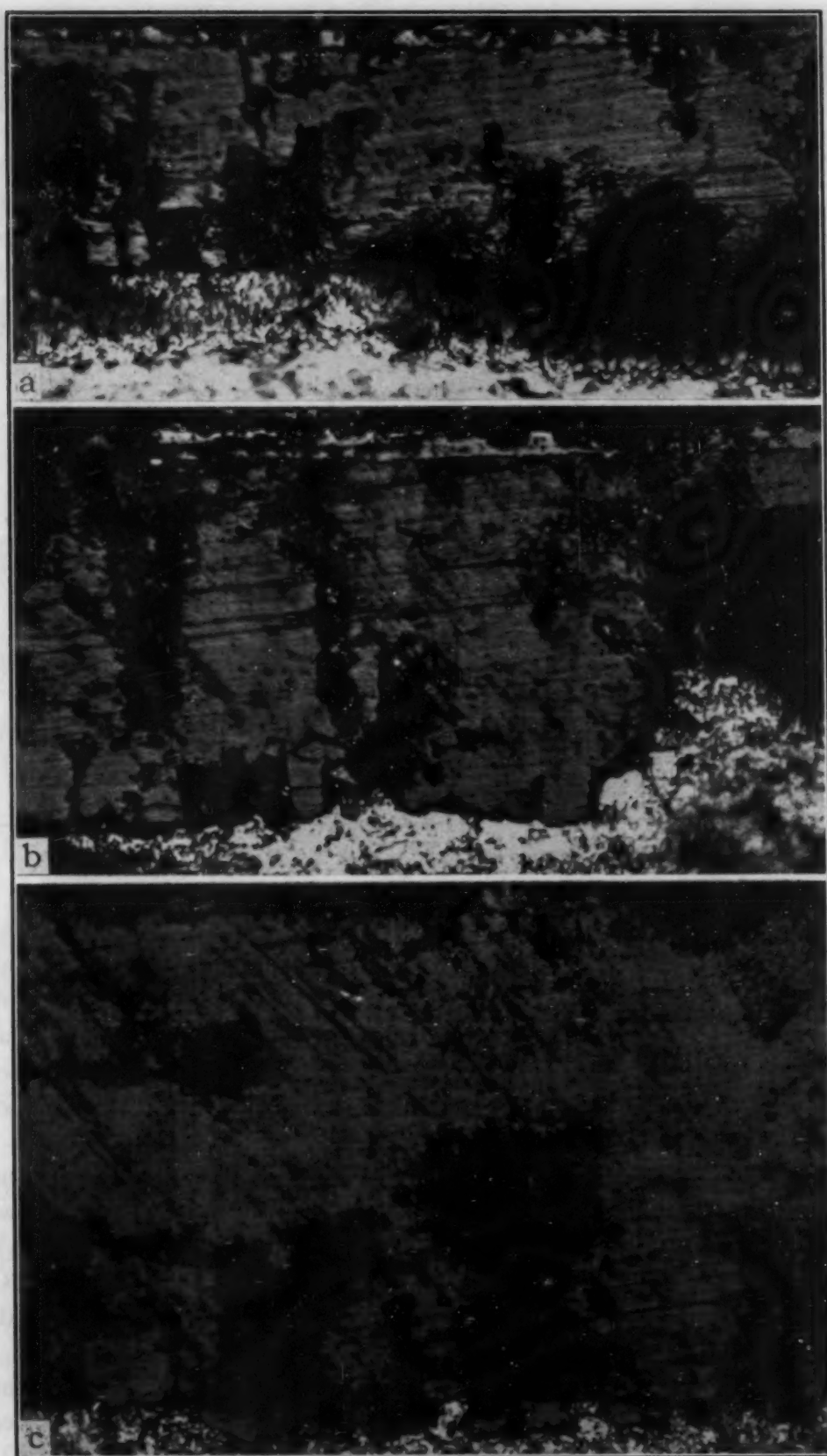


Fig. 7—Oxide Layers Formed on Pure Iron at 700 °C (1290 °F).  $\times 1000$ . a—15 minutes; b—30 minutes; c—60 minutes.

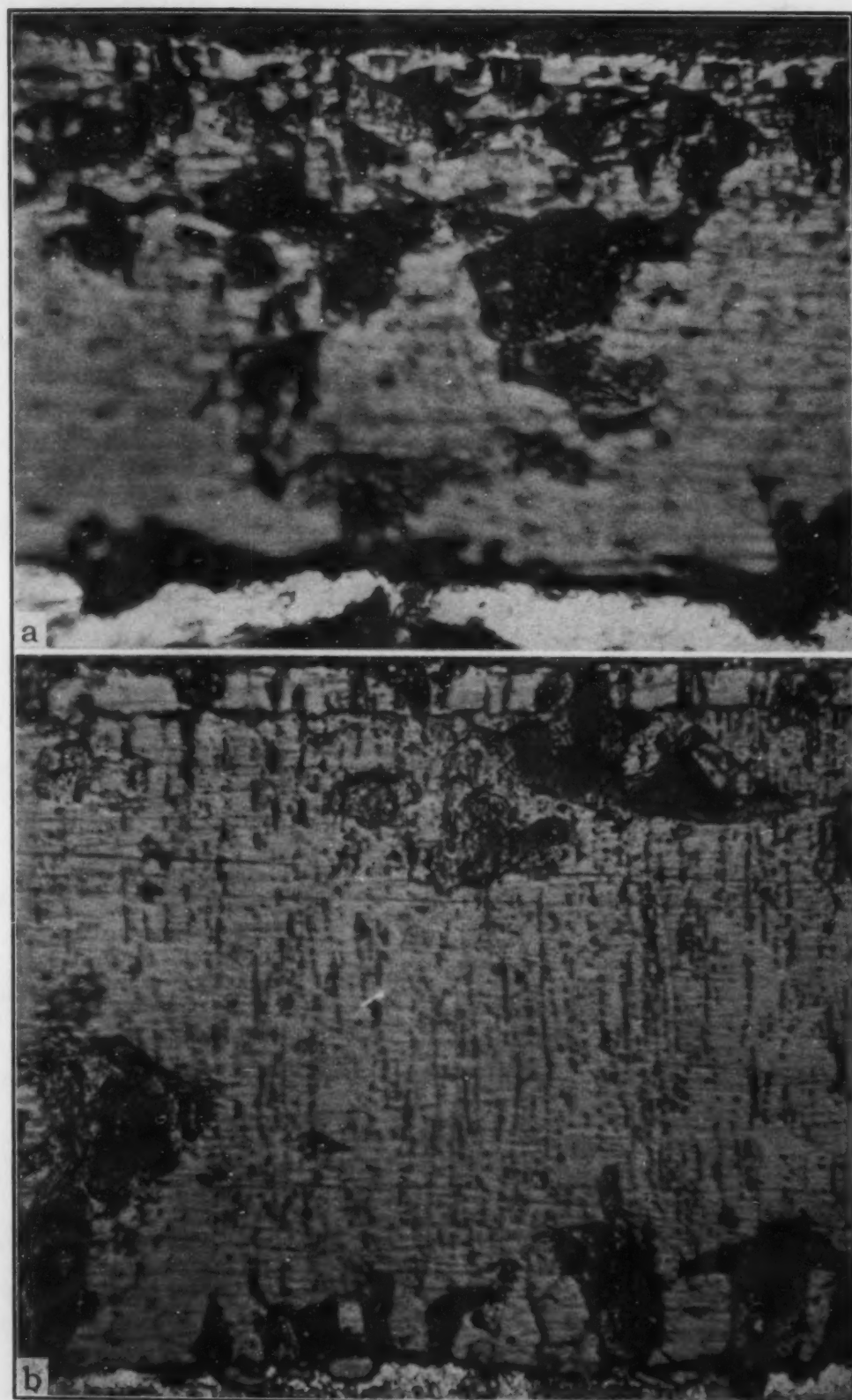


Fig. 8—Oxide Layers Formed on Pure Iron at 800 °C (1470 °F).  $\times 1000$ . a—15 minutes; b—30 minutes.



Fig. 8 (cont.)—Oxide Layers Formed on Pure Iron at 800 °C (1470 °F).  $\times 500$ .  
c—60 minutes; d—120 minutes.

to get reflections, and the composite thickness of the three oxides is still sufficiently thin that some radiation penetrates to the iron, giving diffraction lines.

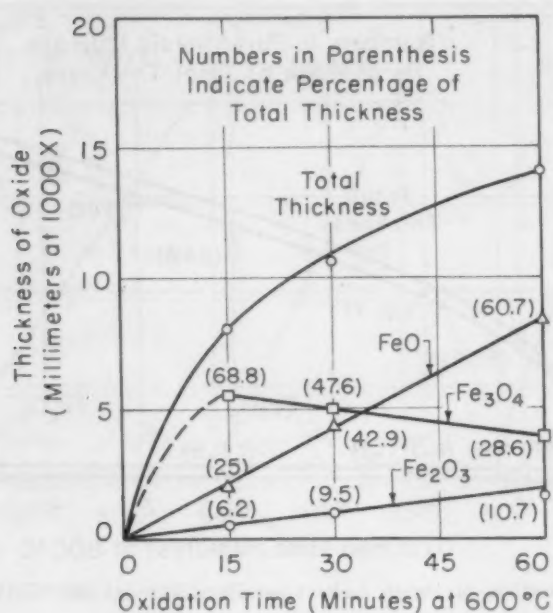


Fig. 9—Formation of Oxide Layers on Pure Iron at 600°C (1110°F).

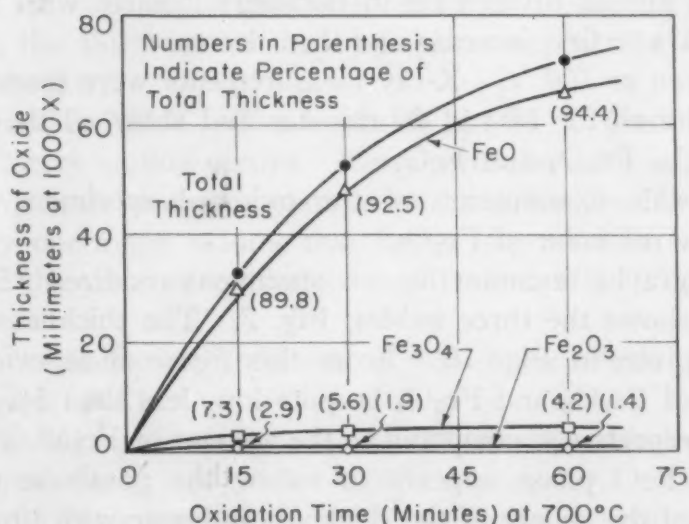


Fig. 10—Formation of Oxide Layers on Pure Iron at 700°C (1290°F).

Visual examination of the surface oxide indicates a blue-black oxide which does not serve to identify the oxide, since  $\text{Fe}_2\text{O}_3$  may be this color. Fortunately, the oxide is resolved at  $\times 1000$  and can be differentiated from the other two oxides.

Metallographic examination at  $\times 1000$  shows the three oxide layers, Fig. 6. Measurements on the thickness of each oxide indicate very thin layers of  $\text{Fe}_2\text{O}_3$  (from 5 to 10% of the total thickness) but rather heavy layers of  $\text{Fe}_3\text{O}_4$  and  $\text{FeO}$ . The thicknesses of the respective oxides are given in Fig. 9; the figures in parentheses at



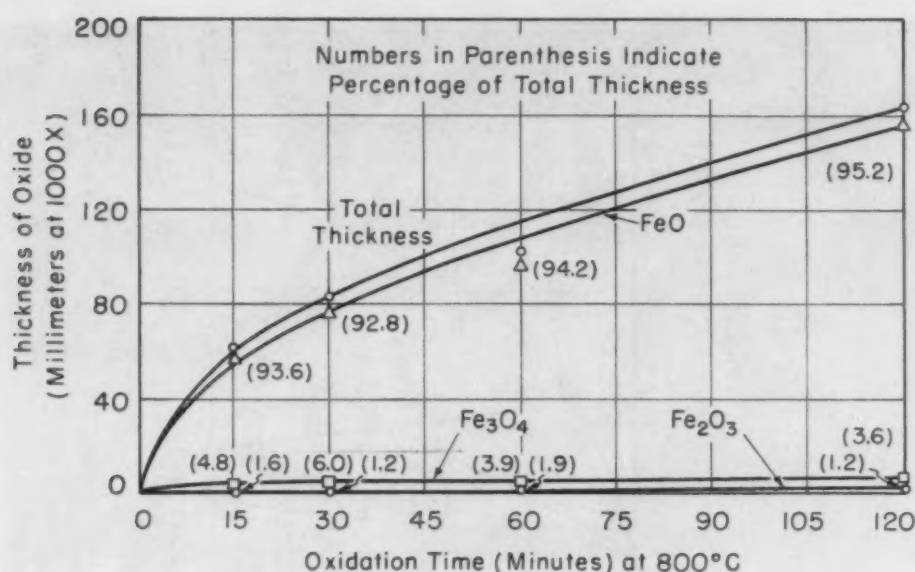


Fig. 11—Formation of Oxide Layers on Pure Iron at 800 °C (1470 °F).

each point are the per cent of the total thickness. The  $\text{Fe}_2\text{O}_3$  and  $\text{FeO}$  phases appear to increase in thickness linearly with time; the  $\text{Fe}_3\text{O}_4$  appears to first increase and then decrease.

*Oxidation at 700 °C*—X-ray measurements were made only on the iron oxidized for 15 and 30 minutes and show all the expected oxides,  $\text{Fe}_2\text{O}_3$ ,  $\text{Fe}_3\text{O}_4$  and  $\text{FeO}$ .

The visible examination of the oxidized specimens shows a characteristic red color of  $\text{Fe}_2\text{O}_3$ .

Metallographic examination on specimens oxidized 15, 30 and 60 minutes shows the three oxides, Fig. 7. The thicknesses of the oxides are given in Fig. 10. From this figure it is evident that the amount of  $\text{Fe}_2\text{O}_3$  and  $\text{Fe}_3\text{O}_4$  is quite low, less than 5% and less than 10%, respectively, compared to the amount of  $\text{FeO}$ . The thickness of the  $\text{FeO}$  phase appears to follow the parabolic rate law, since a plot of the square of the thickness is linear with time.

*Oxidation of 800 °C*—X-ray examination shows only the  $\text{Fe}_3\text{O}_4$  and  $\text{FeO}$  and no  $\alpha\text{-Fe}_2\text{O}_3$ . This is surprising, since the  $\text{Fe}_2\text{O}_3$  is found for the 700 °C (1290 °F) oxidation. This situation may have something to do with the greater bulk of the substrate which may affect the intensities of the  $\text{Fe}_2\text{O}_3$ .

The  $\text{Fe}_2\text{O}_3$  layer, however, is found by visual observation. A red oxide layer so characteristic of this oxide forms on the surface and, by metallographic examination, there is definitely the  $\alpha\text{-Fe}_2\text{O}_3$  oxide layer. See Fig. 8.

The thicknesses of the respective oxides formed at this temperature are given in Fig. 11. Once again, as noted for the oxidation

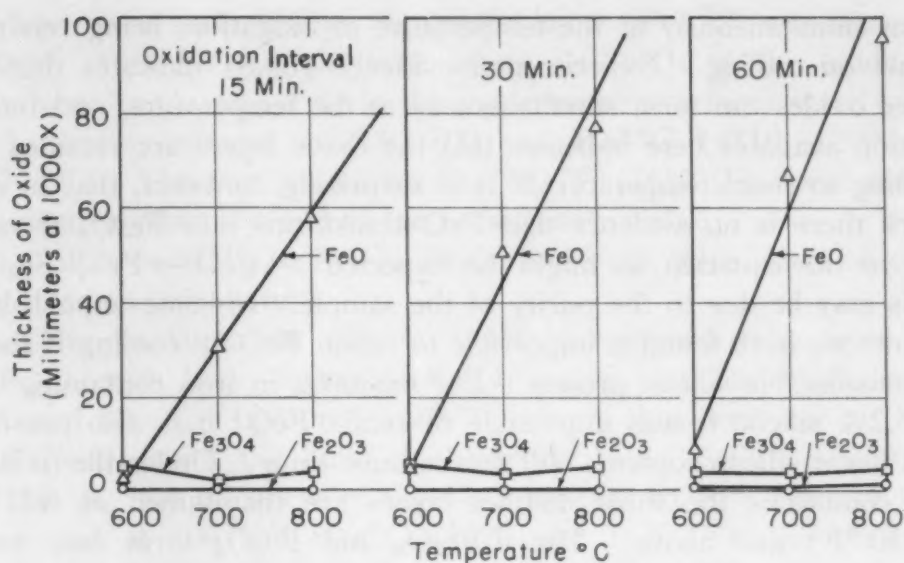


Fig. 12—Thickness of Oxide Layers With Increasing Temperature.

at 700 °C, the bulk of the oxide is FeO. Only a small amount of Fe<sub>2</sub>O<sub>3</sub> (less than 2% of the thickness) and Fe<sub>3</sub>O<sub>4</sub> (about 5%) forms. Here again the thickness of the FeO phase appears to follow the parabolic rate law.

*Oxidation at 900 °C*—The oxidation at 900 °C (1650 °F) is so severe that heavy scaling occurs. X-ray measurements were possible on the heavy scale and they showed patterns for Fe<sub>3</sub>O<sub>4</sub> and FeO. By inference one might assume that Fe<sub>2</sub>O<sub>3</sub> is present in small quantities as in the case of oxidation at 700 and 800 °C (1290 and 1470 °F).

Visual examination indicates a blue-black oxide which, of course, proves little.

No metallographic work was possible on the samples oxidized at this temperature.

From the preceding discussion of the oxide structure and composition at the various temperatures, it is obvious that temperature influences greatly the respective thicknesses of the oxide layers formed on iron at and above 600 °C (1110 °F). The large effect of temperature is shown in Fig. 12 where the thickness of the oxide layers is plotted against temperature for constant oxidation times. From this figure it is seen that at the higher temperatures FeO is the oxide which appears to be growing and not the other two oxides.

An interesting question is posed by the results of these experiments. Excluding the oxidation of iron at 500 °C, one might inquire as to whether the oxide layer is all FeO at the oxidation temperature, transforming into layers on cooling, or whether all three oxides

form simultaneously at the temperature of oxidation, being retained intact on cooling. Experimental evidence (6, 8) indicates that all three oxides can form simultaneously at the temperature, and information available here indicates that the oxide layers are retained on cooling to room temperature. It is surprising, however, that in our work there is no evidence that FeO transforms into  $\text{Fe}_3\text{O}_4$  according to the equation as might be expected:  $4\text{FeO} \rightarrow \text{Fe} + \text{Fe}_3\text{O}_4$ . This may be due to the purity of the sample. In some unpublished results we have found it impossible to retain FeO on cooling if there is considerable silicon present. For example, in iron containing 1.9 to 5.2% silicon it was impossible to retain FeO; it is also possible that lower silicon contents will do the same thing. Under the oxidizing conditions the three distinct layers are maintained at 600 °C (1110 °F) and above. The  $\alpha\text{-Fe}_2\text{O}_3$  and  $\text{Fe}_3\text{O}_4$  form only very thin layers at 700 °C (1290 °F) and above, remaining essentially constant in thickness, while the FeO, being the bulk of the oxidation product, increases according to a parabolic rate law and very rapidly (probably exponentially) with temperature.

#### SUMMARY

The oxidation of high-purity iron from 500 to 900 °C (930 to 1650 °F) in air was found to follow the common parabolic rate law:  $W^2 = Kt + C$ , where  $W$  is the weight gain,  $t$  is time, and  $K$  and  $C$  are constants.

The oxidation process as a function of temperature follows the usual exponential law. The parabolic rate constant,  $K$ , shows the following temperature dependence

$$K = Ae^{-Q/RT}$$

where  $Q$  is the activation energy,  $R$  the gas constant,  $T$  the absolute temperature, and  $A$  a proportionality constant. In our case the activation energy was found to be 33,000 calories per gram mol.

The nature of the oxide films was studied using the Geiger counter X-ray spectrometer. The oxide formed at 500 °C (930 °F) was essentially  $\text{Fe}_3\text{O}_4$ , but at 600, 700, 800 and 900 °C (1110, 1290, 1470 and 1650 °F) the other oxides,  $\alpha\text{-Fe}_2\text{O}_3$  and FeO, were found. From the samples oxidized at 500 °C it was also possible, due to the thin film, to pick up the iron lines, and for this reason a calculation of the lattice parameter of the iron was made. A value of 2.869 Å was obtained, which is in reasonable agreement with values found in the literature.

By a careful metallographic technique, the oxide layers formed



on iron were made visible. Only one layer ( $\text{Fe}_3\text{O}_4$ ) was found at 500 °C (930 °F) but all three layers ( $\alpha\text{-Fe}_2\text{O}_3$  at the oxide-gas interface,  $\text{Fe}_3\text{O}_4$ , and FeO at the oxide-metal interface) were found for samples oxidized at 600, 700 and 800 °C (1110, 1290 and 1470 °F). The samples oxidized at 900 °C (1650 °F) could not be mounted successfully due to the loose heavy scale.

All three oxides,  $\alpha\text{-Fe}_2\text{O}_3$ ,  $\text{Fe}_3\text{O}_4$  and FeO, were intact on cooling to room temperature.

The oxidation at 600 °C (1110 °F) shows thin layers of  $\alpha\text{-Fe}_2\text{O}_3$  with heavy layers of  $\text{Fe}_3\text{O}_4$  and FeO. The oxidation at 700 and 800 °C (1290 and 1470 °F) shows thin layers of  $\alpha\text{-Fe}_2\text{O}_3$  and  $\text{Fe}_3\text{O}_4$ , with the bulk of the oxide being FeO. At 600 °C (1110 °F) the thickness of the FeO appears to vary linearly with time, but at 700 and 800 °C (1290 and 1470 °F), the thickness appears to follow the parabolic rate law.

#### ACKNOWLEDGMENT

The authors wish to acknowledge the help of Mr. R. McKelvey, who carried out the oxidation of the iron, and Mr. R. L. Anderson, whose suggestions made possible the metallographic technique used for obtaining the oxide photographs.

#### References

1. N. B. Pilling and R. E. Bedworth, "The Oxidation of Metals at High Temperatures", *Journal, Institute of Metals*, Vol. 29, 1923, p. 529-591.
2. J. Bénard and J. Talbot, "The Kinetics of the Reaction of Iron in Its Initial Phase", *Comptes Rendus*, Vol. 226, 1948, p. 912-914.
3. K. Heindlhofer and R. M. Larsen, "Rates of Scale Formation in Iron and a Few of Its Alloys", *TRANSACTIONS, American Society for Steel Treating*, Vol. 21, 1933, p. 865-895.
4. O. A. Tesche, "An X-ray Study of Scale Formation on Iron Between 400 and 700 °C", *TRANSACTIONS, American Society for Metals*, Vol. 42, 1950, p. 641.
5. U. R. Evans, "Oxidation of Iron in the Range 100-400 °C", *Nature*, Vol. 164, 1949, p. 909-111.
6. E. A. Gulbransen and J. W. Hickman, "Electron-Diffraction Study of Oxide Films Formed on Fe, Co, Ni, Cr, and Cu at High Temperatures", *Metals Technology*, Vol. 13, 1946, TP 2068.
7. R. Jackson and A. G. Quarrell, "An Electron-Diffraction Study of Oxide Films on Iron", *Iron and Steel Institute, Special Report No. 24*, Vol. 65, 1939.
8. J. W. Hickman, "Oxide Films Formed on Metals and Binary Alloys", *Transactions, American Institute of Mining and Metallurgical Engineers*, Vol. 180, 1949, p. 547-564.
9. E. A. Gulbransen, R. T. Phelps and J. W. Hickman, "Electron Diffraction and Electron Microscope Study of Oxide Films Formed on Metals and Alloys at Moderate Temperatures", *Industrial and Engineering Chemistry, Analytical Edition*, Vol. 18, 1946, p. 391-400.



10. L. B. Pfeil, "The Oxidation of Iron and Steel at High Temperatures", *Journal*, Iron and Steel Institute, Vol. 119, 1929, p. 501-548.
11. L. B. Pfeil, "Constitution of Scale", *Journal*, Iron and Steel Institute, Vol. 123, 1931, p. 123-142.
12. H. J. Goldschmidt, "The Crystallographic Structure of Fe, FeO and Fe<sub>3</sub>O<sub>4</sub> and Their Interrelations", *Journal*, Iron and Steel Institute, Vol. 146, 1942, p. 157-173.
13. M. J. Bénard, "Mechanism of the Surface Oxidation of Iron at High Temperatures", *Journal de chimie physique et de physico-chimie biologique*, Vol. 44, 1947, p. 266-268.
14. J. Bénard and O. Coquelle, "Nouvelles Recherches par la Methods Micrographique sur l'oxydation du Fer aux Temperatures Elvees", *Comptes Rendus*, Vol. 222, 1946, p. 786-797.
15. G. Valensi, "Theoretical and Experimental Investigations About Conjugated Formation of Several Layers in Dry Corrosion", Pittsburgh International Conference on Surface Reactions, Corrosion Publishing Co., Pittsburgh, 1948, p. 156-164.
16. C. S. Barrett, "Structure of Metals", App. VII, McGraw-Hill, New York, 1943.
17. C. M. Farquhar, H. Lipson and A. R. Weill, "An X-ray Study of Iron-Rich Iron-Silicon Alloys", *Journal*, Iron and Steel Institute, Vol. 152, 1945, p. 457-472.
18. A. Taylor, "An Introduction to X-ray Metallography", Table XLVI, Chapman and Hall, London, 1945.
19. W. Jost, "Diffusion und Chemische Reaktion in Festen Stoffen", 1937, p. 160, Verlag von T. Steinkopff, Dresden und Leipzig.

## DISCUSSION

**Written Discussion:** By Bruce W. Dunnington, research associate, The Ohio State University Corrosion Laboratories, Columbus, Ohio.

Dr. Stanley and his co-workers have successfully begun the attack on a very difficult problem, the metallographic examination of iron oxides. Before discussing these interesting photographs I would like to raise several questions. The authors have used cold-rolled iron for their rate measurements, which means that the oxidation rates are different from those of annealed iron. This has been found to be true in our own laboratories for 18-8, and by Bénard and Talbot<sup>4</sup> for iron and copper. Also, the furnace atmosphere has been described as air with a relative humidity of 52 to 75%. It is known from the work of Siebert and Donnelly<sup>5</sup> that the oxidation rate of iron increases with humidity of the atmosphere. We must, therefore, keep in mind that these experiments have been run under special conditions and the results cannot be directly compared with those for annealed metal in dry air.

The most interesting finding of the authors is the variation in relative thickness of the oxides with time at a constant temperature. In view of the close agreement between Tesche's data at 15 minutes and Bénard's at 5 hours, such a variation is unexpected. It may also be said to be contrary to Wagner's<sup>6</sup> statements concerning the growth of multilayered

<sup>4</sup>J. Bénard and J. Talbot, "Effect of Crystal Orientation on the Hot Oxidation of Iron and Copper", *Comptes Rendus*, Vol. 225, No. 9, 1947, p. 411.

<sup>5</sup>C. A. Siebert and H. G. Donnelly, "The Effect of Humidity of Air on the Oxidation of a Low Carbon Steel", *TRANSACTIONS*, American Society for Metals, Vol. 28, 1940, p. 372.

<sup>6</sup>C. Wagner, "Handbuch der Metallphysik", Band I, Teil II. Thermodynamik metallischer Mehrstoffsysteme, p. 144, published by Akademische Verlagsgesellschaft, Becker and Erler Kom.—Ges., Leipzig, 1940.

films. The relative thicknesses of the layers should be directly proportional to the specific diffusivities, and since these diffusivities will remain essentially constant at a given temperature, the relative thicknesses of the oxides must likewise remain constant. A possible explanation of these unusual results may be an uncontrolled variation of testing temperature. At 700 and 800 °C (1290 and 1470 °F) the data agree well with those of Tesche and Bénard. The measured variation with time at these two temperatures is not greater than 5%, which may be about the limit

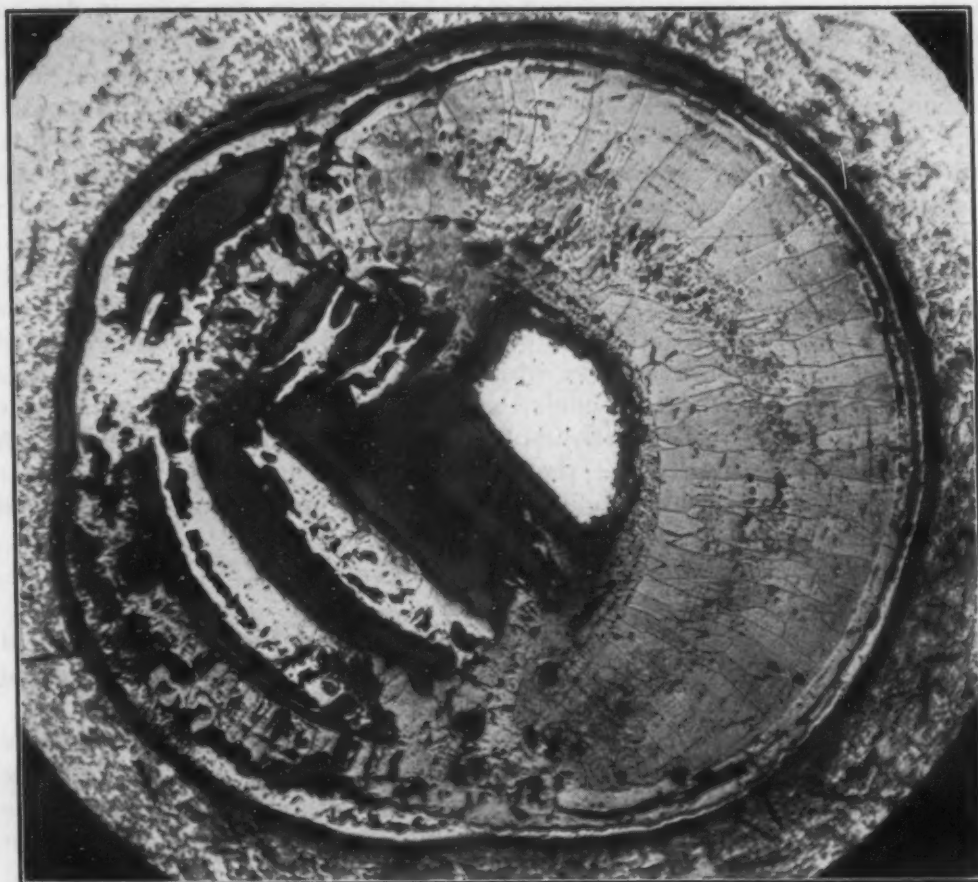


Fig. 13—Iron Wire Oxidized 14 Hours at 1500 °F in Air.

of accuracy of the metallographic method. At 600 °C (1110 °F) there is as much as 40% variation, but on consulting Bénard's data it appears that the change with temperature is so rapid in this region that a 30 °C error in test temperatures would give the measured variation in thickness.

The authors conclude from these data that  $\text{Fe}_2\text{O}_3$  and  $\text{Fe}_3\text{O}_4$  films remain essentially constant in thickness during oxidation above 700 °C (1290 °F). Our experiments at The Ohio State University Corrosion Laboratories are in disagreement on this point. We have observed a concomitant increase in thickness of all three layers with time at 815 °C (1500 °F).

My understanding is that these relative thickness measurements are made with the thought that they provide a fundamental method of de-

scribing the oxidation, one that could be generally applied if only we could avoid the effects of differential specific volume such as cracking and blistering. This is true only to the extent that we are willing to limit our examination to a segment of the oxidation phenomenon. We know that the diffusion of iron out contributes overwhelmingly more movement of mass than the diffusion of oxygen in. Therefore, as oxidation proceeds by diffusion of metal out through the oxide, a void or voids must form somewhere within the envelope of oxide. Fig. 13 is a specimen whose geometry is specially chosen to illustrate the consequences of the diffusion. It is the structure resulting from oxidizing an iron wire in dry air at 815 °C (1500 °F) for 14 hours. It is evident that the iron separates from the oxide along one side and diffuses through the opposite side, leaving a void behind it. The oxide left stranded continues to approach the equilibrium state of  $\text{Fe}_2\text{O}_3$ , and occasionally, when it cracks, oxygen rushes in to attack the retreating surface of iron. The process repeats itself and results in a series of little oxide bridges. Something similar must happen when any surface oxidizes, but it is not usually so conveniently condensed. It cannot be argued that the study of ideally adhering sections represents the true picture of oxidation, for such areas are at liberty to act as observed only because of the immediately related phenomenon of void formation which may occur at a greater or lesser distance. Thus, we must conclude that the relative amounts of each oxide formed are different from those observed on the adherent sections. A more complete statement of these ideas will be published in the near future as part of a more detailed study of diffusion phenomena observed during the oxidation of pure iron.

**Written Discussion:** By C. A. Phalnikar and W. M. Baldwin, Jr., Case Institute of Technology, Cleveland.

Congratulations are certainly due these authors for such an excellent paper. The photomicrographs, considering the great difficulties involved in this type of work, are superb.

We should like to suggest that the relationship between log rate constant and reciprocal absolute temperature is not a simple straight line as the authors have indicated in their Fig. 3, but rather follows a more complicated course. To support this suggestion we offer herewith a plot of log rate constant versus reciprocal absolute temperature including not only the authors' data, but also Tesche's data presented before this society last year, as well as some data of our own soon to be published (Fig. 14). All three sets of data are best described by a crenated curve rather than a straight line. For example, the data points for 600 and 900 °C (1110 and 1650 °F) of Stanley et al which fall below the straight line of Fig. 3, and the data point for 700 °C (1290 °F) which falls above the straight line, are confirmed by these independently determined points. We are led to assume that the deviation of the points experimentally determined by Stanley et al from the straight line is not due to experimental error but is in fact a real effect and that the assumption of the straight line is in error.

The crenated curve can be justified on the basis of additional data which Stanley et al report. On the basis of the excellent micrographic evidence adduced in this paper as well as on the basis of Tesche's and



Bénard and Coquelle's data (Fig. 15), it appears that in the temperature range up to circa 550 °C (1020 °F) the oxide coat is predominantly  $\text{Fe}_3\text{O}_4$ ; in the range from circa 650 °C (1200 °F) to circa 900 °C (1650 °F), the oxide coat is predominantly  $\text{FeO}$ , above approximately 900 °C (1650 °F)  $\text{FeO}$  disappears, yielding to both  $\text{Fe}_3\text{O}_4$  and  $\text{Fe}_2\text{O}_3$ . The actual limits to these temperature ranges appear to depend upon the purity of the iron

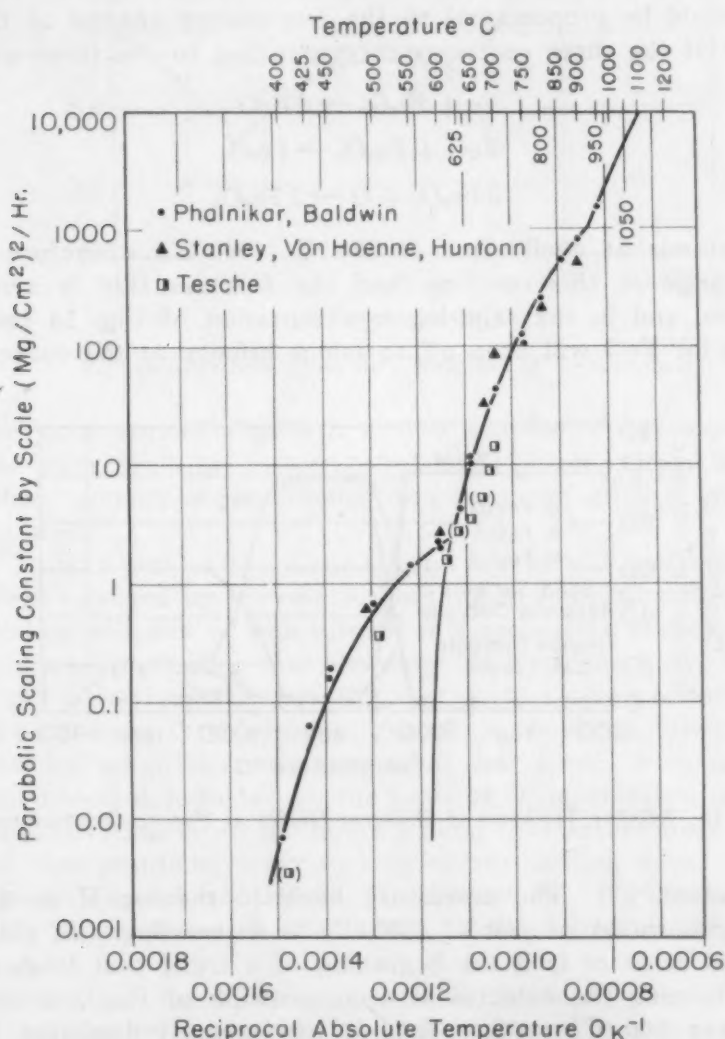


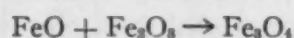
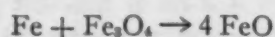
Fig. 14—Parabolic Scaling Rate Constant as a Function of Temperature.

(cf. the thickness percentages of the various scales formed in 15 minutes at 600 °C as reported in the authors' Fig. 9 with the thickness percentages of the various scales reported by Tesche for 15 minutes for 600 °C (1110 °F) in Fig. 15) and time (cf. the different curves in the authors' Fig. 9). Thus that portion of the log  $K$  vs  $1/T$  curve below 550 °C (1020 °F) must be set by  $\text{Fe}_3\text{O}_4$ , the scallop of the log  $K$  —  $1/T$  curve between 650 and 900 °C (1200 and 1650 °F) must be set by  $\text{FeO}$ , and the small portion of the curve above 900 °C (1650 °F) must be set by both  $\text{Fe}_3\text{O}_4$  and  $\text{Fe}_2\text{O}_3$ . The fact that the log  $K$  vs  $1/T$  curve shows three



distinct segments over three distinct temperature ranges where three distinct scales predominate appears more logical than if a straight line existed over all three temperature ranges, for this would require the extreme coincidence that the three oxides would yield the identical values of  $A$  and  $Q$  in the Arrhenius equation given by the authors on page 444.

The curves can be rationalized still further. From general principles, or, specifically, from the Wagner equation, we know that the rate of scaling should be proportional to the free-energy change of the scaling reaction. Of the three reactions corresponding to the three scale layers



the first stands at equilibrium at 570 °C (1060 °F) wherefore the free-energy change of this reaction, and the reaction rate is zero at that temperature, and in the semi-log representation of Fig. 14 the reaction rate curve for FeO will drop off to minus infinity as the curve descends

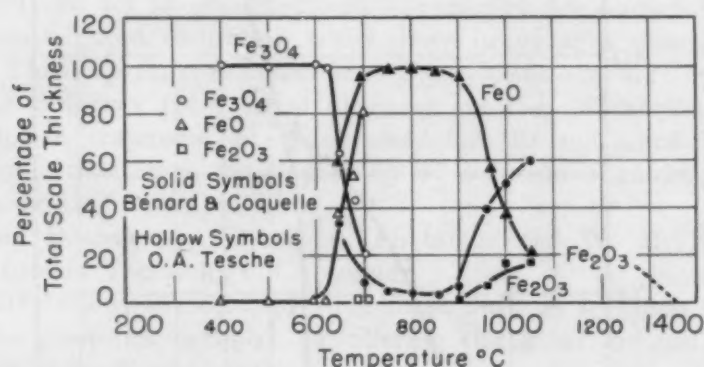


Fig. 15—Relative Thickness of Different Oxides at Various Temperatures.

to 570 °C (1060 °F). The downward hook to the  $\log K$  vs  $1/T$  curve in the neighborhood of 400 °C (750 °F) is interesting. Is this due to experimental error or is it the beginning of a trend that leads to minus infinity, indicating the eutectoidal decomposition of  $\text{Fe}_3\text{O}_4$  at some temperature (say 360 °C) so low that it has escaped detection by other means?

The authors mentioned that Valensi has treated the case of multiple-layered scaling. They undoubtedly recall that Valensi has demonstrated that under a number of restrictive assumptions multi-layered scales should obey the Pilling and Bedworth parabolic law. One of these assumptions was that all layers start growing by the diffusion process at the same instant from an absolutely clear metallic surface. Under these conditions, the parabolic law is not only obeyed but the ratio of thicknesses between the various layers should remain constant. The fact that the thickness ratios do not remain constant at 600 °C (1110 °F) (cf. Fig. 9) indicates that iron should not oxidize parabolically at this temperature. Heindlhofer and Larsen's curves show nonparabolic growth in this temperature

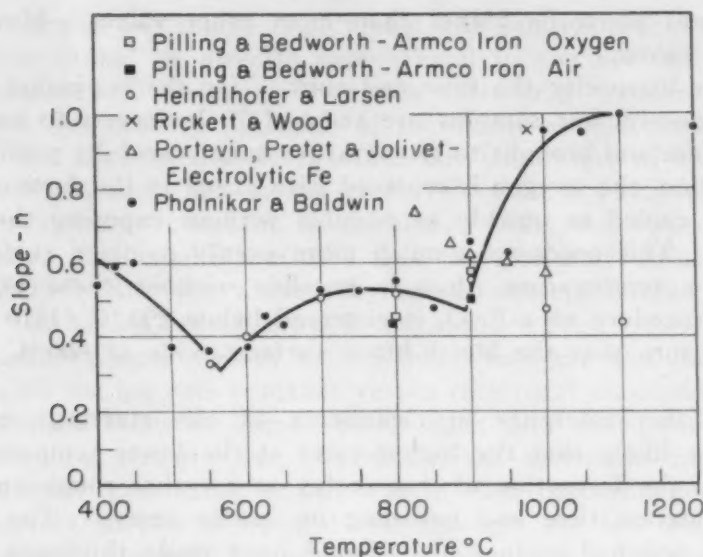


Fig. 16—Parabolic Slope as a Function of Temperature.

range but good parabolic growth at 700 and 800 °C (1290 and 1470 °F) where the layer thickness ratios are relatively stable. Other investigators' curves show systematic deviations from parabolic growth around 600 °C (1110 °F) also.

Fig. 16 is a plot of the slope of the log weight increase versus log time curves reported by various authors, again indicating the segmenting of the scaling behavior of iron into three temperature ranges.

The discussers realize that the slope of a log-log curve in oxidation work is not a fundamental quantity, but it does serve to emphasize this question of at least three separate growth mechanisms. Incidentally, the isothermal log weight increase versus log time curves from which Fig. 16 was plotted were determined on the basis of, in most cases, several dozen data points covering up to 100 hours scaling time rather than on the basis of two to four points covering an hour or two scaling time.

**Written Discussion:** By M. T. Simnad, M. H. Davies and C. E. Birchenall, Metals Research Laboratory, Carnegie Institute of Technology, Pittsburgh.

The study of the kinetics of iron oxidation by the metallographic method and the verification of the phases formed in the scale by X-ray analysis are in keeping with the excellent precedent set by Bénard and Coquelle, and Tesche. The data will be useful as a supplement to these earlier works.

We have had a similar study in progress for a considerable period involving variations in technique which we hope are refinements. It might be useful to point out a few of these and the differences appearing to arise therefrom in anticipation of the full account to be published later.

The first change is in atmosphere control. The two works mentioned above and the present paper used air, subject to normal day-to-day variations, especially in humidity. Our runs in pure oxygen show good agreement for over-all rates with most previously published data for air and with the present paper's two upper points, whereas the lower points

in the present paper lie higher than most other values. More will be said of this below.

In order to specify the time and surface for the beginning of oxidation more closely, our samples are reduced in hydrogen to remove the air-formed film and brought to temperature under carefully purified argon. After oxidation, the oxygen is replaced with argon in the furnace and the samples are cooled as quickly as possible without exposing them to the atmosphere. This produces a much more evenly oxidized surface, especially at low temperature, than is possible without these precautions. With this procedure no  $\alpha$ - $\text{Fe}_2\text{O}_3$  is observed below 800 °C (1470 °F). Are the authors sure that the bluish-black surface oxide at 600 °C (1110 °F) is really  $\text{Fe}_2\text{O}_3$ ?

Despite the difference in cleanliness of the starting surfaces, it appears more likely that the higher rates at the lower temperatures are the result of the formation of thin scales on a rather rough surface due to short oxidation time and polishing on coarse emery. The use of a more highly polished surface also should have made thickness measurements easier. Improved adherence might have permitted metallography of scales at 900 °C (1650 °F) as well.

Finally, it seems inadvisable to us to draw a straight line through five points (Fig. 3) which involve at least two changes in the products of reaction, particularly in view of the scatter in these points.

#### Authors' Reply

The authors are gratified at the interest and activity in the field of oxidation, particularly with pure metals, since they believe that a better understanding of the oxidation mechanism can best be obtained by work on high-purity materials. The discussion raised is very much appreciated because this interchange of ideas is conducive to the assay of results and is a prerequisite to increasing the rate of progress to be made in work of this nature. The oxidation of iron, as reported here, is only a small part of a large investigation on the nature of oxide films formed on iron-rich iron-silicon alloys, which will be reported on in the near future.

The discussers point out that the oxidation was not carried out under as ideal conditions as one might have used. This criticism is well taken, although it should be pointed out that the work reported here was carried out in such a way as to simulate commercial conditions such as might exist when one would oxidize iron-silicon alloys to obtain electrically insulating oxides. Another desire to be satisfied was to see what happens to pure iron, with which the writers have been doing considerable work, when such material is placed into an air muffle furnace for forging or hot rolling.

Dunnington indicates that the use of cold-rolled iron may lead to variable oxidation rates due to the existing preferred orientation originating from the cold reduction. This of course is a possibility but how serious an error it would introduce is not known to the authors.

The authors are aware of the fact that the oxidation rate is increased with increasing humidity in the atmosphere. For this reason the humidity was obtained as the work was carried out and no obvious ambiguities appeared in the range of the observed humidities.



Theoretically one might expect that the relative thicknesses of the oxide layers should be directly proportional to the specific diffusivities, and since these diffusivities will remain essentially constant at a given temperature, the relative thickness of the oxides should remain constant. However, the experimental fact, under our conditions of experiment, is that the  $\alpha$ -Fe<sub>2</sub>O<sub>3</sub> and Fe<sub>3</sub>O<sub>4</sub> layers at 700 °C (1290 °F), and above, remain thin and reasonably constant in thickness, while the FeO layer grows very rapidly. One might postulate that the iron ions diffuse rapidly to the Fe<sub>3</sub>O<sub>4</sub>-FeO interface where they are effectively filtered out so that the other two layers cannot grow in thickness.

The authors were pleased indeed that Phalnikar and Baldwin found the points on the log rate constant versus reciprocal absolute temperature plot fitted their crenated curves better than they fitted our plot which was drawn as a straight line. Certainly, the activation energy for the growth of each layer must be different in each case and hence it is not strictly correct to plot a straight line through the few points obtained here. However, one may be permitted to obtain an activation energy for the over-all oxidation process of iron; this figure will eventually serve as a base-line to which one can refer other data, principally those which show the effect of silicon on the oxidation of iron.

Simnad, Davies and Birchenall have adopted an admirable technique in preparing their samples and oxidizing them under such carefully controlled conditions. Under such ideal conditions they observe no  $\alpha$ -Fe<sub>2</sub>O<sub>3</sub> below 800 °C (1470 °F) and are prone to ask whether the authors are sure that they observe  $\alpha$ -Fe<sub>2</sub>O<sub>3</sub> at 600 °C (1110 °F). The authors believe that they observe Fe<sub>2</sub>O<sub>3</sub>; certainly three distinct layers were observed metallographically.

The authors wish to thank the various discussers for their remarks and will be looking forward to the detailed accounts of each group's research, since all have some very important and critical work in progress.



## A HARDENABILITY TEST FOR DEEP HARDENING STEELS

BY WILLIAM WILSON, JR.

### *Abstract*

*A new criterion of equivalent cooling conditions is proposed for the correlation of hardenability tests with the cooling curves measured during actual quenching. Equivalent cooling conditions exist only when the cooling curves may be superimposed between the upper critical temperature or the solution temperature—which ever is the lower—and the  $M_s$  temperature.*

*With the aid of this criterion, a hardenability test for deep hardening steels was designed to reproduce commercial oil quenching. The test described is suitable for steels having an ideal diameter less than 21 inches. Operational details and a correlation of the test with actual oil quenching practice are given. Representative results with commercial steels are included.*

IN view of the clarification of hardenability by the Jominy test, it was believed desirable to extend this type of testing to include the deep hardening grades of steel. It is well known that some steels harden throughout larger sections than those to which the Jominy test is equivalent. For these cases, the standard Jominy test gives no information concerning the limiting hardenability of the steel.

In view of the difficulties encountered with some predictions made from the Jominy hardenability test results (1),<sup>1</sup> a more restrictive criterion of equivalent cooling conditions was adopted. It is proposed that two sections have equivalent cooling conditions, when, and only when, the cooling curves can be superimposed between the upper critical temperature or the solution temperature—which ever is the lower—and the  $M_s$  temperature.

Two tests have been described in the literature which might be considered useful for studying the hardenability of deep hardening steels. These are the Post et al. "Air Hardenability Test" (2) and the De Vries "End-Quenched Bar for Deep Hardening Steels" (3). From theoretical heat transfer considerations, it was concluded that

<sup>1</sup>The figures appearing in parentheses pertain to the references appended to this paper.

A paper presented before the Thirty-second Annual Convention of the Society, held in Chicago, October 21 to 27, 1950. The author, William Wilson, Jr., is research metallurgist, Armour Research Foundation of Illinois Institute of Technology, Chicago. Manuscript received April 21, 1950.

the Post test would not reproduce the quenching curves observed in practice, because the retarded cooling is provided by a slug at one end of the bar. The De Vries test, when applied to most deep hardening steels, involves practically isothermal austenite transformation. However, the isothermal transformation may be affected by transformation and nucleation effects occurring during the initial rapid cooling. Limited knowledge of the relationship between the transformation of austenite, isothermally and during quenching, is one of the primary incentives for the development of a hardenability test. The De Vries test does not provide information concerning the transformation during continuous cooling and, therefore, will not be considered further.

#### SPECIFICATIONS FOR THE NEW HARDENABILITY TEST

The literature survey showed that the need was for a test that: (a) made possible the study of deep hardening steels; (b) provided cooling curves satisfying the proposed criterion of equivalent cooling conditions; (c) was reproducible; and (d) included the Jominy test range for comparative purposes. No simple analytical approach to this problem was available. It was a problem of elimination by trial and error to secure a set of testing conditions which would meet these specifications.

#### DETAILS OF THE HARDENABILITY TEST

The test specimen is  $1\frac{1}{4}$  inches in diameter by 11 inches long. This specimen is machined from  $1\frac{1}{2}$ -inch round stock allowing  $\frac{1}{8}$  inch of stock removal to eliminate any prior decarburization. Each specimen is provided with seven thermocouple wells; these are drilled radially through the center of the bar and to a depth of  $\frac{1}{16}$  inch from the opposite side of the bar. The specimen is provided at its top with an extension rod for supporting it in the quenching fixture. These constructional details for the specimen are shown in Fig. 1.

Water at room temperature is used to quench one end of the hardenability bar and is directed vertically from a  $\frac{1}{2}$ -inch diameter jet orifice with a velocity corresponding to a free jet height of  $3\frac{1}{2}$  inches.

The quenching fixture is considerably more elaborate than that used for the Jominy hardenability test. An annular transite plate, attached to the jet orifice with suitable brackets, supports a tubular furnace over the jet. The specimen is supported from the top of this furnace and is practically surrounded by the furnace during the test.

The furnace was a Hevi-Duty Electric Co. type M-2011S,

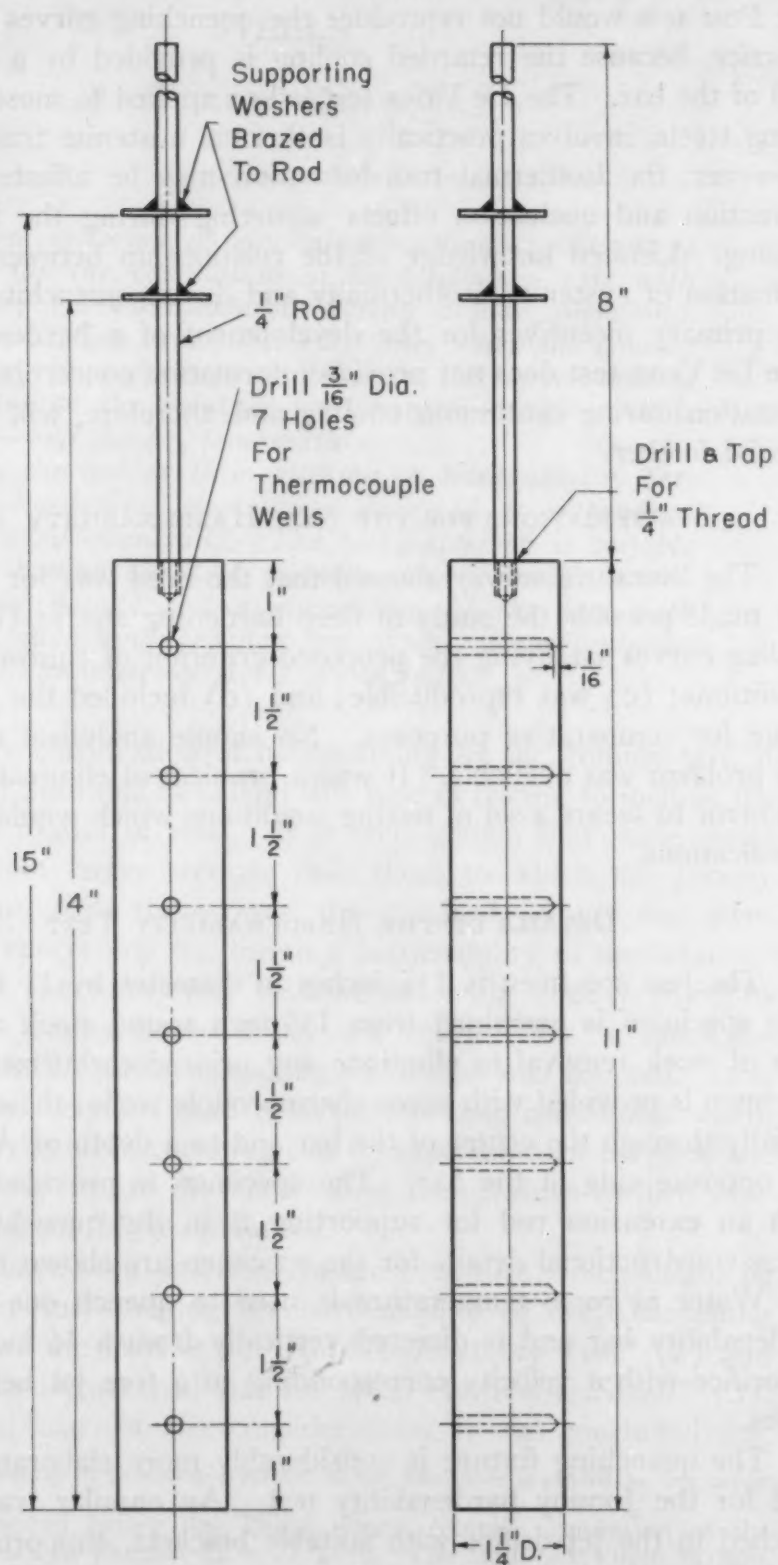


Fig. 1—Specimen for the New Hardenability Test.



remodeled for this testing. A 1¼-inch-thick outer lining of 2000 °F (1100 °C) refractory brick is used. Inside this refractory liner, hair-pin cooling coils of ¼-inch stainless steel tubing are used. These cooling coils are of varying lengths and are connected in series. An inner lining of 2300 °F (1250 °C) refractory brick is used between the cooling coils and the original refractory heating element retainers. The original heating elements, consisting of three pairs of elements, are used. Each pair is externally controlled by a variable transformer. A stainless steel equalizer tube is used immediately inside the heating elements. Fig. 2 shows the hardenability furnace open. Two of the plates have been removed to show the refractory liners and a portion of the heating element. In the right-hand side of the furnace, the hardenability bar is supported in its heating position; the seven thermocouples are inserted in the bar and extend through the top of the furnace. In the left-hand side of the photograph, the equalizer tube is shown. The specimen would normally be supported inside the equalizer tube.

In preparation for the heating cycle, a thick transite plate, with a small recessed heating element, is inserted between the bottom of the furnace and its supporting ring. This plate will be noted on the stand at the bottom of Fig. 3. With the specimen in place, and with all thermocouples connected to a multiple-point recorder, heating is started by controlling the voltage applied to the various sections of the furnace and to the small heating element in the plate. The latter heating element serves to make up end losses from the furnace. During the development stages of this test, the complete heating cycle was manually controlled with variable transformers. Recently, the furnace has been connected, as shown in Fig. 4, to operate on two pyrometers. The lower 9-inch length of the hardenability bar, with manual control, could be maintained within  $\pm 10$  °F of the desired austenitizing temperature. The uppermost 2-inch length of the specimen is to be disregarded, because over this length there is a drop in the austenitizing temperature. Normal operation includes holding the bar at the austenitizing temperature for 1 hour.

In preparation for quenching, the inserted transite plate is withdrawn, allowing the equalizer tube to rest on the steel pins in the annular transite support. The hardenability bar is lowered to its quenching position; the voltage applied to the two lower pairs of heating elements is reduced to zero. At this time, three simultaneous operations are performed, the pump or jet is started, water is admitted to the cooling coils, and the recorder chart is marked. The voltage applied to the top pair of heating elements is reduced in



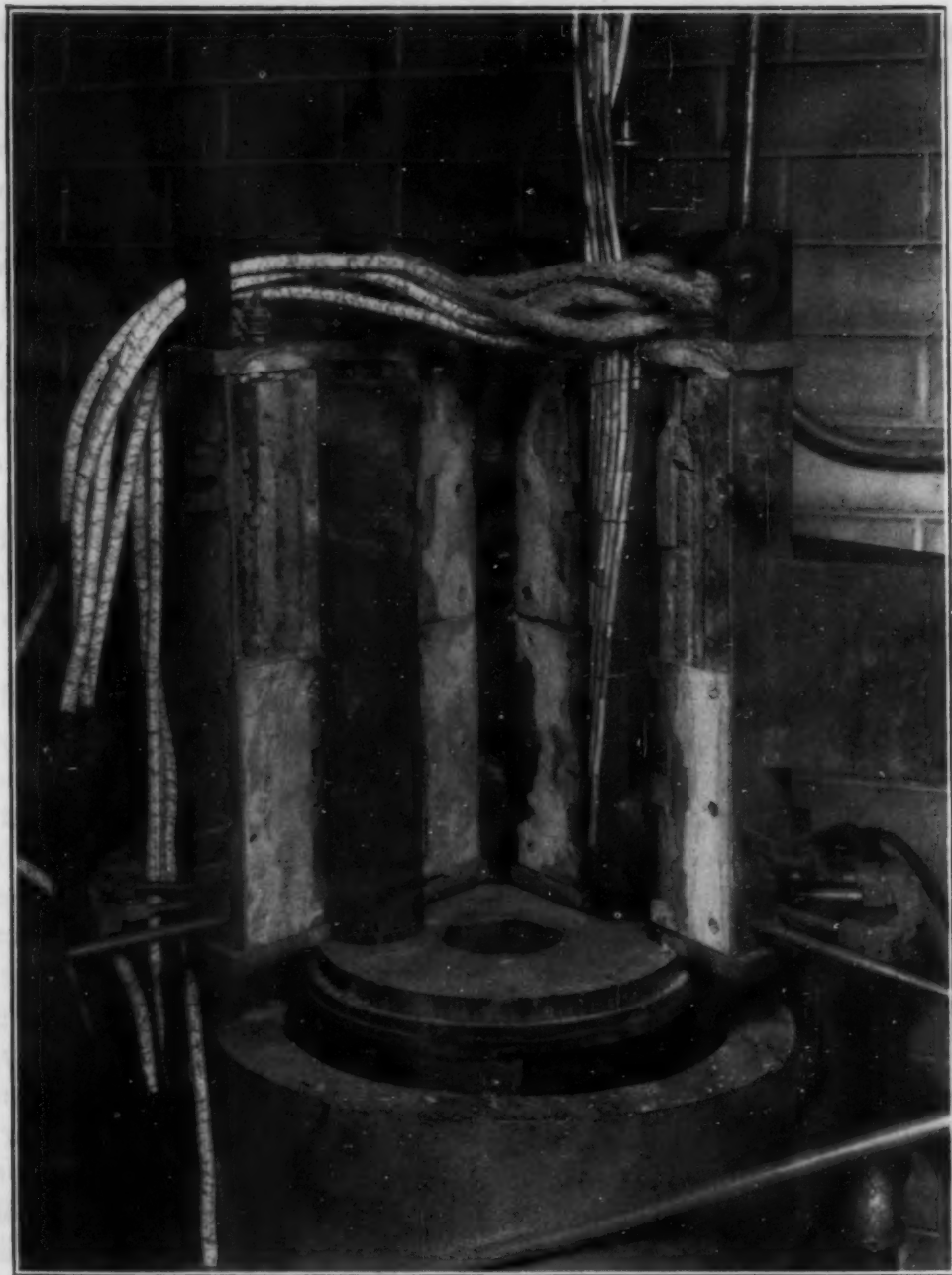


Fig. 2—The Tubular Furnace—"Open".

accord with the program in the "Outline of Operating Procedure" in the Appendix. The total quenching time is 90 minutes, after which time the bar may be left in the furnace without experiencing any reheating.

Four longitudinal flats are ground at 90-degree intervals, removing 0.030 inch per flat. A preliminary Rockwell "C" hardness survey is made at  $\frac{1}{2}$ -inch intervals. In intervals where an abrupt change of hardness is noted, readings are taken at smaller intervals.

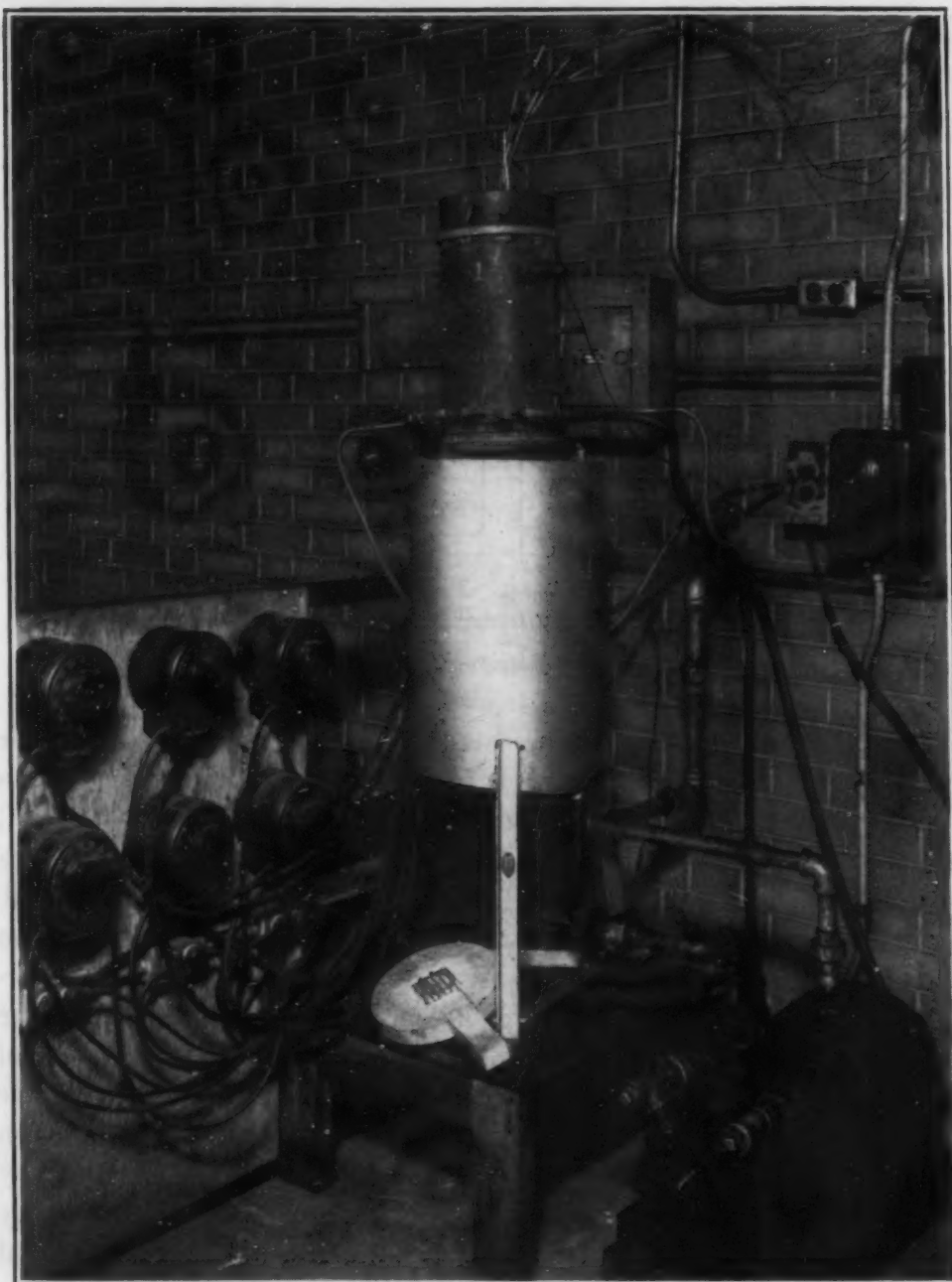


Fig. 3—The Hardenability Furnace and Auxiliary Equipment.

#### COOLING CURVES AND CORRELATION

Figs. 5 and 6 show three sets of typical cooling curves obtained with the hardenability test. These cooling curves are for steels X-5, U-9 and a plain carbon AISI 1040. The cooling curves for steel U-9 have been included in both Figs. 5 and 6, to make them directly comparable. Although a small amount of scatter is believed normal, certain definite observations can be made from these cooling curves.

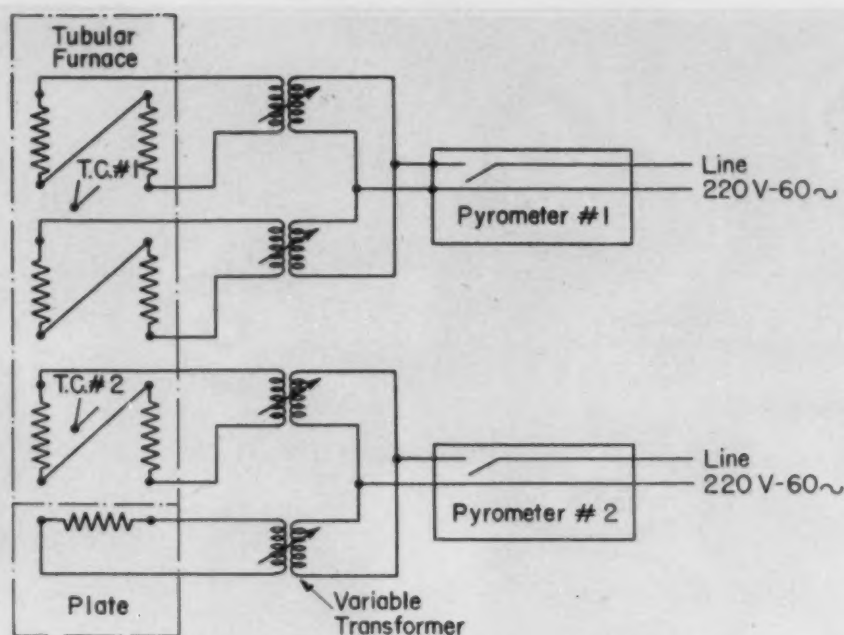


Fig. 4—Schematic Wiring Diagram for Automatic Temperature Control.

It should be mentioned that steel U-9 hardened throughout the full length of the hardenability bar. Therefore, its cooling curves show no heat effects of austenite transformation above the  $M_s$  temperature, at approximately 500 °F (260 °C). Steel X-5 hardens approximately to a depth of 1½ inches from the quenched end. The steel X-5 undergoes transformation in the bainite transformation range. The effect of this transformation cannot be thermally detected at its early stages but is readily noted at 8½ inches from the quenched end. As generally observed, with decreasing rates of cooling, the transformation takes place over a smaller temperature range, and the heat of transformation causes a pronounced inflection of the cooling curve in this range. The steel AISI 1040 is very shallow hardening when compared to X-5 and U-9 and normally should not be studied with this test. Similarly to X-5, the thermal

Table I  
Chemical Analyses of the Steels Tested for Hardenability

Serial No.	Alloying Element, %							
	C	Mn	Si	Cr	Ni	Mo	V	Cu
H-1	0.54	0.79	....	1.06	....	0.43	0.10	....
X-3	0.54	0.83	0.35	0.96	0.90	0.29	....	....
X-4	0.54	0.82	0.27	1.01	1.52	0.32	....	....
X-5	0.49	0.72	0.28	0.96	0.89	0.29	....	....
X-7	0.57	0.76	0.26	0.94	0.91	0.31	....	....
U-3	0.48	0.56	0.19	0.76	1.56	0.30	....	1.76
U-7	0.51	0.55	0.29	0.76	1.68	0.30	....	1.85
U-9	0.49	0.50	0.23	0.78	1.58	0.35	....	1.84

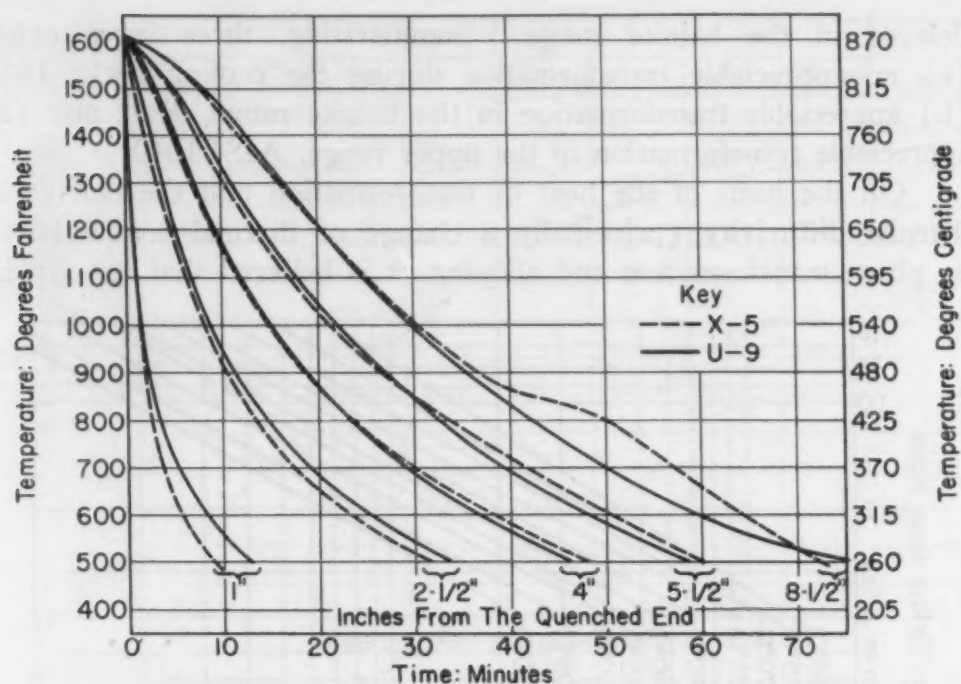


Fig. 5—Typical Hardenability Bar Cooling Curves.

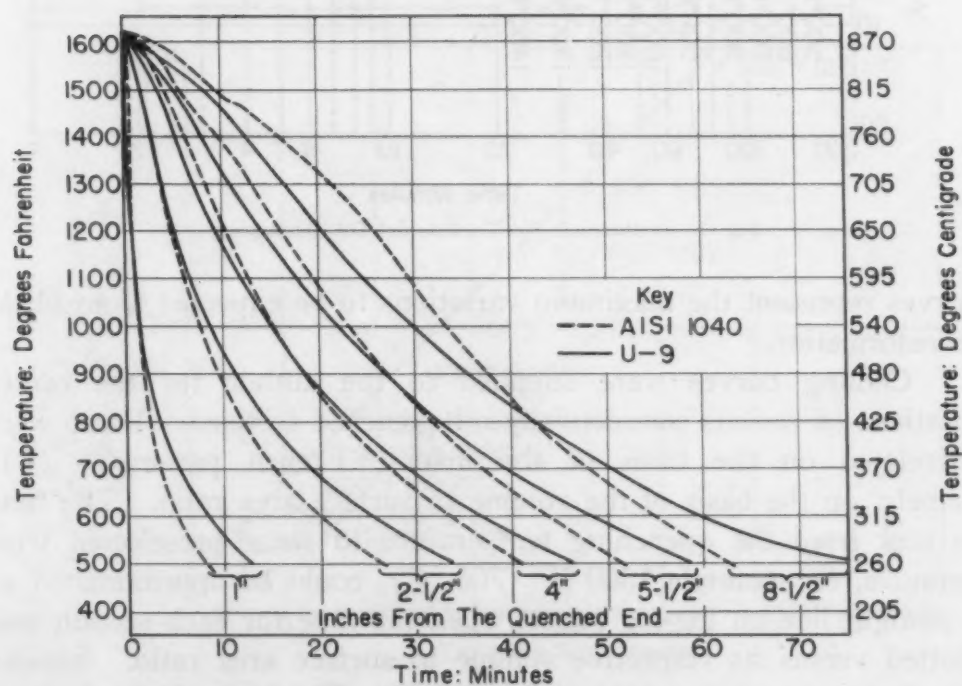


Fig. 6—Typical Hardenability Bar Cooling Curves.

effect of its transformation on cooling is more readily observed at greater distances from the quenched end.

The steels X-5 and U-9 have similar cooling curves until marked effects of the transformation are noted in X-5. Steel AISI 1040 is delayed in the upper transformation range, whereas X-5 is



delayed in the bainite range. Summarizing, three cases exist: (a) no appreciable transformation during the cooling cycle, U-9; (b) appreciable transformation in the bainite range, X-5; and (c) appreciable transformation in the upper range, AISI 1040.

On the basis of the heat of transformation and the change of thermal diffusivity (principally a change of thermal conductivity) by phase transformation and alloying, it is believed that the typical

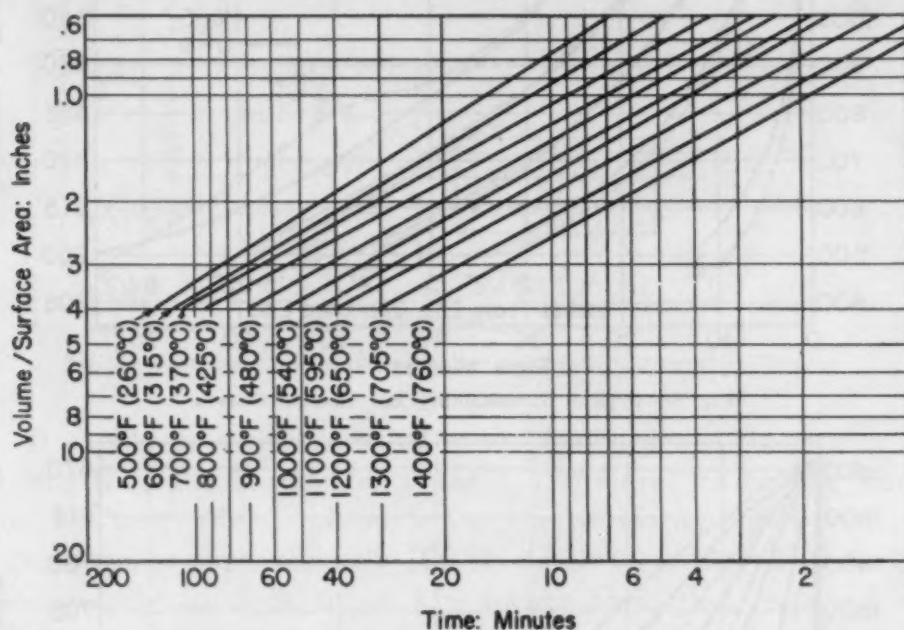


Fig. 7—Isothermals for Commercial Oil Quenching.

curves represent the maximum variations to be expected from phase transformation.

Cooling curves were supplied to the author for the center locations of various commercially oil-quenched sections. These were correlated on the basis of the inverse French parameter (4); namely, on the basis of the volume to surface area ratio. The time to cool from the quenching temperature to some preselected temperature, for example 1300 °F (705 °C), could be approximated as a straight line on log-log paper, when the time for each section was plotted versus its respective volume to surface area ratio. Similar correlations were carried out in 100 °F (55 °C) increments from 1400 °F (760 °C) to 500 °F (260 °C). The results are shown in Fig. 7.

Using the adopted criterion, the hardenability bar was correlated with the average commercial cooling curves by a simple graphical method. On ordinary rectangular coordinate paper, the times for the two cooling curves to reach the same temperature are plotted as

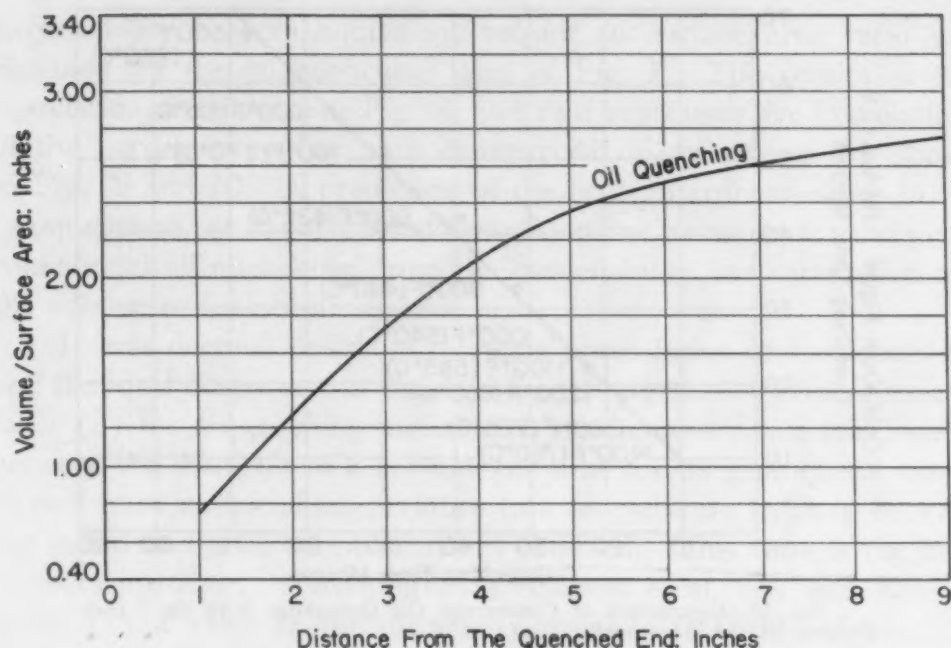


Fig. 8—Correlation of Commercial Oil Quenching With the Hardenability Bar [Solution Temperature 1620 °F (880 °C)].

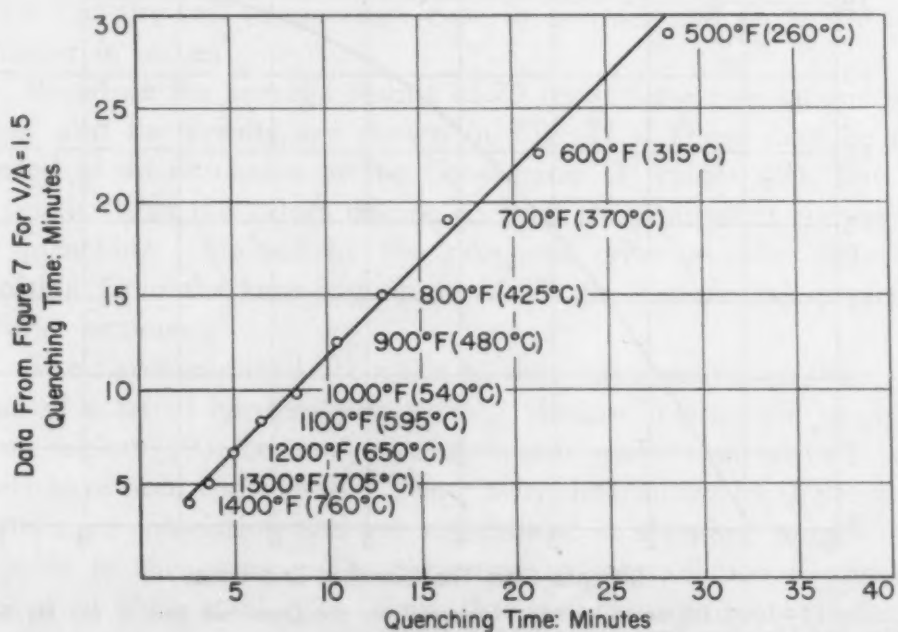


Fig. 9—Comparison of Commercial Oil Quenching With the 2.5-Inch Position of the Hardenability Bar.

the coordinates of each point. For example, along one axis the time for the hardenability bar to cool from the critical point of the steel to 1300 °F (705 °C) is plotted; along the other axis, for a point in the section under consideration, the time to cool from the critical point to 1300 °F (705 °C) is plotted. These two time values

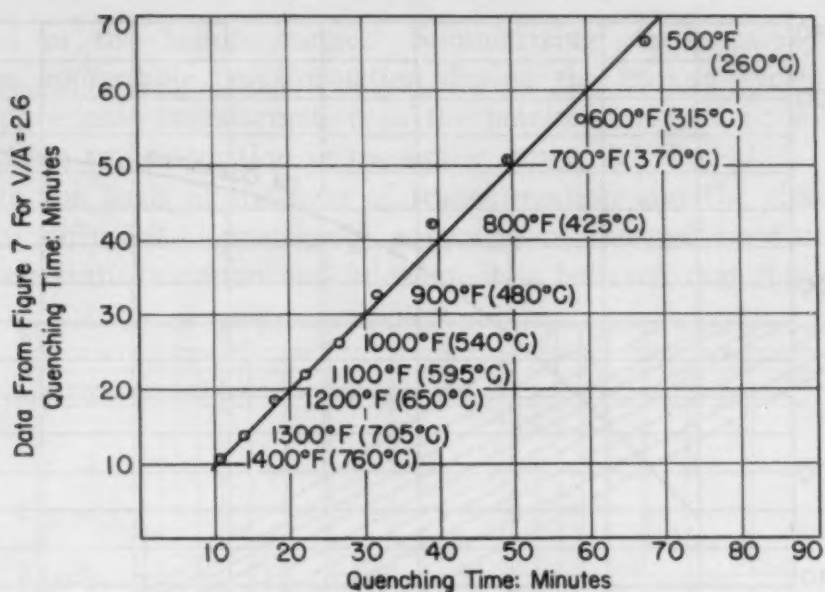


Fig. 10—Comparison of Commercial Oil Quenching With the 7-Inch Position of the Hardenability Bar.

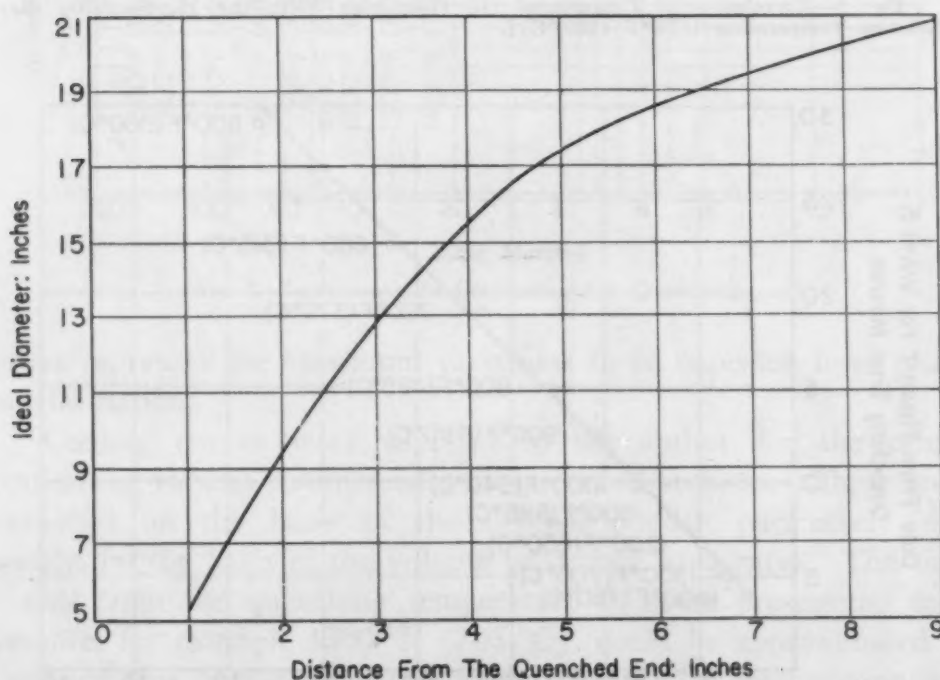


Fig. 11—Ideal Diameter Versus Distance From the Quenched End of the Hardenability Bar [Solution Temperature 1620 °F (880 °C)].

represent the coordinates of a point in which the temperature is considered to be the parameter of the plotted point. Similarly, successively lower temperatures are plotted until the  $M_s$  temperature is reached. Then if a 45-degree line can be drawn through the array of points, it may be said that the cooling curves under consideration are equivalent. Hence, for each thermocouple in the

hardenability bar, an equivalent volume to surface area ratio was obtained for the oil quenching data of Fig. 7. The results of this correlation are shown in Fig. 8, and two representative correlations of the hardenability bar with commercial oil quenching are shown in Figs. 9 and 10. A prediction of the center hardness either in the "as-quenched" or "as-tempered" condition can be made, for the given commercial oil quenching, from the hardenability bar correlation and the volume to surface area ratio.

It was deemed desirable to retain some index of hardenability, and the ideal diameter was retained for this purpose. From Russell's table (5) for a quenching medium of infinite severity, a relationship between the diameter of a bar and the time for its geometrical center to cool from its initial temperature to a temperature halfway between the initial and final temperatures is obtained. This time is the half-temperature time. Assuming with Asimow et al. (6) and Kramer et al. (7) a value of the diffusivity equal to 0.00900 in.<sup>2</sup>/sec., the ideal diameter may be calculated by the expression

$$D_I = 3.29 \sqrt{t}$$

where  $t$  is the half-temperature time in minutes and  $D_I$  is the ideal diameter in inches.

Based on the average results of 75 tests, these calculations were made, and the results are shown in Fig. 11. These may be considered as an extension of the Grossmann  $D_I$  values (8), but will be smaller than the values calculated from the equivalent commercial oil quenching, obtained by the proposed criterion—the difference resulting from the time lag observed in the commercial quenching of large sections.

The hardenability tests made to date have permitted the evaluation of a set of hardenability factors, similar in principle to Grossmann factors (9), but only the chromium-nickel-molybdenum alloy steels have been considered. These were determined by the methods of multiple correlation and are too limited in chemical ranges to be included in this paper. These factors, in contradiction to the conclusion of Post et al. (2), show the same sensitivity to variations in chemical composition that is observed in the low and medium alloy steels.

## RESULTS

Three steels, X-4, X-5, and H-1, were studied by the Jominy, Post, and this new test. Samples for the three tests of each steel were taken from adjoining locations in the same bar. The results



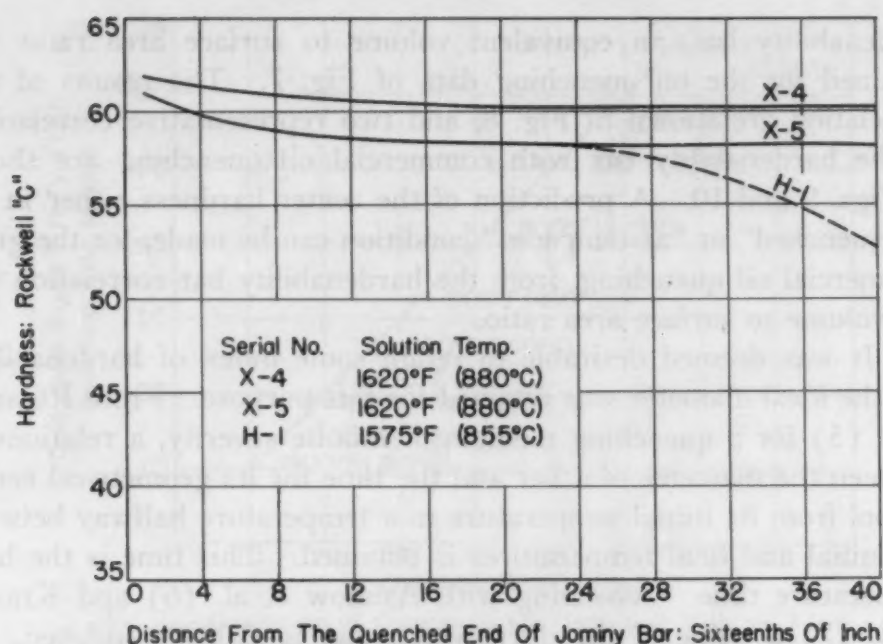


Fig. 12—Jominy Hardenability Test Results for Steels X-4, X-5, and H-1.

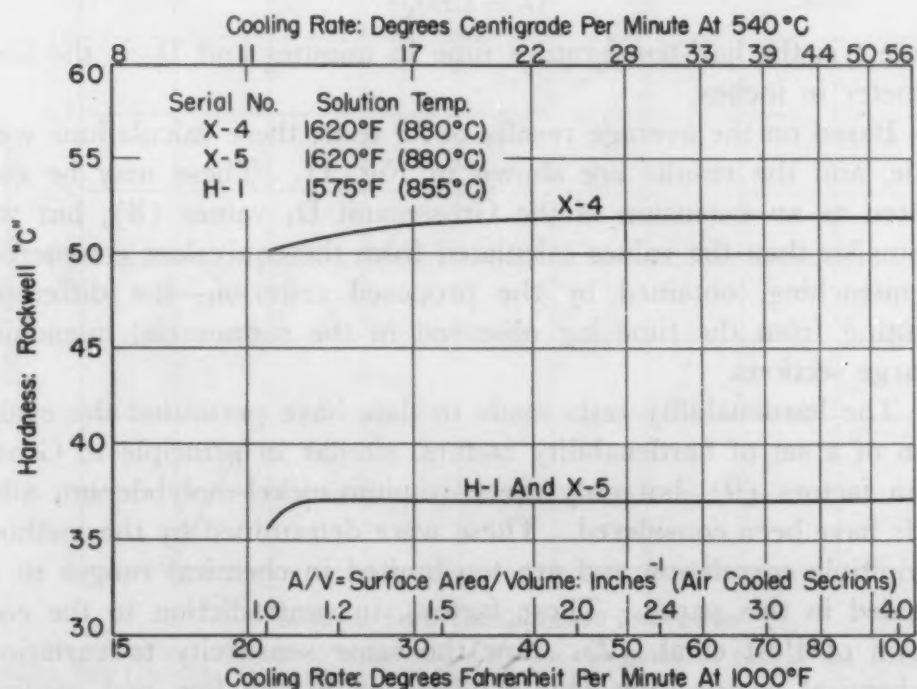


Fig. 13—Post Air Hardenability Test Results for Steels X-4, X-5, and H-1.

of the Jominy tests are shown in Fig. 12; Post tests are shown in Fig. 13; new tests in Fig. 14. Chemical analyses are given in Table I for all of the steels studied.

No significant variations in hardenability between the three steels are revealed by the Jominy tests. A slight tendency for H-1

to drop in hardness is noted beyond the 1½-inch position on the Jominy bar. A difference in maximum hardness also is noted.

The Post air hardenability tests show that X-4 has either a higher hardenability or a much higher maximum hardness than X-5 or H-1; the latter steels are predicted as identical. In these tests, the hardenability curves show a plateau at respective hardness levels.

Fig. 14 shows hardenability data secured with the new test. Except for H-1, the hardenability test results show steep hardness

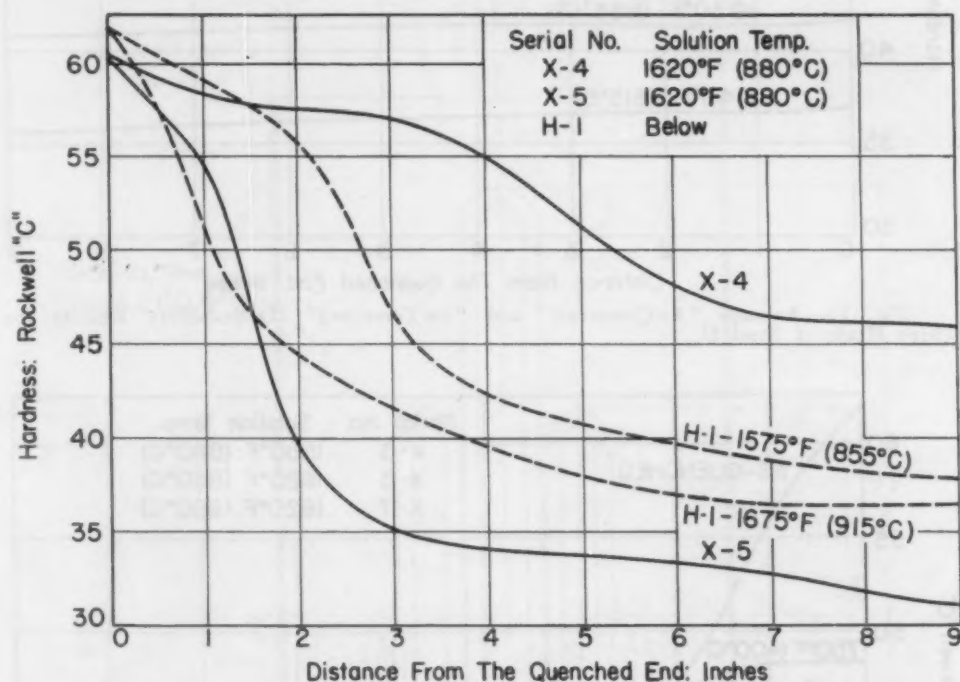


Fig. 14—New Hardenability Test Results for Steels X-4, X-5, and H-1.

gradients at the hardness values for which the Post test suggests plateaus. Steel H-1 ultimately reaches the predicted plateau hardness. If the plateau hardness values of the Post test results are plotted on the respective curves of Fig. 14, a wide scatter will be noted. Since it has been established that the cooling curves of the new test are similar to those of practice, it is suggested that the Post test cooling curves are dissimilar as theoretically presupposed.

Combining the above discrepancies with the Post et al. observation of hardenability insensitive to minor alloy variations suggests that the cooling curves of the Post test approach isothermal transformation.

The test results shown in Fig. 14 indicate X-4 to be the highest in hardenability of the three steels. One of the shortcomings of the test is shown by steel H-1, which has been tested from two different

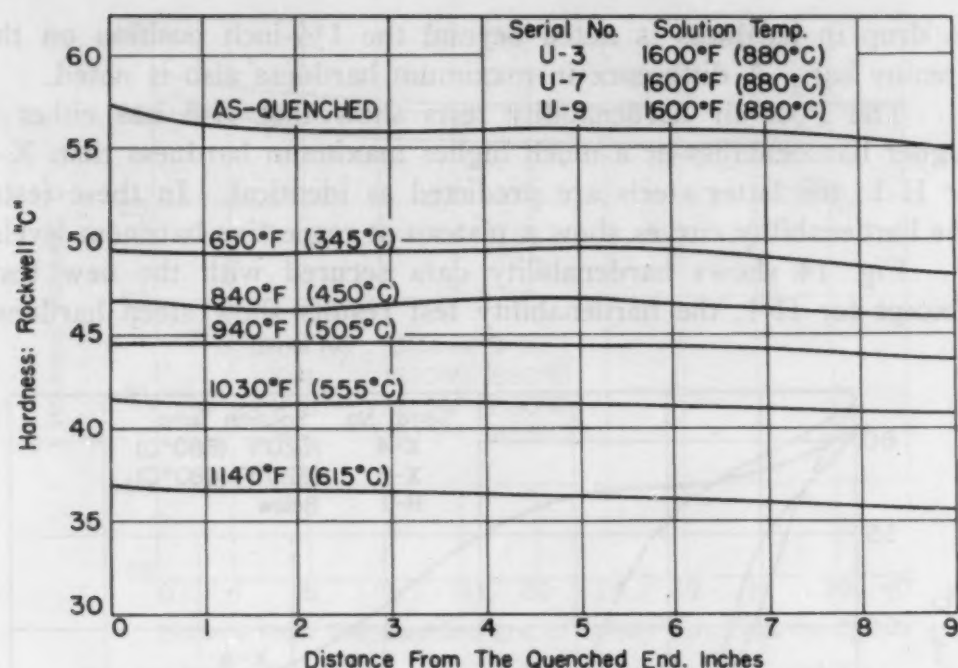


Fig. 15—Average "As-Quenched" and "As-Tempered" Hardenability Results for Three Heats of Steel U.

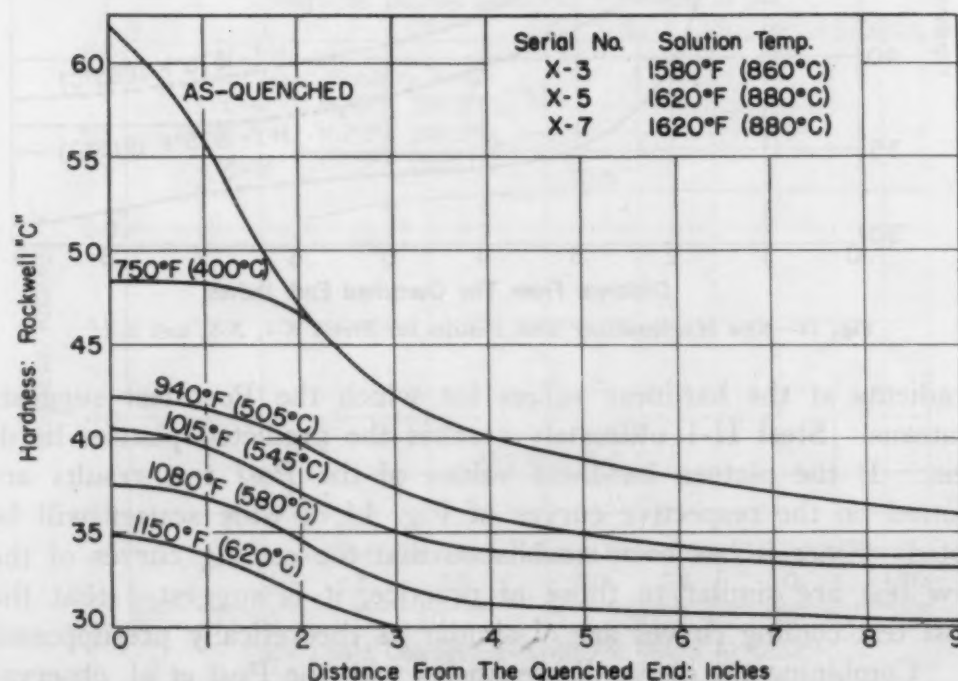
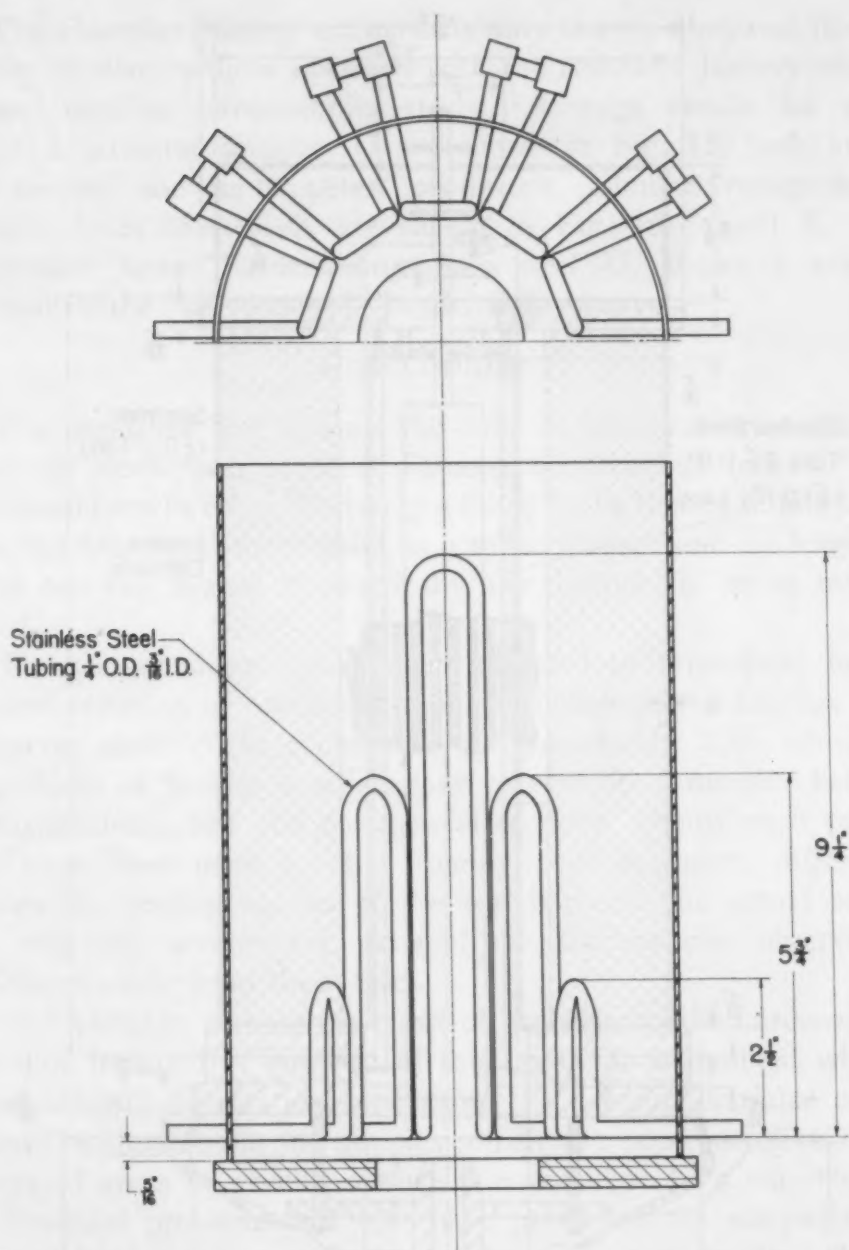


Fig. 16—Average "As-Quenched" and "As-Tempered" Hardenability Results for Three Heats of Steel X.

solution temperatures. There is an apparent decrease in hardenability when the steel is tested with a higher solution temperature. This apparent decrease in hardenability is attributed to a greater heat storage in the furnace; this effect makes a correlation of the

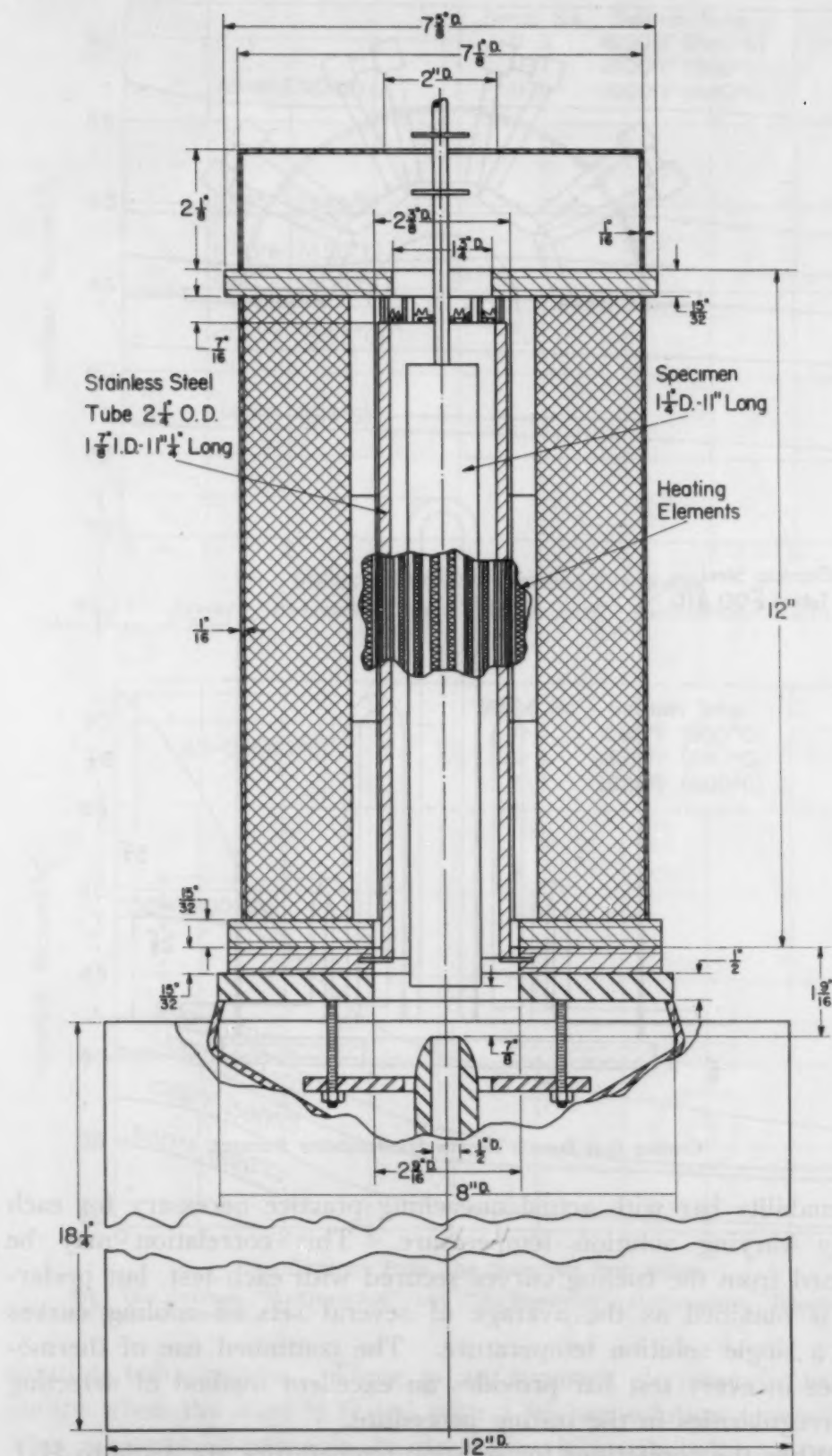


Cooling Coil Details for the Hardenability Furnace.

hardenability bar with actual quenching practice necessary for each widely varying solution temperature. This correlation may be obtained from the cooling curves secured with each test, but preferably is obtained as the average of several sets of cooling curves from a single solution temperature. The continued use of thermocouples in every test bar provides an excellent method of detecting any irregularities in the testing procedure.

When the corrections for solution temperature are made to H-1, the  $D_I$  value is slightly greater than that of X-5.





Quenching Fixture Details for the Hardenability Test.

The characteristics of all hardenability curves observed to date are very similar to those obtained with the standard Jominy test on low and medium hardenability steels. Average results for three heats of a patented analysis U are shown in Fig. 15, both in the "as-quenched" and "as-tempered" conditions. Similar average results for three heats of steel X are shown in Fig. 16. Steel X, of a considerably lower hardenability than steel U, shows a marked inflection in the "as-quenched" hardenability curve.

### CONCLUSIONS

The described test extends the field of hardenability testing to include all steels with an ideal diameter less than 21 inches. This value should not be considered to be a limit, for by the use of additional controlled heating element pairs in a taller furnace and by lengthening the test bar, a steel of practically any desired  $D_I$  value may be studied.

The test conditions have been adjusted to reproduce, by the proposed criterion of equivalent cooling conditions, the average cooling curves observed in commercial oil quenching. This eliminates the problem of finding a satisfactory correlation parameter between the hardenability test and commercial sections. Many such parameters have been used for the Jominy test; however, differences between the cooling curves of the test bar and the actual section exist and may account for some of the discrepancies observed in predictions made from these tests.

One variable, namely the effect of pressure on the hardenability, cannot be included in any test of this type. It is doubted whether any significant information concerning the pressure variable can be obtained without securing samples which are representative of the segregated areas in which pressure is assumed to be a variable.

Practical problems and cost have precluded the comparison of "as-quenched" sections with the hardenability test results. Microstructural examinations of several hardened and tempered sections have been compared with the hardenability test results, and these appear to support the proposed correlation. Except for this rather meager evidence, the correlation must stand on the similarity of the cooling curves, over the pertinent temperature range.

This hardenability test has been satisfactorily applied to over 100 heats of steel. In every instance, the quenching curves were checked and the reproducibility of this test was confirmed. Reproducibility between similar hardenability quenching fixtures cannot be considered because only one testing apparatus has been built.

The Jominy hardenability test range is condensed into essentially the first inch of this hardenability bar.

#### ACKNOWLEDGMENTS

The author wishes to acknowledge the sponsorship of the A. Finkl & Sons Company, Chicago, which made possible this development as a part of their research program at the Foundation. Especially, he wishes to express his appreciation to Messrs. William and Alfred Finkl for permission to publish this work, and to their chief metallurgist, Mr. Theodore Ledin, for securing the cooling curves which were used in the development of this hardenability test.

Further, the author wishes to acknowledge the contributions of innumerable members of the Metals Research Division of the Armour Research Foundation.

#### References

1. H. Allsop and W. Steven, "A Study of the Relationship Between End-Quench Hardenability Curves and the Hardness of Bars Quenched in Oil", Special Report No. 36, 1946, p. 199, The Iron and Steel Institute, London, England.
2. C. B. Post, M. C. Fetzer and W. H. Fenstermacher, "Air Hardenability of Steels", *TRANSACTIONS, American Society for Metals*, Vol. 35, 1945, p. 85.
3. G. De Vries, "An End-Quenched Bar for Deep Hardening Steels", *TRANSACTIONS, American Society for Metals*, Vol. 41, 1949, p. 678.
4. H. J. French, "Effects of Size and Shape of Sample on the Cooling in Different Media", *TRANSACTIONS, American Society for Steel Treating (ASM)*, Vol. 17, 1930, p. 675.
5. T. F. Russell, "Some Mathematical Considerations on the Heating and Cooling of Steel", Special Report No. 14, 1936, p. 149, The Iron and Steel Institute, London, England.
6. M. Asimow, W. F. Craig and M. A. Grossmann, "Correlation Between Jominy Test and Quenched Round Bars", *Journal, Society of Automotive Engineers*, Vol. XLIX, 1941, p. 283.
7. I. R. Kramer, S. Siegel and J. G. Brooks, "Factors for the Calculation of Hardenability", *Transactions, American Institute of Mining and Metallurgical Engineers*, Vol. CLXVII, 1946, p. 670.
8. M. A. Grossmann, M. Asimow and S. F. Urban, "Hardenability of Alloy Steels", 1939, p. 124, The American Society for Metals.
9. M. A. Grossmann, "Hardenability Calculated from Chemical Composition", *Transactions, American Institute of Mining and Metallurgical Engineers*, Vol. CL, 1942, p. 227.

#### Appendix

##### OUTLINE OF OPERATING PROCEDURE

- A. Adjust free jet height to  $3\frac{1}{2}$  inches.
- B. Insert bottom heating plate.
- C. Insert thermocouples and wire same to hardenability bar.



D. Insert hardenability bar in furnace—support on lower washer.

E. Heat bar to austenitizing temperature (Variacs set slightly above the minimum required voltage when using automatic control).

F. Hold austenitizing temperature 1 hour.

G. Withdraw bottom heating plate.

H. Lower hardenability bar to upper washer.

I. Turn power "off" to bottom and middle sections.

J. Simultaneously

1. Turn on pump;

2. Turn on cooling coils;

3. Mark recorder chart.

K. Reduce top zone Variacs.

Quenching Time, Minutes	Variat Settings (at the Indicated Times)	
	110-Volt	220-Volt
0	as for heating	as for heating
4.5	50	100
14	25	50
34	10	20
39	0	0

L. Stop test 90 minutes after starting the quench.

M. Grind 4 flats 90 degrees apart by removing 0.030 inch per flat.

N. Make a plot of Rockwell "C" hardness versus distance from the quenched end.

## DISCUSSION

**Written Discussion:** By D. Niconoff, Metallurgical Laboratory, Republic Steel Corp., Central Alloy District, Canton, Ohio.

The author is to be congratulated for developing an ingenious method for overcoming the principal limitation of the end-quench hardenability test as applied to deep hardening steels. The effective length of the conventional Jominy specimen corresponds to the center hardness of only 4-inch round bar, and a greater specimen length is obviously required for the determination of hardenability of steels capable of complete hardening in larger cross sections, but the length cannot be increased indefinitely without introducing an air quenching effect at the slowly cooled end of the specimen.

The latter effect is common in the end-quenched specimens possessing considerable ratio of length to diameter. In the early days of developing the end-quench test, when experiments were conducted with  $\frac{1}{4}$ -inch diameter by 3-inch test pieces, the air quenching effect was found to be very pronounced and an attempt was made to overcome it by shielding the sides of the specimen with an asbestos sleeve. With larger specimens such a remedy would be impractical, and either the length and diameter



would have to be increased proportionally, until the specimens become unwieldy, or a resort must be made to artificial retardation of the cooling rate at one end of the specimen by applying controlled heat.

This method was obviously designed for alloys possessing uncommonly high hardenability, such as air hardening die steels, but this fact does not preclude the possibility of its use on some of the constructional steels possessing the ideal critical diameter in excess of 7 inches, the conventional Jominy curve of which is usually represented by a straight, horizontal line offering scant information regarding their thermal characteristics. The hardenability curves given by the author in Fig. 14 for three steels of similar character show high sensitivity of this method to relatively small variation in the alloy contents, and it would be interesting to see how the 4340-type compares with them. It would also be of interest to know the degree of reproducibility of the results obtained by this method.

Even if the reproducibility of the author's results obtained with a single fixture is good, it is doubtful whether the data obtained with several units of this type would be in satisfactory agreement because of the inherent difficulty of matching their heat storing and heat dissipating characteristics. The nature of the furnace refractories, arrangement of the cooling tubes, and rate of circulation of the coolant would be just as important in this case as the control of the power input observed by the author in his experiments.

It is conceivable that these variables could be fixed and compensated by determination of a series of correlating curves for each individual furnace. Remembering, however, the cooperative time and effort spent in standardizing the Jominy test—a test that hardly could be improved in its simplicity—it appears to be improbable that the present method for determination of the hardenability of deep hardening steel would ever become a production tool although undoubtedly it could be used to good advantage for research purposes.

**Written Discussion:** By Gerrit De Vries, metallurgist, U. S. Naval Ordnance Test Station, Pasadena, Calif.

The author is to be congratulated for his new test. A test that will reproduce the average cooling curves observed in commercial oil quenching can be very useful. However, it appears that the composition of the steel and the solution temperature may influence the correlation between the test bar and commercial oil quenching too much to have this test accepted generally.

It is shown in Figs. 5 and 6 that a difference in composition causes a change in the cooling curves given by the test. Therefore, exact correlation of the cooling curves cannot be expected unless the composition of the hardenability bar and that of the oil-quenched sections are the same or similar.

Apparently an increase in the solution temperature causes a decrease in the cooling rate of the hardenability bar. It is known that at a given temperature the cooling rate at the center of a section increases with quenching temperature. Therefore, the correlation of cooling curves for hardenability comparison can only be had if the oil-quenched sections and the hardenability bar are quenched from the same temperature. Since the test apparatus was designed to reproduce the cooling curves found

in oil quenching when quenched from 1620 °F, it may be necessary to establish new cooling conditions for each quenching temperature if correlation between oil-quenched rounds and the hardenability bar is desired.

The making of a similar hardenability fixture to reproduce the results given by the author would be difficult, as the apparatus is complex and there are many factors that may influence the cooling rate, such as the temperature and the velocity of the cooling water and the surrounding air; also, the line voltage supplied to the Variac during cooling and the efficiency of the insulation surrounding the furnace.

The test should be helpful to those using large quantities of similar deep hardening steels. In such cases standards can be established and correlated with production experience from commercial quenching.

#### Author's Reply

The discussion of Messrs. Niconoff and De Vries is acknowledged gratefully. The original paper was confined to the constructional details, operational details, and typical results of the best testing method developed. However, a complete reply to the discussion requires a brief consideration of the heat transfer involved in this test.

The stainless steel tube, if not end-quenched, would reduce the radiant heat transfer rate, between the furnace and the specimen, to one-half of its value in the absence of the tube.

However, no net heat flow between the furnace and the bar would be experienced, if each cylindrical element of the specimen could be contained in a tubular element which experiences the same temperature-time cycle as the corresponding element of the specimen. By end quenching the tube, its time-dependent longitudinal temperature distribution approaches that of the specimen more closely than it would by radiation alone. The net heat transfer rate between the furnace and the specimen is reduced from one-half, for the tube alone, to some smaller fraction by end quenching the tube.

In practice, the ideal temperature-time distribution in the tube is not attained because of practical limitations. Temperature measurements show that the heat supplied during the quenching cycle is not sufficient to counterbalance all of the losses from the top of the furnace. Heat transfer calculations also indicate that the specimen loses heat to the tube at distances greater than 4 inches from the quenched end of the specimen. Conversely, at distances between 1 and 4 inches from the quenched end of the specimen, the bar gains heat from the tube. As would be predicted, the efficiency of the cooling coils is low.

The net rate of heat transfer from the furnace to the tube is increased by end quenching the tube. Except for the heat transferred from the tube to the bar, as described above, the heat stored in the furnace is transferred to the cooling water which strikes the end of the tube, or is lost by radiation. Much of the heat storage of the furnace is dissipated in this manner.

In the light of the above heat flow considerations, the author is inclined to believe the discussers underestimated the true importance of the end-quenched tube. If this tube were absent, the author most certainly

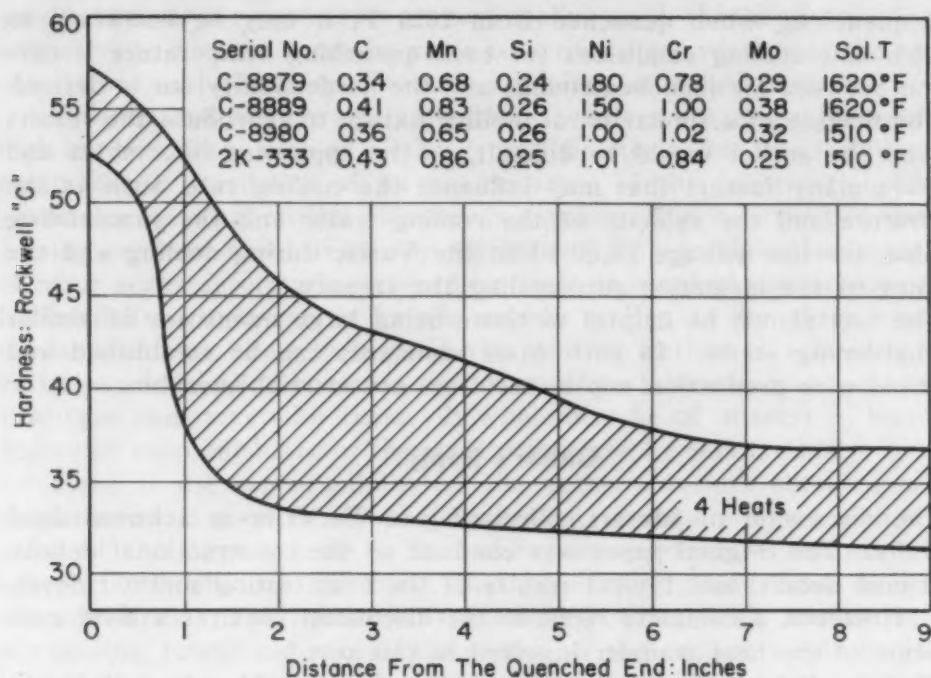


Fig. 17—Hardenability Band for Steel C.

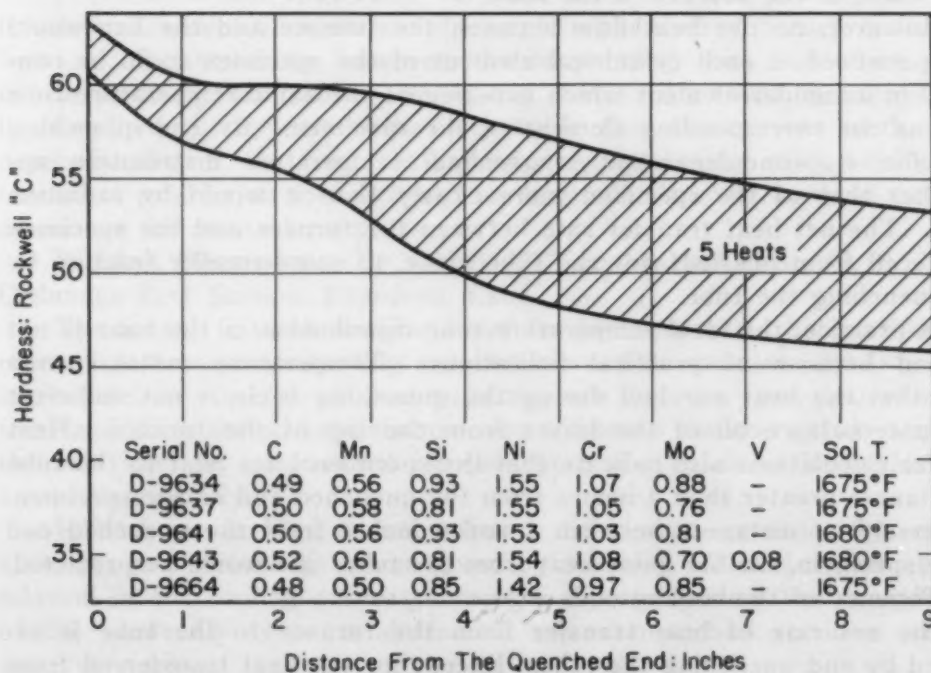


Fig. 18—Hardenability Band for Steel D.

would agree with their conclusion that the hardenability bar cooling curves are determined by the furnace characteristics.

The reproducibility of this test is shown in two ways. Figs. 17, 18 and 19 show hardenability bands based on a limited number of heats of three commercial steels. The hardenability band of Fig. 17 is enlarged



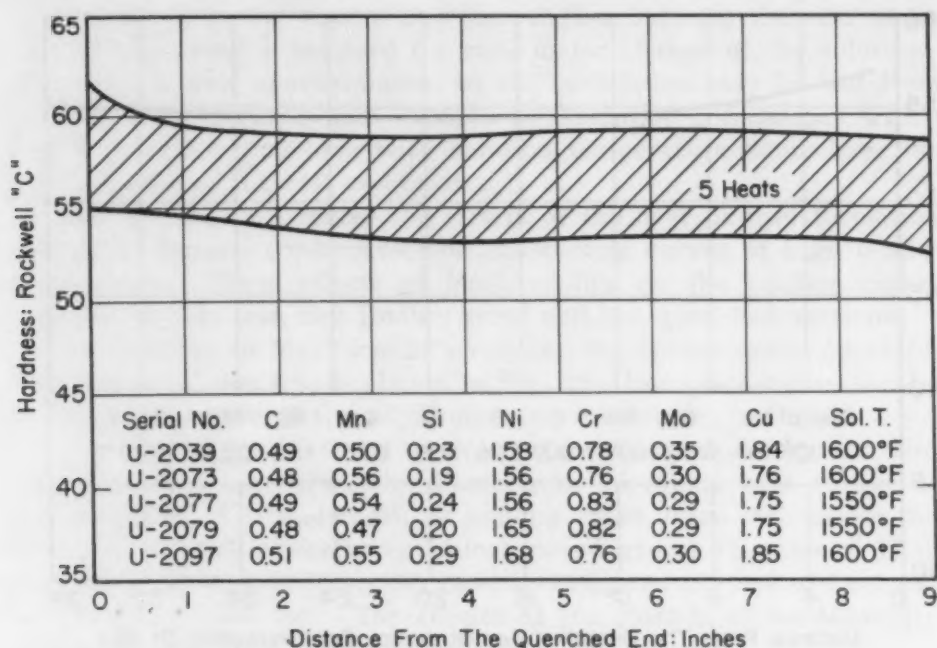


Fig. 19—Hardenability Band for Steel U.

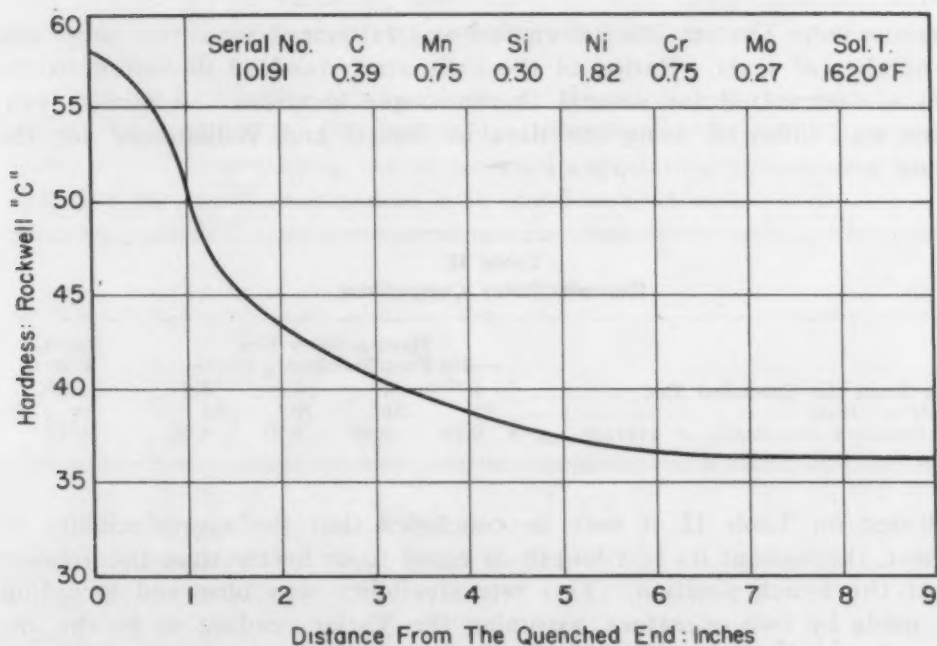


Fig. 20—New Hardenability Test Results for Type 4340.

by the range of solution temperatures included in it. The heat analyses are given and, due to normal segregation, the bar compositions may be somewhat different. No sensitivity of the method to small variation in alloy content is noted.

Table II contains quantitative information for comparing the reproducibility of this test with the Jominy test. For thirty routine tests, the time for each of the observed temperature-time curves to reach 900 °F



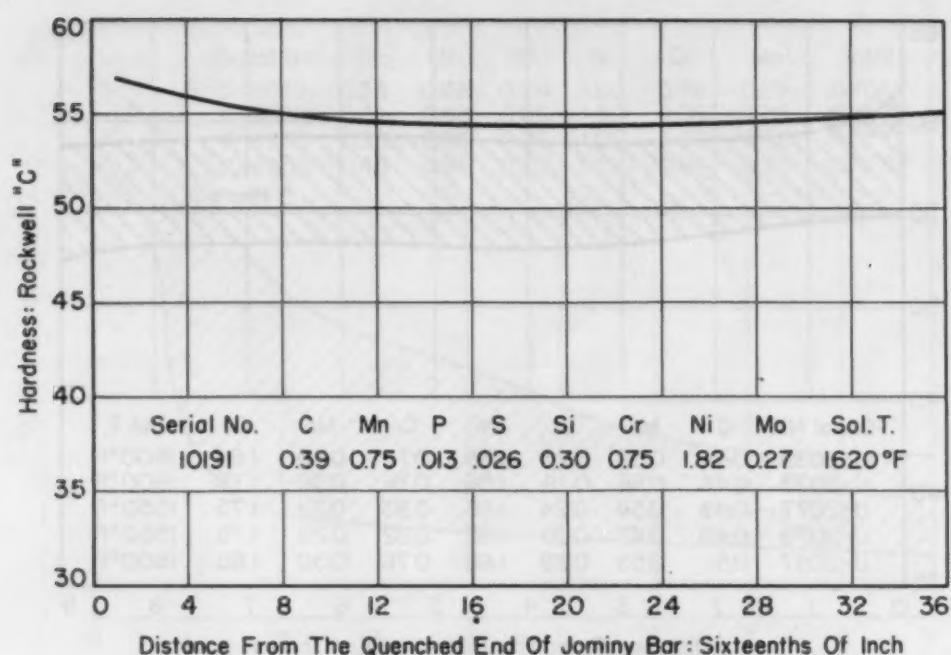


Fig. 21—Jominy Hardenability Test Results for Type 4340.

was recorded. The standard deviation was estimated from the range and the number of tests. Ratios of the estimated standard deviation to the mean are presented for several thermocouple locations. A similar procedure was followed using the data of Russel and Williamson<sup>2</sup> for the Jominy test.

Table II  
Reproducibility Comparison

Inches From the Quenched End .....	Hardenability Test —for Deep Hardening Steels—				Jominy Test <sup>2</sup>
	1	4	7	8.5	
Number of Tests .....	30	30	30	30	9
(Est. Standard Deviation) ÷ average $t_{900}^{\circ}\text{F}$ .....	0.18	0.09	0.07	0.08	0.17

Based on Table II, it may be concluded that the reproducibility of this test, throughout its test length, is equal to or better than the Jominy test at the 1-inch position. This reproducibility was observed including tests made by two operators, assuming the Variac reading to be the applied voltage, allowing the combined coolant flow to vary between 1.5 and 2.0 liters or quarts per minute, using direct tap water for the cooling coils, neglecting the ambient temperature, and neglecting the change of resistance of the heating elements with age. The neglect of these variables makes the testing procedure relatively simple, and provides further support for the author's conclusion that the testing procedure is not sensitive to the furnace characteristics.

<sup>2</sup>T. F. Russel and J. C. Williamson, "Surface Temperature Measurements During the Cooling of a Jominy Test Piece", Special Report No. 36, 1946, p. 34. The Iron and Steel Institute, London, England.

As stated in the text, a new correlation between the test and commercial quenching is required for each major change of the solution temperature. A first approximation to the correlation may be had from the cooling curves secured with each test. Tentative correlations with commercial oil quenching over wide solution temperature limits have not required changing the test conditions.

Mr. De Vries attributes the effects of the heat of transformation and change of thermal conductivity on the cooling curves of Figs. 5 and 6 to composition. These effects of hardenability on the cooling curves are common to this test, the Jominy test,<sup>2</sup> and the quenched sections.

In response to Mr. Niconoff's request, the hardenability curve of 4340 determined by this test is shown in Fig. 20. For comparison, the Jominy hardenability curve of the adjoining sample is shown in Fig. 21.

As alternate procedures to overcome surface radiation, Mr. Niconoff suggests either increasing the diameter or supplying heat to one end of the specimen. The midlength air cooling curve, 0.125 inch below the surface, of a 3.5-inch diameter by 14-inch round gave a  $D_1$  value of 17 inches. Post et al (2) and De Vries (3) have investigated the use of heat supplied to one end of the bar. The results of the Post et al hardenability test were compared with those of this test in the paper.

The complexity of the quenching fixture is outweighed by the practical limitations of securing these data by any other means. Actually, hardenability data on steel sections weighing 1000 pounds or more may be secured with this test.

It is believed that the problems of standardizing this test would be simpler than those for the Jominy test because of the limited group concerned with these steels, the absence of correlating parameters, and because of the experience gained with the Jominy test.

## AN EXAMINATION OF THE QUENCHING CONSTANT, $H$

BY D. J. CARNEY AND A. D. JANULIONIS

### *Abstract*

*The purpose of this investigation was to examine the quenching constant,  $H$ , in greater detail. A brief review of the development of the term,  $H$ , is given along with a review of recent experimental work.  $H$  values were calculated from cooling curves of various sizes of stainless steel bars quenched in water and oil.  $H$  increases as the round diameter is decreased and, within a single round,  $H$  increases from the center to the surface. Also, in an end-quench bar,  $H$  increases sharply near the quenched end. This latter effect yields an apparent hardenability which is greater than is actually obtained in larger-size rounds. These variations in  $H$  appear to be due to variations in the surface heat abstraction coefficient.*

UNPUBLISHED work, carried out by S. F. Urban and M. Baeyertz at the South Works Research Laboratory of the Carnegie-Illinois Steel Corp. during studies in 1944 on the effects of various elements on the hardenability of steel, indicated quite definitely that the severity of quench, or  $H$  value, as determined by the method of Grossmann and Asimow (1)<sup>1</sup> was not always the same for the same quenchant. In general, much higher  $H$  values were obtained with sections less than 1 inch in diameter; in fact, it appeared that the quench obtained was nearly infinite for a series of 1/2-inch rounds quenched in water. The present study was undertaken to determine quantitatively the variations in  $H$  values, since it was felt that the observed changes of  $H$  could be the cause of some of the anomalous results which were obtained in quenching steel.

A brief review of how the term " $H$  value" arose and how it has been used in connection with quenching steel is as follows:

As far back as 1822, Fourier (2), using the assumption of Newton's law of cooling, solved the differential equation for an infinitely long bar cooled symmetrically about its axis. For simplification, it was necessary in his solution to assume that the thermal conductivity,  $k$ ,

<sup>1</sup>The figures appearing in parentheses pertain to the references appended to this paper.

A paper presented before the Thirty-second Annual Convention of the Society, held in Chicago, October 21 to 27, 1950. The authors, D. J. Carney and A. D. Janulionis, are associated with United States Steel Co., Chicago. Manuscript received April 13, 1950.



and the surface heat abstraction coefficient,  $C^*$  did not vary with temperature. These two constants were later combined into one letter "h", which was defined as being equal to  $C/k$ . "h" is the measure of the severity of quench when one calculates cooling rates in quenched rounds.

Heindlhofer (3), in 1922, reviewed the mathematics of the various hypotheses on rapid cooling. He showed that the assumption of Newton's law of cooling is not always valid under common conditions of quenching. Heindlhofer stated that whereas this law is substantially valid for relatively small temperature differences at low temperatures, it does not hold for large temperature differences at high temperatures, such as occur in quenching steel.

In spite of this objection, three different authors more recently have successfully used the same type of mathematical solution. Scott (4), in 1934, showed that the calculated cooling curves and the actual cooling curves obtained from center thermocouples of quenched steel rounds agreed quite closely.

In 1936, Russell (5) covered the mathematical solution in detail and presented condensed tables for applying the calculations to quenched plates and cylinders. Later, in 1946 (6, 7), he showed that the mathematical calculations could successfully be applied to end-quench bars.

Grossmann and co-workers (1), in 1939, went a step further than the others and showed that hardnesses in quenched steel rounds correlated well with the cooling times calculated by using the same type of mathematical solution. For convenience, these authors preferred to use diameters instead of radii. Consequently, they defined  $H = \frac{1}{2} "h" = \frac{1}{2} C/k$ . The  $H$  as used in this report is the heat transfer coefficient which has been defined as above by Grossmann and Asimow.

Rose (8), and Krainer and Swoboda (9), in Germany, used mathematical calculations in connection with cooling curves obtained from small, quenched silver balls. Rose determined the heat transfer factor of a number of quenching media as a function of temperature. Krainer and Swoboda attempted with only fair success to correlate the results of the silver-ball test with hardnesses obtained in quenched steel cylinders.

In 1947, Jones and Pumphrey (10) presented a very interesting paper in which they attempted to correlate hardnesses obtained in quenched steel rounds with cooling curves obtained in silver and stainless steel rounds. The hardness correlations were not very successful. One of the reasons for this was that the  $H$  value was not

\* $C$  is the constant of proportionality in Newton's law of cooling.



**Table I**  
**Effective Values of H for Different Temperature Ranges**  
**and Specimen Sizes (Jones and Pumphrey)**

Dia. of Specimen, in.	Effective Value of H for Temperature Range	
	700 - 600 °C (1292 - 1112 °F)	300 - 200 °C (572 - 392 °F)
$\frac{3}{4}$	Much greater than 0.9	Approximately equal to 0.9
$1\frac{1}{4}$	Slightly greater than 0.9	Less than 0.9
$3\frac{1}{2}$	Less than 0.9	Much less than 0.9

constant with temperature. Their results showed that the value of the heat transfer coefficient varied considerably with temperature and for the purpose of hardness correlation the effective value of H was found to depend on specimen size. Some of their data are given in Table I. They stated, "The usual assumption made in mathematical considerations of quenching, that H is constant, should therefore be regarded with suspicion."

#### PROCEDURE

Rounds of stainless steel of the following composition were used in this investigation: C 0.10%, Mn 0.92%, P 0.029%, S 0.009%, Si 0.28%, Cu 0.02%, Ni 9.76%, Cr 16.76%. Specimens for quenching were forged from  $3\frac{1}{2}$ -inch diameter stock and machined into five different cylindrical sizes— $\frac{1}{2}$  by 2, 1 by 4,  $1\frac{1}{2}$  by 6,  $2\frac{1}{4}$  by 9, and 3 by 12 inches. The  $\frac{1}{8}$ -inch diameter holes for the thermocouples were drilled longitudinally from the top of the specimens to a point midway along the length of the bars. At this position the bars could be assumed to be of infinite length. Small beads were made on chromel-alumel thermocouples and the couples welded to the bottom of the drilled holes by means of an arc welding process. Steel pipes were welded to the top of the specimens to protect the couples from the quenchant. The construction of the specimens is shown in Fig. 1.

From one to three thermocouples were attached to each specimen, usually one at the center and the others, if any, at positions closer to the surface. The chromel-alumel thermocouples were checked occasionally before and after use and found to have altered calibration by less than 4 °F.

The specimens were heated in a resistance furnace in a muffle with an atmosphere produced by spent carburizing compound. The steel was placed in this furnace after the furnace had attained a temperature of 1550 °F (845 °C). When the steel was at the temperature of the furnace for 20 minutes, it was taken out rapidly and quenched. The time required to remove the specimen from the furnace to immersing it in the quenching media was approximately 1 second.

The specimens were quenched by hand in circulated water and in

oil. In quenching, the specimens were moved in a circular path in a 5-foot diameter quenching tank.

Three Gilbert amplifiers and three Esterline-Angus recorders

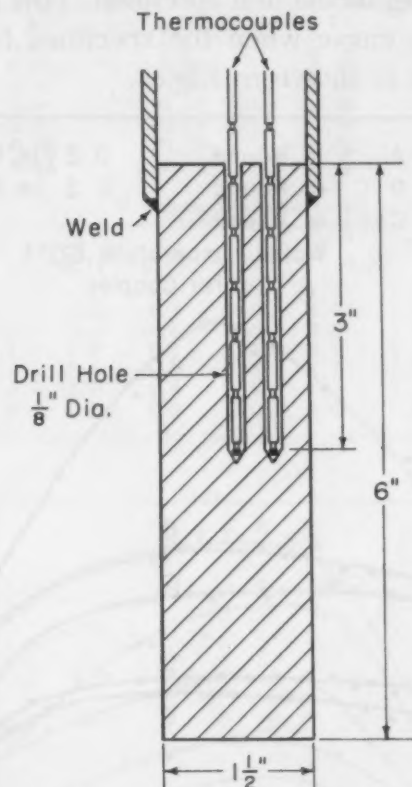


Fig. 1—Construction of a Typical Specimen for Cooling Rate Measurements.

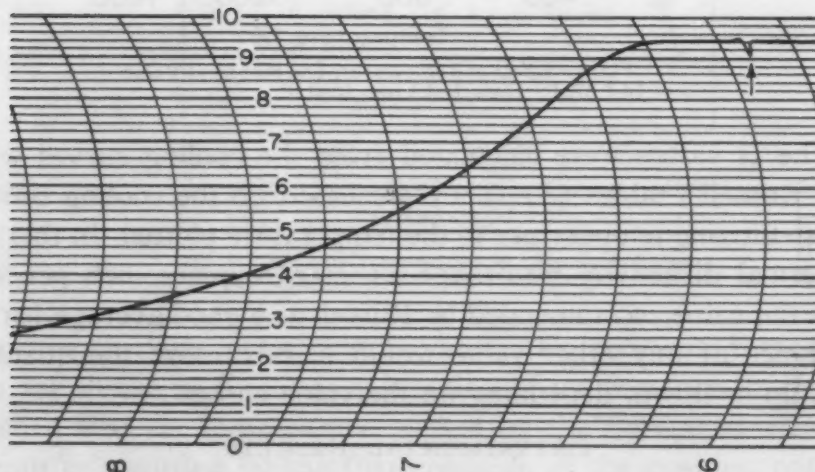


Fig. 2—Cooling Curve for Center Couple of 1 1/2-Inch Round Showing Jog in Curve at the Beginning of Water Quench.

were used to follow the rapidly varying emf of the thermocouple. The recording mechanism was of the variable-speed type, with chart speeds

of 3, 6 and 12 inches per minute. Three instruments were used in the cases where three couples were attached to one specimen. The timing of the beginning of quench was effected by a thyatron trigger circuit through the quenching media and specimen. This mechanism produced a jog in the cooling curve when the specimen hit the quenchant. A typical cooling curve is shown in Fig. 2.

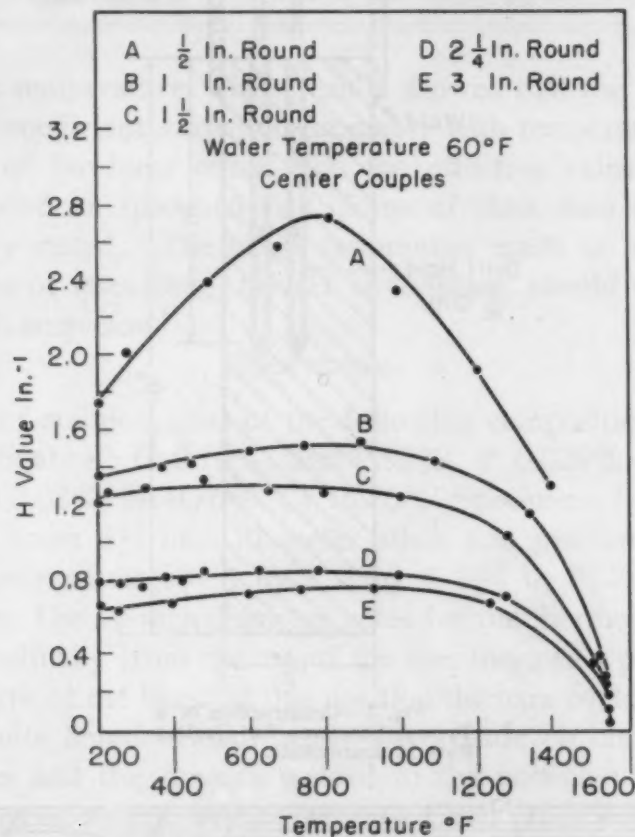


Fig. 3—Effect of Temperature and Size on H Value for 18-8 Water-Quenched From 1550°F.

The H values were calculated from the cooling curves with the aid of Russell's tables (5). They are based on the cooling time from the austenitizing temperature to the temperature plotted. In this report, the thermal diffusivity was taken as 0.0099 square inch per second. This is the value recommended by Russell as a good average for steels. The choice of any other value would merely move the quantitative results up or down, depending on the value chosen.

#### EXPERIMENTAL RESULTS

##### (a) Variation of H With Temperature and With Size of Quenched Round

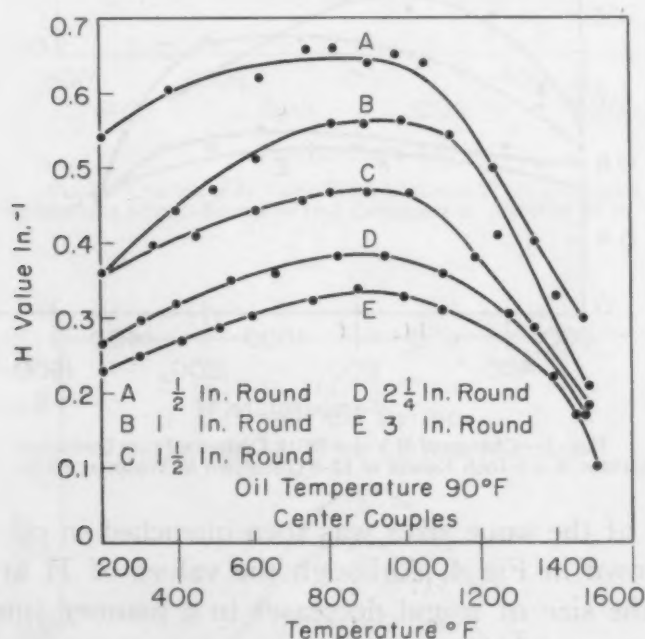
Five rounds of stainless steel with diameters of 1/2, 1, 1 1/2, 2 1/4, and 3 inches were quenched in water, and cooling curves were recorded

**Table II**  
**H Values From All the Thermocouples of the 3-Inch Rounds Quenched in Water**

Temperature, °F	H value, center couples Specimen Number				
	3	4	2	5	6
1400	0.67	0.65	0.65	0.40	0.80
1200	0.85	0.80	0.85	0.72	0.95
1000	0.85	0.80	0.85	0.72	0.90
800	0.86	0.80	0.80	0.70	0.90
600	0.85	0.74	0.80	0.70	0.80
400	0.80	0.70	0.75	0.70	0.80
200	0.65	0.70	0.70	0.65	0.70

Inches from surface	H values, positions closer to surface Specimen Number									
	6	6	4	2	4	3	5	3	5	2
	0.09		0.11	0.15	0.21	0.33		0.43	0.49	1.02
1400 °F	...	...	...	...	...	1.2	1.2	0.8	1.3	0.9
1200	...	...	...	1.2	1.0	1.6	1.7	1.5	1.3	0.9
1000	...	...	...	1.6	1.6	2.0	1.75	1.5	1.3	1.0
800	...	3.1	2.7	1.7	1.7	1.9	1.7	1.5	1.3	0.95
600	3.6	3.5	3.4	1.6	1.5	1.5	1.5	1.4	1.2	0.9
400	3.1	2.5	2.7	1.4	1.4	1.2	1.2	1.1	1.0	0.9
200	1.8	1.6	1.7	1.0	1.0	1.0	1.0	1.0	0.9	0.8



**Fig. 4—Effect of Temperature and Size on H Value for 18-8 Oil-Quenched From 1550°F.**

from center thermocouples. The  $H$  values obtained from these cooling curves are shown in Fig. 3 as a function of temperature. It should be mentioned that the temperature plotted on the horizontal axis is the temperature recorded by the thermocouple at the position noted and not the surface temperature. It can be seen that  $H$  varies with temperature and appears to go through a maximum and that  $H$  increases as the size of round decreases, with the biggest increase occurring between 1-inch and  $1\frac{1}{2}$ -inch rounds.



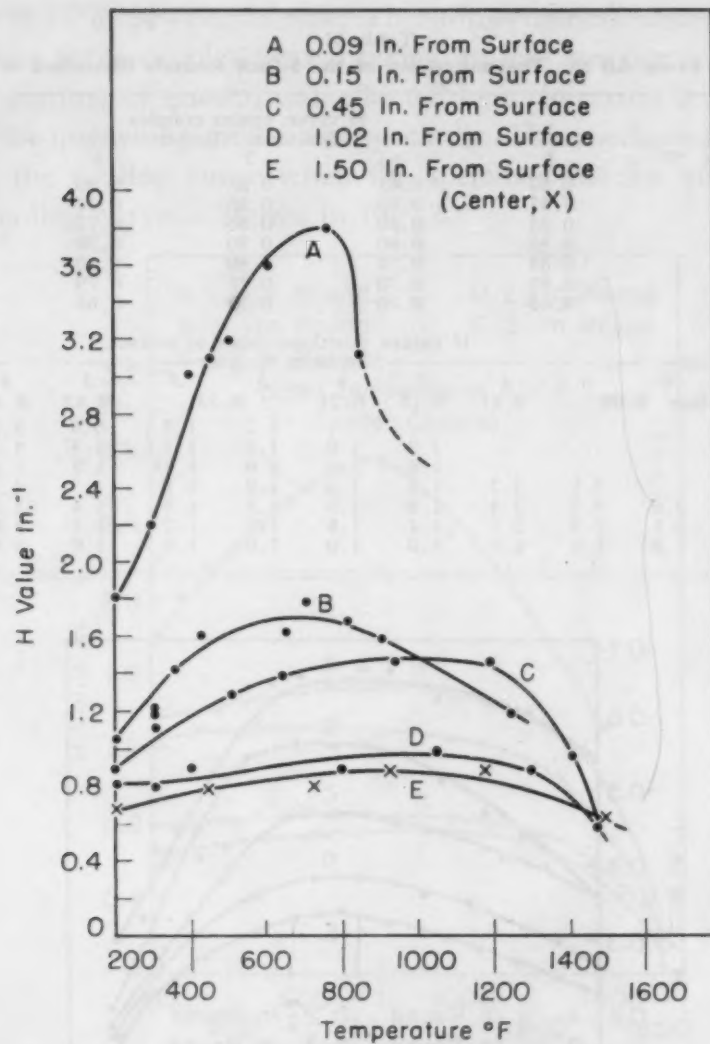


Fig. 5—Change of H Value With Distance From Quenched Surface of a 3-Inch Round of 18-8 Quenched in Water at 60°F.

A series of the same sizes was then quenched in oil, and the H values are shown in Fig. 4. Although the values of H are lower, H increases as the size of round decreases in a manner similar to that found on water quenching.

*(b) Variations of H Within a Single Quenched Round*

Five stainless rounds, 3 inches in diameter, were machined so that each had a center thermocouple and two other couples at points closer to the surface. All five specimens were quenched in water and the cooling curves recorded. The location of the couples and the results of the H values are shown in Table II. Five of the locations are plotted in Fig. 5. It is seen that the H value increases as one approaches the surface within a single round quenched in water. The rate of increase of H is not linear but increases sharply as one gets closer to the surface.

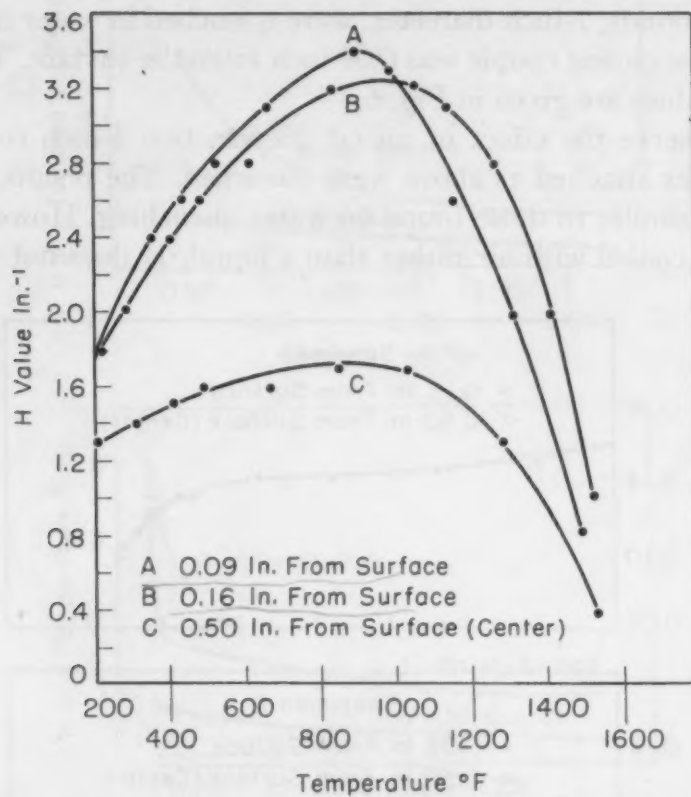


Fig. 6—Change of  $H$  Value With Distance From Quenched Surface of a 1-Inch Round of 18-8 Quenched in Water at  $60^{\circ}\text{F}$ .

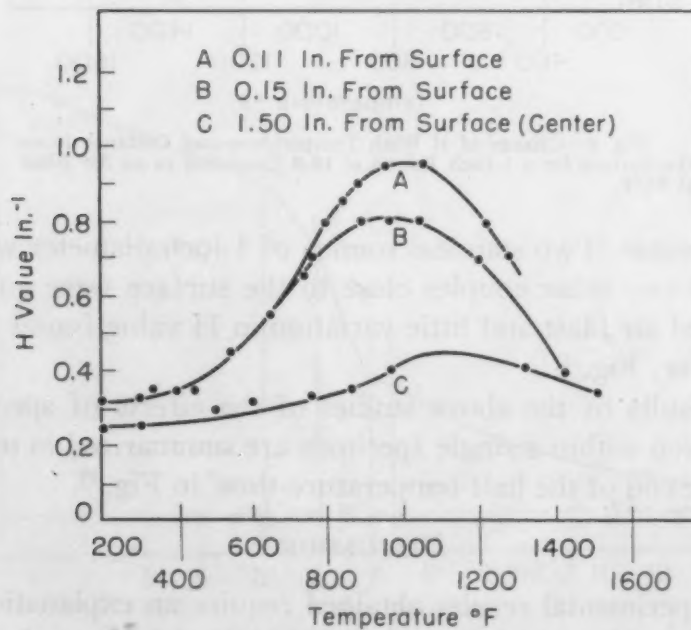


Fig. 7—Change of  $H$  With Distance From Quenched Surface of 3-Inch Round of 18-8 Quenched in Oil at  $100^{\circ}\text{F}$ .

Two rounds, 1-inch diameter, were quenched in water in the same manner. The closest couple was 0.09 inch from the surface. The results of the H values are given in Fig. 6.

To observe the effect of an oil quench, two 3-inch rounds with three couples attached as above were quenched. The results, shown in Fig. 7, are similar to those found on water quenching. However, if the rounds are cooled with air rather than a liquid, H does not vary from

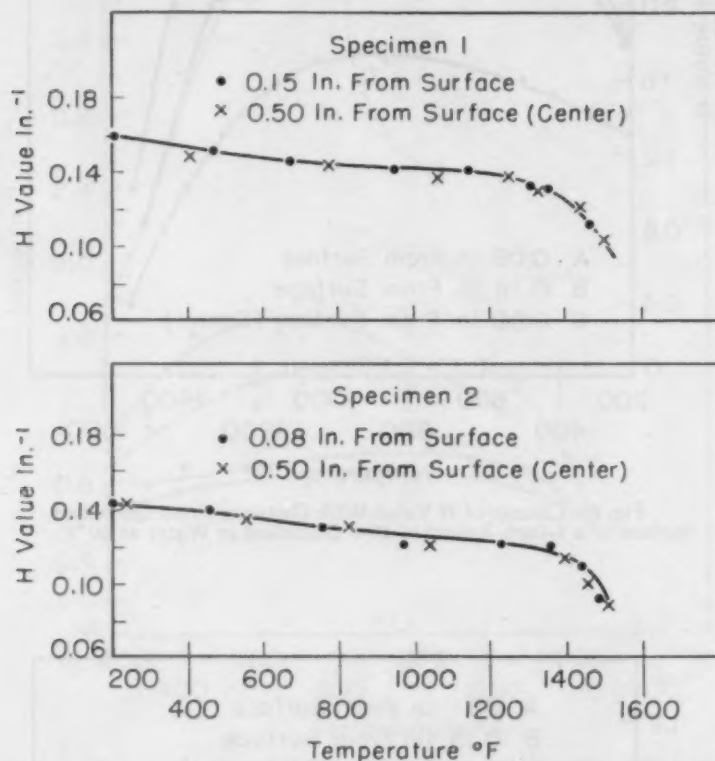


Fig. 8—Change of H With Temperature and Distance From the Surface for a 1-Inch Round of 18-8 Quenched in an Air Blast at 82°F.

surface to center. Two stainless rounds of 1-inch diameter with center couples and two other couples close to the surface were quenched in a compressed air blast and little variation in H value found from surface to center. Fig. 8.

The results of the above studies of the effects of specimen size and of location within a single specimen are summarized in terms of H values at the end of the half temperature-time<sup>2</sup> in Fig. 9.

#### DISCUSSION

The experimental results obtained require an explanation of (a) the change of H with temperature, (b) the increase of H with a

<sup>2</sup>The time to cool to  $\frac{1}{2}$  the temperature difference between the initial temperature of the bar and the temperature of the quenchant.

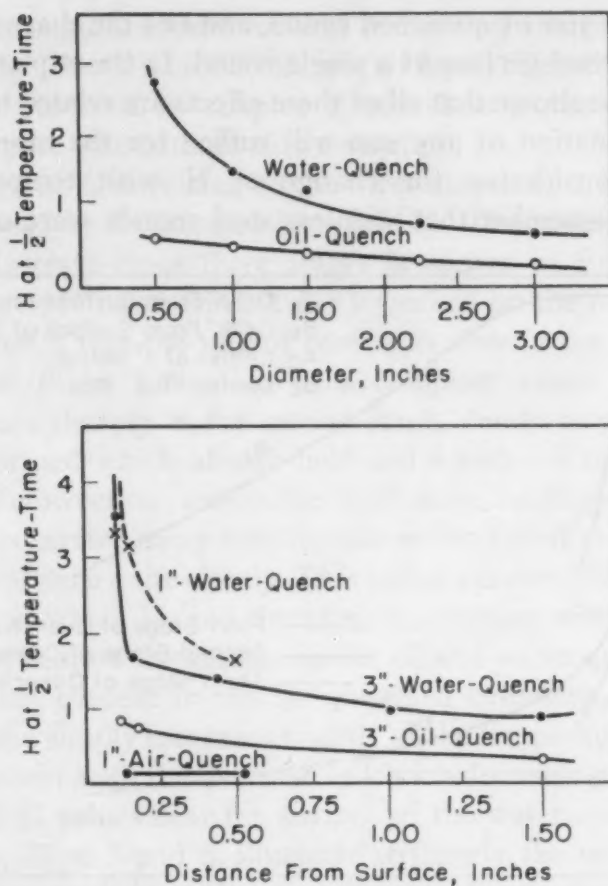


Fig. 9—Effect of Specimen Size and Location Within a Single Specimen on the  $H$  Value at the End of the  $\frac{1}{2}$  Temperature-Time.

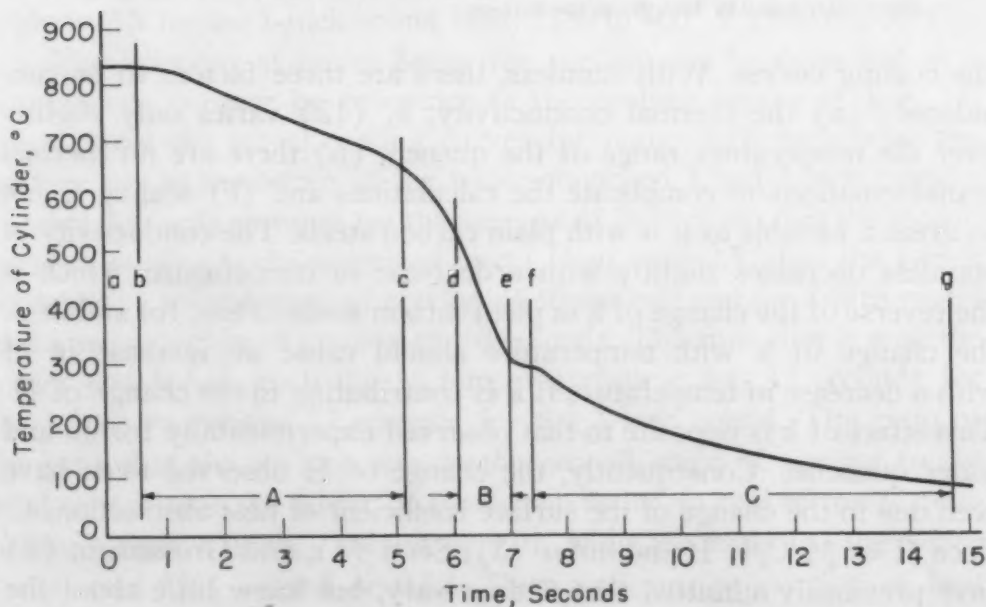


Fig. 10—Typical Cooling Curve for Small Cylinder During Quenching in Still Liquid Showing Three Stages of Quenching A, B, and C. (Curve Taken From Pilling and Lynch.)



decrease in the size of quenched round, and (c) the sharp increase in  $H$  near the quenched surface of a single round. In the explanation offered below, it will be shown that all of these effects are related to one another and the explanation of any one will suffice for the others.

Before considering the change of  $H$  with temperature, it is important to remember that stainless steel rounds were used to obtain

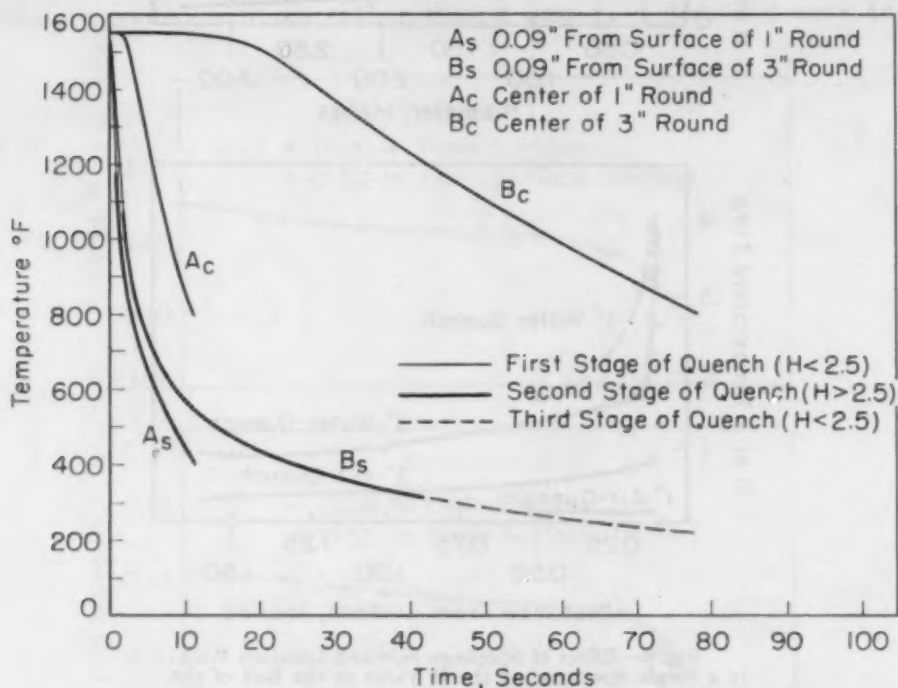


Fig. 11—Cooling Curves for Water-Quenched 1-Inch and 3-Inch Rounds at the Center and 0.09 Inch From the Surface.

the cooling curves. With stainless, there are three factors to be considered: (a) the thermal conductivity,  $k$ , (12) varies only slightly over the temperature range of the quench, (b) there are no thermal transformations to complicate the calculations and (c) scaling is not so great a variable as it is with plain carbon steels. The conductivity of stainless decreases slightly with a decrease in temperature, which is the reverse of the change of  $k$  in plain carbon steels. Thus, for stainless, the change of  $k$  with temperature should cause an increase in  $H$  with a decrease in temperature if  $k$  is contributing to the change of  $H$ . This effect of  $k$  is opposite to that observed experimentally for oil and water quenches. Consequently, the change of  $H$  observed must have been due to the change of the surface coefficient of heat abstraction,  $C$ , since  $H = \frac{1}{2} C/k$ . Heindlhofer (3), Scott (4), and Grossmann (1) have previously admitted that  $C$  does vary, but knew little about the magnitude of its variation with temperature during a quench. This work indicates that  $C$  varies considerably, starting with a fairly low

value, going through a maximum and decreasing sharply to another low value. Since  $C$  is a surface coefficient of heat abstraction, its effects should be best observed by couples placed close to the surface. The data in this report substantiate this deduction.

The change of  $C$  is related to the three stages of a quench which has been proposed by Pilling and Lynch (13). The cooling curve used by them to illustrate these three stages is shown in Fig. 10. Later, Rose (8), Scott (14) and Russell (15) worked on the same problem. Their theory states that the rate of cooling is slow in the first stage of a quench, due to the formation of a complete vapor blanket; the cooling increases sharply in the second stage, due to small pockets of vapor being formed which absorb heat and which are rapidly carried away by liquid convection; and in the third stage, cooling is again slow, since the heat is carried away only by convection currents in the liquid.  $C$  follows this pattern quite closely. This pattern is very plainly reflected in the manner in which  $H$ , and therefore  $C$ , changes with temperature for the couples nearest the surface in the oil and water quenches. It is, furthermore, not evident in the air-quenched cylinders. In the latter case, the  $H$  value simply increases slightly as the temperature decreases, which is consistent with the decrease in  $k$  with decreasing temperature. The high peak  $H$  values near the surface of the water-quenched 1 and 3-inch rounds, Figs. 5 and 6, illustrate strikingly the very rapid heat abstraction characteristic of the second stage of quenching with liquid quenchants. At a distance of 0.09 inch from the surface, the  $H$  for the 3-inch round is above 2.5 from 1070 to 318 °F (575 to 160 °C) and is above 2.5 for the 1-inch round from 1180 to 400° F (640 to 205°C).

The behavior at points below the surface can be explained in a nonrigorous manner by reference to the cooling curves of Fig. 11. These show the actual cooling curves for points 0.09 inch from the surface and at the center of the water-quenched 1 and 3-inch rounds. If one arbitrarily assumes for the purpose of illustration that the second stage of cooling is characterized by an  $H$  of over 2.5, then the 1-inch round had a second stage of cooling of 10 seconds and the 3-inch round had a second stage of cooling of 40 seconds. The time that it took the center couples to reach the  $\frac{1}{2}$  temperature-time was 11 seconds for the 1-inch round and 77 seconds for the 3-inch round. The ratio of the time that the surface was in the second stage of cooling to the total time it took the center of the 1-inch round to cool to the  $\frac{1}{2}$  temperature-time was  $\frac{10}{11}$  second or 0.91, while the ratio for the 3-inch round was  $\frac{40}{77}$  second or 0.52. Thus a greater proportion of heat from the center of the 1-inch than of the 3-inch round passes out to the surface while it is in the second stage of cooling and therefore the

H value for the center of the 1-inch round is higher than that for the 3-inch round.

This same type of reasoning explains both the increase of  $H$  with a decrease in diameter of round and the increase in  $H$  as one approaches the surface in a single quenched round. The cooling curves measured by internal thermocouples are but a reflection of surface conditions during the quench. The closer one is to the surface and the higher the conductivity, the clearer is the reflection of the early portion of the quench when the surface has a high  $C$  value.

This change of  $C$  or  $H$  is important from a practical point of view. It is possible that one could obtain full hardening in one particular thin section and have little hardening in the same quenchant if the section size were increased only slightly. This is possible, since the total amount of heat in the thinner section size could be such that the majority of the heat passes out through the surface while it has a high  $C$  value, while in the slightly larger section size the additional heat capacity could be such that most of the heat has to go out through a surface while it has a low surface heat abstraction coefficient or low  $C$  value.

In an end-quench bar,  $H$  increases sharply near the quenched end in a manner similar to the increase in  $H$  near the surface of a single quenched round. Additional work is being done on rounds and end-quenched bars of low alloy steels and will be reported in the near future.

#### CONCLUSIONS

1. The heat transfer equivalent,  $H$ , increases as the round diameter is decreased when  $H$  is calculated from cooling curves obtained from center thermocouples.
2.  $H$  varies within a single quenched round, increasing from the center to the surface, with the sharpest increase occurring near the quenched surface.
3. In an end-quench bar,  $H$  increases sharply near the quenched end.
4. The above variations in  $H$  appear to be due to the variation in the surface heat abstraction coefficient,  $C$ , with the three stages of a quench.

#### References

1. M. A. Grossmann, M. Asimow and S. F. Urban, "The Hardenability of Alloy Steel", p. 124, Cleveland, Ohio, 1939. Published by the American Society for Metals.
2. J. B. Fourier, "The Analytical Theory of Heat", Cambridge University Press, 1878. English Translation by Alexander Freeman.



3. K. Heindlhofer, "Quenching: A Mathematical Study of Various Hypotheses in Rapid Cooling", *Physical Review*, Vol. 20, 1922, p. 221-242.
4. H. Scott, "Some Problems of Quenching Steel Cylinders", *TRANSACTIONS, American Society for Metals*, Vol. 22, 1934, p. 68.
5. T. F. Russell, "Some Mathematical Considerations on the Heating and Cooling of Steel", Iron and Steel Institute, Special Report No. 14, 1936, p. 149.
6. T. F. Russell, "Some Theoretical Considerations of the Jominy Hardenability Test", Iron and Steel Institute, Special Report No. 36, 1946, p. 25.
7. T. F. Russell and J. C. Williamson, "Surface Temperature Measurements During the Cooling of a Jominy Test Piece", Iron and Steel Institute, Special Report No. 36, 1946, p. 34.
8. A. Rose, "The Cooling Power of Quenching Agents for Steel", *Archiv für das Eisenhüttenwesen*, Vol. 13, February 1940, p. 345.
9. V. H. Krainer and K. Swoboda, "The Role of the Quenchant in the Hardening of Alloy Steel", *Archiv für das Eisenhüttenwesen*, Vol. 17, 1944, p. 163.
10. F. W. Jones and W. I. Pumphrey, "Some Experiments on Quenching Media", *Journal*, Iron and Steel Institute, Vol. 156, Part I, May 1947, p. 37.
11. M. Asimow, W. F. Craig and M. A. Grossmann, "Correlation Between Jominy Test and Quenched Round Bars", *S.A.E. Journal*, Vol. 49, 1941, p. 283.
12. S. M. Shelton, "Thermal Conductivity of Some Steels and Iron Over the Temperature Range 100 to 500 °C", *Bureau of Standards Journal of Research*, Vol. 12, 1934, p. 441.
13. N. B. Pilling and T. D. Lynch, *Transactions, American Institute of Mining and Metallurgical Engineers*, Vol. 62, 1920, p. 665.
14. H. Scott, "The Problem of Quenching Media for the Hardening of Steel", *TRANSACTIONS, American Society for Metals*, Vol. 22, 1934, p. 577.
15. T. F. Russell, "Some Tests on Quenching Oils", Iron and Steel Institute, Special Report No. 24, 1939, p. 283.

## DISCUSSION

**Written Discussion:** By L. T. Wright and C. H. Samans, Engineering Research Dept., Standard Oil Company (Indiana), Chicago.

The authors are to be congratulated on an excellent paper based on highly accurate experimental data. Although it long has been thought that " $H$ " varied with temperature and size, they are to be commended for having pointed out these variations so clearly.

There are two questions which we should like to raise concerning this paper. First, although the " $H$ " plotted by the authors is symbolically the same as Grossmann's " $H$ ", is it really the same term? The same mathematical derivation, based on a constant value of  $H$ , is used in either case. The authors' " $H$ " is based on actual temperature-time curves at various fixed points within the bar and on an assumed value of the thermal diffusivity " $a$ ". Grossmann's " $H$ " is based on hardness measurements and the assumption that the half-temperature cooling times are equal at the surfaces of the unhardened cores in bars of different sizes quenched in a given medium. Thus the two methods of determining " $H$ " are averaging processes starting with differing initial data. It would be



interesting to see a comparison of the two methods carried out experimentally on common test specimens.

In the present work, the authors selected a value for thermal diffusivity for use in computing "H". This raises, therefore, a second question as to the significance, in magnitude, temperature and position variability of "H", of an incorrect selection of the value for thermal diffusivity. This question is important, since a computation of thermal diffusivity, based upon what appeared to be the best available data for 18-8 stainless steel, indicated that a figure of 0.006 square inch per second at room temperature and a figure of about 0.008 square inch per second at 1470 °F (800 °C) would be more representative than the value of 0.0099 square inch per second used by the authors.

In order to examine the effect of varying the selected value of thermal diffusivity, values of "H" were computed by the authors' method. The results are tabulated below for both Curve E and Curve B in Fig. 5 of the paper (water-quenched, 3-inch round).

	For Curve "E" (Center of Bar)			For Curve "B" (0.15 In. From Surface)		
	a = 0.006	0.008	0.0099	0.006	0.008	0.0099
1400 °F	∞	2.3	0.70	3.3	1.6	0.95
1200	∞	1.6	0.84	3.3	2.0	1.25
1000	20	1.5	0.88	3.3	2.3	1.50
800	6.7	1.3	0.90	3.3	2.6	1.66
600	4.1	1.2	0.82	3.3	2.3	1.68
400	3.3	1.1	0.76	3.3	2.0	1.48

NOTE: The values of ∞ merely mean that "a" could not have been that small.

It will be seen at once that the proper selection of "a" value of the thermal diffusivity is more important for points near the center of the bar. Obviously the room temperature value of 0.006 square inch per second is too small for the center point and high temperatures. The higher diffusivity value is probably more representative at the center, since the center of the bar remains at high temperature for a considerable period of time. For positions near the surface the effective diffusivity will be lower, due to the lower average temperature.

A possible method of determining both "H" and the proper value of "a" for a given position in the bar is to plot, on log-log graph paper, the "reduced temperature" (as used in Russell's tables) against time from the experimental data. On a transparent graph paper plot Russell's data for the point in question, showing curves of "reduced temperature" against "reduced time" for various values of "H". By superposing the transparent graph over the graph of experimental data, one can determine which "H" value gives the curve shape most nearly approaching the experimental one, and, at the same time, the corresponding values of actual and "reduced" time are shown. This time comparison allows "a" to be calculated. This comparison was made for the bar positions represented by Curves E and B of Fig. 5 with the following results:

Curve E  
Effective H = 0.8  
Effective a = 0.010 sq.in./sec.

Curve B  
Effective H = 3.3  
Effective a = 0.006 sq.in./sec.

Now, obviously, the severity of the quench is strictly represented by the rate of cooling at the surface of the bar. Why does the "H" value at the

center turn out to be so low? This is explained by the lower effective thermal diffusivity of the surface layers. The temperature gradients near the surface are very steep, due to this low diffusivity, and therefore the center of the bar is more protected from the severe quench which exists at the surface.

#### Authors' Reply

Drs. Wright and Samans' valuable comments are greatly appreciated. Their first question is: "Are Grossmann's ' $H$ ' and the ' $H$ ' plotted in this paper the same?" At present, it can only be said that the " $H$ " values determined by the two methods are of the same order of magnitude for both oil and water quenches. It is true, however, that although the " $H$ " value determined in both methods is based on the same mathematical derivation, " $H$ " is not determined in the same manner. Grossmann and co-workers made an additional assumption of the  $\frac{1}{2}$  temperature cooling time being related to the hardness of the quenched rounds. More experimental evidence is necessary to determine the degree of correlation between the " $H$ " values determined by the two methods. Grossmann's " $H$ " is an average " $H$ " over the three or more particular  $Du/D$  positions in the three or more different size rounds quenched. Cooling curves need be measured at approximately the same positions in the same three bars in order to make proper comparison of the " $H$ " value determined by both methods.

The second question is concerned with the problem of the choice of the proper average diffusivity value in making calculations of " $H$ " values from cooling curves. This is an extremely difficult problem, since the diffusivity is known not to be constant, but varies with temperature during the quench. A single average diffusivity value was chosen. To be precise, because of the different temperature gradients at different positions within a quenched bar, a different average value should have been chosen for the different positions within the same bar. Drs. Wright and Samans have devised a method of choosing this average diffusivity value for the different locations. It involves making the best match between actual cooling curves and mathematically derived curves. Since the mathematically derived curve assumes that the diffusivity and surface heat abstraction coefficient are constant, a perfect fit can never be obtained. The degree of misfit depends upon the variation in the so-called constants. This method, however, is better than the calculation of an average diffusivity value based on the use of known data on thermal conductivity, specific heat and density. This is evident from Wright and Samans' calculations using 0.006 square inch per second for the center cooling curve of the 3-inch round which yields entirely erroneous " $H$ " values. Their matching method yielded an average diffusivity of 0.010 for the center couples, which was the same as the value used in this paper. For the couple 0.15 inch from the surface of a 3-inch round, their method yielded an average diffusivity of 0.006. If a perfect match were made using their method, then the " $H$ " value would have been constant with temperature, as they recorded in their table. But actually a perfect fit is not obtained and the degree of misfit is shown by the " $H$ " values

obtained using the 0.006 average diffusivity for this cooling curve. These values are listed below:

Temp., °F	"H" (in.-1)
1200	2.0 (extrapolated)
1000	2.6
800	2.8
600	2.9
400	2.4
200	2.0

This merely raises the curve as plotted in the paper. The use of a lower diffusivity for other positions near the surface raises the curves in a similar manner to higher "H" values than plotted in the paper. The conclusions reached in the paper remain unchanged.



## THE TEMPERING OF CHROMIUM STEELS

BY R. W. BALLUFFI, MORRIS COHEN AND B. L. AVERBACH

### Abstract

*The second, third, and fourth stages of tempering have been studied in a series of chromium steels by means of dilatometric, magnetic, and metallographic techniques used in conjunction with an electrolytic method for the extraction of carbides. It has been shown that, in the second stage of tempering which occurs between 400 and 600 °F (205 and 315 °C), the retained austenite is decomposed into the same products as would be obtained from the transformation of primary austenite at the same temperature. The transformation rate, however, is accelerated by the presence of the tempered martensite. The third stage of tempering starts at about 400 °F (205 °C) and involves the formation of cementite which, at first, has a higher iron content than stoichiometric  $\text{Fe}_3\text{C}$ . The kinetics of this reaction indicate that the diffusion of carbon in ferrite is not the rate-limiting factor in the process. During the fourth stage which sets in at 1000 °F (540 °C),  $(\text{Cr,Fe})_7\text{C}_3$  is precipitated while the cementite goes back into solution. The alloy carbide is coarse and spheroidal compared to the fine, plate-like form of the cementite being replaced, and is not very effective in inhibiting plastic deformation. The role of chromium in retarding softening on tempering comes into play during the third stage by restricting the growth and spheroidization of the cementite platelets.*

MUCH previous work has been done on the decomposition of martensite and retained austenite during the tempering of plain carbon and low alloy steels (1-6),<sup>1</sup> and as a result, the tempering process can be divided into four well-defined but overlapping stages:

1). Immediately after quenching, the matrix of the hardened steel consists of untempered martensite and retained austenite. If the quenched steel is then heated at temperatures up to approxi-

<sup>1</sup>The figures appearing in parentheses pertain to the references appended to this paper.

This work represents a portion of a thesis submitted by R. W. Balluffi in partial fulfillment for the requirements for the degree of Doctor of Science at the Massachusetts Institute of Technology, February 1950.

A paper presented before the Thirty-second Annual Convention of the Society, held in Chicago, October 21 to 27, 1950. Of the authors, R. W. Balluffi is associated with the Research Laboratory, Sylvania Electric Products Inc., Bayside, Long Island, N. Y., Morris Cohen is professor of metallurgy, and B. L. Averbach is assistant professor of metallurgy, Massachusetts Institute of Technology, Cambridge, Mass. Manuscript received April 14, 1950.



mately 400 °F (205 °C), a carbon-rich transition product (not cementite) is precipitated from the martensite, and the reaction has been called the first stage of tempering. During this period of carbon rejection, the martensite lattice contracts in volume and becomes less tetragonal.

2). At temperatures between 400 and 600 °F (205 and 315 °C), the retained austenite is decomposed into bainite. This transformation, which is the second stage of tempering, tends to increase the volume of the steel.

3). As the temperature is raised beyond 400 °F (205 °C) the early precipitate is converted to cementite, and this conversion is regarded as the third stage of tempering. It is marked by a considerable decrease in volume, and overlaps the austenite decomposition reaction of the second stage.

4). At still higher temperatures, above about 1000 °F (540 °C), complex alloy carbides form at the expense of the cementite in steels containing a sufficiently high content of stable carbide-forming elements. This process is designated as the fourth stage of tempering.

The kinetics of the first and second stages of tempering have been analyzed quantitatively elsewhere (6) by means of precision-length measurements to trace the course of the reactions. Accordingly, the present work was concentrated on the third and fourth stages, although the second stage had to receive considerable attention in order to disentangle the third stage. Because of the large volume changes attending these processes, it was possible to follow the corresponding length variations with a dilatometer, which is a much less tedious approach than the precision-length technique (6). In addition, the conversion of the transition precipitate into cementite during the third stage was studied by means of magnetic measurements. This was feasible because the intensity of magnetization and the Curie point of the transition precipitate are both markedly higher than those of the cementite (2).

Chromium steels were deliberately chosen for this investigation to permit a detailed analysis of the fourth stage of tempering in view of the fact that the kinetics and mechanism of this process have not been established. Electrolytic extraction, X-ray diffraction, specific volume determinations, quantitative metallography and electron microscopy were used to study this problem.

#### MATERIALS INVESTIGATED

The compositions of the steels studied are listed in Table I.

Table I  
Composition of Steels

Steel	C	Si	Mn	S	P	Cr	V
K	1.07	0.23	0.25	0.014	0.011	—	—
T	1.00	0.35	0.37	—	—	1.56	0.21
Z	1.11	0.25	0.25	—	—	4.11	—
Y	0.67	0.28	0.31	0.009	0.014	4.00	—

Steels K and T are commercial grades and are the same as those previously investigated for the first and second stages (6). Steels Z and Y were prepared as 30-pound laboratory heats by the Vanadium-Alloys Steel Company. All four materials were received in the spheroidized condition.

The Y composition was specifically chosen because, at temperatures just below the critical range,  $(\text{Cr,Fe})_7\text{C}_3$  is the only stable carbide that exists in this alloy (7). Hence, any cementite that may form during the third stage of tempering should disappear completely during the fourth stage of tempering.

#### SECOND AND THIRD STAGES OF TEMPERING

*Experimental Details*—The reactions involved in the second and third stages of tempering occur more and more rapidly as the temperature is raised, and therefore the dilatometer assembly used for tracing the changes must be capable of being heated quickly to the predetermined tempering temperature. Otherwise, a large part of the transformation may take place during the heating, and the observed changes will not represent a true isothermal tempering process. Consequently, the quenching dilatometer described by Averbach and Cohen (6) was employed, with some modifications, to facilitate quenching upward from the ambient to the tempering temperature.

The specimens were thin-walled tubes, 3 inches long by 0.277 inch O.D. by 0.217 inch I.D. Thermocouple wires were spot-welded to the inner surface, and the temperature was recorded by means of a string galvanometer. For each run, a hardened specimen was loaded into the dilatometer at room temperature, and quenched upward to the tempering temperature in a liquid metal bath. Only 20 seconds were required to reach temperature.

Two austenite-martensite mixtures were obtained in each steel by hardening to room temperature and to  $-320^\circ\text{F}$  ( $-195^\circ\text{C}$ ), as indicated in Table II. The changes in length on tempering such a pair of specimens at any given temperature were substituted into simultaneous equations (6) to solve for the expansion due to the

**Table II**  
**Volume Per Cent of Retained Austenite and Undissolved Carbides**  
**in Hardened K, T, and Z Steels**

Steel		Volume Per Cent Undissolved Carbides*	Volume Per Cent Retained Austenite†
K (1.07% C)	Austenitized at 1450 °F, brine quenched to RT	3.0	7.8
	Austenitized at 1450 °F, refrigerated in liquid nitrogen	3.0	3.8
T (1.00% C - 1.56% Cr)	Austenitized at 1550 °F, oil-quenched to RT	8.0	10.0
	Austenitized at 1550 °F, refrigerated in liquid nitrogen	8.0	2.0
Z (1.11% C - 4.11% Cr)	Austenitized at 2000 °F, oil-quenched to RT	0.0	75.0
	Austenitized at 2000 °F, refrigerated in liquid nitrogen	0.0	25.0

\*From lineal analysis (9)

†From X-ray intensities (10)

transformation of the retained austenite and the contraction due to the decomposition of the martensite. These calculations were carried through for steels K, T, and Z.

Further information on the conversion of the transition precipitate to cementite in the third stage of tempering was obtained by magnetic intensity measurements, using the ballistic-galvanometer technique (8). Specimens, 4 inches long by 1/4-inch diameter, of the K steel were water-quenched from 2000 °F (1095 °C) to dissolve all the carbides, cooled immediately to -320 °F (-195 °C) to eliminate most of the retained austenite, and were then tempered at 450 to 1100 °F (230 to 595 °C) for various times. After this, each specimen was heated slowly from room temperature in the magnetometer and the intensity of magnetization was determined as a function of temperature in a field of 400 oersteds. Thus, the Curie point of the existing carbide phase was ascertained by this procedure without causing any further tempering.

*Discussion of Results*—The transformation of the retained austenite in steels K, T, and Z is shown in Figs. 1, 2, and 3, as a function of tempering temperature and time. There is not much difference in the curves for steels K and T. The rate of transformation increases rapidly with temperature in this second stage of tempering, and at 700 °F (370 °C) the reaction is essentially complete before the earliest measurement can be made. The product of the reaction is bainite, as would be the case if the primary austenite were hot-quenched into this temperature range. Figs. 1 and 2 indicate that the bainitic product is not stable and undergoes a slight contraction on holding at temperature. This phenomenon becomes



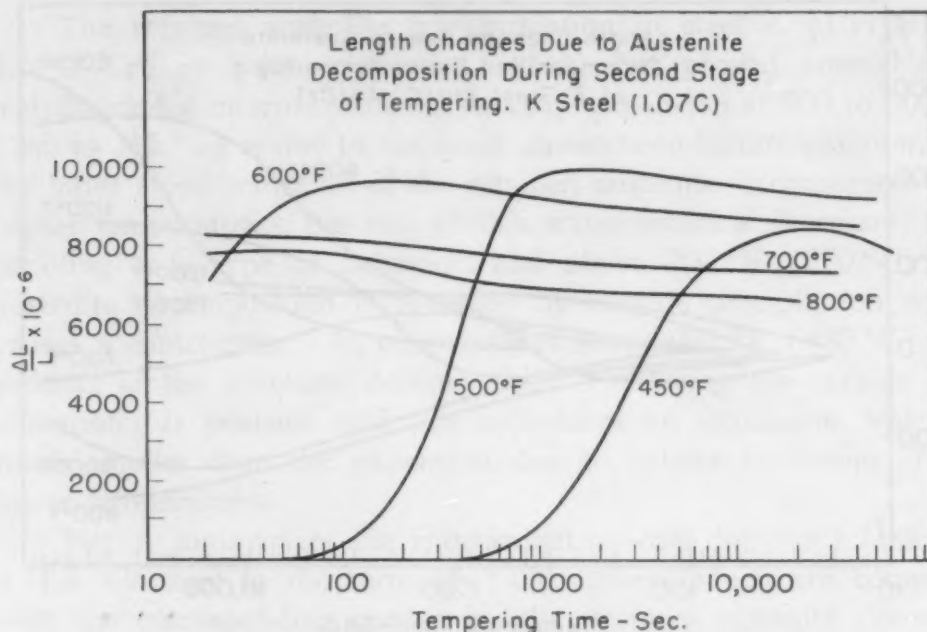


Fig. 1—Length Changes Due to Austenite Decomposition During Second Stage of Tempering—K Steel (1.07% Carbon).

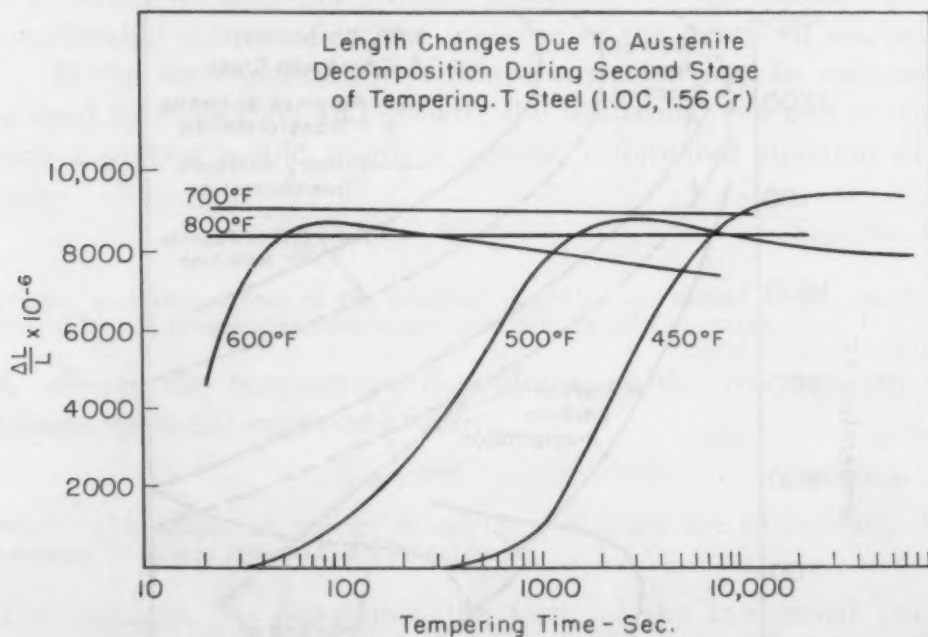


Fig. 2—Length Changes Due to Austenite Decomposition During Second Stage of Tempering—T Steel (1.0% Carbon, 1.56% Chromium).

more pronounced at the lower tempering temperatures. Bainite is undoubtedly an aggregate, but magnetic measurements reveal no cementite Curie point after tempering well into the second stage (2). It is conceivable, therefore, that the bainitic contraction in Figs. 1 and 2 denotes the gradual conversion of a transition precipitate in the bainite to the more stable cementite.



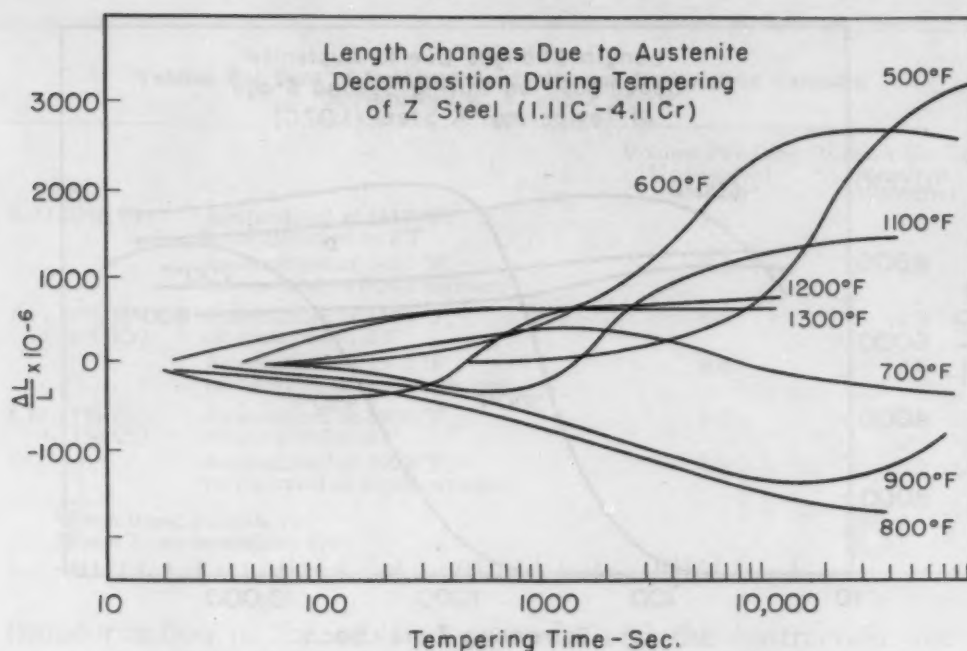


Fig. 3—Length Changes Due to Austenite Decomposition During Tempering of Z Steel (1.11% Carbon, 4.11% Chromium).

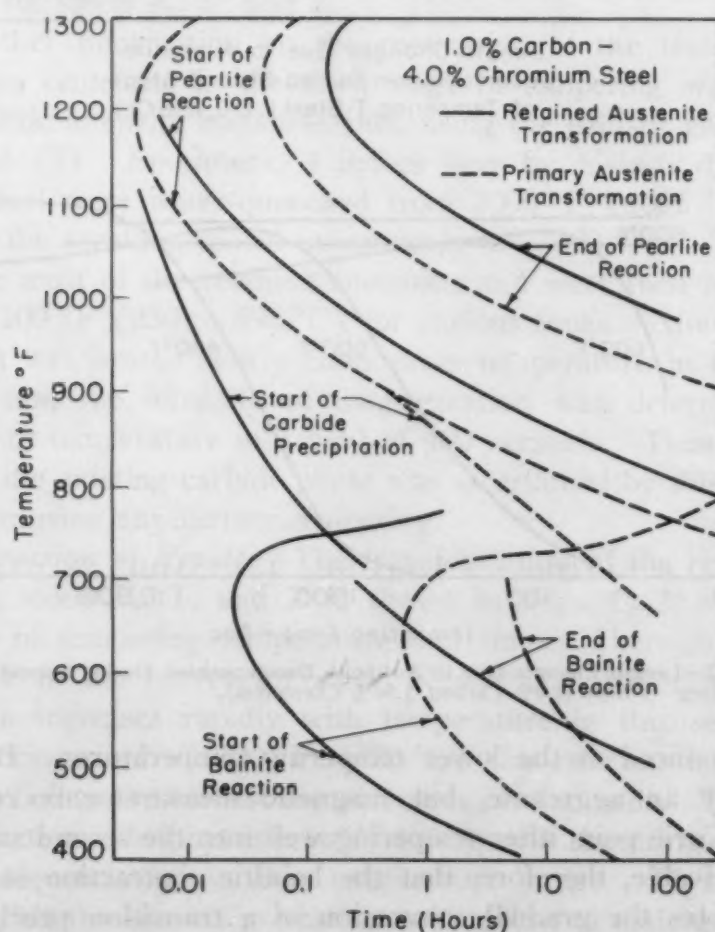


Fig. 4—Transformation Data for the 1.11% Carbon, 4.11% Chromium Steel in the Form of TTT Curves.

The retained austenite transformation in steel Z (1.11% C-4.11% Cr) is quite complex (Fig. 3) but proved amenable to metallographic interpretation. The large expansion at 500 to 600 °F (260 to 315 °C) is due to the usual austenite-to-bainite reaction, but the latter stops before all of the retained austenite is consumed. At higher temperatures, the rate of this transformation decreases, thus denoting a C type of behavior, and above 700 °F (370 °C) the austenite decomposition is preceded by carbide precipitation which causes a contraction. At temperatures above 900 °F (480 °C), the product of the austenite decomposition (following the carbide precipitation) is pearlite, and this introduces an expansion which is much smaller than the expansion due to bainite formation at the lower temperatures.

Fig. 4 summarizes the transformation data for the 1.11% C-4.11% Cr steel in the form of TTT curves, which are compared with the corresponding curves for the primary austenite decomposition (11). Retained austenite decomposes into the same series of products as does the primary austenite but the reaction rate is considerably influenced by the presence of the tempered martensite.

If the decomposition of retained austenite may be assumed to proceed by nucleation and growth, the isothermal reaction curve for such a process would follow a general differential equation of the type:

$$\frac{dy}{dt} = k(a - y)t^m \quad \text{Equation 1}$$

where:  $a$  = total extent of the reaction possible,  $y$  = extent of the reaction at time  $t$ ,  $k$  = a temperature-dependent constant,  $m$  = a constant.

$K$  reflects the temperature dependence of the reaction rate and follows the usual exponential form:

$$k = Ae^{-Q/RT} \quad \text{Equation 2}$$

where:  $Q$  = activation energy in cal/mole,  $T$  = absolute temperature,  $A$  = a constant,  $R$  = gas constant = 1.99 cal/mole.

The constant,  $m$ , determines the form of the isothermal reaction curve and has been used by Zener (12) as a criterion for the shape of the precipitating particle. In the well-known nucleation and growth equation of Johnson and Mehl (13),  $m$  has a value of 3.

In the integral form, Equation 1 becomes

$$\log \log \left( \frac{a}{a - y} \right) = (m + 1) \log t + \log \frac{k}{2.3} \quad \text{Equation 3}$$

To evaluate this equation, it is assumed that the change in unit length is proportional to the extent of the reaction and that the

maximum change in unit length corresponds to the completion of the reaction. If  $\log \log \left( \frac{a}{a-y} \right)$  is plotted as a function of  $\log t$ , a straight line with a slope of  $(m+1)$  should be observed. Fig. 5 shows the validity of this formulation for the K (1.07% C) and T (1.0% C, 1.56% Cr) steels, and the slope of the line yields a value

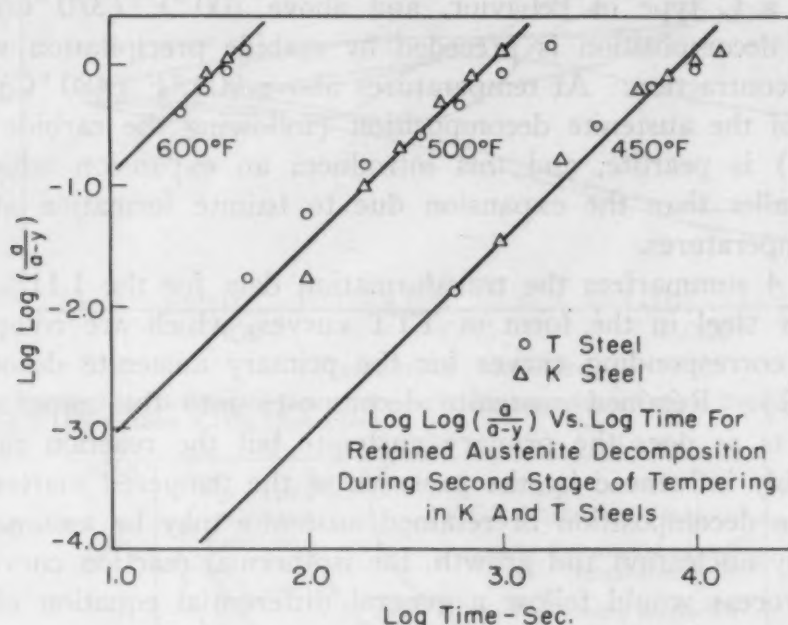


Fig. 5—Log Log  $\left( \frac{a}{a-y} \right)$  Versus Log Time for Retained Austenite Decomposition During Second Stage of Tempering in K and T Steels.

of 0.6 for  $m$ . The reaction apparently involves a nucleation and growth process of the type which proceeds after an incubation time. It is difficult, however, to say more about the nature of the precipitate or the mechanism of the reaction from the kinetic data alone. The kinetics of the austenite decomposition in the Z steel (1.11% C, 4.11% Cr) were not studied in detail because of the complexity of the reaction products.

The reaction constant,  $k$ , for both steels was found to have the same temperature dependence (Fig. 6), with the heat of activation for the process being 58,000 cal/mole. However, this value refers to a quantity with dimensions of  $(\text{time})^{-1.6}$ . On the more usual basis of  $(\text{time})^{-1}$  for the reaction constant, dimensional analysis (14) shows that the activation energy is 36,000 cal/mole. The latter figure is in good agreement with the value of 38,000 cal/mole obtained by Averbach and Cohen (6) and is of the same order as the activation energy for the diffusion of carbon in austenite (15).

The calculated curves for the decomposition of 100% martensite

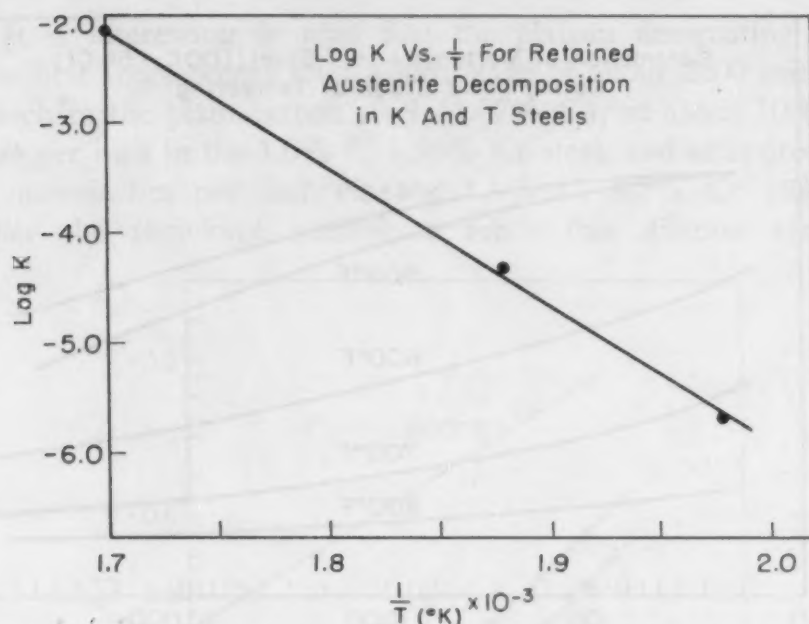


Fig. 6—Log K Versus  $\frac{1}{T}$  for Retained Austenite Decomposition in K and T Steels.

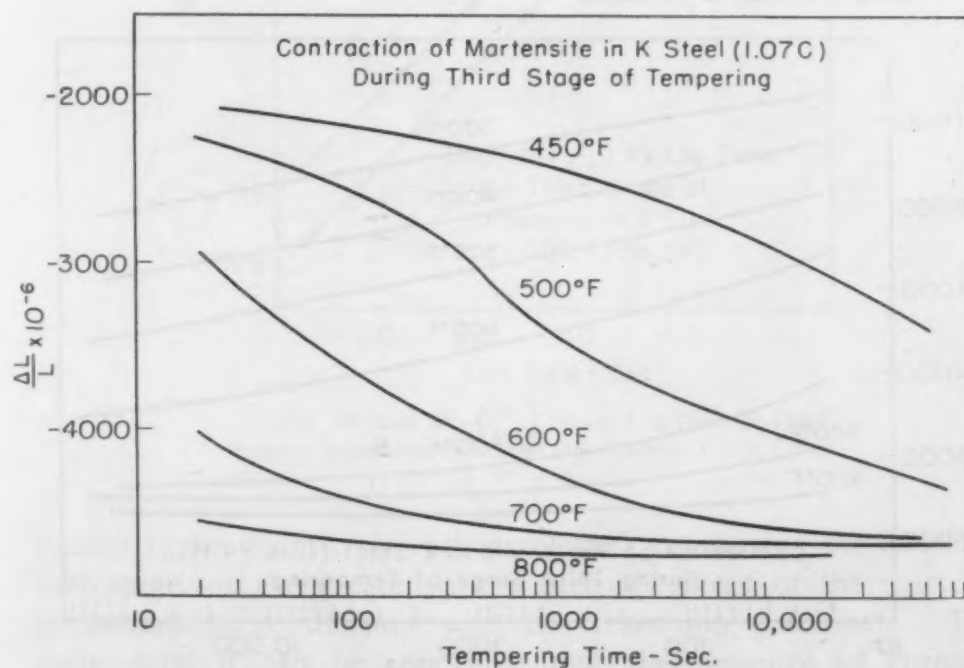


Fig. 7—Contraction of Martensite in K Steel (1.07% Carbon) During Third Stage of Tempering.

in the K, T, and Z steels are presented in Figs. 7, 8, and 9. The third stage in the K (1.07% C) and T (1.0% C, 1.5% Cr) compositions forms a continuation of the first-stage behavior (6). At the end of the first stage of tempering, the shrinkage curves show a plateau which represents a metastable equilibrium between the



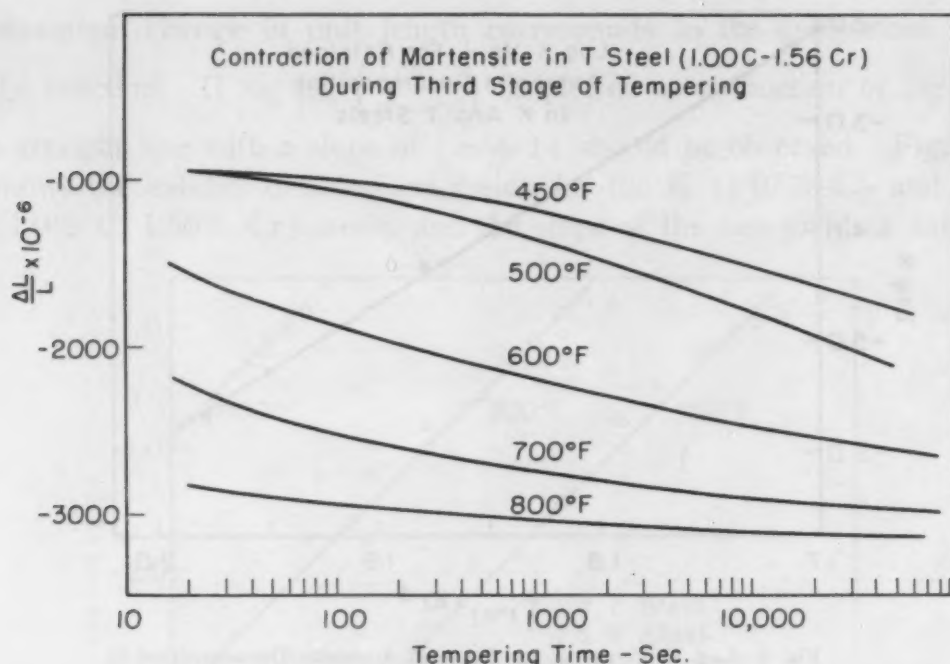


Fig. 8—Contraction of Martensite in T Steel (1% Carbon, 1.56% Chromium) During Third Stage of Tempering.

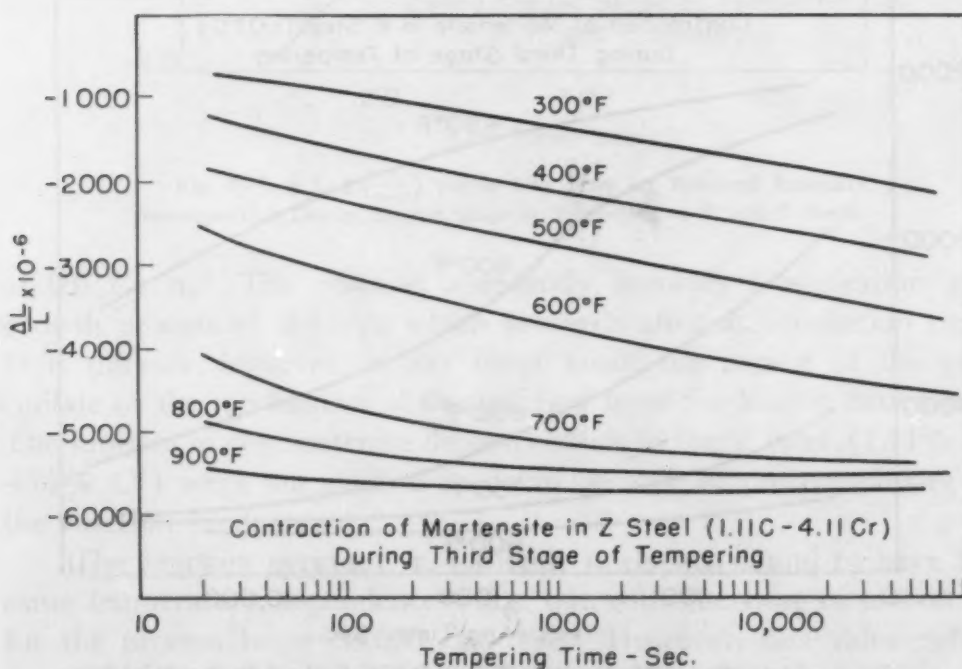


Fig. 9—Contraction of Martensite in Z Steel (1.11% Carbon, 4.11% Chromium) During Third Stage of Tempering.

martensitic lattice and the transition precipitate. In Figs. 7 and 8, this stage is barely indicated by the retarded shrinkage at short times at 450 and 500 °F (230 and 260 °C). The conversion to cementite occurs rapidly at these temperatures and is essentially complete within 24 hours at 800 °F (425 °C).

It is interesting to note that the plateau designating the end of the first stage occurs after a shrinkage of about 2000 microinches per inch in the plain carbon steel (1.07% C), at about 1000 microinches per inch in the 1.0% C, 1.56% Cr steel, and at approximately 800 microinches per inch<sup>2</sup> in the 1.1% C, 4.1% Cr steel. The smaller the shrinkage needed to reach this dilation arrest, the

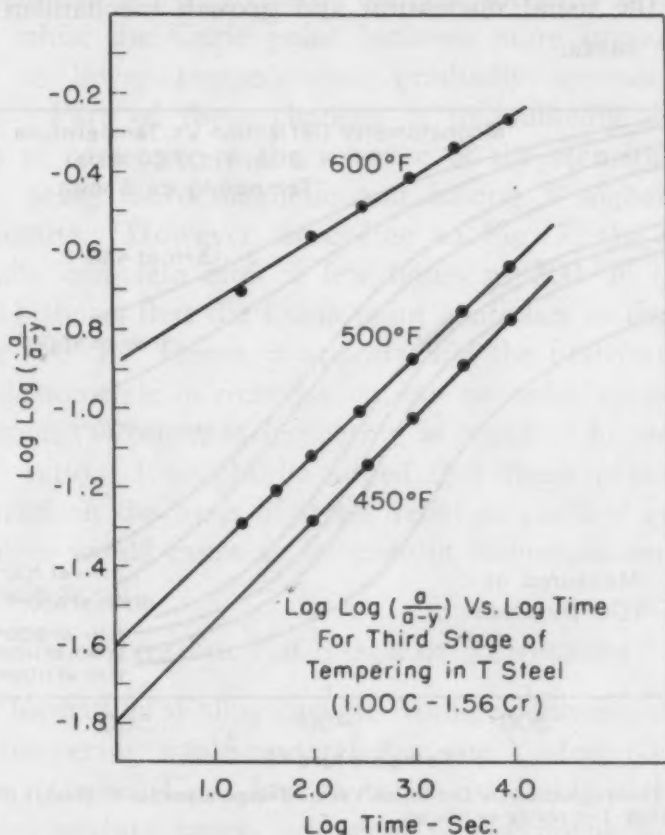


Fig. 10—Log Log ( $\frac{a}{a-y}$ ) Versus Log Time for Third Stage of Tempering in T Steel (1% Carbon, 1.56% Chromium).

smaller is the quantity of carbon rejected in attaining the end of the first stage, or the greater is the carbon content of the martensite in metastable equilibrium with the transition precipitate. From these data, it can be concluded that the presence of chromium increases the amount of carbon in the martensite at the end of the first stage. This corresponds to a decrease in the thermodynamic activity of carbon in the presence of chromium and an increase in the solubility of carbon in the martensitic lattice coexisting with the transition precipitate.

Using the curves in Figs. 7 and 8 as a measure of the extent

<sup>a</sup>This has been confirmed by precision-length measurements after tempering at lower temperatures.

of the third-stage reaction, the data were analyzed in accordance with Equation 3. Fig. 10 indicates that straight lines are obtained, the average value of  $m$  being  $-0.8$ . A negative quantity for  $m$  indicates that the reaction is extremely rapid at the beginning (see Equation 1) and that there is no incubation period. The same characteristics were found for the first stage (6) and this may indicate that the usual nucleation and growth mechanism does not apply in these cases.

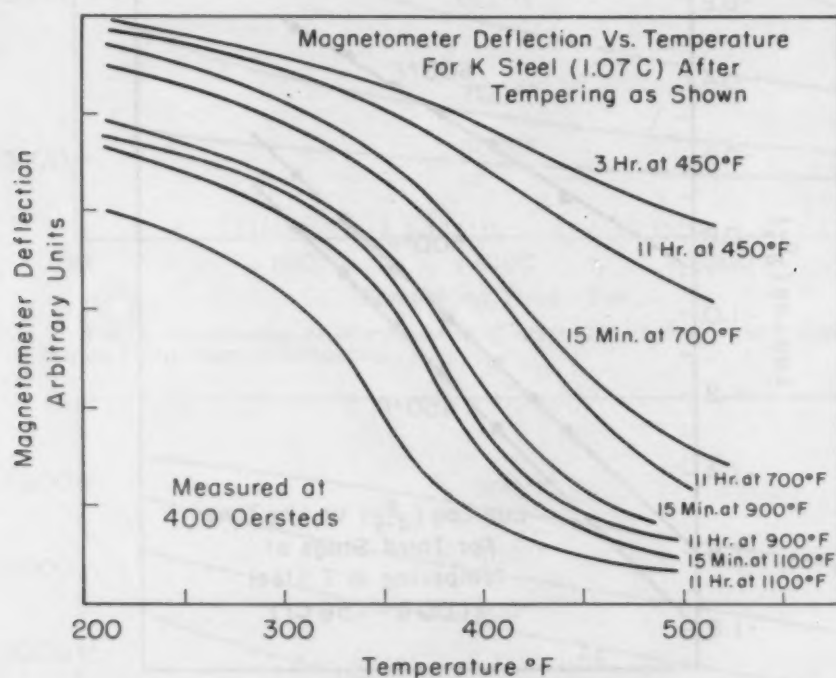


Fig. 11—Magnetometer Deflection Versus Temperature for K Steel (1.07% Carbon) After Tempering as Shown.

Activation energies for the reaction constant of the third stage on the basis of  $(\text{time})^{-1}$  were found to be 42,300 cal/mole for the K steel (1.0% C) and 57,500 cal/mole for the T steel (1.0% C, 1.5% Cr). These values are considerably larger than the activation energy of 18,100 cal/mole reported by Stanley (16) for the diffusion of carbon in ferrite, and thus it seems that the diffusion of carbon is not the controlling factor in the kinetics of the third stage of tempering.

The conversion of the transition precipitate to cementite is indicated magnetically in Fig. 11 for specimens of the K steel (1.07% C) which was tempered sufficiently to bring them into various portions of the third stage. The magnetic measurements were made, after the tempering, on slow heating from room temperature in order to reveal the Curie point of the carbide phase. Pure

cementite ( $\text{Fe}_3\text{C}$ ) passes through its Curie point at about  $400^\circ\text{F}$  ( $204^\circ\text{C}$ ), and is denoted by a rapid decrease in magnetization on heating. The specimen tempered for 11 hours at  $1100^\circ\text{F}$  ( $595^\circ\text{C}$ ) contains well-formed cementite, and Fig. 11 illustrates the corresponding magnetic behavior.

As the tempering temperature is increased above  $450^\circ\text{F}$  ( $230^\circ\text{C}$ ), the curves in Fig. 11 show that the intensity of magnetization decreases while the Curie point becomes more pronounced and is displaced to lower temperatures, gradually approaching that of cementite. Part of these changes is undoubtedly caused by the formation of cementite at the expense of the transition precipitate, the latter being more magnetic and having a higher Curie point than cementite. However, according to Fig. 7, the third stage is substantially complete after a few hours at  $700^\circ\text{F}$  ( $370^\circ\text{C}$ ), and yet Fig. 11 shows that the Curie point continues to drop on tempering above  $700^\circ\text{F}$ . Hence, it appears that the first-formed cementite is not stoichiometric in composition, but probably contains an excess of iron atoms. Prolonged tempering is required in order to achieve the  $\text{Fe}_3\text{C}$  ratio. It might be added that these phenomena cannot be explained on the basis of stress relief or particle growth because such changes would cause an increase in magnetization and a raising of the Curie point.

#### THE FOURTH STAGE OF TEMPERING

The formation of alloy carbide from cementite during the fourth stage of tempering was investigated in the Y steel (0.67% C, 4.0% Cr) since  $(\text{Cr,Fe})_7\text{C}_3$  is known to be the stable carbide below the critical temperature range. A series of specimens was austenitized at  $2000^\circ\text{F}$  ( $1095^\circ\text{C}$ ), refrigerated in liquid nitrogen, and then tempered for different times in the range of  $1000$  to  $1400^\circ\text{F}$  ( $540$  to  $760^\circ\text{C}$ ). The austenite retained after refrigeration was entirely transformed during the early part of these tempering treatments. Moreover, the formation of cementite  $(\text{Fe,Cr})_3\text{C}$  during the third stage of tempering was virtually completed before the first measurements in this temperature range were made.

*Metallographic Studies*—It was found that a boiling  $\text{KMnO}_4$ – $\text{NaOH}$  etch (17) darkened the  $(\text{Cr,Fe})_7\text{C}_3$  carbide and left the coexisting  $(\text{Fe,Cr})_3\text{C}$  and matrix unaffected. The progressive formation of the alloy carbide was thus observed, and could be determined quantitatively by lineal analysis (9). It is evident from Fig. 12 that very little of the alloy carbide is produced at  $1000^\circ\text{F}$  ( $540^\circ\text{C}$ ), most of the carbon being present as cementite. After



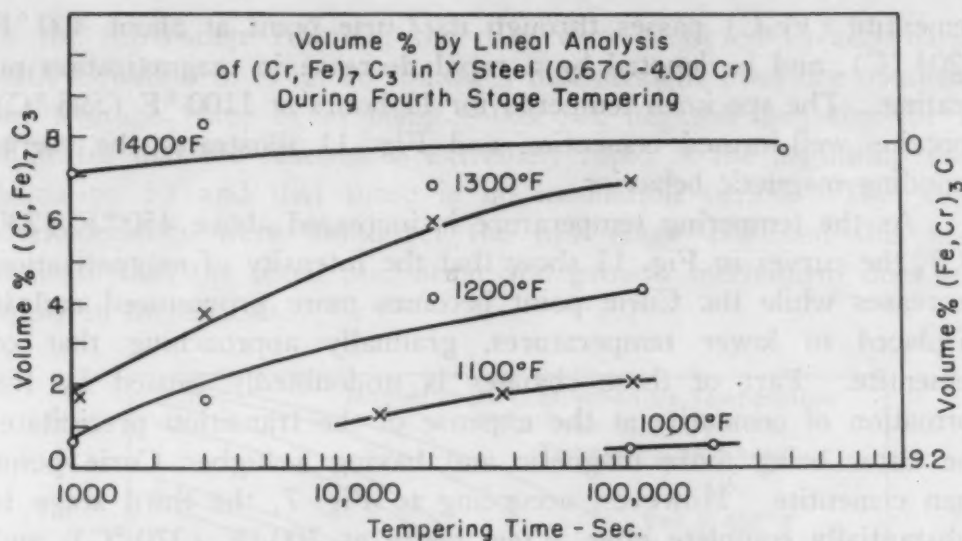


Fig. 12—Volume Per Cent by Lineal Analysis of  $(Cr, Fe)_7C_3$  in Y Steel (0.67% Carbon, 4% Chromium) During Fourth Stage of Tempering.

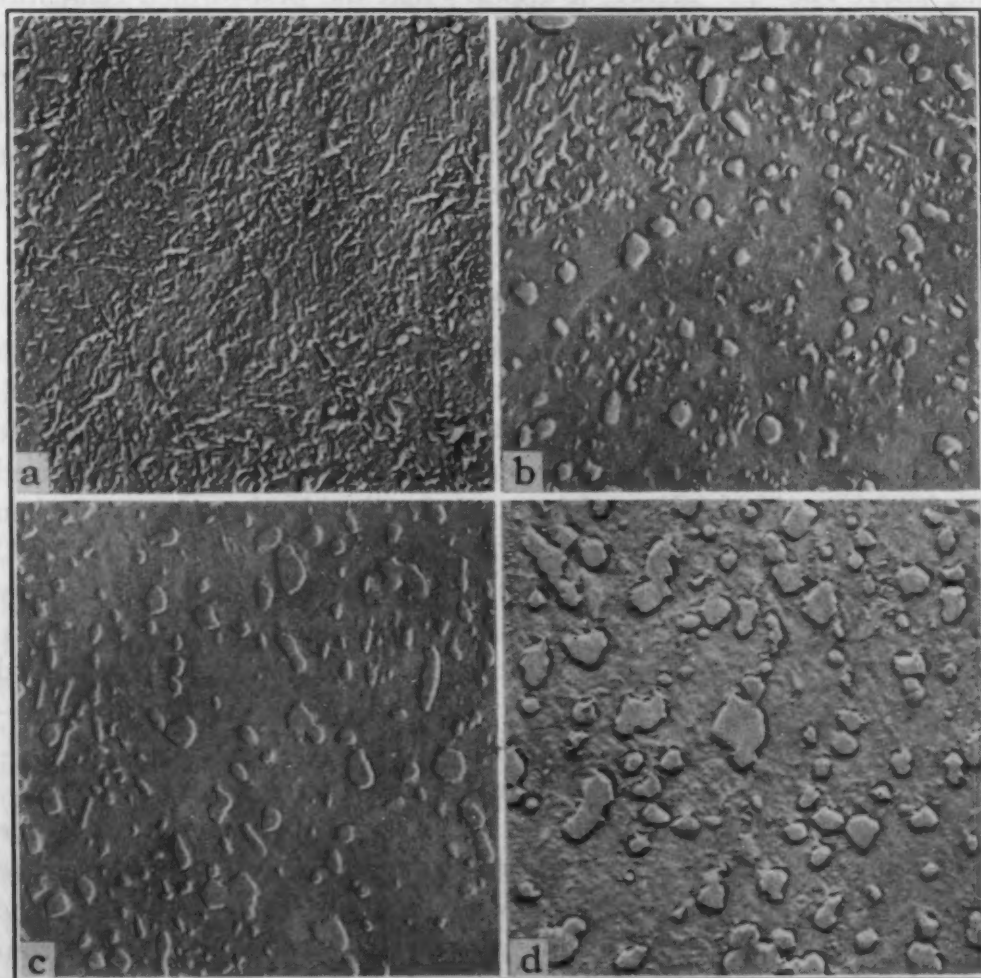


Fig. 13—Electron Micrographs of Y Steel (0.67% Carbon, 4% Chromium) After Tempering for 28 Hours at Temperatures Indicated.  $\times 12000$ . a—1000°F; b—1190°F; c—1310°F; d—1405°F.

28 hours at 1300 °F (705 °C), however, nearly all of the  $(\text{Fe,Cr})_3\text{C}$  is converted to  $(\text{Cr,Fe})_7\text{C}_3$ .

The mode of formation of the alloy carbide at the expense of the cementite during these tempering studies is revealed by the electron micrographs in Fig. 13. These pictures were taken by Prof. D. H. Whitmore of Northwestern University, who used a collodion replica which had been shadow-cast with chromium.<sup>3</sup> Fig. 13a indicates that the cementite existing at 1000 °F (540 °C) has a plate-like shape which is inherited from the third stage of tempering. Figs. 13b and 13c show that, as the tempering proceeds during the fourth stage, there is a gradual disappearance of the plate-like  $(\text{Fe,Cr})_3\text{C}$  while the amount of  $(\text{Cr,Fe})_7\text{C}_3$  increases, the latter having a distinctly spheroidal form. After tempering at 1405 °F (760 °C) (Fig. 13d), the structure consists entirely of well-rounded spheroids of the alloy carbide in a ferritic matrix.

It is important to note that the size, shape and distribution of the  $(\text{Fe,Cr})_3\text{C}$  particles are quite different from those of the  $(\text{Cr,Fe})_7\text{C}_3$  particles during the fourth stage of tempering. Many small particles of cementite are replaced by relatively few large particles of the alloy carbide, and regions around the latter are frequently devoid of cementite. This strongly suggests that the  $(\text{Fe,Cr})_3\text{C}$  does not transform into  $(\text{Cr,Fe})_7\text{C}_3$  in situ (by virtue of an increase in the chromium content) but actually dissolves in the ferritic matrix while the more stable carbide grows elsewhere. Therefore, cementite formation during the third stage of tempering should not be regarded as a preparatory step toward the ultimate precipitation of the alloy carbide; rather, it is essentially a competitive process which happens to occur more rapidly than the formation of the more stable carbide.

It may also be significant that the  $(\text{Cr,Fe})_7\text{C}_3$  particles are spheroidal instead of plate-like. Evidently, the precipitation temperature is sufficiently high so that coherency with the matrix is not maintained and the particles assume a shape of minimum interfacial area. This may explain why the formation of  $(\text{Cr,Fe})_7\text{C}_3$  during the tempering of chromium steels does not cause secondary hardening (18).

*Specific Volume*—The specific volume changes during the fourth stage of tempering were measured by the weight-in-air, weight-in-water method (19) with an accuracy of  $\pm 0.00002$  cc/gm, and the results are given in Fig. 14. On comparison with Fig. 12, it is evident that a contraction accompanies the conversion of cementite

<sup>3</sup>The experimental details connected with these electron micrographs are described by Professor Whitmore in a written discussion of this paper.

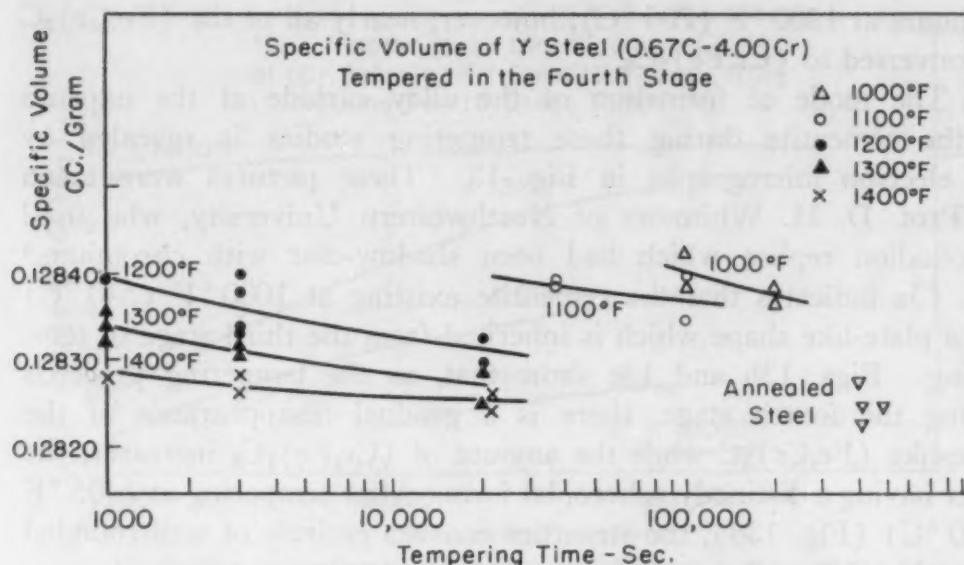


Fig. 14—Specific Volume of Y Steel (0.67% Carbon, 4% Chromium) Tempered in the Fourth Stage.

to the alloy carbide. There has been some question on this point in the past (20). The contraction is caused, not by a greater density of the alloy carbide, but by the depletion of chromium from the matrix when the alloy carbide forms.

*Electrolytic Isolation of the Carbides*—The carbides existing in the fourth stage of tempering were extracted from the Y steel by electrolysis (21, 22), using the sodium citrate type of cell (22). The carbides were sufficiently fine and reactive so that quantitative results could not be obtained with the simple hydrochloric acid cell. Table III shows the weight percentages and chemical analysis of the carbide residue as a function of tempering time and temperature.

Because of partial oxidation of the residues, the sum of the elements listed in Table III does not total 100%, but this discrepancy becomes less, the greater the degree of tempering. Consequently, to correct the weight percentage of the carbides, it is necessary to multiply the experimental values by  $\frac{\text{total analysis}}{100}$ . The corrected values are given in Table III.

The carbon contents of the series in Table III were found to be somewhat erratic, and hence it was considered preferable to calculate the carbon content from a weight balance (Weight per cent carbon in carbides =  $100 \frac{\text{Weight per cent carbon in steel}}{\text{Corrected weight per cent carbides in steel}}$ ). This expression is based on the fact that practically all of the carbon in the steel is in the carbide phase (whether cementite or alloy carbide)



**Table III**  
**Weight Per Cent and Chemical Analysis of Carbide Residues From Tempered Y Steel**  
**(0.67% C - 4.00% Cr) Obtained With the Sodium Citrate Cell**

Temp. °F	Temp. (sec.)	Experimental Results					Total Analysis	Corrected Results	
		Wt. % Carbides	Wt. % Fe	Wt. % Cr	Wt. % Mn	Wt. % C		Wt. % Carbides	Wt. % Carbon
1000	100,000	10.3	61.05	18.37	1.16	7.41	87.99	9.1	7.4
1000	200,000	10.2	62.39	21.63	1.24	7.34	92.60	9.4	7.1
1100	11,800	10.0	60.72	23.31	1.18	7.21	92.42	9.2	7.3
1100	35,000	9.5	54.12	20.09	1.40	8.18	92.79	8.8	7.6
1100	100,000	9.0	51.15	34.65	1.56	7.91	95.27	8.6	7.8
1200	1,000	9.9	59.73	22.05	1.04	7.64	90.96	9.0	7.4
1200	3,000	9.5	55.44	27.30	1.06	8.18	91.98	8.7	7.7
1200	20,000	8.7	49.17	35.28	1.48	8.32	94.25	8.2	8.2
1200	100,000	8.2	43.56	41.05	1.52	8.68	94.81	7.8	8.6
1300	1,000	9.2	54.78	29.61	1.20	7.91	93.50	8.6	7.8
1300	3,000	8.6	51.48	34.65	1.20	8.18	95.51	8.2	8.2
1300	20,000	8.1	46.53	39.59	1.36	8.73	96.21	7.8	8.6
1300	100,000	7.8	46.20	41.27	1.40	8.73	97.60	7.6	8.8
1400	1,000	8.4	48.84	36.33	1.06	8.95	94.68	8.0	8.4
1400	3,000	8.2	48.84	38.11	1.24	8.32	96.51	7.9	8.5
1400	20,000	7.8	48.10	39.51	1.23	8.43	97.27	7.6	8.8
1400	360,000	7.5	47.53	40.32	1.20	8.86	97.91	7.4	9.0

during the fourth stage of tempering. These calculated carbon contents are also shown in Table III.

As the tempering proceeds in the fourth stage, the weight per cent of carbide *decreases*. This is to be expected because the  $(\text{Cr,Fe})_7\text{C}_3$  which forms at the expense of the  $(\text{Fe,Cr})_3\text{C}$  is richer in carbon than the latter (9.0% versus 6.7%) and, therefore, a given supply of carbon ties up fewer metallic atoms in the alloy carbide than in cementite. Since the atomic weights of iron and chromium are quite similar, the per cent of carbon in each carbide remains substantially constant despite considerable variation in the iron:chromium ratio. Thus, it is possible to calculate the fraction of  $(\text{Fe,Cr})_3\text{C}$  and of  $(\text{Cr,Fe})_7\text{C}_3$  present in each carbide mixture from the corrected carbon contents of the residues in Table III. As a next step, the weight per cent of each carbide in the steel can be evaluated.

Fig. 15 shows how the weight percentages of the two carbides change on tempering. The agreement with the volume percentage curves in Fig. 12 is good. The time-temperature dependence of this fourth-stage reaction corresponds to an activation energy of 60,000 cal/mole, based on  $(\text{time})^{-1}$  units, which is about the value expected for the diffusion of chromium in alpha iron. This would suggest that the rate of alloy carbide formation is controlled by the diffusion rate of the chromium through the ferrite matrix. No equations like Equations 1 and 3 were found to fit the transformation curves in Fig. 15.

No adequate method was found for separating the iron, chromium



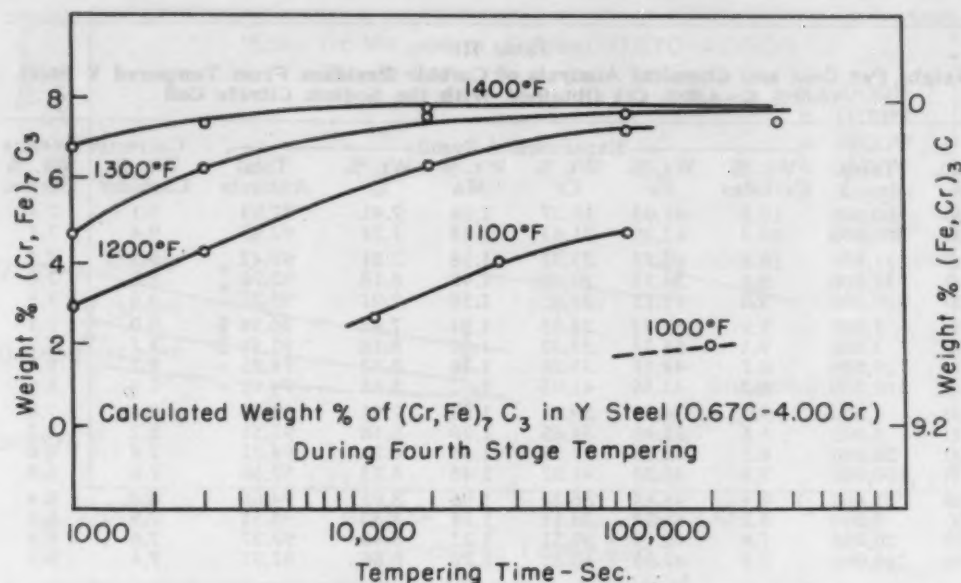


Fig. 15—Calculated Weight Per Cent of  $(Cr, Fe)_7C_3$  in Y Steel (0.67% Carbon, 4% Chromium) During Fourth Stage of Tempering.

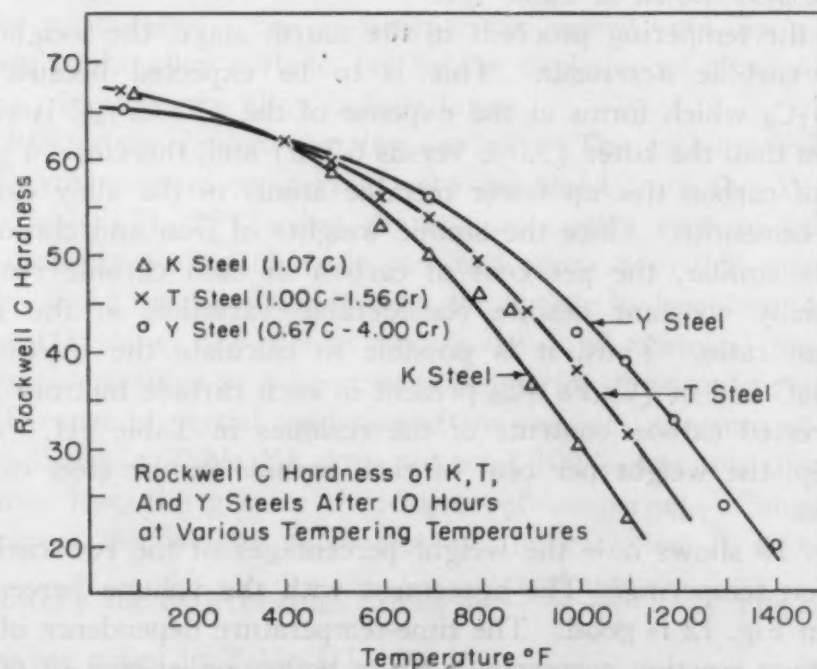


Fig. 16—Rockwell C Hardness of K, T, and Y Steels After 10 Hours at Various Tempering Temperatures.

and manganese contents in Table III according to the individual carbides. Nevertheless, it is apparent that the chromium increases markedly, and the manganese slightly, in the carbide phase during this stage of tempering. The chromium change is due primarily to the formation of the chromium-rich carbide in place of the

cementite, but even after this conversion is complete, there is some further build-up of chromium in the alloy carbide.

#### HARDNESS CHANGES

The effect of chromium in retarding the softening due to tempering is shown in Fig. 16. No secondary hardening is observed, and this is true even with chromium contents above 4% (18). By comparing the hardness curves in Fig. 16 with the stages of tempering as herein defined, one sees that the principal influence of chromium in resisting softening comes in the third stage. In chromium steels, the cementite particles remain small and plate-like throughout the third stage, whereas in plain carbon steels, the cementite particles grow and begin to spheroidize under similar tempering conditions. Curie point measurements indicate that the cementite in the Y steel (0.67% C, 4.0% Cr) has about the same chromium percentage as the martensite from which it forms, and that the chromium content of the cementite does not change much on tempering up to 1000 °F (540 °C). Above this temperature, the chromium content starts to increase, but the alloy carbide makes its appearance in this range and the cementite dissolves in the matrix.

It is now clear that the formation of the alloy carbide is not responsible for the well-known retention of hardness on tempering of high chromium steels. Such retention usually persists up to about 900 to 950 °F (480 to 510 °C), while the fourth stage of tempering does not set in until about 1000 °F (540 °C). Furthermore, when the  $(\text{Cr,Fe})_7\text{C}_3$  finally does precipitate, there is no corresponding secondary hardening because the large spheroidal alloy carbide particles are less effective in obstructing plastic deformation than the fine dispersion of cementite platelets which are replaced. At the same time, chromium is drained from the matrix and part of the solid solution hardening effect is thereby lost.

#### CONCLUSIONS

1. The effect of chromium on the second, third and fourth stages of tempering has been studied by means of dilatometric, magnetic, X-ray, metallographic, specific volume and electrolytic extraction methods.
2. Retained austenite decomposes during the second stage of tempering into the same products as does the primary austenite on direct isothermal transformation. When the chromium content is sufficiently high so that a well-defined bainite C-curve appears in

the primary transformation diagram, the retained austenite decomposition also exhibits a C-curve behavior.

3. The formation of cementite during the third stage of tempering has been traced by Curie point measurements. The indications are that the cementite, when first formed, is richer in iron than the formula  $\text{Fe}_3\text{C}$ , but gradually approaches this composition as the tempering proceeds.

4. The fourth stage of tempering occurs above 1000 °F (540 °C) with the precipitation of  $(\text{Cr,Fe})_7\text{C}_3$  and the simultaneous solution of the cementite produced during the third stage.

5. The kinetics of the above reactions were analyzed, and heats of activation were determined. Modified nucleation and growth equations were found to fit the transformation curves for the second and third stages, but not the fourth stage.

6. Chromium retards softening during tempering because it inhibits the growth of the cementite particles in the third stage. The alloy carbide precipitates above 1000 °F (540 °C) in a relatively coarse spheroidal form (compared to the existing fine dispersion of plate-like cementite), and is therefore attended by softening.

#### ACKNOWLEDGMENTS

This investigation was sponsored by grants-in-aid from the Republic Steel Corp. and the Union Carbide and Carbon Co.

The authors are also grateful to Prof. Donald H. Whitmore of Northwestern University for the electron micrographs and to Mr. L. S. Castleman for the numerous retained austenite determinations. The assistance of Mr. Edward LaRocca in specimen preparation and of Miss Miriam Yoffa in the metallographic work is appreciated. The Vanadium-Alloys Steel Company kindly furnished the two laboratory steels investigated.

#### References

1. Arbusow and G. Kurdjumov, "The Condition of Carbon in Tempered Steel", *Journal of Physics*, USSR, Vol. 5, 1941, p. 101.
2. D. P. Antia, S. G. Fletcher and M. Cohen, "Structural Changes During the Tempering of High Carbon Steels", *TRANSACTIONS, American Society for Metals*, Vol. 32, 1944, p. 290.
3. S. G. Fletcher and M. Cohen, "The Effect of Carbon on the Tempering of Steel", *TRANSACTIONS, American Society for Metals*, Vol. 32, 1944, p. 333.
4. D. P. Antia and M. Cohen, "The Tempering of Nickel and Nickel-Molybdenum Steels", *TRANSACTIONS, American Society for Metals*, Vol. 32, 1944, p. 363.
5. G. Kurdjumov and L. Lyssak, "The Application of Single Crystals to the Study of Tempered Martensite", *Journal, Iron and Steel Institute*, Vol. 156, Part I, 1947, p. 29.



6. B. L. Averbach and M. Cohen, "The Isothermal Decomposition of Martensite and Retained Austenite", *TRANSACTIONS, American Society for Metals*, Vol. 41, 1949, p. 1024.
7. W. Crafts and C. N. Offenhauer, "Carbides in Low Chromium Steel", *Transactions, American Institute of Mining and Metallurgical Engineers*, Vol. 150, 1942, p. 275.
8. O. Zmeskal and M. Cohen, "Simultaneous Measurements of Magnetic and Dilatometric Changes", *Review of Scientific Instruments*, Vol. 13, 1942, p. 346.
9. R. T. Howard and M. Cohen, "Quantitative Metallography by Point Counting and Lineal Analysis", *Transactions, American Institute of Mining and Metallurgical Engineers*, Vol. 172, 1947, p. 413.
10. B. L. Averbach and M. Cohen, "X-ray Determinations of Retained Austenite by Integrated Intensities", T.P. 2342, *Metals Technology*, February 1948.
11. T. Lyman and A. R. Troiano, "Transformation of Austenite in One Percent Carbon High Chromium Steels", *Transactions, American Institute of Mining and Metallurgical Engineers*, Vol. 162, 1945, p. 196.
12. C. Zener, "Theory of Growth of Spherical Precipitates from Solid Solution", *Journal of Applied Physics*, Vol. 20, 1949, p. 950.
13. W. A. Johnson and R. F. Mehl, "Reaction Kinetics in Processes of Nucleation and Growth", *Transactions, American Institute of Mining and Metallurgical Engineers*, Vol. 135, 1939, p. 416.
14. C. Zener, Discussion of reference 6.
15. C. Wells, W. Batz and R. F. Mehl, "Diffusion Coefficient of Carbon in Austenite", *Transactions, American Institute of Mining and Metallurgical Engineers*, Vol. 188, March 1950, p. 553.
16. J. K. Stanley, "The Diffusion and Solubility of Carbon in Alpha Iron", *Journal of Metals, American Institute of Mining and Metallurgical Engineers*, Vol. 1, October 1949, p. 752.
17. E. C. Groesbeck, "Metallographic Etching Reagents. Part III, For Alloy Steels", *Scientific Papers, Bureau of Standards*, Vol. 20, 1925, No. 518, p. 527-586.
18. W. Crafts and J. Lamont, "Secondary Hardening of Tempered Martensitic Alloy Steel", *Transactions, American Institute of Mining and Metallurgical Engineers*, Vol. 180, 1949, p. 471.
19. S. G. Fletcher and M. Cohen, Authors reply to paper "The Effect of Carbon on the Tempering of Steel", *TRANSACTIONS, American Society for Metals*, Vol. 32, 1944, p. 333-357.
20. R. W. Balluffi and M. Cohen, Discussion to reference 18.
21. W. Koch, "Electrolytic Isolation of Carbides in Alloyed and Unalloyed Steels", *Stahl und Eisen*, Vol. 69, January 1949, p. 1.
22. D. J. Blickwede and M. Cohen, "The Isolation of Carbides from High Speed Steel", *Transactions, American Institute of Mining and Metallurgical Engineers*, Vol. 185, 1949, p. 578.

## DISCUSSION

**Written Discussion:** By D. P. Antia, the Indian Institute of Metals, Calcutta, India.

The authors are to be congratulated in presenting yet another paper on the fundamental aspects of transformation of steels during tempering. In the original paper submitted by Antia, Fletcher and Cohen there was some doubt about the second stage and it was not certain whether the retained austenite decomposed into bainite as does the primary austenite



on direct isothermal transformation. This may perhaps be due to the presence of chromium in the steels under study while in the original paper only plain carbon and nickel steels were studied.

This paper is certainly a great contribution to our knowledge of the why and wherefores of heat treatment, and in this case it has been definitely shown that chromium inhibits growth of cementite particles in the third stage, thus retarding softening during tempering.

**Written Discussion:** By D. H. Whitmore, Northwestern University, Evanston, Ill.

It is gratifying to have the results of this excellent and comprehensive study of the second, third, and fourth stages of tempering in chromium steels. This investigation points up the need for marshalling several experimental attacks in solving a metallurgical problem as complex as the tempering of hardened steel. Electron microscopy is a powerful research technique, which has proved useful in investigating structures of metals below the limit of resolution of the light metallograph. Despite the potentialities of this technique for thus supplementing the more familiar research methods, it has received rather limited usage by the metallurgist, undoubtedly due to the difficulties of replicating the surfaces of metals and interpreting the resulting electron micrographs. However, it is to be expected that, as techniques improve and interpretation of micrographs becomes more straightforward, electron microscopy will assume a more prominent role in metallurgical research.

The details of the experimental technique successfully applied at Northwestern University to the authors' Y steel (0.67% C, 4.0% Cr), tempered in the range where the fourth stage is encountered, will be briefly described here. The specimens were polished mechanically, etched lightly with a picral solution, and replicated with a dilute solution of collodion in amyl acetate and acetone. A negative plastic replica was made by flowing a drop of the collodion solution over the prepared metal surface and rapidly draining off the excess solution.<sup>4</sup> When the collodion film has dried, a 200-mesh, woven, stainless steel screen, 1/8-inch diameter, is positioned over the surface of the metal sample; both the replica and screen, whose function is to support the replica film, are then stripped from the sample with a piece of scotch tape. The replica, now supported by the screen, is shadow-cast with chromium in an evaporation unit at an oblique angle of deposition. It has been clearly demonstrated by Williams and Wyckoff<sup>5</sup> that the contrast of an electron micrograph is vastly improved by means of shadow casting, a process of condensing in vacuum a thin film of a suitable metal from vapor of the same composition onto the surface of the plastic replica. The shadowed replica is next transferred to a special holder, which is introduced into the column of an RCA Model EMU electron microscope; the column is evacuated; and a representative area of the replica is photographed.

Based upon a careful study of a series of fourteen electron micrographs of different samples of the authors' Y steel, tempered in the range 1000 to 1420 °F, this discussor is in full agreement with the authors' con-

<sup>4</sup>V. J. Schaefer and D. Harker, *Journal of Applied Physics*, Vol. 13, 1942, p. 427.

<sup>5</sup>R. C. Williams and R. W. G. Wyckoff, *Journal of Applied Physics*, Vol. 15, 1944, p. 712.

clusions regarding the mechanism of carbide conversion occurring during the fourth stage of tempering of this steel. The gradual formation of the nearly spheroidal  $(\text{Cr,Fe})_7\text{C}_3$  particles with the simultaneous disappearance of the tiny, plate-like  $(\text{Fe,Cr})_3\text{C}$  particles, as described by the authors, is even more evident when the entire series of micrographs is examined. No evidence was found in these to suggest that  $(\text{Fe,Cr})_3\text{C}$  transforms to  $(\text{Cr,Fe})_7\text{C}_3$  in situ; rather, as suggested by the authors, the evidence indicates that the  $(\text{Fe,Cr})_3\text{C}$  dissolves in the ferrite, and the alloy carbide,  $(\text{Cr,Fe})_7\text{C}_3$ , springs up in other areas of the ferrite.

Encouraged by the agreement of the results of this electron microscope study with the authors' data obtained from other experimental attacks, work is now in progress extending this investigation to lower temperatures where further clarification of the structures of the phases developed during tempering is sorely needed.

**Written Discussion:** By Otto Zmeskal, Illinois Institute of Technology, Chicago.

The authors have presented the results of a research job that is, in the writer's opinion, an unusually excellent one.

A great deal of groundwork previously done by Dr. Cohen and his associates is represented in the measurements and analytical treatment of data presented in this paper. Because of the principles that have been so clearly brought forward by the Cohen teams during the past years, the conclusions of this paper fall in perfect pattern and order.

The role of chromium in retarding the softening during tempering has been convincingly demonstrated.

Would the authors care to show us the photomicrographs they have prepared in this study? It would be interesting to see the various transformation structures produced during the different tempering treatments of the retained austenite and to be able to compare the electron micrographs of Fig. 13 with the light micrographs.

Also, are transformation curves, similar to Fig. 4, available for steels K, T, and Y, and if they are, could they be presented?

**Written Discussion:** By Walter Crafts, chief metallurgist, and John L. Lamont, research metallurgist, Union Carbide and Carbon Research Laboratories, Inc., Niagara Falls, N. Y.

This paper represents a much-needed contribution to the understanding of the tempering of alloy steels. We are particularly gratified to have the uncertainty removed regarding the volume changes at elevated temperatures, where we found expansion that presumably was caused by austenite decomposition rather than by carbide changes.

The inference that the presence of chromium increases the amount of carbon in the martensite at the end of the first stage is suggestive of a hypothesis that in steels that are capable of secondary hardening (molybdenum or vanadium, but not chromium), a martensite-like constituent is stable to high tempering temperatures and produces secondary hardening when it decomposes. Although some structures lend some support to the conception, it is somewhat difficult to accept and it would be appreciated if the authors could explain further the significance of their conclusion.

The authors report that dilation tests indicated disappearance of the

transition carbide ( $\text{Fe}_3\text{C}$ ) at a temperature much lower than that indicated by magnetic tests for the full development of cementite ( $\text{Fe}_3\text{C}$ ) and have explained the difference by assuming that the first-formed cementite contained an excess of iron. Inasmuch as we have observed X-ray diffraction lines associated with the  $\text{Fe}_3\text{C}$  phase after tempering at temperatures as high as 1000 °F for 2 hours in the electrolytically extracted carbide of a steel with 0.5% carbon and 8% chromium, we question whether the  $\text{Fe}_3\text{C}$  phase is not more persistent than is indicated by dilatometric data.

It has also appeared to us that the  $\text{Fe}_3\text{C}$  phase is more persistent in steels that show marked secondary hardening behavior, such as vanadium and molybdenum steels, than in chromium steels that exhibit no true secondary hardening. However, at tempering temperatures below 1000 °F the chromium steels soften much less readily than steels with strong secondary hardening tendencies so that resistance to softening does not appear to be directly associated with the persistence of the  $\text{Fe}_3\text{C}$  phase. It is hoped that the authors will be able to continue their efforts to rationalize the tempering reactions and the associated hardness changes in alloy steels.

**Written Discussion:** By Edward A. Loria, Senior Fellow, Mellon Institute of Industrial Research, Pittsburgh.

The transformation data for the 1.11% carbon, 4.11% chromium steel in the form of TTT curves presented as Fig. 4 are of particular interest. According to the authors, the retained austenite transformation in this steel is quite complex but proved amenable to metallographic interpretation, and a brief description of the reaction sequences is given. Notwithstanding that the comment may be that the observed structures are straightforward, the writer believes that, in view of the known inadequacy of the present nomenclature for the decomposition products of austenite and the variations in microstructures observed in alloy steels, it is necessary to resort to micrographs in order to classify some of the microstructures. The work of Hultgren on the morphology of the reaction sequences in alloy steels bears out such a contention.

This particular steel is analogous in composition to that studied by Lyman and Troiano (11). The nature of the complex structures existing in the bainite shelf and in the bay or intermediate region above is shown in several micrographs by these investigators. Also their TTT diagram delineates a two-stage reaction in the bainite transformation region, and it is to be noted further in a comparison of the two diagrams that, in the present one, the start curves for primary austenite transformation are shifted markedly to the left (shorter times), the time factor being more than 1000 at the tip of the pearlite knee or the tip of the bainite knee. Both steels were austenitized at practically the same temperature.

The writer would like to see a few high magnification micrographs of the retained austenite transformation in the bay following the precipitation of the carbides of plate-like habit and in the bainite region, both for the case where the acicular carbide first appears followed by separate ferrite and carbide reactions and the case, at lower temperatures, where the typical bainite structures are found. No doubt, the tempered martensite plates nucleated the retained austenite transformation products and influenced the reaction rate. Finally, would the authors comment



on the occurrence of a two-stage reaction in the primary austenite-to-bainite transformation and what effect, if any, it would have on the course of the retained austenite transformation both for the temperature range of 500 to 700 °F (260 to 370 °C) where the end of the bainite reaction is delineated and above 700 °F (370 °C) where the end of the bainite reaction is not defined in the TTT diagram?

#### Authors' Reply

The authors appreciate the additional detail that Professor Whitmore has provided on the methods used in obtaining the electron micrographs shown in the paper. It is also encouraging to know that he plans to extend these techniques to a study of the precipitates which are formed during the earlier stages of tempering. More data are needed on the identity and the shape of the transition precipitate, and one may expect that the improved methods of electron microscopy will be helpful in this problem.

The photomicrographs of the tempered structures requested by Professor Zmeskal were not included because they added little to the discussion given in the paper. However, a few of the more interesting ones are included in connection with Mr. Loria's comments.

With regard to Professor Zmeskal's second question, transformation curves for the decomposition of retained austenite in the plain carbon and the low chromium steels are presented in Fig. 1 of the paper. The transformation rate increases so rapidly with temperature that no C-curve behavior could be detected. In fact, all of the retained austenite was converted before the first measurements could be made at 700 °F (370 °C) and above. Thus it was not possible to work out TTT curves like those in Fig. 4 for the K and T steels. The decomposition characteristics of retained austenite in steel Y were not determined, in view of the more complete investigation on this point in steel Z. Steel Y was selected specifically for the fourth-stage studies involving the formation of the alloy carbide.

The lack of secondary hardening in the chromium steels, in contrast to the marked secondary hardening observed in some of the molybdenum or vanadium steels, is pointed out by Drs. Crafts and Lamont, and is an important subject that deserves further attention. The findings of this paper indicate that the resistance to softening on tempering the chromium steels results from the cementite particles remaining relatively small before (and while) the alloy carbide forms. The chromium carbide seems to form directly (or grow rapidly) as comparatively large spheroids. It is unlikely that these particles are coherent with the matrix, and thus virtually no additional hardening due to their precipitation is obtained. In fact, there are two sources of softening at this stage: (a) the removal of the fine dispersion of cementite, and (b) the reduction of the solid solution hardening due to depletion of chromium from the ferritic matrix.

On the other hand, if the alloy carbide were precipitated in the form of fine platelets, it is possible that such particles could be coherent with the matrix and hence could cause additional hardening. This might be



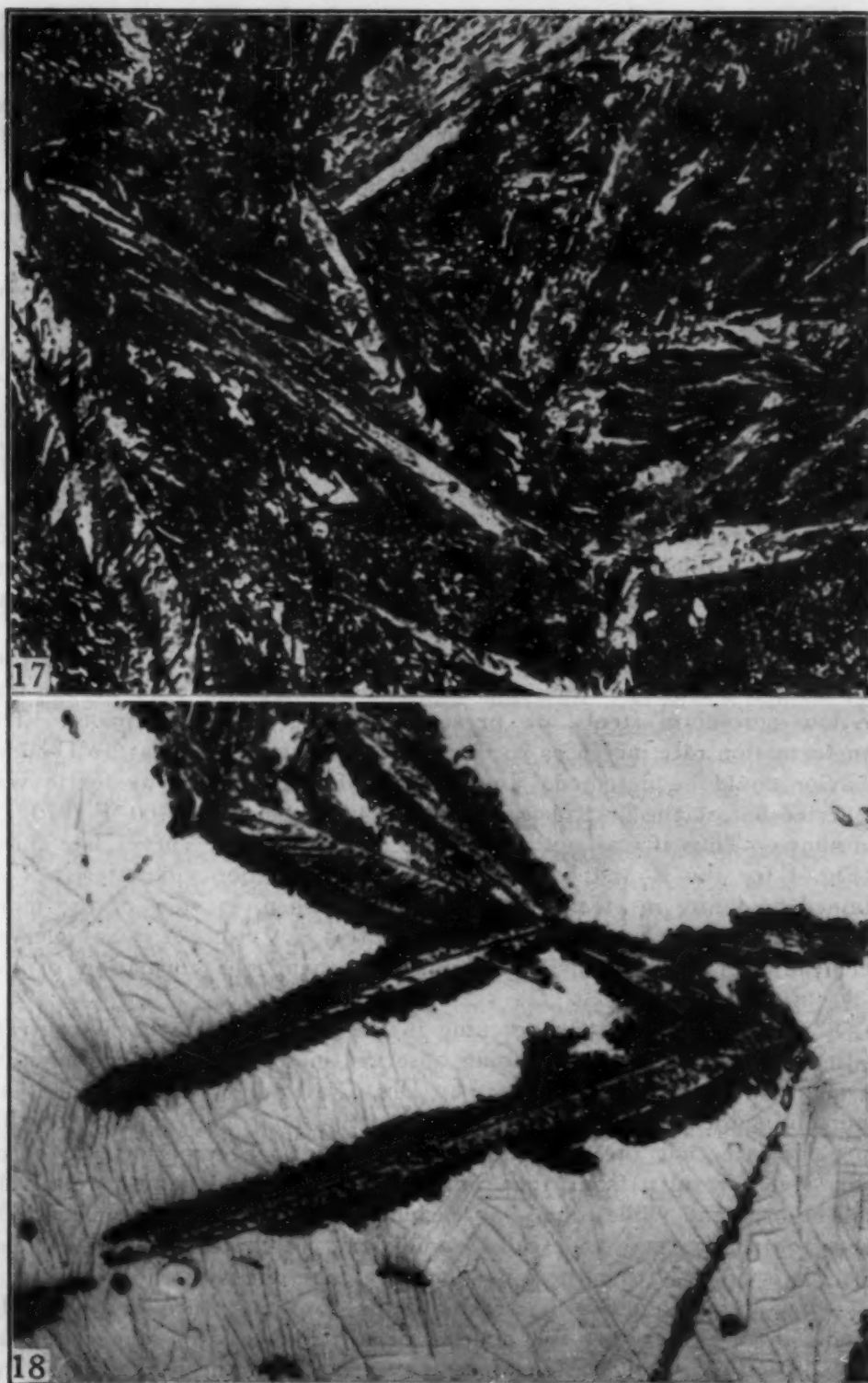


Fig. 17—Structure of Z Steel (1.11% C-4.11% Cr) After Hardening and Tempering at 500 °F (260 °C) for 28 Hours. Tempered martensite, bainite, and trace of retained austenite. Etched with 2% nital.  $\times 1500$ .

Fig. 18—Structure of Z Steel (1.11% C-4.11% Cr) After Hardening and Tempering at 700 °F (370 °C) for 28 Hours. Tempered martensite, bainite, carbide, and retained austenite. Etched with 2% nital.  $\times 1500$ .

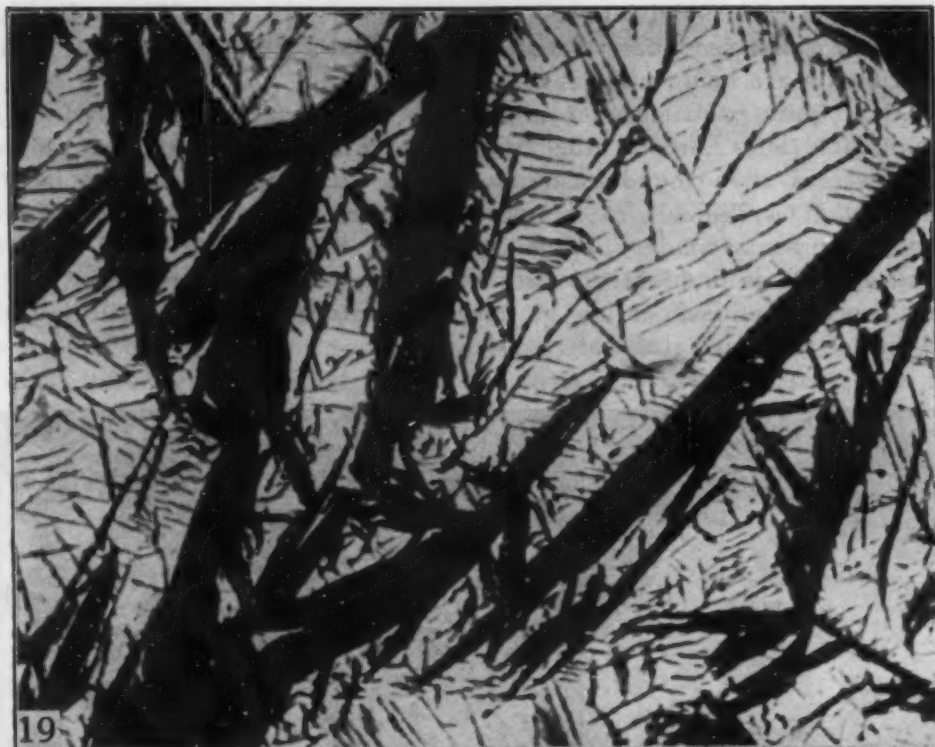


Fig. 19—Structure of Z Steel (1.11% C - 4.11% Cr) After Hardening and Tempering at 800 °F (425 °C) for 28 Hours. Tempered martensite, carbide and retained austenite. Etched with 2% nital.  $\times 1500$ .

Fig. 20—Structure of Z Steel (1.11% C - 4.11% Cr) After Hardening and Tempering at 900 °F (480 °C). Tempered martensite, carbide, low temperature (arborescent) pearlite, and retained austenite. Etched with 2% nital.  $\times 1500$ .

the case in the molybdenum or vanadium steels and, if so, it would account for the secondary hardening observed in these materials. Such experiments are being undertaken at M.I.T.

It is quite probable that in the 8% chromium steel referred to by Drs. Crafts and Lamont, the transition carbide may persist to higher temperatures than found in the lower chromium steels studied by the authors. It is difficult to imagine, however, how this phase could be responsible for secondary hardening in the vicinity of 1000 °F (540 °C) because (a) it is undoubtedly present in only minor amounts, and (b) it is in process of disappearing in this temperature range, constituting the tail-end of the third stage of tempering.



Fig. 21—Structure of Z Steel (1.11% C - 4.11% Cr) After Hardening and Tempering at 1200 °F (650 °C) for 40 Seconds. Tempered martensite, nodular pearlite, and retained austenite. Etched with 2% nital.  $\times 1500$ .

Mr. Loria points out the difficulties in nomenclature regarding the austenitic decomposition products. However, the authors feel that such matters cannot be settled by tempering studies, wherein the available (retained) austenite comprises only a fraction of the structure. On the other hand, it is quite in order to report that the decomposition products formed on tempering are the same as those formed during the primary austenitic transformation in the corresponding temperature range, while relying on the latter type of investigation to establish the real identity of the products. In comparing the secondary products of the present paper with the primary products observed by Lyman and Troiano (11), the authors appropriately used the terminology of these investigators,



and believe that no misunderstanding is likely to occur for the purposes at hand. Examples are given in the accompanying photomicrographs, as requested by Mr. Loria. (Figs. 17 to 21.)

These figures illustrate various tempered structures in the 1.11% C–4.11% Cr steel (steel Z) after austenitizing at 2000 °F (1095 °C) and oil quenching to room temperature. For comparison purposes, frequent reference should be made to the TTT curves in Fig. 4. Fig. 17 (tempered at 500 °F for 28 hours) shows the martensitic plates that are present *prior* to tempering and the bainite that is produced from the retained austenite *during* the tempering. The acicular nature of the bainite is just barely discernible because of the completeness of the retained austenite conversion. Fig. 18 (tempered at 700 °F for 28 hours) demonstrates how the bainite reaction sets in preferentially around the existing martensite, although some of the bainite does appear to form “in the clear”. The bainite reaction does not go to completion at this temperature, but the subsequent precipitation of the carbide directly from the austenite is clearly visible.

In Fig. 19 (tempered at 800 °F for 28 hours), the carbide precipitation takes place first. Neither bainite nor pearlite is present in this case because 800 °F corresponds to the bay region between the bainite and pearlite C curves. Fig. 20 (tempered at 900 °F for 28 hours) shows both the carbide precipitation and the beginnings of pearlite formation,<sup>6</sup> in addition to the existing martensite. Finally, Fig. 21 (tempered at 1200 °F for 40 seconds) illustrates the pearlite reaction taking precedence over the carbide precipitation. Here the pearlite assumes its typical nodular appearance and seems to be nucleated by the existing martensite.

To avoid possible misunderstanding, it should be emphasized that the “end of bainite reaction” curve indicates where the bainite reaction stops, but not necessarily where all of the austenite is consumed. In both the primary (11) and secondary austenitic transformations, the percentage of bainite formed between the “start” and the “end” curves decreases with increasing temperature. Presumably a temperature is reached in the upper region of the bainitic C curves where the percentage of bainite becomes zero. Any further comment on this point would involve some speculation on the nature of bainite, which lies outside the scope of the present paper.

<sup>6</sup>The term pearlite is used loosely here to designate the dark-etching ferrite-carbide aggregate that is associated with the lower branch of the pearlite C curves. This structure has been called “arborescent” by Jolivet (*Journal, Iron and Steel Institute*, Vol. 140, 1939, p. 95).



## EFFECT OF REHEAT TREATMENT ON TRANSVERSE DUCTILITY IN WROUGHT STEEL PRODUCTS

BY PAUL E. BUSBY, CHARLES V. KLIMAS AND CYRIL WELLS

### *Abstract*

*The effect of (a) a retemper and (b) a re-quench and temper treatment on the transverse reduction of area quality of quenched and tempered forgings and seamless tubes has been investigated. Forgings of large and small sizes and seamless tubes of an intermediate size have been used in this study. A typical composition is SAE 4335. Results indicate that at a given yield strength (a) a retemper or (b) a re-quench and temper usually improves transverse reduction of area quality only slightly, if at all. Where the improvement is definite and large, the reheat treatment generally follows a first treatment that was not properly performed. When a re-quench and temper raises the average transverse reduction of area quality, this frequently means that the second quench was more effective than the first, and evidence of this fact is shown by an increase in yield strength – tensile strength ratio. Evidence is also given showing that even when the improvement of transverse reduction of area quality resulting from reheat treatment is relatively small, the increase in percentage of acceptance of forgings or seamless tubes may be quite large. The degree to which a small improvement increases the percentage of accepted product depends on the transverse reduction of area quality of the material inspected and specification requirements.*

THIS paper is the third of a series entitled "Transverse Mechanical Properties in Heat Treated Wrought Steel Products". The first publication (1)<sup>1</sup> consists primarily of a summary and covers briefly several subjects, one of which is "The Effect of Reheat Treatment on Transverse Reduction of Area Quality". In the pres-

<sup>1</sup>The figures appearing in parentheses pertain to the references appended to this paper.

This paper is based on work done for the Office of Scientific Research and Development under Contract NDCre-120, OEMsr-771 with the Carnegie Institute of Technology, Pittsburgh, Pa., and on work done for the Ordnance Corps, Department of the Army, under contracts with the same institution.

Of the authors, Paul E. Busby and Cyril Wells are associated with the Metals Research Laboratory, Carnegie Institute of Technology, Pittsburgh, and Charles V. Klimas is associated with the Carnegie-Illinois Steel Corporation, Duquesne, Pa. Manuscript received August 31, 1950.

**Table I**  
**Chemical Composition of Individual Tubes or Solid Forgings\***

Company and Forging or Seamless Tube No.	Size Range No.	Per Cent of Element						
		C	Mn	Si	Ni	Cr	Mo	V
15-9	1	0.34	0.60	0.25	1.86	0.89	0.25	....
15-10	1	0.34	0.63	0.20	1.91	0.95	0.27	....
15-11	1	0.36	0.62	0.21	1.90	0.90	0.27	....
15-12	1	0.34	0.63	0.20	1.91	0.95	0.27	....
14-7	2	0.36	0.75	0.26	1.89	0.80	0.38	....
5-2	6	0.38	0.80	0.21	0.41	1.51	0.44	0.15
5-3	6	0.34	0.84	0.21	0.47	1.22	0.49	0.16
5-4	6	0.35	0.72	0.24	0.22	1.40	0.50	0.17

\*All steels were fine-grained; those to which vanadium was not added were aluminum-killed.

P and S each below 0.03%.

ent paper, many times the number of data previously published on this subject are presented and discussed, earlier conclusions are further substantiated, and new ones are added. One of these earlier conclusions (1) which has been further substantiated is "a reheat treatment consisting of either (a) a retemper or (b) a requench and temper over and above a normal quench and temper treatment probably has a small but usually insignificant effect on the transverse reduction of area quality of forgings, providing the forgings are tempered to the same yield strength before and after reheat treatment and during quenching the austenite is transformed essentially to martensite".

#### MATERIAL AND HEAT TREATMENT

Material used in this study consists in part of basic open-hearth seamless tubes and in part of acid open-hearth and basic electric forgings. Chemical compositions usually fall between the following limits:

C	Mn	P	S	Si	Ni	Cr	Mo	V
0.25	0.50	<0.03	<0.03	0.20	0.20	0.50	0.20	0.00
0.45	1.00	<0.03	<0.03	0.40	3.00	2.00	0.60	0.20

Specific chemical compositions of each of seven individual forgings and one seamless tube designated 14-7 are given in Table I.

Seamless tubes vary in size roughly from 5-6 inches OD, 1½ inches ID, and 90 inches long to 6½-7½ inches OD, 2½ inches ID, and 160 inches long, while forgings vary from about 2.5-5.5 inches OD and 85 inches long to about 17-25 inches OD, 8½ inches ID, and 340 inches long. For convenience, the forgings have been divided into six classes (Table II) and are arranged in order of increasing wall thickness. All seamless tubes are in Class 2.

In order to summarize the numerous heat treatments for future

**Table II**  
**Approximate Dimensions and Heat Treatment of Seamless Tubes,**  
**Bored-Out Forgings, and Solid Forgings**

No.	Max. OD (In.)	ID (In.)	Wall (In.)	Length (In.)	Prior Treatment						Quench		Temper	
					1 °F	T.†	2 °F	T.†	3 °F	T.†	°F	T.†	°F	T.†
1	2.5-5.5	S.F.*	...	70-85	After forging, forging was cooled and heated for quench.						1625	6	1080	10
2	6-10	1.5-2.5	2-3	50-160	1700	8	....	..	....	..	1500	5	1150	10
3	10-13	2.5-5.5	3-4	70-180	1750	12	....	..	1225	15	1600	15	1150	15
4	11-15	2.5-5.5	4-5	180-290	1700	14	....	..	1225	15	1600	10	1250	8
5	15-27	2.5-14	6-7	200-750	1640	16	1520	16	1150	12	1600	8	1200	10
6	17-25	3-8.5	7-8.5	250-350	1640	21	1520	20	1200	14	1680	10	1200	12

\*Solid forging.

†Time at temperature (hours).

After each prior treatment (1, 2, or 3), forgings were furnace-cooled or air-cooled to at least below their transformation range before being heated for the quench.

After tempering, tubes were either air- or furnace-cooled.

All tubes were quenched in water.

A reheat and temper usually consisted of a duplication of the first quench and temper noted above; a retemper treatment usually consisted of a duplication of the first tempering treatment. Occasionally, when the yield strength of a forging was too high, the temperature was slightly increased for the retemper operation.

reference in this paper, a tabulation of a typical heat treating cycle is given for forgings (or seamless tubes) in each size range; size ranges are indicated in Table II and are listed by number. Reference to the forging (or seamless tube) size number in subsequent tables of this publication should therefore be sufficient to indicate the approximate size and heat treatment of the forgings studied. With few exceptions, reheat treatments referred to in this investigation consisted of a duplication of either the first quench and temper or the first temper treatment.

Estimates of the effect of reheat treatments on mechanical properties are based on (a) results of a large number of tests made on individual forgings before and after reheat treatment and (b) acceptance test data which were supplied by the forging manufacturers from production records. Testing of individual forgings was carried out in the laboratory after the regular commercial heat treatments (and reheat treatments) had been performed by the producer. Laboratory test specimens were 0.252 inch in diameter; industrial data were determined from either 0.357-inch diameter specimens (forgings of size range No. 1 and seamless tubes of size range No. 2) or 0.505-inch diameter specimens (all other sizes). Specimens from the solid forgings consisted of midradius material, while those from the remaining forgings and the seamless tubes consisted of midwall material. Specimens from all forgings and tubes came from positions sufficiently far from ends to be uninfluenced by end effects.<sup>2</sup>

<sup>2</sup>Sometimes midwall and midradius material located close to the ends of quenched and tempered forgings has a better RAT quality at a given yield strength than that of similar material located at greater distances from the ends. This is due to a more rapid cooling of end midwall and midradius material during the quench.



## PROCEDURE

In order to study the effect of reheat treatment on the transverse reduction of area (RAT) quality<sup>3</sup> of a forged product which was originally quenched essentially to martensite, it is necessary to consider first what variation of yield strength and transverse reduction of area is to be expected in such products. It has already been shown (1) that the variation of RAT in a high-quality forging is much higher than is generally recognized. On the average, the difference between the maximum and minimum RAT values for a large number of specimens taken from a single forging is about 30%; the difference in the maximum and minimum yield strength values determined from these specimens is usually about 10,000 psi. Furthermore, there is a small but finite probability that the results of two adjacent tensile tests ( $\frac{1}{2}$  to 1 inch center to center) will be the maximum and minimum RAT values among a large number of tests cut from the forging; the yield strengths determined on such specimens rarely differ by more than 2000 psi. From an engineering viewpoint a variation of 10,000 psi in yield strength is often negligible and a single yield strength value is usually representative of the true yield strength of the material. However, a variation of 30% in transverse reduction of area obviously precludes the possibility that the reduction of area value determined from one or two tensile test results will always accurately indicate the true ductility of the forging tested.

For these reasons, it is necessary in analyzing company data to consider whether a reheat treatment had been made because of low RAT or because of yield strength values outside the specified range. Company data, therefore, are separated in the following tables according to the specified properties which motivated the reheat treatment. In addition, the data listed in these tables are divided into three groups. Results of tests which were the cause of reheat treatment are designated Group A. Group B data include the results of tests on those forgings which were reheat treated (requenched and tempered or retempered) on the basis of the results of tests included in Group A. Group C data include all tests which were made on all forgings in the heat or practice. Reasons for this subdivision of the data should be apparent from a later general discussion wherein the effect of bias (associated with Group A data) on conclusions is considered. The interpretation of the results for forgings

<sup>3</sup>Transverse reduction of area (RAT) quality of a unit of product is defined arbitrarily as the distribution of reduction of area values for all transverse specimens of standard size which can be taken from the unit at specified positions. A discussion of the definition of RAT quality is given in an earlier publication [(1), page 718].



which were tested in the laboratory is simplified because of the relatively large number of unbiased data available on each forging.

In order to carry out the analysis, sample yield strength and RAT averages were computed and in the case of individual tubes, sample standard deviation ( $\sigma_{\text{RAT}}$ ) values were calculated.<sup>4</sup> An estimate of the average RAT quality of each reheat treated unit at the same yield strength (Y psi) as the quenched and tempered unit was also made on the basis of the assumption that a 5000-psi decrease of yield strength is accompanied by a 1.5% increase in transverse reduction of area.<sup>5</sup> In addition, the yield strength to tensile strength ratio was computed for each unit investigated.

Where computed odds<sup>6</sup> based on the assumption that samples were randomly drawn from normal populations<sup>7</sup> are 19 or more to 1 that a difference is not a chance occurrence, the difference is accepted as being significant. A significant difference is designated by S in the tables. When the difference between two estimated averages is significant, it is concluded that the units have different average RAT quality; when the difference between two sample standard deviations is significant, it is concluded that the variation of RAT quality within one unit is different from that in the other.

#### RESULTS AND THEIR INTERPRETATION

Results are given in Tables III to IX, inclusive. These show the effects of (a) a retemper (Tables III, IV, V) and (b) a re-quench and temper (Tables VI to VIII, inclusive) on the RAT quality of quenched and tempered forgings and seamless tubes. They show also the effect of certain multiple reheat treatments on the RAT quality of quenched and tempered forgings (Table IX).

<sup>4</sup>Methods for calculating an average (arithmetic mean) and a standard deviation are discussed by Olds and Wells [(2), pages 851 and 852]. Wells and Mehl [(1), page 737] demonstrated that the standard deviation ( $\sigma$ ) for RAT determined from the results of a large number of tests on a single forging or from a number of forgings from the same heat is usually about 5%. It is believed that the average standard deviation among a large number of heats from a given practice is also approximately 5%.

<sup>5</sup>It has been observed [(1), page 744] that within yield strength range limits of about 100,000 and 180,000 psi, an increase of 5000 psi in yield strength in a quenched and tempered seamless tube was accompanied by a decrease of 1.5% in RAT; this tube was quenched essentially to martensite before being tempered. Forgings such as 5-2, 5-3, and 5-4, which are quite large in cross section, are not quenched essentially to martensite before the temper. An increase of 5000 psi in yield strength in each of these forgings may not be accompanied by a decrease of 1.5% in RAT. However, because of the limited yield strength range over which this relation is used, it is believed that the estimated average RAT quality of the forgings (at a given yield strength) is not seriously in error because of the assumption made.

<sup>6</sup>Examples showing how to make these computations are given in many texts and technical papers. See paper by Olds and Wells, section on "Tests of Significance" [(2), pages 855 to 860], and texts by Croxton and Cowden [(3), page 347], and Snedecor [(4), pages 218 to 226].

<sup>7</sup>Actually RAT populations sampled in this investigation are neither normal nor randomly sampled; however, they are usually sufficiently normal and randomly sampled to support the belief that odds in favor of conclusions drawn being correct are quite high. Strong evidence supporting this opinion is given in an earlier publication (1).

**Table III**  
**Data Showing the Effect of Retempering on the RAT Quality of Each of Three Quenched and Tempered Forgings**

Company and Forging No.	Size Range No.	Heat Treatment	No. of Tests	Average YS (1 unit = 1000 psi)	YS TS	Average RAT (%)	Average RAT (%) at YS of Y* psi	Difference†	$\sigma_{RAT}$ (%)	Difference†
15-11	1	QT	47	132	0.90	33.6	33.6}	NS	8.1}	NS
		QTT	48	122	0.89	38.4	35.4}		7.0}	
5-3	6	QT	16	107	0.78	43.1	43.1}	NS	4.9}	NS
		QTT	16	103	0.77	44.9	43.7}		3.6}	
5-4	6	QT	32	108	0.78	41.1	41.1}	S	3.3}	NS
		QTT	32	105	0.78	44.9	44.0}		3.5}	

Y\* = the average of all yield strength values for specimens taken from each quenched and tempered unit.

† = S denotes the difference between bracketed values is significant; NS denotes no significant difference.

TS = tensile strength.

YS = yield strength measured at 0.01% offset.

$\sigma_{RAT}$  = standard deviation of sample consisting of RAT values.

QT = quenched and tempered.

QTT = quenched, tempered, and retempered.

In order to show briefly and as clearly as possible how results have been interpreted, certain data listed in Table III have been selected for illustrative purposes.

The difference between any two RAT averages bracketed together (Column 8) is accepted as the best estimate of the effect of retempering on the average RAT quality of a unit and the difference between any two standard deviations bracketed together (Column 10) is accepted as the best estimate of the effect of retempering on the variation of RAT quality within a unit. Thus it is estimated that retempering improved the average RAT quality of forging 15-11 by 1.8% and decreased variation within the forging (standard deviation,  $\sigma_{RAT}$ , decreased by 1.1%). One is likely to have some confidence in the estimate that retempering improved average RAT quality, but practically none in the estimate that retempering decreased the variation of RAT quality. Since neither of the two differences is significant,<sup>8</sup> the authors have not drawn the conclusion that retempering improved the RAT quality of forging 15-11 more than would be expected as a result of lowering yield strength by 10,000 psi. When a conclusion is drawn, it is expected that the odds in favor of its being correct are rarely lower than 5 to 1, quite frequently about 10 to 1, and usually 20 to 1 or higher.

It may be observed from the table that the average yield strength and RAT values for thirty-two specimens taken from a large quenched and tempered forging (forging 5-4) are 108,000 psi and 41.1%, respectively, and that the estimated average of thirty-two

<sup>8</sup>A significant difference is defined as being such that this or a larger difference would be observed only 5% or less of the time if the samples were randomly drawn from a normal population an infinite number of times.

**Table IV**  
**Data Showing the Effect of Retempering on the RAT Quality of Each of Several Groups of Quenched and Tempered Forgings Which Were Subsequently Retempered in Commercial Practice for the Purpose of Decreasing Yield Strength**

Company No.	Size Range No.	Approximate No. of Tubes	Group	No. of Tests	Average YS		Average RAT (%)	Average RAT (%) at a YS of Y psi	Difference
					(1 unit = 1000 psi)	TS			
4	2	14	A	28	81	0.78	50.5	50.5	NS
		14	B	28	75	0.75	51.2	49.4	
7	3	4	A	18	81	0.76	41.6	41.6	NS
		4	B	18	78	0.77	44.5	43.6	
17	3	3	A	12	107	0.85	39.6	39.6	NS
		3	B	12	97	0.84	43.6	40.6	
5*	4	58	A	232	88	0.81	44.9	44.9	S
		58	B	232	79	0.80	48.7	46.0	
5†	4	8	A	32	86	0.81	48.7	48.7	NS
		8	B	32	76	0.80	52.0	49.0	
5	5	23	A	95	82	0.80	38.7	38.7	S
		23	B	95	78	0.79	41.8	40.6	

\*Acid open-hearth steel.

†Basic electric steel.

Two tests per tube, size range No. 2; four tests per tube for tubes of larger sizes.

RAT values for specimens taken from the same forging after retempering is 44.0%, assuming a yield strength of 108,000 psi. The difference between these averages is significant, and it is concluded that retempering raised the average RAT quality of this forging. Actually this conclusion would have been accepted if the difference had been only 1.7%; therefore it is rather certain that an improvement of at least 1.2% resulted from the tempering treatment.

*Effect of Retempering—Individual Forgings:* From results given in Table III it appears that retempering (a) raised the average RAT quality of all three quenched and tempered forgings by an amount slightly greater than would be expected from the lowering of yield strength and (b) decreased the variation of RAT quality on the average by a very small amount. It is estimated that if the retemper had not affected yield strength, the average RAT quality of the reheat treated material would have been on the average higher than that of the quenched and tempered material by about 1.8%. The average decrease in the computed standard deviations is only 0.7%. As is apparent from results already discussed in the preceding section, evidence is strong that the retemper definitely improved the average RAT quality of large forging 5-4.

*Effect of Retempering—Groups of Forgings:* Data given in Table IV show that the average RAT quality of material in each of all groups of quenched and tempered forgings, except one, appears to have been improved (as a whole) by a retemper slightly more than would be expected from the lowering of yield strength. The



authors estimate that if retempering had not affected yield strength, the RAT quality of these products would have been improved on the average by 0.9%.

It may be noted that the difference of 1.1% between the two averages of 44.9% and 46.0% (Column 9) and the difference of 1.9% between the two averages of 38.7% and 40.6% are significant. Actually if the one difference had been 0.9% instead of 1.1% and the other 1.4% instead of 1.9%, both would still be significant. This information, together with that material given in the table, supports the conclusion that as a result of retempering (a) the average RAT quality of quenched and tempered acid open-hearth steel forgings in size range No. 4 and coming from Company 5 was improved (as a group) by at least 0.2% (1.1%–0.9%) and (b) the average RAT quality of quenched and tempered forgings in size range No. 5 coming from the same company was improved by at least 0.5% (1.9%–1.4%) above that expected from the lowering of yield strength.

From the results listed in Table V one may observe that the average RAT quality of retempered material in each of four of the B groups is apparently higher than that of quenched and tempered material in the four comparable C groups. Four differences (three of which are significant) between bracketed averages support the above statement. The three significant differences are 3.2% (Item 3), 1.9% (Item 7), and 3.3% (Item 10). Since much smaller differences of (a) 1.7%, (b) 0.9%, and (c) 0.8%, respectively, would still be significant, it is concluded that a retemper improved the average RAT quality of each of these materials: the first by at least 1.6%, the second by at least 1.0%, and the third by at least 2.5%.

It may be noted in the table that the RAT quality of the retempered product is often significantly lower than that of the quenched and tempered material. The difference results not from retempering but from the fact that forgings or seamless tubes which were retempered in an effort to improve RAT quality tended on the average to have poorer RAT quality than other products made in the same practice.

*Effect of Requench and Temper—Individual Forgings or Seamless Tubes:* Data in Table VI show the effect of a requench and temper on the RAT quality of each of four quenched and tempered forgings and one quenched and tempered seamless tube. If (a) a requench and temper had about the same effect on each product and (b) yield strength were not affected by the requench and temper,



**Table V**  
**Results Showing the Effect of Retempering on the RAT Quality of Each of Several Groups of Quenched and Tempered Seamless Tubes and Forgings Which Were Subsequently Retempered in Commercial Practice in an Effort to Improve RAT Quality**

Company No.	Size Range No.	Approximate No. of Tubes	Group	No. of Tests	Average YS (1 unit = 1000 psi)	YS TS	Average RAT (%)	Average RAT (%) at a YS of Y psi	Difference
15	1	20	B	32	121	0.86	34.0	31.9}	NS
		23	C	23	128	0.87	31.0	31.0}	
16	1	56	A	56	132	....	26.8	25.6	S
		56	B	56	131	....	35.2	33.7}	
		500	C	604	136	....	37.6	37.6}	
3	2	21	A	42	97	0.79	37.5	38.4	S
		21	B	42	92	0.79	46.5	45.9}	
		100	C	278	94	....	42.7	42.7}	
9	2	60	A	120	95	0.80	36.9	37.2	S
		60	B	120	91	0.80	42.6	41.7}	
		175	C	482	94	....	43.7	43.7}	
14	2	15	A	30	117	0.86	33.8	33.5	S
		15	B	30	114	0.86	41.3	40.1}	
		300	C	771	118	....	42.1	42.1}	
17	2	52	A	104	131	0.90	29.7	30.9	S
		52	B	104	127	0.90	31.8	31.8}	
		250	C	644	127	....	37.3	37.3}	
1	3	35	A	146	75	0.73	34.2	34.8	S
		35	B	146	73	0.73	40.3	40.3}	
		150	C	649	73	....	38.4	38.4}	
8	3	41	A	164	106	0.77	39.6	40.5	NS
		41	B	164	101	0.77	43.8	43.2}	
		88	C	352	103	....	43.6	43.6}	
12	3	22	A	88	109	0.87	35.0	36.5	NS
		22	B	88	102	0.85	39.5	38.9}	
		132	C	720	104	....	39.5	39.5}	
17	4	46	A	184	74	0.80	36.2	36.5	S
		46	B	184	71	0.80	43.8	43.2}	
		150	C	662	73	....	39.9	39.9}	

Group A consists of quenched and tempered seamless tubes or forgings which failed to meet specification requirements for RAT.

Group B consists of retempered Group A product.

Group C includes all seamless tubes or forgings made in the practice considered over a time period including that during which Group A product was made.

one would estimate from results given in the table that the reheat treatment would have raised the average RAT quality of the five products by 1.5% and would have lowered the variation of RAT quality very slightly. The average difference in computed sample standard deviations is 0.4%.

The RAT quality of the reheat treated portion of the seamless tube is apparently lower than that of the quenched and tempered portion. The difference between averages (44.6%–42.5%) and the difference between standard deviations (5.7%–2.3%) are both significant. These differences are such as to justify the conclusion that both the average RAT quality is lower and the variation of RAT quality is larger in the reheat treated portion than in the quenched and tempered portion of the seamless tube. The authors believe that factors other than reheat treatment—perhaps a combination of non-

**Table VI**  
**Data Showing the Effect of a Requench and Temper Treatment on the RAT Quality of Each of Four Forgings and One Seamless Tube (14-7)**

Company and Tube No.	Size Range No.	Heat Treatment	No. of Tests	Average YS		Average RAT (%)	Average RAT (%) at a YS of Y psi	Difference	$\sigma_{RAT}$ (%)	Difference
				(1 unit = 1000 psi)	YS TS					
15-9	1	QT	47	124	0.89	39.4	39.4	NS	8.1	S
		QT-QT	44	123	0.91	41.6	41.3		2.4	
15-10	1	QT	48	130	0.90	32.3	32.3	S	7.6	NS
		QT-QT	48	144	0.93	34.4	38.6		7.4	
15-12	1	QT	50	122	0.83	40.3	40.3	NS	3.3	NS
		QT-QT	50	132	0.86	38.3	41.3		4.0	
14-7	2	QT	52	115	0.88	44.6	44.6	S	2.3	S
		QT-QT	52	119	0.89	41.3	42.5		5.7	
5-2	6	QT	31	89	0.73	49.3	49.3	NS	2.7	NS
		QT-QT	32	95	0.74	47.7	49.5		2.7	

QT = Quenched and tempered.

QT-QT = Quenched, tempered, requenched, and tempered.

metallic inclusions and position in ingot—are responsible for the poorer quality of the reheat treated portion of the tube.

The average of RAT values for 48 specimens from quenched and tempered portions of forging 15-10 is 32.3%, and the average of RAT values for 48 specimens from reheat treated portions of forging 15-10 at the same yield strength (130,000 psi) is estimated to be 38.6%. The difference, 6.3%, is significant. However, out of 48 RAT values for specimens from quenched and tempered portions of the forging, 10 unusually low values were for specimens from one small region of the tube. No such series of low values were obtained for specimens from any other region. When the section of the forging not reheat treated is divided into four equal parts, one observes that the averages based on 12 RAT values per part are 33.0, 35.1, 25.5, and 35.7%, respectively. The averages of the 36 values for specimens from the three parts which appear to be reasonably alike in RAT quality is 34.6%, and the difference between this and the estimated average (38.6%) of the RAT quality for the reheat treated parts is 4.0%. Since a difference of 3.3% would also have been significant, it is concluded that reheat treatment improved the average RAT quality of the forging by at least 0.7%.

From results given in the table it appears that the variation of RAT quality in parts of forging 15-9 which were quenched and tempered is much larger than that in parts which were reheat treated. The difference between the standard deviations 8.1% and 2.4% is significant. Based on statistical considerations, it is estimated that the difference between the standard deviations of the populations from which the two samples were drawn is at least 4%. The much larger variation of RAT quality in the portion of the forging which

**Table VII**  
**Results Showing the Effect of a Requench and Temper Treatment on the RAT Quality of Each of Several Groups of Quenched and Tempered Seamless Tubes and Forgings Which Were Subsequently Requenced and Tempered in Commercial Practice for the Purpose of Increasing Yield Strength**

Company No.	Size Range No.	Approximate No. of Tubes	Group	No. of Tests	Average YS (1 unit = 1000 psi)	YS TS	Average RAT (%)	Average RAT (%) at a YS of Y psi	Difference
15	1	61	A	61	109	0.81	38.6	38.6}	S
		61	B	61	124	0.88	41.1	45.6}	
3	2	12	A	24	86	0.75	44.2	44.2}	NS
		12	B	24	94	0.80	42.9	45.3}	
4	2	8	A	24	66	0.69	56.3	56.3}	NS
		8	B	16	75	0.77	56.8	59.5}	
14*	2	35	A	81	88	0.76	50.3	50.3}	NS
		35	B	81	103	0.82	46.1	50.6}	
14**	2	5	A	10	106	0.82	45.8	45.8}	NS
		5	B	10	116	0.86	45.7	48.7}	
17	2	40	A	91	114	0.89	44.1	44.1}	NS
		40	B	102	124	0.90	41.6	44.6}	
5	3	8	A	32	100	0.77	38.1	38.1}	NS
		8	B	32	108	0.78	38.1	40.5}	
5†	4	18	A	74	78	0.78	48.4	48.4}	S
		18	B	74	83	0.82	49.5	51.0}	
5††	4	7	A	28	75	0.79	52.0	52.0}	NS
		7	B	28	76	0.81	52.3	52.6}	
5	5	8	A	42	84	0.81	43.3	43.3}	NS
		8	B	42	79	0.79	45.0	43.5}	

\*Tubes approximately 6 inches OD, 2 inches ID, and 90 inches long.

\*\*Tubes approximately 8.5 inches OD, 2.5 inches ID, and 115 inches long.

†Acid open-hearth steel.

††Basic electric steel.

was not reheat treated is attributed to factors such as nonmetallic inclusions and position in ingot, but not to reheat treatment.

*Effect of Requench and Temper—Groups of Forgings or Seamless Tubes:* Data listed in Table VII indicate that a requench and temper treatment resulted in an estimated improvement of 2.1% in the average RAT quality of the combined products listed. The improvement is believed to result primarily from administering a more drastic quench when the forgings (or seamless tubes) were requenched. A more drastic quench which in the subsequently tempered product results in higher average RAT quality at a given yield strength, especially when that yield strength is high, is expected to raise the yield strength-tensile strength ratio of the quenched and tempered product. It may be noted that the one time when the yield strength-tensile strength ratio is lower after reheat treatment, the beneficial effect of reheat treatment on average RAT quality at a given yield strength appears to be least.

In one instance, where as a result of a requench and temper the improvement of average RAT quality at a given yield strength was most marked, the yield strength-tensile strength ratio was



increased from 0.81 to 0.88. The largest improvement occurred in a group of forgings quenched and tempered to a relatively high average yield strength level.

The products considered to have been improved most definitely by a re-quench and temper are (a) the size range No. 1 forgings from Company 15 and (b) the size range No. 4 acid open-hearth steel forgings from Company 5. The difference between the estimated average RAT quality for the quenched and tempered size range No. 1 forgings and the estimated average RAT quality for the re-quenched and tempered forgings is 7.0%, and the corresponding difference for the size range No. 4 forgings is 2.6%. Both these differences are significant and in fact would have been considered significant if the one, 7.0%, had been only 1.8% and the other, 2.6%, had been only 1.6%. From the above information and results given in the table, it is concluded that the re-quench and temper treatment would have increased the average RAT quality of the smaller forgings, considered together as a group, by at least 5.2% and the RAT quality of the larger forgings by at least 1% if after the re-quench the smaller forgings had been tempered to a yield strength of 109,000 psi and the larger ones to a yield strength of 78,000 psi.

The analysis of results listed in Table VIII is quite similar to that used in analyzing the results in Table V. It is believed that the RAT quality of four of the reheat treated products (B groups—Items 1, 3, 4, 6) referred to in the table would be definitely poorer than that in the four corresponding C groups at a given yield strength, not because of reheat treatment but because, in commercial practice, forgings (or seamless tubes) which were re-quenched and tempered in an effort to improve RAT quality had on the average a poorer RAT quality at a given yield strength than had other forgings (or seamless tubes) made in the same practice.

The conclusion that on the average a re-quench and temper raised the average RAT quality of size range No. 4 forgings from Company 17 appears to be justified, since the difference between the two averages 40.8% and 41.9% (Column 9, Item 7) is significant; the smallest difference between the averages which would be considered significant is 1.0% (actual difference 1.1%).

*Effect of Re-quench and Temper—Heats of Seamless Tubes:* Strong evidence supporting the viewpoint that RAT quality is unlikely to be raised perceptibly by a re-quench and temper may be obtained by considering individually the fourteen heats which comprise the data for Company 14 listed in Table VIII. The practice



**Table VIII**  
**Data Showing the Effect of a Requench and Temper on the RAT Quality of Each of Several Groups of Quenched and Tempered Seamless Tubes and Forgings Which Were Subsequently Requenced and Tempered in an Effort to Improve RAT Quality**

Company No.	Size Range No.	Approximate No. of Tubes	Group	No. of Tests	Average YS (1 unit = 1000 psi)	YS TS	Average RAT (%)	Average RAT (%) at a YS of Y psi	Difference
15	1	61	A	61	125	0.87	26.0	26.3	
		61	B	61	124	0.87	35.1	35.1	
		832	C	832	124	....	37.1	37.1	S
3	2	36	A	72	93	0.78	39.6	39.6	
		36	B	72	93	0.81	42.0	42.0	
		350	C	440	93	....	42.3	42.3	NS
14	2	200	A	420	118	0.87	30.9	31.2	
		200	B	487	116	0.87	36.3	36.0	
		1500	C	3602	117	....	38.6	38.6	S
17	2	65	A	136	124	0.89	31.7	31.7	
		65	B	136	127	0.90	34.7	35.6	
		400	C	475	124	....	38.7	38.7	S
1	3	5	A	23	71	0.74	35.6	35.3	
		5	B	20	72	0.74	42.1	42.1	
		22	C	90	72	....	39.9	39.9	NS
12	3	22	A	88	104	0.84	33.8	33.8	
		22	B	88	107	0.86	36.6	37.5	
		150	C	744	104	....	39.5	39.5	S
17	4	23	A	92	71	0.79	35.8	35.5	
		23	B	92	68	0.75	43.1	41.9	
		300	C	1200	72	....	40.8	40.8	S
5	5	10	A	10	80	0.79	40.1	40.4	
		10	B	10	81	0.80	42.6	43.2	
		60	C	60	79	....	40.9	40.9	NS

in which these tubes were made was well controlled so that (a) each tube was quenched essentially to martensite, (b) practically all tubes were tempered to within  $\pm 5000$  psi or so of the practice yield strength average (120,000 psi) and (c) all tubes in a heat had practically the same RAT quality (1, 5).

Because of space restrictions a tabulation of the data is not presented, but from a table similar in form to those already presented one may observe the following facts: (a) Thirteen out of fourteen differences between two averages are insignificant and the average of these fourteen differences is  $-0.4\%$ ; (b) thirteen out of fourteen differences between two standard deviations are insignificant and the average of these fourteen differences is  $+0.04\%$ ; (c) the only significant difference between averages is  $3.0\%$  ( $47.8\%$ – $44.8\%$ )—the smallest difference which would be considered significant is  $2.6\%$ ; (d) the only significant difference between standard deviations is  $1.8\%$ <sup>9</sup> ( $5.1\%$ – $3.3\%$ ); (e) nine differences between averages are negative, three are positive, and two are zero; (f) eight differences between standard deviations are negative, four are posi-

<sup>9</sup>This difference would normally be accepted as evidence that the standard deviation of the population representing the RAT quality of the reheat treated material was lower than that of the population representing the RAT quality of the unreheat treated material by at least  $0.5\%$  if the data in the two samples were the only data available.

Table IX  
Results Showing the Effect of Certain Multiple Heat Treatments on RAT Quality

Approximate No. of Tubes	Heat Treatment	No. of Tests	Average YS (1 unit = 1000 psi)	$\frac{YS}{TS}$	Average RAT (%)	Average RAT (%) at a YS of Y psi	Difference
100	QT	460	74	0.74	38.4	38.4	NS
65	QTT	296	74	0.73	38.0	38.0	NS
30	QOTT	141	76	0.73	37.6	38.2	S
7	QTTT	28	73	0.72	41.4	41.1	S
12	QOTTT	52	72	0.73	41.4	40.8	S
15	QOTTTT	68	72	0.72	40.4	39.8	

QT — Quench, temper.  
 QTT — Quench, double temper.  
 QOTT — Double quench, double temper, etc.

tive, and one is zero; (g) the maximum difference between averages is 3.3% and the minimum -2.3%; and (h) the maximum difference between standard deviations is 2.0% and the minimum -1.0%.

In general, the information given above is at least approximately that which would be expected if each pair of samples considered had been taken from the same normal population and if the values making up each sample had been randomly selected. In view of this fact it is concluded that a re-temper and re-temper did not appreciably affect either the average RAT quality of or the variation of RAT quality within the seamless tubes studied in the present investigation.

**Multiple Heat Treatments:** Results given in Table IX show the effect of certain multiple heat treatments on the RAT quality of size range No. 3 forgings coming from Company 1 and having a yield strength of about 74,000 psi. Three of the differences between bracketed averages are significant and indicate that the average RAT quality of each group of reheat treated tubes is probably higher than that of the group of quenched and tempered tubes. The three significant differences are 2.7% (33.3%-30.6%), 2.4% (33.0%-30.6%), and 1.4% (32.0%-30.6%); computed minimum differences considered significant are 1.9, 1.4, and 1.3%, respectively. It is concluded on a basis of the above results that (a) a quench and triple temper, (b) a double quench and triple temper, and (c) a double quench and quadruple temper improved average RAT quality by at least 0.8, 1.0, and 0.1%, respectively.

#### GENERAL DISCUSSION

**Odds That Conclusions Are Correct:** From the discussion of results just completed it should be clear that conclusions are based on tests of significance. A significant difference has been so de-

fined<sup>10</sup> that odds are 19 or more to 1 in favor of conclusions being correct, providing assumptions of normal populations and random sampling are valid. The question now to be discussed is: What are the actual odds when the assumptions are not valid? This question cannot be answered precisely, but pertinent information disclosed by results of sampling of (a) a known typical population representing the RAT quality of a forging and (b) populations representing the RAT qualities of groups of seamless tubes made in a well-controlled practice support the belief that these odds are quite high—probably rarely less than 5 to 1 and quite frequently 10 to 1 or higher.

The known population consists of RAT values for 277 specimens taken from Forging 1, Company 12 [(1), page 719]. The frequency curve representing the RAT quality of this forging is typical of those representing the RAT qualities of other forgings in that it is not normal and is skewed in the direction of low values. Twenty samples, each consisting of fifty values selected essentially in a random manner from the population, were obtained. The difference between averages and the difference between standard deviations for samples 1 and 2, 3 and 4, and so on were noted and tests of significance between averages and between standard deviations were applied. None of the ten differences between averages and only one of the ten differences between standard deviations were significant. In another experiment, 264 of the 277 values were arranged in groups of four, values 1 to 4 in group 1, values 5 to 8 in group 2, etc. The difference between averages and the difference between standard deviations for groups 1 and 2, groups 3 and 4, etc., were noted. Then, as before, the tests of significance between averages and between standard deviations were applied. In this instance one of the thirty-three differences between averages and four of the differences between standard deviations were significant.

*Effect of Bias on Conclusions:* While in some instances reheat treatments have actually improved the RAT quality of quenched and tempered forgings by a considerable amount, sometimes claims of improvement due to reheat treatment are made when no such improvement has resulted from this cause. Such an erroneous conclusion frequently is based on biased and misinterpreted data. In an effort to show how bias has at least sometimes led metallurgists to erroneous conclusions concerning the effect of reheat treatment on the RAT quality of a product, certain data have been selected for illustrative purposes and are discussed herewith.

<sup>10</sup>See footnote 8.



Table X

Shows the Effect on the Percentage of Material Accepted and Rejected (on the Average) When the Average RAT Quality Is Increased From 36.0% by 0.0, 1.5, 2.0, 2.5, and 3.0%, Respectively, and When the RAT Quality Inspected and Specification Requirements Are as Described Below

Procedure*	Quenched and Tempered Tubes		Reheat Treated Tubes									
			Assumed Improvement of Average RAT Quality (%)									
	Acc.† (%)	Rej.‡ (%)	0.0		1.5		2.0		2.5		3.0	
	Acc.† (%)	Rej.‡ (%)	Acc.† (%)	Rej.‡ (%)	Acc.† (%)	Rej.‡ (%)	Acc.† (%)	Rej.‡ (%)	Acc.† (%)	Rej.‡ (%)	Acc.† (%)	Rej.‡ (%)
Step 1	35.9	64.1	....	....	....	....	....	....	....	....	....	....
Step 2	58.9	41.1	....	....	....	....	....	....	....	....	....	....
Step 3	....	....	73.7	26.3	81.0	19.0	83.5	16.5	85.8	14.2	88.0	12.0
Step 4	....	....	83.1	16.9	91.2	8.8	93.4	6.6	95.1	4.9	96.5	3.5

\*Procedure: Step 1—Secure two RAT values, 1 and 2, per tube. Accept if both values are 35% or higher; otherwise reject.

Step 2—Secure two RAT values, 3 and 4, per tube rejected in Step 1. Accept if both values are 35% or higher; otherwise reject.

Step 3—Reheat tubes treated and rejected in Step 2. Secure two RAT values, 5 and 6, per reheat treated tube. Accept if both values are 35% or higher; otherwise reject.

Step 4—Secure two RAT values, 7 and 8, per tube rejected in Step 3. Accept if both values are 35% or higher; otherwise reject.

Each population is assumed to be normal, to be randomly sampled, and to have a standard deviation ( $\sigma_{\text{RAT}}$ ) of 4%.

†Accepted.

‡Rejected.

Of RAT values for 104 specimens from 104 quenched and tempered tubes, 65 are above and 39 (37.5% of total) below 35% (the specification minimum); after reheat treating the 39 tubes, 15 of the 39 values (38.5%) are below 35%. The values from the 39 tubes average 29.0% before reheat treatment and 34.7% after, a difference of 5.7%. Furthermore, of the two values per tube, one obtained before and one after reheat treatment, that for the specimen from the reheat treated tube is higher than the other 33 times out of 39. On a basis of data such as the above, certain metallurgists have concluded that reheat treatment improves RAT quality considerably. This conclusion would be justified in the present instance if the RAT variation within tubes were zero ( $\sigma_{\text{RAT}} = 0$ ) or were at least much smaller than it really is. Actually  $\sigma$  is so large that the differences observed are believed to result not from reheat treatment but almost, if not entirely, from biased sampling.

This belief is supported by the results of a sampling study on a population consisting of the 277 RAT values from Forging 1, Company 12 [ (1)—page 719]. These values were written on chips and were randomly sampled until 1054 values had been selected; 906 of these were 40% or above, and a new value was randomly drawn from the population for each of those which were below 40%.

Of the 1054 first values, 148 (14%) are below 40%; after selecting new values for these 148, 22 of the 148 (14.9%) are below



40%. The 148 values first selected average 35.9%; and after re-sampling, the average is 44.7%, a difference of 8.8%.<sup>11</sup> In addition, the second value selected is higher than the first 139 times out of 148.

*Relation Between RAT Quality and Percentage of Accepted Product:* Sometimes average RAT quality is improved 1 or 2% and occasionally even more as a result of (a) a retemper or (b) a re-quench and temper. Results in Table X show, at least approximately, the effect of such an improvement on the percentage of material accepted when the specified requirement is as indicated in the table. Apparently an improvement of 2 or 3% in average RAT quality may be quite important to a producer, even though it may be relatively unimportant to the design engineer; this is especially true when the average RAT quality of the product is not much higher than the minimum value specified, as is the case in the example given. Normally one thinks of an improvement of 1 or 2% in average RAT quality as being rather unimportant.

#### MISCELLANEOUS GENERAL DISCUSSION

It appears from results as a whole that the small forgings (size range No. 1) were improved in RAT quality by reheat treatment as much or more than were the large forgings (size ranges 5 and 6). However, if small and large forgings had always been tempered to the yield strength level of the small forgings (about 125,000 psi), then the resulting improvement might have been much more marked in the large than in the small forgings.

An earlier publication (1) pointed out: "Acceptance of the conclusion that the transverse reduction of area quality of quenched and tempered wrought steel products of certain sizes and compositions is rarely improved by reheat treatments has already resulted in a drastic reduction of such treatments and in a modification of the design of certain specifications." In one instance after the present information became available, the percentage of reheat treatments was reduced from about 20% to less than 1%; in a second instance, from about 2% to practically zero; and in a third, from 100% (practice was formerly to double quench) to practically zero.

In the discussion of the above paper [(1), page 815] the statement is made that the practice of reheat treatment operations has not been discontinued as a result of this research because (a) there have been too many instances where a second quench accomplished

<sup>11</sup>The difference in the average values obtained from such comparisons depends on the relative values of the average RAT quality of the material inspected and the specification minimum. When the average quality of the material tested is well above specification requirements, the apparent improvement is large in the few forgings which would normally be reheat treated.

what a first had not and (b) repeated tempering treatments are sometimes found effective for the removal of retained austenite as well as for final stress removal. Two other discussers of the same paper [(1), pages 807-808] believe martensite may be present in some of the quenched and tempered products investigated and apparently think that, should martensite be present, a retemper would increase RAT quality at a given yield strength. Still another discussor [(1), page 811] believes that a re-quench may improve RAT quality of large forgings, since such treatment tends to give deeper hardening than a single quenching and tempering treatment.

The present authors are of the opinion that the practice of making reheat treatments is not likely to be, and should not be, discontinued as a result of the present research. However, there is no doubt that many reheat treatments made do practically no good. If the particular products which are being re-quenched and tempered have high quench cracking susceptibilities (6, 7), the reheat treatments may actually do harm.

While a heat treater may find it difficult to decide when a reheat treatment will appreciably improve RAT quality in a forging at a given yield strength, it is believed his decisions will be more reliable if advantage is taken not only of his experience, but also of the information disclosed in this paper. It would seem, for example, that if in the practice established by Company 15 a specimen had a yield strength-tensile strength ratio of 0.80 and a yield strength of 105,000 psi, a re-quench and temper should normally be recommended if an improvement of RAT quality at the same yield strength is desired. Many other conditions exist in practice and justify reheat treatment. However, no description of these is given here because (a) they are numerous and frequently too difficult to evaluate and (b) because of space restrictions.

#### SUMMARY

1. Samples drawn from populations representing the transverse reduction of area (RAT) qualities of (a) quenched and tempered and of (b) reheat treated materials investigated in the present research are in general sufficiently large and representative that the information they provide through statistical analyses forms a sound basis for conclusions relating to the effect of reheat treatment on the RAT qualities of the products investigated. These products consist of more than 4000 forgings and 3000 seamless tubes made in several practices and supplied by twelve companies. Some of the forgings are solid, some bored-out; all are cylindrical and tapered. The

forgings and seamless tubes together vary considerably in size (minimum 2.5 to 5.5 inches in OD and 85 inches long, and maximum 17 to 25 inches OD, 8.5 inches ID, and 340 inches long). Compositions vary somewhat; an SAE 4335 composition is typical. Carbon contents range from about 0.30 to 0.45%, and alloying elements from 1.5 to 4.5%.

2. Data presented in this paper support the previously published conclusion (1) that "Normally, a commercial heat treatment consisting of a normalize, a quench to martensite and a subsequent temper is sufficient to develop in units of fine-grained wrought steel products a transverse reduction of area quality which cannot be significantly improved by additional heat treatments involving (a) a retemper or (b) a re-quench and temper, providing the units are always tempered to essentially the same yield strength level."

3. The transverse reduction of area quality of more than 3000 quenched and tempered SAE 4335 seamless tubes, which were very severely water-quenched (probably essentially to martensite) and which were obtained in an unusually well-controlled heat treatment practice, is either not increased at all or only slightly as a result of a retemper or a re-quench and temper treatment.

4. Transverse reduction of area quality of more than 4000 forgings was on the average improved more by reheat treatment than that of the seamless tubes, probably because in general the forgings were not and in many cases could not be quenched so completely to martensite as were the seamless tubes.

5. It is estimated that on the average (a) a retemper improved the average transverse reduction of area quality of forgings by only 1 or 2% and had practically no effect on transverse reduction of area variation within forgings, and (b) a re-quench and temper raised the average transverse reduction of area quality by an amount between  $1\frac{1}{2}$  and  $2\frac{1}{2}$ % and affected transverse reduction of area variation imperceptibly.

6. Only occasionally when tests of significance were applied to data did these tests indicate that the differences observed (a) between averages or (b) between standard deviations were sufficiently large to convince the authors that a real improvement had resulted from reheat treatments. Odds of 10 or higher to 1 in favor of an improvement of transverse reduction of area quality in the particular forging having resulted from a reheat treatment convince the authors that the improvement is real.

7. One group of small quenched and tempered SAE 4335 forgings, about 85 inches long and varying in diameter from 2.5 to 5.5



inches, is estimated to have been improved in average transverse reduction of area quality by 7% (45.6%–38.6%) as a result of a re-quench and temper. Tests of significance show that with odds of probably better than 10 to 1, the actual increase of average transverse reduction of area quality in this instance is at least 5.2%. Here the second quench and temper treatments were, at least on the average, much more effective than the first, and this accounts for the unusually large improvement of average transverse reduction of area quality resulting from the reheat treatments.

8. An improvement of transverse reduction of area quality resulting from a re-quench and temper treatment is generally associated with a higher yield strength–tensile strength ratio in the reheat treated material than in the quenched and tempered material.

9. In many practices yield strength–tensile strength ratio information might be used to better advantage than transverse reduction of area data by heat treaters responsible for making decisions as to whether or not forgings should be re-quenched and tempered.

10. Improvement of transverse reduction of area quality resulting from either a retemper or a re-quench and temper of quenched and tempered forgings appears to be in the present investigation more pronounced in small (2.5 to 5.5 inches in diameter) than in large (more than 15 inches OD and having a wall thickness of 6 inches or more) forgings. One should note that the large forgings were usually quenched and tempered to relatively low yield strength levels (average 90,000 psi), while the small forgings were quenched and tempered to much higher yield strength levels (average 127,000 psi).

11. The effect of an improvement in average transverse reduction of area quality of 1.5, 2, 2.5, and 3% on the percentage of accepted product has been computed assuming conditions which, at least sometimes, were approximately those existing in practice.

#### ACKNOWLEDGMENTS

The program of research leading to results published in this paper was conceived and developed as a result of close cooperation among the following groups: (a) War Metallurgy Committee of NDRC, (b) an advisory committee functioning under the War Metallurgy Committee, (c) armed services, (d) Carnegie Institute of Technology, (e) industrial concerns, and (f) technical advisors.

The authors are indebted to many in each of these groups and wish to express appreciation for their valuable contributions.

Research assistants whose help has been especially valuable



include I. Broverman, A. H. Grobe, C. C. Busby, and M. A. Redmerski. Gratitude is also felt toward J. R. Johnson and L. Redmerski, laboratory assistants, for their aid in tabulating data and executing laboratory work.

#### References

1. Cyril Wells and R. F. Mehl, "Transverse Mechanical Properties of Heat Treated Wrought Steel Products", *TRANSACTIONS, American Society for Metals*, Vol. 41, 1949, p. 717.
2. Edwin G. Olds and Cyril Wells, "Statistical Methods for Evaluating the Quality of Certain Wrought Steel Products", *TRANSACTIONS, American Society for Metals*, Vol. 42, 1950, p. 845-899.
3. F. E. Croxton and D. J. Cowden, *Applied General Statistics*, 1939, Prentice-Hall, Inc., New York.
4. G. W. Snedecor, *Statistical Methods*, Fourth Edition, 1946, Iowa State College Press, Ames, Iowa.
5. C. Wells, R. F. Mehl, C. V. Klimas, I. Broverman and P. E. Busby, "Improvement in Wrought Gun Tubes: Part I—Operating Characteristics of Specification WVXS-78", Serial No. M-537, Aug. 6, 1945, Vols. I and II. Published by the Office of Technical Services, Department of Commerce, Washington 25, D. C.
6. Cyril Wells, C. F. Sawyer, I. Broverman and R. F. Mehl, "A Quench Cracking Susceptibility Test for Hollow Cylinders", *TRANSACTIONS, American Society for Metals*, Vol. 42, 1950, p. 206.
7. J. W. Spretnak and Cyril Wells, "An Engineering Analysis of the Problem of Quench Cracking in Steel", *TRANSACTIONS, American Society for Metals*, Vol. 42, 1950, p. 233.

# NOTCHED AND UNNOTCHED TENSILE AND FATIGUE PROPERTIES OF TEN ENGINEERING ALLOYS AT 25 °C AND -196 °C

BY J. W. SPRETNAK, M. G. FONTANA AND H. E. BROOKS

## *Abstract*

*The effect of notches on the tensile and fatigue properties at 25 °C (77 °F) and -196 °C (-321 °F) of ten engineering alloys was investigated. The materials studied were the following: 24S-T and 75S-T aluminum alloys, FS-1 magnesium alloy, SAE 2330 steel (150,000 psi tensile strength), NE (SAE) 8630 steel (150,000 psi tensile strength), 18-8S stainless steel (210,000 psi tensile strength), titanium, Hy-Tuf steel (230,000 psi tensile strength), and SAE 4340 steel (150,000 and 230,000 psi tensile strength). The Vickers hardness and Charpy key-hole impact strength of these materials were determined at room temperature and at temperatures down to that of liquid hydrogen, -253 °C (-423 °F).*

THE use of engineering metals and alloys of very low temperatures is increasing continuously and is becoming of significant technical importance. Accordingly, information is needed on mechanical properties (particularly tensile and fatigue) of these metals and alloys at very low temperatures for engineering design data. The unnotched tensile and unnotched fatigue properties of several engineering alloys at temperatures down to -196 °C (-321 °F) were presented in a previous paper (1),<sup>1</sup> along with Vickers hardness values and Charpy impact strengths down to the temperature of liquid hydrogen, -253 °C (-423 °F). This previous paper should be referred to for detailed descriptions of experimental techniques used in the current studies.

The purpose of the present investigation was to determine the effect of notches on the tensile and fatigue properties of ten engineering alloys at room temperature and at the temperature of liquid nitrogen, -196 °C (-321 °F). Included also are some additional data on hardness and impact strength at the low temperatures. The test-

<sup>1</sup>The figures appearing in parentheses pertain to the references appended to this paper.

Of the authors, J. W. Spretnak is associate professor of metallurgy and research associate, Ohio State University Research Foundation, M. G. Fontana is professor of metallurgical research, and chairman, department of metallurgy, The Ohio State University, and H. E. Brooks is research engineer, Ohio State University Research Foundation. Manuscript received April 14, 1950.

ing procedures employed were essentially the same as those used in the previous work reported, with some minor modifications. Suitably designed notched tensile and notched fatigue specimens were used in the investigation.

### MATERIALS TESTED

The metals and alloys studied in the current investigation were the following: 24S-T and 75S-T aluminum alloys, Dowmetal FS-1 magnesium alloy, SAE 2330 steel heat treated to 150,000 psi tensile strength, NE (SAE) 8630 steel at 150,000 psi tensile strength, 18-8 S type stainless steel cold drawn to 210,000 psi tensile strength, titanium metal in the hot-swaged condition, Hy-Tuf steel heat treated to a tensile strength of 230,000 psi, and SAE 4340 steel heat treated to tensile strength levels of 150,000 and 230,000 psi. The compositions of the metals and alloys are presented in Tables I and II.

**Table I**  
Composition of the Nonferrous Metals and Alloys

Metal	Speci- fication	% Si	% Fe	% Cu	% Mn	% Al	% Mg	% Zn	% Cr	% Ni	Other
24S-T Aluminum <sup>1</sup>	QQ-A-354	0.16	0.43	3.8- 4.4	0.6- 0.9	bal.	1.2- 1.7	<0.10	....	<0.05	<0.05 Bi Pb
75S-T Aluminum <sup>1</sup>	AN-A-9a	0.20	0.45	1.50	0.15	bal.	2.80	5.70	0.30	....	0.05 Ti
FS-1 Magnesium	AN-M-27	<0.01	<0.001	<0.01	0.49	3.10	bal.	1.05	<0.001		
Titanium <sup>2</sup>	.....	Not Available									

<sup>1</sup>Commercially heat treated and aged.

<sup>2</sup>Received in hot-swaged condition as  $\frac{1}{4}$ -inch rounds with Vickers hardness number of 250.

**Table II**  
Compositions of the Steels

Steel	Specification	% C	% Mn	% P	% S	% Si	% Ni	% Cr	% Mo
SAE 2330 <sup>1</sup>	AN-QQ-S-589	0.28- 0.33	0.60- 0.80	<0.026	<0.030	0.20- 0.35	3.25- 3.75	....	...
NE(SAE) 8630 <sup>2</sup>	AN-S-14a	0.27- 0.33	0.70- 0.90	<0.022	<0.033	0.20- 0.35	0.48- 0.67	0.49- 0.56	0.18
Type 304 Stainless Steel (18-8) <sup>3</sup>	.....	0.054	0.49	0.019	0.015	0.42	8.82	18.50	...
Hy-Tuf <sup>4</sup>	.....	0.259	1.26	0.016	0.017	1.37	1.91	0.09	0.43
SAE 4340 <sup>5</sup>	AN-QQ-S-756A	0.46	0.70	0.018	0.031	0.288	1.78	0.95	0.23

<sup>1</sup>Received as normalized. Austenitized at 1500°F, oil-quenched, and tempered at 925°F to 150,000 psi tensile strength.

<sup>2</sup>Received as normalized. Austenitized at 1500°F, oil-quenched, and tempered at 850°F to 150,000 psi tensile strength.

<sup>3</sup>Cold drawn to 210,000 psi tensile strength.

<sup>4</sup>Received as normalized.

<sup>5</sup>Received as normalized. Austenitized at 1550°F, oil-quenched and tempered at (a) 1200°F (150,000 psi tensile strength) and (b) 800°F (230,000 psi tensile strength).

The cold drawn 18-8S stainless steel was obtained from the Allegheny-Ludlum Steel Corporation, the SAE 4340 and Hy-Tuf steels were obtained from The Crucible Steel Company of America,



and the titanium was supplied by The Remington Arms Company. The remaining metals and alloys were supplied by the Materials Laboratory, Wright-Patterson Air Force Base. All the material was received as  $\frac{3}{4}$ -inch rounds except the titanium, which was in the form of  $\frac{5}{8}$ -inch rounds.

#### EQUIPMENT AND PROCEDURES

*Tensile Tests*—A four-screw, 60,000-pound capacity, Olsen Universal testing machine was used in the tensile tests. It is a mechanically loaded type equipped with a pendulum-lever weighing system and autographic strain recorder. The tests in liquid nitrogen were carried out by enclosing the test specimen in a metal Dewar flask which was kept filled with liquid nitrogen.

The tensile strain in this study was measured by means of SR4-Al wire strain gages. Two gages were used on opposite sides of each specimen to compensate for any eccentric loading. The gages were connected in series, so that the values obtained for single readings were averages for the two gages. The temperature compensation was made by means of a "dummy" gage maintained at the temperature of testing. This gage consisted of an SR4-Al gage cemented to an unstressed bar kept at the temperature of testing. The compensating gage was connected so as to "electrically buck" the live wire gage.

Standard threaded end tensile test specimens were used with the gage length equal to four times the gage diameter. In the unnotched tests, the following gage diameters were used: 0.505 inch for 24S-T and 75S-T aluminum alloys and FS-1 magnesium alloy, 0.30 inch for SAE 2330 steel, NE (SAE) 8630 steel, 18-8S stainless steel, Hy-Tuf steel, and SAE 4340 steel, and 0.25 inch for titanium. The varying size of bars resulted from the limitations of the testing machine and the as-received bar size. In the notched tests, the corresponding major diameters were 0.555, 0.35, 0.30 inch for the root diameters of 0.505, 0.30, and 0.25 inch respectively. The circumferential notches had a notch angle of 60 degrees, a constant depth of 0.025 inch and a notch radius of 0.010 inch.

Notched and unnotched tensile tests were made at room temperature and at  $-196^{\circ}\text{C}$  on the ten metals and alloys. The temperature of  $-196^{\circ}\text{C}$  was obtained by surrounding the specimen with a metal Dewar flask filled with liquid nitrogen. The specimens were soaked in the cooling medium for about 15 minutes before starting the test. At least two specimens were tested at each temperature.

The modulus of elasticity was determined by taking strain read-



ings with SR4-A1 strain gages at 500-pound increments of load until a total load of 5000 pounds or one-half of the yield strength (whichever was the least) was reached. The machine was stopped for each reading. Three determinations of the modulus were made at both testing temperatures in order to obtain an average representative value.

In the unnotched tests, after the modulus was determined, the specimen was loaded further and readings were taken at sufficiently small intervals to definitely establish the stress-strain curve. The machine was again stopped for each reading. The yield strength values were obtained from the stress-strain curves at an offset of 0.2%.

After the stress-strain curve was sufficiently established to obtain the offset yield strengths, the specimen was stressed continuously at a crosshead speed of 0.1 inch per minute until the specimen ruptured. The ultimate strength is the maximum load divided by the original cross sectional area. The nominal fracture stress was calculated by dividing the breaking load by the area of the cross section of the bar at the fracture after rupturing had occurred.

All measurements for the determination of the elongation and the reduction of area were made after the test specimens returned to room temperature. In the unnotched tests, the elongations were determined in a gage length equal to four times the diameter. In the notched bar tests, the only ductility values reported are those for reduction of area. Two values of reduction of area values were recorded, one for the root diameter and the other just adjacent to the notch on the major diameter. These ductility values reported are specific for these notched bars and should not be directly compared to results from unnotched specimens.

*Fatigue Tests*—Redesigned Krouse cantilever beam machines of the constant deflection type were used in the fatigue testing. This type of machine is usually used for the flexure testing of plate specimens. The principal modification consisted of a 90-degree rotation of the supporting beam for the vise so that the specimen is in a vertical instead of a horizontal position. Another modification was the substitution of a glass fabric laminate supporting beam for the metal beam in order to decrease the consumption of liquid coolants by decreasing the thermal conductivity of the supporting beam. The testing speed employed was 2000 rpm. This modified arrangement is advantageous because the specimen and the coolant can be contained easily in the Dewar flask surrounding the specimen. Previous tests (1) comparing results of the cantilever test and the rotat-

ing beam test showed close agreement between the two methods.

Three sizes of fatigue test specimens were used in the study. The minimum cross sectional area was varied as the strength of the material varied because of the limited capacity of the testing machine. The 24S-T and 75S-T aluminum alloys and the FS-1 magnesium alloy were tested as specimens with a minimum diameter of 0.5 inch. The notched specimens in all cases had the root diameter identical with the minimum diameter of the unnotched tests. The notch in all notched specimens was constant, with an angle of 60 degrees, depth of 0.025 inch, and root radius of 0.010 inch. All of the remaining materials except titanium were tested in bars of minimum diameter of 0.30 inch. Titanium was tested as bars with minimum diameter of 0.25 inch.

The bar stock as received was cut into sections of proper length. The center portions of these bars were then turned down, leaving about 0.004 inch on the diameter for polishing. The reduced section was then highly polished with a polishing wheel having the same radius as the specimen profile, using 180-grit abrasive and keeping the plane of the wheel parallel to the longitudinal axis of the specimen.

The desired stress was applied to the specimen by hanging the corresponding dead weight from the connecting rod bearing. An electronic indicator was used to determine the point to which the beam deflected under the given load. The connecting rod was then attached to the beam, and the eccentric shaft was adjusted to produce the same deflection. The specimen was carefully aligned in the machine so the reversed stress was of the same magnitude.

After the initial deflection for a given load was determined, the machine was turned about ten cycles manually and another calibration made. If there was an appreciable change in the deflection, the procedure was repeated until the deflection approached a constant value. The motor was then used to drive the machine, and checks were made at progressively longer intervals until the deflection was constant or the specimen failed. The speed of testing was kept constant at 2000 revolutions per minute.

*Hardness Tests*—A Vickers pyramid hardness testing machine was used for making hardness measurements in this investigation. The specimen was contained in a metal dish with a bottom rigid enough to withstand the necessary loads. When liquid nitrogen or liquid hydrogen was used as the coolant, the considerable volume of gas released agitated the liquid and the specimen was efficiently cooled. A simple metal-lined wooden dish proved to be a satisfactory container for the coolant and specimen. Cylinders about  $\frac{1}{2}$  inch

thick were cut from the  $\frac{3}{4}$ -inch diameter bars for hardness tests. The ends were faced in a lathe and polished down to a 2/0 grit paper.

Five impressions were made with the Vickers diamond pyramid at regular intervals along two radii of the specimen, at 90 degrees to each other. The hardness number reported is the average of these ten determinations. Impressions were made at room temperature,  $-78$ ,  $-196$ , and  $-253$  °C. In the low temperature tests the specimen was placed in a metal-lined wooden dish filled with the cooling medium. The impressions were made while the specimens were immersed in the coolant and the impressions were measured after the specimens were brought back to room temperature. Tests were made in which the impressions were made and measured while the specimen was immersed in liquid nitrogen. These tests indicated that the increase in diagonal length caused by thermal expansion did not significantly change the hardness number.

*Impact Tests*—All of the impact tests were made on a Riehle impact testing machine using the 220-foot-pound initial position (striking velocity 18.1 feet per second). The specimens were thoroughly cooled in the liquid coolant and quickly transferred to the machine for the test. All the tests were made on the standard Charpy keyhole notch specimens. These specimens were made according to Federal Specification QQ-M-151a. Each specimen was cut from the center of the bar to assure uniformity of test conditions.

Impact tests were made at room temperature,  $-78$  °C (dry ice and acetone),  $-196$  °C (liquid nitrogen), and  $-253$  °C (liquid hydrogen). All the specimens were soaked in the bath at the desired temperature for half an hour before testing. The specimens, after the soaking period, were transferred quickly to the anvil of the impact machine and were broken immediately. Previous work has demonstrated that no perceptible increase of temperature occurs in the impact bars between the time they leave the bath and the time they are broken (about 5 seconds).

## RESULTS AND DISCUSSION

*Tensile Tests*—The modulus of elasticity values for the ten materials are summarized in Table III. In all cases, the modulus of elasticity increased as the testing temperature was decreased from  $25$  °C ( $77$  °F) to  $-196$  °C ( $-320$  °F). The average increases in the modulus are as follows:

Aluminum and Magnesium Alloys . . . .	$1.1 \times 10^6$ psi
Steels . . . . .	$1.5 \times 10^6$ psi
18-8S Stainless . . . . .	$4.1 \times 10^6$ psi
Titanium . . . . .	$2.2 \times 10^6$ psi



**Table III**  
**Modulus of Elasticity of the Engineering Alloys at Various Temperatures**

Material	Modulus of Elasticity, $\text{psi} \times 10^{-6}$	
	25 °C	-196 °C
24S-T Aluminum	10.9	12.0
75S-T Aluminum	10.3	11.6
FS-1 Magnesium	6.4	7.3
SAE 2330 Steel (150,000 psi)	29.2	31.6
NE 8630 Steel (150,000 psi)	29.8	32.4
18-8S Stainless (210,000 psi)	23.6	27.7
Titanium (93,000 psi)	16.7	19.0
Hy-Tuf Steel (230,000 psi)	29.8	31.3
SAE 4340 Steel (150,000 psi)	30.9	31.8
SAE 4340 Steel (230,000 psi)	30.7	30.9

The largest increase in the modulus was observed in the 18-8S stainless steel ( $4.1 \times 10^6$  psi) and the smallest in the SAE 4340 steel heat treated to 230,000 psi tensile strength ( $0.2 \times 10^6$  psi).

The 0.2% offset yield strength values for the ten metals and alloys are summarized in Table IV. Yield points were observed at both test temperatures in SAE 2330 steel, and SAE 4340 steel treated to 150,000 psi tensile strength. In these unnotched tests, reduction of the testing temperature to -196 °C brings about an average increase of about 30% for the aluminum alloys and the steels. FS-1 magnesium and titanium show an unusually high increase in yield strength at the low temperature (61.9 and 146.0% respectively).

The ultimate strength values in the unnotched and notched tests at 25 °C and -196 °C are summarized in Table V. In the unnotched tests, the ultimate strength values parallel the yield strength values in their temperature dependence. At -196 °C the aluminum alloys and the steels show an average increase of 29.5% in the ultimate strength. Again the FS-1 magnesium and titanium exhibit the highest temperature dependence (increase of 57.0 and 108.9% respectively). At 25 °C, the ultimate strength values are increased by the presence of a notch in all the materials tested. In the notched tests,

**Table IV**  
**Unnotched Yield Strength of the Engineering Alloys at Various Temperatures**

Material	Yield Strength, $\text{psi}^*$		Per Cent Increase
	25 °C	-196 °C	
24S-T Aluminum	48,500	63,100	30.1
75S-T Aluminum	72,200	89,500	23.9
FS-1 Magnesium	29,900	48,400	61.9
SAE 2330 Steel (150,000 psi)	139,300	186,300	33.8
NE 8630 Steel (150,000 psi)	121,500	166,500	37.0
18-8S Stainless (210,000 psi)	148,800	189,000	27.1
Titanium (93,000 psi)	72,150	177,500	146.0
Hy-Tuf Steel (230,000 psi)	196,250	233,000	18.7
SAE 4340 Steel (150,000 psi)	136,000	199,500	46.7
SAE 4340 Steel (230,000 psi)	214,000	267,000	24.8

\*0.2% offset



**Table V**  
**Ultimate Tensile Strength of the Engineering Alloys at Various Temperatures**

Material	Ultimate Tensile Strength, psi					Per Cent Increase
	Unnotched 25 °C	Unnotched -196 °C	Per Cent Increase	Notched 25 °C	Notched -196 °C	
24S-T Aluminum	69,900	87,300	24.9	70,600	82,900	17.4
75S-T Aluminum	83,900	99,500	18.6	87,200	103,500	18.7
FS-1 Magnesium	40,100	62,800	57.0	43,000	52,900	23.0
SAE 2330 Steel (150,000 psi)	145,300	186,300	28.3	178,800	240,300	34.4
NE 8630 Steel (150,000 psi)	142,000	192,100	35.2	190,500	234,000	22.8
18-8S Stainless (210,000 psi)	212,400	296,250	39.6	267,000	340,000	27.3
Titanium (93,000 psi)	89,650	186,500	108.9	116,800	212,800	82.8
Hy-Tuf Steel (230,000 psi)	231,510	283,000	22.2	294,000	304,500	3.5
SAE 4340 Steel (150,000 psi)	146,000	208,000	42.5	185,800	254,000	36.5
SAE 4340 Steel (230,000 psi)	231,000	288,000	24.7	283,000	271,500	-4.5

**Table VI**  
**Nominal Fracture Stress of the Engineering Alloys at Various Temperatures**

Material	Fracture Stress, psi					Per Cent Increase
	Unnotched 25 °C	Unnotched -196 °C	Per Cent Increase	Notched 25 °C	Notched -196 °C	
24S-T Aluminum	96,100	107,000	11.4	74,500	87,900	17.9
75S-T Aluminum	111,300	116,700	4.8	90,300	105,500	16.7
FS-1 Magnesium	56,600	69,300	23.2	44,600	55,200	25.0
SAE 2330 Steel (150,000 psi)	243,500	291,000	19.7	211,500	257,500	21.8
NE 8630 Steel (150,000 psi)	239,000	307,500	28.9	204,800	242,000	18.1
18-8S Stainless (210,000 psi)	301,000	538,700	79.1	270,000	367,500	36.1
Titanium (93,000 psi)	133,500	221,500	65.7	124,500	223,000	78.4
Hy-Tuf Steel (230,000 psi)	346,000	383,500	10.9	312,000	309,500	2.5
SAE 4340 Steel (150,000 psi)	250,000	311,000	24.4	209,500	271,500	29.6
SAE 4340 Steel (230,000 psi)	315,000	323,000	2.5	294,000	279,500	-4.7

**Table VII**  
**Unnotched Tensile Elongation of Engineering Alloys at Various Temperatures**

Material	Per Cent Elongation*		Per Cent Change
	25 °C	-196 °C	
24S-T Aluminum	20.0	21.5	+2.5
75S-T Aluminum	13.5	12.0	-11.1
FS-1 Magnesium	16.5	6.5	-60.6
SAE 2330 Steel (150,000 psi)	17.5	20.5	+17.1
NE 8630 Steel (150,000 psi)	15.5	18.0	+16.1
18-8S Stainless (210,000 psi)	12.0	29.5	+145.8
Titanium (93,000 psi)	27.5	13.8	-49.8
Hy-Tuf Steel (230,000 psi)	11.8	12.0	+2.1
SAE 4340 Steel (150,000 psi)	20.4	20.0	-1.9
SAE 4340 Steel (230,000 psi)	11.8	4.0	-65.9

\*Elongation in gage length equal to four times the gage diameter.

the temperature dependence of the ultimate strength is less than that in the unnotched tests. Titanium, however, still exhibits a relatively high increase in notched ultimate strength at -196 °C of 82.8%. The SAE 4340 steel at the 230,000 psi tensile strength level shows a slight decrease in notched ultimate strength at -196 °C.

The nominal fracture stress values of the ten materials in the unnotched and notched tests at 25 °C and -196 °C are summarized in Table VI. These values were obtained by dividing the breaking load by the cross sectional area of the fractured section, measured

Table VIII  
Tensile Reduction of Area of Engineering Alloys at Various Temperatures

Material	Unnotched Per Cent Red. of Area		Notched			
	25 °C	-196 °C	Per Cent Red. of Area at Root of Notch		Per Cent Red. of Area Outside Notch	
	25 °C	-196 °C	25 °C	-196 °C	25 °C	-196 °C
24S-T Aluminum	30.5	20.5	7.0	6.5	1.8	4.8
75S-T Aluminum	28.0	15.0	2.3	2.3	1.5	1.5
FS-1 Magnesium	36.5	8.0	11.3	4.0	7.5	2.3
SAE 2330 Steel (150,000 psi)	59.5	40.0	22.0	6.8	8.8	1.8
NE 8630 Steel (150,000 psi)	59.5	50.0	13.3	3.3	6.8	0.8
18-8S Stainless (210,000 psi)	54.5	45.5	11.5	7.3	8.5	5.0
Titanium (93,000 psi)	24.0	14.8	12.5	5.0	7.8	1.0
Hy-Tuf Steel (230,000 psi)	44.3	32.8	7.5	2.5	5.0	1.3
SAE 4340 Steel (150,000 psi)	59.7	44.5	17.0	6.3	13.5	3.8
SAE 4340 Steel (230,000 psi)	45.8	11.0	3.5	2.8	2.5	1.8

after fracture. In the unnotched tests, the fracture stress was increased in all cases by dropping the testing temperature to  $-196^{\circ}\text{C}$ . The most attractive increases of fracture stress in lowering the temperature were observed in the 18-8S steel and in titanium (increase of 79.1 and 65.7% respectively). At  $25^{\circ}\text{C}$ , the presence of the notch decreased the fracture stress in all cases. In the notched tests, reduction of the temperature from  $25^{\circ}\text{C}$  to  $-196^{\circ}\text{C}$  increased the fracture stress with one exception. Titanium exhibited the largest increase of 78.4%. The SAE 4340 steel heat treated to 230,000 psi tensile strength decreased 4.7% in the notched fracture stress in reducing the testing temperature from  $25^{\circ}\text{C}$  to  $-196^{\circ}\text{C}$ .

The elongation values for the ten materials in the unnotched tensile tests at  $25^{\circ}\text{C}$  and  $-196^{\circ}\text{C}$  are summarized in Table VII. These values exhibit an erratic dependence on the testing temperature. Decreasing the temperature to  $-196^{\circ}\text{C}$  resulted in three general behaviors: (a) elongation essentially unchanged (24S-T and 75S-T aluminum alloys, Hy-Tuf steel, SAE 4340 at 150,000 psi tensile strength), (b) elongation decreased (FS-1 Mg, titanium, SAE 4340 steel at 230,000 psi tensile strength), and (c) elongation increased (SAE 2330 steel, NE 8630 steel, 18-8S stainless steel).

The reduction of area values in the unnotched and notched tensile tests at  $25^{\circ}\text{C}$  and  $-196^{\circ}\text{C}$  for the ten materials are presented in Table VIII. In the unnotched tests, the reduction of area values all decreased in lowering the temperature to  $-196^{\circ}\text{C}$ . The sharpest decreases occurred in FS-1 magnesium and SAE 4340 steel at 230,000 psi tensile strength. The presence of a notch at  $25^{\circ}\text{C}$  produces a significant decrease in reduction of area in all cases. In the notched tests, the general effect of reducing the temperature to  $-196^{\circ}\text{C}$  is to reduce the reduction of area values both at the root of the notch and just outside of the notch on the major diameter.

**Table IX**  
**Endurance Limits in Fatigue at 25 °C and -196 °C**  
**For N = 10<sup>7</sup> Cycles**

Material	Unnotched		Fatigue Stress, psi Per Cent Increase	Notched		Per Cent Increase
	25 °C	-196 °C		25 °C	-196 °C	
24S-T Aluminum	25,500	45,000*	76	11,000	20,000	82
75S-T Aluminum	30,000	55,500*	85	15,000	20,000	33
FS-1 Magnesium	19,000	25,000*	32	8,000	10,000	25
SAE 2330 Steel (150,000 psi)	75,000	125,000*	67	17,500	40,000	129
NE 8630 Steel (150,000 psi)	70,000	125,000*	79	30,000	35,000	17
18-8S Stainless (210,000 psi)	110,000	155,000*	45	23,000	40,000	74
Titanium (93,000 psi)	73,500	100,000	36	27,500	40,000	45
Hy-Tuf Steel (230,000 psi)	88,400	120,000	36	38,000	46,000	16
SAE 4340 Steel (150,000 psi)	74,000	116,000	56	20,000	20,000	0
SAE 4340 Steel (230,000 psi)	89,200	121,500	36	49,000	36,000	-14

\*Extrapolated from 10<sup>6</sup> cycles.

*Fatigue Tests*—The fatigue curves (S-N curves) for the ten materials in the unnotched and notched tests at 25 °C and -196 °C are presented in Figs. 1 to 10. The curves for 24S-T aluminum are essentially parallel and exhibit no knee; the notched fatigue curves for 75S-T aluminum alloy at 25 °C and -196 °C converge at high stress levels. The curves for FS-1 magnesium exhibit no knee, but the unnotched curve at 25 °C is somewhat flatter than the other three curves. The curves for SAE 2330 steel exhibit a knee as in the curves typical of steels. Of interest to note in the curves for the notched fatigue at 25 °C and -196 °C is that the endurance limit is higher at -196 °C but the fatigue strength at high stress levels is higher at 25 °C (i.e., the curves cross). The same type of crossing

**Table X**  
**Fatigue Strength at 25 °C and -196 °C**  
**For N = 10<sup>6</sup> Cycles**

Material	Unnotched		Fatigue Stress, psi Per Cent Increase	Notched		Per Cent Increase
	25 °C	-196 °C		25 °C	-196 °C	
24S-T Aluminum	58,200	81,500	40	44,000	47,000	7
75S-T Aluminum	68,000	90,000	32	44,000	45,000	2
FS-1 Magnesium	30,000	44,500	48	23,300	25,500	9
SAE 2330 Steel (150,000 psi)	133,000	203,000	53	115,000	100,000	-13
NE(SAE) 8630 Steel (150,000 psi)	125,000	192,000	54	114,000	84,000	-26
18-8S Stainless (210,000 psi)	168,000	222,000	32	103,000	96,000	-7
Titanium (93,000 psi)	101,000	139,000	38	67,000	80,000	19
Hy-Tuf Steel (230,000 psi)	188,000	185,000	-2	136,000	90,000	-34
SAE 4340 Steel (150,000 psi)	140,000	193,000	38	128,000	100,000	-22
SAE 4340 Steel (230,000 psi)	192,000	205,000	7	118,000	60,000	-49
<b>For N = 10<sup>6</sup> Cycles</b>						
24S-T Aluminum	42,200	65,000	54	29,500	34,000	15
75S-T Aluminum	44,000	70,500	60	29,300	33,000	13
FS-1 Magnesium	24,300	32,700	35	14,000	16,500	18
SAE 2330 Steel (150,000 psi)	83,000	157,000	89	52,000	46,000	-15
NE(SAE) 8630 Steel (150,000 psi)	86,000	144,000	67	62,000	59,000	-5
18-8S Stainless (210,000 psi)	118,000	181,000	53	45,000	50,000	11
Titanium (93,000 psi)	76,000	106,000	39	49,000	63,000	29
Hy-Tuf Steel (230,000 psi)	128,000	152,000	19	61,000	74,000	21
SAE 4340 Steel (150,000 psi)	88,000	144,000	64	57,000	48,000	-16
SAE 4340 Steel (230,000 psi)	132,000	167,000	27	54,000	45,000	-17



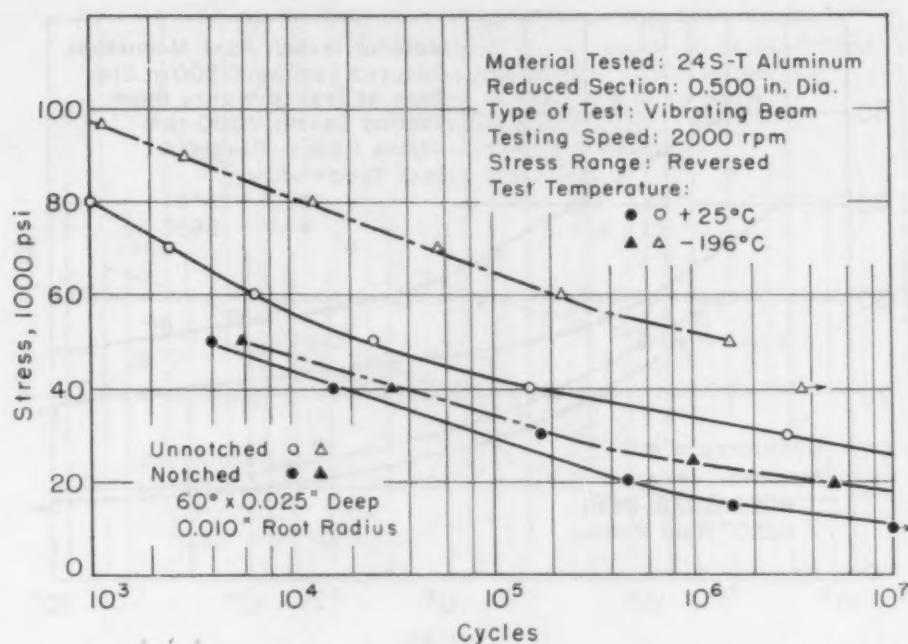


Fig. 1—Results of Vibrating Beam Tests of Notched and Unnotched 24S-T Aluminum Specimens.

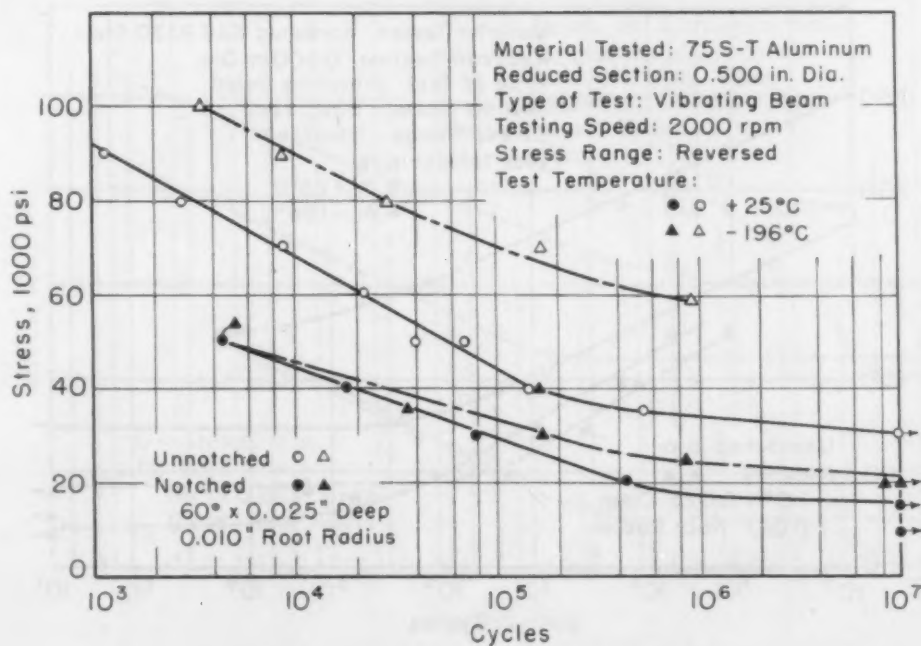


Fig. 2—Results of Vibrating Beam Tests of Notched and Unnotched 75S-T Aluminum Specimens.

of the curves for the notched tests is evident in the curves for NE (SAE) 8630 steel, 18-8 stainless steel and Hy-Tuf steel. The endurance limits of the notched tests on SAE 4340 steel (150,000 psi) are so nearly alike as to cause some uncertainty in deciding whether or



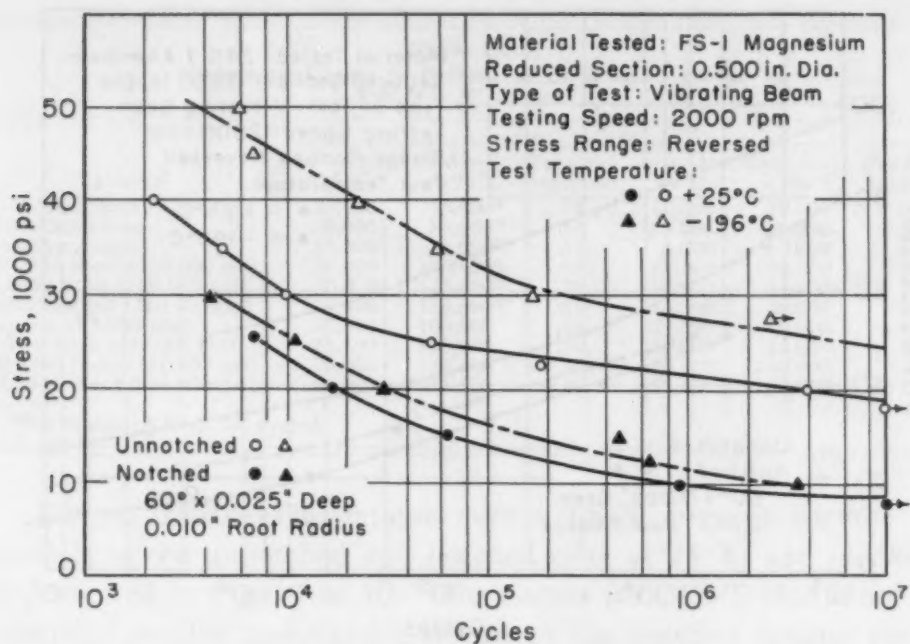


Fig. 3—Results of Vibrating Beam Tests of Notched and Unnotched FS-1 Magnesium Specimens.

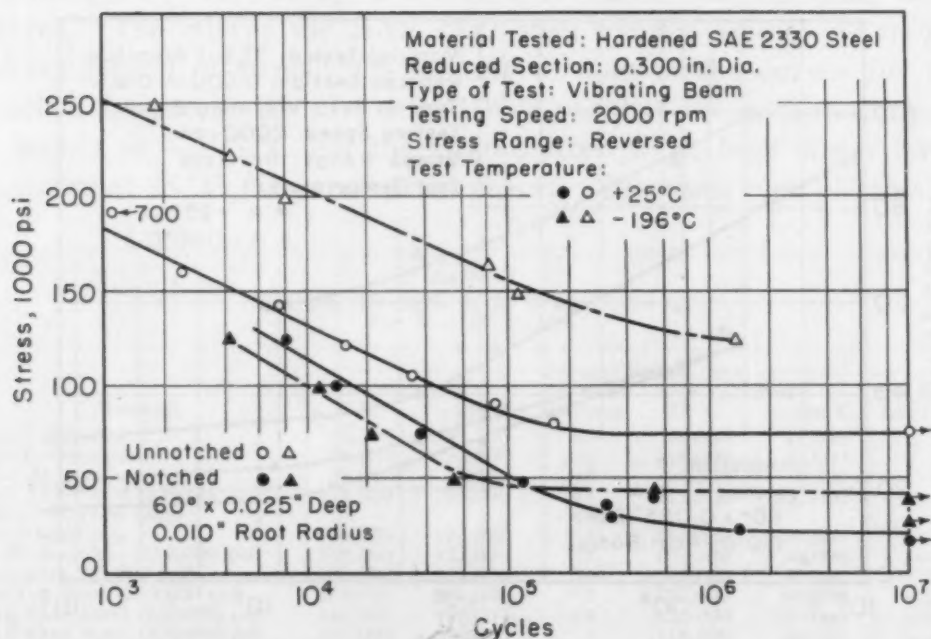


Fig. 4—Results of Vibrating Beam Tests of Notched and Unnotched Hardened SAE 2330 Steel Specimens.

not the curves cross. The S-N curves for titanium are characterized by a knee, but less sharp than those observed in curves for steel.

The endurance limits (for  $10^7$  cycles) for the ten materials are summarized in Table IX. In all cases in the unnotched tests, reduc-

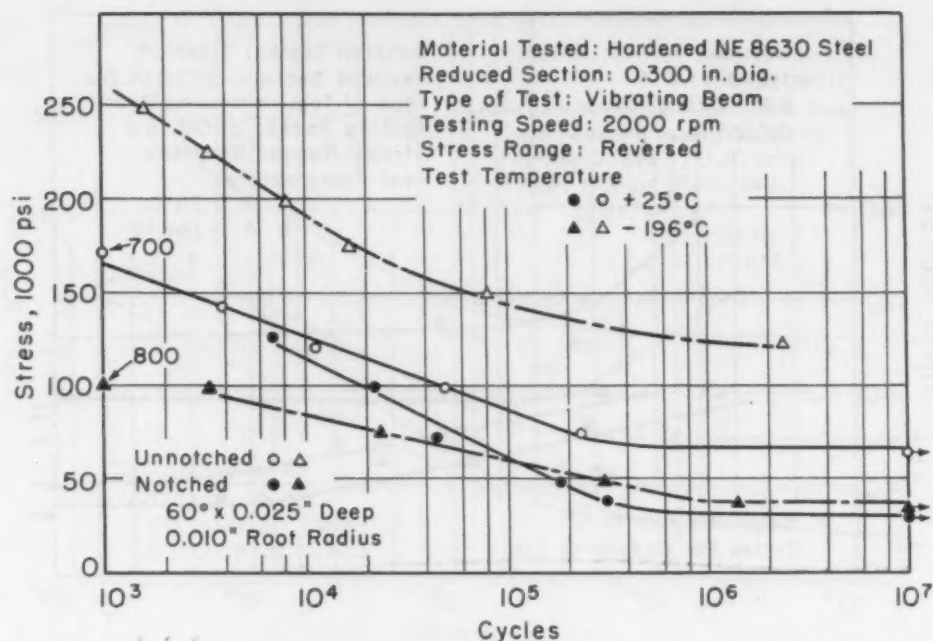


Fig. 5—Results of Vibrating Beam Tests of Notched and Unnotched Hardened NE 8630 Steel Specimens. (150,000 psi tensile strength.)

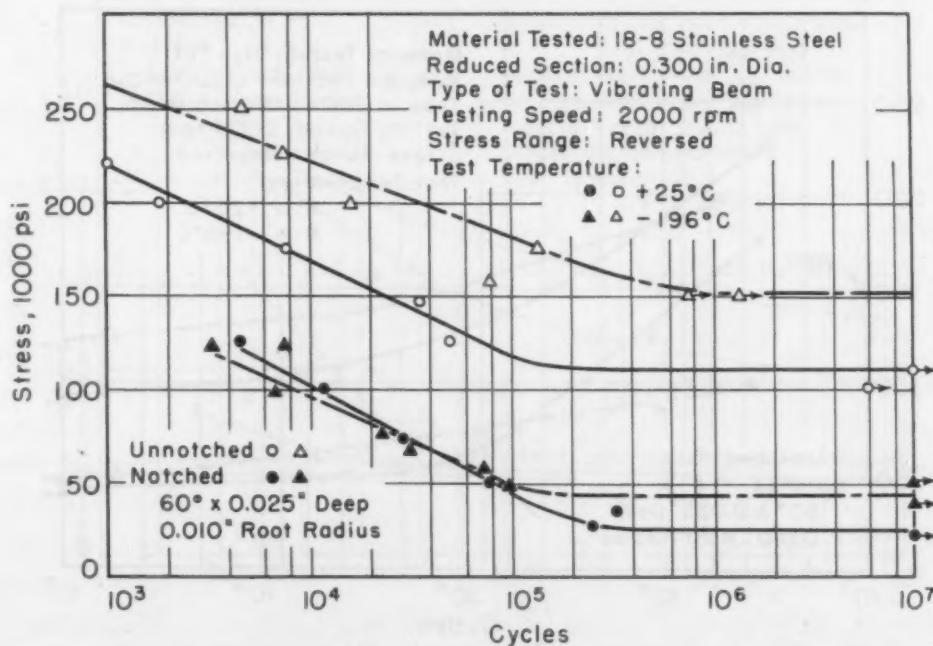


Fig. 6—Results of Vibrating Beam Tests of Notched and Unnotched 18-8 Stainless Steel Specimens. Cold-worked to 230,000 psi tensile strength.

ing the testing temperature to  $-196^{\circ}\text{C}$  brought about an increase in the fatigue strength. The largest increase occurred in the 75S-T aluminum alloy (85%), and the smallest in the FS-1 magnesium alloy (32%). The average increase for all materials is 55%. The

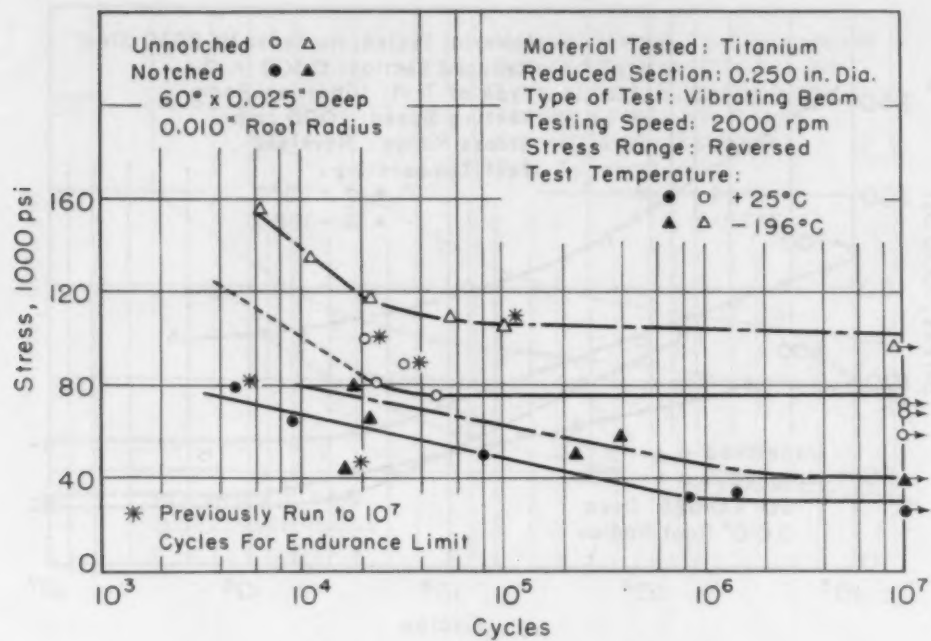


Fig. 7—Results of Vibrating Beam Tests of Notched and Unnotched Titanium Specimens. (93,000 psi tensile strength.)

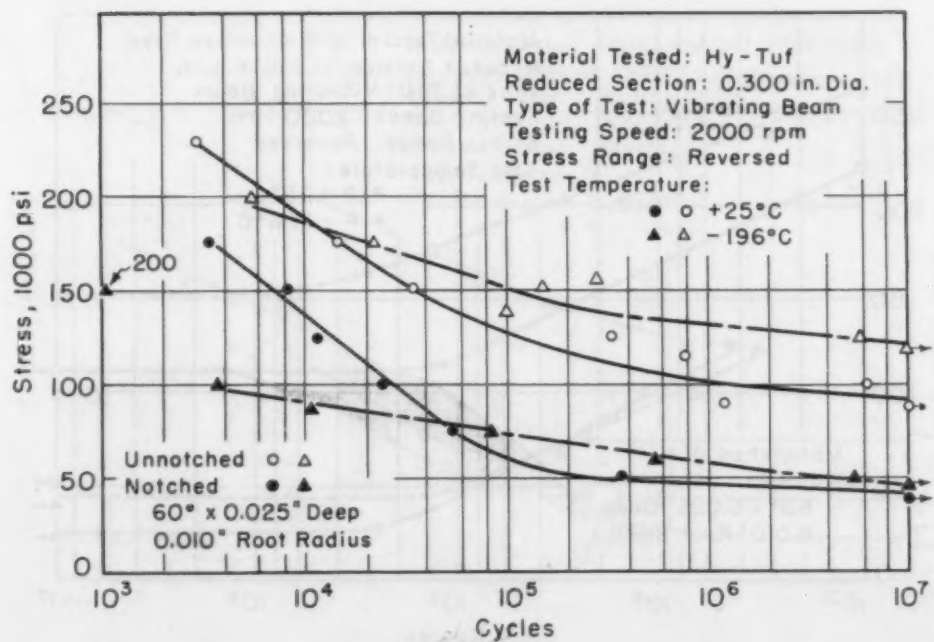


Fig. 8—Results of Vibrating Beam Tests of Notched and Unnotched Hy-Tuf Steel. (230,000 psi tensile strength.)

presence of notches significantly reduces the endurance limit at room temperature in all cases. The average decrease for all materials is 64%. The notched endurance limit in all cases except for SAE 4340 steel increased when tested at  $-196^{\circ}\text{C}$ . The largest increase oc-

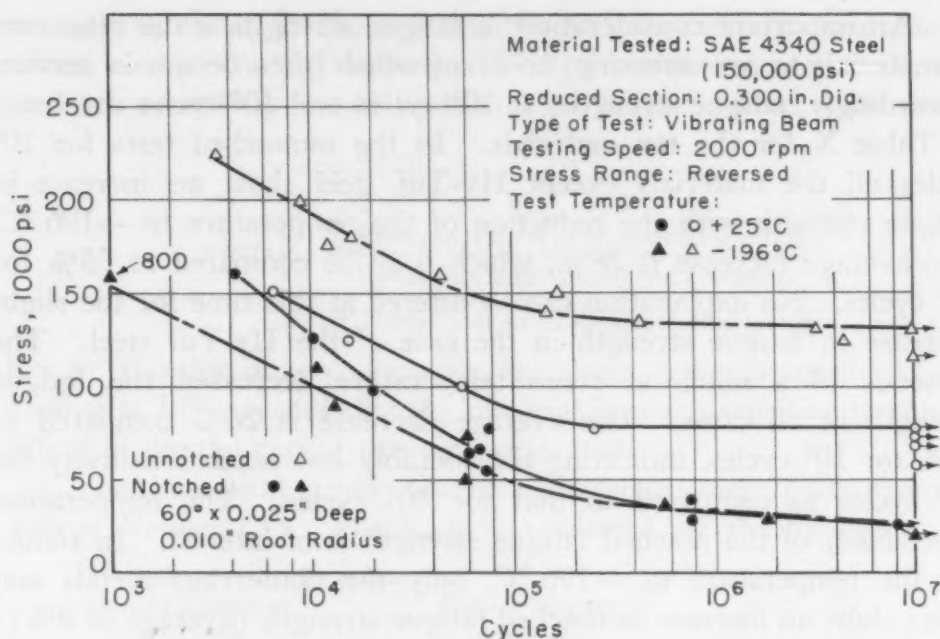


Fig. 9—Results of Vibrating Beam Tests of Notched and Unnotched SAE 4340 Steel (150,000 psi) at Various Temperatures.

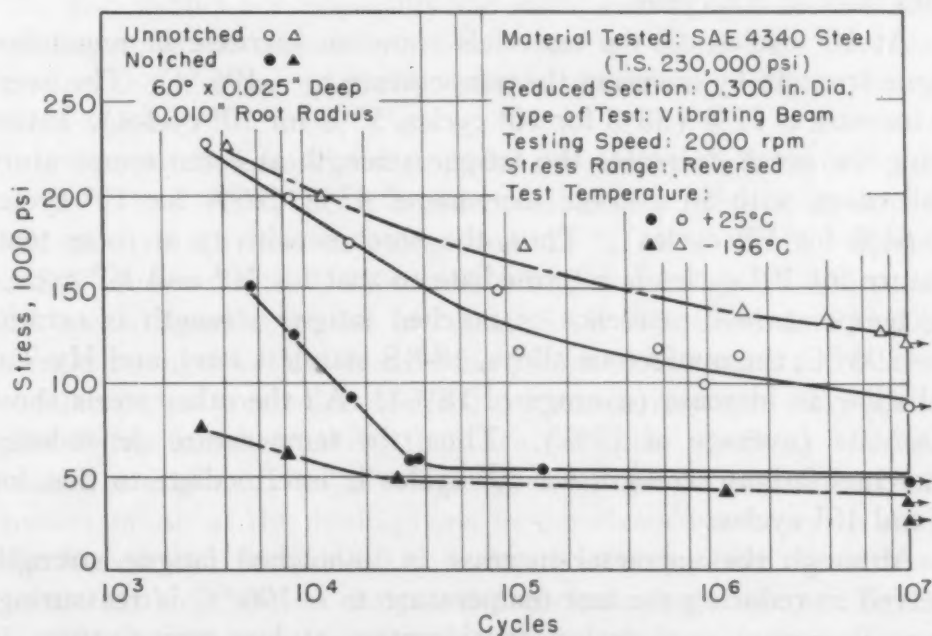


Fig. 10—Results of Vibrating Beam Tests of Notched and Unnotched SAE 4340 Steel (Tensile Strength 230,000 psi).

curred in the SAE 2330 steel (129%), whereas the SAE 4340 steel at 150,000 psi tensile strength showed no change and at 230,000 psi tensile strength suffered a decrease of 14%. No reason is apparent for the behavior of the notched endurance limits of this steel at -196 °C.



An important consideration in fatigue strength is the resistance of materials to overstressing, an event which often occurs in service. Accordingly, fatigue strengths at  $10^4$  cycles and  $10^5$  cycles are listed in Table X for the ten materials. In the unnotched tests for  $10^4$  cycles all the materials except Hy-Tuf steel show an increase in fatigue strength with the reduction of the temperature to  $-196^\circ\text{C}$ . The average increase is 38%, which is to be compared to 55% for  $10^7$  cycles. No explanation can be offered at this time for the slight decrease in fatigue strength in the case of the Hy-Tuf steel. The presence of a notch at room temperature decreased the fatigue strength in all cases. The average decrease is 26% compared to 64% for  $10^7$  cycles, indicating considerably less notch sensitivity for  $10^4$  cycles as compared to that for  $10^7$  cycles. The temperature dependency of the notched fatigue strength is of interest. In reducing the temperature to  $-196^\circ\text{C}$ , only the nonferrous metals and alloys show an increase in notched fatigue strength (average of 9%); all the steels show a decrease (average of 26%). Thus, the materials in notched fatigue are more sensitive to low temperatures at  $10^4$  cycles than at  $10^7$  cycles.

At  $10^5$  cycles, all the materials show an increase in unnotched fatigue strength by lowering the temperature to  $-196^\circ\text{C}$ . The average increase is 51% (38% for  $10^4$  cycles, 55% for  $10^7$  cycles). Introducing the notch decreases the fatigue strength at room temperature in all cases, with an average increase of 45% (26% for  $10^4$  cycles and 64% for  $10^7$  cycles). Thus, the notch sensitivity at room temperature for  $10^5$  cycles is intermediate to that for  $10^4$  and  $10^7$  cycles. The temperature dependence of notched fatigue strength is erratic. At  $-196^\circ\text{C}$ , the nonferrous alloys, 18-8S stainless steel, and Hy-Tuf steel show an increase (average of 18%). All the other steels show a decrease (average of 13%). Thus, the temperature dependency of notched fatigue strength for  $10^5$  cycles is intermediate to that for  $10^4$  and  $10^7$  cycles.

Although the universal increase in unnotched fatigue strength observed in reducing the test temperature to  $-196^\circ\text{C}$  is reassuring, a very important engineering consideration at low temperatures is the notch sensitivity in fatigue. Stress raisers are often introduced inadvertently through design, fabrication, heat treatment, and service conditions. To obtain a more quantitative analysis of this notch sensitivity, the fatigue strength data were analyzed in two ways in order to sort out the ten metals and alloys according to their notch sensitivity. The "fn" and "q" values were used in this analysis. The "fn" values are simply the fraction of the unnotched fatigue

strength exhibited in the notched test, or the reciprocals of the  $K_t$  values used in the "q" values. The "fn" value for a material with no notch sensitivity would be 1.0. The "q" (2) value is defined as

$$q = \frac{K_t - 1}{K_t - 1}$$

$$\text{where } K_t = \frac{\text{Endurance limit of unnotched specimen}}{\text{Endurance limit of notched specimen}}$$

$K_t$  = Theoretical stress concentration factor.

For a "q" value of zero, the materials show no notch sensitivity, and a value of 1.0 indicates that the material is notch sensitive to the full extent of the theoretical stress concentration.

The theoretical stress concentration factors were taken from the data of Neuber (3). The  $K_t$  values selected are the following:

Test Bar		
Major Diameter	Root Diameter	$K_t$
0.55 inch	0.50 inch	3.15
0.34 inch	0.30 inch	2.75
0.30 inch	0.25 inch	2.65

The two factors act essentially the same in sorting the materials according to notch sensitivity. Since the "q" values take into consideration the test-bar geometry, further discussions will be based on these values.

The notch sensitivity factors for the endurance limit ( $10^7$  cycles) at 25 °C and -196 °C are listed in Table XI. The notch sensitivity increases in all cases in going from 25 °C to -196 °C, except for 24S-T aluminum, SAE 2330 steel, 18-8S stainless steel, and titanium. Of special interest is the fact that SAE 4340 steel at 230,000 psi tensile strength is less notch-sensitive at both temperatures than is the same steel treated to 150,000 psi tensile strength. Hy-Tuf steel also is less notch-sensitive than are the other steels at 150,000 psi tensile strength. The "q" values greater than 1.0 encountered are a manifestation of the assumptions in the elasticity theory in deriving the  $K_t$  values. In Table XII is the increasing order of notch sensitivity ( $10^7$  cycles) in fatigue for the ten materials at 25 °C and -196 °C. At room temperature, the notch sensitivity is lowest for the aluminum and magnesium alloys and SAE 4340 and Hy-Tuf steels heat treated to 230,000 psi tensile strength. At -196 °C, the order is essentially the same except for the improved positions of titanium, SAE 2330 steel, and 18-8S stainless steel because of their decreased sensitivity at the low temperature. Despite the decrease in notch sensitivity of 18-8S stainless steel, it is very notch-sensitive at both temperatures.

**Table XI**  
**Notch Sensitivity Factors in Fatigue at 25 °C and -196 °C**  
**For N = 10<sup>7</sup> Cycles**

Material	"fn" <sup>(1)</sup>		K <sub>t</sub>		"q" <sup>(2)</sup>	
	25 °C	-196 °C	25 °C	-196 °C	25 °C	-196 °C
24S-T Aluminum Alloy	0.43	0.44	2.318	2.250	0.61	0.58
75S-T Aluminum Alloy	0.50	0.36	2.000	2.775	0.47	0.83
FS-1 Magnesium	0.42	0.40	2.375	2.500	0.64	0.70
SAE 2330 Steel						
(150,000 psi T.S.)	0.23	0.32	4.285	3.125	1.88	1.21
NE(SAE) 8630 Steel						
(150,000 psi T.S.)	0.43	0.28	2.333	3.571	0.76	1.47
18-8S Stainless Steel						
(210,000 psi T.S.)	0.21	0.26	4.783	3.875	2.16	1.64
Titanium Metal						
(93,000 psi T.S.)	0.37	0.40	2.673	2.500	1.01	0.91
Hy-Tuf Steel						
(230,000 psi T.S.)	0.43	0.3	2.326	2.608	0.76	0.92
SAE 4340 Steel						
(150,000 psi T.S.)	0.27	0.17	3.730	5.800	1.56	2.74
SAE 4340 Steel						
(230,000 psi T.S.)	0.55	0.30	1.820	3.375	0.47	1.36

<sup>(1)</sup> fn = fraction of unnotched fatigue strength in notched test.

$$\text{q} = \frac{K_t - 1}{K_t - 1}$$

K<sub>t</sub> = Fatigue Strength of Unnotched Specimen  
 Fatigue Strength of Notched Specimen

K<sub>t</sub> = Theoretical stress concentration factor.

**Table XII**  
**Increasing Order of Notch Sensitivity in Fatigue at 25 °C and -196 °C**  
**For N = 10<sup>7</sup> Cycles**

Order (Increasing Sensitivity)*	25 °C	-196 °C
1	75S-T Aluminum	24S-T Aluminum
2	SAE 4340 Steel** (230,000 psi)	FS-1 Magnesium
3	24S-T Aluminum	75S-T Aluminum
4	FS-1 Magnesium	Titanium
5	Hy-Tuf Steel (230,000 psi)	Hy-Tuf Steel (230,000 psi)
6	NE(SAE) 8630 Steel (150,000 psi)	SAE 2330 Steel (150,000 psi)
7	Titanium	SAE 4340 Steel (230,000 psi)
8	SAE 4340 Steel (150,000 psi)	NE(SAE) 8630 Steel (150,000 psi)
9	SAE 2330 Steel (150,000 psi)	18-8S Stainless (210,000 psi)
10	18-8S Stainless (210,000 psi)	SAE 4340 Steel (150,000 psi)

\*Based on "q" values.

\*\*Tensile strength at room temperature.

The notch sensitivity factors in overstressing (10<sup>4</sup> and 10<sup>5</sup> cycles) at 25 °C and -196 °C are listed in Table XIII. At 10<sup>4</sup> cycles, all the materials show an increase in notch sensitivity in reducing the temperature to -196 °C. The increasing order of notch sensitivity at the two temperatures is given in Table XIV. It is interesting to note that at room temperature, the least notch sensitivity is exhibited by the steels treated to 150,000 psi tensile strength. However, at -196 °C the best resistance to notches is exhibited by the non-ferrous alloys. Thus, at a high degree of overstressing, the non-ferrous alloys are definitely less sensitive to notches at low temperatures.



**Table XIII**  
**Notch Sensitivity Factors in Fatigue at 25 °C and -196 °C**  
**For N = 10<sup>4</sup> Cycles**

Material	$f_n^{(1)}$		$K_t$		$q^{(2)}$	
	25 °C	-196 °C	25 °C	-196 °C	25 °C	-196 °C
24S-T Aluminum Alloy	0.76	0.58	1.323	1.734	0.15	0.34
75S-T Aluminum Alloy	0.65	0.50	1.545	2.000	0.25	0.47
FS-1 Magnesium	0.78	0.57	1.288	1.745	0.13	0.35
SAE 2330 Steel						
(150,000 psi T.S.)	0.86	0.49	1.157	2.030	0.09	0.59
NE(SAE) 8630 Steel						
(150,000 psi T.S.)	0.91	0.44	1.097	2.286	0.06	0.73
18-8S Stainless Steel						
(210,000 psi T.S.)	0.61	0.43	1.631	2.313	0.36	0.75
Titanium Metal						
(93,000 psi T.S.)	0.66	0.58	1.507	1.738	0.31	0.45
Hy-Tuf Steel						
(230,000 psi T.S.)	0.72	0.49	1.382	2.055	0.22	0.60
SAE 4340 Steel						
(150,000 psi T.S.)	0.91	0.32	1.094	3.147	0.05	1.23
SAE 4340 Steel						
(230,000 psi T.S.)	0.61	0.29	1.627	3.417	0.36	1.38
<b>For N = 10<sup>5</sup> Cycles</b>						
24S-T Aluminum Alloy	0.70	0.52	1.431	1.912	0.20	0.42
75S-T Aluminum Alloy	0.67	0.47	1.501	2.136	0.23	0.53
FS-1 Magnesium	0.58	0.50	1.736	1.982	0.34	0.46
SAE 2330 Steel						
(150,000 psi T.S.)	0.63	0.29	1.596	3.413	0.34	1.38
NE(SAE) 8630 Steel						
(150,000 psi T.S.)	0.72	0.41	1.387	2.441	0.22	0.82
18-8S Stainless Steel						
(210,000 psi T.S.)	0.38	0.28	2.622	3.620	0.93	1.50
Titanium Metal						
(93,000 psi T.S.)	0.64	0.59	1.551	1.683	0.33	0.41
Hy-Tuf Steel						
(230,000 psi T.S.)	0.48	0.49	2.098	2.054	0.63	0.60
SAE 4340 Steel						
(150,000 psi T.S.)	0.65	0.33	1.544	3.000	0.31	1.14
SAE 4340 Steel						
(230,000 psi T.S.)	0.41	0.27	2.444	3.711	0.83	1.55

<sup>(1)</sup>  $f_n$  = fraction of unnotched fatigue strength in notched test.

$$^{(2)} q = \frac{K_t - 1}{K_t - 1}$$

$K_t$  = Fatigue Strength of Unnotched Specimen

$K_t$  = Fatigue Strength of Notched Specimen

$K_t$  = Theoretical stress concentration factor.

**Table XIV**  
**Increasing Order of Notch Sensitivity in Fatigue at 25 °C and -196 °C**  
**For N = 10<sup>4</sup> Cycles**

Order (Increasing Sensitivity)*	25 °C	-196 °C
1	SAE 4340 Steel** (150,000 psi)	24S-T Aluminum
2	NE(SAE) 8630 Steel (150,000 psi)	FS-1 Magnesium
3	SAE 2330 Steel (150,000 psi)	Titanium
4	FS-1 Magnesium	75S-T Aluminum
5	24S-T Aluminum	SAE 2330 Steel (150,000 psi)
6	Hy-Tuf Steel (230,000 psi)	Hy-Tuf Steel (230,000 psi)
7	75S-T Aluminum	NE(SAE) 8630 Steel (150,000 psi)
8	Titanium	18-8S Stainless (210,000 psi)
9	SAE 4340 Steel (230,000 psi)	SAE 4340 Steel (150,000 psi)
10	18-8S Stainless (210,000 psi)	SAE 4340 Steel (230,000 psi)

\*Based on "q" values.

\*\*Tensile strength at room temperature.



**Table XV**  
**Increasing Order of Notch Sensitivity in Fatigue at 25 °C and -196 °C**  
**For N = 10<sup>5</sup> Cycles**

Order (Increasing Sensitivity)*	25 °C	-196 °C
1	24S-T Aluminum	Titanium
2	NE(SAE) 8630 Steel** (150,000 psi)	24S-T Aluminum
3	75S-T Aluminum	FS-1 Magnesium
4	SAE 4340 Steel (150,000 psi)	75S-T Aluminum
5	Titanium	Hy-Tuf Steel (230,000 psi)
6	FS-1 Magnesium	NE(SAE) 8630 Steel (150,000 psi)
7	SAE 2330 Steel (150,000 psi)	SAE 4340 Steel (150,000 psi)
8	Hy-Tuf Steel (230,000 psi)	SAE 2330 Steel (150,000 psi)
9	SAE 4340 Steel (230,000 psi)	18-8S Stainless (210,000 psi)
10	18-8S Stainless (210,000 psi)	SAE 4340 Steel (230,000 psi)

\*Based on "q" values.

\*\*Tensile strength at room temperature.

Examining the notch sensitivity factors for intermediate overstressing for 10<sup>5</sup> cycles (Table XIII), increases in notch sensitivity at -196 °C are noted in all cases except that for Hy-Tuf steel. As is the case for 10<sup>4</sup> cycles, the SAE 4340 steel at 150,000 psi tensile strength is less notch-sensitive than is the same steel at 230,000 psi tensile strength. Thus, except for Hy-Tuf steel, in the case of overstressing, the steels treated to a lower tensile strength have superior resistance to notches than have the steels treated to high tensile strength level. The increasing order of notch sensitivity for 10<sup>5</sup> cycles at 25 °C and -196 °C are summarized in Table XV. At 25 °C, the best resistance to notches is exhibited by the nonferrous alloys and the steels treated to 150,000 psi tensile strength. At -196 °C, the least notch sensitivity is exhibited by the nonferrous alloys and Hy-Tuf steel (titanium at -196 °C has the least notch sensitivity). Thus, in intermediate overstressing, the nonferrous alloys are less notch-sensitive at low temperature.

To summarize, at the endurance limit (10<sup>7</sup> cycles) the nonferrous alloys and steels heat treated to 230,000 psi tensile strength are least sensitive to notches at 25 °C and -196 °C. In the case of overstressing (10<sup>4</sup> and 10<sup>5</sup> cycles), the steels treated to 150,000 psi tensile strength show the least notch sensitivity at 25 °C. However, at -196 °C the least notch sensitivity is exhibited by the nonferrous alloys. Steels treated to 230,000 psi tensile strength are superior to those treated to 150,000 psi tensile strength only for 10<sup>7</sup> cycles. In the case of overstressing, the steels at the lower strength level have superior resistance to notches. It must be recalled that these observations are based on certain test-bar geometry and the type of notch used. Other test-bar geometries and notches could alter the conclusions made on the tests in this investigation.

Table XVI  
Results of Vickers Hardness Tests at Various Temperatures

Material	Vickers Pyramid Hardness			
	25 °C	-78 °C	-196 °C	-253 °C
24S-T Aluminum	143	151	166	...
75S-T Aluminum	...	...	...	...
FS-1 Magnesium	104	114	130	...
SAE 2330 Steel (150,000 psi)	321	359	384	...
NE 8630 Steel (150,000 psi)	302	327	377	...
18-8S Stainless (210,000 psi)	422	480	610	...
Titanium (93,000 psi)	257	337	414	537
Hy-Tuf Steel (230,000 psi)	523	559	598	896
SAE 4340 Steel (150,000 psi)	335	368	418	637
SAE 4340 Steel (230,000 psi)	504	540	582	829

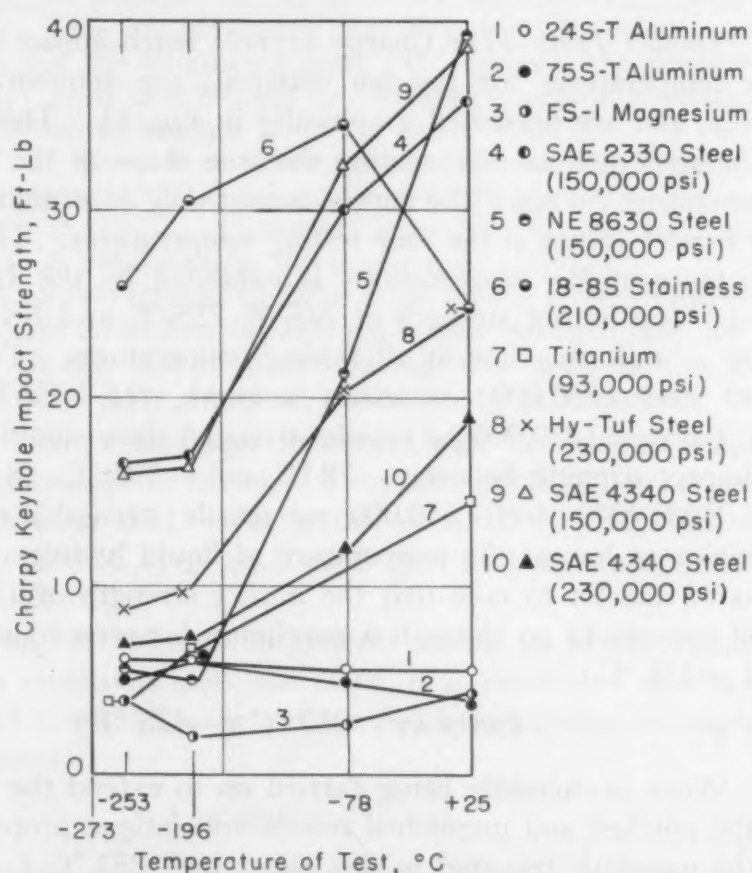


Fig. 11—Charpy Keyhole Impact Strength of the Engineering Alloys at Various Temperatures.

**Hardness**—The hardness data at the various temperatures are summarized in Table XVI. In all cases, the hardness increased with decreasing temperatures. The increase is continuous except for a few exceptions. Sharp increases in hardness are noted in the following cases: (a) 18-8S stainless steel,  $-78^{\circ}\text{C}$  to  $-196^{\circ}\text{C}$ , (b) Hy-Tuf steel,  $-196^{\circ}\text{C}$  to  $-253^{\circ}\text{C}$ , (c) SAE 4340 steel at both strength levels,  $-196^{\circ}\text{C}$  to  $-253^{\circ}\text{C}$ .

**Table XVII**  
**Results of Charpy Keyhole Notch at Various Temperatures**

Material	Absorbed Energy, ft-lbs			
	25°C	-78°C	-196°C	-253°C
24S-T Aluminum	5.5	5.5	6.0	6.0
75S-T Aluminum	4.0	5.0	6.0	5.0
FS-1 Magnesium	4.2	2.6	2.0	3.7
SAE 2330 Steel (150,000 psi)	35.8	30.0	16.8	16.4
NE 8630 Steel (150,000 psi)	39.1	21.0	5.0	5.4
18-8S Stainless (210,000 psi)	24.7	34.5	30.3	25.9
Titanium (93,000 psi)	14.5	....	6.6	3.8
Hy-Tuf Steel (230,000 psi)	24.8	20.2	9.7	8.6
SAE 4340 Steel (150,000 psi)	38.7	32.3	16.4	16.0
SAE 4340 Steel (230,000 psi)	19.0	12.0	7.4	6.9

*Impact Tests*—The Charpy keyhole notch impact values at various temperatures for the ten materials are summarized in Table XVII, and are presented graphically in Fig. 11. This figure is not to be construed as representing the true shape of the impact versus temperature curves. The curves consist only of straight lines joining the impact values at the four testing temperatures. The best impact resistance of low temperatures is exhibited by the 18-8S stainless steel. The impact strength of 24S-T, 75S-T, and FS-1 magnesium alloy is uniformly low at all testing temperatures. Titanium, SAE 4340 steel (230,000 psi tensile strength, NE (SAE) 8630 steel, Hy-Tuf steel (230,000 psi tensile strength) show significant decreases in impact strength between  $-78^{\circ}\text{C}$  and  $-196^{\circ}\text{C}$ . SAE 2330 steel and SAE 4340 steel (150,000 psi tensile strength) exhibit ductile behavior as low as the temperature of liquid hydrogen ( $-253^{\circ}\text{C}$ ). It is of interest to note that the impact strength of 18-8S stainless steel appears to go through a maximum between room temperature and  $-253^{\circ}\text{C}$ .

#### TESTS AT $-253^{\circ}\text{C}$ ( $-425^{\circ}\text{F}$ )

Work is currently being carried on to extend the determination of the notched and unnotched tensile and fatigue properties of some of the materials reported in this paper to  $-253^{\circ}\text{C}$  ( $-423^{\circ}\text{F}$ ). It is planned to present these data in the near future.

#### SUMMARY

The general conclusions resulting from this investigation are the following:

1. In the unnotched tensile tests, the modulus of elasticity, yield strength, ultimate strength and nominal fracture stress all increase with decreasing temperature. Ductility values have an erratic dependence on temperature.



2. The effect of a notch is to increase the ultimate strength in tension, which also increases with decreasing temperature. However, notches decrease the fracture stress both at 25 °C and -196 °C. Notches, in general, significantly reduce the tensile reduction of area.

3. In the unnotched fatigue tests, the following average increases in fatigue strength at -196 °C over that at 25 °C occurred: 55% for  $10^7$  cycles, 45% for  $10^5$  cycles, and 38% for  $10^4$  cycles.

4. In the notched fatigue tests at 25 °C and -196 °C the following conclusions are drawn:

(a) The average decrease in fatigue strength at 25 °C caused by the presence of the notch are the following: 64% for  $10^7$  cycles, 45% for  $10^5$  cycles, and 26% for  $10^4$  cycles.

(b) At the endurance limit ( $10^7$  cycles), the nonferrous alloys and steels heat treated to 230,000 psi tensile strength are least sensitive to notches at 25 °C and -196 °C.

(c) In the case of overstressing ( $10^4$  and  $10^5$  cycles), the steels treated to 150,000 psi tensile strength show the least notch sensitivity at 25 °C. However, at -196 °C, the least notch sensitivity is exhibited by the nonferrous alloys.

(d) Steels treated to 230,000 psi tensile strength are superior to those treated to 150,000 psi tensile strength only for  $10^7$  cycles. In the case of overstressing, the steels at the lower strength level have superior resistance to notches.

5. The Vickers hardness increases with decreasing temperature. Sharp increases in hardness are noted in the following cases: (a) 18-8S stainless steel, -78 °C to -196 °C, (b) Hy-Tuf steel, -196 °C to -253 °C, (c) SAE 4340 steel at both strength levels, -196 °C to -253 °C.

6. The impact strength in general shows an inverse relationship to notch sensitivity and, therefore, it is concluded that impact strength is not a reliable criterion for notch sensitivity in fatigue at low temperatures.

#### ACKNOWLEDGMENTS

This investigation was made possible by the support and the continued interest of the Materials Laboratory, Engineering Division, Wright-Patterson Air Force Base. The work was done under Contract No. W33-038-ac-15698 between Ohio State University Research Foundation and the Wright-Patterson Air Force Base, with D. A. Shinn acting as project engineer. The liquid nitrogen and liquid hydrogen were furnished by The Ohio State University Cryogenic Laboratory. The valuable assistance of J. L. Zambrow and Mrs. W. Buckingham is appreciated.



## References

1. J. L. Zambrow and M. G. Fontana, "Mechanical Properties, Including Fatigue, of Aircraft Alloys at Very Low Temperatures", *TRANSACTIONS, American Society for Metals*, Vol. 41, 1949, p. 480-518.
2. *Metals Handbook*, 1948 edition, American Society for Metals, p. 245.
3. H. Neuber, "Theory of Notch Stresses: Principles for Exact Stress Calculation", Translation 74, The David W. Taylor Model Basin, United States Navy, November 1945.

# THE INFLUENCE OF TEMPERATURE UPON THE TIME DELAY FOR YIELDING IN ANNEALED MILD STEEL

BY D. S. WOOD AND D. S. CLARK

## Abstract

*The results of an experimental investigation of the time required for the initiation of plastic deformation in an annealed low carbon steel subjected to rapidly applied tensile stress at four temperatures are presented. The stress is applied to a test specimen in a continuous manner within a period of about 7 milliseconds and is maintained substantially constant thereafter. The extension of the specimen is measured as a function of time.*

*A well-defined period of time is found to elapse between the instant the stress reaches its full value and the instant plastic deformation begins. This time is designated as the "delay time". The delay time is measured as a function of the applied stress at temperatures of  $-75$ ,  $73$ ,  $150$ , and  $250^{\circ}\text{F}$  ( $-60$ ,  $23$ ,  $65$ , and  $121^{\circ}\text{C}$ ). At any given temperature the relation between the logarithm of the delay time and the applied stress is represented by two connected straight lines. One is a line of constant stress; the other is a line along which the delay time decreases as the stress is increased to values above the constant stress line. The line of constant stress is identified with the static upper yield stress of the material. It is shown that the temperature dependence of the delay time cannot be adequately described by a simple thermal activation function of the form  $t = e^{Q/RT}$ .*

IN a previous paper (1)<sup>1</sup> the present authors described experiments in which it was shown that a definite time delay is required for the initiation of plastic deformation in an annealed mild steel. The technique used was to apply a predetermined tensile stress, exceeding the static yield point stress, to a specimen within a total time of about 5 milliseconds and to maintain the stress constant thereafter. The delay time for the initiation of plastic deformation was found by measuring the extension of the specimen as a function of time. The delay time was observed to vary continuously from 5 milliseconds at a stress of about 51,000 psi to

<sup>1</sup>The figures appearing in parentheses pertain to the references appended to this paper.

Of the authors, D. S. Wood is assistant professor and D. S. Clark is associate professor of mechanical engineering, California Institute of Technology, Pasadena, Calif. Manuscript received June 12, 1950.

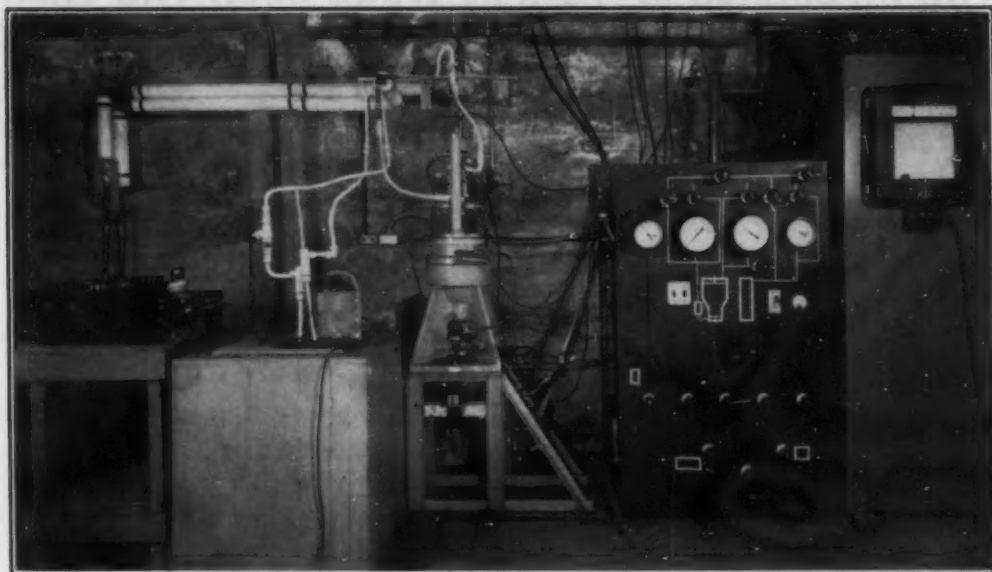


Fig. 1—General View of Equipment.

6 seconds at a stress of about 37,000 psi for an annealed 0.19% carbon steel having a static upper yield stress of 36,000 psi.

The purpose of this paper is to present the results of further experiments which have been made to aid in determining the nature of the mechanism associated with the delay time for yielding in mild steel. The method used is to investigate the dependence of the delay time upon temperature as well as stress. The rapid load tensile testing machine developed for the previous investigation is employed with modification to permit testing at various temperatures. From the results of this investigation, a quantitative determination may be made of the relation of the activation energy to the delay phenomenon.

#### EQUIPMENT

*Rapid Load Testing Machine*—The rapid load testing machine used in this investigation has been previously described (1). Briefly, the machine consists of a piston attached to one end of the specimen. The piston operating in a cylinder is actuated by compressed air on one face adjusted to the desired pressure prior to the test. Fluid at the same pressure acts on the other face of the piston. The load is applied to the specimen by releasing the fluid pressure by means of a small piston. The rate of release of fluid pressure and hence the application of load by the predetermined air pressure can be controlled within limits. The machine and accessories are shown in Fig. 1. The machine is analogous to a simple single degree of freedom mechanical oscillator with

viscous damping. The damping is provided by the viscous fluid which moves with the loading piston and flows through a nest of very small tubes. This arrangement prevents undesirable overshooting and oscillation of the load acting on the specimen. The damping required depends upon the mass of the machine and the material and dimensions of the specimen. Critical damping is secured by changing the viscosity of the fluid (glycerin and water) so that the load on the specimen rises to its final value in the

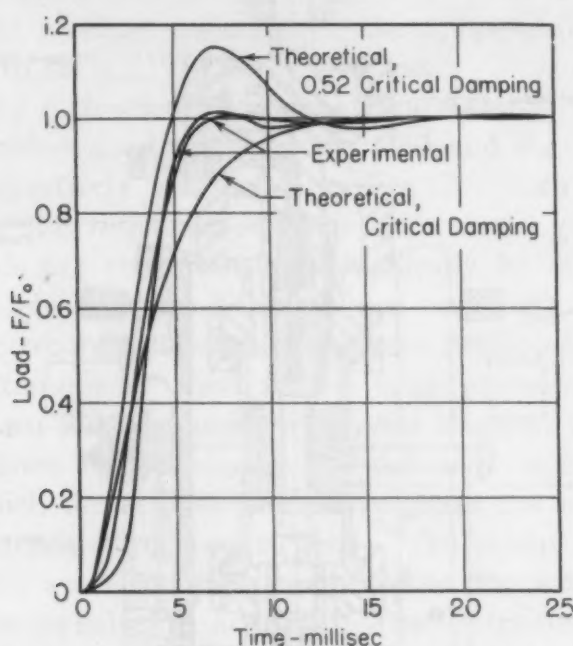


Fig. 2—Theoretical and Experimental Load Versus Time for Free Loading With Elastic Specimen.

desired time without overshooting. Theoretical and experimental load rise curves for the machine as used in the present investigation are shown in Fig. 2.

*Specimen Heat Exchanger*—The tests presented in this paper required that the specimen be maintained at constant temperature. The heat exchanger, shown in Fig. 3, consists of a bellows-type jacket surrounding the specimen, headers at each end of the bellows, and water jackets to prevent heating or cooling of adjacent portions of the testing machine. The total extension of the specimen is limited to 0.05 inch by stops so that the bellows are not damaged during the test. The fluid for heating or cooling is circulated into and out of the bellows through the headers.

Thermocouples inserted through suitable stuffing boxes in the heat exchanger provide for the measurement of the specimen tem-



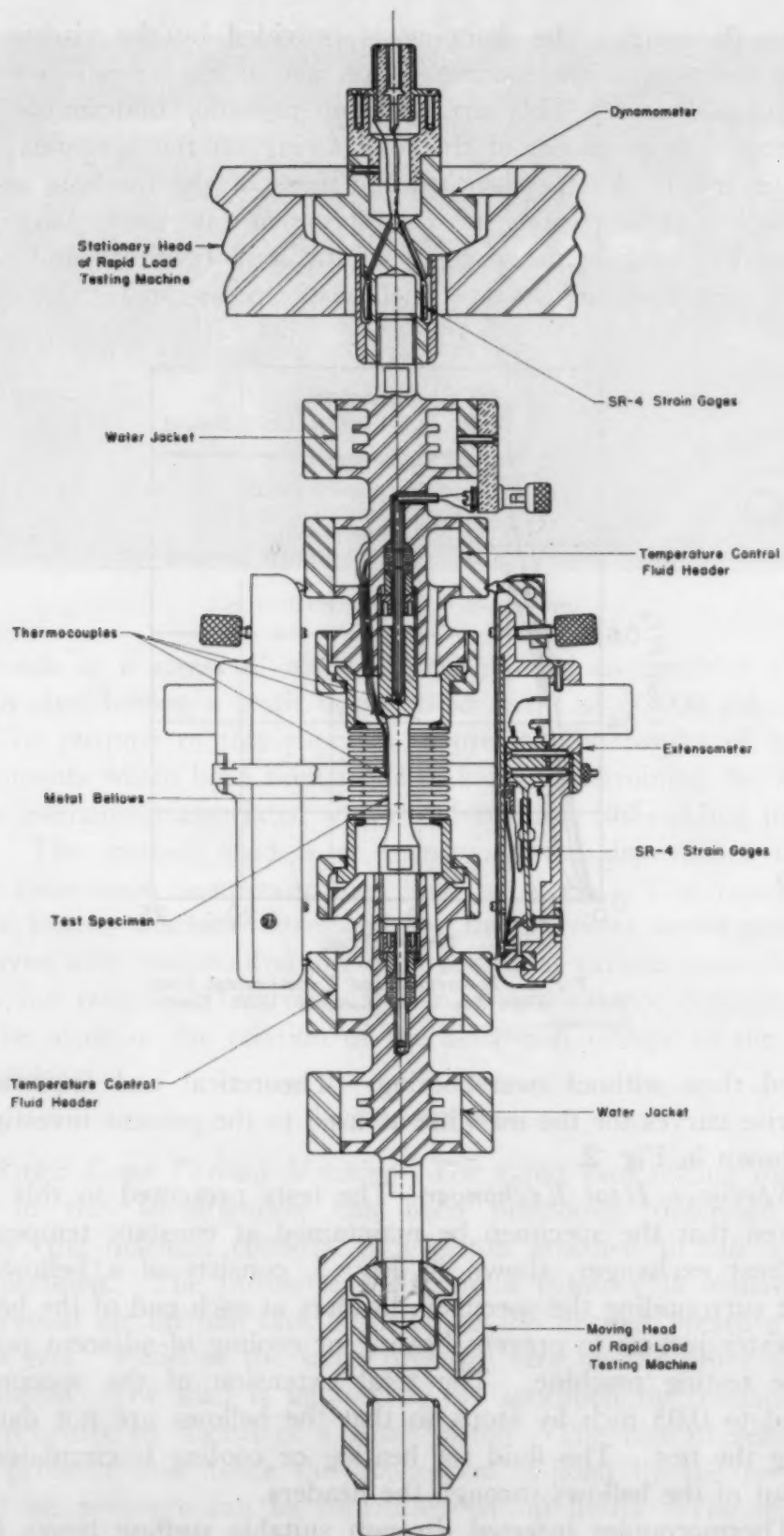


Fig. 3—Arrangement for Controlled Temperature Tests in Rapid Load Testing Machine.

perature. Copper-constantan couples were used with the beads taped to the specimen at two points, one at the center of the gage section and the other on one of the fillets. A portable precision potentiometer was used to measure the e.m.f. of the thermocouples. The thermocouple wire was calibrated at four fixed temperature points—namely, freezing chloroform ( $-82.3^{\circ}\text{F}$ ), freezing mercury ( $-38.0^{\circ}\text{F}$ ), freezing carbon tetrachloride ( $-9.2^{\circ}\text{F}$ ), and body temperature ( $98.6^{\circ}\text{F}$ ). The difference in temperature between the two thermocouples was found to be  $1^{\circ}\text{F}$  ( $0.6^{\circ}\text{C}$ ) or less in all tests, and the absolute accuracy of the temperature measurements is estimated to be  $\pm 2^{\circ}\text{F}$  ( $1.2^{\circ}\text{C}$ ) or less.

*Load and Extension Measuring Equipment*—The dynamometer and extensometer used to detect the load and the extension of the specimen respectively are shown in Fig. 3. Both of these instruments are of the resistance-sensitive wire strain gage type. Their output signals are recorded photographically by means of cathode-ray oscillographs utilizing direct-coupled amplifiers. The dynamometer and the recording system have been previously described (1).

The extensometer used in the tests presented in this paper consists of two identical units which are clamped on opposite sides of the specimen heat exchanger. Each unit incorporates a small beam on which the resistance-sensitive gages are mounted. As the specimen extends, these beams bend. The strain gage elements of the two units are electrically connected in the same bridge circuit so that their signals are additive. The instrument has a natural frequency of about 2800 cycles per second, and its calibration is linear and equal to  $5.75 \times 10^{-3}$  inch per ohm. It is estimated that the error in the measurements of load and extension using these instruments is not more than  $\pm 4\%$ .

*Alcohol Cooling and Circulating Unit*—For the tests made at temperatures below room temperature, circulating denatured ethyl alcohol is used as the heat exchange fluid. This alcohol transfers heat from the specimen to an alcohol-solid carbon dioxide cooling unit. The temperature of the test specimen is controlled by proper adjustment of the rate of flow of coolant.

*Oil Heating and Circulating Unit*—For tests made at temperatures above room temperature, SAE 10 lubricating oil heated by an electric immersion heater is used as the temperature control fluid. The tank in which the oil is heated and the circulating pump and necessary valves and controls are assembled together to form a convenient portable unit. The oil temperature is controlled by an industrial temperature control unit which operates a contactor sup-

plying power to the immersion heater.

#### MATERIAL TESTED AND TEST SPECIMEN

The 0.17% carbon steel used in this investigation was obtained from the Columbia Steel Company, Torrance, Calif., in the form of hot-rolled bars  $\frac{5}{8}$  inch in diameter from one billet of heat number 32882. The analysis as given by the mill is as follows:

Carbon %	Manganese %	Phosphorus %	Sulphur %
0.17	0.39	0.017	0.040

Test specimens, of the form shown in Fig. 4, were machined from this material. The gage section of the specimens was finished

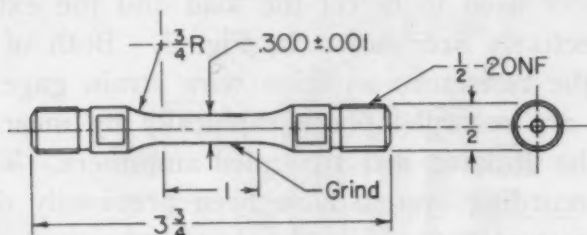


Fig. 4—Test Specimen.

by grinding, and after machining they were annealed in dry hydrogen. The furnace schedule was as follows:

- Heat from room temperature to 1300 °F at normal furnace rate under full power.
- Heat from 1300 to 1600 °F at 2.4 °F per minute.
- Hold at 1600 °F for 49 minutes.
- Cool from 1600 to 1300 °F at 2.3 °F per minute.
- Cool from 1300 to 1000 °F at 3.1 °F per minute.
- Cool from 1000 °F to room temperature at normal furnace rate with power off.

The metallographic structure of a finished specimen is shown in the two photomicrographs of Fig. 5.

The hardness of ten test specimens, selected at random, was found to range from Rockwell B-47 to 59. The maximum range of hardness in any single specimen was 3 Rockwell B numbers.

The surface finish of ten specimens, selected at random, ranged from 8 to 13 microinches r.m.s. as determined by means of a Brush Surface Analyzer.

#### EXPERIMENTAL RESULTS

*Static Tension Tests*—At least two static tests were made at temperatures of -75, 73, 150, and 250 °F (-60, 23, 65, and 121 °C). Stepwise loading was used, allowing approximately 2

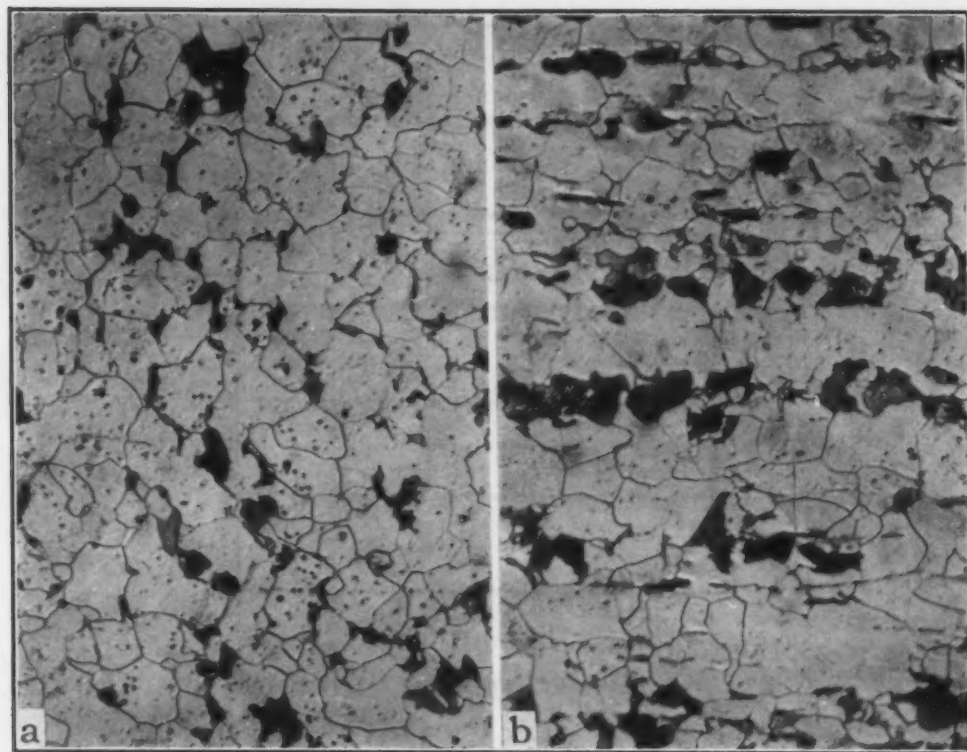


Fig. 5—Metallographic Structure of Material Tested. a—Transverse section, Nital etch.  $\times 200$ . b—Longitudinal section, Nital etch.  $\times 200$ .

minutes to elapse between points. Approximately 10 points were taken in the elastic range, and from 10 to 60 points in the range of plastic deformation up to a total strain of 5%. Two tests at room temperature were continued to failure, while all other static tests were stopped after 5% strain.

These tests were made in a 30,000-pound Riehle universal testing machine having a least reading of 10 pounds or 140 psi for the specimen gage section. The specimen heat exchanger, extensometer, alcohol cooling and circulating unit, and oil heating and circulating unit employed in the rapid load tests were also used for maintaining controlled temperatures in the static tests. The resistance changes of the extensometer were measured by means of a Wheatstone bridge and sensitive galvanometer. The measured extensions were converted to strain in the specimen gage section by making suitable corrections for the elastic extensions which occur in the heads of the heat exchanger and in the shoulders of the specimen.

The static stress-strain relations which were obtained at the four temperatures are shown in Figs. 6, 7, 8, and 9, respectively. The complete stress-strain curves for two tests at room temperature



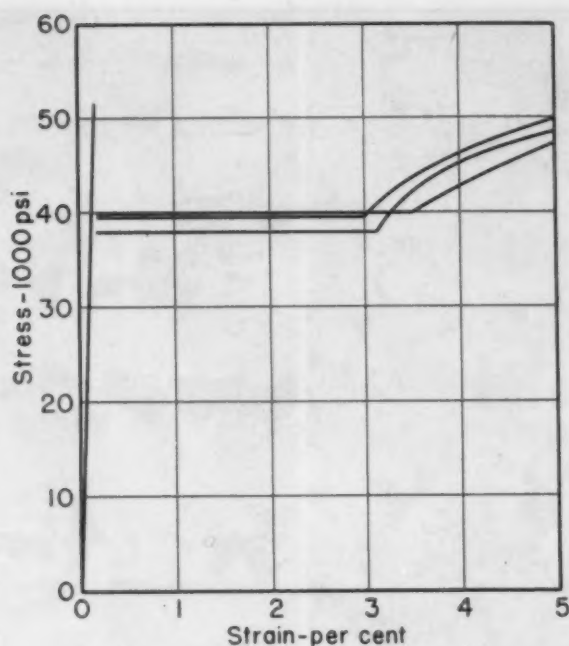


Fig. 6—Static Stress Versus Strain,  $-75^{\circ}\text{F}$  ( $-60^{\circ}\text{C}$ ).

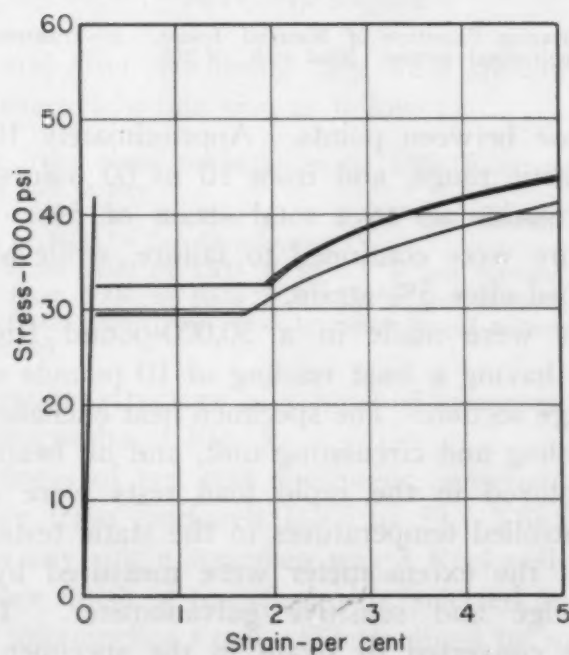


Fig. 7—Static Stress Versus Strain,  $73^{\circ}\text{F}$  ( $23^{\circ}\text{C}$ ).

( $73^{\circ}\text{F}$ ) are shown in Fig. 10. All values of stress and strain are conventional engineering values based upon initial cross sectional area and initial length. The values of upper and lower yield stress and the yield strain for all the static tests are given in Table I.

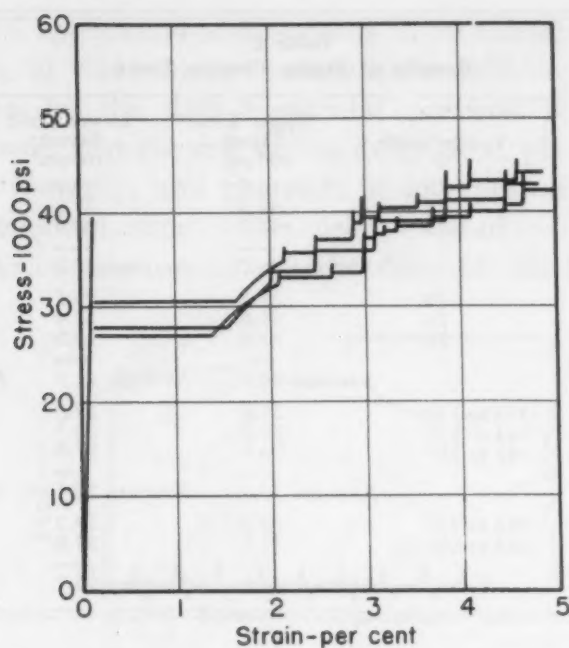


Fig. 8—Static Stress Versus Strain, 150 °F (66 °C).

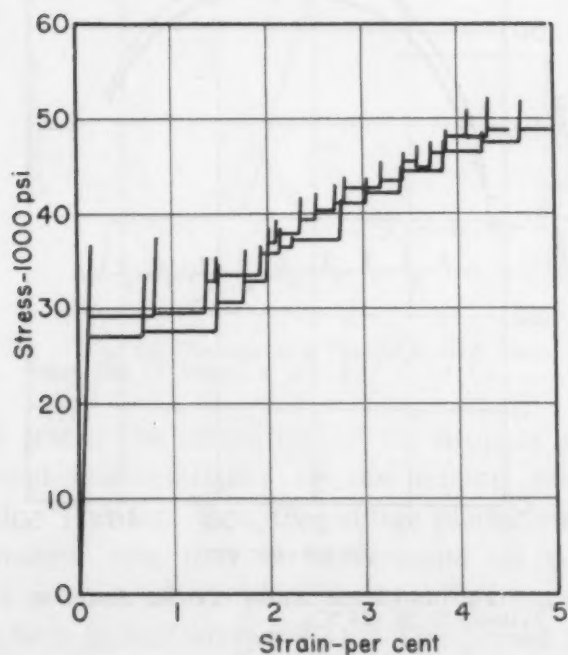


Fig. 9—Static Stress Versus Strain, 250 °F (121 °C).

It will be noted that the static stress-strain relations obtained at 150 and 250 °F (65 and 121 °C) show clearly the phenomenon of strain aging. At these temperatures appreciable strain aging evidently takes place in the approximately 2-minute interval between

**Table I**  
**Results of Static Tension Tests**

Specimen Number	Temperature °F	Upper Yield Stress 10 <sup>3</sup> psi	Lower Yield Stress 10 <sup>3</sup> psi	Yield Strain %
4	-75	51.5	40.0	3.5
95	-75	44.6	39.5	3.0
96	-75	43.9	38.0	3.1
		Average 46.7	Average 39.2	Average 3.2
1	69	35.3	29.5	1.7
164	74	41.0	32.4	1.9
165	75	41.8	32.5	2.0
		Average 39.4	Average 31.5	Average 1.9
158	143 to 153	31.6	27.0	1.4
159	144 to 154	39.7	30.7	1.6
161	148 to 159	36.8	27.9	1.5
		Average 36.0	Average 28.5	Average 1.5
162	248 to 255	32.5	29.2	...
163	249 to 255	36.7	27.0	...
		Average 34.6	Average 28.1	

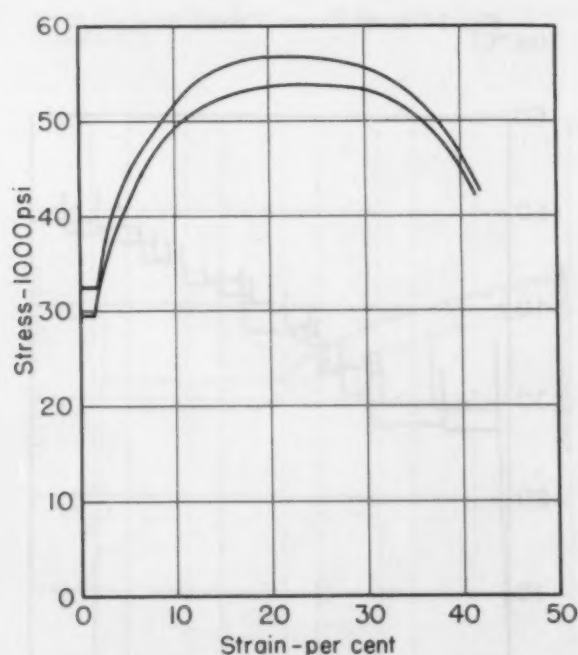


Fig. 10—Static Stress Versus Strain to Failure, 73 °F (23 °C).

successive load increments. During the performance of these tests it was noted, in several instances, that the secondary yield points exhibit a definite delay time for the resumption of plastic deformation.

*Rapid Load Tests*—A tracing of a typical record of a rapid load test is given in Fig. 11. The specimen is elastically deformed

during the load application and remains in an elastic state, to a first approximation, at this constant stress for a definite length of time. This is shown by the first horizontal portions of the load and extension records. At the end of the delay time, plastic deformation begins rather abruptly, and proceeds at an approximately constant rate for a period of time. The drop in load which takes place during this period corresponds to the drop of the beam in a con-

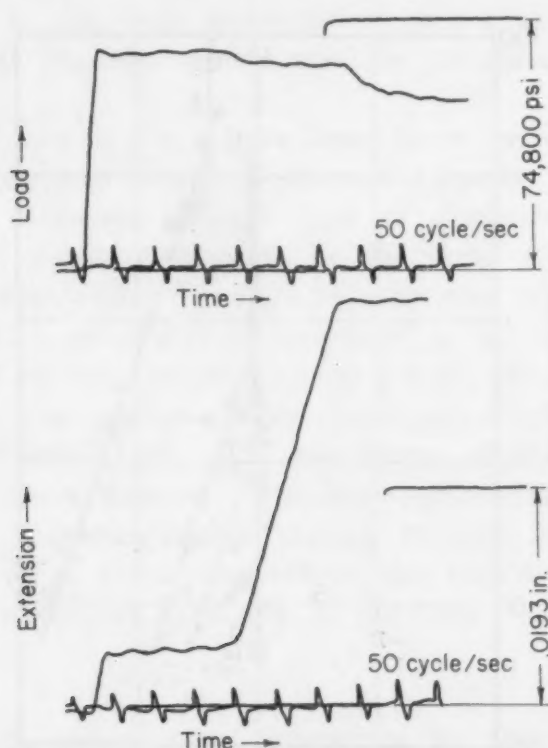


Fig. 11—Tracing of a Typical Record, Specimen No. 63 Tested at  $-74.5^{\circ}\text{F}$  ( $-59^{\circ}\text{C}$ ).

ventional static test. The magnitude of the drop in load is governed by the combined characteristics of the testing machine and the material tested. The fact that the initial plastic deformation proceeds at a constant rate may be understood on the basis of the inhomogeneous nature of the "yield strain" in an annealed low carbon steel, which is well known (2). The period of constant rate of plastic deformation evidently corresponds to the progressive spread of the yielded region throughout the specimen gage section, beginning from one or more localized regions.

The period of constant plastic deformation rate in Fig. 11 is abruptly terminated when the testing machine reaches the limit of its travel. The drop in load at that point represents the stress relaxation of the specimen when deformation suddenly ceases. In



some tests the "yield strain" is completed before the testing machine reaches the limit of its travel. In this case the rate of plastic deformation is observed to decrease progressively after the "yield strain" is completed. This occurs in the cold hardening range of the stress-strain curve.

The results of primary interest for this investigation are the experimental data, obtained at several temperatures, relating the

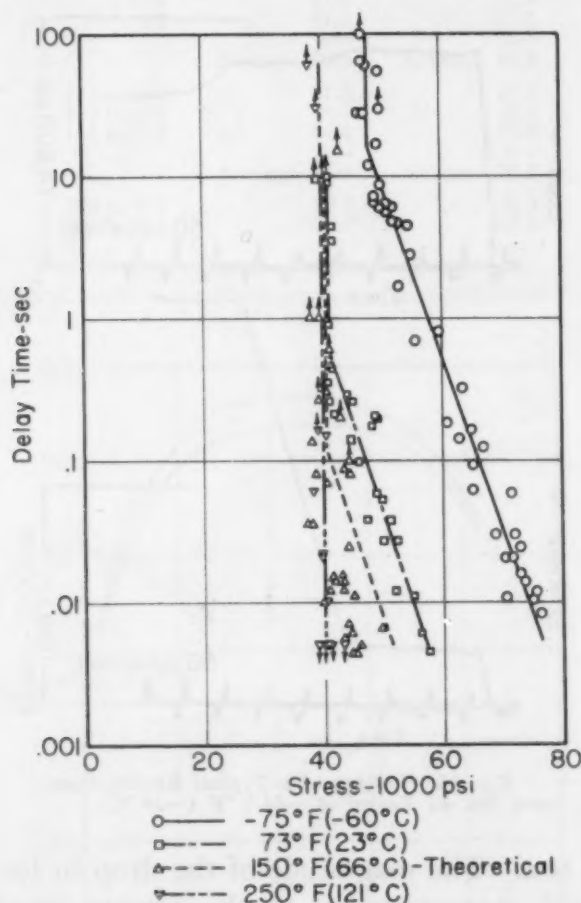


Fig. 12—Delay Time for the Initiation of Plastic Deformation as a Function of Stress.

delay time for the initiation of plastic deformation to the applied stress. These data are shown in Fig. 12. At a given temperature, there is a definite knee in the delay time versus stress relation. At high stresses the logarithm of the delay time increases approximately linearly with decreasing stress. However, at some lower critical stress, the relation changes to a line of essentially constant stress, along which the delay time increases without limit. Previous results (1) at room temperature did not appear to exhibit this knee in the curve. The authors believe that the form of the delay time versus

stress relation shown in Fig. 12 is the correct one. Several possible explanations can be given for the failure to observe this form of the relation in the earlier investigation. First, the specimens used in the first experiments were machined after annealing. The resulting cold-worked surface could have influenced the test results. Second, the number of experimental points obtained in the earlier results may not have been sufficient to define the form of the curve adequately. Finally, it is possible that the knee of the curve for the steel used in the first investigation occurs at a delay time greater than 10 seconds, which was the maximum delay time recorded.

The lines drawn in Fig. 12 are based upon the assumption that for any given temperature the experimental results may be represented by two connected straight lines as discussed above. The line of constant stress is taken to be the mean stress of all the experimental points which appear to be associated with that portion of the curve. This stress will be designated by  $\bar{\sigma}$ . The sloping line was determined by first dividing all the points which appear to be associated with that portion of the curve into two groups at the middle value of delay time. The two means of these two groups of points were then computed. The line representing all the points is taken to be the straight line passing through these two mean points. Thus, for a given temperature, the experimental data are represented by an empirical relation of the form

$$t = t_0 e^{-\sigma/\sigma_0} \quad \text{Equation 1}$$

The constants,  $t_0$  and  $\sigma_0$ , were determined for the results at  $-75$  and  $73^\circ\text{F}$  ( $-60$  and  $23^\circ\text{C}$ ). These constants could not be evaluated for tests made at  $150$  and  $250^\circ\text{F}$  ( $65$  and  $121^\circ\text{C}$ ), because the data do not extend to small enough values of the delay time, as can be seen in Fig. 12. The dashed line in Fig. 12 represents a theoretical extrapolation from the results at  $-75$  and  $73^\circ\text{F}$  ( $-60$  and  $23^\circ\text{C}$ ), and is discussed later. The numerical values of the constants  $t_0$  and  $\sigma_0$  for  $-75$  and  $73^\circ\text{F}$  ( $-60$  and  $23^\circ\text{C}$ ) and the values of  $\bar{\sigma}$  for all four temperatures are given in Table II.

It is reasonable to identify the values of  $\bar{\sigma}$  with the static upper yield stress of the material. If the values of the static upper yield stress given in Table I are compared with the values of  $\bar{\sigma}$  given in Table II, it is seen that at  $-75$  and  $73^\circ\text{F}$  ( $-60$  and  $23^\circ\text{C}$ ) the average values of static upper yield stress are equal to  $\bar{\sigma}$ , within the experimental scatter. However, at  $150$  and  $250^\circ\text{F}$  ( $65$  and  $121^\circ\text{C}$ ) the static upper yield stress values are appreciably

Table II  
Empirical Constants to Fit the Relations  $t = t_0 e^{-\sigma/\sigma_0}$  and  $\sigma = \bar{\sigma}$   
to the Experimental Data

Temperature °F	$t_0$ sec	$\sigma_0$ 10 <sup>3</sup> psi	$\bar{\sigma}$ 10 <sup>3</sup> psi
-75	$4.59 \times 10^6$	3.74	47.8
73	$3.34 \times 10^6$	3.64	41.0
150	.....	....	40.7
250	.....	....	40.0

lower than  $\bar{\sigma}$ . The scatter in values of the static upper yield stress at all four temperatures is considerably greater than the scatter in stress of the rapid load test points corresponding to the critical stress,  $\bar{\sigma}$ , even though the probable errors in load measurement in the static tests are less than the errors in rapid load tests. The explanation of this anomaly is not clear. However, greater bending stresses may have been present in the static tests because the spherical seats through which the load was applied were at a greater distance from the specimen gage section than in the rapid load tests. Hence, a given friction force between the surfaces of the spherical seats would exert a greater bending moment on the specimen in a static test than in a rapid load test. It also seems possible that the different stress-strain histories in the two types of tests may be responsible for the differences observed. In particular, the greater lengths of time during which the material is subjected to stresses at or near the upper yield stress in static tests as opposed to rapid load tests may accentuate the effects of random variations of various kinds between specimens.

The slopes of the lines of Fig. 12 representing the relation between delay time and stress, at stresses greater than  $\bar{\sigma}$  for the temperatures -75 and 73 °F (-60 and 23 °C), are equal within the scatter of the data. This is shown by the nearly equal values of the constant  $\sigma_0$  for the two temperatures which are given in Table II. From this result, it might be assumed that the mechanism associated with the delay time phenomenon is a thermally activated process in which the temperature dependence of the delay time is given by a function of the form

$$t \propto e^{Q/RT}, \quad \text{Equation 2}$$

where  $T$  is the absolute temperature,  $R$  the gas constant, and  $Q$  an activation energy, which is practically independent of stress. By setting the proportionality factor in Equation 2 equal to the stress function previously given to represent the data at a constant temperature (Equation 1), all the data at -75 and 73 °F (-60 and

23 °C) may be represented by a single relation of the form

$$t = \bar{t} e^{-\sigma/\sigma_0} e^{Q/RT}, \quad \text{Equation 3}$$

for stresses greater than the critical stress,  $\bar{\sigma}$ . The numerical values of the constants  $\bar{t}$ ,  $\sigma_0$ , and  $Q$  in this equation which fit the relation to the experimental data are:

$$\begin{aligned} \bar{t} &= 0.036 \text{ second} \\ \sigma_0 &= 3.69 \times 10^8 \text{ psi} \\ Q &= 8000 \text{ calories per mole} \end{aligned}$$

This value of  $\sigma_0$  was taken to be the average of the two values given in Table II for the temperatures  $-75$  and  $73$  °F ( $-60$  and  $23$  °C).

If Equation 3 is valid, it should be possible to predict the test results obtained at other temperatures. The dashed line in Fig. 12 represents Equation 3 for  $150$  °F ( $65$  °C). It is clear from the figure that the test results at  $150$  °F ( $65$  °C) are not compatible with this line. The experimental points have a definite tendency toward smaller delay times than those predicted by Equation 3.

#### SUMMARY AND CONCLUSIONS

As a result of this investigation it has been found that annealed low carbon steel exhibits at least two regimes of behavior, at a given temperature, in the relation between the delay time for the initiation of plastic deformation and the applied stress. In the regime at high stresses the delay time decreases exponentially with increasing stress according to a relation of the form

$$t = t_0 e^{-\sigma/\sigma_0} \quad \text{Equation 1}$$

where  $t_0$  and  $\sigma_0$  are constants. This relation describes the experimental results from the highest stresses investigated down to a lower critical stress,  $\bar{\sigma}$ , at which the other regime of behavior begins. In this second regime the delay time increases without limit at the constant stress,  $\bar{\sigma}$ . Thus, if the stress  $\bar{\sigma}$  is applied to the material, the delay time for yielding is indeterminate, and may have any value ranging from a minimum given by Equation 1 for  $\sigma = \bar{\sigma}$  up to several minutes or longer. This lower critical stress,  $\bar{\sigma}$ , is equal, at least to a first approximation, to the upper yield stress determined in static tests.

It has also been found that the temperature dependence of the delay time at stresses above the lower critical stress cannot be adequately represented by a simple thermal activation function of the form

$$t \propto e^{Q/RT}$$



Although the experimental results obtained at  $-75$  and  $73^{\circ}\text{F}$  ( $-60$  and  $23^{\circ}\text{C}$ ) may be related by such a function if the activation energy,  $Q$ , is chosen to be about 8000 calories per mole, the experimental results obtained at  $150^{\circ}\text{F}$  ( $65^{\circ}\text{C}$ ) do not fit this value of the activation energy.

#### ACKNOWLEDGMENTS

The investigation presented in this paper was conducted at the California Institute of Technology under the sponsorship of the Office of Naval Research. The rapid load testing machine was constructed under a previous contract with the Air Matériel Command, United States Air Force. The authors express their appreciation to these agencies for their support of the work.

#### References

1. D. S. Clark and D. S. Wood, "The Time Delay for the Initiation of Plastic Deformation at Rapidly Applied Constant Stress", *Proceedings*, American Society for Testing Materials, Vol. 49, 1949, p. 717.
2. J. Miklowitz, "The Initiation and Propagation of the Plastic Zone in a Tension Bar of Mild Steel as Influenced by the Speed of Stretching and Rigidity of Testing Machine", *Transactions*, American Society of Mechanical Engineers, *Journal of Applied Mechanics*, Vol. 14, No. 1, 1947, p. A-31.

## EFFECT OF BATH COMPOSITION ON ALUMINUM COATINGS ON STEEL

BY D. O. GITTINGS, D. H. ROWLAND AND J. O. MACK

### *Abstract*

*Antimony, beryllium, bismuth, cadmium, calcium, chromium, cobalt, copper, germanium, lead, magnesium, manganese, nickel, silicon, silver, tin, titanium, vanadium, and zinc were added individually in various amounts to experimental hot-dip aluminum-coating baths. Of these elements, only silicon, copper, and beryllium decreased the thickness of the alloy layer more than 50%. Only silicon and beryllium decreased the average microhardness of the alloy layer. Silicon and beryllium additions improved the flat-bend-test performance of the aluminum coating, but in the concentration ranges studied, beryllium was more effective than silicon. Coatings containing bismuth, calcium, copper, germanium, magnesium, nickel, silicon, tin, or zinc did not have the attractive as-dipped surface appearance characteristic of commercially pure aluminum coatings.*

THE atmospheric corrosion resistance and the oxidation resistance of aluminum have stimulated the development of processes for commercially applying protective aluminum coatings to ferrous materials. For irregular shapes, encouraging results have been attained by spraying, calorizing, cladding, electroplating, and vacuum vaporizing, but for the commercial coating of steel sheets, strip, or wire, the hot dipping process appears to have an economic advantage over that of other aluminizing processes.

In general, hot-dipped coatings on steel are of a duplex nature (1, 2, 3, 4):<sup>1</sup> They contain (a) an alloy layer, which may itself be composed of more than one layer of complex types in which intermetallic compounds usually occur, and (b) a layer of the coating metal superimposed on the alloy. Regardless of the number of layers that might be present in the alloy, they are collectively referred to in the trade as the "alloy layer" of the coating. These coatings, then, are composed of two layers: (a) an alloy layer, which is not

<sup>1</sup>The figures appearing in parentheses pertain to the references appended to this paper.

A paper presented before the Thirty-second Annual Convention of the Society, held in Chicago, October 21 to 27, 1950. The authors, D. O. Gittings, D. H. Rowland and J. O. Mack, are associated with the Research Laboratory, Carnegie-Illinois Steel Corp., Pittsburgh. Manuscript received April 17, 1950.

a cast layer but a diffusion structure that is formed at temperatures well below the melting points of the various phases that compose it, and (b) a coating metal layer, which has solidified from the molten condition and is, therefore, a casting.

Of the many difficulties encountered in the production of commercially acceptable hot-dipped coatings on steel, the problems of adherence and ductility have frequently been the most troublesome. The adherence of a coating is its ability to withstand bending and forming without peeling or flaking.<sup>2</sup> Adherence usually varies inversely as the thickness of the alloy layer, but for the same average thickness, different alloy layers vary in their degree of adherence. Ductility, on the other hand, is a term that applies to the coating as a whole, that is, the coating's ability to elongate without cracking. The outer layer of the coating, the layer superimposed on the alloy, is nearly always more ductile than the alloy, but if this outer layer has poor ductility it may affect the adherence of the alloy layer.

The alloy layers of most hot-dipped coatings on steel have an inherent tendency to be hard and brittle, which are attributes of intermetallic compounds at ordinary temperatures. This brittleness is in some measure associated with thickness, because as the thickness decreases, the apparent brittleness of the alloy layer diminishes. The same phenomenon has been observed with glass, ordinarily a brittle substance. It has been demonstrated many times that sheets of glass, if thin enough, can be bent double without breaking.

Much of the research and development work on hot-dipped aluminum coatings has for some years been directed toward improving the mechanical properties of the alloy layer. The most apparent approach toward the accomplishment of this end is to reduce the thickness, hardness, and brittleness of the layer. Some reduction in thickness can be obtained by decreasing the time of immersion of the steel in the coating bath, by decreasing the bath temperature, by rapid cooling of the coated article after it leaves the bath, or by a combination of these three procedures; but a reduction in hardness can be commercially obtained only with alloying elements.

Inasmuch as experimental data have shown that the alloy layer of commercially pure hot-dipped aluminum coatings on plain-carbon steel is composed of three single-phase layers, the zeta, eta, and theta layers (5), through which the rates of diffusion of iron and aluminum appear to be very rapid even at temperatures as low as 900 °F

<sup>2</sup>The use of the term adherence in this paper differs somewhat from the technical definition of the word but conforms to the idiomatic usage common to the hot-dip coating industry.



(480 °C), a change in the composition of the layer might well result in improved formability through a reduction in both its thickness and its hardness. The only published information in this regard appears to be that of a patent granted to Oganowski, Parks and Coburn (6), in which it is claimed that the addition of silicon to the bath decreases the thickness of the alloy layer.

Because of the scarcity of information concerning bath additions, the present investigation was undertaken to establish the effects of various elements on the microstructure and bend performance of hot-dipped aluminum coatings. Some attention was given, also, to the surface appearance of the as-dipped specimens.

### MATERIALS AND PROCEDURE

The selection of the elements to be added to the bath was limited to those that have some solid solubility in aluminum (7, 8, 9, 10). The aluminum to which the additions were made was commercially pure, 99.86%, and contained as impurities 0.08% silicon

**Table I**  
**Form of Alloy Additions**

Alloying Element	Form of Addition	Alloying Element	Form of Addition
99.86% pure Aluminum		Lead	99.8% Pb bar
Antimony	C.P. Powder*	Magnesium	C.P. bar
Beryllium	5% Be master alloy	Manganese	4.9% Mn master alloy
Bismuth	C.P. granules	Nickel	25% Ni master alloy
Cadmium	C.P. sticks	Silicon	15% Si master alloy
Calcium	C.P. lumps	Silver	C.P. shot
Chromium	3% Cr master alloy	Tin	C.P. stick
Cobalt	C.P. roundels	Titanium	5% Ti master alloy
Copper	C.P. shot	Vanadium	10% V master alloy
Germanium	C.P. powder	Zinc	C.P. stick

\*C.P. means American Chemical Society chemically pure.

and 0.06% iron. The commercially pure aluminum coatings will, in the remainder of this paper, be referred to as basic aluminum coatings. The addition elements were introduced individually into the aluminum baths either as chemically pure metals or as commercial master alloys, Table I. (A master alloy is a commercial alloy of aluminum and the desired alloying element.) Most of the elements with melting points higher than 1800 °F (980 °C) were added as master alloys. When master alloys were not available, the elements were added in the finest form obtainable. These master alloys contained, in some instances, as much as 0.6% silicon and 1.0% iron as impurities, but the authors believe that the effects of these impurities were negligible because of their dilution in the coating bath. As an illustration, the maximum amount of silicon



that ever accumulated in the coating baths was present in the high manganese series, and the final silicon content was only 0.13%, which amount of silicon did not significantly influence the results. To facilitate alloying of these high melting point elements with the aluminum, the baths were heated to temperatures considerably above the melting point of the aluminum. After alloying had been accomplished, the bath temperature was lowered to the desired coating temperature.

Bath temperature measurements were made with a shielded, 18-gage chromel-alumel thermocouple and a portable potentiometer. Bath composition was determined chemically. A prescribed procedure was followed in the preparation, dipping, and cooling of all specimens:

*Grade of Steel*—low-carbon, cold-reduced, box-annealed, 0.035-inch-thick (20-gage) rimmed steel with the following chemical composition in per cent:

C	Mn	P	S	Si	Cu	Ni	Cr
0.08	0.33	0.008	0.023	0.010	0.03	0.03	0.02

*Specimens*—specimens were 1 inch wide by 4 inches long, the long dimension being parallel to the rolling direction.

*Pickling*—3 to 5 minutes' immersion time in a 2% solution of hydrochloric acid at room temperature as a preliminary cleaning operation.

*Fluxing*—60 seconds' immersion time in a molten zinc-ammonium chloride flux at approximately 750 °F (400 °C). Because of the pickup of iron oxide, the flux was replaced periodically.

*Coating Bath*—coating bath consisted of 2.5 pounds of the commercially pure aluminum alloyed with the various elements.

*Coating*—20 seconds' total immersion time in the coating bath at 1250 °F (675 °C).

*Cooling*—in air at room temperature. The specimens were withdrawn from the bath at as nearly the same rate as possible.

The surfaces of the specimens after coating were first examined for smoothness, brightness, and visible polygonal grains. Metallographic specimens were then prepared and studied at magnifications of 100 and 1000 diameters for determination of the thickness and microhardness of the alloy layer. Microhardness tests were made with a Tukon hardness tester using a Knoop indenter with a 25-gram load, the values reported being averages. Bend performance was determined by bending specimens 180 degrees with a zero radius, with the bent edge parallel to the 1-inch width. The tension side of each bend was examined at a magnification of 40 diameters for peeling, flaking, and size and frequency of cracks.

## RESULTS AND DISCUSSION

For convenience in discussing the results obtained with the various elements, the data are divided into four parts: 1. Surface

appearance of coatings; 2. Thickness of the alloy layer; 3. Micro-hardness of the alloy layer; and 4. Bend-test performance.

### *1. Surface Appearance of Coatings*

Inasmuch as an attractive appearance is often desirable in coated products, the influence of addition elements on the surface appearance of the coatings seemed worthy of attention.

Brightness is a requirement for many applications. Commercially pure aluminum coatings are characteristically bright, and they maintain their brightness during weathering longer than most hot-dipped coatings. The surface of a coating should also be smooth; that is, the coating should be free from scruff and pimples, which result when undissolved aluminum compounds are present in the bath. Some addition elements darken an aluminum coating, and this darkening may be, and usually is, undesirable in decorative applications. A description of the surface appearance of each experimental coating is given in Table II. In studying the table it is well to bear in mind that the specimens were hand-dipped; if similar coatings were made on commercial continuous lines, one would expect improved appearance.

The basic aluminum coatings were bright, but a faint polygonal grain pattern, outlined by slightly depressed boundaries, was noticeable. Cadmium, chromium, lead, manganese, silver, tin, or vanadium in the amounts added did not change the appearance of the basic coating. Additions of antimony, beryllium, cobalt, titanium, or zinc produced smooth, bright coatings with no visible surface grains.

Additions of bismuth, calcium, copper, germanium, magnesium, nickel, or silicon produced various changes in the appearance of the basic coating. Magnesium made the surface appear frosty, which decreased its reflectivity to some extent. A greater decrease in reflectivity resulted from additions of bismuth, calcium, silicon, or the lower percentages of copper. Scruffy coatings resulted with the higher concentrations of beryllium, calcium, chromium, cobalt, copper, or manganese. Nickel roughened the surfaces of the coatings, but did not otherwise detract from their brightness. Polygonal surface grains were observed in all of these specimens except those that contained germanium, nickel, silicon, or a low concentration of calcium.

If it should become desirable in commercial hot dipping operations to use addition elements that darken the coating, the darkening could probably be partly controlled by the addition of some brightening element such as magnesium (6).

Table II  
Effects of Alloying Elements on Surface Appearance  
of Hot-Dipped Aluminum Coatings

Alloying Element	Element Concentration in Bath (%)	Surface Appearance of Coatings	Alloying Element	Element Concentration in Bath (%)	Surface Appearance of Coatings
99.86% pure Aluminum			Germanium	0.3	Smooth; bright; light gray
Antimony	0.08	Smooth; grained; * bright		0.7	Smooth; bright; light gray
	0.2	Smooth; bright	Lead	1.4	Smooth; bright; light gray
	0.4	Smooth; bright		0.06	Smooth; grained; bright
	0.6	Smooth; bright		0.1	Smooth; grained; bright
	0.8	Smooth; bright		0.5	Smooth; grained; bright
	1.1	Smooth; bright	Magnesium	1.0	Smooth; grained; bright
	1.5	Smooth; bright		0.9	Smooth; grained; frosty; light gray
Beryllium	0.05	Smooth; bright		1.2	Smooth; grained; frosty; light gray
	0.1	Smooth; bright		4.4	Smooth; grained; frosty; light gray
	0.3	Smooth; bright		8.7	Smooth; grained; frosty; light gray
	0.4	Smooth; bright	Manganese	0.8	Smooth; grained; bright
	0.5	Smooth; bright		1.6	Scruffy; grained; bright
	0.6	Smooth; bright	Nickel	2.0	Rough; bright
	0.7	Smooth; bright		4.0	Rough; bright
	0.8	Slightly scruffy; bright		6.0	Rough; bright
	0.9	Scruffy; bright	Silicon	8.0	Rough; bright
	1.0	Scruffy; bright		0.75	Smooth; bright; light gray
	1.4	Scruffy; bright		1.5	Smooth; bright; medium gray
	1.7	Scruffy; bright		2.25	Smooth; bright; medium gray
	2.0	Scruffy; bright		3.0	Smooth; bright; medium gray
Bismuth	0.07	Smooth; grained; dull gray		3.75	Smooth; bright; medium gray
	0.1	Smooth; grained; dull gray	Silver	6.0	Smooth; grained; bright
	0.7	Smooth; grained; dull gray		0.5	Smooth; grained; bright
	2.4	Smooth; grained; dull gray		2.0	Smooth; grained; bright
Cadmium	0.5	Smooth; grained; bright		5.0	Smooth; grained; bright
	0.97	Smooth; grained; bright	Tin	10.0	Smooth; grained; bright
	2.0	Smooth; grained; bright		1.0	Smooth; grained; bright
	5.0	Smooth; grained; bright		2.5	Smooth; grained; bright
Calcium	0.9	Smooth; grained; dull gray		5.0	Smooth; grained; bright
	1.7	Smooth; dull gray		10.0	Smooth; grained; bright
	3.1	Slightly scruffy; bright; light gray		15.0	Smooth; grained; bright
	6.2	Slightly scruffy; bright; light gray		20.0	Smooth; grained; bright
Chromium	0.2	Smooth; grained; bright	Titanium	0.1	Smooth; grained; bright
	0.5	Slightly scruffy; bright	Vanadium	0.15	Smooth; grained; bright
Cobalt	0.3	Smooth; bright		0.3	Smooth; grained; bright
	0.7	Slightly scruffy; bright		1.2	Smooth; grained; bright
	1.0	Scruffy; bright	Zinc	-2.3	Smooth; bright
Copper	1.8	Smooth; grained; dull gray		3.5	Smooth; bright
	6.4	Smooth; grained; frosty gray		4.6	Smooth; bright
	15.4	Scruffy; bright; light gray		5.8	Smooth; bright
	27.2	Scruffy; bright; light gray		11.5	Smooth; bright

\*Grained means a polygonal grain pattern on surface of coating.



## 2. Thickness of the Alloy Layer

The rate of growth of the iron-aluminum alloy layer, Fig. 1, is essentially a function of the rate of diffusion of iron and of aluminum across the layer at the coating temperature. This diffusion process consists of two stages: (a) the diffusion of atoms through the phase layers and (b) the transfer of atoms across the interfaces between the phases. The influence of an alloying element on the

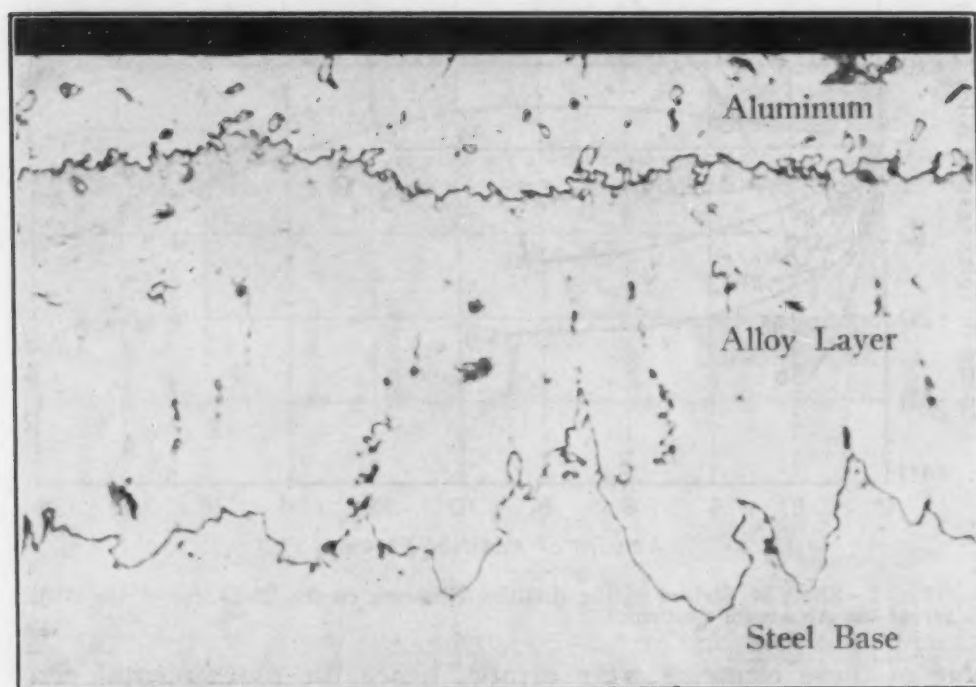


Fig. 1—Cross Section of the Basic Aluminum Coating. Picral and sodium hydroxide etches.  $\times 1000$ .

thickness of the alloy layer is most readily apparent when it affects this diffusion process. If an element reduces the rate of diffusion of iron or of aluminum across the layer, by forming a solid solution or by forming an additional phase or phases, the alloy layer will be reduced in thickness. Notwithstanding the great amount of study that has been devoted to diffusion processes in metals, there is still no basis upon which one may predict the direction and magnitude of the influence of alloying elements on the rate of diffusion of iron and of aluminum across the alloy layer of hot-dipped aluminum coatings.

Of the nineteen elements added to the aluminum baths, sixteen had no significant effect on alloy-layer thickness. These sixteen elements, in the amounts added to the baths, apparently had no



marked effect on the rate of diffusion of iron and of aluminum across the alloy layer; they are antimony, bismuth, cadmium, calcium, chromium, cobalt, germanium, lead, magnesium, manganese, nickel, silver, tin, titanium, vanadium, and zinc. The effect of each of these elements is indicated by the curves of Fig. 2. The data for

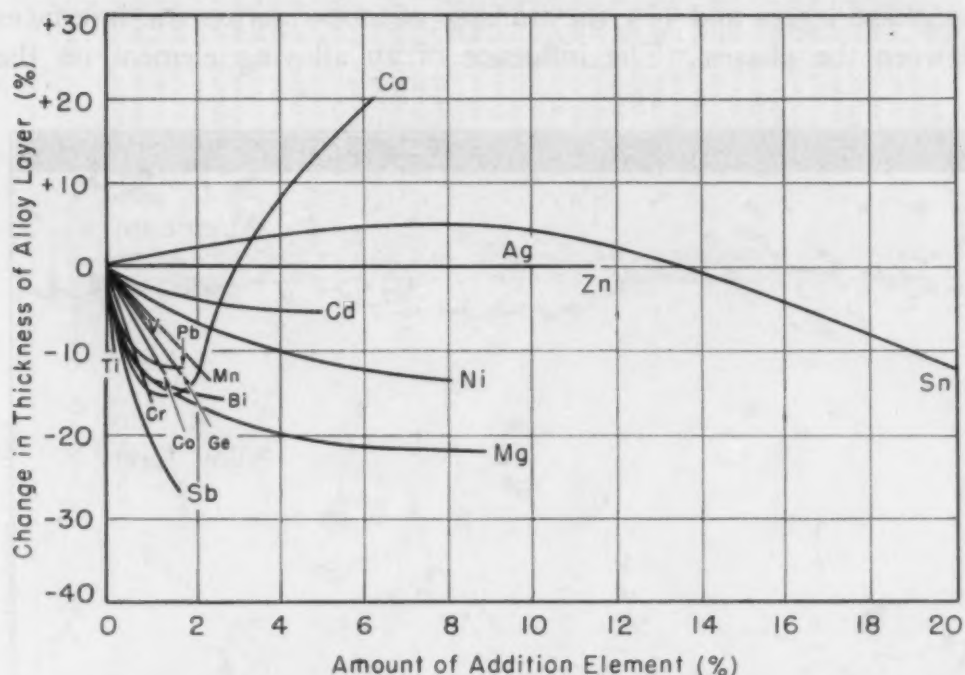


Fig. 2—Effect of Sixteen of the Addition Elements on the Thickness of the Alloy Layer of the Aluminum Coatings.

some of these elements were erratic, hence the experimental error in measuring the change in thickness of the alloy layer was about  $\pm 10\%$ . The remaining three elements, namely silicon, copper, and beryllium, markedly decreased the thickness of the alloy layer, Fig. 3; these elements apparently retard the rate of diffusion of iron and of aluminum across the alloy layer. The data for all nineteen elements are listed in Table III.

Tin contents below about 14% slightly increased the thickness of the alloy layer; above about 14%, however, tin reduced the thickness. Calcium, at a bath concentration of about 6%, produced the only marked increase in alloy-layer thickness; with concentrations of less than about 3% the thickness was reduced.

The data for silver and for zinc indicate that these elements have essentially no effect on the rate of growth of the alloy layer. Antimony, bismuth, cadmium, cobalt, chromium, germanium, magnesium, manganese, nickel, lead, titanium, or vanadium slightly decreases the thickness of the alloy layer.

Table III  
Effects of Various Elements on the Average Thickness and Microhardness  
of the Alloy Layer of Hot-Dipped Aluminum Coatings

Alloying Element	Element Concentration in Bath (%)	Decrease in Average Thickness of Alloy Layer (%)*	Average Microhardness of Alloy Layer (KHN)**	Alloying Element	Element Concentration in Bath (%)	Decrease in Average Thickness of Alloy Layer (%)*	Average Microhardness of Alloy Layer (KHN)**
99.86% pure Aluminum	0.08	Reference Layer	900	Germanium	0.3	-4	...
Antimony	0.2	-6	...	Lead	0.7	+2	...
	0.4	-16	...		1.4	-16	982
	0.6	-8	...		0.06	-10	...
	0.8	-19	...		0.1	-10	902
	1.1	-20	...		0.5	-8	...
	1.5	-23	...		1.0	-8	...
Beryllium	0.05	-26	845	Magnesium	0.9	-18	...
	0.1	-35	807		1.2	-8	...
	0.3	-50	996		4.4	-18	...
	0.4	-71	770		8.7	-24	965
	0.5	-75	715	Manganese	0.8	0	...
	0.6	-77	518	Nickel	1.6	-16	703
	0.7	-83	372		2.0	-18	682
	0.8	-82	310		4.0	-2	...
	0.9	-80	482		6.0	-11	...
	1.0	-82	495		8.0	-13	...
	1.4	-76	560	Silicon	0.75	-42	792
	1.7	-78	684		1.5	-58	792
	2.0	-80	556		2.25	-68	742
Bismuth	0.07	-82	583		3.0	-69	661
	0.1	-14	934		3.75	-72	339
	0.7	-8	...	Silver	6.0	-75	340
	2.4	-12	...		0.5	-6	...
Cadmium	0.5	-4	...		2.0	+4	728
	0.97	0	...		5.0	+6	...
	2.0	-2	...	Tin	10.0	+10	...
	3.0	-6	918		1.0	0	...
	0.9	-14	...		2.5	0	...
	1.7	-14	805		5.0	+4	...
	3.1	0	...		10.0	+1	...
Chromium	6.2	+20	...	Titanium	20.0	-12	891
	0.2	-12	949	Vanadium	0.1	-10	830
	0.5	-6	...		0.15	+2	...
Cobalt	0.3	+7	...		0.3	+2	784
	0.7	+8	...	Zinc	1.2	-11	682
	1.0	-22	1035		2.3	+5	...
	1.8	-25	672		3.5	+5	...
	6.4	-34	807		4.6	+5	...
Copper	15.4	-50	807		5.8	+6	836
	27.2	-66	859		11.5	+2	...

\*As compared with the basic aluminum coatings; + indicates thickness increase, and - indicates decrease in average thickness of alloy layer.

\*\*Knoop Hardness Number, obtained with a 25-gram load.

The limited solubility of chromium, cobalt, germanium, manganese, titanium, and vanadium in liquid aluminum at the coating temperature, 1250 °F (675 °C), did not permit the testing of higher concentrations of these elements. Although small amounts of these five elements had a more marked effect in reducing the thickness of the alloy layer than some of the other elements in Fig. 2, their effectiveness is limited by their low solubility in molten aluminum at practicable coating temperatures.

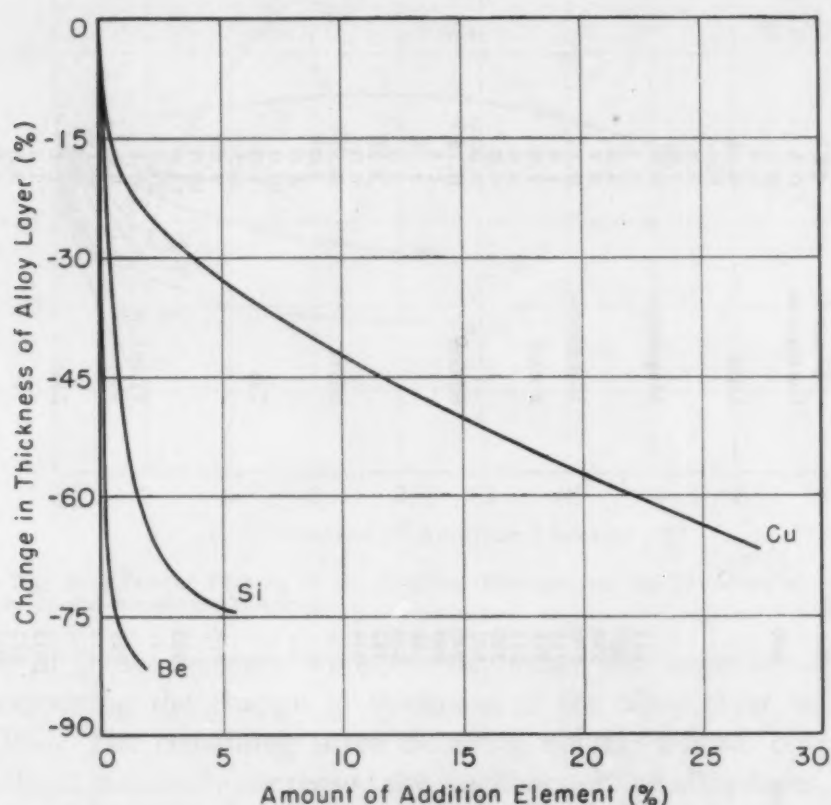


Fig. 3—The Effect of Silicon, Copper, and Beryllium Additions on the Thickness of the Alloy Layer of the Aluminum Coatings.

As compared with the thickness of the alloy layer present in the basic aluminum coatings, 27% copper in the aluminum bath reduced the thickness of the alloy layer about 65%, but additions of copper may not be commercially feasible. One reason is that a high percentage of copper, about 17%, is needed to effect an appreciable reduction in the thickness of the alloy layer, and with copper additions, the excellent corrosion resistance of the aluminum is lost, thus reducing the number of possible applications for aluminum-coated steel. The addition of as low as about 0.25% copper to aluminum appreciably reduces its corrosion resistance (11, 12). In

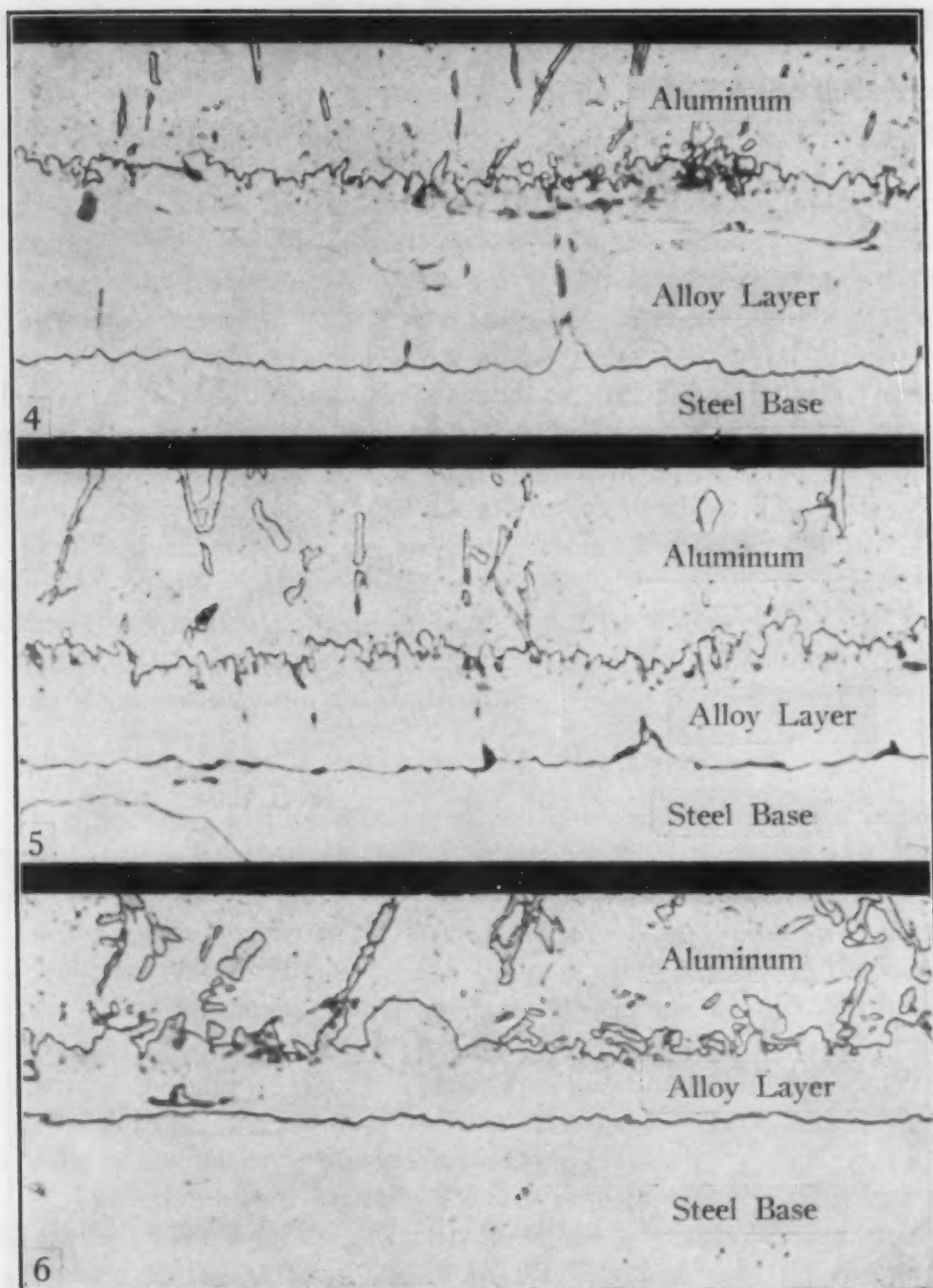


Fig. 4—Cross Section of Aluminum Coating Containing 0.75% Silicon. Picral and sodium hydroxide etches.  $\times 1000$ .

Fig. 5—Cross Section of Aluminum Coating Containing 3% Silicon. Picral and sodium hydroxide etches.  $\times 1000$ .

Fig. 6—Cross Section of Aluminum Coating Containing 6% Silicon. Picral and sodium hydroxide etches.  $\times 1000$ .

fact, sheets of aluminum-copper alloys are frequently clad with commercially pure aluminum or with certain aluminum alloys that offer cathodic protection in corrosive environments. Another reason is



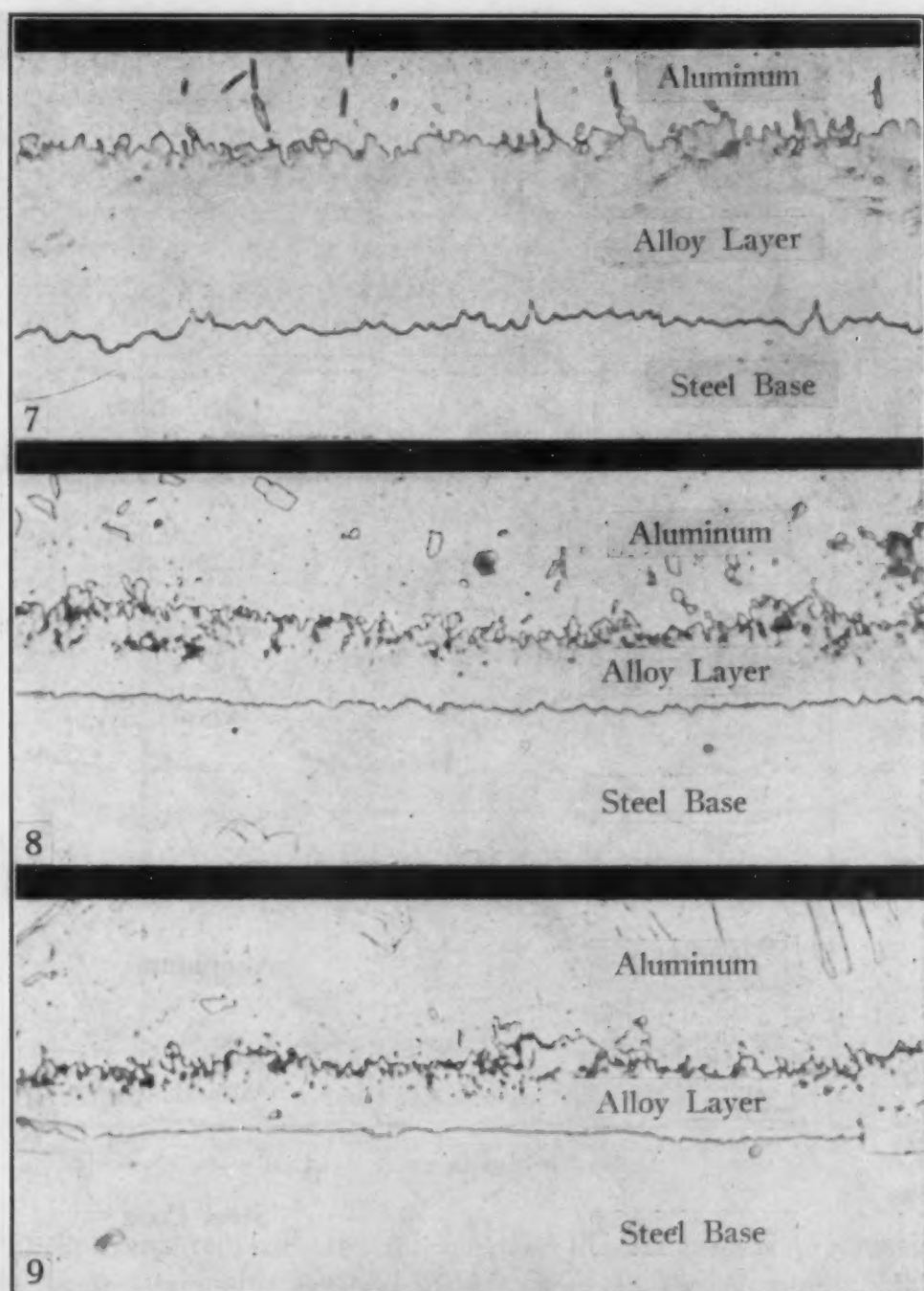


Fig. 7—Cross Section of Aluminum Coating Containing 0.1% Beryllium. Picral and sodium hydroxide etches.  $\times 1000$ .

Fig. 8—Cross Section of Aluminum Coating Containing 0.3% Beryllium. Picral and sodium hydroxide etches.  $\times 1000$ .

Fig. 9—Cross Section of Aluminum Coating Containing 0.6% Beryllium. Picral and sodium hydroxide etches.  $\times 1000$ .

that a eutectic occurs in the aluminum-copper system at 33%, and when copper is added in appreciable amounts, the relatively brittle eutectic structure occurs as a grain-boundary network in the outer

layer of the coating. This brittle constituent lowers the ductility and impairs the formability of the aluminum-coated sheets.

Silicon is more effective than copper in reducing the thickness of the alloy layer; additions of 0.75 to 6.00% silicon to the coating bath reduce the alloy-layer thickness of the basic aluminum coating about 40 to 75%, Figs. 4, 5, and 6. Although aluminum-silicon coatings darken on prolonged exposure to the atmosphere, which makes them unsatisfactory for some applications, they retain their appearance better than aluminum-copper coatings (13), and are also more resistant to other types of corrosion (13, 14).

In the concentration ranges studied, beryllium is even more effective than silicon in reducing the thickness of the alloy layer. Additions of beryllium to the coating bath in amounts up to 0.6% decreased the thickness of the alloy layer as much as 83%, Figs. 7, 8, and 9; further reductions were not obtained with beryllium additions up to 2%. Although the atmospheric corrosion resistance of aluminum coatings containing small amounts of beryllium has not been established, their resistance may not differ substantially from that of the basic aluminum coatings.

### 3. Microhardness of Alloy Layer

Since most of the additions to the aluminum produced a reduction in alloy-layer thickness of less than 25%, and since it was desired to avoid as much unnecessary microhardness testing as possible, only one specimen from each series of additions was tested, namely the specimen having the thinnest alloy layer. If the alloy layer of this specimen showed no marked decrease in microhardness, no additional microhardness tests on the series were made. For the coatings containing silicon, copper, or beryllium, however, microhardness tests were made on all the specimens of each series. The results of the tests are presented in Table III.

The relationship between the decrease in average thickness of the alloy layer and its microhardness, as a result of the various additions to the bath, is shown in Fig. 10; the data on the alloy layer of the basic aluminum coating have been included for comparison. In this figure there are two ranges of microhardness: a higher range that contains values for most of the additions, including some for silicon and beryllium, and a lower range that contains only values for silicon and beryllium additions. The scatter in the higher range may be significant academically, but it is of less practical importance than the difference between the two ranges.

Although an increase in silicon and beryllium contents in the

coating bath resulted in a decrease of both the average alloy-layer thickness and microhardness, there was no straight-line relationship between the two. In fact, no appreciable decrease in average microhardness occurred until a critical amount of either of these elements had been added. A study of the effect of silicon and of beryllium additions on the composition of the alloy layer would have been

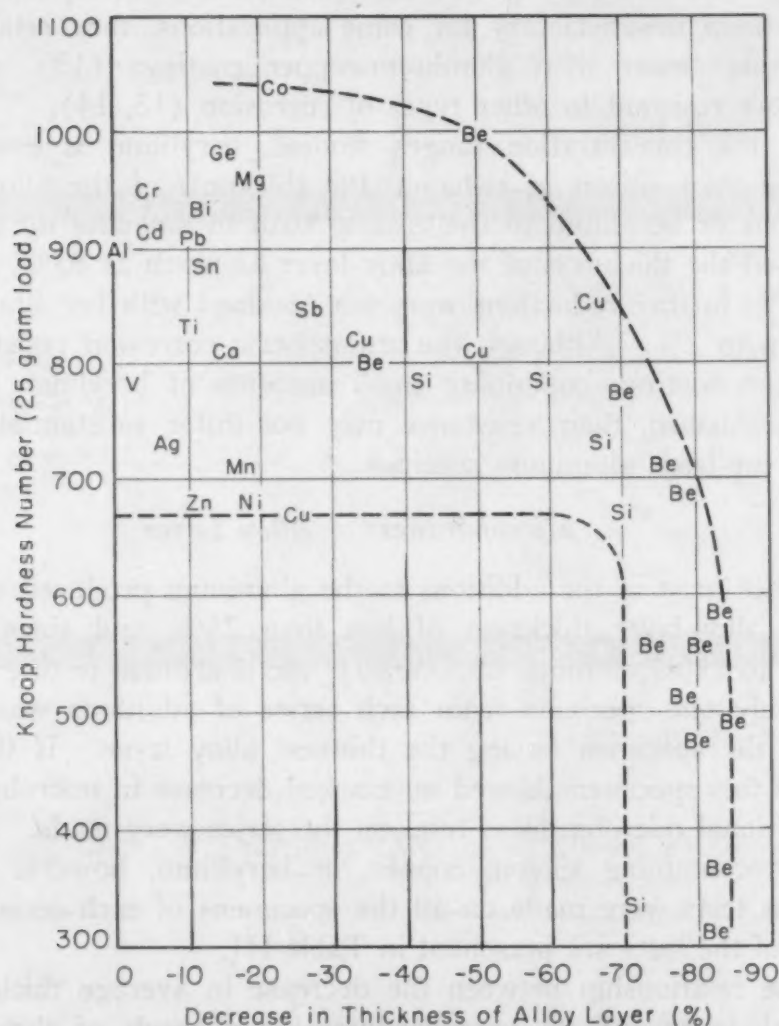


Fig. 10—Correlation Between the Decrease in Average Thickness of the Alloy Layer and Its Microhardness. The dotted lines indicate the spread of the data.

helpful in trying to explain the reason for this decrease in microhardness, but such a study necessitates metallographic procedures capable of differentiating among the phases in the alloy layer. Although a metallographic method for differentiating among the phases in the alloy layer of galvanized coatings has been developed (2), a similar procedure for aluminum coatings containing both



single- and two-phase layers is not available. In the absence of substantiating metallographic data, the authors suggest two possibilities, either of which might account for this decrease in microhardness, but the first seems the more probable explanation.

First, Rhines (3), having investigated diffusion in aluminum-magnesium-zinc and in aluminum-magnesium-silicon systems, reported that the intermediate diffusion layers can usually be predicted as the one- and two-phase regions cut by a line joining the starting compositions on the ternary diagram at the diffusing temperature. By analogy, then, the addition of silicon or of beryllium to the aluminum may have changed the composition of the alloy layer by introducing two-phase layers and perhaps by introducing new one-phase layers. Predictions concerning which phases should theoretically be present in these coatings are not practicable until more complete iron-aluminum-silicon and iron-aluminum-beryllium ternary constitution diagrams are available. Without these diagrams the metallographer is seriously handicapped in the development of new etching reagents for differentiating among the phases because it is necessary for him to know beforehand the number of phases likely to be present, otherwise he has no way of knowing whether his reagents are satisfactory.

Second, as an alternative to possible phase changes, solid-solution effects might have been operative. Silicon or beryllium, by forming solid solutions with the zeta, eta, and theta layers of basic aluminum coatings, may have had an appreciable effect on the rate of diffusion of iron and of aluminum across the alloy layer. If so, the relative thicknesses of the three phases may have been changed. Inasmuch as the additions decreased the total thickness of the alloy layer, they either decreased the thicknesses of the three phases proportionately or decreased the thickness of at least one of the phases more than the others. Consider, for example, the phase next to the steel base, the phase that in hot-dipped coatings is usually harder than any of the others. The appreciable change in microhardness might be explained if this phase were decreased in thickness more than the others by increasing amounts of silicon and beryllium in the coatings. If the microhardness of this phase were to remain relatively constant with increasing additions, the effect of the additions would not be detected so long as the phase is sufficiently thick to hold an entire microhardness indentation. If this phase were to become too thin, part of the microhardness indentation would extend into the adjacent phase, which would be richer in aluminum and would, therefore, be expected to be softer. This condition would result in a composite



**Table IV**  
**Effects of Alloying Elements on Bending Properties**  
**of Hot-Dipped Aluminum Coatings**

Alloying Element	Element Concentration in Bath (%)	Flaking or Peeling	Bend Tests	
			Size	Cracking* Frequency
99.86% pure Aluminum	....	Slight peeling	Large	Numerous
Antimony	0.08	None	Larger	Same
	0.2	None	Larger	Same
	0.4	None	Larger	Same
	0.6	None	Larger	Same
	0.8	None	Larger	Same
	1.1	None	Larger	Same
	1.5	None	Larger	Same
Beryllium	0.05	None	Smaller	Less
	0.1	None	Smaller	Less
	0.3	None	None	None
	0.4	None	None	None
	0.5	None	None	None
	0.6	None	None	None
	0.7	None	Smaller	Less
	0.8	None	Smaller	Less
	0.9	None	Smaller	Less
	1.0	Slight peeling	Smaller	Less
	1.4	None	Smaller	Less
	1.7	None	Smaller	Less
	2.0	None	Smaller	Less
Bismuth	0.07	None	Larger	Less
	0.1	None	Larger	Less
	0.7	None	Larger	Less
	2.4	None	Larger	Less
Cadmium	0.5	None	Same	Same
	0.97	None	Same	Same
	2.0	None	Same	Same
	5.0	None	Same	Same
Calcium	0.9	None	Smaller	More
	1.7	None	Smaller	More
	3.1	None	Smaller	More
	6.2	None	Same	More
Chromium	0.2	Slight peeling	Larger	Less
	0.5	Slight peeling	Larger	Less
Cobalt	0.3	None	Smaller	Same
	0.7	None	Smaller	Same
	1.0	Slight peeling	Same	Same
Copper	1.8	Peeling	Larger	Less
	6.4	Peeling	Same	Same
	15.4	Peeling	Larger	More
	27.2	Slight peeling	Larger	More
Germanium	0.3	None	Larger	Less
	0.7	Slight peeling	Larger	Less
	1.4	Peeling	Larger	Less

\*As compared with 99.86% aluminum reference coatings.

microhardness value for the two phases and would explain the intermediate microhardness values obtained for some of the beryllium additions in Fig. 10. If the phase next to the steel base were to become even thinner, microhardness indentations would be confined primarily to the softer phase; the values for these indentations would be low, as for the silicon and beryllium coatings in the lower microhardness range of Fig. 10.

#### 4. Bend-Test Performance

As was mentioned previously, the relatively poor bending and forming qualities of commercially pure hot-dipped aluminum coat-

Table IV—Continued  
Effects of Alloying Elements on Bending Properties  
of Hot-Dipped Aluminum Coatings

Alloying Element	Element Concentration in Bath (%)	Flaking or Peeling	Bend Tests	
			Size	Cracking* Frequency
Lead	0.06	None	Larger	Less
	0.1	None	Larger	Less
	0.5	None	Larger	Less
	1.0	None	Larger	Less
Magnesium	0.9	Slight peeling	Same	Same
	1.2	Slight peeling	Same	Same
	4.4	Peeling	Larger	Less
	8.7	Peeling	Larger	Less
Manganese	0.8	Slight peeling	Larger	More
	1.6	Slight peeling	Smaller	Less
Nickel	2.0	Slight peeling	Larger	More
	4.0	Slight peeling	Larger	More
	6.0	Slight peeling	Larger	More
	8.0	Peeling; flaking	Larger	More
Silicon	0.75	Peeling	Larger	Less
	1.5	Peeling	Smaller	Less
	2.25	Slight peeling	Smaller	Less
	3.0	Slight peeling	Smaller	Less
Silver	3.75	None	Smaller	Less
	6.0	None	Smaller	Less
	0.5	Slight peeling	Larger	Less
	2.0	Slight peeling	Larger	Less
Tin	5.0	Slight peeling	Larger	Less
	10.0	Slight peeling	Larger	Less
	1.0	None	Smaller	More
	2.5	None	Smaller	More
Titanium	5.0	None	Smaller	More
	10.0	None	Smaller	More
	15.0	None	Smaller	More
	20.0	None	Smaller	More
Vanadium	0.1	Slight peeling	Smaller	More
	0.1	Slight peeling	Same	Same
	0.15	Slight peeling	Same	Same
	0.3	Slight peeling	Same	Same
Zinc	1.2	Slight peeling	Larger	Less
	2.3	Peeling	Larger	Less
	3.5	Peeling	Larger	Less
	4.6	Peeling	Larger	Less
	5.8	Peeling	Larger	Less
	11.5	Peeling; flaking	Larger	Less

\*As compared with 99.86% aluminum reference coatings.

ings on steel are largely attributable to the thick, brittle alloy layer of these coatings. In any investigation to determine improvement in mechanical properties of a coating, through a reduction in the thickness and microhardness of the alloy layer, the ideal test is to subject the coated product to the forming operations required in commercial applications. This is the ultimate test that must finally be made in order to evaluate properly the coated product. But preliminary experimental work, if it is done on a comprehensive basis, is usually conducted with small specimens to minimize costs. The trends obtained with small specimens, utilizing some simple method of evaluation such as the bend test, which is a popular mechanical test for coatings, are often sufficiently informative to enable one to narrow the scope of subsequent, more costly pilot-line investigations.

The results of bend tests are given in Table IV and are based

on comparisons with the basic aluminum coatings. The term cracking means that sections of the coating fractured during bending, but otherwise adhered to the steel base; peeling means that sections of the coating fractured through the alloy layer sufficiently to produce a raised sliver; flaking means that sections of the coating separated completely from the steel base and from the adjoining coating, so that areas of the steel base were exposed.

The only coatings that exhibited satisfactory performance in the flat-bend tests were those containing either silicon or beryllium. Although copper, when added in large amounts, decreased the average thickness of the alloy layer more than 50%, the bend-test performance of the coatings was unsatisfactory because of the brittle, aluminum-copper eutectic in the outer layer of the coatings and because such copper additions did not sufficiently reduce the average microhardness of the alloy layer. The effectiveness of silicon in improving the bending properties of aluminum coatings has been recognized by other investigators (6, 16). They attribute the improvement to the fact that silicon reduces the average thickness of the alloy layer.

Beryllium, in the concentration range 0.3 to 0.6%, was more effective in producing defect-free bends than were the concentrations of silicon studied in this investigation. This improved bend performance associated with beryllium additions appears to be due not only to reductions in the average thickness and microhardness of the alloy layer, but also to a third factor, that is, improved ductility of the aluminum layer of the coatings. Inasmuch as the aluminum layer of the coatings is a cast structure, the influence of alloying elements on the mechanical properties of cast aluminum and of cast aluminum alloys should be applicable, at least qualitatively, to this layer of the coatings. The tensile elongation of cast 99.0% aluminum is about 20%; that of a 0.5% silicon alloy, 18%; and that of a 4.8% silicon alloy, 7.8% (17, 18). These data indicate that an increase in silicon content decreases the ductility of cast aluminum-silicon alloys. In contrast with silicon, beryllium increases the ductility of cast aluminum; 0.5% beryllium increases the tensile elongation to 36% (19). Kroll (10) reports that beryllium-treated aluminum-iron alloys are much more malleable than the beryllium-free compositions. He attributes this to the fact that beryllium tends to neutralize the effect of iron in aluminum alloys. For example, he found that when beryllium is added to iron-bearing aluminum, the  $\text{FeAl}_3$  phase is replaced by the  $\text{Be}_2\text{Fe}$  phase. Perhaps this reaction occurs in a modified form during hot dipping and decreases



the apparent brittleness of the alloy layer of beryllium-bearing aluminum coatings. Therefore the improved bend-test performance of the aluminum-beryllium coatings may be the net result of three factors: 1, a thinner alloy layer; 2, a softer and less brittle alloy layer, and 3, a more ductile aluminum layer.

#### SUMMARY

Of the nineteen elements added individually to commercially pure aluminum baths, only silicon, copper, and beryllium decreased the average thickness of the alloy layer more than 50% of that present without these additions. Silicon and beryllium additions significantly decreased the average microhardness of the alloy layer, but copper and the other elements did not. Small additions of beryllium were more effective than relatively large additions of silicon in reducing the average thickness and microhardness of the alloy layer. Beryllium additions resulted in a more ductile aluminum layer than that obtained with silicon additions. Beryllium did not affect the characteristic brightness of the as-dipped basic aluminum coatings; whereas silicon, in the amounts necessary to obtain a substantial reduction in alloy-layer thickness, gave them a gray appearance.

#### References

1. R. M. Burns and A. E. Schuh, *Protective Coatings for Metals*, 1939, Reinhold Publishing Corporation.
2. D. H. Rowland, "Metallography of Hot-Dipped Galvanized Coatings", *TRANSACTIONS, American Society for Metals*, Vol. 40, 1948, p. 983.
3. F. N. Rhines, "Diffusion Coatings on Metals", *Symposium on Surface Treatment of Metals*, American Society for Metals, 1940, p. 122.
4. R. F. Mehl, "Diffusion in Solid Metals", *Transactions, American Institute of Mining and Metallurgical Engineers*, Vol. 122, 1936, p. 11.
5. Unpublished data, Research and Development Division, Carnegie-Illinois Steel Corporation.
6. K. Oganowski, N. W. Parks and K. G. Coburn, "Coating Ferrous Metals With Aluminum", U. S. Patent No. 2,406,245 (1946).
7. *Metals Handbook*, American Society for Metals, 1948, p. 1145-1240.
8. L. F. Mondolfo, *The Metallography of Aluminum Alloys*, 1943, John Wiley & Sons, Inc.
9. V. Fuss and R. J. Anderson, *The Metallography of Aluminum and Its Alloys*, 1936, The Sherwood Press.
10. W. J. Kroll, "Rare Metals as Constituents in Light Alloys", *Light Metal Age*, Vol. 3, December 1945, p. 23.
11. E. H. Dix, Jr., and J. J. Bowman, "Properties of Aluminum-Copper Alloys", *Metals Handbook*, American Society for Metals, 1948, p. 803.
12. E. H. Dix, Jr., *Corrosion of Metals*, American Society for Metals, 1946, p. 131.
13. L. W. Kempf, "Properties of Aluminum-Silicon Alloys", *Metals Handbook*, American Society for Metals, 1948, p. 805.



14. J. Czochralski, "Silumin—New Light Alloy", *Zeitschrift für Metallkunde*, Vol. 13, 1921, p. 507.
15. H. S. Rawdon, *Protective Metallic Coatings*, 1927, Monograph Series, ACS, Reinhold Publishing Corporation.
16. P. T. Stroup and G. A. Purdy, "Aluminum Coating of Steel—A Comparison of Various Processes", *METAL PROGRESS*, Vol. 57, 1950, p. 59.
17. P. V. Faragher, "Commercial Forms and Applications of Aluminum and Aluminum Alloys", *Proceedings*, American Institute of Mining and Metallurgical Engineers, Institute of Metals Division, 1928, p. 99.
18. R. S. Archer, L. W. Kempf and D. B. Hobbs, "Heat Treatment of Aluminum-Silicon Alloys", *ibid.*, p. 198.
19. R. S. Archer and W. L. Fink, "Aluminum-Beryllium Alloys", *ibid.*, p. 616.

### DISCUSSION

**Written Discussion:** By L. E. Householder, assistant chief metallurgist, Reynolds Metals Co., Richmond, Va.

The authors are to be congratulated on the excellent paper which they have presented. This paper is an important contribution to the metallurgical field of aluminum-coated steel. It also appears to confirm a well-known metallurgical principle of diffusion. The principle to which I refer is that, if the formation of an additional phase by interdiffusion of two metals occurs, a barrier at the interface results which materially decreases the rate of diffusion.

In Figs. 7, 8, and 9, where the coating contains an increased amount of beryllium, the thickness of the alloy layer has not only been decreased, but it is indicated that an additional phase is formed at the interface. The amount of this new phase appears to increase with increased beryllium content of the aluminum. In Mondolfo's book, "Metallography of Aluminum Alloys", the solubility of beryllium in aluminum is only 0.05% at 1195 °F (645 °C) and decreases to 0.005% at 930 °F (500 °C). No pronounced constituent, other than that which can probably be attributed to the iron constituent, is visible in the aluminum alloy coating containing even 0.6% beryllium. Therefore, we assume that either a supersaturated solid solution exists or a very fine precipitate of beryllium constituent is present which is not readily visible in the micrograph. Therefore, in addition to the possibility of forming a complex iron-beryllium or aluminum-iron-beryllium constituent at the interface of the alloy layer and the aluminum, it is quite possible that diffusion of the iron into the aluminum could cause a coalescence of the already only slightly soluble beryllium. If the latter should occur, the phase at the interface could very well be a beryllium or aluminum-beryllium constituent.

I would like to have the authors' opinion concerning the most likely procedure to form the additional phase at the interface of the alloy and aluminum layers in the aluminum-beryllium alloy-coated samples. Also, have the authors carried on any further work in an attempt to definitely identify this new phase?

**Written Discussion:** By T. F. Olt, director, Research Laboratories, The Armco Steel Corp., Middletown, Ohio.

It has been a pleasure to listen to the presentation by the authors relating to the effect of bath composition on aluminum coatings on steel.

Technical information in this field is very limited in the published literature. The authors are to be congratulated for so well defining the problem and systematically exploring it, and the result is certainly in keeping with the excellent quality of performance so characteristic of Dr. Bain's organization.

Over the past ten years we have been utilizing a silicon addition to the aluminum bath in the manufacture of Armco Aluminized sheet steel, and can confirm the authors' findings that a silicon addition decreases the thickness of the primary iron-aluminum alloy layer and also its hardness. Such a product is better able to withstand the rigors of various fabricating operations than an unalloyed pure aluminum coating on steel, which was our reason for changing to that composition of coating.

It is interesting to note that aluminum alloyed with beryllium is equally as effective as silicon in retarding the rate of primary aluminum-iron alloy formation, even at the lower elemental concentration values indicated. It is unfortunate that beryllium is so extremely expensive, costing roughly 500 times as much as silicon. The use of beryllium as a moderator in nuclear reactors has resulted in some increase in beryllium production, which might eventually result in a cost reduction of this metal.

While the aluminum coatings alloyed with silicon withstand fabricating operations to a much greater extent before failure than unalloyed aluminum coatings, at best they still leave much to be desired when compared to the presently available, more ductile and adherent zinc coatings.

The manufacture of aluminum-coated sheet steel is still relatively new, and improvements in the ductility and the adherence of the coating must be made in order to allow the use of such sheets in the more severely fabricated articles.

The authors, in referring to the patent granted to Oganowski, Parks and Coburn as representing the earliest publication of the use of silicon-alloyed aluminum for reducing the thickness and hardness of the alloy layer, evidently were not familiar with the paper by H. Röhrig.<sup>3</sup> Röhrig describes in some detail the variability in primary alloy layers as affected by bath composition, time of immersion, and temperature of the coating bath, and suggested controlling the thickness of the alloy layer by alloying the aluminum. He states that an addition of 5% silicon to the aluminum bath results in a reduction in the thickness of the iron-aluminum intermediate layer to about half of its unalloyed value. This agrees quite well with the data secured by the authors.

I might add that in addition to the variables that have been mentioned, it has been our experience on coatings with a brittle alloy layer that the total thickness of coating is also of importance with respect to freedom from peeling and cracking during fabrication. Other things being equal, the thinner coatings are the more workable.

**Written Discussion:** By Eugene M. Smith, Flat Rolled Products Development Engineer, The Youngstown Sheet & Tube Co., Youngstown, Ohio.

The authors are to be complimented on the presentation of the results of their extensive investigation of the effects of alloying a hot-dip alumi-

<sup>3</sup>H. Röhrig, "Hot-Dipped Aluminum Coatings on Iron", *Zeitschrift für Metallkunde*, Vol. 26, 1934.

num melt. The results presented in this paper may prevent duplication of effort by others and, at the same time, direct attention to the alloy addition agents which show the most promise.

It would be appreciated very much if one of the authors would elaborate on the fluxing procedure. Several questions arise: Assuming the fluxed strip is dry when immersed in the molten aluminum, is there any particular difficulty in flushing the flux from the surface of the strip during the 20-second total immersion time? Is a slow rate of immersion required to allow the flux to melt and float aside? After coating, did appearance indicate uncoated spots which might result from the flux serving as a barrier to the molten aluminum? Was there any evidence of flux being entrapped in the coating? And finally, was coating attempted without the use of a zinc-ammonium chloride flux?

Other questions of interest aside from the fluxing procedure follow: With respect to alloying, was a new melt prepared for each alloy addition or was the smallest quantity of alloying element first added to the bath and then followed by subsequent additions of the desired amount? With respect to coating procedure, how many specimens were coated before the melt was discarded? Was an increase in the iron content of the bath observed or determined? Since coating cannot be accomplished without solution of iron from the article being coated, is the effect of increasing iron concentration expected to materially affect the results reported in this paper? Did all the alloys tried appear to provide completely coated specimens or are some alloys superior in this respect?

**Written Discussion:** By A. Di Giulio, consulting engineer, Detroit.

I wish to compliment the authors on their presentation of very informative data. The many factors involved in producing satisfactory aluminum-coated steel products are numerous and at times not readily understood.

The beneficial additions of silicon and beryllium, as reported by the authors, should be of practical value in commercial fields.

There are some questions which the speaker wishes to ask dealing primarily with the procedure used throughout the experiments: First, were the specimens allowed to cool from the fluxing bath or immersed in the coating bath while hot? Second, has any flux been tried, other than the zinc chloride-ammonium chloride mixture?

As mentioned in the procedure, the flux used had to be periodically replaced. In experiments which the speaker has carried out in which the same flux was used, a deterioration in the appearance of the part was noted: primarily a darkening and a roughening. For this reason a flux of a different composition had to be used. This stable flux insures consistent results over periods of several months of use. Also, on the subject of appearance, the container in which the molten aluminum is kept plays a very important role. Ordinary low carbon steel pots are attacked by molten aluminum and will in time produce rough, gray surfaces. Ceramic pots very effectively eliminate this trouble.

The authors have maintained a constant temperature throughout the experiments, regardless of the composition of the coating alloy. It is important to notice that, in the case of copper and silicon in the range used, the melting point of the alloys decreases by as much as 50°F;



hence, the fluidity of the metal was not the same during the experiments. In the case of beryllium, on the other hand, a 2% addition raises the melting point by approximately 30 °F.

It would seem that the results obtained under these variable conditions are not necessarily comparable if one considers the time necessary to bring the steel to the temperature of the bath (the well-known "cocoon effect" familiar to users of molten salts).

Experiments carried out by the speaker<sup>4</sup> showed that increasing the temperature of immersion will progressively darken the appearance of the coating until at temperatures above 1750 °F (955 °C) the color becomes almost black.

### Authors' Reply

The authors wish to express their appreciation for the discussions of this paper; these pertinent contributions indicate the current interest in the hot-dipped coating of steel.

Mr. Householder has emphasized the complex nature of the diffusion reaction that occurs in the coating of steel with aluminum alloys. We agree that the formation of additional intermediate phases in the alloy layer may create crystallographic barriers to diffusion and thus retard the rate of growth of the alloy layer.

The darkened region between the alloy layer and the aluminum layer (by aluminum layer we mean the coating exclusive of the alloy layer) in Figs. 8 and 9 is the result of polishing and etching and is not to be construed as an additional phase. A precipitate was, however, observed in the aluminum layer of coatings containing more than 0.6% beryllium. This precipitate, as was pointed out by Mr. Householder, is the result of decreased solubility of beryllium in solid aluminum with decreasing temperature.

Mr. Householder suggests the possibility that the formation of a layer of beryllium or of a beryllium-iron phase could be a mechanism that retards the growth of the alloy layer. His suggestions are in agreement with our first proposal that the introduction of new phase layers is a possible reason for the thinner and softer alloy layer. Predictions concerning the processes by which such phases might be formed must be withheld, however, until we obtain ternary phase diagrams that are more nearly complete, and until we obtain suitable etching or X-ray techniques for distinguishing among the intermediate phases. Attempts have been made in our laboratory to distinguish among the phases by means of etching, but the identity and the number of the phases have not been established unequivocally.

We agree with Mr. Olt that the total thickness of a coating influences its ability to withstand forming operations. It is gratifying to note the agreement between our results and those obtained by Röhrig. It is true that beryllium costs more than silicon, but, at the present market prices, a pound of aluminum containing 0.5% beryllium costs only 2½ times as much as a pound of aluminum containing 8% silicon. The increasing demand for beryllium alloys may further reduce its cost.

<sup>4</sup>A. Di Giulio, "Aluminum Coating of Steel Products", *Wire and Wire Products*, Vol. 23, August 1948.



In reply to Mr. Smith, the zinc-ammonium-chloride flux was easily flushed from the strip by agitating it during immersion in the aluminum bath. All the coatings were free of uncoated spots and of entrapped flux particles. When no flux was used, only nonuniform coatings were produced. Other fluxes were not tried.

The alloys were produced by preparing the most dilute bath first and then by increasing the alloy concentrations in the required steps.

Possible contamination of the baths with iron and silicon was recognized, hence precautions were taken to maintain very low iron concentrations. For example, to avoid unnecessary contamination of the bath with iron, graphite instead of iron crucibles were used; to minimize the solution of iron from the samples, only four specimens were coated at each alloy concentration; and to minimize the amount of iron salts carried over into the bath from the flux, the flux was replaced periodically.

Dr. Di Giulio's questions concerning the fluxing practice have been answered in replying to Mr. Smith's discussion.

Dr. Di Giulio states that although the coating temperature was constant, the liquidus temperature of the various coating alloys varied; hence the fluidities of the coating baths were not constant in our experiments. It is generally agreed that an increase in bath fluidity increases the drainage of a coating metal; therefore it seems reasonable to believe that when the fluidity of the aluminum bath is increased, the thickness of the aluminum layer of the coatings would be decreased. The effect of fluidity on the thickness of hot-dipped coatings has not been considered sufficiently important to warrant any more than a few qualitative studies by various investigators. In most of these studies, the fluidity was varied about 100 or 200% by increasing the bath temperature, whereas fluidity changes associated with individual additions of silicon, copper, magnesium, tin, and nickel, as in our experiments, have been reported to be about 0 to 37%.<sup>5, 6</sup>

We believe, however, that the bath fluidity has no significant effect on the thickness of the alloy layer. Inasmuch as the thickness varies directly with bath temperature and immersion time, the control of the temperature and immersion time is considerably more important than is the control of bath fluidity.

Dr. Di Giulio also mentions the possibility that when the liquidus temperature of the aluminum alloy is near the bath temperature, the bath would have a greater tendency to solidify on the specimen immediately after its immersion than when the liquidus temperature of the aluminum alloy is well below the bath temperature. This has been termed the "cocoon effect". In our experiments, a 20-second immersion time was experimentally determined as being long enough to overcome the "cocoon effect".

<sup>5</sup>E. E. Stonebrook and W. E. Sicha, "Correlation of Cooling Curve Data with Casting Characteristics of Aluminum Alloys", *Transactions, American Foundrymen's Society*, Vol. 57, 1949, p. 489.

<sup>6</sup>L. W. Eastwood and L. W. Kempf, "The Measurement of Fluidity of Aluminum Casting Alloys", *Transactions, American Foundrymen's Society*, Vol. 47, 1939, p. 571.

# THE EFFECT OF COLD ROLLING ON THE CREEP PROPERTIES OF SEVERAL ALUMINUM ALLOYS

By O. D. SHERBY AND J. E. DORN

## Abstract

*The creep and stress rupture properties of the following alloys were obtained for 90, 212, 300, and 400 °F up to 1000 hours rupture time:*

*99.6% Al Alloy: H12 and H18 tempers*

*2S Alloy: H12 and H18 tempers*

*4S Alloy: H32 and H38 tempers.*

*In general, the H18 and H38 tempers of the above-mentioned alloys had superior creep resistances to the H12 and H32 tempers respectively up to about 212 °F, but above 212 °F the less severely cold-rolled materials exhibited the better creep resistances.*

DATA on the creep and stress rupture properties of aluminum alloys are now available for some sheet materials in the precipitation-hardened state (1)<sup>1</sup> and annealed and cold-rolled conditions (2) as well as for some casting and forging alloys (3). In view of the increasing interest in the application of aluminum alloys to elevated temperature service, the current investigations on the creep and stress rupture of the following aluminum sheet alloys were initiated:

99.6% Al-H12<sup>2</sup>  
2S-H12  
4S-H32

99.6% Al-H18  
2S-H18  
4S-H38

Creep and stress rupture properties were evaluated at 90, 212, 300 and 400 °F and the stresses were selected so as to cause the rupture time to vary from several minutes to about 1000 hours. Some attempt was also made to stress the specimens so that creep rates as low as about  $10^{-7}$  per hour could be approximated.

The following data were obtained for each alloy that was investigated at the four temperatures which were employed in this program of research:

<sup>1</sup>The figures appearing in parentheses pertain to the references appended to this paper.

<sup>2</sup>The first digit after H indicates specific combinations of basic operations (1 represents a strain-hardened state only; 3 represents strain-hardened and then stabilized). The second digit indicates the final degree of strain hardening (2 indicates  $\frac{1}{4}$  hardened, 8 indicates fully hardened).

Of the authors, O. D. Sherby is research engineer and J. E. Dorn is professor of metallurgy, University of California, Berkeley, Calif. Manuscript received April 14, 1950.

1. Creep strain as a function of time for various appropriate stresses.
2. Stress versus the time to rupture and stress versus the secondary creep rate.

### MATERIALS

All of the 0.064-inch thick sheet materials that were used in this investigation were supplied by the Aluminum Company of America from their standard production stock. Reference to Table I reveals that the actual chemical compositions of the alloys which were inves-

**Table I**  
**Chemical Compositions of Alloys Investigated**

Alloy and Temper	Composition	Element, Per Cent							Other Elements	
		Al (Min)	Si	Fe	Cu	Mn	Mg	Zn	Each	Total
99.6% Al-H12	Actual <sup>1</sup>	....	0.07	0.26	0.004	0.003	0.003	....	<0.05	<0.15
99.6% Al-H18	Actual <sup>1</sup>	....	0.07	0.25	0.004	0.003	0.007	....	<0.05	<0.15
	Specified <sup>2</sup>	99.6	Si + Fe = <0.4		<0.05	....	....	....	<0.05	<0.15
2S-H12	Actual <sup>1</sup>	....	0.07	0.57	0.16	0.005	0.001	....	<0.05	<0.15
2S-H18	Actual <sup>1</sup>	....	0.08	0.56	0.10	0.01	0.002	<0.10	<0.05	<0.15
	Specified <sup>3</sup>	99.0	Si + Fe = <1.00		<0.20	<0.05	<0.05	<0.10	<0.05	<0.15
4S-H32	Actual <sup>1</sup>	....	0.16	0.52	0.15	1.20	0.96	0.03	<0.05	<0.15
4S-H38	Actual <sup>1</sup>	....	0.16	0.49	0.16	1.10	0.94	<0.10	<0.05	<0.15
	Specified <sup>4</sup>	....	<0.30	<0.70	<0.20	1.0-1.5	0.8-1.3	<0.10	<0.05	<0.15

<sup>1</sup>Spectrochemical analysis data furnished by the Aluminum Company of America.

<sup>2</sup>Specified values are from ASTM Specification B-178-47T.

<sup>3</sup>Specified values are from Federal Specification QQ-A-561A and Navy Department Specification 47A3E. The latter specification, however, permits 0.25% maximum zinc.

<sup>4</sup>Specified values are from ASTM Specification B-209-48T.

tigated are within the various specification limits that have been established.

An effort was made to select materials whose mechanical properties were in close agreement with typical values for commercial stock. For purposes of characterizing the material, the actual mechanical properties were determined as recorded in Table II. A comparison of the actual values with the specified values reveals that these materials fall within the limits of the specifications. Microstructures in both the longitudinal and transverse directions were found to be normal and representative of commercial sheet materials of the respective alloys and tempers.

### EXPERIMENTAL TECHNIQUE AND TESTING PROCEDURES

A detailed description of the creep equipment and methods of testing has been presented in previous reports (1, 2) and will not be repeated here. Sheet specimens of the design shown in Fig. 1 were



**Table II**  
**Mechanical Properties**

Alloy and Temper	Properties	Longitudinal				
		Tensile Strength psi	Tensile Yield Strength <sup>1</sup> psi	Elong. in 2 In. %	Compressive Yield Strength <sup>1</sup> psi	Shearing Strength psi
99.6% Al-H12	Actual	13,000	12,400	13.0	10,800	9,200
	Specified <sup>2</sup>	11,000	.....	12.0	.....	.....
99.6% Al-H18	Actual	23,100	21,400	7.8	17,600	12,700
2S-H12	Actual	15,300	14,800	10.8	12,700	10,800
	Specified <sup>3</sup>	14,000	.....	8.0	.....	.....
	Typical <sup>5</sup>	15,500	14,000	12.0	.....	10,000
2S-H18	Actual	25,600	23,800	5.5	21,100	14,400
	Specified <sup>3</sup>	22,000	.....	4.0	.....	.....
	Typical <sup>5</sup>	24,000	22,000	5.0	.....	13,000
4S-H32	Actual	32,500	27,700	8.8	23,400	18,800
	Specified <sup>4</sup>	28,000	.....	5.0	.....	.....
	Typical <sup>5</sup>	31,000	22,000	10.0	.....	17,000
4S-H38	Actual	45,000	42,400	7.8	37,300	24,800
	Specified <sup>4</sup>	38,000	.....	4.0	.....	.....
	Typical <sup>5</sup>	40,000	34,000	5.0	.....	21,000
		Transverse				
99.6% Al-H12	Actual	12,600	12,000	10.0	13,000	.....
99.6% Al-H18	Actual	24,000	21,000	5.8	22,400	.....
2S-H12	Actual	16,200	15,400	8.2	15,800	.....
2S-H18	Actual	26,400	24,200	5.2	25,200	.....
4S-H32	Actual	32,400	24,900	8.2	26,200	.....
4S-H38	Actual	45,200	40,800	7.5	45,600	.....

<sup>1</sup>Offset equals 0.2%.

<sup>2</sup>Specified values are from ASTM Specification B-178-47T.

<sup>3</sup>Specified values are from Federal Specification QQ-A-561A and Navy Department Specification 47A2E.

<sup>4</sup>Specified values are from ASTM Specification B-209-48T.

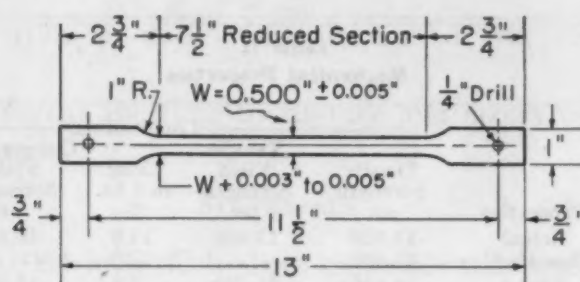
<sup>5</sup>Typical values are from "Alcoa Aluminum and Its Alloys", 1947 edition.

prepared with the long axis of the specimen in the rolling direction. The rack and pinion type of extensometers that were used permitted the evaluation of strains over the 6-inch long gage section to be determined within  $\pm 0.00008$ . Each specimen was mounted in the furnace approximately 1 hour prior to the time of application of the load in order to permit the specimen to acquire the testing temperature before subjecting it to creep.

### EXPERIMENTAL RESULTS

All of the creep strain versus time data were originally plotted on cartesian coordinate paper to facilitate the evaluation of the secondary creep rate and the creep intercept. Three typical creep curves of this type are shown in Fig. 2. At the higher stresses and temperatures, creep curves of the type shown in Fig. 2A were obtained. Here, following the initial primary stage of creep, a short secondary stage is noted wherein the strain increases almost linearly with the





Gage Length: 6 Inches

Sheet Thickness: 0.064 In. (Nominal)

Direction of Stress: With Grain

Taper: Gradual Taper From Ends of Reduced Section to Middle

Fig. 1—Stress Rupture and Creep Specimen.

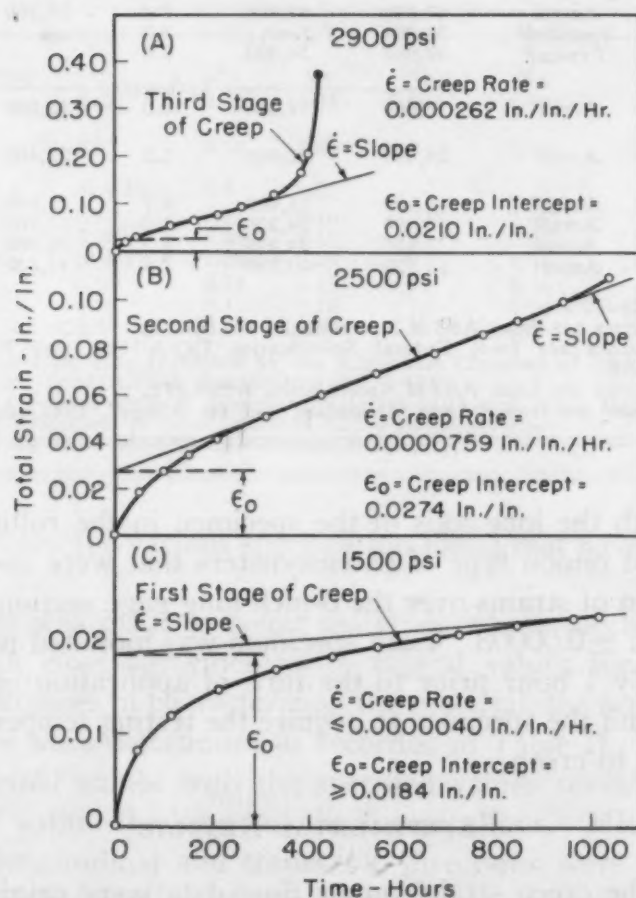


Fig. 2—Creep Curves of 2S-H18 Alloy at 400 °F  
Typifying the Three Stages of Creep.

time. After the short secondary creep stage there is a rapid transition to the tertiary stage which is terminated by rupture. The rupture point is designated by the solid circle at the end of the curve. Curves of the type shown in Fig. 2B were obtained at lower

stresses and at lower temperatures. Here, the primary stage of creep, giving a monotonically decreasing creep rate, is extended over a longer time interval; the secondary stage of creep, exhibiting almost a constant creep rate, becomes well defined and finally the increasing creep rate of the third stage is obtained. At the higher stress levels and temperatures, the third stage of creep terminated in rupture, but at the lower values of stress and temperatures the tests were discontinued at 1000 hours, as shown in Fig. 2B, before rupture occurred.

Some attempt was made to obtain data yielding secondary creep rates approximating  $10^{-7}$  per hour. However, when lower stresses or lower temperatures are applied, the primary stage of creep often extends beyond 1000 hours. As shown in Fig. 2C, it is only possible to state that the secondary creep rate is less than some estimated value approximating the minimum creep rate which was observed.

#### DISCUSSION OF RESULTS

Curves of the logarithm of the creep strain versus the logarithm of the time were plotted in order to permit rapid comparison of all of the original creep data as shown in Figs. 3 to 8. In addition, conventional logarithmic curves of the stress versus the secondary creep rate and the stress versus the time to rupture are recorded for each alloy that was investigated in Figs. 9 to 14. Most of these data are satisfactorily self-consistent, with the possible exception of those for Al-H12 alloy which exhibited some scatter. The reason for this scatter is not known but it is significant to note that Al-H18, which yielded very consistent creep data, was rolled from the same ingot from which the Al-H12 material was prepared.

At 90 °F the harder rolled Al-H18 alloy withstood higher creep stresses than the less severely cold-rolled Al-H12 alloy at the same secondary creep rates. But the stress versus secondary creep rate curve for harder rolled Al-H18 alloy decreases more rapidly with decreasing creep rate than the curve for Al-H12 alloy. The data indicate that the two curves not only converge but actually cross each other at a secondary creep rate of somewhat less than  $10^{-7}$  per hour, so that at yet slower secondary creep rates, the softer rolled Al-H12 might actually resist higher stresses at the same strain rate than the harder rolled Al-H18 alloy.

The inversion of the creep resistance as a function of the secondary creep rate for the two differing tempers of cold-rolled aluminum is clearly demonstrated by the data at 212 °F. Whereas the harder rolled Al-H18 will resist higher stresses for the same secondary creep rate than the softer rolled Al-H12 alloy for all secondary creep

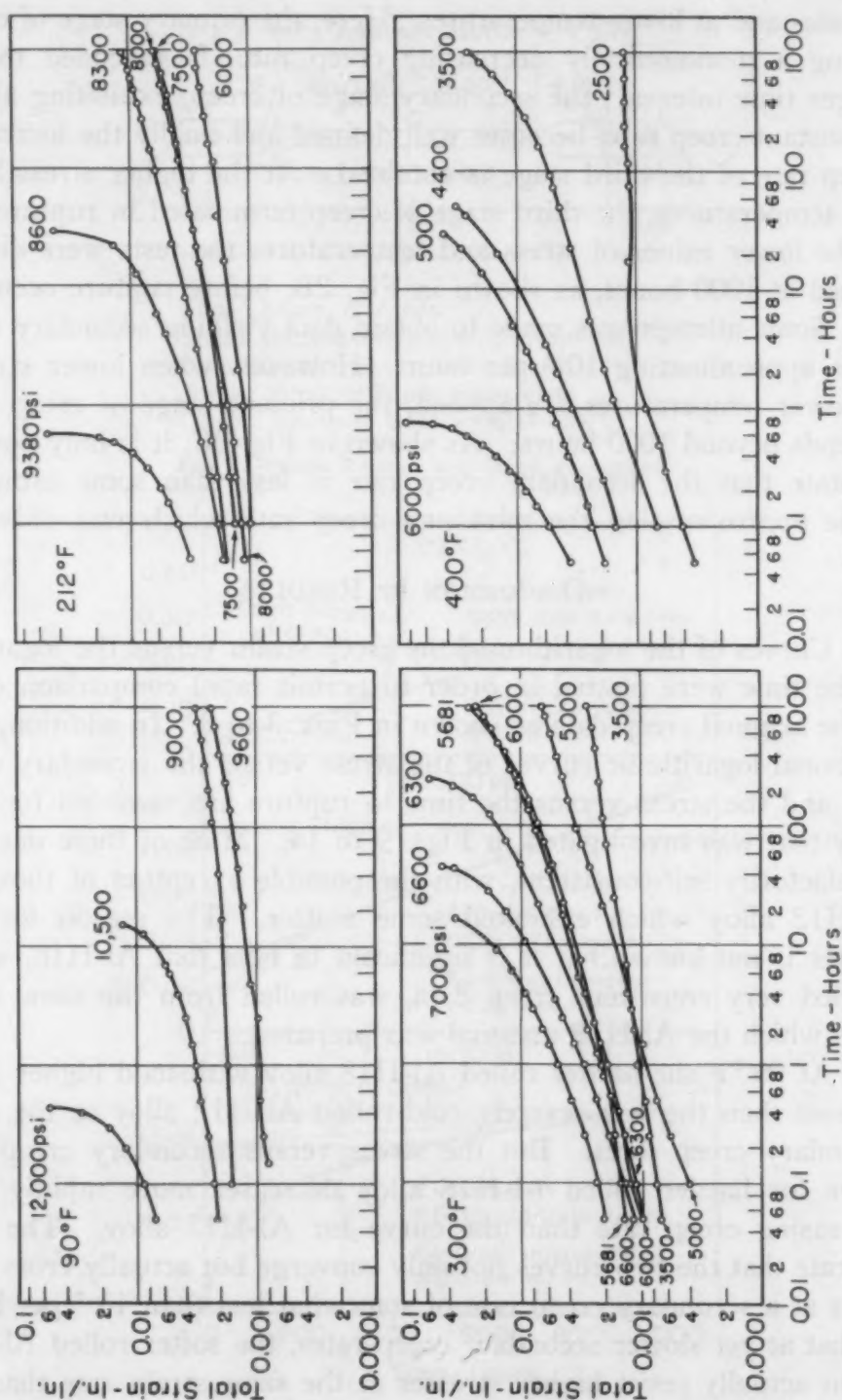


Fig. 3—Total Creep Strain as a Function of Time for 99.6% Al-H12 Alloy.

rates above about  $6 \times 10^{-6}$  per hour, the softer rolled Al-H12 alloy will resist higher stresses than the Al-H18 alloy for all lower secondary creep rates which were investigated.

At successively higher temperatures the transition secondary creep rate (above which the harder rolled material is superior to the

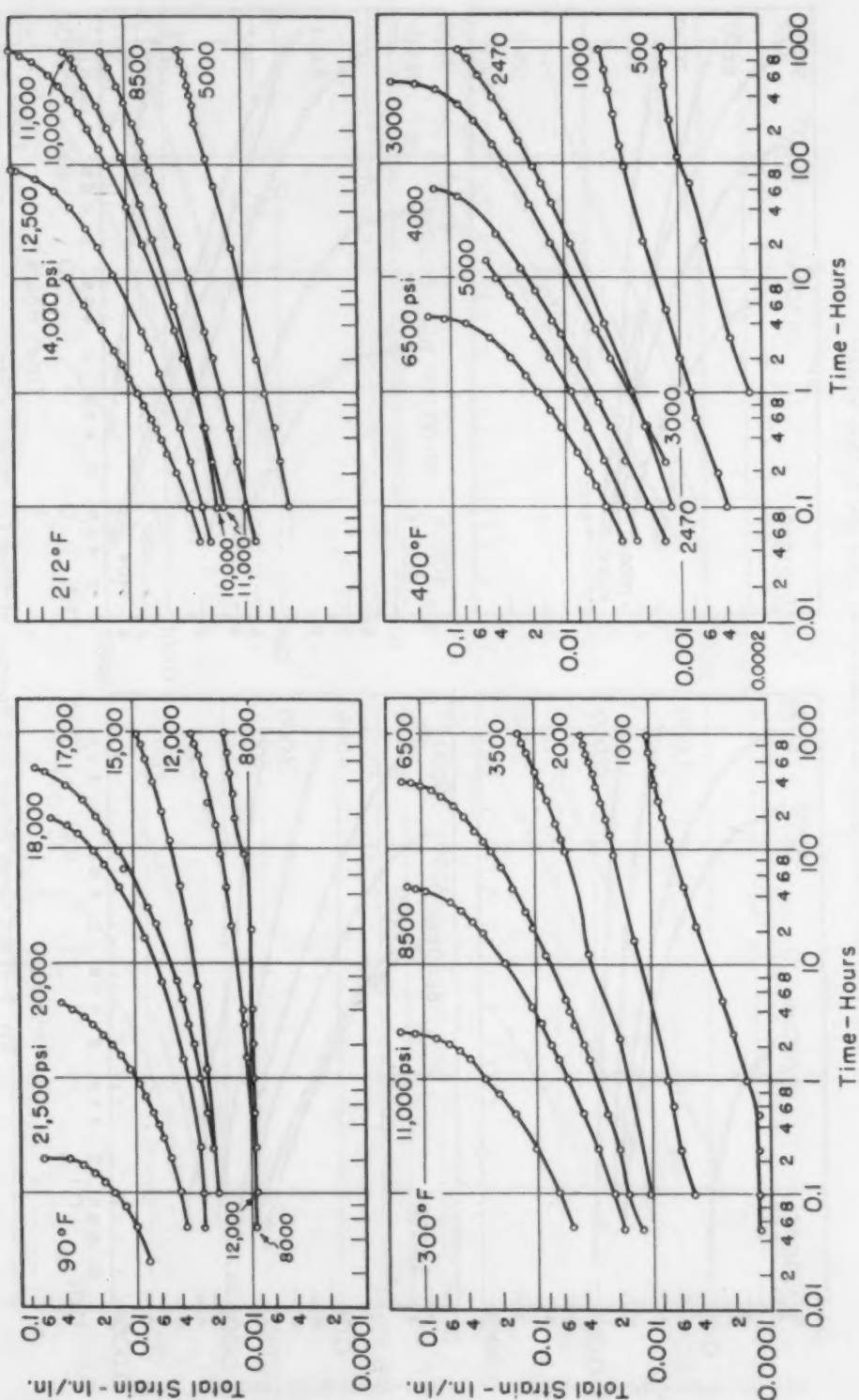


Fig. 4—Total Creep Strain as a Function of Time for 99.6% Al-H18 Alloy.

less severely cold-rolled stock and below which the less severely cold-rolled stock resists higher stresses for the same secondary creep rate than the harder rolled material) shifts to higher values. This trend is plotted in Fig. 15. It is interesting to note that the relationship



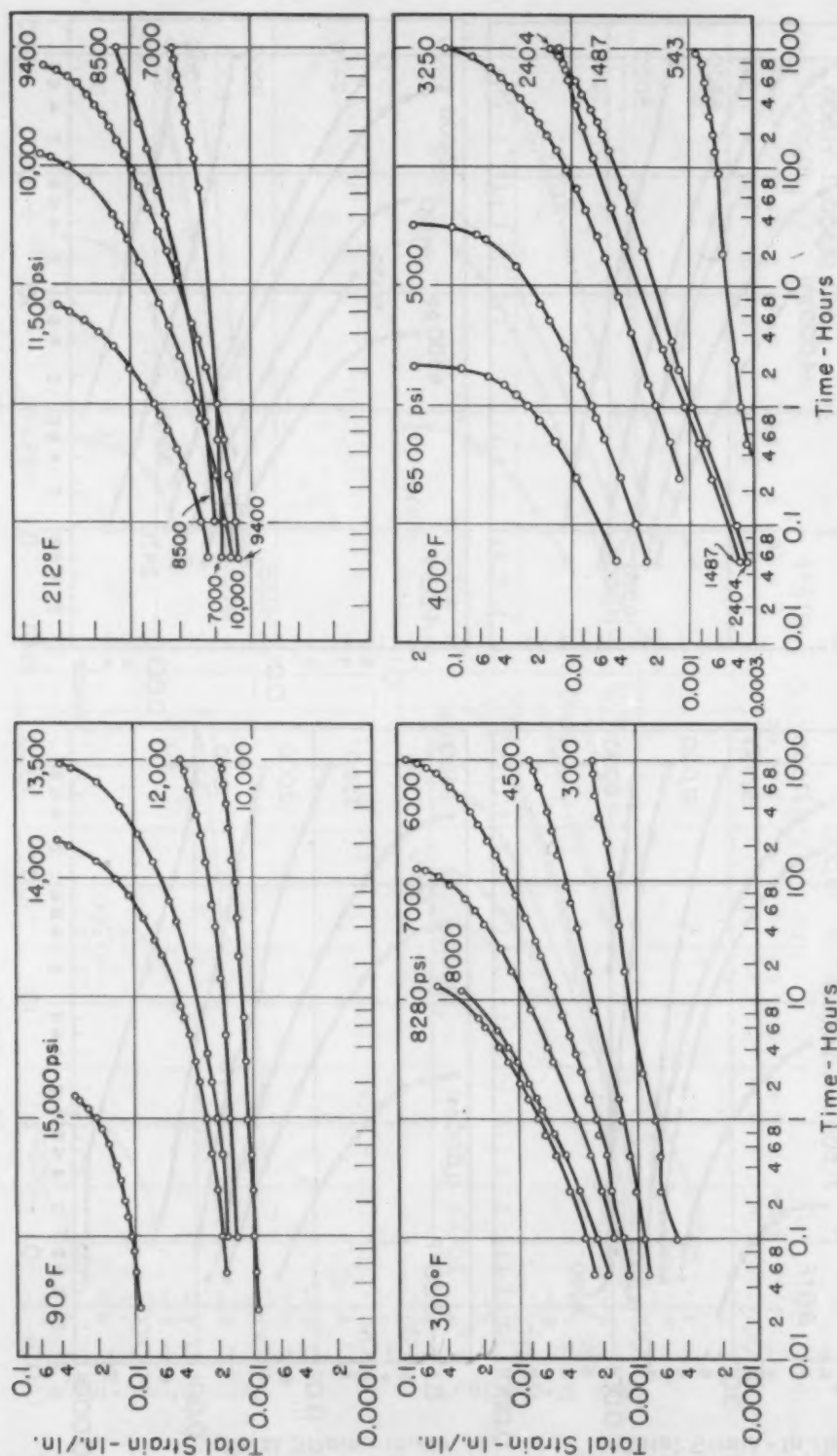


Fig. 5—Total Creep Strain as a Function of Time for 2S-H12 Alloy.

between the temperature and the strain rate at which inversion in the relative creep resistances of Al-H12 and Al-H18 alloys occurs is given by an equation of the form

$$\dot{\epsilon} e^{Q/RT} = \text{Constant}$$

Equation 1

as shown by the linear curve of Fig. 15.

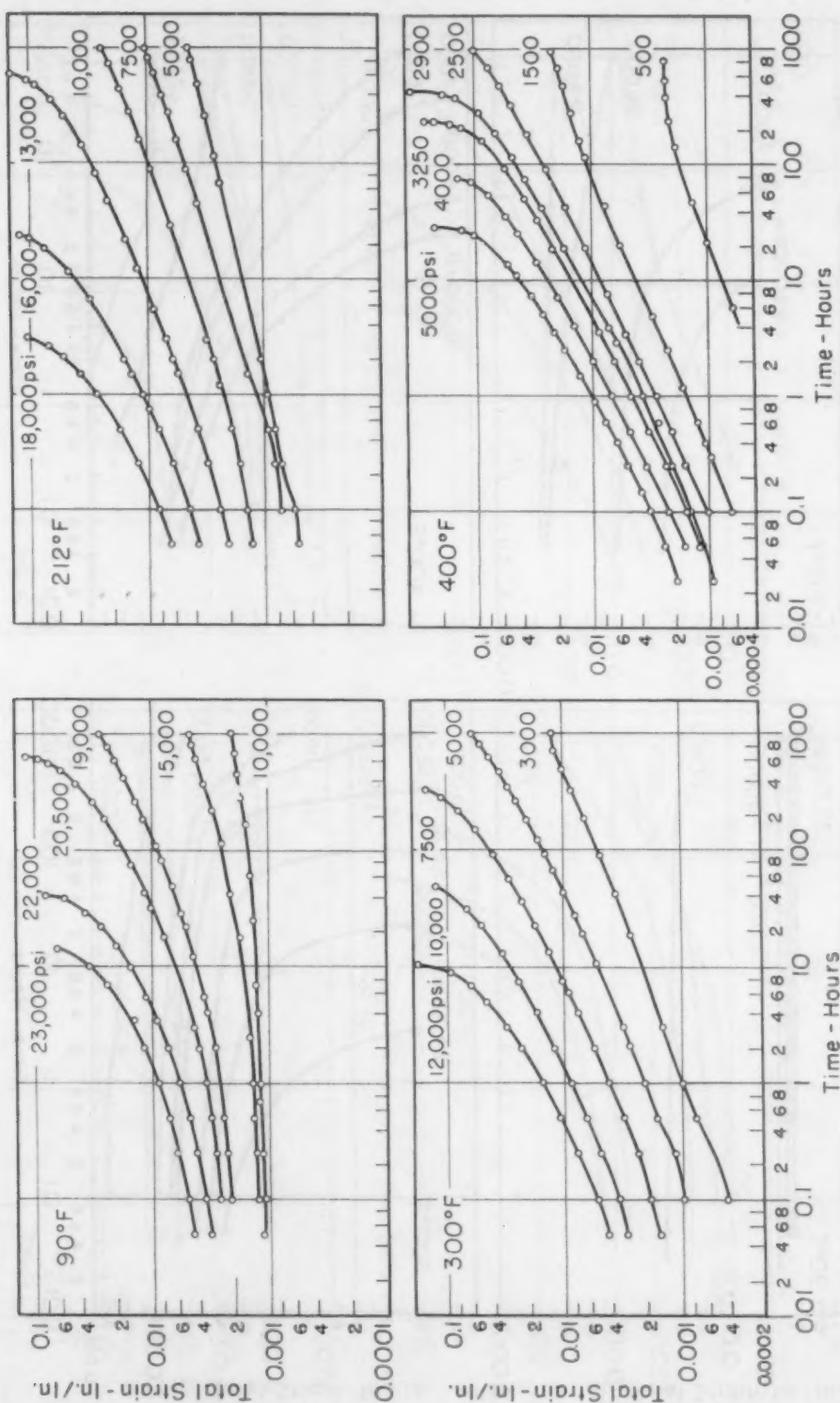


Fig. 6—Total Creep Strain as a Function of Time for 2S-H18 Alloy.

Undoubtedly the creep data recorded here for Al-H12 and Al-H18 are somewhat affected by recovery and possibly recrystallization even at the lowest temperature of 90 °F. It is not easily possible, however, to ascribe the inversion in the creep resistances of

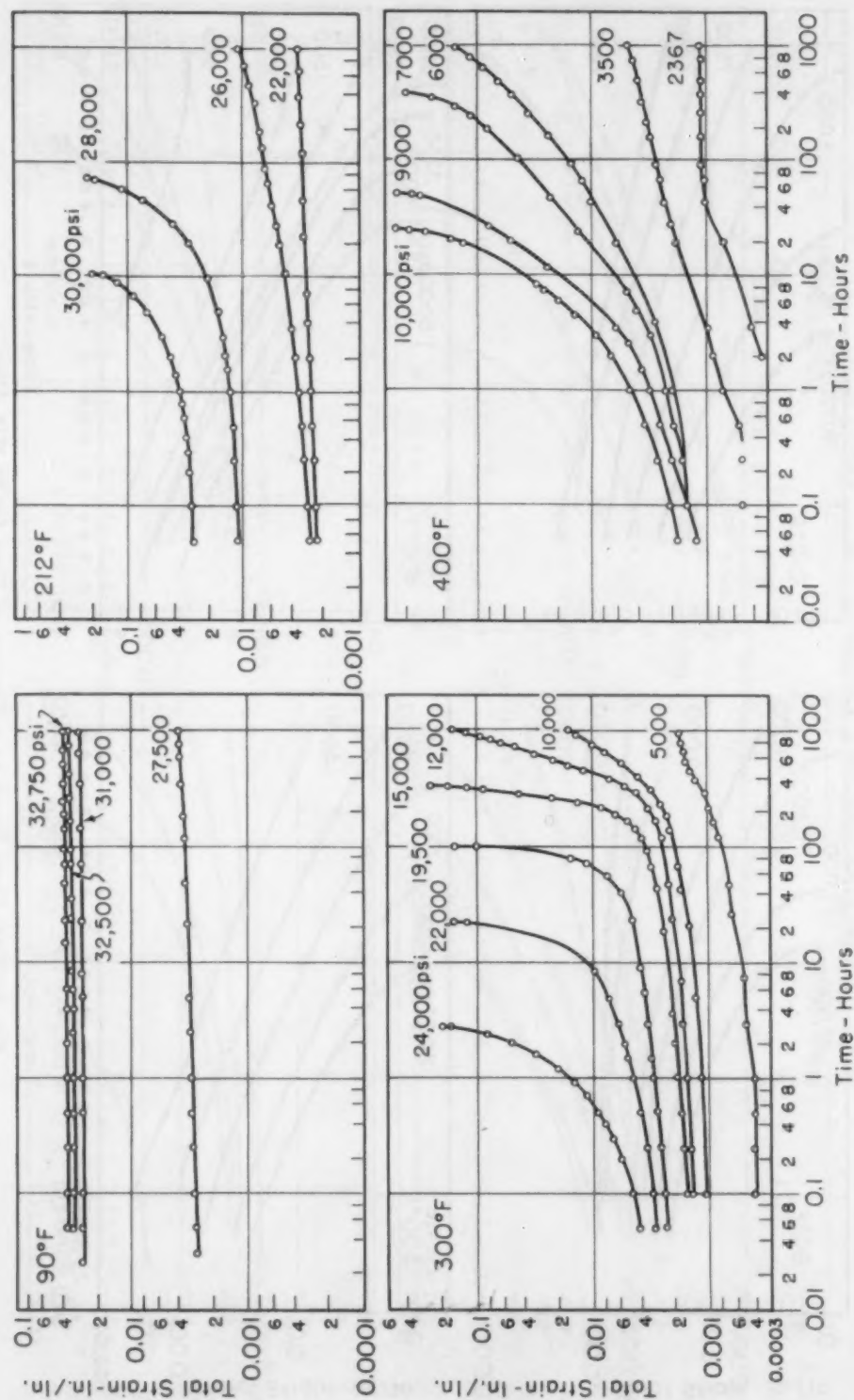


Fig. 7—Total Creep Strain as a Function of Time for 4S-H32 Alloy.

Al-H12 and Al-H18 exclusively to these phenomena. Although the recovery rate of Al-H18 might initially exceed that of Al-H12 because of its initially higher cold-worked state, it is inconceivable that as the two strain-hardened states begin to approximate each other,

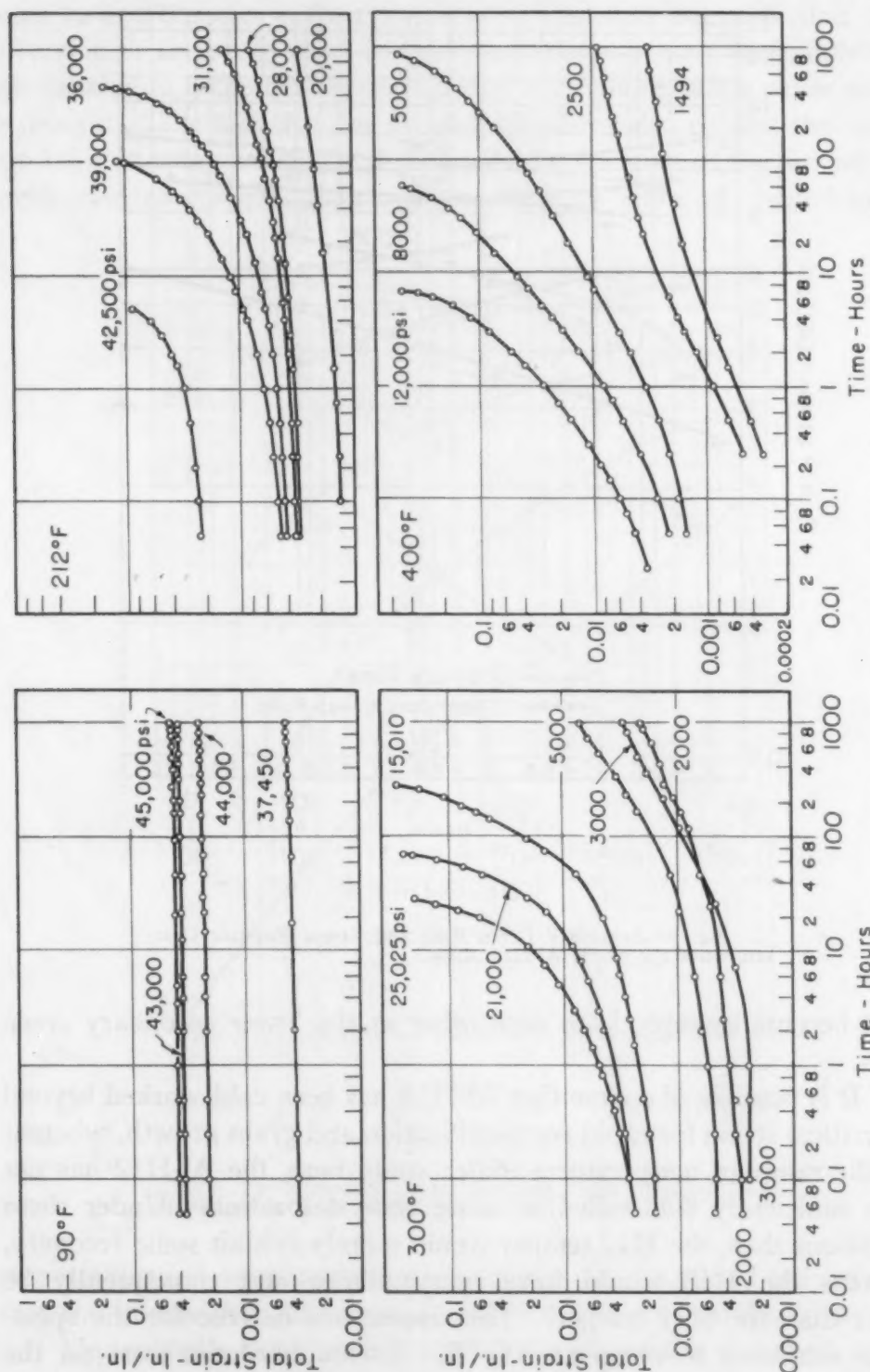


Fig. 8—Total Creep Strain as a Function of Time for 4S-H38 Alloy.

the softening rate of Al-H18 will continue to exceed that of Al-H12 so that eventually Al-H18 will become softer than that of Al-H12. Reflections on recovery therefore suggest that the creep resistances of an alloy in two different initial work-hardened states should at



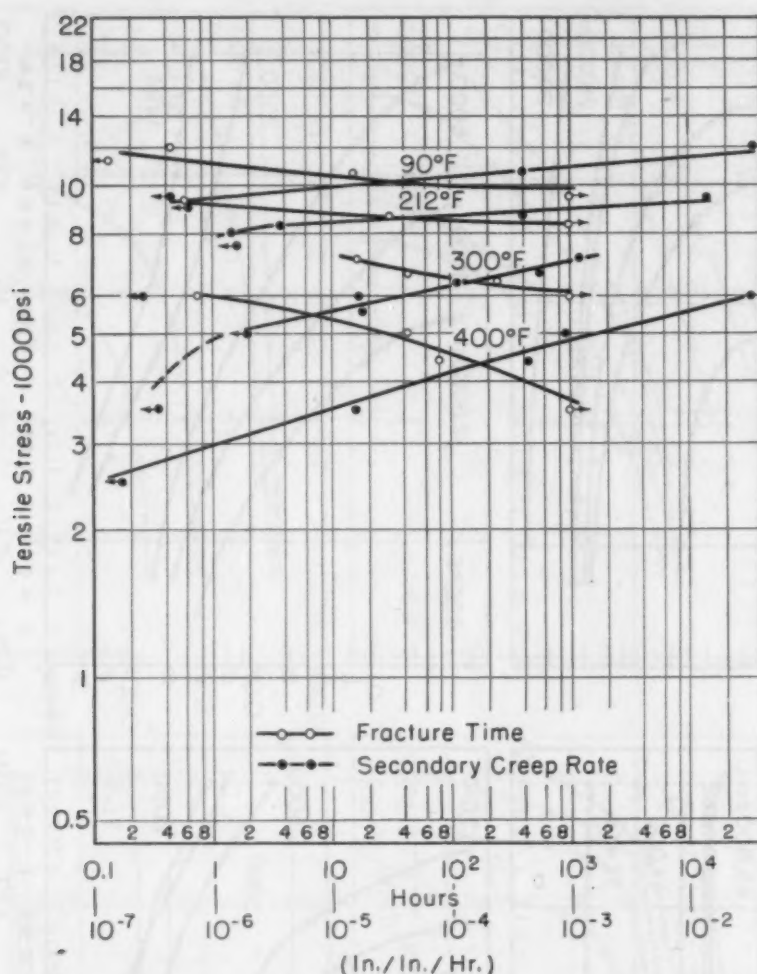


Fig. 9—Secondary Creep Rate and Stress Rupture Characteristics for 99.6% Al-H12 Alloy.

most become asymptotic to each other at the lower secondary creep rates.

It is possible of course that Al-H18 has been cold-worked beyond the critical strain for rapid recrystallization and grain growth, whereas for the range of temperatures under study here, the Al-H12 has not been sufficiently cold-rolled to cause recrystallization. Under these conditions then, the H12 temper would merely exhibit some recovery, whereas the H18 would have recrystallized and consequently be softer than the H12 temper. This appears to be true for the specimens subjected to creep at 400 °F. Knoop hardness tests on the specimens after creep at this temperature reveal that the hardness of all of the H18 specimens was measurably lower than that for the H12 specimens. But at 300 °F and at all lower temperatures the H18 temper material remained harder than the H12 temper even over the range of secondary creep rates where the H18 had lower resist-

ance to a creep stress than the H12. This fact suggests that the inversion in the creep rates of the two tempers cannot be completely attributable to recrystallization and that some more subtle cause must be sought. The fact that the 2S and 4S alloys also exhibit the same inversion of creep resistance at about the same values of the secondary creep rate as the 99.6% aluminum alloy in spite of their higher

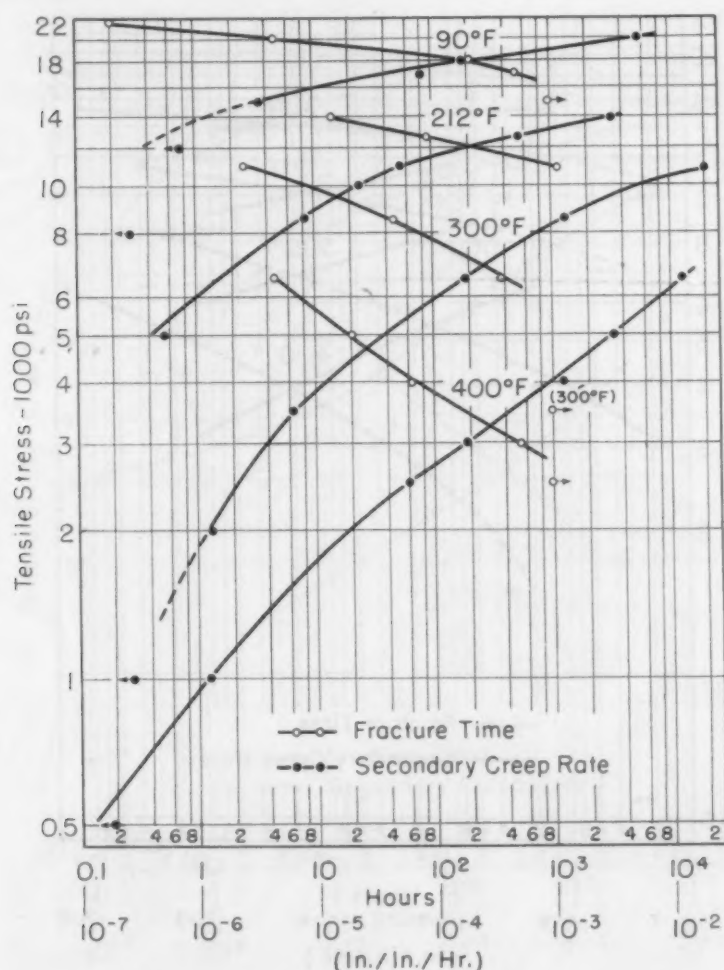


Fig. 10—Secondary Creep Rate and Stress Rupture Characteristics for 99.6% Al-H18 Alloy.

recrystallization temperatures also appears to disqualify the concept that the inversion in creep resistance is due to recrystallization.

Undoubtedly the elucidation of the origin of the observed inversion phenomenon will require further extensive investigations. It is nevertheless interesting to reflect on possible explanations of inversion. One theory which appears to be consistent with many of the current observations assumes that cold rolling modifies in some way the crystal structure so as to give the metal higher resistance to higher

creep rates but lower resistance to slower creep rates. This explanation of course could not be true if creep occurred by a single mechanism. But if two mechanisms of creep do occur and one predominates at the higher creep strain rates, whereas another predominates at the lower creep strain rates, the observed inversion becomes feasible. Under these conditions the microstructural changes attending

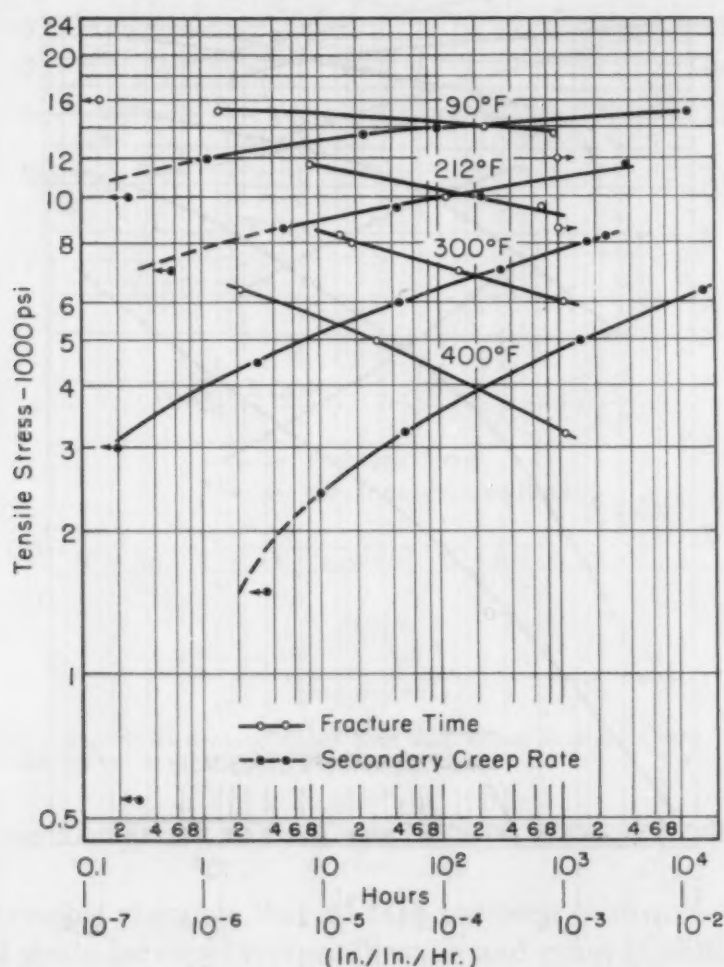


Fig. 11—Secondary Creep Rate and Stress Rupture Characteristics for 2S-H12 Alloy.

cold rolling and annealing cause the resistance to creep by the first mechanism at high creep rates to increase, whereas the same or other microstructural changes attending cold rolling and annealing cause the creep resistance by the second mechanism at slow creep rates to decrease. Furthermore, this effect would not only cause the stress - creep rate curves for the harder rolled material to intersect with those for the less severely cold-rolled material, but it would also cause the stress - creep rate curves of the harder rolled material to be steeper

than those of the softer rolled material, in agreement with the current observations. Of course, the greater steepness of the creep curves for the harder rolled stock might also be partially attributable to higher recovery or recrystallization rates it might undergo. Added weight to the possible value of the proposed theory for inversion is gained from recent investigations by Wood (4) who has reported two distinctly different mechanisms for creep of aluminum. At low

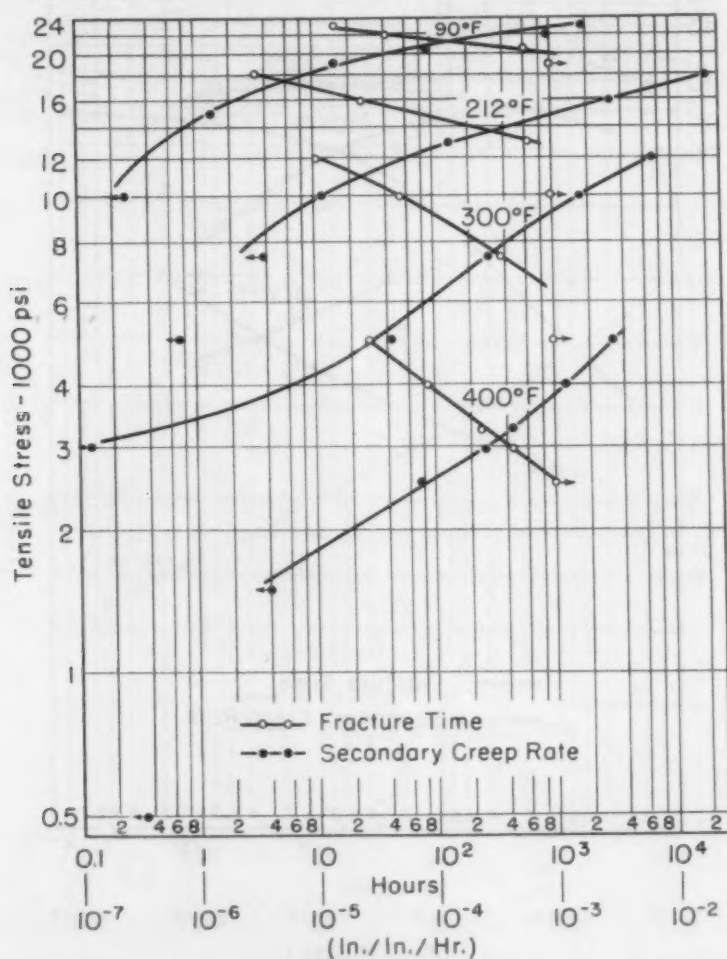


Fig. 12—Secondary Creep Rate and Stress Rupture Characteristics for 2S-H18 Alloy.

temperatures creep appears to be predominantly a slip mechanism, whereas at elevated temperatures slip is repressed and the creep strain is primarily attributable to rotation of elements of a substructure within the grain. If these mechanisms are stimulated by activation processes, it necessarily follows that decreasing the strain rate has an analogous effect to increasing the temperature. Thus, the transition from the low temperature mechanism to the high temperature mechanism should be shifted to higher secondary creep rates at the



higher temperatures in complete accord with the shift in the inversion conditions which are shown in Fig. 15.

Although the proposed theory for the inversion of the creep resistance of Al-H12 and Al-H18 appears valid and interesting, additional confirmation will be required before its unqualified acceptance is justified. For example, recent observations on the damping capac-

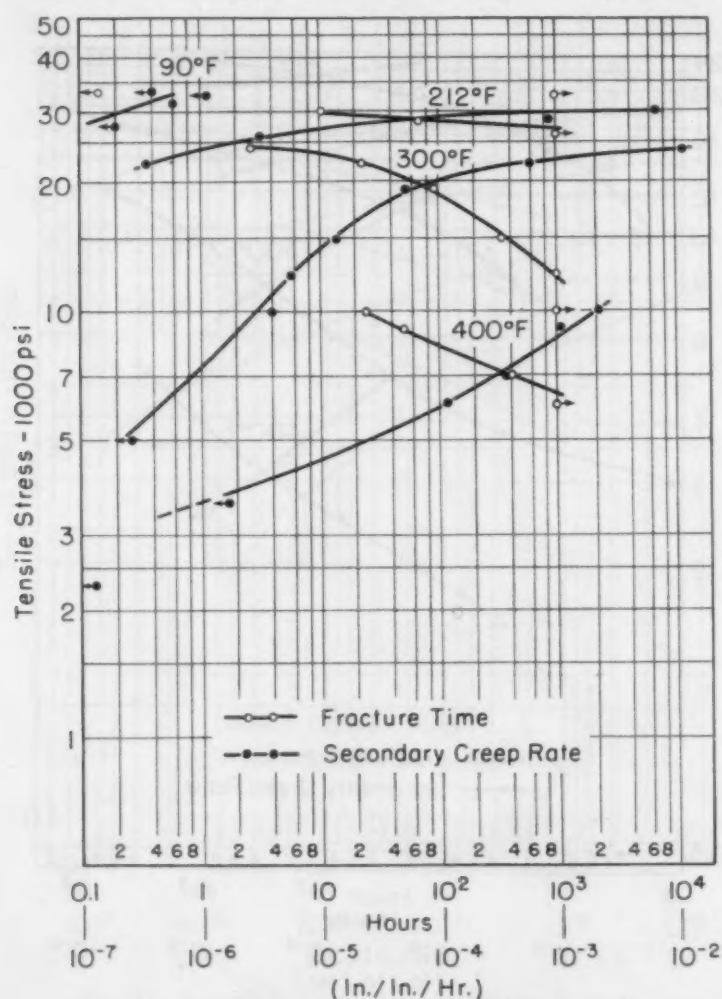


Fig. 13—Secondary Creep Rate and Stress Rupture Characteristics for 4S-H32 Alloy.

ity of aluminum by Kê (5) reveal that the more severely cold drawn aluminum wire has lower viscous-like resistance to grain boundary rotation or shear than less severely cold drawn wire, even after complete recrystallization and correction for the grain size differences. Consequently, the effects of cold work on grain boundary shear strains are retained, even after recrystallization. If it could be demonstrated that the effects observed by Kê are attributable to the boundaries of the elements of the substructure within the grains

detected by Wood, the present observations on the effect of cold work on the secondary creep rate would be materially clarified.

The alloy pair 2S-H12 and 2S-H18 as well as the pair 4S-H32 and 4S-H38 also exhibit evidence of inversion as shown by comparison of the data in Figs. 11 and 12 as well as those in Figs. 13 and 14. In general, 2S-H18 alloy has superior creep resistance to 2S-H12

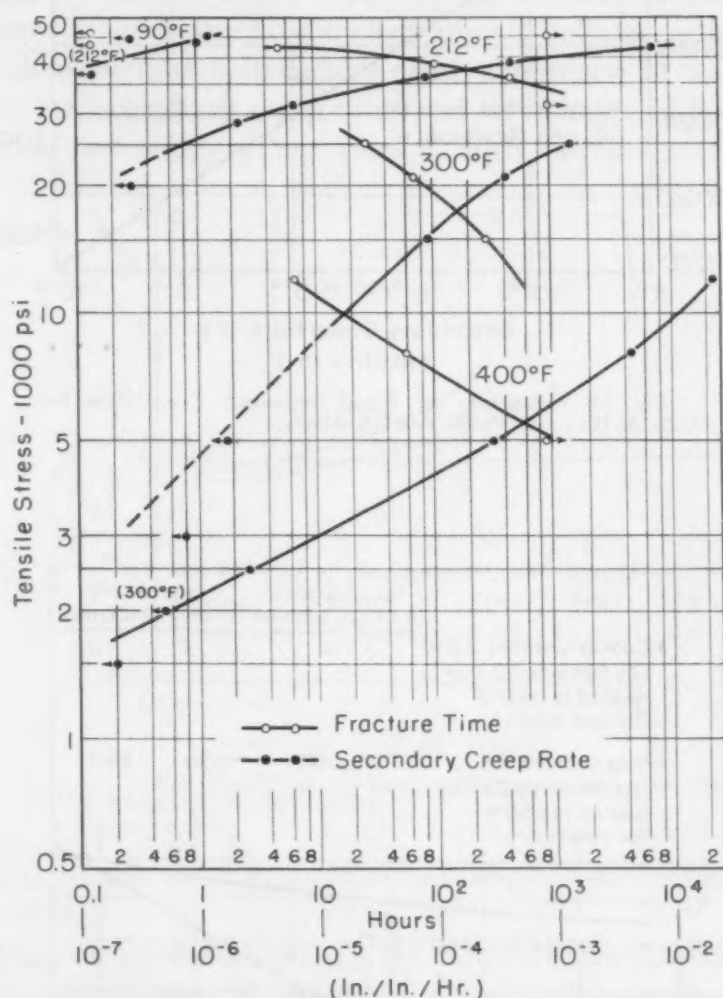


Fig. 14—Secondary Creep Rate and Stress Rupture Characteristics for 4S-H38 Alloy.

alloy at 90, 212 and 300 °F over the range of secondary creep rates which were investigated. At 400 °F, however, 2S-H12 has slightly higher creep resistance than 2S-H18. The 4S-H38 alloy has better creep resistance than 4S-H32 at 90 and 212 °F. At 300 and 400 °F, 4S-H32 is superior to 4S-H38 in creep resistance.

Obviously many factors play a role in determining the creep rates of metals and it is not always possible to isolate the effects of each factor, or to attribute observed effects unquestionably to one or

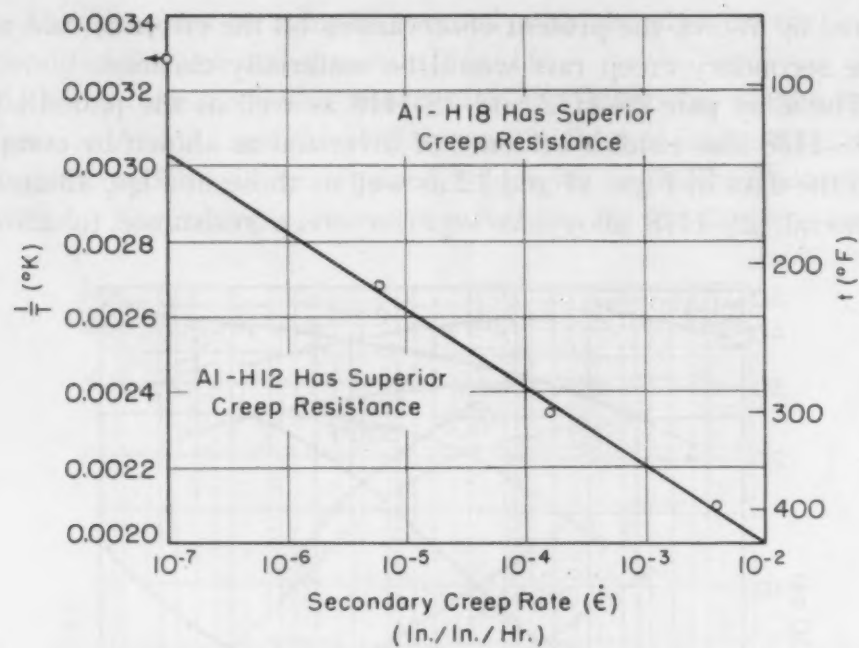


Fig. 15—Conditions for Equal Secondary Creep Rate for 99.6% Al-H12 and 99.6% Al-H18 Alloys.

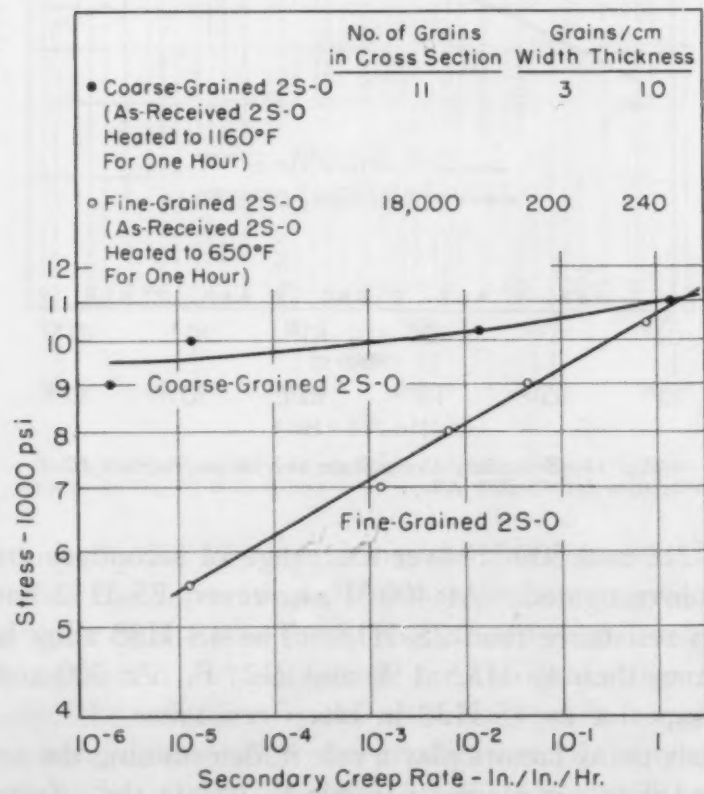


Fig. 16—Comparison of the Creep Properties of Fine and Coarse-Grained 2S-O Aluminum at 212 °F.

another factor. Investigations (6) have shown that grain size of 2S-O might influence its creep rate materially. As shown in Fig. 16, the coarser-grained 2S-O alloy has a higher resistance to creep than the finer-grained 2S-O at all conditions which were investigated. But the data clearly indicate that the finer-grained 2S-O alloy has a higher creep resistance than the coarse-grained 2S-O alloy at creep rates in excess of about 1.5 per hour. Thus the effect of finer grain size is somewhat analogous to the effect of cold rolling on the creep properties, inasmuch as both factors cause a decrease in the creep resistance at low secondary creep rates and an increase in creep resistance at higher secondary creep rates. Such parallel trends might be

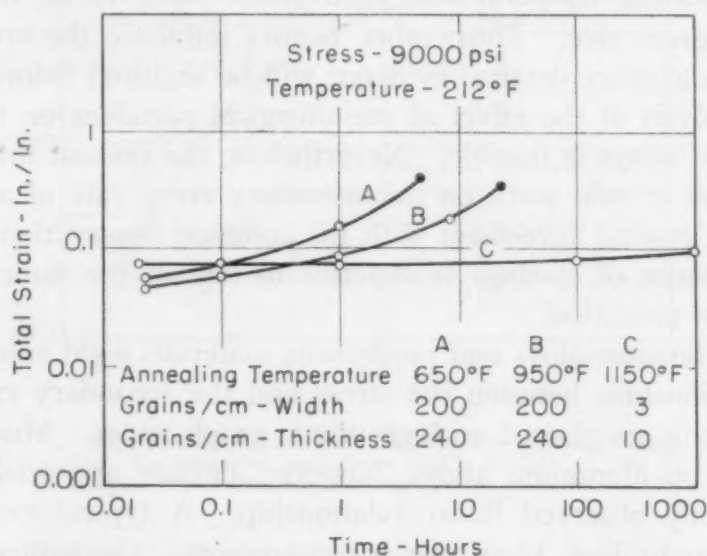


Fig. 17—Effect of Annealing Temperature on the Creep Resistance of 2S-O Alloy.

ascribed to the finer grain size resulting from fragmentation upon cold rolling.

Factors other than grain sizes, however, are also known to affect the creep properties of aluminum alloys. This is illustrated by the creep curves for 2S-O alloy at 212 °F and a stress of 9000 psi as shown in Fig. 17. Specimens A, B, and C were annealed respectively, for about 1 hour, at 650, 950 and 1150 °F (345, 510 and 620 °C) before the creep tests were made. Although specimen C had relatively coarse grains following the annealing treatment, specimens A and B exhibited approximately the same grain size. The creep curves of the fine-grained specimens A and B are distinguished from those of the coarse-grained specimen C in accordance with the general observations of effect of grain size on the creep properties of metals; whereas the initial creep strain for the coarse-grained speci-



men C was greater than that for the finer-grained specimens, B and C, the creep rate was less and consequently the total creep strain for the coarser-grained specimen, C, was less than those for the finer-grained specimens beyond about 0.3 hours. But in spite of the fact that specimens A and B exhibited about the same grain sizes, the creep curve for specimen B, which was annealed at the higher temperature, fell below that for specimen A. Similar differences between the creep data of specimens A and B were also obtained from tests performed at 400 °F (205 °C) and stresses of 3000 and also 5000 psi. Consequently, the annealing temperature itself modifies the structure of metals in such a way as to induce higher creep resistance for the higher annealing temperatures, even when there is no observable change in grain size. Thus, other factors influence the creep rates of metals, and more detailed evidence will be required before a satisfactory analysis of the effect of metallurgical variables on the creep resistance of alloys is feasible. Nevertheless, the present information on the effect of cold work on the secondary creep rate of aluminum alloys is in general agreement with the common observation that the creep resistance of castings is superior to that of the same alloy in the wrought condition.

Many ferrous alloys and nonferrous materials yield substantially linear relationships between the stress and the secondary creep rate when the data are plotted on logarithmic graph paper. Much of the creep data on aluminum alloys, however, deviate appreciably from the commonly observed linear relationship. A typical example of this is given in Fig. 13 of the present report. Consequently, any extrapolation of these data, and, therefore, presumably any other creep data, beyond the range of investigation must be done judiciously and with caution. If a satisfactory theory of creep were available, it would be possible to establish more accurate methods of extrapolation. The first step in this direction concerns possible causes of the nonlinearity of the logarithm of the stress versus the logarithm of the secondary creep rate. Of course, metallurgical instability resulting in overaging, recovery and recrystallization will be less complete under the higher secondary creep rates; consequently, when materials that exhibit these phenomena are subjected to successively lower secondary creep rates the stresses might well decrease more rapidly than linearly, on logarithmic plots. But there is some justification in believing that, even in the absence of such structural instability, nonlinear creep curves will be obtained.

The linear logarithmic plots suggest that the stress is related to the secondary creep rate by the equation

$$\dot{\epsilon} = A \sigma^n$$

Equation 2

where  $A$  and  $B$  are parameters, whereas reaction rate theory (7) suggests that the relationship in its simplest formulation be somewhat analogous to

$$\dot{\epsilon} = A \sinh B\sigma \quad \text{Equation 3}$$

where  $A$  and  $B$  are parameters that are functions of the temperature and the state of the metal during secondary creep. Although some evidence exists which suggests that  $A$  and  $B$  change with differing

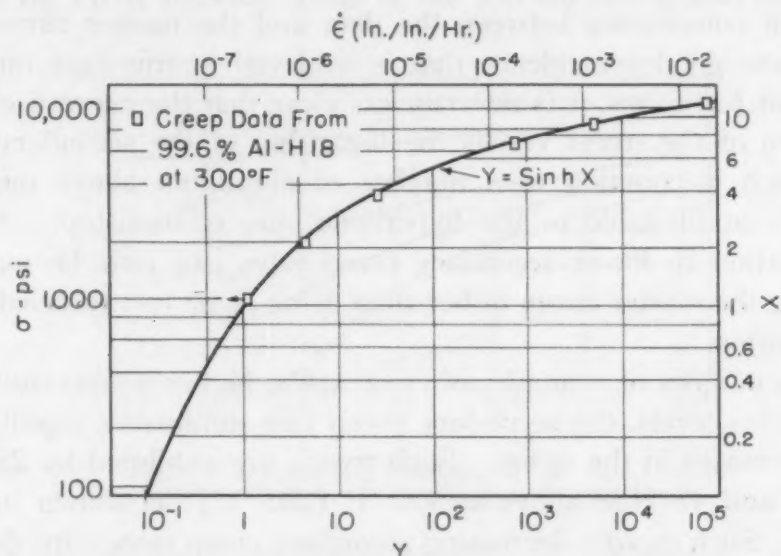


Fig. 18—Hyperbolic Sine Relationship on Logarithmic Paper. Experimental data from 99.6% Al-H18 at 300 °F is compared with theoretical curve.

values of  $\dot{\epsilon}$ , even for the same test temperature, it will be convenient to assume for the present that such changes will not seriously modify the pattern of the relationship given in Equation 3 between  $\dot{\epsilon}$  and  $\sigma$ . Consequently, the simplification that  $A$  and  $B$  are substantially constant for a constant test temperature will be invoked here. Deviations from this assumption will not seriously alter the conclusions to be developed in the following argument.

In Fig. 18 is shown a plot of

$$y = \sinh x \quad \text{Equation 4}$$

on logarithmic coordinates as given by the solid line. A comparison of Equations 3 and 4 reveals that

$$\frac{\dot{\epsilon}}{A} = y \text{ and } B\sigma = x$$

Consequently,

$$\log \dot{\epsilon} = \log y + \log A$$

and

$$\log \sigma = \log x - \log B$$

Therefore, a  $\log \sigma$  versus  $\log \dot{\epsilon}$  curve should have the same general shape of the  $\log y$  versus  $\log x$  curve except that its origin is shifted on the  $y$  scale by  $\log A$  and on the  $x$  scale by  $-\log B$ . If then  $\sigma$  versus  $\dot{\epsilon}$  were also plotted on Fig. 18, it should be possible to shift this plot vertically and horizontally until these data fit the solid master curve.

For purposes of illustration the data for Al-H18 at 300 °F (150 °C) were plotted on the same scale as Fig. 18 and then shifted to permit coincidence between the data and the master curve. Although the good coincidence that is achieved in this case might be somewhat fortuitous, it is nevertheless clear that the curvature in the logarithm of the stress versus the logarithm of the secondary creep rate which is common to a number of aluminum alloys might be primarily attributable to the hyperbolic sine relationship. A safer extrapolation to lower secondary creep rates can now be made by following the master curve rather than using some less justified linear extrapolation.

In a number of examples of creep at the higher temperatures and lower stress levels, the secondary creep rate diminishes rapidly with small decreases in the stress. Such trends are exhibited by 2S-H18, 4S-H32 and 4S-H38 alloys at 400 °F (205 °C), as shown in Figs. 12 to 14. Such rapidly decreasing secondary creep rates with decreasing stresses might at first appear to disqualify the hyperbolic sine law, since this relationship demands an almost linear decrease in the logarithm of the secondary creep rate with a decrease in the logarithm of the stress at the lower stress levels as shown in Fig. 18. Although the actual cause for this effect has not yet been uncovered, it is possible that such data are merely reflections of the existence of a threshold stress below which a secondary creep rate is not achieved. The fact that this effect has only been detected at the lowest stress levels in part supports this thesis. Furthermore, it is well known that the second law of thermodynamics demands a threshold value of the stress in cases where irreversible changes in the microstructure attend deformation. Consequently, the theoretical justification for the existence of a threshold stress for secondary creep is well established, even though such a value has not yet been found experimentally.

If a threshold stress for secondary creep be admissible, Equation 3 would be rewritten as

$$\dot{\epsilon} = A \sinh B (\sigma - \sigma_0) \quad \text{Equation 5}$$

in its simplest form where  $\sigma_0$  is the threshold stress level. That such a relationship causes a rapid decrease in the secondary creep rate



with decreasing stress analogous to that which has been observed for some aluminum alloys is shown by the curves of Fig. 19.

In conclusion it is necessary to emphasize the crudity and simplicity of the analyses that were presented. First, the data are not quite suitable for theoretical analyses inasmuch as they refer to constant load rather than constant true stress conditions. Secondly, the secondary creep rate determinations are influenced not only by reductions in the cross sectional areas of the specimens but also by recov-

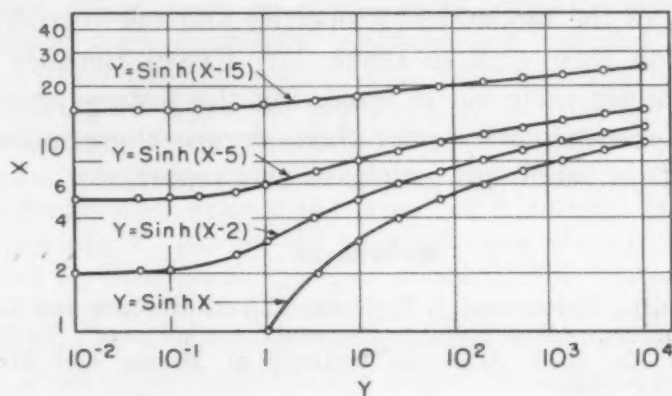


Fig. 19—Hypothetical Examples of the Effect of a Threshold Stress on the Hyperbolic Sine Relationship.

ery and possibly recrystallization phenomena. Therefore, the state of the metal is very likely different at the secondary creep rate, not only for different temperatures of test but even for different initial stresses at the same temperature of test. Thirdly, the mechanism of creep itself probably is different at the different temperatures and strain rates. Consequently, the quantitative accuracy of the preceding discussion is highly questionable. But nevertheless the general qualitative aspects of the analysis are not only interesting but appear to have some theoretical and experimental justification. The results certainly emphasize the need for a more fundamental approach to the solution of creep problems.

#### CONCLUSIONS

1. Creep and stress rupture properties have been determined for the following aluminum sheet materials over the range of 90 to 400 °F:

99.6% Al Alloy: H12 and H18  
2S Alloy: H12 and H18  
4S Alloy: H32 and H38

2. Cold working to obtain the fully hardened state improved the creep resistance of the materials tested up to about 212 °F, but



beyond 212 °F maximum cold working decreased the creep properties.

3. An attempt was made to analyze the results of this investigation in terms of qualitative theoretical considerations.

#### ACKNOWLEDGMENTS

This investigation was sponsored by the Aluminum Company of America. The authors wish to thank the Alcoa Laboratories for preparation of the specimens, for the chemical analyses and for the determination of the mechanical properties and microstructures.

In addition they wish to thank Mr. Erwin Berliner and Mr. M. Kawaguchi for their aid in executing the testing program, and to Mrs. G. Pelatowski they offer their sincere appreciation for the preparation of the numerous graphs of this report.

#### References

1. A. Flanigan, L. Tedsen and J. E. Dorn, "Stress Rupture and Creep Tests on Aluminum Alloy Sheet at Elevated Temperatures", Technical Publication No. 2033, American Institute of Mining and Metallurgical Engineers, 1946.
2. J. E. Dorn and T. E. Tietz, "Creep and Stress Rupture Investigations on Some Aluminum Alloy Sheet Materials", *Proceedings, American Society for Testing Materials*, 1949.
3. O. D. Sherby, T. E. Tietz and J. E. Dorn, "The Creep Properties of Some Forged and Cast Aluminum Alloys", University of California Engineering Research Project Report, Dec. 1, 1949.
4. W. A. Wood and W. A. Rachinger, "The Mechanism of Deformation in Metals, with Special Reference to Creep", *Journal, Institute of Metals*, November 1949.
5. Ting-Sui Kê, "A Study of Recrystallization and Grain Growth by Measurements of Internal Friction", *Journal of Metals*, March 1950.
6. O. D. Sherby, "The Effect of Grain Size on the Creep Properties of 2S-O Aluminum", M.S. Thesis, University of California, Berkeley, 1949.
7. Walter Kauzman, "Flow of Solid Metals from the Standpoint of the Chemical-Rate Theory", *Transactions, American Institute of Mining and Metallurgical Engineers*, Vol. 143, 1941.

# GRAIN REFINEMENT OF ALUMINUM-SILICON (5% Si) AND ALUMINUM-SILICON-MAGNESIUM (7% Si, 0.3% Mg) CASTING ALLOYS

BY VINCENT DEPIERRE AND HAROLD BERNSTEIN

## *Abstract*

*Small rivet-shaped castings of the aluminum-silicon alloys, containing graduated amounts of the refining elements, were made in a preheated graphite mold. The castings were sectioned, polished and macroetched, and their grain sizes were measured. The added elements had similar effects upon the grain size of the two alloys tested. Boron, columbium, titanium, zirconium, tantalum, molybdenum, tungsten, chromium, and beryllium, in that order of effectiveness, refined the grain size of the two aluminum-silicon alloys. Boron, the most effective grain refiner, produced its maximum effect at about 0.05% boron concentration by weight. Microscopic examination of the aluminum-silicon alloys with added grain refiners showed that the grain refiners altered the shape and distribution of the silicon constituent in the microstructure of the alloys.*

VARIOUS elements are used as grain refiners of aluminum alloy castings, in order to obtain desirable manufacturing and mechanical properties associated with fine grain size in aluminum alloys. Previous work described the effect of alloying elements on the grain size of aluminum - 4.5% copper (1),<sup>1</sup> and a study of grain refinement in commercial purity aluminum (2). This investigation is concerned with the merits of various grain refiners as applied to aluminum-silicon (5% silicon) and aluminum-silicon-magnesium (7% silicon, 0.3% magnesium) casting alloys, covered by Classes 2 and 3, respectively, of Navy Department Specification 46Alf. The elements boron, beryllium, columbium, chromium, molybdenum, tantalum, titanium, tungsten, and zirconium were selected for investigation on the basis of their effects on commercially pure aluminum.

## PROCEDURE AND TEST RESULTS

### *Raw Materials*

Aluminum-silicon (5% silicon) alloy melts were prepared with

<sup>1</sup>The figures appearing in parentheses pertain to the references appended to this paper.

Of the authors, Vincent DePierre is senior metallurgist and Harold Bernstein is metallurgist, United States Naval Gun Factory, Washington, D. C. Manuscript received June 6, 1950.

Table I  
Analyses of Raw Materials

Material	Al	Cu	Fe	Mg	Mn	Si	Zn	Other
Aluminum	Bal.	0.01	0.08	.....	0.01	0.09	...	.....
Silicon	.....	.....	0.65	.....	.....	Bal.	...	.....
Magnesium	.....	.....	.....	99.5	.....	.....	...	.....
Al-Beryllium	Bal.	0.01	.....	0.02	.....	0.06	...	4.59 Be
Al-Boron	Bal.	.....	0.07	.....	.....	0.08	...	1.54 B
Al-Columbium	Bal.	.....	.....	.....	.....	.....	...	0.80 Cb
Al-Chromium	Bal.	.....	.....	.....	.....	.....	...	2.95 Cr
Al-Molybdenum	Bal.	.....	.....	.....	.....	.....	...	1.0 Mo
Al-Tantalum	Bal.	.....	.....	.....	.....	.....	...	1.0 Ta
Al-Titanium	Bal.	0.05	0.34	.....	0.02	0.15	...	2.47 Ti
Al-Tungsten	Bal.	.....	.....	.....	.....	.....	...	1.0 W
Al-Zirconium	Bal.	.....	.....	.....	.....	.....	...	2.03 Zr

commercial aluminum (99.81%), silicon (99%), and master alloy additions.

Aluminum-silicon-magnesium (7% silicon, 0.3% magnesium) alloy melts were prepared from ingot metal containing no grain refiners, and master alloy additions. The ingot metal was previously prepared from commercial aluminum, silicon and magnesium, in a 100-pound melt which was pigged for remelting.

The chemical analyses of the raw materials used are listed in Table I.

#### MELTING AND CASTING PRACTICE

The alloys were melted in batches of 350 grams in No. 4118 Dixon plumbago crucibles, size 1, without covers. The furnace used was a Hevi-Duty pit-type electrical resistance furnace equipped with Leeds and Northrup Micromax recorder and controller. Furnace temperature was maintained at 1300 °F (705 °C). The refining agents in the form of aluminum master alloys were added in steps. After each addition, the melt was stirred with a graphite rod, held at temperature for 15 minutes and removed from the furnace to pour one casting. Subsequently, the melt was returned to the furnace and the next addition of master alloy made. Approximately 80 grams of metal were poured into a vertical graphite mold, preheated to 750 °F (400 °C). The mold was held in a transite flask. Mold temperature was determined by means of a thermocouple located at mid-wall thickness of the mold. The castings are rivet shaped, with a 3/4-inch diameter, 2-inch long shank. Fig. 1 shows the transite flask, graphite mold, and a specimen casting. From each melt, four castings were poured; each casting, in turn, representing an increase in concentration of addition agent.

#### SPECIMEN PREPARATION

A 3/4-inch long section was cut from the small end of each cast-

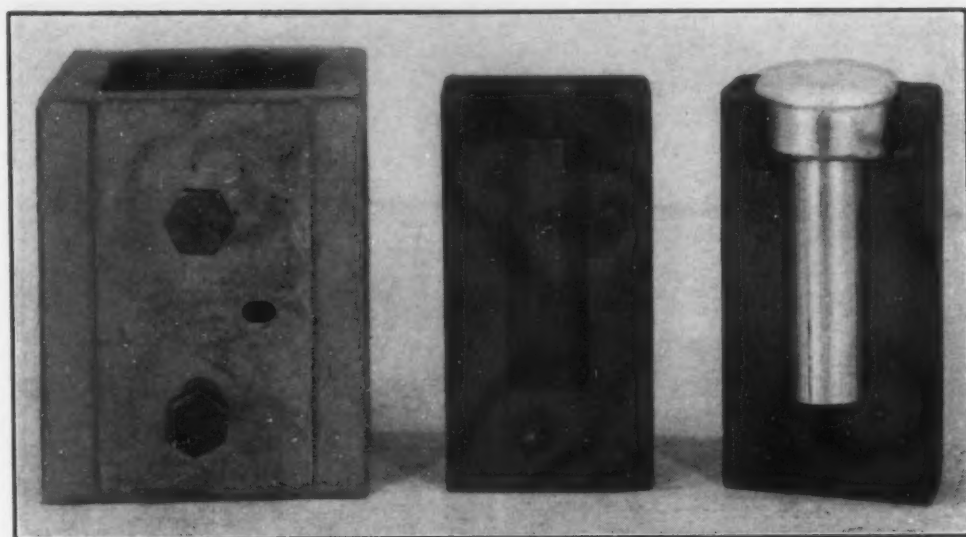


Fig. 1—Transite Flask, Split Graphite Mold, and Aluminum Alloy Casting Used for Grain Size Determinations. Approximately  $\times 0.5$ .

ing, and faced off in a lathe. The machined face was ground on a belt surfacer, followed by hand polishing on 0, 00, and 000 emery papers. The specimens were etched in aqua regia to which 1% HF had been added. The macroetched cross sections of four castings representing the range of grain size explored may be seen in Fig. 2.

#### GRAIN SIZE MEASUREMENT

The grain diameters were measured using a bench microscope equipped with 48-mm objective; and the Bausch and Lomb ASTM grain size measurer for an eyepiece. The magnification was approximately 15 diameters. The average grain diameter was arrived at by scanning the cross section with the various size grids and selecting the grid conforming most nearly to the grain dimensions. The grain sizes, expressed in inches, are listed in Tables II and III. The refining effects of boron, titanium, and zirconium on aluminum-silicon-magnesium alloy are demonstrated in Fig. 3, where grain size has been plotted against concentration of added element.

#### CHEMICAL ANALYSIS

One specimen from each batch of four was selected for chemical analysis. In each case, it was the specimen which represented the leveling off point of refinement. For example, the second specimen in the boron series of the aluminum-silicon-magnesium alloy was analyzed. To determine the extent of dilution of the primary alloying elements, the last specimen in the tantalum series of the aluminum-silicon-magnesium alloy, and in the columbium series of the



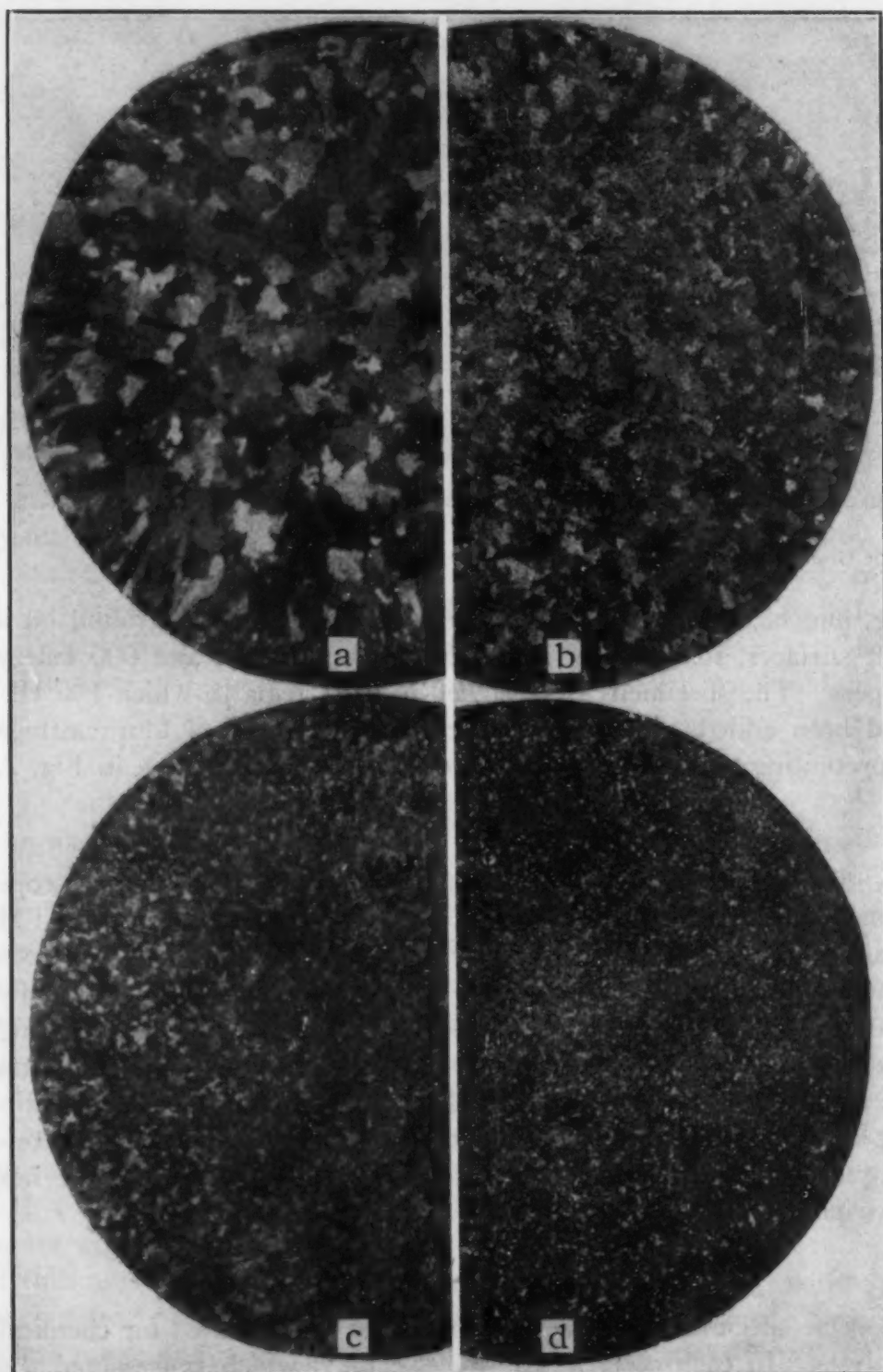


Fig. 2—Grain Size of Various Specimens of Aluminum - 7% Silicon-Magnesium Alloy. Approximately  $\times 4$ . a—Base metal. b—0.25% chromium added. c—0.05% columbium added. d—0.04% boron added.

**Table II**  
**Aluminum-5% Silicon Alloy**  
**Casting Analyses and Grain Size Measurements**

	Si	Fe	Cu	Zn	Mg	Al	Grain Size
Base Material—5.70-4.51	0.22	0.02	0.01	0.02	Bal.		0.037
% Addition (Nominal)	Grain Size (Inches)	% Addition (Nominal)	Grain Size (Inches)	% Addition (Nominal)	Grain Size (Inches)		
<i>Boron</i>		<i>Zirconium</i>		<i>Beryllium</i>			
0.01	0.019	0.05	0.037	0.02	0.031		
0.02	0.013	0.15	0.037	*0.10	0.022		
*0.04	0.008	*0.22	0.013	0.14	0.022		
0.08	0.008	0.28	0.013	0.33	0.022		
<i>Columbium</i>		<i>Tantalum</i>		<i>Tungsten</i>			
0.01	0.022	0.01	0.031	<0.01	0.026		
0.02	0.022	0.02	0.026	0.01	0.022		
0.03	0.015	*0.03	0.013	*0.02	0.019		
*0.04	0.013	0.05	0.013	....	....		
<i>Titanium</i>		<i>Chromium</i>		<i>Molybdenum</i>			
0.02	0.019	0.01	0.037	<0.01	0.031		
0.05	0.013	0.06	0.037	0.01	0.026		
*0.16	0.009	*0.14	0.022	*0.03	0.019		
0.25	0.009	0.25	0.022	0.05	0.019		

\*Chemical analysis.

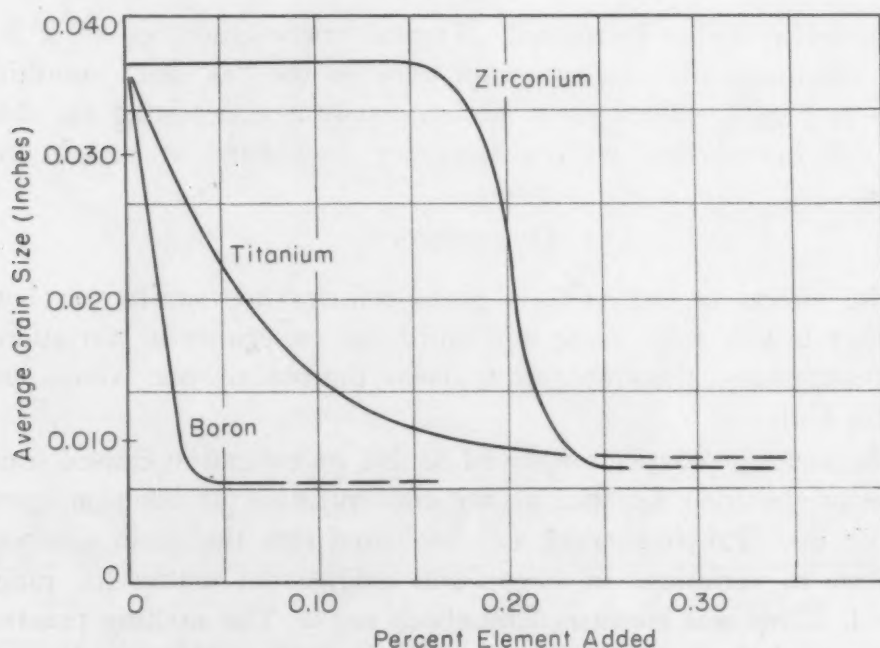


Fig. 3—Effect of Refining Elements Upon Grain Size of Aluminum-7% Silicon-Magnesium.

aluminum-silicon alloy, was analyzed. Twenty-five grams of millings from the midlength of each casting served for chemical analysis. The results are listed in Tables II and III.

#### MICROEXAMINATION

One rivet from each batch of four was selected for microexamination. A cross section near the middle of the shank was polished

**Table III**  
**Aluminum - 7% Silicon - Magnesium Alloy**  
**Casting Analyses and Grain Size Measurements**

	Si	Fe	Cu	Zn	Mg	Al	Grain Size
Base Material—7.78-6.76	0.28	0.01	0.02	0.41-0.34	Bal.		0.037
% Addition (Nominal)	Grain Size (Inches)	% Addition (Nominal)	Grain Size (Inches)	% Addition (Nominal)	Grain Size (Inches)		
<i>Boron</i>		<i>Zirconium</i>		<i>Beryllium</i>			
0.01	0.026	0.01	0.037	0.02	0.026		
*0.03	0.008	0.05	0.037	0.07	0.019		
0.05	0.008	0.15	0.037	*0.14	0.019		
0.08	0.008	*0.24	0.009	0.33	0.019		
<i>Columbium</i>		<i>Tantalum</i>		<i>Tungsten</i>			
0.01	0.031	0.01	0.031	<0.01	0.026		
0.02	0.019	0.02	0.026	*0.01	0.019		
0.05	0.012	0.05	0.019	0.02	0.015		
*0.07	0.008	*0.07	0.013	....	....		
<i>Titanium</i>		<i>Chromium</i>		<i>Molybdenum</i>			
0.01	0.031	0.03	0.026	0.01	0.019		
0.05	0.022	0.15	0.019	0.02	0.019		
0.14	0.012	*0.26	0.015	0.04	0.015		
*0.25	0.009	0.33	0.015	*0.06	0.013		

\*Chemical analysis.

and etched in Keller's reagent. Typical microstructures at  $\times 500$  of the aluminum-silicon-magnesium alloy in the "as cast" condition appear in Fig. 4. They show silicon constituent outlining the dendritic cell boundaries, with a tendency to cluster at certain cell corners.

#### DISCUSSION

The effects of the various grain refiners are similar on both the alloys tested, with some allowance for experimental variations. The illustrations, therefore, have been limited to one alloy, and serve for both.

The melting practice employed in this investigation caused some dilution of the base material as the concentration of addition agent was built up. Previous work (2) indicated that the grain size was insensitive to variations in silicon and magnesium within the range explored. This was confirmed by check tests. The melting practice also increased the holding time for the first three additions in each batch of four castings. For example, in the third casting, the first addition had been held for 45 minutes, the second addition for 30 minutes. Previous experience with holding times up to one hour indicated no diminution of refining potency.

Examination of the microstructures showed that all of the grain refiners altered the shape and distribution of the silicon constituent. In the base material, this constituent appeared in the shape of small nodules which outlined the dendritic cells, and tended to cluster thickly at the cell corners. In the refined material, the silicon became

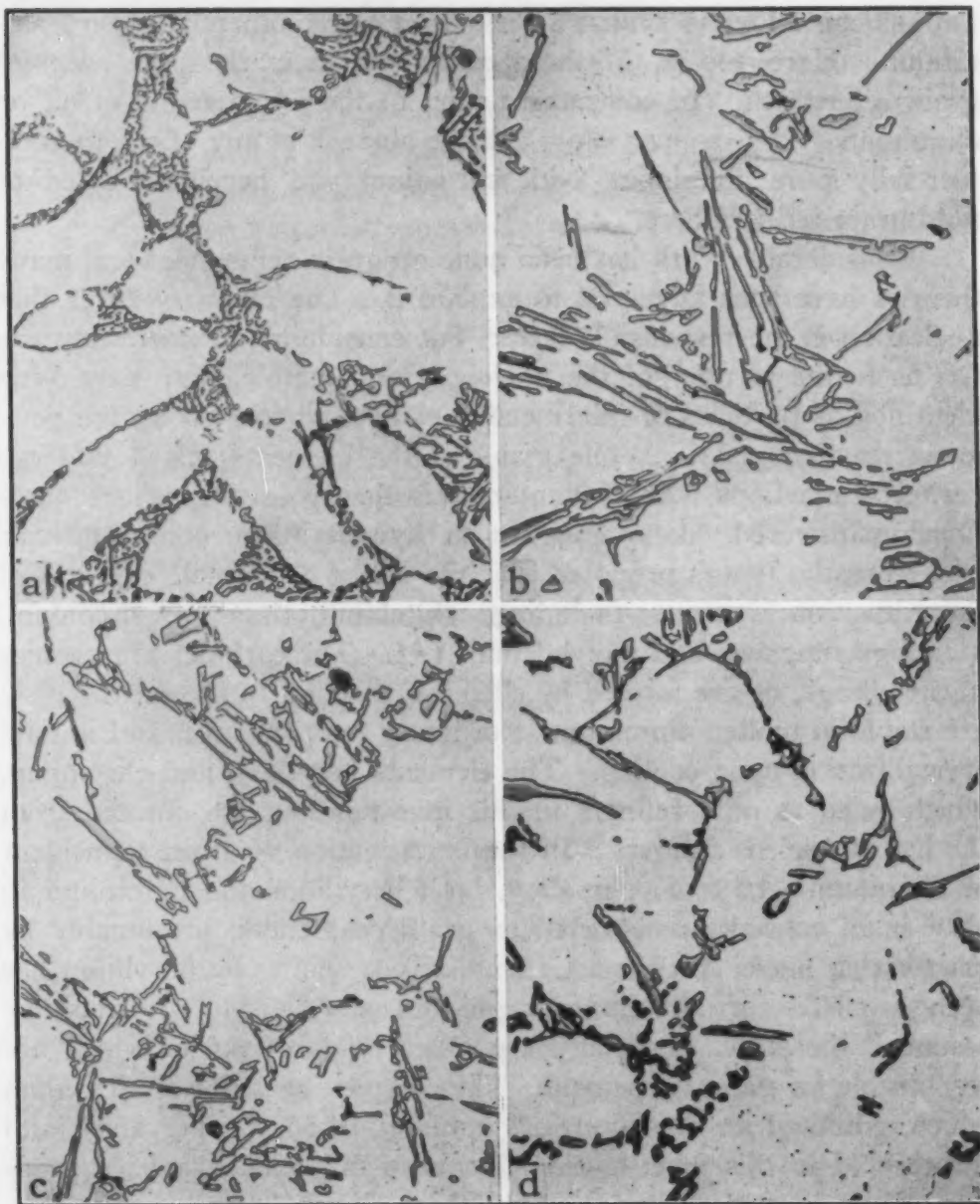


Fig. 4—Microstructures of Various Specimens of Aluminum-Silicon-Magnesium Alloy. Keller's etch.  $\times 500$ . a—Base material. b—0.03% boron added. c—0.14% titanium added. d—0.14% beryllium added.

elongated and irregular, and was more uniformly distributed than in the base material, although still tending to outline the dendritic cells.

The curves of grain refinement with the exception of zirconium are hyperbolic, with the initial additions accomplishing the greatest rate of refinement. Of the elements tested, boron was the strongest refiner with its maximum grain refinement occurring at approximately 0.05% by weight. The behavior of zirconium in the alumi-



num-silicon alloys is similar to its effect on commercially pure aluminum. Here, too, a threshold concentration marked the onset of grain refinement. In contradistinction to their coarsening effect on aluminum-4.5% copper alloy, and the absence of any effect on commercially pure aluminum, both chromium and beryllium acted as mild grain refiners here.

Considerable work has been done on grain refinement and many theories have been advanced to explain it. The majority agree that nucleation is the responsible factor, but considerable controversy exists as to the identity of the nuclei. For example, they have been identified as particles of intermetallic compound formed by the peritectic reactions (3). While many of the elements tested undergo peritectic reactions with aluminum, this theory leaves various questions unanswered, like refinement at hypoperitectic concentrations.

Recently, it was proposed that the nuclei are simple carbides of the transition elements, including columbium, titanium, zirconium, tantalum, tungsten, and molybdenum (4). The carbides are present in the charge, or are formed by chemical reaction in the melt. They are stable in molten aluminum at ordinary temperatures, and initiate crystallization upon cooling. The elements beryllium and chromium, which acted as mild refiners in this investigation, are omitted from the list of nucleus formers. In the investigation of grain refinement of aluminum-4.5% copper alloy, both beryllium and chromium in very small concentrations acted as grain coarseners, presumably by inactivating nuclei in the melt. Similar coarsening by beryllium has been reported for aluminum-magnesium alloys (5). It must be assumed, therefore, that there are other types of nuclei which are responsible for grain refinement. The complex behavior of zirconium which exhibited an inversion in aluminum-4.5% copper alloy, and a threshold in this investigation, seems to fall outside any explanation of simple nucleation.

For the aluminum-4.5% copper alloy, titanium proved to be the best grain refiner. Titanium is also used today as a grain refiner for the aluminum-silicon alloys. Pending check tests on mechanical properties, boron may replace titanium in the aluminum-silicon alloys.

#### CONCLUSION

Under the conditions described herein, boron is the most effective grain refiner for aluminum-silicon alloys, followed by columbium, titanium, zirconium, tantalum, molybdenum, tungsten, chromium, and beryllium.

## ACKNOWLEDGMENTS

For his direction and advice given during the course of this investigation, acknowledgments are due Lewis H. Fawcett, principal metallurgist, and to the personnel of the Laboratory Division, who aided in all phases of the work involved.

This investigation is sponsored by the Office of Naval Research under Project Order 62-47.

## References

1. H. G. Bowen, Jr.; and Harold Bernstein, "Effect of Sixteen Alloying Elements Upon the Grain Size of Cast 4.5% Copper-Aluminum Alloy", *TRANSACTIONS, American Society for Metals*, Vol. 40, 1948, p. 209.
2. Vincent DePierre and Harold Bernstein, "Grain Refinement in Cast Aluminum", *Iron Age*, Vol. 163, No. 3, Jan. 20, 1949.
3. A. Portevin, "Refinement of the Structure of Castings", *Foundry Trade Journal*, Oct. 27, Nov. 10, Nov. 17, 1938.
4. A. Cibula, "The Mechanism of Grain Refinement of Sand Castings in Aluminum Alloys", *Journal, Institute of Metals*, Vol. 17, Part 4, December 1949.
5. G. Gauthier, "Improvement of Cast Aluminum-Magnesium Alloys by Additions of Beryllium and Titanium", *Foundry Trade Journal*, Nov. 17, 1938.

## EFFECT OF STRAIN RATE ON TOUGHNESS OF TEMPER-BRITTLE STEEL

BY D. C. BUFFUM AND L. D. JAFFE

### *Abstract*

*The effect of a change in strain rate upon the transition from ductile to brittle failure was investigated. An SAE 3140 steel was studied in the temper-brittle condition and in the unembrittled condition. V-notched Charpy specimens were tested over a range of testing temperatures at two strain rates differing by 5,000,000:1. Contrary to a report in the literature, the transition temperature was found to be affected by strain rate in both the temper-embrittled and the unembrittled states.*

IT is well known that ferritic steels undergo a transition from tough to brittle behavior as their temperature is lowered, and that this temperature of transition is lowered by reducing the rate of loading (1).<sup>1</sup>

Accordingly, it is most interesting to note that, in a study of temper-brittle and unembrittled steels, Jolivet and Vidal (2) reported rate of loading to have no effect upon the transition temperature. If confirmed, this would apparently mean that the behavior of temper-brittle steel is unlike that of other steel—that the temperature of transition for temper-brittle steel, being independent of rate of loading, may be associated with some transformation taking place in the steel, such as a phase change.

All of Jolivet and Vidal's tests at slow strain rates were performed upon notched bars at room temperature. If one examines the curves given in their paper for energy absorption versus test temperature with impact loading, it will be noted that for nine of the eleven steels tested the transition temperatures are below room temperature. If a reduction in strain rate had lowered the transition temperature, it is evident that room temperature tests at a slow strain rate would not reveal any change in energy value from impact tests at the same temperature, for these steels. A change would be observed only if the transition temperature for specimens broken in impact was at or slightly higher than room temperature.

<sup>1</sup>The figures appearing in parentheses pertain to the references appended to this paper.

A paper presented before the Thirty-second Annual Convention of the Society, held in Chicago, October 21 to 27, 1950. The authors, D. C. Buffum and L. D. Jaffe, are associated with Watertown Arsenal Laboratory, Watertown, Mass. Manuscript received April 24, 1950.

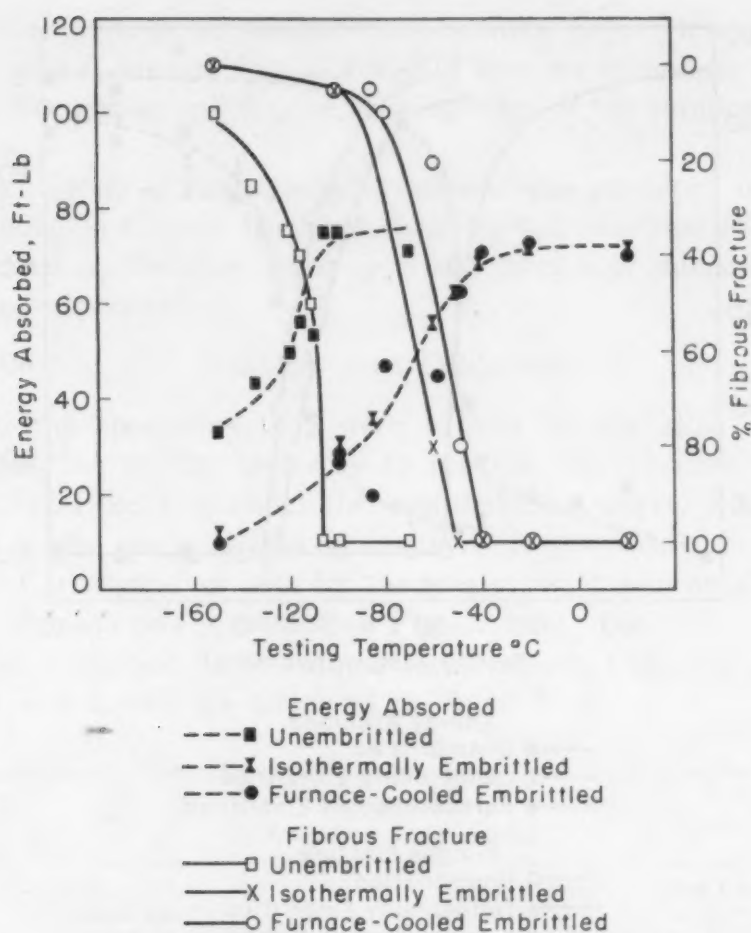


Fig. 1—Transition Curves for Embrittled and Unembrittled SAE 3140 Steel Broken by Slow Bending. Each point represents one test.

In order to verify or disprove the findings of Jolivet and Vidal, complete transition curves were obtained for specimens in the unembrittled and the temper-embrittled states and at both fast and slow strain rates.

#### MATERIAL AND TEST PROCEDURE

Previous work had indicated that a heat of SAE 3140 steel<sup>2</sup> of the following composition (in per cent),

C	Mn	Si	S	P	Ni	Cr	Mo	V	N
0.385	0.79	0.30	0.028	0.015	1.26	0.77	0.02	<0.01	0.006

when heat treated to form tempered martensite, would have its transition temperature within the testing range of the apparatus to be used for slow strain-rate tests. Specimen blanks  $2\frac{3}{16}$  inches long were cut from  $\frac{5}{8}$ -inch round hot-rolled bar stock. These blanks were

<sup>2</sup>This material was supplied by Pennsylvania State College through the courtesy of J. R. Low, Jr. Other experiments on the same heat have been reported (4-7).



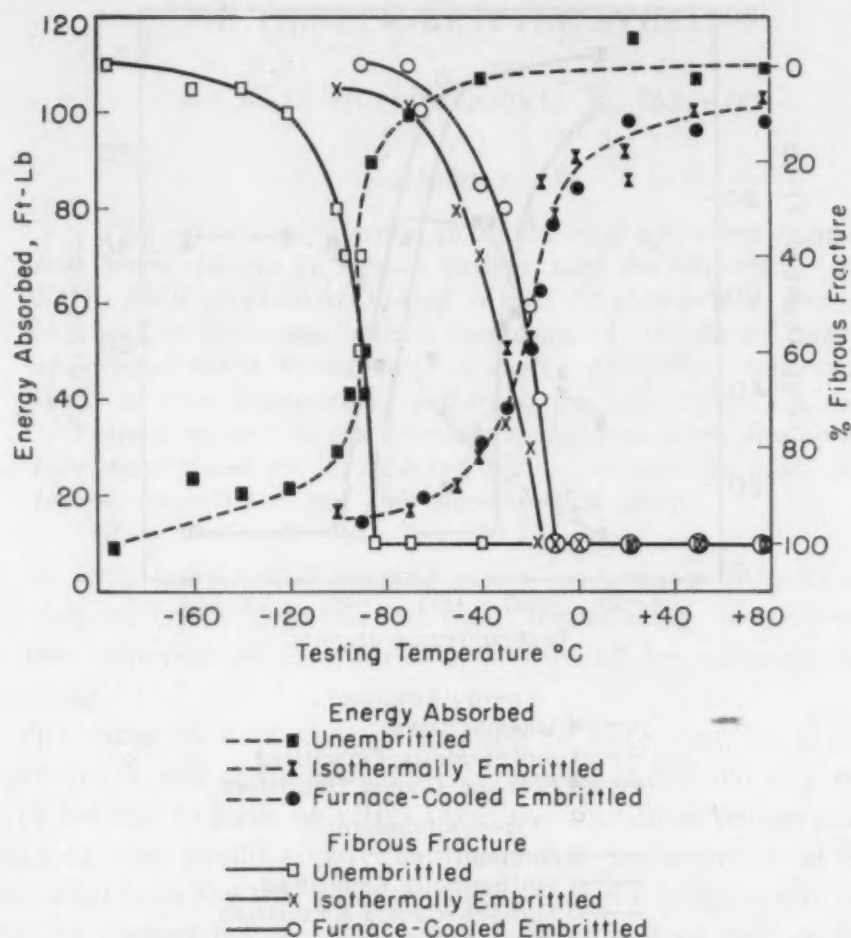


Fig. 2—Transition Curves for Embrittled and Unembrittled SAE 3140 Steel Broken by Charpy Impact Apparatus. Each point represents one test.

austenitized at 900 °C (1650 °F) for 1 hour and water-quenched. They were then divided into three groups and further heat treated as follows:

Groups 1 and 2 were tempered at 675 °C (1250 °F) for 1 hour and water-quenched.

Group 2 was given an additional isothermal embrittling treatment of 48 hours at 480 °C (900 °F) and water-quenched.

Group 3 was tempered at 675 °C (1250 °F) for 1 hour and embrittled by furnace cooling at the rate of 17 °C (30 °F) per hour.

Metallographic examination of the specimens as-quenched showed a microstructure of martensite with no visible carbides and an austenitic grain size of ASTM 8. The Rockwell hardness of the specimens after tempering was C-21 to 23.

Apparatus to be employed in conjunction with a standard tensile testing machine was designed on which bend specimens could be

tested over a range of subzero temperatures (3). The head speed used in this apparatus was  $37.5 \times 10^{-7}$  feet per second as compared to 16.8 feet per second for the striking edge of the standard Charpy machine.

Each group of heat treated specimens was machined into standard V-notched Charpy bars and then divided into two parts which were tested on the slow strain-rate apparatus and standard Charpy machine, respectively.

### RESULTS AND DISCUSSION

On the specimens that were broken by the slow strain-rate apparatus, the energy necessary to fracture the specimens was calculated from the area under the load-deflection curve. This energy, as well as the per cent fibrous fracture,<sup>3</sup> is graphically presented in Fig. 1. Corresponding data for the specimens broken on the Charpy impact machine are presented in Fig. 2.

The transition temperatures<sup>4</sup> were taken from the curves in Figs. 1 and 2, and are tabulated in Table I.

Table I  
Transition Temperatures

	Charpy Impact	Slow Bend
Unembrittled	-85 °C	-106 °C
Isothermally Embrittled	-15 °C	-50 °C
Furnace-Cooled Embrittled	-10 °C	-40 °C

As shown in Table I, the decrease in strain rate caused a decrease in the transition temperature. The effect of the change in strain rate appears to have been somewhat greater for the embrittled specimens than for the unembrittled.

These results are not in accord with the conclusions of Jolivet and Vidal. It is believed that if these authors had performed their slow strain tests over a range of temperatures their conclusions would have been different and possibly would have concurred with those of this report.

### CONCLUSION

Reducing the strain rate lowers the temperature at which the transition from ductile to brittle fracture occurs. Contrary to a

<sup>3</sup>The per cent fibrous was estimated by examining the fractured surface of the specimens with the unaided eye or at a magnification of not more than 24 times.

<sup>4</sup>The transition temperature is here taken as the lowest temperature at which the fracture was 100% fibrous, as read from the plot of per cent fibrous fracture versus testing temperature.

report in the literature, the transition temperature of steel is affected both in the unembrittled state and in the temper-embrittled state. The effect may be somewhat greater for the embrittled specimens.

### References

1. F. F. Witman and V. A. Stepanoff, "Influence of Deformation Speed on Cold Embrittlement of Steel", *Journal of Technical Physics* (U.S.S.R.), Vol. 9, 1939, p. 1070.
2. H. Jolivet and G. Vidal, "Value of the Resilience Test for the Study of Temper Brittleness", *Revue de Metallurgie*, Vol. 41, 1944, p. 378-388 and 403-408.
3. D. Driscoll, "Mechanical Bend Test Device for Autographically Recording of Load-Deflection Diagrams", to be published.
4. L. D. Jaffe and D. C. Buffum, "Temper Brittleness of Plain Carbon Steels", *Transactions, American Institute of Mining and Metallurgical Engineers*, Vol. 180, 1949, p. 513-518.
5. D. C. Buffum, "Investigation of Square Subsize V-Notched Charpy Specimens", *ASTM Bulletin No. 160*, September 1949, p. 45-47.
6. L. D. Jaffe and D. C. Buffum, "Isothermal Temper Embrittlement", *TRANSACTIONS, American Society for Metals*, Vol. 42, 1950, p. 604.
7. L. D. Jaffe and D. C. Buffum, "Retrospection of Temper Brittleness", Presented to Société Française de Métallurgie, 1950. Accepted for publication, *Revue de Métallurgie*.

### DISCUSSION

**Written Discussion:** By Carl A. Zapffe, research metallurgist, Baltimore, Md.

There is scarcely any chance of disagreeing with these findings of Drs. Buffum and Jaffe, for it is a virtual certainty that an increasing velocity of fracture increases the tendency toward elastic, rather than plastic, behavior of most substances, and specifically the ferritic materials under discussion.

While most discussions of rheotropy—as we prefer to call the phenomenon of "transition temperature"—concern carbon or low alloy steels, an excellent material for experimental purposes is provided by the Class II ferritic stainless steels. These display particularly well the fact that rheotropic phenomena are influenced by a number of factors besides temperature, which is the one most frequently discussed. Thus, as chromium increases above approximately 16%, a transition from plastic toward elastic behavior shows itself in ordinary testing, particularly by impact. The high chromium ferritic stainless steels are notoriously unsuited for applications requiring "toughness". Next, temperature affects the rheotropy just as it does with other steels; and a practical application of this fact is demonstrated in the present practice of conducting cold working operations on material which at first is very slightly heated. This, of course, brings the material up over the rheotropic boundary, into a condition where plasticity is again good and the material is readily worked.

As for the effect of strain rate, the point that Drs. Buffum and Jaffe make is readily demonstrated by the simple tests illustrated in Figs. 3

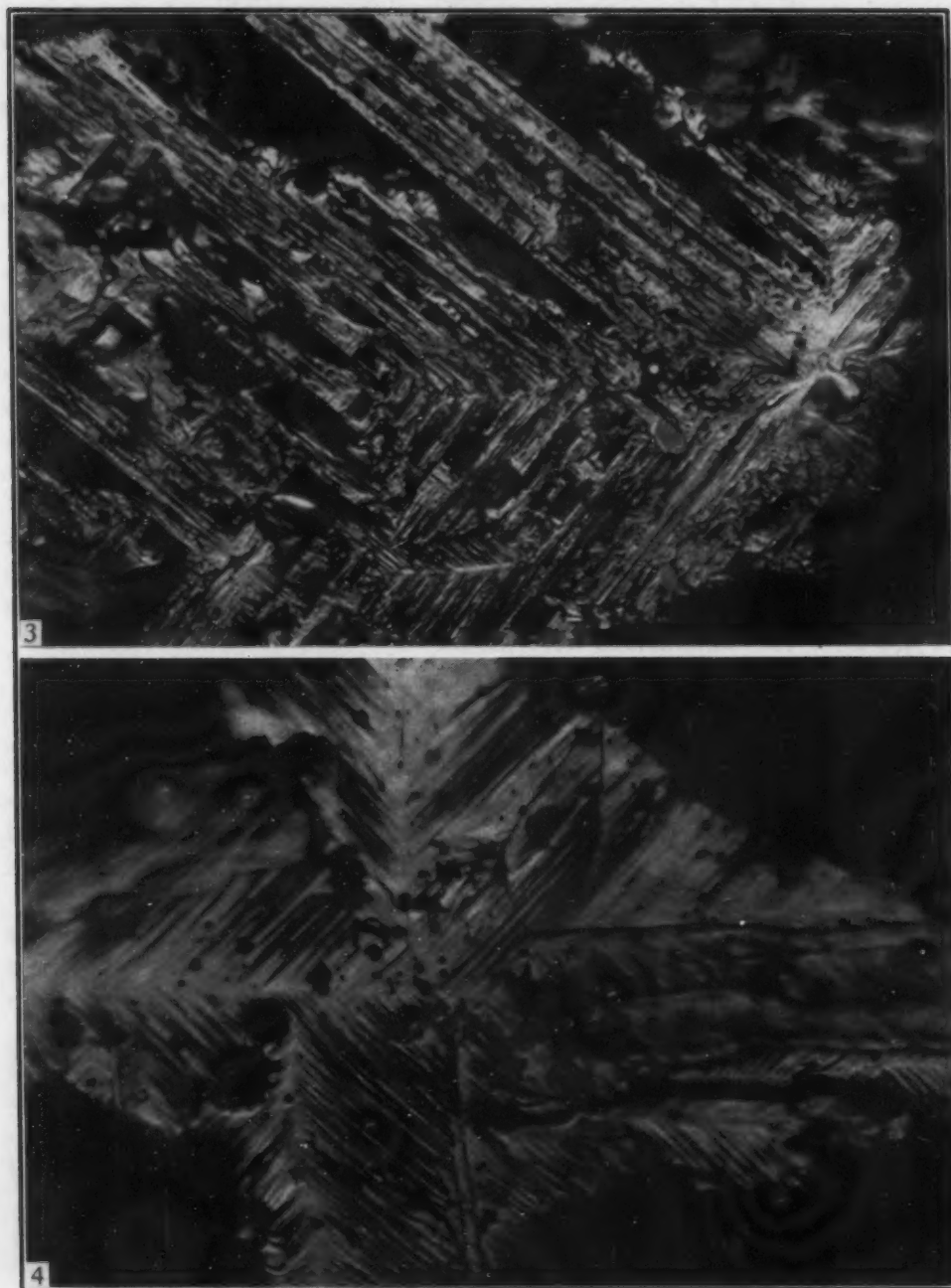


Fig. 3—Fractograph of Type 446 Stainless Steel Fractured by Rifle Fire at 100 °C.  $\times 850$ .

Fig. 4—Duplicate Specimen Fractured by Rifle Fire at 475 °C.  $\times 850$ .

and 4. These are fractographs, and they both refer to a specimen of Type 446 stainless steel containing 26% chromium. The specimens were first uniformly heat treated, and then were fractured under the contrasting conditions of hammer blow and rifle fire, the latter by a 0.22-caliber slug fired against a flattened face on the specimen at a distance of 24 inches from the muzzle. Fig. 3 displays a facet on a fracture made by rifle fire with the specimen heated to 100 °C. The elaborate rectangular



pattern is typical of these steels, and remains essentially as shown here for temperatures up to 100 °C or so, whether fracture is caused by low or high strain rates.

At higher temperatures, however, the metal regains plasticity, as mentioned in an earlier paragraph. This results in a gradual disappearance of fractographically viewable facets as the temperature is increased. Above 400 °C, hammer blow will no longer provide a fracture facet which is suitable for fractographic study.

By way of specific contrast, rifle fire represents a sufficient increase in strain rate such that plastic activities are inhibited, even at temperatures of 475 °C. Fig. 4 shows a facet in a duplicate specimen fractured by rifle fire at 475 °C. The pattern has changed, being no longer markedly rectilinear; and a new set of traces expressing slip movements now appears. Nevertheless, the plastic displacements have been sufficiently limited so that some relatively expansive cleavage traverses remain, such as the one shown.

Incidentally, the choice of the temperature of 475 °C in Fig. 4 followed from the fact that "475 °C embrittlement" was being studied in the research from which these fractographs are taken. That phenomenon does not alter the conclusions here given.

#### Authors' Reply

The authors greatly appreciate the interesting comments by Dr. Zapffe. At present, work is under way by M. R. Norton of this laboratory to study the path of fracture in temper-brittle and unembrittled steels. This work so far has revealed some interesting data on so-called brittle fractures.

On SAE 3140 steel specimens broken at low testing temperatures (down to that of liquid nitrogen), it was noticed that fractures classified as brittle when observed with the unaided eye or slight magnification showed definite indications of ductility when magnified  $\times 200$ . Unembrittled and furnace-cooled embrittled specimens were classified as having brittle fracture at  $-170$  °C and  $-60$  °C respectively. When specimens from these two groups were tested at liquid nitrogen temperature (approximately  $-196$  °C) and the fractures examined at magnification of  $\times 200$ , an appreciable degree of ductility was noted.

It is hoped that further tests at lower testing temperature can be made, thereby producing a completely brittle fracture.

## IRON ORE SMELTING PROBLEMS

(1950 Edward deMille Campbell Memorial Lecture)

By E. C. SMITH

TODAY it is my privilege to present the lecture in honor of the memory of Professor Edward deMille Campbell. A quarter century since his death has made me more able to appreciate his worth and understand the need for teachers of his ability to communicate to those about him, who multiplied his accomplishments. Professor Campbell's men are among us today. The results of his labor, now easily seen in the accomplishments of his students, recall the biblical statement, "By their fruits ye shall know them." It was not my privilege to know Professor Campbell or to work in or about his laboratories. Only by association with his men have I known the wonderful ability of this man as a leader of men of science and industry.

As co-workers in World War I his men and I depended upon each other in aircraft production problems. These friendships, cultivated during the troubled years of boom times and those of bitter depression, remained solid in World War II. As we move into the confusion of a possible World War III it is a great personal satisfaction to know these men are here to pick up the burden. The soundness of their training is more than ever a tribute to their master. Let us hope that our nation turns back to the attitude of respect for hard work and discipline that let a blind professor of chemistry accomplish so much with one generation.

My subject for today, the problems of smelting iron ore, did not escape the studies of Professor Campbell, although his handicap of blindness made it but a minor item in his career. His mind would have been most useful in this field, as smelting problems must be reasoned out without the assistance of visual observation.

The problems confronting the people who smelt iron ore are today four-fold in nature: technical, economic, politico-economic and, finally, outright political. I intend to point out problems which fall into all of these categories.

A war monument that I have seen in Europe carries an inscription which says in effect: "God grows iron that men need not be

---

This is the Twenty-fifth Edward deMille Campbell Memorial Lecture, presented by E. C. Smith, chief metallurgist, Republic Steel Corporation, Cleveland, Ohio. The lecture was presented October 25, 1950, during the Thirty-second Annual Convention of the Society, held in Chicago.

slaves." It is a thought that needs better understanding. No powerful nation exists today except those with big blast furnaces and ample steel production.

The Honorable Oscar Chapman, Secretary of the Interior, recently made a pertinent observation about the role of iron and steel in 20th century America, "The steel industry is as essential to the American economy as the steel reinforcing parts are to a large dam and powerhouse. Every characteristic American business depends upon ample supplies of low cost steel. Beneath the surface of our concrete roads, under the paint of our automobiles, under the porcelain finish on our refrigerators, steel plays the basic role in our daily lives." I will subsequently refer to further quotations from Mr. Chapman upon the same occasion.

Yet the iron smelting industry of today needs men who can arouse the interest of the metal-using world. This very vital part of the metal industry has been left to a mere handful of men, most of whom have devoted but little to serious study of iron smelting. It is with the hope of hastening the day when the nation and the community will be less critical of the business of iron smelting that I undertake this lecture.

Almost a generation ago Dr. William Hatfield gave the third Campbell lecture on "The Application of Science to the Steel Industry". Rather than stress the relation of science to iron smelting, I make a direct request, as a friend of the blast furnace men, that we get acquainted with at least some of their problems, which are by no means limited to technical difficulties. People are more important than things; blast furnace men are people. Some of their most difficult problems concern ideas of those in our time who consider the blast furnace and its operators in what seems to me a hostile frame of mind. Right now we need more people that understand the problems of iron production. We in industry are determinedly seeking means of communication that will let our generation know the truth.

Since iron smelting antedates written history, this study will not try to determine the site or the date of the first fire-smelted iron. Let us discuss some aspects of the modern problem with a bit of background of iron smelting. The Roman times, which are recent in a historical sense, cover that period from 750 B.C. to 400 A.D. It is probable that iron was made on the island of Elba when Rome was founded. Today that island is still a source of good ore. With local adaptations the Elban process, taking root in various parts of the Roman world from Britain to the Black Sea, remained in existence



long after the fall of that Empire. Minor modifications of that process were actually used in Austria up to World War II. It may still be in existence.

Vannoccio Biringuccio in 1540 wrote his "Pirotechnia"; our fellow member, Dr. Cyril Stanley Smith, translated it. The chapters on iron smelting are better records of his day than exist to describe our early furnaces. With but slight modification the chapter on iron ore could describe today's situation. The business is bigger but the problems have not changed.

We agree with Biringuccio that Elban ore was excellent, due to its physical character more than its chemical composition. We cannot agree with his statement that only 40 to 45 per cent was lost, as the slags from those Elban forges are very high in iron. An analysis of slag by my friends Harry Craig Richardson and Sidney W. Poole shows:

FeO	Fe <sub>2</sub> O <sub>3</sub>	MnO	Al <sub>2</sub> O <sub>3</sub>	SiO <sub>2</sub>	CaO	S	P
63.14	15.74	0.016	5.2	14.00	0.38	0.052	0.042

This high iron content is not surprising, for the Catalan forges which still operated in this country about 50 years ago wasted roughly half the iron into the slag. It is most significant that the primary weapons for war, from before the time of Caesar to the Spanish-American War, were produced from similar operations.

The Catalan forge, named from its Spanish home, Catalonia, was a shallow hearth 2 feet by 3 feet and 1½ feet deep. A single tuyere blowing air into the hearth from one side at an angle of 35 degrees terminated about 1 foot above the bottom. Small furnaces worked 300 to 500 pounds of ore per charge. The largest furnaces which worked about double this weight of ore had two tuyeres, one at each end of the hearth. These furnaces using about 350 pounds of charcoal per 100 pounds of iron required up to 8 hours time per charge. The simplest blast source was the water spray trompe, a very ancient device in which the water, discharged into the top of a rectangular box, was sprayed on a baffle board and allowed to fall to the bottom. The entrained air discharged into the tuyere pipe, the water into a spillway.

The Elban furnace, with its Catalan successor, was the predecessor of the bloom furnaces which were about 10 feet high with a stack effect that provided more volume. In such a furnace could be made 400 to 700 pounds of brittle salamander iron, which, never fluid because of lack of heat, was dug out, broken up and refined in a separate finery hearth.

The story of the first furnace that melted this mass of iron is lost



somewhere along the road. The records are at best most controversial, although Swank, in his book on "Iron in All Ages", suggests the Rhine provinces of Germany as a probable place of operation. The exact location is unimportant. The significant fact was that molten iron could be cast from a furnace. Even today it is called the high furnace in Europe and blast furnace in English-speaking lands, and its height, 30 feet is close enough, is determined by the load of ore and limestone crushing the charcoal.

#### SAUGUS

Such a furnace was the first successful American blast furnace, now being dug out foot by foot at Saugus, Mass., under the guidance of Mr. Quincy Bent of Bethlehem Steel, the direction of Mr. Roland Robbins, an archeologist, and the observation of Dr. E. N. Hartley, historian and teacher of history at Massachusetts Institute of Tech-



Excavations of the Saugus Furnace. Photograph by Richard Merrill.

nology. The records are far from complete. It may be that present-day operators of blast furnaces still carry on the age-old tradition that iron is important, skill paramount, and records incidental. In any process which depends upon the skill of the operator and where the moves are carried out on a trial basis, the record is always of secondary interest. There remains the fact that our science has not provided the blast furnace man with a road map.

It must be mentioned that in 1620 an earlier iron project was started in Virginia at Falling Creek, a tributary of the James River, sixty miles above Jamestown and about seven miles below Richmond. An Indian massacre ended this attempt, leaving Saugus as the earliest production, according to records.

The Saugus River is between Boston and Lynn. The choice of this site for an iron works at the head of navigation on the Saugus River was excellent as it combined ore, charcoal, limestone, and water transportation. Water power for blowing the furnace and working the hammers came from ponds on a hill close by.

"The Company of Undertakers for the Iron Works" in 1643 included eleven English gentlemen, who provided £1000 capital to build the Saugus Furnace. The records indicate that John Winthrop, Jr., Thomas Dexter and Robert Bridges were important in this affair. Three years was granted by the court for erection, but legal records indicate production in early 1645. The operation continued until 1688. One commentator of the time summed up the story by saying: "Instead of drawing out bars of iron for the country's use, there was hammered out nothing but contentions and lawsuits."

The labor for furnace operation came from the prisoners of war, captured at Dunbar by the English when they defeated the Army from Scotland. Upon release from captivity of several years, part of these men remained there; descendants of the group still live in that area.

The local bog ore from the nearby ponds was supplemented with an ore from the Rockmine at Nahant, Mass. The Nahant ore reminds me of the remark made during the days of William Jennings Bryan by a commentator who said of silver, "It has all the attributes of money except value." The Nahant ore, very similar to black ore magnetite, did have some iron—12.5% was found in a sample analyzed recently. Until this Rockmine ore was analyzed, the high magnesia content of the slags from this furnace puzzled the investigators. No dolomitic limestone was known in the nearby area, nor did the limestone and coral found on the site indicate the source of the magnesia. The Rockmine ore, upon analysis, proved to be a type of igneous rock rich in magnesia, some samples showing as much as 20% MgO. The low fusibility of this rock leads me to conclude the operators were wise enough to use this for a slag easy to handle. Until operations ceased at Chateaugay, a similar practice used the quite fusible feldspar-bearing gangue rock to get volume of easy flowing slags.

One respects the skill and observation of a group of men who

could make iron from the raw materials available in that location. They deserved a better fate than the series of lawsuits and political pushing around they received. By going out of business they avoided the laws that branded the making of iron in the colonies as a public nuisance that should be abated. Later the Townsend Act of 1750 was violated by colonial ironmakers. Similar political pressure exerted in other lines finally cost England the American Colonies. The War for Freedom was much more concerned with Industrial Freedom and Economic Freedom than many of the ideals we read about.

The men scattered from Saugus when the plant ceased operations. There are records indicating that many of the early iron operations in the New England area had one or more Saugus men involved.

#### STONE-WALLED FURNACES

As long as charcoal was used as the fuel the blast furnaces did not vary much from the 30-foot height. The typical furnace was a stone masonry structure, a sort of truncated pyramid, about 20 to 25 feet square at the base, 15 to 18 feet square at the top. The site selected usually provided approach from a hill and waterpower for blowing. The actual working portion of the furnace, a hearth 3 feet in diameter, widened above the hearth to somewhere between 6 and 10 feet, then at the top narrowed back to 4 feet. This central zone was lined with stone, with a packing of loam and sand to seal the joints.

Through two adjacent sides of the stone pyramid were low tunnel-like entries. One of these openings carried the air from the bellows to the hearth. Through the other the iron was tapped and the slag flushed.

The cycle of operation was to reline and dry the stack—repair the bellows and water wheel—fill the hearth with wood and charcoal—light up—and then blow a gentle blast until the hearth was hot enough to start actual smelting. After that the burdening of the furnace began with layers of charcoal, ore and flux. Such a furnace used about 1700 pounds of charcoal per ton of iron. The slag cinder was flushed as it accumulated and iron cast when required. Blast furnaces from about 1300 to 1650 A.D. generally followed this routine. The identical process was still in use in Sweden until about 50 years ago.

The cast metal was refined to bar iron in the finery fire, which used about 2000 pounds of charcoal per ton of product and wasted



25% of the metal. The bar furnace used 600 pounds of charcoal and wasted 10% of the metal. There may be exceptions as the process varied, but altogether there were required  $1\frac{1}{2}$  tons of iron and 5400 pounds of charcoal per each ton of delivered product. An acre of forest would furnish 7 to 12 tons of charcoal; the weekly requirements for an iron works making one ton per day exceeded this figure. With the navy of the British seafaring people requiring wood for timbers and the difficulty of meeting the needs for domestic fuel, it is small wonder that Queen Elizabeth in 1558 outlawed the making of iron by prohibiting, except at Kent, the cutting of trees for conversion into charcoal for making iron.

The stringent laws against the use of charcoal caused ironmakers to turn to bituminous coal, known as "pit cole" or "sea cole". Patents were issued to various men, such as Simon Sturtevant in 1612, John Rovenson in 1613, and one Gombelton later for an iron works at Lambeth, with failure after failure until Dud Dudley successfully made iron in Worcestershire in 1619. That year is considered the end of the period of medieval iron.

Dud Dudley, in the account of his tribulations published as *Metallum Martis* in 1665, relates that in 1619 he was, at the age of 20 years, "Fetched from Oxford, then of Bayliol Colledge Anno 1618, to look and manage 3 Iron Works of my Father's, 1 furnace and 2 forges in the Chase of Pensnet in Worcester-shire." Due to the scarcity of charcoal he tried "pit cole". After his second trial he made "3 Tuns per week". The letter from his father, Edward Dudley, instructing Parkes, his attorney, to ask for a patent, is dated March 10, 1619.

Dudley's enterprise was bitterly opposed by the long established charcoal smelters who visualized danger to their means of livelihood. Mother Nature helped his enemies by a flood that destroyed his plant within a year after the patent was granted. Rebuilding the plant, he resumed operations only to find his business cited as a monopoly. After weathering this litigation with parental aid, he was allowed to work under his patent for 14 years, when his arch enemies, the charcoal smelters, finally, let us say, persuaded the bar ironmakers to refuse to refine the product of pit cole furnaces. This put him out of business—strangely reminiscent of the monopoly investigations of 1950.

This is apparently the first instance in which an attempt was made to link the words "iron" and "monopoly". It would appear that each generation since has had its share of those who strike out for this goal.



Human affairs, along with political events, repeat themselves. In Congress this year there is an investigation to determine if one or more of the larger steel companies do not constitute a monopoly. It is contended that a steel company should make steel only, not engage in any other business. Putting the steel industry into a position where it controls no raw material, transportation or fabrication would be a repetition of the Dud Dudley experience. We see similar thinking today in England where, under nationalization, the metallurgical coals of steel companies go to the city gas plants. It may be but a coincidence that the Fuel Director for the Midlands of England uses the former home of the present Lord Dudley. Tax conditions forced the owner out; a government employee is supported in the mansion.

Dud Dudley built a new plant in the parish of Sedgley in Staffordshire. He describes it as "27 feet square all of stone". I quote him in the interest of accuracy, "which Cole works being brought into perfection, the Author was by force thrown out of them, and the Bellows of his new Furnace and Invention, by riotous persons cut to pieces, to his no small prejudice, and loss of his invention of making Iron with Pit Cole". Before Dudley finally abandoned his process, due to such bitter opposition, his furnace had made 15 tons per week, a figure seldom bettered in the next hundred years.

#### ANTHRACITE FURNACES

The production did not change in any serious way until James Beaumont Neilson's invention of hot blast in 1828 was started. Production doubled and the fuel per ton was cut in half with 600 °F blast temperature. An important by-product of hot blast was the ability to burn anthracite coal. Tests without hot blast proved anthracite too difficult to use.

A New York City Lutheran clergyman, Dr. Frederick W. Geissenhainer, with twenty years' association with the iron industry, in addition to his ministerial duties, made anthracite iron in 1831. On the basis of a patent issued to him in 1833, he erected a furnace in Schuylkill County, Pa., in 1836, operating it until his death in 1838. When his estate sold the patent rights, the royalty fee was advertised at 25 cents per ton.

Anthracite furnaces really got under way when the famous ironmaster, David Thomas, erected Catasauqua furnace in Pennsylvania. He was the ironmaster of the generation from 1839 until his death in 1882. Thomas' operations, which increased the height of the furnaces to 55 feet and then 80 feet, prepared the industry for the Duquesne revolution, which I shall mention later. Anthracite is now

used only in small amounts that are blended in coke during periods of shortage of coking coals.

#### BY-PRODUCT COKE OVENS

A hundred years after Dud Dudley solved the problems of using coal, iron smelting with coke was accomplished by Abram Darby in 1735 at Colebrookdale. Early coke was made by methods quite similar to charcoal burning. Cokemaking has since passed from the stage of pit coking through that of beehive ovens to by-product ovens. About 1895 the strong cokes of Connelsville, Pa., made in beehive ovens, permitted the operation of the 95-foot furnaces at Duquesne, Pa. These furnaces were so capable that they brought about the "Duquesne Revolution" in the iron industry.

However, another and more drastic revolution had started. European cokemakers had devised a long, narrow, brick chamber in which the coal was subjected to outside heat. The volatile and gaseous parts were driven off, collected as by-products, processed and put to economic use.

Coke could be made by blending different kinds of coal at locations far removed from the mining area. By-product gas could be used to heat the coke oven with a surplus available for gaseous fuel in steel plant operations or in city gas systems. Coke that surpassed the best beehive product was available. Economists selected steel plant locations on the basis of new calculations—haul the ore and coal to the market—make the steel adjacent to the great consumer population areas. This is sound economics and a great benefit to some areas, but it meant relocation of the entire world of industry.

German industry was based on the chemicals made from coal by-products. The steel industry of Germany, using the coke and consuming the by-product gas for fuel, soon eclipsed the English industry, even made steel cheaper than the United States. In my opinion the first World War was fought to keep Continental Europe from coming under German economic control. The German plan involved exactly the same fundamentals that we now face with Russia and for exactly the same reasons. Inside one-sixth of the world's land area is a group of peoples with enough iron ore and coking coal in sight to equip an army that England cannot dominate. World War III is a threat because Soviet Russia controls enough steel production to dominate Asia and its starved peninsula, Europe, that is, unless our steel equips armies with better weapons than the Soviets can build. This war may be the test whether fissionable material or iron dominates as the basic munitions material.

Some parallels are worthy of thought. The British Navy was not much assistance in the Boer War. In 1914 England still called their Army "Contemptibles" and even in 1941 was more concerned with home politics than with the probable disaster they faced in war. Their German neighbors underestimated the British Navy, but German Industry provided weapons for a land army that took the whole world to handle.

The French built the Maginot Line after World War I. The fortifications were almost in and under the French steel area from Metz to Luxembourg. The blast furnaces they rebuilt after World War I in the same area were hand charged, hopelessly out of date and manned by workmen who had been misled by political opportunists. The Maginot Line did not stop the invading armies, nor did French steel industry give much aid to the military. British steel industry, sabotaged by doubtful tax policies and questionable labor politics, was not much support to Great Britain in 1939. Slow-down policy of restricted output was clearly in effect in 1942 when I was in Britain in connection with war steel production and the needs of the British war effort. The United States should not be unduly critical of the effort of some of our Allies, as we have many examples of the same opportunist thinking at home. We may not have a Chamberlain skillful enough to buy us a year for preparation by being willing to die in disgrace in order to lead an enemy away from the real work that he was accomplishing.

The by-product coke oven, while making better coke for the blast furnace, anchored the steel plant within the areas of large population. The political opportunists were not slow to understand the change. Communities dependent upon steelmaking were now part of great population areas. The political portion of the industrial communities saw that a combination of interests of the socialistic-minded labor politicians and the city machine politician could serve each other very well. It was well summarized in Pittsburgh in 1932 when the leading city machine man said, "We are going to split up Andy Mellon's millions and you might as well get some." A part of Andy Mellon's millions was the Koppers Company.

The community lawsuits of today to eliminate the coke oven from populated areas may be only the work of unscrupulous local lawyers, but they have a strange similarity to the persecution of the local street railways of a generation ago and the wave of anti-industry persecution that came to England about 1900. Since we seem to follow the path of our English cousins, remember that an industrial nation needs a standard of machine perfection as well as a standard of living.



Over the years there has been much mental and physical energy expended to develop a substitute for the iron blast furnace which would eliminate the seemingly inefficient double refining process on which today's steel industry is based.

The major iron smelting problem concerns the principal raw material, iron ore. When the first ore was shipped from the Mesabi Range it was presumed to be an ore source which would last centuries. Yet after three generations, which included the Spanish-American and two World Wars, we find the blast furnace man wondering what ore he will be using next year. Not only do we frequently hear that our supply of ore is nearing exhaustion, but some are suggesting that there is need of government control to insure equitable distribution of what is left.

I would like to quote from the statement made by Secretary of the Interior Chapman in April, 1950, before the so-called Celler Committee studying possible changes in the anti-trust laws. Said Mr. Chapman:

"A problem facing the nation with respect to the steel industry associated with concentration of control is the lag between the rate at which the steel industry is expanding and the long-run rate at which the nation's economy is growing. The increase in steel production capacity is not expected to exceed 1% annually for the next few years, where the national economy, as noted, is expanding at the rate of about 3% per year. The capacity of the steel industry should be expanded to conform with those larger requirements of our expanding economy."

I would like to inject here the fact that the nearly 30 million tons of steel lost during strike periods in the last five years have been a more important cause of deficit than lack of expansions.

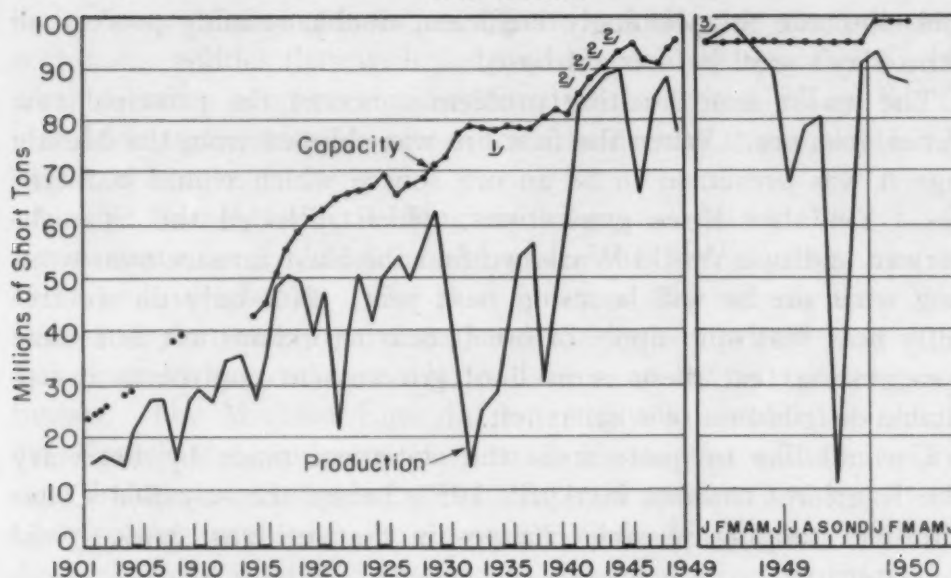
Mr. Chapman then points out that the degree of expansion which he suggests "is dependent to a great degree upon the availability of suitable raw materials". But he adds this rhetorical question: "Are there raw materials for any company to continue?"

My answer to Mr. Chapman's statement, if it had been directed to me, would have been a firm "Yes". I cannot agree that we are nearing the end of blast furnace ore in North America. Mr. Chapman's word "suitable" is somewhat like "virtuous"—the exact definition depends upon who defines it. The blast furnace man has behind him 500 years of history, proving that "suitable" is an ambiguous word.

The lowest iron content ore that I have observed in commercial blast furnace use was the 19.3% iron content ores used at Scun-



U.S. Capacity and Production of Steel Ingots and Steel for Castings  
1901 to 1950



• Capacities for Other Years Not Available

1/ The Figures for 1934 and Subsequent Years Include Only That Portion of Steel for Castings Made by Foundries Which Were Operated by Companies Producing Steel Ingots

2/ Average Annual Capacity as of January 1 and July 1

3/ Monthly Figures at Annual Rates

Source: American Iron and Steel Institute

thorpe, England, during 1942. The actual local ore with 16% iron had been combined with the comparatively rich Corby ore which had 29% iron. The Corby plant of Stewart & Lloyd was designed by H. A. Brassert and co-workers in the early thirties to use this rich 29% iron ore. It is today an excellent steel plant. The Scunthorpe furnaces of United Steel were McKee designed to handle the leaner ores of Lincolnshire. These excellent furnaces with outstanding performance records are leading the way in carbon lining for big furnaces. If this country ever gets humble enough to quit crying and go to work we need not use any 16% iron content for several hundreds of years. The coke blast furnace is a flexible tool in industry. It is effective—not necessarily efficient. What it can actually use has never been clearly established.

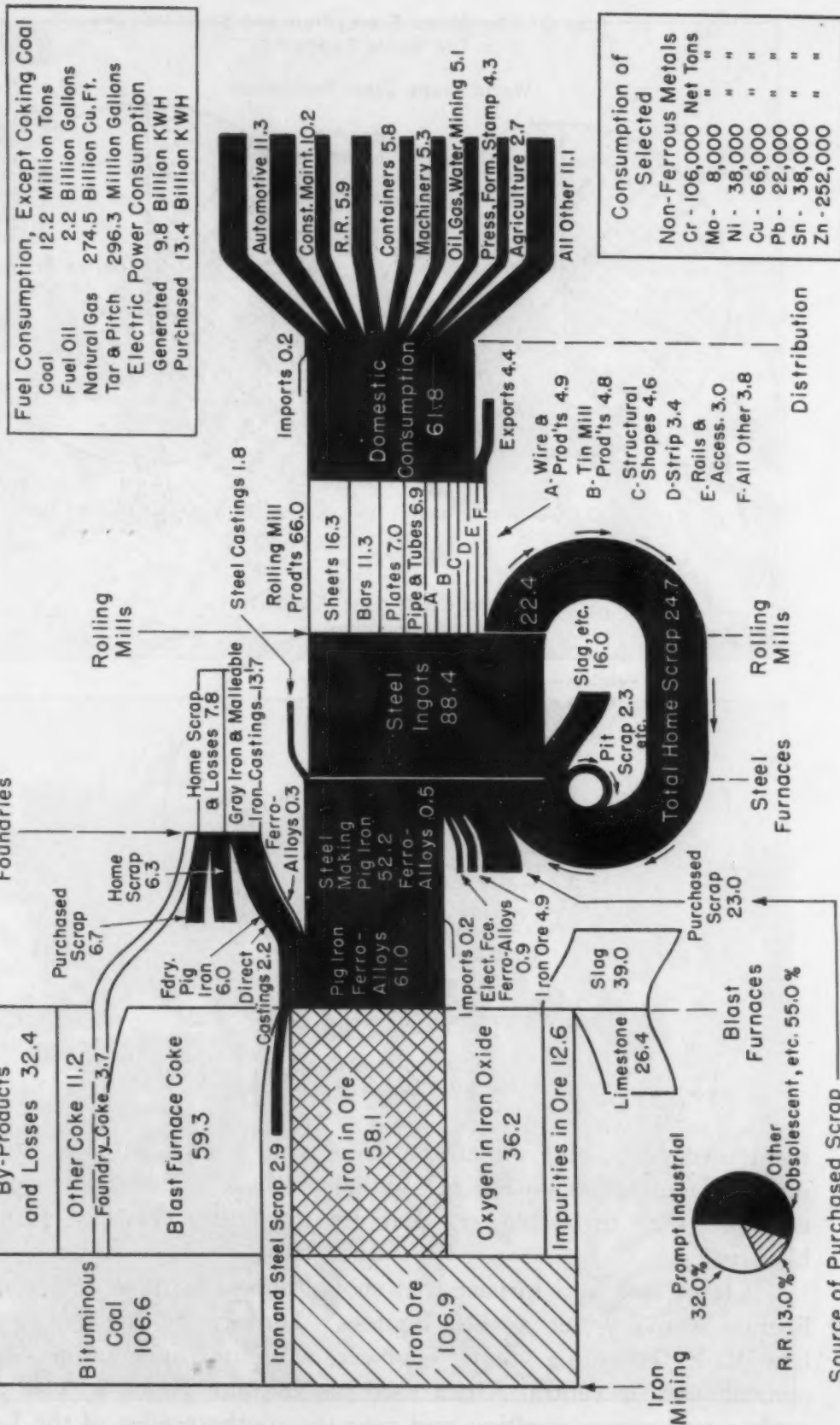
#### AFRICAN ONE-MAN FURNACES

One current political thought is based on the premise that all large industrial operations are inherently bad. The tendency to sanctify small operations is purely a smoke-screen set up by those who preach that all industrial production should be under govern-

# United States Iron and Steel Industry

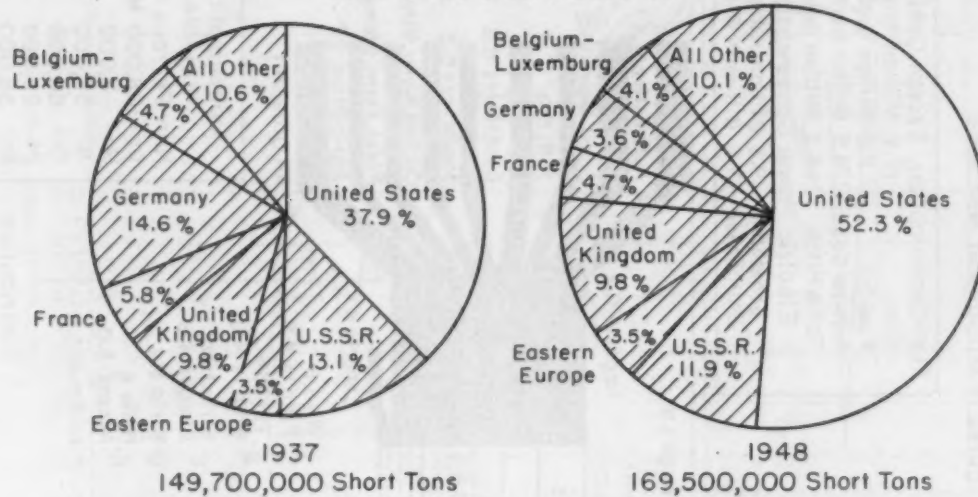
## Physical Flow From Raw Materials to Finished Products - 1948

(All Figures in Millions of Net Tons)

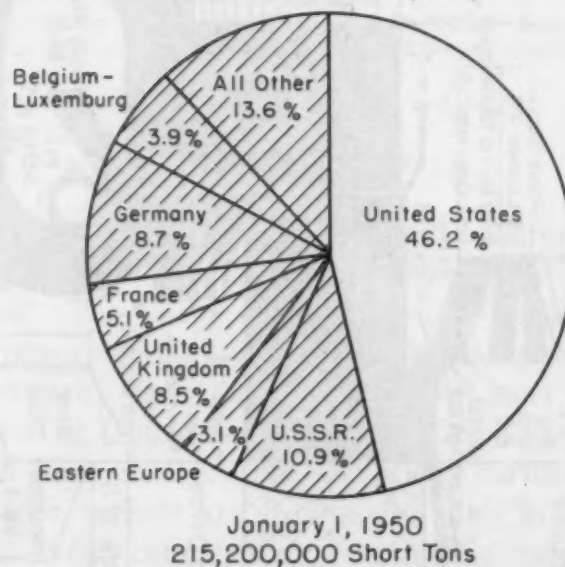


### Role Of The United States Iron and Steel Industry in The World Economy

#### World Crude Steel Production



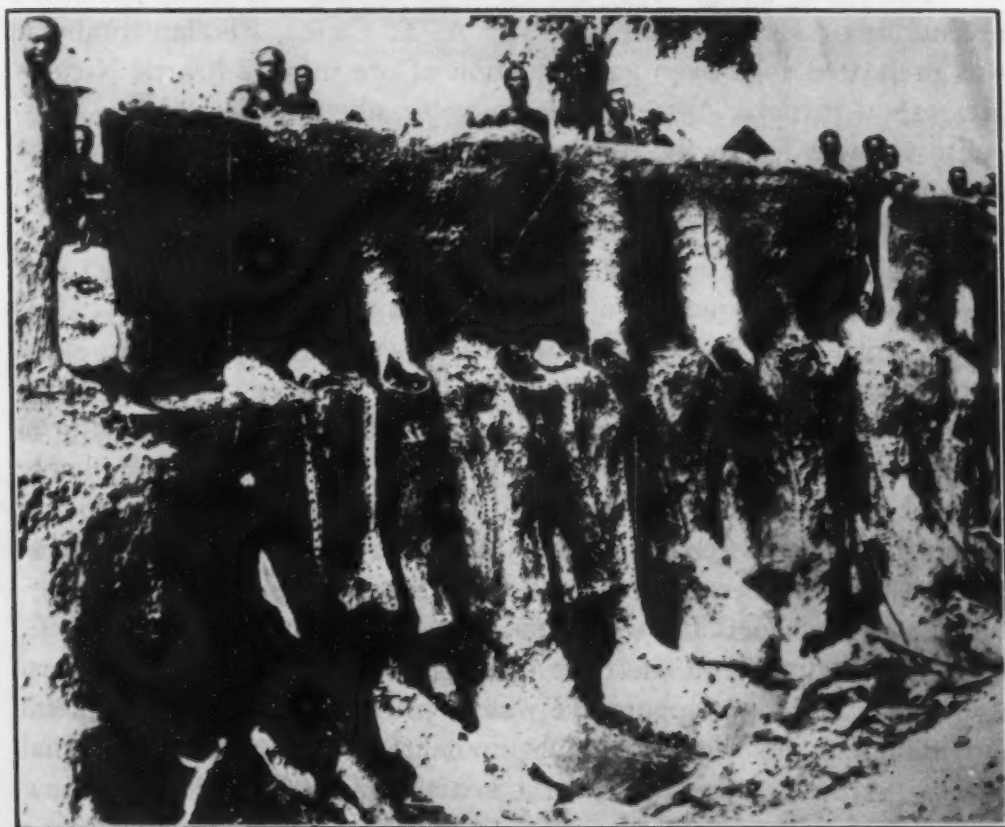
#### World Crude Steel Capacity



ment ownership, and yet at the same time point with glee at the unusual tonnage obtained in southern Russia from big furnaces equipped with turbo blowers that are the largest in blast furnace history.

Let us look at a furnace that should appeal to those self-termed liberals who cry out against bigness. During World War I the late W. E. Thorne, a mining engineer, while on copper mine development work in central Africa used his vacation period to visit and study a native iron smelting unit near the southern edge of the Lake





African One-Man Furnaces, Lake Chad Area, 1917. *Courtesy W. J. McCaughey.*



Chad area. The illustrations of this operation were made from photographs sent to Prof. W. J. McCaughey of Ohio State University.

The African blast furnace consists of a mud tube 8 inches in diameter made by plastering a bundle of reeds. While still damp this tube is set in place in the edge of a soft rock formation in a half round gutter in the rock face which supports the tube.

The operation consists of drying the tube in position, filling it with charcoal and ore, keeping the blast going while more charcoal and ore are added. The resultant lump of reduced spongy iron is moved to a forge fire, reheated and forged to remove slag and is then reformed into small bars for use by the natives.

#### BRASSERT-CAPE

Direct reduction to sponge iron appeals to many who feel that modern industry is too big and complicated. Since it was my lot to be on the losing side of our direct reduction test at Warren, Ohio, it may be well to explain what we encountered. Even those who lose the battle may record their side of the fight, although this is not the usual procedure.

The plant, designed by H. A. Brassert and his men, combined inventions of Mr. Brassert and Mr. A. T. Cape. Fundamentally it was preheated coke oven gas reduction of ore in a 12-hearth Nichols Herreshoff furnace, 20 feet inside diameter, about 53 feet high. Magnetite ore was fed to the top hearth after drying. This furnace was designed to handle daily 140 tons of ore from which would be produced 85% reduced melting stock, at the daily rate of 100 tons. Republic's Canton Electric Furnace Shop was to use the product and this amount was about 3% of the charge at that time.

A word about the reasons for this experiment will serve to eliminate the myth that we expected unusual results. We needed material for reboiling electric furnace steels during the war. Such material would be desirable if it was free from alloy, not quite completely reduced and yet heavy enough to sink through the slag and submerge in the metal. We felt we could justify the more expensive direct-reduced material because of its freedom from alloy contamination.

Under instructions we started at low temperature, 1150 °F, where the hydrogen of the coke oven gas was to combine at a very high rate. The low temperature was to prevent welding of the metal and minimize the wear on the equipment. We got so little actual metallic reduction (0.5%) with the hearths at 1100 °F that we knew the big furnace was not agreeing with the laboratory. Upon slowing down the feed and holding the ore on the hearths we finally got 21%

reduction. As soon as we satisfied the inventors that we were not getting results, we moved to our top amounts of gas flow and got 38% reduction. Unable to better this, we added approximately 1% soda ash, kicked the temperature up to 1250 °F hearth temperature and got about 85% reduction.

With good reduction our briquette plant, which was a pair of rolls, promptly welded the sponge iron on the roll face and smashed

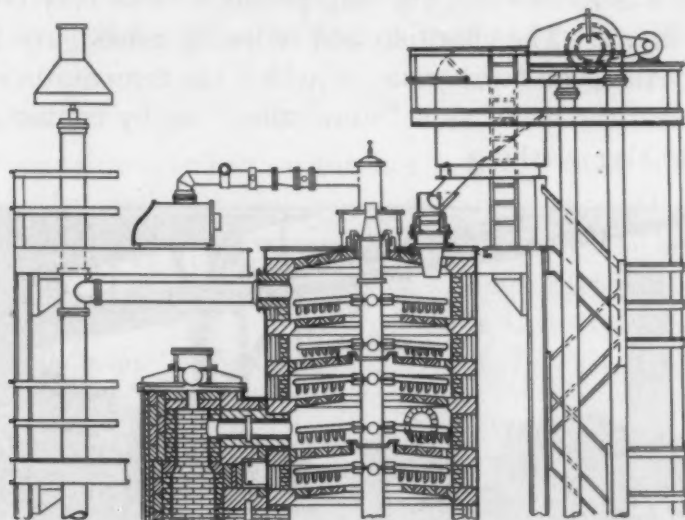


Diagram of Brassert-Cape Furnace.

the machine. Since it was impossible on account of war needs to get a plunger-type briquette press, we continued to use the rolls with much mechanical delay.

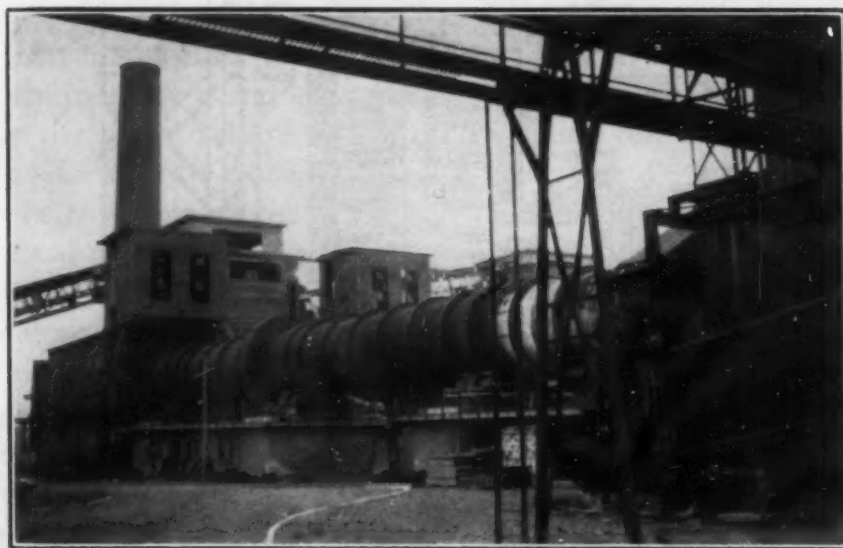
We finally got production to about one-third the planned output. The product, fragile, high in sulphur, disliked by the steelmelters, was charged into the blast furnace with the exception of small trial lots made into electric furnace steel at Canton. In fairness to all concerned, the lack of a proper hydraulic briquette press was the worst obstacle we met.

#### KRUPP RENN

Another small unit of modern vintage is the Krupp Renn Luppen furnace. On the basis of previous experience with handling high iron content zinc ores in the Waelz process, the German iron industry about 1930 undertook a series of studies to provide means of smelting certain lean iron ores. The invention of F. Johannsen (U. S. Patent 2,228,702) of a rotating kiln furnace similar to a cement kiln was the result of this work. Known as the Krupp Renn, it was well explained both as to purpose and product by Houdremont in 1939. This furnace produced iron for melting scrap, also recov-

ered nickel from very lean nickel silicate ores, and could have produced manganese-rich slags. It is a furnace very difficult to operate, but useful in war, a tool possible for use in the United States in case of submarine warfare.

The Field Information Agency Technical Report 799 describes them as 230 feet long, 13.8 feet in diameter, brick lined, using oil or coal for fuel. The process reduced the iron but did not melt it. The gangue was melted and the slag produced was very corrosive to the furnace lining. The charging and reducing zones gave little trouble, but the balling or finish zone, in which the temperature was high enough to weld the metal as it "snowballed" up by contact, was subject to liquid slag washing.



Krupp Renn Furnace.

The metal product, called Luppen—an old European name for a lump or small bloom of iron—was so variable in size, from tiny particles to lumps weighing several pounds, that it is difficult to present any dimensions.

The slagging of the outgoing end was such a problem that the furnaces were considered by the Germans and Japanese as wartime units, too difficult for peacetime use. It is of interest that only the furnace of the Russian satellite area of Silesia is now being operated. The slags range from 55 to 65%  $\text{SiO}_2$ , 15 to 30%  $\text{Al}_2\text{O}_3$  and from 12 to 25% of  $\text{CaO}$ ,  $\text{MgO}$  and  $\text{FeO}$ . Houdremont indicates 57%  $\text{SiO}_2$ , 25%  $\text{Al}_2\text{O}_3$  and 18% bases as typical. This would indicate the need for a siliceous refractory lining and the firestone used in acid Bessemer lining is very similar to the material that was most useful.



From the studies made of the operations of the Goering Werke it appears that the Krupp firm built, operated and maintained the Renn Feuers, as they were called. The simplicity of forcing such a burden on a private corporation in order that the difficulties would not embarrass the administration should appeal to government ownership advocates.

Krupp Renn furnaces may be used in this country for the beneficiation of manganese ore, or to smelt lean nickel ore. It is unlikely they will be used for the smelting of iron except in times of stress.

#### WIBERG

A proper direct-reduction furnace for very small output is operated in Sweden and is useful where certain economic conditions are present. Direct reduction of iron ore with fuel is the oldest method of production. There are interesting savings that might be the reward of the inventor of a really effective direct-reduction process. Efficiency in the use of fuel, particularly of the character of charcoal, coke, or petroleum carbon, is indicated.

The commercial furnace invented by Prof. Martin Wiberg of Sweden is today the lowest fuel consumer in the iron reduction business. The fuel consumption of 9,000,000 Btu per ton of product is offset in industry by the very small capacity, which is about 30 tons per day. This capacity is possible because of very select ore. The furnace will reduce ordinary ore well, but for its very limited output small amounts of high-grade ore are used.

The process has been well described by E. Ameen and P. E. Cavanaugh and others. It has reduced American ore in the experiments with Steep Rock Lake hematite. The usual Swedish materials are the excellent Kiruna Lump and such sinters as Vintjarn. The product has been the source of melting stock for high-grade steel for many years.

The Wiberg process and its accomplishment should be on the study list of any new sponge iron inventor. Its 9,000,000 Btu per ton figure is the best measuring stick yet afforded for any new process. Inventors who turn up with lower fuel requirement should be sure of their figures. The pounds of iron per cubic foot of working volume per day Eketorp estimates as 54. This is about equal to an American blast furnace but is far below the Domnarvet furnaces of Sweden which make about 90 pounds of iron per cubic foot per day.

The iron as reduced is very low in sulphur, for the reducing gases are cleaned before entering the tall, narrow shaft. Much of the material is below 0.010 sulphur, which is excellent for making electric



furnace steel. Its value in fuel-fired furnaces such as a basic open-hearth would be less. In Sweden, with acid open-hearth and electric furnaces as the usual conversion process, the material is excellent.

The very small diameter shaft required to zone the furnace will be a serious obstacle to large production from single units. To multiply the units is not impossible for the countries that have excellent iron ore and very limited coke supply. Since the process reduces by gas, it might be said that any source of carbonaceous gas of reducing nature could supply the fuel. This is not exactly correct, as the amount of hydrogen that can be handled has real limitations. The reduction of iron ore with methane is distinctly a high temperature furnace operation.

The furnace offers many chances to study the reduction process; the ore does not melt nor is slag formed in more than minute amounts. We can learn what goes on in the big blast furnace above the smelting line, a privilege we rarely get in big furnaces. Small furnaces have been stopped and cooled with inert nitrogen, but the big furnaces are too difficult to handle. We see what is in a big furnace only when a catastrophe stops it very quickly.

#### ORE BENEFICIATION

Biringuccio's instruction that one "must provide an experienced, intelligent sorter who will carefully sort the pure from the impure and will separate them according to the indications of their appearance and by breaking them" is useful today. We mine ore with a considerable degree of selection on the part of the miner. Even the open pit ore is subject to much selection, mixing and blending. Since modern magnetic separation makes Biringuccio's lodestone a particularly useful iron ore, science has evidently progressed in five hundred years.

Two of the new beneficiation projects in iron ore have moved far enough to warrant discussion, although there are many who say neither is economically sound at this time. Southern ores are being beneficiated, sintered and used today in Republic's Southern operations. Whether they can compete with imported ores or new beneficiation methods, only time will tell. In the North, the magnetic taconites of Minnesota, the magnetite concentrates of the Adirondacks, and the magnetite ore of the Cornwall Mine have been used to produce pellets that worked well in full size blast furnace tests.

Pelletmaking history extends back more than a generation when the Swedish tackled the problem of blast furnace ore from magnetite slimes finer than 300 mesh. Results this year from several tests indi-

cate pellets can be made about as economically as sinter. Studies of both sinter and pellets indicate the pellet has some very desirable characteristics. The three outstanding are:

1. Pellets can be substantially all the easily reducible oxide hematite.
2. They are porous and reduce easily.
3. The silica gangue of the ore does not produce large amounts of Fayalite or iron silicate glass.

Shipments of pellets totaling 10,000 tons have been made without undue breakage. We have no doubt that similar handling qualities will be shown by shipments throughout several seasons.

The taconite from which the present pellet development, or other better products, will come is a very siliceous rock with small amounts of magnetite. The ore will run slightly under 30% iron. Large-scale operations, including mining, concentrating, pelletizing, and shipping are expected to be done for about present ore price.

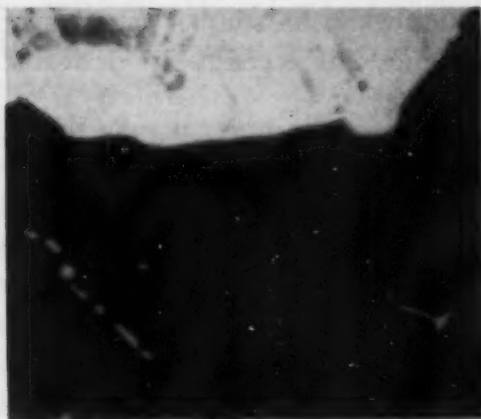
The nonmagnetic lean ores, such as the Western Mesabi taconites and the lean Marquette (Michigan) ores, we can leave for the iron men of the year 2500. Where coarse-grained magnetites are involved it seems quite reasonable to predict that sintering will be used. There seems no logical reason to grind fine enough to make the pellet type of product.

#### ORE BENEFICIATION—SOUTHERN

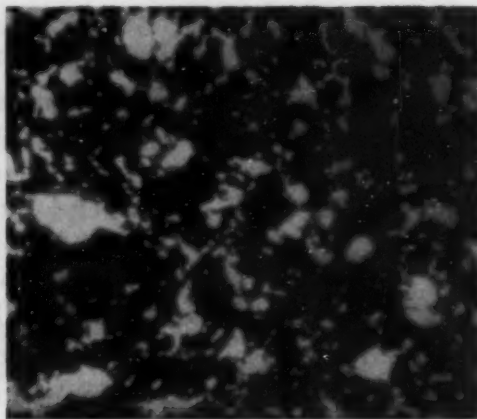
The Southern iron ore of Red Mountain near Birmingham, Alabama, presents a problem of working with a softer ore. The Clinton formation holds the Big Seam, the important, workable ore body. It is from 10 to 22 feet in thickness, dips off to the southeast and the complete extent is not known at this time. The probable recoverable ore is certainly a guess as the overlying Fort Payne chert is a water-bearing strata. Faulting has broken the formations in such a manner that the water hazard is very real; water pressures approach 1000 pounds per square inch.

At the northeast end of Red Mountain outcrop, ore is definitely high in silica due to leaching out of the lime. Such ore is now being beneficiated at the Spaulding Mine of Republic Steel. Sinter from this operation is used both at Birmingham and Gadsden plants.

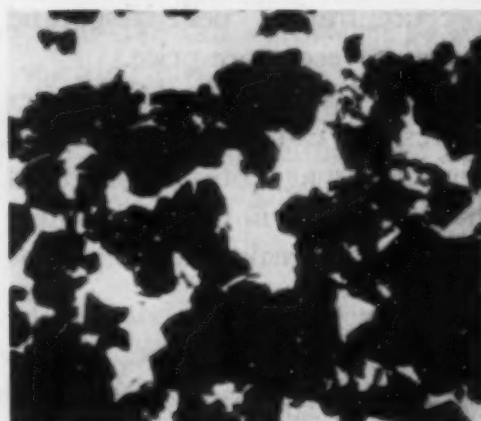
The Big Seam ore is oolitic. The problem of ore dressing involves the separation of very soft hematite from a fossil beach made up of beautiful particles of sand, fossil remains of tiny creatures of the seas of Silurian times and dispersed through the whole is clay so fine that it has not been possible to separate for identification. The ore must be crushed to a size where the hematite can be rubbed off



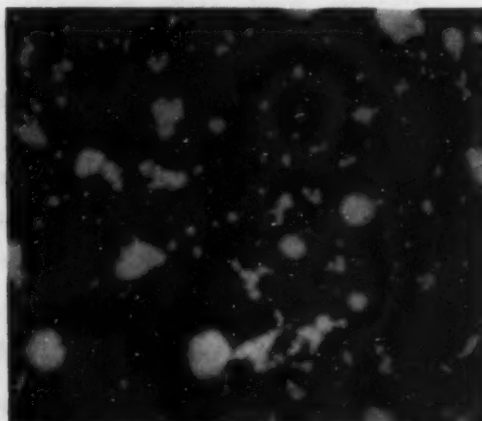
Coarse Grain Magnetite,  
Fisher Hill Mine, New York.



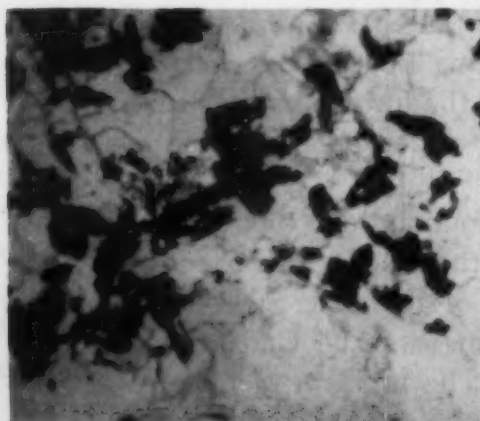
Pellet Port Henry (New York) Ore.



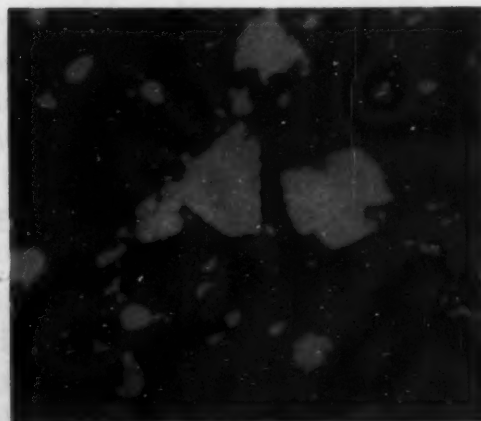
Medium Grain Magnetite,  
Cornwall Mine, Pa.



Pellet Cornwall, Lebanon, Pa.



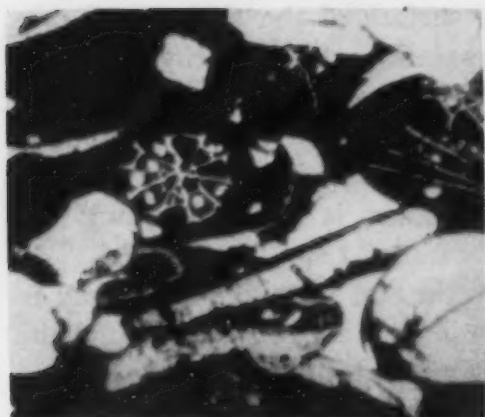
Fine Grain Magnetite,  
Magnetic Taconite, Minn.



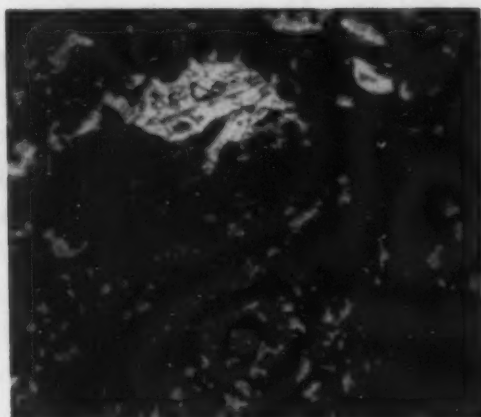
Pellet Magnetic Taconite,  
Minn.

Petrographic Sections of Ores and Resulting Sinters. Magnification  $\times 20$ .

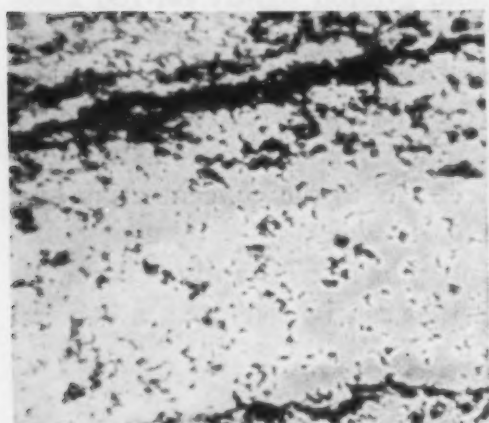
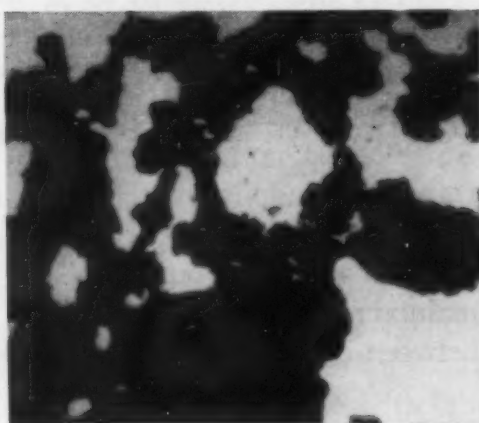




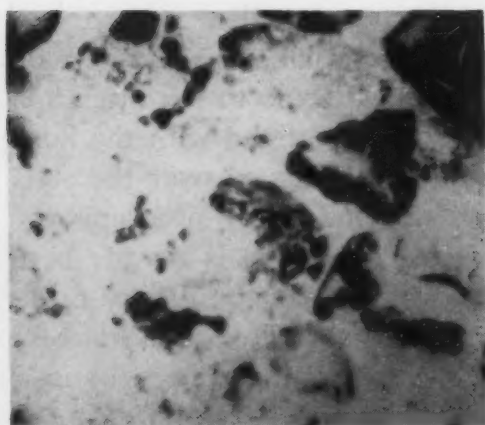
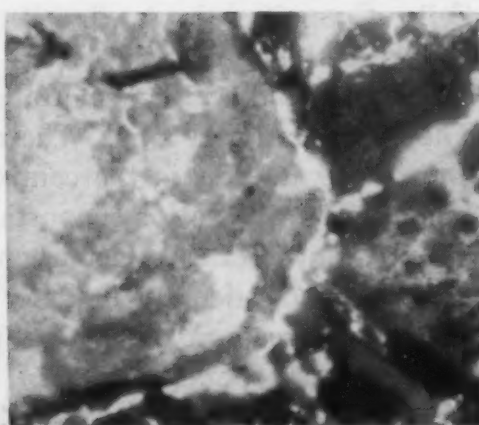
Hematite, Spaulding Mine, Ala.



Hard Burned Sinter, Canton, O.

Lean Hematite Ore,  
Negaunee, Mich.

Swedish Sinter.

Hematite (Minn.),  
Non-Magnetic Taconite.Blast Furnace Hearth, Buffalo, N. Y.  
Iron Penetration.  
*Courtesy W. J. McCaughey and  
J. O. Lord.*

Petrographic Sections of Ores and Sinters. Magnification  $\times 20$ . Hearth bottom with iron penetration.



the sand grain, as well as from the surface of the skeleton of pre-historic, tiny, sea creatures. The separation of this sticky, red mud from the sand, chert and the hard portions of the ore is difficult. Equally difficult is the separation of the water from the mud to a degree that permits sintering. The sintering of slimy mud is considered impractical. The resultant product is not self-fluxing nor does the phosphorus change much.

The blast furnace men are uncertain that this is the best way to prepare this ore. No other producer in the area has duplicated the plant. Beneficiation studies are being pushed, but, as in other times, the blast furnace operator has made the best of the material available.

For the record, a short, technical description of the Spaulding concentrate process devised by Mr. Oscar Lee is included:

Dry ore is crushed to  $\frac{1}{4}$  inch and ground lightly on rod mills with 8-mesh screens to minimize overgrinding. The screen under-size is de-slimed in bowl classifiers and the slime de-watered to concentrates. Classifier sands, after further hydraulic classification into 8 size bands, go to shaker tables. Granular hematite goes as concentrates, the middling is reground and returns to the concentrating circuit, and the tailings are rejected. The de-watering equipment bulks large in the plant outlay. The tailing pile is constantly studied to maintain, within the limits of the cost that can be tolerated, a balance between concentrates and tailings.

#### DR. JAMES BOYD'S STATEMENT ON IRON ORE

The statement Dr. Boyd of the Bureau of Mines made to the Celler Committee in April, 1950, provides an excellent summary of the present ore supply problem. His tables provide the best data on supply, demand and transportation that have come to my attention. They merit critical study. These tables are presented with the hope of arousing interest in the controversy now going on over the steel supply and iron ore for supporting present and future programs.

Dr. Boyd stated a fact when he said, "The time is already here when the domestic steel industry would have serious difficulty operating at full capacity from the present domestic iron ore sources; in fact, at an operating rate of 100% capacity, inadequacy of iron ore supply is indicated for 1950."

Included to assist evaluation are part of the charts presented to the Celler Committee in April, 1950, by Mr. H. B. McCoy, Director, Office of Domestic Commerce, Department of Commerce.

Dr. Boyd enumerates the contributing factors as follows:

1. The heavy drain upon the iron reserves of the Mesabi Range during World War II and the high demand during postwar years.
2. Inadequacy of the shipping capacity on the Great Lakes and the delay necessary to expand and modernize the Great Lakes fleet. Shipyard capacity is available for only 6 boats every 18 months.
3. The continued high demand for steel production accompanied by substantial increases in steel-producing capacity.
4. The necessary delays in developing new sources of iron ore.
5. The preponderant concentration of steelmaking capacity in the areas adjacent to the Great Lakes transportation.

There are 265 boats in this type of service, so our shipping capacity can hardly be made adequate unless new shipyards are built. We have ore. We must develop new mines, provide adequate transportation. This will require a change of political views in many places.

#### FIREBRICK-LINED FURNACES

My personal interest in blast furnaces started fifty years ago when I burned a bare foot while exploring the mysteries of a cast house in New Castle, Pa., long before the days of safety regulations and plant protection forces. That cast house had many interesting points for a small boy. My next serious look at a blast furnace was years later in Columbus during Ralph H. Sweetser's time. Another of my friends of that time was Wilbur Stout, who became an expert in the archeology of Ohio charcoal furnaces during his time with Ohio Geological Survey. Under the sponsorship of Prof. D. J. Demorest,

**Table I**  
**Total United States Iron Ore Requirements at Assumed Steel Production Rates, 1950-70**  
(in millions of tons)  
Statement of Dr. James Boyd, April 17, 1950

Janu- ary 1	Steel Capacity (Net Tons)	Produc- tion at 85% Capacity (Net Tons)	Pig Iron Require- ments at 85% Steel Capacity (Net Tons)	Iron Ore Require- ments at 85% Steel Capacity (Gross Tons)	Pig Iron Require- ments at 100% Steel Capacity (Net Tons)	Iron Ore Require- ments at 100% Steel Capacity (Gross Tons)	Iron Ore Supplies at 100% Steel Capacity (Gross Tons)
1950	99.4	84.5	57.5	96.0	67.6	112.9	104.2
1951	100.0	85.0	57.8	96.5	68.0	113.6	103.4
1952	101.0	85.9	58.4	97.5	68.7	114.7	102.9
1953	101.0	85.9	58.4	97.5	68.7	114.7	105.0
1954	101.0	85.9	58.4	97.5	68.7	114.7	109.4
1955	102.0	86.7	59.0	98.5	69.4	115.9	114.9
1956	103.0	87.6	59.6	99.5	70.0	116.9	113.9
1957	104.0	88.4	60.1	100.4	70.7	118.1	124.9
1958	106.0	90.0	61.2	102.2	72.1	120.4	127.2
1959	108.0	91.7	62.4	104.2	73.4	122.6	129.2
1960	110.0	93.5	63.6	106.2	74.8	124.9	129.1
1965	117.0	99.5	67.7	113.1	79.6	132.9	124.0
1970	125.0	106.3	72.3	120.7	85.0	142.0	119.4

**Table II**  
**United States Iron Ore Supplies and Deficiencies Under Assumed Conditions, 1950-70**  
 (in millions of gross tons)  
 Statement of Dr. James Boyd, April 17, 1950

	1950	1951	1952	1953	1954	1955	
Maximum iron ore supplies:							
At normal (85%) steel prod.	Ore available to meet all requirements						
At full steel production	104.2	103.4	102.9	105.0	109.4	114.9	
Emergency (restricted imports)	102.2	101.4	100.9	103.0	107.4	112.9	
Deficiency of supply:							
At normal (85%) steel prod.	none	none	none	none	none	none	
At full steel production	8.7	10.2	11.8	9.7	5.3	1.0	
Emergency (restricted imports)	10.7	12.2	13.8	11.7	7.3	3.0	
	1956	1957	1958	1959	1960	1965	1970
Maximum iron ore supplies:							
At normal (85%) steel prod.	Ore available to meet all requirements						
At full steel production	113.9	124.9	127.2	129.2	129.1	124.0	119.4
Emergency (restricted imports)	111.9	122.9	125.2	127.2	127.1	122.0	117.4
Deficiency of supply:							
At normal (85%) steel prod.	none	none	none	none	none	4.1	21.5
At full steel production	3.0	0	0	0	0	13.9	27.6
Emergency (restricted imports)	5.0	0	0	0	0	15.9	29.6

**Table III**  
**Maximum Iron Ore Supplies for the United States, 1950-70**  
 (million of gross tons)  
 Statement of Dr. James Boyd, April 17, 1950

Source:	1950	1951	1952	1953	1954	1955	1956	1957	1958	1959	1960	1965	1970
<i>Domestic</i>													
Southeastern States	8.0	8.0	8.0	8.0	8.0	8.0	8.0	8.0	8.0	8.0	8.0	7.0	6.0
Western States	5.0	5.0	5.0	5.0	5.0	5.0	5.0	5.0	5.0	5.0	5.0	6.0	7.0
Northeastern States	4.0	4.0	4.0	4.0	4.0	4.0	4.0	4.0	4.0	4.0	4.0	5.0	6.0
Lake Superior Dist.	82.7	81.4	79.4	77.9	77.5	75.7	72.1	71.1	69.6	67.6	67.0	47.4	33.8
Taconite Concentr.	...	...	...	...	2.5	6.0	6.5	7.0	10.0	13.0	13.5	22.0	25.0
Total Domestic	99.7	98.4	96.4	94.9	97.0	98.7	95.6	95.1	96.6	97.6	97.5	87.4	77.8
<i>Foreign</i>													
Canada:*													
Lake Superior Dist.	...	...	...	1.1	1.1	2.0	2.0	2.0	2.0	2.0	2.0	2.0	2.0
Quebec-Labrador	...	...	...	...	...	...	...	10.0	10.0	10.0	10.0	15.0	20.0
Chile	2.5	2.5	2.5	2.0	0.6	0.6	0.6	0.6	0.6	0.6	0.6	0.6	0.6
Sweden	1.0	1.0	1.0	1.0	1.0	1.0	1.0	1.0	1.0	1.0	1.0	1.0	1.0
Liberia	...	...	1.0	1.0	1.0	1.0	1.0	1.0	1.0	1.0	1.0	1.0	1.0
Venezuela	...	0.5	1.0	4.0	7.7	10.6	12.7	14.2	15.0	16.0	16.0	16.0	16.0
Other	1.0	1.0	1.0	1.0	1.0	1.0	1.0	1.0	1.0	1.0	1.0	1.0	1.0
Total Foreign	4.5	5.0	6.5	10.1	12.4	16.2	18.3	29.8	30.6	31.6	31.6	36.6	41.6
GRAND TOTAL	104.2	103.4	102.9	105.0	109.4	114.9	113.9	124.9	137.2	129.2	129.1	124.0	119.4

\*Net U.S. Supply (imports minus exports).

my undergraduate thesis was a series of load tests on blast furnace firebrick, a correlation of the size of the different clays with the compressive strength of varied mixtures. I have had occasion in recent years to remember that initial experience with the imperfect matching of bond clays.

#### LINING PROBLEMS

Blast furnace firebricks, the resultant of some hundreds of years of trial and error, represent the blending of different clays. The



**Table IV**  
**Iron Ore Reserves of the United States, January 1, 1950 (in Gross Tons)**  
 Statement of Dr. James Boyd, April 17, 1950  
 (Prepared by United States Geological Survey)

	Grade % Fe <sup>3</sup>	Commercial <sup>1</sup> Tonnage (Measured, Indicated and Inferred)	Submarginal <sup>2</sup> Tonnage
Northeastern <sup>4</sup>	60 <sup>5</sup>	1,600,000,000 <sup>6</sup>	200,000,000
Southeastern <sup>4</sup>	35	1,100,000,000	800,000,000
Lake Superior <sup>7</sup>	51.5	1,600,000,000	61,000,000,000
Western <sup>8</sup>	50	800,000,000	250,000,000
Total	....	5,100,000,000	62,250,000,000

<sup>1</sup>Material of such nature and geographic and geologic distribution as to be considered usable under present economic and technologic conditions. (See submarginal column.)

<sup>2</sup>Material that may become usable under future conditions. This includes: Material of lower grade than is now being mined. Material of usable grade but in deposits less than minable size. Deposits of minable size but containing impurities in harmful quantities. Deposits technologically satisfactory but too remote from transportation and blast furnaces for present use.

<sup>3</sup>Approximate.

<sup>4</sup>The commercial reserves of the Northeastern States are in New Jersey, New York and Pennsylvania; the submarginal material includes the low-grade ores of Maine and Ohio.

<sup>5</sup>Concentrates. From Geo. W. Hewitt, Iron ore supply for future: American Iron and Steel Institute Meeting, May 21-22, 1947, p. 7.

<sup>6</sup>Nine-tenths of the commercial ores of the Southeastern States are in Alabama; the other tenth is in Georgia, Kentucky, North Carolina, Tennessee, Virginia, and West Virginia. Submarginal ores are divided between Alabama and the other Southern States.

<sup>7</sup>The enormous taconite resources are included in the "Submarginal" column.

<sup>8</sup>In the States west of the Mississippi River, Utah and Texas have five-eighths of the commercial reserves.

**Table V**  
**Active Foreign Iron Ore Interests of United States Firms**  
 (United States Geological Survey)

Country and Deposit	Reserves Tons	Grade	Interested United States Companies	Operating Companies
<i>Chile</i>				
El Tofo	85,000,000	50-60% Fe	Bethlehem Steel Corp.	Bethlehem-Chile Iron Mines Co.
El Romeral	20,000,000	60% Fe		
<i>Liberia</i>				
Bomi Hills	14,835,000 108,100,000	66-67% Fe 42% Fe	Republic Steel Corp.	Liberian Mining Co.
<i>Venezuela</i>				
Cerro Bolivar (and 25 others)	Greatly in excess of 1,000,000,000	Of highest grades	United States Steel Corp.	Orinoco Mining Co.
El Pao (and 19 others)	60,000,000	60% Fe	Bethlehem Steel Corp.	Iron Mines Co. of Venezuela
<i>Canada</i>				
Quebec-Labrador	Close to 400,000,000 indicated at present with further possibilities.	About 60% Fe	M. A. Hanna Co. Republic Steel Corp. Wheeling Steel Corp. Youngstown Sheet & Tube National Steel Corp. Armco Steel Corp. and Canadian Companies	Iron Ore Co. of Canada
Steep Rock	282,000,000	55% Fe	U.S. Stockholders Inland Steel ("C" body concession)	Steep Rock Iron Mines Ltd. Not operating yet.
Michipicoten area:			Jones & Laughlin Steel Corp. Option	Not operating yet.
Michipicoten	100,000,000	35% Fe		
Ruth mine	28,600,000	26-35% Fe		
Lucy mine	"Moderate"	About 35 (low silica)		



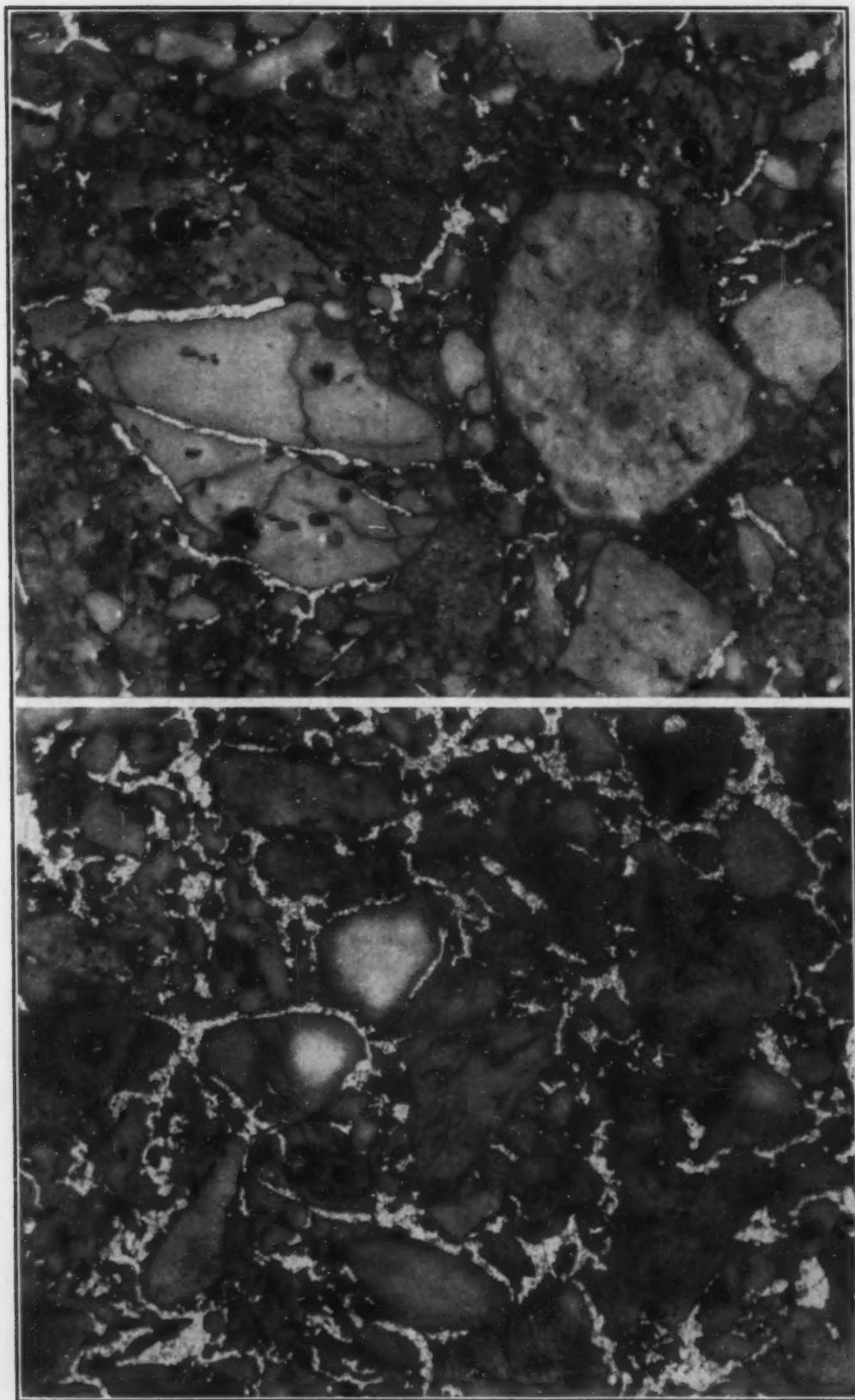
usual combination consists of a clay with good refractory properties and indifferent bonding qualities mixed with another clay that may have mediocre refractory properties but excellent bonding ability. The whole business, the exact particle size of each clay, the amount of ingredients, the molding, drying, burning, inspection, and shipping, is a mixture of art, science, skill and commerce.

Since a blast furnace hearth is expected to be in service many years, any reasonable precaution is justified. Every care possible is given to making and testing. Special masons, moving from company to company, lay the brick. The furnace operator uses the best judgment and skill available in blowing in the furnace. In spite of all known precautions, we have significant variations in the same furnace with different linings from the same brick company, with everything as nearly identical as customary testing could determine. In recent years a lining in one furnace lasted a week. Another furnace, after a full campaign, still had a hearth so nearly perfect that the salamander iron was less than 100 tons. That is the blast furnace man's problem in its nasty aspects. He is expected to get at least 2,000,000 tons of iron or more production from a hearth. Republic has several furnaces with that production out of the present hearths. It is a serious disaster when a hearth goes out in a week or even two months.

The lining that failed prematurely showed upon examination that internal fissuring in the brick permitted iron to penetrate the bricks. The combination of clays was not exactly correct. The brick simply disintegrated and the result was a hearth breakout. It is interesting to observe the iron penetration into the brick and realize that molten iron is not a very sturdy bond for the flint clay particles which make up the real body of the brick. Such failures, although very rare, explain in part why the European blast furnace men risked carbon blocks in their hearths and the reason behind the present experiment with carbon hearths in the United States.

#### CARBON HEARTH

The Thomas Basic Bessemer process of Europe requires an iron, high (2%) in phosphorus, that is more fluid than the lower phosphorus irons we use in American steelmaking. Hearth breakouts were more of a problem in blast furnaces making such fluid iron. A generation ago the European furnaces began carbon linings and they are more commonly used there. While our experience in the United States is too limited for conclusions, it may be said that, with more than 2,000,000 tons of iron on some American carbon hearths, this construction is here to stay.



Examples of Metal Penetration Into Refractory Brick in Blast Furnace Linings. (Upper) Clay hearth that failed in 6 days. (Lower) Clay hearth that failed in 60 days. Courtesy W. J. McCaughey and J. O. Lord.

There have been several quite serious failures; some of these failures have not been adequately explained. Personal observations of some of these linings at time of failure indicate no problems impossible of solution. It is my opinion that we will continue to use much carbon block construction. The working face of carbon-lined hearths has given little trouble. The saw cutting marks have been observed on carbon blocks in a hearth after making hundreds of thousands of tons of iron. Trouble has occurred at the iron notch area with wet notch clay and resultant steam destruction as the probable explanation. In Republic's carbon hearths we now install brick at the tap hole. We do have two furnaces with carbon block iron notch construction still in service with no indication of trouble.

Damage to the carbon blocks away from the working face has been explained by oxidation from steam as a probable cause, along with oxidation due to air infiltration. Our present construction is to provide a tight brick outer shell. While we attempt to prevent access of air to the hot carbon, we are more concerned about leaking water about the hearth. We have many problems still to solve. When we get a bit more experience and feel safe, we can direct our efforts toward higher production rates.

The carbon hearth may have arrived at the proper time. After studying the probable ore supply for future ironmaking in the United States, one can anticipate less alumina for the slag systems involved. In at least two recent hearth breakouts the lack of alumina (9 to 10%  $\text{Al}_2\text{O}_3$  slags) caused the furnace to slag the lining to satisfy the need for alumina. As in many other industrial moves the accessory protection of the nonslagging carbon block may well be more important than the primary saving envisioned at the time of installation.

#### PRESSURE OPERATION

The modern turbo blower for a blast furnace may be said to be able to deliver 100,000 cubic feet of air per minute at 30 to 35 pounds per square inch pressure. There have been larger blowers for some years in Europe; the largest, reported as 140,000 cubic feet per minute, were built by the Germans for Russian plants before World War II. The latest Russian-built turbo blowers have been reported as approximately the same size as the 125,000-cubic-foot blowers installed recently at Republic, Cleveland. The Russian turbo blowers were reported as able to operate at 42 pounds per square inch pressure, indicating they can use high top pressure.

The normal operation of a coke blast furnace requires a blast pressure that exceeds the approximate 18 pounds per square inch



pressure drop through the stack by enough to force the gas out of the furnace through the cleaning and into the gas system.

The pressure at the top of the furnace is about 2 pounds; furnaces that are being pushed rarely exceed 4 pounds pressure at the top. There are many operating reasons why this pressure has not been exceeded but the most important is excessive dust loss.

High pressure operation of blast furnaces was developed under the invention of Julian Avery. In 1938 Avery, then with Arthur D. Little Co., suggested in a paper on blast furnace operation that pressure operation be achieved by controlling the outflow of gas. The operation he suggested could be carried out at one or two atmospheres pressure above the normal. His invention concerned the automatic throttle valve at the outlet. As no furnace was equipped to carry such pressure, the demonstration awaited the war with its shortage of iron which justified the trial.

The Defense Plant Corporation furnace, adjacent to the Cleveland plant of Republic Steel, was operated as No. 5 Furnace of Republic by the blast furnace group under Mr. J. H. Slater, whose untimely death before this development was fairly started deprived the blast furnace industry of one of this generation's most capable men. The general foreman of this furnace, Mr. Walter Montgomery, has been with this operation since the start.

Cost calculations indicated that with Lake ore the furnace could be pushed until the dust loss exceeded 350 pounds of dust per net ton of iron. Such an operation did not require any change. To effect top pressure operation, and provide for blower capacity to test the theory, required controlled gas flow by Askania regulated valves in the gas main behind the washer. Extra wind by turbo blowers in series was made available.

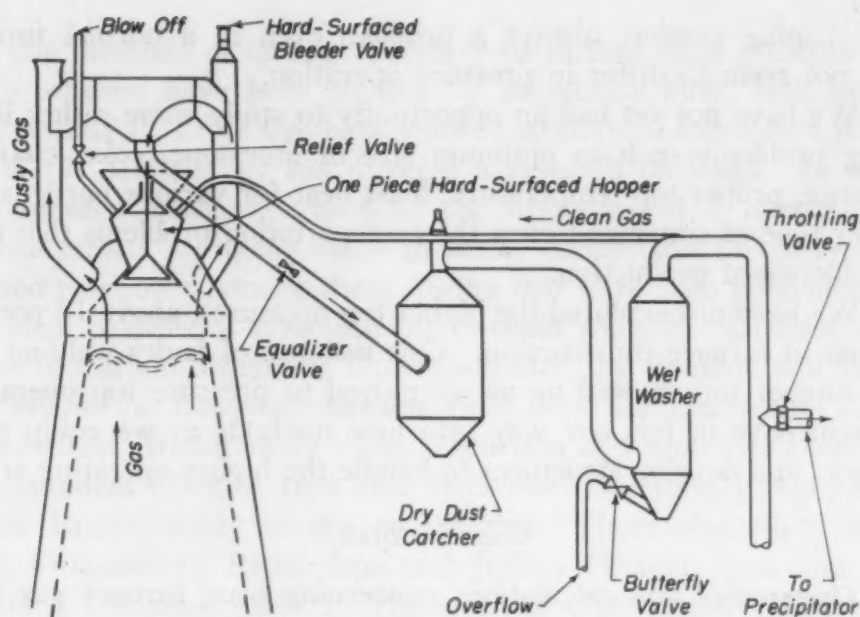
Although early operation under the observation of the War Metallurgy Committee indicated an excellent normal operating stack, pressure operations resulted in a series of problems. Numerous gas leaks allowed damage by grit blasting. Gas washer seals were inadequate. The new pressure regulating device was not well understood. When the furnace was finally able to operate, it was found that dust loss was very small, also that the furnace could handle the additional wind without getting rough in operation.

Joe Slater and Walter Montgomery, who had pushed the furnace during normal operating experiments to establish an upper limit of wind regardless of dust, were satisfied that less than 90,000 cubic feet per minute of wind could be used with straight Lake ore burden. Mr. Slater's most important criterion of test was simple: "Would the





Republic Steel's Pressure Blast Furnace in Cleveland.



Blast Furnace Alterations for Pressure Operation.

furnace settle down and drive smoothly when higher wind and top pressure were tried?" Blast furnace men are by nature determined people. Before Slater died he and Montgomery had blown 110,000 cubic feet of wind per minute with 11 pounds top pressure and had a smooth furnace on straight Lake ore. At an interesting meeting of blast furnace men it is related that Slater issued the ultimatum that he would show the furnace to anyone but answer no more questions in meetings except those from furnace men blowing more than 100,000 cubic feet of wind per minute on straight Lake ore.

The first lining finished its usefulness in the early days of October, 1950, and finally the first chapter of history can be written. We know we can operate for normal periods of time. We will provide additional furnaces as we can afford the equipment cost.

The practical operations test, now of four years' duration, has been under the observation of the Arthur D. Little Co. men, as have operations at Republic's Youngstown No. 3. The recent work has concerned a comprehensive study of how to sample gas from a blast furnace and make use of the data obtained. Further studies on high pressure operation are planned. Additional instrumentation is contemplated so that a more critical analysis of this new operation can be made.

We have behind us the actual operating experience. We have before us many problems such as better methods of handling the grit blasting gas leaks. The bell and hopper wear have been brought under control by equalizing pressure between the bells with cleaned

gas. Lining erosion, always a problem even in a normal furnace, does not seem to differ in pressure operation.

We have not yet had an opportunity to study some rather interesting problems such as optimum size of limestone, coke, charging sequence, proper top temperature, blast heat for various burdens, the proper type of sinter and even the transportation problems that arise with increased production.

We have not explored the higher top pressures, above 12 pounds, because of furnace construction. One instance of faulty welding in a dust catcher top showed up as we moved to pressure top operation. We will have to feel our way into new methods as we equip more furnaces and develop structures to handle the higher operating stress.

### GAS STUDIES

The studies and calculations concerning blast furnace gas have gone hand in hand with furnace development. Sampling has been an outstanding problem, analysis of the gas not particularly difficult, interpretation of results as variable as the schools of furnace operators. The Bureau of Mines studies of some years ago furnished a mass of well-handled measurements to blast furnace men. Interpretation of these data is still a matter of personal opinion. The present interest in gas study is important because of the relative increase in coke cost and operating expense. Ore and transportation costs have gone up but not in proportion to coke cost.

Borrowing from the oil industry the continuous sampler and developing an automatic analyzer have been the objective of a task group of Arthur D. Little Co., who have studied blast furnace gas for some years. The article entitled "Blast Furnace Control by Top Gas Composition" by Messerle gives an equation that satisfies most of the known variables for which data are obtained. It falls far short of the need, since it does not attempt to include the reducibility of the iron ore. It has been known for hundreds of years that limonites, hematites and siderites reduce with less trouble than magnetite. In Biringuccio's time, the magnetites were not considered ore in that area. The Swedish furnaces had solved the problem of reduction of magnetite many years earlier. Dense hematite ores were known to be difficult to reduce unless crushed to small particle size. Reduction studies to arrive at some measure of reducibility have been made in many laboratories. There have been many full-size furnace runs which give gross figures. All these tests are useful to the furnace operation but none permits him to burden his furnace except on an empirical basis.



The methods of testing necessary to further high pressure furnace operation have been studied by Republic's men; task groups from Arthur D. Little Co. have worked steadily in Republic's plants. Dr. W. J. McCaughey has directed a research on slags. In every blast furnace operating group of the whole world it appears that unusual efforts are being made to better understand this very complicated reaction. Among these studies that have been published and that seem of especial value are the German study of "Disintegrating Effect of Carbon Monoxide Upon Iron Ore" by Baukloh and Jaeger (*Archiv für das Eisenhüttenwesen*, 1939, Brucher Translation 2250), the excellent British study "The Reduction of Lump Ore" by Wild and Saunders (British Iron and Steel Institute, June 1950) and an earlier British study of the equilibrium "Thermodynamics of the Blast Furnace" by Richardson and Jeffres (British Iron and Steel Institute, December 1949). The work of our Bureau of Mines on gaseous reduction and that of other American laboratories, much still unpublished, has indicated that the porous, highly oxidized sinter or pellet is very easily reduced. These and many other studies such as the radon tracer timing of gas flow through the English blast furnace by E. W. Voice (British Iron and Steel Institute, November 1949) are all driving at fundamentals. Every industrial nation of the world needs more iron and it must be gotten by better operation of the present furnaces.

Since much of the work in blast furnace gas study is of the preliminary survey character, a large portion of the results has not been prepared for publication. In our gas studies at Republic, we are, as previously noted, about ready to equip a furnace for another chapter of this work. In a report presented to the Eastern States Blast Furnace and Coke Oven Association at Pittsburgh in 1945, Dr. D. E. Babcock presented a portion of the results of our work mainly for study as to possible use to blast furnace men. He expanded the use of the Messerle equation and directed his attention to a more critical use of the top gas analysis as a means of furnace operating control.

Dr. Babcock's paper "Blast Furnace Gas Composition and Its Interpretation" moved from the Messerle equation and developed the basis of additional interpretation in which the variable humidity within the furnace is more completely related.

The Messerle equation is made up to two terms. The first gives the quantity of oxygen from the charge by indirect reduction of each unit of carbon gasified; the second term gives the same for direct reduction.



The Messerle equation as presented was as follows:

$$\frac{32/22.4 \times 0.5 (\text{CO}_2\text{-CO}_2 \text{ flux})}{12/22.4 \times (\text{CO}_2\text{-CO}_2 \text{ flux} + \text{CO} + \text{CH}_4)} =$$

$$\frac{32/22.4 \times [0.5 (\text{CO}_2\text{-CO}_2 \text{ flux}) + 0.5 \text{CO} - 0.27 \text{N}_2]}{12/22.4 \times (\text{CO}_2\text{-CO}_2 \text{ flux} + \text{CO} + \text{CH}_4)}$$

This form of accounting for the gas does not give enough weight to the water problems within the blast furnace. Dr. Babcock included some of the observations of the problems of water as vapor and the resulting reaction products. In the intervening five years, our gas interpretation studies have been directed toward developing a gas analysis machine that could continuously analyze for CO, CO<sub>2</sub>, hydrogen and CH<sub>4</sub>. With this as an objective, the task force of Arthur D. Little has built up, around the Cambridge Institute Company analyzer, a unit that provides the results of relating CO/CO<sub>2</sub> and H<sub>2</sub>O/H<sub>2</sub>. The actual operation uses the factor obtained by the relation of CO/CO<sub>2</sub>/H<sub>2</sub> which we refer to as Gas Index. That this relation could be useful was indicated in Dr. Babcock's figures at Pittsburgh where he matched the CO/CO<sub>2</sub> ratio with the H<sub>2</sub> in the top gas.

September 1945 Gas Data	
CO/CO <sub>2</sub> Ratio	H <sub>2</sub> % Top Gas
1.20/1.39	6.7%
1.40/1.59	3.6
1.60/1.79	3.1
1.80/1.99	2.7
2.00/over	2.3

We have included in the instrumentation of the Cleveland No. 5 Furnace continuous humidity recording so that we may divide the weather humidity from water introduced into the furnace by water leaks, steam addition to blast, combined water of the burden and water carried in with the stock. Since each furnace has certain operating characteristics it is to be expected that no universal formula will appear.

Dr. Babcock's Pittsburgh figures indicated that with blast heat at approximately 1000 °F, each increased gram of moisture in the blast air will result in the following changes when making basic iron of about 1% silicon:

Silicon drop	= 0.10%
Hearth heat drop	= 1.24%
Sulphur increase	= 0.0012%

By adjusting the blast temperature upward approximately 60 °F, this increase of 1 gram of moisture can be overcome. This form of

adjustment has severe limitations because many ores, especially those easily reduced, will not tolerate high blast temperature. The stock column in the furnace hangs up and operations become practically impossible.

To go in the opposite direction and use dry blast has been tried in many places. The problem seems simple—use dry blast, save coke for reducing ore, get more production. Practically, the result of moisture is to provide hydrogen at the expense of heat. As the furnace temperature increases, hydrogen is a better reducer, although expensive in heat units. As the furnace cools, the carbon monoxide is a better reducer. By a combination of both, the furnace has self-adjusting characteristics. Until we find a method of making the furnace operate uniformly, dry blast will find many practical limitations besides the cost of refrigeration. A wise use of steam in the blast is at times a valuable tool for control of furnace operation.

In our studies of gas analysis in Cleveland it has been determined that several hours elapse between significant changes of gas chemistry and the corresponding changes of analysis of the iron. The British radon tracer experiments indicate a few seconds travel time for gas. Wall gas samples from the furnace for radon showed significant count in less than 2 seconds with peak activity at about 6 seconds. The center of the stock column was slower, 4 to 6 seconds to start and 8 or 9 to peak.

Furnace performance changes slowly. Five hours after the gas warning, the iron from the furnace at Cleveland gives confirmation. During that period we can make changes in the operation such as higher blast heat, change of burden. The dramatic way that a water leak of consequence shows up permits repair to be undertaken in minutes. The major burden changes still require hours. Extra coke at the top is seven hours ahead of significant gas changes. Wind rate changes show very quickly because of altered  $\text{CO}/\text{CO}_2$  ratio. The combination of Messerle's work, Dr. Babcock's calculation, the Arthur D. Little task groups instrumentation and Walter Montgomery's utilization of the information has produced much more uniform analysis iron. Our best test period was one in which Walter Montgomery predicted correctly his cast conditions over 80% of the time and his operating changes hours in advance, resulting in many more casts of iron of desired chemistry.

It is of interest at this point to comment that an extremely serious problem, for which we have no idea of solution, is that a blast furnace may store up iron for days, even weeks, then reverse the cycle and for days we get more than we charge. An average cycle is about

20 days. The original task assignment to the Arthur D. Little group was that continuous gas analysis meant 24 hours a day for at least one month. This was to insure analysis for a full cycle of iron holdup. This has been accomplished. We expect to turn the operation over to the furnace crew with the instrument indicating both in the cast house and supervisor's office along with the roomful of these indicators that now keep score on the furnace.

### SLAGS

With the decline of the charcoal furnace production about one hundred years ago, the slags involved in smelting shifted from glassy to stony in appearance. They resembled volcanic lava and it was natural that the geologists and mineralogists became interested. The scientists interested in earth history were evolving a logical geological picture. The mineralogists of that time recognized in blast furnace slags the same minerals that were present in igneous rocks. In the glassy charcoal slags, mineralization was not important and, since the wood ash flux produced a series of glass-like slags, there was little in the naturally occurring minerals to provide a base for study.

About 75 years ago serious study of the minerals of the blast furnace slags began in Sweden, England and other places in Europe. These studies have continued through the years in universities. The Geophysical Laboratory in Washington has been an important source of such information. The studies of the late Professor McCaffrey at the University of Wisconsin a generation ago were an important addition to the fund of information. The studies of Professor McCaughey at Ohio State have gone on for about 25 years and have added much to the fund of knowledge, especially in the methods of interpretation and use of the data.

In the work of Akerman, also Vogt, in the early 1880's it was noted that minerals not then known in nature were present. A great controversy arose when Professor McCaffrey reported new minerals in his slags about a generation ago and proposed that they be classified and named. Other experimenters tried to duplicate the work of McCaffrey but did not obtain the same results. In the uproar over the supposed mistake by Professor McCaffrey, all the good that might have accrued was lost. Professor McCaffrey ended his career a disappointed man. His records lay in the cabinets at Madison, his men scattered and nearly all went into other work. It looked very much as if the science of blast furnace slagmaking were to await more generations before commercialization would be accomplished. This may still be the hard fact, for today there is only a small use of the scien-



tific data accumulated in the past hundred years. It is a tribute to the faith in the work of Professor McCaffrey that the men at Madison retained his records. Over the last three years Professor Barker has photocopied the store of work sheets and records. Thirty years of storage was not in Professor McCaffrey's original plans. Copying was imperative because of deterioration of paper and plastic used to record results. Interpretation and use are moving slowly. But Professor McCaffrey's work will be available as a foundation on which to build. The reproduction in Professor McCaughey's laboratory of the controversial mineral Madisonite is a fact. It is to be hoped that Professor McCaughey can find time to present a paper on this phase of his slag studies soon. At least we can say that Madisonite exists in more places than "in the mind of Professor McCaffrey", where a contemporary scientist placed it a generation ago.

The use of thermo-chemical data in the making of cement, glass, ceramics and slags is moving more rapidly each year. The equilibrium diagrams of silicate systems are as common as the corresponding diagrams in the alloy systems and in some industries as well understood. The facts are now available in a limited way; the commercialization is but a matter of time. Results obtained in the glass industry will aid in the steel industry. The increasing use of beneficiated ores, coke from washed coal in the blast furnace, will force the study of silicate systems, for beneficiated raw materials will no longer carry the natural slagmaking constituents. Lining damage due to lowered alumina (9%  $\text{Al}_2\text{O}_3$ ) has been pointed out earlier in this paper. It is no longer practical to depend on natural ore, such as the Mesabi Scranton grade. The carbon block hearth and eventual bosh from carbon brick will cope with this damage problem. Viscosity of slag will force the development of slag systems that are workable, even where they do not damage the furnace. It is the prime business of the furnace to reduce the iron to the metallic state but the slag in many areas of the world exceeds the weight of iron. Silicate chemistry is more important than iron on a weight basis and bids fair to be more critical in operation. In the Saar, at Corby in England, and in the Salzgitter area of Germany, slag systems that would flush from the furnace governed the operation. The removal of sulphur from the iron was a second operation where soda slags in the iron ladles accomplished this part of the refining.

#### BLAST FURNACE COMMENT

In a letter to one of my associates about a year ago from a man who does not think the big blast furnace is anything to be worshipped,



there were some interesting thoughts. Some of that letter expresses so well the thoughts of many that I am recording a part of it.

"The steel industry has never, alas, understood the ethical significance of the blast furnace. The moral definition of the blast furnace is that it is a millstone hung about the neck of the steel industry in punishment for its sins against research. It is the scarlet letter that proclaims to all and sundry that here are those unfortunates who have lived impure lives. The blast furnace is not efficient and under existing circumstances can scarcely be a money maker, provided the bookkeeping is honest. It has but one virtue—size. There are a goodly number of individuals who think that anything large must necessarily be the acme of efficiency and nothing can be done about such personal preferences. The blast furnace is an affliction sent on the industry for reasons not yet understood."

With the comment that the blast furnace is not efficient I can agree, but the critic forgets that every day we are willing to give ground technically for effective economic performance. In my opinion the writer missed, and the public seems to miss, this very evident fact that no working unit in any metal industry can match the blast furnace in tons of useful product per unit of time. The dead weight of iron produced each year is about 15 times the weight of all the rest of the metal industry combined. Talk of substitution is a waste of breath. Studies concerning replacement of iron in our lives is a waste of time and substance.

What we need in this country is to provide the transportation facilities to move the ore we know is available. We need some reasonable assurance that coal will be mined to provide the required coke. We need the communities, now thriving because of steel plants, to recognize that the coke oven and blast furnace are industry's economic guarantee of their future.

A tax system that does not provide for replacement of worn-out equipment could wreck our plants as effectively as bombing. A tax system that works against the development of iron ore reserves has our key munitions industry always in doubt as to what the real ore situation will be in times of stress.

The British plants of the late 1930's depressed me when I saw the preparations for World War II as early as 1936. I told the manager of the alloy steel plant which impressed me most that I would not grade his equipment as heavy melting scrap if it were cut and ready to melt up. That plant was then making critical items for British defense. In August of 1942, on the day of the Dieppe raid, a black hour in British history, I was at that plant. With obsolete

equipment, a crew of arrogant workmen and poor raw materials, due to capable management it was making the finest alloy steel I was privileged to see in Britain. The manager asked me whether I still thought his equipment was scrap; I repeated the statement of the earlier visit. We in America should study the lessons that Britain can teach us. I repeat once more, an industrial nation needs a standard of machine perfection as well as a standard of living. No nation in our time has more ruthlessly built up machine power at the expense of living standards than the present Soviet masters. In our land subversives have skillfully sabotaged our preparation programs by loud propaganda, causing our workmen to resent and to fight the new machines. To the people of this audience it is my earnest plea that the real story be told. We in the steel industry need more transportation, an assured supply of coal, an operating group that is not misled by propaganda. We are all in this boat together, and while the blast furnace crew may be only the "black gang" on this boat, they, too, are important.

To my friends among blast furnace men I wish to convey my humble appreciation for the hours they have spent to open my eyes to their problems. To my teachers living and dead, particularly to the other Professor Campbell, William Campbell of Columbia and Professors McCaughey and Demorest of Ohio State, I owe a debt.

To my present associates, the operating group of Republic Steel, I wish to give credit for their permission to present these studies and to thank them for the assistance I have received. To Joseph H. Slater and Frank C. Janeczek, now gone, Walter J. Montgomery, Robert P. Liggett, Donald E. Babcock, Walter Carroll, John J. Hazel, Sidney W. Poole, Michael P. Fedock and others, I acknowledge my debt. The Arthur D. Little Co. men, under Dr. Bruce Old, who have lived with us are part of the group.

Some present will remember the Montaigne quotation Schumacher used to close his Institute of Metals lecture early this year: "I have gathered me a posy of other men's flowers, only the thread that binds them is my own."

## SOME ASPECTS OF GRAPHITIZATION IN STEEL

BY G. V. SMITH, J. A. MACMILLAN AND E. J. DULIS

### *Abstract*

*Several experiments have been made in an effort to reveal some of the fundamental factors which play a role in the graphitization of steels; particular attention has been paid to the important effect of aluminum deoxidation. The experiments have related primarily to the nucleation aspect of the problem, and have included the effect of the heat treating atmosphere. It has been shown that penetration of nitrogen from the atmosphere into the steel inhibits the inversion of carbide to graphite. This suggests that the role of aluminum deoxidation lies in the "residual" aluminum, presumed to exist in solid solution in the metal, rather than in the deoxidation products.*

IRON carbide ( $\text{Fe}_3\text{C}$ ) in steels is thermodynamically unstable below about 2000 °F and in some instances inverts to graphite and iron. Of the many variables which affect this inversion, deoxidation with aluminum is of particular importance. If a steel, free from carbide-stabilizing elements, such as chromium, is deoxidized with a relatively large amount of aluminum, one pound or more per ton of steel, it may be readily graphitized; in contrast, if the steel is deoxidized with 0.5 pound, or less, of aluminum per ton of steel, it is difficult, and in some cases apparently impossible, to cause graphitization.

Graphitization proceeds by nucleation and growth. Of these two processes, the former is generally considered the more important and is, perhaps, in many cases the determining factor. Accordingly, it seems in order to seek the role of aluminum in nucleation.

### MATERIALS AND PROCEDURE

Two plain carbon eutectoid steels deoxidized with aluminum and silicon as indicated in Table I, which may be graphitized in relatively short time, were investigated. Both were employed in the initial phases of the investigation, but in the later stages only one was used.

Preliminary experiments were made to determine the initial microstructure most susceptible to graphitization and also the optimum graphitizing temperature for an arbitrary heating period of 10 days.

A paper presented before the Thirty-second Annual Convention of the Society, held in Chicago, October 21 to 27, 1950. The authors, G. V. Smith and E. J. Dulis, are associated with the Research Laboratory, U. S. Steel Co., Kearny, N. J. J. A. MacMillan, formerly at Research Laboratory, now returned to National Tube Company, Lorain, Ohio. Manuscript received March 13, 1950.



Table I  
Chemical Composition of Test Steels

Steel	C	Mn	P	S	Si	Ni	Cr
1	0.79	0.62	0.011	0.025	0.23	0.02	0.02
2	0.75	0.55	0.025	0.032	0.20	0.02	0.04
Steel	Mo	Ti	Al	Al <sub>2</sub> O <sub>3</sub>	V	Cu	Zr
1	0.00	0.01	0.069	0.004	0.00	0.03	0.01
2	0.00	0.01	0.046	0.006	0.00	0.06	0.01

Samples of both steels were heated in air for 0.5 hour at 1600 °F (870 °C), either furnace-cooled, air-cooled or water-quenched, reheated in air for 10 days at 1100, 1200 or 1300 °F (595, 650 or 705 °C), and examined microscopically for graphite. On the basis of these tests, water quenching was selected as producing the most susceptible microstructure, and 1200 °F (650 °C) as being the optimum graphitizing temperature; they were therefore employed in the subsequent experiments. Samples in these experiments and also those described below were half-disks  $\frac{1}{4}$  to  $\frac{3}{8}$  inch thick of 1-inch round bar, unless otherwise stated.

Experiments were also made to determine the effect of austenitizing temperature. Sample of both steels were heated in air for 0.5 hour at 100 °F intervals from 1400 to 2300 °F (760 to 1260 °C), water-quenched, reheated in crushed coke for 10 days at 1200 °F (650 °C), and the number of graphite nodules was counted.

Table II  
Summary of Experiments on Effect of Atmosphere

Austenitizing Treatment			Graphitizing Treatment			Thickness of Carbide-Stable Rim, Inches
Atmosphere	Time, Hours	Temp. °F	Atmosphere	Time, Days	Temp. °F	
Air	0.5	2000	Deoxidized Lead	10	1200	0.025
Air	0.5	2000	Air	10	1200	0.025
Air	0.5	2000	{ Air	1	1200	0.014
			{ Deoxidized Lead	9		
Crushed Coke	0.5	2000	Deoxidized Lead	10	1200	0.016
Crushed Coke	0.5	2000	Air	10	1200	0.010
Crushed Coke	0.5	2000	{ Air	1	1200	0.005
			{ Deoxidized Lead	9		
Purified Helium	24	1800	Purified Helium	10	1200	None
Purified Helium	24	1800	Air	10	1200	None
Purified Nitrogen	2	1800	Purified Helium	10	1200	0.003
Purified Nitrogen	4	1800	Purified Helium	10	1200	0.007
Purified Nitrogen	8	1800	Purified Helium	10	1200	0.017
Purified Nitrogen	24	1800	Purified Helium	10	1200	0.039
Purified Nitrogen	2	1800	Air	10	1200	None
Purified Nitrogen	4	1800	Air	10	1200	0.002
Purified Nitrogen	8	1800	Air	10	1200	0.011
Purified Nitrogen	24	1800	Air	10	1200	0.035
Crushed Coke	1	2000	Purified Helium	10	1200	0.016
Crushed Coke	1	2000	Purified Nitrogen	10	1200	0.017
Crushed Coke	1	2000	Air	10	1200	0.012
Crushed Coke	1	2000	Undeoxidized Lead	10	1200	0.012
Purified Nitrogen	6	2000	Purified Helium	10	1200	0.028
Purified Nitrogen	6	2000	Purified Nitrogen	10	1200	0.028
Purified Nitrogen	6	2000	Air	10	1200	0.024
Purified Nitrogen	6	2000	Undeoxidized Lead	10	1200	0.025



In these experiments, a surface rim free of graphite, but containing carbide, was observed. This led to a study of the effect of atmosphere during austenitizing and graphitizing. Experiments were made with Steel 1 in various atmospheres including air, crushed-coke-atmosphere, purified helium, and purified nitrogen. The purification of helium and nitrogen was effected by passing the gas over heated copper gauze and through phosphorus pentoxide. The specific austenitizing and graphitizing treatments are given in Table II.

In the planning of these experiments on the effect of atmosphere, we were influenced by results of Austin and Fetzer (1),<sup>1</sup> who had observed rim effects during graphitization studies, as described in the Discussion.

## RESULTS

### *Effect of Initial Microstructure and Subcritical Heating Temperature on Graphitization*

No graphite developed in the furnace-cooled or air-cooled samples, but a relatively large amount formed in all the water-quenched samples, i.e., those which had a martensitic microstructure. The variation of graphitization of these latter samples with graphitizing temperature is shown in Fig. 1. The extent in either steel was about the same at 1100 and 1200 °F (595 and 650 °C), but was somewhat less at 1300 °F (705 °C). For subsequent experiments, a temperature of 1200 °F was chosen.

### *Effect of Austenitizing Temperature*

The variation with austenitizing temperature of graphitization near the center (i.e., remote from apparent surface effects) of samples of Steel 1 is shown by photomicrographs in Fig. 2. The nodule density and austenite grain size varied with austenitizing temperature, as shown in Fig. 3, for both steels.

### *Effect of Austenitizing Atmosphere*

The results of the experiments on the effect of atmosphere are given in Figs. 4 to 10 and Table II. It should be pointed out that for the thickness measurements of Table II, the rim was considered to be the portion clearly affected by the atmosphere, even though this portion was not entirely graphite-free, as illustrated in Fig. 8e.

Fig. 4 shows that the graphite-free rim observed in the study of effect of austenitizing temperature was not caused by decarburization. The variation of the rim thickness with austenitizing temperature in these experiments is shown in Fig. 5.

<sup>1</sup>The figures appearing in parentheses pertain to the references appended to this paper.

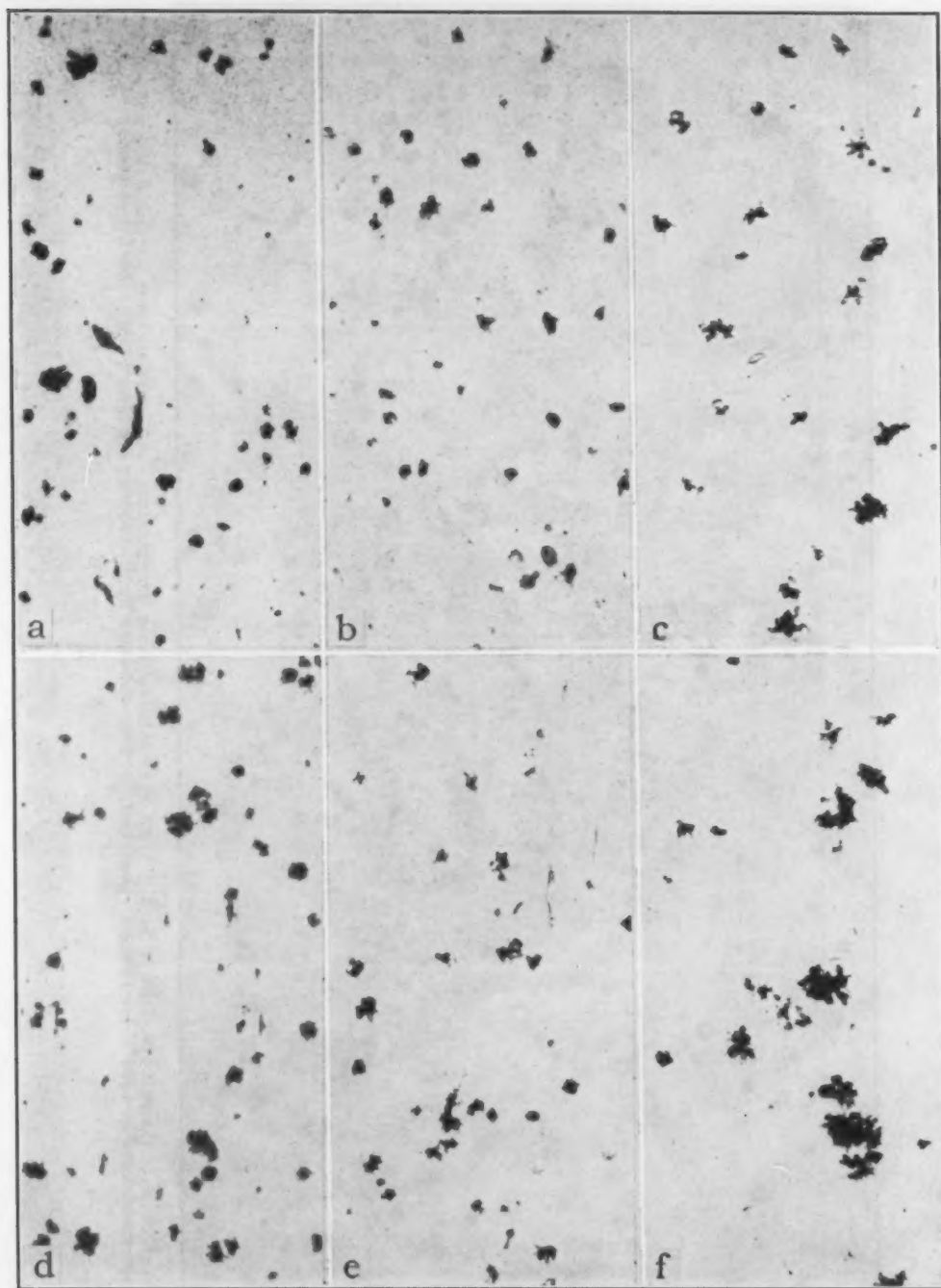


Fig. 1—Variation of Graphitization of Two Plain Carbon Eutectoid Steels, Initially Water-Quenched After 0.5 Hour at 1600°F, With Subcritical Reheating Temperature, the Holding Time Being 10 Days in Each Case. Unetched.  $\times 250$ . (a), (b) and (c)—Steel 1 at 1100, 1200 and 1300°F respectively. (d), (e) and (f)—Steel 2 at 1100, 1200 and 1300°F respectively.

The effect of austenitizing in air and crushed coke and of graphitizing in air, deoxidized lead, or partially in air and partially in deoxidized lead, is shown in Fig. 6 and in Table II. A carbide-stable surface rim developed for either austenitizing anneal, but was thicker for the

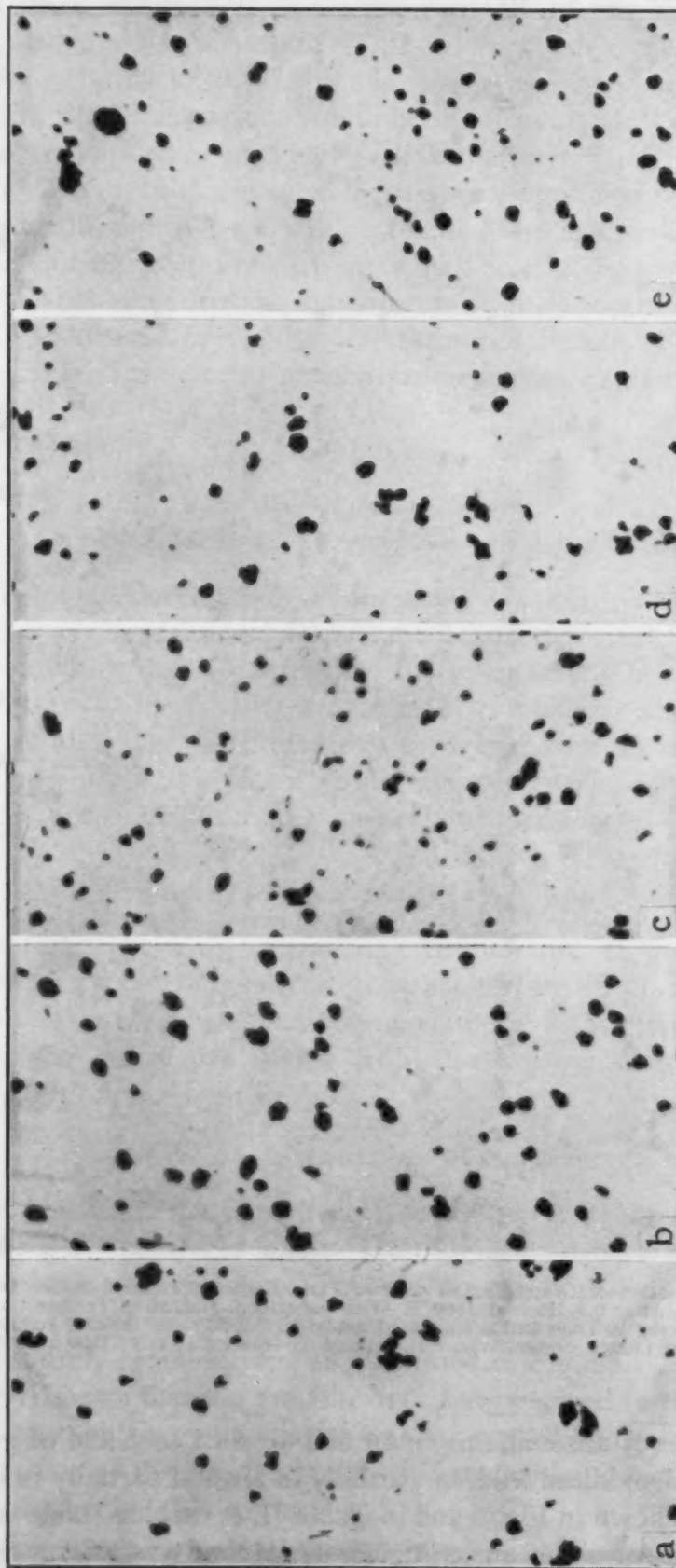


Fig. 2—Variation of Number and Size of Graphite Nodules in Steel 1 With Prior Austenitizing Temperature. All samples heated at indicated temperature for  $\frac{1}{2}$  hour, quenched to martensite, and heated at 1200°F for 10 days. Unetched.  $\times 250$ . (a) 1400°F; (b) 1500°F; (c) 1600°F; (d) 1700°F; (e) 1800°F.

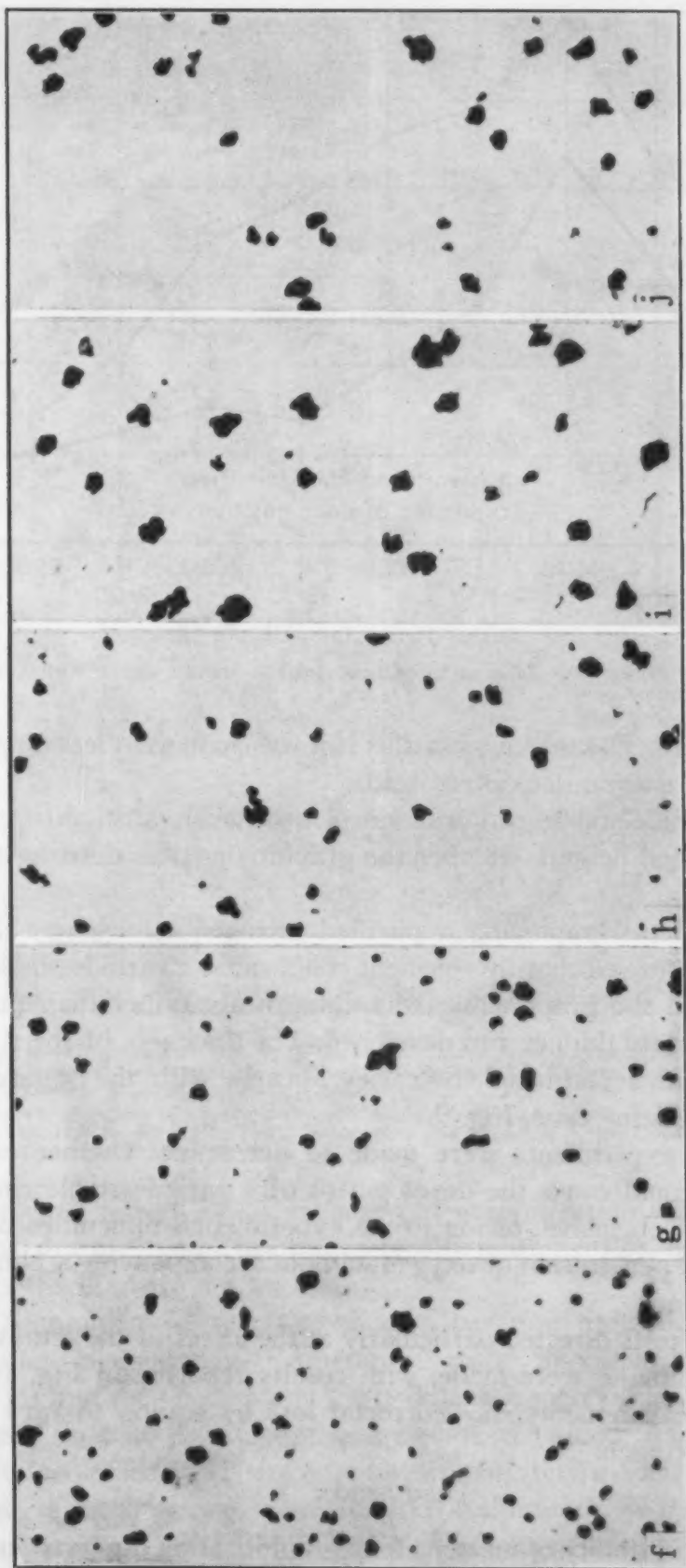


Fig. 2—(Continued)—Variation of Number and Size of Graphite Nodules in Steel 1 With Prior Austenitizing Temperature. All samples heated at indicated temperature for  $\frac{1}{2}$  hour, quenched to martensite, and heated at 1200°F for 10 days. Unetched.  $\times 250$ . (f) 1900°F; (g) 2000°F; (h) 2100°F; (i) 2200°F; (j) 2300°F.



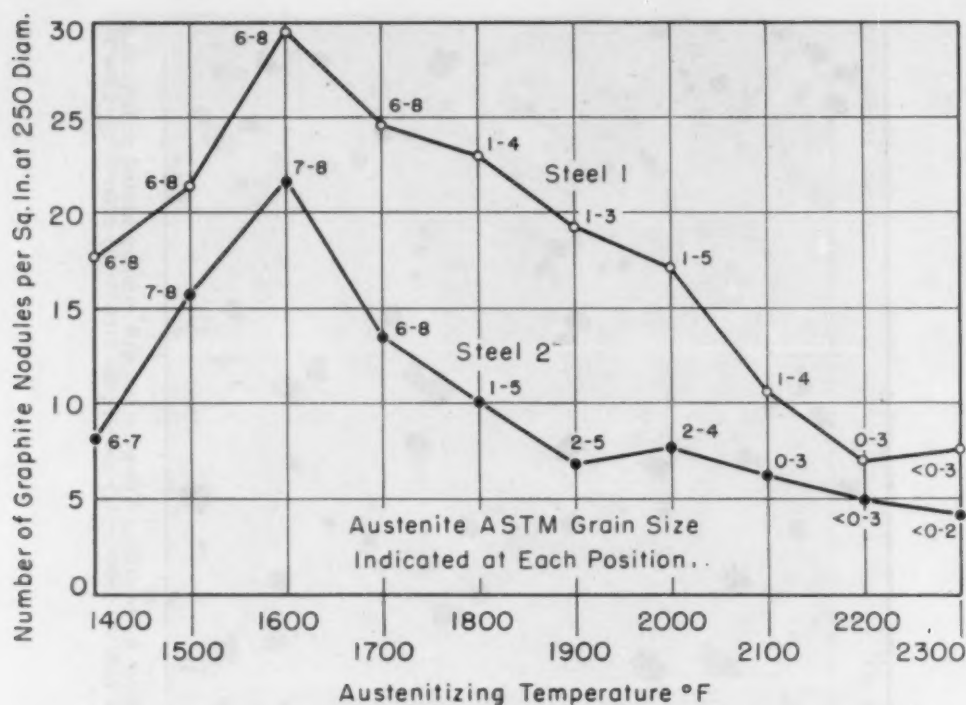


Fig. 3—Variation of Number of Graphite Nodules in Steels 1 and 2 With Austenitizing Temperature.

air atmosphere. The thickness of this rim was somewhat less on graphitizing in air than in deoxidized lead.

No carbide-stable rim was developed when austenitizing was done in purified helium, whether the graphitizing was done in helium or air, Fig. 7.

Experiments employing a purified nitrogen atmosphere during austenitizing proved that this element could cause a carbide-stable rim, Fig. 8. When the graphitizing was done in air rather than purified helium, a slightly thinner rim developed. The thickness of the rim for either graphitizing atmosphere varies linearly with the square root of the austenitizing time, Fig. 9.

Several experiments were made to determine whether oxygen penetration could cause the development of a carbide-stable rim, but these were inconclusive, owing to the experimental difficulties of getting sufficient penetration of oxygen without accompanying scaling and decarburization.

Further tests directed particularly at the effect of the atmosphere during graphitizing were made, with results reported in Fig. 10 and Table II. Measurements showed metal loss by scaling to vary from 0.002 to 0.006 inch.

#### DISCUSSION

The susceptibility of martensite to graphitization observed in these

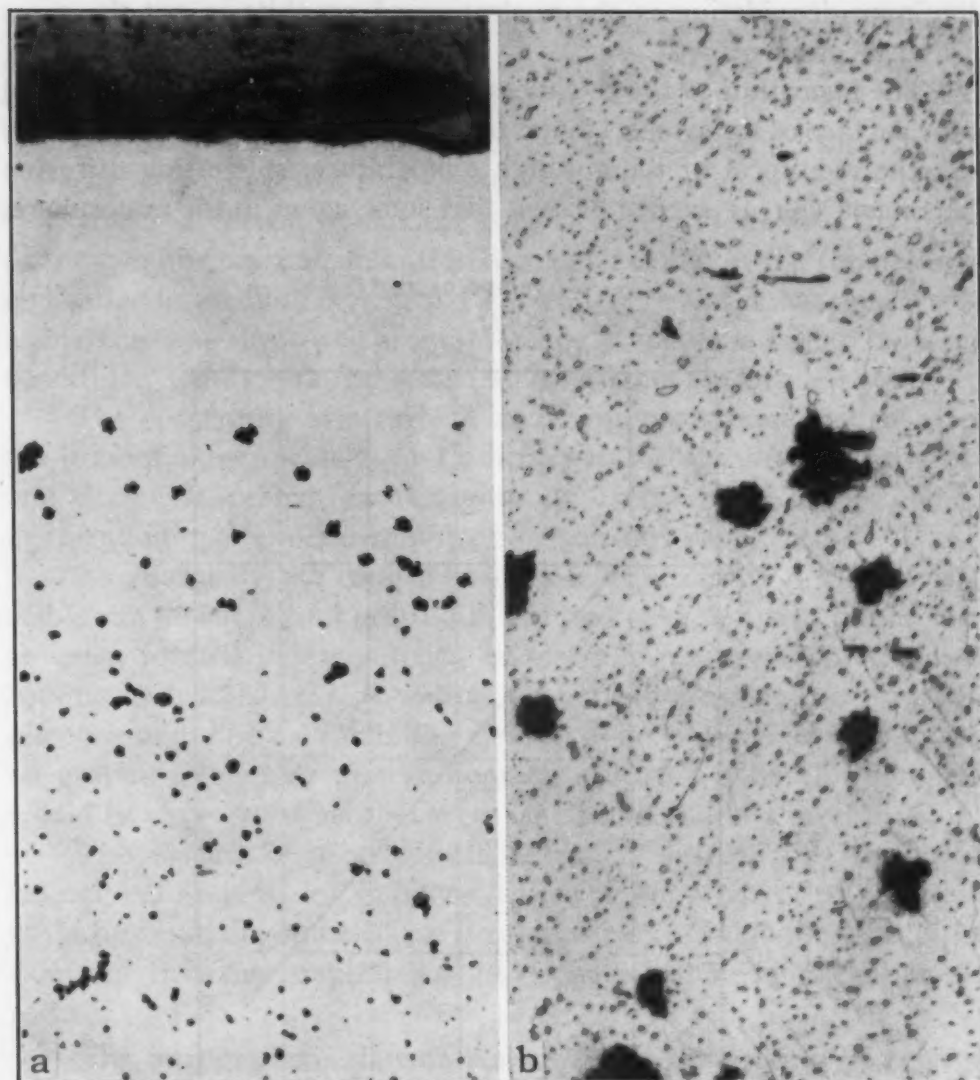


Fig. 4a—Graphite-Free Rim at Surface of Sample of Steel 1 Heated  $\frac{1}{2}$  Hour in Air at 2000 °F, Quenched to Form Martensite, and Then Reheated in Crushed Coke for 10 Days at 1200 °F. Unetched.  $\times 100$ .

Fig. 4b—Junction of Graphitized and Ungraphitized Zones in Fig. 4a, Showing a Plentitude of Carbide in the Stable Zone, Hence That the "Rim" Is Not a Consequence of Decarburization. Picral etch.  $\times 500$ .

experiments, as well as the variation of graphitization with graphitizing temperature, confirms previous observations (2), although the reasons therefor are not known.

The number of graphite nodules per unit area increased with increasing austenitizing temperature to a maximum at 1600 °F (870 °C) and then decreased; the nodule size increased as the number decreased so that the amount of graphite remained nearly constant, as estimated visually. There was no discontinuity associated with the sudden grain coarsening, characteristic of aluminum-deoxidized steels, that occurred at 1800 °F (980 °C). This suggests that the role of

aluminum deoxidation in the nucleation of graphite is not the same as that in grain growth.

The logarithm of the thickness of the graphite-free rim observed at the surface of the samples in the foregoing experiment varied linearly with the reciprocal of the absolute temperature, suggesting diffusion phenomena (3). It seemed evident that some agent in the atmosphere,

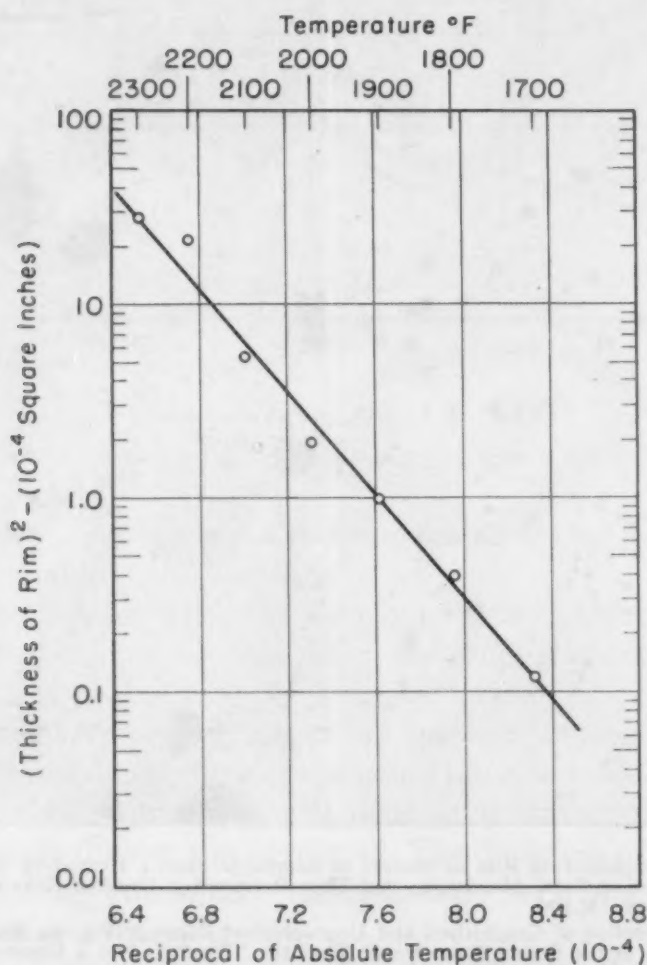


Fig. 5—Variation of the Logarithm of the Square of the Carbide-Stable Rim Thickness With Reciprocal of Absolute Temperature of Austenitizing; for Samples of Steel 1 Heated in Air for  $\frac{1}{2}$  Hour, Quenched, and Graphitized in Crushed Coke for 10 Days at 1200°F.

probably oxygen or nitrogen, or both, had diffused into the steel during austenitizing and had somehow inhibited the carbide-graphite inversion.

A carbide-stable rim had been previously observed by Austin and Fetzer (1), who reported that "a stable rim was obtained at the peripheral parts of a sample of steel which normally graphitized, if the specimen was protected from oxidation during annealing above the critical range, by surrounding it with charcoal granules. Similar results

were obtained when the austenitizing was conducted in vacuum." Evidence that a diffusion process was involved is offered by the fact that rim thickness, as measured from photomicrographs in their paper, varies linearly with the square root of the austenitizing time, Fig. 9. These authors suggested that the atmosphere surrounding steel packed in charcoal is carbon monoxide, which renders ineffective the nuclei of the graphite reaction, but offered no explanation of the rim observed on heating in vacuum. Austin and Fetzer also reported that the carbide-stable rim was destroyed if graphitizing were done under oxidizing conditions. Oddly, the rim was destroyed from the inside outward.

The occurrence of a carbide-stable rim on austenitizing in air in the present experiments is contradictory to the observations of Austin and Fetzer or, perhaps more accurately, their interpretation, and led to the additional experiments described in this paper.

As shown by the comparison experiments of Fig. 6, a carbide-stable rim developed on heating in crushed coke, but was not as thick as when formed by austenitizing in air. The occurrence of a rim on heating in crushed coke as well as when heating in air suggested that nitrogen might be the inhibiting element. The rim was slightly thinner on graphitizing in air than in deoxidized lead, but hardly more than would be expected if account were taken of metal loss by scaling.

The absence of a carbide-stable rim on austenitizing in purified helium and graphitizing in either helium or air proved that something in the austenitizing atmosphere is responsible for inhibiting graphitization and that the graphitizing atmosphere is not significant in this regard.

The nitrogen experiments revealed that penetration of nitrogen can inhibit graphitization, but the oxygen experiments were inconclusive. Again, graphitizing in air gave a slightly thinner rim than graphitizing in helium.

The problem of diffusion accompanied by phase change, of which the penetration of nitrogen or oxygen into steel containing readily nitrided or oxidized alloying elements is a special case, has been treated mathematically by Darken (4). Accordingly, it seemed desirable to calculate, if possible, the penetration to be expected in various instances, and to compare it with that observed on the assumption that the measured thickness of rim represented the depth of diffusion penetration and "subscale" precipitation. This has been possible in the case of nitrogen, using unpublished data for the solubility and diffusivity obtained by L. S. Darken and R. P. Smith in this Laboratory. A similar calculation has not been possible in the case of oxygen.

The relation developed by Darken (4), which is applicable to



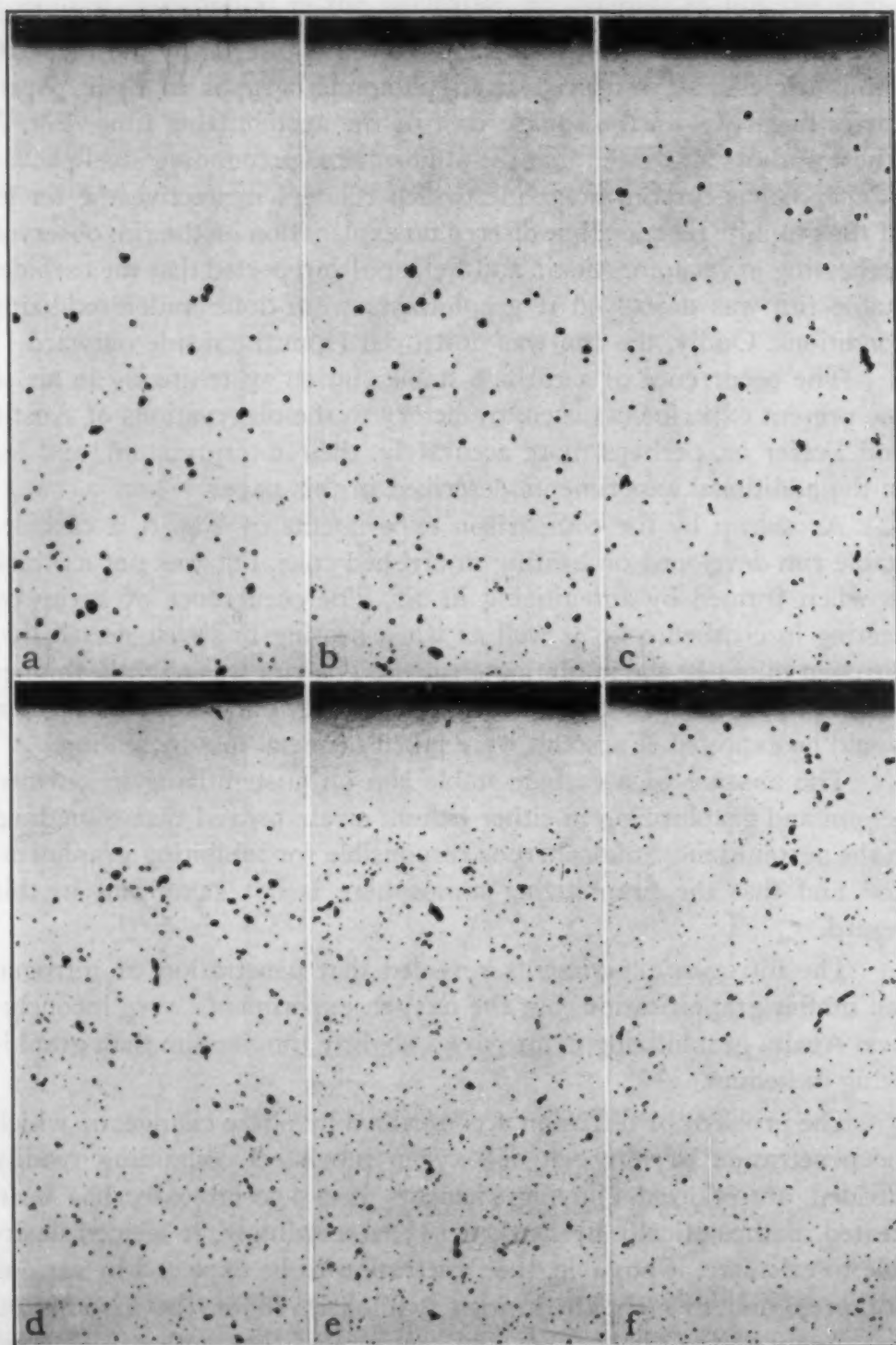


Fig. 6—Effect of Austenitizing in Air (a, b and c) and in Crushed-Coke-Atmosphere (d, e and f) on Development of a Carbide-Stable Surface Rim, and the Effect of Graphitizing in Air on the Destruction of This Rim. Austenitized  $\frac{1}{2}$  hour at 2000°F in indicated atmosphere, quenched to martensite, and graphitized 10 days at 1200°F as indicated. Unetched.  $\times 50$ . (a and d) Graphitized 10 days in deoxidized lead; (b and e) graphitized 1 day in air, 9 days in deoxidized lead; (c and f) graphitized 10 days in air.

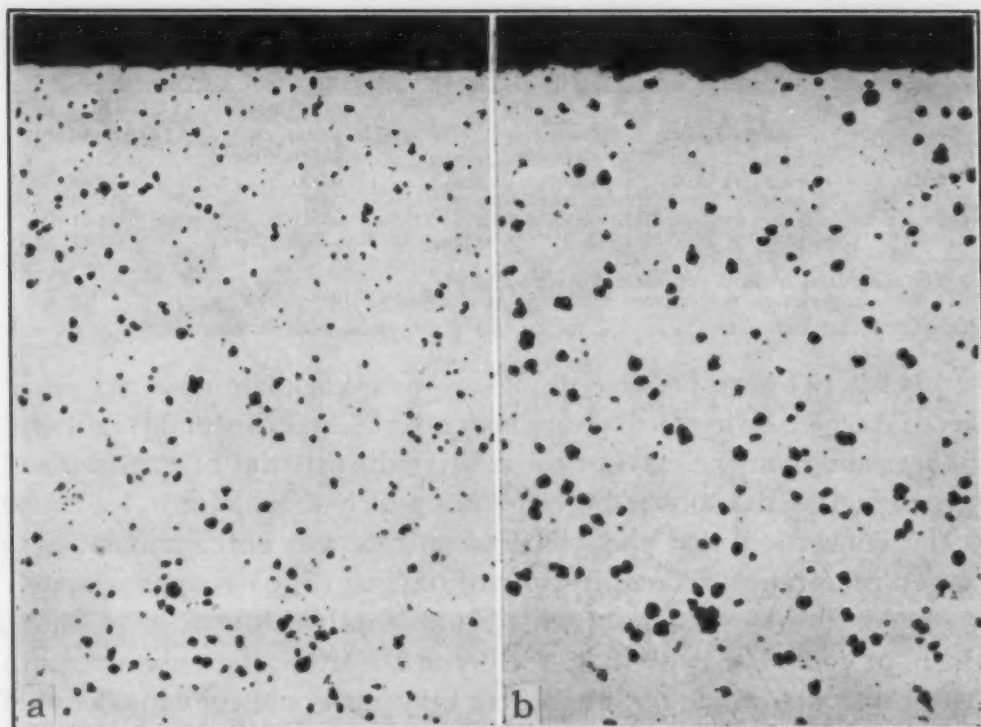


Fig. 7—Effect of Austenitizing in Purified Helium on Subsequent Graphitization Characteristics. Samples austenitized 24 hours at 1800°F, quenched to martensite, and graphitized 10 days at 1200°F. Unetched.  $\times 150$ . (a) graphitized in purified helium; (b) graphitized in air.

experiments in which nitrogen penetration is presumed to occur (specifically subscale formation unaccompanied by scale formation), may be expressed as follows:

$$X = \left( 2 D_N \frac{U_N^\circ}{U_N} t \right)^{1/2}$$

where  $X$  = depth of penetration in cm.

$D_N$  = diffusion coefficient of nitrogen in steel in  $\text{cm}^2/\text{sec}$ .

$U_N^\circ$  = solubility of nitrogen in steel in weight per cent

$U_N$  = mean concentration of nitrogen in subscale; assuming the precipitate to be  $\text{AlN}$  this is taken to be  $\frac{1}{2} U_N^\circ + 14/27 X$  (weight per cent aluminum in steel)

$t$  = time in seconds

Using this relation, the penetration to be expected in various instances, assuming nitrogen as the diffusing element, has been calculated. These results are listed with the corresponding observed rim thickness in Table III.

For samples austenitized in nitrogen, the agreement of calculated and observed rim thickness seems fairly good. A similar conclusion may be made in case of samples austenitized in crushed coke, except that the observed effect of time is inconsistent in itself. The greatest difference between observation and calculation is to be noted in the case of the air-austenitized sample.

**Table III**  
**Comparison of Observed and Calculated Rim Thickness**

Case	Austenitizing Treatment	Observed Rim Thickness, cm*	Calculated Rim Thickness, cm†
1	6 hours at 2000 °F in nitrogen .....	0.071	0.10
2	24 hours at 1800 °F in nitrogen .....	0.099	0.128
3	½ hour at 2000 °F in crushed coke .....	0.041	0.029
4	1 hour at 2000 °F in crushed coke .....	0.041	0.041
5	½ hour at 2000 °F in air .....	0.063	0.029

\*Graphitizing atmosphere nonoxidizing.

†Assuming rim to result from nitrogen penetration.

It has not been possible to make similar calculations for penetration of oxygen, owing to the complexity of the experimental conditions, but reasoning, on the basis of the relative diffusivities of nitrogen and oxygen and of the subscale precipitates which should form, leads one to the conclusion that the observed effects are not attributable to oxygen penetration. The diffusivity of oxygen (5, 6) is approximately one-hundredth that of nitrogen. Thus, if other things were equal, which, of course, they are not, a penetration of oxygen only one-tenth that of nitrogen would be anticipated. Oxygen would combine not only with aluminum but also with silicon and, since silicon is present in relatively large amount (0.23%), the subscale penetration would be correspondingly slowed. Thus, it seems quite certain that the depth of oxygen penetration in the experiments considered herein would be considerably smaller than the observed rim thickness and therefore that the stable rim, even in specimens austenitized in air, is a consequence of nitrogen rather than oxygen penetration. It is possible that oxygen could produce a similar effect, but the depth of rim would be expected to be considerably less than was observed in our experiments.

In the final experiments, directed particularly at the effect of graphitizing atmosphere, an effort was made to measure the metal loss during scaling. Although this could not be done with great precision because of the change in density in the metal, the observed loss of 0.002 to 0.006 inch is of the same order as the decrease in rim thickness. This loss of metal is also not out of line with rough calculations based on gain in weight scaling measurements of Day and Smith (7). The observations fail to confirm those of Austin and Fetzer.

This investigation has clearly established that the diffusion penetration of nitrogen during austenitizing inhibits the subsequent inversion of carbide to graphite in otherwise readily graphitizable aluminum-deoxidized steel during a subcritical graphitizing anneal. It is not unreasonable to expect that oxygen penetration, in the absence of nitrogen, would yield a similar effect, but this has not been proved. Although only one steel has been thoroughly studied in this investigation, it seems



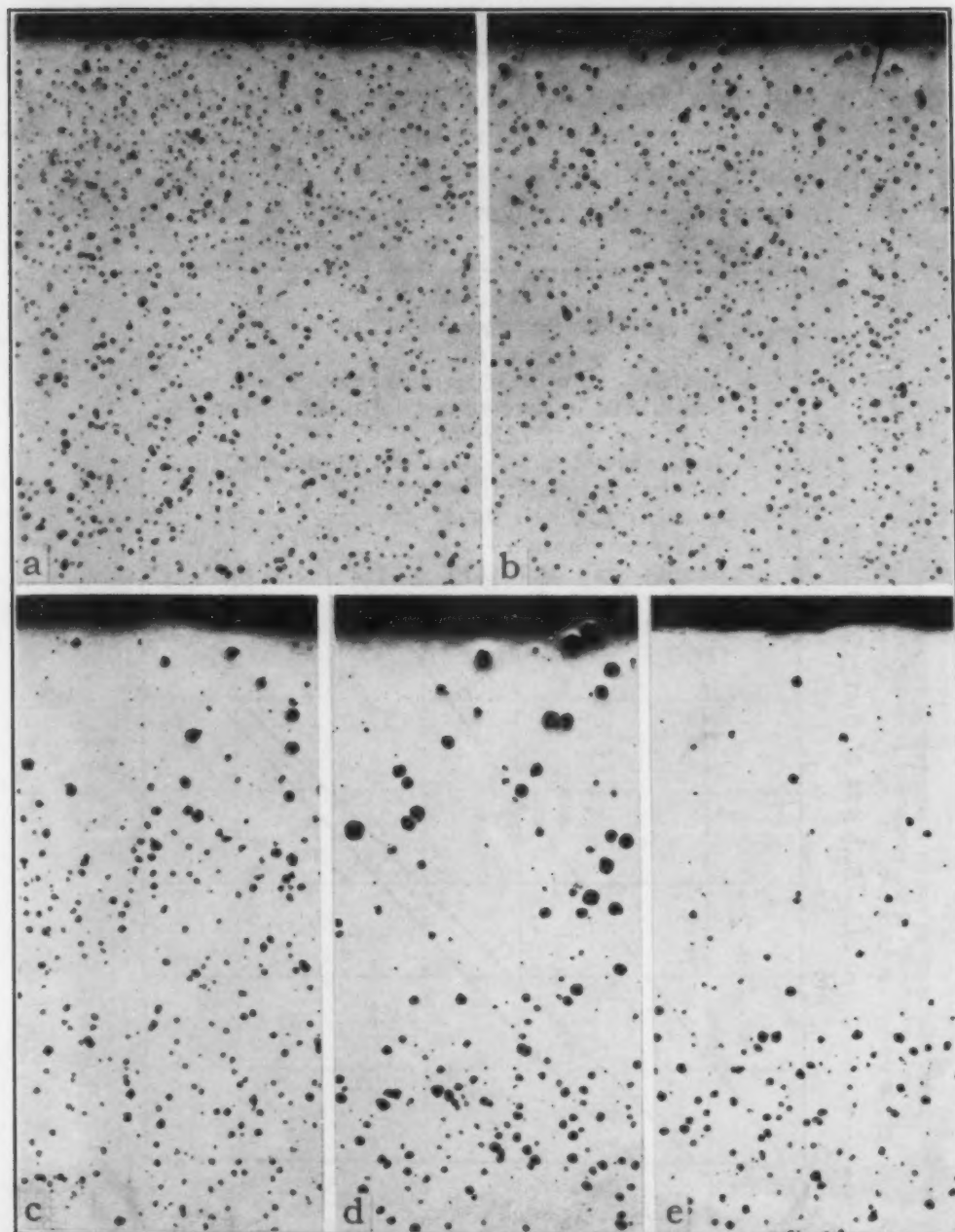


Fig. 8—Effect of Austenitizing in Purified Nitrogen on the Development of a Carbide-Stable Surface Rim. Samples (a, b, c, and d) austenitized 2, 4, 8 and 24 hours respectively, at 1800°F, quenched to martensite, and graphitized 10 days at 1200°F in purified helium. (e) Austenitized 24 hours, graphitized in air. Unetched.  $\times 50$ .

reasonable to consider the observed phenomenon to be general, especially inasmuch as Austin and Fetzer (1) have reported somewhat similar effects for a number of steels, though they interpret them differently and, we judge, incorrectly.

In the light of the experiments reported herein, it is of interest to consider the manner in which aluminum deoxidation increases susceptibility to graphitization. The aluminum added to molten steel



for deoxidation combines with the dissolved oxygen to form deoxidation products such as aluminum oxide ( $\text{Al}_2\text{O}_3$ ), reducing the dissolved oxygen to quite low concentration. The deoxidation products either rise into the slag or are trapped within the solidifying metal and appear on microscopic examination as so-called nonmetallic inclusions. Not only does the aluminum-oxygen combination occur, but it is now gen-

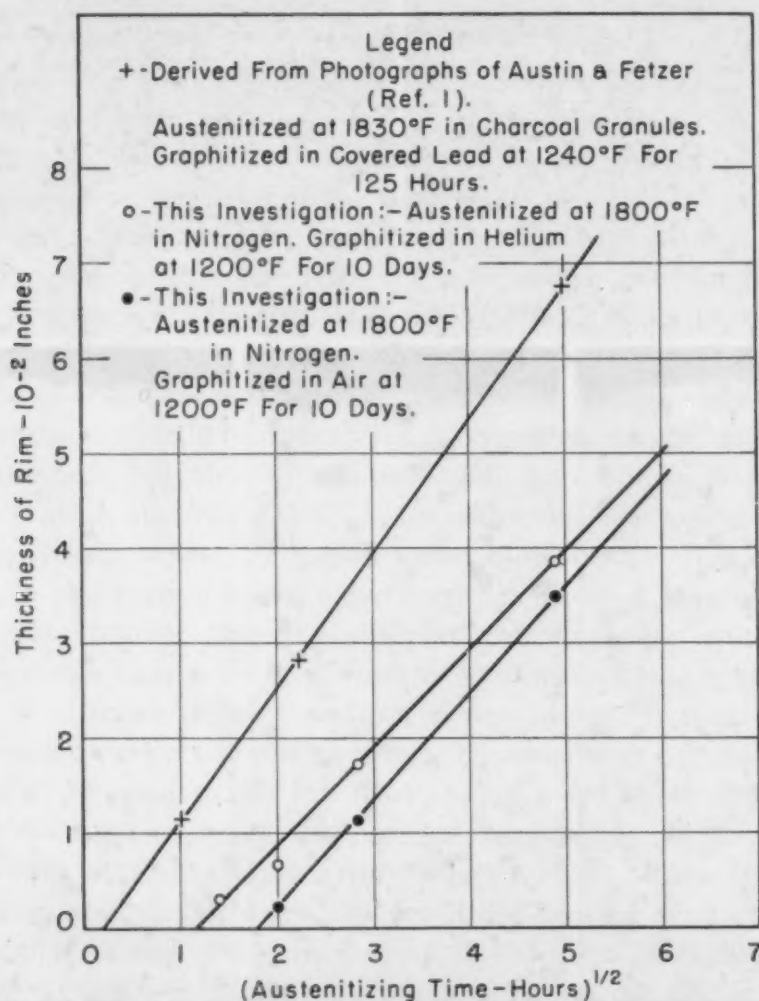


Fig. 9—Variation of Rim Thickness With Square Root of Time in Various Atmospheres.

erally thought that combination also takes place with nitrogen ( $\text{AlN}$ ). The excess aluminum beyond that which combines to form "deoxidation" products dissolves in solid solution in the metal; this portion is often called metallic or residual aluminum.

Thus the role of aluminum deoxidation in promoting graphitization may logically be sought in either or both the deoxidation products and the solid solution aluminum. In the former instance, the semi-inert deoxidation products may be considered as nucleation sites for the

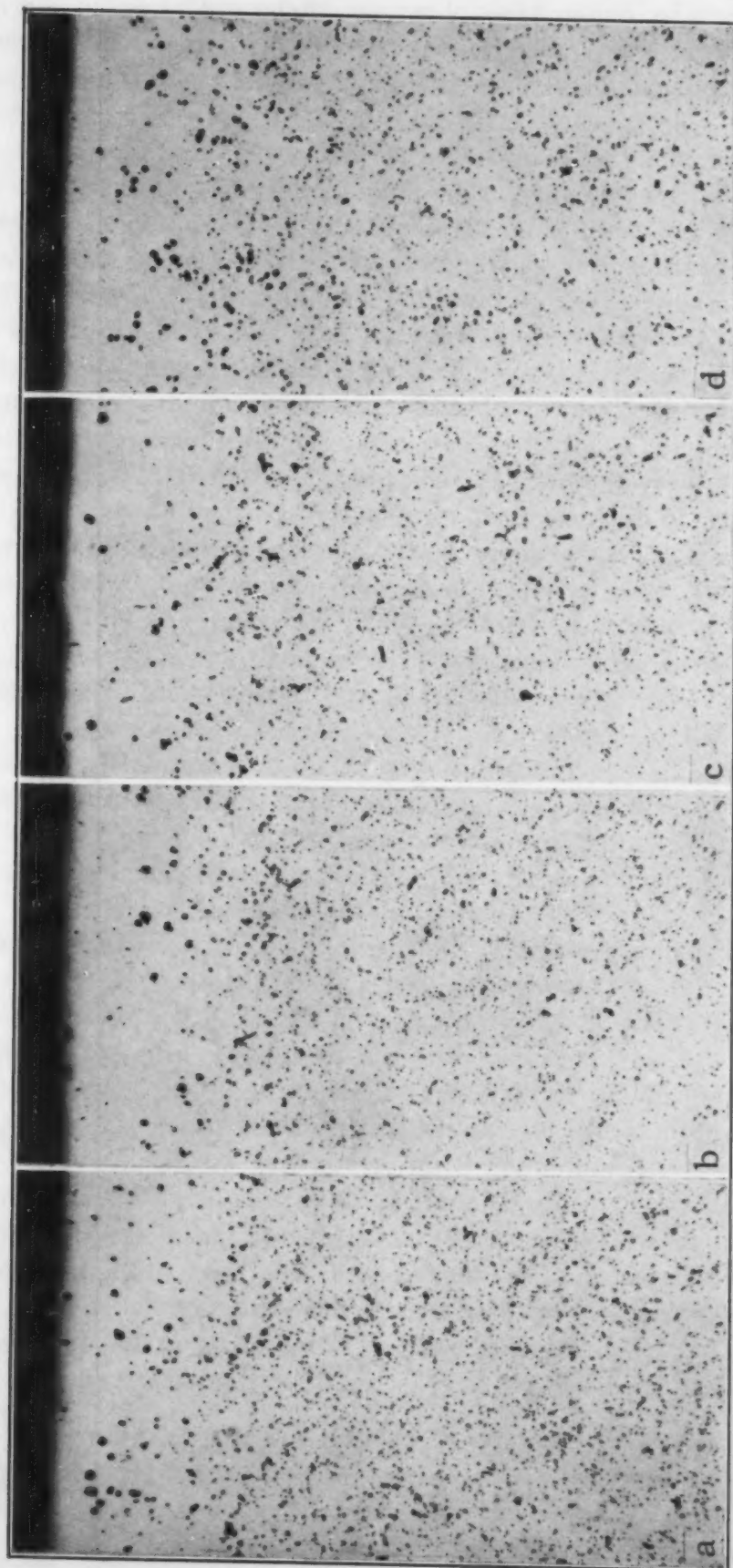


Fig. 10.—Effect of Atmosphere During Graphitizing Anneal on Carbide-Stable Rim Developed by Austenitizing at 2000°F in: (1) Crushed Coke for 1 Hour; and (2) in Purified Nitrogen for 6 Hours. Unetched. X 50. Specimens (a and c) graphitized in purified helium; specimens (b and d) graphitized in purified nitrogen; specimens (c and g) graphitized in air; specimens (d and h) graphitized in unoxidized lead.

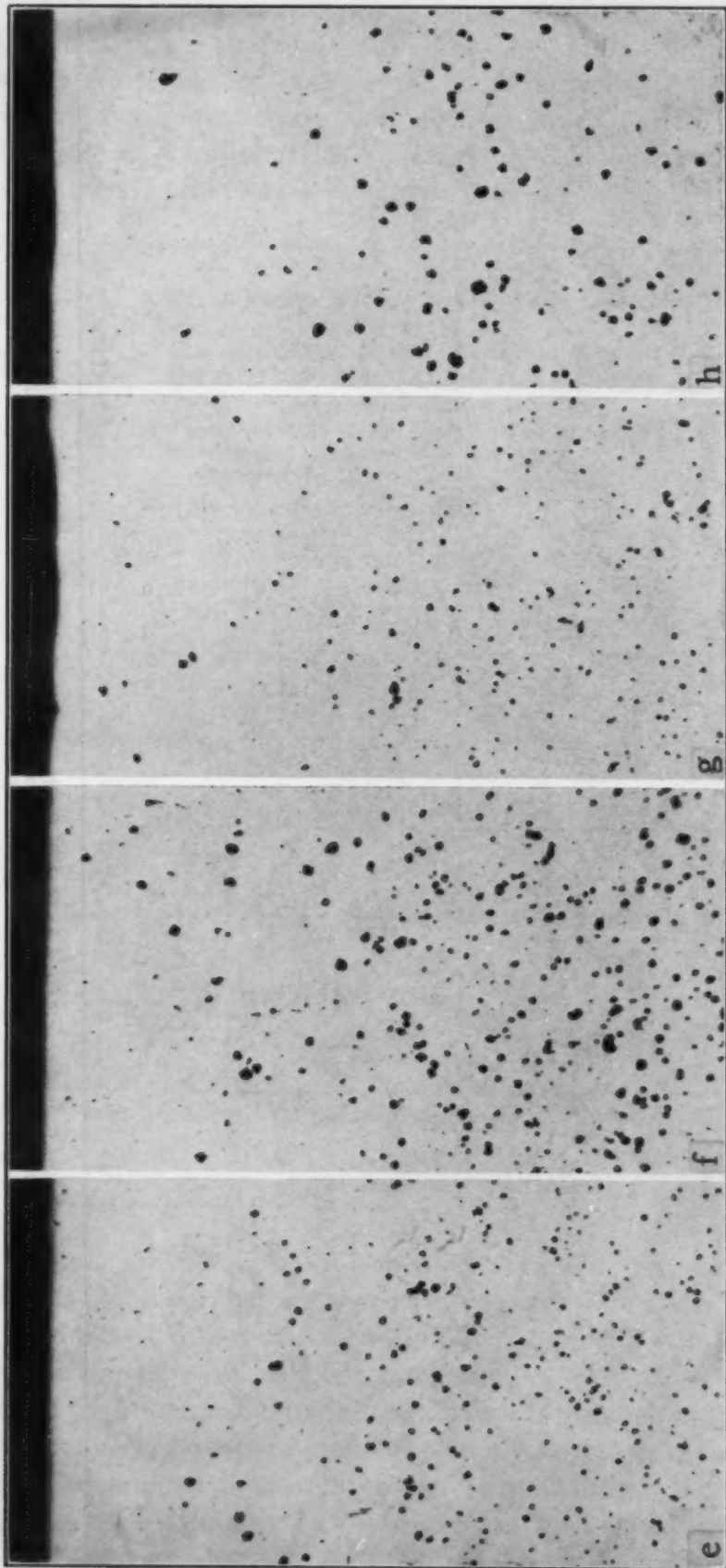


Fig. 10—(Continued)—Effect of Atmosphere During Graphitizing Anneal on Carbide-Stable Rim Developed by Austenitizing at 2000 °F in: (1) (a, b, c, d) Crushed Coke for 1 Hour; and (2) (e, f, g, h) in Purified Nitrogen for 6 Hours. Unetched, X 50. Specimens (a and e) graphitized in purified helium; specimens (b and f) graphitized in purified nitrogen; specimens (c and g) graphitized in air; specimens (d and h) graphitized in deoxidized lead.



carbide-graphite inversion; no ready explanation of the action of metallic aluminum is apparent, especially in view of the very small amount—less than perhaps 0.07%—of this element usually encountered in commercial steels.

It would appear that the inhibition of subsequent graphitization by the penetration of nitrogen during austenitizing, as observed in this investigation, must result from the tying up of the metallic aluminum,<sup>2</sup> and that the susceptibility of aluminum-deoxidized steels is attributable to the presence of aluminum, not alumina or other deoxidation products. It is very doubtful that such diffusion could affect in any significant way the inclusions already present. Presumably, however, the aluminum in solid solution would react with the inwardly diffusing nitrogen (and oxygen) to form products similar to those originating at the time of deoxidation. An effort was made to find microscopic evidence of a subscale in the carbide-stable rim of the samples of this investigation, but no such evidence was noted, presumably owing to the small quantities of the reactants. Such a subscale has been observed, however, in this Laboratory by E. W. Filer for a sample of an experimental steel containing somewhat higher aluminum heated in a nitrogen atmosphere. The occurrence of oxide subscales is well known (4, 8).

It is of interest to note that the importance of the metallic or residual aluminum in promoting graphitization, as shown here, supports claims (2) which have been advanced on the basis of comparison of amounts of "combined" and "uncombined" aluminum, determined chemically, but which previously were not completely substantiated.

The conclusion of Austin and Fetzer (1) that the carbide-stable rim may be destroyed by performing the graphitizing anneal in an oxidizing environment has not been substantiated by the experiments described here. The observed diminution in rim thickness in our experiments apparently is accounted for by metal loss by scaling. In fact, it is not unreasonable to expect that, if oxygen penetrates during a graphitizing anneal, it might result in further carbide stabilization.

The mechanism whereby residual aluminum exerts its very important effect on susceptibility to graphitization is obscure. Indeed, in this respect it would have been simpler had the deoxidation products such as alumina been proved important, for it is possible to conceive of them as acting as nucleation sites. The role of aluminum is especially difficult to comprehend because only small percentages of this element are involved, perhaps 0.01 to 0.07 weight per cent. Also

<sup>2</sup>Other combinations as with silicon may also be expected to occur, but those with aluminum are apparently the significant ones in view of the fundamental role of aluminum deoxidation. At some other level of graphitization susceptibility, such as may be presumed for silicon-killed steels or other steels in which no aluminum is added, it may be possible that similar subscale phenomena involving silicon or other elements may be similarly significant.



puzzling in respect to the mechanism of the aluminum effect is the observation that the number of graphite nodules, i.e., graphite nuclei, decreases with increasing time and temperature of austenitizing, as though the effective agent is either agglomerating or dissolving to an increasing degree.

The widely differing susceptibility to graphitization of different initial microstructures, as well as the effect of graphitizing temperature, are also of considerable interest in respect to the mechanism of graphitization. It is planned to devote further study to these and other aspects of the graphitization problem.

#### SUMMARY

Samples of aluminum-deoxidized eutectoid carbon steels were austenitized 0.5 hour at 1600 °F (870 °C), either furnace-cooled, air-cooled, or water-quenched, resulting in coarse pearlite, fine pearlite and martensite, respectively, then subjected to an arbitrary graphitizing treatment of 10 days at 1100, 1200 or 1300 °F (595, 650 or 705 °C). No graphite developed in either the furnace-cooled or air-cooled samples, but a relatively profuse quantity developed in the water-quenched samples, i.e., those initially martensitic. The variation of the extent of graphitization with reheat temperature was not very pronounced, but exhibited an apparently significant maximum at 1200 °F (650 °C), Fig. 1.

The variation of number of graphite nodules (nuclei) with austenitizing temperature was determined with results summarized in Figs. 2 and 3. Samples were heated for 0.5 hour at intervals of 100 °F in the range 1400 to 2300 °F (760 to 1260 °C), water-quenched, and graphitized 10 days at 1200 °F (650 °C). The number of graphite nodules increased to a maximum at about 1600 °F (870 °C), then declined with further increase of temperature, with no apparent correlation with the grain coarsening behavior of the austenite. As the number of nodules decreased, their size increased in such a manner that the total amount of graphite did not change, as judged by visual means.

In these experiments, the occurrence of a rim of stable carbide was noted on the surface of the samples, Fig. 4. Extensive studies of the effect of various atmospheres including purified helium on the development of this rim proved that it can result from the penetration of nitrogen into the metal during austenitizing; although it seems probable that oxygen penetration would have a similar effect, the experiments did not yield positive proof. These elements are considered to combine with the residual or dissolved aluminum remaining from de-

oxidation. The observations indicate that the role of aluminum deoxidation in promoting susceptibility to graphitization is played through the residual aluminum and not by the alumina or other products of deoxidation. The exact mechanism of this effect, however, remains obscure, and further experiments are planned.

#### ACKNOWLEDGMENT

The authors wish to acknowledge helpful discussions with L. S. Darken and other members of the laboratory staff.

#### References

1. C. R. Austin and M. C. Fetzer, "Factors Controlling Graphitization of Carbon Steels at Subcritical Temperatures", *TRANSACTIONS, American Society for Metals*, Vol. 35, 1945, p. 485-535.
2. G. V. Smith, "Graphitization of Low-Carbon Low-Alloy Steel; an Appraisal of the Literature", *Welding Journal Research Supplement*, Vol. 13, 1948, p. 277-284.
3. R. F. Mehl, "Diffusion in Solid Metals", *Transactions, American Institute of Mining and Metallurgical Engineers*, Vol. 122, 1936, p. 11-56.
4. L. S. Darken, "Diffusion in Metal Accompanied by Phase Change", *Transactions, American Institute of Mining and Metallurgical Engineers*, Vol. 150, 1942, p. 157-169.
5. A. Bramley, F. W. Haywood, A. T. Cooper and J. T. Watts, "The Diffusion of Non-Metallic Elements in Iron and Steel", *Transactions, Faraday Society*, Vol. 31, 1935, p. 707.
6. T. E. Brower, B. M. Larsen and W. E. Shenk, "Critical Studies of a Modified Ledebur Method for Determination of Oxygen in Steel, II", *Transactions, American Institute of Mining and Metallurgical Engineers*, Vol. 113, 1934, p. 61-81.
7. M. J. Day and G. V. Smith, "Iron Alloy Scaling", *Industrial and Engineering Chemistry*, Vol. 35, 1943, p. 1098-1103.
8. F. N. Rhines, "A Metallographic Study of Internal Oxidation in the Alpha Solid Solutions of Copper", *Transactions, American Institute of Mining and Metallurgical Engineers*, Vol. 137, 1940, p. 246.

---

#### DISCUSSION

**Written Discussion:** By B. F. Brown, research associate, Department of Engineering Research, North Carolina State College, Raleigh, N. C.

This demonstration that a carbide stabilizing effect can enter solid metal from gaseous nitrogen will be of interest not only to graphitization in steel but to graphitization in cast irons as well; it should also be of value in understanding the principles involved in the effect of alloying elements on the stability of cementite.

Many experiments have shown that the addition of aluminum to steel is associated with increased rates of graphitization, the common explanation being that aluminum oxide inclusions formed by the deoxidation reaction act as sites of easier nucleation of graphite. The present authors have not been fully satisfied with this explanation and have suggested that aluminum is itself inherently a graphitizer and that the effect of adding it

is not through the formation of inclusions but rather through the presence of residual aluminum.

The effect of alloying elements on the rate of graphitization reactions is of course of prime importance to the metallurgy of the cast irons, and a study of the extensive cast iron literature on the subject affords a clue to a third possible explanation of the effect of aluminum: As aluminum is added to cast iron in increasing quantities, the effect is first to increase the rate of graphitization; but beyond about 3% aluminum, the effect of further additions is to decrease the rate of graphitization, although the cementite is presumably fundamentally the same. One infers from this that aluminum is acting intrinsically not as a graphitizer but rather as a carbide stabilizer. Again in cast irons, it is observed that boron acts as a graphitizer when present in small amounts (of the order of 0.001%), but that in larger concentrations it too acts as a carbide stabilizer. Likewise manganese, when added to irons containing sulphur, acts first to increase the rate of graphitization; but shortly after the sulphur is balanced stoichiometrically with manganese, further additions of manganese act to stabilize the cementite. A number of other elements, such as titanium and zirconium, appear to act similarly.

If it is true that aluminum and these other elements are intrinsically carbide stabilizers, as they do appear to be, then why do they speed graphitization when present in small amounts?

All of these elements are known to be scavengers—desulphurizers, deoxidizers, dehydrogenizers, or denitrogenizers—and the elements they remove (sulphur, oxygen, hydrogen, and probably nitrogen) are carbide stabilizers.

It therefore seems in order to suggest that in reality aluminum acts as a graphitizer because it acts as a deoxidizer. It does not seem possible, however, to say with certainty at this time that the graphitizing effect is limited to removal of a carbide stabilizer and to rule out the possibility that the inclusions formed may assist by providing for easier nucleation, for the various experiments in the literature appearing to demonstrate the absence of such an effect of  $Al_2O_3$  have been somewhat short of fully conclusive, and we should be prepared to draw other conclusions if more decisive future studies should present contradictory evidence.

The findings of this current paper will be as valuable and as welcome to the metallurgy of all the cast irons as it is to graphitization in steel.

**Written Discussion:** By Carl A. Zapffe, consulting metallurgist, Baltimore, Md.

In thermodynamic discussions of carbon in steel, a temperature is usually named below which the carbide  $Fe_3C$  becomes unstable. This temperature is usually placed in the neighborhood of 1290 °F (700 °C), which raises a question, in passing, as to the figure of 2000 °F (1095 °C) which the authors here choose.

However, the point that I wish to make is that the thermodynamics for the solution of carbon in iron are more properly expressed in terms of  $f$  ( $T$ ,  $X$ ,  $P$ ), for pressure is very likely an important variable in the Fe-C system just as it is for those systems of other interstitially dissolving components: N, H, O, and so forth. When the reasoning of



thermodynamics was first applied to metallurgy, a short-cut was adopted for a two-variable system, because substitutionally dissolving elements such as metals are only negligibly affected by pressure. The time has come, however, when a stricter consideration should be given. The gas-metal systems cannot be understood at all without regard for pressure. On the basis of  $f(T, X, P)$  reasoning, a number of current difficulties with the Fe-C system immediately disclose possible explanations. While we expect to go into this in detail in a later publication, attention will be called to the fact that within an iron matrix there is available a pressure range extending from the high order of the internal pressure of the metal down to values in the order of atmospheric pressures wherever a break in the lattice results. If iron carbide is then presumed to be pressure-sensitive, one can relate its behavior to changes in internal pressure. The same results reported by the present authors for steel are also found with cast iron, where stresses due to quenching are known to expedite graphitization. That this results from local decreases in the internal pressure is indicated by two further sets of phenomena. One is described here, where the addition of an element, such as aluminum, favors graphitization. Included nonmetallic particles—inclusions—would present to the matrix local points for reversion of the carbide to graphite. A particularly suggestive experiment with cast iron provides confirming results. It has been found that hydrogen gas dissolved into white iron favors graphitization, and particularly after the gas has first been removed. It is known that hydrogen precipitates internally to open and distend minute rifts which do not readily heal after the gas has been removed. It is likely that cold working would increase graphitization in experiments such as those conducted by the present authors, and this should be investigated.

We have prepared a three-dimensional model for the iron-carbon system which incorporates pressure as a third variable, and we find that most of the "anomalies" described in the literature are then readily explained, and specifically the long-standing puzzle of the "double diagram" for the Fe-C system.

**Written Discussion:** By A. M. Hall, Battelle Memorial Institute, Columbus, Ohio.

The authors have significantly advanced our understanding of the part played by aluminum in the decomposition of the iron carbide in a graphitizable steel, into iron and graphite, when such a steel is held at subcritical temperatures. They are to be congratulated for the experimental approach they chose; it was especially well suited to the problem.

The authors' results indicate very strongly that the role of aluminum deoxidation, in promoting susceptibility to graphitization, is played through residual solid-solution aluminum, rather than by alumina or other deoxidation products. In a project being conducted at Battelle Memorial Institute for the Joint ASTM-ASME High-Temperature Committee a very similar viewpoint has developed. The method is that of extracting and analyzing the carbide residues of several plain-carbon steels of different known degrees of susceptibility to graphite formation. A paper covering the latter study will be presented at the next annual meeting of the ASME by E. E. Fletcher and the writer.



The authors' results supply added confirmation that microstructure has a strong influence on graphitization. The concentration of graphite found in 1943 in the low temperature region of the weld heat-affected zone of the Springdale steam pipe<sup>3</sup> immediately stimulated speculation as to a relationship between microstructure and graphitization susceptibility. As yet, however, no clear-cut statement of this relationship has been promulgated. The authors' finding that the martensitic structure was the most susceptible of the structures studied seems logical, since it was certainly the least stable.

**Written Discussion:** By W. K. Bock, research engineer, National Malleable and Steel Castings Co., Cleveland.

The statement is made that graphitization proceeds by nucleation and growth. The latter term must embody three separate processes: decomposition of cementite, migration of carbon and deposition of carbon on a nucleus or growing graphite nodule. The nature of the nucleus is quite uncertain. The deoxidation products of aluminum, manganese sulphide, local energy increase, due to strain and increased interfacial area, are possibilities which have been suggested.

To confuse the picture of the nucleus still more, the action of elements like aluminum or of treatments like quenching can be thought to aid the decomposition of cementite as well as forming nuclei. For example, aluminum may form alumina and the latter become a nucleus. On the other hand, aluminum may deprive the oxycementite of its oxygen and thus increase its tendency to decompose.

The fact that the steel must be water-quenched to be graphitized shows that the aluminum alone is not responsible for graphite formation. By quenching, the free energy of the system could be raised either by strain energy, increase in interfacial energy, or both. Here, there would be increased driving force tending to convert the steel to the stable system. Locally, this energy might be high enough to cause the decomposition of cementite in sufficient amount to free carbon atoms so close to one another that they could form a lattice and so become a nucleus.

In line with the discussion above, the austenite grain sizes shown in Fig. 3 are of less interest than the strain energy and relative fineness of the martensite formed on quenching.

The authors suggest that nitrogen and possibly oxygen penetrate into the sample during austenitizing treatment, react with aluminum and so cut down graphite formation near the surface. This presupposes an effect of aluminum on graphitization which may be correct. However, if one considers the role of carbon migration in graphitization, another interpretation is possible. Considering Table II and neglecting any possible effect of oxygen in stabilizing cementite, it is noted that, at 2000 °F (1095 °C) austenitizing temperature, air in ½ hour and nitrogen in 6 hours produce carbide-stable rims of the order of 0.025 inch thick, while crushed coke in ½ and 1 hour produces carbide-stable rims of slightly over half as great. Since the nitrogen atom is probably smaller than an oxide of carbon molecule, it could penetrate deeper. The presence of the gas molecules or atoms in the outer layer could, by taking up space

<sup>3</sup>R. W. Emerson, "Carbide Instability of Carbon-Molybdenum Steel Piping", *Transactions*, American Society of Mechanical Engineers, Vol. 66, 1944, p. 5.

which is needed for passage of carbon, materially affect the migration of carbon and so stop graphitization. The small helium atom would be quite mobile and, according to this theory, would have to offer little impediment to carbon migration to explain the absence of rims when the steel has been austenitized in that gas.

Some of the effect of the various treatments on graphitization in the body of the piece may be masked by the lack of graphite analyses. It has been our experience that even when small amounts of graphite are formed, metallographic estimation of the amount of graphite is unreliable.

These comments are not offered as contradiction or denial of the authors' conclusions but rather to present alternate conclusions in an effort to further discussion of this interesting problem of graphitization.

**Written Discussion:** By J. J. Heller, research engineer, Engineering Research Institute, University of Michigan, Ann Arbor, Mich.

The results of this paper add another section to the over-all picture which should eventually tell the complete story of graphitization in steel.

I would like to add a few comments concerning the relation between the results of this work and a graphitization hypothesis by J. J. Kanter as presented in the Addendum to the Summary Report on Carbide Extraction Studies of Plain Carbon Steels to Project No. 29 of the Joint ASTM-ASME Committee on the Effect of Temperature on the Properties of Metals.

The authors state that they observed a carbide-stable (low graphitization susceptibility) rim on specimens austenitized in air. They concluded that this rim can result from the penetration of nitrogen into the surface of the metal during austenitizing. The development of the carbide-stable rim serves to emphasize the hypothesis of Mr. Kanter. Under this hypothesis, graphitization susceptibility is intimately related to the solubility of carbon in the ferrite matrix; thus the higher the carbon solubility the more susceptible is the steel to graphite formation, and vice versa. Nitrogen in solid solution in ferrite is believed to reduce the solubility of carbon in the ferrite. Thus solid-solution nitrogen would act to reduce graphitization susceptibility by reducing carbon solubility. Aluminum would remove nitrogen from solid solution by the formation of the insoluble aluminum nitride, thus increasing carbon solubility and thereby increasing the susceptibility of the steel to graphitization. Generally, the steel used for this investigation is readily susceptible to pronounced graphite formation under the test conditions. The carbide-stable rim (e.g., free from graphite) may be explained, following Mr. Kanter's hypothesis, by the idea that enough nitrogen penetrated into the surface of the metal so that there was an excess over that required to combine with the aluminum to form aluminum nitride. This excess would presumably be in solid solution in the ferrite matrix, thus reducing the solubility of the carbon in the ferrite and thereby making the steel at the surface of the sample more resistant to graphitization.

The authors also made mention of the fact that under certain conditions the carbide-stable rim is destroyed from the inside outward. The fact that this carbide-stable rim was found to be destroyed from the inside outward can also be explained under this hypothesis. It would be expected that once the carbide-stable rim was established, a gradual

diffusion reaction would occur. That is, more of the residual aluminum would find its way to the surface and come into contact with the inside edge of the carbide-stable rim. The aluminum would then combine with the nitrogen that had been in solid solution. Eventually this reaction would destroy the carbide-stable rim by taking the nitrogen out of solid solution and thereby allowing graphitization to occur.

It would be interesting to note the results of comparative nitrogen analysis on the surface portions of the following samples:

- (a) a sample in the original, untreated condition
- (b) a sample containing the carbide-stable rim
- (c) a sample that has had the carbide-stable rim destroyed.

#### Authors' Reply

In the interest of brevity, we refrained from speculation in the paper and simply reported the experimental observations, the principal one of which was that the role of aluminum deoxidation in promoting graphitization must be tied up not with the deoxidation products such as  $\text{Al}_2\text{O}_3$ , but with the residual aluminum. It seemed obvious to us, however, that the aluminum acts in either one of two ways: (a) as a direct graphitizing element (acting like such elements as nickel and silicon are popularly held to act); and (b) as a scavenger for some other element (or elements) which acts to stabilize carbide. It seemed to us that the role of  $\text{Al}_2\text{O}_3$ , which has often been suggested as providing nucleation sites for graphite, could not be an important one in our experiments, since this constituent was presumably equally abundant in the carbide-stable rim and in the graphitizable interior. Either of the two first-mentioned mechanisms would appear possible on the basis of our results on penetration of nitrogen, and in an effort to determine which is correct, we are proceeding to prepare Fe-C alloys of a high degree of purity with different concentrations of nitrogen and aluminum.

We are not aware that large amounts of aluminum act to stabilize carbide, as Dr. Brown states; if true, this, of course, suggests that the carbide-stable rim in our experiments was a consequence of nitrogen acting as a stabilizer, and that the role of aluminum deoxidation is to scavenge nitrogen (and possibly other elements as well). It would appear desirable, however, to check this mechanism by the experiments suggested in the preceding paragraph.

The suggestion of Dr. Zapffe that consideration of the pressure variable will elucidate the question of the stability of iron carbide relative to graphite is an interesting one, but since he chooses only to make the suggestion and to reserve a detailed picture until a later publication, we can hardly consider it here. When the details of his theory appear, we will, of course, consider them. It might be pointed out in this connection that whereas carbon steels graphitize more rapidly when they possess a quenched structure, this prior treatment is not necessary to graphitization. Dr. Zapffe's suggested experiment of studying the effect of cold work has been performed a number of times, and it is now well known that cold work accelerates graphitization. Whether or not the pressure variable is important to graphitization, it should be emphasized that we were concerned not with explaining the metastability of  $\text{Fe}_3\text{C}$  but were attempt-



ing to discover how aluminum deoxidation promotes graphitization. Further, whereas nonmetallic inclusions unquestionably play an important role in graphitization in some cases, as Dr. Zapffe points out, our experiments indicate that this is not a prominent one in steels. In regard to the temperature below which  $\text{Fe}_3\text{C}$  is unstable, this temperature is at least 2000 °F (1095 °C), and very probably higher, contrary to Dr. Zapffe, and whereas there may be some argument as to the exact temperature, we hardly think anyone else would place it as low as 1300 °F (705 °C), which he proposes.

Mr. Hall's discussion does not require any comment, except to point out that the least stable microstructure in molybdenum steels does not appear to be martensite as in the carbon steels.<sup>4</sup>

In reply to Mr. Bock, it is not necessary to quench to get graphite, although this treatment accelerates graphitization in plain carbon steels. As we understand Mr. Bock's alternative explanation of the carbide-stable rim, molecules of CO and  $\text{CO}_2$  are considered to exist within the steel and to prevent the migration of carbon, thereby preventing graphitization. This hypothesis is untenable inasmuch as molecules, including CO and  $\text{CO}_2$ , are not known to exist as such in metals. Contrary to Mr. Bock, we find that the metallographic detection of graphite is most reliable and in fact more sensitive than the chemical means. It is, of course, necessary that the sample for microscopic examination be properly prepared, so that the graphite is retained, not torn away.

Mr. Heller's explanation of the carbide-stable rim is based on a suggestion that graphitization susceptibility varies directly with the carbide solubility in ferrite, and that this is reduced by the presence of nitrogen. This hypothesis has not been proved, so far as we are aware, and we doubt that it could be demonstrated; that is, one would expect the change in solubility of carbide by the presence of nitrogen to be so small as to be undetectable. But in any event it hardly seems appropriate to consider solubility which is only an associated aspect of the primary question, namely the thermodynamic stability of the phases. In other words, why not simply state that nitrogen stabilizes the carbide phase, which is one of the possibilities discussed above.

In regard to the decrease in rim thickness on graphitizing in an oxidizing atmosphere, we have shown by experimental measurements described in the paper that this is a consequence of scaling loss and therefore that the destruction of the rim from the inside outward is only apparent, not real. Whereas the mechanism suggested by Mr. Heller would lead in the same direction as the observed effect, we would predict that the diffusivity of aluminum would be too slight at 1200 °F (650 °C) to produce an observable effect. In any event, Mr. Heller's explanation would not account for the difference between graphitizing in an inert and in an oxidizing atmosphere, which, of course, is the essential point, and which can be simply explained as a scaling loss in the oxidizing atmosphere. The nitrogen analyses about which Mr. Heller inquires would indeed be desirable but the specimens and the penetrations were too small for such study.

<sup>4</sup>G. V. Smith, "Graphitization of Low-Carbon Low-Alloy Steel; an Appraisal of the Literature", *Welding Journal*, Vol. 27, 1948; *Welding Research Supplement*, p. 277s-284s.



# KINETICS OF THE AUSTENITE TRANSFORMATION IN CERTAIN ALLOY STEELS

BY EDWARD A. LORIA

## *Abstract*

*Results obtained in an investigation of the isothermal transformation characteristics and structural features of complex alloy steels are described. The TTT-diagrams of six commercial steels are presented and discussed. Photomicrographs and hardness data are included as aids in the analysis of these diagrams. The steels are arranged in two groups on the basis of similar chemical composition. In one group are three nickel-chromium-molybdenum steels of 4.84 to 5.10% total alloy content and in the other are three chromium-molybdenum-manganese steels of 2.47 to 2.66% total alloy content. Variations in carbon and alloy content permit the comparison of the transformation velocities and provide information on hardenability and slack-quenched structures in these steels. The TTT-diagrams show a complete break, or region of relatively stable austenite, between the pearlite and bainite transformations. Further, the top of the bainite range is marked by a horizontal shelf extending to short reaction times, and the effects of carbon and alloy contents on the time for the initial decomposition at any temperature are clearly indicated.*

## INTRODUCTION

THIS contribution is the third of a series (1, 2)<sup>1</sup> dealing with the decomposition of austenite at subcritical temperatures in complex alloy steels. The first paper (1) described the nature and mode of formation of the acicular structure found within the intermediate transformation range of two particular alloy steels with appreciable amounts of a number of carbide-forming elements. In a slightly hypereutectoid steel containing nickel, chromium, molybdenum and manganese, the initial transformation was a carbon-rich plate which decomposed or tempered slowly to a carbide-ferrite aggregate after long holding periods at temperature. In a chromium-molybdenum-manganese hypoeutectoid steel the primary precipitate was acicular ferrite containing entrapped particles of carbide and

<sup>1</sup>The figures appearing in parentheses pertain to the references appended to this paper.

The author, Edward A. Loria, is Senior Fellow, Mellon Institute of Industrial Research, Pittsburgh. Manuscript received September 19, 1950.

austenite (martensite on quench). The second paper (2) summarized the results of isothermal transformation studies on the chromium-molybdenum-manganese hypoeutectoid steel and another nickel-chromium-molybdenum hypereutectoid steel. Both TTT-diagrams showed a full knee for the pearlite reaction and a second, lower knee for the bainite reaction, separated by a bay of extremely slow reaction.

The object of this investigation is to extend the present knowledge of the transformation characteristics of complex alloy steels which have been so admirably defined by Troiano (3-7) and Hultgren (8). The TTT-diagrams for six steels of high alloy content are presented and arranged in two groups on the basis of similar chemical analysis. For such compositions, a TTT-diagram with a complete break, indicating a region of relatively stable austenite separating the pearlite and bainite transformation ranges, is generally expected. In this type of diagram the top of the bainite range is marked by a clearly defined horizontal shelf. The best method available to describe the kinetics of the decomposition of austenite in steel is still the original method used by Davenport and Bain (9), which consists of plotting the start and end of transformation as a function of time at constant temperature. While this method does not yield the complete kinetics of the reactions, it provides a sound basis for comparing the velocities of transformation as affected by the many variables, such as alloying elements, austenite grain size and austenite heterogeneity. It has been adopted in the present work, and the tool utilized to determine the fraction transformed was the metallographic examination of the specimens reacted at various time intervals. In this way the effects of carbon and alloy contents on transformation behavior and hardenability can be revealed in a comparison of the start of transformation curves obtained for the various steels.

#### EXPERIMENTAL PROCEDURE

The composition of the steels studied is given in the following tabulation, together with a code letter for each steel to facilitate subsequent reference:

Steel	C	Ni	Cr	Mo	Mn	Si	V	P	S
A	0.60	2.75	1.25	0.50	0.60	0.30	0.12	0.035	0.024
B	0.59	....	1.06	0.54	0.96	0.28	0.12	0.032	0.022
C	0.86	2.47	1.21	0.50	0.66	0.38	....	0.040	0.024
D	0.42	2.71	1.00	0.48	0.67	0.31	....	0.030	0.022
J	0.39	....	1.00	0.56	1.10	0.29	0.12	0.015	0.013
K	0.31	....	0.99	0.52	0.76	0.27	0.11	0.016	0.013

Steels A, C and D contain appreciable amounts of nickel, chromium, molybdenum and manganese. The differences between them are that steel A has an intermediate carbon content and the highest amount of nickel, whereas steel C has the highest carbon content with the lowest nickel content and steel D has the lowest carbon and chromium contents. Steel J is essentially a manganese-chromium-molybdenum steel and steel K is of somewhat similar composition but with lower carbon and manganese. The TTT-diagrams and the structural features of steels J and K have been investigated by Troiano (3) and are included here for direct comparison with the transformation characteristics of steel B, which has a similar alloy but a higher carbon content. All compositions were commercially made acid open-hearth steels and were processed in the form of forged rounds.

The prior treatment for steels A to D consisted of normalizing at 1700 °F (925 °C) and tempering at 1200 °F (650 °C), while steels J and K were just normalized at 1650 °F (900 °C). Rounds of 1/2-inch diameter, which were cut into disks about 1/4-inch thick, were used for the isothermal and hardness studies. All austenitizing was done in an atmosphere furnace. Steels A, C and D were austenitized for 1 hour at 1550 °F (845 °C), steel B for 1 hour at 1650 °F (900 °C), and steels J and K for 1 hour at 1650 and 1600 °F (900 and 870 °C), respectively. These temperatures were selected because they approximate those employed in the commercial heat treatment of these steels. The as-quenched grain sizes resulting from these austenitizing treatments are indicated on the appropriate transformation diagrams. The  $A_1$ ,  $A_3$  and  $A_{cm}$  critical points were determined by the standard microscope method.

As in the earlier work, upon austenitizing, the specimens were quickly transferred to lead or salt baths controlled to  $\pm 5$  °C and, after suitable periods of time, quenched into water. Progress of transformation was measured microscopically at several temperature levels. Rockwell C hardness numbers on the diagrams represent not only the measured hardness but also indicate by their position some of the temperature levels investigated. In general, the over-all accuracy of the microscopic determinations is believed to be of the order of 10 to 15 °F. The normal inhomogeneities of commercial steels preclude the possibility of greater accuracy.  $A_{cm}$  for high carbon steel C could not be determined by the standard microscope method since it was virtually impossible to detect and identify the first small carbide particles to precipitate below  $A_{cm}$ . Indeed, there are many alloy steels whose value of carbon content for eutectoid



composition is unknown and thus the upper critical temperature cannot be properly designated as  $A_{cm}$  or  $A_3$  according to present convention.

### EXPERIMENTAL RESULTS

The TTT-diagrams for the different steels are shown in Figs. 1, 2, 3, 9, 10 and 11. The diagrams have been drawn in the customary manner where the beginning line indicates approximately less than  $\frac{1}{2}\%$  transformation and the ending line somewhat more

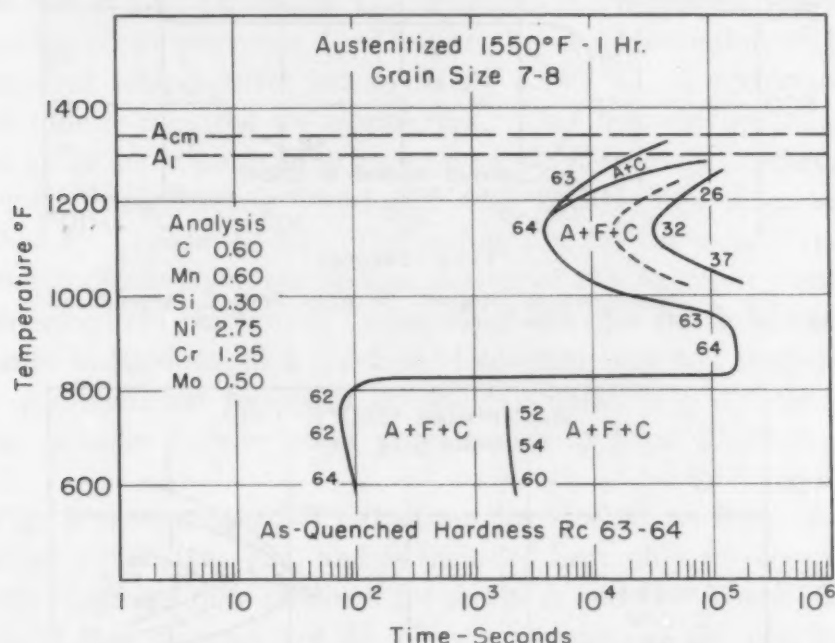


Fig. 1—Transformation Diagram for Alloy Steel A, Austenitized at 1550 °F (845 °C).

than 99% decomposition of the austenite. The three transformation products of austenite (pearlite, bainite and martensite), although different in structure and properties, are all basically mixtures of ferrite and carbide and are therefore all indicated on the TTT-diagram by the notation  $F + C$ . The thin dotted line within the  $A + F + C$  field represents, for each temperature level, the time at which half of the total austenite has transformed.

The TTT-diagram developed for steel A in Fig. 1 shows a full knee for the pearlite reaction and a second, lower knee for the bainite reaction separated by a bay of extremely slow reaction. The effect of the alloying elements in shifting the eutectoid point to the left was sufficient enough to make steel A slightly hypereutectoid, the  $A_{cm}$  being found at 1340 °F (725 °C).  $A_1$  was located at 1300 °F (705 °C). Since the 1550 °F (845 °C) austenitizing temperature was

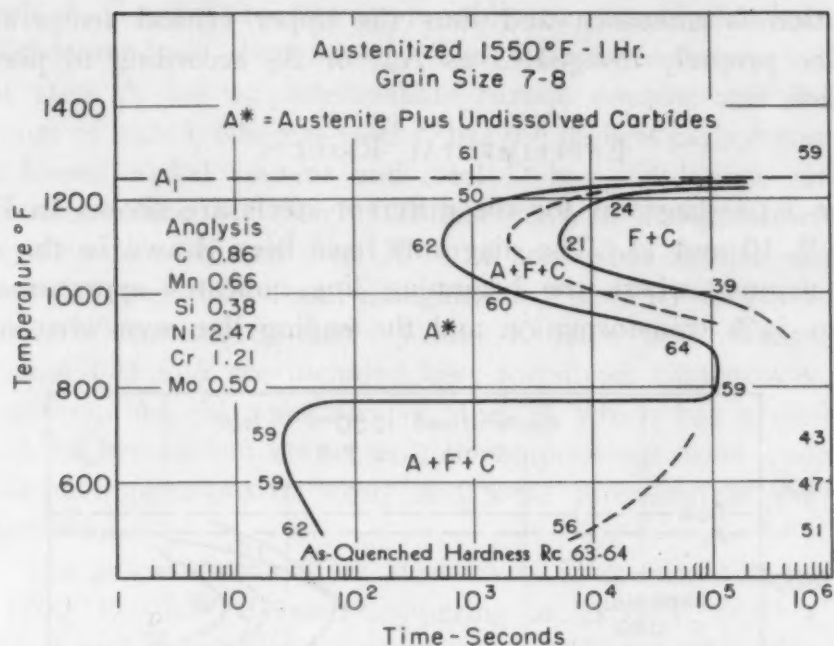


Fig. 2—Transformation Diagram for Alloy Steel C, Austenitized at 1550°F (845°C). After Loria (2).

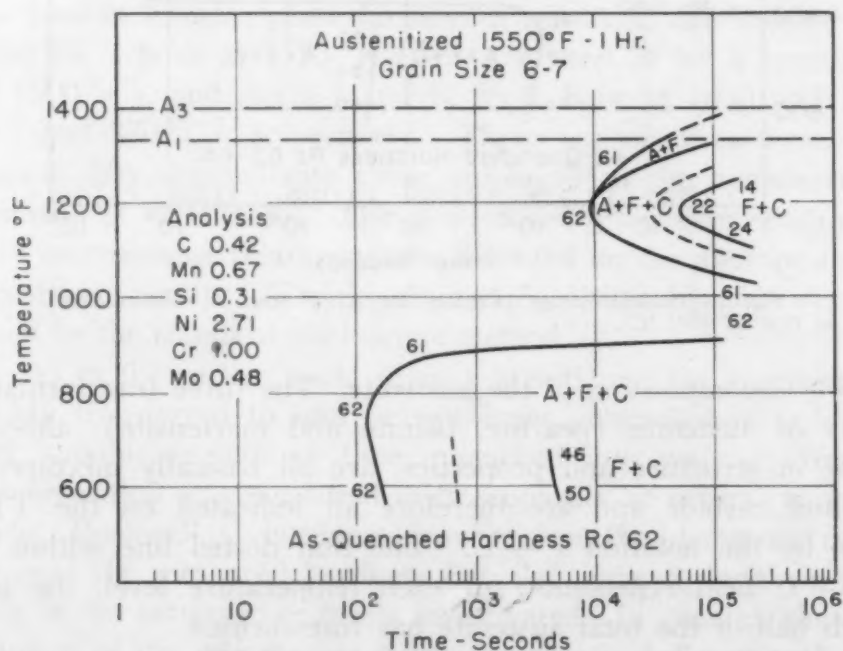


Fig. 3—Transformation Diagram for Alloy Steel D, Austenitized at 1550°F (845°C).

not quite high enough to effect their complete solution, minute segregated carbides were observed in some of the transformation products. At temperatures below  $A_1$ , proeutectoid carbide first resulted as an outline of the former austenite grain boundaries and

with much less facility than ferrite forms in hypoeutectoid steels. The carbide that forms grows more slowly but is otherwise similar to ferrite in that it grows preferentially along grain boundaries and has the same characteristic morphological relations to dendrite formation. The apex of the pearlite knee or the temperature of most rapid reaction occurs at 1140 °F (615 °C). Above 950 °F (510 °C) the transformation product was fine pearlite, the lamellar spacing of which increased with rising temperature. The bainite shelf occurs at a temperature of 830 °F (445 °C). The acicular structures occurring in the bay of extremely slow reaction were studied previously and portrayed in reference 1. Despite the rapid initiation of transformation at temperatures below 830 °F (445 °C), a prolonged period of time is required for completion. This behavior is characteristic of many steels containing an appreciable percentage of chromium and molybdenum and is associated with a two-stage reaction first described by Troiano (3-6). The ending line for the bainite reaction does not indicate complete decomposition of the austenite; only the first intermediate reaction is disclosed. Undoubtedly these products do change in hardness as a function of reaction time and temperature. Their conformation has been shown previously (1, 2), the dark-etching, acicular bainite being very similar to Figs. 25-26 in reference 2.

Fig. 2 presents the TTT-diagram for steel C, as determined in an earlier publication (2), and is included here only for comparison with the diagrams now obtained for steels A and D. The significant aspects of this diagram are the clear separation of the pearlite and bainite reactions with respect to temperature and the intermediate temperature range in which neither reaction will occur within reasonable time. The 1550 °F (845 °C) austenitizing temperature was not high enough to bring about complete solution of the alloy carbides. As a consequence undissolved carbides were found in the decomposition products and  $A_{cm}$  could not be determined microscopically.  $A_1$  was located at 1250 °F (675 °C). The tip of the pearlite knee occurs at 1100 °F (595 °C) and the top of the bainite reaction is at 775 °F (415 °C). Again two types of structure arise on isothermal transformation at various levels in this region; the end of the intermediate reaction is not delineated in the diagram.

The TTT-diagram developed for hypoeutectoid steel D is set forth in Fig. 3. From the standpoint of composition, steel D has lower carbon and chromium contents than steels A or C.  $A_3$  occurs at 1400 °F (760 °C) and  $A_1$  at 1335 °F (725 °C). Above 1200 °F (650 °C) a deposit of proeutectoid ferrite is observed at the



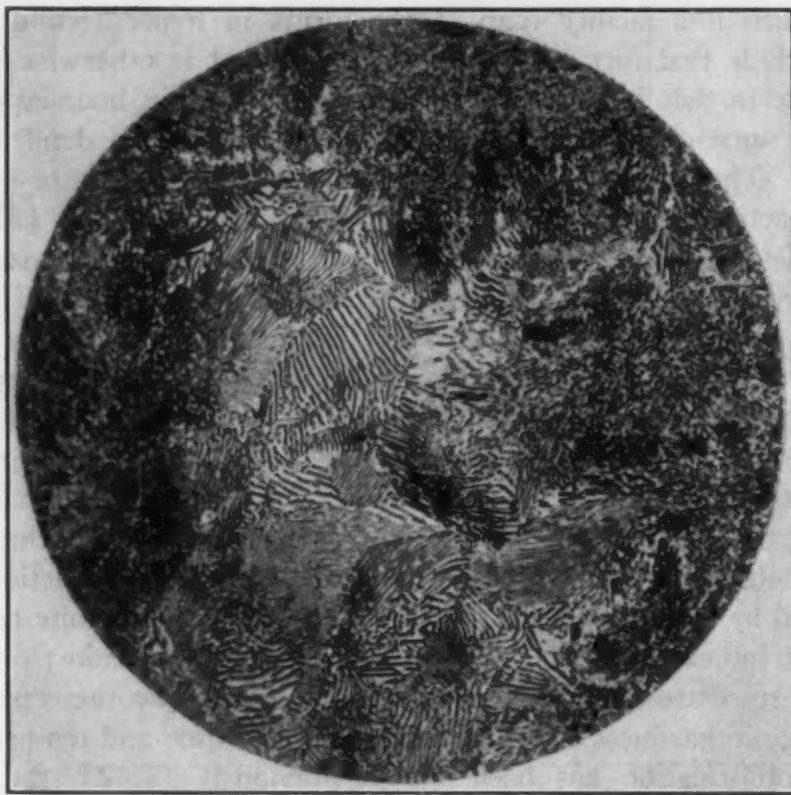


Fig. 4—Alloy Steel D Transformed at 1200 °F (650 °C) for 17 Hours. Modified picral etch.  $\times 1000$ .

former austenite grain boundaries and precedes the reaction to pearlite in decreasing magnitude to the tip of the pearlite knee that appears at 1185 °F (640 °C). At and below the knee only fine pearlite is formed. The structure depicted in Fig. 4 for the 1200 °F reaction temperature shows both lamellar and granular pearlite. Then a region of stable austenite exists between 900 and 1030 °F (490 and 555 °C); the quenched martensite structure on holding steel D for 25 hours at 960 °F is illustrated in Fig. 7. The initiation of the bainite reaction is not delayed to the same degree as the pearlite transformation; the bainite knee projects to the left below the 900 °F (480 °C) shelf. The nature of the acicular ferrite containing small carbides formed at 800 °F (425 °C) is presented in Fig. 5. The rapid beginning and extremely slow ending of transformation in the vicinity of 750 to 900 °F (400 to 480 °C) are explained by the transformation to two different types of reaction product. As is common to most alloy steels, the microstructural appearance of the bainite changes markedly as a function of temperature. In the lower temperature range, 680 to 570 °F (360 to 300 °C), only the dark-etching, acicular bainite forms and the re-

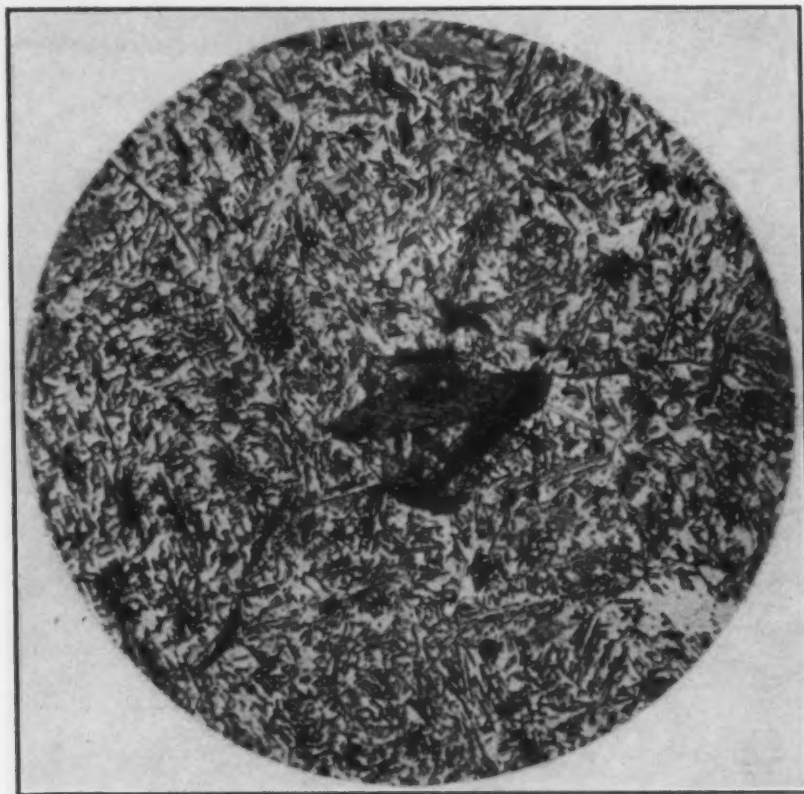


Fig. 5—Alloy Steel D Transformed at 800 °F (425 °C) for 10 Hours. Modified picral etch.  $\times 1000$ .

action goes to completion within a relatively short time, as can be seen in Fig. 6.

So as to consider the transformation characteristics of a steel with lower alloy content, the TTT-diagram for chromium-molybdenum-manganese hypoeutectoid steel B is set forth in Fig. 9. It is apparent that, even without nickel, the reactions to pearlite and bainite are completely separated, both as to temperature and time. The structural features in the transformation of austenite in this steel were previously shown and discussed (2). Briefly,  $A_3$  and  $A_1$  appear at 1385 °F (640 °C) and 1350 °F (730 °C). The extent of the proeutectoid ferrite reaction is much more reduced than that observed in steel D, which, of course, had a lower carbon but a higher alloy content. The apex of the pearlite reaction is found at 1200 °F (650 °C). Again the pearlite knee is transposed far to the right on the time axis by the alloy content, while the bainite knee juts out to the left below the 930 °F (500 °C) shelf. In the 700 to 925 °F (370 to 495 °C) range, transformation starts rather promptly but is extremely sluggish in going to completion. The second dashed line in this part of the diagram indicates only the

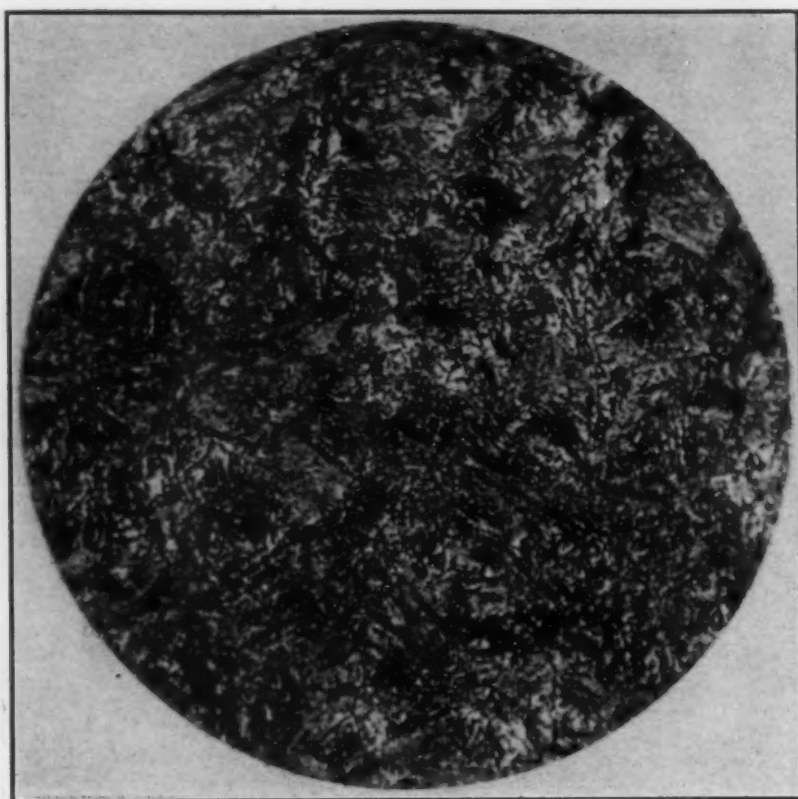


Fig. 6—Alloy Steel D Transformed at 600 °F (315 °C) for 75 Minutes. Modified picral etch.  $\times 1000$ .

completion of the first intermediate reaction of the two-stage bainite reaction.

The TTT-diagrams determined by Troiano (3) for analogous steels J and K are included for comparison purposes as Figs. 10 and 11. Steel J is essentially a manganese-chromium-molybdenum hypoeutectoid steel and steel K is of somewhat similar analysis but with lower manganese and carbon. The reaction sequences observed in these steels can be compared to those obtained in steel B to show the effect of a higher carbon content in the latter and in steel D to show the effect of a high percentage of nickel when added to the base (alloy) composition of steels J and K. In his report (3) Troiano directs special attention to the unusual character of the TTT-diagram for steel J and to its high hardenability. In contrast to steel K, the pearlite and bainite transformations are clearly separated, and, with falling temperature, the proeutectoid ferrite reaction veers sharply to longer times in line with the pearlite reaction. Then the bainite reaction begins at much lower temperatures than in the case of steel K. Troiano emphasizes that the results obtained in this range are of great importance. The intermediate reaction starts



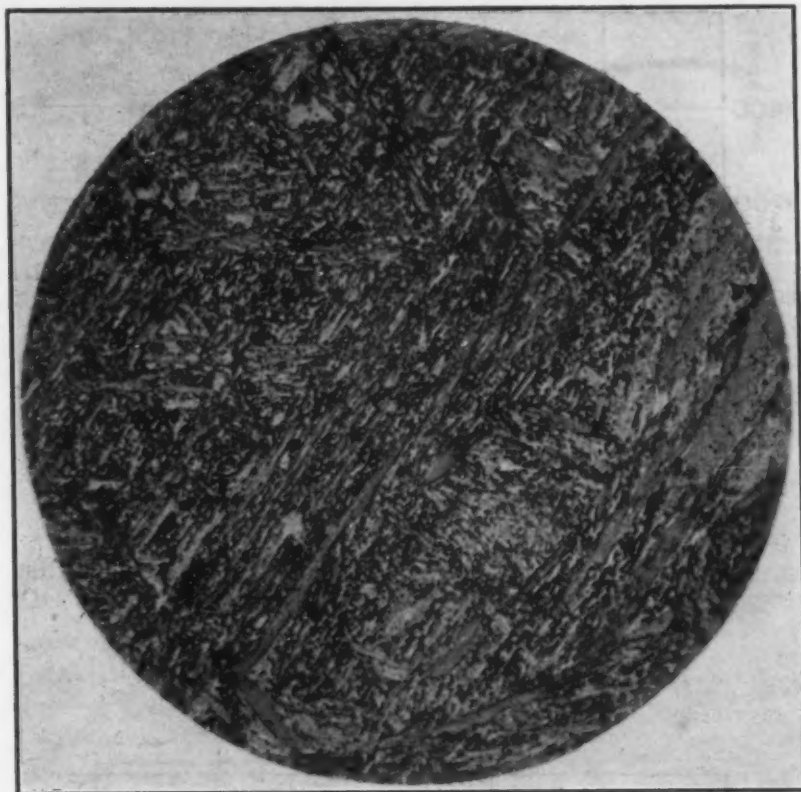


Fig. 7—Alloy Steel D Transformed at 960 °F (515 °C) for 25 Hours. Modified picral etch.  $\times 1000$ .

after a very short time (less than 1 minute) and comes to apparent completion within several minutes. The solid line indicating the completion of the bainite reaction is this apparent completion of the reaction, which, however, does not represent complete decomposition of the austenite. It was not practical within the scope of Troiano's investigation to attempt to determine the time for the beginning or completion of the second intermediate reaction, except to find that in all cases (4340 type steels) the time for beginning is of the order of magnitude of days and weeks and for completion the time is probably of the order of months. In other words, only the first intermediate reaction is indicated; there must be at least a second reaction to allow the remaining unstable austenite to decompose.

In the pearlite transformation range, one should note that the initial reaction is the formation of proeutectoid ferrite at temperatures both above and below the temperature of the pearlite knee. Thus in steels J and K, which have a sufficiently low carbon content, the ferrite reaction exhibits a knee of its own and precedes the pearlite reaction by an appreciable period of time. Ferrite forms over the temperature range 1120 to 1290 °F (605 to 700 °C) and is the initial transformation rather than pearlite, which was the case for steels A

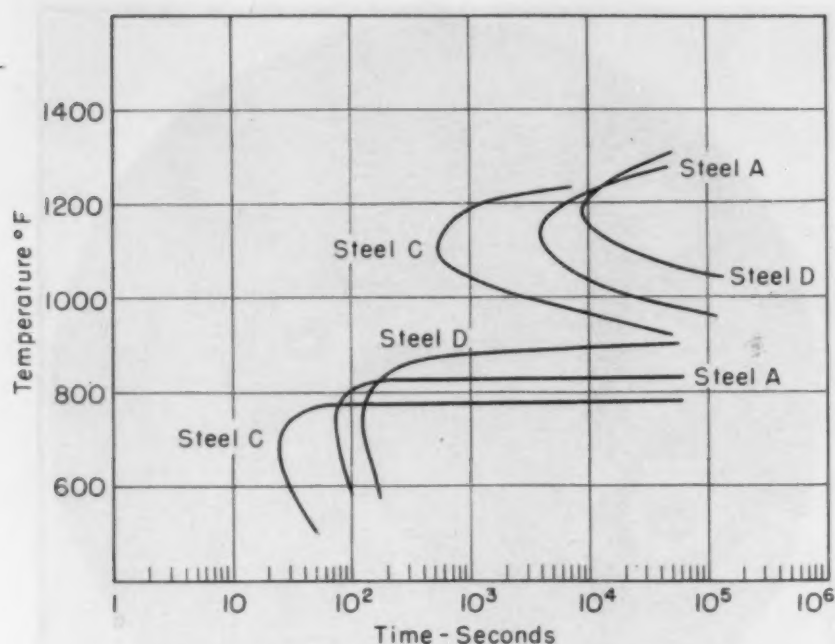


Fig. 8—Comparison of Start of Transformation Curves for Alloy Steels A, C and D.

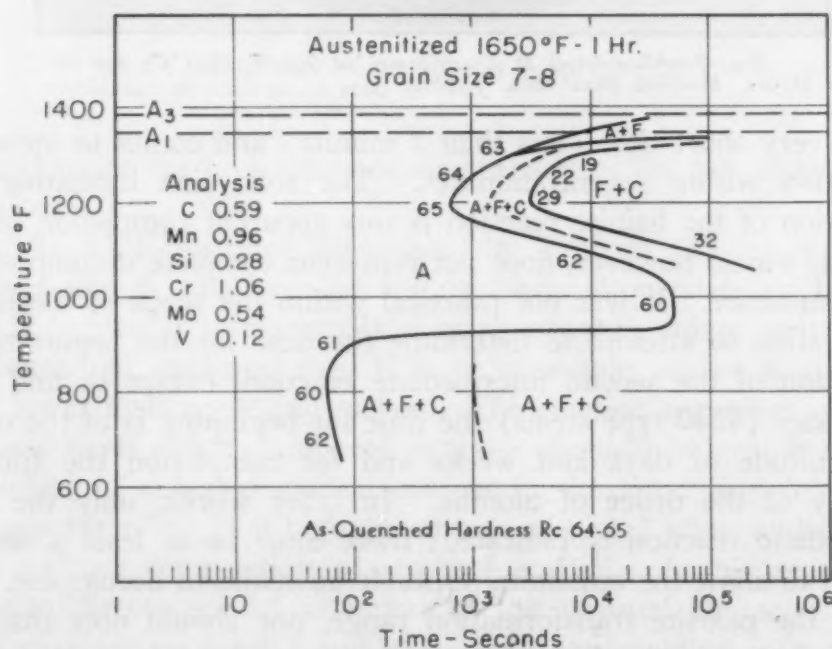


Fig. 9—Transformation Diagram for Alloy Steel B, Austenitized at 1650 °F (900 °C). After Loria (2).

to D. In steel J the ferrite and pearlite knees both occur at 1235 °F (670 °C) and the bainite shelf is located in the 940 to 970 °F (505 to 520 °C) range, whereas in steel K they occur at 1235 and 1065 °F (670 and 575 °C), respectively.

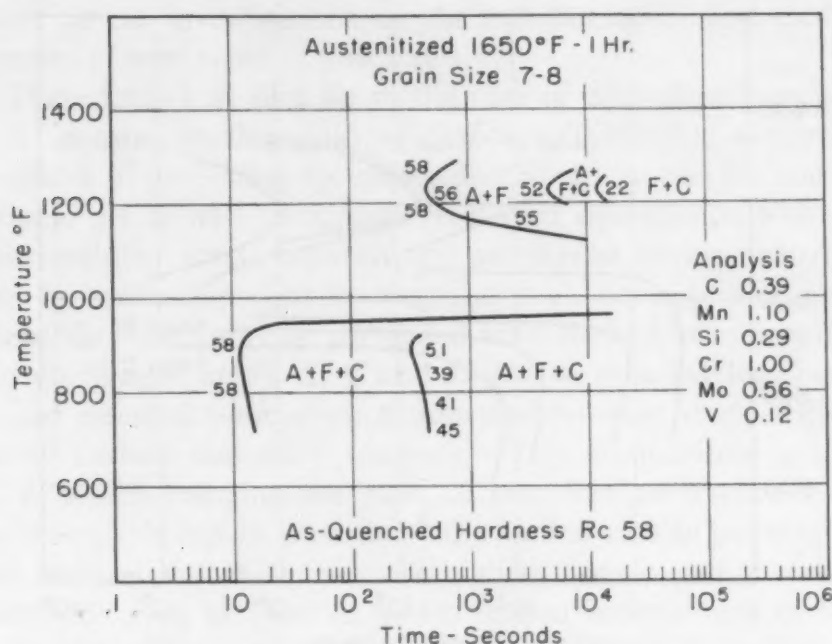


Fig. 10—Transformation Diagram for Alloy Steel J, Austenitized at 1650 °F (900 °C). After Troiano (3).

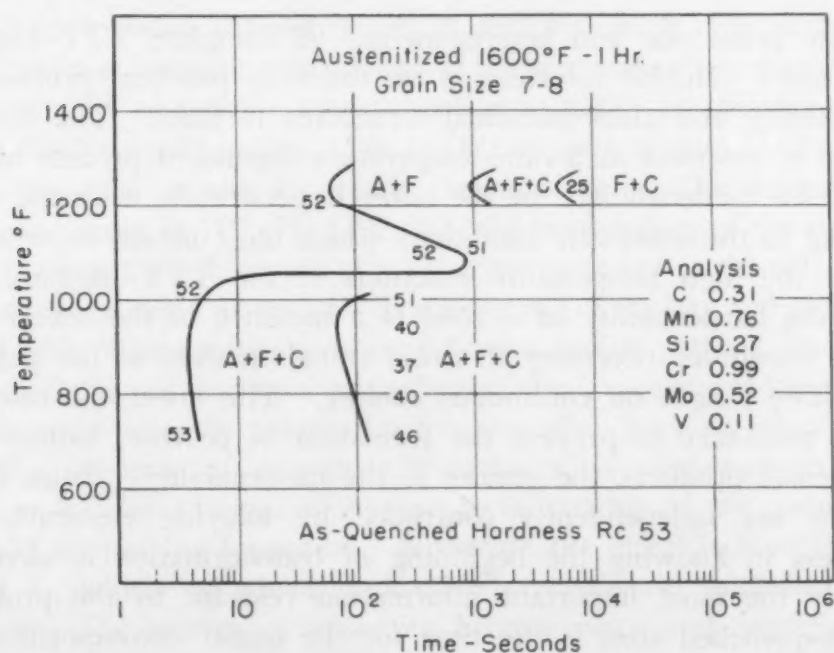


Fig. 11—Transformation Diagram for Alloy Steel K, Austenitized at 1600 °F (870 °C). After Troiano (3).

### DISCUSSION

Now that the TTT-diagrams for the six steel compositions have been constructed, a comparison can be made of the velocities of transformation between them as affected by the alloying elements,



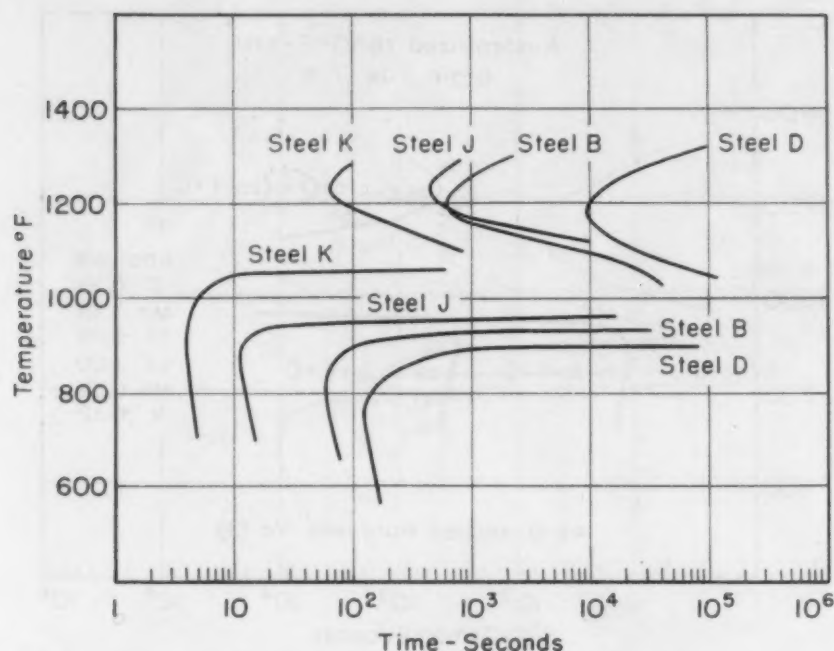


Fig. 12—Comparison of Start of Transformation Curves for Alloy Steels B, D, J and K.

austenite grain size and heterogeneity. A complete TTT-diagram yields much valuable information on the very practical problem of hardenability and slack-quenched structures in steel. The decomposition of austenite as a time-temperature-dependent process hinges directly on hardenability, for the latter is generically a kinetic term referring to the kinematic conditions which must obtain in order to prevent the high temperature reactions in the TTT-diagram. In effect, the hardenability of a steel is a measure of the severity of cooling conditions necessary to avoid transformation in the pearlite and bainite ranges on continuous cooling. The lower the rates of cooling necessary to prevent the formation of pearlite, bainite and proeutectoid products, the greater is the hardenability. Since these reactions are independently controlled by alloying elements, the usefulness in knowing the beginning of transformation is obvious. Probably the most important information relevant to the problem of slack-quenched steel is the time for the initial decomposition of austenite at any temperature and the nature of the product or products of decomposition at that temperature. This information will allow at least a qualitative analysis of the structure observed as a result of a slack-quench. It is understood, of course, that the slack-quenched structures form over a range of temperatures, which range is primarily dependent upon the results of true isothermal decomposition. Troiano (3) and Edlund (10) have followed this approach

in their recent investigations on the metallographic and mechanical properties of new types of gun steels.

These facts lead directly to the idea of equivalent compositions, that is, various combinations of carbon and alloying elements that are capable of producing the same effect upon the pearlite and bainite reactions. It is well recognized that such equivalence with respect to hardenability exists between and among the various alloying elements in multicomponent commercial steels for which quantitative hardenability data may be correlated with chemical composition.

Accordingly, steels A, C and D can be grouped together, since they are essentially nickel-chromium-molybdenum steels with variations in carbon and alloy contents. This comparison is made in Fig. 8, which contains the start of transformation curves for the three steels. It can be seen that the reaction rate to pearlite is most rapid in steel C, which has the highest carbon and lowest nickel content, followed by steel A, which has an intermediate carbon and the highest nickel, and ending with steel D, which has the lowest carbon and chromium contents. The actual differences are 0.18% carbon and 0.25% chromium between steels A and D, 0.26% carbon and 0.28% nickel between steels A and C, and 0.44% carbon and 0.24% nickel between steels C and D. The curves show that the time for the start of pearlite transformation at 1200 °F (650 °C) varies from 1000 seconds in steel C to 10,000 seconds in steel D, decreasing by a factor of 10 with increasing carbon content. The decrease is of the same order at 1100 °F (595 °C), the temperature of the tip of the pearlite knee, which occurs at a lower temperature as the carbon content of these steels increases. The lowering of the bay and the bainite shelf with respect to temperature follows a similar pattern. The results indicate that an increase in carbon content accelerates the pearlite reaction, moving the pearlite knee to the left. Such an effect, caused by the presence of proeutectoid carbides, is presumed to be the reason for the reversal in hypereutectoid steels of the influence of carbon on pearlite formation. No doubt the effect is accentuated in steel C, which contained undissolved carbides to nucleate the reaction. The matter of austenite heterogeneity and segregation of alloy carbides is an important consideration in any analysis of the results. On the other hand, the effect of austenite grain size developed by the austenitizing treatment is minute, since steel D had a rating only one index number lower than that obtained for steels A and C. The bainite reaction starts quite rapidly for these steels, the time difference at 720 °F (380 °C) ranging from 25 seconds in steel C to 150 seconds in steel D, or a factor of 6 between steels C and D and only about 2 between steels A and D.

The second grouping that can be made consists of steels B, J and K, which are essentially chromium-molybdenum-manganese steels of variable carbon and alloy contents. Steel D can be included in the comparison to show the added effect of an appreciable quantity of nickel on the base composition of steels J and K. The comparison of the start of transformation curves for these steels is given in Fig. 12. At the outset it should be noted that the curves for steels J and K in the 1100 to 1300 °F (595 to 705 °C) temperature range are for the reaction to ferrite rather than pearlite, which is the case for steels B and D. Also these steels produced only an as-quenched hardness of 58 and 53, compared to 64 and 62 for the latter. The curves show clearly the influence of increasing carbon content in suppressing transformation within the pearlite range and its marked effect in lowering the bainite shelf and delaying transformation in that region. Thus the difference in 0.08% carbon and 0.34% manganese between steels J and K was sufficient to delay the start of the proeutectoid ferrite reaction from 65 to 450 seconds, or a factor of about 7, and to separate the pearlite and bainite reactions by lowering the bainite shelf about 110 °F. The addition of 0.20% more carbon in steel B initiated the direct transformation to pearlite at a later time instead of proeutectoid ferrite obtained in steels J and K. Also the bainite transformation was lowered slightly and delayed considerably. At 800 °F (425 °C) the reaction starts in less than 15 seconds in steel J versus 60 seconds in steel B, a four-fold increase. The potent effect of 2.71% nickel as an additional alloying element in steel D compared to steels B and J is demonstrated by the appreciable time delay in the start of the pearlite reaction and by the lowering and delaying of the bainite reaction as well. The tip of the pearlite knee in steel D begins at 9500 seconds, compared to 625 seconds in steel B and 550 seconds in steel J, a time factor greater than 10. The bainite reaction temperature is lowered by 30 to 60 °F. Again the reaction below the shelf starts rapidly, the time difference at 720 °F (380 °C) ranging from 15 seconds in steel J to 140 seconds in steel D, or a factor of almost 10 between steels J and D, and a factor of only 2 between steels B and D. In regard to austenite grain size, it can be said that the austenitizing treatments produced the same rating in steels B, J and K, whereas steel D had only one lower index number.

#### References

1. E. A. Loria and H. D. Shephard, "Acicular Transformations in Alloy Steel", *TRANSACTIONS, American Society for Metals*, Vol. 40, 1948, p. 758-774.



2. E. A. Loria, "Isothermal Transformation of Austenite in Two Alloy Steels", *TRANSACTIONS, American Society for Metals*, Vol. 41, 1949, p. 1248-1260.
3. A. R. Troiano, "Final Report on an Investigation of the Metallographic and Physical Properties of New Types of Gun Steels", OSRD Report No. 3513, Serial No. M-239, April 1944.
4. T. Lyman and A. R. Troiano, "Influence of Carbon Content upon the Transformations in 3% Chromium Steel", *TRANSACTIONS, American Society for Metals*, Vol. 37, 1946, p. 402-448.
5. A. R. Troiano and J. E. DeMoss, "Transformations in Krupp-Type Carburizing Steels", *TRANSACTIONS, American Society for Metals*, Vol. 39, 1947, p. 788-800.
6. A. R. Troiano, "The Transformation and Retention of Austenite in SAE 5140, 2340 and T1340 Steels of Comparable Hardenability", *TRANSACTIONS, American Society for Metals*, Vol. 41, 1949, p. 1093-1112.
7. J. P. Sheehan, D. A. Julien and A. R. Troiano, "The Transformation Characteristics of Ten Selected Nickel Steels", *TRANSACTIONS, American Society for Metals*, Vol. 41, 1949, p. 1165-1184.
8. A. Hultgren, "Isothermal Transformation of Austenite", *TRANSACTIONS, American Society for Metals*, Vol. 39, 1947, p. 915-1005.
9. E. S. Davenport and E. C. Bain, "Transformation of Austenite at Constant Subcritical Temperature", *Transactions, American Institute of Mining and Metallurgical Engineers*, Vol. 90, 1930, p. 117-154.
10. D. L. Edlund and T. L. Oberle, "Final Report on Development of High Strength Gun Steels", OSRD Report No. 6597, Serial No. M-434, January 1946.

## GRAIN AND GRAIN-BOUNDARY COMPOSITIONS: MECHANISM OF TEMPER BRITTLENESS

BY J. W. SPRETNAK AND RUDOLPH SPEISER

### *Abstract*

*The thermodynamics of interfaces and surface adsorption of solute atoms is examined. It is demonstrated that concentration or depletion of the solute atom at grain boundaries of polycrystalline solid solutions can be explained by use of the adsorption isotherm. Furthermore, the effect of temperature changes on the adsorption is formulated. The role of surface (grain boundary) adsorption in several grain-boundary phenomena in metals is examined.*

*Consideration of the positive adsorption of carbon atoms at the austenite grain boundaries (increasing with increasing temperature) leads to a new and very promising theory of the mechanism of temper brittleness. The carbon-enriched grain-boundary regions give rise to retained austenite in the quench. Subsequent tempering causes precipitation of carbides from the retained austenite, depleting the carbon content so as to give fresh martensite on cooling down to room temperature. It is proposed that the embrittling phase is a thin layer of martensite at the prior austenite grain boundaries which acts as an effective barrier to the propagation of stresses across the grain boundaries. Alloying elements delay the precipitation of carbides and enhance the resistance to tempering of the grain-boundary martensite; plain carbon steels embrittle at a very high rate.*

IT is well recognized that grain-boundary phenomena are of prime interest in their effects on the properties and behavior of polycrystalline metals, in which interfaces between grains are an inherent part of the structure. Many examples of such grain-boundary effects can be cited. Among these could be mentioned the general effect on the kinetics of nucleation in solid-solid reactions, the embrittlement of copper by bismuth, the boron hardenability effect in steel, temper brittleness in steel, sensitizing of austenitic stainless steel to intergranular corrosion, and embrittlement of molybdenum by carbon and oxygen.

A paper presented before the Thirty-second Annual Convention of the Society, held in Chicago, October 21 to 27, 1950. The authors, J. W. Spretnak and Rudolph Speiser, are associate professors, Department of Metallurgy, The Ohio State University, Columbus, Ohio. Manuscript received April 6, 1950.

It becomes ultimately apparent that, to understand these grain-boundary phenomena, it is imperative to answer the question as to what is the expected equilibrium distribution of the solute element within the grain and how this distribution is affected by the temperature and by the nature of the solvent and solute atoms. It is the purpose of this paper to investigate the thermodynamics of interfaces and to attempt to deduce the expected distribution of the solute element under various circumstances, and finally to apply these deductions to some grain-boundary reactions of particular technical interest.

### THERMODYNAMIC PROPERTIES OF INTERFACES

The thermodynamics of surface phases as developed by Gibbs, although generally applied to liquid-vapor or liquid-liquid interfaces, can equally well be applied to solid-solid interfaces. However, it must be recognized that the rate of approach to equilibrium is slow in solids compared to the rate in liquids. Furthermore, several mechanisms<sup>1</sup> of diffusion are possible in solids which have different activation energies and lead to widely varying rates of diffusion. Consequently, this treatment will yield the limiting state of the system at equilibrium and, since most systems of interest are not in thermodynamic equilibrium, the state of the system at any particular instant will depend upon the previous history of the sample.

Guggenheim (1)<sup>2</sup> has improved the Gibbs theory of surface adsorption by considering a more easily physically visualized surface phase. Gibbs pictured the interface or "dividing surface" separating two homogeneous phases as a two-dimensional heterogeneous discontinuity, whereas Guggenheim, more realistically, ascribes a definite volume to the surface phase.

If  $\gamma$  denotes the surface tension,  $S^\sigma$  the entropy per unit area in the surface phase,  $\tau$  the thickness of the surface phase,  $\Gamma_i^\sigma$  the excess of solute of species  $i$  in the surface over that in the homogeneous phase,  $\mu_i^\sigma$  the chemical potential of species  $i$  in the surface, then Guggenheim has shown that

$$d\gamma = -S^\sigma dT + \tau dP - \sum_i \Gamma_i^\sigma d\mu_i^\sigma \quad \text{Equation 1}$$

Except for the term  $\tau dP$  in Equation 1, this equation corresponds to the Gibbs equation for the change in surface tension with a change in pressure, temperature, and composition in the system.

<sup>1</sup>The proposed mechanisms of diffusion are (a) simple exchange, (b) cyclic exchange, (c) diffusion of holes and (d) interstitial diffusion.

<sup>2</sup>The figures appearing in parentheses pertain to the references appended to this paper.



The change in surface tension at constant temperature and pressure can then be written as

$$d\gamma = -\sum_i \Gamma_i^\sigma d\mu_i^\sigma \quad \text{Equation 2}$$

and for a two-component system

$$d\gamma = -\Gamma_1^\sigma d\mu_1 - \Gamma_2^\sigma d\mu_2 \quad \text{Equation 3}$$

where sub-index 1 refers to the solvent and 2 to the solute.

(In the Gibbs treatment the dividing surface is placed so that  $\Gamma_1^\sigma$  vanishes and  $d\gamma = -\Gamma_2^\sigma d\mu_2$ .)

If the Gibbs-Duhem relation is applied, then Equation 3 becomes ( $N_1$  = mole fraction in the homogeneous phase)

$$-d\gamma = \left(\Gamma_2^\sigma - \frac{N_2}{N_1} \Gamma_1^\sigma\right) d\mu_2 \quad \text{Equation 4}$$

or

$$N_2 \left( \frac{\Gamma_2^\sigma}{N_2} - \frac{\Gamma_1^\sigma}{N_1} \right) = - \frac{\partial \gamma}{RT \partial \ln(f_2 N_2)} \quad \text{Equation 5}$$

where  $f_2$  is the activity coefficient of species two in the homogeneous solution.

The positive adsorption of the solute (surface excess) can then be defined as occurring when

$$\frac{\Gamma_2^\sigma}{N_2} > \frac{\Gamma_1^\sigma}{N_1} \quad \text{Equation 6}$$

and negative adsorption (surface deficiency) as

$$\frac{\Gamma_2^\sigma}{N_2} < \frac{\Gamma_1^\sigma}{N_1} \quad \text{Equation 7}$$

It can be seen that when  $\left[ \frac{\partial \gamma}{\partial \ln(f_2 N_2)} \right]_T$  is negative, the adsorption will be positive and when  $\left[ \frac{\partial \gamma}{\partial \ln(f_2 N_2)} \right]_T$  is positive the adsorption is negative. Since the activity coefficient is always positive, it follows that  $\partial \ln(f_2 N_2)$  always increases with an increase in concentration so that the sign of  $\left[ \frac{\partial \gamma}{\partial \ln(f_2 N_2)} \right]_T$  depends upon the direction of the change of the surface tension. That is, if the surface tension decreases as the mole fraction of solute in the homogeneous phase is increased, an excess of solute will be present in the surface phase, whereas if the surface tension increases, there will be a deficiency of solute in the interface.

Thus, it is possible to have segregation of the solute element

in the grain boundary without precipitation; similarly in the case of negative adsorption, depletion of the solute in the grain boundary without precipitation in the interior of the grain.

If the temperature is allowed to vary at constant composition and constant pressure, the expression for the change in surface tension with a change in temperature deduced from Equation 1 is (for a two-component system)

$$\frac{d\gamma}{dT} = -S^\sigma - \Gamma_1^\sigma \frac{d\mu_1^\sigma}{dT} - \Gamma_2^\sigma \frac{d\mu_2^\sigma}{dT} \quad \text{Equation 8}$$

But

$$-S^\sigma = \frac{dG^\sigma}{dT} = \mu_1 \frac{d\Gamma_1^\sigma}{dT} + \mu_2 \frac{d\Gamma_2^\sigma}{dT} + \Gamma_1^\sigma \frac{d\mu_1}{dT} + \Gamma_2^\sigma \frac{d\mu_2}{dT} \quad \text{Equation 9}$$

where  $G^\sigma$  is the surface free energy

Combining Equations 8 and 9 and assuming that

$$\mu_1 \frac{d\Gamma_1^\sigma}{dT} \approx 0, \text{ we have}$$

$$\mu_2 \frac{d\Gamma_2^\sigma}{dT} = \frac{d\gamma}{dT} \quad \text{Equation 10}$$

It is evident from Equation 10 that the temperature coefficient of  $\Gamma_2$  is positive when the temperature coefficient of the surface tension is negative ( $\mu_2$  is always negative) and vice versa. A positive  $\frac{d\Gamma_2}{dT}$  means that more solute will go into the surface phase as the temperature is increased and a negative value means that the solute will leave the boundary and pass into the interior of the grain as the temperature is increased.

In general, the surface tension for liquids decreases with an increase in temperature and varies approximately linearly with the temperature. That is

$$\gamma = \gamma_0 - bT \quad \text{Equation 11}$$

where  $\gamma_0$  and  $b$  are constants. At the critical temperature  $bT_c = \gamma_0$ . It would be expected that in general the surface tension of solids would also decrease with an increase in temperature. Positive temperature coefficients of the surface tension have been reported (1) for several liquid metals but these reports must be substantiated.

An interesting form of Equation 5 can be obtained if one assumes that the homogeneous solid phase can be considered as a regular solution (2), then since

$$\ln a_2 = \ln N_2 + \frac{1}{2}\beta N_1^2 \quad \text{Equation 12}$$

where  $\beta$  is related to the heat of solution, and  $a_2$  is the activity of the solute,

$$d \ln a_2 = \frac{d N_2}{N_2} + \beta N_1 d N_1 = \left( \frac{1}{N_2} - \beta N_1 \right) d N_2 \quad \text{Equation 13}$$

Then Equation 5 becomes

$$RT(1 - \beta N_1 N_2) N_2 \left( \frac{\Gamma_2^s}{N_2} - \frac{\Gamma_1^s}{N_1} \right) = - \frac{\partial \gamma}{\partial \ln N_2} \quad \text{Equation 14}$$

This expression shows that the positive adsorption at the interface is greater, the greater the positive deviation of the homogeneous phase from Raoult's law. Furthermore, if the positive deviation becomes large enough, phase separation takes place so that immiscibility can be considered as a case of extreme physical adsorption at the interface.

A reverse argument leads to the conclusion that negative deviations from Raoult's law ( $\beta < 0$ ) results in a diminished adsorption at the grain boundary. Very large negative deviations lead to compound formation and the solute may then be fixed in the interior of the grain. Thus the addition of substances that cause compound formation with the solute may prevent the migration of the solute element to the grain boundary, provided that the added substance has a low mobility and is in sufficient excess. An example of this is in 18-8 stainless steel in which carbon is fixed by the addition of titanium or columbium, strong carbide formers, which prevent the diffusion of carbon to the grain boundary. The adsorption of carbon at the grain boundary is the underlying mechanism of the continuous precipitation of chromium carbides at the grain boundary, leading to the intergranular corrosion of stainless steels under these conditions. It is also possible, in some alloys, that there are two diffusible solute elements present in rather high dilution which can interact to form compounds. In this case it is plausible to assume that both components would be first concentrated by positive adsorption at the grain boundary and then react to form the compound at the grain boundary. This can take place without exceeding the solubility of either solute or compound in the bulk phase.

If in Equation 14,  $\beta = 0$ , then Raoult's law is obeyed and the expression reduces to the usual form.

$$RT N_2 \left( \frac{\Gamma_2^s}{N_2} - \frac{\Gamma_1^s}{N_1} \right) = - \frac{\partial \gamma}{\partial \ln N_2} \quad \text{Equation 15}$$



## THE MECHANISM OF TEMPER BRITTLENESS

The type of embrittlement of hardened steels resulting from the tempering operation, universally termed "temper brittleness", has been a prime metallurgical puzzle for the last three decades. Considerable study of this embrittlement (References 3 through 13) has yielded much useful information concerning this malady but has not yielded a satisfactory explanation of its mechanism. The consideration of the quasi-equilibrium distribution of the solute element within a crystal grain and the effect of temperature on this distribution leads to a theory of temper brittleness which shows exceptional promise in explaining the various observations concerning this phenomenon.

A satisfactory theory of temper brittleness must explain the following experimental evidence concerning it:

(a) The increase of susceptibility to temper brittleness with increasing austenitizing temperature (3).

(b) The effect of composition on susceptibility (5). Steels with carbon contents below 0.20% are relatively insensitive. Also, steels of higher carbon content, but with low alloy content, are also relatively insensitive.

(c) The occurrence of the embrittlement along the prior austenite grain boundaries.

(d) The kinetics of the embrittlement reaction (5, 8, 9).

(e) The recovery of ductility by a high temperature tempering operation (9). This is sometimes interpreted as a manifestation of the reversibility of the embrittlement reaction.

The basis of the current theory of temper brittleness is the distribution of carbon atoms in the austenite grains during the austenitizing treatment. In other words, the cause of temper brittleness is basically the concentration of carbon at the grain boundary of austenite grains before the quench by the mechanism of surface adsorption.

In considering the distribution of carbon in austenite grains, reference is again made to Equation 10 which gives the temperature coefficient of the change in the degree of grain-boundary adsorption.

The sign of the change depends on the sign of  $\frac{dy}{dT}$ . The general behavior is a decrease in surface tension with increasing temperature. From these considerations it seems likely that carbon should show the expected increase in positive adsorption at the austenite grain boundaries. Another general principle controlling the degree of positive adsorption is the deviation from Raoult's law. The tendency is higher, the higher the positive deviation from Raoult's law.

Recent evidence shows that carbon in austenite exhibits a marked positive deviation from Raoult's law (14).

Experimental evidence suggests that carbon does indeed undergo positive adsorption in austenite to a degree which increases with increasing temperature. For example, studies on overheating and burning in steels (15, 16) indicate that both carbon and sulphur are driven to the austenite grain boundary to an increasing extent with increasing temperature. Both elements reduce the melting point and can cause burning if the temperature is sufficiently high. The chief difference in the behavior of sulphur and carbon lies in their mobilities. Carbon has very high mobility compared to sulphur. Sulphur begins to move to the grain boundary when the temperature has attained the overheating range, and on fairly rapid cooling it is precipitated in the grain boundaries. To prevent overheating effects, very slow cooling must be used to allow the sulphur to diffuse back into the grain.

A beautiful example of increasing positive adsorption of an interstitial solute element in austenite with increasing temperature is that of boron (17). To develop the boron precipitate in steel, the sample is austenitized at a very high temperature and quenched rapidly to the transformation temperature at which a ferrite outline is formed. It becomes evident that a sufficiently high temperature must be attained to force enough boron to the grain boundary to be in excess of the solubility within the range of the subcritical transformation temperature. The austenitizing temperature required to produce the precipitate was found to decrease with increasing boron content. Because of the high mobility of boron, the cooling rate must be sufficiently high to prevent the migration back into the grain, since the adsorption decreases with decreasing temperature.

The result of positive adsorption of carbon at the austenite grain boundary caused by the austenitizing treatment is then a grain-boundary region with carbon concentration considerably higher than the average composition. The excess carbon should increase with increasing austenitizing temperature, which is in line with the observed increased sensitivity with increased austenitizing temperature. It also explains why carbon contents under 0.20% are relatively insensitive to temper brittleness. The probable explanation is that the surface excess of carbon in this case is not sufficiently high to alter significantly the transformation characteristics of the grain-boundary material. Such a situation also explains the considerably lower sensitivity of normalized steels as compared to quenched steels, because in this case cooling down in the austenite

range allows diffusion of carbon back into the austenite grain.

It is next in order to consider what happens in the quenching operation. The transformation characteristics of the grain-boundary region and the body of the grain are illustrated schematically in Fig. 1. Because of the excess of carbon, it may be postulated that in essence the grain-boundary material is a hypereutectoid steel, with the  $M_s$  temperature below room temperature. The expected

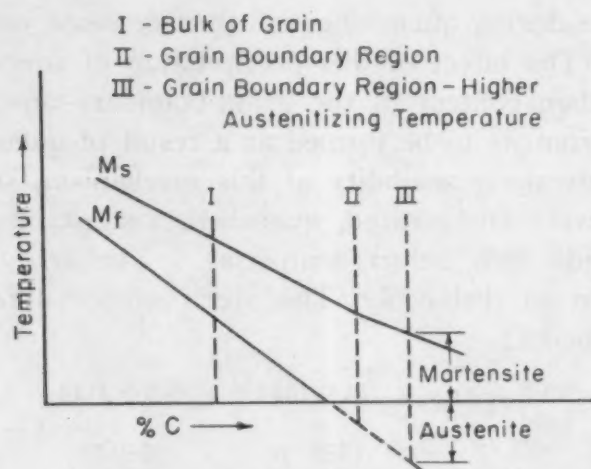


Fig. 1—Effect of Carbon Content on Martensite Transformation Characteristics of Grain Boundary and of Bulk of Grain.

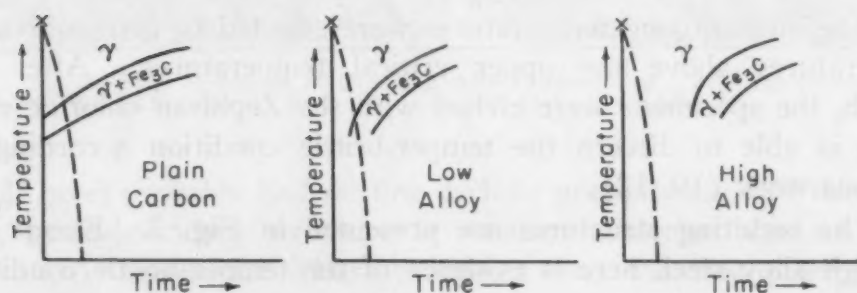


Fig. 2—Effect of Alloying Elements on the Kinetics of Carbide Precipitation From Austenite.

structure after quenching accordingly will be martensite of average composition in the bulk of the grain, and in the grain boundary high carbon martensite and retained austenite. A key factor in determining the amount of retained austenite under a given set of conditions in the quench is the kinetics of the precipitation of cementite during the quench. The effect of alloying elements on the precipitation of cementite is depicted schematically in Fig. 2. In plain carbon steel it is impossible to suppress the precipitation of cementite. The amount of cementite precipitated from the high



Table I  
Steel Compositions

SAE No.	C	Mn	Cr	Ni	Mo
1020	0.20	0.90	0.06	0.19	0.03
1045	0.42	0.86	0.11	0.15	0.02
3140	0.39	0.73	0.63	1.21	0.07
3335	0.36	0.48	1.51	3.42	0.06

(P < 0.020, S < 0.027, Si < 0.30)

carbon austenite during quenching will then decrease with increasing alloy content. The effect of this precipitation of course will be to deplete the carbon content of the grain-boundary austenite and to cause more martensite to be formed as a result of quenching.

To illustrate the plausibility of this mechanism, small samples of four steels were austenitized, quenched, and examined with the Zephiran chloride etch before tempering. The analyses of these steels are given in Table I. The steels were subjected to the following treatments:

Steel	SAE 1020	SAE 1045	SAE 3140	SAE 3335
Austenitizing Temperature	1650 °F (900 °C)	1550 °F (840 °C)	1550 °F (840 °C)	1550 °F (840 °C)
Time	½ Hour	½ Hour	½ Hour	½ Hour
Type of Quench	Brine	Brine	Oil	Oil

The austenitizing temperatures were selected to give equivalent temperatures above the upper critical temperatures. After the quench, the specimens were etched with the Zephiran chloride etch, which is able to discern the temper-brittle condition according to previous work (10, 12).

The resulting structures are presented in Fig. 3. Except for the high alloy steel, here is evidence of the temper-brittle condition in the as-quenched state! None of the common etchants for steel reproduced this grain-boundary effect. Repolishing these structures for 1 minute leaves the grain-boundary effect very much evident after the details of the bulk structure have been removed. The degree of attack by the Zephiran chloride etch varies in the approximate decreasing order—SAE 1045, 3140, 1020, and 3335. From previous considerations, the relatively slight response to the etch in the case of SAE 1020 reflects the smaller amount of carbon segregation at the grain boundary as a result of the lower carbon content. Considering the kinetics of carbide precipitation, it is possible to make some speculations as to what structure is attacked by Zephiran chloride. Because of the high alloy content, the SAE

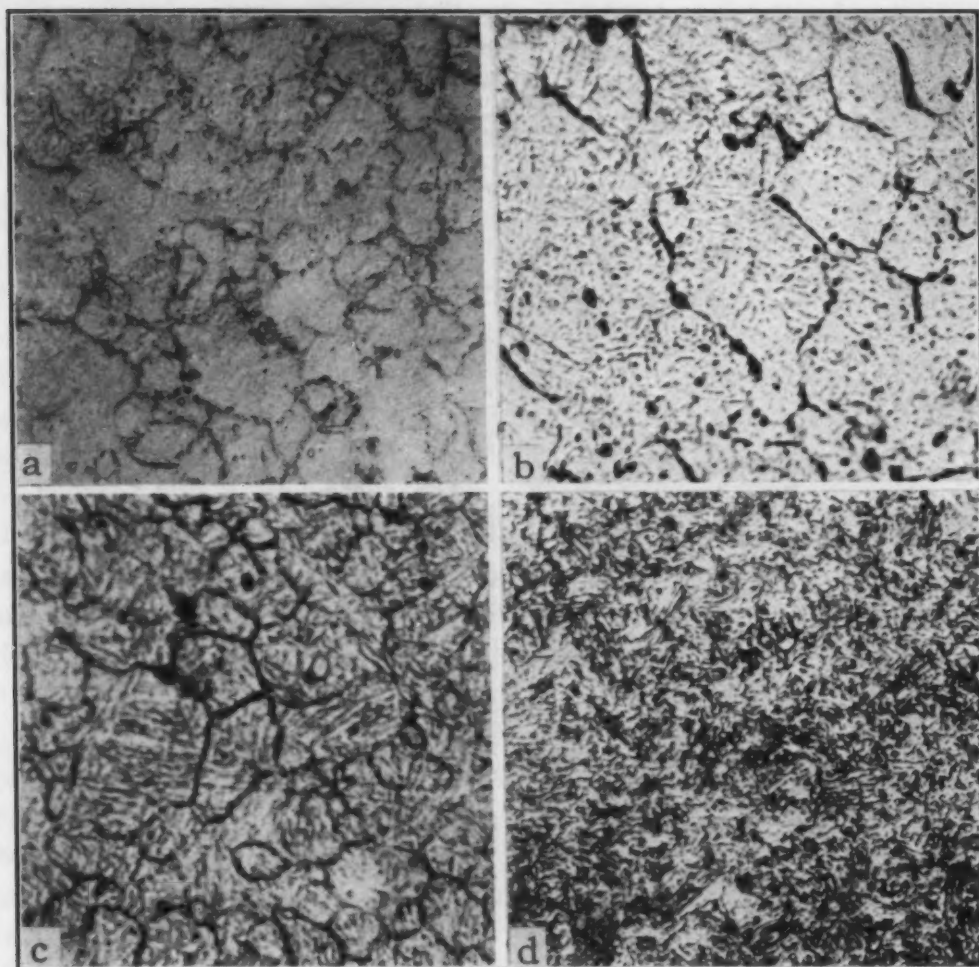


Fig. 3—Steel Structures As-Quenched After Austenitizing. Zephiran chloride etch.  $\times 600$ . (a) SAE 1020; (b) SAE 1045; (c) SAE 3140; (d) SAE 3335.

3335 steel probably had no fine carbide precipitation and the resulting grain-boundary structure is retained austenite plus martensite or 100% austenite. Thus it appears that the fine precipitate of carbide is a requisite for the response to the etchant. The question next arises as to whether the sensitive structure is fine carbides associated with austenite or with martensite. As will be discussed later, subsequent embrittling tempering treatments can only lead to an increasing amount of fine carbide and martensite, and yet the response to the etchant increases with increasing embrittlement. Thus it is tentatively concluded that the structure sensitive to the Zephiran etch is a dispersion of fine carbides associated with martensite, giving etching characteristics similar to what is termed body-centered martensite, or dark martensite. The surface-active constituent of the etchant probably accounts for the pronounced grain-boundary attack.

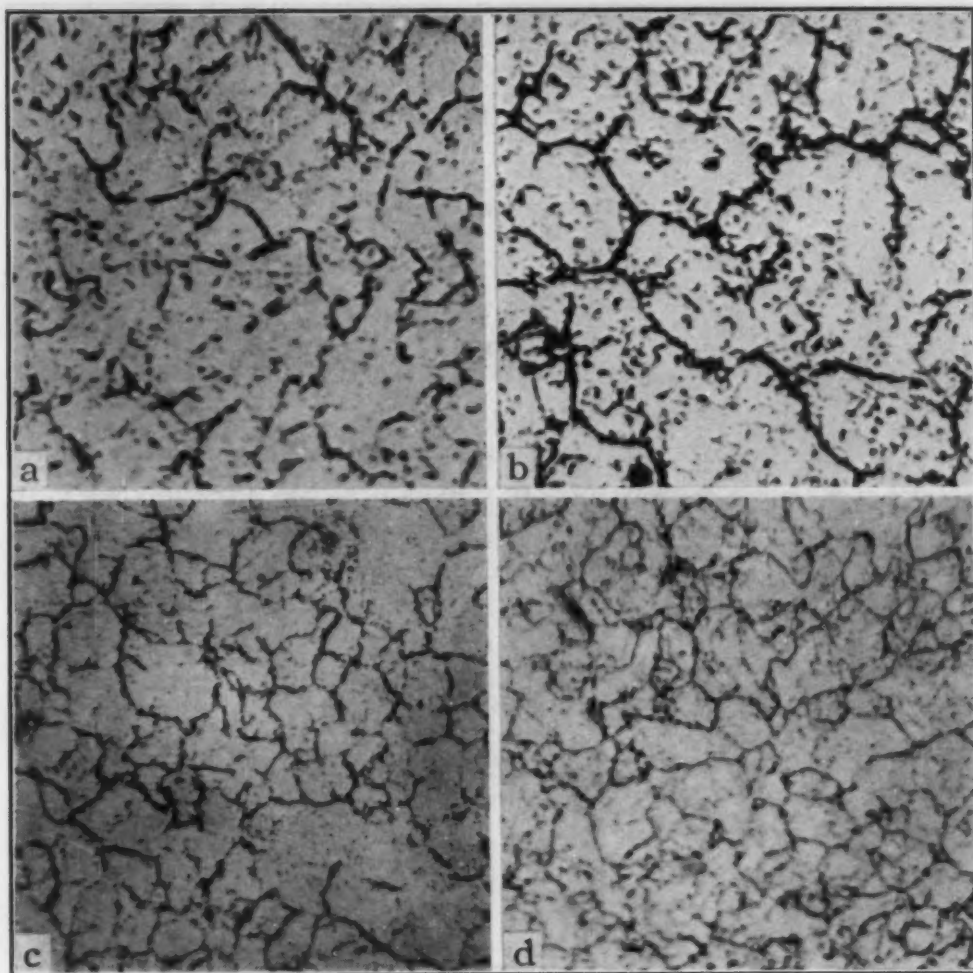


Fig. 4—Steel Structures After Tempering. Treatment consisted of austenitizing, quenching, tempering 24 hours at 900 °F (480 °C), followed by a brine quench. Zephiran chloride etch, repolished approximately 1 minute.  $\times 600$ . (a) SAE 1020; (b) SAE 1045; (c) SAE 3140; (d) SAE 3335.

The structures of Fig. 3 substantiate nicely the postulate of Jaffe and Buffum (11) stating that the effect of alloying elements is to retard the rate of embrittlement and that plain carbon steels embrittle at such a high rate that it is impossible to prevent this condition in these steels. In other words, the temper-brittle condition is the expected one for plain carbon steels. As subsequent embrittling treatments in tempering were carried on, the response to the etch increased in all specimens but at a much higher rate in the plain carbon steels. Fig. 4 shows the structure of the four steels after tempering 24 hours at 900 °F (480 °C) followed by a brine quench. The nonuniform grain-boundary effect often observed in etched temper-brittle specimens is probably a manifestation of the dependence of surface tension on orientation. Born and Stern (18) have calculated the surface tensions of the (111), (110), and (100)



planes of rock salt. The calculations yielded the following ratios of the surface tension:  $\sigma_{111}:\sigma_{110}:\sigma_{100} = 5.81:2.71:1$ . Kê (19) also found evidence of distinctly heterogeneous precipitation of bismuth in grain boundaries of copper.

Let us consider next the reactions during tempering in the embrittling temperature range. In the case of the plain carbon and low alloy steels, the structure at the grain boundary carried into the tempering operation will consist of fine carbides, martensite, and retained austenite. Two main reactions are to be considered. The first is the tempering of the martensite. The degree of tempering will depend on the carbon and alloy content. The second reaction is the "conditioning" of the retained austenite as a result of the precipitation of carbides. This "conditioning" process thus reduces the carbon content of the retained austenite, raising its  $M_s$  and  $M_f$  temperature. As a result, when the steel is cooled to room temperature, fresh martensite is formed at the grain boundary, the amount depending on the degree of depletion of carbon by the carbide precipitation.

Consequently, it is proposed that temper brittleness is a result of a thin film of hard-brittle martensite structure which acts as an effective barrier to the propagation of stresses across the grain boundaries. The effectiveness of this barrier increases with the amount of martensite in the grain boundary. The action of martensite formed during a previous operation in a subsequent temper depends on its resistance to tempering. If this resistance is high, further martensite formation will be an additive effect. Thus, the effect of alloying elements is two-fold. The first effect is that on the kinetics of carbide precipitation from the austenite. The typical time-temperature-embrittlement diagrams, illustrated in Fig. 5, duplicate closely the effect of alloying elements on the kinetics of precipitation of carbide from austenite. Manganese and molybdenum are particularly effective in delaying the carbide precipitation. The second important effect of alloying elements is the enhancement of the resistance of the martensite to tempering. A tempering operation at a given temperature results in two opposing tendencies, the precipitation of carbides leading to more fresh martensite on cooling to room temperature, and the tempering of any existing martensite. The more the resistance to tempering, the more additive will be the effect of forming more martensite.

The maximum degree of embrittlement possible in a steel should depend mainly on the carbon content and the austenitizing temperature, assuming a sufficiently drastic quench. The over-

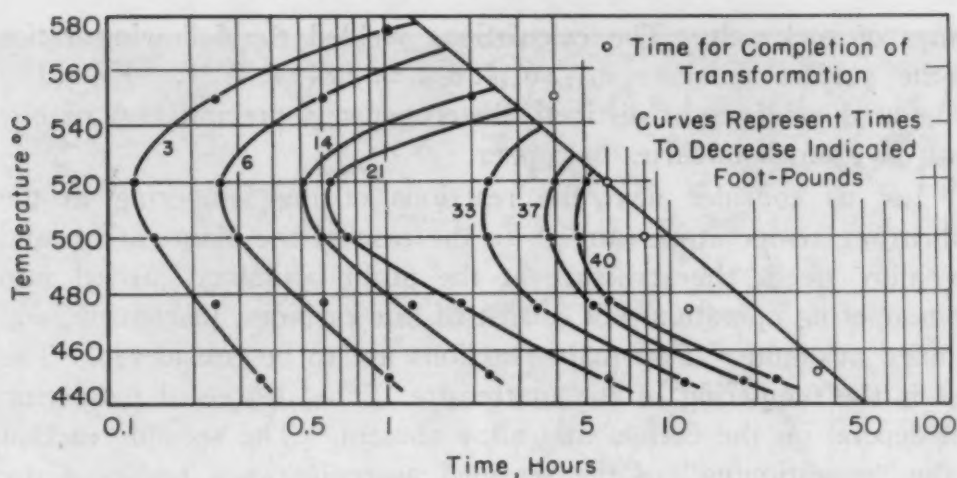


Fig. 5—Kinetics of Temper Embrittlement. (Plot by Hollomon of data by Greaves and Jones.)

coming of temper brittleness by a high temperature draw can be explained simply as attaining a temperature sufficiently high to effectively temper the grain-boundary martensite. This treatment has been referred to previously as a demonstration of the reversibility of temper brittleness. The approach to a comparable value at a given tempering temperature by a brittle and a ductile specimen observed by Greaves and Jones (5) can be reconciled by the opposing tendencies of tempering existing martensite and the precipitation of carbides leading to the formation of fresh martensite.

Additional support for this proposed general mechanism for temper brittleness is given by the fact that the Zephiran reagent did not attack in the characteristic fashion the microstructure of the SAE 1045 steel which was normalized from the austenitizing temperature, nor again after tempering at 900 °F (480 °C). This observation is interpreted as the result of diffusion of the excess carbon at the austenite grain boundary back into the grain during cooling (as predicted by Equation 10) through the austenite temperature range in the normalizing treatment.

#### SUMMARY

1. The thermodynamics of interfaces and surface adsorption of solute atoms is examined. It is demonstrated that concentration or depletion of the solute atom at the surface can be explained by use of the adsorption isotherm. Furthermore, the effect of temperature changes on the adsorption is formulated.
2. The positive surface adsorption increases with increasing positive deviation of the solute from Raoult's law.

3. The role of surface (grain boundary) adsorption in several grain-boundary phenomena is examined.

4. Consideration of the positive adsorption of carbon at the austenite grain boundaries during the austenitizing treatment (increasing with increasing austenitizing temperature) gives rise to a new and very promising theory on the mechanism of temper brittleness.

5. The high carbon concentration at the grain-boundary regions causes retained austenite to be formed on the quench. Evidence is presented to show that the Zephran chloride etch gives indications of the embrittled condition in the as-quenched state for all the steels studied except the high alloy steel.

6. Subsequent tempering operations lead to precipitation of carbides, depleting the retained austenite of carbon, causing fresh martensite to be formed on cooling to room temperature.

7. It is proposed that the embrittling phase in temper brittleness is a thin shell of martensite (and perhaps slightly tempered martensite) around the prior austenite grains.

8. The role of alloying elements is two-fold: (a) to delay the precipitation of carbides, and (b) to enhance the resistance to tempering of the martensite. Plain carbon steels embrittle at a very rapid rate as compared to alloy steels.

9. The recovery of ductility as a result of a high temperature tempering operation is explained simply as the attainment of a temperature sufficiently high to effectively temper the grain-boundary martensite.

#### ACKNOWLEDGMENTS

The metallographic work on the four steels discussed in the text was done as part of a thesis for the Bachelor's degree in metallurgical engineering at The Ohio State University by Charles E. Fiala and Richard J. Clifford, currently with Republic Steel Corporation, Canton, Ohio, and the National Tube Company, Lorain, Ohio, respectively.

#### References

1. E. A. Guggenheim, "The Thermodynamics of Interfaces in Systems of Several Components", *Transactions, Faraday Society*, Vol. 36, 1940, p. 397.  
N. K. Adams, "The Physics and Chemistry of Surfaces", Third Edition, 1941, Chapter III, Oxford University Press, London: Humphrey Milford.
2. J. H. Hildebrand, "Solubility of Non-Electrolytes", Second Edition, 1936, p. 188, Reinhold Publishing Corporation, New York.



3. R. H. Greaves, "Temper-Brittleness of Nickel-Chrome Steel", *Journal, Iron and Steel Institute*, Vol. 100, No. II, 1919, p. 329.
4. R. H. Greaves, M. Fell and Sir Robert Hadfield, Bart., "Further Communication on Temper-Brittleness of Nickel-Chrome Steel", *Journal, Iron and Steel Institute*, Vol. 100, No. II, 1919, p. 340.
5. R. H. Greaves and J. J. A. Jones, "Temper-Brittleness of Nickel-Chromium Steels", *Journal, Iron and Steel Institute*, Vol. 102, No. II, 1920, p. 171.
6. R. H. Greaves and J. J. A. Jones, "Temper-Brittleness of Steel; Susceptibility to Temper-Brittleness in Relation to Chemical Composition", *Journal, Iron and Steel Institute*, Vol. 111, No. I, 1925, p. 231.
7. W. T. Griffiths, "Note on Nitrogen as a Possible Factor in Temper-Brittleness", *Journal, Iron and Steel Institute*, Vol. 111, No. I, 1925, p. 257.
8. J. H. Hollomon, "Temper-Brittleness", *TRANSACTIONS, American Society for Metals*, Vol. 36, 1946, p. 473.
9. W. S. Pellini and B. R. Queneau, "Development of Temper-Brittleness in Alloy Steels", *TRANSACTIONS, American Society for Metals*, Vol. 39, 1947, p. 139.
10. J. B. Cohen, A. Hurlich and M. Jacobson, "A Metallographic Etchant to Reveal Temper-Brittleness in Steel", *TRANSACTIONS, American Society for Metals*, Vol. 39, 1947, p. 109.
11. L. D. Jaffe and D. C. Buffum, "Temper Brittleness of Plain Carbon Steels", *Transactions, American Institute of Mining and Metallurgical Engineers, Institute of Metals Division*, Vol. 180, 1949, p. 513.
12. D. McLean and L. Northcott, "Micro-Examination and Electrode-Potential Measurements of Temper-Brittle Steels", *Journal, Iron and Steel Institute*, Vol. 158, 1948, p. 169.
13. L. D. Jaffe, "Carbide Distribution as a Possible Cause of Temper Brittleness", *Journal, Iron and Steel Institute*, Vol. 164, Part 1, January 1950, p. 1.
14. R. P. Smith, "Equilibrium of Iron-Carbon Alloys with Mixtures of  $\text{CO-CO}_2$  and  $\text{CH}_4\text{-H}_2$ ", *Journal, American Chemical Society*, Vol. 68, 1946, p. 1163.
15. A. Preece, J. Nutting and A. Hartley, "The Overheating and Burning of Steel: Part III—The Influence of Excessive Reheating Temperatures on the Mechanical Properties and the Structure of Alloy Steels", *Journal, Iron and Steel Institute*, Vol. 164, Part 1, January 1950, p. 37.
16. T. Ko and D. Hanson, "Grain-Boundary Phenomena in Severely Heated Steel", *Journal, Iron and Steel Institute*, Vol. 164, Part 1, January 1950, p. 46.
17. R. A. Grange and T. M. Garvey, "Factors Affecting the Hardenability of Boron-Treated Steels", *TRANSACTIONS, American Society for Metals*, Vol. 37, 1946, p. 136.
18. M. Born and O. Stern, "Surface Energy of Crystals and Its Influence on Crystal Form", *Sitzungsberichte der preussischen Akademie der Wissenschaften, Physikalisch-mathematische Klasse*, Vol. 48, 1919, p. 901.
19. T'ing-Sui Kê, "Grain-Boundary Relaxation and the Mechanism of Embrittlement of Copper by Bismuth", *Journal, Applied Physics*, Vol. 20, 1949, p. 1226.

## DISCUSSION

**Written Discussion:** By D. C. Buffum, Watertown Arsenal, Watertown, Mass.

The authors state that steels with carbon content of less than 0.20% are relatively insensitive to temper brittleness; Hum, Parker, Hultgren

and Prindle<sup>3</sup> did extensive work on the AISI 3100 series of steel using carbon contents of 0.12, 0.02 and 0.01%. They found that the steel containing 0.12% carbon was highly susceptible and the 0.02 and 0.01% carbon steels were appreciably susceptible.

In regard to the authors' statement that reversibility is caused by tempering the grain boundary martensite, a series of tests was made at the Watertown Arsenal Laboratory,<sup>4</sup> in which an embrittled SAE 3140 steel was reheated to the tempering temperature for periods up to 240 hours. These data indicated that the phenomenon known as retrogression took place. In other words, the embrittlement that was developed during an isothermal treatment of 48 hours at 500 °C (930 °F) almost completely disappeared when the steel was retempered a short time at 675 °C (1250 °F). However, as the length of time at 675 °C increased, the amount of embrittlement increased until after 240 hours at 675 °C the embrittlement was almost equivalent to that developed with a 48-hour treatment at 500 °C.

Next, it is stated that increasing the austenitizing temperature increases the carbon concentrated in the grain boundaries. Studies have been made at the Watertown Arsenal Laboratory<sup>5</sup> of the effect of grain size on temper brittleness and it was found that specimens austenitized at 1150 °C (2100 °F) have much higher transition temperatures than those austenitized at 900 °C (1650 °F), which corroborates the present authors' findings. However, when specimens were austenitized at 1150 °C (2100 °F), cooled to 900 °C (1650 °F), and held for 1 hour and 40 minutes before quenching, the transition temperature was the same as for those bars quenched straight from 1150 °C (2100 °F). If the authors' theory was correct, it would seem likely that the 900 °C (1650 °F) treatment would have reduced the concentration of carbon in the grain boundaries, thereby reducing the transition temperature. Such was not the case, and it appears as though the increase in grain size was the cause of the increase in transition temperature.

The usual method of isothermally embrittling specimens is to reheat the bars to a given embrittling temperature after they have been quenched from the temper and hold for an allotted time before water quenching again. At the Watertown Arsenal Laboratory<sup>6</sup> specimens have been embrittled by various other heating, holding and cooling cycles, one being to cool from the tempering temperature directly to the embrittling temperature, holding the allotted time and water quenching. Specimens were embrittled for the same time at the same temperature; one group received the usual embrittling method and the other received the embrittling method stated above. On testing, both groups had the same transition temperature and so were embrittled to the same extent. Furthermore, groups that were given like treatments, except furnace-cooled to room temperature from the embrittling temperature, were embrittled to a greater extent. This would seem to indicate that the authors' theory

<sup>3</sup>J. K. Y. Hum, E. R. Parker, R. R. Hultgren and W. R. Prindle, unpublished work at University of California.

<sup>4</sup>L. D. Jaffe and D. C. Buffum, "Retrogression in Temper Brittleness", accepted for publication by Société Française de Métallurgie.

<sup>5</sup>L. D. Jaffe and D. C. Buffum, unpublished work at Watertown Arsenal.

<sup>6</sup>D. C. Buffum and L. D. Jaffe, unpublished work at Watertown Arsenal.

of quenched martensite in the grain boundaries being the cause of temper brittleness is invalid.

Etching studies<sup>7</sup> conducted at Watertown Arsenal Laboratory have shown that grain boundary outlines can be revealed in unembrittled as well as in embrittled specimens of both plain carbon and alloy steels, provided that etching time is prolonged sufficiently. This has been found to be true not only for the Zephiran chloride etch, but also for other etching reagents. These results lead to speculation concerning the lack of grain boundary outlines in the quenched structure of Fig. 3d. Is it possible that increased etching time may have revealed grain boundaries in this steel too?

**Written Discussion:** By Samuel J. Rosenberg, metallurgist, National Bureau of Standards, Washington, D. C.

The theory advanced by the authors—namely, that austenite retained at the grain boundary regions after quenching transforms to martensite on subsequent tempering, thus accounting for temper brittleness—is rather difficult to accept.

If austenite actually is retained at the grain boundaries (and it must be emphasized that metallographic examination of hardened steels containing retained austenite usually shows it to be intermixed with the martensite), it would be expected that this austenite would decompose isothermally at the tempering temperature into either upper bainite or fine pearlite. Published TTT diagrams for carbon steels show the decomposition of austenite to be substantially complete in less than a minute in the temperature range where temper brittleness occurs.

Assuming, however, that austenite is retained at the grain boundaries and is conditioned by the tempering treatment for subsequent transformation to martensite on cooling, the rate of cooling should have no effect on temper brittleness. Considerable data are available in the published literature to prove that the  $M_s$  temperature is not affected by the rate of cooling. Yet steels which exhibit temper brittleness on slow cooling after tempering frequently do not show temper brittleness if rapidly cooled. This would appear to indicate that whatever is the grain boundary constituent that causes temper brittleness, it is not martensite.

The authors also state that temper brittleness does not occur after a high temperature draw because the temperature is sufficiently high to effectively temper the grain boundary martensite. It is hard to conceive just how this martensite forms from austenite during heating to the high tempering temperature. Possibly the authors meant to imply that the austenite retained at the grain boundaries decomposes into ferrite and carbides at these high tempering temperatures. It is, however, well known that steels susceptible to temper brittleness are embrittled by slow cooling through the temper-brittle range, even though tempered at a higher temperature. If, therefore, grain boundary martensite were the actual cause of temper brittleness, we would have the interesting but doubtful phenomenon of an aggregate of ferrite and carbide transforming to martensite on slow cooling.

**Written Discussion:** By Carl A. Zapffe, research metallurgist, Baltimore.

<sup>7</sup>M. R. Norton, unpublished work at Watertown Arsenal.



The authors are to be congratulated for bringing into metallurgy an advanced understanding of thermodynamics which is certain to lead to much further work.

Of the many possible interesting applications of their theory, one of the most tantalizing, also the most challenging, is certainly the phenomenon of sensitization in the austenitic stainless steels. The complex involvements of chromium, nickel, and other alloy contents have never been satisfactorily explained. It is virtually impossible to establish an acceptable reasoning for sensitization based upon two-variable thermodynamics in terms of  $f(T, X)$ . The data clearly show that chromium reacts with carbon to form carbide throughout the entire range of chromium contents used in stainless steels, but that the carbides preferentially deposit in the grain boundaries when nickel is present, and with a deleterious effect virtually regardless of either chromium or nickel content within the stainless range. Expanding the thermodynamic concept from  $f(T, X)$  to  $f(T, X, P)$  also provides no new ready explanations. However, the further expansion to considerations of  $f(T, X, P, \rho)$ , which is essentially the thermodynamics discussed by the present authors, definitely opens an entirely new and acceptable area of study. There is no question that surface tension is a variable where grain boundaries are concerned; and surface tension, of course, is as much a part of the thermodynamics of a system as any one of the more common variables. The reasonings of these authors would probably then be extended to show that the presence of nickel upsets the composition gradient measured across body and surface of the grain, enabling those concentrations to occur at the grain boundary, which account for the phenomenon of sensitization.

This is a most fruitful line of thought, and their later publications will be watched with much interest.

**Written Discussion:** By A. R. Entwisle and G. C. Smith, Department of Metallurgy, University of Cambridge, Cambridge, England.

The segregation of elements, to or away from austenite grain boundaries during heating prior to hardening, is a phenomenon which may contribute directly to temper brittleness. In the present state of knowledge, however, it seems difficult to state with any certainty exactly which of the elements present in a steel will exhibit these segregation effects most markedly. The authors have done a service by drawing attention to such possibilities, but the final mechanism they propose seems open to several objections.

In the first place, the authors assume that plain carbon steels are susceptible to temper embrittlement, and this hypothesis forms an integral part of their theory. It is argued that however rapidly a plain carbon steel is cooled after tempering, the embrittling reaction proceeds nearly to completion. Some information on this point can be obtained by fracture studies. One of the characteristic features of temper brittleness as exhibited by low alloy steels is the intergranular nature of the fracture produced in the notched-bar test at low temperature. This type of fracture is quite distinct from the cleavage-type fracture of nonembrittled low alloy steels at low temperatures. If plain carbon steels are temper-brittle in the same sense as low alloy steels, an intergranular fracture should be produced when they are fractured in a brittle manner in the

notched-bar test. Experiments have been carried out which prove that this is not the case. An examination was made of the brittle fractures produced in the notched-bar test of two steels, British Standards E.N. 8 and E.N. 23. The former of these is a 0.4% plain carbon steel (Mn 0.65%) and the latter a nickel-chromium steel, similar to SAE 3335. These were treated as shown in Table II.

Table II

Specimen	Steel	Austenitizing Temperature*	Quench	Tempering Treatment	Embrittling Treatment
a	E.N. 23	1250 °C	Oil	1 hour, 640 °C	8 hours, 520 °C
b	E.N. 23	1250 °C	Oil	1 hour, 640 °C	Nil
c	E.N. 8	1000 °C	Brine	1 hour, 630 °C	24 hours, 480 °C
d	E.N. 8	1000 °C	Brine	1 hour, 630 °C	Nil

\*High austenitizing temperatures were used, to facilitate examination of the fractures.

After tempering, the specimens were notched, and fractured at  $-180^{\circ}\text{C}$ . The fracture surfaces were then carefully examined. Fig. 6a showed

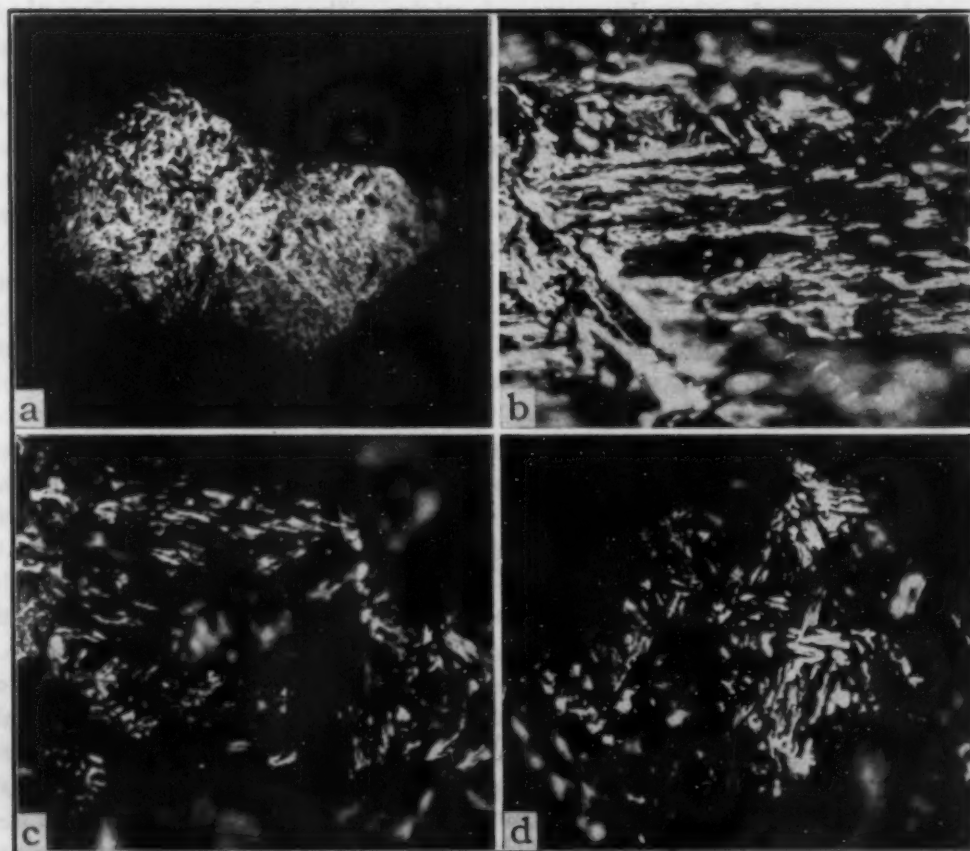


Fig. 6—Fracture Surfaces of E.N. 23 and E.N. 8 Steels.  $\times 430$ . (See Table II.)

curved surfaces with particles, characteristic of an intergranular fracture. Fig. 6b exhibited cleavage surfaces, quite different in appearance from the intergranular fracture of Fig. 6a. Figs. 6c and 6d, i.e., the plain carbon steels, also show these cleavage facets. Fig. 6c does show a trace of

intergranular fracture but the amount is very small, about 5%. This evidence shows that the type of fracture experienced by plain carbon steels is different from that of alloy steels in the temper-brittle condition. It cannot, therefore, be considered that plain carbon steels are temper-brittle in the same sense as low alloy steels.

Secondly, the phenomenon of reversibility is an important characteristic of the temper embrittling reaction, but it is one which seems difficult to explain on the basis of the present authors' theory. Houdremont and Schrader<sup>8</sup> demonstrated that the reaction is, in fact, reversible for at least eight heating and cooling cycles. If temper brittleness were due to a "thin film of hard brittle martensite structure", the breakdown of the martensite on tempering at a high temperature (above 600 °C) would not be reversible. It would thus be impossible to make the steel brittle again, which is in contradiction to Houdremont and Schrader's results.

Finally, the conclusions drawn from examination of the steels etched with Zephiran chloride etch can have only a very limited significance at the present time, as the action of the reagent is not well understood. The authors assume that the action is specific, but it is not known whether in fact this is the case. Thus the grain boundary attack in the quenched steels may arise from a cause different from that in the embrittled steels.

**Written Discussion:** By M. J. Sinnott, associate professor of metallurgical engineering, University of Michigan, Ann Arbor, Mich.

The authors have presented a somewhat novel theory to explain the cause of temper embrittlement, but there seem to be quite a few discrepancies between their theory and available experimental data. I am inclined to agree with the authors that there are concentration gradients existing between the boundaries and the grain proper, but that these gradients give rise to retained austenite and subsequently martensite is highly unlikely in view of the data that have been published.

The work of J. A. Jones<sup>9</sup> on a 3.0% nitrogen-0.8% chromium-0.33% carbon steel showed that this material when hardened, then tempered at 640 °C (1185 °F) for 4 hours and water-quenched, had an impact strength of 86 foot-pounds Izod. If furnace-cooled from the tempering temperature, the impact strength dropped to 16 foot-pounds. These same materials were then tempered at 600 °C (1110 °F) for 1 hour, one sample being water-quenched and another air-cooled. This treatment was repeated for 10, 20, 30, and 60 cycles. In all cases the water-quenched samples retained their impact strength while the furnace-cooled specimens showed embrittlement. The sample which had been tempered sixty times at 600 °C (1110 °F) and water-quenched was tempered again at 600 °C (1110 °F) and air-cooled and this material showed embrittlement. These treatments certainly would have removed any austenite or martensite that might have been present, yet the steel still shows temper embrittlement.

Similarly the work of Borel<sup>10</sup> with a 0.22% carbon-1.0% manganese steel shows that temper embrittlement in this steel can be obtained by air cooling from 850 to 650 °C (1560 to 1200 °F), then slowly cooling to

<sup>8</sup>E. Houdremont and H. Schrader, *Archiv für das Eisenhüttenwesen*, Vol. 7, 1933, p. 49.

<sup>9</sup>J. A. Jones, *Metal Treatment*, Vol. 4, No. 15, 1938, p. 97.

<sup>10</sup>Borel, *Revue de Metallurgie*, Vol. 31, 1934, p. 14-34.



room temperature. This type of treatment certainly should yield no retained austenite or martensite at the boundaries to account for the brittleness.

Recent work by Jacquet<sup>11</sup> with a 3.25% nitrogen-1.65% chromium-0.3% carbon steel showed that by suitable treatments he could pass from a brittle to a tough condition or from a tough to a brittle condition, indicating the reversibility of the embrittling process at temperatures below the critical as was found by Jones. It is the irreversibility of the mechanism proposed by the authors that leads me to believe that their theory is not an acceptable one for explaining temper embrittlement.

The statement is made in the paper that "Manganese and molybdenum are particularly effective in delaying carbide precipitation." I would infer from this that these elements are effective then in stopping or delaying the onset of embrittlement. Data are available to indicate that this is true of molybdenum but not for manganese.<sup>12</sup>

I would also like to ask the authors if they have done sufficient work with the Zephrian etch to be convinced of the reliability of this test in detecting the presence of embrittlement. Some investigators have had only indifferent success in the use of this etch, although this might be due to faulty technique.

**Written Discussion:** By H. C. Turner, graduate student and assistant, Department of Mining and Metallurgical Engineering, University of Illinois, Urbana, Ill.

The authors state the belief that retained austenite at the grain boundaries is responsible for temper brittleness. From this it might be anticipated that a cold treatment in liquid nitrogen following quenching would decrease the amount of austenite and thus reduce the degree of embrittlement. Investigation of a series of specimens from a heat of SAE 3335 steel failed to show any such difference as determined by the Zephrian chloride etchant.

All specimens were quenched in oil from the austenitizing temperature, but in addition one group of specimens was given a liquid nitrogen treatment immediately after quenching. Photomicrographs of four specimens are shown in Figs. 7 and 8. Fig. 7 shows the microstructures as etched, and Fig. 8 illustrates the same specimens when repolished (for 1 minute) to more clearly define the attack at the grain boundaries. Microstructures c and d of Figs. 7 and 8 were given the liquid nitrogen treatment and show the same degree of grain boundary attack as the corresponding specimens a and b which were not subjected to the cold treatment. This indicates that temper brittleness has not been decreased by the liquid nitrogen treatment.

The photomicrographs also show the reversibility of the temper brittleness reaction. Microstructures a and c of Figs. 7 and 8 have been tempered at a temperature which should produce maximum embrittlement. Microstructures b and d have been given the same treatment and, subsequently, a temper above the region of maximum embrittlement and quenched. In the resulting structures the grain boundaries are not as

<sup>11</sup>Jacquet, *Comptes Rendus*, Vol. 230, 1950, p. 650-651.

<sup>12</sup>S. A. Hervese and A. R. Elsea, *Journal of Metals*, Vol. 185, 1949, p. 366-370; Discussion by H. V. Joyce, *TRANSACTIONS, American Society for Metals*, Vol. 39, 1947, p. 153.

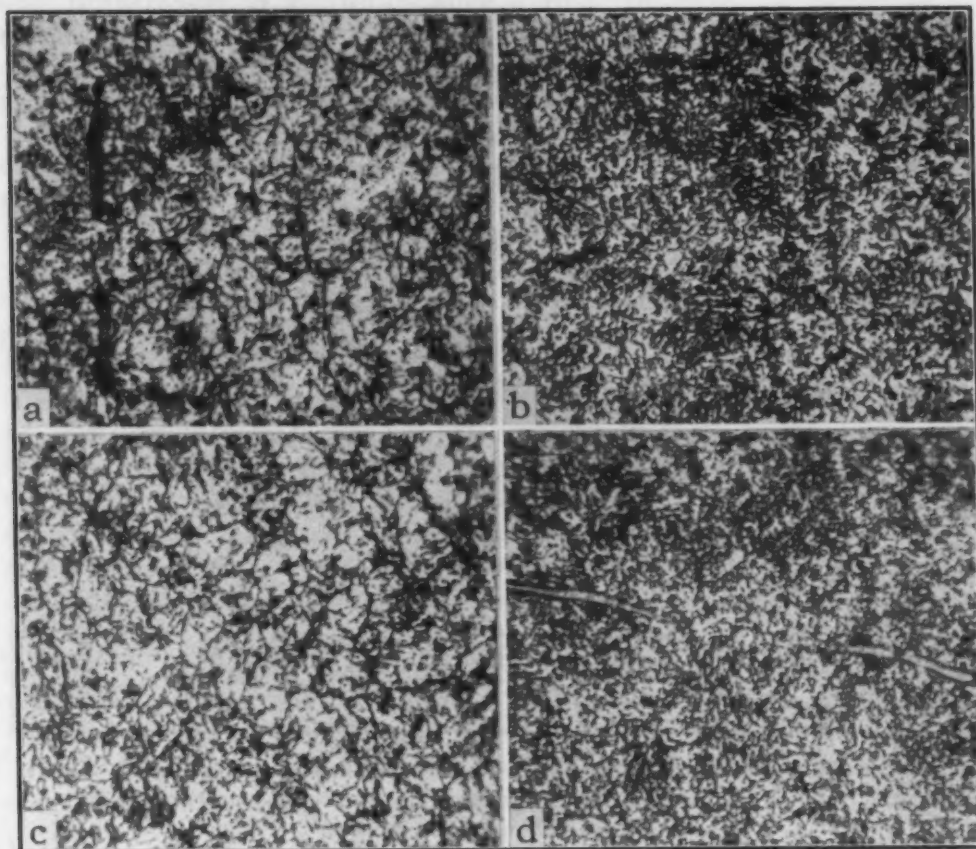


Fig. 7—Microstructures of SAE 3335 Austenitized at 1450 °F (790 °C), Quenched and Tempered as Indicated, Followed by a Water Quench. Zephiran chloride etch.  $\times 1200$ . a—Oil-quenched and tempered at 900 °F (480 °C) for 24 hours. b—Same as a but also tempered for 12 hours at 1100 °F (590 °C). c—Oil-quenched followed by immediate cold treatment in liquid nitrogen and tempered at 900 °F (480 °C) for 24 hours. d—Same as c but also tempered for 12 hours at 1100 °F (590 °C).

severely attacked by the etchant as in the former case. Embrittlement caused by the initial tempering has been diminished by the second treatment.

#### Authors' Reply

The authors are grateful for the interest and contributions of the several discussers as evidenced by their painstaking and thorough discussions of several points of interest concerning the perplexing phenomenon of temper brittleness in steel. It should be pointed out that the principal purpose of writing the paper was to examine thermodynamically the role of interfaces in influencing the position of solute atoms in solid solutions. The, perhaps unfortunate, choice of temper brittleness as an example of a phenomenon in which surface adsorption probably plays a vital role has tended to obscure the primary purpose of the paper. However, since the interest of the discussers, aside from Dr. Zapffe, apparently lies in temper brittleness, the closure will be mainly restricted to this subject.

A few general remarks appear to be in order at this point. It has become fashionable to evaluate the degree of temper embrittlement by the use of the transition temperature range in the impact test. At best,

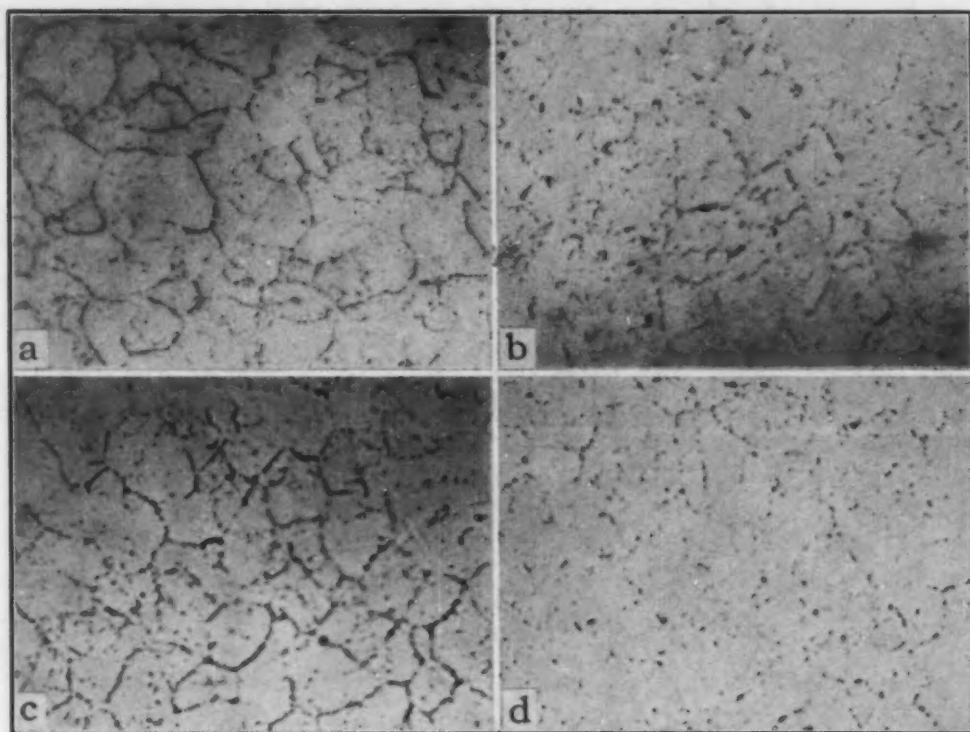


Fig. 8—Microstructures of Specimens in Fig. 7 When Repolished for 1 Minute.  $\times 1200$ .

the conditions in the impact test are complex and not readily evaluated, involving such factors as stress state, stress concentration, and strain rate. The factors affecting low temperature impact behavior are complex and numerous, among which should be listed austenite grain size, deoxidation effects, composition effects, structural effects, size and shape of ferrite grains in the tempered steels, and various aging effects. The effect of composition is by no means an easy factor to study if other variables are to be held constant, as evidenced by the painstaking research of Rinebolt and Harris.<sup>13</sup> The importance of the effect of ferrite grain size on transition temperature was recently illustrated in the timely contribution of Hodge, et al.<sup>14</sup> Finally, it is to be mentioned that the possibility of austenite formation in tempering below the nominal  $A_{c1}$  temperature should not be overlooked.<sup>15</sup> Consideration of these factors and evaluation of claims made by various investigators lead to the inescapable conclusion that the initial problem is an accurate definition of "temper brittleness"—where does the phenomenon start and end, and how many different mechanisms should our definition include? In the current paper the viewpoint was taken that temper brittleness refers to an embrittling process resulting from the quenching of a heat treatable steel to tetragonal martensite and tempering the steel in such a way that it is

<sup>13</sup>J. A. Rinebolt and W. J. Harris, Jr., "Effect of Alloying Elements on Notch Toughness of Pearlitic Steels", see this volume of *TRANSACTIONS*, p. 1175.

<sup>14</sup>J. M. Hodge, R. D. Manning and H. M. Reichhold, "The Effect of Ferrite Grain Size on Notch Toughness", *Transactions, American Institute of Mining and Metallurgical Engineers*, Vol. 185, 1949, p. 233.

<sup>15</sup>E. F. Bailey and W. J. Harris, Jr., "Austenite Formation During Tempering and Its Effect of Mechanical Properties", *Journal of Metals*, October 1950, p. 997.



held isothermally in a critical range during tempering or cooled slowly through this critical range after tempering. Doubt is raised among the discussers as to whether carbon steels embrittle by the same mechanism as do alloy steels. Also, a somewhat startling claim is made that iron with 0.01 and 0.02% carbon is susceptible to temper brittleness. Certainly these compositions are not heat treatable in the ordinary sense of the term and we should look to aging effects in these commercially pure irons.

Rather than to answer each discussor individually, a general answer will be made. The authors are firmly convinced that the key to temper brittleness lies in interfacial energy effects, namely the adsorption of solute atoms, particularly carbon, to interfaces in order to minimize the free energy of the system. The paper itself is concerned with what will be called the primary mechanism of temper brittleness concerned with adsorption effects in austenite. The role of austenite as regards its treatment, such as the austenitizing temperature, rate of cooling, and embrittlement around the prior austenite grains, is too well established experimentally to be ignored. The heterogeneous etching effect of Zephiran chloride<sup>10</sup> indicates clearly a dependency of adsorption effects on relative orientations of adjoining grains, as would be expected. The proposed mechanism also explains adequately the kinetics of primary embrittlement as illustrated in Fig. 5 of the paper. Contrary to some claims, this primary embrittlement can occur isothermally in the critical range or by continuously cooling through the range.

The chief objection to this primary mechanism seems to lie in the somewhat confused concept of "reversibility" of the reaction. The effect of heating in primary embrittlement in any tempering range is (a) to temper any fresh martensite formed by a previous treatment, and (b) to condition any retained high carbon austenite. Nowhere in this mechanism is it proposed that martensite is forming from ferrite and carbide as suggested by S. J. Rosenberg. The primary mechanism can hold forth only as long as any retained austenite remains. Thus, it is doubtful if the primary mechanism is operative for more than a very few cycles. Retrogression as described by D. C. Buffum can be explained by initial tempering of fresh martensite at 675 °C (1250 °F) and subsequent conditioning of retained austenite by slowly precipitating carbides at this temperature.

How then can we interpret the completely "reversible" type of embrittlement described by Messrs. Entwisle and Smith, and Sinnott? In essence, a steel may be repeatedly tempered at such a temperature as 600 °C (1110 °F), and if quenched from the temperature it will be ductile, and if slow-cooled it will be brittle. Such is the case up to as many as 60 cycles, as indicated in the discussion. Certainly after such cycling, any structures carried over from the original quench and temper will be "washed out" and a structure of spheroidized carbide in a matrix of ferrite will be formed. The authors wish to propose that this behavior is a result of a second mechanism of embrittlement, which for convenience shall be termed secondary temper embrittlement. As previously indicated, the secondary brittleness in cycling cannot be explained by gross structure considerations. The most likely explanation is that it is a result of

<sup>10</sup>In answer to questions about the Zephiran chloride etch, no research was done concerning its action. The instructions of Cohen, Hurlich and Jacobson were followed.

adsorption effects in the ferrite grains, most likely of carbon. The real interfaces in tempered structures are those of ferrite grains and any subsequent adsorption effects should occur at the ferrite grain boundaries. The effect of holding at such a temperature as 600 °C (1110 °F) would be then to yield an excess of carbon atoms at ferrite grain boundaries through the mechanism of surface adsorption. Through the recent brilliant research of Wert,<sup>17</sup> reliable data are available for the solubility of carbon in ferrite as a function of temperature. At 600 °C (1110 °F), his data indicate a solid solubility of 0.01 weight per cent and at room temperature a solubility of  $10^{-7}$  weight per cent. Thus, having an excess of carbon at the interfaces at high temperatures, quenching may lead to a retained supersaturated solution, whereas slow cooling may lead to an aging reaction giving rise to secondary embrittlement. This is probably the explanation of the observation reported by Buffum that iron with 0.01 and 0.02% carbon are susceptible to temper brittleness. Any residual stress not removed by the treatments could also lead to adsorption at certain crystallographic planes, which might have some bearing on cleavage fractures mentioned by Messrs. Entwisle and Smith. Thus, it is suggested that in research on temper brittleness, one must consider at least two different mechanisms. The possibility of forming austenite at these high temperatures also should not be overlooked as an occasional auxiliary reaction.

This laboratory has not carried out extensive work on temper brittleness in the past, nor does not contemplate doing so in the near future. Accordingly, it may appear presumptuous for the writers to suggest some key experiments concerning temper brittleness. However, for what it may be worth, it is suggested that the kinetics of embrittlement after several cycles (secondary embrittlement) be determined and compared to the familiar "C" type curve for primary embrittlement. If the kinetics are distinctly different, then truly two mechanisms are involved. Also, further work on fracture studies is needed to determine if fracture in primary embrittlement is associated with the prior austenite grain size, and if that in secondary embrittlement is associated with the ferrite grain structure.

<sup>17</sup>C. A. Wert, "Solid Solubility of Cementite in Alpha Iron", *Journal of Metals*, October 1950, p. 1242.

## THE INFLUENCE OF CHROMIUM ON THE MECHANICAL PROPERTIES OF PLAIN CHROMIUM STEELS

BY W. O. BINDER AND HOWARD R. SPENDELOW, JR.

### *Abstract*

*Mechanical properties of a series of annealed vacuum- and air-melted chromium steels are shown for chromium contents from 0.3 to 55%. The influence of carbon and nitrogen on the toughness of ferritic chromium steels has been determined as a function of chromium content, and the effect of chromium in lowering the transition temperature of the alloys is discussed. It is concluded that the lowering of the impact strength of ferritic chromium steels as the chromium content is raised above about 20% chromium is not due to chromium of itself, but is associated with other factors, namely the carbon and nitrogen contents of these steels. In the virtual absence of carbon and nitrogen, increasing chromium from 12 to 25% has a toughening influence on the matrix of these steels lowering the transition temperature about 65 °C (115 °F).*

*While extremely low carbon and nitrogen contents are prerequisite to very high impact strength in steels containing above about 20% chromium, the addition of some 0.10 to 0.25% nitrogen to these steels reduces their grain size and improves their ductility and impact strength, though not to the very high level obtained in the very low carbon, low nitrogen alloys.*

THE reduction in toughness which occurs in plain chromium stainless steels when the chromium content is increased above about 20% has, for many years, been associated with chromium, per se. It has generally been considered that this decrease occurs regardless of the heat treatment or carbon and nitrogen contents of the steels, and that the transition temperature is raised with increasing chromium content (1).<sup>1</sup> The influence of chromium on the properties of chromium steels has been under study for a number of years at the Union Carbide and Carbon Research Laboratories, Inc. (2-7), and during the course of this investigation it was discovered that chromium-iron alloys, containing up to at least 35% chromium, could be made with a room-temperature Izod impact

<sup>1</sup>The figures appearing in parentheses pertain to the references appended to this paper.

A paper presented before the Thirty-second Annual Convention of the Society, held in Chicago, October 21 to 27, 1950. The authors, W. O. Binder and Howard R. Spendelow, Jr., are research metallurgists, Union Carbide and Carbon Research Laboratories, Inc., Niagara Falls, N. Y. Manuscript received April 15, 1950.



strength of the order of 80 to 100 ft-lbs. This was accomplished by lowering the carbon and nitrogen content of the alloys through a vacuum-melting process below certain critical amounts which are a function of the chromium content of the alloys.

For 25% chromium steels of very high toughness, the maximum tolerance for carbon plus nitrogen is about 0.035%, while in 18% chromium steels the tolerance is about 0.055%. To a certain extent, these results have been corroborated by Hochmann (8), who in 1948 reported improving the toughness of 25% chromium-iron alloys by reducing the total carbon and nitrogen contents of the alloys below 0.01%. At the present time, the levels of carbon and nitrogen required for an impact strength of the order of 80 to 100 ft-lbs in the 18 and 25% chromium alloys cannot be obtained except by vacuum melting or melting under an inert atmosphere using selected raw materials. In normal air melting practice, where these low levels of carbon and nitrogen cannot be obtained, the impact strength and ductility of steels containing upward of 20% chromium can be improved by the addition of some 0.10 to 0.25% nitrogen (3, 5).

#### STEELMAKING PRACTICE

All the experimental steels used in this investigation were melted in a basic-lined, high-frequency induction furnace. Some steels were made with electrolytic chromium and iron, while low carbon ferrochromium and ingot iron were used for making others. When desired, silicon and manganese were added as silicon metal and low carbon manganese metal, and carbon was added in the form of crushed furnace electrodes. High nitrogen ferrochromium was the source of nitrogen in the air-melted steels, while nitrogen was introduced into the vacuum-melted steels by finishing the heat under a partial pressure of nitrogen gas.

In making the air-melted steels, all the iron was melted and deoxidized with a portion of the silicon and manganese to be added. Ferrochromium was then added, followed by any nitrogen and carbon additions. The heat was then deoxidized with the remainder of the manganese and silicon, and cast into a 2-inch square ingot mold.

In the vacuum-melted steels, all the components of the charge were melted together, as no facilities were available for making any further additions to the heat after the initial charging. The molten charges were held at pressures of 300 to 400 microns for about 20 minutes to insure degassification, and then cast. Lower operating pressures were not employed because of chromium losses due to

evaporation, and even at these pressures, manganese could not be retained in the steels above about 0.02%.

No special precautions were necessary in hot working or heat treating the alloys, as it was established that significant nitrogen pickup from the air did not occur in the solid state. All the steels containing less than 20% chromium were heated for 1 hour at 900 °C (1650 °F), followed by a 3-hour anneal at 735 °C (1350 °F). The higher chromium alloys were heated for 6 hours at 900 °C (1650 °F), and water-quenched. This latter temperature was chosen as sufficiently high to avoid the formation of sigma phase, FeCr, during heat treatment, and yet not so high as to cause any marked grain growth in the alloys. Typical microstructures of the vacuum-melted alloys, at two levels of chromium, are shown in Fig. 1, along with commercial alloys of similar compositions for comparison.

#### MECHANICAL PROPERTIES OF PLAIN CHROMIUM-IRON ALLOYS

Room temperature tensile and impact test data for vacuum-melted 0.3 to 55% chromium-iron alloys are presented as a function of chromium content in Figs. 2 to 4. Most of the steels were made with electrolytic chromium and iron, but a few 25% chromium alloys were made with low carbon ferrochromium and ingot iron. In no case was any carbon, nitrogen, manganese, or silicon added intentionally to these alloys, although those made with ferrochromium contain up to about 0.25% silicon derived from the ferrochromium. Since the high silicon alloys are confined to the 25% chromium level, the curves in Figs. 2 to 4 represent the properties of binary chromium-iron alloys. The range of impurity content in these vacuum-melted chromium-iron alloys is given in Table I.

Table I  
Impurities in Vacuum-Melted Chromium-Iron Alloys

Carbon	less than 0.01% average—0.015% maximum
Nitrogen	less than 0.005% average—0.01% maximum
Manganese	less than 0.02%
Silicon	less than 0.02%, except in steels made with ferrochromium and ingot iron, which contain up to 0.25%
Oxygen	0.04% average
Sulphur	0.016% average
Phosphorus	0.008% average

Fig. 2 shows that the hardness of the vacuum-melted chromium-iron alloys increases steadily from Rockwell B-0 at 0.35% chromium to about Rockwell B-100 at 55% chromium. The scatter of hardness data at the 25% chromium level is due, in part, to the effects of the higher silicon contents. It will be noted that there is a differ-

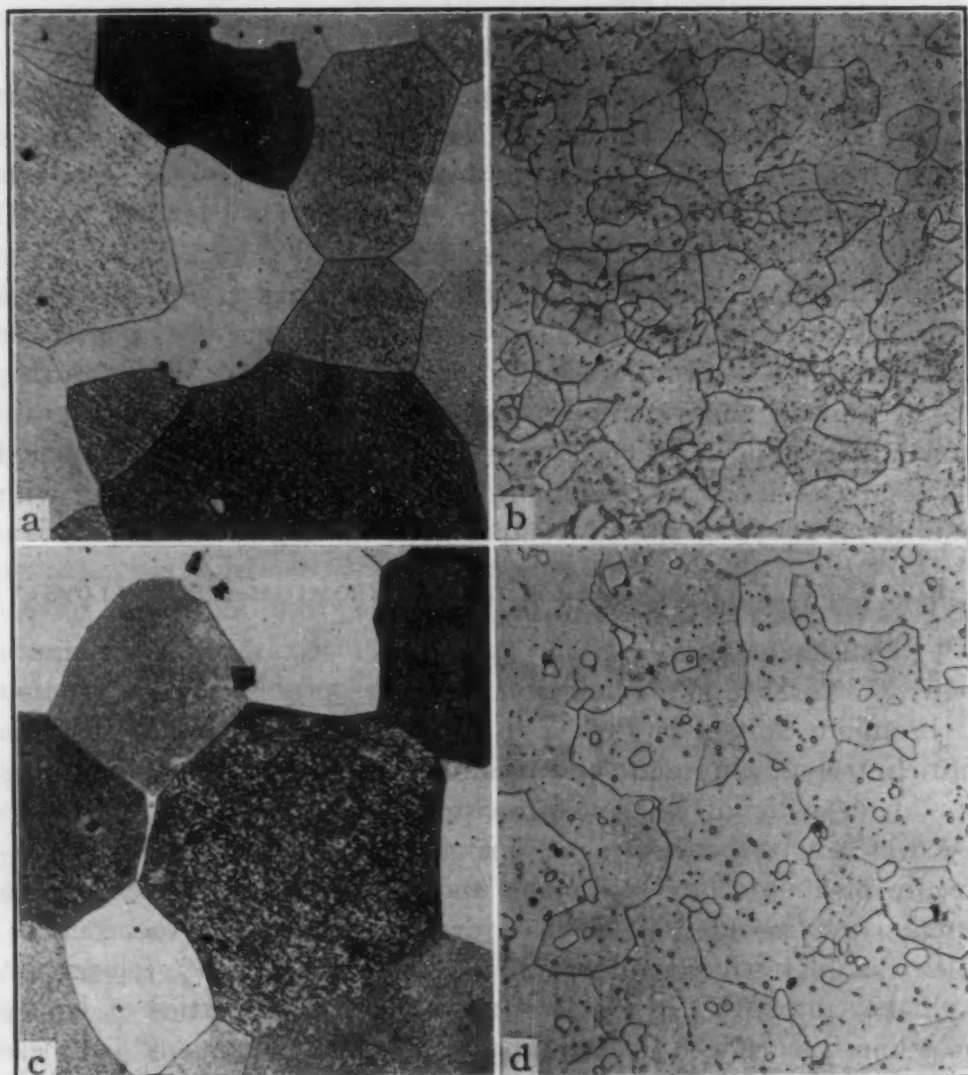


Fig. 1—Photomicrographs of Vacuum-Melted and Commercial Chromium Steels. 25% HCl in alcohol etch.  $\times 250$ . a—Vacuum-melted steel, 18.57% chromium, trace of manganese, trace of silicon, 0.0047% carbon, 0.002% nitrogen. b—Commercial steel, 18.12% chromium, 0.66% manganese, 0.42% silicon, 0.04% carbon, 0.034% nitrogen. c—Vacuum-melted steel, 25.10% chromium, trace of manganese, trace of silicon, 0.007% carbon, 0.005% nitrogen. d—Commercial steel, 28.50% chromium, 0.56% manganese, 0.60% silicon, 0.24% carbon, 0.12% nitrogen.

ence in hardness of about 15 Rockwell B points between 12 and 25% chromium alloys. This agrees closely with the difference in hardness between commercial steels of these chromium contents, shown in Table II, although the absolute hardness of the vacuum-melted alloys is somewhat lower.

The tensile strengths of the vacuum-melted alloys are also lower than those of commercial steels of equivalent chromium contents, but in the range where comparisons may be drawn, increasing the chromium content of both commercial and experimental alloys a given amount produces about the same increase in the tensile



Table II  
Typical Properties of Annealed Chromium Steels

AISI Type	Chromium, %	Carbon, %	Yield Strength, psi	Tensile Strength, psi	Elongation, %	Reduction in Area, %	Hardness, Rockwell B	Izod Impact Strength, ft-lbs
410	11.5-13.0	0.15 max.	40,000	75,000	35	70	74-83	115-95
430	14.0-18.0	0.12 max.	40,000	75,000	35	70	76-85	35-15
442	18.0-23.0	0.35 max.	45,000	75,000	30	60	80-88	15-5
446	23.0-27.0	0.35 max.	50,000	80,000	35	45	83-90	5-1

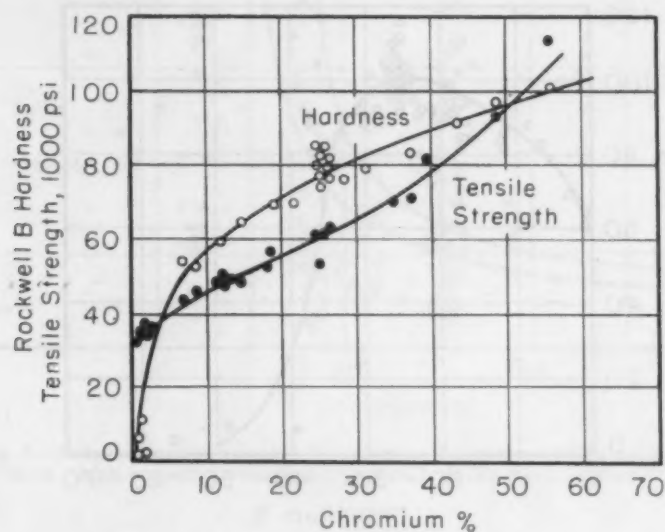


Fig. 2—Hardness and Tensile Strength of Vacuum-Melted Chromium-Iron Alloys.

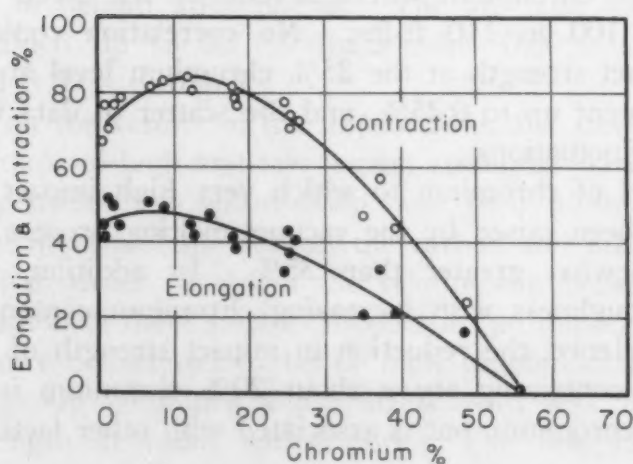


Fig. 3—Ductility of Vacuum-Melted Chromium-Iron Alloys.

strength. The ductility data shown in Fig. 3 may be similarly compared to that of Table II. To summarize, the effect of chromium on the strength of the base metal is about the same for both vacuum-

melted and commercial steels, and the greater strength of the latter is probably due to the effects of carbon and nitrogen.

The impact strength of vacuum-melted chromium-iron alloys is shown as a function of chromium content in Fig. 4. The lower impact strength of the alloys lean in chromium is probably a reflection of their lower tensile properties. The toughness of the alloys increases as the chromium content is raised, reaching a maximum

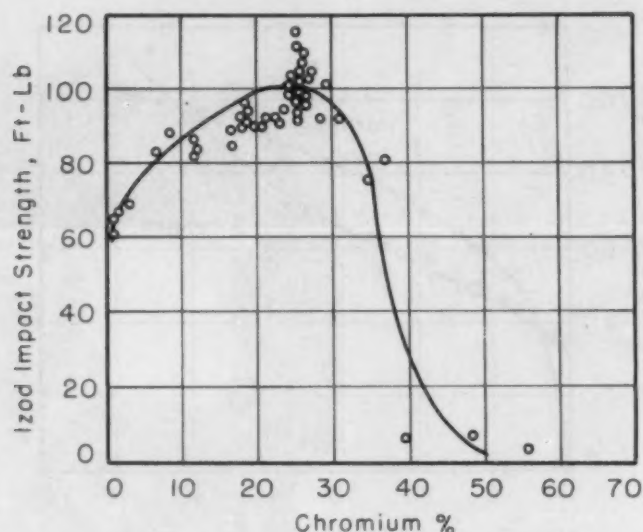


Fig. 4—Impact Strength of Vacuum-Melted Chromium-Iron Alloys.

at about 26% chromium, where several of the steels had impact strengths of 100 to 110 ft-lbs. No correlation could be found between impact strength at the 25% chromium level and variations in silicon content up to 0.25%, and the scatter of data is attributed to statistical fluctuations.

The level of chromium to which very high impact strength is retained has been raised by the vacuum-melting process from about 20% to somewhat greater than 35%. In addition, these steels increase in toughness with increasing chromium contents up to at least 26%. Hence, the reduction in impact strength of normal air-melted steels containing above about 20% chromium is not necessarily due to chromium, but is associated with other factors.

#### EFFECT OF CARBON AND NITROGEN ON THE TOUGHNESS OF CHROMIUM-IRON ALLOYS

The essential difference between normal air-melted steels and the vacuum-melted alloys just discussed is in their carbon and nitrogen contents. In order to determine the effect of these elements

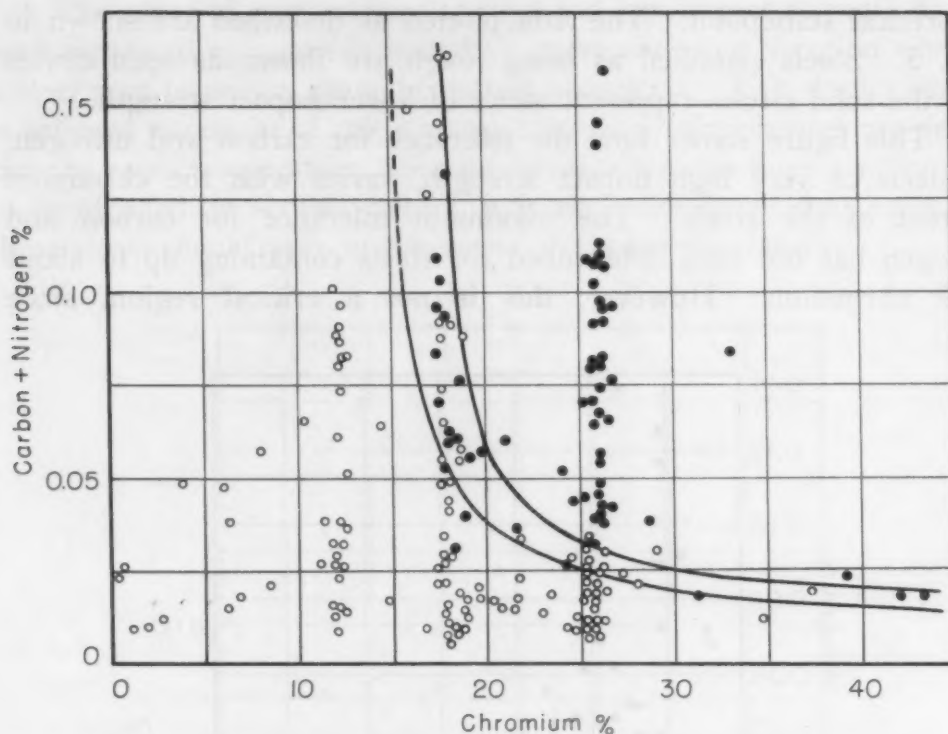


Fig. 5—Influence of Carbon and Nitrogen on Toughness of Chromium-Iron Alloys. Open circles—high impact strength alloys; solid circles—low impact strength alloys.

on toughness, room temperature impact tests were made on a series of 12 to 40% chromium-iron alloys with higher carbon and nitrogen contents. The tests covered steels made in vacuo, and in air, in argon, and in helium atmospheres. The air- and inert-gas-melted steels contained up to 0.75% manganese, 0.50% silicon, 0.10% carbon, and 0.10% nitrogen.

Based on the results of the impact tests, the steels were classified into groups of high and low impact strength. Using the appropriate designation, this information was then plotted against the chromium content and the sum of the carbon and nitrogen contents of the steel in order to obtain the relationship between toughness and composition of these steels. Steels with an impact strength over 50 ft-lbs were considered to be of high toughness, while the low toughness group contained those steels with less than 10 ft-lbs impact strength at room temperature. The few steels of intermediate toughness were disregarded in this analysis. To facilitate plotting of the data, carbon and nitrogen were assumed to be equivalent in their effect on the toughness of the steels, since both form interstitial-type solid solutions in ferrite. Furthermore, the atomic radii and weights of the two are nearly the same, so that the assumption of equivalency does not seem unreasonable from a



theoretical standpoint. The data plotted as described are shown in Fig. 5. Steels classified as being tough are shown as open circles and the solid circles represent steels of lower impact strength.

This figure shows how the tolerance for carbon and nitrogen, in steels of very high impact strength, varies with the chromium content of the steels. The maximum tolerance for carbon and nitrogen has not been determined for steels containing up to about 15% chromium. However, this is not a critical region, since

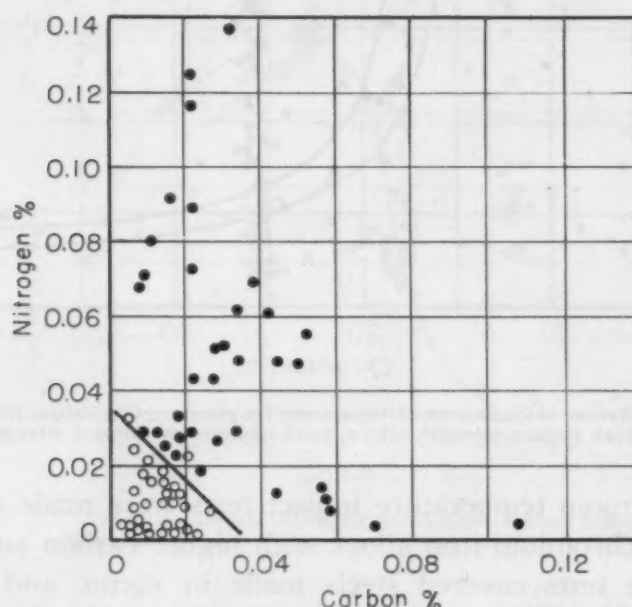


Fig. 6—Effect of Carbon and Nitrogen on the Toughness of 24 to 26% Chromium-Iron Alloys. Open circles—high impact strength alloys; solid circles—low impact strength alloys.

normal air-melted steels of these chromium contents, with carbon and nitrogen contents up to 0.12 and 0.05%, respectively, have a high level of impact strength. The tolerance for carbon and nitrogen in very tough steels decreases extremely rapidly as the chromium content is raised from 15 to 20%, and then less rapidly with further increases in chromium content. The marked decrease in the tolerance for carbon and nitrogen occurs over the same range of chromium contents in which normal air-melted chromium steels lose impact strength, and this curve, in effect, represents the toughness of such steels as a function of chromium content. These data strengthen the previous conclusion that increasing chromium alone is not responsible for the decrease in toughness of ferritic chromium steels, and show that the carbon and nitrogen contents of the steels are closely related to lowering toughness.

The zones of compositions of high and low impact strength have been separated by a double boundary curve enclosing a region where a steel may possess a range of impact properties. This duplex zone is believed to consist of steels whose transition temperatures are very close to room temperature. Since transition temperatures are known to be affected by several factors, it is not inconsistent that some of these steels should vary in toughness at room temperature.

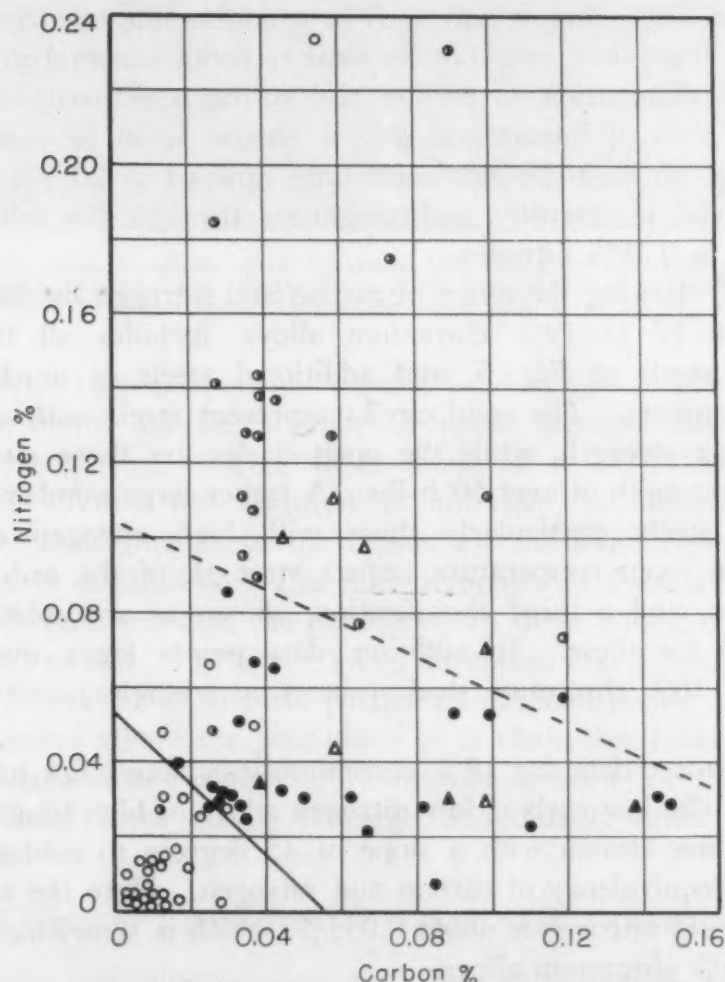


Fig. 7—Effect of Carbon and Nitrogen on the Toughness of 17 to 19% Chromium-Iron Alloys. Open circles—high impact strength alloys; solid circles—low impact strength alloys; semi-solid circles—intermediate impact strength alloys; triangles represent commercial arc-melted steels.

The individual effects of carbon and nitrogen were determined at two levels of chromium, 18 and 25%. This was accomplished by preparing supplementary "scatter plots" based on toughness at room temperature and using the carbon and nitrogen contents of the steels as coordinates. These are shown in Figs. 6 and 7.

The solid circles in Fig. 6 represent vacuum- and air-melted 24 to 26% chromium steels with impact strengths of less than 10 ft-lbs at room temperature, while the open circles represent steels with an impact strength of over 50 ft-lbs. A straight line of a 45-degree slope may be drawn to separate the zones of high and low toughness, indicating that the assumption of equivalency of carbon and nitrogen in Fig. 5 was a reasonable one. This line intercepts the carbon and nitrogen axes at about 0.035%, and though drawn as a single line, it may well be a double line to include those steels with transition temperatures close to room temperature. While the virtual elimination of carbon and nitrogen is necessary for a very high level of impact strength, it should again be pointed out that normal air-melted steels containing upward of 20% chromium are improved in ductility and toughness through the addition of some 0.10 to 0.25% nitrogen.

Fig. 7, showing the effect of carbon and nitrogen on the impact strength of 17 to 19% chromium alloys, includes all the 18% chromium steels of Fig. 5, and additional steels of much higher nitrogen contents. The solid circles represent steels with up to 15 ft-lbs impact strength, while the open circles are those steels with an impact strength of over 50 ft-lbs. A rather large number of 18% chromium steels, particularly those with high nitrogen contents, possessed a room temperature impact strength of the order of 30 to 50 ft-lbs, and a third classification, shown as semisolid circles, is included for these. In addition, data points for a number of commercial 18% chromium steels (shown as triangles) are included in Fig. 7.

The impact data for 18% chromium-iron alloys fall into three divisions. The low carbon, low nitrogen alloys of high toughness lie beneath a line, drawn with a slope of 45 degrees to conform with the idea of equivalency of carbon and nitrogen. Here the tolerance for carbon and nitrogen is about 0.055%, which is somewhat greater than for 25% chromium alloys.

Directly above this zone lies one wherein the majority of the steels possess less than 15 ft-lbs impact strength. The presence of a few steels of higher impact strength in this region is again believed to be due to a slight shift in the transition temperature of the alloys. The upper limit of this region is defined by a line intercepting the nitrogen axis at 0.105%, and which, if fully extended, would intercept the carbon axis at about 0.26%. However, since no data are available for steels containing more than about 0.15% carbon, the continuation of the boundary line beyond



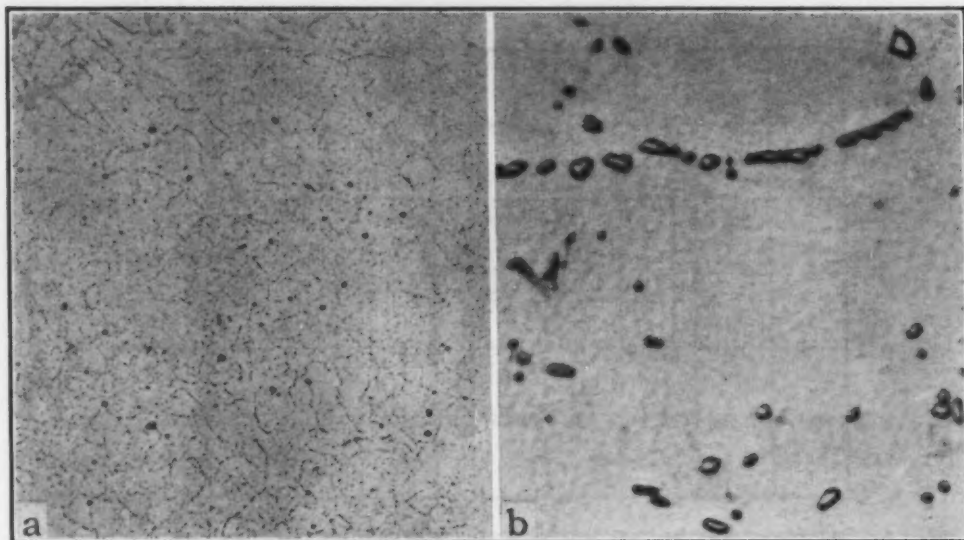


Fig. 8—Photomicrographs of an Air-Melted 18% Chromium Steel Containing 0.037% Carbon and 0.107% Nitrogen. Heated 1 hour at 900 °C (1650 °F) and air-cooled and 3 hours at 735 °C (1350 °F) and air-cooled. 25% HCl in alcohol etch. a— $\times 250$ . b— $\times 2800$ .

that level of carbon is not considered valid at this time.

Above this line lies a group of higher nitrogen steels of intermediate toughness, ranging from about 30 to 50 ft-lbs in impact strength. While the addition of nitrogen to these steels has improved their toughness, the reason for the improvement has not been clearly established. The microstructure of these alloys, shown in Fig. 8, indicates that the precipitate in these alloys, after heating for 1 hour at 900 °C (1650 °F) and air-cooled and 3 hours at 735 °C (1350 °F), exists as discrete particles and small pools. In the very few instances where the precipitate is in chain-like form, the chains are broken and not complete. This may account for the improved toughness of these alloys, although undoubtedly other factors are involved.

#### EFFECT OF CHROMIUM ON TRANSITION TEMPERATURE

In the preceding sections, the effect of chromium on toughness had been considered only at room temperature, and it remained to determine whether the transition temperature of vacuum-melted higher chromium alloys had merely been depressed to about room temperature or whether a steel had been produced which retained its toughness at considerably lower temperatures.

Only vacuum-melted alloys, made with electrolytic chromium, electrolytic iron and silicon were used for this phase of the investigation. Silicon was added in varying amounts up to about 0.75% in an attempt to determine its influence on transition temperature

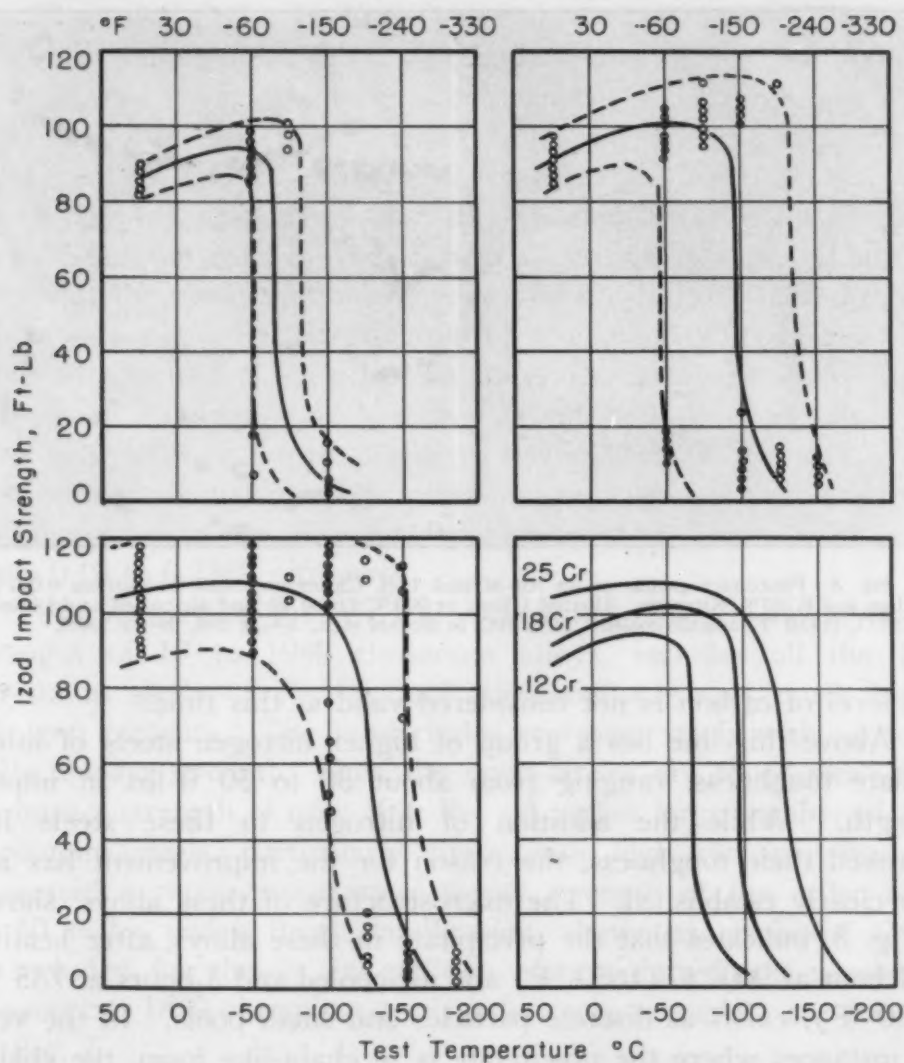


Fig. 9—Effect of Chromium on the Transition Temperature of Vacuum-Melted Chromium-Iron Alloys. Upper left—12% chromium steels; Upper right—18% chromium steels; Lower left—25% chromium steels; Lower right—summary curves.

at different levels of chromium. No correlation was indicated by these data, so the silicon-containing alloys were included with the plain chromium-iron alloys in order to provide more data for analysis to determine the effects of chromium on the transition temperature of chromium-iron alloys.

Since other uncontrollable variables might have some influence on the transition temperature of an individual steel, it was anticipated that the approach to the problem should be statistical in nature. For this reason, the results of subzero impact tests on a number of steels at chromium levels of 12, 18, and 25% were grouped together and plotted as shown in Fig. 9. The broken lines encompass all the data points obtained, while the solid curve is the line

of best fit through each set of data. The latter curves for the three levels of chromium, when plotted on the same coordinates, reveal a marked influence of chromium in lowering the transition temperatures of the alloys. At the 12, 18, and 25% chromium levels, the indicated average transition temperatures are  $-65$ ,  $-90$ , and  $-130$  °C ( $-85$ ,  $-130$ , and  $-200$  °F), respectively. These data show that increasing the chromium content up to at least 25% has a strong toughening effect on the ferrite matrix.

#### SUMMARY AND CONCLUSIONS

The influence of chromium on the mechanical properties of vacuum-melted chromium-iron alloys, containing less than 0.015% carbon and 0.01% nitrogen, has been studied in alloys containing up to 55% chromium. In the range where these alloys may be compared with normal air-melted stainless steels, increasing the chromium content a given amount produces about the same increment in hardness and tensile strength in both types of alloy, although the absolute values of hardness and tensile strength are lower in the vacuum-melted alloys. The vacuum-melted alloys retained a notched Izod impact strength at room temperature of 80 to 100 ft-lbs at chromium contents up to at least 35%.

The effect of carbon and nitrogen on the toughness of plain chromium stainless steels was determined as a function of chromium content. At the 25% chromium level, the tolerance for these elements in steels of very high impact strength is about 0.035% total. Within this limit, carbon and nitrogen appear to be equivalent. At the 18% chromium level, the tolerance for carbon and nitrogen in very tough steels is increased to about 0.055%, with the two elements again appearing equivalent. The addition of more than 0.10 to 0.12% nitrogen to air-melted 18% chromium steels resulted in an impact strength consistently in the range of 30 to 50 ft-lbs in steels containing up to at least 0.12% carbon.

The high impact strength of initially tough vacuum-melted chromium-iron alloys was retained at lower and lower temperatures as their chromium content was increased, up to at least 25%. At the 12, 18, and 25% chromium levels, the indicated average transition temperatures were found to be  $-65$ ,  $-90$ , and  $-130$  °C ( $-85$ ,  $-130$ , and  $-200$  °F), respectively.

These data support the general conclusion that the reduction in toughness of normal air-melted ferritic stainless steels above about 20% chromium content is not due to chromium alone but is associated with other factors such as their carbon and nitrogen



contents. Of itself, chromium has a strong toughening influence on the ferrite matrix, as shown by its reduction of the transition temperature of vacuum-melted alloys.

#### ACKNOWLEDGMENT

The authors are pleased to acknowledge the cooperation and assistance of Mr. Russell Franks, Development Manager, Technical Service and Development Department, Electro Metallurgical Division, and of Mr. Walter Crafts, Chief Metallurgist, Dr. W. D. Forgeng, Messrs. R. Gerby, J. Thompson, and L. De'Aeth of the Union Carbide and Carbon Research Laboratories, Inc., in conducting this work.

#### References

1. V. N. Krivobok, "Alloys of Iron and Chromium", *TRANSACTIONS, American Society for Metals*, Vol. 23, 1935, p. 1-60.
2. C. E. MacQuigg, "Some Commercial Alloys of Iron, Chromium, and Carbon in the Higher Chromium Ranges", *Transactions, American Institute of Mining and Metallurgical Engineers*, Vol. 69, 1923, p. 831-847.
3. R. Franks, "Chromium Steels Improved by Nitrogen", *Iron Age*, Vol. 132, Sept. 7, 1933, p. 10-13.
4. F. M. Becket and R. Franks, "Titanium and Columbium in Plain High Chromium Steels", *Transactions, American Institute of Mining and Metallurgical Engineers*, Vol. 113, 1934, p. 126-142.
5. R. Franks, "Chromium Steels of High-Nitrogen Content", *TRANSACTIONS, American Society for Metals*, Vol. 23, 1935, p. 968-994.
6. A. B. Kinzel and W. Crafts, "The Alloys of Iron and Chromium", Vol. 1, 1937, McGraw-Hill Book Company.
7. A. B. Kinzel and R. Franks, "The Alloys of Iron and Chromium", Vol. 2, 1940, McGraw-Hill Book Company.
8. J. Hochmann, "Sur l'amélioration des valeurs de la résilience des alliages ferritiques à 25% de chrome par la méthode de fusion sous vide", *Comptes Rendus*, Vol. 226, 1948, p. 2150-2151.

#### DISCUSSION

**Written Discussion:** By Carl A. Zapffe, Baltimore, Md.

Joseph Hochmann, to whom the present authors make reference, submitted in June 1950 a thesis to the University of Paris for his Doctorate.<sup>2</sup>

His research, conducted in the laboratory of J. Holtzer at Unieux, France, was restricted more or less to a consideration of 25% chromium alloys; but he also describes the astonishing increase in toughness afforded by the chromium content when the interstitial alloying elements are kept at a minimum. He then goes on to uncover a number of other phenomena, making his thesis well worth reading.

It is not often that something completely new crops up in metallur-

<sup>2</sup>J. Hochmann, "Influence De La Fusion Sous Vide Sur Les Propriétés Des Ferrites A 25% De Chrome", Thesis presented to University of Paris, June 20, 1950, No. 292, 70 pages.

gical discussions; and it is especially surprising to have the field suddenly reversed with regard to rheological changes caused by chromium content in the ferritic stainless steels, for the loss in toughness at chromium contents above 16 to 20% has been accepted virtually without question for a couple of decades.

Just as the present authors have considered the separate effects of nitrogen and carbon, Hochmann studied nitrogen, carbon, oxygen, and also hydrogen, although he found this last element almost impossible to control. He found that 0.03 to 0.04% carbon added to the vacuum-cast metal erased its advantage over that melted in air. This is identical with the findings of the present authors. Nitrogen, according to Hochmann, shows some distinctions from carbon. If the steel was heat treated at 900 °C (1650 °F) for 30 minutes and quenched in water, then nitrogen in amounts of 0.045 to 0.055% still did not appreciably lower the impact strength. However, additions of only 0.023% severely affected the toughness if the metal was annealed at 1200 °C (2190 °F). This is aside from the effect of that treatment upon grain size. Oxygen similarly greatly reduced the notch-impact values after a treatment at 1200 °C (2190 °F), and also appreciably after the 900 °C (1650 °F) treatment. With carbon and nitrogen kept to a few thousandths of a per cent, hydrogen showed a destructiveness equal to that of any of the elements, but the data were irregular because of difficulties in control.

I would like to point out that these ferritic stainless steels are particularly fruitful for fractographic study, providing easily viewed facets which are rich in detail. Anyone examining the cleavage patterns of these alloys will find an attractive piece of research awaiting him.

**Written Discussion:** By M. E. Nicholson, assistant section head, physical metallurgy, Engineering Research Department, Standard Oil Company (Indiana), Chicago.

The results of this careful and detailed investigation of Messrs. Binder and Spendelow are extremely interesting. If high chromium steels having high notch impact strengths at room temperatures could be produced commercially, they undoubtedly would be used extensively for refinery applications.

It is common knowledge that commercial high chromium steels (containing normal percentages of carbon and nitrogen), which have low notch impact strengths at room temperatures, are further embrittled when aged at sigma-forming temperatures or in the temperature range of 885 °F (475 °C). I wonder if the authors have any information concerning the embrittling effects of aging between 885 and 1400 °F on their low carbon and low nitrogen alloys? Further, does the presence of silicon accelerate the rate of embrittlement of these alloys in this temperature range, as it does in alloys containing normal percentages of carbon and nitrogen?

**Written Discussion:** By J. Hochmann, Jacob Holtzer Co., Unieux, Loire, France.

I congratulate the authors on their excellent paper and am happy to find that their results confirm some tests which I carried out in the laboratories of Jacob Holtzer and Co., in Unieux.

It appears certain now that the brittleness of ferritic alloys from 20 to 30% chromium is not an inherent property of the iron-chromium solid

solution, but that this brittleness is due to the presence of slight amounts of impurities of which the most deleterious is carbon.

I found, as did the authors, that nitrogen contributed to brittleness, but that nitrogen contents in the range of 0.023 to 0.055% did not embrittle the alloys when heat treated at 900 °C (1650 °F), although such alloys would be embrittled if heat treated at 1200 °C (2190 °F).

My results show that oxygen also contributes in good measure to the brittleness of iron-chromium alloys.

A short summary of my tests is given here. Steels of the following composition were melted in a high-frequency furnace:

C .....	0.027/0.036	Cr ...	24.9 /25.2	Al .....	<0.002
Si .....	0.03 /0.06	S ....	0.002/ 0.005	O .....	0.054/0.060
Mn .....	0.005	P ....	0.018/ 0.025	N .....	0.050/0.058

Small ingots of this steel were remelted under a vacuum of about 0.001 mm in a resistance-wound graphite furnace, in alumina, beryllia, and magnesia crucibles.

The vacuum melting effected a thorough decarburization, denitrogenation and deoxidation of the metal as the following tabulation shows:

	Carbon %	Oxygen %	Nitrogen %
Metal remelted under vacuum			
Alumina crucible .....	0.002-0.003	0.002-0.003	0.005-0.008
Beryllia crucible .....	0.002-0.003	0.001-0.002	0.002-0.003
Magnesia crucible .....	<0.002	0.012	0.006

It should be pointed out that deoxidation in magnesia crucibles was not very thorough.

Table III  
Impact Strengths (in Kg/m/cm<sup>2</sup>) of Metal Remelted Under Vacuum

	Heat Treatment	
	30 Min. at 900 °C Water Quench	30 Min. at 1200 °C Water Quench
(A) Beryllia Crucibles		
Melt 1 .....	29.4	31.6
Melt 2 .....	28.4	33.8
Melt 3 .....	29.5	28.9
Melt 4 .....	27.8	27.8
(B) Alumina Crucibles		
Melt 1 .....	26.8	27.8
Melt 2 .....	28.9	24.0
Melt 3 .....	27.8	24.6
Melt 4 .....	25.1	23.0
On samples cut from the as-cast ingot without any forging, the following values were obtained:		
	21.4	25.7
(C) Magnesia Crucibles		
	23.0	2.9-3.5
Impact Strengths (in Kg/m/cm <sup>2</sup> ) of Metal Melted in Air		
	0.6	0.3

Table III lists the impact strength values of the metal remelted under vacuum. The specimens were 10 by 10 mm in cross section with a 5-mm deep notch and a notch radius of 1 mm. Excellent results were obtained—comparable to values with the best austenitic steels of the 18-8 type. The figures are very high, even for alloys heated to 1200 °C (2190 °F), which yielded a large grain size and even in as-cast alloys that were not forged. Only the alloy melted in magnesia showed any brittleness



after the 1200 °C (2190 °F) heat treatment (but this metal was not thoroughly deoxidized).

To determine the factors affecting the brittleness in these alloys, we deliberately added one of the three elements, oxygen, nitrogen or carbon, to metal that had been previously remelted under vacuum. The oxygen was added by lining the alumina crucible with chromium oxide paste.

The following table shows how 0.032% carbon is sufficient to embrittle the steel. Nitrogen embrittles alloys heat treated at 1200 °C (2190 °F). It is also seen that oxygen renders the alloys brittle.

Table IV  
Impact Strengths of Metal Remelted in Vacuum and Then Alloyed With Carbon, Nitrogen or Oxygen (Impact Strengths Given in Kg/m/cm<sup>2</sup>)

Carbon Additions	Alumina Crucibles		Remarks
	Heat Treatment		
	30 Min. at 900 °C Water Quench	30 Min. at 1200 °C Water Quench	
Melt 1 (C = 0.037)	1.3	0.8	(O = 0.003% ; N = 0.004%)
Melt 2 (C = 0.032)	1.5	1.0	
Melt 3 (C = 0.040)	2.6	1.7	(Ingot homogenized 4 hours at 1400 °C under vacuum)
Nitrogen Additions			
Melt 1 (N = 0.055)	18.8	8.1	(O = 0.002% ; C = 0.003%)
Melt 2 (N = 0.040)		{5.9}	
		{2.3}	
		{1.5}	
Melt 3 (N = 0.023)		7.4	
Melt 4 (N = 0.045)	{25.9}	5.7	(Ingot homogenized for 4 hours at 1400 °C in argon atmosphere)
	{26.9}		
Oxygen Additions			
Melt 1 (O = 0.037)	9.0	1.5	(N = 0.007% ; C = 0.003%)
Melt 2 (O = 0.048)	7.0	1.0	
Melt 3 (O = )	{5.3}	2.3	(Ingot homogenized for 4 hours at 1400 °C under vacuum)
	{7.6}		

Since these data bring the old ghost of the inherent brittleness of chromium ferrites to rest, it is perhaps not too much to hope that the brittleness of other alloy ferrites that do not transform, such as Fe-Al, Fe-Ti, Fe-Mo and Fe-Tu, can be overcome. Here is a large and fruitful field of study for the experimental investigator.

#### Authors' Reply

Dr. Zapffe's discussion of Dr. Hochmann's work and the latter's written discussion in which he summarizes his Doctoral thesis are much appreciated. While the present work differs to some extent from Dr. Hochmann's as to the specific effects and limits of certain impurities in high chromium ferrites, it is in complete agreement in that the low toughness of ferritic alloys containing 20 to 30% chromium is not an inherent property of the iron-chromium solid solution, but rather due to the presence of small amounts of impurities.

Dr. Hochmann cites carbon, nitrogen, and oxygen as the principal impurities contributing to low toughness in 25% chromium ferrites. His data showing the effect of carbon agree well with those obtained during this investigation, although his indicated nitrogen tolerance is somewhat higher. We agree with the statement that melts made in magnesia crucibles are poorly deoxidized, but take exception to his contention that

oxygen above about 0.04% is detrimental to the toughness of chromium ferrites.

Fig. 10 shows the silicon-oxygen relationship for a number of vacuum-melted 25% chromium alloys made during this investigation. All these alloys were melted in magnesia crucibles and all possessed Izod impact strengths (notched) of the order of 100 foot-pounds at room temperature.

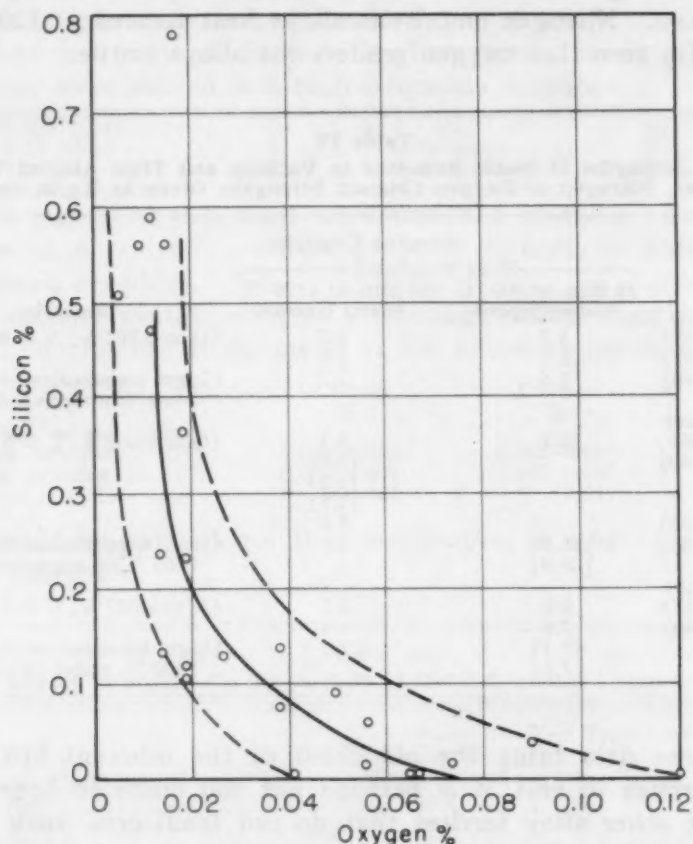


Fig. 10—Silicon-Oxygen Relationship for Vacuum-Melted 25% Chromium-Iron Alloys.

These data show that steels of high room temperature impact strength can be made with oxygen contents up to at least 0.12%. The discrepancy between Dr. Hochmann's and our data with respect to oxygen may be related to the mode of occurrence of oxygen in the alloys rather than to the total oxygen content.

While oxygen does not appear to have a significant effect on the room temperature toughness of the alloys, it could have an embrittling influence with respect to their subzero temperature properties. In Table V, the impact toughness of several 25% chromium alloys containing up to 0.028% total carbon and nitrogen is shown as a function of their oxygen contents. All the alloys shown here were vacuum-melted in a magnesia crucible using electrolytic chromium and iron with small amounts of silicon added to control the oxygen content. The impact specimens were water-quenched from 900 °C (1650 °F). These data indicate that variations in oxygen content up to 0.12% have no influence on

Table V  
Subzero Toughness of 25% Chromium Alloy Ferrites

Heat No.	Per Cent					Izod Impact Strength—Foot-Pounds—				
	O	Si	C	N	Total C + N	R. T.	—50	—75	—100	—125
L-763	0.016	0.78	0.005	0.003	0.008	112	119	...	119	8
K-726	0.021	0.40*	0.005	0.002	0.007	106	...	...	53	...
L-672	0.028	0.13	0.008	0.001	0.009	101	106	110	110	112
K-490	0.038	0.14	0.014	0.002	0.016	100	100	...	100	13
K-480	0.041	Trace	0.014	0.003	0.017	100	100	...	100	10
K-721	0.055	0.02	0.009	0.003	0.012	97	106	...	113	...
L-671	0.056	0.06	0.010	0.003	0.013	96	98	104	109	13
K-239	0.066	Trace	0.010	0.002	0.012	96	100	108	51	...
L-761	0.09	0.05	0.007	0.005	0.012	93	100	109	107	6
L-683	0.12	0.01	0.012	0.016	0.028	92	...	102	20	9

\*Approximate.

the room temperature toughness of the alloys and that there is also no correlation with respect to subzero impact values.

Dr. Hochmann's data tend to show that higher temperature heat treatments have a greater embrittling effect than the 900 °C (1650 °F) water quench used on all our higher chromium alloys. Impact tests were recently made on several 25% chromium alloys that were quenched from a 30-minute heat treatment at 1200 °C (2190 °F), and the results are shown in Table VI, along with the data for the same alloys quenched from 900 °C (1650 °F).

Table VI  
Effect of Annealing Temperature on Toughness of 25% Chromium Alloy Ferrites

Heat No.	Composition, %				Room Temperature	
	O	Si	C	N	Izod Impact Strength—Ft.-lb.*—	900 °C Quench 1200 °C Quench
L-763	0.016	0.78	0.005	0.003	112	115
L-781	0.017	0.36	0.007	0.003	98	107
L-672	0.028	0.13	0.008	0.001	101	105
P-171	0.049	0.09	0.006	0.003	100	100
K-721	0.055	0.02	0.009	0.003	97	102
L-671	0.056	0.06	0.010	0.003	96	103
K-525	0.072	0.02	0.018	0.003	98	100
L-761	0.090	0.05	0.007	0.005	91	94
L-683	0.120	0.01	0.012	0.016	92	94

\*Double-notched specimens—average of two breaks.

These data do not indicate any difference in toughness between alloys quenched from 900 and 1200 °C (1650 and 2190 °F). Even the alloy tested with the highest oxygen content has a toughness akin to that of the best austenitic grades of stainless steel.

In reply to Dr. Nicholson's discussion, the high-purity 25% chromium alloys are susceptible to loss of toughness when heated at temperatures below 900 °C (1650 °F). In this respect, they are like normal air-melted steels; however, the loss of toughness occurs at a much slower rate. No systematic study of the effect of silicon on the rate of toughness loss has been made, but it has been observed that higher silicon contents increase the rate of loss in high-purity alloys, just as in normal air-melted steels.



## RHEOTROPIC EMBRITTLEMENT OF STEEL

By E. J. RIPLING AND W. M. BALDWIN, JR.

### Abstract

*The term "rheotropic embrittlement" was introduced to describe a type of brittleness under severe service conditions which can be overcome by cold working under mild service conditions.*

*A large part of the low temperature ductility deficiency of SAE 1340 when furnace-cooled as well as when quenched and tempered in the vicinity of 600 °F was found to be rheotropic. The low notched ductility of SAE 1340 at high strength levels was also shown to be a result of this type of brittleness.*

*Rheotropic embrittlement was found to account for the dangerously high transition temperature in both heat treated SAE 1340 and annealed steels.*

*The condition which causes this type of brittleness was shown to be either not cumulative under low temperature straining, or else cumulative but readily washed out by room temperature deformation.*

IN an effort to aid in unraveling the mysteries surrounding the mechanical behavior of metals, a number of investigations have been carried out wherein metals are first deformed under one set of physical conditions and then further deformed to failure (or tested) under another set of physical conditions. One of the more popular experiments of this type has consisted in stretching a tensile specimen an arbitrary amount at room temperature—the deformation so effected being usually termed a prestrain—and then continuing the stretching to failure (or testing) after the specimen has been cooled to a lower temperature.

Data obtained on tests of this kind are generally represented by plotting the ductility<sup>1</sup> retained at the low temperature as an ordinate

<sup>1</sup>The ductility value that is most convenient for this work is the maximum natural strain ( $\epsilon_1$ ) where this quantity is defined as:

$$\epsilon_1 = \ln \frac{\text{original area}}{\text{final area}}$$

This investigation is one in a series in a research program conducted at the Metals Research Laboratory, Department of Metallurgical Engineering, Case Institute of Technology, Cleveland, in cooperation with the Office of Naval Research, U. S. Navy.

A paper presented before the Thirty-second Annual Convention of the Society, held in Chicago, October 21 to 27, 1950. Of the authors, E. J. Ripling is research associate and W. M. Baldwin, Jr., is research professor, Metals Research Laboratory, Department of Metallurgical Engineering, Case Institute of Technology, Cleveland. Manuscript received March 7, 1950.

against the prestrain as an abscissa. The data resulting from these tests when so plotted have so far revealed two basic types of behavior. The first type is characterized by a smooth curve joining a point on the ordinate axis with one on the abscissa axis. The point on the ordinate axis is represented by the ductility of the metal at the low temperature ( $\epsilon_B$ ) when no prestrain has been effected while

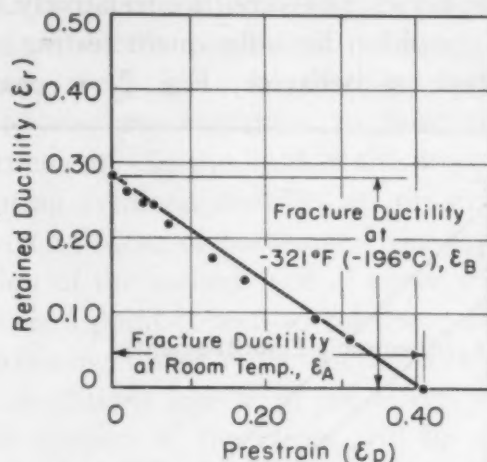


Fig. 1—Simplest Relationship Between Retained Ductility and Prestrain Obtained by Prestraining the Aluminum Alloy 24S-T4 at Room Temperature Followed by Testing at  $-321^{\circ}\text{F}$  ( $-196^{\circ}\text{C}$ ) [Liu (1)].

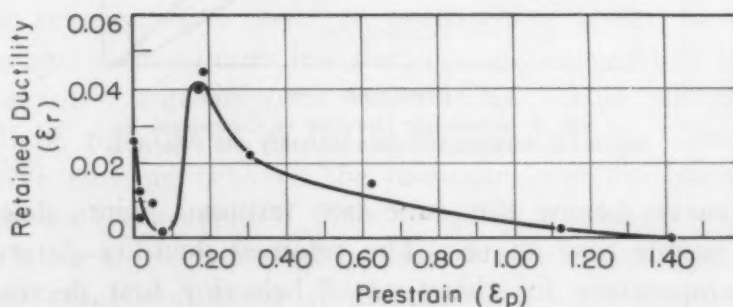


Fig. 2—Compound Relationship Between Retained Ductility and Prestrain Obtained by Prestraining an Annealed 2.75% Silicon Steel at Room Temperature Followed by Testing at  $-321^{\circ}\text{F}$  ( $-196^{\circ}\text{C}$ ) [Ripling and Sachs (5)].

the point on the abscissa axis is represented by the ductility of the metal at room temperature when prestraining by tension has been carried to the extreme limit of fracture ( $\epsilon_A$ ). This type of curve is illustrated in Fig. 1 and is the prototype for the aluminum alloy 24S-T4 (1)<sup>2</sup> and for a steel heat treated by quenching to a martensitic condition and tempering at a rather high temperature (2).

This simple relationship between prestrain and retained ductility is expected to be the general behavior for deformations in which

<sup>2</sup>The figures appearing in parentheses pertain to the references appended to this paper.

prestraining has been conducted under a ductile condition, with the subsequent straining to failure being performed under a less ductile condition. Thus Bridgman (3) found both pearlitic and martensitic steels evidenced this type of curve when he substituted relatively high hydrostatic pressures for relatively high (room) temperatures as the more ductile condition in prestraining, and relatively low hydrostatic (atmospheric) pressures for relatively low temperatures as the less ductile condition for subsequent testing.

The second type of behavior, Fig. 2, is characterized by an

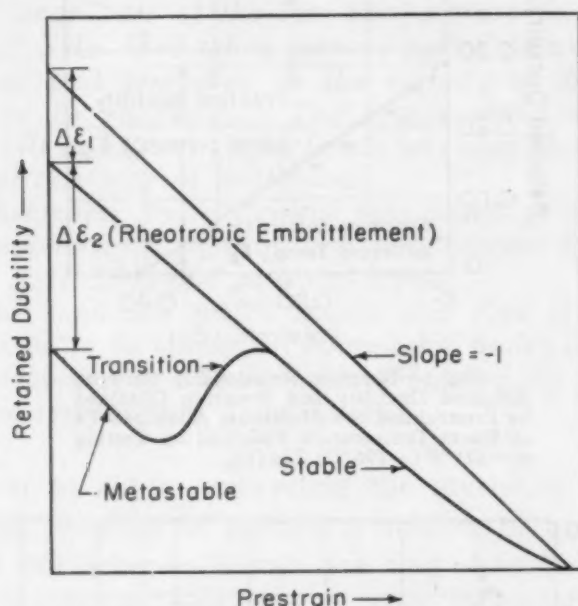


Fig. 3—Schematic Drawing of Compound Relationship Between Retained Ductility and Prestrain.

irregular curve joining the same two terminal points discussed in the more simple case above. The retained ductility determined at the low temperature for this type of behavior first decreases at a rather fast rate with increasing prestrain. The ductility then passes through a minimum, increases, and passes through a maximum before decreasing smoothly to the second terminal point. This type of trend curve is evidenced by a large number of annealed<sup>3</sup> steels when they are strained various amounts at room temperatures and subsequently tested to failure at a low temperature (4).

It is suggested here that curves of the first type represent the simplest reaction of a metal to prestraining under more ductile conditions and testing under less ductile conditions. The ordinate value (retained ductility at zero prestrain,  $\epsilon_B$ ) is less than the abscissa value (room temperature ductility,  $\epsilon_A$ ) by an amount

<sup>3</sup>Annealed steels, as used here, include all steels other than martensitic and bainitic steels.



$\Delta\epsilon_1 = \epsilon_A - \epsilon_B$ , but the relationship between these terminal points is quite simple. In the second case, it is hypothesized that the less ductile conditions serve not only to depress the terminal ordinate point in a simple manner ( $\Delta\epsilon_1$  of Fig. 3), but, in addition, engender some impediment within the metal which further reduces its ductility ( $\Delta\epsilon_2$ ). Over and above this, it is hypothesized that this impediment and the brittleness which it effects ( $\Delta\epsilon_2$ ) are removed by prestraining under more ductile conditions. Since the embrittlement under consideration ( $\Delta\epsilon_2$ ) is to be distinguished from embrittlement in general by its responsiveness to flow, it will be termed *rheotropic* embrittlement. In the light of this hypothesis, the second type of curve relating retained ductility to prestrain is seen to be compounded, in part at least, of portions of the first type of simpler curve. That portion of the second type of curve from the maximum to the terminal abscissa point is seen to represent the simple reaction of a metal to prestraining under more ductile conditions, and testing under less ductile conditions free from the effects of a superimposed impediment. This portion of the curve will be referred to as the stable branch of the curve and retained ductility values falling on the stable branch will be referred to as strain-stabilized ductility values. That portion of the second type of curve from the initial terminal ordinate point to the minimum is seen to represent the metastable reaction of a metal to prestraining under more ductile conditions and testing under less ductile conditions, while still under the burden of a superimposed impediment. This portion of the curve will be referred to as the metastable branch. That portion of the curve running between the minimum and maximum will be referred to as the transition branch. It is conceivable that rheotropic brittleness in some cases need evidence no metastability, whence the compound curve would show an immediate increase in retained ductility values with prestrain from the original terminus to the stable branch of the curve.

It will be noticed then that the proposition assumes that the low ductility of annealed steels at subzero temperatures is—in part, at least—rheotropic. It is seen further that the concept of transition temperature—those temperatures above which steels are relatively ductile, and below which they are relatively brittle—is part of this proposition because of the assumption that low temperature brittleness is in part rheotropic.

*Purpose of Present Investigation*—To investigate the conditions surrounding rheotropic embrittlement, it was felt that heat treated steels might be used, since these materials are more versatile than

annealed steels. By tempering a martensitic steel to different strength levels, it is possible to impart to a particular steel either a high ductility at both room temperature and at some low temperature, or a high room temperature ductility and a low ductility at the subzero temperature. Furthermore, if the abnormally low ductility of annealed steels at subzero temperatures is partly rheotropic, it would be interesting to compare the behavior of this pearlitic material with a martensitic steel which becomes brittle at low

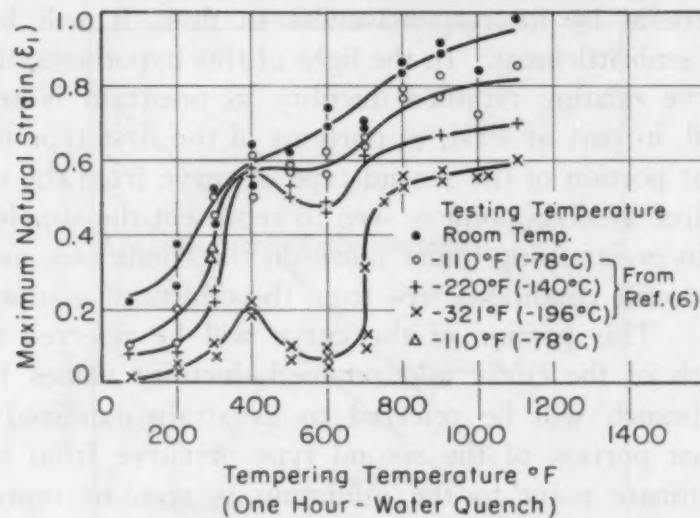


Fig. 4—Effect of Tempering Temperature on the Ductility of Quenched and Tempered SAE 1340 Steel at Various Testing Temperatures.

temperatures. This comparison would be most valid if the same steel were used in both the heat treated and annealed condition so that the microstructure could be varied while the chemistry of the steel was kept constant.

Data recently presented on the low temperature properties of quenched and tempered SAE 1340 indicate that this alloy might be satisfactory for this investigation, Fig. 4 (6). Unnotched tensile tests made on this steel as oil-quenched from 1525 °F (830 °C), and tempered for 1 hour over a temperature range of room temperature to 1100 °F (595 °C) revealed virtually a smooth relationship between ductility at fracture and tempering temperature for tests conducted at room temperature. This smooth relationship, however, was marred when the tensile tests were conducted at lower temperatures, in that specimens tempered in the temperature range between 400 and 750 °F (205 and 400 °C) exhibited an abnormally low ductility. The ductility within this tempering range was found to be only a fraction of the value that would have been expected by

interpolating a curve from the data obtained on specimens which were tempered at higher and lower temperatures.

The present research to investigate rheotropic embrittlement was, therefore, carried out by prestraining a series of SAE 1340 specimens (in both the quenched and tempered condition and the annealed condition) by various amounts at room temperature, and then testing these prestrained specimens to failure at the temperature of boiling nitrogen ( $-321^{\circ}\text{F}$  or  $-196^{\circ}\text{C}$ ). Other specimens were also tested under the reversed conditions of straining, that is, prestraining at the low temperature with subsequent testing at room temperature. A few other test pieces were also prestrained by drawing through a die at room temperature and then testing this cold-worked steel at  $-321^{\circ}\text{F}$  ( $-196^{\circ}\text{C}$ ). In still another series of tests, the specimens were prestrained in simple tension at room temperature and then tested in a notched condition to failure, again at room temperature.

#### RESULTS AND DISCUSSION

The heat treating and testing procedures used in this investigation are described in detail in the Appendix.

*Heat Treated Steels*—Test specimens which were quenched and then tempered at various temperatures between 300 and 1100  $^{\circ}\text{F}$  were prestrained at room temperature and subsequently tested at  $-321^{\circ}\text{F}$  ( $-196^{\circ}\text{C}$ ). The results of these tests with retained ductility plotted as a function of the prestrain are shown in Fig. 5. The shape of these curves indicates that the manner in which tempered martensites deform at a low temperature depends upon the temperature at which material was tempered. Those specimens which were tempered at the high temperatures (800 and 1100  $^{\circ}\text{F}$ ) yielded relations of the first type; that is, they showed no evidence of rheotropic embrittlement. This behavior is similar to that typified by the aluminum alloy 24S-T4 (Fig. 1). At the lower tempering temperatures (400 to 700  $^{\circ}\text{F}$ ), however, the retained ductility as a function of prestrain varied in the more complex manner which was previously referred to as the second type, and typified by an annealed steel. For the material which was tempered at 500, 600, and 700  $^{\circ}\text{F}$ , it was possible to obtain retained ductility data for prestrains all the way from zero prestrain to a prestrain value close to the fracture ductility. Consequently, it was possible to obtain the metastable, transition, and stable branches of these curves. Specimens which were tempered at the two lowest temperatures (300 and 400  $^{\circ}\text{F}$ ) strained so rapidly at room temperature after



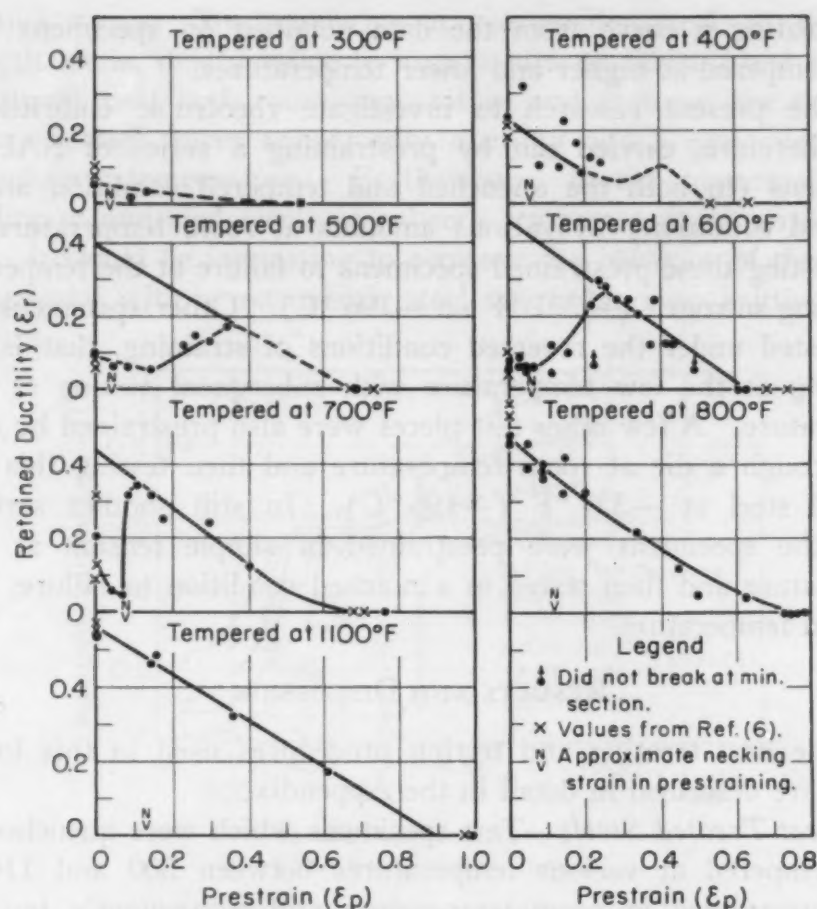


Fig. 5—Effect of Tempering Temperature and Prestraining at Room Temperature on the Retained Ductility of Martensitic SAE 1340 Steel at  $-321^{\circ}\text{F}$  ( $-196^{\circ}\text{C}$ ).

the necking strain was exceeded, that it was not possible to obtain prestrain values close to the room temperature ductility without causing specimen breakage. However, large enough sections of the stable curves for the steel tempered at 500, 600 and 700  $^{\circ}\text{F}$  (260, 315 and 370  $^{\circ}\text{C}$ ) were obtained to make it possible to extrapolate this branch of the curves back to a prestrain of zero. This type of extrapolation will be referred to as extrapolation Type A.<sup>4</sup> The ordinate values obtained by these extrapolations are the ductility values that these tempered products would possess if the material were free from any rheotropic impediment. These extrapolated values, when plotted as a function of tempering temperature, fall along a curve that would represent a natural extension of the ductility values obtained at the high tempering temperatures, as shown in Fig. 6. This suggests that an alternate way to determine the ductility values that these tempered products would possess in

<sup>4</sup>Since a large number of extrapolations will be used in the remainder of this discussion, it will be convenient to label them.

the absence of any rheotropic impediment would be an extrapolation of the ductility values obtained at the high tempering temperatures to those at lower tempering temperatures. Such an extrapolation will be referred to as extrapolation Type B. The horizontal component of the length of the metastable branch, and the slope of the transition branch, Fig. 5, indicate in a qualitative way how far the

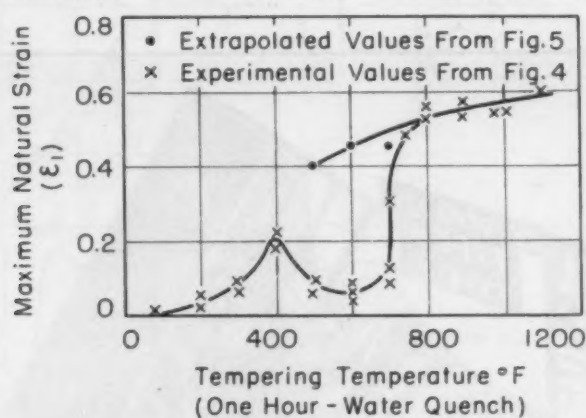


Fig. 6—Low Temperature Ductility of Martensitic SAE 1340 in the Absence of Disturbing Condition That Causes 600°F Embrittlement.

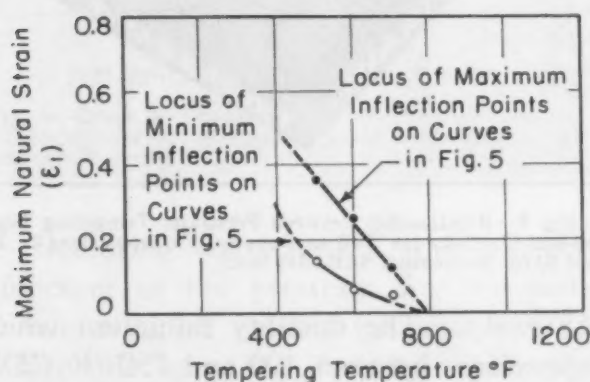


Fig. 7—Relationship Between Maxima and Minima and Tempering Temperature for Retained Ductility-Prestrain Curves.

steel is from a strain-stabilized condition at any tempering temperature. As the tempering temperature was increased, the room temperature prestrain necessary to effect a stable behavior at the low temperature became less, until at a tempering temperature of 800°F (425°C), the material which was given a prestrain of zero was stable, as shown in Fig. 7.

The inter-relationship between the various points discussed above is integrated into the three-dimensional plot in Fig. 8 with tempering temperature, prestrain, and retained ductility as the axes.

The limiting prestrain possible at room temperature is determined by the fracture strain at room temperature as a function of the tempering temperature (see Fig. 4). This curve then is the base of the diagram in Fig. 8. The right-hand wall of the model is the retained ductility as a function of prestrain for the material tempered at 1100 °F (595 °C) (Fig. 5), while the other wall represents the low temperature ductility as a function of tempering

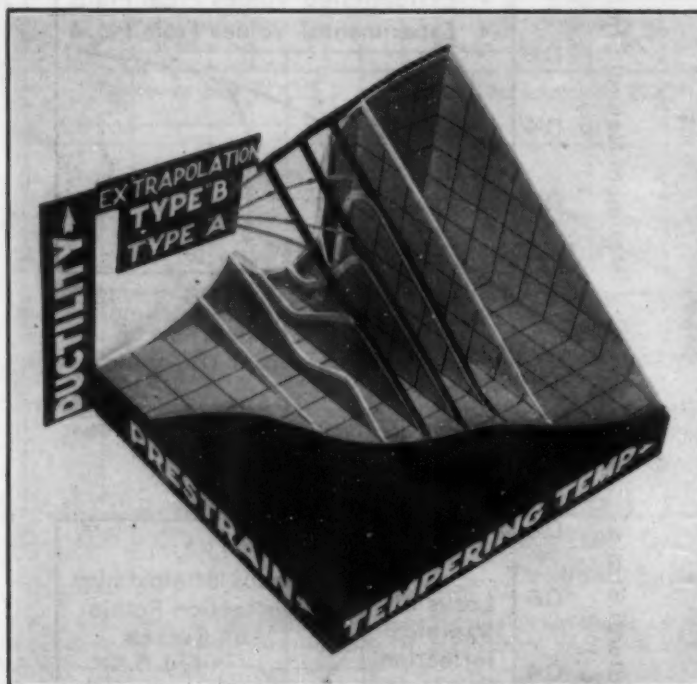


Fig. 8—Relationship Between Prestrain, Tempering Temperature and Ductility (as Well as Between Extrapolations of Types A and B) for Martensitic SAE 1340 Steel.

temperature (Fig. 4). The ductility minimum which occurred at tempering temperatures between 400 and 750 °F (205 and 400 °C) for the material which was not prestrained is found to move into the diagram on the horizontal plane and at a slight angle to the prestrain axis. This was shown in Fig. 7 by the movement of the curve minima to higher prestrains as the tempering temperature was reduced while the transition branches of the curves became less steep. It should be noted that the valley shown in Fig. 8 does not affect the steel when it is tempered at temperatures of 300 °F (150 °C) or less, since the depression would intersect the 300 °F tempering temperature plane at a prestrain greater than the room temperature ductility of the steel at that tempering temperature. The relationship between extrapolations of Types A and B are also shown in Fig. 8.



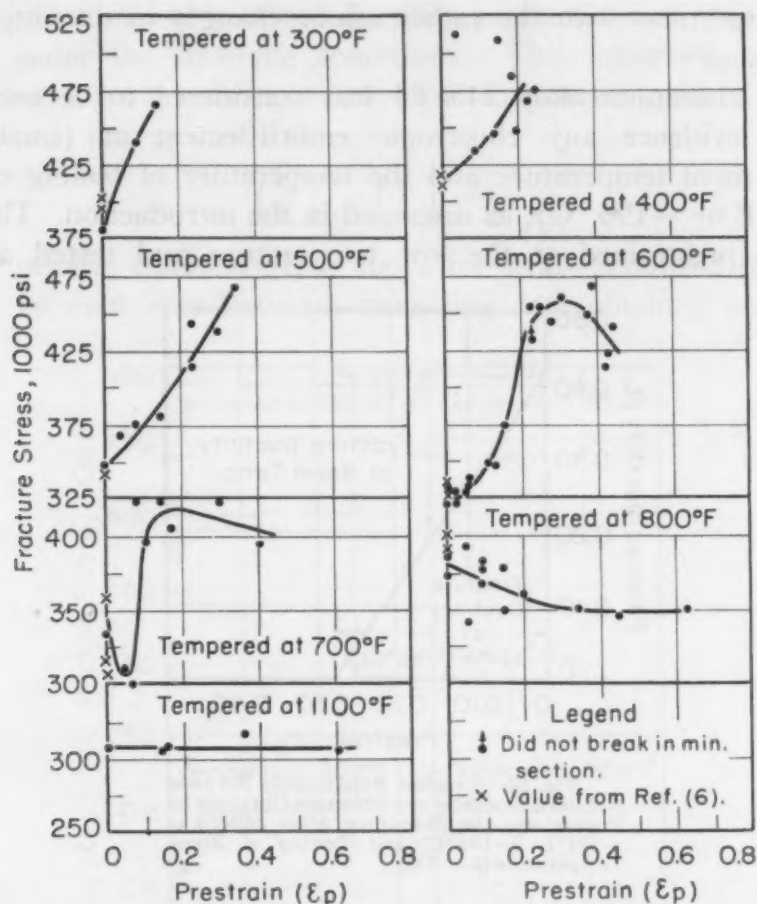


Fig. 9—Effect of Tempering Temperature and Prestraining at Room Temperature on the Fracture Stress of Martensitic SAE 1340 Steel at  $-321^{\circ}\text{F}$  ( $-196^{\circ}\text{C}$ ).

The other fracturing characteristic, the fracture stress,<sup>5</sup> was plotted as a function of the prestrain for the material after oil quenching and tempering at various temperatures (Fig. 9). The fracture stress depends upon the ductility of the steel as well as on the yield strength and strain hardening rate. Consequently, the maxima and minima in the retained ductility—prestrain curves of Fig. 5 could become evident only in the fracture stress—prestrain curve when the ductility varied greatly over the range of prestrains investigated, since it was necessary for the changes in ductility to overshadow the changes in yield strength and strain hardening rate. These ductility changes were large enough to show maxima and minima only for the material tempered at 600 and 700 °F (315 and 370 °C). At the lower tempering temperatures, the strain hardening rate must have been quite high to account for the rapid increase

<sup>5</sup>The fracture stress is defined as the breaking load divided by the cross sectional area of the broken specimen at the fracture.

in fracture stress with the rather minor changes in ductility shown in Fig. 5.

The aluminum alloy 24S-T4 was considered to be one which did not evidence any rheotropic embrittlement at temperatures between room temperature and the temperature of boiling nitrogen ( $-321^{\circ}\text{F}$  or  $-196^{\circ}\text{C}$ ), as discussed in the introduction. This alloy was also prestrained at the low temperature and tested at room

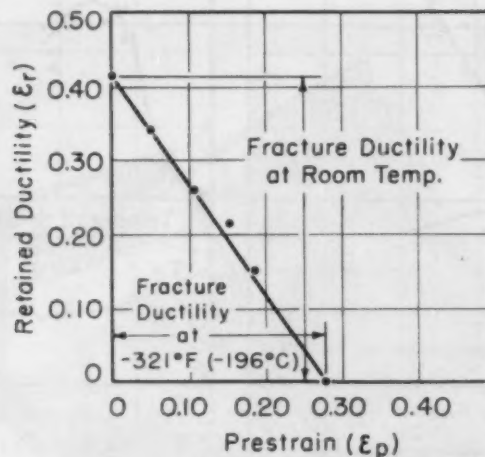


Fig. 10—Simplest Relationship Between Retained Ductility and Prestrain Obtained by Prestraining the Aluminum Alloy 24S-T4 at  $-321^{\circ}\text{F}$  ( $-196^{\circ}\text{C}$ ) and Testing at Room Temperature [Liu (1)].

temperature by Liu (1), to obtain the relationship between prestrain and retained ductility shown in Fig. 10. It can be seen here that reversing the prestraining and testing temperatures produces a curve whose abscissa and ordinate values were reversed from Fig. 1. This curve shown in Fig. 10 is considered to be the behavior characteristic of materials free from rheotropic embrittlement where the prestraining conditions produced a lower ductility than the testing conditions. This behavior may be described by stating that straining a metal at one temperature will decrease the ductility of the metal at the other temperature by an amount that is proportional to the ratio of the ductilities of the metal under two conditions of straining. That is:

$$\epsilon_r = \frac{\epsilon_B}{\epsilon_A} (\epsilon_A - \epsilon_p)$$

where:  $\epsilon_r$  = retained ductility in the second straining operation  
 $\epsilon_A$  = fracture ductility at the temperature of first strain  
 $\epsilon_B$  = fracture ductility at the temperature of second strain  
 $\epsilon_p$  = prestrain.

This equation might also be written in the form  $\epsilon_p/\epsilon_A + \epsilon_r/\epsilon_B = 1$ . This has the advantage that the components of the equation repre-

sent the prestrain and retained ductility as fractions of the fracture ductility under the straining conditions. This latter equation can also be put into a more general form for curves which are not straight lines, i.e.,

$$\left(\frac{\epsilon_p}{\epsilon_A}\right)^m + \left(\frac{\epsilon_r}{\epsilon_B}\right)^n = 1$$

The general equation given above for strain-stabilized behaviors can now be used as a basis for analyzing data obtained under any

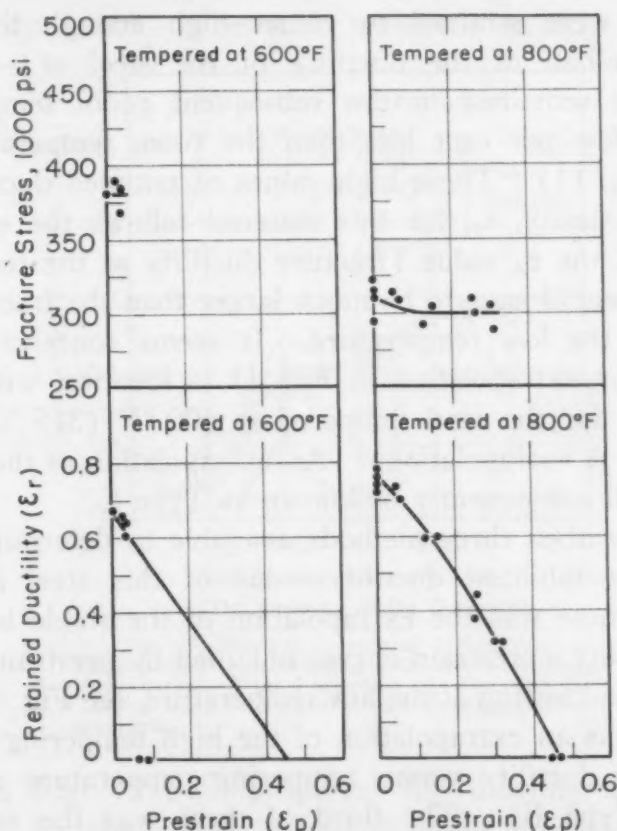


Fig. 11—Effect of Tempering Temperature and Prestraining at  $-321^{\circ}\text{F}$  ( $-196^{\circ}\text{C}$ ) on the Fracturing Characteristics of Martensitic SAE 1340 Steel at Room Temperature.

condition of prestraining. It is found to be particularly helpful in discussing prestraining at the low temperature ( $-321^{\circ}\text{F}$  or  $-196^{\circ}\text{C}$ ) and testing at room temperature.

Specimens of SAE 1340 were quenched and tempered at 600 and  $800^{\circ}\text{F}$  ( $315$  and  $425^{\circ}\text{C}$ ) and then subjected to this reversed condition of straining in the hope of obtaining additional information about the impediment which caused rheotropic embrittlement at low temperatures. The retained ductility and fracture stress obtained on these specimens are plotted as a function of the prestrain in



Fig. 11. The retained ductility-prestrain curve for the steel tempered at 800 °F showed a behavior similar to that which would be expected from the above equation excepting that it was slightly concave downward. It should also be mentioned that under the conditions of straining, shown in Fig. 5, the data obtained on this material showed a slight upward concavity.

Only very small prestrains could be investigated for the material tempered at 600 °F because of the low ductility of this material at -321 °F (-196 °C). However, when specimens tempered at this temperature were strained to values high enough to exhaust as much as one-half of the ductility of the steel at -321 °F, the ductility that remained in the subsequent room temperature test was only a few per cent less than the room temperature fracture ductility (Fig. 11). These high values of retained ductility indicate that if the quantity,  $\epsilon_r$ , for this material follows the equation suggested above, the  $\epsilon_A$  value (fracture ductility at the temperature of first strain) would have to be much larger than the fracture ductility measured at the low temperature. It seems conceivable that this  $\epsilon_A$  obtained by extrapolation in Fig. 11 is identical with the extrapolated value for the steel tempered at 600 °F (315 °C) shown in Fig. 5 (Type A extrapolation). An extrapolation of the type shown in Fig. 11 will subsequently be known as Type C.

There are then three methods available to determine the hypothetical strain-stabilized ductility value of this steel at -321 °F. The first of these was the extrapolation of the stable branch of the retained ductility-prestrain curves obtained by prestraining at room temperature and testing at the low temperature, see Fig. 5 (Type A). The second was an extrapolation of the high tempering temperature branch of the ductility versus tempering temperature curve shown in Fig. 4 (Type B). The third of these was the very doubtful extrapolation shown in Fig. 11 of the retained ductility-prestrain curve obtained by prestraining at -321 °F and testing at room temperature (Type C).<sup>6</sup> All three of these extrapolations indicate that the ductility of SAE 1340 tempered at 600 °F (315 °C) when tested at -321 °F (-196 °C) in the absence of the rheotropic impediment should be approximately  $\epsilon_1 = 0.45$ .

The high values of ductility retained at room temperature obtained on this steel after it had been tempered at 600 °F and prestrained at -321 °F give an indication of the nature of the impediment that causes brittle behaviors in this material at low

<sup>6</sup>Although the data in Fig. 11 are limited to such a narrow range of prestraining as to make the accuracy and validity of the Type C extrapolation highly doubtful in that particular case, it will be seen below that in those cases where the data are more extensive, the extrapolation is quite legitimate.

temperatures. The factor that causes rheotropic embrittlement either (a) does not build up gradually with low temperature straining, but affects the fracturing behavior suddenly at a particular strain, or (b) if the condition is built up during the low temperature straining, the condition is rapidly washed out by room temperature straining.

The effect of testing temperature on the material which was tempered at temperatures of 800 °F (425 °C) and higher was such that the curves in Fig. 4 could be related to each other by a proportionality factor. The data presented in Fig. 4 have been

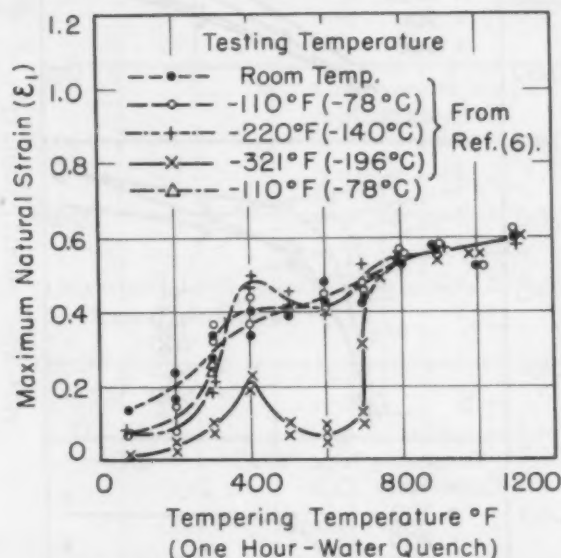


Fig. 12—Effect of Tempering Temperature on the Ductility of Martensitic SAE 1340 at Various Temperatures After Correcting the Ductility for Testing Temperature at the High Tempering Temperatures.

replotted in Fig. 12 by multiplying the ductility at each testing temperature by the proper proportionality constant so that the curves became coincident at the higher tempering temperatures. It can then be seen that in addition to the low temperature ductility deficiency that exists at tempering temperatures between 400 and 700 °F (205 and 370 °C), the ductility at tempering temperatures less than 400 °F is lower at the subzero testing temperatures than would be expected from the proportionality correction. Consequently, at these low tempering temperatures a second disturbing factor may be causing an abnormally low ductility at subzero temperatures. It is not known at present whether this disturbing influence is metastable or not. Nor, as a matter of fact, can one be sure that a proportionality type of correction for testing temperatures is proper over this entire range of tempering temperatures.

The high ductility of this steel when tempered at 400 °F and tested at -321 °F then results from the fact that this tempering temperature lies between the tempering temperatures at which the two embrittling effects are most active. If either or both of these embrittling conditions were effective over a wider tempering range, or if the tempering temperature at which they were most active were moved closer to 400 °F, the peak in ductility at a tempering

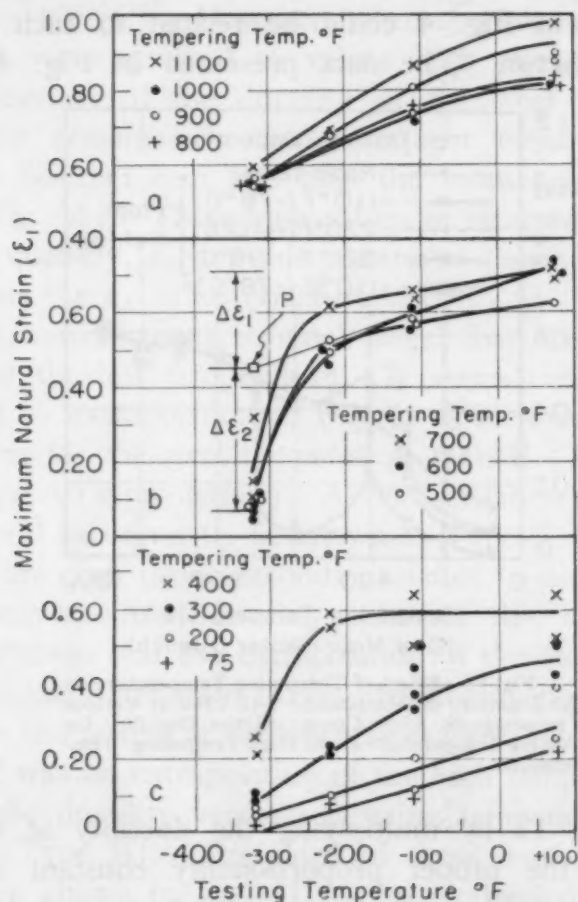


Fig. 13—Effect of Testing Temperature on the Low Temperature Ductility of SAE 1340 Steel Tempered Between Room Temperature and 1100 °F [Ripling (6)].

temperature of 400 °F would not exist. Many steels do not show this ductility peak at low tempering temperatures, according to W. F. Brown, Jr. (7).

*Rheotropic Embrittlement and Transition Temperature*—The ductility—testing temperature curves for SAE 1340 steel reported in a previous investigation (6) are replotted in terms of natural strain in Fig. 13. Those steels, tempered at 400, 500, 600 and 700 °F, are seen to evidence dangerously high transition tempera-



tures.<sup>7</sup> The hypothetical value of ductility free from rheotropic embrittlement for the steel tempered at 600 °F as evaluated by extrapolations of Types A, B and C is entered in Fig. 13b at point "P". It is seen that this value falls on a natural extension of the relatively high ductility values obtained at the higher testing temperatures and indicates that the high transition temperature is due to rheotropic embrittlement. The relatively slight embrittlement,  $\Delta\epsilon_1$  in Fig. 13b, represents the simple depression of ductility with lowered testing temperature, whereas the relatively large embrittlement,  $\Delta\epsilon_2$  in Fig. 13b, represents the additional embrittlement effected by the rheotropic impediment.

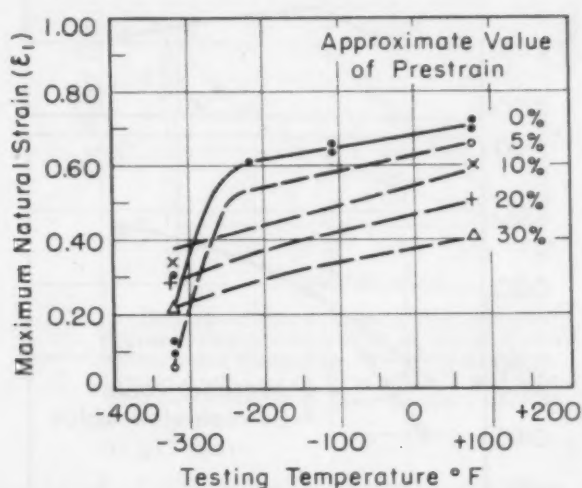


Fig. 14—Effect of Testing Temperature and Prestraining at Room Temperature on the Ductility of SAE 1340 Quenched and Tempered at 700 °F.

It is not as yet known whether the large fraction of the ductility deficiency at low temperatures ( $\Delta\epsilon_2$  in Fig. 13b), caused by the rheotropic embrittlement, can be readily overcome by some simple treatment. On the other hand, since small amounts of cold work (prestrain) increase the ductility of steel and eliminate the dangerously high transition temperature, there may be some practical applications for using strain as a method of overcoming the rheotropic impediment. The data shown in Fig. 5 for SAE 1340 tempered at 700 °F are replotted in Fig. 14 with prestrain as the parameter. Prestretching about 10% or more appeared to eliminate the transition temperature effects within this testing temperature range.

<sup>7</sup>Although these transition temperatures are reasonably low, it must be realized that a more severe stress condition (such as the presence of a notch) would raise these values above room temperature. Actually, it had been reported that a transition temperature also existed in this testing temperature range for the quenched steel when it was tempered at 300 °F. Additional data obtained at this tempering temperature indicate that this conclusion was not correct (see Fig. 4).

The fact that point "P" falls on an extension of the high ductility branch of the curve in Fig. 13b suggests another alternate method of extrapolation to determine hypothetical ductility values for materials free from rheotropic embrittlement. An extension of the high ductility branch of a ductility-testing temperature curve to lower temperatures as shown in Fig. 13b will subsequently be referred to as a Type D extrapolation.

Although the curves shown in Fig. 13a show no transition

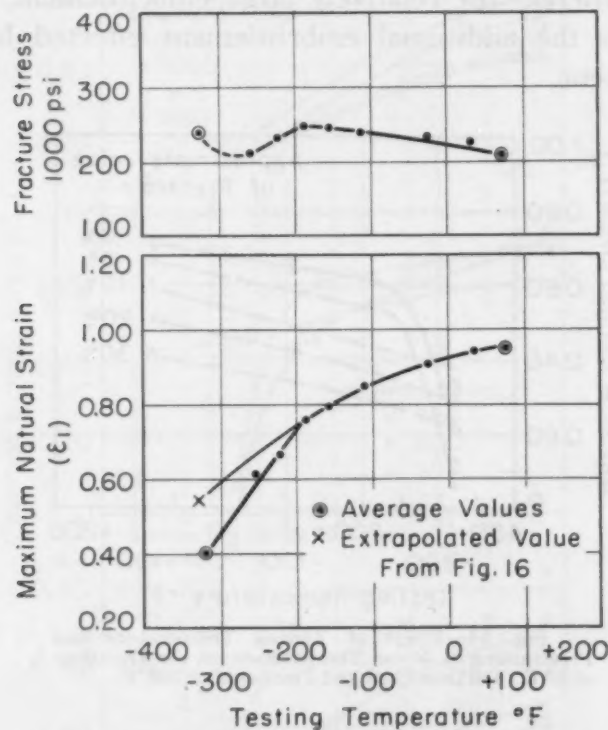


Fig. 15—Fracturing Characteristics of Annealed (Furnace-Cooled) SAE 1340 Steel as a Function of Testing Temperature.

temperature, it must be remembered that the simple unnotched tensile test imposes quite mild test conditions and that a transition temperature at temperatures lower than that reported is not improbable. Indeed, Baeyertz, Craig and Sheehan (8) using a more severe criterion—a V-notch Charpy test—report transition temperatures of approximately  $-100^{\circ}\text{F}$  ( $-75^{\circ}\text{C}$ ) for SAE 1340 steels tempered at 800 to 1100  $^{\circ}\text{F}$  (425 to 595  $^{\circ}\text{C}$ ) as compared with transition temperatures of approximately  $+150^{\circ}\text{F}$  ( $+65^{\circ}\text{C}$ ) for the same steels tempered in the range of 600  $^{\circ}\text{F}$ . It is felt that while rheotropic embrittlement will account for the dangerously high transition temperatures of steels tempered in the range of 600  $^{\circ}\text{F}$ , it might not affect the transition temperature of steels tempered at 800  $^{\circ}\text{F}$  and higher.

These remarks need not be confined to heat treated steels alone, but may be applied to annealed steels as well, since, as has been developed above, they likewise exhibit rheotropic brittleness at low temperatures and not at high temperatures.

*Annealed Steels*—To investigate the influence of rheotropic brittleness on the transition temperature behavior of annealed steels, pieces of SAE 1340 were heated to 1675 °F (915 °C) and furnace-

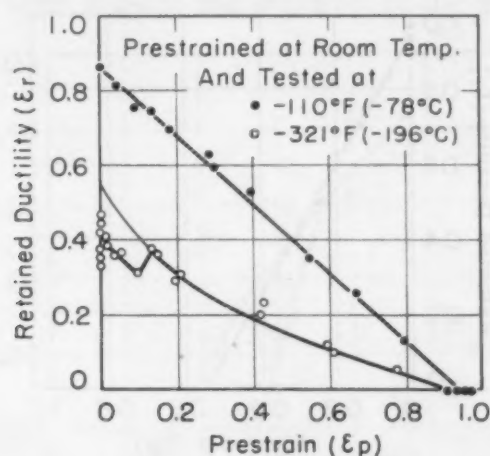


Fig. 16—Effect of Prestraining Annealed (Furnace-Cooled) SAE 1340 at Room Temperature and Testing at One Stable Straining Temperature (−110°F or −78°C) and One Metastable Straining Temperature (−321°F or −196°C).

cooled. Specimens of this pearlitic steel were then tested at temperatures between room temperature and −321 °F (−196 °C). The fracture stress and fracture ductility as a function of the testing temperature for the annealed material are shown in Fig. 15.<sup>8</sup>

It can be seen that both of these fracturing characteristic curves show a break at a testing temperature of about −190 °F (−123 °C). In view of the behavior of heat treated steels, it is expected that the metal would be rheotropically embrittled below −190 °F and not above. Convenient testing temperatures above and below this critical temperature of −190 °F were −110 °F (dry ice in isopentane) and −321 °F (boiling nitrogen). Retained ductility–prestrain curves for the furnace-cooled steel after prestraining at room temperature and testing at these two low temperatures are shown in Fig. 16. Straining at the higher temperature showed a stable behavior at all prestrains, while at the lower temperature a prestrain of approximately  $\epsilon_1 = 0.15$  was necessary to effect stable straining. The stable branch of the retained ductility–prestrain

<sup>8</sup>The increase in fracture stress at a testing temperature of −321 °F as compared to the value at −255 °F is due to a rapid increase in yield strength in this temperature range. This effect had been previously discussed in some detail (9).



curve for the material tested at  $-321^{\circ}\text{F}$  was again extrapolated to a prestrain of zero in order to determine the magnitude of the effect of the impediment at a testing temperature of  $-321^{\circ}\text{F}$ . The extrapolated value representing an impediment-free ductility at this temperature was then plotted in Fig. 15. This extrapolated point along with the experimental data points obtained at temperatures higher than  $-190^{\circ}\text{F}$  ( $-123^{\circ}\text{C}$ ) produce a curve which represents

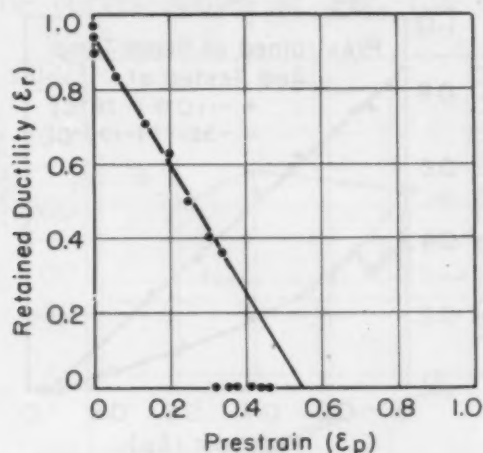


Fig. 17—Effect of Prestraining Annealed (Furnace-Cooled) SAE 1340 Steel at  $-321^{\circ}\text{F}$  on the Retained Ductility at Room Temperature.

the effect of testing temperature on ductility for furnace-cooled SAE 1340 in the absence of rheotropic embrittlement.

Although the furnace-cooled SAE 1340 showed rheotropic brittleness at  $-321^{\circ}\text{F}$ , the ductility of the material at this testing temperature was still quite high. Consequently, it was possible to check the extrapolation of Type D in Fig. 15 by prestraining this material at  $-321^{\circ}\text{F}$  ( $-196^{\circ}\text{C}$ ) and testing it at room temperature. The retained ductility-prestrain curve for this condition of straining is shown in Fig. 17. Since quite a long length of this curve could be obtained experimentally, and since the curve was a straight line, the extrapolation to the prestrain axis (Type C) was considered to be quite accurate. Here again (as was the case with martensitic steels) the extrapolated value, which should yield the maximum prestrain possible at the low temperature, was higher than the low temperature ductility of the metal. The extrapolated ductility (Type C) of  $\epsilon_1 = 0.55$  at  $-321^{\circ}\text{F}$  was in good agreement with the extrapolation of the Type A in Fig. 16. These more reliable data obtained on the furnace-cooled steels, prestrained at a low temperature and tested at room temperature, substantiate the description of the behavior of the rheotropic impediment, given above

in the discussion of martensitic steels. In other words, the source of the embrittlement is either not cumulative as low temperature straining progresses, or else the source is cumulative, but is readily washed out with room temperature straining.

The general proposition of rheotropic brittleness allows a fuller interpretation of the data previously presented on the low temperature properties of an annealed 2.75% silicon steel (5). The data presented for this steel include the ductility of the steel as a function

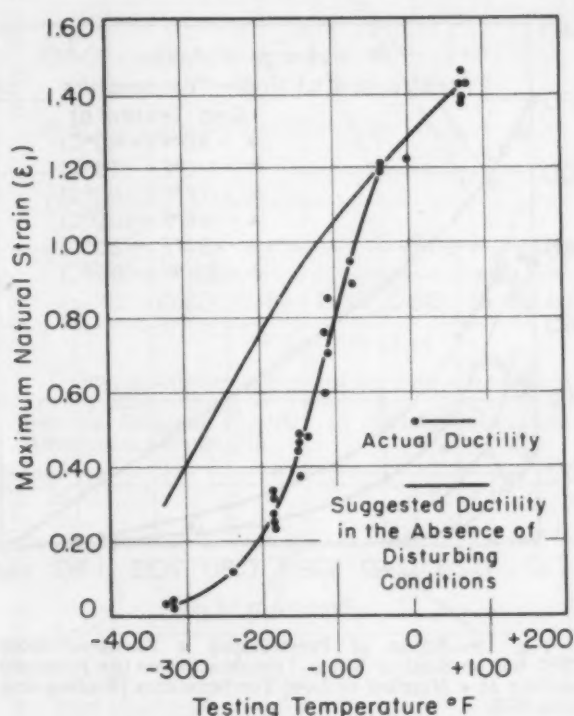


Fig. 18—Ductility of Annealed (Furnace-Cooled) 2.75% Silicon Steel as a Function of Testing Temperature [Ripling and Sachs (5)].

of testing temperature, Fig. 18, the retained ductility of the annealed material at a number of low temperatures as a function of room temperature prestrain, Fig. 19, as well as the retained ductility at room temperature as a function of the prestrain at a number of low temperatures, Fig. 20.

The shape of the retained ductility—prestrain curve, Fig. 19, obtained when the steel was prestrained at room temperature and tested at  $-40^\circ\text{F}$ , indicates that the steel behaves simply at this testing temperature. At all the testing temperatures lower than this, however, the steel at zero prestrain is subject to rheotropic brittleness. Furthermore, the very deep upward concavity in the lower temperature curves of Fig. 19 indicates that the extrapolated strain-stabilized values on the retained ductility axis for this steel would be

very high. No attempt to extrapolate these curves to a prestrain of zero was made, since the curves were too steep in the vicinity of the retained ductility maxima. Nevertheless, since the values extrapolated from the stable branch of the compound curves should be rather high over the range of testing temperatures investigated, it is suggested that the effect of testing temperature on the impediment-free ductility of this steel should be as shown in the upper curve of Fig. 18. This wide difference between the experi-

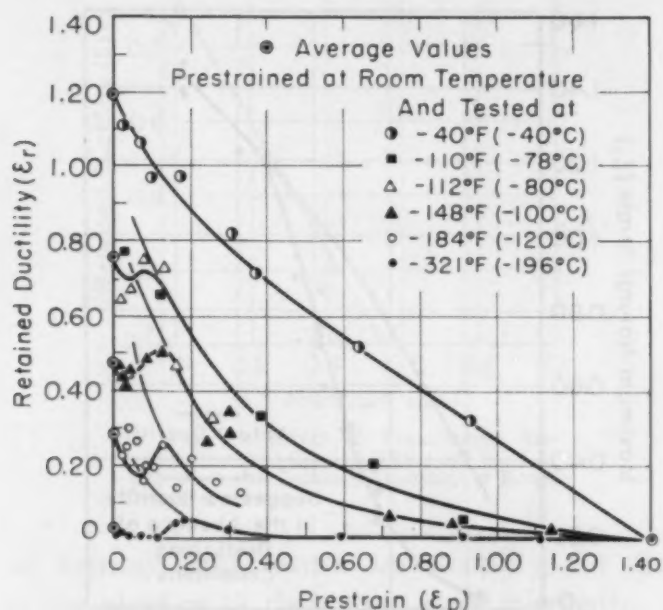


Fig. 19—Effect of Prestraining a Furnace-Cooled 2.75% Silicon Steel at Room Temperature on the Retained Ductility at a Number of Low Temperatures [Ripling and Sachs (5)].

mental curve and the extrapolated curve indicates that the impediment is highly effective in this steel.

Since the extrapolated values (Type A, Fig. 19) are high for testing temperatures down to  $-321^\circ\text{F} (-196^\circ\text{C})$ , it is now not surprising to find the ductility values in Fig. 20 to be also quite high.

It had been suggested previously that the complex shape of the retained ductility-prestrain curve for annealed steels which were prestretched at room temperature and tested at a low temperature might be related to the unique manner in which these materials yielded during a tensile strain (5). When these materials are stretched in simple tension, they exhibit a yield jog. The range of plastic strain over which this nonuniform flow exists is of the same order of magnitude as the range of prestrains corresponding to the metastable branch of the retained ductility-prestrain curve for these steels. It had been felt that the nonuniform deformation



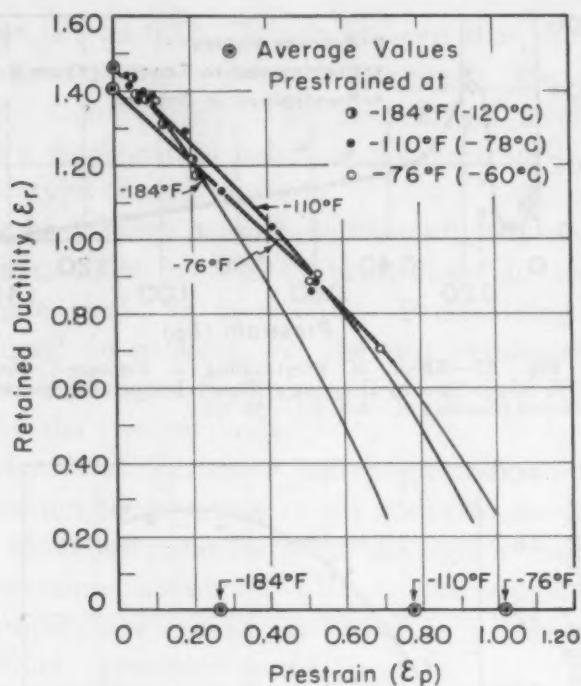


Fig. 20—Effect of Pretraining a Furnace-Cooled 2.75% Silicon Steel at Various Low Temperatures on the Retained Ductility at Room Temperature [Ripling and Sachs (5)].

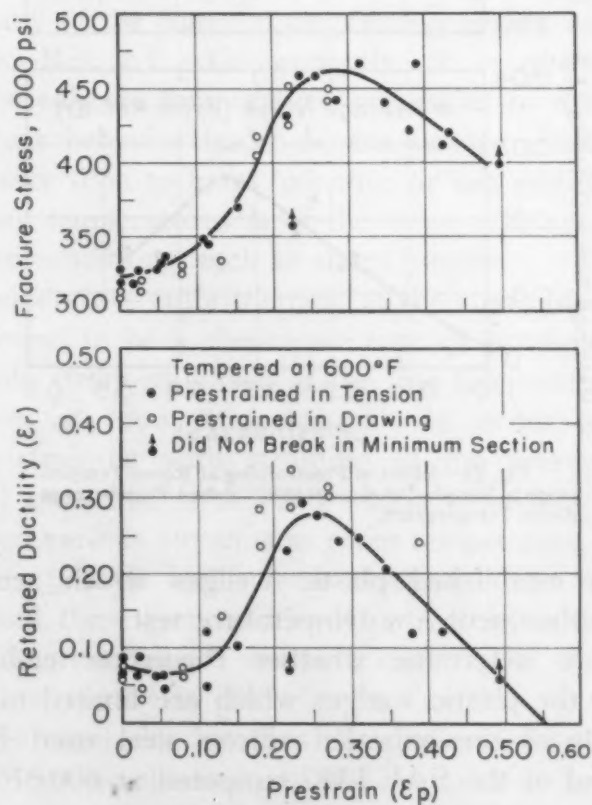


Fig. 21—Effect of Pretraining Martensitic SAE 1340 by Drawing at Room Temperature on the Fracturing Characteristics at -321°F (-196°C).

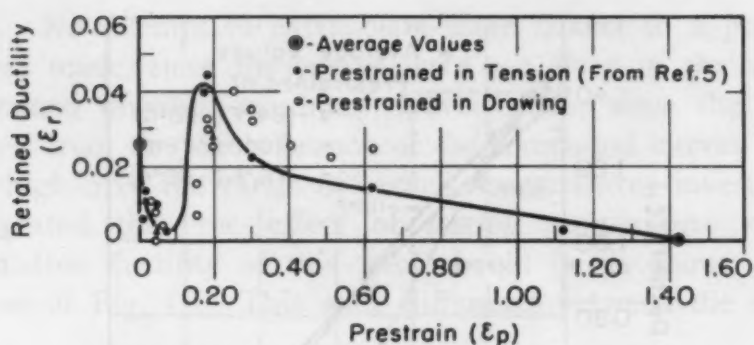


Fig. 22—Effect of Prestraining a Furnace-Cooled 2.75% Silicon Steel by Drawing at Room Temperature on the Retained Ductility at  $-321^\circ\text{F}$  ( $-196^\circ\text{C}$ ).

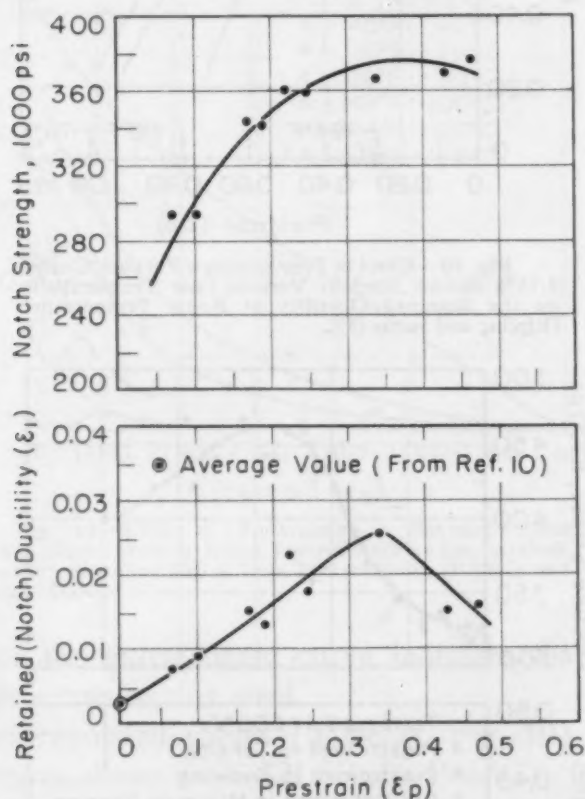


Fig. 23—Effect of Prestraining at Room Temperature in Simple Tension on the Notched Properties at Room Temperature.

in prestraining established plastic wedges which acted as stress raisers in the subsequent low temperature test.

In order to determine whether rheotropic embrittlement is associated with the plastic wedges which are limited to prestraining in tension, rods of the annealed silicon steel used in an earlier investigation and of the SAE 1340 tempered at  $600^\circ\text{F}$  were drawn through a die at room temperature and subsequently tested at  $-321^\circ\text{F}$  ( $-196^\circ\text{C}$ ). The results of these two series of tests are

shown in Figs. 21 and 22. It can be seen that, for both materials, prestraining in drawing produced practically the same results as prestretching. Consequently, this behavior of steels must be considered to be a fundamental behavior not necessarily associated with any particular type of cold working.

It might be further noted here how slightly necking influenced the test results. The SAE 1340 prestrained in tension necked at an approximate strain of  $\epsilon_1 = 0.05$ . Prestraining in drawing, of course, produced no necking, yet the test results after prestraining up to an  $\epsilon_1 = 0.25$  agreed within a few per cent for the specimens prestrained by the two methods.

Davidenkov and Sakharov had presented a few data showing that the transition temperature of an annealed steel which was prestretched at room temperature went through a maximum when the steel was prestrained about 5% (10). This would suggest that the transition temperature-prestrain curve is a mirror image of the retained ductility-prestrain curve.

*Notched Tests*—Much of the interest in the low temperature performance of steels is based on the fact that they are considered to behave in a similar manner when subjected to straining in the presence of any of the common embrittling agents (see for example, discussion to Ref. 6). Consequently, it is often convenient to determine the subzero temperature properties of materials in order to predict their behavior under severe service conditions. It is of vital importance then to know whether or not embrittlement caused by low testing temperatures is of the same type as that effected by severe service conditions, such as sharp notches.

Low temperature embrittlement of the steels investigated in this study was found to be a rheotropic type of brittleness. The steels could be made strain-stabilized at the low temperature by first cold working them at room temperature. In order to compare low temperature straining with straining in the presence of a notch, specimens of quenched SAE 1340 which were tempered at 600 °F were stretched various amounts at room temperature. Sharp notches (notch radius  $\leq 0.001$  inch) were machined into these prestrained specimens, and these were strained to fracture again at room temperature. The retained, or notched, ductility of these bars as well as the notch strength<sup>9</sup> is plotted as a function of the prestrain in Fig. 23. The similarity between the shape of these curves and the shape of the curves obtained on this material at low temperatures,

<sup>9</sup>The notch strength is equal to the maximum load divided by the initial area. The maximum load and breaking load at these low ductilities are the same and the area at fracture is not much different from the original area so that the notch strength was approximately equal to the fracture stress.



as shown in Figs. 5 and 9, indicates that here again embrittlement is a rheotropic condition.

### SUMMARY AND CONCLUSIONS

1. It is proposed that the brittleness in steels and other metals at low temperatures can be removed in part by cold work at relatively high temperatures. Such brittleness is termed rheotropic.
2. Specifically, the low temperature brittleness of steels at high strength levels (tempered in the vicinity of  $\sim 600^{\circ}\text{F}$ ) is shown to be rheotropic.
3. A large part of the deficiency in ductility of annealed steels at low temperatures has also been found to be rheotropic.
4. The nature of cold work necessary to remove rheotropic brittleness is not specific; it has been found that stretching or cold drawing through a die is about equally effective.
5. Several methods for determining the magnitude of rheotropic embrittlement presented themselves. All of these methods yielded the same values.
6. Rheotropic embrittlement was found to be the source of dangerously high transition temperatures in a heat treated steel (SAE 1340) and in annealed steels.
7. The condition which causes rheotropic embrittlement is either not cumulative under low temperature straining or else it is cumulative and is readily washed out by room temperature deformation.
8. Embrittlement caused by other severe service conditions, e.g. sharp notches, is also preponderantly rheotropic.

### Appendix

#### MATERIAL AND PROCEDURE

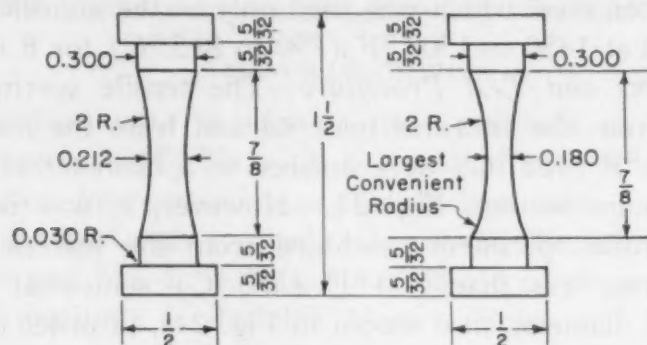
*Material*—Two different steels were used in this investigation. The first of these was the low alloy medium carbon steel, SAE 1340, which was used in both the furnace-cooled and the quenched and tempered conditions. The low temperature tensile properties of this steel in the quenched and tempered condition had been investigated previously (6). The other steel was an annealed 2.75% silicon

Table I  
Composition of Steels Tested

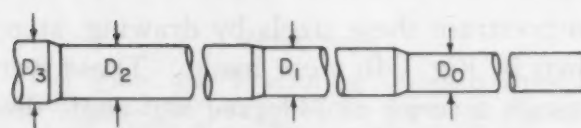
Alloy	Composition, %								
	C	Mn	P	S	Si	Ni	Al	Cu	Sn
SAE 1340	0.42	1.81	0.023	0.022	0.24	.....	.....	.....	.....
2.75% Silicon	0.031	0.12	0.011	0.015	2.73	0.098	0.23	0.116	0.008

steel whose low temperature properties have also been described earlier (5). The composition of these two steels is shown in Table I.

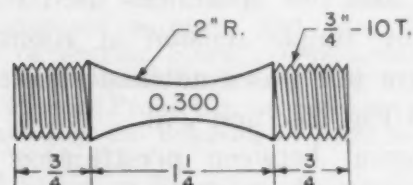
*Heat Treatment*—Rods ( $\frac{3}{4}$ -inch diameter) of SAE 1340 were given a normalizing heat treatment which consisted of heating to



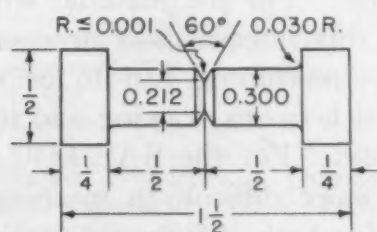
(a) Tensile Test Specimens



(b) Drawing Specimens



(c) Prestrain Specimen For Notched Test



(d) Test Specimen Notch Test

Fig. 24—Prestrain and Test Specimens.

1675 °F (915 °C) for  $\frac{1}{2}$  hour and air cooling. This was followed by a stress relief at 1200 °F (650 °C) for 4 hours with furnace cooling. Tensile specimens, of the type shown in Fig. 24a, were machined from this normalized and stress-relieved material, leaving sufficient stock on the pieces for finish grinding. The specimens were then austenitized at 1525 °F (830 °C) for 1 hour, oil-quenched,

tempered at the desired temperature for 1 hour, and finish ground.

Other pieces of the SAE 1340 were annealed by heating to 1675 °F (915 °C) for ½ hour followed by a furnace cool. Tensile specimens, again of the type shown in Fig. 24a, were then machined from this annealed material.

The silicon steel which was used only in the annealed condition was annealed at 1450 to 1500 °F (790 to 815 °C) for 8 hours.

*Specimens and Test Procedure*—The tensile specimens which were made from the annealed material and from the material tempered at 800 °F (425 °C) were finished to a diameter of 0.212 inch at the minimum section, Fig. 24. However, it was necessary to make the tensile specimens machined from the material tempered at temperatures less than 700 °F (370 °C) somewhat smaller at the minimum diameter, also shown in Fig. 24a, in order to minimize fracturing at the specimen shoulders and to avoid damage to the testing equipment.

In order to prestrain these steels by drawing, stepped specimens of the type shown in Fig. 24b were made. These were then drawn in 5% steps through a series of 7-degree half-angle dies, after which tensile specimens were machined from the rods.

The prestrain and test specimens used for the series in which prestraining was by simple tension at room temperature and in which the subsequent test was a notched tensile test at room temperature are shown in Fig. 24c and 24d.

The time interval between prestraining and testing for the material which was prestrained and tested both in tension was between 3 and 4 hours excepting for those specimens which were subjected to a notch test. For the material which was prestrained by drawing, however, this interval was necessarily longer, since a considerable amount of machining had to be done on the drawn rods. The time interval between drawing and testing for the silicon steel was about 40 hours. For the SAE 1340 tempered at 600 °F (315 °C), which was more difficult to machine, this aging period was about 175 hours for both the drawn specimens and for those specimens tested in a notched condition.

All the tensile strains made in this study were obtained on a 10,000-pound Riehle tensile testing machine. The room temperature strains were accomplished with the use of a specially designed loading fixture which yielded an eccentricity of less than 0.001 inch and a radial strain gage reading in 0.0001 inch (11). These same loading fixtures were adapted to the low temperature work under which conditions the eccentricity was slightly higher. A remote reading



mechanical gage also reading in 0.0001 inch was developed to be used with this apparatus. A detailed description of this equipment is given elsewhere (12).

The fracture strain (or "retained ductility") as well as the magnitude of the prestrain were obtained by taking diameter measurements with a microcomparator before and after each strain.

#### ACKNOWLEDGMENTS

The authors wish to express their gratitude to the Office of Naval Research, U. S. Navy, in cooperation with whom this work was conducted, for permission to publish these data.

They further wish to thank Dr. A. R. Troiano for his kind suggestions and Mr. L. J. Ebert for his aid in preparing the text. A debt of gratitude is also due Messrs. Howe and Mayersky for conducting many of the tests and to the General Electric Company for supplying the liquid nitrogen used as a coolant in this study.

#### References

1. S. I. Liu, "The Flow and Fracturing Characteristics of the Aluminum Alloy 24S-T4 as Affected by Strain-Thermal History", Case Institute of Technology, ONR Tech. Report No. 19, Contract No. N6-ori-273/I, November 1949.
2. D. J. McAdam, Jr., G. W. Geil and R. W. Mebs, "Influence of Plastic Deformation, Combined Stresses, and Low Temperatures on the Breaking Stress of Ferritic Steels", *Transactions, American Institute of Mining and Metallurgical Engineers*, Vol. 172, 1947, p. 323.
3. P. W. Bridgman, "Plastic Properties of Steels—On the Effect of Prestraining in Tension on the Behavior of Steel in Tension", Watertown Arsenal Report WAL III/7-6.
4. G. Sachs, "Effect of Strain on Fracture", *Fracturing of Metals*, published by American Society for Metals, Cleveland, 1948, p. 51.
5. E. J. Ripling and G. Sachs, "The Effect of Strain-Temperature History on the Flow and Fracture Characteristics of an Annealed Steel", *Journal of Metals*, Vol. 1, No. 2, 1949, p. 78.
6. E. J. Ripling, "Tensile Properties of a Heat Treated Low Alloy Steel at Subzero Temperatures", *TRANSACTIONS, American Society for Metals*, Vol. 42, 1950, p. 439.
7. W. F. Brown, Jr., Discussion to Reference 6.
8. M. Baeyertz, W. F. Craig, Jr., and J. P. Sheehan, "Effect of Alloying Elements on Impact Properties of Quenched and Tempered Steels", Armour Research Foundation, ONR Tech. Report No. 22, Contract N6-onr-274/I, September 1949.
9. G. L. Tuer, E. J. Ripling and G. Sachs, "The Low Temperature Static Notch Tensile Characteristics of a 2¾ Per Cent Silicon Steel", Case Institute of Technology, ONR Tech. Report No. 16, Contract N6-ori-273/I.
10. G. Sachs, L. J. Ebert and W. F. Brown, Jr., "Comparison of Various Structural Alloy Steels by Means of the Static Notch-Bar Tensile Test", *Transactions, American Institute of Mining and Metallurgical Engineers*, Vol. 172, 1947.
11. G. Sachs, J. D. Lubahn and L. J. Ebert, "Notched-Bar Tensile Test Characteristics of Heat Treated Low Alloy Steels", *TRANSACTIONS, American Society for Metals*, Vol. 33, 1944, p. 340-395.
12. E. J. Ripling and G. Tuer, "An Apparatus for Low Temperature Tensile Testing", *Product Engineering*, Vol. 20, No. 1, 1949, p. 103.

## DISCUSSION

**Written Discussion:** By Wendell P. Roop, research consultant, Swarthmore College, Swarthmore, Pa.

The authors have discovered a systematic relation between the two stages of strain toward fracture in a simple tensile test when the first stage (prestrain) is accomplished at room temperature and the second stage at  $-321^{\circ}\text{F}$ .

In the normal case the total natural strain at fracture is a simple average between the values obtained in tests all made at each of the two temperatures. But in the "rheotropic case" the combined effect is not an arithmetic mixture of two simple effects. Small prestrain may be followed by disproportionate loss of cold ductility. And even, what seems anomalous, cold brittleness can be diminished by prestrain.

In Fig. 4 are given the results of some earlier tests each made at a single temperature. The section on the abscissa marked 1000 shows a gradual loss of ductility with reduced temperature of test, while at abscissa 600 is seen an abrupt drop in ductility of the sort found in ship steel.

In Fig. 5 it is seen that at abscissa 600, prestrain up to 25% causes a quick rise in total strain at fracture from 5% at the necking point to about 50% total at 25% prestrain. This is contrary to the shipyard idea that cold working has an embrittling effect. It is noted that in Fig. 5 (700) a sharp loss in cold ductility is caused by prestrain to necking value. This is regarded in the shipyards as normal behavior, but it is the sort of thing they do not like.

The procedure for study of rheotropic brittleness by means of tests at a single low temperature is more convenient than the use of a whole series of temperatures which cannot be assigned in advance. If inferences about transition temperatures could be drawn from the curves on variable prestrain, it would save work. However, this seems not to be the case, since all the cited data on transition temperature come from tests at a series of temperatures. Possibly the suggested relation between the curve of transition temperature of prestrain and the curve of retained ductility on prestrain could be developed in this direction.

The further suggestion, as to the effect of notching on rheotropic embrittlement, leads me to inquire how far the authors would be willing to go in linking the phenomenon of rheotropism with the behavior of steel in notches. In several different kinds of tests for cold brittleness, a preliminary phase of ductile action precedes fractures which otherwise are brittle. May we suppose that early high strains near the notch can wash out the brittleness there, possibly at a local temperature raised by the straining?

Here we approach one of the mysteries in testing for cold brittleness. The fact is that in many cases an open crack appears at an early stage in the apex of the notch and this crack looks much the same whether the fracture, when it advances, does so in the brittle or ductile mode. The choice between ductility and brittleness is made in the presence of the sharpest notch possible—namely, a natural crack. I would be grateful for any explanation that might be given for this.

Or, conversely, is it possible that some of the apparently anomalous effects of prestrain could arise in unobserved preliminary fractures? Most of the present data were taken with simple tensile test specimens, and a great part of the range of strain covered lies at strain values beyond the necking point.

At some stage before final rupture a preliminary crack opens up on the axis of such a specimen, and no one knows just when. However, in comparable situations where it can be seen, the crack appears at a very early stage. It seems to me reasonable to suppose that even when it cannot be seen it still may be there to breach the continuity of the metal at a stage earlier than has been supposed.

The presence of such an opening on the axis of a tensile test specimen would upset the values both of stress and of strain in our curves of "true stress on natural strain" over the whole range of values beyond the point of its beginning. We know that this point of beginning precedes final rupture, though not long in time in the ordinary test, yet far down the stress-strain curve; but I am not aware that any attempt has been made to correct the curve for this fact. It seems to me not impossible that the beginning of the crack might even coincide with the beginning of the necking process.

Do the new data now presented by the authors give us any light on this matter?

**Written Discussion:** By W. A. Pennington, chief chemist and metallurgist, Carrier Corp., Syracuse, N. Y.

It is always a pleasure to read a technical paper which is highly concentrated in useful information. Not only is this paper in this class, but it is written in a clear and attractive style. The authors are to be congratulated.

Most scientists prefer to find something really practical in the papers they read. The authors have satisfied this desire by demonstrating that rheotropic embrittlement at extremely low temperatures can be removed in part by suitable cold work performed at higher temperatures.

The interpretation of the data, particularly with respect to the extrapolations, is interesting and in general quite acceptable. However, exception must be taken to the so-called extrapolation of Type C shown in Fig. 11. The authors refer to this as a very doubtful extrapolation. One cannot extrapolate a curve until he has the curve. Certainly the four points between 0.6 and 0.7 retained ductility, where the tempering temperature was 600 °F, do not determine a definitely placed line. If the line is determined by law of least squares, the intercept on the abscissa will be nearer 0.35 than 0.45. The authors point out in footnote 6 that better data are to follow further within the paper to justify the Type C extrapolation. Even so, it is not justified in Fig. 11.

**Written Discussion:** By Carl A. Zapffe, consulting metallurgist, Baltimore, Md.

My attention was called to this paper particularly because of the authors' use of "rheotropic", since we have recently been using this word and its derivatives in a slightly different sense.

"Rheotropy" is certainly a word which is due for wide usage in metallurgy. It is based upon two Greek stems, the one (rheo-) literally meaning



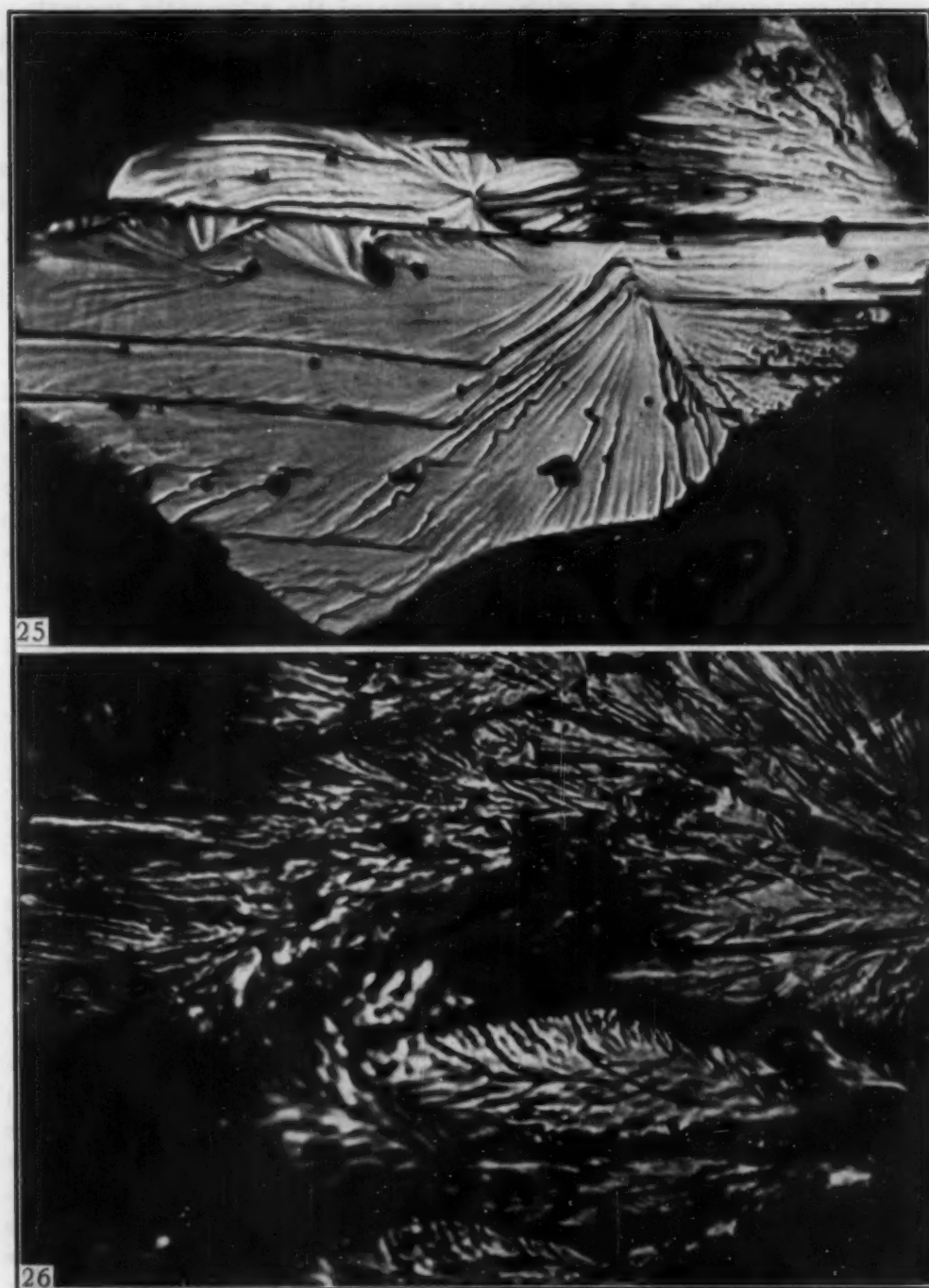


Fig. 25—Fractograph of Mild Steel Fractured at  $-196^{\circ}\text{C}$ . Condition: Annealed  $1000^{\circ}\text{C}$  ( $1830^{\circ}\text{F}$ ) for 2 hours. Furnace-cooled.  $\times 800$ .

Fig. 26—Fractograph of Material in Fig. 25, but Cold-Worked to Approximately 50% Reduction Previous to Fracture at  $-196^{\circ}\text{C}$ .  $\times 800$ .

(Figs. 25 and 26 reduced  $33\frac{1}{4}\%$  in reproduction.)

“current”, but used today in its sense of flow; and the other (-trope) meaning reversal or change. Rheology is the science of the deformation and flow of matter, and this word has become well entrenched in the past decade or two by the establishment of organizations for studies of rheology.

In metallurgy, a long-standing interest in deformation and flow has been capped within the last few years by a particular interest in those factors causing changes in rheological behavior. The term most used today is "transition temperature". However, because of the confusion of the word "transition" with allotropic changes in metals and alloys, we suggested the adoption of "slip-transition temperature", particularly because the phenomenon in question specifically concerns the operation or non-operation of the slip mechanism. This suggestion was later modified by proposing "rheotropic temperature" as a preferred technical expression. This specifically designates a fundamental change in rheological behavior, the boundary of the two conditions here identified as temperature. Since factors other than temperature can likewise effect the rheological change, the terminology is adaptable to "rheotropic velocity" (of fracture), "rheotropic composition", and so forth. Drs. Ripling and Baldwin recognize this appropriateness of the term, and their expression "rheotropic embrittlement" is probably in line with what we regard as proper usage.

During our work with the Office of Naval Research, particularly on the rheotropic problem, the fractographic patterns of several steels were studied under conditions similar to those discussed by the present authors. Figs. 25 and 26 are submitted here because they provide visual evidence of an interesting sort for the phenomenon described by Ripling and Baldwin. Both fractographs refer to a mild steel, such as used for ship-plate construction. A specimen has been heated at 1830 °F (1000 °C) for 2 hours and furnace-cooled. It was fractured in liquid nitrogen ( $-321^{\circ}\text{F}$  or  $-196^{\circ}\text{C}$ ) by hammer blow. The facet in Fig. 25 is smooth and expansive, giving visual indication of a relatively unimpeded cleavage traverse. Crystallographic markings also appear, which are characteristic of clastic tendencies. This steel would show a high rheotropic temperature.

In Fig. 26, this identical material is shown, again fractured at  $-321^{\circ}\text{F}$  ( $-196^{\circ}\text{C}$ ), but this time after first cold working the specimen by pounding with a hammer at room temperature until the section was reduced to approximately 50%.

In marked contrast to Fig. 25, the fracture traverse is now much roughened on both a micro and macro scale. Only slight indications of crystallographic traces remain. The pattern reveals that fracture has been continuously impeded in traversing this grain; and the observation is consistent with the fact that the steel now exhibits a greater resistance to fracture, with rheotropic effects as described by Ripling and Baldwin. These fractographic patterns, of course, record the exact path taken by the fracture, and their details are accordingly strictly pertinent to studies of rheology and fractology.

#### Authors' Reply

The authors wish to thank the discussers for the interest they have shown in this paper.

Captain Roop's attempts to correlate the phenomenon discussed in this report with ship-plate behaviors are particularly stimulating. His statement that the "natural strain at fracture is a simple average between the values obtained in tests all made at each of two temperatures" (for the nonrheotropic case) is virtually true. However, "a simple average"

implies that the relationship between prestrain and retained ductility is linear. That this is not necessarily the case is shown by some of the data in Fig. 19. It is for this reason that the authors chose the words "smooth curve" to describe the retained ductility-prestrain curves found in the simplest case.

A necessary part of the phenomenon that we describe is that the first strain be above the transition temperature (for the strain rate, and hydrostatic tensile stresses under the prestrain conditions). Consequently, it would be expected that "high strains near the notch" could not wash out brittleness there if the brittleness were caused by the transition temperature effects.

Captain Roop's suggestion that ductile behaviors are found even in the presence of a natural crack (the sharpest notch possible) means simply that for some materials even this very sharp notch cannot cause the transition temperature to be above the testing temperature. The suggestion, that some of the effects of prestrain may be appreciably influenced by the crack that formed internally in necked tensile bars, apparently overlooks the fact that the same low temperature retained ductility was obtained when the prestraining was by stretching or by drawing (see Figs. 21 and 22). It is realized that internal cracks might form in drawing as well as in stretching, but these cracks do not form in drawn products until the reductions are quite high.

Dr. Pennington takes exception to our extrapolation of Type C in Fig. 11. The authors realized that this experimental curve was much too short for the extrapolation shown in Fig. 11 and the extrapolation was made only because other data in the report indicated that it was feasible. These facts are pointed out in the text.

Dr. Zapffe's use of the stem "rheo" to mean flow is the same interpretation that we used. The stem "trope", however, was used by us as "a combining form used to signify 'turning'" or sensitive to. The use of the term "transition temperature" to signify the temperature at which behaviors change from ductile to brittle seems so well entrenched in the literature that a change to "rheotropic temperature" now would lead to no end of confusion.

It is gratifying to learn that results similar to those reported here have been observed by Dr. Zapffe in his fractographic studies.

The authors further wish to point out the very minor part played by residual stresses in rheotropic behaviors. This conclusion is arrived at as a consequence of the fact that, first, prestraining by drawing and by stretching produced the same retained ductility at the low testing temperature, while the residual stress patterns for these two methods of deformation are quite different. Furthermore, at the low temperature there was almost always some ductility retained and it requires only rather slight strains to wipe out residual stress patterns.



## EMBRITTLMENT OF STAINLESS STEEL BY STEAM IN HEAT TREATING ATMOSPHERES

BY C. A. ZAPFFE AND R. L. PHEBUS

### *Abstract*

*The special bar-bend test described in a previous paper is applied to a number of Class I (hardenable) stainless steels which are hardened over a range of temperatures from various atmospheres of (a) dry helium, (b) normal air, and (c) steam.*

*By means of bendability (measured as angle of bend sustained without fracture in this single-bend test), there is demonstrated a powerful and heretofore unrecognized effect of steam in embrittling the steel through the hydrogenizing effect of the metal-steam reaction. Steels which sustain a full bend of 180 degrees when hardened from a dry atmosphere fail at angles as low as 20 degrees when steam is admitted to the furnace atmosphere during heat treating; and steels which fracture at a given angle when quenched from normal air can be markedly improved by drying the furnace atmosphere.*

*These results confirm the theory of the "hydrogen potential" of steam-metal reactions, earlier advanced by the senior author, and explain numerous problems of cracking and poor ductility on the basis of the common presence of steam in furnace atmospheres as humidity and/or a reaction product of fuel combustion. Attention is called to the practical aspects of the discovery as well as the theoretical.*

**M**OISTURE has become generally recognized as the most important source of hydrogen absorbed by steel during melting. In the basic open-hearth process, "flakes" caused by hydrogen (a source of considerable trouble during World War I) have been largely eliminated by drying the materials in the charge, particularly the lime. In the ferritic grades of stainless steel, a strong tendency toward gassiness and "bleeding" in ingots and castings has been reduced by similar precautions. In welding, the new "low hydrogen" electrodes avoid the inferior ductility, cracking, and "fish-eyes" caused by moisture. In fact, many ferrous processes today have been modified to overcome this role of moisture.

---

Work performed in the Laboratory of the senior author under contract with the Office of Naval Research.

---

A paper presented before the Thirty-second Annual Convention of the Society, held in Chicago, October 21 to 27, 1950. Of the authors, C. A. Zapffe is research metallurgist, Baltimore, Md., and R. L. Phebus is research assistant, Towne Scientific School, University of Pennsylvania, Philadelphia. Manuscript received March 23, 1950.

The hydrogenizing effect of moisture on solid metal is less generally recognized. A recent article by the senior author (1)<sup>1</sup> developed calculations for the "hydrogen potential" of steam in contact with a number of metal systems and showed that the general rule is for an increased potential to occur with decreasing temperatures. Typical calculations showed  $P_{H_2}$  values in the hundreds and thousands of atmospheres for an equivalent of one atmosphere of  $H_2O$ . While these figures are uncorrected for imperfect gas behavior, no reasonable fugacity coefficient can change their essential significance. It should be noted that the values are based upon the atomic H component as developed by the steam-metal reaction, and as calculated to theoretical  $P_{H_2}$  values through the quadratic relationship between  $P_H$  and  $P_{H_2}$ .

Perhaps the fact that the hydrogenizing effects encountered in industry are considerably less than indicated by these figures is due not so much to errors in the theory as to the kinetic conditions of steam-metal reactions. Immediately upon generation of the reaction potential, an oxide film is simultaneously formed and smothers further reaction. A large momentary injection of hydrogen may occur, but its integrated or total action would fall far short of the metal-steam calculations when the surfacial system converts to oxide-steam. During melting, considerably smaller potentials can exert a greater total hydrogenizing effect because the mobile system provides a constantly renewed metal-steam interface.

Nevertheless, the hydrogenizing of solid steel by steam has been clearly demonstrated in at least one industrial application, as described by Solberg and his co-workers (2) for the upper temperature ranges of commercial steam plants; in the lower ranges of boiler operation, it has been noted in connection with the phenomenon of "boiler embrittlement" (3).

In virtually every furnace used today for hardening and heat treating steels, the atmosphere contains  $H_2O$  derived from combustion of fuel or from environmental sources. Many steels sensitive to injury from hydrogen are therefore exposed to  $H_2O$  throughout their entire history, yet the only effect commonly considered is the oxidation it causes.

In this paper we shall consider the hydrogenizing effect of steam, measured quantitatively by means of a specially designed bend test. Materials tested are the Class I<sup>2</sup> stainless steels exposed to various hardening heat treatments.

<sup>1</sup>The figures appearing in parentheses pertain to the references appended to this paper.

<sup>2</sup>Terminology according to book, "Stainless Steels", by Carl Zapffe, published by American Society for Metals, 1949.

## EXPERIMENTAL PROCEDURE

The details of the "bar-bend test" have been given in a previous article (4). Essentially, the method involves bending a round bar at a constant angular rate around a radius and measuring the angle at which fracture occurs. In the present research a  $\frac{1}{4}$ -inch bar is bent around a pin of the same diameter. The Class I stainless steels studied in the foregoing research (4) are used, wherein "standard" behavior was established as heat treated in a normal air atmosphere. The six specimens to be discussed are listed in Table I.

Table I  
Analyses of Specimens

AISI Type No.	Per Cent						
	Cr	C	Mn	Si	P	S	Ni
403	12.44	0.101	0.41	0.31	0.013	0.021	....
410	12.63	0.102	0.50	0.26	0.020	0.023	....
414	12.49	0.119	0.56	0.35	0.020	0.010	1.75
416	13.02	0.099	0.73	0.25	0.016	0.252	....
431	16.31	0.155	0.63	0.39	0.022	0.017	1.86
440-C	16.88	1.012	0.34	0.50	0.026	0.025	....

Triplicate specimens were used in each test. They were cut in approximately 4-inch lengths from commercial bar with a cold drawn finish. The specimens were placed in a horizontal Globar-heated tube furnace (1.5 inch I.D.) previously brought to the hardening temperature, held for 30 minutes, and quenched in oil. They were then tested in the bend machine without any further treatment (such as the stress-relief treatment common in commercial practice for the more hardenable grades).

Three types of furnace atmospheres were compared, requiring three series of tests. Ordinary air was used in the first series, and the results were reported in the preceding paper (4). The second series utilized an atmosphere of approximately 100% steam. This atmosphere was provided by connecting a flask of boiling water to one end of the furnace tube, so that steam continuously exhausted at the other end. The results of this second series, as compared with the first, provide the principal material for the present discussion. The third series used carefully dried helium to provide a comparison for the effect of the normal moisture present in the air.

In Figs. 1 through 5, bendability curves from the first series of tests for heat treating in air are reproduced from the foregoing study (4), and the individual points are therefore not shown. Data for the curves for helium and air are indicated on the graphs. The



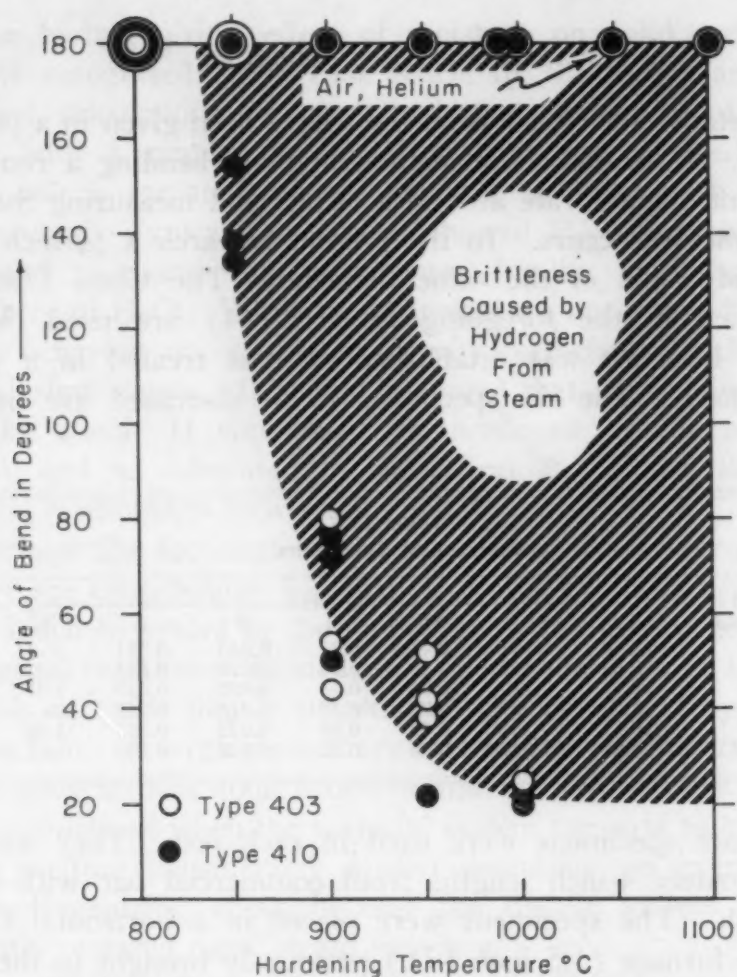


Fig. 1—Bend Values for Stainless Steels—Types 403 and 410—Oil-Quenched From Atmospheres of (a) Dry Helium, (b) Normal Air and (c) Steam.

areas representing embrittlement are variously shaded to depict more clearly the effect of steam and of air versus helium. All graphs follow the convention established in the previous study, wherein the hardening temperature along the abscissa is varied over a wide range of the austenite field, while the bend angles are plotted along the ordinate.

## RESULTS

### *Types 403 and 410*

Fig. 1 provides a striking verification of the steam-hydrogen theory, and points to a behavior having both theoretical and practical significance.

Data for two grades of stainless steel are plotted—Types 403 and 410. In the previous experiments with heat treatment in air these steels developed no measurable brittleness, regardless of hard-

ening temperature. This is indicated by the "air" points along the 180-degree bend line at the top of the diagram.

Tests in helium confirmed the experiments in air, all of the specimens likewise bending 180 degrees after hardening.

In steam, however, both grades immediately displayed brittleness. Brittleness occurred at all hardening temperatures just above 800 °C (1470 °F), which is close to the lower limit of the gamma field. In the range of commercial hardening near 1000 °C (1830 °F) the bend angles dropped to very low values. Steels which would bend 180 degrees after hardening in air fractured at only 20 degrees of bend after a duplicate hardening treatment in an atmosphere of steam.

Thus the shaded area in Fig. 1 indicates the damage to these steels caused by steam present during the heat treating operation. The close conformity of the two sets of points follows logically from the fact that Types 403 and 410 are virtually identical steels, Type 403 merely representing metal more closely specified and inspected for special service in steam turbines.

#### *Type 414*

In Fig. 2, a steel of greater bend-sensitivity—Type 414—reveals a distinction between the air and the helium treatments not apparent in Fig. 1. Since the air used in these experiments contained normal atmospheric humidity, the data in Fig. 2 indicate the scope of the hydrogen embrittlement problem as presented by moisture in normal atmospheres.

This graph shows that air treatment led to bend failures at hardening temperatures above 850 °C (1560 °F), whereas in helium the same steel maintained a 180-degree bend up to hardening temperatures of 1000 °C (1830 °F). The downsweep of these bendability curves with increasing temperature, of course, primarily reflects the increasing proportion of the austenite-martensite transformation—the more fully hardened the specimen the more readily it will be damaged by a given hydrogen content. The temperature displacement of the curves thus indicates the severity of the hydrogenizing condition.

When hardened from 950 °C (1740 °F) in helium, the Type 414 stainless steel bent a full 180 degrees, but when the heat treatment was conducted in a normal air atmosphere, it fractured at bends of only about 30 degrees. No humidity reading was recorded for these air tests, because they were conducted during the preliminary study of the general bendability behavior for normal proc-

essing, when such marked effects were not expected. Quantitative aspects of humidity will be reserved for later treatment, attention here being directed instead toward the extremes of the steam phenomenon as disclosed by treatments in dry helium and pure steam.

For Type 414 in steam, the data in Fig. 2 show greatly increased embrittlement. Analogous to the comparison between helium and air treatments, the damage from an atmosphere of steam far

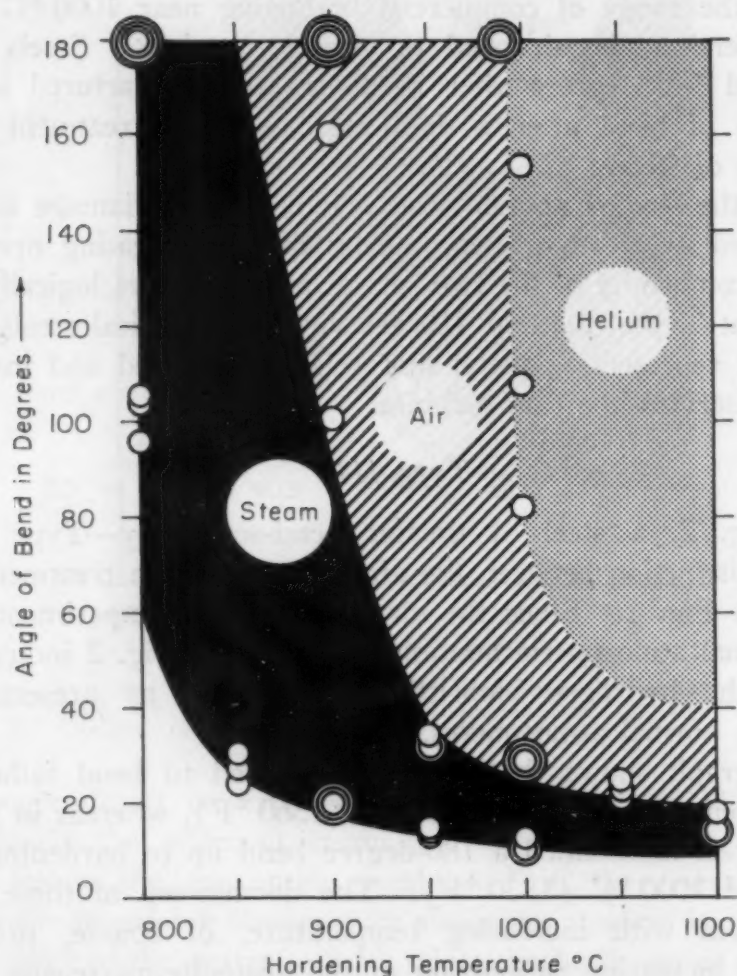


Fig. 2—Bend Values for Stainless Steel—Type 414—Hardened by Heat Treatment in Helium, Air and Steam.

exceeds that caused by air. In air at 900 °C (1650 °F) most bars will bend 180 degrees, whereas in steam at the same temperature all bars fracture at angles close to 20 degrees. At higher hardening temperatures these bend angles drop even further.

Such results certainly hold significance for commercial handling of this grade of steel, because much of the heat treating is conducted in the atmospheres of oil- or gas-fired furnaces where water vapor is a prominent product of combustion. The differences in bend-



ability disclosed in Fig. 2 should have important consequences in the drawing, coiling, and handling of Type 414 in the mill.

### Type 431

Type 431 is a grade of steel similar to Type 414 in having a nickel content of 1 or 2%, but differs in having a two-phase constitution of austenite and ferrite caused by an increased chromium

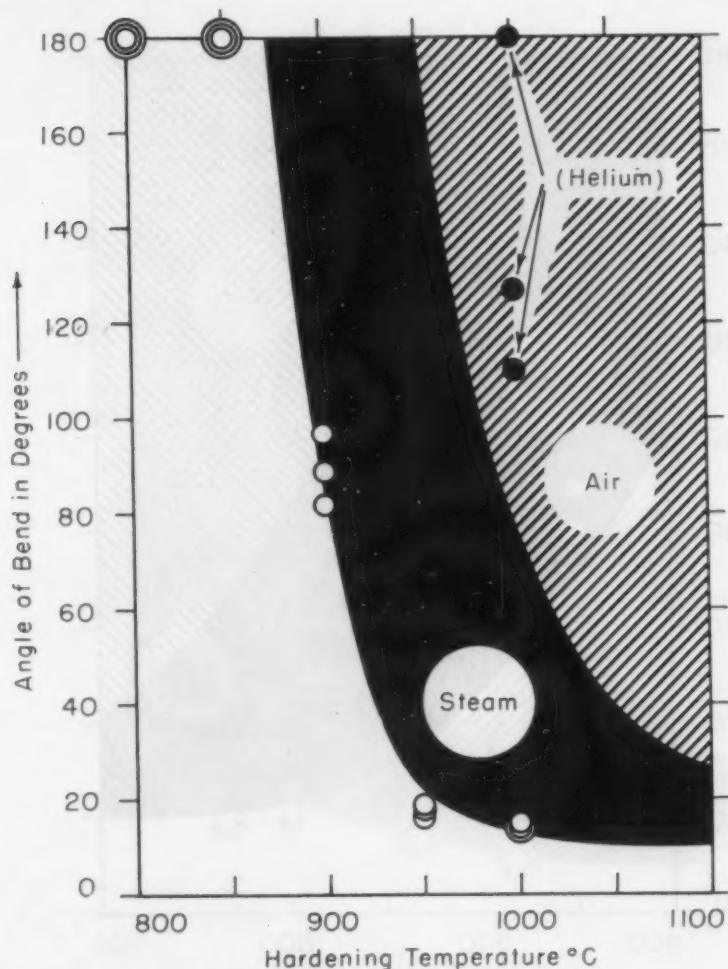


Fig. 3—Bend Values for Stainless Steel—Type 431—Oil-Quenched From Treatments in Various Atmospheres.

content. Its behavior, shown in Fig. 3, is similar to that for Type 414 shown in the previous figure. This metal has maximum bendability when heated in helium, slightly inferior bendability when treated normally in air, and markedly lowered bendability when exposed to steam during heat treatment. The steam and air curves are shifted to the right, which is consistent with the fact that Type 431 is not fully hardenable by the martensite reaction, as is Type 414. However, the helium curves for the two alloys are virtually

identical. In other words, the intrinsic bendabilities of Types 414 and 431 compare closely, but Type 414 is more seriously damaged by moisture than is Type 431. It is not clear whether this results from the greater proportion of martensite in Type 414, or from the protective effect of the higher chromium content in Type 431.

Here again the data show that this is a steel which should have excellent bendability (which is presumed to be a measure of general

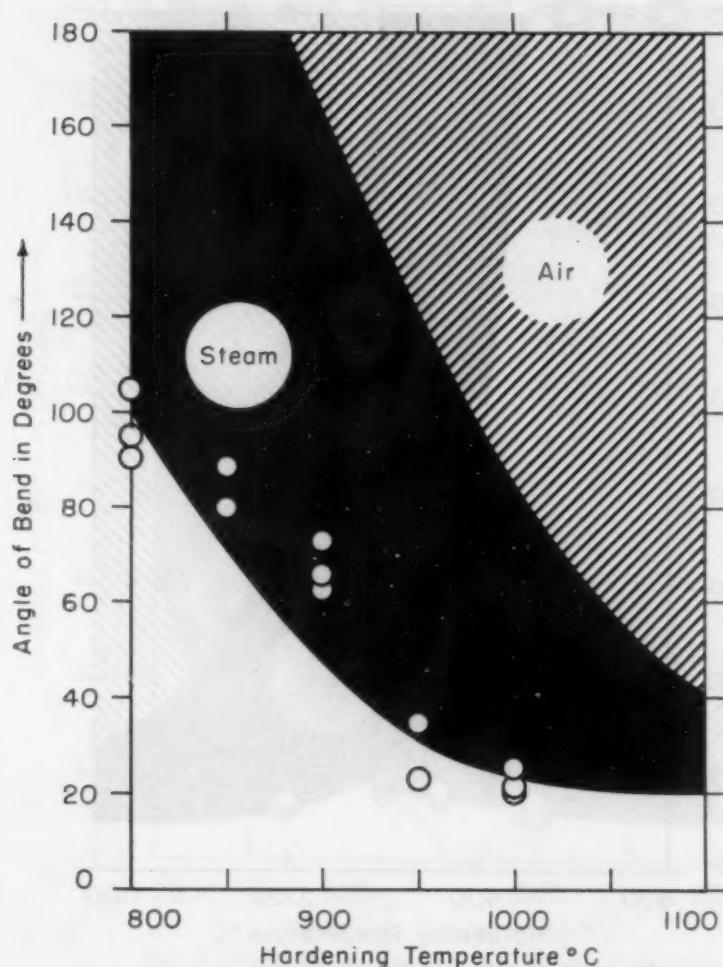


Fig. 4—Bend Values for Stainless Steel—Type 416—Oil-Quenched From Hardening Treatments in Air and Steam.

ductility) when heat treated in the absence of moisture but, on the other hand, is readily susceptible to fracture when exposed to moisture during heat treatment. Plant experience confirms this conclusion, for these grades are plagued by brittleness. The particularly destructive effect of bright-annealing atmospheres rich in hydrogen (e.g., cracked ammonia) is convincing evidence of their sensitivity to hydrogen.

## Type 416

The bend data for Type 416 presented in the previous paper (4) showed that all specimens fractured at hardening temperatures above 900 °C (1650 °F). This is in notable contrast to the behavior of Types 403 and 410, which showed no embrittlement, regardless of hardening temperature. The latter steels differ constitutionally

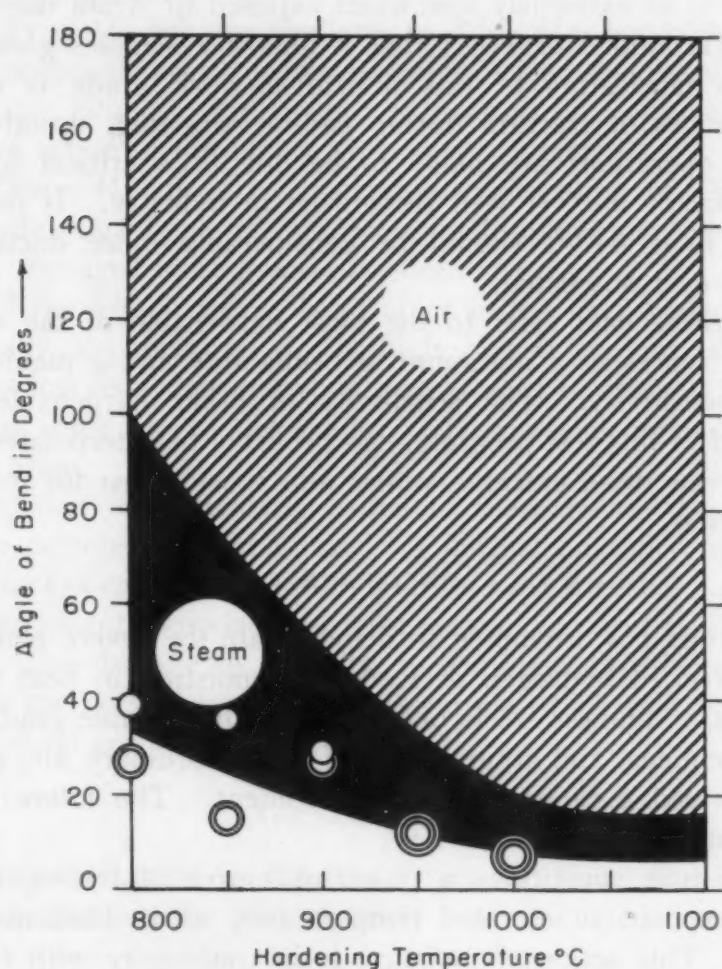


Fig. 5—Bend Values for Stainless Steel—Type 440-C  
—Oil-Quenched From Air and Steam Atmospheres.

from Type 416 only in sulphur content, Type 416 being the free-machining modification.

The bend values also were erratic, undoubtedly because of the heterogeneous structure produced by the sulphides. For this reason the curve for the air atmosphere in Fig. 4 should not be interpreted strictly. The data for steam also show relatively poor conformity, and the curve was drawn somewhat arbitrarily. Nevertheless, it is clear that the values for the steam treatment all lie far below the



family of curves for air, and that they corroborate the preceding data regarding the deleterious effect of steam.

#### *Type 440-C*

A final series of tests with a high carbon stainless steel, Type 440-C, again gives the same type of results (see Fig. 5). This steel is brittle upon oil quenching from all hardening ranges; its bendability is so extremely low when exposed to steam during heat treatment (around 5 degrees) that it almost resembles glass. The warning to fabricators of this difficult-to-work grade is obvious. Many instances of fracture during coiling, drawing, upsetting and other cold operations are likely to be due to a critical hydrogen content, a factor not yet well recognized in industry. If free from hydrogen, Type 440-C should be considerably more ductile than anyone has ever suspected.

Since these data refer to the most hardenable of the stainless steels, they represent a minimum in bendability and a maximum in hydrogen sensitivity. The sensitivity of other hardenable steels, not included in this test program, can probably be interpolated somewhere between these extreme values and those given for grades of lower hardness.

#### CONCLUSION

This study has attempted to demonstrate the severe embrittling action on steel of hydrogen derived from moisture in heat treating atmospheres. Stainless steels of the Class I hardenable grades were used as specimens, and atmospheres of steam, ordinary air, and dry helium provided a range of moisture content. The following tentative conclusions can be drawn:

1. Moisture constitutes a powerful source of hydrogen when steels are exposed to elevated temperatures, as in hardening heat treatments. This action of moisture is in conformity with the concept of the hydrogen potential in steam-metal reactions previously developed by the senior author.
2. Measured in terms of bendability (the angle to which a specimen quenched from a given atmosphere will bend before fracture), embrittlement is a maximum for an atmosphere of pure steam, and a minimum for dry helium; for normal air the values lie in between, apparently indicating the effect of moisture present as humidity.
3. Types 403 and 410 bend a full 180 degrees when quenched from air or dry helium over the entire hardening range, but will

fracture throughout that same range when the hardening treatment is conducted in steam. For commercial treatments at about 1000 °C (1830 °F) bend values may be as low as 20 degrees.

4. Type 414 can be hardened from temperatures up to about 1000 °C (1830 °F) in dry helium without loss of 180-degree bendability, but this steel will fracture at 30 degrees following an air treatment, and at only 10 degrees following a steam treatment at the same temperature.

5. Type 431 behaves similarly to Type 414, but higher temperatures are necessary to produce a given effect by moisture. This may be due either to the smaller proportion of martensite, or to a protective action of the higher chromium content.

6. Type 416, the free machining modification of Type 410, is less ductile than Type 410 under normal conditions and is proportionately damaged more greatly by steam.

7. Type 440-C, whose bendability in the hardened condition is intrinsically low because of the high carbon content, shows bend values as low as 5 degrees when heat treated in steam. This is the minimum value for all the grades and represents virtually a glass-like condition.

Attention is particularly called to these results because, aside from the demonstrated importance of normal humidity, water vapor is a product of combustion in oil- and gas-fired furnaces, and is therefore a prominent component of most commercial heat treating atmospheres. The damage to ductility, as expressed by decreased bendability in the present tests, has a magnitude which is striking in both its theoretical and its practical aspects.

#### ACKNOWLEDGMENT

Acknowledgment is due the Office of Naval Research under whose sponsorship the present study was conducted.

#### References

1. C. A. Zapffe, "Concept of the Hydrogen Potential in Steam-Metal Reactions", *TRANSACTIONS, American Society for Metals*, Vol. 40, 1948, p. 315-352; discussion, p. 352-354.
2. H. L. Solberg, G. A. Hawkins and A. A. Potter, "Corrosion of Unstressed Steel Specimens and Various Alloys by High-Temperature Steam", *Transactions, American Society of Mechanical Engineers*, Vol. 64, 1942, p. 303-313; discussion, p. 313-316.
3. C. A. Zapffe, "Boiler Embrittlement", *Transactions, American Society of Mechanical Engineers*, Vol. 66, 1944, p. 81-117; discussion, p. 117-126.
4. C. A. Zapffe, R. L. Phebus and F. K. Landgraf, "A Bar-Bend Test and Its Application to Stainless Steel", *TRANSACTIONS, American Society for Metals*, Vol. 42, 1950, p. 666.

### DISCUSSION

**Written Discussion:** By G. A. Moore, assistant professor of metallurgy, University of Pennsylvania, Philadelphia.

The authors appear to have demonstrated beyond question their thesis that steam has a commercially important damaging effect on the ductility of the hardenable stainless steels. Perhaps they have insufficiently emphasized that the claim is being made only for the hardenable types, since all available evidence clearly indicates that hydrogen present in solid austenitic steels has no observable damaging effect. While this writer is satisfied that the observed effect is due to hydrogen supplied by the decomposition of steam, it might be legitimately objected that the effect could be due to the introduction of surface notches by grain boundary corrosion. It would be helpful if the authors could eliminate this possibility by presenting micrographic evidence of the absence of such notches, by showing the same embrittlement in bars polished after treatment, or by showing the absence of an effect on fully austenitic stainless steel.

Certain observations of embrittlement in welds and in alloy steel have been explained by the contention that when a steel is incompletely transformed, hydrogen concentrates in the austenite. If the austenite transforms after a delay, the effect of the hydrogen is concentrated in a few martensite crystals and a little hydrogen has more than a normal effect, while if the austenite is retained permanently, the hydrogen has abnormally little effect. Such an effect appears to be shown by the data on Types 414 and 431, but the observation is confused by the fact that the two steels presumably were not tested at the same hardness. Perhaps the authors have data which would permit comparing the bend angles at equal hardnesses, rather than at equal heat treating temperatures?

The bar-bend test, as shown by the current and preceding reports from Dr. Zapffe, appears to be a sensitive detector of embrittlement. Unfortunately, it appears impossible for the reader to translate these results into terms which are more familiar in measuring ductility. It would not appear too laborious to make experimental calibrations for the machine, one for each combination of pin and bar diameter, by which the bend angles could be expressed as elongation or as natural strain at the outer fiber, or at the point of initiation of the first crack if the crack does not start at the outer surface. If the authors can supply this calibration, the results will have far greater significance.

The hydrogen embrittlement of alloy steels has been only superficially investigated by comparison with the comprehensive and conclusive works which have been done on iron and on simple steels. No doubt the presence of several additional phases, and the probable variations in hydrogen solubility, will introduce many new complications. The authors are to be complimented for starting such a difficult study, which most certainly will lead to many interesting findings, and which it is hoped will be continued on an expanding scale.

### Authors' Reply

Dr. Moore's questions apparently arise from following a train of logic similar to our own in conducting these tests. A very great number of



variables and necessary controls confront the investigator conducting experimentation even with gas-metal systems under equilibrium conditions. When the further complication of a kinetic system is added, the problem becomes one which can only be treated one step at a time.

Accordingly, the present paper is little other than an introduction to the discovery that steam can cause hydrogen embrittlement in certain steels as a result of exposure during conventional heat treatments. In subsequent phases of the research, several of which are described in current or pending publications, a number of questions are answered such as those placed by Dr. Moore. Identification of the defect as a function of hydrogen embrittlement is simple and conclusive. First, the gas can be observed escaping from the specimen if it is immersed in hot oil or glycerin following the quench. Second, bendability is little affected, whether one polishes the surface after quenching, or leaves it as oxidized. Third, the bendability recovers by simple aging processes, quite regardless of surface condition.

As for the significance of the bendability results as measures of a mechanical property, two aspects suggest themselves: (a) That bendability probably deserves considerably more attention than it has heretofore received as an informative mechanical property, and (b) that calibration experiments will be necessary, such as Dr. Moore suggests. We have already conducted a limited number of these, some of which were reported one year ago in the introductory paper on the bar-bend test. Hardness measurements seem to conform, so far as interpretation is concerned, with bendability measurements in certain areas of treatment; but there are other conditions for which the bendability seems to be a specifically sensitive and informative measurement.

## THE TERNARY SYSTEM CHROMIUM-MOLYBDENUM-IRON

BY J. W. PUTMAN, R. D. POTTER AND N. J. GRANT

### *Abstract*

*A series of chromium-iron-molybdenum alloys was made up by induction melting under an inert atmosphere and purified by vacuum melting. Thermal analyses were made and liquidus temperatures determined for these alloys. The effects of several heat treatments on the solid alloys were observed and ternary isothermal sections drawn at 1300, 1100 and 900 °C (2370, 2010 and 1650 °F) from the data obtained. X-ray diffraction data on  $Fe_3Mo_2$  and the iron-molybdenum-sigma phase are given.*

THE experimental work reported herein was carried out as part of the program of investigation of materials for high temperature applications being sponsored by the United States Navy Department, Bureau of Aeronautics.

In the search for structural metals which are useful at the high operating temperatures encountered in gas turbines, the problem of developing alloys which will perform satisfactorily at temperatures above 1500 °F (815 °C) is becoming more and more important.

Without prior knowledge of the properties of its alloys, one would have reason to believe that the chromium-molybdenum-iron system might be the source of useful high temperature alloys because of the high melting points of molybdenum and chromium. Since there is no binary eutectic between either chromium and molybdenum or chromium and iron, the extent of the iron-molybdenum eutectic might be expected to be somewhat localized, avoiding low melting point eutectics. The presence of chromium would, of course, enhance the oxidation resistance of alloys containing it in appreciable quantities.

Furthermore, alloys of this system would be useful extensively because of the abundant supply of iron and chromium and the relatively large supply of molybdenum in this country.

Interest in this system has been further heightened by the devel-

---

A paper presented before the Thirty-second Annual Convention of the Society, held in Chicago, October 21 to 27, 1950. Of the authors, J. W. Putman is research assistant, Massachusetts Institute of Technology, Cambridge, Mass., R. D. Potter is assistant professor of metallurgy, University of California, Berkeley, Calif., and N. J. Grant is associate professor, Massachusetts Institute of Technology, Cambridge, Mass. Manuscript received April 27, 1950.

opment of certain very strong, almost successful alloys (1)<sup>1</sup> which are described below.

## REVIEW OF PREVIOUS WORK

### Ternary Alloys

Parke and Bens (1) made a scattered but extensive study of the stress-rupture properties of chromium-base alloys, as the alloys in this system are commonly termed, and giving consideration to both high

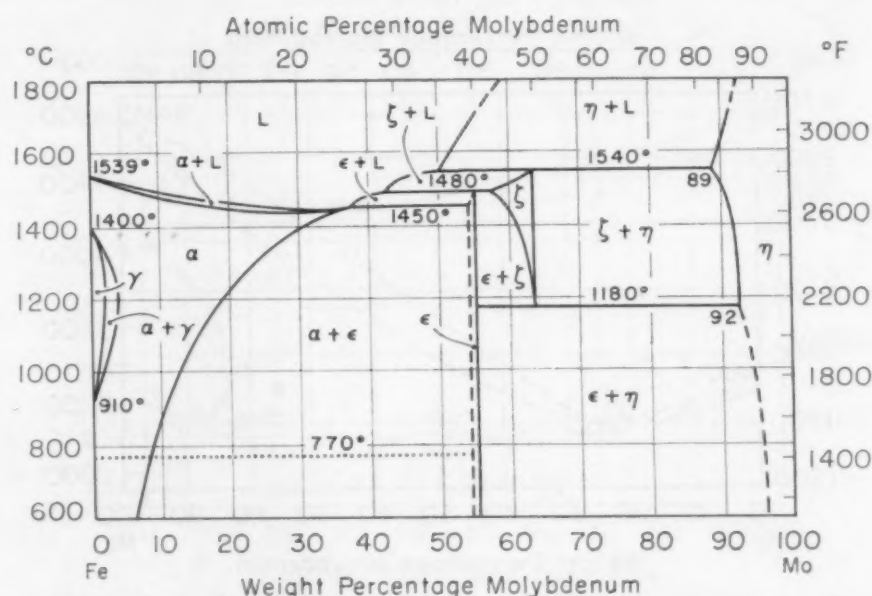


Fig. 1—The Iron-Molybdenum Binary System. *Metals Handbook* (1948).

temperature strength and ductility, suggested the composition 60 chromium - 25 molybdenum - 15 iron as being the most promising at 1600 °F (870 °C).

Battelle Memorial Institute (2) has found that this alloy, which consists for the most part of a body-centered cubic solid solution, develops a phase having the structure of iron-chromium sigma upon aging or stress-rupture testing at 1600 °F (870 °C).

### The Binary System

**Iron-Molybdenum.** The iron-molybdenum system was studied by Sykes (3), Takei and Murakami (4), and Arnfelt (5). The binary diagram of Fig. 1 given by Sykes in the *Metals Handbook* (1948) appears to be a summary of these investigations. There are two intermetallics in the system, both forming by peritectic reactions.

The epsilon phase ( $\epsilon$ ) occurring at 40 atomic per cent molybde-

<sup>1</sup>The figures appearing in parentheses pertain to the references appended to this paper.



num was shown by Arnfelt to be trigonal in structure and to have the empirical formula  $\text{Fe}_3\text{Mo}_2$ .

The occurrence of the zeta phase ( $\zeta$ ) at 50 atomic per cent molybdenum was established by Takei and Murakami, and this phase has recently been shown by Goldschmidt (6) to have the same structure as  $\text{FeCr}$ , the iron-chromium sigma phase. The zeta or sigma phase in the iron-molybdenum system decomposes at  $1180^\circ\text{C}$  ( $2156^\circ\text{F}$ ) by a eutectoid reaction to form  $\text{Fe}_3\text{Mo}_2$  and eta ( $\eta$ ), the molybdenum terminal solid solution.

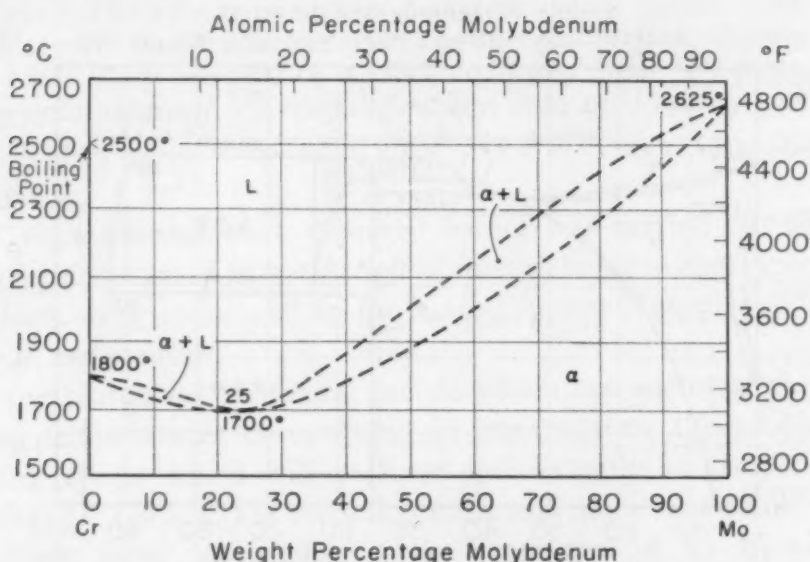


Fig. 2—The Chromium-Molybdenum System. *Metals Handbook* (1948).

**Chromium-Molybdenum.** The chromium-molybdenum system is generally considered to be a continuous series of solid solutions, as shown in Fig. 2 from the *Metals Handbook* (1948). The most recent work is that of Parke and Herzig (7) who found by pressing together blocks of molybdenum and chromium and heating for a long time at  $1260^\circ\text{C}$  ( $2300^\circ\text{F}$ ) that only continuous solutions were formed. Trzebiatowski, Ploszek and Lobzowski (8) formed chromium-molybdenum alloys by sintering fine powders. They report the melting point of chromium as  $1770^\circ\text{C}$  ( $3218^\circ\text{F}$ ) and a liquidus minimum between chromium and molybdenum at  $1700^\circ\text{C}$  ( $3218^\circ\text{F}$ ) and 25% molybdenum. X-ray studies of the alloys showed the presence of only one phase, the body-centered cubic solid solution. According to the literature, the melting point of chromium is between  $1500$  and  $1900^\circ\text{C}$  ( $2732$  and  $3452^\circ\text{F}$ ). The *Metals Handbook* (1948) has adopted the figure of  $1800^\circ\text{C}$  ( $3272^\circ\text{F}$ ), while Brenner, Burkhead and Jennings (9) of the Bureau of Standards recommend the deter-

mination of Grube and Knabe (10) which gives 1890 °C (3434 °F) as the melting point.

*Iron-Chromium.* The familiar iron-chromium diagram as given in the *Metals Handbook* by Bain and Aborn and reproduced in Fig. 3 is well established, with the possible exception of the high-chromium boundaries of the sigma and the sigma-plus-alpha fields. It is interesting to note that the iron-chromium sigma is essentially a low temperature phase decomposing above 820 °C (1508 °F), while FeMo,

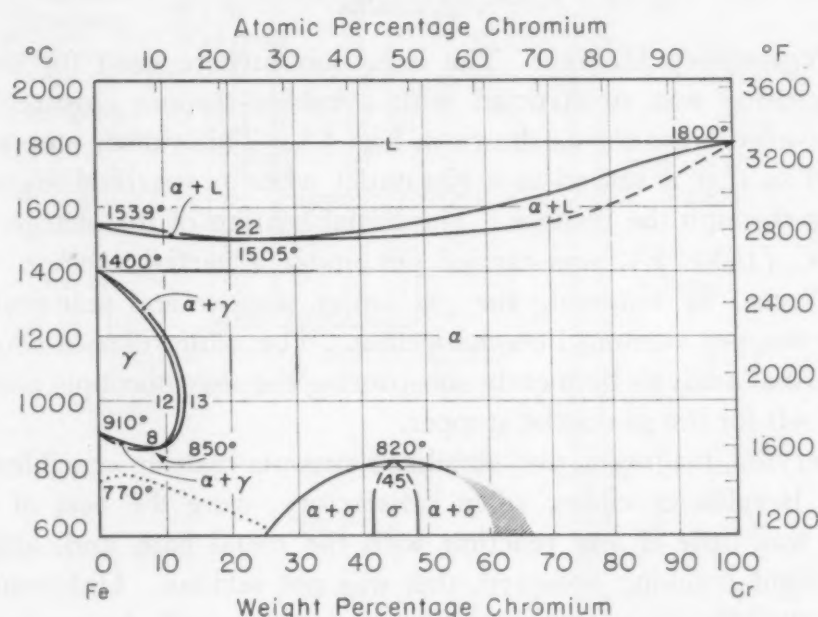


Fig. 3—The Iron-Chromium Binary System. *Metals Handbook* (1948).

although isomorphous with FeCr, is a high temperature phase being stable up to its melting point and unstable below 1180 °C (2156 °F). In this respect, FeMo is also distinct from the cobalt-chromium sigma (CoCr) described by Sully and Heal (11) and iron-vanadium sigma (FeV) described by Wever and Jellinghaus (12), both of which are stable at room temperatures and unstable at elevated temperatures.

## EXPERIMENTAL WORK

### *Summary of Procedure*

A series of chromium-molybdenum-iron alloys covering at approximately 10% intervals the range of composition of from 10 to 70% chromium, from 10 to 60% molybdenum, and from 10 to 70% iron was made up by melting under an inert atmosphere in an induction furnace. The alloys were further refined by remelting under vacuum. Liquidus temperatures were then determined by thermal

analysis using thermocouple pyrometry. After thermal analysis, the alloys were analyzed chemically for composition. The alloys were then subjected to various heat treatments followed by metallographic and X-ray examination for the purpose of delineating the extent of the various phases at various temperatures.

*Materials.* The materials used were electrolytic chromium and iron containing approximately 0.5% oxygen and the high purity, lamp-filament grade of molybdenum.

### *Apparatus*

*Preliminary Melting.* The induction furnace used for preliminary melting was constructed with a rubber-stopper closure in the water-cooled brass top as shown in Fig. 4A. This rubber stopper was pierced so that it served as a gas outlet when prepurified argon was flowing through the furnace. The initial heating of the charge, up to 1000 °C (1830 °F), was carried out under a partial vacuum. This was effected by removing the gas outlet stopper and substituting a rubber-stopper vacuum line connection. The same furnace was used for thermal analysis by merely substituting the thermocouple assembly of Fig. 4B for the gas outlet stopper.

Beryllia, magnesia, and stabilized zirconia melting crucibles were tried. Beryllia crucibles, when satisfactory, were the best of these. There was little if any reaction with the metal bath and, although some slight cracking occurred, this was not serious. Unfortunately, these crucibles were not consistent performers and the majority of them cracked severely, spilling the melt. This condition could not be rectified, in spite of the best efforts of the suppliers, and beryllia crucibles were abandoned.

Magnesia crucibles usually cracked during the melting cycle. Moreover, the use of these crucibles in the vacuum-melting step resulted in several mild explosions when air was admitted to the furnace after cooling.

Stabilized zirconia crucibles were finally adopted as the most suitable for the purpose. There was some reaction with the melt and some cracking, but the reaction zone could be ground off the ingot without any hazard to health, which was not the case with ingots melted in beryllia.

The molybdenum crucible cover was used to prevent bridging of the melt and did this effectively.

*Vacuum Melting.* The crucible arrangement in the vacuum-melting induction furnace was substantially the same as that in the argon furnace. A condenser consisting of an inverted, small Alundum



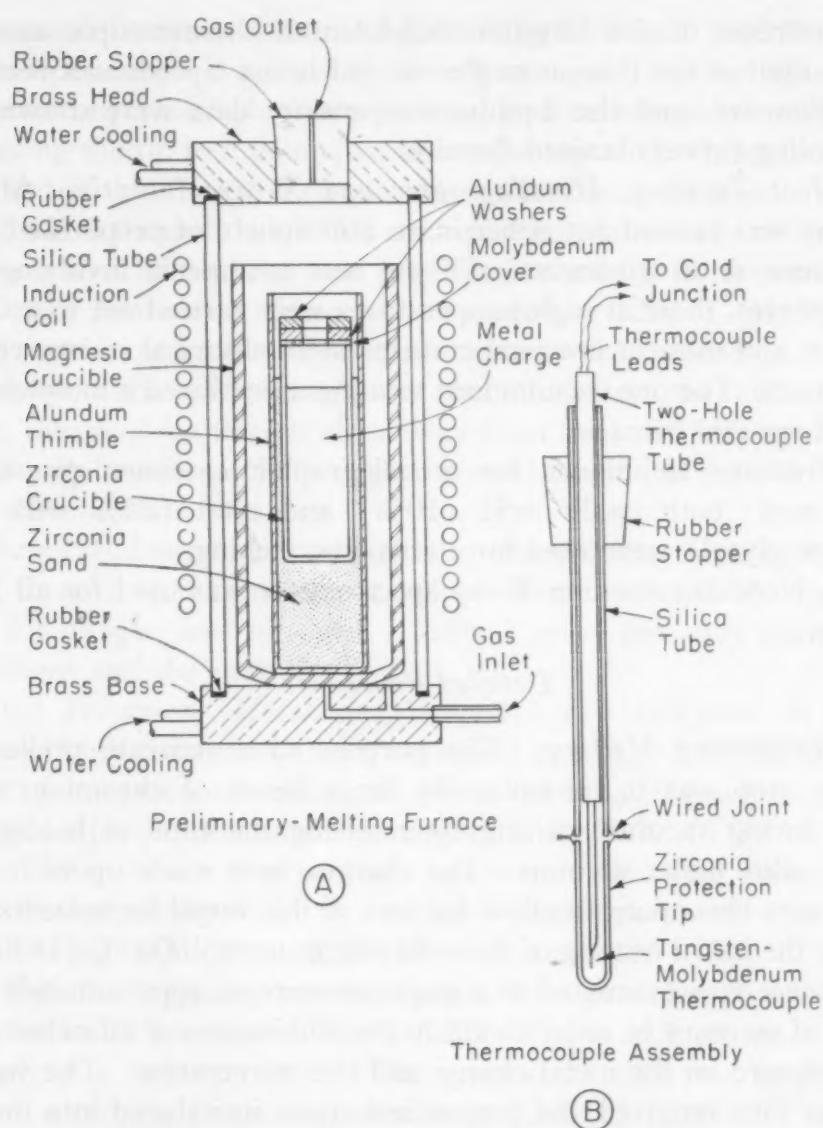


Fig. 4A—Section Through Furnace Used in Preliminary Melting and Thermal Analysis. Fig. 4B—Details of Thermocouple Assembly.

crucible with a pierced bottom was placed on top of the melting crucible for the purpose of minimizing the escape of chromium vapor into the vacuum system. The furnace top was equipped with a sight glass and prism for optical temperature measurement.

The vacuum system consisted of a high-vacuum mechanical pump backing up two mercury diffusion pumps. It was possible to reduce the absolute pressure in the system to less than  $10^{-5}$  millimeters of mercury at room temperature and to just above  $10^{-4}$  millimeters at  $1200^{\circ}\text{C}$  ( $2190^{\circ}\text{F}$ ).

**Thermal Analysis.** Thermal analysis was carried out in the same furnace as the preliminary melting operation, the only difference being

the insertion of the tungsten-molybdenum thermocouple assembly. The output of the thermocouple was fed into a Speedomax recording potentiometer, and the liquidus-temperature data were drawn from the cooling curves obtained thereby.

*Heat Treating, Metallographic and X-ray Analysis.* All heat treating was carried out either in an atmosphere of prepurified argon or helium, or in a vacuum. Of the heat treatments involving inert atmospheres, those at high temperatures were carried out in a Globar furnace, and those at low temperatures in an electrical resistance muffle furnace. The one vacuum heat treatment employed a molybdenum-wound vacuum furnace.

Ordinary techniques for metallographic specimen preparation were used; both oxalic acid (10%) and nital (20% with 20% ethylene glycol) were used for electrolytic etching.

A Norelco recording X-ray spectrometer was used for all X-ray studies.

#### *Detailed Procedure*

*Preliminary Melting.* The purpose of a separate preliminary melting step was to minimize the large losses of chromium which occur during vacuum melting by reducing the time of holding the molten alloy under vacuum. The charges were made up with about 20% extra chromium to allow for loss of this metal by volatilization. During the initial heating of the solid charge up to 1000 °C (1830 °F), the furnace was evacuated to a gage pressure of approximately -30 inches of mercury in order to aid in the elimination of adsorbed gases and moisture on the metal charge and the refractories. The vacuum line was then removed and prepurified argon introduced into the furnace for the remainder of the fusion process. The alloy was permitted to solidify in the crucible and both were removed for the vacuum melting.

*Vacuum Melting.* The alloy in its crucible was then placed in the vacuum-melting furnace, the system evacuated, and the temperature raised at a moderate rate to about 1400 °C (2550 °F). Then the temperature was raised rapidly to 1800-2000 °C (3270-3630 °F) and held for 1 to 3 minutes before the power was shut off and the melt allowed to cool under vacuum. After cooling, the alloy ingot, still in the same crucible, was returned to the preliminary melting furnace for thermal analysis.

*Thermal Analysis.* The charge was again heated under a partial vacuum to about 1000 °C (1830 °F) before argon was started through the furnace. Heating continued until the charge melted and reached

a temperature between 1800 and 2200 °C (3270 and 3990 °F), at which temperature it was held for 4 or 5 minutes. During this time, the thermocouple assembly was inserted and permitted to warm up by lowering the tip to a point just above the top of the induction coil. At the end of this time, the couple was lowered into the melt. When the recorder indicated that it had attained a constant temperature, the power was shut off and the melt permitted to solidify by free cooling. Occasionally heats were reheated and cooled to 1200 °C (2190 °F) several times in order to recheck points, but it was preferred to avoid this because of the continuous loss of chromium from the melt. After cooling, the crucibles were broken away from the solidified ingots, the crucible-metal surfaces of the ingots ground away and samples taken for the chemical analysis.

*Chemical Analysis.* In addition to determining the composition of the three major constituents, alloys were analyzed by vacuum fusion for oxygen and nitrogen. Table I gives the alloy numerical designations and the analyses.

*Heat Treatment, Metallographic and X-ray Analysis.* A small number of high chromium alloys were held at 1370 °C (2500 °F) for 24 hours in a vacuum furnace and permitted to cool slowly at a rate of 2 degrees per minute until a temperature of 800 °C (1470 °F) was attained, after which free cooling was permitted. The alloys were etched electrolytically in nital, examined metallographically, and the presence of sigma in certain of the alloys was noted.

All of the remaining heat treatments were preceded by a solution treatment for 24 hours, at 1300 °C (2370 °F), in an inert atmosphere followed by a water quench. The purpose of this was to provide data for a ternary isothermal section at 1300 °C (2370 °F) and to provide microstructural data which would serve as references by means of which the effects of all subsequent heat treatments on microstructures could be judged.

Duplicate samples of each ternary alloy were solution heat treated for the 1300 °C (2370 °F) isothermal section. One sample of each alloy was prepared for X-ray examination, either by crushing or by filing, and the remaining sample prepared for metallographic examination. Phase identification in this series of alloys was a matter of correlating X-ray and metallographic data.

Solution heat treated samples of each ternary alloy were reheated to 1100 °C (2010 °F), held for 24 hours, and water-quenched and examined metallographically. Since the 1300 °C (2370 °F) isothermal section had already been established, it was felt that phase identification could be accomplished by referring the 1100 °C



Table I  
Chemical Analyses of the Alloys After Thermal Analysis

Melt Number	Cr	Mo	Fe	O <sub>2</sub>	N <sub>2</sub>
219	23.27	49.07	25.19	0.127	0.048
23	64.77	24.10	10.62	0.396	0.015
24	19.32	11.07	69.41	0.053	0.023
25	11.45	30.26	57.14	0.030	0.011
26	.....	55.74	44.22	0.157	0.016
27	10.47	21.60	68.29	0.035	0.010
28	8.63	40.67	50.42	.....	.....
29	10.44	50.26	38.90	.....	.....
30	10.13	57.87	32.30	0.116	0.017
31	18.62	20.66	80.79	0.072	0.003
32	21.08	28.53	50.06	.....	.....
33	18.51	40.26	39.50	.....	.....
34	19.13	52.00	29.11	.....	.....
35	18.38	59.60	19.60	0.129	0.005
36	27.23	17.37	55.59	.....	.....
37	31.46	26.26	43.66	0.106	0.005
38	25.68	36.80	36.10	.....	.....
39	24.56	47.74	27.99	.....	.....
40	26.09	57.74	15.67	.....	.....
41	43.18	8.80	48.05	0.041	0.011
42	41.89	22.13	36.36	.....	.....
43	36.52	31.34	31.90	0.088	0.019
44	41.62	39.20	20.01	.....	.....
45	26.09	63.87	10.41	0.195	0.003
46	50.50	9.53	39.18	0.173	0.003
47	50.78	19.47	29.39	0.124	0.009
48	53.17	28.00	19.37	0.239	0.006
49	41.42	47.07	11.75	0.179	0.005
50	58.44	11.27	30.79	0.163	0.011
51	63.01	18.67	19.17	0.205	0.006
52	55.85	34.14	11.75	.....	.....
53	66.69	10.60	21.13	0.126	0.036
54	90.67	9.27	.....	0.344	0.006
254	84.63	15.37*	.....	0.714	0.039
55	75.96	24.04*	.....	.....	.....
56	68.67	31.33*	.....	.....	.....
256	73.53	26.47*	.....	.....	.....
57	70.06	29.94*	.....	.....	.....
257	66.33	33.67*	.....	.....	.....
58	44.74	55.26*	.....	.....	.....
59	90.12	.....	10.78	0.530	0.030
60	79.34	.....	19.74	.....	.....
61	11.36	.....	89.02	.....	.....
62	20.76	.....	78.94	.....	.....
63	33.48	.....	68.30	.....	.....
64	37.14	.....	60.46	.....	.....
65	.....	63.61*	36.39	.....	.....
66	.....	45.42*	54.58	.....	.....
67	70.69	.....	31.36	.....	.....
69	.....	57.60	43.10	.....	.....
70	.....	41.20	59.61	.....	.....
71	.....	31.14*	68.86	.....	.....
72	58.63	41.37*	.....	.....	.....
73	90.35	9.65*	.....	.....	.....
74	43.53	56.47*	.....	.....	.....

\*By difference from 100%.

(2010 °F) microstructures back to the corresponding structures existing at 1300 °C (2370 °F). For this reason, a complete X-ray analysis of the alloys of this and the following series was not made.

A third set of solution heat treated ternary alloys was reheated to 900 °C and held for 5 days at that temperature. The longer holding time was adopted to allow for the increased sluggishness of solid-state reactions in this system at low temperatures. These alloys

Table II  
Comparison of Measured Interplanar Spacings of  $\text{Fe}_3\text{Mo}_2$  With Those Calculated From Published Data

Author's Data		Arnfeld Data (5)	
I*	Cr $K_\alpha$ 'd'	I*	Fe $K_\alpha$ and $K_\beta$ 'd'
S	2.39	S	2.36-2.32
M	2.28	..	...
S	2.19	S	2.17-2.18
VS	2.15	S	2.14
VS	2.09	S	2.07
M	2.06	W	2.05
S	2.04	S	2.02
S	1.97	M	1.95
M	1.925	M	1.90
W	1.83	W	1.82
W	1.80	W	1.79

\*—Relative Intensities; VS—Very Strong; S—Strong; MS—Medium Strong; M—Medium; MW—Medium Weak; W—Weak; VW—Very Weak.

were also examined metallographically and the extent of the various phase regions at this temperature was noted.

#### Other Experiments

Alloy 71 containing 31% molybdenum and 69% iron was decomposed electrolytically in a 1:1 HCl electrolyte. The  $\text{Fe}_3\text{Mo}_2$  residue, after washing in water and alcohol, was dried, sealed in an evacuated quartz tube and annealed for 96 hours at 870 °C (1600 °F). An X-ray pattern of the residue was made using chromium K-alpha radiation. The interplanar spacings so determined and those given by Arnfeld are compared in Table II.

Alloy 65 containing 64% molybdenum and 36% iron was water-quenched from 1400 °C (2550 °F). This specimen was then crushed and an X-ray pattern made. The interplanar spacings found are compared with those of Goldschmidt for  $\text{FeMo}$  in Table III.

The interplanar spacings corresponding to three major lines in the  $\text{FeMo-FeCr}$  X-ray pattern were plotted for all ternary alloys consisting of single-phase sigma at 1300 °C (2370 °F) as a function of the atomic percentage of molybdenum. The effect of molybdenum on these interplanar spacings is shown in Fig. 21.

### EXPERIMENTAL RESULTS

#### Liquidus Temperatures

The liquidus temperatures measured by the thermal analysis method are given in Fig. 5. The liquidus surface has a region of low melting (about 1460 °C) alloys which extends inward from the iron-molybdenum eutectic to an approximate composition of 60 iron - 20 chromium - 20 molybdenum.

**Table III**  
**Comparison of Measured Interplanar Spacings of FeMo With Published Data**

Author's Data		Goldschmidt Data (6)	
I*	Cr K $\alpha$ 'd'	I*	Co K $\alpha$ 'd'
W	2.46	W	2.46
W	2.35	MW	2.35
M	2.18	S	2.21
M	2.14	M	2.13
MS	2.09	M	2.08
MS	2.04	MS	2.04
W	1.99	S	1.99

\*—Relative Intensities; VS—Very Strong; S—Strong; MS—Medium Strong; M—Medium; MW—Medium Weak; W—Weak; VW—Very Weak.

The concavity of the liquidus in this region is quite slight and the data do not appear to be sufficiently accurate to determine whether the liquidus minimum slopes downward upon entering the ternary or whether it slopes slightly upward. The former would indicate a ternary eutectic type of reaction in this region, while the latter would suggest a ternary peritectic reaction.

The melting points of chromium-molybdenum alloys as determined here are higher than those given in the binary diagram of Fig. 2. The melting point of chromium was measured as 1892 °C (3435 °F). The data indicate that the liquidus minimum in this binary system is an extended flat at about 1860 °C (3380 °F), covering a range of chromium contents from 15 to 30%. In the iron-molybdenum binary alloys in the region of 55 to 60% molybdenum, the measured liquidus temperatures are lower than the published data of Fig. 1 by about 100 degrees. However, the measured melting temperatures of the iron-molybdenum alloys in the region of the eutectic are quite in line with these data.

#### *Effect of Thermal Treatments on Solid-Phase Distribution*

*Alloys Quenched From 1300 °C.* Fig. 6 summarizes the data obtained from the metallographic and X-ray studies of these alloys. The data indicate that the influence of Fe<sub>3</sub>Mo<sub>2</sub> in the ternary is quite localized at 1300 °C (2370 °F), since none of this phase was found in alloys containing as little as 9% chromium. For this reason, the fields involving this phase are indicated by dashed lines merely to indicate their existence.

The diagram of Fig. 6 shows the considerable effect of chromium in increasing the range of composition of the iron-molybdenum sigma phase. It also shows that the high temperature stability of the sigma phase in iron-chromium alloys would be enhanced by the addition of



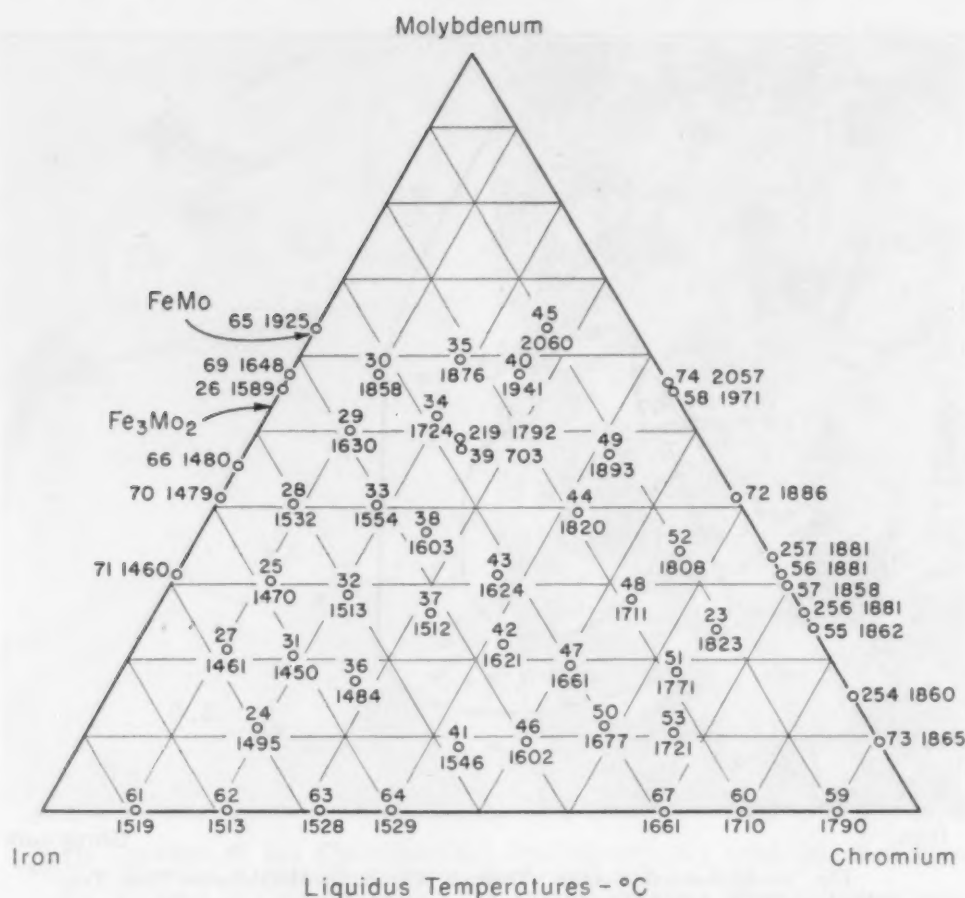


Fig. 5—Ternary Plot of Chromium-Molybdenum-Iron Liquidus Temperatures.

molybdenum. This is further borne out in the lower temperature heat treatments to be described below.

Fig. 7 shows that the 1300 °C (2370 °F) structure of Alloy 28 (8.6 chromium – 40.7 molybdenum – 50.4 iron) consists wholly of the sigma phase. The structure of Alloy 35 (18.4 chromium – 59.6 molybdenum – 19.6 iron) is shown in Fig. 8. The irregular white etching patches are primarily molybdenum solid solution in a sigma matrix. The small globules within the solid solution patches are sigma which has precipitated on cooling from the melt due to decreasing solubility of iron and chromium. The large black areas in the sigma matrix are holes from which sigma particles were torn during the metallographic preparation.

Alloy 30 (10.1 chromium – 57.9 molybdenum – 32.3 iron) has the same type of structure at 1300 °C (2370 °F) as Alloy 35, except that the amount of molybdenum solid solution is quite minute, as shown in Fig. 9.

Another two-phase sigma plus solid solution structure is exhib-

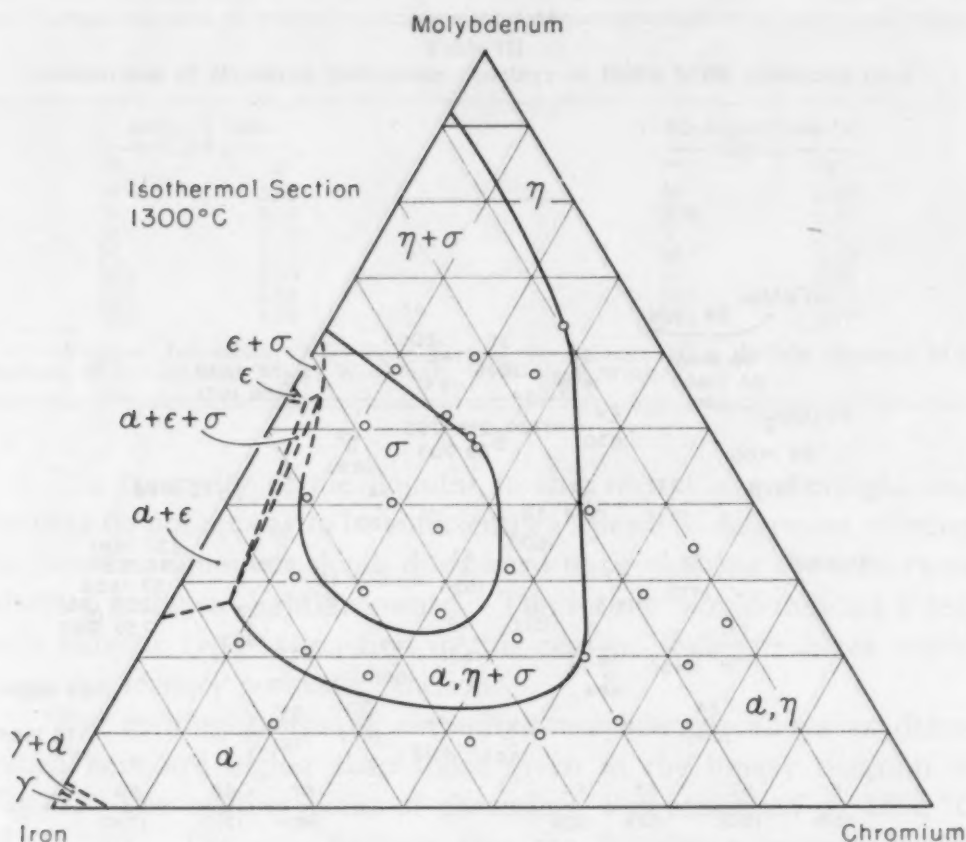


Fig. 6—Isothermal Section Through Chromium-Molybdenum-Iron Ternary at 1300 °C (2370 °F).

ited by Alloy 219 (23.3 chromium – 49.1 molybdenum – 25.2 iron) in Fig. 10. The absence of precipitated sigma within the solid solution seems to indicate a rather slight decrease in the solubility of iron and chromium in this particular solution. The manner in which cracks in the sigma matrix frequently terminate themselves upon reaching the more ductile second phase is also illustrated by this photomicrograph.

*Alloys Quenched From 1100 °C.* Metallographic data obtained from this series of alloys are given in the isothermal section of Fig. 11. Both the sigma and sigma plus solid solution fields are expanded toward the chromium-molybdenum side, the chromium corner, and the iron-chromium side of the ternary. The eutectoid decomposition of high molybdenum sigma, which occurs at 1180 °C (2155 °F) for FeMo, is reflected in the appearance of two new fields: molybdenum solid solution plus epsilon, and molybdenum solid solution plus epsilon plus sigma. The two-phase sigma plus epsilon field and the three-phase alpha plus sigma plus epsilon fields are also expanded by the shrinking of the sigma field from the iron-molybdenum side of the

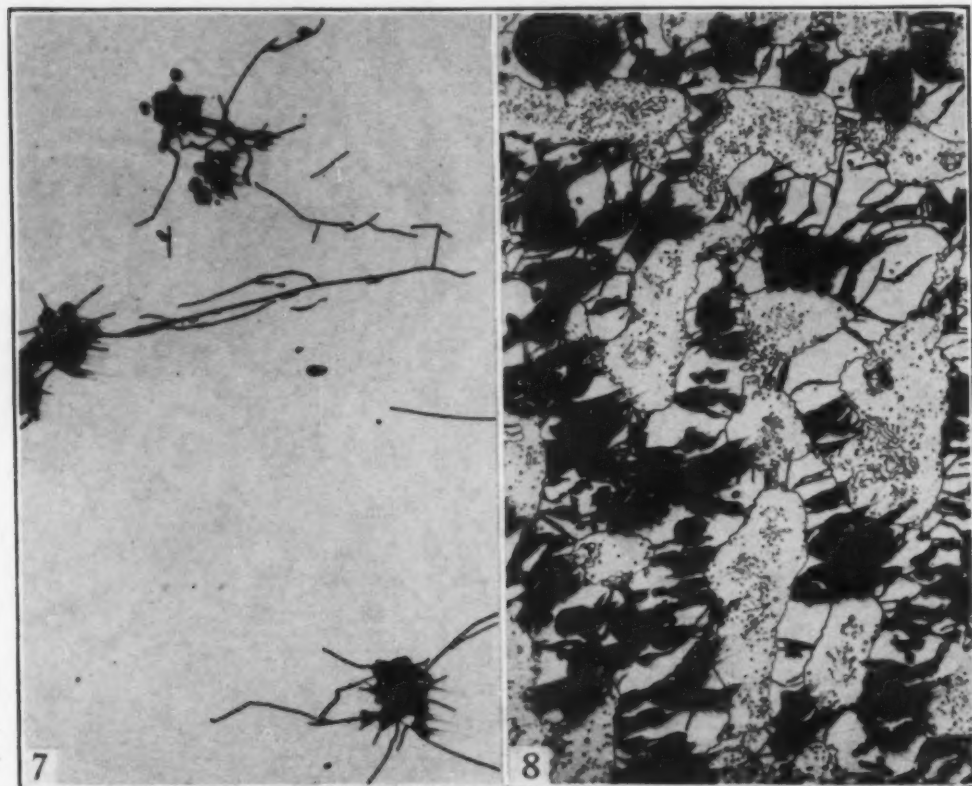


Fig. 7—Alloy 28 (8.6 Chromium—40.7 Molybdenum—50.4 Iron) Quenched From 1300 °C. Structure is single-phase sigma. Oxalic acid etch.  $\times 150$ .

Fig. 8—Alloy 35 (18.4 Chromium—59.6 Molybdenum—19.6 Iron) Quenched From 1300 °C. The irregular light-etching patches are primary molybdenum solid solution in a cracked sigma matrix. Oxalic acid etch.  $\times 150$ .

ternary. The boundaries of these fields are again shown with dashed lines because they contain an insufficient number of alloys to determine their limits with any degree of accuracy.

Alloy 25 (11.4 chromium—30.3 molybdenum—57.1 iron) consists of three phases at 1100 °C (2010 °F), as shown in Fig. 12. The sharp-cornered particles having heavy black boundaries are ferrite. The light-etching phase which appears to have precipitated in the matrix is epsilon, and the matrix itself is the sigma phase.

Fig. 13 shows the microstructure of Alloy 30 (10.1 chromium—57.9 molybdenum—32.3 iron) at 1100 °C (2010 °F). The dark speckled regions appear to be the solid solution plus epsilon eutectoid. The white etching particles in the sigma matrix are probably epsilon.

Alloy 41 (43.2 chromium—8.8 molybdenum—48.0 iron) contains at least 50% sigma at 1100 °C (2010 °F), as shown in Fig. 14. The rounded gray patches are ferrite.

An acicular precipitate of the sigma phase in Alloy 44 (41.6 chromium—39.2 molybdenum—20.0 iron) is seen in Fig. 15.



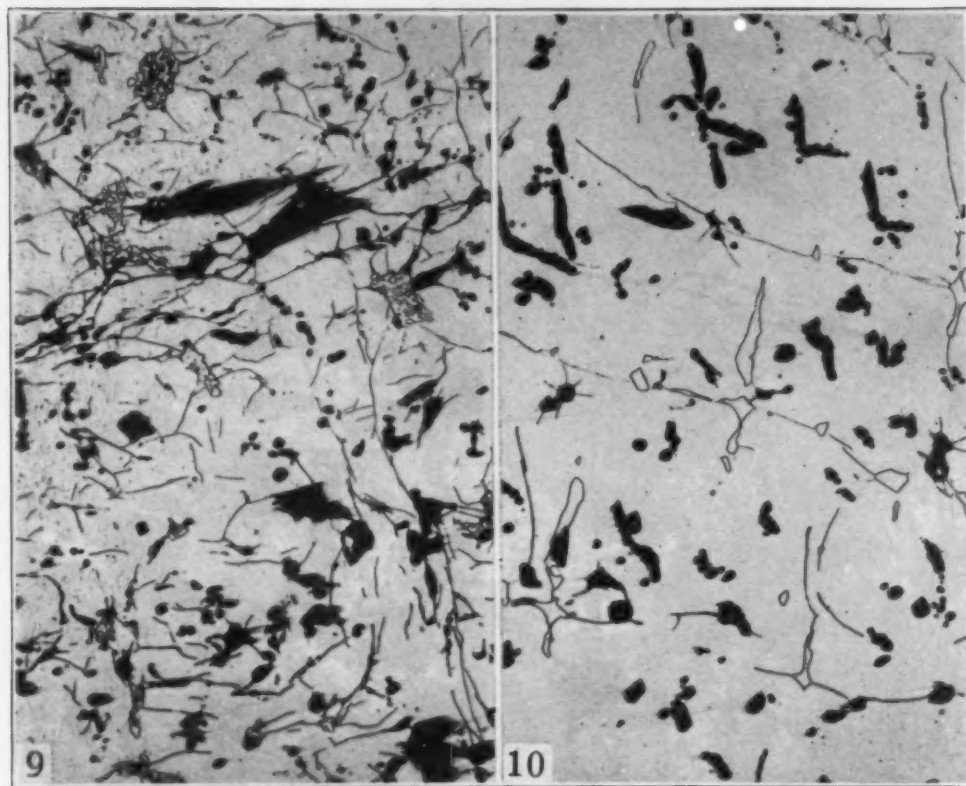


Fig. 9—Alloy 30 (10.1 Chromium—57.9 Molybdenum—32.3 Iron) Quenched From 1300 °C. Similar in structure to Alloy 35 except much less molybdenum solid solution. Oxalic acid etch.  $\times 150$ .

Fig. 10—Alloy 219 (23.3 Chromium—49.1 Molybdenum—25.2 Iron) Quenched From 1300 °C. Solid solution in sigma matrix. Note different appearance from solid solution of Alloy 30. Oxalic acid etch.  $\times 150$ .

*Alloys Quenched From 1300 °C and Aged 5 Days at 900 °C.* The isothermal section showing the distribution of the various phases in the ternary after this heat treatment is given in Fig. 16. The three-phase fields and the two-phase sigma plus epsilon field are again expanded toward higher chromium contents because of the low temperature decomposition of the sigma and the shrinking of the sigma field away from the iron-molybdenum side of the ternary. The extent of the sigma and the sigma plus solid solution fields toward the chromium-molybdenum side and the chromium corner of the ternary is *less* than that at 1100 °C (2010 °F). This would seem to indicate that the alloys in this region are extremely sluggish and that equilibrium was not at all attained in the aging time of 5 days at temperature. Hence, the sigma boundaries are dashed lines in this region, with arrows indicating the direction of movement for equilibrium.

Fig. 17 shows the microstructure of Alloy 43 (36.5 chromium—31.3 molybdenum—31.9 iron) after this heat treatment. This alloy was completely transformed to sigma in the 1100 °C (2010 °F) heat

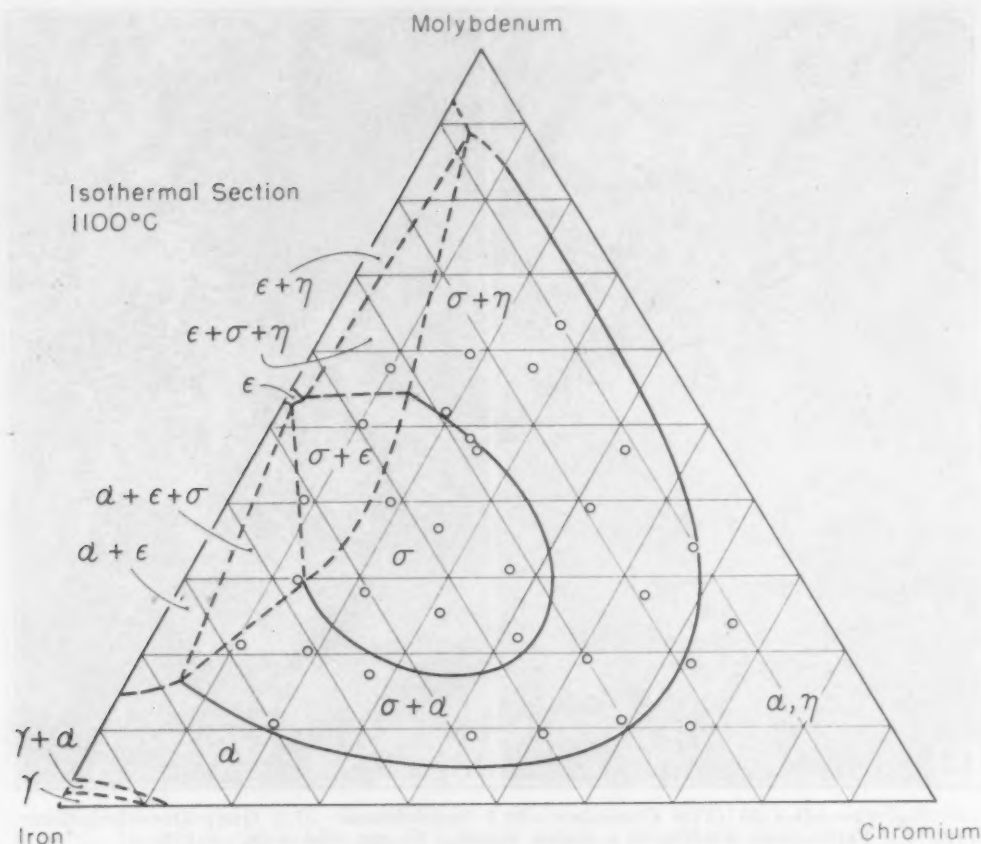


Fig. 11—Isothermal Section Through Chromium-Molybdenum-Iron Ternary at 1100 °C (2010 °F).

treatment. The grayish patches are the remnants of solid solution particles which have not yet completely decomposed to form sigma.

On the other hand, Alloy 45 (26.1 chromium–63.9 molybdenum–10.4 iron) developed considerably more sigma at 900 °C (1650 °F) than in the 1100 °C (2010 °F) aging treatment. The microstructure of this alloy is found in Fig. 18. It will be noted that the white sigma areas appear to be growing in a dendritic fashion. This may be due either to concentration gradients or to preferred crystallographic growth direction.

The microstructure of Alloy 25 (11.4 chromium–30.3 molybdenum–57.1 iron) after the 900 °C (1650 °F) treatment is shown in Fig. 19 and is much different in appearance from that after the 1100 °C (2010 °F) treatment. However, this still appears to be a three-phase alloy. It is magnetic, and both the white patches and the gray matrix have about the same high hardness. It is concluded, therefore, that the gray matrix is largely sigma and that the white areas contain a conglomerate of epsilon and ferrite, the ferrite being in a finely divided form, as indicated by the black dots.

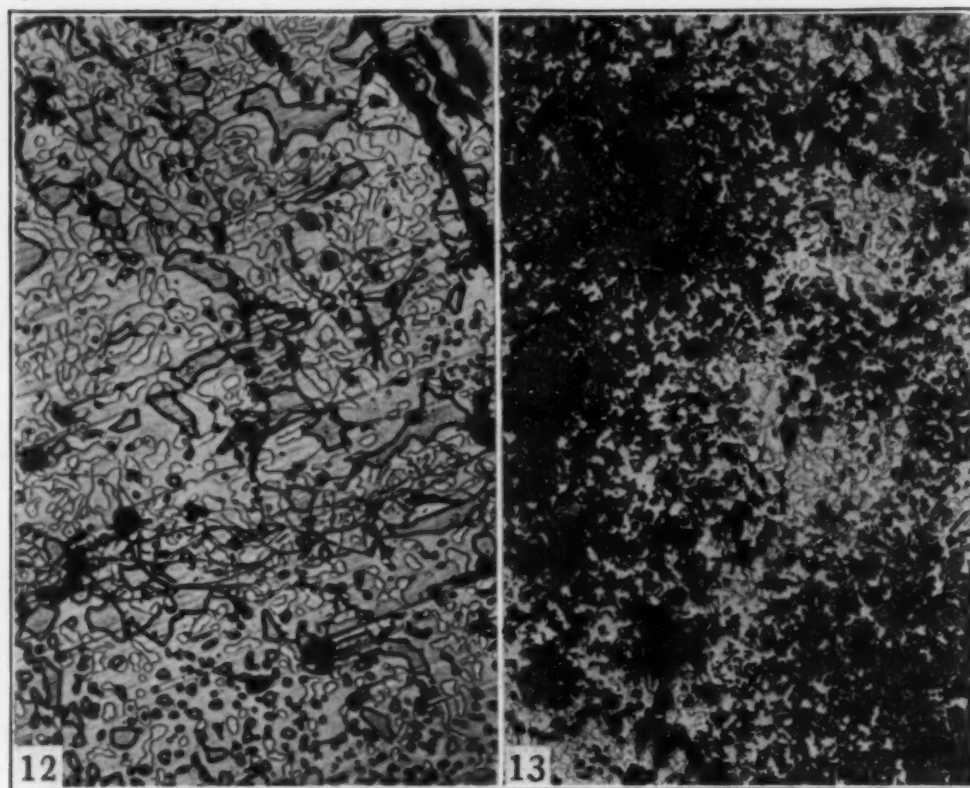


Fig. 12—Alloy 25 (11.4 Chromium - 30.3 Molybdenum - 57.1 Iron) Quenched From 1100 °C. Ferrite and  $\text{Fe}_3\text{Mo}_2$  in a sigma matrix. Oxalic acid etch.  $\times 150$ .

Fig. 13—Alloy 30 (10.1 Chromium - 57.9 Molybdenum - 32.3 Iron) Quenched From 1100 °C. Eutectoid of solid solution plus  $\text{Fe}_3\text{Mo}_2$  in sigma matrix which also appears to contain massive epsilon. Oxalic acid etch.  $\times 150$ .

*Alloys Slow Cooled From 1370 °C.* The purpose of this experiment was to determine the extent of the region of alloys containing sigma toward the chromium-molybdenum side and the chromium corner of the ternary under conditions of continuous slow cooling. The data obtained are shown in Fig. 20. Because of the sluggishness of sigma formation, less sigma was formed on direct cooling of these alloys from 1370 °C (2500 °F) than was formed on holding the same alloys at 1100 °C (2010 °F) for 24 hours.

#### *X-ray Data*

*$\text{Fe}_3\text{Mo}_2$ .* The X-ray measurements of certain interplanar distances of this phase are compared with those given by Arnfelt in Table II. It will be seen that the matching of these data is fair, but there is a shift in the pattern toward higher 'd' values in the data determined here. This might be due to composition differences between the specimens used in the two determinations. It was found that annealing the electrolytically separated  $\text{Fe}_3\text{Mo}_2$  residues improved



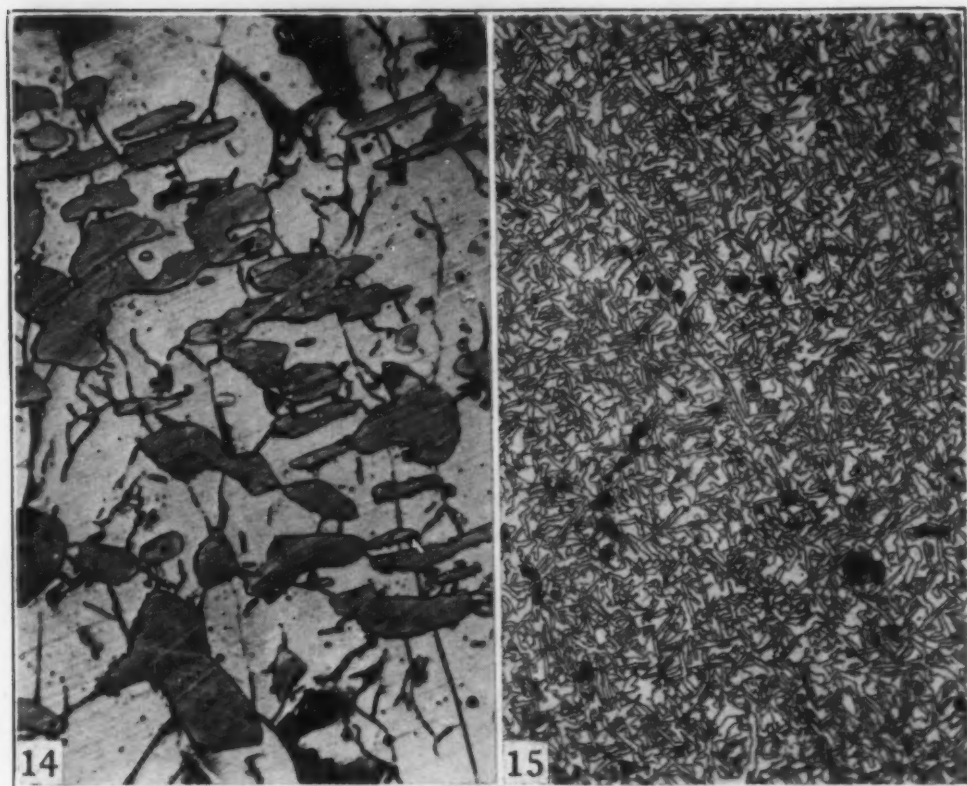


Fig. 14—Alloy 41 (43.2 Chromium—8.8 Molybdenum—48.0 Iron) Quenched From 1100 °C. Gray particles are ferrite in a sigma matrix. Oxalic acid etch.  $\times 150$ .

Fig. 15—Alloy 44 (41.6 Chromium—39.2 Molybdenum—20.0 Iron) Quenched From 1100 °C. Acicular precipitate of sigma phase in solid solution matrix. Oxalic acid etch.  $\times 150$ .

the matching. The maximum benefits from annealing were obtained in less than 96 hours.

*Sigma Phase.* The X-ray pattern of FeMo as determined here was in good agreement with that of Goldschmidt (6). The matching of the data is shown in Table III.

In an effort to determine the effect of molybdenum on the interplanar spacings in the sigma lattice, 'd' values were calculated for three of the most prominent lines in the patterns of those specimens which consisted of single-phase sigma at 1300 °C (2370 °F). These 'd' values were then plotted as a function of the atomic percentage of molybdenum in their respective specimens. The curves were then extended to include the corresponding 'd' values given by Duwez (14) for FeCr. These latter 'd' values would correspond to zero atomic percentage of molybdenum. The atomic ratio of iron to chromium was not constant from alloy to alloy. However, since the iron and chromium atomic radii are quite similar, it was thought that these two elements might act as one in their effect upon the lattice.

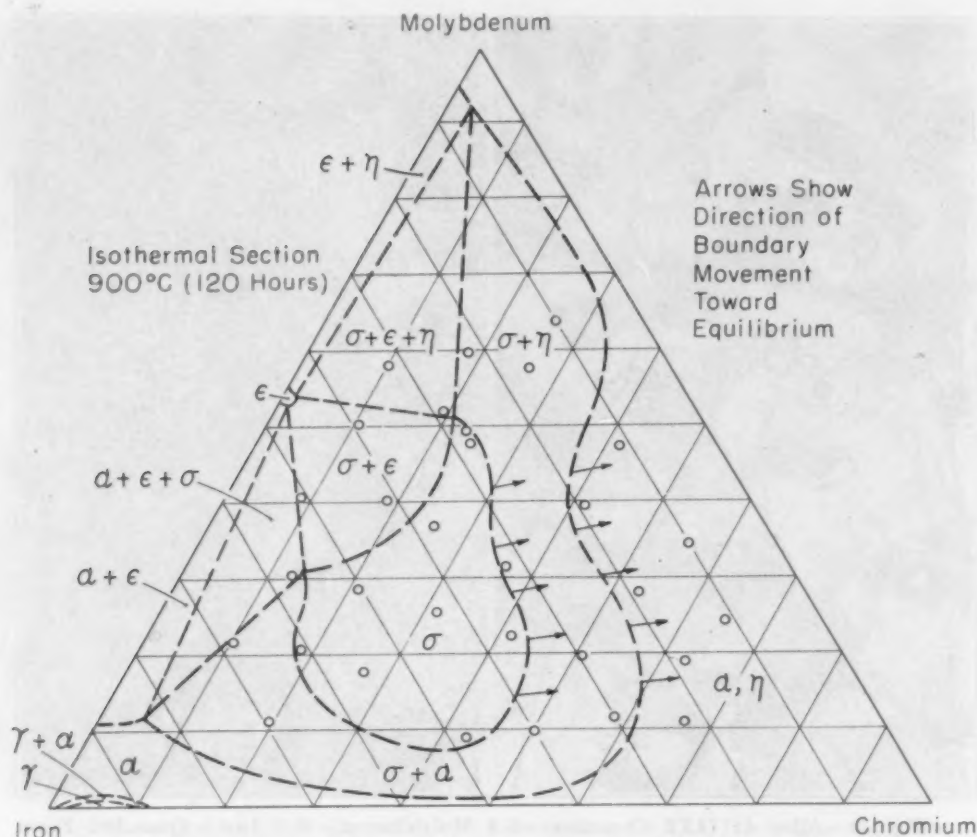


Fig. 16—Isothermal Section Through Chromium-Molybdenum-Iron Ternary at 900 °C (1650 °F).

This plot is shown in Fig. 21. It will be seen that the 'd' values increase almost linearly with increasing molybdenum.

#### DISCUSSION OF RESULTS

As can be seen from the ternary diagrams of Figs. 6, 11, 16 and 20, sigma is the major intermediate phase in the chromium-molybdenum-iron system. Its extensive occurrence puts rather severe limitations on the range of compositions which would be useful for high temperature duty, if one desires an alloy which does not develop the sigma phase in service.

Fig. 22 shows a vertical section through the ternary from the composition 100% iron to the composition 70% chromium and 30% molybdenum. It is unfortunate that it was necessary to extrapolate the high chromium sigma and sigma plus alpha boundaries because of the nonequilibrium condition of the pertinent alloys after aging for 5 days at 900 °C (1650 °F). However, even a conservative extrapolation serves to demonstrate the considerable extent of the solid

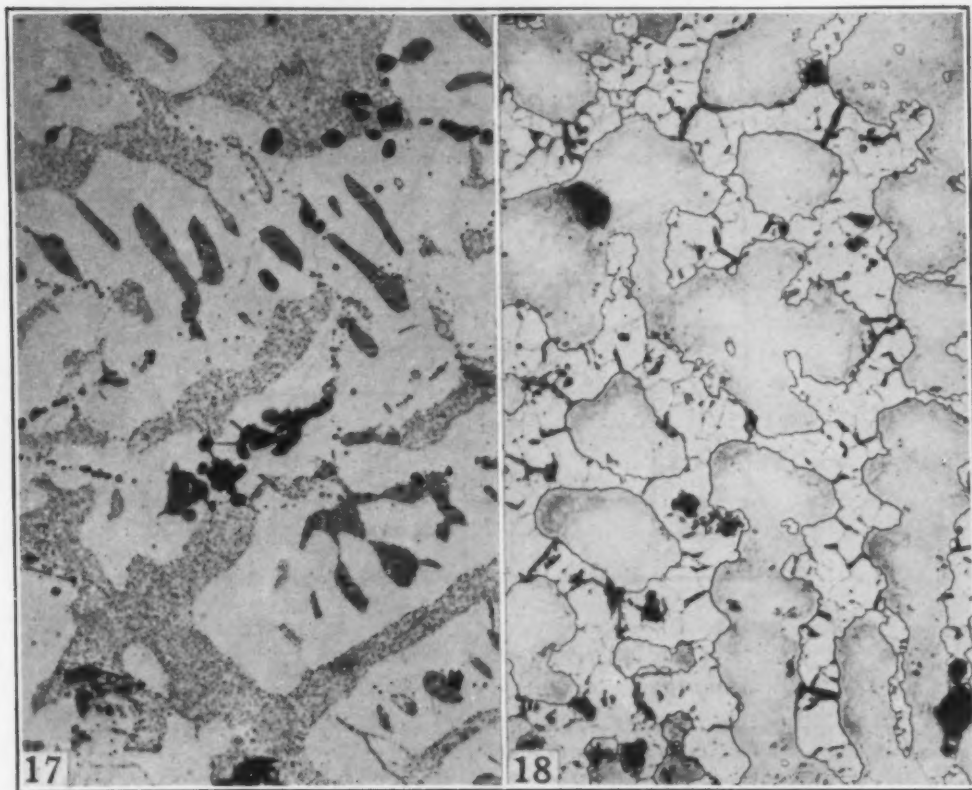


Fig. 17—Alloy 43 (36.5 Chromium—31.3 Molybdenum—31.9 Iron) Aged 5 Days at 900 °C. Sigma matrix containing particles of solid solution which have not as yet been transformed. Oxalic acid etch.  $\times 150$ .

Fig. 18—Alloy 45 (26.1 Chromium—63.9 Molybdenum—10.4 Iron) Aged 5 Days at 900 °C. Very white areas are sigma phase which is in a solid solution matrix. Oxalic acid etch.  $\times 150$ .

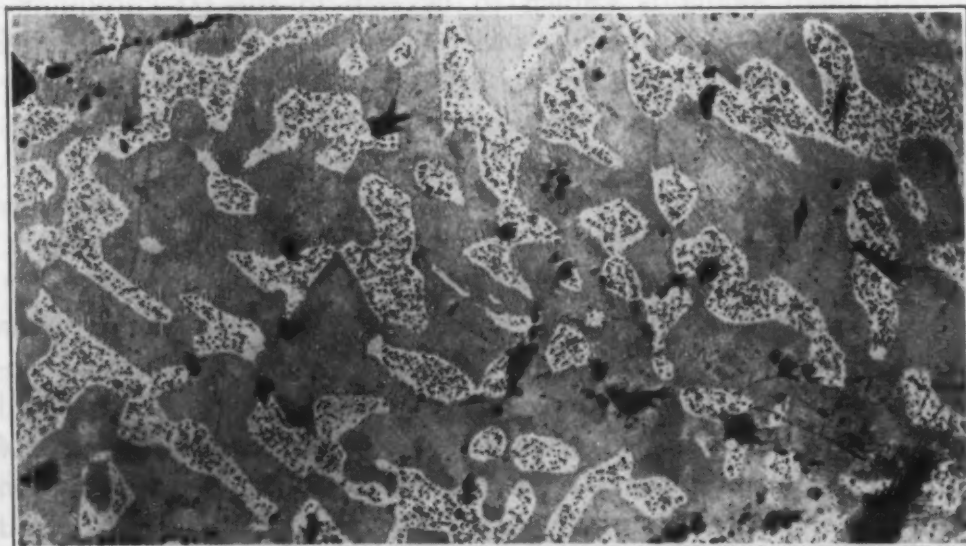


Fig. 19—Alloy 25 (11.4 Chromium—30.3 Molybdenum—57.1 Iron) Aged 5 Days at 900 °C. Gray matrix probably sigma. White patches  $\text{Fe}_3\text{Mo}_3$  containing ferrite shown by black spots. Oxalic acid etch.  $\times 150$ .



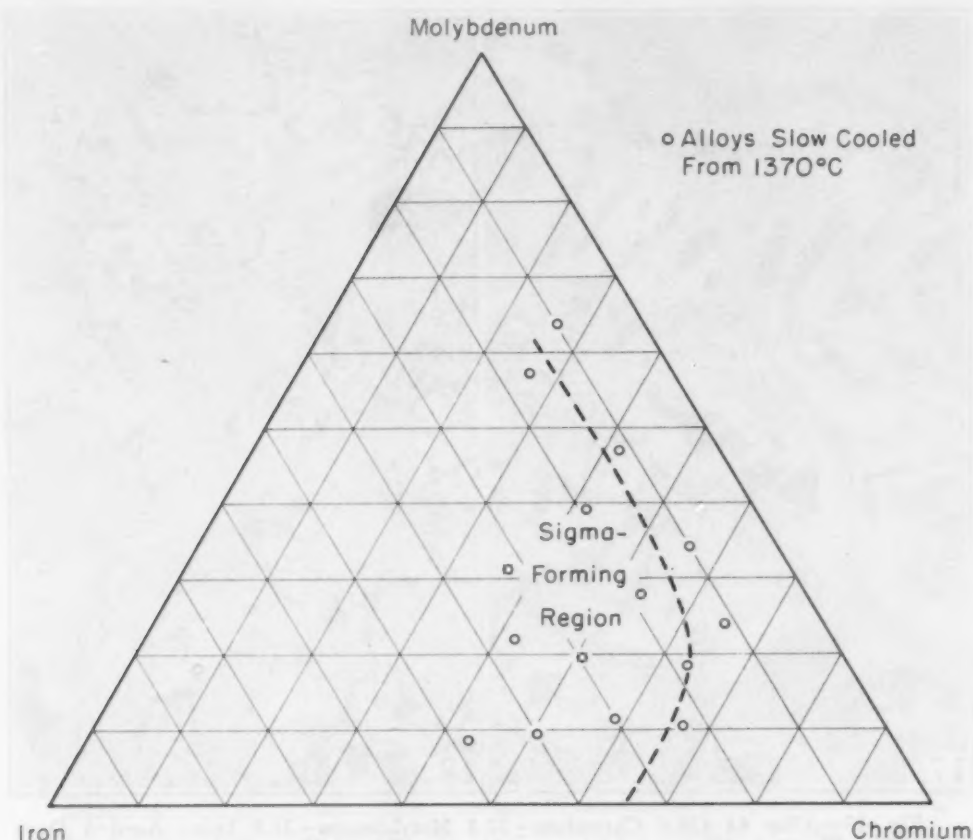


Fig. 20—Ternary Plot Showing Extent of Sigma Region in Chromium-Molybdenum-Iron Alloys Slow Cooled From 1370 °C (2500 °F).

solution plus sigma phase space toward the chromium-molybdenum side of the ternary.

Although sigma is known to develop in the 60 chromium–25 molybdenum–15 iron alloy, there is no real evidence that this phase is alone responsible for the brittleness exhibited by that alloy. Some of the high chromium alloys such as Alloy 48 (53.2 chromium–28.0 molybdenum–19.4 iron) were found to be so brittle that cracking and fragmentation occurred when hardness measurements were made with the Rockwell tester, even after quenching from 1300 °C (2370 °F), when no sigma could be found to be present.

The effect of molybdenum in stabilizing iron-chromium sigma at high temperatures is illustrated in Fig. 23 which is a vertical section through the ternary from 100% molybdenum to 50% iron and 50% chromium. This effect probably explains the persistence of sigma in the 20 chromium–14 nickel–4 molybdenum steels solution treated at temperatures between 1050 and 1150 °C (1920 and 2100 °F) (13).

The large amount of sigma in Alloy 45 (26.1 chromium–63.9

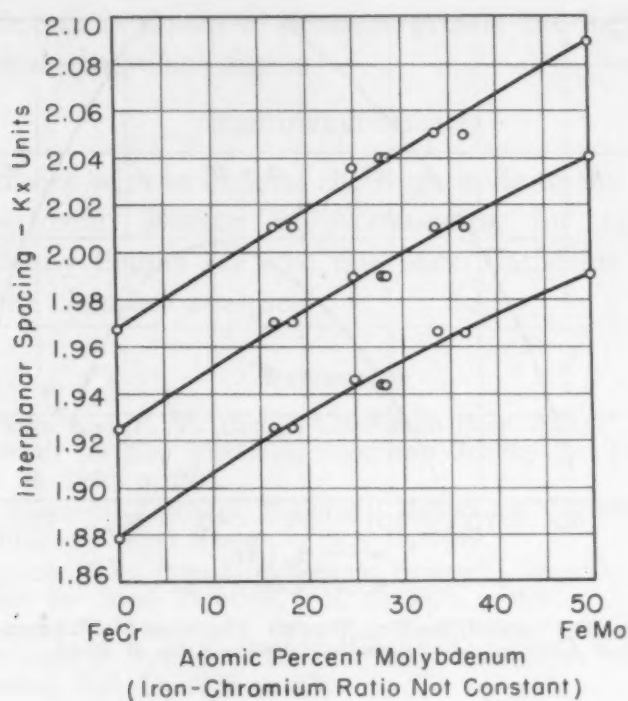


Fig. 21—Interplanar Spacing Versus Atomic Percentage Molybdenum for Chromium-Molybdenum-Iron Sigma Phase.

molybdenum – 10.4 iron) at 900 °C (1650 °F) might at first suggest the possibility of an undiscovered sigma phase existing in the chromium-molybdenum binary near the composition CrMo. On the other hand, the microstructure (Fig. 18) suggests, because of the dendritic appearance of the sigma, that there was considerable segregation during solidification. If this were the case, the primary dendrites would be rich in molybdenum, while the last liquid to solidify would be rich in iron and chromium. If such an inhomogeneity were not eliminated in the 1300 °C (2370 °F) solution, it might be expected that the sigma phase would take on such a dendritic (or interdendritic) appearance.

The curves of sigma-phase interplanar spacings versus the atomic percentage of molybdenum seem to follow Vegard's law.

#### SUMMARY

Liquidus temperatures of the chromium-molybdenum-iron system have been measured over the range of compositions of from 10 to 70% chromium, 10 to 60% molybdenum, and 10 to 70% iron. All ternary alloys containing less than 30% iron were found to have melting points above 1650 °C (3000 °F).

Isothermal sections through the ternary at 1300, 1100 and

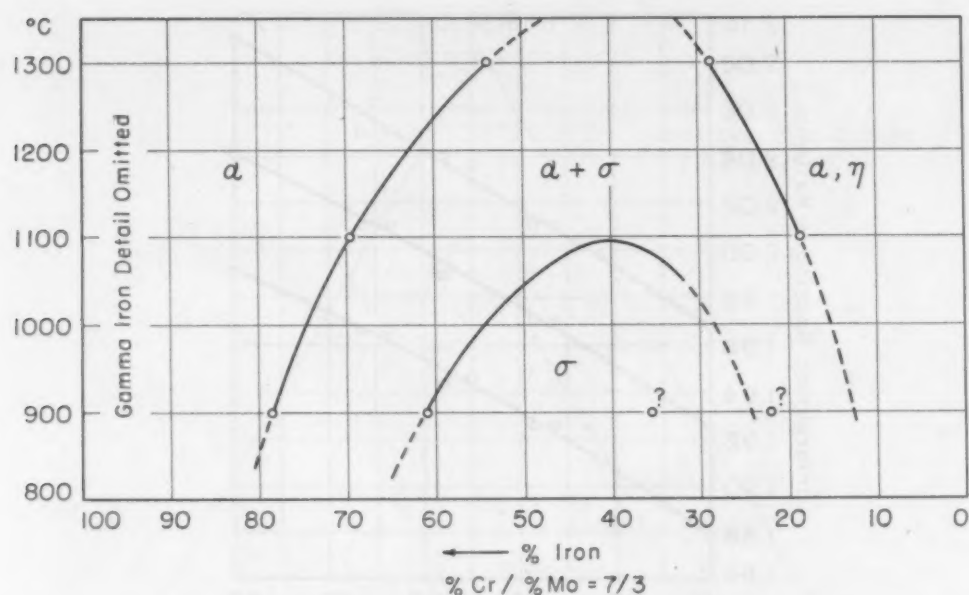


Fig. 22—Vertical Section Through Chromium-Molybdenum-Iron Ternary at Constant Chromium-Molybdenum Ratio of 70-30.

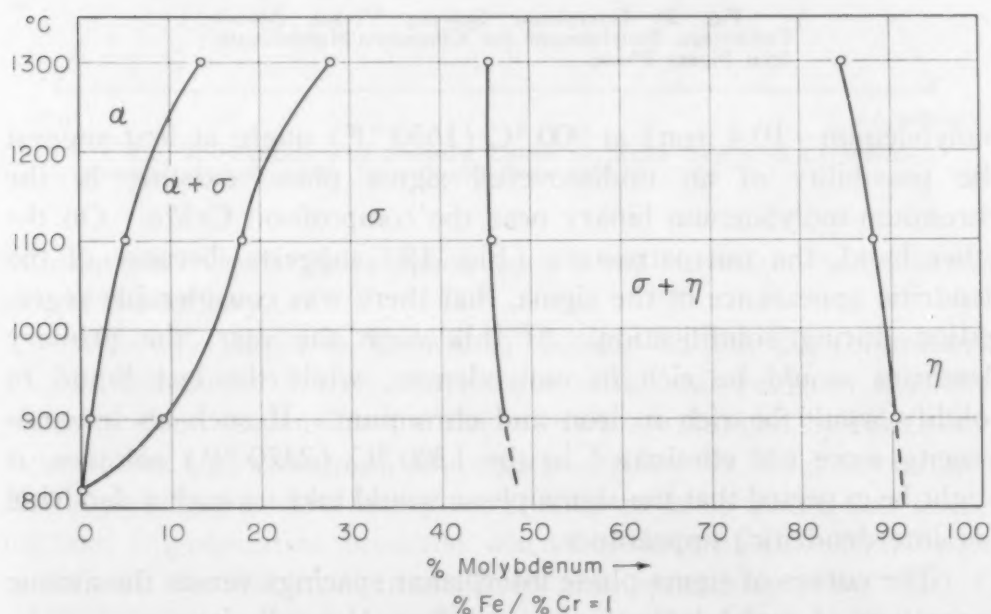


Fig. 23—Vertical Section Through Chromium-Molybdenum-Iron Ternary at Constant Iron-Chromium Ratio of 50-50.

900 °C (2370, 2010 and 1650 °F) are given and these show that the sigma phase is the major intermediate phase. At 1100 °C (2010 °F), phase spaces involving sigma extend to within 35% of the chromium-molybdenum and iron-chromium sides of the ternary. The extent of these sigma-phase spaces is increased further upon aging at 900 °C (1650 °F).



Molybdenum is shown to promote greatly the high temperature stability of iron-chromium sigma.

#### ACKNOWLEDGMENT

The authors wish to express their gratitude to the United States Navy Department, Bureau of Aeronautics, for sponsoring this research. Many thanks are also due Mrs. Catherine Pigford, who performed the chemical analyses.

#### References

1. R. M. Parke and F. P. Bens, "Chromium-Base Alloys", *Symposium on Materials for Gas Turbines*, American Society for Testing Materials, June 24, 1946, p. 80.
2. Battelle Memorial Institute, Summary Report on Chromium-Base Alloys to Office of Naval Research, Oct. 15, 1949.
3. W. P. Sykes, "The Iron-Molybdenum System", *TRANSACTIONS*, American Society for Steel Treating, Vol. 10, 1926, p. 839.
4. T. Takei and T. Murakami, "On the Equilibrium Diagram of the Iron-Molybdenum System", *TRANSACTIONS*, American Society for Steel Treating, Vol. 16, 1929, p. 339.
5. H. Arnfelt, "On the Constitution of the Iron-Tungsten and the Iron-Molybdenum Alloys", Iron and Steel Institute (London), *Carnegie Scholarship Memoirs*, Vol. 17, 1928, p. 13.
6. H. J. Goldschmidt, "A Molybdenum Sigma Phase", *Research*, Vol. 2, No. 7, 1949, p. 343.
7. R. M. Parke and A. J. Herzig, "Final Report on Heat Resisting Metals for Gas Turbine Parts, Chromium-Base Alloys", Climax Molybdenum Co., N.D.R.C.-O.S.R.D. No. 6547, Jan. 21, 1948.
8. W. Trzebiatowski, H. Ploszek and L. Lobzowski, "X-Ray Analysis of Chromium-Molybdenum and Chromium-Tungsten Alloys", *Analytical Chemistry*, Vol. 19, No. 2, 1947, p. 93.
9. A. Brenner, P. Burkhead and C. Jennings, "Physical Properties of Electrodeposited Chromium", *Journal of Research*, National Bureau of Standards, Vol. 40, 1948, p. 31.
10. G. Grube and R. Knabe, "The System Palladium-Chromium", *Zeitschrift für Elektrochemie*, Vol. 42, 1936, p. 793.
11. A. H. Sully and T. J. Heal, "An Electron Compound in Alloys of Transition Metals", *Research*, Vol. 1, 1948, p. 288.
12. F. Wever and W. Jellinghaus, "The Two-Compound System Iron-Vanadium", *Mitteilungen aus dem Kaiser-Wilhelm-Institut für Eisenforschung*, Düsseldorf, Vol. 12, 1930, p. 317.
13. "Investigations into Corrosion Resisting Cast Chromium-Nickel Steel with Special Reference to the Sigma Phase", *Sulzer Technical Review*, 1949, No. 2, p. 1-8.
14. P. Duwez and R. Baen, "X-Ray Study of the Sigma Phase in Various Alloy Systems", Preprint No. 47, 1950, American Society for Testing Materials.

#### DISCUSSION

**Written Discussion:** By Walther L. Havekotte, Firth-Sterling Steel and Carbide Corporation, McKeesport, Pa.

This paper is of considerable interest, because from 1945 through

March 1950 we conducted research on some of these alloys, especially the 60Cr-15Fe-25Mo-type alloy. This work was sponsored by O.N.R. and conducted at Battelle Memorial Institute.<sup>2</sup> We found that all of the alloys studied were very brittle, and we were unable to associate brittleness with the presence or absence of sigma in the microstructure. Our work indicated that the alloy's lack of ductility was caused by the brittleness of the chromium-rich solid-solution matrix phase.

It is well known that chromium crystallizes with a body-centered cubic lattice, as does the 60Cr-15Fe-25Mo-type alloy. Chromium of commercial purity is brittle and has the same type of fracture as that of the chromium-base alloy, yet the commercial grade of chromium does not contain sigma phase. Certain chromium-nickel alloy steels contain sigma in much larger quantities than we found in the 60Cr-15Fe-25Mo-type alloy, and yet the steels are reasonably ductile.

Ultra-pure chromium (0.014% oxygen, 0.009% carbon, and 0.002% nitrogen) has been found ductile at room temperature when loaded at low strain rates. Samples loaded in compression were reduced about 40% before cracking occurred. When the mechanisms of the effects of impurities which produce brittleness in chromium are understood, possibly this knowledge will permit production of ductile chromium-base materials. However, these future, ductile, chromium-base alloys may become brittle when heated to elevated temperatures because of the absorption of nitrogen.

The authors stated that the alloys were melted three times before the thermal-analysis study. Since carbon was not added to the charge for purposes of deoxidation, what was the purpose of the second melting cycle? Was there not a large loss of chromium during this melting cycle at such low pressures?

**Written Discussion:** By Pol Duwez, associate professor of mechanical engineering, California Institute of Technology, Pasadena, Calif.

The authors are to be congratulated for a study which, without doubt, required a great deal of time and patience. A former student of mine at California Institute of Technology, Captain Spencer R. Baen, has carried out a study of the phase boundaries in the same ternary system at 650 °C (1200 °F). Although this study was limited to one temperature, it was more exhaustive and more accurate than the work of the present authors. About 180 alloy compositions were used and the phase boundaries were established by the well-known method of intersection of lattice parameter contours and tie lines. The results of this work will be published shortly.

Since our own section of the diagram lies at a temperature below the lowest one of Messrs. Putman, Potter and Grant, it is interesting to see whether this low temperature cut is compatible with an extrapolation of the present work. In general, such an extrapolation did not reveal any major disagreement. The reason for this apparent agreement, however, is that the phase boundaries given in this paper may be displaced quite appreciably and still account for the observed structures in the alloys studied. As a concrete example, our results have been added to the vertical cut presented in Fig. 22 of the paper. The results are presented in

<sup>2</sup>W. L. Havekotte, C. T. Greenidge and H. C. Cross, "Chromium-Base Alloys", A.S.T.M., Atlantic City, 1950.

Fig. 24. The boundary between the alpha region and the alpha-plus-sigma region seems to fall exactly on the extrapolated curve of the authors. The boundaries of the sigma phase at 650 °C (1200 °F) are, according to our study, at 38 and 55% iron. If the limits of the sigma field given by the authors at 900 °C (1650 °F) are correct, that would mean that the sigma-phase field in the vertical cut considered in Fig. 24 would increase its width with increasing temperature. This seems improbable, since at 1100 °C (2010 °F) the sigma field has vanished and the shape given in Fig. 1 is the most logical one to expect.

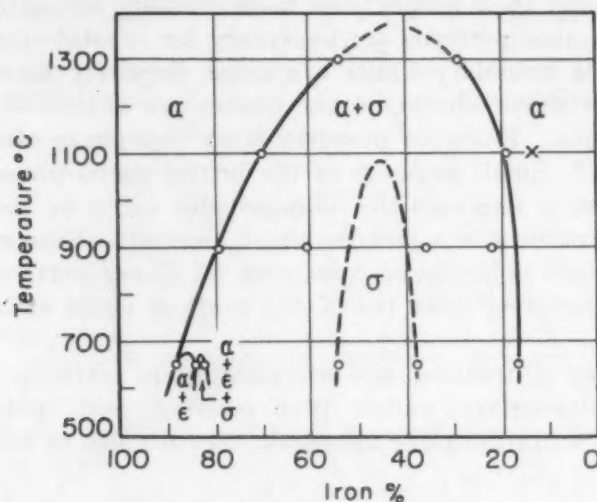


Fig. 24—Same Vertical Section as in Fig. 22 to Which Results at 650 °C (1200 °F) Have Been Added.

It would be possible, however, to retrace the sigma-field boundary at 900 °C (1650 °F) (Fig. 16) so that it is compatible with the sigma field outlined in Fig. 24. This would first require that the alloy containing 61% iron, 19% chromium, and 20% molybdenum would be in an alpha-plus-sigma field instead of in the sigma field. With the technique used by Messrs. Putman, Potter and Grant, it is quite probable that in an alloy which lies close to a phase boundary the presence of a second phase (in this case alpha) was not detected. It is indeed difficult, especially by means of an X-ray spectrometer of the type used by the authors, to detect a small amount of alpha in an alloy containing a large quantity of sigma.

The other discrepancies between the authors' results and our results at 650 °C (1200 °F) may also be corrected by displacing slightly the phase boundaries of the sigma and the alpha-plus-sigma fields in the authors' diagrams of Figs. 11 and 16.

**Written Discussion:** By E. L. Kamen, Armour Research Foundation, Chicago.

The results of this work showing the large extent of the sigma phase in Cr-Mo-Fe alloys are surely of great value. It is noteworthy to observe the small number of alloys used in the survey of this system and the wide application of the metallographic evidence. It should be interesting to compare the results of this investigation with that of a more detailed project.



Dr. Duwez in discussing this paper has described the X-ray diffraction method as being a superior means of surveying phase diagrams. Undoubtedly metallographic examination of a larger number of alloys would permit a more accurate determination of the isothermal phase boundaries. Therefore, the comparison between the results of this survey, using only 31 alloys, with the X-ray investigation of Dr. Duwez, using over 100 alloys, does not seem warranted.

Bradley and Goldschmidt have stated<sup>3</sup> in regard to phase diagram determination that "The powder photographs enable the phases present to be identified and their proportions to be roughly estimated." Certainly the X-ray diffraction patterns are necessary for crystal structure identification, but phase boundary limits are more definitely located by microstructures which show whether other phases are absent or present, even in low proportions. Filing of powders from two-phase alloys is open to many objections.<sup>4</sup> Small amounts of the brittle sigma phase which would be obtained as very fine particles in a powder could be lost or oxidized, and even when retained in a powder, small amounts of second phases may not diffract enough radiation to appear in an X-ray pattern. Dr. Hume-Rothery has questioned<sup>5</sup> that the X-ray method could estimate one part in one hundred.

Today, X-ray diffraction and metallographic methods are being accepted as complementary, rather than isolated, and application of the combination is a more desirable approach than the use of either one alone.

#### Authors' Reply

Mr. Havekotte states that he and his associates have found that brittleness in the present 60Cr-25Mo-15Fe-type alloys is unrelated to the presence or absence of sigma phase. This is in agreement with the authors' comments on the subject found on page 844 of the paper. The brittleness of the chromium-rich solid solution is apparently related to the brittleness of the commercially pure chromium. Current opinion is that the brittleness of the chromium may be caused by small amounts of impurities such as carbon, oxygen, and nitrogen. Mr. Havekotte's results on ultra-pure chromium seem to strengthen this belief.

The alloys were melted three times, including the thermal analysis study. The first melt was to obtain a melt with minimum loss of chromium; the second, or vacuum melting cycle, was intended only to remove gaseous impurities by reducing the total pressure above the melt to a value less than the equilibrium partial pressures of the various dissolved gases. The loss of chromium was indeed large during the vacuum melting and approximated 20% of the chromium charged, depending on the composition.

Since submission of this paper for publication, the authors have completed a 1000-hour aging experiment at 900 °C (1650 °F) on all of the ternary alloys containing over 30% chromium. The results of this experiment are shown in Fig. 25. The sigma and sigma-plus-chromium solid

<sup>3</sup>Bradley and Goldschmidt, *Journal, Iron and Steel Institute*, Vol. CXL, 1939.

<sup>4</sup>Hume-Rothery, *Journal of Scientific Instruments*, Vol. 18, 1941, p. 74.

<sup>5</sup>Hume-Rothery, *Journal of the Institute of Metals*, Vol. LXIX, 1943, p. 1.

solution boundaries have been shifted toward appreciably higher chromium contents, as was expected.

Dr. Duwez has compared the results presented here with those obtained by him at 650 °C (1200 °F), and he finds that agreement can be obtained by displacing the given phase boundaries without contradicting

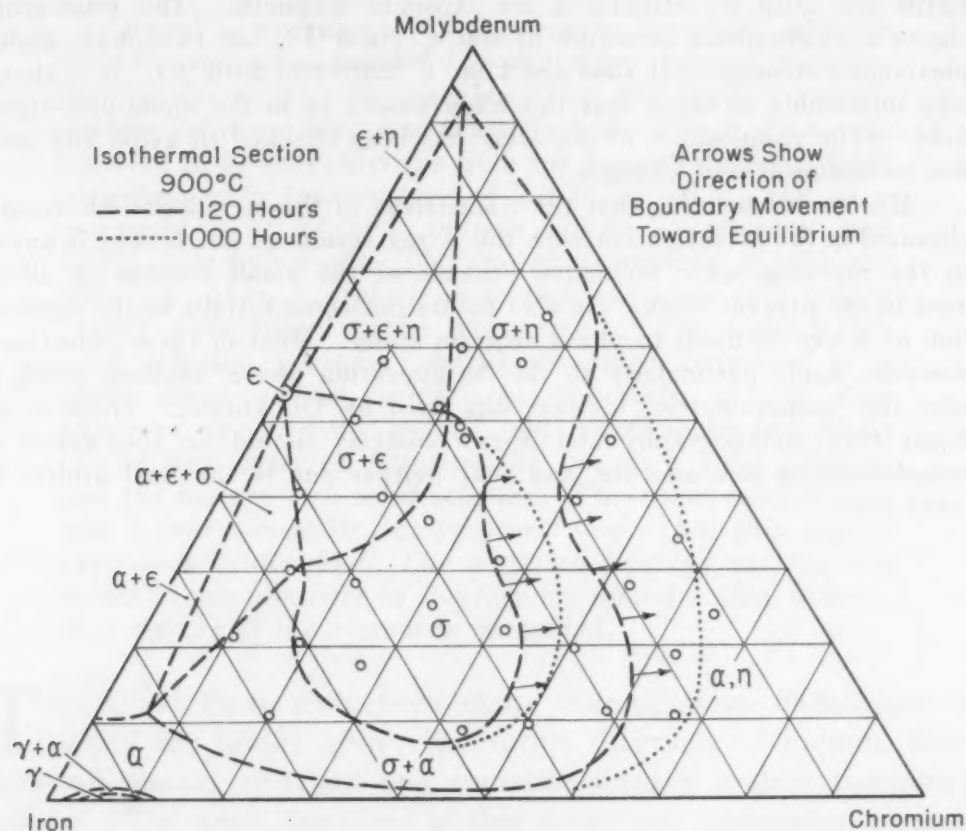


Fig. 25—Ternary Plot of Alloys Containing Over 30% Chromium. Aged 1000 hours at 900 °C (1650 °F).

any of the evidence contained in the paper. In addition to merely noting what phases were present in the alloys, the authors, when possible, made rough visual estimates of the relative amounts of these phases. These estimates were then used to assist in locating the phase boundaries. While not rigorous, this procedure may have resulted in the location of the phase boundaries with somewhat more accuracy than the small number of specimens used would indicate. This does not apply to the alloys of the three-phase fields, because in such cases reasonable estimates were not possible. In Fig. 24, there seems to be a genuine discrepancy between the data at 900 °C (1650 °F) and those at 650 °C (1200 °F). The discrepancy on the high chromium side of the diagram is increased if the more recent data from Fig. 25 are applied to this plot. Dr. Duwez does not state the length of time that his alloys were held at 650 °C (1200 °F), and the authors wonder if his data at 650 °C (1200 °F) might not represent alloys farther from equilibrium than those of the present work at 900 °C (1650 °F) for 1000 hours.

With regard to the discrepancy at the high iron side of Fig. 24, Dr.

Duwez puts the alloy with 61% iron, 19% chromium, and 20% molybdenum in the sigma-plus-alpha field instead of the sigma field. The 1300, 1100, and 900 °C (2370, 2010, and 1650 °F) structures of this alloy have been rechecked by the authors, both metallographically and magnetically. The 900 °C (1650 °F) structure is nonmagnetic, while the 1300 and 1100 °C (2370 and 2010 °F) structures are strongly magnetic. The microscope shows a single-phase structure at 900 °C (1650 °F), but two-phase alpha-plus-sigma structures at 1300 and 1100 °C (2370 and 2010 °F). It is therefore impossible to agree that this alloy should be in the alpha-plus-sigma field. (The composition of the alloy has been checked to avoid any shift due to compositional changes.)

Mr. Kamen believes that the comparison of the metallographic results obtained in the investigation with the X-ray results of Dr. Duwez is unfair to the metallographic technique because of the small number of alloys used in the present work. He also points out some pitfalls in the application of X-ray methods to phase diagram study. Most of these objections, however, apply particularly to the "disappearing phase" method which is why the "isoparametric" method was used by Dr. Duwez. There is no doubt that metallography and X-ray analysis should be considered as complementing one another, and that neither one is the final arbiter in every case.



# THE TERNARY SYSTEM INDIUM-CADMIUM-ZINC

BY S. C. CARAPPELLA, JR., AND E. A. PERETTI

## Abstract

*From a knowledge of the binary diagrams already reported and an additional 120 alloys for thermal, metallographic, X-ray and hardness analyses, the ternary system indium-cadmium-zinc has been studied. The system was revealed to be eutectiferous with the ternary eutectic point occurring at a temperature of  $116.0 \pm 1.0^\circ\text{C}$  and at a composition of 74.00% indium, 24.25% cadmium and 1.75% zinc by weight. The one-phase regions of both the zinc-rich phase (alpha) and the cadmium-rich phase (beta) were found to be quite small. The indium-rich solid solution (gamma phase) dissolved cadmium to a fairly large extent, while the solubility of the zinc appeared to be very small. An appreciable two-phase region was detected between the zinc-rich solid solution and the indium-rich solid solution. The room temperature and ternary eutectic temperature limits for this region have been established. The zinc-rich liquidus surface was found to predominate in the ternary model. Also, a hardness survey of the system is presented.*

THOUGH there have been many investigations undertaken to study the binary alloy constitution diagrams of indium, there does not appear recorded any complete ternary system containing indium. The work described in this paper was undertaken to start filling the gap of this aspect in our knowledge of indium alloy behavior.

## HISTORICAL SURVEY

Preliminary to the work done on the ternary system indium-zinc-cadmium, an evaluation was made of the information available on the respective binary systems. A review of the literature reveals that much work has been done on the zinc-cadmium system (1-6),<sup>1</sup> the indium-cadmium system (7-9) and the indium-zinc system (10-12). A brief discussion of the diagrams will be undertaken to single out their respective salient features.

<sup>1</sup>The figures appearing in parentheses pertain to the references appended to this paper.

A paper presented before the Thirty-second Annual Convention of the Society, held in Chicago, October 21 to 27, 1950. Of the authors, S. C. Carapella, Jr., was formerly O'Brien Fellow, University of Notre Dame, now research metallurgist, American Smelting and Refining Co., Barber, N. J., and E. A. Peretti is professor of metallurgy, University of Notre Dame, Notre Dame, Ind. Manuscript received April 14, 1950.

**Cadmium-Zinc**—In Fig. 1, the diagram for the system cadmium-zinc as taken from Hansen's compilation of binary diagrams (13) is presented. The composite plot of the liquidus values obtained by the numerous investigators results in a smooth curve. The accepted value for the eutectic point is 266 °C (511 °F) and at a composition of 82.6 weight per cent cadmium. The fixing of the mutual solubility limit of zinc and cadmium at the eutectic temperature has led to many controversial discussions. Investigations have been conducted for the specific purpose of establishing the respective

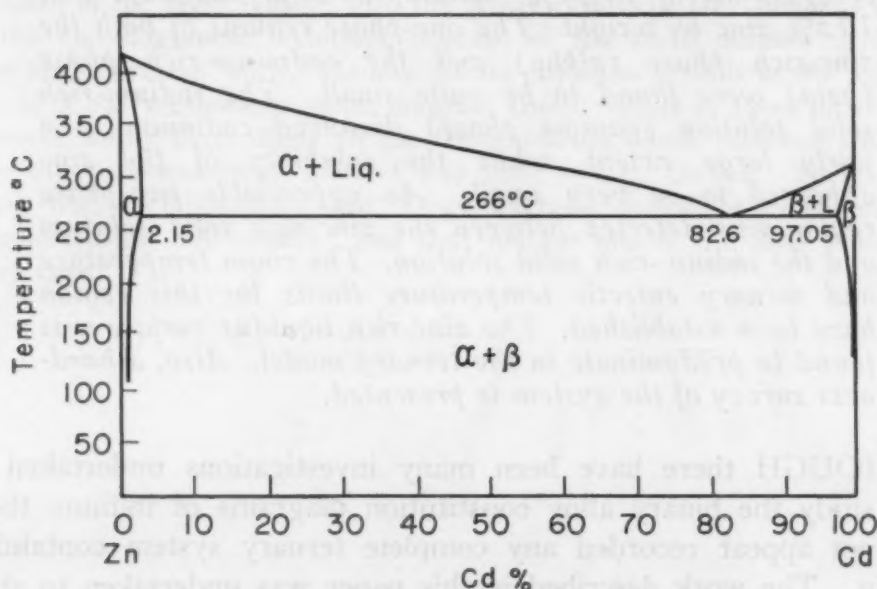


Fig. 1—The Zinc-Cadmium Phase Diagram.

limits of the single-phase fields. Boas' work (5) consists of an extensive X-ray analysis on the determination of the solubility of cadmium in zinc over a range of temperatures and has been used in the construction of the diagram. The evaluation of the cadmium-rich solvus was made by Stockdale (4) and is also included in the diagram. The mutual solubility of both zinc and cadmium drop precipitously below 100 °C to values of less than 0.1 weight per cent cadmium in zinc (6) and 0.2 weight per cent of zinc in cadmium at room temperature.

**Indium-Cadmium**—The system indium-cadmium has been investigated by Wilson and Wick (7) and also reported by Valentiner (11). Betteridge (9) confined his investigation to the saturation value of cadmium in indium at 100 °C and room temperature. The liquidus values given by Wilson and Wick and those obtained by Valentiner do not in general agree. The results are plotted in Fig. 2,

and the liquidus curve of Wilson and Wick indicates that appreciable supercooling had taken place during thermal analysis. The value given by both investigators for the eutectic temperature and eutectic composition is in good agreement.

The solubility of indium in cadmium is quite small, as indicated from the microscopic work of Wilson and Wick and the X-ray observations of Betteridge. Both investigators report a saturation value of cadmium in indium at the eutectic temperature of 18.0 weight per cent using their respective techniques. Valentiner detected eutectic temperature arrests beyond this value, while Wilson and Wick show a smooth solidus curve to this point. Again,

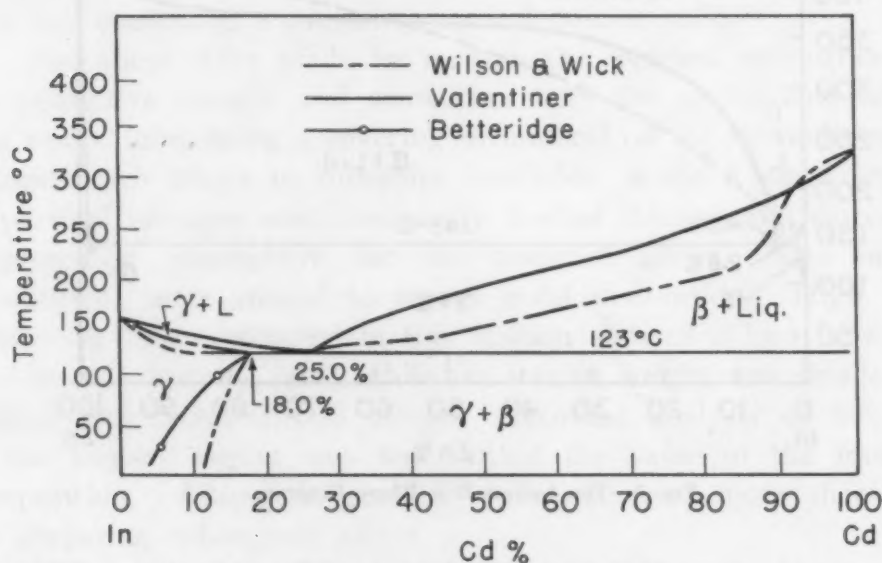


Fig. 2—The Indium-Cadmium Phase Diagram.

some controversy appears in fixing the saturation limit of cadmium in indium at room temperature. Wilson and Wick have placed the room temperature limit at 15 weight per cent cadmium by microscopic means, while the value reported by Valentiner, based on electrical measurements, was less than 8 atomic per cent cadmium. Betteridge, from the results of X-ray analysis, fixes the limit at  $4.5 \pm 0.5$  atomic per cent of cadmium.

Due to the disagreement in the course of the solidus and the room temperature saturation value of cadmium in indium, a series of alloys was prepared in the respective vicinities to establish the proper values. Thermal studies of alloys in the vicinity of the solidus, by suspending a strip of the alloy in a furnace and observing the temperature of intercrystalline fracture (14, 15) with a certified thermometer, resulted in values which were in qualitative agreement



with those indicated by Wilson and Wick. Microscopic studies of alloys to fix the room temperature value of the solvus corroborated the value of  $4.5 \pm 0.5$  atomic per cent of cadmium obtained by Betteridge from X-ray analysis.

**Indium-Zinc**—The results of the indium-zinc phase diagram are incorporated in Fig. 3. The diagram reported by Rhines and Grobe (12) has been prepared from the results obtained from an exhaustive survey of alloys. The values determined by Valentiner (11) are in good agreement with those of Rhines and Grobe, both, however,

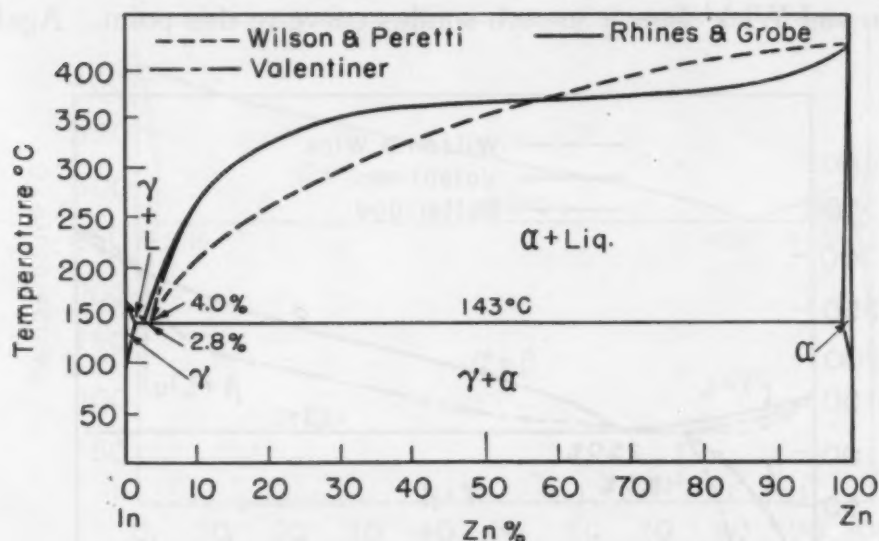


Fig. 3—The Indium-Zinc Phase Diagram.

differing with original work of Wilson and Peretti (10). Though the value of the eutectic temperature reported in the three investigations is in excellent agreement, the composition of the eutectic differs. The work of Wilson and Peretti, and Valentiner, results in a eutectic value of 4 weight per cent zinc as compared with 2.8 weight per cent zinc given by Rhines and Grobe. The solubility of indium in zinc is agreed to be quite small at both the eutectic temperature and room temperature. From the work of Rhines and Grobe, the solubility of zinc in indium at the eutectic temperature is 1.2 weight per cent zinc and at room temperature about 0.2 weight per cent zinc.

Experimental work was carried out to clarify the discrepancy of the reported eutectic value, and a new composition of  $2.0 \pm 0.1$  weight per cent was established by metallographic analysis for this point (16).

## EXPERIMENTAL PROCEDURE AND RESULTS

*Materials:* The cadmium and zinc<sup>2</sup> used for the investigation were purchased from the J. T. Baker Chemical Company. The indium<sup>2</sup> was furnished by the Indium Corporation of America. In order to use the indium on hand judiciously, alloys weighing about 70 grams were prepared along sections containing a constant indium content. The proposed sections contained 80, 65, 50, 35 and 15 weight per cent indium, respectively. Later it was found advantageous to use a supplemental section containing a constant 1.4 weight per cent zinc. The compositions of the alloys in the constant indium sections were mapped out so that they would, in general, lie on a line containing a constant cadmium-to-zinc ratio.

The alloys were made by melting the weighed proportions of the respective metals, and sometimes both the metals and alloys, in a pyrex tube, using a covering of mineral oil for the indium and cadmium-rich alloys to minimize oxidation, while a small stream of purified nitrogen was continually flushed through the system as a protective atmosphere for the zinc-rich alloys. The molten constituents were stirred to insure good dissolution. High zinc-containing alloys prepared in this fashion showed a loss in weight as low as 3 parts in 7000, while the loss in weight was smaller for indium and cadmium-rich alloys. Chemical analysis of an alloy in the ternary region was well within the value of the intended composition. Alloys, in general, were not used more than once for preparing subsequent alloys.

The furnace used for obtaining thermal data was the same as the one described in an earlier investigation (17). Alloys were analyzed under a controlled cooling rate of  $\frac{1}{2}$  to 2 °C per minute using a calibrated iron-constantan thermocouple. Thermal analysis of the alloys was carried out under the same atmospheres used for melting. Direct rate plots were used to determine the temperature of the reactions. Inverse rate plots were employed to detect phase changes. It was found necessary to stir the alloy throughout the analysis, otherwise some of the reactions would be obscured by supercooling. Two runs were made on each alloy and were found to agree to  $\pm 2$  °C. The temperature values of some of the alloys in the two-phase region of the section of constant indium content were obtained by suspending a strip of the alloy in tension and observing the temperature of intercrystalline fracture by means of

<sup>2</sup>The cadmium was analyzed and the following impurities were reported: Pb—0.025%; Cu—0.0035%; Zn—0.01%; Ti—0.005%. The label analysis given for the zinc is: Insol in H<sub>2</sub>SO<sub>4</sub>—0.01%; Pb—0.001%; Fe—0.001%. The indium had a guaranteed purity of 99.97% with the following analysis: Cu—0.002%; Pb—0.006%; Sn—0.01%; Zn—0.01%.

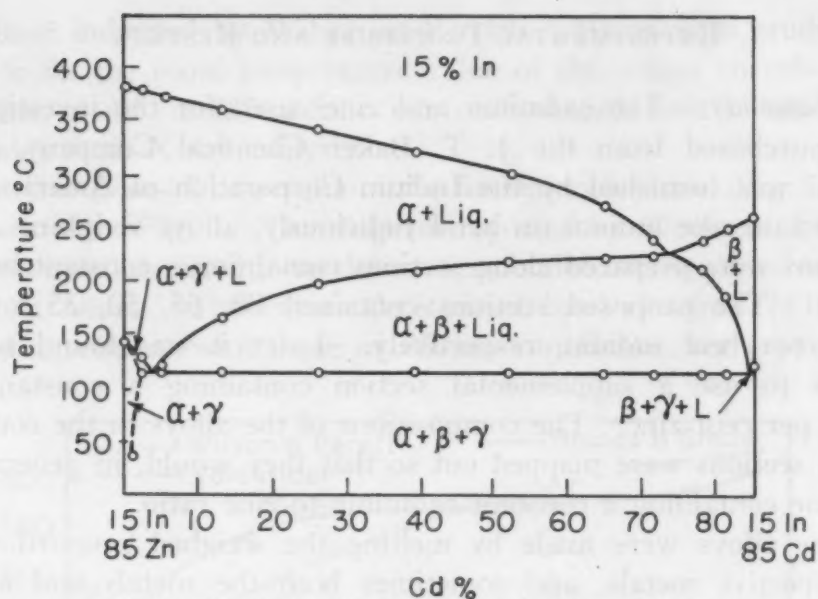


Fig. 4—The 15% Indium Section of the Phase Diagram.

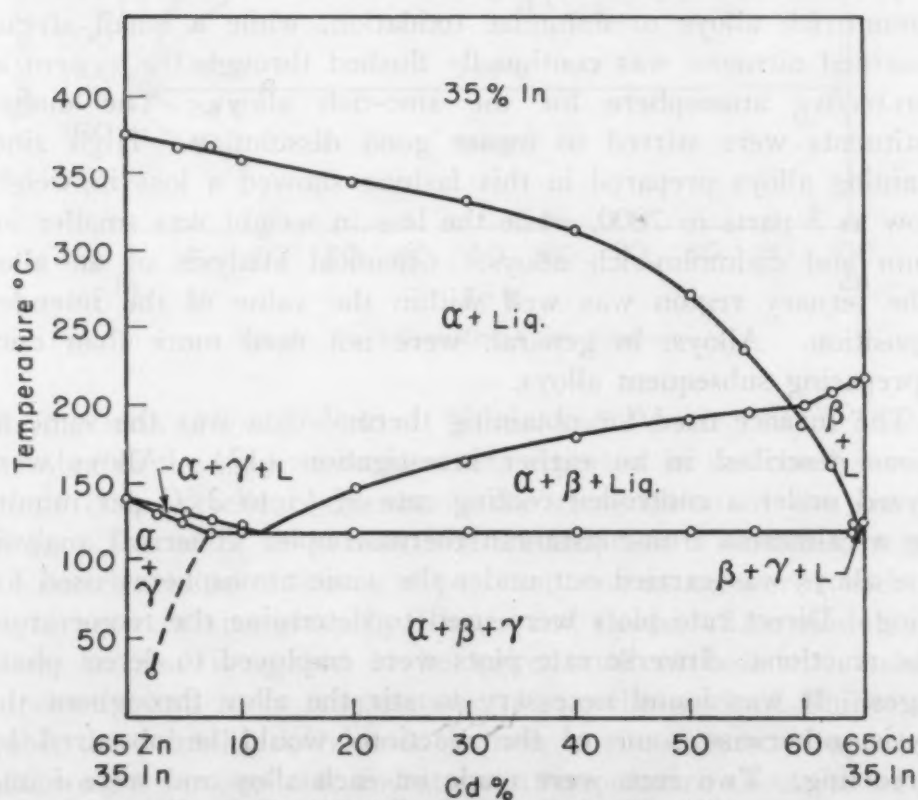


Fig. 5—The 35% Indium Section of the Phase Diagram.

a certified thermometer. The eutectic temperature value of an alloy obtained from this method of analysis was found to check within  $\pm 2^\circ\text{C}$  with the value obtained by the conventional method of thermal analysis. The average value of the two runs obtained by thermal analysis is incorporated in Figs. 4 to 9.



The metallographic preparation of zinc and cadmium alloys could be carried out in the conventional manner. A procedure has been developed for the preparation of indium and indium-rich alloys (18). To differentiate the respective primary phases in the microstructures, certain characteristics of each phase were noted. For example, the zinc-rich phase could be selectively darkened by etching with warm alkaline sodium picrate, whereas the cadmium and

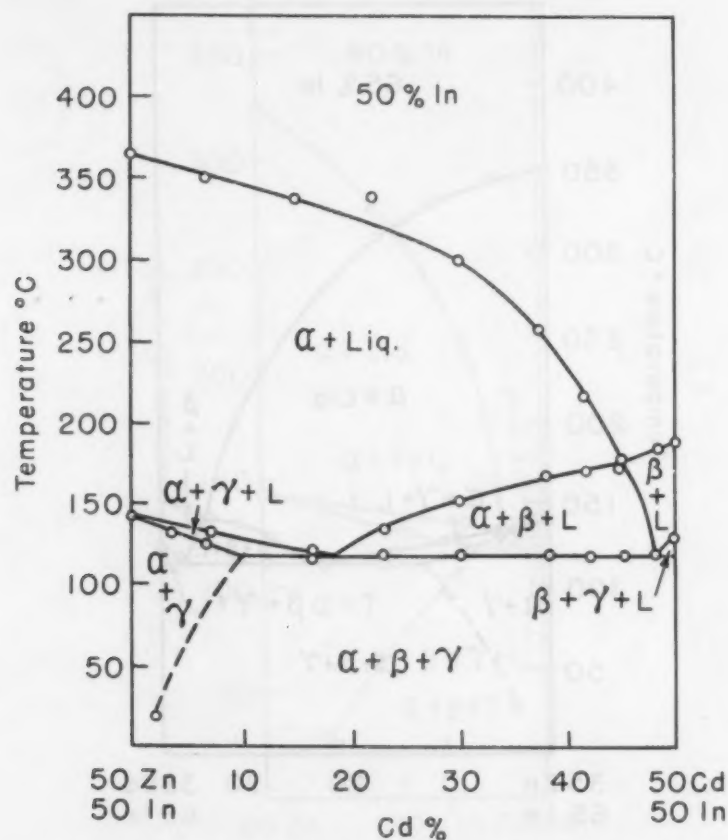


Fig. 6—The 50% Indium Section of the Phase Diagram.

indium would be unaffected. The cadmium and indium could be distinguished from each other, since cadmium polishes in relief. In general, Vilella's reagent was used for indium and cadmium-rich alloys.

Metallographic studies of the ternary alloys were important in substantiating the results of the thermal data. Structural observations were made of a series of alloys in the anticipated one-phase regions to establish these limits. The alloys were worked, homogenized at 110 °C (230 °F) for several days and furnace-cooled at a rate of about 10 °C per hour to room temperature. The zinc-rich region was found to be quite limited, since a heterogeneous structure

resulted from the addition of as little as 0.3 weight per cent each of cadmium and indium. Likewise, a similar observation was made for the addition of the same quantities of zinc and indium to cadmium. Indium-rich alloys containing zinc and cadmium indicate that the solubility of zinc is less than 0.2 weight per cent. It is difficult to establish the amount of cadmium in solid solution because of the influence of such a small amount of zinc toward the formation

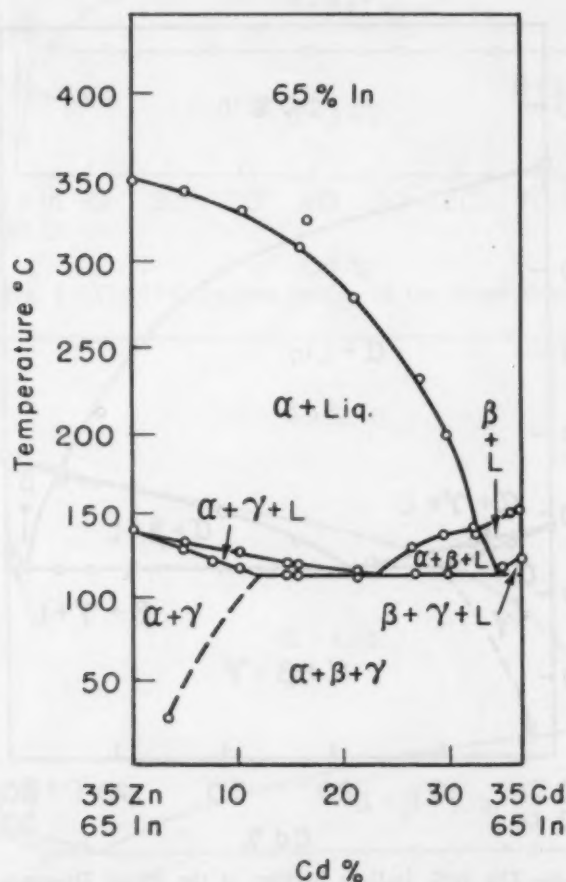


Fig. 7—The 65% Indium Section of the Phase Diagram.

of a heterogeneous structure. All of these alloys were re-treated at 110 °C (230 °F) and quenched for room temperature studies. No noticeable change in the structure was noted. The ternary eutectic composition was found to contain 74.00% indium, 24.25% cadmium, and 1.75% zinc by weight.

From preliminary work done in the cadmium and zinc-rich regions of the ternary diagram and the saturation limits of the one-phase fields indicated in the binary diagrams, it was inferred that the single-phase regions were quite limited. Instead of studying the limits of the one-phase fields in the ternary model by X-ray

analysis, the extent of the two-phase regions was investigated. To do this, a series of alloys was prepared along various sections of the diagram in such a fashion that the planar reflections of interest in the respective phases would be prominent. This could be done, since measurable systematic changes of the interplanar spacings would be continuous from the saturation value of the given phase

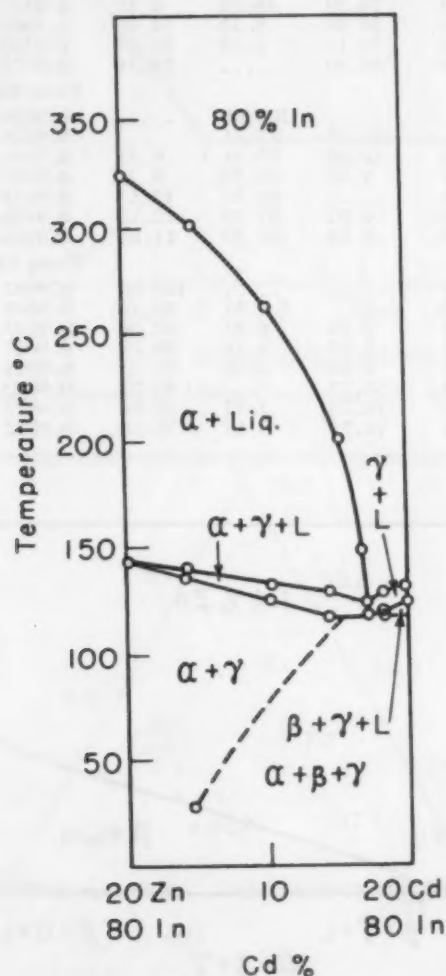


Fig. 8—The 80% Indium Section of the Phase Diagram.

in the binary alloy through the two-phase field of the ternary diagram to the saturation value of the same phase in the three-phase field where the interplanar spacing becomes constant.

The alloys used for this phase of the investigations were melted under a covering of mineral oil and drawn up into a capillary tube and quenched into water. The specimens were worked and inserted into tubes which were then evacuated and sealed. The alloys were placed in a furnace and annealed at a temperature near the ternary eutectic value (110 °C) for 3 to 6 days and furnace-cooled at a rate



**Table I**  
**X-Ray Data**  
**Interplanar Spacings of Alloys Given in Kx Units for Cobalt K $\alpha$  Radiation**

Composition of Alloy			Atomic, %			"d" Value		
Cadmium	Weight, % Zinc	Indium	Cadmium	Zinc	Indium	Plane 21.1	Plane 21.2	
100.00	.....	.....	100.00	.....	.....	0.9587	0.9189	
90.00	10.00	.....	83.96	16.04	.....	0.9573	0.9186	
80.00	19.50	0.50	70.16	29.40	0.43	0.9572	0.9186	
80.00	19.00	1.00	70.39	28.74	0.86	0.9571	0.9186	
81.73	3.27	15.00	80.09	5.51	14.40	0.9603	0.9186	
78.60	1.40	20.00	78.13	2.39	19.47	0.9569	0.9186	
85.00	.....	15.00	85.26	.....	14.74	0.9575	0.9189	
						Plane 20.3	Plane 10.5	Plane 11.4
.....	100.00	.....	.....	100.00	.....	0.9434	0.9075	0.9045
20.00	80.00	.....	12.69	87.31	.....	0.9426	0.9074	0.9045
19.50	80.00	00.50	12.38	87.31	0.31	0.9426	0.9074	0.9045
2.50	82.50	15.00	1.57	89.19	9.24	0.9425	0.9075	0.9045
.....	80.00	20.00	.....	87.53	12.47	0.9424	0.9072	0.9045
0.50	80.00	19.50	0.32	87.53	12.15	0.9426	0.9075	0.9045
1.00	80.00	19.00	0.64	87.52	11.84	0.9426	0.9075	0.9045
						Plane 333		
.....	.....	100.00	.....	.....	100.00	0.9041		
.....	2.80	97.20	.....	4.81	95.19	0.9039		
1.00	4.00	95.00	0.99	6.81	92.20	0.9035		
4.00	4.00	92.00	3.96	6.81	89.23	0.9027		
5.00	4.00	91.00	4.95	6.81	88.23	0.9024		
15.00	.....	85.00	15.27	.....	84.73	0.9022		
18.60	1.40	80.00	18.72	2.42	78.86	0.9022		
15.00	5.00	80.00	14.71	8.43	78.86	0.9022		

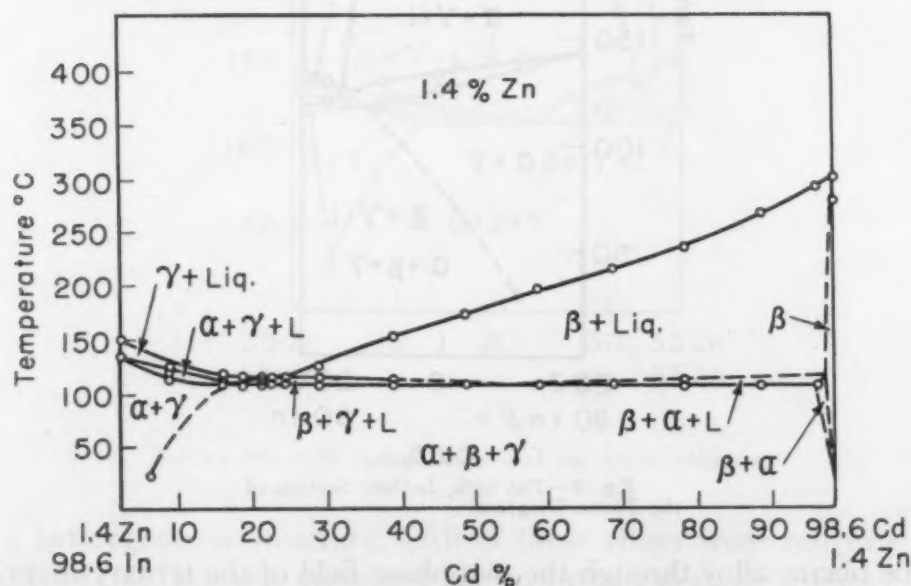


Fig. 9—The 1.4% Zinc Section of the Phase Diagram.

of about 10 °C per hour. Debye-Scherrer diffraction patterns were taken of these alloys using a cobalt target (19) and employing K $\alpha$  radiation. Four observations were made of each pattern and the average value was used to calculate the respective "d" values (interplanar spacings) of the planes reported in Table I. The "d" values were reproducible to  $\pm 0.0002$  Kx units. Since the indium-rich

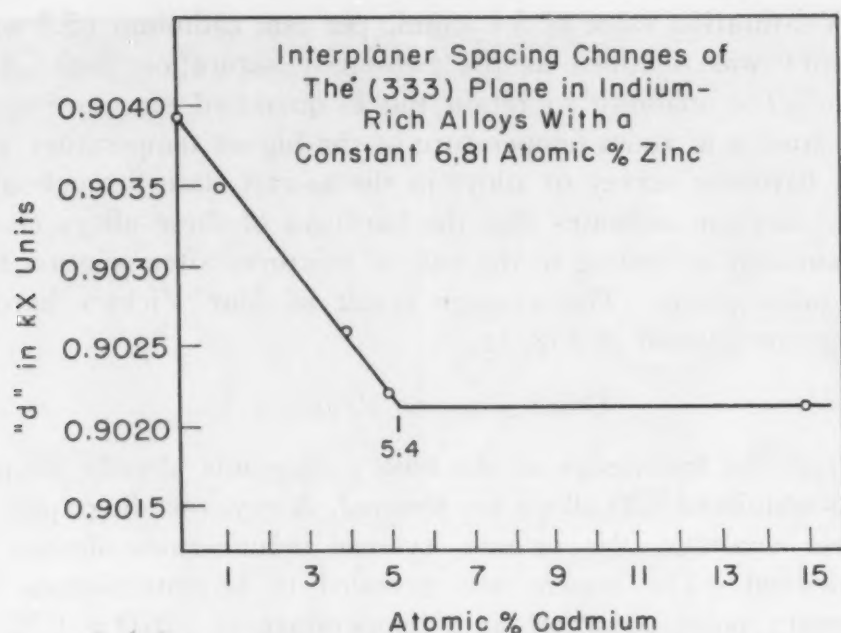


Fig. 10—Interplanar Spacings of Alloys Containing 6.81 Atomic Per Cent Zinc.

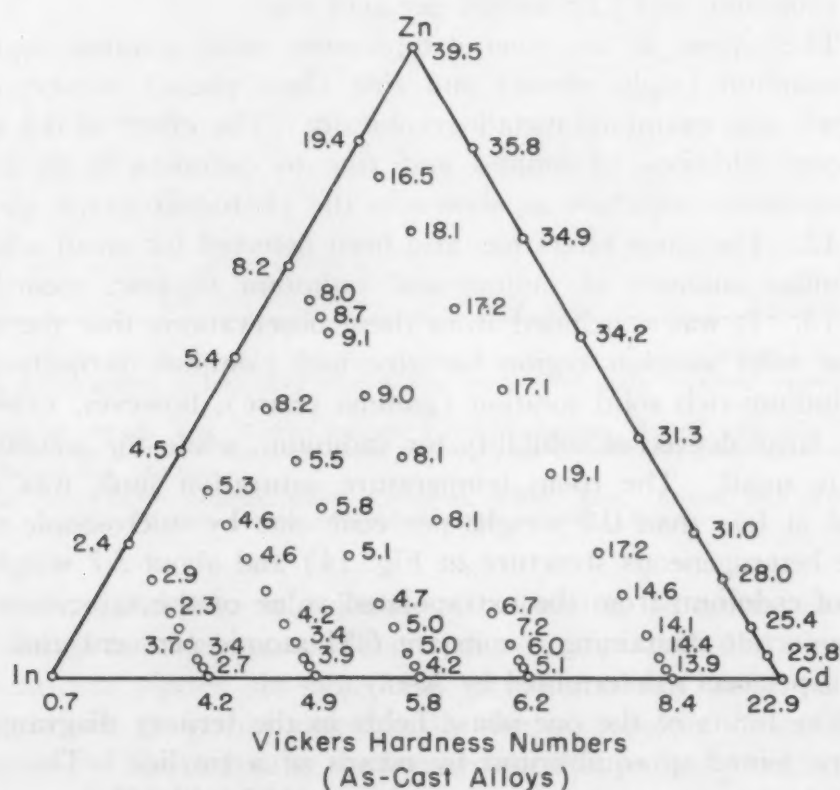


Fig. 11—Hardness Survey of Indium-Zinc-Cadmium Alloys.

phase in a section containing a constant 6.81 atomic per cent zinc (4.00 weight per cent) was the only one to show any consistent change in the two-phase field, the values have been plotted in Fig.

10. A saturation value of 5.4 atomic per cent cadmium (5.3 weight per cent) was obtained as the two-phase saturation limit of this section. The inability to retain the as-quenched structure limited X-ray studies at room temperature of the higher temperature value.

A hardness survey of alloys in the as-cast state throughout the ternary diagram indicates that the hardness of these alloys changes approximately according to the rule of mixtures after solution hardening takes place. The average result of four Vickers hardness readings are plotted in Fig. 11.

#### DISCUSSION OF RESULTS

From the knowledge of the binary diagrams already discussed and an additional 120 alloys for thermal, X-ray, metallographic and hardness analyses, the ternary system indium-zinc-cadmium has been defined. The system was revealed to be eutectiferous with the ternary point occurring at a temperature of  $116.0 \pm 1^\circ\text{C}$  and at a composition of 74.00 weight per cent indium, 24.25 weight per cent cadmium, and 1.75 weight per cent zinc.

The extent of the room temperature solid solution region in the cadmium (alpha phase) and zinc (beta phase) corners of the diagram was examined metallographically. The effect of 0.3 weight per cent additions of indium and zinc to cadmium is to form a heterogeneous structure as shown in the photomicrograph given in Fig. 12. The same effect has also been detected for small additions of similar amounts of indium and cadmium to zinc, recorded in Fig. 13. It was concluded from these observations that the extent of the solid solution region for zinc and cadmium is quite small. The indium-rich solid solution (gamma phase), however, exhibits a fairly large degree of solubility for cadmium, while the solubility of zinc is small. The room temperature saturation limit was determined at less than 0.2 weight per cent zinc by microscopic means (note heterogeneous structure in Fig. 14) and about 5.7 weight per cent of cadmium from the extrapolated value of the saturation limit of the section containing a constant 6.81 atomic per cent zinc (4.00 weight per cent) determined by X-ray.

The limits of the one-phase fields in the ternary diagram, Fig. 15, are joined in equilibrium by means of a tie line. The course of the tie line at room temperature was determined by X-ray analysis. Since X-ray studies of the zinc-rich alloys yielded no consistent change in "d" values, it was inferred that the tie line joined an almost pure zinc phase with the indium-rich phase. The other two-phase regions between the indium and cadmium-rich phases, and



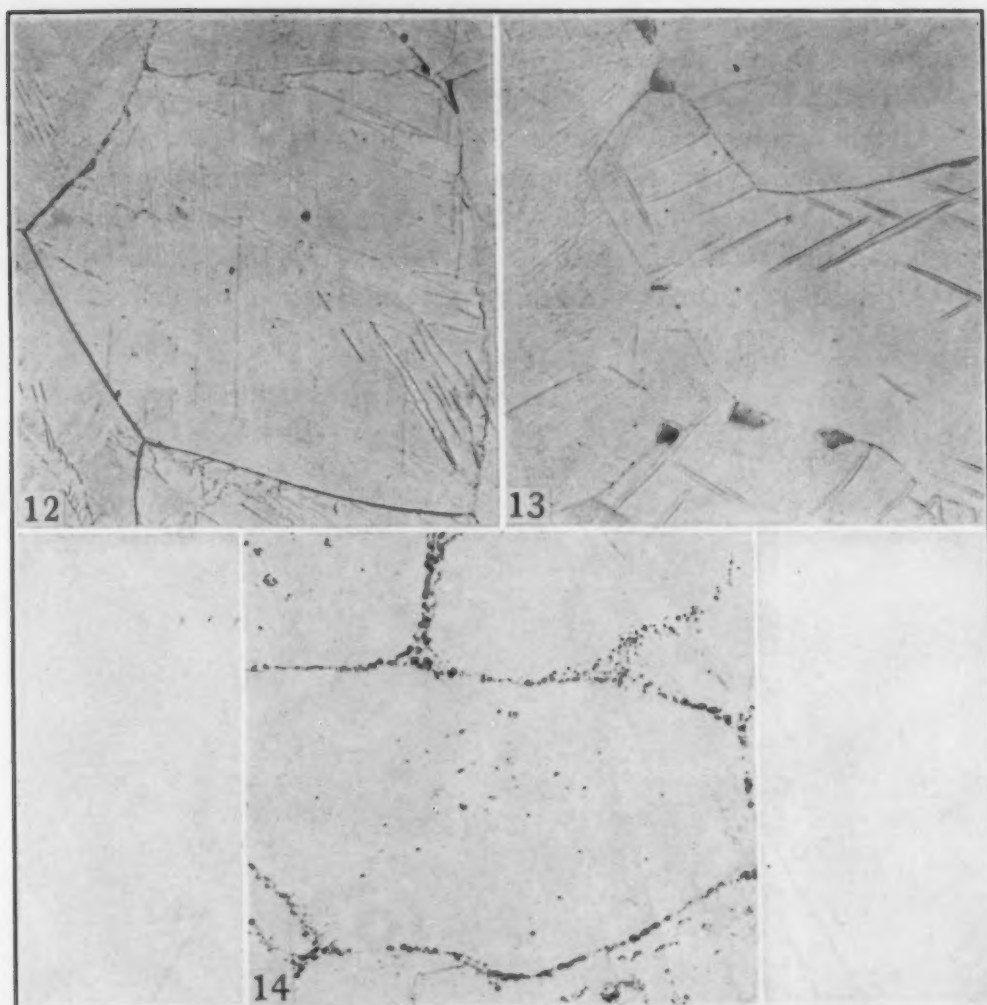


Fig. 12—99.4% Cadmium, 0.30% Zinc, 0.30% Indium. Etched with Vilella's reagent,  $\times 100$ . Large grains of beta solid solution plus unidentified grain boundary constituent. As-cast.

Fig. 13—99.4% Zinc, 0.30% Indium, 0.30% Cadmium. Etched with 2% Nital,  $\times 100$ . Large grains of the alpha solid solution plus eutectiferous constituent at the grain boundaries. As-cast.

Fig. 14—95.80% Indium, 4.00% Cadmium, 0.20% Zinc. Etched with Vilella's reagent.  $\times 100$ . Primary gamma solid solution plus eutectic. As-cast.

the cadmium and zinc-rich phases were found to be quite restricted from X-ray measurements. This indicates that both the zinc and cadmium-rich phases do not have any significant solid solution region, which is in agreement with the microscopic observations. The course of the tie line at the ternary eutectic temperature between the zinc-rich phase (alpha) and the indium-rich phase (gamma) was fixed by means of the values obtained for the saturation limit at the eutectic temperature of the two-phase field in the various sections of constant indium content. The tie line joins a phase of almost pure zinc with an indium-rich solid solution which contains

about 16.0% cadmium determined by the extension of the tie line through the determined points of the constant indium sections and probably slightly less than 0.2 weight per cent zinc.

Metallographic studies supported the findings of thermal analysis that the system was eutectiferous. Several photomicrographs of alloys from the section of constant 15 weight per cent indium are shown in Figs. 16 to 20. Fig. 16 represents an alloy which belongs to the region of primary cadmium solidification. In this alloy a

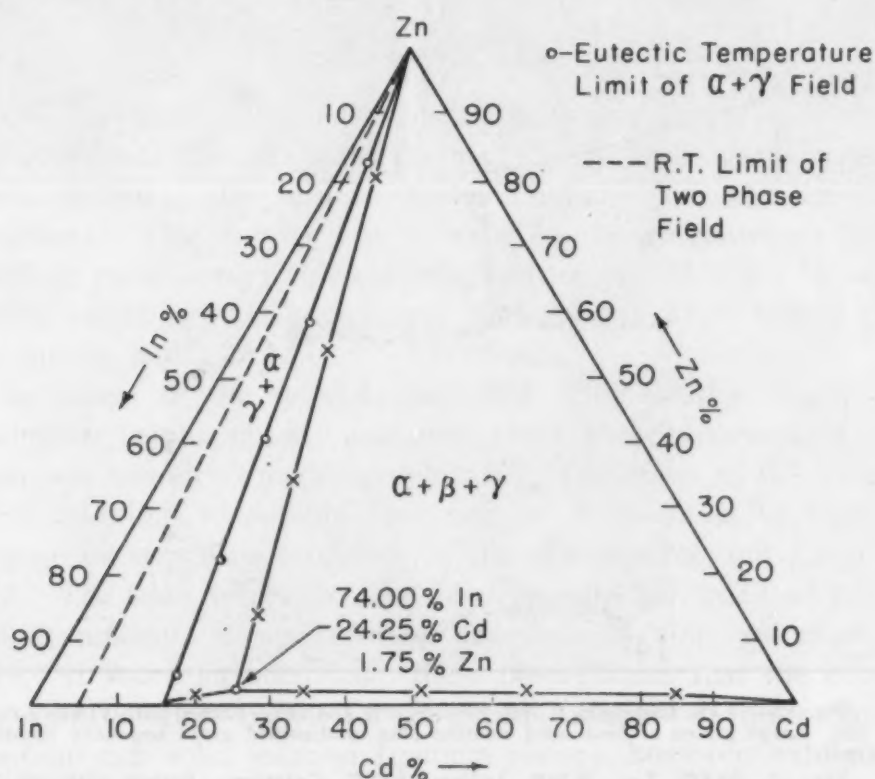


Fig. 15—The Phase Fields at Room Temperature and the Eutectic Temperature.

noticeable degree of divorcement is noted of the zinc-rich phase, the dark constituent, which ordinarily should have gone to form univariant eutectic surrounding the primary phase. This divorcement may be attributed to supercooling. Likewise, a similar observation has been made of the divorced cadmium in the primary zinc-rich alloys, photographed in Figs. 17 to 20. The amount of divorced cadmium is seen to diminish with increasing zinc content and disappears in the alloy given in Fig. 20. This alloy lies on the limit of the two-phase saturation and, therefore, cadmium should be rejected in the form of a precipitate which is difficult to resolve in this photomicrograph. There does not appear to be any obvious divorcement in the primary indium alloy shown in Fig. 21, which

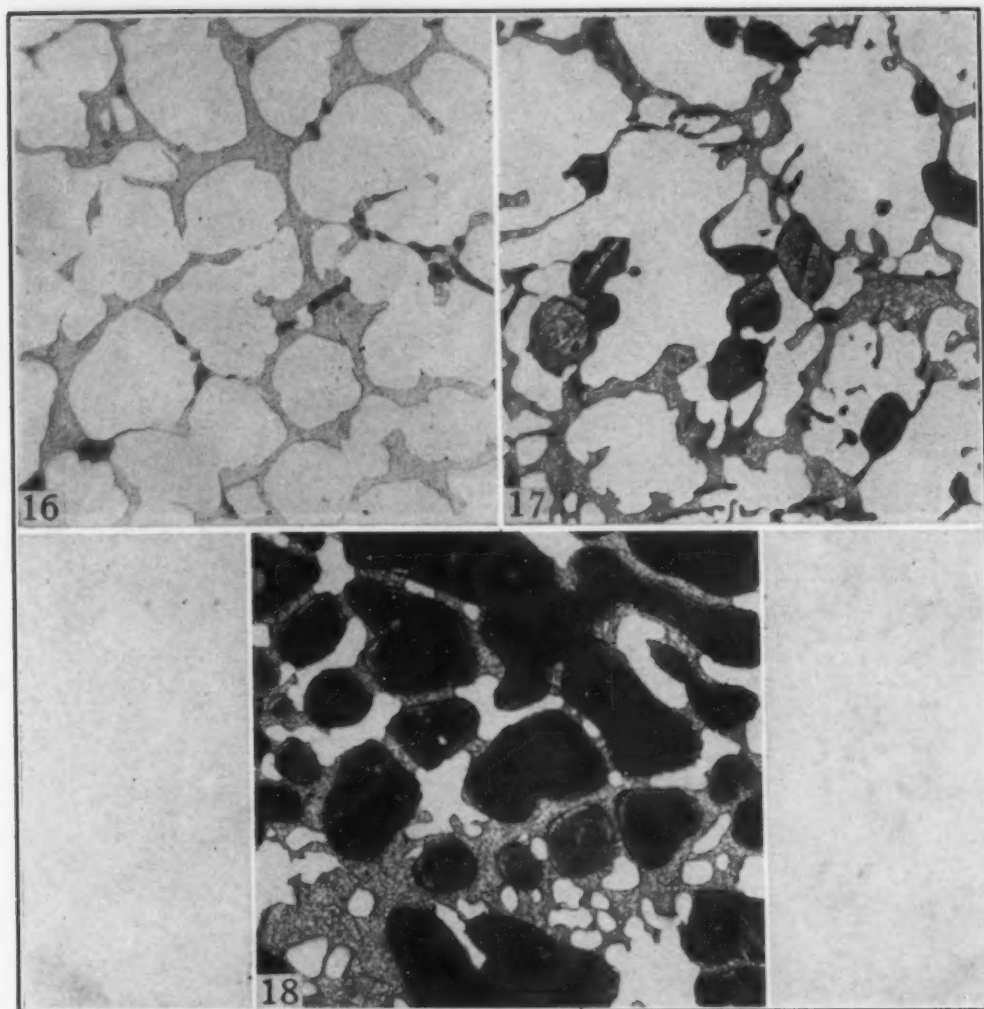


Fig. 16—3.27% Zinc, 81.73% Cadmium, 15.00% Indium. Etched with warm alkaline sodium picrate,  $\times 100$ . The light grains are primary beta solid solution; the dark particles are zinc-rich alpha in a matrix of eutectic.

Fig. 17—32.69% Zinc, 53.21% Cadmium, 15.00% Indium. Etched with warm alkaline sodium picrate,  $\times 100$ . The dark grains are primary alpha, the light are beta in a ground mass of eutectic. As-cast.

Fig. 18—58.86% Zinc, 26.14% Cadmium, 15.00% Indium. Etched with warm alkaline sodium picrate,  $\times 100$ . Dark primary alpha with light colored beta plus eutectic. As-cast.

shows a fairly well-defined univariant eutectic microconstituent surrounding the primary phase. The ternary eutectic structure is shown in Fig. 22.

It proved to be quite feasible to use vertical sections of constant indium content to determine the ternary system indium-zinc-cadmium, since all these sections were quite similar in nature. From the results of these sections and known geometric relationships of the ternary alloy system, the ternary eutectic composition could presumably be determined. The limits of the alpha plus gamma regions of these diagrams were fixed from thermal and X-ray studies.



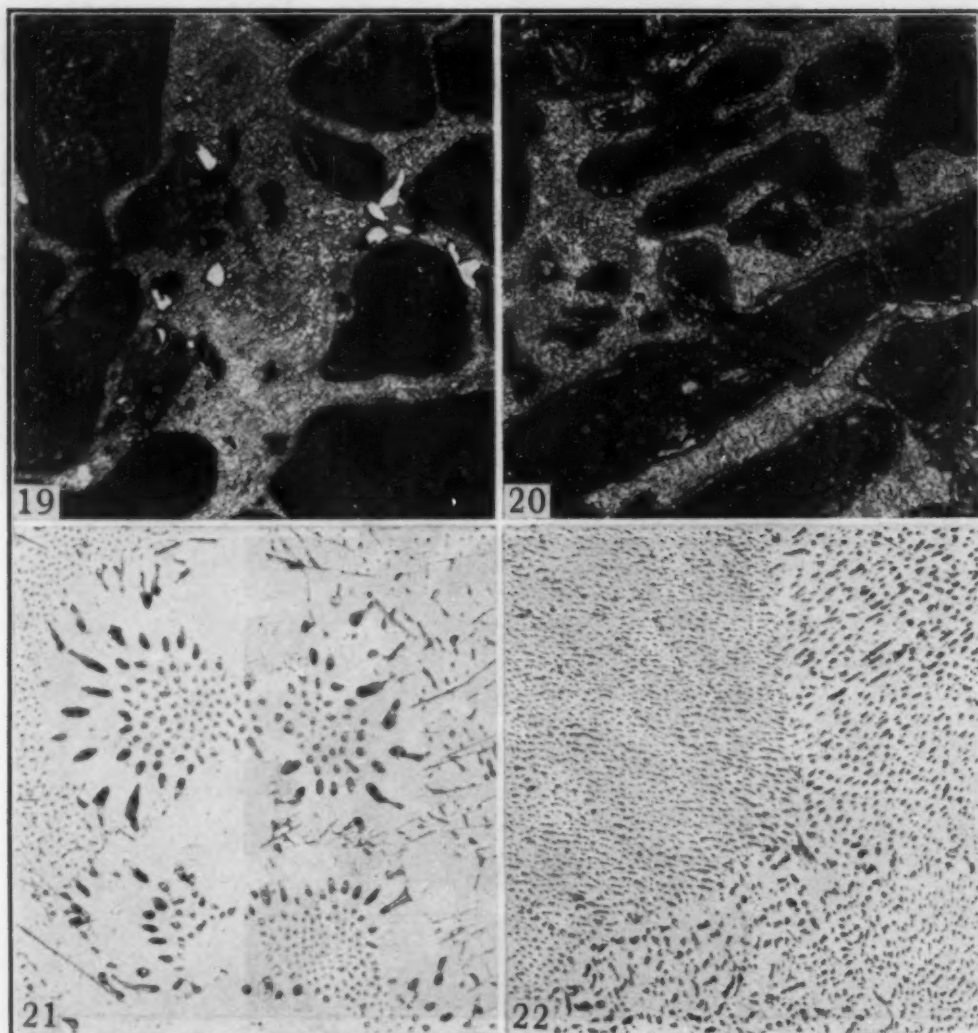


Fig. 19—80.00% Zinc, 5.00% Cadmium, 15.00% Indium. Etched with warm alkaline sodium picrate,  $\times 100$ . Dark primary alpha with light colored beta plus eutectic. As-cast.

Fig. 20—85.20% Zinc, 2.50% Cadmium, 15.00% Indium. Etched with warm alkaline sodium picrate,  $\times 100$ . Dark primary alpha plus eutectic. As-cast.

Fig. 21—75.00% Indium, 23.50% Cadmium, 1.5% Zinc. Etched with Vilella's reagent,  $\times 100$ . Primary gamma plus eutectic. As-cast.

Fig. 22—The Ternary Eutectic—74.00% Indium, 24.25% Cadmium, 1.75% Zinc. Etched with Vilella's reagent,  $\times 100$ .

Fig. 23 shows a method developed for plotting the thermal values of the liquidus curves from the various sections of constant indium content. From this plot, information can be obtained for plotting the isotherms of the liquidus surface. To do this, a horizontal line is drawn through the temperature desired, as indicated by the discontinuous line in Fig. 23, and the composition of a series of points on the isotherm is established. For example, the amount of indium is immediately known from the constant content indium section intersected by the horizontal line, and the cadmium content

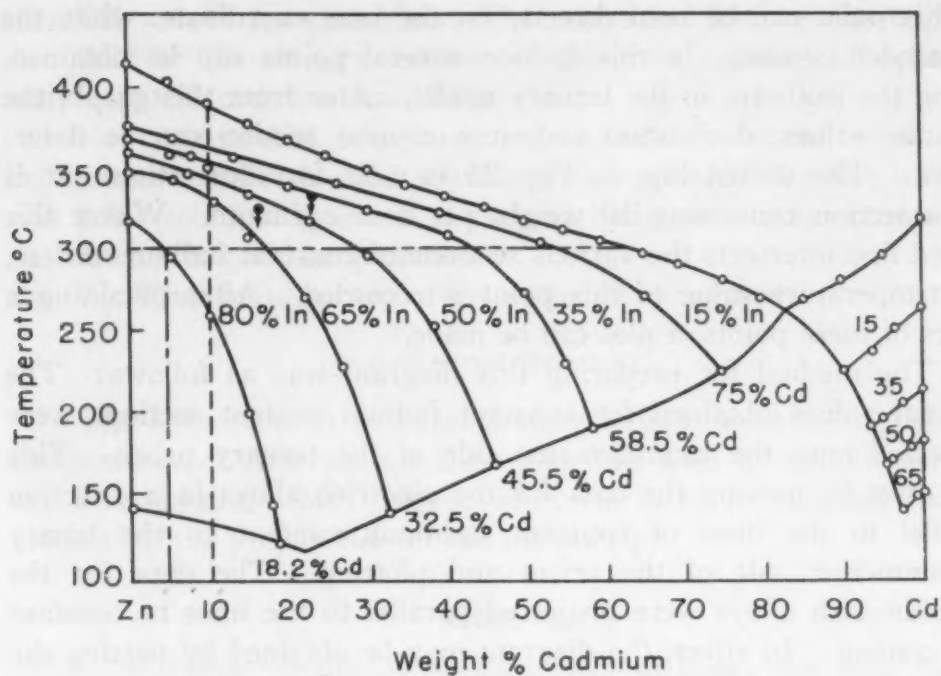


Fig. 23—Graphical Portrayal of Liquidus Sections.

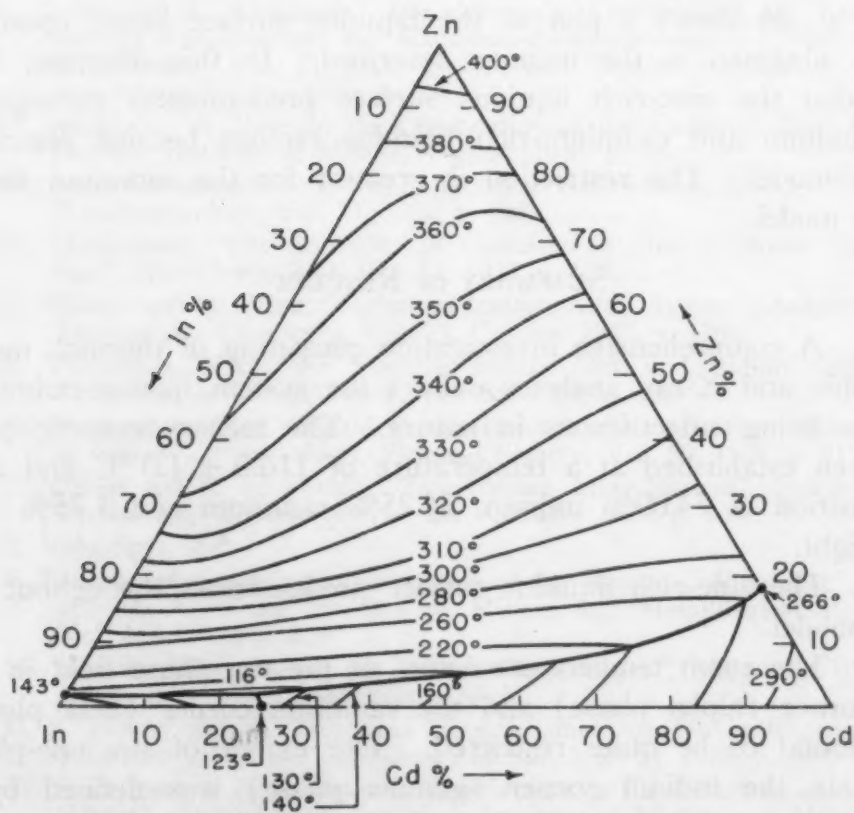


Fig. 24—The Liquidus Isotherms.

at this point can be read directly on the base coordinate, while the remainder is zinc. In this fashion several points can be obtained, fixing the isotherm in the ternary model. Also from this graph, the liquidus values of constant cadmium content section can be determined. The dotted line in Fig. 23 is used for illustration. It is for a section containing 10 weight per cent cadmium. Where this dotted line intersects the various sections of constant indium content, the temperature value of this point is recorded. After obtaining a series of these points, a plot can be made.

The method for preparing this diagram was as follows: The thermal values obtained for constant indium content sections were projected onto the cadmium-zinc side of the ternary prism. This was done by moving the data for the zinc-rich alloys in a direction parallel to the lines of constant cadmium content to the binary cadmium-zinc side of the prism and plotting. The data for the cadmium-rich alloys were projected parallel to the lines to constant zinc content. In effect, the diagram may be obtained by parting the ternary triangle at the ternary eutectic value along the univariant eutectic valley, using the zinc-cadmium eutectic composition as a pivot point until the other binary sections are 90 degrees to it instead of the original 60 degrees.

Fig. 24 shows a plot of the liquidus surface based upon the values obtained in the manner described. In this diagram, it is seen that the zinc-rich liquidus surface predominates throughout. The indium and cadmium-rich liquidus regions become restricted in the model. The restriction is greatest for the cadmium region of the model.

#### SUMMARY OF RESULTS

1. A comprehensive investigation consisting of thermal, metallographic and X-ray analyses defines the system indium-cadmium-zinc as being eutectiferous in nature. The ternary eutectic point has been established at a temperature of  $116.0 \pm 1.0$  °C and at a composition of 74.00% indium, 24.25% cadmium and 1.75% zinc by weight.

2. The zinc-rich liquidus surface predominates throughout the space model.

3. The room temperature limits of the one-phase field in the zinc corner (alpha phase) and the cadmium corner (beta phase) were found to be quite restricted. The extent of the one-phase region in the indium corner (gamma phase) was defined by a composition of 5.7 weight per cent cadmium and by slightly less



than 0.2 weight per cent zinc. The saturation limit of the indium-rich field at the ternary eutectic temperature consists of approximately 16.0% cadmium and 0.2% zinc.

4. A detectable two-phase region was found to exist only between the zinc-rich solid solution (alpha phase) and the indium-rich solid solution (gamma phase) at both room temperature and the ternary eutectic temperature.

5. A hardness survey of the system is presented.

#### ACKNOWLEDGMENT

The authors wish to express their indebtedness to the Indium Corporation of America for their generous loan of indium used in the investigation. Mr. Eugene Hoffman is to be thanked for his aid during the preparation of the manuscript.

#### References

1. W. M. Peirce, "Studies on the Constitution of Binary Zinc-Base Alloys", *Transactions, American Institute of Mining and Metallurgical Engineers*, Vol. 68, 1922, p. 769.
2. C. H. M. Jenkins, "The Constitution and the Physical Properties of the Alloys of Cadmium and Zinc", *Journal, Institute of Metals*, Vol. 36, 1926, p. 63.
3. G. Grube and A. Burkhardt, "Die elektrische Leitfähigkeit, die Korrosion und die Vergutbarkeit der Kadmium-Zinklegierungen", *Zeitschrift für Metallkunde*, Vol. 21, 1929, p. 231, and English translation: *Metals and Alloys*, Vol. 1, 1929, p. 294.
4. D. Stockdale, "A Note on the Constitution of the Cadmium-Zinc Alloys", *Journal, Institute of Metals*, Vol. 44, 1930, p. 75.
5. W. Boas, "Determination of the Solubility of Cadmium in Zinc by X-Rays", *Metallwirtschaft*, Vol. 11, 1932, p. 603.
6. M. Straumanis, "The Solubility of Cadmium in Zinc at Room Temperature", *Metallwirtschaft*, Vol. 12, 1933, p. 175.
7. C. Wilson and O. Wick, "Cadmium-Indium Alloy System", *Industrial and Engineering Chemistry*, Vol. 29, October 1927, p. 1164.
8. S. Valentiner, "Über die Systeme Indium-Zink und Indium-Kadmium", *Zeitschrift für Metallkunde*, Vol. 35, 1943, p. 250.
9. W. Betteridge, "The Crystal Structure of Cadmium-Indium Alloys Rich in Indium", *Proceedings, Physical Society*, Vol. 50, 1938, p. 519.
10. C. Wilson and E. A. Peretti, "Zinc-Indium Alloy System", *Industrial and Engineering Chemistry*, Vol. 28, February 1936, p. 204.
11. S. Valentiner, *ibid.*
12. F. Rhines and A. Grobe, "Constitution of the System Indium-Zinc", *Transactions, American Institute of Mining and Metallurgical Engineers*, Vol. 156, 1944, p. 253.
13. M. Hansen, "Der Aufbau der Zweistofflegierungen", Lithoprint 1943, Edwards Bros., Inc., Ann Arbor, Mich.
14. C. E. Homer and H. Plummer, "Embrittlement of Tin at Elevated Temperatures", *Journal, Institute of Metals*, Vol. 64, 1939, p. 169.
15. W. S. Pellini and F. N. Rhines, "Constitution of Lead-Rich Lead-Antimony Alloys", *Transactions, American Institute of Mining and Metallurgical Engineers*, Vol. 152, 1943, p. 65.

16. S. C. Carapella, Jr., and E. A. Peretti, "Metallographic Re-evaluation of the Indium-Zinc Eutectic Composition", *Journal, Institute of Metals*, Vol. 188, June 1950, p. 890.
17. E. A. Peretti and S. C. Carapella, Jr., "The Indium-Bismuth Phase Diagram", *TRANSACTIONS, American Society for Metals*, Vol. 41, 1949, p. 947.
18. S. C. Carapella and E. A. Peretti, "Metallography of Indium and Indium-Rich Alloys", *METAL PROGRESS*, Vol. 56, No. 5, 1949, p. 666.
19. L. A. Carapella, "A Graphical Method for Selecting Suitable Radiations for Precision Determination of Noncubic Lattice Constants and for Indexing Back-Reflection Lines in X-ray Photograms", *Journal of Applied Physics*, Vol. 11, No. 12, 1940, p. 800.

# THE DETERMINATION OF SOLIDUS TEMPERATURES IN MAGNESIUM ALLOYS BY DILATOMETRIC MEASUREMENTS

BY HEINRICH ADENSTEDT AND JAY R. BURNS

## *Abstract*

*A demonstration is given of the feasibility of measuring solvus and solidus temperatures of magnesium alloys through the use of a dilatometer. The method has been used to determine the solidus temperatures of binary magnesium-aluminum alloys in the range 4 to 13%, and agreement with published results is good. Binary magnesium-zinc alloys in the range 4 to 10% zinc were investigated with a resultant upward displacement of the previously accepted solidus temperatures.*

THE dilatometer has been used frequently for constitutional diagram research, for determination of lattice transformations (ferrous alloys), precipitation hardening and solution phenomena ( $\text{CuAl}_2$  in aluminum), and magnetic property changes (nickel alloys). The publications to date have been concerned only with measurements of the changes which occur in the solid state. The comment has been made that measurements were found impractical in the region of the solidus, or above, because the measuring pressures collapsed the specimens. Some authors, however, working with dilatometers of low contact pressure for measuring specimen lengths, have reported marked dilatations in the region of the solidus which they ascribed to the formation of a liquid phase and its consequent expansion of the specimen. Because the solidus temperature is generally considered an absolute maximum for heat treatment temperatures, its measurement is of practical importance. It was with this viewpoint in mind, and its possible application to new and polynary magnesium alloys, that the following experimental work was done.

## APPARATUS

The dilatometer employed was designed by Franz Bollen-

A paper presented before the Thirty-second Annual Convention of the Society, held in Chicago, October 21 to 27, 1950. Of the authors, Heinrich Adenstedt is associated with the Air Materiel Command, Wright-Patterson Air Force Base, Dayton, Ohio, and Jay R. Burns is associated with the Dow Chemical Co., Midland, Mich., formerly with Air Materiel Command, Wright-Patterson Air Force Base, Dayton, Ohio. Manuscript received April 12, 1950.



rath (1)<sup>1</sup> and constructed by E. Leitz. It records a continuous dilation graph on photographic paper as reproduced in Fig. 2.

The furnace controller is operated from a thermocouple placed adjacent to the furnace heating element. The heating and cooling program was predetermined by a prepared template inserted into the controller.

The dilatometer heating chamber was connected to an evacuation system through a dry ice - alcohol cold trap. Use of a high vacuum at temperatures in excess of the solidus points resulted in selective sublimation of alloy phases. For this reason, argon of 99.9% purity and sulphur dioxide were used in the heating chamber at slightly more than one atmosphere pressure. The sulphur dioxide partial pressure, from the cold trap, was approximately 10 mm.

### MATERIALS

Cast and machined magnesium alloy specimens were used for the major portion of the work, although a few extruded samples were also run. The metal for the cast specimens was melted in a normal manner in steel pots under flux. Either 1/4-inch diameter pencils or 1/2 by 1/2-inch bars were poured in a warm cast iron mold. The chemical analyses of specimens tested are shown in Table I. Nominal analyses figures are used in the text and figures when referring to the alloys.

Table I  
Chemical Composition of Alloys Used

Mg-Al Binaries		Analyzed, %						
Melt No.	Nominal % Al	Al	Zn	Mn	Fe	Cu	Pb	Total Other
9022	5	5.2	...	...	...	...	...	...
8993	9	9.2	...	...	...	...	...	...
9023	13	13.1	...	...	...	...	...	...
Mg-Zn Binaries								
Melt No.	Nominal % Zn							
9035	4.5	<0.03	4.1	0.02	0.04	0.001	0.003	<0.02
9024	6.0	...	5.7	...	...	...	...	...
9036	7.5	<0.03	7.5	0.02	0.04	<0.001	0.002	<0.02
8954	10.0	<0.03	9.9	0.02	0.03	0.002	0.003	<0.02
Extruded sample from Dow Chemical Co. ...		...	6.3	...	...	...	...	...

Note—Analyses for impurities in the magnesium-aluminum alloys were not made but purity is believed to be same as measured in magnesium-zinc alloys.

Photographic reproduction of the dilatometer curves obtained are shown on the left side of Figs. 1, 2, 3, 5, and 6. The corresponding first derivative is plotted on the right side of each of the figures. A magnifying glass, straightedge and protractor were used to measure

<sup>1</sup>The figures appearing in parentheses pertain to the references appended to this paper.

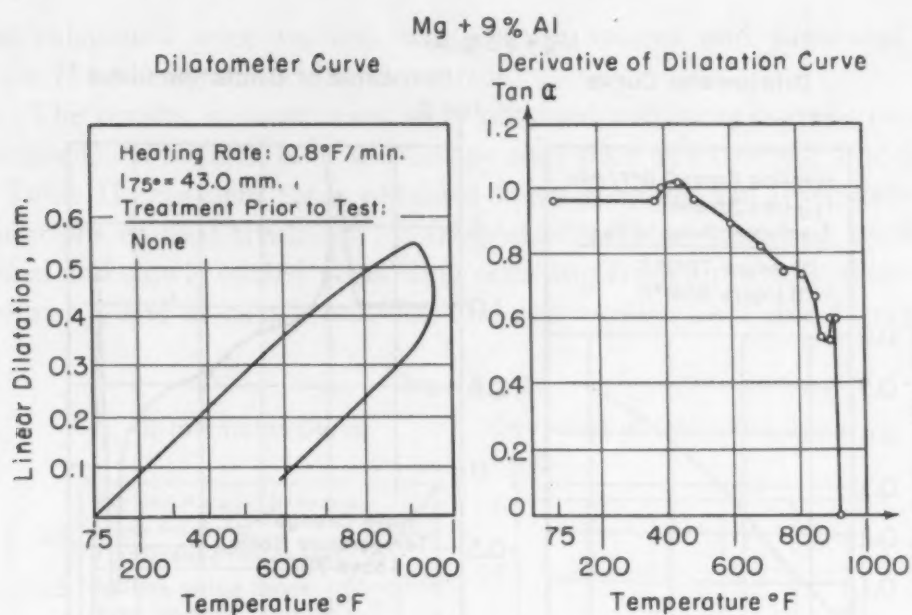


Fig. 1—Left: Dilatometer Curve of Magnesium Plus 9% Aluminum Alloy. Right: Derivative of dilatation curve.

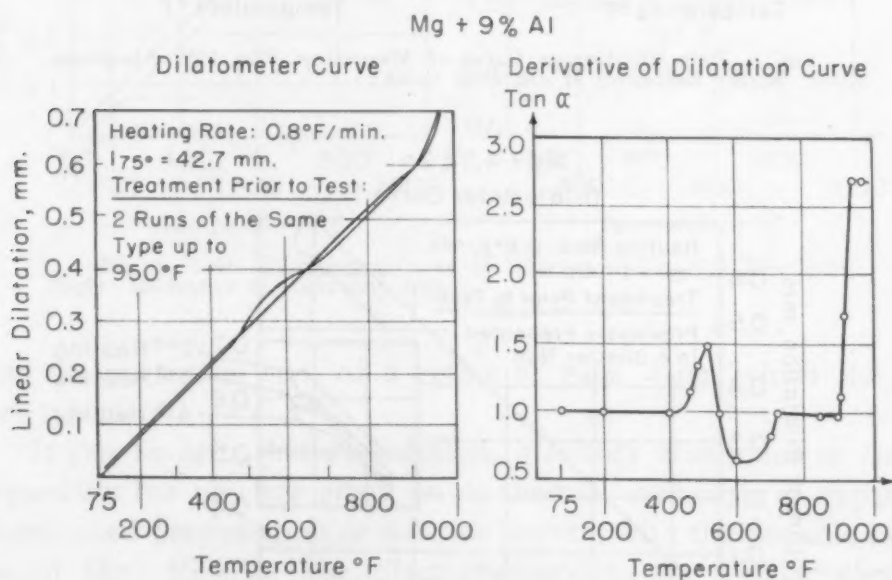


Fig. 2—Left: Dilatometer Curve of Magnesium Plus 9% Aluminum Alloy. Right: Derivative of dilatation curve.

the slope of the dilation curve at desired points. Through repetitious reading of the slope by the same and different observers, the precision was found to be  $\pm 10$  minutes, except at very sudden slope changes as in Fig. 3 in the range 800 to 815 °F (430 to 435 °C). The tangent value of the measured angle is directly proportional to the ratio of the coefficient of expansion of the test material to the coefficient of expansion of pure aluminum at any chosen temperature. Expansion of a pure aluminum sample produced displacement of the dilatometer light

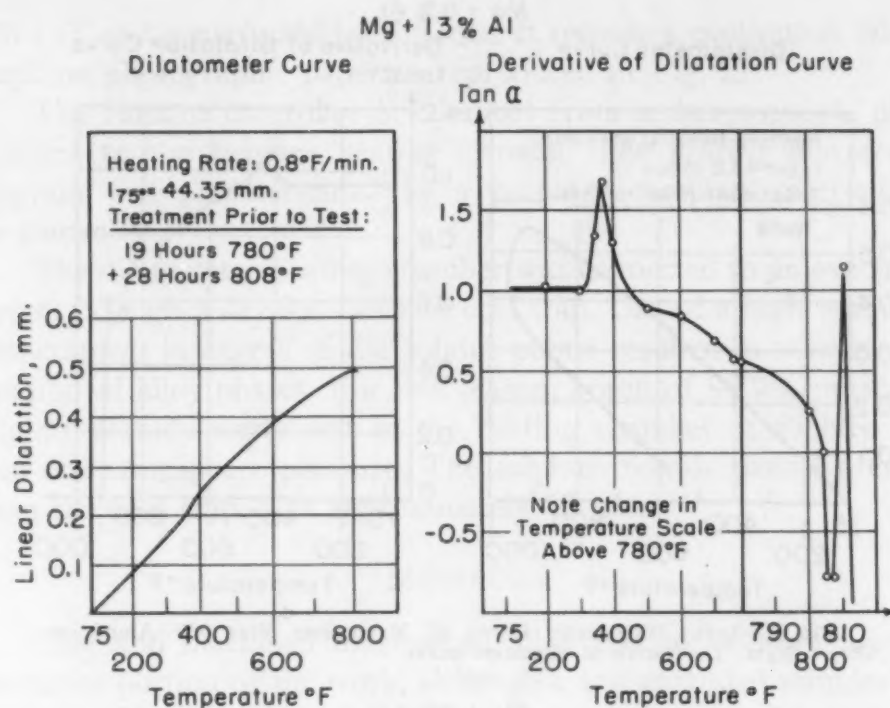


Fig. 3—Left: Dilatometer Curve of Magnesium Plus 13% Aluminum Alloy. Right: Derivative of dilatation curve.

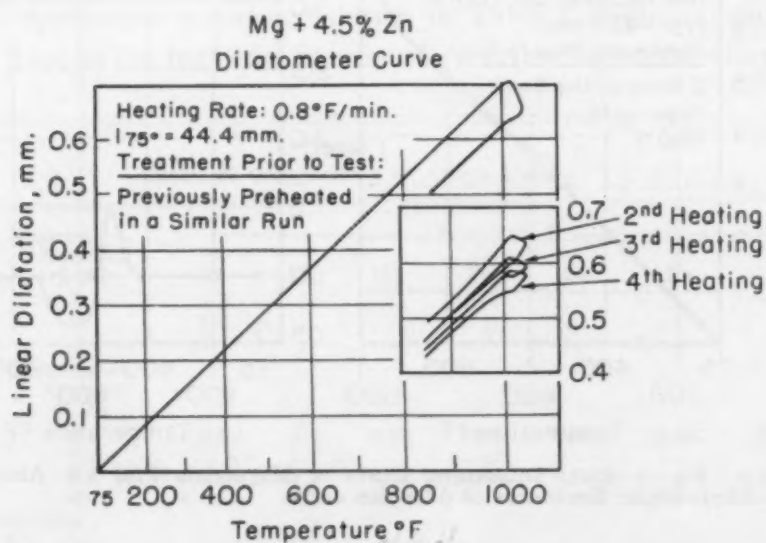


Fig. 4—Dilatometer Curve of Magnesium Plus 4.5% Zinc Alloy.

beam along the temperature axis. The proportionality factor is a function of the two specimen lengths. The true thermal coefficients of expansion of the magnesium alloy samples could thus be calculated using the known true coefficient of expansion for aluminum. For practical purposes, the mean coefficient of expansion of the different alloys



was calculated over various temperature ranges and presented in Table II as being of incidental interest.

The results, in most cases, were obtained with very coarse-grained specimens. Some effects of anisotropy may thus be expected. The data in Table II represent those obtained from specimens in three general conditions of heat treatment: homogenized and air-quenched, homogenized and slowly cooled (condition resulting from a previous dilatometer run), and as-cast condition. The run number in Table II repre-

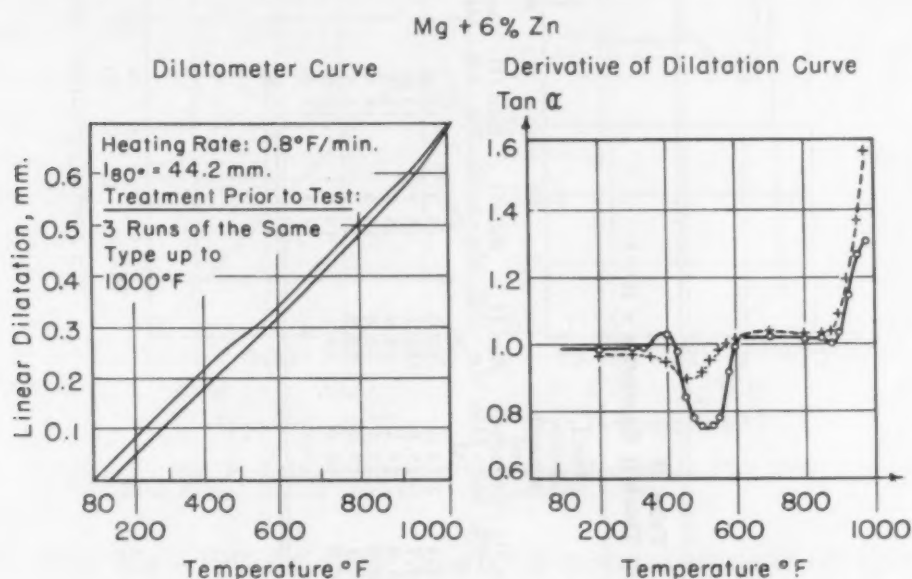


Fig. 5—Left: Dilatometer Curve of Magnesium Plus 6% Zinc Alloy. Right: Derivative of dilatation curve.

sents the particular run, of a series of runs, from which the data were taken.

It can be seen that the addition of either aluminum or zinc to magnesium has no clear effect on its thermal coefficient of expansion except when precipitation or solution occurs, with the possible exception of Mg-10%Zn. The effect produced by the alloying elements passing in or out of solution overshadows any other differences, as can be seen by comparing the results on Mg-13%Al for a homogenized and quenched sample with results on a slowly cooled sample. The large amount of aluminum precipitating from solution in the quenched sample results in a greater coefficient of thermal expansion. The increase is due only to the precipitation process, however. An example of the effect of considerable amounts of precipitated zinc returning into solution is illustrated in Run III on a Mg-6.3%Zn extruded sample. The result is a mean coefficient of thermal expansion less than that for pure magnesium.

Table II  
Mean Coefficient of Thermal Expansion  $\times 10^6/^{\circ}\text{F}$

Temp. Range, $^{\circ}\text{F}$	Run I 99.8% Mg	Run II 99.8% Mg	Run I, Homo- genized and quenched, Mg-5% Al	Run III As Cast, Mg-9% Al	Run I Homo- genized and quenched, Mg-13% Al	Run II Mg-13% Al	Run II Mg-4.5% Zn	Run III Mg-6% Zn	Run I, Homo- genized and quenched, Mg-7.5% Zn	Run I, Homo- genized and quenched, Mg-10% Zn	Run III, Extruded, Mg-6.3% Zn
75-200	15.1	....	15.6	15.3	15.6	15.0	15.2	15.2	15.5	16.4	15.2
75-300	15.1	....	15.7	15.4	15.8	15.1	15.2	15.3	15.6	16.2	15.1
75-400	15.4	15.4	15.7	15.5	17.5	15.4	15.4	15.5	15.9	16.2	15.2
75-500	....	15.6	15.8	16.0	17.3	15.8	15.8	15.4	16.1	16.4	14.8
75-600	15.9	15.9	16.1	16.2	17.0	15.8	16.2	15.1	16.4	16.7	14.0
75-800	16.3	16.4	16.7	16.0	16.2	16.1	16.8	16.0	17.0	....	14.8
75-1000	16.7	16.9	17.0	....	....	....	17.4	17.3	....	....	....

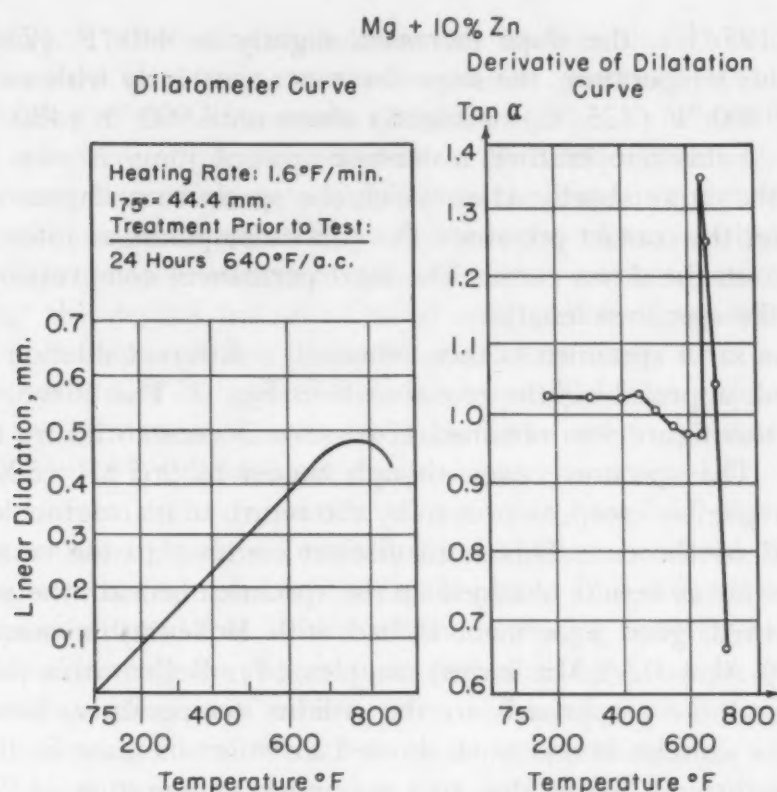


Fig. 6—Left: Dilatometer Curve of Magnesium Plus 10% Zinc Alloy. Right: Derivative of dilatation curve.

The Mg-10%Zn alloy showed a mean coefficient of thermal expansion which was always greater than that for pure magnesium and seems, therefore, to be the only alloy in which the thermal coefficient is different from that of pure magnesium, aside from the precipitation or resolution phenomena.

Most of the tests were made with a heating and cooling rate of  $0.9 \pm 0.1$  °F (0.5 °C) per minute. It can be seen by comparison of the heating and cooling curves, and a comparison of runs made with different heating rates, that this heating rate is sufficiently slow to permit at least a very close approach to equilibrium conditions in the solidus regions. The applied heating rates were generally too high for accurate measurement of solvus temperatures.

#### RESULTS AND DISCUSSION

The results obtained on Mg + 9%Al are presented first and the interpretations made will be found generally applicable to the subsequent data. The results from this alloy are the most amenable to interpretation. The curve obtained on heating and cooling an as-cast specimen is shown in Fig. 1. No deviations from a uniform expansion exist in the temperature range 75 to 380 °F (25 to 195 °C). Beginning at



380 °F (195 °C), the slope increases slightly to 440 °F (230 °C). Beyond this temperature, the slope decreases constantly with an acceleration at 800 °F (425 °C) or slightly above until 900 °F (480 °C) is reached. At this temperature, a definite upward jump is seen in the slope of the curve shortly after which the specimen collapses due to creep under the contact pressures. No particular points of interest are to be seen on the down-curve. The total permanent compression was 0.6% of the specimen length.

If the same specimen is then reheated, a different dilation curve is obtained, approaching the one shown in Fig. 2. The curve reproduced in this figure was obtained after several runs to insure reproducibility. The specimen, even though heated to 965 °F (520 °C), exhibits negligible creep, as proven by the return to its original length, at the end of the run. This is in distinct contrast to the results in Fig. 1. As far as results obtained on the specimen beneath the solidus are concerned, good agreement is had with Bollenrath's results on Mg + 10%Al + 0.5%Mn forged samples (2). Bollenrath's samples collapsed on their approach to the solidus temperature, however, whereas the samples in this work showed a distinct increase in dilation on passing through the solidus, to a maximum temperature of 965 °F (520 °C) or even 1000 °F (540 °C) in the case of one Mg + 9%Al run.

Referring to the derivation of the dilation curve of Fig. 2, the first maximum beginning at 400 °F (205 °C), or slightly above, and ending at 545 °F (285 °C), represents precipitation of the Mg-Al compound from solution. At a temperature of 545 °F (285 °C), the dilation becomes less than normal, indicating that the compound is being redissolved. The process of solution of all of the aluminum is completed at 720 °F (380 °C), indicating this to be the solvus temperature. Duplicate runs and various heating rates showed that approximately equilibrium conditions were had at the measured solvus temperature in this case. Between 720 and 905 °F (380 and 485 °C), a range of constant dilation rate exists, indicating the range of homogeneous solid solution. At 905 °F (485 °C), a large increase in dilation rate reveals the solidus temperature. A magnesium-aluminum liquid solution forms at certain regions in the sample. The percentage of aluminum dissolved in the remaining solid matrix becomes progressively less and the dilation of this solid matrix consequently takes place at an increasing rate.

The increased coefficient of expansion above the solidus is due to the expansion of the still solid matrix as its composition changes, and possibly due to the formation of a liquid phase with consequent

expansion. The relative contribution of each of these mechanisms is not known. Calculations of the expansion produced by changes in composition of the solid matrix, above the solidus, show that this factor alone will account for the increase in thermal expansion. Similarly, the greater expansion rate of magnesium-aluminum binaries, compared with magnesium-zinc binaries, above the solidus, can be accounted for by the relative effects of the aluminum and zinc atoms in contracting the crystal lattice of solid magnesium. Expansion due to alloying elements passing in or out of solution under near equilibrium conditions would be expected to be reversible. The expansion produced by formation of a liquid phase from solid components is not known for the conditions and compositions encountered. It is believed, however, that if the formation of a liquid phase had contributed to the expansion, plastic deformation would have occurred, due to the heterogeneous dispersion of the liquid phase. It is difficult to conceive of expansion produced in this manner as being reversible.

Upon cooling the magnesium-9% aluminum sample from above the solidus, aluminum returns into solid solution and remains in solution during the slow cool to room temperature.

Cooling at an especially slow rate, or holding the sample at some suitable temperature during cooling, will, however, permit precipitation to occur during the cooling cycle, as was demonstrated during the work. A fast heating rate of 4.2 °F (2.3 °C) per minute resulted in a characteristic precipitation hump that is flatter and located about 40 °F (20 °C) higher than normal. No effect occurred on the location of the solidus temperature at 900 °F (480 °C) on the heating curve.

The typical dilation curve (e.g., Fig. 2) can be obtained on the first run if the specimen is first homogenized just below the solidus.

Two experimental conditions are believed necessary to permit extension of the dilation curve to temperatures well beyond the solidus without collapse of the specimen. First, a continual and gradual readjustment of the metallographic structure must occur upon heating in order that near-equilibrium conditions exist at all times. Secondly, the grain size must be very large—typical of a germinated magnesium structure. Single grains were estimated to occupy 10 to 20% of the specimen volume.

The first condition is necessary to prevent excessive diffusion over any short-time interval. It is believed that excessive diffusion causes a temporary reduction in creep strength and resultant breakdown of the specimen (diffusion plasticity).

The second condition, that of an extremely coarse grain size (approaching a single crystal specimen), contributes directly to the

creep strength, at least below the solidus. It is further believed, from the observations made during this work, that the very coarse grain structure is responsible for a desirable melting phenomena in magnesium-aluminum alloys above the solidus. Instead of molten material forming on the grain boundaries and thus separating the grains by a liquid phase, it occurs in a highly dispersed and isolated manner within the grain. The solid portions of the sample thus retain their connections and sustain small deforming pressures against the sample.

Fig. 3 shows the typical dilatometer curve for magnesium - 13% aluminum. Precipitation in this high aluminum alloy began at 320 °F (160 °C) and the range of resolution extended to the eutectic temperature of 808 °F (430 °C), instead of 815 °F (435 °C) as reported in the literature. This deviation is probably a result of the impurities present in the specimens. Above the eutectic temperature, a reproducible and definite, but short, uptrend is seen and immediately afterwards the specimen collapses. A second run on the same sample gives the same curve. As might be expected, the desired large grain size could not be produced in this composition.

#### MAGNESIUM-ZINC ALLOYS

More difficulty was experienced in obtaining usable results in the magnesium-zinc alloys than with magnesium-aluminum compositions. This was, in part, due to the fact that grain diameters could not be made as large as in the magnesium-aluminum alloys and also due to the increased sublimation and oxidation tendencies of these alloys in the neighborhood of the solidus. Aside from these difficulties, the dilatometric methods seemed applicable to this alloy system.

Some preliminary germination tests were made on magnesium-zinc alloys with zinc contents of 3, 4, 5, 6, and 7.5%. Chill cast bars with a 1/2 by 1/2-inch cross section were severely cold bent in one direction and then homogenized for 42 hours at 950 °F (510 °C). Additional samples, in the low zinc range, were bent and homogenized 12 hours at 1000 and 1050 °F (540 and 565 °C). The sample containing 6% zinc showed the most extensive germination, and this in a region apparently critically strained. The 7.5% zinc sample similarly showed germination but not so extensive. The 4.5 and 3% zinc samples showed no definite germination. None of the samples germinated so quickly or extensively as did magnesium-aluminum alloys, however. This fact probably explains the difficulties experienced in obtaining the desired specimen stability above the solidus. The final grain diameters and stability above the solidus of dilatometer samples corresponded with



the foregoing tests. The grain diameters measured on the dilatometer specimens after running are as follows:

Mg - 4.5% Zn	= 0.006 inch
Mg - 6% Zn	= ~ specimen diameter = 0.125 inch
Mg - 7.5% Zn	= 0.080 inch
Mg - 10% Zn	= 0.020 inch
Mg - 6.34% Zn	= 0.030 inch

No success was had in attempting to achieve a germinated grain size in the 4.5% zinc dilatometer samples through simple homogenization and, therefore, all samples collapsed just over the solidus line. The upper curve of Fig. 4 shows the first run on magnesium - 4.5% zinc after it had been previously heated over the same cycle. Fig. 4 also shows the same specimen cycled 3 more times between 850 and 1040 °F (455 and 560 °C). In every case, the heating rate was the same. It can be seen that the point of breakdown of the specimen is at the same temperature in every case; and since creep began and ended abruptly at this temperature, the temperature was taken as being a first approximation to the solidus. The creep subsequent to the breakdown was less with each succeeding run, as evidenced by the fact that the slope becomes flatter each time above the solidus and the displacement of the down-curve at the solidus temperature is less each cycle. However, the grain size never coarsened satisfactorily with continued runs and the desired creep resistance above the solidus was not obtained as with the magnesium-aluminum alloys.

Tests were extensive with the magnesium - 6% zinc composition and the nature of the results very much in keeping with those on magnesium-aluminum alloys. The dilations connected with structural changes were not so large, however. Fig. 5 shows the fourth slow run made on a sample, demonstrating the curve obtained and its similarity to magnesium - 9% aluminum. The solidus is indicated at 890 °F (475 °C) on the heating curve and 880 °F (470 °C) on the cooling curve. The solvus point was found to be in the range 580 to 600 °F (305 to 315 °C).

The character of the results on magnesium - 7.5% zinc were very much like those on 6% zinc except that precipitation, coalescence, and resolution in the solid state are not indicated to a pronounced degree on the dilation curve.

The results obtained with magnesium - 10% zinc are shown in Fig. 6. The sample was given a preliminary homogenization treatment of 24 hours at 640 °F (340 °C). The solidus is indicated at 640 °F (340 °C) and the sample could be heated to 800 °F (425 °C) before it collapsed.

## EXTRUDED MAGNESIUM - 6.3% ZINC

A binary alloy containing 6.3% zinc was received from the Dow Chemical Company in the as-extruded condition. Following a procedure described by E. Schmid and G. Siebel (3), the 6.3% zinc sample was treated to produce abnormally coarse grains. The treatment was as follows:

homogenize 65 hours at 640 °F (340 °C)  
 room temperature strain 8%  
 homogenize 24 hours at 700 °F (370 °C)  
 room temperature strain 0.2%  
 homogenize 24 hours at each of the following temperatures successively: 700, 750, 800, 850 °F (370, 400, 425, 455 °C)

The grain size could not be coarsened to the same extent as that achieved in the cast alloys. The subsequent dilation curve showed an

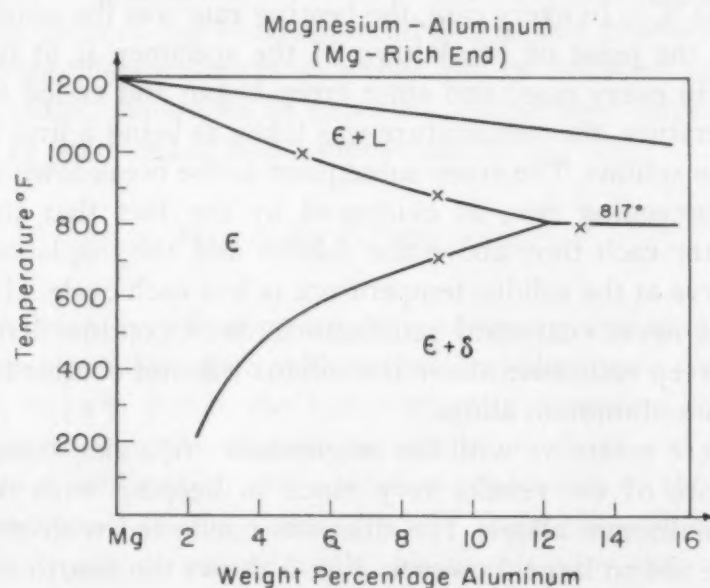


Fig. 7—Magnesium-Rich End of the Magnesium-Aluminum Constitutional Diagram.

increased expansion rate on heating over the temperature range 870 to 940 °F (465 to 505 °C), indicating entry into the  $\alpha +$  liquid field. At 940 °F (505 °C) the specimen began to creep rapidly. The solidus was indicated at a somewhat higher temperature on the heating curve than on the cooling curve, demonstrating that a heating and cooling rate of less than 1.6 °F per minute is desirable for the Mg-Zn binaries.

#### COMPARISON OF RESULTS WITH PUBLISHED EQUILIBRIUM DIAGRAMS

Fig. 7 shows the magnesium-rich end of the magnesium-aluminum constitutional diagram as reported by M. Hansen (4). The results

Table III  
Mechanical Properties on HTA Mg-Zn Alloy Cast Test Bars

Alloy	Heat Treatment				% E	TYS	UTS
	Hrs.	°F	Hrs.	°F			
Mg - 5.9% Zn	20	800	20	347	2.3	22,500 psi	31,500 psi
Mg - 5.9% Zn	20	850	20	347	2.2	23,200 psi	31,300 psi
Mg - 5.9% Zn	20	900	20	347	5.5	23,000 psi	36,300 psi
Mg - 5.9% Zn	20	925	20	347	3.4	22,600 psi	34,400 psi
Mg - 5.9% Zn	20	950	20	347	0.8	.....	16,000 psi

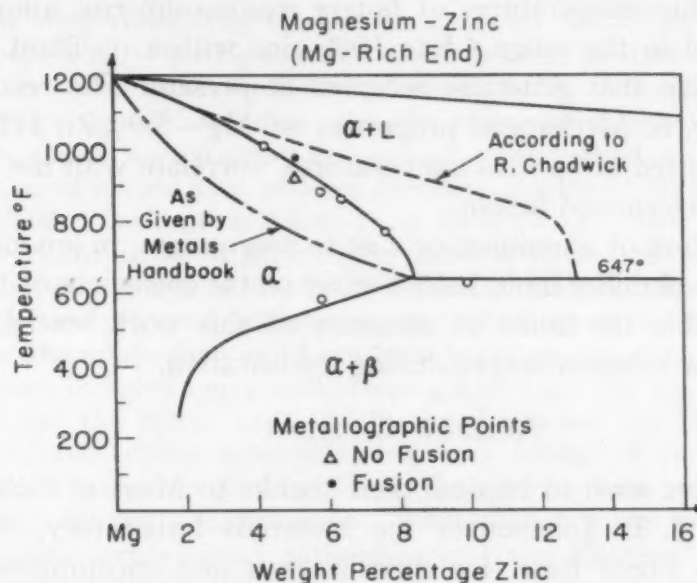


Fig. 8—Magnesium-Rich End of the Magnesium-Zinc Constitutional Diagram.

obtained from this work have been placed on the diagram and are in good agreement.

Fig. 8 shows the magnesium-rich end of the magnesium-zinc constitutional diagram. Many controversial results have been reported for this diagram.

The maximum solubility of zinc has been reported to be as little as 6% and as much as 13% (5, 6). The work of Schmidt and Seliger (7) on the equilibrium solid-phase solubility of zinc is considered to be correct, however, and their solvus and maximum solid solubility figures are used. The solidus line from the *ASM Metals Handbook* (8) and the solidus determined by Chadwick (6), who reported 13% maximum solubility, are shown in Fig. 8. The results obtained from this work are plotted with small circles. Very brief metallographic examination of samples of a magnesium-5% zinc extruded alloy, heated to various temperatures, confirmed the dilatometric results as shown in Fig. 8. Some practical substantiation was



found for the solidus line herein determined, from tensile testing binary alloys homogenized at various temperatures and then aged. The results are shown in Table III.

#### CONCLUSIONS

A continuously recording dilatometer, with small contact pressures, may be satisfactorily used for measurement of solidus temperatures of magnesium alloys.

The solidus temperatures of binary magnesium-zinc alloys have been measured in the range 4.5 to 10% zinc with a resultant solidus line higher than that generally accepted at present. The results are plotted in Fig. 8. Mechanical properties of Mg-5.9%Zn HTA test bars, homogenized at various temperatures, correlate with the solidus temperature determined herein.

The addition of aluminum or zinc to magnesium, in amounts less than the solid solubility limit, has no effect on the coefficient of thermal expansion within the limits of accuracy of this work, except when precipitation or solution occurs during mensuration.

#### ACKNOWLEDGMENT

The writers wish to express their thanks to Messrs. Richard R. Kennedy and J. B. Johnson of the Materials Laboratory, Wright-Patterson Air Force Base, for their interest and encouragement of this work and for permission to publish the results. Appreciation is extended to the Dow Chemical Company for extruded samples and permission to do some of the metallographic and analytical work in their laboratories.

#### References

1. F. Bollenrath, "A New Optical Dilatometer", *Zeitschrift für Metallkunde*, Vol. 7, 1933.
2. F. Bollenrath, "Precipitation from Cold-Worked Supersaturated Solid Solutions, as Evidenced by Thermal Expansion Measurements", *Metallwirtschaft*, Vol. 12, No. 40, 1933, p. 569.
3. E. Schmid and G. Siebel, *Zeitschrift für Elektrochemie*, Vol. 37, 1933, p. 455.
4. M. Hansen, "The Constitution of Binary Alloys", Berlin, 1936.
5. W. Schmidt, *Zeitschrift für Metallkunde*, Vol. 19, 1927, p. 454.  
M. Hansen, *Journal, Institute of Metals*, London, Vol. 39, 1928, p. 298.
6. R. Chadwick, *Journal, Institute of Metals*, London, Vol. 39, 1928, p. 285.
7. E. Schmid and H. Seliger, "Investigations of Binary Solid Solutions of Magnesium", *Metallwirtschaft*, Vol. 11, 1932, p. 409.
8. J. B. Hess, "Magnesium-Zinc", *ASM Metals Handbook*, 1948 edition, p. 1227.

## DISCUSSION

**Written Discussion:** By R. S. Busk, Magnesium Laboratories, Dow Chemical Co., Midland, Mich.

The authors present a very marked correction to the previously accepted solidus for Mg-rich Mg-Zn alloys. The correction is so large that we felt obliged to check its accuracy and prepared a Mg + 3.5% Zn alloy made from distilled magnesium and high-purity zinc. In the present paper the authors worked with commercial grade magnesium which contained substantial quantities of manganese and iron. Therefore we made a second alloy containing Mg + 3.5% Zn + 1% Mn. The melting point of the pure binary lies between 1050 and 1055 °F as determined metallographically. The ternary solidus is lowered 10 °F. This is excellent confirmation of the authors' data, and the new solidus should be accepted.

This seems an excellent example of perpetuation of error through duplication of earlier data without adequate checking. The solidus in the *ASM Metals Handbook* is taken from Beck<sup>2</sup> which gives an apparently accurate curve. The literature references in Beck lead one finally to a discussion of a paper of Chadwick's<sup>3</sup> by Dr. Hansen given in 1928. As well as I can determine, all subsequent solidus curves for magnesium-zinc alloys at the magnesium end have been based on this discussion in which Dr. Hansen included two points showing melting. The subject of the discussion was the solvus line, and in the discussion Dr. Hansen made it clear that the solidus determinations were incidental and probably not reliable. In his subsequent treatise on binary diagrams published in 1936, he himself did not use the points. Nevertheless other investigators, including even such eminent authorities as Hume-Rothery,<sup>4</sup> have accepted this curve without question.

We are indebted to the present authors for correcting this error and it is to be hoped that standard reference books will note the data given here.

<sup>2</sup>*The Technology of Magnesium and Its Alloys*, edited by E. H. Adolf Beck, translation by F. A. Hughes & Co., Limited, London, 1940.

<sup>3</sup>R. Chadwick, "The Constitution of the Alloys of Magnesium and Zinc", *Journal, Institute of Metals*, Vol. 39, 1928, p. 285.

<sup>4</sup>W. Hume-Rothery and E. O. Rounsefell, "The System Magnesium-Zinc", *Journal, Institute of Metals*, Vol. 41, 1929, p. 119.

## CONSTITUTION AND MECHANICAL PROPERTIES OF ZIRCONIUM-IRON ALLOYS

BY E. T. HAYES, A. H. ROBERSON AND W. L. O'BRIEN

### *Abstract*

*A diagram for the zirconium-iron system has been developed which shows a eutectoid at 2.5% iron and 800 °C (1470 °F), and a eutectic at 16% iron and 934 °C (1715 °F). The maximum solubility of iron in beta zirconium is 5.5%; solubility in the alpha, or hexagonal, form is less than 0.02% iron.*

*Alloys containing up to 7% iron can be worked at 850 °C (1560 °F).*

*Tensile data are given for hot-rolled, quenched, drawn and cold-worked alloys. Heat resistance and hot strength are also included.*

THE United States Bureau of Mines has developed a commercial process for the production of ductile zirconium and at the present time is producing over 300 pounds of the metal per week. A number of reports outlining the production (1),<sup>1</sup> melting (2), heat resistance (3), and fabrication and physical properties (4) have already been published. There is a widespread interest in the use of this material, particularly in regards to its corrosion resistance.

The Northwest Electrodevelopment Laboratories of the Bureau of Mines in cooperation with the Air Matériel Command have been investigating zirconium alloys for the past two years and the results of this preliminary survey have been the subject of a Report of Investigations (5). Although the primary purpose of this preliminary survey was to determine the suitability of zirconium alloys for medium temperature applications, data also were obtained on the mechanical properties of these alloys. One of the more interesting, as well as promising, was the zirconium-iron series. It is interesting both from the standpoint of improving the physical properties of zirconium metal and because iron is a nuisance element

<sup>1</sup>The figures appearing in parentheses pertain to the references appended to this paper.

Published by permission of the Director, Bureau of Mines, United States Department of Interior, Washington, D. C.

A paper presented before the Thirty-second Annual Convention of the Society, held in Chicago, October 21 to 27, 1950. The authors, E. T. Hayes, A. H. Roberson and W. L. O'Brien, are metallurgists, Northwest Electrodevelopment Laboratory, Albany, Oregon. Manuscript received April 22, 1950.



in zirconium metal production. In order to properly evaluate the zirconium-iron system it was necessary to develop an equilibrium diagram that would provide a basis for a complete investigation of the system.

Although phase diagrams for the zirconium-iron system have been published, the major portion of such work has been directed toward the iron-rich sections. Vogel and Tonn (6) developed a complete diagram, but since their alloys were prepared by melting

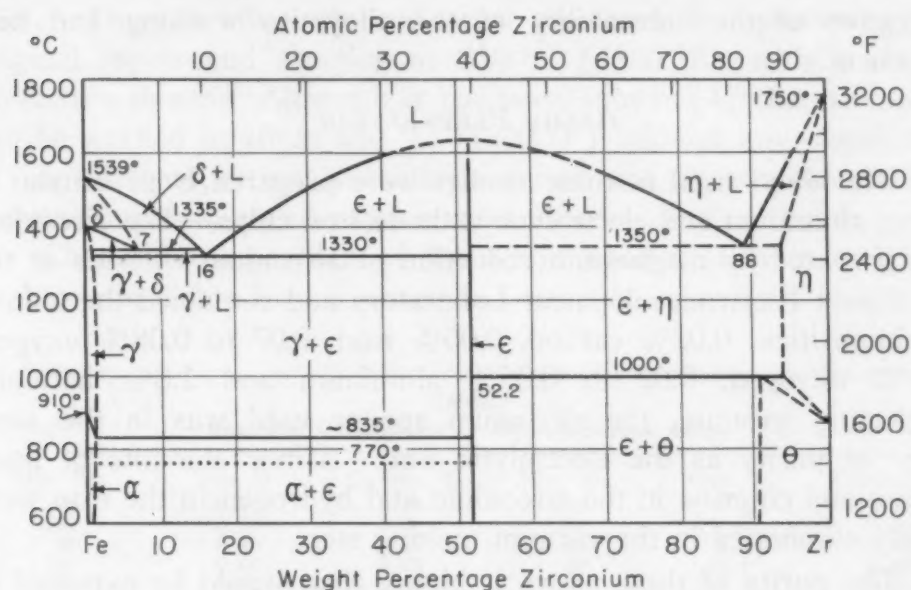


Fig. 1—Iron-Zirconium System. (ASM Metals Handbook.)

in alumina crucibles, the higher zirconium alloys were so contaminated that the results are of doubtful value.

It has been reported by several investigators (7, 8) that molten zirconium, like titanium, is practically a universal solvent and either reduces or dissolves alumina crucibles with subsequent embrittlement of the metal. It has been recognized for over 25 years that a few tenths of a per cent of oxygen or nitrogen destroys the ductility of the metal.

Allibone and Sykes (9) restricted their studies to alloys containing less than 30% zirconium. Wallbaum (10) prepared a few high zirconium alloys by melting in alumina and made only a cursory study of the system. The most probable diagram based on the work of these investigators is shown in Fig. 1 as reproduced from the *Metals Handbook* (11). It is to be noted that most of the lines on the zirconium-rich end are dotted to show that final placement of the phase boundaries has not been made. It will be shown in this paper

that the eutectic temperature and solid phase relationships for the zirconium-rich alloys are drastically different from those proposed by previous investigators.

The major portion of this investigation was confined to a study of the phase relationships in the solid state with only a small amount of effort being directed to obtaining the liquidus lines. Data were obtained by metallographic examination, thermal analysis, X-ray studies, and tensile properties. It is believed that the phase diagram presented here is substantially correct, and that the tensile data are indicative of the amenability of the alloys to working and heat treatment.

#### ALLOY PREPARATION

The alloys used in these studies were prepared from Bureau of Mines zirconium and electrolytic cathode iron chips. The zirconium was prepared by magnesium reduction of zirconium chloride at the Northwest Electrodevelopment Laboratory and contained the following impurities: 0.02% carbon, 0.06% iron, 0.07 to 0.08% oxygen, 0.01% nitrogen, 0.02 to 0.05% aluminum and 1.8% hafnium. Neglecting hafnium, the zirconium sponge used was in the same order of purity as the electrolytic iron. Minor amounts of magnesium and chlorine in the zirconium and hydrogen in the iron were largely eliminated in the vacuum melting step.

The purity of these alloys is higher than would be expected in commercial practice and much better than any reported in the literature. Two ingots were prepared by arc melting in a helium atmosphere but the tungsten introduced (0.1 to 0.3%) was more objectionable than the carbon in regard to physical properties and metallographic structures and hence all alloys reported were prepared by melting in graphite. It has been shown previously (5) that the addition of 0.3 to 0.4% carbon has no harmful effects on the properties of zirconium metal; in fact, it produces an increase in strength. The effect of hafnium has not been determined, but work in these laboratories on zirconium metal containing 0.1 to over 2% hafnium has failed to disclose any variation in properties that could be assigned to its presence.

Alloys containing less than 0.2% iron were chosen from zirconium ingots containing abnormally large amounts of incidental iron. This iron is a result of a carry-over from the chloride refining step and pickup from the iron reduction pot in the zirconium production cycle. Above 0.2% the iron was added as cathode chips incorporated in the briquetted sponge. Melting was carried out

under vacuum (0.1 micron) in a three-phase, split-resistor, graphite furnace using a graphite crucible with the melt being allowed to solidify in the melting crucible. After removal from the furnace, the graphite was removed by turning in a lathe. The scalped ingot was about 2 inches in diameter, 3 inches long and weighed about 2 pounds.

This ingot was encased in a close fitting piece of heavy-wall iron tubing and end plugs welded in place, after which it was forged and rolled at 850 °C (1560 °F) to produce sheet of desired thickness. Three-eighths-inch rod was produced by quartering the original ingots and swaging at 850 °C (1560 °F) with a similar protective sheath. Although it has been shown (4) that zirconium can be worked in air at 650 °C (1200 °F) without any impairment of physical properties, this alloy's series was sheath protected to reduce the possibility of oxygen contamination to a minimum.

Chemical composition of the alloys used in this investigation is shown in Table I.

Table I  
Chemical Composition of Zirconium-Iron Alloys

Alloy No.	Iron, %	Carbon, %	Alloy No.	Iron, %	Carbon, %
29	0.24	0.26	240	5.5	0.09
197	0.39	0.05	203	7.55	0.05
80	0.45	0.17	88	8.5	0.09
110	0.66	0.23	89	13.1	0.09
233	0.97	0.09	90	16.8	0.36
111	1.15	0.18	170	20.3	0.12
118	1.73	0.15	171	30.0	0.39
263	2.5	0.05	107	44.2	0.96
169	2.9	0.08	106	46.1	0.16
239	3.3	0.11	109	51.6	0.79
264	4.6	0.04	108	59.6	0.67
87	5.16	0.15			

The carbon content, which varied from 0.05 to 0.96%, was the result of carbon pickup from the graphite melting crucible. All the carbon occurred as zirconium carbide and no evidence was found that indicated a solubility of the carbide in the metal. The carbide grains which were scattered at random were disregarded as a phase during the metallographic analysis.

The three alloys containing more than 0.4% carbon were in the brittle range so that only metallographic and X-ray examinations could be made. The metallographic structures of Alloys 106 and 107 were similar, except for the amount of carbide present, and no marked structural difference was observed which could be ascribed to the variation in carbon content.

Sheet was prepared by hot rolling to an alloy content of 5.5%



iron, and rod was produced by hot forging up to 7% iron. Above this 7% limit the alloys were too brittle to be worked, and above 13.5% iron they were too friable to allow hardness readings to be made.

All hot working was performed at 850 °C (1560 °F), with frequent reheating during the process, followed by a 30-minute reheat and air cooling after the last pass. Subsequent heat treatment was carried out either in high vacuum (0.1 micron) or a helium atmosphere. In this manner oxygen or nitrogen contamination was confined to negligible amounts. In the few instances where metallographic specimens showed slight surface discoloration, due to the presence of small amounts of oxide picked up during heat treatment, no variation in microstructure was observed which could be attributed to oxides or nitrides. Segregation was a minor problem after the above working procedure, and all the worked alloys were homogeneous.

Metallographic specimen preparation closely followed previously published techniques (12), the etchant being 6 parts glycerine, 2 parts HF, and 1 part conc.  $\text{HNO}_3$ . The etchant was applied by swabbing for 2 or 3 seconds.

## RESULTS

### *Alpha Field*

The solubility of iron in the alpha form of zirconium is quite low. Alpha zirconium, the normal room temperature form, has a hexagonal close-packed structure. At 862 °C this transforms to beta zirconium, a body-centered cube. Zirconium specimens containing 0.013 to 0.2% iron were furnace-cooled in vacuum from 750 to 900 °C at 50-degree intervals. Metallographic examination showed that the specimens containing 0.013% iron had a homogeneous structure with no evidences of an intergranular phase or a second constituent other than scattered carbides. However, the 0.02% iron alloys showed the presence of a very fine intergranular constituent which increased regularly with increasing iron content. Fig. 2 shows a typical area of the 0.02% iron specimen and illustrates the appearance of this new phase. The maximum solubility at the eutectoid temperature could not be determined on quenched specimens due to difficulties encountered in metallographic interpretation. However, thermal analysis of specimens containing 0.09 and 0.12% iron showed a eutectoid arrest at 800 °C (1470 °F). This would indicate that the solubility at 800 °C is considerably less

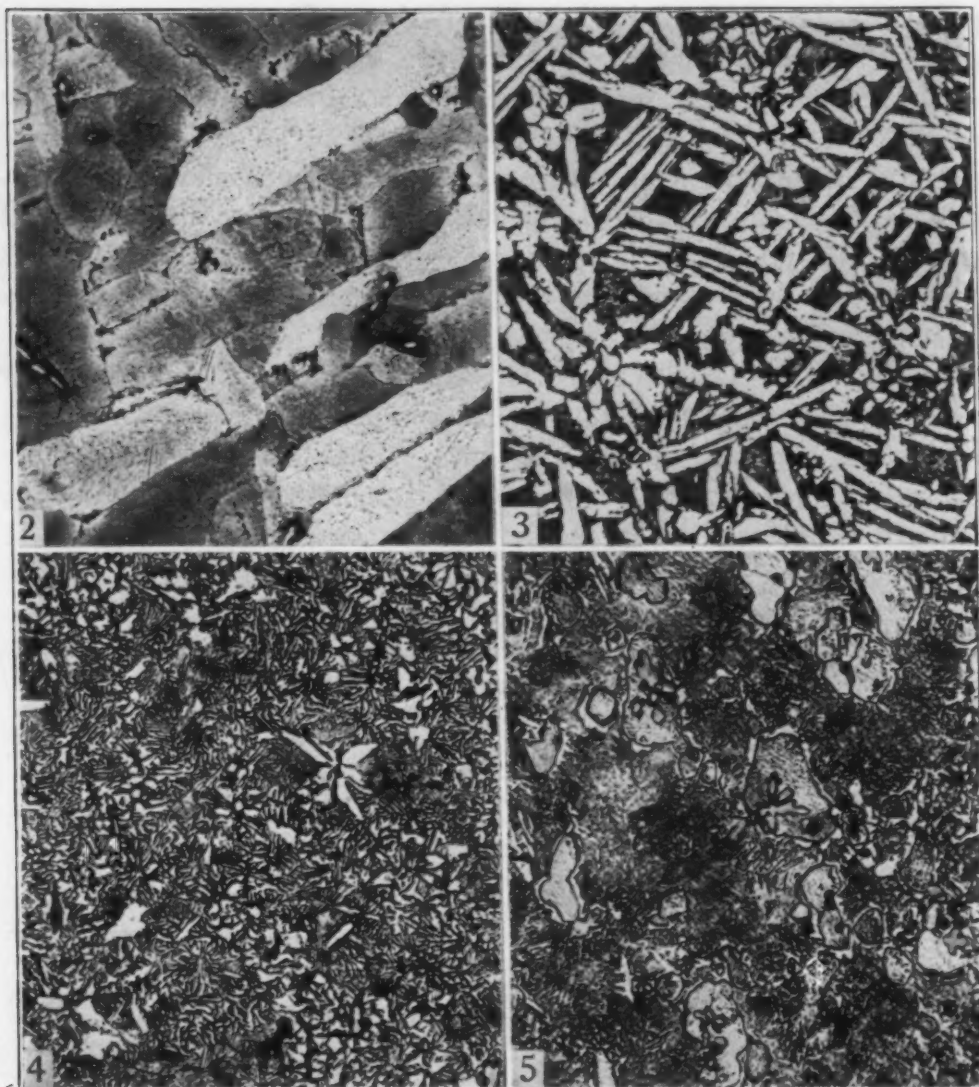


Fig. 2—0.02% Iron, Furnace-Cooled, Showing First Traces of Eutectoid.  $\times 250$ .

Fig. 3—1.7% Iron, Rapid Cool, Alpha Needles and Eutectoid.  $\times 250$ .

Fig. 4—2.5% Iron, Rapid Cool, Eutectoid.  $\times 250$ .

Fig. 5—3.3% Iron, Rapid Cool, Eutectoid and Gamma Grains.  $\times 250$ .

All specimens etched with Vilella's reagent.

than 0.09% iron. It is concluded that the solubility of iron in alpha zirconium at room temperature is less than 0.02% and probably not much greater than this amount at 800 °C (1470 °F).

#### *Beta Field*

The beta field was established on the basis of thermal analysis and metallographic examination of heat treated samples. This was complicated somewhat by the fact that the beta form cannot be retained by quenching, even after the addition of 5% iron. Alloys

quenched from this field have a Widmanstätten-type pattern of acicular needles which were shown by X-ray diffraction patterns to be alpha zirconium. Since iron did not stabilize the beta form, the presence of Widmanstätten needles was taken as indicative of the presence of beta at temperature. Thus specimens showing a continuous Widmanstätten structure were considered to have been all beta at the quenching temperature, while the presence of bright alpha grains surrounded by this acicular structure showed alpha plus beta.

Thermal analysis was performed in a helium atmosphere at heating and cooling rates of 5 °C per minute. Differential readings were made between the specimen and a nickel neutral body. The chromel-alumel couples were checked against a similar secondary standard couple calibrated by the Bureau of Standards. Table II gives the results of four such runs:

Table II  
Thermal Analysis of Zirconium-Iron Alloys

Iron, %	Thermal Arrest			
	Heating		Cooling	
	°C	°F	°C	°F
0.25	798	1468	801	1474
0.66	798	1468	801	1474
1.15	798	1468	802	1474
2.9	800	1470	800	1470

The eutectoid temperature therefore is placed at  $800 \pm 5$  °C (1470 °F).

Preliminary investigations indicated that the beta solid solution decomposed eutectoidally. Cooling at rates of 2 and 9 °C per minute gave discordant results, due to the rapid rate of decomposition of the eutectoid. These rates produced either a spheroidized or extremely coarse pearlitic structure. Increasing the cooling rate to 50–90 °C per minute through the critical temperature resulted in a fine-grained but well-defined eutectoidal pattern. The eutectoid produced in the 1.7, 2.5, and 3.3% iron alloys under these conditions is illustrated in Figs. 3, 4, and 5. The 1.7% alloy consists of about 50% acicular alpha grains surrounded by this fine eutectoid. The 2.5% alloy is practically 100% eutectoid. The hypereutectoid composition, 3.3% iron, shows irregular islands of a new phase (gamma) in this matrix. In this specimen the carbide grains appear to have been the nuclei for gamma formation, since the carbides are within the gamma grains. Metallographic examination of alloys



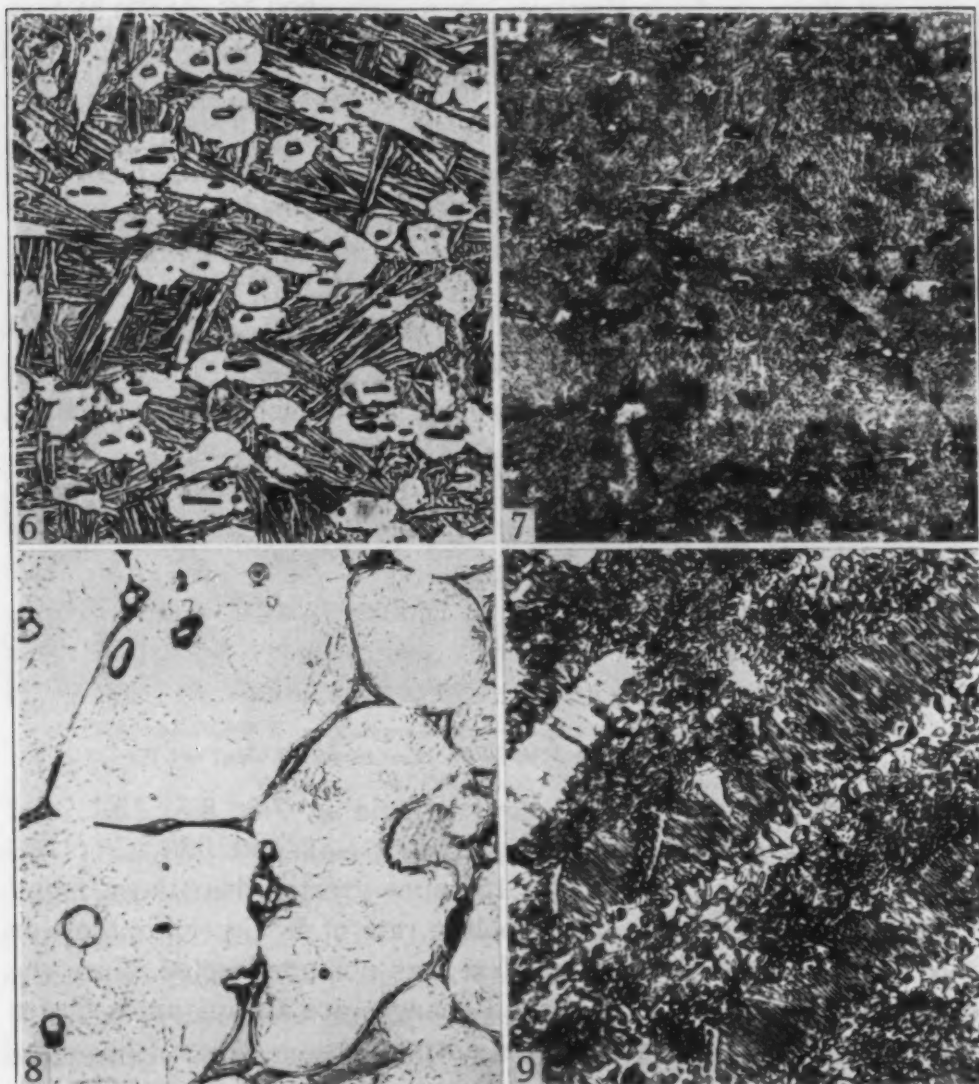


Fig. 6—0.97% Iron Quenched From 850 °C—Alpha Plus Beta Field.  $\times 250$ .

Fig. 7—3.3% Iron Quenched From 950 °C. Fine Widmanstätten needles in residual beta grains.  $\times 250$ .

Fig. 8—5.5% Iron, Heated to 950 °C, Showing Melting in Grain Boundaries.  $\times 250$ .

Fig. 9—16.8% Iron, Furnace-Cooled, Eutectic and Gamma Phase.  $\times 250$ .

All specimens etched with Vilella's reagent.

containing up to 5.5% iron which were slow-cooled from the beta field placed the eutectoid composition at 2.5% iron.

The beta field could not be delineated so nicely by quenching experiments. Although DeBoer and Fast (13) have shown that the presence of oxygen raises the transformation temperature of zirconium, in this investigation this effect was considered less important than the speed at which the transformation takes place. The alpha plus beta structure of the 0.97% iron alloy quenched from 825 °C is shown in Fig. 6. Although the addition of iron to zirconium

depresses the transformation temperature to 800 °C (1470 °F) at 2.5% iron, and it would be expected that this alloy should be entirely beta, this two-phase structure persisted in specimens quenched from slightly above the beta boundary and it was necessary to quench from temperatures 50 to 70 °C above the critical before they were all beta. As the iron content increased, the Widmanstätten pattern persisted in quenched samples up to the maximum solubility at 5.5% iron.

X-ray analyses were made on numerous samples vacuum-quenched from the beta field at temperatures as high as 1100 °C (2010 °F). Powder and wedge specimens showed only alpha zirconium, with no change from the basic lattice parameter.

The solidus line of the beta field was determined by melting-point studies. The 5.5% iron alloy heated to 950 °C (1740 °F) had just started to melt, as shown in Fig. 8. The 4.6% iron alloy had a similar appearance after being heated to 1000 °C (1830 °F). Again, all specimens with lower iron content were heated to these temperature levels to verify the first signs of melting.

### *Eutectic*

Thermal analysis of the alloys containing 7.5, 8.5, 13.1, and 30.0% iron gave thermal arrests between 931 and 936 °C (1708 and 1717 °F), which were 10 to 15 times greater than those found for the eutectoid when the same cooling rate of 5 °C per minute was used. This increase in heating effect was not unexpected, since the effects obtained between liquid-solid changes are always much larger than those involving solid-solid transformations.

Operating data from the zirconium production unit supports the 934 °C (1715 °F) value for the eutectic temperature. During the distillation cycle, in which magnesium chloride and excess magnesium are removed from the zirconium sponge, nodules or "tears" form on the walls of the iron distillation pot when the temperature exceeds 935 °C (1715 °F). Analyses of these nodules give consistent values of 16%. Metallographic examination of these nodules showed that they were entirely eutectic.

Examination of the 13.1, 16.8, 20.3, and 30.0% iron alloys placed the eutectic composition near 16%. Fig. 9 shows the appearance of the eutectic with minor amounts of the gamma phase in the 16.8% iron alloy. Fig. 10 shows the eutectic with an equal amount of gamma in the 29.6% iron alloy.

X-ray analysis of the 13.1 and 16.8% iron alloys slow-cooled from 950 to 900 and 850 °C (1740 to 1650 and 1560 °F) and

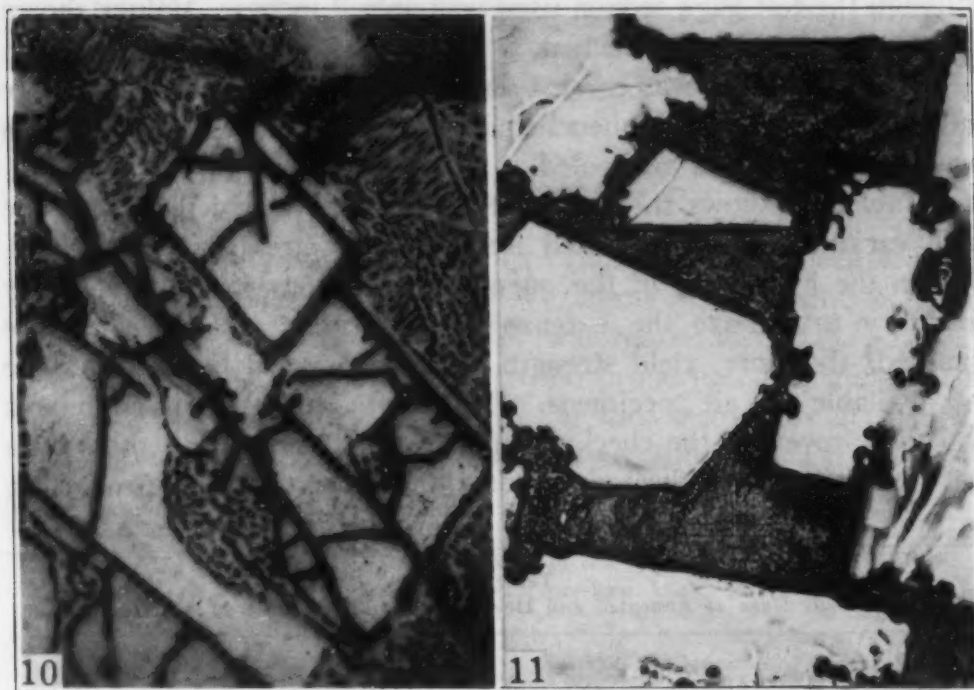


Fig. 10—29.6% Iron, Furnace-Cooled, Eutectic and Gamma Phase.  $\times 250$ .

Fig. 11—59.6% Iron, Furnace-Cooled, Gamma Phase and Iron-Rich Eutectic.  $\times 250$ .  
All specimens etched with Vilella's reagent.

then oil-quenched showed only alpha zirconium and the gamma phase instead of the expected beta solid solution and gamma. Thus it appears that the addition of the maximum amount of iron soluble in beta zirconium, 5.5%, is not sufficient to stabilize the beta form.

The greatest amount of gamma phase was observed near 45% iron, which corresponds closely with Vogel and Tonn's (6) value of 47.8% iron and indicates the gamma phase is  $Zr_2Fe_3$ . Beyond the gamma phase an iron-rich eutectic was observed in the 59.6% iron specimen. Fig. 11 shows a representative area with angular grains of gamma surrounding an iron-rich eutectic. These alloys were quite brittle and could be easily powdered. X-ray analysis of the 44.2% alloy as quenched (sealed in quartz under a partial pressure of helium) from 900 °C (1650 °F) showed a face-centered cube with  $a_0 = 7.040 \text{ \AA}$ .

#### MECHANICAL PROPERTIES

Tensile properties were determined on three representative alloys from the projected heat treatable range (beta field) in the original hot-rolled condition and after heat treatment.

All tests were made with standard ASTM sheet specimens with a 0.5 by 0.064-inch cross section and a 4-inch gage length,



although the test gage section used was only 2 inches. Values shown are an average of two specimens.

Heat treatment was carried out in a purified helium atmosphere and the specimens were quenched in water. Drawn specimens were heated in helium and air-cooled.

Table III shows the properties of the alloys and illustrates the wide variations which resulted from the heat treatments indicated. Due to the brittleness of the quenched specimens it was frequently necessary to remove the extensometer before complete data were obtained; therefore, yield strength and proportional limit values are not available for all specimens. The limited number of specimens available prevented the checking of divergent results, and the values are listed to show indicated trends rather than absolute properties.

Table III  
Tensile Data of Annealed and Heat Treated Zirconium-Iron Alloys

Alloy		Yield Strength, 0.2% Offset psi X 1000	Ultimate Strength, psi X 1000	Proportional Limit, 0.01% Offset psi X 1000	Elongation, % in 2 Inches	Hard- ness
Zirconium Sheet HR 850 °C		41.5	63.2	24.2	14.2	B-86
0.97% Fe						
HR at	850 °C	49.0	79.5	31.4	10.5	B-90
Quenched from	950 °C	86.2	96.5	68.2	10.0	100
Drawn at	400 °C	83.3	99.6	57.0	7.5	98
	500 °C	60.3	86.6	46.9	10.0	95
	600 °C	53.9	80.8	37.1	13.5	92
3.3% Fe						
HR at	850 °C	68.7	93.8	41.3	8.2	B-96
Quenched from	950 °C	....	132.2	....	0	C-46
Drawn at	400 °C	104.4	106.0	64.0	0.5	C-31
	500 °C	....	119.6	51.5	3.7	C-25
	600 °C	71.7	104.0	42.5	6.1	C-20
5.5% Fe						
HR at	850 °C	71.5	84.1	44.6	3.2	C-20
Quenched from	900 °C	....	103.0	....	0	C-55
	400 °C	....	92.0	62.2	0.2	C-32
	500 °C	....	87.7	51.0	0.7	C-29
	600 °C	62.5	77.8	40.0	1.5	C-19

In general, complete annealing was accomplished with the 600 °C (1110 °F) draw, and properties of the 850 °C (1560 °F) hot-rolled material restored.

### Cold Working

The 2.5 and 4.6% alloys were cold-rolled 20, 40, 60, and 80% to 0.030-inch finished sheet which was tested for mechanical properties.

In the 2.5% alloy, maximum properties were developed in the 60% cold-worked material where the yield strength was 100,000 psi, ultimate 122,500 psi, and elongation 5.5%. The modulus of elasticity for the 20% cold-reduced sheet was  $13.5 \times 10^6$  psi.

Similar results were obtained in the 4.6% alloy where the specimens rolled 80% were overworked and the 60% reduction gave the following values: yield, 94,000 psi, ultimate 113,800 psi, with 1.4% elongation.

### Hot Strength

Tensile properties at 650 °C (1200 °F) were determined on 1/4-inch round specimens by the Air Matériel Command at Wright Field. One specimen of each alloy was heated to 650 °C (1200 °F) for at least 30 minutes and the tensile properties determined at that temperature. The rate of loading in this series was 2000 pounds per minute. The results of these tests are shown in Table IV.

Table IV  
Tensile Properties of Zirconium-Iron Alloys at 650 °C

Alloy No.	% Fe	Yield Strength 0.2% Offset psi × 1000	Ultimate Strength psi × 1000	Elongation, %	Reduction in Area, %
80	0.45	3.71	12.4	81	74
110	0.66	6.07	17.4	75	86
111	1.15	4.38	15.7	88	89
118	1.83	6.98	20.5	87	92
169	2.9	6.17	21.6	75	83
87	5.16	6.70	23.3	51	62

In general, there was a progressive increase in both yield and ultimate strengths with increasing iron. Any variations were attributed to the fact that only one specimen for each composition was tested.

### HEAT RESISTANCE

Heat resistance was determined on cast, swaged, rolled and heat treated alloys by heating specimens in a muffle furnace with holes in the door and rear wall to provide air circulation and prevent oxygen impoverishment. In this study a gain of 600 mg per square decimeter per 24 hours (mdd), which corresponds to a corrosion rate of 0.1 inch per year of zirconium, was taken as a criterion of serviceability.

Table V is a tabulation of the data obtained by heating specimens in air at 650 °C for 1 and 24 hours.

In general, the heated alloys were covered with an adherent black or brown surface layer at the end of an hour. Extended heating periods produced a white nonadherent powdery oxide which spalled readily, especially in the lower iron alloys.

Table V  
Heat Resistance of Zirconium-Iron Alloys in Air at 650 °C

Iron, %	Condition	Weight Gain, Mg/dm <sup>2</sup>	
		1 Hour	24 Hours
0.5	Cast	400	73*
1.15		280	296*
1.75		370	182*
5.16		48	51
9.0	1/4-inch Swaged Rod	16	48
13.1		12	26
0.5		365	..*
9.0		42	..*
0.97	Sheet, Hot-rolled at 850 °C	96	900
	Oil-quenched from 950 °C	85	815
	Drawn at 400 °C	69	345
	500 °C	70	325
	600 °C	54	380
	Annealed at 950 °C	91	895
3.3	Sheet, Hot-rolled at 850 °C	96	240
	Oil-quenched from 950 °C	92	300
	Drawn at 400 °C	78	210
	500 °C	59	215
	600 °C	44	215
	Annealed at 950 °C	109	640
5.5	Sheet, Hot-rolled at 850 °C	103	430
	Oil-quenched from 900 °C	100	290
	Drawn at 400 °C	84	255
	500 °C	76	265
	600 °C	78	290
	Annealed at 900 °C	112	570

\*High oxide loss prevented accurate values.

Metallographic examination showed that the oxides were confined to the surface, with the exception of the swaged rods, where there was some penetration at the ends along cold-worked lines. Oxidation proceeded, due to the spalling of the oxides which exposed fresh surfaces for oxygen attack.

Based on the tentative maximum of 600 mdd, none of the cast alloys up to 1.75% iron had a satisfactory heat resistance. Above 5% the cast alloys were superior to the fabricated sheet, with the 13.1% specimen showing a weight gain of only 26 mdd. Compared with 18-8 stainless steel, however, even the smallest gains were high, since the average for stainless check specimens was about 4 mdd.

The fabricated alloy containing 0.97% iron exceeded the tentative maximum of 600 mdd in specimens which had been hot-rolled at 850 °C (1560 °F), quenched from 950 °C (1740 °F), and reheated to 950 °C in helium after quenching from the same temperature. Specimens quenched and reheated to 400, 500 and 600 °C (750, 930 and 1110 °F) were well below the allowable values.

Weight gains for the 3.3% alloy were all within acceptable limits except the specimen annealed at 950 °C (1740 °F) after being quenched from the same temperature. The 5.5% alloy showed good heat resistance for all conditions, with hot-rolled, quenched and reheated specimens showing maximum values, all of which were within allowable limits.



These data indicate that the best heat resistance was obtained in cast specimens. Heating the alloys to 850–950 °C (1560–1740 °F) during fabrication materially reduced their usefulness for heat resisting alloys. For fabricated sheet the best properties were obtained by quenching from the beta field, followed by annealing at 400 or 500 °C (750 or 930 °F).

### DISCUSSION

The equilibrium diagram for zirconium-rich, zirconium-iron alloys is shown in Fig. 12. Major differences from previous investigators is lowering of the eutectic temperature by over 400 °C

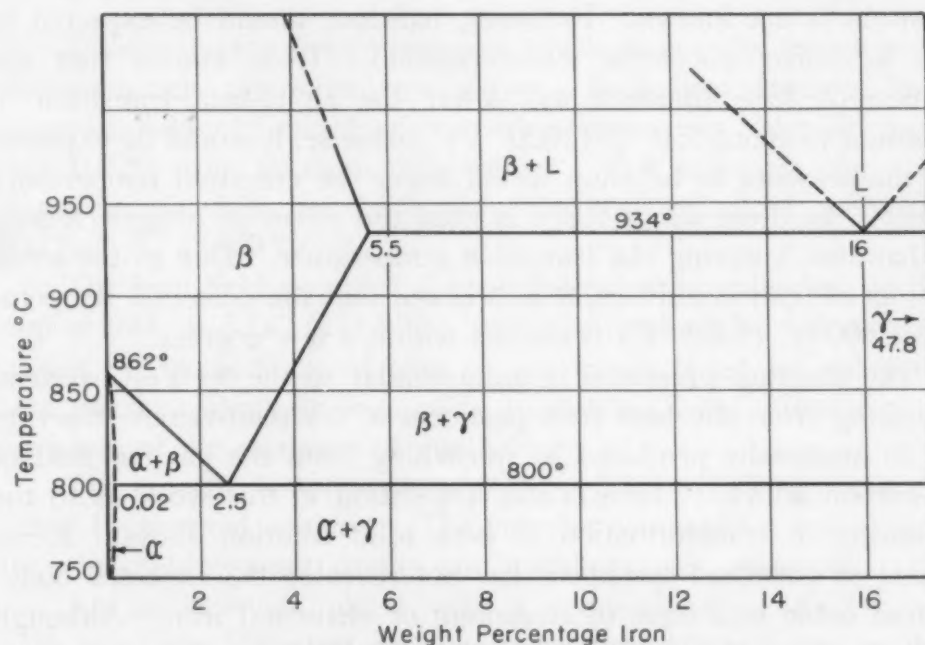


Fig. 12—Equilibrium Diagram of the Zirconium-Iron System.

(750 °F) and the definite establishment of a eutectoid field rather than a suggested peritectoid. Vogel and Tonn's eutectic at 12% iron and 1350 °C (2460 °F) as well as their transformation at 1000 °C (1830 °F) shows some relation to the eutectic found at 16% iron and 934 °C (1715 °F) in this work. The considerable differences in temperature between the two observations must be attributed to contamination resulting from the use of alumina crucibles. These same impurities completely obscured the eutectoid reaction.

Fast (13) has shown that the addition of 0.75% oxygen will raise the beta transformation point of zirconium from 862 °C

(1585 °F) to well over 1000 °C (1830 °F). This amount of oxygen could be easily added by dissolution of an oxide-type crucible or exposure of the alloys to air at temperatures above 700 °C (1290 °F). Vogel and Tonn do not give an oxygen analysis of their alloys, but presumably it was of the order of 1%. On the other hand, the oxygen content of the alloys used in this work was about 0.08% and it is doubtful that this figure would be lowered if iodide-deposited zirconium was used as a base material.

Detailed studies of ductile zirconium containing up to 2% hafnium indicate that it is completely soluble, since no structural or mechanical changes have been observed that could be assigned to the presence of hafnium. The effect of hafnium on the alpha-beta transition is not known. However, hafnium should be expected to have a similar allotropic transformation. It is known that the addition of 35% titanium will lower the alpha-beta transition of zirconium to about 550 °C (1020 °F); likewise, it would be expected that the presence of hafnium would lower the eutectoid temperature slightly. In these alloys there is then the effect of oxygen raising and hafnium lowering the transition temperature. Due to the small amounts of both impurities, it is believed that the eutectoid temperature of 800 °C (1470 °F) is correct within a few degrees.

The diagram presented is quite similar to the Fe-Fe<sub>3</sub>C system. Quenching from the beta field produces a Widmanstätten structure akin to martensite produced by quenching from the gamma field of iron-carbon alloys. There is still a question in this work as to the mechanism of transformation of beta solid solution alloys. X-ray analysis of quenched specimens has not revealed the expected body-centered cubic beta form of zirconium or elemental iron. Although metallographic examination shows that the Widmanstätten structure becomes finer with increasing iron content, it does not aid in showing the disposition of the iron after quenching from the beta field.

There are a number of similarities between the zirconium-iron diagram developed in this investigation and the titanium-nickel diagram recently announced (14). Titanium and zirconium have similar crystal structures and even transform from hexagonal to cubic forms within 20 °C of each other. As might be expected in alloys involving the transition elements, the equilibrium diagrams are of the same type. Titanium as well as zirconium is highly sensitive to oxygen contamination, and the diagram for titanium-nickel alloys is considerably changed from the earlier one proposed by Wallbaum on the basis of studies of impure alloys. For instance, the eutectic temperature was shown to be over 300 °C (570 °F)

lower than Wallbaum's when a good grade of titanium was used and precautions taken to avoid contamination in alloy production.

Slow-cooled beta alloys are quite amenable to cold working. The alloys can be quenched and drawn to produce a considerable variation in mechanical properties. From the standpoint of low iron content it appears that iron has little effect on the normal properties of ductile zirconium. The iron alloys up to 5.5% iron may find application in cases where corrosion resistance is a problem. However, they will be restricted to uses below a temperature of 1000 °C (1830 °F).

#### SUMMARY

A diagram has been presented which shows the constitution of zirconium-rich, zirconium-iron alloys. Its salient features include an alpha field of limited width with a maximum solubility of less than 0.02% iron at room temperature. The eutectoid composition was determined to be 2.5% iron and the eutectoid temperature  $800 \pm 5$  °C (1470 °F).

The beta field occupied a quadrilateral area extending to 5.5% iron at  $934 \pm 5$  °C (1713 °F) and was outlined by metallographic studies. The addition of iron to zirconium failed to stabilize the beta phase, making it impossible to obtain X-ray diffraction confirmation of the existence of this field.

The eutectic temperature of  $934 \pm 5$  °C (1713 °F) was established by thermal analysis. The eutectic composition was placed at 16% by melting-point studies and metallographic observation.

An intermediate phase with a composition of  $\text{Fe}_3\text{Zr}_2$ , about 47% iron, was identified metallographically and confirmed by X-ray analysis. This phase, designated as gamma, is a large face-centered cube with  $a_0 = 7.04$  Å.

The diagram resembles the Fe-Fe<sub>3</sub>C system and, hence, offers a number of possibilities in regard to heat treatment of the alloys. Ultimate strengths of the order of 100,000 psi were developed by quenching from the beta field. These quenched alloys could be drawn to produce strengths intermediate between the quenched and annealed condition.

Alloys containing up to 7% iron can be worked at 850 °C (1560 °F) when protected from oxidation. Alloys containing as much as 4.4% iron can be reduced 60% by cold working.

Heat resistance and hot strength data indicate the alloys will be restricted to uses below 550 °C (1020 °F).



## ACKNOWLEDGMENTS

The authors wish to thank the Air Matériel Command, United States Air Force, for permission to publish this work.

The authors are indebted to Dr. W. J. Kroll for his advice and assistance. Other members of the Northwest Electrodevelopment Laboratory who assisted in the work are: V. V. Donaldson, alloy preparation, and D. M. Mortimore, X-ray analyses.

## References

1. W. J. Kroll, C. T. Anderson, H. P. Holmes, L. A. Yerkes and H. L. Gilbert, "Large-Scale Laboratory Production of Zirconium", *Journal, Electrochemical Society*, Vol. 49, No. 1, 1948.
2. W. J. Kroll and H. L. Gilbert, "Melting and Casting Zirconium Metal", *Journal, Electrochemical Society*, Vol. 96, No. 3, 1949, p. 158.
3. E. T. Hayes and A. H. Roberson, "Some Effects of Heating Zirconium in Air, Oxygen and Nitrogen", *Journal, Electrochemical Society*, Vol. 96, No. 3, 1949, p. 142.
4. E. T. Hayes, E. D. Dilling and A. H. Roberson, "Fabrication and Mechanical Properties of Ductile Zirconium", *TRANSACTIONS, American Society for Metals*, Vol. 42, 1950, p. 619.
5. C. T. Anderson, E. T. Hayes, A. H. Roberson and W. J. Kroll, "A Preliminary Survey of Zirconium Alloys"—to be published as a Report of Investigation, U. S. Bureau of Mines.
6. R. Vogel and W. Tonn, *Archiv für das Eisenhüttenwesen*, Vol. 5, 1932, p. 387.
7. W. J. Kroll and H. L. Gilbert, "Melting and Casting Zirconium Metal", *Journal, Electrochemical Society*, Vol. 96, No. 3, September 1949.
8. J. D. Fast, "The Transition Point Diagram of the Zirconium-Titanium System", *Recueil des Travaux Chimiques des Pays-Bas*, Vol. 58, 1939, p. 973-983.
9. T. E. Allibone and C. Sykes, *Journal, Institute of Metals*, Vol. 37, 1928, p. 173.
10. H. J. Wallbaum, "The Systems of the Iron Metals with Titanium, Zirconium, Columbium, and Tantalum", *Archiv für das Eisenhüttenwesen*, Vol. 14, 1941, p. 521-526.
11. American Society for Metals—*Metals Handbook*, 1948, p. 1221.
12. A. H. Roberson, "Metallography of Zirconium and Zirconium Alloys", *METAL PROGRESS*, Vol. 56, November 1949, p. 667-669.
13. J. H. DeBoer and J. D. Fast, "The Influence of Oxygen and Nitrogen on the Alpha-Beta Transition of Zirconium", *Recueil des Travaux Chimiques des Pays-Bas*, Vol. 59, 1940, p. 161-167.
14. J. R. Long, E. T. Hayes, D. C. Root and C. E. Armantrout, "A Tentative Titanium-Nickel Diagram", U. S. Bureau of Mines Report of Investigations 4463 (1949).

## DISCUSSION

**Written Discussion:** By M. Hansen, supervisor, Nonferrous Metals Research, Armour Research Foundation, Chicago.

I would like to call attention to a paper by H. J. Wallbaum.<sup>2</sup> By X-ray studies, Wallbaum has shown that an alloy of the composition

<sup>2</sup>H. J. Wallbaum, *Archiv für das Eisenhüttenwesen*, Vol. 14, 1941, p. 521-526.

corresponding to the formula  $\text{Fe}_3\text{Zr}_2$  consists of two phases. He found that the phase coexisting with alpha and beta zirconium solid solutions is  $\text{Fe}_3\text{Zr} = \epsilon$ , which has a cubic lattice of the  $\text{MgCu}_2$  type, and another intermediate phase,  $\eta$ , exists approximately 7 atomic per cent richer than iron, having a hexagonal lattice of the  $\text{MgNi}_2$  type. The latter phase apparently is formed by a peritectic reaction:



#### Authors' Reply

The authors found no X-ray or metallographic evidence of another intermediate phase of compound of the type  $\text{ZrFe}_3$ . The alloys prepared by Wallbaum were of doubtful purity, since they were melted in alumina or silicon carbide crucibles, and no analysis is given of the finished zirconium-iron alloy. The introduction of small amounts of oxygen or nitrogen would certainly complicate the study of the intermediate phases of this system.

A critical review of the alloys studied in this paper has led the authors to believe that the zirconium-rich intermediate phase is  $\text{ZrFe}_2$  (face-centered cube) and not  $\text{Zr}_2\text{Fe}_3$  as at first believed and described elsewhere by Vogel and Tonn (6). No attempt was made to delineate the gamma field but the appearance of another eutectic in the 59.6% iron alloy is considered as proof that the right-hand boundary cannot be another compound such as  $\text{ZrFe}_3$ .

## FRACTURING OF SILICON-FERRITE CRYSTALS

BY C. F. TIPPER AND A. M. SULLIVAN

### *Abstract*

*Neumann lamellae formation associated with cleavage fracturing was studied in tensile tests of a 3.5% silicon ferrite having large grains of similar orientation. Neumann lamellae were not observed to form except in conjunction with the cleavage type of fracturing. It is shown that Neumann lamellae are unlikely origins or causes for cleavage but that shock loading accompanying discontinuous cleavage may cause formation of Neumann lamellae.*

*X-ray verification was made of cleavage on the (100) and (112) planes.*

REFERENCE has been made in many investigations of samples of fractured mild steel to two characteristic features.

One of these is that cleavage fracture does not occur in all the grains of a predominantly brittle fracture (13, 19, 20).<sup>1</sup> The other relates to the occurrence of Neumann lamellae in the vicinity of both service fractures and those produced in the laboratory (2, 13, 19, 20).

The effect of orientation on the tendency to cleave rather than deform plastically has been studied in certain single crystals, notably zinc and magnesium, in which the change has also been found to be sensitive to temperature (14).

The possibility of a preferred orientation being the explanation of a marked tendency to cleavage in mild steel plates was early recognized, but an X-ray investigation of some of these plates did not reveal such an orientation. On the other hand, there is a marked tendency for cleavage to occur in groups of similarly oriented grains, i.e., when the boundaries are indistinct.

This is observed also in the fracture of impact test-pieces, particularly when the steels under test have been cooled slowly from above  $A_3$  to room temperature (6), in which condition they are particularly prone to notch brittleness. Groups of crystals of similar

<sup>1</sup>The figures appearing in parentheses pertain to the references appended to this paper.

A paper presented before the Thirty-second Annual Convention of the Society, held in Chicago, October 21 to 27, 1950. Of the authors, C. F. Tipper is associated with the Engineering Department, Cambridge University, England, and A. M. Sullivan is metallurgist, Mechanics Division, Naval Research Laboratory, Washington, D. C. Manuscript received April 5, 1950.



orientation might be formed by the transformation of large austenite grains, and a connection between fracture appearance and austenite grain size has already been noted (15). Mott (9) has drawn attention to the necessity of re-initiating fracture in each grain of differing orientation for propagation to proceed. Hence, a group of grains of closely similar orientation makes for easy fracture.

Preliminary experiments (19, 20) on notched iron crystals at low temperatures have shown that cleavage occurs on planes of indices  $\{100\}$ , however the grains are placed relative to the notch and falling hammer, although the determination of energy to fracture in different orientations is still unknown.

It was considered that a preliminary investigation of the influence of orientation on fracture might be obtained by studying fracture of large crystals in thin plate, and at the same time by observing the initiation of fracture by inspection of the surface during the course of testing.

The other matter to which attention has been given in this investigation is that of the occurrence of Neumann lamellae. These bands are formed on the  $\{112\}$  planes of the alpha iron crystals (4, 10, 11), more often by shock at low temperatures, but they also occur in static loading, especially in silicon ferrite (2). Difference of opinion exists on whether the bands are true twins or are zones of slip, in which deformation has proceeded further or on different planes than in intermediate regions. There is evidence that sometimes the deformation is such that the material within the bands has sheared so that it is in a position crystallographically twinned with respect to the main crystal. There is equally convincing evidence that the material within the bands is not necessarily twinned (1, 10, 11, 22). Both such structures are encountered in the deformation of metals other than alpha iron and in some instances the bands are true twins, confirmed by means of X-ray analysis, and in others they are better described as deformation bands produced by different slip mechanisms.

It is generally agreed that the composition planes in iron are parallel with  $\{112\}$  planes in the crystal, while in other examples of banded structures the plane of separation may not be a possible slip or twin plane of the lattice. It is sometimes stated that Neumann lamellae are formed before plastic deformation takes place, and that plastic deformation may inhibit their formation. This can hardly be true, since the bands as observed on the surface are marked by differences of level. They are not readily formed after considerable plastic deformation has occurred, but one example has been obtained

during the present experiments of a band forming in a highly deformed zone.

The importance of temperature and composition on the initiation of Neumann lamellae has been studied specially by Barrett, Ansel and Mehl (2) on alloys of silicon in iron. There may also be a critical stress for twinning as there is for slip. It has been shown that  $\{112\}$  planes are one of the possible planes of slip in the body-centered cubic lattice, although with higher silicon contents or lower temperatures in silicon ferrite, there is a tendency for slip to be on  $\{110\}$  planes, while twinning still persists.

It has been suggested that fracture by cleavage is facilitated by the severe local distortion that may occur on the boundaries of Neumann lamellae. This view has been put forward by Shevandin (16) and also by Zapffe (22), who has shown evidence of concentrated deformation along these directions and, on heating, recrystallization may begin there.

Against this, however, may be cited the fact that cleavage fractures have been observed in mild steel without the presence of Neumann lamellae (19). Hence, it may be concluded that although the same conditions promote both cleavage fracture and Neumann lamellae formation, the one is not necessary for the other to take place. Lamellae formation without fracture is often encountered.

#### MATERIAL STUDIED

A suitable material for such investigation was available in the form of a silicon-ferrite, containing 3.5% silicon. This was supplied by Dr. C. G. Dunn, The General Electric Company, Pittsfield, in the form of sheet, 0.015-inch thick, made by the Allegheny Ludlum Steel Company.

This material has been used by Dunn (5) in several investigations. After suitable heat treatment the grain size is very large and has a marked preferred orientation. Dunn has shown this to be such that a  $[001]$  direction is in the direction of rolling and a  $\{110\}$  plane in the plane of rolling. The marked preferred orientation imposes restrictions upon the use of this material for the purpose of investigating orientation effects and the results of the tests to be described are of a preliminary nature only.

Shaped test-pieces were milled from the plate. The machined edges were ground and polished. This was found to be essential to remove notches that were introduced in the preparation of the test-pieces. One face of the test-piece was also rubbed with fine emery and finished on a buffing wheel with a dry polish, this material

**Table I**  
**Tensile Test-Pieces of Silicon Ferrite**

No.	Ultimate Stress, psi	Type of Fracture	Remarks
1	48,600	Cleavage	In shoulder
2	54,300	Ductile	
3	54,400	Ductile	
4	49,250	Cleavage	Fracture arrested at boundary
5	Test-piece pulled through at pin in clamp.		
6	55,900	Cleavage	In shoulder
7	56,100	Ductile	
8	47,600*	Cleavage	Specimen notched one side
9	25,000*	Cleavage 3 steps	Specimen notched one side
10	50,300*	Ductile not across	Specimen notched one side
11	51,200*	Ductile	Specimen notched one side

\*On notched area.

being readily tarnished by wet polishing. No attempt was made to obtain a perfect metallographic polish.

After treatment, the dimensions of the test-pieces were as follows: thickness 0.013 to 0.0145 inch, width 0.8 inch, parallel section approximately 2 inches. Fine lines were scribed in order to measure extension, but this proved to be so nonuniform that the figures had little significance.

The enlarged ends were drilled and held in a clamp by means of a bolt and nut which passed through the hole and the nut was tightened only after a small load had been applied. This method insured a reasonable measure of axial loading. Only in one instance did the bolt tear through the plate.

The clamps were held in the normal wedge grip attachment of a 30,000-pound Baldwin-Southwark tensile testing machine.

A microscope, which could be traversed in two directions, was mounted so that the whole of the test-piece could be kept under observation during test.

Tests were carried out at room temperature, the load being slowly applied and sometimes stopped for a close inspection of the specimen to be made.

#### EXPERIMENTAL RESULTS

The tests were all made at room temperature, between 75 and 85 °F. The results are summarized in Table I. Extension figures are not included because of the fact that a number of specimens broke outside the gage marks and the extension was very non-uniform. It was about 15% in the ductile fractures.

Two types of fracture were encountered: (a) It was slow and proceeded in a series of steps at varying angles to the axis of the



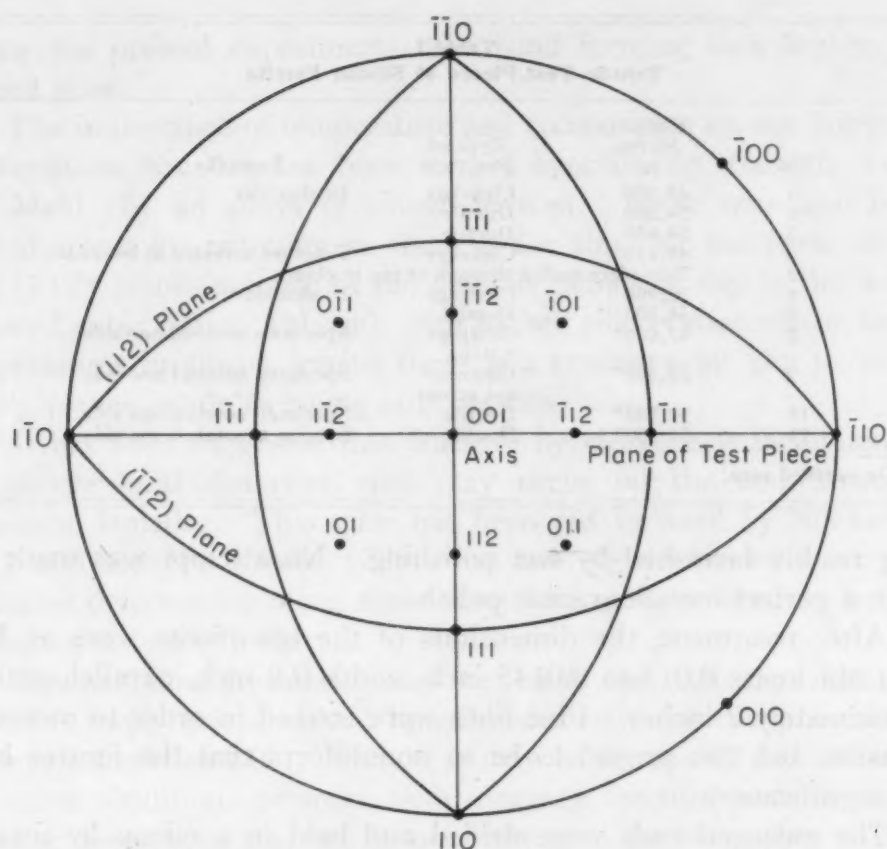


Fig. 1—Projection of Test-Piece Relative to Crystal Axis.

specimen, the rate of propagation depending upon the rate at which the machine was operated; (b) it occurred with great suddenness, with a "click", and was an unmistakable cleavage fracture. Both fractures started from the edge of the specimen or from a notch when present, except the ductile fractures, which on certain occasions were observed to be re-initiated ahead of the advancing crack and to be linked by marked deformation zones which ultimately developed into fractures at 100 to 115 degrees to these.<sup>2</sup> Owing to the distortion, this angle could not be measured accurately. Typical examples of such fractures are shown in Figs. 2 and 3. A photograph at a higher magnification of an interrupted fracture is shown in Fig. 4. A piece of mirror was placed behind the specimen in order to distinguish between the regions which had parted and those in which there was no visible separation. These zones are marked on a tracing made from the photograph, Fig. 4a.

An extreme case of a second fracture being initiated some distance in front of the main advancing crack was observed in Specimen

<sup>2</sup>Angles between traces of planes of indices {112} in the plane of the specimen should be approximately 110 degrees in a perfectly oriented crystal.



Fig. 2—Ductile Fracture Through Three Crystals.  $\times 4$ .



Fig. 3—Interrupted Ductile Fracture.  $\times 5$ .

3. A crystal boundary was situated more than halfway across and when the fracture had progressed some distance a new crack was observed to start at the boundary. Both cracks then spread in the same direction until the test was stopped. When unloading to remove the specimen, the bridge between the two fractures broke suddenly with a cleavage-type fracture. The difference in appearance of the fractures is clearly shown in Fig. 5.

Examination of the surface of fracture shown in Fig. 5 also confirmed that it had the typical appearance of a cleavage and that it had been initiated at both pre-existing cracks with a sharp line of demarcation in the middle corresponding to a slight nick visible on the surface, shown in Fig. 6. The angle which the cleavage-type fracture makes with the first section of ductile fracture is about 29



Fig. 4—Area in Fig. 3 at Higher Magnification Showing Regions Which Have Separated and Those Which Have Not.  $\times 100$ .

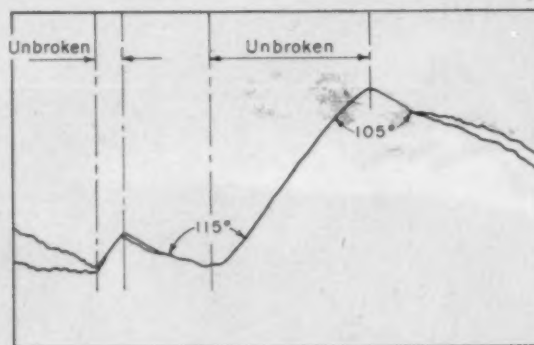


Fig. 4a—Diagram Made From Fig. 4 Indicating Regions Discussed.

degrees as marked on the drawing of Fig. 5a. The theoretical angle between the traces of planes of (112) form is 33 degrees 33 minutes.

X-ray evidence for this grain shows that the cube pole (001) is displaced from the rolling direction ( $\alpha = 14$  degrees;  $\phi = 12$  degrees).

The short segment of cleavage fracture in this specimen is identified from its traces in two surfaces 90 degrees apart as occurring on a plane of the (112) type. Cleavage of this type has been reported by Barrett (2) and more recently by Klier (8).

Positive identification of the planes operating to give the ductile part of this fracture could not be made. On the face of the specimen the trace of the ductile fracture coincides with a trace of the (112)-type plane; however, the polished section 90 degrees from this face



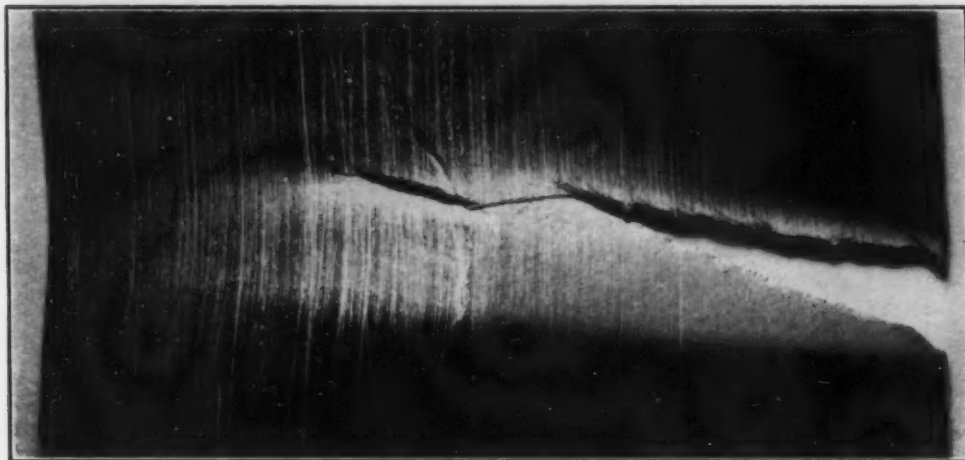


Fig. 5—Discontinuous Ductile Fracture, the Two Parts of Which Were Joined by Cleavage.  $\times 5$ .

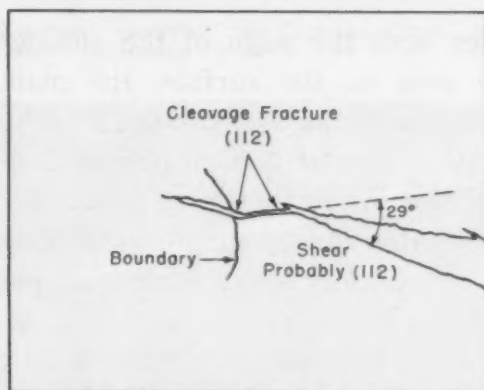


Fig. 5a—Diagram Made From Fig. 5 Indicating Regions Discussed.

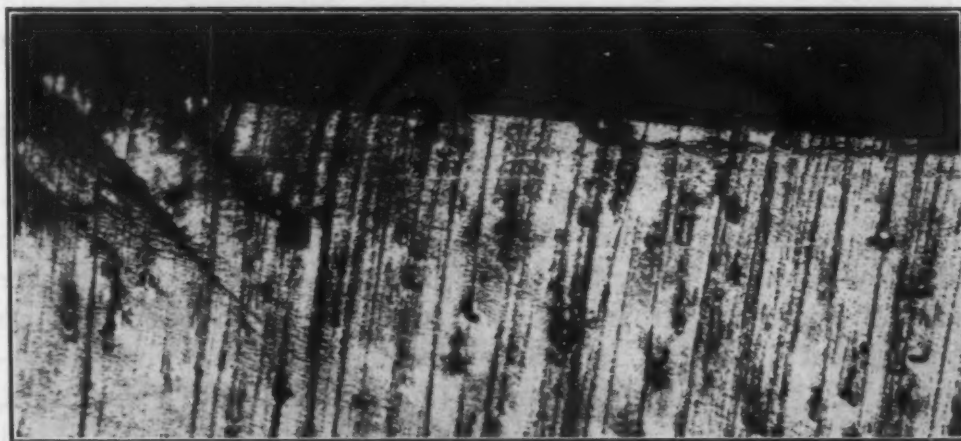


Fig. 6—Cleavage Fracture of Fig. 5 at Higher Magnification. Note slip bands and two very faint Neumann lamellae near fracture edge.  $\times 100$ .

shows the thin sheet to be so distorted that no fracture trace could be accurately identified.

Two faint Neumann lamellae appeared in this region, Fig. 6,



Fig. 7—Cleavage Fracture and Neumann Lamellae.  $\times 4$ .

making small angles with the edge of the cleavage fracture. Slip bands can also be seen on the surface, the main direction being approximately parallel with the fracture edge. This has been found to be the main direction observed on all plastically deformed crystals, except near the fracture, when they may follow the line of fracture. They were wavy and often indeterminate in direction, such as might be expected if the direction of shear were in a plane perpendicular to the plane of the test-piece (18).

A projection of the test specimen relative to the crystal directions has been made in Fig. 1 placing the [001] direction in the axis of straining and the (110) plane in the plane of the surface. This is the preferred orientation found by Dunn, although some deviation from this orientation has been noted by him and is seen in the results now obtained.

Barrett (2) has investigated the directions of slip, twinning and cleavage in silicon ferrite, and has found that below 4% silicon, slip may be on {110}, {112} and {123} planes at room temperature and, as in alpha iron, the surface markings are very broken and wavy unless the direction of slip lies in the plane of the surface under observation. It is strongly suggested from the markings observed that the commonest slip planes and directions would therefore be ( $\bar{1}\bar{1}2$ ) in the [111] and (112) in the [ $\bar{1}\bar{1}1$ ] directions, while when at the point of fracture, the (1 $\bar{1}2$ ) plane in the [ $\bar{1}\bar{1}1$ ] or the [ $\bar{1}12$ ] in the [1 $\bar{1}1$ ] may participate in the final breakdown.

Turning to the other type of fracture encountered, an entirely different sequence of events must occur. In the first place, there is an almost entire absence of surface markings, i.e., wavy slip lines, although some plastic deformation generally preceded fracture as



Fig. 8—Both Neumann Lamellae and Cleavage Crack, Beneath Main Fracture, Change Direction at Grain Boundary.  $\times 250$ .



Fig. 9—Cleavage Fracture and Neumann Lamellae Start From Notch. Path of indistinct fracture shown in Fig. 10a.  $\times 6$ .

the crystal boundaries showed in relief. Fracture took place very rapidly with a distinct noise and was associated with the appearance of a large number of Neumann lamellae on the surface. Sometimes the fracture could be arrested before it was complete. Two examples of such test-pieces are shown in Fig. 7, Specimen 4, and Fig. 9, Specimen 9. In Specimen 4, the fracture was arrested at a crystal boundary, but in Specimen 9 the whole section was one crystal.

Attention should be drawn to the direction of fracture which generally was close to 90 degrees to the axis of the specimen. The biggest deviation was in Specimen 9. X-ray evidence for this grain shows that the cube pole (001) is displaced from the rolling direction ( $\alpha = 14$  degrees;  $\phi = 10$  degrees) and that cleavage has occurred on the (001) plane. The Neumann lamellae follow the





Fig. 10—Area in Fig. 9 at Higher Magnification. Note absence of Neumann lamellae in first section of fracture, Fig. 10a, Point 1-2.  $\times 20$ .

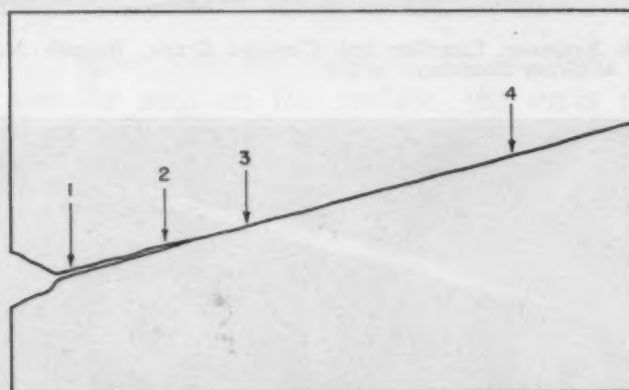


Fig. 10a—Diagram of Fig. 10 Indicating Regions Discussed.

fracture closely and change direction at a crystal boundary; they are almost absent near the point of initiation of fracture; they extend beyond the end of the crack and tend to die away at some distance beyond this. Fig. 11 shows that the lamellae are not parallel with the fracture; they were observed to make small angles with the fracture, except in Specimen 9, where the two coincided. In this crystal, traces of the (001) and the (112) type nearly coincide. Fig. 11 also illustrates another characteristic. The fracture path may be interrupted and restarted, leaving bridges of unbroken metal adhering to both halves of the test-piece. Local distortion occurs at the base of the connecting links, which eventually pull apart as the gap widens. Fig. 11 shows one of these small sections adhering to one surface of the fracture. It will be noted that the upper surface is rougher than the lower. It is considered that the upper surface is not a true cleavage surface, that it remained attached and was finally torn from the main body of the

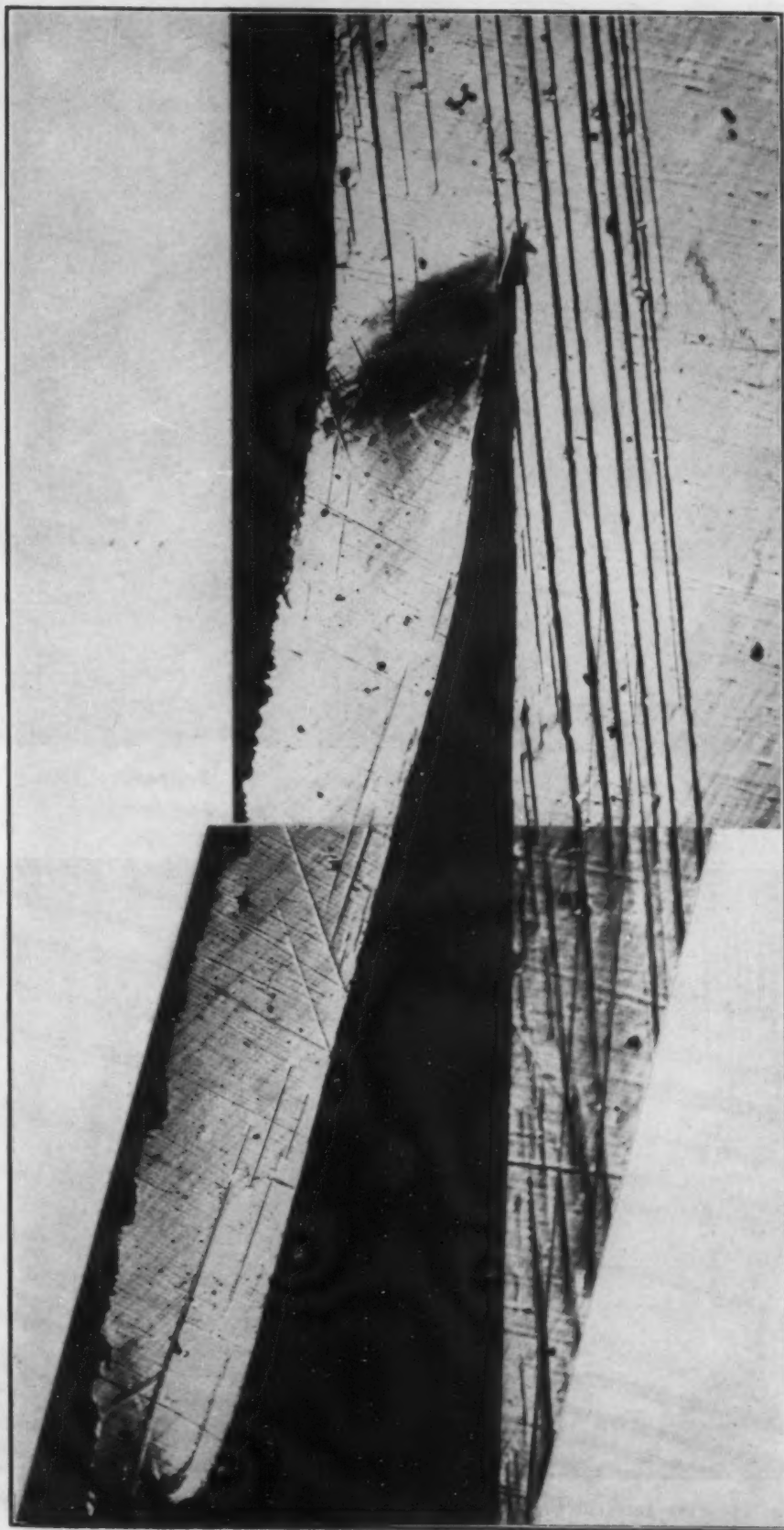


Fig. 11—Cleavage Fracture Stops and Starts Again Leaving "Bridge" Which Finally Breaks. Note fine slip bands and distortion at each end of bridge.  $\times 100$ .

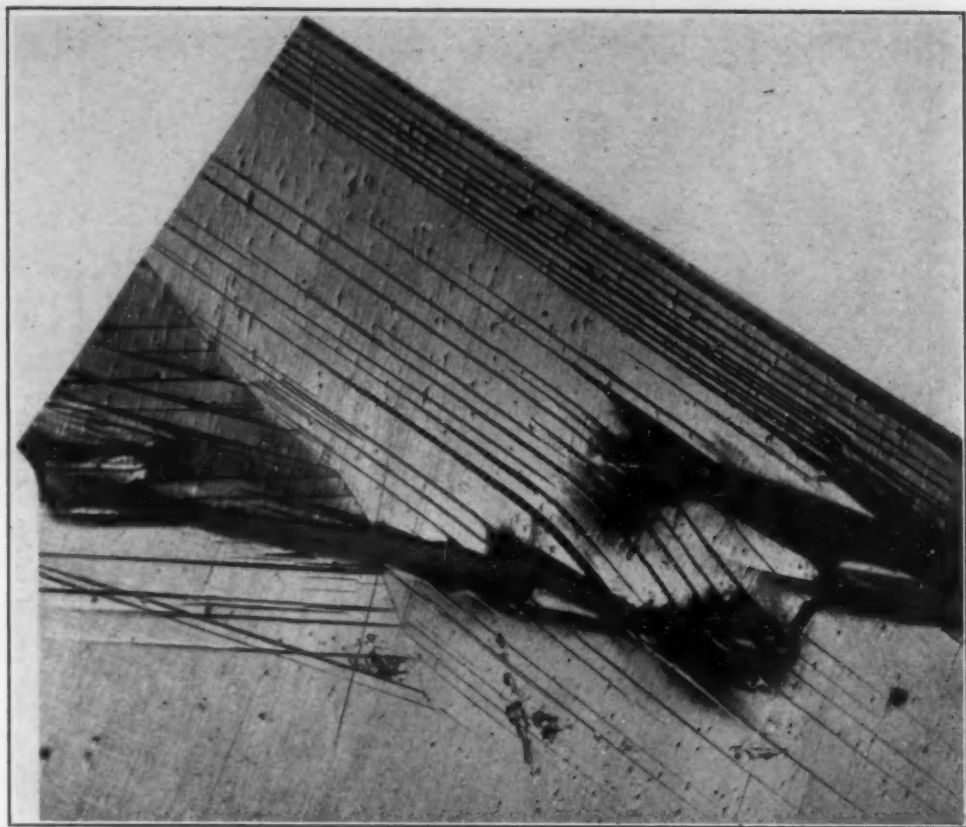


Fig. 12—Composite Picture Showing Two Sides of Same Fracture.  $\times 100$ .

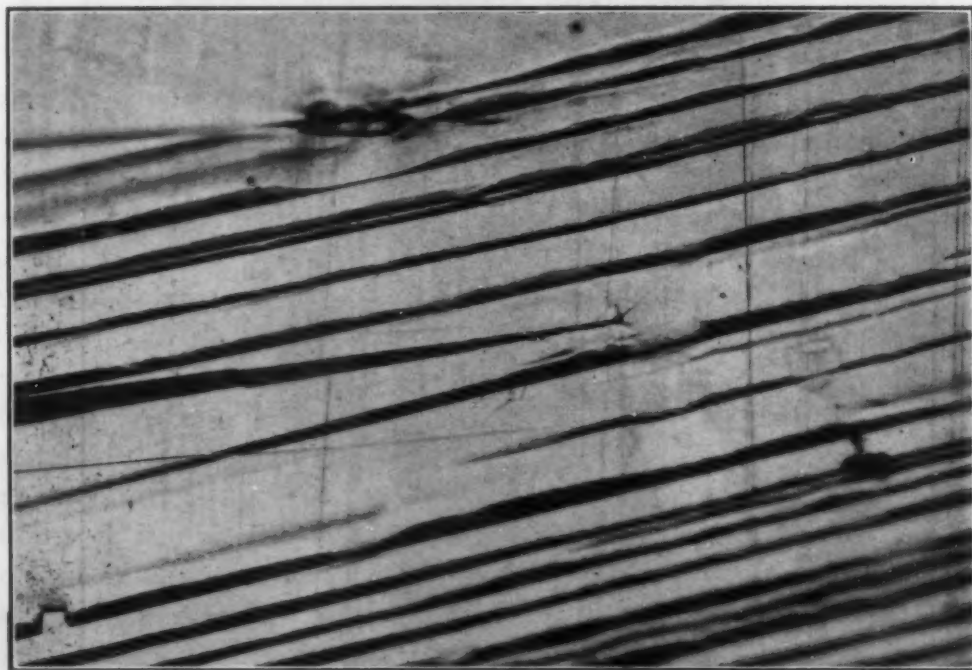


Fig. 13—Fine Internal Crack Makes Small Angle With Neumann Lamellae. Note distortion at end of crack.  $\times 250$ .



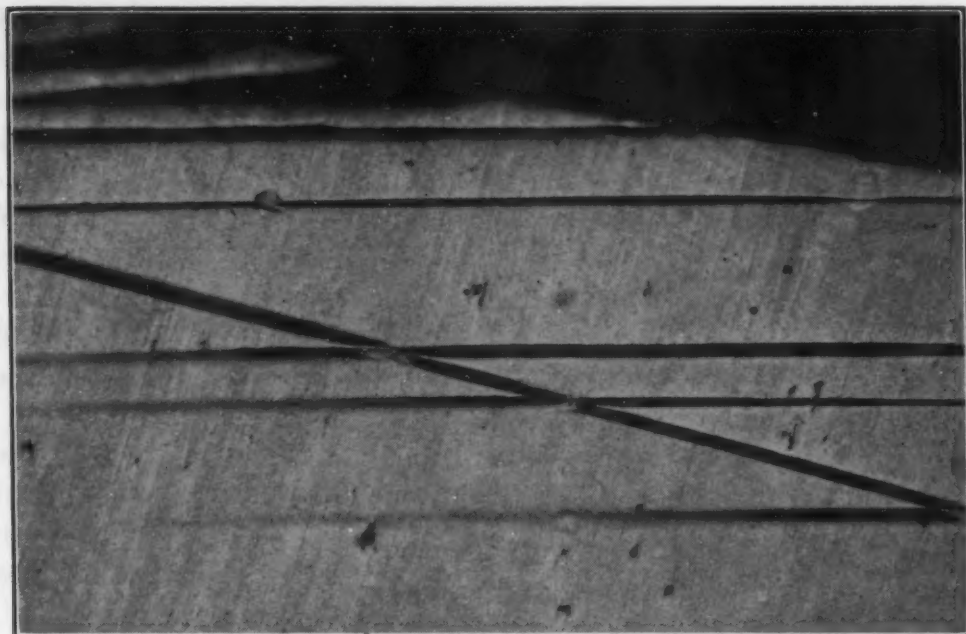


Fig. 14—Neumann Lamellae Make Small Angle With Fracture. Note intersecting and "fading away" at ends of lamellae.  $\times 250$ .

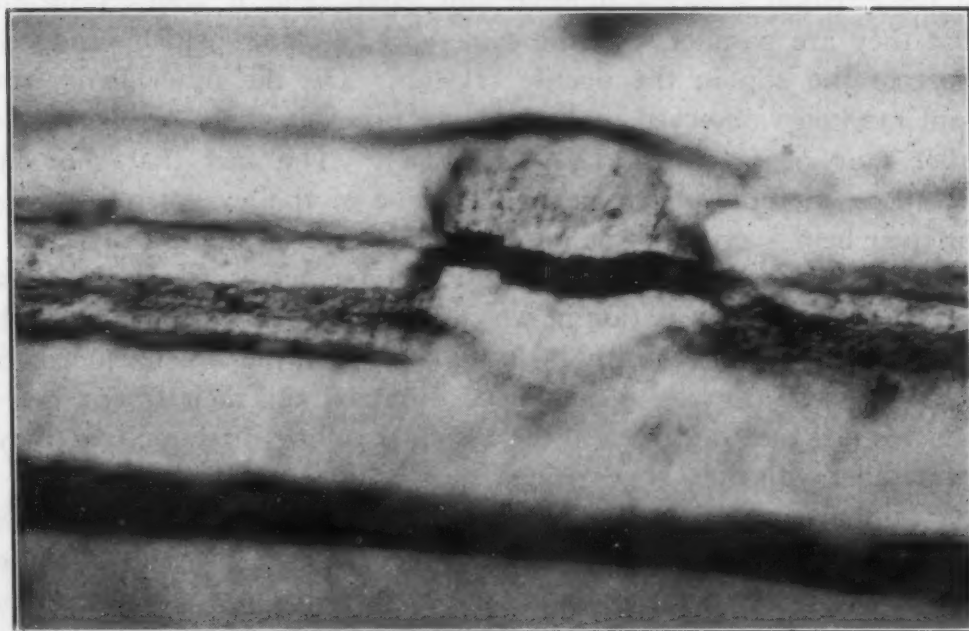


Fig. 15—Carbide Inclusion Cracked. Note roughness in Neumann lamellae due to slip bands.  $\times 1000$ .

crystal. Straight slip lines on this tongue are visible with considerable plastic deformation at the root. The rest of the surface shows very faint, straight markings, apart from striae made by the rather crude method of polishing.

Fig. 12, showing two halves of the same fracture in Specimen 4, also depicts the nature of the surface and small projections formed by the stopping and starting of the fracture. It is not difficult to see how such a process tends to maintain the mean fracture path both along a crystal direction and at right angles to the tensile stress. Similar observations have been made in the fracture of plastics and glass.

The formation of internal cracks independent of the main fracture is illustrated in Figs. 8 and 13. The distortion to the right of Fig. 8 is the plastic deformation caused by the opening out of the fracture and its arrest at the boundary described above.

These photographs show quite clearly that the direction of the Neumann lamellae is distinct from that of the fractures, and that both change direction at a boundary, Fig. 8. The plastic deformation at the end of the fine crack in Fig. 13 is clearly visible and will be discussed later.

#### *Neumann Lamellae*

The lamellae are characteristic in appearance. They are zones of deformation showing internal slip bands, and it seems probable that they are parallel with the same  $(112)$  planes which produced most of the slip in the ductile crystals. On the other hand, the faint markings observed in Fig. 11 are probably those of one of the other pair of planes,  $(1\bar{1}2)$  or  $(\bar{1}12)$ . The fact that the slip directions in these planes lie in the plane of the specimen accounts for their being very faint or in other samples even invisible.

If the lamellae are on the  $\{112\}$  type planes according to a perfect preferred orientation in which the  $(110)$  plane coincides with the plate surface and the  $[001]$  in the axis, then the lamellae normals are inclined 55 degrees to the  $[110]$  direction and their traces intersect this face at 90 degrees to the assumed rolling direction, i.e., they are parallel with the  $(100)$  plane.

If, however, the orientation is slightly displaced from this position, as it is shown to be by X-ray evidence, the traces of these planes may not coincide and angles between them of 5 to 10 degrees, such as are observed, are to be expected.

Confirmation that the bands are regions of severe deformation is afforded by the displacement and cracking of small inclusions. A large number of small slag inclusions added to the difficulty of obtaining a good polished surface. In addition, there were small, bright inclusions which darkened on boiling in alkaline sodium picrate and were identified as carbides. Many of them cracked when

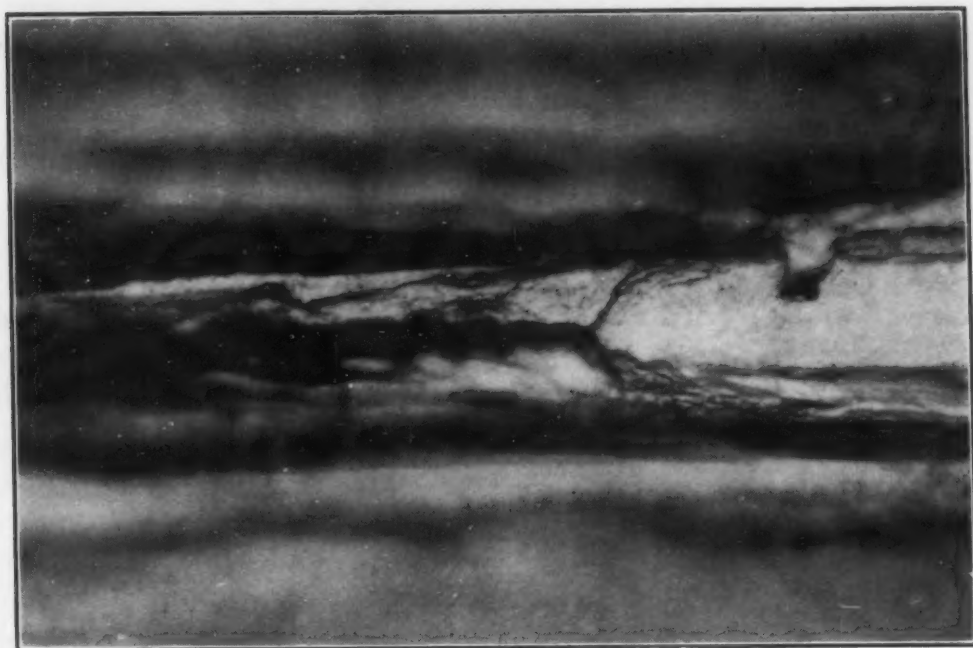


Fig. 16—End of Fracture Illustrated in Fig. 10a.  $\times 1000$ .

they were in the path of a Neumann lamella. Fig. 15 shows such an inclusion, traversed by a fissure in the neighborhood of a lamella. The internal structure of the Neumann lamella is also brought out.

At the ends of the bands, however, there is a tapering off, both in width and in difference of level. This is clearly seen in Fig. 14. This photograph also shows the kind of distortion produced at the intersection of lamellae. It is difficult to reconcile the fading out of the lamellae with the idea that they are true twins, in which the shear has been a constant amount throughout.

#### *Structure of Fractured Surface*

Markings on the surface of cleavage fractures are of two kinds: coarse striae which are usually nearly parallel with the plane of the plate, and fine markings which may assume a variety of patterns. The surface is rarely smooth and consists of planes on several levels.

The coarse parallel markings can be associated with the Neumann lamellae and have been followed from the plate surface to the fracture surface. Fig. 14, for example, shows how the lamellae form a slight discontinuity on the fracture edge. The planes (112) and ( $\bar{1}\bar{1}2$ ) of Fig. 1 intersect the plane of fracture (001) at 35 degrees 16 minutes on either side and it is considered that the parallel markings traversing the fracture plane parallel with the plate surface are formed by the intersections of these planes with the (001) plane. It will be recalled that the first region of





Fig. 17—Surface of Fracture Illustrated in Fig. 10a. Fracture from left to right.  $\times 100$ .

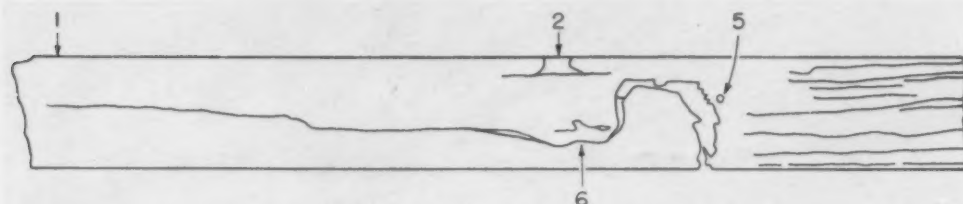


Fig. 17a—Diagram of Fig. 17 Indicating Regions Discussed.

fracture in Specimen 9 was free from these lamellae. The section shown in Fig. 17 represents the surface starting from the notch at the extreme left, Point 1 in Fig. 10a, and there are few such markings until Point 2 is reached, where some discontinuity arose causing plastic deformation on the surface (seen at a higher magnification in Fig. 19). Near Point 1, in the diagram, markings at right angles to the plate surface were observed. It is probable that they represent deformation bands near the notch bottom which formed before fracture was initiated.

The markings on the first part of the fracture are similar to those encountered on many fracture surfaces. At Points 5 and 6 in Fig. 17, shown at higher magnifications in Figs. 18 and 21, striations running from inclusions are clearly visible. It is almost certain that fracture was separately initiated at the inclusion at Point 5. It is possible that the large curved lines in this region may represent the position of crystal boundaries before final recrystallization.

Beyond Point 2 in the sample, Neumann lamellae appear both on the surface and in the section. In this section, Fig. 22, in regions between lamellae, the material shows a structure found also in plastics and glass, the velocity of propagation of the fracture being greatest in the center of the bands between the lamellae. This is evidence against the theory that fracture propagates along the interfaces of Neumann lamellae and the unaffected metal.

#### *The Structure at the Ends of Cracks*

It has already been stated that some fractures ended near a boundary and in this region, even when the fracture was chiefly crystalline, there was evidence of plastic deformation. This is apparent at the end of even the finest crack shown in Fig. 13, and the form of these crack ends, shown more clearly in Figs. 16 and 20 which correspond to Point 4 in Fig. 10a, is identical with that observed on a large scale on the surface of plate through which a fracture is propagating from a notch or crack. (See Fig. 9 in *Metallurgia*, Ref. 20.)

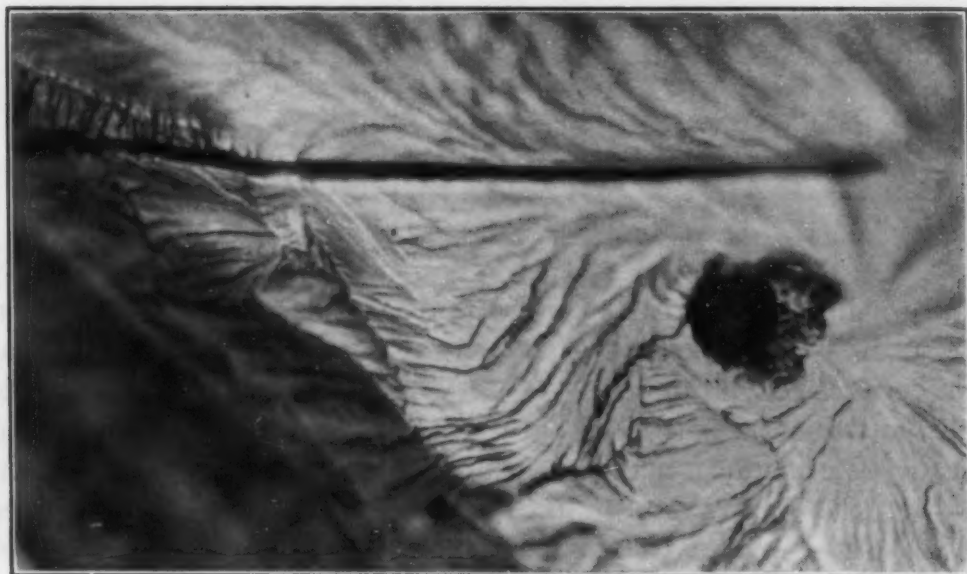


Fig. 18—Point 5 in Fig. 17a.  $\times 1000$ .

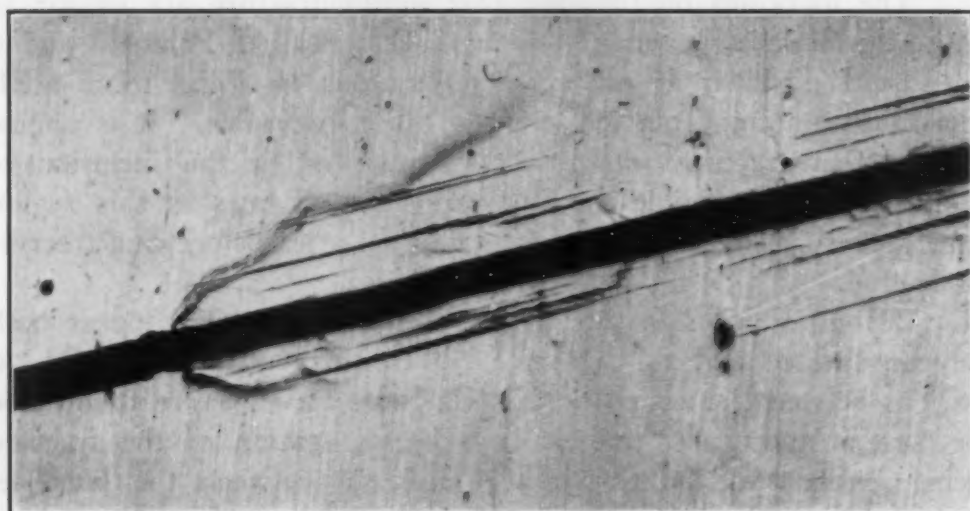


Fig. 19—Point 2 in Fig. 10a.  $\times 100$ .

The question naturally arises, does plastic deformation always precede fracture, or are the fractures arrested because the velocity of propagation falls below a certain critical value and plastic deformation absorbs the elastic strain energy in the system? It is difficult to explain the striae on the fractured surfaces (as distinct from Neumann lamellae and "steps" due to separation along intersecting crystal planes) without resort to some flow on these surfaces. In fact, the partial replacement of wavy markings by rectilinear, when iron crystals are embrittled by hydrogen or broken at low temperatures (23), is evidence in favor of flow in the parting of the material,



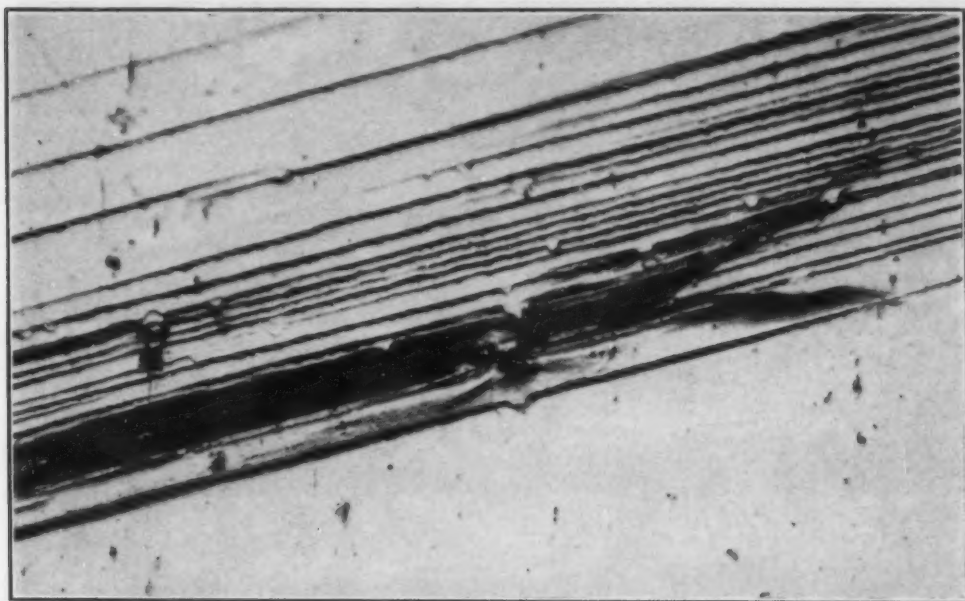


Fig. 20—Point 4 in Fig. 10a.  $\times 100$ .

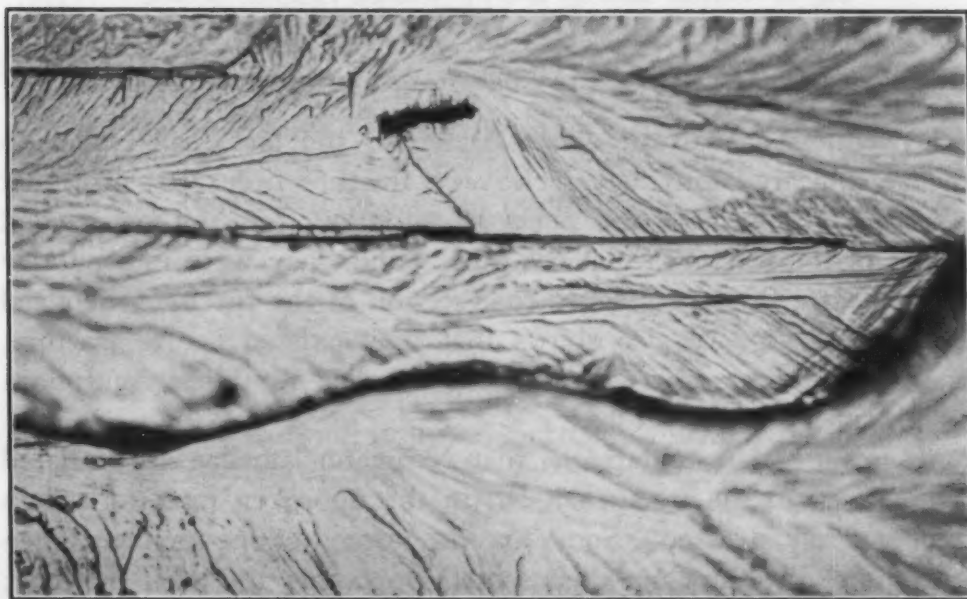


Fig. 21—Point 6 in Fig. 17a.  $\times 500$ .

confined to layers of the order of the width of slip bands. It is unlikely, however, that the markings produced on the surfaces of fractured glass can be attributed to flow on these surfaces. It is a matter for further investigation.

The significance of these markings is also discussed in a paper by Kies and Sullivan (7).

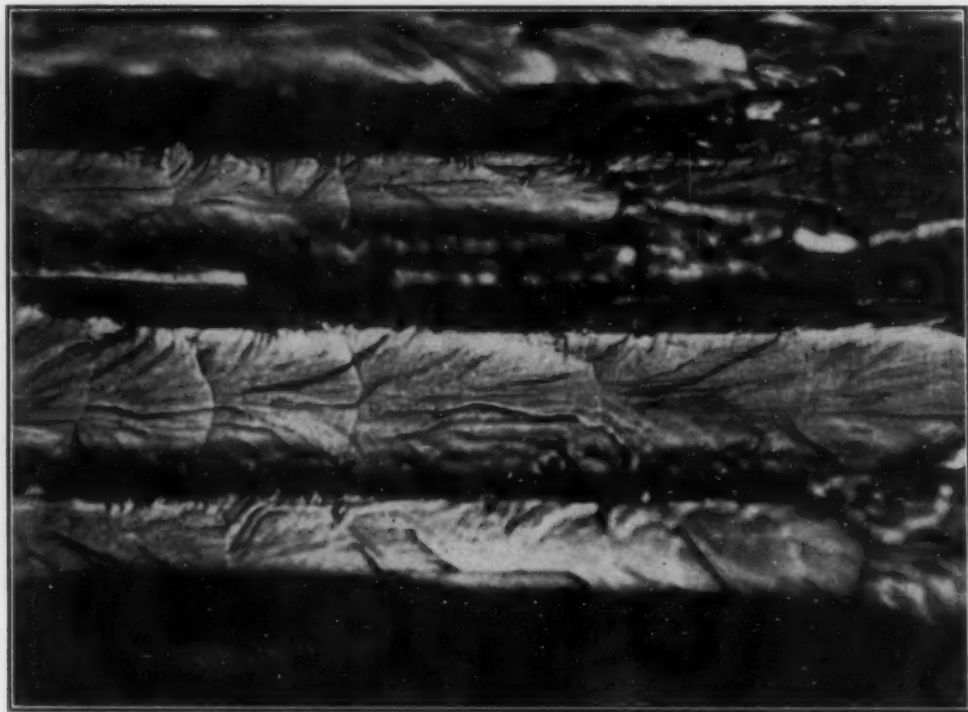


Fig. 22—Surface Markings Between Neumann Lamellae.  $\times 1000$ .

#### *Sequence of Events in the Formation of Neumann Lamellae*

Attention has already been drawn to the fact that Neumann lamellae appeared only when cleavage fracture occurred; also that they were absent near the point of initiation, but ran on beyond the end of the fracture. On the other hand, they were indisputably present before fracture reached that section of the specimen depicted in Fig. 22. Fig. 12 also shows that they existed before fracture, since it is unlikely otherwise that the lamellae would be continuous on both sides of the fracture.

It is suggested, tentatively, that Neumann lamellae are initiated by the shock of the fracture itself, in the unbroken material which is still severely stressed. Some may be formed at the moment when the first break occurs or when something occurs to check fracture; a shock would be given to the metal in either case. The traces of the lamellae in the fracture plane all lie very nearly parallel to the direction of propagation so that they do not cut across the path of the fracture. It is difficult to explain their formation without knowing the sequence of events, which is also complicated by inability to stop the straining mechanism of the machine sufficiently rapidly to insure that no plastic deformation occurs after the initial high speed fracture has taken place.

## SUMMARY AND DISCUSSION OF RESULTS

Neumann lamellae associated with fracturing occur only when the fractures are of the cleavage type. Similar bands, which may or may not be true twins, are commonly produced in alpha iron, if the metal is subjected to shock, when they are not formed under static conditions of loading. The evidence is in favor of the formation of the lamellae by cleavage, rather than that they contribute to the onset of cleavage. This view agrees with the observation that many ship-plate fractures in which a large number of crystals have broken in cleavage do not show Neumann bands while others show them only in selected regions.

An X-ray investigation was made to check the orientation of the crystals in two specimens. Slip markings, directions of fracture in the ductile crystal and Neumann lamellae appear to coincide with possible {112} planes. The fracture plane in cleavage is seen to be (112) for Specimen 3 and (100) for Specimen 9.

Insufficient evidence is at hand to show the effect of orientation on the method of fracture. Further studies are under way to clarify this.

The fractured surface is marked by a large number of wavy lines, indicative of the direction in which the fracture has propagated, and of regions of initiation and arrest. There are, in addition, bands of distorted material nearly parallel with the plate surface which are considered to be the intersections of Neumann lamellae in this plane.

## ACKNOWLEDGMENTS

This work was carried out in the Mechanics Division, Naval Research Laboratory, Washington, D. C. One of us (C. F. T.) had the privilege of working in this Department during part of September and up to November 1949, for which leave of absence was kindly given by Prof. J. F. Baker, O.B.E., Sc.D., Head of the Department of Engineering, University of Cambridge.

## References

1. C. S. Barrett, "Structure of Iron after Compression", *Transactions, American Institute of Mining and Metallurgical Engineers*, Vol. 135, 1939, p. 296.
2. C. S. Barrett, G. Ansel and R. F. Mehl, "Slip, Twinning, and Cleavage in Iron and Silicon Ferrite", *TRANSACTIONS, American Society for Metals*, Vol. 25, 1937, p. 702.
3. M. Baeyertz, W. F. Craig, Jr., and E. S. Bumps, "A Metallographic Description of Fracture in Impact Specimens of a Structural Steel", *Metals Transactions, American Institute of Mining and Metallurgical Engineers*, Vol. 185, 1949, p. 481.



4. W. E. Carrington and M. L. V. Gayler, "Changes in Microstructure Caused by Deformation Under Impact at High Striking Velocities", *Proceedings of the Royal Society, Series A*, Vol. 194, 1948, p. 323.
5. C. G. Dunn, "Recrystallization and Twin Relationships in Silicon Ferrite", *Transactions, American Institute of Mining and Metallurgical Engineers*, Vol. 158, 1944, p. 372.
6. J. Görrissen, "Some Notes on Brittleness in Mild Steel", *Journal, Iron and Steel Institute*, Vol. 162, May 1949, p. 16.
7. J. A. Kies and M. Sullivan, "Fracture Markings in Plastics", paper presented at American Physical Society Meeting, New York, February 1950.
8. E. P. Klier, "A Study of Cleavage Surfaces in Ferrite", Pennsylvania State College, School of Mineral Industries, Final Report to ONR, Oct. 15, 1949.
9. N. F. Mott, "Fracture of Metals: Some Theoretical Considerations", *Engineering*, Vol. 16, 1948, p. 16.
10. H. O'Neill, "Deformation Lines in Large and Small Crystals of Ferrite", *Journal, Iron and Steel Institute*, Vol. 113, 1926, p. 417.
11. L. B. Pfeil, "Deformation of Iron with Particular Reference to Single Crystals", *Carnegie Scholarship Memoirs*, Iron and Steel Institute, Vol. 15, 1926, p. 319; "Effect of Cold Work on the Structure and Hardness of Single Iron Crystals and the Changes Produced by Subsequent Annealing", *Carnegie Scholarship Memoirs*, Iron and Steel Institute, Vol. 16, 1927, p. 153.
12. E. Poncelet, "Fracture", *Verre et Refractaire*, August 1948, p. 203; June 1949, p. 149; October 1949, p. 289.
13. A. E. Ruark, W. J. Ferguson, H. L. Smith, G. A. Hornbeck, I. R. Kramer, P. E. Shearin, R. M. Trimble and H. N. Michie, "Ductility and Fracture Resistance of Ship-Plate", Naval Research Laboratory Report No. O-2796, November 1946.
14. E. Schmid and I. W. Boas, *Kristallplastizität*, Julius Springer, Berlin, p. 176 ff.
15. B. F. Shepherd, "The P-F Characteristic of Steel", *TRANSACTIONS, American Society for Metals*, Vol. 22, 1934, p. 979.
16. E. Shevandin, "The Spreading of a Brittle Fracture Crack", *Technical Physics, U.S.S.R.*, Vol. 5, 1938, p. 279.
17. J. W. J. Smith, A. A. Dee and J. Young, "Mode of Formation of Neumann Bands. Part I—The Mechanism of Twinning in the Body-Centered Cubic Lattice", *Proceedings of the Royal Society*, Vol. 121, 1928, p. 477.
18. G. I. Taylor and C. F. Elam, "The Distortion of Iron Crystals", *Proceedings of the Royal Society*, Vol. 112, 1926, p. 337.
19. C. F. Tipper, "Admiralty Ship Welding Committee Report, No. R.3", H. M. Stationery Office, 1948.
20. C. F. Tipper, "The Fracture of Metals", *Metallurgia*, Vol. 39, January 1949, p. 133.
21. H. Wallner, "Linienstrukturen an Bruchflächen", *Zeitschrift für Physik*, Vol. 144, 1939, p. 368.
22. Carl A. Zapffe, "Neumann Bands and the Planar-Pressure Theory of Hydrogen Embrittlement", *Journal, Iron and Steel Institute*, Vol. 154, 1946, p. 123.
23. C. A. Zapffe and C. O. Worden, "Deformation Phenomena on a Cleavage Facet of Iron", *METAL PROGRESS*, Vol. 55, May 1949, p. 640.

## DISCUSSION

**Written Discussion:** By A. J. Opinsky and R. Smoluchowski, Carnegie Institute of Technology, Pittsburgh.

In connection with the very interesting research reported by the authors, we would like to mention some of our recent results to appear shortly in the "Pittsburgh Conference on Plastic Deformation in Solids", 1950. We studied the crystallographic aspect of slip in body-centered cubic lattices and compared the theoretical conclusions with experimental data on single crystals of 3.4% silicon ferrite. From the sequence of appearance of various slip planes as a function of orientation of the tensile axis, an accurate determination can be made of the ratios of the critical shear stresses. In particular, whenever the tensile axis is very close to the [100] direction, then only the {211} type of plane should be active in accord with the results reported in this paper.

**Written Discussion:** By Carl A. Zapffe, consulting metallurgist, Baltimore, Md.

This question of Neumann bands comes up again in the paper by Dr. Klier to follow this one. The identity of Neumann bands has been argued for more than half a century, and they are not yet well understood. The history was reviewed in Ref. 22 cited by Dr. Tipper and Miss Sullivan. At that time the phenomenon was studied fractographically, both in pure iron and silicon ferrite; and it was concluded that the markings ascribed to Neumann bands are primarily a shearing movement along {112}, accompanied by more or less latticular rupture, and that twinning of the included material may or may not develop. It appears that Dr. Tipper and Miss Sullivan have a similar opinion, believing that the deforming stress may in some cases exceed a threshold value sufficient for causing twinning, and in other cases may not.

Two fractographs (Figs. 23 and 24) are submitted here to indicate the complexity of the Neumann-band phenomenon, and aspects which remain to be clarified. Fig. 23 shows a "V"-shaped intersection of two of the {112} traces. The illumination obliqued from the left clearly shows the faulted surfaces of these bands, such that the V-shaped block in the center lies at a lower level. The light has shaded one band and illuminated the other showing this faulting. Since the fracture has followed the pattern of the fractograph, it is clear that one of two things has happened: (a) the V-shaped block has moved by a faulting or twinning operation into the body of the metal or (b) fracture has proceeded downward along the band at the left and upward again along the band at the right. In either case, cleavage for at least a short distance along the band is clearly indicated.

In Fig. 24, a second complication appears in the stepwise lamellar formation, here shown at a magnification of  $\times 4000$ . Whether this refers to some internal rearrangement, as by slip within the band itself, is not yet known. However, at least two cleavage families have obviously been operative to develop this stepwise effect. In the cited Ref. 22, some further information on these bands was added by experiments passing hydrogen gas through banded metal, and observing the emission of the gas beneath an oil film on a fractured surface. The results proved that the body of the Neumann band contains hiatuses of sufficient size to house occlu-

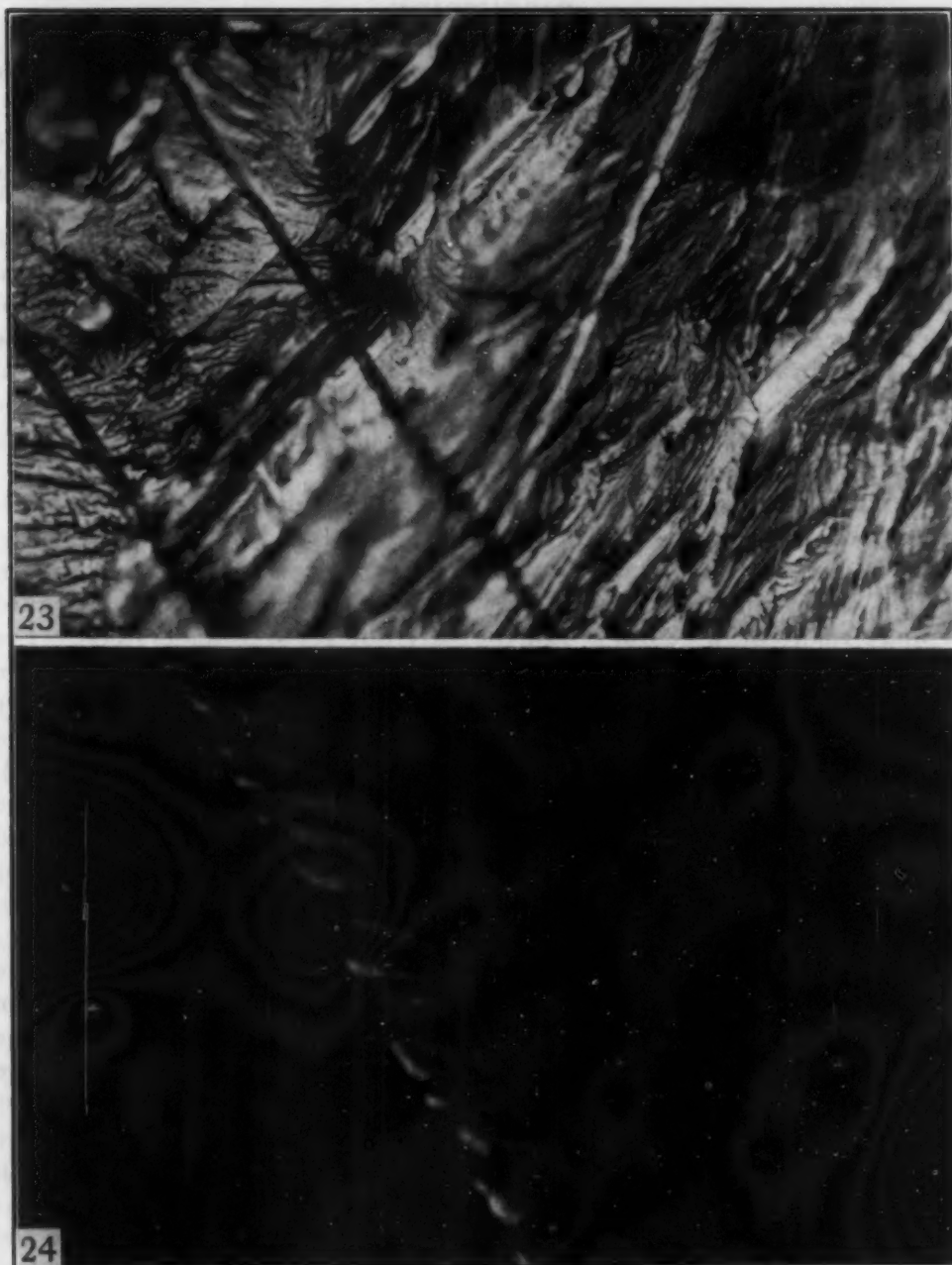


Fig. 23—Fractograph of Silicon Ferrite, Showing Intersecting Neumann Bands by Means of Oblique Light Coming From the Left.  $\times 1000$ .

Fig. 24—Neumann-Band Detail Observed Fractographically With Oblique Light, Showing Fine-Scale Stepwise Structure.  $\times 4000$ .

sions of gas; and they also proved that these formations provide favored passages for the gas diffusing through the steel.

It is reassuring to find such capable investigators as Dr. Tipper and Miss Sullivan turning their attention to these problems; and we shall await with much interest their further publications.

**Written Discussion:** By G. W. Geil, metallurgist, National Bureau of Standards, Washington, D. C.



The authors of this paper have suggested a sequence of events in the formation of Neumann lamellae. They suggest, tentatively, that "Neumann lamellae are initiated by the shock of the fracture itself, in the unbroken material which is still severely stressed. Some may be formed at the moment when the first break occurs or when something occurs to check fracture; a shock would be given to the metal in either case."

Some data obtained recently at the National Bureau of Standards in tension tests of ingot iron at low temperatures<sup>3</sup> apparently do not conform

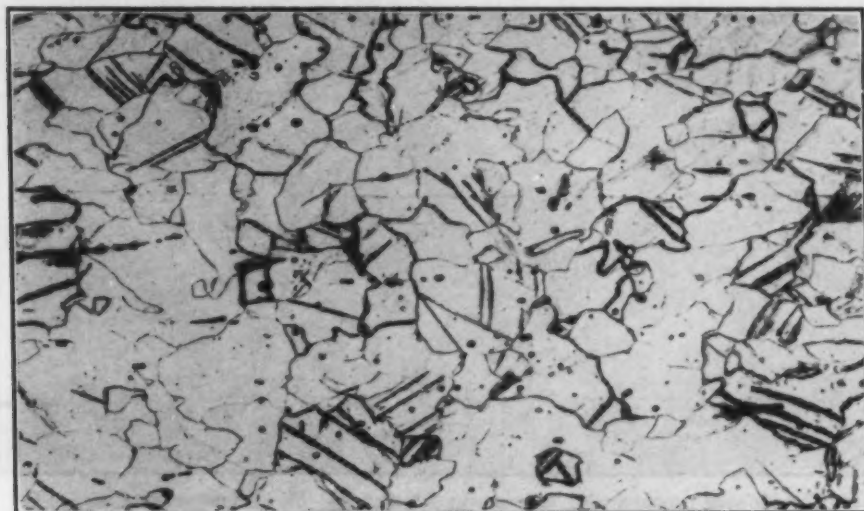


Fig. 25—Photomicrograph of a Portion of the Reduced Section of a Tension Test Specimen of Ingot Iron Initially as Hot-Rolled and Subsequently Extended in Tension at  $-196^{\circ}\text{C}$  to the Maximum Load. Etched in 4% Nital.  $\times 100$ .

to the sequence of events in the formation of Neumann lamellae as proposed by the authors. Neumann lamellae were observed in ingot iron specimens slowly deformed under tension at  $-196^{\circ}\text{C}$  and not extended to fracture. Fig. 25 is a photomicrograph of a portion of the reduced section of a tension test specimen of ingot iron, initially as hot-rolled and extended in tension at  $-196^{\circ}\text{C}$  to the maximum load (a true strain of 0.14). Numerous Neumann lamellae were present, as indicated in this photomicrograph. Neumann lamellae were also present in specimens that had been extended slowly to very small strains. These data indicate that the shock of fracture itself is not necessary for the initiation of Neumann lamellae.

**Written Discussion:** By W. H. Bruckner, associate professor, University of Illinois, Urbana, Ill.

This paper is of interest as an experimental exploration of a theory by Shevandin that Neumann bands facilitate cleavage failure. I would infer from the authors' discussion that Shevandin's theory postulates the propagation of fracture along the twin interface. The authors state that under the conditions of their experiments the Neumann lamellae have no effects such as Shevandin postulated. This could be granted on the basis of the evidence given in their paper; however, if a general statement is

<sup>3</sup>G. W. Geil and N. L. Carwile, "Tensile Properties of Ingot Iron at Low Temperatures", *Journal of Research*, National Bureau of Standards, RP 2119, August 1950.

made as by the authors that this applies to fracture of ferrite in general, I feel compelled to draw attention to a paper which I presented before the American Welding Society.<sup>4</sup>

My paper described some impact tests made with varied initial energy to obtain a metallographic sequence of fracture in polycrystalline structural steels and Armco iron. The fracture mechanism which was suggested for the experimental materials by the data obtained in the preparation of

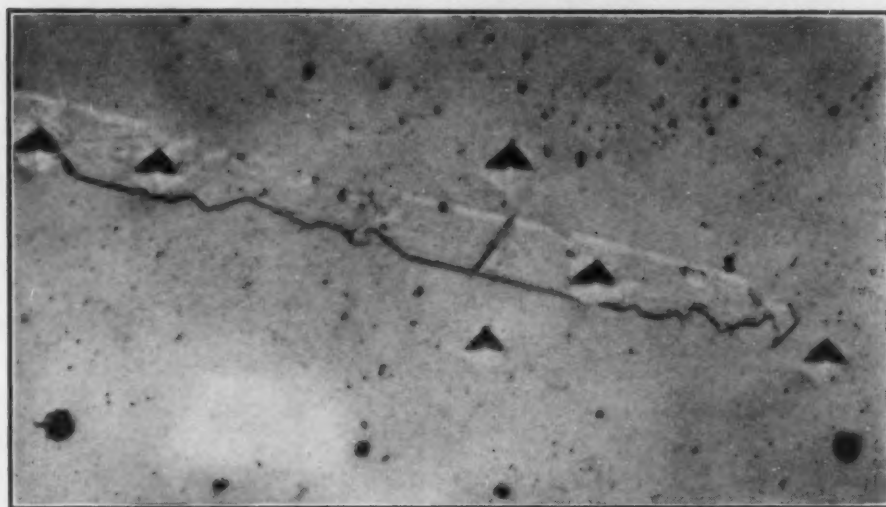


Fig. 26—Microhardness Indents in Mechanical Twin and Surrounding Ferrite. Etchant, 5% Nital.  $\times 900$ .

the paper led to an opposite conclusion to that given by Tipper and Sullivan. It was shown in the paper that Neumann lamellae could initiate cleavage and that the presence of the lamellae could determine the path of fracture. The cleavage fracture was always across the twin and was found in some cases to be confined to the mechanical twin and in others to have propagated into the ferrite surrounding the twin.

In attempting to account for the initiation of the cleavage fracture in the twin, it was thought that the region had absorbed a large amount of energy. Accordingly, some twins in a ferrite grain remote from the fracture were indented with a  $1\frac{1}{4}$ -gram load on a Vickers-type diamond indenter employed in the Hanemann Micro-Hardness Tester. As shown in Fig. 26, the hardness of the twin region is not perceptibly different from that in the surrounding ferrite. However, when it was possible to place an indent on the twin interface, the smaller indentation produced was easily discernible. The experiment suggests that the twinning operation does not absorb a large amount of energy and that whatever increase in energy is produced is mainly in the interface. We, therefore, suspect that the causative factor operative in cleavage initiation in the twin must be sought at the twin interface.

Since it was not possible for me to use an X-ray diffraction method for orientation studies of fracture in the polycrystalline material, it was necessary to employ etch pits which delineate the (100) planes in alpha

<sup>4</sup>W. H. Bruckner, "The Micro-Mechanism of Fracture in the Tension Impact Test", *Welding Journal*, Vol. 29, September 1950, p. 467s-476s.

iron. In these studies I have never seen a major cleavage in ferrite on any other plane than the (100) series. On occasion some slight tearing or parting was noted along a twin interface but only as a small section of the fracture interposed between the traces of (100) cleavages. It was suggested in the discussion by Zapffe that secondary, tertiary and other cleavages could take place; Klier too has found secondary cleavage on the {112} plane.<sup>5</sup> These data may possibly exist only for single crystals or ferrite of large grain size for which the time factor in the propagation of cleavage fracture may have more significance than for the commercial structural steels of relatively small grain size.

The tests which these authors have made are of value in indicating the behavior of silicon ferrite of large grain size when subjected to a biaxial tension stress system. When the data are compared with the behavior of polycrystalline ferrite of small grain size in sufficient mass to cause inhibition of shear deformation and in which mass each grain may be surrounded by others which exercise mutual restraint, would the authors expect the same behavior as they have indicated for the thin sheets of silicon ferrite?

#### Authors' Reply

It is gratifying to the authors to find so much interest taken in their paper and they would like to thank all those who have contributed to the discussion.

Criticism has been made on two grounds confined to the tentative explanation which the authors put forward to explain their observations.

These criticisms are mainly that (a) since Neumann lamellae can develop in some instances in slow loading, long before fracture is imminent, therefore a high strain rate does not enter into their formation and (b) there is evidence that their presence facilitates cleavage fractures and such fractures originate in Neumann lamellae.

It was never intended to convey the opinion that lamellae could not be formed independently of fracture. In fact the opposite view was expressed on page 907, paragraph 4, although attention was drawn to the undisputed evidence that they occur more readily when the metal is subjected to shock. It would be very interesting to know if the material tested by Dr. Geil had a marked yield. The formation of Neumann lamellae in individual grains has some resemblance to Luders' band formation in polycrystalline metals in that the deformation is discontinuous. It is known that twin formation is accompanied by a sudden drop in the load, similar to that at the yield point in mild steel when tested in a suitable machine.<sup>6</sup> Such a drop signifies a very high strain rate and conditions approaching those produced by impact loading, and Chalmer's<sup>7</sup> work on tin suggests that twinning requires a minimum amount of stored elastic strain energy.

Whether Neumann lamellae are true twins or only bands of deformation produced by shear parallel with certain crystal planes, they may be expected to show slight differences in hardness due to the plastic deformation which, however, may easily be masked by orientational differences

<sup>5</sup>E. P. Klier, "A Study of Cleavage Surfaces in Ferrite", see this volume, p. 935.

<sup>6</sup>E. Schmid and I. W. Boas, *Kristallplastizität*, p. 170.

<sup>7</sup>C. Chalmer, *Proceedings, Physical Society*, Vol. 47, 1935, p. 733.



between the bands and the grain within which they form. Both Professor Bruckner and Dr. Zapffe show evidence that the material within the band is strained and it may be inferred that the interface is also in a state of strain. Professor Bruckner's photomicrographs,<sup>4</sup> Figs. 17 and 21, do not show fracture along the boundary, however, as postulated by Shevandin, but across the lamellae. The fact that some lamellae fracture before the main body of the grain may be fortuitous and due entirely to the difference of orientation between them relative to the operative stress system. It does not imply that cleavage fractures in general are always initiated by cracks in the lamellae. As already pointed out, many instances of cleavage fractures have been seen without Neumann lamellae.

The hypotheses that cleavage fractures both initiate Neumann lamellae and sometimes start in them are not incompatible and the evidence is in favor of both being valid.

## A STUDY OF CLEAVAGE SURFACES IN FERRITE

BY E. P. Klier

### *Abstract*

*The structures at cleavage surfaces in ferrite have been examined by X-ray, fractographic and metallographic procedures. It has been found that plastically-strained metal exists at such surfaces in coarse-grained ferrite over a wide range of testing conditions.*

**S**TUDIES of cleavage surfaces in metals by metallographic methods have been highly refined in recent years, largely through the efforts of Zapffe and associates (1).<sup>1</sup> X-ray studies of such surfaces, however, are largely lacking. The present paper is a preliminary report on the X-ray analysis of the structures at cleavage surfaces in ferrite.

In the study of surface cleavage effects by X-ray analysis, two methods are available—namely, low glancing angle diffraction and back-reflection techniques. In the present work the back-reflection technique has proven advantageous, since it provides high resolution for line width measurements, readily shows up fibering, and provides a means of estimating surface film thicknesses, while the beam can be confined to a small area of the surface under investigation.

Back-reflection X-ray studies are usually conducted using Laue or focusing conditions of diffraction. For Laue diffraction, a single crystal and white radiation are employed, while for focusing conditions, a polycrystal and characteristic radiation are used. In general, when characteristic radiation is used under conditions for Laue diffraction, no diffraction pattern—or at best, a very incomplete one—is obtained. Under ordinary experimental conditions, however, there is a white component to the impinging X-radiation, so that for a single-crystal specimen, a weak Laue diffraction pattern will be obtained, while the characteristic radiation will be dissipated largely by incoherent scattering. For a specimen made up of a single crystal on which a film of disturbed or highly divided metal exists, the diffraction pattern, therefore, will consist of two parts—the Laue spots and a Debye-Scherrer ring. The Laue spots arise as

<sup>1</sup>The figures appearing in parentheses pertain to the references appended to this paper.

A paper presented before the Thirty-second Annual Convention of the Society, held in Chicago, October 21 to 27, 1950. The author, E. P. Klier, is associate professor, Department of Chemical Engineering, University of Maryland, College Park, Md. Manuscript received April 17, 1950.

indicated above, while the Debye-Scherrer ring will arise from the diffraction of the characteristic radiation by the divided metal surface. The density of the Laue spots will be determined by the thickness of the divided surface layer which would scatter the continuous radiation in such a way as to contribute to the general background. Results which seemingly conform to this case have been reported for coarse-grained ferrite broken brittlely under liquid air (2).

From a preliminary study of coarse-grained ferrite, it was concluded that the surface of the fracture consisted of a film of particles

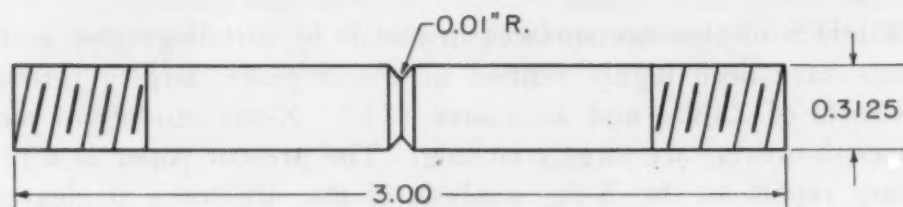


Fig. 1—Cleavage Fracture Test Specimen.

about  $10^{-5}$  cm in diameter. Since the Laue diffraction spots were also obtained on the pattern, it was estimated that the film of particles might be strain free, in which case the line width measurements could be used directly to determine the particle size of the ferrite.

It is evident that further data on these phenomena are needed, and preferably should be obtained on cleavage facets of single grains so that directional effects may be isolated.

#### EXPERIMENTAL PROCEDURE

*Material*—The ferrite used was in the form of round bar stock of the following composition: Mn 0.03%; C 0.02%; P 0.010%; S 0.013%; Co 0.005%; Mo 0.004%; Ni 0.032%; Cr 0.003%; Si 0.0035% and balance Fe (3). This ferrite was obtained by melting hydrogen-annealed electrolytic iron in magnesia crucibles in a high-frequency induction unit under an atmosphere of purified dry hydrogen (3). The molten iron was allowed to freeze in the crucible, then reheated to just above the melting temperature, and again allowed to freeze in the crucible. The ingots were forged and rolled to  $\frac{5}{16}$ -inch round stock.

The ferrite grain size was greater than ASTM No. 1, and frequently the fracture surface obtained comprised the cleavage facets of only one grain. Of these cleavage facets normally only one was suitably aligned for study.

The specimen used, shown in Fig. 1, could be broken in tension



impact or in bending. From the numerous specimens broken, the most interesting results were obtained from those tested as follows:

Spec. No.	Test Procedure	Temperature
1	Slow Bend	-190 °C (-310 °F)
2	Impact Bend	-70 °C (-94 °F)
3	Tension Impact	-70 °C (-94 °F)
4	Tension Impact	25 °C (77 °F)
A	Tension Impact	25 °C (77 °F)

Specimens were not tested at temperatures above 25 °C because this appeared to be the maximum temperature at which cleavage fractures could be formed readily in the large-grained ferrite. A specimen tested in static tension at 25 °C failed in shear.

*Microscope Examination*—The broken specimens were supported in a special fixture and the cleavage surfaces were examined metallographically. Appropriate fracture surfaces were nickel-plated after X-ray examination, and sectioned normal to the cleavage facet. The fracture edge and microstructure were examined after etching in 10% nital. Specimen No. 1 was given a flash copper plate prior to the nickel plate.

*X-Ray Examination*—The cleavage facets were oriented in a uniform manner with reference to the direction of the X-ray beam. This was necessary in order that the effects of fibering could be detected. The continuous and K-radiations of chromium were used in conjunction with a back-reflection-type camera in which both the specimen and the film were stationary.

*Electron Microscopy*—One of the specimens tested in tension impact at 25 °C was examined with the electron microscope. Replicas of the fracture surface were prepared by the polystyrene-silica technique.

## RESULTS

*Specimen No. A*—This specimen was subjected to a series of tests to determine whether or not the disturbed metal revealed in the X-ray diffraction patterns was restricted to the cleavage surfaces in the grains under observation.

In Figs. 2 and 3 are presented the back-reflection Laue pattern and fractograph of the specimen as fractured. From the X-ray pattern it would appear that extensive plastic distortion has occurred in the specimen.

As is indicated in Figs. 4 and 5, etching the cleavage surface in 10% nital has not removed the material which gives rise to the Debye-Scherrer conditions for diffraction. However, by etching in 10% HNO<sub>3</sub> plus water, the Debye-Scherrer ring has been eliminated (Fig. 6). This demonstrates that the Debye-Scherrer diffraction

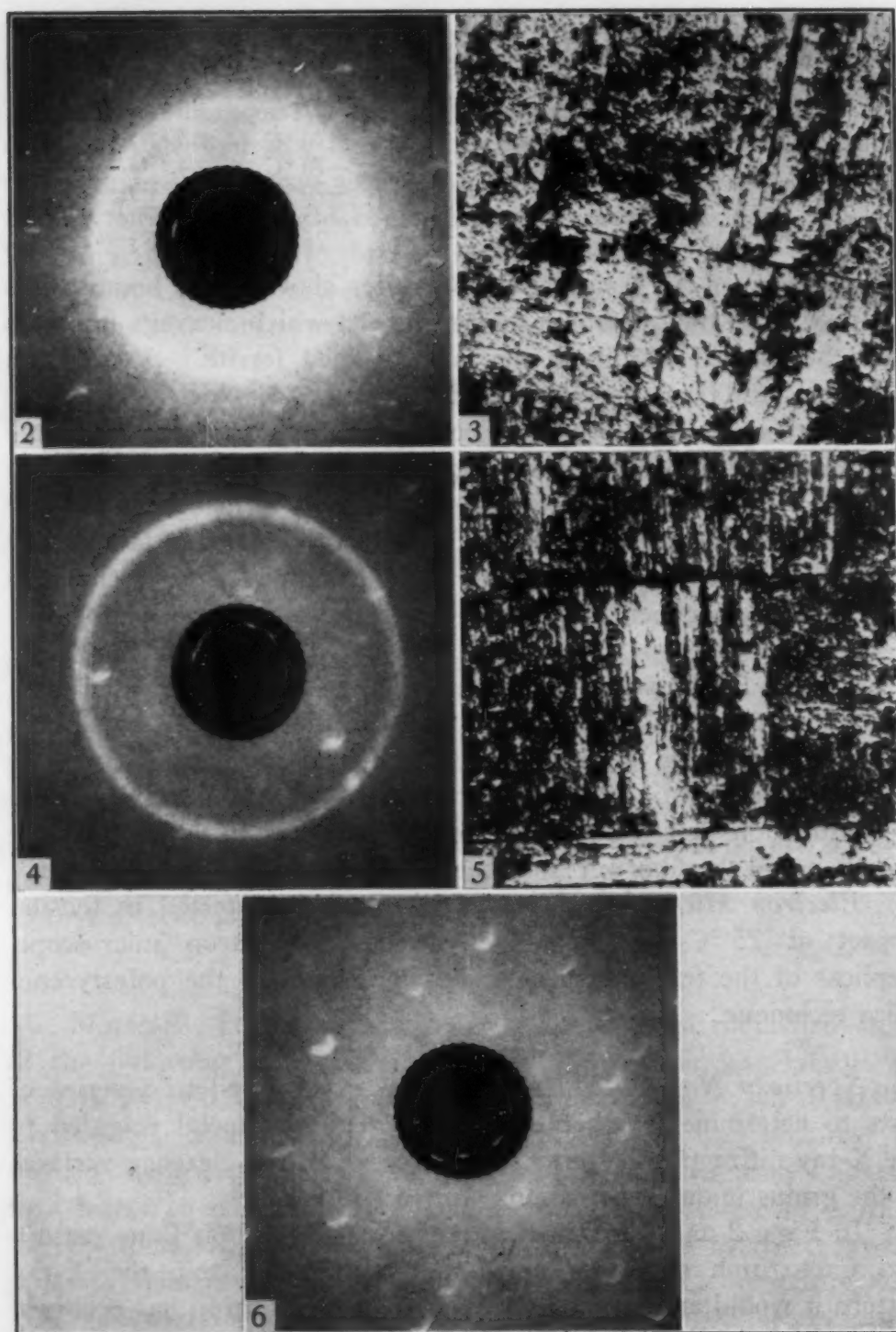


Fig. 2—Back-Reflection X-Ray Pattern, Specimen A, as Fractured.

Fig. 3—Fractograph  $\times 250$ , Specimen A, as Fractured.

Fig. 4—Back-Reflection X-Ray Pattern, Specimen A, Etched 10% Nital.

Fig. 5—Fractograph  $\times 250$ , Specimen A, Etched 10% Nital.

Fig. 6—Back-Reflection X-Ray Pattern, Specimen A, Etched 10%  $\text{HNO}_3 + \text{H}_2\text{O}$ .

effects arise from strained metal largely present at the fracture surface and are not characteristic of the grain as a whole.

Additional evidence that the disturbed metal, responsible for the Debye-Scherrer diffraction, lies largely at the cleavage surface has been obtained for Specimen No. 1, discussed below. This specimen after sectioning on a plane normal to the cleavage plane was subjected to an X-ray analysis on the new surface. The Debye-Scherrer diffraction ring was not developed, thus indicating the absence of the fragmentation effect noted at the cleavage surface.

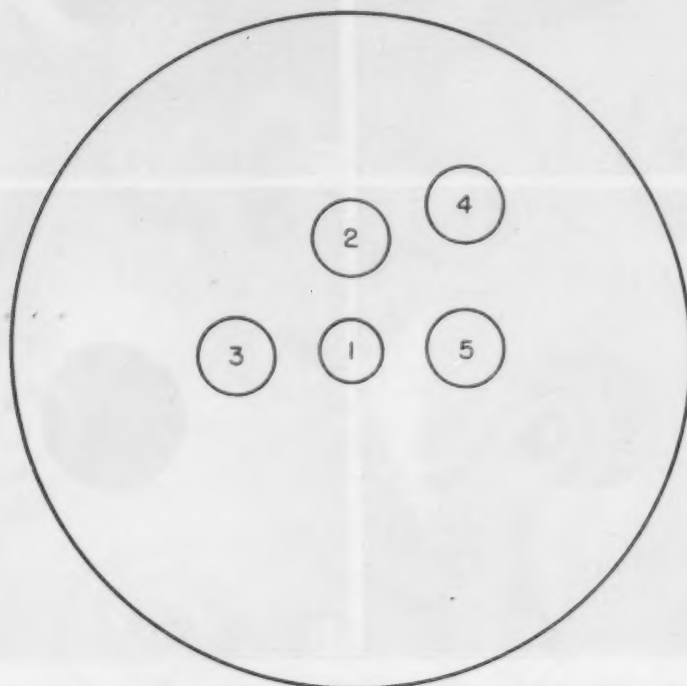
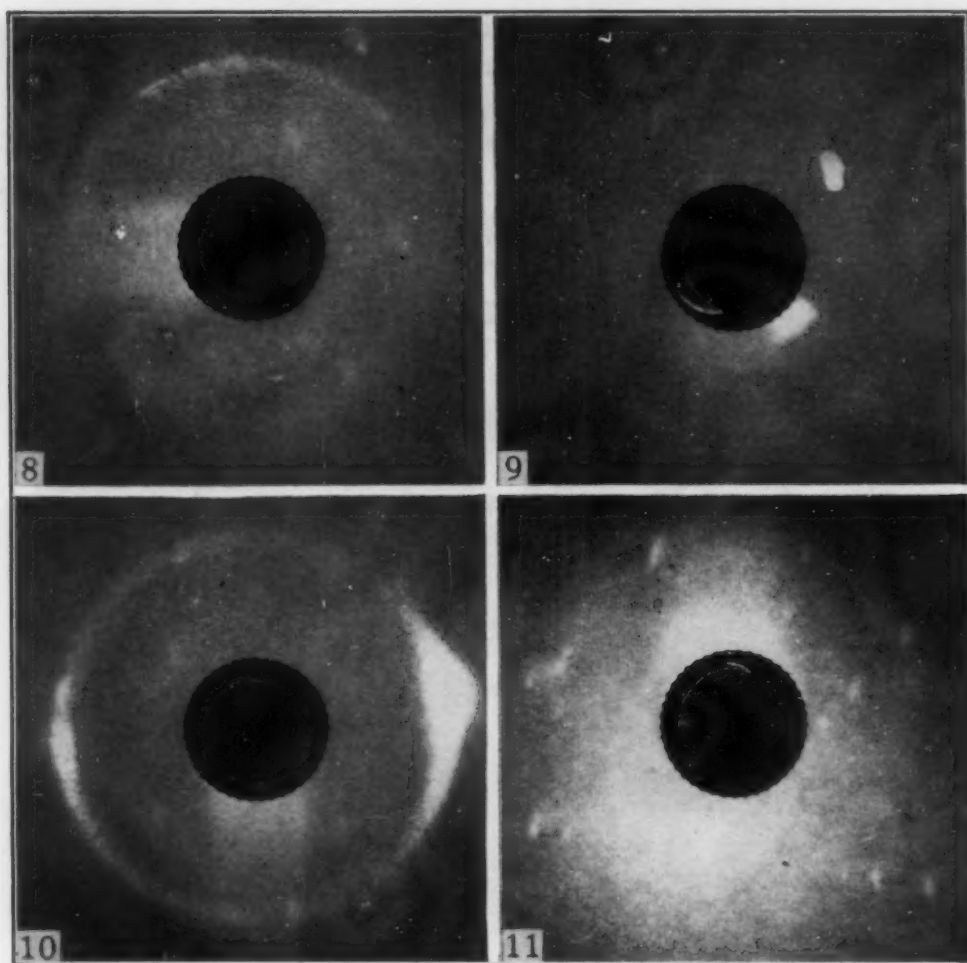


Fig. 7—Stereographic Plot of Incident Beam Orientations.

*Specimen No. 1*—This specimen was cooled in liquid air and was then broken with a sharp hammer blow. The hammer blow was nearly in the  $[0\bar{1}1]$  direction of the crystal of ferrite which made up the cross section of the specimen. The fracture possibly was not propagated in the  $[0\bar{1}1]$  direction because the fracture facet examined was tilted at about 45 degrees to the axis of the specimen. If it is assumed, however, that fibering of the disturbed surface metal would be normal to the direction of crack propagation, the X-ray results should indicate that crack propagation was close to the  $[0\bar{1}1]$  direction in this crystal.

Five X-ray patterns were taken on the cleavage surface to check this postulated fiber structure. The incident beam-crystal face angle for each of these exposures is indicated in the stereographic plot, Fig. 7. Suitable diffraction patterns are presented in Figs. 8 to 11.





Figs. 8 to 11—X-Ray Diffraction Patterns, Specimen No. 1. Fig. 8—Orientation 1, Fig. 7; Fig. 9—Orientation 2, Fig. 7; Fig. 10—Orientation 3, Fig. 7; Fig. 11—Orientation 4, Fig. 7.

It is evident, first of all, that the Debye-Scherrer ring indicating a disturbed surface layer on the ferrite crystal is not obtained with uniform intensity for all incident-beam angles. This is as would be expected for a fiber structure. However, the diffraction data are not in full accord with the fiber structure indicated and can be best accounted for by restricting the fiber pattern to a preferred orientation structure with limited rotation in a direction indicated in Fig. 12 by the dotted arrow. The nonexistence of the Debye-Scherrer ring for certain incident-beam angles can be understood by reference to Fig. 12.

The reflection circle is drawn on the projection at two pertinent locations. These locations correspond to the diffraction patterns presented in Figs. 10 and 11. The location giving the pattern in Fig. 10 lies in a zone of high expectancy for  $\{112\}$  reflections, and as a consequence a strong Debye-Scherrer ring is obtained. The

location giving the pattern in Fig. 11 lies in a zone of low expectancy for  $\{112\}$  reflections and the Debye-Scherrer ring is here absent.

In Fig. 11 it is evident that no appreciable Debye-Scherrer ring exists. On the other hand, the Laue diffraction spots are quite pronounced. This should not be the case if the postulate is valid that the Debye-Scherrer ring arises from a surface layer of disturbed metal. Rather, to a close approximation, the intensity of the Laue spots should be nearly constant from pattern to pattern, as the

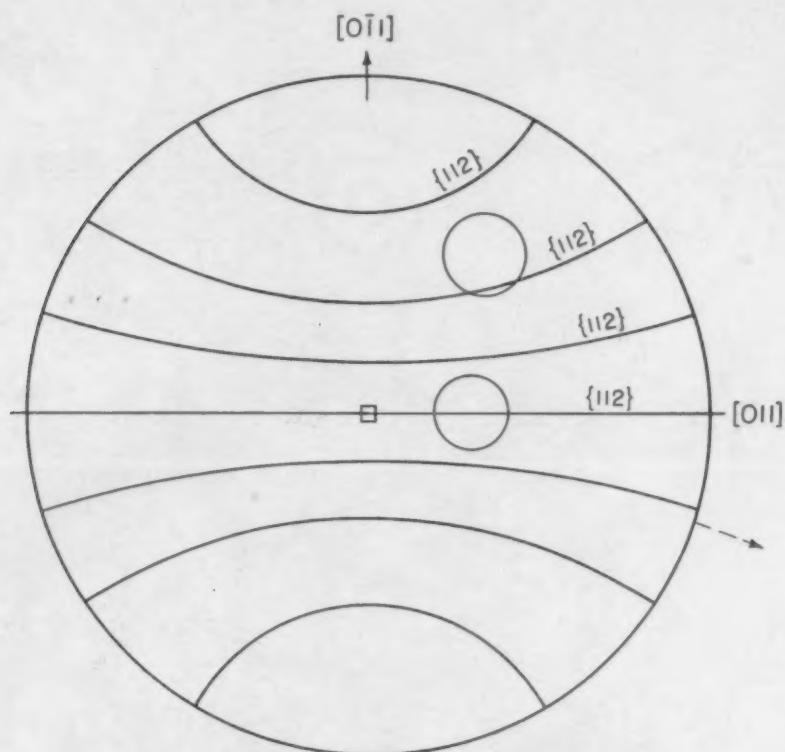
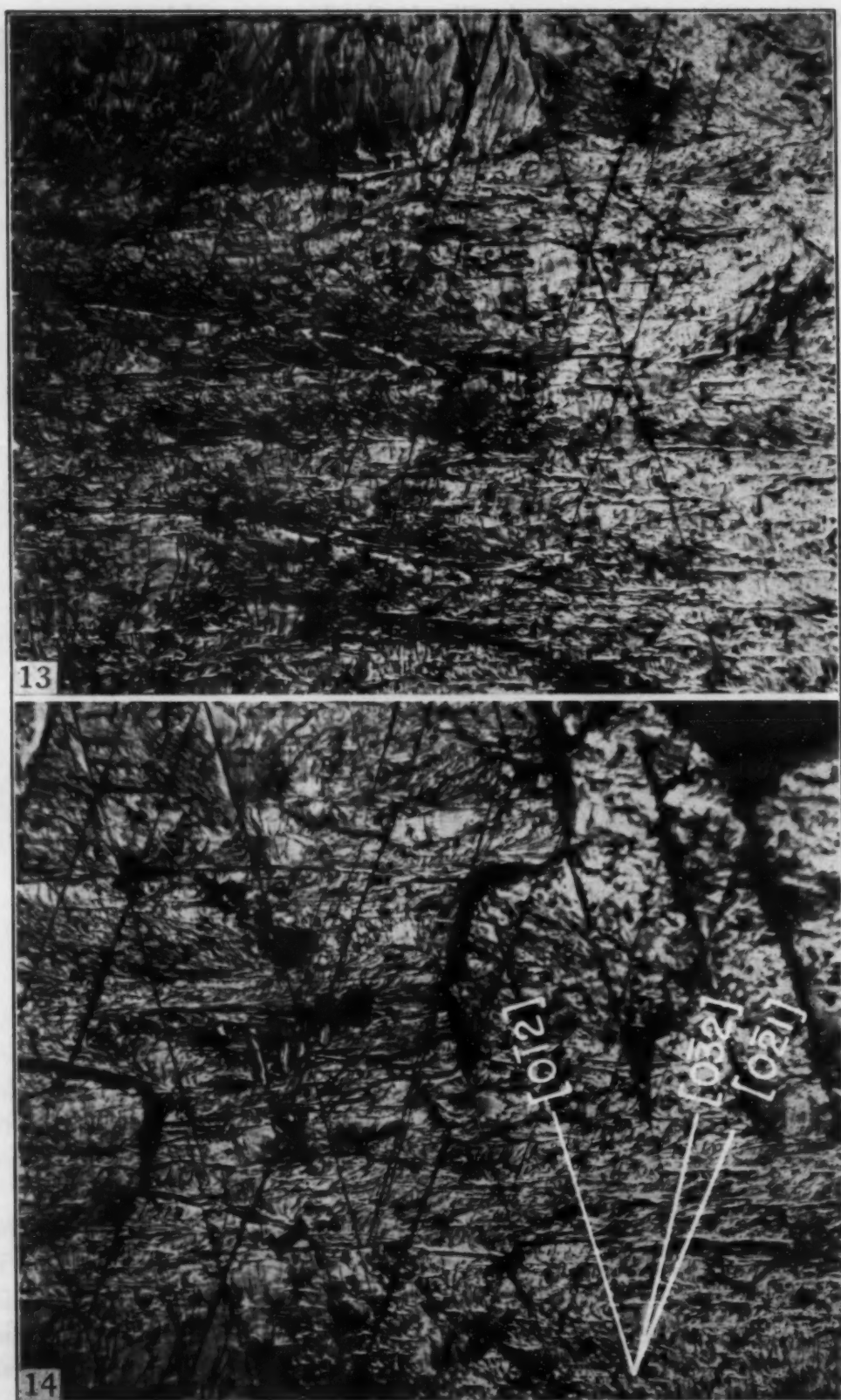


Fig. 12—A Fiber Pattern Which Will Account for Diffraction Data Presented in Figs. 8 to 11.

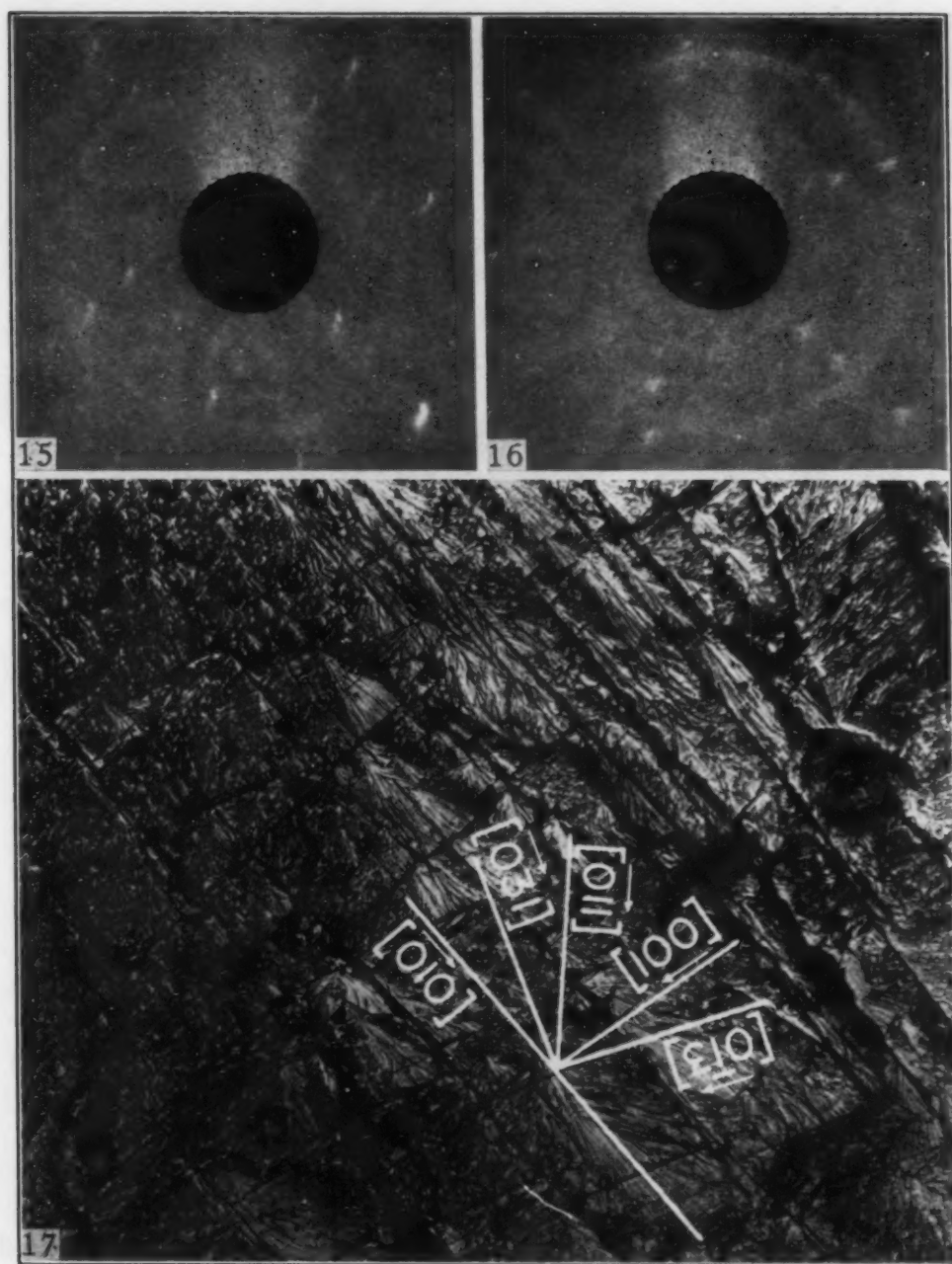
experimental conditions for Laue diffraction for the respective exposures have remained nearly constant. It appears then that the disturbed metal is not present as a uniform layer at the fracture surface. In a further analysis of this effect, the fractographs of the surface are examined (Figs. 13 and 14).

The probable direction of crack propagation is indicated by the arrow. The structure of interest in relation to the X-ray data is the laminated structure evident throughout the fractographs but in particular in the lower left-hand corner of Fig. 13. The grain seemingly has been laminated in the path of the fracture and these laminations have been pulled apart and broken across in the process of the fracture propagation.



Figs. 13 and 14—Fractographs  $\times 250$ , Specimen No. 1 With Indicated Trace Directions. Crack propagation  $\rightarrow$ .



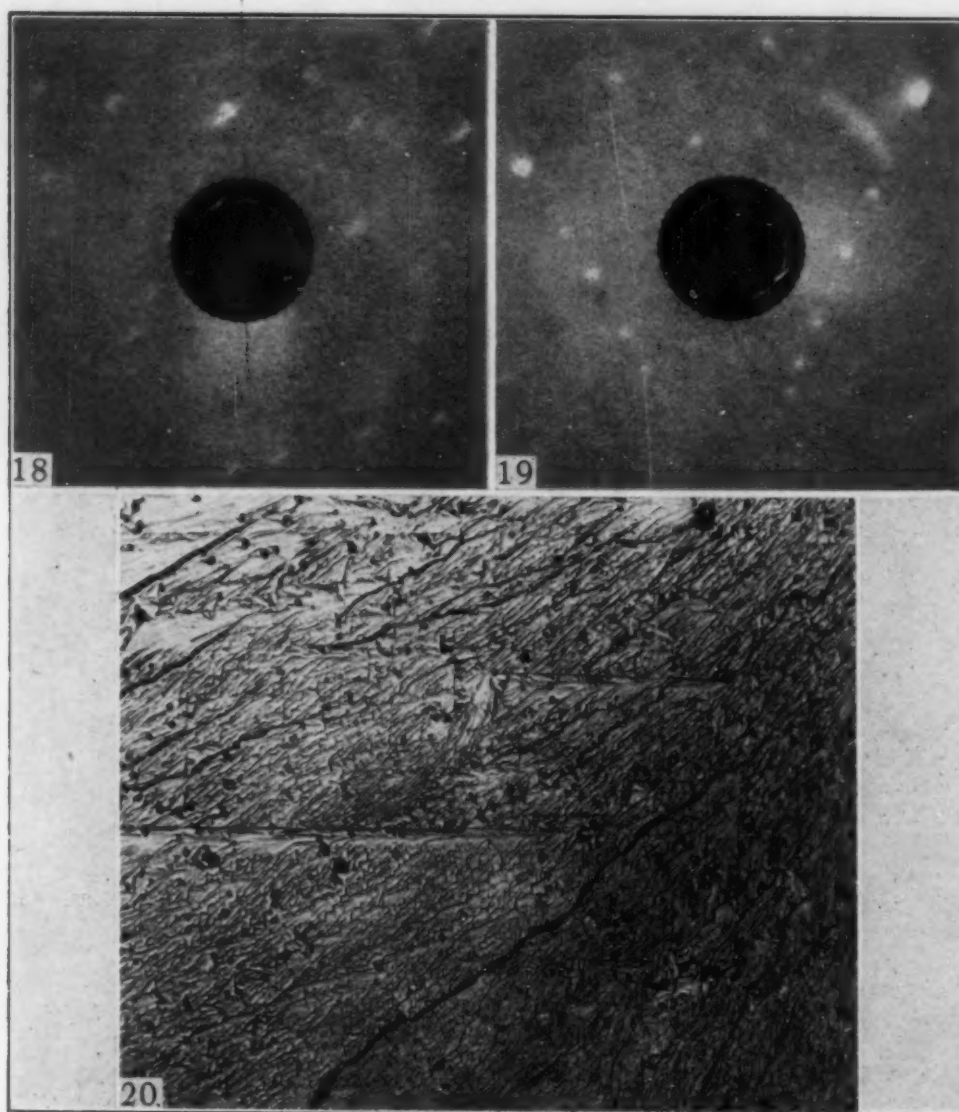


Figs. 15 and 16—X-Ray Diffraction Patterns, Specimen No. 2. Fig. 15—Orientation 1, Fig. 7; Fig. 16—Orientation 4, Fig. 7.

Fig. 17—Fractograph  $\times 250$ , Specimen No. 2 With Indicated Trace Directions.

Before this phenomenon is considered further, the X-ray and fractographic data for the remaining specimens are presented.

*Specimen No. 2*—This specimen was broken in impact bending at  $-70^{\circ}\text{C}$ . A preliminary survey had indicated that a specimen tested in tension impact at this temperature did not reveal cleavage surface alterations as indicated by the presence of the Debye-Scherrer

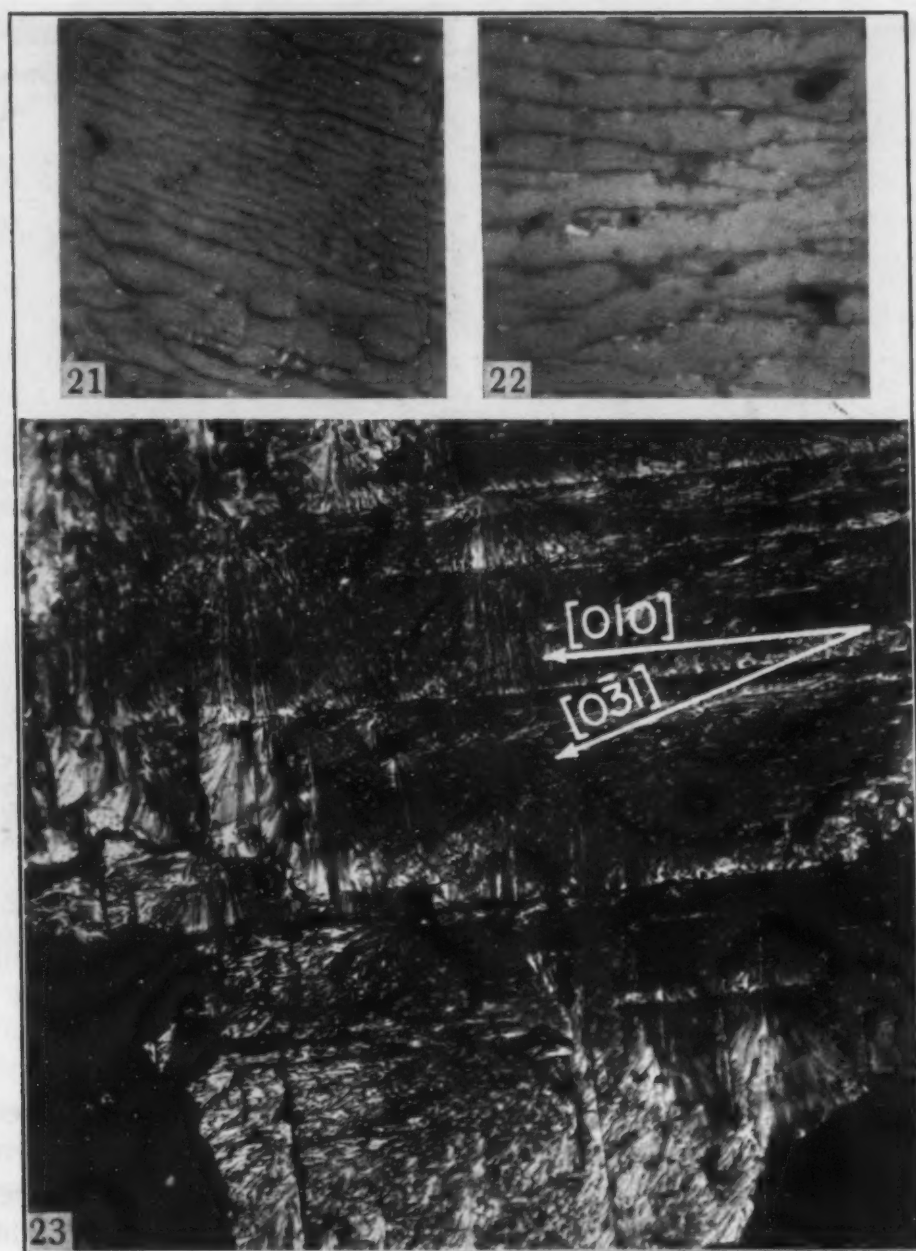


Figs. 18 and 19—X-Ray Diffraction Patterns, Specimen No. 3. Fig. 18—Orientation 1, Fig. 7; Fig. 19—Orientation 4, Fig. 7.  
Fig. 20—Fractograph  $\times 250$ , Specimen No. 3.

ring in the X-ray diffraction pattern. In the X-ray pattern obtained for the impact bend specimen for an incident X-ray beam normal to the cleavage surface (Fig. 15), the traces of the Debye-Scherrer ring are so faint that they do not show up in the reproduction of the pattern. By a rotation such that the incident beam is nearly parallel to the  $(1\bar{1}1)$  plane of the crystal, the Debye-Scherrer ring is observed (Fig. 16). This is also true after a rotation of about 20 degrees in the  $[0\bar{1}2]$ .

The fractograph of this specimen is shown in Fig. 17.

*Specimen No. 3*—The tension impact test at  $-70^\circ\text{C}$  was repeated. The two X-ray patterns obtained are reproduced in Figs.



Figs. 21 and 22—Electron Fractographs, Specimen No. 4. Approximately  $\times 5000$ .

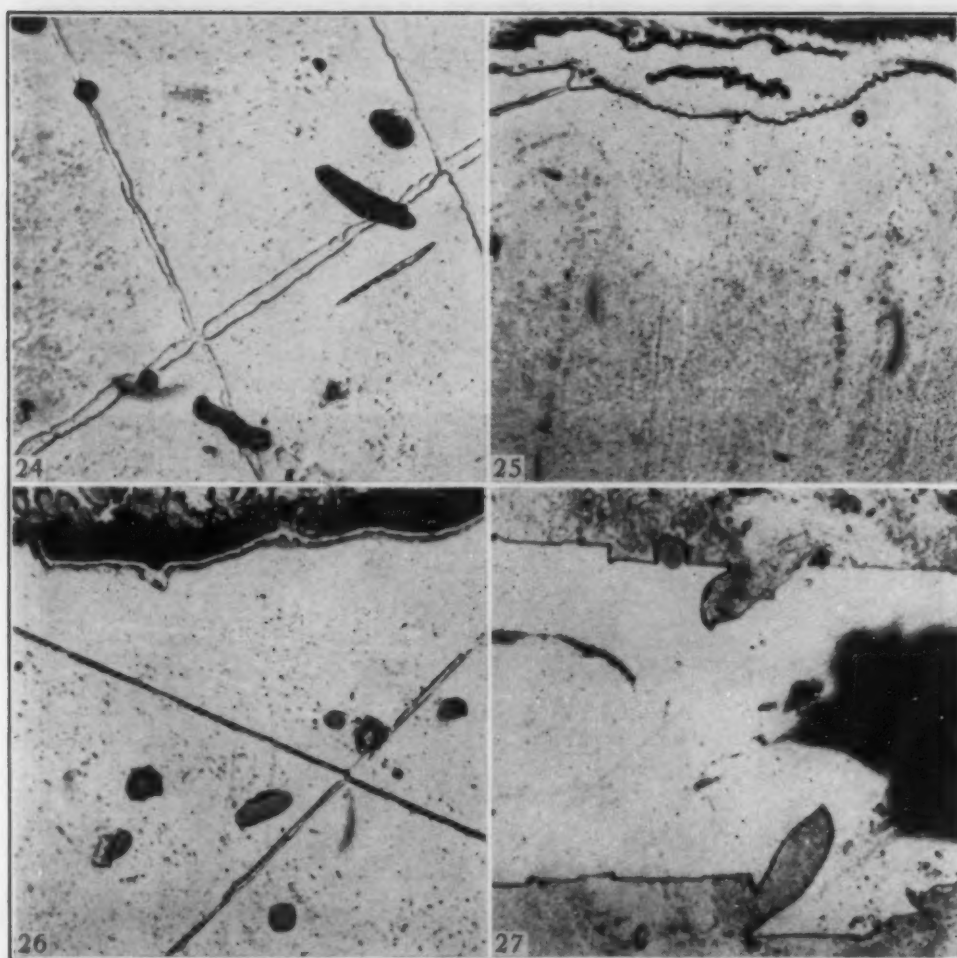
Fig. 23—Fractograph  $\times 250$ , Specimen No. 4.

18 and 19. In Fig. 18 a faint Debye-Scherrer ring is observed. There is little evidence of such a ring in Fig. 19.

The fractograph of this specimen is presented in Fig. 20.

*Specimen No. 4*—A repeat specimen was tested in tension impact at 25 °C. This specimen differed from Specimen No. A in that the fracture surface was tilted at about 60 degrees to the axis of the specimen, while the fracture in Specimen A was normal to the axis of the specimen. Both fractures were cleavage fractures.



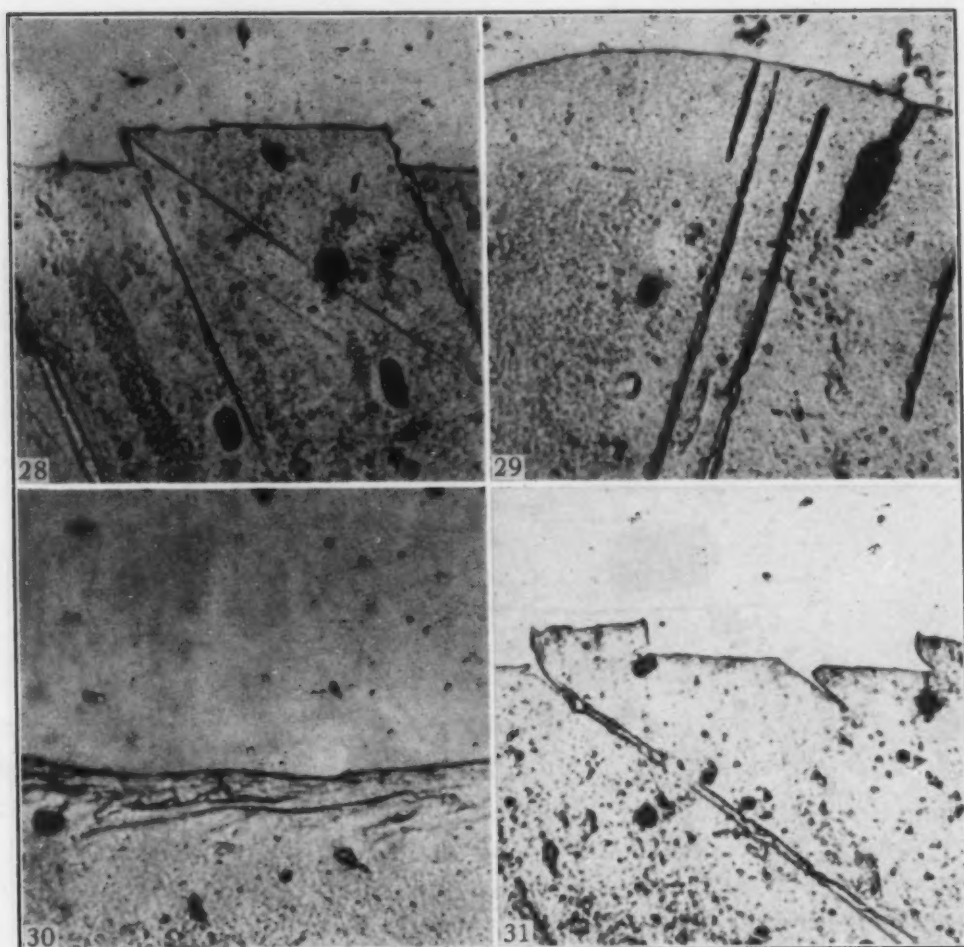


Figs. 24 to 27—Structures Revealed on Micrographic Sections Normal to the Fracture Plane.  $\times 1000$ . Figs. 24 to 26—Specimen No. 1; Fig. 27—Specimen No. 2.

The X-ray patterns obtained for Specimen No. 4 were in general agreement with the patterns obtained for Specimen No. A, with a difference, however, in the intensity of the Debye-Scherrer rings. For Specimen No. 4 the Debye-Scherrer rings were so faint that no effort has been made to reproduce them. It is evident from this that the volume of strained metal present at the cleavage surface may be subject to wide variations, especially if the conditions of fracturing are not highly controlled.

Electron and regular fractographs of Specimen No. 4 are shown in Figs. 21 to 23.

To obtain further information on the character of the cleavage surfaces, metallographic sections normal to the cleavage facets were prepared. Pertinent photomicrographs obtained from Specimen No. 1 are shown in Figs. 24 to 26. It is evident that the crack has not followed a well-defined crystallographic path across the

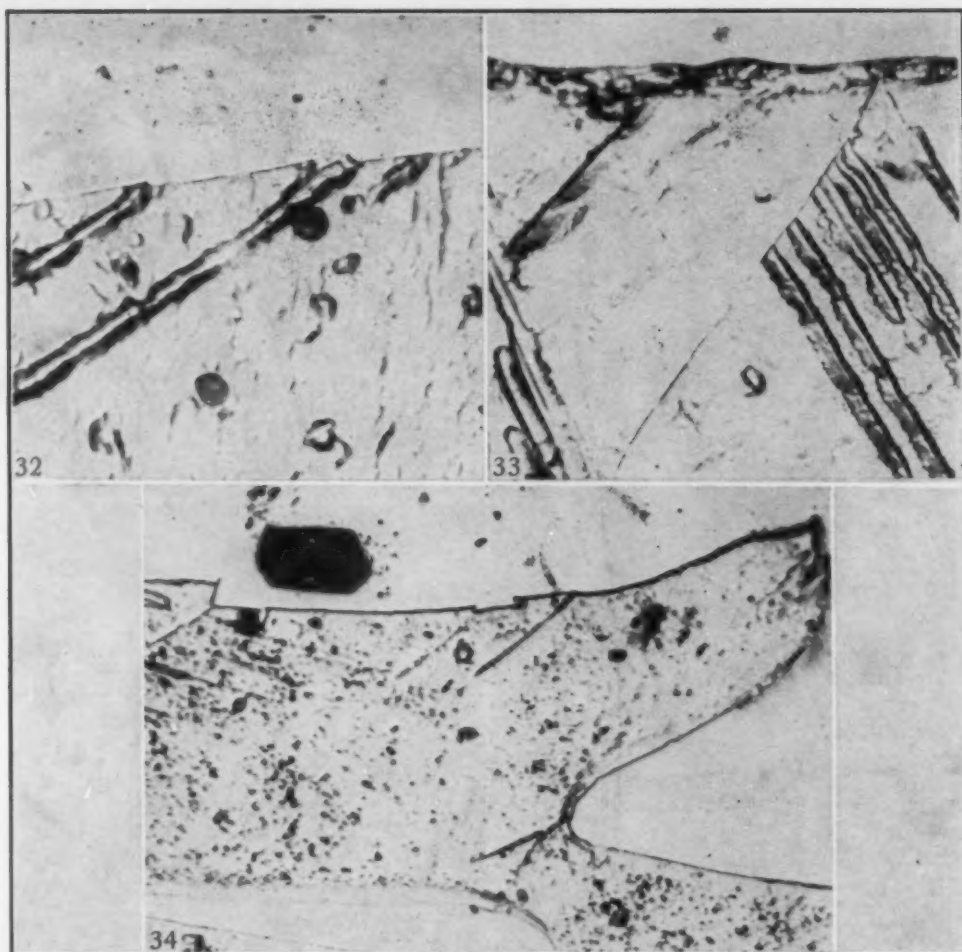


Figs. 28 to 31—Structures Revealed on Micrographic Sections Normal to the Fracture Plane.  $\times 1000$ . Specimen No. 2.

single grain. The crack surface was found to consist of a straight segment in only a few instances. The fracture surface for this specimen does not appear to be truly laminated as postulated from an examination of the fractographs. It is true that a serrated effect is revealed in Fig. 25, but this is a minor surface effect compared to the irregularities developed on a large scale.

On occasion a laminated fracturing effect under suitable testing conditions is observable, as is indicated in Figs. 27 and 34, and to a lesser degree in Fig. 31. However, strained metal is regularly present at the fracture surface as indicated in Figs. 30 and 33, in which the zones of the plastically strained metal are clearly revealed. This zone of plastically strained metal is highly restricted, however, being of the order of 0.005 mm thick.<sup>2</sup> The depth of distortion arising in the formation of laminations (Fig. 34) may extend to appreciably greater depths.

<sup>2</sup>An X-ray micrograph of a similar structure has been reported by Barrett (8).



Figs. 32 to 34—Structures Revealed on Micrographic Sections Normal to the Fracture Plane.  $\times 1000$ . Figs. 32 and 33—Specimen No. 3; Fig. 34—Specimen No. 4.

#### DISCUSSION OF RESULTS

An analysis of the X-ray data is assisted by a consideration of Figs. 35 and 36.<sup>3</sup> Fig. 35 represents an idealized laminated fracture surface, while Fig. 36 is a simulation of the fracture edge presented in Fig. 26. By means of either of these constructions the data presented for the fracture specimens may be explained.

For Specimen No. 1 the pertinent construction is obviously that given in Fig. 36.

From a consideration of the fractographs for Specimen No. 1 (Figs. 13 and 14), it appears that the fibering produced in the fracturing process is sufficiently well developed that the fiber pattern indicated in Fig. 12 may be used satisfactorily. On the basis of these two constructions, four types of diffraction patterns become

<sup>3</sup>A similar construction is found in reference 4.



possible, in which (a) the Debye-Scherrer ring or (b) the Laue pattern is pronounced or (c) both are equally pronounced, or (d) both are suppressed.

A pattern in which both the Laue and Debye-Scherrer patterns are pronounced would be obtained if the incident beam is so oriented that the distorted and undistorted portions of the crystal are equally

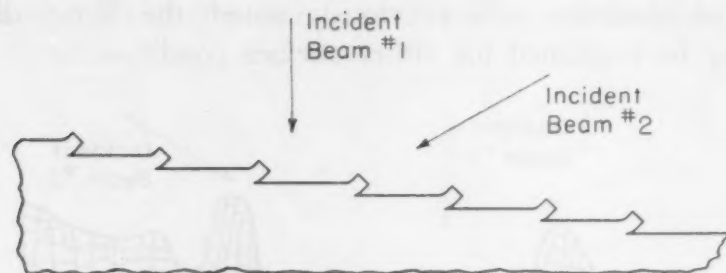


Fig. 35—Idealized Laminated Structure Showing Relationship Between Incident Beam Angle and Surface Irradiated.

irradiated, and the  $\{112\}$  reflection circle is in a zone of high expectancy on the fiber pattern (Fig. 36, incident beam 1) (cf. Fig. 8).

A pattern in which the Debye-Scherrer ring has been suppressed would result from an appropriate rotation in the plane perpendicular to the direction of crack propagation. This would serve to rotate the reflection circle into a zone in which the expectancy for  $\{112\}$  reflections is low. The rotation, however, would not change the surface of the specimen accessible to the continuous X-radiation, and so the Laue diagram would be obtained relatively unaltered in intensity (cf. Fig. 11).

The Laue diffraction spots could be suppressed, while the Debye-Scherrer ring remains unaltered by an appropriate rotation in the direction of the crack propagation or origin. Such a rotation would introduce a change in geometry (Fig. 36, incident beam No. 2) for the diffracting surface so that the unaltered crystal is no longer effectively irradiated. The  $\{112\}$  reflection circle, however, could be retained in a zone of high expectancy for  $\{112\}$  reflections and the Debye-Scherrer ring would be obtained (cf. Fig. 10). From this last orientation it is possible to rotate the crystal in such a way that the  $\{112\}$  reflection circle falls into a zone of low expectancy for  $\{112\}$  reflections, while the surface geometry of the crystal precludes the effective development of the Laue pattern. In this case no diffraction pattern would be obtained. Experimental verification of this last case is seemingly indicated in Fig. 9.

In an examination of Figs. 8 and 10 it will be noted that there exists an appreciable variation in the intensities of the respective Debye-Scherrer rings. This indicates that the restrictions on the locations of  $\{112\}$  reflections are greater than would be required for the existence of a fiber texture only.

From the photomicrographs, Figs. 27 and 30, it is indicated that the surface conditions in both Figs. 35 and 36 may be found in the same specimen. As previously noted, the X-ray diffraction effects may be explained for either surface condition.

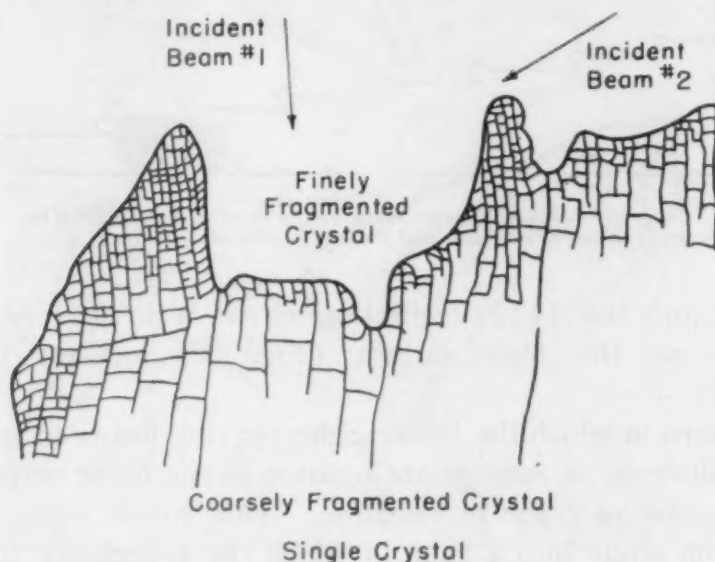


Fig. 36—Schematic Representation of Fragmented Crystal at Fracture Surface, Specimen No. 1. (Fracture edge in Fig. 26 simulated with ordinate expanded five times.)

*Cleavage Planes in Ferrite*—The cleavage planes in ferrite have been determined as of the family  $\{100\}$  (5). The results obtained here for X-ray analysis are in agreement with this conclusion. From the metallographic and fractographic evidence, however, it is apparent that the specimens have opened up on other planes than the  $\{100\}$ . It is desirable that the identity of these other planes of failure be determined.

The fractographic evidence of secondary cleavage is not in general unambiguous, but it is believed that the heavy slanting lines on the fractograph in Fig. 14 arise in large measure from such secondary cleavage. The directions of these and other crystallographically oriented lines in the  $(100)$  are indicated by the arrows at the side of the fractographs.

As indicated in Fig. 14, the secondary planes of failure cut the  $(100)$  in the  $\langle 012 \rangle$ . Important planes which cut the  $(100)$  in





*Slip Planes in Ferrite*—The slip planes known to operate in ferrite are of the  $\{110\}$ ,  $\{112\}$  and  $\{123\}$  (7). Each of these types of planes can cut the (100) in only a limited number of directions. Such traces are indicated in Fig. 37.

It is evident from this figure that when all traces of a given form are present, it is possible to identify positively the slip planes operating. If the traces of a given form are not all present, some ambiguity as to the identity of the operative slip plane may arise. Thus, planes of the form  $\{110\}$  and  $\{123\}$  have traces in common with  $\{112\}$  planes in the (100). However, traces of the form  $\langle 100 \rangle$  and  $\langle 032 \rangle$  and/or  $\langle 031 \rangle$  will positively identify slip planes of the forms  $\{110\}$  and  $\{123\}$ , respectively.

In an examination of the respective fractographs, it is evident that certain of the traces are unambiguously generated through the operation of the slip mechanism (Fig. 17). This is indicated by a lateral displacement of traces at intersection points. Such displacement has been positively identified in the fractographs of Specimens Nos. 1, 2, and 4. From these data it appears that slip in Specimen No. 1 has been certainly in planes of the  $\{123\}$  and probably in planes of the  $\{112\}$ . This conclusion is based on the fact that no traces of the  $\langle 011 \rangle$  have been observed while those of the  $\langle 031 \rangle$  and  $\langle 032 \rangle$  have been identified along with traces of the  $\langle 012 \rangle$ .

Slip plane traces<sup>4</sup> identified in Specimens Nos. 2 and 4 indicate that slip has taken place on the  $\{110\}$ ,  $\{112\}$  and  $\{123\}$ . Slip traces were not fully apparent on the fracture formed under tension impact at  $-70^\circ\text{C}$ .

#### SUMMARY AND CONCLUSIONS

1. It has been shown by X-ray analysis that in the generation of a cleavage fracture in ferrite, plastically deformed metal is obtained at the fracture surface for a variety of test conditions. This plastically strained metal may be present at the fracture surface in a finely serrated form or it may be present in the form of a fragmented layer of irregular thickness. The X-ray data may be accounted for by either surface structure.

2. The plastically strained metal at a cleavage surface may be fibered in the direction of crack propagation.

3. The fracturing process in ferrite is complex, and involves cleavages on the  $\{100\}$  and probably  $\{112\}$ . Possibly twin bands are important in a consideration of the fracture problem. In Fig.

<sup>4</sup>Ambiguity exists here between the  $\langle 011 \rangle$  and  $\langle 001 \rangle$ . It is evident, however, that traces of the  $\{110\}$ ,  $\{112\}$  and  $\{123\}$  exist on the cleavage surfaces of both Specimens Nos. 2 and 4.

29 a noncrystallographically oriented fracture surface is indicated which occurs seemingly in the absence of plastic strain. On a microscopic scale, the fracture surface is noncrystallographic in the presence of plastic strain.

4. Slip plane traces in the (100) indicate that slip at  $-190^{\circ}\text{C}$  for Specimen No. 1 has been certainly on the {123} and probably on the {112}. At the higher temperatures the {110}, {112} and {123} are active.

#### ACKNOWLEDGMENT

The author acknowledges indebtedness to the Office of Naval Research for sponsoring this research program, to Mr. J. Bryner for making the replica of the fracture surface for the electron fractograph, and to Miss L. Tarr for obtaining the normal fractographs.

#### References

1. C. A. Zapffe and M. Clogg, Jr., "Fractography—A New Tool for Metallurgical Research", *TRANSACTIONS, American Society for Metals*, Vol. 34, 1945, p. 71. This is an early work of Dr. Zapffe on fractures. Subsequent work from his laboratory may be found in *TRANSACTIONS, American Society for Metals*; *Transactions, American Institute of Mining and Metallurgical Engineers*, and in *METAL PROGRESS*.
2. E. P. Klier, D. E. Nulk and F. C. Wagner, "The Structure at a Cleavage Surface in Ferrite", Technical Note No. 110-E, AIME. (In press.)
3. C. R. Austin, "Effect of Elements in Solid Solution on Hardness and Response to Heat Treatment of Binary Alloys", *TRANSACTIONS, American Society for Metals*, Vol. 31, 1943, p. 321.
4. J. Bénard, P. Lacombe and T. Chaudron, "The Superficial Hardening of Aluminum and Iron by Abrasion. The Use of X-ray Reflections for the Study of Surface Conditions", *Comm. tech etats et proprietes surface metaux, Journees etats surface (Paris)*, October 1945, p. 73-81.
5. C. A. Edwards and L. B. Pfeil, "The Production of Large Crystals by Annealing Strained Iron", *Journal, Iron and Steel Institute*, Vol. 109, 1924, p. 129.
6. E. Schmidt and W. Boas, "Kristallplastizitat", Julius Springer, 1935.
7. C. S. Barrett, "The Structure of Metals", McGraw-Hill Book Company, 1943.
8. C. S. Barrett, Seminar—Naval Research Laboratory, Washington, D. C. cf. "A New Microscopy and Its Potentialities", *Transactions, American Institute of Mining and Metallurgical Engineers*, Vol. 161, 1945, p. 15.

#### DISCUSSION

**Written Discussion:** By W. H. Bruckner, associate professor, University of Illinois, Urbana, Ill.

Dr. Klier has presented convincing evidence in this paper of the existence of a deformation layer on the cleavage surface as indicated from the X-ray diffraction patterns before and after etching. The reader is, how-

ever, left in doubt as to the information obtainable from some of the micrographs shown. For example, in Fig. 31 a cleavage fracture is shown parallel and to the right of the Neumann band and this cleavage is considered by the author to be on the  $\{112\}$  plane. However, if the orientation of the particular grain of Fig. 31 were such as to make the polishing plane normal to a diagonal of the unit cube [a (111) pole] the trace of a cleavage fracture on (100) could be parallel or normal to the trace of the twin on the polishing plane. Whether this was the case or not for Fig. 31 could have been determined by producing etch pits in the polished section. A triangular etch pit would indicate that the polishing plane has cut across the corner of the cubic lattice. In every case under my observation, cleavages and mechanical twins were parallel only when the orientation of the lattice with respect to the polishing plane was such as to give triangular etch pits. More usually the etch pits had a square or other rectangular shape.

Fracture studies have been made<sup>5</sup> on polycrystalline material of relatively small grain size for which the etch pit method is the only feasible one for determining orientation. Nevertheless, it was possible to discover through metallographic evidence that cleavage and mechanical twinning are interrelated as suggested by Klier throughout his paper. Micrographs are presented in the discussor's paper which give proof that cleavage may be initiated in the twin deformed region and that the path of fracture causing failure may in fact be determined by regions of high twin density.

In closing I should like to ask whether the noncrystallographically oriented fracture shown in Fig. 29 could possibly be a separation at the ferrite grain boundary which frequently occurs in impure ferrite?

**Written Discussion:** By Carl A. Zapffe, consulting metallurgist, Baltimore, Md.

In the past several years an increasing number of investigators outside our own group have turned their attention to fractographic patterns, but this is the finest contribution yet coming to our attention.

Dr. Klier's photographs are splendid from both a photographic and a technical standpoint. He has in addition brought the important tool of X-ray diffraction to bear upon the problem, also the electron microscope.

We have studied the fractographic structures of iron and iron alloys, but only with the optical microscope. The last volume of *TRANSACTIONS* carries an article of ours on ingot iron, in which patterns are shown similar to those published by Dr. Klier. In more recent work, yet unpublished, we have carried the study from pure iron on through a wide range of alloying with other elements. Throughout these investigations, as Dr. Klier also observes, there is definite evidence of secondary cleavage in iron and ferrous alloys on the icositetrahedral family. Iron which is pure or only slightly alloyed with ferritizing elements, such as chromium and silicon, shows increasing activity on  $\{112\}$  as rheological changes set in favoring clastic rather than plastic activities. Neumann bands, to which the  $\{112\}$  movements usually refer, become increasingly evident as (a) fracture velocity increases, (b) temperature of fracture decreases, (c) alloying content increases. In a paper on Neumann bands given before

<sup>5</sup>W. H. Bruckner, "Micro-Mechanism of Fracture in the Tension-Impact Test", *Welding Journal*, Vol. 29, September 1950, p. 467s-476s.



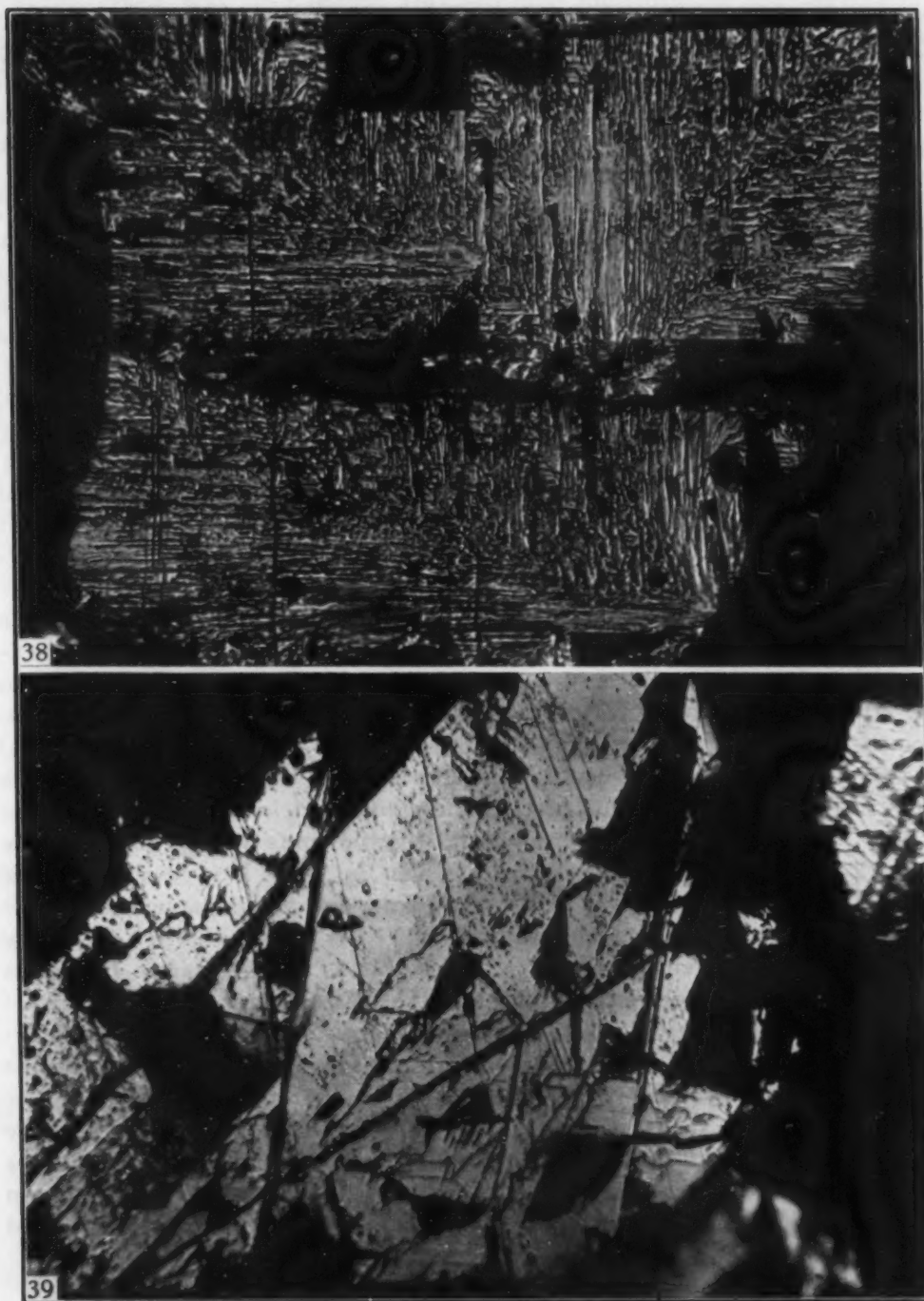


Fig. 38—Fractograph of 55% Chromium Ferrite, Showing the Typical Cubic Cleavage Predominating Throughout the Iron-Rich Side of the System. Specimen fractured at room temperature. Original  $\times 500$ , reduced  $\frac{1}{4}$ .

Fig. 39—Fractograph of 70% Ferrochromium, Disclosing Cleavage on (112). Specimen fractured at room temperature. Original  $\times 350$ , reduced  $\frac{1}{4}$ .

the British Iron and Steel Institute,<sup>6</sup> the long controversy regarding the nature of these markings was renewed, and evidence was given that the

<sup>6</sup>C. A. Zapffe, "Neumann Bands and the Planar-Pressure Theory of Hydrogen Embrittlement", *Journal, Iron and Steel Institute*, Vol. 154, No. 2, 1946, p. 123-130; disc., p. 130-131.

phenomenon is not strictly a twinning operation. A current paper by Tipper and Sullivan being given this week also confirms this. Apparently a great deal of strain is produced by the movements giving rise to  $\{112\}$  activity; and this may result in enforced twinning, also to weaknesses leading to what mineralogists have long called "parting", but which can be understood as secondary cleavage.

In the work with iron-chromium alloys, it has been found that  $\{100\}$  cleavage by far predominates throughout the iron-rich side of the diagram. This is true, for example, throughout the range of the ferritic stainless steels. Two fractographs are submitted here (Figs. 38 and 39) and Fig. 38 refers to a specially made alloy containing 55% chromium. The fracture pattern is obviously cubic, no angles registering other than 90 degrees. In Fig. 39, however, the chromium content has been raised to 70%, and now few if any cubic markings are present. Instead, the angles are exactly those which conform to  $\{112\}$  registrations upon a (112) fracture plane. This fractograph is representative of alloys containing chromium in amounts of 60% or more. Occasionally a cubic pattern is observed, but the angles still belong to the  $\{112\}$  family, both in facet and in intersecting registrations.

We have not yet specifically studied the iron-rich alloys for evidence of secondary icositetrahedral cleavage. However, there are many indications that it occasionally occurs. Some suspicion accordingly attaches to Dr. Klier's Fig. 14. Angles are prominent which are close to 30 degrees. Computations for registrations of  $\{123\}$  on either cubic or icositetrahedral cleavage faces have not yet been attempted; but we have tabulated the registrations for the various interrelationships which might occur among  $\{100\}$ ,  $\{110\}$ , and  $\{112\}$ . There are no relationships among any of these which can explain the angles shown in his Fig. 14. However, there are registrations of  $\{112\}$  on an icositetrahedral face which have the similar angle of  $30^\circ, 49' 31''$ . It is not clear from Dr. Klier's text whether his X-ray study of this specimen definitely identified this as a (001) face. He refers to Pfeil's work, which concerned only the obvious primary cleavage of iron. Of course, if the diffraction analysis identified this as a (001) cleavage, that is final; and the markings must then refer to combinations involving the  $\{123\}$  family.

Fractographic study of iron and its alloys will immediately convince anyone that a great amount of new information is presented on these facets, and information which will become considerably important in developing the understanding of the rheology and fractology of iron and steel.

#### Author's Reply

The problem of Neumann band formation has assumed a role of considerable importance in the discussion of our paper, and Professor Bruckner considers Neumann band formation to be connected intimately with the problem of cleavage failure. The work which we have presented can hardly be used for a suitable discussion of Neumann band formation, other than to indicate that the role of such bands in leading to cleavage failure must in general be a minor one. In the present instance, for example, the Neumann bands formed prior to the formation of the crack, and the

cleavage crack was propagated through the specimen to the Neumann band. However, it is certainly to be expected that the circumstances which lead to the formation of a Neumann band, as in the material and specimens studied by Professor Bruckner, may well lead to the formation of a crack in that Neumann band.

Professor Bruckner questions the trace orientations elicited from Fig. 31 and suggests that the plane of polish here is  $\{111\}$ . This inference is not correct and the plane of polish is close to  $\{100\}$ .

The noncrystallographic fracture in Fig. 29 is believed not to be a grain boundary.

In answer to Dr. Zapffe's question concerning trace identification in Fig. 14, it is indicated that this specimen failed in such a way that a cube corner was exposed. All measurements were made from appropriate edges of the cube face studied, so that there is no question that the traces are properly identified. Angular measurements have not been reported, as the crystal was distorted in breaking to such an extent that such measurements alone are not of value. It is necessary to consider as well the relative positions of the traces.



## FRACTOGRAPHIC REGISTRATIONS OF FATIGUE

By C. A. ZAPFFE AND C. O. WORDEN

### *Abstract*

*Fatigue fractures of 75S-T6 aluminum alloy, mild steel, and alloy steel are studied fractographically. Two distinctive patterns common to all specimens are found which characterize a condition of damage from fatigue stressing, one apparently representing a preliminary stage, and the second a final stage. The structures giving rise to the two patterns are referred to as platy and fine lamellar, respectively, and are found on the facets of subsequent impact fractures to extend for a distance into the parent metal corresponding to the stressed zone. Their relationships to cyclic count and to proximity to the zone of maximum stress are briefly examined. The patterns clearly display a subdivided or mosaic constitution of the grain, with a structural reorganization caused by fatigue.*

*Besides providing a new viewpoint for such phenomena as the known increase of damping with onset of fatigue, these patterns promise to reveal the fundamental nature of fatigue itself, and perhaps also to provide a metallographic technique by which the occurrence and even the stages of fatigue failures can be recognized. A tentative explanation for fatigue is offered on the basis of the recently announced micellar theory for the solid state.*

IN the course of an investigation of deformation and fracture phenomena using the fractographic microscope technique, attention was given several fatigue failures from commercial installations. Immediately there appeared a fractographic pattern type which was highly distinctive and which has not previously been observed.

To define this pattern at least tentatively and to relate it directly to the metallurgical phenomenon of fatigue, some typical ferrous and nonferrous specimens were subjected to fatigue testing in a laboratory machine, and the fractures were examined for characteristic patterns.

---

From research conducted in the laboratory of the senior author under partial sponsorship of the Office of Naval Research.

A paper presented before the Thirty-second Annual Convention of the Society, held in Chicago, October 21 to 27, 1950. The authors, C. A. Zapffe and C. O. Worden, are consulting metallurgists, Baltimore. Manuscript received April 13, 1950.

## MATERIALS

In Table I, nine fatigue specimens are described. They include 75S-T6 aluminum alloy, mild steel, and a low alloy steel. Each represents a specimen tested to destruction in a Sonntag constant-stress machine with completely reversed bending (mean stress  $S = 0$  and the ratio  $r = \frac{S_{\max.}}{S_{\min.}} = -1$ ). The resulting fatigue-fracture facets were studied first, and then certain other facets which will be described in the course of the discussion.

Table I  
Description of Specimens

Specimen	Material	Stress (psi)	Cycles	Remarks
A	75S-T6	45,000	18,000	Aluminum alloy, 0.188-inch sheet
B		35,000	119,000	
C		25,000	336,000	
D	SAE 1010	40,000	30,000	Plain carbon steel, annealed
E		40,000	31,000	
F		30,000	315,000	
G	SAE 4130	30,000	504,000	Low alloy steel, oil-quenched and drawn to Rockwell C-23
H		75,000	25,000	
I		45,000	2,074,000	

## FRACTURE PATTERNS

Fractographic study, to be particularly informative, usually requires specimens having facets which favorably expose the internal architecture of the grain; and it is common to produce optimum facets by some sort of impact fracture. Fatigue fractures may impose a special difficulty on fractography when they lack those expansive facets which are especially important to good photography. In addition, aluminum and its alloys inherently resist fractographic study because of a difficulty in obtaining any kind of fracture with readily viewable facets. The fractographs to be presented are therefore poor photographically, and must be examined rather carefully to disclose their details.

*Platy Structure*

In Table I, the first three specimens of the 75S-T6 aluminum alloy represent a range of fatigue stressing which varies about twenty-fold in number of cycles to failure, and changes correspondingly in the applied stress.

In Fig. 1, the upper fractograph conveys a proper general impression of the severely broken fields provided by this metal. The

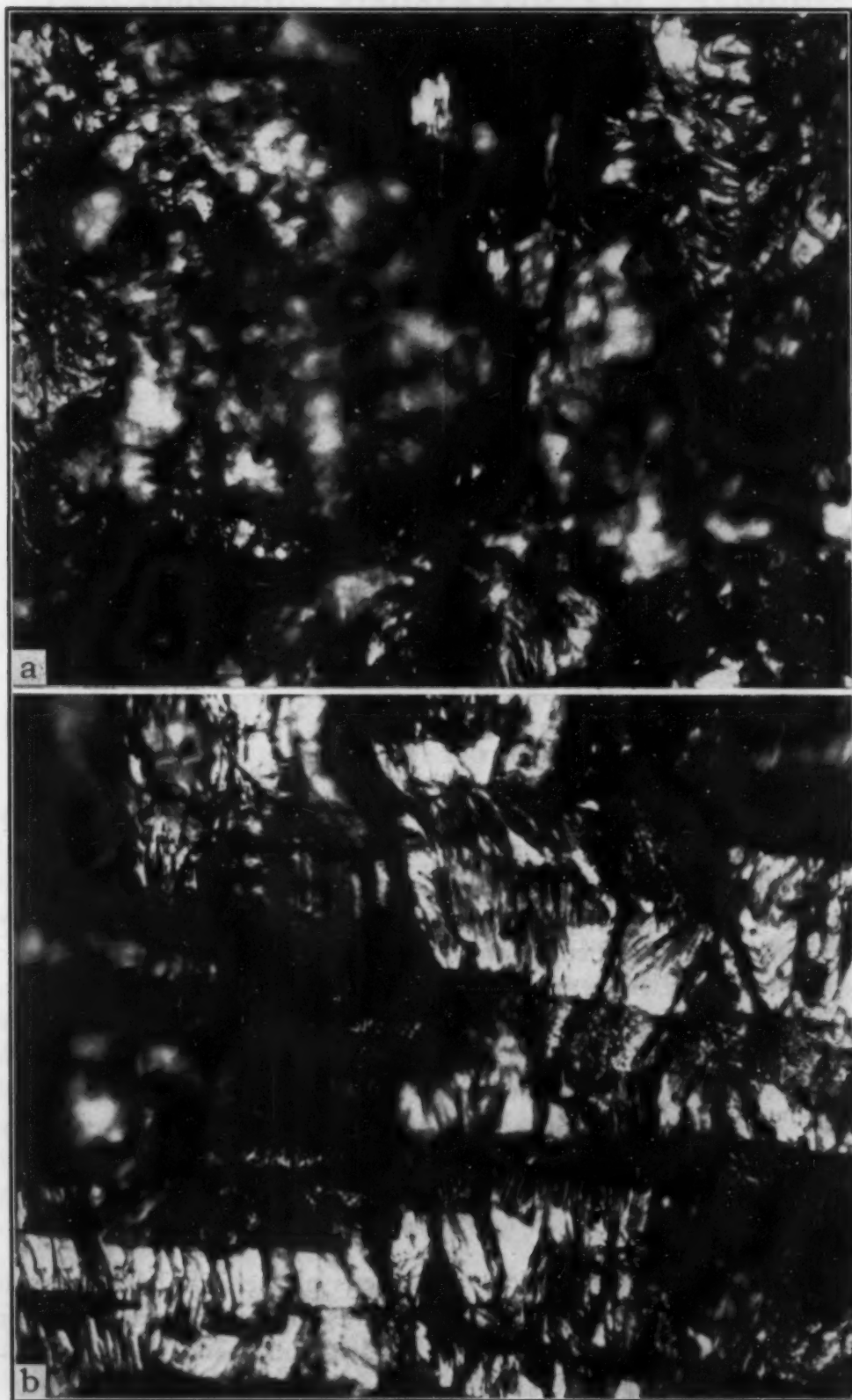


Fig. 1—Fractographs of Fatigue Fractures in 75S-T6 Aluminum Alloy, Showing Onset of Coarse Platy Pattern. (a) 18,000 cycles. (b) 336,000 cycles. Both fields  $\times 475$ .



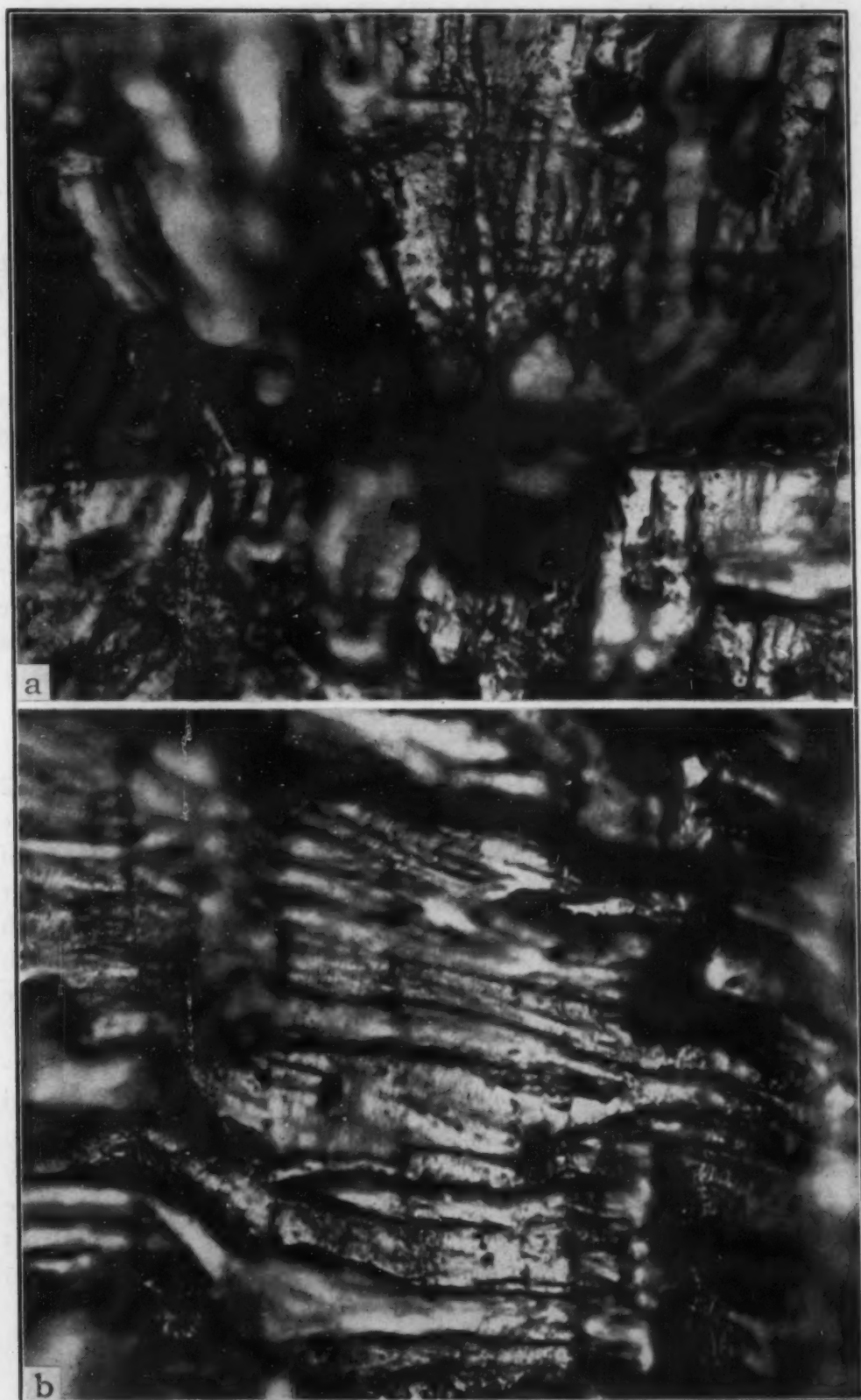


Fig. 2—Platy Pattern in Fatigue Fractures at Higher Magnification. (a) Specimen A at  $\times 850$ . (b) Specimen C at  $\times 1050$ .

specimen is A in Table I, which had the least number of cycles applied before fracture; and the field would be disregarded as uninformative if it were not for later patterns causing one's attention to return to the fact that a very slight columnar or platy effect is apparent as a vertical streaking in the fractograph.

In specimen B, which endured about 7 times as many cycles before rupture, this platy pattern becomes more strongly delineated; and in specimen C it is at a maximum for the series, in keeping with its maximum cyclic treatment. The lower fractograph in Fig. 1 displays the pronounced platy pattern in the fatigue fracture of specimen C.

At higher magnification, in Fig. 2, further fields are shown for these same two specimens—the end-members of their series; and here the platy effect is more clearly displayed in the fracture of A. Nevertheless, the broad comparison of the patterns for the two specimens is better given in the previous Fig. 1. The platy pattern in this Fig. 2, incidentally, is that which is horizontal in the upper fractograph and vertical in the lower, reversing the order of the previous figure. The transecting markings are believed to be of another origin, and they will be ignored in the present discussion.

#### *Lamellar Structure*

On very close examination of the lower fractograph in Fig. 2 (possibly not visible in the reproduction), an extremely fine-scale pattern appears. The two fractographs in Fig. 3, both taken of specimen C, show this structure to better advantage. The upper fractograph shows a small field, the lower a much larger field. Each is entirely subdivided by minute striae or lamellae. The fractograph in Fig. 4 taken at the limiting resolving power of the microscope shows the markings in more detail.

This *fine lamellar structure* seems clearly to be a fatigue phenomenon, suggesting a stage of minute structural ordering advanced beyond the grosser platy structure, and apparently favored by an increasing number of stress cycles. The lamellae are approximately parallel to the platy markings; and both sets of markings lie approximately in the bending plane perpendicular to the stress motion, as one would expect for a structural rearrangement due to this type of flexion.

#### *Fracture of Parent Metal*

If these platy and lamellar patterns are characteristic phenomena of fatigue-type stressing, fractographic study of the parent metal

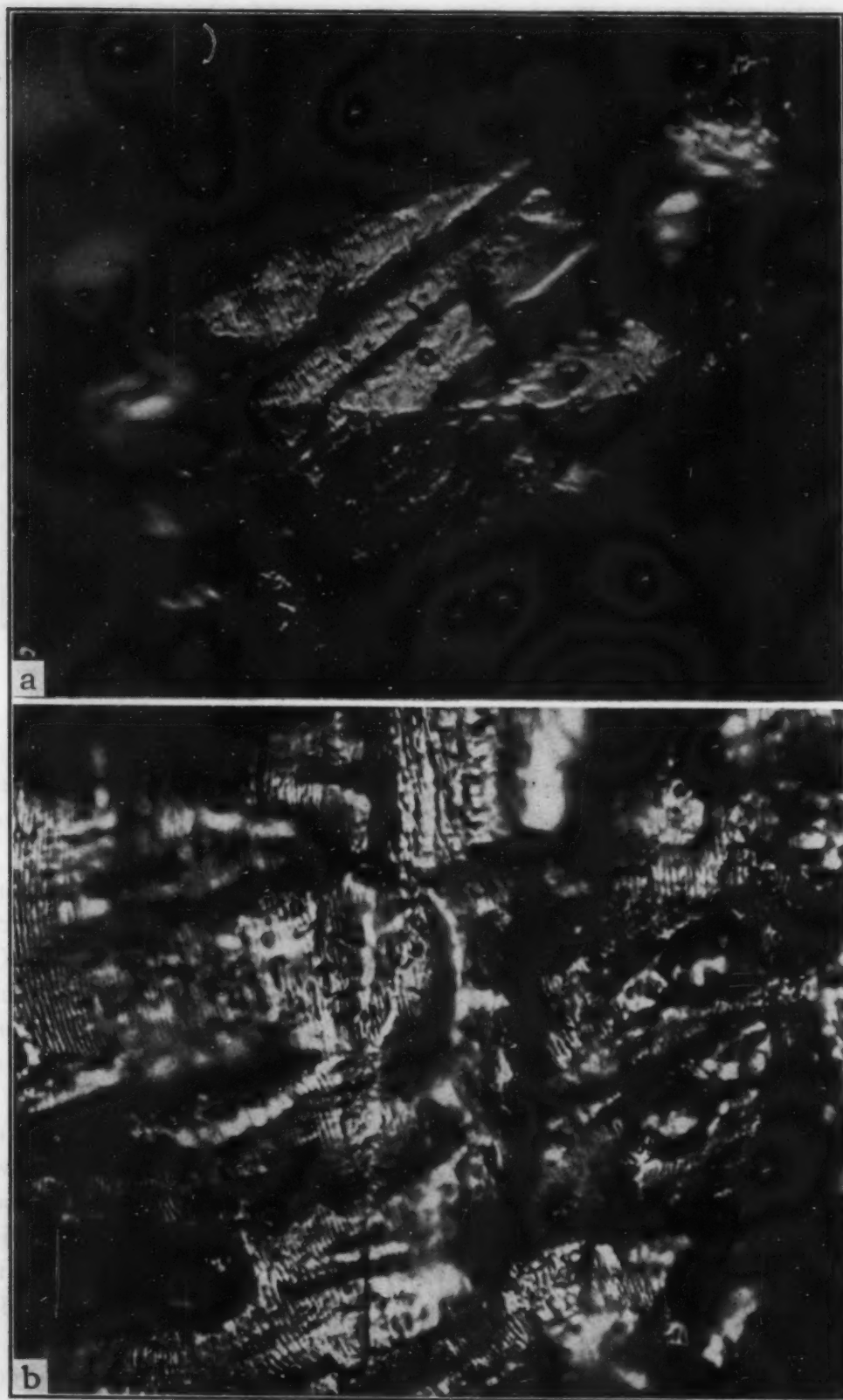


Fig. 3—Fine Lamellar Structure Composing Entire Fields in Specimen C. (a) Small field.  $\times 850$ . (b) Larger field.  $\times 1050$ .



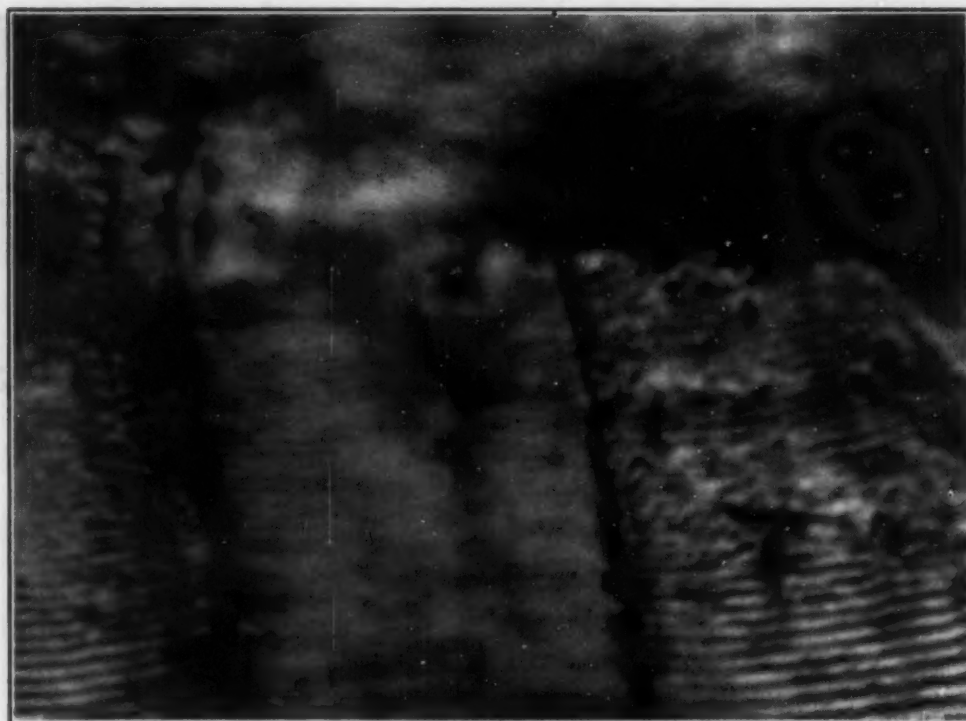


Fig. 4—Lamellar Fatigue Structure at High Magnification.  $\times 3400$ .

receding from the stressed zone back into the relatively unstressed metal should provide a needed comparison. These same specimens were therefore next broken in various directions by impact to expose the fracture pattern at significant locations.

In Fig. 5, two fractographs convey the essential information derived from a number of tests. The upper field shows an impact fracture face 0.25 inch back from the fatigue facet of specimen C and parallel to it. The platy feature is still much in evidence, but the fine lamellae are virtually absent. This confirms the opinion that the lamellae represent an advanced structural change, and a high level of damage.

In the lower fractograph there is shown the field of a second impact fracture made parallel again to the fatigue facet, but now 0.60 inch back into the parent metal. Virtually no trace is to be found of either the coarse or the fine fatigue registrations. This is a typical fractograph for the aluminum alloy in its normal condition, and the unattractiveness of the pattern from a photographic standpoint underscores the remark given in the introduction.

Fractures of specimen A made 0.25 inch back already showed a disappearance of both fatigue registrations, in keeping with the lesser cycles given this specimen and the general trend of the pre-

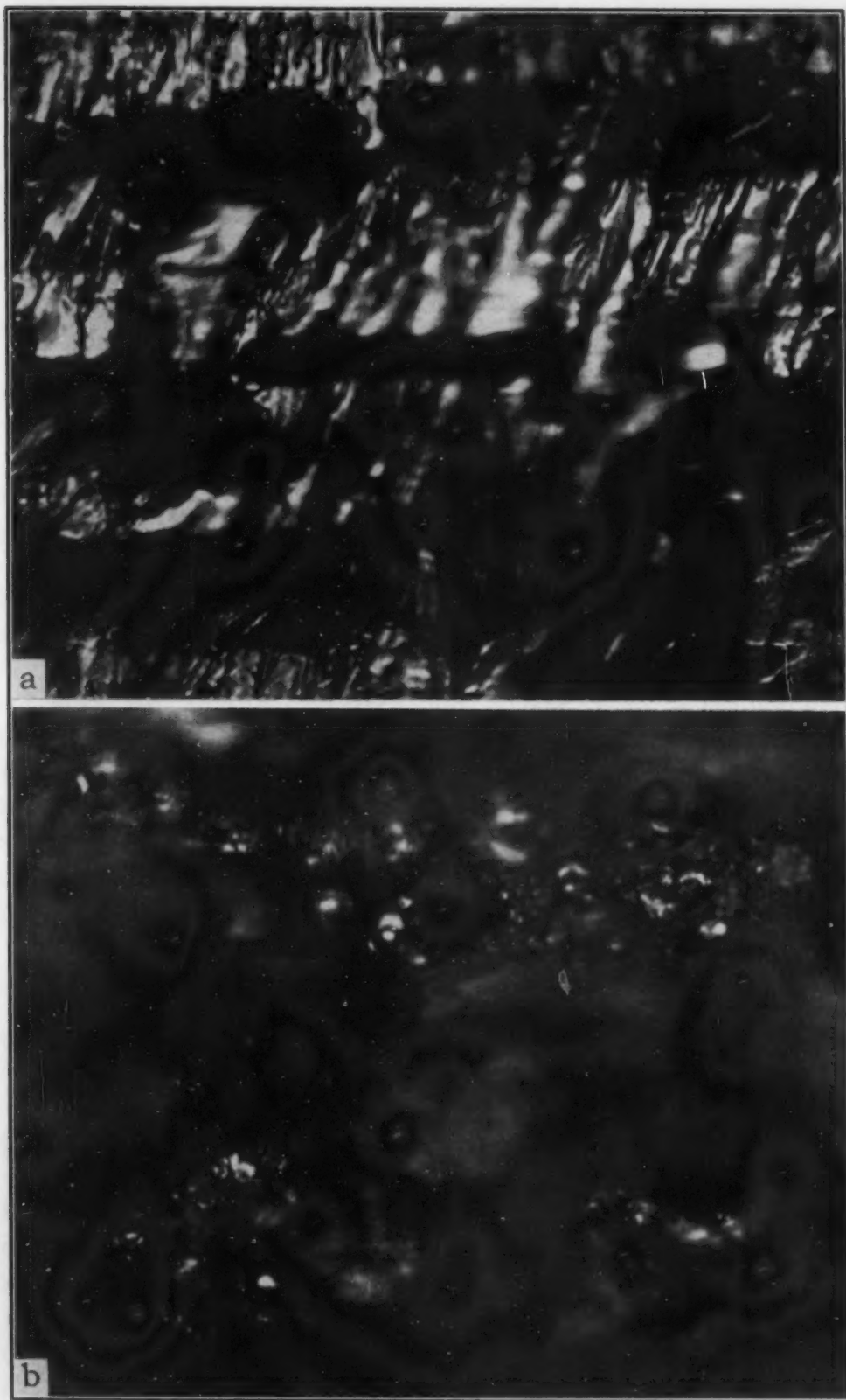


Fig. 5—Patterns of Impact Fractures in the Parent Metal of Specimen C Parallel to the Fatigue Facet. (a) 0.25 inch from surface. (b) 0.60 inch from surface. Both fields  $\times 850$ .

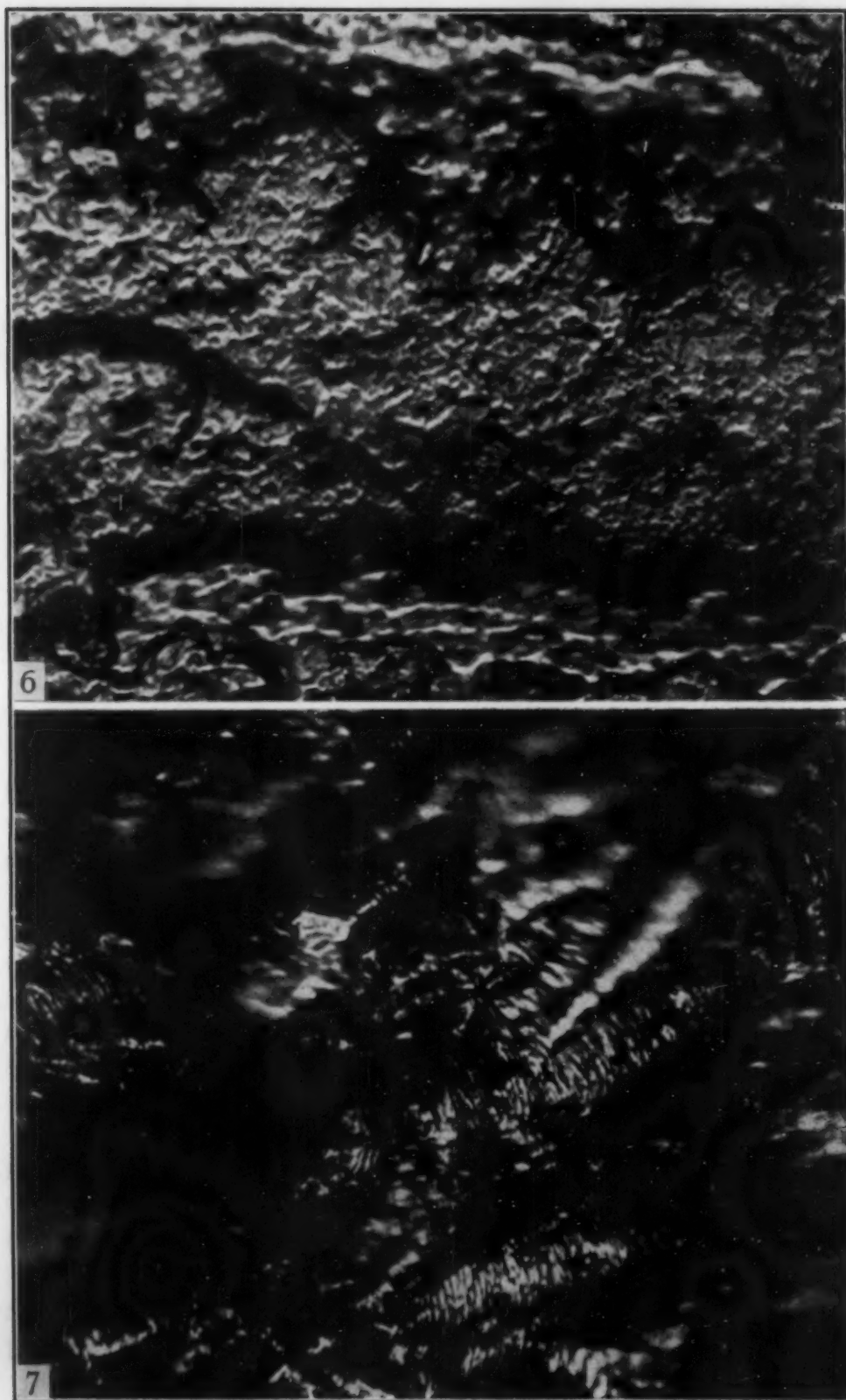


Fig. 6—Fracture Pattern Parallel to Platelets in 75S-T6 Alloy.  $\times 850$ .  
Fig. 7—Lamellar Fatigue Registrations in SAE 1010 Iron.  $\times 850$ .



ceding information. The pattern appeared exactly as in the lower fractograph of Fig. 5 and is therefore not reproduced.

As a somewhat exceptional instance, specimen C also happened to contain a small area of horizontal fracture (perpendicular to the fatigue facet and in the plane of the strip), thus providing an *inter-platelet* pattern, which is shown in Fig. 6. This can be understood as a separation of the individual plates in previous figures. Comparing it to the pattern in lower Fig. 5, which is quite typical of the original aluminum alloy fractured in any direction, one will readily note the pronounced micromechanical effect of the fatigue stressing in developing the layer-like pattern.

#### *Ferrous Materials*

Specimens D through I in Table I are ferrous materials, alloyed and unalloyed. While a great deal more work must be done before a satisfactory interpretation can be made of the fractographic fatigue patterns, one is immediately impressed that the general registrations of fatigue are common to steel and its alloys as well as to aluminum alloys. Fig. 7 displays an abundance of fine lamellar detail strictly analogous to that found in the previous Figs. 3 and 4. This is specimen No. 4, which received only 30,000 cycles, a minimum for the steel series. All other specimens showed more or less of this same distinctive pattern. Their fractographs are not reproduced because Fig. 7 typifies the group, and also because the alloy steels and those SAE 1010 specimens having greatly increased cyclic counts displayed such a comminution of facets that photography was particularly difficult.

#### DISCUSSION

These patterns are novel and striking, but they immediately carry any discussion into aspects of solid-state physics which are far from being understood today.

Accordingly, the authors shall only record here certain preliminary opinions which may be helpful, at least, in initiating further thought by other investigators. We regard the phenomena depicted in the fractographs as a demonstration of the subdivisive nature of the solid state presumed by numerous "mosaic" theories, and specifically postulated by the recently announced "micellar theory" (1).<sup>1</sup> The suggestive periodic spacing of the fine lamellae and the order of the lamellar thicknesses conform to the micellar theory; and the action of the fatigue stressing on the development of the lamellar formation is strictly in keeping with the micellar concept.

<sup>1</sup>The figures appearing in parentheses pertain to the references appended to this paper.

Whether the matrix begins with a micellar constitution or not, the obvious laminated form of the fatigue-stressed metal makes certain that the damaged state involves a subdivided constitution. This conforms with, and in turn probably explains, the known fact that damping strongly increases with fatigue stressing (2).

More importantly, it suggests a new approach for the explanation of fatigue failures, and in addition a possible metallographic means for identifying the occurrence and even the stages of such failures.

### CONCLUSION

From this preliminary study of fracture patterns in steels and aluminum alloy ruptured under conditions of fatigue stressing, the following conclusions can be drawn:

1. Fractographic study of fatigue facets immediately reveals characteristic patterns by which certain aspects of the failure can be identified;

2. Two of these patterns are pronounced in 75S-T6 aluminum alloy, and at least one of them is common to steel, and probably to ferrous and nonferrous alloys in general;

3. In 75S-T6 aluminum alloy, a coarse platy structure develops as a preliminary stage in fatigue damage;

4. A fine lamellar formation follows this as an advanced stage, and one which especially denotes a condition of fatigue damage in all metals studied;

5. These two fractographic patterns decrease in clarity along subsequent impact fracture surfaces extending from the fatigue facet back into the parent metal, disappearing entirely at some depth, depending largely upon the cyclic count of the test;

6. This displayed fact of a structurally subdivided and rearranged matrix (a) accounts for the effect of fatigue on damping capacity, (b) promises a new approach for explaining the puzzling metallurgical phenomenon of fatigue, and (c) provides a metallographic technique for identifying the occurrence and even the stages of such failures;

7. The periodic spacing of the fine lamellae, their thickness, and the whole matter of their appearance and development strongly suggest a micellar constitution for the solid state as recently postulated by the senior author.

### ACKNOWLEDGMENT

The Office of Naval Research sponsored this work in part; the fatigue testing was performed at the Glenn L. Martin Co. of Baltimore; and the samples were kindly provided this Laboratory by Mr. Paul W. Boone, metallurgist of that Company.

### References

1. C. A. Zapffe, "A New Theory for the Solid State", *TRANSACTIONS, American Society for Metals*, Vol. 42, 1950, p. 387.
2. A. Karius, E. Gerold and E. H. Schulz, "Changes in Material Under Fatigue Stress", *Archiv für das Eisenhüttenwesen*, Vol. 18, 1944, p. 113-124.

---

### DISCUSSION

**Written Discussion:** By Gilbert E. Doan, head, Department of Metallurgical Engineering, Lehigh University, Bethlehem, Pa.

Metallurgists come to rely on standard methods for investigating metallic structures—microscopic, radiographic, diffraction, visual fracture, etc. Fractography combines two of these: microscopy and fractures. As a body of knowledge is built up correlating fractographic appearances with compositions, treatments, and properties, relationships are certain to appear, and in particular cases fractographic examination will no doubt give superior results. The pioneering work in developing this body of knowledge comes from Dr. Zapffe's laboratory. The present case, showing a layer-like pattern accompanying fatigue, illustrates the promise of the method.



## THE STRESS-STRAIN ENERGY RELATIONSHIP FOR METALS

By D. J. McADAM, JR.

### *Abstract*

*Attention is confined almost entirely to oxygen-free copper, a metal that is practically free from structural changes other than those due solely to plastic strain.*

*The lower the temperature, the more rapid is the increase of intrinsic strength with strain. Diagrams show the influence of temperature on the stress-strain relationship for constant intrinsic strength and for constant total strain. The influence of temperature on the flow stress involves two factors: (a) a direct temperature effect; (b) the influence of temperature on the rate of increase of intrinsic strength with strain. The effects of these two factors on the flow stress should be expressed in terms of flow-stress ratios.*

*Diagrams show the influence of plastic strain on latent energy, and on the ratios of latent energy to total strain energy and work hardening energy. Other diagrams show how these energies vary with temperature. The fundamental stress-strain energy relationship is the influence of temperature on the rate of increase of latent energy with strain. The increase of latent energy with strain is a function of the strain, not of the total strain energy.*

IN a previous paper (5),<sup>1</sup> the author discussed the influence of temperature on the stress-strain energy relationship for copper and a nickel-copper alloy. The present paper presents a more general treatment of the subject, including a more thorough study of the influence of temperature and plastic strain on total energy and latent energy. Evidence is presented to show that prevalent views about the influence of plastic strain on latent energy are incorrect, and diagrams have been constructed to show the correct relationship between these two variables. A study is also made of the influence of temperature and plastic strain, and of the relationship between intrinsic strength and latent energy.

<sup>1</sup>The figures appearing in parentheses pertain to the references appended to this paper.

A paper presented before the Thirty-second Annual Convention of the Society, held in Chicago, October 21 to 27, 1950. The author, D. J. McAdam, Jr., is a consultant, Washington, D. C., formerly chief of section on thermal metallurgy, National Bureau of Standards. Manuscript received April 15, 1950.

Although attention is confined almost entirely to the properties of oxygen-free copper, it is believed that the information obtained is applicable to metals in general. For this purpose it is advantageous to use a metal, such as copper, that is practically free from structural changes other than those due solely to plastic strain. Another advantage in the use of copper is that the direct temperature effect on the flow stress is relatively small, as indicated by the slight effect of temperature on the yield stress.

#### INTRINSIC STRENGTH AS AFFECTED BY TEMPERATURE AND PLASTIC STRAIN

In general use, the word "strength" designates a property that varies with the temperature, as indicated by the variation of the flow stress and other strength indices. Intrinsic strength or strength state, however, is a property independent of temperature, provided that change in temperature causes no change in structure. As shown in a previous paper by the author (5), the lower the temperature, the more rapid is the increase of intrinsic strength with plastic strain. For a comparison of intrinsic strengths by means of flow stresses, therefore, the flow stresses must be determined at the same temperature.

The influence of temperature and plastic strain on the intrinsic strength of oxygen-free copper may be studied by means of the upper diagrams of Figs. 1 and 2. The lower diagrams show the influence of temperature and plastic strain on the strain energy. Strain is expressed in terms of  $A_0/A$ , in which  $A_0$  and  $A$  represent the initial and current areas of cross section. Since values of  $A_0/A$  are represented on a logarithmic scale, abscissas are proportional to true strains. Figs. 1 and 2 are based on data presented in papers by the author and previous associates (2, 3, 4). Attention will now be given to the upper diagrams.

Curves  $F_0$  in each figure represent continuous flow under unidirectional tensile stress. Beyond point M representing the beginning of local contraction, however, such a curve cannot be obtained by means of a single tension test, but must be established by indirect methods. These methods are illustrated in Figs. 9 and 10 of a paper by the author and associates (4), and are described in a previous paper by the author (5). By this method, this part of the  $F_0$  curve for room temperature has been established definitely, and the corresponding portions of the  $F_0$  curves for low temperatures have been established with sufficient accuracy for a study of the influence of temperature and plastic strain on intrinsic strength.

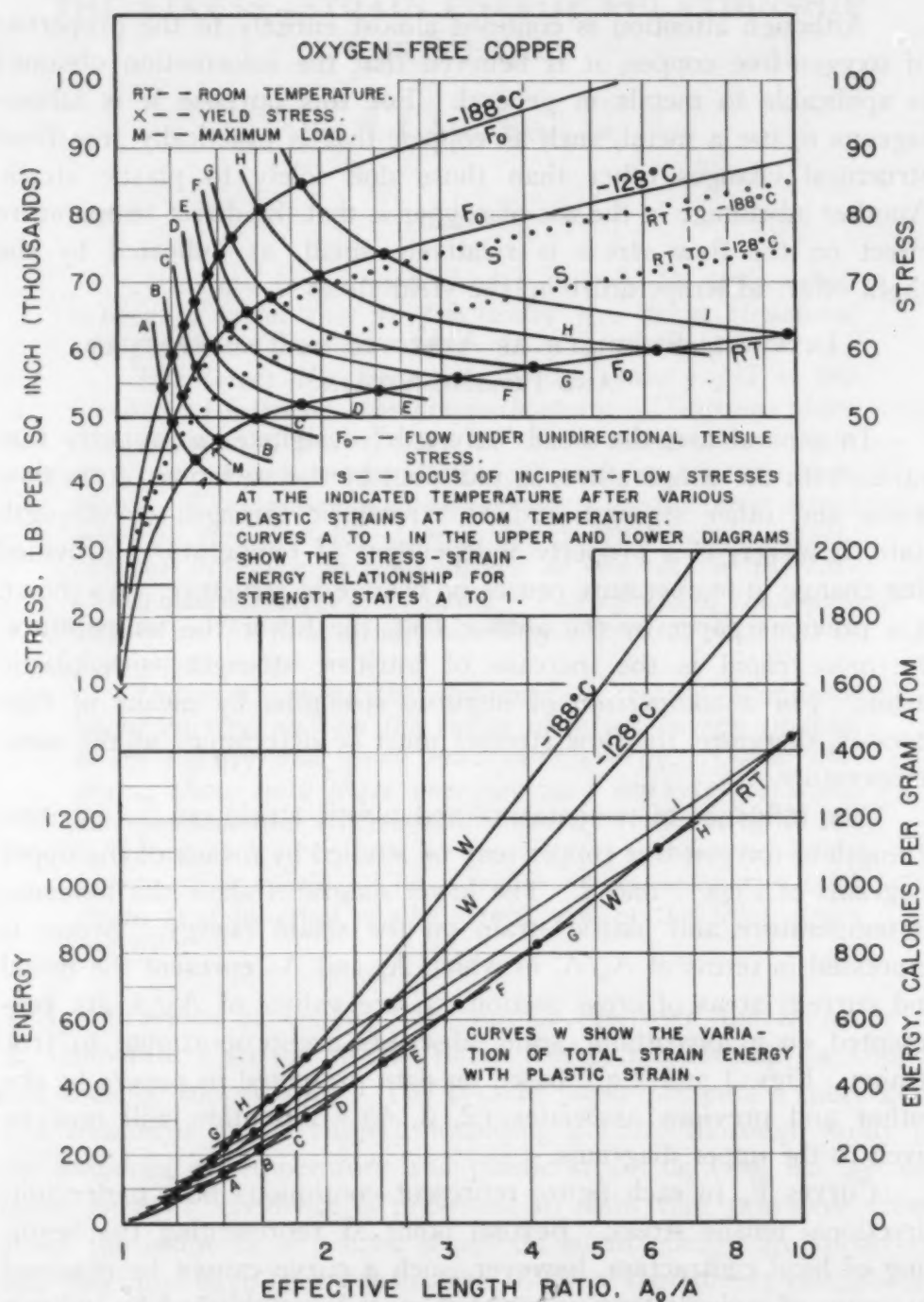


Fig. 1—Influence of Temperature and Plastic Strain on the Intrinsic Strength of Oxygen-Free Copper.

Curves S in Fig. 1 have been derived from the  $F_0$  curve for room temperature and from some points (not indicated) representing ultimate stresses of severely cold-rolled copper at the two low temperatures. The method of derivation is described in a previous paper (5). Each curve S represents the locus of incipient-flow stresses at



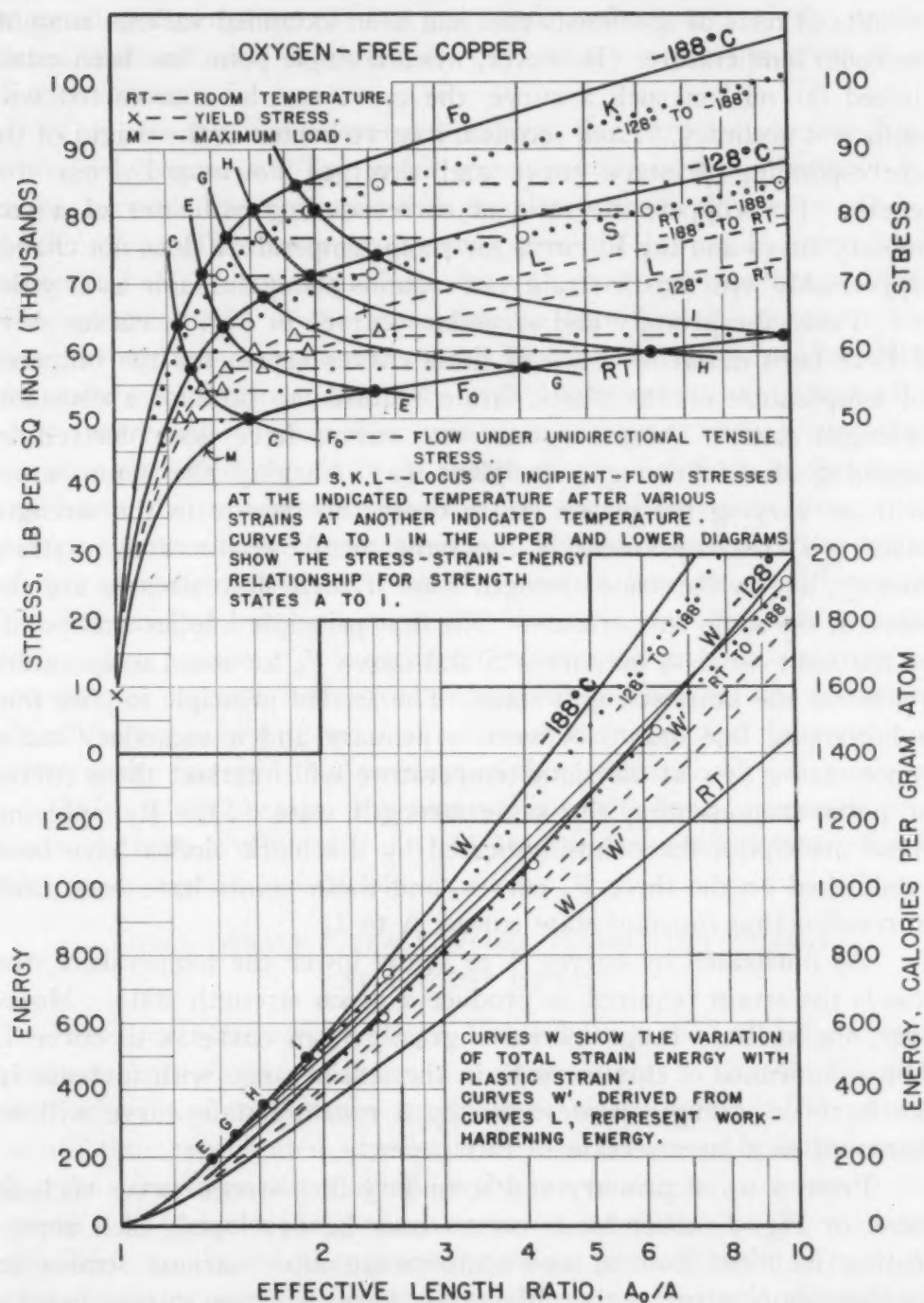


Fig. 2—Influence of Temperature and Plastic Strain on the Intrinsic Strength of Oxygen-Free Copper.

the indicated low temperature after various plastic strains at room temperature. Such curves, although they do not represent continuous flow, have been termed "secondary flow-stress curves" to distinguish them from the primary curves from which they are derived. For accurate determination, a secondary curve should be based on

results of tests of specimens that had been extended various amounts at room temperature. However, when a single point has been established far out on such a curve, the curve can be constructed with sufficient accuracy. Each secondary curve begins at the origin of the corresponding primary curve and diverges downward from that curve. For copper, the ratio of corresponding ordinates of a secondary curve and the  $F_0$  curve for room temperature does not change appreciably with plastic strain, but remains about the same as at yield.

From the primary and secondary curves in Fig. 1, curves A to I have been derived. Each of these curves represents the influence of temperature on the plastic strain required to produce a constant-strength state. These constant-state curves have been derived by applying the following principles: (a) Varying the temperature without varying the plastic strain causes no change in the strength state; (b) two specimens of the same metal, whatever their strain history, are in the same strength state if their flow stresses are the same at the same temperature. The first principle implies that points at the same abscissa on curves S and curve  $F_0$  for room temperature represent the same strength state. The second principle implies that a horizontal line drawn between a primary and a secondary curve representing flow at the same temperature will intersect these curves at points representing the same strength state (5). By applying these principles, the points indicated by the black circles have been established on the three  $F_0$  curves, and these points have been used in constructing constant-state curves A to I.

As illustrated by curves A to I, the lower the temperature, the less is the strain required to produce a given strength state. Moreover, the abscissa range increases greatly from curve A to curve I. The significance of this increase in the strain range with increase in the intrinsic strength represented by a constant-state curve will be discussed in a later section of this paper.

From a set of primary and secondary flow-stress curves such as those in Fig. 1, other locus curves may be developed, each representing incipient flow at one temperature after various strains at another temperature, either higher or lower. These curves can be established in exact correlation with the primary and secondary curves, and extended throughout the strain range of the curves from which they are derived. Examples of such "tertiary" flow-stress curves are those designated K and L in Fig. 2. These curves are derived by a graphical method essentially the same as that used in establishing the constant-state curves. The procedure is indicated by the horizontal lines extending to the open circles and triangles.

A detailed description of this graphical method, and of the arithmetical method used in extending the tertiary curves, is given in a previous paper (5).

The primary, secondary and tertiary flow-stress curves in Fig. 2 are in two groups. The upper group comprises the uppermost  $F_0$  curve, curve K and curve S; this group represents flow at  $-188^\circ\text{C}$  ( $-306^\circ\text{F}$ ). The lower group comprises the lowest  $F_0$  curve and curves L; this group represents flow at room temperature. Ordinates of the curves at the same abscissa in either the upper or the lower group are proportional to the intrinsic strengths produced by the same total strain at the three different temperatures. Since the temperatures of primary flow were the same for both groups, the intrinsic strengths should be in the same proportion in each group, and hence the ordinates for each group should be in the same proportion. Intrinsic strengths, therefore, should be compared in terms of flow-stress ratios rather than in terms of flow-stress differences. The influence of temperature on the flow stress involves two factors: (a) a direct effect; (b) an effect of temperature on the rate of increase of intrinsic strength with strain. Each of these factors should be expressed in terms of a flow-stress ratio, and the combined effect of the factors is the product of these ratios.

With plastic strain, the intrinsic strength ratio increases continuously from a value of 1 at yield, but the direct temperature factor for copper remains practically constant.

#### TOTAL STRAIN ENERGY, WORK HARDENING ENERGY AND LATENT ENERGY

The lower diagrams in Figs. 1 and 2 show the influence of temperature and plastic strain on the strain energy. Curves W show the variation of total strain energy with plastic strain. The energy values thus represented are derived from the areas beneath curves  $F_0$ ; the areas were determined by the use of original unreduced diagrams (20 inches wide), which were on coordinate paper with fine subdivisions. In calculating energy values per unit volume from the areas, a factor was used to convert abscissas to natural strains, and other factors were used to determine the energy equivalent per unit area in calories per gram atom. Curves W' in Fig. 2 show the influence of plastic strain on work hardening energy. Just as the influence of temperature on the primary flow stress involves a direct temperature factor and an intrinsic strength factor, so the influence of temperature on the total strain energy involves corresponding factors. One of these factors is the energy corresponding to the



direct effect of temperature on the flow stress; the other factor is the influence of temperature on the work hardening energy, the energy remaining after allowance for the influence of the direct temperature factor. Curves  $W'$  thus are derived from the areas beneath curves  $L$  in the upper diagram of Fig. 2. Curves  $W'$  and the lowest curve  $W$  thus correspond to the previously discussed lower group of flow-stress curves in the upper diagram; the dotted curves and the uppermost curve  $W$  in the lower diagram correspond to the dotted curves and the uppermost curve  $F_0$  in the upper diagram. Corresponding ordinate ratios for either the upper or the lower group of curves in the lower diagram represent the influence of temperature on work hardening energy. The influence of temperature on work hardening energy, therefore, should be expressed in terms of energy ratios rather than energy differences.

Since the ordinate ratios for curves  $F_0$  increase with plastic strain, the ordinate ratios of the derived curves  $W$  also increase. However, the increase in the ordinate ratios is nearly completed within the range of strain between yield and maximum load; with additional strain, the ratios change very little. There is a similar variation in the ordinate ratios for curves  $W'$ . Throughout the strain range beyond the points representing the maximum load, the ordinate ratio for the curves representing flow at  $-188^\circ\text{C}$  ( $-306^\circ\text{F}$ ) and at room temperature is about 1.6 for curves  $W$  and about 1.2 for curves  $W'$ .

Curves  $A$  to  $I$  in the lower diagram of Fig. 1 are derived from the correspondingly designated curves in the upper diagram. The black circles on the curves in the lower diagram are directly below the corresponding circles in the upper diagram. Since each constant-state curve in the upper diagram represents the influence of temperature on the total strain required to produce a specific strength state, the corresponding curve in the lower diagram represents the influence of temperature on the total strain energy required to produce the same strength state. Moreover, since each of those curves in the lower diagram represents constant intrinsic strength, a reasonable assumption is that each curve also represents constant latent energy. By "latent energy" is meant the portion of the total energy that is not converted into heat, but is involved in the work hardening. On the assumption that each constant-state curve in the lower diagram represents constant latent energy, the course of each curve shows the influence of temperature on the latent energy ratio, the ratio of the latent energy  $E$  to the total energy  $W$ . The course of each curve thus indicates that  $E/W$  increases with decrease in the temperature

at which the metal flows. Moreover, a comparison of the curves in terms of ordinate ratios shows that the influence of temperature on  $E/W$  varies greatly with the intrinsic strength represented by a constant-state curve. For strength state I,  $E/W$  evidently is about three times as great for flow in liquid air as for flow at room temperature. For strength state A, however, the corresponding ratio of values of  $E/W$  is only about 1.6.

In the lower diagram of Fig. 2, each of the constant-state curves E to I represents the influence of temperature on the work hardening energy required to produce a constant amount of latent energy. Although such curves could be derived from curves  $W'$ , they would be too crowded for clear discernment. The constant-state curves in the lower diagram of Fig. 2, therefore, have been derived from the group comprising the uppermost curve W and the two dotted curves. Curves E to I in the lower diagram thus correspond to the horizontal dot-and-dash lines extending between the black circles and the open circles in the upper diagram. The course of each constant-state curve in the lower diagram, therefore, shows the influence of temperature on the ratio of the latent energy E to the work hardening energy  $W'$ . Comparison of curves E to I shows that the influence of temperature on the latent energy ratio  $E/W'$  varies with the intrinsic strength. For strength state I, the latent energy ratio is about 3.8 times as great when the flow is at  $-188^{\circ}\text{C}$  ( $-306^{\circ}\text{F}$ ) as when the flow is at room temperature; for strength state E, the corresponding ratio is about 3.2. For strength state A (not represented in Fig. 2), the corresponding ratio is not more than 2.

#### INFLUENCE OF PLASTIC STRAIN ON LATENT ENERGY AND ON THE LATENT ENERGY RATIO

The relation between the latent energy and the total strain energy at room temperature has been investigated by Farren and Taylor (7), Taylor and Quinney (8), and Rosenhain and Stott (6). In each of these investigations, the total strain energy and the evolved heat were determined directly, and the latent energy was determined by difference. Results obtained in these investigations have been assembled in Fig. 4. These results are indicated by the small circles, triangles and squares. The curves in the lower left diagram have been reproduced from Fig. 3, which is derived from the lower diagrams of Figs. 1 and 2.

In the investigation by Farren and Taylor (7) the specimens were strained by tension. For various stages during the straining, the increments of applied energy and latent energy were determined.

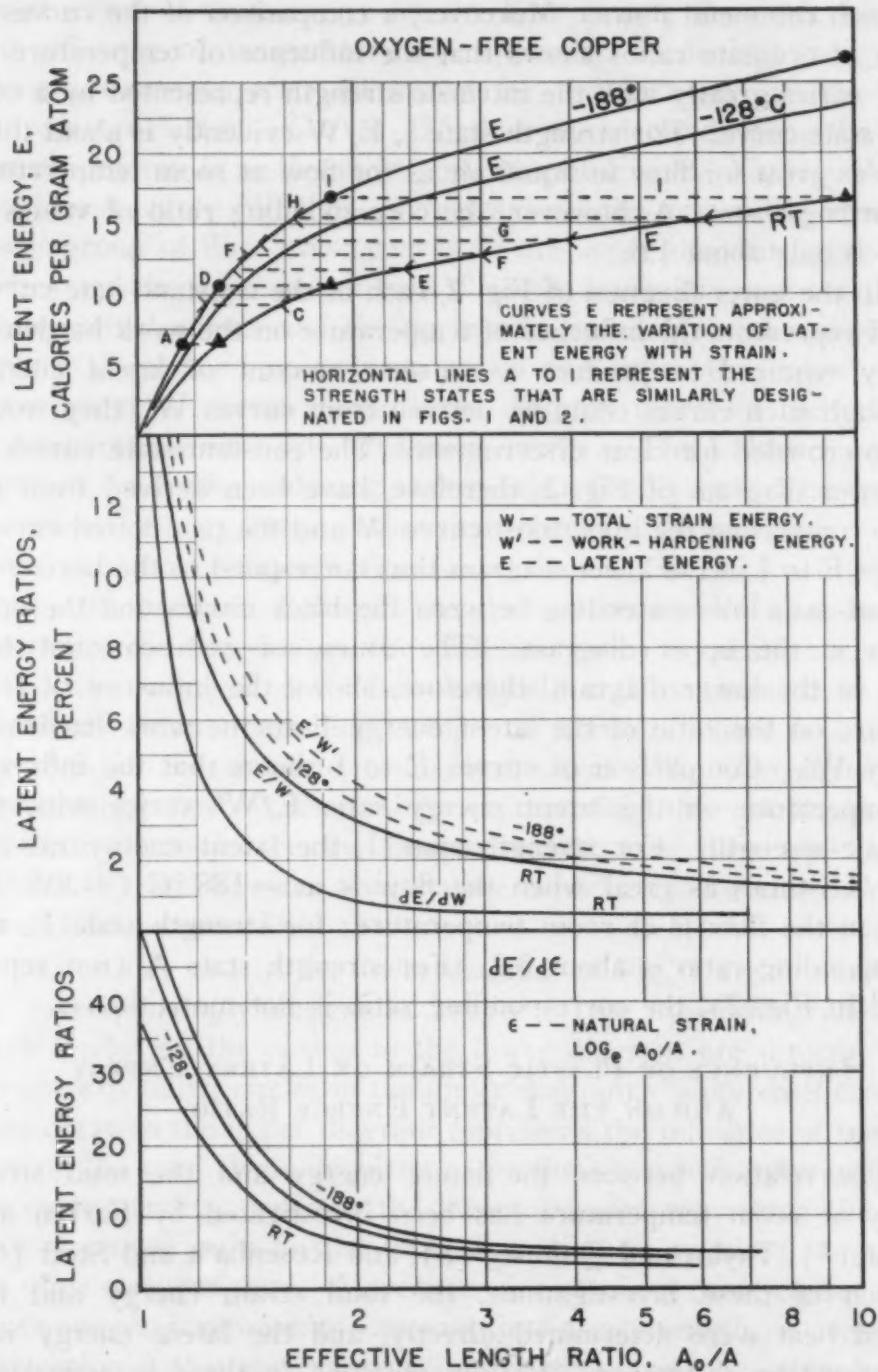


Fig. 3—Variation of Latent Energy With Strain on Oxygen-Free Copper.

The results for copper and aluminum are represented in the lower diagrams of Fig. 4. The evidence thus assembled suggests that  $dE/dW$  decreases with increase in plastic strain. Taylor and Quinney (8), however, regarded these results as inconclusive because of the wide scatter, and because of the relatively small strain at which



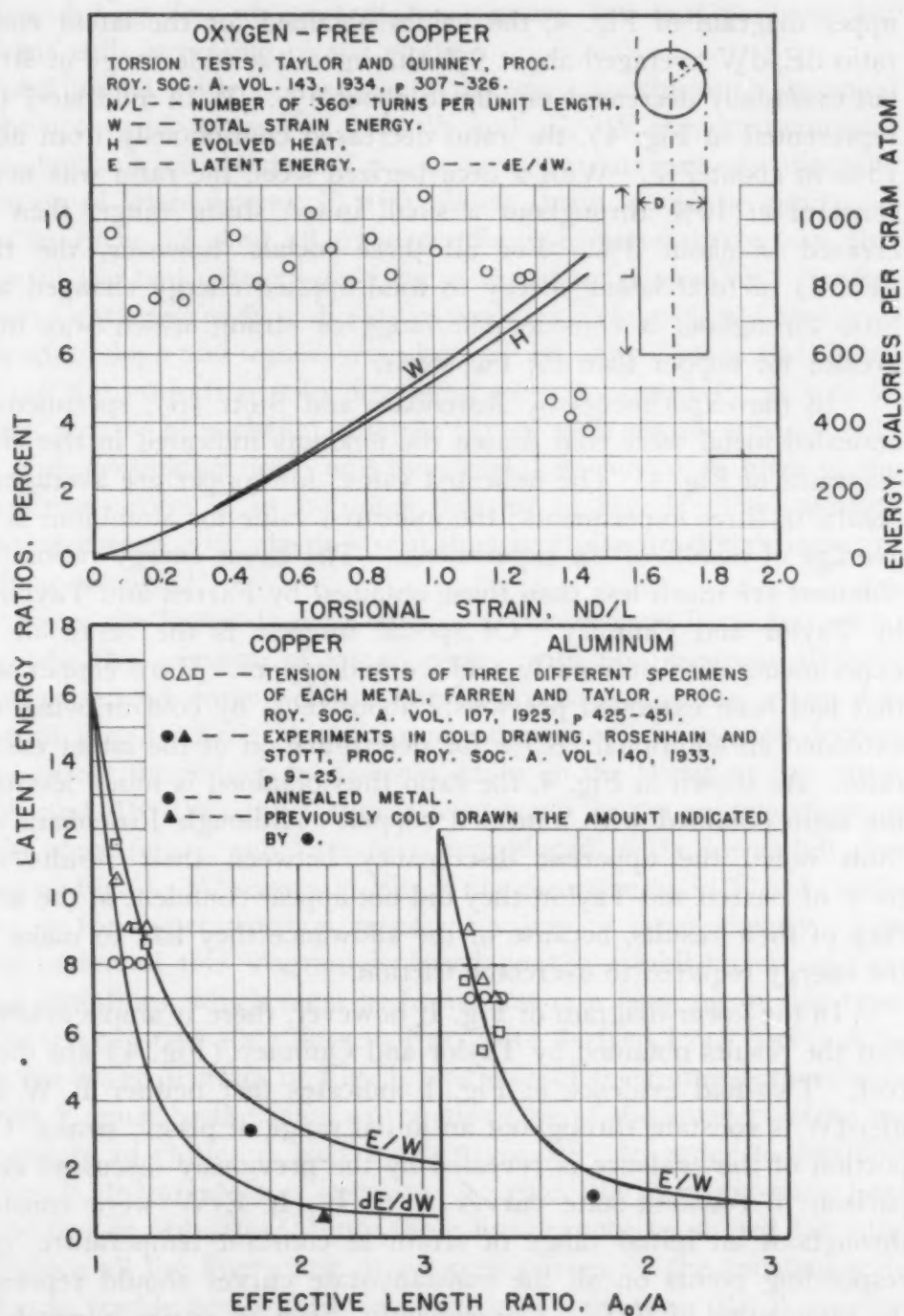


Fig. 4—Influence of Plastic Strain on Latent Energy and on the Latent Energy Ratios.

local contraction began and terminated each experiment. In the experiments by Taylor and Quinney, therefore, the straining was by torsion, and thus the strain range was much greater than in the experiments by Farren and Taylor. Moreover, improvements were made in the measurement of the evolved heat. As shown in the

upper diagram of Fig. 4, the values obtained for the latent energy ratio  $dE/dW$  averaged about 9% throughout a wide range of strain, but eventually decreased rapidly to about 4%. With mild steel (not represented in Fig. 4), the ratio decreased continuously from about 13% to about 7%. With a decarburized steel, the ratio was nearly constant at 10% throughout a small initial strain range, then decreased to about 3%. For all three metals, however, the ratio ( $E/W$ ) of total latent energy to total applied energy changed very little throughout a considerable range of strain, which was much greater for copper than for the steels.

In the experiments by Rosenhain and Stott (6), specimens of annealed metal were cold drawn the amounts indicated in the lower diagrams of Fig. 4. The indicated values for copper are averages of results of three experiments; the indicated value for aluminum is the average of results of six experiments. The latent energy ratios thus obtained are much less than those obtained by Farren and Taylor or by Taylor and Quinney. Of special interest is the result of the experiments with previously cold-worked copper. Hard copper wire that had been extended previously about 69% by cold drawing was extended an additional 28.5% for determination of the latent energy ratio. As shown in Fig. 4, the ratio thus obtained is much less than the ratio obtained with annealed copper. Although Rosenhain and Stott noted the apparent discrepancy between their results and those of Farren and Taylor, they did not appear confident of the accuracy of their results, because of the allowance they had to make for the energy required to overcome friction.

In the lower diagram of Fig. 1, however, there is ample evidence that the results obtained by Taylor and Quinney (Fig. 4) are incorrect. Two-fold evidence in Fig. 1 indicates that neither  $E/W$  nor  $dE/dW$  is constant throughout an initial range of plastic strain. One portion of the evidence is revealed by the previously discussed comparison of constant-state curves A to I. If  $E/W$  were constant throughout an initial range of strain at constant temperature, corresponding points on all the constant-state curves should represent the same value of  $E/W$ . Consequently, since  $W$  varies inversely as  $E/W$ , corresponding ordinates for all the constant-state curves should be in the same proportion. However, as shown in the lower diagram of Fig. 1, the range of ordinate ratios in a constant-state curve increases from curve A to curve I. Moreover, the increase in the range of ordinate ratios is greatest between curves A and B, decreases with increase in the intrinsic strength, and is slight between curves H and I. The evidence thus indicates that  $E/W$  decreases rapidly

at first during flow at constant temperature, but that the decrease slackens with increasing plastic strain.

Additional evidence leading to the same conclusion is revealed by the upturn of curves W. If  $E/W$  and  $dE/dW$  remained constant throughout an initial range of plastic strain, a curve representing the variation of latent energy  $E$  with plastic strain would be similar in form to curve W, and all corresponding ordinates throughout this range of the two curves would be in the same proportion. Such a curve of variation of  $E$  with plastic strain, therefore, would rise with *increasing* slope and would end abruptly at what Taylor and Quinney call the saturation point for latent energy. However, as will be shown, a curve of variation of latent energy with plastic strain should rise with *decreasing* slope, and thus would be similar in form to the flow-stress curves  $F_0$  in the upper diagram of Fig. 1. The variation of latent energy with plastic strain thus is similar to the variation of intrinsic strength.

From the lower diagram of Fig. 1 curves have been derived to represent the variation of latent energy with plastic strain at three different temperatures. These curves are shown in the upper diagram of Fig. 3. From this diagram, other curves have been derived to represent the influence of plastic strain on the latent energy ratios  $E/W$  and  $dE/dW$ ; these curves are shown in the middle diagram of the same figure, and have been reproduced in the lower left diagram of Fig. 4. Abscissas in Fig. 3 are the same as in Fig. 1; ordinates in the upper diagram represent values of latent energy. The construction of this diagram is based on the establishment of constant-state lines, which must be horizontal in a diagram of this type. Since the constant-state lines in Fig. 3 are derived from curves A to I in the lower diagram of Fig. 1, abscissas of their intersections with curves E must be the same as the abscissas of the corresponding intersections of curves A to I with curves W. In order to establish curves E, therefore, it is necessary to place the constant-state lines at the proper ordinates. Since these lines cannot be shifted laterally, and since all the lines must fit between curves E, the constant-state lines can readily be assembled so as to give a diagram that is approximately correct.

As a starting point for construction of this diagram, it is necessary to establish approximately the intersection of line A with the curve E representing the variation of latent energy with strain at room temperature. As shown in Fig. 3, the abscissa in terms of  $A_0/A$  at this point is 1.3. An approximate value for  $E$  at this point has been derived from the lower left diagram of Fig. 4. When  $A_0/A$



is 1.2, the value of  $E/W$  evidently is about 8.5%. When  $A_0/A$  is 1.3, the approximate value of  $E/W$ , as indicated by the curve designated  $E/W$ , is about 6.7%. Since the corresponding value of  $W$  (Fig. 1) is about 105 calories per gram atom, the corresponding value of  $E$  is about 7 calories per gram atom. This value has been used in establishing not only the intersection of line  $A$  with the lower curve  $E$  in Fig. 3, but also the intersection of this line with the other  $E$  curves.

The next step is the placing of lines  $D$  and  $I$  in proper relation to line  $A$ . The left end of line  $D$  must be directly above the right end of line  $A$ , and the left end of line  $I$  must be directly above the right end of line  $D$ . By using the proper ordinate ratios at these vertically opposite points, it is possible to establish three points each on the upper and lower curves  $E$ . On the reasonable assumption that the ordinate ratios should be the same at these two abscissas, various ordinate ratios were tried. If the ordinate ratio were much greater than 1.6, curves  $E$  would be very different in form from ordinary flow-stress curves, and would even have reversal of curvature. When the ratio is made 1.6, and when approximately the same ratio is used throughout the entire length of curves  $E$ , all the other constant-state lines fit into unique positions between curves  $E$ , as shown in the upper diagram of Fig. 3. The diagram thus established, therefore, is believed to be an approximately correct representation of the influence of plastic strain on the latent energy at the three indicated temperatures.

It is worthy of note that the ordinate ratio 1.6 is the same as the previously mentioned ordinate ratio for the upper and lower curves  $W$  in Fig. 1. The evidence thus implies that  $E/W$  for copper at constant strain varies only slightly with temperature. This relationship will be discussed later in connection with the lower left diagram of Fig. 7.

The variation of  $E/W$  with plastic strain is represented by the indicated curve in the middle diagram of Fig. 3. This curve is derived from the lower curve  $E$  of Fig. 3 and the lower curve  $W$  of Fig. 1. It, therefore, represents the variation of  $E/W$  with strain at room temperature. However, as implied in the preceding paragraph, the position of such a curve would vary only slightly with temperature. The variation of  $dE/dW$  with plastic strain is represented by another indicated curve in the middle diagram of Fig. 3. This curve is derived from a curve (not shown) of variation of  $E$  with  $W$ . The curves for  $E/W$  and  $dE/dW$  have been reproduced in the lower left diagram of Fig. 4, for comparison with the results of

the investigations by Farren and Taylor and by Rosenhain and Stott. As shown in the description of the method of deriving the upper diagram of Fig. 3, the upper part of the curve for  $E/W$  in the lower left diagram of Fig. 4 has been drawn in accord with the results obtained by Farren and Taylor. The rest of the curve is derived by the previously described method from the completed upper diagram of Fig. 3.

As shown in Fig. 4, the point representing the results obtained by Rosenhain and Stott with annealed copper is in fair agreement with the curve for  $E/W$ , especially since this point may be a little too low (6). As would be expected, since this point represents a ratio of total latent energy to total applied energy, the point is in much better agreement with the curve for  $E/W$  than with the curve for  $dE/dW$ . The result obtained by Rosenhain and Stott by additional extension of previously cold drawn copper represents the ratio of increments of  $E$  and  $W$ . As would be expected, therefore, the corresponding point in Fig. 4 is in much better agreement with the curve for  $dE/dW$  than with the curve for  $E/W$ .

In the lower right diagram of Fig. 4, the curve for  $E/W$  is based entirely on the results obtained by Farren and Taylor and by Rosenhain and Stott with aluminum. As represented by this curve, the results obtained by Farren and Taylor clearly indicate an initial rapid decrease of  $E/W$  with plastic strain. The curve has been extended on the assumption that the point representing the results obtained by Rosenhain and Stott is a little too low. The evidence indicates that the ratio of latent energy to total strain energy is generally less for aluminum than for copper.

The upper diagram of Fig. 4, based on results obtained by Taylor and Quinney (8), evidently gives an incorrect picture of the influence of plastic strain on  $dE/dW$  and  $E/W$ . The incorrectness of this diagram may be attributed partly to the serious disadvantages in the use of torsion tests for an investigation of this kind, and partly to the use of an incorrect method in the calculations of total strain energy. Whereas, in straining by tension or by cold drawing, the strain at any instant is nearly constant statistically throughout the cross section, in straining a cylinder by torsion the strain varies linearly with distance from the axis. If the latent energy ratio were nearly constant throughout an initial range of strain, as the upper diagram of Fig. 4 implies, this strain gradient would not affect adversely the results of an investigation of latent energy by means of torsion tests. However, since the latent energy ratio varies greatly with plastic strain, the strain gradient in a cylin-

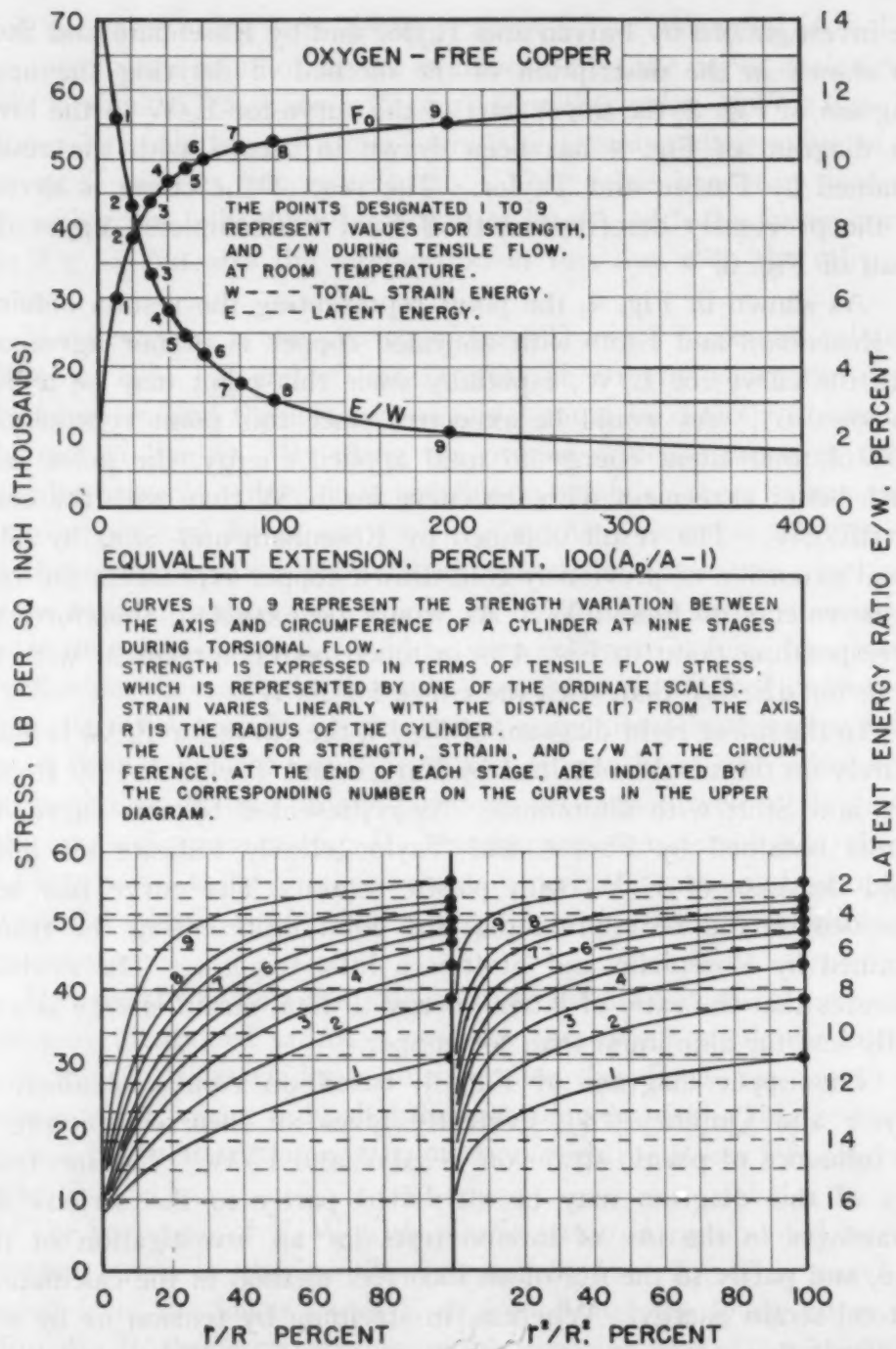


Fig. 5—Theoretical Picture of the Radial Variation of Strength and the Latent Energy Ratio at Nine Stages During the Torsional Straining of a Copper Cylinder.

der under torsion is associated with a radial variation of strength and of the latent energy ratio. This radial variation is illustrated in Fig. 5.

Fig. 5 presents a theoretical picture of the radial variation of strength and the latent energy ratio at nine stages during the tor-



sional straining of a copper cylinder. Since this figure has been designed for merely qualitative representation, strength is expressed in terms of the tensile flow stress instead of the shearing flow stress, and strain is expressed in terms of extension instead of shearing strain. In the upper diagram, curve  $F_0$  represents the variation of the tensile flow stress with extension, and the other curve represents the corresponding variation of  $E/W$ . In the lower diagrams, curves 1 to 9 represent the variation of strength between the axis and circumference at nine stages during torsional flow. The values for strength, strain and  $E/W$  at the circumference, at the end of each stage, are indicated by the corresponding numbers on the curves in the upper diagram. The ordinate scale at the left of the lower diagram represents tensile flow stresses. The horizontal broken lines represent corresponding values of  $E/W$ , as indicated by the ordinate scale on the right. Since the strain during torsion remains nil at the axis, and varies linearly from the axis to the circumference, each curve in the lower diagram has been derived, with appropriate change of abscissa scale, from the corresponding portion of curve  $F_0$ ; this portion extends from the origin to the correspondingly numbered point.

In the lower left diagram of Fig. 5, each curve shows the variation of strength and  $E/W$  between the axis and circumference of the cylinder. With distance from the axis, the strength increases and the latent energy ratio decreases. At the end of a stage, therefore, the experimentally determinable value for  $E/W$  is the mean of the values represented by the corresponding curve. However, since the area of cross section of a cylinder varies as the square of the radius, the mean value of  $E/W$  cannot be calculated directly from a curve in the lower left diagram, but can be calculated directly from a curve in the lower right diagram, in which abscissas represent squares of radial distances.

Comparison of the curves in the lower right diagram of Fig. 5 shows that the variation of the mean value of  $E/W$  differs greatly from the variation of  $E/W$  at the circumference of the cylinder. Near the beginning of plastic strain, the mean value of  $E/W$  decreases *less* rapidly than the value of  $E/W$  at the circumference. Eventually, however, the mean value decreases *more* rapidly than the value at the circumference. This relationship probably would account for an initial delay and an eventual acceleration in the descent of a curve for  $E/W$  determined by torsional tests, but could not account for apparent constancy of  $dE/dW$  throughout a wide range of plastic strain, as indicated in the upper diagram of Fig. 4.

The incorrectness of this diagram in Fig. 4 probably is due chiefly to an erroneous method of calculating values of the total strain energy. Taylor and Quinney derived values of stress from values of torque by use of the formula  $q = 12 G / \pi D^3$ , in which  $G$  represents the torque,  $D$  represents the diameter of the cylinder and  $q$  is assumed to be the "average shear stress over the cross section". As shown in the lower right diagram of Fig. 5, however, correct values of the average flow stress at various stages of torsional flow cannot be derived from values of torque by the use of a single formula. With plastic strain, the true average flow stress first increases more rapidly, then less rapidly, than the average stress obtained by the formula used by Taylor and Quinney. This error in the calculated variation of the flow stress with strain would cause a similar error in the calculated variation of total strain energy, and thus would affect the course of curve  $W$  in the upper diagram of Fig. 4.

The divergence of curve  $W$  from curve  $H$  probably should be more rapid near the origin, but should gradually become less rapid until the curves are almost parallel. Since values of  $E$  are calculated from differences between corresponding ordinates of these two curves, a small error in the course of curve  $W$  would cause a large error in curves derived to represent the variations of  $E$ ,  $E/W$  and  $dE/dW$  with plastic strain. The influence of plastic deformation on latent energy and on the latent energy ratios is believed to be represented correctly by the curves in Fig. 3 and in the lower diagrams of Fig. 4, not in the upper diagram of Fig. 4.

#### INFLUENCE OF TEMPERATURE ON STRAIN ENERGY

Fig. 6 shows the influence of temperature on the strain energy for constant intrinsic strength, and Fig. 7 shows the influence of temperature on the strain energy for constant total strain. Temperatures are plotted as abscissas. The temperature scale is the same that has been used in papers by the author and previous associates (3, 4, 5). Temperatures in degrees K are plotted on a logarithmic scale. Since abscissas are proportional to the logarithm of the degrees K, the scale is the same in principle as Kelvin's original thermodynamic scale.

In Fig. 6 the letters adjacent to curves represent the strength states that are similarly designated in Figs. 1, 2 and 3. The upper left diagram shows the variation of total strain energy with temperature for the six indicated strength states, and the upper right diagram shows the variation of work hardening energy for the five

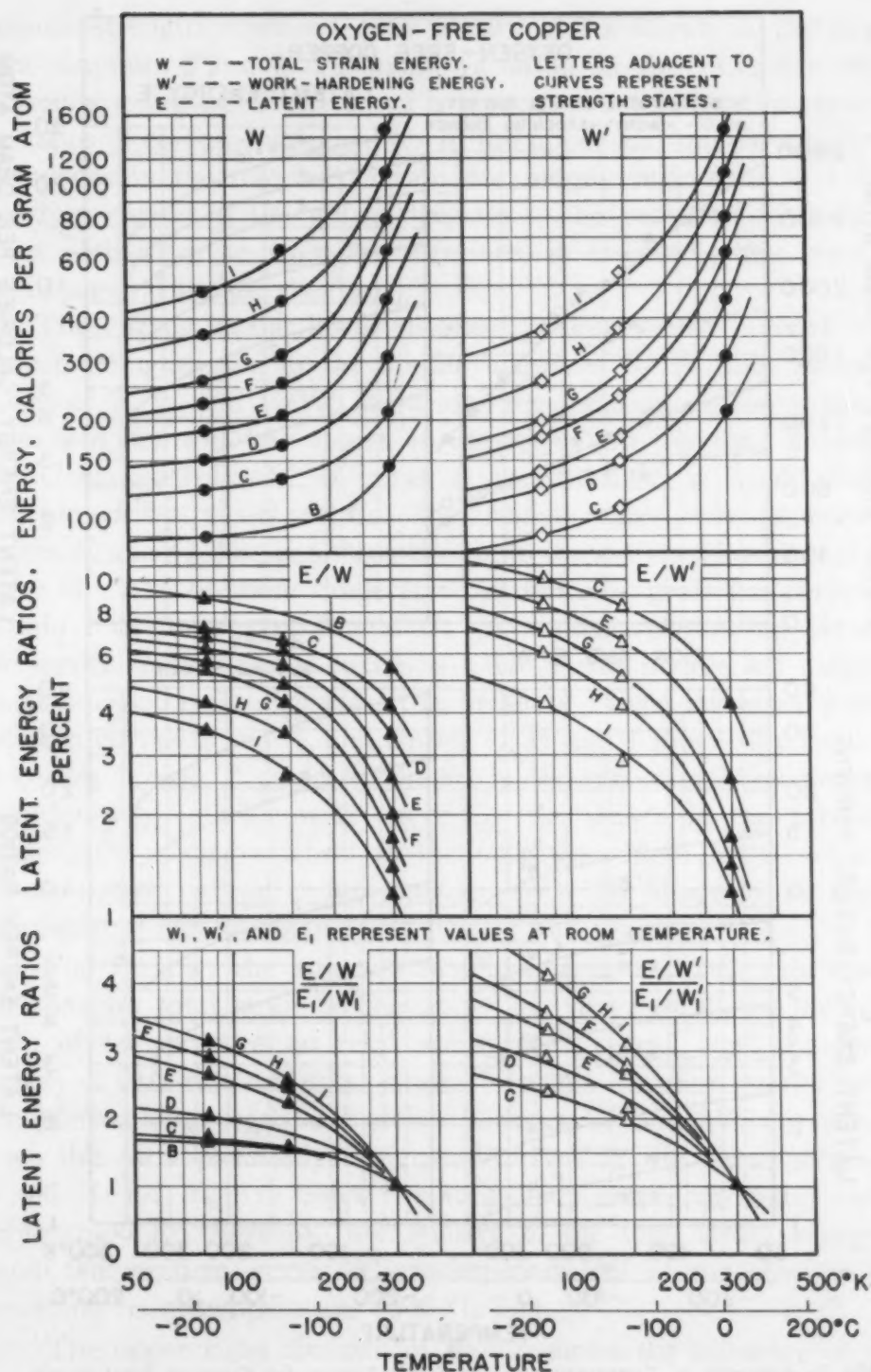


Fig. 6—Influence of Temperature on the Strain Energy for Constant Intrinsic Strength.

indicated strength states. The middle diagrams show the corresponding variations of  $E/W$  and  $E/W'$ . Since a logarithmic scale of ordinates is used for the upper and middle diagrams, these dia-



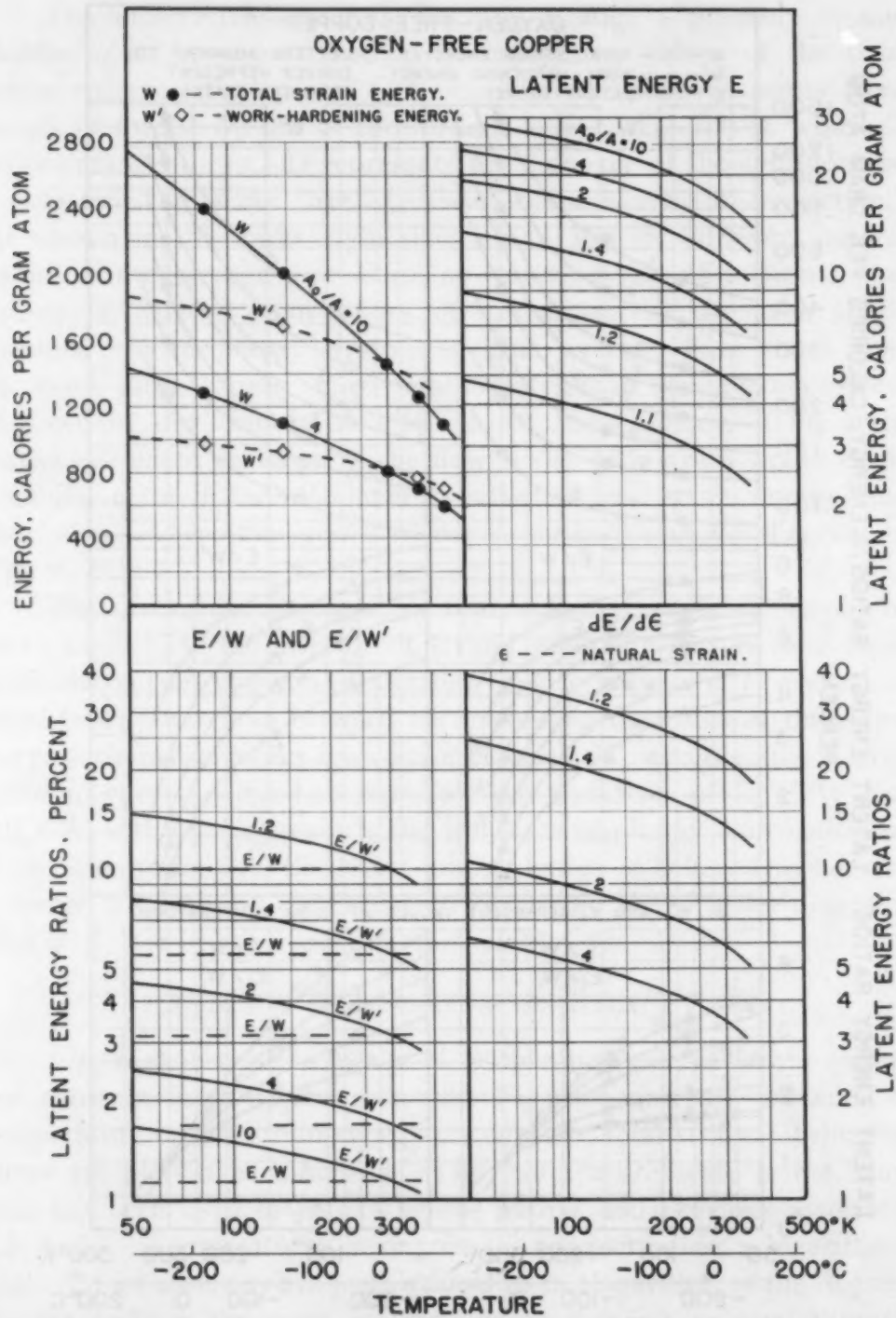


Fig. 7—Influence of Temperature on the Strain Energy for Constant Total Strain.

grams reveal directly and clearly the influence of temperature and intrinsic strength on ordinate ratios. As shown in the upper left diagram, the ratio between the total strain energies at room temperature and  $-188^{\circ}\text{C}$  ( $-306^{\circ}\text{F}$ ) increases greatly with increase in the

intrinsic strength represented by a curve. As shown in the upper right diagram, there is a similar variation in the ratio for work hardening energies. Since there is a reciprocal relationship between the ratios of corresponding curves in the upper and middle diagrams, the curves in the middle diagram are merely inversions of corresponding curves in the upper diagram. The variation of ordinate ratios with intrinsic strength, therefore, is essentially the same in the upper and middle diagrams.

The curves in the lower diagram of Fig. 6 are derived from corresponding curves in the middle diagrams by plotting ratios of values of  $E/W$  and  $E/W'$  at various temperatures to the values at room temperature. As shown in the lower left diagram, curves B and C almost coincide; if curve A were drawn, it would almost coincide with curves B and C. The ordinate range increases between curves C and G, but is almost the same for curves H and I as for curve G. The ordinate range is about twice as great for curves G, H and I as for curves B and C. A similar relationship between the vertical ranges of the curves is found in the middle left diagram. In the lower right diagram, the ordinate range increases greatly between curves C and G, and curves G, H and I practically coincide. If curves A and B could be drawn in this diagram, they probably would nearly coincide with curve C. As shown in the preceding section, the great variation in the ordinate ranges for a series of constant-state curves is incompatible with the diagram in Fig. 4 representing results obtained by Taylor and Quinney (8).

Fig. 7 shows the influence of temperature on the strain energy for constant total strain. The upper left diagram shows the influence of temperature on total strain energy and work hardening energy at two indicated total strains. In this diagram, energy values are plotted on a cartesian scale. Curves W and W' are derived from the correspondingly designated curves in Fig. 2, at strains of 4 and 10 for  $A_0/A$ . Since the values for work hardening energy represented by curve W' are relative to the total strain energy at room temperature, curve W' crosses curve W at the abscissa representing room temperature (300 °K).

The upper right diagram of Fig. 7 shows the influence of temperature on the latent energy for constant total strain. The curves show the variation of latent energy at the five indicated total strains. These curves are derived from the upper diagram of Fig. 3. As shown in the description of the development of this diagram, the ordinate ratios at constant strain were kept nearly constant throughout the length of the curves. Because of the logarithmic scale used in the

upper diagram of Fig. 7, therefore, all the curves have about the same vertical range and are of the same form. The vertical range between room temperature and  $-188^{\circ}\text{C}$  ( $-306^{\circ}\text{F}$ ) represents a ratio of about 1.6 for the corresponding values of  $E$ .<sup>2</sup>

The lower left diagram of Fig. 7 shows the variation of the latent energy ratios  $E/W$  and  $E/W'$  with temperature at the five indicated values of total strain. These curves have been drawn so as to be in proper correlation with the curves designated  $E/W$  and  $E/W'$  in the middle diagram of Fig. 3. Since, as previously shown, the ordinate ratio at constant total strain for the upper and lower curves  $E$  in Fig. 3 is about the same as the corresponding ratio for curves  $W$  in Fig. 1, temperature evidently would have little effect on the position of the curve for  $E/W$  in the middle diagram of Fig. 3. In the lower diagram of Fig. 7, therefore, the influence of temperature on  $E/W$  is represented approximately by the horizontal broken lines. The curves for  $E/W'$ , however, indicate that temperature has much effect on that ratio. These curves and the corresponding curves in the middle diagram of Fig. 3 have been derived by correlating values of  $E$  represented in the upper diagram of Fig. 3 with corresponding values of  $W$  represented in Fig. 2.

The curves in the lower diagram of Fig. 3 represent the influence of plastic strain on the rate of increase of latent energy  $E$  with natural strain  $\epsilon$ . The values of  $dE/d\epsilon$  used in deriving these curves were obtained from curves  $E$  in the upper diagram of this figure. The curves for  $dE/d\epsilon$  in Fig. 3 have been used to derive the curves in the lower right diagram of Fig. 7. These show the influence of temperature on  $dE/d\epsilon$  at the five indicated values of total strain. These curves, as would be expected, are identical in form with each other, and with the curves in the upper right diagram. The effect of temperature, expressed in terms of ratios, evidently varies little with plastic strain.

The relationship represented in the lower diagram of Fig. 3 and in the lower right diagram of Fig. 7 is the fundamental stress-strain energy relationship. The increase in latent energy with plastic strain is a function of the strain, not of the total energy. As previously shown, the *total* energy is affected greatly by another factor, which varies with the metal, namely, the direct effect of temperature on the flow stress. The fundamental latent energy ratio, therefore, is  $dE/d\epsilon$ , not  $E/W$  or  $dE/dW$ . Since values of work hardening

<sup>2</sup>In Fig. 10 of a preceding paper (5), the curves  $E$  are much steeper. At that time, however, the author had not discovered that the results of the investigation by Taylor and Quinney are incorrect. The curves, therefore, are based on the assumption that the latent energy ratio  $E/W$  remains constant throughout a wide initial range of strain. For this reason, curves  $E$  in Fig. 10 of the preceding paper are much too steep.



energy have been derived by making allowance for the direct temperature effect, the ratios of latent energy to work hardening energy are much more important than ratios involving total energy.

#### SUMMARY

1. The influence of temperature on the flow stress involves two factors: (a) a direct temperature effect; (b) the influence of temperature on the rate of increase of intrinsic strength with strain. The lower the temperature, the more rapid is the increase of intrinsic strength with strain.

2. The effects of the direct temperature factor and the intrinsic strength factor on the flow stress should be expressed in terms of flow-stress ratios rather than in terms of flow-stress differences. The product of these two ratios represents the combined effect of the two factors on the flow stress.

3. The lower the temperature, the less is the plastic strain required to produce a given strength state (intrinsic strength). The range of strain, for a constant strength state and a constant temperature difference, increases with the intrinsic strength.

4. A constant strength state implies constant latent energy. For constant latent energy, the ratio range of the total energy increases with increase of the intrinsic strength by cold work.

5. The variation of these ratio ranges with intrinsic strength is incompatible with the prevalent idea that the latent energy ratios  $E/W$  and  $dE/dW$  for copper are nearly constant throughout an initial range of plastic strain. The form of the curve of variation of the total strain energy  $W$  with natural strain leads to the same conclusion.

6. A diagram has been developed to represent approximately the variation of latent energy  $E$  with plastic strain at three different temperatures. With plastic strain, the latent energy *increases* at a decreasing rate, and the latent energy ratios  $E/W$  and  $dE/dW$  *decrease* at a decreasing rate.

7. A diagram has been developed to illustrate the effects of torsional strain on strength and on the latent energy ratio  $E/W$ . Reasons are given for the incorrectness of the results of the investigation by Taylor and Quinney.

8. Diagrams are presented to show the influence of temperature on total energy, work hardening energy and latent energy, for constant strength states.

9. Diagrams are presented to show the influence of temperature on total strain energy, work hardening energy, latent energy,

and three different latent energy ratios, for constant total strains.

10. The fundamental temperature-strain energy relationship is the influence of temperature on the rate of increase of latent energy with plastic strain. The increase of latent energy with plastic strain is a function of the strain, not of the total stress or total energy. The fundamental latent energy ratio, therefore, is  $dE/d\epsilon$ , not  $E/W$  or  $dE/dW$ . ( $\epsilon$  represents natural strain.)

11. The ratio of latent energy to work hardening energy ( $W'$ ) is much more important than ratios involving the total energy ( $W$ ).

### References

1. J. E. Dorn, A. Goldberg and T. E. Tietz, "The Effect of Thermo-mechanical History on the Strain Hardening of Metals", *TRANSACTIONS, American Institute of Mining and Metallurgical Engineers*, Vol. 180, *Metals Technology*, September 1948, T.P. 2445. Discussion, *Transactions, Journal of Metals*, May 1949, p. 325.
2. D. J. McAdam, Jr., and R. W. Mebs, "An Investigation of the Technical Cohesive Strength of Metals", *Transactions, American Institute of Mining and Metallurgical Engineers*, Vol. 162, 1945, p. 474-536.
3. D. J. McAdam, Jr., and R. W. Mebs, "The Technical Cohesive Strength and Other Mechanical Properties of Metals at Low Temperatures", *Proceedings, American Society for Testing Materials*, Vol. 43, 1943, p. 661-703.
4. D. J. McAdam, Jr., G. W. Geil and Frances Jane Cromwell, "Flow, Fracture and Ductility of Metals", *Transactions, American Institute of Mining and Metallurgical Engineers*, Vol. 175, p. 306. *Metals Technology*, January 1948, T.P. 2296.
5. D. J. McAdam, Jr., "Influence of Temperature on the Stress-Strain Energy Relationship for Copper and Nickel-Copper Alloy", *AIME Metals Transactions*, Vol. 185, 1949, p. 727-740, T.P. 2703.
6. W. Rosenhain and V. H. Stott, "The Energy Absorbed in the Cold Working of Metals", *Proceedings of the Royal Society, Series A*, Vol. 140, 1933, p. 9-25.
7. W. S. Farren and G. I. Taylor, "Heat Developed During Plastic Extension of Metals", *Proceedings of the Royal Society*, Vol. A-107, 1925, p. 425-451.
8. G. I. Taylor and H. Quinney, "The Latent Energy Remaining in a Metal after Cold Working", *Proceedings of the Royal Society*, Vol. A-143, 1934, p. 307-326.

# TENSION-COMPRESSION BIAXIAL PLASTIC STRESS-STRAIN RELATIONS FOR ALUMINUM ALLOYS 24S-T AND 2S-O

BY JOSEPH H. FAUPEL AND JOSEPH MARIN

## Abstract

*In this paper the mechanical behavior of aluminum alloys 24S-T and 2S-O subjected to biaxial tension-compression stresses is considered. Plastic stress-strain relations are obtained for both constant and variable principal biaxial stress ratios.*

*On the basis of the results obtained, it is concluded that a generalized deformation theory may be used to predict, approximately, stress-strain relation for both constant and variable principal stress ratios. Furthermore, the tests indicate that failure by yielding is predicted in accordance with the distortion energy or von Mises-Hencky theory of failure.*

IN engineering applications of materials, a structure or member may be considered to be subjected to static, fatigue or impact loads. Furthermore, the material may be subjected to high temperatures so that creep of the material is produced. Moreover, the loads may be applied in such a way that either uniaxial or combined stresses are produced within the material. In this paper, the behavior of aluminum alloys 24S-T and 2S-O when subjected to combined static stresses is discussed.

Interest in the plastic stress-strain relations for metals subjected to combined stresses has risen out of attempts to predict ductility and fracture strengths of metals undergoing various forming operations such as deep drawing or undergoing plastic straining in service applications such as aircraft structural members. A specific outcome of the researches on plastic flow of metals under states of combined static stress is the determination of mechanical properties,

A paper presented before the Thirty-second Annual Convention of the Society, held in Chicago, October 21 to 27, 1950. Of the authors, Joseph H. Faupel is associated with the Engineering Research Laboratory, E. I. duPont de Nemours & Company, Inc., Wilmington, Delaware; formerly duPont post-graduate fellow in mechanical engineering at The Pennsylvania State College. Joseph Marin is professor of engineering mechanics and research professor of engineering materials, The Pennsylvania State College, State College, Pa. Manuscript received April 4, 1950.



such as yield and fracture strengths and ductility. Another outcome is the theoretical determination of combined loading stress-strain relations in the plastic range in terms of simple tension values. The theory used to express combined loading stress-strain relations in terms of simple tension values will be designated as the generalized deformation theory (1, 2).<sup>1</sup> By the use of this theory, it is possible to approximately predict stresses and strains in the plastic range for states of combined stress in terms of simple tension stress-strain values.

During the past few years, three types of theories have been proposed: "deformation", "flow", and "slip" theories (4-7). It is not the purpose of this paper, however, to discuss the relative merits of the various types of theories. The analyses made in this paper have utilized a deformation-type theory because of its simplicity and because previous investigations have shown it to be a good first approximation of the test results.

Most of the research work to date on the problem of determining mechanical properties and stress-strain relations in the plastic range for metals subjected to combined static stresses has dealt with the biaxial state of tensile stresses. In most of these investigations the ratios of the principal stresses were maintained essentially constant, as were also the directions of the principal stresses. In this paper, a state of combined static stress is considered where the directions of the principal stresses do not remain constant. Furthermore, both constant and variable principal stress ratios are considered for the case of tension-compression biaxial stress-strain relations.

Three theories are used for comparing experimental and theoretical yield strengths: the maximum stress, maximum shear and distortion energy theories of failure. The derivations of these theories are well known and are reported elsewhere.

Although tests on materials subjected to combined stresses are rather difficult to perform, many investigations have been conducted in order to study the behavior of metals when subjected to such stresses (8-10). However, the majority of the tests reported have been on specimens subjected to combinations of loads that produced two positive principal stresses. In these investigations, the ratios of the principal stresses as well as their directions were maintained essentially constant. Furthermore, in some of the early work in this field the tests were conducted on solid specimens subjected to torsion or a combination of torsion and bending. In these latter

<sup>1</sup>The figures appearing in parentheses pertain to the references appended to this paper.

tests, a nonuniform stress distribution existed by virtue of lower stressed inner fibers tending to restrain yielding of the higher stressed outer fibers. Because of the presence of nonuniform stress distribution, much of the early data are difficult to evaluate. Morrison (11), for example, working with mild steel found a 3 to 4% drop in yield strength for each 1% increase in thickness of bars in bending for the range of thickness 0.1 to 0.5 inch.

Relatively few tests have been conducted on materials subjected to a combination of positive and negative stresses (1, 11-24). Most of the reported data were obtained under conditions of constant principal stress ratios; Hohenemser and Prager (19) conducted a limited number of tests under conditions of variable principal stress ratios.

Some general conclusions that may be made on the basis of previous investigations are:

1. Brittle materials fail in accordance with the maximum stress theory.
2. Ductile materials yield in accordance with the distortion energy theory or fracture in accordance with values determined by the generalized deformation theory.
3. Stress-strain relations in the plastic range may be approximated by the generalized deformation theory (or Nadai's Octahedral Shear Stress-Strain Relation).

#### MATERIAL TESTED

The materials used for the static combined tension-torsion tests were aluminum alloys 24S-T and 2S-O. Constant principal stress ratio tests on the former material were conducted under the sponsorship of the U. S. Army Air Forces, Wright Field, Dayton, Ohio, and the results reported in Reference 1. Constant principal stress ratio tests on 2S-O and variable principal stress ratio tests on both 24S-T and 2S-O are described in the present paper.

Aluminum alloy 24S responds to precipitation hardening and contains, nominally, 4.4% copper, 1.5% magnesium and 0.6% manganese. In the fully heat treated condition this alloy has the strength

Table I  
Conventional Mechanical Properties of Aluminum Alloys Tested

Alloy	Tensile Strength (psi)	Yield Strength (0.2% Offset)	Modulus of Elasticity (psi)	% Elongation in 2 Inches	Poisson's Ratio
24S-T	68,000	46,000	10,600,000	19 to 22	0.33
2S-O	13,000	5,000	10,000,000	35 to 45	0.33

of structural steel and is designated 24S-T. Aluminum alloy 2S is commercially pure aluminum and can be hardened only by cold working. In the fully annealed condition, it is designated 2S-O.

All of the material tested was supplied in tubular extruded form in lengths of 16 feet with an internal diameter of 1 inch and a wall thickness of  $\frac{1}{4}$  inch. The mechanical properties of these materials as supplied are given in Table I.

#### TEST PROCEDURE

*Test Specimens*—The biaxial stress test specimens were machined from tubular sections having an inside diameter of 1 inch and a wall thickness of  $\frac{1}{4}$  inch. The dimensions of the machined

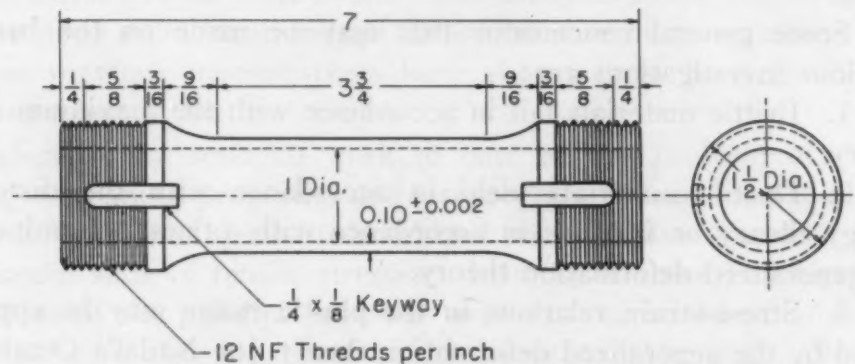


Fig. 1—Tension-Torsion Specimen.

specimens are shown in Fig. 1. The specimens used had an over-all length of 7 inches, with an intermediate length of 3.75 inches of reduced wall thickness equal to approximately 0.10 inch. The wall thickness was determined at 48 places on each specimen to an accuracy of 0.0001 inch by the use of equipment described in Reference 2. The wall thickness-diameter ratio was approximately 0.1, so that the biaxial stresses throughout the wall were essentially uniform. It was found that a wall thickness of 0.1 inch for a specimen length of 7 inches was necessary in order to eliminate failure by buckling for the alloy 24S-T. However, for the alloy 2S-O, buckling occurred for specimens having a wall thickness of 0.175 inch.

*Testing Machine*—The combined stress testing machine used in the investigation described in Reference 1 was used. In this machine, tubular specimens can be subjected simultaneously to tension and torsional stresses. Fig. 2 is a photograph of the machine. The axial tensile load is applied manually to the specimen (S) by means of a gear unit (W) through a load transmitting bar



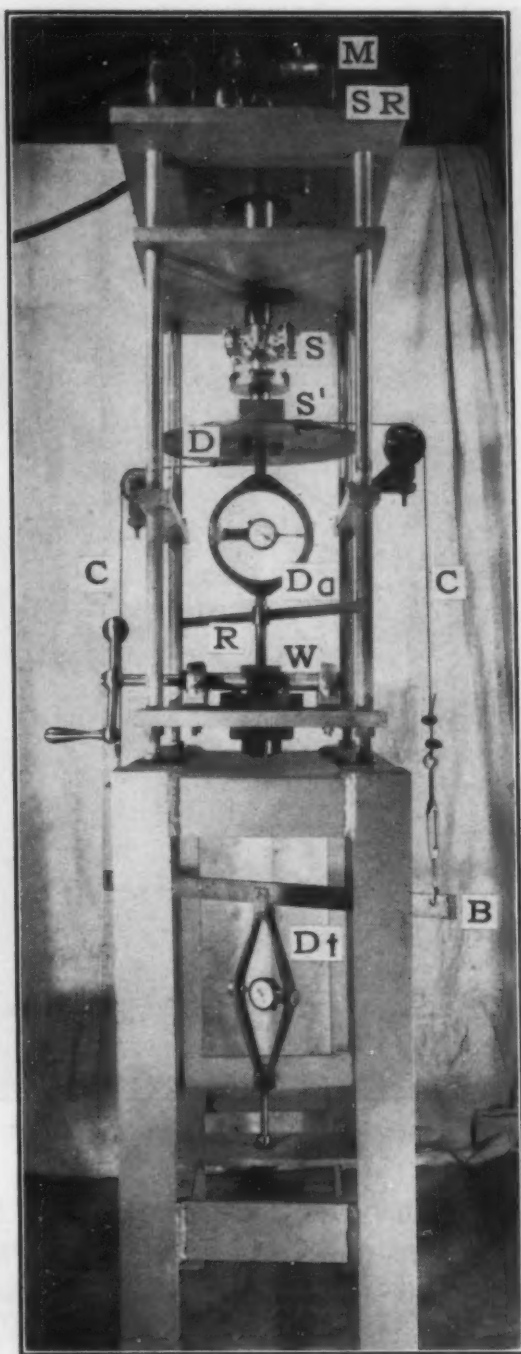


Fig. 2—Combined Tension-Torsion Machine.

(R). The axial load is measured by means of a dynamometer (Da). The rod (R) transmits the load to the specimen through a bearing with a spherical seat (S') to assure axiality of loading.

The torsional moment is applied automatically by a  $\frac{3}{4}$ -HP motor (M) equipped with a speed reducer (SR) and a rheostat for regulating the speed. To the lower part of the specimen a disk (D)

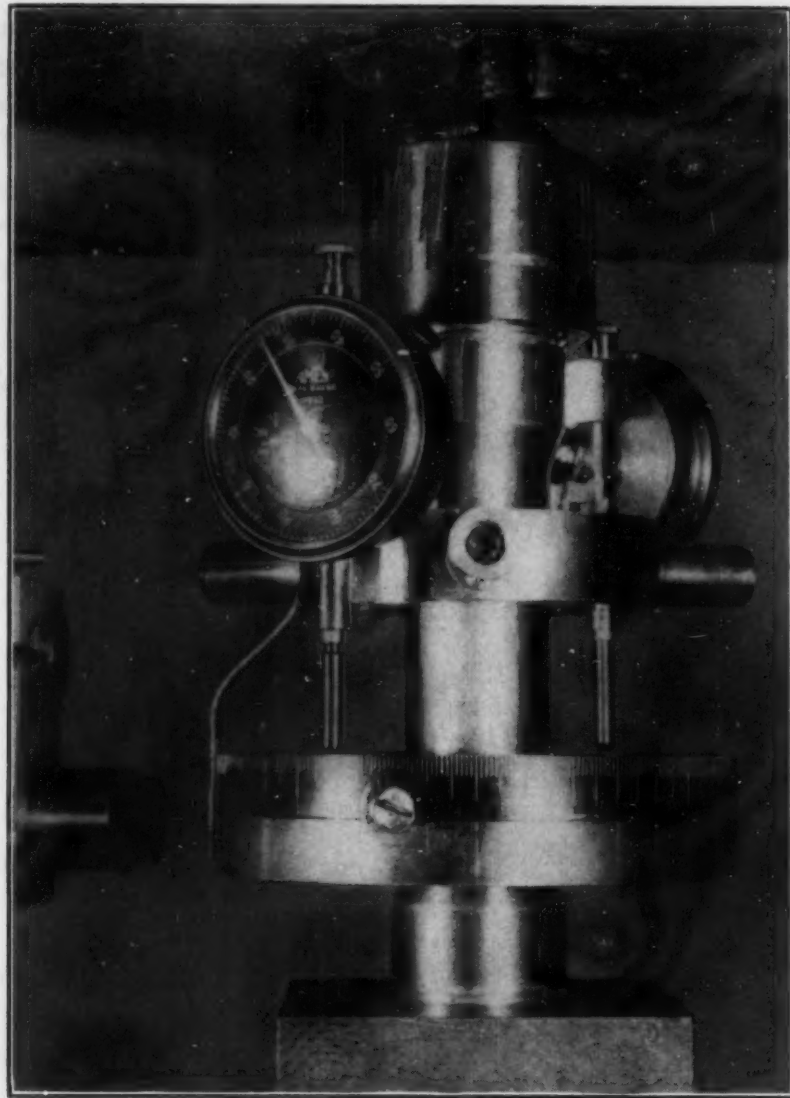


Fig. 3—Strain Gage for Combined Stresses.

is attached to which cables (C) are connected. The cables pass over essentially frictionless pulleys to a bar (B). The dynamometer (Dt) attached to the bar (B) and base of the testing machine is used to measure the torsional load.

*Method of Measuring Strains*—A combination axial strain-angle of twist strain gage was used to measure strains in both the elastic and plastic ranges. The axial tensile strains were measured over a 2-inch gage length by two 0.0001-inch dial gages placed 180 degrees apart as shown in Fig. 5. The angles of twist were measured for a 2-inch gage length by the twistmeter part of the strain gage. Axial strains and angles of twist could be measured in the plastic range by having three rods spaced 120 degrees apart which bear

on the specimen at one end and are connected by a preload spring to the strain gage at the other end. By adjusting the preload compression in the spring when the strain gage is initially attached to the specimens, compression in the springs can be maintained throughout the test. This provision is necessary, since the diameter of the specimen is reduced in the plastic range by tensile loads.

*Methods of Testing*—The wall thickness and external diameter of the specimens were first measured and the strain gage was then attached to the specimen. After the specimen was placed between the threaded holders of the testing machine, the load and strain readings were adjusted to their zero values. For the constant principal stress ratio tests, the loads were then simultaneously applied to predetermined values of nominal constant principal stress ratio, and readings were taken of axial strain and angle of twist. For the 24S-T specimens, the last set of readings recorded represented, in most cases, approximately the loads at fracture. For the 2S-O specimens, the last readings represent failure by buckling of the specimens.

For the variable principal stress ratio tests, two variations in loading procedure were employed. In one case the axial tensile load was applied to some predetermined value and then held constant at that nominal stress while torque was then gradually applied until fracture or buckling occurred. In the other method, the shear stress was applied to some predetermined value and then held constant at that nominal shear stress while axial tensile load was gradually applied until failure by fracture or buckling occurred. Thus, in these latter tests each set of readings recorded represented a different principal stress ratio. The method of measuring strains was exactly the same as for the constant principal stress ratio tests.

#### TEST RESULTS

*Tension tests* were made on tubular specimens (Fig. 1) of the same dimensions as used for the combined stress tests, in order to consider the effect of shape and size of specimen. In the interpretation of the combined stress results, it was also necessary to obtain true stress-strain relations in simple tension. The observed data for the tension specimens are plotted in Fig. 4. In this case, the principal stress ratio is  $\sigma_2/\sigma_1 = 0$ . From the elastic range portion of the stress-strain diagram as plotted in Fig. 6, the nominal values of the mechanical properties were determined. These nominal values are shown in Table II and include modulus of elasticity, strength, and ductility values. The true values of strength and ductility as



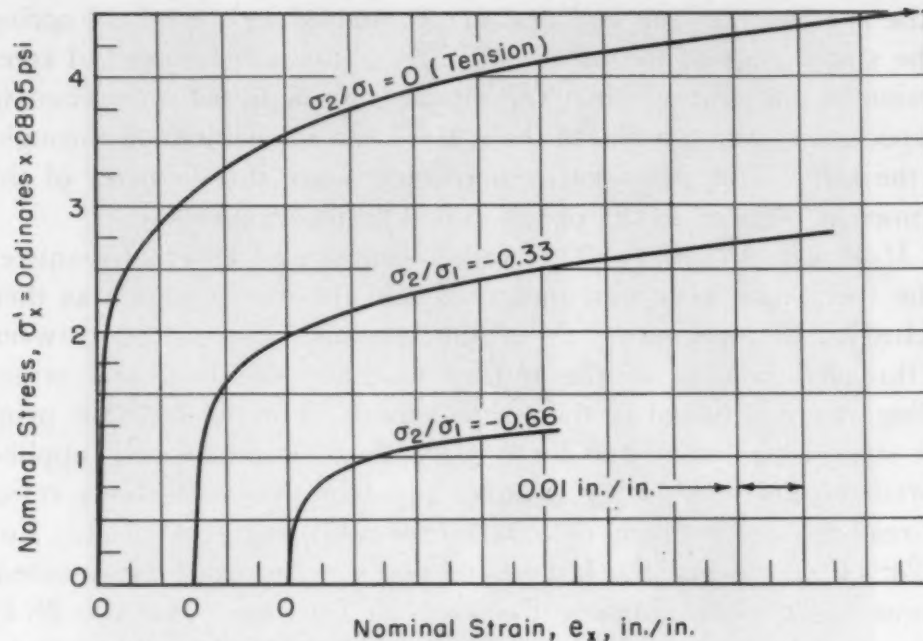


Fig. 4—Nominal Normal Stress-Strain Relations for Alcoa 2S-O.

obtained from the true stress-strain diagram of Fig. 9 are also given.

In plotting the true stress-strain diagram of Fig. 9, the true strain and true stress are defined respectively by the relations (1)

$$\epsilon = \log (1 + e_0) \quad \text{Equation 1}$$

$$\sigma = \frac{P}{A_0} (1 + e_0) \quad \text{Equation 2}$$

where  $e_0$  is the nominal unit axial strain,  $P$  is the axial load and  $A_0$  is the initial cross sectional area.

Many test data for simple tension can be expressed by the parabolic relation

$$\sigma = K \epsilon^n \quad \text{Equation 3}$$

where:  $K$  = strength coefficient;  $n$  = strain hardening exponent.

Average values of  $K$  and  $n$  as obtained from a log-log plot of the stress and strain are given in Table II.

Table II  
Mechanical Properties of Aluminum Alloy 2S-O Tubing in Simple Tension

	Mechanical Property (average of three tests)	Test Results
Nominal Values	Yield Strength (0.2% offset), psi	6,750
	Ultimate Strength, psi	13,700
	Modulus of Elasticity, psi	10,000,000
	% Elongation in 2 Inches	29 (at ultimate strength)
True Values	Fracture Strength, psi	18,000
	Axial Ductility	0.26
	Constant $K$ , psi	25,000
	Strain Hardening Coefficient, $n$	0.244

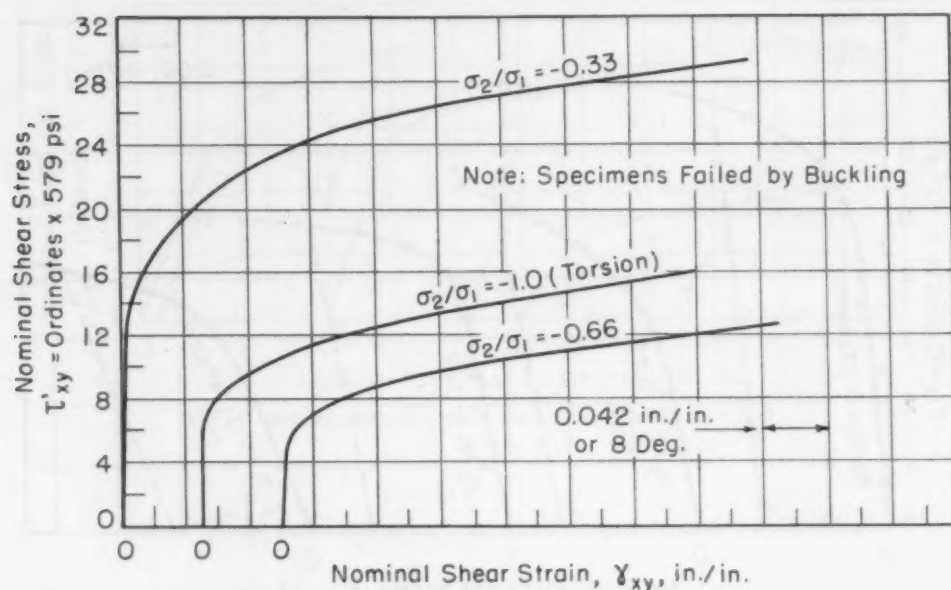


Fig. 5—Relation Between Nominal Shear Stress and Shear Strain for Alcoa 2S-O.

*Constant Stress Ratio Test Results*—Nominal stress-strain diagrams for both the elastic and plastic ranges were obtained for 2S-O tubes. These results are plotted in Figs. 4 and 5, for the various constant principal stress ratios considered. In Fig. 4, the relations between the nominal axial stress ( $\sigma_x^1$ ) and nominal strain ( $e_x$ ) are shown. In Fig. 5, relations between the nominal shear stress ( $\tau_{xy}^1$ ) and nominal shear strain ( $\gamma_{xy}$ ) are shown. The approximate values of the nominal axial and shearing stresses used in plotting Figs. 4 and 5 are, respectively,

$$\sigma_x^1 = \frac{P}{\pi t(d+t)} \quad \text{Equation 4}$$

$$\tau_{xy}^1 = \frac{2M_t}{\pi dt(d+t)} \quad \text{Equation 5}$$

where  $P$  = the axial load,  $M_t$  = the twisting moment,  $d$  = the internal diameter of the specimen, and  $t$  = the wall thickness.

The nominal axial and shear strains, in terms of the measured strains, are, respectively,

$$e_x = \frac{\delta_{1x} + \delta_{2x}}{2L_o} \quad \text{Equation 6}$$

$$\gamma_{xy} = \frac{\pi}{720} (d+2t) \int \quad \text{Equation 7}$$

where  $\delta_{1x}$ ,  $\delta_{2x}$  = the measured axial strains on two sides of the specimen,  $L_o$  = the gage length, and  $\int$  = the angle of twist in degrees.

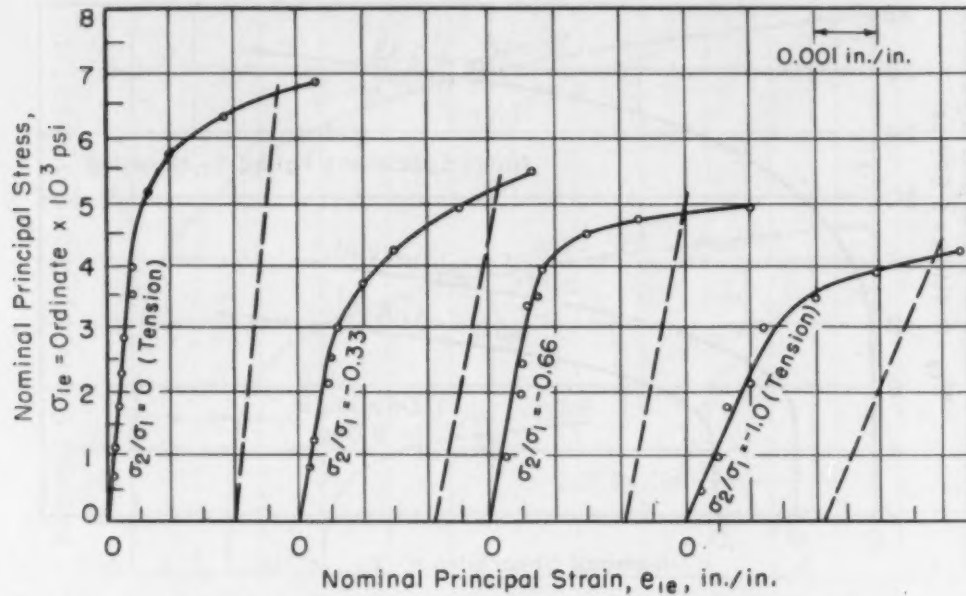


Fig. 6—Elastic Stress-Strain Relations for Alcoa 2S-O.

*Elastic Combined Stress-Strain Relations*—Using values of nominal stresses ( $\sigma_x^1$ ) and ( $\tau_{xy}^1$ ) and the nominal strains ( $e_x$ ) and ( $\gamma_{xy}$ ), the nominal principal stresses and elastic strains can be calculated. The values of the nominal principal stresses and strains have been shown to be, respectively,

$$\left. \begin{matrix} \sigma_{2e} \\ \sigma_{1e} \end{matrix} \right\} = \frac{\sigma_x^1}{2} \pm \sqrt{\frac{(\sigma_x^1)^2}{4} + (\tau_{xy}^1)^2} \quad \text{Equation 8}$$

$$\left. \begin{matrix} e_{1e} \\ e_{2e} \end{matrix} \right\} = \frac{e_x + e_y}{2} \pm \sqrt{\frac{(e_x - e_y)^2}{4} + \frac{\gamma_{xy}^2}{4}} \quad \text{Equation 9}$$

For alloy 2S-O the relations between the nominal principal stresses and nominal principal strains for various constant ratios of biaxial stresses are shown in Figs. 6 and 7. In calculating values of the nominal principal stresses and strains, values of stresses and strains from the average stress-strain relations in Figs. 4 and 5 were used. By means of Figs. 6 and 7 it is possible to obtain the principal nominal stress values at yield,  $\sigma_{1y}$  and  $\sigma_{2y}$ , for each constant principal stress ratio. For simple tension with  $\sigma_{2e}/\sigma_{1e} = 0$ , the yield stress  $\sigma_y$  is  $\sigma_{1e}$  and  $\sigma_{2e}$  is zero. The yield stress for simple tension was defined by an offset strain of 0.002 inch per inch as shown in Fig. 6. For the other constant principal stress ratios an equivalent offset strain, suggested by Marin (27), corresponding to the value of 0.002 inch per inch for simple tension was used. The equivalent offset strains  $e_{1e}$  and  $e_{2e}$  have been shown to be



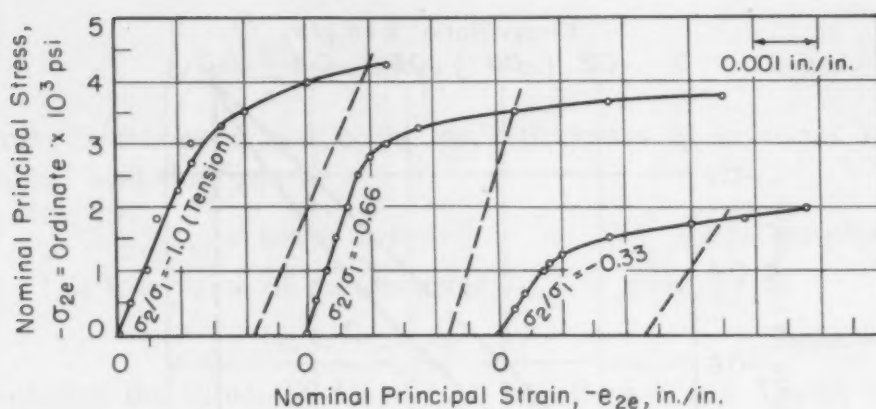


Fig. 7—Elastic Stress-Strain Relations for Alcoa 2S-O.

$$e_{01} = \frac{\sigma_y}{E} \left[ 1 - \frac{1 - m\alpha}{\sqrt{1 - \alpha + \alpha^2}} \right] + e_t \quad \text{Equation 10a}$$

$$e_{02} = \frac{\sigma_y}{E} \left[ 1 - \frac{\alpha - m}{\sqrt{\alpha^2 - \alpha + 1}} \right] + e_t \quad \text{Equation 10b}$$

where  $\sigma_y$  is the yield stress in simple tension, psi, corresponding to an offset  $e_t$ ,  $E$  is the modulus of elasticity,  $\sigma_{2e}/\sigma_{1e}$  is the principal stress ratio  $\alpha$ , and  $m$  is Poisson's ratio.

The values of the equivalent offset strains  $e_{01}$  and  $e_{02}$  are calculated for each constant principal stress ratio by Equations 4 and 5. These values of offset strain are then used as shown in Figs. 6 and 7 to determine the yield stresses  $\sigma_{1y}$  and  $\sigma_{2y}$  for each principal stress ratio. The values of the yield stresses  $\sigma_{1y}$  and  $\sigma_{2y}$  so obtained are given in Table III.

Table III  
Yield Strengths of 2S-O Alloy for Various Ratios of Biaxial Stresses

Biaxial Stress Ratio	Yield Stress $\sigma_{1y}$ , psi	Yield Stress $\sigma_{2y}$ , psi	Stress Ratios*	
			$x = \sigma_{1y}/\sigma_y$	$y = \sigma_{2y}/\sigma_y$
0 (Tension)	6,750	0	1.00	0
-0.33	5,300	-1,800	0.79	-0.27
-0.66	4,900	-3,500	0.73	-0.52
-1.00 (Torsion)	4,650	-4,500	0.62	-0.62

\* $\sigma_y$  is the yield strength in simple tension at 0.2% offset.

For 2S-O, Fig. 8 shows the relation between the yield stress ratio  $x = \sigma_{1y}/\sigma_y$  and  $y = \sigma_{2y}/\sigma_y$  as listed in Table III. The relations between the yield stress ratios  $X$  and  $Y$  as predicted by the maximum shear, maximum stress and distortion energy theories are also shown. A comparison of the test results and the distortion energy theory (as given in Fig. 8) shows that this theory of failure gives an

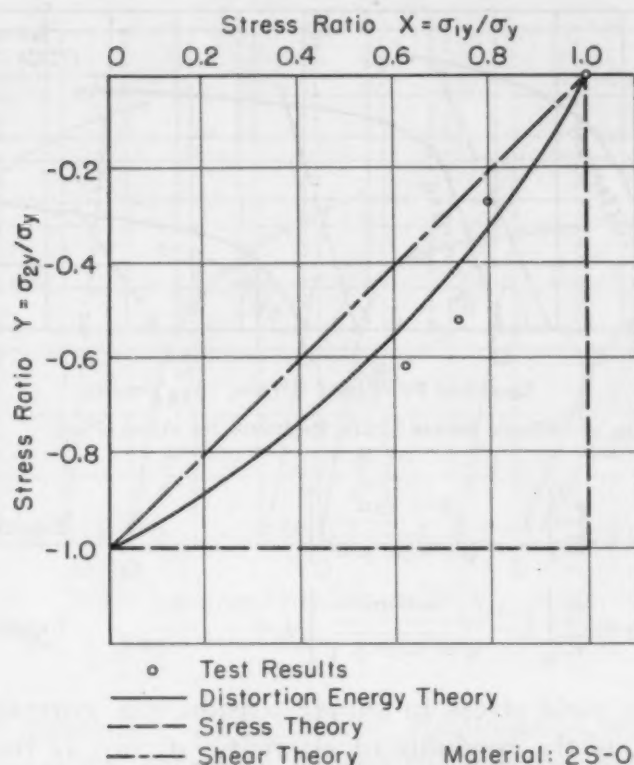


Fig. 8—Comparison of Yield Strengths for Various Biaxial Stress Ratios With Theories of Failure.

approximate prediction of the yield strengths. It is evident that yield strength decreases with decreasing principal stress ratio. For the 2S-O alloy, however, buckling obscures the influence of biaxiality on true ductility.

*Plastic Combined Stress-Strain Relations*—To determine the plastic stress-strain relations, the changes in the dimensions of the specimens must be considered. In the plastic range these changes in dimensions are appreciable and the stresses and strains can no longer be based on the original dimensions and gage length. True stresses and strains based on change in dimensions must now be used in place of the nominal values given by Equations 4 and 5.

The true stress components  $\sigma_x$  and  $\tau_{xy}$  can still be defined by Equations 4 and 5, provided the original values of  $d$  and  $t$  in these equations are replaced by their true values.

To determine the true value of wall thickness ( $t_p$ ) we can write, using Equation 1, the true strain in the direction of the wall thickness as

$$\epsilon_x = \log_e (1 + \epsilon_x) = \log_e t_p/t \quad \text{Equation a}$$

If the volume is assumed to remain constant in the plastic range,  $\epsilon_x + \epsilon_y + \epsilon_z = 0$ . Since  $\sigma_y = 0$  and  $\sigma_z = 0$ , then  $\epsilon_y = -\epsilon_x$  or

$$\epsilon_x = -\frac{\epsilon_x}{2} = -\frac{1}{2} \log_e (1 + e_x) \quad \text{Equation b}$$

From Equations a and b the wall thickness  $t_p$  in terms of the original wall thickness is

$$t_p = t / (1 + e_x)^{1/2} \quad \text{Equation c}$$

The true value of the diameter ( $d_p$ ) is given by

$$\epsilon_s = \log_e d_p / d \quad \text{Equation d}$$

Replacing the values of  $d$  and  $t$  in Equations 4 and 5 with  $d_p$  and  $t_p$  from Equations c and d, the true stress components  $\sigma_x$  and  $\tau_{xy}$  are

$$\sigma_x = \frac{P}{\pi t(d+t)} (1 + e_x) = \sigma_x^1 (1 + e_x) \quad \text{Equation 11}$$

$$\tau_{xy} = \frac{2M_t}{\pi d t(d+t)} (1 + e_x)^{3/2} = \tau_{xy}^1 (1 + e_x)^{3/2} \quad \text{Equation 12}$$

The true principal stresses corresponding to the true stress components  $\sigma_x$  and  $\tau_{xy}$  are

$$\left. \begin{matrix} \sigma_1 \\ \sigma_2 \end{matrix} \right\} = \frac{\sigma_x}{2} \pm \sqrt{\frac{\sigma_x^2}{4} + \tau_{xy}^2} \quad \text{Equation 13}$$

The directions of the planes of principal stresses are defined by the values

$$\theta_1 = \frac{1}{2} \left[ \tan^{-1} \left( \frac{-2\tau_{xy}}{\sigma_x} \right) \right] \quad \text{Equation 14}$$

$$\theta_2 = \frac{\pi}{2} + \theta_1$$

The values of  $\theta_1$  and  $\theta_2$  determine the direction of the planes perpendicular, respectively, to the stresses  $\sigma_1$  and  $\sigma_2$ .

The true principal strains will be defined as the strains in the direction of the true principal stresses. The values of the principal strains in terms of the nominal strains  $e_x$  and  $\gamma_{xy}$  have been determined by a geometric method using the condition that the deformations are large. This analysis shows that the nominal principal strain values are (1):

$$e_1 = \sqrt{[e_x^2 + (\tan \gamma_{xy} - \frac{e_x}{2} \cot \beta_1)^2] \sin^2 \beta_1 - \sin^2(\beta_1 - \alpha_1) + \cos(\beta_1 - \alpha_1) - 1}$$

$$e_2 = \sqrt{[e_x^2 + (\tan \gamma_{xy} - \frac{e_x}{2} \cot \beta_2)^2] \sin^2 \beta_2 - \sin^2(\beta_2 - \alpha_2) + \cos(\beta_2 - \alpha_2) - 1}$$

$$e_3 = -(e_1 + e_2) \quad \text{Equation 15}$$



where

$$\begin{aligned} \alpha_1 &= \tan^{-1} \left[ \frac{e_x + 1}{\cot \beta_1 + \tan \gamma_{xy} - \frac{e_x}{2} \cot \beta_1} \right] \\ \alpha_2 &= \tan^{-1} \left[ \frac{e_x + 1}{\cot \beta_2 + \tan \gamma_{xy} - \frac{e_x}{2} \cot \beta_2} \right] \\ \beta_1 &= \left( \theta_1 + \frac{\pi}{2} \right), \quad \beta_2 = \left( \theta_2 + \frac{\pi}{2} \right) \end{aligned} \quad \text{Equation 16}$$

and  $\theta_1$  and  $\theta_2$  are the directions of the planes of principal stress as given by Equation 14. With values of  $e_1$  and  $e_2$  determined by Equations 15 and 16, the true principal strains are by Equation 1

$$\begin{aligned} \epsilon_1 &= \log_e (1 + e_1) \\ \epsilon_2 &= \log_e (1 + e_2) \\ \epsilon_3 &= -(\epsilon_1 + \epsilon_2) \end{aligned} \quad \text{Equation 17}$$

Taylor and Quinney (14) used the *strain quadric method* for determining the principal strains. Using this procedure the nominal principal strains become

$$\begin{aligned} e_1 &= \frac{1}{4} \left[ e_x + \sqrt{\left( \frac{d+2t}{L_0} \right)^2 \left( \frac{\rho \pi}{180} \right)^2 + 9e_x^2} \right] \\ e_2 &= \frac{1}{4} \left[ e_x - \sqrt{\left( \frac{d+2t}{L_0} \right)^2 \left( \frac{\rho \pi}{180} \right)^2 + 9e_x^2} \right] \\ e_3 &= -(e_1 + e_2) \end{aligned} \quad \text{Equation 18}$$

where  $e_x$  is defined by Equation 6 and the other terms in Equation 18 are as previously defined. With values of the nominal principal strains determined from Equation 18, Equation 17 can be used to find the true principal strain. In calculating the values of the true principal stresses  $\sigma_1$  and  $\sigma_2$  and the true strains  $\epsilon_1$  and  $\epsilon_2$ , values of the stresses ( $\sigma_x^1$ ) and ( $\tau_{xy}^1$ ) and strains ( $e_x$ ) and ( $\gamma_{xy}$ ) are selected from the average curves of Figs. 4 and 5. These resulting true stress-strain relations for the constant principal stress ratio tests are shown in Figs. 9 and 10. The principal strains were evaluated both by reference to strain quadrics (3) and by a geometrical method. Fig. 11 is a plot of principal stress versus principal strain for various stress ratios based on calculations performed by both methods. Fig. 11 shows that the two methods are in good agreement. The last points in these figures represent failure of the tubes by buckling. The ratio of the principal stresses in these figures is based on

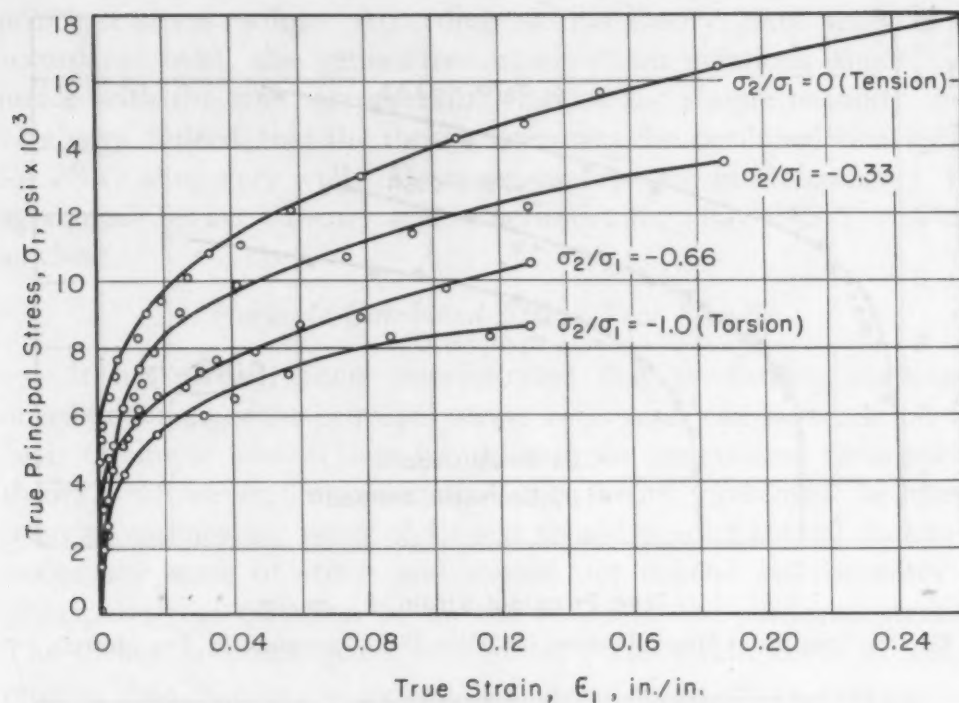


Fig. 9—True Stress - True Strain Relations. Material: Alcoa 2S-O.

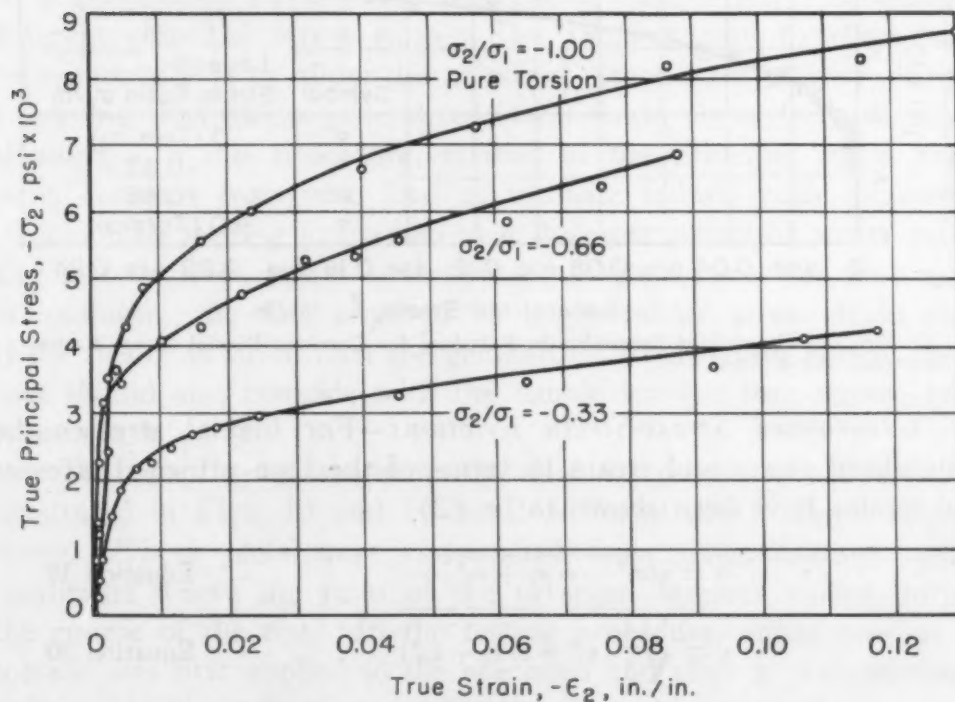


Fig. 10—True Stress - True Strain Relations. Material: Alcoa 2S-O.

nominal values; however, for all practical purposes the ratios calculated on this basis are close enough to the true values to warrant their use.

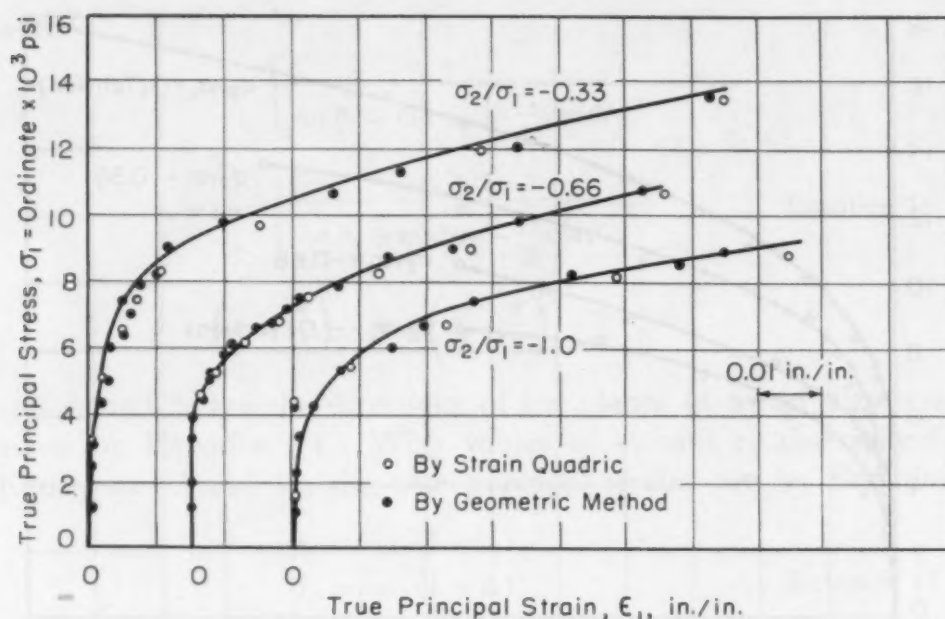


Fig. 11—True Stress-Strain Relations for Alcoa 2S-O Determined by Two Methods.

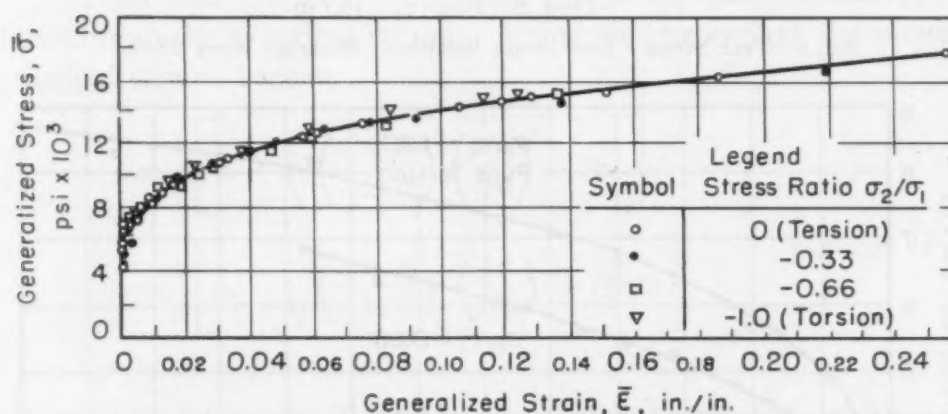


Fig. 12—Generalized Stress-Strain Relations for Constant Biaxial Stress Ratios. Material: Alcoa 2S-O.

*Generalized Stress-Strain Relations*—For biaxial stresses the generalized stress and strain in terms of the true principal stresses and strains have been shown to be (2)

$$\bar{\sigma} = \sqrt{\sigma_1^2 - \sigma_1 \sigma_2 + \sigma_2^2} \quad \text{Equation 19}$$

$$\bar{\epsilon} = \sqrt{\frac{4}{3} (\epsilon_1^2 + \epsilon_1 \epsilon_2 + \epsilon_2^2)} \quad \text{Equation 20}$$

The generalized stresses and strain are identical with the significant or effective stresses and strains used by other investigators. Furthermore, the octahedral stress and strain are equal to the values of  $\bar{\sigma}$  and  $\bar{\epsilon}$  except for a numerical constant. The generalized stress  $\bar{\sigma}$  and generalized strain are plotted in Fig. 12 for the various constant



principal stress ratios. According to this theory, data analyzed in accordance with the generalized stress-strain relations should coincide with the true stress-strain relations for simple tension. Fig. 12 shows, indeed, that the theory interprets the combined stress data for 2S-O alloy very well. However, as reported in Reference 1, the agreement between theory and experiment for alloy 24S-T was not as close.

#### *Variable Combined Stress Test Results*

It has already been demonstrated that predictions of biaxial ductility for constant principal stress ratio tests can be made on the basis of simple tension data by utilizing the generalized deformation theory. However, in order that the theory presented be useful from an engineering point of view it should predict biaxial ductilities under any state of stress and should not depend on constancy of principal stress direction or on the ratios of the principal stresses. The theory proposes that a true stress-true strain curve of simple tension data is also the generalized stress-strain curve representing data obtained under any state of stress. Consequently, each point on a generalized stress-strain plot could, theoretically, represent a different principal stress ratio. The simplest way to check this experimentally is to allow the principal stress ratio to vary during a test and then plot a generalized stress-strain curve from the data obtained. In this procedure, instead of the principal stress ratio being constant from zero load to ultimate failure, each increment of combined loading gives rise to a different principal stress ratio. The instantaneous values of the principal stress ratios are then used in computing the data required for a generalized stress-strain plot. If the theory is valid, then the generalized stress-strain plot of these data should also coincide with the simple tension true stress-true strain curve.

That the theory is apparently valid for the materials tested is illustrated in Figs. 13 and 14 for 24S-T and 2S-O alloys, respectively. These plots were constructed from data obtained under conditions where the ratio of the principal stresses varied during the course of the test. In the testing procedure, either tension or torsion was first applied to the specimen and after a predetermined value of axial or shear stress was reached, this nominal stress was maintained constant; the torque or axial load was then continuously applied until fracture (24S-T) or buckling (2S-O) occurred. In Fig. 13, for example, the open circles represent data from a test in which pure torsion ( $\sigma_2/\sigma_1 = -1.0$ ) was initially applied to the

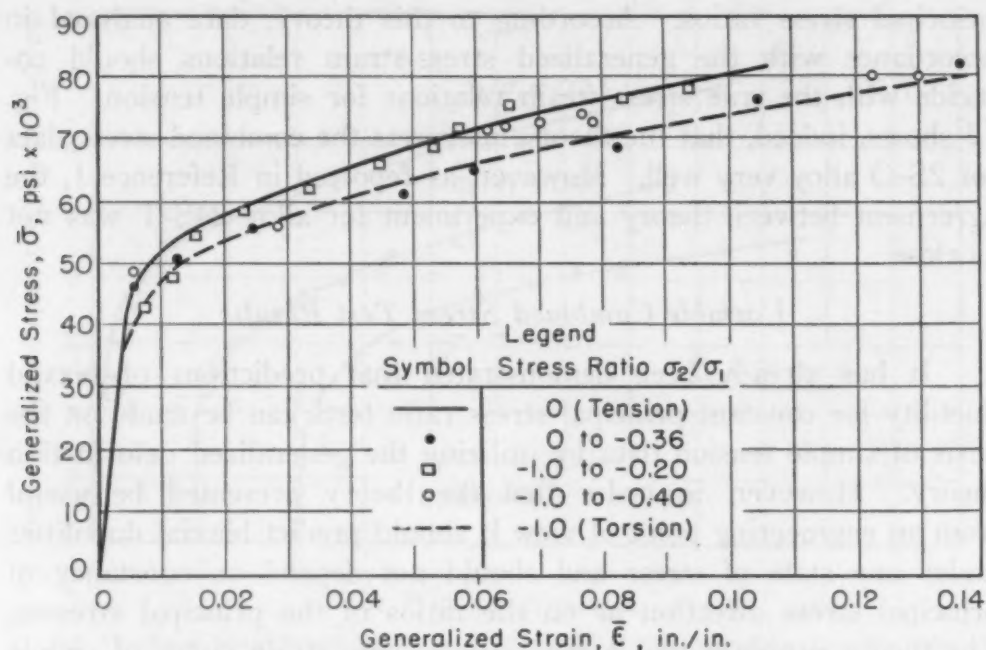


Fig. 13—Generalized Stress-Strain Relations for Variable Biaxial Stress Ratios. Material: Alcoa 24S-T.

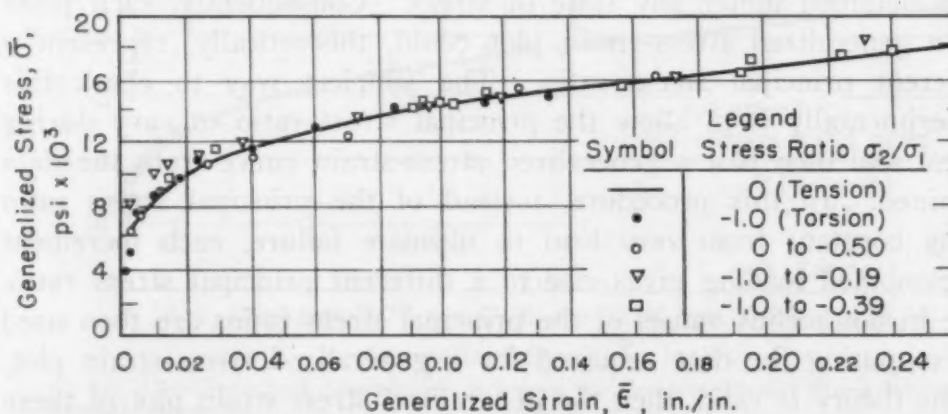


Fig. 14—Generalized Stress-Strain Relations for Variable Biaxial Stress Ratios. Material: Alcoa 2S-O.

specimens until a predetermined shear stress was reached; at this stress, tension was applied ( $\sigma_2/\sigma_1 = 0$ ) while the shear stress was held constant. Additional increments of tension loading then had the effect of raising the principal stress ratio from  $-1.0$  to  $-0.4$ , at which point buckling occurred.

### SUMMARY

In the present investigation aluminum alloy 24S-T was subjected to variable principal stress ratio tests of the tension-compression type as an extension of data obtained in Reference 1. In addition, both constant and variable principal stress ratio tests

were conducted on aluminum alloy 2S-O. In Reference 1, for 24S-T, it is shown that both yield and fracture strengths for material subjected to tension-compression biaxial stresses are lowered while ductility is increased as the stress ratio is decreased. For alloy 2S-O, yield strength is decreased with decreasing stress ratio but the occurrence of buckling obscures the influence of biaxiality on ductility. Yielding, however, takes place in accordance with the distortion energy theory of failure, and stress-strain relations in the plastic range are represented very well by the generalized deformation theory for both alloys under conditions of constant and variable principal stress ratios.

#### ACKNOWLEDGMENTS

The experimental work reported in this paper utilized equipment developed in a project sponsored at The Pennsylvania State College by the U. S. Army Air Forces (1). Appreciation is expressed to this organization for permission to use the equipment and make reference to the data obtained. Thanks are also due to the E. I. duPont de Nemours & Company, Inc., Wilmington, Delaware, who sponsored the research reported in this paper through a Fellowship in the School of Engineering at The Pennsylvania State College. This paper represents, in part, a thesis submitted by J. H. Faupel to The Pennsylvania State College for the degree of Ph.D. in Engineering Mechanics.

#### References

1. J. Marin, J. H. Faupel and V. L. Dutton, AF Tech. Report 5694, April 1948; also see J. Marin, "Stress-Strain Relations in the Plastic Range for Biaxial Stresses", *Journal, Franklin Institute*, Vol. 248, 1949, p. 231-249.
2. J. Marin, J. H. Faupel, V. L. Dutton and M. W. Brossman, "Biaxial Plastic Stress-Strain Relations for 24S-T Aluminum Alloy", N.A.C.A. Technical Note No. 1536, May 1948.
3. A. E. H. Love, "A Treatise on the Mathematical Theory of Elasticity", Fourth Edition, 1944, Dover Publications, Inc., New York, N. Y.
4. W. Prager, "Recent Developments in the Mathematical Theory of Plasticity", *Journal of Applied Physics*, Vol. 20, No. 3, March 1949, p. 235-241.
5. W. Prager, "Theory of Plastic Flow versus Theory of Plastic Deformation", *Journal of Applied Physics*, Vol. 19, No. 6, June 1948, p. 540-543.
6. W. Prager, "An Introduction to the Mathematical Theory of Plasticity", *Journal of Applied Physics*, Vol. 18, No. 4, April 1947, p. 375-383.
7. S. B. Batdorf and B. Budiansky, "A Mathematical Theory of Plasticity Based on the Concept of Slip", N.A.C.A. Technical Note No. 1871, April 1949.
8. J. Marin, "Mechanical Properties of Materials and Design", 1942, McGraw-Hill Book Co., Inc., New York, N. Y.



9. J. H. Hollomon, "The Problem of Fracture", 1946, The American Welding Society, New York, N. Y.
10. M. Gensamer, E. Saibel, J. T. Ransom and R. E. Lowrie, "Fracture of Metals", 1947, The American Welding Society, New York, N. Y.
11. J. L. M. Morrison, "The Yield of Mild Steel with Particular Reference to the Effect of Size of Specimen", *Proceedings*, Institution of Mechanical Engineers (London), Vol. 142, No. 3, 1940, p. 193-223.
12. G. Cook and A. Robertson, "The Strength of Thick Hollow Cylinders Under Internal Pressure", *Engineering* (London), Vol. 92, 1911, p. 786-789.
13. M. Ros and A. Eichinger, "Versuche zur klärung der Frage der Bruchgefahr", Bericht No. 34, *Eidgenoessiche Material Prüfungsanstalt*, Zurich, Switzerland, 1929.
14. G. I. Taylor and H. Quinney, "The Plastic Distortion of Metals", *Transactions*, Royal Society of London, Vol. 23, Series A, 1931, p. 323-361.
15. J. Seigle and F. Cretin, "Limite élastique et resistance des aciers doux recruits dans le cas d'efforts combines de traction et de torsion", *Revue de Metallurgie, Memoirs*, June 22, 1925, p. 374-382.
16. E. A. Davis, "Combined Tension-Torsion Tests on a 0.35 Per Cent Carbon Steel", *Transactions*, American Society of Mechanical Engineers, Vol. 62, No. 7, October 1940, p. 577-586.
17. E. G. Thomsen and J. E. Dorn, "The Effect of Combined Stresses on the Ductility and Rupture Strength of Magnesium-Alloy Extrusions", *Journal of the Aeronautical Sciences*, Vol. 11, No. 2, April 1944, p. 125-136.
18. P. W. Bridgman, "On Torsion Combined with Compression", *Journal of Applied Physics*, Vol. 14, No. 6, June 1943, p. 273-283.
19. K. Hohenemser and W. Prager, "Beitrag zur Mechanik des bildsamen Verhaltens von Flusstahl", *Zeitschrift für Angewandte Mathematik und Mechanik*, Vol. 12, 1932, p. 1-14.
20. W. Lode, "Versuche ueber den Einfluss der mittleren Hauptspannung auf das Fliessen der Metalle Eisen, Kupfer und Nickel", *Zeitschrift für Physik*, Vol. 36, 1926, p. 913.
21. R. Schmidt, "Ueber den Zusammenhang von Spannungen und Formaenderungen im Verfestigungsgebiet", *Ingenieur-Archiv*, Vol. 3, No. 3, 1932, p. 215-235.
22. A. Nadai and E. A. Davis, "Plastic Behavior of Metals in the Strain Hardening Range", Parts 1 and 2, *Journal of Applied Physics*, Vol. 8, No. 3, March 1937, p. 205-217.
23. J. Marin and R. L. Stanley, "Failure of Aluminum Subjected to Combined Stresses", Supplement, *Journal*, American Welding Society, Vol. 5, No. 2, February 1949, p. 74-80.
24. J. H. Hollomon, "Tensile Deformation", *Metals Technology*, Technical Paper No. 1879, Vol. 12, No. 4, June 1945.
25. J. R. Low and F. Garofalo, "Precision Determination of Stress-Strain Curves in the Plastic Range", *Transactions*, Society for Experimental Stress Analysis, Vol. 4, No. 2, 1947, p. 16-24.
26. "Alcoa Aluminum and Its Alloys", The Aluminum Company of America, 1947, Pittsburgh, Pa.
27. J. Marin, "A Method of Defining Failure in Members Subjected to Combined Stresses", *TRANSACTIONS*, American Society for Metals, December 1941, p. 1013-1021.
28. A. Nadai, "Plasticity", 1931, McGraw-Hill Book Company, Inc., New York, N. Y.

# HOT FORMING OF ALUMINUM AND MAGNESIUM ALLOYS

BY T. E. PIPER

## *Abstract*

*Extensive development work in forming high strength aluminum and magnesium alloys at elevated temperatures has made possible substantial savings in production fabrication. Results of experimentation at Northrop Aircraft, Inc., have been assembled and are discussed in this paper.*

*Methods of heating and their limitations, effect of time and temperature on mechanical properties, heating time versus cross sectional area, methods of temperature control, and a comparison of hot forming in the heat treated condition versus forming in the annealed condition are all discussed.*

*In general, limited room temperature forming can be accomplished in the heat treated and work-hardened conditions of aluminum and magnesium alloys; however, elevated temperature forming limits comparable to annealed material in certain conditions of forming may be realized without appreciable reduction in strength. This reduces fabrication to a single operation and eliminates all check and straightening resulting from heat treat warpage.*

*The resistance and oil bath methods of heating proved to be the most satisfactory for the fabrication at elevated temperatures of 75S-T6 aluminum alloy and AZ31X-h (FS1-h) magnesium alloy. Both alloys may be hot formed at 300 °F (150 °C).*

WITH the advent of 75S high strength aluminum alloys for aircraft design applications, a great production savings in man-hours may be realized and closer-tolerance parts produced in the forming processes by taking advantage of the inherent hot forming characteristics of 75S in the heat treated condition. When the parts were formed before heat treating, relief of induced stresses during heat treating, as well as nonuniform cooling afterward, resulted in serious warpage and dimensional changes. To correct the distorted shapes, mechanical straightening and makeshift shop practices were used. These in turn caused indeterminate prestress-

<sup>1</sup>The figures appearing in parentheses pertain to the references appended to this paper.

A paper presented before the Thirty-second Annual Convention of the Society, held in Chicago, October 21 to 27, 1950. The author, T. E. Piper, is chief materials and process engineer, Northrop Aircraft, Inc., Hawthorne, Calif. Manuscript received April 17, 1950.

ing, reduced mechanical properties, and overburdening of production facilities to an extent that output was retarded.

During World War II many development projects were conducted in various fields of aircraft production, namely to improve production techniques. Among the projects under study was the fabrication of light metal alloys at elevated temperatures. Startling results were reported for magnesium and some aluminum alloys. This work was done on an experimental basis; consequently, correlation between experimental results and applied production results have not yet been fully evaluated. It is important in aircraft production to find a method of producing fuselage formers, skins and other structural components in the heat treated or fully hard condition, since heat treating of these parts produces excessive warpage.

While the definite advantages of hot forming are often overlooked, the disadvantages of this process are sometimes overemphasized. The greatest advantages are: (a) that hot forming in the heat treated condition requires only one operation, while in the annealed condition at room temperature several operations are necessary; (b) in forming annealed material at temperatures up to 600 °F (315 °C) many parts can be formed in one piece, whereas in forming at room temperature, it may be necessary to make the part in several pieces.

The technical problem involved in hot forming is that of selecting temperature and heating methods that will enable the production department to use the hot forming technique without burdening itself with additional hazards and at the same time retard production to the point where the entire merits of the method are lost.

#### HOT FORMING TEMPERATURE RANGE

The technical problem in hot forming is to maintain a critical temperature range. The effect of temperature is illustrated in Figs. 1, 2 and 3 on the mechanical properties of heat treated 75S aluminum alloys and the work hardened AZ31X (FS1) magnesium alloy at temperature and at room temperature after heating. The forming temperature must be low enough so that there is no adverse effect on the strength properties of the finished part due to overaging or annealing. However, if the forming temperature is too low because of inadequate heat or through cooling, the parts cannot be properly formed.

For 75S-T6, the most generally used of the high strength heat treatable aluminum alloys, a temperature of 300 °F (150 °C) appears to have no appreciable effect on strength. At 400 °F (205 °C)



appreciable overaging takes place. (See Figs. 1 and 3.) Magnesium alloys also have inherent hot forming characteristics similar to 75S-T6 except higher temperatures are required for hot forming. A temperature of 275 to 400 °F (135 to 205 °C) is recommended for most forming operations on high strength magnesium alloys. For AZ31X-h (FS1-h), the most commonly used work hardenable

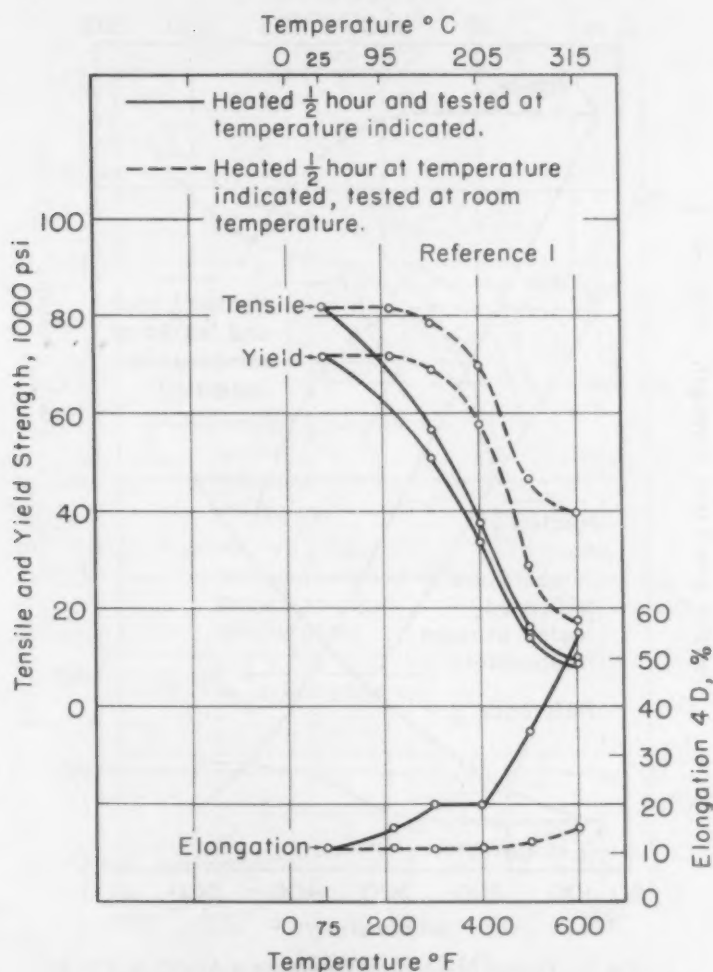


Fig. 1—Typical Mechanical Properties of 75S-T6 Aluminum Sheet at Elevated Temperatures and at Room Temperature After Heating.

magnesium alloy in aircraft, a temperature of 300 °F (150 °C) produces little or no loss in strength characteristics (see Fig. 2).

It was found that excellent results by hot forming could be obtained on heat treated 75S aluminum alloy and magnesium alloys in the full hard condition because of their improved formability at elevated temperatures. The forming limits of 75S-T6 at 300 °F (150 °C) compare favorably with 75S-O at room temperature under certain conditions of forming: stretch forming, bending, joggling.

## HEATING METHODS

Since temperature is a critical factor, methods that permit uniform heating throughout the mass of the part are necessary. Conventional furnace heating methods are unsatisfactory. The time involved in heating is lengthy and methods of handling are awk-

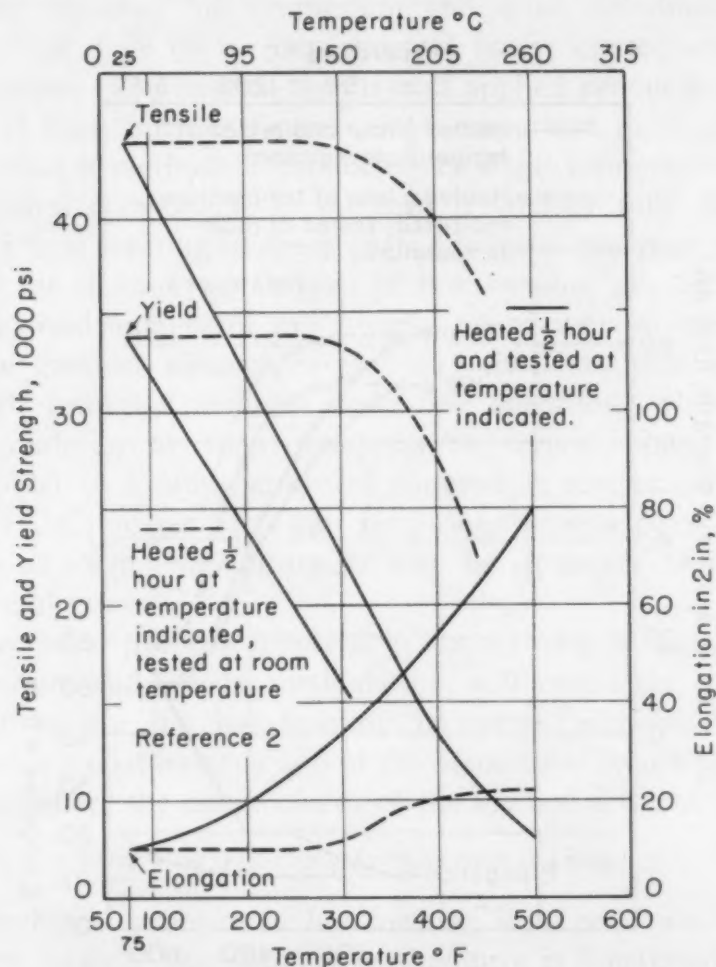


Fig. 2—Typical Mechanical Properties of AZ31X-h (FS1-h) Magnesium Sheet at Elevated Temperature and at Room Temperature After Heating.

ward. Because of the rapidity of heating, adequate temperature control could not be maintained and, hence, induction heating was not practical. Electrical resistance heating then appeared to offer greatest promise. With this method the heat developed would be uniform throughout the part, except where there were severe variations in size and shape of the cross section. In the latter case, hot oil bath heating was the method found most advantageous.

To determine the optimum temperature to which the part should be heated by resistance heating, extensive tests were conducted (see

Figs. 4, 5, 6, 7, 8 and 9). For test purposes, hat sections (0.051 Alclad sheet) and extrusions (0.594-square-inch cross sectional area) of 75S in the heat treated condition were used as specimens (see Figs. 4 and 5). Fig. 6 presents the mechanical properties of extrusions when heated to 300 °F (150 °C), using either A.C. or D.C. electrical equipment. As shown, there were no significant

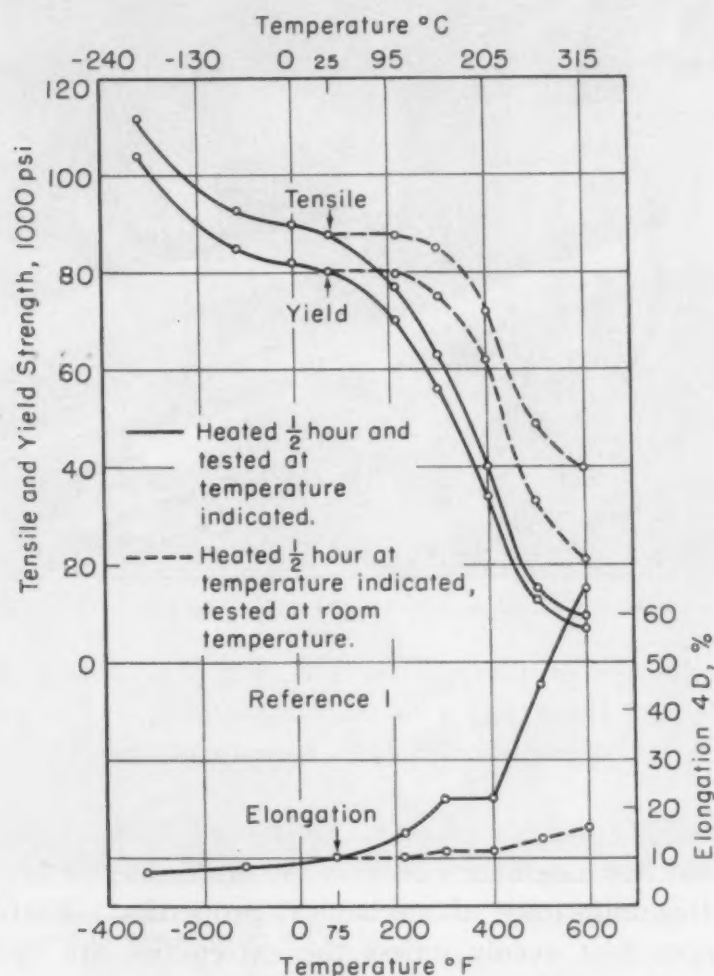


Fig. 3—Typical Mechanical Properties of 75S-T6 Aluminum Extrusions at Elevated Temperatures and at Room Temperature After Heating.

mechanical property losses nor did the final mechanical properties of the material fall below the minimum requirements of the material specification standards of Northrop Aircraft, Inc. The values presented in Fig. 6 are those after the material has been heated only once. Reheating of the 75S-T6 material will successively reduce the mechanical properties because the overaging effects are cumulative.

Heating 75S-T6 extrusions to 400 °F (205 °C) produces sub-



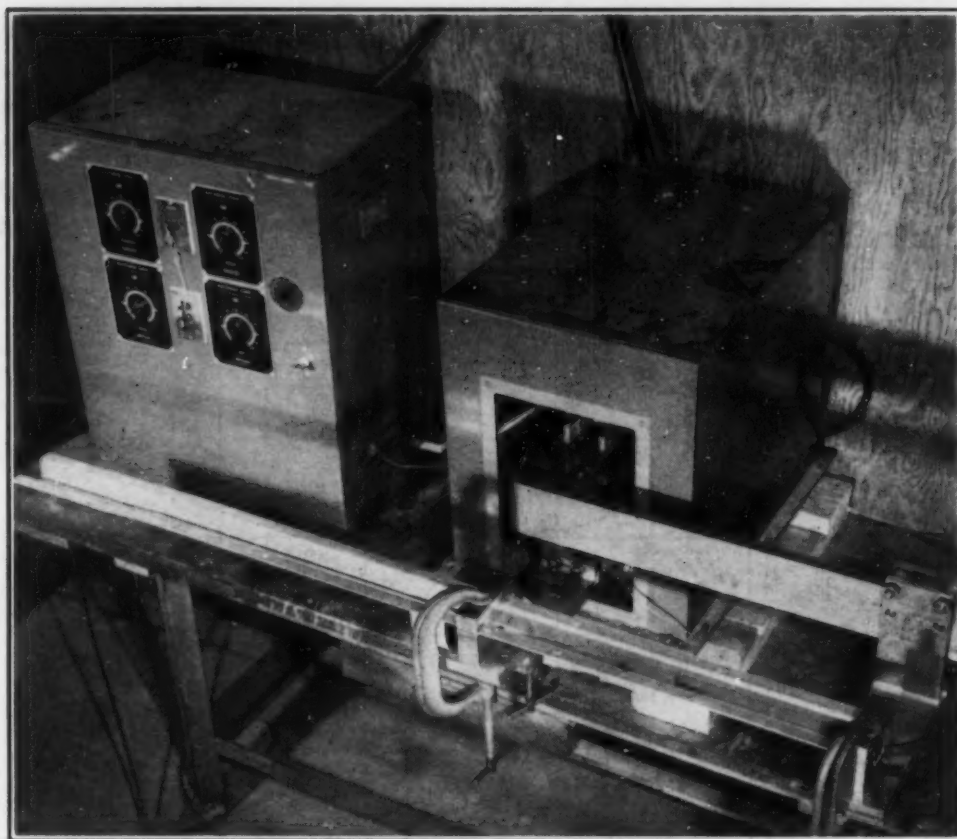


Fig. 4—Experimental Electrical Resistance Heating by A-C Method of 75S-T6 Alclad Sheet.

stantial mechanical property losses (see Fig. 7). Using A.C. electrical equipment, there was a loss of approximately 6% in ultimate and tensile yield strength; with D.C. equipment, this loss was about 5%.

Location of the extrusion to be heated with respect to the magnetic field has a definite effect on the uniformity of heating and, hence, on the uniformity of mechanical properties. Extrusions of various shapes heat evenly unless the extremities are rather thin. By experimenting with extrusions of various shapes, it was determined that a satisfactory heat gradient could be obtained by locating the thickest part of the extrusion within the inductive loop formed by the bus bar and the piece, and keeping the thinnest section away from the loop. Other factors affecting uniformity include surface area, room temperature, voltage, and length of part.

Where severe variation exists in size and shape of the cross section of the parts, the hot oil bath method of heat should be employed. In the Hot Forming Temperature Range section, page 1014, heating heat treatable and work hardening alloys by any method will produce losses in mechanical properties if temperature of the

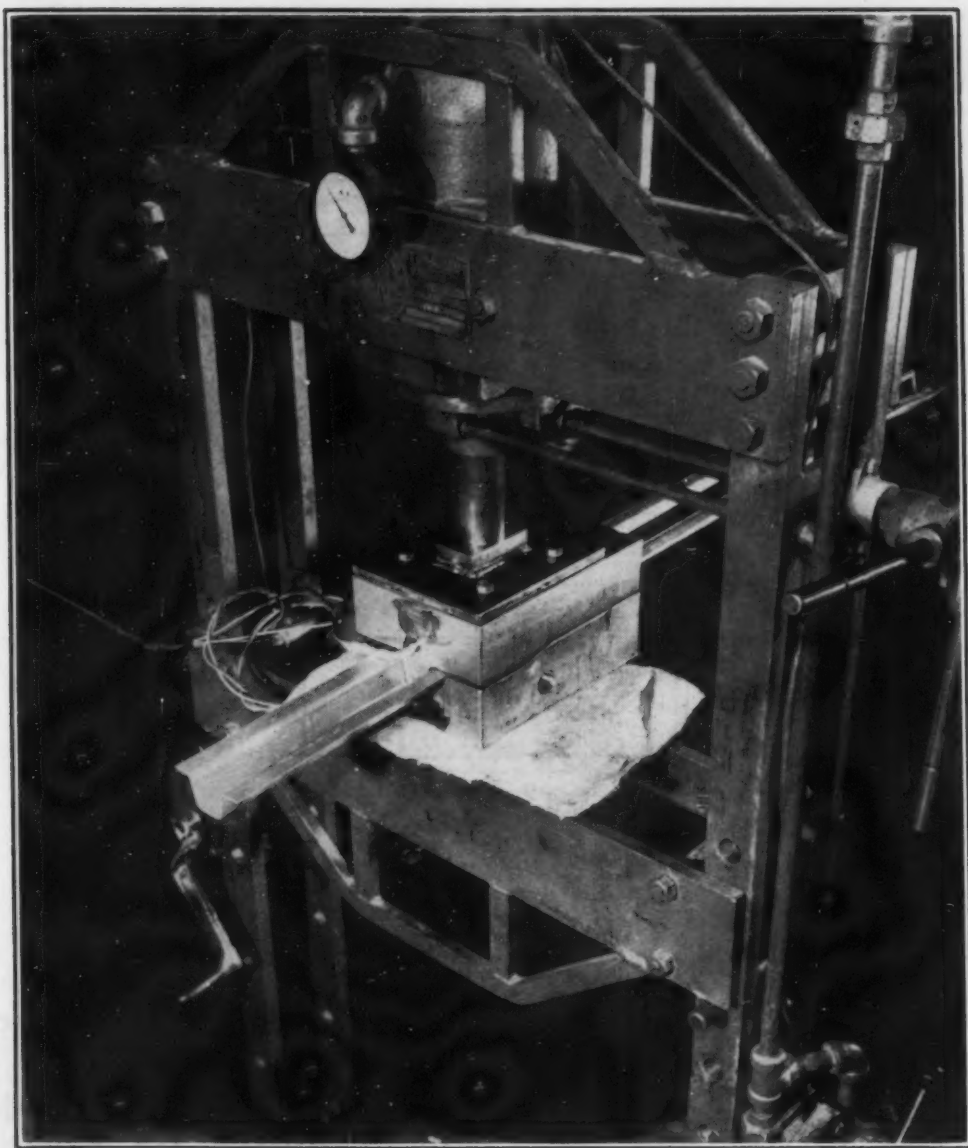


Fig. 5—Experimental Hot Forming 75S-T6 Alclad Hat Section Using Heated Dies. Section preheated by method shown in Fig. 4.

heating medium is too high and/or time at temperature is too long. Numerous tests have been run on this phase of hot forming, and graphs as shown in Figs. 1, 2 and 3 depict consequences of overheating. Thorough heating of parts can be accomplished by the hot oil bath immersion method with very accurate control of temperatures so that reproducible formability characteristics can be obtained.

#### TEMPERATURE EFFECTS

In addition to determining the effect of resistance heating on the physical properties of the material, the relative effects of A.C.

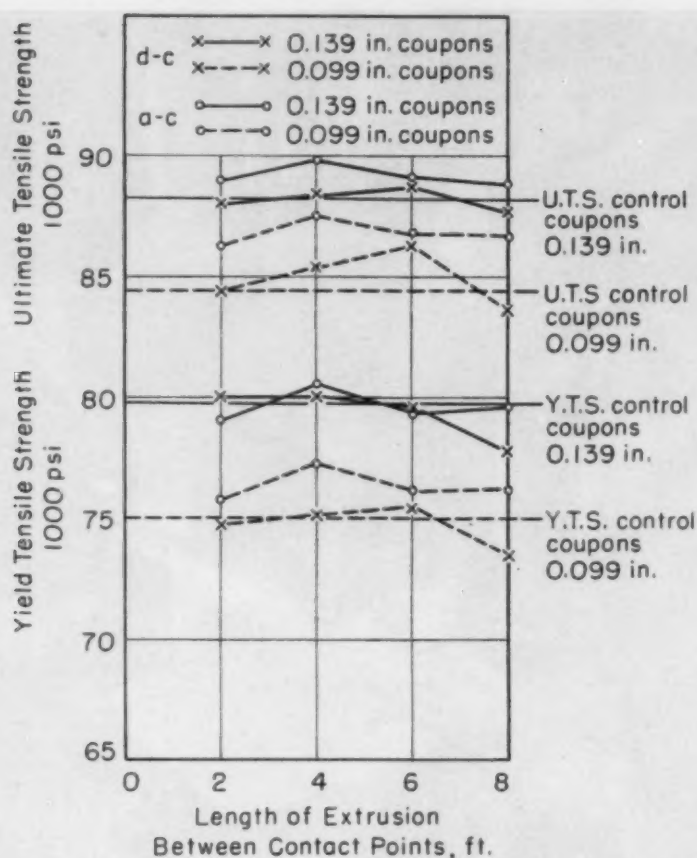


Fig. 6—Effect of Length on Mechanical Properties at Room Temperature of 75S-T6 Zee Extrusions Heated to 300°F (150°C) by Electrical Resistance Method on A-C and D-C Equipment.

and D.C. methods, as well as different temperatures, were also investigated.

The A.C. electrical equipment consisted of a single-phase, 60-cycle A.C. transformer, rated at approximately 40 kva; a phase shift control was used ahead of the transformer to control the primary voltage. The D.C. equipment included a tri-phase transformer rated at approximately 75 kva, and ahead of the transformer a panel that controlled phase shift, rate of D.C. pulses per second and off time between pulses.

Although 300°F (150°C) was the proposed allowable temperature for production heating of parts, the tests were also run at 400°F (205°C), to accentuate any difference between results produced by A.C. and D.C. equipment. To control temperature, a temperature-indicating lacquer was used at 300°F (150°C); in the series of tests at 400°F (205°C), electrical recorders were used in addition to the temperature-indicating lacquers.

The sharpest difference in property results caused by heating



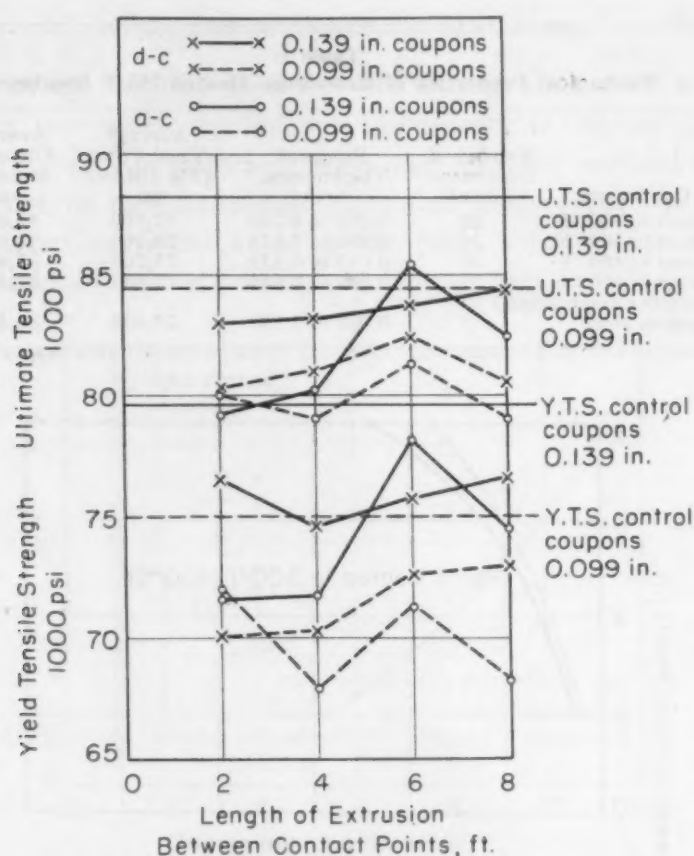


Fig. 7—Effect of Length on Mechanical Properties at Room Temperature of 75S-T6 Zee Extrusions Heated to 400 °F (205 °C) by Electrical Resistance Method on A-C and D-C Equipment.

at 300 and 400 °F (150 and 205 °C) can be seen in the elongation values. Heating the extrusion to 300 °F (150 °C) produced an average gain of 4.75% over the control values; yet there was an average loss of 17.4% in elongation when heated to 400 °F (205 °C) by either method. This can be attributed to the stress relieving action that takes place without overaging at 300 °F (150 °C), resulting in an increase in elongation at room temperature. At 400 °F (205 °C), overaging or coalescence of the age hardening precipitate occurs, lowering the tensile properties but also causing a decrease in elongation. These data are presented in Table I.

With special reference to part length, Figs. 6 and 7 show these mechanical property results by means of curves, for two selected thicknesses, and various heating conditions.

An important problem in resistance heating was local overheating of the part at the point of contact. This was overcome by using the solid copper bus bar, which conducted the secondary current from the transformer and provided area of contact and support

**Table I**  
**Mechanical Properties of Resistance Heated 75S-T Specimens**

Heating Conditions	Number of Specimens Tested	Range of Thicknesses, inch	Average Yield Point (2% Offset) psi	Average Ultimate Strength psi	Average Elongation in 2 Inches, %
D.C. equipment to 300 °F	20	0.098 to 0.139	77,100	86,600	13.4
A.C. equipment to 300 °F	20	0.098 to 0.139	78,100	88,600	13.0
D.C. equipment to 400 °F	20	0.098 to 0.139	73,700	82,400	10.3
A.C. equipment to 400 °F	20	0.099 to 0.139	72,600	81,300	10.5
Control Specimens (no heating) from random stock	4	0.099 to 0.139	77,600	86,400	12.6

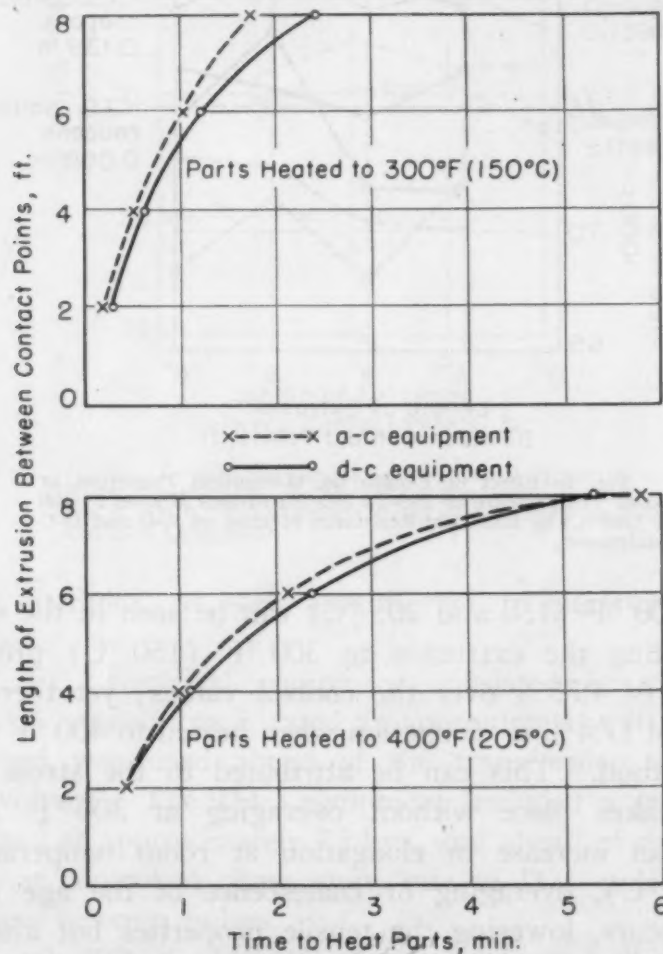


**Fig. 8—Length of 75S-T6 Extrusion Versus Heating Time by Resistance Heating Using A-C and D-C Equipment.**

for the parts to be heated. It was also found that the method of clamping at contact points with sufficient pressure and clean surfaces was of the utmost importance. When the parts were of odd shape, as the hat section in Fig. 4, copper dies conforming to the part were used with successful results.

## COMPARISON OF HEATING METHODS

In comparing the two methods of heating aluminum and magnesium alloys, one of the main items to consider is the time required to heat parts. For the electrical resistance heating method the time to bring a part to the maximum allowable temperature is a direct function of cross sectional area of the part, area of the inductive loop, magnitude of current flow and power factor. Fig. 8 shows

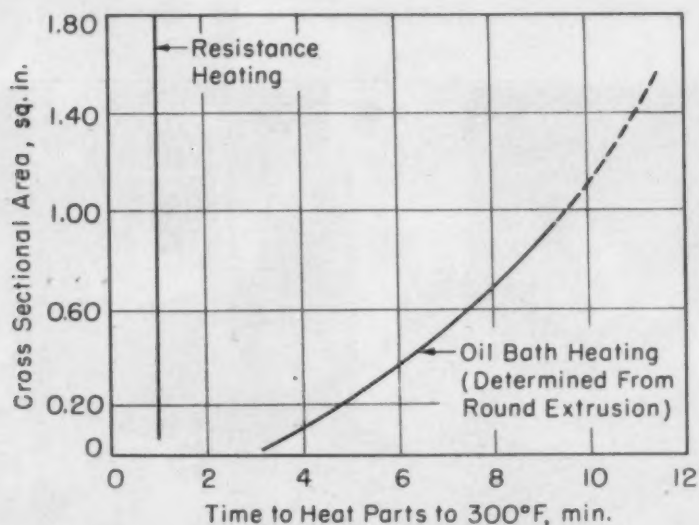


Fig. 9—Comparison of Electrical Resistance and Oil Bath Heating of 75S-T6 Extrusions to 300°F (150°C).

the comparative curves of heating time versus length of part for A.C. and D.C. electrical equipment in resistance heating to 300 and 400 °F (150 and 205 °C). However, greater flexibility of the A.C. setup can be obtained with the use of phase shift control. By phase shift control, greater speed of heating can be obtained if needed, which is desirable when heating parts of odd lengths and special shapes. For the hot oil bath heating method the time to bring a part to the maximum allowable temperature is a direct function of thickness of the part and the temperature of the heating medium. Therefore, with adjustable controls on resistance heating equipment, it is possible to heat any cross sectional area of material, within limits of the equipment, to 300 °F (150 °C) in 1 minute, while heating by oil to the same temperature the time required increases as cross sectional area increases. (See Fig. 9.)

A limited number of tests were made to determine if variation in soaking time after a part reached the forming temperature would cause a change in the formability of the material. The conclusion arrived at was that the time necessary to insure thorough heating



of the part was all that was required, since the variation in formability was negligible. This would also reduce the possibility of overaging or annealing the material by overheating, i.e., temperature or time.

As was previously pointed out, one of the main reasons for forming alloys in the heat treated condition was to eliminate warpage due to heat treatment, which increases the number of man-hours required for fabrication. An example in the saving of man-hours required for fabrication is exemplified by the fabrication in a



Fig. 10—Farquhar Hydraulic Press Forming 75S-T6 Extrusions Preheated by Hot Oil Immersion Method.

Farquhar hydraulic press of 75S spar caps for the XF-89 airplane by hot forming in the "T6" condition as compared to forming in the SO condition. An order of 20 parts would require approximately (a) 1 man-hour fabrication time using the resistance heating method, (b) 4 man-hours for hot oil immersion method, and (c) 60 man-hours by forming in the "SO" or "AQ" condition.

#### PRODUCTION APPLICATION

Typical examples of the use of elevated temperature as applied to production forming at Northrop Aircraft, Inc., are herewith discussed.

For the forming of an extruded 75S-T6 aluminum alloy spar cap, a 75-ton Farquhar hydraulic press is used. The extrusion is heated to 300 °F (150 °C) by immersing in a gas-fired oil bath

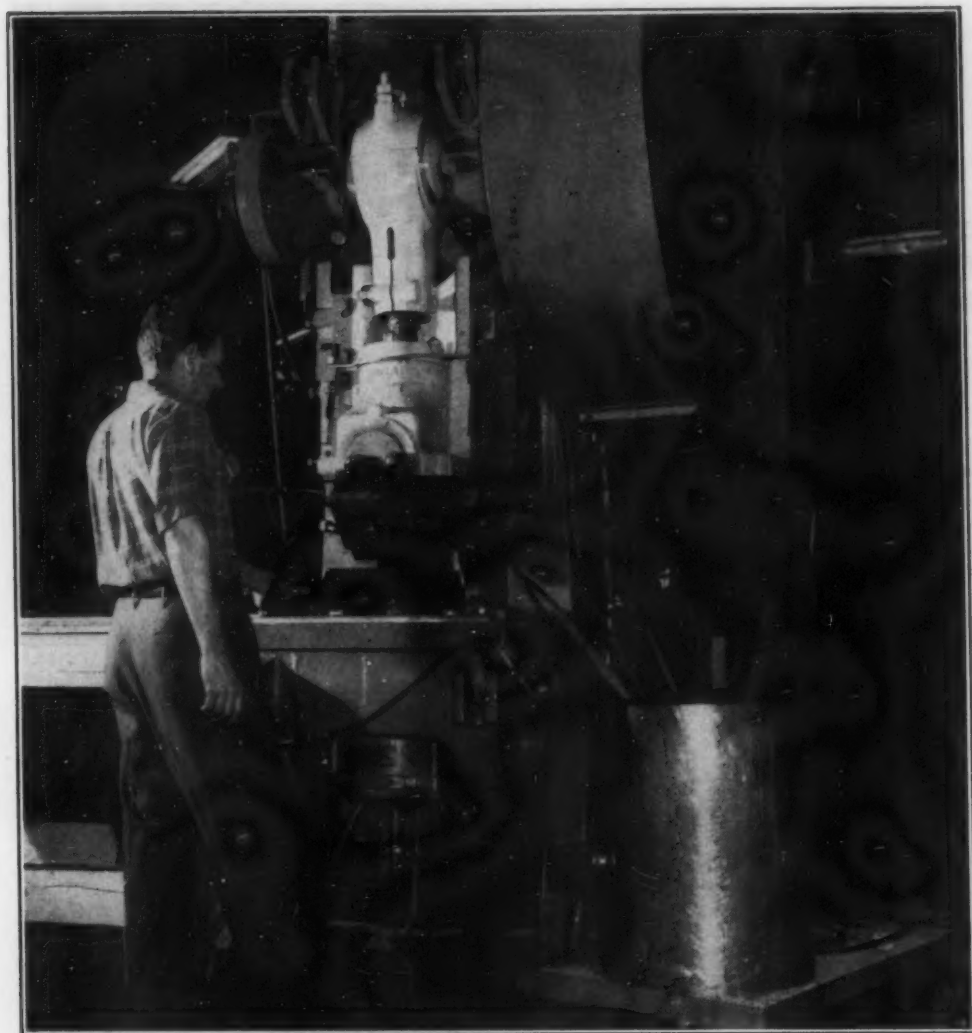


Fig. 11—Punch Press Forming 75S-T6 Extrusions Preheated by Hot Oil Immersion Method.

operating at 300 °F (150 °C). A fixed-depth-type joggle die, preheated to 300 °F (150 °C) by cartridge-type heaters, produces a 0.188-inch joggle with a washout of six times the joggle depth. See Fig. 10.

In joggling a 75S-T6 aluminum alloy L-section extrusion on a 30-stroke, a 75-ton Niagara punch press is employed. The extrusion is heated to 300 °F (150 °C). An adjustable depth house-top joggle die, preheated to 300 °F (150 °C) by cartridge-type heaters, is used, which joggles all standard L-section extrusions to a maximum depth of 0.250 inch. See Fig. 11.

In the press forming of a 75S-T6 aluminum alloy extrusion which has been heated by the electric resistance method to 300 °F (150 °C), a Farquhar hydraulic press is used. The heater used

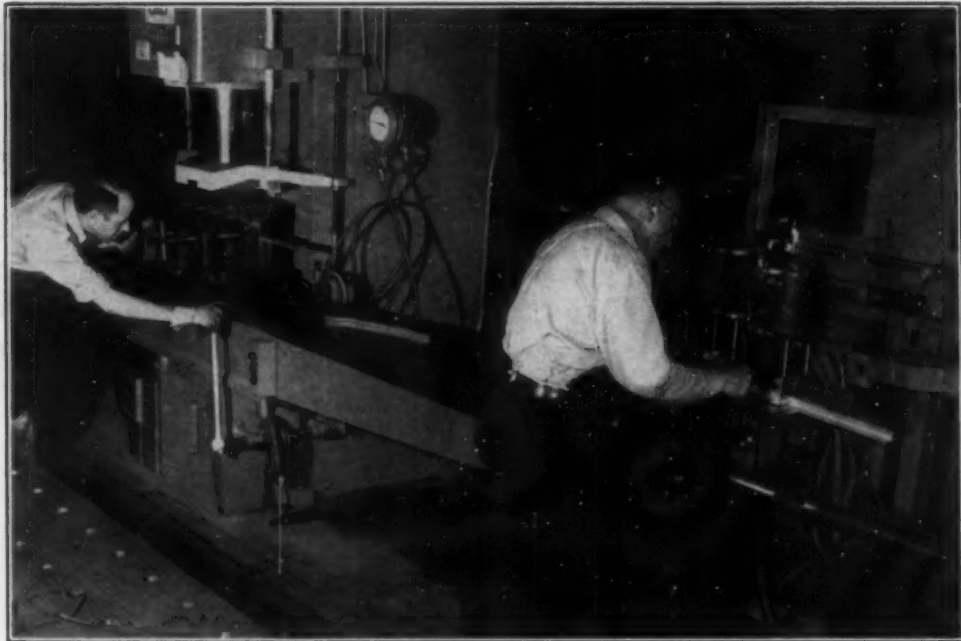


Fig. 12—Punch Press Forming 75S-T6 Extrusions Preheated by Resistance Heating Method.

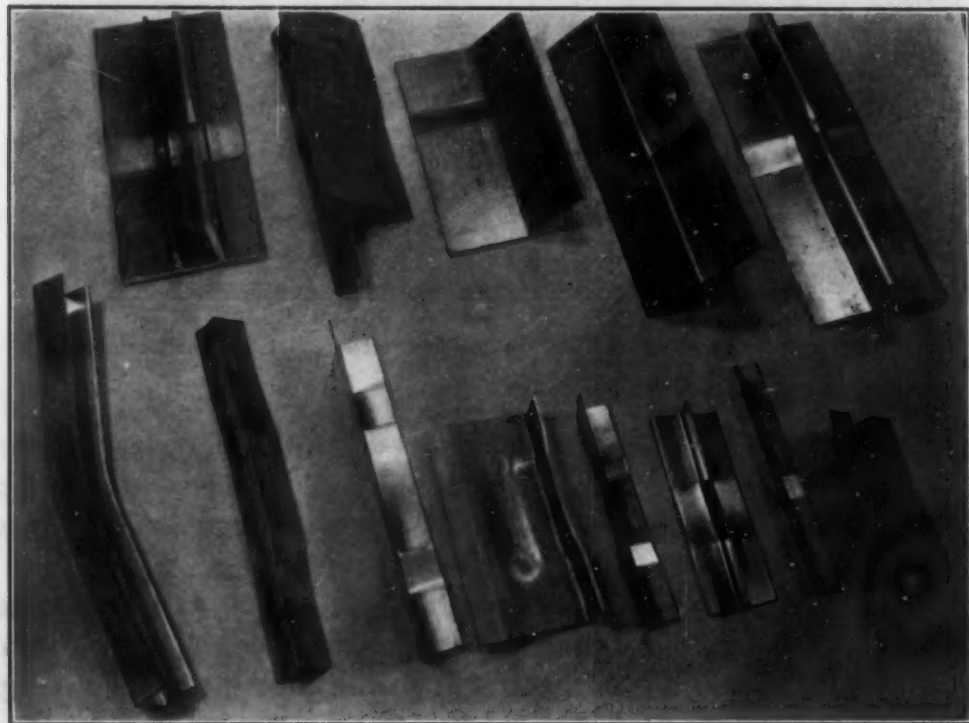


Fig. 13—Typical 75S-T6 Extrusions Hot-Formed at 275 to 300°F (135 to 150°C).

consists of a single-phase, 60-cycle A.C. transformer, rated at approximately 30 kva, and a phase shift control ahead of the transformer to control the primary voltage. A solid copper bus bar is



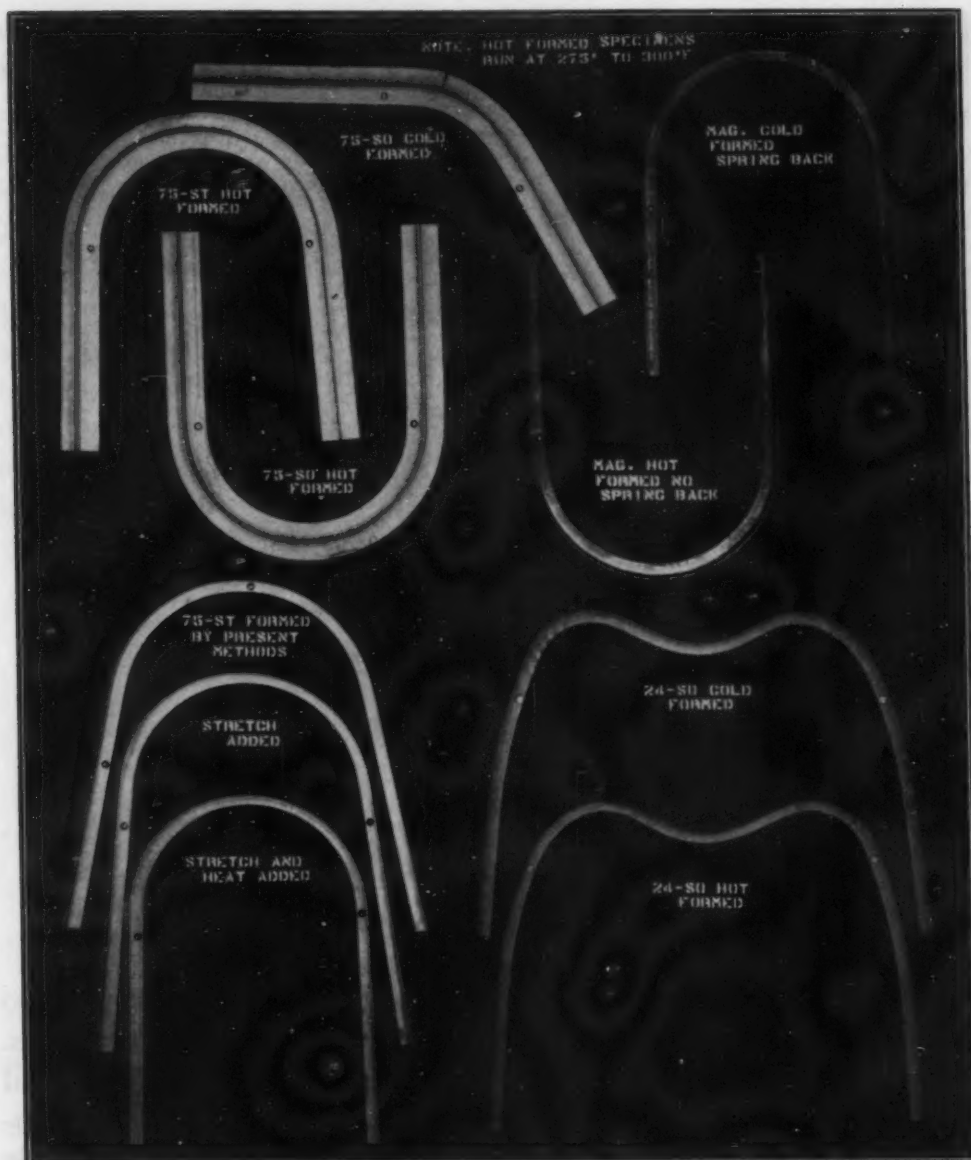


Fig. 14—Increased Formability of High Strength Aluminum and Magnesium Alloys by the Application of Elevated Temperatures in Forming.

used in lieu of flexible cables for transmission of electrical energy, since the heater is used in a fixed installation. See Fig. 12.

Fig. 13 illustrates typical elevated temperature applications in forming various shapes of 75S-T6 aluminum alloy extrusions. The joggling and bending operations were performed on either the hydraulic presses or punch presses, and heating to 300 °F (150 °C) was accomplished by hot oil immersion and/or electrical resistance methods.

The merits of hot forming aluminum and magnesium alloys by the stretch wrapping operation are shown in Fig. 14. The advan-

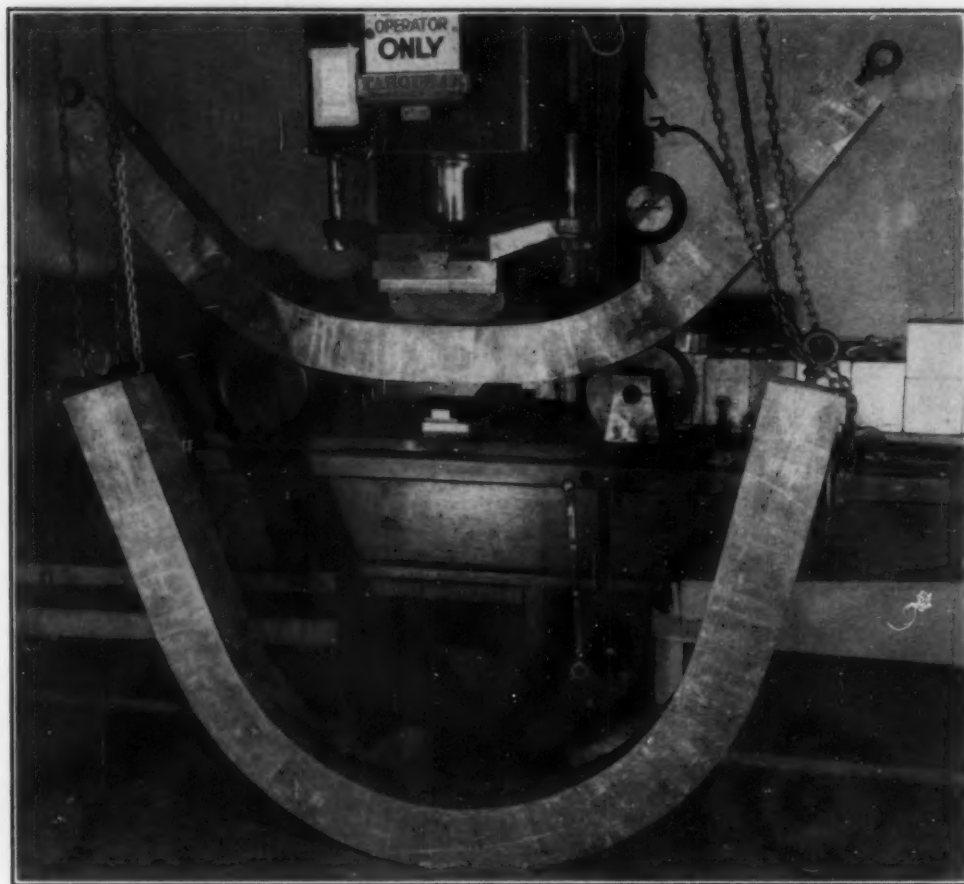


Fig. 15—14S Hand Forgings Preheated to 600°F (315°C) in Air Furnace and Formed on Hydraulic Press.

tage of elevated temperatures in increasing formability applies to 75 S-O and 24S-O as well as 75S-T6 and magnesium extrusions. In these applications the increase in formability allows 75S-T6 and 75S-O to be formed to a smaller radii without fracturing accompanied with a marked decrease in springback; i.e., the allowable stretch in the outer fibers is increased.

The use of elevated temperatures in fabrication of aluminum alloys applies to 14S in the annealed condition as well as to 75S. Fig. 15 illustrates a 6.5-inch square 14S hand forging that was originally designed to be machined out of billet stock. By pre-heating this forging in an electric air-circulating furnace to 600 °F (315 °C) it was possible to contour it to a 24-inch radius using rocker-type dies on a 75-ton Farquhar hydraulic press.

#### CONCLUSIONS

1. Forming at elevated temperatures is suitable for production fabrication of high strength aluminum and magnesium alloys, with substantial savings in time and man-hours. By employing temper-

atures in the order of 300 °F (150 °C) within time restrictions, mechanical property losses are negligible.

2. Electrical resistance and hot oil bath heating methods have proven successful for elevated temperature forming applications. In some instances, where large parts are involved, electrical air circulating furnaces are required.

3. In general, only limited room temperature forming can be accomplished in the heat treated and work-hardened conditions of aluminum and magnesium alloys; however, elevated temperature forming limits comparable to annealed material in some conditions of forming may be realized. This reduces fabrication to a single operation and eliminates all check and straightening resulting from heat treat warpage.

#### References

1. E. C. Hartmann, F. M. Howell and R. L. Templin, "How To Use High-Strength Aluminum Alloy", *Aviation Week*, Oct. 10, 1949, p. 21-28, 34, 35.
2. Dow Chemical Company, Original data on file in Dow laboratories.
3. G. Sachs, G. Espey and G. V. Kasik, "Hot Roll Forming of Various Aluminum Alloys", *TRANSACTIONS, American Society for Metals*, Vol. 37, 1946, p. 449-467.
4. G. Sachs and G. Espey, "Forming of the Aluminum Alloy 75S", *TRANSACTIONS, American Society for Metals*, Vol. 37, 1946, p. 468-496.

#### DISCUSSION

**Written Discussion:** By E. H. Schuette, Technical Department, Magnesium Division, The Dow Chemical Company, Midland, Mich.

The author, in his excellent treatment of a subject currently receiving a great deal of attention, states that the room temperature properties of FS1-H24 (former designation: FS1-h) are not appreciably affected by exposure in forming to a temperature of 300 °F (150 °C). Fig. 2 of the paper gives curves of properties related to temperature, for half-hour exposures.

Data recently compiled by The Dow Chemical Company make it possible to determine the effect of the forming temperature on both the forming characteristics and the properties, with full consideration for the additional variable of exposure time. These data are presented in Dow Technical Memorandum No. 14, "Bend Radii of Magnesium-Alloy Sheet", and Dow Technical Memorandum No. 16, "Effect of Forming Temperature on Properties of Dowmetal FS1-H24 Sheet". Some of the information available from these two papers is presented in Fig. 16.

The lower curve shows design values of die radii, in terms of sheet thickness, for various forming temperatures; values shown are such as to produce a scrap rate of one in a thousand. The improved formability with increasing temperature is evident. The upper curves, based on the data



in Technical Memorandum No. 16, show the time limitations necessary to hold property levels above specified minimum values. The limitations, as will be noted, are slightly different, depending on whether the compressive yield or tensile yield is the critical property that must be maintained. The curve for specification tensile strength is not shown; it would be above both of the curves given.

A few examples will serve to illustrate the use of curves like these. If forming is done at 300 °F (150 °C), the lower curve shows a minimum die radius of 5.3t can be used, and the upper curves indicate that the exposure to this temperature can be for as long as 20 hours (1200 minutes). With platen heaters installed close to the forming equipment, it may be possible to limit the time of elevated temperature exposure to,

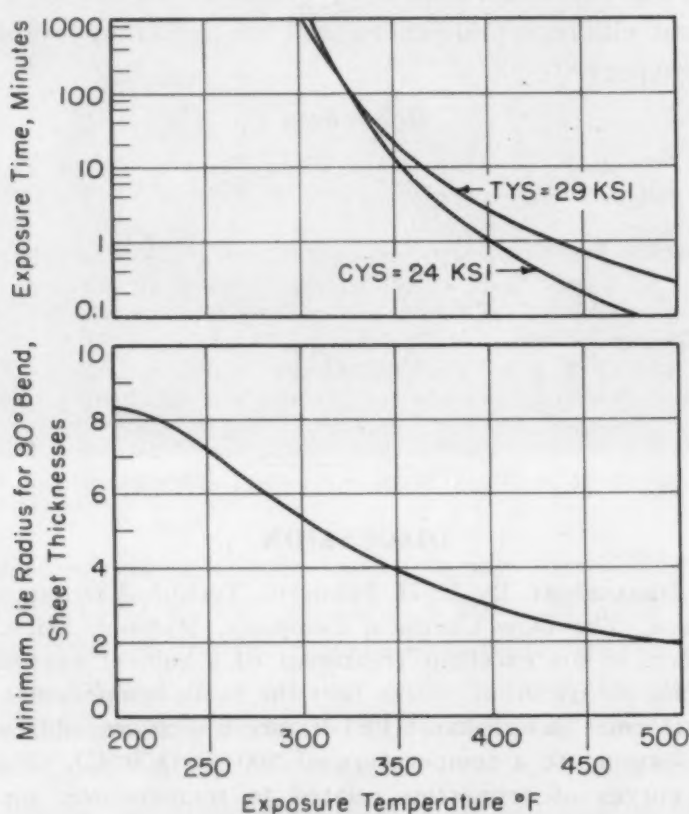


Fig. 16—Permissible Exposure Times and Die Radii for Various Forming Temperatures for FS1-H24 Sheet.

say, 5 minutes. If this is done, a temperature of 360 °F (180 °C) can be tolerated if the compressive yield is critical, or 380 °F (195 °C) if the tensile yield is critical. The die radii for these temperatures are, respectively, 3.7t and 3.3t. If the time can be further limited to 1 minute, the permissible forming temperatures are 400 and 430 °F. Corresponding die radii are 3.0t and 2.6t.

The curves given here represent only a summary of the available information. The complete reports also make possible a determination of suitable design property values if, for some reason, exposure times or temperatures beyond the limitations here given should be found necessary.

**Written Discussion:** By J. W. Sweet, chief metallurgist, Boeing Airplane Company, Seattle, Wash.

The author, Mr. Piper, has very adequately presented a subject of considerable interest to the airplane industry and we at Boeing Airplane Company are in general agreement with his findings.

Aluminum alloy 24S, which is at present the most widely used duralumin-type alloy, satisfactorily withstands certain forming operations at room temperature in the 24S-T3 or 24S-T4 condition; namely, stretch forming, bending, and joggling. With the advent of 75S alloy it was soon learned that only minor straightening operations could be accomplished in the 75S-T6 condition. The higher ultimate strength accompanied with lower elongation and smaller spread between ultimate strength and yield strength made forming operations of 75S-T6 at room temperature prohibitive. This led to the investigation of the hot-forming characteristics of aluminum alloys. As noted by Mr. Piper, experimental work was undertaken during World War II on the fabrication of light metal alloys at elevated temperature. The aircraft industry has taken an active interest in the development of forming operations. Tests performed at Boeing Airplane Company have resulted in the establishment of a hot-forming temperature of 300 °F (150 °C) for 75S-T6 material which is in agreement with Mr. Piper's findings. We have limited the time at temperature to 15 minutes, so as to guard against losing any of the room temperature strength. Fig. 1 of the text shows some loss of properties after one-half hour at 300 °F (150 °C); after 15 minutes we find essentially no loss of properties.

The heat is applied locally through suitable fixtures between hot plates or locally or totally by submersion in hot oil or salt at 300 °F (150 °C). In the case of the hot plates, the fixture temperature is maintained at 300 °F (150 °C). Heated forming dies may be used. The die temperature must be maintained at 325 °F (165 °C) and the time of contact before forming is limited to 30 seconds. It is required that the part be automatically removed from the die. The temperature must be thermostatically controlled and the length of heat application is to be regulated by an automatic timer. In applications where an air furnace has to be used, the parts are preheated to 250 °F (120 °C) before raising the furnace to 300 °F (150 °C).

It has been our experience that the forming characteristics of 75S-T6 at 300 °F (150 °C) is comparable to 24S-T4 at room temperature. To say it compares favorably with 75S-O at room temperature may be somewhat misleading; however, certain operations such as stretch forming, bending and joggling can be satisfactorily accomplished.

Hot forming of magnesium alloys in both the annealed and hard-rolled condition is the preferred procedure at Boeing Airplane Company. A maximum temperature of 550 °F (290 °C) for a total time of 1 hour is allowed for FS1 annealed material. The FS1 hard material and ZK60 aged material may be heated to 325 °F (165 °C) for a time not to exceed 15 minutes.

Mr. Piper's very interesting paper thoroughly covers the advantages of the hot-forming operation. The problems which may occur are clearly presented. The information included in Mr. Piper's paper is a worthwhile

contribution to the metal-forming problems encountered in aircraft construction.

### Author's Reply

In regard to the discussion by E. H. Schuette, we believe his comments are an excellent addition to the paper and nothing further can be added at this time.

Concerning the discussion of J. W. Sweet, we should like to comment as follows: In regard to the last sentence in paragraph 2, further tests at Northrop indicate that 1 hour at 300 °F (150 °C) did not have any detrimental effect on the room temperature mechanical properties. Therefore, we have set up 1 hour as the maximum soaking time (single or cumulative heats), and minimum soaking times in the oil bath to bring part to forming temperature of 300 °F (150 °C) have been set up as follows:

Thickness (Inches)	Time (Minutes)
Up to 0.081	5
0.082 to 0.125	10
0.126 to 0.250	15
0.251 to 0.500	20

In regard to paragraph 3 of Mr. Sweet's discussion, very little work has been done on the use of hot plates at Northrop, but this method should be applicable to heating sheet stock. We definitely agree that the temperature must be thermostatically controlled and the length of heat application be regulated by an automatic timer.



# STRAIN HARDENING OF MILD STEEL IN THE TORSION TEST AS A FUNCTION OF TEMPERATURE

BY HUGO LARSON AND E. P. KLIER

## Abstract

*In studying the strain hardening characteristics of two ship-plate steels it was found that reliable tension data could not be obtained at very low temperatures because brittle failure occurred after slight deformation. However, the same steels tested in torsion showed extensive ductility to temperatures as low as  $-188^{\circ}\text{C}$  ( $-306^{\circ}\text{F}$ ). The torsion data were treated, using the generalized plastic flow concept, to convert the experimental torque twist results to effective stresses and effective strains. The results can be expressed by the equation  $\sigma = K\delta^n$  in which  $K$  is the strength coefficient and  $n$  is the strain hardening exponent. The values for  $K$  and  $n$  thus obtained compare favorably with the results from tension tests, for temperatures at which the latter data were available. The additional values obtained at  $-188^{\circ}\text{C}$  ( $-306^{\circ}\text{F}$ ) indicate that the strain hardening exponent decreases with temperature. The form of the curve resembles that found for the transition from ductile to brittle behavior in the impact test.*

ONE of the most important characteristics of metals is the property of plasticity or the ability to undergo permanent deformation under a suitably applied load. Of the tests commonly used to measure plasticity the tension test is one of the most important. In recent years the stress-strain relationships in the tension test have been put on a more fundamental basis by the consideration of the true stress-true strain diagram. For many metals the resulting diagram is to a high degree parabolic and, therefore, the stress-strain curve can be described by an analytic expression of the form  $\sigma = K\delta^n$ . For steels this represents an

\*The material presented here has been taken from a thesis submitted by Hugo Larson to the Division of Metallurgy, The Pennsylvania State College, in partial fulfillment of the requirements for the degree of Master of Science in Metallurgy, January 1949.

A paper presented before the Thirty-second Annual Convention of the Society, held in Chicago, October 21 to 27, 1950. Of the authors, Hugo Larson is a graduate student in metallurgy, Massachusetts Institute of Technology, Cambridge, Mass., and E. P. Klier is associate professor, Department of Chemical Engineering, University of Maryland, College Park, Md. Manuscript received April 13, 1950.

important simplification in the study of plasticity, since it is now possible to describe pertinent stress-strain characteristics by stating the two constants  $K$  and  $n$ , the strength coefficient and the strain hardening exponent, respectively.

Another important contribution to the knowledge of the plastic behavior of metals has been made by the introduction of the generalized theory of plastic flow. This theory, based on an analogy to flow in noncrystalline solids, postulates that the flow curve of a metal under any stress system can be made to coincide with the tension curve if the states of stress and strain are understood for the stress system under consideration. Most experimental results reported in the literature support this theory, particularly at small strains.

Because the constants  $K$  and  $n$  are of fundamental importance, it is desirable to know their variation with temperature. References in the literature (1, 2)<sup>1</sup> state that the strain hardening exponent,  $n$ , increases at lower temperatures. On the other hand, tension tests performed on Navy ship-plate steels under U. S. Navy Contract NObs-31217 (3) indicate that the strain hardening exponent for certain steels decreases at lower temperatures. For the steels studied, pronounced embrittlement was encountered in the range of liquid air temperatures, and this embrittlement curtailed the study of the strain hardening of these steels at the lowest accessible temperatures.

The transition from ductile to brittle behavior occurs at a lower temperature for the torsion test than for the tension test. By combining this experimental situation with the concepts of the theory of plastic flow, it should be possible to obtain a pseudo-tension diagram from the torsion test data. In this way it should be possible to study the behavior of  $K$  and  $n$  over a temperature range inaccessible to the tension test.

#### THE THEORY OF PLASTIC FLOW

If plastic flow of metals can be assumed to be governed by the same rules as isotropic amorphous solids, certain fundamental relationships exist between the stresses and strains (4):

1. The axes of the principal stresses and strains coincide throughout deformation.
2. The density remains constant.
3. The principal shear strains are directly proportional to the principal shear stresses.

With these assumptions it is possible by rather simple algebraic manipulation to obtain the so-called plasticity equations:

<sup>1</sup>The figures appearing in parentheses pertain to the references appended to this paper.

$$\delta_1 = \frac{1}{3C} [\sigma_1 - \frac{1}{2} (\sigma_2 + \sigma_3)]$$

$$\delta_2 = \frac{1}{3C} [\sigma_2 - \frac{1}{2} (\sigma_1 + \sigma_3)]$$

$$\delta_3 = \frac{1}{3C} [\sigma_3 - \frac{1}{2} (\sigma_1 + \sigma_2)]$$

$\sigma$  and  $\delta$  are the principal true stress and true strain and  $C$  is a function of strain. By further analysis and without any new assumptions, the generalized flow equation can be obtained:

$$\frac{1}{\sqrt{2}} [(\sigma_1 - \sigma_2)^2 + (\sigma_2 - \sigma_3)^2 + (\sigma_3 - \sigma_1)^2]^{1/2} = 3C [\frac{2}{3} (\delta_1^2 + \delta_2^2 + \delta_3^2)]^{1/2}$$

This can be simplified to  $\bar{\sigma} = f(\bar{\delta})$  where  $\bar{\sigma}$  and  $\bar{\delta}$  are the effective or significant stress and strain as defined by the preceding equation.

If these equations are applied to the case of simple tension, in which case  $\sigma_1 = \sigma$ ,  $\sigma_2 = \sigma_3 = 0$  and  $\delta_1 = \delta$ ,  $\delta_2 = \delta_3 = -\frac{1}{2}\delta$ , the equations  $\bar{\sigma} = \sigma$  and  $\bar{\delta} = \delta$  are obtained. Thus the generalized flow curve is identical to the tension curve, and stress-strain data for any test will fall on the curve for simple tension if the corresponding stress and strain data can be expressed in terms of effective stress and strain.

It is important to note that the final relationships between effective stress and strain were based on an analogy to plastic flow in isotropic amorphous materials. Gensamer (5) has discussed deviations due to the failure to retain isotropy, and he states that stress is a function not only of strain but also of the anisotropy resulting from strain. Barrett (6) has surveyed the anisotropy caused by preferred orientation for drawing, swaging, extrusion, compression, and tension. This preferred orientation develops gradually during the test and is not detected by X-rays until the cross section of the specimen has been reduced by a third or a half. The type and amount of preferred orientation is characteristic of the metal and the magnitude of the three principal strains.

Other evidence of the nonhomogeneity of flow is offered by evidence of a strain gradient from grain boundary to grain center (7). Discontinuous or stepwise strain has been found by McReynolds for aluminum (8). In this case, deformation proceeded in a wavelike manner through the specimen. This evidence suggests that strain is not isotropic, at least at high strains.

It is recognized that the mechanism of deformation in metals is quite different from that in amorphous solids. Nevertheless, it is usually assumed that, although deformation is inhomogeneous in



any one grain, the neighboring grains deform by approximately equal amounts so that the flow equations will hold true over a region large compared to the size of a single grain.

Experiments on a cold-rolled 0.2% carbon steel and a cold drawn, tough pitch copper support this concept of a generalized theory of plastic flow (9). After prestraining under combined stresses, the specimens were strained further under simple tension. If the prestrain, expressed as an effective strain, is added to the subsequent tensile strain, the resulting stress-strain curve coincides with the curve for a specimen tested entirely in tension.

Lankford (10), using his own data and that of Prater and Low (11), obtained excellent agreement between flow curves determined by tension, compression, and balanced and unbalanced biaxial tension.

E. A. Davis (12) found that data from torsion and tension tests coincide to a strain of 0.2. However, even at a strain of 0.6, which is beyond the point of necking in the tension test, the two curves differ by no more than 10%.

Schmidt (13) conducted combined torsion and tension tests on mild steel and copper, using various constant ratios of tensile and torsional strain. He found that all the points fell on a common curve when the data were expressed as effective stresses and strains.

Davidenkov and Spiridinova (14) found good agreement between the two types of straining.

#### EXPERIMENTAL PROCEDURE

From the foregoing it is evident that a suitable mathematical apparatus exists which will allow the conversion of torsional strain hardening data into tensile strain hardening data. Because of brittle failure in tension below a minimum temperature, these converted values characterize pseudo-tensile data, but are nonetheless valid. To check the conversion operation, the strain hardening data obtained in torsion were checked against comparable data obtained in tension (3) for two steels. These two steels were selected, as they were known to possess a transition in the strain hardening exponent, and the approximate temperature range of these transitions was known. Thus, with the experimental apparatus available, it would be possible to check in the tension and torsion tests the correlation of  $n$  and  $K$  above and through the transition range in the tensile test, while the character of the transition could be investigated in the torsion test to lower temperatures.

Strain hardening data in the tensile test were available for

Table I  
Chemical Analyses

	C	Mn	S	P	Si	Al	Ni	Cu	Cr	Mo	N <sub>2</sub>
Steel C	0.24	0.48	0.026	0.012	0.05	0.016	0.02	0.03	0.03	0.005	0.009
Steel R	0.20	0.33	0.020	0.013	0.01	0.009	0.15	0.18	0.09	0.018	0.005

Mill Physical Results				
Steel C				
Gage (in.)	Y. P. (psi)	T. S. (psi)	Elong. (%)	
1/2	41,200	68,400	26.5	
3/8	40,410	68,100	25.0	
Steel R				
	Y. P. (psi)	T. S. (psi)	Elong. in 8 in. (%)	
	38,000	62,500	28	

temperatures of 25,  $-75$  and  $-150^{\circ}\text{C}$  for Steels C and R listed in Table I. Torsion tests for Steels C and R were run at these temperatures and at  $-188^{\circ}\text{C}$  ( $-306^{\circ}\text{F}$ ). The torsion tests at  $-150^{\circ}\text{C}$  were not successful because of thermal variations during the test.

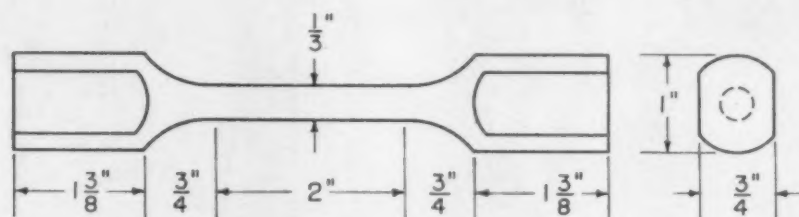


Fig. 1—Torsion Specimen.

Specimens were cut from  $3/4$ -inch plate so that the axis of the specimen was in the rolling direction. They were  $6\frac{1}{4}$  inches long and had a 2-inch gage length with a diameter of  $1/3$  inch. A drawing of the specimen is shown in Fig. 1.

The method of gripping and loading the specimens can be seen in Fig. 2. The upper grip rotated on ball bearings in the end plates A and B. The lower grip, 8 inches long and 2 inches in diameter, was fixed in the end plate C. For tests at low temperatures, the insulated can could be raised to surround the specimen. It was filled with acetone and dry ice for tests at  $-75^{\circ}\text{C}$  ( $-103^{\circ}\text{F}$ ) and with liquid air for those at  $-188^{\circ}\text{C}$  ( $-306^{\circ}\text{F}$ ). Weights were added to the weight pan, and the torque was applied to the specimen through the flexible cable to a wheel mounted on the movable grip.

The strain gages shown in Fig. 3 were designed to permit observation of the twisting over the 2-inch gage length when the specimen was submerged in the cooling bath. The upper gage consisted of a ring graduated in degrees onto which an adjustable mirror

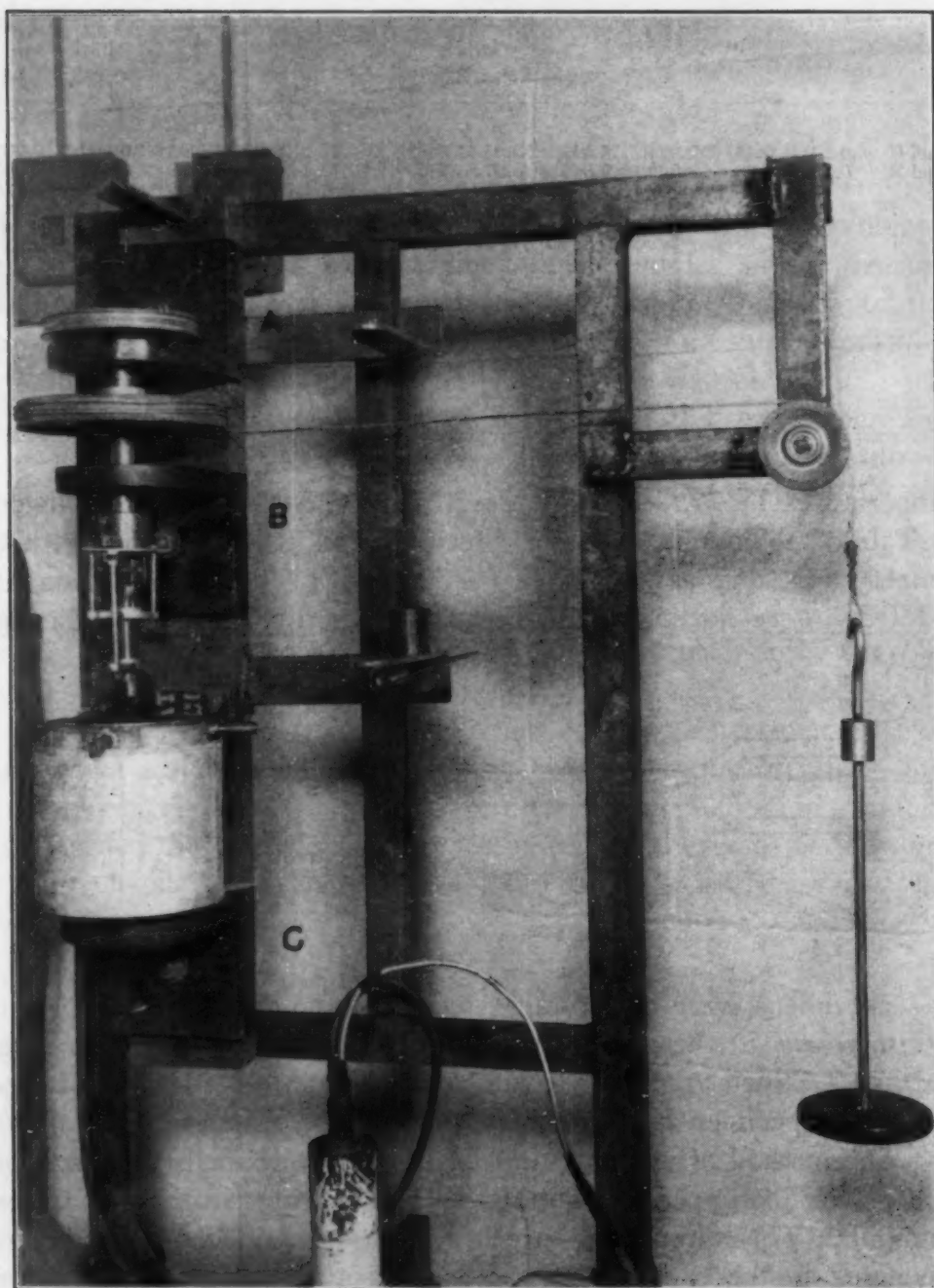


Fig. 2—Torsion Apparatus.

was fastened. The lower strain gage terminated in a pointer and mirror. In the elastic range and for small plastic strains, the twisting was measured by an optical system consisting of the two mirrors, a telescope, and a scale graduated in millimeters. By proper manipulation of the telescope and the upper mirror, the image of the scale was reflected by both mirrors into the telescope. An accurate determination of the angular twisting after each load increment could be



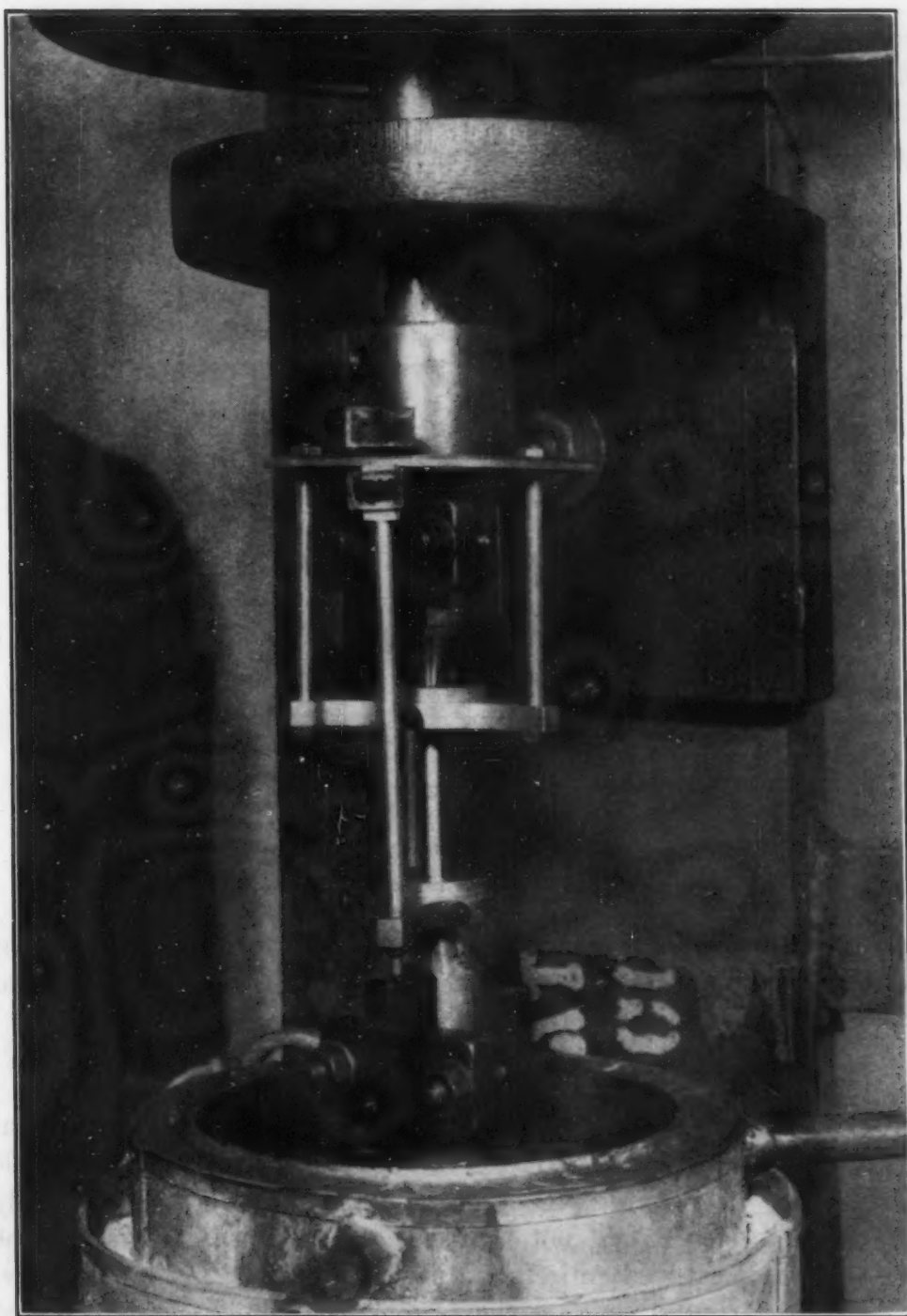


Fig. 3—Strain Gages.

obtained from the two scale readings. After several degrees of deformation, which was well beyond the elastic limit, the mirrors twisted off scale. Beyond this point the strains were determined by the reading on the upper graduated ring opposite a line scribed on the pointer of the lower strain gage. The angular twisting could

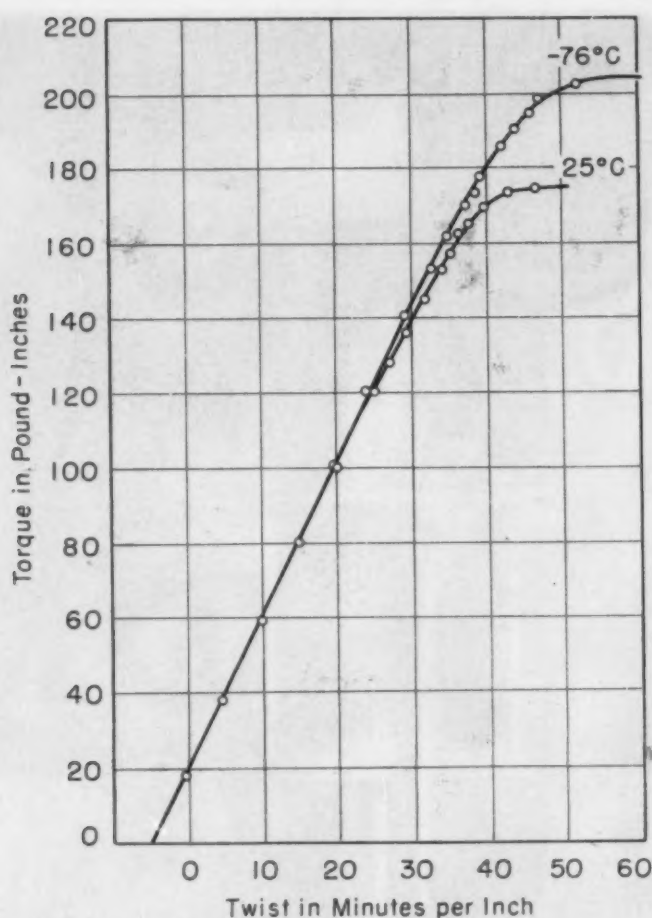


Fig. 4—Torque-Twist Data for Steel C at Small Strains.

be read to tenths of a degree with an accuracy of  $\pm 0.1$ . This was quite adequate in view of the extensive ductility exhibited even at the lowest testing temperature.

### RESULTS

Torque-twist data at small strains are shown for Steel C at room temperature and at  $-75^{\circ}\text{C}$  in Fig. 4, and for Steels C and R at  $-188^{\circ}\text{C}$  in Fig. 5. At  $-188^{\circ}\text{C}$  the mirrors fogged so badly the optical system could not be used, and at this temperature the twisting was measured entirely with the pointer and graduated scale.

The shearing stresses at the proportional limit were calculated from the formula  $S_s = \frac{2T}{\pi r^3}$ , in which  $S_s$  is the shearing stress,  $T$  is the torque at the proportional limit, and  $r$  is the radius of the bar. These values, together with various other observations, are listed in Table II. Although it is difficult to detect the departure from elastic behavior with any great accuracy, the increased strength at lower temperatures is quite obvious.

Interesting yield point phenomena were observed. This is shown most clearly in Fig. 4 but may also be seen in Figs. 7 and 8. After straining beyond the elastic limit, the initial stages of plastic deformation could be followed quite easily with the optical strain measuring setup. Load increments were made as small as possible in this region. For example, the elastic limit for Steel C at 25 °C was approximately 160 pound-inches and the load was increased in steps of 4 pound-inches. After successive load increments had produced a total plastic deformation of several tenths of a degree, a torque was reached which resulted in a twisting of several degrees at constant load. For Steel C this so-called yield point twisting

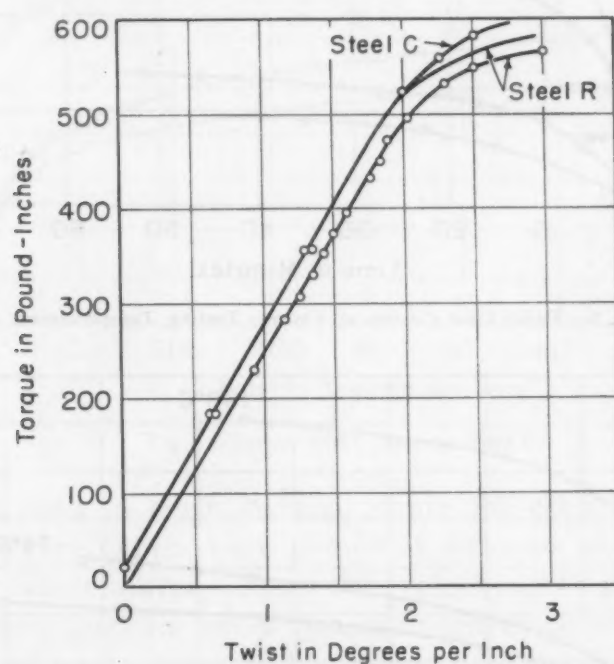


Fig. 5—Torque-Twist Data at Small Strains for Steels C and R at  $-188^{\circ}\text{C}$ .

Table II  
Mechanical Properties of Steels C and R Determined From Torsion Tests

	Steel C			Steel R		
	25 °C	-75 °C	-188 °C	25 °C	-76 °C	-188 °C
Shearing Stress at Proportional Limit (psi)	18,900	21,000	70,000	17,500	21,000	63,000
Torque at Yield Point (psi)	175	205	650	163	191	590
Yield Point Twisting (degrees/inch)	7.0	7.2	23.5	6.5*	7.1	
Torque at Fracture (pound-inches)	530	617	907	520	613 & 610	
Twist to Fracture (degrees/inch)	705	620	451	742	672 & 700	
Strain Hardening Exponent	0.222	0.212	0.099	0.207	0.216	0.133
Strength Coefficient (psi)	102,000	120,000	175,000	101,000	118,000	174,000

\*Extrapolated value.



amounted to 7, 7.2, and 23.5 degrees per inch of gage length at 25,  $-75$ , and  $-188^{\circ}\text{C}$  respectively. For the first few tests the load increments were too great in this region and the effect was not detected. Consequently the value for Steel R at  $25^{\circ}\text{C}$  was estimated

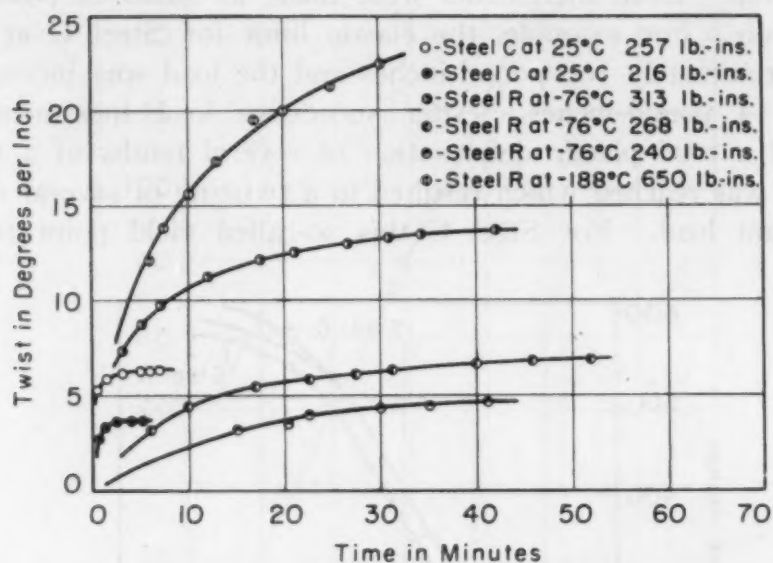


Fig. 6—Twist-Time Curves at Various Testing Temperatures.

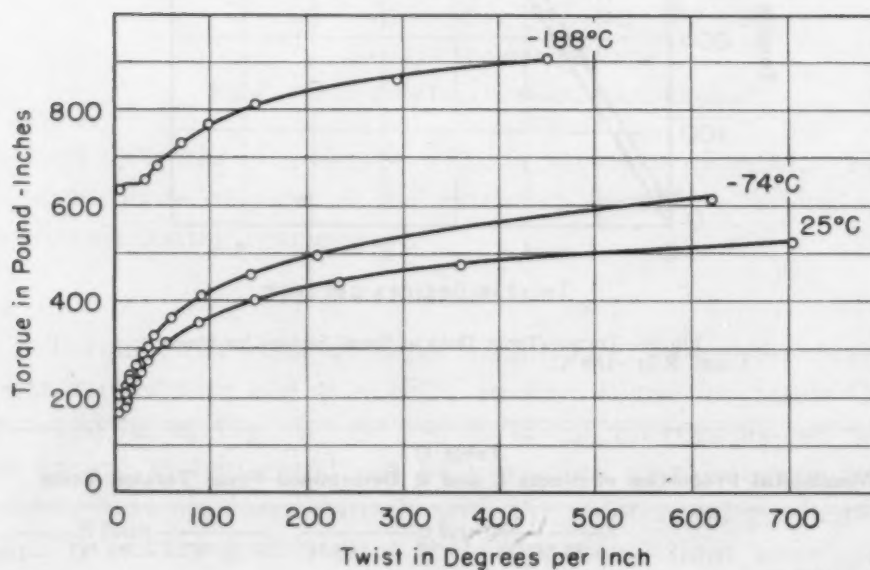


Fig. 7—Torque-Twist Data for Steel C.

by extrapolating the torque-twist data in the plastic range backward to a torque midway between the last point in the elastic region and the first one in the region of plastic deformation. The test on Steel R at  $-188^{\circ}\text{C}$  had to be discontinued when the liquid air was exhausted. However, the specimen had already twisted 17 degrees

per inch and would probably have reached a value similar to that found for Steel C. During subsequent tests on Steel R the test bar was loaded more rapidly through this region. This permitted the obtaining of the complete torque-twist curve before the liquid air was completely used.

It was evident after the first test that considerable scatter in the torque-twist data would result if insufficient time were allowed

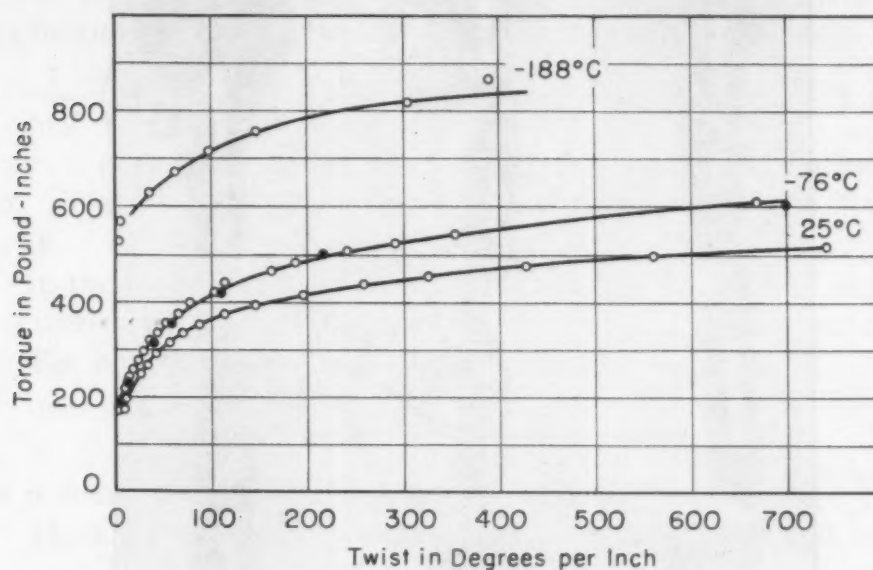


Fig. 8—Torque-Twist Data for Steel R.

for the specimen to reach its final strain for each load increment. Many strain-time curves were plotted at different torque values and at different temperatures. From the typical curves shown in Fig. 6 it can be seen that the effect became much more noticeable at the lower testing temperatures. The times required for the tests increased proportionally. It was particularly disturbing at  $-188^{\circ}\text{C}$ , at which temperature the time was limited by the available supply of liquid air.

The complete torque-twist curves are shown in Figs. 7 and 8. The strength increased considerably at  $-188^{\circ}\text{C}$  compared to room temperature, and the ductility decreased. This change in ductility in the torsion test is small compared to that occurring in the tension test. For both steels the ductility in tension decreased from a true strain of 1.0 at  $25^{\circ}\text{C}$  to approximately 0.02 to 0.05 at  $-188^{\circ}\text{C}$ .

Although extensive ductility was exhibited at all temperatures, the fracture characteristics were not identical. At room temperature and at  $-75^{\circ}\text{C}$  the fractures occurred on a transverse plane (Fig. 9) which was also one of the planes of maximum shear stress. The

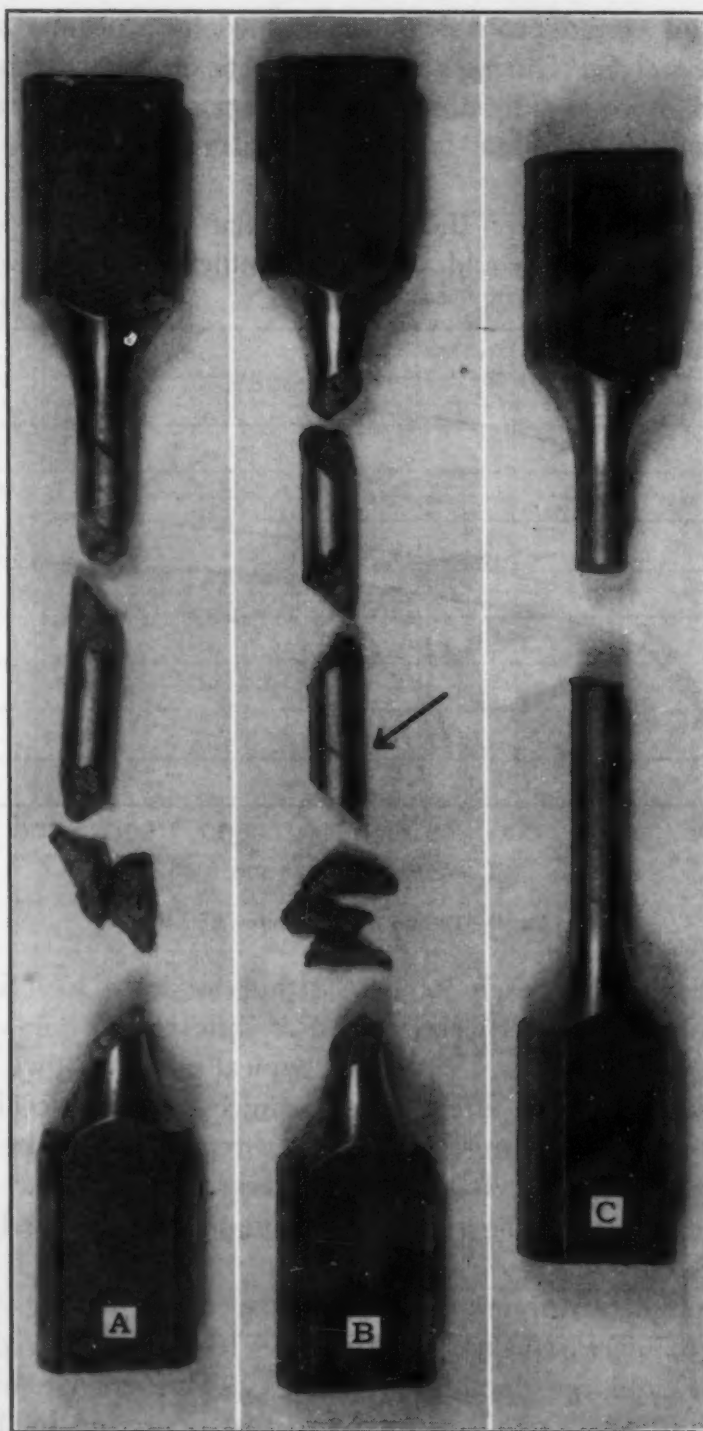


Fig. 9—Typical Fractures. A—Steel R at  $-188^{\circ}\text{C}$ ; B—Steel C at  $-188^{\circ}\text{C}$ ; C—Steel R at  $-71^{\circ}\text{C}$ . The arrow indicates a line drawn along the longitudinal axis before the test was begun.

fracture surfaces were smooth, but they had a rather smeared fibrous appearance. At  $-188^{\circ}\text{C}$  fracture occurred on several helical planes simultaneously, and both Steels C and R broke into several pieces.



Although rupture was preceded by considerable deformation, the fracture surfaces exhibited a crystalline or granular appearance characteristic of brittle failures. Fig. 9 shows that one of the fracture surfaces was parallel to a line scribed longitudinally along the bar before the test was begun.

#### TREATMENT OF DATA

At any given torque the shearing stress at the surface of a cylindrical test bar can be calculated from the formula (4),

$\tau = \frac{1}{2na^3} \left( 3T + \theta \frac{dT}{d\theta} \right)$  in which  $\tau$  is the shearing stress,  $T$  is the torque,  $a$  is the radius, and  $\theta$  is the angular twisting in radians per inch. The nominal shear strain is calculated from the formula  $\gamma = a\theta$ .

In the torsion of a uniform cylindrical bar the state of stress is represented by  $\sigma_1 = -\sigma_3$ ,  $\sigma_2 = 0$ . Since  $\tau = \frac{1}{2}(\sigma_1 - \sigma_3)$ ,  $\tau = \sigma_1$ . The effective stress is calculated from the equation

$$\bar{\sigma} = \frac{1}{\sqrt{2}} [ (\sigma_1 - \sigma_2)^2 + (\sigma_2 - \sigma_3)^2 + (\sigma_3 - \sigma_1)^2 ]^{1/2}$$

and is found to be  $\bar{\sigma} = \sqrt{3} \sigma_1 = \sqrt{3} \tau$ .

The state of strain is represented by  $\delta_1 = -\delta_3$ ,  $\delta_2 = 0$ . Since  $\gamma = \delta_1 - \delta_3$ , the effective strain is found to be  $\bar{\delta} = \frac{2}{\sqrt{3}} \delta_1 = \frac{\gamma}{\sqrt{3}}$ .

The use of  $\gamma = a\theta$  at high strains has been questioned. Saibel (15) has developed a different relationship,  $\bar{\delta} = \frac{1}{\sqrt{3}} [\gamma^2 + \frac{1}{2}\gamma^4]^{1/2}$ . However, if  $\gamma$  is small, this reduces to  $\bar{\delta} = \frac{\gamma}{\sqrt{3}}$ .

Nadai expresses the generalized flow equations in terms of octahedral stresses and strains, a different but equivalent notation (16). If his expression for octahedral strain is transformed into effective strain, the equation  $\bar{\delta} = \frac{1}{\sqrt{3}} \ln [1 + \frac{\gamma^2}{2} + \gamma (1 + \frac{\gamma^2}{4})^{1/2}]$  is obtained.

This equation also reduced to  $\bar{\delta} = \frac{\gamma}{\sqrt{3}}$  for small strains.

On the other hand, it is likely that increasing anisotropy at high strains invalidates the assumptions made in deriving the flow equations. In these tests the use of  $\gamma = a\theta$  gave a satisfactory correlation between torsion and tension data to reasonably high strains.

The effective stress-effective strain data were plotted on log-log coordinates as seen in Figs. 10 and 11. In general, the data are

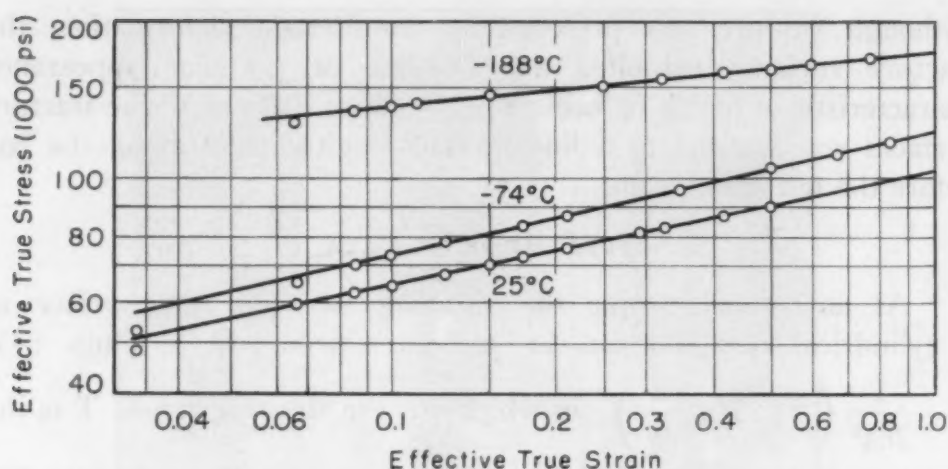


Fig. 10—Effective Stress - Effective Strain Data for Steel C.

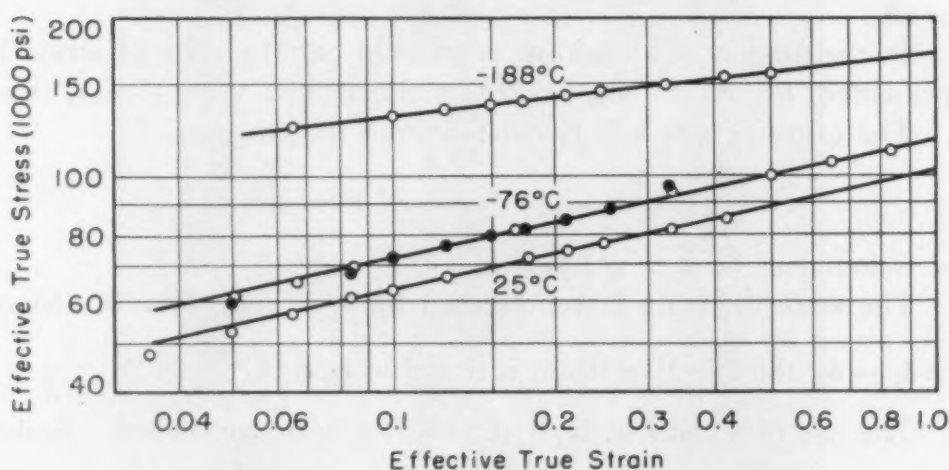


Fig. 11—Effective Stress - Effective Strain Data for Steel R.

represented quite well by straight lines. The points for Steel C at small strains do not fall on the curve drawn. However, if the yield point strain is subtracted from each strain value, the data fall on the curve drawn through the points at higher strains. The data for Steel R are shown as corrected in this manner. The yield point strain is an important correction only at small strains. At higher strains it is a small part of the total strain, and it has a negligible effect on the position of the line drawn through the points. Fig. 11 indicates that duplicate tests on Steel R at  $-75^{\circ}\text{C}$  gave a satisfactory comparison.

Original plans did not include the obtaining of accurate strain data at high strains. In view of the possible limitations imposed by the assumption of isotropy throughout straining, a good correlation between torsion and tension data was not expected as the specimens became appreciably work-hardened. For this reason it

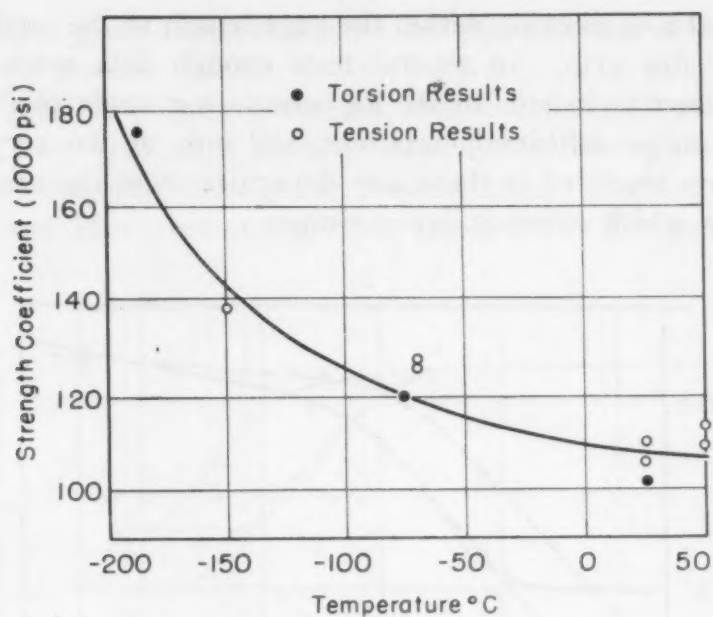


Fig. 12—Variation of Strength Coefficient of Steel C With Temperature.

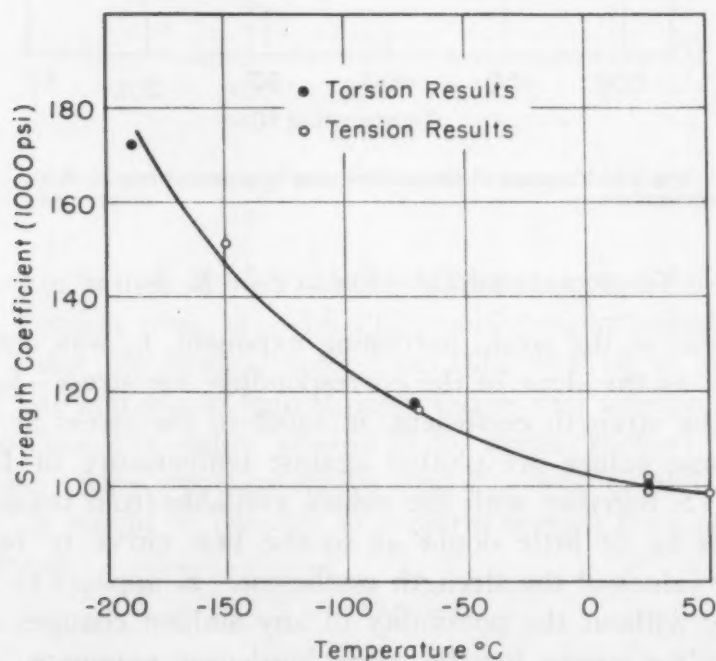


Fig. 13—Variation of Strength Coefficient of Steel R With Temperature.

seemed permissible to remove the strain gages after the specimens had been twisted about 500 degrees to prevent their being damaged when the specimen fractured. However, the total twisting to fracture was measured by noting the rotation of the upper, movable grip and correcting this figure by a factor of 0.86 which was found

to be the ratio of twisting within the gage length to the total rotation of the movable grip. In several tests enough data were obtained in this manner to include in the log stress-log strain plots. These data seem to be sufficiently accurate, and only at the very highest strain values recorded is there any departure from the straight-line relationship which exists at lower strains.

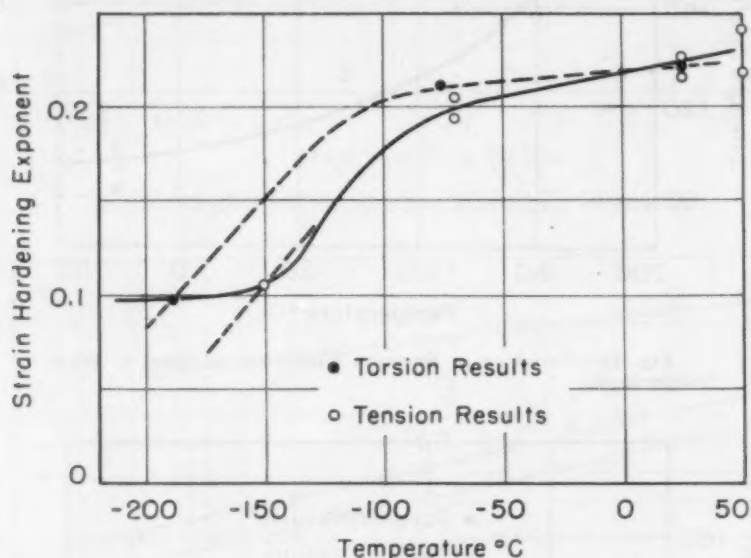


Fig. 14—Variation of Strain Hardening Exponent of Steel C With Temperature.

#### TEMPERATURE DEPENDENCE OF $K$ AND $n$

The value of the strain hardening exponent,  $n$ , was determined for each test as the slope of the corresponding log stress-log strain curve;  $K$ , the strength coefficient, is equal to the stress at a strain of 1.0. These values are plotted against temperature in Figs. 12, 13, 14 and 15, together with the values available from tension tests. There seems to be little doubt as to the best curve to be drawn through the values of the strength coefficient.  $K$  appears to increase continuously without the possibility of any sudden changes of slope as shown by the curves for the strain hardening exponent.

The values of  $n$  from torsion and tension experiments checked reasonably well at both room temperature and  $-75^{\circ}\text{C}$ . The value of  $n$  found for the torsion test at  $-188^{\circ}\text{C}$  was identical to the tension value at  $-150^{\circ}\text{C}$ . Thus the solid curve in Figs. 14 and 15 would appear to represent the temperature-dependence of the strain hardening exponent. This interpretation would be in line with the generalized theory of plastic flow which states that  $n$  is a "universal"



constant for a given metal at a given temperature and is independent of the stress system.

The possibility exists, however, that  $n$  depends upon the stress system. Two lines must then be drawn, one through the torsion results and the other through the tension lines. The dotted lines in Figs. 14 and 15 represent the latter possibility. The correct inter-

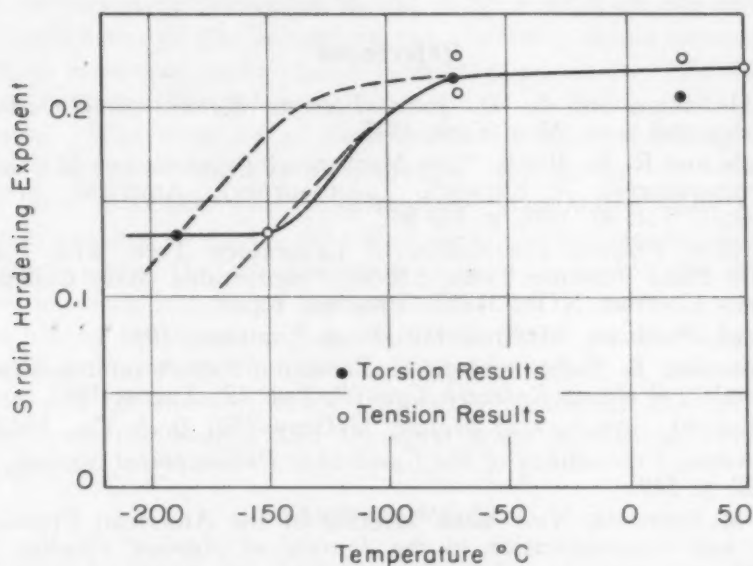


Fig. 15—Variation of Strain Hardening Exponent of Steel R With Temperature.

pretation can be determined only by further test at different temperatures. Torsion tests at  $-150^{\circ}\text{C}$  would be particularly valuable. If the  $n$  value for Steel C were from 0.12 to 0.14, it would lie on the solid line and would lend support to the first interpretation. On the other hand, a value around 0.20 would support the second hypothesis. Also since extensive ductility was exhibited down to  $-188^{\circ}\text{C}$ , it would be possible to perform torsion tests at still lower temperatures.

#### CONCLUSIONS

Values for the strength coefficient,  $K$ , and the strain hardening exponent,  $n$ , were determined from torsion tests at room temperature,  $-75^{\circ}\text{C}$ , and  $-188^{\circ}\text{C}$ . At room temperature and at  $-75^{\circ}\text{C}$  the values so obtained could be compared to the values already available from tension tests; and it was found that the two sets of results compared favorably within the supposed experimental error. Having obtained this good correlation at the two higher temperatures it might be assumed that the values of  $K$  and  $n$  at  $-188^{\circ}\text{C}$  are valid

as well. This assumption is permissible only with certain reservations which can be decided only by tests run in the intermediate temperature range.

While the question of full correlation between the tensile and torsional test data is still open, it is evident that the torsion test affords an additional and important means for studying the strain hardening characteristics of mild steels at low temperatures.

### References

1. J. H. Hollomon and L. D. Jaffe, *Ferrous Metallurgical Design*, John Wiley and Sons, New York, 1947.
2. L. Seigle and R. M. Brick, "The Mechanical Properties of Metals at Low Temperatures: A Survey", *TRANSACTIONS, American Society for Metals*, Vol. 40, 1948, p. 813-862.
3. U. S. Navy Project, Correlation of Laboratory Tests with Full Scale Ship Plate Fracture Tests, SR-96, Pennsylvania State College, U. S. Navy Contract NObs-31217. Progress report.
4. A. Nadai, *Plasticity*, McGraw-Hill Book Company, 1931.
5. M. Gensamer, E. Saibel and J. T. Ransom, "Report on the Fracture of Metals", *Welding Research Council*, Vol. 12, August 1947, p. 443-471.
6. C. S. Barrett, *Structure of Metals*, McGraw-Hill Book Co., 1943.
7. R. L. Aston, *Proceedings of the Cambridge Philosophical Society*, Vol. 23, 1927, p. 549.
8. A. W. McReynolds, New York Meeting of the American Physical Society and Communication to the *Journal of Applied Physics*, January 1948.
9. L. R. Jackson, "Work Hardening and Rupture in Metals", *Metals Technology*, Vol. 13, October 1946.
10. W. T. Lankford, J. R. Low and M. Gensamer, "The Plastic Flow of Aluminum Alloy Sheet Under Combined Loads", *Metals Technology*, Vol. 14, August 1947.
11. J. R. Low and T. A. Prater, "Plastic Flow of Aluminum Aircraft Sheet Under Combined Loads—II", Final Report OSRD No. 4052, Serial No. N-328, August 1944.
12. E. A. Davis, "Plastic Behavior of Metals in the Strain Hardening Range—Part II", *Journal of Applied Physics*, Vol. 8, 1937, p. 213-217.
13. R. Schmidt, *Dissertation, Goettingen*, Julius Springer, Berlin, 1932.
14. N. N. Davidenkov and N. I. Spiridinova, "Mechanical Methods of Testing", *Proceedings, American Society for Testing Materials*, Vol. 46, 1946, p. 1147-1158.
15. E. A. Saibel, "Final Report on the Extension of the Thermodynamic Theory of the Strength of Metals", Contract NObs-34023, Job Order No. 1, July 1946.
16. A. Nadai, "Plastic Behavior of Metals in the Strain Hardening Range—Part II", *Journal of Applied Physics*, Vol. 8, 1937, p. 205-213.

### DISCUSSION

**Written Discussion:** By G. W. Geil, metallurgist, National Bureau of Standards, Washington, D. C.

The torque-twist data obtained for Steel C at small strains are shown in Figs. 4 and 5 of the authors' paper. The slope of the elastic portion of

the torque-twist curve obtained for Steel C tested at  $-188^{\circ}\text{C}$  is approximately one-half that of the torque-twist curves obtained for the steel tested at  $-76$  and  $25^{\circ}\text{C}$ . These data indicate that the modulus of rigidity of the steel at  $-188^{\circ}\text{C}$  is about one-half of the value of the modulus at  $-76$  or  $25^{\circ}\text{C}$ . Normally, one would expect a small increase or very little change in the strength moduli with a decrease in temperature from room to  $-188^{\circ}\text{C}$ . Do the authors have any explanation for this behavior of the steel?

The authors have presented in Fig. 6 their data on the effect of the time of application of the torque on the resulting strain produced in the specimen, as measured by the twist in degrees per inch. Additional information on the experimental procedure used in obtaining these data would be welcome. Was each set of data presented for a specified torque obtained on a specimen initially subjected to that torque or were the data obtained on a specimen which had received prior deformation under successively increasing torques? As these steels showed appreciable so-called yield point twisting, the interpretation of the data would depend upon the prior torque-strain history of the specimen.

It is indeed unfortunate that the torsion tests conducted at  $-150^{\circ}\text{C}$  were not successful as the torsion data for tests at this temperature apparently are the most vital for an answer to the question of full correlation between the tensile and torsional work hardening exponents for these steels.

#### **Authors' Reply**

We wish to thank Mr. Geil for calling our attention to the apparent discrepancy in the modulus of rigidity for the specimens tested at  $-188^{\circ}\text{C}$ . The abscissa in Fig. 5 was incorrectly labeled; each abscissa value should be divided by two. This doubles the modulus calculated from these curves and brings the values at  $-188^{\circ}\text{C}$  into agreement with those at higher temperatures.

The strain-time curves in Fig. 6 were obtained during the progress of the test. They do not represent tests on new unstressed specimens. They were obtained when an incremental load was added to a specimen which had been subjected to successively increasing loads.

We also regret that it was necessary to conclude the project before we were successful in performing tests at  $-150^{\circ}\text{C}$ .

## THE POWDER METALLURGY OF BERYLLIUM

BY HENRY H. HAUSNER AND NORMAN P. PINTO

### *Abstract*

*The powder metallurgy of beryllium has been studied in detail. Methods have been developed for pressing and sintering beryllium powder, and the physical properties of such material have been determined. The behavior of powder compacts under thermal and mechanical treatments has been studied and the resultant properties established. The powder with which the studies were made has been characterized thoroughly.*

*The fundamental ductility of beryllium is discussed, and it is proposed that the pure metal may be inherently more ductile than data on currently available metal indicate.*

*Compacts sintered in vacuo at temperatures slightly below the melting point exhibit optimum properties, including maximum density and slight ductility. Vacuum sintering results in rapid evaporation from the surface of the compact. Argon sintering under similar conditions produces lower densities, no ductility, and less evaporation loss. Grain size of the sintered compact may be controlled by varying sintering time and/or temperature.*

*It was found that vacuum-sintered compacts may be cold-rolled 9% without fracture. Mechanical twins are developed which disappear after a 30-minute anneal at 800 °C (1470 °F); higher temperatures produce grain growth. Compacts may be hot-rolled readily through over 80% reduction.*

*The method for polishing of metallographic specimens of powder metallurgical bars is presented.*

**B**ERYLLIUM metal is of considerable commercial importance because of its mechanical, chemical, and nuclear properties. Its low neutron capture properties, together with other properties, make beryllium a useful metal in the construction of nuclear reactors. This metal may well find extensive use in particular applications because of its low density, good resistance to corrosion, and high relative strength; its strength-to-weight ratio is significantly superior to those of other engineering materials, such as aluminum, magnesium, titanium, or stainless steel. However, beryllium, as now produced, appears to inherently lack room-temperature ductility.

A paper presented before the Thirty-second Annual Convention of the Society, held in Chicago, October 21 to 27, 1950. Of the authors, H. H. Hausner is section head and N. P. Pinto is senior engineer, Metallurgical Laboratories, Sylvania Electric Products Inc., Bayside, Long Island, N. Y. Manuscript received April 13, 1950.



Most previous investigators (1-10)<sup>1</sup> used casting and extrusion methods for the manufacture of beryllium test pieces. We concentrated our investigations on the powder metallurgical methods for the production of the solid metal and the test bars and have studied especially compacts pressed at room temperature and then sintered, without including those pressed at elevated temperatures.

#### THE FUNDAMENTAL DUCTILITY OF BERYLLIUM

Beryllium of sufficiently high purity has not yet been produced on which to measure properties definitively; most beryllium metal contains 1 to 5% oxygen. Moreover the theory of deformation of metals has not advanced to the stage where reliable predictions can be made of the elastic or plastic properties of pure beryllium.

Deductions or conclusions made by metallurgical analogies are extremely hazardous, and reasoning based on apparently sound theories and experience with other metals often produces deductions having little basis in fact. The production of ductile titanium and zirconium has lent credence to the concept of ductility which assigns the cause of brittleness (when present) to the presence of oxygen and nitrogen in solid solution. Inasmuch as zirconium is crystallographically almost identical with beryllium, both having closed-packed hexagonal structures with very low axial ratios ( $c/a = 1.589$  and  $1.585$  for zirconium and beryllium, respectively), possibly the removal of oxygen or  $\text{BeO}$  from the beryllium lattice will yield ductile beryllium.

The mechanical behavior of metals and alloys is presumably conditioned by the crystalline symmetry and the interatomic forces. Only the first of these factors has been adequately studied so that we may partially assess its importance. In metals, plastic deformation takes place by slip along the planes of closest packing and greatest interplanar spacing. Generally, the higher the crystalline symmetry, the more easily slip can take place, because with high symmetry there are many planes along which slip can occur. In the hexagonal metals which are of lower symmetry than the face- or body-centered cubic, slip generally occurs only on the basal (0001) planes. The hexagonal metals are then, in general, less ductile than the metals of higher symmetry, but this is partly compensated for by the ease with which the hexagonal metals form deformation twins which orient the slip planes into a more favorable position for slip to occur. This slip may be inhibited in a number of ways, the most important of which for our consideration are: by lattice distortion caused by solid solution formation; by the interatomic cohesive forces which bind the atoms into the

<sup>1</sup>The figures appearing in parentheses pertain to the references appended to this paper.

lattice; and by lattice distortion caused by mechanical strain.

Little is known concerning the interatomic forces which resist slip by holding the atoms together, but the comparison of heats of sublimation or heats of fusion, which have been used by various investigators as measures of cohesive forces in metal deformation, does not place beryllium in an unfavorable position from the standpoint of ductility. The rough inverse relationship between atomic volume and hardness may indicate, however, that pure beryllium will be harder than other hexagonal metals by virtue of its small atomic volume.

Alexander, Swinton and Pidgeon (2) have pointed out that the ratio of absolute recrystallization temperature to melting temperature for beryllium is much higher than for other metals, and they imply that lack of malleability is characteristic of beryllium.

We therefore suggest that any inherent nonductility of beryllium has not yet been proven beyond doubt and that future investigation, possibly in the field of powder metallurgy, may produce evidence establishing or defining ductility.

#### EXPERIMENTAL WORK

##### *Raw Materials*

*Particle Characteristics*—The beryllium powder used for these tests was the -200-mesh product of the Brush Beryllium Co. (Cleveland) and was made by lathe chipping of vacuum-cast beryllium billets followed by comminution in a rolling mill and an attrition mill.

The results of sieve analysis of the as-received powder (Table I) reveal approximately 60% of the particles smaller than  $44\mu$  and 96%

Table I  
Particle Size Distribution of Beryllium Powder\*

Mesh Size	-60+100	-100+200	-200+250	-250+325	-325+400	-400
Per Cent	0.5	3	12	24	5	55

\*Particle size distribution determined by screening.

finer than  $74\mu$ . Microscopic analyses checked these data satisfactorily.

Attempts to determine the particle size distribution by photometric methods have shown considerable difference between spatulated and unspatulated powders. Fig. 1 shows the effect of spatulation time and illustrates the correlation between microscopic tests and photometric tests on unspatulated powders.

The average particle size was determined by sub-sieve sizer as  $14.7\mu$ , compared with  $17.7\mu$  determined by photometer.

*Purity*—The powder used in these investigations contained impu-

urities, present in significant amounts, which were carried over as tramp constituents from the raw material or were added during processing. The spectrographic analysis showed the following concentrations in parts per million:

Si .....	600	Ni .....	~30	Cd .....	<0.3
Mg .....	1700	Mn .....	110	Cr .....	150
Al .....	2000	Sn .....	~3	B .....	1.5
Fe .....	1450	Pb .....	~60		
Cu .....	~60	Ca .....	360		

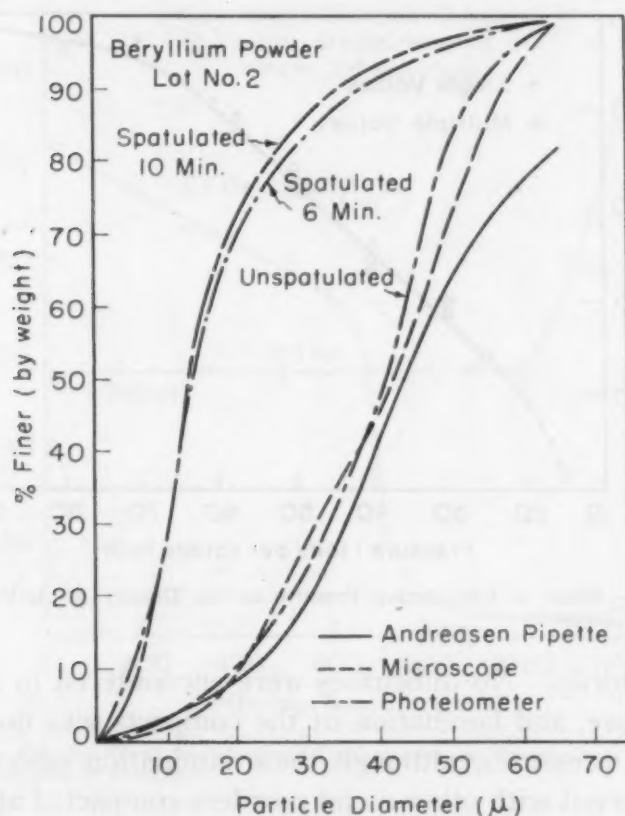


Fig. 1—Comparison of Particle Size Distribution as Determined by Various Methods.

The raw material contained nonmetallic impurities, particularly BeO and slag; the latter was substantially eliminated by vacuum melting. The BeO content, approximately 0.15 to 0.20% in vacuum-cast billets, increased during the comminution of the billets, and particularly during attrition milling, to about 1.5%; this increase was occasioned by the continual exposure of fresh surfaces to the atmosphere and the increase of surface area as particle size was reduced. A check of the effect of particle diameter on BeO content showed  $5\mu$  and  $29\mu$  particles containing 3.43 and 2.83% BeO, respectively. It has also been

shown that the storage of beryllium, even in sealed containers, permits an increase of approximately 3.7% BeO in six months.

### Compacting

Beryllium powder, as described above, was compacted under varying conditions to determine optimum compacting conditions. It was compacted in a steel die, in a hydraulic press at 15 to 90 tsi, for a constant pressing time of 1 minute. Tests have shown that compacting at 10 tsi or below is not practical, since the powder particles do not

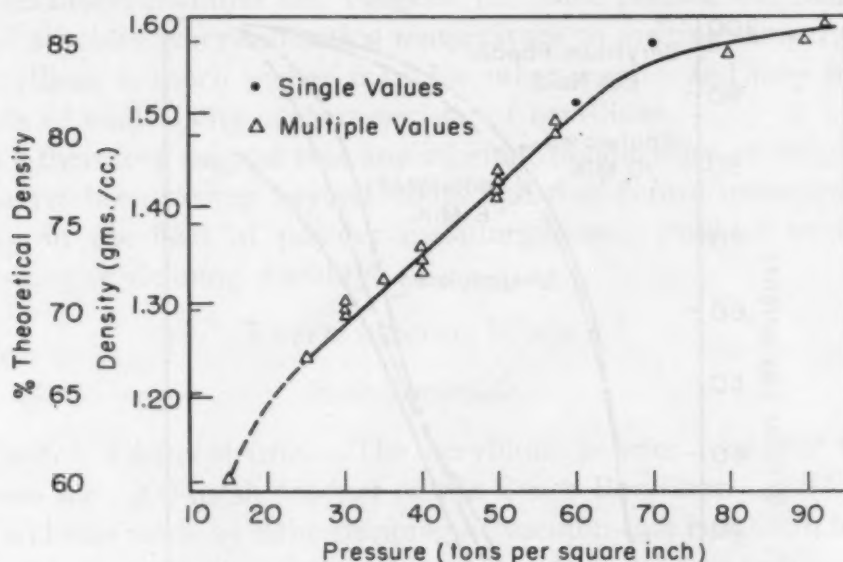


Fig. 2—Effect of Compacting Pressure on the Density of As-Pressed Beryllium Compacts.

adhere satisfactorily. No difficulties were encountered in compacting at 15 tsi or above, and lamination of the compacts was not observed, even at higher pressures, although these lamination effects can frequently be observed with other metal powders compacted at high pressures. Fig. 2 shows the densities of the compacts in the as-pressed state as a function of the compacting pressure. The density of the specimens compacted at 15 tsi was 1.1 grams per cubic centimeter and increased practically linearly with the compacting pressure up to 70 tsi, beyond which the densities increased with a decreasing slope to a density of 1.6 grams per cubic centimeter at 90 tsi. Sintering tests described below showed that the optimal compacting pressure was approximately 55 tsi and that higher pressures contributed very little toward an increase in density of the sintered product.

### Sintering of Beryllium Compacts

*Sintering in Vacuo and in Argon*—In order to evaluate the effect



of sintering conditions on the properties of sintered bars, studies were made using variations of temperature and sintering atmosphere. Further studies were made with regard to grain structure, grain growth and loss of material by volatilization in vacuo.

Vacuum sintering studies were made in a furnace which employs a 3-inch diameter ceramic tube and consistently produces vacua in the order of  $1.0 \times 10^{-5}$  mm of mercury. The tube was degassed before use. The specimens were sintered in beryllia boats, filled with fine-

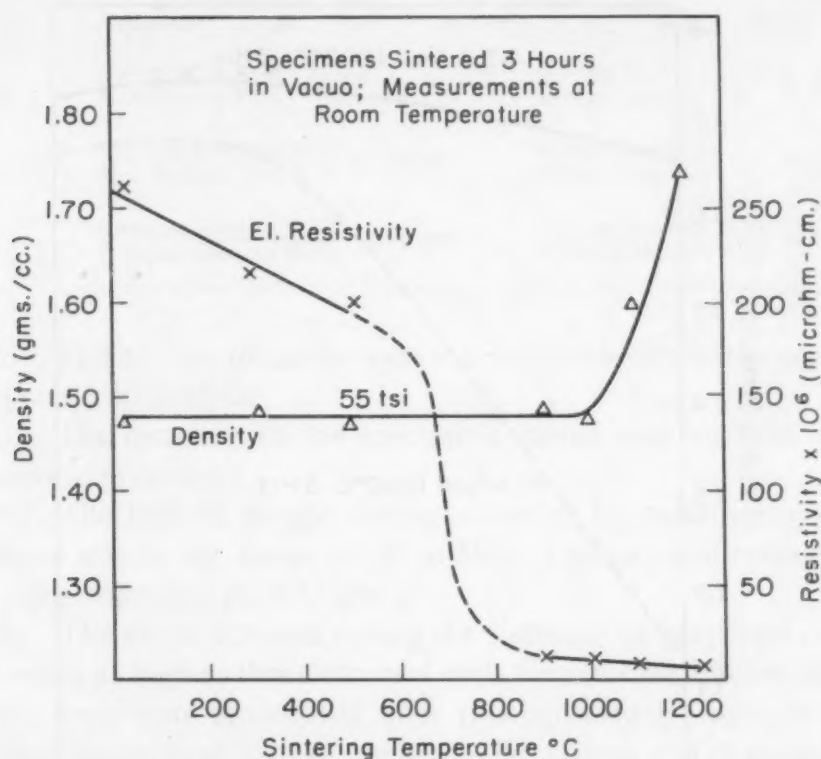


Fig. 3—Effect of Sintering Temperature on Density and Electrical Resistivity of Beryllium.

grained beryllia sand. Temperature measurements were taken with a platinum/platinum-rhodium thermocouple. The temperature increase was at a uniform rate of approximately  $300^\circ\text{C}$  ( $570^\circ\text{F}$ ) per hour and decrease at  $280$  and  $115^\circ\text{C}$  per hour in the first and second hours. For sintering in argon atmosphere, tank argon of 99.8% purity was passed over copper at  $600^\circ\text{C}$  ( $1110^\circ\text{F}$ ), then through a lectrodryer, further through a cold trap of liquid nitrogen and finally over uranium chips at  $750^\circ\text{C}$  ( $1380^\circ\text{F}$ ).

Sintering in vacuum was performed at various temperatures up to  $1250^\circ\text{C}$  ( $2280^\circ\text{F}$ ). Maximum densities of the sintered compacts were obtained with specimens pressed at about 55 tsi. The effect of vacuum sintering temperatures on the densities is shown in Fig. 3. The

densities of the compacts are practically constant up to a sintering temperature of  $1000^{\circ}\text{C}$  ( $1830^{\circ}\text{F}$ ), above which the density increases rapidly and is over 1.70 grams per cubic centimeter after sintering at  $1200^{\circ}\text{C}$  ( $2190^{\circ}\text{F}$ ). Densities as high as 1.8 grams per cubic centimeter were obtained after sintering at approximately  $1250^{\circ}\text{C}$  ( $2280^{\circ}\text{F}$ ), where several of the specimens began to melt. The possibility of densification at lower temperatures induced by variations of

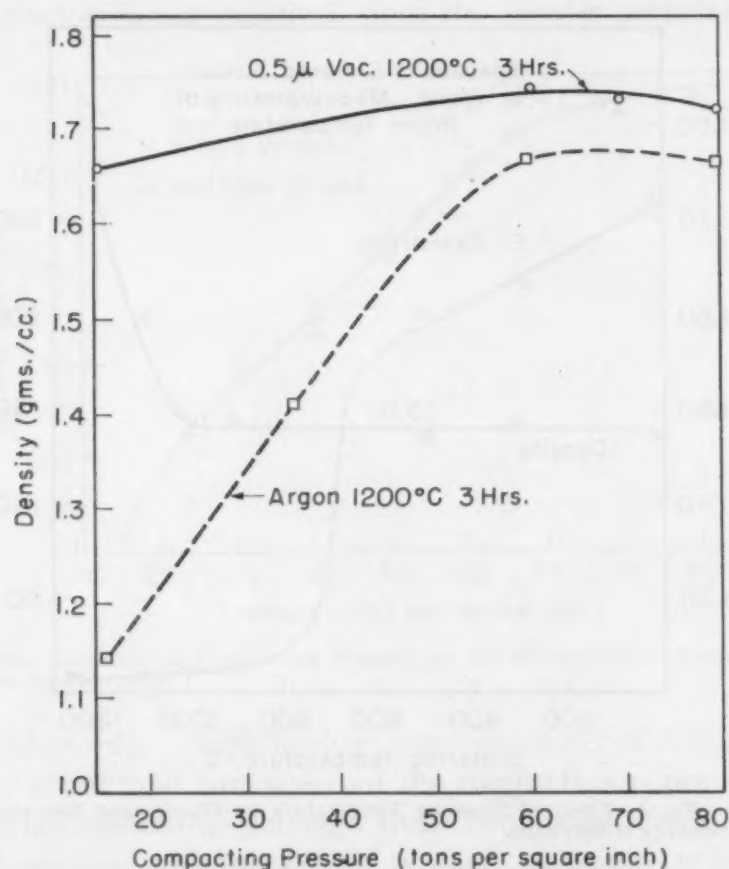


Fig. 4—Comparison of Argon-Sintered and Vacuum-Sintered Beryllium Compacts.

compacting pressure was studied; a series of bars compacted between 10 and 65 tsi and sintered in vacuo at  $900^{\circ}\text{C}$  ( $1650^{\circ}\text{F}$ ) for 3 hours showed no change in density after sintering.

The vacuum sintering of beryllium was investigated and the effect of temperature on density is shown in Fig. 4. Microstructures of vacuum- and argon-sintered bars are discussed below. Vacuum sintering at  $1200^{\circ}\text{C}$  ( $2190^{\circ}\text{F}$ ) showed the following results:

1. The densities of the specimens varied from 1.68 to 1.72 grams per cubic centimeter.

**Table II**  
**The Evaporation of Beryllium Compacts During Sintering In Vacuo**

Sample No.	State	Surface Area— Exposed to Vacuum		Volume cu. in.	Weight g.	Density g/cc	Weight Loss During Sintering g. %	
		Total sq. in.	sq. in.					
B-21	As Compacted	3.02	2.46	0.330	7.33	1.35	....	....
	As Sintered	2.15	.....	0.199	5.38	1.67	1.95	26.5
B-23	As Compacted	1.57	0.968	0.072	1.66	1.36	....	....
	As Sintered	1.01	.....	0.038	0.911	1.47	0.75	45
Surface Area B-23			= 1:2		Volume B-23		= 1:4.6	
Surface Area B-21					Volume B-21			
Exp. Surface Area B-23			= 1:2.55		Weight Loss B-23		= 1:2.6	
Exp. Surface Area B-21					Weight Loss B-21			
Compact Density B-22			= 1:1.007		Sintered Density B-21		= 1:0.88	
Compact Density B-23					Sintered Density B-23			

2. The highest densities were reached with specimens compacted in the range 50 to 60 tsi.

3. The densities of the specimens varied only slightly with the compacting pressure.

4. The loss of weight during sintering by volatilization of the beryllium was in the range of 18 to 50%. Losses were reduced when bars were imbedded in BeO grain.

5. The vacua attained during the sintering of beryllium compacts were never as high as those attained with the same equipment and other metals; beryllium evaporated at a rate sufficiently high to prevent attaining better than  $0.1\mu$  of mercury. Beryllium was observed to deposit at sites remote from the maximum temperature zone, and there was high pick-up in the diffusion pump.

A comparison of vacuum and argon sintering is given in Fig. 4. The difference in densities of sintered bars is much greater when low compacting pressures are used, although argon-sintered densities are never as high as those of vacuum sintering.

Beryllium compacts sintered in high vacua showed a measurable ductility which was not observed in the specimens sintered in argon and which will be discussed below.

*Evaporation of Beryllium During Sintering in Vacuo*—The high rate of evaporation was studied to determine whether evaporation from particle surfaces or compact surfaces determined the extent of loss.

Loss during sintering at 1235 °C (2255 °F) was determined by weight difference (Table II). The ratio of the weight losses of the two

samples was 1:2.6 and therefore practically the same as that obtained by comparison of exposed surfaces (1:2.55). Thus, the weight loss for the beryllium compacts during sintering in vacuo is a function of the exposed area rather than a function of the volume.

The rate of evaporation and vapor pressure of beryllium based on these data agree with the findings of Holden, Speiser and Johnston (8) and the extrapolated data of Schuman and Garrett (11).

Inasmuch as the pores are continuous in a pressed compact, all particle surfaces were exposed to vacuum until a temperature of about 1000 °C was reached, when densification began. This temperature was about 200 °C higher than the temperature at which evaporation was first observed; this early evaporation may have been the more volatile impurities magnesium or calcium. Although evaporation occurs uniformly throughout the sample, the weight loss has been shown to be a function of the exposed surface area of the bar, and any metal which evaporates from the particles is retained, probably by condensation within the bar, after the pores are constricted or closed.

*Electrical Resistivity of Sintered Beryllium*—The development of sintering, particularly the earlier stages, is evidenced more sensitively by changes in electrical properties than in mechanical properties, such as density or strength.

Electrical resistivity measurements were taken on beryllium compacts as pressed (room temperature) and as sintered at 300 to 1200 °C. Fig. 3 shows a density increase at sintering temperatures of 1000 °C and above and that the density below this temperature virtually did not change. The change in electrical resistivity, however, occurred much earlier, due to the improvement of the bond between the particles, presumably by the breaking of the BeO barrier between particles. This did not affect pore volume and thus the density of the compact remained unchanged. Further, a substantial drop in resistivity occurred between the sintering temperatures of 500 and 900 °C.

Similar results were obtained by R. H. Myers (12), who recently described his work on sintering of electrolytic tantalum powder. He observed that sintering of tantalum in vacuo changes the electrical resistivity of the compact in certain steps without any changes in density. Trzebiatowski (13) has observed similar behavior on metals which form oxide, e.g., copper, and not on nonoxide-forming elements, e.g., gold; like effects are reported for nickel by Grube and Schlecht (14).

*Metallographic Study of Sintering*—The phenomena effecting the sintering of powder compacts may be observed conveniently by a study of microstructures. The compact in the as-pressed state, Fig. 5, showed



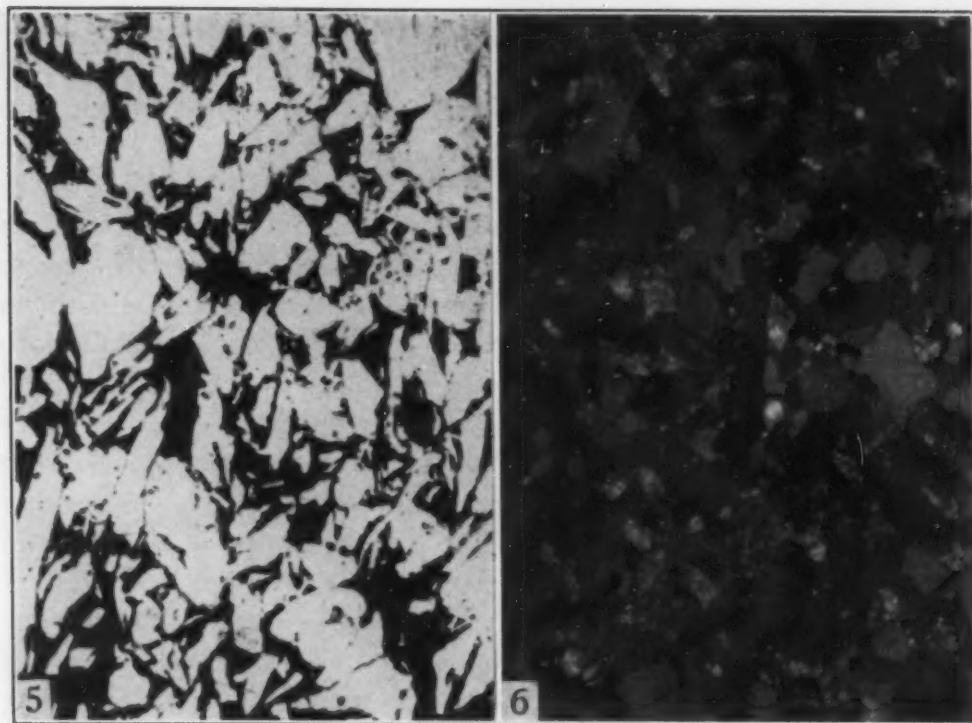


Fig. 5—Compact Pressed at 50 tsi, Not Sintered. This as-pressed compact shows the needle- or plate-like shape of the 200-mesh particles and their relative orientation. Bright field, unetched.  $\times 250$ .

Fig. 6—Compact Pressed at 50 tsi, Sintered  $\frac{1}{2}$  Hour at 1050°C in Argon. Polarized light, unetched.  $\times 250$ .

particles of a plate- or needle-shaped form with the major dimension usually perpendicular to the pressing direction. The density of the pressed compacts varies with pressures as shown in Fig. 2.

In order to observe structural changes during sintering, series of bars were sintered in vacuo and in purified argon. Sintering below 500 °C did not produce an observable change of structure or density, although electrical resistivity decreased.

Changes in microstructure were observed after sintering at 1000 °C, at which temperature the specimens began to shrink dimensionally. In the bars sintered between 1000 and 1250 °C, the typical recrystallization and grain growth processes occurred. After sintering at 1000 °C, the structure still contained some of the original powder particles, but occasional particles were present which apparently had been stressed more than others during the pressing operation and had recrystallized during sintering. These recrystallized particles were small, mostly less than  $10\mu$ . The area of contact between particles in the as-pressed compact was fairly small; during sintering at 1000 °C, this contact area was increased greatly so that most of the particle surface area became interface area. The void volume was still large and was dispersed as small areas.

After sintering at 1050 °C (Fig. 6), the area occupied by voids was less and the density increased. Few of the original particles could be recognized; fairly uniform, equiaxed grains of approximately 5 to 15 $\mu$  diameter characterized this stage of sintering.

At a sintering temperature of 1100 °C (2010 °F) grain growth became pronounced. The grains were larger and more uniform in shape and size; the original plate and needle shape had been destroyed, and the voids appeared as larger and more concentrated areas. Complete recrystallization and crystal growth up to grains of 10 to 30 $\mu$  size occurred at this temperature, and the grains had the characteristically polygonal shape. Practically all of the agglomerates of BeO were arranged at the grain boundaries and most of the larger ones were located in the areas where three boundaries intersect.

During sintering at 1150 °C (2100 °F) the density of the material increased further and the grains grew to an average diameter of approximately 50 $\mu$ . Spheroidization of the voids started at this temperature. After sintering at 1150 °C (2100 °F) the inclusions (probably BeO) still appeared concentrated at the grain boundaries. At 1200 °C (2190 °F) the grains grew beyond these mechanical barriers and some of the voids and inclusions were distributed within the grains.

At 1225 °C (2240 °F) the grain diameter increased to approximately 150 $\mu$ , and some of the holes and inclusions were still located at the grain boundaries. These hole areas are fairly large, whereas the smaller void-inclusion areas are scattered throughout the cross section. At 1250 °C (2280 °F) the specimens started to melt, and grains grew to several hundred microns diameter.

All the above-described microstructures are characteristic for sintering in purified argon at the above-mentioned temperature for a period of 30 minutes. Whereas the sample sintered 30 minutes at 1200 °C (2190 °F) showed an average grain size of approximately 75 microns, an increase in sintering time to 1 hour resulted in grain growth to an average size of 100 to 120 $\mu$ .

The oxide film covering the surface of beryllium particles is tenacious and stable and probably restricts the bonding of particles during the earlier stages of sintering. At a temperature between 500 and 900 °C, the particle bond was improved many-fold, without change in compact density. This improvement was occasioned probably by the diffusion of beryllium and BeO, the latter agglomerating. At 900 °C (1650 °F) the vapor pressure of beryllium is in the order of 1 $\mu$  of mercury, and vapor transport may participate in the improvement of bond, as was suggested by Rhines, Birchenall and Hughes (16) in their study of copper sintered between 800 and 1000 °C; the vapor pressure – tem-

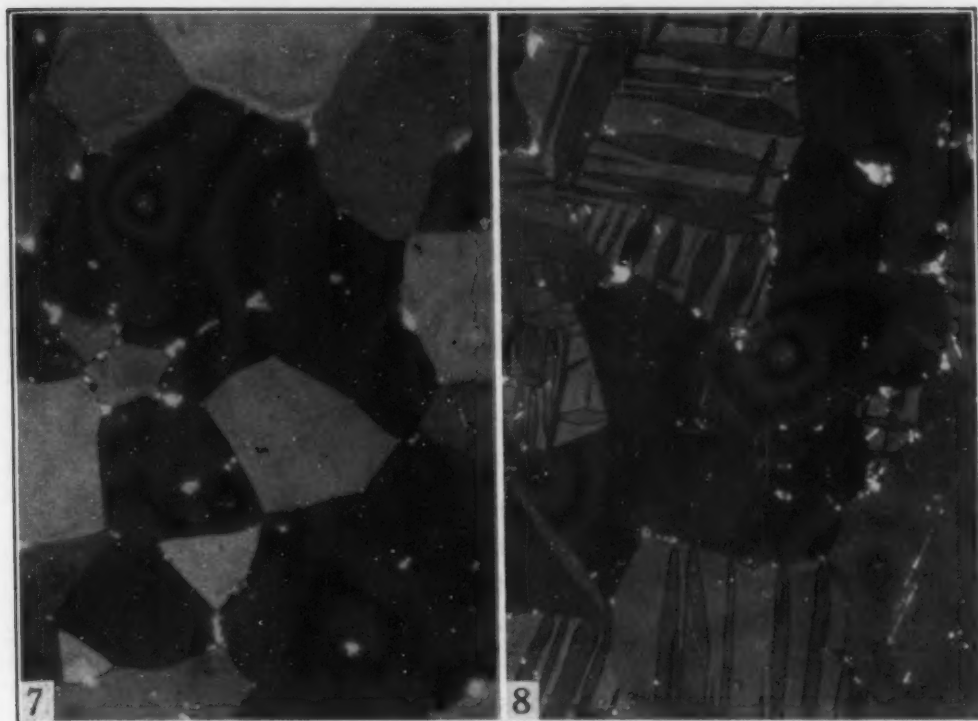


Fig. 7—Compact Pressed at 50 tsi, Sintered 3 Hours at 1220°C in Vacuo. Characteristic structure before cold working. Polarized light, unetched.  $\times 250$ .

Fig. 8—Compact Pressed at 50 tsi, Sintered 3 Hours at 1220°C in Vacuo; Cold-Rolled 9%. Characteristic cold-worked structure showing mechanical twins. Polarized light, unetched.  $\times 250$ .

perature relationship of beryllium and copper are similar. At higher temperatures these mechanisms are augmented by atomic transport or viscous flow, which are responsible for the densification of the compact.

Fig. 7 shows the microstructure of a compact sintered at 1220°C for 3 hours in vacuo. The void inclusion areas of this and other vacuum-sintered beryllium specimens were located primarily at the grain boundaries. Fewer nonmetallic impurities (including voids) could be observed in the vacuum-sintered specimens than in the argon-sintered samples. This observation is checked by density data, Fig. 4.

*Bending of Sintered Beryllium*—Earlier tests have shown that beryllium compacts sintered in purified argon were extremely brittle, whereas vacuum-sintered compacts exhibited a certain ductility. In order to compare these low orders of ductility, the specimens were bent. These tests have indicated that vacuum-sintered beryllium bars of 0.125-inch thickness can be bent without fracture about a radius of 1.9 inches, which corresponds to an elongation of the outer fibers of about 6.4%; cold rolling of these specimens was possible as described below. Beryllium compacts of like dimensions sintered under similar temperature and time conditions but in an atmosphere of highly puri-



**Table III**  
**Electrical Resistivity of Specimens of Vacuum-Sintered Beryllium**

Sample No.	State	Resistivity in Ohm-Cm	
		Convex Side	Concave Side
B-30	Straight before rolling	$6.0 \times 10^{-6}$	$6.0 \times 10^{-6}$
B-23	Bent	$5.6 \times 10^{-6}$	$5.8 \times 10^{-6}$
B-34	Bent	$5.8 \times 10^{-6}$	$6.1 \times 10^{-6}$

fied argon could not be bent or rolled to any measurable degree without breaking.

The fact that a slightly porous material such as the above-described beryllium specimens could be bent to the degree indicated does not necessarily permit the conclusion that the material is ductile. It is known that certain porous or fibrous materials can be bent, or rolled, slightly without being ductile because the presence of non-metallics permits discontinuous cracks without complete bar fracture. The electrical resistivities of the vacuum-sintered beryllium bars were measured in order to check this possibility.

Table III shows the resistivities of two bent specimens and for comparison the resistivity of a straight sample. Voltage drop measurements were taken on both sides of the specimens. Although resistance measurements of this type show average figures of resistance, these average figures are affected to a certain extent by the resistance of the surface on which the voltage drop is measured. Loosening of bonds between the crystals or cracks on the outer (convex) side of the bent samples should result in a greater voltage drop (resistance increase) on the outer side than on the inner (concave) side. Resistivity changes due to microstructural changes, twinning, are considered minor relative to those due to the development of cracks. Table III shows that the resistance of the bent samples was not substantially different when measured on the concave and on the convex side, indicating that no cracking occurred on the convex side. Similar results may be obtained when the measurements are made on a bent specimen of material known to be ductile.

#### *Mechanical and Thermal Treatment of Sintered Beryllium*

*Cold Rolling and Annealing of Sintered Beryllium*—Further investigations into the ductility of vacuum-sintered beryllium bars were made by cold rolling. A two-high reversible rolling mill with 8-inch diameter by 12-inch flat rolls was used for these tests. The beryllium specimens were approximately  $\frac{1}{8}$  by  $\frac{3}{8}$  by 8 inches. These bars were compacted at 50 tsi, sintered at 1220 °C (2230 °F) for



3 hours in vacuo of  $0.1\mu$  mercury. The reduction was approximately 1.5 to 2 mils per pass.

The maximum decrease in thickness without cracking was approximately 9%. After a reduction of approximately 9%, surface and edge cracks appeared.

Cold rolling affects greatly the microstructure of beryllium compacts. The structure of the vacuum-sintered compacts, Fig. 7, consisted of randomly oriented grains without lines or bands. After a reduction of 1 to 2% (one to two passes through the rolls), structure changed materially and bands were formed which could be recognized as mechanical twins. Further rolling and decrease in thickness of  $7\frac{1}{2}$  to 9% revealed increased mechanical twinning and twins on practically every grain, as shown in Fig. 8. The degree of cold working on sintered beryllium can be recognized by the amount of mechanical twinning.

It appeared also that some grains underwent more severe working than others, probably a function of orientation, and that most of the work was absorbed by them.

The bands have been shown to be mechanical twins and to disappear completely without the formation of annealing twins when heated to temperatures over  $800^\circ\text{C}$ . Heating to higher temperatures resulted in rapid grain growth.

Temperatures up to  $600^\circ\text{C}$  apparently produced no stress relief or change in structure. However, at  $700^\circ\text{C}$  many of the twins disappeared, grain growth was not appreciable, and the original structure was restored. Some twins persisted at  $800^\circ\text{C}$  (Fig. 9) and grain growth had advanced, in some cases beyond the original grain boundaries defined by the oxide-void network. At  $900^\circ\text{C}$ , no trace of mechanical twins remained; grains were larger and occupied areas comparable to areas formerly occupied by several grains. At  $1000^\circ\text{C}$ , the only traces of the original structure were the ghost networks of oxides and voids superimposed at random on the structures of large, randomly oriented grains.

Although we have not attempted to check the recrystallization point of  $810^\circ\text{C}$  ( $1490^\circ\text{F}$ ) as determined by Alexander et al (2), these results confirm their value. It is still possible that this value may be much higher than the true recrystallization temperature of beryllium. It has been shown that the recrystallization temperatures of metals in the form of powder metal compacts are characteristically higher than the same metals fabricated by casting and shaping. The recrystallization temperature of sintered platinum, for example, is 200 to  $600^\circ\text{C}$  higher than that of regular platinum (15). This difference may be

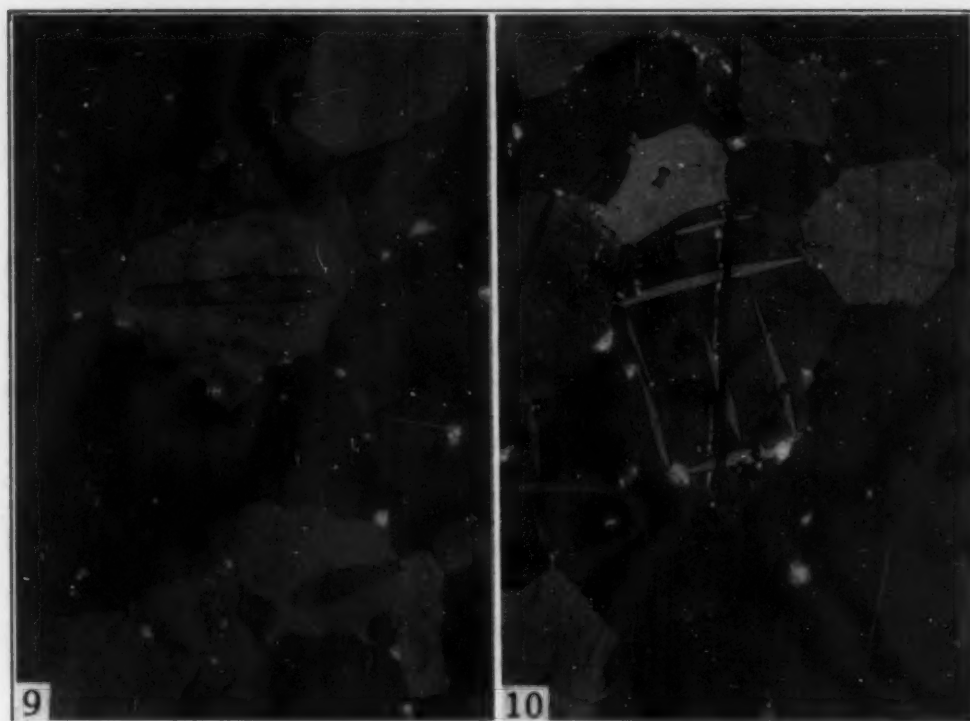


Fig. 9—Compact Pressed at 50 tsi; Sintered 3 Hours at 1220°C in Vacuo; Cold-Rolled 6%; Heated  $\frac{1}{2}$  Hour at 800°C in Argon and Water-Quenched. Most twins have disappeared; grains have started to increase in size. Polarized light, unetched.  $\times 250$ .

Fig. 10—Compact Pressed at 50 tsi, Sintered 3 Hours at 1220°C in Vacuo; Cold-Rolled 2  $\frac{1}{2}$ %; Annealed 3 Hours at 500°C in Vacuo. Scratch hardness test made with Bergman hardness tester using 1-gram load. The extent of mechanical twinning is characteristic of this reduction. The impression of the indenter appears shallower where it crosses bands or band-matrix interfaces. Polarized light, unetched.  $\times 250$ .

accounted for by the fact that, in powder compacts, the voids present at grain-boundary intersections reduce effectively the angle of intersection and the energy at that point available for the initiation of recrystallization. If such an effect could be assigned beryllium, its recrystallization temperature to melting point ratio mentioned by Alexander et al (2) and referred to previously might be reduced and this indication of inherent brittleness nullified.

As with other hexagonal metals, annealing twins were not formed from the mechanical twins. Although an occasional twin persisted after annealing, it is difficult to describe them definitely as persistent mechanical twins, annealing twins, or new mechanical twins occasioned by stresses due to quenching. It is not yet possible to correlate, with these limited data, reduction with the recrystallization temperature, although such studies are underway.

It was found possible to cold roll vacuum-sintered beryllium still further by the interposition of an intermediate annealing treatment. It is apparently important that the annealing time and temperature be controlled to avoid excessive grain growth. Specimens cold-rolled 6% could be reduced another 6% after annealing at 1000 °C.

The cold rolling tests, like other tests, showed that the vacuum-sintered beryllium specimens behaved differently from the specimens sintered in argon. In the cold rolling of argon-sintered beryllium specimens, 1 to 2% was the maximum decrease in thickness, and surface cracks could be observed at a very early stage; correspondingly fewer mechanical twins were observed.

The fact that beryllium can be hot-rolled is well known. The material was hot-rolled in this investigation to study the grain structure of these specimens and to compare it with the structure of the material as sintered and as cold-rolled. Vacuum-sintered beryllium bars were completely jacketed in 0.040-inch cold-rolled steel and the assemblies heated in hydrogen atmosphere up to 1000 °C and rolled at this temperature in the above-described rolling mill. The reduction in thickness per pass was approximately 10% and no difficulties were encountered at reductions of 50 to 80%. Original grains were distorted and grain growth was evident; no twinning could be observed. The grains were elongated in the direction of rolling, and the void-inclusion areas especially showed this elongation. As the per cent reduction increased the void-inclusion areas tended to become more closely aligned, finally appearing as oxide stringers.

*Hardness of Beryllium Compacts*—Previous work on determining the hardness of beryllium bars has shown that cold working and cracking occur near the indenter impression when loads are applied. The usual Rockwell loads occasion mechanical twins characteristically 60 degrees apart and often produce microscopic cracks. Hence, hardness tests employing major loads of this order of magnitude are of use for comparison only; the reliability of the absolute numbers is questionable and their use is therefore empirical. The standard superficial Rockwell 15-T scale was adopted for the comparison of bars, despite the difficulty of conversion to more familiar systems. The hardness of as-pressed compacts was in the range of 65 to 70 15-T, corresponding to 58 to 67 BHN (500-kg load). As sintered, the compacts varied from 73 to 76 (66 to 80 BHN), depending on the sintering temperature, with a melted specimen showing 84.5 (132 BHN).

Heat treating experiments showed that the cold-rolled hardness of 81.5 (114 BHN) could be reduced to the original as-pressed hardness after annealing above the recrystallization point.

A scratch test was made on a specimen of cold-rolled beryllium, using a 1-gram load on a diamond pyramid. Fig. 10 shows the impression crossing crystals, boundaries, and twins. It appears that the impression was less deep as it traversed individual twin bands and grain boundaries. Although this evidence is not conclusive, micro-



hardness tests showed that the twins were harder than the crystal matrix. Twins were thus consumed by the matrix during annealing, as is generally observed in recrystallization.

### *Metallography of Powder Compacts*

In an earlier stage of this investigation, formation of dark needle-shaped markings was observed in many cases within the grains of a sintered beryllium compact. These polishing defects are known to occur frequently in brittle materials and are probably caused by chipping of the surface along definite cleavage lines. In order to eliminate them, H. W. Woods developed the following polishing technique. After polishing the bakelite-mounted specimens on 2/0 and 3/0 kerosene-lubricated paper on rotating disks, they are polished further on a silk-covered disk using an aqueous solution of Linde Grade A polishing powder with about 10% oxalic acid. Polishing time is approximately 3 minutes. The final polish which eliminates all the markings is done on a Gamal cloth covered disk, using the Grade B suspension as before, for 3 to 4 minutes.

### CONCLUSIONS

Although the above-described tests were made with an impure material, some conclusions can be drawn which will be helpful, not only for the further development of the powder metallurgy of beryllium but also for the development of the metallurgy of beryllium in general.

1. Beryllium powder can be compacted at room temperature without difficulties, and no binder is necessary to form the compacts.
2. In order to obtain a material of fairly high density, the beryllium compacts may be sintered in a high vacuum or in a protective atmosphere, such as argon, at temperatures below the melting point of beryllium.
3. Sintered beryllium compacts reveal microstructures of equiaxed grains and random orientation.
4. Beryllium sintered in vacuo reveals measurable ductility, whereas argon-sintered beryllium compacts are brittle.
5. Vacuum-sintered beryllium can be reduced 9% in thickness by cold rolling; mechanical twins are formed, which disappear after annealing. Annealing after cold rolling permits further deformation.

### ACKNOWLEDGMENTS

The authors wish to acknowledge the work of H. W. Woods in the metallographic preparation of specimens. We appreciate the efforts



of B. Kopelman and C. C. Gregg in the development of analytical techniques and the study of particle characteristics. We are indebted to R. P. Angier for contributions in the earlier stages of these investigations and to B. H. Alexander for his very helpful discussions and recommendations. The comments and suggestions of W. E. Kingston have been most helpful.

This work was performed under Atomic Energy Commission Contract No. AT-30-1-GEN-224. This report is published by permission of the A.E.C.

### References

1. W. Kroll, "Is Beryllium Ductile?", *Metals and Alloys*, Vol. 8, 1937, p. 348-353.
2. W. A. Alexander, J. K. Swinton and L. M. Pidgeon, "The Recrystallization Temperature of Beryllium", *Transactions, Canadian Institute of Mining and Metallurgy*, Vol. 50, 1947, p. 657-664.
3. H. A. Sloman, "Researches on Beryllium", *Journal, Institute of Metals*, Vol. 44, 1932, p. 365-391.
4. L. Tarnopol, "Hexagonal Slip in Beryllium Crystal", *METAL PROGRESS*, Vol. 52, 1947, p. 391.
5. G. V. Raynor, "Beryllium, Beryllium Alloys and the Theoretical Principles Affecting Alloy Formation with Beryllium", *Journal, Royal Aeronautical Society*, Vol. 50, 1946, p. 390-415.
6. D. W. Lillie, P. Gordon and A. R. Kaufman, "The Mechanical Properties of Beryllium", *Journal of Metallurgy and Ceramics*, Vol. 1, 1948, p. 64-89.
7. F. Fichter and K. Jablczynski, *Berichte*, Vol. 46, 1913.
8. R. B. Holden, R. Speiser and H. L. Johnston, "The Vapor Pressures of Inorganic Substances. I—Beryllium", *Journal, American Chemical Society*, Vol. 70, 1948, p. 3897.
9. A. R. Kaufman, P. Gordon and D. W. Lillie, "The Metallurgy of Beryllium", *TRANSACTIONS, American Society for Metals*, Vol. 42, 1950, p. 785-844.
10. W. Hausser, A. Bardehle and G. Heisen, *Fortschritte auf dem Gebiete der Röntgenstrahlen*, Vol. 35, 1926.
11. R. Schuman and A. B. Garrett, "The Vapor Pressure of Beryllium at 1170-1340 °K", *Journal, American Chemical Society*, Vol. 66, 1944.
12. R. H. Myers, "The Sintering of Electrolytic Tantalum Powder", *Metallurgia*, Vol. 38, 1948, p. 307-310.
13. W. Trzebiatowski, *Zeitschrift für physikalische Chemie*, Vol. 87, 1934.
14. G. Grube and H. Schlecht, *Elektrochem.*, Vol. 44, 1938.
15. A. B. Middleton, L. B. Pfeil and E. C. Rhodes, "Pure Platinum of High Recrystallization Temperature, Produced by Powder Metallurgy", *Journal, Institute of Metals*, Vol. 75, 1934.
16. F. N. Rhines, C. E. Birchenall and L. A. Hughes, "Behavior of Pores During the Sintering of Copper Compacts", *Journal of Metals*, February 1950.

### DISCUSSION

**Written Discussion:** By W. W. Beaver, technical assistant to director of development, The Brush Beryllium Co., Cleveland.

This paper is of interest to the beryllium metal industry of which

The Brush Beryllium Company is an important part. The authors' contribution in determining grain growth as a function of temperature in cold-pressed beryllium powder is especially appreciated.

In considering Fig. 4 of this paper, in which argon-sintered and vacuum-sintered beryllium compacts are compared, we should like to ask the authors if the dew point of the argon entering the sintering furnace was known, and if the BeO content of the compacts after sintering was determined. It appears from Fig. 4 that the argon used for sintering these compacts may not have been as pure as might be expected from the elaborate purification to which it was subjected. In the compacts made at lower compacting pressures, the low density could be caused by the particle surfaces oxidizing faster than sintering could take place. More surface would appear to be available for oxidation of the compacts made at lower pressure because of a greater connected pore volume. The lack of ductility found for argon-sintered compacts, as well as their disintegration on cold rolling, also seems to point out typical effects of particle oxidation.

Our experience with apparent ductility in beryllium powder consolidated at less than maximum density corresponds to that found by the authors, and we agree that little information of value on the ductility of beryllium compacts can be determined unless at maximum density, which, of course, changes with the oxide content of the powder. The resistivity values of  $5.6 \times 10^{-6}$  to  $6.1 \times 10^{-6}$  ohm-cm compared with figures of  $4.02 \times 10^{-6}$  to  $4.30 \times 10^{-6}$  for extruded or swaged beryllium at maximum density that have been reported<sup>2</sup> also indicate that maximum density had not been achieved.

In the bending tests for sintered beryllium described on page 1064, a value of 6.4% for elongation of the outer fibers was found, apparently, assuming no deformation of the fibers on the inner circumference of the bend. We would like to suggest that a better comparison between ductility obtained as tensile elongation with that obtained from bend tests can be found by assuming appropriate inner fiber deformation. Timoshenko's<sup>3</sup> formula for unit elongation of fiber with Dr. Hausner's data is used as follows:

$$\text{Ex (extension)} = \frac{y \text{ (the distance between the neutral axis and the fiber)}}{r \text{ (the radius of bending)}}$$

$$y = \frac{0.125 \text{ (thickness)}}{2} = 0.0625$$

$$r = 1.9 \text{ (bending radius)} + 0.0625 = 1.9625$$

$$\text{Ex} = \frac{0.0625}{1.9625} = 3.18\%$$

This value for per cent elongation can then be compared with

<sup>2</sup>C. B. Sawyer and B. Kjellgren, "Beryllium and Some of Its Aluminum Alloys", *Metals and Alloys*, 1940; A. R. Kaufmann, P. Gordon and D. W. Lillie, "The Metallurgy of Beryllium", *TRANSACTIONS, American Society for Metals*, Vol. 42, 1949, p. 785-844.

<sup>3</sup>S. Timoshenko, "Strength of Materials", Part I, 1930, p. 88.

the elongation data of 1 to 5% available in the unclassified literature<sup>4</sup> on beryllium for extruded rods made from powdered, flake and cast beryllium.

#### Authors' Reply

Argon sintering was performed using argon purified as described and having a dew point lower than  $-75^{\circ}\text{C}$ ; the oxygen content of the argon was not determined and may be more significant than water vapor contamination. Thermodynamic calculations<sup>5</sup> show that the oxygen pressure in the reaction  $\text{Be} + \text{O}_2 \rightleftharpoons \text{BeO}$  is in the order of  $10^{-50}$  atmospheres, definitely encouraging the formation of oxide at even the highest attainable vacua. The pressure ratio  $p_{\text{H}_2}/p_{\text{H}_2\text{O}}$  in reaction  $\text{Be} + \text{H}_2\text{O} \rightleftharpoons \text{BeO} + \text{H}_2$  is of the order  $10^{15}$ , indicating that lowest obtainable dew points favor the formation of oxide. We may conclude that the conditions encountered in the sintering of beryllium in any available atmosphere permit the formation of BeO. The BeO is, however, dispersed differently in argon- and in vacuum-sintered bars, which may account for the difference in ductility.

Timoshenko's simplified formula takes no cognizance of differences between compressive and tensile properties. Since these properties are not known for sintered beryllium, only approximations are possible and precise calculations must await better data or methods.

<sup>4</sup>See Kaufmann et al, above.

<sup>5</sup>Louis Gold, "Growth and Perfection of Beryllium Crystals", AECD-2643, July 20, 1949.

## THE DIMENSIONAL BEHAVIOR OF INVAR

BY B. S. LEMENT, B. L. AVERBACH AND MORRIS COHEN

### *Abstract*

*The dimensional changes which occur during the aging of invar have been studied as functions of time, temperature, heat treatment and chemical composition. Starting from a quench-anneal, it is found that a contraction takes place on aging because of stress relief. However, there is also a superimposed expansion due to a lattice change which occurs on prolonged aging in the temperature range 20 to 95 °C (70 to 205 °F).*

*The solubility of carbon in invar, as determined by X-ray diffraction, is 0.18 weight per cent at 830 °C (1525 °F), and is vanishingly small at room temperature. Any excess carbon exists as graphite.*

*The expansion coefficient has been studied over the range -40 to +40 °C (-40 to 105 °F) as a function of composition and heat treatment, and a heat treatment which results in good dimensional stability and a low expansion coefficient has been devised.*

THE 64-36 iron-nickel alloy called "invar" was discovered by Guillaume (1)<sup>1</sup> in 1896, and has proved of considerable scientific and practical interest because of its low coefficient of thermal expansion at room temperature. Shockley (2) has applied the band theory of solids to explain this unusual property in terms of the magnetic behavior of the alloy. Although invar is austenitic (face-centered cubic), it is ferromagnetic at room temperature, having a Curie point of about 260 °C (500 °F). On heating from absolute zero to the Curie point, the characteristic decrease in ferromagnetism is accompanied by a tendency toward a decrease in atomic spacing (2) which is superimposed upon the normal dilation due to the rising temperature. These two opposing effects happen to counterbalance each other almost completely in the vicinity of room temperature and thereby result in a low expansion coefficient. The

<sup>1</sup>The figures appearing in parentheses pertain to the references appended to this paper.

This paper is taken from a thesis submitted by Bernard S. Lement in September 1949 in partial fulfillment of the degree of Doctor of Science in Metallurgy at the Massachusetts Institute of Technology.

A paper presented before the Thirty-second Annual Convention of the Society, held in Chicago, October 21 to 27, 1950. Of the authors, B. S. Lement is assistant professor of metallurgy, University of Notre Dame; B. L. Averbach is assistant professor of physical metallurgy, Massachusetts Institute of Technology, and Morris Cohen is professor of physical metallurgy, Massachusetts Institute of Technology. Manuscript received April 7, 1950.



coefficient increases with temperature until the Curie point is reached and remains fairly constant at still higher temperatures.

The coefficient of thermal expansion of invar is markedly influenced by thermal and mechanical treatments (3-6). Quenching from about 800 °C (1470 °F) produces a lower coefficient than does furnace cooling. The coefficient is further reduced by cold working, and even negative values have been reported (6). However, the low coefficients obtained by cold working are found to increase with time at room temperature. Similarly, low temperature aging treatments cause an increase in the coefficient of either the quenched or cold-worked invar.

Although invar possesses a low coefficient of thermal expansion at room temperature, the alloy is subject to isothermal dimensional changes which occur on aging at and above room temperature. Guillaume (7) spent over thirty years of research in attempting to determine the cause and cure of this dimensional instability. In brief, he found two types of dimensional behavior: (a) an expansion which he named the "progressive change", and (b) a contraction which he named the "transitory change". Guillaume attributed these dimensional effects to the presence of carbon in commercial heats of invar. He suggested that carbon is combined in the form of cementite ( $\text{Fe}_3\text{C}$ ) which undergoes a volume change on transforming from the paramagnetic to the ferromagnetic state or vice versa. In support of this theory, he demonstrated that dimensional instability increases with increasing carbon content and decreases with increasing amounts of strong carbide-forming elements. However, the presence of cementite in invar has not been established and, in any case, it is not likely that the Curie point of such a phase would change spontaneously on aging at room temperature.<sup>2</sup>

Although invar has been used successfully for geodetic tapes, clock parts and thermostatic strips, even more exacting requirements are necessitated by modern precision equipment in which dimensions must remain constant with respect to time as well as temperature. To meet this challenge, it is essential to obtain an understanding of the metallurgical phenomena that are responsible for the dimensional behavior of invar. The present investigation is concerned with this problem, and places particular emphasis upon the factors that enter into the time-dependent instability of invar. From a practical point of view, considerable attention is devoted to the attainment of maximum dimensional stability with minimum expansion coefficient.

<sup>2</sup>A comprehensive review of the literature on invar is given in Reference 1.

## ALLOYS STUDIED

Iron-nickel-carbon alloys in the form of 0.250 and 0.375-inch diameter cold drawn rods were used in this investigation. Two series of invars were studied. The first, a commercial grade, contained 36.8% nickel, 0.44% manganese and 0.24% silicon, and the carbon content was varied by carburization or decarburization in a gas train similar to that described by Low and Gensamer (8). Carbon contents ranging from 0.01 to 0.84% were obtained in this way. The alloys were homogenized for 24 hours at 1095 °C (2000 °F) after each gas treatment, and the difference in carbon content between the center and surface of a 0.250-inch diameter specimen was always less than 0.02%. No significant changes in oxygen and nitrogen content occurred during the gas treatments, as is illustrated by the following analysis taken before and after decarburization:

Treatment	% Carbon	% Oxygen	% Nitrogen
As-received	0.070	0.0027	0.0058
24 hours at 1095 °C in wet H <sub>2</sub>	0.011	0.0036	0.0077

The second series of invars consisted of six laboratory heats containing 36.0% nickel, 0.10% manganese, and 0.10% silicon, with carbon contents from 0.02 to 0.58%. Both the commercial and the laboratory heats also contained approximately 0.009% phosphorus and 0.02% sulphur.

## DIMENSIONAL CHANGES DURING AGING

*Precision Length Measurements*—All precision length determinations, whether before or after aging, were made at  $20 \pm 1$  °C, with a 5000 $\times$  comparator in the same way as previously described by the authors in connection with their work on gage steels (9). The specimens were 4 inches long by 0.250-inch diameter with spherically-ground ends. For each reading, the temperatures of the specimen and standard block were measured to within  $\pm 0.05$  °C; the observed lengths were then corrected to a reference temperature of exactly 20 °C and are believed accurate to about  $\pm 2$  microinches per inch. In making this correction due account was taken of the difference between the thermal expansion coefficient of the steel gage block and that of the invar specimen.

*Aging Following Quenching From 830 °C*—The first dimensional stability runs were conducted on commercial invar at aging temperatures of 20 to 205 °C (68 to 400 °F) after water quenching from 830 °C (1525 °F). The latter treatment corresponds to the

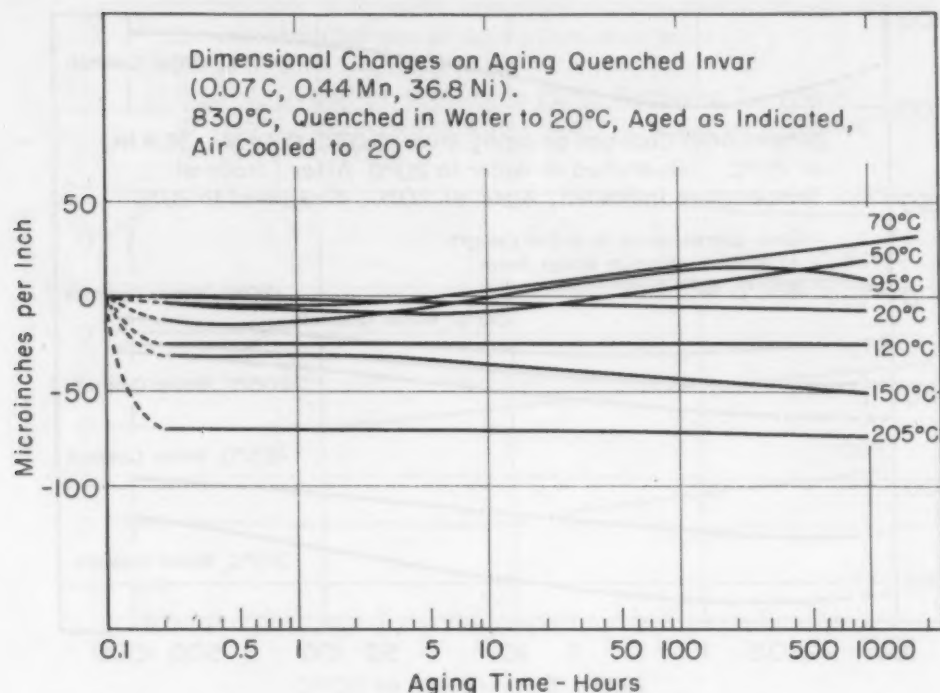


Fig. 1—Dimensional Changes on Aging Quenched Invar (0.07% Carbon, 0.44% Manganese, 36.8% Nickel). 830 °C, quenched in water to 20 °C, aged as indicated, air-cooled to 20 °C.

usual practice and tends to suppress such precipitation processes as may occur during slower cooling. The specimens were air-cooled from the aging temperature to 20 °C for the length measurements.

As shown in Fig. 1, at least two phenomena take place on aging at temperatures up to 205 °C (400 °F). One causes a contraction [the "transitory change" of Guillaume (7)] which increases with increasing aging temperature; the other causes an expansion [the "progressive change" of Guillaume (7)] and occurs at aging temperatures up to at least 95 °C. It will be demonstrated later that the contraction is due to stress relief, the stresses having been introduced by the quenching from 830 °C (1525 °F). For convenience, the expansion will be referred to as the  $\gamma$ -expansion; it occurs to a maximum extent at 70 °C (158 °F).

*Aging at 70 °C Following Quenching From Various Temperatures*—The curves for this series are plotted in Fig. 2. The starting condition in each case is a water quench from 830 °C. Before the aging at 70 °C it is evident that increasing initial contractions result on quenching from temperatures up to 315 °C (600 °F). However, quenching from 425 °C (800 °F) produces less of a contraction than from 315 °C (600 °F), and quenching from 540 °C (1000 °F) causes a substantial expansion. The contraction is the same stress-relief phenomenon that is observed in Fig. 1, except



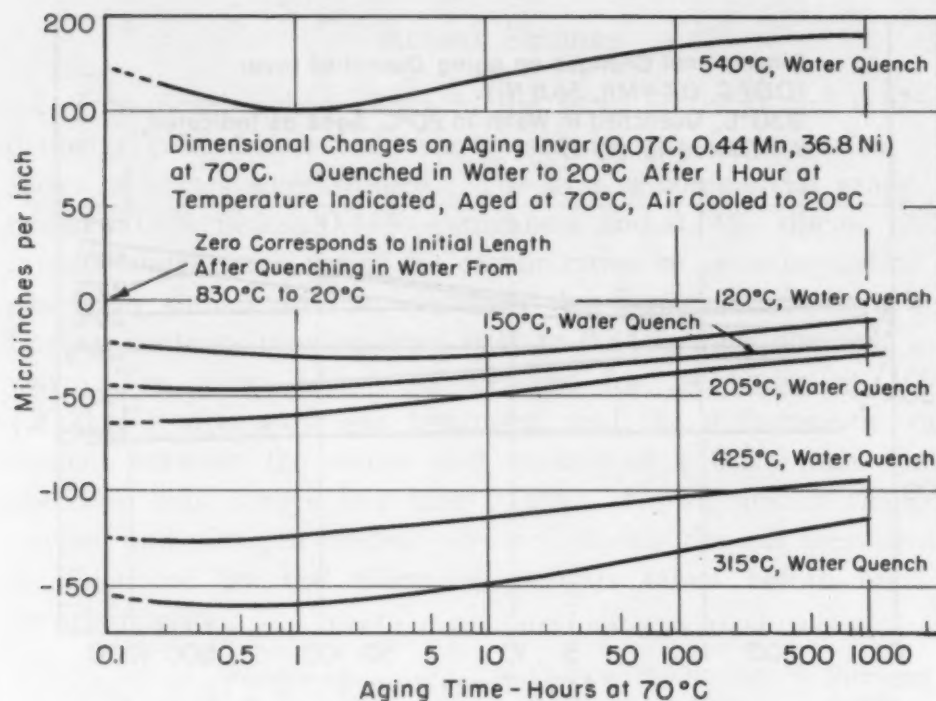


Fig. 2—Dimensional Changes on Aging Invar (0.07% Carbon, 0.44% Manganese, 36.8% Nickel) at 70°C. Quenched in water to 20°C after 1 hour at temperature indicated, aged at 70°C, air-cooled to 20°C.

that the magnitude is now greater because of the higher temperatures involved. However, when the quenching temperature is increased above 315 °C, any stress relief that may take place relative to the previous 830 °C quench is obscured by the new length changes that are introduced by the second quench.<sup>3</sup> This is why an actual expansion is found on quenching from 540 °C.

On subsequent aging at 70 °C after the above quenching treatments (Fig. 2), there is an initial contraction (stress relief) followed by the  $\gamma$ -expansion. The magnitude of this expansion is greater following quenching from above 205 °C (400 °F) than from below this temperature.

Practically no change in length occurs at 50 °C after prolonged aging at 70 °C. Specimens were first quenched from 830 °C (1525 °F), aged for 1000 hours at 70 °C, and then aged at 50 °C. No change in length was observed after several thousand hours at the latter temperature, and this suggests that after the process responsible for the  $\gamma$ -expansion has been carried out at 70 °C no further effect will be observed on aging at a lower temperature.

*Aging Following Quenching From 205 °C*—On the basis of Fig. 2, a quenching temperature of 205 °C (400 °F) was selected

<sup>3</sup>Stresses are relieved more effectively the higher the temperature, if the subsequent cooling is slow. When quenching is used, new stresses are set up, particularly if temperatures above 315 °C (600 °F) are employed.



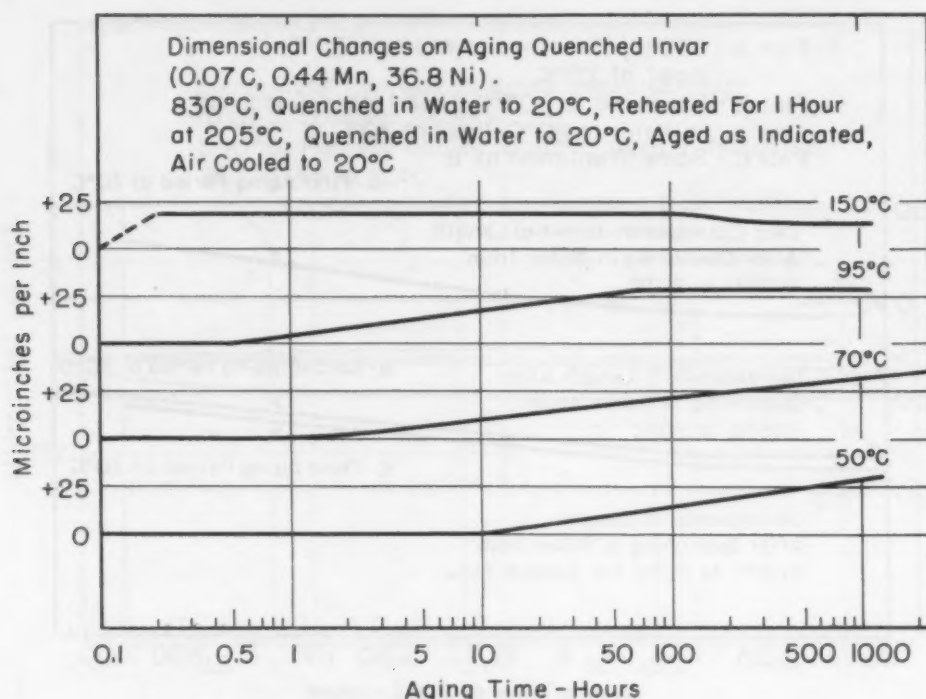


Fig. 3—Dimensional Changes on Aging Quenched Invar (0.07% Carbon, 0.44% Manganese, 36.8% Nickel). 830 °C, quenched in water to 20 °C, reheated for 1 hour at 205 °C, quenched in water to 20 °C, aged as indicated, air-cooled to 20 °C.

for stress relieving purposes, after the 830 °C water quench, in order to minimize the contraction effect on subsequent aging at lower temperatures. This treatment was designed to reveal the  $\gamma$ -expansion to better advantage. The result is shown in Fig. 3.

The expansion in question starts in 10, 1, 0.5 and <0.2 hours respectively on aging at 50, 70, 95 and 150 °C (120, 158, 200 and 300 °F). As in the case of Fig. 1, the maximum expansion occurs at 70 °C. The interposed treatment at 205 °C (400 °F) noticeably suppresses the previously observed contraction due to stress relief, but it does not suppress the  $\gamma$ -expansion.

*Multiple Aging at 205 and 70 °C*—Since invar is able to undergo the  $\gamma$ -expansion after a water quench from 205 °C (400 °F) as well as from 830 °C (1525 °F), it appeared probable that reheating to 205 °C after the  $\gamma$ -expansion might cause an equivalent contraction and put the alloy back into condition for re-expansion at 70 °C, without introducing new quenching stresses. This expectation was confirmed.

Plot A in Fig. 4 is the same as the 70 °C curve in Fig. 1 and shows the changes in length on aging at 70 °C after quenching from 830 °C. On reheating to 205 °C (400 °F) for 1 hour and water quenching, a contraction takes place which is larger than can be

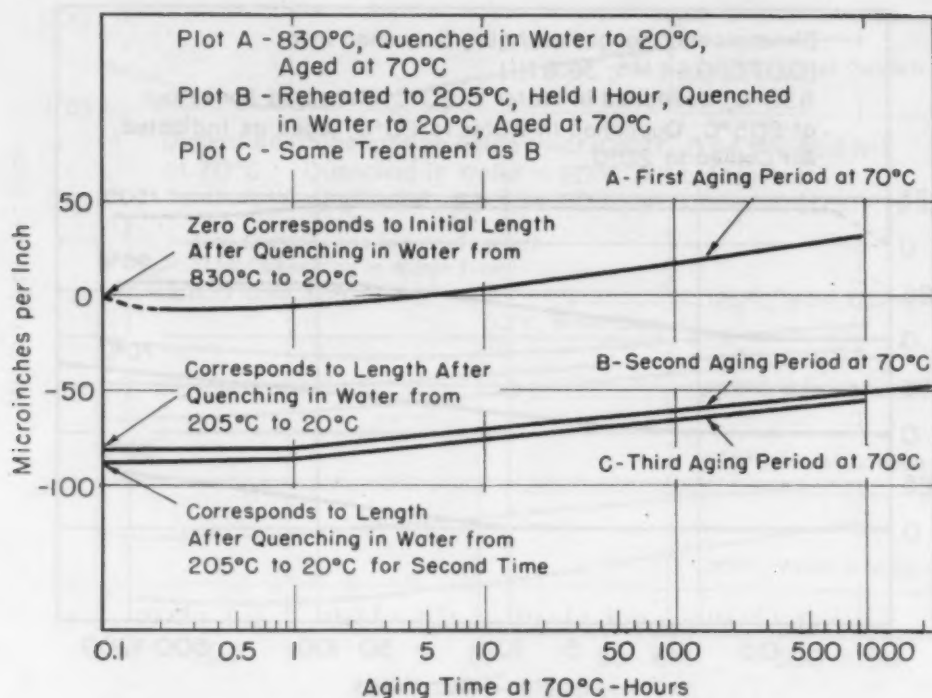


Fig. 4—Dimensional Changes on Aging Quenched Invar (0.07% Carbon, 0.44% Manganese, 36.8% Nickel) at 70 °C. Plot A—830 °C, quenched in water to 20 °C, aged at 70 °C. Plot B—Reheated to 205 °C, held 1 hour, quenched in water to 20 °C, aged at 70 °C. Plot C—Same treatment as B.

attributed to stress relief on the basis of Fig. 1. The excess of the actual contraction over stress-relief contraction is approximately equal to the expansion which occurred during the first aging at 70 °C. This suggests that the  $\gamma$ -expansion and the contraction in excess of that due to stress relief at higher aging temperature may be related.

During the second aging period at 70 °C, an expansion ensues (Plot B) which follows rather parallel to the expansion of Plot A. On reheating to 205 °C (400 °F) for 1 hour a second time, a contraction results which is approximately equal to the expansion that previously took place at 70 °C. This second contraction is smaller than the first contraction at 205 °C because very little additional stress relief occurs during the second treatment. On aging at 70 °C a third time (Plot C), an expansion similar to Plot B takes place.

These observations indicate that the  $\gamma$ -expansion denotes a reversible reaction that can be repeated over and over again by reheating to 205 °C. In fact, the reversibility of the reaction was verified by subjecting higher carbon invar (in which the effect is enhanced) to ten such cycles. This phenomenon is quite analogous to retrogression in age hardening systems (10). The contraction that occurs on reheating to 205 °C is the reversible counterpart

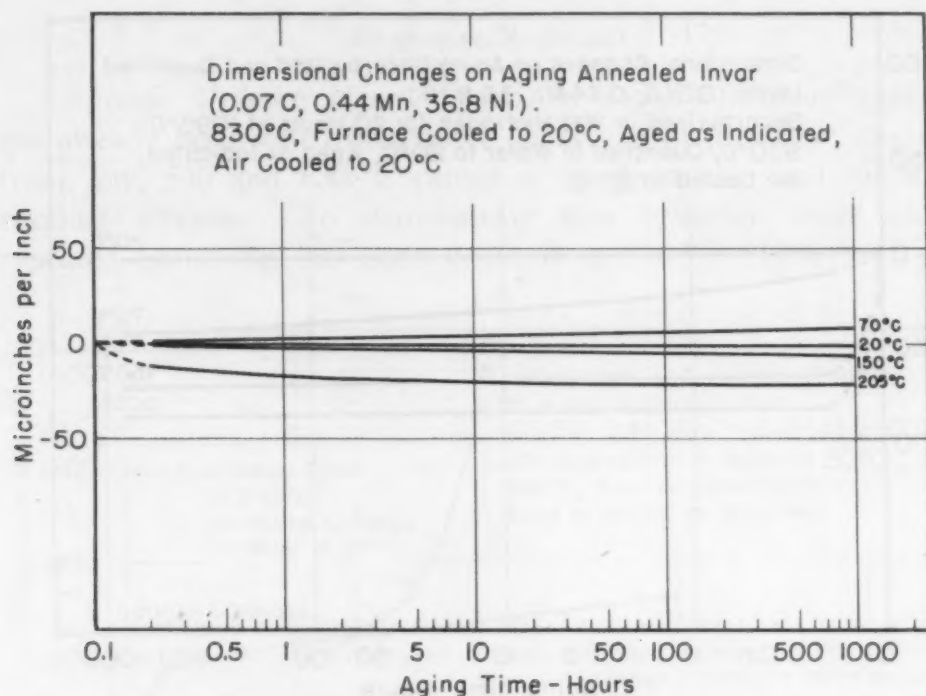


Fig. 5—Dimensional Changes on Aging Annealed Invar (0.07% Carbon, 0.44% Manganese, 36.8% Nickel). 830 °C, furnace-cooled to 20 °C, aged as indicated, air-cooled to 20 °C.

of the  $\gamma$ -expansion, and will be designated hereafter as the  $\gamma$ -contraction. Even when the specimens are initially furnace-cooled from 830 °C instead of being water-quenched, aging at 205 °C conditions the alloys for the  $\gamma$ -expansion. It should be noted that aging directly at 205 °C after quenching from 830 °C causes a large contraction (Fig. 1) but this is due to stress relief and is not reversible on cycling between 205 and 70 °C.

*Effect of Cooling Rate From 830 °C*—The length changes on aging at temperatures of 20 to 205 °C after furnace cooling from 830 °C (1525 °F) are illustrated in Fig. 5. These results are not altered appreciably by air cooling instead of furnace cooling. Compared to the curves for water-quenched invar in Fig. 1, the slower cooling rates yield expansion and contraction effects of considerably smaller magnitude. Whereas the  $\gamma$ -expansion is attributable to the same cause in both Figs. 1 and 5, it is doubtful that the contraction appearing at 150 and 205 °C (300 and 400 °F) in Fig. 5 can be due to stress relief, in view of the slow cooling from 830 °C. This contraction turns out to be the same phenomenon as the reversible 205 °C contraction identified in the previous section. Part of the  $\gamma$ -expansion actually sets in during the slow cooling from 830 °C to room temperature, and this makes it possible for the reverse contraction to occur during the subsequent aging at 150 and 205 °C.

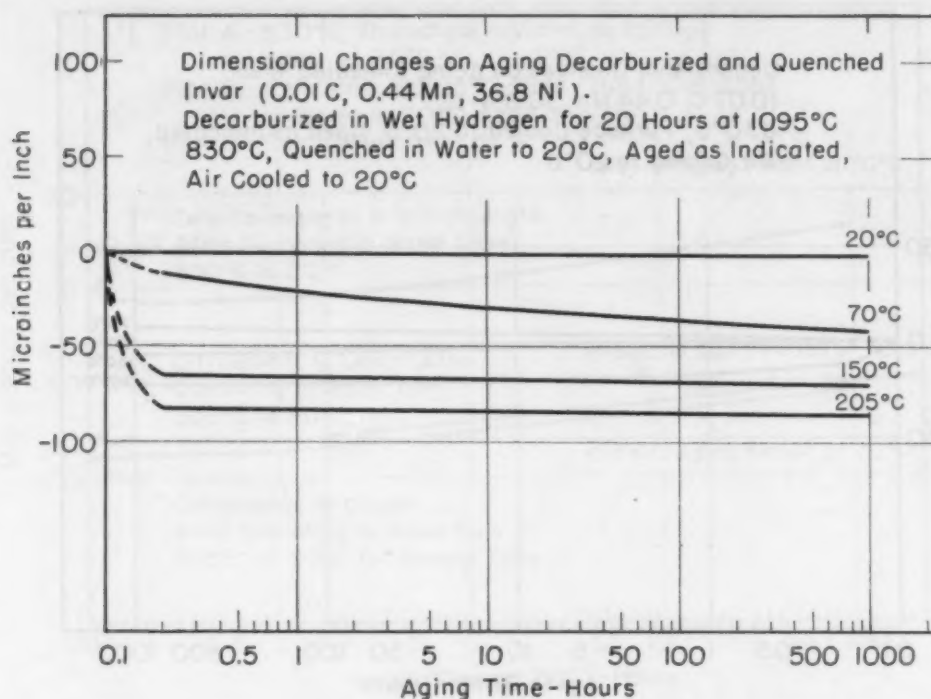


Fig. 6—Dimensional Changes on Aging Decarburized and Quenched Invar (0.01% Carbon, 0.44% Manganese, 36.8% Nickel). Decarburized in wet hydrogen for 20 hours at 1095°C. 830°C, quenched in water to 20°C, aged as indicated, air-cooled to 20°C.

The 20°C curve in Fig. 5 indicates that invar is dimensionally stable at room temperature after furnace cooling, but as will be discussed later, the thermal expansion coefficient is appreciably larger in this condition than in the water-quenched state.

*Aging of Low Carbon Invar*—The aging curves for quenched low carbon invar (reduced from 0.07 to 0.01% carbon by a wet hydrogen treatment) are shown in Fig. 6. It is evident that the  $\gamma$ -expansion is no longer present and therefore must be a carbon-dependent phenomenon. On the other hand, the contractions due to stress relief remain in the picture, inasmuch as the initial quenching from 830°C introduces stresses whether the carbon is low or not.

When the very low carbon invar is furnace-cooled from 830°C (1525°F), no stresses are set up, and there is no subsequent contraction due to stress relief on aging. Small contractions of about 3 microinches per inch appear in 1000 hours at 150 and 250°C. These contractions are similar in kind to those of the 0.07% carbon invar in Fig. 5, but are reduced in magnitude. This is to be expected because the contraction in question is the reversible counterpart of the  $\gamma$ -expansion and the latter was demonstrated to be carbon-dependent in the previous section.



## RESIDUAL STRESSES

*Specific Volume Versus Precision Length Measurements*—It has already been stated that water quenching of the invar specimens from, say, 540 and 830 °C causes a net expansion and introduces residual stresses. To demonstrate this behavior more clearly, repeated quenching was carried out from 540 °C (1000 °F), start-

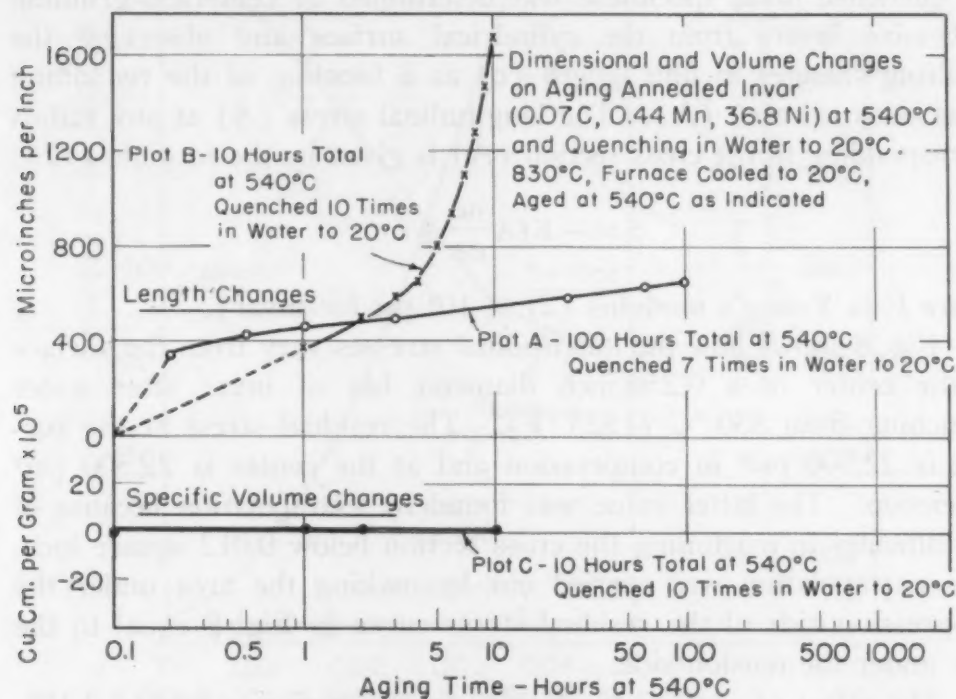


Fig. 7—Dimensional and Volume Changes on Aging Annealed Invar (0.07% Carbon, 0.44% Manganese, 36.8% Nickel) at 540 °C and Quenching in Water to 20 °C. 830 °C, furnace-cooled to 20 °C, aged at 540 °C as indicated.

ing with furnace-cooled commercial invar. The specific volumes as well as the lengths of the specimens were measured in order to ascertain whether the length changes were attended by corresponding volume changes. (The specific volumes were determined by the weigh-in-water, weigh-in-air technique (11) to an accuracy of  $\pm 2 \times 10^{-5}$  cu. cm. per gm.)

The data in Fig. 7 reveal that ten 1-hour aging and quenching treatments produce much more expansion than a total of 100 hours at temperature with only seven intermediate quenches. In other words, the expansion is more dependent on the number of quenching operations than the cumulative time of heating. Furthermore, there is virtually no change in volume, even after a total linear expansion of 1700 microinches per inch (which would correspond to an easily detectable volume increase of  $62 \times 10^{-5}$  cu. cm. per gm.).

In view of these findings, it is clear that the length changes under consideration here do not result from phase transformations, but from thermal gradients in the quenching process which cause plastic flow and residual stresses. These length changes do not affect the density appreciably because they are accompanied by compensating changes in the lateral dimensions.

*Residual Stress Distribution*—The actual stress distribution in the quenched invar specimens was determined by centerless-grinding successive layers from the cylindrical surface and observing the resulting changes in unit length ( $\epsilon$ ) as a function of the remaining cross sectional area ( $A$ ). The longitudinal stress ( $S$ ) at any radius corresponding to the cross section ( $A$ ) is given by the formula (12):

$$S = -E(A \frac{d\epsilon}{dA} + \epsilon)$$

where  $E$  is Young's modulus ( $21 \times 10^6$  psi for invar).

Fig. 8 shows how the longitudinal stresses vary from the surface to the center of a 0.250-inch diameter bar of invar after water quenching from  $830^\circ\text{C}$  ( $1525^\circ\text{F}$ ). The residual stress at the surface is 22,500 psi<sup>4</sup> in compression and at the center is 22,500 psi<sup>4</sup> in tension. The latter value was found by extrapolation because of the difficulty in machining the cross section below 0.012 square inch. This extrapolation was carried out by making the area under the compression side of the residual stress curve in Fig. 8 equal to the area under the tension side.

The effect of various treatments on the surface stress of 0.375-inch diameter invar bars is indicated in the following tabulation:

Bars of 0.10% Manganese, 36.0% Nickel Invar Subjected to Various Treatments		
Carbon Content	Treatment	Residual Compressive Stress at Surface, psi
0.02	$830^\circ\text{C}$ , $\frac{1}{2}$ hr., Water Quench	24,000
0.40	$830^\circ\text{C}$ , $\frac{1}{2}$ hr., Water Quench	21,000
0.02	$830^\circ\text{C}$ , $\frac{1}{2}$ hr., Water Quench, $315^\circ\text{C}$ , 1 hr., Air Cool	7,000
0.40	$830^\circ\text{C}$ , $\frac{1}{2}$ hr., Water Quench, $315^\circ\text{C}$ , 1 hr., Air Cool	10,000
0.02	$830^\circ\text{C}$ , $\frac{1}{2}$ hr., Furnace Cool, $540^\circ\text{C}$ , 1 hr., Water Quench	13,000
0.40	$830^\circ\text{C}$ , $\frac{1}{2}$ hr., Furnace Cool, $540^\circ\text{C}$ , 1 hr., Water Quench	13,000

The high compressive stress caused by the quench from  $830^\circ\text{C}$  is considerably relieved by heating for 1 hour at  $315^\circ\text{C}$  ( $600^\circ\text{F}$ ). It will be remembered that the latter treatment causes a linear contraction, while the stress-producing quench causes an expansion. Water quenching from  $540^\circ\text{C}$  ( $1000^\circ\text{F}$ ) introduces a surface stress of somewhat more than half that resulting from the  $830^\circ\text{C}$  ( $1525^\circ\text{F}$ ) quench.

*Shock Tests*—It was noted that a relatively large contraction occurred when a bar of invar containing residual stresses was sub-

<sup>4</sup>The numerical identity of these values is coincidental.

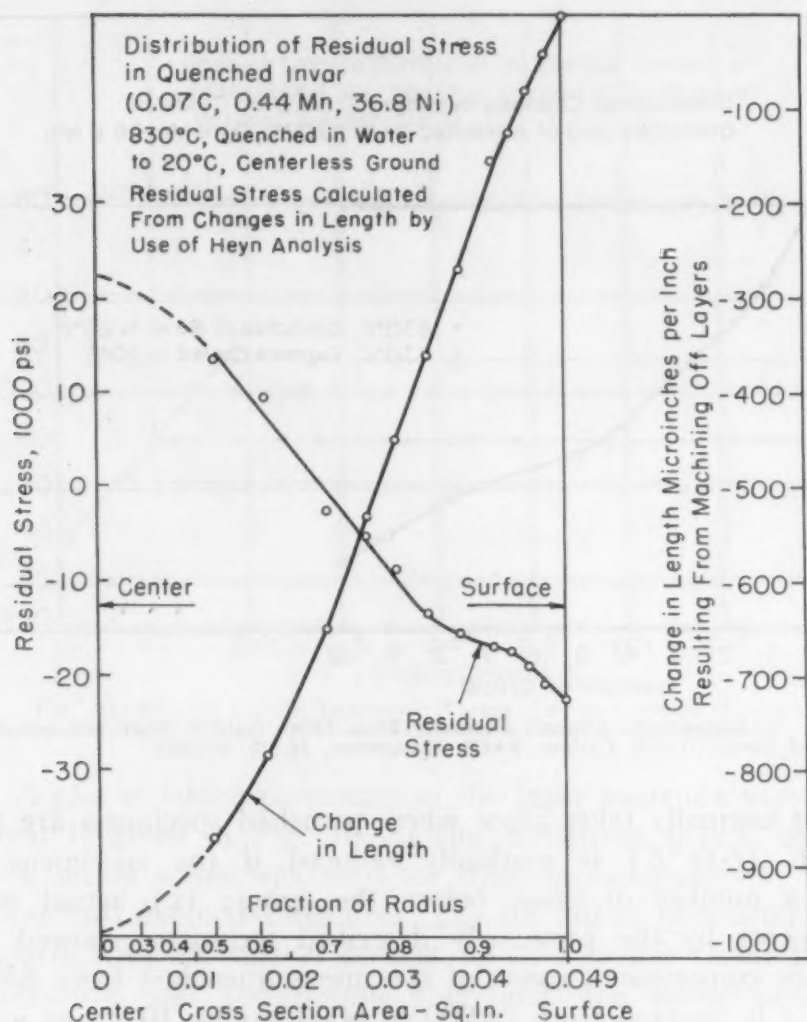


Fig. 8—Distribution of Residual Stress in Quenched Invar (0.07% Carbon, 0.44% Manganese, 36.8% Nickel). 830 °C, quenched in water to 20 °C, centerless ground. Residual stress calculated from changes in length by use of Heyn analysis.

jected to shock by dropping on the floor. To inquire further into this behavior, 0.375-inch diameter specimens were suspended by an electromagnet and were allowed to fall in a horizontal position through a height of 5 feet to strike a concrete floor. The spherical ends of the rods were not disturbed in any way by this treatment. Precision length measurements were conducted before and after each drop to determine the change in length.

As demonstrated by Fig. 9, increasing contractions are caused by repeated dropping, suggesting that progressive stress relief is achieved by these shock treatments. This conclusion is substantiated by the following observations: (a) Furnace-cooled (unstressed) samples do not undergo any appreciable change in length (Fig. 9) when dropped repeatedly; (b) the large contraction due to stress

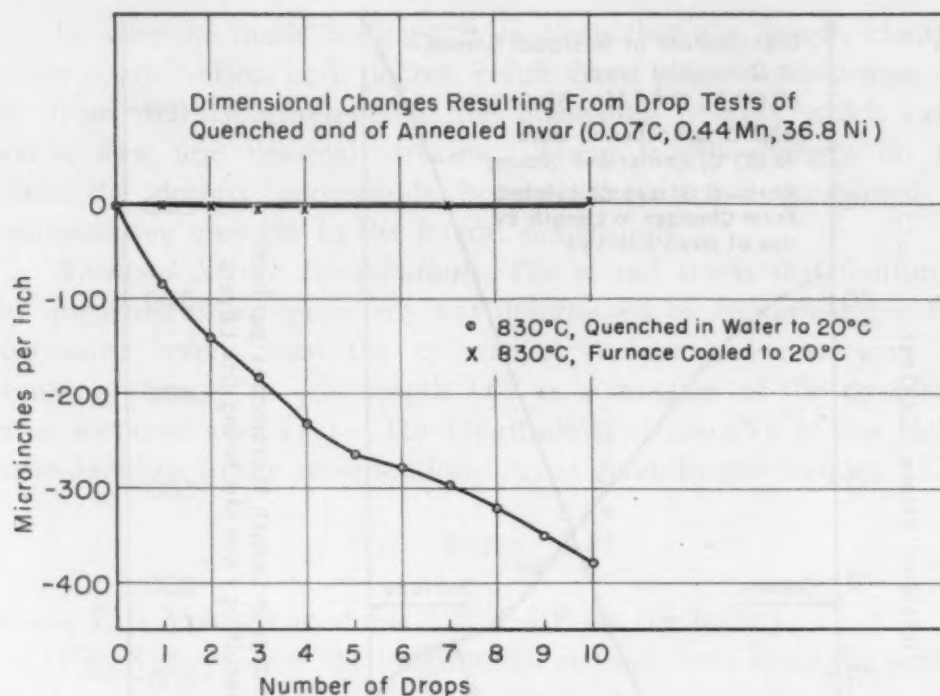


Fig. 9—Dimensional Changes Resulting From Drop Tests of Quenched and of Annealed Invar (0.07% Carbon, 0.44% Manganese, 36.8% Nickel).

relief that normally takes place when quenched specimens are aged at 315 °C (600 °F) is markedly reduced if the specimens are dropped a number of times before the aging; (c) actual stress measurements by the previously described technique showed that the surface compressive stress of specimens quenched from 830 °C (1525 °F) is lowered from 24,000 to 6000 psi by 10 drops in the case of 0.02% carbon invar, and from 21,000 to 13,000 psi in the case of 0.40% carbon invar.

It is worth stating here that the stress relief resulting from the shock treatments has no material influence on the  $\gamma$ -expansion during subsequent aging in the vicinity of 70 °C. The latter phenomenon is obviously not a stress or stress-relief effect.

#### CARBON SOLUBILITY IN AUSTENITE

*Solubility Limit*—Inasmuch as the  $\gamma$ -expansion (at  $\sim 70$  °C) and the corresponding  $\gamma$ -contraction (at  $\sim 205$  °C) were found to be carbon-dependent, it was deemed advisable to determine the carbon solubility limit in 64-36 iron-nickel austenite as a function of temperature. For this purpose, the standard precision lattice-parameter technique was adopted, using cobalt radiation and a 10-centimeter diameter back-reflection focusing camera. With extrapolation methods, an accuracy of about  $\pm 0.0003\text{\AA}$  was obtained.



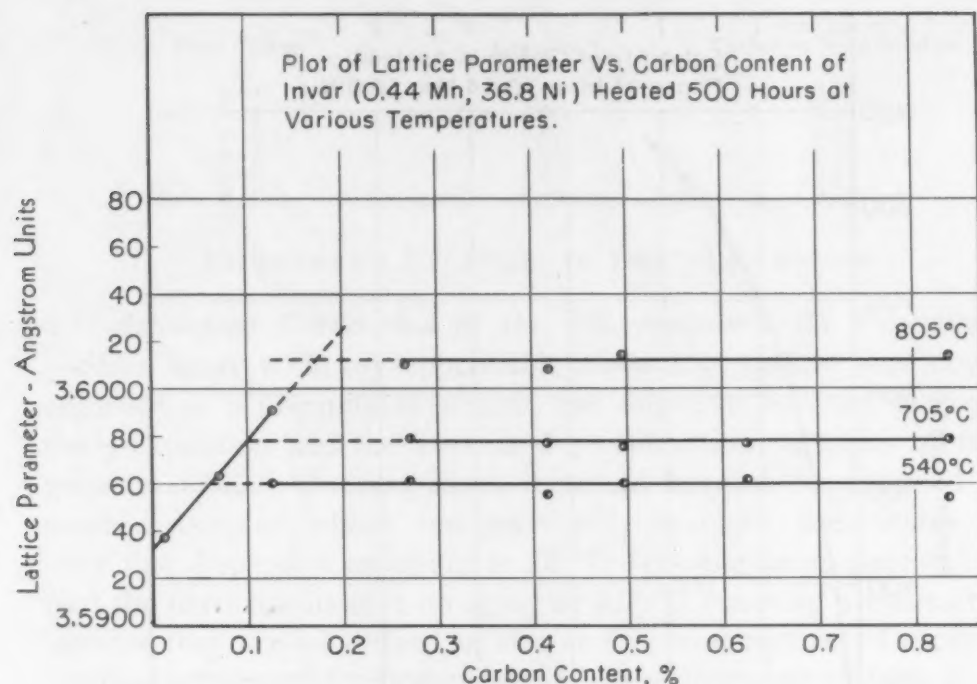


Fig. 10—Plot of Lattice Parameter Versus Carbon Content of Invar (0.44% Manganese, 36.8% Nickel) Heated 500 Hours at Various Temperatures.

A plot of lattice parameter of the invar austenite versus carbon content is given in Fig. 10. (The carburized 0.44% manganese, 36.8% nickel series was used for these measurements.) The data disclose two distinctive features: (a) the lattice parameter increases regularly with the carbon content up to a definite limit at a given temperature, and (b) beyond this limit, the lattice parameter is independent of the carbon content at a given temperature.

When the above limits are plotted against the temperature, the solubility curve in Fig. 11 is obtained. The lowest experimental point was determined at 540 °C (1000 °F); below this temperature level, equilibrium could not be assured by the 500-hour heating period used. Consequently, the solubility curve was extrapolated to lower temperatures on the ideal-solution assumption that the logarithm of the mole fraction of solute at saturation is proportional to the reciprocal of the absolute temperature. This extrapolation indicates that carbon is virtually insoluble at 20 °C. Even 0.01% carbon in solution supersaturates invar at room temperature; 0.05% carbon is soluble at 500 °C (930 °F), while at 830 °C (1525 °F), 0.18% carbon is soluble.

*Occurrence of Graphite*—The alloys lying to the right of the solubility curve in Fig. 11 contain saturated austenite and a carbon-rich phase, which was established as graphite. In the first place, the fact that the austenitic lattice parameter is constant for carbon

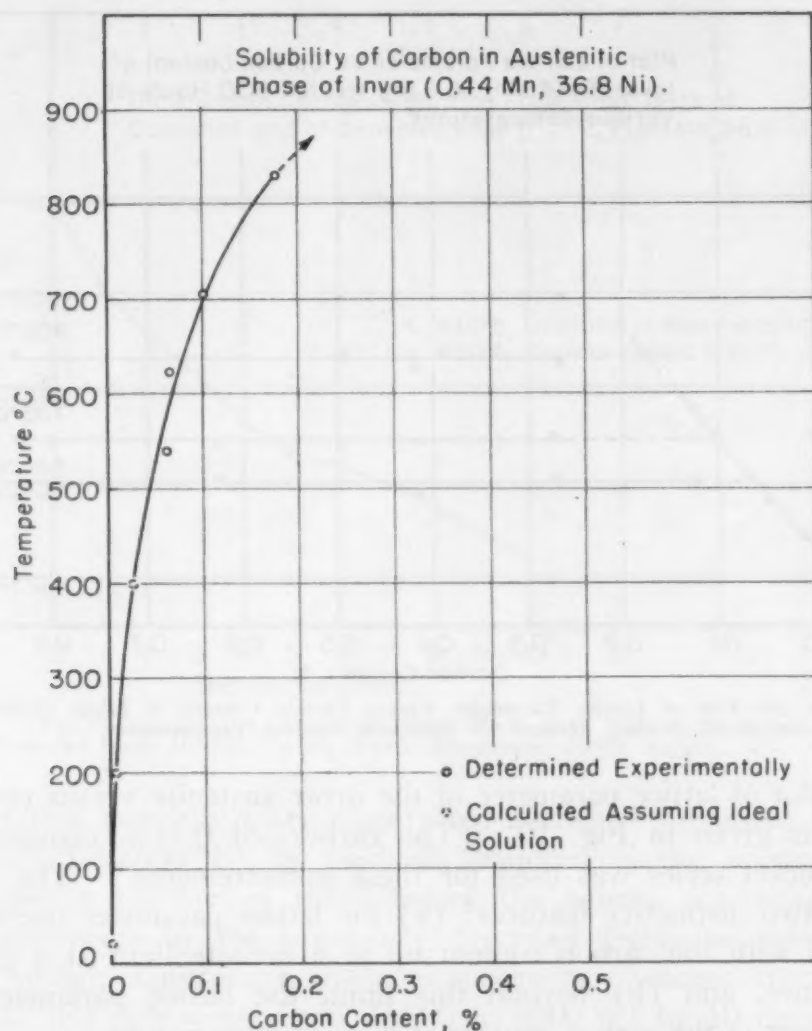


Fig. 11—Solubility of Carbon in Austenitic Phase of Invar (0.44% Manganese, 36.8% Nickel).

contents exceeding the solubility limit (Fig. 10) signifies that the second phase must be either graphite or a carbide that has approximately the same iron-nickel ratio as the ternary solid solution; otherwise the lattice parameter of the latter would change with increasing carbon content. An iron-nickel carbide of composition  $\text{Fe}_2\text{NiC}$  fulfills this requirement, but its existence has not been ascertained despite many attempts to do so.

In the second place, the presence of graphite was not only verified by metallographic examination, but was found by chemical analysis. As shown in the following tabulation, graphite can be detected chemically at carbon contents beyond 0.15% in specimens quenched from 830 °C, and the calculated carbon in solid solution lies between 0.17 and 0.20%. This is in good agreement with the X-ray findings (Fig. 11).

Total Carbon %	Graphite %	Calculated Carbon in Solid Solution %
0.02	0.00	0.02
0.10	0.00	0.10
0.15	0.00	0.15
0.25	0.05	0.20
0.40	0.23	0.17
0.58	0.40	0.18

### PHENOMENA RELATING TO THE $\gamma$ -EXPANSION

#### *Attempted Correlation of the $\gamma$ -Expansion With Precipitation*

—Since invar with any appreciable amount of carbon may now be regarded as a precipitable system, one might be tempted to explain the  $\gamma$ -expansion and the associated  $\gamma$ -contraction in terms of retrogression (10). On this basis, it would have to be assumed that some carbon-rich phase, not necessarily graphite, precipitates in a very fine dispersion on aging at 70 °C (causing an expansion) and that the particles dissolve on aging at 205 °C (causing a contraction) because they are subcritical in size at this temperature. Despite the intriguing nature of this explanation, its validity may be questioned on the following grounds.

The variation of the austenitic lattice parameter with respect to carbon (Fig. 10) and nickel (13) content is known. This information enables one to calculate the change in unit length that should be expected from the precipitation of the supersaturated carbon in any given form. Table I presents the calculated unit length changes for an invar containing 0.05% carbon, 36.00% nickel and 63.95% iron, assuming that all the carbon precipitates from the austenite as (a) graphite, (b) cementite, (c) nickel carbide, or (d) iron-nickel carbide. In no case does an expansion attend the pre-

**Table I**  
Calculation of Length Changes Due to Precipitation of Graphite or Carbide in Invar

Assumed Precipitated Phase	Specific Volume, Cu Cm/Gm	Reaction	Unit Change in Length, Micro- inches/Inch
Graphite	0.44500	1 gram A $\rightarrow$ 0.9995 gram A <sub>1</sub> + 0.0005 gram C	-170
Cementite	0.13000	1 gram A $\rightarrow$ 0.9925 gram A <sub>2</sub> + 0.0075 gram Fe <sub>3</sub> C	-410
Nickel Carbide	0.12608	1 gram A $\rightarrow$ 0.9922 gram A <sub>3</sub> + 0.0078 gram Ni <sub>3</sub> C	-600
Iron-Nickel Carbide	0.13000*	1 gram A $\rightarrow$ 0.9924 gram A <sub>4</sub> + 0.0076 gram Fe <sub>2</sub> NiC	-440

#### Calculated Chemical Compositions and Specific Volumes of Austenitic Phases

Austenitic Phase	C	Ni	Fe	Specific Volume Cu Cm/Gm
A	0.05	36.00	63.95	0.12257
A <sub>1</sub>	0.00	36.00	64.00	0.12234
A <sub>2</sub>	0.00	36.30	63.70	0.12236
A <sub>3</sub>	0.00	35.54	64.46	0.12232
A <sub>4</sub>	0.00	36.00	64.00	0.12234

\*Specific volume of this hypothetical carbide is assumed to be the same as for cementite.

precipitation process. Even the precipitation of graphite, which has the largest specific volume, results in a contraction.

In order to determine the temperature range of graphite precipitation, aging of supersaturated invar was carried out for 350 hours at higher and higher temperatures until graphite could actually be determined by chemical analysis. Graphite was first detected at 315 °C (600 °F), reached a maximum amount between 425 and 540 °C (800 and 1000 °F), and started to redissolve at still higher temperatures. In accordance with the calculations (Table I), the graphite precipitation caused a contraction, and its re-solution caused an expansion. Clearly, then, precipitation of the stable graphite phase does not appear to be a likely explanation for the  $\gamma$ -expansion.

*X-Ray Measurements During the  $\gamma$ -Expansion*—In order to determine whether the formation of either ferrite or martensite might be responsible for the  $\gamma$ -expansion, 12-hour X-ray exposures were made on 0.40% carbon invar with monochromatic iron K $\alpha$  radiation and a modified Debye camera (14). Specimens were X-rayed after the following treatments: (a) water quenched from 830 °C (1525 °F), (b) quenched and then aged 500 hours at 70 °C, and (c) furnace-cooled from 830 °C. In each case, only austenitic diffraction lines appeared, from which it is estimated that the amount of ferrite or martensite, if present at all, could not have exceeded 0.5%.

While it is conceivable that the formation of up to 0.5% ferrite or martensite on aging at 70 °C could account for the observed expansion, this explanation must be rejected. Increasing carbon should enhance the stability of the austenite and thus render it *less* liable to decompose at 70 °C; yet the  $\gamma$ -expansion is known to increase with the carbon content. Furthermore, it is difficult to imagine that such a transformation could be reversed by heating at 205 °C (400 °F), and this reversion is one of the main characteristics of the phenomenon.

Precision lattice-parameter determinations were then performed on a series of invar powders in order to ascertain whether the  $\gamma$ -expansion is associated with a true volume change and whether such a change is accompanied by an alteration in the atomic spacing of the austenite. The powder specimens were water-quenched from 830 °C and aged for 500 hours at 70, 95 and 205 °C (158, 200 and 400 °F). The fractional changes in length as calculated from the lattice-parameter measurements were found to be in reasonably good agreement with the directly-measured expansions of bar specimens after correction for the stress-relief contractions. Typical results



are given below:

	500 hrs. at 70 °C		500 hrs. at 95 °C		500 hrs. at 205 °C	
	0.27% C	0.42% C	0.27% C	0.42% C	0.27% C	0.42% C
Calculated from Austenitic Lattice Parameters	+110	+240	+140	+140	0	+30
Precision Length Measurements (Corrected for stress-relief contraction)	+170	+170	+160	+150	+40	+40

It may be concluded that the  $\gamma$ -expansion represents a true volume effect of the austenite per se.

It was previously shown that the length changes calculated for various types of precipitation are incompatible with the actual measurements of the  $\gamma$ -expansion. Now it becomes evident that this expansion reflects some phenomenon going on *within* the austenitic phase and that the magnitude of the expansion is entirely accounted for by this change in the austenite without assuming the occurrence of undetected precipitation or transformation processes. As will be discussed later, it is believed that this carbon-dependent phenomenon is due to a reversible redistribution of the carbon atoms within the austenitic solid solution.

*Magnetic and Hardness Changes Accompanying the  $\gamma$ -Expansion*

—The intensity of magnetic saturation was measured (15) at a field strength of 1100 oersteds, which is well above the saturation value for invar. The Curie temperature was also obtained by measuring the saturation magnetization of quenched invar on both heating and cooling through the magnetic transformation.

Table II indicates that there is a small but definite increase in saturation magnetization which accompanies the  $\gamma$ -expansion. The magnitudes of both the expansion and increase in magnetization remain virtually unchanged for invars containing from 0.25 to 0.58% carbon after a water quench from 830 °C (1525 °F). This is to be expected, since only 0.18% carbon is soluble in invar at this temperature. If the quenching temperature is raised to 1205 °C (2200 °F), a greater  $\gamma$ -expansion would be anticipated because more carbon is dissolved, and this is confirmed in Table II. The change in magnetization accompanying the  $\gamma$ -expansion is also increased as a result of the higher temperature quench.

As suggested by Table II, there appears to be a slight hardening associated with the  $\gamma$ -expansion. However, the effect is so small that it can be detected only in the higher carbon invars quenched from the higher temperature.

The Curie temperature of invar quenched from 830 °C (1525 °F) is found to depend on the carbon content. With 0.02% carbon present, the magnetic inversion occurs at 250 °C (480 °F),

**Table II**  
**Changes in Length, Hardness, and Magnetization on Aging Quenched Invar at 70 °C**

Carbon %		Change in Length Micro-inches/Inch	Hardness Rockwell B	Intensity of Saturation Magnetization (Gauss)
0.25	(a) 830 °C, Water-Quenched	0	86	1050
	(b) 500 hours at 70 °C	148	86	1080
	(a) 1205 °C, Water-Quenched	0	85	1055
	(b) 500 hours at 70 °C	152	85.5	1085
0.40	(a) 830 °C, Water-Quenched	0	84	1060
	(b) 500 hours at 70 °C	140	84	1090
	(a) 1205 °C, Water-Quenched	0	87.5	1090
	(b) 500 hours at 70 °C	180	89	1130
0.58	(a) 830 °C, Water-Quenched	0	83	1025
	(b) 500 hours at 70 °C	143	83	1055
	(a) 1205 °C, Water-Quenched	0	90.5	1085
	(b) 500 hours at 70 °C	173	91.5	1125

with 0.10% carbon at 255 °C (490 °F), and with 0.40% carbon at 273 °C (525 °F). There is virtually no hysteresis in the magnetization curves on heating and cooling, and the average increase in Curie temperature with carbon content amounts to approximately 0.6 °C per 0.01% carbon. No evidence of a cementite Curie point was found; hence Guillaume's theory that the  $\gamma$ -expansion is associated with the magnetic change in cementite could not be confirmed.

Magnetic measurements were also made on a series of invars with varying carbon contents after furnace cooling from 830 °C (1525 °F). In this condition, part of the  $\gamma$ -expansion takes place during the slow cooling. If these specimens are subsequently heated to 205 °C (400 °F) and then quenched, the portion of the  $\gamma$ -expansion which has been completed is reversed and a contraction is observed, whose magnitude is a function of the carbon content (Table III). Subsequent aging at 70 °C re-introduces the  $\gamma$ -expansion. Generally, there is a slight decrease in magnetization attending the contraction at 205 °C and a subsequent increase in magnetization attending the  $\gamma$ -expansion on aging at 70 °C. These data confirm the fact that the  $\gamma$ -expansion is reversible and that it is associated with a change in magnetization.

#### VARIATIONS IN THERMAL EXPANSION COEFFICIENTS

*Method of Measurement*—The usual quartz dilatometer is not sufficiently sensitive to determine changes in the expansion coefficient of invar and hence the procedure of Souder and Hidnert (16) was adopted for this work. The measurements were made on rods, 4 inches long by  $\frac{3}{8}$ -inch or  $\frac{1}{4}$ -inch diameter, in an agitated silicone oil bath which could be maintained at temperatures from -50 to +50 °C (-58 to 122 °F). Two small invar arms were attached

Table III  
Changes in Length and Magnetization on Aging of Furnace-Cooled Invar  
at 205 and 70 °C

Carbon %	Treatment	Change in Length Micro-inches/Inch	Length Change Due to $\gamma$ -Expansion at 70 °C, Micro- inches/Inch	Intensity of Saturation Magnetization (Gauss)
0.02	Furnace-Cooled	0		1005
	205 °C, Water-Quenched	0		1010
	500 hours at 70 °C	0	0	1005
0.10	Furnace-Cooled	0		1040
	205 °C, Water-Quenched	-32		1035
	500 hours at 70 °C	+28	+60	1040
0.15	Furnace-Cooled	0		1040
	205 °C, Water-Quenched	-55		1030
	500 hours at 70 °C	+45	+90	1040
0.25	Furnace-Cooled	0		1060
	205 °C, Water-Quenched	-80		1050
	500 hours at 70 °C	+15	+95	1070
0.40	Furnace-Cooled	0		1100
	205 °C, Water-Quenched	-105		1050
	500 hours at 70 °C	+25	+130	1105
0.58	Furnace-Cooled	0		1060
	205 °C, Water-Quenched	-110		1045
	500 hours at 70 °C	+20	+130	1070

to the ends of the specimen with set screws, and extended vertically through openings in the cover of the bath. The end faces of the arms had been metallographically polished and a reference mark consisting of a Knoop indentation was impressed on each face. As the specimen was heated and cooled, the displacements of the reference marks were observed through two fixed microscopes equipped with calibrated filar eyepieces.

All of the supporting members of the apparatus were made of invar and the entire instrument was operated in a room maintained at  $20 \pm 0.5$  °C. The expansion coefficients were measured over at least two complete heating and cooling cycles from -40 to +40 °C, and the accuracy of the average coefficient obtained in this way was estimated to be  $\pm 0.1 \times 10^{-6}$  per °C. The expansion curves were all reversible and linear in this temperature range and no hysteresis effects were observed.

*Results of Thermal Coefficient Measurements*—It is evident from Table IV that the coefficient of thermal expansion of invar varies appreciably with the content of minor elements, particularly in the annealed condition. Carbon, manganese and possibly silicon appear to have a deleterious effect. However, in each case, the coefficient can be greatly reduced by water quenching from 830 °C (1525 °F). Unfortunately, this treatment leads to dimensional instability and poses the need for a stabilizing operation after the quenching that will not raise the expansion coefficient.



**Table IV**  
**Coefficient of Thermal Expansion of Invar**

Composition				Expansion Coefficient $\times 10^6 / ^\circ\text{C}$ ( $-40$ to $+40$ $^\circ\text{C}$ )		
C	Mn	Si	Ni	Annealed*	Water Quenched†	Water Quenched and Stabilized‡
0.07	0.44	0.24	36.8	1.9	0.9	1.1
0.02	0.09	0.01	36.0	0.8	-0.1	0.0
0.10	0.12	0.08	36.1	1.0	0.1	0.0
0.15	0.08	0.17	36.0	1.3	0.1	0.0
0.25	0.05	0.20	36.6	1.4	0.0	1.0

\*830  $^\circ\text{C}$  (30 minutes), furnace cool

†830  $^\circ\text{C}$  (30 minutes), water quench

‡Treatment consists of:

a. 830  $^\circ\text{C}$  (30 minutes), water quench

b. 315  $^\circ\text{C}$  (1 hour), air cool

c. 95  $^\circ\text{C}$  (48 hours), air cool

In the light of the known dimensional behavior, a series of heat treatments was designed to improve the stability of quenched invar, using the 0.07% carbon, 0.44% manganese, 0.24% silicon, 36.8% nickel alloy that showed the highest coefficient in Table IV. According to Table V, it is clear that aging for 48 hours at 95  $^\circ\text{C}$  (which is sufficient to complete the  $\gamma$ -expansion) has practically no effect on the expansion coefficient. This is also true for heating at 205  $^\circ\text{C}$  (which reverses the  $\gamma$ -phenomenon) and at 315  $^\circ\text{C}$  (which is a stress relieving treatment). On subsequent aging at 95  $^\circ\text{C}$  for 48 hours, there is still relatively little change in the coefficient, but if the invar is annealed by furnace cooling from 830  $^\circ\text{C}$  (1525  $^\circ\text{F}$ ) (which gives excellent stability), the coefficient increases by almost 100% over the previous values. This increase is probably due to presence of graphite which precipitates during the slow cooling from 830  $^\circ\text{C}$ . However, variations in the cooling rate from 315  $^\circ\text{C}$  and below have a negligible effect on the expansion coefficient. These results make it possible to achieve an excellent combination of low expansion coefficient and high dimensional stability, as will be discussed in the next section.

**Table V**  
**Effect of Heat Treatment in the Expansion Coefficient of Commercial Invar**

(36.8% Ni, 0.07% C, 0.44% Mn, 0.24% Si, 0.011% S, 0.007% P, bal. Fe)  
Treatments were given in succession as indicated. Coefficients apply to temperature range of  $-40$  to  $+40$   $^\circ\text{C}$ .

Treatment	Expansion Coefficient $\times 10^6 / ^\circ\text{C}$	Treatment	Expansion Coefficient $\times 10^6 / ^\circ\text{C}$
830 $^\circ\text{C}$ (30 min.), water quench	0.9	830 $^\circ\text{C}$ (30 min.), water quench	0.9
95 $^\circ\text{C}$ (48 hrs.), air cool	1.0	95 $^\circ\text{C}$ (48 hrs.), air cool	1.0
205 $^\circ\text{C}$ (1 hr.), water quench	0.8	205 $^\circ\text{C}$ (1 hr.), air cool	1.2
315 $^\circ\text{C}$ (1 hr.), water quench	0.8	315 $^\circ\text{C}$ (1 hr.), furnace cool	1.0
95 $^\circ\text{C}$ (48 hrs.), air cool	1.0	95 $^\circ\text{C}$ (48 hrs.), air cool	1.0
830 $^\circ\text{C}$ (30 min.), furnace cool	1.9		



## DISCUSSION OF RESULTS

This investigation has demonstrated that the following factors play significant roles in the dimensional stability of invar:

1. Residual stresses and stress relief
2. The  $\gamma$ -expansion phenomenon
3. The formation of graphite.

*Residual Stresses and Stress Relief*—It has been shown that quenching introduces longitudinal compressive stresses at the surface and tension stresses in the interior of bar specimens. On rapid cooling, the surface temperature is lowered first, but the shrinkage of the surface layer is opposed by the interior which is under hydrostatic pressure and resists flow. Therefore, the surface layer is initially put in tension and undergoes plastic deformation when the stresses become sufficiently large. As the interior cools, it tends to contract further, but this contraction is resisted by the cold surface layer. When temperature equilibrium is finally established, the bar has undergone a net elongation and the surface is in compression while the center is in tension. Since the resultant condition is due primarily to plastic deformation, there is no appreciable change in volume.

On aging, relief of the residual stress occurs. If the quenched condition is taken as the reference length, stress relief produces a contraction, which is to be expected. During heating, the surface reaches the stress relieving temperature before the interior, and undergoes compressive flow while the interior is still under elastic tension. This not only relieves the tension in the interior but also results in an over-all decrease in length.

It has been demonstrated that stress relief proceeds very slowly at room temperature, but that it becomes appreciable at temperatures as low as 205 °C (400 °F). If invar is heated to 315 °C (600 °F) and then quenched, it is possible to obtain considerable stress relief without setting up new quenching stresses. From above 315 °C, however, it is necessary to cool slowly in order to achieve substantial stress relief.

It was found that stress relief can also be attained by mechanical shock. When quenched invar rods are dropped onto a concrete floor, measurable stress relief results. Apparently the elastic waves set up by the impulse are sufficient to cause plastic flow in some regions, thus lowering the elastic stresses.

*The  $\gamma$ -Expansion Phenomenon*—The  $\gamma$ -expansion is a reversible process which has the following characteristics:

Starting with invar quenched from 830 °C (1525 °F),

1. The  $\gamma$ -expansion occurs and has its maximum value on prolonged aging in the range of 50 to 95 °C (120 to 205 °F). Approximately 50 hours are required to complete the process at 95 °C, while at 70 °C the process is still underway in 2000 hours. The total net expansion is about 50 microinches per inch in commercial invar.

2. The reaction can be reversed by heating at 205 °C (400 °F), and a comparable contraction takes place. The  $\gamma$ -expansion may then be obtained once more by heating at 70 °C, after which the process can be reversed again by reheating at 205 °C. This cycle has been repeated 10 times with no apparent hysteresis.

3. The  $\gamma$ -reaction is carbon-dependent. With 0.02% carbon present the expansion is not observed, and the magnitude of the effect can be related to the solubility of carbon in invar at the quenching temperature.

4. The  $\gamma$ -expansion is a true volume effect, since it is completely accounted for by a corresponding increase in lattice parameter.

5. There is a small increase in magnetization, and possibly in hardness, associated with the  $\gamma$ -expansion.

Since the  $\gamma$ -expansion is produced by an increase in the lattice parameter of the invar, it seems that the effect is probably caused by some reaction within the austenitic lattice. Inasmuch as the phenomenon is also carbon-dependent, the process likely involves a distribution of carbon atoms into preferred positions in the austenite during the low temperature aging. Conceivably if Guinier-Preston zones were being formed, as a pre-precipitation process, some lattice parameter changes might be expected, but it is difficult to predict, *a priori*, whether it should be an increase or a decrease. However, the clustering of carbon atoms, corresponding to Guinier-Preston zones, might well account for the slight hardening tendency during the  $\gamma$ -expansion. Furthermore, such clustering could be wiped out on heating (say at 205 °C where the temperature is still too low for the occurrence of any appreciable decomposition of the supersaturated austenite) to cause the observed contraction and to set the stage for the recurrence of the  $\gamma$ -expansion on subsequent aging in the vicinity of 70 °C. An attempt is being made to detect Guinier-Preston zones in single crystals of invar, after aging at 70 °C.

The increase in magnetization accompanying the  $\gamma$ -expansion can be partially explained on the basis of the band theory of invar (2). An increase in lattice parameter at a given temperature below the Curie point is equivalent to a partial reversion to the ferromagnetic condition existing at absolute zero. Such a reversion would be accompanied by an increase in magnetization.

*The Formation of Graphite*—The solubility of carbon in invar at 830 °C (1525 °F) is 0.18%. Any excess carbon exists as graphite. If an alloy with, for example, 0.15% carbon is quenched from 830 °C and then reheated at low temperatures for prolonged periods of time (e.g., 350 hours), no graphite is detected until an aging temperature of 315 °C (600 °F) is reached. The maximum amount of graphite is precipitated between 425 and 540 °C (800 and 1000 °F) and re-solution occurs at higher temperatures. Despite the voluminous nature of graphite, its precipitation is attended by a net contraction in the invar, this contraction being caused by the decrease in lattice parameter of the austenite as it rejects carbon from the lattice.

The graphite precipitation is well separated in temperature from the  $\gamma$ -expansion and there seems to be no direct connection between the two processes. It is difficult to conceive of a pre-precipitation stage for graphite which would first produce an expansion in the austenite at about 70 °C, then disappear with further heating at about 205 °C, and finally cause a net contraction by precipitating as graphite at temperatures above 315 °C.

*Stabilization Treatment*—The presence of graphite raises the coefficient of thermal expansion as indicated by the high values found after furnace cooling. This necessitates a water quench from the solution temperature to suppress the formation of graphite. The dimensional instability introduced thereby can be alleviated by a stress relieving treatment, but the temperature is limited by the possibility of graphite precipitation. It has been shown that appreciable stress relief can be attained at 315 °C (600 °F) with negligible graphite formation. Furthermore, this treatment has little effect on the expansion coefficient.

However, after such stress relief, invar is capable of undergoing the  $\gamma$ -expansion, and this leads to dimensional instability again. Hence, it is desirable to age invar after stress relieving so that the  $\gamma$ -expansion may be consummated before the alloy is machined to final dimensions and placed in service. The time rate of the  $\gamma$ -expansion increases with the aging temperature, but the maximum extent decreases, and this makes it necessary to select an optimum aging temperature. Forty-eight hours at 95 °C (205 °F) is appropriate and, moreover, exerts little influence on the expansion coefficient.

Accordingly, the stabilization treatment for achieving good dimensional stability consistent with minimum expansion coefficient involves the following sequence:



- a. 830 °C (1525 °F), 30 minutes, water quench
- b. 315 °C (600 °F), 1 hour, air cool
- c. 95 °C (205 °F), 48 hours, air cool

This treatment has been applied to all the invar alloys listed in Table IV with excellent results. In each case, the expansion coefficient is appreciably lower than in the annealed condition, and the dimensional stability is quite good.

#### CONCLUSIONS

1. The dimensional behavior of invar has been studied with respect to its coefficient of thermal expansion, as well as its stability versus time.

2. The solubility of carbon in invar has been determined. At 830 °C (1525 °F), it is 0.18% carbon and becomes vanishingly small as room temperature is approached.

3. Quenching from a solution temperature of 830 °C produces an appreciably lower expansion coefficient than does furnace cooling, but leads to dimensional instability.

4. On aging quenched invar at 20 to 95 °C (68 to 205 °F), two overlapping dilation effects occur. One is an expansion (called the  $\gamma$ -expansion) and appears to result from a redistribution of the carbon atoms in solid solution. The other is a contraction due to the relief of quenching stresses.

5. The  $\gamma$ -expansion can be reversed at 205 °C (400 °F) with a corresponding contraction, and this makes it possible for the  $\gamma$ -expansion to re-occur at lower temperatures. This cycle has been repeated 10 times.

6. The quenching stresses are relieved more effectively the higher the temperature, but above 315 °C (600 °F) graphite may precipitate, thus raising the expansion coefficient, and new quenching stresses may be introduced if the cooling is too rapid.

7. Based on these findings, a stabilization treatment has been developed to achieve an optimum combination of low expansion coefficient and high dimensional stability:

- a. 830 °C (1525 °F), 30 minutes, water quench
- b. 315 °C (600 °F), 1 hour, air cool
- c. 95 °C (205 °F), 48 hours, air cool

Step (a) is a solution treatment for the graphite, step (b) is a stress relieving operation, and step (c) accomplishes the  $\gamma$ -expansion before the invar is finished to size and placed in service.



## ACKNOWLEDGMENTS

This investigation was carried out in cooperation with the Instrumentation Laboratory of the Massachusetts Institute of Technology. The authors wish to thank Professor John T. Norton for his advice on the X-ray stages of this study, and they are also indebted to John M. Fitzpatrick, Walter Fitzgerald, Leonard Sudenfield, Harold Ludwig and Mrs. Annette Lement for assistance in various phases of the work. The authors are also especially grateful to C. Sheldon Roberts for his efforts in gathering the data on expansion coefficients. The Driver-Harris Company of Harrison, N. J., kindly supplied the special heats of invar.

## References

1. J. Marsh, "Alloys of Iron and Nickel, Vol. I", McGraw-Hill Book Co., 1938.
2. W. Shockley, "The Quantum Physics of Solids—I", Monograph B-1184, Bell Telephone Laboratories.
3. C. E. Guillaume, "Changements Passagers et Permanents des Aciers au Nickel" (Transitory and Permanent Changes of Nickel Steels), C. R. Acad. Sci., Paris, Vol. 136, 1903, p. 356.
4. H. Scott, "Expansion Characteristics of Low-Expansion Nickel Steels", TRANSACTIONS, American Society for Steel Treating, Vol. 13, 1928, p. 829.
5. T. F. Russell, "Low Expansion Nickel Steel", *Engineering* (London), Vol. 128, 1929, p. 400.
6. M. A. Hunter, "Low-Expansion Alloys", *Metals Handbook*, American Society for Metals, Cleveland, 1948, p. 601.
7. C. E. Guillaume, "Recherches Metrologiques sur les Aciers au Nickel" (Metrologic Researches on Nickel Steels), *Travaux et Memoires du Bureau International des Poids et Mesures*, Vol. 17, 1927, p. 113.
8. J. R. Low and M. Gensamer, "Aging and the Yield Point in Steel", *Transactions*, American Institute of Mining and Metallurgical Engineers, Vol. 158, 1944, p. 207.
9. B. S. Lement, B. L. Averbach and M. Cohen, "The Dimensional Stability of Steel, Part IV—Tool Steels", TRANSACTIONS, American Society for Metals, Vol. 41, 1949, p. 1001.
10. R. F. Mehl and L. K. Jetter, "The Mechanism of Precipitation from Solid Solution", Symposium on the Age-Hardening of Metals, American Society for Metals, 1939, p. 342.
11. S. G. Fletcher and M. Cohen, "The Effect of Carbon on the Tempering of Steel", TRANSACTIONS, American Society for Metals, Vol. 32, 1944, p. 333. See Authors' Reply to Discussion, p. 358.
12. E. Heyn, "Internal Strains in Cold Wrought Metals, and Some Troubles Caused Thereby", *Journal*, Institute of Metals, Vol. 12, 1914, No. 2, 3.
13. E. A. Owen and A. H. Sully, "The Equilibrium Diagram of Iron-Nickel Alloys", *Philosophical Magazine*, Series 7, Vol. 27, 1939, p. 614; "On the Migration of Atoms in Iron-Nickel Alloys", *Philosophical Magazine*, Vol. 31, 1941, p. 340.
14. B. L. Averbach and M. Cohen, "X-ray Measurements of Retained Austenite by Integrated Intensities", *Transactions*, American Institute of Mining and Metallurgical Engineers, Vol. 176, 1948, p. 401.
15. O. Zmeskal and M. Cohen, "Simultaneous Measurement of Magnetic and Dilatometric Changes", *Review of Scientific Instruments*, Vol. 13, August 1942, p. 346.
16. W. Souder and P. Hidnert, "Measurements on the Thermal Expansion of Fused Silica", *Science Papers*, Bureau of Standards, Vol. 21, 1926, No. 524.

## PREPARATION AND PROPERTIES OF TITANIUM-CHROMIUM BINARY ALLOYS

BY D. J. MCPHERSON AND M. G. FONTANA

### *Abstract*

*The preparation of titanium-chromium binary alloys by induction and arc melting was investigated. Two furnaces developed for this work are described. Various types of refractory crucibles were investigated for induction melting of these alloys. Low porosity thoria, beryllia and carbon were found to be the most promising materials. Arc-melted alloys were used for property evaluation. Titanium-rich alloys, containing 0 to 20% chromium, were found to constitute the forgeable range of the system, by open-die drop forging methods. Property evaluation was concentrated on the binary alloys of this forgeable range. Chemical, spectrographic, and vacuum-fusion analyses, hardness and hot hardness, room temperature tensile and impact properties, stress-rupture properties, elevated temperature oxidation resistance, and metallographic and X-ray studies are reported. The outstanding property of the forgeable titanium-chromium alloys was very high room temperature strength in combination with low specific gravity. These alloys could not be considered for high temperature, high strength applications in air based on results of oxidation, hot hardness, and stress-rupture tests.*

THE relatively recent development of production methods for "ductile" titanium has resulted in widespread interest regarding possible engineering applications for this metal. The effects of various alloying agents upon titanium present a wide field for current study. The objective of the present investigation was to evaluate some of the engineering characteristics of binary alloys of titanium with chromium. The choice of chromium as a second component was based on the known value of this metal in stainless steels and in most heat resisting alloys. Titanium and chromium have high melting points, 3300 and 3430 °F (1820 and 1890 °C), respectively. The density of titanium is 4.5 grams per cubic centimeter, while that of chromium is 7.1 grams per cubic

This paper is based on McPherson's thesis in partial fulfillment of the requirements for a Ph.D. degree.

A paper presented before the Thirty-second Annual Convention of the Society, held in Chicago, October 21 to 27, 1950. Of the authors, D. J. McPherson is associated with Armour Research Foundation, Chicago, and M. G. Fontana is professor and chairman, Department of Metallurgy, The Ohio State University, Columbus, Ohio. Manuscript received April 13, 1950.

centimeter. These metals should be expected to yield a series of light, but refractory alloys.

Alloys were prepared for exploratory work in a vacuum-induction furnace, employing various refractory crucibles. The problem of choosing a melting container for the metals chromium and titanium is a difficult one, particularly for the latter. The problems have been discussed in the literature by Parke and Bens (1),<sup>1</sup> Adcock (2), Vogel and Wenderott (3), Kroll (4, 5), Powell (6), Brace (7) and Sutton (8). After considerable work was done with the induction furnace, the size limitations and low reproducibility of results due to crucible materials were deemed unsatisfactory for evaluation of the binary alloys. Accordingly, an arc furnace employing a water-cooled copper crucible and adjustable tungsten electrode was constructed. This paper will be primarily concerned with the alloys produced in the arc furnace. Use of the induction furnace was continued after the successful operation of the arc furnace, but chiefly for the purpose of evaluating crucible materials for use with titanium-chromium alloys.

#### SURVEY OF THE LITERATURE

The literature dealing with titanium-chromium binary alloys is limited. The constitution diagram has been determined only for the range 0 to 57 weight per cent titanium. This work was done by Vogel and Wenderott (3). The intermetallic compound  $\text{Cr}_2\text{Ti}_3$  is placed at 57% titanium and 43% chromium. A eutectic between chromium and  $\text{Cr}_2\text{Ti}_3$  occurs at 42% titanium and 2550 °F (1400 °C). At this temperature the solid solubility of titanium in chromium is given as 26 weight per cent. Parke and Herzig (9) prepared two chromium-base alloys containing 7 and 10% titanium in connection with the search for gas turbine blade alloys. Brittle properties caused this system to be abandoned. Some preliminary data on a 10% chromium alloy with titanium was reported by E. I. Larson et al (10). Powder metallurgy techniques were used, and melting was reported in a 90 Ti – 10 Cr bar vacuum-sintered at 2190 °F (1200 °C). After sintering at 2060 °F (1125 °C) the bar was reduced 26% by cold rolling. After a vacuum anneal, it was further reduced in thickness 9% before cracking occurred. The hardness of the sintered bar was Rockwell C-24. An increase in electrical resistance indicated the probability that some solid solution exists. Data from a paper by Brace (11) indicate that titanium-chromium alloys containing equi-atomic ratios of molybdenum and tungsten possess considerably better tensile properties at 1750 °F (955 °C) than do the straight Ti-Cr binary alloys.

<sup>1</sup>The figures appearing in parentheses pertain to the references appended to this paper.



The most extensive published data concerning these binary alloys were found in a report to Project RAND by Battelle Memorial Institute (12). Most of the data were obtained from materials fabricated by powder metallurgy methods, but some information was included on alloys prepared by arc melting and forging. Titanium-base binary alloys containing chromium, molybdenum, tungsten, columbium and tantalum in amounts up to 20% by weight were studied. At the 10% addition level, the alloy containing chromium showed the highest ultimate (137,000 psi) and yield (124,000 psi) strengths. In the 20% chromium alloy, the strength fell off "because of the excessive amount of intermetallic compound present". The chromium alloys also showed the greatest hardness and strength response to cold working and the greatest hardening response to heat treatment of all the combinations tested. From an examination of microstructures it was estimated that the limit of solubility of chromium in alpha titanium is less than 2.5%. Annealing a 2.5% chromium alloy at 1830 °F (1000 °C) yielded a structure composed almost entirely of alpha needles, with a small amount of untransformed beta phase between the needles. Quenching the alloy from this temperature yielded a structure composed entirely of transformed beta phase, a fine acicular structure with the original beta grain boundaries clearly visible. This structure was said to be the result of a martensitic type of transformation during the quench. At quenching temperatures lower than 1470 °F (800 °C) and at higher chromium contents, the martensitic transformation no longer occurred and the beta phase was retained, not transformed, according to the report. Complete retention of the cubic beta phase was noted in quenched 10% chromium alloys. It was found that the beta phase, either retained or transformed, was appreciably harder and less ductile than the alpha phase.

#### APPARATUS AND MATERIALS

Fig. 1 is a photograph of the induction melting unit developed for this work. The furnace tube is 3 inches I.D. by 15 inches long. Alloy melts weighing up to one pound can be prepared in this unit. The furnace is mounted in such a manner that it may be moved up and down within the induction coil, allowing considerable flexibility in the heating zone. The unit is adaptable to either vacuum or special atmosphere runs. Power for melting is provided by a 50-KW motor-generator set.

W. Kroll (4) first applied arc furnace techniques to the production of titanium and its alloys, on a small scale. Arc furnaces for larger-scale operation have been developed by Battelle Memorial



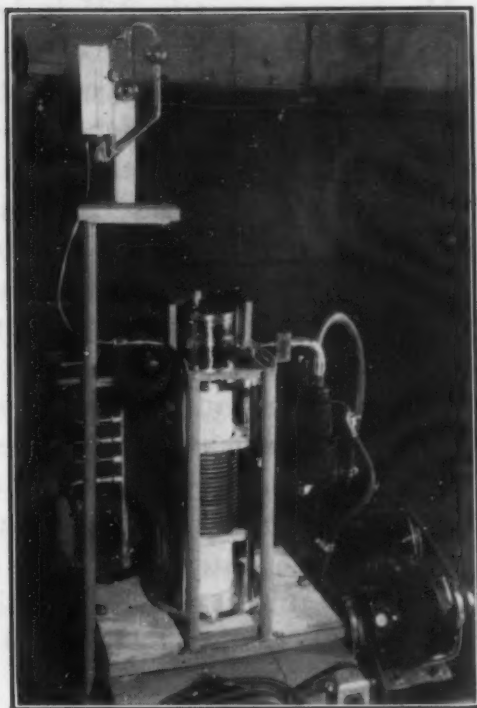


Fig. 1—Vacuum and Controlled Atmosphere Induction Melting Furnace.

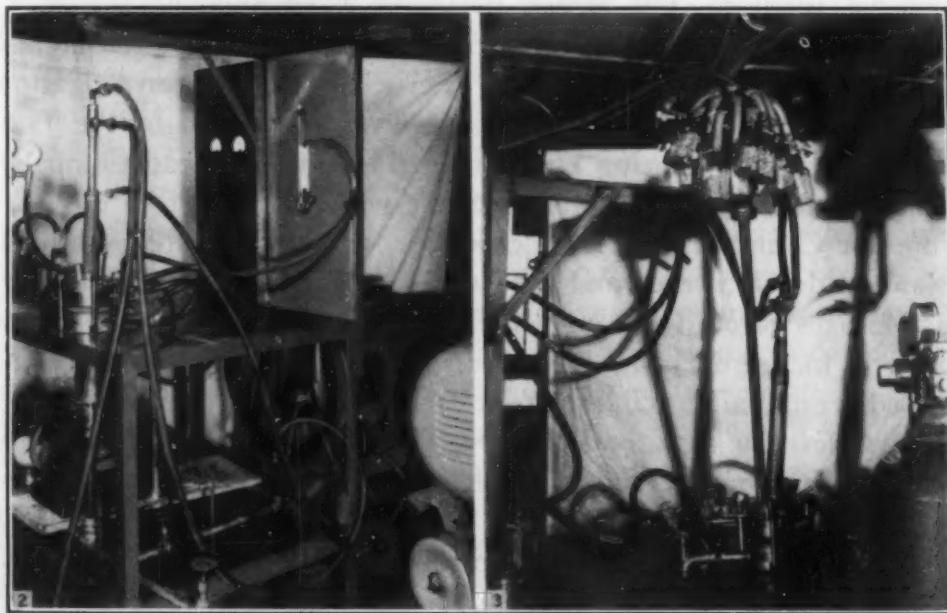


Fig. 2—Arc Melting Furnace. Fig. 3—View of Arc Furnace Charging Device.

Institute (13). A modification of this type of furnace designed for either positive pressure or vacuum melting has been developed for the present work.

Fig. 2 is a photograph of the arc melting unit. Fig. 3 is a side view of the apparatus showing the charging device employed. The water-

cooled copper crucible is approximately 2.25 inches in diameter by 6 inches deep. A double thrust bearing is located at the top of the bellows. The upper ring of this bearing is secured to the electrode by set-screws, thus allowing 360-degree rotation of the electrode within the bellows and furnace. The sidewise motion of the adjustable electrode is restricted by a brass ring in the head. This is so arranged that the electrode cannot approach closer to the crucible side wall than 0.5 inch. The electrode is supported at the top by a pulley system which counterbalances the electrode weight and atmospheric pressure when the furnace is evacuated. The furnace charge tube is  $\frac{3}{4}$ -inch copper tubing. The large number of individual feed nipples was provided since, in the interest of alloy homogeneity, it was necessary to restrict charge increments to about 50 grams. This amount can easily be held molten in the water-cooled crucible. A mercury pressure seal is designed to maintain argon pressure in the system at 2 inches of mercury above atmospheric. The power for this furnace is supplied by two 300-ampere D.C. welding generators connected in parallel and synchronized for identical operating characteristics.

*Refractory Crucibles for Induction Melting*—Various grades of beryllia crucibles were obtained from M. W. Mallett of Battelle Memorial Institute, The Brush Beryllium Company and the A. C. Sparkplug Division of General Motors Corporation. The latter also provided alundum, zircon and thoria crucibles for the investigation. Stabilized zirconia and titania containers were provided by the Titanium Alloy Manufacturing Division of the National Lead Company. A silicon carbide-faced graphite crucible was obtained from the Carborundum Company. Graphite crucibles were made from National Carbon grade C. S. rods and fired at 3200 °F (1760 °C) for 1 hour. Crucible sizes varied from  $\frac{7}{8}$ -inch I.D. by 3 inches deep to 2.25 inches I.D. by 6 inches deep. Molybdenum sheet, 5 mils in thickness, was wrapped around all crucibles except carbon to serve as a "heater".

*Materials for the Arc Furnace*—The arc furnace crucibles were spun from high-purity copper sheet in two parts, cups and flanges. The silver-soldered joint occurred near the top, out of the melting zone. Crucibles were spun with hemispherical and flat-bottom shapes. Flat-bottom crucibles were adopted for the manufacture of all large ingots which were to be forged.

Hot-swaged and annealed  $\frac{3}{4}$ -inch tungsten rods were employed for the cathode tips. The stainless steel bellows had 1-inch I.D., 1.5-inch O.D., 8-inch free length and 64 total convolutions. These bellows allowed a 2.75-inch thrust in both directions from the equilibrium position of the electrode. Argon gas of 99.93% purity served as the melting atmospheres without further purification.

*Melting Stock*—Considerable preliminary work was carried out to evaluate the various grades of chromium and titanium metal available for melting stock. Electrolytic chromium of 99% minimum purity was obtained in powdered form and as  $\frac{3}{4}$ -inch maximum plates. It was used in both forms for induction melting work. The plates were sized to  $\frac{1}{8}$  inch for arc furnace feed. This grade of chromium contains as principal impurities about 0.50% oxygen and 0.03% hydrogen. The hydrogen is easily removed by warm extraction in vacuo. Attempts to reduce the oxygen content by premelting and by reducing with carbon yielded charge material which gave no better alloy ingots than the as-received plate. Accordingly, the latter was adopted as melting stock.

Bureau of Mines titanium powder was used for induction melting work. Du Pont sponge titanium (99.8% pure) became available at the time the arc melting phase of the investigation was undertaken and was used as melting stock for this work. The sponge was sized to the range  $\frac{1}{8}$  to  $\frac{1}{3}$  inch in a gyratory crusher for charge material.

#### EXPERIMENTAL PROCEDURES

All alloys prepared by induction melting were allowed to solidify in the crucibles. The majority of melts were made in vacuum. It was found that about 50 microns (0.050 mm of mercury) was the highest vacuum which could be tolerated in melting these alloys without excessive vaporization of chromium. Melting was accomplished rapidly and the molten alloys were held at 50 microns pressure for several minutes for refining. Other melting atmospheres investigated were positive and partial pressures of purified hydrogen or helium gas. Refractory crucibles were outgassed in a good vacuum for 1 hour at 3000 °F (1650 °C) prior to use. Chemical analysis, microscopic examination, hardness and hot forgeability were used to evaluate the effects of various crucible materials on the alloys.

Arc furnace melts weighing up to 150 grams were made from a single batch charge. Preparation of larger ingots required the use of the charging device. Such ingots, weighing up to 3 pounds, could be made without breaking the arc or suspending the operation. After the alloy charge was prepared and added to the furnace, the system was twice evacuated and flushed with argon. Argon pressure was then maintained nearly static at 2 inches of mercury above atmospheric. Cooling water was adjusted to the proper flow, and an arc was struck on the melt at about 300 amperes and 30 arc volts. The arc length was usually maintained at about 0.5 inch. Each charge increment was finished-off at a power input of approximately 600 amperes and



25 arc volts, the electrode being gyrated to play the arc over the entire surface of the melt. Charge additions were made by withdrawing the electrode to a distance of 2 or 3 inches and pouring the contents of a charge-bottle into the furnace via the hopper and feed tube. An arc length of 4 inches could easily be maintained in this atmosphere. About 30 minutes was required for the preparation of a 2.5-pound ingot. The furnace could be opened and the ingot removed within 15 to 30 minutes after the power was shut off. Charge weights, power input, water flow, argon flow and melting times were varied somewhat to achieve optimum conditions for various alloy compositions.

Vacuum melting was investigated briefly. Unstable arc conditions and "glow-discharge" phenomena were encountered when high vacuum was employed. The furnace was evacuated and argon was bled in to various pressures in order to determine possible operating conditions. Pressures of at least 8 centimeters of mercury were required in this furnace to achieve a reasonably stable arc. No advantages were noted for this type of vacuum operation, so positive-pressure argon atmospheres were adopted for alloy production.

*Forging*—Arc-melted ingots were lightly surface-ground on the sides and bottom to remove cold shuts or seams which might be present. The ingots were heated to a temperature range of 1700 to 2000 °F (925 to 1095 °C) for forging in air. Most of the 2-pound ingots were forged to  $\frac{5}{8}$ -inch square bars for testing purposes. Generally, three heatings were sufficient for forging an ingot 2.25 inches in diameter and 3 inches long to a  $\frac{5}{8}$ -inch square bar 30 inches long. The bars were cooled in air after forging.

*Gas Contents*—Gas analyses for oxygen, nitrogen and hydrogen contents of representative arc-melted products by vacuum fusion were provided by the Titanium Alloy Manufacturing Division of National Lead Company in Niagara Falls. Conventional vacuum fusion methods have been regarded as very uncertain for titanium, due to the high stability of the compounds titanium oxide and titanium nitride. The method used for these determinations was similar in principle to that described by Sloman (14), involving reaction of the sample in a bath of gas-free iron saturated with carbon.

*Hot Hardness*—Hot hardness tests were run on selected compositions of arc-melted and forged alloys at Battelle Memorial Institute. The apparatus used has been described by Bergh (15). The tester consisted essentially of a high temperature vacuum furnace having a 130-degree pyramid diamond indenter mounted on the top plate. The specimen rested on an anvil which was actuated by a hydraulic system. The pressure exerted in indenting the specimen could be controlled



by the amount of air admitted to the hydraulic system, and was read on a mercury manometer. Approximately 200-gram loads were applied for all indentations. The furnace contained a specimen charge chute and gear-driven positioner rod so that numerous specimens could be tested without opening the apparatus. Each reading reported is averaged from ten indentations. Readings were taken after specimens had cooled to room temperature. The error incurred by indenting at high temperature and measuring the indentation at room temperature has been discussed by Bens (16). He pointed out that even with copper the maximum error amounts to only two Vickers hardness numbers and that it is safe to neglect the error for most materials.

*Tensile Tests*—The ASTM standard  $\frac{1}{4}$ -inch test-piece, having a 0.250-inch gage diameter and 1-inch gage length, was used for tensile strength data on these alloys. A Baldwin SR-4, Model K, strain indicator was employed and a single Baldwin SR-4, Type A-7, strain gage was used on each test bar. An unalloyed titanium dummy specimen was used with the strain indicator for temperature compensation. Modulus of elasticity values are averaged from three sets of readings. Yield strengths are taken at 0.2% offset. True ultimate strength is calculated from breaking load and fracture area. The strength-weight ratio is a pure number obtained by dividing ultimate strength in psi by density in grams per cubic centimeter.

*Impact Tests*—Standard ASTM Charpy keyhole-notch specimens were used to evaluate notched-bar impact properties of the arc-melted and forged compositions. Each alloy was tested in duplicate in a Riehle testing machine using 220 ft-lbs of energy, which corresponds to a striking velocity of 18.1 feet per second. The impact tests were conducted at room temperature.

*Stress-Rupture Tests*—Stress-rupture test specimens were machined from forged bars of selected arc-melted compositions. The test coupons were 2.75 inches in over-all length, having a 0.150-inch gage diameter, 1-inch gage length, and  $\frac{1}{4}$ -inch threaded diameter  $\frac{1}{2}$  inch long. Tests were run in stress-rupture equipment at the Titanium Alloy Manufacturing Division of National Lead Company.

*Oxidation Tests*—Oxidation test specimens consisted of  $\frac{1}{4}$ -inch thick slices cut from the  $\frac{5}{8}$ -inch square forged alloy bars. Surfaces were prepared by sanding, finishing on 120-grit emery cloth, and by washing in acetone. Tests were run at 1000, 1200, 1350 and 1500 °F (540, 650, 730 and 815 °C) in still air in an electric furnace. Types 304 and 316 stainless steels were run with each set of tests for comparison purposes. Small porcelain crucibles were placed in an inverted position over the test-pieces when they were removed from the furnace.

so that the scale, which tended to flake off of these alloys upon cooling, would not be lost. After the test-pieces had cooled to room temperature, each was weighed with its collected scale. The gain in weight divided by surface area was reported as the extent of oxidation.

*X-Ray Diffraction*—A number of 100 to 200-gram arc-melted alloys were prepared for X-ray diffraction studies. Coupons from these ingots were heated to 1400 °F (760 °C) in one lot, held for 2 hours, and furnace-cooled. Powdered samples were prepared and exposed in a Debye-Scherrer-type camera. Copper  $K\alpha$  radiation was employed for this work. The copper  $K\beta$  radiation was removed by the use of a cylindrical nickel-foil filter within the camera.

### RESULTS AND DISCUSSION

*Induction Melting—Crucible Materials*—Only that phase of the induction melting program which relates to evaluation of crucible materials for titanium-chromium alloys will be discussed in this report. It may be noted that arc-melting procedures, which completely avoid the use of refractory containers, are considered superior for the production of titanium-rich alloys.

In this work low-porosity crucibles of zircon ( $ZrO_2 \cdot SiO_2$ ), alumina and titania were badly attacked by the molten alloys. The portions of the crucibles in contact with the alloys were almost entirely eaten away. Stabilized zirconia crucibles generally yielded ingots low in zirconium content, but considerable reaction was apparent from crucible discoloration. Microstructures of alloys prepared in these crucibles frequently revealed unaccountable three-phase structures and most of these alloys were hard and brittle. Over 1% silicon and 0.2% carbon were found in the alloy melted in silicon carbide. A three-phase structure was observed and the alloy was exceedingly hard. Alloys which analyzed less than 0.2% carbon were prepared in dense, high-fired graphite crucibles, but ingot quality was relatively poor and the molten alloys displayed a strong tendency to climb the container wall. This tendency was also noted to a lesser degree with some of the metallic oxide refractories. This effect is least in the case of the refractories most inert to titanium when they are fabricated into the densest bodies. The use of graphite containers was deemed questionable for work such as the present investigation. The commercial beryllia crucibles tested gave very poor results. Beryllium analyses ranging from 2.5 to 5.0% were obtained on ingots melted in these containers. Specially prepared, low-porosity beryllia and thoria crucibles yielded the most promising results of all materials tested. Several thoria-melted ingots yielded no traces of thorium in chemical analyses.

Beryllium pickups of only 0.02 and 0.03% were noted for two alloys melted in beryllia. Alloys melted in thoria and beryllia also displayed the greatest degree of hot forgeability and the lowest hardness values of all induction-melted ingots. Unfortunately, however, results varied

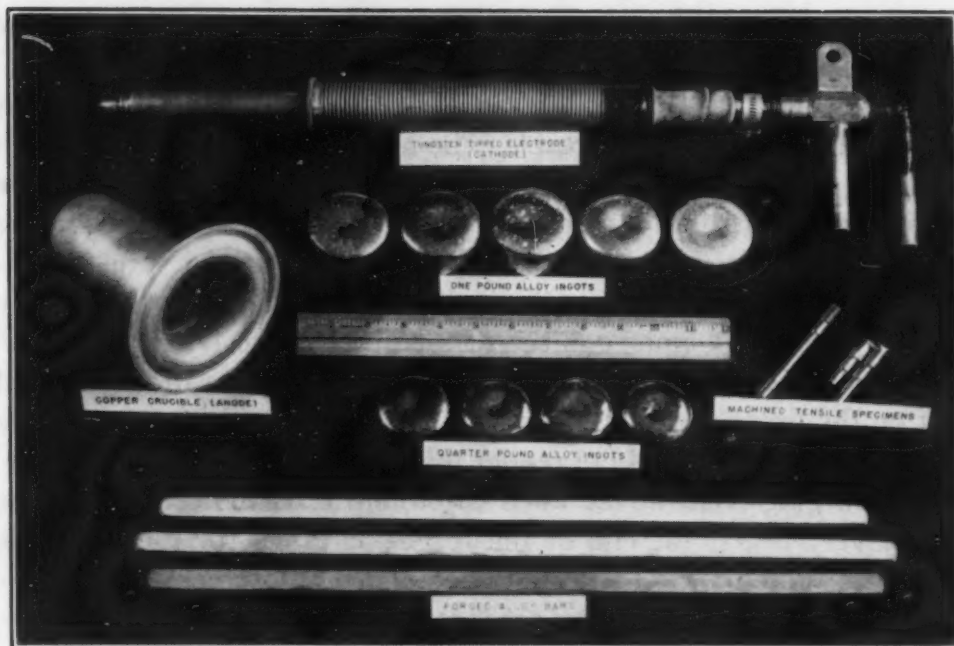


Fig. 4—Arc Furnace Electrode, Crucible and Products.

widely from lot to lot of these special crucibles and acceptable performances were not always obtained.

*Arc Melting and Forgeability*—Approximately seventy melts were made in the arc furnace, of which the first twenty-five were designed to establish techniques and evaluate base materials. No trouble was experienced in removing ingots from the copper crucibles. Merely inverting the crucible usually caused the ingot to fall out. Ingot quality of the arc-melted alloys was very good. No blow-holes or shrinkage cavities were found. The only defects noted were: (a) an occasional dent in the top surface due to the "boring" effect of the arc into the molten alloys; this was minimized by rapid gyration of the electrode as the power was shut off; (b) occasional inclusion of unmelted chromium particles at the cold surfaces in contact with the crucible; (c) frequent shallow cold shuts around the sides, indicating that the arc had not been played about the edges sufficiently during the finishing-off of additions. Fig. 4 is a photograph of the furnace crucible and electrode, several ingots as removed from the furnace, three forged bars and two machined tensile specimens.



The high-chromium compositions were considerably more difficult to prepare than the titanium-rich alloys. This was due in part to the expulsion of gases by the electrolytic chromium which made the arc less stable. Higher power input and a slight positive flow of argon gas were necessary in melting the chromium-rich alloys, whereas normal operation called for a static atmosphere in order to minimize the impurities (principally nitrogen) introduced with the gas.

It was apparent from initial tests that only the titanium-rich alloys of this system would be forgeable. The high-chromium alloys, though relatively soft, behaved in a brittle manner. In order to establish the approximate limit of the forgeable range, 1-pound ingots containing 10% increments of chromium were prepared and tested. These compositions up to and including 20% chromium could be satisfactorily forged by a power hammer in the temperature range 1700 to 1900 °F (925 to 1040 °C). The 30 and 40% chromium compositions cracked apart on the first or second hammer blow. Increasing the temperature to 2100 °F (1150 °C) did not render the latter compositions forgeable. Further forging trials at the 20% chromium level indicated that this must be very nearly the end of the forgeable range for the materials used, since some of the bars showed a tendency to crack. The forgeable range could probably be extended through the use of higher-purity titanium and chromium.

The depth of the zone affected by heating ingots to 2000 °F (1095 °C) in air for forging was very shallow and the surface scale could be easily ground or machined off. Forging seams were not deep except in several bars at the high-chromium end of the forgeable range.

The study of properties was concentrated principally on the forgeable alloys of the titanium-chromium system, viz., titanium-base alloys containing up to 20% chromium.

*Chemical Purity of Arc-Melted Alloys*—Chemical analyses of a number of arc-melted alloys are presented in Table I. The alloys which were analyzed for both titanium and chromium averaged 99.54% of these two elements. The average of eighteen random analyses gave 0.09% tungsten in the arc-melted products. Iron, manganese, and in some cases, tin, appear from spectrographic checks to comprise the major metallic impurities other than tungsten. These elements are residuals in the melting stock. Pickup of copper from the crucible was considerably less than 0.01% in all cases. The chromium contents varied from intended figures by an average of 1.06% chromium for the entire group of alloys.

Vacuum-fusion analyses of selected titanium-chromium compositions are indicated in Table II. The data show that the oxygen content



Table I  
Chemical Analyses of Arc-Melted Alloys

Ingot No.	Condition	Intended Cr, %	Ti, %	Cr, %	W, %
18	Forged	0	.....	.....	0.09
X-1	Forged	0	.....	.....	0.08
X-2	Forged	2	97.12	2.51	0.17
X-3-E	Forged	4	95.25	4.55	0.07
X-3-M	Forged	4	.....	4.00	0.16
X-3-EE	Forged	4	.....	4.08	.....
X-4	Forged	6	93.26	6.02	0.22
X-5	Forged	8	90.41	9.29	0.08
X-6	Forged	10	.....	9.48	.....
XG-2	Forged	10	89.35	10.03	0.15
X-7-E	Forged	12	.....	11.11	.....
X-7-M	Forged	12	.....	11.14	0.04
X-7-EE	Forged	12	.....	11.88	.....
X-8	Forged	14	.....	14.18	.....
X-9	Forged	16	.....	13.02	.....
X-10	Forged	18	.....	15.93	.....
X-11	Forged	20	.....	17.63	0.01
XG-3	Forged	20	79.40	20.07	0.15
4	As-Cast	0	.....	.....	0.03
19	As-Cast	0	.....	.....	0.02
XR-1	As-Cast	5	.....	5.22	.....
26	As-Cast	10	.....	10.39	0.05
XR-2	As-Cast	15	.....	14.28	.....
59	As-Cast	20	.....	19.73	0.07
XR-3	As-Cast	25	.....	23.54	.....
60	As-Cast	30	.....	29.07	.....
XR-4	As-Cast	35	.....	35.54	0.04
65	As-Cast	40	.....	38.46	.....
XR-5	As-Cast	45	.....	42.26	.....
64	As-Cast	50	.....	47.68	.....
XR-6	As-Cast	55	.....	52.11	.....
66	As-Cast	60	.....	57.62	0.11
XR-7	As-Cast	65	.....	63.41	.....
62	As-Cast	70	30.18	.....	.....
XR-8	As-Cast	75	25.19	.....	.....
63	As-Cast	80	19.32	.....	.....
XR-9	As-Cast	85	14.05	.....	0.05
67	As-Cast	90	8.76	.....	.....
XR-10	As-Cast	95	4.50	.....	.....

Table II  
Vacuum Fusion Analyses of Arc-Melted Titanium, Chromium, and Selected Alloys

Specimen	Composition	Condition	Gas Content, Weight %		
			Oxygen	Nitrogen	Hydrogen
19	Titanium	As-Cast	0.228	0.0530	0.0095
24	Chromium	As-Cast	0.480	0.0268	0.0116
26	90 Ti - 10 Cr	As-Cast	0.167	0.0500	0.0180
59	80 Ti - 20 Cr	As-Cast	0.201	0.0503	0.0145
XG-2	90 Ti - 10 Cr	Forged	0.229	0.0444	0.0193
XG-3	80 Ti - 20 Cr	Forged	0.237	0.0316	0.0410

of electrolytic chromium is reduced little or none by arc melting. Oxygen content increases slightly with the amount of chromium in the alloys. The oxygen content of the as-forged material is slightly higher than that of as-cast alloys of the same composition. A small amount of nitrogen is picked up by titanium, chromium and the binary alloys by arc melting in 99.93% argon. These increases amount to 0.01%N<sub>2</sub> for chromium and 0.03%N<sub>2</sub> for titanium, over the nitrogen contents of the respective charge materials. The gas contents (particularly oxygen) are higher than might be desired, but since ductility of

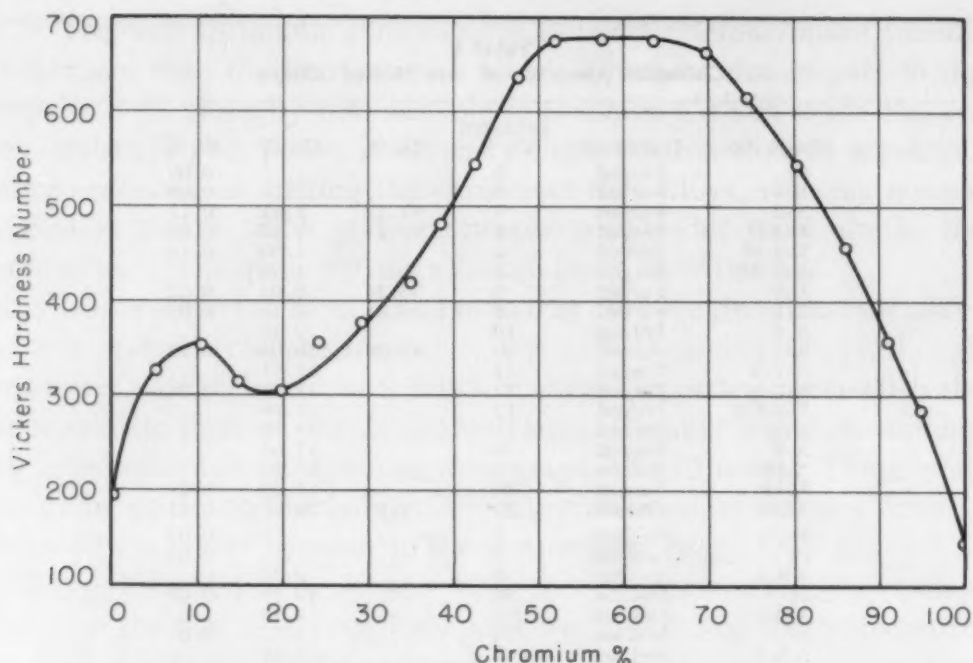


Fig. 5—Hardness of As-Cast Arc-Melted Alloys.

the forgeable alloys was found to be good, the harmful effect is apparently not too great. In addition, nitrogen and oxygen undoubtedly contributed to the high strength values obtained.

*Hardness*—The average room temperature hardnesses of a series of as-cast alloys, varying in composition by 5% chromium (nominal) from pure titanium to pure chromium are shown in Fig. 5. Average hardness values for arc-melted and forged alloys are presented in Fig. 6. It may be noted that the trend of the as-forged hardness curve is identical to that of the as-cast hardness curve of Fig. 5 for the same composition range, and further, that the hardness values are changed only slightly by forging the ingots.

Maximum hardness for as-forged alloys occurs at approximately 9% chromium content. Annealing these alloys at 1400 °F (760 °C) slightly softens compositions containing less than 9% chromium, but hardens alloys in the 10 to 18% chromium range. Water quenching the alloys from 1800 °F (980 °C) hardens all compositions, and the maximum hardening response occurs at the 6% chromium level. In order to check the hardness response of this 6% chromium alloy to quenching temperature, coupons from a forged bar were water-quenched from six temperatures in the range 1200 to 2000 °F (650 to 1095 °C). Fig. 7 shows that the hardness increases with increasing quenching temperature. Structures produced are discussed in a later section.

*Hot Hardness*—The results of hot hardness tests on alloys in the forgeable range are tabulated in Table III. The values are quite low.

Table III  
Hot Hardness Data for As-Forged Arc-Melted Alloys

Bar No.	Composition Cr, %	Average Diamond Pyramid Hardness No.*			
		80°F	1200°F	1350°F	1500°F
X-1	Pure Ti	168	36	22	14
X-3	4.2	233	46	22	10
X-5	9.3	346	39	21	13
X-7	11.4	299	53	32	17
X-9	13.0	284	60	34	21
X-11	17.6	299	70	51	28

\*50-Kg load for 80°F values.

200-gram load for elevated temperature values.

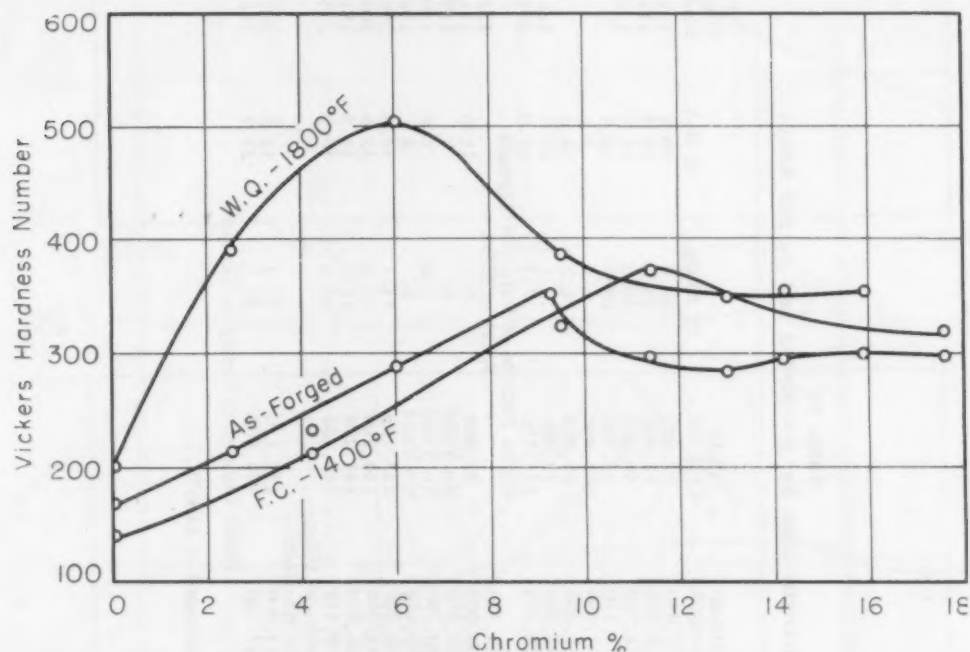


Fig. 6—Hardness of Forged Arc-Melted Alloys.

On a basis of the linear relationship between hot hardness and load carrying ability of metals and alloys at elevated temperatures described by Bens (16), even the best of these alloys should be relatively weak at the temperatures investigated.

Fifteen indentations were made on unalloyed titanium at room temperature in the hot hardness tester in order to compare the microhardness values with standard Vickers Pyramid Hardness numbers. An average value of 169 DPH was obtained using 200-gram loads in the hot hardness tester, and an average value of 168 VPN was shown on the same specimen by the Vickers tester, using a 50-kilogram load. The correlation is excellent, so the hardness values reported for room temperature are standard Vickers determinations.

*Tensile Tests*—The results of room temperature tensile tests on arc-melted and forged alloys are listed in Table IV. Fig. 8 is a plot of



Table IV  
Tensile Strength Data for Arc-Melted and Forged Alloys

Specimen*	Composition Weight %	Density	Ultimate Strength	Yield 0.2% Off.	% Elong.	% R.A.	True Ultimate Strength	Strength- Wgt. Ratio	Modulus $\times 10^6$
X-1-F	Pure Ti	4.50	77,950	72,460	20.3	60.9	131,000	17,300	16.8
X-1-Q	Pure Ti	4.50	64,900	52,800	25.0	58.5	119,000	14,400	16.6
X-1-A	Pure Ti	4.50	71,580	56,410	26.6	63.3	137,000	15,900	19.2
X-2-F	2.5 Cr	4.55	91,170	74,950	10.9	10.9	**	20,050	16.2
X-2-Q	2.5 Cr	4.55	104,530	102,820	3.1	3.1	**	22,950	15.8
X-3-F	4.2 Cr	4.58	111,800	98,340	6.2	16.1	**	24,400	16.5
X-3-A	4.2 Cr	4.58	98,500	79,000	28.1	45.2	126,500	21,500	16.2
X-4-F	6.0 Cr	4.60	128,280	115,150	17.2	61.0	211,500	27,900	15.5
X-4-Q	6.0 Cr	4.60		Broke Because of Defect in Threads					
X-5-F	9.3 Cr	4.65	133,540	93,000	3.1	11.0	133,540	28,700	17.2
X-5-A	9.3 Cr	4.65	100,000	No Yield	Broke at Fillet	0	114,000	21,500	16.4
X-6-F	9.5 Cr	4.67	159,370	No Yield	0	0	159,370	34,100	14.7
X-6-Q	9.5 Cr	4.67	140,790	No Yield	1.6	1.6	140,790	30,100	18.1
X-7-F	11.4 Cr	4.70	179,670	No Yield	0	0	179,670	38,200	17.8
X-7-A	11.4 Cr	4.70	166,320	153,180	14.1	39.3	256,760	35,400	17.4
X-8-F	14.2 Cr	4.75	148,250	144,560	14.1	38.6	209,030	31,200	14.9
X-8-Q	14.2 Cr	4.75	144,250	141,270	17.2	31.6	181,680	30,400	14.0
X-9-F	13.0 Cr	4.73	150,410	147,430	12.5	46.0	221,480	31,800	15.1
X-9-A	13.0 Cr	4.73	Broke at Fillet						16.7
X-10-F	15.9 Cr	4.78	No Specimen	135,110	17.2	43.5	207,270	29,800	15.9
X-10-Q	15.9 Cr	4.78	142,200	134,860	20.3	35.7	188,310	29,100	16.0
X-11-F	17.6 Cr	4.82	137,260	Broke Because of Defect in Threads					
X-11-A	17.6 Cr	4.82							17.4

\*F—as-forged; Q—water-quenched from 1800 °F; A—annealed at 1400 °F.

\*\*Breaking load not observed accurately.

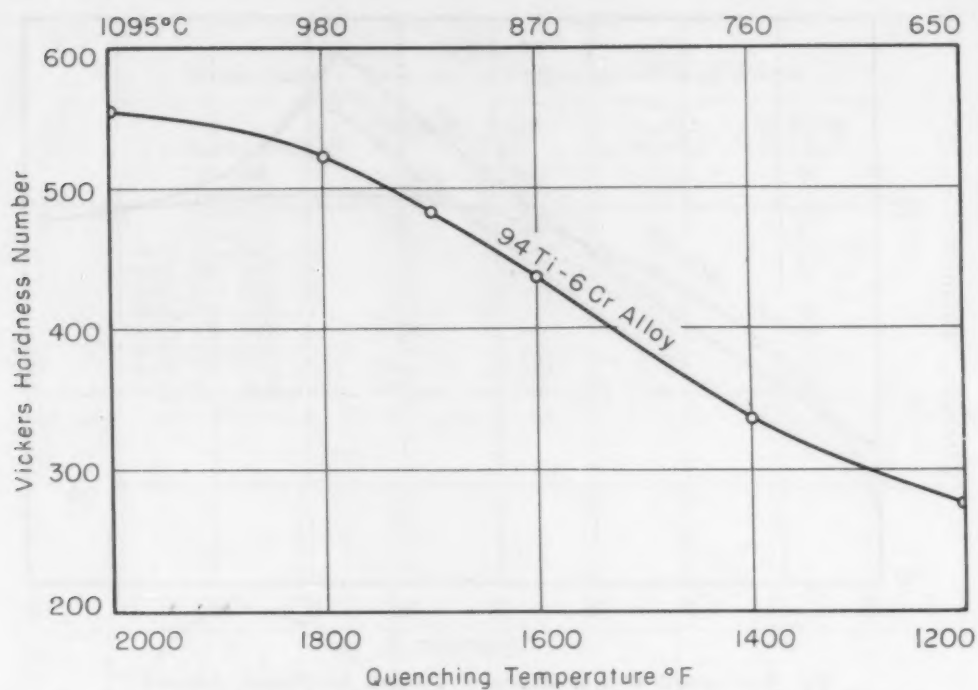


Fig. 7—Effect of Quenching Temperatures on the Hardness of 94% Ti – 6% Cr Alloy.

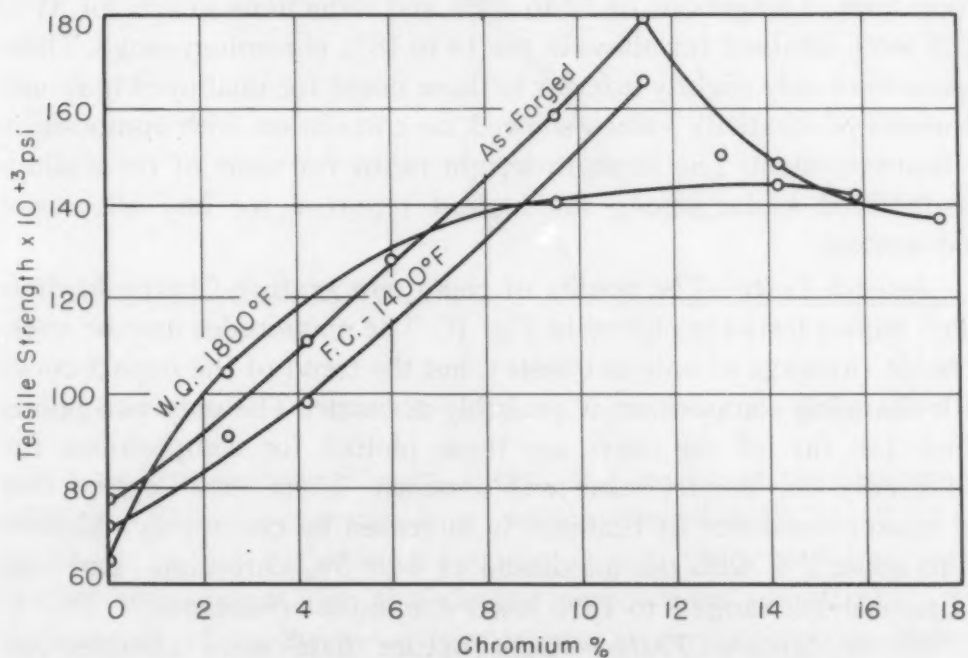


Fig. 8—Tensile Strength of Forged Arc-Melted Alloys.

tensile strength versus composition, and Fig. 9 depicts strength-weight ratio versus composition of the alloys. Those alloys at the highest strength level, containing 9 to 11% chromium, showed no yielding and fractured in a brittle manner. The ductility functions, elongation and reduction of area, were quite good except at the peak strength – compo-

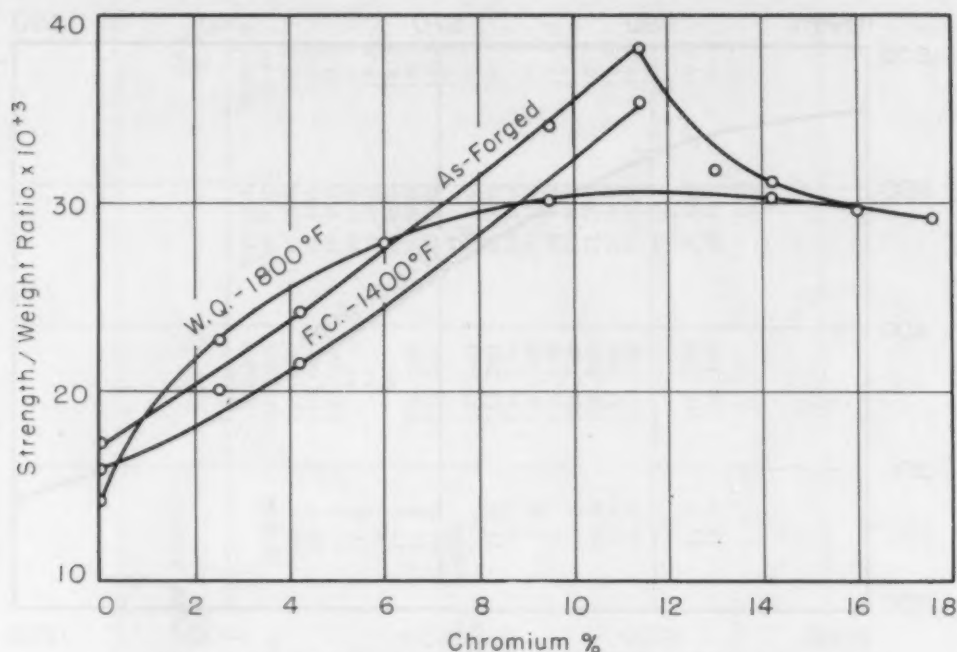


Fig. 9—Strength-Weight Ratios of Forged Arc-Melted Alloys.

sition level. Elongations of 12 to 20% and reductions in area of 31 to 46% were obtained for alloys in the 14 to 18% chromium range. These values were only slightly inferior to those noted for unalloyed titanium. Modulus of elasticity values showed no correlation with composition or heat treatment. The strength-weight ratios for some of these alloys are believed to be among the highest reported for any alloys not cold-worked.

*Impact Tests*—The results of room temperature Charpy keyhole notch impact tests are plotted in Fig. 10. The magnitudes may be questionable (average of only two tests), but the trend of the impact curve with changing composition is probably accurate. The only two points which fall far off the curve are those plotted for compositions for which only one impact value was obtained. These data suggest that the impact resistance of titanium is increased by chromium additions up to about 7% with the maximum at 4 or 5% chromium, and that additions in the range 8 to 18% lower the impact resistance.

*Stress-Rupture Tests*—Stress-rupture data were obtained on selected forgeable compositions over a range of temperatures and stresses. The data are shown in Table V. Chromium additions enhance the stress-rupture properties of titanium, but these materials would not be suitable for use at high temperatures and high stresses.

*Oxidation Tests*—Tests were made to evaluate the relative resistance to oxidation at elevated temperatures of titanium and forgeable titanium-chromium alloys. Tests were run at a constant time, 6 hours, at

Table V  
Stress-Rupture Data on As-Forged Arc-Melted Alloys

Composition	Temp., °F	Stress, psi	Hours to Rupture	% Elong. in 1 Inch
Titanium	1250	13,000	1	48
Titanium	1250	10,000	14	21
Titanium	1150	8,000	7	47
Titanium	1050	8,000	16	52
90% Ti-10% Cr	1250	13,000	1	74
90% Ti-10% Cr	1150	15,000	21	31
90% Ti-10% Cr	1150	12,000	48	..
90% Ti-10% Cr	1150	10,000	791	22
80% Ti-20% Cr	1250	13,000	25	64
80% Ti-20% Cr	1150	15,000	100	33
80% Ti-20% Cr	1150	13,000	118	48
80% Ti-20% Cr	1150	11,500	418	54

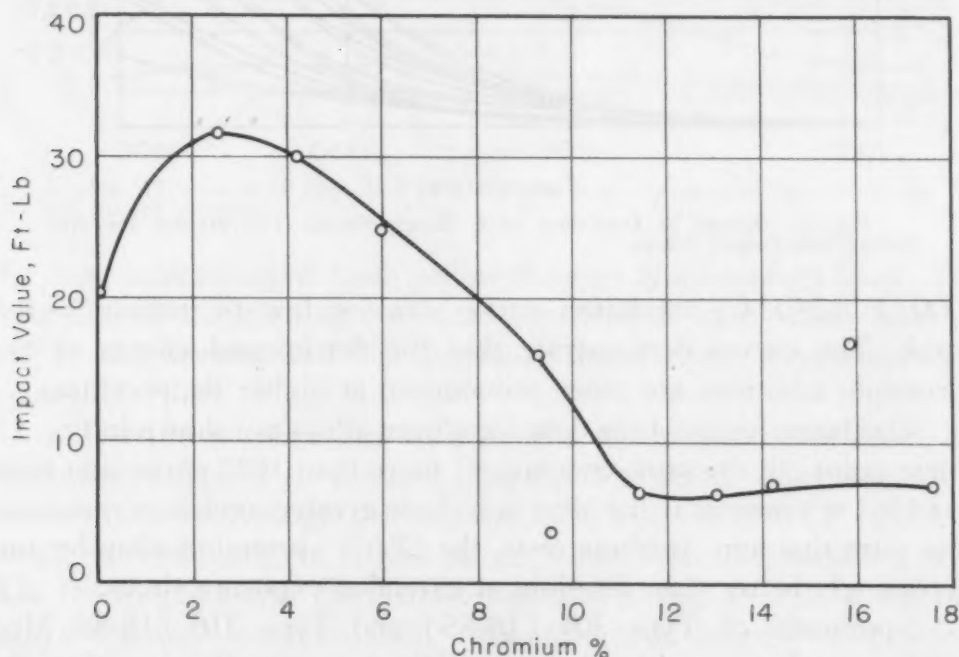


Fig. 10—Keyhole-Notch Charpy Impact Values for As-Forged Arc-Melted Alloys.

the four temperatures chosen. Then, at a constant temperature of 1500 °F (815 °C), exposure times were increased to 12, 24, 48, 72 and 96 hours. In Fig. 11, extent of oxidation in 6 hours is plotted versus testing temperature for the eleven compositions investigated. The dependence of oxidation on temperature is very nearly logarithmic. These data show that the oxidation resistance of unalloyed titanium is adversely affected by chromium additions up to 16% chromium. The lower chromium additions seem to be most harmful. Improvement is gradually obtained with further increase of chromium content until at 16% chromium the extent of oxidation is again close to that of unalloyed titanium. Above 16% chromium, the oxidation is less than that for titanium. These relationships are emphasized by Fig. 12. The



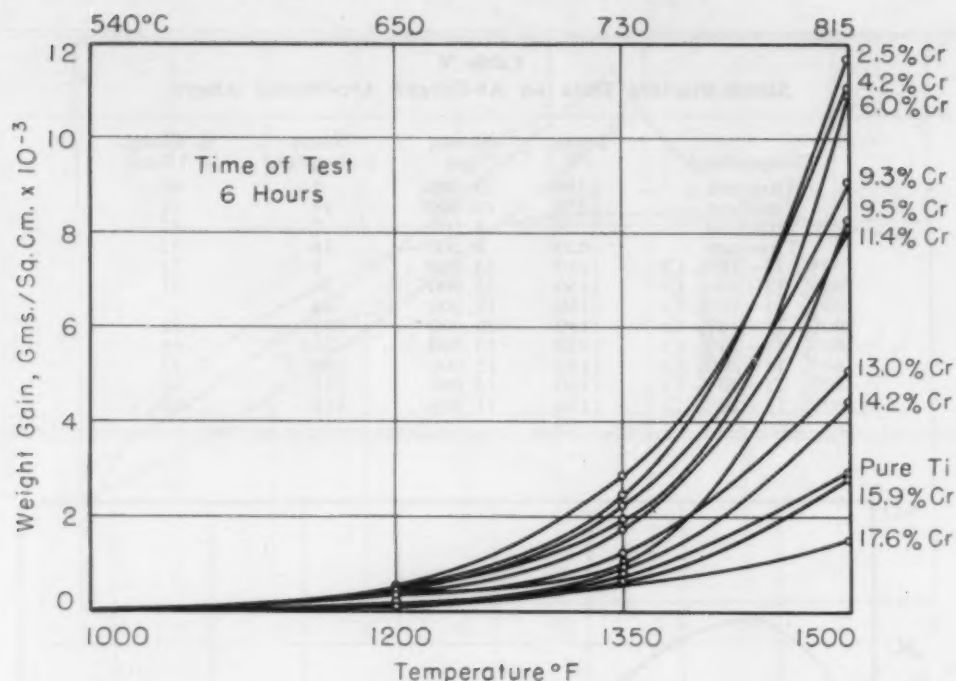


Fig. 11—Extent of Oxidation in 6 Hours Versus Temperature for Arc-Melted and Forged Alloys.

1000 °F (540 °C) oxidation curve was too low to include in this graph. The curves demonstrate that the detrimental effects of low chromium additions are more pronounced at higher temperatures.

Oxidation-versus-time data for eleven alloys are shown in Fig. 13. These point out the same conclusion: more than 16% chromium must be added to titanium if the alloy is to have greater oxidation resistance than pure titanium. In these tests, the 17.6% chromium alloy became increasingly better than titanium at extended exposure times.

Specimens of Type 304 (18-8S) and Type 316 (18-8S Mo) stainless steels, run with all tests, oxidized at rates far less than the titanium-chromium alloys and could not be depicted in the graphs. At 1500 °F (815 °C), after 96 hours in air, the weight gained per square centimeter due to oxidation of the most resistant of the forgeable titanium-chromium alloys tested (17.6% chromium) was about 60 times that of Type 304 stainless steel and approximately 15 times that of Type 316.

The relatively poor oxidation resistance of the forgeable titanium-chromium alloys was undoubtedly due to the formation of porous, nonadhesive scales. Many of the scales formed on these alloys at 1500 °F (815 °C) tended to flake off when the specimens were cooled. This tendency was minimum in the highest chromium content alloys. Scales consisting of at least two separate layers were formed. The inner scales were generally green to greenish-brown in color, while

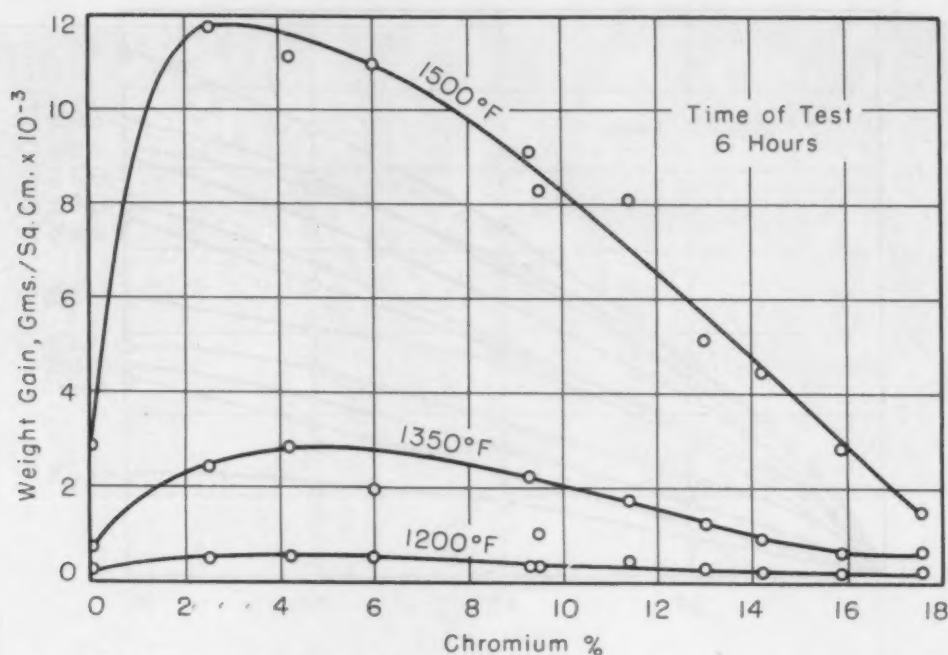


Fig. 12—Extent of Oxidation in 6 Hours Versus Composition for Arc-Melted and Forged Alloys.

the outer scales ranged from yellow through blue-violet to black. The colors noted suggest that the outer nonadhesive layers were titanium oxides and nitrides and that the inner dense layers were chromium oxides.

After the above results were known, it was decided to check the oxidation resistance of the cast alloys (20 to 100% chromium) in a cursory manner. A single test was run for 6 hours at 1500 °F (815 °C) on eleven compositions in this range. These data are combined with that for forged alloys (top curve, Fig. 12) in Fig. 14. All of the cast alloys showed less oxidation than the best forged composition. Chromium metal displayed the greatest oxidation resistance of all compositions in the binary system, but its performance in this test was inferior to the two stainless steels. Accordingly, the titanium-chromium binary alloys cannot be generally recommended for high temperature applications in air, from the standpoint of scaling resistance.

*Alloy Structures*—A few selected photomicrographs of structures encountered in the forgeable alloys are presented in Figs. 15 through 20. The structural features reported by Battelle in the RAND report (Literature Survey) are largely confirmed by this work. Apparently about 10% or more of chromium stabilizes the cubic beta solid solution down to low temperatures, since the Widmanstätten plates of hexagonal alpha titanium are no longer evident, even in air-cooled alloys. This structural change undoubtedly accounts for the sharp breaks in the mechanical property curves for these forged alloys.

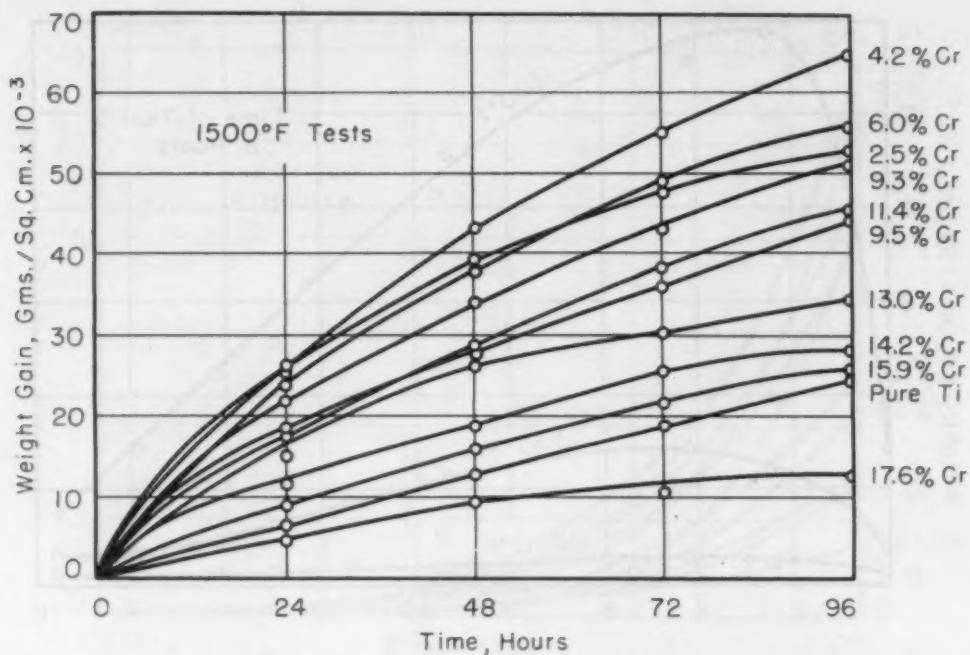


Fig. 13—Extent of Oxidation at 1500 °F (815 °C) Versus Time for Arc-Melted and Forged Alloys.

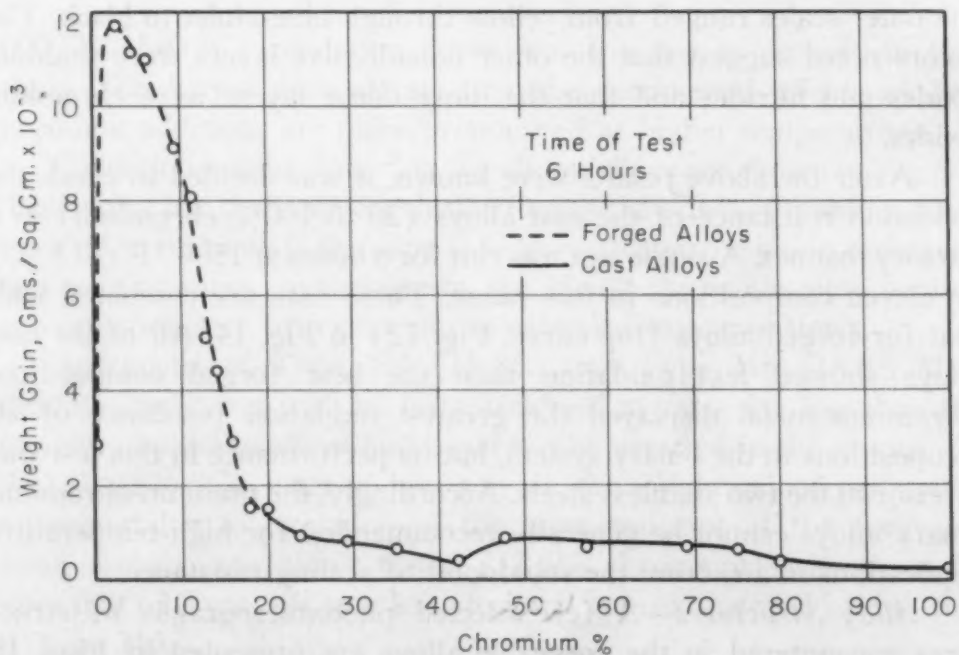


Fig. 14—Extent of Oxidation in 6 Hours at 1500 °F Versus Composition for Arc-Melted Titanium-Chromium Alloys.

Such breaks were noted in tensile, impact and hardness curves with increasing chromium content. Increases in strength and hardness result as the original plate-like alpha decreases and the amount of transformed beta (acicular alpha) increases. A rather sudden decrease in strength and hardness occurs when the structure consists almost



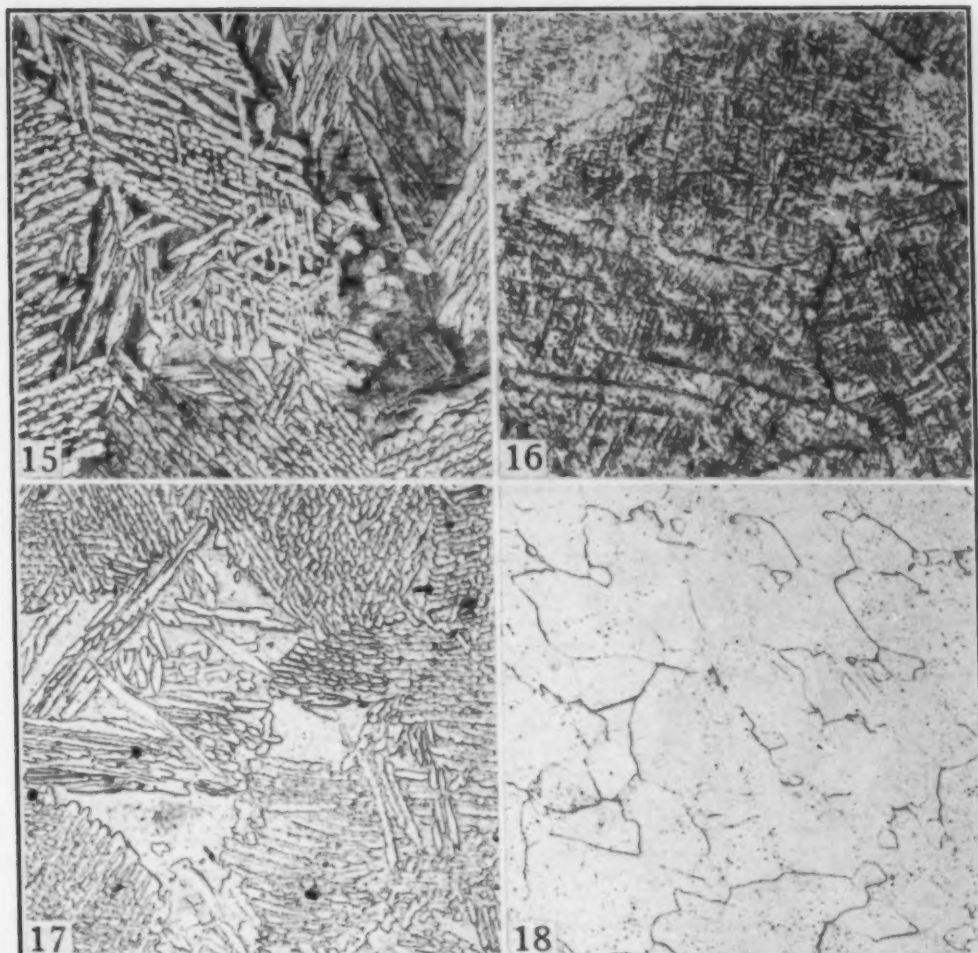


Fig. 15—Structure of 2.51% Chromium Alloy, Forged and Air-Cooled, Then Reheated to 1800 °F (980 °C) and Water-Quenched. Platelets of alpha, which were in equilibrium with beta at the quenching temperature, in a matrix of transformed beta. The original beta grain boundaries are evident. Etchant: 3% HF, 2% HNO<sub>3</sub> in water.  $\times 100$ .

Fig. 16—Structure of 4.16% Chromium Alloy, As-Forged and Air-Cooled. Decomposition product of beta solid solution within original beta grain boundaries. Etchant: 3% HF, 2% HNO<sub>3</sub> in water.  $\times 100$ .

Fig. 17—Structure of 6.02% Chromium Alloy, Forged and Air-Cooled, Then Reheated to 1800 °F (980 °C) and Water-Quenched. Widmanstätten arrangement of alpha plus considerable retained beta phase. Etchant: 3% HF, 2% HNO<sub>3</sub> in water.  $\times 100$ .

Fig. 18—Structure of 9.48% Chromium Alloy, As-Forged and Air-Cooled. Apparently consists almost entirely of retained beta phase. Etchant: 3% HF, 2% HNO<sub>3</sub> in water.  $\times 100$ .

entirely of retained beta phase, as in slowly cooled alloys above approximately 10% chromium. When the amounts of a new phase, probably an intermetallic compound, become appreciable at still higher chromium contents, the hardness curve begins to rise again. Above this point, about 20% chromium, the alloys become increasingly brittle. The curvilinear form of the property curves for water-quenched alloys is believed due to the fact that retained rather than transformed beta phase is present in alloys containing less than 10% chromium when they are quenched. The structural change at the 10% chromium level



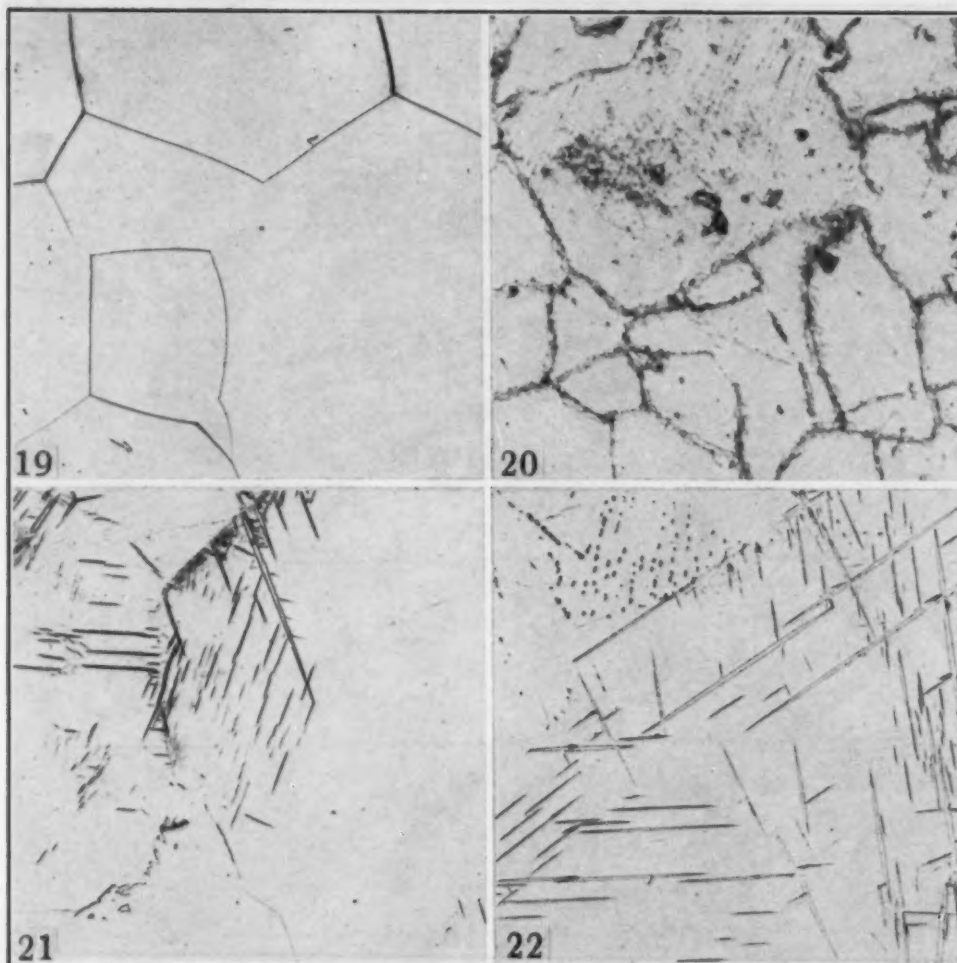


Fig. 19—Structure of 15.93% Chromium Alloy, Forged and Air-Cooled, Then Reheated to 1800 °F (980 °C) and Water-Quenched. Largely retained beta, plus globules of a second phase. Etchant: 3% HF, 2% HNO<sub>3</sub> in water.  $\times 100$ .

Fig. 20—Structure of 17.63% Chromium Alloy, Forged and Air-Cooled, Then Reheated to 1400 °F (760 °C), Held 1 Hour, and Furnace-Cooled. Retained beta and considerable amounts of the second phase, occurring mainly at the grain boundaries. This phase is probably the intermetallic compound, Cr<sub>2</sub>Ti<sub>3</sub>.  $\times 100$ .

Fig. 21—Structure of 6% Chromium Alloy, Forged and Air-Cooled, Then Reheated to 1800 °F (980 °C), Held 1 Hour, and Water-Quenched. Largely retained beta. All alpha dissolved on holding at temperature. Small amount of acicular beta transformation product formed on quenching through transformation temperature. Etchant: 3% HF, 2% HNO<sub>3</sub> in water.  $\times 100$ .

Fig. 22—Structure of 6% Chromium Alloy, Forged and Air-Cooled, Then Reheated to 1700 °F (925 °C), Held 1 Hour, and Water-Quenched. Considerably more of the acicular transformed product than in Fig. 21. Slight amount of alpha in equilibrium with beta after 1 hour at temperature is represented by the dark, dashed lines. Etchant: 3% HF, 2% HNO<sub>3</sub> in water.  $\times 100$ .

is, therefore, not as sharp as it is in the case of annealed and air-cooled alloys. The actual mechanisms of structural and property changes for these alloys cannot be treated accurately until a constitution diagram is available.

Figs. 21 through 24 show the structures obtained upon water quenching specimens of a 94 Ti–6 Cr alloy from a series of temperatures. Hardness values for these specimens are shown in Fig. 7. The

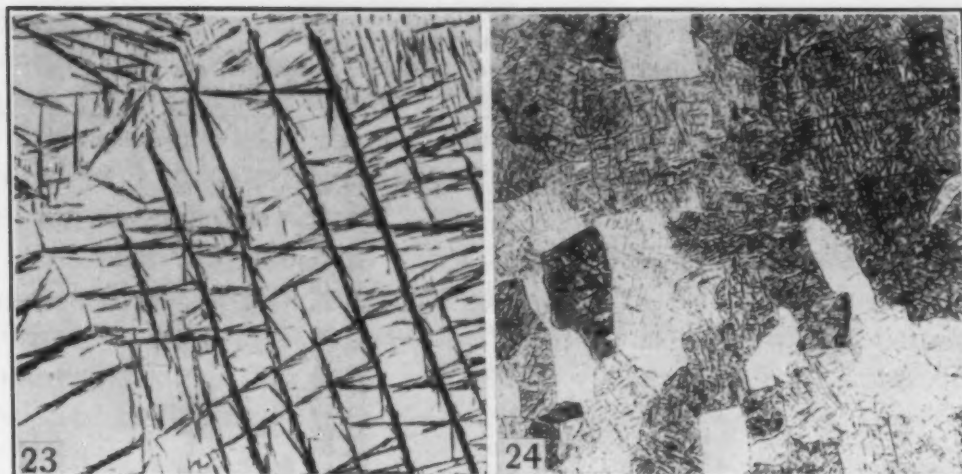


Fig. 23—Structure of 6% Chromium Alloy, Forged and Air-Cooled, Then Reheated to 1600 °F (870 °C), Held 1 Hour, and Water-Quenched. Heavy occurrence of beta transformation product. Balance is retained beta. All alpha taken into solution during heating. Etchant: 3% HF, 2% HNO<sub>3</sub> in water.  $\times 100$ .

Fig. 24—Structure of 6% Chromium Alloy, Forged and Air-Cooled, Then Reheated to 1400 °F (760 °C), Held 1 Hour, and Water-Quenched. The beta has apparently completely transformed. Etchant: 3% HF, 2% HNO<sub>3</sub> in water.  $\times 100$ .

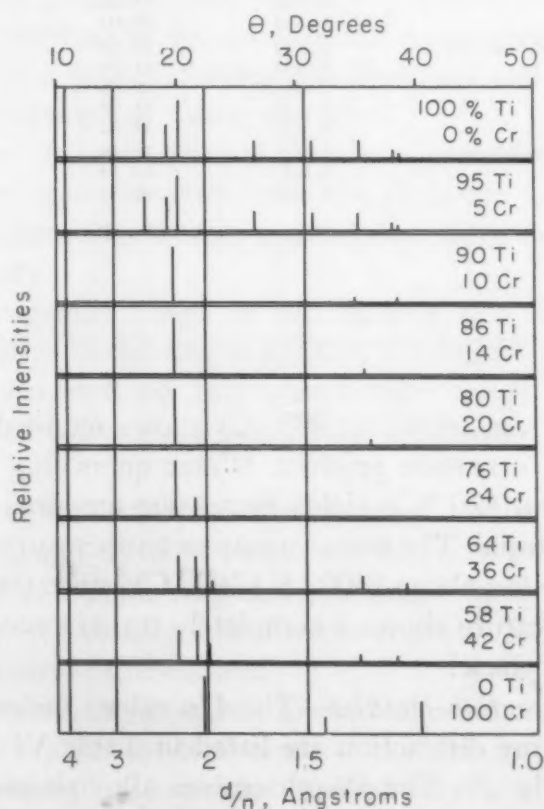


Fig. 25—X-Ray Diffraction Patterns for Titanium, Chromium, and Several Binary Alloys, Using Copper K $\alpha$  Radiation.

**Table VI**  
**X-ray Diffraction Patterns of Titanium, Chromium, and**  
**Several Binary Alloys, Using Copper K $\alpha$  Radiation**

Material	d/n, Å	$\theta^\circ$	I*
Titanium	2.549	17.55	m
	2.337	19.20	m
	2.237	20.10	s
	1.720	26.54	w
	1.471	31.51	w
	1.330	35.31	w
	1.244	38.18	f
	1.228	38.76	vf
95 Ti - 5 Cr	2.545	17.58	m
	2.337	19.20	m
	2.236	20.11	s
	1.720	26.54	w
	1.472	31.49	w
	1.332	35.26	w
	1.248	38.03	f
	1.232	38.61	vf
90 Ti - 10 Cr	2.253	19.95	s
	1.33	35.5	vf
	1.23	38.5	vf
86 Ti - 14 Cr	2.268	19.81	s
	1.313	35.84	f
80 Ti - 20 Cr	2.258	19.90	s
	1.303	36.15	vf
76 Ti - 24 Cr	2.250	19.98	s
	2.090	21.58	vf
64 Ti - 36 Cr	2.226	20.20	m
	2.079	21.70	m
	1.989	22.74	vf
	1.328	35.38	f
	1.221	39.03	vf
58 Ti - 42 Cr	2.237	20.10	m
	2.092	21.56	m
	2.004	22.56	w
	1.331	35.28	f
	1.232	38.62	vf
Chromium	2.027	22.29	s
	1.437	32.34	w
	1.187	40.37	m

\*s—strong.  
m—medium.  
w—weak.  
f—faint.  
vf—very faint.

alloy quenched from 1800 °F (980 °C) shows retained beta and a few needles of transformation product. Water quenching from 1700 and 1600 °F (925 and 870 °C) yields increasing amounts of this acicular transformed material. The transformation temperature for this composition apparently lies above 1400 °F (760 °C), since the alloy quenched from this temperature shows a completely transformed structure, and no retained beta phase.

*X-Ray Diffraction Results*—The d/n values for each of the alloys examined by X-ray diffraction are listed in Table VI and plotted for comparison in Fig. 25. The 5% chromium alloy shows the same lines as unalloyed titanium, slightly shifted. This pattern is absent in the case of alloys containing 10% or more of chromium, as predicted by photomicrographic evidence. The strong line for the beta solid solution

persists in alloys containing 10 to 24% chromium, above which content it begins to diminish appreciably in intensity. At 24% chromium a new pattern appears and this phase is quite strong in alloys containing approximately 40% chromium. None of the lines of this new phase correspond to those for unalloyed chromium; it is presumed to be an intermetallic compound.

Copper  $K_{\alpha}$  radiation was not entirely suitable for this alloy system. Exposures of some compositions failed to produce readable diffraction patterns. A molybdenum tube would be preferable but was not available for this work. The results are reported to the precision believed justifiable.

#### SUMMARY AND CONCLUSIONS

1. An arc furnace of 3-pound melting capacity and an induction furnace of 1-pound capacity were developed for the preparation of titanium-chromium binary alloys. Arc melting in an argon atmosphere is recommended for titanium alloy production until suitable refractories are developed.

2. Specially prepared, low-porosity crucibles of thoria, beryllia and carbon appeared to be the most effective containers for induction melting. There is a need for rigid specifications and standardization of crucible fabrication for this application.

3. The arc furnace yielded binary alloys of 99.5% chemical purity. Tungsten contamination from the electrode was held to a low value, and gas contents, though appreciable, were not greatly detrimental to ductility.

4. The forgeable range in the system was found to be the titanium-rich alloys containing 0 to 20% chromium. Property evaluation was concentrated on this composition range. The testing of alloys in the 20 to 100% chromium range was limited because of their brittleness.

5. The forgeable alloys were subjected to the following tests: hardness at room and elevated temperatures, room temperature tensile and impact tests in various conditions of heat treatment, elevated temperature oxidation characteristics, stress-rupture, and metallographic and X-ray structural examination.

6. The outstanding property of the forgeable titanium-chromium alloys was very high room temperature strength in combination with low specific gravity. Chromium proved extremely efficacious in strengthening titanium. The tensile strength of titanium was nearly doubled by additions of 13 to 18% chromium, with little loss of ductility and only slight increase in weight.



7. It was shown that chromium additions up to 16% chromium decrease the elevated temperature oxidation resistance of titanium. All alloys of higher chromium content oxidized at lesser rates than titanium in air, but no alloy in the system approached the performance of commercial austenitic stainless steels.

8. Hot hardness values for the forgeable alloys in the temperature range 1200 to 1500 °F (650 to 815 °C) were extremely low. These alloys showed relatively poor stress-rupture properties in the temperature range 1050 to 1250 °F (565 to 675 °C). These facts, combined with the oxidation results given above, establish the fact that forgeable titanium-chromium alloys could not be recommended for use as high temperature, high-stress materials.

9. These alloys might be considered for moderate-temperature (less than 1000 °F or 540 °C), moderate-stress (less than 10,000 psi) applications in cases involving low specific gravity as a criterion.

#### ACKNOWLEDGMENT

The interest and support of the Materials Laboratory, Engineering Division, Wright-Patterson Air Force Base, is greatly appreciated. This work was carried out under Contracts W33-038-ac-16368 and W33-038-ac-21339 (20377) between the Air Force and The Ohio State University Research Foundation. Gratitude is expressed to Dr. S. F. Urban and the Titanium Alloy Manufacturing Division of National Lead Company for an unstinted supply of helpful materials and for the performance of special tests. The help of staff members of Battelle Memorial Institute in making available special equipment and for guidance in arc furnace technology is gratefully acknowledged. The United States Bureau of Mines provided a liberal supply of titanium for the induction melting work.

Mr. Leonard Johnson and Mr. Richard Rhoney gave able assistance in furnace construction and maintenance and in the performance of tests. Dr. Rudolph Speiser and Mr. David Cross provided material aid and guidance in the X-ray program.

#### References

1. R. M. Parke and F. P. Bens, "Chromium-Base Alloys", Symposium on Materials for Gas Turbines, American Society for Testing Materials, 1946.
2. F. Adcock, "Alloys of Iron Research. Part 5—Preparation of Pure Chromium", *Journal, Iron and Steel Institute*, Vol. 115, 1927, p. 369.
3. R. Vogel and B. Wenderott, "The Constitution Diagram Iron-Chromium-Titanium", *Archiv für das Eisenhüttenwesen*, Vol. 14, 1940, p. 279.
4. W. Kroll, "Production of Ductile Titanium", *Transactions, Electrochemical Society*, Vol. 78, 1940, p. 35.

5. W. Kroll, C. T. Anderson and H. L. Gilbert, "A New Graphite Resistor Vacuum Furnace and Its Application in Melting Zirconium", American Institute of Mining and Metallurgical Engineers, T.P. 2310, *Metals Technology*, Vol. 15, No. 1, January 1948.
6. A. R. Powell, "Minor Metals", *Metal Industry*, June 29, 1945, Vol. 66, No. 26, p. 406.
7. P. H. Brace, "Reactions of Molten Titanium with Certain Refractory Oxides", *Journal*, Electrochemical Society, Vol. 94, No. 4, October 1948, p. 170.
8. J. B. Sutton, "Induction Melting of Titanium Metal in Graphite", *Report of Symposium on Titanium*, Paper 9, Office of Naval Research, Department of the Navy, Washington, D. C., March 1949.
9. R. M. Parke and A. J. Herzig, "Heat Resisting Metals for Gas Turbine Parts (N-102): Chromium-Base Alloys", (Final Report), *Office of Scientific Research and Development*, No. 6547, Serial No. M-656, January 1946.
10. E. I. Larson, E. F. Swazy, L. S. Busch and R. H. Freyer, "Some Preliminary Data on Alloys of Titanium", *Report of Symposium on Titanium*, Paper 12, Office of Naval Research, Department of the Navy, Washington, D. C., March 1949.
11. P. H. Bracé, "Some Aspects of the Metallurgy of Titanium Alloys", *Report of Symposium on Titanium*, Paper 14, Office of Naval Research, Department of the Navy, Washington, D. C., March 1949.
12. "Titanium and Titanium-Base Alloys", Project RAND, Douglas Aircraft Company, Inc., *Report R-131*, March 15, 1949.
13. O. W. Simmons, C. T. Greenidge and L. W. Eastwood, "The Production and Arc Melting of Titanium", *Report of Symposium on Titanium*, Paper 10, Office of Naval Research, Department of the Navy, Washington, D. C., March 1949.
14. H. A. Sloman, "The Determination of Oxygen, Hydrogen, and Nitrogen in Titanium", *Research No. 5066—Gaseous Constituents and Inclusion in Metals*, *Report No. 1504*, National Physical Laboratory, Metallurgy Division, Teddington, England, Oct. 9, 1947.
15. P. S. Bergh, "High Temperature Micro Hardness Tester", *Technical Report No. M-5*, The Kellex Corporation, Silver Spring Laboratory, Dec. 23, 1948.
16. F. P. Bens, "Hardness Testing of Metals and Alloys at Elevated Temperatures", *TRANSACTIONS*, American Society for Metals, Vol. 38, 1947, p. 505.

# STATISTICAL ANALYSIS OF THE EFFECT OF ALLOYING ELEMENTS ON MECHANICAL PROPERTIES OF SEAMLESS STEEL TUBES

By W. T. ROGERS

## Abstract

*This paper presents the results of a multiple regression analysis which evaluates the relation of carbon, manganese, phosphorus, silicon, titanium and molybdenum to the mechanical properties, yield strength, tensile strength and elongation of seamless steel tubes. Independent relations are shown separately, followed by a complete set of multiple estimating equations using the common elements carbon, manganese, phosphorus and silicon for the determination of yield strength, tensile strength and elongation. The equations developed have been applied in practice for the past two years and proved accurate within the probability limits of established standard errors.*

THE relation of the chemical constituents, carbon, manganese, phosphorus, silicon and various alloying elements, to the mechanical properties of yield strength, tensile strength and elongation of various steels has been the object of a great deal of study and research for the past half century. It is found, however, that the greater portion of effort in this connection has been directed toward a specific type of alloy which in most cases has involved some sort of heat treatment. The fact that most research students have been prone to be thus specific has tended toward a deficiency in published knowledge about the most commonly used type of steel, namely the "as-rolled" plain carbon steel which sometimes contains relatively small amounts of residual alloys.

A review of past literature on this subject indicates that the works of W. R. Webster in 1894 (1)<sup>1</sup> and H. H. Campbell in 1895 (2) are the most comprehensive literature presently available. In Webster's work, the evaluations of the various elements studied were confined to a chemical range of 0.06 to 0.19% carbon and 0.16 to 0.73% manganese, and while in Campbell's studies the exact range of individual heats is not given, it is apparently contained within the values of 0.07 to 0.52% carbon and 0.30 to 0.70% manganese.

<sup>1</sup>The figures appearing in parentheses pertain to the references appended to this paper.

A paper presented before the Thirty-second Annual Convention of the Society, held in Chicago, October 21 to 27, 1950. The author, W. T. Rogers, is metallurgical statistician, National Tube Co., United States Steel Corporation Subsidiary, Lorain Works, Lorain, Ohio. Manuscript received April 19, 1950.



Webster's work was done on plates, and Campbell's results were apparently obtained from bars. The conclusions presented in this study are based on routine tests obtained from hot-rolled seamless steel tubes.

In the manufacture of seamless tubes for line pipe or oil country use, practically all material is made from deoxidized or "killed" basic open-hearth steel with a small, but ever-increasing, proportion being made from deoxidized acid Bessemer steel. Recent developments in the field of pipe-line engineering have resulted in a demand for material with increasingly higher mechanical properties than have been furnished in the past. This, together with the fact that weldability requirements have placed such stringent carbon and manganese limitations on this class of product, makes it essential for the metallurgists to know, with a high degree of accuracy, just what can be obtained in the way of mechanical properties from each 0.01% of carbon, manganese, or other of the chemical constituents.

There are basically two ways of attacking this problem: the research method or the statistical method. When the research method is used, it is the usual procedure to make a series of steels in which all elements have been held constant except the one being studied and to vary the amount of this one element over a prescribed range and thus by a series of successive experiments arrive at a factor from which the effect of this one element on the mechanical property being investigated may be evaluated. This approach is excellent from an academic standpoint and has been the starting point for a large proportion of metallurgical developments in the past. However, there are three objections which make it undesirable from a practical standpoint. The first objection and the most serious is that it is economically impossible to equip a laboratory which can produce the various conditions found in actual manufacturing practice in a finishing mill. The second fault is that the time and expense involved in preparing the various samples to meet the required conditions precludes the possibility of securing sufficient tests to formulate a reliable conclusion. This is particularly true in the case of mechanical properties having sources of variability other than chemical composition. The third objection is that in order to overcome the difficulty which arises from the limitations in the number of samples which can be processed, it is necessary to produce and test steels of unorthodox analysis that will probably never be produced in actual manufacturing practice. In summarizing these objections, it can be stated that the variability of the mechanical properties under consideration is such that the influence of chemical



constituents in the normal commercial ranges cannot be economically evaluated by laboratory experimentation.

The second line of approach is the statistical method and particularly that part of statistical procedure which deals with the application of multiple correlation analysis (3). This method makes it possible, by the use of data from routine test reports, to deal with normal commercial ranges of chemistry and to evaluate the effect of normal increment increases of each chemical constituent. It not only gives the quantitative effect of each related variable but also furnishes equations which can be used to evaluate the effect of any combination of the factors considered. The objections to this method are, first, a large amount of data are required before a study can be undertaken and, second, the time and labor required are prohibitive. These may be valid objections, but it is pointed out that very few steel manufacturing concerns with more than one year of production history suffer from lack of data, especially that pertaining to chemical and mechanical properties. The labor involved can also be reduced to a minimum by employing punch card tabulating equipment from which approximately 75% of the calculating work may be carried out mechanically.

The statistical method was used in this study. Inasmuch as the method is only incidental to the actual results, and also due to the fact that the mathematical mechanics employed are commonly available and may be obtained from the appended references, the detail of the development of various statistical constants is not included, as this is believed to be subordinate to the purpose of this paper. The factors included in this study which are considered to be related to the as-rolled mechanical properties of yield strength, tensile strength, and per cent elongation in 2 inches are the chemical constituents carbon, manganese, phosphorus and silicon. The analysis consists of developing successive linear regression coefficients with each of these independent variables for each mechanical property. Actual averages were then plotted as deviations from calculated averages as developed by the various estimating equations and are presented in the included graphs (3). In addition to the variables included in the multiple regression analysis, a limited amount of data on titanium and molybdenum were also available and, while no definite conclusions are made, the apparent effect of these elements is presented as a matter of further information. Table I presents a statistical summary of the data used. This paper will discuss the effect of each related independent factor individually with a summary showing a complete regression or estimating

**Table I**  
**Summary of Variables Included in Study Showing Average, Range**  
**and Standard Deviation**

	Number of Items	Average	Standard Deviation	Range
Carbon.....	8391	0.242%	0.064%	0.09-0.49%
Manganese.....	8391	0.596%	0.260%	0.30-1.60%
Phosphorus.....	8391	0.0136%	0.0150%	0.006-0.094%
Silicon.....	8391	0.052%	0.0069%	0-0.260%
Titanium.....	8	0.0215%	.....	0.009-0.080%
Molybdenum.....	60	0.270%	0.008%	0.25-0.30%
Yield Strength.....	8391	46,699 psi	8,003 psi	30,000-104,000 psi
Tensile Strength.....	8391	70,383 psi	10,850 psi	53,000-124,000 psi
Elongation in 2 Inches..	8391	38.48%	4.69%	22.0-53.0%

equation and a presentation of the apparent effects of the alloys on which limited data are available.

#### PROCEDURE

The records of the mechanical testing laboratory at Lorain Works of National Tube Company have been punched on International Business Machine tabulating cards for the past ten years. The information carried on these cards includes the complete chemical analysis and mechanical testing results of each heat of steel processed into seamless pipe. The data on which this study is based include 8391 test results on as-rolled pipe in sizes from 4½ to 26 inches outside diameter for the complete year of 1947. A multiple correlation was set up in which carbon, manganese, phosphorus and silicon were the independent variables, and yield strength, tensile strength and per cent elongation in 2 inches were the dependent variables. The work involved in obtaining the necessary sums of squares and product sums was performed on tabulating equipment up to the point of obtaining the first extensions, and thereafter the corrections and the solving of the necessary equations were performed on automatic calculators. The simultaneous equations were solved by the Doolittle System, from which it was also possible to develop the multiple correlation coefficients and the standard errors. The distributions of the various variables necessary for testing the linear regression lines for curvilinearity were obtained from tabulating equipment. Following the working of the problem, the results were checked against similar data for the entire year of 1948, and no significant differences from 1947 results were apparent.

#### THE EFFECT OF CARBON

The range of carbon included in the data is from 0.09 to 0.49%, and the effects of this element on the mechanical properties involved

are in close agreement with those of other investigators and are stated as independent relations in the following equations:

$$\begin{aligned}\text{Yield Strength} &= 36,396 + 42,540 \times \text{Per Cent Carbon} \\ \text{Tensile Strength} &= 46,239 + 99,770 \times \text{Per Cent Carbon} \\ \text{Per Cent Elongation in 2 Inches} &= 49.00 - 43.44 \times \text{Per Cent Carbon}\end{aligned}$$

Fig. 1 shows these relations graphically. It is apparent that there is close agreement with the linear equations over the entire range of carbon, which tends to refute the contentions of some observations that as carbon increases its effect varies in magnitude.

#### THE EFFECT OF MANGANESE

The range of manganese is from 0.30 to 1.60%, and the relation of mechanical properties to this element is as represented by the following equations:

$$\begin{aligned}\text{Yield Strength} &= 38,339 + 14,028 \times \text{Per Cent Manganese} \\ \text{Tensile Strength} &= 58,313 + 20,252 \times \text{Per Cent Manganese} \\ \text{Per Cent Elongation in 2 Inches} &= 40.87 - 4.00 \times \text{Per Cent Manganese}\end{aligned}$$

The graphic representations of these equations are shown in Fig. 2. From these curves it is evident that the coefficients developed are representative of the actual relations throughout the complete range of manganese involved. There is no evidence that the coefficients for manganese should be different for various carbon contents or that the constants used in the equations should be related to carbon.

#### THE EFFECT OF PHOSPHORUS

The data on phosphorus ranged from 0.006 to 0.039% on open-hearth steel and from 0.060 to 0.094% on Bessemer steel, with independent relations as follows:

$$\begin{aligned}\text{Yield Strength} &= 45,089 + 118,400 \times \text{Per Cent Phosphorus} \\ \text{Tensile Strength} &= 67,894 + 183,000 \times \text{Per Cent Phosphorus} \\ \text{Per Cent Elongation in 2 Inches} &= 39.91 - 105 \times \text{Per Cent Phosphorus}\end{aligned}$$

Fig. 3 shows the plot of the actual data on the respective regression lines. An examination of these graphs shows that the linear regression expressed by the equations checks very well in the range of 0.006 to 0.039% obtained on open-hearth steel, and it is also evident that the equations hold true when extended from the open-hearth range to the Bessemer range, but within the Bessemer range itself there is no indication of an increase in yield strength and tensile strength or a decrease in elongation with increasing phosphorus.

#### THE EFFECT OF SILICON

The relations with silicon are shown in Fig. 4, where it is



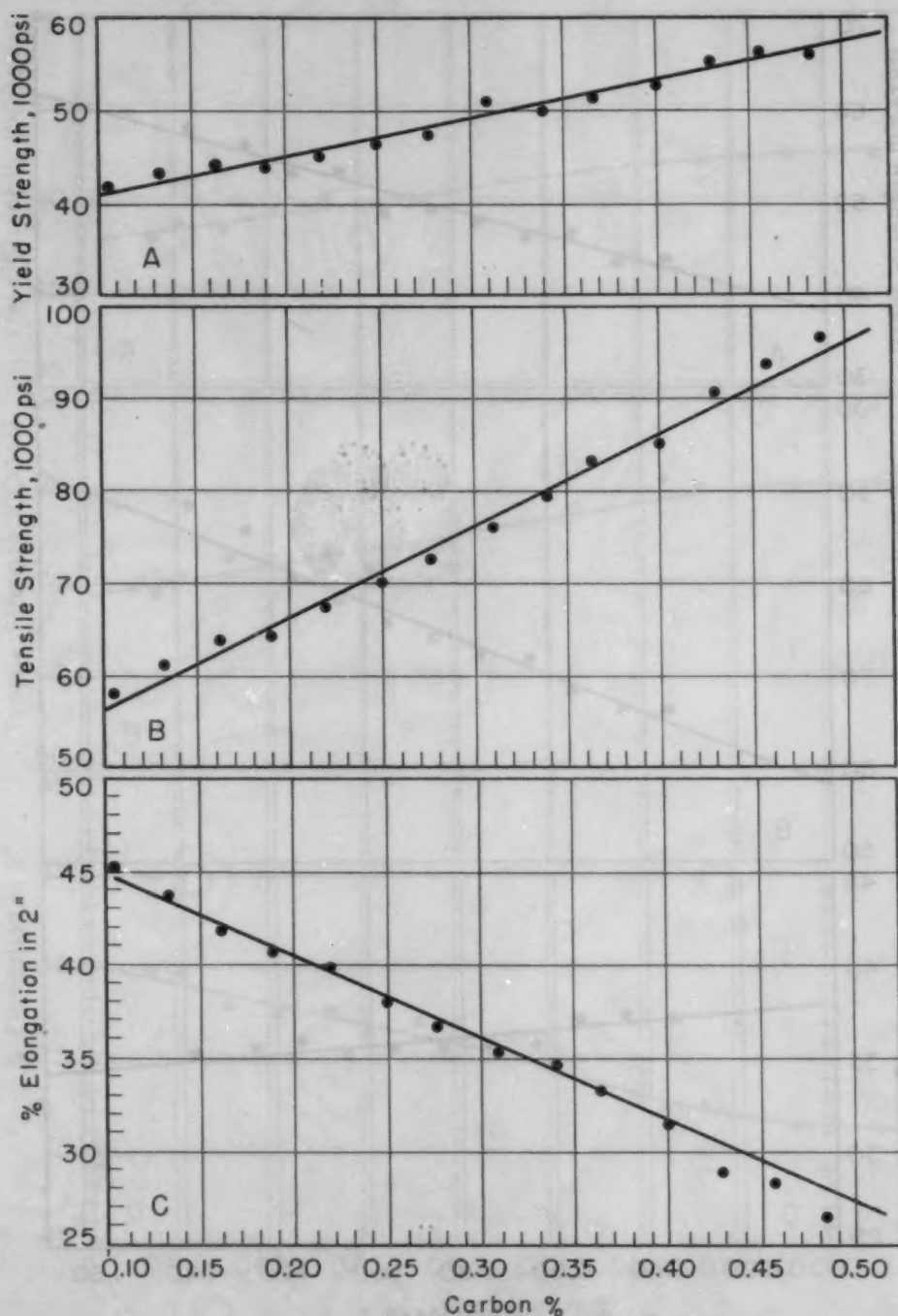


Fig. 1—(A) Independent Relation Between Per Cent Carbon and Yield Strength; (B) Independent Relation Between Per Cent Carbon and Tensile Strength; (C) Independent Relation Between Per Cent Carbon and Elongation in 2 Inches.

evident that increased proportions of this element in the range under consideration (0.0 to 0.26%) have a tendency to increase slightly the yield strength and tensile strength and lower the per cent elongation. These relations are expressed as follows:



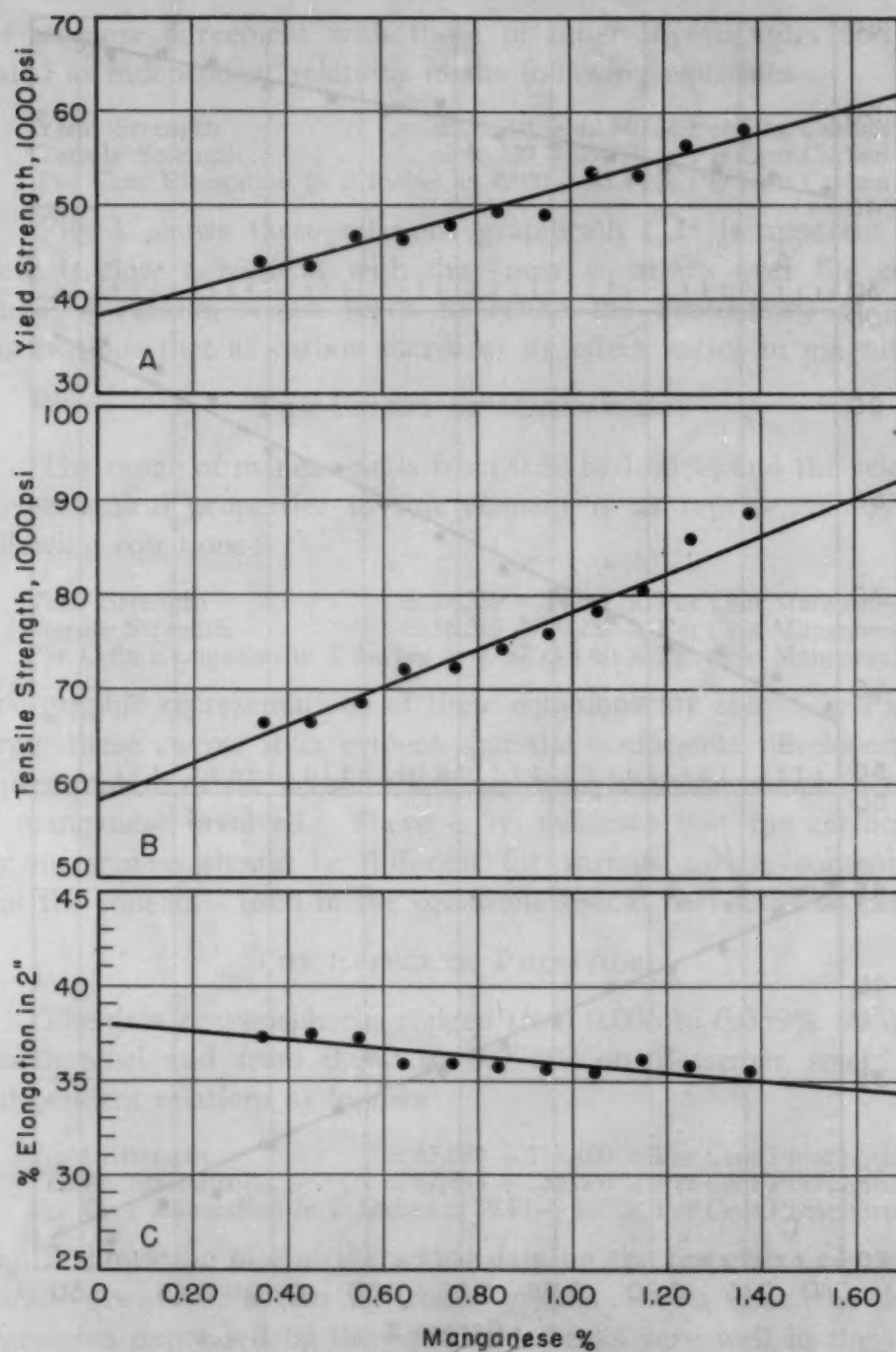


Fig. 2—(A) Independent Relation Between Per Cent Manganese and Yield Strength; (B) Independent Relation Between Per Cent Manganese and Tensile Strength; (C) Independent Relation Between Per Cent Manganese and Elongation in 2 Inches.

$$\begin{aligned} \text{Yield Strength} &= 46,431 + 5,160 \times \text{Per Cent Silicon} \\ \text{Tensile Strength} &= 69,767 + 11,840 \times \text{Per Cent Silicon} \\ \text{Per Cent Elongation in 2 Inches} &= 38.74 - 4.94 \times \text{Per Cent Silicon} \end{aligned}$$

#### THE EFFECT OF TITANIUM

The relations with titanium are based on 8 heats of deoxidized

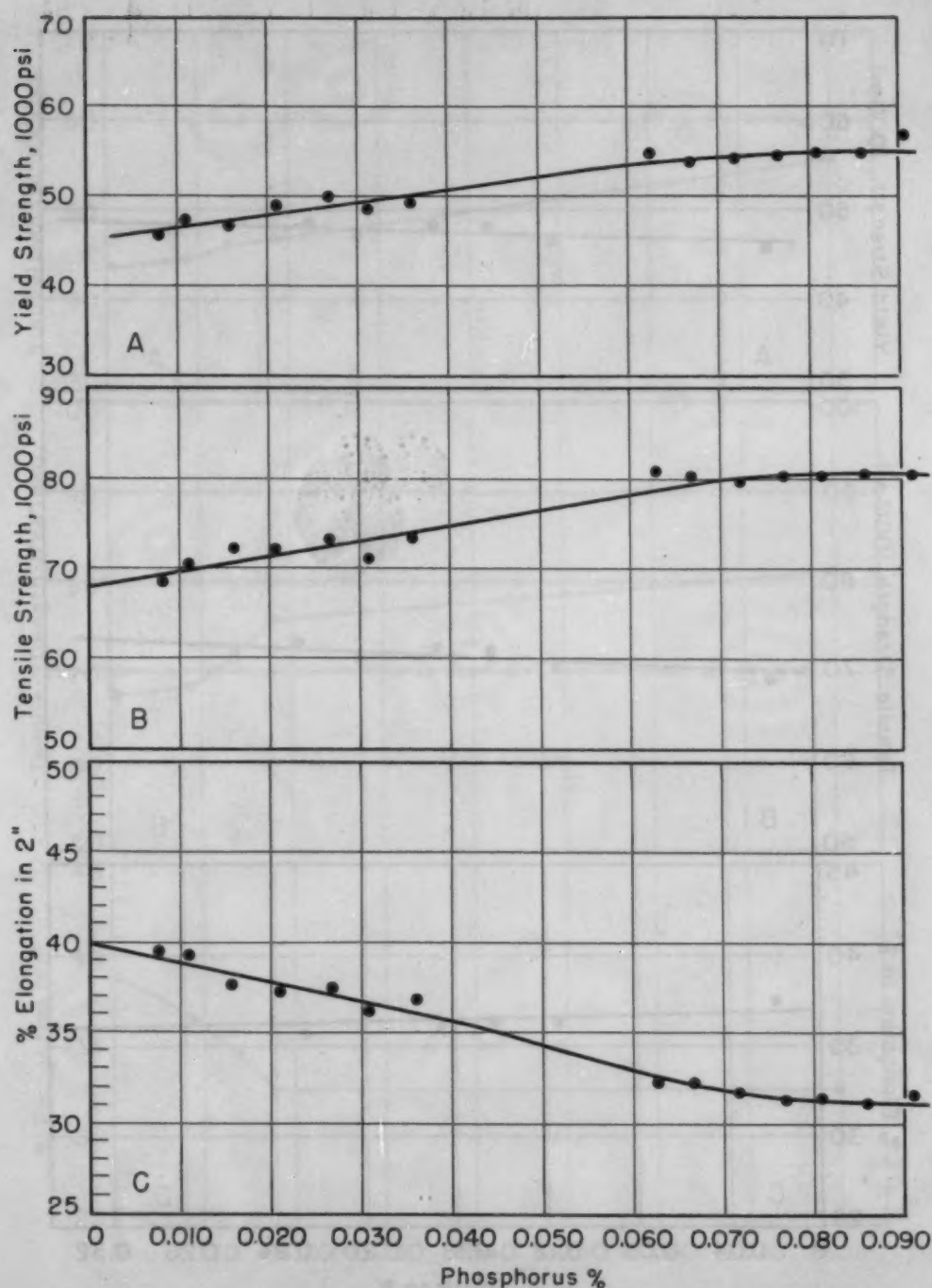


Fig. 3—(A) Independent Relation Between Per Cent Phosphorus and Yield Strength; (B) Independent Relation Between Per Cent Phosphorus and Tensile Strength; (C) Independent Relation Between Per Cent Phosphorus and Elongation in 2 Inches.

Bessemer steel in the range of zero to 0.08% titanium and are shown in Fig. 5. All heats were adjusted to a common value for carbon, manganese, phosphorus and silicon with the differences for various increments of titanium being plotted as independent relations. The figures presented indicate that the yield strength increases

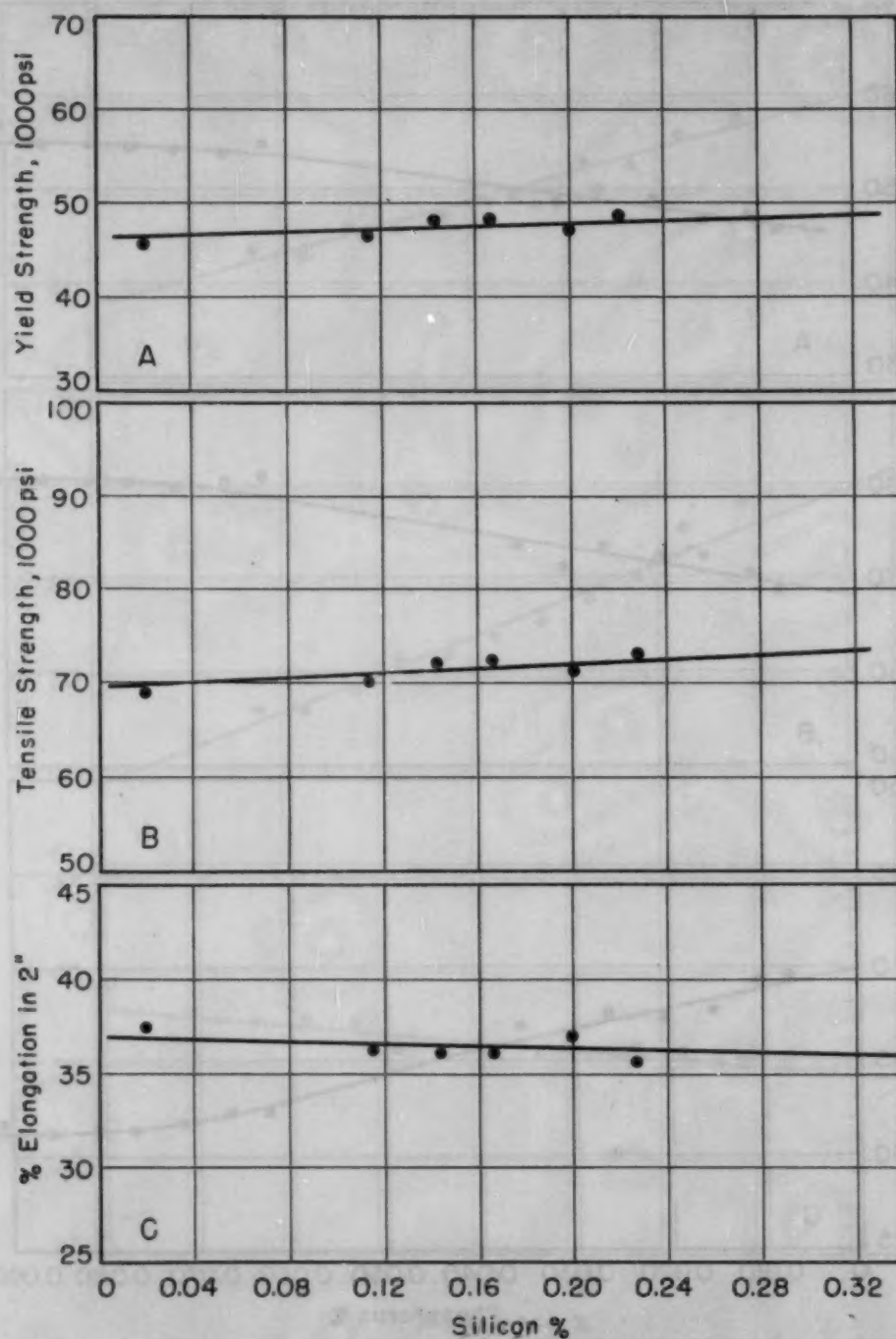


Fig. 4—(A) Independent Relation Between Per Cent Silicon and Yield Strength; (B) Independent Relation Between Per Cent Silicon and Tensile Strength; (C) Independent Relation Between Per Cent Silicon and Elongation in 2 Inches.

approximately 1500 psi for each 0.01% titanium, and tensile strength increases 8500 psi from zero to 0.018% titanium, and 5000 psi from 0.018 to 0.080%. The percentage elongation is reduced 6.25% from zero to 0.018% titanium, and thereafter remains unchanged up to 0.080% titanium, indicating that increased



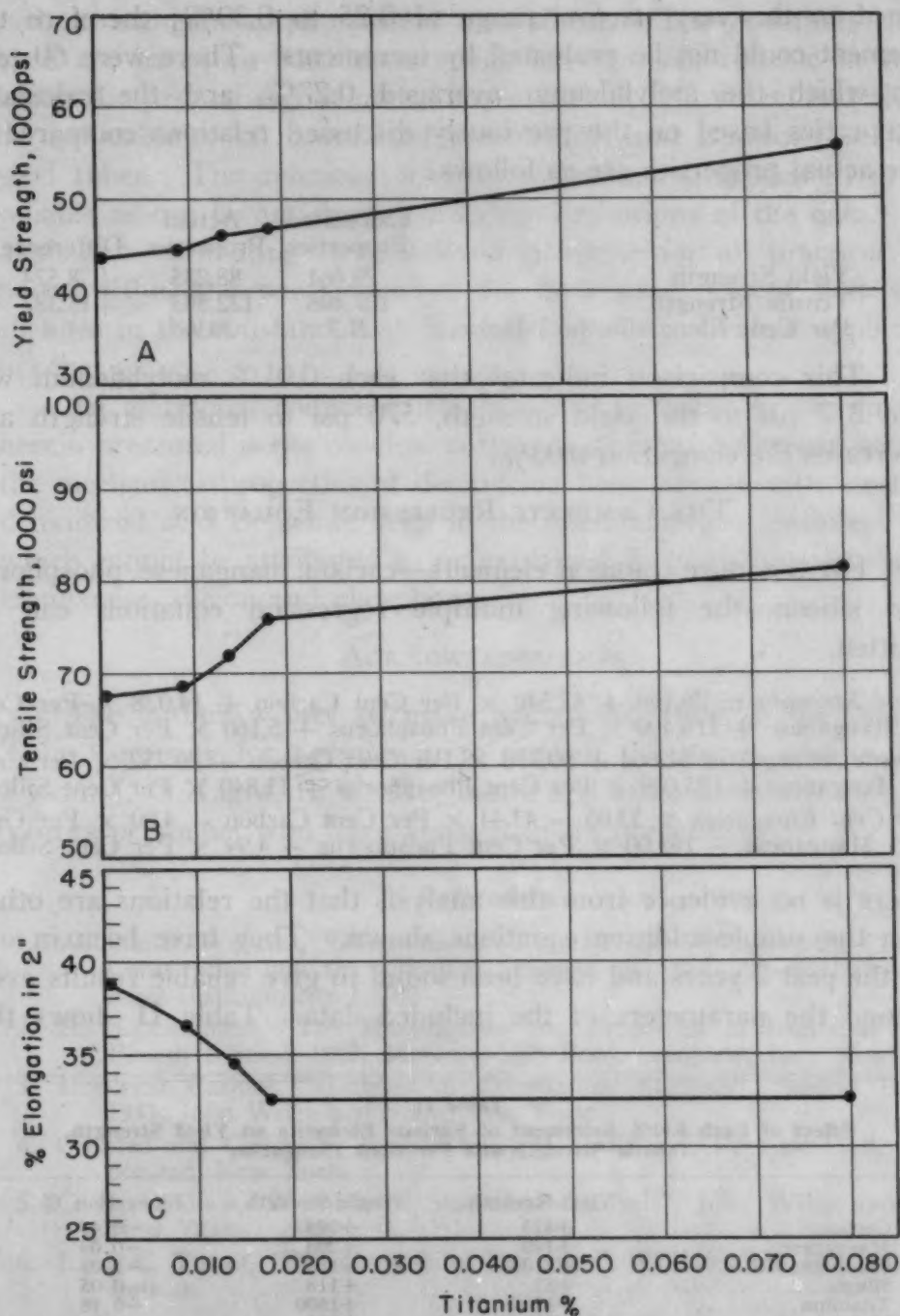


Fig. 5—(A) Independent Relation Between Per Cent Titanium and Yield Strength; (B) Independent Relation Between Per Cent Titanium and Tensile Strength; (C) Independent Relation Between Per Cent Titanium and Elongation in 2 Inches.

strength may be anticipated from increased titanium without impairing the elongation properties.

#### THE EFFECT OF MOLYBDENUM

The data on molybdenum in the as-rolled condition were con-

fined to the very narrow range of 0.25 to 0.30%; therefore this element could not be evaluated by increments. There were 60 tests on which the molybdenum averaged 0.27%, and the calculated properties based on the previously discussed relations compared to the actual properties are as follows:

	Calculated Properties	Actual Properties	Difference
Yield Strength	79,661	88,235	+ 8,574
Tensile Strength	107,496	122,893	+15,387
Per Cent Elongation in 2 Inches	21.7	30.9	-0.8

This comparison indicates that each 0.01% molybdenum will add 317 psi to the yield strength, 570 psi to tensile strength and decreases the elongation 0.03%.

#### THE COMPLETE REGRESSION EQUATION

For the more common elements—carbon, manganese, phosphorus and silicon—the following multiple regression equations can be written.

$$\begin{aligned} \text{Yield Strength} &= 26,166 + 42,540 \times \text{Per Cent Carbon} + 14,028 \times \text{Per Cent Manganese} \\ &+ 118,400 \times \text{Per Cent Phosphorus} + 5,160 \times \text{Per Cent Silicon} \\ \text{Tensile Strength} &= 31,064 + 99,770 \times \text{Per Cent Carbon} + 20,252 \times \text{Per Cent Manganese} \\ &+ 183,000 \times \text{Per Cent Phosphorus} + 11,840 \times \text{Per Cent Silicon} \\ \text{Per Cent Elongation} &= 53.05 - 43.44 \times \text{Per Cent Carbon} - 4.00 \times \text{Per Cent Manganese} \\ &- 105.00 \times \text{Per Cent Phosphorus} - 4.94 \times \text{Per Cent Silicon} \end{aligned}$$

There is no evidence from this analysis that the relations are other than the simple additive equations shown. They have been in use for the past 2 years and have been found to give reliable results even beyond the parameters of the included data. Table II shows the

Table II  
Effect of Each 0.01% Increment of Various Elements on Yield Strength, Tensile Strength and Per Cent Elongation

	Yield Strength	Tensile Strength	Elongation, %
Carbon.....	+425	+998	-0.43
Manganese.....	+140	+203	-0.04
Phosphorus.....	+1184	+1830	-1.05
Silicon.....	+52	+118	-0.05
Titanium.....	+1500	+1800	-0.78
Molybdenum.....	+317	+570	-0.03

actual increase in psi which will result from an increase of 0.01 in a given chemical element.

#### CONCLUSION

This paper has presented a method of calculating the mechanical properties of seamless steel pipe from the chemical constituents

carbon, manganese, phosphorus and silicon. The equations developed are based on 8391 tests which have proven reliable in calculating the properties considered for a period of 2 years, and should be applicable to all deoxidized open-hearth and Bessemer seamless steel tubes. The relations with titanium and molybdenum are as reliable as can be anticipated from the limitations of the data. The method of estimating is considered adequate for all practical purposes within the parameters of the data used, except that slight changes in the constants may be necessary for individual application in other plants.

An additional comment which is felt pertinent to the findings herein presented is the conclusion that there is no difference between the mechanical properties of deoxidized basic open-hearth steel and deoxidized acid Bessemer steel in the manufacture of seamless pipe, which cannot be attributed to or explained by variations in carbon, manganese, silicon and phosphorus.

#### ACKNOWLEDGMENTS

The author wishes to make acknowledgment to the National Tube Company for permission to publish this paper and to J. D. Tyson, J. O. Light, R. C. McQuattie and other members of Lorain Works personnel who have assisted in its preparation.

#### References

1. William R. Webster, "Observations on the Relations Between the Chemical Constitution and the Ultimate Strength of Steel", *Journal, Iron and Steel Institute*, No. 1, 1894.
2. H. H. Campbell, "The Manufacture and Properties of Iron and Steel", Fourth Edition, 1907, McGraw-Hill Book Company, Inc., New York.
3. Mordecai Ezekiel, "Methods of Correlation Analysis", Second Edition, 1941, John Wiley and Sons, New York.
4. Croxten and Cowden, "Applied General Statistics", Prentice-Hall, Incorporated, New York.
5. C. H. Goulton, "Methods of Statistical Analysis", John Wiley and Sons, New York.
6. L. H. C. Tippett, "The Methods of Statistics", Williams and Horgate, Ltd., London.

#### DISCUSSION

**Written Discussion:** By E. W. Earhart, metallurgical engineer, Alan Wood Steel Co., Conshohocken, Pa.

Mr. Rogers is to be complimented on his able presentation of his subject matter which is of fundamental interest to so many in various fields of the metal industry. Certainly the wide scope of data handled



in deriving the relationships between chemistry levels and physical values should be appreciated and does lend further emphasis to the findings of the author. We should like Mr. Rogers' opinion on the following points which occur to the writer after reviewing the paper at hand.

In discussing the effect of phosphorus on the various physical values, the author states that the equation derived for phosphorus at the level of values customarily obtained for basic open-hearth steels likewise holds true when extended into the range of phosphorus in Bessemer steels. Mention is not made of the widely different nitrogen levels in the two steels. Data presented by Graham<sup>2</sup> show an increase in tensile strength of approximately 5000 psi by raising the nitrogen level 0.010%. Other data<sup>3</sup> show higher physical values for Bessemer steel as compared with basic steel at the same phosphorus level. From Table I in the paper at hand, the standard deviation shown for phosphorus (0.0150%) being higher than the average 0.0136% would imply two distinct and widely separated distributions being involved. I would appreciate the author's thoughts on that point and also his opinion on whether truer formulas would be anticipated if basic open-hearth and Bessemer steels were treated separately with recognition being given to the higher nitrogen level in Bessemer steel.

No mention is made of wall thickness classification with respect to chemistry versus physical values. In computing tensile, yield and per cent elongation for a specific item, would it not be necessary to correct for wall thickness in the wide range of pipe sizes covered? It is rather common, in the production of flat-rolled products to guaranteed physical ranges, to adjust chemistry upward as the gage increases. Is such adjustment made in the manufacture of seamless pipe and, if so, would it not have its effect in developing the formulas shown?

**Written Discussion:** By W. D. Gilder, project engineer and chief metallurgist, The Weatherhead Co., Cleveland.

The author is to be commended for the excellent presentation of his practical solution to a highly essential control problem. Not only the rule of thumb, but also numerous empirical derivations have been used in the evaluation of physical properties derived from unit additions of the chemical composition to that of the iron base in steel. All have been found limited and lacking.

It is well recognized and proven that physical effects produced by addition of components will be largely governed by either their chemical combination, or solubility, or both, as the case may be for each element. The addition of manganese to iron increases the strength relatively little in the dissolved state; however, with the presence of sufficient carbon to utilize the entire manganese content as combined carbides, the resulting values are greatly enhanced, while an addition of sulphur acts negatively by making the combined manganese ineffective. Consequently, the addition of each unit of composition to produce a straight-line function must necessarily "wash out" these characteristics in this method and result in an over-all statistical average. The above is also borne out conclusively with the wide range of K values (tensile strength 46,239 to 67,894) for

<sup>2</sup>H. W. Graham, "The Acid Bessemer Process of 1940", AIME Technical Publication No. 1232, October 1940, page 14 of preprint.

<sup>3</sup>F. T. Sisco, "Alloys of Iron and Carbon", Vol. II, p. 93.

individual elements and K value drops (tensile strength 31,064) in the complete regression equations. Also note that neither titanium nor molybdenum adheres strictly to straight-line functions. Would the author have any other explanation for the lack of a single K value for the base strength of iron? Elucidating an example, in the absence of any other elements, an infinitesimal addition of carbon would result in 46,239 psi tensile strength and under the same conditions an infinitesimal addition of phosphorus would result in 67,894 psi, while infinitesimal additions of each element—carbon, manganese, phosphorus, silicon, etc.—would result in 31,064 psi tensile strength.

Obviously, the discrepancies will be greatest in numerical values where relative combinations of individual elements deviate widely from the statistical average values of all the elements summarized. Therefore, these values cannot be regarded correct for other conditions than those experienced in the sphere of the author's data and unfortunately are not to be employed universally for hot-rolled carbon steel in general. The developed equations, which have been proven reliable in calculating the physical properties, should be augmented for general use if at all possible. The author has shown the comprehensive data necessary to evaluate such a study, and facilities are not readily available other than those of statistical nature.

**Written Discussion:** By W. R. Weaver, director, Steel Conservation and Quality Control, Republic Steel Corp., Cleveland.

The wisdom of allowing this paper to remain almost entirely free of the "statistical" attachments which customarily accompany a paper of this type, and presenting merely the useful interpretations, must be commended. There has been omitted, however, one very valuable and useful factor as part of the interpretation. This is the "standard error of estimate", or the amount by which the actual value of tensile strength, reduction of area, etc., can lie, either above or below the value as calculated from the equation. The points shown on the charts appear to hold to very close agreement, but these represent large groups of heats and not individual heats. The true usefulness of such a tool depends upon how closely the physical values for an individual heat or lot of steel can be predicted from the chemistry, rather than predictions about averages of large numbers of heats or lots.

Data on both open-hearth and bessemer grades have been treated in one lump, assuming that there were no particular reasons for analyzing one separately from the other. Results of a multiple correlation of this type are interpreted as straight-line, or linear, relationships. The charts for phosphorus show a curved line, or curvilinear relationships, existing. It is suggested, therefore, that a more precise evaluation might be obtained by treating these two grades of steel separately, recognizing basic differences in the two processes, such as, for instance, nitrogen and phosphorus contents, as justifying such an attack. It is possible that the formula developed may not prove valid for the Bessemer grades.

**Written Discussion:** By W. K. Bock, research engineer, National Malleable and Steel Castings Co., Cleveland.

Some years ago we began a study of the properties of cast steels. The method of attack to the problem was a combination of the two out-

lined by Mr. Rogers. A limited number of heats—twenty-five—were made using regular production equipment operated by plant personnel, and the data were analyzed by the methods of statistics. A number of our conclusions have been published.

In an article by Schwartz and Bock,<sup>4</sup> an equation is developed relating tensile strength to carbon, silicon, manganese, nickel, chromium, molybdenum, vanadium and copper. It was found useful to introduce into the equation another variable, the hardenability computed by Grossmann's famous relations. Comparison of the coefficients for carbon, silicon and manganese from the reference paper with those reported for tensile strength by Mr. Rogers here gives:

	Wrought Steel	Cast Steel
Carbon	99700	144960
Silicon	11840	7380
Manganese	20252	41750

It is probably too much to expect that the coefficients should check, but it is interesting to note that the elements listed in order of decreasing strengthening effect are carbon, manganese and silicon in both cases. That this was not predictable can be seen by considering that silicon is more effective in strengthening ferrite than manganese, as was shown by Schwartz and Bock.<sup>5</sup> In both the work on cast steel and that on ferrite, the additive effect of the various elements was found as it was in Mr. Rogers' work.

Mr. Rogers noted that the coefficient for manganese was not affected by carbon content. In our work on steel we found the same thing.

The relations which were established for cast steel have been determined on heats made by acid electric or basic open-hearth processes and there was never any possibility of separating them according to melting practice. Mr. Rogers notes that his equations should be applicable to all deoxidized open-hearth and Bessemer steels.

Finally, there is one bit of information that would be useful. What are the standard errors of estimate of each of the equations?

We are glad to have this opportunity to compare our work on cast steel with Mr. Rogers' study of wrought steel. The parallels which were found are especially interesting in light of the view so often expressed that what is true of cast steel is not necessarily true of wrought steel.

**Written Discussion:** By Harold Hessing, metallurgist, National Bureau of Standards, Washington, D. C.

Mr. Rogers' paper is welcome, both for the information on the effect of a wide range of chemical composition on the mechanical properties of steel and for the application of statistical analysis to metallurgy. I would welcome his clarification of a few points.

Mr. Rogers states on page 1128 that "actual averages were then plotted as deviations from calculated averages . . . . in the included graphs". It would appear that the points in the graphs are averages plotted as themselves rather than as deviations. Assuming that these points are averages, the question of the distribution of the specimens is raised. How

<sup>4</sup>H. A. Schwartz and W. K. Bock, "Tensile Properties Versus Composition of Double Normalized Cast Steel", *Transactions, American Foundrymen's Society*, Vol. 56, 1948, p. 446-451.

<sup>5</sup>H. A. Schwartz and W. K. Bock, "Effect of Alloying Elements in Malleable Iron", *Transactions, American Foundrymen's Society*, Vol. 56, 1948, p. 458-461.



many specimens does each point represent? If the four points in Fig. 1b below 0.15% carbon and above 0.45% carbon represent a majority of the specimens, then the increased weighting due to a large number of specimens at the extremities of the range would indicate that the derived line is too low.

The fundamental point of Mr. Rogers' work is that the equations have been useful and checked as valid in the production work of his company. For any other application, his equation would seem of limited value without some statement of the deviation of the observed from the predicted values. If there were enough duplicates within heats, a measure of the significance of the deviation would be an F-test applied to the ratio of the variance between duplicates to the variance between calculated and observed values.

The use of regression equations seems predicated on a straight-line relationship, free of curvilinearity or degree higher than one. To use statistical terminology, there should be no interaction. However, one equation frequently quoted for the tensile strength of as-rolled steel shows manganese with a small carbon-interaction effect in addition to its additive effect. The simple additive effect of "alloying" elements could have been demonstrated more clearly to the metallurgist by a plot of mechanical properties against manganese content for several carbon contents on the same figure. If these lines were parallel, there would be no question of interaction.

The six averages plotted in Fig. 4 (effect of silicon) appear widely enough dispersed about sensibly horizontal lines to lead me to question whether dropping the silicon term from the complete regression equation would appreciably lower the precision or accuracy of the multiple regression equation.

The data on which this analysis is based were obtained from pipe from 4½ to 26 inches outside diameter. It would seem that the cooling rate through the critical range would vary enough with different sizes of pipe to affect the mechanical properties as much as small changes in chemical composition. Could some correlation be made with pipe size? Would such correlation improve the accuracy of the regression equations?

**Written Discussion:** By Frank R. Hicks, metallurgist, Kobe, Incorporated, Huntington Park, Calif.

Mr. Rogers is to be complimented for his excellent paper on the development of multiple equations for the calculation of physical properties from chemical composition of seamless steel tubes. Purely mechanical details of the development have been justifiably omitted from the discussion. However, certain incidental details would be of interest to many readers in applying Mr. Rogers' formulas to the products of other mills. Specifically:

1. How were physical tests made? Were full specimens, ASTM flat specimens, ASTM round specimens, or combinations of these used?
2. What method was used to determine yield strength?
3. How was chemical sampling accomplished? Was it found necessary to sample near each tensile fracture?
4. What was the normal spread, or range, of physicals for a given chemical composition?

We have made full specimen tensile tests on 1¼-inch tubing from two suppliers other than National Tube Company, and have also used Mr. Rogers' formulas for calculating ultimate strength and elongation. (Our chemical sampling was not necessarily adjacent to the tensile failure.)

The maximum deviation of the calculated values from our test values were:

Supplier "A"—Ultimate strength, plus 4.4%.

Supplier "B"—Ultimate Strength, minus 9.9%; Elongation, plus 19%.

We are wondering if these deviations are normal, or whether our testing technique, or possibly the suppliers' mill practice, might be responsible for the deviations encountered. Incidentally, the chemical compositions of the tubes giving the total spread of 14.3% noted above would have predicted a spread of only 2% between the two samples.

#### Author's Reply

The volume and range of subject material brought out by the discussion on this paper is gratifying in that it shows a deep interest in the relation of factors associated with mechanical properties of "as-rolled" steels in general and the multiplicity of variables which affect these mechanical properties. I am very grateful to the several gentlemen who have taken the time to inquire further into this problem, and while some of the comment offered departs from the scope of this investigation, it does point out that additional work lies ahead if our knowledge in respect to the variables encountered is to be increased. Inasmuch as more than one comment is on the same subject, my reply will be by subject rather than by author.

Nitrogen has long been a controversial element with respect to its effect on mechanical properties. Recently Enzian<sup>6</sup> discussed the effect of nitrogen on the mechanical properties of Bessemer steel. In this work the yield point and tensile strength were greater in the steels containing a larger proportion of nitrogen; the steels dealt with in Enzian's investigation, however, were not thoroughly killed with aluminum and were in the normalized condition. It is well known, in studying the influence of nitrogen in steel, that deoxidation practice and heat treatment are important factors which influence the behavior of this element. In the present study a comprehensive attempt has been made to throw additional light on the effect of this element. In general, the results indicate that nitrogen in a steel properly deoxidized with aluminum is not significant in its association with yield strength, tensile strength and elongation. It should be clearly understood that in studying the properties of ordinary Bessemer steel, we are not dealing with a steel which has been thoroughly deoxidized; on the other hand, deoxidized Bessemer steel described by Wright,<sup>7</sup> Price<sup>8</sup> and Wilder<sup>9</sup> is thoroughly deoxidized with silicon and

<sup>6</sup>G. H. Enzian, "Some Effect of Phosphorus and Nitrogen on Properties of Low Carbon Steel", *Journal of Metals*, February 1950; *Transactions, American Institute of Mining and Metallurgical Engineers*, Vol. 188, p. 346.

<sup>7</sup>E. C. Wright, "Manufacture and Properties of Killed Bessemer Steel", *Transactions, American Institute of Mining and Metallurgical Engineers*, Vol. 158, 1944, p. 107.

<sup>8</sup>E. G. Price, "Advantages of Bessemer Steel in Producing Tubular Products", *Steel*, Nov. 15, 1948.

<sup>9</sup>A. B. Wilder, "The Bessemer Converter Process", *Journal of Metals*, November 1949 and December 1949.

aluminum and its behavior therefore is entirely different from ordinary Bessemer steel. Further, it has been shown by Wilder<sup>9</sup> that nitrogen, in a commercial low carbon steel properly deoxidized, does not adversely affect the toughness characteristics of the steel. In studying the influence of nitrogen, the important factor to consider is whether or not the steel has been deoxidized so as to "fix" or render inactive the nitrogen present.

The graph for phosphorus shows that an extension of the linear equation from the open-hearth range would pass through the Bessemer range, but within the Bessemer range itself there is an apparent flattening out of the relation, and while this must be given some weight in our thinking, there is not sufficient evidence through a wide enough range of phosphorus content to assume that an equation other than a straight line would apply.

It is agreed that the standard error is an integral part of any regression analysis, but it is pointed out that a standard error does not have the same characteristics as a regression coefficient, and the standard error of one manufacturer in this case may not be adaptable to the product of another manufacturer. It therefore goes without saying that this figure, if quoted, would serve no useful purpose. Pipe diameter and wall thickness of pipe may be related to mechanical properties, but a discussion of these relationships is not within the scope of this paper.

The inference that the constants shown present a value which may be considered as the strength of pure iron is erroneous. These constants are only a statistic which enables the equations to be balanced within the parameters of the variables included.

The analogy to cast steel is interesting and informative, particularly the observation that findings with regards to the effect of manganese at various carbon levels were similar. The procedure of plotting physical properties against manganese content for various levels of carbon was done as a check against the statement that "there is no evidence that the coefficients for manganese should be different for various carbon contents".

Testing procedure was carried out in accordance with ASTM standards.

Although it is apparent that the effect of silicon is slight and leaving it out would not materially affect the accuracy of the estimating equation, the general interest in this common alloying element is felt sufficient to justify its inclusion.



## GRINDABILITY OF TOOL STEELS

By L. P. TARASOV

### *Abstract*

*The grindability, or the relative ease of grinding, was determined for a large number of tool and die steels. A useful method of rating the steels is by means of a grindability index equal to the volume ratio of material removed in grinding to wheel wear. The higher this index, the easier the steel is to grind. The power or energy consumed in grinding cannot be used to predict the grindability of tool steels, since these quantities can be the same for steels known to be extremely difficult to grind as for those comparatively easy to grind. However, curves of grinding energy versus grindability index are useful in studying the factors affecting grindability.*

*The grindability index for tool steels heat treated to ordinary commercial requirements is about 200 times greater for the easiest steel to grind than for the most difficult one. For steels in the same hardness range, the hardness of the carbide particles is the most important factor in determining the grindability. The higher the chromium content of nondeforming steels or the higher the vanadium content of high speed steels, the lower is the grindability index. The grindability of a tool steel improves as its Rockwell hardness is decreased, the percentage improvement being far greater for low than for high grindability steels.*

*Neither the surface finish obtained nor the susceptibility of the steel to surface cracking during or after grinding can be related in general to the ease of removing stock. To avoid confusion, it is necessary to exclude the concepts of finishability and grinding sensitivity from that of grindability.*

**A**LTHOUGH the term machinability can be used to denote the relative ease of removing material by any machining method, including grinding (1),<sup>1</sup> certain distinctive features of the grinding process make it highly desirable to use a separate word, *grindability*, to describe that portion of machinability which has to do with grinding.

<sup>1</sup>The figures appearing in parentheses pertain to the references appended to this paper.

A paper presented before the Thirty-second Annual Convention of the Society, held in Chicago, October 21 to 27, 1950. The author, L. P. Tarasov, is associated with the Research and Development Department, Norton Company, Worcester, Mass. Manuscript received April 26, 1950.

One of the important respects in which grinding differs so markedly from all operations with metallic cutting tools is that a controlled amount of wear is necessary for the proper functioning of the grinding wheel; otherwise, the abrasive grains in the cutting surface of the wheel become dull and generate excessive heat in the work surface when the rate of feed is fixed. Wear of the grinding wheel is the mechanism whereby the dull grains are replaced by sharp ones, either by fracture of the grains themselves or by fracture of the bond posts holding them in place (2). Metallic cutting tools, on the other hand, become dull when they wear, so that every effort is made to minimize tool wear consistent with maintaining the rate of production at the desired level. Thus the methods that have been used for evaluating machinability are not necessarily applicable to the study of grindability.

In dealing with grindability, it is necessary to differentiate between fixed-feed (or precision) grinding and constant-pressure grinding, the latter being represented by snagging, or by offhand grinding on a bench stand. The wheel action may be quite different in the two cases. In fixed-feed grinding, the wheel is forced to remove a depth of stock equal to the feed minus the radial wheel wear, while in constant-pressure grinding the rate of stock removal for a given wheel depends on the pressure exerted by the wheel on the surface and on the sharpness of the wheel face. Whether or not a group of materials ground by the two methods would be rated in the same order, with respect to grindability, would have to be determined by experiment.

Some work on the grindability of a variety of steels (plain carbon, low alloy, and austenitic) has been reported briefly by Volskii (3), but the results are expressed in terms of an undefined productivity index, and the steel analyses are not provided, so the meager data are of limited utility. The type of microstructure and the degree of alloying were found to affect the quantity used as a measure of grindability, but no relationship could be established between this and the various common mechanical properties.

The need for detailed information on the grindability of hardened tool and die steels arose in attempting to provide the best grinding recommendations for a wide variety of these steels, a number of which have been developed in the past few years. It is known from long experience that the various types of tool steels cannot be ground in exactly the same manner, even though they have been heat treated to about the same hardness. In order to keep the testing program within reasonable limits, a few representative steels had to be

selected from a very large number of types and subtypes, to say nothing of competitive brands. A decision had to be made as to the minimum number of steels required and as to which steels should be chosen for exhaustive testing in various grinding operations.

The studies described in this paper not only made it possible to classify and select the steels in the desired manner, but they also answered, at least in preliminary fashion, a number of important questions about grindability: How broad a field should be covered by the concept of grindability? What are the measurable and significant variables in terms of which it can be defined in a satisfactory manner? To what extent do tool steels vary in grindability? What are the factors responsible for the differences? How may grinding conditions affect grindability? It is with the answers to these questions that this paper is concerned.

#### EXPERIMENTAL PROCEDURE

*Steels Tested*—The tool and die steels were furnished by several cooperating tool steel manufacturers in the form of hardened and tempered blocks, 6 by 1½ by 1½ inches, except for some of those used for investigating the effect of Rockwell hardness, which were only ½ inch in thickness. Most of the blocks were heat treated by the manufacturers in accordance with the normal recommendations for the individual brands; the rest were processed similarly in a commercial heat treating shop. A block of AISI 52100 steel was included in this study.

The steels are listed in Table I in accordance with the letter designations assigned to them. The various types are described by whatever method is most appropriate in each instance, and the ASM designations are given when such exist. The high speed steels are described by their approximate W-Cr-V or W-Mo-Cr-V percentages; in addition, the T or M designations used in the automotive industry are given in parentheses if available. The compositions are mostly nominal, although where these did not happen to be available for individual brands, either typical or actual analyses are given. Nominal analyses are sufficiently accurate, since the present study is exploratory in character. The Rockwell hardness values are averages obtained during the grindability tests other than those in which the effect of hardness on grindability was investigated.

The letter designations for the *high speed* steels are in the form of a code describing the approximate composition. The first letter classifies the steels on the basis of tungsten and molybdenum: A for about 18% tungsten; B for about 14% tungsten; C for about 8%



Table I  
Description of Steels Investigated

Steel Designation	Description	Type of Steel	ASM Type*	Approximate Analysis, %						Hardness, Rockwell C
				C	W	Mo	Cr	V	Other	
High Speed Steels										
AA <sub>1</sub>	18-4-1	(T1)	5C1	0.7	18.1	—	4.0	1.1	—	64
AA <sub>2</sub>	18-4-1	(T1)	5C1	0.7	18.3	—	4.0	1.2	—	64
AB	18-4-2	(T2)	5C2	0.8	18.5	0.8	4.0	2.1	—	63
ABA	20-4-2, 12 Co	(T6)	5D4	0.8	20.5	0.6	4.2	1.6	12.2 Co	63
AC	18-4-3	(T3)	5C3	1.1	17.4	1.1	4.2	3.3	—	62
AD	18-4-4	—	—	1.2	18.5	0.8	4.0	4.0	—	64
BB	14-4-2	(T7)	—	0.7	14.0	—	4.0	2.0	—	63
BC	14-4-3	—	—	1.0	14.0	0.8	4.0	3.0	—	63
BEA	13-5-5, 5 Co	(T15)	—	1.5	12.5	—	5.0	5.0	5.0 Co	67
CA	2-8-4-1	(M1)	5A2	0.8	1.7	8.5	3.8	1.2	—	64
CB	0-8-4-2	(M10)	5A1	0.8	—	8.0	4.0	1.9	—	64
DAB	6-5-4-1, 1 Cb	(M8)	—	0.8	6.1	4.9	4.3	1.5	1.3 Cb	64
DB-1	6-5-4-2	(M2)	5A3	0.8	6.5	5.0	4.0	1.9	—	64
DB-2	6-6-4-2	—	—	1.0	6.2	6.2	4.0	2.4	—	65
DC	6-6-4-3	(M3)	—	1.1	5.9	5.7	4.0	3.0	—	64
DD	6-5-5-4	(M4)	5A4	1.3	5.5	4.5	4.5	4.0	—	65
Miscellaneous Tool Steels										
EA	Plain carbon		1A	1.1	—	—	—	—	—	63
EB	Nondeforming, oil hardening, low alloy		2A2	0.9	—	—	—	—	1.7 Mn	58
EC	Nickel-chromium		6E	0.7	—	—	1.0	—	1.8 Ni	61
ED	Nondeforming, air hardening, low alloy		2B1	0.7	—	1.4	1.0	—	2.0 Mn	59
EE	Shock resisting		3B	0.5	—	0.5	—	—	1.0 Si	60
EF	Hot work		4B	0.4	—	1.4	5.0	0.9	1.1 Si	50
EG	Nondeforming, air hardening, medium alloy		2B2	1.0	—	1.0	5.0	—	0.7 Mn	60
EH	Hot work		4F1	0.3	9.0	—	3.5	0.4	—	53
EJ	Finishing		6K	1.3	3.5	—	—	—	—	61
High C, High Cr Die Steels										
FA <sub>1</sub>	Oil hardening		2C1	2.1	—	—	12.5	—	0.5 Ni	62
FA <sub>2</sub>	Oil hardening		2C1	2.1	—	—	12.5	—	0.5 Ni	64
FB	Air hardening		2D2	1.5	—	0.8	12.0	—	—	59
FC	Air hardening, high vanadium		—	2.4	—	1.1	12.8	4.0	—	65
Graphitic Tool Steels										
GA	Nondeforming, oil hardening		—	1.5	—	0.3	—	—	—	63
GB	Water hardening (shallow)		—	1.5	—	—	—	—	0.2 Al	65
GC	Air hardening		—	1.5	—	0.5	0.5	1.8 Ni	1.0 Si	63
GD	Water hardening (medium)		—	1.5	2.8	0.5	—	—	—	63
AISI Steels										
HA	52100		—	1.0	—	—	1.5	—	—	64

\*ASM METALS HANDBOOK, 1948, p. 656.

molybdenum; and D for about 6% each of tungsten and molybdenum. The second letter corresponds to the vanadium content, A signifying 1%, B—2%, and up through E for 5%. Cobalt or columbium is denoted by a third letter. Subscripts serve to differentiate between two brands or hardness levels of the same type of steel.

The other types of tool steels are grouped under self-explanatory headings. The first letter in the steel designation is common to each group, while the second one is a serial mark.

Before the grindability studies were started, the blocks were surface ground on all sides to remove scale and decarburization, and to make them flat and parallel.

*Grinding Conditions*—Surface grinding was selected for evaluating the grindability of tool steels because rectangular test blocks are much cheaper to prepare than those needed for other methods of grinding, such as cylindrical; moreover, the surface dimensions of a rectangular block do not change during the course of a test. As the study progressed, it was found desirable to modify the grinding conditions from time to time, both because the grindability of the steels tested varied over such a wide range and because the effect upon grindability of certain factors other than the composition of the steel needed investigation.

The 6 by 1½-inch surfaces of the steel blocks were ground lengthwise, one at a time, under the conditions listed in Table II.

Table II  
Grinding Conditions

---



---

Machine—Norton 6 by 18-inch surface grinder; horizontal spindle, reciprocating work chuck
Wheel specifications—32A46-18VBE* (32A46-G12VBEP, 32A60-M8VBE)
Wheel diameter—8 inches at start; discarded at 7 inches
Wheel width—0.470 inch (½ inch nominal)
Wheel speed (idling)—6000 surface feet per minute (5500)
Unit crossfeed—0.050 inch after each table traverse
Unit downfeed—0.001 inch after each complete crossfeed (0.0005, 0.002)
Total downfeed—0.020 inch (0.010, 0.040, 0.100)
Table speed—720 inches per minute (430)
Grinding fluid—soluble oil in water, 1:40
Dressing—sharp, with special diamond, as described in text.

---



---

\*This is a Norton 32 Alundum wheel (aluminum oxide), 46-grit size, I grade, No. 8 structure, vitrified bond of the BE type; it is a wheel often used for surface grinding hardened steels. The strength of the bonding, which determines the hardness of the wheel, increases in alphabetical sequence with the grade letter, while the spacing of the abrasive grains increases slowly with the structure number. A special porous-type structure is denoted by the letter P at the end of the specification.

---



---

The conditions considered standard in much of the work, and to which many of the data obtained under modified conditions could be readily adjusted, are given first; other conditions, used in various combinations, appear in parentheses.

Whatever the grinding conditions, the wheel was dressed wet with a diamond prior to each run, the diamond being traversed several times across the wheel face at a moderately rapid speed. The wheel was left in a sharp and free-cutting condition by feeding it down 0.001 inch each time. The dressing action of the diamond, which was offset ½ inch from the vertical centerline of the wheel, was kept the same throughout all the work by turning the diamond 30 degrees in its holder every ten wheel dressings so that it always retained its initial shape of a twelve-sided pyramid with a very obtuse

apex angle. Previous experience had shown that this technique imparted a highly reproducible degree of sharpness to the wheel face. Originally, the diamond had been ground to the shape of a cone with the same apex angle, and the pyramidal surface was generated in dressing other wheels.

After each dressing, the wheel was broken in by a preliminary grind on the same block of steel that was to be tested, in order to get the wheel face into a relatively stable condition. The same grinding conditions were used as in the test run except for the total downfeed needed for breaking the wheel in properly, as determined in some auxiliary tests. The various quantities measured in this study either remained fairly constant after the preliminary run or else they changed rather slowly and in a uniform manner.

*Measured and Calculated Quantities*—Since nothing was known at the beginning of this investigation as to the most satisfactory way of expressing grindability, it was necessary to make several types of measurements from which various potentially useful functions could be calculated. The wheel wear and the net power consumed in grinding were the two basic quantities measured, both because they have a definite practical significance and because they can be readily obtained in a regular surface-grinding test.

A decrease in wheel wear is always desirable in fixed-feed grinding (provided it does not lead to unsatisfactory grinding effects), since it not only lowers wheel and time costs but also makes it possible to grind to greater dimensional accuracy. The net power consumption is an indication of the freeness of cut. The lower the power, the freer is the cut and the less is the heat introduced into the work. Keeping the heat to a minimum is always desirable, since this lessens the possibility of distortion, burn and surface cracking.

The wheel wear was determined from the average of two diameters at right angles, measured at the start and end of each run with an 8-inch micrometer caliper read to 0.0001 inch. The volumetric wheel wear is readily calculated from the radial wheel wear, the wheel width and the diameter. The material removed in grinding is equal to the area of the test block, multiplied by the total downfeed less the radial wheel wear.

The power input to the direct-current motor of the surface grinder was recorded graphically on an Esterline-Angus recording wattmeter. The average power for each completed crossfeed, obtained by visual inspection of the chart, was averaged for all the successive downfeeds in a run and was corrected for the idling power. The electrical losses in the motor are not taken into account



in this correction, and the mechanical losses are not exactly the same during grinding as during idling, so that the average net power value determined from the chart differs somewhat from the average power actually consumed in the grinding operation. However, the two quantities are closely related, an increase in one corresponding to an increase in the other. Thus, although the calculated power value is actually the net input to the motor required for grinding, it also serves as a somewhat distorted measure of the power absorbed in the grinding operation, the amount of distortion being unknown.

Because the wheel wear was extremely high for steels that were very resistant to grinding, the power was correspondingly low. Correction of the power to a standard depth of material removed led to the use of energy consumed in removing a unit volume of material. The grinding energy, as this was called for short, was readily calculated from the power and the volume of material removed in unit time, and it was expressed in HP min./cu. in.

Some other types of data were also recorded in the course of this study. In many, but not all, instances, the surface finish existing at the end of a run was measured on a profilometer. The depth of overtempering caused by grinding heat was determined for some of the steels during the initial part of the work. The Rockwell hardness was measured repeatedly to keep track of any gradient below the original surface and by this means to determine how far down the shallow hardening steels could safely be ground. In testing the shallow hardening steels, both top and bottom surfaces of several blocks were ground in order to provide sufficient material of reasonably uniform hardness for testing.

#### EVALUATION OF GRINDABILITY

Any quantities intended to be useful measures of the grindability of tool steels must rate the steels in the same order that they are rated on the basis of valid tool room and production experience; otherwise, even though the quantities are of interest in elucidating the factors involved in grindability, it will be difficult, if not impossible, to make use of the ratings in actual practice. A steel is considered easy to grind when it can be ground rapidly to the desired accuracy of form and dimension. Rapid stock removal is associated with low wheel wear; of course, the wheel has to wear at a sufficient rate to remain free cutting so as to avoid the generation of excessive heat. Thus a steel for which both time and wheel costs are low is considered easy to grind and can be said to have a high grindability.

As will be seen shortly, the volume ratio of material removed to wheel wear increases in accordance with the relative grindability rating of a steel based on shop experience, and for that reason it is called the grindability index in this paper. However, this does not preclude the development of other grindability indices which may also be useful in rating materials.<sup>2</sup> Originally, wheel wear was

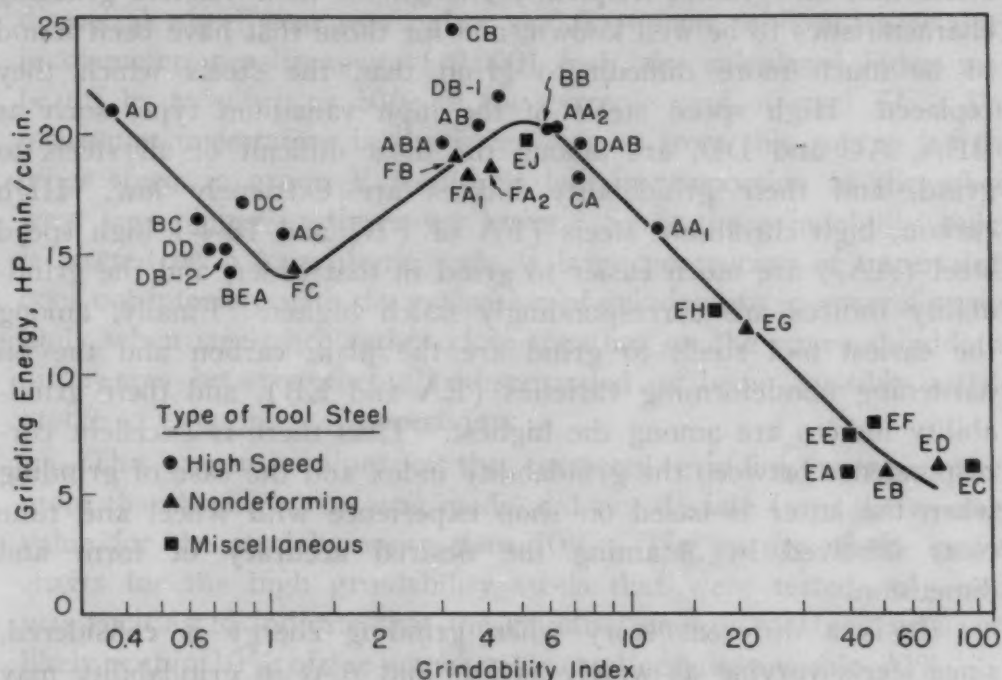


Fig. 1—Grindability Data for a Variety of Tool and Die Steels Heat Treated in Normal Fashion and Ground With a 32A46-I8VBE Wheel. Grindability index is volume ratio of material removed to wheel wear.

used as a measure of grindability (2), but this led to the association of low wear with high grindability and it appeared to be more satisfactory to develop an index which increased when the grindability or ease of grinding increased.

In order to determine how grindability can best be evaluated, it is convenient to plot the grinding energy, which is a measure of freeness of cut, as a function of the grindability index just mentioned. The data for all the steels of Table I except those in the G and H groups are recorded in Fig. 1. The grindability index is always plotted logarithmically to allow for the extremely wide variation between low and high grindability steels without squeezing

<sup>2</sup>For example, instead of using the volume ratio of material removed to wheel wear under the same grinding conditions for the grindability index, the volume ratio at the same power consumption (and heat generation) might be used. To obtain the latter volume ratio would require interpolating results from experiments with wheels of several grades. There are theoretical advantages to such an index, but they are outweighed by the greatly increased cost of obtaining the necessary data. The steels would still be rated in the same general order but the relative values would be different.

all the points together for the steels with low grindability indices.

Before proceeding to a detailed discussion of the experimental points and the curve connecting them, it is desirable to establish first that the grindability index does indeed rate the steels in the same order as they are commonly rated in the shop with respect to ease of grinding. This comparison can be made only for those steels that are ground frequently enough for their relative grinding characteristics to be well known, and for those that have been found to be much more difficult to grind than the steels which they replaced. High speed steels of the high vanadium type, such as BEA, AC and DD, are among the most difficult of all steels to grind, and their grindability indices are extremely low. High carbon, high chromium steels (FA or FB) and 18-4-1 high speed steel (AA<sub>1</sub>) are much easier to grind in that order, and the grindability indices are correspondingly much higher. Finally, among the easiest tool steels to grind are the plain carbon and the oil hardening nondeforming varieties (EA and EB), and their grindability indices are among the highest. Thus there is excellent correspondence between the grindability index and the ease of grinding when the latter is based on shop experience with wheel and time costs involved in obtaining the desired accuracy of form and dimension.

It is a different story when grinding energy is considered, since steels varying as widely as DD and AA<sub>1</sub> in grindability may have the same grinding energy associated with them. The overlapping of the grinding energy values for steels of entirely different grinding characteristics means that grinding energy cannot be used by itself as a measure of grindability. However, the use of grinding energy in conjunction with the grindability index may well lead to a better understanding of grindability.

Some comments are necessary in regard to how the experimental points were obtained, what the order of accuracy is likely to be, and why the curve is drawn in the manner indicated. Several 32A46-I8VBE wheels were used and enough steels were ground with each of the wheels to permit all the original data to be corrected to a standard set of grinding conditions. One of the wheels was arbitrarily chosen to serve as the standard. The steels tested with this wheel were ground in succession and then a second run was made in the same order. Thus values for two different wheel diameters were obtained for each of the steels and it was then possible to correct them satisfactorily to a standard nominal diameter of 7.50 inches. The other grinding conditions were the ones listed



first in Table II. The data obtained with the other wheels were similarly corrected to these same standard conditions.

The corrected values of the grindability index for the low and medium grindability steels generally did not deviate from the final average value for each steel by more than 10%, except for two steels which showed a maximum deviation of about 20%. Some of the highest grindability steels were run only once and since the diametral wheel wear was as low as 0.0004 inch, with an uncertainty in diameter measurement of 0.0001 inch, the calculated index may be off by as much as 50% in the extreme case of steel EC. The maximum uncertainty in the index arising from this source for the other steels in group E would be less in proportion as the wheel wear was higher or the index lower. Since the grindability index is plotted on a logarithmic scale, a large percentage of uncertainty does not interfere with the evaluation of grindability in general terms. Only when steels are rather close together on the curve should the differences between them be disregarded as being possibly attributable to experimental uncertainty.

The extreme values of the corrected grinding energy, when more than a single run was made, did not deviate from the average value for the steel by more than 10%. The nature of the power charts for the high grindability steels that were tested only once was such as to indicate that the grinding energy obtained was very likely within 10% of the actual value, and certainly within 20%.

The experimental points fall fairly close to a grindability curve which rises with decreasing grindability index, then drops and finally rises again. The only exception is steel CB, which is considerably farther from the other points or from the curve than could be accounted for by experimental error. It is not certain that this curve is the correct way of depicting the relationship between the experimental points, since they could also be represented by two separate sloping bands, roughly from EB to CB and from FC to AD, in conformity with the definite gap between the two sets of points. However, the continuous-curve representation is favored at the present time, since when a much harder wheel was used for grinding four of the steels, the points fell on the single continuous curve of Fig. 6.

The condition of the surface produced by grinding is sometimes considered to have a bearing on how a steel should be rated with respect to ease of grinding. Hardened steels may be difficult to grind, not because they are resistant to the grinding operation but because they are susceptible to surface cracking. Grinding sensi-

tivity, as this is called, is now known to be dependent on the response of the steel to heat treatment (2). A steel heat treated one way may be highly sensitive so that it has to be ground with extreme care to avoid the appearance of fine surface cracks, and yet the same steel may be made completely insensitive at the same Rockwell hardness by modifying its heat treatment. Since the grindability index and the grinding energy may be the same for the two heat treatments, it is best to exclude sensitivity from the concept of grindability. To use a single word for two unrelated phenomena would simply lead to unnecessary confusion.

Ease of grinding is also sometimes taken to imply the relative ease of obtaining a good surface finish. However, as will be shown later, the ease of obtaining a good finish and of removing stock do not go together. To avoid confusion, the former should be termed the finishability, in accordance with a suggestion by Ernst (4). Thus, grindability will be used in the narrow sense of the relative ease of removing stock by grinding without reference to the sensitivity or the finishability of the steel.

#### EFFECTS OF VARIOUS FACTORS ON GRINDABILITY

*Quenching Medium*—The data of Fig. 1 show definitely that the medium in which the steel is quenched has no bearing on its grindability. Steels EA, EB and ED at the right are water, oil and air hardening, respectively, and the difference in grindability index and grinding energy is not great enough to be of any significance in view of the experimental uncertainty mentioned earlier. All three steels, as well as the other three in that vicinity, must be considered as having essentially the same grindability characteristics. Similarly, steels EJ, FA and FB, which are near the peak of the curve, are water, oil and air hardening, respectively, and they also belong together from the standpoint of grindability.

Since grinding recommendations are necessarily related to the grindability of a steel, it follows that it is not possible to make such recommendations solely on the basis of how the steel is normally quenched.

*Alloying Elements*—In order to ascertain the effects that the various principal alloying elements found in tool and die steels may have on their grindability, it is desirable to consider separately two principal groups, the nondeforming and the high speed steels.

The grindability index is plotted in Fig. 2 as a function of the chromium content of the nondeforming steels. The points fall close to a straight line, showing that the logarithm of the grindability

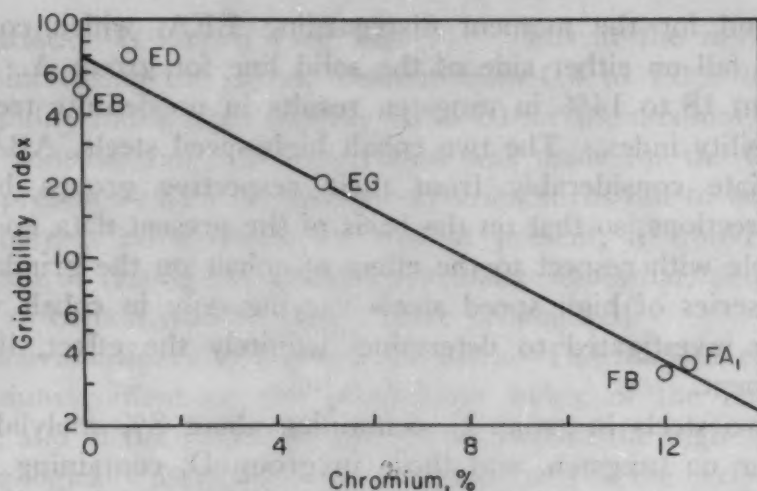


Fig. 2—Effect of Chromium Content on the Grindability Index of Nondeforming Steels.

index decreases linearly with increasing percentage by weight of chromium. Steel FC is omitted from consideration, even though it is in the nondeforming group, because it contains 4% vanadium, which markedly affects the grindability, as shown by the data for the high speed steels in Fig. 3.

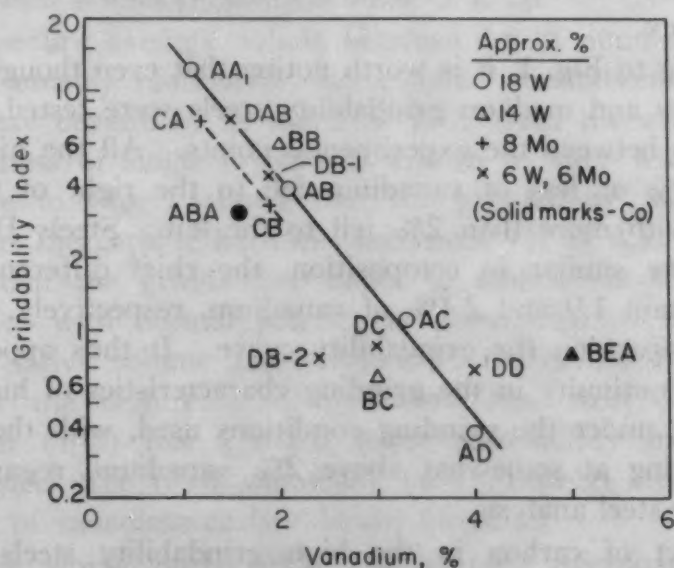


Fig. 3—Effect of Vanadium Content on the Grindability Index of High Speed Steels.

The high speed steels fall into four groups distinguished by the initial letter of their designation. The sharp decrease in grindability index with increasing vanadium content is immediately apparent. The steels in group A, containing roughly 18% tungsten, fall very close to a straight line with the exception of ABA, which contains 12% cobalt. The two in group B, containing about 14%



tungsten and for the moment disregarding BEA, which contains 5% cobalt, fall on either side of the solid line for group A. Thus a drop from 18 to 14% in tungsten results in no definite trend in the grindability index. The two cobalt high speed steels, ABA and BEA, deviate considerably from their respective groups but in opposite directions, so that on the basis of the present data no trend is discernible with respect to the effect of cobalt on the grindability index. A series of high speed steels varying only in cobalt would have to be investigated to determine definitely the effect, if any, of this element.

The two steels in group C, containing about 8% molybdenum and little or no tungsten, and those in group D, containing about 6% each of tungsten and molybdenum, are close to the solid line for the straight tungsten steels in group A, the only exception being DB-2. The observed scatter about the solid line may well be due to effects arising from other differences in constituents between steels, not capable of being taken into account at present. The substitution of part or most of the tungsten in high speed steel by molybdenum does not have any definite effect on the grindability index. The addition of 1% columbium, as in DAB, also does not affect the index.

Returning to Fig. 1, it is worth noting that even though a large number of low and medium grindability steels were tested, there is a definite gap between the experimental points. All the high speed steels with 2% or less of vanadium fell to the right of this gap, while those with more than 2% fell to the left. Steels DB-1 and DB-2 are very similar in composition, the chief difference being that they contain 1.9 and 2.4% of vanadium, respectively, yet they are very far apart on the grindability curve. It thus appears that there is a discontinuity in the grinding characteristics of high speed steels, at least under the grinding conditions used, with the discontinuity occurring at somewhat above 2% vanadium, regardless of the rest of the steel analysis.

The effect of carbon in the high grindability steels can be deduced approximately from a comparison of steels EF and EG, which contain 5% chromium and are reasonably similar except for the carbon contents, these being 0.4 and 1.0%, respectively. The measured grindability index of EF was 48 at a hardness of Rockwell C-50. Had the hardness been C-60, as was that of EG, the index would have been somewhat less, perhaps 40, if the reasonable assumption is made that the index of EF varies in the same manner with Rockwell hardness as that of EB, for which the magnitude of

the variation is known (see Fig. 5). Thus at the same hardness level, increasing the carbon content from 0.4 to 1.0% lowered the grindability index from roughly 40 to 20 for the medium alloy steels under consideration. No correction was made for the 0.9% vanadium present in EF. If such a correction turns out to be necessary, and there is no evidence for that at present, it would be in the direction of raising the grindability index somewhat, and hence the effect of carbon would be even more pronounced.

*Microhardness of Carbide Particles*—The marked effect of the chromium content on the grindability index of the nondeforming steels, and of the vanadium content on that of the high speed steels, can be logically ascribed to the microhardness of the carbide particles present in these steels (5). In a nondeforming steel not containing any chromium, such as EB, these particles are iron carbide, which has a Knoop hardness at 25 g. load of 1150. In the high carbon, high chromium steel FA, they are in the form of a complex iron-chromium carbide, for which the value on the same hardness scale is 1820, about 50% harder than iron carbide. In a high vanadium, high speed steel like BEA, the particles are predominantly vanadium carbide, with a Knoop hardness value of 2520.

These are average values obtained for a number of particles with presumably random crystallographic orientations. The actual values may deviate by as much as 10% from the average because the hardness of single crystals is known to vary with orientation. Reference to Fig. 1 shows that the grindability index decreases rapidly as the carbide hardness increases. It is thus reasonable to assume that the grindability index of tool steels heat treated in accordance with normal practice is determined to a large extent by the relative volume and hardness of the carbides present. The fact that the high carbon, high chromium steel containing 4% vanadium (FC) has a much lower grindability index than the similar steel free from vanadium (FA) can be attributed to the presence of vanadium carbide in the former.

It is worth noting that the average microhardness of the vanadium carbide particles in steel BEA is slightly higher than that of the aluminum oxide abrasive used in grinding—2520 versus 2440. However, aluminum oxide is highly anisotropic with respect to hardness, which can vary in the range of 1900 to 2900, while the hardness of vanadium carbide falls in the considerably narrower range of 2300 to 2700. Thus in some directions aluminum oxide is harder than vanadium carbide, even though on the average it is slightly softer. Were it not for this fact, the high vanadium, high

speed steels might be even more difficult to grind than they are.

The pronounced gap in the grindability index found to exist between the low and medium grindability high speed steels indicates the likelihood of a corresponding jump in carbide particle hardness rather than a continuous transition in the commercially available steels.

Although vanadium carbide is appreciably softer than silicon carbide, wheels made of this abrasive have usually been found to be somewhat inferior to the most suitable aluminum oxide wheels for grinding the low grindability high speed steels. The reason is that by far the greater portion of the steel consists of martensite, which long experience has shown to be ground much more satisfactorily with aluminum oxide wheels. Any advantage presumably gained from grinding the vanadium carbide with the harder silicon carbide abrasive is more than offset by the greater advantage of grinding the martensitic matrix with aluminum oxide. Occasional reports that silicon carbide is superior indicate that under some grinding conditions the advantage may be the other way.

Carbide segregation can have an important effect on the grindability of a steel. It was observed that the power varied in an unexpected manner when steel AA<sub>2</sub> was ground. Normally the power varies in a uniform manner as the test block is fed across the wheel, 0.050 inch at the end of each table traverse. The power may stay substantially constant, or it may rise or drop gradually, or it may first rise and then drop during the course of a complete crossfeed, depending on the steel and the wheel being tested. For steel AA<sub>1</sub>, the power remained substantially uniform during a cross-feed, but for steel AA<sub>2</sub>, which was of the same 18-4-1 type, the power was lower for the central portion of the test block (in the direction of its width) than for the rest of it; however, the average power was consistently higher than for AA<sub>1</sub>. A macroetch showed pronounced carbide segregation in the central portion.

These results were obtained when the bar was down to about half its original thickness of 1½ inches as a result of other grinding experiments. The grindability index obtained under these conditions was much lower than for AA<sub>1</sub>, which did not show any marked carbide segregation in the portion for which the grinding data were obtained. Carbide segregation may well be the reason why in actual grinding practice a particular steel does not always respond to grinding in the manner considered normal for it and why in such cases the grinding conditions may have to be modified to get satisfactory results.



*Graphitic Tool Steels and AISI 52100*—In order to obtain the desired accuracy for these steels, most of which were very easy to grind, the grinding conditions were modified considerably to obtain sufficient wheel wear. The total downfeed was increased to as much as 0.100 inch, and the unit downfeed was 0.002 inch, twice as high as formerly. The resulting grinding energy and grindability index, plotted in Fig. 4, could not be converted to the standard grinding

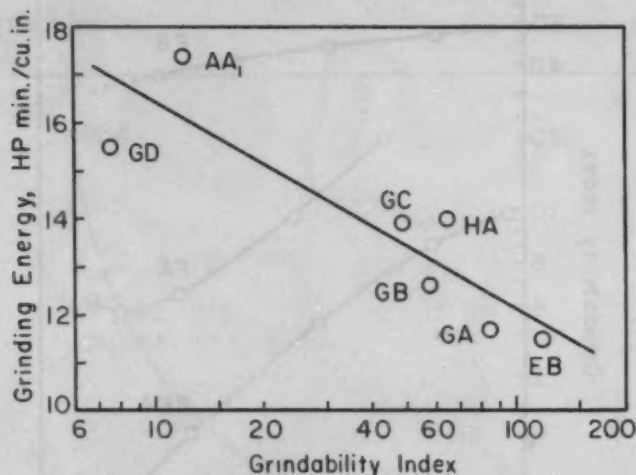


Fig. 4—Grindability Data for Graphitic Tool Steels and AISI 52100 Steel.

conditions used up to this point, because the new conditions were too dissimilar. However, steels EB and AA<sub>1</sub> were retested under the new conditions to furnish a basis for comparison. Except for GD, the graphitic steels, as well as AISI 52100 (steel HA), were somewhat less grindable than the oil hardening tool steel EB, but they were still in the high grindability class. Steel GD, containing almost 3% tungsten, had about the same grindability characteristics as the 18-4-1 high speed steel AA<sub>1</sub>. Before any conclusions can be drawn as to the possible effect of free graphite on the grindability of tool steels, it would be necessary to test steels free from graphite that are in other respects more similar to the graphitic steels than the ones that were available.

*Rockwell Hardness*—The effect of this variable was investigated for steels EB, FA and BEA, one from each of the major grindability groups. The softest of the BEA bars was in the annealed condition, while all the rest were quenched and tempered to the required hardness. They were ground with a 32A46-I8VBE wheel, the unit downfeed being 0.002 inch. The total downfeed was 0.100 inch for EB and 0.040 inch for the other two steels.

The grindability index, corrected as necessary to a standard

set of grinding conditions, is plotted for each steel as a function of the Rockwell hardness. Because the downfeeds were different from those used in obtaining the data of Fig. 1, the grindability indices of the steels in the C-60 range are not necessarily in agreement in the two plots. However, this does not affect the validity of the conclusions to be drawn.

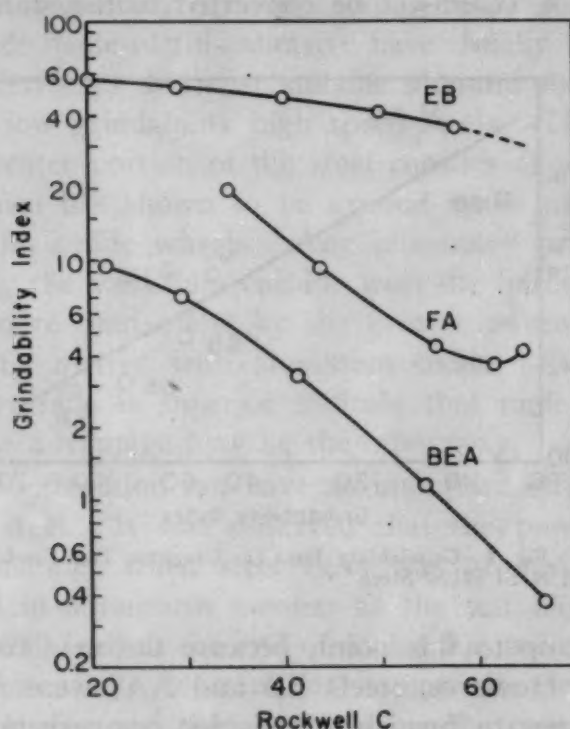


Fig. 5—Effect of Rockwell Hardness on Grindability Index.

It is immediately apparent from Fig. 5 that the lower the grindability of the steel in its normal high hardness range, the more rapidly does the grindability index increase with decreasing Rockwell hardness. A decrease in hardness from C-65 to C-20 doubles the grindability index of EB, but it increases the index over twenty-fold for BEA. This shows why it may be highly advantageous to rough grind the high vanadium, high speed steels in the soft condition when circumstances permit, leaving only the minimum amount of stock for finish grinding after heat treatment.

The minimum in the FA curve is a real one, since it was observed not only in the present experiment but also in each of the five runs on the C-62 and C-64 test blocks used in obtaining the data for Fig. 1. The reason for this slight reversal is not known.

The sharp rise in grindability index with decreasing Rockwell hardness, observed for steels BEA and FA, can probably be attrib-

uted to the softening of the martensitic matrix, in which the carbide particles are imbedded. The carbides remain just as hard but their effect on the wheel rapidly becomes less as the surrounding matrix becomes able to deform more readily with decreasing hardness.

The variation of grinding energy with Rockwell hardness was highly erratic for these steels, and a satisfactory explanation of this phenomenon is not available at present. This behavior furnishes additional evidence that grinding energy by itself is not a satisfactory measure of grindability.

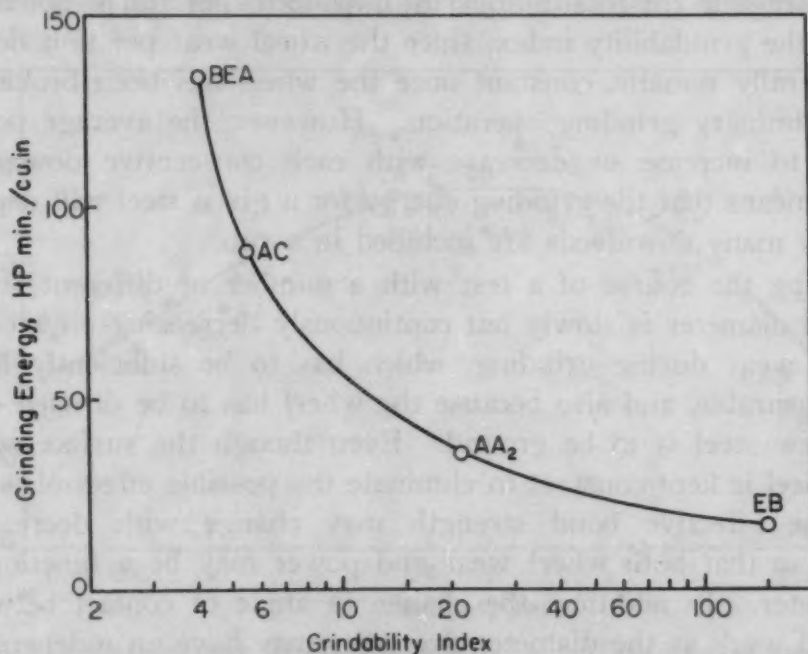


Fig. 6—Grindability Data for Four Steels Ground With an Extremely Hard Wheel, 32A60-M8VBE.

*Grinding Variables*—Provided that other grinding conditions are the same, a slight change in the grade of the wheel used does not affect very much the relative grinding energy and grindability index of a group of steels. When seven selected steels were ground with a 32A46-G12VBEP wheel, which is known to be quite similar to 32A46-I8VBE in its grinding characteristics except that the former produces a rougher finish, the grinding energy and grindability index fell reasonably close to the curve of Fig. 1.

However, when a 32A60-M8VBE wheel was used, which is much harder than is consistent with good surface grinding practice for hardened tool steels, the results shown in Fig. 6 were obtained. The unit and total downfeed were different for each of the four steels tested, so the points are not as reliable as those in Fig. 1, but the resultant uncertainty is not great enough to change the



general character of the curve appreciably. The curve is a satisfactory schematic representation of what happens when an extremely hard wheel is used.

The grinding energy rises very rapidly as the grindability index decreases, and there is no evidence of any discontinuity or change of direction in the curve, such as occurs in Fig. 1. The ratio of the grinding energies for BEA and EB is several times greater for the M than for the I grade wheel, while the ratio of the grindability indices is less for the former.

A change in the total number of downfeeds per run is not likely to affect the grindability index, since the wheel wear per unit downfeed generally remains constant once the wheel has been broken in by a preliminary grinding operation. However, the average power is likely to increase or decrease with each consecutive downfeed, and this means that the grinding energy for a given steel will depend upon how many downfeeds are included in a run.

During the course of a test with a number of different steels, the wheel diameter is slowly but continuously decreasing on account of wheel wear during grinding, which has to be sufficiently large to be measurable, and also because the wheel has to be dressed each time a new steel is to be ground. Even though the surface speed of the wheel is kept constant to eliminate the possible effect of wheel speed, the effective bond strength may change with decreasing diameter so that both wheel wear and power may be a function of the diameter. In addition, the change in angle of contact between wheel and work as the diameter decreases may have an independent effect on the wear and power.

One way of allowing for changing diameter is to grind a standard test block as often as appears to be necessary, and then to correct the data for the other steels in accordance with the trend shown by the steel used as a standard. However, this procedure is based upon the assumption that all the steels tested will exhibit the same trend, and this assumption is not always justified. For this reason, it is better to retest all the steels at several diameters and obtain the desired quantities for some common diameter by interpolation.

Other operating variables, such as wheel specifications, wheel speed, table speed, unit downfeed and unit crossfeed, may also affect the grindability data. The same is true if the nature of the operation is changed, as from surface to cylindrical grinding. The curve of grinding energy versus grindability index will vary with the grinding conditions, but the relative position of the various steels with respect to the others can be expected to remain roughly the same.

Of course, steels having similar grinding characteristics may appear in a somewhat different order on various curves, but the greater the difference between the grindability of the steels, the less likely is this to happen. These generalizations are based partly on other laboratory data and partly on shop experience.

#### FINISHABILITY AND OTHER RESULTS

*Factors Affecting Finishability*—When the grindability data recorded in Fig. 1 were being obtained, the surface roughness at the end of each run was measured on a profilometer. The results were

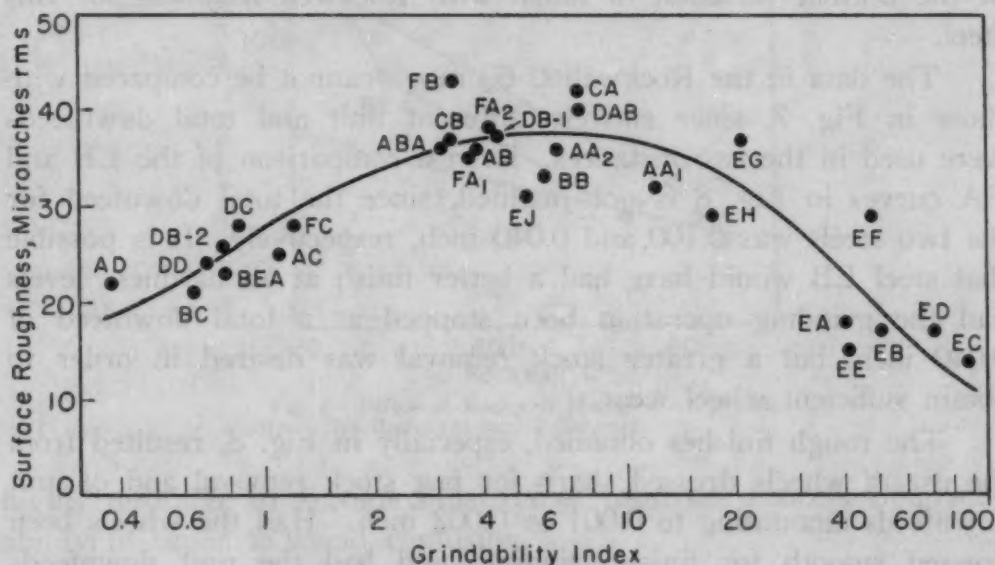


Fig. 7—Finishability Data for Same Steels as in Fig. 1. Unit downfeed was 0.001 inch.

corrected to a standard set of grinding conditions and the average value for each steel is plotted against its grindability index in Fig. 7. Although there is considerable scatter, it is evident that the medium grindability steels had the poorest finish, since the profilometer reading in microinches rms was the highest. The best finish was obtained with some, but not all, of the highest grindability steels, and an intermediate finish with the low grindability steels. This behavior can perhaps be explained in terms of the glazing or dulling of the abrasive grains, which is favored both by a decrease in the wheel wear and by the presence of extremely hard carbide particles in the steel.

The surface roughness tends to increase with grinding energy, but there is a great deal of scatter because the curves of Fig. 1 and Fig. 7 are dissimilar in the low grindability region.

It should be noted that the surface finish is extremely sensitive

to grinding conditions. Occasionally, the profilometer reading was very much higher for a given steel in one run than in all the others, yet the power and wear data were in good agreement. Such inconsistent finish data were not used in obtaining the average values.

The study of the effect of the Rockwell hardness on the grindability index of three steels also provided surface finish data, which are plotted in Fig. 8. In general, the softer the steel, the poorer is the finish, but this trend is reversed for the hardest specimen of steel BEA. Only a single surface was available at each hardness level, so this reversal in direction is not necessarily representative of the normal variation of finish with Rockwell hardness for this steel.

The data in the Rockwell C-60 range cannot be compared with those in Fig. 7, since entirely different unit and total downfeeds were used in the two instances. Even a comparison of the EB and FA curves in Fig. 8 is not justified, since the total downfeed for the two steels was 0.100 and 0.040 inch, respectively. It is possible that steel EB would have had a better finish at all hardness levels had the grinding operation been stopped at a total downfeed of 0.040 inch, but a greater stock removal was desired in order to obtain sufficient wheel wear.

The rough finishes obtained, especially in Fig. 8, resulted from the use of wheels dressed sharp for fast stock removal and of unit downfeeds amounting to 0.001 or 0.002 inch. Had the wheels been dressed smooth for finish grinding, and had the unit downfeeds been decreased to 0.0005 inch or less, considerably lower profilometer readings would have been obtained. With a properly selected wheel, all the steels in Fig. 7 can be finish ground to essentially the same high degree of finish, in the range of 5 to 10 microinches rms. However, a drop in Rockwell hardness, as in Fig. 8, is likely to result in a poorer finish, even under finish grinding conditions.

It is instructive to consider the relationship between grindability index and finishability. An *increase* in the index caused by a drop in Rockwell hardness is associated with a *decrease* in finishability (or increase in profilometer reading). The change is in the same direction as that in the left-hand portion of the curve in Fig. 7, where the change is caused by a change in the steel analysis and resulting microstructure; however, the relationship between the grindability index and finishability is reversed for the right-hand portion of the same curve, where an *increase* in the index is associated with an *increase* in finishability. Thus finishability may vary in the same direction as the grindability index.



or it may vary in the opposite direction, depending on circumstances. Since a change in the material that makes it easier to remove stock may make it either more or less difficult to attain a good finish when the wheel has been dressed sharp for rapid stock removal, and since in finish grinding the relationships between surface roughness and grindability index are still different, it is

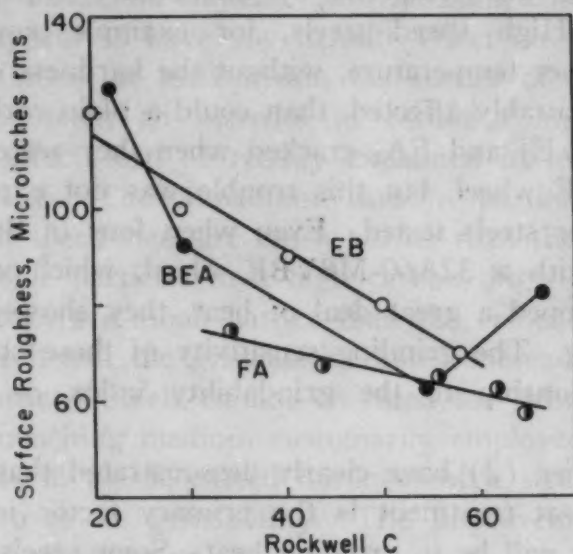


Fig. 8—Effect of Rockwell Hardness on Finishability. Unit downfeed was 0.002 inch.

highly desirable to exclude finishability from the concept of grindability in order to avoid confusion.

*Burn Depth and Surface Cracking*—At the outset of this study, it was thought that the relative depth of burn resulting from the use of a 32A46-I8VBE wheel might be helpful in interpreting grindability. The depth of burn was determined by suitably etching the slightly tapered surface of a test block (6). The taper was obtained by shimming up one end of the block the required amount on the surface grinder and then grinding it very gently with a very soft wheel. Steels AA<sub>2</sub>, BEA, DD, FA<sub>1</sub>, FB and all those in the miscellaneous group E were examined in this manner, but it was not possible to establish any correlation whatever with power consumption or with grindability index.

Although the etching technique was modified as appeared necessary in order to bring out the darkening associated with overtempering, the ground surfaces of the various steels responded so differently to etching that the apparent burn depth, which was generally under 0.001 inch, may have been seriously in error. Metallographic and microhardness examinations might have been

more satisfactory in establishing possible correlations, but destruction of the test blocks would have been involved. The depth of burn in a steel, if it were determined by these methods, would undoubtedly depend not only on the power consumed in grinding, which would bear some relation to the maximum temperatures attained at various small depths below the ground surface, but also on the extent to which the steel was tempered by momentary exposure to these temperatures. High speed steels, for example, could attain an appreciably higher temperature, without the hardness or microstructure being measurably affected, than could a plain carbon tool steel.

Steels EG, EJ and FA<sub>1</sub> cracked when they were ground with a 32A46-I8VBE wheel, but this trouble was not experienced with any of the other steels tested. Even when four of the other steels were ground with a 32A60-M8VBE wheel, which was much too hard and developed a great deal of heat, they showed no signs of surface cracking. The grinding sensitivity of these steels obviously bears no relationship to the grindability index or the grinding energy.

Other studies (2) have clearly demonstrated that the response of a steel to heat treatment is the primary factor in determining how sensitive it will be to grinding heat. Some steels, like EJ, are well known to be susceptible to surface cracking and greater care has to be taken in grinding them than most other tool steels. It is interesting to note that steel FA<sub>1</sub>, which is normally not particularly sensitive, cracked when it was first ground but the cracks were successfully ground out and did not reappear in subsequent grinding, which was of equal severity. Evidently the sensitive region in this test block was limited to a region near the original surface.

#### CONCLUSIONS

The grindability of tool and die steels, and presumably of other heat treatable varieties, can be expressed conveniently and usefully in terms of a dimensionless index which equals the volume ratio of the material removed to wheel wear. The numerical value of the index depends primarily on the grinding wheel used, since a soft one will wear more rapidly than a hard one, but it can also be affected by other variations in grinding conditions. An increase in the index for a given set of grinding conditions corresponds to an improvement in the grindability.

The grinding energy per unit material removed does not agree with shop experience in rating many of the tool steels from the standpoint of ease of grinding and thus is not, by itself, a useful

measure of grindability. However, when it is plotted against the grindability index defined above, the resulting grindability curve is very helpful in deciding how the various steels should be grouped with respect to grindability and in studying the factors affecting it.

The grindability index of nondeforming steels decreases rapidly with increasing chromium content and that of high speed steels with increasing vanadium content. Molybdenum, cobalt and columbium do not appear to have any definite effect on the grindability of high speed steels, at least within the scatter of the results. In 5% chromium steels, an increase in carbon content lowers the index. These effects can be readily explained in terms of carbide particle hardness. The vanadium carbide particles in a high vanadium, high speed steel are much harder than the complex iron-chromium carbide particles in a high carbon, high chromium steel and these in turn are much harder than the cementite particles in carbon tool steel, and the grindability index increases very rapidly in the same order. Steels cannot be rated for grindability on the basis of the quenching medium customarily employed.

A decrease in the Rockwell hardness of a steel by tempering generally improves its grindability. The improvement is greatest for the low grindability steels.

An increase in the grindability index may correspond either to an improvement or deterioration in the surface finish obtained. Under the surface grinding conditions used, in which the wheel was dressed sharp for fast stock removal, the medium grindability steels had a poorer finish than either the low or the high grindability steels. For the same steel, a decrease in Rockwell hardness generally leads to a rougher surface.

There is no relationship between the grindability of a steel and the extent to which it is burned under sufficiently severe grinding conditions, nor between grindability and grinding sensitivity.

#### ACKNOWLEDGMENTS

The cooperation of the following steel manufacturers in providing the heat treated test blocks used in this study is gratefully acknowledged: The Carpenter Steel Company, Crucible Steel Company of America, Latrobe Electric Steel Company, The Timken Roller Bearing Company, Universal-Cyclops Steel Corporation, and Vanadium-Alloys Steel Company. The author also wishes to thank Mr. H. L. Erikson for performing all the experimental work, and Mr. H. W. Wagner and Dr. L. H. Milligan for numerous helpful discussions during this investigation.



### References

1. O. W. Boston, "Machinability of Steel", *Metals Handbook*, American Society for Metals, 1948, p. 360.
2. L. P. Tarasov, "Some Metallurgical Aspects of Grinding", *Machining—Theory and Practice*, American Society for Metals, 1950, p. 409.
3. N. I. Volskii, "Grindability of Steel", *Stanki i Instrument*, Vol. 19, July 1948, p. 20.
4. H. Ernst, "Physics of Metal Cutting", *Machining of Metals*, American Society for Metals, 1938, p. 32.
5. L. P. Tarasov, "The Microhardness of Carbides in Toolsteels", *METAL PROGRESS*, Vol. 54, 1948, p. 846.
6. L. P. Tarasov and C. O. Lundberg, "Nature and Detection of Grinding Burn in Steel", *TRANSACTIONS*, American Society for Metals, Vol. 41, 1949, p. 893.

### DISCUSSION

**Written Discussion:** By W. R. Frazer, chief metallurgist, Union Twist Drill Co., Athol, Mass.

The author has added another chapter to the important factual knowledge regarding grinding of steels which he and his associates are assembling for the use of industry. This paper presents a yardstick for measuring the ease of grinding the various steels studied under laboratory-controlled conditions.

It is interesting to learn that finishing steel EJ containing 3.5% tungsten is ten times more difficult to grind than carbon tool steel EA and three times more difficult to grind than 5% chromium die steel EG, placing it in the much higher alloy group.

The author's observation regarding the effect of carbide segregation and its effect on grindability, as demonstrated by the two samples of 18-4-1 high speed steel, is of great importance. We note that the segregated area required less power to grind, which is the opposite of what we would expect. Since the average power required to grind the segregated sample was greater and the grindability lower, we would expect a larger carbide particle size was present. Did the author find this difference between the two samples? Also, did carbide particle size or distribution affect the location of points AD and CB in Fig. 1, since they seem to be out of place with respect to other steels of similar chemistry?

The tremendous value of vanadium in producing abrasion-resistant properties in tool steels is clearly shown by the grouping of the high vanadium steels at the left of Fig. 1. The grindability index, as determined by studies of surface grinding with a standard grade wheel, indicates that these steels are about five times more difficult to grind than conventional lower vanadium types. When first introduced, they did present a grinding problem to industry, but through the cooperation of the grinding wheel manufacturer and toolmaker, wheels have been developed that are successfully grinding these steels.

The introduction of high vanadium, high speed steel tools to industry during recent years has developed production records that have well established these steels as essential to the economic manufacture of consumer goods. The grinding wheel manufacturers have met the chal-

lence of the greatly increased wear resistance and can recommend the most suitable wheels for various grinding operations.

**Written Discussion:** By A. O. Mason, research metallurgist, Ternstedt Division, General Motors Corp., Detroit.

In the first place, since the working surfaces of practically all tools and dies are finished by grinding, the importance of this work would be difficult to overestimate.

It is customary for the toolmaker to grind his tools according to his own judgment. This judgment is based principally on his own limited experience and is guided by past failures where tools have been ruined by improper grinding.

Unfortunately, where the tools are only moderately damaged by grinding, the toolmaker seldom hears of it and he consequently assumes that his grinding practice is satisfactory. A comment by Dr. Tarasov or others on the probable truth of this statement would be appreciated. Dr. Tarasov's investigation makes it clear that good grinding of the various types of tool steels is a very complicated subject. The toolmaker with his limited knowledge of metallurgy and physics would perhaps be more confused than helped by conclusions such as the 200-to-1 variation in grindability shown by Dr. Tarasov.

It is believed, however, that a few quite limited grinding process specifications for hardened tool steel could be written, now that they are badly needed, and that their general use could be promoted without great effort or expense.

In his paper Dr. Tarasov used a testpiece 6 by 1½ by 1½ inches, and ran his tests by surface grinding. If Dr. Tarasov will recommend grinding conditions for surface grinding such a testpiece for 1% carbon, extra quality, carbon tool steel of medium hardenability, it is believed that the specification will have great value. Rough and finish grinding should, of course, be covered.

Toolmakers are highly intelligent and resourceful and it is believed that they will modify the specification in the right direction when grinding tools of different size and form.

Similar information for one oil hardening low alloy steel such as Dr. Tarasov's EB, an air hardening steel such as his FB, a hot work steel such as his EF, and a couple of high speed steels such as his DB-1 and his AA-1 would also be of great value.

It is believed that sound information on grinding the six steels listed will apply closely on over 90% of the tool steel used in this country.

Grinding specifications on these steels sponsored by an authoritative source can be adopted by master mechanics of large plants and managers of tool shops, and their actual use can consequently be promoted by those in authority where the tools are made.

Master mechanics know that grinding probably is the weakest factor in their tooling. It is, therefore, confidently expected that they will welcome and use such information.

The need for the grinding specifications outlined above has been discussed with Dr. Tarasov from time to time for several years. In view of his exhaustive investigation it is hoped that they can be supplied soon. He is doing a great service for industry and indirectly for the nation.

**Written Discussion:** By C. K. Baer, metallurgist, Sanderson-Halcomb Works, Crucible Steel Company of America, Syracuse, N. Y.

I congratulate the author for giving us a numerical measure of a complex attribute.

Both the user and the producer of tool steel should benefit by a scheme that evaluates the ease of grinding. The user's gain is obvious. To the producer, knowledge of his product's behavior in the consumer's operations, including grinding, is vital to the successful application of those products. Moreover, steels which resist the abrading action of a grinding wheel and hence have low grindability indices might be expected to resist also the abrading agents encountered in service and hence have high anti-wear properties. In fact, the grindability indices reported for the various tool steels are roughly in the same direction as the wear resisting characteristics displayed by those steels in service. Thus the author's work might furnish the tool steel man with the means to predict wear resistance in service. With a measure of grindability now available, and with the possibility of securing sufficient evidence that that measure correlates with resistance to wear in service, however, the author has set an immediate goal of increasing the grindability index without sacrificing anti-wear properties in service.

Such a purpose leads at once to the question of why the grindability index differs from steel to steel. In this connection I would like to comment on the author's brief reference to the part played by microstructure in influencing grindability.

It does not seem reasonable that the hardness of the carbides alone can account for the wide differences in grindability, as stated on p. 1157. Later in the text (p. 1161), in fact, the author hints that other structural factors may be important. This notion seems worthy of more emphasis and study. For example, steel BEA in the annealed condition (Fig. 5) presents to the grinding wheel just as many hard vanadium carbides as it does at the high hardness levels, yet the grindability index decreases sharply with increasing hardness. Even if the hardest carbides are the ones still undissolved when the steel itself is quite hard, these same carbides are also undissolved when the steel is soft. It seems proper, therefore, to endorse the suggestion that the hardness and strength of the martensitic matrix have a significant effect. We might even visualize that analogous actions cause the metal loss in grinding and the abrasive loss of the grinding wheel itself. High bond strength in a grinding wheel usually means high wheel hardness and low wheel wear. Similarly, the high bond strength of the martensite in the steel being ground could mean a greater ability to hold the hard carbides in place, thus forcing the particles of the grinding wheel to contact them more frequently, and thereby lowering the grindability. On the other hand, in the annealed steel the ferritic bond is weak and releases the hard carbides easily. This line of speculation may also partly explain the trend toward improved finishability with low grindability index.

**Written Discussion:** By Edward E. Hall, chief metallurgist, Cyclops Division, Universal-Cyclops Steel Corp., Titusville, Pa.

Dr. Tarasov's paper is an interesting contribution to a subject which has been flooded with opinions, but on which there is recorded very little



factual data. He is to be congratulated on his work, which is a start on a subject of great importance to users of tool steels.

Considerable thought has undoubtedly been given to the selection of the grindability index, but it is my suggestion that an index which increases as grinding difficulties increase would be more useful and less confusing to those who consider this subject only infrequently.

The grindability index has generally placed the several steels in the order in which they are commonly rated in the shop with respect to ease of grinding, but there seem to be slight discrepancies in the placement of some of the high speed steels. Referring to Figs. 1 and 3, it is my belief that the opinions of experienced grinders would not agree with the relationship shown between DB-1, DB-2, DC and BEA. Fig. 1 shows DB-1 to have a grindability index of approximately 4.5, while the other steels referred to are all in the vicinity of 0.7. A variety of shop grinding experiences, I believe, would rate DB-2 and DC between DB-1 and BEA, but definitely closer to DB-1, with the index decreasing in relation to the increase in vanadium and carbon.

Dr. Tarasov concluded that ease of grinding decreases according to the increase in volume and hardness of the carbide particles present. This would undoubtedly be correct if all other factors were equal, but it should be kept in mind that the volume of carbide particles present is greatest in the annealed condition where grinding is relatively easy. It seems to me that along with the hardness of the carbide particles, the ability of the matrix to hold these particles in place is very important. A question arises as to whether carbides are actually fractured or cut during grinding or are they pushed deeper into the matrix in the case of soft materials and possibly pulled out in the case of hard materials. The pulling out of carbides during the grinding of hardened steel might possibly explain the reversal of the curve for steel FA in Fig. 5. It is conceivable that at high hardnesses the matrix lacks sufficient toughness to hold in place the large carbide particles for which this type of steel is noted. The pulling out of carbides and their size might also explain some of the results listed in the finishability data.

It is hoped that Dr. Tarasov will continue his studies to further enlarge upon this very interesting subject.

**Written Discussion:** By A. O. Schmidt, research engineer, Kearney & Trecker Corp., Milwaukee.

The grindability of tool steels as reported in this paper presents data highly interesting to the production engineer. Although new cutting tool materials of the cast alloy and tungsten-titanium carbide type are available to industry, tool steels which will permit good production still are very much in demand. They are less brittle and usually permit the use of positive rake angles which minimize work hardening when machining alloy steels. The values plotted in Fig. 1 suggest that those steels which are harder to grind may, in operation, have a better tool life. It might be assumed that high speed steels which are harder to grind should have more wear resistance which would be synonymous with improved tool life in most cases.

Comparative tests, in which the high speed steel materials AA<sub>1</sub> and DC respectively were used as blades in a 12-bladed, 5-inch diameter face

mill, were conducted. When milling 350 Bhn dieblock steel in short-time tests at 120 to 185 feet per minute with these cutters, very little difference between the materials could be established. At 185 feet per minute material DC stood up better and at 120 feet per minute the cutter with blades of AA<sub>1</sub> gave better results. No coolant was used in either case.

However, in a production test, when milling forgings of SAE 4615 at 120 feet per minute the cutter with blades of DC material gave an average of 100% more pieces when used in comparison with cutters having blades of 18-4-1 type. An emulsion 40:1 was used as a coolant.

Since it was not possible to test all the high speed steel tool materials used in the grindability tests, this milling test is limited. Other reports might help to give a more complete picture of the relationship between grindability and high speed steel tool life.

#### Author's Reply

The questions raised and the comments offered by the discussers, who represent both the makers and users of tool steels, will be very helpful in the planning of further studies of grindability, whether by ourselves or by other experimenters. The measurement of grindability is not particularly difficult but there are so many metallurgical and grinding factors capable of affecting grindability that it is hoped this paper will stimulate others to investigate some of the factors of especial interest to them.

The questions raised by Dr. Frazer with regard to the possible effects of carbide particle size and distribution cannot be answered at present, since the test blocks had to be reserved for other studies involving grinding recommendations, and thus could not be sectioned for metallographic examination. The drop in power observed as the wheel moved into the carbide-rich portion of the segregated high speed steel block AA<sub>2</sub> indicates that the wheel began to cut more freely, perhaps because it wore more rapidly than before and thus presented sharper cutting points. Further experimentation under carefully controlled conditions is necessary to determine whether or not this explanation is correct and also why the average power was simultaneously considerably greater than for the unsegregated test block AA<sub>1</sub>.

Mr. Mason's remarks indicate clearly the importance of furnishing tool and die makers with improved grinding recommendations for a number of commonly used steels. The necessary data from which such recommendations can be made are now being obtained, but it must be realized that a great deal of work has to be done in order for the new recommendations to be an actual improvement over those now existing, based as they are upon years of field experience.

As Mr. Mason has pointed out, improper grinding that results in tool spoilage can be readily recognized by the toolmaker, but when the damage is only moderate, the useful life of the tool or die may be considerably shortened without anyone becoming aware of the underlying cause. However, even slight damage can generally be detected by means of well-established inspection techniques, some of which involve metallographic studies. This means that the plant metallurgist, where one is available, should be brought into the grinding picture. Close cooperation between the metallurgist and the tool-engineer is necessary if grinding practice

is to be improved so that tool and die life can be increased by eliminating the type of damage which at present remains undetected.

Mr. Baer brings up the possibility of establishing some sort of correlation between grindability and wear in service. While resistance to wear and resistance to grinding are observed to be associated in a general way, there is no simple relationship between the two and it is not likely that the relative wear resistance of various types of steels can be predicted on the basis of grindability data. Wear is an extremely complicated phenomenon, and the same is true of the grinding process, which involves both wheel wear and metal removal. The wear resistance of a steel under service conditions will be affected by a variety of factors, and so will its resistance to grinding, as measured by wheel wear or grindability index, but it is not likely that the major factors will be the same in the two cases. However, if the samples to be tested are quite similar in their make-up, such as different lots of the same material, it may be possible to find a reasonably good correlation between wear resistance and grindability.

Dr. Schmidt's preliminary results show clearly that two steels may differ much more with respect to grindability index than with respect to wear resistance as measured by tool life. The grindability index of steel AA<sub>1</sub> was 14 times as large as that of steel DC, which is another way of saying that the wheel wear resulting from the grinding of DC was 14 times that for AA<sub>1</sub>, assuming equal metal removal. In spite of this, the DC tool lasted only twice as long as the AA<sub>1</sub> tool when the die blocks were milled wet, and there was very little difference between the two high speed steels when the milling was done dry.

Even though two tool steels differ much more in their grindability than in their wear resistance in a particular application, as in the foregoing instance, a moderate gain in wear resistance may be enough to compensate for a considerably lower grindability index. The thing that matters is the total cost of machining the work, which includes time and tool costs, the latter involving the cost of the finished tool and of regrinding it when it dulls. In spite of the higher grinding costs, a lower grindability tool steel may give sufficiently longer tool life to warrant its use on the basis of over-all economy. A great deal of experimental work is obviously needed to determine the relationships that may exist between resistance to grinding and resistance to wear in service.

Both Mr. Baer and Mr. Hall discuss the important effect of the matrix hardness upon the grindability index in greater detail than was done in the paper. The question as to what actually happens in grinding to the carbide particles in tool steels varying in Rockwell hardness can be answered only after further experimentation.

In answer to Mr. Hall's suggestion that it would be better to have the grindability index increase with the difficulty of grinding rather than with the ease of grinding, we have simply followed the accepted terminology in the field of machinability studies, where an increase in the machinability index always corresponds to greater ease of machining. Since grindability is a special form of machinability, it is desirable to preserve consistency in terminology wherever possible.

Mr. Hall has raised the interesting point that on the basis of shop



experience high speed steels DB-2 and DC should be closer to DB-1 than to BEA with respect to grindability index than is indicated by Fig. 1. One possible explanation for the supposed discrepancy between shop and laboratory evaluation of these steels is that the grinding conditions may have been significantly different. Results obtained with a fairly large test block, like that used to determine grindability, may not be parallel to those obtained when the cut is frequently interrupted, as is the case when small tools are ground.

Another possibility is that the shop evaluation of grinding difficulty is based partly on the relative ease of finding satisfactory grinding conditions and partly on the relative wheel wear for a standard set of grinding conditions, rather than entirely on the latter. Laboratory experience with low grindability steels has shown that it is much easier to find satisfactory grinding conditions for some of these steels than for certain others having essentially the same grindability characteristics. Further study will be necessary to clarify the relationship between grindability as measured in the laboratory and the ease of grinding as vaguely defined in the shop. The present work is only a first step in that direction.

Some supplementary data have been obtained very recently, too late for inclusion in Fig. 1, which substantiate in a general way the shape of the grindability curve between index values of 1 and 6, and fill the gap between the low and medium grindability steels. Two experimental wear-resistant steels were tested in the heat treated condition. The high carbon, high chromium, high vanadium type fell halfway between FC and FB, just slightly below the line joining them. The values for the grindability index and the grinding energy were 2.2 and 16.4 respectively. The other steel, lower in chromium, fell considerably above the curve, the corresponding values being 1.9 and 20.0. No explanation is available at present why the value of grinding energy for this steel, just as for CB, is much higher than for the other steels with the same grindability index. Perhaps the line sloping downward to the left in the curve of Fig. 1 should be widened into a band whose upper boundary is a line through DC and BC. As more data are accumulated, the shape of the grindability curve (or band) for a given set of grinding conditions will become better defined.

## EFFECT OF ALLOYING ELEMENTS ON NOTCH TOUGHNESS OF PEARLITIC STEELS

BY J. A. RINEBOLT AND W. J. HARRIS, JR.

### *Abstract*

*The effects of alloying elements on Charpy V-notch properties were investigated. Al, B, C, Cr, Cu, Mn, Mo, Ni, P, S, Si, Ti, and V were added singly to a base composition of 0.30% carbon, 1.00% manganese, and 0.30% silicon. All specimens had a coarse pearlitic microstructure which was held as constant as possible.*

*The transition temperature in Charpy V-notch tests was lowered by manganese and nickel and raised by carbon, copper, molybdenum, phosphorus, and silicon. Effects of the other additions were complex. In addition to changing transition temperature, additions were found to change maximum energy and the shape of the curve. The effects of carbon, manganese, and nickel were approximately additive.*

*No exact correlation was found between tensile properties and transition temperature, but a good correlation was found between maximum energy and reduction of area.*

THE present study was initiated to establish the quantitative effects of alloying elements on tensile properties and notch toughness of pearlitic steels, with variables other than composition held as constant as possible. It was felt such an investigation might delineate clearly some of the factors which control impact resistance, might contribute to an understanding of the mechanism by which alloying elements affect brittle and ductile fracturing, and might lead to discovery of steels having improved low temperature ductility.

### EXPERIMENTAL PROCEDURE

#### *Melting and Forging Practice*

Eighty-nine small ingots of steel were made by melting approximately 250 pounds in a 300-pound capacity, basic-lined, high-frequency furnace. These melts were split into four or five ingots

---

This paper represents only the personal opinions of the authors and in no way reflects the official attitude of the U. S. Navy. Published with permission of the U. S. Navy Department.

A paper presented before the Thirty-second Annual Convention of the Society, held in Chicago, October 21 to 27, 1950. The authors, J. A. Rinebolt and W. J. Harris, Jr., are associated with the Ferrous Alloys Branch, Metallurgy Division, Naval Research Laboratory, Washington, D. C. Manuscript received April 19, 1950.

of about 55 pounds each. One of the splits, generally the first, was made to a base composition for use as a check on uniformity of melting practice from heat to heat. Increasing amounts of a single alloy addition were added to subsequent splits to cover the range of compositions desired. The same melting practice was used on all heats. Armco iron was first charged in the furnace. After it became molten, which required about 55 minutes, the slag was skimmed off, ferrosilicon (97%) was added, and then additions of electrolytic manganese and Mexican graphite (87% carbon) were made to give the base composition. Just before pouring, the heats were killed with 1.5 pounds of aluminum per ton of steel. Immediately after the first ingot was poured, the desired alloying addition for the second ingot was made, and immediately after that addition went into solution, the second ingot was poured. This procedure was carried out for the balance of the ingots. Delay between pours averaged 2 minutes, while the time between meltdown and final pour was approximately 15 minutes. All ingots were poured at 2850 °F (1565 °C) into big-end-up, cast iron chill molds provided with hot tops and a pouring cup.

The ingots, which were 4 by 4 by 18 inches, were sawed into blanks 4 by 4 by 1½ inches. These blanks were homogenized at 2300 °F (1260 °C) for 1 hour and then forged to 5/8-inch square bars. Forging was done on all four sides of the bars without reheating.

#### *Composition and Sampling Methods*

The chemical composition is shown in Table I.\* The base analysis of all the melts was 0.30% carbon, 1.00% manganese and 0.30% silicon. Chips for chemical analysis were taken from the hot top adjacent to the ingot. This sampling technique was checked on each ingot by analyzing a random Charpy blank and comparing it with that from the chips taken from the hot top. Differences between the two analyses averaged less than 0.01% carbon, 0.02% manganese, and 0.01% silicon. Differences for other additions were from 0.001 to 0.03%. A further check made by taking chips from the top, center, and bottom portions of four ingots showed the extent of segregation to be very small.

#### *Heat Treatment*

In the course of establishing a heat treatment which would produce constant microstructure, isothermal and continuous cooling

\*Additional heats made for studies of the effects of carbon, chromium, cobalt, nitrogen and silicon are reported in the first paragraph of the authors' reply.



Table 1  
Composition, Pearlite (%), Grain Size and Temperatures of Transformation  
During Continuous Heating and Cooling

Steel	C %	Mn %	Si %	S %	P %	N <sub>2</sub> %	Element Varied %	Pearlite %	ASTM Ferrite Grain Size	Ac <sub>1</sub>	Ac <sub>3</sub>	Ar <sub>3</sub>	Ar <sub>1</sub>	Ac <sub>1</sub> -Ar <sub>1</sub>
Al 1	0.28	1.01	0.29	0.018	0.005	0.0045	(Al) 0.001	46	6	1340	1500	1320	1180	160
Al 2	0.29	1.02	0.29	0.016	0.006	0.0045	0.019	39	7	1350	1480	1350	1220	130
Al 3*	0.28	0.98	0.26	0.012	0.005	0.0045	0.050	36	7	1350	1480	1350	1210	140
Al 4	0.28	0.96	0.25	0.016	0.006	0.0045	0.092	40	8	1350	1480	1350	1210	140
B-1*	0.29	1.06	0.27	0.02	0.005	0.005	(B) 0.0005	38	8	1350	1480	1350	1200	150
B-2	0.29	1.07	0.26	0.02	0.005	0.005	0.0011	37	8	1350	1480	1350	1200	150
B-3	0.29	1.05	0.25	0.02	0.005	0.005	0.0022	36	8	1350	1480	1350	1215	135
B-4	0.28	1.01	0.24	0.02	0.005	0.005	0.0044	42	7	1350	1500	1350	1215	135
C-1	0.01	0.99	0.24	0.02	0.006	0.0045	(C) 0.01	0	6	1600	1650	1550	1510	90
C-2	0.11	0.99	0.24	0.02	0.01	0.0045	0.11	13	8	1365	1580	1445	1320	45
C-3	0.27	0.98	0.22	0.02	0.01	0.0045	0.22	29	8	1365	1540	1390	1205	160
C-3*	0.31	1.01	0.30	0.02	0.006	0.0045	0.31	40	8	1365	1475	1335	1210	155
C-6	0.43	1.02	0.28	0.02	0.006	0.0045	0.43	68	8	1350	1420	1280	1230	120
C-7	0.53	1.02	0.28	0.02	0.005	0.0045	0.53	82	8	1365	1420	1250	1200	165
C-8	0.63	0.99	0.26	0.02	0.004	0.0045	0.63	97	8	1360	1410	1250	1220	140
C-4	0.67	0.99	0.22	0.02	0.008	0.0045	0.67	100	8	1350	1380	1225	1230	120
Cr 1*	0.26	1.15	0.19	0.018	0.008	0.005	(Cr) 0.005	38	8	1350	1475	1350	1200	150
Cr 2	0.26	1.11	0.18	0.022	0.009	0.005	0.48	51	8	1370	1480	1330	1225	145
Cr 3	0.26	1.09	0.17	0.020	0.007	0.005	0.95	69	7	1380	1480	1315	1230	150
Cu 1*	0.32	1.06	0.25	0.018	0.003	0.005	(Cu) 0.03	43	8	1345	1460	1330	1210	135
Cu 2	0.32	1.04	0.27	0.02	0.003	0.005	0.50	46	8	1345	1460	1330	1210	135
Cu 3	0.34	1.00	0.27	0.02	0.003	0.005	1.02	45	8	1345	1460	1330	1210	135
Cu 4	0.35	1.02	0.27	0.019	0.004	0.005	1.60	53	8	1345	1460	1330	1210	135
Cu 5	0.34	1.01	0.27	0.018	0.004	0.005	2.00	58	8	1325	1425	1250	1180	145
Mn 1	0.27	0.30	0.31	0.02	0.006	0.005	(Mn) 0.30	22	8	1370	1510	1410	1275	95
Mn 2	0.28	0.49	0.30	0.02	0.006	0.005	0.49	31	8	1365	1520	1400	1240	125
Mn 3*	0.31	1.01	0.28	0.02	0.006	0.006	1.01	45	7	1350	1460	1330	1200	150
Mn 10	0.27	0.41	0.31	0.02	0.005	0.0035	0.41	23	8	1370	1520	1415	1260	110
Mn 11	0.29	0.80	0.31	0.02	0.005	0.0035	0.80	37	7	1370	1520	1415	1260	110
Mn 12*	0.30	1.09	0.30	0.02	0.005	0.0035	1.09	41	7	1370	1520	1415	1260	110
Mn 13	0.30	1.55	0.30	0.02	0.005	0.0035	1.55	51	8	1340	1470	1290	1150	190

\*Base analysis.

†No ferrite present.

Table I—Continued  
Composition, Pearlite (%), Grain Size and Temperatures of Transformation  
During Continuous Heating and Cooling

Steel	C %	Mn %	Si %	S %	P %	N <sub>2</sub> %	Element Varied % (Mo)	Pearlite %	ASTM Ferrite Grain Size	Ac <sub>1</sub>	Ac <sub>3</sub>	Ar <sub>3</sub>	Ar <sub>1</sub>	Ac <sub>1</sub> -Ar <sub>1</sub>
Mo 1*	0.30	0.98	0.23	0.02	0.006	0.0035	0.0	40	8	1350	1480	1315	1180	170
Mo 2	0.29	0.98	0.21	0.019	0.006	.....	0.11	36	8	.....	.....	.....	.....	.....
Mo 3	0.29	0.94	0.19	0.017	0.006	.....	0.18	34	7	.....	.....	.....	.....	.....
Mo 4	0.29	0.90	0.15	0.017	0.006	.....	0.29	41	7	1360	1500	1340	1240	120
Ni-1*	0.31	1.07	0.25	0.022	0.005	0.006	(Ni)	44	7	1350	1500	1325	1200	150
Ni-2	0.30	1.06	0.25	0.02	0.005	0.005	0.40	45	8	1340	1480	1320	1190	150
Ni-3	0.30	1.05	0.25	0.02	0.005	.....	1.00	43	8	1300	1440	1300	1160	140
Ni-4	0.30	1.02	0.23	0.02	0.005	.....	1.32	49	8	1320	1420	1260	1140	180
Ni-5	0.29	1.01	0.22	0.017	0.006	.....	3.15	53	8	1290	1400	1150	1035	255
Ni-6*	0.30	1.00	0.28	0.024	0.004	0.005	0.02	39	8	1350	1470	1350	1220	130
Ni-7	0.30	1.01	0.27	0.015	0.005	.....	0.16	42	8	.....	.....	.....	.....	.....
Ni-8	0.30	1.00	0.25	0.024	0.005	.....	0.32	38	8	.....	.....	.....	.....	.....
Ni-9	0.30	1.00	0.23	0.023	0.005	.....	1.80	41	8	1300	1400	1230	1100	200
P 1*	0.29	1.00	0.30	0.020	0.005	0.005	(P)	38	8	1335	1475	1315	1200	135
P 2	0.29	1.01	0.29	0.019	0.05	.....	0.05	36	8	1350	1500	1350	1220	130
P 3	0.28	1.01	0.28	0.020	0.12	.....	0.12	41	8	1350	1520	1370	1220	130
P 4	0.28	0.98	0.26	0.019	0.21	.....	0.21	38	7	1380	1520	1400	1220	160
P 5*	0.28	1.08	0.32	0.017	0.004	0.0045	0.004	40	8	1355	1490	1350	1220	135
P 6	0.27	1.02	0.30	0.02	0.015	.....	0.015	36	8	.....	.....	.....	.....	.....
P 7	0.28	1.02	0.31	0.02	0.030	.....	0.030	34	8	.....	.....	.....	.....	.....
P 8	0.27	1.01	0.32	0.016	0.042	.....	0.042	38	7	1355	1500	1370	1200	155
S 1*	0.28	1.05	0.31	0.026	0.007	0.005	(S)	38	8	1350	1480	1350	1210	140
S 2	0.28	0.99	0.29	0.047	0.007	.....	0.047	41	8	.....	.....	.....	.....	.....
S 3	0.28	1.00	0.28	0.063	0.005	.....	0.063	33	8	.....	.....	.....	.....	.....
S 4	0.27	0.99	0.27	0.137	0.006	.....	0.137	28	8	1350	1500	1390	1210	140
S 5*	0.28	1.04	0.28	0.007	0.006	0.004	0.007	39	7	1350	1480	1350	1210	140
S 6	0.28	1.03	0.27	0.015	0.006	.....	0.015	39	8	.....	.....	.....	.....	.....
S 7	0.26	1.02	0.26	0.021	0.006	.....	0.021	35	8	.....	.....	.....	.....	.....
S 8	0.26	0.98	0.27	0.028	0.006	.....	0.028	34	8	1350	1510	1360	1200	150

\*Base analysis.

Table 1—Continued  
Composition, Pearlite (%), Grain Size and Temperatures of Transformation  
During Continuous Heating and Cooling

Steel	C %	Mn %	Si %	S %	P %	N <sub>s</sub> %	Element Varied %	Pearlite %	ASTM Ferrite Grain Size	Ac <sub>1</sub>	Ac <sub>3</sub>	Ar <sub>3</sub>	Ar <sub>1</sub>	Ac <sub>1</sub> -Ar <sub>1</sub>
Si 1*	0.31	0.98	0.26	0.02	0.003	0.0045	(Si)	39	8	1360	1480	1350	1220	140
Si 2	0.32	0.97	1.03	0.02	0.003	.....	0.26	49	8	1385	1525	1365	1235	150
Si 3	0.32	0.96	1.81	0.02	0.003	.....	1.03	55	7	1420	1450	1410	1260	160
Si 4	0.33	0.98	2.52	0.02	0.004	.....	1.81	52	7	1450	1470	1300	1280	170
Si 5	0.34	0.99	3.05	0.02	0.004	.....	2.52	44	8	1465	1480	1300	1280	185
Si 6*	0.27	0.96	0.30	0.02	0.008	0.0045	0.30	35	8	1350	1500	1360	1215	135
Si 7	0.27	0.95	0.60	0.02	0.008	.....	0.60	31	8	1375	1520	1375	1220	155
Si 8	0.27	0.97	1.27	0.02	0.008	.....	1.27	42	7	1400	1550	1405	1240	160
Si 9	0.28	1.04	2.67	0.02	0.008	.....	2.67	34	7	1450	1470	1270	1260	190
Ti-1*	0.30	0.92	0.21	0.02	0.007	0.005	(Ti)	36	7	1360	1480	1355	1230	130
Ti-2	0.30	0.94	0.20	0.017	0.007	0.005	0.06	34	7	1350	1480	1370	1230	120
Ti-3	0.29	0.93	0.23	0.014	0.006	0.005	0.23	33	8	1350	1520	1400	1230	120
Ti-4	0.29	0.96	0.28	0.013	0.007	0.005	0.39	27	8	1350	1550	1410	1225	125
V-1*	0.29	0.98	0.28	0.018	0.007	0.0045	(V)	40	8	1355	1480	1350	1225	130
V-2	0.29	0.98	0.27	0.019	0.007	.....	0.07	44	7	1360	1500	1350	1210	150
V-3	0.29	0.98	0.26	0.02	0.007	.....	0.14	39	7	1370	1500	1370	1210	160
V-4	0.29	0.93	0.22	0.02	0.007	.....	0.21	28	7	1370	1525	1400	1210	160
C-Mn 1	0.11	0.57	0.31	0.013	0.004	.....	(C-Mn)	6	8	1460	1600	1500	1390	70
C-Mn 2	0.18	0.56	0.31	0.012	0.006	.....	0.11 0.57	18	8	1380	1550	1420	1220	160
C-Mn 3	0.20	1.12	0.31	0.011	0.004	.....	0.18 0.56	30	8	1350	1520	1380	1200	150
C-Mn 4*	0.32	1.05	0.29	0.012	0.004	0.0045	0.20 1.12	47	8	1360	1480	1330	1210	150
C-Ni 1	0.11	1.15	0.28	0.01	0.005	0.0045	0.32 1.05	14	8-9	1340	1540	1375	1260	80
C-Ni 2	0.20	1.17	0.28	0.007	0.003	.....	(C-Ni)	25	8	1330	1500	1340	1160	170
C-Ni 3	0.20	1.19	0.25	0.012	0.003	.....	0.11 0.52	31	8	1300	1440	1240	1060	240
C-Ni 4	0.29	1.05	0.22	0.018	0.003	.....	0.20 0.52	51	8	1300	1400	1180	1080	220
Mn-Ni 1	0.28	0.53	0.31	0.02	0.003	0.006	0.29 2.04	32	8	1360	1500	1400	1250	110
Mn-Ni 2	0.29	0.50	0.31	0.02	0.003	.....	(Mn-Ni)	33	8	1350	1480	1350	1220	130
Mn-Ni 3	0.28	1.02	0.31	0.02	0.002	.....	0.53 0.03	39	8	1340	1460	1310	1180	160
Mn-Ni 4	0.26	1.04	0.28	0.02	0.002	.....	0.50 0.54	38	8	1305	1420	1240	1080	225
							1.02 0.54							
							1.04 2.07							

\*Base analysis.



cycles were investigated. Normal pearlites were found after continuous cooling, while partially spheroidized carbides were present after isothermal transformation. It was determined that a cooling rate of 25 °F per minute from 1650 to 800 °F (900 to 425 °C) did lead to nearly constant microstructure, and that it could be obtained in an asbestos-lined stainless steel box loaded to give a constant mass and cooled in still air.

All Charpy and tensile blanks were given a normalizing treatment which consisted of holding at 1650 °F (900 °C) for 1 hour and air cooling.

The normalized blanks were given one of the following treatments:

a. *A Treatment*—Austenitized for 4 hours at 1650 °F (900 °C) and cooled at a rate of approximately 25 °F per minute. Frequent checks were made on the cooling rates at the center and at the edges and corners of the box to make certain that cooling was uniform.

b. *B Treatment*—Same as for A, followed by tempering for 4 hours at 900 °F (485 °C) and then cooling at a rate of 25 °F per minute.

#### *Dilatometric Technique*

Temperatures of transformation during continuous cooling at the rate used for Treatment A were established by use of a dilatometer. Care was taken to eliminate temperature gradients, slip, and other experimental errors. Dilation measurements were made with a dial gage calibrated to  $10^{-4}$  inches. Specimens were 1 inch long and 0.500 inch in diameter with a  $\frac{1}{8}$ -inch central hole in which the conical end of the rod used to measure dilation was firmly seated. Temperature was read from an indicating controller connected to thermocouple leads welded to the specimens. Oxidation was prevented by providing an inert atmosphere of purified nitrogen.

#### *Metallography*

Specimens for microexamination were cut either from the ends of Charpy bars broken at room temperature or from the threaded ends of broken tensile bars. Grain size was measured by projecting the magnified image of the specimen on a ground glass and comparing it with ASTM grain size charts. The percentage of pearlite was measured with a Hurlbut counter (3)<sup>1</sup> attached to the mechanical stage of a bench microscope.

No absolute measurements of pearlite spacing were made, since this spacing was kept constant, but comparisons of the spacings of

<sup>1</sup>The figures appearing in parentheses pertain to the references appended to this paper.

the base analysis and several of the more highly alloyed steels were made using the resolution method (4).

### *Charpy V-Notch Impact Tests and Tensile Tests*

Twenty standard V-notch Charpy specimens were prepared for each composition and heat treatment. The depth and angle of the notch of approximately 20% of all specimens were checked by projecting an image of the notch magnified 50 diameters on ground glass and checking it against a transparent template inscribed with lines at the limits of tolerance of the notch.

Impact testing was carried out at temperatures between  $-315$  and  $600^{\circ}\text{F}$ . These temperatures were obtained by the following methods:

370 to	600 $\pm 5^{\circ}\text{F}$	Furnace.
80 to	360 $\pm 2^{\circ}\text{F}$	Glycerine and heaters.
- 94 to	80 $\pm 2^{\circ}\text{F}$	Dry ice and alcohol.
-260 to	-100 $\pm 3^{\circ}\text{F}$	Freon 12 and liquid nitrogen.
-315	$\pm 2^{\circ}\text{F}$	Liquid nitrogen.

After being held for 15 minutes at temperature, the specimens were broken immediately<sup>2</sup> in a pendulum-type impact testing machine of 264 ft-lb capacity with a striking velocity of 16.5 ft/sec. Data taken were energy absorbed, fracture appearance and temperature of test.<sup>3</sup>

Duplicate tensile tests were made at room temperature on all alloys. Threaded end, 0.357-inch diameter tensile specimens with a gage length of 1.4 inches were used. The stress to give 0.2% strain was taken as the yield strength.

## RESULTS

### *Microstructure and Transformations*

The ferrite grain size given in Table I is ASTM 7 to 8 for all alloys except for the 0.01% carbon steel and the 0% aluminum steel. Table I also includes the percentage of pearlite which changes as the amount of carbon changes or as alloying elements modify the eutectoid carbon content. Checks were made on the spacing of pearlite in the base analysis and in several of the more highly alloyed steels. As far as could be determined, the spacings were uniform for the heat treatment used.

Transformation temperatures, shown in Table I, were deter-

<sup>2</sup>Tests with a stop-watch revealed that the complete operation could be carried out in not more than 4 seconds. Temperature change during this interval was found to be negligible.

<sup>3</sup>Curves were drawn through a plot of energy or fracture appearance versus temperature, and the transition temperatures were recorded. The fracture appearance was a visual estimate of the per cent of the broken surface occupied by cleavage facets.

mined for the majority of the alloys as a check on the uniformity of pearlite spacing, since it has been shown (4) that spacing is dependent on the difference between the critical temperature and the temperature of transformation. Although the transformation range includes both ferrite and pearlite reactions, it was apparent from the appearance of the dilation curves that the pearlite transformation occurred in a narrow temperature range at or near the temperature of completion of transformation.

In the base compositions the temperature difference between the beginning of transformation on heating and the end of transformation on cooling varied from 130 to 170 °F. Of the other steels, 58 out of 68 fell within a range of 120 to 180 °F. Those falling outside these limits were the low carbon and low manganese steels and the high nickel and high silicon steels. None of these showed abrupt changes in impact properties when they were compared with others in the series. The temperature of completion of transformation varied from 1180 to 1230 °F (640 to 665 °C) for the base analysis. Of the other steels, 56 out of 69 fell within a range from 1180 to 1240 °F (640 to 670 °C). Again those outside were the low carbon and low manganese steels and the high silicon and high nickel steels. The uniformity of the temperature difference between the start of transformation on heating and completion of transformation on cooling as well as the similarity of the temperature of the completion of transformation indicates that the pearlite spacings are similar.

### *Tensile Tests*

The effects of alloying elements on tensile properties are given in Table II. These results are for heat treatment A, which was a slow cool of 25 °F per minute from an austenitizing temperature of 1650 °F (900 °C). The data are discussed later in terms of their correlations with impact properties.

### *Impact Tests*

(a) *Definition of Transition Temperature*—Four of the more commonly used definitions for transition temperature are shown in Fig. 1. These cover a wide range of absolute values of temperature; at present there is no agreement that one has more merit than the others. Using all four definitions of Fig. 1, Fig. 2 gives the effect of composition on uncorrected transition temperature for four alloying additions. While the absolute value of the temperature depends on the definition selected, the trends are similar. The greatest devia-



Table II  
Tensile Properties and Transition Temperatures for All Steels

Steel No.	Element Varied %	Tensile Strength psi	Yield Strength psi	Elong. in 1.4 Inch, %	Reduction of Area, %	Average Energy T. Temp. (°F)	Adjusted Av. Energy† T. Temp. (°F)	50% Brittle T. Temp. (°F)	First Sign of Brittleness Trans. Temp. (°F)	15 Ft-Lb Trans. Temp. (°F)	Max. Energy Ft-Lbs	Min. Energy Ft-Lbs
Al 1A	Al	80,000	43,100	35	57	80	92	120	275	— 50	87	5
Al 1B	0.001	80,450	42,650	32	58	77	89	124	200	— 4	85	4
Al 2A	0.019	80,600	48,350	37	64	18	26	40	120	— 60	97	6
Al 3A	0.050	79,300	48,100	35	63	18	30	40	120	— 48	101	7
Al 4A	0.092	77,800	48,500	35	62	16	27	34	100	— 4	106	6
Al 4B	0.092	77,000	48,900	36	63	18	29	54	120	— 42	95	5
B 1A	B	80,200	49,050	34	63	16	30	35	100	— 58	94	8
B 2A	0.0011	79,850	45,850	35	61	30	46	57	130	— 50	97	3
B 3A	0.0022	79,300	44,800	34	63	37	52	63	140	— 43	92	4
B 4A	0.0044	77,150	40,350	35	61	41	58	64	150	— 39	95	4
C 1A	C	48,350	30,050	49	86	—102	—97	—98	—95	—115	240	4
C 1B	0.01	47,050	28,500	52	80	—120	—115	—115	—115	—127	230	5
C 2A	0.11	60,350	38,900	48	75	— 75	— 70	— 72	— 60	— 85	238	2
C 3A	0.22	71,450	45,200	39	66	6	12	24	75	— 58	134	6
C 5A	0.31	83,800	49,650	33	61	24	15	70	145	— 50	83	6
C 5B	0.31	84,350	51,850	36	61	32	23	63	130	— 40	88	6
C 6A	0.43	96,350	51,200	28	53	118	122	128	200	0	74	6
C 7A	0.53	106,000	52,500	26	49	150	154	182	230	72	49	5
C 7B	0.53	105,000	53,500	26	50	166	170	180	220	64	50	6
C 8A	0.63	121,125	55,200	18	35	212	215	252	320	168	35	5
C 4A	0.67	118,900	50,850	19	32	232	239	262	350	196	31	6
C 4B	0.67	120,800	53,500	19	34	240	243	260	320	200	29	8
Cr 1A	Cr	77,400	49,000	39	66	— 17	29	17	70	— 86	105	10
Cr 1B	0.005	77,575	49,000	38	66	— 20	26	6	70	— 118	110	2
Cr 2A	0.48	83,900	49,000	31	66	— 23	20	14	100	— 92	116	3
Cr 3A	0.95	90,050	57,250	28	67	52	94	108	200	— 6	100	4
Cu 1A	Cu	82,200	48,100	32	60	18	19	44	90	— 52	92	4
Cu 1B	0.03	78,550	48,000	33	63	18	19	40	106	— 60	96	6
Cu 2A	0.50	86,600	53,800	31	60	26	23	50	116	— 68	85	5
Cu 3A	1.02	96,050	63,400	30	57	68	51	94	130	— 36	75	7
Cu 4A	1.60	102,950	74,400	25	53	90	70	112	180	— 5	65	6
Cu 5A	2.00	112,750	79,650	21	50	128	112	165	210	8	60	5
Cu 5B	2.00	108,300	80,950	19	49	170	153	196	220	54	58	6

†Transition temperature adjusted to 0.30% carbon, 1.00% manganese and 0.30% silicon except where these elements were varied and then only the other two were adjusted to the base composition.

Table II—Continued  
Tensile Properties and Transition Temperatures for All Steels

Steel No.	Element Varied %	Tensile Strength psi	Yield Strength psi	Elong. in 1.4 Inch, %	Reduction of Area, %	Average Energy T. Temp. (°F)	Adjusted Av. Energy† T. Temp. (°F)	50% Brittle T. Temp. (°F)	First Sign of Brittleness Trans. Temp. (°F)	15 Ft.-Lb. Trans. Temp. (°F)	Max. Energy Ft.-Lbs	Min. Energy Ft.-Lbs
Mn 1A	Mn 0.30	67,350	42,100	40	59	78	92	98	160	9	100	4
Mn 1B	Mn 0.30	67,400	41,850	36	60	82	96	102	180	18	100	5
Mn 2A	Mn 0.49	70,350	46,000	38	61	50	60	80	140	24	100	5
Mn 2B	Mn 0.49	70,350	44,600	38	61	56	66	67	140	10	103	4
Mn 3A	Mn 1.01	83,700	53,625	35	62	26	23	50	120	50	99	6
Mn 3B	Mn 1.01	82,850	47,950	38	62	36	34	70	140	30	92	5
Mn 10A	Mn 0.41	68,200	41,500	36	60	64	78	82	100	10	99	4
Mn 11A	Mn 0.80	76,950	47,550	34	60	40	44	56	140	40	90	3
Mn 12A	Mn 1.09	83,200	52,200	32	62	18	18	40	100	68	93	6
Mn 13A	Mn 1.55	91,500	61,000	31	68	15	15	10	82	110	105	5
Mo 1A	Mo 0.0	78,400	46,450	36	62	16	21	56	120	48	96	6
Mo 1B	Mo 0.0	78,700	47,600	36	62	4	9	44	120	64	98	4
Mo 2A	Mo 0.11	77,250	48,150	40	59	48	60	85	160	14	92	4
Mo 3A	Mo 0.18	77,800	49,300	34	57	80	90	120	200	14	87	4
Mo 4A	Mo 0.29	81,250	46,850	31	55	86	96	124	230	12	82	3
Mo 4B	Mo 0.29	79,050	50,200	31	55	84	94	124	160	0	88	2
Ni 1A	Ni 0.04	83,300	49,325	35	61	16	23	54	100	56	92	6
Ni 1B	Ni 0.04	83,450	49,500	35	59	16	23	44	80	49	95	5
Ni 2A	Ni 0.40	83,000	54,500	30	63	2	9	24	88	78	103	9
Ni 3A	Ni 1.00	85,500	57,700	30	65	2	8	32	110	105	105	4
Ni 4A	Ni 1.32	91,400	59,300	34	65	—	5	20	80	110	100	3
Ni 5A	Ni 3.15	97,500	65,175	35	66	22	8	10	48	154	100	7
Ni 5B	Ni 3.15	91,650	64,500	29	66	30	16	8	80	168	105	4
Ni 6A	Ni 0.02	82,100	52,600	33	63	14	16	40	90	70	90	5
Ni 7A	Ni 0.16	82,800	51,900	33	64	10	18	26	77	80	95	5
Ni 8A	Ni 0.32	83,000	54,500	34	63	14	15	30	90	70	90	4
Ni 9A	Ni 1.80	91,000	60,700	30	64	4	3	10	80	120	93	5

†Transition temperature adjusted to 0.30% carbon, 1.00% manganese and 0.30% silicon except where these elements were varied and then only the other two were adjusted to the base composition.

Table II—Continued  
Tensile Properties and Transition Temperatures for All Steels

Steel No.	Element Varied %	Tensile Strength psi	Yield Strength psi	Elong. in 1.4 Inch, %	Reduction of Area, %	Average Energy T. Temp. (°F)	Adjusted Av. Energy† T. Temp. (°F)	50% Brittle T. Temp. (°F)	First Sign of Brittleness Trans. Temp. (°F)	15 Ft-Lb Trans. Temp. (°F)	Max. Energy Ft-Lbs	Min. Energy Ft-Lbs
P 1A	P 0.005	80,300	50,950	37	62	18	23	50	110	— 44	97	6
P 1B	P 0.005	80,750	49,400	36	63	18	23	36	116	— 62	98	6
P 2A	P 0.05	85,350	50,050	34	60	76	83	110	190	— 30	98	4
P 3A	P 0.12	90,375	50,750	33	59	176	189	220	290	— 80	88	5
P 4A	P 0.21	95,550	58,400	30	53	260	272	305	370	160	85	5
P 4B	P 0.21	94,700	57,300	30	54	290	302	325	400	162	82	6
P 5A	P 0.004	79,750	50,700	37	65	2	18	30	90	— 70	109	4
P 6A	P 0.015	81,900	50,850	35	64	5	22	20	95	— 52	105	6
P 7A	P 0.030	82,800	51,800	36	63	32	43	54	100	— 44	101	3
P 8A	P 0.042	83,400	49,650	33	61	84	98	100	200	— 2	94	4
S 1	S 0.026	81,700	52,400	28*	64	5	19	20	70	— 70	105	6
S 2	S 0.047	79,650	51,150	29*	62	10	0	26	70	— 90	80-110	6-6
S 3	S 0.063	79,350	51,350	28*	62	—	0	—	60	— 70	70-130	4-4
S 4	S 0.137	74,350	47,500	29*	55	—	1	—	70	— 58	60-160	4-4
S 5	S 0.007	78,900	48,800	33	63	—	14	20	70	— 74	110	4
S 6	S 0.015	78,300	49,500	34	64	0	16	20	90	— 78	110	4
S 7	S 0.021	77,350	51,250	34	65	—	20	10	80	— 80	100	4
S 8	S 0.028	75,750	49,550	35	63	—	7	0	70	— 65	92	4
Si 1A	Si 0.26	79,800	48,650	34	61	6	3	48	96	— 62	96	4
Si 1B	Si 0.26	76,600	46,450	35	63	22	19	48	112	— 68	103	6
Si 2A	Si 1.03	95,100	55,100	30	58	112	99	146	208	0	75	6
Si 3A	Si 1.81	105,000	62,600	28	57	220	206	250	312	96	67	6
Si 4A	Si 2.52	114,900	73,000	25	46	302	285	340	420	204	52	6
Si 5A	Si 3.05	121,500	82,100	29	46	352	331	406	430	252	52	3
Si 5B	Si 3.05	121,600	81,200	23	44	354	333	400	420	220	51	2
Si 6A	Si 0.30	77,100	48,950	36	63	0	11	10	60	— 62	106	4
Si 7A	Si 0.60	83,400	52,550	35	63	35	45	60	100	— 56	97	6
Si 8A	Si 1.27	92,200	54,900	33	60	120	132	140	200	0	86	5
Si 9A	Si 2.67	109,000	73,500	29	53	300	314	320	380	176	69	4
Ti 1A	Ti 0.0	79,800	49,750	38	63	16	17	27	120	— 56	97	5
Ti 1B	Ti 0.0	78,950	48,150	38	62	10	11	38	120	— 64	100	5
Ti 2A	Ti 0.06	79,400	49,450	35	62	60	64	98	180	— 16	113	5
Ti 3A	Ti 0.23	77,350	49,600	36	63	28	33	76	130	— 48	122	6
Ti 4A	Ti 0.39	77,000	52,450	35	66	7	10	28	80	— 76	132	6
Ti 4B	Ti 0.39	77,250	51,700	39	60	12	15	42	70	— 62	128	8

\*Elongation in 2-inch gage length.

†Transition temperature adjusted to 0.30% carbon, 1.00% manganese and 0.30% silicon except where these elements were varied and then only the other two were adjusted to the base composition.



Table II—Continued  
Tensile Properties and Transition Temperatures for All Steels

Steel No.	Element Varied %	Tensile Strength psi	Yield Strength psi	Elong. in 1.4 Inch, %	Reduction of Area, %	Average Energy T. Temp. (°F)	Adjusted Av. Energy† T. Temp. (°F)	50% Brittle T. Temp. (°F)	First Sign of Brittleness Trans. Temp. (°F)	15 Ft-Lb Trans. Temp. (°F)	Max. Energy Ft-Lbs	Min. Energy Ft-Lbs
V 1A	0.006 V	79,500	49,450	36	63	2	7	36	80	-60	100	6
V 1B	0.006 V	80,075	50,250	38	63	16	21	38	100	-54	98	7
V 2A	0.07	85,250	53,700	31	58	66	72	90	180	-	80	5
V 3A	0.14	94,000	62,500	26	55	118	125	134	200	-26	69	4
V 4A	0.21	91,800	65,450	28	57	86	86	126	180	-8	87	5
V 4B	0.21	92,700	67,800	29	56	68	74	105	185	-12	87	3
C-Mn-1	0.11 0.57 Mn	56,400	36,700	47	73	52	51	48	-40	-62	240	4
C-Mn-2	0.18 0.56	65,000	40,950	37	66	4	3	20	70	-48	140	2
C-Mn-3	0.20 1.12	72,450	47,000	42	69	32	21	16	20	-92	152	6
C-Mn-4	0.32 1.05	84,450	51,700	33	61	30	26	60	90	-52	100	4
C-Ni-1	0.11 0.52 Ni	66,350	45,850	42	75	102	85	115	-85	-170	248	2
C-Ni-2	0.20 0.52	77,250	53,200	40	72	62	43	40	10	-160	154	5
C-Ni-3	0.20 2.03	84,550	60,900	36	73	80	56	66	-	-192	153	7
C-Ni-4	0.29 2.04	94,400	64,750	31	66	18	5	8	80	-126	106	6
Mn Ni-1	0.53 0.03 Mn Ni	71,700	43,100	35*	60	42	51	70	160	-28	87	3
Mn Ni-2	0.50 0.54	77,000	49,100	29*	57	50	54	82	135	-30	89	6
Mn Ni-3	1.02 0.54	83,500	54,500	28*	64	10	1	13	90	-75	104	5
Mn Ni-4	1.04 2.07	90,650	63,900	28*	65	40	14	14	40	-160	109	4

\*Elongation in 2-inch gage length.

†Transition temperature adjusted to 0.30% carbon, 1.00% manganese and 0.30% silicon except where these elements were varied and then only the other two were adjusted to the base composition.

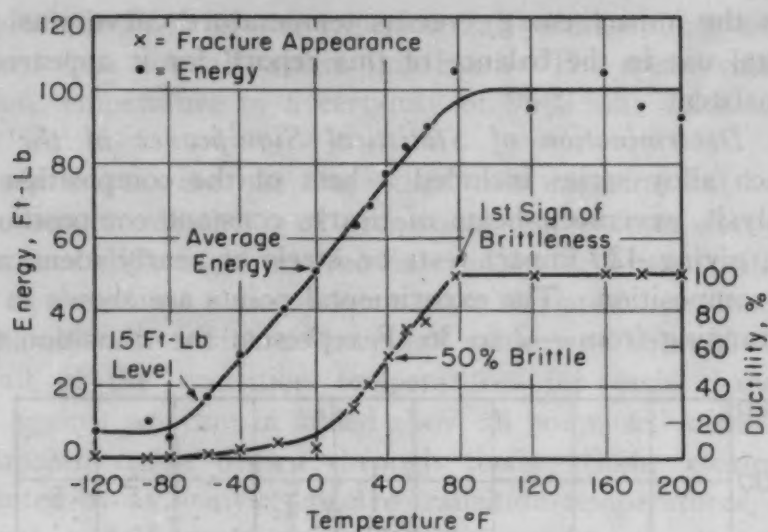


Fig. 1—Typical Curve Showing Different Transition Temperatures on Steel V1A.

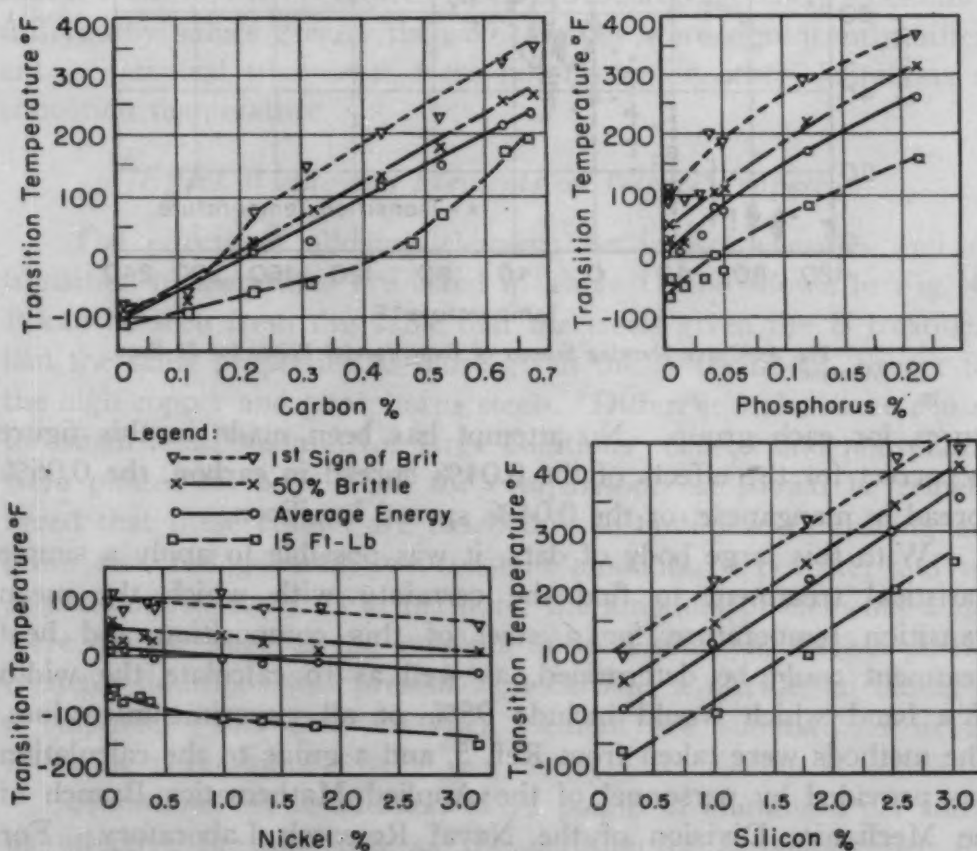


Fig. 2—Comparison of Effects of Alloying Elements (C, P, Ni, and Si) on Transition Temperature Using Different Definitions.

tions are for the carbon and the nickel steels, using the 15-ft-lb definition.

The temperature based on the intersection of the average energy

line with the impact energy versus temperature curve was selected for general use in the balance of this report, for it appeared to be more consistent.

(b) *Determination of Statistical Significance of the Data*— Since each alloy series included a heat of the composition of the base analysis, seventeen heats of nearly constant composition were available, giving 420 impact tests on steels of nearly identical grain size and composition. The experimental points are shown in Fig. 3. Crosses ranging from  $-2$  to  $36^{\circ}\text{F}$  represent the transition temper-

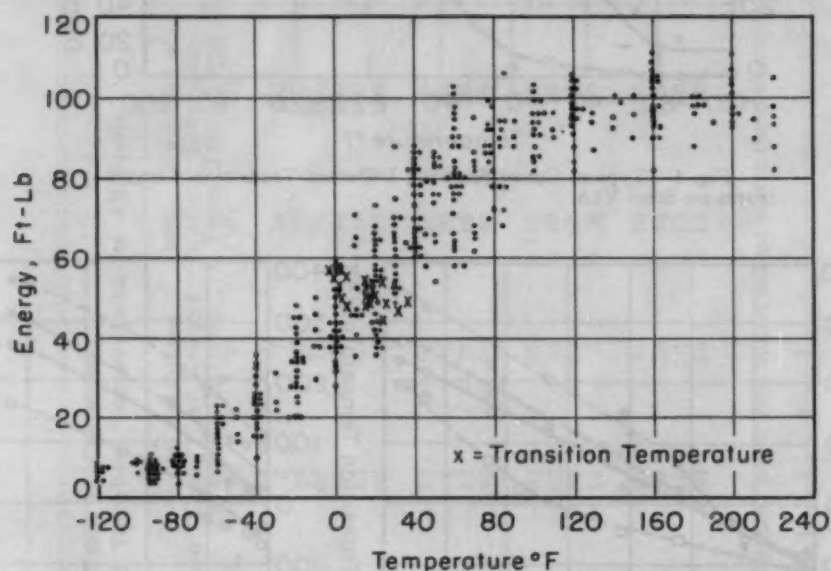


Fig. 3—Curve Showing Scatter of Experimental Points for 21 Base Analyses.

atures for each group. No attempt has been made in this figure to correct for the effects of the 0.04% spread in carbon, the 0.06% spread in manganese, or the 0.04% spread in silicon.

With this large body of data, it was possible to apply a simple statistical treatment to find the certainty with which the mean transition temperature for a steel of this composition and heat treatment could be determined, as well as to calculate the width of a band which would include 95% of all experimental values. The methods were taken from Ref. 5, and a guide to the calculation was provided by personnel of the Applied Mathematics Branch of the Mechanics Division of the Naval Research Laboratory. For these calculations, the adjusted transition temperatures given in Table II for the base compositions for both A and B heat treatment were used. The arithmetical average transition temperature was  $20^{\circ}\text{F}$  with a root mean square deviation of  $7.5^{\circ}\text{F}$ . Assuming a Gaussian distribution, a band of plus or minus twice this value



should include 95% of the experimental points. Only one of the 21 values does not fall within this band. The mean value of the transition temperature to a certainty of 95% was calculated to be  $20 \pm 5^\circ\text{F}$ .

Since there were not more than two experimental values (A and B heat treatments) of transition temperature for steels of compositions differing from the base analysis, it was neither practicable to determine a root-mean-square deviation nor to determine the certainty with which the average value was known. However, when all of the transition temperatures for each element were plotted against per cent of added alloy, all points fell within  $\pm 15^\circ\text{F}$  of a smooth curve drawn through them. Some elements were represented by as many as twelve transition temperatures, considering the A and B treatments and additional heats melted for study of intermediate compositions. From these results, it was considered that if transition temperatures based on the average energy definition differed by values greater than  $30^\circ\text{F}$ , they were significantly different. Statistical treatments were not made for other definitions of transition temperature.

#### *Effect of Alloying Elements on Impact Properties*

The effects of alloying elements on impact energies and on transition temperatures are listed in Table II and shown in Fig. 4.<sup>4</sup> It can be seen from this table that the steels given the B treatment had the same properties as those given the A treatment, except for the high copper and phosphorus steels. Different scales were chosen for small additions and for large additions; carbon and phosphorus were plotted on both scales for comparison. It should be remembered that these results are based on constant pearlite spacing and grain size and generally on constant amounts of pearlite, and not at constant strength. Furthermore, the amounts of elements added were not the same as the amounts in solid solution, since a portion of many additions was present as a carbide, a nitride, an oxide, or a sulphide. The data for each element are summarized in the following paragraphs.

**Aluminum**—The addition of  $\frac{1}{2}$  pound of aluminum per ton is as effective in this steel as the addition of 2 pounds per ton. Absence of aluminum contributes to a slight increase in the grain size, which may explain the higher transition temperature of the heat which contains no aluminum. Other possible explanations

<sup>4</sup>The curves are based on corrected values obtained by adjusting the experimental transition temperatures to constant values of carbon, manganese, and silicon, except when these were intentionally varied.

involve the effect of aluminum on oxygen and nitrogen.

*Boron*—Boron additions were so small that although boron seems to increase transition temperature rapidly and regularly, the points for all boron heats fell within the scatter band. Within the experimental error, then, boron in the small amounts added has no effect on transition temperature.

*Carbon*—Although carbon changes the microstructure by addition of pearlite, its effect on transition temperature is quite uniform. It increases transition temperature 6 °F per 0.01% above 0.30% carbon and 5 °F per 0.01% below 0.30% carbon. Since the 0.01% carbon steel had a larger grain size than the other members of the carbon series, its comparison with the finer-grained steels may be misleading, since, according to the works of Hodge et al. (2), its transition temperature may be 40 to 80 °F higher than that of an 0.01% carbon steel with the grain size equal to that of other steels in this series. Carbon lowers maximum energy.

*Chromium*—Chromium has little effect on transition temperature. For chromium contents above 0.9%, the microstructure is different from that of the base analysis and the results are not comparable. For revised comments on the effect of chromium, see discussion.

*Cobalt*—For effects of cobalt, see discussion.

*Copper*—Copper raises transition temperature slightly. Although the solid solubility limit was exceeded, no marked increase in transition temperature was noted, nor was any grain-boundary precipitate observed. From Table II, it can be seen that Cu 5B which was tempered at 900 °F (480 °C) for 4 hours has a higher transition temperature than Cu 5A. This suggests that the high copper steel is supersaturated with the copper-rich phase after cooling at the standard cooling rate of 25 °F per minute. Copper decreases maximum energy.

*Manganese*—Manganese up to 1.5% decreases transition temperature at a rate of approximately 1.0 °F per 0.01%. It does not change maximum energy. Amounts smaller than 0.30% were not studied. A steel with 2.00% of manganese heat treated identically with the less highly alloyed heats had a transition temperature in excess of 200 °F but a very different microstructure; therefore, it was not included in this study.

*Molybdenum*—Molybdenum increases transition temperature almost as rapidly as carbon, and it decreases maximum energy.

*Nickel*—Nickel is slightly beneficial. Although all of the data fall on a very smooth curve, the maximum difference between the

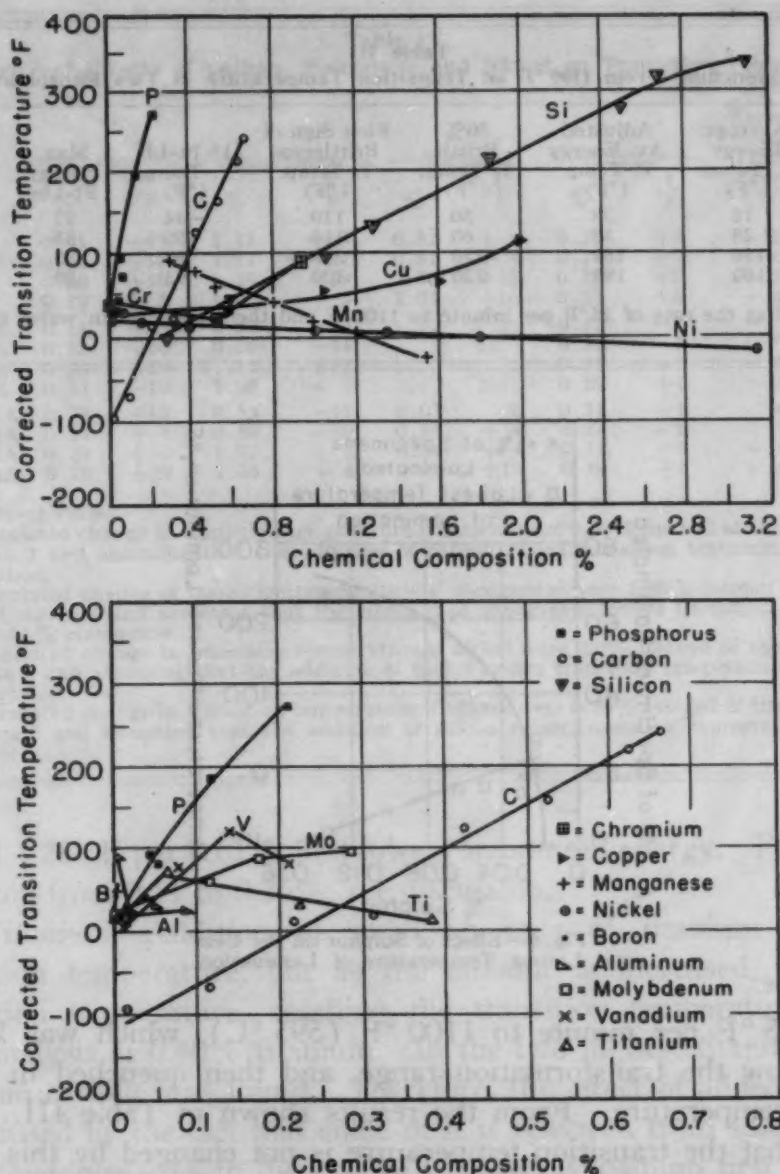


Fig. 4—Effect of Chemical Composition on Transition Temperature

steel with the highest nickel content and the base analysis is 30 °F, which is just equal to the experimental scatter. It should be emphasized again, however, that Fig. 2 shows the effect of nickel to be greater when a transition temperature criterion based on the 15-ft-lb level is adopted.

**Nitrogen**—For effects of nitrogen, see discussion.

**Phosphorus**—Phosphorus increases transition temperature at a rate of 13 °F per 0.01%. In view of the fact that phosphorus has been shown to increase the susceptibility to temper embrittlement most recently by Baeyertz and Craig (6), specimens of the base analysis and the high phosphorus steel were cooled at the standard



Table III  
Effect of Quenching From 1100 °F on Transition Temperature in Two Phosphorus Heats

Steel No.	Average Energy T. Temp. (°F)	Adjusted Av. Energy T. Temp. (°F)	50% Brittle T. Temp. (°F)	First Sign of Brittleness T. Temp. (°F)	15 Ft-Lb T. Temp. (°F)	Max. Energy Ft-Lbs	Min. Energy Ft-Lbs
P1A	18	23	50	110	-44	97	6
P1X*	28	33	60	116	-50	88	6
P3A	176	189	220	290	80	88	5
P3X*	180	193	220	300	93	89	2

\*Cooled at the rate of 25 °F per minute to 1100 °F and then quenched in water to room temperature.

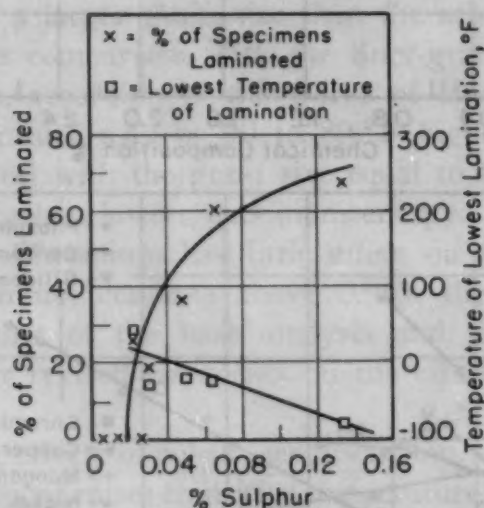


Fig. 5—Effect of Sulphur on Per Cent and Lowest Temperature of Lamination.

rate of 25 °F per minute to 1100 °F (595 °C), which was known to be below the transformation range, and then quenched in water to room temperature. From the results shown in Table III, it can be seen that the transition temperature is not changed by this treatment. Phosphorus also reduces maximum energy.

**Sulphur**—It was not feasible to include the effects of sulphur in Fig. 4, for sulphur increases the tendency toward lamination, and laminations result in large scatter. Fig. 5 indicates that as sulphur is added, the lowest temperature at which laminations occur decreases, and the percentage of specimens which are laminated increases. Sulphur increases the energy absorption when it induces laminations but appears to lower the maximum energy for specimens which fracture without laminations. It seems to have little effect on the transition temperature of unlaminated specimens and no effect on the portion of the Charpy curve below the minimum temperature for laminations.

**Silicon**—Silicon increases transition temperature regularly at a

Table IV  
Additivity of Effects of Carbon, Manganese and Nickel on Transition Temperature

Steel No.	Carbon		Manganese		Nickel		Silicon		Experimental Trans. Temp. (°F)	Calculated Trans. Temp. (°F)
	%	*°F	%	†°F	%	‡°F	%	§°F		
★ C-Ni 1A	0.11	+95	1.15	+15	0.52	+4	0.28	+2	-102	14
C-Ni 2A	0.20	+50	1.17	+17	0.52	+4	0.28	+2	-62	11
C-Ni 3A	0.20	+50	1.19	+19	2.03	+16	0.25	+5	-80	10
C-Ni 4A	0.29	+5	1.05	+5	2.04	+16	0.22	+8	-18	16
C-Mn 1A	0.11	+95	0.57	-43	.....	.....	0.31	-1	-52	-1
C-Mn 2A	0.18	+60	0.56	-44	.....	.....	0.31	-1	-4	11
C-Mn 3A	0.20	+50	1.12	+12	.....	.....	0.31	-1	-32	29
C-Mn 4A	0.32	-10	1.05	+5	.....	.....	0.29	+1	30	26
Mn-Ni 1A	0.28	+10	0.53	-47	0.03	0	0.31	-1	42	4
Mn-Ni 2A	0.29	+5	0.50	-50	0.54	+4	0.31	-1	50	8
Mn-Ni 3A	0.28	+10	1.02	+2	0.54	+4	0.31	-1	-10	5
Mn-Ni 4A	0.26	+20	1.04	+4	2.07	+16	0.28	+2	-40	2

★Element varied.

\*Calculated change in transition temperature if carbon were 0.30% instead of the value given in Column 2 and assuming that the addition of carbon raised transition temperature 5°F per 0.01% carbon.

†Calculated change in transition temperature if manganese were 1.00% instead of the value given in Column 4 and assuming that the addition of manganese lowers transition temperature 1°F per 0.01% manganese.

‡Calculated change in transition temperature if nickel were 0.0% instead of the value given in Column 6 and assuming that the addition of nickel lowers transition temperature 0.08°F per 0.01% nickel.

§Calculated change in transition temperature if silicon were 0.30% instead of the value given in Column 8 and assuming that the addition of silicon raises transition temperature 1°F per 0.01% silicon.

rate of 1.25 °F per 0.01% and lowers maximum energy. For effects of silicon from 0.11 to 0.26%, see discussion.

**Titanium**—Addition of small amounts of titanium increases transition temperature, but as the amount is increased, it lowers transition temperature, reaching the transition temperature of the base analysis at 0.40% titanium. In the two highest titanium steels, titanium carbide was found. Therefore, the effect of added titanium is confused by the fact that some of it is removed from solution.

**Vanadium**—As in the case of titanium, vanadium first increases transition temperature, and then appears to lower it.

#### Additivity of Effects of Composition on Transition Temperature

In an attempt to establish whether or not the changes in transition temperature caused by alloy additions could be predicted for complex alloys from the data collected by varying one element at a time, twelve heats were made in which two elements were varied simultaneously. Factors based on the effect of single element additions were taken from Fig. 4, and the assumption was made that no interactions occurred. After the transition temperature of the complex alloy was determined, the difference between the amount of each alloy in the complex heats and the amount of each alloy

in the base analysis was calculated. This difference was multiplied by the factor for the change in transition temperature per 0.01% of alloy. In Table IV are shown the compositions of the heats in which manganese and carbon, manganese and nickel, and nickel and carbon were varied, the experimental transition temperatures, the calculated change in transition temperature necessary to adjust the amount of each element to the amount present in the base analysis, and the final calculated transition temperatures. Remembering that the base analysis had a transition temperature range of from 5 to 35 °F, it can be seen that nine of the twelve values fall within this

		Yield
% Pearlite	% Carbon	Strength, psi
x 40-82	0.31-0.67	49-61,000
□ 18-30	0.17-0.30	41-49,000
○ 0-13	0.01-0.11	30-39,000

Note: The Carbon Contents of These Points is 0.30% not 0.31%

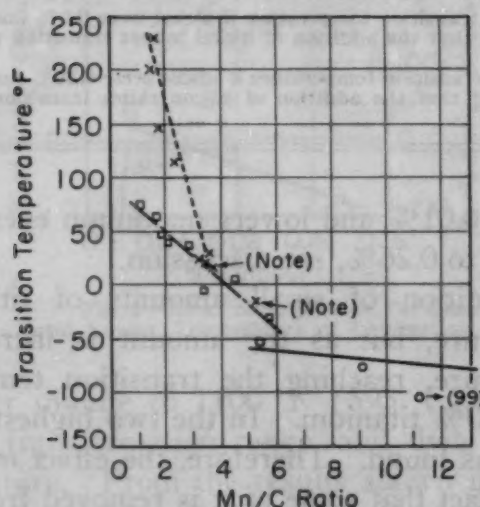


Fig. 6—Effect of Mn/C Ratio on Transition Temperature at Constant Yield Stress.

range, and the others fall outside by a maximum of 6 °F, although the experimental transition temperatures vary from -102 to 50 °F. Additivity of composition effects is not proved conclusively by these data, but it does appear that calculation of transition temperature from composition may be possible for coarse pearlitic steels. Further work on this phase of the problem is required, using different combinations of alloying elements.

#### *Effect of Manganese-Carbon Ratio on Transition Temperature*

High manganese-carbon ratios have frequently been mentioned as being beneficial in ferritic steels. From the remarks of the pre-



Table V  
Additivity of Effects of Manganese and Carbon on Transition Temperature  
at Various Manganese/Carbon Ratios

Steel No.	Carbon %	Manganese %	Mn/C Ratio	Experimental Trans. Temp. °F	Calculated Trans. Temp. °F	Yield Strength psi	Pearlite %
Mn 1	0.27	0.30	1.1	78	22	42,100	22
C 4	0.67	0.99	1.5	232	17	50,850	100
Mn 10	0.27	0.41	1.5	64	19	41,500	23
C 8	0.63	0.99	1.6	212	17	55,200	97
Mn 2	0.28	0.49	1.8	50	9	46,000	31
C 7	0.53	1.02	1.9	150	16	52,500	82
Mn Ni 1	0.28	0.53	2.0	42	4	43,100	32
C 6	0.43	1.02	2.4	118	44	51,200	68
Mn 11	0.29	0.80	2.8	40	24	47,550	37
C Mn 2	0.18	0.56	3.1	-4	11	40,950	18
C Mn 4	0.32	1.05	3.3	30	26	51,700	47
Mn 3	0.31	1.01	3.3	26	24	53,625	45
C 5	0.31	1.01	3.3	24	20	49,650	40
Mn 12	0.30	1.09	3.6	18	27	52,200	41
C 3	0.22	0.98	4.4	6	52	45,200	29
Mn 13	0.30	1.55	5.1	-15	40	61,000	51
C Mn 1	0.11	0.57	5.2	-52	-1	36,700	6
C Mn 3	0.20	1.12	5.6	-32	29	47,000	30
C 2	0.11	0.99	9.0	-75	25	38,900	13
C 1†	0.01	0.99	99.0	-120	30	30,050	0

\*Element varied.

†C1B used instead of C1A because C1B had a finer grain size which more closely approximated the other steels.

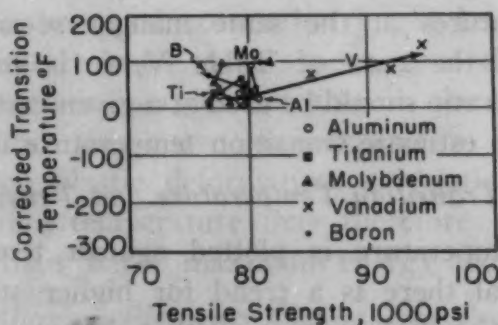
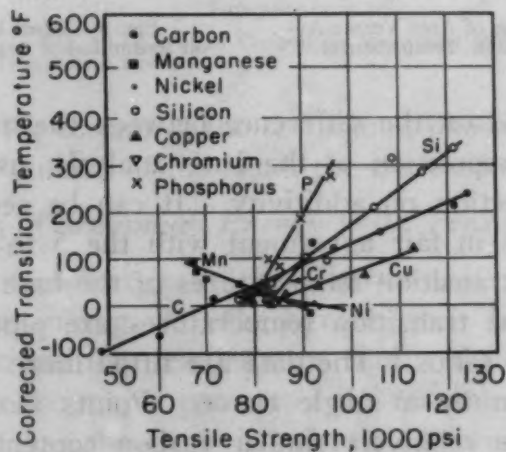


Fig. 7—Effect of Tensile Strength on Transition Temperature.

ceding section on additivity of composition effects, it is apparent that transition temperature will be lower with a high manganese-carbon ratio, for both lowering carbon and raising manganese lower transition temperature. In this study, alloys of manganese-carbon ratios varying from 1.1 to 99 were available for consideration of this effect. In Table V the compositions and the experimental transition temperatures are listed, together with calculated transition

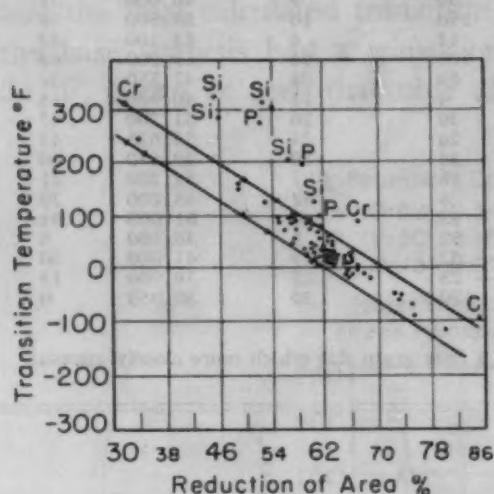


Fig. 8—Reduction of Area Versus Average Energy Transition Temperature.

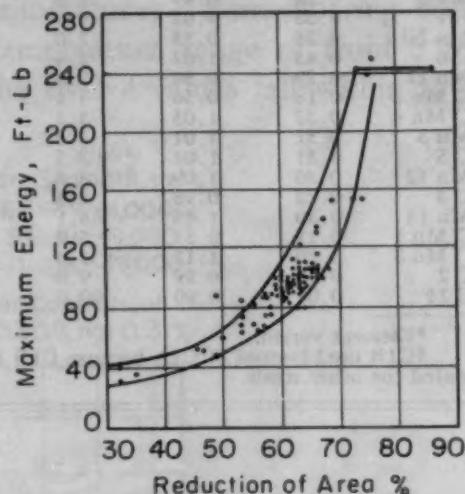


Fig. 9—Effect of Maximum Energy on Reduction of Area.

temperatures based on the difference between the measured composition and the composition of the base analysis, using the method outlined in the section on additivity. It can be seen that the calculated values are in fair agreement with the 5 to 35 °F range of the experimental transition temperatures of the base analysis.

In Fig. 6, the transition temperatures are plotted against the manganese-carbon ratios. The data are fitted more closely by three straight lines than by a single curve. Points along each of the straight lines have relatively similar carbon contents, pearlite contents or yield strengths. It is possible to get a series of values of transition temperatures at the same manganese-carbon ratio. In view of this and the data of Table V, it is believed that the manganese-carbon ratio should be used at a given carbon content if an attempt is made to estimate transition temperature using this factor.

#### *Correlation of Transition Temperature and Tensile Properties*

Transition temperature is plotted against tensile strength in Fig. 7. In general there is a trend for higher strength steels to have higher transition temperatures, although manganese and nickel decrease transition temperature while they increase strength. It

does not appear feasible to correct transition temperature values for changes in strength as the addition of an alloy is made, for the slope of the transition temperature-tensile strength curves vary with alloys. Thus it does not appear to be practicable to compare the effects of alloying elements on transition temperature at both constant microstructure and constant strength.

Transition temperature is plotted against reduction of area in

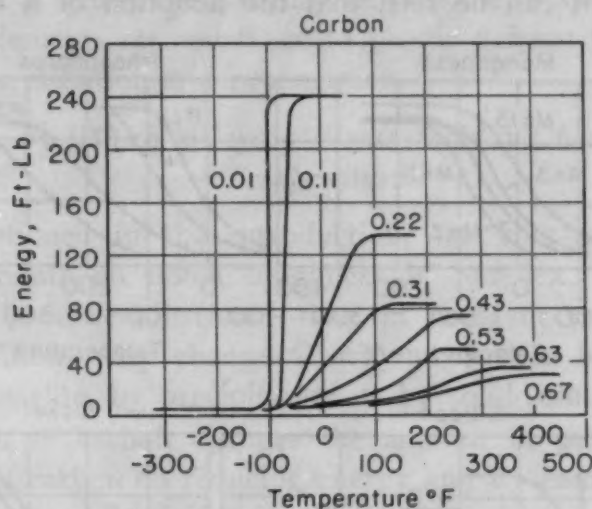


Fig. 10—Effect of Carbon on the Shape of the Transition Curve.

Fig. 8. Except for certain of the chromium, phosphorus, and silicon series which fall outside of the band, the correlation is fair.

#### *Correlation of Maximum Energy With Tensile Properties*

The maximum energy in the Charpy test is plotted against reduction of area in Fig. 9. The agreement is better than for the correlation of transition temperature and reduction of area. It seems likely that the major portion of the maximum energy with its ductile fracture is absorbed in plastic deformation and, since reduction of area is a measure of the ability of a steel to flow without fracture, this good correlation might be anticipated. The transition temperature used in this portion of the study is based not only on maximum energies but also on the shape of the transition curve. Since this curve may depend on other factors than ability to undergo plastic deformation, correlation of reduction of area and transition temperature may therefore be expected to be less satisfactory than that of maximum energy and reduction of area.

#### *Effects of Alloying Elements on Shape of Transition Curve*

Since the energy in the Charpy impact test goes into bending,



initiation of a crack, and propagation of a crack, it is possible that alloying elements may have different effects on the energy required for these various events and therefore may have different shapes of energy versus temperature curves. By study of Figs. 10 and 11, it can be seen that different shapes of transition curves do exist. Addition of carbon, for example, raises transition temperature, but it also lowers maximum energy and widens the temperature range. From Fig. 11, it can be seen that the adoption of a definition of

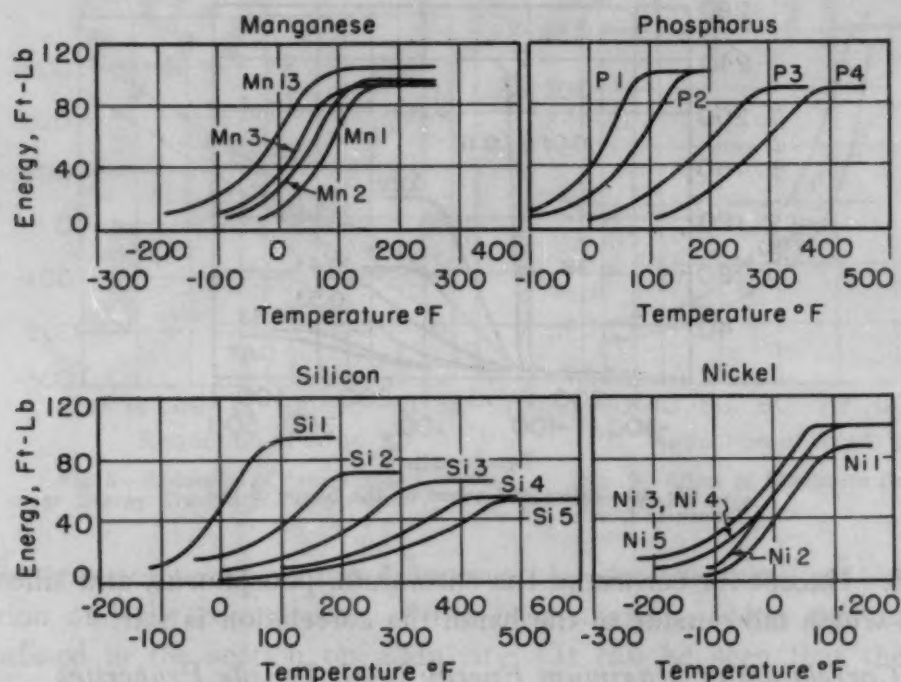


Fig. 11—Effect of Manganese, Nickel, Silicon and Phosphorus on the Shape of the Transition Curve.

transition temperature based on a 15-ft-lb energy level would compare the low carbon steel at 6% of the maximum energy with the high carbon steel at 40% of its maximum energy. In view of this discrepancy, it is not surprising that Fig. 2 showed the effects of carbon transition temperature to be different for the 15-ft-lb definition than for the other criteria.

In the nickel steels, it can be seen in Fig. 11 that the upper portions of the curves are very similar but that there is a definite trend below the 40-ft-lb level for the energy values of high nickel steels to drop less rapidly as temperature of testing is lowered. As indicated in Fig. 2, the effect of nickel is greater when it is measured by the 15-ft-lb definition.

As shown in Fig. 11, phosphorus and silicon decrease the maximum energy and widen the range of the transition zone. They change the shape of the curves gradually.

Addition of manganese, however, shifts the entire curve to lower temperature without changing its shape, according to Fig. 11. The maximum energy, the lower end of the curve, and the width of the transition zone all stay the same.

From these considerations, it is important to note that metallurgical variables affect the entire energy curve as well as transition temperature. Perhaps, when the distribution of energy in breaking a Charpy bar is determined, it may be possible to specify the effects of alloying elements on resistance to plastic deformation and resistance to crack initiation and propagation.

#### *Mechanisms by Which Alloying Elements May Change Transition Temperature*

As mentioned in the introduction, the role of the effect of alloying elements on notch toughness is complex. It is believed that it has been demonstrated that, at constant pearlitic spacing, alloying additions may change Charpy properties by changing the amount of pearlite, by precipitation or by solid-solution effects.

Addition of carbon changes the amount of pearlite markedly. The effects of carbon on reducing energy and widening the transition range can be explained if this pearlite is considered both to start and to stop cracks. With large amounts of pearlite, cracks start easily at high temperature because of restraint of the ferrite and a high probability that a platelet is properly oriented to crack. However, since the crack can also be stopped or retarded by properly oriented platelets, the transition range is wide. As the amount of pearlite is reduced, the effectiveness of pearlite in starting and stopping cracks is reduced, and the properties of the ferrite become more important. In a steel with no pearlite, the transition range is very narrow because there are no structures present to stop cracks once they start. The drop in maximum energy which occurs as the amount of pearlite increases is probably related to the reduction of ductility observed in going from completely ferritic to completely pearlitic structures.

Precipitation probably accounts for the increase in transition temperature noted after tempering of the high copper and phosphorus steels, as shown by the A and B treatments in Table II for Cu 5 and P 4. However, Table III shows that the high transition temperature of the high phosphorus steel cannot be suppressed by quenching from 1100 °F (595 °C). In view of this, it is doubtful that precipitation accounts for the brittleness of normalized high phosphorus steels.

Silicon, manganese, and nickel change transition temperature by dissolving in the ferrite. They have no tendency to precipitate, nor do they change the amount of pearlite markedly. Therefore, an explanation of their effects must be sought by further study of the properties of solid solutions.

#### SUMMARY AND CONCLUSIONS

1. The effects of alloying elements on ductility of pearlitic steels were investigated by making alloy additions to an aluminum-killed steel having a base composition of 0.30% carbon, 1.00% manganese, 0.30% silicon steel. Aluminum, boron, carbon, copper, chromium, manganese, molybdenum, phosphorus, silicon, sulphur, titanium, and vanadium, were systematically varied.

2. All steels investigated were cooled at a rate of 25 °F per minute from the austenitizing temperature. This treatment produced a coarse pearlitic structure of equivalent pearlite spacing for all the alloys investigated.

3. After study of several definitions of transition temperatures, the average energy transition temperature of Charpy V-notch specimens broken over a range of temperatures was selected as the criterion for evaluating the effects of alloy additions.

4. The following tabulation shows the effect on transition temperature with an increase in alloying element.

Increase T.T.	Decrease T.T.	Raise and Then Lower T.T.	Lower and Then No Change
B			
C	Mn	Ti	Al
Cr	Ni	V	
Cu			
Mo			
P			
Si			

5. The effects of carbon, manganese, and nickel on transition temperature appeared to be nearly additive.

6. The only tensile property which showed even a fair correlation with transition temperature was reduction of area.

7. A good correlation was established between maximum energy and reduction in area.

8. Alloying elements affect the entire energy versus temperature curve in different ways. Therefore, a study of a single transition temperature may neglect many important effects.



## ACKNOWLEDGMENTS

The authors wish to express their appreciation to Dr. O. T. Marzke, Division Superintendent of the Metallurgy Division, for his interest and many contributions to this investigation.

The assistance of W. S. Kenton, who carried out many of the tests, is gratefully acknowledged. Members of the Division whose help has also been valuable include G. G. Gregg, D. H. Price, C. R. McCollum, R. E. Raring, R. Dunphy, A. R. Donaldson, F. W. Friske, C. M. Bible, O. Mylting and S. Cress, as well as the melting, forging and stenographic groups. The calculations of statistical averages made by the Applied Mathematics Branch, Mechanics Division, are also appreciated.

## References

1. L. Seigle and R. M. Brick, "Mechanical Properties of Metals at Low Temperatures, A Survey", *TRANSACTIONS, American Society for Metals*, Vol. 40, 1948, p. 813-869.
2. J. M. Hodge, R. D. Manning and H. M. Reichhold, "Effects of Ferrite Grain Size on Notch Toughness", *Journal of Metals*, Vol. 1, No. 3, 1949, p. 233.
3. R. T. Howard and M. Cohen, "Quantitative Metallography by Point Counting and Lineal Analysis", *Transactions, American Institute of Mining and Metallurgical Engineers*, Vol. 172, 1948, p. 413.
4. G. E. Pellissier, H. F. Hawkes, W. A. Johnson and R. F. Mehl, "The Interlamellar Spacing of Pearlite", *TRANSACTIONS, American Society for Metals*, Vol. 30, 1942, p. 1049-1086.
5. H. Arkin and R. R. Colton, "An Outline of Statistical Methods", Fourth Edition, Barnes and Noble, Inc., New York, 1939.
6. M. Baeyerztz, W. F. Craig and J. P. Sheehan, *Journal of Metals*, Vol. 188, No. 2, 1950, p. 389.

## DISCUSSION

**Written Discussion:** By R. H. Frazier, Battelle Memorial Institute, Columbus, Ohio.

The authors have presented a paper containing a vast quantity of impact data in a most understandable manner. It is not always easy to apply impact test results in engineering and to explain why the various elements in steel affect the transition temperature in the Charpy impact test as they do. The work by the authors has helped materially in advancing our knowledge of the notched-bar behavior of steel.

It is interesting to compare the data the authors have presented here on killed steels with data obtained at Battelle Memorial Institute on semi-killed steels processed in a somewhat similar fashion. Battelle's data were reported before the Annual Meeting of the American Welding Society on Tuesday, October 24, 1950. The semikilled steels were tested using key-hole-notched specimens, and the transition temperature was determined as that at which the energy level reached 20 foot-pounds. This definition of

the transition temperature, as compared with the criteria used by the authors, was, of course, taken into account in making the comparison.

The influence of carbon, manganese, and phosphorus in the semikilled steels is almost identical with their influence in killed steels. It might be well to point out, however, in the case of phosphorus that its influence, in semikilled steels of ship-plate type containing very low phosphorus, is not so great as might be indicated by the curves in Fig. 4 of the paper. This is shown in Fig. 12 where the authors' results on killed steel and results

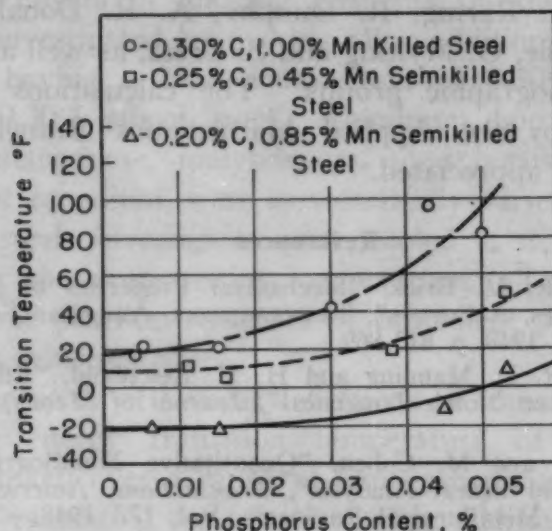


Fig. 12—Influence of Phosphorus on Transition Temperature.

on two semikilled steels of lower carbon and manganese contents are plotted.

A comparison of the influence of silicon in the two types of steel is shown in the following tabulation:

Type of Steel	Composition, %		Range of Silicon Content, %	Effect on Transition Temperature
Semikilled	0.25	0.45	0.02-0.31	Lowers slightly
Semikilled	0.20	0.85	0.02-0.16	Lowers
Semikilled	0.20	0.85	0.16-0.29	Raises
Killed	0.30	1.00	0.26-3.05	Raises

In the semikilled steel, with 0.20% carbon and 0.85% manganese, a minimum value for the transition temperature was obtained at about 0.16% silicon. Either raising or lowering the silicon content from this value caused the transition temperature to increase. One might, therefore, ask whether the transition temperature in killed steel would not also reach a minimum value somewhere below 0.26% silicon. In view of the interesting observations as to the effect of silicon on the transition temperature of the semikilled steel with 0.20% carbon and 0.85% manganese, one might also speculate on how much more silicon would be needed in the semikilled steel with 0.25% carbon and 0.45% manganese to cause its transition temperature to be raised.

Within the range of 0.06 to 0.19% vanadium, the effect of vanadium in the semikilled steels was to raise the transition temperature perceptibly

in much the same manner as vanadium was found by the authors to affect the killed steels. Whether or not additional amounts of vanadium in the semikilled steel would lower the transition temperature, as the authors observed with killed steels of more than 0.20% vanadium, has not been determined.

The effects of such elements as silicon, manganese, vanadium, and aluminum seem to throw considerable light on the possible influence of oxygen and nitrogen and their mode of existence on the notched-bar behavior of steel over a range of temperatures.

**Written Discussion:** By Morgan L. Williams, metallurgist, National Bureau of Standards, Washington, D. C.

In the first reference cited by the authors, there appears the statement: "The ideal experiment of adding controlled amounts of single alloying elements to pure ferrite has not yet been performed." From the practical point of view, the authors have improved on this "ideal experiment" by using, instead of pure ferrite, a base composition which is nearer to the realities of commercial practice.

The data showing the effect of the different alloying elements on the shape of the transition curve, on the maximum energy, and on the transition temperatures as defined by different criteria, are especially significant. This information may help to resolve some of the apparent discrepancies in results obtained using different definitions of the transition temperature, and will lead to a better theoretical understanding of notch toughness.

It is to be hoped that this work will be continued and expanded to include a few additional elements and a wider range of compositions. Tin and arsenic, for example, are often found as residual elements in commercial steels, and a knowledge of the effects of these elements on the notch toughness would be helpful. Some of the elements were investigated only in the relatively high ranges of alloy content, and it is possible that, in the lower ranges, there may be a reversal in the effects of these elements, as the authors have shown for titanium and vanadium. Our knowledge of the properties of some of the specialized and less common alloy steels seems to be greater than our knowledge of the commonly used low alloy structural steels. I believe that further investigation of the lower ranges of alloying or residual elements commonly found in commercial steels would be profitable.

The authors are to be congratulated for their excellent presentation of this extensive and important fundamental research.

**Written Discussion:** By M. Baeyertz, Armour Research Foundation, Chicago, W. F. Craig, Jr., Climax Molybdenum Co., Chicago, and J. P. Sheehan, Armour Research Foundation, Chicago.

The task of evaluating the effect of alloying elements on notch toughness of steels is an enormous one. The authors are to be commended both for their courage in undertaking this assignment and for the work they have thus far completed.

When work of the scope of the paper by Rinebolt and Harris is encountered, it is natural to attempt to apply the findings to commercial steels and their use. In many cases, however, the authors have stopped short of evaluations of importance to such application of their data. In practice, one is not so much concerned with the effect of an addition of



a single element in such a way as to maintain a structure of coarse pearlite as with the more complex problem of balancing a combination of elements to give the best over-all performance. The end result may represent an integration of microstructural, solid solution, and precipitation effects, the complexity of which suggests a word of caution in any attempted application of the authors' data to the general case of alloy steels in the unhardened state, that is, hot-rolled, normalized, or normalized and tempered, as contrasted to those annealed to give a specific structure of coarse pearlite. The authors have carefully avoided any implication that this can be done; however, the appearance of simple addition of the effects on transition temperature of carbon, manganese, and nickel might lead one to attempt to push this principle too far. One example will illustrate the difficulties to be encountered.

Ref. 6 of the paper pertains to work of the present discussers dealing with AISI-SAE 1340, 5140, and molybdenum modifications of these grades in which transition temperatures for the fully quenched and tempered steels were given. Subsequently, transition temperatures have been determined for these same steels in the unhardened (normalized and tempered) condition, and it seemed of interest to examine these results in the light of the data of Rinebolt and Harris. Alloy steels are, of course, more fre-

**Table VI**  
**Analyses**

Grade	Composition, %					
	C	Mn	P	S	Si	Cr
5140	0.44	0.73	0.020	0.025	0.26	0.80
Mo-Cr	0.40	0.79	0.021	0.021	0.26	0.44
5140	0.42	0.76	0.036	0.027	0.27	0.77
Mo-Cr	0.42	0.80	0.041	0.019	0.24	0.50
1340	0.40	1.90	0.028	0.019	0.34	
Mo-Mn	0.38	1.29	0.025	0.019	0.24	0.18

**Table VII**  
**Normalized and Tempered Hardnesses**

Grade	Phosphorus %	Hardness After	Hardness After	Hardness After
		Normalizing	Tempering Treatment A	Tempering Treatment B
		R <sub>C</sub>	R <sub>B</sub>	R <sub>B</sub>
5140	0.020	10 (91 R <sub>B</sub> )	87	88
Mo-Cr	0.021	21	91	92
5140	0.036	19	91	92
Mo-Cr	0.041	25	95	95
1340	0.028	24	94	94
Mo-Mn	0.025	24	95	94
Normalizing		Air-cooled from 1550 °F in impact specimen blank size.		
Tempering Treatment A		Tempered 7 to 10 hours at 1150 to 1175 °F and water-quenched. (Cycle adjusted to give same hardness as Treatment B.)		
Tempering Treatment B		Tempered 1 hour at 1150 °F and cooled to 700 °F at ¼ °F per minute. Air-cooled to room temperature.		

quently used in the normalized and tempered than in the annealed state. Analyses of the steels and details of the heat treatments are given in Tables VI and VII. V-notch Charpy transition temperatures according to two of the criteria used by the authors are listed in Table VIII.

While the authors observed that molybdenum increased transition temperature almost as rapidly as carbon when added to their base composition, the data in Table VIII indicate that, when molybdenum replaced part of the chromium in 5140 or manganese in 1340, in no case was the transition temperature raised. On the contrary, by effectively preventing temper embrittlement under conditions in which it would otherwise have occurred (5140, 0.036% phosphorus and 1340, 0.028% phosphorus, not quenched from the tempering temperature), the use of molybdenum brought about a marked reduction in transition temperature. Because phosphorus increases susceptibility to temper embrittlement, the effect on transition temperature of other elements which enter into this phenomenon would presumably vary in accordance with the phosphorus content in the steel. It is to be noted the authors' steels, excepting the phosphorus series, had extremely low phosphorus contents (0.002 to 0.010%). Temper brittleness would thereby be minimized in these steels. (The authors checked for embrittlement in two members of the plain carbon phosphorus series. However, plain carbon steels ordinarily exhibit little temper brittleness by the usual criterion of a difference between specimens water-quenched and those more slowly cooled from above the embrittling range. Jaffe<sup>5</sup> has suggested that both sets are embrittled.)

Table VIII  
V-Notch Charpy Transition Temperatures

Grade	Phosphorus %	Transition Temperatures, °F			
		Average Energy Criterion		First Sign of Brittleness Criterion	
		Treatment A	Treatment B	Treatment A	Treatment B
5140	0.020	30	40	75	85
Mo-Cr	0.021	25	10	60	75
5140	0.036	50	125	100	190
Mo-Cr	0.041	30	35	65	75
1340	0.028	10	135	75	200
Mo-Mn	0.025	5	0	75	75

An increase in manganese from 1.55 to 2.00% or of chromium from 0.48 to 0.95% in the authors' steels sharply increased transition temperature in contrast to the effect of these elements in smaller amounts. Transition temperatures in Table VIII for the steels which were not temper-embrittled evidently reflect a balancing of the effect of the molybdenum addition by that of the reduction of chromium or manganese. When the opportunity for temper embrittlement exists, the effects no longer balance, and the molybdenum steels exhibit lower transition temperatures.

As the authors point out, in attempting to predict the behavior of complex steels from the individual effects of adding or varying single elements, the assumption is made of no interaction among elements. Temper brittleness, however, is one example of an interaction which can occur in unhardened alloy steels. No doubt other types of interaction need also to be considered. It seems evident that much work is needed to unravel the effects on transition temperature of different combinations

<sup>5</sup>L. D. Jaffe and D. L. Buffum, "Temper Brittleness of Plain Carbon Steels", *AIIME Metals Technology*, Vol. 15, No. 8, December 1948, T.P. 2482.

of elements, and it is hoped some of the authors' future work will be directed toward this goal.

**Written Discussion:** By G. M. Boyd, Lloyd's Register of Shipping, London, England.

The paper is important in that it throws considerable light on the effects of composition on the notch sensitivity, but its value depends, as does that of many allied investigations, on the choice of a criterion for notch sensitivity, or notch ductility.

In a recent (unpublished) study intended to compare the notch ductilities of a large number of samples, the writer made a critical survey of the criteria which have from time to time been suggested, but came to the conclusion that few, if any, of these were related to service performance. A new criterion was therefore developed on the following reasoning.

It is assumed that the total energy recorded in a notch impact test at a given temperature is a measure of the resistance of the material to fracture at that temperature. Moreover, it is known that over a wide range of temperatures embracing the normal service range, the impact energy increases with temperature. Consequently, if two steels are tested at a given temperature, the steel giving the higher energy is to be preferred. Also, if two steels show a given energy level at different temperatures, the steel which shows it at the lowest temperature is to be preferred.

To take these points into account it is necessary to attach different "weights" to the energy values at different temperatures, the weights increasing with decrease in temperature.

Logically, the weights should be related to the liability of the steel to be subjected to the various temperatures in service, having due regard to the liabilities for the simultaneous occurrence of fracture-conducive conditions such as notches, high stresses, etc. The available data are insufficient to enable logical weight factors to be deduced from such considerations, but, for the purpose of comparison only, any arbitrary weighting system would serve, provided that it bears some reasonable resemblance to the logical system, and that it is consistently applied.

In the recent study referred to, the following weighting factors were adopted:

For temperatures up to and including $-30^{\circ}\text{C}$ ( $-22^{\circ}\text{F}$ )	3.00
For temperatures up to and including $-20^{\circ}\text{C}$ ( $-4^{\circ}\text{F}$ )	2.18
For temperatures up to and including $-10^{\circ}\text{C}$ ( $+14^{\circ}\text{F}$ )	1.66
For temperatures up to and including $0^{\circ}\text{C}$ ( $+32^{\circ}\text{F}$ )	1.35
For temperatures up to and including $+10^{\circ}\text{C}$ ( $+50^{\circ}\text{F}$ )	1.12
For temperatures $20^{\circ}\text{C}$ ( $+68^{\circ}\text{F}$ ) and over	1.00

The reciprocals of these weight factors vary in a linear manner from 0.33 at  $-30^{\circ}\text{C}$  to 1.00 at  $20^{\circ}\text{C}$ .

The criterion suggested is the mean weighted energy over a temperature range from  $-30$  to  $+30^{\circ}\text{C}$  ( $-22$  to  $+86^{\circ}\text{F}$ ).

This criterion is in no sense a "transition temperature", but is a measure of the extent to which the energy is maintained as temperature is reduced, and enables an assessment to be made of the relative merits of energy-temperature curves which intersect.

It has been found that this criterion gives a good correlation with judgments made from combinations of other criteria on a "common sense" basis.



This mean weighted energy criterion in its present form can be applied only to tests in which the energy required for rupture is measured, or can be deduced, and moreover it rests upon purely arbitrary "weighting". It is to be hoped, however, that more rational weight factors will be developed as more knowledge becomes available. In the meantime it would probably be instructive if the authors could re-plot their results against the mean weighted energy to ascertain whether the correlations they have found are improved or modified.

Presumably the authors have recorded the percentage cleavage in all the tests and, if so, they would no doubt find it instructive to study plots of percentage fibrous against energy absorption. The writer has found that for many steels the relationship is sensibly linear, apart from deviations near the origin for the tests made at low temperatures, which deviations might be accounted for by a "ductility transition" as suggested by Vanderbeck and Gensamer.<sup>9</sup>

**Written Discussion:** By N. P. Allen, superintendent, Metallurgy Division, National Physical Laboratory, Teddington, Middlesex, England.

The authors of this paper are to be congratulated in presenting results on the effect of a number of alloying elements on the tough to brittle transition in impact of a particular type of steel at a time when both steelmakers and users find only scant information in the literature. It is apparent that a large amount of work has been carried out very carefully and it is gratifying to note that the information has been condensed into a form that is easily assimilated.

Only manganese and nickel have been found to have a distinct effect in lowering the transition temperature, and the extent of the influence of nickel is small. The elements having the largest effects in raising the transition temperature have been found to be carbon, phosphorus, and silicon. From this it would appear that an important conclusion to be drawn is that these elements should be kept at low levels in steels with a ferrite-pearlite microstructure that are required to have low transition temperatures. Silicon presumably raises the transition temperature by its effect on the ferrite, but there is a suggestion that precipitation may account for the influence of phosphorus. Is it not possible that phosphorus behaves by a similar mechanism to that of silicon? The effect of carbon, which is attributed to the proportion of pearlite in the structure, is particularly striking in that the steels having the lowest transition temperatures of all in Fig. 2 are those containing less than about 0.2% carbon. This, combined with the influence of manganese, supports the policy of keeping the carbon content low and maintaining the required strength by means of manganese in steels for ship-plate and other uses where conditions of service are such that brittle fracture may occur. In view of the importance of this work, it seems that consideration might profitably be given to carrying out confirmatory tests at a lower carbon level.

The results on the effect of Mn/C ratio given in Fig. 6 are interesting, but it is not easy to see why the steels should fall into three groups. One wonders whether this may not be a coincidence and that further work might reveal that the behavior conforms equally well to a simpler scheme.

<sup>9</sup>R. W. Vanderbeck and M. Gensamer, "Evaluating Notch Toughness", *Welding Journal*, Vol. 29, No. 1, 1950, p. 37s.

The authors are to be commended for exercising some reserve on the question of calculation of transition temperature on the basis of additivity of effects of different alloying elements. In this connection, there is a suggestion in the results of work on the effects of alloying elements in ferrite in progress at the National Physical Laboratory that two elements may have a combined effect which is not accounted for by their effects when present individually.

Finally it is to be noted that these results refer to steels which are effectively deoxidized. The behavior of steels which are not completely deoxidized might be very different; and this possibility needs to be carefully considered in view of the large output of "balanced" and "rimming" steels.

**Written Discussion:** By M. L. Becker and T. Dennison, Metallurgy Division, British Iron and Steel Research Association, London, England.

On page 1189, the authors rightly draw attention to the fact that "... the amounts of elements added were not the same as the amounts in solid solution, since a portion of many additions was present as a carbide, a nitride, an oxide, or a sulphide." This emphasizes one of the major difficulties associated with an attempt to study the effect of individual alloying additions in the manner described in the paper, and the approach we are adopting in this country is a systematic examination of the effect of alloying additions to pure iron. It is recognized that this approach to the problem is complementary to that adopted by the authors. The British work is being carried out at the Metallurgy Division of the National Physical Laboratory, under a research contract from The British Iron and Steel Research Association. An interim report, describing the technique employed for the large-scale production of pure iron and iron alloys, and on the tensile and impact properties of iron and some iron alloys of high purity, is being prepared for publication, and will shortly be submitted to the Iron and Steel Institute.

Regarding the effect of manganese-carbon ratio on transition temperature (p. 1194 to 1196 and Fig. 6), the original recommendation put forward by Barr and Tipper<sup>7</sup> was that for ordinary shipbuilding steels of 26 to 33 tons psi tensile strength, the manganese-carbon ratio should not be less than 3. The qualification is often overlooked and the recommendation extended to apply to steels of other than ordinary shipbuilding quality. Rinebolt and Harris have expressed this qualification in another way by suggesting (p. 1196) "... that the manganese-carbon ratio should be used at a given carbon content if an attempt is made to estimate transition temperature using this factor." Structural steel for shipbuilding purposes has a tensile strength of 26 to 33 tons psi and is manufactured from steels with carbon contents of 0.12 to 0.24%, so that the original recommendation of Barr and Tipper was intended to apply to conditions similar to those represented by the middle curve of Fig. 6. According to this curve, increasing the manganese-carbon ratio from 1 to 3 lowers the transition temperature from about 75 °F to about 20 °F, which substantiates the British recommendation.

It is not surprising that no close correlation was found between

<sup>7</sup>W. Barr and C. F. Tipper, "Brittle Fracture in Mild-Steel Plates", *Journal, Iron and Steel Institute*, Vol. 157, October 1947, p. 223.

ordinary tensile properties at room temperature and the transition temperature determined from impact tests (p. 1196 to 1197), as steels of quite different notch sensitivity may have very similar ordinary tensile properties. Better correlation might be expected using the results of notch tensile tests.

The work on the effect of alloying elements on the properties of pure iron, carried out for The British Iron and Steel Research Association at the National Physical Laboratory, shows that a feature of the impact energy-temperature curves for pure iron and high-purity alloys is a very sharply defined transition temperature, comparable to that for the 0.01% carbon alloy in Fig. 10 of the paper by Rinebolt and Harris. As the carbon content of the iron is increased to 0.05%, the lower part of the transition curve begins to spread over a wider temperature range. The addition of up to 2% of manganese to an iron containing 0.05% carbon has the effect of substantially lowering the transition temperature, while the lower part of the transition curve becomes progressively sharper. This should be compared with the statement at the top of page 1199 that the "Addition of manganese, however, shifts the entire curve to lower temperatures without changing its shape."

Regarding the additivity of the effects of carbon, manganese, and nickel, on the transition temperature (p. 1193 to 1194), comparison of the results for iron-manganese alloys of high purity with those for iron-carbon and iron-carbon-manganese alloys, also of high purity, shows that the combined effect of manganese and carbon in lowering the transition temperature is greater than when manganese is present alone. Whereas there are inconsistencies in the results to be published, it is clear that the relationship between transition temperature and variations in the carbon or manganese contents is not linear. The lowering of the transition temperature due to the addition to iron of up to 2% manganese is roughly five times as great in the presence of 0.05% carbon as when the manganese is added alone. Furthermore, the equivalent increase in transition temperature due to the addition to pure iron of up to 0.05% carbon alone is about six times the value of 5 °F per 0.01% carbon obtained by the authors on a more complex material. This emphasizes the empirical nature of the additivity of composition effects. Such conclusions should be treated with caution, and regarded as only of limited practical validity.

**Written Discussion:** By C. F. Tipper, Engineering Department, Cambridge University, Cambridge, England.

The authors are to be congratulated on the long and laborious investigation which they have completed in the course of which they have established some much-needed facts. Some modification may be required when applying these results to commercial steels, but the relative effects of the different alloying elements have been determined without dispute.

So much factual information is packed into this paper that there is little to discuss, but much upon which to speculate. This applies particularly to Figs. 10 and 11 depicting families of curves for different amounts of the same element. There are good grounds for saying that most of the energy absorption in notch impact tests takes place during the initial stages of the test when the fracture is partly or chiefly crystalline. Hence, a gradually sloping energy/temperature curve is an indication that the



material is less susceptible to temperature brittleness than if the curve is steep. A low energy level may be due to low tensile strength or poor ductility—chiefly the latter—or to the curtailment of the ductile zone at the base of the notch. A study of the fractures would help to decide which of the two factors were operative and would probably account for the shapes of the curves observed. What is rather puzzling is that the shapes of the curves for carbon and silicon are of the same type and yet the pearlite percentages differ considerably so that the explanation given on page 1199 of the role of pearlite in fracture initiation and arrest cannot be used for the silicon alloys. This point merely emphasizes the complexity of the problem.

I would like to endorse the opinion expressed on page 1197 relating to correlation of notch impact tests with tensile test results. There is no logical reason known at present for connecting transition temperatures with tensile test results, but every reason to connect maximum energy with tensile properties.

**Written Discussion:** By H. W. G. Hignett, superintendent, Development and Research Department Laboratory, The Mond Nickel Co., Ltd., Birmingham, England.

The Birmingham Laboratory of The Mond Nickel Co., Ltd., has devoted considerable attention to the influence of chemical composition on impact transition temperatures. So far, however, only hardened and tempered steels have been considered and the writer does not, therefore, feel competent to comment in detail on the obviously careful and valuable work of Rinebolt and Harris. These investigators may, however, care to have the data presented in Table IX, which demonstrate that nickel depresses the transition temperatures of normalized steels containing large amounts of free ferrite and also those of hardened and tempered steels in which the carbide is uniformly dispersed.

Table IX

Mark	Chemical Composition, %							Heat Treatment*	
	C	Si	Mn	S	P	Ni	Cr		
A	0.15	0.16	0.54	0.024	0.016	2.01	0.21	1650 °F, A.C.	
								1580 °F, O.Q., 1020 °F, W.Q.	
B	0.15	0.25	0.44	0.024	0.020	3.04	0.27	1650 °F, A.C.	
								1545 °F, O.Q., 1020 °F, W.Q.	
C	0.16	0.38	0.39	0.027	0.012	4.70	0.15	1650 °F, A.C.	
								1470 °F, O.Q., 1200 °F, W.Q.	
Mark	Hardness (D.P.N.)		Maximum Energy (Ft.-lb)		Minimum Energy (Ft.-lb)		Average Energy Transition Temperature (°F)		15 Ft.-lb Transition Temperature (°F)
A	172/180		93		2		+ 43		- 33
	222/234		93		2		+ 5		- 85
B	169/176		88		2		+ 5		- 71
	222/233		94		3		-148		-215
C	179/189		97		2		- 62		-186
	217/222		126		13		-188		-310

\*Steels heat treated as  $\frac{3}{8}$ -inch diameter bar.

#### Authors' Reply

The authors appreciate the comments made by all of the discussers. As Mr. Frazier indicates, it is interesting to note that the effects of most

alloying elements are the same in the 0.20% carbon semikilled steels which he and his co-workers have studied and in the 0.30% carbon aluminum-killed steels investigated by the authors. Although it is possible, as he points out, that phosphorus below 0.03% may have less effect per point than when it is present in greater amounts, scatter in the data makes it difficult to establish such behavior with absolute certainty. Mr. Frazier's finding, that increases of silicon content from 0.02 to 0.16% decrease transition temperature, is partially confirmed by data collected by the authors after this paper was published. These data, shown in Fig. 13 and Table X, indicate that silicon in the range from 0.11 to 0.26% does not increase transition temperature. Mr. Frazier found that addition of vanadium up

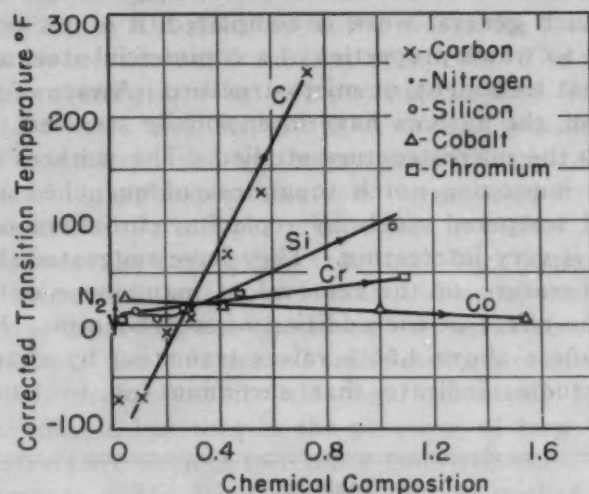


Fig. 13—Effects of Carbon, Silicon, Chromium, Cobalt and Nitrogen on Transition Temperature.

to 0.20% increased transition temperature. The decrease in transition temperature for vanadium contents above 0.14% in the authors' steels has been attributed by the authors to the removal of vanadium from ferrite by the formation of vanadium carbides. In 0.20% carbon steels, more than 0.21% vanadium might be required for formation of the carbides. Therefore, it is considered likely that Mr. Frazier would have observed a decrease in transition temperature if he had continued to increase vanadium contents.

The authors agreed with Mr. Frazier's suggestion that the effects of such elements as aluminum, manganese, silicon, and vanadium might be influenced by oxygen and nitrogen, until results of studies on the effect of nitrogen became available after publication of the preprint. These data, which are shown in Fig. 13 and Table X, demonstrate that nitrogen has little effect on notch toughness and, therefore, may not modify the behavior of other alloying elements.

The authors are grateful to Dr. Williams for his comments regarding the importance of studies of commercial steels. However, his suggestion that the work be expanded to include studies of effects of residual elements such as tin and arsenic, and small amounts of the more common elements, will be followed in future studies of alloys of high purity. In the steels

used in this report, many alloying elements had such small effects that they were masked by scatter until additions were made in amounts in excess of commercial limits.

Dr. Baeyertz and Messrs. Craig and Sheehan have commented on the difficulties to be encountered in applying results of the present study to commercial steels. The authors agree that variations in microstructure, heat treatment, as well as composition, may affect notch toughness and that for a given heat treatment changes in composition influence microstructure. However, the present work was intended to establish the effects of alloying elements at constant microstructure (the microstructure developed in a 2-inch normalized plate). Later studies will include effects of composition in other microstructures and in the presence of embrittling reactions. Until such general work is completed, it is not possible to determine the extent to which properties of a commercial steel are dependent on composition, heat treatment, or microstructure. Aware of the complexities of the problem, the authors have intentionally stressed that their results apply only to the microstructure studied. The work of Dr. Baeyertz and Mr. Craig on improving notch toughness of quenched and tempered or normalized and tempered steels by replacing chromium or manganese with molybdenum is very interesting. They have suggested that the effect on transition temperature of the removal of manganese or chromium is compensated by the effect of the addition of molybdenum. However, the addition of manganese above 1.55% raises transition by changing microstructure. New studies indicate that chromium up to 1.10% increases

Table X  
Composition of New Heats

Steel No.	Per Cent						Corr. Average Energy T. Temp. °F.
	C	Mn	Si	S	P	Element Varied (C)	
C 9	0.02	0.99	0.30	0.02	0.005	0.02	-74
C 10	0.12	0.98	0.28	0.02	0.005	0.12	-70
C 11	0.21	0.96	0.27	0.02	0.005	0.21	-6
C 12	0.30	0.97	0.28	0.02	0.005	0.30	9
C 13	0.30	1.05	0.32	0.02	0.004	0.30	16
C 14	0.43	1.06	0.31	0.02	0.005	0.43	65
C 15	0.57	1.05	0.31	0.02	0.004	0.57	127
C 16	0.74	1.05	0.31	0.02	0.005	0.74	244
(Co)							
Co 1	0.30	1.04	0.34	0.02	0.004	0.04	24
Co 2	0.30	1.03	0.31	0.02	0.004	0.41	17
Co 3	0.31	1.01	0.30	0.02	0.004	1.00	14
Co 4	0.32	1.07	0.30	0.02	0.004	1.55	5
(Cr)							
Cr 5	0.30	1.06	0.31	0.02	0.004	0.05	5
Cr 6	0.30	1.06	0.31	0.02	0.004	0.48	30
Cr 7	0.29	1.03	0.29	0.02	0.004	1.10	47
(N <sub>2</sub> )							
N <sub>2</sub> 1	0.28	1.06	0.28	0.02	0.004	0.004	8
N <sub>2</sub> 2	0.29	1.09	0.27	0.02	0.004	0.008	-2
N <sub>2</sub> 3	0.30	1.08	0.26	0.02	0.004	0.015	-8
N <sub>2</sub> 4	0.30	1.12	0.25	0.02	0.003	0.018	27
(Si)							
Si 10	0.30	1.03	0.10	0.02	0.005	0.10	13
Si 11	0.31	1.03	0.18	0.02	0.005	0.18	6
Si 12	0.31	1.03	0.28	0.02	0.007	0.28	17
Si 13	0.31	1.11	1.06	0.02	0.006	1.06	96



transition temperature approximately  $\frac{1}{2}$  °F per 0.01% as shown in Fig. 13 instead of more rapidly as suggested by the preprint. Taking these findings into account, it would be expected that, even in the unembrittled state, the molybdenum steels should have higher transition temperatures than the manganese or chromium steels. The findings of Dr. Baeyertz and Mr. Craig can probably be explained only by assuming that molybdenum leads to the developing of tougher microstructures as well as the suppression of embrittling reactions.

In connection with the observations of Dr. Baeyertz and Messrs. Craig and Sheehan that plain carbon steels do not exhibit temper embrittlement by the usual criterion, it is necessary to explain more fully why such steels were checked for temper embrittlement. These comments also apply to the question raised by Dr. Allen as to the reason for considering the effect of phosphorus to be different from that of silicon. The authors found that phosphorus increased transition temperature rapidly. In view of earlier work by Dr. Baeyertz and Mr. Craig, it seemed possible that this phosphorus effect was introduced by temper embrittlement. Therefore, specimens of low and high phosphorus steels were cooled from 1650 to 1100 °F at the standard rate of 25 °F per minute and quenched from 1100 °F in an attempt to suppress the embrittling reaction. No change in properties was observed. However, it was found that additional embrittlement in the high phosphorus steel but not the low phosphorus steel was achieved by tempering at 900 °F for 4 hours. These results were interpreted to mean that phosphorus probably embrittles pearlitic steels by a solid solution effect as does silicon, but that in the presence of large amounts of phosphorus such steels are subject to temper embrittlement.

The comments of Mr. Boyd indicate that he wishes to take account of the impact energy throughout the entire transition range. The authors have indicated their belief that comparison of steels by a single transition temperature may be inadequate, since steels have quite different transition curves. A representation of the transition curve by a single value through the use of Mr. Boyd's weighting factors is an interesting suggestion. However, such a procedure is probably applicable only to steels with very similar shapes of transition curves. Nonetheless, Mr. Boyd's suggestion will be kept in mind during subsequent analyses of the data. His observations that the relation between fibrous fracture area and energy absorption is linear except at the low energy end of the curve will be checked by the authors in future analysis of their data.

The authors agree with Dr. Allen that improvements in notch toughness are to be achieved to a greater extent by removing phosphorus, carbon, and silicon than by adding nickel or manganese. It should be mentioned that, as shown in Fig. 13 and Table X, cobalt is a third alloying element which has a tendency to lower transition temperature. The authors agree that their data support the policy of keeping carbon low and maintaining strength by adding manganese in order to lower transition temperature. As suggested by Dr. Allen, confirmatory studies are being made at a lower carbon level. The original effects of carbon were confirmed by two new heats, as shown in Fig. 13. The authors suggest that Dr. Allen's hope for finding a single relation between Mn/C ratio and transition temperature instead of the three relations found by the authors

may be difficult to achieve whenever simple additivity applies because, as shown in Table V of the preprint, at a Mn/C ratio of 1.5, transition temperature may vary from 64 to 232 °F, with the higher transition temperature occurring in the 0.67% carbon steel. These findings are in accord with the remarks of Dr. Dennison and Mr. Becker who indicate that Mn/C ratio alone does not specify transition temperature except within limited ranges of carbon or manganese contents or tensile strengths. It is agreed, as Drs. Allen and Dennison and Mr. Becker point out, that additivity of effects of alloying elements is not likely to be generally applicable. In answer to Dr. Allen's last comment on the influence of deoxidation practice on the effects of composition changes, the authors wish to refer to the earlier comments of Mr. Frazier which indicate that many alloying elements have the same effects on transition temperature in both killed and semikilled steels.

The authors agree with Dr. Tipper that the mechanisms by which alloying elements modify the shapes of the transition curves may be revealed by detailed study of the fracturing process, particularly crack initiation. Results of such studies will be presented by the authors in the near future. Dr. Tipper's suggestion that there is no general mechanism by which pearlite influences the shape of the transition curves is probably correct. The authors appreciate the endorsement by Drs. Tipper and Dennison and Mr. Becker of the opinion that there is poor correlation between tensile properties and transition temperature but good correlation between tensile properties and maximum energy.

The authors are in full agreement with Dr. Dennison and Mr. Becker that studies of notch toughness of pure binary ferrites should accompany investigations of more complex alloys and steels. The interim report of the National Physical Laboratory is awaited with interest, particularly since additions of carbon and manganese to pure iron appear to have quite different effects on shifts and shapes of the transition curves from their effects in 0.30% carbon steels.

The work of Mr. Hignett on the effect of nickel has been done at more rapid cooling rates than those adopted by the authors. In view of the large effect of nickel on hardenability, it is suggested that the microstructures of Mr. Hignett's nickel steels differ, with the pearlite becoming progressively finer. Hence the more rapid lowering of transition temperature by nickel observed by Mr. Hignett may not be directly comparable with the work of the authors, which was based on comparison at essentially constant microstructure.

## THE STRESS-STRAIN ENERGY RELATIONSHIP FOR ALUMINUM

By D. J. McADAM, JR.

### *Abstract*

*Strain aging during tension tests of aluminum, duralumin, nickel and brass affects the results of tests at temperatures above and below a range between about 150 and 200 °K. The effect of temperature on the flow stress involves a direct effect and an effect on the rate of increase of intrinsic strength with strain. The effects of these two factors should be expressed in terms of flow-stress ratios. The lower the temperature, the more rapid is the increase of intrinsic strength with strain. This effect of temperature on the true rate of work hardening is much greater for aluminum than for copper, Monel or nickel. With plastic strain, the direct temperature factors for aluminum and copper are practically constant; the factor for Monel is practically constant after slight initial strain. The direct temperature factors for aluminum, duralumin, copper, Monel and nickel are not very different. Curves have been derived to represent the influence of temperature on the stress-strain relationship for constant intrinsic strength. Other curves have been derived to represent the influence of temperature and plastic strain on total strain energy, work hardening energy and latent energy of aluminum.*

IN previous papers, the author has discussed the stress-strain energy relationship for Monel (13)<sup>1</sup> and oxygen-free copper (13, 14). Within the range from -188 °C to room temperature, these metals are practically free from structural changes other than those due solely to plastic strain; they show no evidence of crystal recovery or strain aging. The present paper considers the stress-strain energy relationship for some metals that are subject to strain aging. Although chief attention is given to aluminum alloy 2S, containing 99.4% aluminum, some attention is given to high-purity aluminum, duralumin 24S-T and other metals.

Much evidence for strain aging of aluminum and its alloys is found in the literature. Strain aging of metals probably is a manifestation of precipitation hardening induced by plastic strain. The

<sup>1</sup>The figures appearing in parentheses pertain to the references appended to this paper.

The author, D. J. McAdam, Jr., is a consultant, Washington, D. C., formerly chief of section on thermal metallurgy, National Bureau of Standards. Manuscript received September 1, 1950.



increase in the flow stress of a strain aging metal during plastic strain, therefore, is the resultant of two factors: (a) the increase due solely to the plastic strain; (b) the increase due to the strain aging. Variations in the strain rate have opposite effects on these two factors. Whereas an increase in the strain rate causes an increase in factor (a), it causes a decrease in factor (b). Probably because of these opposing effects of variation in the strain rate, metals subject to strain aging exhibit discontinuities in the stress-strain curve. These discontinuities may appear as single yield points, as a succession of yield points giving a serrated stress-strain curve, or as a "stair-step" curve. They also tend to cause Luders lines.

Serrated stress-strain curves have been reported by Portevin and Le Chatelier (19) for duralumin at room temperature, and by Sutoki (23) for duralumin at 20 to 100 °C. Luders lines in duralumin have been reported by Portevin and Le Chatelier (19), by Fell (4), and by Stang, Greenspan and Newman (22). McReynolds (16), using constant loading rates, obtained stair-step curves with commercial aluminum (2S) at temperatures between -30 and 60 °C. With aluminum alloys containing 0.1 and 0.5% copper, stair-step curves were obtained at temperatures between 10 and 120 °C and between 10 and 150 °C. With high-purity aluminum (99.996%), smooth curves were obtained under the conditions of their experiments, but single yield-point elongations were obtained when tests were resumed after interruptions. Since McReynolds' experiments involved only about 2.5% extension of annealed metal, they do not establish the entire temperature ranges for discontinuities in the stress-strain curves, nor do they establish the entire ranges for strain aging.

Direct determination of the temperature ranges for strain aging may be obtained by a study of curves of variation of strength with temperature. Such curves, based on the results of tension tests, have been assembled in Fig. 1.

#### INFLUENCE OF TEMPERATURE ON THE ULTIMATE STRESS AND YIELD STRESS FOR VARIOUS NONFERROUS METALS

Fig. 1 shows curves of variation of ultimate stress and yield stress with temperature. The temperature scale is the same that has been used in papers by the author and previous associates (8-11, 13-15). Temperatures in degrees K are plotted on a logarithmic scale. Since abscissas are proportional to the logarithm of degrees K, the scale is the same in principle as Kelvin's original thermodynamic scale. The temperature range represented includes the boiling point of liquid hydrogen (20.5 °K) and the melting points of the metals represented.

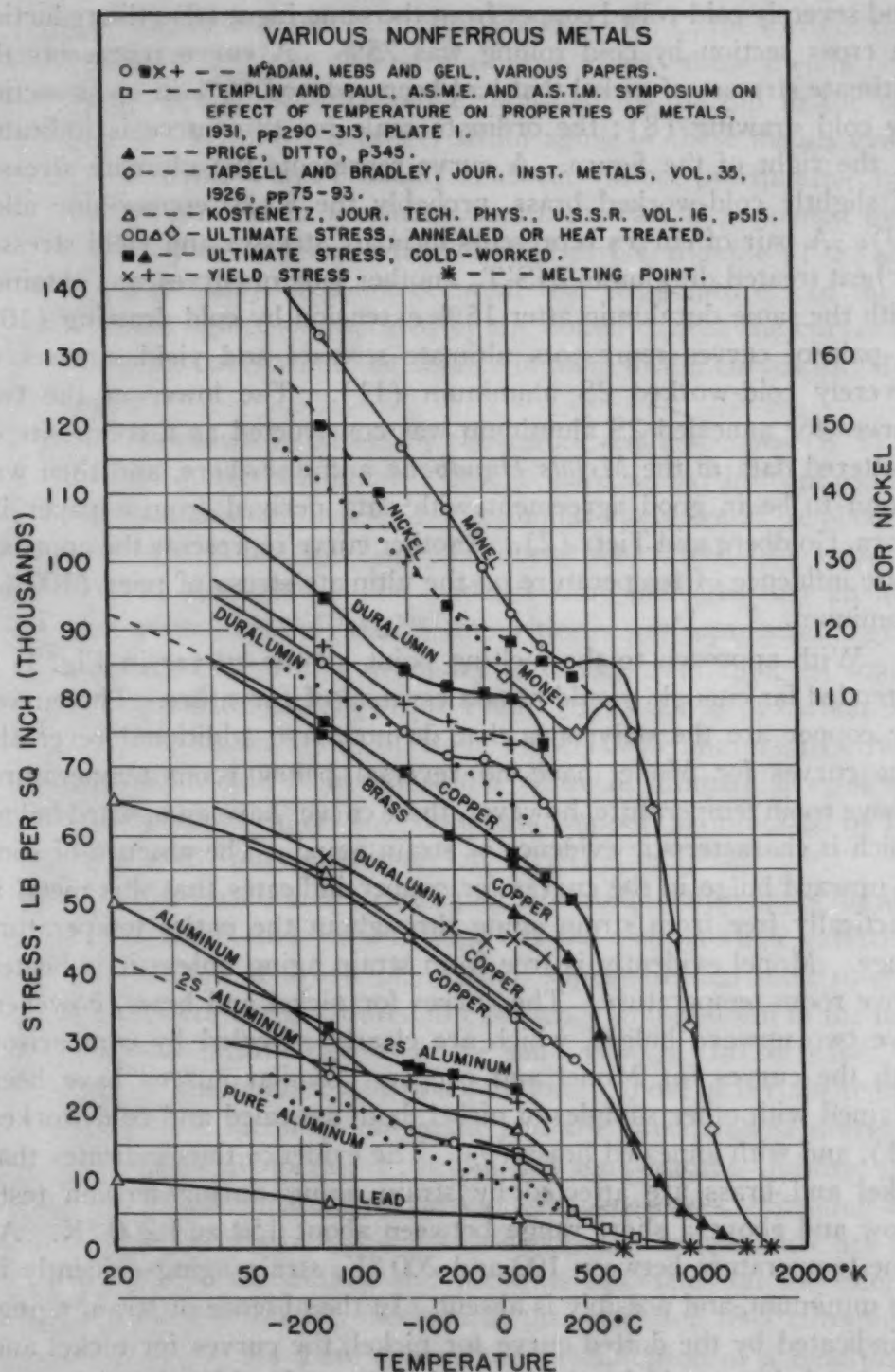


Fig. 1—Influence of Temperature on the Ultimate Stress and Yield Stress of Various Metals.

Two confluent curves represent ultimate stresses of annealed Monel (8). Four confluent curves represent ultimate stresses of oxygen-free copper. Two of these curves were obtained with annealed

and severely cold-rolled copper from the same ingot (8); the reduction in cross section by cold rolling was 75%. A curve represents the ultimate stresses of nickel that had been reduced 60% in cross section by cold drawing (8); the ordinate scale for this curve is indicated at the right of the figure. A curve represents the ultimate stresses of slightly cold-worked brass, probably the 80-20 copper-zinc alloy (9). A pair of curves represents ultimate stresses and yield stresses of heat treated duralumin 24S-T; another pair of curves was obtained with the same duralumin after 15% extension by cold drawing (10). A pair of curves represents ultimate stresses and yield stresses of severely cold-worked 2S aluminum (11). The lower of the two curves for annealed 2S aluminum was constructed as a composite of scattered data in the *Metals Handbook* and elsewhere, and then was found to be in good agreement with data derived from a paper by Dorn, Goldberg and Tietz (2). Another curve represents the approximate influence of temperature on the ultimate stress of pure (100%) aluminum.

With approach to the melting point all the curves in Fig. 1, if extended far enough, would have a reversal of curvature. The curves for copper are the only ones that do not have additional reversals. The curves for Monel have no reversal below room temperature. Above room temperature, however, these curves have an upward bulge, which is characteristic evidence of strain aging. The absence of such an upward bulge in the curves for copper indicates that this metal is practically free from strain aging throughout the entire temperature range. Monel evidently is free from strain aging unless it is heated above room temperature. The curves for nickel and brass, however, have two upward bulges, which are clearly revealed by comparison with the curves for Monel and copper. Similar curves have been obtained with other samples of nickel, both annealed and cold-worked (11), and with annealed brass (9). The evidence thus indicates that nickel and brass are affected by strain aging during tension tests below and above a short range between about 150 and 200 °K. At some temperature between 100 and 200 °K, strain aging evidently is at a minimum, and possibly is absent. In the absence of strain aging, as indicated by the dotted curve for nickel, the curves for nickel and brass probably would be similar to the curves for Monel and copper.

The curves for 2S aluminum and duralumin are similar in form to the curves for nickel and brass. Each of these curves has upward bulges below and above a short range between about 150 and 200 °K. In view of the previously mentioned evidence that duralumin is subject to strain aging at room temperature, and that aluminum is subject to



strain aging at temperatures as low as  $-30^{\circ}\text{C}$ , the form of the curves in Fig. 1 suggests that strain aging affects these metals below and above the temperature range indicated by the dip in the curves in Fig. 1. Within this range, strain aging of these metals evidently is at a minimum, and probably is absent. Since precipitation hardening of duralumin after a solution treatment can be prevented by holding this alloy at the temperature of solid carbon dioxide ( $195^{\circ}\text{K}$ ), strain aging probably does not occur at that temperature. In the absence of strain aging, as indicated by the dotted curves, the curves for these alloys probably would be similar in form to the curves for Monel and copper.

As shown in papers by the author and associates (8, 11), curves for high-purity aluminum (99.97%) are similar in form to the curves for 2S aluminum in Fig. 1. A similar curve could be obtained from data in a paper by Dorn, Goldberg and Tietz (2) with annealed 99.98% aluminum. The evidence thus indicates that an aluminum alloy containing only 0.02% impurities is subject to strain aging. The amount of impurities necessary to cause strain aging of some metals is very small. As shown by Pfeil (18), 0.003% of carbon is enough to cause strain aging of iron. For 100% aluminum, strain aging probably would be absent and a curve of ultimate stresses would be similar to the curves for Monel and copper, as indicated by the curve designated "pure aluminum" in Fig. 1.

The variation of strain aging indicated by the curves for aluminum alloys, nickel and brass in Fig. 1 is the characteristic variation of the precipitation of a new phase from supersaturated solid solution. As the temperature is lowered, the tendency to formation of the new phase increases, but the rigidity of the solid solution also increases, and thus opposes the tendency to precipitation. Above a certain temperature, the second factor is dominant and the precipitation decreases with decrease in temperature; below this temperature, the first factor becomes dominant and the precipitation increases. Striking examples of increase of strain aging with decrease in temperature are shown in a paper by the author and previous associates on the effect of low temperatures on the mechanical properties of 18-8 chromium-nickel steel (15). As there shown, the precipitation of a new phase from the metastable solid solution during a tension test increases rapidly with decrease below room temperature. For this alloy, however, the temperature for minimum strain aging evidently is above room temperature. The evidence thus indicates that the variation of strain aging indicated by the curves in Fig. 1 is not uncommon.

As shown in Fig. 1, the curves for yield stress of 2S aluminum

and duralumin are similar in form to the curves for ultimate stress. Similar curves for the yield stress of nickel and brass, either annealed or cold-worked, could be derived from previous papers (9, 11). The form of these curves for yield stress thus indicates that they, like the curves for ultimate stress, are affected by strain aging. The slight strain corresponding to the observed yield stress evidently can cause enough strain aging to affect the course of a curve of variation of the yield stress with temperature.

As shown in previous papers (13, 14), the influence of temperature on the flow stress involves two factors: a direct temperature factor and an intrinsic strength factor. The intrinsic strength is unchanged when the temperature of a metal specimen is varied without increase of plastic strain, provided that the variation of temperature causes no structural change. The variation of the flow stress with the temperature of such a specimen reveals the influence of the direct temperature factor. Increase of plastic strain, however, causes an increase of intrinsic strength. The lower the temperature, the more rapid is the increase of intrinsic strength with plastic strain. Each of these factors should be expressed in terms of flow-stress ratios, not in terms of flow-stress differences.

The influence of the direct temperature factor is revealed by the curves of yield stress in Fig. 1. Since each curve of yield stresses represents the effect of temperature with only slight variation of plastic strain, the ratio of the indicated yield stresses at  $-188^{\circ}\text{C}$  and room temperature represents approximately the direct temperature factor for that temperature range. This ratio would be about the same whether it is derived from the experimentally determined curve or from a curve corrected for the influence of strain aging. An important relationship is revealed by a comparison of the direct temperature factors thus obtained from the yield-stress curves in Fig. 1. For the severely cold-worked 2S aluminum and the heat treated duralumin, the factor is about 1.25; for the duralumin that had been heat treated and cold drawn, the value obtained is about 1.20. For annealed 2S aluminum no curve of yield stresses has been drawn. Although values reported in the literature seem to indicate that the yield stresses at  $-188^{\circ}\text{C}$  and room temperature are about the same, it appears probable that the direct temperature factor is about the same for annealed as for severely cold-worked aluminum. As shown in previous papers (13, 14), the direct temperature factor for oxygen-free copper is practically unaffected by prior plastic strain, and the factor for Monel is practically constant after slight initial plastic strain.

Direct temperature factors can be derived from the ultimate-stress curves for severely cold-worked copper and nickel in Fig. 1. Since the plastic strain required for determining the ultimate stresses varied little with temperature, and was slight in relation to the prior plastic strain at room temperature, the ultimate-stress curves for these metals in Fig. 1 represent the stress-temperature relationship for constant intrinsic strength. The ratios of the ultimate stresses at  $-188^{\circ}\text{C}$  and room temperature, therefore, represent the direct temperature factors for that stress range. For the cold-worked copper and nickel, the values thus obtained are about 1.33 and 1.35 respectively. For most exact determination, the direct temperature factors should be obtained from flow-stress curves. A value so derived for copper is about 1.31. For Monel, after slight initial plastic strain, the factor is about the same as for copper. The evidence thus indicates that the direct temperature factors for these three metals differ only slightly, and are not much greater than the values for aluminum and duralumin. The great differences in the melting points of these metals evidently have little effect on the direct temperature factors below room temperature.

The slope of a curve of ultimate stresses of annealed metal depends not only on the direct temperature factor, but also on the variation of the intrinsic strength with the temperature at which the metal has been strained. The ratio of the ultimate stresses of annealed copper at  $-188^{\circ}\text{C}$  and room temperature is about 1.6. This ratio represents the product of the direct temperature factor (1.31) and an approximate value of the intrinsic strength factor. The intrinsic strength factor for that amount of plastic strain, therefore, is about 1.22. For Monel, the corresponding value, derived from flow-stress curves in a previous paper (13), is about 1.19. The evidence in another previous paper (11) seems to indicate that the corresponding value for nickel is only about 1.1. The ratio of the ultimate stresses for annealed 2S aluminum at  $-188^{\circ}\text{C}$  and room temperature is about 1.92. Since the direct temperature factor is 1.25, the corresponding value of the intrinsic strength factor is about 1.54. The effect of this range of temperature evidently is much greater for aluminum than for copper, Monel and nickel. It is worthy of note that the intrinsic strength ratios for these four metals are in the inverse order of their melting points. The lower the melting point, the more rapid is the increase of intrinsic strength with plastic strain.

An accurate value of the direct temperature factor for aluminum cannot be obtained from the ultimate-stress curve for severely cold-



worked aluminum. Because of the great influence of temperature on the rate of increase of the intrinsic strength of aluminum with plastic strain, the ultimate-stress curve for the severely cold-worked aluminum is affected by an increase of intrinsic strength with decrease in temperature. For the heat treated duralumin, however, the slope of the ultimate stress curve is only slightly greater than the slope of the yield-stress curve. The precipitation hardening, while it increased the strength, has greatly decreased the rate of work hardening, and thus has decreased the influence of temperature on the rate of increase of intrinsic strength with strain.

#### INTRINSIC STRENGTH AND THE DIRECT TEMPERATURE FACTOR AS AFFECTED BY PLASTIC STRAIN

Quantitative evaluation of the intrinsic strength factor and the direct temperature factor should be made in terms of flow stresses, as illustrated in Fig. 2. Each upper diagram shows the influence of plastic strain on the tensile flow stress at two different temperatures; each lower diagram shows the influence of plastic strain on the intrinsic strength ratio and the direct temperature factor. Strain is expressed in terms of  $A_0/A$ , in which  $A_0$  and  $A$  represent the initial and current areas of cross section. Since values of  $A_0/A$  are represented on a logarithmic scale, abscissas are proportional to natural strains. Moreover, the natural strains representing prior plastic deformation and those representing subsequent strain during a tension test are directly additive.

The curves in the upper left diagram are derived from results obtained by Dorn, Goldberg and Tietz (2) with 2S aluminum. Curves F represent continuous flow at the indicated temperatures; the right end of each of these curves represents the flow stress and strain at the beginning of local contraction. Curve S is the locus of points representing incipient flow stresses at  $-195^\circ\text{C}$  after various strains at room temperature. Such curves, although they do not represent continuous flow, have been termed "secondary flow - stress curves" to distinguish them from the primary curves with which they are to be compared (13, 14). Comparison of corresponding ordinates of curve S and the lower curve F reveals the influence of the direct temperature factor; comparison of curve S with the upper curve F reveals the influence of the intrinsic strength factor. These factors should be expressed in terms of flow-stress ratios (13, 14).

The lower left diagram of Fig. 2 shows the influence of plastic strain on three flow-stress ratios. Ordinates of curve FSR represent ratios of corresponding ordinates of the two curves F in the upper

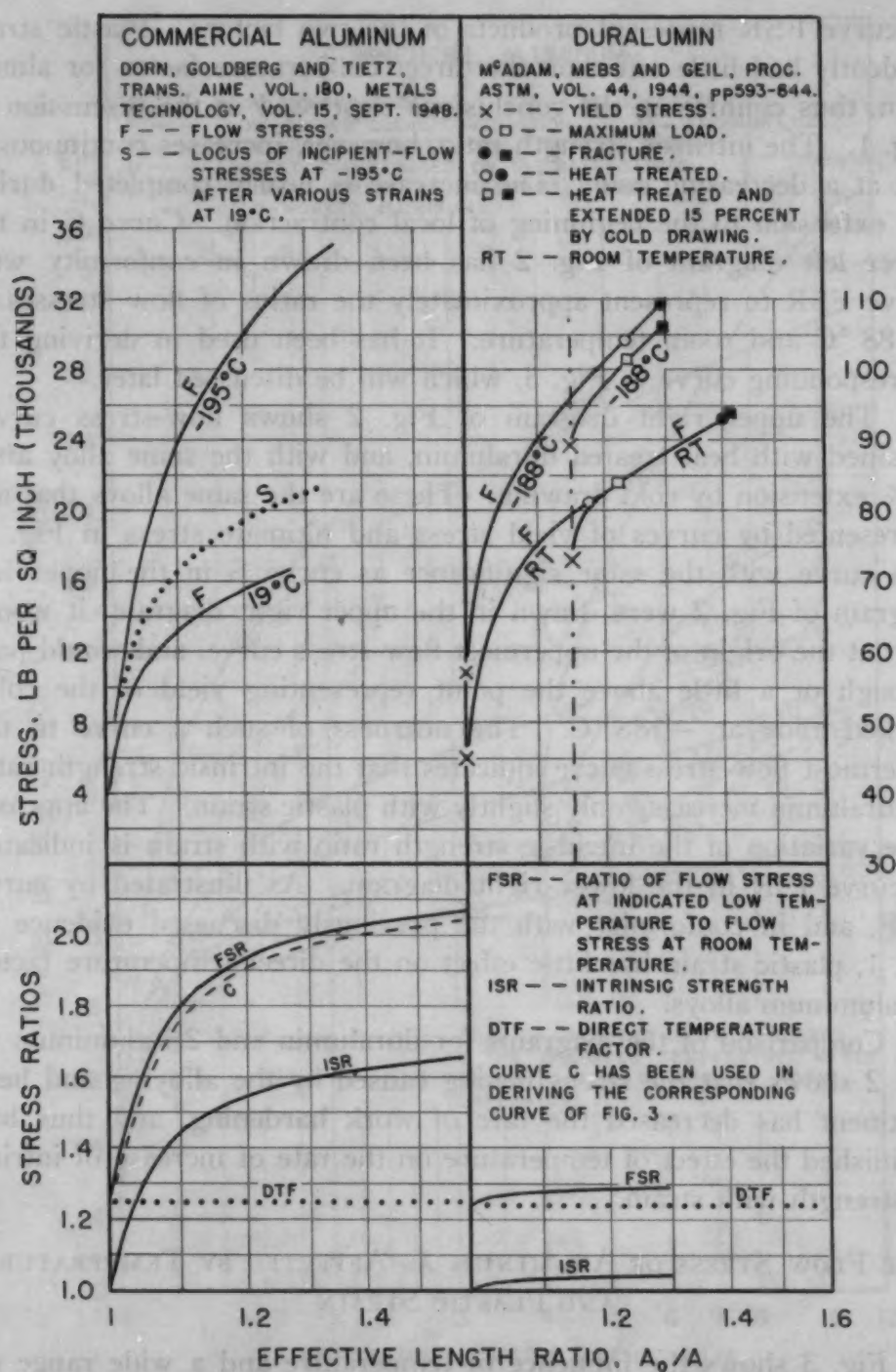


Fig. 2—Influence of Plastic Strain on the Direct Temperature Factor and Intrinsic Strength Factor for 2S Aluminum and Duralumin.

diagram. Curve ISR represents ratios of ordinates of the upper curve F and curve S, and curve DTF represents ratios of ordinates of curve S and the lower curve F. Ordinates of curves ISR thus represent values of the intrinsic strength ratio, ordinates of curve DTF represent values of the direct temperature factor, and ordinates

of curve FSR represent products of the two factors. Plastic strain evidently had little effect on the direct temperature factor for aluminum, thus confirming the conclusions expressed in the discussion of Fig. 1. The intrinsic strength ratio, however, increases continuously, but at a decreasing rate. The increase is nearly completed during the extension to the beginning of local contraction. Curve C in the lower left diagram of Fig. 2 has been drawn in conformity with curve FSR to represent approximately the ratios of flow stresses at  $-188^{\circ}\text{C}$  and room temperature. It has been used in deriving the corresponding curve in Fig. 3, which will be discussed later.

The upper right diagram of Fig. 2 shows flow-stress curves obtained with heat treated duralumin, and with the same alloy after 15% extension by cold drawing. These are the same alloys that are represented by curves of yield stress and ultimate stress in Fig. 1. If a curve with the same significance as curve S in the upper left diagram of Fig. 2 were drawn in the upper right diagram, it would start at the origin of the uppermost flow-stress curve, and would pass through or a little above the point representing yield of the cold-worked alloy at  $-188^{\circ}\text{C}$ . The nearness of such a curve to the uppermost flow-stress curve indicates that the intrinsic strength ratio of duralumin increases only slightly with plastic strain. The approximate variation of the intrinsic strength ratio with strain is indicated by curve ISR in the lower right diagram. As illustrated by curve DTF, and in conformity with the previously discussed evidence in Fig. 1, plastic strain has little effect on the direct temperature factor for aluminum alloys.

Comparison of the diagrams for duralumin and 2S aluminum in Fig. 2 shows that the strengthening caused by the alloying and heat treatment has decreased the rate of work hardening, and thus has diminished the effect of temperature on the rate of increase of intrinsic strength with strain.

#### THE FLOW STRESS OF ALUMINUM AS AFFECTED BY TEMPERATURE AND PLASTIC STRAIN

Fig. 3 shows the influence of temperature and a wide range of plastic strain on the flow stress of 2S aluminum. In establishing this diagram, attention was given first to the four primary flow-stress curves within the strain range from yield of annealed metal to the points representing true stress at the maximum load. The course of a flow-stress curve near this point can be determined accurately when the ultimate stress is known (13, 14). At the point representing the stress at maximum load, a flow-stress curve must be tangent



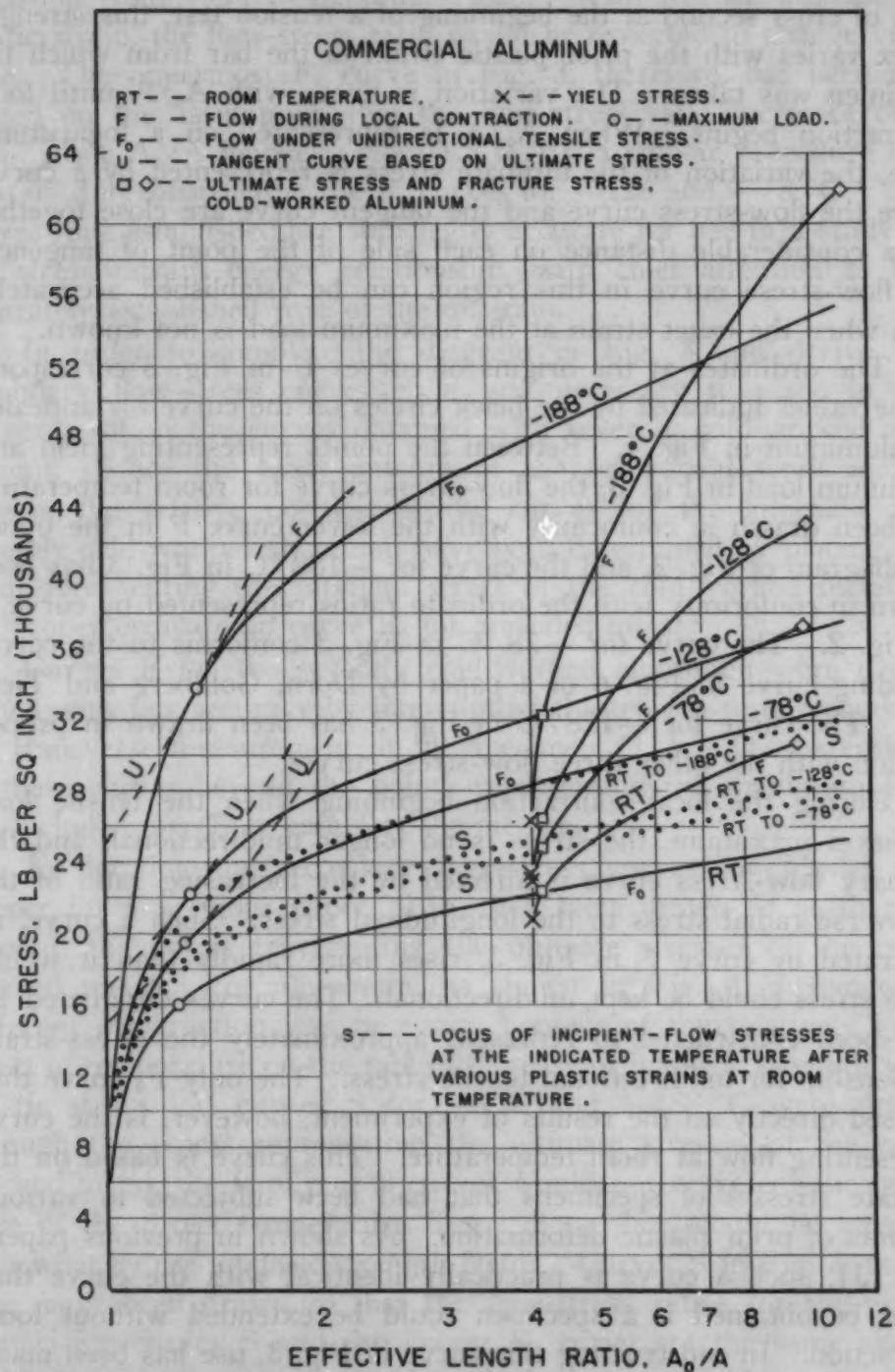


Fig. 3—Influence of Temperature on Primary and Secondary Flow-Stress Curves for 2S Aluminum.

to a curve of variation of the ultimate stress with prior plastic strain. In Fig. 3, therefore, three of the four primary flow-stress curves are tangent to curves U, which start at points representing ultimate stresses of annealed aluminum; the tangent curve for room temperature has been omitted. Since the ultimate stress is based on the

area of cross section at the beginning of a tension test, this strength index varies with the prior plastic strain of the bar from which the specimen was taken. The variation is linear with  $A_0/A$  until local contraction begins. When  $A_0/A$  is represented on a logarithmic scale, the variation of the ultimate stress is represented by a curve. Since the flow-stress curve and the tangent curve are close together for a considerable distance on each side of the point of tangency, the flow-stress curve in this region can be established accurately, even when the exact strain at the maximum load is not known.

The ordinates at the origins of curves U in Fig. 3 correspond to the values indicated by the black circles on the curve for annealed 2S aluminum in Fig. 1. Between the points representing yield and maximum load in Fig. 3, the flow-stress curve for room temperature has been drawn in conformity with the lower curve F in the upper left diagram of Fig. 2, and the curve for  $-188^\circ\text{C}$  in Fig. 3 has been drawn in conformity with the ordinate ratios represented by curve C in Fig. 2. The curve for  $-78^\circ\text{C}$  in Fig. 3 conforms to the corresponding curve in Fig. 6 of a paper by Dorn, Goldberg and Tietz (2). The curve for  $-128^\circ\text{C}$  in Fig. 3 has been drawn in proper relation with the other three flow-stress curves.

During the local contraction beginning when the tensile load reaches a maximum, the stress is no longer unidirectional, and the ordinary flow-stress curve is affected by the increasing ratio of the transverse radial stress to the longitudinal stress. Such a curve, as illustrated by curve F in Fig. 3, rises more rapidly than it would if the stress could be kept unidirectional. The curves designated  $F_0$  have been constructed to represent approximately the stress-strain relationship for unidirectional tensile stress. The only  $F_0$  curve that is based directly on the results of experiment, however, is the curve representing flow at room temperature. This curve is based on the ultimate stresses of specimens that had been subjected to various amounts of prior plastic deformation. As shown in previous papers (12, 13), such a curve is practically identical with the curve that would be obtained if a specimen could be extended without local contraction. In constructing this curve in Fig. 3, use has been made of data on page 771 of the *Metals Handbook* (17) and in a paper by Templin (26). Since no such experimental basis is available for the  $F_0$  curves representing flow at low temperatures, these curves have been constructed by application of the principle illustrated by the course of curve C in the lower left diagram of Fig. 2. As illustrated by this curve, the increase in the ratio of the flow stresses at  $-188^\circ\text{C}$  to the flow stress at room temperature is nearly completed during the

extension from yield to maximum load. With further increase in plastic strain, the flow-stress ratio would be expected to change very little. The uppermost  $F_0$  curve in Fig. 3, therefore, has been extended on the assumption that the flow-stress ratio increases only 10%, while  $A_0/A$  increases from 1.3 to 10; a similar procedure has been used in constructing the  $F_0$  curves for  $-128$  and  $-78^\circ\text{C}$ . The curves thus established are sufficiently accurate for use in a study of the stress-strain energy relationship, with chief attention to the accurately established part of the diagram.

In order to complete the diagram in Fig. 3 and derive the secondary flow-stress curves  $S$ , it was necessary to place in the proper position the curves obtained with severely cold-worked aluminum. Since the exact amount of the prior cold work is not known, the relative position of the curves for the annealed and severely cold-worked aluminum have been determined by placing the point representing the ultimate stress of the cold-worked metal at the proper ordinate on curve  $F_0$  for annealed metal.<sup>2</sup>

Curves  $F$  for the severely cold-worked aluminum were determined with fair accuracy by interrupting the tension tests frequently for transverse measurement of the specimen (11). The extensions of these curves beyond the points representing the maximum load are included merely to complete the picture.

In deriving the secondary flow-stress curves for Monel and copper for a previous paper (13), they were drawn so as to pass through the points representing the ultimate stresses of the cold-worked metal. For aluminum, as shown in Fig. 3, a somewhat different construction was necessary because of the relatively great effect of temperature on the rate of increase of intrinsic strength with plastic strain. If curves  $S$  for  $-128$  and  $-188^\circ\text{C}$  were drawn through the points representing the ultimate stresses of the cold-worked metal, the family of  $S$  curves would not represent the influence of the direct temperature factor alone, but would be affected somewhat by the intrinsic strength factor. Curves  $S$  in Fig. 3, therefore, have been drawn so that the flow-stress ratios for the group comprising curves  $S$  and the lowest  $F_0$  curve are the same as the yield-stress ratios for the cold-worked aluminum. Moreover, for reasons given in the discussion of Figs. 1 and 2, these ratios have been kept the same throughout the entire strain range represented in Fig. 3. The ordinate ratios for these curves represent direct temperature factors; the ordinate ratios for corresponding primary

<sup>2</sup>As shown in the literature (17, 26), cold work beyond about 20% reduction in cross section causes little increase in the ratio of yield stress to ultimate stress. The ultimate stress for severely cold-worked metal, therefore, is the flow stress.



and secondary flow-stress curves represent intrinsic strength ratios.

From curves  $F_0$  and the secondary flow-stress curves of Fig. 3, curves of other types have been derived and are represented in Figs. 4 to 8.

#### THE STRESS-STRAIN-TEMPERATURE RELATIONSHIP FOR VARIOUS STRENGTH STATES

The upper diagram in Fig. 4 shows the relationship between plastic strain, temperature and flow stress for various strength states; the lower diagram shows the corresponding relationship between plastic strain, temperature and strain energy. Consideration will be given first to the upper diagram. Curves  $F_0$  and  $S$  in this diagram have been reproduced from Fig. 3. From the relationship between these primary and secondary flow-stress curves, other curves of two kinds have been derived, and are shown in the upper diagram of Fig. 4. Attention will be given first to curves A to H, which represent a series of strength states. These constant-state curves have been derived by applying the following principles: (a) Varying the temperature without varying the plastic strain causes no change in the strength state. (b) Two specimens of the same metal, whatever their strain-temperature history, are in the same strength state if their flow stresses are the same at the same temperature.<sup>3</sup> The first principle implies that points at the same abscissa on the lower  $F_0$  curve and curves  $S$  represent the same strength state. The second principle implies that a horizontal line drawn between a primary and secondary curve representing flow at the same temperature will intersect these curves at points representing the same strength state. By applying these principles, as illustrated by the horizontal dot-and-dash lines in Fig. 4, the points indicated by the black circles have been established on the four  $F_0$  curves, and these points have been used in constructing constant-state curves A to H. The intersections of all the constant-state curves with curve  $F_0$  for  $-188^\circ\text{C}$  are within the range between yield and maximum load, and thus are in the most accurately established part of this flow-stress curve.

The abscissa range for a constant-state curve, expressed in terms of ratios of natural strain, increases greatly from curve A to curve H. In this respect, aluminum is similar to copper, as illustrated in Fig. 1 of a previous paper (14). The significance of this increase in the abscissa range will be discussed later in connection with the lower diagram of Fig. 4.

A curve representing a constant strength state does not repre-

<sup>3</sup>This principle implies that the direct temperature factor does not vary with plastic strain.

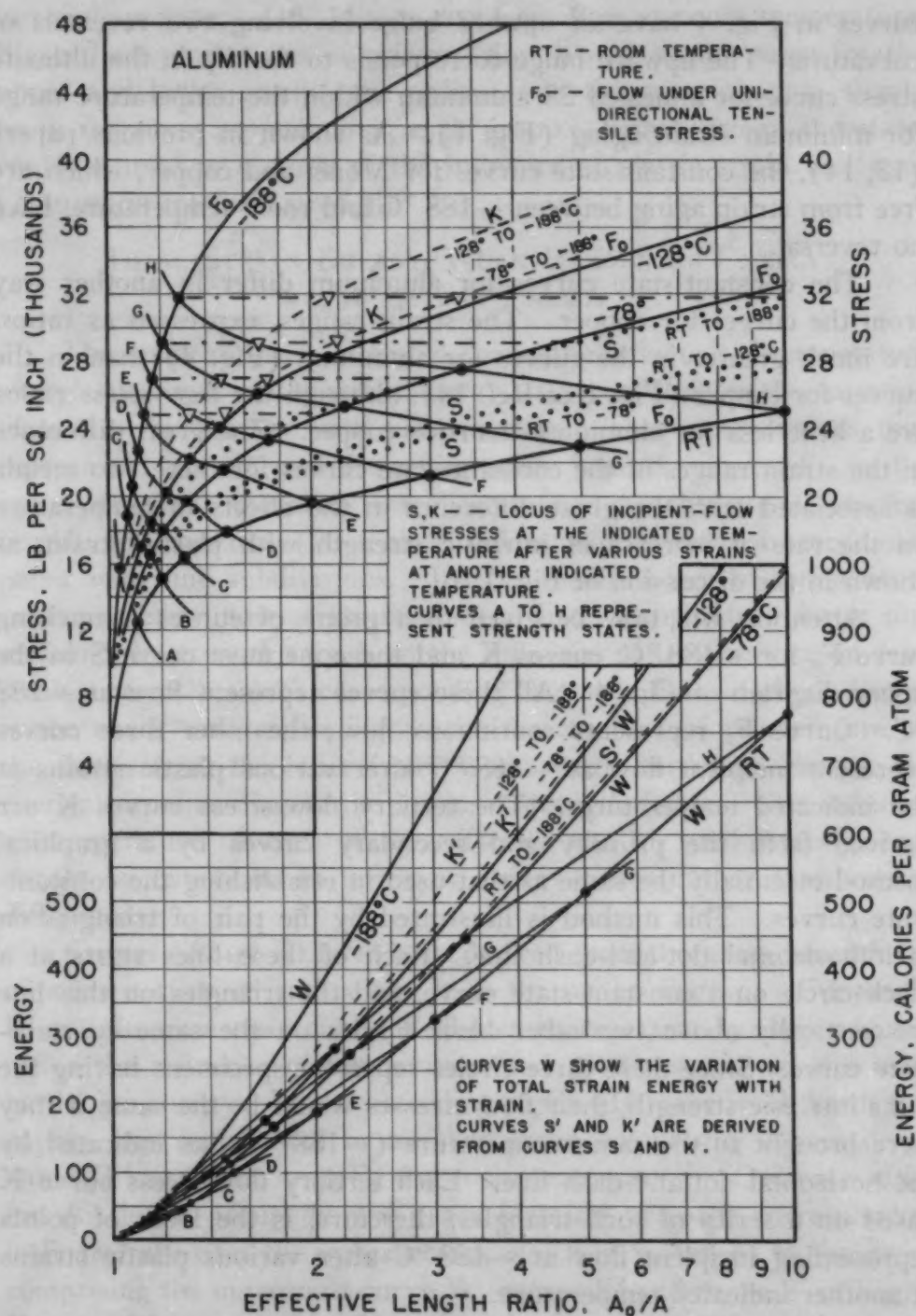


Fig. 4—Influence of Temperature on the Stress-Strain Energy Relations for Various Strength States.

sent a constant structural state, even when strain aging is absent. Since strain aging in varying degree affects the flow-stress curves for aluminum, it affects the form of the derived curves representing constant strength states. Because of strain aging, the constant-state

curves in Fig. 4 have an upward bulge involving two reversals of curvature. The upward bulge corresponds to the dip in the ultimate stress curve for annealed 2S aluminum within the temperature range for minimum strain aging (Fig. 1). As shown in previous papers (13, 14), the constant-state curves for Monel and copper, which are free from strain aging between  $-188^{\circ}\text{C}$  and room temperature, have no reversal.

The constant-state curves for aluminum differ in another way from the curves for copper. The strain ranges, expressed as ratios, are much greater in the curves for aluminum (Fig. 4) than in the curves for copper (Fig. 1 of Ref. 14), although the flow-stress ratios are a little less for aluminum than for copper. The great difference in the strain ranges of the constant-state curves for these two metals is associated with the great difference in the effects of temperature on the rate of increase of intrinsic strength with plastic strain, as shown in the discussion of Fig. 1.

Attention will now be given to a group of curves comprising curve  $F_0$  for  $-188^{\circ}\text{C}$ , curves K and the uppermost curve S in the upper diagram of Fig. 4. All these curves represent flow at  $-188^{\circ}\text{C}$ . Curve  $F_0$  represents continuous flow; the other three curves represent incipient flow at  $-188^{\circ}\text{C}$  after various plastic strains at the indicated temperatures. The tertiary flow-stress curves K are derived from the primary and secondary curves by a graphical method essentially the same as that used in establishing the constant-state curves. This method is illustrated by the pair of triangles on each horizontal dot-and-dash line. Each of these lines starts at a black circle on a constant-state curve, and the triangles on this line are vertically above two other black circles on the same constant-state curve. Since these three circles represent specimens having the same intrinsic strength, their flow stresses would be the same if they were brought to the same temperature ( $-188^{\circ}\text{C}$ ), as indicated by the horizontal dot-and-dash line. Each tertiary flow-stress curve K based on a series of such triangles, therefore, is the locus of points representing incipient flow at  $-188^{\circ}\text{C}$  after various plastic strains at another indicated temperature.

Since the four curves of this group represent flow at the same temperature, they may be used in a study of the influence of plastic strain and temperature on intrinsic strength. If the ordinates of the curves of this group be compared at the same abscissa, these ordinates will be proportional to the intrinsic strengths produced by the indicated primary strain at the indicated temperatures. By a similar graphical method another group of curves could be constructed, as



in previous papers (13, 14), to represent flow at room temperature. Since the temperatures of primary flow would be the same for the upper and lower groups, the ordinates at the same abscissa should be in the same proportion in each group. Either group, therefore, could be used in a study of the influence of plastic strain and temperature on intrinsic strength.

#### TOTAL STRAIN ENERGY, WORK HARDENING ENERGY AND LATENT ENERGY

The lower diagram of Fig. 4 shows the influence of temperature and plastic strain on the strain energy. Curves W show the variation of total strain energy with plastic strain. The energy values thus represented are derived from the areas beneath curves  $F_0$  in the upper diagram; the areas were determined by the use of original unreduced diagrams (20 inches wide), which were on coordinate paper with fine subdivisions. Just as the influence of temperature on the primary flow stress involves a direct temperature factor and an intrinsic strength factor, so the influence of temperature on total strain energy involves corresponding factors. One of these factors is the energy corresponding to the direct effect of temperature on the flow stress; the other factor is the work hardening energy, the energy corresponding to the intrinsic strength factor. The influence of temperature on each of these factors and on total strain energy should be expressed in terms of energy ratios rather than energy differences.

Curves  $S'$  and  $K'$  have been derived from the areas beneath the uppermost curve  $S$  and curves  $K$  in the upper diagram. Curves  $S'$ ,  $K'$  and the uppermost curve  $W$ , therefore, represent by their ordinate ratios the influence of temperature and plastic strain on the work hardening energy. In the preceding paper (14), the work hardening energy was represented by another group comprising curves designated  $W'$  and the curve  $W$  for room temperature. Ordinate ratios for this lower group, however, are identical with the corresponding ordinate ratios for the upper group, which is analogous to the group comprising the uppermost curve  $W$ , curves  $K'$  and curve  $S'$  in Fig. 4. From either group, therefore, the other group may be derived, and either group may be used in deriving values of work hardening energy for use in diagrams of different types.

Curves  $B$  to  $H$  in the lower diagram of Fig. 4 are derived from the correspondingly designated curves in the upper diagram; the black circles on the curves in the lower diagram are directly below the corresponding circles in the upper diagram. Each of these curves

in the lower diagram, therefore, shows the influence of temperature on the total strain energy required to produce a constant strength state. As would be expected in view of their derivation, the curves have an upward bulge and two reversals of curvature, and thus differ from the corresponding curves for copper (14). In the two previous papers (13, 14), it was assumed that, when a curve represents constant intrinsic strength, it also represents constant latent energy. By "latent energy" is meant the portion of the total strain energy that is not evolved as heat, but is involved in the work hardening. For copper, however, the latent energy is due solely to the plastic strain, and is not affected by the structural changes involved in strain aging. Though the constant-state curves for aluminum are affected by strain aging, it appears justifiable to assume that each constant-state curve in Fig. 4 represents approximately constant latent energy.

On this assumption, the course of each curve shows the influence of temperature on the latent energy ratio, the ratio of the latent energy  $E$  to the total strain energy  $W$ . The course of each curve thus indicates that  $E/W$  increases with decrease in the temperature at which the metal flows. Moreover, a comparison of the curves in terms of ordinate ratios shows that the influence of temperature on  $E/W$  varies greatly from curve B to curve W. As shown in the preceding paper (14), this variation is incompatible with a prevalent view with regard to the variation of  $E/W$  with plastic strain. Whereas evidence presented by Taylor and Quinney (25) has been interpreted to mean that  $E/W$  for copper is nearly constant throughout an initial range of plastic strain, the evidence in the preceding paper and confirmed by the previously mentioned evidence in the lower diagram of Fig. 4 indicates that  $E/W$  decreases continuously with plastic strain.

#### INFLUENCE OF PLASTIC STRAIN AND TEMPERATURE ON LATENT ENERGY AND LATENT ENERGY RATIOS

For a study of the latent energy of aluminum, the lower diagram of Fig. 4 has been correlated with published results of direct determinations of latent energy. Diagrams based on this correlation are shown in Fig. 5. Direct determinations of latent energy were made by Farren and Taylor (3), Rosenhain and Stott (21), and Taylor and Quinney (25). Their experiments consisted of determinations of the total strain energy and evolved heat; the values of latent energy thus were determined by difference. Fig. 4 of the preceding paper (14) contains plotted results of their experiments, with abscissas representing plastic strains. The lower right diagram of that

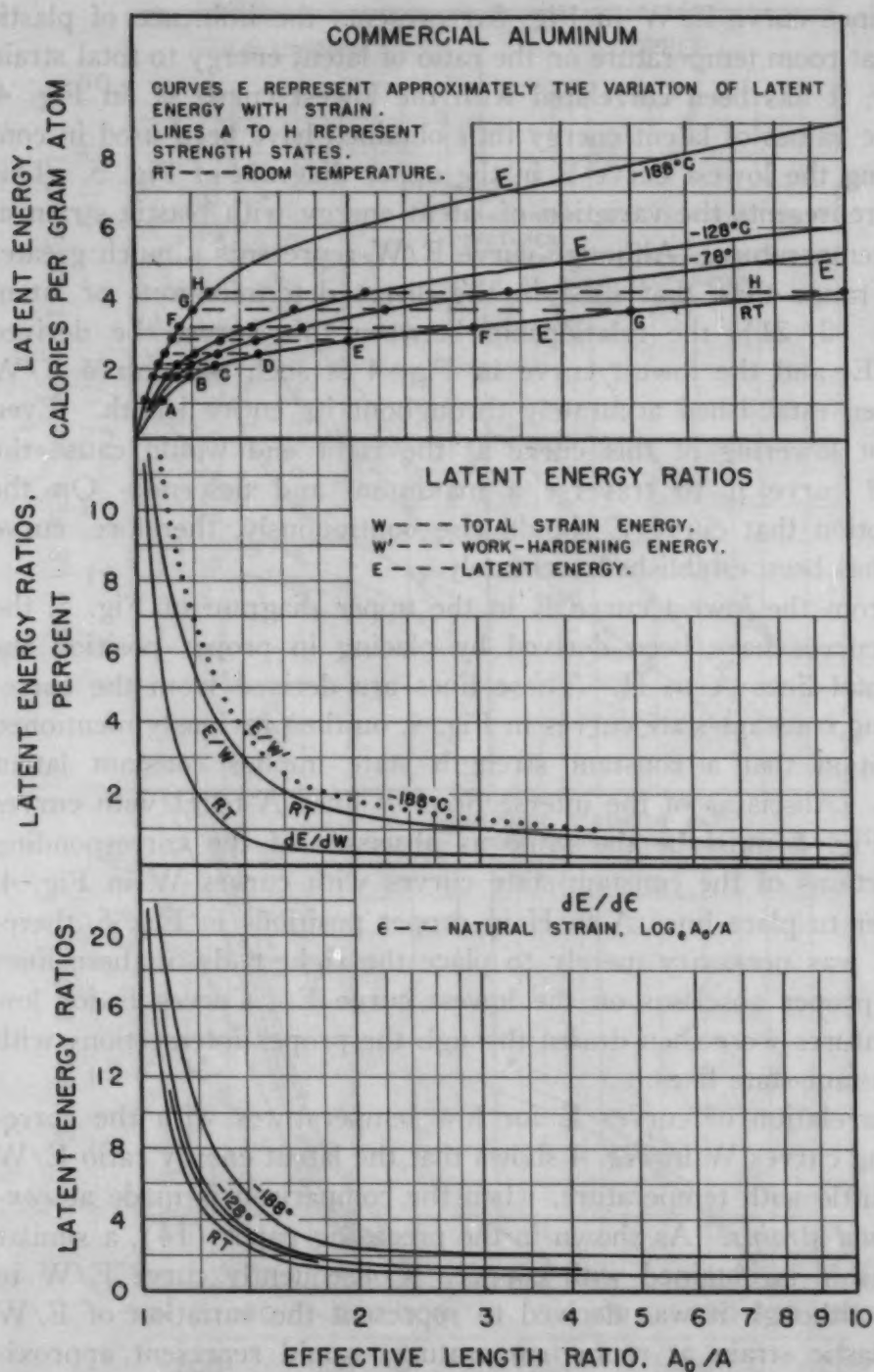


Fig. 5—Influence of Strain at Various Temperatures on Latent Energy and Latent-Energy Ratios.

figure shows results obtained by Farren and Taylor (3) and by Rosenhain and Stott (21) with commercial aluminum. The diagram also contains a curve representing the present author's interpretation of the evidence. This curve, designated  $E/W$ , has been reproduced and prolonged in the middle diagram of Fig. 5 of the present paper.

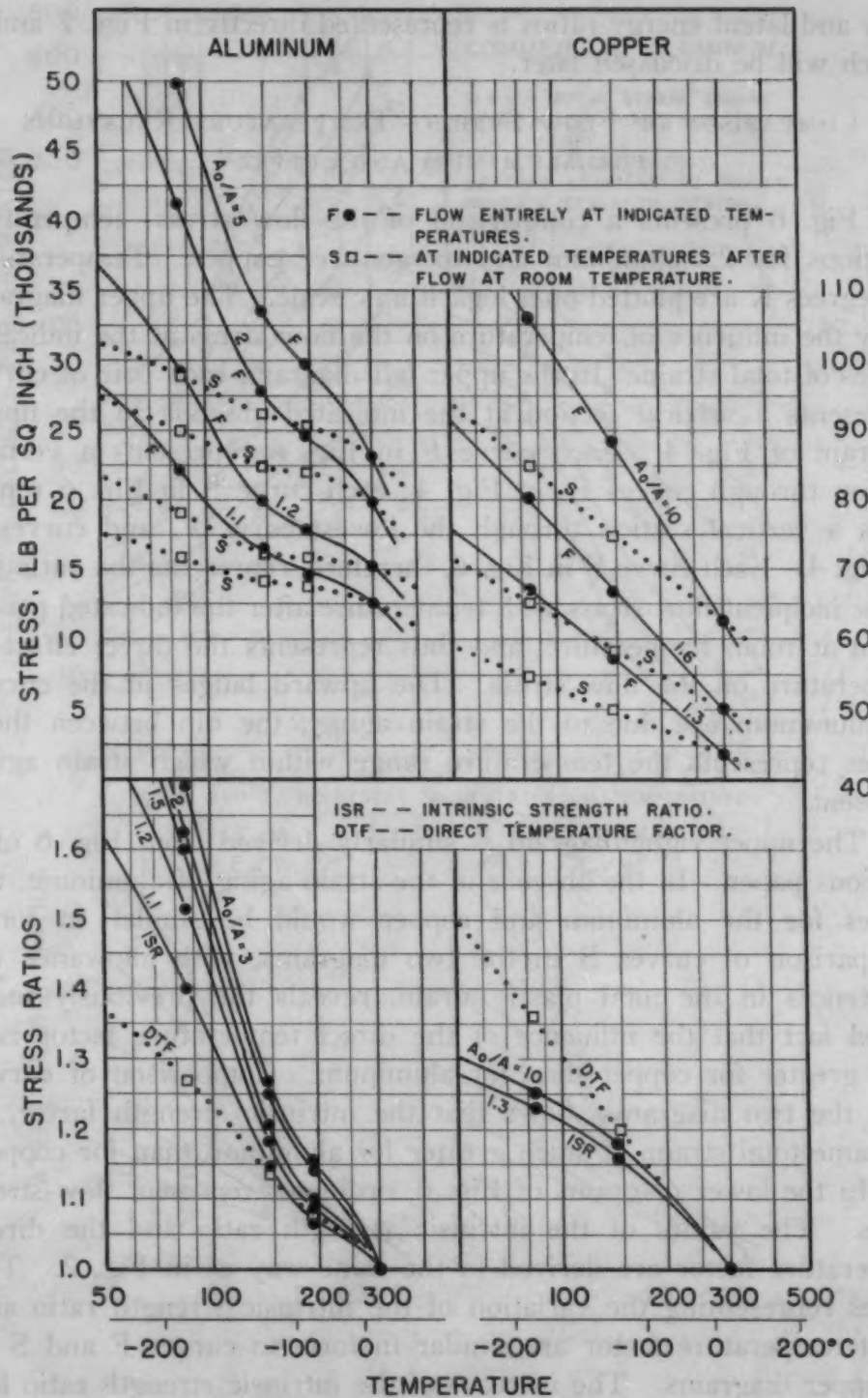


Since curve  $E/W$  in Fig. 5 represents the influence of plastic strain at room temperature on the ratio of latent energy to total strain energy, it has been correlated with the lowest curve  $W$  in Fig. 4, and the values of latent energy thus obtained have been used in constructing the lowest curve  $E$  in the upper diagram of Fig. 5. This curve represents the variation of latent energy with plastic strain at room temperature. Although curve  $E/W$  represents a much greater strain range than that used in the direct determinations of latent energy (3, 21), the relationship between this curve, the derived curve  $E$ , and the lowest curve in Fig. 4 is such that curve  $E/W$  has been established accurately throughout its entire length. Even a slight lowering of this curve at the right end would cause the derived curve  $E$  to traverse a maximum and descend. On the assumption that curve  $E$  should rise continuously, therefore, curve  $E/W$  has been established accurately.

From the lowest curve  $E$  in the upper diagram of Fig. 5, the other curves have been derived by placing in proper position the horizontal lines  $A$  to  $H$ . These lines are derived from the corresponding constant-state curves in Fig. 4, on the previously mentioned assumption that a constant strength state implies constant latent energy. Abscissas of the intersections of lines  $A$  to  $H$  with curves  $E$  in Fig. 5 must be the same as abscissas of the corresponding intersections of the constant-state curves with curves  $W$  in Fig. 4. In order to place lines  $A$  to  $H$  in proper positions in Fig. 5, therefore, it was necessary merely to place the right ends of these lines at the proper abscissas on the lowest curve  $E$ . Curves  $E$  for low temperatures were then drawn through the proper intersections with the constant-state lines.

Correlation of curves  $E$  for low temperatures with the corresponding curves  $W$  in Fig. 4 shows that the latent energy ratio  $E/W$  varies little with temperature, when the comparison is made at *constant total strains*. As shown in the preceding paper (14), a similar relationship is obtained with copper. Consequently curve  $E/W$  in Fig. 5, although it was derived to represent the variation of  $E/W$  with plastic strain at room temperature, would represent approximately the variation of  $E/W$  at temperatures down to  $-188^{\circ}\text{C}$ . The ratio of latent energy to work hardening energy  $W'$ , however, varies considerably with temperature, as indicated by a comparison of curves  $E/W$  and  $E/W'$  in Fig. 5.

From the varying slope of curve  $E$  for room temperature, a curve has been derived to represent the influence of plastic strain on  $dE/dW$ . This curve is shown in the middle diagram of Fig. 5. In



the lower diagram of Fig. 5 are curves representing the influence of plastic strain on the rate of increase of the latent energy with natural strain. As illustrated by the four curves, this ratio varies considerably with temperature. The influence of temperature on latent en-

ergy and latent energy ratios is represented directly in Figs. 7 and 8, which will be discussed later.

#### COMPARISON OF FLOW STRESS - TEMPERATURE RELATIONS FOR ALUMINUM AND COPPER

Fig. 6 presents a comparison of the flow stress - temperature relations for 2S aluminum and oxygen-free copper. Temperatures in degrees K are plotted on a logarithmic scale. The upper diagrams show the influence of temperature on the flow stress at the indicated values of total strain. In the upper left diagram, each pair of curves represents a vertical section at the indicated abscissa in the upper diagram of Fig. 4. Each curve F in Fig. 6 represents a vertical section through curves  $F_0$  in Fig. 4; each curve S in Fig. 6 represents a vertical section through the lowest curve  $F_0$  and curves S in Fig. 4. Each curve S in Fig. 6, therefore, represents the variation of the incipient-flow stress with temperature after the indicated plastic strain at room temperature, and thus represents the direct effect of temperature on the flow stress. The upward bulges in the curves for aluminum are due to the strain aging; the dip between these bulges represents the temperature range within which strain aging is absent.

The upper right diagram is similarly derived from Fig. 6 of a previous paper. In the absence of the strain aging of aluminum, the curves for the aluminum and copper would be similar in form. Comparison of curves S in the two diagrams, with allowance for differences in the total plastic strain, reveals the previously mentioned fact that the influence of the direct temperature factor is a little greater for copper than for aluminum. Comparison of curves F in the two diagrams shows that the intrinsic strength factor, at the same total strain, is much greater for aluminum than for copper.

In the lower diagrams of Fig. 6, ordinates represent flow-stress ratios. The values of the intrinsic strength ratio and the direct temperature factor are derived in the same way as in Fig. 2. The curves representing the variation of the intrinsic strength ratio and direct temperature factor are similar in form to curves F and S in the upper diagrams. The increase of the intrinsic strength ratio between room temperature and  $-188^\circ\text{C}$  is much greater for aluminum than for copper. Since, as previously shown, the direct temperature factor for both aluminum and copper varies little with plastic strain, only one curve has been used in Fig. 6 to represent the direct temperature factor for each of these metals. These ratios are expressed in terms of the intrinsic strength at room temperature.





be given first to Fig. 7, which represents various strain energy relations for strength states B to H, the same strength states that are represented in Fig. 4.

The upper left diagram in Fig. 7 shows the influence of temperature on total strain energy and work hardening energy. The values of work hardening energy are derived by the use of ordinate ratios for the uppermost curve W, curves K' and curve S' in Fig. 4. Since energy values are plotted on a logarithmic scale in Fig. 7, vertical distances are proportional to energy ratios. Because vertical distances between curves W and W' represent the influence of the direct temperature factor, and because this factor varies little with plastic strain, corresponding vertical distances are the same for each pair of curves. The constant-state curves in this diagram are affected by strain aging, and thus have two reversals, whereas the corresponding curves for copper (14) have no reversal between  $-188^{\circ}\text{C}$  and room temperature. Moreover, the ratio range of energy values for constant state is much greater for aluminum than for copper. This difference between the two metals may be correlated with the difference in the effect of temperature on the intrinsic strength factor.

The upper right diagram of Fig. 7 shows the influence of temperature on the latent energy ratio  $E/W$ . Because of the reciprocal relationship between these curves and the curves in the upper left diagram, corresponding curves in the two diagrams are identical in form and vertical range on the logarithmic scale. The vertical range increases greatly from curve B to curve H. As shown in the preceding paper (14), this variation of the vertical range is incompatible with the view (25) that the latent energy ratio  $E/W$  is nearly constant throughout an initial range of plastic strain.

The lower two diagrams in Fig. 7 show the influence of temperature when  $E/W$  and  $E/W'$  are expressed in terms of the value at room temperature. These curves have been derived from corresponding curves in the upper diagrams. The latent energy ratios represented in the lower diagrams are much greater than the corresponding ratios for copper (14).

Fig. 8 shows the influence of temperature on various energy relations for the indicated values of total strain. The upper left diagram, derived from the lower diagram of Fig. 4, shows the influence of temperature on total strain energy and work hardening energy. The upper right diagram, derived from the upper diagram of Fig. 5, shows the influence of temperature on latent energy. The lower left diagram shows the influence of temperature on the latent energy ratios  $E/W$  and  $E/W'$ .—As shown in the discussion of Fig. 5,





lower left diagram of Fig. 8, the ratio of latent energy to work hardening energy increases with decrease in temperature.

The lower right diagram of Fig. 8 shows the influence of temperature on the rate of increase of latent energy with strain. As shown in this diagram and in the lower diagram of Fig. 5, this ratio increases with decrease in temperature, but decreases with increase in plastic strain. As stated in the preceding paper (14), the increase of latent energy with plastic strain is a function of the strain, not of the total strain energy.

#### CRYSTAL RECOVERY AFTER COLD WORK

Since the diagrams in Figs. 1 to 8 are based on the results of ordinary tension tests, they contain no evidence of crystal recovery after cold work. However, evidence for the softening effect of crystal recovery of 2S aluminum and high-purity aluminum (99.97%) was given in a paper by the author and previous associates (11). Tension tests at low temperatures were interrupted several times for measurement of the diameter of the specimen at room temperature in order to obtain values of the true stress and strain. When the load was applied again after cooling to the low temperature, the stress at the resumption of flow was less than the stress at the interruption. These differences in the flow stress were greatest at  $-188^{\circ}\text{C}$ , but lesser differences were obtained at  $-128$  and  $-78^{\circ}\text{C}$ . The recovery thus indicated was greater for the high-purity aluminum than for the 2S aluminum.

Additional evidence for the recovery of aluminum after cold work at low temperatures has been obtained by Tietz and Dorn (28). Their experiments were made with high-purity aluminum (99.987%). After extension at  $-195^{\circ}\text{C}$  to 0.075 true strain, a specimen was kept for 7 days at  $90^{\circ}\text{F}$ . When the test was resumed at  $-195^{\circ}\text{C}$ , the flow stress had decreased from 12,000 to 9300 psi, whereas the flow stress at the same strain at room temperature would be about 6500 psi. However, no estimate was made of the loss of intrinsic strength during the interval at  $90^{\circ}\text{F}$ . When allowance is made for the direct temperature factor, by the method illustrated in Fig. 2, it becomes evident that nearly all the excess intrinsic strength produced by the straining at  $-195^{\circ}\text{C}$  was removed by the stay at  $90^{\circ}\text{F}$ .

As a result of their experiments, Tietz and Dorn reached the following conclusion: "Prestraining at lower temperatures to identical flow stresses results in higher recovery rates of the flow stress . . . ." This statement, however, is too general, even if the word

"strains" be substituted for the word "stresses". The statement might be interpreted to imply that any metal that has been strained at  $-195^{\circ}\text{C}$  would lose much of its intrinsic strength if kept at room temperature. The statement even appears to imply that any metal, cold-worked at any temperature, would lose some of its intrinsic strength if kept at any higher temperature. However, important softening after cold work occurs only when a metal is heated into a temperature range for softening by recovery. The lower limit of the softening range sometimes is far above the temperature at which the metal has been cold-worked. The lower limit of the range varies with the melting point, and is greatly affected by alloying; the upper limit is the recrystallization range. The width of the softening range varies greatly with the metal. For steels, nickel and Monel, the range is wide; for copper it is relatively narrow.

As shown in Fig. 1, room temperature for aluminum is equivalent to much higher temperatures for copper and Monel. The previously mentioned softening of aluminum at room temperature after strain hardening at lower temperatures indicates that the recovery range for aluminum extends below room temperature. Moreover, there is evidence for crystal recovery of aluminum at room temperature after strain hardening at the same temperature. By the use of electron diffraction methods, Heidenreich (5) has investigated the structure of cold-worked high-purity aluminum and an alloy of aluminum with 4% copper. Freshly cold-worked aluminum was found to consist of two structures differing greatly in fineness. The coarser of these was a mosaic of "domains" ranging from 1 to 2 microns in size; the finer structure was a granular detail consisting of disoriented regions 200 to 800 angstroms in size. After a time at room temperature, however, the granular structure had disappeared, but the domains were still present. Annealing above the recrystallization temperature eliminated the domains. The cold-rolled alloy containing 4% copper contained only the granular structure; the domains had not yet been formed. The presence of the domains in the high-purity aluminum evidently indicates partial recovery after cold work. The absence of domains in the alloy containing 4% copper indicates that recovery had not yet begun.

For pure aluminum that has been strain-hardened at the temperature of liquid air, the lower limit of the softening range probably is far below room temperature. Moreover, the lower limit of the softening range possibly is not much lower for pure aluminum than for 2S aluminum. It appears possible that this limit may be near the temperature range within which strain aging is absent.

If zinc and some other metals that melt at low temperatures were strain-hardened at  $-188^{\circ}\text{C}$ , they probably would recrystallize at room temperature. For such a metal, the upper limit of the softening range is below room temperature. There is good reason to believe that metals with high melting points, after strain hardening at low temperatures, retain practically all their excess intrinsic strength after return to room temperature. When the previously described interrupted tension tests at low temperatures were applied to nickel (11) and copper (8), there was no evidence of softening when the tests were resumed at the low temperatures after various intervals at room temperature. In this respect, therefore, these metals behaved very differently from aluminum. The evidence thus indicates that, after strain hardening at  $-188^{\circ}\text{C}$ , the lower limit of the softening range for metals with high melting points is above room temperature, and that this limit for some metals is far above room temperature.

#### CONCLUSIONS

1. Strain aging during tension tests of aluminum and duralumin affects the results of tests at temperatures below and above a range between about 150 and  $200^{\circ}\text{K}$ . Strain aging thus affects the flow stress, the ultimate stress, and even the yield stress. At some temperature between 150 and  $200^{\circ}\text{K}$ , strain aging is at a minimum, and probably is absent.
2. The variation of strain aging with temperature is about the same for nickel and brass as for aluminum. Such a variation of strain aging with temperature probably would be found with many other metals.
3. The influence of temperature on the flow stress involves two factors: (a) a direct temperature factor; (b) the influence of temperature on the rate of increase of intrinsic strength with plastic strain. The lower the temperature, the more rapid is the increase of intrinsic strength with strain.
4. The effects of these two factors on the flow stress should be expressed in terms of flow-stress ratios.
5. With plastic strain, the intrinsic strength factor increases continuously, but the direct temperature factors for aluminum, duralumin and copper are practically constant. The direct temperature factor for Monel is practically constant after slight initial plastic strain.
6. The direct temperature factors for aluminum, duralumin, copper, Monel and nickel do not differ greatly throughout the range from room temperature to  $-188^{\circ}\text{C}$ .



7. The effect of temperature on the rate of increase of intrinsic strength with plastic strain is much greater for aluminum than for copper, Monel and nickel. The intrinsic strength factors for these metals, at constant total strain within the range from room temperature to  $-188^{\circ}\text{C}$ , are in the inverse order of the melting points. The precipitation hardening due to the heat treatment of duralumin decreases the rate of work hardening, and thus decreases the influence of temperature on the rate of increase of intrinsic strength with plastic strain.

8. The lower the temperature, the less is the plastic strain required to produce a given strength state (intrinsic strength). The curves representing the influence of the temperature of aluminum on the stress-strain relationship, for either constant intrinsic strength or constant total strain, are affected by the influence of strain aging. These curves, unlike the curves for copper, have an upward bulge and two reversals of curvature.

9. The influence of temperature on total strain energy involves two factors. One of these is the energy corresponding to the direct temperature factor; the other is the work hardening energy, the energy corresponding to the intrinsic strength factor. The total strain energy is the product of these two factors.

10. On the assumption that a constant strength state represents constant latent energy, curves have been derived to represent the influence of plastic strain and temperature on latent energy and on the ratios of latent energy to total energy and work hardening energy.

11. With plastic strain, the latent energy increases continuously, at a decreasing rate. With plastic strain, the ratios of the latent energy to the total energy and work hardening energy decrease continuously, at a decreasing rate.

12. The influence of strain aging affects the curves representing the influence of temperature on total strain energy, work hardening energy, and the latent energy ratios. All these curves, unlike the curves for copper, have two reversals.

13. For constant total strain, the ratio of latent energy to total energy varies little with temperature, but the ratio of latent energy to work hardening energy increases as the temperature is lowered.

14. The increase of latent energy with plastic strain is a function of the strain and temperature, not of the total strain energy.

15. Since the various diagrams representing the stress-strain energy relationship are based on the results of ordinary tension tests, these diagrams reveal no evidence of crystal recovery of cold-worked aluminum throughout a range from  $-188^{\circ}\text{C}$  to room temperature.

However, the literature contains evidence for crystal recovery of aluminum within this temperature range.

16. When aluminum has been strain-hardened at  $-188^{\circ}\text{C}$ , the temperature range for softening due to crystal recovery extends far below room temperature. The excess intrinsic strength due to strain hardening of high-purity aluminum at  $-188^{\circ}\text{C}$  disappears almost entirely during a few days at room temperature.

17. When metals with high melting points are strain-hardened at  $-188^{\circ}\text{C}$ , practically all the intrinsic strength is retained at room temperature.

### References

1. E. W. Colbeck and W. E. MacGillivray, "The Mechanical Properties of Metals at Low Temperatures", *Transactions*, Institution of Chemical Engineers, Vol. 11, 1933, p. 107-120.
2. J. E. Dorn, A. Goldberg and T. E. Tietz, "The Effect of Thermal-Mechanical History on the Strain Hardening of Metals", *Transactions*, American Institute of Mining and Metallurgical Engineers, Vol. 180; *Metals Technology*, September 1948, T.P. 2445.
3. W. S. Farren and G. I. Taylor, "Heat Developed During Plastic Extension of Metals", *Proceedings*, Royal Society, A, Vol. 107, 1925, p. 425-451.
4. E. W. Fell, "Yielding Phenomena and Distortion in Iron, Steel, Aluminum Alloys and Other Metals Under Stress", Iron and Steel Institute, *Carnegie Scholarship Memoirs*, Vol. 26, 1937, p. 123-163.
5. R. D. Heidenreich, "Structure of Slip Bands and Cold-Worked Metal", *Seminar on the Cold Working of Metals*, American Society for Metals, 1949, p. 57-64.
6. V. J. Kostenetz, "Mechanical Properties of Metals and Alloys in Tension at Low Temperatures", *Journal*, Technical Physics, U.S.S.R., Vol. 16, 1946, p. 515-554.
7. D. J. McAdam, Jr., and R. W. Mebs, "An Investigation of the Technical Cohesive Strength of Metals", *Transactions*, American Institute of Mining and Metallurgical Engineers, Vol. 162, 1945, p. 474-536.
8. D. J. McAdam, Jr., and R. W. Mebs, "The Technical Cohesive Strength and Other Mechanical Properties of Metals at Low Temperatures", *Proceedings*, American Society for Testing Materials, Vol. 43, 1943, p. 661-703.
9. D. J. McAdam, Jr., and G. W. Geil, "The Variation of the Strength, Resistance to Oxidation and Electrical Conductivity of Metals With Temperature", *TRANSACTIONS*, American Society for Metals, Vol. 33, 1944, p. 514-534.
10. D. J. McAdam, Jr., R. W. Mebs and G. W. Geil, "The Technical Cohesive Strength of Some Steels and Light Alloys at Low Temperatures", *Proceedings*, American Society for Testing Materials, Vol. 44, 1944, p. 593-624.
11. D. J. McAdam, Jr., G. W. Geil and R. W. Mebs, "Effects of Combined Stresses and Low Temperatures on the Mechanical Properties of Some Nonferrous Metals", *TRANSACTIONS*, American Society for Metals, Vol. 37, 1946, p. 497-537.
12. D. J. McAdam, Jr., G. W. Geil and Frances Jane Cromwell, "Flow, Fracture and Ductility of Metals", *Transactions*, American Institute of Mining and Metallurgical Engineers, Vol. 175, p. 306; *Metals Technology*, January 1948, T.P. 2296.

13. D. J. McAdam, Jr., "Influence of Temperature on the Stress-Strain-Energy Relationship for Copper and Nickel-Copper Alloys", *Transactions, American Institute of Mining and Metallurgical Engineers*, Vol. 185, 1949, p. 727-740, T.P. 2703.
14. D. J. McAdam, Jr., "The Stress-Strain Energy Relationship for Metals", *TRANSACTIONS, American Society for Metals*, Vol. 43, 1951, p. 970-992.
15. D. J. McAdam, Jr., G. W. Geil and Frances Jane Cromwell, "Influence of Low Temperatures on the Mechanical Properties of 18-8 Chromium-Nickel Steel", *TRANSACTIONS, American Society for Metals*, Vol. 41, 1949, p. 609-645.
16. A. W. McReynolds, "Plastic Deformation Waves in Aluminum", *Transactions, American Institute of Mining and Metallurgical Engineers, Journal of Metals*, Vol. 1, January 1949, p. 32-45, T.P. 2499 E.
17. *METALS HANDBOOK*, American Society for Metals, 1948, p. 771.
18. L. B. Pfeil, "The Change in Tensile Strength Due to Aging of Cold-Drawn Iron and Steel", *Journal, Iron and Steel Institute*, Vol. 118, 1928, No. 2, p. 167-194.
19. A. Portevin and F. Le Chatelier, "Heat Treatment of Aluminum-Copper Alloys", *TRANSACTIONS, American Society for Steel Treating*, Vol. 5, 1924, p. 457-478.
20. W. B. Price, "Properties of Copper and Some of Its Important Industrial Alloys", American Society of Mechanical Engineers and American Society for Testing Materials, *Symposium on Effect of Temperature on Properties of Metals*, 1931, p. 340-350.
21. W. Rosenhain and V. H. Stott, "The Energy Absorbed in the Cold-Working of Metals", *Proceedings, Royal Society, A*, Vol. 140, 1933, p. 9-25.
22. A. H. Stang, M. Greenspan and S. G. Newman, "Poisson's Ratio of Some Structural Alloys for Large Strains", *Journal of Research, National Bureau of Standards*, Vol. 37, 1946, p. 211-221.
23. Tomiya Sutoki, "On the Serrated Elongation in Different Metals", *Science Reports, Tohoku Imperial University*, Vol. 29, 1944, p. 673-696.
24. N. J. Tapsell and J. Bradley, "The Mechanical Properties at High Temperatures of an Alloy of Nickel and Copper", *Journal, Institute of Metals*, Vol. 35, No. 1, 1926, p. 75-93.
25. G. I. Taylor and H. Quinney, "The Latent Energy Remaining in a Metal After Cold-Working", *Proceedings, Royal Society, A*, Vol. 143, 1934, p. 307-326.
26. R. L. Templin, "Effects of Cold-Working on Physical Properties of Metal", American Institute of Mining and Metallurgical Engineers, Preprint, Cleveland Meeting, September 1929.
27. R. L. Templin and D. A. Paul, "The Mechanical Properties of Aluminum and Magnesium Alloys at Elevated Temperatures", American Society of Mechanical Engineers and American Society for Testing Materials, *Symposium on Effect of Temperature on Properties of Metals*, 1931, p. 290-313.
28. T. E. Tietz and J. E. Dorn, "The Effect of Strain History on the Work Hardening of Metals", *Seminar on the Cold Working of Metals*, American Society for Metals, 1949, p. 163-179.



14. The American Society of Climate Engineers, 1957. *Journal of the American Society of Climate Engineers*, Vol. 1, No. 1, pp. 1-10.

15. The American Society of Climate Engineers, 1957. *Journal of the American Society of Climate Engineers*, Vol. 1, No. 1, pp. 11-20.

16. The American Society of Climate Engineers, 1957. *Journal of the American Society of Climate Engineers*, Vol. 1, No. 1, pp. 21-30.

17. The American Society of Climate Engineers, 1957. *Journal of the American Society of Climate Engineers*, Vol. 1, No. 1, pp. 31-40.

18. The American Society of Climate Engineers, 1957. *Journal of the American Society of Climate Engineers*, Vol. 1, No. 1, pp. 41-50.

19. The American Society of Climate Engineers, 1957. *Journal of the American Society of Climate Engineers*, Vol. 1, No. 1, pp. 51-60.

20. The American Society of Climate Engineers, 1957. *Journal of the American Society of Climate Engineers*, Vol. 1, No. 1, pp. 61-70.

21. The American Society of Climate Engineers, 1957. *Journal of the American Society of Climate Engineers*, Vol. 1, No. 1, pp. 71-80.

22. The American Society of Climate Engineers, 1957. *Journal of the American Society of Climate Engineers*, Vol. 1, No. 1, pp. 81-90.

23. The American Society of Climate Engineers, 1957. *Journal of the American Society of Climate Engineers*, Vol. 1, No. 1, pp. 91-100.

24. The American Society of Climate Engineers, 1957. *Journal of the American Society of Climate Engineers*, Vol. 1, No. 1, pp. 101-110.

25. The American Society of Climate Engineers, 1957. *Journal of the American Society of Climate Engineers*, Vol. 1, No. 1, pp. 111-120.

26. The American Society of Climate Engineers, 1957. *Journal of the American Society of Climate Engineers*, Vol. 1, No. 1, pp. 121-130.

27. The American Society of Climate Engineers, 1957. *Journal of the American Society of Climate Engineers*, Vol. 1, No. 1, pp. 131-140.

# INDEX OF AUTHORS

## VOLUME XLIII

### TRANSACTIONS OF AMERICAN SOCIETY FOR METALS

1951

#### A

Adenstedt, Heinrich ..... 873  
Averbach, B. L. ....497, 1072

#### B

Baldwin, W. M., Jr. .... 778  
Balluffi, R. W. .... 497  
Beck, F. H. .... 404  
Bernstein, Harold ..... 635  
Bever, M. B. ....342, 378  
Bindari, A. E. .... 226  
Binder, W. O. .... 759  
Boss, G. H. .... 122  
Brooks, H. E. .... 547  
Buffum, D. C. .... 644  
Burns, Jay R. .... 873  
Busby, P. E. .... 526

#### C

Carapella, S. C., Jr. .... 853  
Carney, D. J. .... 480  
Childs, W. J. .... 105  
Clark, D. S. .... 571  
Cline, J. E. .... 105  
Cohen, Morris ....497, 1072

#### D

DePierre, Vincent ..... 635  
Dorn, J. E. .... 611  
Dulis, E. J. .... 692

#### E

Eberly, W. S. .... 243

#### F

Faupel, J. H. .... 993  
Floe, C. F. ....342, 378  
Fontana, M. G. ....404, 547, 1098

#### G

Geisler, A. H. .... 70  
Gilman, J. J. .... 161  
Gittings, D. O. .... 587  
Grant, N. J. .... 824

#### H

Harris, W. J., Jr. .... 1175

Hausner, H. H. .... 1052  
Hayes, E. T. .... 888  
Huntoon, R. T. .... 426

#### J

Jaffe, L. D. .... 644  
Janulionis, A. D. .... 480

#### K

Kinsey, H. V. .... 193  
Kisner, W. M. .... 105  
Klier, E. P. ....935, 1033  
Klimas, C. V. .... 526  
Koh, P. K. .... 226

#### L

Larson, Hugo ..... 1033  
Lement, B. S. .... 1072  
Light, J. O. .... 323  
Loria, E. A. .... 718

#### M

Mack, J. O. .... 587  
MacMillan, J. A. .... 692  
Mahla, E. M. .... 290  
Marin, Joseph ..... 993  
Miller, O. O. .... 260  
Moeller, R. D. .... 39  
McAdam, D. J., Jr. ....970, 1215  
McCullough, H. M. .... 404  
McPherson, D. J. .... 1098

#### N

Nicholson, M. E. .... 142  
Nielsen, N. A. .... 290

#### O

O'Brien, W. L. .... 888

#### P

Peretti, E. A. .... 853  
Phebus, R. L. .... 811  
Pinto, N. P. .... 1052  
Piper, T. E. .... 1013  
Post, C. B. .... 243  
Potter, R. D. .... 824  
Putman, J. W. .... 824

## R

Rengstorff, G. W. P. ....	342, 378
Rinebolt, J. A. ....	1175
Ripling, E. J. ....	778
Roberson, A. H. ....	888
Rogers, W. T. ....	1126
Rowland, D. H. ....	587

## S

Schonfeld, F. W. ....	39
Sherby, O. D. ....	611
Shortsleeve, F. J. ....	142
Smith, E. C. ....	651
Smith, G. V. ....	692
Speiser, Rudolph ....	734
Spendelow, H. R., Jr. ....	759
Spretnak, J. W. ....	547, 734
Stanley, J. K. ....	426
Stewart, M. T. ....	193
Sullivan, A. M. ....	906

## T

Tarasov, L. P. ....	1144
Tipper, C. F. ....	906
Tipton, C. R., Jr. ....	39

## V

vonHoene, J. ....	426
-------------------	-----

## W

Waber, J. T. ....	39
Wells, Cyril ....	526
Wilder, A. B. ....	323
Wilson, William, Jr. ....	454
Wood, D. S. ....	571
Worden, C. O. ....	958
Wulff, John ....	105

## Z

Zapffe, C. A. ....	811, 958
Zmeskal, Otto ....	226



## SUBJECT INDEX

### Activation energy

- stainless steels .....405, 419-420
- type 304 ..... 419
- type 410 .....419-420
- type 430 ..... 419
- steel
- for isothermal grain
- growth .....279-280

### Adhesion

- of molybdenum coatings
- to copper .....120-121
- to nickel .....115-121
- to steel .....115, 120-121

### Allotropy

- of silver chloride ..... 58

### Alloying

- of silver chloride .....58-61

### Aluminum

- role in magnet alloys ..... 77
- ultimate stress
- effect of temperature .1217-1218

### Aluminum alloys

#### Alcoa 2S

- stress-strain energy relationship .....1215-1242
- ultimate stress
- effect of temperature
- .....1217-1218
- yield stress
- effect of temperature
- .....1217-1220

#### Alcoa 2S-O

- stress-strain relations for
- biaxial tension-compression stress. See under
- Stress-strain relations.
- copper-magnesium alloys (24S)
- retained ductility .779-780, 788
- copper-magnesium alloys (24S-T)
- stress-strain relations for
- biaxial tension-compression stress. See under
- Stress-strain relations.
- tensile and fatigue properties
- effect of notches at 25
- °C and -196 °C...547-560
- creep properties
- Al-H12 .....615-627

### Aluminum alloys (cont.)

#### creep properties

- Al-H18 .....615-623
- 2S-H12 .....618, 623-625
- 2S-H18 .....613-615, 619, 625
- 2S-O .....628-630
- 4S-H32 .....620, 626-627
- 4S-H38 .....620, 621, 627

#### magnesium alloy (52S)

- recovery and cold work-
- ing of .....122-138

#### mechanical properties ..... 613

- Al-H12 ..... 613
- Al-H18 ..... 613
- 2S-H12 ..... 613
- 2S-H18 ..... 613
- 4S-H32 ..... 613
- 4S-H38 ..... 613

#### zinc-magnesium-copper alloys (75S)

- fractographic study of fa-
- tigue .....958-968
- hot forming of 75S-T6
- .....1013-1032
- tensile and fatigue prop-
- erties
- effect of notches on at
- 25 °C and -196 °C.547-570

### Aluminum coating

#### on steel .....587-605

- adherence of coating .... 588

- alloy layers .....587-588

#### bending properties of

- coating .....602-605

- effect of alloying ele-
- ments .....603-605

- effect of beryllium .... 604

- effect of copper ..... 604

- effect of silicon ..... 604

#### cracking

- definition ..... 604

- ductility of aluminum..604-605

- effect of beryllium ..604-605

- effect of silicon .....604-605

- ductility of coating..... 588

- effect of thickness on

- ductility ..... 588

#### flaking

- definition ..... 604

- methods of coating..... 587

## SUBJECT INDEX

### Aluminum coating (cont.)

- on steel
  - microhardness of the alloy
    - layer ....595, 599-602, 605
  - effect of alloying elements ..... 595
  - effect of beryllium ....
    - ..... 595, 599-602, 605
  - effect of copper ....595, 605
  - effect of silicon .....
    - ..... 595, 599-602, 605
  - relationship to thickness
    - .....599-600
- peeling
  - definition ..... 604
  - procedure .....589-590
  - surface appearance.591-592, 605
  - effect of alloying elements .....591-592, 605
  - thickness of alloy layer..
    - ..588-589, 593-600, 605-607
  - effect of alloying elements .....593-599
  - effect of bath temperature ..... 588
  - effect of beryllium ....
    - ..594-596, 598-599, 605, 606
  - effect of cooling rate .. 588
  - effect of copper .....594-599
  - effect of silicon .....
    - 589, 594-597, 599, 605, 607
  - effect of time of immersion ..... 588
  - relationship to microhardness .....599-600

### Aluminum-silicon alloys

- grain refinement of .....635-643

### Aluminum-silicon-magnesium alloys

- grain refinement of .....635-643

### Annealing

- of Alcoa aluminum alloy 52S
  - effect of temperature on grain size .....130-138
  - effect of temperature on properties .....124-129
  - effect of time .....126-127
- silver chloride .....52-54
- steels, high chromium
  - effect of annealing temperature on relative magnetic susceptibilities ..... 188

### Annealing (cont.)

- steels, high chromium
  - effect on grain size ..... 181
  - influence on rate of sigma formation .....181, 185-186
  - relationship of initial ferrite content and annealing temperature ..... 181

### Annual Address of the President 7

### Annual Dinner of ASM ..... 23

### Annual Meeting of ASM .... 7

### Annual Report of the Secretary 15

### Annual Report of the Treasurer 11

### Austenite transformation

- in chromium-molybdenum-manganese steels
  - TTT diagrams .....725-729
- in nickel-chromium-molybdenum steels
  - TTT diagrams .....721-725

### Austenitic stainless steels

- See also Stainless steels.

### Beryllium

- in aluminum-silicon alloy
  - effect on grain size ...639, 642
- in aluminum-silicon-magnesium alloy
  - effect on grain size ....640-641
- ductility ..... 1053
- metallography of powdered
  - compacts ..... 1068
- powder metallurgy ....1052-1069
- bend tests of sintered
  - compacts .....1063-1064
- electrical resistivity of
  - specimens ..... 1064
- cold rolling of sintered
  - compacts .....1064-1067
- effect of annealing.1065-1066
- influence on microstructure .....1065-1066
- compacting ..... 1056
- electrical resistivity of
  - sintered compacts .... 1060
- hardness of sintered compacts .....1067-1068

## SUBJECT INDEX

### **Beryllium (cont.)**

- powder metallurgy
  - microstructures of sintered compacts .....1060-1063
  - effects of sintering temperature .....1061-1062
- sintering
  - in argon ..... 1057
  - effect of sintering temperature on density..1057-1058
  - effect of sintering temperature on electrical resistance .....1057, 1060
  - evaporation of beryllium .....1059-1060
  - in vacuum ..... 1057
- recrystallization temperature .....1065-1066

### **Biaxial tension-compression stresses**

- applied to aluminum alloys
  - 2S-O and 24S-T
  - effect on mechanical behavior .....993-1012

### **Biringuccio's lodestone** ..... 670

### **Boron**

- in aluminum-silicon alloy
  - effect on grain size ...639, 642
- in aluminum-silicon-magnesium alloy
  - effect on grain size.638, 640-642

### **Brass**

- ultimate stress
  - effect of temperature.1217-1218

### **Brassert-Cape furnace** .....666-667

### **Bromine-methanol method**

- of isolating carbides in stainless steel ....293, 312, 316-317

### **Cadmium-zinc**

- constitution diagram ..... 854

### **Carbide isolation**

- methods ..... 293
  - bromine-methanol technique .....293, 312

### **Carbon**

- in chromium steels
  - effect on toughness .....
    - .....764-769, 771-777

### **Carbonitriding**

- advantages claimed for ...348-349
- carbon sources ..... 347
- composition of cases
  - austenite (retained) gradients .....395-397
  - procedure for determining ..... 395
- carbon gradients .....
  - .....383-386, 394-396
  - effect of temperature of carbonitriding ....383-386
- effect of temperature of carbonitriding .....347, 367
- nitrogen gradients .....
  - .....382-386, 394-397
  - effect of temperature of carbonitriding ....383-386
- constitution of cases ....378-397
  - effect of temperature of carbonitriding ..389-393, 396
  - effect of tempering ....389-393
  - literature survey .....378-381
  - phases by X-ray diffraction.389-393, 396-397, 400-402
  - procedure for determining ..... 381-382, 386-388
- depth of case
  - effect of temperature of carbonitriding .....
    - .....352-353, 358, 361-362
  - effect of tempering ....363-365
  - effect of time of carbonitriding .....358-359
  - effect of water vapor.... 360
- depth-hardness
  - effect of temperature of carbonitriding .....355-356
- epsilon carbonitride phase..
  - ..... 379-380, 389-390
- preferred orientation ..389-390
- exhaust gas
  - composition ..... 360
- furnace, diagram ..... 351
- history and development.343-344
- microhardness of case
  - effect of temperature of carbonitriding .....
    - .....355, 360, 363-365
  - effect of tempering....363-367
  - effect of water vapor ... 360



## SUBJECT INDEX

- Carbonitriding (cont.)**  
 microstructure of case 352-356,  
 359-360, 362-363, 365, 371-376  
 effect of cooling rate ..362-363  
 effect of gas composition  
 .....359, 371-374  
 effect of temperature of  
 carbonitriding .....352-356  
 effect of tempering .....  
 .....362, 363, 365  
 effect of water vapor ...  
 .....359, 360, 371-376  
 microstructure of core ..366, 368  
 effect of cooling rate..366, 368  
 effect of temperature of  
 carbonitriding ..... 366  
 nitrogen sources ..... 347  
 process .....342-352  
 relation to carburizing and  
 nitriding .....344-348  
 surface hardness of case  
 effect of cooling rate...362-363  
 effect of gas composition. 359  
 effect of temperature of  
 carbonitriding .....356-357  
 effect of tempering ....366-367
- Carbon-molybdenum steels**  
 Charpy impact  
 after exposure to elevated  
 temperatures ..... 333
- Carburizing**  
 effect of water vapor ..... 345  
 energizers .....343, 346  
 process .....344-345  
 relation to carbonitriding  
 and nitriding .....344-348  
 temperature ..... 345
- Castings**  
 of silver chloride .....48-51
- Cementite**  
 crystal structure ...379, 394, 395
- Charpy impact**  
 after exposure at elevated  
 temperatures .....333-335  
 carbon-molybdenum steels 333  
 chromium-molybdenum  
 steels ..... 333  
 chromium-molybdenum-  
 vanadium steels ..... 333  
 exposure factors ..... 334
- Charpy impact (cont.)**  
 after exposure at elevated temp.  
 molybdenum-vanadium  
 steels ..... 333  
 steel, SAE 3140 .....646-648  
 titanium-chromium alloys  
 .....1114-1115
- Charpy impact properties**  
 pearlitic steels .....1175-1214
- Chromium**  
 in aluminum-silicon alloy  
 effect on grain size ...639, 642  
 in aluminum-silicon-magnesium  
 alloy  
 effect on grain size ...638, 640  
 effect on mechanical properties of  
 chromium steels 761-764, 771  
 as function of carbon and  
 nitrogen contents .....  
 .....765-767, 771  
 effect on transition temper-  
 atures of chromium steels  
 .....769-772  
 melting point ..... 1098  
 role in retarding softening  
 of steel .....514-516, 521, 524
- Chromium carbide**  
 crystal structure .....318-320
- Chromium-iron** .....142-143  
 phase diagram ..... 143
- Chromium-molybdenum**  
 constitution diagram ....826-827
- Chromium-molybdenum-iron**  
 constitution diagram. See under  
 Constitution diagrams.
- Chromium-molybdenum steels**  
 creep-rupture properties .340-341  
 effect of molybdenum ... 340  
 elevated temperature tests  
 .....327, 331-333, 337  
 decarburization ..... 327  
 effect of post-welding heat on  
 graphitization .331, 332, 337  
 graphite rating of welds. 327  
 effect of aluminum deoxi-  
 dation ..327, 334, 336, 337  
 effect of molybdenum  
 variation ..... 327  
 photomicrographs ...328-329

## SUBJECT INDEX

### Cr-Mo steels (cont.)

- elevated temperature tests
  - hardness ..... 334
  - oxidation ..... 327, 332
  - sigma phase ..... 330
  - spheroidization ..... 327-329
  - tensile properties ..... 339
- microstructure
  - effect of elevated temperatures on carbides ... 327-328

### Chromium-molybdenum-vanadium steels

- Charpy impact
  - after exposure to elevated temperatures ..... 333
- elevated temperature tests ..... 331-335
- graphitization ..... 331, 335
- hardness ..... 334
- oxidation ..... 332
- spheroidization ..... 331

### Chromium-nickel-molybdenum steel

- sigma phase
  - etchants ..... 164
  - microstructures ..... 164-165

### Chromium steel

- carbide precipitation .... 144-145
- relationship to formation
  - of sigma ..... 144-145
- chromium-iron carbide
  - rate of formation . 144-145, 154
- compositions ..... 144
- ferrite to ferrite plus sigma
  - ..... 146-148, 154, 155
  - rate of reaction ..... 146-148, 154, 155
  - effect of carbon . 147, 148, 155
  - effect of temperature .. 147
  - time-temperature transformation curves ..... 148
- ferrite/ferrite plus sigma boundary . 145-148, 150-152, 154, 158
- determination ..... 145-146
- heat treatment to establish ..... 145
- influence of carbon ..... 150, 151, 154, 158
- influence of manganese .. 151, 152, 154
- influence of minor elements ..... 150-152

### Chromium steel (cont.)

- ferrite/ferrite + sigma boundary
  - influence of nitrogen ... 158
  - influence of silicon 151, 152, 154
  - influence of temperature ..... 147, 148
- sigma phase
  - embrittlement ..... 158
  - solubility of carbon in . 150, 151
- sigma phase formation
  - threshold time ..... 145, 148-150, 153-154, 156-158
  - effect of carbon 153, 154, 156
  - effect of chromium ... 147-149, 154, 157, 158
  - effect of cold work ... 145, 149, 150
  - effect of manganese .. 154
  - effect of pretreatment ..... 159-160
  - effect of silicon ..... 154
  - effect of temperature 148-149
  - temperature of minimum 149
- tempering. See under Tempering of

### Chromium steels, plain

- effect of carbon on toughness ..... 764-769, 771-777
- photomicrographs ..... 769
- effect of chromium on mechanical properties .. 761-764, 771
- as function of carbon and nitrogen contents ..... 765-767, 771
- typical microstructures 761-762
- effect of chromium on transition temperatures ... 769-772
- effect of nitrogen on toughness ..... 764-769, 771-777
- as function of heat treatment temperature .. 773-777
- photomicrographs ..... 769
- effect of oxygen on toughness ..... 773-777

### Cleavage fracture

- in silicon-ferrite. See under Fracture.

### Cleavage planes

- in fractured ferrite ..... 950-953

## SUBJECT INDEX

### Cleavage surfaces

- in ferrite
  - electron microscope examination .....937, 945-946
  - experimental procedure for determining .....936-937
  - fibering .....939-952
  - fractographic examination .....941-953
  - metallographic examination .....937, 946-948
  - planes of cleavage....950-953
  - plastically deformed metal
    - forms of .....937-952
  - slip planes in ferrite...952-953
  - X-ray examination ....935-953

### Coating

- molybdenum. See Molybdenum plating.

### Cobalt

- role in magnet alloys.....77-79

### Coefficient of expansion

- of magnesium alloys
  - dilatometric determination of .....876-878

### Coefficient of surface heat abstraction

- use in determining H factor .....480-496

### Coercive force

- definition of ..... 72
- of permanent magnet materials ..... 72

### Cold work

- of silver chloride ..... 51
- effect on hardness .....45-46

### Columbium

- in aluminum-silicon alloy
  - effect on grain size ..... 639
- in aluminum-silicon-magnesium alloy
  - effect on grain size....638, 640

### Composition

- of permanent magnet materials ..... 71

### Constitution

- of permanent magnet alloys
  - Alnicos .....73-74, 78

### Constitution (cont.)

- of permanent magnet alloys
  - Cunico .....85-86
  - Cunife .....85-86

### Constitution diagrams

- cadmium-zinc ..... 854
- chromium-molybdenum .826-827
- chromium-molybdenum-iron
  - chemical analysis .....831-832
  - extent of sigma phase..842-846
  - effect of aging at 900 °C 846
  - iron-chromium sigma phase
    - effect of molybdenum on high temperature stability .....844, 846-847
    - effect of molybdenum on interplanar spacing .. .....841-842, 845
  - isothermal sections
    - at 900 °C ..838-842, 850-851
    - at 1100 °C ..836-837, 839-841
    - at 1300 °C .....834-838
  - metallographic analysis 830-833
  - typical microstructures .....837-838, 840-841, 843
  - thermal analysis of ....829-830
  - liquidus temperatures.833-835
  - thermal treatments
    - effect on solid phase distribution .....834-842
  - X-ray diffraction analysis .....831-833
  - data on Fe<sub>3</sub>Mo<sub>2</sub> .833, 840-841
  - data on iron-molybdenum
    - sigma phase ..... .....833-834, 841-842
- indium-cadmium .....854-856
- indium-cadmium-zinc
  - chemical analysis ....857, 862
  - hardness survey .....863-864
  - metallographic analysis .....859-860, 864-868
  - one-phase limits 859-860, 864
  - typical microstructures .....866-868
  - phase fields at room and eutectic temperatures.864-866
  - ternary eutectic composition ..... 860
  - microstructure ..... 868
  - thermal analysis of ..... .....857-862, 868-870



## SUBJECT INDEX

### Constitution diagrams (cont.)

- indium-cadmium-zinc
  - thermal analysis of
    - distribution of phases 858-862
    - liquidus temperatures 869-870
  - type of system ..... 864
  - X-ray diffraction analysis
    - .....860-867
    - data on interplanar spacings .....862-863
    - extent of two-phase regions .....861-867
- indium-zinc ..... 856
- iron-chromium .....143, 827
- iron-molybdenum .....825-826
- nickel-aluminum .....201-202
- zirconium-iron .....901-903
- development of diagram
  - alloy preparation ...890-892
  - composition of alloys used ..... 891
  - by metallographic examination .....892-896
  - by thermal analysis..892-896
  - by X-ray studies ...894-897
- differences compared with
  - earlier work .....901-902
- eutectic .....896, 901-902
- eutectoid .....894, 901-902
- gamma field ( $Zr_2Fe_3$ ) .... 897
- maximum solubilities
  - in alpha field .....892-893
  - in beta field .....894-895
- previous work .....889-890
- solidus line .....896, 901-902

**Constitutional diagrams.** See also Constitution.

silver chloride .....59-61

### Cooling curves

- use in determining H factor
  - .....482-492
- use in new hardenability test .....459-465

### Copper

- role in magnet alloys .....81-82
- ultimate stress
  - effect of temperature 1217-1218

### Corrosion resistance

- stainless steel, type 304
  - effect of cold work ....310-312

### Corrosion resistance (cont.)

- stainless steel, type 304
  - effect of heat treatment 310-312
  - effect of interrupted quench from annealing temperature on ..... 305
  - effect of sensitization temperature .....294-299

### Creep

- aluminum alloys .....611-634
- Al-H12 .....615-627
  - creep strain as a function of time ..... 616
  - effect of cold work..615-627
  - effect of stress ..... 616
  - effect of temperature.. 616
  - secondary creep rate
    - versus stress .....615-622
  - secondary creep rate
    - versus temperature 615-622
  - stress-rupture characteristics ..... 622
- Al-H18 .....615-623
  - creep strain as a function of time ..... 617
  - effect of cold work..615-627
  - effect of stress ..... 617
  - effect of temperature.. 617
  - secondary creep rate
    - versus stress .....615-623
  - secondary creep rate
    - versus temperature 615-623
  - stress-rupture characteristics ..... 623
- 2S-H12 .....618, 623-625
  - creep strain as a function of time ..... 618
  - effect of cold work ...
    - .....618, 623-625
  - effect of stress ..... 618
  - effect of temperature.. 618
  - secondary creep rate
    - versus stress ..... 624
  - stress-rupture characteristics ..... 624
- 2S-H18 .....613-615, 619, 625
  - creep strain as a function of time ..... 619
  - effect of cold work ...
    - .....619, 623-625
  - effect of stress..613-615, 619

## SUBJECT INDEX

### Creep (cont.)

- aluminum alloys
  - 2S-H18
    - effect of temperature..
      - .....613-615, 619
    - secondary creep rate
      - versus stress ..... 625
    - stress-rupture characteristics ..... 625
  - 2S-O
    - effect of annealing temperature .....629-630
    - effect of grain size ..628-629
  - 4S-H32 .....620, 626-627
    - creep strain as a function
      - of time ..... 620
    - effect of cold work ..620, 627
    - effect of stress ..... 620
    - effect of temperature .. 620
    - secondary creep rate
      - versus stress ..... 626
    - stress-rupture characteristics ..... 626
  - 4S-H38 .....620, 621, 627
    - creep strain as a function
      - of time ..... 621
    - effect of cold work ..620, 627
    - effect of stress ..... 621
    - effect of temperature.. 621
    - secondary creep rate
      - versus stress ..... 627
    - stress-rupture characteristics ..... 627

### Creep properties

- aluminum alloys
  - effect of cold rolling on 611-634
  - mechanisms of ....617-627, 633
  - specimen ..... 614
  - stress versus logarithm of
    - secondary creep rate 630-633
  - threshold stress ..... 632
  - effect on solidus temperature
    - determinations with dilatometer .....880-886

### Creep-rupture test

- nickel-aluminum-molybdenum
  - alloys .....194-199, 215-216
  - specimen ..... 195

### Crystal recovery

- aluminum, 2S
  - after cold work .....1240-1242

### Crystal structure

- cementite ..... 379
- iron carbide ..... 379
- iron-nitrogen phases ....379-380
- martensite ..... 381
- silver chloride ..... 58

### Curie point measurements

- in studying tempering of
  - chromium steels .....
    - .....498, 501, 509, 516

### Curie temperature

- Invar
  - effect of carbon content..
    - .....1089-1090

### Debye patterns

- sigma phase .....234-235

### Deep hardening steels

- hardenability test. See Hardenability test.

### Deformation

- of Alcoa aluminum alloy 52S
  - differences in during rolling
    - and stretching .....122-139

### Density

- chromium ..... 1098
- titanium ..... 1098

### Diffraction patterns

- titanium-chromium alloys 1121

### Diffusion

- mechanism of ..... 735

### Dilatometer

- use in determining solidus temperatures of magnesium alloys.
  - See under Solidus temperatures.
- use in studying tempering of
  - chromium steels .....
    - .....498-502, 505-508

### Direct temperature factors

- aluminum, 2S ..... 1220
  - influence of plastic strain
    - .....1222-1224
- copper .....1220-1221
- duralumin ..... 1220
- effect of prior plastic strain 1220
- Monel .....1220-1221
- nickel ..... 1221

### Domnarvet furnace ..... 669

## SUBJECT INDEX

### Ductility

- beryllium .....1053-1054
- of chromium steels. See Chromium steels, plain.
- steel, SAE 3140
  - effect of strain rate ...644-650
  - transverse of wrought steel products
    - effect of reheat treatment on. See Reheat treatment.

### Ductility, retained

- definition of .....778-779
- versus prestrain in steel 779-810
- two basic types of behavior 779

### Duralumin

- ultimate stress
  - effect of temperature ....
  - .....1217-1218, 1220
- yield stress
  - effect of temperature ....
  - .....1217-1218, 1220

### Election of Officers ..... 22

### Electrical resistance

- of silver chloride .....63-64

### Electrolytic method

- for extraction of carbides
- in chromium steels ....512-515

### Electron microscope

- use in studying cleavage surfaces in ferrite ....937, 945-946
- use in studying tempering of chromium steels .....
  - .....510-511, 518-519

### Electron microscopy

- preparation of specimens 293-294

### Elevated temperature

- forming of aluminum and magnesium alloys. See under Hot forming of.

### Elevated temperature properties

- carbon-molybdenum steels
  - .....327-329, 331-334, 336-337
- chromium-molybdenum steels
  - .....327, 330-335, 339-341
- chromium-molybdenum-vanadium steels .....331-335
- molybdenum-vanadium steels
  - .....327, 330-333, 337

### Elevated temp. properties (cont.)

- nickel-aluminum-molybdenum
  - alloys .....196, 215-218, 224
  - effect of molybdenum ... 196
  - fatigue ..... 224

### Embrittlement

- of stainless steels
  - by normal moisture or steam
    - in heat treating atmosphere
      - bar-bend test for ..... 813
    - compositions of steels
      - tested ..... 813
    - experimental procedure
      - .....813-814
    - results for types 403 and 410 steels..814-815, 820-821
    - results for type 414 steel
      - .....815-817, 821
    - results for type 416 steel
      - .....818-821
    - results for type 431 steel
      - .....817-818, 821
    - results for type 440C steel
      - .....819-821
  - of steel
    - rheotropic. See Rheotropic embrittlement of steel.

### Endurance limits

- for ten engineering alloys at
  - 25 °C and -196 °C, notched and unnotched ..556, 558-561
  - fatigue curves (S-N curves)
    - .....556-561

### Energy product

- definition of ..... 72
- of permanent magnet materials 72

### Equilibrium diagrams

- See Constitution diagrams.

### Etch pits

- in silver chloride ..... 51

### Expansion properties

- type 430 stainless steel ....
  - .....248-249, 258-259
- type 446 stainless steel ....
  - .....243-245, 257-259
- effect of nitrogen in ..... 245

### Fabrication

- of silver chloride .....45-46



## SUBJECT INDEX

### Fatigue

- fractographic study of
  - fractographs of Alcoa 75S alloy .....959-966
  - fractographs of SAE 1010 iron .....966-967
- fracture patterns
  - depth of patterns ...962-967
  - lamellar structure ..... 962
  - materials studied ..... 959
  - micellar theory as explanation for fatigue 967-968
  - correlation with damping behavior ..... 968
  - platy structure .....959-962
  - possible uses for ..... 968
  - relationship to stage of fatigue ...962, 964, 967-968

### Fatigue properties at low temperatures

- of ten engineering alloys, notched and unnotched .....556-566

### Ferrite

- cleavage surfaces in. See Cleavage surfaces.

### Ferrite/ferrite plus sigma boundary

- steel, chromium .....
  - ....145-148, 150-152, 154, 158
- determination .....145-146
- heat treatment to establish 145
- influence of carbon .....
  - .....150-151, 154, 158
- influence of manganese ..
  - .....151-152, 154
- influence of minor elements
  - .....150-152
- influence of nitrogen .... 158
- influence of silicon 151-152, 154
- influence of temperature
  - .....147, 148

### Ferrite to ferrite plus sigma

- steel, chromium..146-148, 154-155
- rate of reaction .....
  - .....146-148, 154-155
- effect of carbon 147, 148, 155
- effect of temperature .. 147
- time-temperature transformation curves ..... 148

### Ferritic stainless steels

- See also Stainless steels.

### Ferritic stainless steels, trade designation

- type 446 .....243-259

### Fibering

- at cleavage surfaces in ferrite
  - .....939-952

### Finishability

- tool steels
  - effect of hardness ...1164-1165
  - surface roughness versus grindability index ..1163-1165

### Flow stress

- aluminum, 2S
  - influence of temperature
    - .....1224-1228, 1235-1236
  - primary curves .....1224-1227
  - secondary curves .....
    - .....1225, 1227-1228
- copper
  - influence of temperature
    - .....1235-1236
  - ratios ..... 1222
  - influence of plastic strain 1222
- in stressed metals
  - effect of temperature on 975

### Flow stress ratios

- aluminum, 2S
  - influence of temperature
    - .....1235-1236
- copper
  - influence of temperature
    - .....1235-1236

### Forgings

- steel
  - effect of reheat treatment on transverse ductility. See Reheat treatment.

### Fractography

- use in studying cleavage surfaces in ferrite .....941-953
- use in studying fatigue fractures. See under Fatigue.

### Fracture

- fatigue
  - fractographic study of. See under Fatigue.
- of silicon-ferrite crystals
  - material studied .....908-909

## SUBJECT INDEX

### Fracture (cont.)

- of silicon-ferrite crystals
  - Neumann bands formed
    - during .....910-927
    - nature of Neumann bands
      - .....907-908
    - relationship to cleavage-
      - type fracture .....910-927
    - sequence of formation
      - .....926-927
  - structure at the end of
    - cracks .....923-926
  - structure of fractured
    - surface .....921-923
  - tensile results ..... 909
  - types of fractures .....
    - .....906-907, 909-912
  - X-ray study of cleavage
    - fractures .....912-921

### Grain boundary

- adsorption of solute atoms
  - .....735-747
- effect of temperature
  - changes on .....735-747
- in producing temper brittle-
  - ness .....739-747
- role in several grain bound-
  - ary phenomena .....738, 740
- phenomena .....734-735

### Grain growth, rate of

- steel
  - influence of austenitizing
    - temperature .....279-280
  - influence of grain size ...
    - .....278-280, 284

### Grain refinement

- aluminum alloys
  - preparation of specimens
    - .....636-637
- aluminum-silicon alloys ..635-643
- aluminum-silicon-magnesium
  - alloys .....635-643
  - microstructures ..... 641

### Grain size

- aluminum alloys
  - 2S-O
    - effect on creep resistance
      - .....628-629
- aluminum-silicon alloys ..639-642
  - effect of beryllium on..639, 642
  - effect of boron on ....639, 642

### Grain size (cont.)

- aluminum-silicon alloys
  - effect of chromium on 639, 642
  - effect of columbium on .. 639
  - effect of molybdenum on . 639
  - effect of tantalum on .... 639
  - effect of titanium on ..639, 642
  - effect of tungsten on .... 639
  - effect of zirconium on ...
    - .....639, 641-642
- aluminum-silicon-magnesium
  - alloys .....638-642
  - effect of beryllium on ..640-641
  - effect of boron on 638, 640-642
  - effect of chromium on 638, 640
  - effect of columbium on 638, 640
  - effect of molybdenum on 640
  - effect of tantalum on .... 640
  - effect of titanium on ..640-642
  - effect of tungsten on .... 640
  - effect of zirconium on ... 640
- of recrystallized Alcoa 52S
  - alloy .....127-138
  - after rolling .....130-133
  - after stretching .....133-138
  - effect of annealing temper-
    - ature on .....130-138
  - effect of type of deforma-
    - tion on .....136-138

### Grain size, austenite

- steel
  - influence of austenitizing
    - temperature .....260-285
  - influence of austenitizing
    - time .....263-285
  - influence of carbides ..277, 285
  - influence of deoxidation
    - practice .....273-276, 285
  - influence of inclusions ...
    - .....273-276, 285, 289
  - influence of nitrogen .... 276

### Graphitization

- steel .....692-711
  - carbon-stable rim ....700-
    - 701, 705, 707-709, 715, 717
  - effect of oxygen penetra-
    - tion ..... 709
  - diffusion process .....700-701
  - nitrogen penetration ..
    - .....701, 703-704
  - oxygen penetration\* .....704

## SUBJECT INDEX

### Graphitization (cont.)

- steel
  - effect of aluminum deoxidation .....705-706, 709-710
  - effect of austenitizing atmosphere ....693-695, 698-709
  - nitrogen atmosphere .....701, 703, 705, 707-708
  - effect of austenitizing temperature ....693-694, 696-699
  - effect of cold work ..... 716
  - effect of graphitizing atmosphere ..... 704
  - effect of graphitizing temperature .....692-695
  - effect of initial microstructure ..... 694
  - effect of stress .....713-714
  - inhibition by penetration of nitrogen .....
    - ...701, 703, 709, 711, 714-716
  - mechanism of effect of residual aluminum ...709-710

### Grindability

- tool steels .....1144-1174
- compositions ..... 1147
- depth of burn .....1165-1166
- method of determining 1165
- effect of alloying elements .....1154-1157
- effect of chromium content .....1154-1155
- effect of hardness ...1159-1161
- effect of martensitic matrix .....1170, 1173
- effect of quenching medium .....1154
- effect of vanadium content .....1155, 1156
- evaluation .....1150-1154
- procedure for evaluating .....1146-1150
- relation to wear resistance .....1170, 1173
- types of measurements ..
  - .....1149-1150
- versus tool life .....1171-1172

### Grindability index

- tool steels .....1151, 1154-1165
- definition .....1151, 1154

### Grindability index (cont.)

- tool steels
  - effect of carbide hardness .....1151, 1157, 1170-1171
  - effect of carbide segregation .....1158
  - effect of carbon content .....1156-1157
  - effect of chromium content .....1154-1155
  - effect of cobalt content .. 1156
  - effect of columbium ..... 1156
  - effect of hardness ...1160-1161
  - effect of molybdenum ... 1156
  - effect of tungsten ...1155-1156
  - effect of vanadium content .....1155-1156
  - effect of wheel hardness .....1161-1162
  - microhardness of carbide particles ..... 1157
  - versus grinding energy .....1151, 1159, 1161-1162
  - versus surface roughness .....1163-1165

### Grinding

- sensitivity .....1153-1154, 1166
- effect of heat treatment .....1154, 1166
- relation to grindability index ..... 1166
- relation to grinding energy 1166
- surface cracking ....1165-1166
- surface finish ..... 1154

### Grinding wheels

- aluminum oxide versus silicon carbide ..... 1158

### Growth equations

- for transformation curves in studying tempering of chromium steels 503-505, 508

### Hardenability

- of chromium-molybdenum-manganese steels ..720, 725-729
- definition of ..... 730
- of nickel-chromium-molybdenum steels .....721-725
- relationship to isothermal transformation ..... 730



## SUBJECT INDEX

### **Hardenability (cont.)**

of steel

H factor. See H factor in  
hardenability of steels.

### **Hardenability test**

for deep hardening steels 454-479

composition of steels tested 460

correlation with oil quench-  
ing practice ....462, 468-472

correlation with quench cool-  
ing curves ..459-465, 471-472

details of test..455-460, 469-470

disadvantages of test..473-475

heat flow considerations 475

limitations of existing tests

.....454-455, 471-472, 479

operating procedure ...472-473

representative results ...

.....467-471, 476-479

reproducibility of test..475-479

scope of test ..... 471

specifications of test .... 455

### **Hardness**

beryllium compacts ..... 1067

nickel-aluminum-molybdenum

alloys .....209-211

steels, high chromium .....

168-171, 173, 180, 183, 185-186

comparison of cast and

wrought material ...183, 186

correlation with average

austenite path ..... 171

correlation with mean fer-

rite path ..... 171

dependence on sigma dis-

tribution ..... 171

effect of annealing ..... 180

effect of holding at sigma

formation temperature 190

effect of repeated recrystal-

lization ..... 185

mixed phase hardening 168-170

comparison with age

hardening ..... 169

microstructures showing 170

relation to sigma content 173

of ten engineering alloys

at room and lower temper-

atures ..... 567

titanium-chromium alloys ..

.....1110-1111, 1113

### **Heating methods**

for hot forming aluminum

and magnesium alloys

.....1016-1021, 1027

comparison of methods ..

.....1022-1024

### **Heat of activation**

for decomposition of retained

austenite in chromium steels

.....504, 508, 513

### **Heat resistance**

of zirconium-iron alloys ...

.....899-901, 903

### **Heat transfer equivalent, H. See**

H factor in hardenability of steels.

### **Heat transfer factor. See Coefficient**

of surface heat abstraction.

### **Heat treating atmospheres**

embrittling effect on stainless

steels

of normal air .....814-821

of steam .....814-821

### **Heat treatment**

reheat treatment of wrought

steel products

effect on transverse ductility.

See Reheat treatment.

### **H factor in hardenability of steels**

development of term, H

effect of variations in thermal

diffusivity .....494-496

procedure in determining 482-484

review of recent experimental

work .....480-482

variation of H

with size of quenched round

.....484-486, 492

explanation for .....488-492

with temperature..484-486, 492

explanation for .....488-492

within a single quenched

round .....484-486, 492

explanation for .....488-492

### **High temperature**

forming of aluminum and

magnesium alloys. See under

Hot forming of.

## SUBJECT INDEX

- Hot forming of**
  - aluminum and magnesium alloys (75S-T6 and AZ31X-h)
  - advantages 1013-1014, 1026-1027
  - savings in fabricating time ..... 1024
  - applicability to other alloys ..... 1026
  - comparison of heating methods ..... 1022-1024
  - heating methods ..... 1016-1019, 1027
  - electric resistance—effect of length on mechanical properties ..... 1017-1018, 1020-1021
  - hot oil bath ..... 1018-1019
  - hot forming temperature range ..... 1014-1017, 1027
  - effect of temperature on properties ..... 1015-1017
  - production applications ..... 1024-1029
  - similarity to room-temperature forming of 75S-O ..... 1015
  - temperature effects .. 1019-1022
- Hot hardness**
  - steels, high chromium
  - correlation with average austenite path ..... 171
  - correlation with room temperature hardness .. 171
  - effect of sigma formation 172
  - titanium-chromium alloys .. 1104-1105, 1110-1111
- Hot strength**
  - of zirconium-iron alloys 899, 903
- Hydrogen embrittlement**
  - of stainless steels. See Embrittlement.
- Impact values**
  - of ten engineering alloys at room and lower temperatures ..... 567-568
- Indium-cadmium**
  - constitution diagram .... 854-856
- Indium-cadmium-zinc**
  - constitution diagram. See under Constitution diagrams.
- Indium-zinc**
  - constitution diagram ..... 856
- Interdiffusion**
  - of molybdenum coatings
  - on copper ..... 120
  - on nickel ..... 115-120
  - on steel ..... 115-120
- Interplanar spacings**
  - of indium-cadmium-zinc alloys ..... 862-863
- Intrinsic strength factors**
  - aluminum 2S ..... 1221
  - influence of plastic strain ..... 1222-1223
  - copper ..... 1221
  - duralumin ..... 1221
  - effect of plastic strain ..... 1220, 1222-1224
  - effect of temperature ..... 1220, 1222-1224
  - Monel ..... 1221
  - nickel ..... 1221
- Invar**
  - carbon solubility in austenite ..... 1084
  - effect of temperature .... 1085
  - lattice parameter versus carbon content ..... 1085
  - Curie temperature
  - effect of carbon content.. ..... 1089-1090
  - dimensional changes ..... 1074-1077, 1079, 1081-1085, 1093
  - aging at various temperatures ..... 1074-1075
  - annealed material ..... 1079
  - aging following quenching from various temperatures ..... 1075-1077
  - effect of cooling rate .... 1079
  - effect of heat treatment.. ..... 1082-1083
  - effect of residual stresses and stress relief .... 1081-1084, 1085, 1093
  - effect of shock treatment ..... 1082-1084
  - multiple aging ..... 1077
  - expansion coefficient ..... 1073-1075, 1079-1081, 1091-1093

## SUBJECT INDEX

### Invar (cont.)

- expansion coefficient
  - effect of carbon content..
    - .....1073, 1080
  - effect of cold working ... 1073
  - effect of cooling rate ....
    - .....1073, 1079-1080
  - effect of heat treatment..
    - .....1073, 1091-1093
  - effect of room temperature
    - aging ..... 1073
    - length measurements .... 1074
    - progressive change ..1073, 1075
    - specific volume versus
      - length ..... 1081
    - transitory change ..1073, 1075
  - $\gamma$ -expansion .....
    - ...1075, 1077-1079, 1093-1095
  - correlation with precipitation
    - .....1087-1089
  - effect of multiple aging ..
    - .....1077-1079, 1094
  - effect of carbon content .
    - .....1080, 1094
  - effect of cooling rate .... 1079
  - hardness changes accom-
    - panying .....1089-1090, 1094
  - magnetic changes accom-
    - panying .....1089-1091, 1094
  - X-ray measurements during
    - .....1088-1089, 1094
  - literature survey .....1072-1073
  - occurrence of graphite ....
    - .....1085-1087, 1095
  - stabilization treatment ....
    - .....1092, 1095-1096
  - thermal expansion coefficients
    - .....1090-1092
    - effect of minor elements
      - .....1091-1092
    - methods of measurement 1090
  - Young's modulus ..... 1082

### Iron

- effect on properties of ductile
  - zirconium ..... 903
- lattice parameter ..... 435

### Iron carbide

- crystal structure ..... 379

### Iron-chromium

- constitution diagram .....
  - .....142-143, 827

### Iron-molybdenum

- constitution diagram ....825-826

### Iron-nitrogen

- phases .....379-380, 389-390
- crystal structures .....379-380
- diagram ..... 380

### Iron ore smelting .....651-691

- African one-man furnaces ..
  - .....662, 664-666
- capacity
  - United States, 1901-1950 662
  - World, 1950 ..... 664
- carbon hearth .....678, 680
- direct reduction .....666-667
  - Brassert-Cape furnace 666-667
  - diagram ..... 667
  - Wiberg furnace .....669-670
- Domnarvet furnace ..... 669
- effect of moisture in air blast
  - on composition .....686-687
- firebrick-lined furnaces ..675-678
  - lining problems .....676, 678
- gas studies .....684-688
  - gas index ..... 686
  - Messerle equation .....684-686
- history .....651-662
  - anthracite furnaces ....658-659
  - by-product coke ovens 659-662
  - Catalan forge .....653-654
  - Catasauqua furnace ..... 658
  - Duquesne revolution .... 659
  - Elban forge .....652-653
  - pit cole furnace .....657-658
  - Saugus furnace .....654-656
  - stone-walled furnaces 656-658
- Krupp Renn furnace ....667-669
  - Luppen ..... 668
- ore beneficiation ....670-671, 674
  - pelletmaking .....670-671
  - desirable characteristics 671
  - sintering ..... 670
  - southern ore .....670-674
    - concentration process 674
- ore deficiencies, 1950-1970.. 676
- ore requirements, 1950-1970 675
- ore reserves, 1950 ..... 677
- ore supplies, 1950-1970 .... 676
- ore supply problem .....674-675
- pressure operation .....680-684
  - blast furnace alterations for 683



## SUBJECT INDEX

- Iron ore smelting (cont.)**  
 production  
   United States, 1901-1950 662  
   World, 1937, 1948 ..... 664  
 raw materials to finished  
   products—1948 ..... 663  
 slags ..... 688-689  
   madisonite ..... 689  
 United States  
   interests in foreign ores.. 677  
   ore deficiencies ..... 676  
   ore requirements ..... 675  
   ore reserves ..... 677  
   ore supplies ..... 676  
   ore supply problem .... 674-675
- Iron oxides**  
 formed at various temperatures ..... 427
- Iron percarbide ..... 379**
- Isothermal transformation**  
 in chromium-molybdenum-manganese steels  
   compositions ..... 719  
   effect of alloying elements ..... 725-727, 730, 732  
   experimental procedure 719-721  
   hardness data .... 720, 725-729  
   TTT diagrams of ..... 725-729  
 in nickel-chromium-molybdenum steels  
   composition ..... 719  
   effect of alloying elements ..... 723, 730-732  
   experimental procedure 719-721  
   hardness data ..... 720-725  
   photomicrographs .... 724-727  
   TTT diagrams of ..... 721-725  
   relationship to hardenability 730  
   relationship to slack-quenched structures ..... 730-731
- Jominy test**  
 compared with new hardenability test ..... 465-472, 479
- Krupp Renn furnace ..... 667-669**
- Latent energy**  
 aluminum, 2S  
   influence of plastic strain ..... 1232-1235
- Latent energy (cont.)**  
 aluminum, 2S  
   influence of temperature ..... 1232-1235, 1237-1240  
 definition ..... 1232  
 of stressed metals  
   effect of plastic strain on ..... 977-986  
   latent energy ratio  
     influence of plastic strain on ..... 977-986  
   latent energy relationships ..... 975-977
- Latent energy ratios**  
 aluminum, 2S  
   influence of plastic strain ..... 1232-1236  
   influence of temperature ..... 1232-1240
- Lattice constants**  
 of magnet alloys  
   Alnicos ..... 75, 80-81  
   Cunico ..... 87, 90  
   Cunife ..... 87, 90  
   Silmanal ..... 90, 92-94  
   Vectolite ..... 94-95  
   Vicalloys ..... 95-96
- Lattice strain**  
 role in permanent magnetism ..... 70, 76-77, 83-84, 87-99
- Liquidus temperatures**  
 in chromium-molybdenum-iron alloys ..... 833-835  
 in indium-cadmium-zinc alloys ..... 869-870
- Luppen ..... 668**
- Machinability**  
 of silver chloride ..... 58
- Magnesium alloys**  
 solidus temperatures  
   dilatometric determination of. See under Solidus temperatures.
- Magnesium alloys, trade designation**  
 AZ31X-h  
   hot forming ..... 1013-1032

## SUBJECT INDEX

- Magnesium alloys, trade designation (cont.)**  
 FS-1 magnesium alloy  
   tensile and fatigue properties  
   effect of notches on at 25 °C  
   and -196 °C .....547-570
- Magnet alloys**  
 Alnicos .....71-85  
 Cunico .....85-90  
 Cunife .....85-90  
 Silmanal .....90-94  
 Vectolite .....94-95  
 Vicalloys .....95-97
- Magnetic measurements**  
 in studying tempering of chromium steels .....  
   .....498, 500-502, 508-509
- Magnetic susceptibilities**  
 steels, high chromium ...188-190  
   effect of annealing temperature ..... 188  
   effect of holding at sigma formation temperature 189-190
- Magnetostriction**  
 in permanent magnet alloys  
   ..... 84, 98-99
- Marble's reagent** ..... 200
- Martensite**  
 crystal structure ..... 381
- Measuring equipment**  
 for rapid load tests  
   dynamometer ..... 575  
   extensometer ..... 575
- Mechanical properties. See Properties.**  
 aluminum alloys  
   Al-H12 ..... 613  
   Al-H18 ..... 613  
   2S-H12 ..... 613  
   2S-H18 ..... 613  
   4S-H32 ..... 613  
   4S-H38 ..... 613
- Melting point**  
 chromium ..... 1098  
 titanium ..... 1098
- Messlerle equation** .....684-686
- Metallic characteristics**  
 of silver chloride .....39-69
- Metallographic**  
 study of cleavage surfaces  
   in ferrite .....937, 946-948
- Metallographic analysis**  
 of chromium-molybdenum-iron alloys .....830-833  
 of indium-cadmium-zinc system .....859-860, 864-868  
 of zirconium-iron system.892-896
- Metallography**  
 of chromium steels  
   use in studying tempering  
   .....503, 509-511, 521-525  
 of permanent magnet alloys  
   Alnicos .....76, 79-80, 82-84  
   Cunico .....87-88  
   Cunife .....87-88  
   Silmanal .....90-92  
 of silver chloride .....46-48
- Micellar theory**  
 as explanation for fatigue 967-968  
   correlation with damping  
   behavior ..... 968
- Microhardness**  
 carbide particles in tool  
   steels ..... 1157  
   effect on grindability .... 1157  
 stainless steel, 19-9 W-Mo  
   sigma phase ..... 235  
 steels, high chromium  
   constituents ..... 173
- Microstructure**  
 of chromium-molybdenum-iron alloys ...837-838, 840-841, 843  
 of indium-cadmium-zinc alloys .....866-868  
 of molybdenum coatings ... 111  
 of plain chromium steels ..  
   ..... 761-762, 769
- Modulus of elasticity**  
 for ten engineering alloys 552-553
- Moisture**  
 as source of hydrogen in embrittlement of stainless steels  
   .....811-812, 814-821

## SUBJECT INDEX

### **Molybdenum**

- in aluminum-silicon alloy
  - effect on grain size ..... 639
- in aluminum-silicon-magnesium alloy
  - effect on grain size ..... 640

### **Molybdenum-nickel alloys**

- constitution diagram ..... 205

### **Molybdenum pentachloride**

- use in molybdenum plating ..... 105-121

### **Molybdenum plating**

- adhesion of the plate .... 114-120
- on copper ..... 120-121
- disadvantages of previous methods ..... 106-107
- microstructure ..... 110-120
- on nickel ..... 115-121
- possible usefulness of ..... 105
- properties of the plating ..
  - ..... 112-113, 118-120
- on steel ..... 115, 120-121
- structure of the plate.... 110-114
- study of plating procedure
  - ..... 107-110

### **Molybdenum-vanadium steels**

- Charpy impact
  - after exposure to elevated temperatures ..... 333
- elevated temperature tests
  - ..... 327, 330-332, 337
- effect of heat treatment prior to welding on graphitization ..... 331
- graphite rating of welds
  - ..... 327, 330, 331, 337
- oxidation ..... 332

### **Monel**

- ultimate stress
  - effect of temperature 1217-1218

### **Murakami etch ..... 164**

### **Neumann bands**

- in silicon-ferrite 907-908, 910-927

### **Neumann lamellae. See Neumann bands.**

### **Nickel**

- role in magnet alloys ..... 77
- ultimate stress
  - effect of temperature 1217-1218

### **Nickel-aluminum alloys**

- constitution diagrams ... 201-202
- identification of constituents ..... 200-204
- photomicrographs ..... 203

### **Nickel-aluminum-molybdenum**

- alloys** ..... 193-225
- chemical analyses .. 196, 213, 216
- creep-rupture life versus tensile strength ..... 215
- creep-rupture properties ..
  - ..... 194-199, 215-216
- effect of cobalt ..... 199
- effect of molybdenum ... 196
- effect of nickel to aluminum ratio ..... 196
- effect of tungsten ..... 199
- influence of composition variations ..... 194-199
- influence of solution treatment ..... 211-212
- time versus per cent elongation curves. 198-199, 212, 214
- elevated temperature properties ..... 215-218
- effect of molybdenum on 196
- fatigue ..... 224
- etchants ..... 200
- hardness
  - of solution-treated and aged specimens ..... 200-211
- identification of constituents ..... 200-207
- metallographic characteristics ..... 199-207
- microstructures
  - effect of cobalt ..... 211
  - effect of heat treatment
    - ..... 207-209
  - photomicrographs .. 208, 210
- nickel-aluminum ratio versus log rupture time ..... 215-216
- photomicrographs ..... 206
- rupture life ..... 223
- specifications (tentative) 218-220
- tensile properties ..... 217



## SUBJECT INDEX

### Nitriding

- atmosphere ..... 346
- process ..... 346
- relation to carburizing and  
  carbonitriding ..... 344-348
- temperature ..... 346
- time ..... 346

### Nitrogen

- in cementite ..... 394
- in chromium steels
  - effect on toughness .....  
                    .....764-769, 771-777
  - as function of heat treat-  
  ment temperature 773-777
- in stainless steel, AISI type 446
  - effect on expansion prop-  
  erties ..... 245
  - effect on grain size ..... 244
  - effect on tensile properties 244

**Nitrogen-iron.** See Iron-nitrogen.

### Notches

- effect on properties of ten engi-  
  neering alloys
- alloys tested .....548-549
- Charpy keyhole impact values  
  at room and lower tem-  
  peratures .....567-568
- equipment and procedure  
  .....549-552
- fatigue properties at 25 °C and  
  -196 °C
- fatigue (S-N) curves.556-561
- notch sensitivity ....562-566
- resistance to over-  
  stressing .....556, 562
- summary of endurance  
  limits .....556, 558-561
- tensile properties at 25 °C  
  and -196 °C .....552-555
- modulus of elasticity  
  values .....552-553
- Vickers hardness values at room  
  and lower temperatures 567

### Notch sensitivity

- of ten engineering alloys at  
  25 °C and -196 °C ....562-566

### Nucleation equations

- for transformation curves  
  in studying tempering of  
  chromium steels.503-505, 508

### Order-disorder

- in magnet alloys
- Vicalloy .....95-96

### Ore beneficiation

- pelletmaking .....670-671
- desirable characteristics . 671
- sintering .....670, 671, 674
- Spaulding concentrate proc-  
  ess ..... 674

### Oxidation

- iron
  - at 500 °C .....436-437
  - at 600 °C .....437, 440-442
  - at 700 °C .....438, 441-442
  - at 800 °C .....439, 440, 442
  - thickness of oxide versus  
    oxidation time ..... 442
  - at 900 °C ..... 443
  - effect of humidity ....446, 452
  - effect of silicon in iron on  
    oxide film ..... 444
  - effect of time and tem-  
    perature .....429-431
  - literature survey .....426-428
  - composition of oxides . 427
  - kinetics of the reaction 427
  - mechanism of reaction 428
  - structure of oxides ... 427
  - oxide films .....431-443
  - diffraction patterns .433-434
  - identification .....431-434
  - metallography .....435-436
  - thickness ..... 436
  - oxides formed at various  
    temperatures .....427-428
  - effect of thickness .... 427
  - relative thickness ..443, 450
  - parabolic rate law ...427, 444
  - rate constant .....427, 444
  - rate constant versus recip-  
    rocal of temperature.430-431
  - stainless steel, type 304
    - pretreatment to form pref-  
  erential oxides ....415-417
    - effect of oxygen con-  
    centration ..... 416
    - effect of partial pressure  
    of oxygen on rate..409-411
    - effect of temperature on  
    rate .....410-411
    - effect of time on rate 409-412

## SUBJECT INDEX

### Oxidation (cont.)

- stainless steel, type 410
  - effect of structure on oxidation characteristics 417-418
  - effect of temperature ..417-418
- stainless steels .....
  - .....405, 410-411, 417-418
- equipment for determining .....406-407
- literature survey .....405-406
- mathematical representation
  - of rate law ...410, 417-419
  - exponent n versus temperature .....418-419
- procedure for determining .....407-409
- rupture of scales .....411-413
  - effect of composition on time for rupture...412-413
  - effect of rate of oxide formation ..... 411
- variation with temperature.405
- equation ..... 405

### Oxidation tests .....1114-1117

- stainless steels ..... 1116
  - type 304 ..... 1116
  - type 316 ..... 1116
- titanium-chromium alloys
  - .....1114-1118

### Oxides

- stainless steel, type 304....
  - .....413-415, 421
  - composition .....414-415, 421
  - effect of oxidation time 414
- stainless steel, type 430.... 415
  - composition ..... 415
  - effect of oxidation time 415

### Pearlitic steels

- Charpy impact ..... 1181
  - effect of alloying elements
    - .....1183-1186, 1189-1200
- impact energy versus temperature .....1187-1188
- maximum energy versus reduction in area of tensile test ..... 1196
- shape of transition curves 1197
  - effect of alloying elements ...1187, 1197, 1199
  - effect of carbon .....
    - .....1187, 1197-1198

### Pearlitic steels (cont.)

- Charpy impact
  - shape of transition curves
    - effect of manganese...
      - .....1198-1199
    - effect of nickel ...1187, 1198
    - effect of phosphorus ..
      - .....1187, 1198
    - effect of silicon...1187, 1198
  - transition temperatures
    - .....1182-1189
  - additivity of composition effects .....1193-1194
  - additivity of effects of manganese and carbon...1195
  - definition .....1182, 1187
  - effect of aluminum .... 1189
  - effect of boron ..... 1190
  - effect of carbon .....
    - .....1187, 1190, 1207, 1211
  - effect of chromium ...
    - .....1190, 1205, 1211-1213
  - effect of cobalt .....
    - .....1190, 1211, 1213
  - effect of composition ..
    - .....1182, 1187, 1191
  - effect of copper ..... 1190
  - effect of manganese ...
    - .....1190, 1205, 1207
  - effect of manganese-carbon ratio .....1194, 1196, 1208
  - effect of molybdenum
    - .....1190, 1205, 1213
  - effect of nickel .....
    - 1187, 1190, 1207, 1210, 1214
  - effect of nitrogen ..... 1211
  - effect of phosphorus ..
    - 1187, 1191-1192, 1202, 1211
  - effect of silicon .....
    - 1187, 1192-1193, 1202, 1211
  - effect of sulphur ..... 1192
  - effect of tensile strength
    - .....1195-1197
  - effect of titanium ..... 1193
  - effect of vanadium ....
    - .....1193, 1202, 1211
  - mechanisms by which alloying elements may change ...1199-1200, 1207
  - versus reduction of area of tensile test...1196-1197
  - composition .....1176-1179, 1212

## SUBJECT INDEX

### Pearlitic steels (cont.)

- effect of sulphur on lowest temperature of lamination 1192
- effect of sulphur on per cent lamination .....
- grain size .....1177-1181
- per cent pearlite .1177-1179, 1181
- temperatures of transformation .....1177-1182
- tensile properties .....1182-1186

### Permanent magnetism

- theory regarding .....
- .....70, 74, 76-77, 84, 97-99

### Phase diagrams. See Constitution diagrams.

### Photomicrographs

- of nickel-chromium-molybdenum steels during isothermal transformation .....724-727

### Plastic deformation

- associated with cleavage surfaces in ferrite .....937-952

### Plastic flow

- equations .....1035, 1045
- theory .....1034-1036

### Plastic strain

- in stressed metals
- effect on intrinsic strength .....971-975
- influence on latent energy and the latent energy ratio .....977-986

### Plating

- molybdenum. See Molybdenum plating.

### Post test

- compared with new hardenability test .....465-472

### Powder metallurgy

- beryllium .....1052-1069
- bend tests of sintered compacts .....1063-1064
- electrical resistivity of specimens ..... 1064
- cold rolling of sintered compacts .....1064-1067
- effect of annealing.1065-1066

### Powder metallurgy (cont.)

- beryllium
- cold rolling of sintered compacts
- influence on microstructure ..... 1065
- compacting ..... 1056
- effect of pressure on density ..... 1056
- electrical resistivity of sintered ..... 1060
- hardness of sintered compacts ..... 1067
- metallography of compacts ..... 1068
- microstructures of sintered compacts .....1060-1063
- effects of sintering temperature .....1061-1062
- particle size .....1054-1055
- purity .....1054-1056
- sintering .....1056-1060
- in argon ..... 1057
- effect of sintering temperature on density..1057-1058
- effect of sintering temperature on electrical resistance .....1057, 1060
- evaporation of beryllium .....1059-1060
- in vacuum ..... 1057
- twinning .....1065-1066

### Precipitation

- role in magnet alloys
- Alnicos .....73-85
- Cunico .....85, 87-90
- Cunife .....85, 87-90
- general theory .....70, 97-99
- Silmanal .....90-94
- Vectolite .....94-95
- Vicalloys .....95-97

### Preferred orientation

- carbonitrided case
- epsilon phase .....389-390

### President's Annual Address.. 7

### Prestraining

- versus retained ductility of steel .....778-792

### Properties

- of Alcoa aluminum alloy 52S
- after stretching .....124-129



## SUBJECT INDEX

### Properties (cont.)

- effect of hot forming on mechanical properties
  - of aluminum alloy 75S-T6 .....1015-1017
  - of magnesium alloy AZ31X-h .....1015-1017
  - of molybdenum coatings .....112-113, 118-120
  - of permanent magnet material ..... 72
  - of plain chromium steels
    - tensile and impact ....761-777
  - of silver chloride
    - elastic constants .....55-58
    - mechanical .....55-58
    - physical .....62-63
  - of ten engineering alloys at 25 °C and -196 °C
    - Charpy keyhole impact.567-568
    - tensile and fatigue, both notched and unnotched .....552-556
    - Vickers hardness values.. 567
  - transverse ductility of wrought steel products
    - effect of reheat treatment on. See Reheat treatment.
  - of zirconium-iron alloys
    - heat resistance ...899-901, 903
    - hot strength .....899, 903
    - tensile data .....898-899
    - workability ..... 903

### Puron

- composition ..... 428

### Quenching

- three stages in .....490-492

**Quenching constant, H.** See H factor in hardenability of steels.

### Rapid load testing

- arrangement for controlled
  - temperature tests ..... 574
- circulating unit ..... 575
  - alcohol cooling ..... 575
  - oil heating .....575-576
- equipment ..... 572
  - photograph ..... 572
- measuring equipment ..... 575
  - dynamometer ..... 575
  - extensometer ..... 575

### Rapid load testing (cont.)

- period of constant plastic deformation rate ..... 581
- plastic deformation
  - delay time for initiation.581-585
  - effect of stress ..... 582
  - delay time versus stress
    - relation .....582-585
    - effect of temperature.583-585
- procedure .....571-576
- relation between logarithm of delay time and applied stress .....582-585
- specimen ..... 576
  - heat exchanger .....573-575
- static upper yield stress..583-585
- typical record of ..... 581

### Recovery

- of Alcoa aluminum alloy
  - 52S .....122-138
- definition of .....122-123
- results of ..... 122

### Recrystallization

- of Alcoa aluminum alloy
  - 52S .....127-138
- of silver chloride .....51-52

### Reheat treatment

- effect on transverse ductility of wrought steel products
  - calculation of standard deviations ..... 530
- composition of tubes and forgings ..... 527
- heat treatments employed .....527-528
- material tested .....527-528
- other possible advantages of reheat treatment ...542-543
- reasons for not reheat treating .....543-545
- relationship to product
  - acceptability ..... 542
- reliability of conclusions .....539-542
- results and their interpretation
  - multiple heat treatments .....530-532, 539
  - re-quench and temper groups of forgings or tubes .....530-532, 536-537

## SUBJECT INDEX

### Reheat treatment (cont.)

- effect on transverse ductility of wrought steel products
- results and their interpretation
- requench and temper heats
  - of tubes ..530-532, 537-539
- requench and temper individual forgings or tubes
  - .....530-536
- ret tempering groups of forgings .....530-533
- ret tempering individual forgings .....530-532
- summary of results ..543-545
- test procedure .....529-530

### Residual induction

- definition of ..... 72
- of permanent magnet materials ..... 72

### Rheotropic embrittlement of steel

- definition .....779-781
- effect of tempering temperature on ductility ..782-783, 785-792
- effect of tempering temperature on fracture stress .....787-792
- heat treatment of material
  - .....803-804
- material used .....802-803
- of notched specimens ...801-802
- purpose of investigation..781-783
- retained ductility versus prestrain
  - definition of retained ductility .....778-779
- heat treated SAE 1340 steel .....783-792
- three portions of curves.. 781
- two basic types of behavior ..... 779
- specimens and test procedure .....804-805
- and transition temperature of annealed steels ...795-801
- drawing versus prestretching .....800-801
- and transition temperature of SAE 1340 steel .....792-795

### Rolling

- of Alcoa aluminum alloy 52S
- recovery and recrystallization after .....122-138

### Seamless tubes

- steel
  - effect of reheat treatment on transverse ductility. See Reheat treatment.
  - mechanical properties
    - effect of alloying elements .....1129-1137
    - effect of carbon ...1130-1131
    - equations ..... 1130
    - effect of manganese .. .....1130, 1132
    - equations ..... 1130
    - effect of molybdenum.. .....1135-1136
    - effect of nitrogen ..... ....1138-1139, 1142-1143
    - effect of phosphorus .. .....1130, 1133
    - equations ..... 1130
    - effect of silicon ..... ....1130-1132, 1134
    - equations ..... 1132
    - effect of titanium .1132-1135
    - regression equation ... 1136

### Secretary's Annual Report ... 15

### Sensitization

- stainless steels
  - definition ..... 293

### Sigma phase

- in chromium-molybdenum-iron alloys .....833-834, 841-847
- chromium-nickel-molybdenum steel
  - effect of aging time ...164-165
  - microstructures .....163-165
  - effect of aging temperature .....164-165, 167
  - effect of molybdenum ... 166
  - manner of growth ..... 168
  - relation to apparent ferrite content .....165-166
  - transformation of ferrite .....166-167
  - embrittlement ..... 162
  - etchants for detecting ..... 164
  - stainless steel, 19-9 W-Mo
    - Debye diffraction patterns .....234-235
    - literature survey .....226-227

## SUBJECT INDEX

### Sigma phase (cont.)

- stainless steel, 19-9 W-Mo
  - magnetic intensity to detect .....232-233
  - effect of aging temperature .....232-233
  - effect of aging time..232-233
  - effect of solution treatment .....232-233
  - effect of strain hardening .....232-233
- magnetic measurements
  - for detecting ..... 228
- mechanism of formation .....232-233, 235, 237-242
- microhardness ..... 235
- microstructure .....229-232
  - effect of aging temperature .....229-232
  - effect of aging time..229-232
  - effect of solution treatment .....231-232
  - effect of strain hardening .....229-231, 236
- steel, chromium
  - embrittlement ..... 158
  - solubility of carbon in..150-151
- wrought heat resisting steel, 19-9 W-Mo .....226-242

### Sigma phase formation

- steels, high chromium .....
  - .....173-186, 189-190
  - effect of age hardening.173-174
  - effect of alloying elements .....174-175
  - effect of composition on temperature range .... 176
  - effect on macrohardness. 173
  - effect of manganese on tendency ..... 176
  - effect of molybdenum on temperature range .... 176
  - effect of stability of austenitic matrix .....189-190
- rate
  - comparison of cast and wrought material ...
    - .....183-184, 186
  - effect of annealing ..180, 186
  - effect of cold work..178, 185
  - effect of ferrite .....176-178

### Sigma phase formation (cont.)

- steels, high chromium
  - rate
    - effect of manufacturing variables .....181-184, 186
    - effect of rate of solidification .....182-184
    - effect of repeated recrystallization ..... 185
    - effect of rolling temperature .....181-182, 186
    - influence of carbon ... 175
    - influence of free energy 174
    - influence of nitrogen .. 175
    - relation to ferrite in initial structure ..... 174
    - temperature dependence 179
  - threshold time .....145, 148-150, 153-154, 156-158
  - effect of carbon.153-154, 156
  - effect of chromium....
    - .....147-149, 154, 157-158
  - effect of cold work ...
    - .....145, 149-150
  - effect of manganese ... 154
  - effect of pretreatment 159-160
  - effect of silicon ..... 154
  - effect of temperature 148-149
  - temperature of minimum 149

### Silicon-ferrite

- study of fracture of crystals. See under Fracture.

### Silver chloride

- analogy to metals permitting use as transparent metallurgical tool
- alloying of silver chloride 58-61
- castings .....48-51
- cold-worked silver chloride 51
- crystal structure and
  - allotropy ..... 58
- dissimilarities .....63-64
- fabrication .....45-46
- machinability ..... 58
- mechanical properties and
  - elastic constants .....55-58
- melting and casting .....41-45
- metallography .....46-48
- physical properties .....62-63
- recrystallization .....51-52
- stress relief anneal .....52-54



## SUBJECT INDEX

### Slip planes

in fractured ferrite .....952-953

### Solidus temperatures

dilatometric determination for  
magnesium alloys  
apparatus employed ...873-874  
comparison with published  
results .....884-886  
compositions of alloys used 874  
determination of coefficient  
of expansion ...877, 880-886  
dilatometer curves ....874-879  
interpretation of curves  
.....875-886  
effects of creep .....880-886  
factors controlling creep  
.....881-883  
first derivative of dilatometer  
curves .....874-886  
results for magnesium-  
aluminum alloys ....879-882  
results for magnesium-zinc  
alloys .....882-884  
solvus temperatures ..880, 883

### Solvus temperatures

in magnesium alloys  
dilatometric determination of.  
See under Solidus tempera-  
tures.

### Spaulding concentrate process 674

### Specific volume measurements

in studying tempering of  
chromium steels .....511-512

### Spectrophotometer

use in measuring absorption  
spectrum of silver chloride  
.....42-43

### Stainless steels. See also Ferritic stainless steels.

Class I type  
embrittlement during heat  
treatment  
compositions of steels  
tested .....813  
effect of normal moisture  
and steam .....814-821  
magnetic intensity  
apparatus for measuring 228

### Stainless steels (cont.)

oxidation .....404-420  
activation energy..405, 419-420  
equations ..... 405  
18-8S stainless  
tensile and fatigue properties  
effect of notches on at 25 °C  
and -196 °C .....547-570

### Stainless steel, trade designation

19-9 W-Mo  
sigma-phase formation 226-242  
type 304  
carbide form  
effect of cold work ..310-312  
effect of heat treatment  
.....310-312  
effect of interrupted  
quench from annealing  
temperature ..... 302  
effect of sensitization  
time .....299, 305-307  
photomicrographs .....  
299-300, 303-304, 306-307, 311  
carbide precipitation in 290-322  
compositions .....292, 408  
cooling versus heating to  
sensitization temperature  
on rate of carbide  
nucleation .....302-305  
corrosion resistance  
effect of interrupted  
quench from annealing  
temperature ..... 305  
effect of cold work and heat  
treatment on corrosion  
rate .....310-312  
effect of sensitization  
temperature on carbide  
form .....294-300  
effect of sensitization  
temperature on corrosion  
rate .....294-299  
effect of time of sensitization  
on carbide form ..... 299  
electron photomicrographs  
299-300, 303-304, 306-307, 311  
electron photomicrographs  
.....295-297, 299-  
300, 303-304, 306-308, 311, 315  
locus of carbide precipitation  
.....308-309

## SUBJECT INDEX

### Stainless, trade designation (cont.)

- type 304
  - locus of carbide precipitation
  - electron photomicrographs
    - ..... 308
  - method of carbide isolation 293
  - sensitization by interrupted
    - quench from annealing
    - temperature .....305-306
- type 410
  - composition ..... 408
- type 430 .....245-246, 248-249
  - composition .....246, 408
  - critical points ..... 249
  - expansion properties ....
    - .....248-249, 258-259
  - effect of austenite on ..
    - .....248-249, 258-259
- type 446 .....243-250
  - austenite-forming elements
    - in .....244, 248
  - austenite phase .....
    - ..244-245, 247-248, 251, 254
  - effect of composition ..
    - .....245, 251, 254
  - effect on expansion
    - properties .....247-248
  - effect of temperature 251, 254
  - influence of nitrogen .. 244
  - treating temperature versus
    - available chromium to
      - form .....251, 252
  - chromium equivalent of im-
    - purity elements ...252-253
  - comparison of multiplying
    - factors ..... 253
  - commercial applications
    - ....243-244, 254-255, 258-259
  - composition .....243, 245, 248
  - effect of nitrogen on
    - expansion properties .. 245
  - effect of nitrogen on grain
    - size ..... 244
  - effect of nitrogen on tensile
    - properties ..... 244
  - expansion characteristics
    - .....243-245, 257-259
  - effect of austenite formation
    - on .....247-248, 257-259
  - ferrite-forming elements in
    - .....244, 248

### Stainless, trade designation (cont.)

- type 446
  - ferrite/ferrite-austenite
    - boundary
      - effect of composition .. 252
      - effect of temperature .. 252
  - grain size
    - effect on nitrogen ..... 244
  - high temperature oxidation
    - resistance ..... 243
  - microstructure 246-251, 256-257
    - effect of carbon ..... 249
    - effect of manganese ... 249
    - effect of nickel ..... 250
    - effect of silicon ..... 250
    - effect of temperature on
      - .....249-250, 256-257
  - tensile properties
    - effect of nitrogen ..... 244

### Static stress versus strain

- mild steel
  - effect of temperature ..577-580

### Static tension

- test procedure .....576-577

### Statistical analysis

- seamless steel tubes
  - effect of alloying elements
    - on mechanical properties
      - .....1126-1137
  - effect of 0.01% increment
    - of various elements .. 1136
  - literature survey ..1126-1127
  - procedure ..... 1129

### Steam

- in heat treating atmospheres
  - embrittling effect on stainless
    - steels .....814-821

### Steel

- activation energy for isothermal
  - grain growth .....279-280
- aluminum coating of ....587-605
- austenite grains
  - effect of shape on growth
    - .....281-285, 288-289
  - influence of time at
    - austenitizing temperature
      - on shape .....279-285
- austenitizing time vs. reciprocal
  - absolute temperature .....281

## SUBJECT INDEX

### Steel (cont.)

- chromium. See Chromium
- steels, plain.
- tempering of. See under Tempering of.
- chromium-molybdenum-manganese
  - isothermal transformation. See under Isothermal transformation.
- coarse grain type
  - influence of austenitizing temperature on grain size ...263, 268-269, 271, 275, 284
  - influence of austenitizing time on grain size .....263-267, 275, 284
  - isothermal austenite grain growth ..... 277
- deep hardening
  - hardenability test. See Hardenability test.
- fine grain type
  - influence of austenitizing time on grain size ... ..263-266, 269-275, 284
  - photomicrographs ..... 264
- grain growth, rate of
  - influence of austenitizing temperature .....279-280
  - influence of grain size ... ..278-280, 284
- grain size (austenite)
  - influence of austenitizing temperature .....260-285
  - influence of austenitizing time .....263-285
  - photomicrographs ..... 264
  - influence of carbides ..277, 285
  - influence of deoxidation practice .....273-276, 285
  - influence of inclusions ... ..273-276, 285, 289
  - influence of nitrogen .... 276
  - influence of the steelmaking process .....276, 285
  - isothermal growth in coarse-grained steels ..277-278, 285
  - relation between grain coarsening and residual aluminum .....274-276, 285
  - graphitization .....692-711

### Steel (cont.)

- H factor. See H factor in hardenability of steels.
- Hy-Tuf steel
  - tensile and fatigue properties
  - effect of notches on at 25 °C and -196 °C .....547-570

### Steel, mild

- nickel-chromium-molybdenum
  - isothermal transformation. See under Isothermal transformation.
- rheotropic embrittlement in. See Rheotropic embrittlement of steel.
- strain hardening characteristics at low temperature ..1033-1050
- temper brittleness. See Temper brittleness.
- time delay for yielding ..571-586
- influence of temperature .....571-586

### Steel, trade designation

- NE 8630
  - tensile and fatigue properties
  - effect of notches on at 25 °C and -196 °C .....547-570
- SAE 1010
  - fractographic study of fatigue .....958-959, 966-967
- SAE 2330
  - tensile and fatigue properties
  - effect of notches on at 25 °C and -196 °C .....547-570
- SAE 3140
  - composition ..... 645
  - effect of strain rate on ductility .....644-650
  - effect of strain rate on transition temperature .....644-648
  - energy absorption versus test temperature .... 646
  - Charpy impact .....646-648
  - slow bend test .....645-648
- SAE 4130
  - fractographic study of fatigue .....958-959, 967



## SUBJECT INDEX

### Steel, trade designation (cont.)

- SAE 4340
  - tensile and fatigue properties
  - effect of notches on at 25 °C and -196 °C .....547-570
- wrought
  - effect of reheat treatment on transverse ductility.
  - See Reheat treatment.

### Strain aging

- aluminum
  - high-purity ..... 1219
  - 2S .....1218-1219
- brass .....1218-1219
- copper .....1218-1219
- duralumin .....1218-1219
- effect of temperature ..... 1219
- literature survey .....1215-1216
- Monel .....1218-1219
- nickel .....1218-1219

### Strain energy

- aluminum, 2S
  - influence of temperature .....1229, 1231, 1237-1240
  - variation with plastic strain .....1229, 1231
- of stressed metals
  - effect of temperature on .....986-991
  - total strain energy relationships .....975-977

### Strain rate

- SAE 3140 steel
  - effect on transition temperature .....644-648

### Strength

- intrinsic strength of metals
  - as affected by plastic strain and temperature ....971-975

### Stresses, biaxial tension-compression

- applied to aluminum alloys
  - 2S-O and 24S-T
  - effect on mechanical behavior .....903-1012

### Stress relief

- of silver chloride .....52-54

### Stress rupture

- specimen ..... 614

### Stress rupture (cont.)

- titanium-chromium alloys .....1114-1115

### Stress-strain

- energy relationship for metals
  - fundamental stress-strain energy relationship ..990-991
- influence of plastic strain
  - on latent energy and the latent energy ratio ..977-986
- influence of temperature
  - on flow stress ..... 975
- influence of temperature
  - on strain energy ....986-991
- intrinsic strength as affected
  - by temperature and plastic strain .....971-975
- total strain energy, work
  - hardening energy and latent energy .....975-977

### Stress-strain curves

- for silver chloride .....40, 54-56

### Stress-strain energy relations

- for various strength states .....1228-1231
- influence of temperature .....1229-1231

### Stress-strain relations

- for biaxial tension-compression
  - of aluminum alloys 2S-O and 24S-T
  - constant stress ratio test results ..... 1001
  - determination in terms of simple tension values 994
  - elastic combined stress-strain relations ..1002-1004
  - generalized deformation theory for ..994-995, 1011
  - generalized stress-strain relations .....1008-1009
  - material tested .....995-996
  - mechanical properties 995-996
  - method of measuring strains .....998-999
  - methods of testing .... 999
  - plastic combined stress-strain relations ..1004-1007
  - production applicability of relations .....993-994

## SUBJECT INDEX

### Stress-strain relations (cont.)

- for biaxial tension-compression  
of Al alloys 2S-O and 24S-T  
tension test results..999-1000
- testing machine .....996-998
- test specimens used ... 996
- variable combined stress  
test results .....1009-1010

### Stretching

- of Alcoa aluminum alloy 52S  
recovery and recrystallization  
after .....122-138

### Structure

- of molybdenum plate ....110-120
- of permanent magnet alloys
- Alnicos .....74-75
- Cunico .....86-89
- Cunife .....86-89
- Silmanal .....92-94
- Vectolite .....94-95
- Vicalloys .....95-96

### Surface tension

- grain boundary  
equations for changes in  
.....735-738

### Tantalum

- in aluminum-silicon alloy  
effect on grain size ..... 639
- in aluminum-silicon-magnesium  
alloy  
effect on grain size ..... 640

### Technical Program and Reports of

- Officers, ASM—32nd Annual  
Convention, Chicago, October  
21 to 27, 1950 ..... 1

### Temper brittleness

- in steel  
theory of mechanism ..739-747
- effect of alloying elements  
.....741-742
- typical microstructures  
.....742-744

### Tempering of

- chromium steels  
hardness changes ..... 515
- effect of chromium on  
.....514-516, 521, 524

### Tempering of (cont.)

- chromium steels  
materials investigated 498-499
- structural components of  
.....499-500
- structural changes during  
first stage .....497-498
- definition of first stage  
.....497-498
- structural changes during  
fourth stage .....509-516
- definition of fourth stage 498
- electrolytic isolation of  
the carbides .....512-515
- electron microscopy of  
.....510-511, 518-519
- heat of activation of  
decomposition ..... 513
- metallographic study of  
.....509-511, 521-525
- specific volume measure-  
ments in studying..511-512
- structural changes during  
second stage .....  
.....498-509, 515-516
- decomposition equations  
.....503-505
- definition of second stage  
..... 498
- dilatometer measurements  
in studying .....499-502
- heat of activation of  
decomposition ....504, 508
- magnetic measurements  
in studying .....500-502
- metallographic study of  
.....503, 521-525
- structural changes during  
third stage ...498-509, 516
- decomposition equations  
.....503-505, 508
- definition of third stage  
..... 498
- dilatometer measurements  
in studying .....  
.....499-502, 505-508
- heat of activation of  
decomposition ....504, 508
- magnetic measurements  
in studying .....  
.....500-502, 508-509

## SUBJECT INDEX

- Tempering of (cont.)**  
 chromium steels  
   struct. changes during 3rd stage  
   metallographic study of  
     .....503, 521-525  
 steel  
   effect of temperature on  
     ductility ....782-783, 785-792  
   effect of temperature on  
     fracture stress .....787-792
- Tensile properties**  
 at low temperatures  
   of ten engineering alloys,  
   notched and unnotched  
     .....552-555  
 nickel-aluminum-molybdenum  
   alloys ..... 217  
 pearlitic steels .....1182-1186  
 stainless steel, type 446.... 244  
   effect of nitrogen ..... 244  
 titanium-chromium alloys ..  
   .....1111-1114
- Tensile strain**  
 relation to torsional strain..  
   .....1035-1036
- Tensile stress**  
 aluminum 2S  
   influence of plastic strain..1222
- Tensile test**  
 strain hardening exponent  
   variation with temperature  
     .....1048-1049  
 strength coefficient  
   variation with temperature  
     .....1047-1048
- Tension-compression biaxial stresses**  
 applied to aluminum alloys  
   2S-O and 24S-T  
   effect on mechanical behavior  
     .....993-1012
- Testing for**  
 H factor in hardenability of  
   steels .....480-496
- Tests**  
 bar-bend test  
   use in studying embrittlement  
     of stainless steel  
   by normal moisture and  
   steam .....814-821
- Tests (cont.)**  
 hardenability. See Harden-  
   ability test.  
 Jominy. See Jominy test.  
 Post. See Post test.
- Thermal analysis**  
 of chromium-molybdenum-iron  
   alloys .....829-830, 833-842  
 of indium-cadmium-zinc alloys  
   .....857-862, 868-870  
 of zirconium-iron system.892-896
- Thermal conductivity**  
 use in determining H factor  
   .....480-496
- Thermal diffusivity**  
 use in determining H factor  
   .....480-496
- Thermal expansion coefficients**  
 Invar .....1072-1096
- Thermal treatments**  
 of chromium-molybdenum-iron  
   alloys  
   effect on solid phase dis-  
   tribution .....834-842
- Thermodynamics**  
 of interfaces .....735-738
- Titanium**  
 in aluminum-silicon alloy  
   effect on grain size....639, 642  
 in aluminum-silicon-magnesium  
   alloy  
   effect on grain size ....640-642  
 density ..... 1098  
 melting point ..... 1098  
 role in magnet alloys .....79-80  
 tensile and fatigue properties  
   effect of notches on at 25  
   °C and -196 °C .....547-570
- Titanium-chromium alloys**  
 arc furnace melting .....  
   .....1100-1102, 1107-1110  
 chemical purity of alloys  
   .....1108-1110  
 crucibles .....1102, 1107  
 Charpy impact .....1114-1115  
 diffraction patterns ..... 1121  
 forgeability .....1104, 1108



## SUBJECT INDEX

### Titanium-chromium alloys (cont.)

- forgeability
  - method ..... 1104
  - range ..... 1108
  - temperatures ..... 1108
- gas contents
  - methods of analyses .... 1104
- hardness ..... 1110-1111, 1113
  - effect of annealing... 1110-1111
  - effect of forging..... 1110-1111
  - effect of quenching temperature ..... 1110, 1113
- hot hardness 1104-1105, 1110-1111
  - forged alloys ..... 1110-1111
  - methods ..... 1104-1105
- induction furnace for melting ..... 1100-1101
- literature survey ..... 1099-1100
- methods of preparation 1103-1104
- oxidation tests ..... 1114-1117
  - effect of composition 1115-1118
  - effect of testing temperature ..... 1115-1117
  - effect of time ..... 1116, 1118
- refractory crucibles for induction melting .1102, 1106-1107
  - effect on ingot composition ..... 1106-1107
- stress-rupture properties ..... 1114-1115
- structures ..... 1117-1122
  - effect of composition. 1117-1122
  - effect of treatment .. 1118-1122
- tensile properties ..... 1111-1114
  - effect of composition. 1113-1114

### Tool steels

- compositions ..... 1147
- finishability ..... 1163-1165
- grindability ..... 1144-1174
- grindability index 1151, 1154-1165

### Torsional strain

- relation to tensile strain 1035-1036

### Torsion test

- apparatus ..... 1037-1039
- effective stress versus effective strain ..... 1045-1046
- steel, mild
  - fractures ..... 1043-1045
  - effect of temperature.. ..... 1043-1045

### Torsion test (cont.)

- steel, mild
  - mechanical properties ... 1041
  - torque versus twist.. 1040-1043
    - effect of temperature.. ..... 1040-1043
  - twist versus time ..... 1042
    - effect of temperature.. ..... 1042-1043
  - yield point twisting.. 1041-1042
- strain gages ..... 1037-1039
- strain hardening exponent
  - variation with temperature ..... 1048-1049

### Transformation - temperature - time diagrams for steel. See also

- isothermal transformation.
- chromium-molybdenum-manganese steels ..... 725-729
- nickel-chromium-molybdenum steels ..... 721-725

### Transition temperature

- of annealed steels
  - and rheotropic embrittlement ..... 795-801
- of SAE 1340 steel
  - and rheotropic embrittlement ..... 792-795
- SAE 3140 steel
  - effect of strain rate ... 644-648

### Transparency

- of silver chloride ..... 42-45
  - effect of chlorination on.. 43-45
  - effect of fluorescent lighting on ..... 42-43

### Treasurer's Annual Report .. 11

### Tubes

- seamless steel
  - effect of reheat treatment on transverse ductility. See Reheat treatment.

### Tungsten

- in aluminum-silicon alloy
  - effect on grain size ..... 639
- in aluminum-silicon-magnesium alloy
  - effect on grain size ..... 640

## SUBJECT INDEX

### Ultimate stress

- aluminum
  - effect of temperature 1217-1218
- aluminum 2S
  - effect of temperature 1217-1218
- brass
  - effect of temperature 1217-1218
- copper
  - effect of temperature 1217-1218
- duralumin 24S-T
  - effect of temperature ... 1217-1218, 1220
- Monel
  - effect of temperature 1217-1218
- nickel
  - effect of temperature 1217-1218
- slope of curve
  - influence of direct temperature factor .....1220-1221
  - influence of intrinsic strength factor .....1220-1222

### Vanadium

- role in magnet alloys .....95-96

### Vilella's reagent .....164, 177, 200

### Wiberg furnace .....669-670

### Workability

- of zirconium-iron alloys ... 903

### Work hardening energy

- aluminum 2S
  - influence of temperature .....1231, 1237-1238
  - influence of plastic strain 1231
- relationship of stressed metals .....975-977

### Wrought steel

- effect of reheat treatment on transverse ductility ...526-546

### X-ray

- diffraction analysis
  - of chromium-molybdenum-iron alloys 831-834, 840-842
  - of indium-cadmium-zinc alloys .....860-867

### X-ray (cont.)

- study of cleavage
  - of silicon-ferrite crystals .....912-921
- study of cleavage surfaces
  - in ferrite .....935-953
- study of magnet alloys
  - Alnicos .....73-75, 79
  - Cunico .....86-87
  - Cunife .....86-87
  - Silmanal .....90, 92
  - Vectolite .....94-95
  - Vicalloys .....95-96
- study of recrystallization in Alcoa 52S alloy .....127-131, 133-135
- study of zirconium-iron system .....894-897

### Yield stress

- aluminum 2S
  - effect of temperature 1217-1218
- duralumin 24S-T
  - effect of temperature ... 1217-1218, 1220

### Young's modulus

- Invar ..... 1082

### Zirconium

- in aluminum-silicon alloy
  - effect on grain size..... 639, 641-642
- in aluminum-silicon-magnesium alloy
  - effect on grain size ..... 640

### Zirconium-iron alloys

- constitution diagram ....901-903
- development of .....888-901
- effect of iron on properties 903
- heat resistance .....899-901, 903
- hot strength .....899, 903
- tensile data
  - for cold-worked alloys .898-899
  - for drawn alloys ..... 898
  - for hot-rolled alloys ..... 898
  - for quenched alloys ..... 898
- workability ..... 903

